QL
401
.M15X
12

MALACOLOGIA

International Journal of Malacology

ol. 57(1)
2014

MALACOLOGIA
http://malacologia.fmnh.org

World's Leading Malacological Journal
Journal Impact Factor 1.592 (2012)

Founded in 1961

EDITOR-IN-CHIEF
GEORGE M. DAVIS

Editorial Office
Malacologia
P.O. Box 1222
West Falmouth, Massachusetts 02574, U.S.A.
georgedavis99@hotmail.com

Business & Subscription Office
Malacologia
P.O. Box 385
Haddonfield, New Jersey 08033, U.S.A.
malacologia@comcast.net

Copy Editor
EUGENE COAN
Santa Barbara Museum of Natural History
Santa Barbara, California, U.S.A.
genecoan@gmail.com

Associate Editor
JOHN B.BURCH
University of Michigan
Ann Arbor, Michigan, U.S.A.
jbburch@umich.edu

Managing Editor
CARYL HESTERMAN
Haddon Heights, New Jersey, U.S.A.
malacologia@comcast.net

Composition Editor
CLAUDIA WILKE
Giessen, Germany
claudiawilke@hotmail.com

Graphics Editor
THOMAS WILKE
Justus Liebig University
Giessen, Germany
tom.wilke@allzool.bio.uni-giessen.de

MALACOLOGIA is published by the INSTITUTE OF MALACOLOGY

Board of Directors - U.S.A.:

President

PAULA M. MIKKELSEN
Paleontological Research Institution, Ithaca, New York

Vice President

DIARMAID Ó FOIGHIL
University of Michigan, Ann Arbor

Secretary and Treasurer

GEORGE M. DAVIS
West Falmouth, Massachusetts

Members

RÜDIGER BIELER
Field Museum, Chicago, Illinois

JOHN B. BURCH
University of Michigan, Ann Arbor

CAROLE S. HICKMAN
University of California, Berkeley

ALAN KOHN
University of Washington, Seattle

ELLEN STRONG
National Museum of Natural History, Washington D.C.

Copyright © 2014 by the Institute of Malacology
ISSN: 0076-2997 (Print)
ISSN: 2168-9075 (Online)

VOL. 57, NO. 1 EDITORIAL BOARD 2014

J. A. ALLEN
Marine Biological Station
Millport, United Kingdom

T. ASAMI
Shinshu University
Matsumo, Japan

T. BACKELJAU
University of Antwerp
Antwerp, Belgium

B. BAUR
Universität Basel
Basel, Switzerland

D. BLAIR
James Cook University
Townsville, Australia

P. BOUCHET
Muséum National d'Histoire Naturelle
Paris, France

R. A. D. CAMERON
University of Sheffield
Sheffield, United Kingdom

J. G. CARTER
University of North Carolina
Chapel Hill, North Carolina, U.S.A.

R. CIPRIANI
California State University
Fullerton, California

T. COLLINS
Florida International University
Miami, Florida, U.S.A.

R. H. COWIE
University of Hawaii
Honolulu, Hawaii, U.S.A.

G. CUEZZO
Universidad Nacional de Tucumán
Tucumán, Argentina

B. DAYRAT
University of California
Merced, California, U.S.A.

B. DEGNAN
University of Queensland
Brisbane, Australia

D. J. EERNISSE
California State University Fullerton
Fullerton, California, U.S.A.

D. GEIGER
Santa Barbara Museum of Natural History
Santa Barbara, California, U.S.A.

G. GIRIBET
Harvard University
Cambridge, Massachusetts, U.S.A.

E. GITTENBERGER
Naturalis Biodiversity Center
Leiden, The Netherlands

F. GIUSTI
Università di Siena
Siena, Italy

M. GLAUBRECHT
Museum of Natural History Berlin
Berlin, Germany

D. GRAF
University of Wisconsin
Stevens Point, Wisconsin, U.S.A.

E. HARPER
University of Cambridge
Cambridge, United Kingdom

G. HASZPRUNAR
Zoologische Staatssammlung München
München, Germany

K. HAYES
University of Hawaii
Honolulu, Hawaii, U.S.A.

K. E. HOAGLAND
Independent Consultant
Falmouth, Massachusetts, U.S.A.

M. HORSAK
Masaryk University
Drno, Czech Republic

C. ITUARTE
Museo Argentino de Ciencias Naturales
Buenos Aires, Argentina

M. S. JOHNSON
University of Western Australia
Crawley, Australia

SMITHSONIAN
AUG 25 2015
LIBRARIES

G. KAMENEV
Institute of Marine Biology
Vladivostok, Russia

Y. KANTOR
Russian Academy of Sciences
Moscow, Russia

F. KOEHLER
Australian Museum
Sydney, Australia

T. KONDO
Osaka Kyoiku University
Osaka, Japan

K. A. LUTAENKO
Institute of Marine Biology
Vladivostok, Russia

C. LYDEARD
Western Illinois University
Macomb, Illinois, U.S.A.

BRUCE A. MARSHALL
Museum of New Zealand Te Papa Tongarewa
Wellington, New Zealand

J. NEKOLA
University of New Mexico
Albuquerque, New Mexico, U.S.A

T. OKUTANI
Tokyo University of Fisheries
Tokyo, Japan

L. PAGE
University of Victoria
Victoria, BC, Canada

G. PAULEY
Florida Museum of Natural History
Gainesville, Florida, U.S.A.

R. PIPE
The Marine Biological Association
Plymouth, United Kingdom

W. F. PONDER
Australian Museum
Sydney, Australia

T. RAWLINGS
Cape Breton University
Nova Scotia, Canada

T. SASAKI
University Museum, University of Tokyo
Tokyo, Japan

L. R. L. SIMONE
Museu de Zoologia da Universidade
de São Paulo, Brazil

P. TATTERSFIELD
Tideswell, Buxton
United Kingdom

C. THIRIOT
University Pierre et Marie Curie
Paris, France

S. TILLIER
Muséum National d'Histoire Naturelle
Paris, France

Á. VALDÉS
California State Polytechnic University
Pomona, California, U.S.A.

J. VOIGHT
Field Museum Natural History
Chicago, Illinois, U.S.A.

A. WARÉN
Museum of Natural History
Stockholm, Sweden

M. WU
Hebei University
Hebei, China

ELECTRONIC ACCESS TO *MALACOLOGIA*

Malacologia is available on line, with volumes 1 (1962) to 48 (2006) freely accessible via the *Biodiversity Heritage Library* (BHL; a consortium of natural history and botanical libraries that cooperate to digitize and make accessible the legacy literature of biodiversity held in their collections), and most recent numbers obtainable from *BioOne*, a global not-for-profit collaboration of scientific publishers and libraries:
BHL (www.biodiversitylibrary.org): *Malacologia* grants open access to electronic copies of all pre-2007 volumes, which can be read and downloaded at http://www.biodiversitylibrary.org/bibliography/12920.

BHL
Biodiversity Heritage Library

BioOne (www.bioone.org): *Malacologia* is part of the BioOne.2 collection of scientific journals. Access is available to institutions and consortia holding BioOne subscriptions (see the BioOne web site for details). In addition, subscribers to the *Malacologia* print edition are given access to this journal on BioOne. To be granted such individual access, contact the subscription office at malacologia@comcast.net.

BioOne™ RESEARCH EVOLVED

ANNOUNCEMENT

The J Frances Allen Institute of Malacology Outstanding Student Publication Award

The Board of Directors of the Institute of Malacology, publisher of the academic journal *Malacologia*, is pleased to announce the creation of the J Frances Allen Institute of Malacology Outstanding Publication Award. This cash award of $500 will be presented for an outstanding paper published in *Malacologia* by a student, with the timing dependent on the superior quality of the student paper as judged by a committee of the IM Board. There is no formal application or deadline. A student submitting a manuscript must be sole or senior author of the paper, and should indicate that the paper being submitted stems from Master's or Ph.D. research to confirm his or her eligibility for the award. The Allen Publication Award was established in 2011 to honor J Frances "Jady" Allen, who provided indispensable help and guidance in establishing the journal *Malacologia*, first published in 1962.

MALACOLOGIA, 2014, 57(1): 1–97

DECONSTRUCTING *DENDROPOMA*: A SYSTEMATIC REVISION OF A WORLD-WIDE WORM-SNAIL GROUP, WITH DESCRIPTIONS OF NEW GENERA (CAENOGASTROPODA: VERMETIDAE)

Rosemary E. Golding[1,2], Rüdiger Bieler[1*], Timothy A. Rawlings[3] & Timothy M. Collins[4]

ABSTRACT

Identifying natural groups within the caenogastropod family Vermetidae has proven challenging. The sessile lifestyle of vermetids, with associated xenomorphically distorted, overgrown and corroded shells, has resulted in a long and confused taxonomic history based primarily on adult shell characters. In this study, we use morphological, anatomical and molecular data to clarify systematics and phylogenetic relationships within the genus *Dendropoma s.l.* We assess generic names previously used in the Dendropoma group for availability and recognize *Veristoa* Iredale, 1937, as a junior synonym of *Dendropoma* Mörch, 1861. We describe 21 species, eight of which are new, place them into four robustly supported genera (*Dendropoma s.s.*; *Novastoa* Finlay, 1926; *Ceraesignum* n. gen.; *Cupolaconcha* n. gen.), and outline the current state of knowledge of the distribution of these taxa. The genus *Dendropoma s.s.* is well supported in our phylogenetic analysis and is additionally supported by features of the operculum, reproductive traits and a novel mitochondrial gene order. Among the four genera, members of *Dendropoma s.s.* alone maintain unstalked egg capsules in the mantle cavity rather than attaching them to the shell via a slit in the female mantle. The opercula of examined species within the genus *Novastoa* are characterized by a well-developed mammilla on the internal surface and upright tightly packed spiral lamina on the external surface. In *Ceraesignum* n. gen., the operculum lacks a mammilla and displays a fingerprint-like texture on its inner surface. The genera *Ceraesignum* n. gen. and *Novastoa* form a well-supported monophyletic group with the genus *Dendropoma s.s.*, although sister group relationships among these genera are not resolved. The fourth genus, *Cupolaconcha* n. gen. is more closely related to the vermetid genera *Eualetes* Keen, 1971a, *Thylaeodus* Mörch, 1860, and *Petaloconchus* Lea, 1843, demonstrating that *Dendropoma s.l.* is not a monophyletic group. The calcified operculum of *Cupolaconcha* n. gen. is unique in the Vermetidae and examined species in this genus are also characterized by a translocation of the valine mitochondrial tRNA. Further study will encompass the full range of morphological diversity in the Vermetidae to clarify the major lineages within this remarkable family of snails.

Keywords: Taxonomy, evolution, reef-forming organisms, protoconch morphology, gene sequence order, molecular phylogeny.

INTRODUCTION

The caenogastropod family Vermetidae comprises at least 160 extant species of sessile, suspension-feeding, irregularly coiled marine snails found in warm temperate and tropical oceans around the world. The taxonomy and nomenclatural history of this family of "worm-snails" is notoriously confused (Keen, 1961; Bieler & Petit, 2011), however, in part because their uncoiled and attached tubes defy traditional classifications based on adult shell characters, in part because of a long and complex history that commingled nominal gastropod and polychaete taxa. Among the now recognized subgroups of Vermetidae is the genus *Dendropoma* Mörch, 1861, a name introduced by Mörch (1861: 153) as a Section of *Siphonium* (see below) and based on the type species, by subsequent designation of Keen (1961: 189), *Siphonium* (*Dendropoma*) *lituella* Mörch, 1861.

[1]Invertebrates, Field Museum of Natural History, 1400 Lake Shore Drive, Chicago, Illinois 60605, U.S.A.
[2]Malacology, Australian Museum, 6 College Street, Sydney, NSW 2010, Australia
[3]Department of Biology, Cape Breton University, 1250 Grand Lake Road, Sydney, Nova Scotia, B1P 6L2, Canada
[4]Department of Biological Sciences, Florida International University, 11200 SW 8th St., Miami, Florida 33199, U.S.A.
*Corresponding author: rbieler@fieldmuseum.org

The *Dendropoma* group is thought to include a wide range of vermetid species and morphologies, ranging from the large and conspicuous coral reef dweller *Dendropoma maximum* (G. B. Sowerby I, 1825) of the Indo-Pacific (with a concave, corneous saucer-shaped operculum), to gregarious *Dendropoma corrodens* (d'Orbigny, 1841) of the Caribbean (with a conical operculum constructed of a spiral corneous lamella), to *Dendropoma meroclistum* Hadfield & Kay, 1972, from the Hawaiian Islands (with a bi-layered, partly calcified operculum).

Focusing on aspects of protoconch morphology, Bandel & Kowalke (1997: 260 ff.) separated *Dendropoma s.l.* (specifically including *D. maximum* and *D. meroclistum*) from the remaining Vermetidae in a new subfamily "Dendropominae" (emended to Dendropomatinae by Bieler & Petit, 2011: 11). The new nominal subfamily was described as including "vermetid gastropods with irregular teleoconch and regular protoconch with a cancellate sculpture").

There are probably at least a few dozen living species belonging to *Dendropoma s.l.*, but their number cannot yet be estimated with any confidence for three reasons: (1) Historic under-sampling: these sessile and often cryptic organisms are rarely collected during general collecting efforts and often excluded from regional biodiversity studies. (2) Taxonomic uncertainty: original species descriptions (and type specimens that often consist of tube fragments from vaguely indicated localities) cannot always be clearly recognized and linked to living populations. Their sessile mode of life allows rafting on natural and man-made structures and thus potential dispersal across oceans, confounding regional revisionary studies. Also, the past near-random allocation of generic names, including both gastropods and polychaetes (e.g., genus *Serpula* Linnaeus, 1758, type of polychaete family Serpulidae) makes it extremely difficult to recognize subsets among the some 1,300 species-group names that have been in use for worm-snails (Bieler & Petit, 2011). (3) Hidden diversity in species complexes; recent molecular work by Calvo et al. (2009) has shown that the "well-recognized" reef building species *Dendropoma petraeum* (Monterosato, 1884) represents a species complex. Likewise, Faucci (2007) appears to have identified numerous cryptic species within her phylogeographic survey of six vermetid species across the Pacific.

The lack of a reliable taxonomic infrastructure for the Vermetidae has proved particularly challenging for marine ecologists given that vermetids are a significant element of many marine warm temperate and tropical ecosystems. Within these environments, vermetids are well recognized for their role in habitat creation and modification, as well as interactions with other sessile animals. For instance, various species of *Dendropoma* are gregarious and form structurally complex platforms ("trottoirs") and reefs in the subtropical and tropical waters of the Mediterranean, Bermuda, Brazil, Cape Verde Islands and Mexico (e.g., Antonioli et al., 1999). While otherwise poorly studied, these biogenic structures are known to greatly enhance regional fish diversity and support a rich community of endolithic organisms, including crustaceans, polychaetes, sponges, sipunculids and bivalves (Thomas & Stevens, 1991; Goren & Galil, 2001). Reef-building vermetids have thus been considered critical "ecosystem engineers" in the marine environment (Coleman & Williams, 2002) – organisms that through morphological complexity have profound effects on local biodiversity. Changes in the abundance and distribution of reef-building vermetids can also have broader effects by influencing water flow, sedimentation and larval settlement patterns. Such responses have been noted with the loss of the rim of *Dendropoma* reefs along the rocky Mediterranean shores of Israel and the associated proliferation of invasive Red Sea mussels *Brachidontes pharaonis* (P. Fischer, 1870) (Rilov et al., 2004).

Vermetids, including *Dendropoma s.l.*, are also well represented in sensitive and threatened marine habitats, including coral reefs (e.g., Peyrot-Clausade et al., 1992; Gischler & Ginsburg, 1996). Although their interactions with other coral reef organisms are poorly understood, *Dendropoma maximum* and a guild of other vermetids including *D. platypus*, *D. meroclistum* and *D. gregarium*, appear to negatively affect the growth, morphology and survival of reef building corals (Zvuloni et al., 2008; Shima et al., 2010, 2013). Such responses may be the direct or indirect effects of mucus "feeding nets" deployed by reef-dwelling vermetids (Zvuloni et al., 2008). Although such deleterious effects on corals can be ameliorated locally when protective guard crabs are present (Stier et al., 2010), reefs in the Red Sea and South Pacific are currently experiencing marked increases in vermetid density, a possible byproduct of human activities in coastal waters (e.g., eutrophication, species introductions, coastal development) (Zvuloni et al., 2008; Shima et al., 2013). This dramatic change in baseline community structure underscores the need to understand more fully the complex set of interrelationships among vermetids, corals, and other reef-dwelling organisms.

Knowledge of vermetid systematics and ecology is also becoming increasingly important to the field of paleoclimatology. Vermetids are extremely reliable tools for interpreting past sea-level, sea temperature and productivity (e.g., Schiaparelli et al. 2006; Vescogni et al., 2008; Sisma-Ventura et al., 2009), and consequently, of great importance for predicting future climatic trends. For instance, *Dendropoma* spp. and *Petaloconchus varians*, with their low intertidal distribution and purported narrow bathymetric ranges, have provided sea level estimates for the Brazilian coast spanning the entire Holocene period (e.g., Laborel et al., 2000), with a hypothesized precision of 0.40–1.00 m (e.g., Angulo et al., 1999, 2002). Similar paleoclimatological studies have been conducted in the Mediterranean based on *D. petraeum* (e.g., Morhange & Pirazzoli, 2005). Because of their often ubiquitous occurrence in temperate zones (in contrast to stony corals) and the possibility of performing ^{14}C age determinations, vermetids are now formally used as Sea Surface Temperature (SST) proxies (Silenzi et al., 2004). Confusion regarding species' identities and their true bathymetric ranges, however, is leading to concern over the widespread and uncritical use of vermetids as reliable paleoclimatic indicators, reinforcing the need for further systematic work (e.g., Schiaparelli et al., 2006).

To date, a molecular approach has not been formally employed as part of a systematic revision of the Vermetidae or its component groupings. Molecular tools and techniques have been applied to vermetids over the past decade, however, in an effort to interpret species boundaries (Calvo et al., 2009; Weinberger et al., 2010), explore phylogeographic structure (Faucci, 2007), as well as to place the Vermetidae within the context of caenogastropod evolution (e.g., Colgan et al., 2007; Criscione & Ponder, 2012). Such studies have convincingly demonstrated the utility of fast evolving mitochondrial DNA (mtDNA) genes (*COI*, *rrnS*, *rrnL*) and nuclear genes (*H3*, *28S rRNA*, *ITS*) in helping to discriminate among populations and species of vermetids (Faucci, 2007; Calvo et al., 2009), to identify cryptic species (Faucci, 2007; Calvo et al., 2009), to highlight cases of likely species introductions (Faucci, 2007; Weinberger et al., 2010), as well as to infer the role of physical processes on the pattern of speciation and divergence of vermetid taxa (Faucci, 2007). Evidence of multiple mitochondrial gene order rearrangements within the Vermetidae has also suggested the possibility of using derived mtDNA gene order patterns to define monophyletic lineages of vermetids (Rawlings et al., 2001, 2010). A molecular approach thus holds great potential for helping to build a stable taxonomic framework for this family.

This study aims to examine the systematic diversity and evolutionary relationships of the group of worm-snails currently assigned to *Dendropoma*. The taxa included herein were chosen to represent the breadth of morphological diversity in this group, but this study does not yet provide a comprehensive systematic revision of all species in this complex. The primary aim of this study is to generate morphological/anatomical data suitable for a genus-level revision of the group, sampling across the newly recognized morphological diversity. In order to re-evaluate the composition of genera, previously introduced genus-group taxa will be assessed. In addition to the development of a set of morphological characters to distinguish each group, we will use a molecular phylogeny to examine the monophyly of *Dendropoma* and other newly morphologically defined groups. We intend to develop a molecular framework and a set of morphological characters to distinguish each group and to allow for the accurate systematic placement of established and previously undescribed species of *Dendropoma s.l.*

MATERIALS AND METHODS

Material

The specimens examined during this study were sourced primarily from the collections of the Field Museum of Natural History (FMNH; based on numerous vermetid-focused expeditions, see below) and the Australian Museum (AM). Additional material was loaned by the Florida Museum of Natural History at the University of Florida (UF), the California Academy of Sciences (CASIZ) and the Museum of New Zealand Te Papa Tongarewa (NMNZ). Further specimens for this study were donated to the Field Museum collections by M. Calvo and J. Templado (material from the Mediterranean); L. Gosselin (material from western Canada); M. G. Hadfield, A. Faucci, R. Strathmann and M. Strathmann (material from the Hawaiian Islands); I. Kappner (material from Jordan and

Cape Verdes); P. M. Mikkelsen (material from Bahamas, Barbados and Florida); J. Norenberg (material from California); A. Pacheco (material from mainland Chile); N. Phillips and S. Schiaparelli (material from French Polynesia); U. Safriel (material from Sinai); J. D. Taylor (material from the Maldives and Kenya); and J. Worsfold (Bahamas). The Material Examined sections of the systematic descriptions presented here include specimen counts in some cases. However, where the examined lot comprises a chunk of "vermetid crust" (referred to here as an aggregate matrix) removed from the surface of the substratum, it was usually not possible to provide a precise specimen count and the count is estimated as "many".

Field Work

The material and observations on which this study is based come from vermetid-focused field work in many locales, including: Bahamas (Grand Bahama, New Providence; April 1993, August 1994 [RB]; Andros, March 2004 [TR]; Abaco August 2012 [RB, TC]); Barbados (August 2010 [RG, TR]); Belize (Carrie Bow Cay; 1986 [RB], 2011 [RB, RG, TC, TR]); Bermuda (Bermuda Biological Station/Aquarium; March 1983, May 1988 [RB]); British Virgin Islands (Guana; August 2010 [RB, TC]); Cayman Islands (Grand Cayman; January 2011 [Lauren Dombowsky for this project]); Chilean offshore Islands (Juan Fernandez Archipelago and Desventuradas Islands; 1997 [RB]); Dominica, August 1978 [RB]; East Florida and the Florida Keys (Smithsonian Marine Station, Ft. Pierce; Summerland Mote Lab, etc.; 1985–2012 [RB]; Peanut Island; 1997 [TR]); Hawaiian Islands (Oahu; Kewalo Marine Laboratory, etc.; December 1986, March 1988, June 1995 [RB]); Netherlands Antilles (Saba; August 1996, October 2010 [RB]; St. Martin, August 1996 [RB]); St. Lucia, August 1978 [RB]; U.S. Virgin Islands (West Indies Laboratory, St. Croix; February 1987 [RB]); Venezuela (INTECMAR station, Puerto Cabello, etc.; 1986 [RB]); Western Australia (Houtman Abrolhos Archipelago; May 1994 [RB]).

Worm-snails were collected during field work using a variety of specialized techniques tailored to maximize the success of locating and obtaining intact specimens. Intertidal or shallow subtidal vermetid habitat was accessed by snorkeling (Fig. 1) and deeper sites were surveyed using SCUBA (Fig. 2). In both cases, specimens were located by eye, and a hammer and chisel (or screwdriver) were used to remove either the specimen alone, a chunk of substratum with the vermetid attached, or a section of "vermetid crust" in the case of reef-forming species. Care was taken to retrieve the specimen with an intact shell whenever possible. Dead worm-snail shells were obtained by collecting objects on the shoreline that had been utilized as substratum by vermetids (Fig. 3), such as larger gastropod shells or echinoderm tests. Key vermetid habitats include stones, coral rubble, living coral heads (Fig. 4) and gorgonian stems and holdfasts (Fig. 5).

Anatomical and Morphological Studies

Where possible, animals were collected alive and photographed to record coloration of the head-foot and mantle. In most cases, this was not possible, and only preserved material was available. The systematic anatomical descriptions below are based on both dry and wet (ethanol and formalin preserved) specimens. If only dry material was available, individual dried bodies were removed from their shells and rehydrated in distilled water to allow partial description of the soft tissue anatomy.

Individual shells and clusters of shells attached to the substratum were photographed using a digital camera (attached to a stereo microscope if very small) or alive in the field using a digital camera in an underwater housing. Shell measurements were made using digital calipers to record the following parameters: (1) maximum aperture diameter; (2) length of shell (i.e. greatest length in any direction); (3) diameter of last whorl (sometimes equal to length of shell, if concentrically coiled). The coiling pattern was categorized as: (1) concentric; (2) initially concentric but becoming off-center; (3) "*Turritella*-squeezed-sideways", a recognizable pattern unique to some vermetids [a term first applied to a species of *Petaloconchus* by Carpenter (1857: 309)]; or (4) irregular. Protoconchs were sometimes obtained directly from adult shells, but overgrowth by the postlarval shell often hindered obtaining a clean specimen. In most cases, recently settled juveniles were removed from the substratum around adult worm-snails and – often after comparison with hatchlings or adult protoconchs – presumed to belong to the same species. Intracapsular larval shells were also examined when found, and although they may not have reached settlement size they were clean and ideal for observing sculpture. Opercula were photographed using a digital camera attached to a microscope to record color.

Shells, protoconchs and opercula were cleaned of encrusting algae by immersion in an ultrasonic water bath and examined using SEM to observe sculpture and protoconch shape. Buccal masses were extracted manually from dissected specimens and radulae cleaned by soaking in 10% NaOH solution for about four hours at 60°C, then rinsed in distilled water and ethanol. At least two radulae were examined by SEM from each species and the maximum number of rows and length of the ribbon were recorded. Specimens to be imaged by SEM were mounted on conductive carbon tabs, coated in gold and examined using a Leo EVO 60 SEM.

The anatomical descriptions based on dissected specimens include aspects of the external morphology (including coloration in life, if possible, and in preserved specimens), pallial anatomy (including the pallial reproductive system), and egg capsules recovered from brooding females. Specimens were dissected under a stereomicroscope and illustrated using a drawing tube attachment. Anatomy was studied in two to ten specimens, except where only one specimen was available.

Comparative descriptions of each genus and species in the Systematic Part are limited to characters that are informative for distinguish-

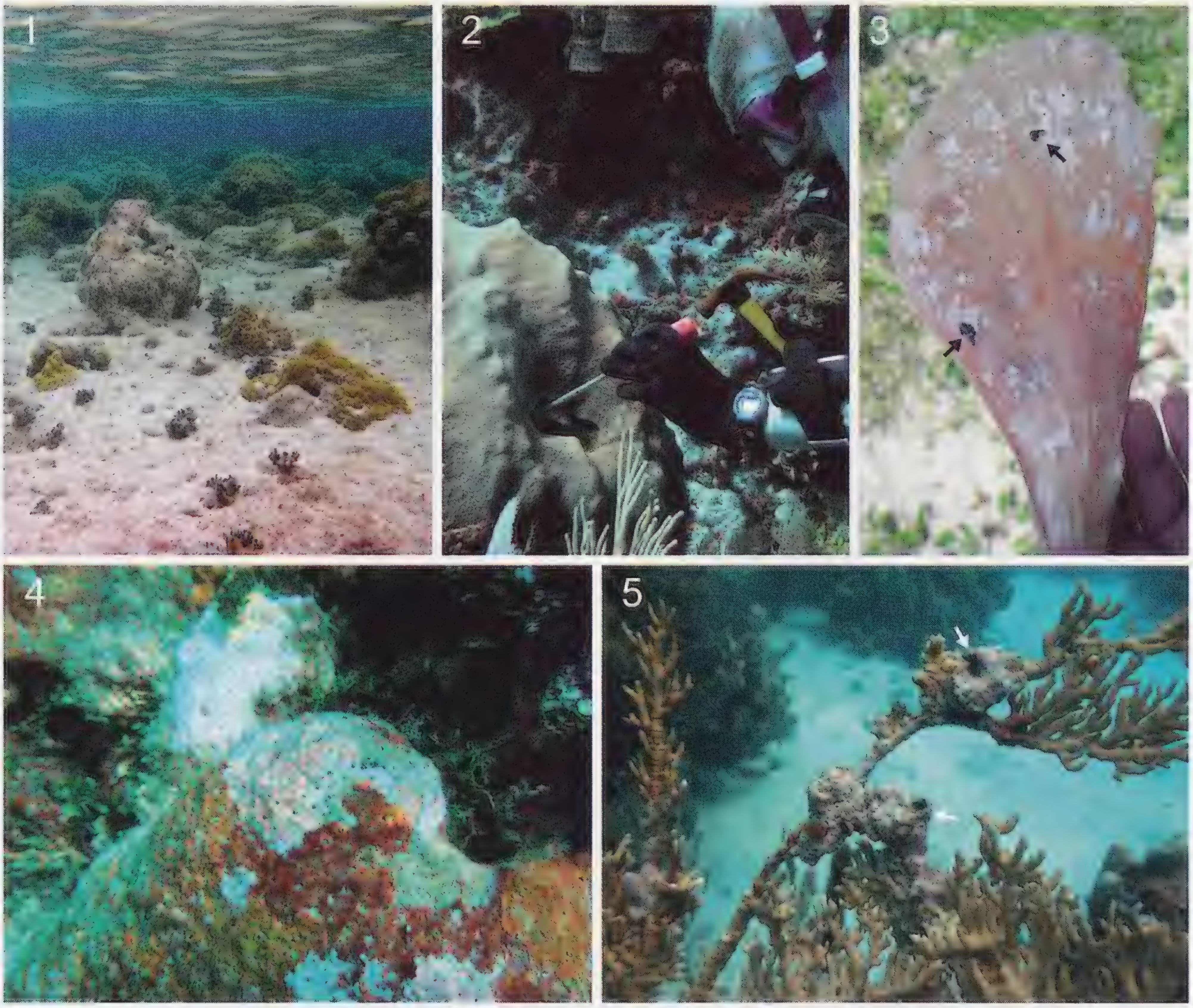

FIGS. 1–5. Photographs of collecting methods employed and habitat utilized by Caribbean species of *Dendropoma*, *Novastoa* and *Cupolaconcha* at Carrie Bow Cay, Belize (April 2011). FIG. 1: Shallow subtidal reef where *D. corrodens*, ***C. guana*** n. sp. and ***N. pholetor*** n. sp. occur on the exposed surfaces of living and dead coral heads; FIG. 2: Collecting *D. nebulosum* by SCUBA, using a hammer and screwdriver to remove specimens intact from the substratum in crevices between living coral tissue; FIG. 3: Empty shell of *Pinna* sp. collected from beach drift with shells of ***C. guana*** attached (arrows); FIG. 4: Dead coral head encrusted with coralline algae and dense aggregation of *D. corrodens*; FIG. 5: *D. nebulosum* (arrows) and *D. corrodens* co-occurring on the stems of a gorgonian covered with milleporid "fire coral".

ing taxa at the equivalent level. Characters that are variable within a population or consistent within a genus are not included in species-level descriptions.

Molecular Systematics

Specimens preserved in 70–95% ethanol or RNAlater were used for DNA extraction. A complete list of taxa sampled, including locality details and collector information, is provided in Table 1. Whenever possible, tissue was sampled from the same lots as those examined for morphological and anatomical characters. Additional representatives of other vermetid genera (*Eualetes, Petaloconchus, Thylacodes, Thylaeodus, Vermetus*) were also included in our analysis to determine their relationship to focal *Dendropoma s.l.* taxa.

For most animals, DNA was extracted from pieces of the head/foot region; however, in cases of particularly small vermetids (e.g., *Dendropoma corrodens* and *Cupolaconcha meroclista*), the whole body was occasionally used. Two different methods of DNA extraction were routinely employed: (1) the standard CTAB and phenol chloroform extraction protocol described in Collins (1996) for molluscan tissue, and (2) QIAGEN's silica gel membrane DNA-binding protocol as implemented in its DNeasy Tissue Kit (catalogue #: 69504) for animal tissues.

For DNA amplification and sequencing, we targeted both mitochondrial (mtDNA) and nuclear gene regions. For mtDNA, we amplified a > 1.5 kb fragment spanning domains III–IV of the small-subunit rRNA (*rrnS*), an intervening tRNA valine (*trnV*), and domains I–IV of the large-subunit rRNA (*rrnL*) (Rawlings et al., 2001). Substantial interspecific variation exists at the nucleotide level within this region of the genome, including changes in gene order within and among vermetid genera (Rawlings et al. 2001, 2010). In addition, we targeted a ~1,100 bp portion of the nuclear *28S rRNA* gene. While much less variable than mtDNA, we have documented up to 2.5% difference (uncorr.-P distances) in nucleotide sequence of this gene region within the Vermetidae based on sampling so far (Rawlings et al., unpublished data).

We amplified the mtDNA region in 2–3 overlapping chunks, since attempts at amplifying this region in one piece were rarely successful with standard PCR amplification kits. Given the gene order changes that have occurred within this region, the size of the total product amplified was highly variable across taxa, ranging from 1621–2505 bp in length. For two-piece amplifications, we typically employed the following primer pairs, based on universal primers listed in Palumbi (1996): Fragment A – 12SA (5'-AAACTGGGATTAGATACCCCACTAT-3') or 12Sai (5'-AAACTAGGATTAGATACCCTATTAT-3') in association with 16SA (5'-ATGTTTTTGATAAACAGGCG-3'); and Fragment B – 12SF (reverse complement of Palumbi's 12Sb' primer; 5'-GCACACATCGCCCGTCGCTCT-3') in combination with 16SBr (5'-CCGGTCTGAACTCAGATCACGT-3'). In some instances, however, these primer combinations were not successful; consequently additional primers were designed and different primer combinations attempted. A full listing of the primer combinations used and the sizes of the resulting amplification products can be obtained from the authors.

The region of the *28S rRNA* gene was amplified using primer pairs 28SD1F (5'-GGGACTACCCCCTGAATTTAAGCAT-3') and 28SD6R (5'-CCAGCTATCCTGAGGGAAACTTCG-3') designed by Park & Ó Foighil, 2000. Amplifications of this gene region were relatively straightforward, although some taxa exhibited length heteroplasmy resulting in stutters/overlapping chromatograms beyond a specific point in the sequence. In such instances, we typically cloned the PCR amplification and sequenced the resulting clonal products with good results; alternatively, to avoid cloning, we designed internal sequencing primers to bind on the downstream side of the variable region on both forward and reverse strands.

Amplification of PCR products occurred in molecular labs spanning two different institutions (Florida International University, Cape Breton University) and utilizing different thermal cyclers and PCR chemistries. The general protocols for successful amplification of targeted gene regions, however, were as follows. For each amplification, 1 µl of 1x or 1/10x dilutions of each genomic DNA extraction was used as the template in a 25–50 µl reaction volume that consisted of 1.5–2.0 mM $MgCl_2$, 1x PCR buffer, 0.5 µM of each primer, 200 µM of each dNTP, and 0.5–1.5 units of Taq DNA polymerase (depending on reaction volume). PCRs were performed in MJ peltier thermal cyclers (MJ Research PTC-200, MJ Mini) or a Stratagene Robocycler Gradient 96 thermal cycler. PCR conditions followed the general procedures outlined in Mikkelsen et al. (2006).

TABLE 1. Material used in the molecular phylogeny. Museum registration numbers for voucher specimens (where available), locality, collector and GenBank accession data are given.

Species	Reg. #	Locality	Collector/Year	GenBank Acc. # mtDNA	 28SrDNA
Dendropoma Mörch, 1861					
Dendropoma mejillonense Pacheco & Laudien, 2008	FMNH 312173	Chile: Peninsula Mejillones, 17 m, Anemones Wall, 23.470°S, 70.619°W [from original syntype lot]	AP; 2006	KC583421	KC583387
Dendropoma nebulosum (Dillwyn, 1817)	FMNH 315538	U.S.A., Florida: 7 m, patch reef off Marathon, Key Vaca, Monroe County, Florida Keys, 24.659°N, 81.015°W	RB; 1997	AF338147	KC583388
	FMNH 335070	Bahamas: 10–12 m, outside barrier reef off Walker's Key, reefs NE of Great Abaco Island, 26.641°N, 77.037°W	RB, PS; 2012	KC583422	KC583389
Dendropoma platypus (Mörch, 1861)	–	U.S.A., Hawaii: Oahu, Kaneohe Bay, 21.436°N, 157.791°W [Precipitated DNA – no reference specimen seen]	AF; 2004	KC583423	KC583390
Dendropoma petraeum (Monterosato, 1884)	FMNH 327231	Spain, Murcia: Cabo de Palos, 37.633°N, 0.699°E	JT; 1999	AF338148	KC583391
Dendropoma corrodens (d'Orbigny, 1842)	FMNH 293171	U.S.A., Florida: Missouri Key, Florida Keys, 24.675°N, 81.239°W	RB, PMM; 1994	AF338144	KC583392
	FMNH 327142	Belize: 2 m, SW from boat launch, Carrie Bow Cay, 16.802°N, 88.083°W	RB, RG, TR, TC, PS; 2011	KC583424	KC583393
	FMNH 327095	Barbados: limestone rocks and base of cliffs, River Bay, East coast, 13.323°N, 59.596°W	RG, TR, CMc; 2010	KC583425	KC583394
	FMNH 327096	Barbados: fringing reef, Six Men's Bay, West coast, 13.268°N, 59.645°W	RG, TR, CMc; 2010	KC583426	KC583395
	FMNH 326712	British Virgin Islands: 5–6 m, near Monkey Point, White Bay, Guana Island, 18.466°N, 64.572°W	RB, TC; 2010	KC583427	KC583396
	FMNH 326699	British Virgin Islands: 2–3 m, patch reefs, White Bay, Guana Island, 18.471°N, 64.574°W	RB, TC; 2010	KC583428	KC583397
Dendropoma gregarium Hadfield & Kay, 1972	FMNH 318222	U.S.A., Hawaii	MH	HM174252	KC583398
Dendropoma rhyssoconchum Hadfield & Kay, 1972	–	U.S.A., Hawaii: Kaneohe Bay, Oahu, 21.436°N, 157.791°W [precipitated DNA – no reference specimen seen]	AF; 2004	KC583429	KC583399

(continues)

(continued)

				GenBank Acc. #	
Species	Reg. #	Locality	Collector/Year	mtDNA	28SrDNA
Dendropoma psarocephalum Hadfield & Kay, 1972	–	U.S.A., Hawaii: Kaneohe Bay, Oahu, 21.436°N, 157.791°W [precipitated DNA – no reference specimen seen]	AF; 2004	KC583430	KC583400
Novastoa Finlay, 1926					
Novastoa caboverdensis n. sp.	FMNH 301978	Cape Verdes: Pedra Lume, Sal, 16.45°N, 22.53°W	IK, KD; 2003	KC583370	KC583401
Novastoa bahamensis n. sp.	FMNH 327205	Bahamas: intertidal, foreshore off Point of View Villas, Fresh Creek, Andros Island, 24.735°N, 77.793°W	TR; 2004	KC583371	KC583402
Novastoa pholetor n. sp.	FMNH 327172	Belize: lagoon E of Carrie Bow Cay, 16.803°N, 88.082°W	RB, RG, TR, TC, PS; 2011	KC583372	KC583403
Novastoa sp.	MNHNP IM-2000-27249	French Polynesia: Point Tematapu, Rapa Iti Island, 27.604°S, 144.343°W	SS; 2002	KC583373	KC583404
Ceraesignum n. gen.					
Ceraesignum maximum (G. B. Sowerby I, 1825) n. comb.	FMNH 318221	Jordan: Gulf of Aqaba [tissue sample only]	IK; 1999	HM174253	KC583405
	UF 291949	Cook Islands: 0–2 m, Motutapu, Rarotonga Island, 21.24°S, 159.72°W	CM; 2001	KC583374	KC583406
Ceraesignum robinsoncrusoei n. sp.	FMNH 326906	Chile: Isla Róbinson Crusoe, Juan Fernández Archipelago, 33.641°S, 78.823°W	RB; 1997	AF338143	KC583407
Cupolaconcha n. gen.					
Cupolaconcha meroclista (Hadfield & Kay, 1972) n. comb.	FMNH 328505	U.S.A., Hawaii: Kaneohe Bay, Oahu, 21.436°N, 157.791°W	MH; 1998	KC583375	KC583408
	UF 341500	Guam: Pago Bay, Mariana Islands,13.42°N, 144.78°E	WK; 2003	KC583376	KC583409
Cupolaconcha sp.	FMNH 302015	French Polynesia: Point Tematapu, Rapa Iti Island, 27.604°S, 144.343°W	SS; 2002	KC583377	–
Cupolaconcha guana n. sp.	FMNH 327154	Belize: 1–2 m, Little Cat Cay, 16.151°N, 88.200°W	RB, RG, TR, TC, PS; 2011	KC583378	KC583410
	FMNH 335076	Bahamas: 6-8 m, reefs NE of Great Abaco Island, 26.636°N; 77.0352°W	RB, PS; 2012	KC583379	KC583411
	FMNH 326700	British Virgin Islands: 2 m, patch reefs, White Bay, Guana Island, 18.471°N, 64.574°W	RB, TC; 2010	KC583380	KC583412

(continues)

(continued)

Species	Reg. #	Locality	Collector/Year	GenBank Acc. # mtDNA	GenBank Acc. # 28SrDNA
Thylacodes Guettard, 1770					
Thylacodes squamigerus (Carpenter, 1857)	FMNH 318997	U.S.A., California: Corona del Mar, 33.59°N, 117.87°W	JN; 2002	HM174255	KC583413
Thylacodes cf. *decussatus* (Gmelin, 1791)	FMNH 327089	U.S.A., Florida: 7 m, patch reef off Marathon, Key Vaca, Monroe County, Florida Keys, 24.659°N, 81°001'W	RB, PMM; 1997	AF338154	KC583414
Eualetes Keen, 1971a					
Eualetes tulipa (Chenu 1843)	FMNH 318223	U.S.A., Florida: Peanut Island, Palm Beach County, 26.7719°N; 80.0437°W	TR; 1997	HM174254	KC583415
Petaloconchus Lea, 1843					
Petaloconchus varians (d'Orbigny, 1839)	FMNH 327246	U.S.A., Florida: seawall, Hobe Sound, Palm Beach County, 26.956°N, 80.078°	RB, PMM; 1994	KC583381	KC583416
Petaloconchus montereyensis Dall, 1919	FMNH 328504	Canada, British Columbia: low intertidal, in front of the Bamfield Marine Sciences Centre, Bamfield Inlet, 48.8363°N,125.1355°W	LG; 1997	KC583382	KC583417
Thylaeodus Mörch, 1860					
Thylaeodus sp.	FMNH 318224	U.S.A., Hawaii: seawater tables, Kewalo Marine Laboratory, 21.291°N, 157.861°W	MH, RS, MS; 2002	HM174256	KC583418
Vermetus Daudin, 1800					
Vermetus triquetrus Bivona Bernardi, 1832	FMNH 327229	Spain, Murcia: Cabo de Palos, 37.633°N, 0.699°E	JT; 1999	KC583383	KC583419
Vermetus cf. *triquetrus* Bivona Bernardi, 1832 [sensu Bieler, 1995]	FMNH 328506	Azores, São Miguel	AC; 1999	KC583384	KC583420
Outgroups					
Littorina littorea (Linnaeus, 1758)	FMNH 336506	Canada, Nova Scotia: intertidal, Dominion Beach, Cape Breton Island, 46.217°N, 60.038°W	TR; 2012	KC583385	AJ488672
Crepidula fornicata (Linnaeus, 1758)	FMNH 336507	U.S.A., Massachusetts: Surf Drive Beach, Falmouth, 41.538°N, 70.635°W	LC; 1997	KC583386	JF750968

Abbreviations: AC = Ana Costa; AF = Anuschka Faucci; AP = Aldo Pacheco; CM = Christopher Meyer; CMc = Colin McVarish; IK = Isabella Kappner; JN = Jon Norenberg; JT = José Templado; KD = K. Defren; LC = Laurie Collins; LG = Louis Gosselin; MH = Michael Hadfield; MS = Megumi Strathmann; PMM = Paula M. Mikkelsen; PS = Petra Sierwald; RB= Rüdiger Bieler; RG = Rosemary Golding; RS = Richard Strathmann; SS = Stefano Schiaparelli; TC=Timothy Collins; TR=Timothy Rawlings; WK = Walter Kelly.

Annealing temperatures were optimized for each primer pair combination and ranged from 48°C–55°C. A 5 µl aliquot of each PCR product was run out on a 1% agarose gel. When single bands of the appropriate size resulted from these amplifications, the PCR product was prepared for sequencing using Geneclean III (MP Bioproducts Inc.) or Qiagen's QIA Quick PCR Purification Kit (Catalogue 28104). When supernumerary bands were present, the entire PCR product was run out on a 3% Nu-Sieve TAE agarose gel, the band of the correct size was excised under long wavelength ultraviolet light, and purified for sequencing following the protocols in Geneclean III (Catalogue 1001-600). Purified PCR products were either cycle sequenced using BigDye 3.0/3.1 chemistry and analyzed on an ABI 3100 genetic analyzer or sent off campus for sequencing at GeneWiz (New Jersey, U.S.A.; www.genewiz.com). In all cases, the DNA sequence of both strands was obtained before a final consensus sequence was generated for each taxon.

Data Editing and Phylogenetic Analyses

Given that a close caenogastropod sister-group has yet to be identified for the Vermetidae, outgroup selection remains problematic for this family. Recent studies (Colgan et al., 2007; Criscione & Ponder, 2012; Rawlings et al., unpublished data), in combination with the sperm morphological work of Healy (1988), however, support the evolution of vermetids from within the "lower" Hypsogastropoda, with possible ties to members of the Janthinoidea, Stromboidea, Calyptraeoidea, Xenophoroidea and Littorinoidea (Healy, 1988; Criscione & Ponder, 2012; Rawlings et al., unpublished data). In light of this, we chose representatives of two of these superfamilies, *Littorina littorea* (Littorinoidea) and *Crepidula fornicata* (Calyptraeoidea) for rooting our phylogeny. DNA was extracted and amplified for the mtDNA regions for both outgroup taxa; *28S rRNA* nucleotide sequences were obtained from NCBI.

Because of substantial length differences in the amplified fragment of mtDNA across the taxa sampled, we first determined the complement of genes present within these sequences. To begin, we searched all sequences for tRNA genes using tRNAscan-SE (Schattner et al., 2005), using the settings for mtDNA and the invertebrate genetic code. Once tRNA genes were identified, and their boundaries determined, we used MacVector (MacVector, Inc.) to find potential coding sequences of DNA in the intervening stretches of sequence, and BLAST (http://blast.ncbi.nlm.nih.gov/Blast.cgi) to identify these regions based on matches (in identity and length) of the derived amino acid sequence to homologous protein sequences from other gastropod mtDNAs. The start of coding sequence was identified by a standard initiation codon (either ATG, ATA, or GTG). When possible, the first proper stop codon (TAG or TAA) downstream of the initiation codon was chosen to terminate translation; however, to reduce overlap with downstream genes, abbreviated stop codons (T or TA) were selected in some instances. Ribosomal RNA sequences were also identified based on BLAST searches. The precise boundaries of rRNA genes, however, could not be determined due to the lack of sequence conservation at the 5' and 3' ends; therefore, the location of each rRNA gene was assumed to extend from the boundary of the upstream flanking gene to the boundary of the downstream flanking gene.

Once gene identities and boundaries were determined within the sequenced mtDNA fragment, we built gene specific datasets based on identified sequences of *rrnS*, *trnV*, and *rrnL*; other genes that were identified in amplification products of select taxa, including tRNA genes, *trnK*, *trnP*, *trnE*, *trnL*$_{CUN}$, and the protein-encoding gene, *nad6*, were not used in subsequent phylogenetic analyses. Gene specific datasets of the mtdna genes (*rrnS*, *trnV*, *rrnL*) and the nuclear gene sequence (*28S rRNA* gene) were individually aligned using the online version of MAFFT (version 7; http://mafft.cbrc.jp/alignment/server/ref) using E-INS-i – an alignment method recommended for sequences with multiple conserved domains and long gaps – characteristics which typify rRNA genes. Because of uncertainty in several areas of the aligned *rrnS* and *rrnL* dataset associated with length variation among taxa, we created two versions of these alignments: one which included all sites ("complete") and one in which areas of poor alignment (as identified by eye and through confidence evaluation using T-Coffee, Di Tommeso et al., 2011) were excluded ("pruned"). We employed JModeltest2 (Darriba et al., 2012) to determine the best model of sequence evolution based on log likelihood ratio tests for each data partition, and exclusion set, as determined using the Akaike Information Criterion. Because of the short length of the *trnV* gene (70–80 bp in length) sequence from this gene was combined with the *rrnS* dataset for model evaluation in JModeltest2 and subsequent phylogenetic analyses. Alignments of all data sets were incorporated into one data file partitioned into three gene regions: (1) *rrnS* and *trnV*, (2) *rrnL* and (3) *28S rRNA*; this was done for both the complete and pruned datasets.

Base compositional tests were implemented in PAUP* (Swofford, 2002) using chi-squared tests to ensure that there were no significant confounding differences in base composition across taxa. Parsimony-based phylogenetic analyses were also performed in PAUP*, with separate runs performed for each of the three data partitions and the combined dataset for both the pruned and complete alignment. Heuristic searches employed equal weighting of characters, TBR branch swapping, and 100 random sequence additions of taxa. Bootstrap analyses to determine branch support were undertaken using 1,000 pseudoreplicates.

Phylogenetic analyses were also undertaken using Bayesian inference as employed in MrBayes (v3.2.1; Ronquist & Huelsenbeck, 2003). Evaluation of log likelihood ratio tests using the Akaike Information Criterion ranked the GTR + γ + I model of molecular evolution as the best for all data partitions except for *28S rRNA*, for which the TIM3 + γ + I was ranked highest. Consequently, we applied model parameters "nst = 6, invgamma" to each data partition separately, and allowed parameters to vary independently for each partition. Default priors were used in all analyses. Posterior probabilities of phylogenetic trees were based on running 1.5–2x 10^6 generations of MCMC (depending on the dataset), which included two simultaneous runs of 4 chains (1 heated; h = 0.2) starting with a random tree and sampling every 100 generations. Preliminary runs of the data output in Tracer (Rambaut & Drummond, 2007) were used to determine the appropriate burn-in for the dataset and ensure stationarity of the dataset. In total, 1,000 trees (5–7% of the dataset) were excluded as burnin; the remaining 14,000–19,000 trees (depending on the dataset) were used to determine the 50% majority-rule consensus phylogram and estimate Bayesian posterior probabilities.

Synonymies/Chresonymies

Vermetid shells are notoriously difficult to identify and, even when accompanied by a photograph, published records often are not interpretable to specific level. We were thus very selective in adding entries to our synonymy and chresonymy listings, limiting them to (1) those relevant to establishing available names and linking them to past monographs, (2) material personally studied, and (3) clearly recognizable literature data (e.g., pointing to good photographs or other available data).

Terminology/Abbreviations

Protoconch sculpture is referred to as axial or spiral in the traditional sense, but because adult vermetids rarely coil around a defined axis, teleoconch sculpture is described as transverse (= axial) or longitudinal (= spiral). The reproductive system displayed many differences between taxa, but the function of individual components is not well understood. This study did not explore the function of the reproductive system, and simple terms have been used to avoid inferring function. The glandular, pallial section of the reproductive tract is simply referred to as the pallial oviduct or vas deferens and is open in all species examined. Structures containing sperm in the pallial oviduct are referred to as seminal receptacle(s), even if more than one is present.

The following abbreviations are used to label illustrated structures:

ag	accessory gland
an	anus
cm	columellar muscle
co	coelomic oviduct
cr	cartilaginous rod
ct	cephalic tentacle
cvd	coelomic vas deferens
dv	diverticulum of pallial oviduct
ec	egg capsules
ep	expanded distal pocket of pallial oviduct
es	esophagus
fg	food groove
gi	gill
hg	hypobranchial gland
mo	mouth
ms	mantle slit
no	notch in pallial oviduct
op	operculum
os	osphradium
ov	ovary
po	pallial oviduct
pt	pedal tentacle
pvd	pallial vas deferens
re	rectum
sr	seminal receptacle
sv	seminal vesicle
te	testis

The following abbreviations are used for institutions:

AM	Australian Museum, Sydney, Australia
BPBM	Bernice Pauahi Bishop Museum, Honolulu, U.S.A.
FMNH	Field Museum of Natural History, Chicago, U.S.A.
MNHNC	Museo Nacional de Historia Natural de Chile, Santiago, Chile
MNHNP	Museum National d'Histoire Naturelle, Paris, France
NHMUK	Natural History Museum, London, United Kingdom
NMNZ	Museum of New Zealand Te Papa Tongarewa, Wellington
QM	Queensland Museum, Brisbane, Australia
UF	Florida Museum of Natural History, Tallahassee, Florida, U.S.A.
WAM	Western Australian Museum, Perth, Australia
ZMC	Zoologisk Museum, Copenhagen, Denmark

RESULTS

Molecular Data

PCR amplifications were successful for all target taxa and genes except in two instances. For *Dendropoma mejillonense*, we were only able to amplify a small 5' portion (*rrnS*) of the mtDNA target region, approximately 400 bp in length, and were unsuccessful in amplifying the remaining downstream region even with different primer combinations, annealing temperatures, and increased $MgCl_2$ concentrations. In addition, we were unable to amplify the *28S rRNA* gene for *Cupolaconcha* sp. (FMNH 302015). Both taxa were still included in our phylogenetic analyses even though their datasets were not complete.

PCR amplification lengths of our mtDNA dataset were indicative of gene order changes that have occurred within the vermetid mt genome and have been described partly elsewhere (Rawlings et al., 2001, 2010). *Dendropoma corrodens*, *D. nebulosum*, *D. platypus*, *D. gregarium*, *D.* cf. *petraeum*, *D. rhyssoconchum* and *D. psarocephalum*, were all were found to share an indel consisting of *trnK*, *trnP* and *nad6* positioned between *rrnS* and *trnV*, relative to other taxa sampled. Given that *D. mejillonense* was nested within this clade, it is assumed that this taxon also shared this gene rearrangement, although we were not able to confirm this directly for the reasons described above. Members of the genus *Cupolaconcha* were also unique in lacking *trnV* between the *rrnS* and *rrnL*. Alignments with other taxa across the *rrnS-trnV-rrnL* region invariably resulted in a long gap in this region for *Cupolaconcha* suggesting that its *trnV* has been translocated to another region of the genome. *Thylaeodus* also presented a novel gene arrangement. For this taxon, an additional *trnE* was located between *trnV* and *rrnL* (Rawlings et al., 2010). *Thylacodes squamigerus* also exhibited a gene rearrangement in this region involving the presence of *rrnS*, *rrnL* and *nad1* pseudogenes, an extra *trnV* and *trnL*$_{CUN}$ (Rawlings et al., 2010). For all other taxa included in our dataset, the standard gene order of *rrnS-trnV-rrnL* was present.

Gene-specific alignments were 618 bp, 78 bp, 1,577 bp and 1,123 bp in length for the *rrnS*, *trnV*, *rrnL*, and *28S rRNA* gene regions, respectively, and 696 bp for the combined *rrnS* + *trnV* dataset. The complete dataset thus consisted of 3,396 characters, of which 1,494 were parsimony informative. The pruned dataset for the *rrnS* + *trnV* partition was 530 bp in length, 166 bp shorter than the complete alignment, while the pruned *rrnL* dataset was 737 bp in length, over 50% shorter. In total, the combined pruned dataset consisted of 2,390 characters, of which 765 were parsimony informative. Base compositional tests were not significant across taxa for the pruned mtdna datasets or the *28S rRNA* dataset, but significant differences in base composition were evident in the complete *rrnL* dataset ($\chi^2 = 392.5$, df = 105, P = 0.00). These differences did not persist in the pruned *rrnL* dataset ($\chi^2 = 92.9$, df = 105, P = 0.79), indicating that these differences were confined to regions of poor alignment typically associated with sequence length variation across taxa.

Phylogenetic Analyses

The overall pattern of relationships among taxa was largely consistent across data partitions, pruned/complete datasets, and methods of analysis (Parsimony, Bayesian), with relatively few exceptions (Table 2). For clarity, we have presented only the 50% majority rule consensus phylogeny based on a Bayesian analysis of the combined *rrnS* + *trnV*, *rrnL*, and *28S rRNA* pruned dataset with posterior probability values (where > 95%) and parsimony-based bootstrap values (where > 70%) mapped onto their appropriate clades (Fig. 6). Disagreements in the

TABLE 2. Clade support values (PP/BP, in %) resulting from Bayesian and Parsimony-based phylogenetic analyses of individual and combined gene regions using the pruned dataset.

	Clade							
Dataset	*Dendropoma* + *Ceraesignum* + *Novastoa*	*Dendropoma* + *Ceraesignum*	*Dendropoma*	*Ceraesignum* n. gen.	*Novastoa*	*Cupolaconcha* + *Eualetes* + *Thylaeodus* + *Petaloconchus* + *Thylacodes* + *Vermetus*	*Cupolaconcha* + *Eualetes* + *Thylaeodus* + *Petaloconchus*	*Cupolaconcha* n. gen.
rrnS + *trnV*	97/50	< 50/52	100/100	100/78	100/94	< 50/< 50	100/93	100/64
rrnL	100/77	80/54	100/100	100/92	100/99	100/51	98/< 50	100/91
All mtDNA	100/93	62/70	100/100	100/95	100/100	100/51	100/82	100/99
All mtDNA + *28S rRNA*	100/96	56/62	100/100	100/95	100/100	98/< 50	100/86	100/100

results of different data partitions are largely reflected in those major clades with low posterior probability and bootstrap values (Table 2).

Analyses of our molecular dataset, using both parsimony and Bayesian methods, supported a phylogeny consistent with the new taxonomic framework for "*Dendropoma* group" taxa proposed herein. This was true for both the complete dataset and the pruned dataset, which excluded poorly aligned regions across data partitions. Each of the four genera, *Dendropoma*, *Ceraesignum* n. gen., *Novastoa* and *Cupolaconcha* n. gen., formed a strongly supported monophyletic grouping (Fig. 6). High bootstrap (96%) and posterior probability (100%) values also supported the placement of *Dendropoma*, *Ceraesignum* n. gen., and *Novastoa*, within their own clade, separate and distinct from members of the genus *Cupolaconcha* n. gen. (Table 2). Strong genetic differentiation among members of *Dendropoma*, *Ceraesignum* n. gen., and *Novastoa*, as represented by long branch lengths in Figure 6, and morphological differences (see below) were also consistent with recognition of these three groups at the generic level. Members of the genus *Dendropoma* were also defined by a novel pattern of mtDNA genes (*rrnS-trnK-trnP-nad6-trnV-rrnL*) not found in *Ceraesignum* and *Novastoa*. There was no strong evidence of a hierarchical pattern of relationships among these three genera, however: both Bayesian and parsimony analyses of the pruned dataset weakly supported a sister group relationship between *Dendropoma* and *Ceraesignum,* but this pattern was not consistent across data partitions and analyses (Table 2).

Species of *Cupolaconcha* n. gen., in turn, were found to be more closely related to members of the vermetid genera, *Petaloconchus*, *Thylaeodus*, and *Eualetes*, than to *Dendropoma, Ceraesignum* n. gen., and *Novastoa.* The translocation of *trnV* evident in *Cupolaconcha* n. gen. mtdna, however, was confined to this genus alone and was not observed in any members of its sister clade. *Thylacodes* and *Vermetus* were strongly supported as closely related to the *Cupolaconcha* n. gen., *Eualetes*, *Petaloconchus*, and *Thylaeodus* clade in Bayesian analyses of the pruned and complete dataset, but not in parsimony-based results and isolated gene partitions (Table 2). In these analyses, one or both of these genera were more closely allied to the *Dendropoma*, *Ceraesignum* n. gen., *Novastoa* clade or alternatively no strong support was shown for a relationship with either clade.

High levels of genetic differentiation were observed within genera and nominal species of vermetids sampled in our analysis. Within

D. corrodens, for instance, taxa differed up to 18% (uncorr.-P) in nucleotide sequence based on our mtDNA dataset, with 15% difference recorded between two specimens collected from Barbados. Such high levels of genetic differentiation hint of cryptic species residing within this grouping and highlight the need for further study of *D. corrodens*. Within genera, sequence divergence levels in mtDNA exceeded 30% (uncorr.-P) in pairwise comparisons of taxa within *Dendropoma*, *Ceraesignum* n. gen., and *Cupolaconcha* n. gen.

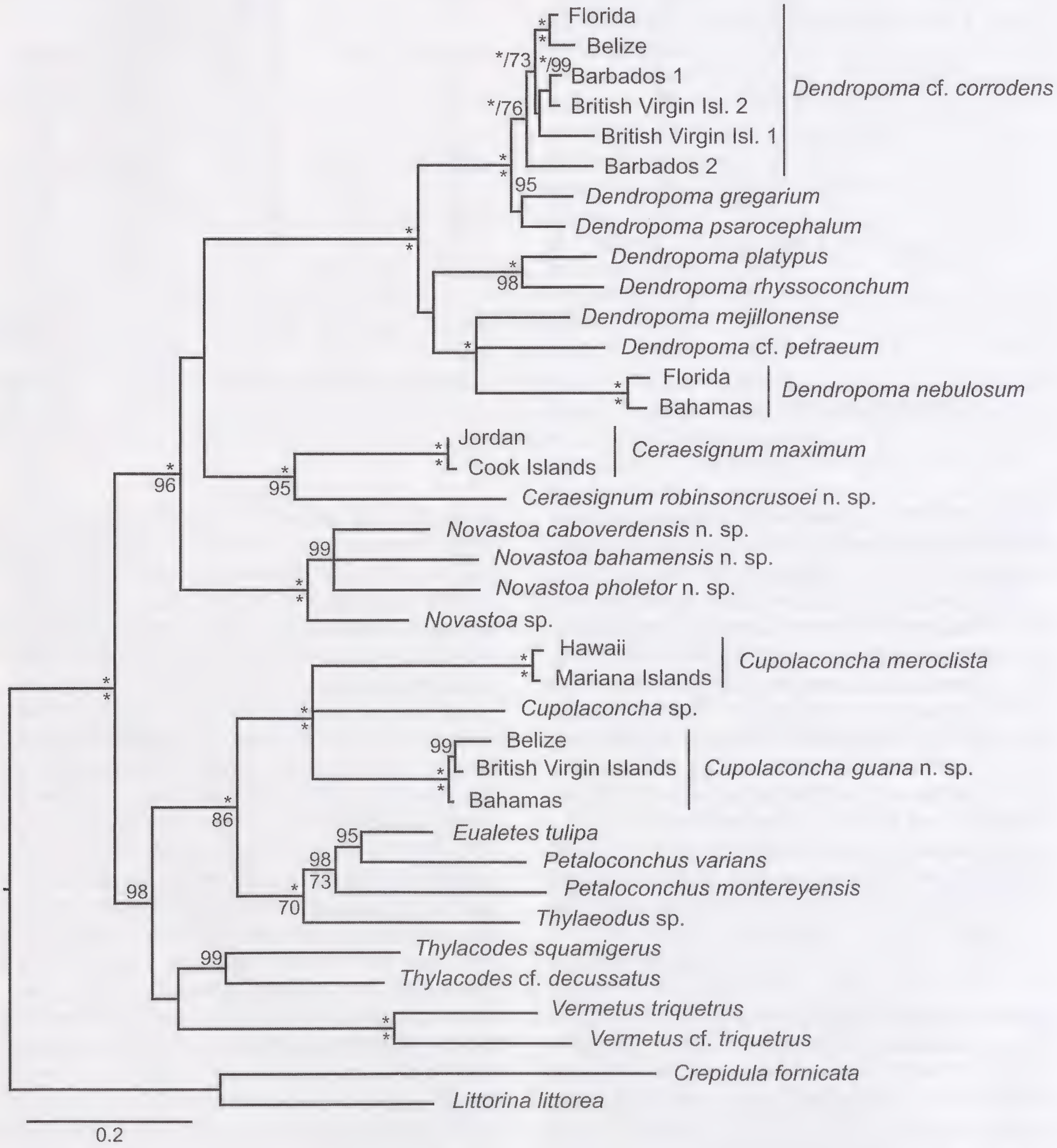

FIG. 6. Phylogenetic relationships among *Dendropoma*, *Ceraesignum*, *Novastoa*, and *Cupolaconcha* and other select vermetid genera, using *Littorina littorea* and *Crepidula fornicata* as outgroups. The phylogram illustrated represents the 50% majority-rule consensus tree from a Bayesian analysis of the combined gene (*rrnS*, *trnV*, *rrnL*, and *28S rRNA* genes), pruned alignment, dataset based on a sampling of 19,001 trees (2,000,000 generations, sample frequency = 100, burnin = 1,000, heat = 0.2). Support values for clades are posterior probabilities (where ≥ 95%, above branches) from the Bayesian analysis and bootstrap percentages (where ≥ 70%; below branches) from a parsimony-based analysis of the same dataset (1,000 pseudoreplicates). Asterisks represent support values of 100%.

SYSTEMATIC PART

Assessment of Genus-Group Names Previously Used in the *Dendropoma* Group

Species now considered as belonging to *Dendropoma sensu lato* have been introduced, or subsequently placed, in a bewildering variety of genus-group names, some of which are now known or thought to belong to polychaete worm groups whereas others are technically unavailable for nomenclatural reasons. Because the current study finds the clade diversity in *Dendropoma s.l.* greater than previously expected, it will be necessary to analyze the availability of generic names in this complex. Keen (1961) assembled a list of assumed synonyms and subgenera of *Dendropoma*, which were further analyzed for availability – in the sense of the I.Z.C.N. [1999] Code – by Bieler & Petit (2011). Expanding on these works we find:

(1) Names that are invalid and cannot be used:

Siphonium "Browne, 1756"

Siphonium "Browne, 1756", is a pre-Linnean name included in the synonymy of *Vermetus* by Gray (1847: 156) but not made available thereby under I.C.Z.N. (1999) Art. 11.5.2. It was also cited as of Browne, sometimes in a slightly different sense in Vermetidae, by numerous authors (e.g., H. Adams & A. Adams, 1854: 356–357; Cossmann, 1912: 134). Gray (1850: 82) can be credited with a formal introduction of the name (type species not designated), but *Siphonium* Gray, 1850, is invalid because preoccupied by *Siphonium* Link, 1807 [Cephalopoda]. For additional discussion of the name *Siphonium*, see Keen (1980).

Spiroglyphus Daudin, 1800

Spiroglyphus Daudin, 1800, was introduced (1800: 39) with two nominal species, *Spiroglyphus politus* Daudin, 1800, and *Spiroglyphus annulatus* Daudin, 1800. The name has been widely used since the 1840s as a molluscan genus and mostly applied to entrenching vermetids in today's concept of *Dendropoma*. Hartman (1959: 47) included *Spiroglyphus* in her list of possible polychaete annelid genera. Keen (1961: 184, 191) stated that the included species "should probably classed as annelids" and for *Spiroglyphus* it is "advisable to set it aside as a *genus dubium*"; and subsequently (Keen, 1980; Keen & Hadfield, 1985) sought suppression of the name under I.C.Z.N. rules. *Spiroglyphus* was placed on the Official Index of Rejected and Invalid Generic Names in Zoology in Opinion 1425 (I.C.Z.N., 1987).

Bivonia Gray, 1842

After describing the genus in 1842 (p. 90), Gray first provided a type species in 1847 (p. 156), *Vermetus glomeratus* Bivona-Bernardi, 1832 – a nominal species later renamed as *Bivonia petraea* Monterosato, 1884 (= *Dendropoma petraeum* herein). Gray's name is invalid because it is preoccupied by *Bivonia* Cocco, 1832 [Crustacea]. It has, however, remained in use until very recently for vermetid taxa (e.g., Bielokrys, 1999). A nominal species described as *Bivonia exserta* Dall, 1881, is discussed below, and its type specimen shown to be a polychaete worm.

Stoa de Seres, 1855

Stoa de Serres, 1855, was introduced (1855: 238) with three new species, *Stoa ammonitiformis*, *S. spiruliformis* and *S. perforans*, without any subsequent type designation. It was considered a synonym of *Spiroglyphus* or subgenus of *Siphonium* in Vermetidae by Mörch (e.g., 1862: 326), and largely fell into disuse. Keen (1961: 184) suggested that *Stoa* species were annelids and subsequently (Keen & Hadfield, 1985) proposed that the name *Stoa* be suppressed under I.C.Z.N. powers. I.C.Z.N. Opinion 1425 (1987) placed it on the Official Index of Rejected and Invalid Generic Names, suppressing it for the purposes of the Principle of Priority but not for those of the Principle of Homonymy.

(2) Names previously considered synonymous but considered *incertae sedis* herein:

Magilina Vélain, 1877

First listed by Vélain (1876: 285) as a *nomen nudum*, *Magilina* was formally introduced in the following year (1877: 105–106) based on *Magilina serpuliformis* Vélain, 1877 (1877: 106–107, figs. 16–18), and an unnamed Miocene species. *Magilina serpuliformis* was described and illustrated as an extremely small-shelled species, with the adult shells measuring 3 to 4 mm in height and 1.25 mm in diameter. Keen (1961: 198) placed the nominal genus in tentative synonymy with *Dendropoma*. However, the original description and illustration of a very small shell with long upright feeding tube and a glossy and smooth protoconch do not match the conditions of the species treated herein. *Magilina* remains *incertae sedis* until type material can be investigated.

Vermitoma Kuroda, 1928

The genus-group name and its type (and only included) species *Vermitoma luchuana* Kuroda, 1928, was introduced in a catalog work by Kuroda (1928: 40) who credited the names to a manuscript by Hirase. The species was subsequently placed in *Dendropoma* by various authors (e.g., Hasegawa in Okutani, 2000: 207), an action that synonymizes *Vermitoma* under *Dendropoma*. However, the original description of *V. luchuana* by Kuroda (1928: 40, footnote in Japanese) described features that do not support this interpretation. Kuroda mentioned that the living specimen does not show affinities with either vermetids or siliquariids, and in particular referred to a scissurellid-like shell slit that was being filled in as growth proceeded but remained open as an elongated oval hole near the aperture. *Vermitoma* thus also remains *incertae sedis* until type material can be investigated.

(3) Name based on an Upper Oligocene fossil species in need of further investigation:

Elliptovermetus Cossmann & Peyrot, 1922, was introduced by its authors (1922: 69) with its type species by original designation, *Vermetus breigneti* Cossmann & Peyrot, 1922, from Aquitanian fossil beds [Early Miocene] of France. The description and figure of the type species depict a tube that is ovate in cross-section, deeply immersed in coral, and showing lamellar growth striae and a raised mid-dorsal crest. Keen (1961: 200) considered it a subgenus of *Dendropoma*. No extant species have been linked to this taxon.

(4) Three available names that can be applied to extant taxa in this group:

Dendropoma Mörch, 1861

Mörch (1861: 153) introduced the genus as a "section" of *Siphonium*. Type species, by subsequent designation of Keen (1961: 189), is *Siphonium* (*Dendropoma*) *lituella* Mörch, 1861, from California. The genus name was placed on the Official List in Opinion 1425 (I.C.Z.N., 1987).

Novastoa Finlay, 1926

Finlay (1926: 386) based his new genus on the type species, by original designation, *Siphonium lamellosum* Hutton, 1873, from New Zealand.

Veristoa Iredale, 1937

Iredale (1937: 254) based *Veristoa*, by original designation, on *Veristoa howensis* Iredale, 1937, from the Tasman Sea.

Few formal attempts have been made to subdivide *Dendropoma* in a systematic manner. Early arrangements (e.g., Mörch, 1860) separated large and solitary forms into "*Siphonium*" and "*Bivonia*," respectively. One hundred years later, Keen (1961: 198–199) similarly recognized two subgenera for the extant species, *Dendropoma s.s.* (for "mainly solitary forms, minute to large") and *Novastoa* (for "colonial forms, usually encrusting rocks in honeycomb-like sheets"). Keen (1961: 200) expressed uncertainty about the validity of this taxonomic distinction based on growth habit, stating in her treatment of *Novastoa* that this "group may be only situs forms, not a true genetic unit, for specimens in the dense clumps may be, to the eye, indistinguishable from solitary specimens as to operculum, nuclear whorls, and sculpture." As will be shown below, the type species of *Dendropoma* and *Novastoa* indeed belong to different clades, although it is not the distinction of solitary versus gregarious life mode that distinguishes them.

Based on analyses of shell morphological and anatomical characters, the studied taxa of the *Dendropoma* group fall into four separate units, here considered genera. The following section describes and arranges 21 species (eight of which are new) into four genera: *Dendropoma* (with *Veristoa* in synonymy), *Novastoa*, *Ceraesignum* n. gen., and *Cupolaconcha* n. gen. Additional species, not morphologically studied in detail, are assigned to these groups based on literature and/or molecular data.

TAXON DESCRIPTIONS

Gastropoda
Caenogastropoda
Vermetoidea Rafinesque, 1815
Vermetidae Rafinesque, 1815

Dendropoma Mörch, 1861

Dendropoma Mörch, 1861: 153 [placed on the Official Lists of Generic Names in Zoology by I.C.Z.N. (1987)].

Spiroglyphus of authors, not of Daudin, 1800 [the latter placed on the Official Index of Rejected and Invalid Names in Zoology; ICZN (1987)].

Stoa of authors, not of Daudin, 1800 [the latter placed on the Official Index of Rejected and Invalid Names in Zoology; ICZN (1987)].

Veristoa Iredale, 1937: 254. With type species, by original designation, *Veristoa howensis* Iredale, 1937 (see below).

Type Species

Siphonium (*Dendropoma*) *lituella* Mörch, 1861, by subsequent designation of Keen (1961: 189).

Diagnostic Description

Teleoconch: Small to medium (maximum dimension 6–40 mm), "tube" narrow or wide (apertural diameter 1.6–11.4 mm), without expanded chamber behind aperture; whorl coiling pattern concentric but sometimes tending to "*Turritella*-squeezed-sideways", either shallowly entrenched in substratum or spiraling vertically through aggregate matrix (composed of conspecific shells); aperture either flush with substratum/aggregate matrix or forming feeding tube above substratum/aggregate matrix; scars from abandoned feeding tubes sometimes present; often encrusted with epifauna. Shell thick; aperture simple. Color variable, sculpture of tall or low transverse lamellae, with or without longitudinal crests/ridges/carinae. Interior surface color variable; sculpture on columellar surface absent; concave septa frequent in abandoned shell.

Protoconch: Settled/hatchling protoconch diameter 410–950 µm, height 360–860 µm. Strong "hook" projection present on apertural lip. Intracapsular growth only evident in protoconch structure; globular with large increase in whorl size; moderately deep suture; 1.3 whorls; sculpture variable; spiral keel(s) at base of whorl absent or present. Color variable, transparent.

Operculum: Circular in axial profile; diameter proportional to shell size, 1.0–7.7 mm. Composed of chitin only; color variable. Varying between conical with concave exterior surface, and "mushroom-shaped" with domed, convex exterior surface. Exterior surface with spiral lamina pressed flat, appearing "stacked" on "mushroom-shaped" opercula; usually encrusted with epifauna. Interior surface either concave or convex, with prominent mammilla conical to nipple-shaped; peripheral surface smooth and glossy; muscle attachment area textured with shallow concentric grooves.

Radula: Taenioglossate, transparent, colorless. Length of ribbon 1.0–2.9 mm; 34–53 rows (proportional to shell size). Trapezoidal rachidian tooth with prominent central cusp flanked on each side by three smaller cusps decreasing in size outwardly. Base of lateral tooth notched to interlock with rachidian and inner marginal teeth; elongate main cusp flanked by 1–2 cusps on inner side, 2–3 cusps on outer side (variable within a population). Inner marginal tooth slender with one cusp on inner side, 2–3 cusps on outer side. Outer marginal tooth smooth on outer side, one or 2–3 cusps on inner side; base simple, without projection.

External Morphology and Color: Body of animal usually stout (length 35 mm), occupying between 1.5 and 3 last whorls of shell; 0.5x body length composed of gonad and digestive gland. Columellar muscle moderately long, extending between 0.5 and one whorl. Pedal tentacles short (in preserved specimens). Head relatively large, cephalic tentacles short (in preserved specimens), broad, with tiny ommatophore bearing eye at outer base; right side of head with food groove with simple margins. Adult male and female mantle undivided. External body coloration variable.

Pallial and Reproductive Anatomy: Gill 0.2x mantle width, full length of mantle cavity; gill leaflets medium height to tall triangular; 13–22 leaflets per mm. Osphradium short to moderately long relative to mantle cavity, 1.1–5.3 mm long; margins smooth; anterior tip straight or curved towards columellar muscle. Rectum running straight or kinked from coelom to anterior right mantle cavity; fecal pellets cigar shaped. Hypobranchial gland pale brown, covering surface of mantle between gill and rectum, sometimes also covering rectum and pallial oviduct. Pallial oviduct notched near midpoint, sometimes with expanded pocket distal to notch; proximal diverticulum sometimes present. Primary and accessory seminal receptacles present, attached to base of proximal oviduct via short duct. Male reproductive system with notch near base of pallial vas deferens; accessory gland present in exhalant channel near anterior tip of pallial vas deferens.

Development and Ecology: 3–8 unstalked egg capsules held in female mantle cavity; double-walled capsule semi-transparent, round to ovoid, diameter increasing with development of embryos; number of eggs/embryos per capsule varying between species. Larval biology with direct development or short planktonic phase. Adults solitary to gregarious or reef-building.

Comparative Remarks

All known species of *Dendropoma s.s.* produce unstalked egg capsules and brood them in the mantle cavity (females lack a pallial slit) rather than attaching the capsules to the shell wall as in the other vermetid genera examined here. This reproductive strategy is unusual in Vermetidae, but it has been reported in *Petaloconchus montereyensis* Dall, 1919 (Hadfield, 1970, 1989), and in two nominal species of *Vermetus*. The latter – studied as *Vermetus alii* Hadfield & Kay, 1972, by Hadfield et al. (1972) from Hawaii and as *Vermetus* sp. by Miloslavich & Penchaszadeh (1992) from Panama – are here both considered as belonging to *Eualetes tulipa* (Chenu, 1843), based on detailed morphological and molecular comparisons to be published in different context. The habit of retaining egg capsules inside the unslit female mantle therefore cannot be considered a unique synapomorphy of *Dendropoma* s. s. However, it is unique to *Dendropoma s.s.* among the group of vermetids examined in this study and is a particularly useful character for differentiating the genus as a subset of the "*Dendropoma* group". *Petaloconchus montereyensis* and *E. tulipa* are dissimilar to *Dendropoma s.s.* in many other regards, and could not be confused with *Dendropoma s.s.* on the basis of reproductive strategy alone.

The *Dendropoma* operculum has two distinct forms: flat to conical with a concave exterior surface, or "mushroom-shaped" with a convex

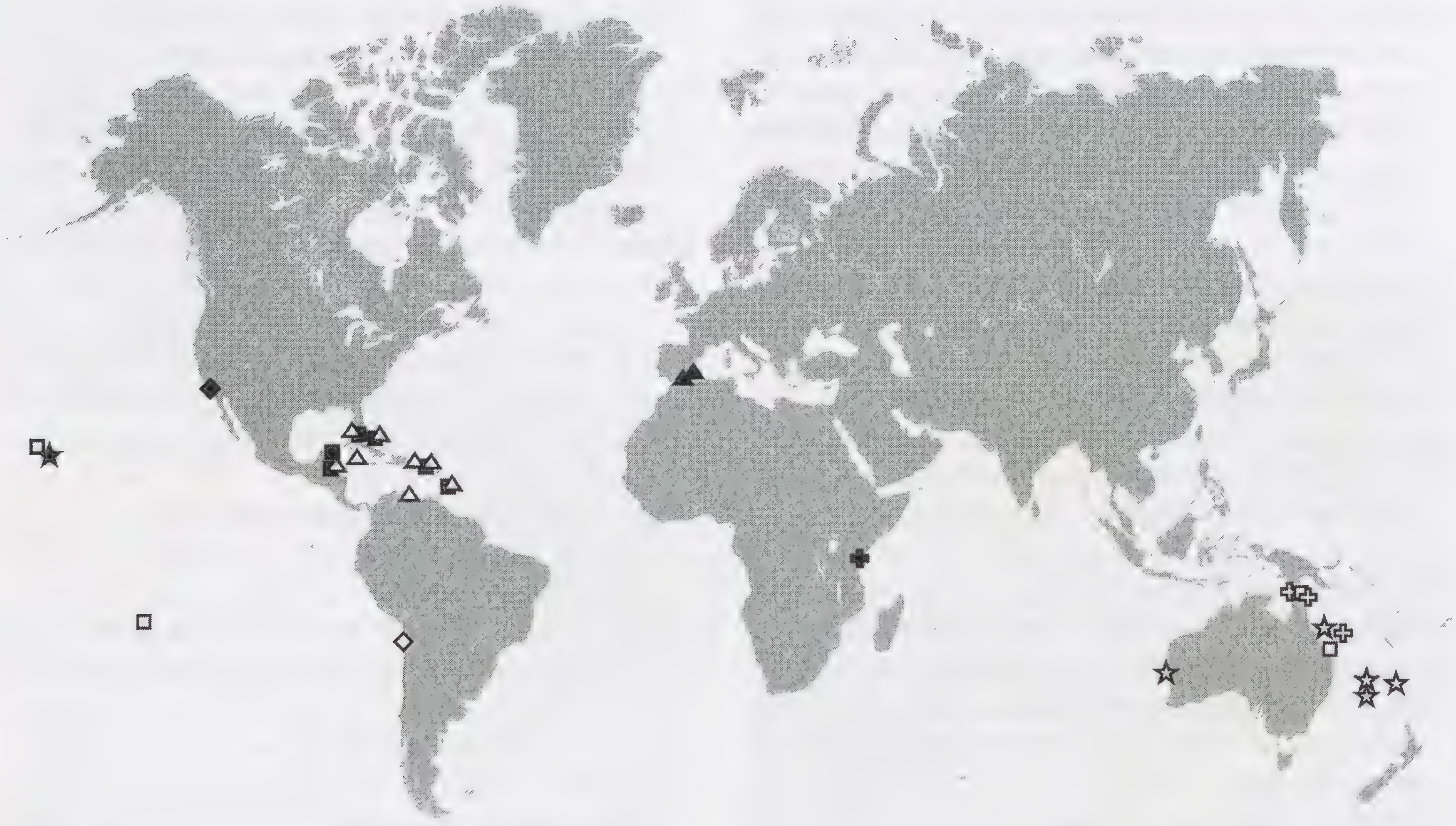

FIG. 7. Distribution map of *Dendropoma* Mörch, 1861 based on material examined in this study. Filled diamond = *D. lituella* (Mörch, 1861); hollow diamond = *D. mejillonense* Pacheco & Laudien, 2008; filled square = *D. nebulosum* (Dillwyn, 1817); hollow square = *D. platypus* (Mörch, 1861); filled triangle = *D.* cf. *petraeum* (Monterosato, 1884); hollow triangle = *D.* cf. *corrodens* (d'Orbigny, 1841); filled star = *D. gregarium* Hadfield & Kay, 1972; hollow star = *D. howense* (Iredale, 1937); filled cross = *D.* cf. *tholia* Keen & Morton, 1960; hollow cross = ***D. expolitum*** n. sp.

exterior surface. The operculum fills the aperture of the shell but does not have a raised, ruffled lamina on the exterior surface, as in *Novastoa*. The lamina on the operculum of *Dendropoma* is multispiral, but is pressed flat when the operculum is concave conical (except in *D. platypus*, where it is sometimes raised for a single revolution) or "stacked" (comprising many horizontal layers) when the operculum is "mushroom-shaped".

The reproductive system also displays some unique characters. For example, the male pallial genital tract is connected to an accessory glandular patch in the exhalant channel, of unknown function but perhaps related to spermatophore production.

Taxonomic Remarks

Dendropoma forms a well-supported, monophyletic clade in the molecular phylogenetic analysis (Fig. 6). Although there are two subclades in *Dendropoma*, we have not introduced subgeneric divisions into the classification. The two subclades approximately correspond to the two different operculum forms, however *D. petraeum* has an intermediate (flat) operculum and is allied with the conical, concave operculate taxa in the molecular phylogeny. These informal groups are referred to here as "concave-operculate" and "convex-operculate" groups. The following systematic descriptions address species belonging to the "concave-operculate" group first, followed by species belonging to the "convex-operculate" group.

Diversity and Distribution (Fig. 7)

Ten species are examined here and included in *Dendropoma s.s.* Only one taxon, from northern Australia, is newly described. There are many other available names in the literature attributed to *Dendropoma* and others that were described in different nominal genera but likely belong here (Bieler & Petit, 2011), but most are poorly described and cannot be placed in this genus with any certainty. *Spiroglyphus stramonitae* Mörch, 1862, originally described from two apparently juvenile specimens and uncertain locality ("Guinea?"), is here considered a member of *Dendropoma s.s.* (Figs. 8, 9). *Dendropoma psarocephalum* Hadfield & Kay, 1972 (Hawaii), and *Dendropoma rhyssoconchum* Hadfield & Kay, 1972 (Hawaii), were included in the molecular phylogenetic analysis, and their generic placement is confirmed. Several other species, for which adequate descriptions and figures are available in the literature, appear to belong in *Dendropoma s.s.* but were not examined in this study, including: *Dendropoma marchadi* Keen & Morton, 1960 (Senegal), *Dendropoma ghanaense* Keen & Morton, 1960 (Ghana), *Dendropoma squamiferum* Ponder, 1967 (New Zealand), and *Bivonia dragonella* Okutani & Habe, 1975 (Japan; based on redescription by Ekawa & Sakashita,

8

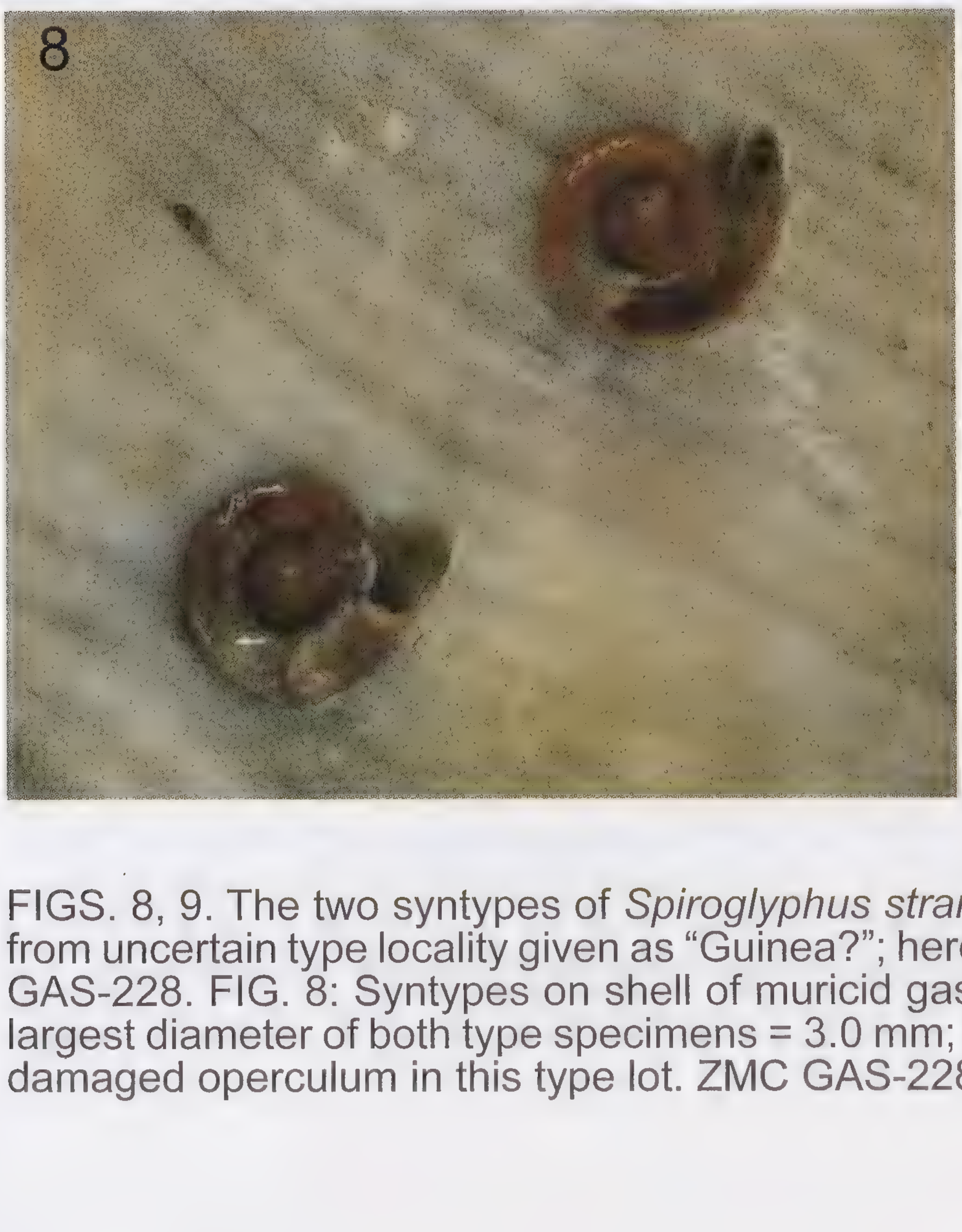

9

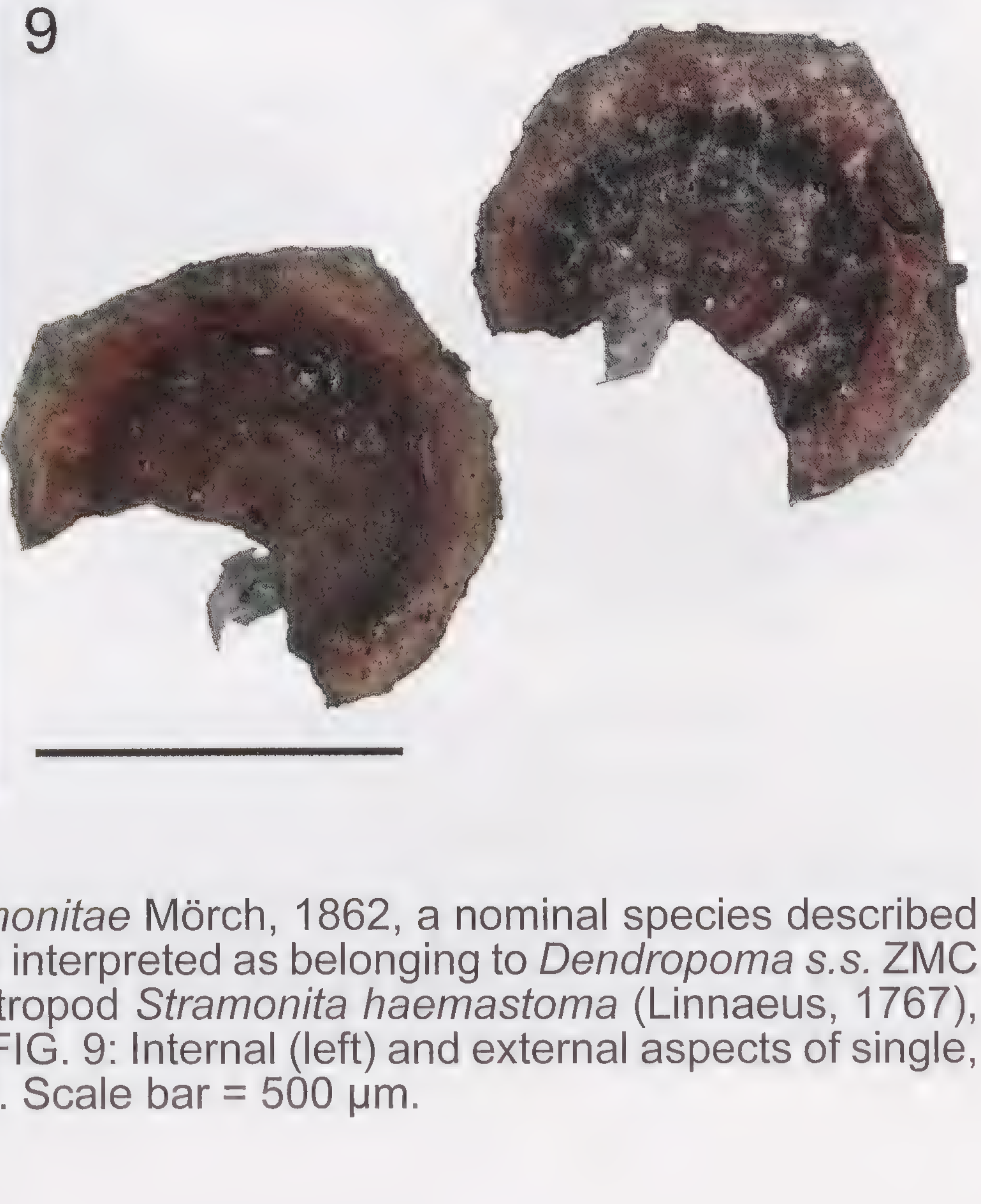

FIGS. 8, 9. The two syntypes of *Spiroglyphus stramonitae* Mörch, 1862, a nominal species described from uncertain type locality given as "Guinea?"; here interpreted as belonging to *Dendropoma s.s.* ZMC GAS-228. FIG. 8: Syntypes on shell of muricid gastropod *Stramonita haemastoma* (Linnaeus, 1767), largest diameter of both type specimens = 3.0 mm; FIG. 9: Internal (left) and external aspects of single, damaged operculum in this type lot. ZMC GAS-228. Scale bar = 500 µm.

2013). Crucially, the available descriptions of the above species include detailed accounts of the operculum and the animal, permitting confirmation of key features distinguishing *Dendropoma s.s.* from *Novastoa*, *Ceraesignum* n. gen. and *Cupolaconcha* n. gen. In most cases, shell characters alone are uninformative for generic assignment.

Dendropoma spp. are distributed globally in tropical and temperate waters. Two nominal species (at least one of which appears to be a species complex) occur sympatrically in the Caribbean.

Dendropoma lituella (Mörch, 1861)

Siphonium (*Dendropoma*) *lituella* Mörch, 1861: 154–155 [placed on the Official List of Specific Names in Zoology by Opinion 1425 (I.C.Z.N. 1987)]; Bieler & Petit, 2011: 44.

Dendropoma (*Dendropoma*) *lituella* – Keen, 1961: 199, 206, text-figs. 26–29, pl. 55, fig. 1 [with selection and illustration of lectotype; Morton, 1965: 588.

Spiroglyphus lituellus [*sic*] – Abbott, 1974: 100.

Dendropoma lituella – Keen, 1983: 10.

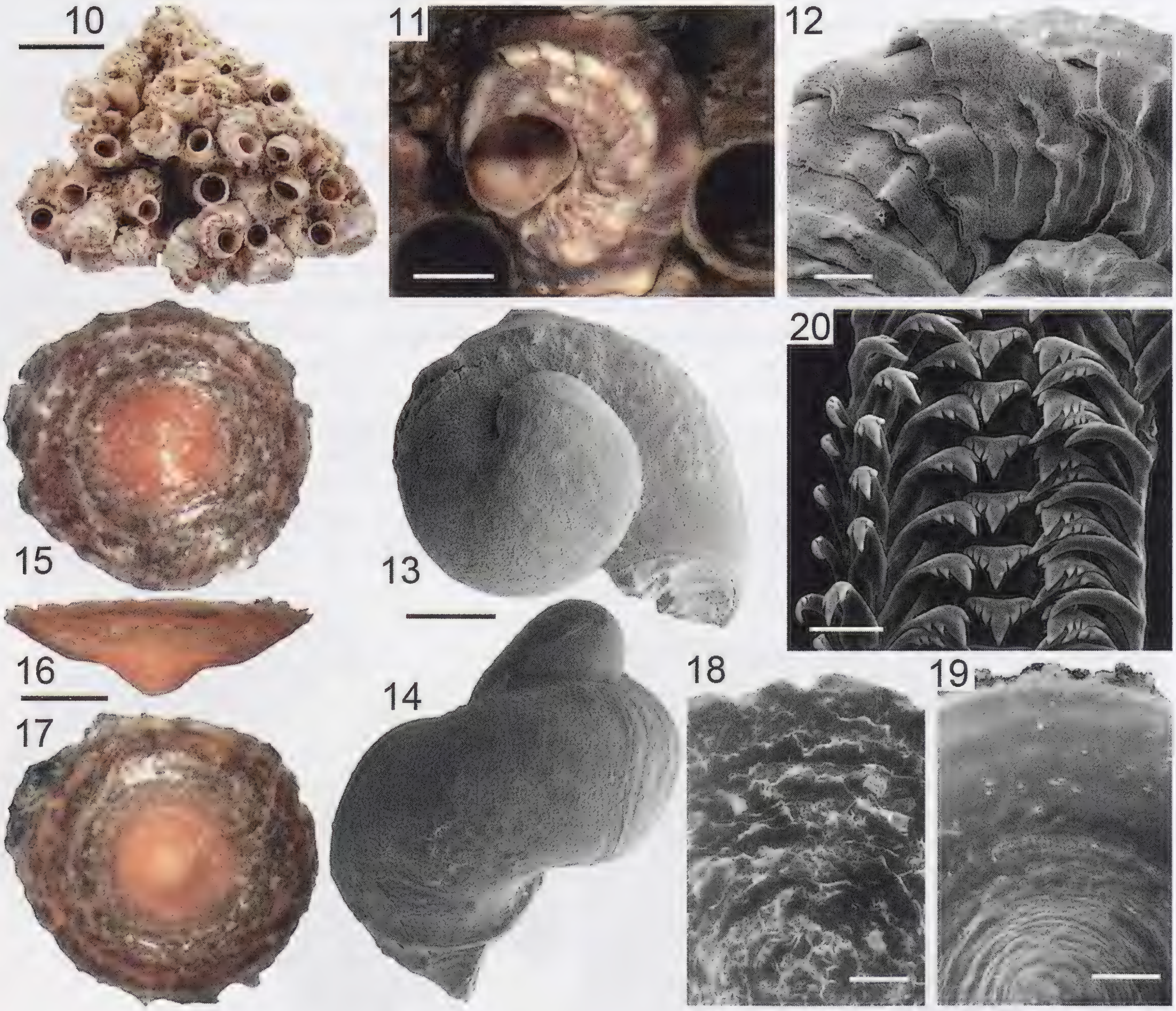

FIGS. 10–20. *Dendropoma lituella* (Mörch, 1861). FMNH 1689, San Diego, U.S.A. FIG. 10: A cluster of specimens removed from substratum. Scale bar = 10 mm; FIG. 11: Individual shell. Scale bar = 2 mm; FIG. 12: SEM image of teleoconch sculpture. Scale bar = 500 μm; FIGS. 13, 14: Protoconchs removed from recently settled juveniles. Scale bar = 200 μm. FIG. 13: Apical view; FIG. 14: Abapertural view; FIGS. 15–17: Operculum. Scale bar = 500 μm. FIG. 15: Exterior surface; FIG. 16: Lateral view; FIG. 17: Interior surface; FIG. 18: SEM image of exterior surface of operculum. Scale bar = 200 μm; FIG. 19: SEM image of interior surface of operculum. Scale bar = 200 μm; FIG. 20: Central section of radula. Scale bar = 50 μm.

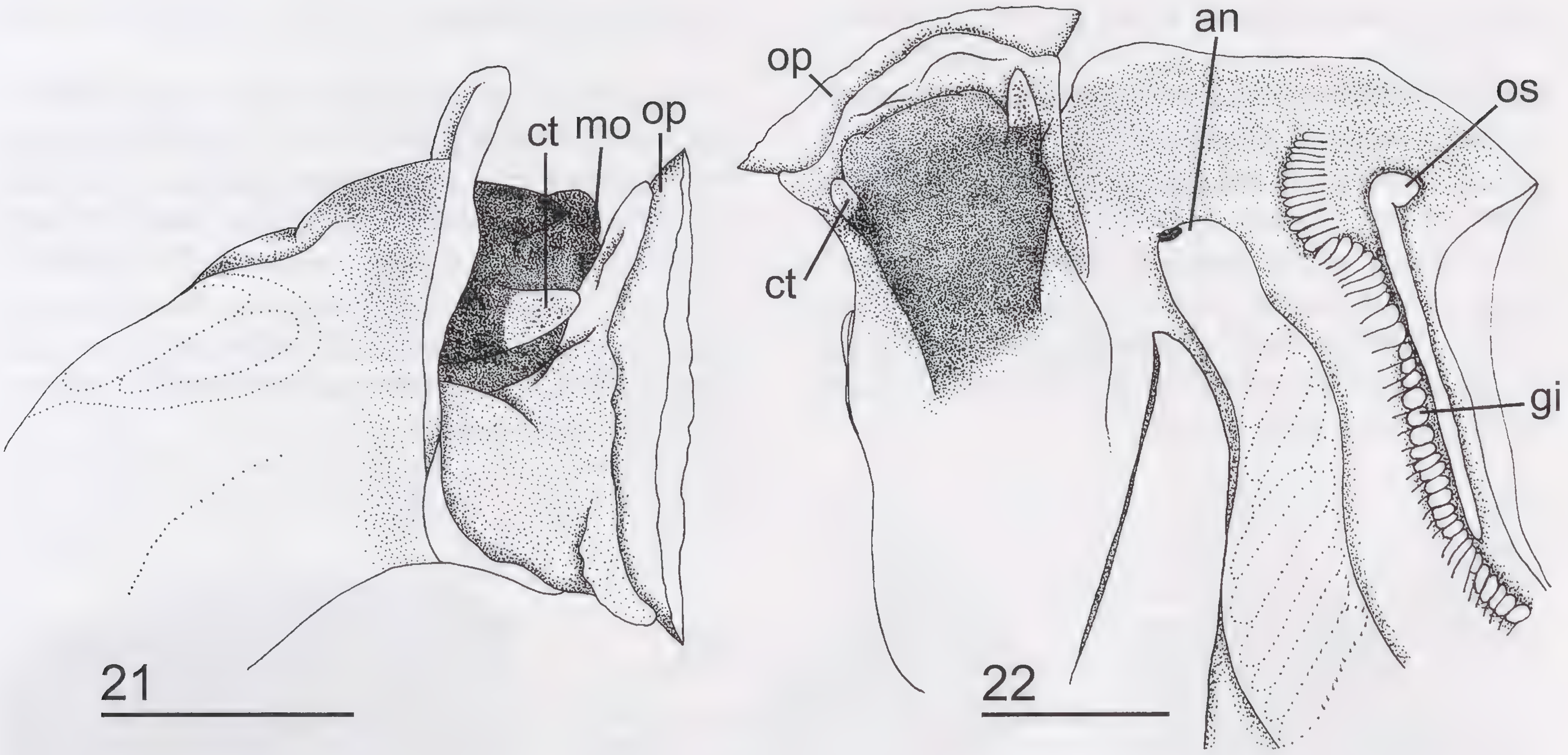

FIGS. 21, 22. Anatomy of *Dendropoma lituella* (Mörch, 1861), based on a partial dried specimen that has been rehydrated. FMNH 1689, San Diego, U.S.A. Scale bars = 1 mm. FIG. 21: Right view of head; FIG. 22: Mantle cavity.

Type Locality

California, imbedded in a *Haliotis* shell; precise locality not known.

Material Examined

Lectotype and paralectotypes: NHMUK 195917.
California, U.S.A.: FMNH 1689: San Diego, purchased from Ward's Natural Science Est., October 1893, dry (many).

Description

Teleoconch (Figs. 10–12): Apertural diameter to 4.1 mm; shell length to 17 mm; diameter of last whorl to 9 mm. Up to four whorls coiled concentrically or slightly off center ("*Turritella*-squeezed-sideways"); shallowly entrenched in substratum; aperture flush with substratum; scars from abandoned feeding tubes absent. Exterior surface cream, with interior surface color faintly showing through; sculpture of low, scale-like transverse lamellae, crossed by longitudinal rib on dorsal surface flanked by 1–2 pairs of smaller ribs on each side. Interior surface cream on ventral surface, dark brown on dorsal surface.

Protoconch (Figs. 13, 14): Settled protoconch diameter to 840 µm, height to 730 µm. Sculpture absent on first whorl, last 0.3 whorl with sculpture of shallow craters, roughly arranged in axial stripes; spiral keel absent. Honey brown.

Operculum (Figs. 15–19): Diameter to 2.7 mm. Shallow conical; opaque pale orange around muscle attachment area, transparent golden peripherally, with ring of dark orange at margin. Lamina on exterior surface flat. Interior surface with low, nipple-shaped mammilla.

Radula (Fig. 20): Length of ribbon 1.2 mm; up to 34 rows. Outer marginal tooth: 2 cusps on inner side.

External Morphology and Color (Fig. 21): Observations of rehydrated specimens: Body occupying at least three whorls of shell. Dorsal surface of head gray, snout pale gray; cephalic tentacles pale gray with dark speckles; foot pale gray; mantle cream with diffuse gray behind anterior margin.

Pallial and Reproductive Anatomy (Fig. 22): Observations of rehydrated specimens: Osphradium moderately long, anterior tip curved towards columellar muscle. Rectum straight.

Development and Ecology: Egg capsules not observed. Adults gregarious.

Comparative Remarks

Belonging to a group of "concave-operculate" *Dendropoma* (*D. lituella*, *D. mejillonense*, *D. nebulosum*, *D. platypus*, *D.* cf. *petraeum* and *D. rhyssoconchum*). Similar to other species in this group with longitudinal sculpture, in particular *D. nebulosum*, which also forms carinae from the transverse lamellae. Distinguished by the unique protoconch sculpture of craters arranged into axial bands.

Taxonomic Remarks

The examined specimens match well with the figured lectotype (Keen, 1961), but are growing more densely and are slightly larger. The shell and operculum match well with Keen's (1961) description. The name lituella is a diminutive of lituus, a Latin noun referring to a cavalry trumpet or an augur's staff used for divination, and apparently describes the snail's coiling pattern. It is a noun in apposition.

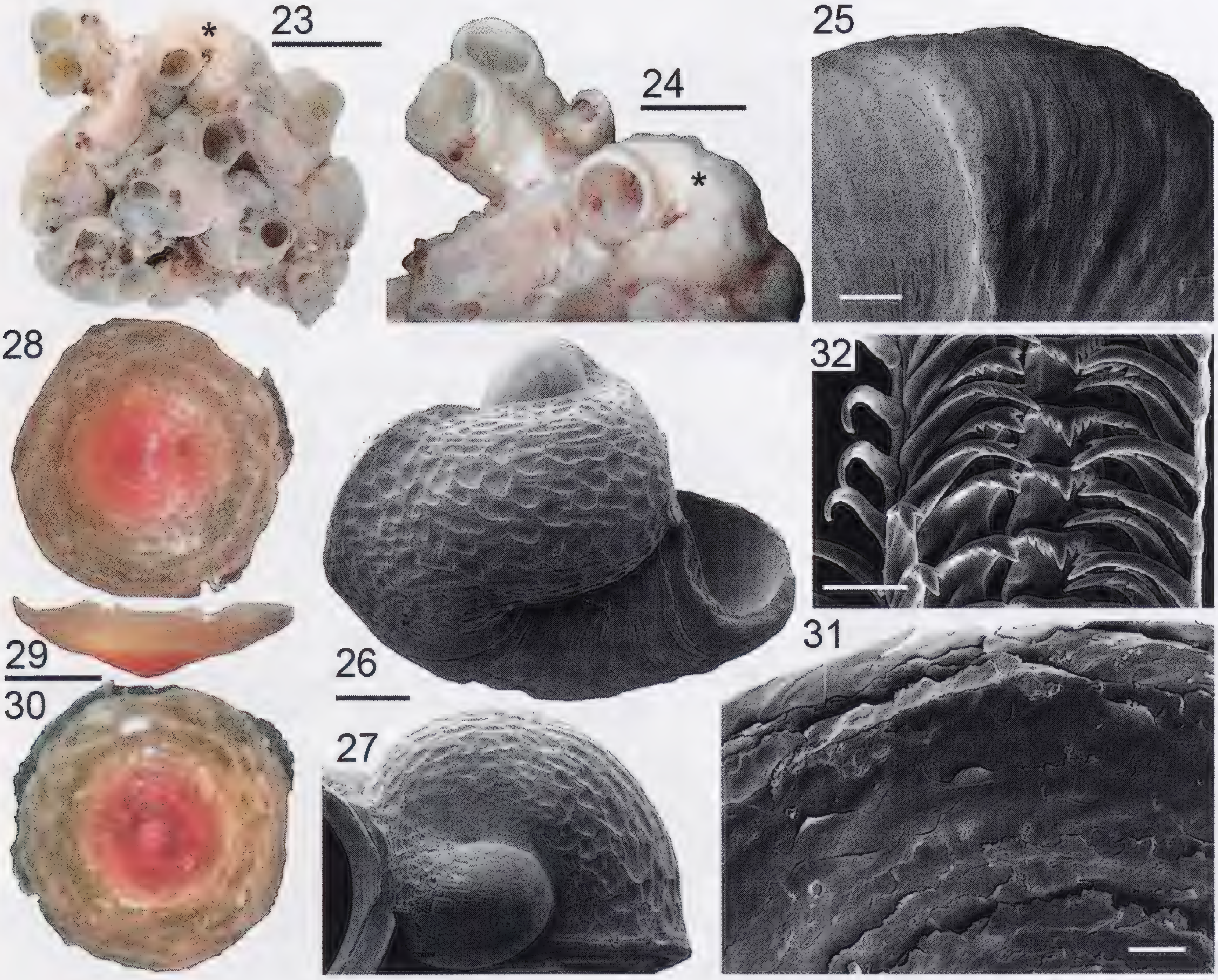

FIGS. 23–32. *Dendropoma mejillonense* Pacheco & Laudien, 2008. FIG. 23: A cluster of specimens removed from the substratum, including lectotype (FMNH 329358, labeled with an asterisk). Paralectotypes, FMNH 312172, Peninsula Mejillones, Chile. Scale bar = 10 mm; Fig. 24: Lectotype (FMNH 329358, labeled with an asterisk) and several other specimens surrounded by numerous recently settled juveniles. Paralectotypes FMNH 312172, Peninsula Mejillones, Chile. Scale bar = 5 mm; FIG. 25: SEM image of teleoconch sculpture. FMNH 312173, Peninsula Mejillones, Chile. Scale bar = 500 µm; FIGS. 26, 27: Protoconchs removed from recently settled juveniles. FMNH 312173, Peninsula Mejillones, Chile. Scale bar = 100 µm. FIG. 26: Abapertural view; FIG. 27: Apical view; FIGS. 28–30: Operculum. FMNH 312173, Peninsula Mejillones, Chile. Scale bar = 1 mm. FIG. 28: Exterior surface; FIG. 29: Lateral view; FIG. 30: Interior surface; FIG. 31: SEM of exterior surface of operculum. FMNH 312173, Peninsula Mejillones, Chile. Scale bar = 100 µm; FIG. 32: Central section of radula. FMNH 312173, Peninsula Mejillones, Chile. Scale bar = 50 µm.

Distribution (Fig. 7)

Examined material from one location (San Diego, California, U.S.A). Distributed from southern California to the southern end of the Gulf of California at La Paz, Baja California (Keen, 1971b: 408).

Dendropoma mejillonense
Pacheco & Laudien, 2008

Dendropoma mejillonensis [*sic*] Pacheco & Laudien, 2008: 219–224, figs. 2, 3; Bieler & Petit, 2011: 46.

Type Locality

17 m, rocky vertical wall known as "Anemones Wall," Peninsula Mejillones, Chile: 23.4695°S, 70.6190°W.

Material Examined

Chile: All from original syntypes: Lectotype: designated herein (Figs. 23, 24), FMNH 329358: coll. by A. Pacheco, July 11, 2006, 70% EtOH (1 specimen attached to paralectotypes); Paralectotypes: FMNH 312172: 70% EtOH (many, attached to lectotype); FMNH 312173: 70% EtOH (many) [DNA sequence data].

Description

Teleoconch (Figs. 23–25): Apertural diameter to 4.5 mm (average 4.29 mm; Pacheco & Laudien, 2008); shell length to 20 mm; diameter of last whorl to 11.5 mm. Initial 2 whorls coiled concentrically, subsequent 1–2 whorls off-center; shallowly entrenched in substratum; aperture sometimes raised 1 cm above substratum as feeding tube; scars from abandoned feeding tubes occasionally present. Exterior surface chalky white to cream; sculpture of low, indistinct transverse lamellae without longitudinal ridges. Interior surface cream on ventral surface, pale fawn on dorsal surface.

Protoconch (Figs. 26, 27): Settled protoconch diameter to 950 µm (770 µm, according to Pacheco & Laudien, 2008); height to 860 µm. Sculpture on all whorls of short, irregularly-shaped "gouge-marks" arranged in roughly spiral bands; spiral keel absent. Pale brown.

Operculum (Figs. 28–31): Diameter to 2.5 mm (average 2.7 mm, according to Pacheco & Laudien, 2008). Shallow conical; opaque reddish-orange around muscle attachment area, transparent golden peripherally. Lamina on exterior surface flat. Interior surface with low, nipple-shaped mammilla.

Radula (Fig. 32): Length of ribbon 2.1 mm; up to 52 rows. Outer marginal tooth: 1 cusp on inner side.

External Morphology and Color (Fig. 33): Body length to 25 mm (average 18 mm according to Pacheco and Laudien, 2008), occupying 2–3 whorls of shell. Columellar muscle extending for 0.5 whorl. Color in life (modified from Pacheco & Laudien, 2008): Head pale grey to reddish with black, white and yellow speckles; foot pale orange with white band around operculum; cephalic tentacles brown or pale gray with black and yellow speckles and distinctive white stripe across base; pedal tentacles pale gray with yellow speckles; mantle pale orange with pale brown band on mantle edge. Color of specimens preserved in 70% EtOH: head-foot and mantle cream to pale gray with scattered black pigment on dorsal surface of head and sides of foot; cephalic tentacles pale gray with white then black stripes at base.

Pallial and Reproductive Anatomy (Figs. 34–37): Gill with 18 leaflets per mm; leaflets medium-height, triangular, breadth equal to height. Osphradium short, 2 mm long; anterior tip curved towards columellar muscle. Rectum straight. Hypobranchial gland extending across rectum and proximal pallial oviduct. Pallial oviduct without expanded distal pocket or proximal diverticulum.

Development and Ecology (Fig. 38): 3–4 unstalked egg capsules per female; 3–10 embryos per capsule (Pacheco & Laudien, 2008). Larval biology not known, but intracapsular larval shells same size as settled protoconchs, suggesting direct development. Adults gregarious.

Comparative Remarks

Similar to other "concave-operculate" *Dendropoma* species, but with weak transverse lamellae and without any longitudinal sculpture

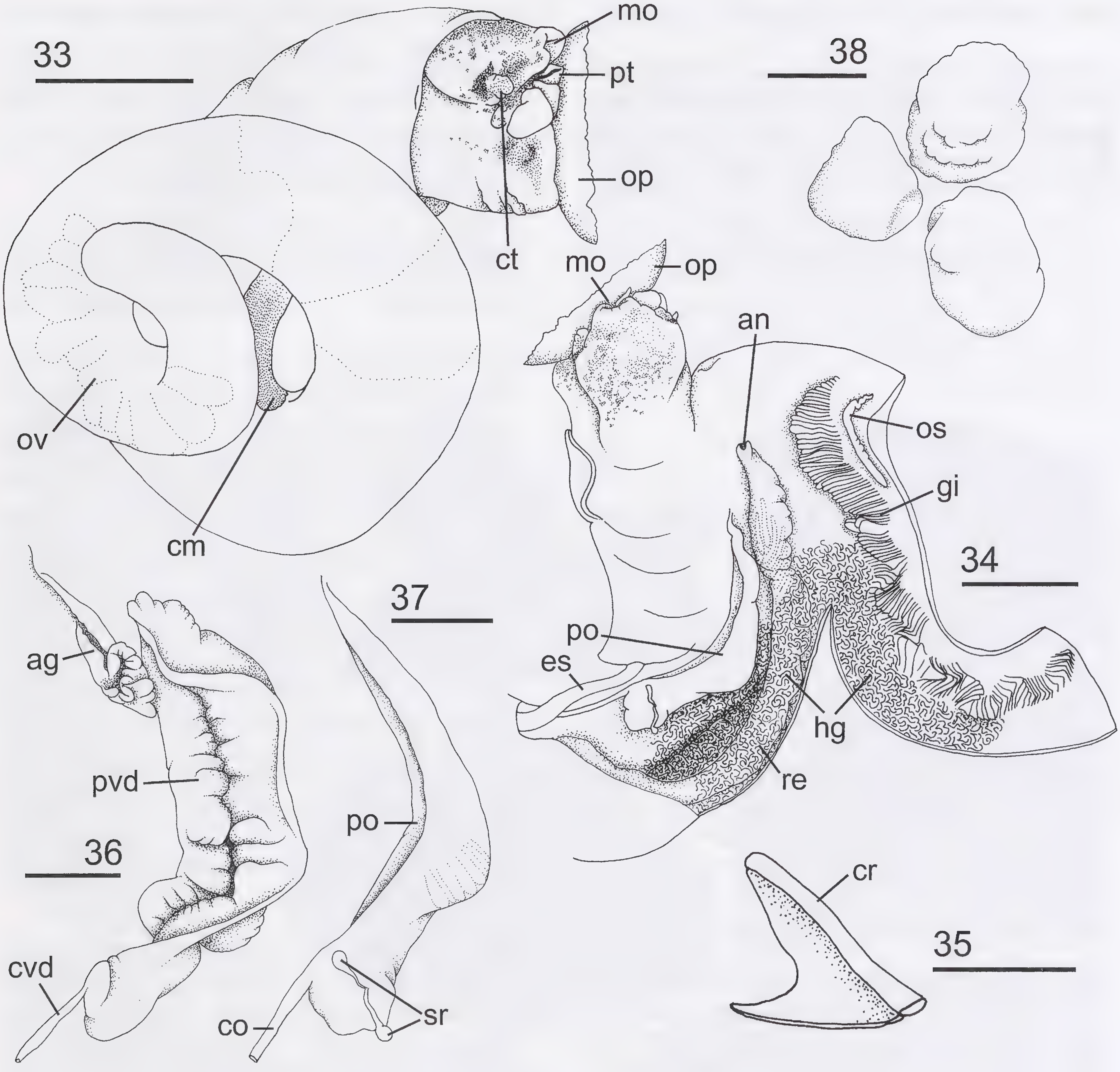

FIGS. 33–38. Anatomy of *Dendropoma mejillonense* Pacheco & Laudien, 2008. FIGS. 33, 34: Female specimen. Scale bars = 2 mm. FIG. 33: Right view of body; FIG. 34: Mantle cavity; FIG. 35: Leaflet from mid-section of gill. FMNH 312172, Peninsula Mejillones, Chile. Scale bar = 500 µm; FIG. 36: Pallial vas deferens. Scale bar = 1 mm; FIG. 37: Pallial oviduct. Scale bar = 1 mm; FIG. 38. Unstalked egg capsules removed from mantle cavity of female. Scale bar = 1 mm. FIGS. 33, 34, 36–38: FMNH 312173, Peninsula Mejillones, Chile.

on teleoconch. The aperture is also raised above the substratum by an extended section of the shell (a feeding tube, but not developed to the extent of some *Petaloconchus* species), which is occasionally removed and extended, resulting in scars from abandoned feeding tubes. The protoconch is highly distinctive and sculptured with short gouges. ***Ceraesignum robinsoncrusoei*** n. sp. is also known from Chile, but occurs in another region and differs in shell, operculum, protoconch and animal morphology.

Taxonomic Remarks

The species epithet is here corrected to *D. mejillonense* to match the neuter generic name. A lectotype has been selected from among the syntypes deposited in the FMNH collections by the original authors (Pacheco & Laudien, 2008).

Distribution (Fig. 7)

Known only from the type locality at Peninsula Mejillones in northern Chile.

Dendropoma nebulosum
(Dillwyn, 1817)

"Tuyaux de mer" Davila, 1767: 562, pl. 4, fig. H [without locality].

"Rugose ridged worm" da Costa, 1770–1771: pl. 11, figs. 8–10 [West Indies; common name and locality from Jackson, 1937: 336].

"Vermiseaux intestins" d'Argenville, 1780: 652, pl. 6 fig. I [American Seas].

"Les Bourras très-raboteux" d'Argenville, 1780: 667, pl. 6, fig. F2.

Serpula nebulosa Dillwyn, 1817: 1076–1077; Wood, 1828: 186, pl. 38, fig. 18; Bieler & Petit, 2011: 49.

Serpula bicarinata G. B. Sowerby II, 1839: 116, fig. 4 [without locality].

Siphonium nebulosum – Mörch, 1859: 357–358 [St. Thomas]; Mörch, 1861: 162–163 (in part; Mörch listed eight infrasubspecific varieties, partly from specimens [Honduras, St. Thomas], partly based on earlier literature); Mörch, 1877: 112–114 [Honduras, St. Thomas]; Clessin, 1902: 52–54; Jong & Coomans, 1988: 42–43, pl. 33, fig. 197 [Curaçao, Aruba, Bonaire; unspecified].

Vermetus (*Siphonium*) *nebulosus* – Tryon, 1886: 184, 440, pl. 54, figs. 87, 88 [the latter fig. = *Serpula bicarinata* of G. B. Sowerby II].

Dendropoma (*Dendropoma*) *nebulosum* – Keen, 1961: 199.

Spiroglyphus (*Novastoa*) *nebulosus* – Abbott, 1974: 101 [as *nomen dubium*].

Dendropoma nebulosum – Rawlings et al., 2001: 1604 [Florida Keys; sequence and gene arrangement data].

Serpulorbis riisei – Zhang, 2011: 69, fig. 126 [Antigua; *non Thylacodes riisei* Mörch, 1862].

Dendropoma irregulare – Zhang, 2011: 69: fig. 128 [Antigua; *non Vermetus irregularis* d'Orbigny, 1841].

Type Locality

American Seas.

Material Examined

Specimens studied by Mörch (1861: 162–163), including his infrasubspecific forms "serrata" (NHMUK 1986.201; Honduras), "rugosa" and "fissurata" (NHMUK 1986.203), and "anaulax" (NHMUK 1986.199; Honduras).

Mexico (Yucatan): FMNH 286235 and 286237: Puerto Morelos, Quintana Roo, approx. 20.83°N, 86.88°W, coll. J. Templado, October 20, 1994, 70% EtOH (total 6 specimens).

Belize: FMNH 326923: patch reef, Carrie Bow Cay, Stann Creek District, 16.80°N, 88.08°W, coll. R. Bieler, March 22, 1986, 70% EtOH (4 adults with egg capsules) (many); FMNH 326934: patch reef, Carrie Bow Cay, Stann Creek District, 16.80°N, 88.08°W, coll. R. Bieler, March 1986, dry (6 specimens).

Bahamas: FMNH 335070: 10–12 m, outside barrier reef off Walker's Key, reefs NE of Great Abaco Island, 26.6410°N, 77.0374°W, coll. R. Bieler & P. Sierwald, August 8, 2012, 95% EtOH and dry [DNA sequence data]; FMNH 326963: Smiths Point, south shore, 4 km SE of Freeport, Grand Bahama Island, 26.5125°N, 078.6083°W, coll. J. Worsfold, January 9, 1989, 70% EtOH (many); FMNH 326964: 3–6 m, circular patch reefs with corals, gorgonians, sponges, known as "School House", off Coral Harbour, SW New Providence Island, 24.97°N, 77.47°W, August 24, 1994, coll. R. Bieler & P. Sierwald, 70% EtOH (5 specimens).

Barbados: FMNH 326965: 18 m, coral reef, off Spring Garden, 13.116°N, 59.638°W, April 18, 1989, coll. P. M. Mikkelsen, 70% EtOH (many).

Florida, U.S.A.: FMNH 326966: 3m, from gorgonians, off Missouri Key, Florida Keys, Monroe County, 24.674°N, 81.238°W, October 15, 1988, R. Bieler & P. M. Mikkelsen, 70% EtOH (2 specimens); FMNH 290043: 5m, spur and groove reef, Looe Key, Lower Florida Keys, Monroe County, 24.5466°N, 81.4133°W, August 10, 1999, coll. R. Bieler & P. M. Mikkelsen, 70% EtOH (many); FMNH 315538, 327090: R/V Floridays, 7 m, "The Slabs" patch reef between outer patches and "coral humps" off Marathon, MM 50, Florida Keys, Monroe County, 24.6588°N, 81.0150°W, July 20, 1997, coll. R. Bieler & P. M. Mikkelsen, 95% EtOH (many), [DNA sequence data]; FMNH 326734: small patch reef, off Newfound Harbor Keys, Monroe County, 24.6162°N, 81.3913°W, coll. R. Bieler & P. Sierwald, September 11, 2010, 70% EtOH (2 specimens), 3.5% glutaraldehyde (1 sample of testis), RNAlater (2 tissue samples); FMNH 326736: ocean side of Ramrod Key, Looe Key forereef, Monroe County, 24.5458°N, 81.4059°W, coll. R. Bieler & P. Sierwald, September 13, 2010, 80% EtOH (2 specimens), 3.5% glutaraldehyde (1 sample of testis), RNAlater (2 tissue samples).

Saba, Netherlands: FMNH 328794: 23 m, dive site "Hole in the Corner" off SE coast of Saba Island, 17.6167°N, 63.2283°W, coll. R. Bieler & P. Sierwald, October 15, 2010, 95% EtOH (5 specimens).

Description

Teleoconch (Figs. 39–42): Size, shape and sculpture highly variable between and within populations. Apertural diameter to 11.4 mm; shell length to 30 mm; diameter of last whorl to 28 mm. Up to four whorls, initial whorls coiled concentrically, sometimes shifting to off-center growth for later whorls; occasionally wrapped around cylindrical substratum (e.g. gorgonian stem); superficially attached to (if gorgonian) or shallowly entrenched in (if rock or shell) substratum; aperture usually flush with substratum, occasionally slightly raised; scars from abandoned feeding tubes absent. Exterior surface chalky white to cream or tan; sculpture of transverse lamellae crossed by 3–7 longitudinal ridges, central ridge dominant, transverse lamellae at apex of ridges forming spinose carinae. Interior surface cream on dorsal surface, dark brown on ventral surface.

Protoconch (Figs. 43–46): Hatchling protoconch diameter to 670 µm; height to 600 µm. Sculpture absent on first 0.5 whorl, last 0.8 whorl with raised "crust" of cratered sculpture; spiral keel absent. Pale brown or colorless.

Operculum (Figs. 47–50): Diameter to 7.7 mm. Shallow conical; opaque dark orange to red around muscle attachment area, transparent golden peripherally, with ring of dark orange at margin. Lamina on exterior surface flat. Interior surface with moderately tall, conical mammilla.

Radula (Fig. 51): Length of ribbon 2.9 mm; up to 45 rows. Outer marginal tooth: one cusp on inner side.

External Morphology and Color (Figs. 52, 53, 55): Body length to 27 mm; occupying 1–2 whorls of shell. Columellar muscle extending for 0.5 whorl. Color in life: Head-foot black with white speckles, especially on snout, sides of head and sides of foot; cephalic and pedal tentacles black, with white speckles; mantle cream with dense, opaque, white pigment; mantle margin with alternating bands of black and white pigment; two morphs present, distinguished by either intense red or yellow pigment on sole of foot and diffuse red or yellow pigment overlaying entire foot and dorsal surface of head. Pigmentation of specimens preserved in 70% EtOH: head-foot cream to pale gray, dorsal surface of head either mottled or entirely dark gray with dark patches on lateral surface of head at base of tentacles; cephalic tentacles pale gray; pedal tentacles dark gray.

Pallial and Reproductive Anatomy (Figs. 56–59): Gill with 22 leaflets per mm; leaflets medium-height, triangular, breadth equal to height. Osphradium short, 3.9 mm long; anterior tip curved towards columellar muscle. Rectum straight. Hypobranchial gland extending across rectum and proximal pallial oviduct. Pallial oviduct with notch at midpoint; proximal diverticulum present.

Development and Ecology (Figs. 54, 60): Up to eight unstalked egg capsules per female; 18–40 embryos per capsule. Late stages as pediveliger with small velar lobes, eye spots, shell suture and inner lip of aperture brown, and larval operculum with distinct orange spiral in center; head and foot in most cases pigmented with fine black spots. Adults solitary or gregarious, often found in association with living coral, gorgonians and *Dendostrea frons*.

Comparative Remarks

Similar to ***Novastoa pholetor***, but without a mantle slit or ruffled lamina on operculum. The protoconch is typical covered by an irregular layer pitted with craters, which does not occur in any other *Dendropoma* species. The operculum is distinct from other "concave-operculate" *Dendropoma* species because the mammilla is conical, not nipple shaped. The egg capsules of *D. nebulosum* contain 30–40 eggs, more than any other species of *Dendropoma*.

Taxonomic Remarks

Dillwyn (1817: 1076) introduced *Serpula nebulosa* based on a figure by Davila (1767: 562, pl. 4, fig. H) and text and figure by "Favanne" [d'Argenville, 1780: 652, pl. 6, fig. I). D'Argenville (1780: 652), who considered the species American and uncommon, referred to Davila's earlier illustration, and Mörch (1859: 357, 1861: 162) interpreted the later figure as a mere copy. Wood (1828: 186, pl. 38, fig. 18) published another, extremely sketchy, copy. Mörch (1859) transferred the species to *Siphonium* and in 1861 recognized it as highly variable and widely distributed in the Caribbean, prompting him to name eight infrasubspecific varieties. He (1859, 1861) synonymized *Serpula bicarinata*

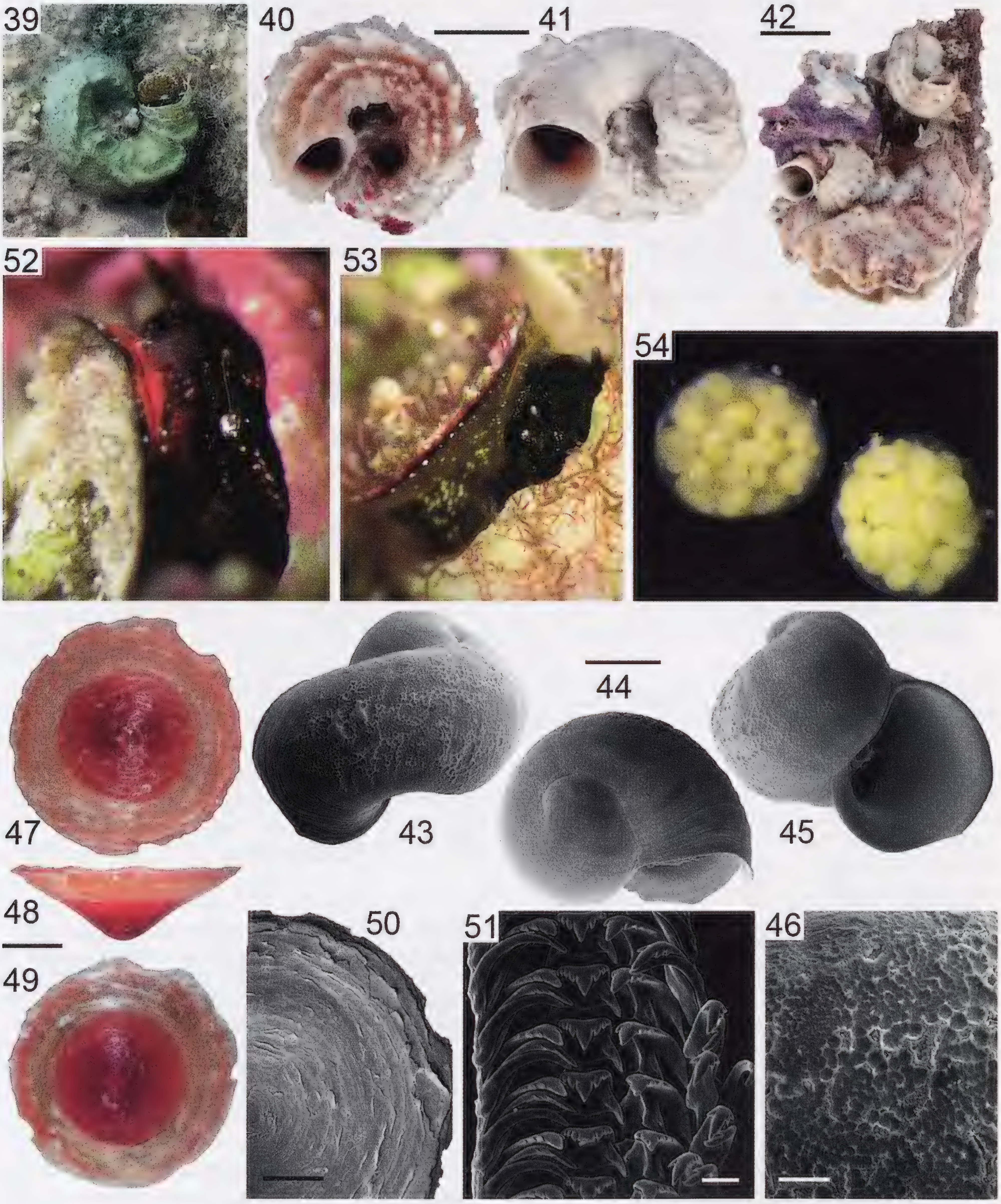

FIGS. 39–54. *Dendropoma nebulosum* (Dillwyn, 1817). FIG. 39: Living animal attached to coral at Carrie Bow Cay, Belize; FIG. 40: Shell with carinate sculpture. FMNH 326934, Carrie Bow Cay, Belize. Scale bar = 10 mm; FIG. 41: Shell without carinate sculpture. FMNH 286237, Yucatan, Mexico; FIG. 42: Specimens growing in clusters on gorgonian stems with *Dendostrea frons*. Scale bar = 10 mm; FIGS. 43–45: Protoconchs removed from recently settled juveniles. FMNH 326963, Grand Bahama Island, Bahamas. Scale bar = 200 µm. FIG. 43: Abapertural view; FIG. 44: Apertural view; FIG. 45: Apical view; FIG. 46: Sculpture on protoconch. Scale bar = 50 µm; FIGS: 47–49: Operculum. FMNH 326963, Grand Bahama Island, Bahamas. Scale bar = 1 mm. FIG. 47: Exterior surface; FIG. 48: Lateral view; FIG. 49: Interior surface; FIG. 50: SEM image of exterior surface of operculum. FMNH 326963, Grand Bahama Island, Bahamas. Scale bar = 500 µm; FIG. 51: Central section of radula. FMNH 326963, Grand Bahama Island, Bahamas. Scale bar = 50 µm; FIGS. 52, 53: Living specimens from Carrie Bow Cay, Belize. FIG. 52: Red morph; FIG. 53: Yellow morph; FIG. 54: Two egg capsules removed from female specimen at Carrie Bow Cay, Belize.

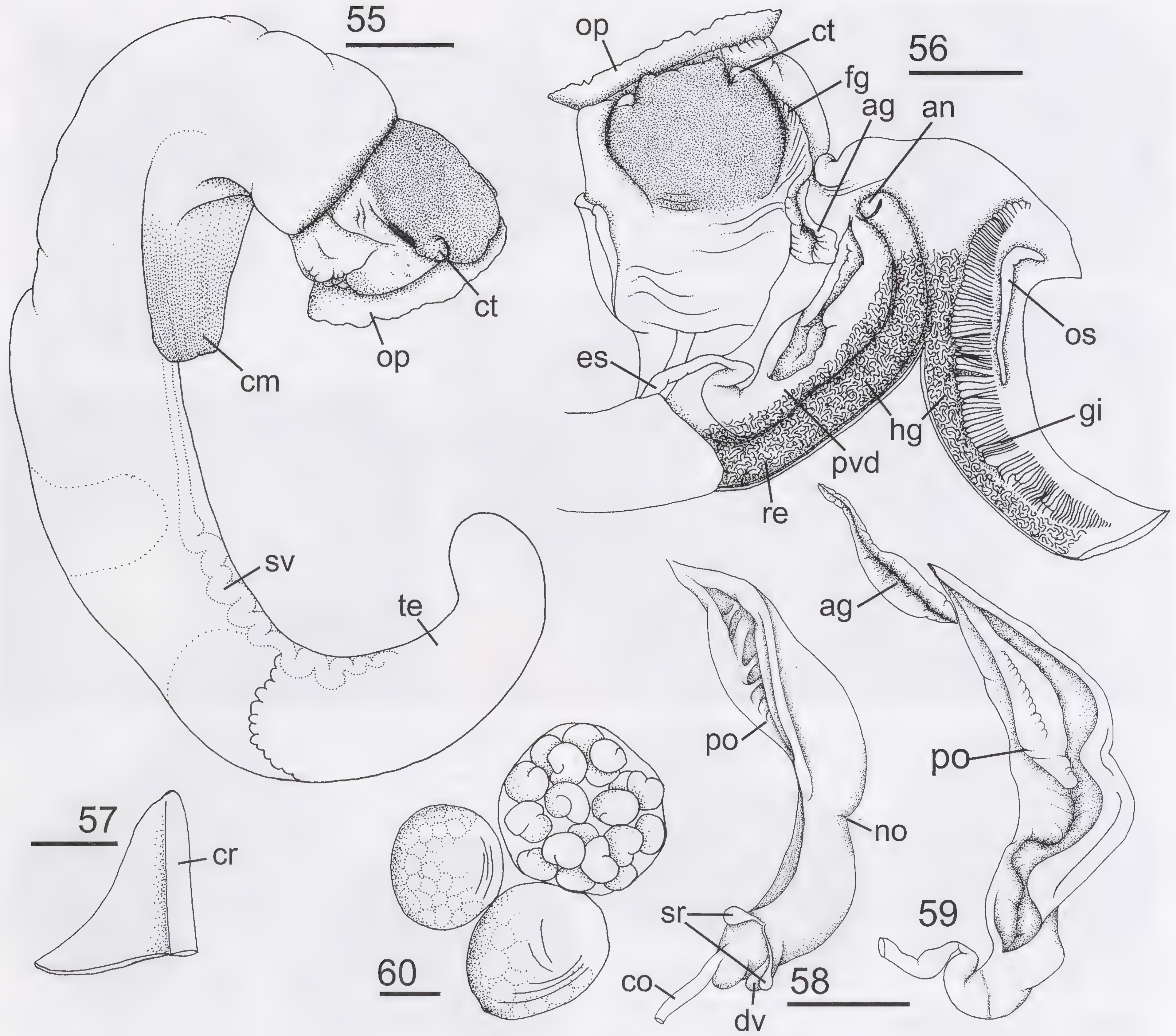

FIGS. 55–60. Anatomy of *Dendropoma nebulosum* (Dillwyn, 1817). FIG. 55: Right view of male specimen. FMNH 326963, Grand Bahama Island, Bahamas. Scale bar = 2 mm; FIG. 56: Mantle cavity of a male specimen. FMNH 326923, Carrie Bow Cay, Belize. Scale bar = 2 mm; FIG. 57: Leaflet from mid-section of gill. FMNH 326963, Grand Bahama Island, Bahamas. Scale bar = 200 µm; FIG. 58: Pallial oviduct. FMNH 326923, Carrie Bow Cay, Belize. Scale bar = 2 mm; FIG. 59: Pallial vas deferens. FMNH 286235, Yucatan, Mexico. Scale bar = 2 mm; FIG. 60: Unstalked egg capsules removed from the mantle cavity of a female, containing embryos at various stages of development. FMNH 326963, Grand Bahama Island, Bahamas. Scale bar = 1 mm.

G. B. Sowerby II, 1839, from unknown locality, and in 1877 Mörch recognized additional historic illustrations, such as d'Argenville's (1780: pl. 6, fig. F2), as belonging to this nominal taxon. The species was rarely mentioned in the subsequent literature, and Abbott (1974: 101) declared it an "undetermined species of dubious identity." Various modern illustrations of this species can be found in the recent literature, misidentified as members of other species (e.g., Zhang, 2011, as "*Serpulorbis riisei*" and "*Dendropoma irregulare*"). *Dendropoma nebulosum* is variable within and between populations. In particular, the presence and prominence of carinose spines on the teleoconch is inconsistent. In at least one population (Carrie Bow Cay, Belize) distinct morphs with either red or yellow coloration on the head-foot were observed alive, but were not otherwise distinguishable.

Distribution (Fig. 7)

Common throughout the Caribbean, Bahamas, and South Florida.

Dendropoma platypus (Mörch, 1861)

Siphonium (*Stoa*) *platypus* Mörch, 1861: 153, 157; Bieler & Petit, 2011: 53.
Siphonium platypus – Clessin, 1902: 48.
Dendropoma (*Dendropoma*) *platypus* – Keen, 1961: 207.
Dendropoma platypus – Hadfield et al., 1972: 84–86, figs. 5, 6, 19H; Kay, 1979: 106, fig. 39B.

Type Locality

Sandwich [Hawaiian] Islands, on a *Chama*; precise locality unknown.

Material Examined

Holotype: NHMUK 195927.
Hawaiian Islands, U.S.A.: FMNH 88577: Mokuoloe Island, Oahu, 157.7861°W, 21.4361°N, coll. T. Dranga, 1925, dry (3 specimens). FMNH 329359: beach rock on reef flats, 0.1 m at low tide, Diamond Head Beach, E Honolulu, Oahu, approx. 21.43°N, 157.79°W, coll. R. Bieler, March 28, 1988, 70% EtOH (2 specimens).
French Polynesia: UF 436992: channel wall with coral and silty slope with rubble, Teruaupou Pass, Moorea Island, Society Islands; 17.5727°S, 149.7884°W, coll. G. Paulay, C. Meyer & S. McPherson, December 7, 2009, 75% EtOH (1 specimen).
Australia: AM C.464334: under beach rock slabs, just below beach, opposite laboratory, Heron Island, Capricorn Group, Queensland, 23.4434°S, 151.9126°E, coll. W. F. Ponder, September 21, 1970, 5% SW formalin (2 specimens); AM C.407534: on semi-exposed boulder bank, Putta Putta Beach, S of Fly Point, Cape York Peninsula, Queensland, 10.7586°S, 142.5994°E, coll. W. F. Ponder & I. Loch, July 11, 1976, 5% SW formalin (many).

Description

Teleoconch (Figs. 61–64): Apertural diameter to 9 mm; shell length to 40 mm; diameter of last whorl to 21 mm. Up to four concentrically coiled whorls, last whorl sometimes straightening out; deeply entrenched in substratum; aperture flush with substratum; scars from abandoned feeding tubes absent. Exterior surface often heavily encrusted, but where exposed white, sometimes mottled brown, purple or green (Hadfield et al., 1972); sculpture of low, thick, transverse lamellae crossed by many (> 10) longitudinal ribs, at apex of each rib transverse lamellae sometimes form carinae. Interior surface of shell white with irregular brown patches on ventral surface.

Protoconch (Figs. 65, 66): Settled protoconch diameter to 560 µm; height to 610 µm. Sculpture of shallow craters on first 0.6 whorl, last 0.7 whorl with tall, widely-spaced axial ribs; spiral keels absent. Pale brown.

Operculum (Figs. 67–72): Diameter to 5 mm. Shallow conical; either dark red around muscle attachment area and colorless peripherally (living Hawaiian specimens, according to Hadfield et al., 1972, and preserved Putta Putta Beach specimens), or opaque orange around muscle attachment area and transparent golden peripherally (preserved Hawaiian and Heron Island specimens). Lamina on exterior surface either flat or raised for approx. one revolution. Interior surface with moderately tall, nipple-shaped mammilla.

Radula (Fig. 73): Length of ribbon 2.8 mm; up to 53 rows. Outer marginal tooth: two cusps on inner side.

External Morphology and Color (Figs. 74, 75): Body length to 35 mm; occupying last 1–2 whorls of shell. Columellar muscle extending for one whorl. Color in life (modified from Hadfield et al., 1972): Head-foot black with yellow and white speckles especially on sides of head; mantle margin with alternating bands of black and bright yellow. Color of specimens preserved in 70% EtOH: Head-foot flesh-colored, dorsal surface of head gray; cephalic tentacles unpigmented with dark gray patches at base; mantle cream with pale grey pigment band behind margin.

Pallial and Reproductive Anatomy (Figs. 76–79): Gill with 17 leaflets per mm; leaflets tall triangular, height twice breadth. Osphradium short-medium length, 5.3 mm long; anterior tip curved towards columellar muscle. Rectum straight. Hypobranchial gland extending partly across rectum. Pallial oviduct without notch at midpoint; proximal diverticulum present.

Development and Ecology: At least five unstalked egg capsules per female; up to 70 larvae per capsule (Hadfield et al., 1972;

based on Hawaiian material). Larval development mixed: laboratory-reared recently hatched larvae with resorbed velum, not capable of swimming (Hadfield et al., 1972), whereas veligers obtained by plankton tow reported by Taylor (1975: 77) were smaller and

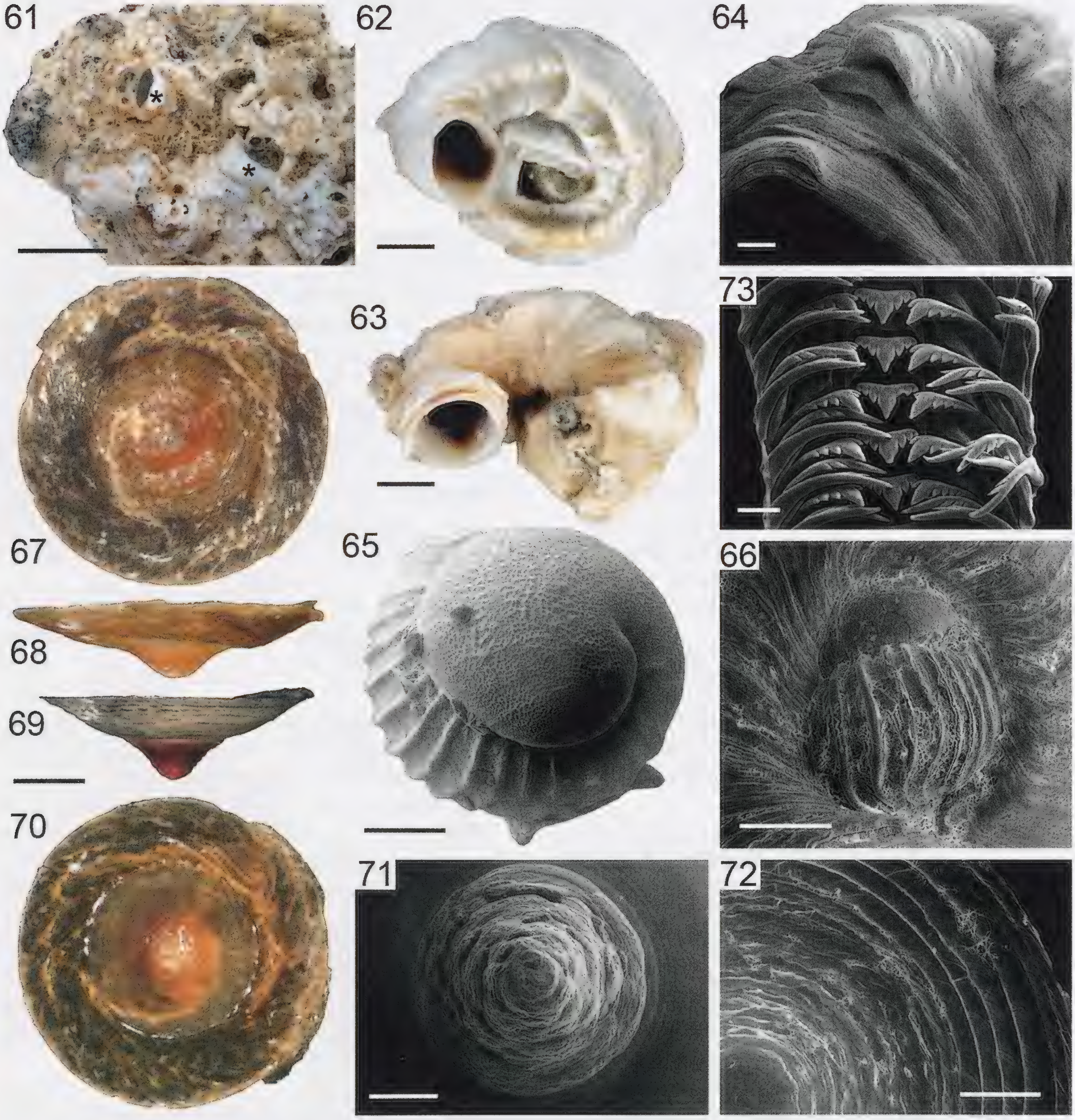

FIGS. 61–73. *Dendropoma platypus* (Mörch, 1861). FIG. 61: Two specimens entrenched in substratum (apertures marked with asterisks) surrounded by *Dendropoma gregarium*. FMNH 329359, Oahu, Hawaii. Scale bar = 10 mm; FIG. 62: Shell with dorsal keel. AM C.407534, Putta Putta Beach, Australia. Scale bar = 5 mm; FIG. 63: AM C.464334, Heron Island, Australia. FIG. 64: SEM image of teleoconch sculpture. AM C.464334, Heron Island, Australia. Scale bar = 500 µm; FIGS. 65, 66: SEM images recently-settled protoconchs. FIG. 65: Apical view. AM C.407534, Putta Putta Beach, Australia. Scale bar = 100 µm; FIG. 66: Abapertural view, partly obscured by later whorls. FMNH 88577, Oahu, Hawaii. Scale bar = 200 µm; FIGS. 67–70: Operculum. Scale bar = 1 mm. FIG. 67: Exterior surface. FMNH 329359, Oahu, Hawaii; FIG. 68: Lateral view. FMNH 329359, Oahu, Hawaii; FIG. 69: Lateral view. AM C.464334, Heron Island, Australia; FIG. 70: Interior surface. FMNH 329359, Oahu, Hawaii; FIGS. 71, 72: SEM images of operculum. AM C.464334, Heron Island, Australia. Scale bar = 500 µm. FIG. 71: Muscle attachment area on interior surface; FIG. 72: Exterior surface; FIG. 73: Central section of radula. FMNH 329359, Oahu, Hawaii. Scale bar = 50 µm.

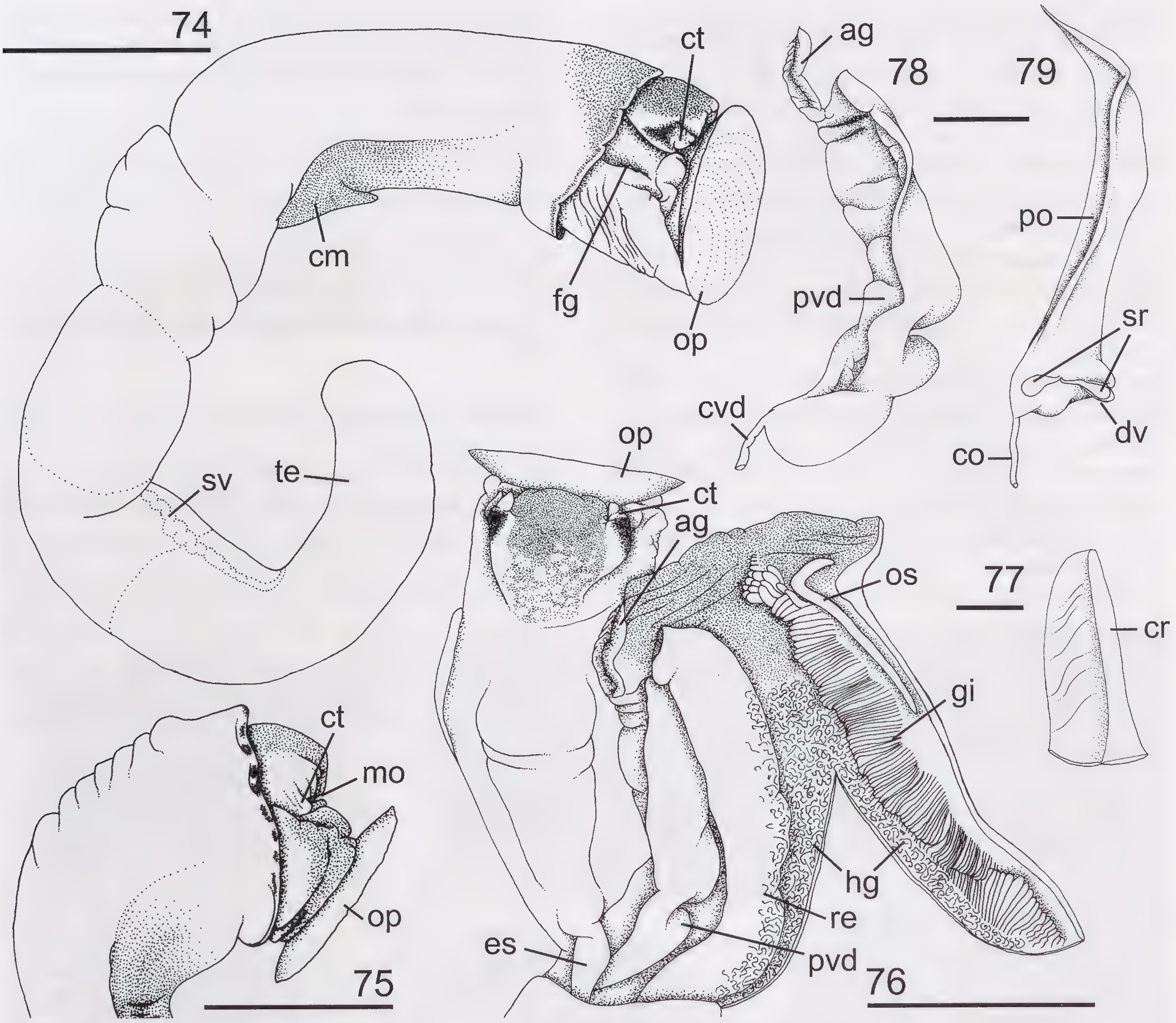

FIGS. 74–79. Anatomy of *Dendropoma platypus* (Mörch, 1861). FIG. 74: Right view of male specimen. FMNH 329359, Oahu, Hawaii. Scale bar = 5 mm; FIG. 75: Right view of anterior body of male specimen. Scale bar = 5 mm. AM C.407534, Putta Putta Beach, Australia; FIG. 76: Mantle cavity of male specimen. FMNH 329359, Oahu, Hawaii. Scale bar = 5 mm; FIG. 77: Leaflet from mid-section of gill. AM C.407534, Putta Putta Beach, Australia. Scale bar = 500 µm; FIG. 78: Pallial vas deferens. FMNH 329359, Oahu, Hawaii. Scale bar = 2 mm; FIG. 79: Pallial oviduct. AM C.464334, Heron Island, Australia. Scale bar = 2 mm.

metamorphosed within hours of collecting. Adults solitary. Healy (1988) studied material originally collected at Fly Point, Somerset, Cape York Peninsula, northern Queensland for sperm (AM C.407534, *vidi*).

Comparative Remarks

Dendropoma platypus is the only "concave-operculate" *Dendropoma* species to have axial ribs on the protoconch, a character that is shared with some "convex-operculate" species of *Dendropoma*. The ribs are tall and widely spaced, unlike other species of "convex-operculate" *Dendropoma* that have low, closely-packed axial ribs on the protoconch, often in combination with spiral sculpture or spiral keels.

Taxonomic Remarks

Material from three different Pacific regions has been assigned here to *D. platypus*. The Hawaiian material most likely belongs to this nominal species as it was collected in the region of the (still broadly stated) type locality and is concordant with the original description. Material from Moorea (French Polynesia) and Australia (Heron Island, Great Barrier Reef and

Putta Putta Beach, Cape York) show some minor differences in anatomy but have been tentatively included in *D. platypus* in order to avoid the premature introduction of new names. This hypothesis should be tested using molecular data and, especially, observations of the color of living animals from these localities and others sites in the South Pacific Ocean. Differences between populations, relative to the Hawaiian material, include: a more deeply concave operculum from Moorea; deep red pigment around the muscle attachment area (Australia); and solid rather than broken pigment around the mantle margin (Heron Island, Putta Putta Beach). However, the protoconchs from at least two localities match those from Hawaii and the shells and animals are generally very similar.

Faucci (2007), in her sampling of cytochrome oxidase subunit 1 (COI) from 170 specimens of *D. platypus* from the Hawaiian archipelago and surrounding Pacific islands, uncovered three strongly supported clades of *D. platypus* separated by large genetic distances (clades A, B, and C in Faucci, 2007). Whether such genetic divergence warrants species level distinction awaits further comparison of the genetics, morphology, and life-history of these specimens. All three clades include specimens collected from the Hawaiian Islands, the broadly stated type locality for this species.

Distribution (Fig. 7)

Central and southern Pacific Ocean between Hawaii, French Polynesia and northern Australia.

Dendropoma cf. *petraeum*
(Monterosato, 1884)
[species complex]

? *Vermetus glomeratus* Bivona-Bernardi, 1832: 7, pl. 2, fig. 5 [see *Bivonia petraea*].

? *Vermetus cristatus* Biondi, 1859: 120, pl. fig. 5.

? *Bivonia petraea* Monterosato, 1884a: 81, 1884b: 61 [introduced as a *nomen novum* for *Vermetus glomeratus* Bivona-Bernardi, 1832 (p. 7, pl. 2, fig. 5) *non Serpula glomerata* Linnaeus, 1758]; Bieler & Petit, 2011: 51.

? *Spiroglyphus glomeratus* – Clessin, 1912: 112, 113, pl. 8 [1901], figs. 1, 2.

? *Dendropoma* (*Novastoa*) *petraeum* Keen, 1961: 200.

? *Dendropoma* (*Novastoa*) *cristatum* (Biondi, 1857 [*sic*]) – Scuderi, 1995: 5.

Dendropoma petraeum – Calvo et al., 1998: 525 ff. (reproductive biology); Rawlings et al., 2001: 1604 ff. (sequence and gene arrangement data).

Dendropoma petraeum [Western clade] – Calvo et al., 2009: 903 ff. (sequence data, larval shell morphology).

Type Locality

Mare di Palermo, Sicily, Italy, Mediterranean Sea.

Material Examined

Spain: FMNH 286238: intertidal, Cabo de Gata, Almeria, 36.780°N, 2.245°W, coll. unknown, February 3, 1995, 70% EtOH (5 specimens); FMNH 327231: Cabo de Palos, Murcia, 37.633°N, 0.699°E, coll. J. Templado, March 29, 1999, 95% EtOH (10 specimens) [DNA sequence data]. This material corresponds with (and are vouchers for) the “CG” and CP” locales in the Calvo et al. (2009) publication.

Description

Teleoconch (Figs. 80–82): Apertural diameter to 3.6 mm; shell length to 13 mm; diameter of last whorl to 7.5 mm. Up to four whorls, initially coiled concentrically, later whorls off-center; shallowly entrenched in substratum; aperture flush with substratum; scars from abandoned feeding tubes absent. Exterior surface bluish-gray; sculpture of low, transverse lamellae crossed by up to five weak longitudinal ribs on dorsal surface, transverse lamellae not forming carinae. Interior surface bluish-gray to dark brown.

Protoconch (Fig. 83): Settled protoconch diameter to 630 μm, height not determined due to overgrowth of teleoconch. Sculpture absent; spiral keels absent. Pale brown.

Operculum (Figs. 84–88): Diameter to 2.6 mm. Flat to slightly domed (flattened “mushroom-shaped”); dark burgundy with transparent margins. Lamina on exterior surface stacked. Interior surface slightly concave, with very low, conical mammilla.

Radula (Fig. 89): Length of ribbon 1.9 mm; up to 40 rows. Outer marginal tooth: 2 cusps on inner side.

External Morphology and Color (Figs. 90, 91): Body slender, length to 37 mm; occupying three whorls of shell. Columellar muscle extending 0.5 whorl. Color of specimens preserved in 70% EtOH: head-foot pale gray, dorsal surface of head with diffuse triangular patch of dark gray pigment behind snout and single stripe of black pigment crossing each cheek, outer surface of tentacle and side of snout; cephalic tentacles otherwise unpigmented; mantle cream with narrow band of black pigment.

Pallial and Reproductive Anatomy (Figs. 92–94): Gill with 18 leaflets per mm. Osphradium short, 1.1 mm long; anterior tip curved towards columellar muscle. Rectum straight. Hypobranchial gland extending across rectum and proximal pallial oviduct. Pallial oviduct without notch at midpoint; proximal diverticulum present.

Development and Ecology: Egg capsules not found in examined material. Calvo et al. (1998) reported that *D. petraeum* from southern Spain produced up to 86 unstalked egg capsules containing one (occasionally two) embryos per capsule. Adults reef-building.

Comparative Remarks

Shell is bluish-gray, unlike other species of *Dendropoma*. The operculum superficially resembles that of the "convex-operculate" *Dendropoma* species, but the "mushroom-shape" is lost and the operculum is almost flat. The stacked layers of the spiral lamina on the

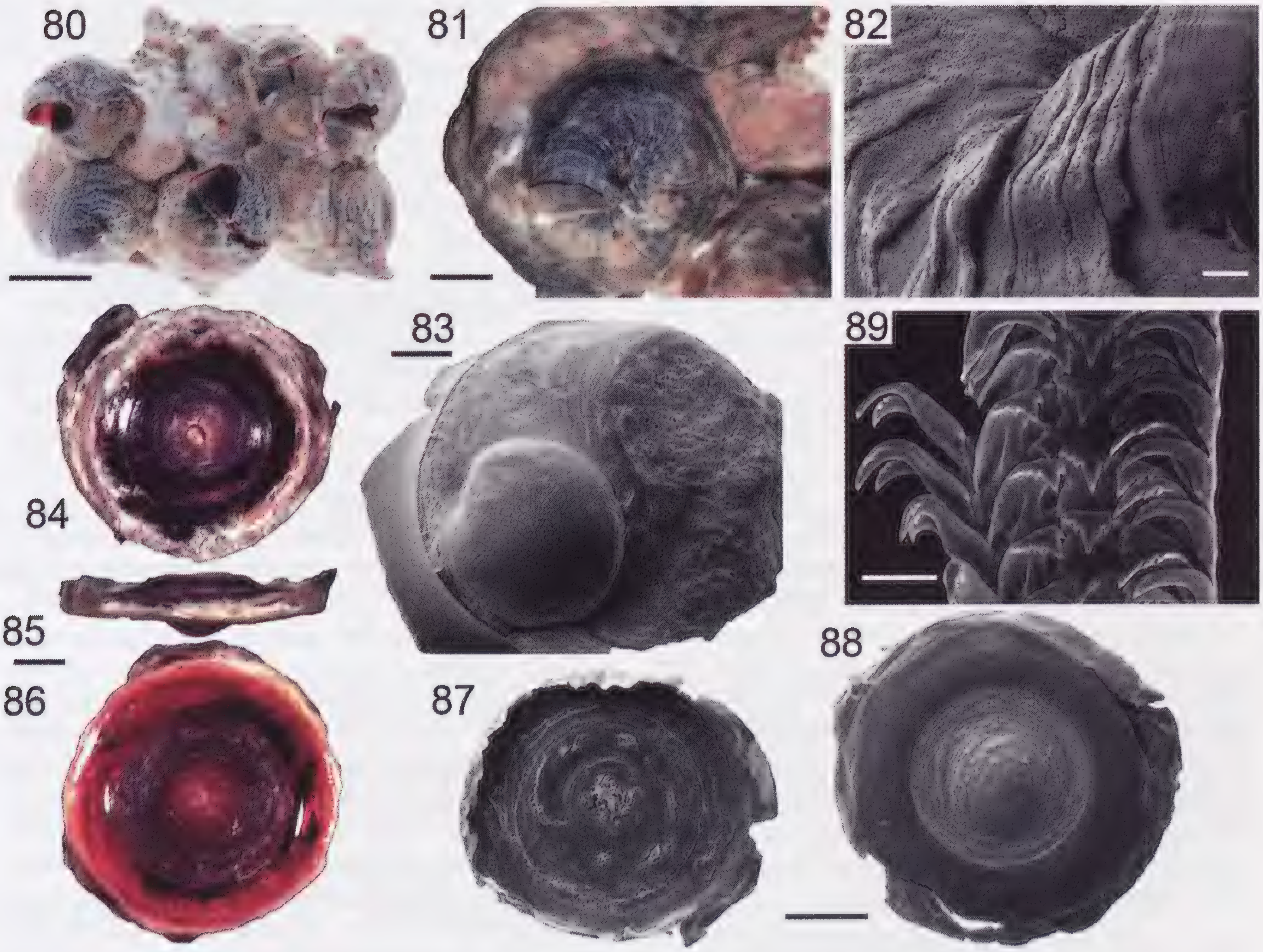

FIGS. 80–89. *Dendropoma* cf. *petraeum* (Monterosato, 1884). FMNH 286238, Cabo de Gata, Spain. FIG. 80: Cluster of specimens removed from substratum. Scale bar = 5 mm; FIG. 81: Adult shell. Scale bar = 2 mm; FIG. 82: SEM image of teleoconch sculpture. Scale bar = 200 µm; FIG. 83: Protoconch removed from adult shell. Scale bar = 100 µm; FIGS. 84–88: Operculum. Scale bars = 500 µm. FIG. 84: Exterior surface; FIG. 85: Lateral view; FIG. 86: Interior surface; FIG. 87: SEM image of exterior surface; FIG. 88: SEM image of interior surface; FIG. 89: Central section of radula. Scale bar = 50 µm.

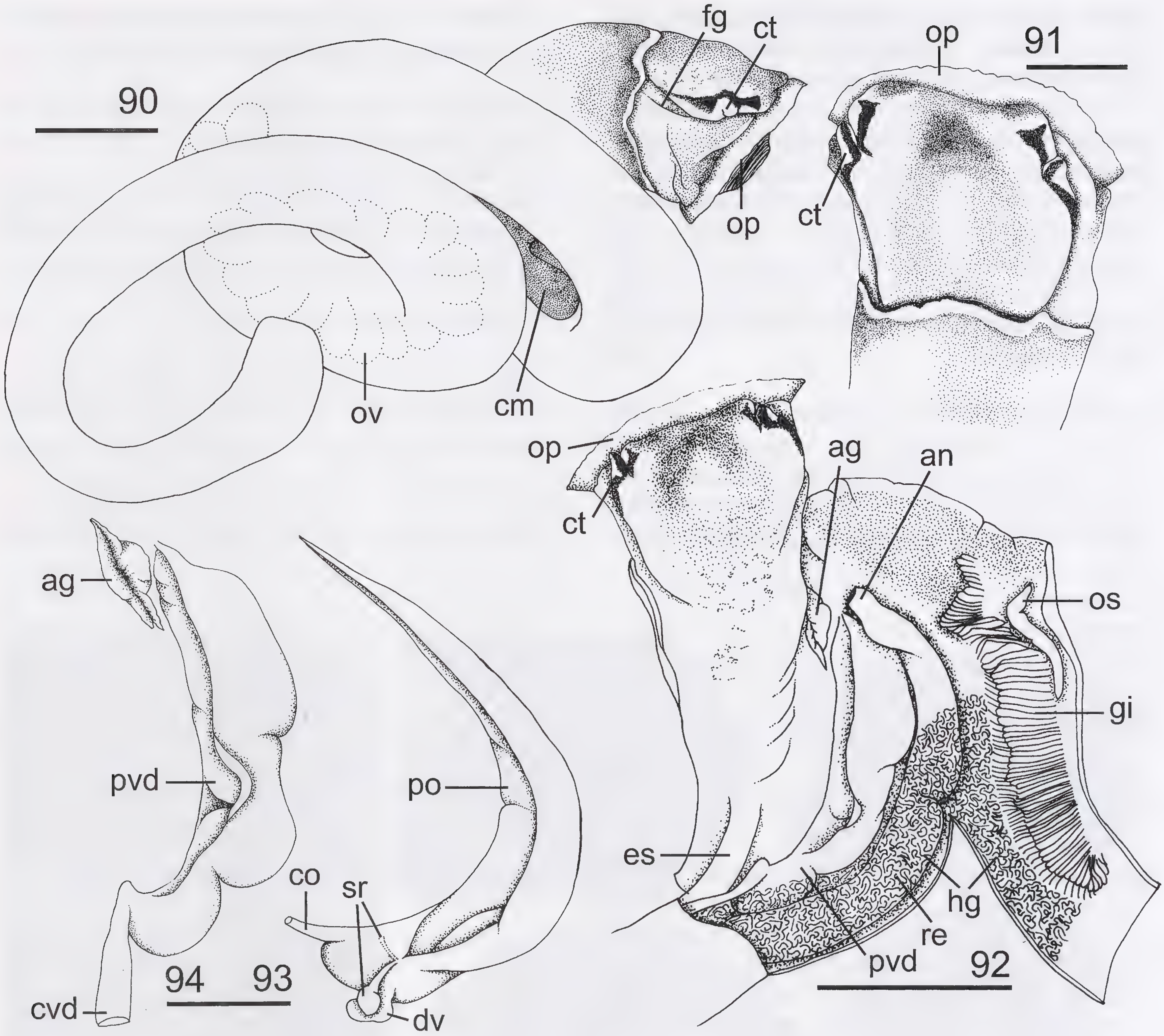

FIGS. 90–94. Anatomy of *Dendropoma* cf. *petraeum* (Monterosato, 1884). FMNH 286238, Cabo de Gata, Spain. FIG. 90: Right view of female specimen. Scale bar = 2 mm; FIG. 91: Dorsal view of head of female specimens. Scale bar = 1 mm; FIG. 92: Anatomy of mantle cavity of a male specimen. Scale bar = 2 mm; FIG. 93: Pallial oviduct. Scale bar = 1 mm; FIG. 94: Pallial vas deferens. Scale bar = 1 mm.

exterior surface are greatly reduced, and the conical mammilla on the interior surface is very low. The presence of multiple longitudinal ribs on the teleoconch, without carinose spines, is also unique in *Dendropoma.*

Taxonomic Remarks

The species identity of *Dendropoma* cf. *petraeum* is uncertain due to a recent molecular analysis that found significant genetic separation between four Mediterranean regions indicative of a cryptic species complex (Calvo et al., 2009). The material used in this study is from southeast Spain, falling within the "western clade" of their analysis, specifically their CG and CP sample groups, which the authors found distinct from a Central clade sampled from Sicily, Malta, and the Tyrrhenian Sea (Corsica and Western Italy). Protoconch morphology varies between "molecular clades", and the protoconchs of the material examined here were smooth, supporting its position in the "western clade." Calvo et al. (2009) described developmental characters separating the clades (egg capsule number, number of eggs per capsule), but few adult-morphological differences. *Dendropoma cristatum* (Biondi, 1859) was recognized as an available senior synonym of *D. petraeum* (Monterosato, 1884) by Scuderi (1995). The type material of both *Vermetus glomeratus* (= *Bivonia petraea*) and

V. cristatus stems from the Central clade region, suggesting a link between these names and that clade, but further investigation of the original material (and, potentially, re-sampling of the exact type localities) will be necessary to properly connect the available names to the clades recognized by molecular studies.

Distribution (Fig. 7)

Examined material from southeast Spain, but see Taxonomic Remarks.

Dendropoma cf. *corrodens* (d'Orbigny, 1841)

Vermetus corrodens d'Orbigny, 1841: 235–236, pl. 18, figs. 1–3 (Cuba and Martinique); Gray, 1854: 14; Clessin, 1912: 116, pl. 15, figs. 1, 3, 4 [after d'Orbigny]; Bieler & Petit, 2011: 32.

Spiroglyphus corrodens – Mörch, 1860: 44.

Spiroglyphus annulatus Daudin, 1800, Mörch, 1860: 44; 1862: 330–331; 1877: 114–116; Clessin, 1912: 108, 109; Morrison, 1968: 45–46; Abbott, 1974: 100; Rehder, 1981: 429, fig. 100 [name placed on the Official Index of Rejected and Invalid Specific Names in Zoology by Opinion 1425 (I.C.Z.N. 1987)].

Spiroglyphus annulatus var. α "dentifera" of Mörch, 1862: 331 [an infrasubspecific name introduced for d'Orbigny's *V. corrodens*].

Spiroglyphus annulatus var. δ "trochicola" of Mörch, 1862: 332 [an infrasubspecific name introduced for material from St. Thomas].

Vermetus (*Spiroglyphus*) *annulatus* var. *corrodens* – Tryon, 1886: 178, 438, pl. 51, fig. 51 [after d'Orbigny, 1841].

Dendropoma (*Dendropoma*) *corrodens* – Keen, 1961: 199, 206.

Dendropoma (*Novastoa*) *irregulare* – Morton, 1965: 588 ff., fig. 4 [gross anatomy, operculum; Jamaica; *non Vermetus irregularis* d'Orbigny, 1841].

Dendropoma corrodens – Rawlings et al., 2001: 1604 ff. [sequence and gene arrangement data].

Type Locality

Cuba and Martinique, precise locality unknown.

Material Examined

Syntypes: NHMUK 54.10.4.159. Original material studied by Mörch (1862: 330–332), including his var. β (NHMUK 1986.205).

Florida, U.S.A.: FMNH 327050: Missouri Key, Florida Keys, 24.674°N, 81.238°W, coll. R. Bieler, September 1989, dry (many); FMNH 326955: shallow-water beach with old coral/beach rock, partly exposed at low tide, Missouri Key, Florida Keys, 24.674°N, 81.238°W, coll. R. Bieler & P. Sierwald, June 10, 1985, 70% EtOH (many); FMNH 326960: shallow-water beach with old coral/beach rock, partly exposed at low tide, Missouri Key, Florida Keys, 24.674°N, 81.238°W, coll. R. Bieler & P. M. Mikkelsen, April 10, 1988, 70% EtOH (many); FMNH 293171: exposed beach rock at low tide and dead gorgonians on beach, Atlantic side of Missouri Key, Florida Keys, 24.6747°N, 81.2392°W, coll. R. Bieler & P. M. Mikkelsen, January 15, 1994, 70% EtOH (many) [DNA sequence data]; FMNH 306129: collected by hand from intertidal rocks at low tide, oceanside Missouri Key, Florida Keys, 24.674°N, 81.238°W, coll. R. Bieler & P. M. Mikkelsen, April 29, 2004, 70% EtOH (many); FMNH 326592: oceanside of Missouri-Ohio Key bridge, Missouri Key, Monroe County, U.S.A., 24.6747°N, 81.2392°W, coll. R. Bieler & P. Sierwald, April 28, 2010, 70% EtOH (many), 3.5% glutaraldehyde (many), 95% EtOH (many), formalin (many) and dry (many).

Bahamas: FMNH 326947: intertidal, Silver Point, Grand Bahama Island, 26.50°N, 78.66°W, coll. J. Worsfold, January 8, 1989, 70% EtOH (many); FMNH 326962: rocks, sand and algae at 2 m depth, near Chub Cay, off Whale Cay, 25.41°N, 77.84°W, coll. P. M. Mikkelsen, October 17, 1987, 70% EtOH (many).

Turks and Caicos Islands: W coast of Salt Cay, 21°19.65'N, 71°12.94'W, coll. R. Bieler & P. Sierwald, April 16, 2004, 70 EtOH (many).

Cayman Islands: FMNH 328947 and 328948: intertidal rocky shore at Spotts Beach, Grand Cayman, 19.2724°N, 81.3159°W, coll. L. Dombowsky, January 11–13, 2011, 70% EtOH (many); FMNH 328949: intertidal rocky shore at East End, Grand Cayman, 19.2934°N, 81.1194°W, coll. L. Dombowsky, January 13, 2011, 70% EtOH (many).

U.S. Virgin Islands: FMNH 326944: Tague Bay, St Croix, 17.757°N, 64.612°W, coll. M. Hadfield & R. Bieler, March 3, 1987, 70% EtOH (many); FMNH 327001: 10–15 m depth, Long Reef, S of Christiansted, St. Croix, coll. R. Bieler & N. Ogden, February 28, 1987, 70% EtOH (many); FMNH 326968: Columbus Landing, St. Croix, 17.779°N, 64.759°W, coll. R. Bieler, March 2, 1987, 70% EtOH (many);

FMNH 326969: reef off Tague Bay, St. Croix, approx. 17.7°N, 64.6°W, coll. M. G. Hadfield, February 28, 1987, 70% EtOH (many); FMNH 327241: Boiler Bay, E of West Indies Laboratory (WIL) of the Fairleigh Dickinson University, St. Croix, 17.7625°N, 64.5786°W, coll. R. Bieler, March 3, 1987.

Guana Island, British Virgin Islands: FMNH 326699: 2–3 m, patch reefs, White Bay, 18.4708°N, 64.5739°W, coll. R. Bieler & T. M. Collins, August 5, 2010, 70% EtOH (many) [DNA sequence data]; FMNH 326712: 5–6 m, near Monkey Point, White Bay, 18.4662°N, 64.5716°W, coll. R. Bieler & T. M. Collins, August 8, 2010, 70% EtOH (10) [DNA sequence data]; FMNH 326709; exposed spit on SW side of bay, across from Pirate's Bight, Normal Island Bay, 18.4788°N, 64.6094°W, coll. R. Bieler & T.M. Collins, August 7, 2010, dry, 70% EtOH (10); FMNH 326718: 5–9 m, Guana Cove, at Iguana Head, 18.4745°N, 64.5823°W, coll. R. Bieler & T. M. Collins, August 9, 2010, 70% EtOH (10).

Saba, Netherlands: FMNH 328792: dive site "Hole in the Corner", near shore, off SE coast of Saba Island, 17.616672°N, 63.226369°W, coll. R. Bieler & P. Sierwald, October 15, 2010, 95% EtOH (many).

Dominica: FMNH 335863, NE coast, St. Andrew Parish, Calibishi Beach, 15.5932°N, 61.3503°W, coll. R. Bieler & P. Sierwald, August 1978, on *Fissurella nodosa* (Born, 1778), many.

St. Lucia: FMNH 335795, NW end of island, Gros Islet Bay, 14.0868°N, 60.9561°W, coll. R. Bieler & P. Sierwald, August 1978, on *Vasum capitellum* (Linnaeus, 1758), many.

Barbados: FMNH 326960: coral reef, 18 m, off Spring Gardens, 13.12°N, 59.638°W, coll. P. M. Mikkelsen, April 18, 1989, 70% EtOH (many); FMNH 327095: limestone rocks and base of cliffs at mouth of estuary, River Bay, 13.3232°N, 59.5958°W, coll. R. Golding, T. Rawlings & C. McVarish, August 10, 2010, 10% SW formalin (many), [DNA sequence data]. FMNH 327096: fringing reef, Six Mens Bay, West coast, 13.2682°N, 59.6451°W, coll. R. Golding, T. Rawlings & C. McVarish, August 11, 2010, 100% EtOH, 10% formalin, [DNA sequence data].

Belize: FMNH 327009: Carrie Bow Cay, Stann Creek District, 16.803°N, 88.082°W, coll. R. Bieler, March 1986, 70% EtOH (many); FMNH 327142: on coral rubble, 2 m, SW from boat launch, Carrie Bow Cay, Stann Creek District, 16.8021°N, 88.0825°W, coll. R. Bieler, R. Golding, T. Rawlings, T. Collins & P. Sierwald, April 14, 2011, dry, 70% EtOH, RNAlater, 95% EtOH (many) [DNA sequence data]; FMNH 327155: on coral boulders on reef crest, 0–1 m, Columbus Reef, Carrie Bow Cay, Stann Creek District, 16.9031°N, 88.0602°W, coll. R. Bieler, R. Golding, T. Rawlings, T. Collins & P. Sierwald, April 18, 2011, dry, 70% EtOH, RNAlater, 95% EtOH, 10% formalin (many).

Venezuela: FMNH 326967: off Quinzandal Beach (INTECMAR station), Puerto Cabello, Carabobo, 10.4747°N, 68.0203°W, coll. R. Bieler & P. Miloslavich, June 1, 1986, 70% EtOH (many).

Description

Teleoconch (Figs. 95–98): Apertural diameter to 1.8 mm; shell length to 10 mm; diameter of last whorl 6 mm. Up to four whorls, coiled concentrically initially, but later whorls tending to straighten; either deeply entrenched in substratum or rising vertically in aggregate matrix; aperture flush with substratum; scars from abandoned feeding tubes absent. Exterior surface dark purplish-brown in life, fading to medium brown; sculpture of tall, closely-packed, vertical, transverse lamellae, "pinched together" to form weak crest on dorsal surface. Interior surface dark brown.

Protoconch (Figs. 99–102): Settled protoconch diameter to 430 µm, height to 450 µm. Sculpture absent on first 0.7 whorl, last 0.6 whorl with low, closely- or widely-spaced axial ribs (varying between populations); three weak spiral keels usually present. Honey brown.

Operculum (Figs. 103–111): Diameter to 1.5 mm. Highly variable in shape between and within populations. Domed, "mushroom-shaped"; dark burgundy with transparent margins. Lamina on exterior surface stacked. Interior surface concave, with low, conical mammilla.

Radula (Fig. 112): Length of ribbon 1.3 mm; up to 35 rows. Outer marginal tooth: two cusps on inner side.

External Morphology and Color (Figs. 95, 113, 114): Body slender, length to 20 mm; occupying 2–3 whorls of shell. Columellar muscle extending 1 whorl. Color in life: Head-foot

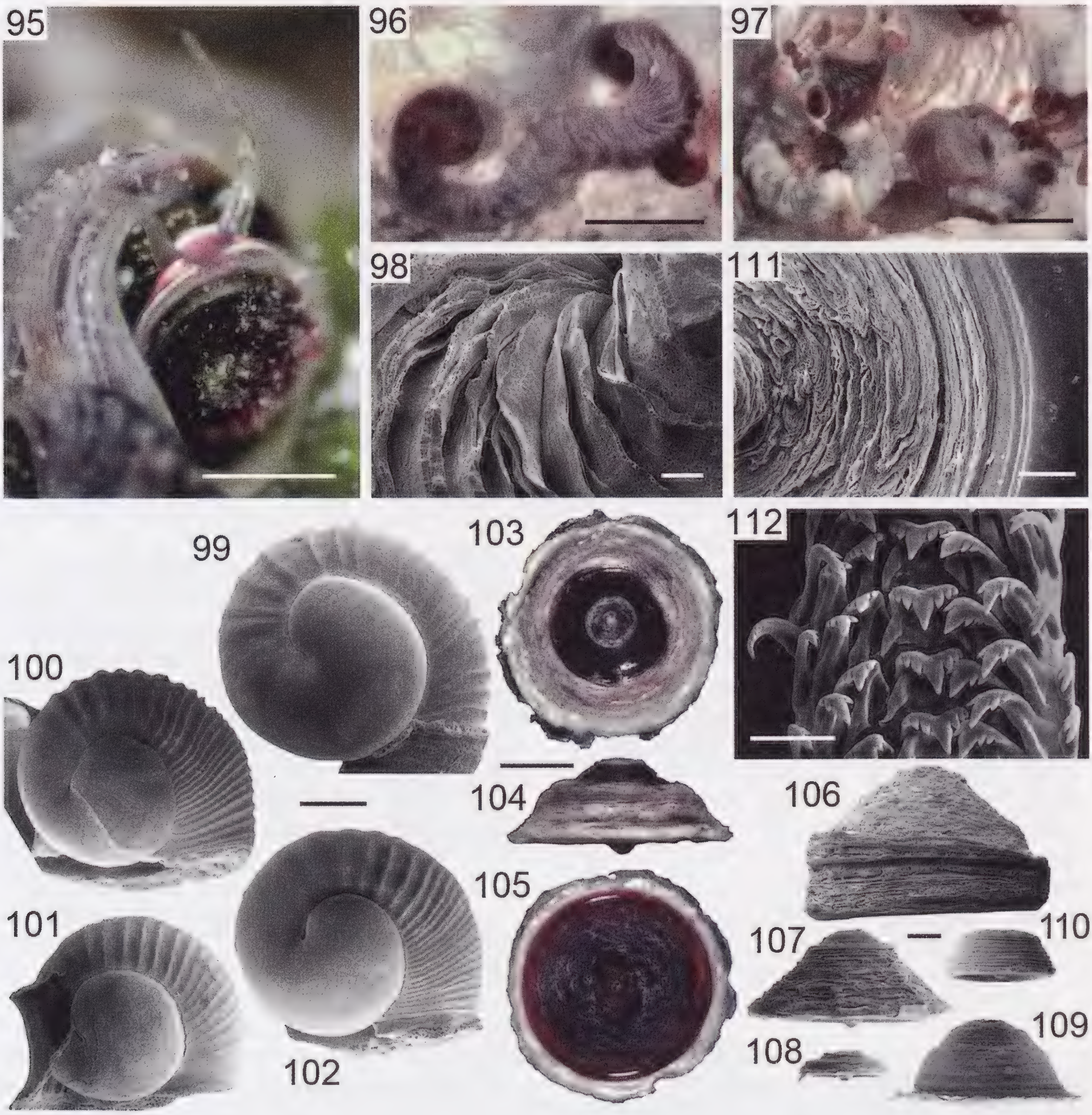

FIGS. 95–112. *Dendropoma* cf. *corrodens* (d’Orbigny, 1841). FIG. 95: Living specimen with pedal tentacles emerging from aperture. FMNH 326592, Florida Keys, U.S.A. Scale bar = 1 mm; FIG. 96, 97: Adult shells. Scale bars = 2 mm. FIG. 96: FMNH 326955, Florida Keys, U.S.A.; FIG. 97: FMNH 326962, Whale Cay, Bahamas; FIG. 98: SEM image of teleoconch sculpture. FMNH 327050, Florida Keys, U.S.A. Scale bar = 200 µm; FIGS. 99–102: SEM images of protoconchs removed from recently settled juveniles from different areas of the Caribbean, apical views. Scale bar = 100 µm. FIG. 99: FMNH 326955, Missouri Key, Florida; FIG. 100: FMNH 326968, St Croix, US Virgin Islands; FIG. 101: FMNH 326699, Guana, British Virgin Islands; FIG. 102: FMNH 328949, Grand Cayman, Cayman Islands; FIGS. 103–105: Operculum. FMNH 326955, Missouri Key, Florida. Scale bar = 500 µm. FIG. 103: Exterior surface; FIG. 104: Lateral view; FIG. 105: Interior surface; FIGS. 106–110: SEM images of opercula from different areas of the Caribbean, lateral views. Scale bar = 100 µm. FIG. 106: FMNH 293171, Missouri Keys, Florida; FIG. 107: FMNH 328949, Grand Cayman, Cayman Islands; FIG. 108: FMNH 326968, St Croix, US Virgin Islands; FIG. 109: FMNH 326962, Whale Cay, Bahamas; FIG. 110: FMNH 327009, Carrie Bow Cay, Belize; FIG. 111: SEM image of muscle attachment area on interior surface of operculum. FMNH 327050, Florida Keys, U.S.A. Scale bar = 100 µm; FIG. 112: Central section of radula. FMNH 306129, Florida Keys, U.S.A. Scale bar = 50 µm.

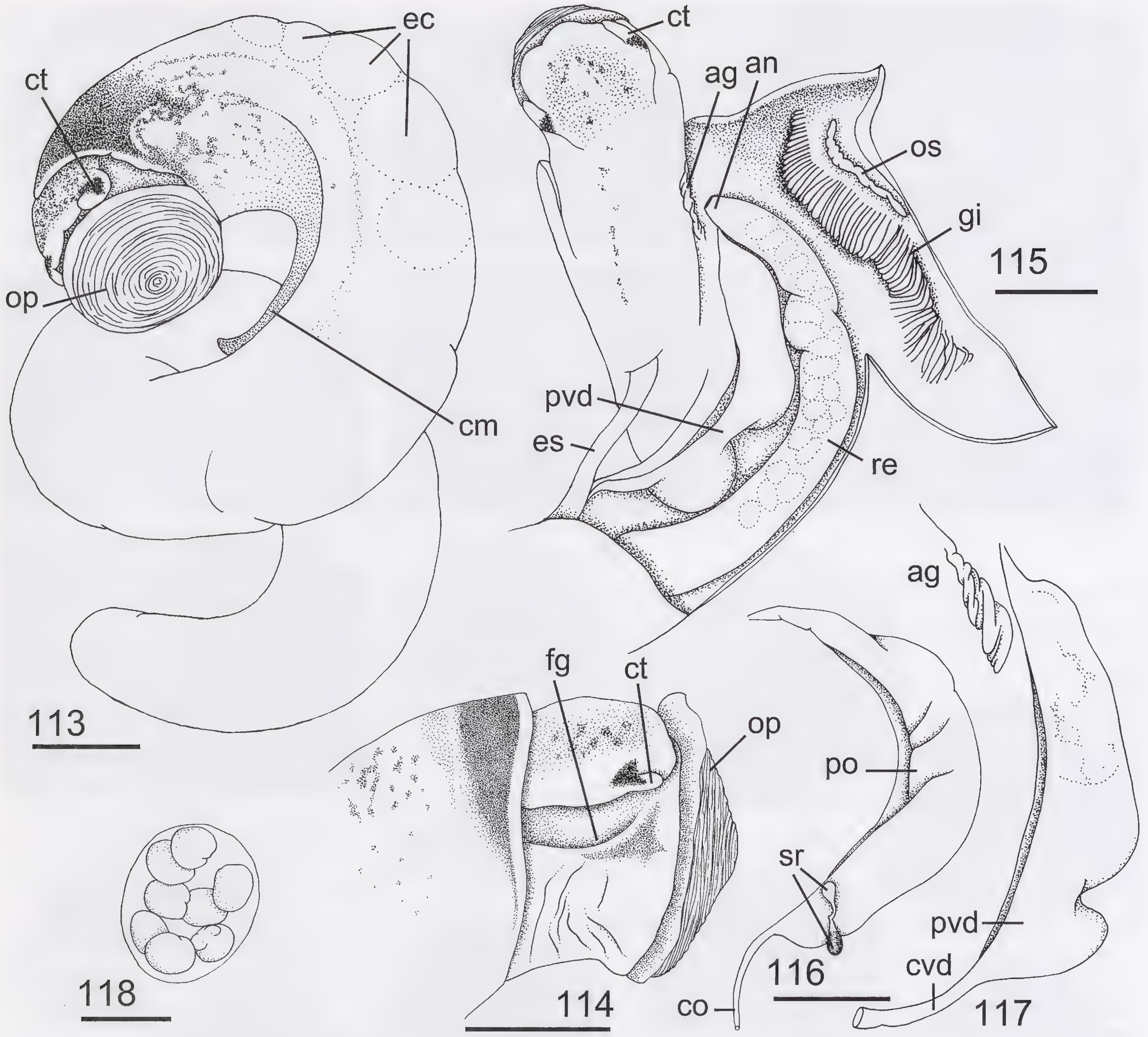

FIGS. 113–118. Anatomy of *Dendropoma* cf. *corrodens* (d'Orbigny, 1841). Scale bars = 1 mm. FIG. 113: Left view of female specimen; FIG. 114: Right view of anterior body. FMNH 326960, Florida Keys, U.S.A.; FIG. 115: Mantle cavity of male specimen; FIG. 116: Pallial oviduct; FIG. 117: Pallial vas deferens; FIG. 118: Unstalked egg capsule removed from female mantle cavity. FIGS. 113, 115–118: FMNH 326592, Florida Keys, U.S.A.

white with mottled black pigment anteriorly; dorsal surface of head with diffuse bright yellow pigment and scattered superficial white speckles, increasing in density around base of tentacles, snout and sides of foot; sole of foot white to rose pink; pedal tentacles transparent with white speckles; cephalic tentacles white with black band at base, surrounded by white pigment patches on surface of head. Color of specimens preserved in 70% EtOH: head-foot mottled grey and white; cephalic tentacles white with black pigment at base; mantle cream.

Pallial and Reproductive Anatomy (Figs. 115–117): Gill with 20 leaflets per mm. Osphradium short, 1.3 mm long; anterior tip curved towards columellar muscle. Rectum straight. Hypobranchial gland not extending across rectum. Pallial oviduct without notch at midpoint or proximal diverticulum.

Development and Ecology (Fig. 118): Up to five unstalked egg capsules per female observed herein (up to eight according to Miloslavich & Penchaszadeh, 1992); 4–9 embryos per capsule. Adults reef-building.

Comparative Remarks

Belonging to the "convex-operculate" group of *Dendropoma* – *D.* cf. *corrodens*, *D. gregarium*, *D. howense*, *D.* cf. *tholia*, *D. psarocephalum* and ***D. expolitum*** n. sp. – that share very similar shell and operculum morphology and similar coloration of the animals (where known). The protoconch of *D.* cf. *corrodens* has closely-spaced axial ribs, like *D. howense*, *D. gregarium* and *D.* cf. *tholia*, but lacks the spiral sculpture of *D. gregarium* and *D.* cf. *tholia*. *Dendropoma* cf. *corrodens* has a purplish-brown shell with prominent, upright transverse lamellae, unlike the pinkish-white shell with relatively smooth transverse lamellae of *D. howense*.

Taxonomic Remarks

The original type localities (given by d'Orbigny as Cuba and Martinique) were not sampled in this study, so we cannot definitely refer the examined material to *D. corrodens*. At the present state of knowledge, we are considering this species to have a pan-Caribbean distribution. However, because of ongoing research in this complex pointing to regional morphological differences (in density and height of axial ribs on the protoconch) and high levels of mtDNA divergence among samples collected to date (up to 18% (uncorr.-P), we are using the tentative name *D.* cf. *corrodens* for our studied material.

Mörch (e.g., 1862: 330–332) considered *V. corrodens* and *Vermetus irregularis* d'Orbigny, 1841, to be members of a single species. The type material of the latter species (also described from Cuba and Martinique; syntypes in MNHUK, *vidi*) does not seem to be conspecific, and even its generic position is presently unresolved.

The name *Spiroglyphus annulatus* Daudin, 1800, was in wide use for this gastropod taxon until it was placed on the Official Index of Rejected and Invalid Specific Names in Zoology by Opinion 1425 (I.C.Z.N., 1987). However, various malacological works figured polychaete worms under this name (e.g., Vokes & Vokes, 1983: pl. 4, fig. 16, as *S. annulatus*; Daccarrett & Bossio, 2011: 245, fig. 358, as "*Dendropoma annulatus*"). The confusion with serpulid worms continues under its present name, *Dendropoma corrodens* (e.g., Tunnell et al., 2010: 136).

Distribution (Fig. 7)

Common throughout the Caribbean, Bahamas, and South Florida.

Dendropoma gregarium
Hadfield & Kay, 1972

Dendropoma gregaria [*sic*] Hadfield & Kay in Hadfield, Kay, Gillette & Lloyd, 1972: 81–83, figs. 1–2, 19A; Kay, 1979: 103, 104, fig. 38.
Dendropoma gregarium – Rawlings et al., 2001: 1604 [sequence and gene arrangement data]; Bieler & Petit, 2011: 40.

Type Locality

On intertidal boulders, Kaheka (near Koloa), Kauai, Hawaii: 21.8750°N, 159.6416°W.

Material Examined

Holotype and paratypes: BPBM 8929.
Hawaiian Islands, U.S.A.: FMNH 326970: Oahu, approx. 21.3°N, 157.9°W, coll. R. Bieler, March 1988, 70% EtOH (many); FMNH 326971: shallow water, old reef flat, Kaneohe Bay, Oahu, 21.45°N, 157.79°W, coll. R. Bieler, December 1986, 70% EtOH (many); FMNH 326972: 0.1 m at low tide, beach rock on reef flats, Diamond Head Beach, Oahu, approx. 21.43°N, 157.79°W, coll. R. Bieler, March 28, 1988, 70% EtOH (many); FMNH 318222: Oahu, coll. M. Hadfield, 70% EtOH (6) [DNA sequence data]; AM C.407557: exposed rocky platform, Diamond Head, Oahu; 21.267°N, 157.817°W., coll. W. F. Ponder & E. A. Kay, April 6, 1974, 10% SW formalin (many).

Description

Teleoconch (Figs. 119, 120): Apertural diameter to 3 mm; shell length to 12 mm; diameter of last whorl to 7 mm. Up to four whorls, coiled concentrically initially, but later whorls tending to straighten; either deeply entrenched in substratum or rising vertically in aggregate matrix; aperture flush with substratum; scars from abandoned feeding tubes absent. Exterior surface deep purplish-black in life (Hadfield et al., 1972), fading to medium brown; sculpture of tall, closely-packed, transverse lamellae, without a longitudinal crest or ridges. Interior surface dark brown.

Protoconch (Figs. 121–123): Hatchling protoconch diameter to 450 μm, height to 360 μm (900 μm by 650 μm according to Hadfield et al., 1972). Sculpture absent on first 0.6 whorl, last 0.7 whorl with very weak axial ribs crossed by broken, spiral threads breaking into pustules near lip; spiral keels absent. Pale brown.

Operculum (Figs. 124–128): Diameter to 2.0 mm. Domed, "mushroom-shaped"; dark burgundy with transparent margins. Lamina on exterior surface stacked. Interior surface concave, with low, conical mammilla.

Radula (Fig. 129): Length of ribbon 1.0 mm; up to 32 rows. Outer marginal tooth: 2–3 cusps on inner side.

External Morphology and Color (Fig. 130): Body slender, length to 20 mm; occupying 2–3 whorls of shell. Columellar muscle extending one whorl. Color in life (modified from Hadfield et al., 1972): Head-foot black with white speckles, especially on sides of head, snout gray; sole of foot either bright pink or light yellow without intergrades; cephalic tentacles black at base, white at tips; pedal tentacles transparent; mantle black except for white speckles on margin. Color of specimens preserved in 70% EtOH: colorless except for pale grey pigment on snout and black pigment at base of tentacles.

Pallial and Reproductive Anatomy (Figs. 131, 132): Gill with 17 leaflets per mm. Osphra-

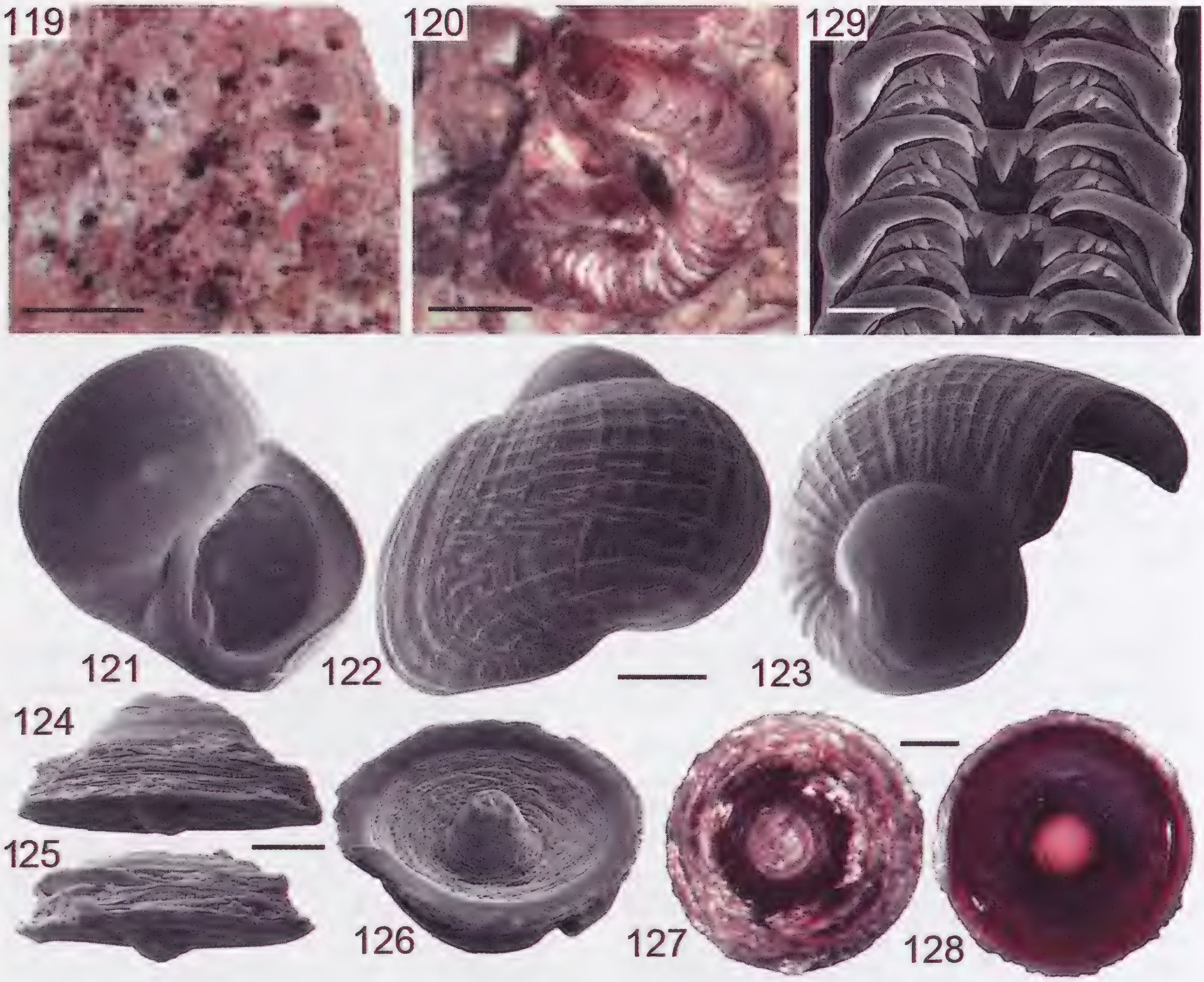

FIGS. 119–129. *Dendropoma gregarium* Hadfield & Kay, 1972. FIG. 119: A cluster of specimens removed from the substratum. Scale bar = 10 mm; FIG. 120: Adult specimen. Scale bar = 2 mm; FIGS. 121–123: SEM images of intracapsular larval shells. Scale bar = 100 µm. FIG. 121: Apertural view; FIG. 122: Abapertural view; FIG. 123: Apical view; FIGS. 124–126: SEM images of opercula. Scale bar = 200 µm. FIGS. 124, 125: Lateral views; FIG. 126: Oblique view of interior surface; FIGS. 127, 128: Operculum. FMNH 407557, Oahu, Hawaii. Scale bar = 200 µm. FIG. 127: Exterior surface; FIG. 128: Interior surface; FIG. 129: Central section of radula. Scale bar = 20 µm. FIGS. 119–126, 129: FMNH 326972, Oahu, Hawaii.

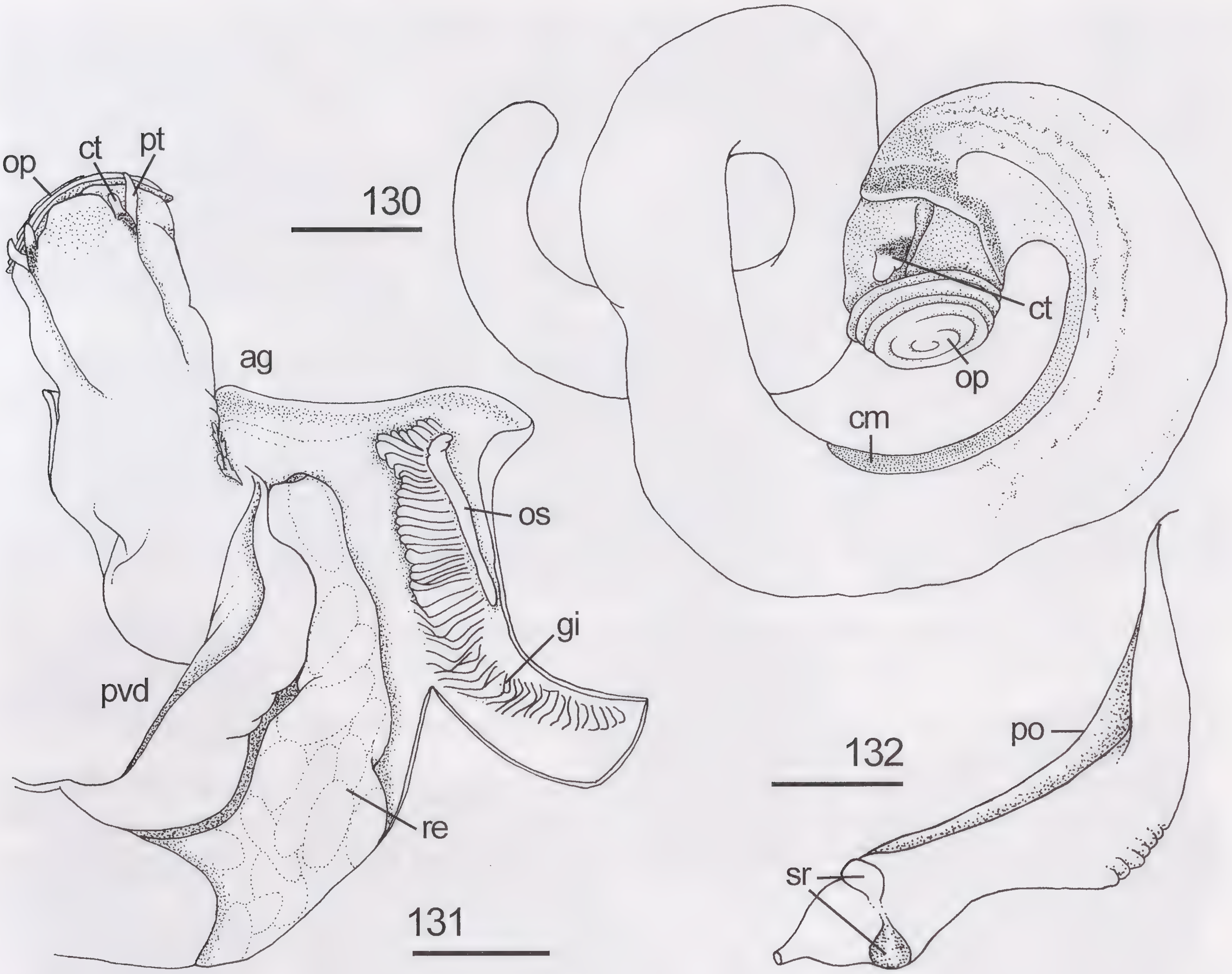

FIGS. 130–132. Anatomy of *Dendropoma gregarium* Hadfield & Kay, 1972. FIG. 130: Left view of female specimen. FMNH 326927, Oahu, Hawaii. Scale bar = 1 mm; FIG. 131: Mantle cavity of male specimen. AM C.4075557, Oahu, Hawaii. Scale bar = 1 mm; FIG. 132: Pallial oviduct. AM C.407557, Oahu, Hawaii. Scale bar = 500 μm.

dium short, 1.5 mm long; anterior tip curved towards columellar muscle. Rectum straight. Hypobranchial gland not extending across rectum. Pallial oviduct without notch at midpoint or proximal diverticulum.

Development and Ecology: 3–4 unstalked egg capsules per female; 6–21 embryos per capsule observed herein; Hadfield et al. (1972) recorded direct development with recently hatched larvae crawling. Adults reef-building.

Comparative Remarks

Belonging to the "convex-operculate" group of *Dendropoma*. The protoconch of *D. gregarium* has characteristic spiral bands of broken threads crossing weak axial ribs.

Faucci (2007) discovered extremely high levels of genetic variation in *COI* sequences among 248 individuals sampled within the Hawaiian Islands and across the Pacific. Many monophyletic groupings of haplotypes were island-specific or restricted to taxa sampled from closely positioned islands, reflecting the lower potential for planktonic dispersal in this direct-developing, albeit geographically widespread, species (Hadfield et al., 1972; Faucci, 2007). The nucleotide sequence of *COI* from the specimen of *D. gregarium* sequenced in our study from Kaneohe Bay, Oahu (FMNH 318222), was most similar to haplotype 69 in Faucci's (2007) phylogenetic analysis (match of 526 bp over a total length of 530 bp). This haplotype was nested within one of several genetically distinct clades of specimens sampled from Oahu.

Distribution

Based on collections by Faucci (2007), *D. gregarium* is common throughout the Hawaiian Islands and Micronesia.

Dendropoma howense
(Iredale, 1937)

Veristoa howensis Iredale, 1937: 254, pl. 17, fig. 8; Keen, 1961: 192; Bieler & Petit, 2011: 40.

Type Locality

Middleton Reef, Tasman Sea, Australia: 29.5°S, 159.2°E.

Material Examined

Syntypes: AM C.060226: from type locality as above, coll. G. P. Whitley, April 1936, dry (many).

Australia: AM C.407559: pools, MTL, Signal Point, Lord Howe Island, New South Wales; 31.525°S, 159.065°E, coll. W. F. Ponder & P. H. Colman, April 21, 1978, 10% SW formalin (many); AM C.407572: on calcarenite rocks, E of cemetery, Point Hunter Reserve, Norfolk Island, 29.067°S, 167.967°E, coll. W. F. Ponder & E. K. Yoo, June 22, 1979, 10% SW formalin (many); AM C.407546: rubble bank and sand flats, Elizabeth Reef, Tasman Sea, 29.923°S, 159.045°E, coll. I. Loch, December 10, 1987, 10% SW formalin (many); AM C.302896, SW of Rat Island, Houtman Abrolhos, Western Australia, 28.72°S, 113.78°E, coll. S. White & C. White, March 1970, 10% SW formalin (many).

Description

Teleoconch (Figs. 133–136): Apertural diameter to 3 mm; shell length to 16 mm; diameter of last whorl to 10 mm. Up to four whorls, coiled concentrically initially, but later whorls tending to straighten; deeply entrenched in substratum; aperture flush with substratum; scars from abandoned feeding tubes absent. Exterior surface medium brown to pinkish-white; sculpture of low, closely-packed transverse lamellae initially upright, flattened in later whorls, without longitudinal crest or ridges. Interior surface medium brown.

Protoconch (Figs. 137–139): Settled protoconch diameter to 480 µm, height to 480 µm. Sculpture absent on first 0.8 whorl, last 0.5 whorl with low, closely-spaced axial ribs; three very weak spiral keels present. Pale brown.

Operculum (Figs. 140–144): Diameter to 1.5 mm. Domed, "mushroom-shaped"; dark burgundy with transparent margins. Lamina on exterior surface stacked. Interior surface concave, with low, conical mammilla.

Radula (Fig. 145): Length of ribbon 1.2 mm; up to 34 rows. Outer marginal tooth: 1 cusp on inner side.

External Morphology and Color: Not known.

Pallial and Reproductive Anatomy: Not known.

Development and Ecology: Developmental biology not known. Adults reef-building.

Comparative Remarks

Belonging to the "convex-operculate" group of *Dendropoma*. The protoconch of *D. howense* is very similar to that of *D. corrodens*, but the adult shells differ in that *D. howense* is very pale and has flattened transverse lamellae. The distribution overlaps with ***D. expolitum*** n. sp., but the protoconch of the latter species is unsculptured and the shell is brown with very coarse transverse lamellae.

Taxonomic Remarks

The type locality of *D. howense* is Lord Howe Island, but material collected from various locations around Australia, including Norfolk Island, Elizabeth Reef and Rat Island (Western Australia) are morphologically similar and are here referred to *D. howense*. Protoconch sculpture is consistent between all examined populations.

Dendropoma howense is the type species of *Veristoa* Iredale, 1937, here confirmed as a junior subjective synonym of *Dendropoma s.s.*

Distribution (Fig. 7)

Tasman Sea from the central Great Barrier Reef (southern extent not known), including Lord Howe and Norfolk Islands, and Rat Island, Houtman Abrolhos, Western Australia. It is not clear whether the distribution is continuous across northern or southern Australia.

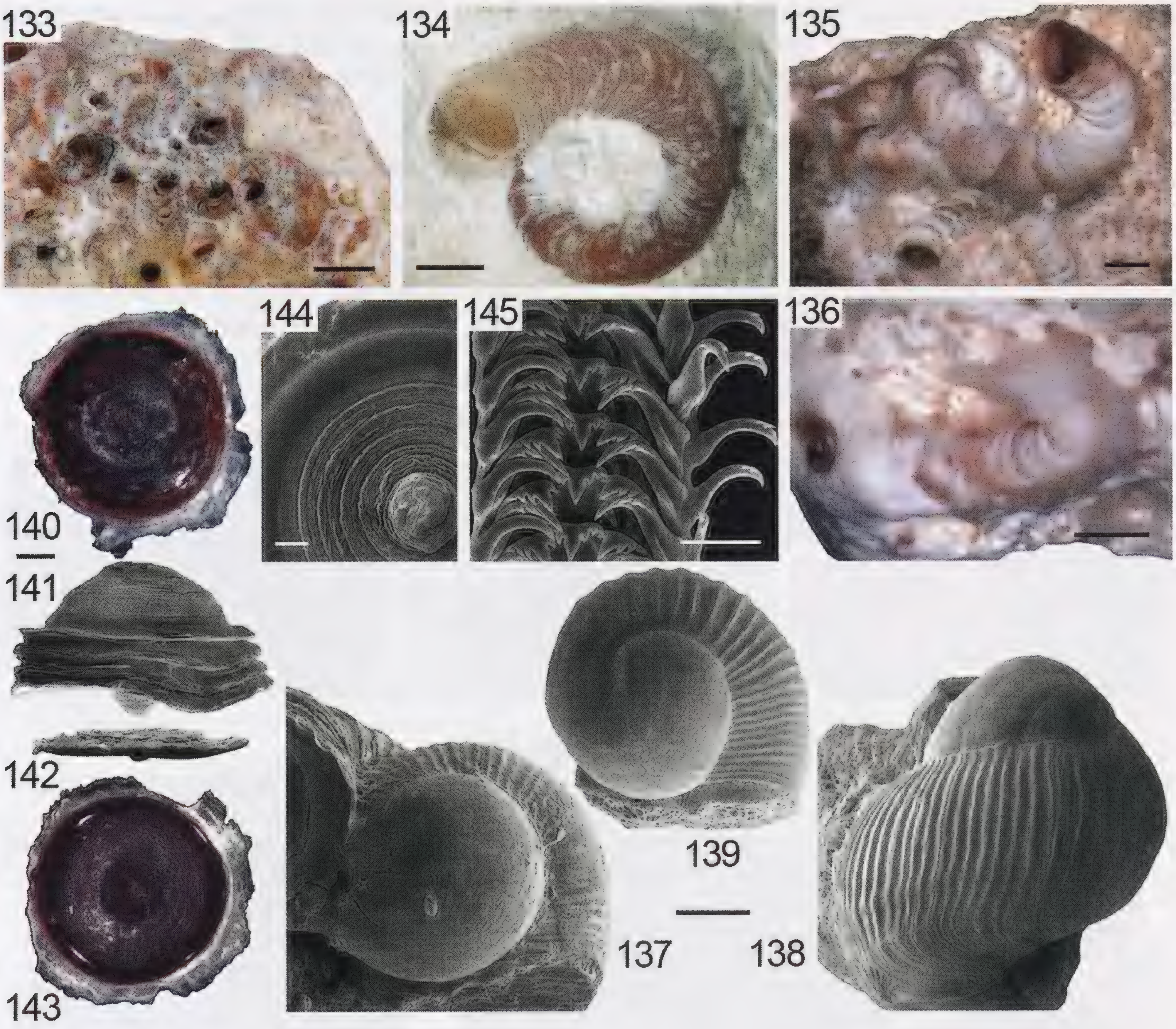

FIGS. 133–145. *Dendropoma howense* (Iredale, 1937). FIG. 133: A cluster of specimens attached to rock substratum. AM C.407559, Lord Howe Island, Australia. Scale bar = 5 mm; FIG. 134: Adult shell. Syntype AM C.060226, Middleton Reef, Tasman Sea, Australia. Sale bar = 1 mm; FIGS. 135, 136: Adult specimens with epifauna and algae partly removed. Scale bars = 2 mm. FIG. 135: AM C.407559, Lord Howe Island, Australia; FIG. 136: AM C.302896, Rat Island, Houtman Abrolhos, Australia; FIGS. 137–139: SEM images of protoconchs removed from recently settled juveniles. Scale bar = 100 µm. FIG. 137: Apical view. AM C.407546, Elizabeth Reef, Tasman Sea, Australia; FIG. 138: Abapertural view. AM C.407572, Norfolk Island, Australia; FIG. 139: Apical view. AM C.302896, Rat Island, Houtman Abrolhos, Australia; FIGS. 140–143: Opercula. Scale bar = 200 µm. FIG. 140: Exterior surface. AM C.407559, Lord Howe Island, Australia; FIG. 141: SEM image of lateral view of operculum. AM C.407559, Lord Howe Island, Australia; FIG. 142: SEM image of lateral view of operculum. AM C.407546, Elizabeth Reef, Tasman Sea, Australia; FIG. 143: Interior surface of operculum. AM C.407559, Lord Howe Island, Australia; FIG. 144: SEM image of muscle attachment area on interior surface of operculum. AM C.407546, Elizabeth Reef, Tasman Sea, Australia. Scale bar = 100 µm; FIG. 145: Central section of radula. AM C.407559, Lord Howe Island, Australia. Scale bar = 50 µm.

Dendropoma cf. *tholia*
Keen & Morton, 1960

? *Dendropoma tholia* Keen & Morton, 1960: 41, pl. 3, text-figs. 6–13, 20–22, 33; Morton, 1965: 588 ff.

? *Vermetus* (*Dendropoma*) *tholia* – Barnard, 1963: 148.

Type Locality

Inhaca Island, off Lorenço Marques, Mozambique.

Material Examined

Kenya: FMNH 328086: mid-littoral rock bench, Kimondo Reef, Diani Beach, 4.36°S, 39.57°E, J. D. Taylor, October 2, 1977, dry (many).

Description

Teleoconch (Figs. 146–148): Apertural diameter to 2.0 mm (Keen & Morton, 1960); remainder of shell entirely encrusted with coralline algae, but shell length at least 6 mm, diameter of last whorl at least 4.5 mm. Unknown number of whorls coiled concentrically, rising vertically through aggregate matrix; aperture flush with substratum; scars from abandoned feeding tubes not visible. Exterior surface pale brown when cleaned; sculpture of low, transverse lamellae, without longitudinal crest or ridges (Keen & Morton, 1960). Interior surface dark brown.

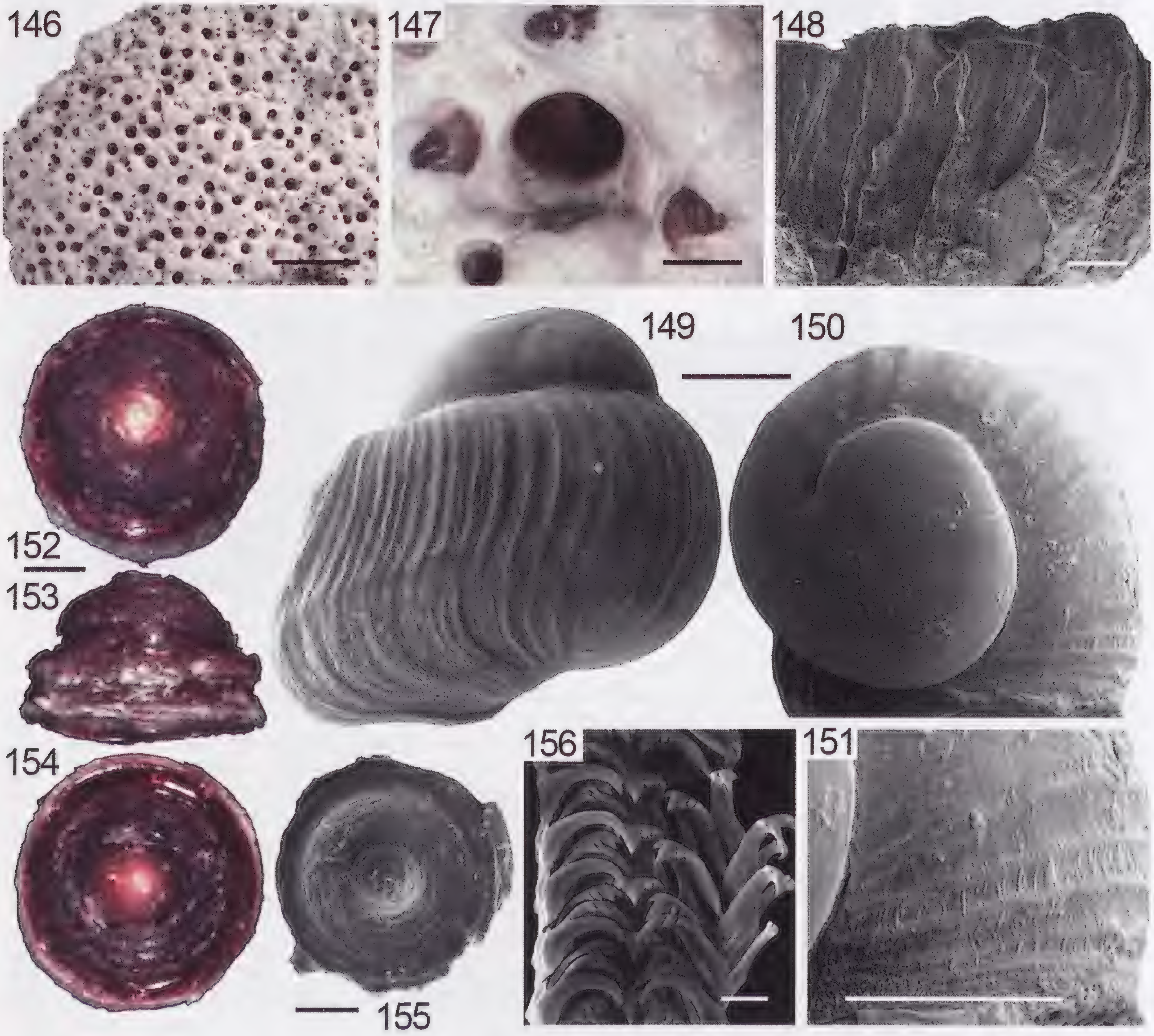

FIGS. 146–156. *Dendropoma* cf. *tholia* Keen & Morton, 1960. FMNH 328086, Kimona, Kenya. FIG. 146: Encrusting layer of coralline algae and *D.* cf. *tholia* removed from substratum, with only apertures visible. Scale bar = 10 mm; FIG. 147: Aperture of a single specimen surrounded by many recently settled juveniles. Scale bar = 1 mm; FIG. 148: SEM image of teleoconch sculpture after removal of encrusting coralline algae. Scale bar = 200 µm; FIGS. 149–151: SEM images of protoconchs removed from recently settled juveniles. Scale bars = 100 µm. FIG. 149: Abapertural view; FIG. 150: Apical view; FIG. 151: Detail of apical view showing sculpture; FIGS. 152–155: Opercula. Scale bars = 200 µm. FIG. 152: Exterior surface; FIG. 153: Lateral view; FIG. 154: Interior surface; FIG. 155: SEM image of interior surface; FIG. 156: Central section of radula. Scale bar = 20 µm.

Protoconch (Figs. 149–151): Settled protoconch diameter to 410 μm, height to 390 μm. Sculpture absent on first 0.8 whorl, last 0.5 whorl with very low axial ribs crossed by numerous spiral bands of pustules near lip; one very weak spiral keel present. Dark brown.

Operculum (Figs. 152–155): Diameter to 1.5 mm. Domed, "mushroom-shaped"; dark burgundy with transparent margins. Lamina on exterior surface stacked. Interior surface concave, with moderately tall, conical mammilla.

Radula (Fig. 156): Length of ribbon 750 μm; up to 33 rows. Outer marginal tooth: one cusp on inner side.

External Morphology and Color: Color of specimens preserved in EtOH (modified from Keen & Morton, 1960): Head-foot black, snout gray; cephalic tentacles black at base, white at tip; pedal tentacles gray.

Pallial and Reproductive Anatomy: Not known.

Development and Ecology: six unstalked egg capsules per female; three embryos per capsule (Keen & Morton, 1960). Adults reef-building.

Comparative Remarks

Belonging to the "convex-operculate" group of *Dendropoma*. Distinguished by the presence of pustulose spiral ribs near the lip of the protoconch. The microsculpture on the protoconch was not documented in the description of the species (Keen & Morton, 1960), but this detail is only visible using SEM (a technique which was not available to the original authors).

Taxonomic Remarks

The type locality for *D. tholia* is on the southern coastline of Mozambique. The examined material was collected 2,500 km north of the type locality, in Kenya. However, there are no other suitable names available for *Dendropoma* species from east Africa, except *D. corallinaceum* (Tomlin, 1939), which according to Keen & Morton (1960) does not extend beyond East London on the southeast coast of South Africa.

The shell, operculum and radula of the examined material agree in most respects with the description of *D. tholia* (Keen & Morton, 1960), supporting the tentative assignment of this material to *D. tholia*.

Distribution (Fig. 7)

East Africa, at least between Mozambique and Kenya.

Dendropoma expolitum n. sp.

Type Locality

Moderately exposed granite shore, Bampfield Pt., W side of Prince of Wales Island, Torres Strait, Queensland, Australia: 10.717°S, 142.117°E.

Material Examined

Australia: Holotype: QM MO.80207: coll. W. F. Ponder & I. Loch, July 1, 1976, 10% SW formalin (1 specimen attached to paratypes; Figs. 156, 157); Paratypes: AM C.464306, QM MO.80208, FMNH 328513, ex AM C.464306: from type locality, coll. W. F. Ponder & I. Loch, July 1, 1976, 10% SW formalin (many); AM C.154222: exposed rocky shore, LT, S side of Fly Point, Cape York Peninsula, Queensland, 10.75°S, 142.6°E, coll. W. F. Ponder & I. Loch, July 11, 1976, 10% SW formalin (many); AM C.464377: attached to bivalve shell, on beach, Frederick Reefs, Coral Sea, 21°S, 154.433°E, coll. K. Gillett, August 1972, dry (many).

Etymology

From the Latin adjective expolitus-a-um, meaning polished, referring to the features of the unsculptured protoconch.

Description

Teleoconch (Figs. 157–159): Apertural diameter to 2.0 mm (Keen & Morton, 1960); shell length to 6 mm, diameter of last whorl to 5 mm. Up to four whorls coiled concentrically; deeply entrenched in substratum; aperture flush with substratum; scars from abandoned feeding tubes absent. Exterior surface medium brown; sculpture of moderately tall, upright, coarse transverse lamellae; longitudinal crest absent. Interior surface dark brown.

Protoconch (Figs. 160, 161): Settled protoconch diameter to 400 µm, height to 420 µm. Sculpture absent; spiral keels absent. Pale brown.

Operculum (Figs. 162–166): Diameter to 1.5 mm. Domed, "mushroom-shaped"; dark burgundy with transparent margins. Lamina on exterior surface stacked. Interior surface concave, with very low, conical mammilla.

Radula (Fig. 167): Length of ribbon 1.0 mm; up to 30 rows. Outer marginal tooth: two cusps on inner side.

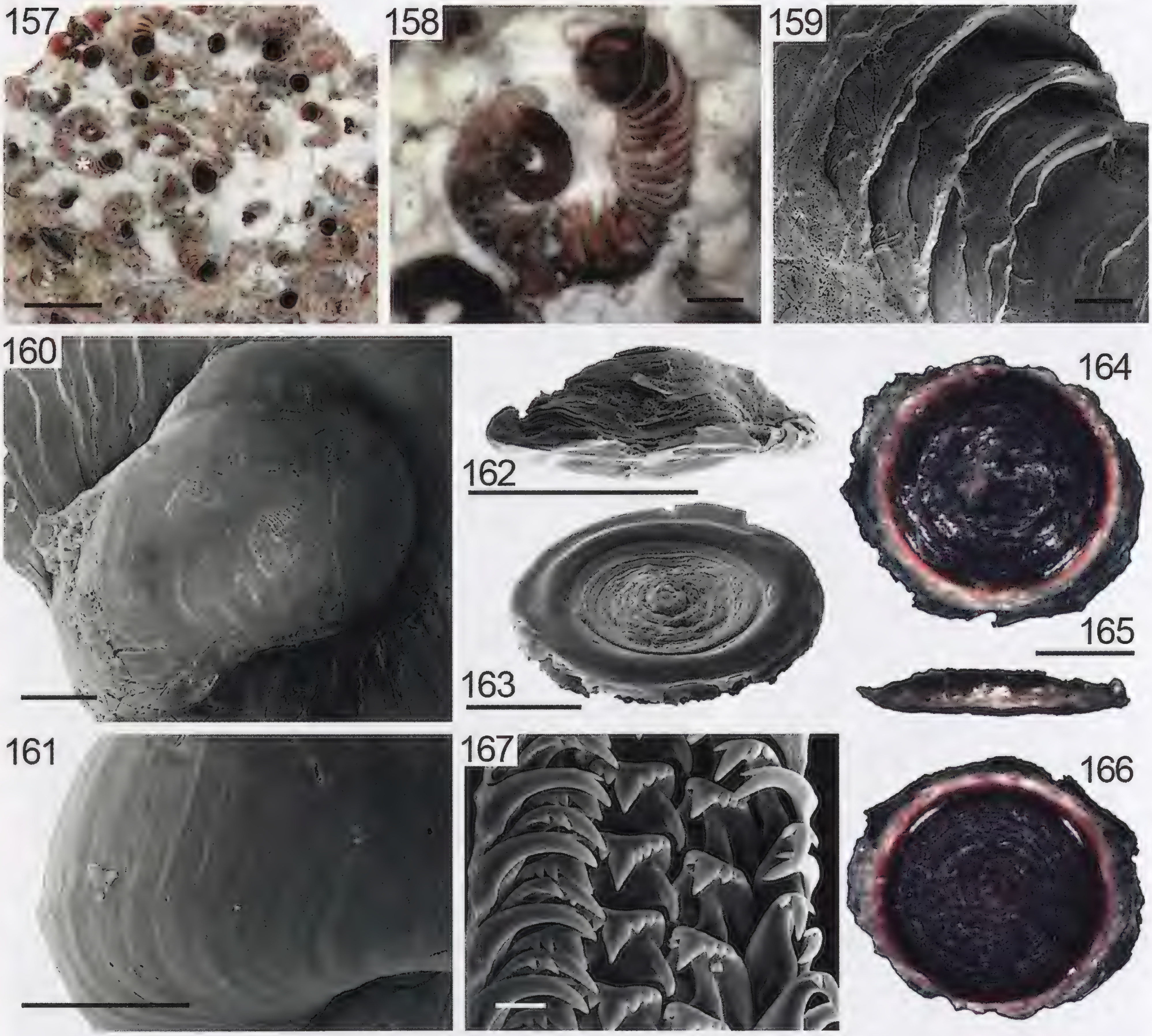

FIGS. 157–167. ***Dendropoma expolitum*** n. sp. FIG. 157: A cluster of specimens including holotype (marked with an asterisk) removed from the substratum, partly encrusted with coralline algae. AM C.464306, Prince of Wales Island, Torres Strait, Australia. Scale bar = 5 mm; FIG. 158: Holotype. QM MO.80207, Prince of Wales Island, Torres Strait. Scale bar = 1 mm; FIG. 159: SEM image of teleoconch sculpture. AM C.464306, Prince of Wales Island, Torres Strait, Australia. Scale bar = 200 µm; FIGS. 160, 161: SEM images of protoconchs removed from recently-settled juveniles. AM C.154222, Fly Point, Cape York, Australia. Scale bars = 100 µm. FIG. 160: Abapertural view; FIG. 161: Detail of protoconch sculpture; FIG. 162: SEM image of lateral view of operculum. AM C.464306, Prince of Wales Island, Torres Strait. Scale bar = 500 µm; FIGS. 163–166: Opercula. AM C.154222, Fly Point, Cape York, Australia. Scale bars = 500 µm. FIG. 163: SEM image of oblique view of interior surface; FIG. 164: Exterior surface; FIG. 165: Lateral view; FIG. 166: Interior surface; FIG. 167: Central section of radula. AM C.464306, Prince of Wales Island, Torres Strait, Australia. Scale bar = 20 µm.

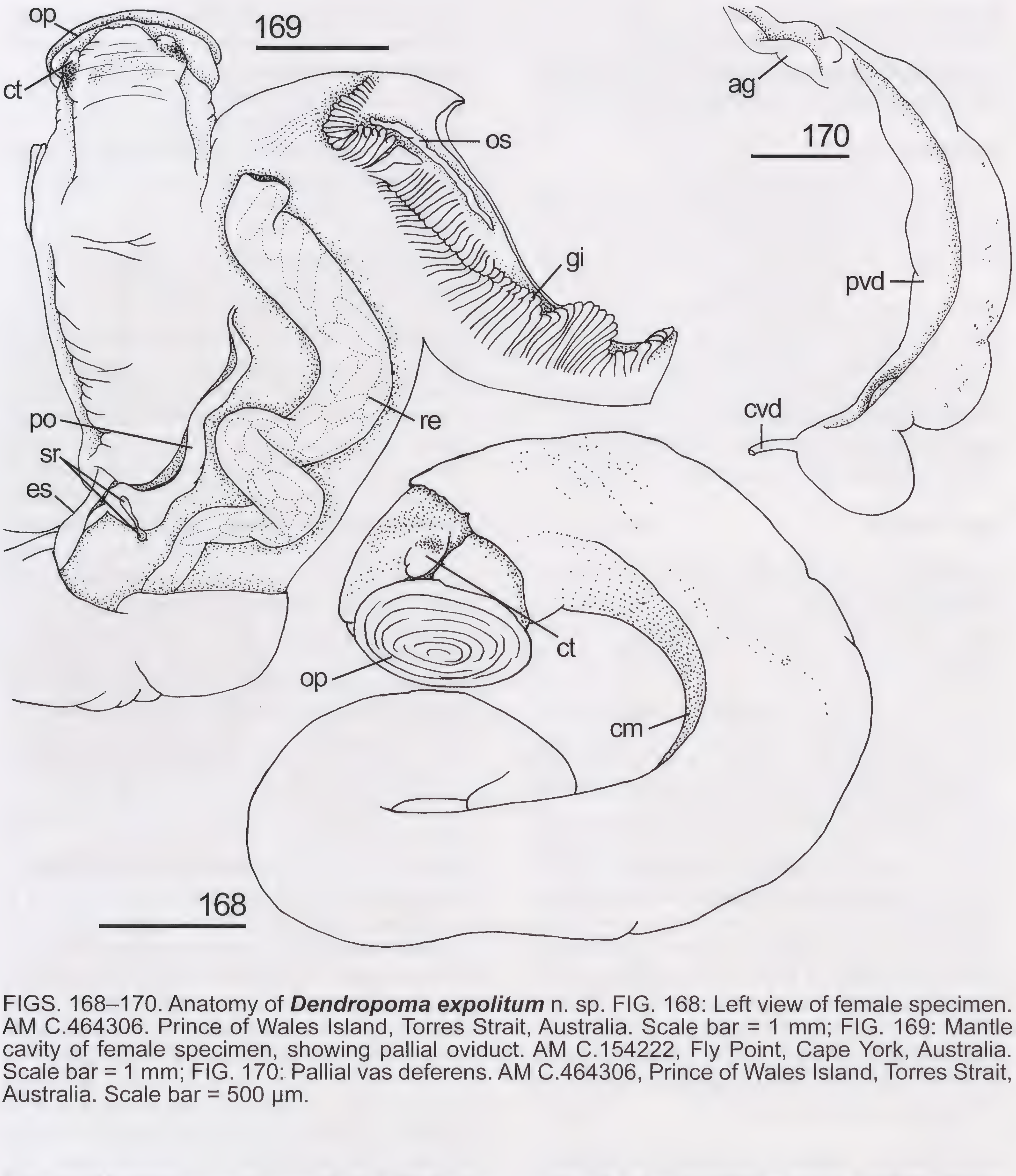

FIGS. 168–170. Anatomy of ***Dendropoma expolitum*** n. sp. FIG. 168: Left view of female specimen. AM C.464306. Prince of Wales Island, Torres Strait, Australia. Scale bar = 1 mm; FIG. 169: Mantle cavity of female specimen, showing pallial oviduct. AM C.154222, Fly Point, Cape York, Australia. Scale bar = 1 mm; FIG. 170: Pallial vas deferens. AM C.464306, Prince of Wales Island, Torres Strait, Australia. Scale bar = 500 µm.

External Morphology and Color (Fig. 168): Body slender, length to 25 mm; occupying 2–3 whorls of shell. Columellar muscle extending one whorl. Color of specimens preserved in 70% EtOH: Colorless except for pale gray pigment on dorsal surface of head and black pigment at base of tentacles.

Pallial and Reproductive Anatomy (Figs. 169, 170): Gill with 17 leaflets per mm. Osphradium short, 1.2 mm long; anterior tip straight. Rectum kinked. Hypobranchial gland not extending across rectum. Pallial oviduct without notch at midpoint or proximal diverticulum.

Development and Ecology: Developmental biology not known. Adults reef-building.

Comparative Remarks

Belonging to the "convex-operculate" group of *Dendropoma*. Distinguished by its unsculptured protoconch.

Taxonomic Remarks

Dendropoma expolitum n. sp. is morphologically consistent from each locality here studied.

Distribution (Fig. 7)

Known from northeast Australia between the central Great Barrier Reef and Cape York.

Novastoa
Finlay, 1926

Novastoa Finlay, 1926: 386; Morton, 1951: 43–51, plate 8, figs. 1, 2, 4b, plate 9, figs 5, 6, text-fig. 1; Bieler & Petit, 2011: 16.
Dendropoma (*Novastoa*) – Keen, 1961: 199–200, text-figs. 30–33.

Type Species

Siphonium lamellosum Hutton, 1873, by original designation.

Diagnostic Description

Teleoconch: Small to medium (maximum dimension 4–28 mm), "tube" wide (apertural diameter 2.3–7.5 mm), sometimes with expanded chamber behind aperture; whorl coiling pattern concentric spiral sometimes tending to straight, shallowly or deeply entrenched or entirely embedded in substratum initially but sometimes elevated in later whorls; aperture flush with substratum or elevated, usually not forming a feeding tube; encrusted or entirely camouflaged with epifauna. Shell thick or thin; aperture simple. Color and sculpture of exterior surface variable. Interior surface color variable; sculpture on columellar surface absent; concave septa frequent in abandoned shell.

Protoconch: Settled protoconch diameter 600–1100 µm, height 500–1000 µm. Weak "hook" projection present on apertural lip. Intracapsular growth only evident in protoconch structure; globular with large increase in whorl size; shallow suture; 1.3 whorls; sculpture variable; spiral keels at base of whorl absent. Color variable, transparent.

Operculum: Circular in axial profile; diameter proportional to shell size, 1.5–6.0 mm. Composed of chitin only; color variable. Exterior surface concave, either shallow saucer-shaped or shallow to deeply conical in lateral profile (excluding mammilla). Exterior surface with tall, upright, multispiral lamina, usually heavily encrusted with epifauna. Interior surface with a prominent mammilla of varying height and profile; surface glossy and smooth peripherally, muscle attachment area (including mammilla) textured with shallow concentric grooves.

Radula: Taenioglossate, transparent, colorless. Length of ribbon 730–2500 µm; 23–44 rows (proportional to shell size). Trapezoidal rachidian tooth with prominent central cusp flanked on each side by three smaller cusps decreasing in size outwardly. Base of lateral tooth notched to interlock with rachidian and inner marginal teeth; elongate main cusp flanked by one cusp on inner side, three cusps on outer side. Inner marginal tooth slender with one cusp on inner side, 2–3 cusps on outer side. Outer marginal tooth smooth on outer side, one cusp on inner side; base simple, without projection.

External Morphology and Color: Body of animal usually very stout (length 7–40 mm), occupying between 1 and 2 last whorls of shell; 0.5x body length composed of gonad and digestive gland. Columellar muscle medium length to very short, extending between 1 and 0.5 whorls. Pedal tentacles short (in preserved specimens). Head relatively large, cephalic tentacles short (in preserved specimens), broad, with tiny ommatophore bearing eye at outer base; right side of head with deep food groove sometimes with convoluted flap on outer margin. Adult female mantle divided by pallial slit (0.5x mantle length) or notch (< 0.3x mantle length) in midline; male mantle undivided. External body coloration variable.

Pallial and Reproductive Anatomy: Gill 0.2–0.3x mantle width, full length of mantle cavity; gill leaflets medium height to tall triangular; 12–16 leaflets per mm. Osphradium short or long relative to mantle cavity, 2.5–5.3 mm; margins irregular or smooth; anterior tip bent 180° or curved towards columellar muscle. Anus either opening within mantle cavity or protruding from mantle aperture; rectum kinked; fecal pellets ovoid or cigar shaped. Hypobranchial gland pale brown (if visible), covering surface of mantle between gill and rectum, sometimes also covering rectum and pallial oviduct. Pallial oviduct notched near midpoint with expanded pocket distal to notch; proximal diverticulum present. Single seminal receptacle attached to base or tip of proximal diverticulum via short duct. Male reproductive system sometimes with notch near midpoint of pallial vas deferens.

Development and Ecology: (At least) 1–5 stalked egg capsules attached to shell wall in a single row corresponding to position of mantle slit/notch in females; double-walled capsule semi-transparent, elongate ovoid to kidney shaped, diameter increasing with development of embryos, size of capsule and number of eggs/embryos per capsule varying between species. Larvae probably direct developing. Adults solitary or gregarious, some species reef-building.

Comparative Remarks

The slit female mantle and method of (stalked) capsule attachment are shared with *Cupolaconcha*, *Ceraesignum* and most members of other vermetid genera. *Novastoa* can be distinguished from these other vermetids by the distinct operculum that has a prominent mammilla on the interior surface (developed to a remarkable degree in some taxa) and a raised, multispiral lamina on the exterior surface of the operculum.

Taxonomic Remarks

Novastoa was introduced by Finlay (1926) at the generic level for *N. lamellosa*, but subsequently reduced to a subgenus of *Dendropoma* by Keen (1961). Keen (1961) provided a diagnosis for the subgenus that conflates some of the features described by Morton (1951) from *N. lamellosa* with those of other, unrelated, *Dendropoma* species, such as an aggregate growth habit and a short spindle on the interior surface of the operculum. The operculum figured by Keen (1961) is redrawn from Morton (1951) but does not closely resemble his description or our own. Keen (1961) included many other species in *D.* (*Novastoa*). Of those examined in this study, none appear to belong in *Novastoa* and mostly are members of *Dendropoma* proper.

Diversity and Distribution (Fig. 171)

Present in all oceans except the Arctic, generally tropical but also known from temperature waters in New Zealand. Six species, including one previously named species, are described below. This is almost certainly an underestimate of the real diversity of *Novastoa*, as the small, deeply embedded shells of several taxa are extremely cryptic and difficult to collect from their reef habitat.

Novastoa lamellosa
(Hutton, 1873)

Siphonium lamellosum Hutton, 1873: 30; Bieler & Petit, 2011: 43.

Novastoa lamellosa – Finlay, 1926: 386; Morton, 1951: 43–51, pl. 8 figs. 1, 2, 4b, pl. 9 figs. 5, 6, text-fig. 1; 1955: 4 ff., fig. 1a, b.

Dendropoma (*Novastoa*) *lamellosum* – Keen, 1961: 199–200, text-figs. 30–33; Morton, 1965: 588 ff., fig. 3 [gross anatomy, operculum; as *D. lamellosa*].

Type Locality

New Zealand, precise locality unknown. Given as "Cook Strait, in deep water" by Suter (1913: 261) and "Chatham Islands" by Powell (1979: 129).

Material Examined

New Zealand: Syntypes (photograph): NMNZ M.000133 [http://collections.tepapa.govt.nz/objectdetails.aspx?oid=753150]. Other: NMNZ M.012245: Kaingaroa, Chatham Islands, 43.73°S, 176.23°W, coll. R. K. Dell, January 27, 1954, 80% EtOH (many), dry (many); NMNZ M.024381: Great Island, Southeast Bay, Three Kings Islands, 34.17°S, 172.13°E, coll. F. Climo, November 28, 1970, 80% EtOH (many), dry (many); NMNZ M.004786: rock face exposed to swell, Noises Islands, Hauraki Gulf, North Island, 36.70°S, 174.97°E, coll. L. Moore, May 1, 1938, dry (many).

Description

Teleoconch (Figs. 172–174): Apertural diameter to 7.5 mm, without an expanded chamber behind aperture; diameter of last whorl to 28 mm. Up to six whorls coiled concentrically, tending to straight in later whorls; early whorls deeply entrenched in substratum; aperture raised above substratum in some dense colonies. Shell thick. Exterior surface purple fading to white; sculpture of tall, delicate, transverse lamellae. Interior surface white with brown patches.

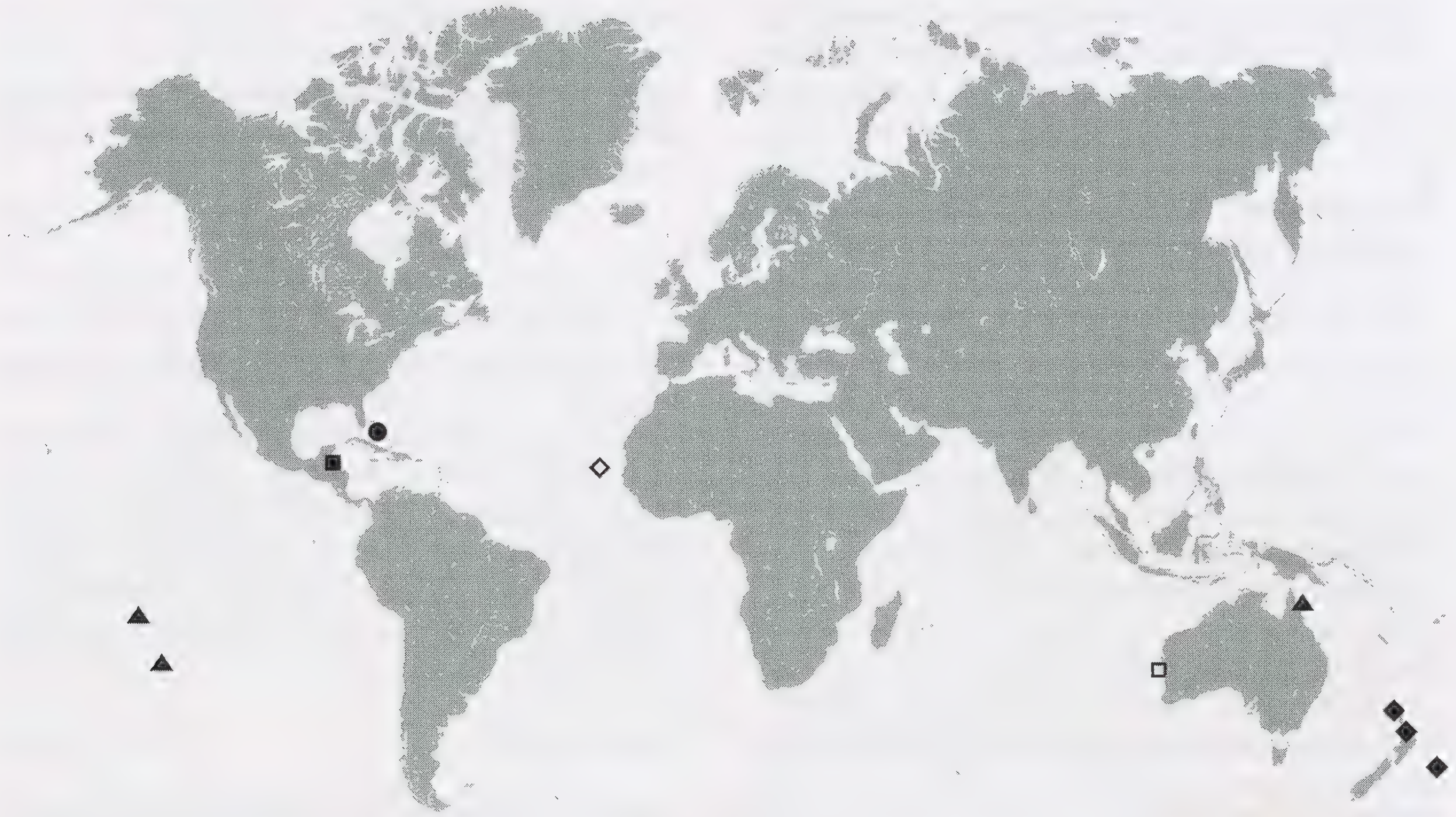

FIG. 171. Distribution map of *Novastoa* Finlay, 1926 based on material examined in this study. Filled diamond = *N. lamellosa* (Hutton, 1873); hollow diamond = ***N. caboverdensis*** n. sp.; filled circle = ***N. bahamensis*** n. sp.; filled square = ***N. pholetor*** n. sp.; hollow square = ***N. batavia*** n. sp.; filled triangle = *N.* sp.

Protoconch (Figs. 175, 176): Settled and hatchling protoconch diameter to 1,100 µm, height to 1,000 µm. Sculpture absent on first whorl, last 0.3 whorl with many wavy, spiral bands of pustules joining to form broken threads near lip. White to pale brown.

Operculum (Figs. 177–181): Diameter to 6 mm. Shallow saucer-shaped; dark caramel brown. Lamina on exterior surface not ruffled. Interior surface with tall, cylindrical mammilla up to 2.5 mm long.

Radula (Fig. 182): Length of ribbon 2.5 mm; up to 34 rows.

External Morphology and Color (Figs. 183, 184): Body length to 40 mm, occupying last two whorls of shell. Columellar muscle medium length, extending one whorl within shell. Food groove with simple outer margin. Adult female mantle divided by pallial slit extending 0.5x mantle length. Color in life (modified from Morton, 1951): dorsal surface of head jet black, lips orange, snout scarlet, cheeks with black patches; cephalic tentacles black with yellow patches near base; pedal tentacles black; foot whitish posteriorly with lateral black patches and orange-brown in food groove; remnant sole of foot orange-red; mantle margin with thin black band, canary yellow then scarlet fading to translucent white. Color of specimens preserved in 80% EtOH: head/foot cream; sides of foot pale grey; pedal and cephalic tentacles black; dorsal surface of head with circular patch of black pigment; mantle edge of mantle grey with band of white pigment on margin; digestive gland faded to cream.

Pallial and Reproductive Anatomy (Figs. 185–187): Gill 0.2x mantle width; gill leaflets tall triangular, breadth half height; 12 leaflets per mm. Osphradium short, 3 mm long; margins irregular; anterior tip curved towards columellar muscle. Anus opening within mantle cavity; fecal pellets not observed. Hypobranchial gland pale brown, covering surface of mantle between gill and extending across rectum and ventral surface of pallial oviduct. Seminal receptacle attached to tip of proximal oviduct. Male reproductive system not observed.

Development and Ecology (Fig. 188): Up to ten stalked egg capsules per female; 6–16 embryos per capsule; up to 2.2 mm diameter. Larval biology not known, but intracapsular larval shells same size as settled protoconchs removed from substratum around adults, suggesting direct development. Adults densely aggregated, forming crusts and reefs on rocky substratum.

Comparative Remarks

Distinct from other vermetids and species in *Novastoa* by the purple shell, presence of very tall transverse lamellae on the teleoconch and a tall, cylindrical mammilla on the interior surface of the operculum.

Taxonomic Remarks

The description here concurs in most respects with the detailed descriptions given by Morton (1951, 1965) and the material examined is almost certainly conspecific. There are a few differences, notably that Morton (1951) did not describe a raised, multispiral lamina on the exterior surface of the operculum. This might have been inadvertently removed when

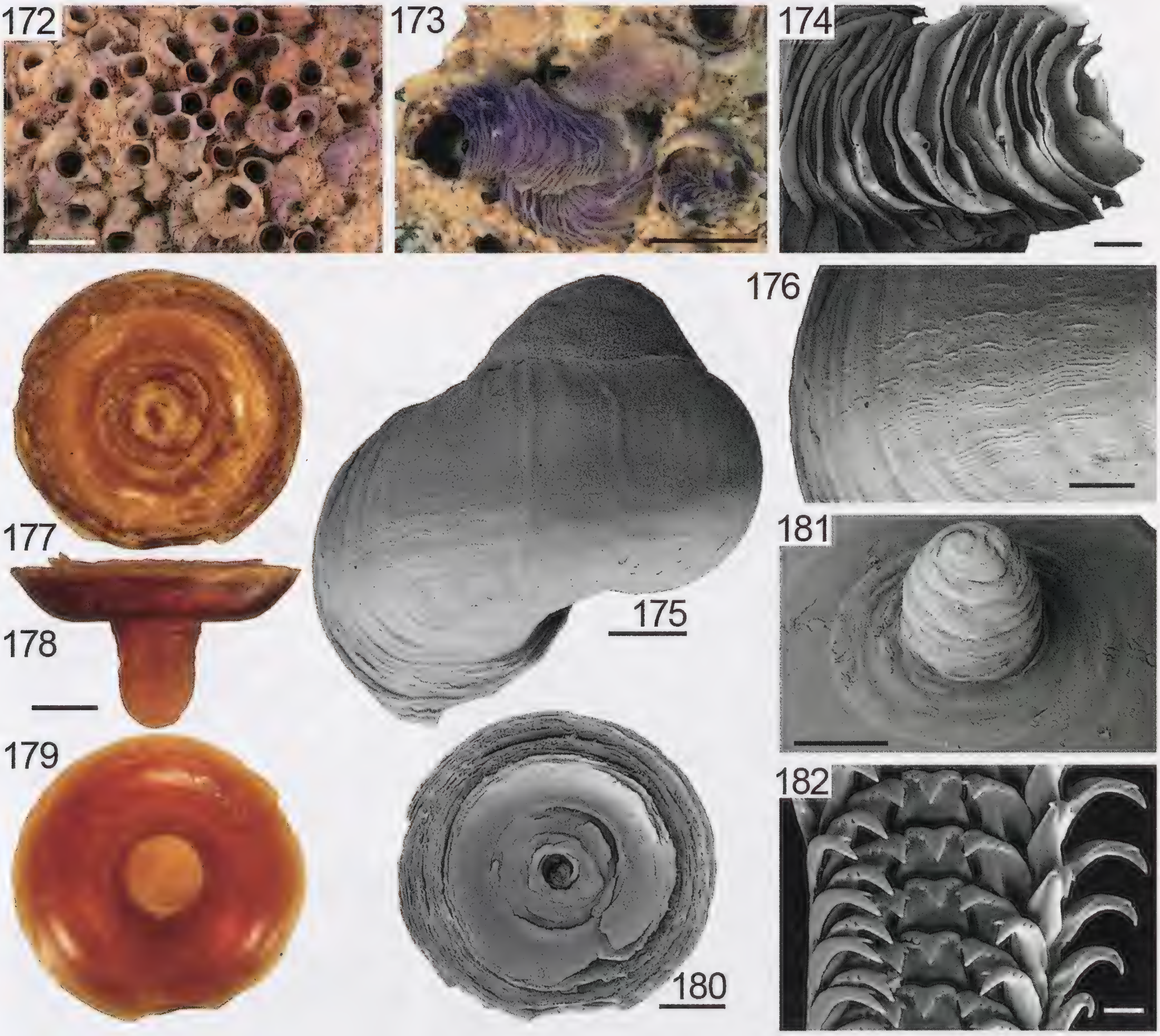

FIGS. 172–182. *Novastoa lamellosa* (Hutton, 1873). FIG. 172: Cluster of specimens. NMNZ M.004786, Noises Islands, New Zealand. Scale bar = 10 mm; FIG. 173: Adult shell attached to substratum. NMNZ M.024381, Three Kings Islands, New Zealand. Scale bar = 5 mm; FIG. 174: SEM image of teleoconch sculpture. NMNZ M.024381, Three Kings Islands, New Zealand. Scale bar = 500 µm, FIGS. 175, 176: SEM images of protoconch. NMNZ M.012245, Chatham Islands, New Zealand; FIG. 175: Abapertural view. Scale bar = 200 µm, FIG. 176: Detail of sculpture. Scale bar = 100 µm; FIGS. 177–179: Operculum. NMNZ M.024381, Three Kings Islands, New Zealand. Scale bar = 500 µm. FIG. 177: Exterior surface; FIG. 178: Lateral view; FIG. 179: Interior surface; FIG. 180: SEM image of exterior surface of operculum. NMNZ M.012245, Chatham Islands, New Zealand. Scale bar = 500 µm; FIG. 181: SEM image of oblique view of mammilla on interior surface of operculum. NMNZ M.024381, Three Kings Islands, New Zealand. Scale bar = 500 µm; FIG. 182: Central section of radula. NMNZ M.012245, Chatham Islands, New Zealand. Scale bar = 50 µm.

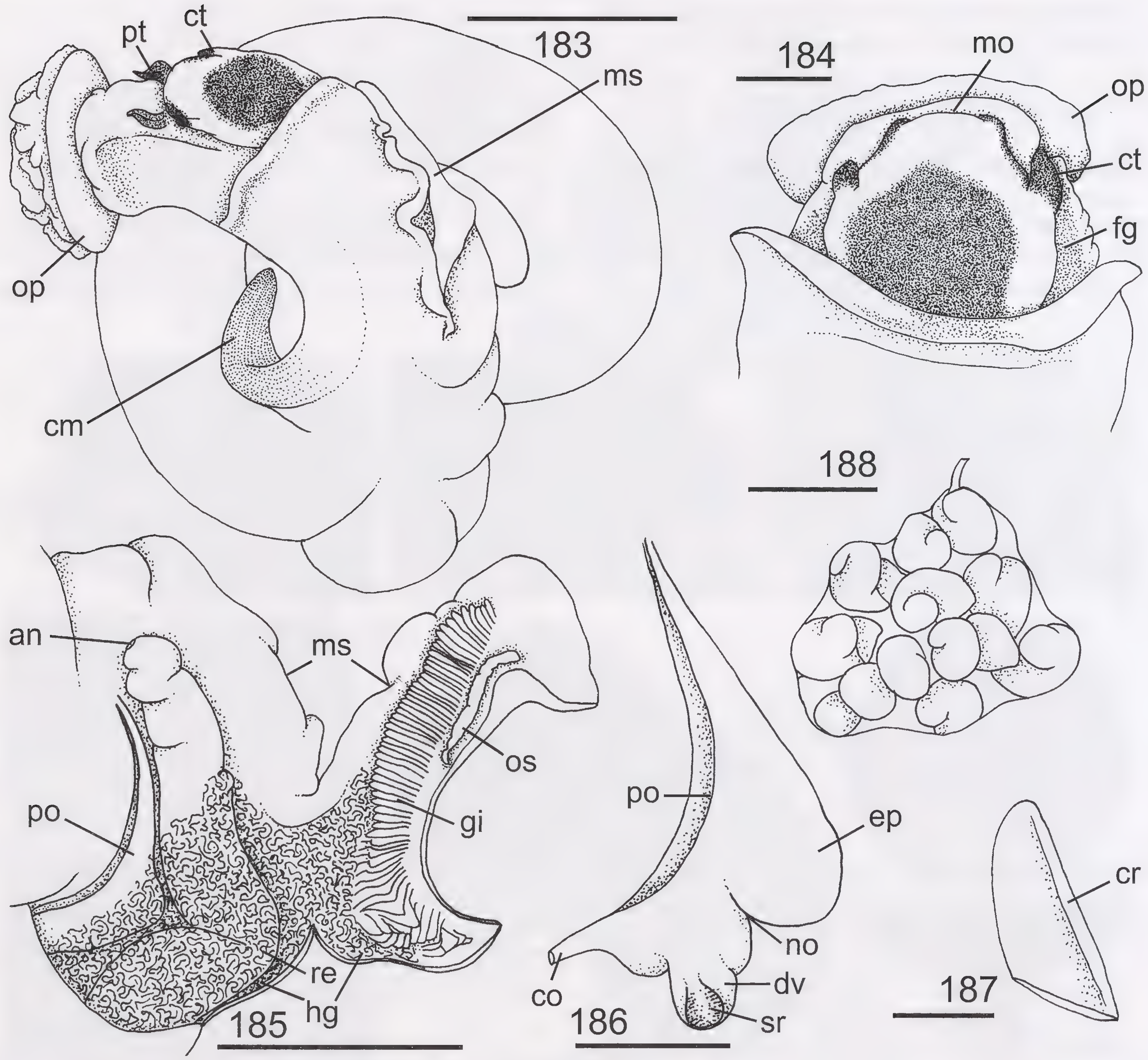

FIGS. 183–188. *Novastoa lamellosa* (Hutton, 1873). NMNZ M.012245, Chatham Islands, New Zealand. FIG. 183: Left view of female specimen. Scale bar = 5 mm; FIG. 184: Dorsal view of anterior body of male specimen. Scale bar = 1 mm; FIG. 185: Mantle cavity of female specimen. Scale bar = 5 mm; FIG. 186: Pallial oviduct. Scale bar = 2 mm; FIG. 187: Gill leaflet. Scale bar = 500 µm; FIG. 188: Stalked egg capsule at late stage of development. Scale bar = 1 mm.

cleaning the operculum to remove encrusting algae. Morton (1951) also did not describe the delicate spiral sculpture on the protoconch, but this is not visible without SEM. The material examined here agreed with Morton's (1951) observation of a slit female mantle, but not with his later conclusion that the female mantle is entire (Morton, 1965).

Distribution (Fig. 171)

Known from New Zealand. Examined material from several locations on the North Island of New Zealand and remote islands northwest (Three Kings Islands) and southeast (Chatham Islands) of New Zealand.

Novastoa caboverdensis n. sp.

Type Locality

Rocky littoral, Pedra Lume, Sal, Republic of the Cape Verde Islands: 16.45°N, 22.53°W.

Material Examined

Holotype: FMNH 301978: from type locality, coll. I. Kappner & K. Defren, April 22, 2003, 95% EtOH (1 male specimen) [DNA sequence data].

Etymology

Named after the type locality in the island nation of Cape Verde (Cabo Verde). Adjective in genitive case.

Description

Teleoconch (Figs. 189, 190): Apertural diameter 5.7 mm, not expanded behind aperture; diameter of last whorl 16 mm. Four whorls coiled concentrically; shallowly entrenched in substratum; aperture flush with substratum. Shell thick. Exterior surface cream with irregular brown discoloration; sculpture of thick, transverse, ruffled lamellae forming approximately 14 longitudinal ribs. Interior surface white with irregular brown patches.

Protoconch: Not known.

Operculum (Figs. 191–194): Diameter 4.9 mm. Shallow conical; bright orange around muscle attachment area fading to white peripherally. Lamina on exterior surface ruffled. Interior surface with short conical to nipple-shaped mammilla.

Radula (Fig. 195): Length of ribbon 2.5 mm, width 320 μm; 44 rows.

External Morphology and Color (Fig. 196): Body length 19 mm, occupying last whorl of shell. Columellar muscle medium length, extending one whorl. Food groove with simple outer margin. Adult female morphology not observed. Color of holotype specimen preserved in 95% EtOH: head/foot white with mottled grey pigment on dorsal and lateral surfaces of head and anterior margin of foot; pedal and cephalic tentacles white; mantle margin dark grey with white trim; digestive gland pale brown.

Pallial and Reproductive Anatomy (Figs. 197–199): Gill 0.2x mantle width; gill leaflets medium height triangular, breadth equal to height; 14 leaflets per mm. Osphradium long, 5.3 mm; margins smooth; anterior tip curved

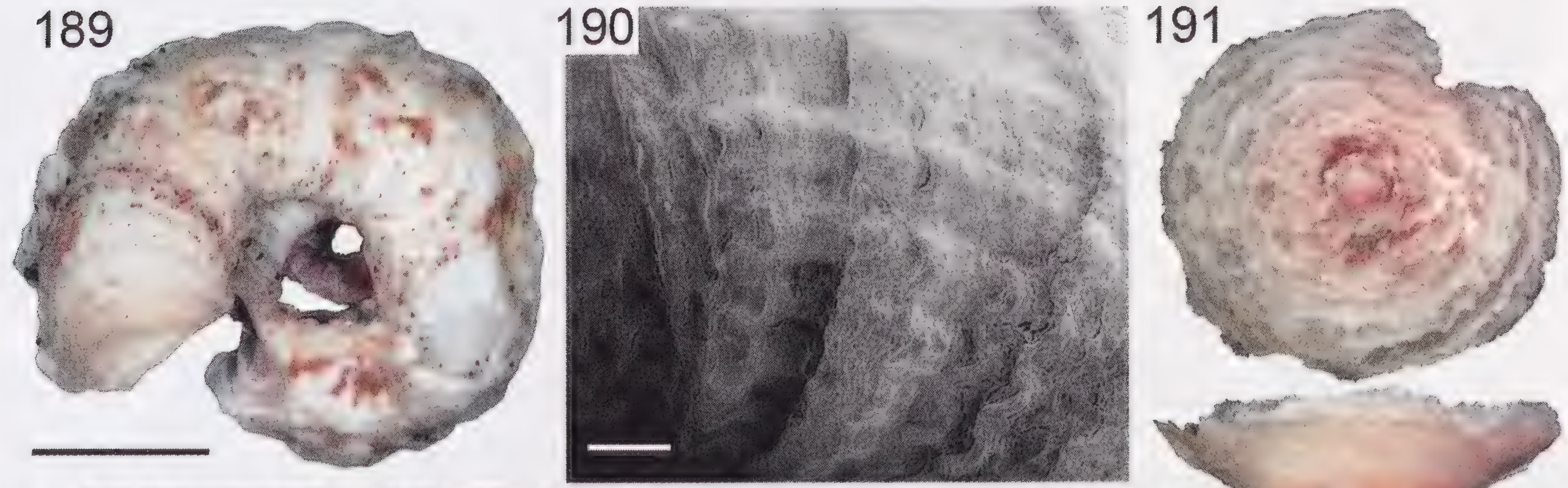

FIGS. 189–195. Holotype of ***Novastoa caboverdensis*** n. sp. FMNH 301978, Pedra Lume, Cape Verde. FIG. 189: Shell removed from substratum. Scale bar = 5 mm; FIG. 190: SEM image of teleoconch sculpture. Scale bar = 500 μm; FIGS. 191–193: Operculum. Scale bar = 1 mm. FIG. 191: Exterior surface; FIG. 192: Lateral view; FIG. 193: Interior surface; FIG. 194: SEM image of muscle attachment area on interior surface of operculum. Scale bar = 500 μm; FIG. 195: Central section of radula. Scale bar = 100 μm.

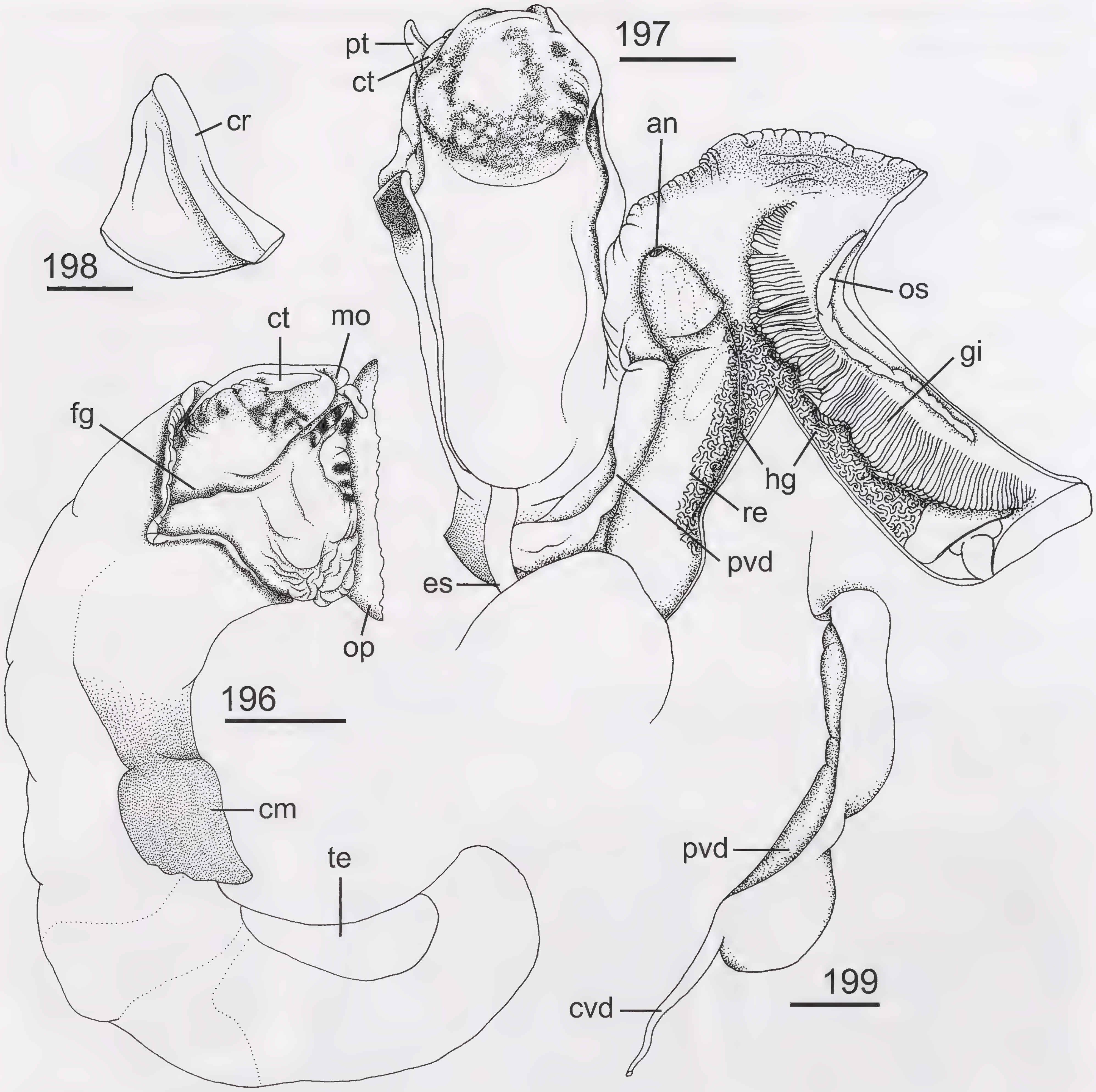

FIGS. 196–199. Anatomy of male holotype of ***Novastoa caboverdensis*** n. sp. FMNH 301978, Pedra Lume, Cape Verde. FIG. 196: Body of male. Scale bar = 2 mm; FIG. 197: Mantle cavity of male. Scale bar = 2 mm; FIG. 198: Gill leaflet from mid-section of gill. Scale bar = 500 μm; FIG. 199: Pallial vas deferens. Scale bar = 1 mm.

towards columellar muscle. Anus opening within mantle cavity; fecal pellets cigar-shaped. Hypobranchial gland pale brown, covering surface of mantle between gill and rectum, covering part of rectum. Female reproductive system not observed. Pallial vas deferens notched near midpoint.

Development and Ecology: Egg capsule morphology and larval biology unknown. Single adult specimen collected, but ecology not known.

Comparative Remarks

Somewhat similar in shell and soft-tissue morphology to *N. lamellosa*, but lacking a cylindrical mammilla on the interior surface of the operculum. *Dendropoma marchadi* Keen & Morton, 1960, occurs nearby in Senegal on mainland Africa. These species can be distinguished by the much larger shell of ***N. caboverdensis*** n. sp. and the presence of a raised, multispiral, ruffled lamina on the exterior surface of the operculum. *Dendropoma marchadi* is known to brood unstalked egg capsules within the mantle cavity. The brooding behavior of ***N. caboverdensis*** n. sp. is not known, but may be similar to other species of *Novastoa* that attach stalked egg capsules to the shell wall.

Distribution (Fig. 171)

Known only from a single specimen from the type locality at Pedra Lume on the island of Sal in Cape Verde.

Novastoa bahamensis n. sp.

Type Locality

Intertidal zone, Silver Point, Grand Bahama Island, The Bahamas: 26.50°N, 78.66°W.

Material Examined

Bahamas: Holotype: FMNH 329355, coll. J. Worsfold, January 8, 1989, 70% EtOH (1 specimen); Paratypes: FMNH 329356, from the type local-

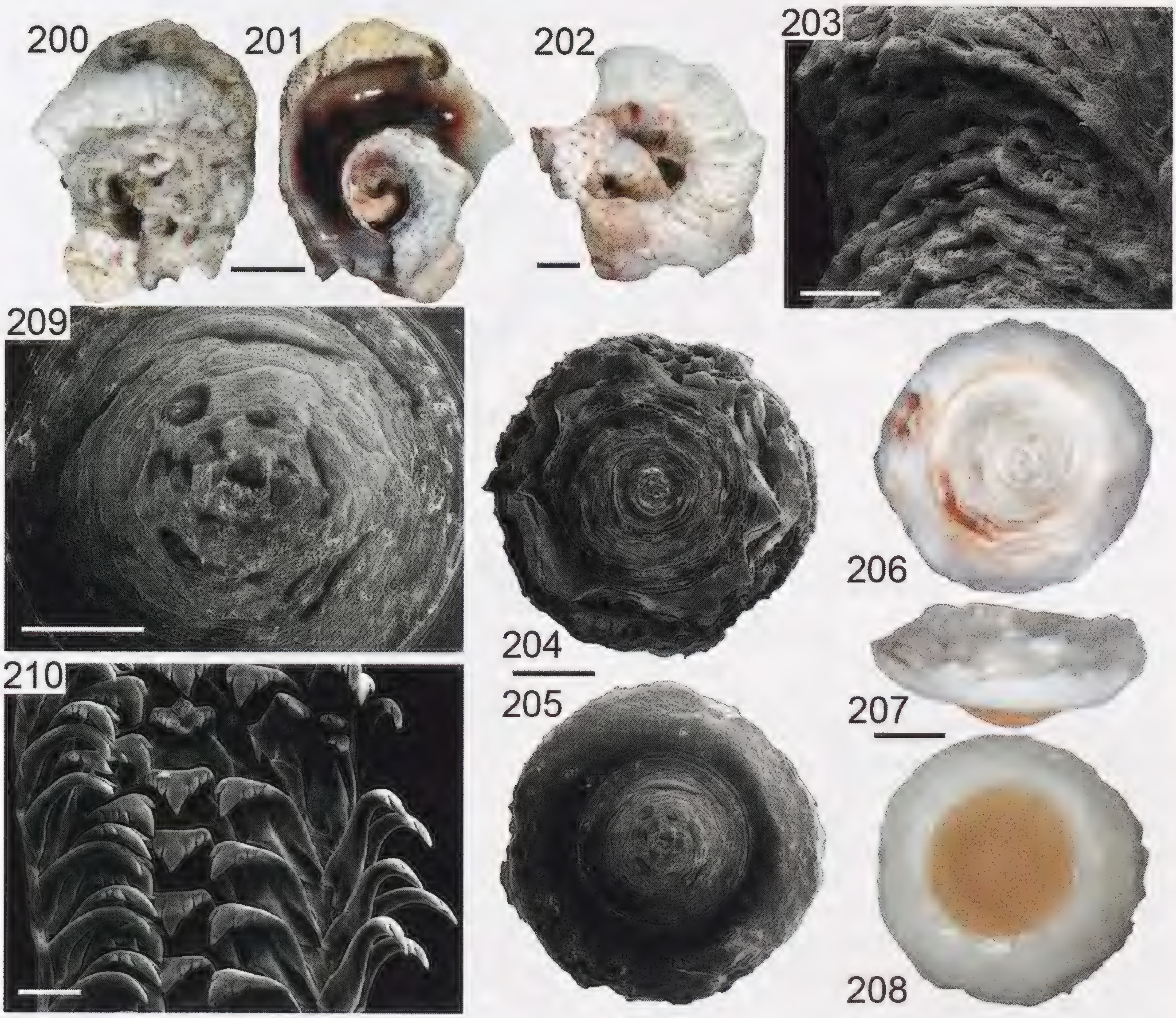

FIGS. 200–210. ***Novastoa bahamensis*** n. sp. FIGS. 200, 201: Part of holotype shell. FMNH 329355, Grand Bahama Island, Bahamas. Scale bar = 5 mm. FIG. 200: Exterior of shell fragment; FIG. 201: Interior of shell fragment; FIGS. 202, 203: Paratype shell. FMNH 329356, Grand Bahama Island, Bahamas. FIG. 202: Exterior of shell. Scale bar = 2 mm; FIG. 203: SEM image of teleoconch sculpture. Scale bar = 500 µm; FIGS. 204–208: Operculum. FMNH 329356. Scale bar = 1 mm. FIG. 204: SEM of exterior surface; FIG. 205: SEM of interior surface; FIG. 206: Exterior surface; FIG. 207: Lateral view; FIG. 208: Interior surface; FIG. 209: SEM image of muscle attachment area on interior surface. FMNH 329356. Scale bar = 500 µm; FIG. 210: Central section of radula. FMNH 329356. Scale bar = 50 µm.

ity, coll. J. Worsfold, January 8, 1989, 70% EtOH (1 specimen); FMNH 327205, oolitic limestone platform in front of Point of View Villas, Fresh Creek, Andros Island, 24.7345°N, 77.7928°W, coll. T. Rawlings, March 26, 2004, 95% EtOH (5 specimens) [DNA sequence data].

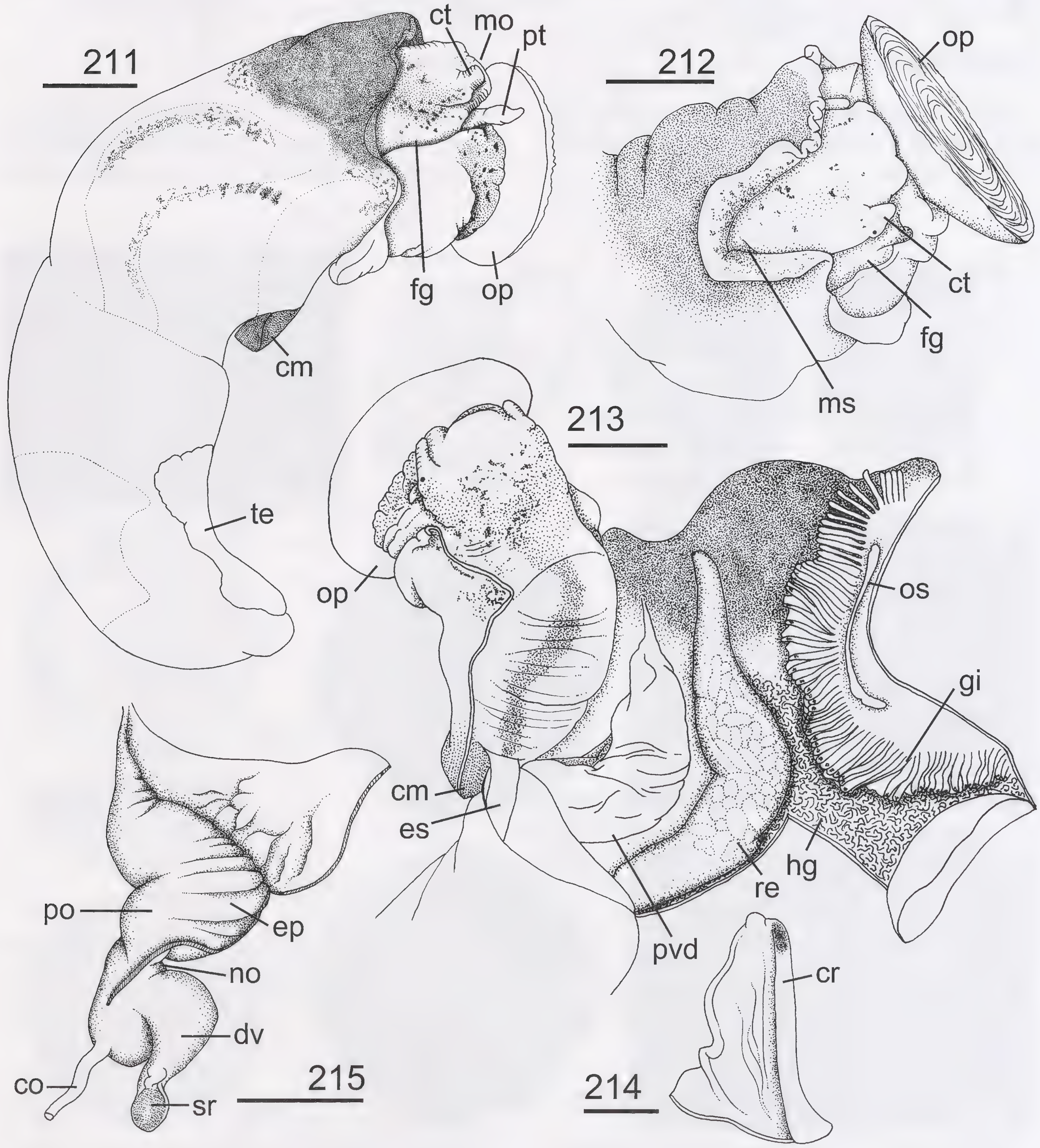

FIGS. 211–215. Anatomy of ***Novastoa bahamensis*** n. sp. FIG. 211: Body of male holotype. FMNH 329355, Grand Bahama Island, Bahamas. Scale bar = 2 mm; FIG. 212: Dorsal view of anterior body, female. FMNH 327205, Andros Island, Bahamas. Scale bar = 1 mm; FIG. 213: Mantle cavity of male holotype. FMNH 329355. Grand Bahama Island, Bahamas. Scale bar = 2 mm; FIG. 214: Gill leaflets from mid and anterior sections of gill. FMNH 327205. Scale bar = 500 µm; FIG. 215: Pallial oviduct with ventral surface of expanded pocket peeled back. Paratype, FMNH 329356, Grand Bahama Island, Bahamas. Scale bar = 1 mm.

Etymology

Named for its occurrence in the Bahamas (adjective).

Description

Teleoconch (Figs. 200–203): Apertural diameter to 6.6 mm, not expanded behind aperture; diameter of last whorl to 17 mm. Up to four whorls coiled concentrically; deeply entrenched in substratum; aperture flush with substratum. Shell thick. Exterior surface white; sculpture of closely-packed, upright, ruffled, transverse lamellae (often heavily worn). Interior surface white with irregular burgundy patches.

Protoconch: Not known.

Operculum (Figs. 204–209): Diameter to 4.2 mm. Shallow saucer-shaped; peripherally white with golden yellow muscle attachment area on interior surface. Lamina on exterior surface ruffled. Interior surface with short, conical mammilla.

Radula (Fig. 210): Length of ribbon to 2.3 mm, width to 275 µm; up to 45 rows.

External Morphology and Color (Figs. 211, 212): Body length to 19 mm, occupying last whorl of shell. Columellar muscle very short, extending < 0.5 whorl. Food groove with convoluted flap on outer margin. Adult female mantle divided by pallial notch extending < 0.3x mantle length. Color of specimens preserved in 70% EtOH: pedal and cephalic tentacles white; head-foot white with mottled grey pigment on sides of foot and dorsal surface of head; mantle dark grey.

Pallial and Reproductive Anatomy (Figs. 213–215): Gill 0.2x mantle width; gill leaflets moderate height triangular, breadth equal to height; 12 leaflets per mm. Osphradium short, 2.5 mm; margins smooth; anterior tip curved towards columellar muscle. Anus opening within mantle cavity; fecal pellets ovoid. Hypobranchial gland pale brown, covering surface of mantle between gill and rectum only. Seminal receptacle attached to tip of proximal diverticulum from pallial oviduct. Pallial vas deferens without notch near midpoint.

Development and Ecology (Fig. 214): Egg capsule morphology and larval biology unknown. Solitary adults living on vertical rock surfaces in intertidal zone.

Comparative Remarks

Superficially similar, in life, to *Dendropoma nebulosum* and ***Novastoa pholetor*** n. sp., both of which also occur in the Caribbean. ***Novastoa bahamensis*** n. sp. occurs on rocks in the intertidal zone, while *D. nebulosum* is found in deeper water (SCUBA depth). Also, the head pigmentation and opercular morphology of ***N. bahamensis*** n. sp. are distinctive and the presence of stalked egg capsules is definitive in distinguishing these taxa. ***Novastoa bahamensis*** n. sp. can be distinguished from ***N. pholetor*** n. sp. by the operculum, which is white and yellow in ***N. bahamensis*** n. sp. but pink and red in ***N. pholetor*** n. sp. These taxa are closely related in the molecular phylogeny and share many morphological characters.

Distribution (Fig. 171)

Known only from two islands in the Bahamas.

Novastoa pholetor n. sp.

Type Locality

1.5 m depth, on coral rubble and living coral heads, Tobacco Reef, Stann Creek District, Belize: 16.8236°N, 88.0812°W.

Material Examined

Belize: Holotype: FMNH 328511, coll. R. Bieler, T. Collins, R. Golding, T. Rawlings & P. Sierwald, April 22, 2011, 70% EtOH (1 specimen); Paratypes: FMNH 327177: from type locality; coll. R. Bieler, T. Collins, R. Golding, T. Rawlings & P. Sierwald, April 22, 2011, RNAlater (4 tissue samples), 95% EtOH (4 tissue samples and egg capsules), 3.5% glutaraldehyde (2 testes), 70% EtOH (many), 5% SW formalin (many), dry (shell fragments). FMNH 327160: 8 m on coral heads, Columbus Reef, Stann Creek District, Belize, 16.9028°N, 88.0554°W, coll. R. Bieler & P. Sierwald, April 18, 2011, RNAlater (1 tissue sample), 95% EtOH (1 tissue sample), 5% SW formalin (1 body and egg capsules), dry (shell fragments); FMNH 327172: 1 m on surface of coral boulders covered with algal "lawn", lagoon E of Carrie Bow Cay, Stann Creek District, 16.8027°N, 88.0816°W, coll.

R. Bieler, T. Collins, R. Golding, T. Rawlings & P. Sierwald, April 21, 2011, RNAlater (2 tissue samples), 95% EtOH (2 bodies without shells), dry (shell fragments), [DNA sequence data]; FMNH 327181: 1 m on surface of coral boulders covered with algal "lawn", lagoon E of Carrie Bow Cay, Stann Creek District, 16.8027°N, 88.0816°W, coll. R. Bieler, T. Col-

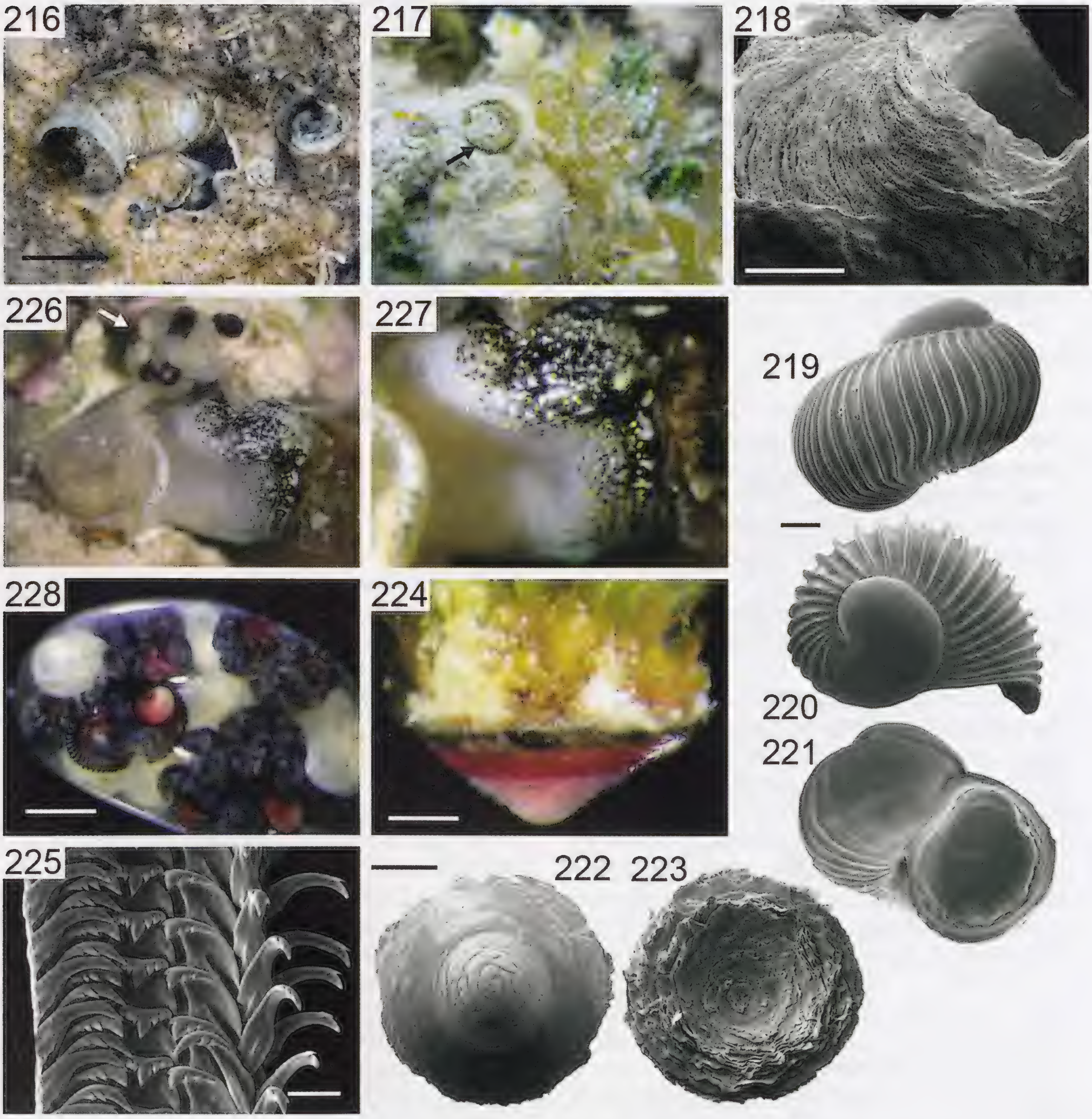

FIGS. 216–228. ***Novastoa pholetor*** n. sp. FIG. 216: Specimen attached to substratum, partly covered by coralline algae. Paratype, FMNH 327177, Tobacco Reef, Belize. Scale bar = 5 mm; FIG. 217: Living specimen *in situ* embedded in substratum, with only aperture and heavily encrusted operculum visible (arrow). Paratype, FMNH 327177; FIG. 218: SEM image of teleoconch sculpture. Paratype, FMNH 327177. Scale bar = 1 mm; FIGS. 219–221: SEM images of intracapsular larval shells. Paratype, FMNH 327177. Scale bar = 100 µm. FIG. 219: Abapertural view; FIG. 220: Apertural view; FIG. 221: Apical view; FIGS. 222, 223: SEM images of operculum. Paratype, FMNH 327177. Scale bar = 1 mm. FIG. 222: Exterior surface; FIG. 223: Interior surface; FIG. 224: Operculum removed from living animal with encrusted layer attached to exterior surface, lateral view. FMNH 327160, Columbus Reef, Belize. Scale bar = 1 mm; FIG. 225: Central section of radula. Paratype, FMNH 327177. Scale bar = 50 µm; FIGS. 226, 227: Living specimen partially removed from shell. Paratype, FMNH 327177. FIG. 226: Female with stalked egg capsule exposed (arrow); FIG. 227: Pigmentation on the head and foot; FIG. 228: Stalked egg capsule containing late-stage embryos in two color morphs. FMNH 327160. Scale bar = 1 mm.

lins, R. Golding, T. Rawlings & P. Sierwald, April 24, 2011, 95% EtOH (1 specimen), 70% EtOH (1 specimen).

Etymology

Named for its deep-hidden, burrowed mode of life. The heavily encrusted operculum matches the surrounding substratum, and when held slightly ajar to permit feeding resembles the camouflaged entrance to the burrow of a trapdoor spider. From the Latin pholetor, for "one who lurks in a hole" (noun in apposition).

Description

Teleoconch (Figs. 216–218): Apertural diameter to 6 mm, not expanded behind aperture; diameter of last whorl to 21 mm. Up to four whorls coiled concentrically; deeply entrenched in substratum (sometimes entirely embedded with only aperture visible); aperture flush with substratum. Shell thick. Exterior surface white; sculpture of closely-packed, upright, ruffled, transverse lamellae (often heavily worn). Interior surface white with brown patches.

Protoconch (Figs. 219–221): Hatchling protoconch diameter to 600 µm, height to 500 µm. Sculpture absent on first 0.6 whorl, last 0.7 whorl with very tall, widely-spaced axial ribs. Either white or dark brown, roughly equal proportions of each color occurring per egg capsule.

Operculum (Figs. 222–224): Diameter to 4.5 mm. Shallow conical; raspberry red periphery fading to pale pink muscle attachment area. Interior surface with short, conical mammilla.

Radula (Fig. 225): Length of ribbon to 2.1 mm, width to 275 µm; up to 41 rows.

External Morphology and Color (Figs. 226, 227): Body length to 21 mm, occupying last whorl of shell. Columellar muscle very short, extending < 0.5 whorl. Food groove with convoluted flap on outer margin. Adult female mantle divided by pallial notch extending < 0.3x mantle length. Color in life: head-foot base color translucent white overlaid with mottled opaque black and white pigment and bright yellow speckles; pedal and cephalic tentacles and lips pale yellow; mantle cream with opaque black and white speckles on lateral edges, anterior edge black with alternating white dots on margin; digestive gland black; ovary cream.

Pallial and Reproductive Anatomy: Not known.

Development and Ecology (Fig. 228): Up to five stalked egg capsules per female; 32–45 eggs/embryos per capsule; up to 1.5 mm diameter. Larval biology not known, but hatchling larvae barely capable of swimming and velum mostly resorbed, suggesting direct development. Proportion of white and dark brown larvae per capsule roughly equal. Adults common in subtidal zone and behind wave-zone on reef crest. Solitary and extremely cryptic.

Comparative Remarks

Superficially similar, in life, to both *Dendropoma nebulosum* and ***Novastoa bahamensis*** n. sp., which have similar Caribbean distributions. ***Novastoa pholetor*** n. sp. generally occurs in shallow subtidal habitat in the wave zone, but ***N. bahamensis*** n. sp. occurs intertidally and *D. nebulosum* in deeper water (SCUBA depth). The head pigmentation and opercular morphology of ***N. pholetor*** n. sp. are highly distinctive and the presence of stalked egg capsules prevents confusion between this species and *D. nebulosum*. Comparison with ***N. bahamensis*** n. sp. shows many morphological similarities, but these species are well-separated by molecular data. They can also be distinguished by the color of the operculum.

Distribution (Fig. 171)

Known only from localities in the vicinity of Carrie Bow Cay, Belize.

Novastoa batavia n. sp.

Type Locality

On dead *Acropora* spp., 6–8 m by SCUBA, reef slope off main dock at Beacon Island station, Goss Channel, Wallabi Group, Houtman Abrolhos, Western Australia, Australia: 28.7090°S, 113.7875°E.

Material Examined

Western Australia: Holotype: WAM S66359 ex FMNH 329357 (Fig. 229): coll. R. Bieler, May 27, 1994, 70% EtOH (1 specimen); Paratypes: FMNH 327038: from type locality, coll. R. Bieler, May 27, 1994, 70% EtOH (4 specimens); FMNH 327047: very protected water with layer of silt on hard bottom, among *Posidonia australis*, W side of West Wallabi Island, Wallabi Group, Houtman Abrolhos, 28.4523°S, 113.7023°E, coll. R. Bieler, May 19, 1994, 70% EtOH (2 specimens).

Etymology

Named for the Dutch East India Company vessel *Batavia* which was infamously shipwrecked in 1629 near the type locality on Beacon Island, in the Houtman Abrolhos of Western Australia. Noun in apposition.

229

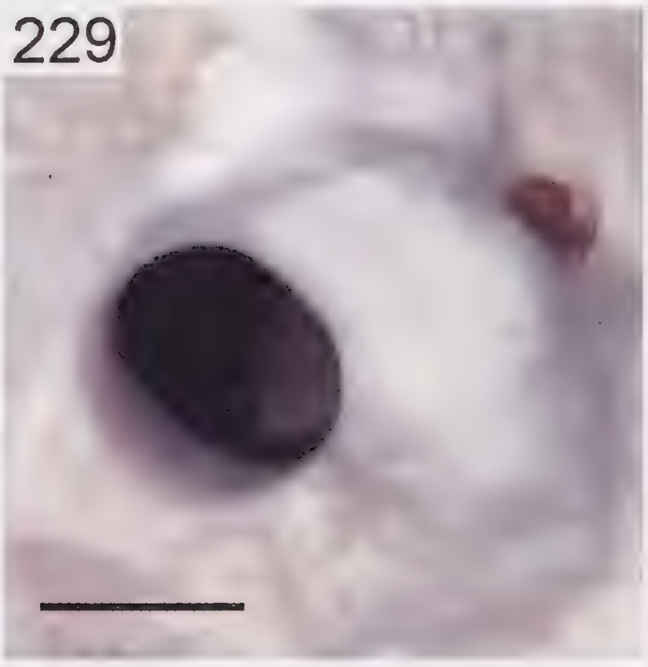

230

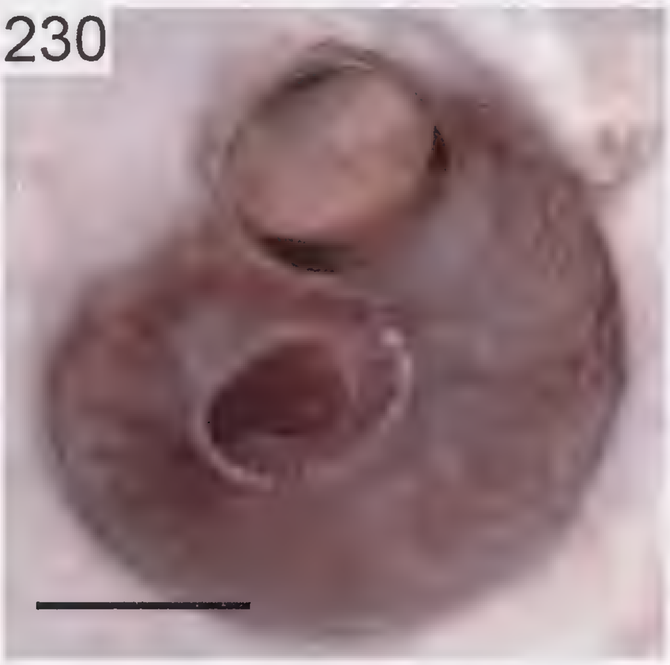

231

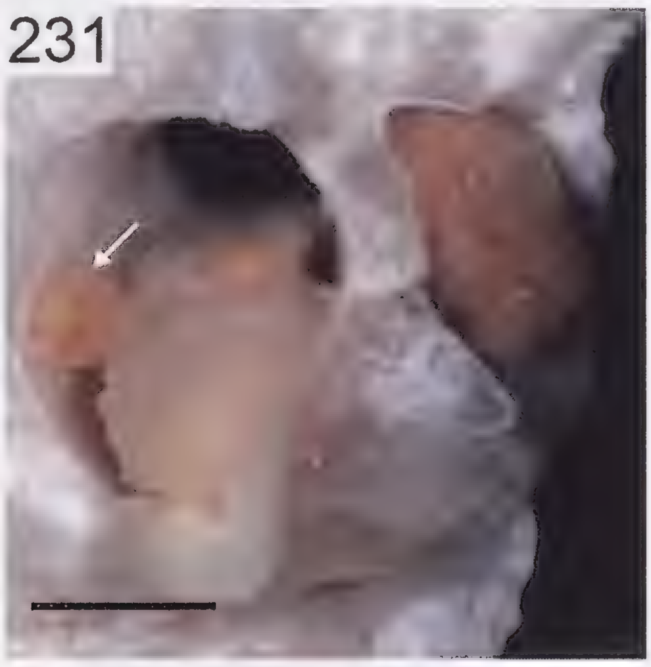

232

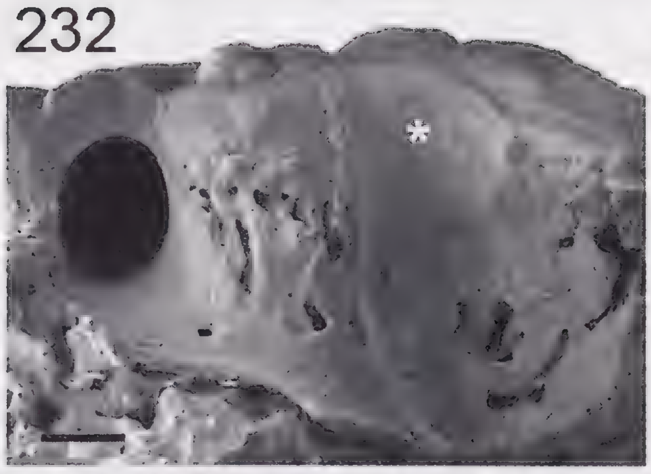

233

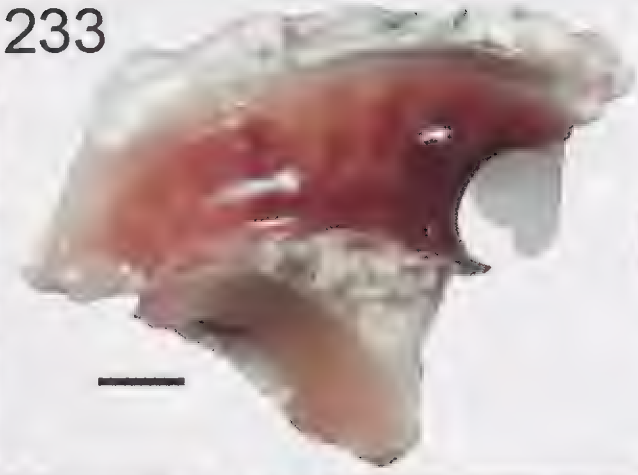

234

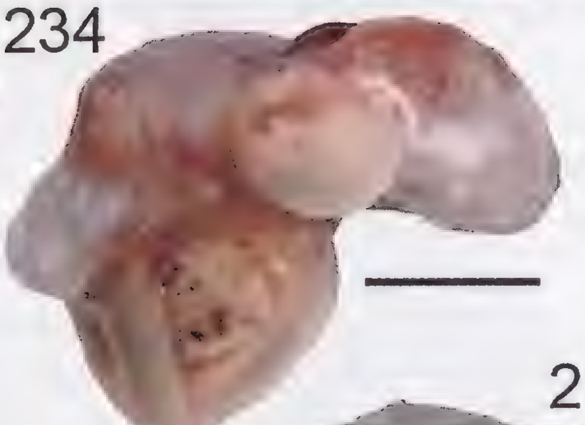

239

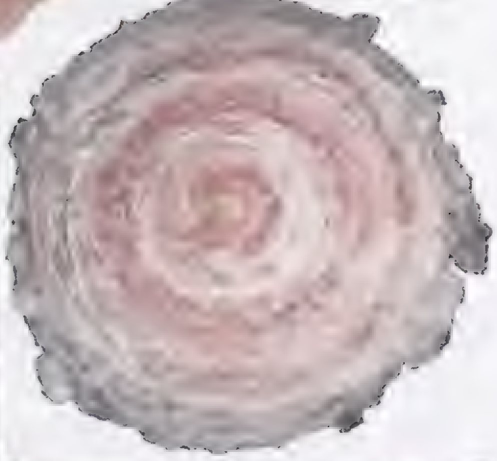

235

236

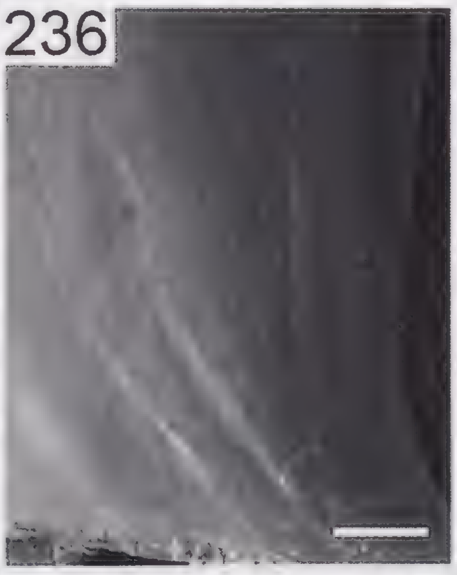

238

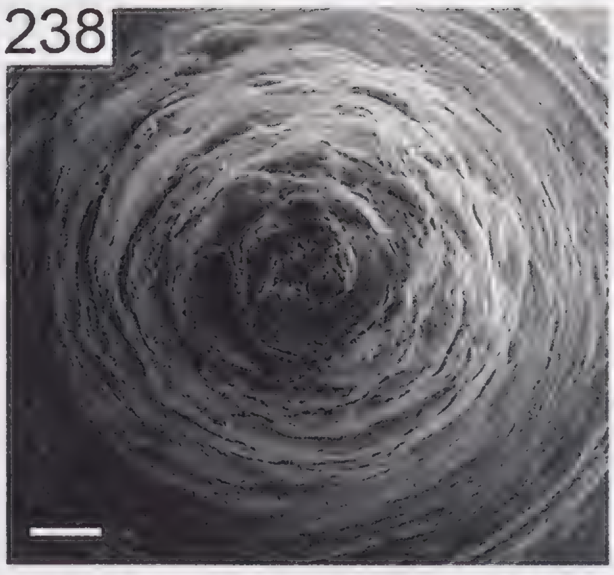

240

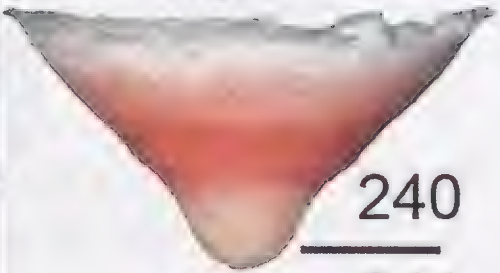

237

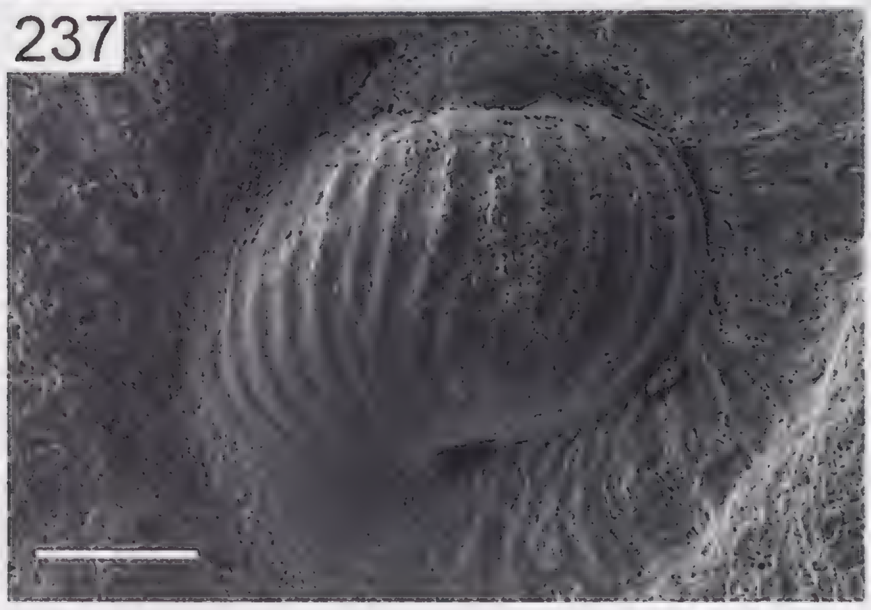

242

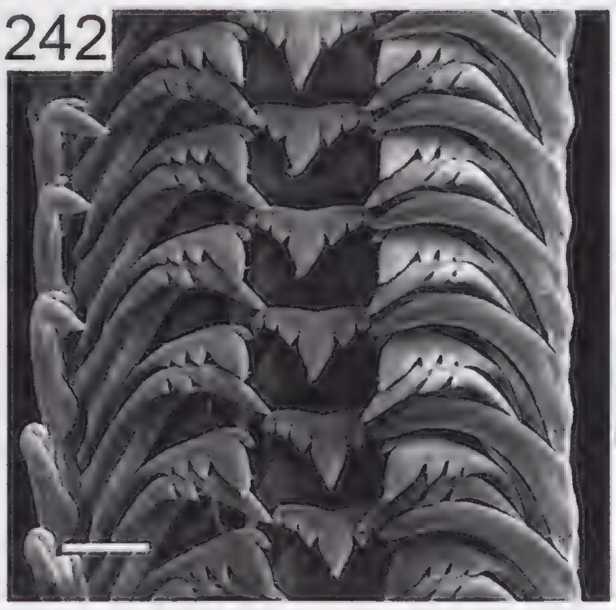

241

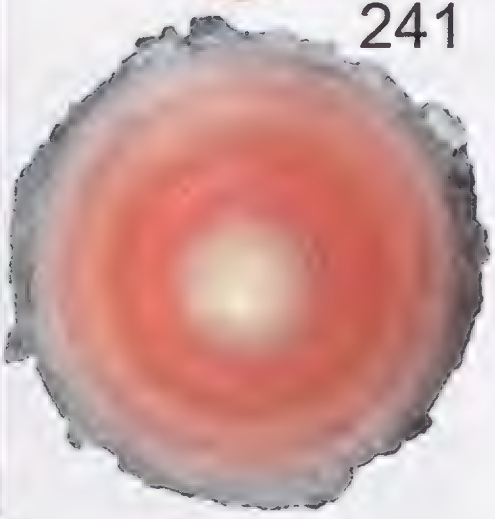

Description

Teleoconch (Figs. 229–236): Apertural diameter to 4.0 mm, diameter of expanded "chamber" behind aperture to 6.3 mm; estimated diameter of shell fragment from largest specimen > 15 mm. Up to three whorls coiled concentrically; entirely embedded in substratum with only aperture and dorsal surface occasionally exposed; aperture flush with surface. Shell thick on exposed dorsal surface but very thin on embedded surfaces. Exterior surface entirely surrounded by substratum matrix or encrusting epifauna, but when cleaned pale brown on exposed dorsal surface and white on embedded surfaces; sculpture of low, transverse lamellae. Interior surface white with transverse stripes of brown on columellar surface of last whorl (in "chamber").

Protoconch (Fig. 237): Settled protoconch diameter (from partially obscured specimen) approx. 630 µm, height 620 µm. Sculpture on last 0.5 whorl of tall, widely-spaced axial ribs. Pale brown.

Operculum (Figs. 238–241): Diameter 4.9 mm. Deeply conical; pale golden mammilla surrounded by ring of dark orange fading to white peripherally. Lamina on exterior surface ruffled. Interior surface with short, nipple-shaped mammilla.

Radula (Fig. 242): Length of ribbon to 2.5 mm, width to 340 µm; up to 43 rows.

External Morphology and Color (Figs. 233, 234, 243–245): Body length to 13 mm, occupying last whorl of shell. Columellar muscle vary short, extending < 0.5 whorl. Food groove with convoluted flap on outer margin. Adult female mantle divided by pallial notch extending < 0.3x mantle length. Color in life: head-foot strikingly mottled with opaque black and white pigment, black predominantly on forehead and around opercular lobe; cephalic tentacles white; forehead, anterior cheeks and mantle region bright yellow; pedal tentacles with black and white flecks, sometimes without black pigment; mantle margin with wide bright yellow band, remainder of mantle with black band interrupted by alternating large and small white patches. Color of specimens preserved in 70% EtOH: entirely white except for scattered flecks of black pigment on dorsal surface of head and around mantle margin.

Pallial and Reproductive Anatomy (Figs. 246–249): Gill 0.3x mantle width; gill leaflets moderate height, breadth equal to height; 14 leaflets per mm. Osphradium long, 5.0 mm; margins smooth; anterior tip bent 180° around columellar muscle. Anus protruding from mantle cavity; fecal pellets not observed.

←

FIGS. 229–242: ***Novastoa batavia*** n. sp. FIG. 229: Adult shell encrusted with coralline algae, only aperture visible. FMNH 327038, Beacon Island, Houtman Abrolhos, Australia. Scale bar = 2 mm; FIG. 230: Juvenile shell and protoconch, not encrusted. FMNH 327038, Beacon Island, Houtman Abrolhos, Australia. Scale bar = 1 mm; FIG. 231: Ventral view of the holotype (female) occupying the "chamber" of its shell and showing a single stalked egg capsule attached to shell wall (indicated by an arrow). WAM S66359, Beacon Island, Houtman Abrolhos, Australia. Scale bar = 2 mm; FIG. 232: SEM image, lateral view of shell deeply embedded in coral substratum, with lateral surface broken away to expose interior of "chamber" (right of image) and cross-section through narrowed aperture (indicated by an asterisk). FMNH 327038, Beacon Island, Houtman Abrolhos, Australia. Scale bar = 500 µm; FIG. 233: Shell fragment showing coloration on interior surface. FMNH 327047, West Wallabi Island, Houtman Abrolhos, Australia. Scale bar = 2 mm; FIG. 234: Lateral view of shell and animal removed from substratum, showing position of body in "chamber" below substratum surface. FMNH 327038, Beacon Island, Houtman Abrolhos, Australia. Scale bar = 1 mm; FIGS. 235, 236: SEM images shell surfaces. FMNH 327038, Beacon Island, Houtman Abrolhos, Australia. Scale bars = 200 µm. FIG. 235: Teleoconch surface after removal of surrounding substratum; FIG. 236: Columellar surface of shell interior; FIG. 237: Abapertural view of protoconch surrounded by first whorl of adult shell. FMNH 327038, Beacon Island, Houtman Abrolhos, Australia. Scale bar = 200 µm; FIG. 238: SEM image of muscle attachment area on interior surface of operculum. FMNH 327047, West Wallabi Island, Houtman Abrolhos, Australia. Scale bar = 500 µm; FIGS. 239–241: Operculum. FMNH 327047, West Wallabi Island, Houtman Abrolhos, Australia. Scale bar = 1 mm. FIG. 239: Exterior surface; FIG. 240: Lateral view; FIG. 241: Interior surface; FIG. 242: Central section of radula. FMNH 327047, West Wallabi Island, Houtman Abrolhos, Australia. Scale bar = 50 µm.

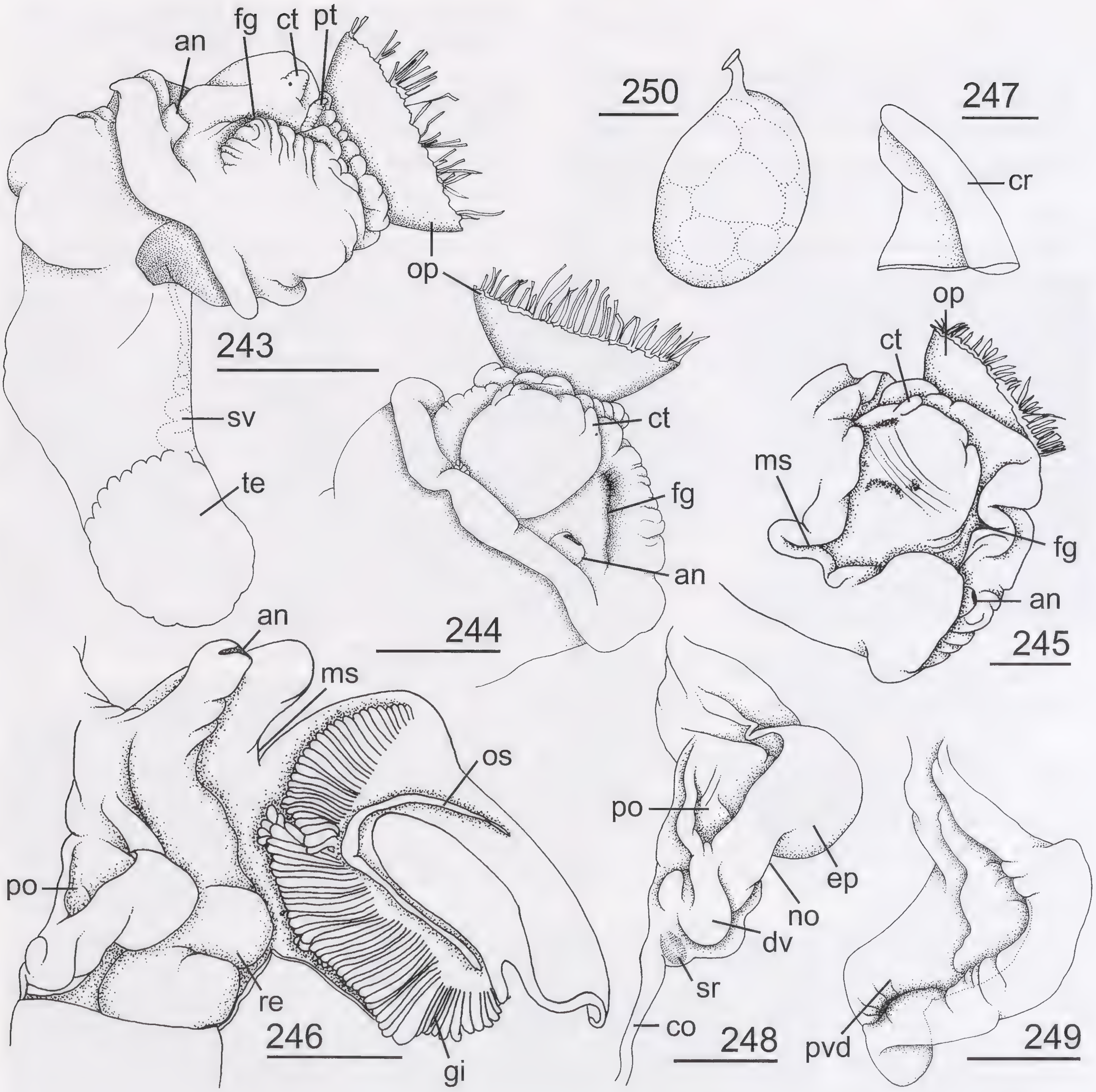

FIGS. 243–250. Anatomy of ***Novastoa batavia*** n. sp. FIGS. 243, 244: Male specimen. Scale bars = 3 mm. FIG. 243: Right view; FIG. 244: Dorsal view of anterior body; FIG. 245: Dorsal view of anterior body of female holotype. WAM S66359, Beacon Island, Houtman Abrolhos, Australia. Scale bar = 1 mm; FIG. 246: Mantle cavity of female specimen. Scale bar = 2 mm; FIG. 247: Leaflet from mid-section of gill. Scale bar = 500 µm; FIG. 248: Pallial oviduct. Scale bar = 1 mm; FIG. 249: Pallial vas deferens with ventral surface peeled back; FIG. 250: Egg capsule removed from holotype. WAM S66359, Beacon Island, Houtman Abrolhos, Australia. Scale bar = 500 µm. FIGS. 243, 244, 246–250: FMNH 327047, West Wallabi Island, Houtman Abrolhos, Australia.

Hypobranchial gland not visible. Seminal receptacle attached to base of proximal diverticulum from pallial oviduct. Pallial vas deferens notched near midpoint.

Development and Ecology (Figs. 231, 250): Single female specimen observed with 1 stalked egg capsule; approx. 20 eggs per capsule; diameter 1.2 mm. Larval biology not known. Adult ecology not known. Shell and operculum often considerably fouled, occasionally entirely embedded in coralline algae.

Comparative Remarks

Most similar to ***Novastoa caboverdensis*** n. sp. and ***N. pholetor*** n. sp., but operculum is intense orange, rather than pale orange (***N. caboverdensis***) or pink (***N. pholetor***), around the muscle attachment area and more steeply concave.

Distribution (Fig. 171)

Known from two islands (Beacon and Wallabi Islands) in the West Wallabi Group of the Houtman Abrolhos, in Western Australia. This is part of the most southerly coral reef on the coastline of Western Australia and is a unique habitat with many endemic species. The northern extent of the range is unknown.

Ceraesignum n. gen.

Dendropoma of authors [in part]. *Non Dendropoma* Mörch, 1861.

Type species

Serpula maxima G. B. Sowerby I, 1825.

Etymology

From the Latin "cera" (= wax) and "signum" (= sign) for the texture on the interior surface of the operculum that resembles the impression of a fingerprint in wax. Noun of neuter gender in Latin.

Diagnostic Description

Teleoconch: Medium to large (maximum dimension 15–450 mm), "tube" wide (apertural diameter 4.5–36 mm); whorl coiling pattern variable, deeply (or entirely) embedded in substratum (living coral or rock); aperture flush with substratum, not forming a feeding tube; encrusted with epifauna or covered by living coral. Shell thick; aperture simple. Color and sculpture of exterior surface variable. Interior surface color variable; sculpture on columellar surface absent; concave septa frequent in abandoned shell.

Protoconch: Settled protoconch diameter 370–700 µm, height 420–710 µm. "Hook" projection present from apertural lip, weak or strong. Intracapsular growth only evident in protoconch structure; globular with varying whorl proportions; 1.25–1.75 whorls; sculpture absent or present as axial and transverse ribs; spiral keels at base of whorl absent or present. Color variable, transparent.

Operculum: Circular in axial profile; diameter proportional to shell size, 2.3–40 mm. Composed of chitin only; transparent, brown. Deep to shallow concave saucer-shaped in lateral profile; without mammilla. Exterior surface sometimes encrusted with epifauna, smooth. Interior surface glossy, smooth except for muscle attachment area textured with "fingerprint" pattern of concentric ridges of varying height.

Radula: Taenioglossate, transparent, colorless or brown. Length of ribbon 2.1–6.5 mm; 49–60 rows (proportional to shell size). Trapezoidal rachidian tooth with prominent central cusp flanked on each side by three smaller cusps decreasing in size outwardly. Base of lateral tooth notched to interlock with rachidian and inner marginal teeth; elongate main cusp flanked by variable number of cusps on inner and outer sides. Inner marginal tooth slender with variable number of cusps on inner and outer sides. Outer marginal tooth smooth on outer side, 1–2 tiny triangular cusps on inner side, base simple, without projection.

External Morphology and Color: Body of animal stout (length 2.8–10 cm in examined wet material), occupying last half of shell (2 whorls where coiled); 0.5x body length (earliest 1 whorl where coiled) composed of gonad and digestive gland. Columellar muscle very short, extending < 0.75 whorls. Pedal tentacles short (in preserved specimens). Head slightly bulbous, cephalic tentacles short (in preserved specimens), broad, with tiny ommatophore bearing eye at outer base; right side of head with food groove sometimes present. Adult female mantle (all large specimens) divided by pallial slit, slightly left of midline; male mantle undivided. External body coloration variable.

Pallial and Reproductive Anatomy: Gill 0.2–0.3x mantle width, full length of mantle cavity; gill leaflets tall or short triangular; 7–16 leaflets per mm. Osphradium short relative to mantle cavity, 1.5–9.0 mm; margins irregular or smooth; anterior tip curled towards columellar muscle. Rectum running from coelom to anterior right edge of mantle cavity in deep curve; fecal pellets ovoid to cigar-shaped. Hypobranchial gland transparent brown to pale yellow, covering mantle surface between gill and rectum, also surface of rectum except tip, and sometimes surface of pallial oviduct.

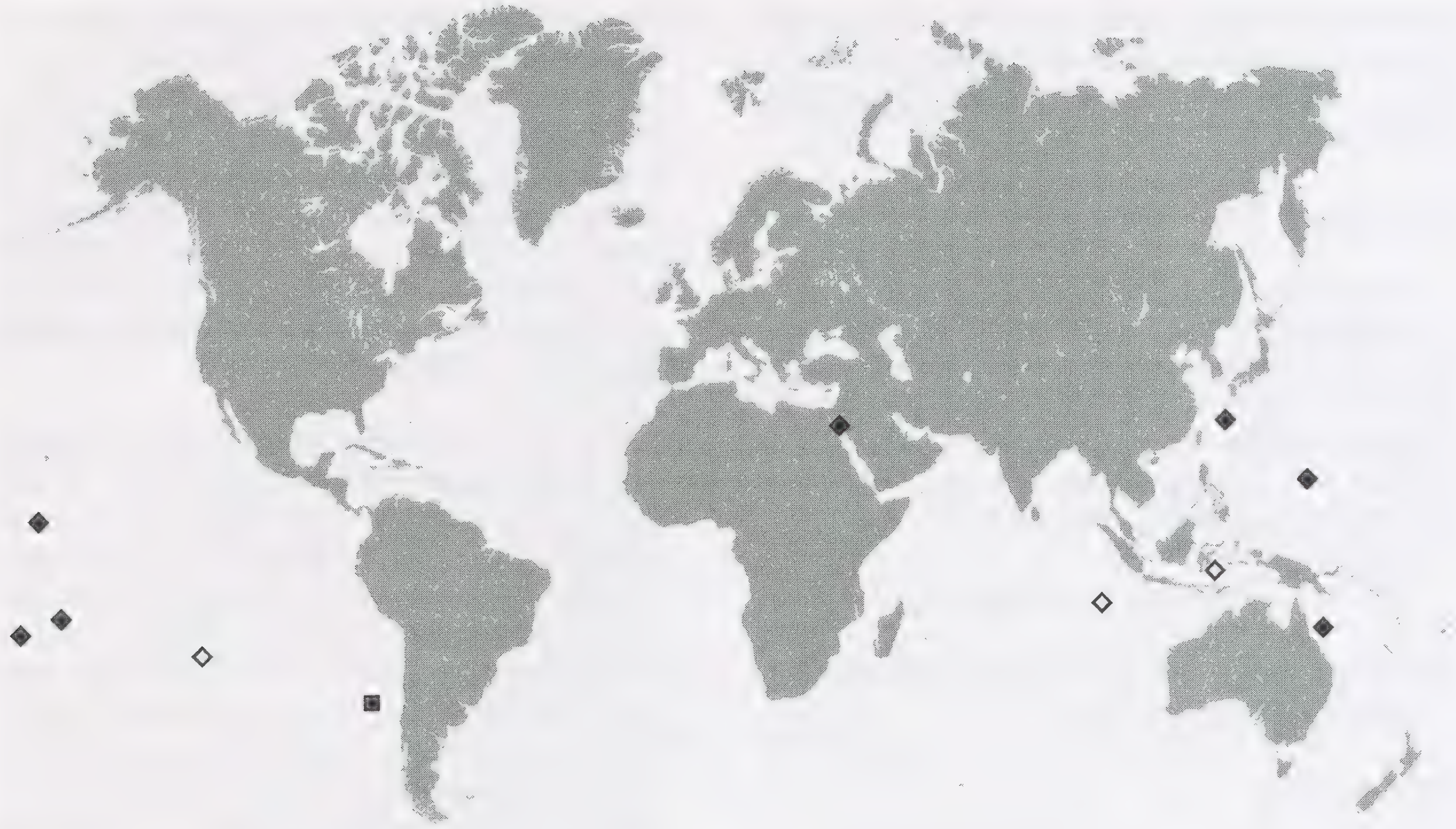

FIG. 251. Distribution map of *Ceraesignum* n. gen. based on material examined in this study and reports in the literature. Filled diamond = *C. maximum* (G. B. Sowerby I, 1825) locations for samples examined during this study; hollow diamond = *C. maximum* reports in the literature; filled square = ***C. robinsoncrusoei*** n. sp.

Posterior end of pallial oviduct broad, tapering to narrow strip anteriorly; proximal diverticulum absent. Seminal receptacles absent (not found in examined specimens). Male reproductive system not examined.

Development and Ecology: 3–58 stalked egg capsules attached to shell wall in single row corresponding to position of mantle slit in females; double-walled capsule semitransparent, elongate ovoid, diameter increasing with development of embryos, size of capsule and number of eggs/embryos per capsule varying between species. Probably protandric. Larval biology varying between species. Adults solitary or living in close proximity to each other.

Comparative Remarks

Like *Cupolaconcha* n. gen., *Novastoa*, and several other vermetid genera, members of *Ceraesignum* have stalked egg capsules attached to the shell wall through the divided female mantle. The animal of *Ceraesignum* is distinct in its saucer-shaped operculum (without a spiral lamina on the external surface or mammilla on the internal surface, but with distinctive "thumbprint" surface texture) and simple, tapering pallial oviduct without obvious seminal receptacle or diverticulum.

Taxonomic Remarks

The type species, *Serpula maxima*, was historically grouped with other large-shelled species (that today are mostly placed in *Thylacodes*), but never before separated into its own genus.

Diversity and Distribution (Fig. 251)

Ceraesignum n. gen. currently contains two species, one of which has been previously described. This low diversity may be genuine, or reflect the lack of knowledge of vermetid diversity in general. There is a noticeable contrast between the distributions of each constituent species, with *C. maximum* widely distributed across the Indo-Pacific and ***C. robinsoncrusoei*** n. sp. restricted to a single remote, offshore island on the eastern rim of the Pacific Ocean. These contrasting demographics presumably reflect different life-history strategies and habitat tolerances/availability.

Ceraesignum maximum
(G. B. Sowerby I, 1825)
n. comb.

Serpula maxima G.B. Sowerby I, 1825: Appendix p. i; Bieler & Petit, 2011: 46.

Vermetus giganteus Quoy & Gaimard, 1834: 294–296, pl. 67 ["65"], figs. 13–15 [Guam]; Bieler & Petit, 2011: 38.

Siphonium maximum – Mörch, 1859: 354; 1861: 166–169; Clessin, 1902: 55–57.

Siphonium giganteum "Quoy and Gaimond" [sic] – Clessin, 1902: 58 [with figs. after Quoy & Gaimard].

Vermetus novaehollandiae – Yonge, 1932: 259–281, figs. 1–6 (*non* Rousseau in Chenu, 1843).

Dendropoma (*Dendropoma*) *maximum* – Keen, 1961: 199; Morton, 1965: 588 ff., fig. 2 [gross anatomy, operculum; Queensland, Australia].

Dendropoma maxima – Kappner, 1998 [ecology, behavior; Gulf of Aqaba]; Kappner et al., 2000: 309 ff. [feeding; Gulf of Aqaba]; Scaps & Denis, 2008: 1 ff., pl. 1 [indicator of coral reef status; Indonesia].

Dendropoma maximum – Hughes & Lewis, 1974: 531 ff. [ecology, reproduction; Red Sea]; Okutani, 2000: 207, pl. 103, figs. [Japan]; Rawlings et al., 2001: 1605 [sequence and gene arrangement data; Gulf of Aqaba]; Phillips & Shima, 2010: 133 ff., figs. 1–4 [reproduction, larvae; French Polynesia]; Phillips, 2011: 2335 ff. [larval development; French Polynesia].

Type Locality

No locality given in original description. Keen (1961: 199) stated "East Indies".

Material Examined

Original material studied by Mörch (1861: 166–169), including his infrasubspecific forms "biangularis" and "praelonga" (NHMUK).

Australia: AM C.326965: with coral in beachrock gutter, SE side of North East Herald Cay, Coral Sea, 16.933°S; 149.183°E, coll. I. Loch, June 17, 1997, 10% SW formalin (1 female).

Republic of Kiribati: UF 410777: 10 m, outer reef slope, S of point S of main reef passage, W side of Kiritimati Atoll, Line Islands, 1.8745°N, 157.5642°E, coll. G. Paulay, August 5, 2005, 95% EtOH (1 specimen).

Guam, U.S.A.: UF 340207, Luminao Reef, Guam Island, Mariana Islands, 13.46°N, 144.65°E, coll. W. Kelly, May 16, 2003, 95% EtOH (1 male).

Cook Islands: UF291949: 0–2 m, Motutapu, Rarotonga Island, 21.24°S, 159.72°W, coll. C.P. Meyer, October 29, 2001, 95% EtOH (1 specimen), [DNA sequence data].

French Polynesia: UF 401093: 0–2 m, in living *Montipora*, outer part of barrier reef between Cooks and Opunohu Bays, Moorea Island, Society Islands, 17.4772°S, 149.8306°W, coll. G. Paulay, July 2006, 75% EtOH (1 juvenile specimen); FMNH 327136: larvae cultured from females removed from coral, lagoon on the northeast shore of Moorea, 149.83°W, 17.5°S, coll. N. Phillips, April–September 2008, 70% EtOH (many larval shells).

Japan: FMNH 328176: Ryukyu Islands, North Pacific Ocean, approx. 26°N, 127°E, coll. R. J. Rogers, 1953–1956, dry (shell fragment).

New Zealand: FMNH 328251: Aitutaki Island, Cook Islands, South Pacific Ocean, approx. 19°S, 160°W, Chancellor-Stuart Field Museum Expedition, 1930, dry (shell fragment).

Jordan: FMNH 318221: Marine Science Station, Gulf of Aqaba, Jordan, 29.4521°N, 24.9704°E, coll. I. Kappner, 1999, 95% EtOH (tissue only), [DNA sequence data].

Description

Teleoconch (Figs. 252–254): Apertural diameter to 3.6 cm (Yonge, 1932); shell length to 45 cm (Keen, 1961). Shell coiling for first few whorls, subsequent whorls irregular tending to straight, often orientated perpendicular to exposed surface of coral (Yonge, 1932). Exterior of shell rarely visible due to encrusting coral, but when exposed: exterior surface matt, white on columellar surface, pale fawn dorsally; sculpture varying from weak transverse striae to low, forward-sloping lamellae with thickened apical ridges. Interior surface white to cream, sometimes with diffuse, pale pink ring inside aperture.

Protoconch (Figs. 255, 256): Hatchling protoconch diameter to 370 μm, height to 420 μm. "Hook" projection weak. Globular, with small increase in whorl size; deep suture; 1.5–1.75 whorls; sculpture on first 0.75 whorl of pocked craters, last 0.75–1.0 whorl with widely–spaced, tall axial ribs crossed by > 20 spiral threads; 3 strong spiral keels present. Colorless.

Operculum (Figs. 257–260): Diameter to 40 mm (Yonge, 1932) (19 mm among examined specimens). Shaped like a deep, concave saucer. "Fingerprint" texture on muscle attachment area composed of tall, closely-spaced, concentric ridges.

Radula (Fig. 261): Colorless to brown. Length of ribbon to 6.5 mm, width to 950 μm, up to 60 rows. Lateral tooth: one cusp on inner side, five cusps on outer side. Inner marginal tooth: two cusps on inner side, three cusps on outer side.

External Morphology and Color (Fig. 262): Body length to 10 mm (in examined specimens). Head flat, small compared to foot muscle; food groove not visible. Color in life (based on Morton, 1965) and specimens preserved in 95% EtOH: head/foot, lips, tentacles cream to pale brown, sole and lateral surfaces of foot, opercular lobe and dorsal surface of head (excluding tentacles) ink black; anterior mantle edge trimmed with cream then black pigment bands; digestive gland dark brown.

Pallial and Reproductive Anatomy (Figs. 263–265): Gill 0.3x mantle width; gill leaflets triangular, tall, height 5x breadth; seven leaflets per mm. Osphradium 9 mm long; margins irregular.

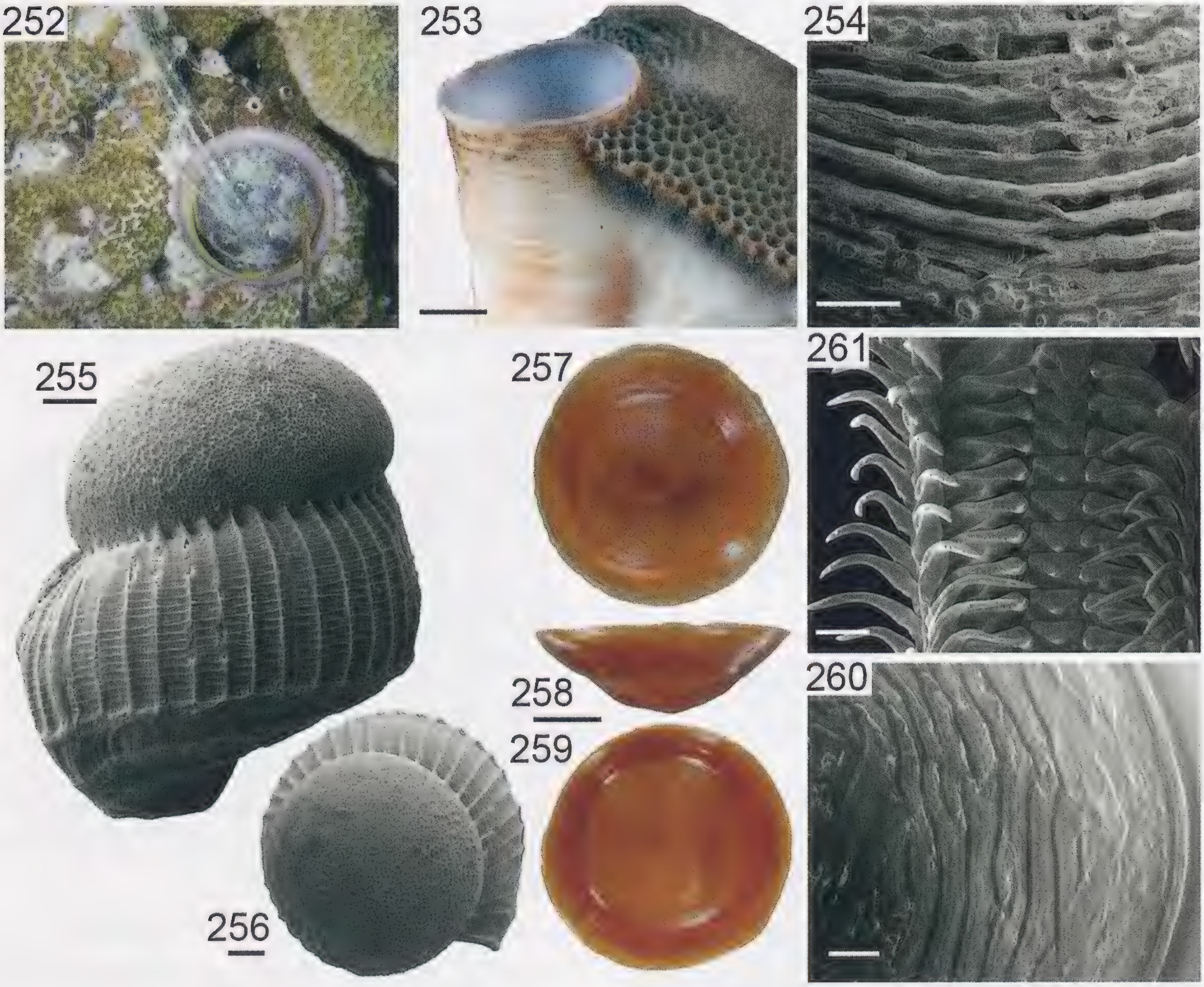

FIGS. 252–261. *Ceraesignum maximum* (G. B. Sowerby I, 1825). FIG. 252: Aperture and mucous feeding net of animal living embedded in a coral head, Fiji. Photographed by W. F. Ponder; FIG. 253: Aperture of shell with surrounding coral partly removed. UF 410777, Kiritimati Atoll, Kiribati. Scale bar = 5 mm; FIG. 254: SEM image of teleoconch sculpture. UF 410777, Kiritimati Atoll, Kiribati; FIGS. 255, 256: Intracapsular larval shells. FMNH 327136, Moorea, French Polynesia. Scale bars = 50 μm. FIG. 255: Abapertural view; FIG. 256: Apical view; FIGS. 257–259: Operculum. AM C.325965, Herald Cays, Coral Sea. Scale bar = 5 mm. FIG. 257: Exterior surface; FIG. 258: Lateral view; FIG. 259: Interior surface; FIG. 260: SEM image of sculpture on muscle attachment area on interior surface of operculum. AM C.325965, Herald Cays, Coral Sea. Scale bar = 500 μm; FIG. 261: Central section of radula. AM C.325965, Herald Cays, Coral Sea. Scale bar = 200 μm.

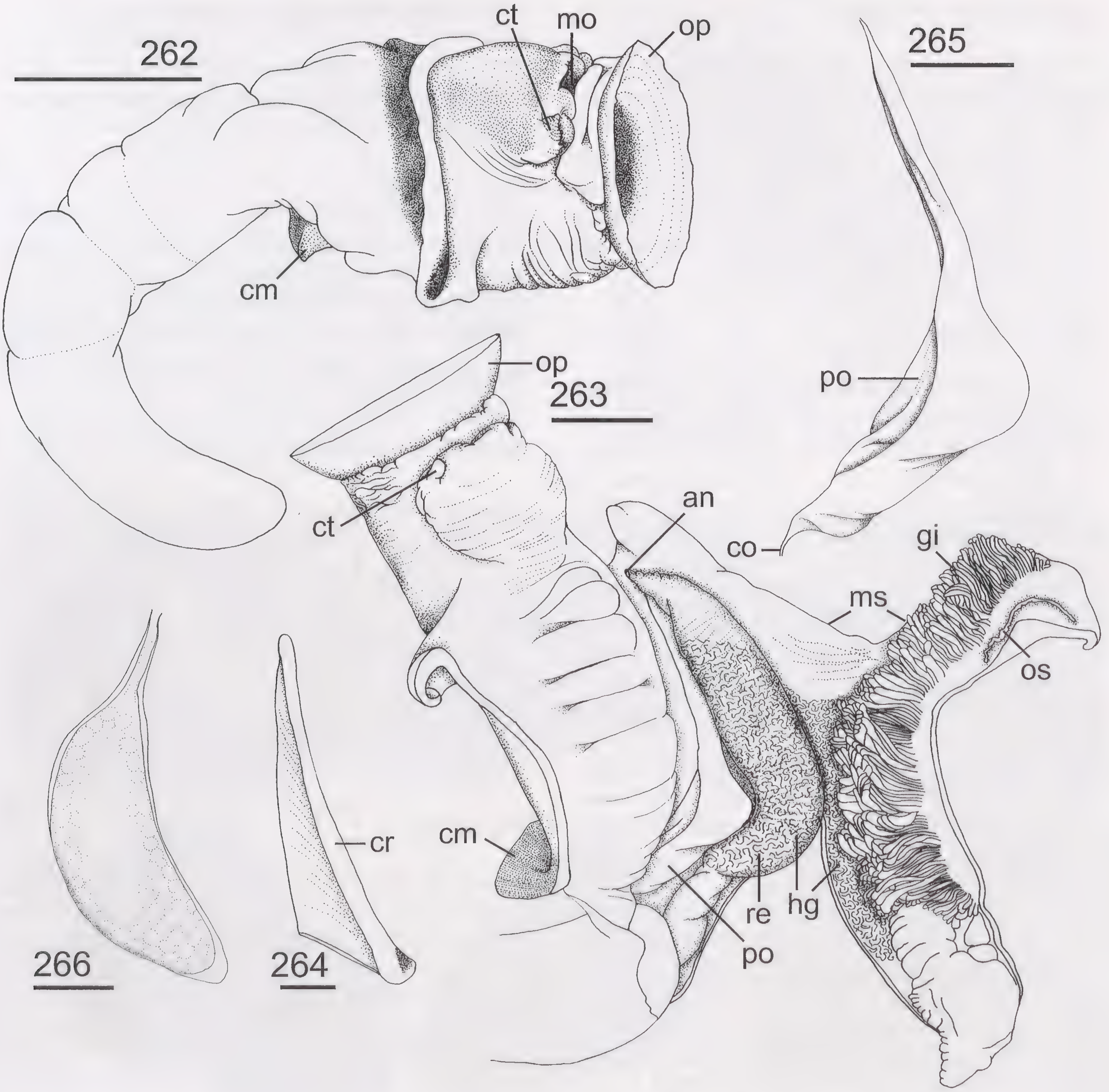

FIGS. 262–266. Anatomy of *Ceraesignum maximum* (G. B. Sowerby I, 1825). FIG. 262: Body of a small specimen, possibly male. UF 340207, Guam. Scale bar = 5 mm; FIG. 263: Anterior body and mantle cavity of female. AM C.325965, Herald Cay, Coral Sea. Scale bar = 20 mm; FIG. 264: Gill leaflet. UF340207, Guam. Scale bar = 500 µm; FIG. 265: Pallial oviduct. AM C.325965, Herald Cay, Coral Sea. Scale bar = 5 mm; FIG. 266: Stalked egg capsule containing embryos at an early stage of development. Redrawn from Hughes & Lewis (1974), Plate 1c. Scale bar = 1 mm.

Fecal pellets cigar-shaped. Hypobranchial gland pale yellow, not covering pallial oviduct.

Development and Ecology (Fig. 266): Based on descriptions of reproduction in population from the Gulf of Aqaba, Red Sea (Hughes & Lewis, 1974) and Moorea, South Pacific (Phillips & Shima, 2010; Phillips, 2011): 1–58 stalked egg capsules at different stages of development per female; each capsule containing 73–571 eggs; to 4 mm long. Hatchlings actively swim, feed on planktonic algae (planktotrophic), surviving for several weeks before metamorphosing in response to settlement cues from coralline algae. The sex ratio is biased towards females with increasing body size, suggesting protandric hermaphroditism. Adults live in areas with high wave activity (Yonge, 1932; Hughes & Lewis, 1974); solitary but often found in great abundances of 22 m^{-2} in the Red Sea and up to 520 m^{-2} in Guam (Smalley, 1984).

Comparative Remarks

Distinguished from ***C. robinsoncrusoei*** n. sp. by its much larger size, deeply concave operculum, complex protoconch sculpture and planktotrophic larval biology. Several other vermetids belonging to *Thylacodes* (formerly *Serpulorbis*) grow to a similar size to *C. maximum*, but lack an operculum and could not be confused if the animal is observed.

Taxonomic Remarks

The anatomy of the specimens examined during the present study generally agrees with earlier accounts that focused on the feeding strategies (and associated structures) of "*Dendropoma maximum*" (Yonge, 1932; Morton, 1965). One point of difference is that the mantle of female specimens examined herein was divided to accommodate the attachment of stalked egg capsules to the shell wall (see also Phillips & Shima, 2010), whereas Yonge (1932) did not record this character (although the condition of the mantle margin was not specified), and Morton (1965) stated that the female mantle was entire. It is unclear whether this inconsistency represents genuine variation within the species, or is due to incomplete knowledge of the morphological and systematic diversity within *Dendropoma s.l.*

Specimens collected from the southern and central Pacific Ocean were used to describe the anatomy and larval biology of *C. maximum*. By contrast, our molecular data come from the extreme western end of the range (Jordan). The capacity for planktotrophic larval dispersal in *C. maximum* supports the hypothesis that it is a single taxon by facilitating medium- to long-range genetic mixing. On the other hand, descriptions of living animals range from feeding exclusively by ciliary currents (e.g., Yonge, 1932; as *Vermetus novaehollandiae*) to feeding by conspicuous mucous net (e.g., Kappner et al., 2000). It will be necessary to examine further wet-preserved material from across the entire range to confirm that this species is cohesive across its range.

Distribution (Fig. 251)

Tropical Indo-Pacific, from the east Pacific Ocean to the Red Sea. Recorded in the literature from various locations including: the Gulf of Aqaba (Kappner, 1998), Indonesia (Scaps & Denis, 2008), the Great Barrier Reef (Yonge, 1932), Pitcairn Islands (Irving, 1995) and the Cocos-Keeling Islands (Maes, 1967).

Ceraesignum robinsoncrusoei n. sp.

Dendropoma "Chile" – Rawlings et al., 2001: 1605 [sequence and gene arrangement data].

Type Locality

Rocky reef at NE point of Cumberland Bay, near Punta Pangal; Robinson Crusoe Island (Isla Róbinson Crusoe), Juan Fernández Archipelago, Chile: ca. 33.641°S, 78.823°W [Islas Océanicas de Chile 1997 Expedition sta. IOC 97-57; B/I *Carlos Porter*].

Material Examined

Juan Fernández Archipelago, Chile: All from station IOC-57 (single collecting event, coll. R. Bieler by SCUBA, March 7, 1997, 3–5 m): Holotype: MNHNC 5988 ex FMNH 329353, 329354, 70% EtOH (one cluster with several attached paratypes , MNHNC 5989; Figs. 282, 283). Paratypes: FMNH 326906, 70% EtOH (many specimens), Bouin's fluid (13 specimens), 100% EtOH (8 specimens), dry (shell fragments) [DNA sequence data].

Etymology

Named after Robinson Crusoe; this fictional character from Daniel Defoe's 1719 novel is the namesake of the type locality (Isla Róbinson Crusoe). Defoe's story was inspired by the travails of Scottish sailor Alexander Selkirk who was rescued from this island in 1708. Noun in genitive case.

Description

Teleoconch (Figs. 267–269): Apertural diameter to 4.5 mm; shell length to 15 mm; diameter of last whorl to 10 mm. Up to six partially or entirely overlapping whorls coiled initially in concentric spiral, straightening towards aperture. Exterior surface matte, white with brown patches showing through from interior surface; sculpture of irregular transverse lamellae. Interior surface white to pale fawn with brown patches.

Protoconch (Figs. 270–272): Settled protoconchs diameter to 700 µm, height to 710 µm. "Hook" projection strong. Globular, with large increase in whorl size; moderately deep suture; 1.25 whorls; sculpture absent. Colorless or pale brown.

Operculum (Figs. 273, 274): Diameter to 2.3 mm, filling about 80–90% of apertural tube diameter. Shaped like shallow, concave saucer. "Fingerprint" texture on muscle attachment area composed of low, widely-spaced, concentric ridges.

Radula (Fig. 275): Colorless. Length of ribbon 1.3–2.1 mm, width 220–250 µm, 32–49 rows. Lateral tooth: two cusps on inner side, 2–3 cusps on outer side. Inner marginal tooth: 1 cusp on inner side, 2–3 cusps on outer side.

External Morphology and Color (Figs. 276, 277): Body length to 28 mm. Head rounded, large compared to foot muscle; shallow, narrow food groove present. Body color of living animal velvety black; with orange band under the transparent rim of the mantle margin; pedal tentacles black, tips of cephalic tentacles lacking pigment; pedal disk around operculum with iridescent green sheen; outer part of operculum appearing lighter-colored from white pigment underneath; forehead between cephalic tentacles with white pigment band. Color of specimens preserved in 70% EtOH: head/foot pale grey; sole of foot, lips, dorsal surface of head and neck dark grey; black speckles radiating from mouth; parallel stripes of black pigment on lateral (including surface of tentacles) and lower surfaces of snout; edge of mantle pale grey fading to

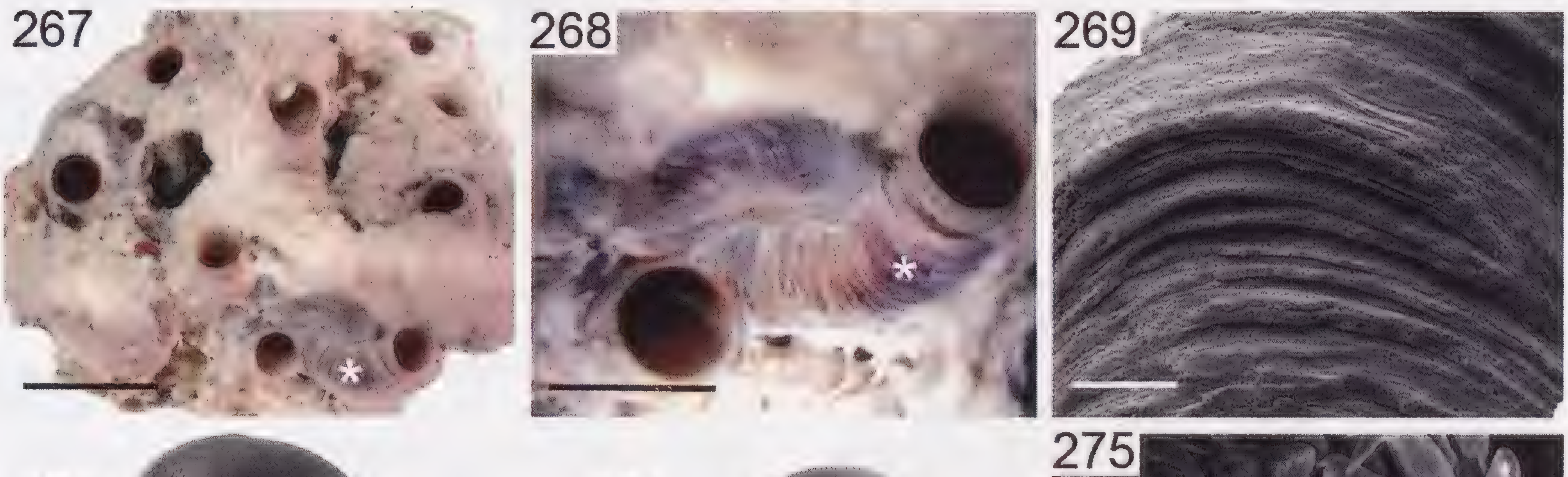

FIGS. 267–275. ***Ceraesignum robinsoncrusoei*** n. sp., Robinson Crusoe Island, Chile. FIG. 267: Cluster of specimens encrusted with coralline algae. Holotype (asterisk) and paratypes, MNHNC 5988, 5989. Scale bar = 20 mm; FIG. 268: Holotype specimen (asterisk). Holotype on right. Scale bar = 10 mm; FIGS. 269–275: Paratypes, FMNH 326906. FIG. 269: SEM image of teleoconch sculpture. Scale bar = 200 µm; FIGS. 270–272: Intracapsular larval shells. Scale bars = 100 µm. FIG. 270: Apertural view; FIG. 271: Abapertural view; FIG. 272: Apical view; FIGS. 273, 274: Operculum. Scale bar = 300 µm. FIG. 273: Interior surface; FIG. 274: Detail of muscle attachment area on interior surface; FIG. 275: Central section of radula. Scale bar = 50 µm.

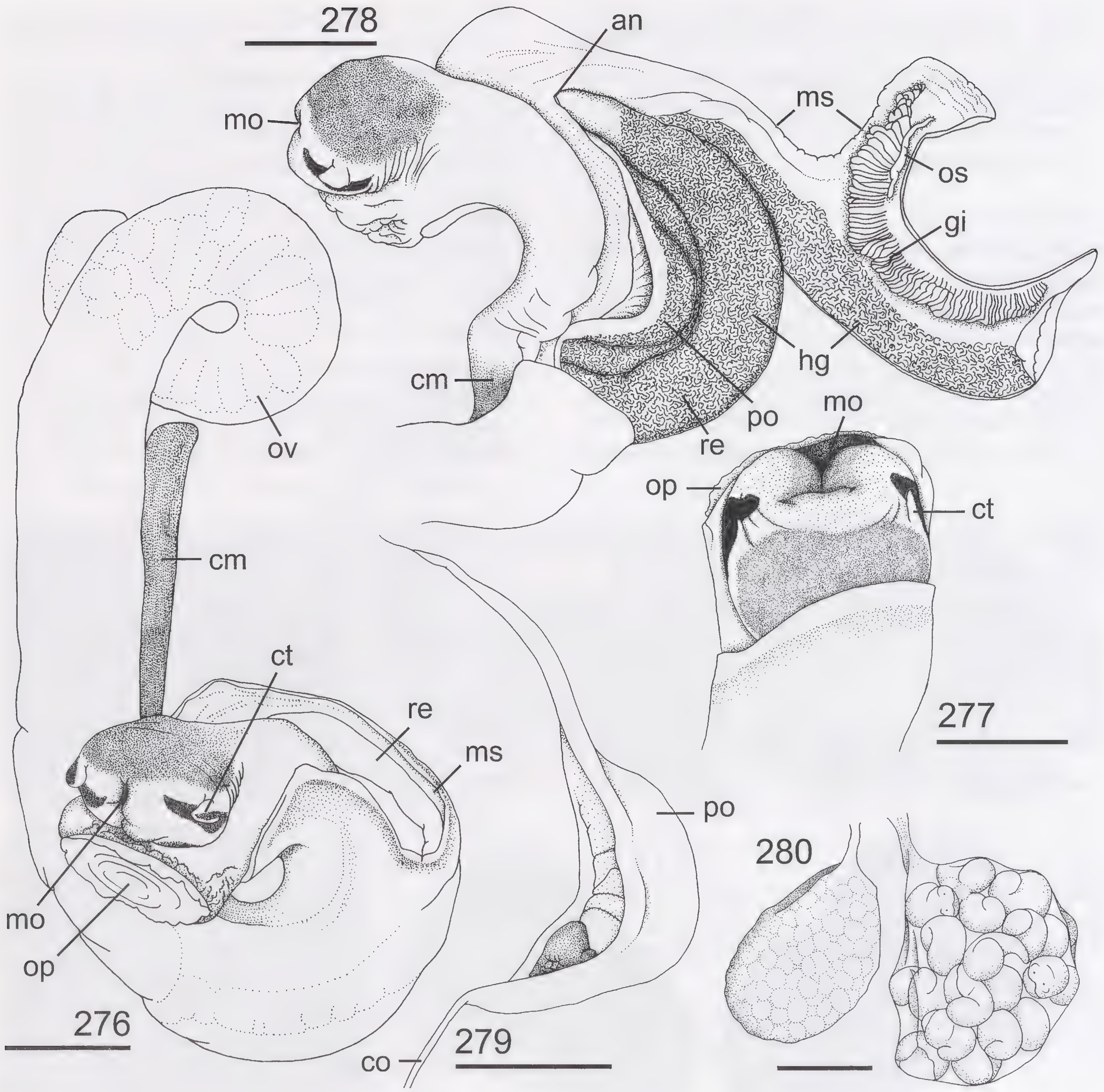

FIGS. 276–280. Anatomy of ***Ceraesignum robinsoncrusoei*** n. sp. Paratypes, FMNH 326906, Robinson Crusoe Island, Chile. FIG. 276: Body of a female brooding egg capsules. Scale bar = 2 mm; FIG. 277: Head and mantle margin of an immature specimen. Scale bar = 1 mm; FIG. 278: Mantle cavity of a brooding female. Scale bar = 2 mm; FIG. 279: Pallial oviduct. Scale bar = 1 mm; FIG. 280: Stalked egg capsules containing embryos at early and late stages of development. Scale bar = 1 mm.

white; digestive gland pale brown with dark brown speckles.

Pallial and Reproductive Anatomy (Figs. 278, 279): Gill 0.2x mantle width; gill leaflets triangular, short, breadth equal to height; 16 leaflets per mm. Osphradium 1.5 mm long; margins smooth. Fecal pellets ovoid. Hypobranchial gland pale brown, covering most of pallial oviduct. Brooding females with mantle slit.

Development and Ecology (Fig. 280): three stalked egg capsules per female; 20–35 embryos per capsule; up to 600 µm diameter; developmental stages in single female spanning from cleaving eggs to pediveligers. Details of larval biology not known, but intracapsular larval shells same size as settled protoconchs removed from substratum around adults, suggesting direct development. Adults living in close proximity to each other, forming crusts on volcanic rock ledges and living bivalve

(*Chama*) specimens. Probably protandric hermaphrodite judged by prevalence of females among large specimens.

Comparative Remarks

Molecular and morphological evidence supports a close relationship with only one other species (*C. maximum*). ***Ceraesignum robinsoncrusoei*** n. sp. can be separated from *C. maximum* by its much smaller size, concentric spiral rather than irregular shell growth, unsculptured protoconch, flatter operculum, and different reproductive strategies. Another species of operculate vermetid, *Dendropoma mejillonense*, was recently described from northern mainland Chile (Pacheco & Laudien, 2008). These two Chilean species are easily distinguished by their opercula, shells and reproductive biology, for example *D. mejillonense* broods its unstalked egg capsules in the mantle cavity and produces distinctively sculptured protoconchs.

Distribution (Fig. 251)

Known only from the type locality at Robinson Crusoe Island in the Juan Fernández Island chain, Chile. The type locality is 160 km from suitable habitat at Alexander Selkirk Island, and 770 km south of the Desventuradas Islands. Despite intensive scuba sampling during the IOC-97 Expedition (resulting in collections of other vermetid species), ***C. robinsoncrusoei*** n. sp. was not found on Alexander Selkirk Island or the Desventuradas islands and is not recorded from mainland Chile. This species might be endemic to Robinson Crusoe Island.

Cupolaconcha n. gen.

Dendropoma sensu Hadfield et al., 1972: 81–98 (in part); Safriel & Hadfield, 1988: 1–13; Gardner, 1989: 250–254. *Non Dendropoma* Mörch, 1861.

Type Species

Dendropoma meroclistum Hadfield & Kay in Hadfield et al., 1972 [as *D. meroclista*].

Etymology

From the distinctive domed aperture of the shell that characterizes the genus. Composed of the architectural term "cupola", describing a domed roof, and the Latin *concha* for molluscan shell. Noun of feminine gender.

Diagnostic Description

Teleoconch: Small (maximum dimension 6.5–14.5 mm), "tube" narrow (apertural diameter excluding dome 1.2–2.5 mm). Tightly-coiled, irregular "*Turritella*-squeezed-sideways" growth form with 5–8 partially or entirely overlapping whorls cemented to, or entrenched in, surface of substratum (shell, rock or coral); aperture often raised above substratum to form a feeding tube; encrusted with calcareous algae except for area around aperture; scars from earlier feeding tubes present. Shell thin; aperture covered by delicate, convex dome with elliptical to lens-shaped slit at apex. Color and sculpture of exterior surface variable. Interior surface color variable; smooth except for crowded, posteriorly-directed denticles covering columellar surface; concave septa present occasionally in early whorls.

Protoconch: Settled protoconch diameter 310–530 µm, height 320–420 µm. Strong "hook" projection present on apertural lip. Biphasic growth evident in some taxa; protoconch shape variable; 1.3–2.5 whorls; sculpture absent or present as spiral pustules or threads; spiral keel(s) at base of whorl absent or present. Colorless or brown, transparent.

Operculum: Slightly oval (subcircular) in axial profile; diameter proportional to shell size, 600–1,100 µm. Composed of two layers; interior layer (attached to surface of foot) delicate, transparent, brown, chitinous disc overlaid by exterior layer of white calcareous substance forming dome-shaped deposit with irregular structure and texture. Margins of chitinous layer protruding from beneath calcareous deposit, rolled towards foot. Interior surface smooth except for slightly convex muscle attachment area on (embedded in foot muscle) with lightly pitted texture.

Radula: Taenioglossate, transparent, colorless. Length of ribbon 350–1,000 µm, width 70–145 µm; 22–42 rows (proportional to shell size). Trapezoidal rachidian tooth with prominent central cusp flanked on each side by 3–4 smaller cusps decreasing in size outwardly. Base of lateral tooth notched to interlock with rachidian and inner marginal teeth; elongate main cusp flanked by variable number of cusps on inner and outer sides. Inner marginal tooth slender with variable number of cusps on inner and outer sides. Outer marginal tooth smooth on outer side, variable number of splayed, digitiform cusps present on inner side; base with prominent semicircular or triangular projection.

External Morphology and Color: Body of animal slender (length 18–24 mm in examined wet material), occupying 4–5 whorls of shell; three earliest whorls composed of gonad and digestive gland. Columellar muscle continuing for ~2 whorls. Pedal tentacles short (in preserved specimens). Head slightly bulbous; cephalic tentacles short (in preserved specimens), broad, with slightly protruding ommatophore bearing eye at outer base; right side of head with broad food groove. Adult female mantle divided by pallial slit varying from shallow notch to deep incision running for half mantle length (brooding females), slightly left of midline. External body coloration variable.

Pallial and Reproductive Anatomy: Gill quarter mantle width, full length of mantle cavity; gill leaflets triangular, breadth greater than height; ~20–30 leaflets per mm. Osphradium short and narrow, 600–800 μm long, margins irregular; anterior tip curled towards columellar muscle. Rectum running from coelom to anterior right edge of mantle opening, without deviations or kinks; fecal pellets spherical to elongate. Hypobranchial gland transparent brown, covering mantle surface between gill and rectum, sometimes also partially covering rectum, greatly developed in brooding females. Pallial oviduct triangular, dimensions variable; proximal, large, glandular diverticulum present, fused to mantle roof. Single spherical seminal receptacle bulb (containing sperm) with short duct present, embedded in ventral glandular lining of pallial oviduct, pointing away from open groove. Male reproductive system unknown.

Development and Ecology: Up to six stalked egg capsules attached to shell wall in single row corresponding to position of mantle slit in females; double-walled capsules semi-transparent, spherical to ovoid, diameter increasing with development of embryos, ~600–1,300 μm; color and number of eggs/embryos per capsule varying between species. Larval biology varying between species. Adults either solitary or gregarious.

Comparative Remarks

Two previously-described species in this group were placed in *Dendropoma*, but are readily distinguished by several major morphological characters. The most conspicuous synapomorphy of *Cupolaconcha* n. gen. is the presence of a calcareous layer on the outer surface of the flat, chitinous operculum. This structure is not found in any other vermetid. Observations of the living animal by M. G. Hadfield (personal communication, 2011) indicate that the calcareous deposit is gradually formed in thin layers by repeatedly "swiping" the foot and operculum inside the mantle margin. This incremental process may explain the irregular and variable structure of the calcareous layer, which when fully developed fits neatly into the shell dome. The shell of *Cupolaconcha* is more elongate and the center of each successive whorl is displaced further sideways than the typical shorter and more-or-less concentric spiral shells typical of *Dendropoma*. The aperture is strikingly different from the typical vermetid (and gastropod) form due to the presence of a dome of shell restricting the aperture to an oval or lens-shaped hole at its apex. The anatomy of *Cupolaconcha* differs from the traditional concept of *Dendropoma* by the presence of a mantle slit in females (associated with the attachment of egg capsules to the interior wall of the shell), a character found in other vermetid genera such as *Thylacodes* (formerly *Serpulorbis*), *Vermetus*, and most species of *Petaloconchus.* However, this study has revealed that *Dendropoma s.l.* comprises several morphologically and genetically distinct groups, some of which share this feature.

Taxonomic Remarks

The description of the proposed type species, *C. meroclista* (Hadfield et al., 1972), acknowledged some discrepancies between "*Dendropoma" meroclista* and other *Dendropoma* species, but did not advocate generic separation. Gardner (1989), in describing a related species from the Pacific coast of Mexico (*C. krypta*), suggested that in future both species should be moved to a distinct subgenus within *Dendropoma* or to a new genus, pending a revision of *Dendropoma*. Molecular data presented here (see Phylogeny section) strongly support the reciprocal monophyly of *Cupolaconcha* n. gen. (including the type species *C. meroclista*) and the group comprising of the remainder of *Dendropoma s.l. Cupolaconcha* n. gen. occupies a different section of the vermetid tree than *Dendropoma*, and is more closely related to *Petaloconchus.*

With the benefit of a molecular phylogeny, comprehensive anatomical information, and the discovery of additional diversity, *Cupolaconcha*

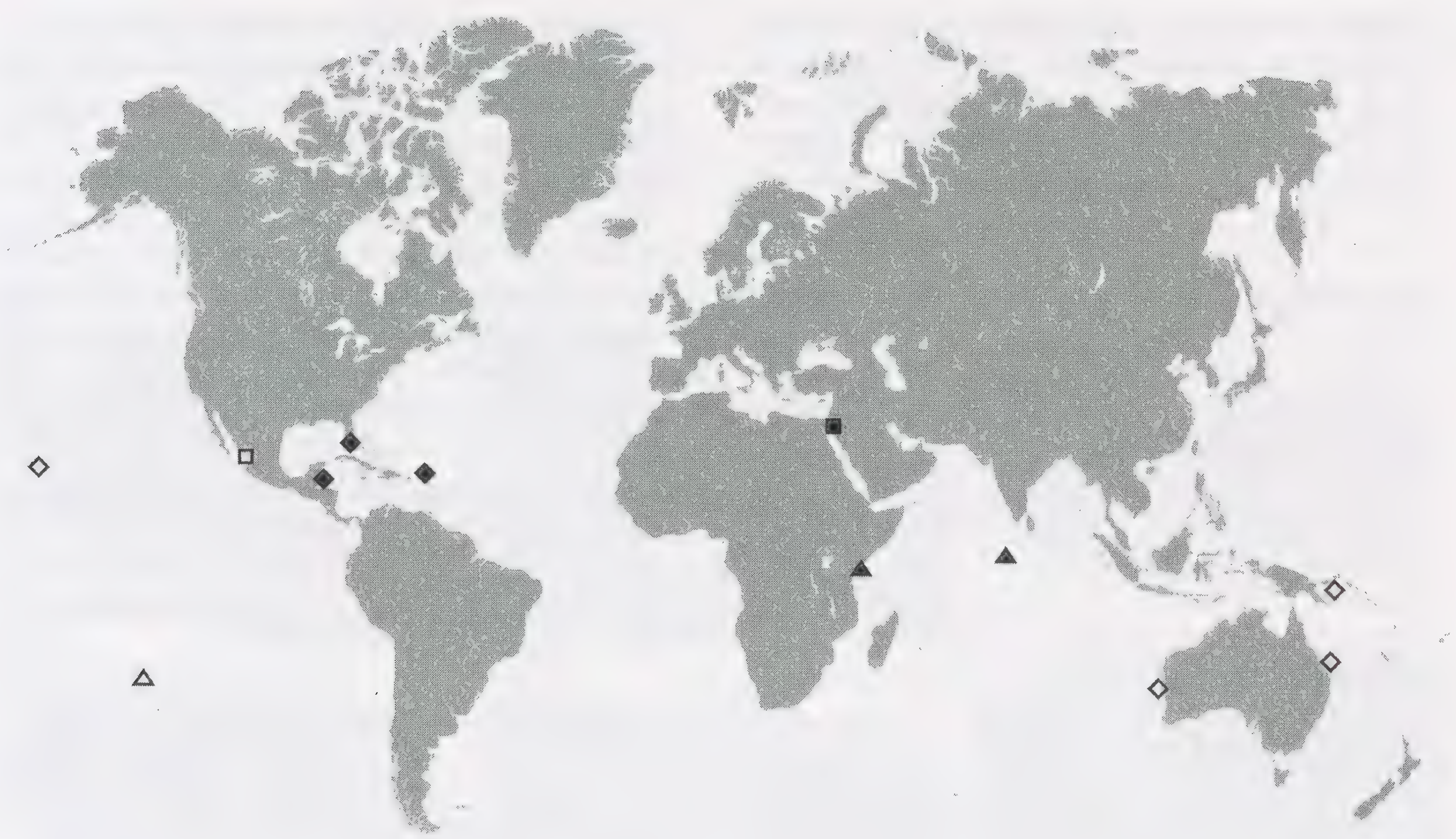

FIG. 281. Distribution map of *Cupolaconcha* n. gen. based on material examined in this study. Filled diamond = ***C. guana*** n. sp.; hollow diamond = *C. meroclista*; filled square = ***C. sinaiensis*** n. sp.; hollow square = *C. krypta*; filled triangle = ***C. maldivensis*** n. sp.; hollow triangle = *Cupolaconcha* sp. (undescribed species included in molecular phylogeny).

n. gen. can be recognized as a distinct genus not closely related to *Dendropoma s.s.*

Diversity and Distribution (Fig. 281)

Two previously-named species are included in *Cupolaconcha* n. gen. Below, we present three new congeneric taxa. The distribution of this group is now known to extend across the tropical Pacific and Indian Oceans and also includes the Red Sea, west coast of Mexico and Caribbean. *Cupolaconcha* n. gen. is not known from the non-Caribbean Atlantic Ocean or from any temperate areas. The animals are found cemented to rock, shell, and coral substratum (Hadfield et al., 1972) in the intertidal to subtidal zone and are known in some areas to form biogenic reefs (Safriel & Hadfield, 1988).

This study is based on a limited number of samples from few locations. The high diversity observed may perhaps be attributed to the combined effects of geographic isolation and (probably) direct development in most species. In the molecular phylogeny, a single specimen of an unknown *Cupolaconcha* species collected at Rapa Iti Island in French Polynesia was found to be sister to, but distinct from, the sequences obtained from a single Hawaiian specimen of *C. meroclista*. This indicates that there is at least one additional undescribed taxon in this species complex. We predict that many more species of *Cupolaconcha* n. gen. will be found in areas where the worm-snail fauna has not been adequately studied.

Cupolaconcha meroclista
(Hadfield & Kay, 1972)
n. comb.

Dendropoma meroclista [*sic*] Hadfield & Kay in Hadfield et al., 1972: 83–84, figs. 3, 4, 19F; Kay, 1979: 104, fig. 39A; Safriel & Hadfield, 1988 (in part): 1–13, figs. 2A, 3, 4A; Bieler & Petit, 2011: 46.

Type Locality

Coralline algal-encrusted reef, Mokuoloe Island (Coconut Island), Kaneohe Bay, Oahu, Hawaii, U.S.A.: 157.7861°W, 21.4361°N.

Material Examined

Holotype: BPBM 8931.

Hawaiian Islands, U.S.A.: FMNH 329347: Honolulu; coll. R. Bieler, 70% EtOH (1 specimen attached to shell of *Eualetes tulipa*); FMNH 329348: shallow water, old reef flat, Kaneohe Bay, Oahu, approx. 21.43°N, 157.79°W, coll. R. Bieler, December 1986, 70% EtOH (many); FMNH 329349: 0.1 m at low tide, beach rock on reef flats, Diamond Head Beach, Oahu, approx. 21.43°N, 157.79°W, coll. R. Bieler, March 28, 1988, 70% EtOH (many); FMNH 328505: Kaneohe Bay, Oahu, 21.436°N, 157.791°W, coll. M. Hadfield, 1998, 95% EtOH (many, bodies only) [DNA sequence data].

Guam: UF341500: Pago Bay, Mariana Islands, 13.42°N, 144.78°E, coll. W. Kelly, June 29, 2003, 95% EtOH (whole body and shell), [DNA sequence data].

Australia: AM C.407574: 0.3 m, near shore in lagoon off E end of Heron Island, Capricorn Group, Great Barrier Reef, QLD, Australia, 23.433°S, 151.95°E, coll. W. F. Ponder, December 24, 1976, 5% SW formalin (many); FMNH 327031: 10 m, on underside of dead coral slab, with other vermetids (*Petaloconchus* and *Thylacodes* spp.), S end of Long Island, Gros Island Channel, Houtman Abrolhos, WA, coll. R. Bieler, F. Wells & C. Bryce, May 23, 1994; 70% EtOH (1 specimen).

Papua New Guinea: AM C.407569: on fringing reef and in lagoon of reef just S of Magulata Pt., NW Kiriwina Island, Trobriand Group, 8.45°S, 151°E, coll. W. F. Ponder & P. H. Colman, June 5, 1976, 5% SW formalin (one specimen attached to shell of *Strombus* sp.).

Description

Teleoconch (Figs. 282–287): Hawaiian and Heron Island populations: apertural diameter to 1.6 mm; shell length to 5.6 mm; diameter of last whorl to 3.7 mm. New Guinea specimen: apertural diameter 2.5 mm; shell length 14.5 mm; diameter of last whorl 3.7 mm. Up to 6 partially or entirely overlapping whorls cemented to, but not deeply entrenched in, substratum; aperture occasionally rising ~1 mm above substratum as short feeding tube; scars from abandoned feeding tubes rarely present. Exterior surface glossy, honey brown to dark purple, semi-transparent around aperture; sculpture of undulating, irregularly-spaced, bulging, transverse folds. Interior surface dark brown to white, sometimes stained green (Hadfield et al., 1972).

Protoconch (Figs. 288–290): Hatchlings and settled protoconch diameter 360 µm [450 µm according to Hadfield et al. (1972)], height 360 µm. No evidence of biphasic growth; globular with small increase in whorl size, shallow suture; 1.3 whorls; sculpture absent on first whorl, sculpture of either variably-developed pustulose sculpture (Hawaiian population) increasing in density towards lip, arranged into 9–15 distinct spiral bands positioned below shoulder, or lacking sculpture entirely (Heron Island, Great Barrier Reef population); single weak spiral keel in lower quarter of whorl present in most specimens from Hawaii. Colorless to very pale brown.

Operculum (Figs. 291–293): Slightly oval in axial profile; diameter to 1,000 µm. Exterior surface of calcareous deposit pitted, irregular but often with coarse, jagged concavity at apex of dome or off-center.

Radula (Fig. 294): Length of ribbon 600–950 µm, width 80–145 µm; 30–42 rows. Lateral tooth: two cusps on inner side, 2–4 cusps on outer side. Inner marginal tooth: 2 cusps on inner side, 3–5 cusps on outer side. Outer marginal tooth: two cusps on inner side; base with prominent semicircular projection.

External Morphology and Color (Figs. 295, 296): Body length to 24 mm. Head-foot, tentacles described by Hadfield et al. (1972) as "dark purple or black with a few superficial markings"; specimens preserved in 5% SW formalin and 70% EtOH entirely devoid of pigmentation except for dorsal surface of head bearing "mosaic" pattern of brown pigment superimposed with white spots; digestive gland olive green with dark brown speckles; ovary pale orange; testis not observed. Living Western Australian specimen (FMNH 327031) flesh-colored, with dark brown patches on foot; mantle margin with red surface pigment and flesh-colored edge with embedded white granular clusters; cephalic and pedal tentacles translucent flesh-colored with few white spots (thus indicating intraspecific variability in coloration or additional unrecognized species diversity).

Pallial and Reproductive Anatomy (Figs. 297, 298): Pallial oviduct narrow; 2.3 mm long, 400 µm wide. Proximal diverticulum curved towards coelomic oviduct, constricted near junction with pallial oviduct.

Development and Ecology (Fig. 299): Stalked egg capsules found in one living and two preserved female specimens: four capsules at different stages of development per female [up to six capsules may occur (Hadfield et al., 1972)]; each capsule containing 4–12 eggs/embryos; eggs/embryos dark yellow when preserved in 70% EtOH. Larval biology not observed, but reported by Hadfield et al. (1972) and Safriel & Hadfield (1988) as direct developing, with crawl-away hatchlings and possibly occasional planktonic larvae. Taylor (1975: 76) hypothesized the veligers as probably "not planktonic for more than a

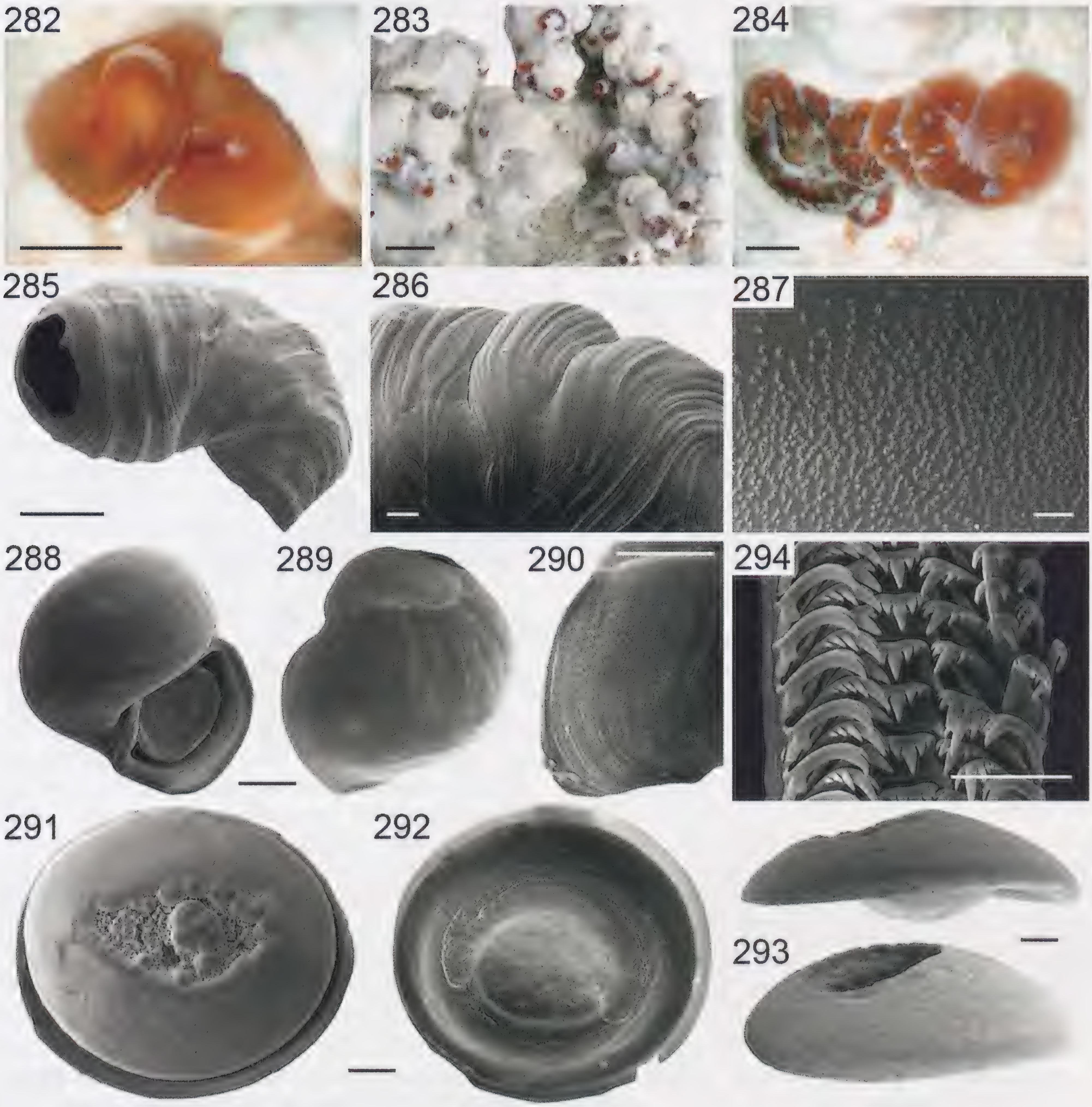

FIGS. 282–294. *Cupolaconcha meroclista* (Hadfield & Kay, 1972). FIG. 282: Specimen partly encrusted with coralline algae. Scale bar = 1 mm; FIG. 283: Coral with many specimens attached. AM C.407574, Heron Island, Australia. Scale bar = 5 mm; FIG. 284: Large specimen cemented to shell of *Strombus* sp. (coralline algae partially removed). AM C.407569, Papua New Guinea. Scale bar = 2 mm; FIG. 285: SEM image of domed aperture and (broken) elliptical slit. Scale bar = 500 µm; FIG. 286: Sculpture on teleoconch. Scale bar = 100 µm; FIG. 287: Sculpture on columellar surface of shell interior. Scale bar = 50 µm; FIGS. 288–290: SEM images of intracapsular larval shells. Scale bars = 100 µm. FIG. 288: Apertural view; FIG. 289: Abapertural view; FIG. 290: Sculpture near aperture; FIGS. 291–293: SEM images of operculum. Scale bars = 100 µm. FIG. 291: Exterior surface. AM C.407574, Heron Island, Australia; FIG. 292: Interior surface; FIG. 293: Lateral and oblique lateral views of calcareous layer (chitinous layer removed); FIG. 294: Central section of radula. Scale bar = 50 µm. FIGS. 282, 285–290, 292–294: FMNH 329349, Oahu, Hawaii.

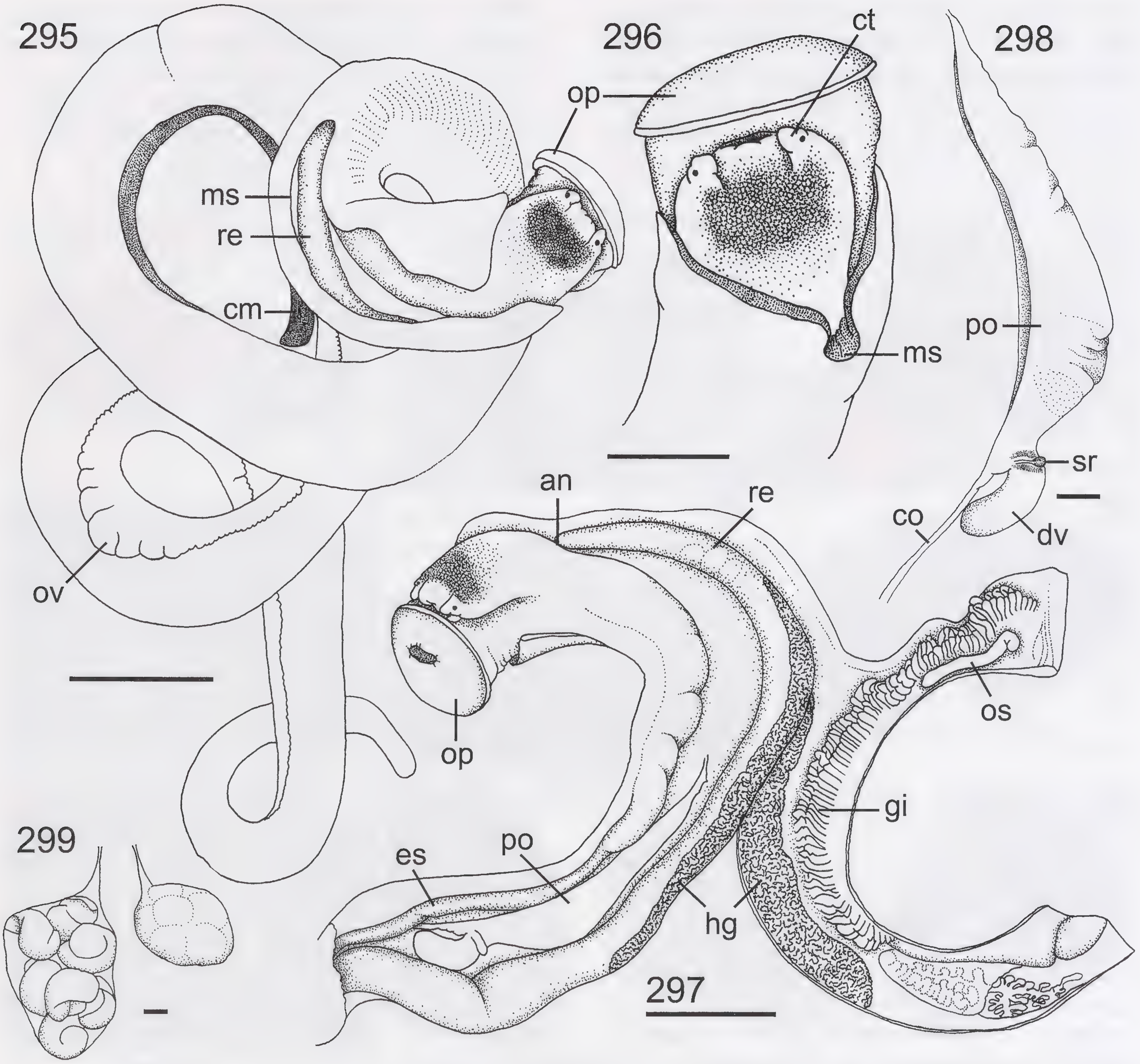

FIGS. 295–299. Anatomy of *Cupolaconcha meroclista* (Hadfield & Kay, 1972). FIG. 295: Body of a female brooding egg capsules. Scale bar = 1 mm; FIG. 296: Head-foot and notched anterior mantle margin of female without egg capsules. FMNH 329347, Hawaii. Scale bar = 500 µm; FIG. 297: Mantle cavity of a brooding female. Scale bar = 1 mm; FIG. 298: Pallial oviduct. Scale bar = 200 µm; FIG. 299: Stalked egg capsules at early and late stages of development. Scale bar = 200 µm. FIGS. 310, 312–314: FMNH 329349, Oahu, Hawaii.

few hours, or at most, a few days." Adults generally solitary, but sometimes settling within 1–2 mm of each other or with other vermetids such as *Dendropoma gregarium*; common in intertidal reef zone attached to rocks and coral (Hadfield et al., 1972).

Comparative Remarks

Shell darker and more purplish than other species of *Cupolaconcha* n. gen.; larger than other species except ***C. guana*** n. sp. Protoconch sculpture variable but pustulose when present and never condensing to form spiral threads as in *C. krypta*; single spiral keel weak. Pigment on head-foot dark purple to black with white markings in life. Egg capsules containing up to six eggs/embryos.

Taxonomic Remarks

Although the anatomy and shell morphology of specimens from the type locality has been described in detail here, there are some discrepancies with outlying populations in Australia and Papua New Guinea. In relation to the

Hawaiian specimens, the shells of specimens from Papua New Guinea are larger and those from Heron Island are smaller. In addition, protoconchs from Heron Island are uniformly without sculpture. Protoconch sculpture was variable between specimens from Hawaii, and some had greatly reduced sculpture, suggesting that this character varies between individuals. These differences were less than those observed between the other species in *Cupolaconcha*, so we have tentatively assigned the non-Hawaiian material to *C. meroclista.*

Faucci (2007) identified four major clades of *Cupolaconcha meroclista* in her phylogeographic analysis of 72 specimens from the Hawaiian archipelago and surrounding Pacific islands. Nucleotide sequence of *COI* from our samples from Kaneohe Bay, Oahu, was identical to her "Haplotype 14" nested in the major clade of specimens sampled from across the Pacific, and including the type locality of this taxon. The existence of three other strongly supported and genetically divergent clades of vermetids with the same general appearance as *C. meroclista*, one including specimens from the Hawaiian Islands, suggests that cryptic species are currently residing under this taxon name (Faucci, 2007).

The species epithet was explained by Hadfield & Kay (1972: 84) as "derived from the Greek, meaning partly closed." The Greek kleistos ("closed") was Latinized to clistus-a-um, a Latin adjective, and combined with the Greek adverbial meros ("partially"). As an adjective, it takes the gender of the genus, and when combined with (neuter) *Dendropoma*, it should have been *Dendropoma meroclistum.*

Distribution (Fig. 281)

Material from Hawaii (including the type locality), the Marshall Islands (Hadfield et al., 1972), Heron Island on the Australian Great Barrier Reef (this study) and Papua New Guinea (this study) are here referred to *C. meroclista*. The species is known from several remote island and mainland locations throughout the tropical central and western Pacific Ocean, but has not been recorded from many areas within its presumed distribution, perhaps due to its inconspicuous appearance. "*Dendropoma*" *meroclista* has been recorded by Kelly (2007; fig. 9c) from Guam and by Fukuda (1993) from the Ogasawara Islands in Japan, but the true identity of material from those locations requires confirmation in light of the additional diversity described here.

Cupolaconcha krypta
(Gardner, 1989)
n. comb.

Dendropoma krypta [sic] Gardner, 1989: 250–254, figs. 1–4; Bieler & Petit, 2011: 43.

Type Locality

Isla Isabela, Nayarit, Mexico (Pacific Ocean): 21.85°N, 105.92°W.

Material Examined

Paratypes: CASIZ 065116: attached to large limpet shell from type locality, coll. G. D. Hanna & E. K. Jordan, CAS expedition ca. 1925, dry (many shells, some with dried animals).

Description

Teleoconch (Figs. 300–304): Apertural diameter to 1.2 mm; shell length to 6.8 mm; diameter of last whorl to 3.5 mm. Up to six partially or entirely overlapping whorls cemented to, but not deeply entrenched in, substratum; aperture occasionally raised ~1 mm above substratum as short feeding tube; scars from abandoned feeding tubes rarely present. Exterior surface matt, pale tan to pinkish brown (not honey brown as described by Gardner, 1989), semi-transparent around aperture; sculpture of undulating, irregularly-spaced, bulging, transverse folds. Interior surface pale brown.

Protoconch (Fig. 305): Settled protoconch diameter 350 µm, height 320 µm. No evidence of biphasic growth; globular with small increase in whorl size, moderately deep suture; 1.5 whorls; sculpture absent on first whorl, sculpture of many (> 30) pustulose to thread-like spiral bands developing towards lip; single spiral keel present in most specimens. Pale brown.

Operculum (Figs. 306, 307): Slightly oval in axial profile; diameter to 600 µm. Exterior surface of calcareous deposit slightly granular, lacking concavity. Interior surface as for genus, not observed to form a distinct plug as described by Gardner (1989).

Radula (Fig. 308): Length of radula ribbon 660 µm, width 100 µm; 27 rows. Lateral tooth: 2–3 cusps on inner side, 2–3 cusps on outer side. Inner marginal tooth: 2–3 cusps on inner side, 2–3 cusps on outer side. Outer marginal tooth: 2–3 cusps on inner side; base with prominent semicircular projection.

External Morphology and Color (Fig. 309): Anterior body of animal known only from 3 rehydrated partial specimens removed from dry paratype lot, confirming some generic features and the following details of pigmentation: head-foot pale brown, with blackish brown pigment covering dorsal surface and sides of head, including most of snout, surrounded posteriorly and laterally by "mosaic" pattern of brown pigment superimposed with white spots; cephalic tentacles and lips white; sparse brown pigment on lateral surfaces of foot and opercular lobe.

Pallial and Reproductive Anatomy: Not known.

Development and Ecology: Egg capsules not known. Adults gregarious, forming a dense, monospecific crust covering the surface of a large limpet (paratypes).

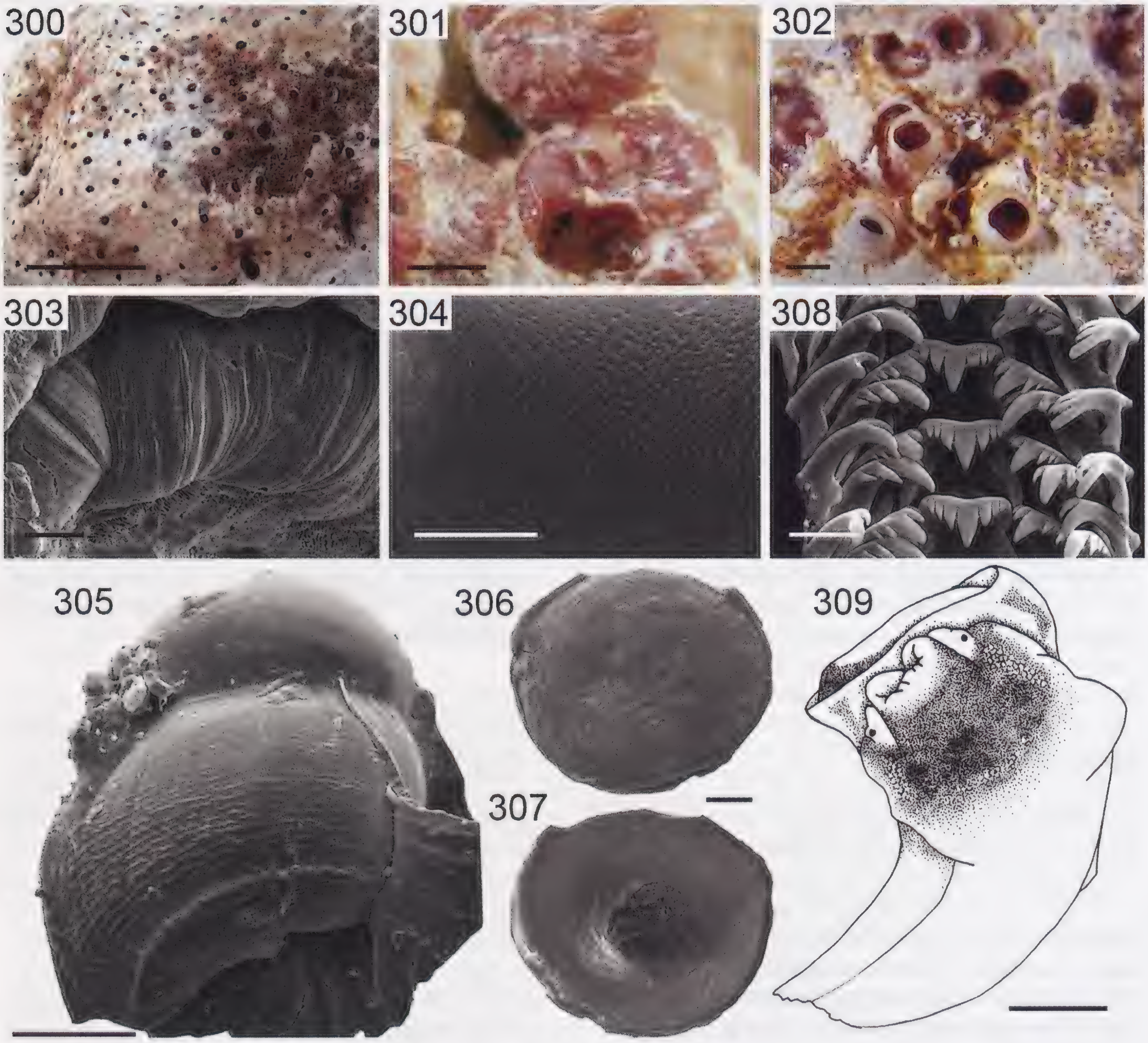

FIGS. 300–309. *Cupolaconcha krypta*. Paratypes, CASIZ 065116, Isla Isabela, Mexico. FIG. 300: Specimens attached to a large limpet shell, only apertures are visible beneath encrusting epifauna. Scale bar = 10 mm; FIG. 301: Partly excavated shells. Scale bar = 2 mm; FIG. 302: Domed apertures with elliptical slits. Scale bar = 1 mm; FIG. 303: SEM image of teleoconch sculpture. Scale bar = 100 µm; FIG. 304: Sculpture on columellar surface of shell interior. Scale bar = 100 µm; FIG. 305: Abapertural view of protoconch. Scale bar = 100 µm; FIGS. 306, 307: SEM images of operculum. Scale bar = 100 µm. FIG. 306: Exterior surface; FIG. 307: Interior surface; FIG. 308: Central section of radula. Scale bar = 20 µm; FIG. 309: Head-foot (without operculum) of a rehydrated specimen. Scale bar = 200 µm.

Taxonomic Remarks

The Greek word krypte was properly Latinized to krypta by the original author, who chose to maintain the spelling with a "k" and explained "from the Greek, meaning hidden, covered, concealed." The resulting adjectival form kryptus-a-um should have been used as *kryptum* in the original combination with (neuter) *Dendropoma.*

Comparative Remarks

Shell paler and smaller than *C. meroclista* and ***C. guana*** n. sp. Protoconch similar to that of *C. meroclista* but spiral bands of pustules condense to form threads near aperture; spiral keel also more strongly developed.

Distribution (Fig. 281)

Cupolaconcha krypta is known only from a single collecting event at Isla Isabela in Mexico. The animals are extremely cryptic because of their minute size and growth under a thick layer of encrustation, and likely are present at other nearby sites on the east Pacific Rim.

Cupolaconcha guana n. sp.

Vermetus conicus "Dillwyn and Wood" var. α *personata* juv. Mörch, 1862: 341–342 [infrasubspecific]; Bieler & Petit, 2011: 52. *Non Serpula conica* Dillwyn, 1817.

Type Locality

5–10 m depth, cove at Iguana Head at SW point of Guana Island: 18.474°N, 64.582°W.

Material Examined

Original material of *Vermetus conicus* var. *personata* of Mörch (1862) from St. Croix, U.S. Virgin Islands (ZMC).

British Virgin Islands: Holotype: FMNH 329350: coll. R. Bieler & T. M. Collins, August 9, 2010, 70% EtOH. Paratypes: FMNH 326719: with holotype, 70% EtOH (9 specimens); FMNH 326713: SE part of White Bay, near Monkey Point, Guana Island, British Virgin Islands, 5–6 m depth, 18.446°N, 64.572°W, coll. R. Bieler & T. M. Collins, August 8, 2010, 70% EtOH (10 specimens). FMNH 326700: 2 m, patch reefs, White Bay, Guana Island, 18.471°N, 64.574°W, coll. R. Bieler & T. M. Collins, August 5, 2010, dry, 70% EtOH (20 specimens) [DNA sequence data].

U.S. Virgin Islands: FMNH 328509: 10–15 m depth, Long Reef S of Christansted, St. Croix, coll. R. Bieler & N. Ogden, February 28, 1987, 70% EtOH (3 specimens).

Belize: FMNH 326930: Carrie Bow Cay, Stann Creek District, 16.803°N, 88.082°W, coll. R. Bieler, March 1986, 70% EtOH (1 animal) and dry (2 shells). FMNH 326932: Carrie Bow Cay, Stann Creek District, 16.803°N, 88.082°W, coll. R. Bieler, March 1986, dry (many, attached to coral substratum); FMNH 327154: attached to coral heads and algae-encrusted coral rubble on shallow subtidal reef, 1–2 m, Little Cat Cay, Stann Creek District, 16.151°N, 88.200°W, coll. R. Bieler, T. Collins, R. E. Golding, T. Rawlings & P. Sierwald, April 17, 2011, RNAlater (8 tissue samples), 95% EtOH (12 animals), 5% SW formalin (many attached to chunks of substratum) [DNA sequence data]; FMNH 327196: Carrie Bow Cay, Stann Creek District, 16.803°N, 88.082°W, coll. R. Bieler, April 2011, dry (many attached to dead shell); FMNH 327169: shallow subtidal coral rubble, under boulders, lagoon E of Carrie Bow Cay, Stann Creek District, 16.803°N, 88.082°W, 20th April 2011, RNAlater (1 animal), 95% EtOH (1 animal), dry (2 shells); FMNH 327185: coral rubble and living coral heads, lagoon E of Carrie Bow Cay, 16.803°N, 88.082°W, April 24, 2011, RNAlater (4 tissue fragments), 95% EtOH (3 animals), 70% EtOH (egg capsules and many specimens attached to chunks of substratum), 5% SW formalin (3 shells with animals).

Bahamas: FMNH 335076: 6–8 m, reefs NE of Great Abaco Island, 26.636°N, 77.0352°W, coll. R. Bieler & P. Sierwald, August 8, 2012, dry and ethanol (many), [DNA sequence data].

Florida, U.S.A.: FMNH 326731: Looe Key reef, Florida Keys, 24.4110°N, 81.4091°W, coll. R. Bieler, September 9, 2011, RNAlater (2 tissue samples), 95% EtOH (2 bodies), dry (2 shells); FMNH 327227: on gorgonians and *Dendostrea frons*, Missouri Key, 24.674°N, 81.238°W, coll. R. Bieler & P. Sierwald, September 2011, dry (many); FMNH 328503: small island oceanside of Bahia Honda Bridge, Florida Keys, 24.6479°N, 81.2842°W, coll. R. Bieler & P. Sierwald, April 9, 2012, dry (many, on lobster trap parts).

Etymology

From the type locality on Guana Island, British Virgin Islands. Noun in apposition.

Description

Teleoconch (Figs. 310–315): Apertural diameter to 2.2 mm; shell length to 7.5 mm; diameter of last whorl to 4.5 mm. Up to eight partially overlapping whorls cemented to, but not deeply entrenched in, substratum; aperture occasionally raised ~1 mm above substratum as short feeding tube; scars from abandoned feeding tubes occasionally present. External surface glossy, either bright orange or dark brown without intergrade colors, opaque;

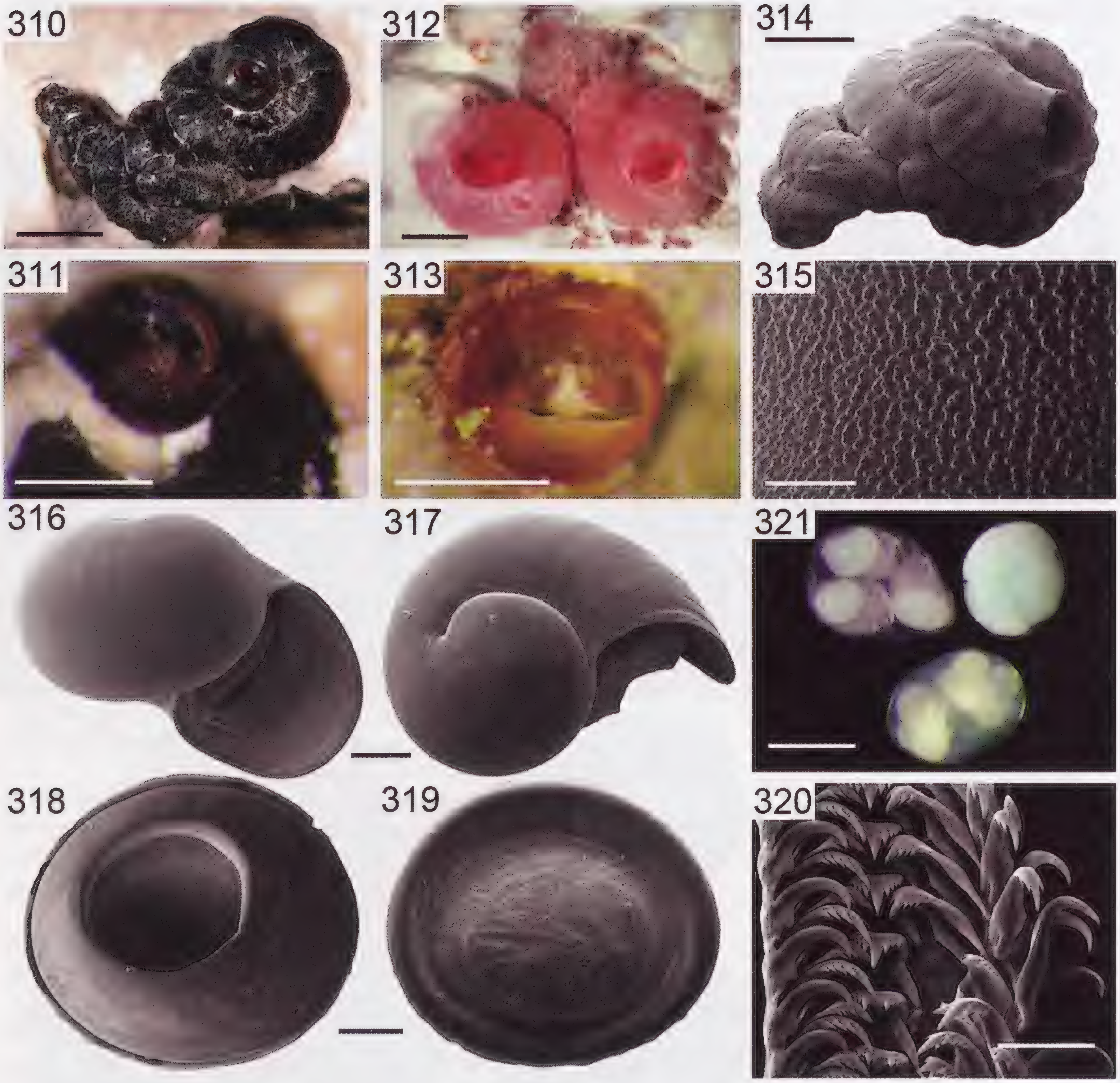

FIGS. 310–321. ***Cupolaconcha guana*** n. sp. FIGS. 310, 311. Dark brown morph. FIG. 310: Holotype, FMNH 329350. Shell cleaned of encrustation. Guana, British Virgin Islands. Scale bar = 2 mm; FIG. 311: Aperture with living animal. Paratype, FMNH 327154, Little Cat Cay, Belize. Scale bar = 1 mm; FIGS. 312, 313. Orange morph. FIG. 312: Paratype FMNH 326719. Scale bar = 2 mm; FIG. 313: Aperture with living animal. Paratype FMNH 327154. Scale bar = 1 mm; FIG. 314: SEM image of shell. Paratype, FMNH 326719. Scale bar = 1 mm; FIG. 315: Sculpture on columellar surface of shell interior. Paratype, FMNH 326713, Guana, British Virgin Islands. Scale bar = 100 µm; FIGS. 316, 317: SEM images of intracapsular larval shells. Paratype FMNH 326719, Guana, British Virgin Islands. Scale bar = 100 µm. FIG. 316: Apertural view; FIG. 317: Apical view; FIGS. 318, 319: SEM images of operculum. Paratype, FMNH 326713, Guana, British Virgin Islands. Scale bar = 200 µm. FIG. 318: Exterior surface; FIG. 319: Interior surface; FIG. 320: Central section of radula. Paratype, FMNH 326713, Guana, British Virgin Islands. Scale bar = 50 µm; FIG. 321: Egg capsules removed from interior shell wall. FMNH 327154. Scale bar = 500 µm.

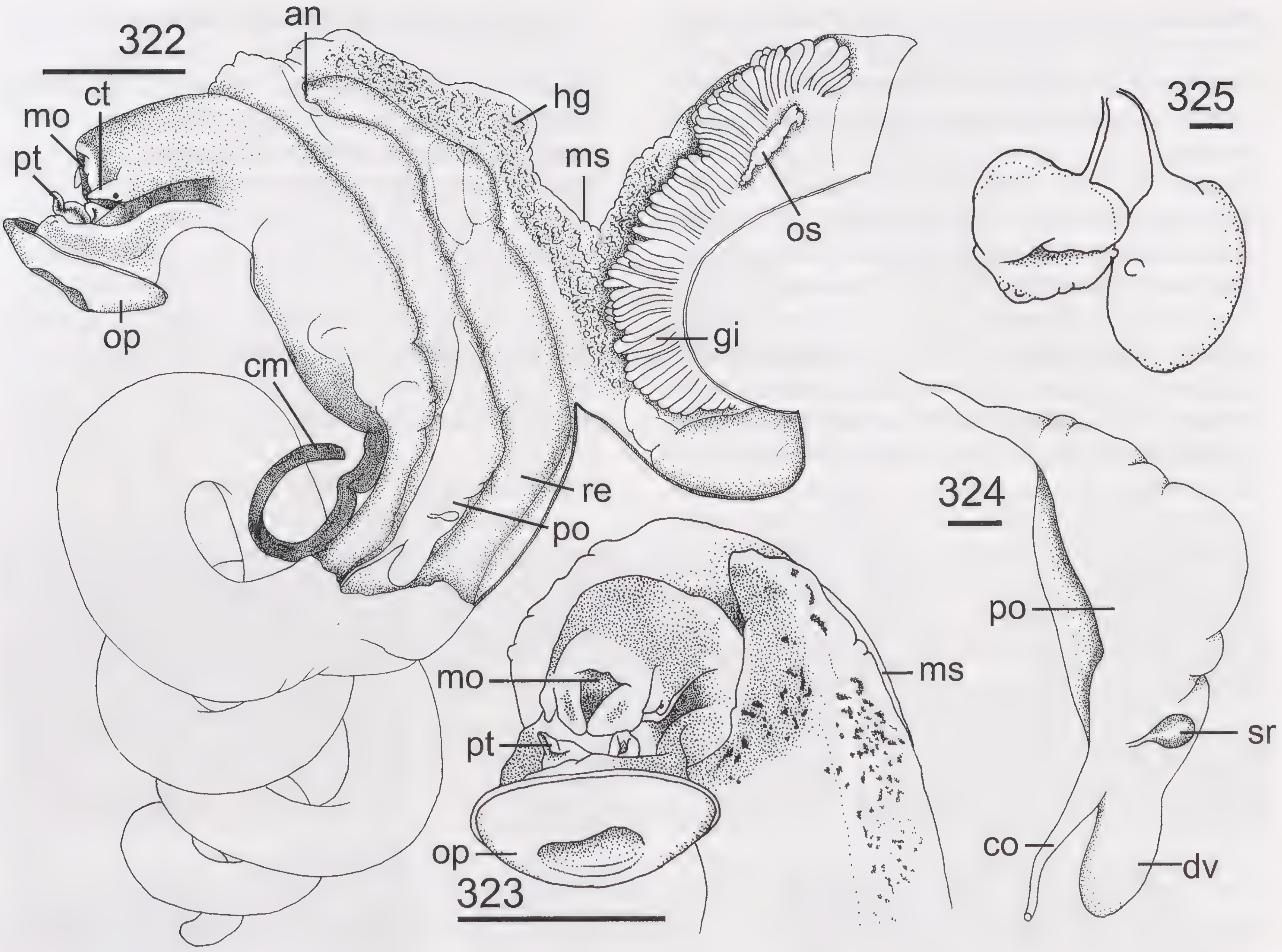

FIGS. 322–325. Anatomy of ***Cupolaconcha guana*** n. sp. FIG. 322: Body and mantle cavity of a female brooding egg capsules. Scale bar = 1 mm; FIG. 323: Anterior body of a female. Scale bar = 1 mm; FIG. 324: Pallial oviduct. Scale bar = 200 µm; FIG. 325: Stalked egg capsules. FMNH 326713, Guana, British Virgin Islands. Scale bar = 200 µm. FIGS. 322–324: FMNH 326719, Guana, British Virgin Islands.

sculpture of undulating, irregularly-spaced, bulging, transverse folds. Interior surface either bright orange or dark brown, matching external shell color.

Protoconch (Figs. 316, 317): Settled protoconch diameter 460–530 µm, height 400 µm. No evidence of biphasic growth; Subplanar, with large increase in whorl size, deep suture; 1.3 whorls; sculpture absent; spiral keel absent. Brown, darkest at suture.

Operculum (Figs. 318, 319): Oval in axial profile; diameter to 1,100 µm. Exterior surface of calcareous deposit mostly smooth, sometimes grainy or coarsely textured, often with concavity at apex of dome or off-center.

Radula (Fig. 320): Length of radular ribbon 340–1,000 µm, width 70–135 µm, 22–36 rows. Lateral tooth: two cusps on inner side, 3–6 cusps on outer side. Inner marginal tooth: two cusps on inner side, 3–4 cusps on outer side. Outer marginal tooth: 2–3 cusps on inner side; base with prominent semicircular projection.

External Morphology and Color (Figs. 311, 313, 322, 323): Body length to 18 mm. Color in life and specimens recently preserved in 70% EtOH: lateral surfaces of foot and neck dark red to rose pink; snout (except lips) and dorsal head diffuse orange-red with fine brown speckles; lips, tentacles and sole of foot cream; anterior edge of mantle brownish-red fading to cream, with dark red pigment speckles on mantle reducing in density posteriorly but especially dense in region of gill; digestive gland olive green with black flecks.

Pallial and Reproductive Anatomy (Figs. 322, 324): Pallial oviduct broad; 1.8 mm long, 600 µm wide. Proximal diverticulum straight, not constricted near junction with pallial oviduct.

Development and Ecology (Figs. 321, 325): Stalked egg capsules found in several preserved and living female specimens: 2–6 capsules at different stages of development per female; each capsule containing 2–3 eggs/embryos; eggs/embryos pale, mint green in life. Hatchlings had resorbed most of the velum and were observed to crawl on the substratum, suggesting that they were not capable of planktonic dispersal. Adults solitary and settling mostly on exposed surfaces of dead coral in the shallow to deep subtidal. Rarely growing adjacent to conspecifics, but often concentrated in large numbers on a particular substratum.

Taxonomic Remarks

Mörch (1862: 341–342) studied specimens of this species from St. Croix and mistakenly considered them to be juveniles of a larger Caribbean species that he called *Vermetus conicus* [(Dillwyn, 1817)]. He (1862: 342) inferred that "the constricted aperture must then, of consequence, become dissolved with age." The varietal name applied to this material by Mörch, "var. α personata juv.," is not available (see also Bieler & Petit, 2011: 6, 52).

Comparative Remarks

Shell color variable, orange morph distinct in genus; larger than other species of *Cupolaconcha* n. gen. except *C. meroclista*. Protoconch planar, unsculptured. Head-foot pigment orange-red in life. Egg capsules containing fewer than three eggs/embryos.

Distribution (Fig. 281)

This is the only representative of *Cupolaconcha* from the Atlantic Ocean, and is not known to occur outside the Caribbean region. Material examined in this study was collected from around the perimeter of the Caribbean Sea at Belize, the Florida Keys and the British Virgin Islands, indicating that ***C. guana*** has a widespread distribution in the region.

Cupolaconcha sinaiensis n. sp.

Dendropoma meroclista – Safriel & Hadfield, 1988 (in part): 1–13, figs. 1, 4B.
Dendropoma sp. Safriel & Hadfield, 1988 (in part): 1–13, fig. 2B, 5.

Type Locality

Gulf of Aqaba, Sinai Peninsula: approx. 29.5°N, 35.0°W.

Material Examined

Israel: Holotype: FMNH 329351: coll. U. Safriel, pre-1987, dry (Fig. 342; 1 shell attached to substratum with paratypes). Paratypes: FMNH 328076: from type locality, coll. U. Safriel, pre-1987, dry (many specimens attached to substratum with holotype). FMNH 328077–328081: from type locality, coll. U. Safriel, pre-1987, dry (many specimens attached to chunks of substratum).

Etymology

Named for the geographic region of the type locality on the Sinai Peninsula. Adjective in genitive case.

Description

Teleoconch (Figs. 326–331): Apertural diameter to 2.3 mm; shell length to 9 mm; diameter of last whorl to 5 mm. Up to six partially overlapping whorls deeply entrenched in substratum; aperture usually raised ~3 mm above substratum as moderately tall feeding tube, especially when growing in dense aggregates; remains of early feeding tubes frequently present. Exterior surface glossy, medium to dark brown, opaque; sculpture of undulating, irregularly-spaced, bulging, transverse folds. Interior surface medium brown to white.

Protoconch (Figs. 332, 333): Hatchlings and intracapsular protoconchs (initial growth phase): diameter 220 µm, [~240 µm according to Safriel & Hadfield (1988)], height 140 µm; settled protoconchs (secondary growth phase): diameter 310 µm; height 350 µm [up to 400 µm (Safriel & Hadfield, 1988)]. Growth divided between intracapsular and pre-settlement (planktonic?) phases with transition evident in protoconch structure; hatchling protoconch almost planar, settled protoconch pupoid, sutures shallow; hatchling protoconch 1 whorl, settled protoconch 2.5 whorls; sculpture absent on first phase, sculpture on second phase of spiral bands of widely-spaced pustules (largest near suture) transitioning to short, oblique threads near lip; 6 spiral keels present. Honey brown.

Operculum: Not observed in this study, but described and figured by Safriel & Hadfield (1988) as identical to that of *C. meroclista* from Hawaii.

Radula: Not observed in this study, but figured by Safriel & Hadfield (1988) showing the following details: Width of radular ribbon 100 µm. Lateral tooth: two cusps on inner side, 2–3 cusps on outer side. Inner marginal tooth: at least one cusp (partially obscured) on inner side, three cusps on outer side. Outer marginal tooth: two cusps on inner side; base with prominent semicircular projection.

External Morphology and Color: Not observed in this study, but described and partially figured by Safriel & Hadfield (1988) as morphologically identical to *C. meroclista* from

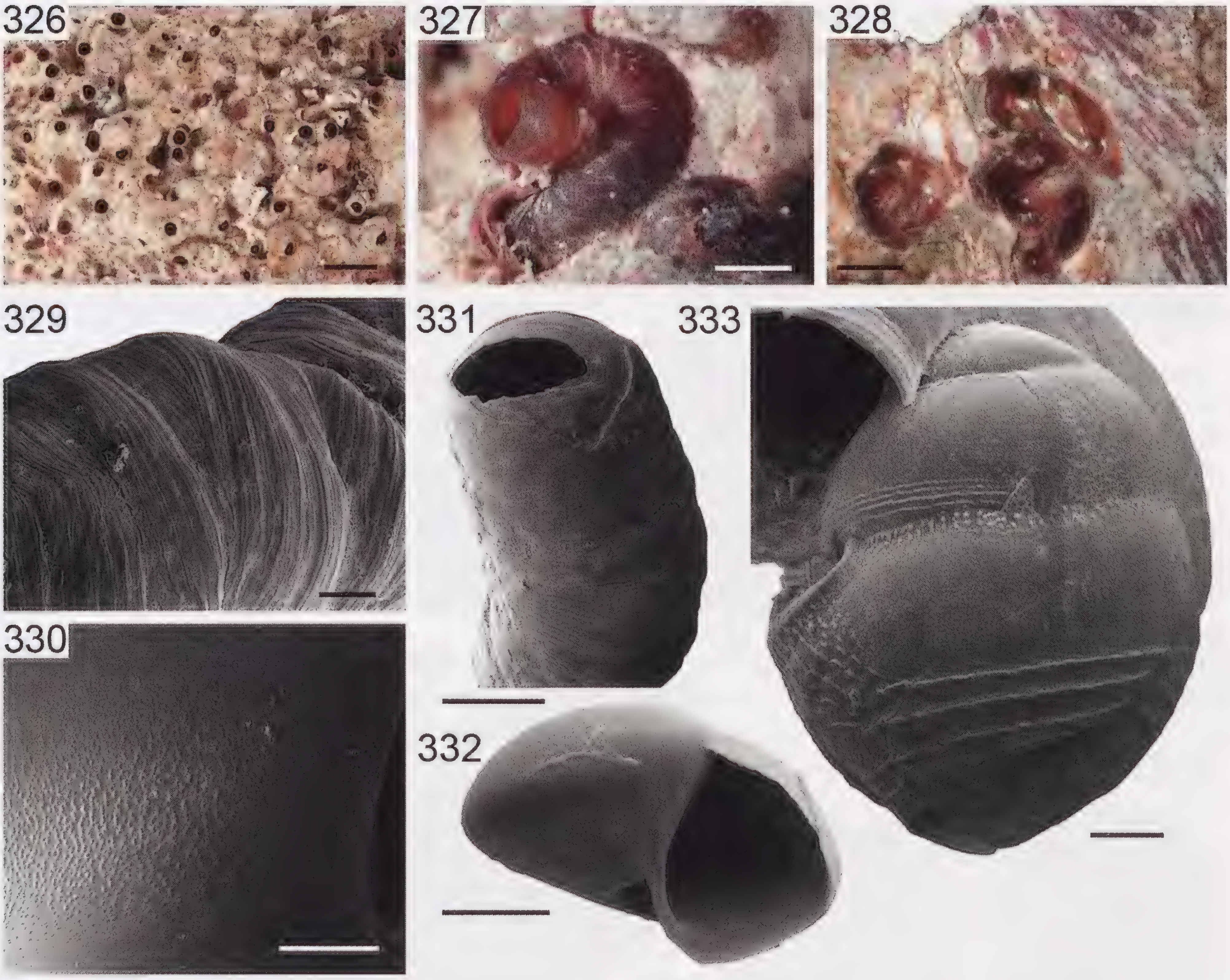

FIGS. 326–333. ***Cupolaconcha sinaiensis*** n. sp. from the type locality at the Gulf of Aqaba, Sinai Peninsula. FIG. 326: A dense aggregate of specimens removed from rock surface. FMNH 328077. Scale bar = 5 mm; FIG. 327: Shell of holotype. FMNH 329351. Scale bar = 1 mm; FIG. 328: Broken specimen deeply entrenched into the surface of a barnacle. FMNH 328077. Scale bar = 2 mm; FIG. 329: SEM image of teleoconch sculpture. FMNH 328079. Scale bar = 200 µm; FIG. 330: Sculpture on columellar surface of shell interior. FMNH 328076. Scale bar = 200 µm; FIG. 331: Feeding tube with domed aperture. FMNH 328079. Scale bar = 500 µm; FIG. 332: Apertural view of intracapsular larval shell. FMNH 328076; FIG. 333: Abapertural view of protoconch from recently-settled juvenile. FMNH 328079. Scale bar = 50 µm.

Hawaii with respect to the following details: head/foot darkly pigmented, snout and tips of cephalic tentacles pale; pedal tentacles dark with pale spots; mantle divided by pallial slit in females.

Pallial and Reproductive Anatomy: Not known.

Development and Ecology: Not observed in this study, but Safriel & Hadfield (1988) described developmental biology of a population from the type locality in considerable detail, noting in particular the following points: females brood up to six stalked egg capsules; each capsule containing 21–134 eggs (x = 65, N = 14). Larvae believed by Safriel & Hadfield (1988) to be capable of sustained planktonic development based on apparent shell growth between hatching and settlement (see above). Highly gregarious, forming a living crust on the intertidal seaward edge of a thick layer of dead vermetid shells cemented together (Safriel, 1966; Safriel & Hadfield, 1988).

Comparative Remarks

Most similar to ***C. maldivensis*** n. sp., in size and propensity to form a living crust of aggregated shells on substratum, but lacking crest and transverse lamellae present in ***C. maldivensis***. Protoconch growth divided into intracapsular and (presumably) planktonic phases, resulting in unique protoconch structure (2.5 whorls, pupoid shape). Egg capsules containing many more eggs/embryos (21–134) than any other species in *Cupolaconcha* n. gen. (maximum 12).

Taxonomic Remarks

Safriel & Hadfield (1988) informally recognized that specimens from the type locality in the Gulf of Aqaba were a distinct species from *C. meroclista*. They used the name "*Dendropoma* sp." in their figure legends, but did not propose a name for this taxon or offer a formal description. Here we introduce ***C. sinaiensis*** n. sp. as a distinct species.

Distribution (Fig. 281)

The description above is based only on material from the type locality. Safriel & Hadfield (1988) reported that specimens from Madagascar were conspecific with those from the Sinai Peninsula, based on protoconch morphology. This remains to be tested, and at present the verified distribution is restricted to the type locality in the Gulf of Aqaba.

Cupolaconcha maldivensis n. sp.

Type Locality

Boulder zone, seaward edge of reef flat, Gan Island, Addu Atoll, Maldives: approx. 0.69°S, 73.14°E.

Material Examined

Republic of Maldives: Holotype: FMNH 329352: coll. J. D. Taylor, 1975, dry (1 shell attached to chunk of substratum with paratypes). Paratypes: FMNH 328083: from the type locality, coll. J. D. Taylor, 1975, dry (many specimens with holotype); FMNH 328082: intertidal reef platform edge, Gan Island, Addu Atoll, Maldives, approx. 0.69°S, 73.14°E, coll. J. D. Taylor, 1975, dry (many).

Kenya: FMNH 328084: edge of fringing reef platform, Likoni, 4.09°S, 39.67°E, coll. J. D. Taylor, 1977, dry (many).

Etymology

Named for the geographic region of the type locality in the Maldive Islands. Adjective in genitive case.

Description

Teleoconch (Figs. 334–337): Apertural diameter to 1.5 mm; shell length to 6.5 mm; diameter of last whorl to 3 mm. Up to five widely-spaced (usually non-overlapping) whorls cemented to, but not deeply entrenched in, substratum; aperture usually raised ~1 mm above substratum as short feeding tube; scars from abandoned feeding tubes frequently present. Exterior surface medium to dark purplish brown, pale brown near aperture, opaque; sculpture of undulating, irregularly-spaced, bulging, transverse folds and scaly lamellae, with crest-like ridge running longitudinally on dorsal surface. Interior surface pale brown to white.

Protoconch (Figs. 338, 339): Settled protoconch diameter 340–370 μm, height 380 μm (Maldives population) to 420 μm (Kenyan population). No evidence of biphasic growth; globular with small increase in whorl size (first whorl disproportionately large in Kenyan population), shallow suture; 1.5 whorls; sculpture absent. Honey brown.

Operculum (Figs. 340, 341): Oval in axial profile; diameter to 740 µm. Exterior surface mostly smooth, sometimes grainy or coarsely textured; irregularly-shaped concavity sometimes present at apex of dome or off-center.

Radula (Fig. 342): Length of radula ribbon 450–600 µm, width 100 µm; 25–31 rows. Lateral tooth: 2–3 cusps on inner side, 2–3 cusps on outer side. Inner marginal tooth: two cusps on inner side, 4–5 cusps on outer side. Outer marginal tooth: 4–5 cusps on inner side; base with prominent triangular projection.

External Morphology and Color (Fig. 343): Anterior body of animal known only from three rehydrated partial specimens removed from dry paratype lot, showing the following features: Head-foot, snout, cephalic tentacles and broad band on mantle margin covered with black pigment, dorsal and lateral surfaces of head posterior to tentacles covered with "mosaic" pattern of black pigment superimposed with white spots; lips white.

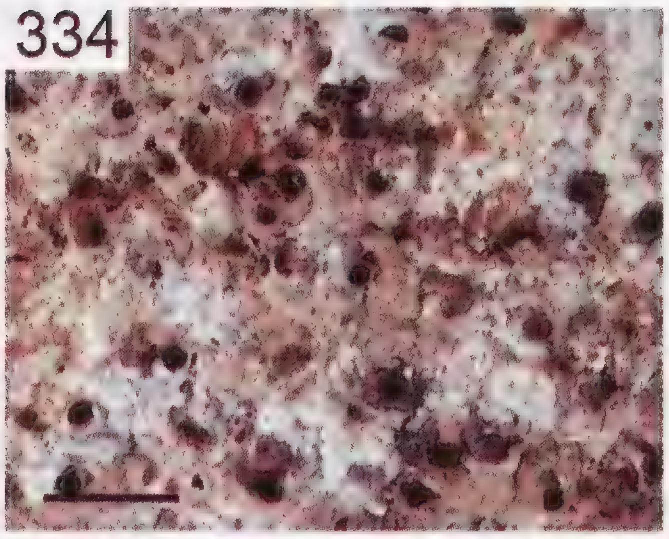

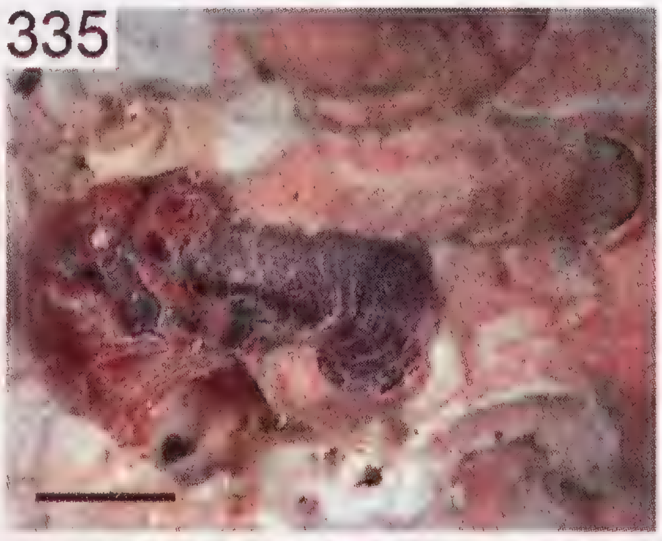

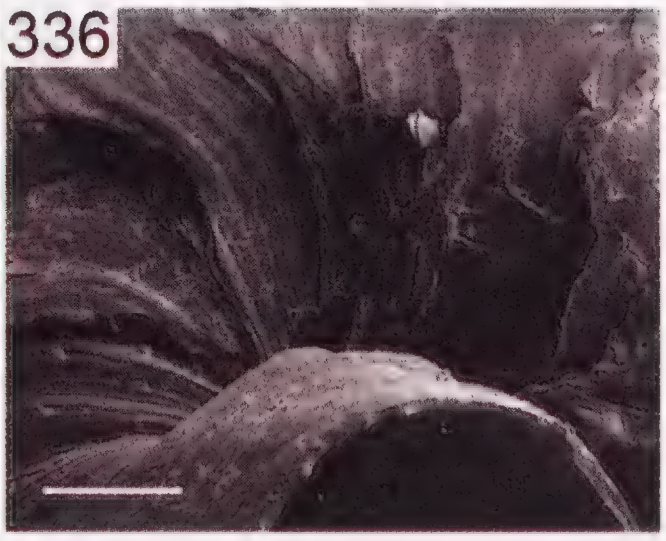

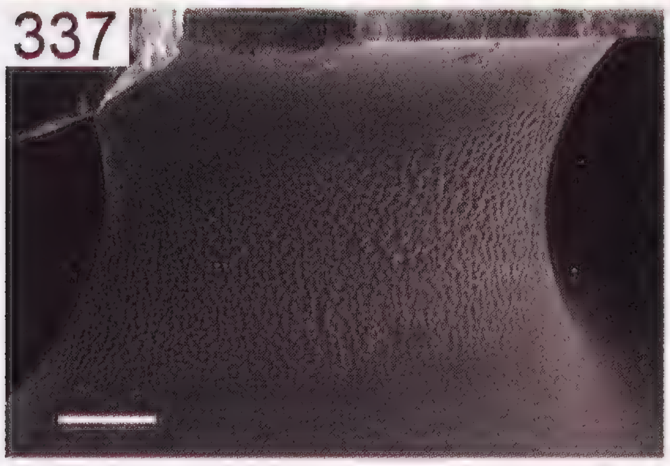

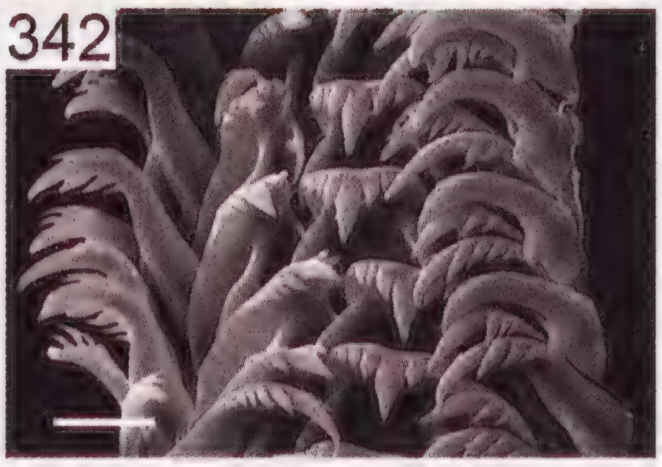

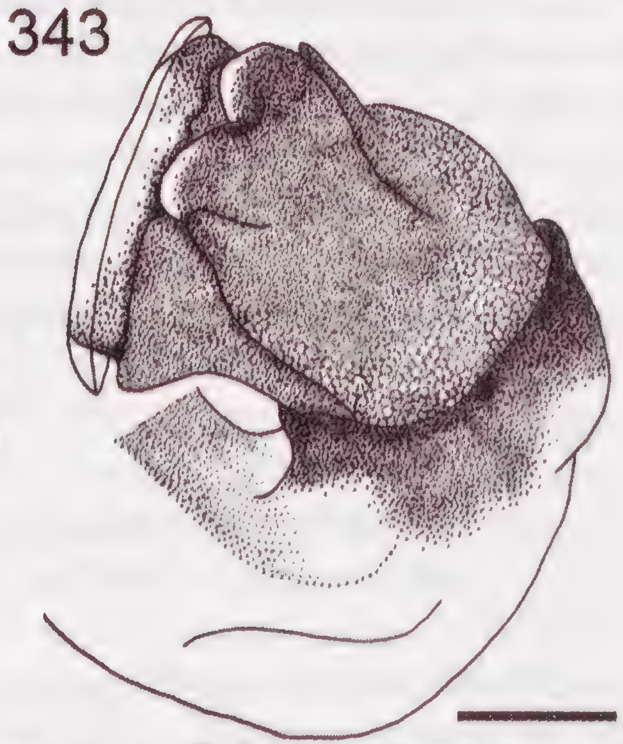

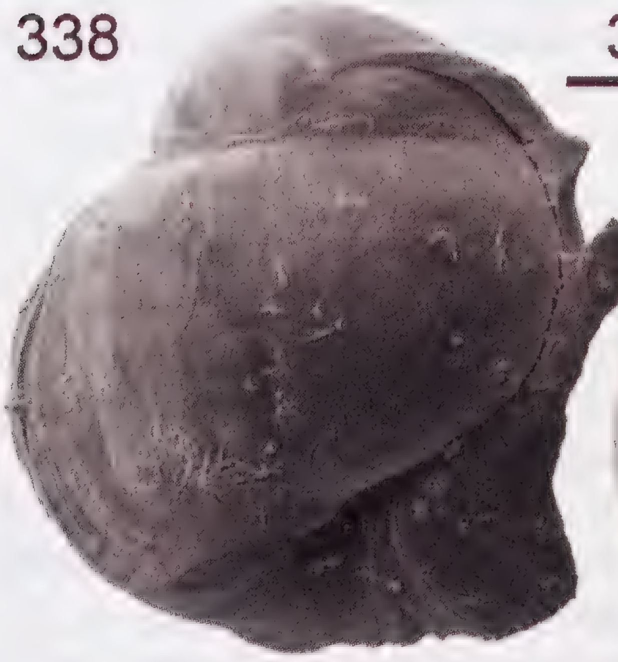

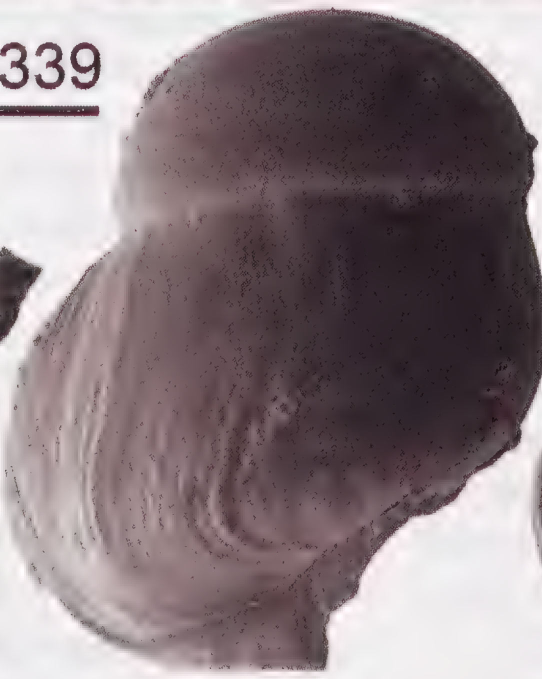

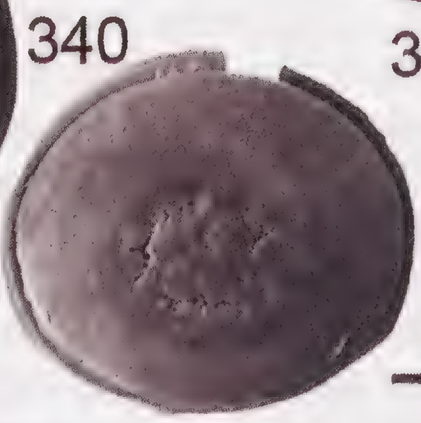

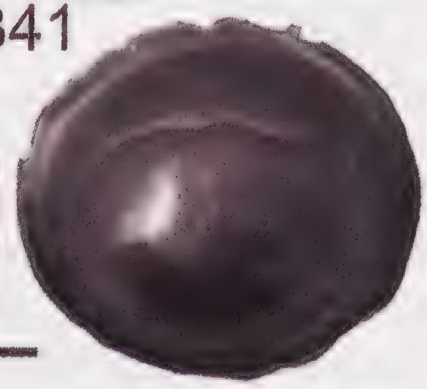

FIGS. 334–343. ***Cupolaconcha maldivensis*** n. sp. FIG. 334: Aggregate of specimens removed from rock surface. Scale bar = 5 mm; FIG. 335: Shell of holotype. FMNH 329352, Gan Island, Maldives. Scale bar = 1 mm; FIG. 336: SEM image of teleoconch sculpture. Scale bar = 200 µm; FIG. 337: Sculpture on columellar surface of shell interior. Scale bar = 100 µm; FIGS. 338, 339: Abapertural view of protoconchs from recently settled juveniles. Scale bar = 50 µm. FIG. 338: Paratypes; FIG. 339: FMNH 328084, Likoni, Kenya; FIGS. 340, 341: SEM images of operculum. Scale bar = 100 µm. FIG. 340: Exterior surface; FIG. 341: Interior surface; FIG. 342: Central section of radula. Scale bar = 20 µm; FIG. 343: Anterior body (without calcareous layer of operculum) of a rehydrated specimen. FIGS. 334, 336–338, 340–343: Paratypes, FMNH 328083, Gan Island, Maldives.

Pallial and Reproductive Anatomy: Not known.

Development and Ecology: Egg capsules not known. Adults gregarious, forming a dense colony encrusting pieces of dead coral and rock.

Comparative Remarks

Similar to ***C. sinaiensis*** n. sp. and *C. krypta* in shell size, but the only species in *Cupolaconcha* n. gen. that has transverse lamellae and a longitudinal crest on the exterior surface of the shell. The protoconch is globular, but lacks any distinct sculpture. Radula dentition is variable, but tends to have a greater number of cusps on the outer side of the inner marginal tooth and the inner side of the outer marginal tooth (4–5) than conspecific taxa; projection on base of outer marginal tooth triangular rather than semicircular.

Taxonomic Remarks

Material from Kenya and the Maldives was examined in the preparation of this description. Despite the considerable distance between these sites in the Indian Ocean, they appear to belong to the same species-level taxon based on morphological data. However, the Kenyan samples were in poor condition, were excluded from the paratype series, and are herein provisionally referred to ***C. maldivensis*** n. sp.

Distribution (Fig. 296)

Known from the Maldives in the central Indian Ocean and Kenya on the east coast of Africa.

The status of "*Dendropoma*" *exsertum* (Dall, 1881)

This nominal species was introduced, as *Bivonia exserta* Dall, 1881, for a single partial shell tube collected as part of the U.S. Coast Survey at Blake Station 20, off Bahia Honda (Cuba: 23°2'30"N, 83°11'W) in ca. 400 m (220 fathoms) depth. Dall (1881: 39) remarked that it "has a remarkable structure sculpture and is only provisionally referred to *Bivonia*, as the operculum is unknown." The species remained unfigured until 1889, when Dall (1889: 264, pl. 26, fig. 6) added a drawing of the holotype and referred to additional material of "*Bivonia ? exserta*" from other locales from Barbados to North Carolina. He concluded that the type specimen was a juvenile shell. Dall's species was uncritically accepted in subsequent regional species listings, e.g., as *Bivonia exserta* by Maury (1922: 132) and as *Dendropoma exsertum* by Rosenberg (2009) and Rosenberg et al. (2009). The holotype specimen (MCZ 7445) is the apertural portion of a polychaete (Serpulidae) worm tube (Figs. 344, 345). The nominal species *Bivonia exserta* Dall, 1881, is here removed from the Mollusca.

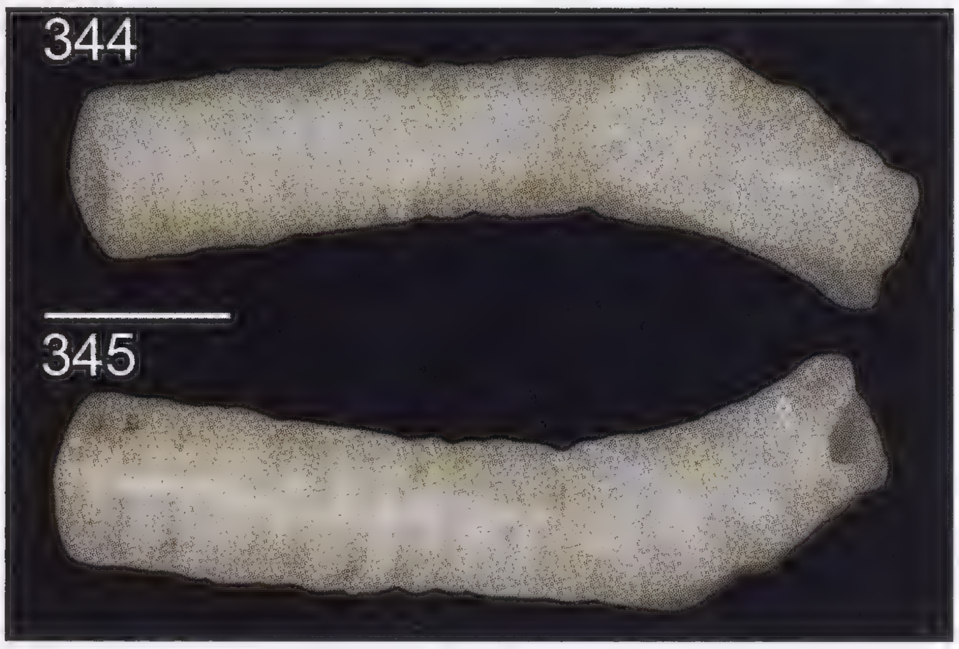

FIGS. 344, 345. Holotype of *Bivonia exserta* Dall, 1881, MCZ 7445, off Bahía Honda, Cuba. FIG. 344: Attached side; FIG. 345: Free side. Scale bar = 2 mm.

DISCUSSION

Genus-Level Systematics

Previous attempts to tackle vermetid evolution (Morton, 1955) and systematics have relied on characters of the adult shell alone (Carpenter, 1857; Mörch, 1861, 1862) or a combination of adult and juvenile shell morphology, growth habit, and partial accounts of the operculum (Keen, 1961). Morton (1965) reinforced and enhanced the classification introduced by Keen (1961) by including morphological descriptions of members of each genus. With each advance in our knowledge of the group, a new concept of the diversity and composition of Vermetidae has emerged. Here, we have proposed a new classification for a subset of the Vermetidae, the "*Dendropoma* group", based on a greatly improved morphological dataset. Crucially, this interpretation has been supported by a new line of evidence with the construction of a molecular phylogeny. The development of a novel systematic framework for these taxa provides an opportunity to examine the morphological and molecular features that define each group and re-examine the evolutionary pathways leading to this diversity.

This systematic revision of *Dendropoma s.l.* is a substantial modification of the prevailing concept of the group, as introduced by Keen (1961) and cemented by Morton (1965). The classification presented here divides the group of taxa previously assigned to *Dendropoma s.l.* into four distinct genera belonging to two separate branches of Vermetidae. Keen (1961) recognized two Recent subgenera of *Dendropoma, Dendropoma s.s.* and *Novastoa*, as well as one extinct subgenus, *Elliptovermetus* (see above). *Dendropoma* (*Dendropoma*) according to Keen (1961) roughly corresponds to the group recognized here as *Dendropoma s.s.*, typified by the Californian species *D. lituella*. However, one of the most conspicuous and ecologically significant species in Keen's version of *Dendropoma*, "*D.*" *maximum*, has been removed to *Ceraesignum* n. gen., together with a newly-described Chilean species, ***C. robinsoncrusoei*** n. sp. Morton (1965) remarked that "*D*". *maximum* was least consistent with his morphology-based concept of *Dendropoma*. The erection of a new genus for these two taxa was determined by their separation from other members of the "*Dendropoma* group" by long branches in the molecular tree, the absence of a major change in mtDNA gene order present in *Dendropoma s.s.* (Rawlings et al., 2001, 2010), and by such morphological characters as a divided female mantle to facilitate the attachment of egg capsules to the shell wall not found in *Dendropoma s.s.* (Table 3).

The second extant subgenus recognized by Keen (1961) was *Dendropoma* (*Novastoa*). The key differences between *Dendropoma* (*Dendropoma*) and *Dendropoma* (*Novastoa*) respectively, as defined by Keen (1961), were a tendency toward solitary and burrowing versus colonial and encrusting growth, attached versus upwardly-spiraling shell forms, and a flat to concave versus convex operculum.

Although *Novastoa* is recognized here as a distinct genus, all species besides the type that Keen (1961) included in *Dendropoma* (*Novastoa*) have now either been placed in *Dendropoma* proper (*D. petraeum*, *D. tholia*), likely belong there (*D. corallinaceum*, *D. ghanaense*), or cannot be placed with certainty in a current genus (*Vermetus irregularis*). Regardless, the description of five new species in this group permits a redefinition of *Novastoa*. The main identifying feature of this genus is the structure of the operculum, which bears a remarkably well-developed mammilla on the internal surface of most species in the genus, including the New Zealand type species *N. lamellosa*. The external surface of the operculum is also composed of tightly packed, upright revolutions of the spiral lamina. This feature is not recorded from any other group of vermetids. The convex operculum that Keen (1961) attributed to *N. lamellosa* was found to be an error inconsistent with Morton's (1951) detailed anatomical description.

The female mantle is undivided in all known species of *Dendropoma s.s.*, allowing retention of the eggs within the mantle cavity even when the animal retracts further into the shell. This character is not uniquely synapomorphic (see generic Remarks), as it is known to occur in at least two other vermetid species, but is diagnostic for *Dendropoma s.s.* when compared to the closely-related taxa examined here. Keen (1961) included the Mediterranean species *D. petraeum* in *Novastoa*, but molecular evidence presented here indicates that this taxon belongs in *Dendropoma s.s.* This conclusion is supported by the structure of the operculum, which is flattened and intermediate between the convex and concave opercular forms.

Hadfield et al. (1972) documented the diversity of Hawaiian vermetids and adopted Keen's (1961) generic classification in assigning their newly-described species. One species presented in that study was *Dendropoma meroclista*, a minute but remarkable worm-snail with several features not previously known in Vermetidae, including a constricted, domed aperture. In light of the previously known morphological differences (such as the presence of a calcified layer on the exterior surface of the operculum and a body capable of retraction deep inside the shell) and many additional characters recognized here (Table 3), it is therefore unsurprising that this species and several other previously unrecognized species have been placed in a new genus, *Cupolaconcha*. The molecular phylogeny supports the conclusion that this group is more closely related to vermetid genera such as *Petaloconchus* than to other members of the "*Dendropoma* group". Based on species examined to date, this genus is also defined by a gene order trait: the absence of a tRNA valine gene between the ribosomal *rrnS* and *rrnL* mtDNA genes. The position of t*rnV*, between these two ribosomal RNA genes appears to be an ancestral position within the Vermetidae, and likely the Gastropoda as a whole (Rawlings et al., 2010).

TABLE 3. Key morphological features separating *Dendropoma*, *Novastoa*, *Ceraesignum* n. gen. and *Cupolaconcha* n. gen.

Shell	*Dendropoma*	*Novastoa*	*Ceraesignum*	*Cupolaconcha*
Shell				
Relative size	Small to medium	Small to medium	Medium to large	Small
Coiling pattern	Concentric, *Turritella*-squeezed-sideways, straight or irregular	Concentric	Concentric, straight or irregular	*Turritella*-squeezed-sideways
Attachment to substratum	Entrenched in substratum or colonial aggregate	Entrenched or entirely embedded in substratum	Entrenched or entirely embedded in substratum	Entrenched in substratum or superficially attached
Feeding tube	Sometimes present, short	Sometimes present, tall	Absent	Present, short or tall
Aperture	Simple	Simple	Simple	Domed with a slit-shaped aperture
Sculpture on columellar surface	Absent	Absent	Absent	Backwards-facing teeth
Operculum				
Axial profile	Circular	Circular	Circular	Oval
Calcified deposit on exterior surface	Absent	Absent	Absent	Present
Shape of chitinous operculum	Conical concave, "mushroom-shaped" or flat	Conical concave	Saucer-shaped	Flat (plus calcareous layers)
Mammilla	Conical or nipple-shaped	Conical, nipple- or spindle-shaped	Absent	Absent
Texture on muscle attachment area	Concentric grooves	Concentric grooves	"Fingerprint pattern"	Dimples
Spiral lamina on exterior surface	Short and flat, or stacked	Tall, ruffled	Smooth	Smooth
Radula				
Cusps on outer marginal tooth	Simple	Simple	Simple	Splayed, digitiform
Base of outer marginal tooth	Simple	Simple	Simple	With a projection
External Morphology				
Length of body relative to shell	Medium	Short to medium	Short to medium	Long
Female mantle margin	Undivided	Divided by long slit or shallow notch	Divided by long slit	Divided by long slit
Reproduction				
Seminal receptacle(s)	Double	Single	Absent	Single
Exhalant channel of males	With "accessory gland"	Simple	Simple	Simple
Egg capsules	Held in mantle cavity, unattached	Attached to shell wall by stalk	Attached to shell wall by stalk	Attached to shell wall by stalk

Significance and Evolution of Morphological Characters

Recognition of species-level diversity in the "*Dendropoma* group" was facilitated by enhancing the dataset of morphological characters introduced by Morton (1965). While shell morphology has been used extensively to differentiate vermetid species, despite difficulties arising from extreme variability, protoconch morphology was found to be particularly useful in discriminating closely related species. Unlike previous genus-level systematic studies of vermetids, the availability of suitable material for SEM provided an excellent source of characters for this study. Some taxa were found to have unique microsculpture, such as the foamy crust on the protoconch of *D. nebulosum* and the distinctive gouges on the protoconch of *D. mejillonense*. The unusually complex protoconch morphology of ***C. sinaiensis*** n. sp. (first recognized by Safriel & Hadfield, 1988) is the primary morphological feature separating this species from related taxa belonging to *Cupolaconcha* n. gen. Future efforts to include a wider range of vermetids may demonstrate the utility of protoconch morphology at the genus level or higher.

Unlike some vermetids, all members of the "*Dendropoma* group" are operculate. Morton (1965) emphasized the significance of operculum morphology in separating *Dendropoma s.l.* from other operculate vermetids (the operculum substantially overhangs the foot and has a distinctive mammilla) and for recognizing three sub-groups within *Dendropoma s.l.* Morton's (1965) subgroups do not directly correlate with any of the genera recognized here. However, results from both the morphological survey and the molecular phylogenetic analysis supported the division of *Dendropoma s.s.* into two distinct subgroups of "concave-operculate" and "convex-operculate" taxa. The former includes the type species and most of the medium-sized species, while the latter comprises of several species that share a conserved morphology and a deeply entrenched colonial growth habit (such as *Dendropoma corrodens*). Although these groups have not been formally named, the concordance between the morphological and molecular datasets suggests that opercular characters are useful for analyzing relationships between groups of species.

Operculum morphology reaches its most extreme in the "*Dendropoma* group" (Figs. 346–358) with *Novastoa* and the "convex-operculate" group of *Dendropoma s.s.*, in which the central mammilla is extended to form a spindle or rod. The functional utility of this character is unclear, although it is likely to be related to their extremely cryptic mode of life and small size relative to other vermetids. Elaboration of the mammilla, deeply anchored in the muscular foot, may improve the animals' ability to prevent removal of the operculum during predatory events. It is interesting to note that *Ceraesignum maximum*, which also lives deeply buried in coral substratum but is by an order of magnitude larger than members of *Novastoa*, has a far simpler operculum that entirely lacks a mammilla on the internal surface.

The calcified operculum of *Cupolaconcha* n. gen. is unique in Vermetidae. The irregular, lopsided calcified layer is fused to the external surface of a simple, flat chitinous operculum. The calcified layer is possibly created by the repeated "wiping" of the operculum inside the mantle margin, resulting in the repeated deposition of thin layers of calcified substance that when fully developed can plug the dome from the inside.

The reproductive biology of species attributed to *Dendropoma s.l.* has been given a mixed account in the literature. Keen (1961) made no remark on the reproductive mode of *Dendropoma s.l.* Morton (1951) originally documented the divided female mantle and attached egg capsules of *Novastoa lamellosa*, but subsequently concluded that *Dendropoma s.l.* (including *Novastoa*) was united by the presence of an undivided female mantle margin, unlike other vermetids (Morton, 1965). Here we have shown that uniquely among "*Dendropoma* group" taxa, *Dendropoma s.s.* broods its unattached egg capsules in the female mantle cavity, protected by an undivided mantle. Most other known vermetids, including *Ceraesignum* n. gen., *Novastoa* and *Cupolaconcha* n. gen. have a female mantle that is slit to varying degrees and attach their egg capsules to the shell wall. Egg capsule size, color and egg count varied between species and are useful for differentiating species. For example, the eggs of ***C. guana*** n. sp. are mint green and contain just two or three eggs per capsule, unlike the six to 12 yellowish eggs included in each capsule of *C. meroclista*. Variation in capsule number is very high, as demonstrated by Calvo et al. (1998) in the *D. petraeum* species complex. Individuals from populations in one region of the Mediterranean can retain up to 86 egg capsules, each usually containing a single egg, while others from a different region brood only 12 egg capsules, each containing 25 eggs.

Species with direct-developing larvae that hatch as crawling juveniles, such as *D. petraeum*, are likely to exhibit a high degree of genetic structure among populations and more intraspecific variation in reproductive characteristics associated with adaptation to local environments. Others such as *C. maximum* with a long lived planktotrophic larva, would be expected to exhibit less genetic variation across locations. There is growing evidence to support this. In her phylogeographic study of six Pacific vermetids, Faucci (2007) demonstrated strong genetic structure even over small spatial scales in *Dendropoma gregarium* and *D. rhyssoconchum* – both species with direct development. In contrast, *Thylacodes variabilis* [as *Serpulorbis*], a species with planktotrophic development, exhibited much less genetic variation across similar geographic scales. There seems to be a high potential for cryptic species in vermetids regardless of reproductive type, however (Faucci, 2007). While more cryptic taxa may be residing within those taxa with direct development (as opposed to mixed and planktotrophic development), the prevalence of cryptic taxa may also simply be reflective of the difficulty in species recognition within this family of sessile irregularly coiled worm-snails.

Radular morphology in Vermetidae is generally assumed to be fairly uniform and of little resolving power between genera. Bandel (1984: 46) stated that because of this great intrafamilial similarity "it seems unwarranted to split the vermetids into many different genera." Morton

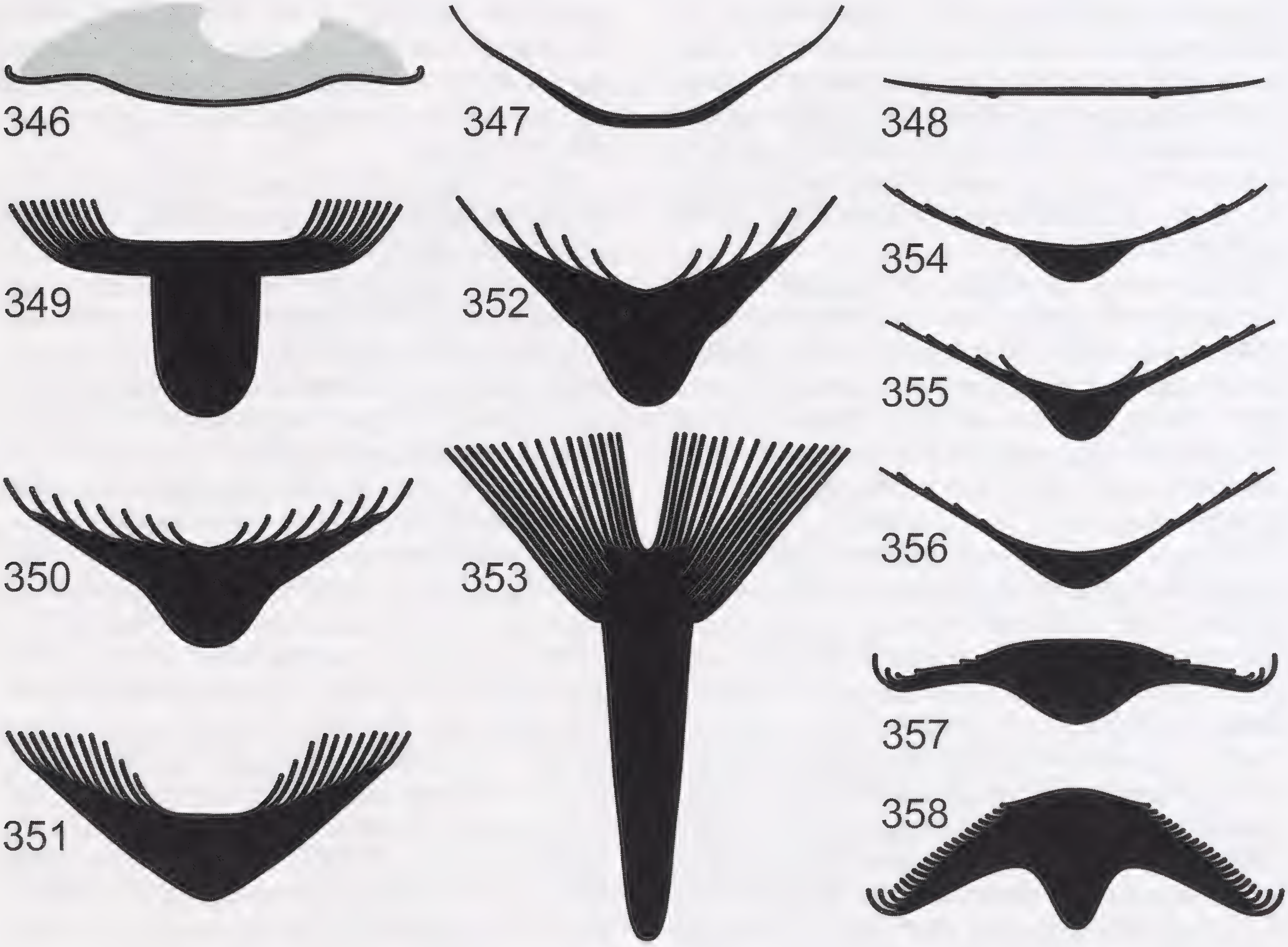

FIGS. 346–358. Cross-sectional diagrams of opercula, not drawn to scale. FIG. 346: *Cupolaconcha* spp., calcareous layer shaded gray; FIG. 347: *Ceraesignum maximum*; FIG. 348: ***Ceraesignum robinsoncrusoei*** n. sp.; FIG. 349: *Novastoa lamellosa*; FIG. 350: ***Novastoa caboverdensis*** n. sp.; FIG. 351: ***Novastoa pholetor*** n. sp.; FIG. 352: ***Novastoa batavia*** n. sp.; FIG. 353: *Novastoa* sp. (as in Table 1); FIG. 354: *Dendropoma lituella* and *Dendropoma mejillonense*; FIG. 355: *Dendropoma platypus*; FIG. 356: *Dendropoma nebulosum*; FIG. 357: *Dendropoma* cf. *petraeum*; FIG. 358: *Dendropoma* cf. *corrodens*, *Dendropoma gregarium*, *Dendropoma howense*, *Dendropoma* cf. *tholia* and ***Dendropoma expolitum*** n. sp.

(1965) recognized that radular morphology is generally conserved in Vermetidae, but identified several minor radular characters as diagnostic for *Dendropoma*. In the present study, radular characters were found to only separate the three genera *Dendropoma s.s.*, *Novastoa*, and *Ceraesignum* from *Cupolaconcha* (and perhaps other groups of vermetids) because of a few minor features on the marginal teeth, but were not useful for differentiating genera or species within those groups.

Phylogenetic Relationships

Our molecular phylogeny, inferred using mtDNA and nuclear gene regions, provided an excellent opportunity to test the integrity of the morphologically defined groups. Strong support indices were recovered for each genus and for several pairs of genera and multi-genus clades (Table 2). Likewise, the presence of a gene order change shared among all *Dendropoma s.s.* provided a robust character supporting placement of taxa within this clade. Unfortunately, the relationships between *Dendropoma s.s.*, *Ceraesignum* n. gen. and *Novastoa* were unresolved, although they form a well-supported clade within Vermetidae. Nevertheless, the results reveal the striking degree of genetic divergence between these genera and reinforce the need to introduce and re-establish genus-level taxa in the group. The sampling, albeit limited, of non-"*Dendropoma* group" taxa was sufficient to conclude decisively that *Cupolaconcha* n. gen. is not closely related to the other three genera included in this systematic revision. Overall, therefore, these molecular results provided good support for our systematic decisions.

This is the first attempt to conduct a molecular phylogenetic analysis of Vermetidae at the genus or family level, and the highly informative results suggest that an expansion of the dataset to include more of the diversity of Vermetidae will be productive. Indeed, the unusual degree of plasticity with the vermetid mtDNA genome (Rawlings et al., 2001, 2010) suggests that gene order rearrangements hold great future potential as robust phylogenetic markers defining major clades of vermetids, as already shown here for *Dendropoma s.s.* and *Cupolaconcha*. Likewise, the high levels of mtDNA sequence divergence observed within and across taxa (Rawlings et al., 2001; Faucci, 2007; Calvo et al. 2009; this study) indicates that mitochondrial gene sequences will likely prove useful in delimiting vermetid taxa (Faucci, 2007; Calvo et al., 2009; Weinberger et al., 2010), exploring biogeographic patterns of diversification (Faucci, 2007), and ultimately, in inferring the evolutionary history of the family. Given that growing evidence suggests that the Vermetidae is harboring more diversity than currently realized (Faucci, 2007; Calvo et al., 2009; this study), molecular data also offer the opportunity to uncover cryptic species of vermetids. Genetic evidence, in concert with supporting morphological and ecological data, should ultimately help us to recognize the true diversity of this family.

ACKNOWLEDGMENTS

Over the many years that led to this study numerous friends and colleagues helped us with obtaining specimens above and below the water line. We especially thank Michael Hadfield (joint field work in U.S. Virgin Islands, Florida, and hosting RB in the Hawaiian Islands); Pablo Penchaszadeh, Patricia Miloslavich and Roberto Cipriani (joint fieldwork and hosting of RB in Venezuela), Paula Mikkelsen (joint field work in Florida and Bahamas, and for providing additional material form Barbados and the Bahamas), Fred Wells (joint fieldwork and hosting of RB in Western Australia), Colin McVarish (valuable field assistance in Barbados) and Petra Sierwald (field help and scuba support in numerous locations).

Additional specimens were contributed to the study by Isabella Kappner (material from Jordan and Cape Verdes), Uriel Safriel (material from Sinai), John D. Taylor (material from the Maldives and Kenya), Stefano Schiaparelli (material from the Indo-Pacific), Jack Worsfold (material from the Bahamas), Aldo Pacheco (material from mainland Chile), Marta Calvo and José Templado (material from Spain), Tony Frias Martins and Ana Costa (material from the Azores), Anuschka Faucci (material from Hawaii and the Pacific Islands), Nicole Phillips (material from Moorea, French Polynesia), Richard and Megumi Strathmann (material from Hawaii), Louis Gosselin (material from western Canada) and Lauren Dombowsky (material from the Cayman Islands).

Formal research station visits, field workshops, and research expeditions were supported by the Bermuda Biological Station and the Bermuda Aquarium (especially Wolfgang Sterrer); Smithsonian Marine Station in Ft.

Pierce, Florida (Mary Rice, Valerie Paul, and staff); INTECMAR station in Puerto Cabello, Venezuela (Pablo Penchaszadeh); Pacific Biomedical Research Center (Michael Hadfield); West Indies Laboratory of the Fairleigh Dickinson University, St. Croix (John and Nancy Ogden); Bellairs Research Institute, Barbados (Judith Mendes, Director); Mote Tropical Research Laboratory, Summerland Key, Florida (David Vaughan); the Seventh International Marine Biological Workshop in the Houtman Abrolhos Islands, Western Australia (Fred Wells and Clay Bryce); Guana (Lianna Jarecki, The Falconwood Foundation); Abaco (Craig Layman and Friends of the Environment); and the Smithsonian Marine Station on Carrie Bow Cay, Belize (Klaus Ruetzler, Zachary Foltz, Scott Jones; Caribbean Coral Reef Ecosystems Program).

Help with loans of type and other museum material and assistance during museum visits was provided by numerous individuals, including Mandy Reid (AMS); Elizabeth Kools (CAS); Regina Kawamoto (BPBM); Sergio Letelier (MNHNC); Bruce Marshall (NMNZ); Kathie Way (NHMUK); Miroslav (Jerry) Harasewych (NMNH/Smithsonian Institution); Darryl Potter (QM); Gustav Paulay and John Slapcinsky (UF); Fred Wells and Corey Whisson (WAM); Ole Tendal and Antonia Vedelsby (ZMC).

Assistance with molecular procedures, including collecting, assembling and annotating nucleotide sequence data, was provided by the following summer research students at Cape Breton University: Samantha Lawrence, Martin MacInnis, Crystal MacLeod, and Kurt Simmons. As so often before, Howard Don Cameron (University of Michigan) and Richard E. Petit (North Myrtle Beach) helped with linguistic and literature questions, respectively. Paul Callomon (ANSP) is thanked for help with translations from Japanese literature. Michael Hadfield and an anonymous reviewer provided valuable critique and suggestions, much but not all was followed herein.

Collecting permits were provided in the context of the listed workshops and expeditions. Fieldwork and specimen acquisition in Florida was partly supported by the Comer Science and Education Foundation, the Negaunee Foundation Ltd, the Grainger Foundation, and Field Museum's Department of Zoology's Marshall Field Fund. Specimen collecting in the protected waters of the Florida Keys was conducted under Florida Keys National Marine Sanctuary Research Permit FKNMS-2009-024 and U.S. Fish and Wildlife Service Special Use Permit 41580-2010-20 (and earlier issues of these permits) for work in the National Wildlife Refuges. RB's participation of the IOC 1997 expedition aboard the R/V Carlos Porter to the Chilean Juan Fernández Archipelago and Desventuras Islands was supported under National Geographic Foundation grant 5257 to Mark Westneat and Brian Dyer. Major funding for this project was provided under National Science Foundation awards DBI-0841760/0841777.

LITERATURE CITED

ABBOTT, R. T., 1974, *American Seashells, 2nd edition.* Van Nostrand Reinhold, New York, U.S.A., 663 pp.

ADAMS, H. & A. ADAMS, 1853–58, *The genera of Recent Mollusca; arranged according to their organization.* John van Voorst, London, 2 vols. [1: 1–256, pls. 1–32 (1853); 1: 257–484 (1854); 2: 1–92, pls. 33–72 (1854); 2: 93–284, pls. 73–96 (1855); 2: 285–412, pls. 97–112 (1856); 2: 413–540, pls. 113–128 (1857); 2: 541–660, pls. 129–138 (1858)].

ANGULO, R. J., P. C. F. GIANNINI, K. SUGUIO & L. C. R. PESSENDA, 1999, Relative sea-level changes in the last 5500 years in southern Brazil (Laguna-Imbituba region, Santa Catarina State) based on vermetid ^{14}C ages. *Marine Geology*, 159: 323–339.

ANGULO, R. J., L. C. R. PESSENDA & M. C. DE SOUZA, 2002, O significado das datações ao ^{14}C na reconstrução de paleoníveis marinhos e na evolução das barreiras quaternárias do litoral paraense. *Revista Brasileira de Geociências*, 32: 95–106.

ANTONIOLI, F., R. CHEMELLO, S. IMPROTA & S. RIGGIO, 1999, *Dendropoma* lower intertidal reef formations and their palaeoclimatological significance, NW Sicily. *Marine Geology*, 161: 155–170.

BANDEL, K., 1984, The radulae of Caribbean and other Mesogastropoda and Neogastropoda. *Zoologische Verhandelingen*, 214: 1–188, pls. 1–22.

BANDEL, K. & T. KOWALKE, 1997, Cretaceous *Laxispira* and a discussion on the monophyly of vermetids and turritellids (Caenogastropoda, Mollusca). *Geologica et Palaeontologica*, 31: 257–274.

BARNARD, K. H., 1963, Contributions to the knowledge of South African marine Mollusca. Part III. Gastropoda: Prosobranchiata: Taenioglossa. *Annals of the South African Museum*, 47(1): 1–199.

BIELER, R. & R. E. PETIT, 2011, Catalogue of the Recent and fossil "worm-snail" taxa of the families Vermetidae, Siliquariidae, and Turritellidae (Mollusca: Caenogastropoda). *Zootaxa*, 2948: 1–103.

BIELOKRYS, L. S., 1999, Small vermetids (Gastropoda) from the Mandrikovka beds. *Paleontologicheskii Zhurnal*, 5: 34–40, pl. 1.

BIONDI, S., 1859 ["1857"], Descrizione di alcune specie malacologiche nuove che vivono nel nostro littorale. Memoria 2.a. *Atti dell' Accademia Gioenia di Scienze Naturali di Catania*, (Ser. 2), 1: 113–123, 1 pl.

BIVONA-BERNARDI, A., 1832, Caratteri di un nuovo genere di conchiglie fossili, estratti dalle Collettanee di Storia naturale, opera manoscritta del barone Antonino Bivona Bernardi. *Effemeridi Scientifiche e Letterarie per la Sicilia*, 1: 55–62, pl. 1; 2: 3–8, pl. 2.

CALVO, M., J. TEMPLADO, M. OLIVERIO & A. MACHORDOM, 2009, Hidden Mediterranean biodiversity: molecular evidence for a cryptic species complex within the reef building vermetid gastropod *Dendropoma petraeum* (Mollusca: Caenogastropoda). *Biological Journal of the Linnean Society*, 96: 898–912.

CALVO, M., J. TEMPLADO & P. E. PENCHASZADEH, 1998, Reproductive biology of the gregarious Mediterranean vermetid gastropod *Dendropoma petraeum*. *Journal of the Marine Biological Association of the United Kingdom*, 78: 525–549.

CARPENTER, P. P. 1857, *Catalogue of the collection of Mazatlan shells in the British Museum collected by Frederick Reigen*. London, xii + 552 pp.

CHENU, J. C., 1843–1845, G[enus] *Vermetus*. *Illustrations Conchyliologiques*. [no text; pl. 1, 1843; pls. 2–5, 1844; pl. 5*, 1845].

CLESSIN, S., 1901–1912, Die Familie Vermetidae. *Systematisches Conchylien-Cabinet von Martini und Chemnitz*, 6(6), 1–124, pls. 1–15. [1–8, pls. 1–12, 1901; 36–80, pl. 13, 1902; 81–104, 1903; pls. 14–15. 1904; 105–124, 1912; pp. 9–35 are on Caecidae].

COCCO, A., 1832, Su di alcuni nuovi crustacei de' mari di Messina. *Effemeridi Scientifiche e Letterarie*, 1(2): 203–209, 1 pl.

COLEMAN, F. C. & S. L. WILLIAMS, 2002, Overexploiting marine ecosystem engineers: potential consequences for biodiversity. *Trends in Ecology and Evolution*, 17: 40–44.

COLGAN, D. J., W. F. PONDER, E. BEACHAM & J. MACARANAS, 2007, Molecular phylogenetics of Caenogastropoda (Gastropoda: Mollusca). *Molecular Phylogenetics and Evolution*, 42: 717–737.

COLLINS, T. M., 1996, Molecular comparisons of transisthmian species pairs: Rates and patterns of evolution. Pp. 303–334, in: J. B. C.Jackson, A. F. Budd & A. G. Coates, eds., *Evolution and environment in tropical America*. University of Chicago Press, Chicago, ix + 425 pp.

COSSMANN, M., 1912, Loxonematacea (fin). *Essais de Paléoconchologie Comparée*. Privately printed, Paris, Livraison 9, 215 pp., 10 pls.

COSSMANN, M. & A. PEYROT, 1922, Conchologie Néogénique de l'Aquitaine. Tome IV Gastropodes (suite). Livraison I. *Actes de la Société Linnéenne de Bordeaux*, 73: 1–322, pls. 1–7.

CRISCIONE, F. & W. F. PONDER, 2012, A phylogenetic analysis of rissooidean and cingulopsoidean families (Gastropoda: Caenogastropoda). *Molecular Phylogenetics and Evolution*, http://dx.doi.org/10.1016/j.ympev.2012.11.026

DACCARETT, E. Y. & V. S. BOSSIO, 2011, *Colombian seashells from the Caribbean Sea*. L'Informatore Piceno, Ancona, Italy, 384 + 16 pp.

[DA COSTA, E. M.], 1770–1771, *Conchology, or natural history of shells*. [London]. 26 pp., 12 pls. [an unfinished anonymous publication, often attributed to Humphrey. See Jackson (1937) and Whitehead (1977).]

DALL, W. H., 1881, [Reports on the results of dredging, under the supervision of Alexander Agassiz, in the Gulf of Mexico (1877–78) and in the Caribbean Sea (1879–80) by the U.S. Coast Survey Steamer "Blake", Lieut.-Commander C. D. Sigsbee, U.S.N., and Commander J. R. Bartlett, U.S.N., commanding.] XV. Preliminary report on the Mollusca. *Bulletin of the Museum of Comparative Zoology*, 9(2): 33–144.

DALL, W. H., 1889, [Reports on the results of dredging, under the supervision of Alexander Agassiz, in the Gulf of Mexico (1877–78) and in the Caribbean Sea (1879–80) by the U.S. Coast Survey Steamer "Blake", Lieut.-Commander C. D. Sigsbee, U.S.N., and Commander J. R. Bartlett, U.S.N., commanding.] XXIX. Report on the Mollusca. Part II. Gastropoda and Scaphopoda. *Bulletin of the Museum of Comparative Zoology*, 18: 1–492, pls. 10–40.

D'ARGENVILLE, A.-J. D. [FAVANNE, J. de & J. G. de FAVANNE], 1780, *La conchyliologie ou histoire naturelle des coquilles de mer, d'eau douce, terrestres et fossile; avec une traité de la zoomorphose, ou représentation des animaux qui les habitent: ouvrage dans lequel on trouve une nouvelle méthode de les diviser*. Troisième édition. 3 vols. De Bure. vol. 1: frontispiece + i–iv + [i] + ai–aiii + i–iv, plate, ix–lx + 1878; vol. 2: frontispiece + 1–848.; vol. 3: frontispiece + pls. 1–80.

DARRIBA, D., G. L. TABOADA, R. DOALLO & D. POSADA, 2012, jModelTest 2: more models, new heuristics and parallel computing. *Nature Methods*, 9: 772.

DAUDIN, F. M., 1800, *Recueil de mémoires et de notes sur des espèces inédites ou peu connues de mollusques, de vers et de zoophytes, orné de gravures*. Fuchs, Treuttel & Wurtz, Paris, i–xviii, 19–50, 4 pls. [pre-5 November 1800].

DAVILA, [P. F.], 1767, *Catalogue systématique et raisonné des curiosités de la nature et de l'art: qui composent le cabinet de M. Davila*. Chez Briasson, Paris, Vol. 1: xxxv + [1] + 571.

DILLWYN, L. W., 1817, *A descriptive catalogue of Recent shells, arranged according to the Linnean method; with particular attention to the synonymy*. J. & A. Arch, London, U.K., Vol. 2: 581–1092 + index.

DI TOMMASO, P., S. MORETTI, I. XENARIOS, M. OROBITG, A. MONTANYOLA, J. -M. CHANG, J. F. TALY & C. NOTREDAME, 2011, T-Coffee: a web server for the multiple sequence alignment of protein and RNA sequences using structural information and homology extension. *Nucleic Acids Research*, 39 (Suppl. 2): W13–W17.

EKAWA, K. & Y. SAKASHITA, 2013, Notes on *Dendropoma dragonella* (Okutani, 1975) (Gastropoda: Vermetidae) from Kagoshima Prefecture, Japan. *Chiribotan*, 42(1–4): 5–10.

FAUCCI, A., 2007, *The influence of larval dispersal potential on speciation, phylogeography, and genetic population structure in two Pacific marine snail groups.* PhD. Dissertation, University of Hawai'i, U.S.A., 136 pp.

FINLAY, H. J., 1926, A further commentary on New Zealand molluscan systematics. *Transactions of the New Zealand Institute*, 57: 320–485, pls. 18–23 [23 December].

FUKUDA, H., 1993, *Marine Gastropoda (Mollusca) of the Ogasawara (Bonin) Islands Part 1: Archaeogastropoda and Neotaenioglossa.* Tokyo Metropolitan University, Tokyo, Japan, 85 pp, 21 pls.

GARDNER, S. M., 1989, A new vermetid from the west coast of Mexico (Gastropoda: Vermetidae). *Venus*, 48: 250–254.

GISCHLER, E. & R. N. GINSBURG, 1996, Cavity dwellers (coelobites) under coral rubble in southern Belize barrier and atoll reefs. *Bulletin of Marine Science*, 58: 570–589.

GOREN, M. & B. S. GALIL, 2001, Fish biodiversity in the vermetid reef of Shiqmona (Israel). *Marine Ecology*, 22: 369–378.

GRAY, J. E., 1842, [*Mollusca*], pp. 48–92. In: *Synopsis of the contents of the British Museum*, [44th Ed.]. British Museum, London, [iv] + 308 pp.

GRAY, J. E., 1847, A list of the genera of Recent Mollusca, their synonyma and types. *Proceedings of the Zoological Society of London*, 15: 129–219.

GRAY, J. E., 1850, [text]. In: M. E. Gray, *Figures of molluscous animals, selected from various authors.* Longman, Brown, Green & Longmans, London, Vol. 4: iv + 219 pp. [August].

GRAY, J. E., 1854, *List of the shells of Cuba in the collection of the British Museum, collected by M. Ramon de la Sagra, described by Prof. Alcide d'Orbigny, in the "Histoire de l'Ile de Cuba."* British Museum, London, 48 pp.

HADFIELD, M. G., 1970, Observations on the anatomy and biology of two Californian vermetid gastropods. *The Veliger*, 12: 301–309.

HADFIELD, M. G., 1989, Latitudinal effects on juvenile size and fecundity in *Petaloconchus* (Gastropoda). *Bulletin of Marine Science*, 45: 369–376.

HADFIELD, M. G., E. A. KAY, M. U. GILLETTE & M. C. LLOYD, 1972, The Vermetidae (Mollusca: Gastropoda) of the Hawaiian Islands. *Marine Biology*, 12: 81–98.

HARTMAN, O., 1959, Catalogue of the polychaetous annelids of the World. *Allan Hancock Foundation Publications Occasional Paper*, 23, Part I: i–vi, 1–353; Part II: i–v, 355–628.

HEALY, J. M., 1988, Sperm morphology in *Serpulorbis* and *Dendropoma* and its relevance to the systematic position of the Vermetidae (Gastropoda). *Journal of Molluscan Studies*, 54: 295–308.

HUGHES, R. N. & A. H. LEWIS, 1974, On the spatial distribution, feeding and reproduction of the vermetid gastropod *Dendropoma maximum*. *Journal of Zoology, London*, 172: 531–547.

HUTTON, F. W., 1873, *Catalogue of the marine Mollusca of New Zealand, with diagnoses of the species.* Colonial Museum and Geological Survey Department, Wellington, xx + 116 pp., 1 pl.

[I.C.Z.N.] International Commission on Zoological Nomenclature, 1987, Opinion 1425. Suppressed: *Spiroglyphus* Daudin, 1800 and *Stoa* De Serres, 1855 (Mollusca, Gastropoda) and specific names published in combination with them. *Bulletin of Zoological Nomenclature*, 44(1): 57–58.

[I.C.Z.N.] International Commission on Zoological Nomenclature, 1999, *International Code of Zoological Nomenclature*, 4th ed. I.T.Z.N., London, xxix + 306 pp.

IREDALE, T., 1937, Middleton and Elizabeth Reefs, South Pacific Ocean. *Australian Zoologist*, 8: 232–261, pls. 15–17.

IRVING, R. A., 1995, Near-shore bathymetry and reef biotopes of Henderson Island, Pitcairn Group. *Biological Journal of the Linnean Society*, 56: 309–324.

JACKSON, J. W., 1937, A letter from George Humphrey to William Swainson, 1815. *Journal of Conchology*, 20(12): 332–337.

JONG, K. M. DE & H. E. COOMANS, 1988, Marine gastropods from Curaçao, Aruba and Bonaire. *Studies on the Fauna of Curaçao and other Caribbean Islands*, 69: 1–261, pls. 1–47.

KAPPNER, I., 1998, *Spatial distribution, population structure and feeding behaviour of the worm-snail* Dendropoma maxima *(Gastropoda, Vermetidae) in the Gulf of Aqaba.* Center for Tropical Marine Ecology (ZMT), Bremen, Germany, M.Sc. Dissertation, University of Bremen, Germany.

KAPPNER, I., S. M. AL-MOGHRABI & C. RICHTER, 2000, Mucus-net feeding by the vermetid gastropod *Dendropoma maxima* in coral reefs. *Marine Ecology Progress Series*, 204: 309–313.

KAY, E. A., 1979, Hawaiian marine shells; reef and shore fauna of Hawaii Section 4: Mollusca. *Bernice P. Bishop Museum Special Publication*, 64(4): xviii + 653 pp.

KEEN, A. M., 1961, A proposed reclassification of the gastropod family Vermetidae. *Bulletin of the British Museum (Natural History), Zoology*, 7(3): 183–213, pls. 54–55.

KEEN, A. M., 1971a, Two new supraspecific taxa in the Gastropoda. *The Veliger*, 13(3): 296.

KEEN, A. M., 1971b, *Sea shells of tropical west America – Marine mollusks from Baja California to Peru*, 2nd ed. Stanford University Press, Stanford, California, xiv + 1064 pp.

KEEN, A. M., 1980, *Siphonium*, an over-used name in Mollusca. *The Festivus*, 12(10): 125–126.

KEEN, A. M., 1983, Vermetidae of the tropical eastern Pacific. *The Western Society of Malacologists Annual Report*, 15(1982): 10.

KEEN, A. M. & M.G. HADFIELD, 1985, *Spiroglyphus* Daudin, 1800 and *Stoa* De Serres, 1855

(Mollusca, Gastropoda, Vermetidae): proposed suppression of two equivocal generic names. Z.N.(S.) 2340. *Bulletin of Zoological Nomenclature,* 42(1): 46–49.

KEEN, A. M. & J. E. MORTON, 1960, Some new African species of *Dendropoma* (Vermetidae: Mesogastropoda). *Proceedings of the Malacological Society of London*, 34(1): 36–51, pls. 2–4.

KELLY, W. C., III, 2007, Three new vermetid gastropod species from Guam. *Micronesica*, 39: 117–140.

KURODA, T., 1928, *Catalogue of the shell-bearing Mollusca of Amami-Ôshima (Ôshima, Ôsumi).* Kagoshima-ken Kyoiku Chosa-kai [Kagoshima Prefectural Educational Investigation Committee], vii + 126 pp.

LABOREL, J., F. LABOREL-DEGUEN, S. PAPAGEORGIOU, J. EVAN, P. A. PIRAZZOLI & C. S. STIROS, 2000, Seismic coastal uplift in a region of subsidence: Holocene raised shorelines of Samos Island, Aegean Sea, Greece. *Marine Geology*, 170: 41–58.

LEA, H. C., 1843, Description of some new fossil shells from the Tertiary of Virginia. *Proceedings of the American Philosophical Society*, (new ser. 3): 162–165.

LINK, H. F., 1807, *Beschreibung der Naturalien-Sammlung der Universität zu Rostock. Mollusken*. Adlers Erben, Rostock, 2–3: 82–160; 4: 6–23.

MAES, V. O., 1967, The littoral marine molluscs of Cocos-Keeling Islands (Indian Ocean). *Proceedings of the Academy of Natural Sciences of Philadelphia*, 119: 93–217.

MAURY, C. J., 1922, Recent Mollusca of the Gulf of Mexico and Pleistocene and Pliocene species from the Gulf States; Part 2: Scaphopoda, Gastropoda, Amphineura, Cephalopoda. *Bulletins of American Paleontology*, 9(38): 33–173.

MIKKELSEN, P. M., R. BIELER, I. KAPPNER & T. A. RAWLINGS, 2006, Phylogeny of Veneroidea (Mollusca: Bivalvia) based on morphology and molecules. *Zoological Journal of the Linnean Society*, 148: 439–521.

MILOSLAVICH, P. A. & P. E. PENCHASZADEH, 1992, Reproductive biology of *Vermetus* sp. and *Dendropoma corrodens* (Orbigny, 1842): two vermetid gastropods from the southern Caribbean. *The Veliger*, 35: 78–88.

MONTEROSATO, T., 1884a, *Nomenclatura generica e specifica di alcune conchiglie mediterranee.* Palermo, Stab. Tipografico Virzi, 152 pp.

MONTEROSATO, T., 1884b, Conchiglie littorali mediterranee. Fam. Vermetidae. *Naturalista Siciliano*, Palermo, 4: 60–63 [a copy of the vermetid text in 1884a].

MÖRCH [as MOERCH], O. A. L., 1859, Études sur la famille des vermets. *Journal de Conchyliologie*, 7: 342–360 (June).

MÖRCH [as MOERCH], O. A. L., 1860, Études sur la famille des vermets (suite). *Journal de Conchyliologie*, 8: 27–48 (January).

MÖRCH, O. A. L., 1861, Review of the Vermetidae (Part I). *Proceedings of the Zoological Society of London*, 1861: 145–181, pl. 25 (September).

MÖRCH, O. A. L., 1862, Review of the Vermetidae (Part II.). *Proceedings of the Zoological Society of London*, 1861: 326–365 (April).

MÖRCH, O. A. L., 1877, Synopsis molluscorum marinorum Indiarum occidentalium imprimis Insularum danicarum. *Malakozoologische Blätter*, 24: 93–123.

MORHANGE, C. & P. A. PIRAZZOLI, 2005, Mid-Holocene emergence of southern Tunisian coasts. *Marine Geology*, 220: 205–213.

MORRISON, J. P. E., 1968, Spiroglyphics: a study in species association. *The American Malacological Union Inc, Annual Reports*, for 1968: 45–46.

MORTON, J. E., 1951, The structure and adaptations of the New Zealand Vermetidae. Part III. *Novastoa lamellosa* and its affinities. *Transactions and Proceedings of the Royal Society of New Zealand*, 79: 43–51, pls. 8, 9.

MORTON, J. E., 1955, The evolution of vermetid gastropods. *Pacific Science*, 9(1): 3–15.

MORTON, J. E., 1965, Form and function in the evolution of the Vermetidae. *Bulletin of the British Museum* (*Natural History*) (*Zoology*), 11(9): 585–630.

OKUTANI, T., ed., 2000, *Marine Mollusks in Japan*. Tokai University Press, Tokyo, xlviii +1,174 pp. [with contributions by multiple authors; Vermetidae (pp. 205–209) by K. Hasegawa].

OKUTANI, T. & T. HABE, 1975, [*The mollusks of Japan. (Sea snails) – I*]. Gakken Illustrated Nature Encyclopedia, Mollusca (I). Gakken, Tokyo, 301 pp.

ORBIGNY, A. D', 1841–1853, Mollusques. In: R.SAGRA, *Histoire physique, politique, et naturelle de l'Ile de Cuba*. 2 vols. and atlas [issued as of 1853, but published in parts earlier, as follows: French edition, 1: 1–264 (1841); 2: 1–112, pts. 1–7 (1842); 113–380, pts. 8–24 (by 1853; exact dates to be clarified). The Spanish ed., with title page dated 1845, translated from and published after the French ed.]

PACHECO, A. & J. LAUDIEN, 2008, *Dendropoma mejillonensis* sp. nov., a new species of vermetid (Caenogastropoda) from northern Chile. *The Veliger*, 50(3): 219–224.

PALUMBI, S.R., 1996, Nucleic acids II: the polymerase chain reaction. Pp. 205–221, in: D. M. HILLIS, C. MORITZ & B. K. MABLE, eds., *Molecular systematics*, 2nd ed. Sunderland, Massachusetts: Sinauer Associates, xvi + 655 pp.

PARK, J.K. & D. Ó FOIGHIL, 2000, Sphaeriid and corbiculid clams represent separate heterodont bivalve radiations into freshwater environments. *Molecular Phylogenetics and Evolution*, 14: 75–88.

PEYROT-CLAUSADE, M., P. HUTCHINGS & G. RICHARD, 1992, Temporal variations of macroborers in massive *Porites lobata* on Moorea, French Polynesia. *Coral Reefs*, 11: 161–166.

PHILLIPS, N. E., 2011, Where are larvae of the vermetid gastropod *Dendropoma maximum* on the continuum of larval nutritional strategies? *Marine Biology*, 158: 2335–2342.

PHILLIPS, N. E. & J. S. SHIMA, 2010, Reproduction of the vermetid gastropod *Dendropoma* *maximum* (Sowerby, 1825) in Moorea, French Polynesia. *Journal of Molluscan Studies*, 76: 133–137.

PONDER, W. F., 1967, A new species of *Dendropoma* from New Zealand (Mollusca: Vermetidae). *Transactions of the Royal Society of New Zealand*, 10(2): 17–20, pl. 1.

POWELL, A. W. B., 1979, *New Zealand Mollusca – Marine, Land and Freshwater Shells*. Williams Collins Publishers Ltd., Auckland, New Zealand, xv + 500 pp.

QUOY, [J. R. C.] & [J. P.] GAIMARD, 1834–1835, *Voyage de découvertes de l'Astrolabe exécuté par ordre du Roi, pendant les années 1826–1827–1828–1829, sur le commandement de M. J. Dumont d'Urville. Zoologie, Mollusques*. J. Tastu, Paris, Vol. 3: 1–366 (1834), 367–954 (1835), atlas 107 pls.

RAMBAUT, A. & A. J. DRUMMOND, 2007, *Tracer v1.4*, available from http://beast.bio.ed.ac.uk/Tracer

RAWLINGS, T. A., T. M. COLLINS & R. BIELER, 2001, A major mitochondrial gene rearrangement among closely related species. *Molecular Biology and Evolution*, 18: 1604–1609.

RAWLINGS, T. A., M. J. MACINNIS, R. BIELER, J. L. BOORE & T. M. COLLINS, 2010, Sessile snails, dynamic genomes: gene rearrangements within the mitochondrial genome of a family of caenogastropod mollusks. *BMC Genomics*, 11: 440. doi:10.1186/1471-2164-11-440

REHDER, H. A., 1981, *The Audubon Society field guide to North American seashells*. Alfred A. Knopf, New York, 894 pp.

RILOV, G., Y. BENAYAHU & A. GASITH, 2004, Prolonged lag in population outbreak of an invasive mussel: a shifting-habitat model. *Biological Invasions*, 6: 347–364.

RONQUIST, F. & J. P. HUELSENBECK, 2003, MrBayes 3: Bayesian phylogenetic inference under mixed models. *Bioinformatics*, 19: 1572–1574.

ROSENBERG, G., 2009, *Malacolog 4.1.1: A Database of Western Atlantic Marine Mollusca*. [WWW database (version 4.1.1)], ULR http://www.malacolog.org/

ROSENBERG, G., F. MORETZSOHN & E. F. GARCÍA, 2009, Gastropoda (Mollusca) of the Gulf of Mexico. Pp. 579–699, in: D. L. FELDER & D. K. CAMP, eds., *Gulf of Mexico – origins, waters, and biota: biodiversity*. Texas A & M Press, College Station, Texas, 1,393 pp.

SAFRIEL, U., 1966, Recent vermetid formation on the Mediterranean shore of Israel. *Proceedings of the Malacological Society of London*, 37: 27–34.

SAFRIEL, U. & M. G. HADFIELD, 1988, Sibling speciation by life-history divergence in *Dendropoma* (Gastropoda; Vermetidae). *Biological Journal of the Linnean Society*, 35: 1–13.

SCAPS, P. & V. DENIS, 2008, Can organisms associated with live scleractinian corals be used as indicators of coral reef status? *Atoll Research Bulletin*, 566: 1–18.

SCHATTNER, P., A. N. BROOKS & T. M. LOWE, 2005, The tRNAscan-SE, snoscan and snoGPS web servers for the detection of tRNAs and snoRNAs. *Nucleic Acids Research*, 2005: W686–W689.

SCHIAPARELLI, S., G. ALBERTELLI & R. CATTANEO-VIETTI, 2006, Phenotypic plasticity of Vermetidae suspension feeding: a potential bias in their use as biological sea-level indicators. *Marine Ecology*, 27: 44–53.

SCUDERI, D., 1995, Il genere *Dendropoma* (Gastropoda, Vermetidae) nel Mediterraneo. *Bollettino Malacologico*, 31(1–4): 1–6.

SERRES, M. DE, 1855, Note sur un nouveau genre d'Annélide tubicole perforant. *Annales des Sciences Naturelles*, (Ser. 4), Zoologie, 3: 238–243, pl. 8.

SHIMA, J. S., C. W. OSENBERG & A. C. STIER, 2010, The vermetid gastropod *Dendropoma maximum* reduces coral growth and survival. *Biology Letters*, 6: 815–818.

SHIMA, J. S., N. E. PHILLIPS & C. W. OSENBERG, 2013, Consistent deleterious effects of vermetid gastropods on coral performance. *Journal of Experimental Marine Biology and Ecology*, 439: 1–6.

SILENZI, S., F. ANTONIOLI & R. CHEMELLO, 2004, A new marker for sea surface temperature trend during the last centuries in temperate areas: vermetid reef. *Global and Planetary Change*, 40: 105–114.

SISMA-VENTURA, G., B. GUSNER, R. YAM, M. FINE & A. SHEMESH, 2009, The reef builder gastropod *Dendropoma petreaum* [sic] – a proxy of short and long term climatic events in the eastern Mediterranean. *Geochimica et Cosmochemica Acta*, 73: 4376–4383.

SMALLEY, T. L., 1984, Possible effects of intraspecific competition on the population structure of a solitary vermetid mollusc. *Marine Ecology Progress Series*, 14: 139–144.

SOWERBY, G. B., I, 1825, *A catalogue of the shells contained in the collection of the late Earl of Tankerville, arranged according to the Lamarckian conchological system; together with an Appendix, containing descriptions of many new species*. London, vii + 92 + xxxiv [Appendix] pp., 9 pls.

SOWERBY, G. B., II, 1839, *A conchological manual*. London, U.K., v + 130 pp., 24 pls. [pre 23 February].

STIER, A. C., C. S. McKEON & C. W. OSENBERG, 2010, Guard crabs alleviate deleterious effects of vermetid snails on a branching coral. *Coral Reefs*, 29: 1019–1022.

SUTER, H., 1913, *Manual of the New Zealand Mollusca*. John Mackay, Wellington, xxiii + 1,120 pp.

SWOFFORD, D. L., 2002, PAUP*. *Phylogenetic Analysis Using Parsimony (*and Other Methods)*. Version 4. Sinauer Associates, Sunderland, Massachussetts, U.S.A.

TAYLOR, J. B., 1975, *Planktonic prosobranch veligers of Kaneohe Bay*. Unpublished PhD dissertation, University of Hawaii, xiii + 593 pp.

THOMAS, L. H. & J. STEVENS, 1991, Communities of constructional lips and cup reef rims in Bermuda. *Coral Reefs*, 9: 225–230.

TOMLIN, J. R. le B., 1939, A new South African vermetid. *Journal of Conchology*, 21(4–5): 145, pl. 12.

TUNNEL, J. W., Jr., J. ANDREWS, N. C. BARRERA & F. MORETZSOHN, 2010, *Encyclopedia of Texas seashells; identification, ecology, distribution, and history.* Texas A & M University Press, College Station, Texas, xi + 512 pp.

TRYON, G. W., 1886, Family Vermetidae. *Manual of Conchology*, 8: 163–191, 224–257 (index and synonymy), 436–446 (plate captions), pls. 30, 49–58.

VÉLAIN, C., 1876, Sur le faune malacologique des îles Saint-Paul et Amsterdam. *Comptes Rendus des Séances de l'Académie des Sciences*, 83: 284–287.

VÉLAIN, C., 1877, Expédition Française aux îles Saint-Paul et Amsterdam. Observations générales sur la faune des deux îles suivies d'une description des mollusques. *Archives de Zoologie Expérimentale et Générale*, 6: 1–143, pls. 1–5.

VESCOGNI, A., F. R. BOSELLINI, M. REUTER & T. C. BRACHERT, 2008, Vermetid reefs and their use as palaeobathymetric markers: new insights from the Late Miocene of the Mediterranean (southern Italy, Crete). *Palaeogeography, Palaeoclimatology, Palaeoecology*, 267: 89–101.

VOKES, H. E. & E. H. VOKES, 1983, Distribution of shallow-water marine Mollusca, Yucatan Peninsula, Mexico. Mesoamerican Ecology Institute Monograph 1. *Middle American Research Institute Publication*, 54: 1–183, incl. 50 pls.

WEINBERGER, V. P., P. MILOSLAVICH & A. MACHORDOM, 2010, Distributional pattern, reproductive traits, and molecular analysis of two coexisting vermetid gastropods of the genus *Petaloconchus*: a Caribbean endemic and a potential invasive species. *Marine Biology*, 157: 1625–1639.

WHITEHEAD, P. J. P., 1977, Emanuel Mendes da Costa (1717–91) and the Conchology, or natural history of shells. *Bulletin of the British Museum (Natural History), Historical Series*, 6(1), 1–24.

WOOD, W., 1828, *Index Testaceologicus; or a catalogue of shells, British and foreign, arranged to the Linnean system; with the Latin and English names, references to authors, and places where found*, 2nd *edition*. Wood, London, xxii + [1] + 212 pp., 38 pls.

YONGE, C. M., 1932, Notes on feeding and digestion in *Pterocera* and *Vermetus*, with a discussion on the occurrence of the crystalline style in the Gastropoda. Great Barrier Reef Expedition 1928–29. *Scientific Reports*, 1: 259–281.

ZHANG, D. Y., 2011, *Antiguan shallow-water seashells – a collection with 18 years study and research of shoreline shells from Antigua and West Indies.* MDM Publishing, Wellington, Florida, xi + 211 pp.

ZVULONI, A., R. ARMOZA-ZVULONI & Y. LOYA, 2008, Structural deformation of branching corals associated with the vermetid gastropod *Dendropoma maxima*. *Marine Ecology Progress Series*, 363: 103–108.

Revised ms. accepted September 28, 2013

MALACOLOGIA, 2014, 57(1): 99–239

HISTOLOGICAL ATLAS OF FRESHWATER MUSSELS (BIVALVIA, UNIONIDAE): *VILLOSA NEBULOSA* (AMBLEMINAE: LAMPSILINI), *FUSCONAIA CERINA* (AMBLEMINAE: PLEUROBEMINI) AND *STROPHITUS CONNASAUGAENSIS* (UNIONINAE: ANODONTINI)

Andrew McElwain* & Stephen A. Bullard

Department of Biological Sciences, College of Liberal Arts and Sciences,
State University of New York at Oswego, 392 Shineman Center,
Oswego, New York 13126, U.S.A.

ABSTRACT

Freshwater mussels (Mollusca: Bivalvia: Unionoida) are a species-rich group of parasitic bivalves comprising approximately 843 nominal species in six families, including 300 species of Unionidae and five of Margaritiferidae in North America. Unionid shells have been studied extensively for the purposes of taxonomy, but less information exists about the cellular anatomy of their "soft tissues" (mantle cavity tissues and visceral tissues). No systematic histological atlas of any unionid has been published in the peer-reviewed literature, and this lack of information hinders basic and applied research topics involving freshwater mussels. Herein, we describe the tissue and cell anatomy of a representative species from each of three lineages (tribes) of Unionidae *sensu* Graf & Cummings (2006) ranging in North America: *Villosa nebulosa* (Ambleminae: Lampsilini), *Fusconaia cerina* (Ambleminae: Pleurobemini) and *Strophitus connasaugaensis* (Unioninae: Anodontini). Based on necropsy observations and light microscopy of serial histological sections, for each species we describe and compare mantle cavity tissues (i.e., tissue enclosed by mantle: mantle, adductor muscle, pedal protractor, pedal retractor, gill, foot, labial palp) and visceral organs (i.e., internal organs: esophagus, digestive diverticulum, stomach, crystalline style sac, intestine, heart, nephridium, cerebral ganglia, pedal ganglia, visceral ganglia, ovaries and testes). We also present a synoptical review of pertinent literature on histological anatomy of unionids. The present study (i) represents the first histological atlas for freshwater mussels, (ii) comprises a baseline for monitoring mussel health in aquatic ecosystems, and (iii) could assist future workers studying freshwater mussel physiology, life history, toxicology, pathology, systematics and ecology.

Key words: Histology, Unionidae, *Villosa nebulosa*, *Fusconaia cerina*, *Strophitus connasaugaensis*, Mobile River Basin.

INTRODUCTION

Diversity

The order Unionoida is a taxonomically and ecologically diverse and geographically widespread group of bivalve mollusks commonly known as "freshwater mussels" including six families (Unionidae, Margaritiferidae, Hyriidae, Etheriidae, Mycetopodidae, Iridinidae), and approximately 161 genera and 843 species, with extant representatives ranging on all continents except Antarctica. Unionidae is the largest family, with approximately 677 species, whereas there are fewer than 100 species in each of the five other mussel families. The greatest concentration of mussel species occurs in the inland waters of North America, with a total of 305 species comprising Unionidae (300 spp.) and Margaritiferidae (five spp.) (Gangloff et al., 2006; Graf & Cummings, 2007; Williams et al., 2009; Jones & Neves, 2010). The southeastern United States is a biodiversity focus for unionids. For example, there are approximately 84–182 unionid species ranging in each of Alabama, Georgia,

---

*Corresponding author: andrew.mcelwain@oswego.edu

Kentucky, Mississippi and Tennessee (Williams & Neves, 1995; Gangloff et al., 2006; Williams et al., 2008, 2009; Jones & Neves, 2010). In addition to their species richness, freshwater mussels are remarkable for their unique life histories. Mussels have a parasitic larval stage (glochidium) that infects fish skin or gill before inhabiting the benthos, and gravid females exhibit parental care by withholding those larvae in their gills for several weeks or months before release. Related to parasitism, some unionids, especially lampsilines, have elaborate modifications of the mantle tissue that mimic specific prey items of the requisite host fish species, essentially acting as a "lure" to hasten transmission of glochidia to the fish (Barnhart et al., 2008). Moreover, freshwater mussels provide an array of well-documented ecosystem services (Vaughn & Hakenkamp, 2001; Atkinson et al., 2011): removing algae and bacteria from stream water, enriching the benthos with organic matter, and comprising a food resource for terrestrial and aquatic animals (Fuller, 1974; Cosgrove et al., 2007).

Conservation Status and Challenges

Many North American unionids are imperiled, specifically an estimated 71% of unionid species in the U.S. are imperiled and 40% of the unionid species in 25 states are imperiled (Williams & Neves, 1995). Furthermore, an estimated 17–37 unionid species already are extinct (Master et al., 2000). Threats to mussel biodiversity and populations include modifications to stream habitat (Hornbach, 2001, and references therein), obliteration of acceptable habitat, toxic contaminants, introduction of exotic bivalve species, and mysterious die-offs (Anderson et al., 1991; Lydeard et al., 2004; McGregor & Garner, 2004; Haag, 2012). Mussel die-offs, short-term high mortality events characterized by multitudes of dead mussels detached from their shells and/or moribund, gaping individuals, are well documented but enigmatic (Pauley, 1968; Ahlstedt & Jenkinson, 1987; Blodgett & Sparks, 1987; Havlik, 1987; Fleming et al., 1995), and most lack a well-established etiological agent or causative mechanism (Pauley, 1968; Neves, 1987). A high diversity of parasites and potential pathogens infect unionids and may impact population levels or the proportion of reproductively viable adults, but the virulence, pathogenicity and epidemiology of these myriad viral, bacterial, fungal and metazoan pathogens (Grizzle & Brunner, 2009) remains understudied relative to related symbionts that infect aquatic vertebrates. Few published descriptions exist of histopathological changes associated with infections or diseases of freshwater mussels (Baker, 1976; Pauley & Becker, 1968; Taskinen et al., 1997; Chittick et al., 2001; Zhong et al., 2011), and although chemical contaminants allegedly cause mussel die-offs, little species-specific information exists on pathological changes to mussel tissues exposed to a toxin (Newton & Cope, 2007).

Need for Histology

The justification for the histological atlas of freshwater mussels presented herein is not fundamentally different from that of an anatomical atlas for any group of organisms: cell and tissue anatomy are "bricks in the foundation" of basic research and contribute to the body of knowledge about a lineage. At present, the literature on freshwater mussels lacks a systematic, comparative atlas of histology with high resolution, color, and labeled micrographs. Herein, we describe the normal appearance, position and overall organization of cells and tissues in three freshwater mussel lineages: Lampsilini, Pleurobemini and Anodontini. Given the conservation status of freshwater mussels and the notion that they are useful as ecosystem indicators, a systematic description of the appearance of normal ("healthy") cells and tissues comprises baseline information for future studies involving not only physiology but also toxicology and histopathology. As such, we think the present study is timely and relevant to conservation biologists and wildlife managers. Beyond them, taxonomists also may find these results useful if comparable data from related species/lineages are published.

ANATOMY OF FRESHWATER MUSSELS

A complete synopsis of the available anatomical information on freshwater mussels is beyond the scope of the present work, but we provide some helpful "first stop" references below, as well as present specific details of their results in order of organ system in the subsequent sections.

Marquee synopses of the biology of freshwater mussels are provided by, among others, Burch (1973), Fuller (1974), Parmalee & Bogan (1998), Bauer & Wächtler (2001), Strayer

(2008), Williams et al. (2008), Watters et al. (2009), Cummings & Graf (2010) and Haag (2012). Anatomical information on freshwater mussels is largely based on shell morphology of adults and glochidia, while details concerning soft tissue structure mainly pertain to the reproductive system including the gill. Most of the earlier published works (late 19th century-early 20th century) consisted of invertebrate textbooks, handbooks or manuals that included a unionid as an examplar bivalve, including illustrations of the mussel and selected organ systems or cells. Work published since the early 1900's contains more detailed, species-specific anatomical treatments that include gross micrographs, histological sections and illustrations. In general, we found that high quality histological micrographs of mussel tissues were sparsely represented in the literature. In fact, with exception to a few works (some of which are detailed below), most either excluded histology or included confirmatory, low resolution histological micrographs that accompanied gross or functional anatomical treatments of the tissue, organ or system being described. The lack of that fundamental information made it difficult for us to sit at the microscope with sections of mussel tissue and reconcile specific cell types, which was an impetus for embarking on this monograph.

Cooke (1895), a general mollusk textbook, generally described gill, foot, mantle, crystalline style, heart, nephridium and gonad of bivalves and compared members of *Anodonta* and *Mytilus* spp. Brooks (1882), Howes (1885) and Girod (1889), also textbooks or dissection manuals, described the general habitus of organs of *Anodonta anatina*, and *Anodonta cygnea*, including dorsal tissues (nephridia, intestine, and adductor muscles), paired nephridia, pericardial cavity, position of intestinal limbs and gill-mantle junction. Simpson (1884) illustrated myofibers of pedal protractors and retractors fanning into the foot of *Pyganodon cataracta* (as *Anodonta fluviatilis*), and provided a helpful nervous system schematic showing ganglia forming a neural circuit and nerve fibers radiating from each ganglion. Raßbach (1912) described mantle morphology, cellular constituents of the epithelium and connective tissue, periostracum secretion and shell structure, including external and internal morphology, mineral layers, regeneration following mechanical damage, and morphology of mineral crystals. Siebert (1913) described incurrent and excurrent apertures, foot, mantle edge, labial palp, ciliated and non-ciliated columnar cells, mucus cells, granular secretory cells and sensilla. Similarly, Gutheil (1912), Splittstößer (1913), Motley (1932), Beedham (1958), Purcheon (1958) and Smith (1988) characterized specific organ systems and their associated tissues; whereas, others have described embryos (Lillie, 1895, 1897, 1898), larvae (Lefevre & Curtis, 1912; Fryer, 1961; Schwartz & Dimock, Jr., 2001), and juveniles (Lefevre & Curtis, 1912; Lasee, 1991). By phylogenetic inference, also helpful to those interested in understanding tissues of freshwater mussels are several synoptical references regarding anatomy and physiology of marine bivalves (Galtsoff, 1964; Norton & Jones, 1992; Eble, 2001; Grizel, 2003).

The unpublished dissertation by Yokley (1968) detailed the shell, mantle tissues and viscera of *Pleurobema cordatum*. Gross photographs accompanied low magnification histological sections of select tissues, and some helpful drawings of select cells highlighted in those sections were provided. Yokley's work comprises the most extensive treatment of cellular anatomy of a freshwater mussel, but we view the present contribution as a much-needed expansion of that work and including three additional unionid species. Another unpublished dissertation, by Lasee (1991), included scanning electron microscopy and some accompanying histology of larval and post-larval development of *Lampsilis cardium* (as *Lampsilis ventricosa*). It also included a study documenting the effects of cadmium on those life history stages, showing marked pathological changes to mantle, ganglia, and digestive gland.

Shell morphology of glochidia and adults is useful towards species-level or higher-level taxonomy (Graf & Cummings, 2006), but some taxonomy is based on viscera morphology (Ridewood, 1903; Ortmann, 1910a, 1911a, b; Purcheon, 1958; Pain & Woodward, 1968; Fuller, 1973; Heard & Dougherty, 1980; Smith, 1988; Mansur & Da Silva, 1990; Graf & Cummings, 2006; Avelar & Cunha, 2009). The visceral mass, gills, and mantle are typically portrayed in a lateral view to show foot, inner and outer gills, labial palps, siphon and adductors (e.g., Pain & Woodward, 1968; Fuller, 1974; Heard & Dougherty, 1980; Mansur & Da Silva, 1990). Three contributions by Ortmann included morphological details of representative species of Anodontini (Anodontinae), Pleurobemini (Unioninae) and Lampsilini

TABLE 1. Major tissue types of Alabama rainbow (*Villsoa nebulosa*), Gulf pigtoe (*Fusconaia cerina*) and Alabama creekmussel (*Strophitus connasaugaensis*).

Tissue types
Mantle edge
Middle mantle
Mantle isthmus
Non-marsupial gill
Marsupial gill
Foot
Pedal protractor/retractor
Adductor
Labial palp
Esophagus
Digestive diverticulum
Stomach
Crystalline style sac
Intestine
Cerebral ganglion
Pedal ganglion
Visceral ganglion
Statocyst
Nerve
Heart
Hemolymph vessel
Pericardial gland
Nephridium
Ovarian acinus
Testicular acinus

(Lampsilinae) (Ortmann, 1923a, b, 1924), focusing on coloration, geometry and sculpture of shell but also position, coloration and shape of the labial palps, gill and siphon papillae. Herein we describe twenty-five major tissues of *Villosa nebulosa* (Conrad, 1834), *Fusconaia cerina* (Conrad, 1838) and *Strophitus connasaugaensis* (Lea, 1858) (Table 1). *Villosa nebulosa* (Conrad, 1834) was originally described as *Unio nebulosus* by Conrad (1834). *Fusconaia cerina* (Conrad, 1838) was originally described as *Unio cerinus* by Conrad (1838). *Strophitus connasaugaensis* (Lea, 1858) was originally described as *Margaritana connasaugaensis* by Lea (1858).

MATERIALS AND METHODS

Mussels were collected by hand while snorkeling, transported to Auburn University in an aerated cooler filled with stream water from the collection site. Specimens of *Villosa nebulosa* were collected from the South Fork of Terrapin Creek near the Cleburne County Road 55 crossing (33°51'36.56"N, 85°31'28.15"W) in May 2010 (n = 36), August 2010 (n = 39) and August 2011 (n = 5), plus Shoal Creek near the Talladega National Forest Road 500 crossing (33°43'30.46"N, 85°36'05.05"W) (Table 2). *Fusconaia cerina* were collected from the Cahaba River, in shoals, upstream and downstream of a canoe launch (33°10'10.04"N, 87°01'12.73"W) located on Slab Road, Shelby County. Specimens of *Fusconaia cerina* were collected in May 2011 (n = 10), August 2011 (n = 28) and June 2012 (n = 7) (Table 3). Specimens of *Strophitus connasaugaensis* were collected from Shoal Creek near the Talladega National Forest Road 500 crossing, in May 2011 (n = 5), January 2012 (n = 3), and from Shoal Creek near the Cleburne County Road 61 crossing (33°46'14.57"N, 85°33'20.59"W), as well as from the South Fork of Terrapin Creek near the Cleburne County Road 55 crossing in August 2011 (Table 3). A separate sample of *V. nebulosa* was collected from pond and recirculating culture systems of the Alabama Aquatic Biodiversity Center (AABC; Marion, Alabama) in July 2010 (n = 20), March 2011 (n = 10) and October 2011 (n = 5) (Table 2). Hatchery-reared specimens of *Strophitus connasaugaensis* were also collected from a pond culture system at the AABC in March 2011 (n = 10) (Table 4).

In the laboratory, each mussel was measured, photographed, and, to minimize the possibility of damaging the microtome blade and simultaneously causing chatter or tears in the paraffin sections, allowed to purge sand and particulate matter for 24 h before fixation. Prior to fixation, the shell of each living mussel was propped open with a wooden dowel to enable adequate infiltration of fixative into the visceral tissues. Mussels were then immersed in 10% neutral buffered formalin for 48 h, rinsed in tap water to remove buffer salts from tissue, and dehydrated in a graded series of ethanols using a Tissue-Tek VIP E300 tissue processor (Sakura Finetek, Inc., Tokyo, Japan). Formalin-fixed mussels with shell then were de-shelled by excising mantle and musculature from the nacre with aid of a scalpel and divided into

TABLE 2. Size, site, and collection dates of Alabama rainbow (*Villosa nebulosa*) specimens used for histology. *Dorsum sectioned in a coronal plane, gonad not sectioned; †Embryos and/or glochidia present in marsupia.

	Shell size					
Specimen code	Length (mm)	Width (mm)	Height (mm)	Sex	Collection site	Collection date
TC-VN-1	31	18	11	♂	Terrapin Creek	May 8, 2010
TC-VN-2	33	22	11	♂	Terrapin Creek	May 8, 2010
TC-VN-3	25	16	9	♂	Terrapin Creek	May 8, 2010
TC-VN-4	24	14	18	♀	Terrapin Creek	May 8, 2010
TC-VN-5	46	26	17	♀†	Terrapin Creek	May 8, 2010
TC-VN-6	48	28	15	♀	Terrapin Creek	May 8, 2010
TC-VN-8	51	30	16	♀	Terrapin Creek	May 8, 2010
TC-VN-9	48	26	17	♀†	Terrapin Creek	May 8, 2010
TC-VN-10	51	29	14	♀	Terrapin Creek	May 8, 2010
TC-VN-11	41	24	12	♂	Terrapin Creek	May 8, 2010
TC-VN-12	51	28	14	♂	Terrapin Creek	May 8, 2010
TC-VN-13	47	28	13	♂	Terrapin Creek	May 8, 2010
TC-VN-14	45	27	11	♂	Terrapin Creek	May 8, 2010
TC-VN-15	45	24	14	♂	Terrapin Creek	May 8, 2010
ABC-VN-9	28	14	11	♀	Alabama Aquatic Biodiversity Center	March 10, 2011
ABC-VN-13	28	9	10	*	Alabama Aquatic Biodiversity Center	March 10, 2011
SC-VN-7	38	23	10	♂	Shoal Creek	May 20, 2011
SC-VN-8	32	19	9	♂	Shoal Creek	May 20, 2011
TC-VN-19	54	32	79	♂	Terrapin Creek	August 3, 2011
TC-VN-20	63	38	20	♂♂	Terrapin Creek	August 3, 2011
ABC-VN-16	41	23	14	♀†	Alabama Aquatic Biodiversity Center	October 25, 2011
ABC-VN-17	38	22	15	♀†	Alabama Aquatic Biodiversity Center	October 25, 2011
TC-VN-21	41	26	17	♀♀	Terrapin Creek	August 3, 2011

pieces by cutting through the visceral mass with aid of a grossing knife. The mussels sampled for histology consisted of 19 wild and four cultured *V. nebulosa* (Table 1), 29 *F. cerina* (Table 2) and 12 wild and 2 cultured *S. connasaugaensis* (Table 3): yielding 57 blocks and 416 slides from *V. nebulosa*, 111 blocks and 397 slides from *F. cerina*, and 49 blocks and 376 slides from *S. connasaugaensis*. Typically, a mussel having a shell length of 40–50 mm would render 4–6 pieces of viscera from anterior to posterior. Each sample was placed into a labeled mega tissue cassette and processed for routine paraffin embedding using the aforementioned automated tissue processor and a Tissue-Tek Thermal Console 4585/7 (Sakura Finetechnical, Tokyo, Japan). Following tissue processing, pieces of visceral mass were embedded in a mega base mold to obtain a whole dorsal to ventral profile of the body.

Before sectioning, paraffin blocks (especially needed for the visceral mass) were immersed for 1–2 min in cold water (5°C) immediately before sectioning. Paraffin blocks were serially sectioned at 4 μm thickness using a Reichert-Jung Biocut 2030 microtome (Wetzlar, Germany), immediately thereafter moved to a Boekel Scientific 145701 lighted tissue floatation bath water (Feasterville, Pennsylvania) at

TABLE 3. Size, site, and collection dates of Gulf pigtoe (*Fusconaia cerina*) specimens used for histology. *Only a small sample of gonad sectioned; †Embryos and/or glochidia present in marsupial; ‡Acini contained a mixture of small, immature ova, and larger degenerative ova.

Specimen code	Shell size Length (mm)	Width (mm)	Height (mm)	Sex	Collection site	Collection date
CR-FC-28	39	37	22	♀♀†	Cahaba River	May 28, 2011
CR-FC-29	47	45	29	♂♂	Cahaba River	May 28, 2011
CR-FC-30	43	39	25	♂♂	Cahaba River	May 28, 2011
CR-FC-31	46	41	26	♀♀†	Cahaba River	May 28, 2011
CR-FC-32	51	46	30	♂♂	Cahaba River	May 28, 2011
CR-FC-33	62	54	35	♂♂	Cahaba River	May 28, 2011
CR-FC-22	53	48	23	♂♂	Cahaba River	May 28, 2011
CR-FC-8	66	56	32	♀♀†	Cahaba River	May 28, 2011
CR-FC-11	66	53	54	♂♂	Cahaba River	May 28, 2011
CR-FC-31	49	42	23	♀♀†	Cahaba River	May 28, 2011
CR-FC-27	76	57	35	♀♀†	Cahaba River	August 15, 2011
CR-FC-22	52	43	24	♂♂	Cahaba River	August 15, 2011
CR-FC-34	58	48	30	♀	Cahaba River	August 15, 2011
CR-FC-35	48	43	27	♀	Cahaba River	August 15, 2011
CR-FC-36	49	46	25	♂	Cahaba River	August 15, 2011
CR-FC-37	50	43	25	♂	Cahaba River	August 15, 2011
CR-FC-6*	54	46	30	♂	Cahaba River	August 15, 2011
CR-FC-10*	41	36	22	♀	Cahaba River	August 15, 2011
CR-FC-12*	70	51	38	♀	Cahaba River	August 25, 2011
CR-FC-15*	55	44	30	♀‡	Cahaba River	August 25, 2011
CR-FC-17*	48	43	29	♀‡	Cahaba River	August 25, 2011
CR-FC-18*	45	41	28	♀	Cahaba River	August 25, 2011
CR-FC-20*	58	53	20	♀	Cahaba River	August 25, 2011
CR-FC-21*	65	55	38	♀	Cahaba River	August 30, 2011
CR-FC-22*	51	42	25	♀	Cahaba River	August 30, 2011
CR-FC-24*	45	38	24	♀‡	Cahaba River	August 30, 2011
CR-FC-26*	72	56	41	♀	Cahaba River	August 30, 2011
CR-FC-34	37	33	23	♀♀†	Cahaba River	July 16, 2012
CR-FC-35	41	39	28	♂♂	Cahaba River	July 16, 2012

43°C and pre-mixed with histology adhesive, and lifted with glass slides. Slides with paraffin sections were heated to 63°C for 45 min to remove excess paraffin, stained in an Sakura Finetek automated slide stainer with fume hood (Tiyoda MFG, Torrance, California, U.S.A.) using Harris's hematoxylin and eosin as per Luna (1968). Stained slides were photographed using a digital single lens reflex camera mounted on a Leica DM 2500 compound microscope (Wetzlar, Germany).

Each mussel was identified to species by the anatomical diagnostic features provided by Burch (1973) and Williams et al. (2008). Nomenclature and higher level systematics of Unionoida follows Graf & Cummings (2007), of *Galba truncatula* follows Bank (2004), and of marine representatives of Bivalvia follows Appeltans et al. (2012).

Morphological terms for Unionidae follows Giribet & Wheeler (2002), Graf & Cummings (2006) and Cummings & Graf (2010). Histologi-

TABLE 4. Size, site, and collection dates of Alabama creekmussel (*Strophitus connasauagaensis*) specimens used for histology. *Glochidia present in marsupial.

	Shell size					
Specimen code	Length (mm)	Width (mm)	Height (mm)	Sex	Collection site	Collection date
ABC-SC-1	25	12	8	♂	Alabama Aquatic Biodiversity Center	March 10, 2011
ABC-SC-2	25	12	8	♂	Alabama Aquatic Biodiversity Center	March 10, 2011
SC-SC-2	69	39	19	♂	Shoal Creek	May 19, 2011
SC-SC-3	73	42	23	♀	Shoal Creek	May 19, 2011
TC-SC-1	31	18	15	♂	Terrapin Creek	August 3, 2011
TC-SC-2	57	30	18	♂	Terrapin Creek	August 3, 2011
TC-SC-4	50	28	14	♀	Terrapin Creek	August 3, 2011
TC-SC-5	31	19	9	♂♂	Terrapin Creek	August 3, 2011
TC-SC-6	56	31	21	♀♀	Terrapin Creek	August 3, 2011
TC-SC-7	31	19	9	♂♂	Terrapin Creek	August 3, 2011
SC-SC-5	48	28	15	♀*	Shoal Creek	February 1, 2012
SC-SC-16	55	30	15	♂	Shoal Creek	May 19, 2011
TC-SC-8	41	25	18	♂	Terrapin Creek	May 8, 2010
TC-SC-9	40	23	15	♀	Terrapin Creek	May 8, 2010

cal terminology for Unionidae follows Ridewood (1903, gill), Gutheil (1912, digestive system), Nelson (1918, digestive system), Motley (1932, cardiovascular system), Atkins (1937, gill), Beedham (1958, mantle), Galtsoff (1964, renal system), Sumner (1966a, digestive system), Yokley (1968, foot, nervous system), Brand (1972, cardiovascular system), Kraemer (1978, nervous system), Woody & Holland-Bartalls (1993, stages of gametogenesis) and Henley (2007, reproductive system). General histological terminology follows Dorland (2007). Shell vouchers for each individual mussel sectioned are retained in the collection of the Aquatic Parasitology Laboratory, Auburn University.

ANATOMICAL PART

Villosa nebulosa

Shell Morphology

Valves of *Villosa nebulosa* are elliptical, moderately thin and slightly compressed. The epidermis is yellow to light brown with thick, green to black interrupted rays. The anterior margin is narrow, rounded and the posterior margin is bluntly pointed to trapezoidal. The dorsal margin is somewhat convex and the ventral shell margin is straight to slightly convex. The umbo is low directed slightly anteriorly. The posterior ridge is low, not deeply furrowed and the posterior slope is flat to concave (Figs. 1, 2) (Williams et al., 2008). The nacre is silver to white with an elliptical pallial line. The anterior adductor scar is deeply inset, perpendicular to the long axis of the shell. The posterior adductor scar is flat and obliquely oriented to the long axis of the shell. The pseudocardinal teeth are triangular, with two slightly divergent teeth on the left valve and one tooth on the right valve. Lateral teeth are long, convex in relation to the dorsal margin, with two teeth on the left valve and one tooth on the right valve (Figs. 3, 4) (Williams et al., 2008).

Gross Anatomical Features of the Mantle Cavity

Unionids can form a reduced and incomplete siphon comprising a pair of incurrent and excurrent apertures. Apertures are formed when the sinistral and dextral mantle edges are cupped and slightly overlap. The incurrent aperture of *V. nebulosa* is papillose, with uniramous, fine papillae and with shorter papillae along the excurrent aperture. Species of *Villosa* have a mottled mantle edge with brown and black transverse bars and the mottling is most pronounced along the siphonal apertures (Williams et al., 2008). Incurrent and excurrent apertures are partitioned by when the mantle edge is slightly curled and forms trapezoidal flaps (Fig. 5).

The mantle edge is pale, orange and mottled with black transverse bars that become conspicuous posteriorly along the siphonal apertures. The middle mantle extends from the pallial line to the umbo cavity and it is pallid, translucent, skin-like tissue. The mantle isthmus is translucent and trapezoidal, extending dorsally into a cleft between the left, right valves. The gills are

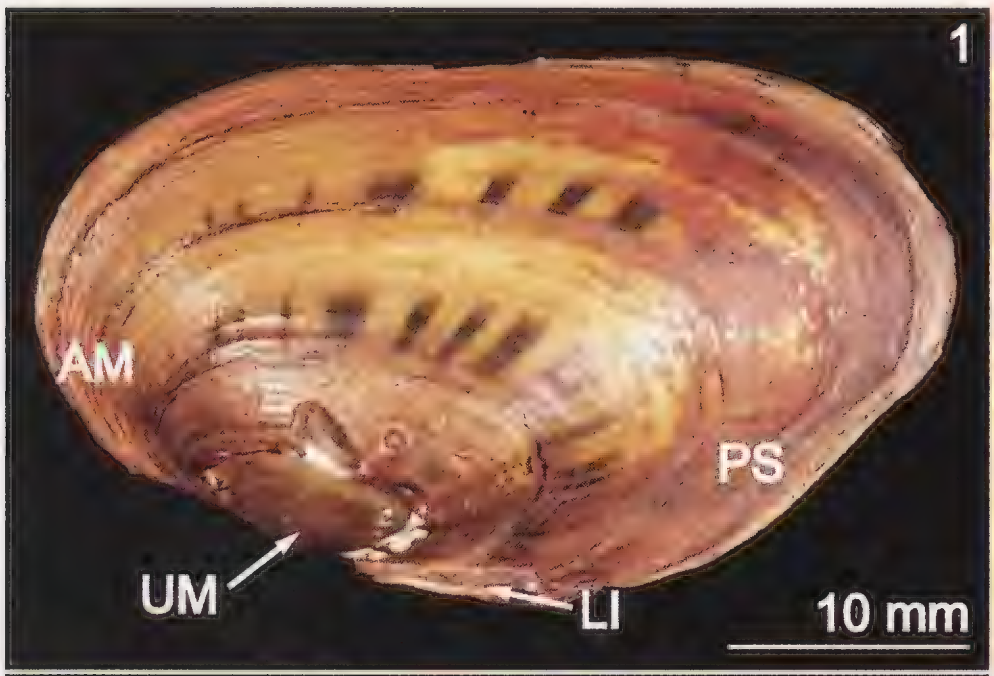

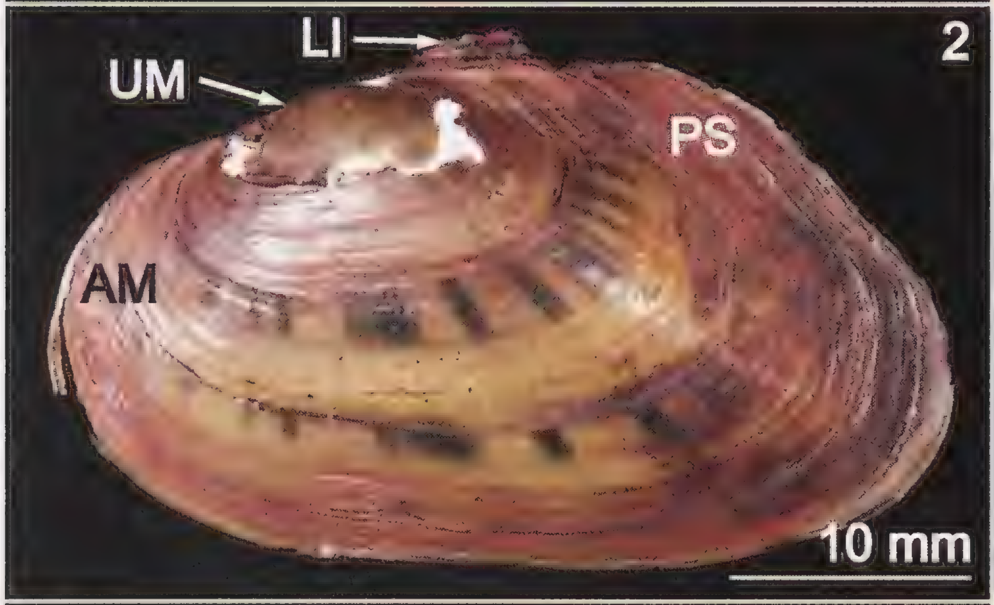

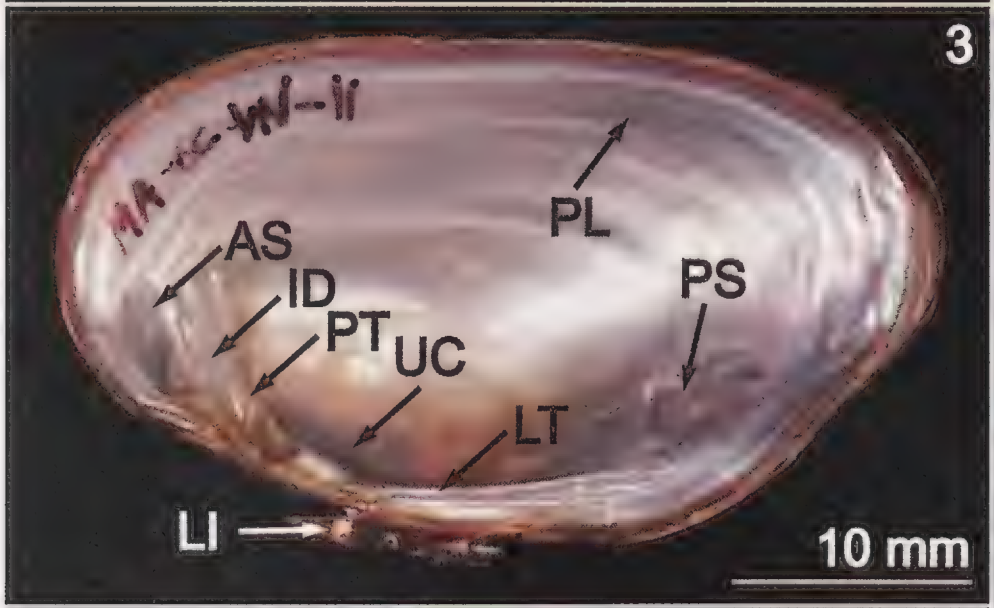

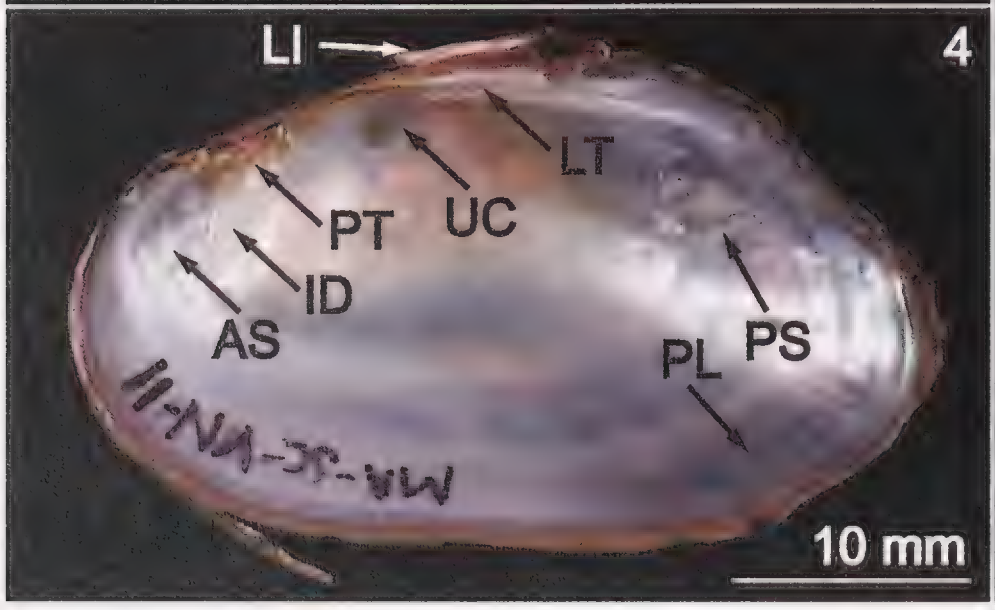

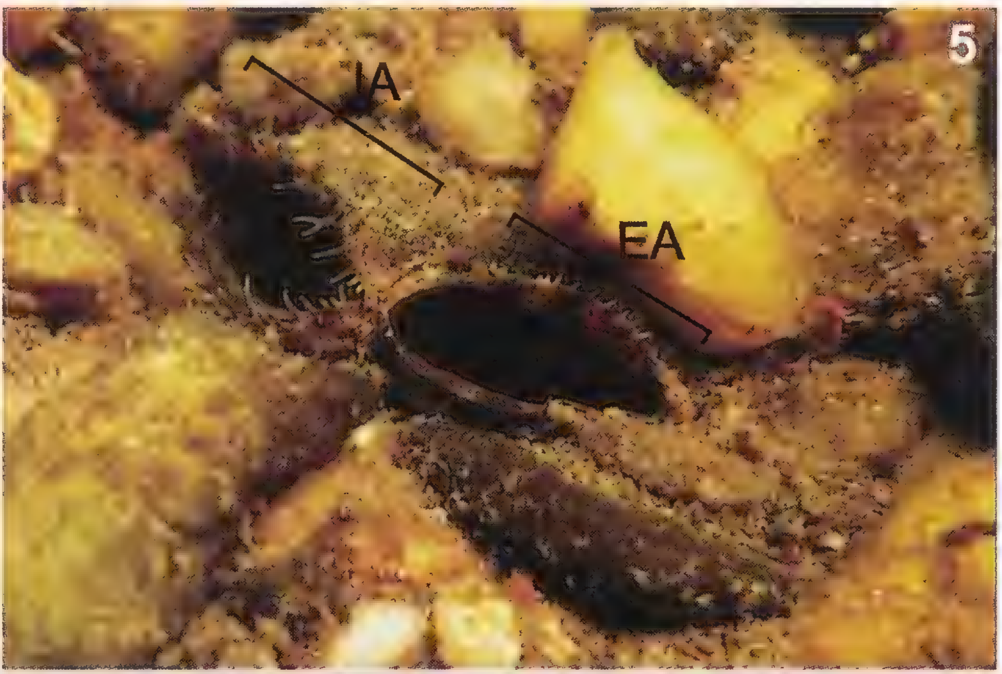

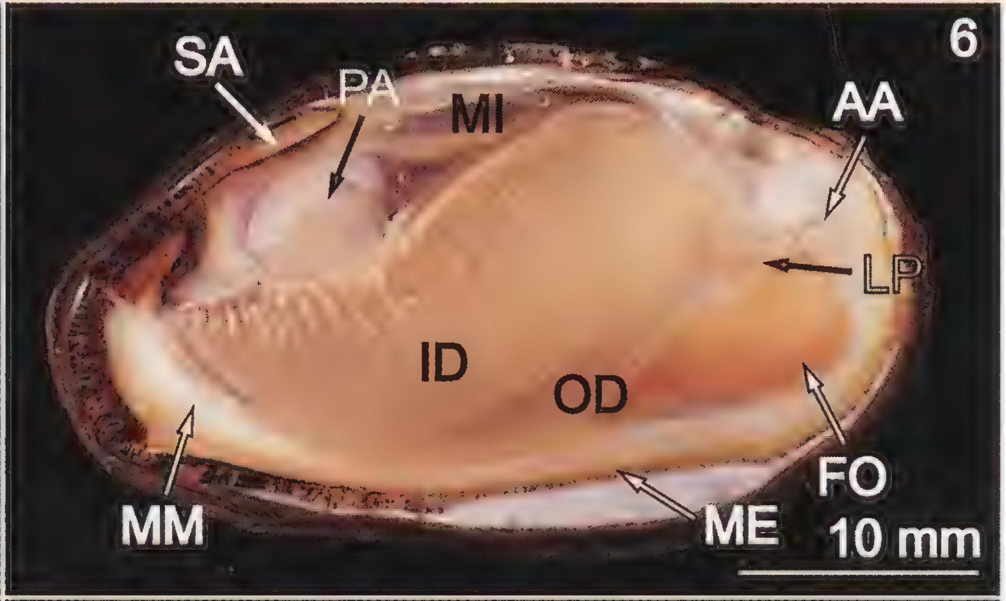

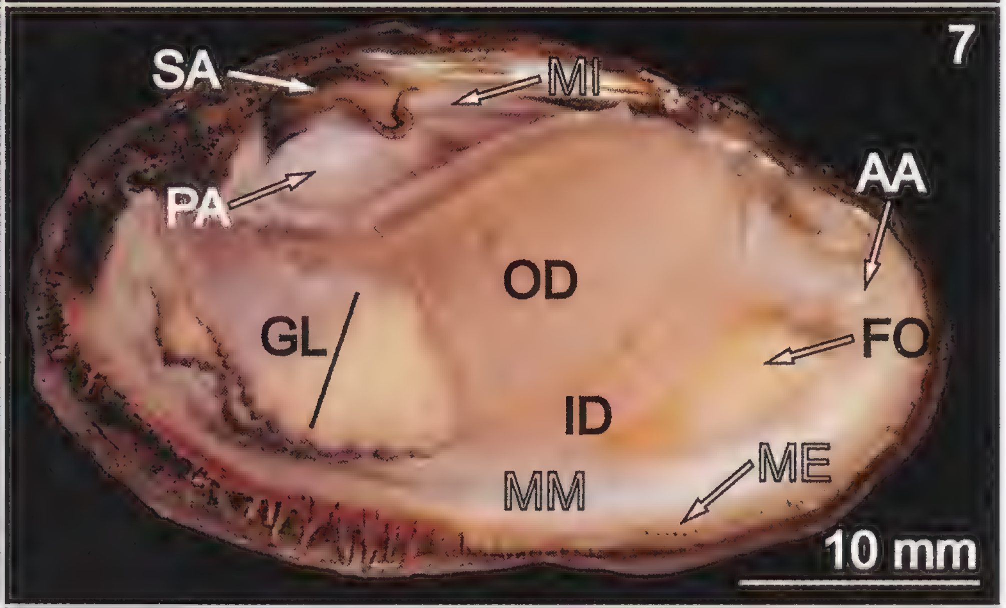

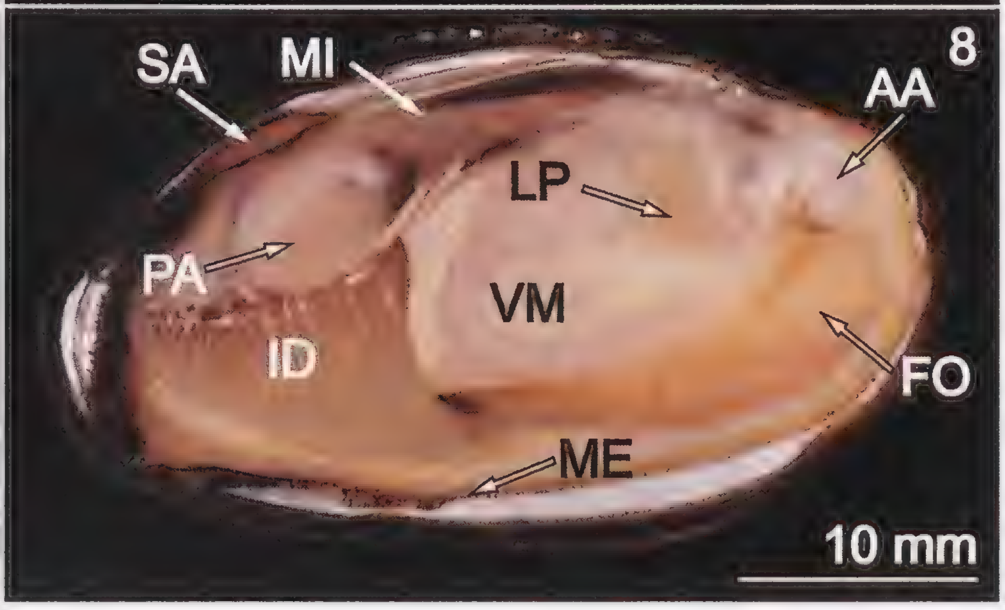

translucent, elongated sheets extending into the mantle cavity. The gills are comprised of two pairs of demibranchs located between the mantle and visceral mass. Each demibranch consists of a series of transversely oriented, ciliated filaments (Figs. 6, 7). Outer gills and inner gills resemble each other in males, but females have an enlarged group of water tubes located along the posterior third of the outer gill. Marsupia have a blackened ventral margin, and the marsupium becomes distended when filled with glochidia (Fig. 7). The apertures are sexually dimorphic; the apertures are flattened in males except for a series of fine branchial papillae. Females however, have enlarged, brown papillae (Fig. 7). The foot of *V. nebulosa* is orange, and there is a black spot located at the posterior margin. The visceral mass is white and extends dorsally to the base of the gills. Labial palps are translucent, triangular lips that extend laterally from the mouth between the foot and visceral mass. The anterior adductor is pale, white, ovular in outline, and oriented vertically between the anterior shell margin and foot. The posterior adductor is grossly identical to the anterior adductor but is parallel with the posterior shell margin (Fig. 8).

Cellular Structure of Mantle

Anterior Mantle Edge: The free distal margin of the mantle edge is lobular, with three epithelial folds, or mantle lobes, extending medially into the mantle cavity (Fig. 9). From ventral to dorsal, there is an outer lobe, a middle lobe and an inner lobe. Mantle lobe morphology varies throughout the length of the mantle edge, but for simplicity only a representative area from the anterior and posterior end will be described. A conspicuous component of the mantle edge is a ribbon of periostracum secreted by a group of cells called the basal bulb located at the base of the outer lobe (Figs. 9–12). Periostracum bends around a semicircular groove called the periostracal groove and extends medially towards the mantle cavity (Figs. 11, 12). Outer lobe is characterized by a flattened ventral margin of columnar cells (Figs. 9, 15), and the epithelium becomes pleated along the dorsal surface for approximately half the length of the outer lobe (Figs. 9, 11, 12). The epithelium becomes pleated again from the base of the middle lobe and plicae extend along the ventral surface of the mantle edge to the junction of the middle mantle (Figs. 9, 13, 14). Columnar epithelial cells of the outer lobe are characterized by a basophilic cytoplasm, and an ovular, monochromatic nucleus (Fig. 11). The simple columnar epithelium terminates at the basal bulb, where it abruptly transitions to a simple, squamous epithelium (Fig. 10). The middle lobe is ventrally flattened, with a simple squamous epithelium, transitioning to columnar epithelium from the distal margin where the slope begins to decline dorsally. Like the outer lobe epithelium, cells lining the middle lobe have monochromatic nuclei, but the cytoplasm is eosinophilic (Fig. 12). The base of the middle lobe is plicate, with several short, broadly rounded epithelial folds. Plicae span the length of the dorsal mantle

←

FIGS. 1−8. Shell morphology, and gross anatomical features of the mantle cavity of *Villosa nebulosa*. FIG. 1: Lateral view of right valve showing the rounded anterior margin (AM), compressed umbo (UM), dorsally located ligament (LI), and posterior slope (PS); FIG. 2: Lateral view of left valve showing the rounded anterior margin (AM), compressed umbo (UM), dorsally located ligament (LI), and posterior slope (PS); FIG. 3: Medial view of the left valve showing the pallial line (PL), anterior adductor scar (AS), posterior adductor scar (PS), pseudocardinal tooth (PT), interdentum (ID), umbo cavity (UC), lateral tooth (LT), and ligament (LI); FIG. 4: Medial view of the left valve showing the pallial line (PL), anterior adductor scar (AS), posterior adductor scar (PS), pseudocardinal teeth (PT), interdentum (ID), umbo cavity (UC), lateral teeth (LT), and ligament (LI); FIG. 5: Ventrolateral view of *Villosa nebulosa* (ca. 50 mm shell length) buried in gravel at Shoal Creek with its mantle cupped forming an incurrent aperture (IA) and excurrent aperture (EA); FIG. 6: Medial view of the mantle cavity with the right valve and right mantle removed to show the position of the mantle edge (ME), middle mantle (MM), foot (FO), anterior adductor (AA), labial palp (LP), inner demibranch (ID), outer demibranch (OD), posterior adductor (PA), mantle isthmus (MI), and supra-anal aperture (SA); FIG. 7: Medial view of the mantle cavity with the right valve and right mantle removed emphasizing the papillose mantle edge (ME), middle mantle (MM), foot (FO), anterior adductor (AA), inner demibranch (ID), outer demibranch (OD), marsupium (MA), glochidia (GL), posterior adductor (PA), mantle isthmus (MI), and supra-anal aperture (SA); FIG. 8: Medial view of the mantle cavity with the right valve, right mantle, and right gills removed revealing the mantle edge (ME), foot (FO), labial palp (LP), visceral mass (VM), anterior adductor (AA), left inner demibranch (ID), posterior adductor (PA), mantle isthmus (MI), and supra-anal aperture (SA).

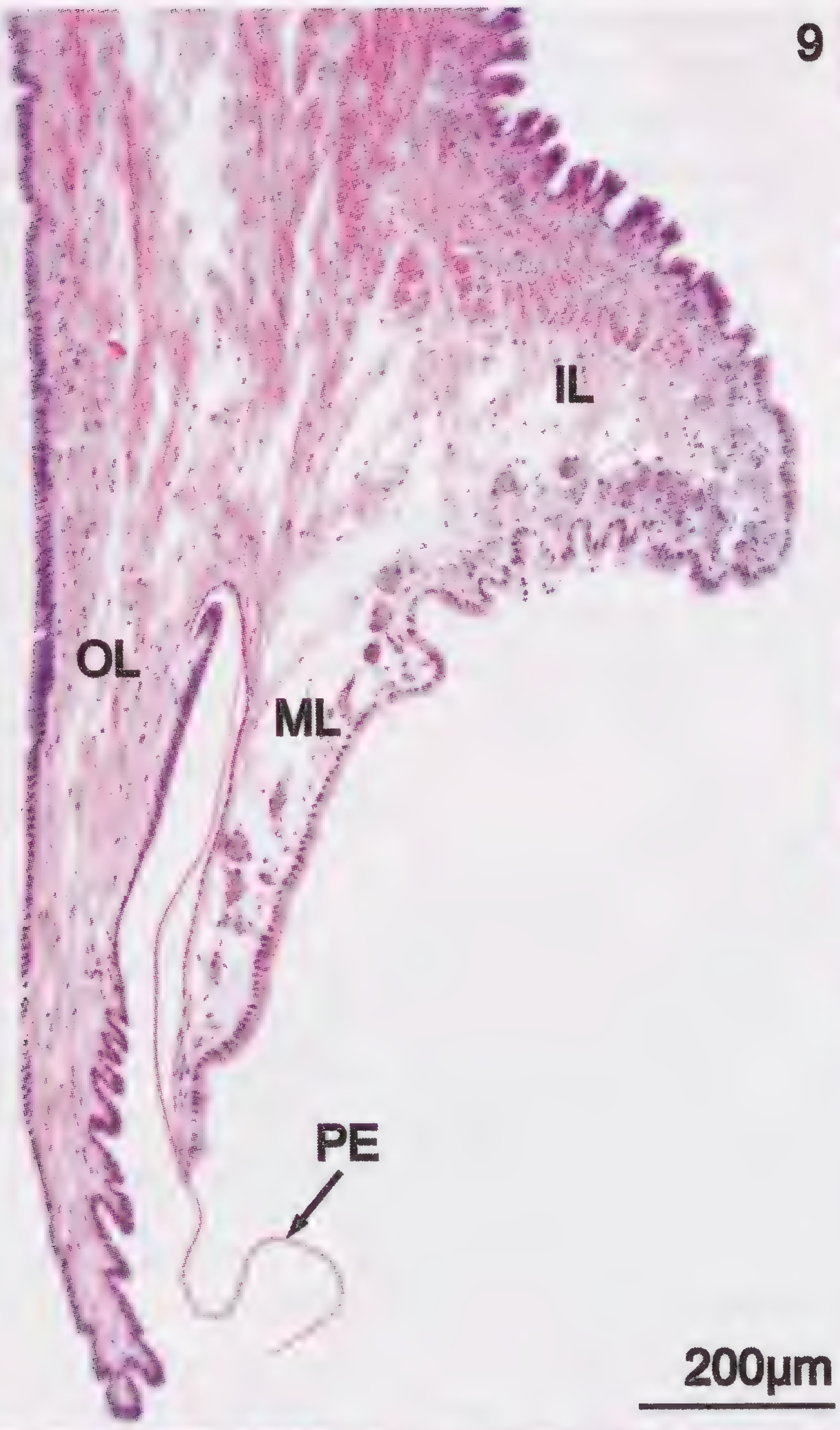
9
IL
OL
ML
PE
200µm

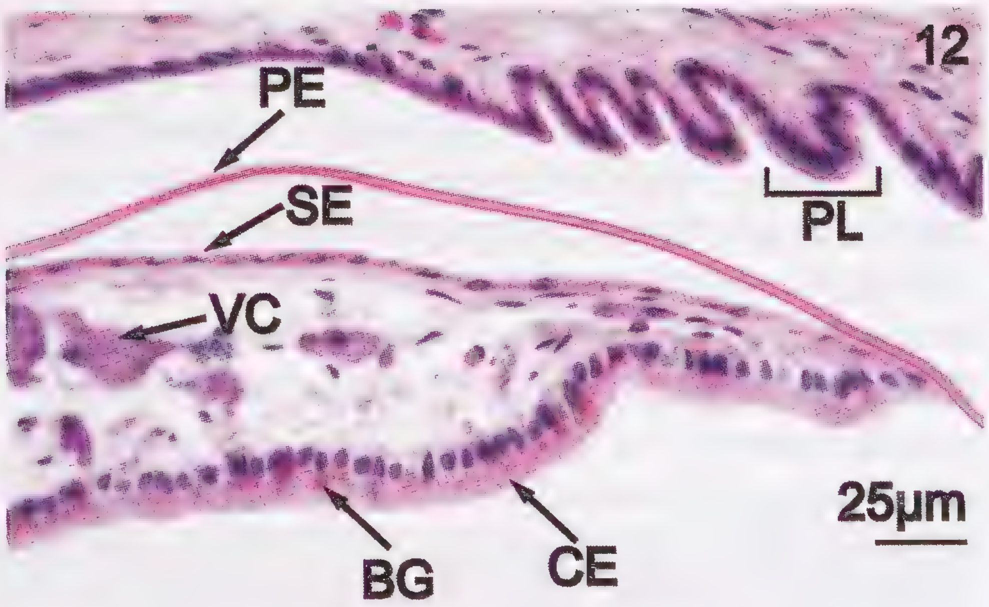
12
PE
SE
PL
VC
25µm
BG
CE

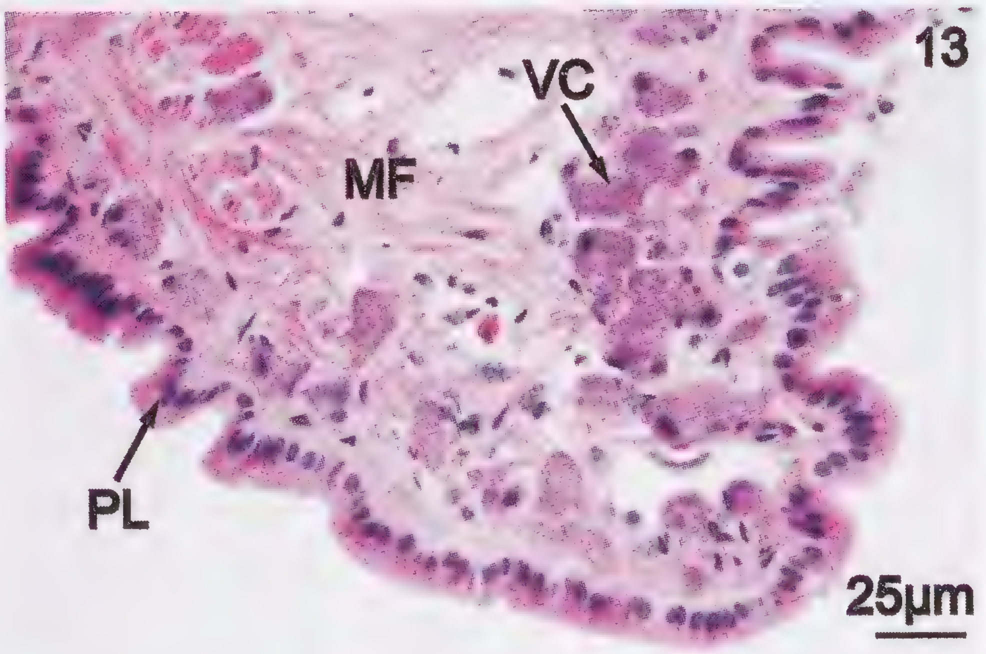
13
VC
MF
PL
25µm

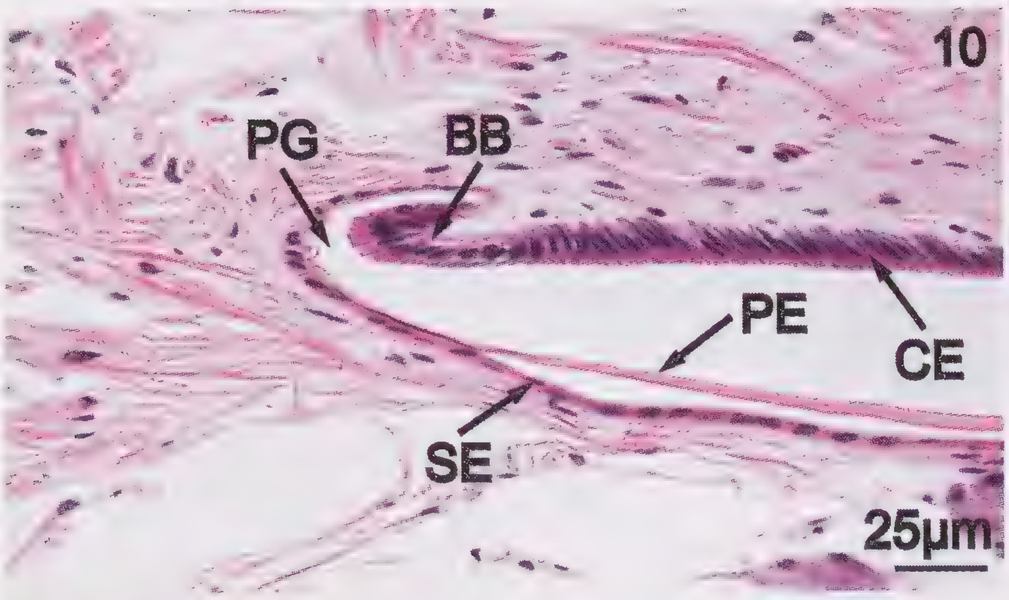
10
PG
BB
PE
CE
SE
25µm

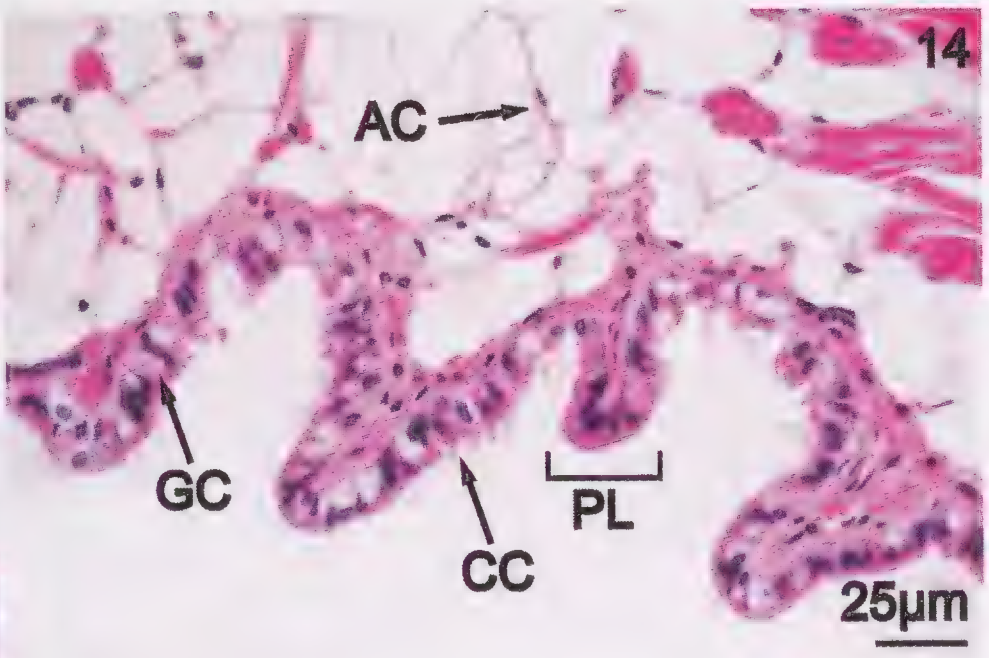
14
AC
GC
PL
CC
25µm

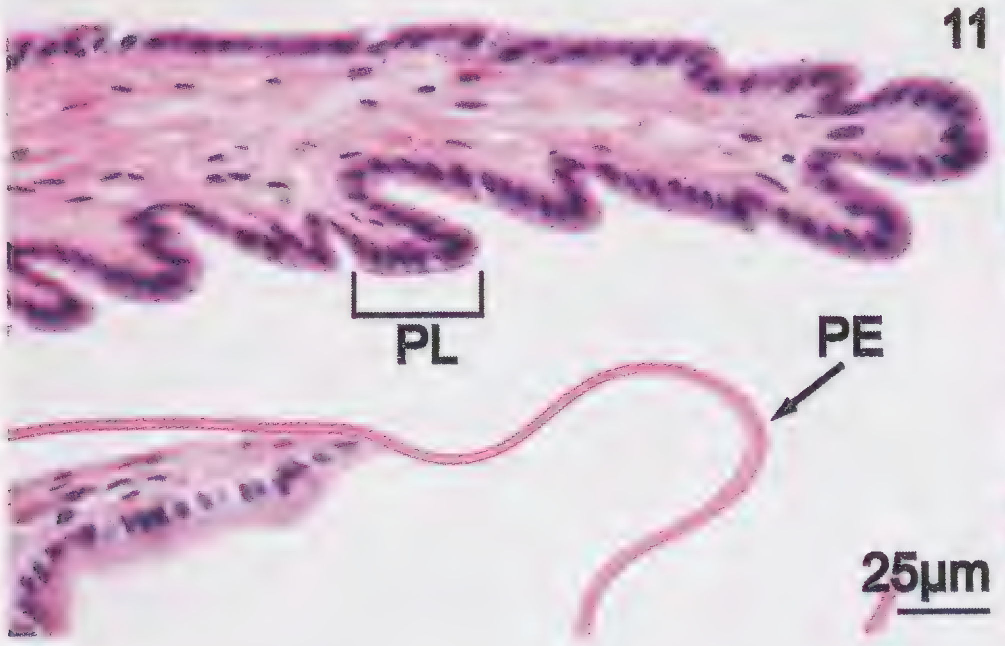
11
PL
PE
25µm

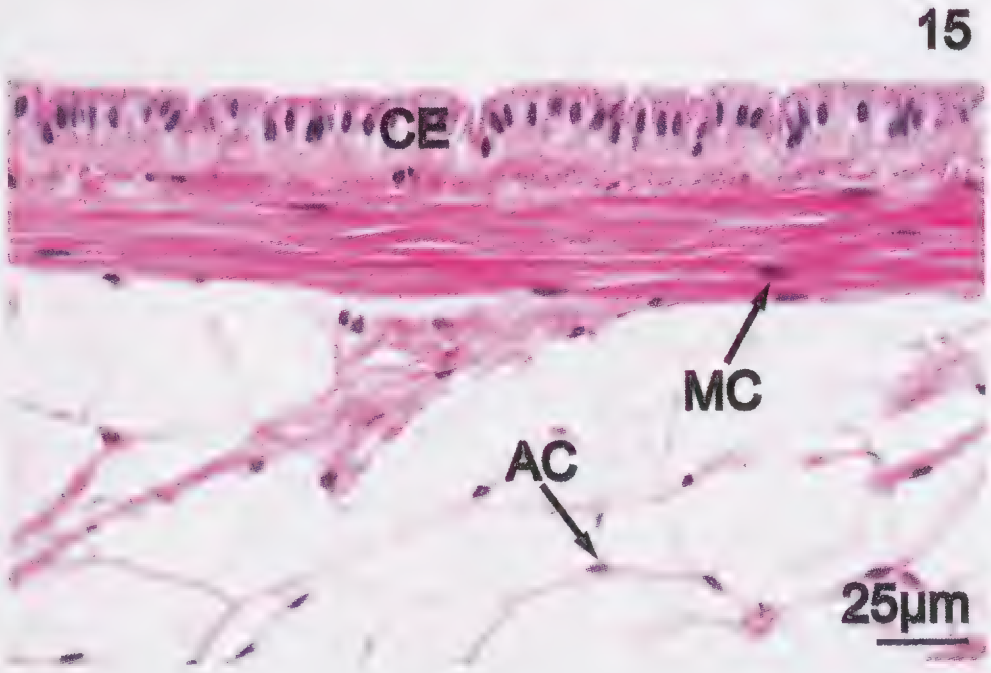
15
CE
MC
AC
25µm

edge surface from the inner lobe to the pallial line, where the dorsal surface of the mantle edge meets the nacre. However, plicae are irregularly spaced and the shape and size of each fold is variable (Fig. 13). Columnar cells continue throughout the length of the mantle edge to the pallial line. In contrast to the columnar epithelium of the outer lobe, cells representing the inner lobe have brown granular inclusions (Fig. 14).

Muscle tissue comprises the main histological constituent of mantle edge with a central region of adipose tissue (Figs. 14, 15). Fibers are organized into dense bands in the straightened, proximal portion of the mantle edge (Fig. 9) and become less regular between each lobe. Small groups of fascicles are scattered throughout a region of adipose tissue in the proximal portion of the mantle edge. Muscle fibers in the outer and middle mantle lobes are wavy but generally regular (Figs. 11, 12). Myofibers in the inner lobe become branched and overlap each other (Fig. 13). Additionally, there are spheroid cells, with a basophilic, granular cytoplasm located directly beneath the epithelium of the middle and inner lobes (Fig. 13).

Posterior Mantle Edge, Middle Mantle and Mantle Isthmus: The mantle edge becomes blackened near the posterior terminus of the visceral mass (Figs. 6–8). Epithelial cells in this region contain brown or black granules, which may be melanin. The concentration of granules in a cell may be so great that the nucleus and cytoplasm may be occluded (Figs. 16–18). Mantle lobe morphology near the posterior adductor muscle is considerably different from the morphological features characterizing the lobes near the labial palps. In the posterior region of the mantle edge, the outer and middle lobes are a forked extension of mantle tissue with each fork appearing equally long. The inner lobe is bulbous and enlarged, with conspicuous plications that have deeper crypts between each peak. Furthermore, epithelial folds around the inner lobe range from single lamellae to forked or branched papillae, giving the inner lobe a high surface area (Fig. 16). Branchial papillae are thin, conical extensions of the mantle located near the narrow, posterior shell margin. Papillae consist of an irregular matrix of muscle and connective tissue fibers surrounding an irregularly shaped hemolymph sinus. Papillae have a highly pleated surface with obliquely oriented epithelial folds directed towards the mantle cavity (Figs. 17, 18).

As the mantle tissue separates from the visceral mass, it is composed of simple, cuboidal epithelium along the shell side, and simple, squamous epithelium along the visceral side (Fig. 19). Middle mantle subepithelium consists of loose connective tissue and hemolymph. The isthmus is a tear drop-shaped extension of the mantle located dorsally in relation to the visceral mass. It originates near the esophageal-digestive gland junction and terminates posterior to the posterior adductor. The isthmus has an irregular surface with simple columnar epithelium and a fibrous subepithelium consisting of muscle and connective tissue. Columnar cells of the isthmus are basophilic with a monochromatic, elliptical nucleus (Figs. 20, 21).

Cellular Structure of Gill

Non-Marsupial Demibranch: Gills, ctenidia or demibranchs of freshwater mussels

←

FIGS. 9–15. Anterior mantle edge of *Villosa nebulosa*. FIG. 9: Transverse section of the anterior portion of the mantle edge showing the position of the outer lobe (OL), periostracal ribbon (PE), middle lobe (ML), and inner lobe (IL); FIG. 10: Transverse section of the mantle edge emphasizing columnar epithelium (CE) of the outer lobe, basal bulb (BB), periostracal groove (PG), squamous epithelium (SE) of the middle lobe, and periostracum (PE); FIG. 11: Transverse section of the distal end of outer and middle mantle lobes where obliquely oriented plicae (PL) line the outer lobe and a periostracal ribbon (PE) leaves the interlobular space; FIG. 12: Transverse section of the middle lobe showing plicae (PL), periostracum (PE), squamous epithelium (SE), violet granulocyte (VC), columnar epithelium of the dorsal surface (CE), and brown intracellular granules (BG); FIG. 13: Transverse section of inner lobe featuring plicae (PL), violet cells (VC), and myofibers (MF); FIG. 14: Transverse section of the dorsal part of the inner mantle edge emphasizing plicae (PL), ciliated columnar cells (CC), goblet cells (GC), and adipocytes (AC); FIG. 15: Transverse section of ventral epithelium of the base of the mantle edge showing columnar epithelum (CE), myocytes (MC), and adipocytes (AC).

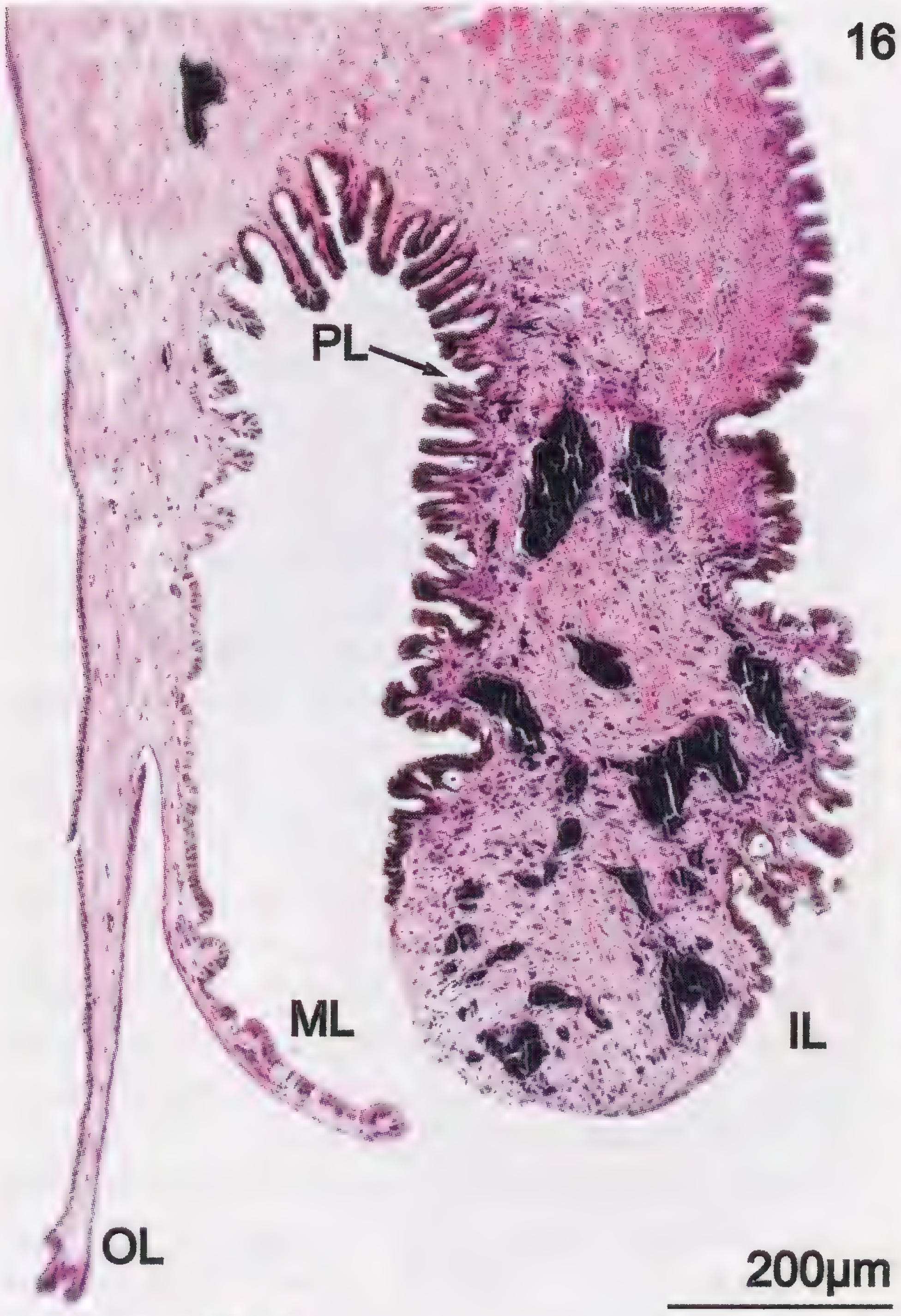
16
PL
ML
IL
OL
200µm

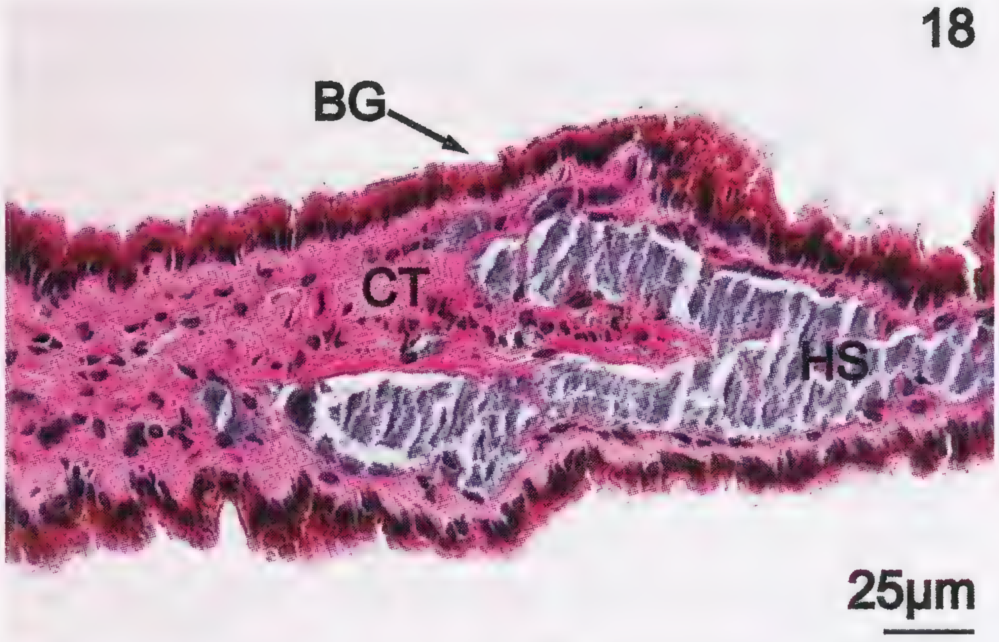
18
BG
CT
HS
25µm

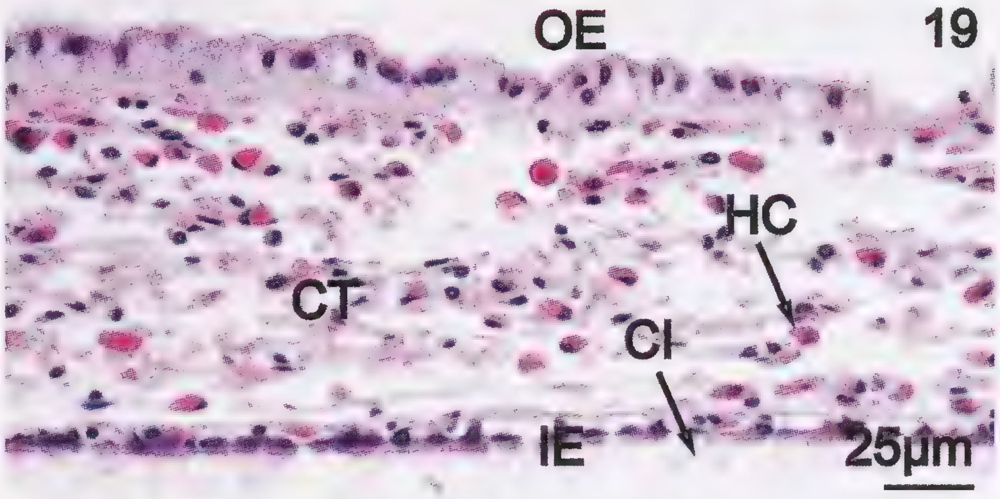
OE
19
HC
CT
CI
IE
25µm

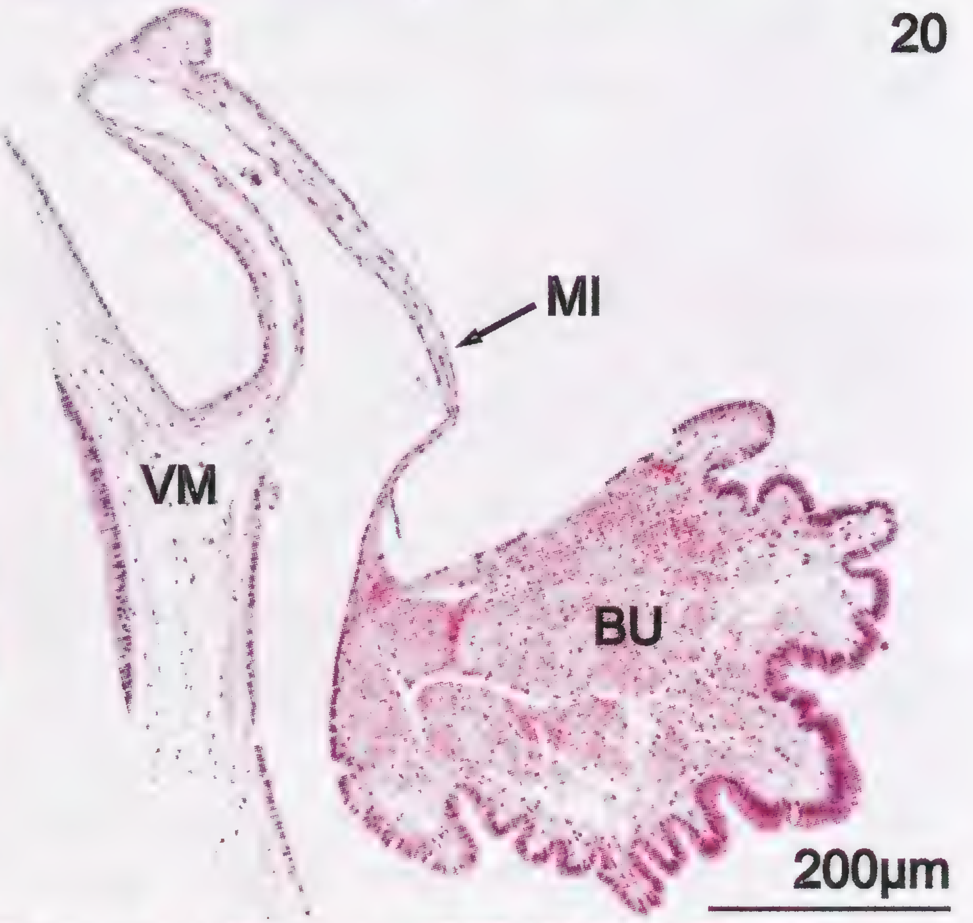
20
MI
VM
BU
200µm

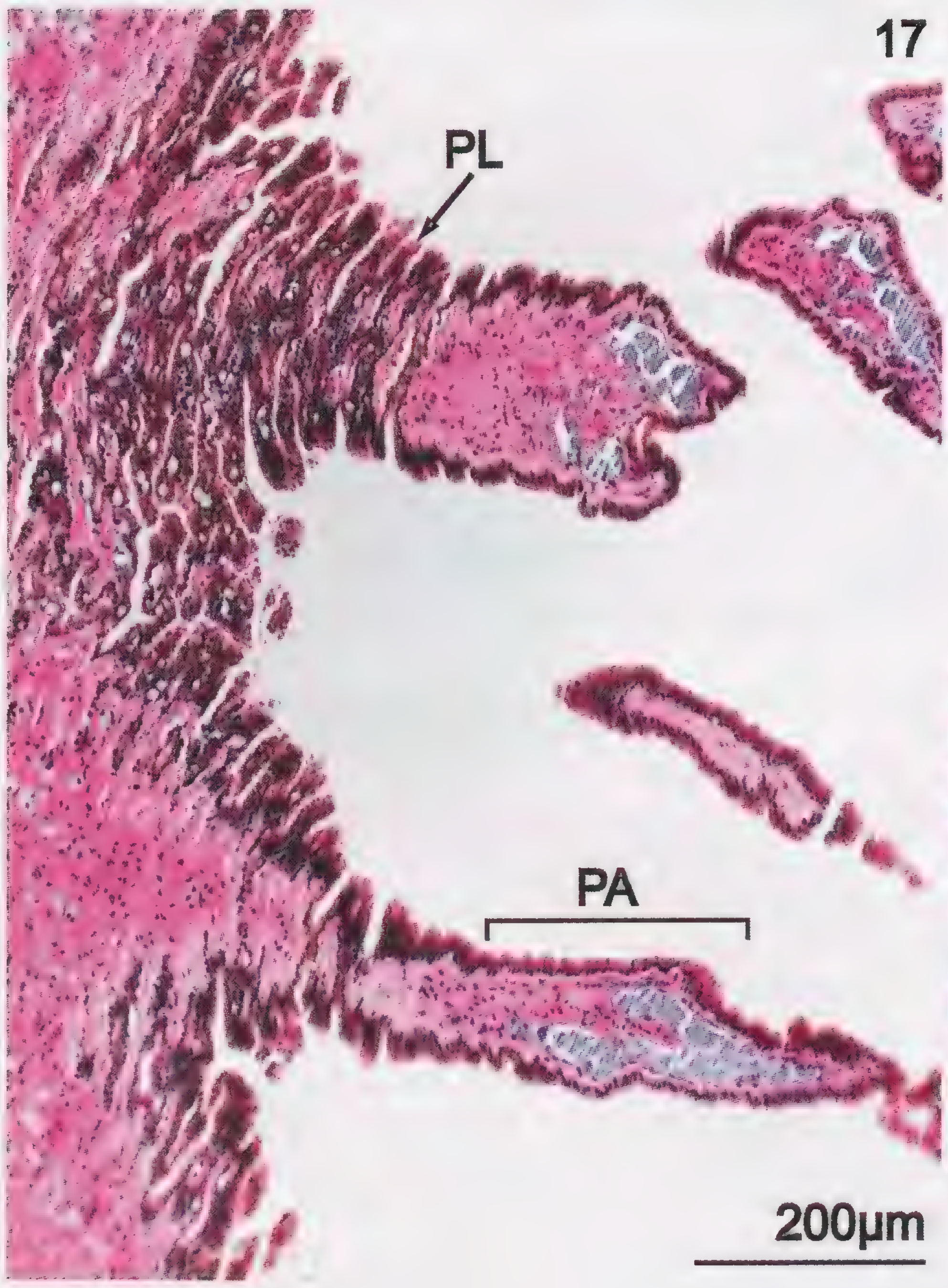
17
PL
PA
200µm

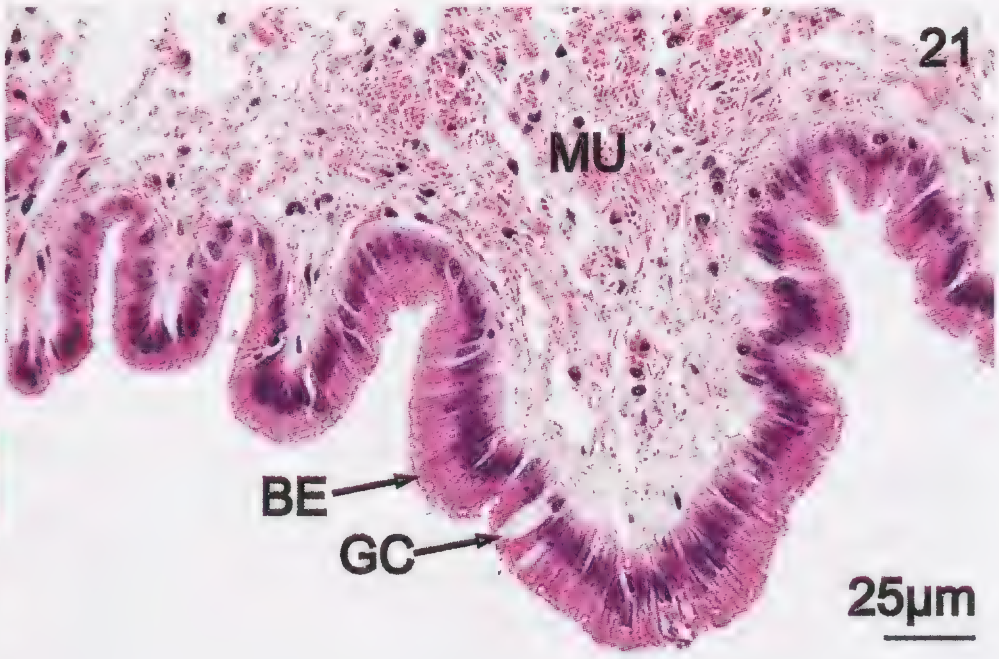
21
MU
BE
GC
25µm

(Unionoida) are paired structures extending into the mantle cavity between the mantle and visceral mass. Outer demibranchs are located medially to the mantle while inner demibranchs are lateral to the visceral mass. Each demibranch consists of an ascending and descending lamella bearing a series of cylindrical filaments running vertically along the lamellar surface. The lateral lamella of an outer demibranch is referred to as ascending whereas the medial lamella of an outer demibranch is referred to as descending. Concerning the inner demibranch, the lateral lamella is descending and the medial lamella is ascending. Ascending and descending lamellae are united by a series of interlamellar septa. When viewed in a transverse orientation, demibranchs are triangular such that one set of outer and inner demibranchs resembles a "W" (Ridewood, 1903; Brusca & Brusca, 2002; Allaby, 2003).

Demibranchs of *V. nebulosa* are nonplicate, with the main functional aspect of a ctenidium consisting of horizontally oriented, cylindrical filaments. Filaments are occasionally separated by pores called ostia (Figs. 22, 23). The inner and outer lamellae of a demibranch are generally separated from each other along the anterior-posterior axis and only joined by a small number of interlamellar septa (Fig. 22). The space between each lamella accommodates water entering through ostia and is referred to as a water tube (Fig. 23). Water travels dorsally and enters the suprabranchial cavity at the dorsal terminus of each demibranch. The superbranchial cavity is a conduit for vertical water currents created by the lateral expansion of the inner and outer lamellae. Each gill is supported with loose connective tissue and large fascicles of muscle located dorsal and lateral to each suprabranchial cavity (Figs. 26–28).

Branchial filaments are cylindrical, bearing cilia organized into three groups (lateral, latero-frontal, and frontal) along the lateral and distal surfaces. A single layer of squamous cells extends along the lateral and medial portions of each filament. Each filament is supported by a set of basophilic skeletal rods located directly under the squamous epithelium, and a pale eosinophilic matrix may be observed throughout the long axis of each filament. The medial portion of each filament contains a hemolymph sinus, or lacuna, where a preponderance of hemocytes is typically observed (Fig. 23). The inner and outer demibranchs appear to be functionally identical (except for marsupial demibranchs, see below) until the free distal tip. Outer demibranchs have a rounded ventral margin (Fig. 24) while the inner demibranchs have a furrow along the ventral surface (Fig. 25).

Ascending lamellae of inner demibranchs are united with the visceral mass anteriorly and become disconnected posteriorly at the gonopores. Ascending lamellae of inner demibranchs are fused posteriorly between the posterior margin of the visceral mass and posterior adductor (Fig. 26). Descending lamellae of inner demibranchs and descending lamellae of outer demibranchs are united with the abdomen. Furthermore, the gill tissue in this region is supported by fascicles spanning the length of the body (Fig. 27). Ascending lamellae of outer demibranchs are united with the abdomen in a medial position to the middle mantle (Fig. 28).

Marsupial Demibranch: Female *V. nebulosa* may be distinguished from males in having

---

←

FIGS. 16–21. Posterior mantle edge, middle mantle, and mantle isthmus of *Villosa nebulosa*. FIG. 16: Sagittal section of posterior mantle edge showing a thin outer lobe (OL) and middle lobe (ML) and a bulbous inner lobe (IL) featuring conspicuous plications (PL); FIG. 17: Sagittal section of posterior mantle edge characterized by conical papillae (PA) with deep, obliquely oriented plications (PL) along the surface; FIG. 18: Sagittal section of a papilla emphasizing a columnar epithelium containing brown intracellular granules (BG) as well as an irregular composition of connective tissue fibers (CT) and hemolymph sinuses (HS) within the subepithelium; FIG. 19: Transverse section of middle mantle displaying a outer epithelium (OE) of columnar cells, inner epithelium (IE) of squamous cells, cilia (CI), subepithelial connective tissue (CT), and hemocytes (HC); FIG. 20: Transverse section of mantle isthmus (MI) portraying a thin dorsal extension of tissue from the visceral mass (VM) and a terminal, dorsally located bulb (BU); FIG. 21: Transverse section of mantle isthmus bulb is emphasizing a basophilic columnar epithelium (BE) with occasional goblet cells (GC) and a subepithelium consisting of irregular muscle fibers (MU).

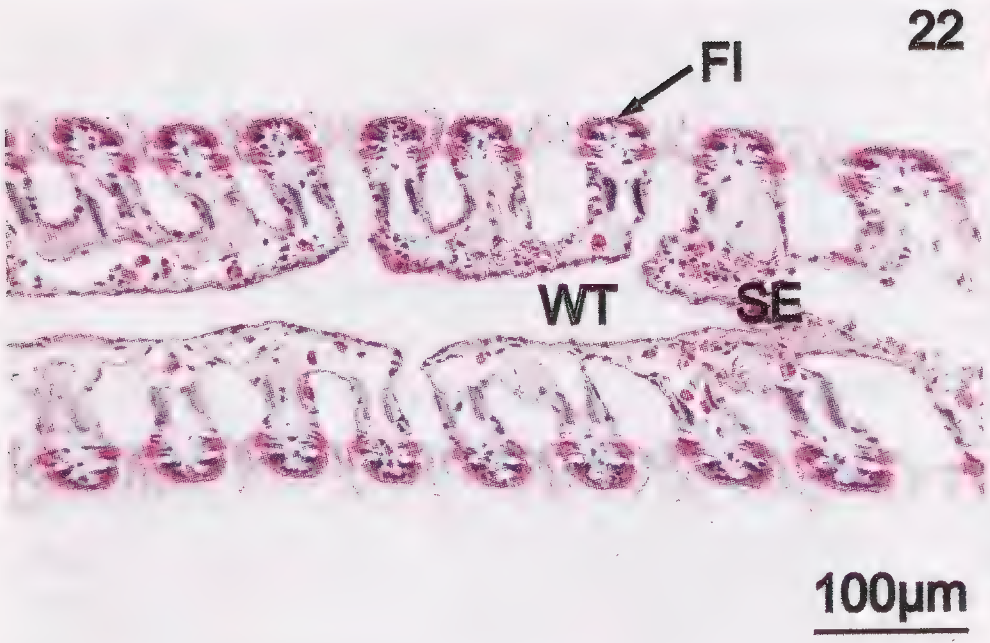
22
FI
WT
SE
100µm

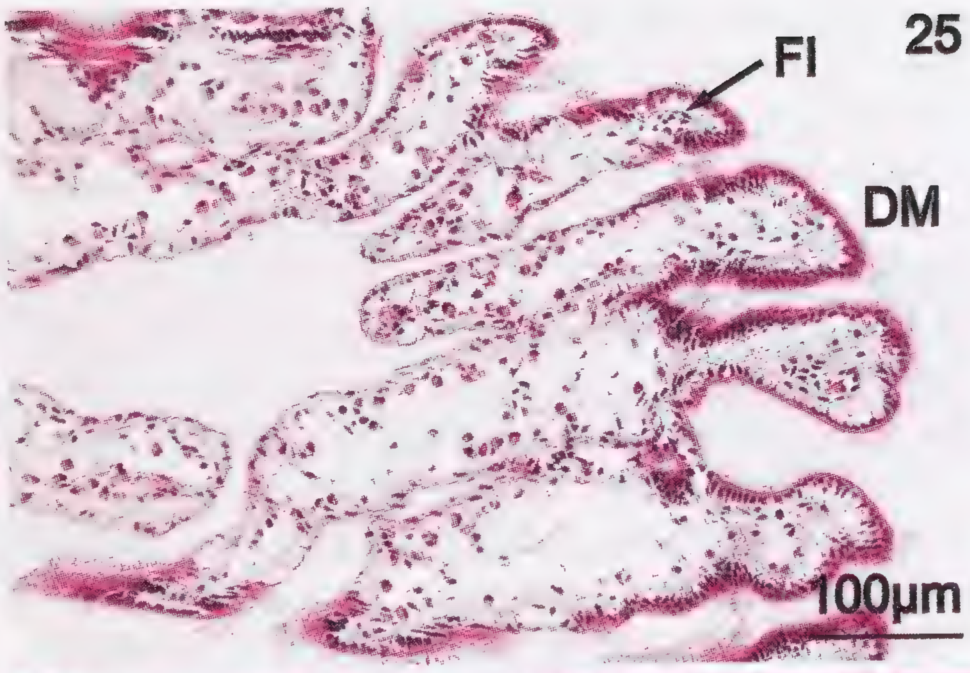
25
FI
DM
100µm

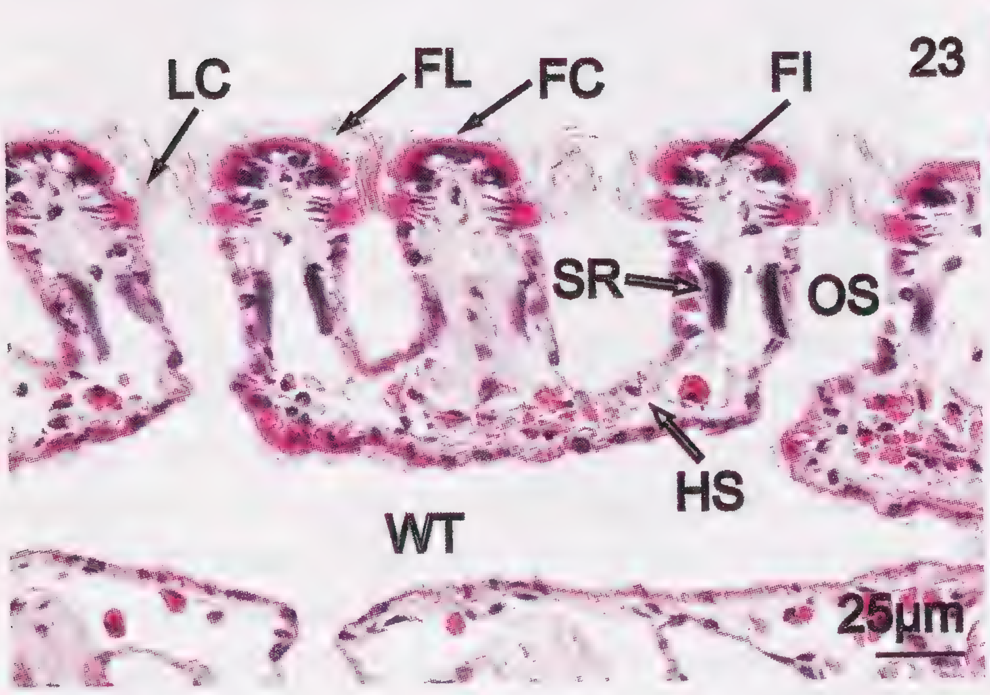
LC
FL
FC
FI
23
SR
OS
HS
WT
25µm

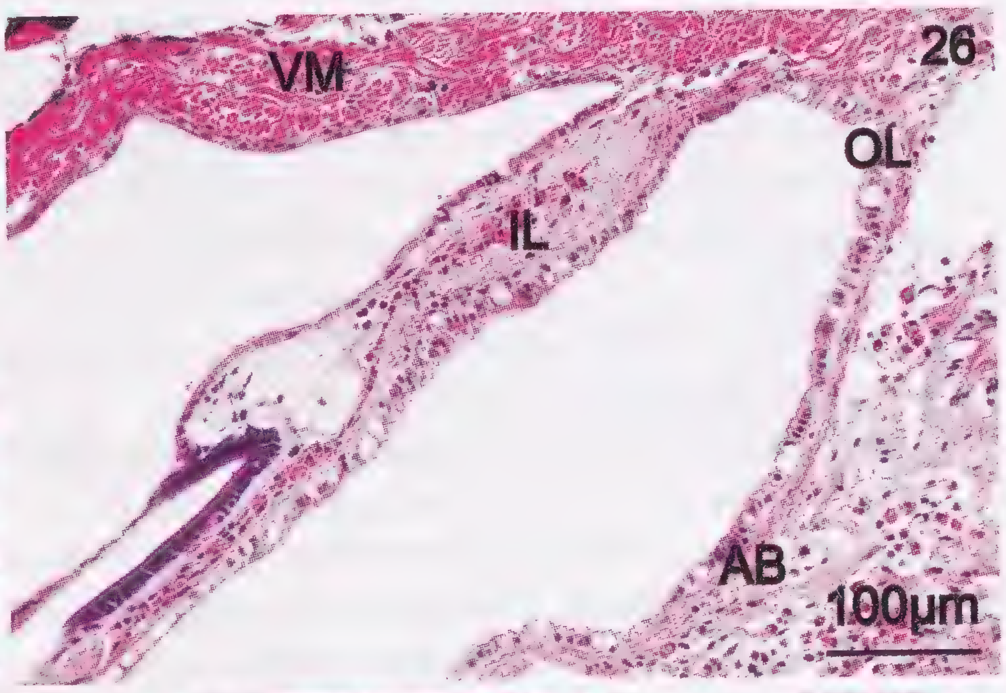
VM
26
IL
OL
AB
100µm

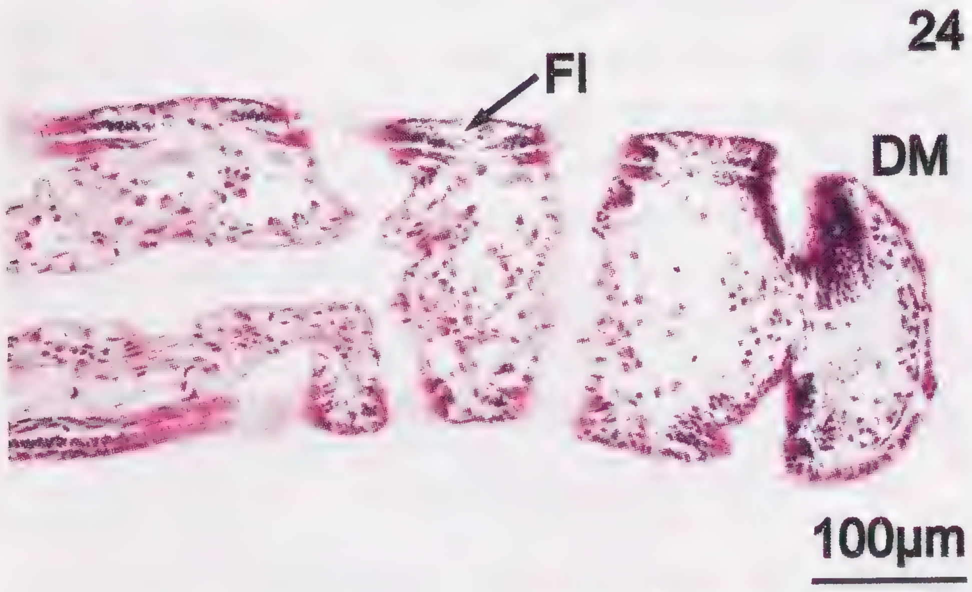
24
FI
DM
100µm

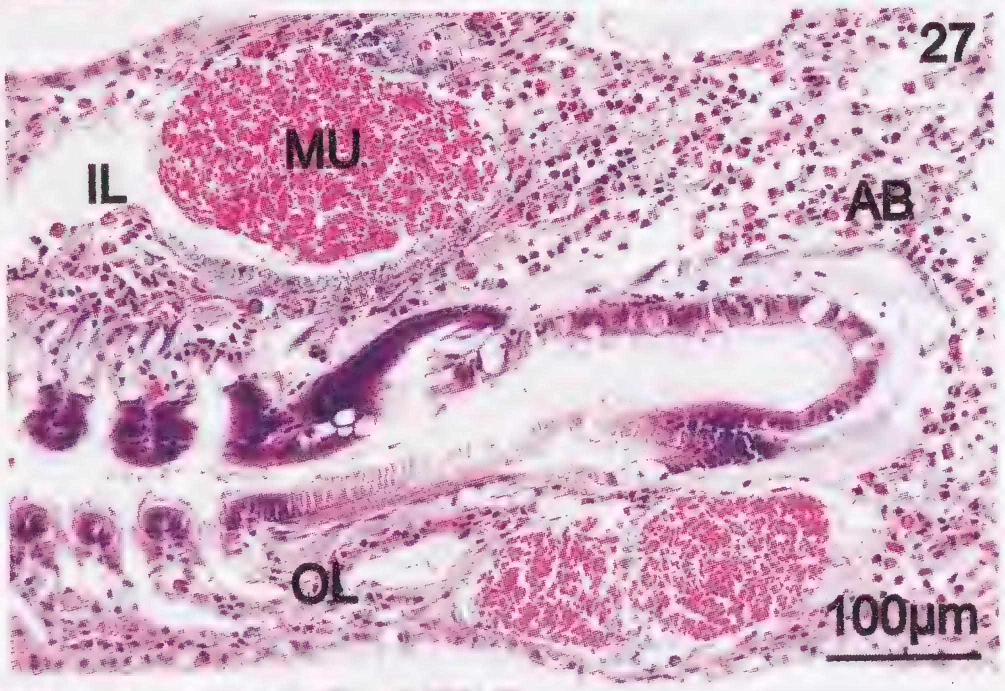
27
MU
IL
AB
OL
100µm

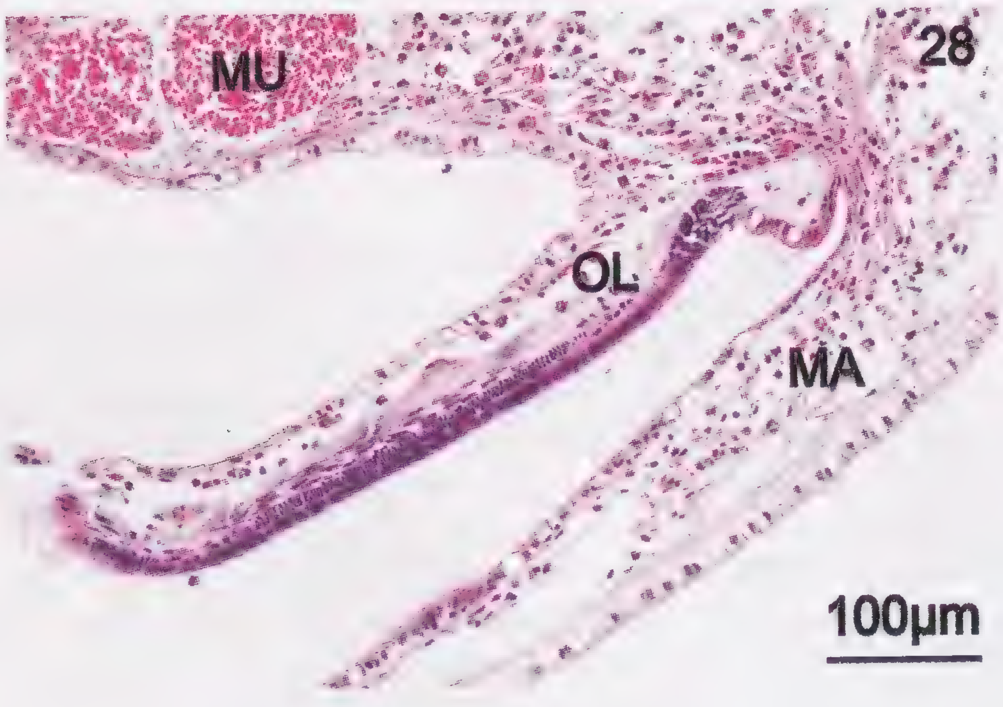
MU
28
OL
MA
100µm

a localized enlargement of the outer demibranch known as a marsupium (Figs. 7, 29). When gravid, the posterior quarter of the ctenidia becomes distended and comprises the distal half of its vertical length. A marsupial demibranch structurally differs from both the anteriorly located non-marsupial outer demibranch, and inner demibranch in many respects. The most obvious characteristic of marsupial gill are the greatly expanded water tubes, which become progressively larger dorsal to ventral. In one individual collected in May 2010, gills were asymmetrically filled allowing a comparison between filled and empty marsupia. The filled marsupium was appeared turgid and symmetrical, while the empty marsupium was flaccid from partially collapsed water tubes (Fig. 29). Glochidia within a filled marsupium appear to be held together by strands of fibrous tissue, possibly representing a binding substance of a conglutinate of embryos (Fig. 30). Walls of marsupial water tubes may be pleated with ciliated plicae. Ciliated plicae also occur along the septa at the base of the marsupium (Fig. 31). The interlamellar septa of the ventral marsupial chambers have a fibrous composition with a lattice of connective tissue (Fig. 32). The epithelium representing the lateral surface of a marsupium appears to be less porous than non-marsupial gill tissue. In contrast to non-marsupial demibranchs, the subepithelium along the vertical surface of the water tubes as well as the septa of marsupia is thickened with connective tissue fibers and a pale staining, ground substance (Figs. 30, 32, 33). The luminal surface of the water tubes is lined with teardrop-shaped, ciliated columnar cells. Ciliated cells lining the lumen marsupial water tubes contain brown intracellular granules, which may explain why the ventral margin of marsupium is blackened (Figs. 7, 30, 32).

Marsupia may contain a mixture of glochidia and spherical to ovular masses of cells representing embryos in various stages of development. Early stage embryos consisted of clusters of eosinophilic, spherical cells within a shapeless, eosinophilic mass. Each cell contains a spherical nucleated mass, surrounded by a heterochromatic, eosinophilic matrix (Fig. 34). Later stage embryos were more differentiated than the largely eosinophilic cellular masses just described. Later stage embryos were ovular, possessing a spherical mass of myocytes, and distinct dorsal and ventral end characterized by basophilic cells. Glochidia were semi-circular with a centrally located adductor muscle flanked by falcate lines of eosinophilic to basophilic tissue presumably representing the mantle (Fig. 35).

Cellular Structure of Foot and Associated Tissues

Pedal Musculature and Byssal Gland: The ventral margin of the foot consists of irregular, overlapping muscle fibers, subepithelial granulocytes, and a highly plicated integument (Fig. 36). Violet staining granulocytes are located directly beneath the pedal epithelium, while pale, blue-staining granulocytes are medial in respect to violet cells (Fig. 37). Foot muscle is composed of regions of irregular and regular muscle fibers. Musculature in the ventral region of the foot has a woven appearance with bundles of fibers arranged

←

FIGS. 22–28. Outer demibranch, and inner demibranch of *Villosa nebulosa*. FIG. 22: Transverse section of inner demibranch displaying transversely oriented filaments (FI), a septum (SE) linking the inner and outer lamina, and a water tube (WT); FIG. 23: Transverse section of the inner lamina of inner ctenidia showing the main tissue components including filament (FI), lateral cilia (LC), frontal lateral cilia (FL), frontal cilia (FC), skeletal rods (SR), and hemolymph sinuses (HS), in addition to ostium pores (OS), and corresponding water tube (WT); FIG. 24: Transverse section of the distal tip of outer gill characterized by a rounded distal margin (DM), resembling the merger of two or more filaments (FI); FIG. 25: Transverse section of the free distal inner gill tip characterized by a bending layer of filaments (FI) around the distal margin (DM) creating a pleated surface; FIG. 26: Transverse section of the inner lamina (IL) and outer lamina (OL) of the inner ctenidia joined separately at the base of the visceral mass (VM); FIG. 27: Transverse section of ctenidia where muscle fascicles (MU) are aligned anterior to posterior where the inner lamina (IL) of inner gill and outer lamina (OL) of outer gill unite with the abdomen (AB); FIG. 28: Transverse section of gill revealing musculature (MU), outer lamina (OL) of outer gill, and mantle (MA).

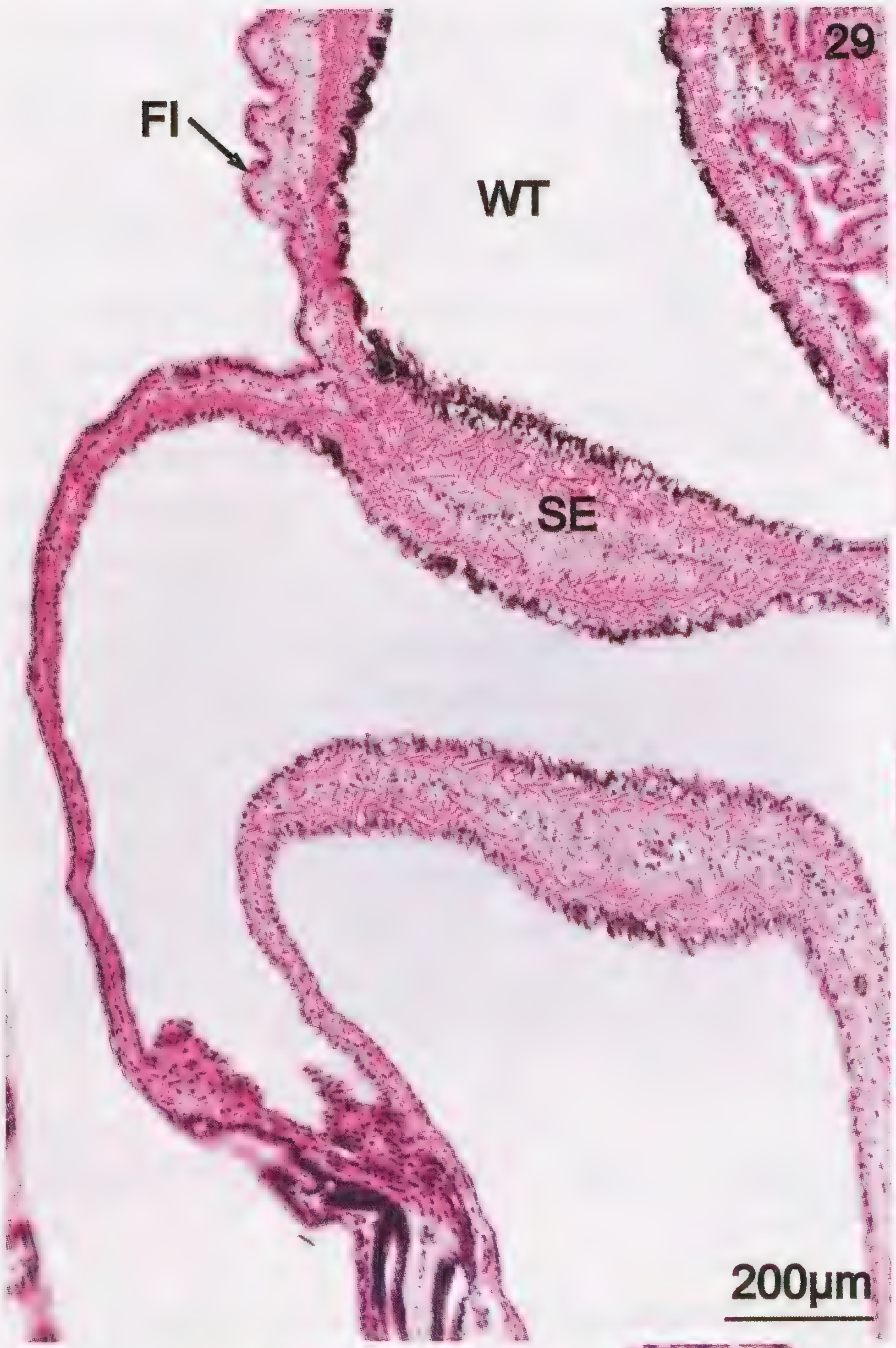
29
FI
WT
SE
200μm

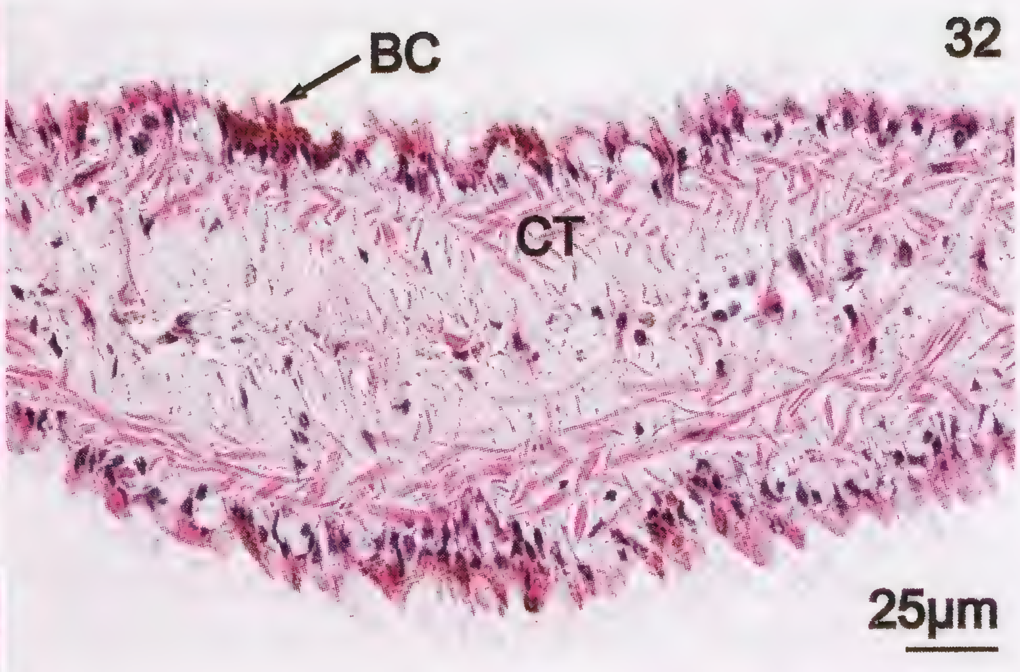
BC
32
CT
25μm

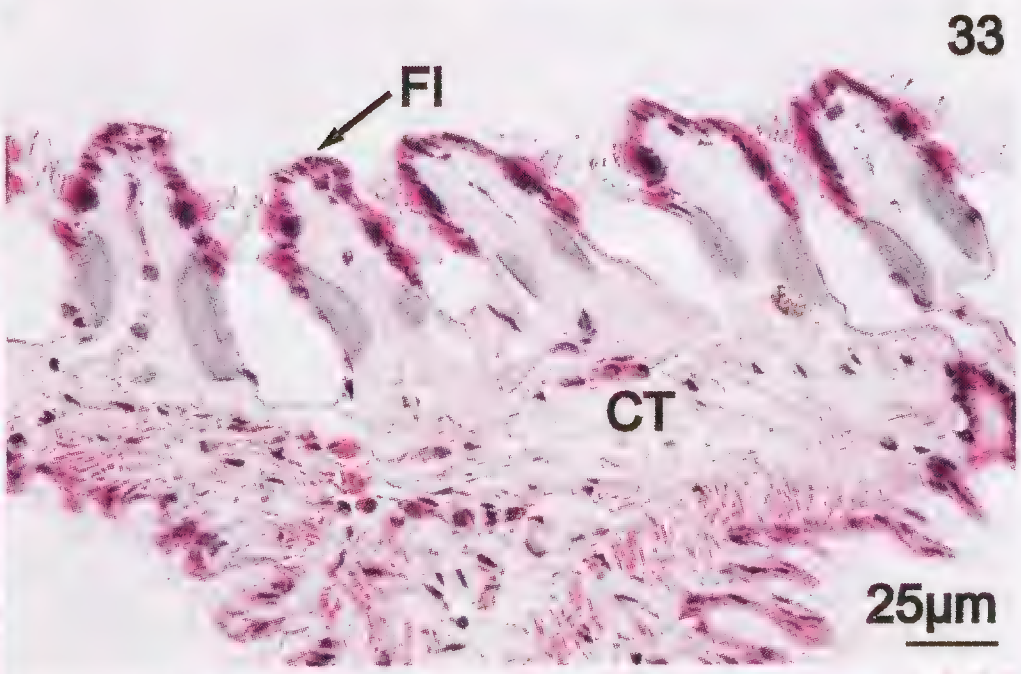
33
FI
CT
25μm

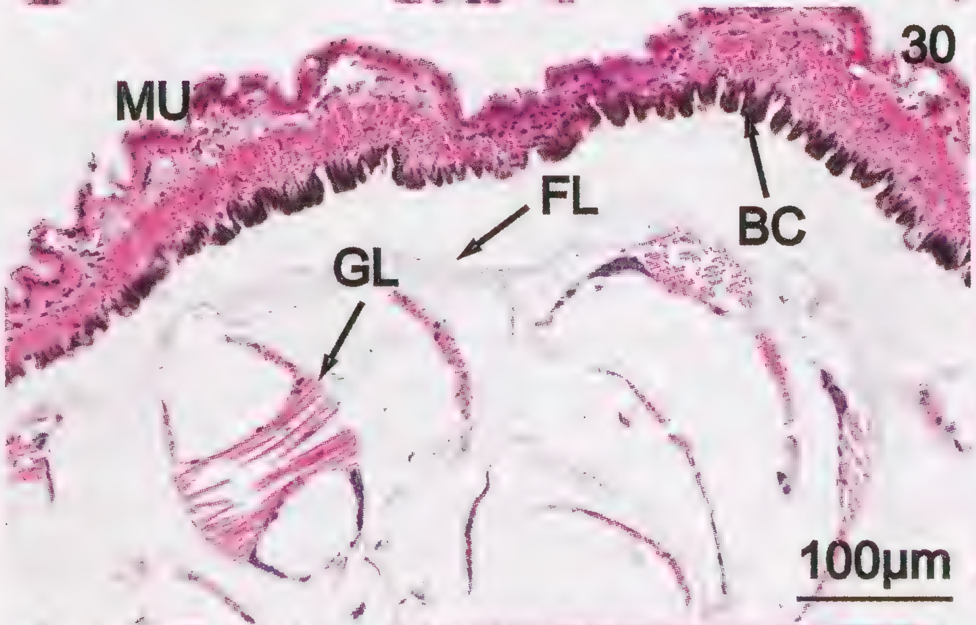
30
MU
FL
BC
GL
100μm

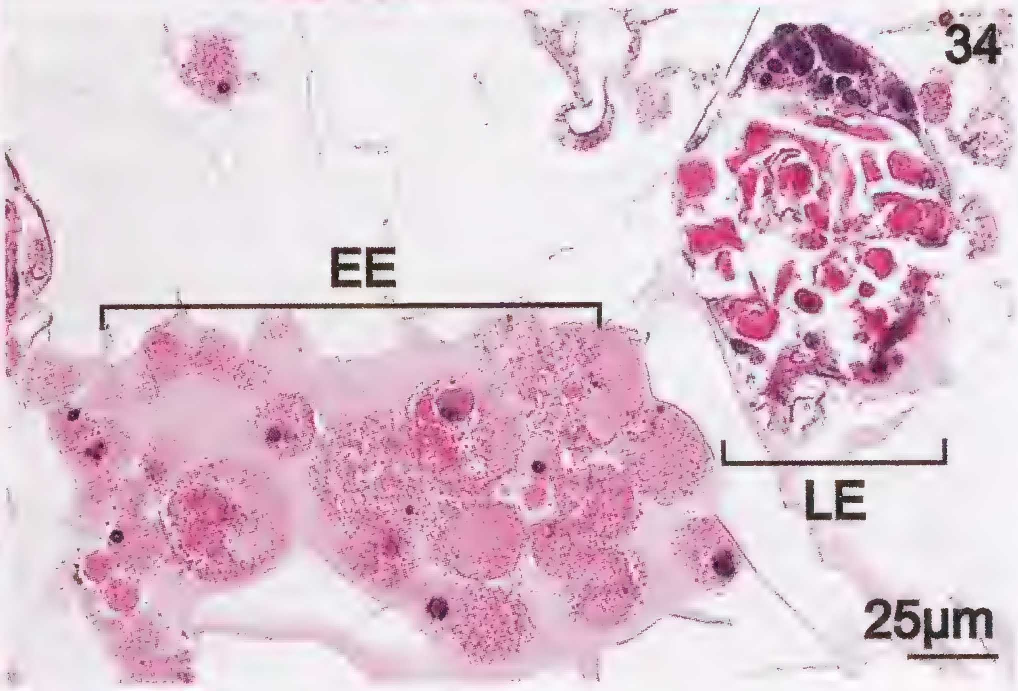
34
EE
LE
25μm

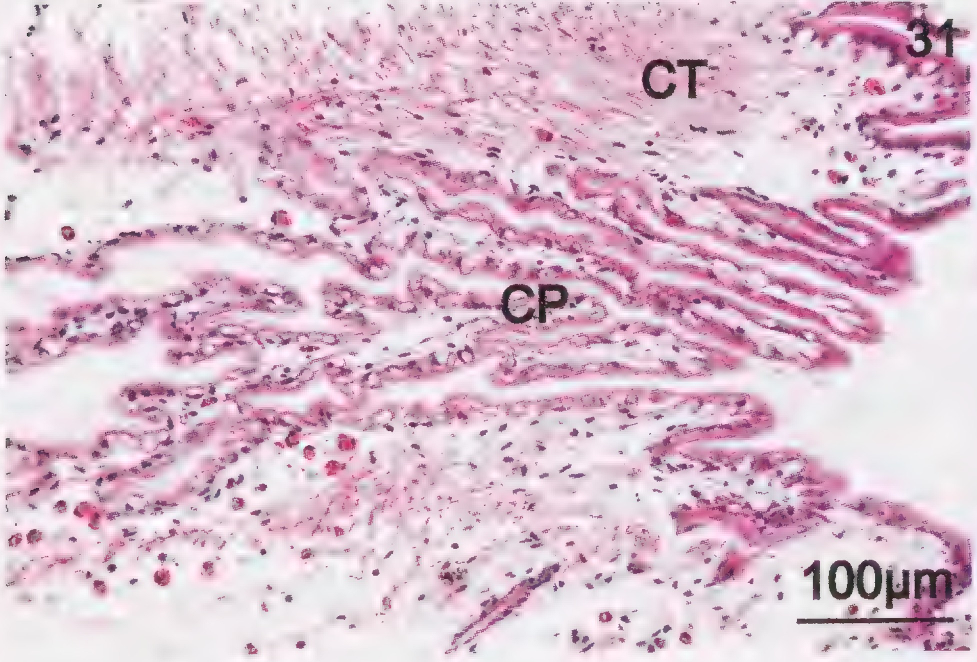
31
CT
CP
100μm

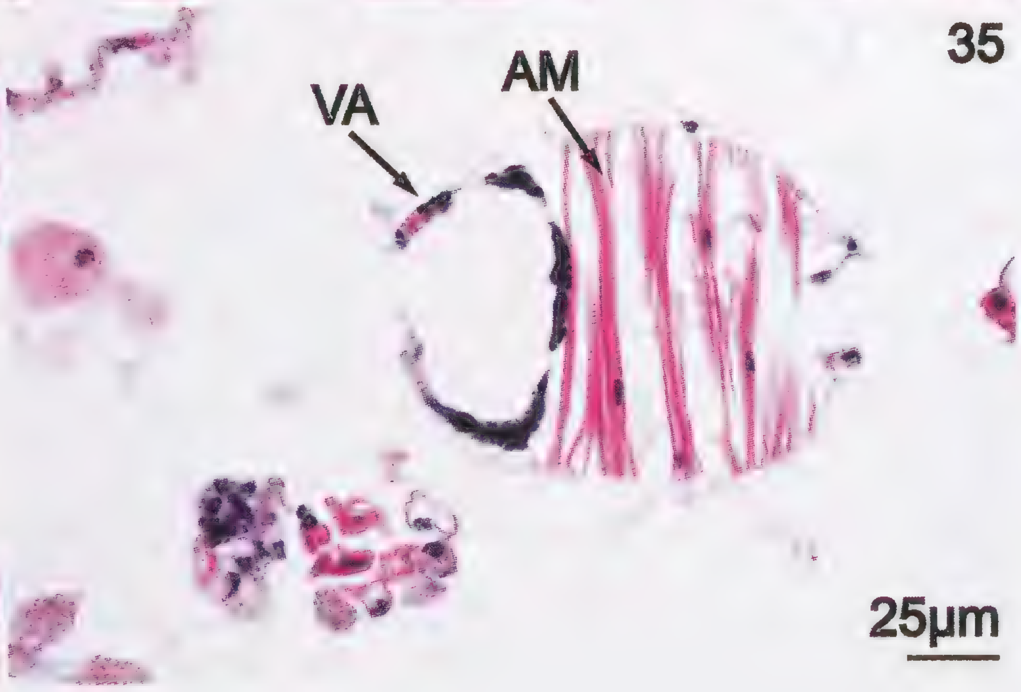
35
VA
AM
25μm

into sagittal and transverse planes, giving the tissue a woven appearance (Fig. 38). In contrast, musculature of the base of the foot is more organized with distinct layers of transverse and sagittal fibers (Fig. 39).

The byssal gland is triangular, located medially at the ventral margin of the coelom, just posterior to the pedal ganglion. The byssal gland has a wide, triangular dorsal chamber and a smaller, ovoid ventral chamber (Fig. 40). The luminal surface of the byssal gland features a simple, ciliated columnar epithelium, and these cells have an eosinophilic cytoplasm and a monochromatic, ovular nucleus. The lumen of the dorsal chamber contains a heterochromatic, eosinophilic mass, possibly representing the remnants of the byssal thread (Fig. 41). The byssal gland of adult *V. nebulosa* is blind-ended, not connected to a dorso-ventral, byssal canal. The byssal canal consists of a series of disconnected, ciliated ducts located medially throughout the pedal musculature. Remnants of the byssal canal have a ciliated columnar epithelium and these cells are surrounded by a pale, eosinophilic matrix of fibrous connective tissue. These ciliated remnants of the byssal canal have an irregular shape and a narrow lumen (Fig. 42).

Pedal Integument and Mesentery: The integument of the foot and visceral mass is pleated, and there are five different epithelial regions ventral to dorsal. In the first two regions, the epithelium appears to be folded and each fold is rounded with some resembling a “Y”. The first region possesses ciliated, columnar cells with a subepithelium consisting of irregular muscle fibers and violet granulocytes (Fig. 43). Ciliated cells have an eosinophilic cytoplasm, similar to the coloration of the underlying muscle tissue, and cilia are short and nearly straight. Epithelial cells in the second region have similar cytological characteristics as region one, however ciliated cells are sparsely distributed. Additionally, muscle tissue beneath the epithelium is generally more regular than in region one, and with fewer violet chromatocytes (Fig. 44). Region three possesses shorter epithelial folds, sparsely distributed ciliated cells, and mucus cells. Unlike epithelia of the first two regions, the basal portion of region three epithelial cells is parallel to the underlying musculature. Muscle underlying type-three epithelium consists an outer, thin, transverse layer and a deeper, thicker, sagitally oriented layer (Fig. 45). The fourth and fifth regions are dorsally located along the oblate portion of the visceral mass. The fourth type of integument surrounding the foot is similar to the third region, but is more irregular and a dark hemolymph sinus is located between the epithelium and muscle (Fig. 46). Region five is located near the junction between visceral mass and inner gill, and has the shortest epithelium of all five regions. Cells representing region five vary in height from a flattened, squamous type to slightly taller, domed to tear drop shaped. Mucus secreting cells also vary in morphology from dome-shaped to tear drop cells (Fig. 47). In a longitudinal orientation the pedal integument has numerous irregular cavities. Additionally, the columnar epithelium at the location of the black spot features brown intracellular granules (Figs. 8, 48).

←

FIGS. 29−35. Marsupium, and embryonic development of glochidia of *Villosa nebulosa*. FIG. 29: Transverse section of an empty marsupium revealing distended water tubes (WT), thickened septa (SE), and reduced filaments (FI) along the distal margin; FIG. 30: Transverse section of a marsupium portraying a wall of concentric musculature (MU), and brown-pigmented columnar cells (BC), and a central mass of fragmented to intact glochidia (GL) enclosed by gray, wispy filaments (FL), possibly representing a substance that binds glochidia together within the conglutinate; FIG. 31: Transverse section of the marsupium at its dorsum, characterized by a thickened base of fibrous connective tissue (CT) and a series of ciliated papillae (CP) extending into the lumen; FIG. 32: Transverse section of a marsupial water tube septum emphasizing a lattice of connective tissue fibers (CT), and brown-pigmented, ciliated cells (BC); FIG. 33: Transverse section of a marsupium showing ctenidial filaments (FI) supported by a continuous subepithelium of connective tissue (CT); FIG. 34: Transverse section of a marsupium containing a mixture of early stage embryos (EE) resembling a mass of spherical cells, and late stage embryos (LE) bearing a resemblance to glochidia; FIG. 35: Transverse section of a marsupium portraying an intact glochidium with well-defined, semicircular valves (VA) and a median adductor muscle (AM).

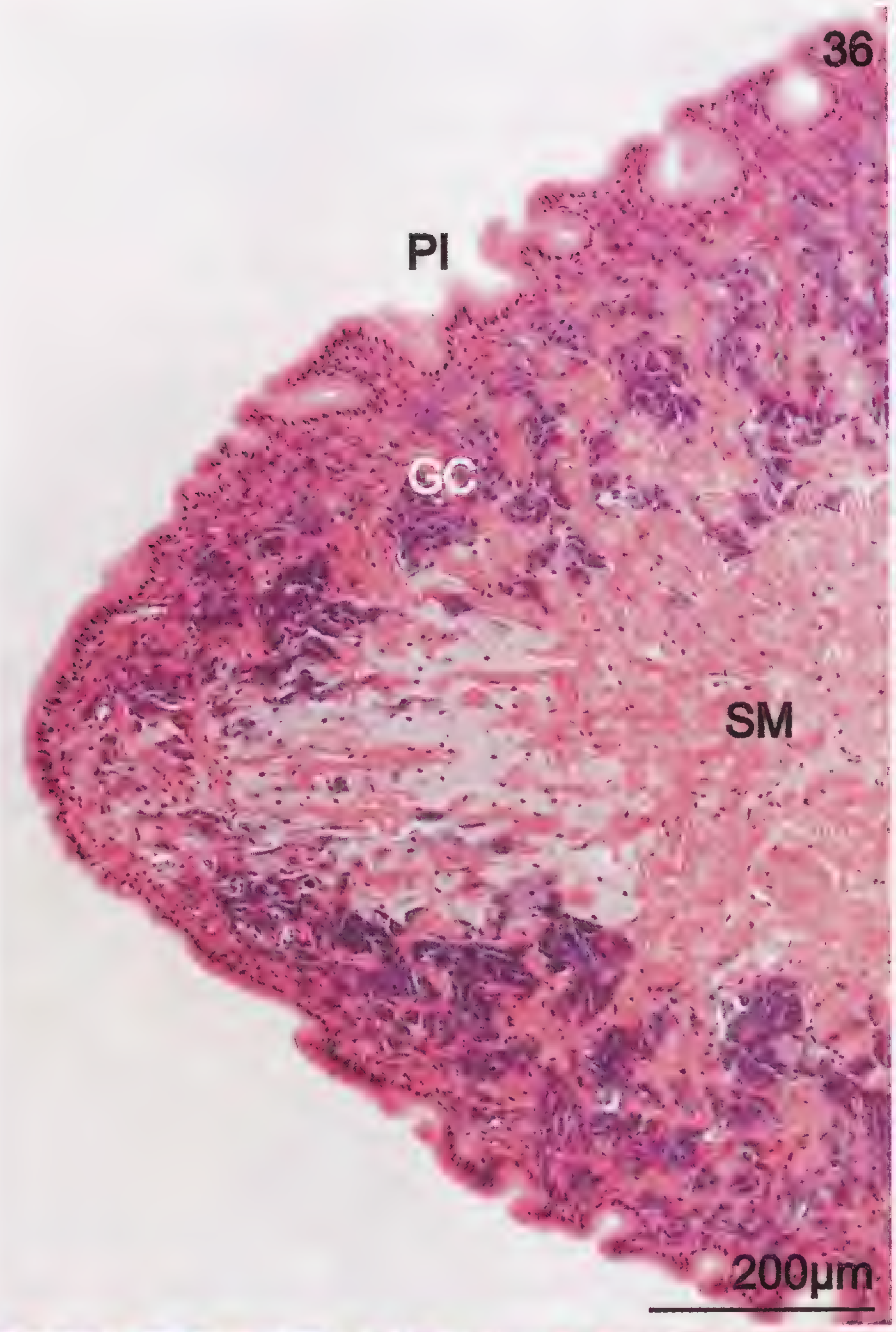
36
PI
GC
SM
200µm

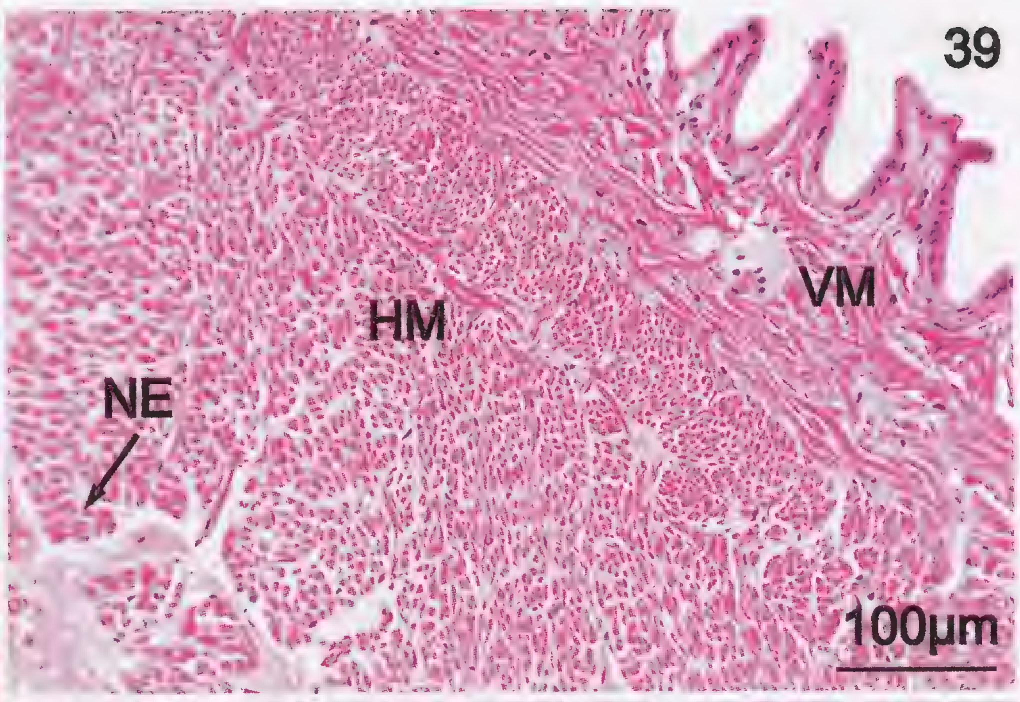
39
HM
VM
NE
100µm

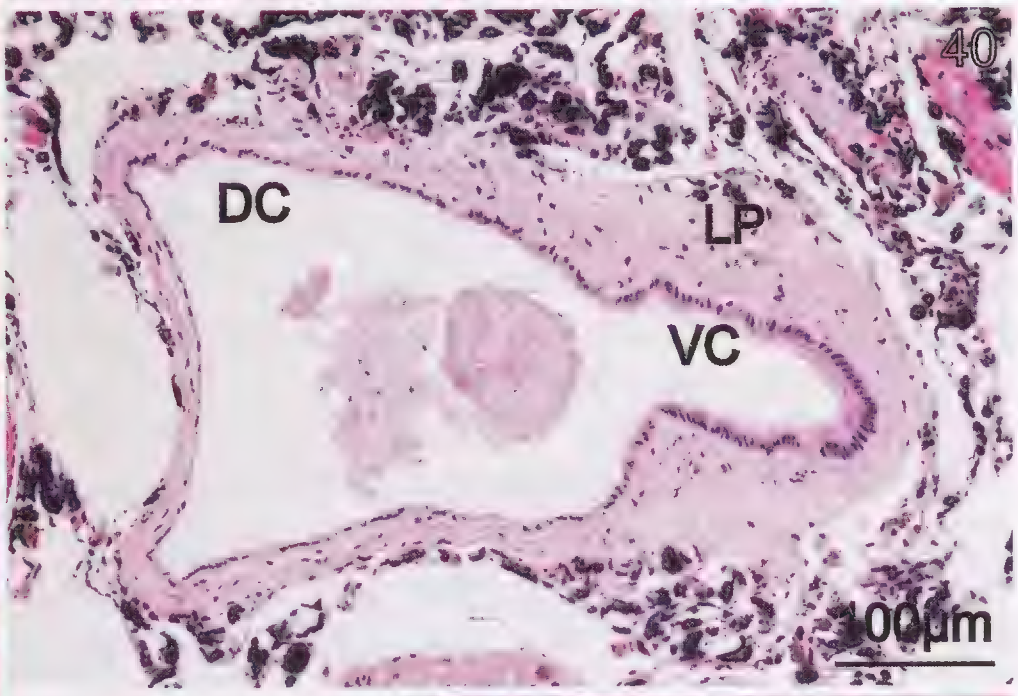
40
DC
LP
VC
100µm

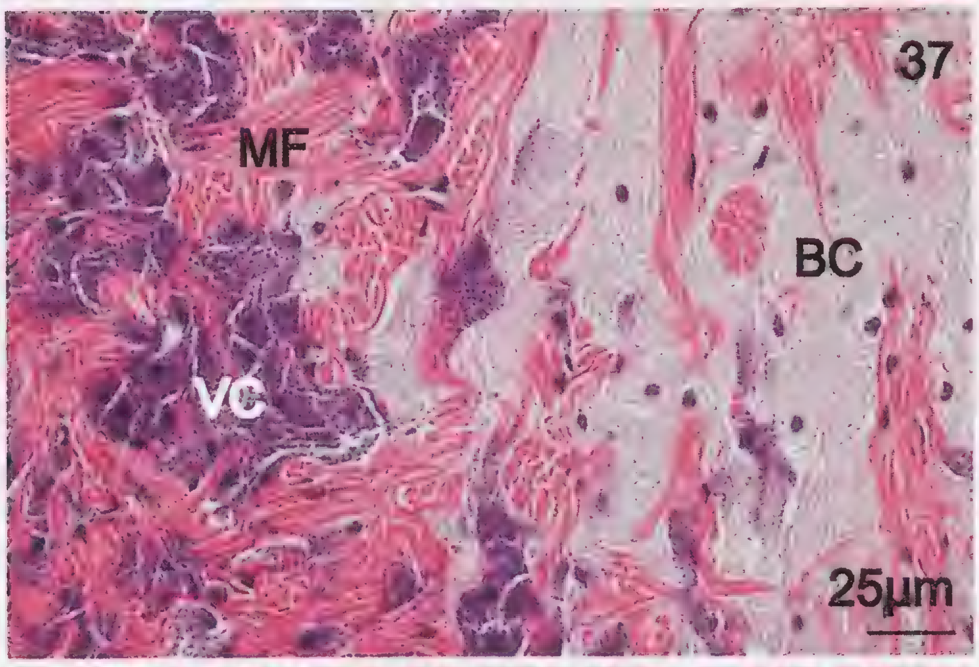
37
MF
BC
VC
25µm

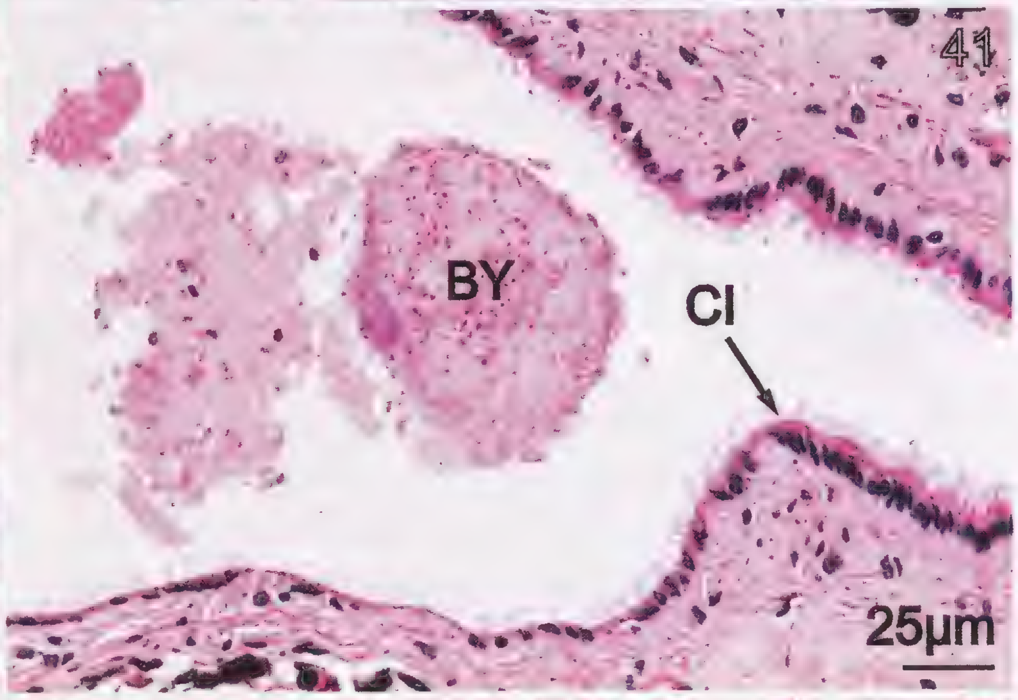
41
BY
CI
25µm

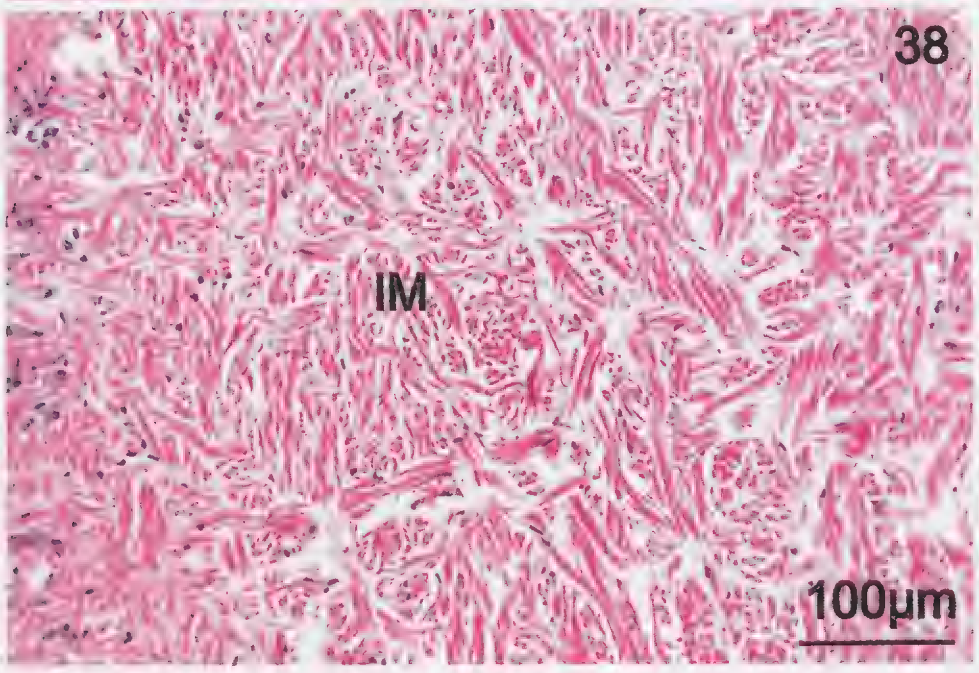
38
IM
100µm

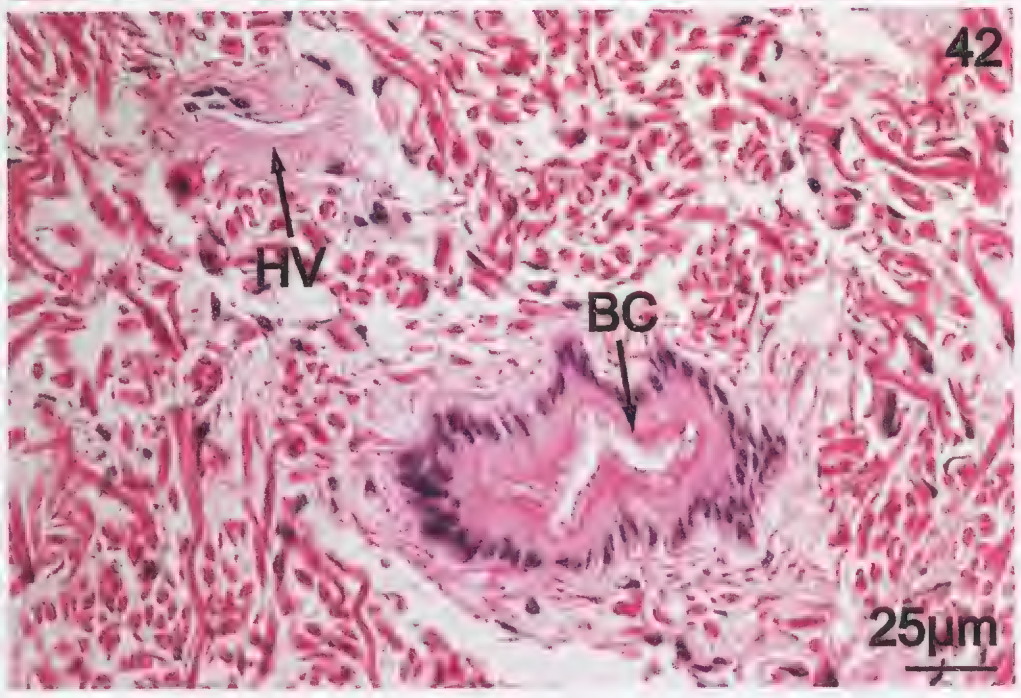
42
HV
BC
25µm

The left and right halves of the visceral mass are united by bundles of mesentery and mesentery fascicles are distributed throughout the hemocoel (Fig. 49). Each fascicle has a heterogeneous composition in terms of the staining characteristics and geometry of its fibrils. Fibrils are eosinophilic, but staining intensity varies from a pale, almost white, to dark red. Each filament is quadrangular, but varies in shape from square, to a triangular. Furthermore, there does not appear to be an obvious pattern of fibril arrangement within a fascicle (Fig. 50).

Labial Palps: Labial palps of *V. nebulosa* have an inner palp surface lined with a series of ciliated, rectangular plicae, whereas the outer surface is generally smooth (Fig. 51). Plicae have a flattened posterior margin and a pleated anterior surface (Fig. 52). Ciliated columnar cells represent the main constituent of the inner palp epithelium and extend along the palp interior until the distal margin of each lip. Ciliated cells of the inner palp surface are characterized by a pale, basophilic cytoplasm and an ovular, monochromatic nucleus. The surface of the free distal palp tip transitions from a ciliated epithelium to a non-ciliated mucosa characterized by basophilic, granular mucus cells (Fig. 53). Although the outer surface of each palp is generally flattened, the integument is composed of teardrop-shaped columnar cells. Teardrop cells of the outer palp surface possess an ovular monochromatic nucleus, an eosinophilic cytoplasm, and a transparent, apical vesicle (Fig. 54). Subepithelial tissue of the palps consists a somewhat dense matrix of pale, eosinophilic fibers within a membranous ground substance, especially the supporting tissue directly beneath the epithelium. However, the medial layers of each palp have a more loose consistency. Additionally, there are a series of well-defined hemolymph sinuses, and wandering hemocytes are widely distributed throughout the subepithelium.

Anterior Adductor and Anterior Pedal Retractors: The anterior pedal retractors are located medial to the labial palps and may be observed in histological sections of palp. Retractor muscle is dark staining and eosinophilic, with distinct fascicles and fasciculi. Furthermore, fibrils are quadrangular and separated by endomysium, however perimysium appears to be more delicate since there are pale, eosinophilic wisps adjacent to fascicles and fasciculi (Fig. 55). Adductor muscle is organized into large fascicles containing dark, red eosinophilic fibers. Adductor myocytes are filamentous with a pale, granular, basophilic nucleus (Fig. 56).

Oral Groove and Esophagus: In transverse sections of the anterior visceral mass, the oral groove resembles a U-shaped canal, travelling dorsally from the labial palps. Oral groove epithelium consists of transversely pleated, ciliated tracts. In a sagittal plane, oral groove appears multinucleated since the walls of the oral groove are curved. Oral groove epithelium is mucociliary with a preponderance of transparent vesicles, especially along the folds (Fig. 57). Additionally, there are wandering hemocytes nestled between columnar cells of the ventral oral groove wall (Fig. 58). Subepithelial tissue of the oral groove consists of a loose meshwork of thin connective tissue fibers and hemocytes. A single layer of cuboidal epithelial cells appears ventrally

---

←

FIGS. 36–42. Pedal musculature, and byssal gland of *Villosa nebulosa*. FIG. 36: Transverse section of the ventral tip of the foot characterized by somatic musculature (SM), granulocytes (GC), and a plicated integument (PI); FIG. 37: Transverse section of foot subepithelium characterized by muscle fibers (MF) pale, blue granulocytes (BC) in the median, and violet cells (VC) between the blue cells and the epithelium; FIG. 38: Transverse section of ventral foot musculature featuring an irregular meshwork (IM) of fibrous tissue; FIG. 39: Transverse section of dorso-lateral foot musculature characterized by vertically oriented myofibers (VM), and horizontally oriented myofibers (HM), and a pedal nerve branch (NE); FIG. 40: Transverse section of the byssal gland featuring a distinct dorsal chamber (DC) and a ventral chamber (VC), surrounded by lamina propria (LP); FIG. 41: Transverse section of the byssal gland displaying ciliated walls (CI) and byssal remnants (BY) within the lumen; FIG. 42: Transverse section of the base of the foot portraying a hemolymph vessel (HV) located in near the vestigial byssal canal (BC).

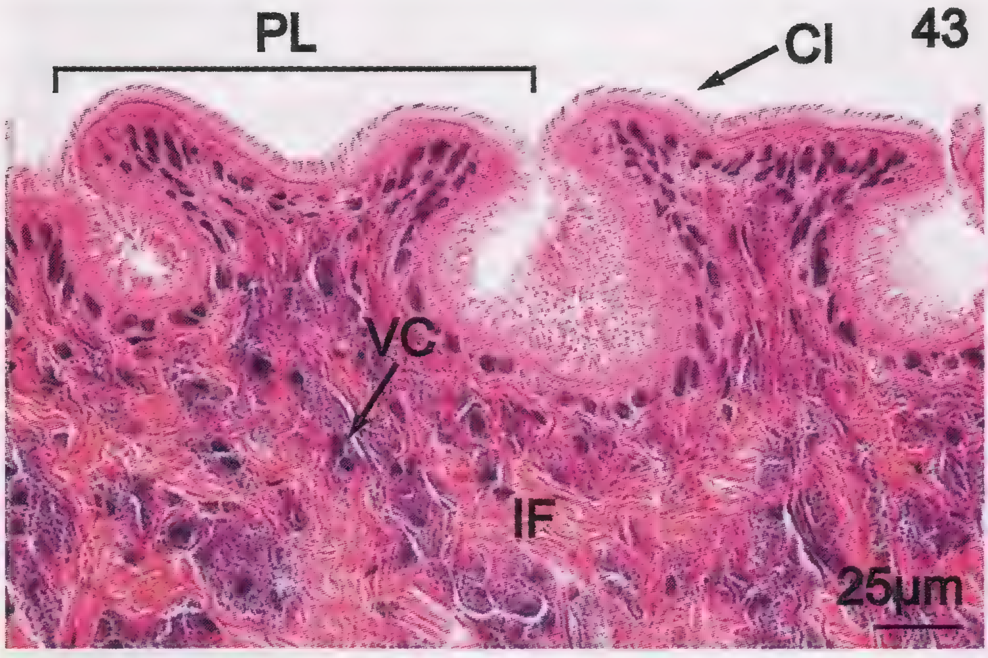
43
PL
CI
VC
IF
25µm

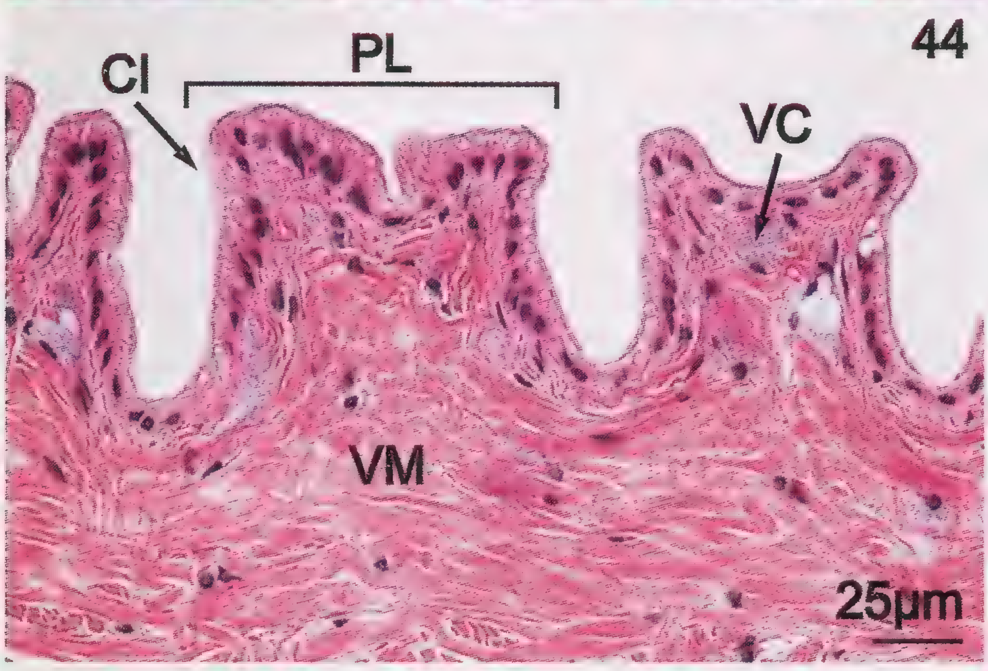
44
CI
PL
VC
VM
25µm

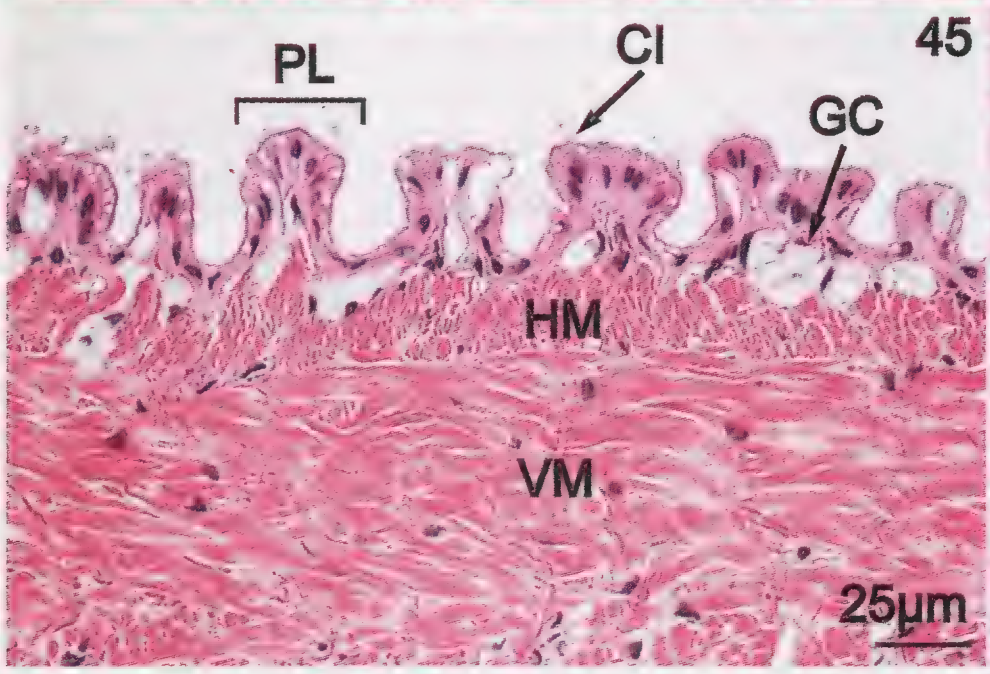
45
PL
CI
GC
HM
VM
25µm

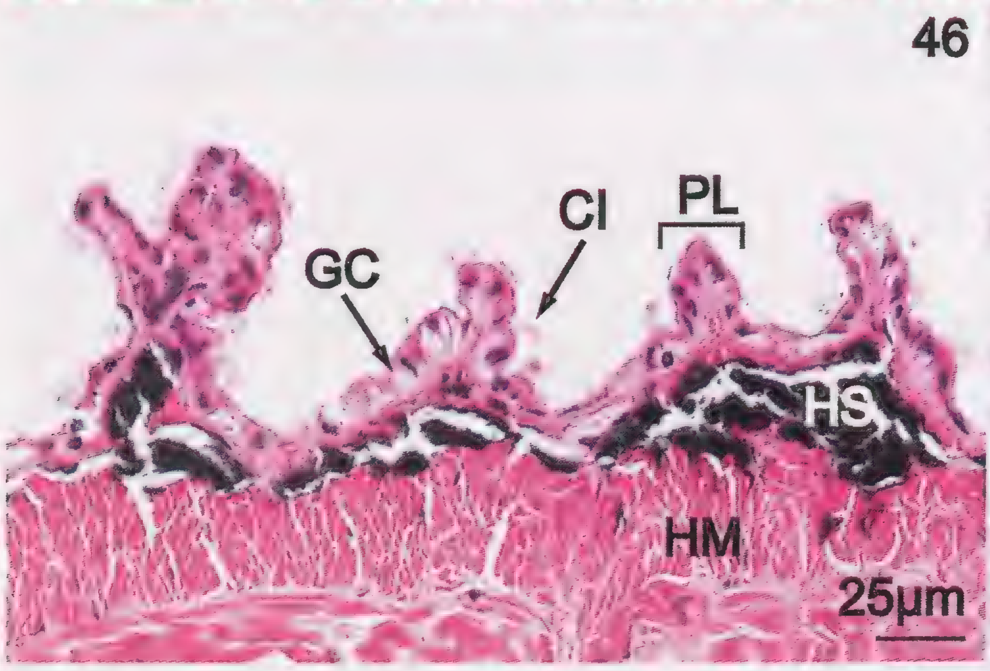
46
CI
PL
GC
HS
HM
25µm

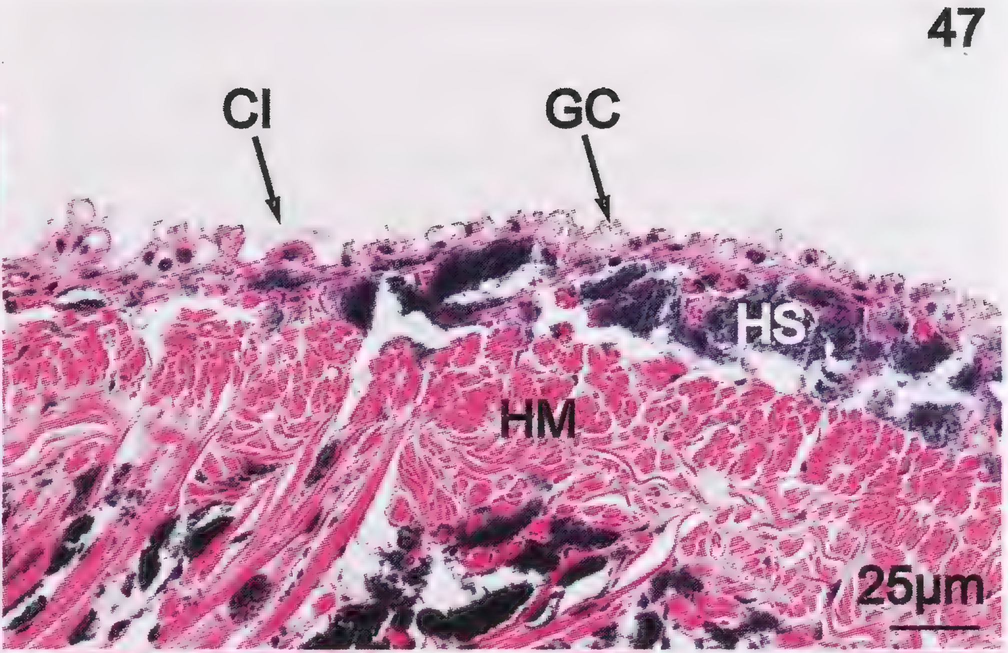
47
CI
GC
HS
HM
25µm

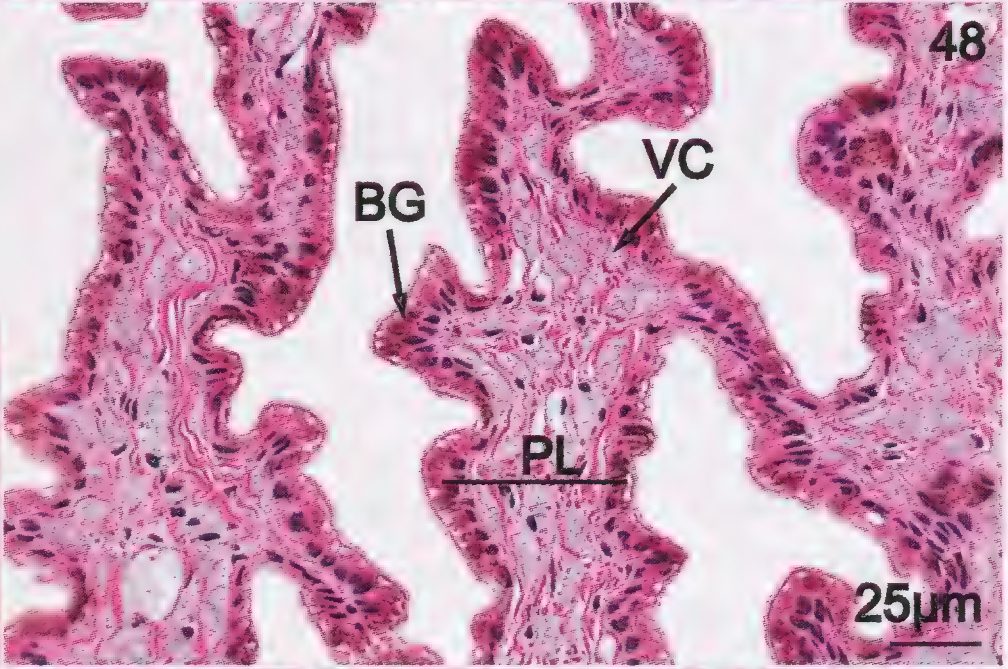
48
VC
BG
PL
25µm

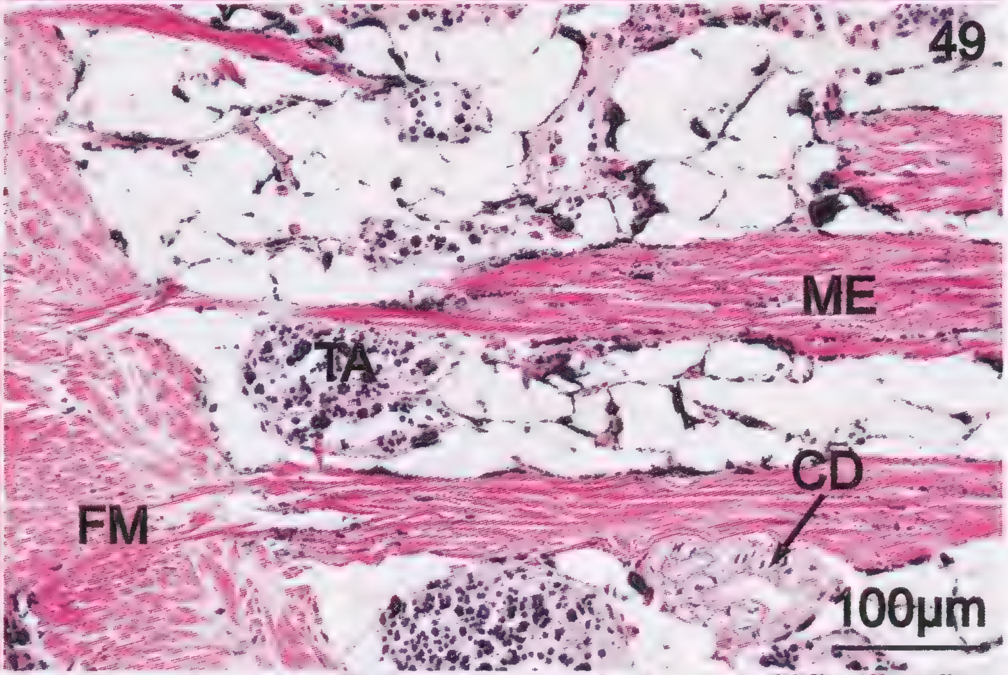
49
ME
TA
CD
FM
100µm

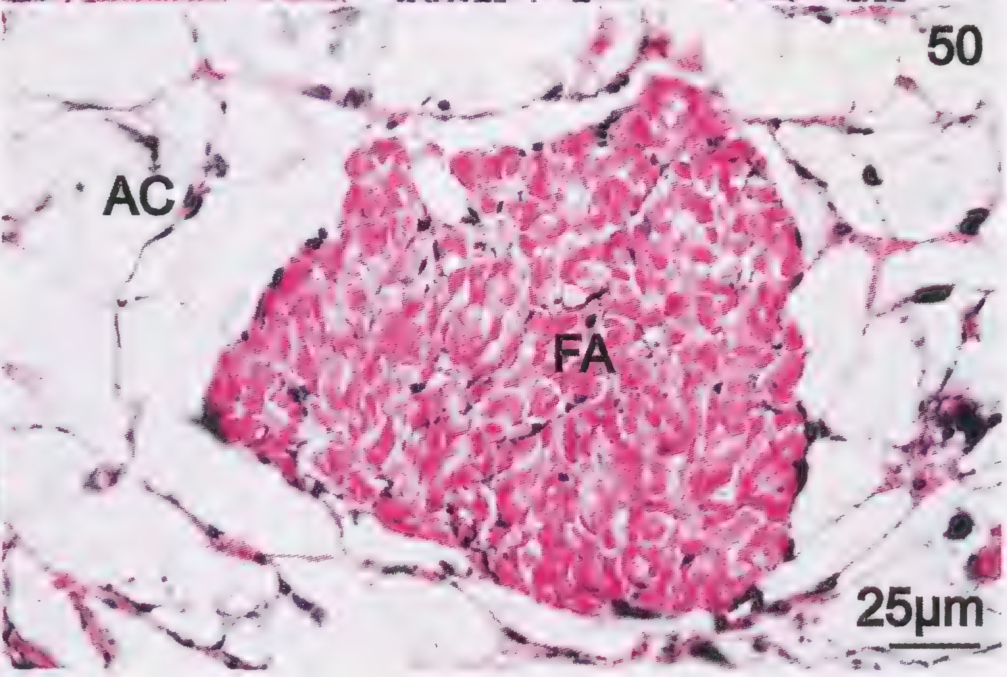
50
AC
FA
25µm

in sections of oral groove, and represents a short stretch of integument between the oral groove and foot (Fig. 59).

The esophagus is essentially a posterior continuation of the oral groove, a short tube connecting the oral groove with the stomach and digestive gland. The esophagus is located at the dorsal end of the visceral mass and is generally between digestive gland tubules and the mantle isthmus (Fig. 60). Ciliated, rectangular folds extend from the dorsal and ventral esophageal walls. Epithelial cells are pseudostratified and ciliated, with an eosinophilic cytoplasm and an elliptical, monochromatic nucleus. Cilia along the apical surface of esophageal cells are short and generally straight. The lumen of the esophagus may contain a shapeless, eosinophilic mass, which may represent mucus and ingested substances. Additionally, the esophageal epithelium is supported by concentric layers of pink and red eosinophilic fibers, creating a heterogeneous lamina propria (Fig. 61).

Cellular Structure of the Alimentary Canal

Digestive Diverticulum: The esophagus expands laterally into a vestibular chamber at the visceral mass dorsum. Particulate matter is transported, by means of ciliary action, through small tubules located on the left and right sides of the body (Fig. 62). There are three types of tubules distinguished by variations in the diverticulum lining. Ciliated primary tubules have folds of epithelial tissue that give tubule walls a wavy or serrated appearance (Figs. 62–64). Primary tubules consist of eosinophilic, columnar cells with cilia. Additionally, primary tubules have low, broadly rounded plicae (Fig. 64). Ciliated epithelium transitions into a microvillar lining in the secondary tubules. Secondary tubules connect to tertiary tubules, which are the most widely distributed diverticulum tubules. Microvillar cells of secondary tubules are characterized by a red, vesiculated cytoplasm, and a pale, basophilic nucleus with a distinct nucleolus (Fig. 65). Tertiary tubules have two types of cells. The most abundant cell type is the vesiculated cell. These cells have a pale, eosinophilic cytoplasm and numerous intracellular vesicles. The second cell type is triangular with a dark staining, basophilic cytoplasm, and a dark staining nucleus containing a distinct nucleolus (Fig. 66).

Stomach: The stomach is a large bag-like chamber located between the digestive diverticulum and style sac. The stomach is somewhat dorsoventrally flattened, with plicated walls and a gelatinous, eosinophilic matrix within the lumen (Fig. 67). The ventral stomach wall features a columnar epithelium with an eosinophilic cuticle (Fig. 68). The lumen may contain a mass of chyme. The composition of chyme may be an irregular eosinophilic mass that has a slightly lighter staining characteristic as compared to the cuticle. Chyme may also consist of darker, eosinophilic granules or spherical objects (Fig. 68). The columnar epithelium has a dense cuticle, embedded in cilia, that is rela-

←

FIGS. 43–50. Pedal integument, and mesentery of *Villosa nebulosa*. FIG. 43: Transverse section of pedal integument type 1, emphasizing broad, Y-shaped plicae (PL) with densely packed cilia (CI) overlying a subepithelium of irregular fibers (IF), and violet cells (VC); FIG. 44: Transverse section of pedal integument type 2 represented by Y-shaped plicae (PL), violet cells (VC), sparse cilia (CI), and supported by an organized layer of vertical musculature (VM); FIG. 45: Transverse section of pedal integument type 3, characterized by short, teardrop-shaped plicae (PL), cilia (CI), goblet cells (GC), horiztonal musculature (HM), and vertical musculature (VM); FIG. 46: Transverse section of pedal integument type 4, characterized by short plicae (PL) with cilia (CI), and goblet cells (GC), and a hemolymph sinus (HS) between the epithelium and horizontal musculature (HM); FIG. 47: Transverse section of pedal integument type 5, featuring epithelial cells with a convex apical surface, cilia (CI), and goblet cells (GC), overlying a hemolymph sinus (HS), and horizontal musculature (HM); FIG. 48: Sagittal section of pedal integument at the black spot along the posterior margin of the foot, emphasizing plicae (PL), with columnar cells containing brown intracellular granules (BG) and a subepithelium of violet cells (VC); FIG. 49: Transverse section of the dorso-lateral aspect of the coelom, portraying fibrous mesentery (ME) extending medially from foot muscle (FM), testicular acini (TA), and ciliated gonadal ducts (CD); FIG. 50: Sagittal section through a fascicle (FA) of mesentery fibers surrounded by adipocytes (AC).

51

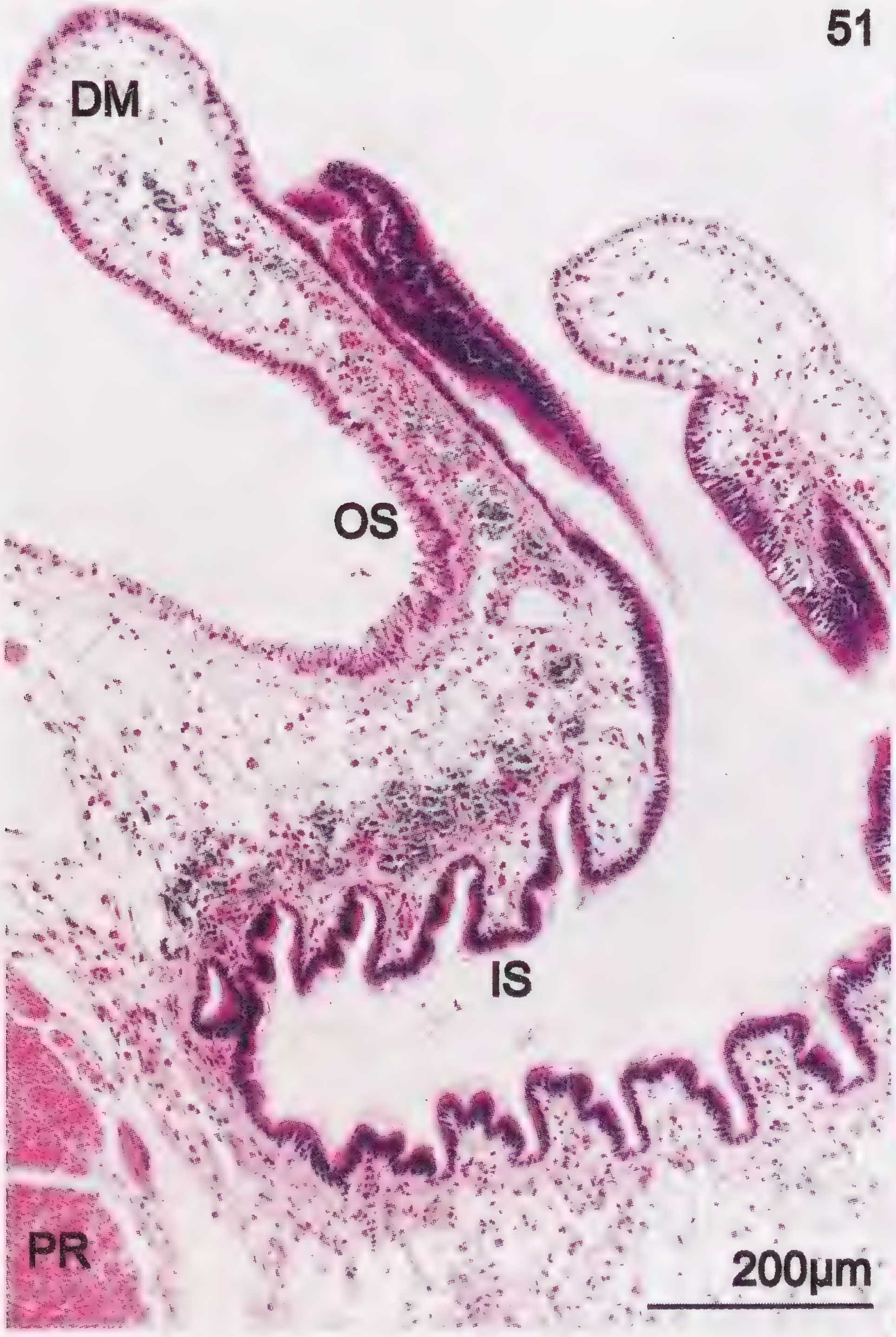

53

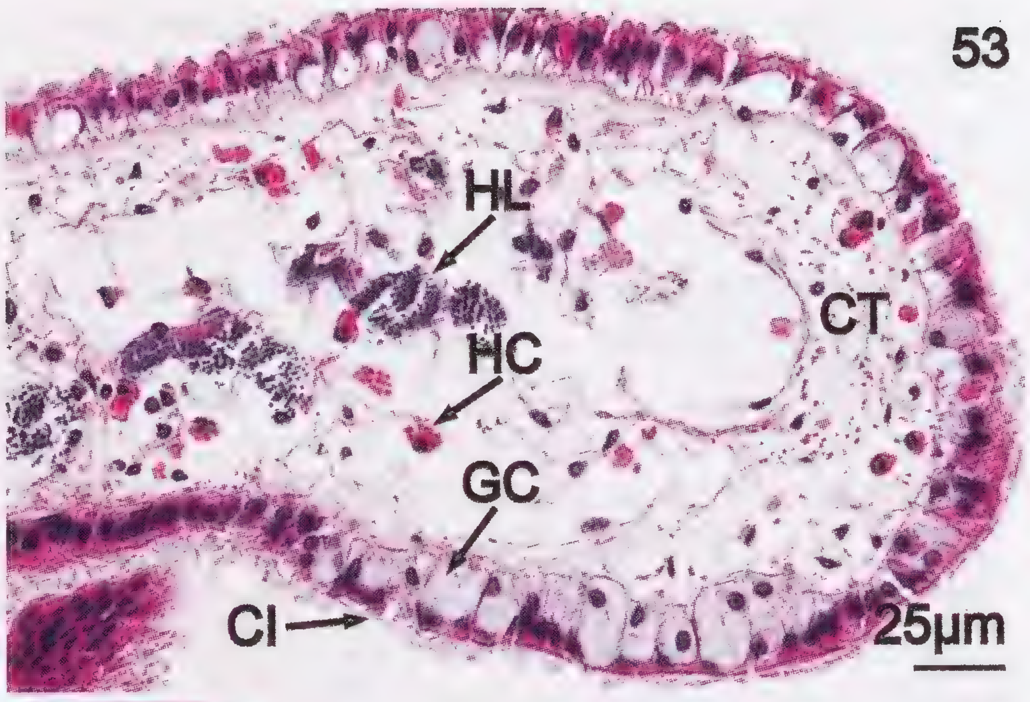

54

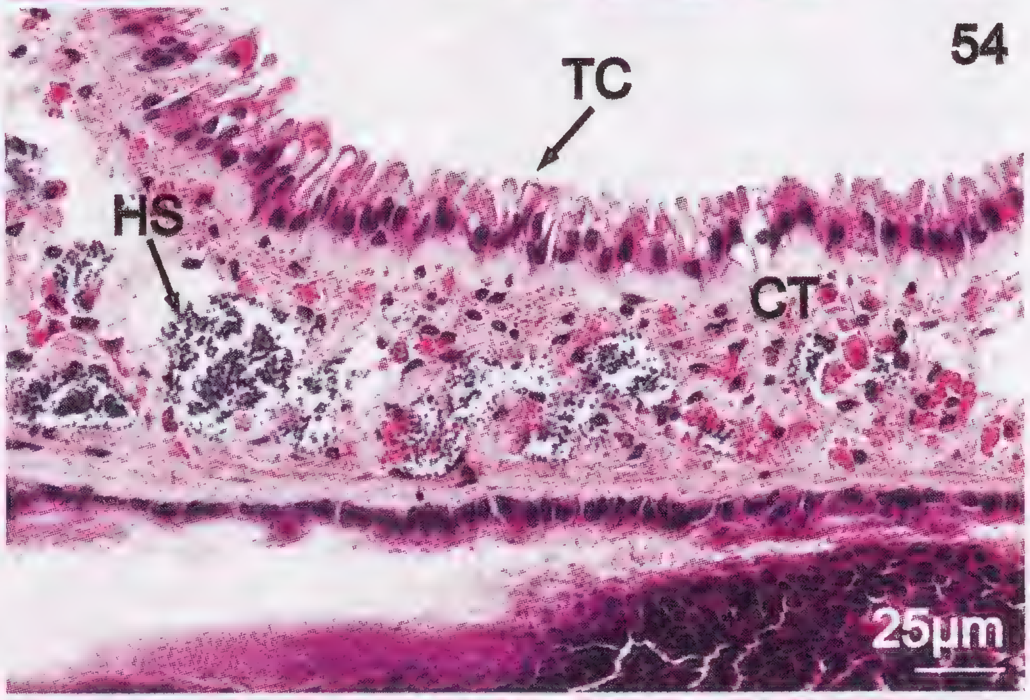

52

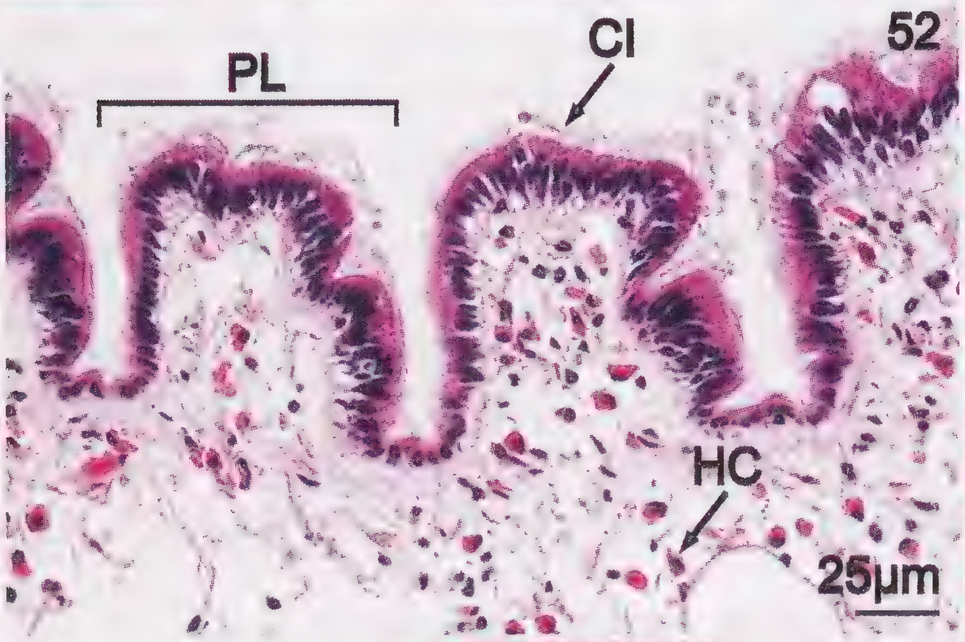

55

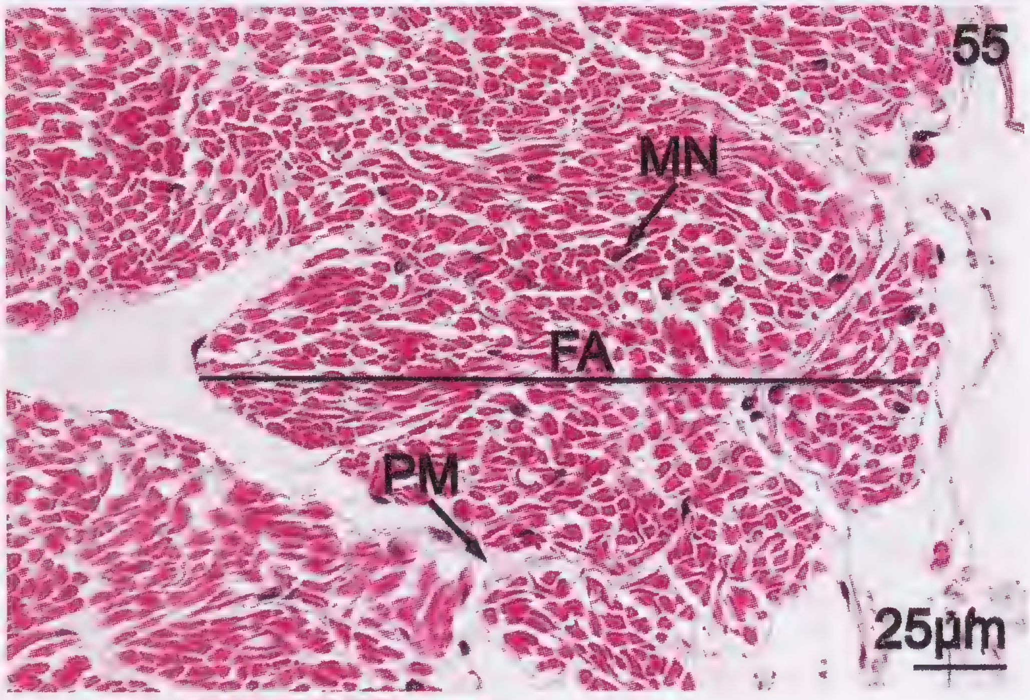

56

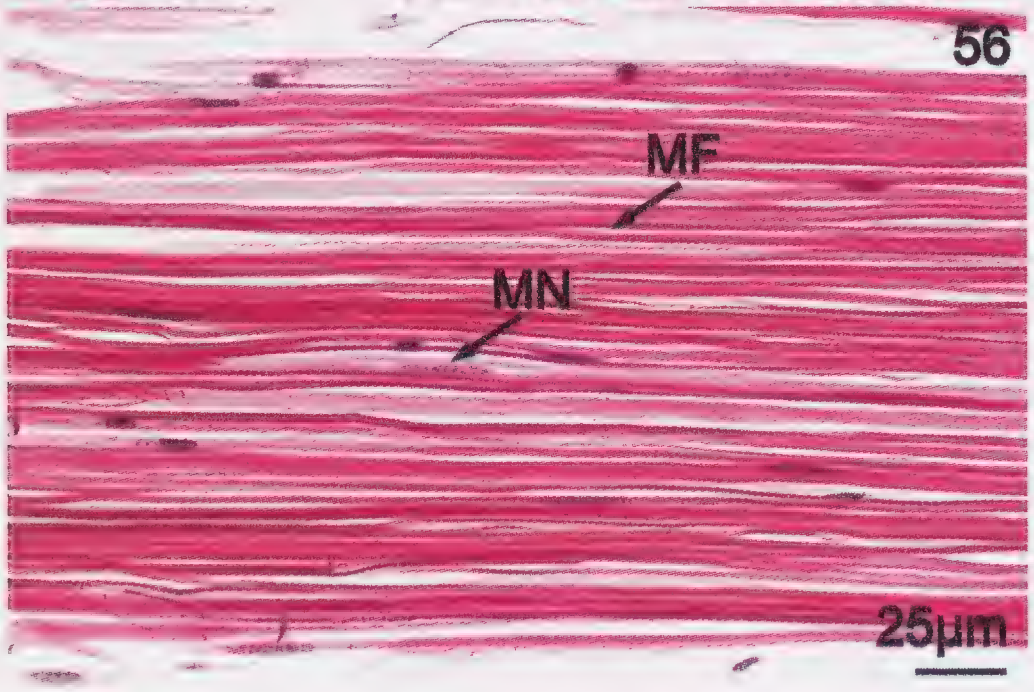

tively uniformly distributed across the apical surface of the epithelium. The cuticle represents the gastric shield and it lines dorsal and ventral surfaces at the posterior end of the stomach. Columnar cells are eosinophilic with an elliptical nucleus and a distinct nucleolus (Fig. 69). The medial aspect of the ventral wall consists of a series of irregular plicae (Fig. 70). The cuticle disappears dextrally where the epithelium becomes pleated (Fig. 71). Plicae are also located along the dorsal aspect of the stomach. Dorsal plicae are tall and narrow in comparison to plicae along the ventral wall (Fig. 72). Additionally, cells lining the dorsal gastric wall may appear vesiculated and may be secretory in nature. The sinistral wall features a rectangular typhlosole extending into the lumen. The typhlosole is slightly forked and possesses a gelatinous cuticle (Fig. 73).

Crystalline Style Sac: The crystalline style is generally a cylindrical rod spanning the visceral mass from the stomach to the posterior margin of the visceral mass. The diagnostic character of the style sac is a pale, eosinophilic rod, the style, within a circular chamber on the sinistral side. The style may be closely associated or attached to ciliated cells along the ventral sac wall, and there are three different types of epithelia throughout the style sac. The crystalline style sac has a lamina propria, and it varies from a thickened connective tissue support underneath the epithelial folds of the style sac, to a thin line of connective tissue surrounding the style sac (Fig. 74).

Type one epithelium is located within the circular portion of the sac and consists of ciliated columnar cells distinguished by a red cytoplasm and a heterochromatic, elliptical nucleus with a distinct nucleolus. The cell membrane along the apical surface of these cells is a thick line and cilia of type one cells are straight and thickened in comparison to cilia of type two epithelia (Fig. 75). Type-two epithelium originates along the left side of the median ventral fold and terminates near the fork. Ciliated cells characterizing this region have a basophilic cytoplasm, an elliptical, heterochromatic nucleus with a distinct nucleolus. The apical portion of the cell membrane is noticeably thinner than the apical membrane of type one cells, and cilia appear to be more flexible than type-one cilia. The ventral fork of the style sac also has a series of ellipsoid, basophilic mucocytes interspersed among ciliated epithelial cells (Fig. 76). The dorsal wall of the style sac, dextral to the median fold, is characterized by a basophilic columnar epithelium. Cells in type-three epithelium appear to be densely packed, supporting thin, flexible cilia similar to cilia featured in type-two epithelium (Fig. 77). The style is eosinophilic, and homogenous except for a series of fine circumferential rings, which may contain fine, black particulate matter (Fig. 78).

Intestine: The crystalline style represents the first limb of the intestine as it curves dorsally along the posterior margin of the visceral mass. The epithelium of the first intestinal limb maintains the same cell types characterizing the horizontal portion of the style sac (Fig. 79). However, the epithelium has large plicae extending into the lumen and the style sac epithelium is convoluted such that each cell type of the style sac may be located on the anterior or posterior wall. The lumen of the descending intestine contains an eosinophilic material likely representing chyme. Within crypts of adjacent folds, and around the distal tips of plicae, chyme appears broken up or shaped according to the contours of the tissue (Fig. 80).

←

FIGS. 51–56. Labial palps, anterior pedal retractor, and anterior adductor of *Villosa nebulosa*. FIG. 51: Sagittal section of labial palps revealing inner plicated surface (IS), distal palp margin (DM), outer palp surface (OS), anterior pedal retractor (PR); FIG. 52: Sagittal section of the inner palp surface featuring plicae (PL), cilia (CI), and hemocytes (HC) in the subepithelium; FIG. 53: Sagittal section of distal labial palp margin portraying cilia (CI), goblet cells (GC), and connective tissue (CT), hemolymph (HL), and hemocytes (HC) of the subepithelium; FIG. 54: Sagittal section of outer palp surface highlighting tear drop-shaped columnar cells (TC), and subepithelial connective tissue (CT), and hemolymph sinuses (HS); FIG. 55: Transverse section of anterior pedal retractor showing a fascicle (FA), with a thin perimysium (PM), and dark-staining myocyte nuclei (MN); FIG. 56: Sagittal section of anterior adductor showing the thin myofibers (MF), and ovular myocyte nuclei (MN).

The second and third intestinal limbs, as seen in transverse sections, are located ventrally in relation to the style sac. The second and third intestinal limbs are characterized by the presence of small to large plicae and both intestinal limbs are histologically identical (Fig. 81). In a longitudinal orientation, the intestine arches along the posterior margin of the visceral mass. The epithelium is lined with a regular series of plicae that appear to

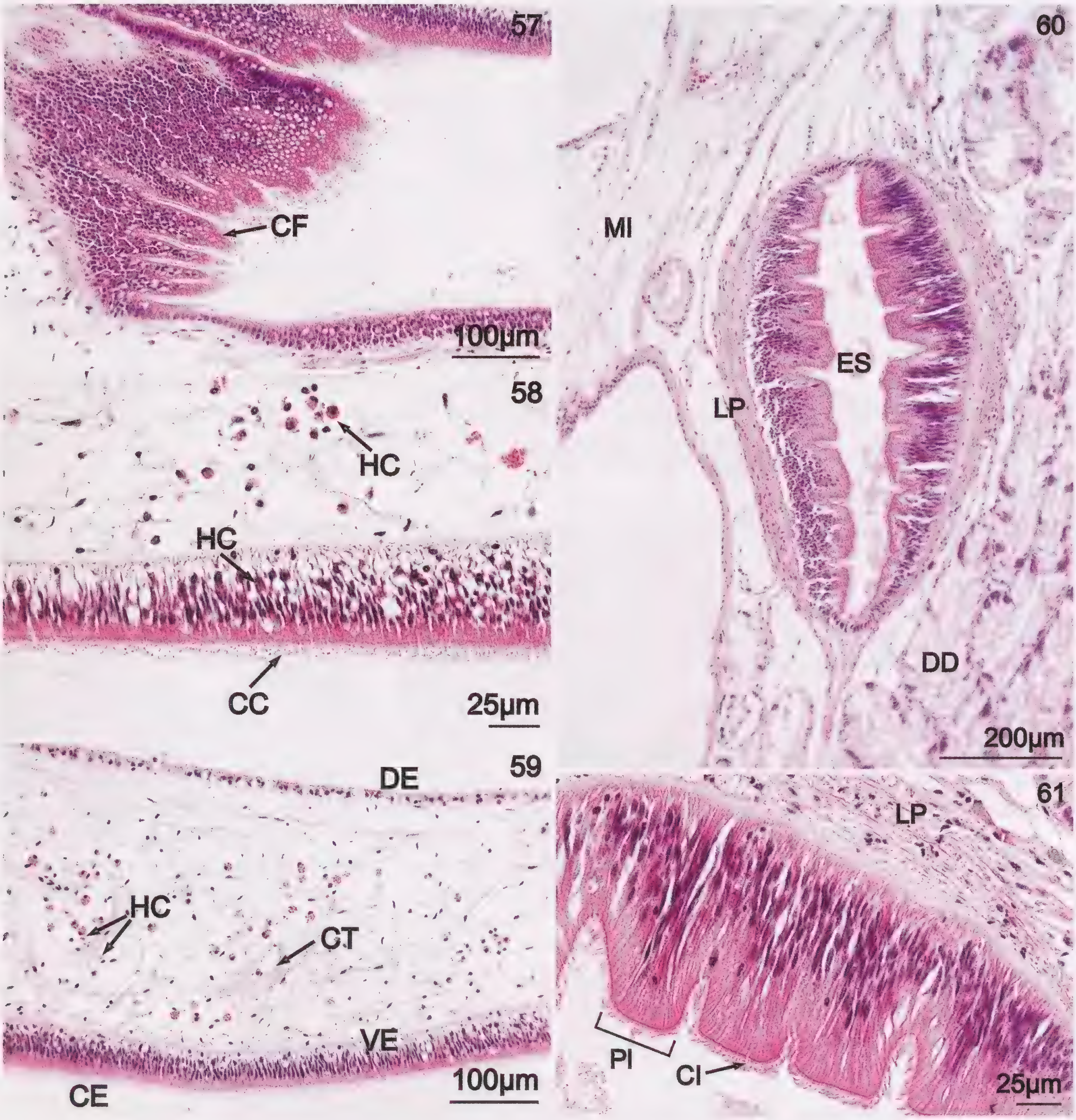

FIGS. 57–61. Oral groove, and esophagus of *Villosa nebulosa*. FIG. 57: Sagittal section of oral groove showing ciliated folds (CF) along the wall; FIG. 58: Sagittal section of the ventral oral groove wall displaying ciliated columnar cells (CC) and hemocytes (HC) within the subepithelium and nestled between epithelial cells of the ventral oral groove wall; FIG. 59: Sagittal section of the ventral oral groove wall displaying ciliated epithelium (CE), a composition of loose connective tissue fibers (CT) and hemocytes (HC) between the ventral epithelium of the oral groove (VE) and the externally located dorsal epithelium (DE); FIG. 60: Transverse section through dorsal aspect of visceral mass revealing the esophagus (ES) encircled by lamina propria (LP), tubules of the digestive diverticulum (DD), and mantle isthmus (MI); FIG. 61: Transverse section of esophagus portraying plicae (PL) with densely packed cilia (CI) and the supporting lamina propria (LP).

be somewhat "Y"-shaped (Fig. 82). Further down the length of the initial limb, villi are replaced by shorter epithelial extensions that are generally plateau-shaped. The lower portion of the first intestinal limb appears to be an area of active secretion and mixing. Plateaus along the anterior and posterior walls are vesiculated and releasing transparent bubbles into the lumen. The center of the lumen has a large mass of fused bubbles surrounded by series of crescent-shaped bubbles (Fig. 83). However, the main constituent of the second and third intestinal limb is the ciliated columnar epithelium. Columnar cells have a

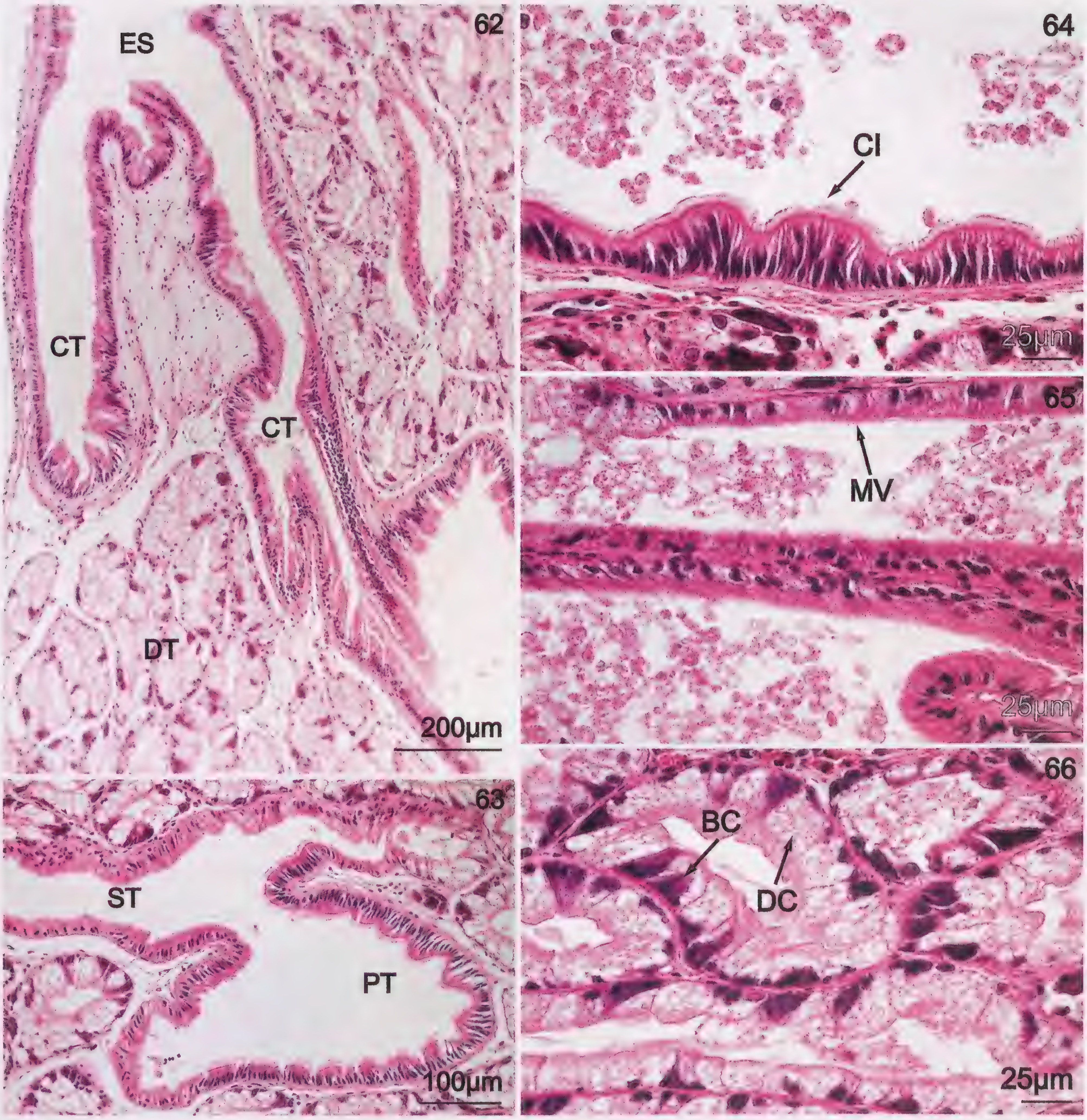

FIGS. 62−66. Digestive diverticulum, and stomach of *Villosa nebulosa*. FIG. 62: Transverse section of the junction between the esophagus (ES) and digestive diverticula highlighting ciliated tubules (CT) leading toward digestive tubules (DT); FIG. 63: Transverse section of digestive diverticulum emphasizing a transition from ciliated primary tubules (PT), to vesiculated secondary tubules (ST); FIG. 64: Transverse section of digestive diverticulum portraying fine structure of primary tubules including cilia (CI); FIG. 65: Transverse section of the digestive diverticulum showing microvilli (MV) of secondary tubules; FIG. 66: Transverse section of digestive diverticulum showing the basophiic basiphil cells (BC), and vesiculated digestive cells (DC).

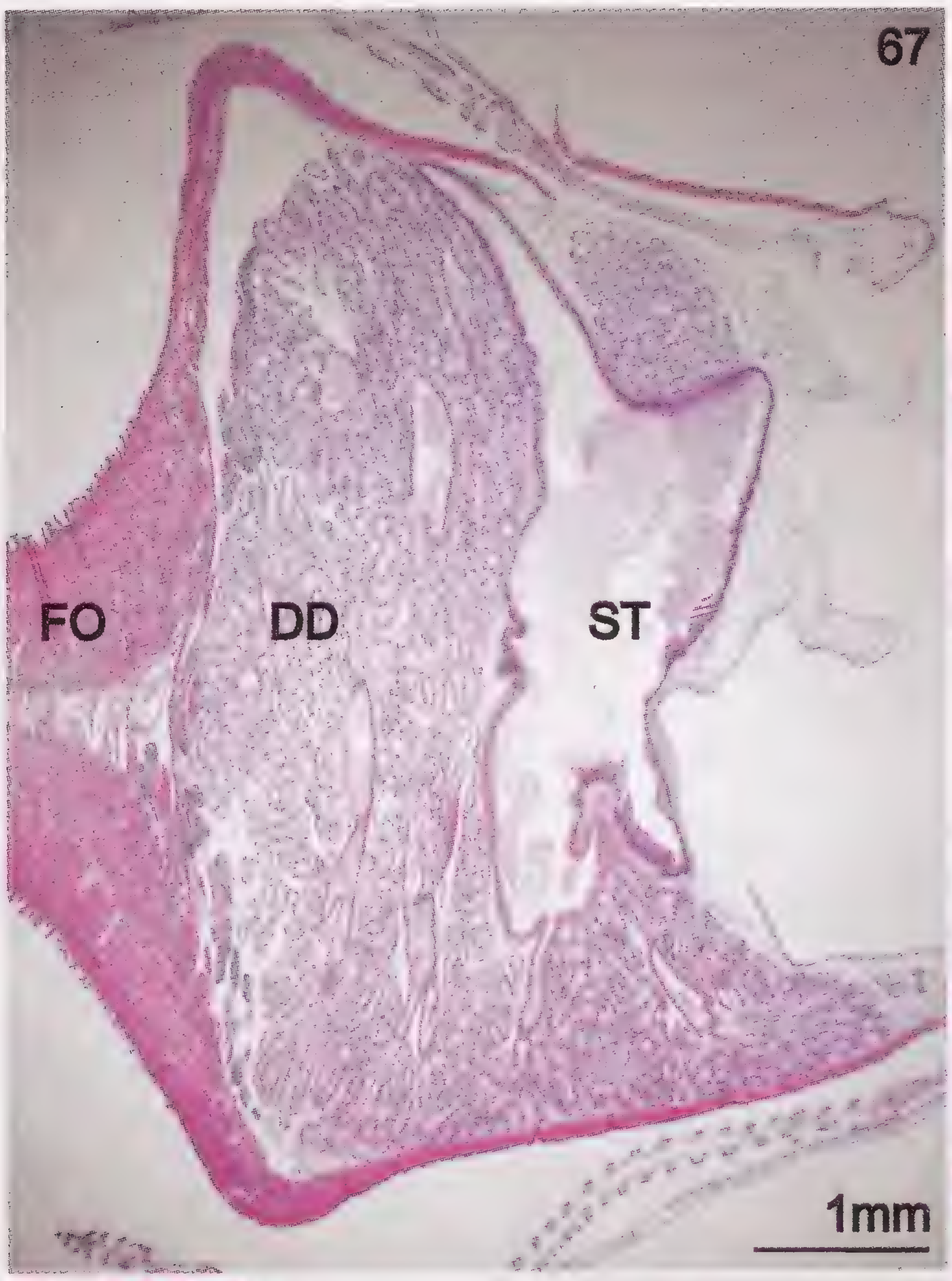
67

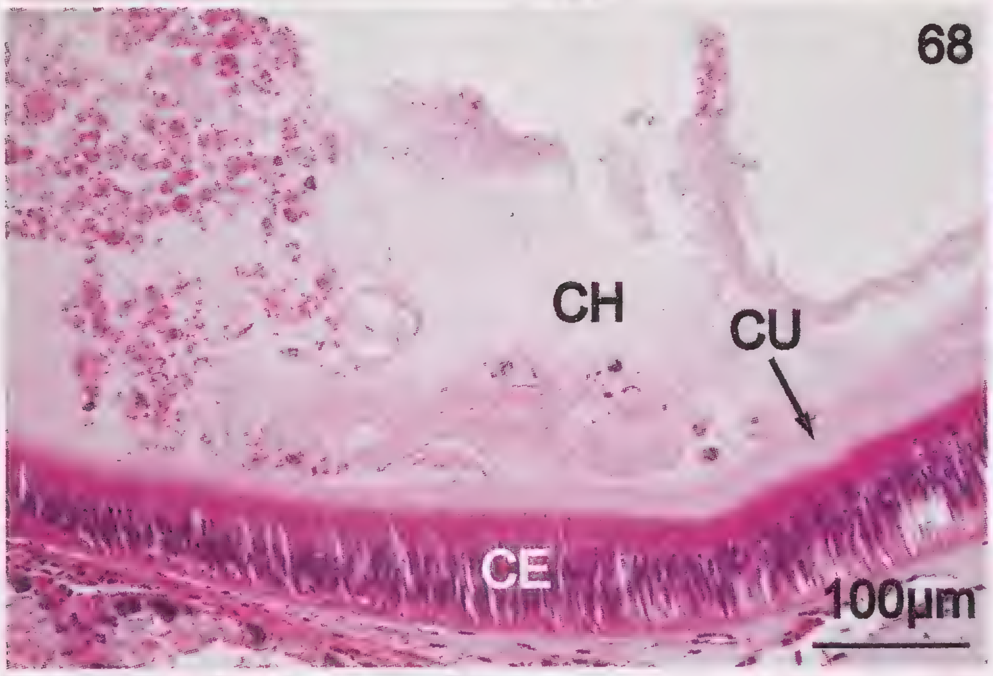
68

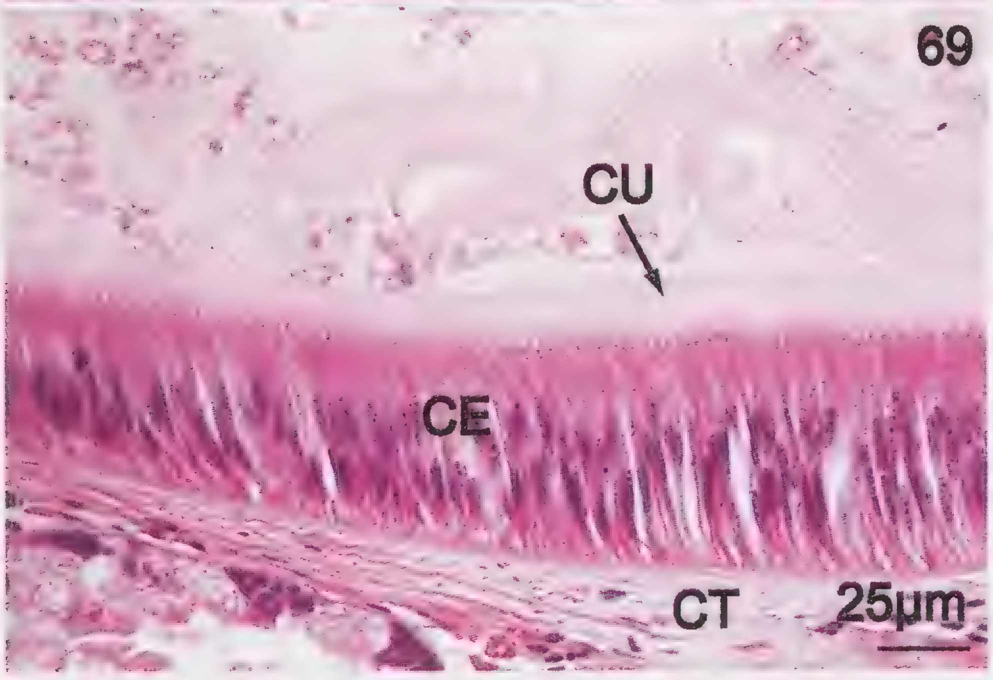
69

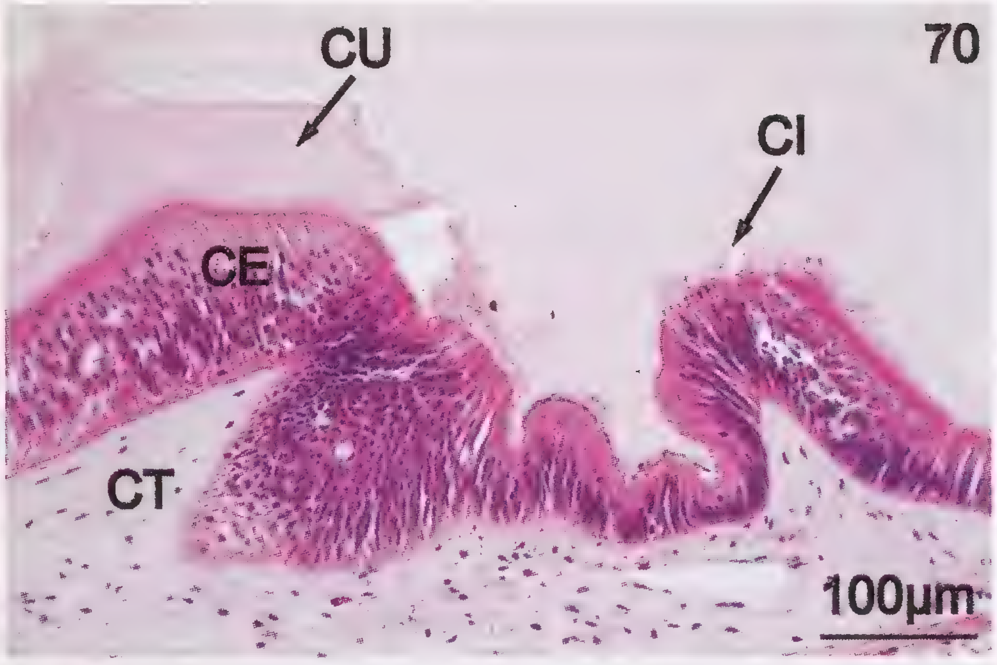
70

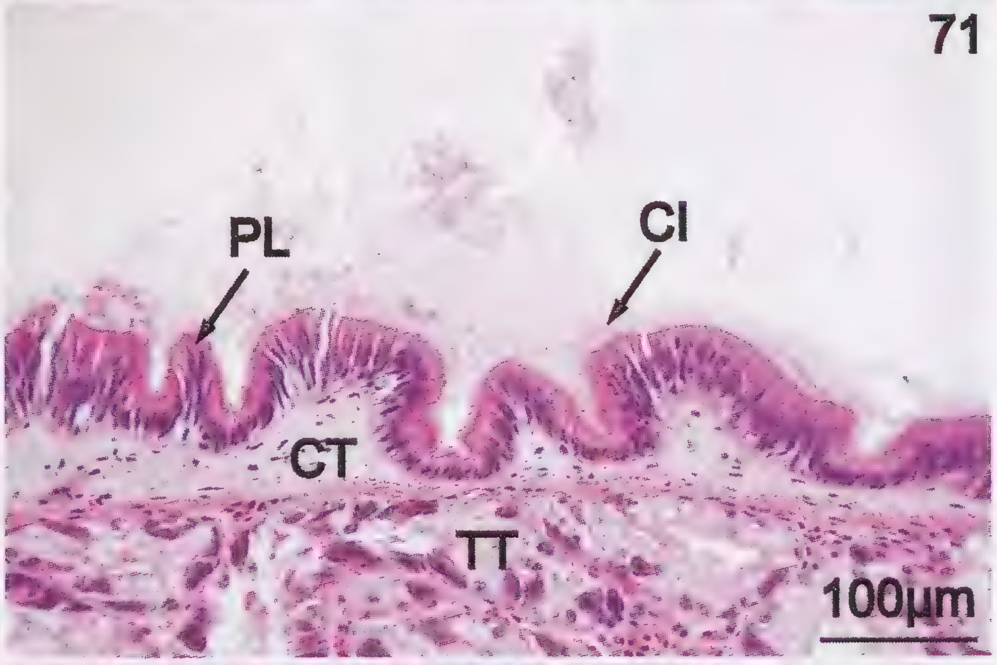
71

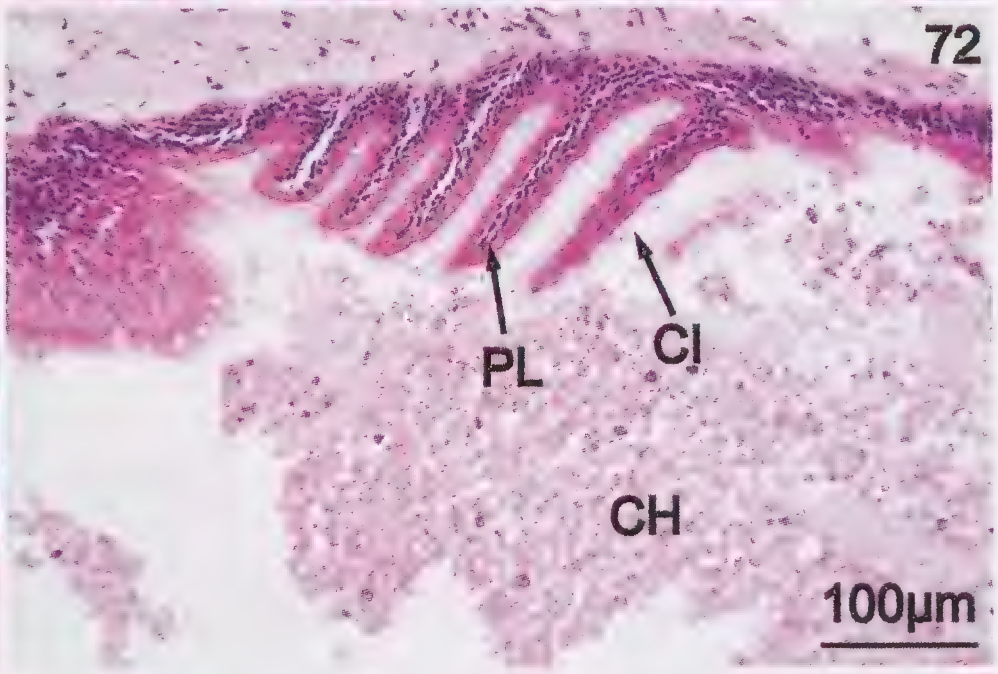
72

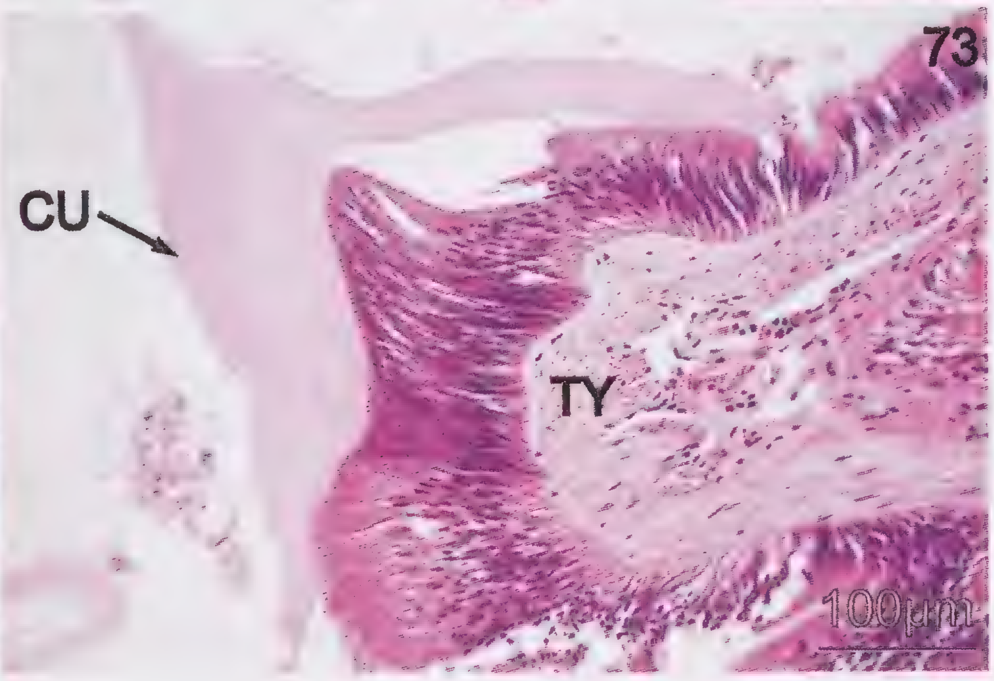
73

pale, eosinophilic cytoplasm, and an ovular nucleus with a distinct nucleolus (Fig. 84).

In sagittal sections of the viscera, the second intestinal limb is posterior to the first limb. The lining of the second intestinal limb consists of short plicae that are generally Y-shaped. Between each Y-shaped structure, there may be a triangular cusp creating a set of oblique crypts between each Y-shaped unit (Fig. 84). Ciliated columnar cells are narrow, eosinophilic with a distinct nucleolus within each nucleus. Additionally, wandering hemocytes are present within the epithelium of the second intestinal limb and typically resemble a spherical mass of eosinophilic vesicles.

The most distinctive feature of the fourth intestinal limb is the centrally located, ventrally directed major typhlosole (Fig. 85). Surrounding the typhlosole, the ventral lining of the intestine is pleated with a series of flattened epithelial folds. The height of each fold, and the length and width of the crypts increases from the base of the typhlosole to the ventrolateral region. Epithelial tissue surrounding the lumen consists of ciliated columnar cells. In general, the cells lining the ventral and dorsal surfaces have similar characteristics. However, the ventral epithelium has a preponderance of red, elliptical granulocytes. The granular component of the columnar cell is tear drop-shaped to elliptical, and apically positioned within the cell (Fig. 86). Granulocytes do not appear to be wandering hemocytes because the granular structure seems to be continuous with the cytoplasm, and there is usually a slight gap surrounding a hemocyte. Furthermore, hemocytes are typically circular, with a distinct, circular nucleus and the cytoplasm may contain prominent vesicles. Cells along the circumference of the typhlosole are well organized, with short bristle-like cilia along the apical surface (Fig. 87). Connective tissue of the fourth intestinal region is represented by a well-defined lamina propria supporting the typhlosole, and a thin wrapping around the lateral and ventral walls. Fibers within the major typhlosole are loosely aggregated, and the tissue has a pale, eosinophilic quality in comparison to the connective tissue surrounding the lateral and ventral walls (Figs. 85–87). The lamina propria is supplied with hemolymph from a series of small sinuses throughout the tissue that are just large enough for a small number of hemocytes to fit within the lumen.

The fifth limb of the intestine is a reflection of intestinal region four in terms of morphological and cytological features (Fig. 88). Morphologically, the intestine is circular along the hinge line, but becomes flattened as it nears the posterior adductor. The lateral and dorsal portions of the intestinal wall are pleated, but the dorsal wall has more plications than the fourth intestinal limb (Fig. 89). The ventral epithelium is a continuation of the typhlosole of the fourth intestinal limb (Fig. 90). Nuclei of the ciliated columnar cells, along the dorsal and ventral walls, are more regular, clearly revealing the presence of a single layer of cells within the ventral and dorsal walls. Unlike region four, granulocytes are absent from the outer wall of the fifth intestinal region. The connective tissue lamina of the typhlosole consists of loose connective tissue and fibroblasts as in region four, but the connective tissue wrapping around the outer wall supports taller epithelial folds than in region four.

←

FIGS. 67–73. Stomach of *Villosa nebulosa*. FIG. 67: Transverse section through visceral mass showing the location of the foot (FO), digestive diverticulum (DD), and stomach (ST), and the gross morphological features of the stomach; FIG. 68: Transverse section of the dextral portion of the ventral stomach wall showing chyme (CH), and a cuticle (CU) attached to the columnar epithelium (CE); FIG. 69: Transverse section of the dextral portion of the ventral stomach wall revealing a dense cuticle (CU) along the surface of the columnar epithelium (CE) and the underlying connective tissue (CT) of the subepithelium; FIG. 70: Transverse section of the medial portion of the ventral stomach wall showing the cuticle (CU), columnar epithelium (CE), cilia (CI), and underlying connective tissue (CT) of the subepithelium; FIG. 71: Transverse section of the ventral stomach wall of the sinistral side of the body revealing cilia (CI), plicae (PL), connective tissue (CT), and tertiary tubules (TT); FIG. 72: Transverse section of the dorsal stomach wall showing plicae (PL), cilia (CI), and chyme (CH); FIG. 73: Transverse section of dextral stomach wall showing a rectangular and forked typhlosole (TY), with an attached cuticle (CU).

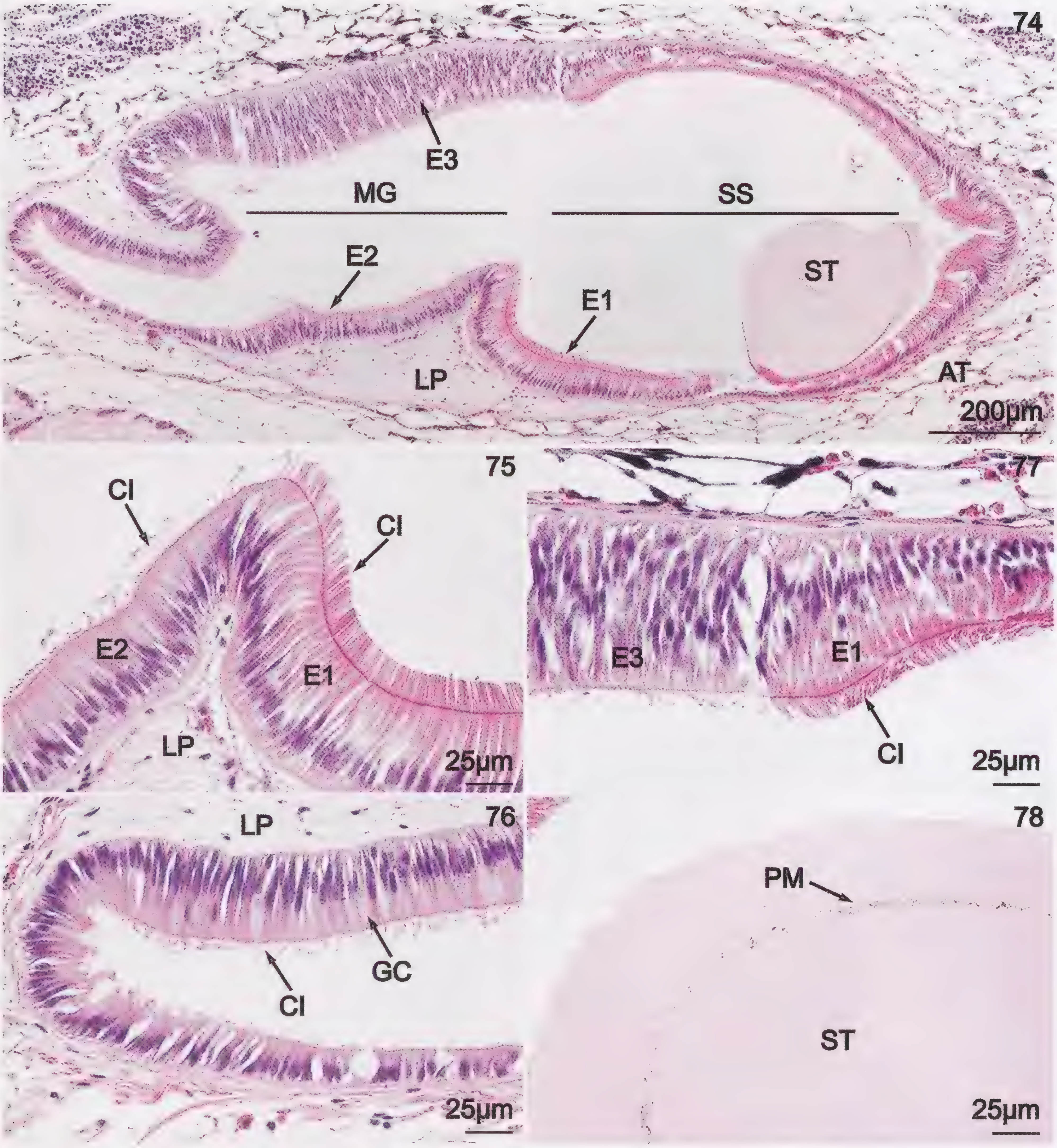

FIGS. 74−78. Crystalline style sac of *Villosa nebulosa*. FIG. 74: Transverse section through the crystalline style sac showing the style sac (SS), crystalline style (ST), midgut (MG), epithelium type 1 (E1), epithelium type 2 (E2), epithelium type 3 (E3), lamina propria LP), and adipose tissue (AT); FIG. 75; Transverse section of the crystalline style sac showing bristle-like cilia (CI) of type-one epithelium (E1), whispy cilia (CI) of type-two epithelium (E2), and the underlying lamina propria (LP); FIG. 76: Transverse section of the crystalline style sac showing wispy cilia (CI) and goblet cells (GC) of type-two epithelium, and the underlying lamina propria (LP); FIG. 77: Transverse section of the crystalline style sac showing the transition from bristle-like cilia (CI) of type-one epithelium (E1), and whispy cilia (CI) of type-three epithelium (E3); FIG. 78: Transverse section of the crystalline style sac showing the gelatinous style (ST) with ring of particulate matter (PM).

Cellular Structure of Cardiovascular System Tissues

Heart: The heart and nephridium are located dorsally in relation to the visceral mass, and cardiac muscle encircles the fifth limb of the intestine from the posterior margin of the visceral mass to the visceral mass midpoint. Bivalves have a three-chambered heart consisting of a laterally positioned pair of auricles and a large medial ventricle (Fig. 91). The ventricle of *V. nebulosa* is conical and contains a distinct epicardium and myocardium (Fig. 92). The epicardium is a sinuous layer of squamous cells, and the myocardium consists of two layers of cardiac muscle. There is a thickened outer region, located directly underneath the epicardium and characterized by a compact network of branched muscle fibers, while the medial portion of the ventricle contains widely separated cardiac myofibers. The heart is situated within a pericardial cavity with a delicate pericardial sac lined with squamous cells. Ventricle contains branched cardiac myocytes having a fibrous consistency and a pale, basophilic nucleus with a distinct nucleolus (Fig. 93). Auricles are generally delicate cylindrical tubes of cardiac muscle and squamous epithelium linking the ventricle to the pericardial sac (Fig. 94). Hemolymph flow between the auricles and ventricle appear to be regulated by auriculoventricular valves. Valves are long, flaps extending into the lumen of the ventricle consisting of a compact layer of irregular muscle fibers surrounded by endothelium (Figs. 91, 95).

Arteries, Veins, Capillaries and Pericardial Gland: Bivalves have an open circulatory system and hemolymph is distributed throughout the body among interstitial spaces and hemolymph sinuses. However, we observed distinct vessels resembling arteries, veins and capillaries. Hemolymph has a distinct cellular and non-cellular component consisting of spherical, eosinophilic hemocytes (e.g., Fig. 93) and black, ink-like granules of hemolymph (e.g., Fig. 96). Hemolymph sinuses are distinct cavities within tissue that are not lined by endothelial cells (e.g., Figs. 59, 86). Hemolymph vessels resemble veins, arteries or capillaries and are lined with squamous cells. Arteries and veins are difficult to distinguish because they each may be circular to ovular or somewhat irregular in shape. Potential arteries have layers of musculature surrounding the lumen (Fig. 96). Veins, however, have thinner walls of fibrous tissue (Fig. 97). Capillaries are simple, circular structures lined with squamous cells and are typically seen in the mantle edge and adductors (Fig. 98).

The pericardial gland is a large network of connective tissue fibers in the dorsal region of the body bordered by gill, mantle isthmus, heart and nephridia. Fibrous connective tissue is located in the dorsal region of the body, anterior to posterior, and is similar to the composition of the middle mantle. The most distinctive feature of this tissue is the preponderance of discolored hemocytes. Eosinophilic hemocytes are present in the sinuses between connective tissue fibers, but many of the hemocytes have a brown or yellow cytoplasm. Discolored hemocytes seemingly have a cytoplasm with a low affinity for eosin given their subtle red coloration, and, additionally, some discolored hemocytes seemingly lack a nucleus or the nucleus appears to be emarginated or slightly separated from the cytoplasm (Fig. 99).

Renal System

Anterior Nephridium: The nephridium is a large tubular organ located dorsally to the left and right of the visceral mass. Nephridial tissue spans the length of the body from the anterior-medial point of the visceral mass to the posterior adductor. Additionally, there are distinct morphological features characterizing the anterior and posterior regions of the nephridia. Anterior nephridia have distinct ventral and dorsal limbs, while the posterior nephridia lacks distinct dorsal and ventral regions (Fig. 100). The ventral nephridial limb is characterized by large plications of the dorsal and ventral walls, while the walls of the dorsal nephridia have fewer plications. Epithelial folds of the ventral limb are composed of columnar cells with an eosinophilic, granular cytoplasm, and a dark-staining, monochromatic nucleus (Fig. 101). The nucleus of a columnar cell is located in the basal portion of the cell, and the apical region may contain a large vesicle. Some columnar cells have a transparent or a pale eosinophilic vesicle, while other cells in the ventral nephridial limb contain a brown vacuole. Subepithelium of the ventral limb consists of connective tissue supporting the epithelium and a hemolymph

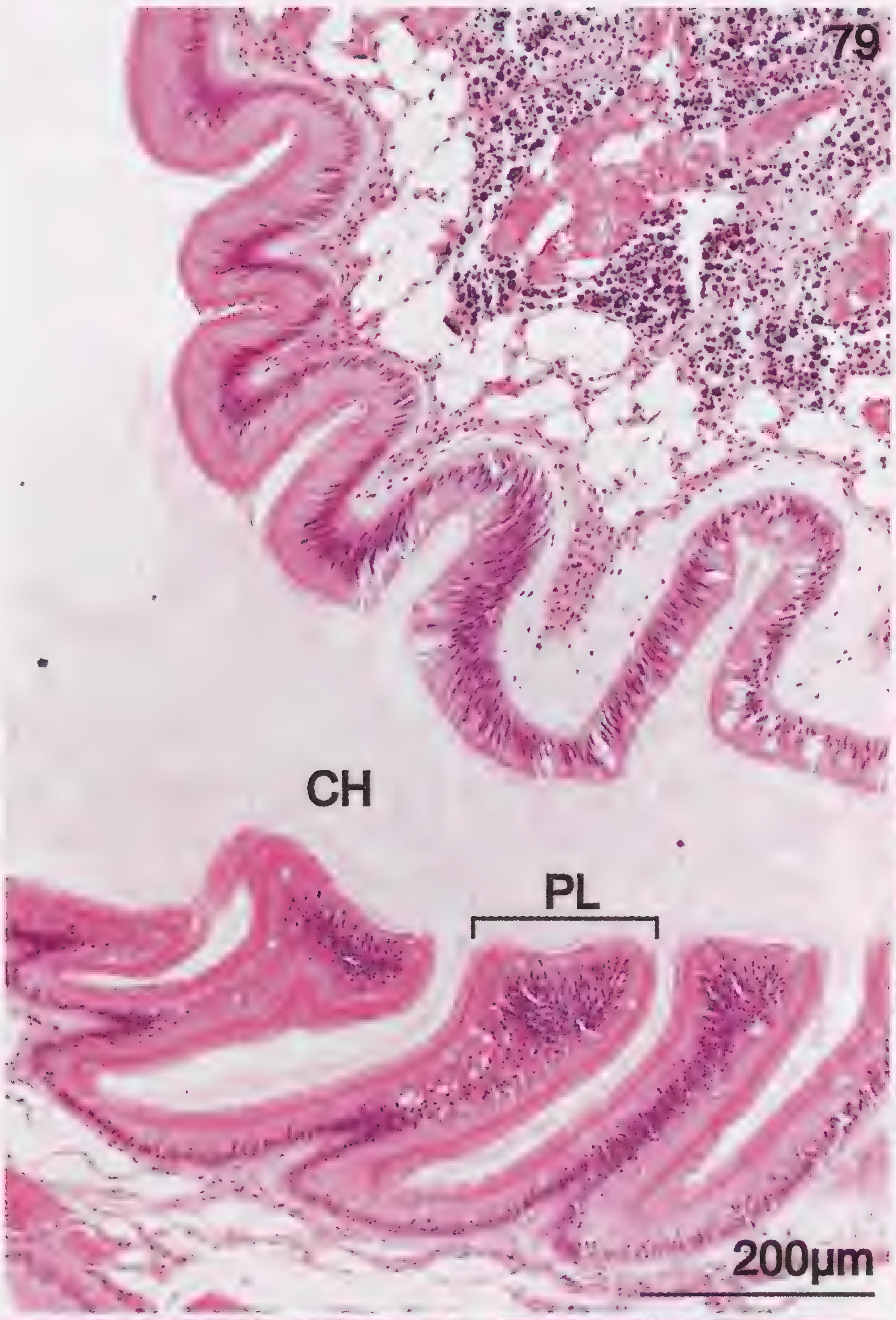
79
CH
PL
200µm

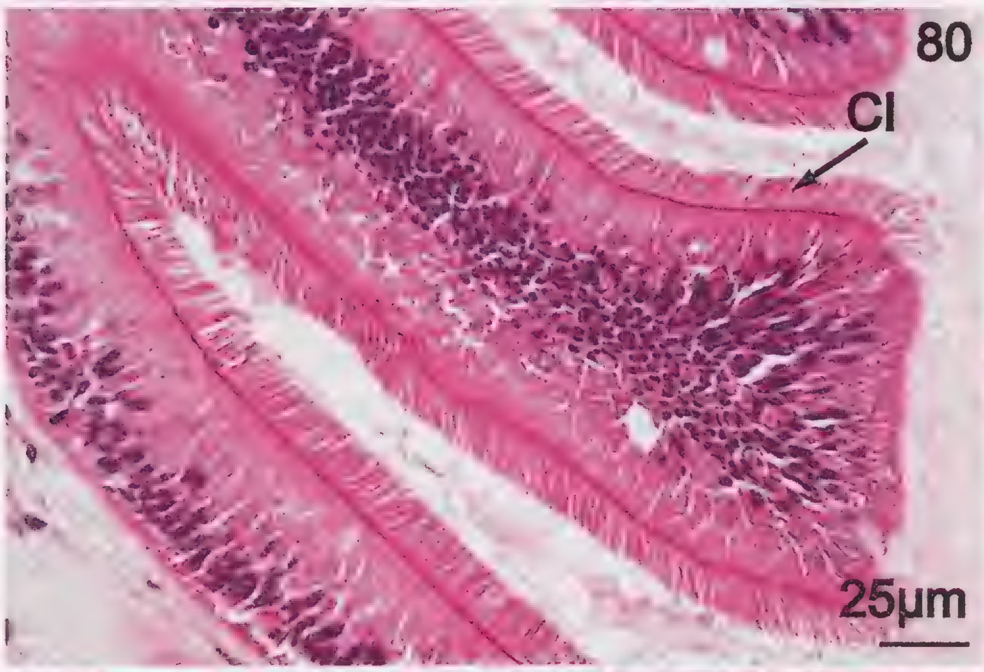
80
CI
25µm

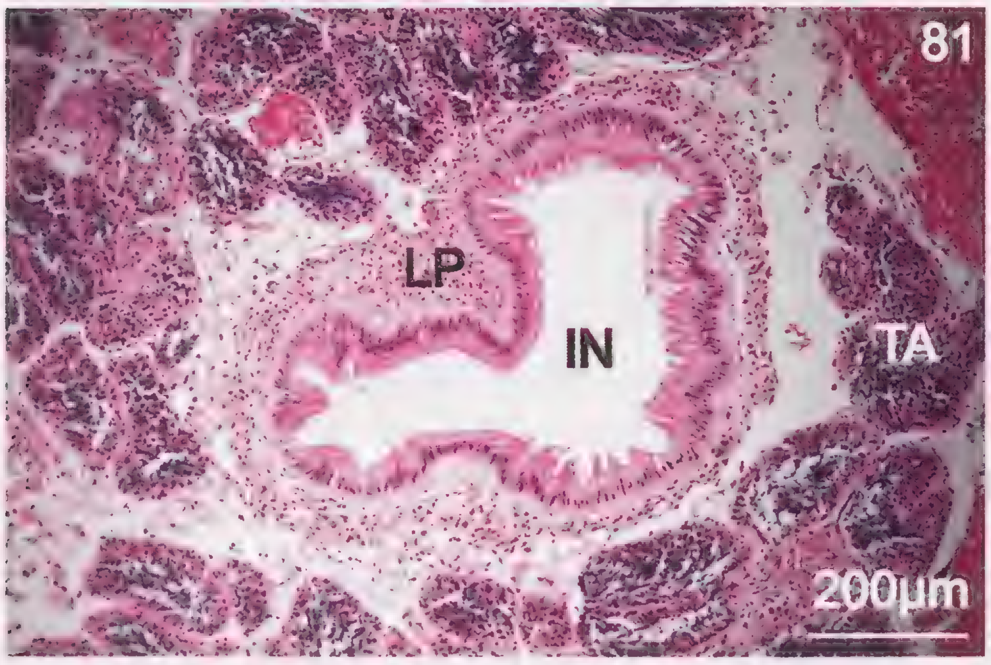
81
LP
IN
TA
200µm

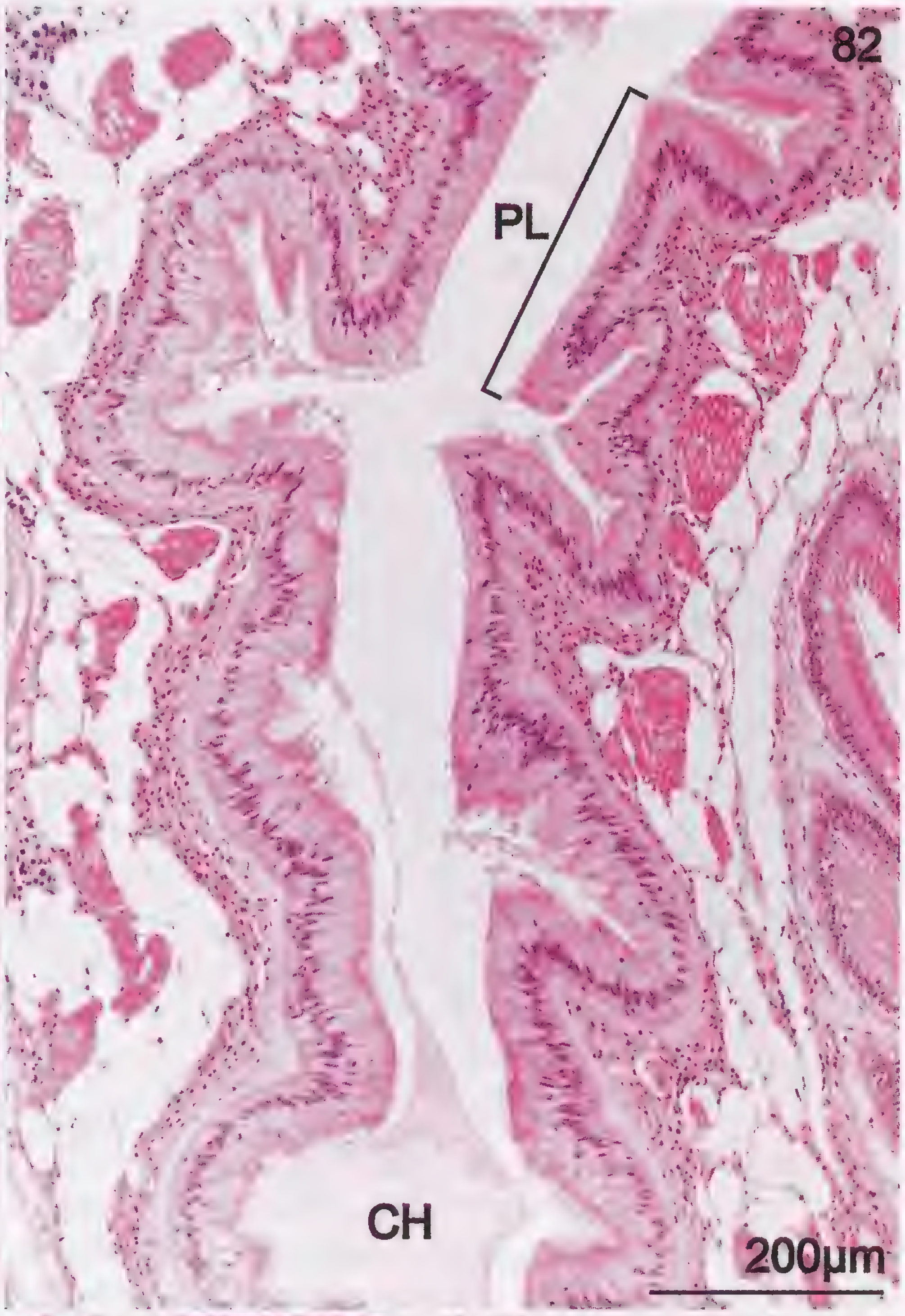
82
PL
CH
200µm

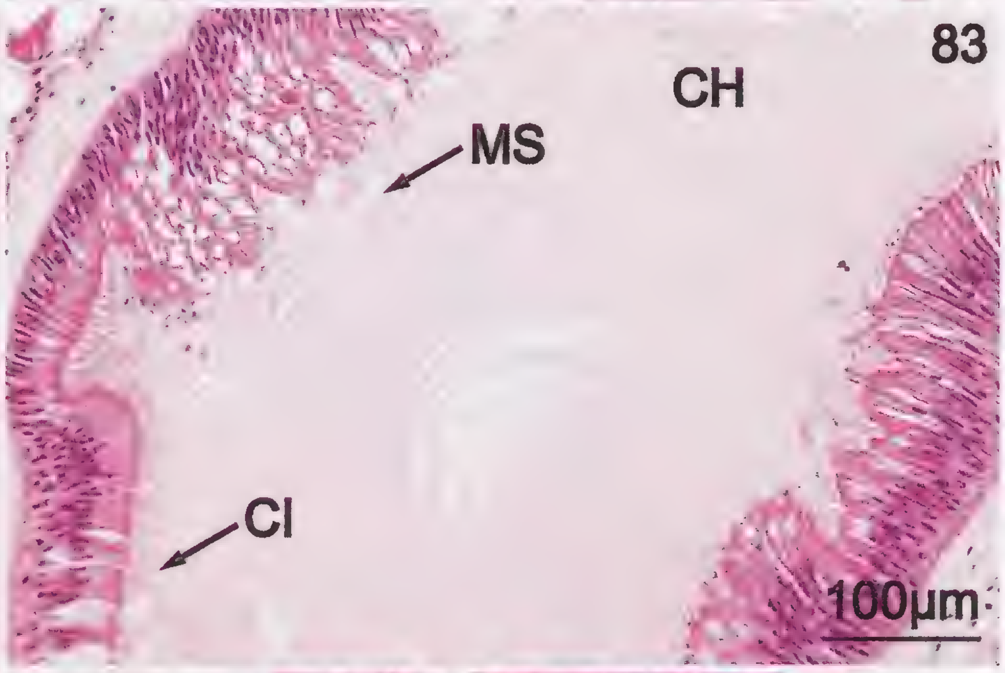
83
CH
MS
CI
100µm

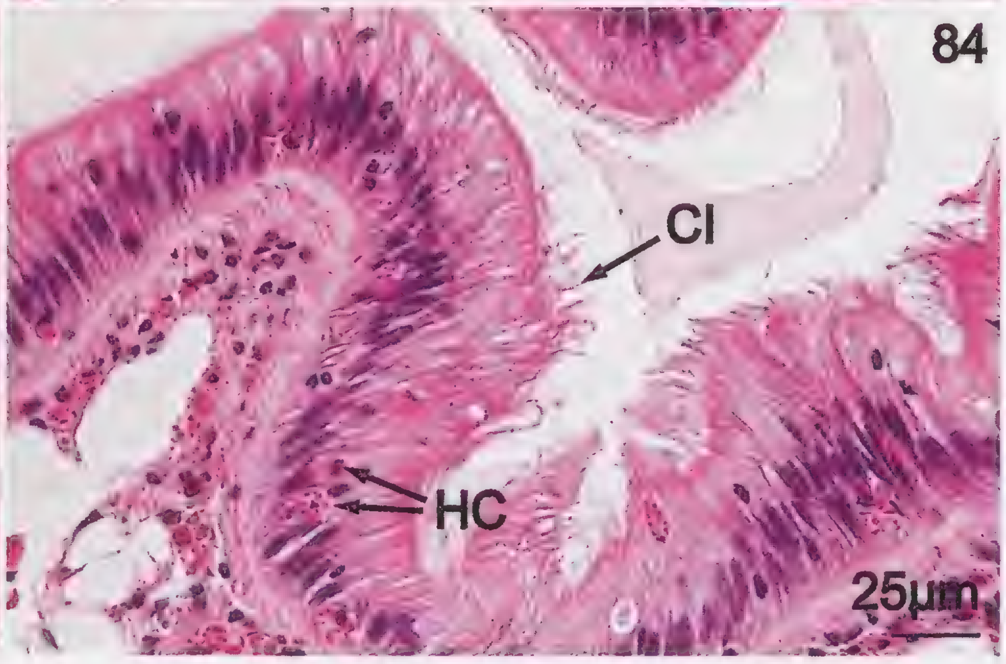
84
CI
HC
25µm

sinus. The lining of the dorsal nephridium is generally flattened, but there are localized regions within the dorsal nephridium is plicated or features teardrop-shaped cells. For example, the ventral wall of the dorsal nephridium has a small number of plicae and the surface of these structures is irregular (Fig. 102). Plicae of the dorsal nephridium are sparsely distributed anterior to posterior. Secondly, the dorsal nephridium contains patches of teardrop-shaped cells with an apical vesicle (Fig. 103). Teardrop cells are typically located at the dorsolateral corners of the dorsal nephridium.

While the above-mentioned features of the walls of the ventral and dorsal limbs of the nephridium are representative of the anterior nephridial region, there are two structures that are unique to the anterior region. The urethra is a communication between the dorsal nephridium and suprabranchial cavity, and located in the anterior end of the nephridium. Additionally, there is a ciliated tubule, the renopericardial canal, located in the lateral portion of the ventral nephridial limb, adjacent to the urethra (Fig. 104). Squamous epithelial cells lining the dorsal nephridial limb change to a ciliated, columnar epithelium at the ventral end of the urethra (Fig. 105). The renopericardial canal is the ciliated tubule at the lateral end of the ventral nephridial limb and transfers fluid from the pericardial cavity to the lumen of the ventral nephridium. The renopericardial canal is composed of conical epithelial folds that extend far into the lumen and these epithelial folds feature ciliated columnar cells, and conspicuous goblet cells. Surrounding the canal is a well-defined lamina propria consisting of concentric layers of fibrous tissue (Fig. 106).

Posterior Nephridium: The nephridium is enlarged between the posterior margin of the visceral mass and posterior adductor. Nephridial epithelium is convoluted, consisting of rounded, and irregular epithelial folds (Fig. 107). Additionally, epithelial folds of the posterior nephridium are typically spaced farther apart from each other than in the anterior nephridium. Regarding the fine structure of posterior nephridial epithelium, cells are columnar, with an eosinophilic, vesicular cytoplasm and a pale, basophilic nucleus typically lacking a well-defined nucleolus (Fig. 108). Additionally, the lumen between the branches has expanded and is significantly larger than the lumen in the anterior region. Nephridial branches have a noticeably different composition from branches within the ventral limb of the anterior nephridium. Epithelial cells characterizing the posterior nephridial branches are columnar and vesiculated and appear to be bubbling at the apical surface. Additionally, the subepithelium of posterior nephridial branches consists of a simple squamous epithelium and hemolymph (Fig. 108). Posterior nephridium has sinistral and dextral limbs divided by a septum of loose connective tissue fibers and a pair of nerves. The posterior nephridial septum also contains a large artery located ventrally in relation to the pedal retractors. The artery is composed of wavy muscle fibers and runs along the hinge line towards the posterior end of the mantle.

Posterior Adductor and Posterior Pedal Retractors: Posterior pedal retractors are located within the nephridial septum, between the posterior adductor and visceral mass. Posterior nephridial branches encircle the posterior pedal retractors (Fig. 109). In transverse sections of the viscera, posterior retractors represent large fascicles. The musculature has a distinct perimysium and endomysium and myofibers are polygonal in outline (Fig. 110). The posterior adductor is located posterior to

---

←

FIGS. 79–84. First intestinal limb, and second intestinal limb of *Villosa nebulosa*. FIG. 79: Sagittal section through the first intestinal limb portraying tall plicae (PL) and chyme (CH) in the intestinal lumen; FIG. 80: Sagittal section of posterior wall of the first intestinal limb emphasizing the tall plicae (PL), with densely ciliated surfaces (CI); FIG. 81: Transverse section through the visceral mass showing the second limb of the intestine (IN), the surrounding lamina propria (LP), and testicular acini (TA); FIG. 82: Sagittal section through the initial portion of the second intestinal limb representing a region of short plicae (PL), and chyme (CH); FIG. 83: Sagittal section of second intestinal limb portraying cilia (CI), mucus secretions (MS), and chyme (CH); FIG. 84: Sagittal section of the second intestinal limb showing cilia (CI) and wandering hemocytes (HC).

85

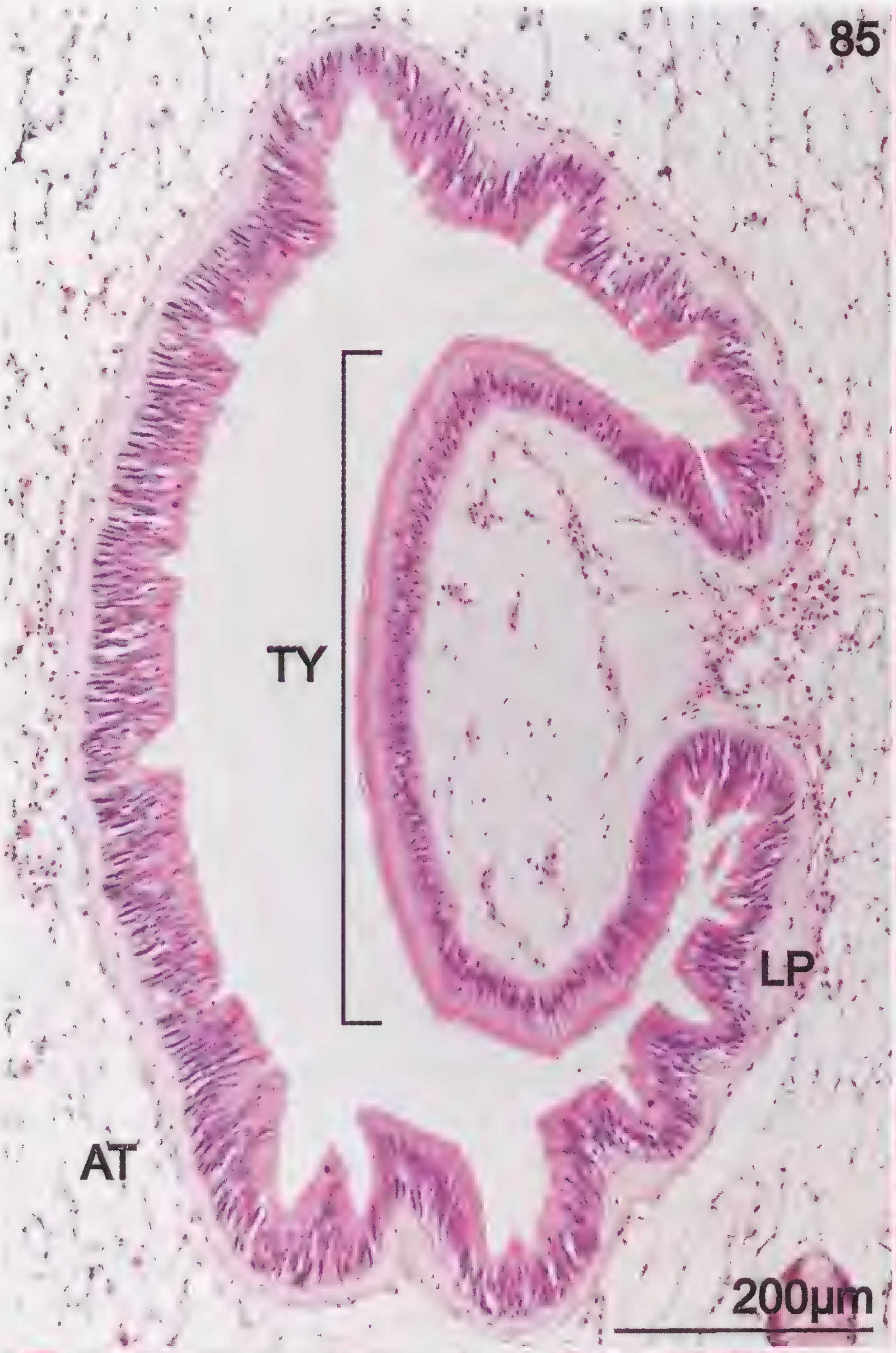

88

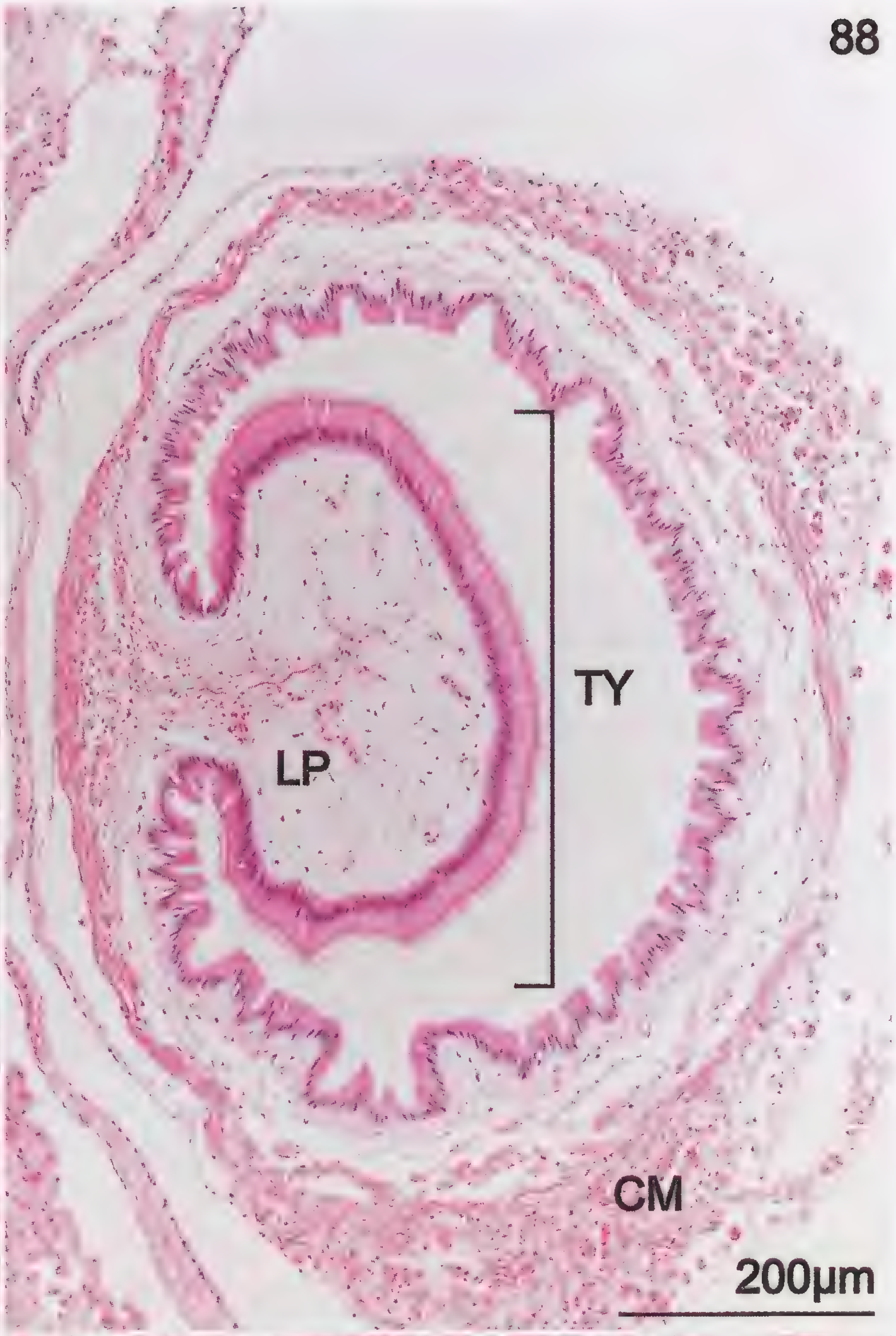

86

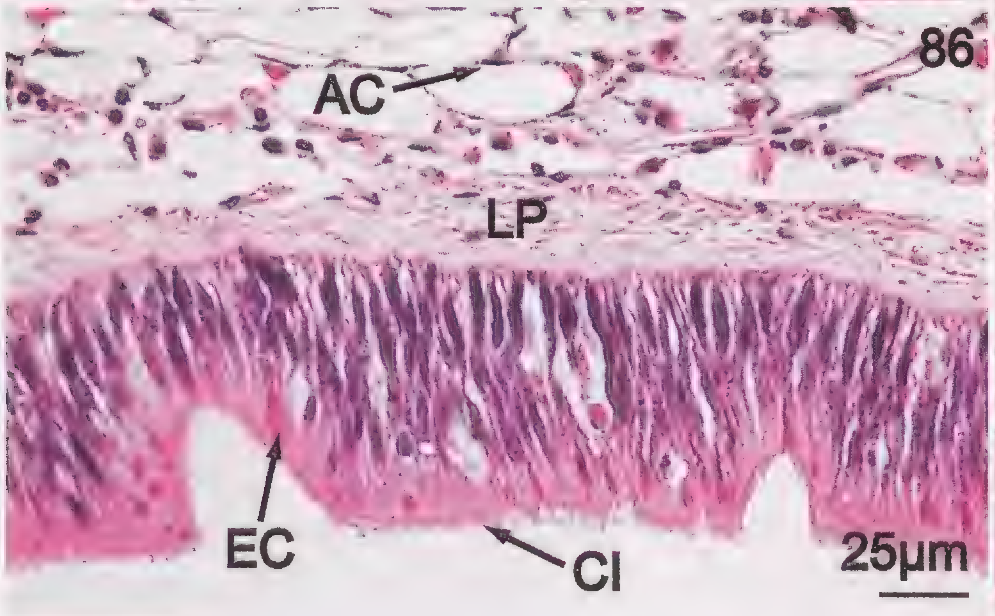

89

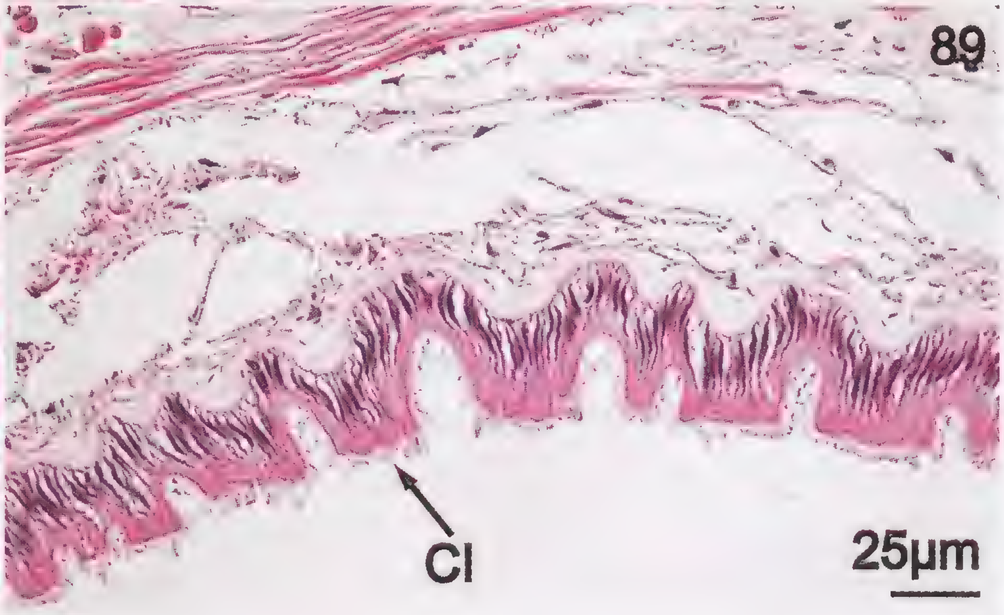

87

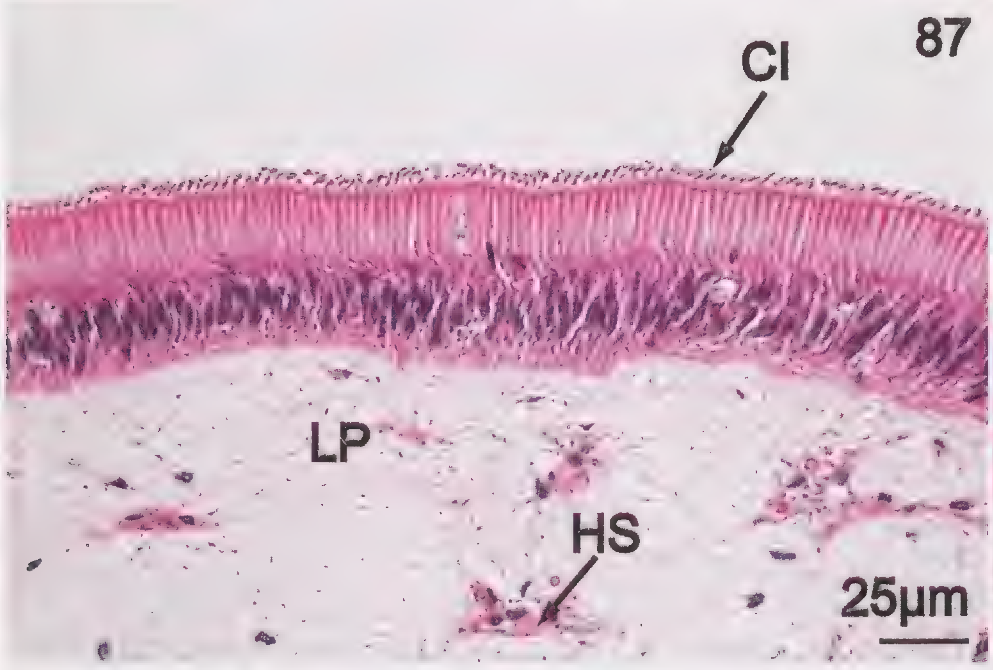

90

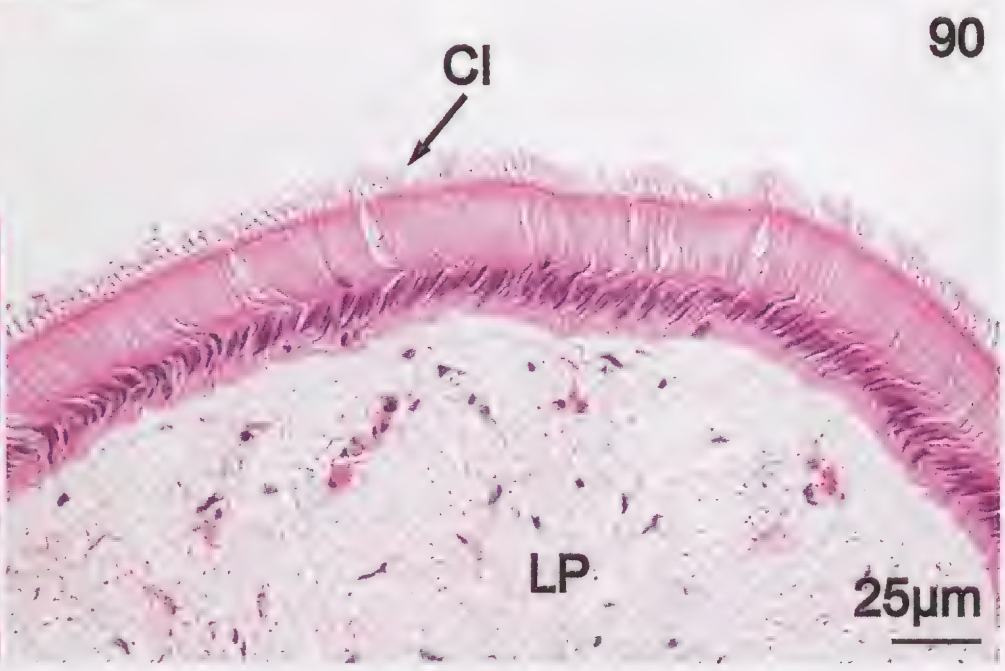

the retractors and oriented perpendicularly in relation to the retractor muscles. Adductor myofibers are organized into large fascicles, with a simple, squamous epimysium and a delicate, fibrous perimysium. Myofibers of the posterior adductor are long, eosinophilic filaments with elliptical, heterochromatic nuclei and a distinct nucleolus (Fig. 111).

Nervous System

Pedal Ganglion, Cerebral Ganglion and Visceral Ganglion: The nervous system of *V. nebulosa* consists of four ganglia, each with a series of nerve fibers that extend throughout the body. There is a pair of ganglia at the anterior end of the visceral mass, each located in the lateral portion of the body between the anterior adductor and labial palp. The third ganglion is the pedal ganglion located in the ventral portion of the hemocoel between the digestive diverticulum and gonad, dorsal to the base of the foot. Finally, the posterior ganglion is situated along the ventral surface of the posterior adductor. Each ganglion has a well-defined outer neural cortex of neuron cell bodies, and a fibrous inner medulla. Furthermore, there is not an obvious difference between the cellular characteristics of all ganglia and therefore the foregoing description of the neural cortex and medulla of the pedal ganglion is representative of the anterior and posterior ganglia.

Pedal ganglion is a bilobed group of neurons at the base of the foot between the gonad and digestive diverticula. Each hemisphere is surrounded by well-defined epineuria, and separated by a median fissure. A series of central commissures communicate horizontally with each hemisphere at the vertical midpoint (Fig. 112). The cortex of the pedal ganglion consists of conical to polygonal cell bodies of unipolar neurons. Neuron cell bodies have a pale, basophilic cytoplasm and a spherical heterochromatic nucleus and a distinct nucleolus. Additionally, neurons have small, brown, granular inclusions located around the nucleus (Fig. 113). Fissures are composed of fibrous connective tissue with a thickened, homogenous appearance. The medulla is distinguished by its web-like appearance formed by overlapping bundles of axons. Glial cells of the medulla have a spherical to spindle shaped nucleus with only a small amount of cytoplasm surrounding the nucleus (Fig. 114). Commissures represent a continuation of the medulla serving to link each half of the ganglion by means of horizontal tracts of axons (Fig. 115). Axons leave the hemispheres via fibrous, lateral extensions of the medulla at the lateral, dorsal and ventral margins of the tissue. Roots along the lateral margins of the pedal ganglion are circular to sinuous bundles of axons and supporting cells (Fig. 116). Histological sections of the visceral mass have revealed ventral pedal nerves threaded through the foot musculature and dorsal pedal nerves extending along the lateral portions of the visceral mass.

The anterior ganglia may be observed in sections of the anterior muscle group and palp. Anterior ganglia appear to control the adductor and retractor muscles since there are nerves inserted into the fascicles of each muscle (Fig. 117). Additional nerves from the anterior ganglia travel through the foot, and mantle edge. Sinistral and dextral nerve centers are also linked to one another by means of a nerve spanning the length of the anterior adductor.

The posterior ganglion is a cylindrical structure along the anteroventral side of the posterior adductor (Fig. 118). Nervous tissue also extends up into the base of the

---

←

FIGS. 85–90. Fourth intestinal limb, and fifth intestinal limb of *Villosa nebulosa*. FIG. 85: Transverse section through the fourth intestinal limb showing a major typhlosole (TY) along the dorsal wall, and surrounding lamina propria (LP), and adipose tissue (AT); FIG. 86: Transverse section of the fourth intestinal limb showing cilia (CI), eosinophilic granulocytes (EC), lamina propria (LP), and adipocytes (AC); FIG. 87: Transverse section through the fourth intestinal limb showing the cilia (CI), lamina propria (LP), and hemolymph sinuses (HS) of the major typhlosole; FIG. 88: Transverse section of the fifth intestinal limb showing the major typhlosole (TY), lamina propria (LP), and cardiac muscle (CM); FIG. 89: Transverse section of the fifth intestinal limb showing cilia (CI) along the surface of plicae; FIG. 90: Transverse section of the fifth intestinal limb emphasizing ciliated columnar epithelium (CI) of the typhlosole.

gill where the outer face of the inner gill and inner face of outer gill unite (Fig. 119). A thin, but dense stratum of fibrous connective tissue surrounds the posterior ganglion, and on the ventral surface there is a simple epithelium of brown, granular cuboidal cells and goblet cells (Fig. 120). Regarding nerves of the posterior ganglion, the pair of nerves seen in histological sections of the nephridia originates at the anterior end of the ganglion, and the sinistral and dextral posterior pallial nerves are rooted in the posterior ganglion

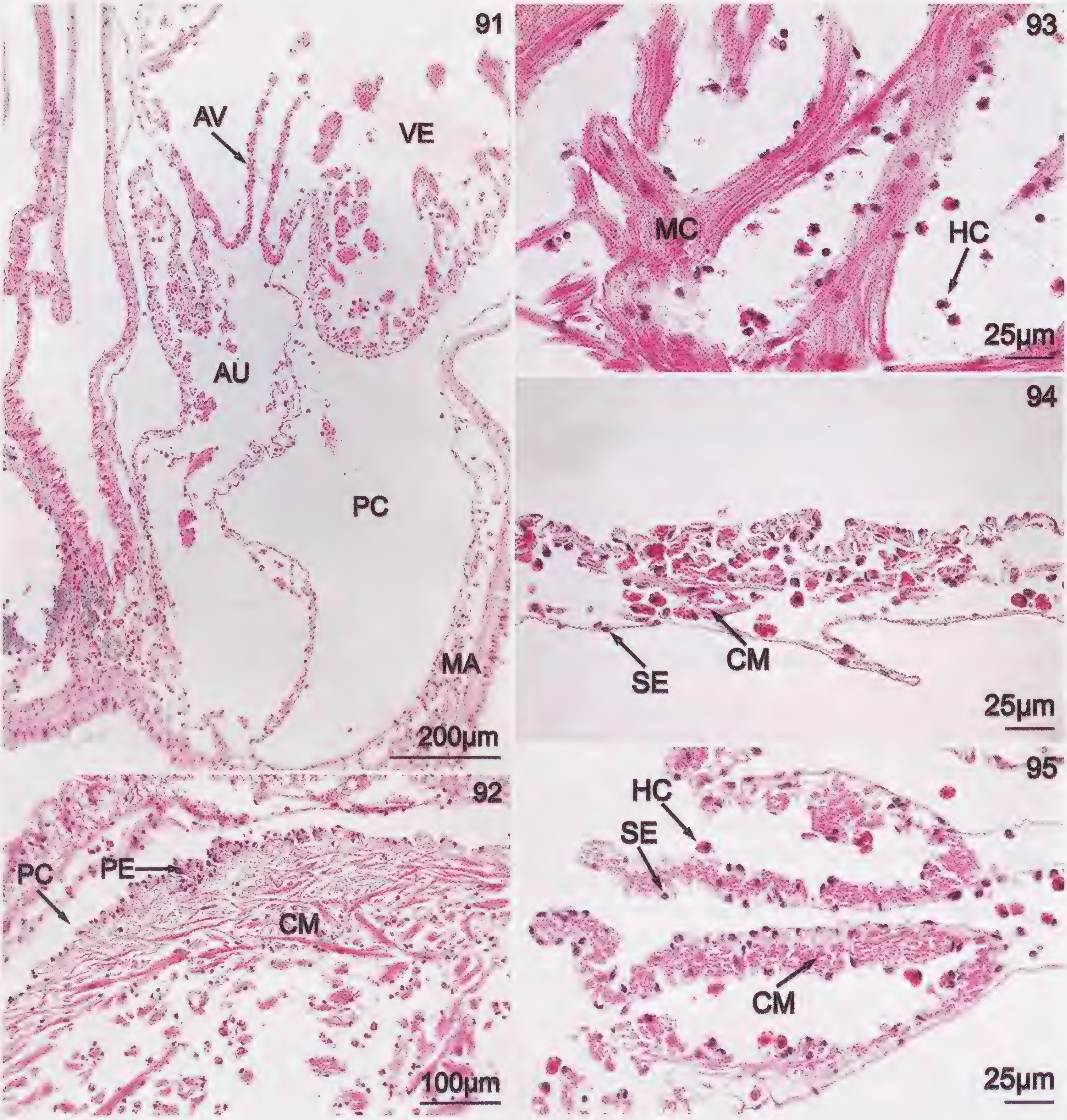

FIGS. 91−95. Heart, and pericardial cavity of *Villosa nebulosa*. FIG. 91: Transverse section through the dorsal portion of the visceral mass revealing the ventricle (VE), auricle (AU), auriculoventricular valve (AV), pericardial cavity (PC), and mantle (MA); FIG. 92: Frontal section of the ventricle emphasizing the irregular cardiac muscle (CM), pericardial epithelium (PE), and pericardial cavity (PC); FIG. 93: Frontal section of the ventricle portraying branched cardiac myocytes (MC) and hemocytes (HC); FIG. 94: Transverse section of the heart and pericardium showing squamous epithelium (SE), and cardiac muscle (CM) of the left auricle; FIG. 95: Transverse section of an auriculoventricular valve, emphasizing squamous epithelium (SE), cardiac muscle (CM), and hemocytes (HC).

Nerves and Statocysts: Nerves are located throughout the body and can be traced from their origin by serial sectioning the body. In a longitudinal orientation, nerves appear as ribbons of fine, eosinophilic filaments that have a slightly wavy appearance. Nerves may be distinguished from connective tissue by observing spindle-shaped gaps between fibers. Additionally, there are small, spindle-shaped nuclei throughout the ribbon of axons, and nuclei have short, brown granular extensions, suggesting these cells are bipolar neurons (Fig. 121). Cross sections of nerves, such as the nephridial nerves, reveal a thick, homogenous, eosinophilic band surrounding the tracts. It appears that this connective tissue wrapping may be myelin or a similar substance and emarginated nuclei are present within this wrapping (Fig. 122).

Statocysts are small sacs located near the lateral margin of the hemocoel and linked to the pedal ganglion via a horizontal band of eosinophilic tissue (Fig. 123). Each statocyst is an ovular chamber formed by a ciliated, columnar epithelium. Epithelial cells lining the sac have a pale, basophilic cytoplasm, and a dark-staining, ovular nucleus. Statocyst epithelium has a stratified appearance, and there are dark-staining, spherical nuclei located in the basal layer of the epithelium. The lumen of the statocyst contains the statolith, a basophilic ring of fluid with a smooth inner surface and a rough outer surface, possibly from ciliary action (Fig. 123).

Reproductive System

Gonadal tissue of *V. nebulosa* is organized into a series of spherical to ovular acini and ciliated gonadal ducts (Fig. 124). Gametogenesis occurred in males and females collected in May 2010, but production was limited in terms of the

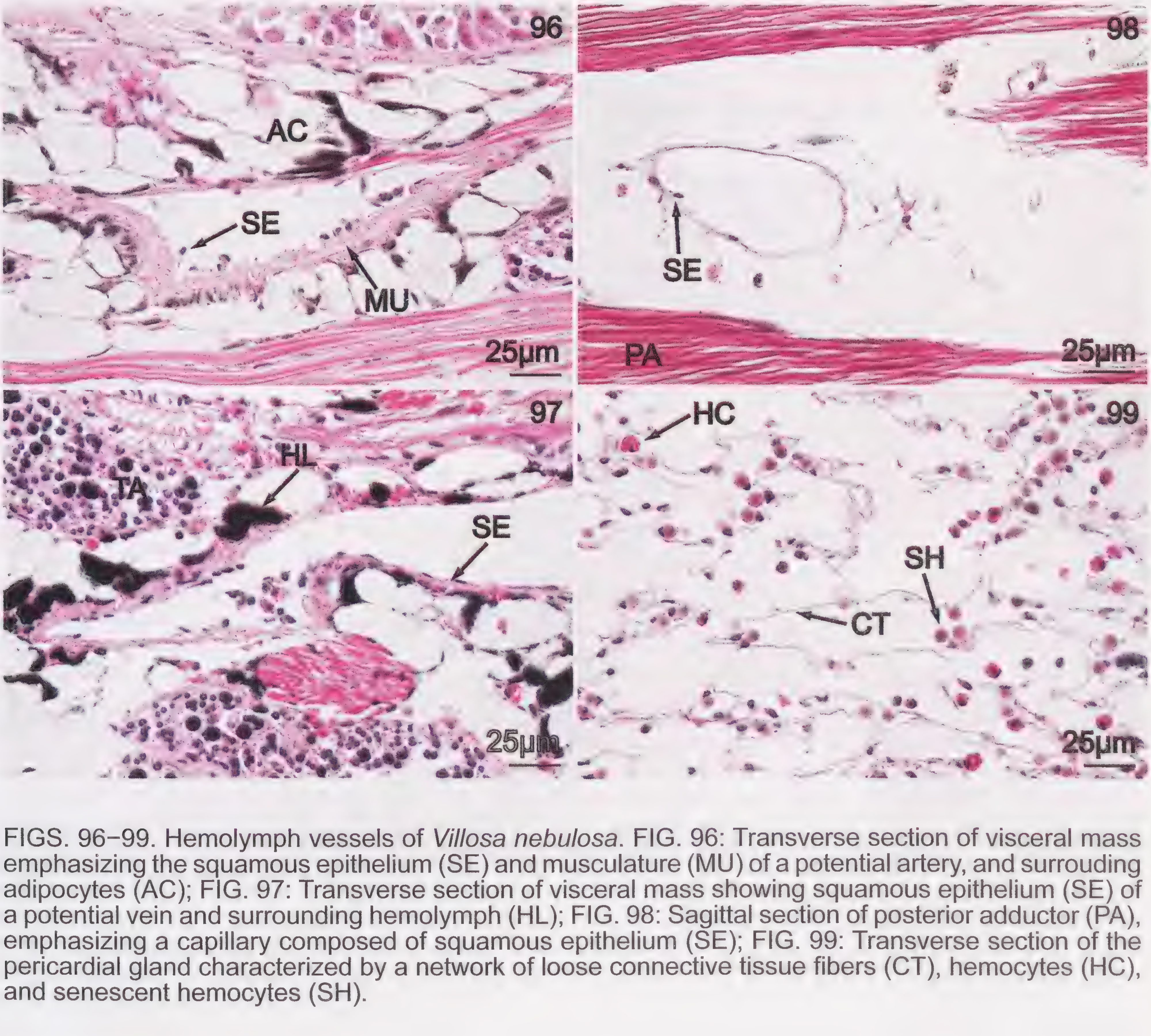

FIGS. 96−99. Hemolymph vessels of *Villosa nebulosa*. FIG. 96: Transverse section of visceral mass emphasizing the squamous epithelium (SE) and musculature (MU) of a potential artery, and surrouding adipocytes (AC); FIG. 97: Transverse section of visceral mass showing squamous epithelium (SE) of a potential vein and surrounding hemolymph (HL); FIG. 98: Sagittal section of posterior adductor (PA), emphasizing a capillary composed of squamous epithelium (SE); FIG. 99: Transverse section of the pericardial gland characterized by a network of loose connective tissue fibers (CT), hemocytes (HC), and senescent hemocytes (SH).

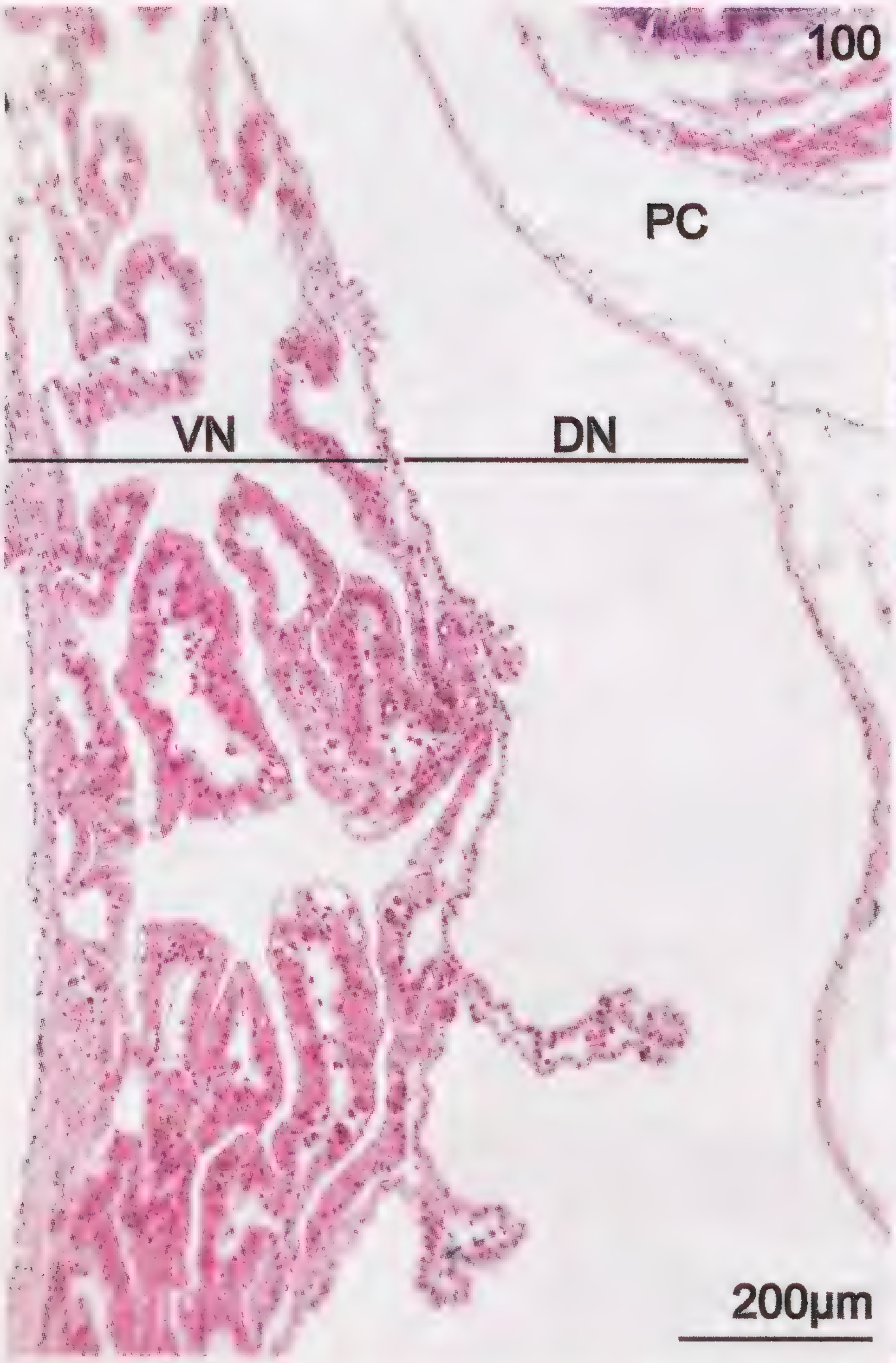

100

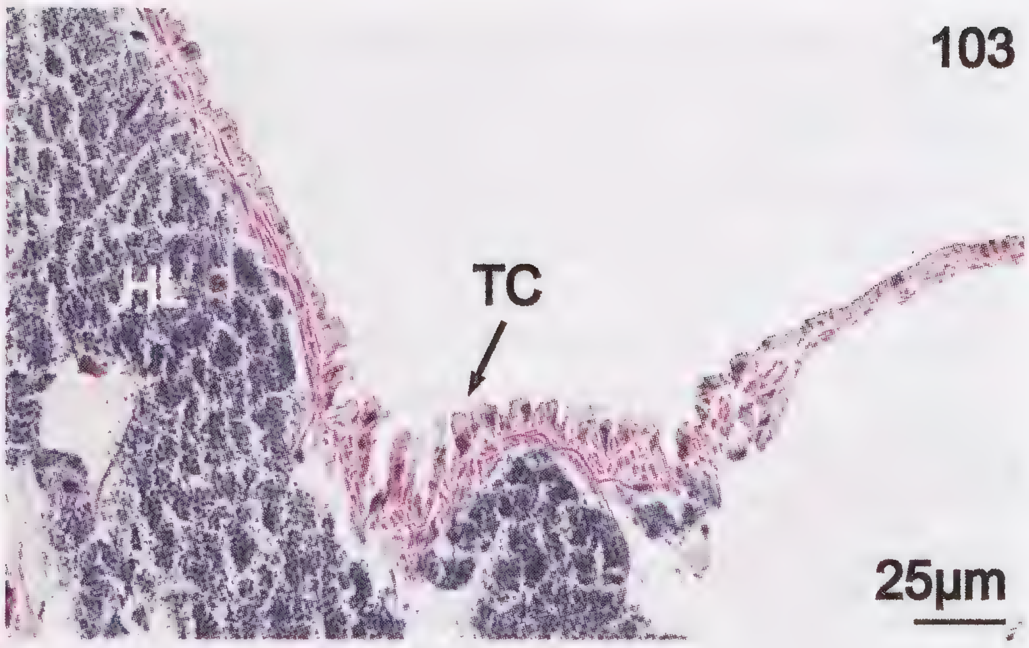

103

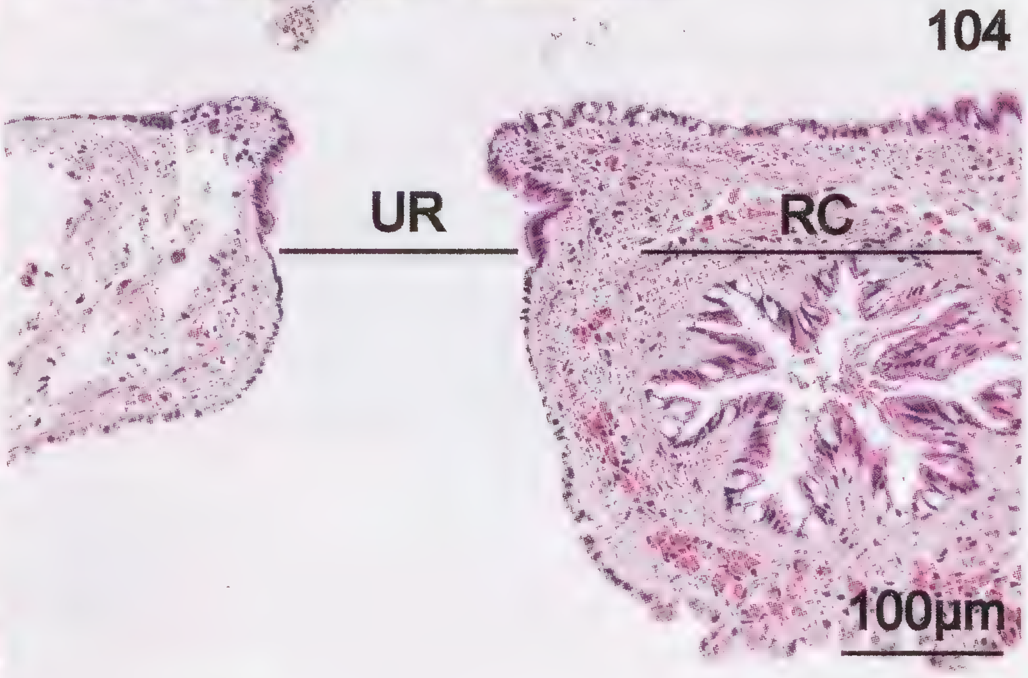

104

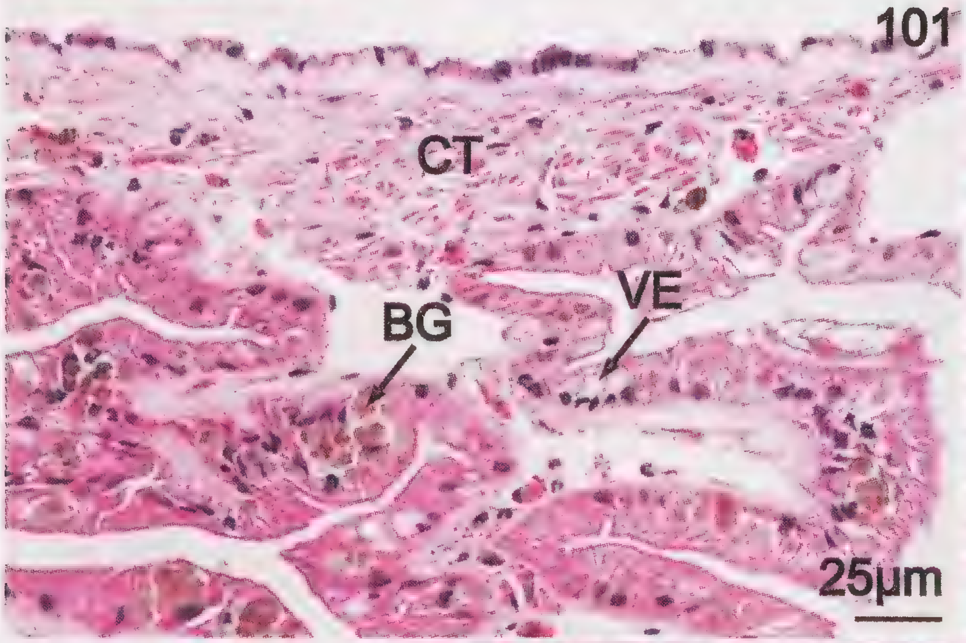

101

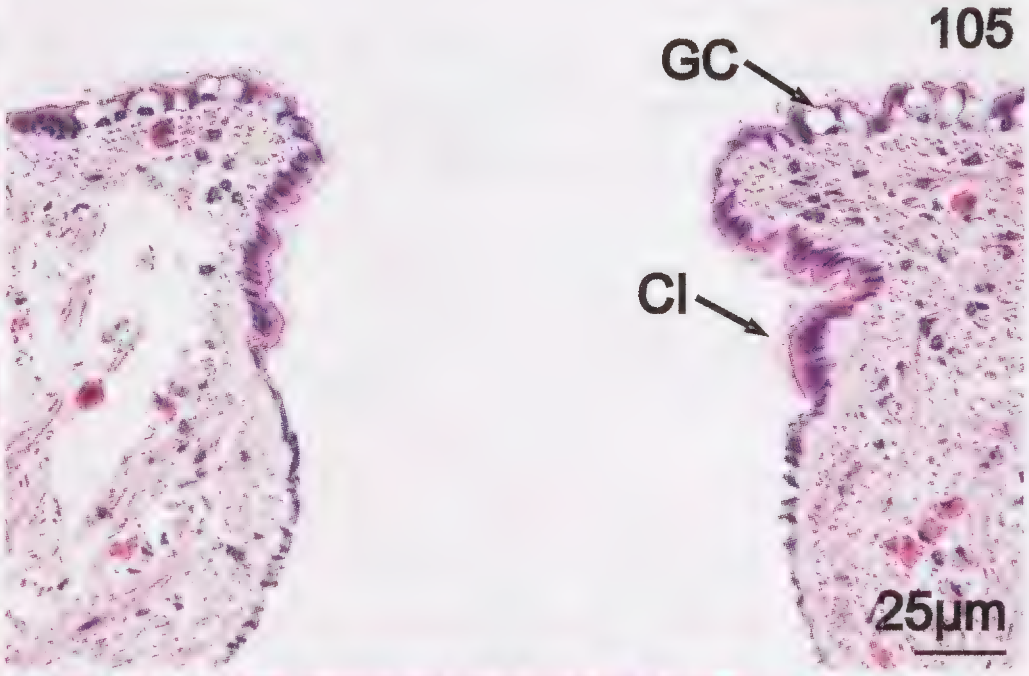

105

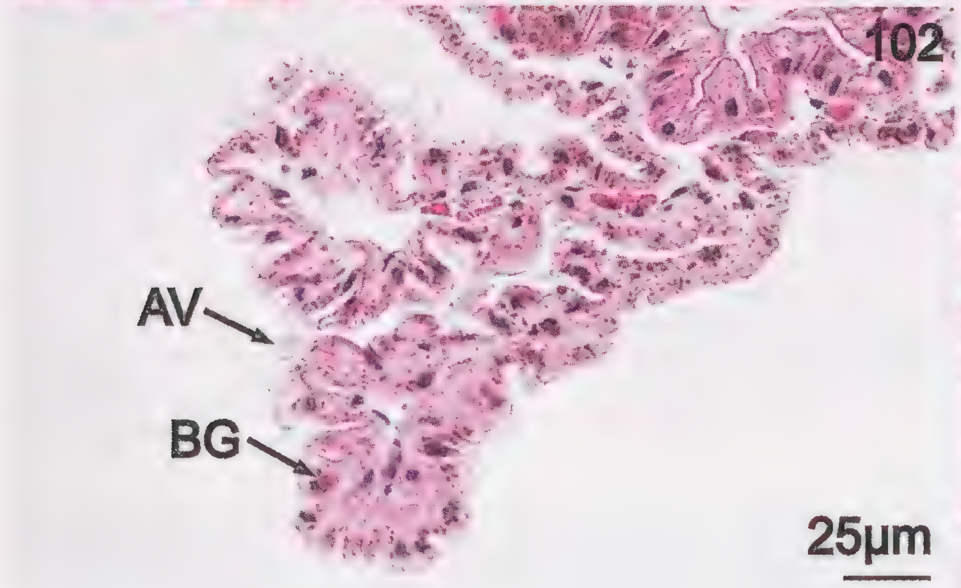

102

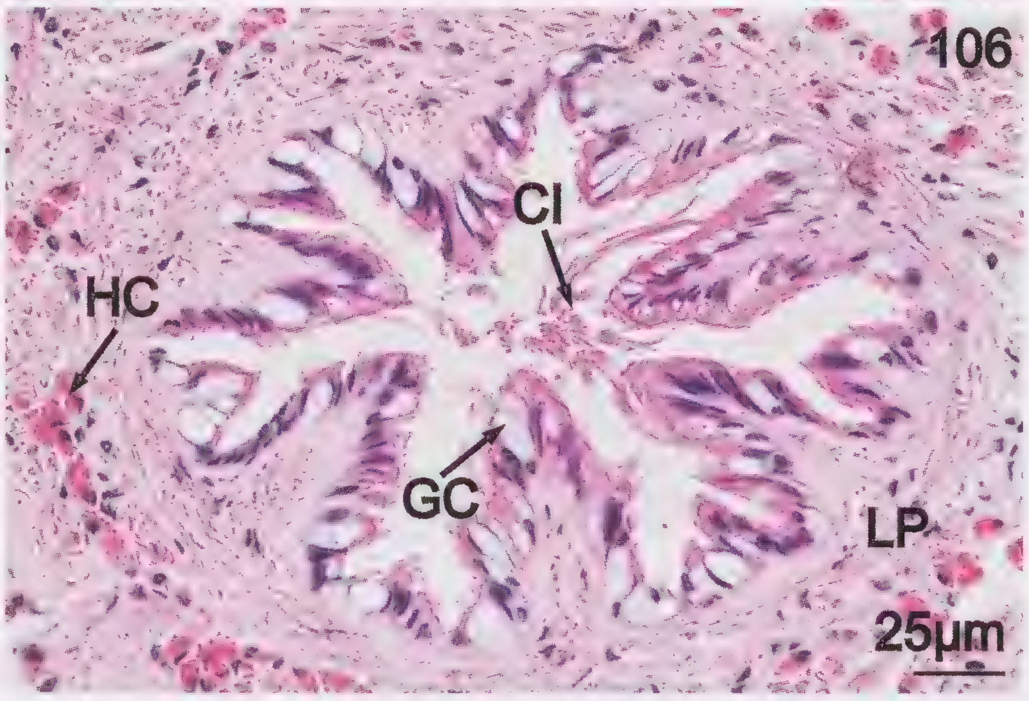

106

number of oocytes and spermatozoa produced as compared to stage 3 individuals collected in August 2010. In females collected in May, ova appeared to develop and arrest at an early stage. Oocytes of stage 1 ovarian acini are basophilic with a distinct, spherical nucleus, and a series of transparent cytoplasmic vesicles. Furthermore, oocytes were typically attached to the inner wall of the acinus and the lumen contained an abundance of spherical, eosinophilic granules. Upon closer inspection, the eosinophilic granules appeared to be apoptotic oocytes given that they were usually enclosed within a membrane, with a small, polygonal nucleus (Fig. 125). Stage 3 females sampled in August possessed a mixture of early stage and late stage oocytes. Oocytes begin as a small basophilic cell with a distinct nucleus and nucleolus. As oocytes mature, they become larger and eosinophilic cytoplasm becomes more prominent. Mature oocytes however, occupied the majority of the acinus volume as they were significantly enlarged. Mature oocytes are enclosed within a membrane that is indistinct and separated from the main part of the oocyte by an expansive fluidic mass. Specifically, the cytoplasm of a mature oocyte is eosinophilic, granular, and contains a pale basophilic nucleus. The nucleus of some oocytes seemingly contained a loose mass of basophilic chromatin, while other oocytes possessed a distinct nucleolus (Fig. 126).

The most distinctive feature of testicular acini from individuals sampled in May 2010 was the preponderance of sperm morula (Fig. 127). Furthermore, these animals exhibited acini in stages 1 and 2. Spermatozoa develop from single-celled spermatocytes and then proceed to divide multiple times and produce a cluster of spherical cells resembling a morula stage embryo. Spermatocytes of sperm morula each differentiate into a pair of ovular spermatozoa. Spermatocytes of a sperm morula are housed within a thin, eosinophilic cytoplasm that is nearly obscured by the strongly basophilic heterochromatin. Furthermore, spermatocytes and sperm morula have such a strong staining quality that individual chromosomes and stages of meiosis are not visible with hematoxylin and eosin preparations. Like stage 1 ovarian acini, testicular acini in males collected in May contained numerous eosinophilic granules, possibly representing apoptotic spermatocytes (Fig. 128). Acini of males collected in August were significantly enlarged and contained a large, central mass of spermatozoa. Additionally, spermatogenesis appeared to be different than in stage 1 individuals. Spermatocytes in stage 3 individuals possessed a pale, basophilic nucleus containing a blend of euchromatin and heterochromatin. Spermatozoa in the lumen of the acini are small, basophilic, and cylindrical, with an eosinophilic flagellum (Fig. 129).

Female and male gonadal tissue contained circular to ovular, ciliated ducts. Gonadal ducts consist of pale, eosinophilic columnar cells with a densely ciliated apical surface (Figs. 124, 128). Ciliated gonadal ducts of stage 3 male *V. nebulosa* contained a condensed mass of spermatozoa traveling towards the dorsal gonadal pore (Fig. 130). The sinistral and dextral gonadal pores are ciliated tubules located at the dorso-lateral margin of the visceral mass between nephridium and inner lamina of the inner gill (Fig. 131).

←

FIGS. 100–106. Anterior nephridium of *Villosa nebulosa*. FIG. 100: Transverse section through dorsal portion of the visceral mass revealing the ventral nephridium (VN), dorsal nephridium (DN), and pericardial cavity (PC); FIG. 101: Transverse section through the ventral nephridium emphasizing a columnar epithelium with vesicles (VE), brown intracellular granules (BG), and connective tissue (CT); FIG. 102: Transverse section of the dorsal nephridial limb showing a branched plication and columnar cells with brown intracellular granules (BG), and transparent apical vesicles (AV); FIG. 103: Transverse section of the dorsal nephridium portraying a patch of teardrop cells (TC) and a hemolymph (HL) sinus beneath the epithelium; FIG. 104: Transverse section of nephridium showing the urethra (UR) and reno-pericardial canal (RC); FIG. 105: Transverse section of a urethra revealing a short stretch of columnar cells bearing cilia (CI), and goblet cells (MC); FIG. 106: Transverse section of a reno-pericardial canal emphasizing conical extensions of epithelial tissue bearing cilia (CI) and goblet ells (GC), encircled by a lamina propria (LP), and hemocytes (HC).

Fusconaia cerina

Shell Morphology

The valves of *Fusconaia cerina* from Cahaba River are circular to rhomboidal, and a well-defined posterior ridge may be present, represented by an obliquely oriented convex line. Shells are typically thick or heavy with a dark brown epidermis. The anterior and posterior margins are broad, but truncated in length. The umbo is broadly conical, high, extending

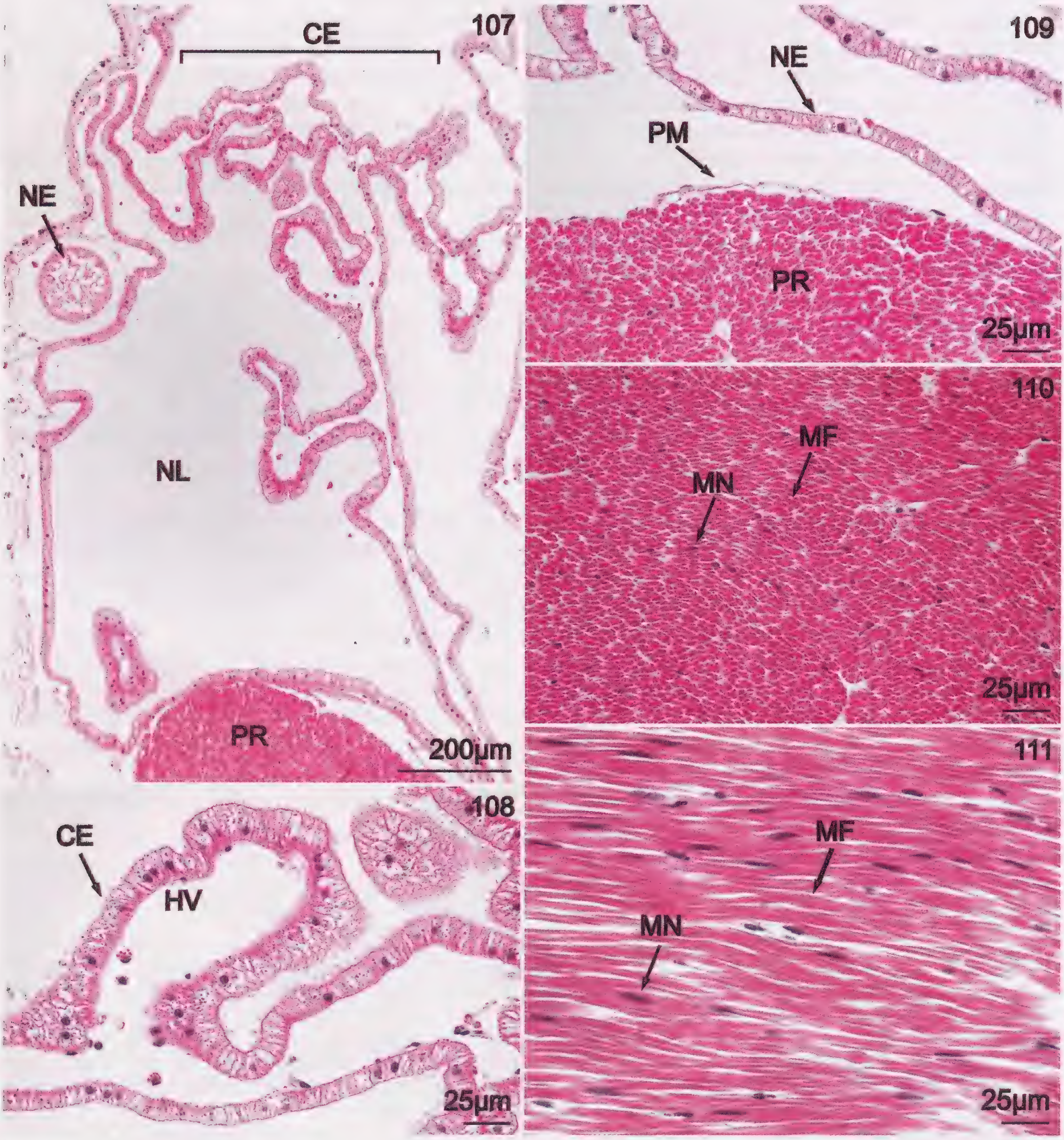

FIGS. 107–111. Posterior nephridium of *Villosa nebulosa*. FIG. 107: Transverse section of the posterior end of the nephridium featuring a convoluted epithelium (CE), expansive nephridial lumen (NL), juxtaposed to the posterior pedal retractor (PR), and a large nerve (NE); FIG. 108: Transverse section of posterior nephridium portraying vesiculated columnar cells of convoluted epithelium (CE), and an underlying hemolymph vessel (HV); FIG. 109: Transverse section of the posterior nephridium showing nephridial epithelium (NE), and the perimysium (PM) of a posterior pedal retractor (PR); FIG. 110: Transverse section of a posterior pedal retractor showing myofibers (MF), and myocyte nuclei (MN); FIG. 111: Sagittal section of posterior adductor displaying thick chords of myofibers (MF), and myocyte nuclei (MN).

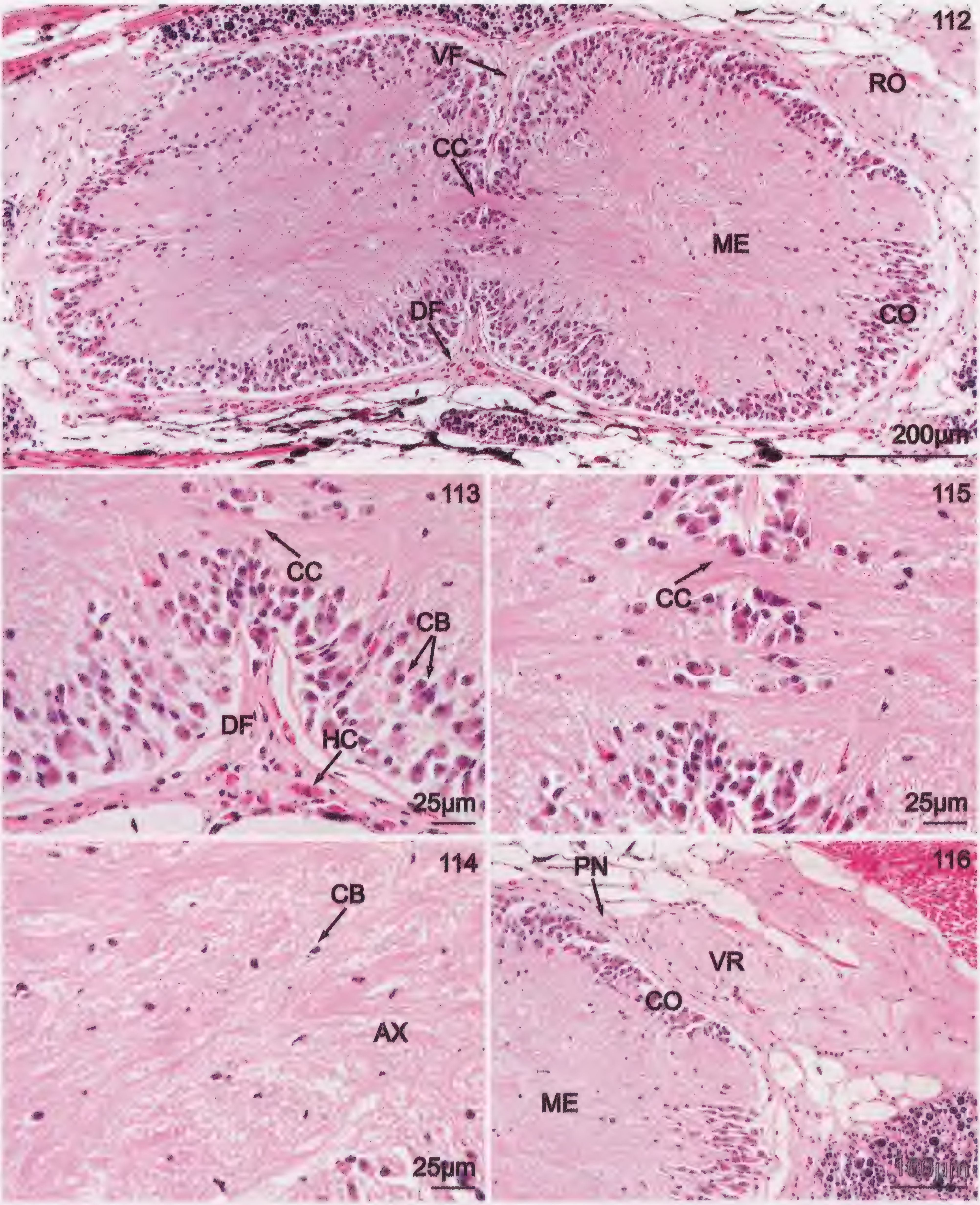

FIGS. 112–116. Pedal ganglion of *Villosa nebulosa*. FIG. 112: Transverse section of pedal ganglion portraying neural cortex (CO), neural medulla (ME), ventral fissure (VF), dorsal fissure (DF), central commissures (CC), and roots (RO); FIG. 113: Transverse section of the dorsal margin of the pedal ganglion revealing the median dorsal fissure (DF), hemocytes (HC), central commissures (CC), and neuron cell bodies (CB); FIG. 114: Transverse section of pedal ganglion medulla displaying cell bodies (CB), and axons (AX); FIG. 115: Transverse section of the pedal ganglion median where central commissures (CC) of axons communicating with the sinistral and dextral hemispheres; FIG. 116: Transverse section of the ventro–lateral aspect of the pedal ganglion revealing the medulla (ME), neural cortex (CO), perineurium (PN), and a ventral root (VR).

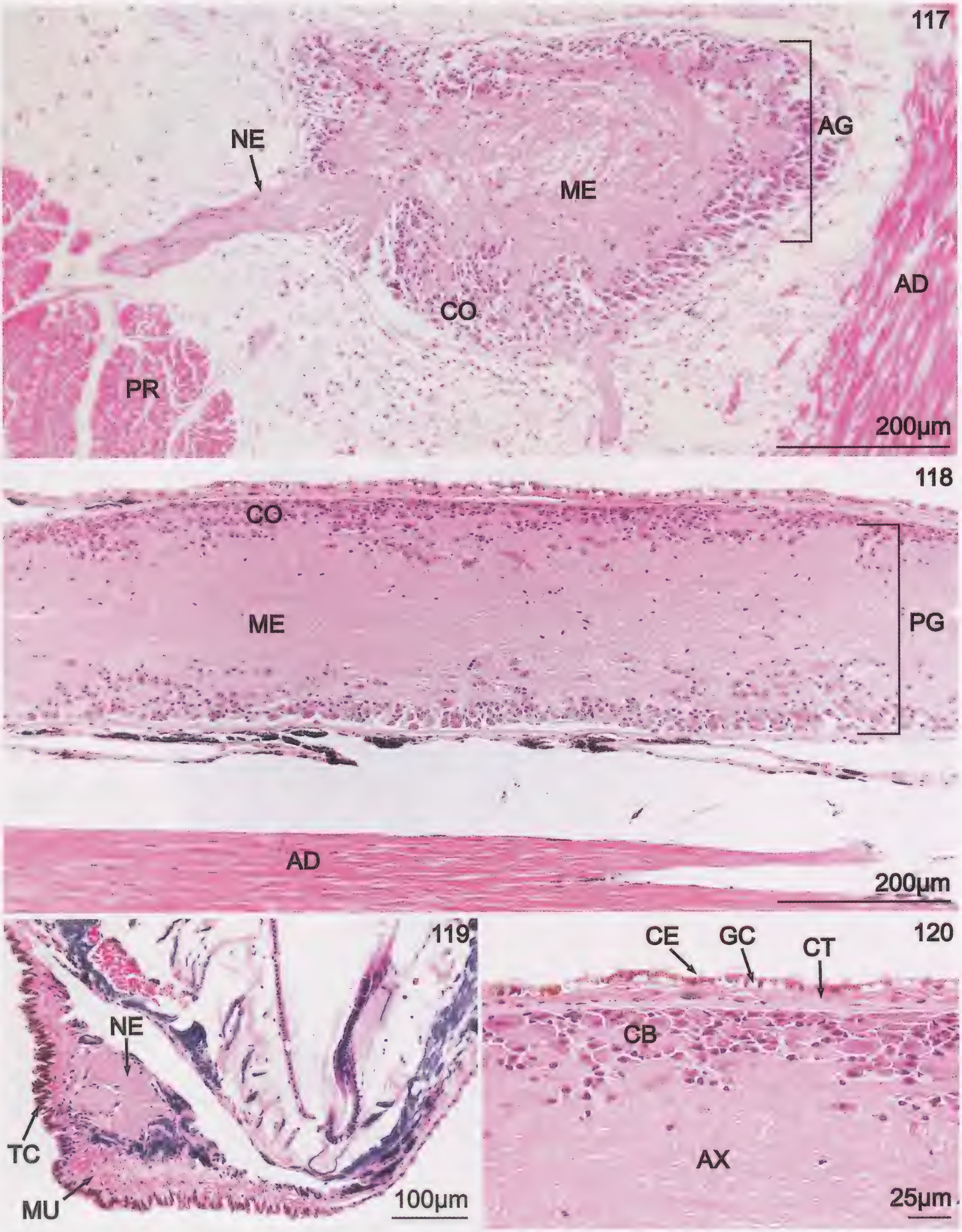

FIGS. 117–120. Cerebral ganglion, and visceral ganglion of *Villosa nebulosa*. FIG. 117: Sagittal section of anterior visceral mass showing the anterior adductor (AD), anterior pedal retractor (PR), and anterior ganglion (AG) with distinct neural cortex (CO), neural medulla (ME), and nerves (NE); FIG. 118: Sagittal section of posterior adductor (AD) emphasizing the posterior ganglia (PG) with distinct neural cortex (CO) and neural medulla (ME) located along the ventral surface of the posterior adductor (AD); FIG. 119: Transverse section of the free dorsal margin of the ctenidia anterior to the posterior adductor, emphasizing nervous tissue (NE) enclosed by musculature (MU) and teardrop cells (TC); FIG. 120: Sagittal section of the ventral margin of the posterior ganglion highlighting neuron cell bodies (CB), axons (AX), connective tissue (CT), goblet cells (GC) and cuboidal epithelium (CE) of the overlying the ganglion.

beyond the hinge line. Furthermore, the shell is typically inflated with an umbo that arches or curls dorsally to meet the hinge line (Figs. 132, 133) (Williams et al., 2008). The nacre is white, with a strongly developed and somewhat cuboidal pallial line. Anterior and posterior adductor scars are conspicuous, with a somewhat irregular surface. Anterior adductor scar is deeply inset and parallel with the anterior margin, while the posterior adductor scar is shallow, parallel with the posterior margin. Pseudocardinal teeth are strongly developed, with two on the left valve and one tooth located on the right valve, pseudocardinal teeth have a rough or grooved surface. Lateral teeth are strongly developed with two on the left valve and one on the right valve. Considering the arched umbo, there is a correspondingly deep umbo cavity. Additionally, the ligament is typically cylindrical, brown, and thickened along the dorsal margin (Figs. 134, 135) (Williams et al., 2008).

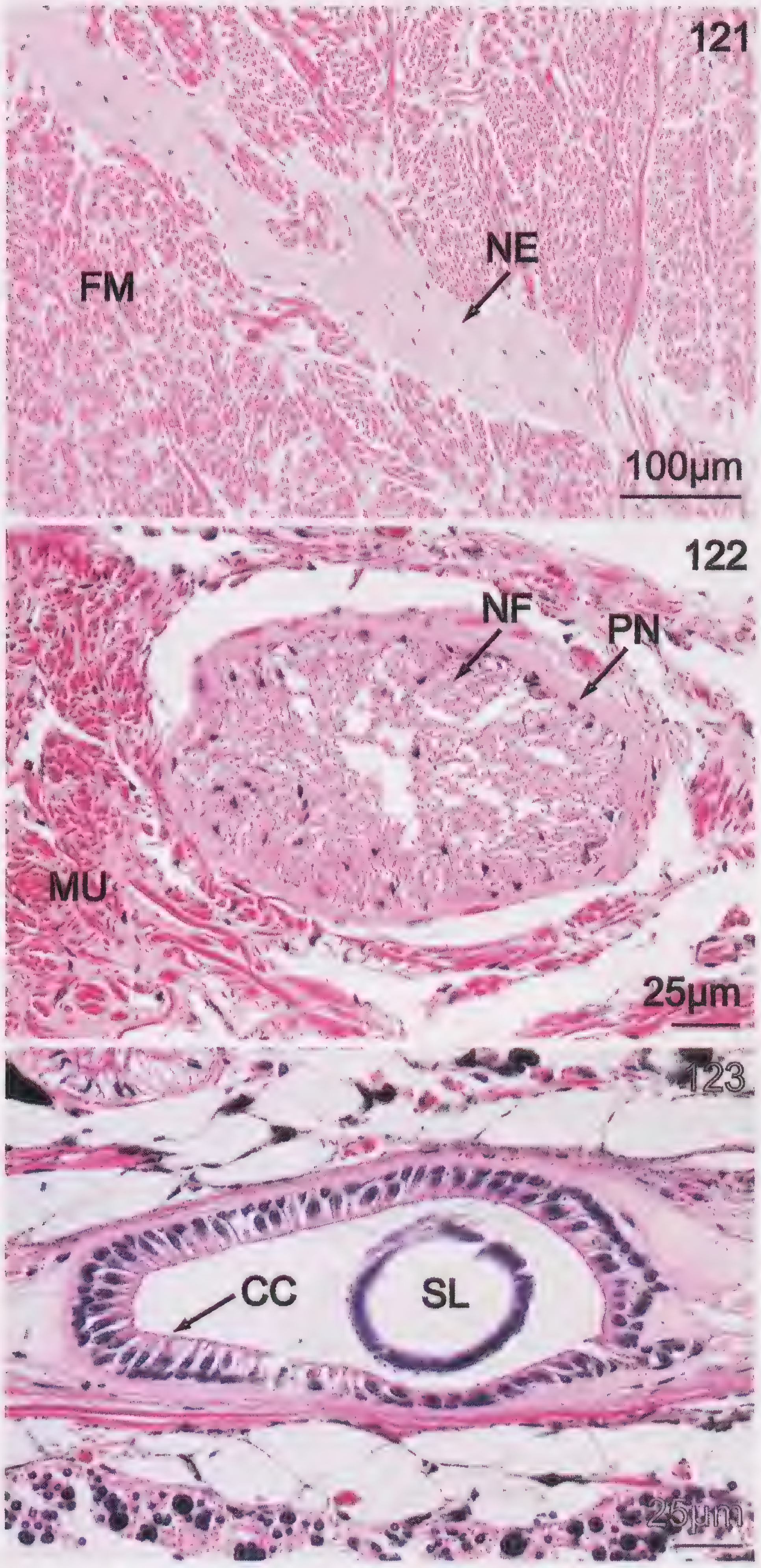

FIGS. 121–123. Nerves, and statocysts of *Villosa nebulosa*. FIG. 121: Transverse section of the lateral margin of the coelom revealing a pedal nerve (NE) running through foot muscle (FM); FIG. 122: Transverse section of a nephridial nerve with a distinct perineurium (PN), nerve fibers (NF) surrounded by concentric layers of musculature (MU); FIG. 123: Transverse section of a statocyst emphasizing the ciliated columnar cells (CC) and a spherical statolith (SL).

Gross Anatomical Features of the Mantle Cavity

Fusconaia cerina were collected in shoal habitats in gravel or sandy substratum. Incurrent and excurrent apertures are lined with papillae and especially along the incurrent aperture, papillae are conical to branched (Fig. 136). The body of *F. cerina* is typically pallid, grey to white. However, the mantle, foot and gill may become red to orange during the spawning season. Inner and outer demibranchs are obliquely oriented posteriorly, as the valves of *F. cerina* are rhomboidal. Females are tetragenous brooders, and each gill may be filled with linear or subcylindrical masses of embryos or conglutinates. Mature conglutinates may be red to orange and fill most of the vertical volume of the marsupial water tubes (Fig. 137). During the summer months, white ovigerous female *F. cerina* may be collected. Conglutinates from white females consist entirely of unfertilized ova, whereas mature, red to orange conglutinates consist of colored, developing embryos or glochidia adhered to unfertilized, white ova (Fig. 138). The mantle edge has a homogenous coloration, with a fine, brown line across the ventral margin. Papillae along the siphonal apertures are located along a truncated posterior margin and appear mottled, brown to white. The foot of *F. cerina* is broad, and the visceral mass is creamy white. The mantle isthmus is broadly rounded and extends deep into the cavity between the sinistral and dextral dorsal margins (Fig. 139).

Cellular Structure of Mantle

Anterior Mantle Edge: The anterior portion of the mantle edge (lateral to labial palps) of *Fusconaia cerina* bears the same cell types as the anterior mantle edge of *Villosa nebu-*

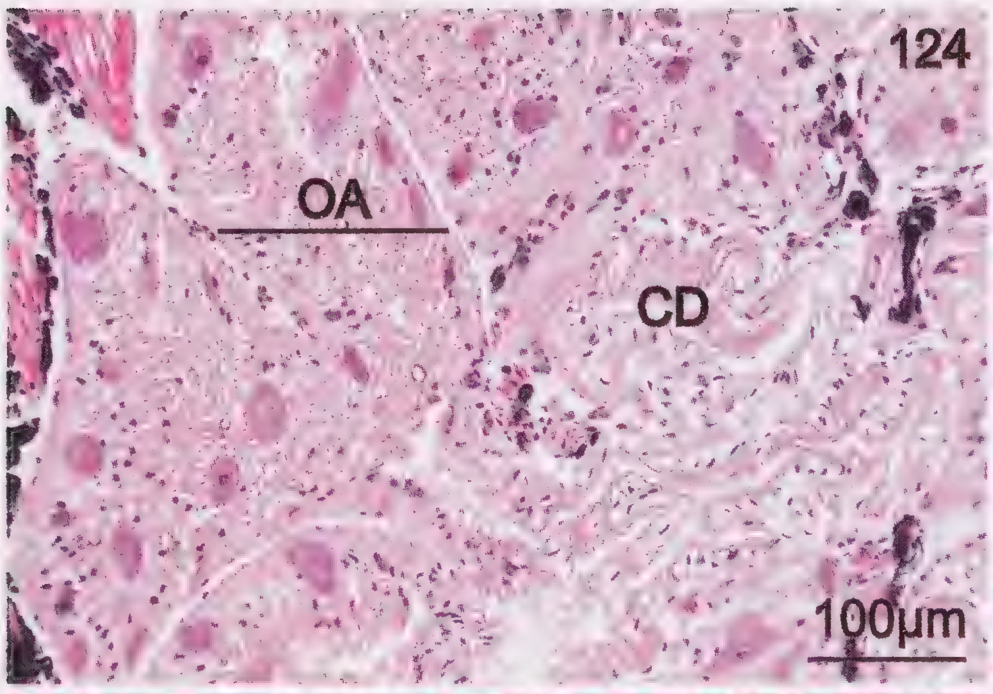
124
OA
CD
100µm

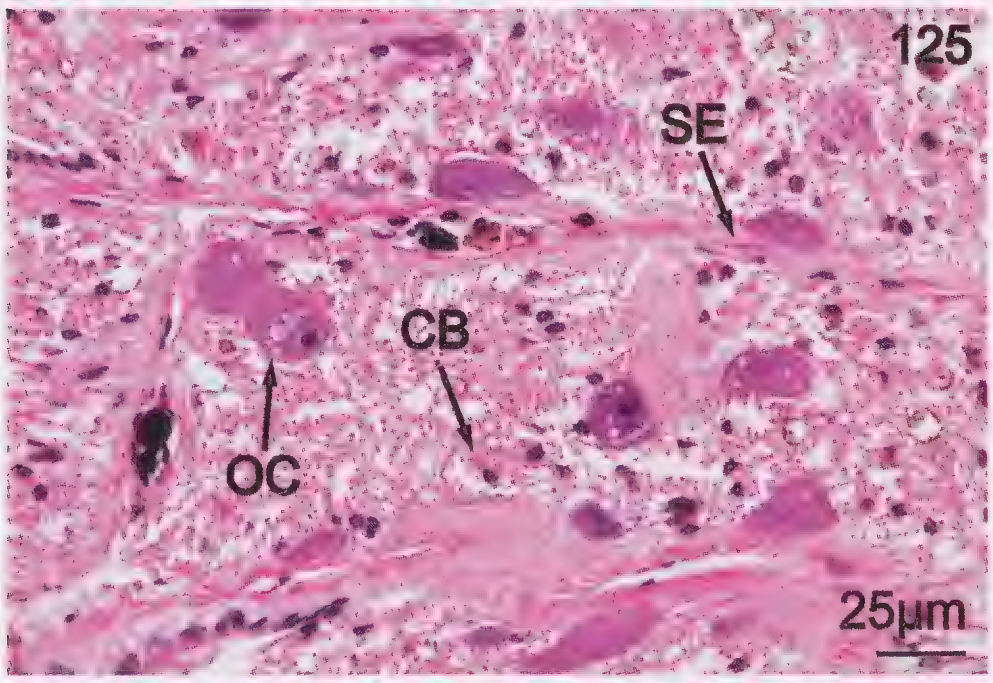
125
SE
CB
OC
25µm

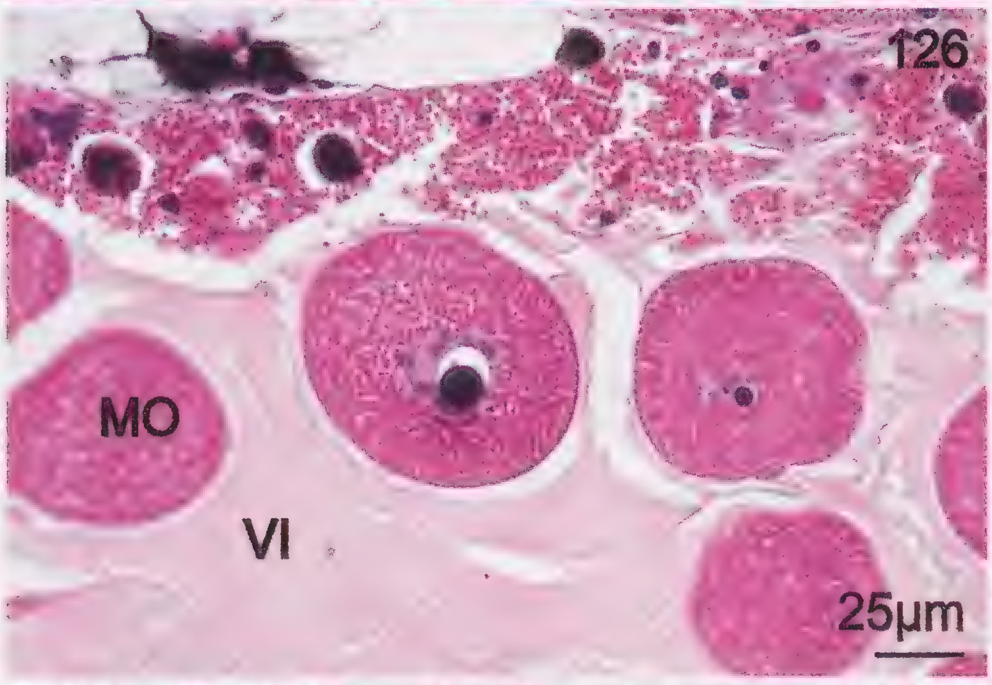
126
MO
VI
25µm

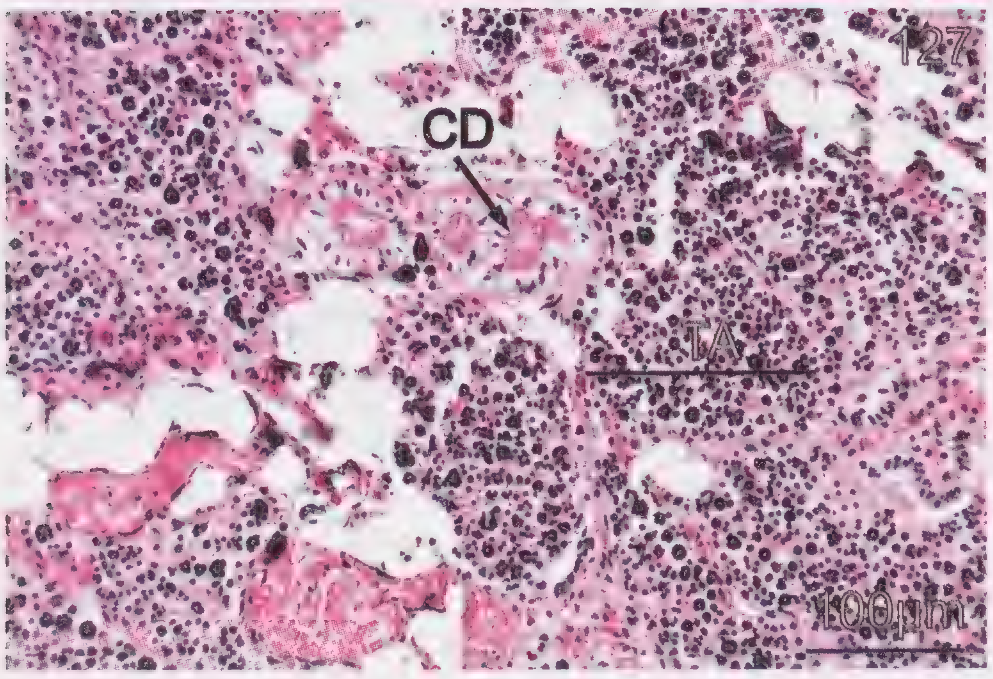
127
CD
TA
100µm

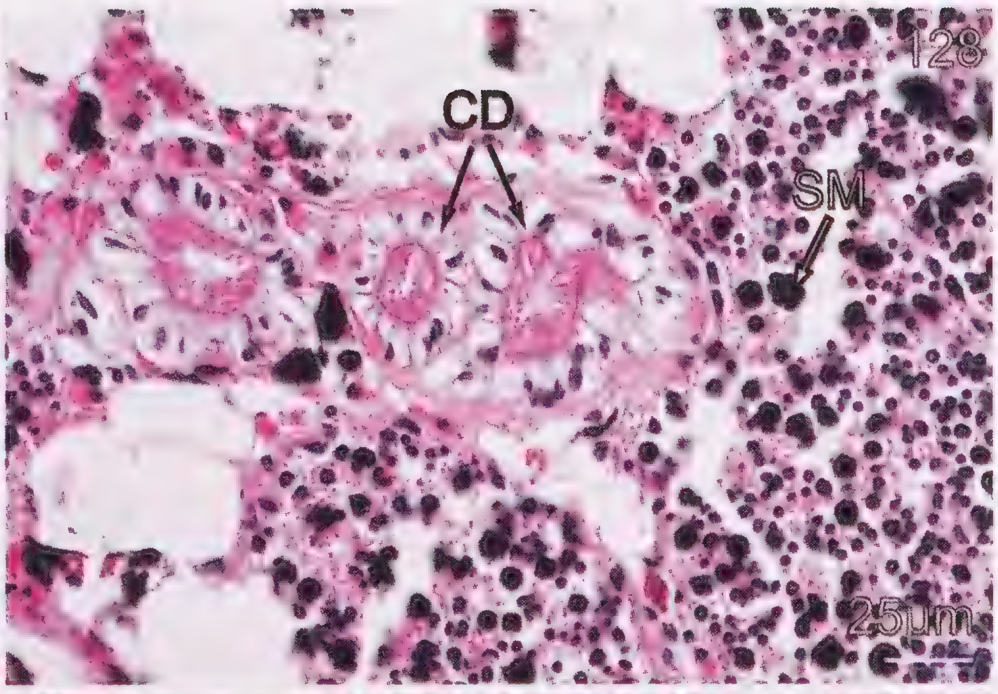
128
CD
SM
25µm

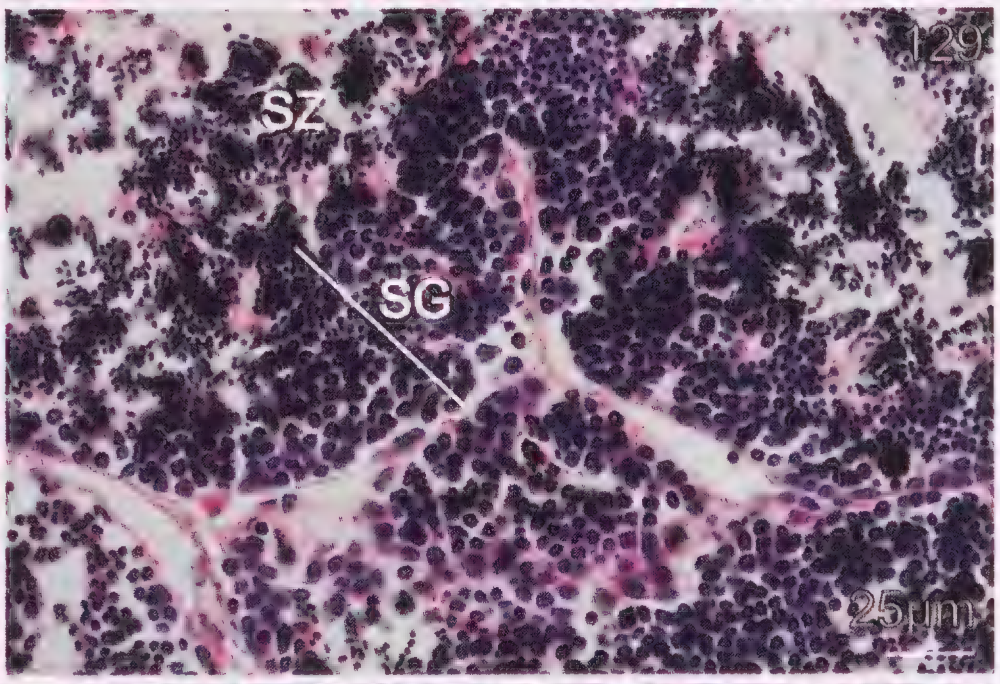
129
SZ
SG
25µm

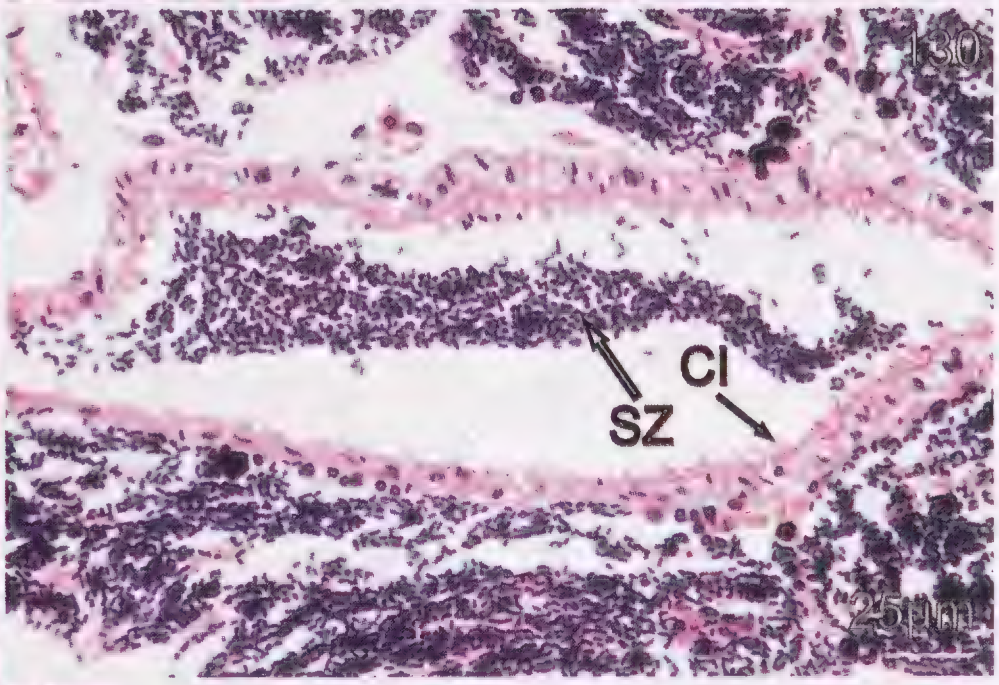
130
SZ
CI
25µm

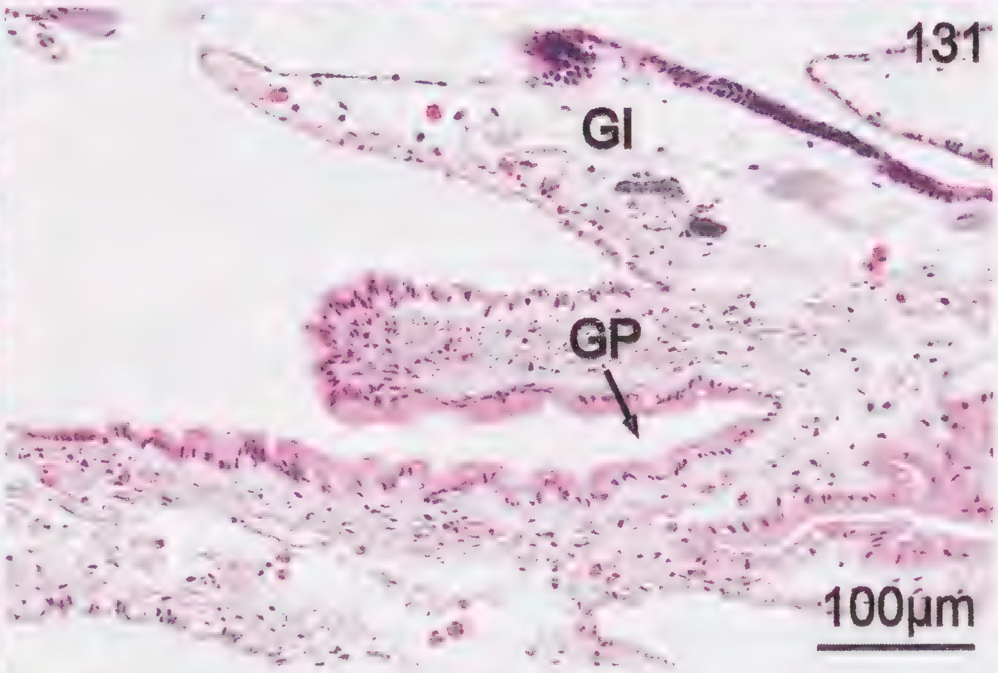
131
GI
GP
100µm

losa. However, there are unique morphological features of mantle edge epithelium of *F. cerina* not observed on *V. nebulosa*. The outer mantle edge epithelium spanning the distance between the pallial line and outer lobe is sinuous, and there are crypts along the ventral surface of the outer mantle lobe (Figs. 140, 141). The outer mantle lobe is branched with as many as three lobes, and the distal tip of each branch is bluntly rounded (Fig. 142). Each branch of the outer mantle lobe is pleated, and plicae are irregular such that each extension of the outer lobe is asymmetrical. The basal bulb of *F. cerina* is located on a triangular plication of columnar cells that is rounded posteriorly (Fig. 141). The middle mantle lobe of *F. cerina* is bulbous with eosinophilic squamous cells extending approximately half the length of the ventral surface before abruptly becoming columnar. Given the abrupt transition from squamous to columnar, and considering how columnar cells maintain the same cytological characteristics as the squamous cells, these two cell types may differ only in orientation (Fig. 143). Inner mantle lobe of *F. cerina* is triangular and plicated, but unlike *V. nebulosa*, the columnar cells along the inner surface of the inner mantle lobe appear to lack brown intracellular granules (Fig. 144). Inner lobe epithelium consists of irregularly shaped plicae, becoming teardrop-shaped along the dorsal surface (Fig. 145). The columnar epithelium along the ventral surface of the mantle edge is wavy, and isolated goblet cells may be interspersed among epithelial cells (Fig. 146).

Posterior Mantle Edge, Middle Mantle and Mantle Isthmus: Posterior mantle edge was sampled adjacent to the posterior adductor. Posterior mantle edge of *F. cerina* maintains the same cell types from the anterior, but the shape of the mantle lobes is different (Fig. 147). Outer lobe is forked with minor epithelial undulations along the dorsal and ventral branches. The middle lobe is cylindrical and pleated along its dorsal surface, and the inner lobe is broader at its base than it is anteriorly. Papillae along the posterior margin of *F. cerina* mantle edge primarily differ from *V. nebulosa* in appearing bluntly rounded to branched (Fig. 148). The columnar epithelium and musculature of *F. cerina* mantle edge papillae is indistinguishable from that of *V. nebulosa* (Fig. 149).

The middle mantle of *F. cerina* has an outer columnar epithelium, inner cuboidal epithelium, and subepithelial strata consisting of loose connective tissue fibers and hemolymph (Fig. 150). The cellular composition of the middle mantle is not different from that of *V. nebulosa*.

Mantle isthmus of *F. cerina* is a well-defined median extension of mantle tissue. The dorsal epithelium around the visceral mass consists of pale eosinophilic columnar epithelial cells similar to the columnar epithelium of middle mantle. Isthmus epithelium is cuboidal along the lateral surfaces and basophilic columnar cells are localized to the dorsal margin (Fig. 151). Additionally, isthmus epithelium features sparsely distributed goblet cells and a wavy subepithelium of connective tissue fibers and hemolymph.

←

FIGS. 124–131. Ovarian acini, testicular acini, and ciliated gonadal ducts of *Villosa nebulosa*. FIG. 124: Transverse section through the visceral mass of an adult female collected in May 2010 displaying a series of stage 1 ovarian acini (OA), and ciliated gonadal ducts (CD); FIG. 125: Transverse section through the visceral mass of an adult female collected in May 2010 emphasizing immature oocytes (OC), cell body (CB), and the squamous epithelial lining of acini (SE); FIG. 126: Transverse section of a stage 3 ovarian acinus of an adult female collected in August 2011 showing mature oocytes (MO), surrounded by vitelline (VI); FIG. 127: Transverse section through the visceral mass of an adult male collected in May 2010 portraying a series of stage 1 testicular acini (TA) and ciliated gonadal ducts (CD); FIG. 128: Transverse section of stage 1 testicular acini of an adult male collected in May 2010 portraying a preponderance of sperm morula (SM) within the acini, and ciliated gonadal ducts (CD) in close proximity to testicular acini; FIG. 129: Transverse section of stage 3 testicular acini of a male collected in August 2011 emphasizing spermatogenesis (SG) and a preponderance of spermatozoa (SZ) in the lumen; FIG. 130: Transverse section through the visceral mass of a stage 3 male collected in August 2011 portraying spermatozoa (SZ) traveling dorsally through a duct by means of cilia (CI); FIG. 131: Transverse section of the dorso-lateral portion of the visceral mass emphasizing the sinistral gonadal pore (GP) dorsal to the gill (GI).

Cellular Structure of Gill

Non-Marsupial Demibranch: Ctenidia of *Fusconaia cerina* feature cylindrical filaments across each ascending and descending lamella, united by septa and vertical water tubes (Fig. 152). Tissue structure of each ctenidial face consists of cylindrical filaments with frontal, frontal-lateral, and lateral groups of ciliated cells across the apical surface. Filaments are occasionally separated by ostia, communicating with medial water tubes, and each filament has a medially located hemolymph sinus. Inner and outer lamellae of each demibranch are joined by a septum, and septa possess teardrop-shaped goblet

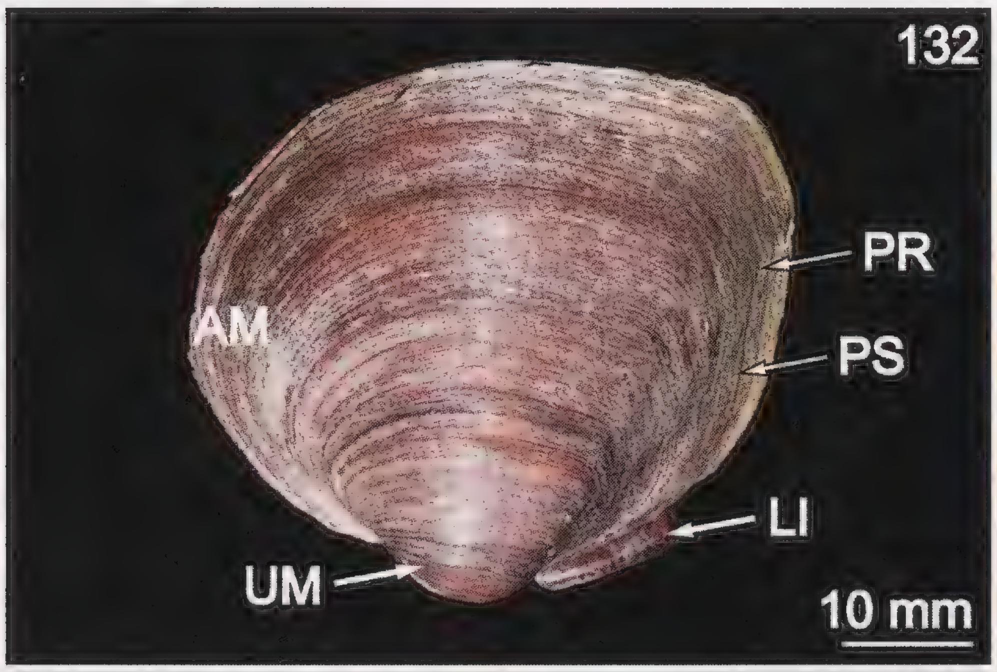

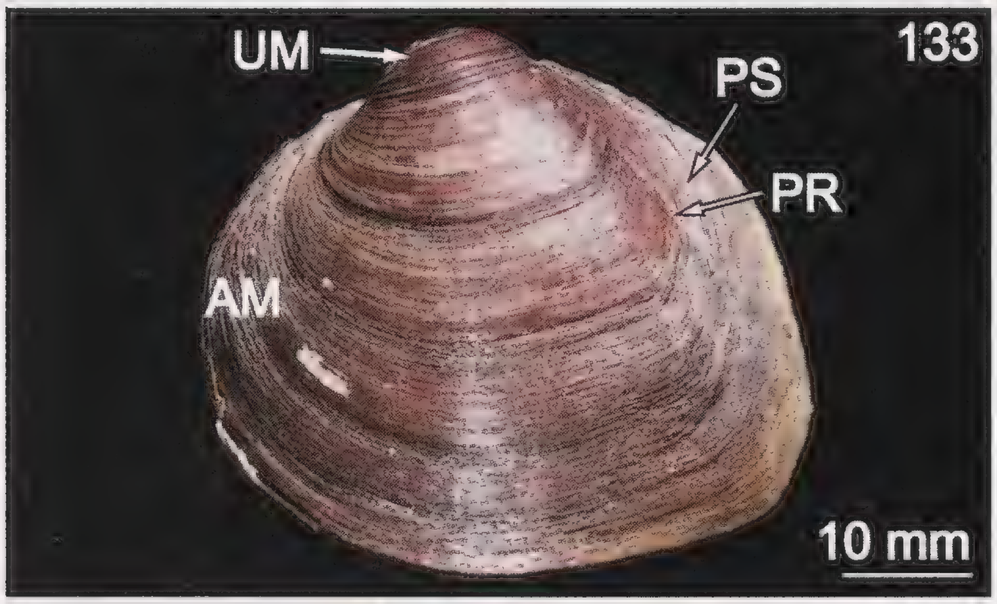

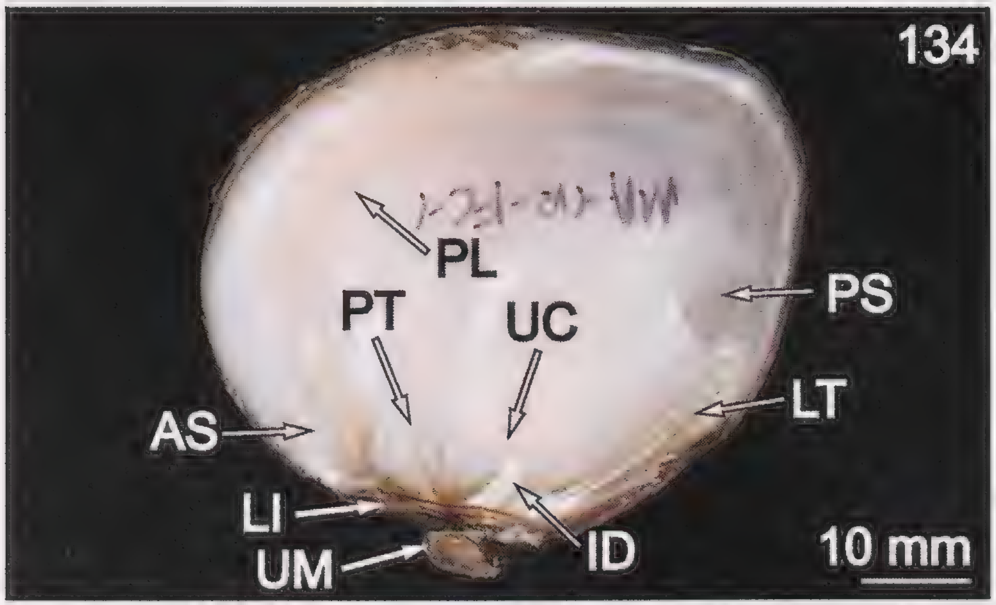

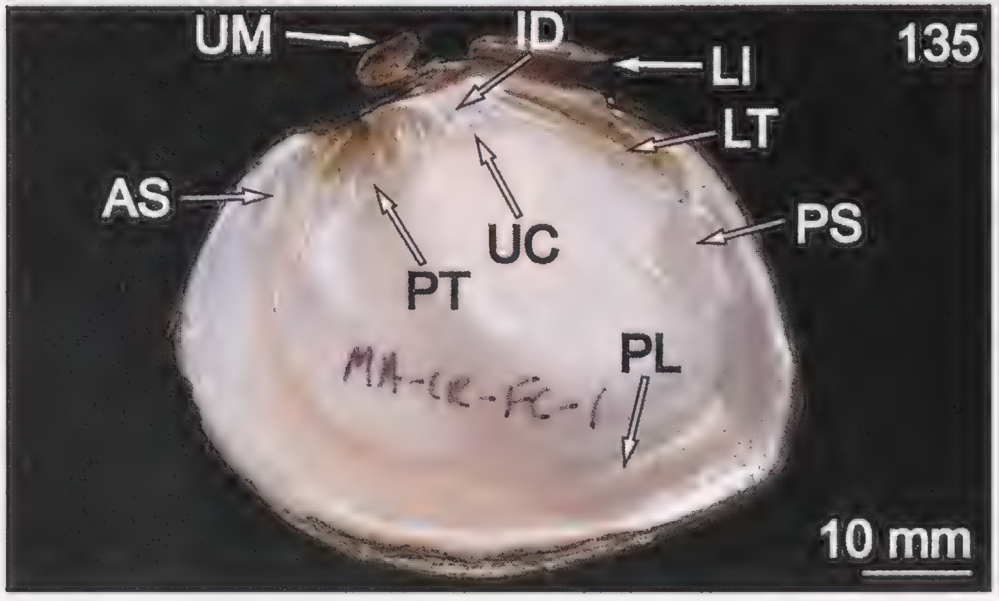

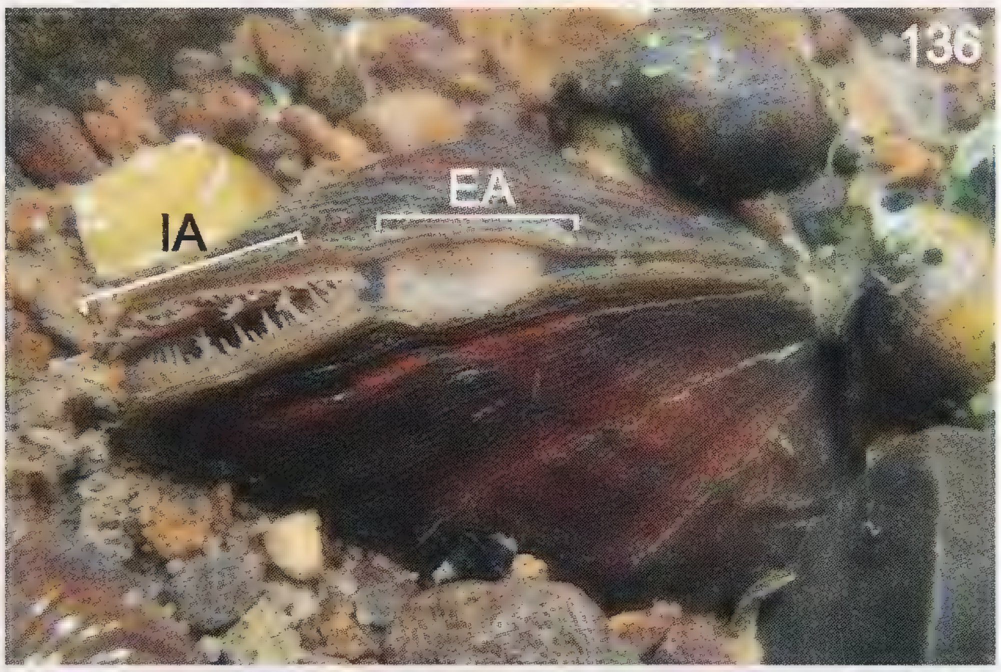

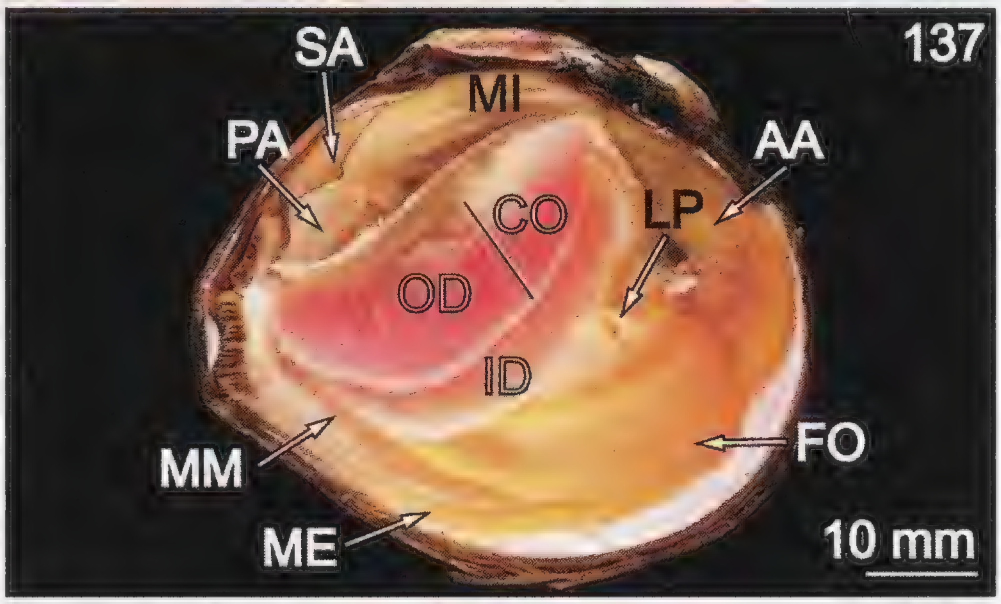

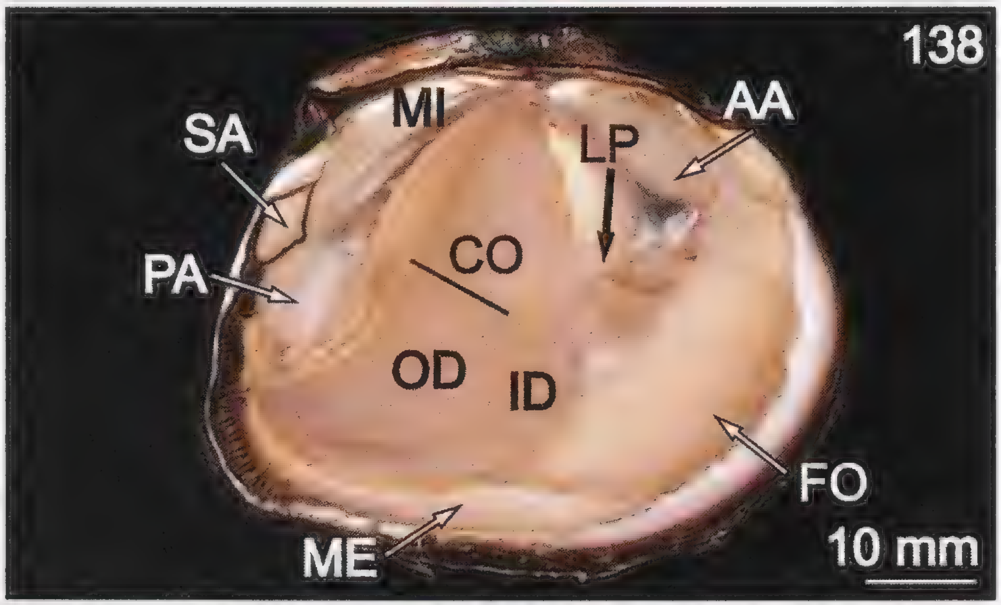

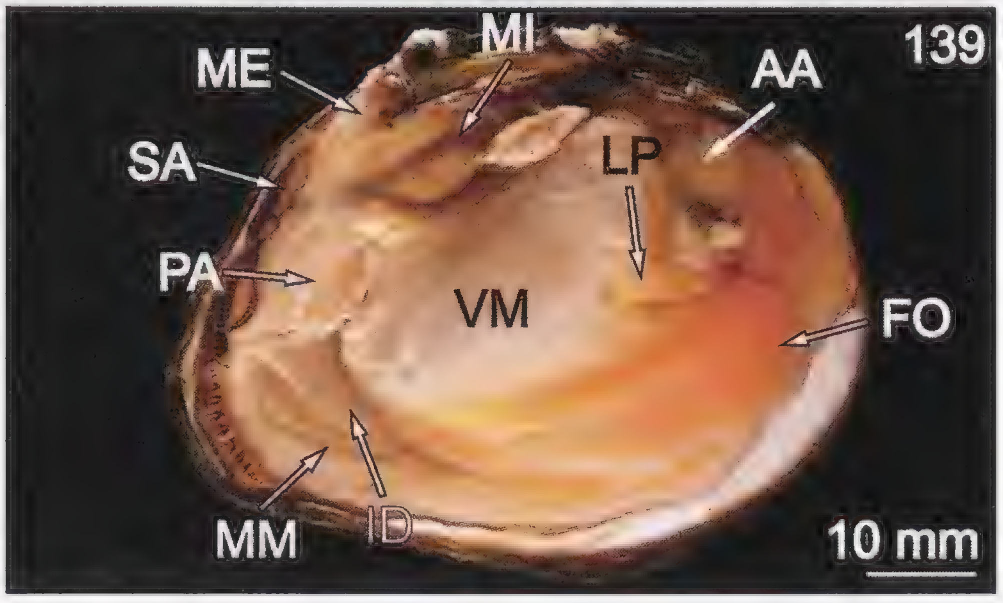

cells (Figs. 153). The distal margin of the outer gill has a rounded surface resembling the fusion of ctenidial filaments, while the inner gill features a median, ciliated furrow (Figs. 154, 155).

The umbo cavity of *F. cerina* is deep, and the visceral mass is a correspondingly arched dorsally and consists of an expansive latticework of loose connective tissue and hemolymph. Ascending lamellae of inner demibranchs are attached at the anterior end of the visceral mass near the labial palps and becomes detached along the length of the body at the anterior end of the nephridium near the urethra (Fig. 156). The ascending lamellae of the inner demibranch are united between the posterior margin of the visceral mass and posterior adductor. Muscle fascicles along the base of the ctenidia of *F. cerina* are most conspicuous in the posterior region of the body between the heart and posterior adductor (Figs. 157, 158). Ascending lamellae of outer demibranchs join the viscera just medial to the middle mantle. The subepithelium dorsal to the outer demibranchs is rich in loose connective tissue and hemolymph (Fig. 159).

Marsupial Demibranch: Female *Fusconaia cerina* utilize both pairs of inner and outer demibranchs for larval incubation. Fertilized and unfertilized ova are packaged into strings or conglutinates and transported into the ctenidial water tubes. Conglutinates may be allocated to nearly all water tubes anterior to posterior and may occupy the entire vertical length of each water tube. Marsupial gills feature enlarged water tubes and interbranchial septa as compared to male demibranchs (Fig. 160). Filaments, ostia and ctenidial vasculature of a marsupium are structurally similar to such structures of male ctenidia (Fig. 161). In gravid female *F. cerina* collected from Cahaba River (Shelby Co., Alabama) in May 2011, water tubes contained clusters of unfertilized ova and spherical, early-stage embryos (Figs. 160–162). Morphologically, the unfertilized ova and early stage embryos are spherical and possess a series of sinuous branches extending from the surface of the ova (Fig. 162).

The main cytological difference between male and female gill is the thickened septa of a marsupium. Septa have a broad, triangular base and generally become narrow at the water tube midline (Figs. 160, 161). Septum epithelium is pleated and typically there is a prominent, median fold extending into the water tube lumen. The epithelium of interbranchial septa consists of teardrop-shaped columnar cells and goblet cells, and septa contain an irregular subepithelium of fibrous tissue and a pale, eosinophilic ground substance (Fig. 163). Branches have a pale, basophilic pigmentation and typically have a sharply defined border similar to the appearance of a ribbon of periostracum. Embryos are typically spherical, while unfertilized ova tend to have an irregular shape in histological sections. Unfertilized ova have an eosino-

---

←

FIGS. 132–139. Shell morphology, and gross anatomical features of the mantle cavity of *Fusconaia cerina*. FIG. 132: Lateral view of the right valve showing the broad anterior margin (AM), arched umbo (UM), ligament (LI), posterior ridge (PR), and posterior slope (PS); FIG. 133: Lateral view of left valve showing the broad anterior margin (AM), conical umbo (UM), well-developed posterior ridge (PR), and posterior slope (PS); FIG. 134: Medial view of the left valve showing the pallial line (PL), anterior adductor scar (AS), posterior adductor scar (PS), strong pseudocardinal teeth (PT), interdentum (ID), deep umbo cavity (UC), lateral teeth (LT), ligament (LI), and umbo extending beyond the dorsal margin (UM); FIG. 135: Medial view of the left valve showing the pallial line (PL), anterior adductor scar (AS), posterior adductor scar (PS), strongly developed pseudocardinal tooth (PT), interdentum (ID), deep umbo cavity (UC), lateral tooth (LT), and well-developed ligament (LI), and umbo (UM); FIG. 136: Ventrolateral view of *Fusconaia cerina* (ca. 60 mm shell length) buried in gravel at Cahaba River with papillose mantle margins cupped to form an incurrent aperture (IA) and excurrent aperture (EA); FIG. 137: Medial view of the mantle cavity with the right valve and right mantle removed showing the orange mantle edge (ME), middle mantle (MM), foot (FO), anterior adductor (AA), labial palp (LP), and tetragenous inner demibranch (ID) and outer demibranch (OD), red conglutinates (CO), posterior adductor (PA), mantle isthmus (MI), and supra-anal aperture (SA); FIG. 138: Medial view of the mantle cavity with the right valve and right mantle removed emphasizing pallid mantle edge (ME), foot (FO), anterior adductor (AA), tetragenous inner demibranch (ID) and outer demibranch (OD), white conglutinates (CO), posterior adductor (PA), mantle isthmus (MI), and supra-anal aperture (SA); FIG. 139: Medial view of the mantle cavity with the right valve, right mantle, and right gills removed revealing the orange mantle edge (ME), middle mantle (MM), foot (FO), labial palp (LP), visceral mass (VM), anterior adductor (AA), left inner demibranch (ID), posterior adductor (PA), mantle isthmus (MI), and supra-anal aperture (SA).

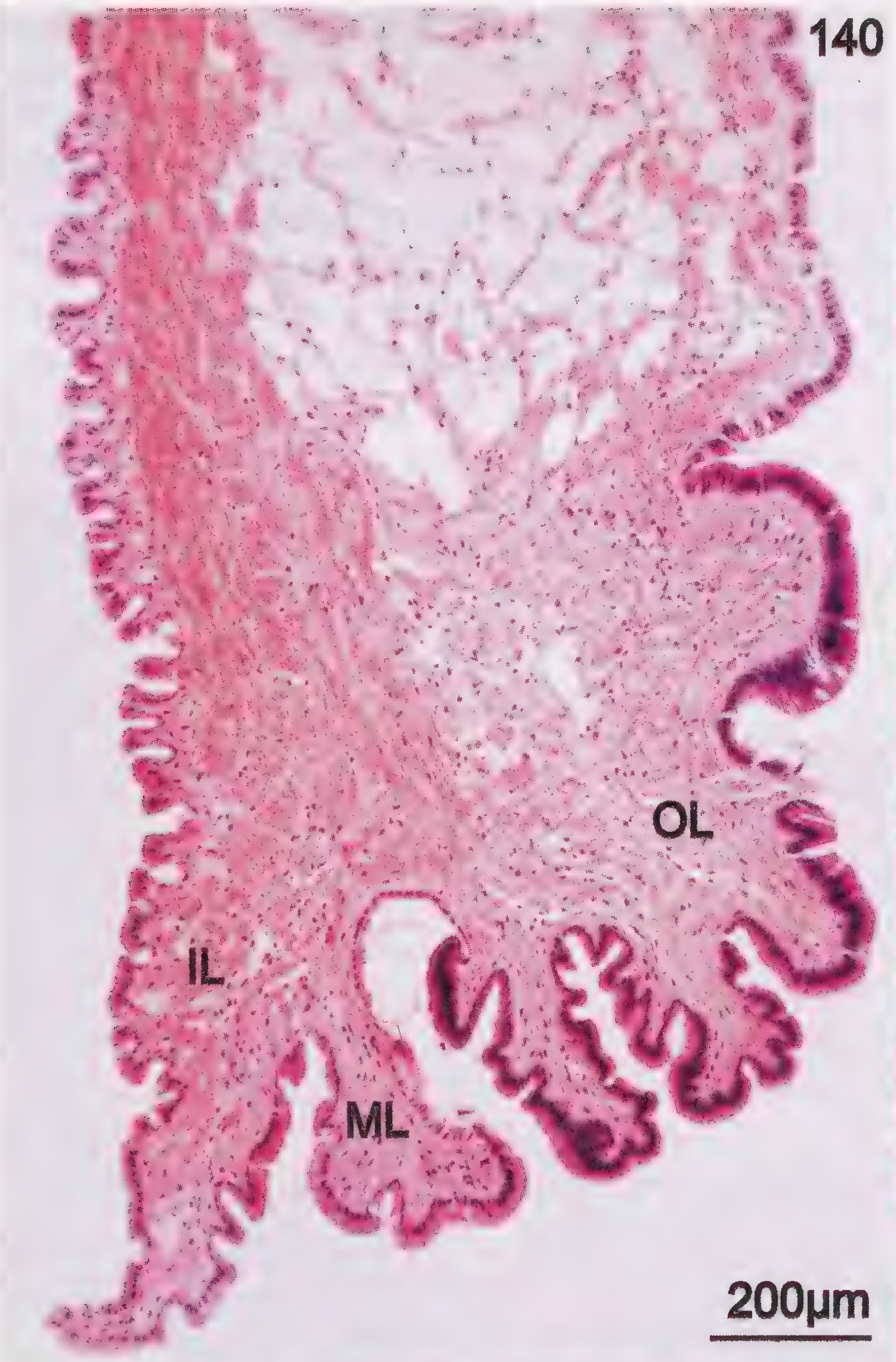
140

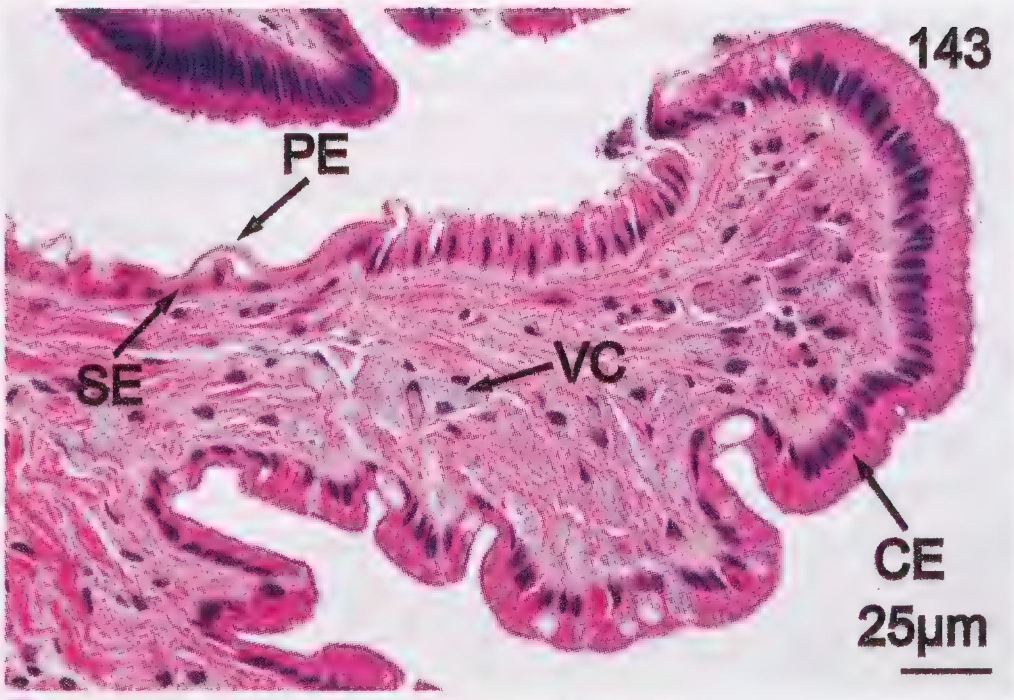
143

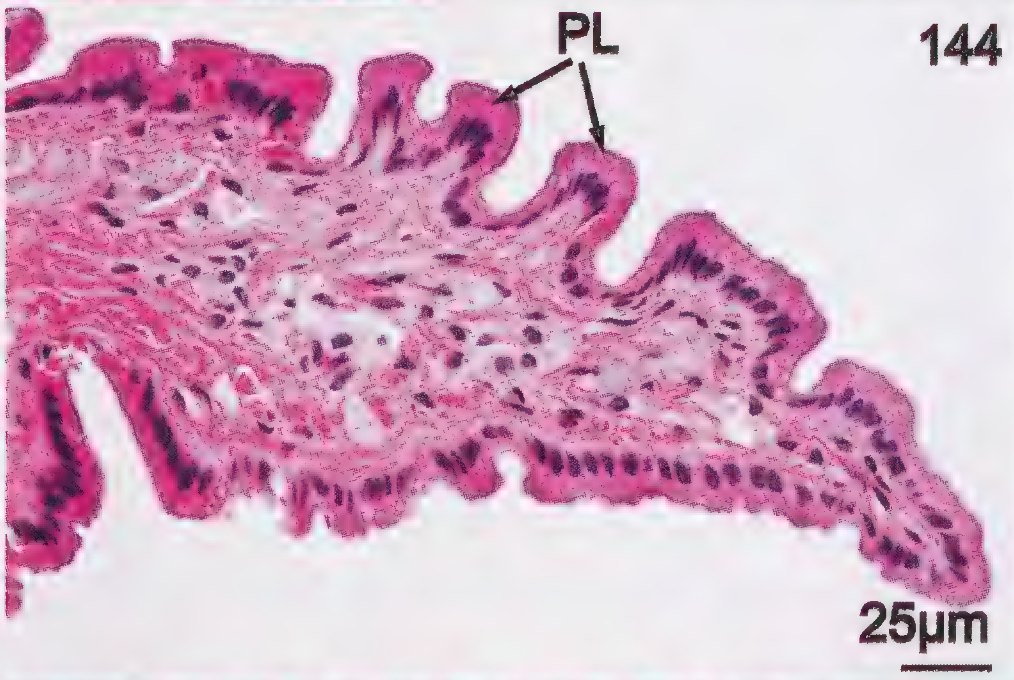
144

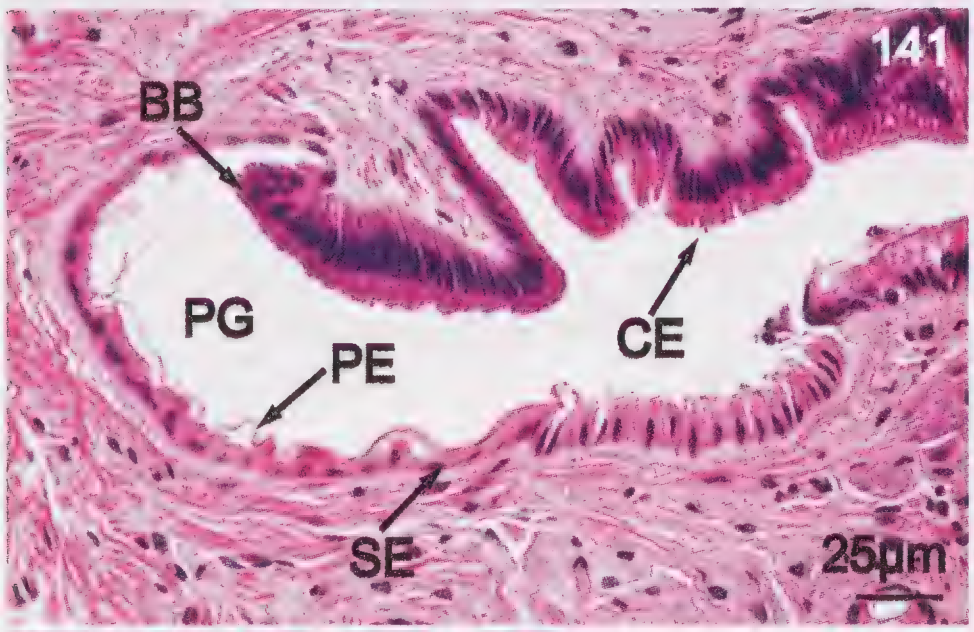
141

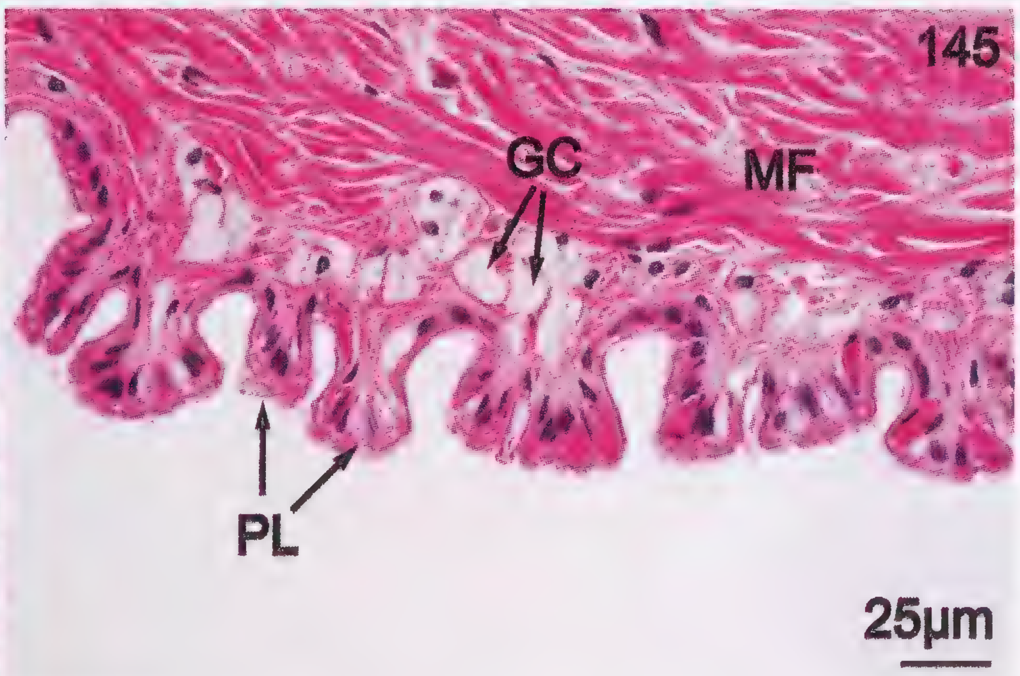
145

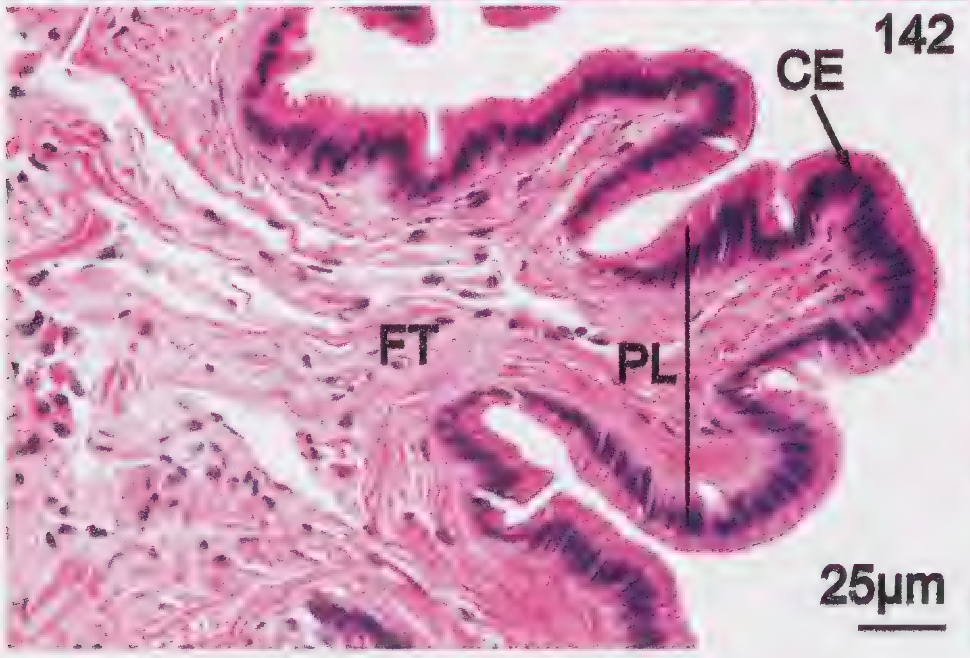
142

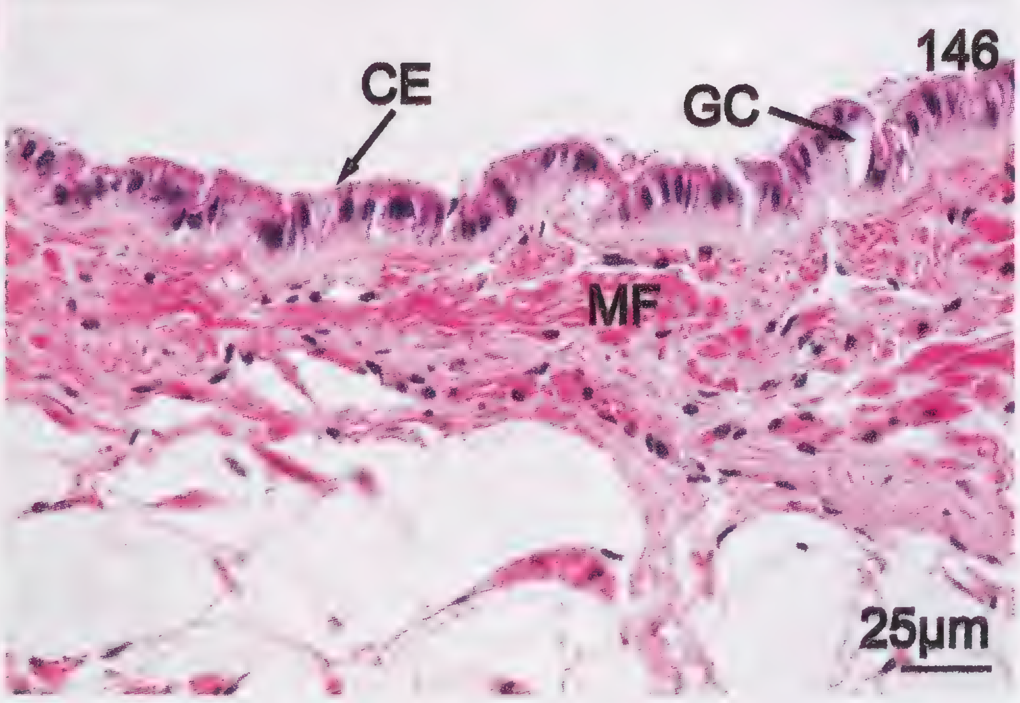
146

philic, homogenously granular composition, while early stage embryos are multinucleated, but lacking apparent cell membranes. Nuclei of early-stage embryos are spherical and a small nucleolus may be observed in some cells. In female *F. cerina* collected from Cahaba River in August 2011, conglutinates had been shed, but the marsupia maintained the same histological characteristics as a filled ctenidium (Fig. 164).

Cellular Structure of Foot and Associated Tissues

Pedal Musculature and Byssal Gland: At low magnification, and in a transverse plane of section, pedal tissue of *Fusconaia cerina* is characterized by a median triangle of somatic musculature flanked by strongly basophilic regions of chromatocytes (Fig. 165). The ventral margin has dark-staining and pale-staining basophilic chromatocytes intertwined among myofibers (Fig. 166). Granulocytes continue dorsally to the terminus of type-three epithelium. Pedal musculature consists of a ventral irregular or woven region with distinct horizontal and vertically oriented myofibers (Fig. 167), while the base of the foot consists of well-defined layers of vertical and horizontally oriented musculature (Fig. 168).

Fusconaia cerina has a diamond-shaped byssal gland located posterior to the pedal ganglion. The luminal surface of the byssal gland is ciliated with an emarginated epithelium and a densely fibrous subepithelium (Figs. 169, 170). There are a series of small, spherical ciliated structures in the posterior region of the foot, possibly representing disconnected remnants of the byssal canal. Sagittal sections of *F. cerina* foot reveal groups of spherical, ciliated structures in an oblique, linear path between the dorsal base of the foot, where the hemocoel joins the pedal musculature and the posterior margin of the pedal integument. Byssal canal remnants consist of a ciliated, columnar epithelium surrounding a lumen filled with debris. Luminal contents of byssal canal may appear to be a shapeless eosinophilic mass material, or a darkened, granular material (Fig. 171).

Pedal Integument and Mesentery: Pedal integument of *F. cerina* consists of five regions from ventral to dorsal. The most distinguishing cytological characteristic of *F. cerina* is the preponderance of violet granulocytes in the ventral portion of the foot. The abundance of granulocytes is so high that histological sections of foot have a distinctive violet tinge (Fig. 172). Type one epithelium is densely ciliated consisting of irregular to rectangular plicae. Granulocytes within the subepithelium of type one plicae appear dorsoventrally compressed. Chromatocytes underlying type one plicae of *F. cerina* are so densely packed that it is difficult to determine the boundaries of some cells. Tall rectangular plicae become narrower and diminish in height between integumentary regions two and three (Figs. 173, 174). Plicae diminish to a simple columnar epithelium featuring subtle undulations in integumentary region four (Fig. 175). Columnar cells of integument four are ciliated, and numerous goblet cells are present. Type four integument of *F. cerina* has a distinct subepithelium of connective tissue

---

←

FIGS. 140–146. Anterior mantle edge of *Fusconaia cerina*. FIG. 140: Transverse section of anterior mantle edge showing the position of the outer lobe (OL), middle lobe (ML), and inner lobe (IL); FIG. 141: Transverse section of mantle edge emphasizing columnar epithelium (CE) of the outer lobe, basal bulb (BB), periostracal groove (PG), squamous epithelium (SE) of the middle lobe, and periostracum (PE); FIG. 142: Transverse section of the distal margin of outer mantle lobe revealing a basophilic columnar epithelium (CE) along branched plicae (PL) and a dense subepithelium of fibrous tissue (FT); FIG. 143: Transverse section of middle mantle lobe revealing a periostracum ribbon (PE) and squamous epithelium (SE), violet cells (VC), characterizing the dorsal margin consisting of a folded columnar epithelium (CE); FIG. 144: Transverse section of the inner mantle lobe edge portraying an irregular epithelium consisting of teardrop-shaped to flattened plicae (PL); FIG. 145: Transverse section of inner epithelium of proximal mantle edge defined by teardrop-shaped plicae (PL), granulocytes (GC), and a well-defined stratum of myofibers (MF); FIG. 146: Transverse section of the outer epithelium of proximal mantle edge characterized by a wavy columnar epithelium (CE), isolated goblet cells (GC), a horizontal lamina of myofibers (MF).

fibers overlying hemolymph sinuses and somatic musculature. Integumentary region five features a simple cuboidal epithelium, goblet cells and sparsely distributed tufts of cilia. Subepithelium of region five features a thin hemolymph sinus juxtaposed upon blocks of somatic musculature (Fig. 176). Overall, the integument around the foot is deeply sinuous at the ventral margin and flattened at the dorsal extent (regions four and five). The ventral

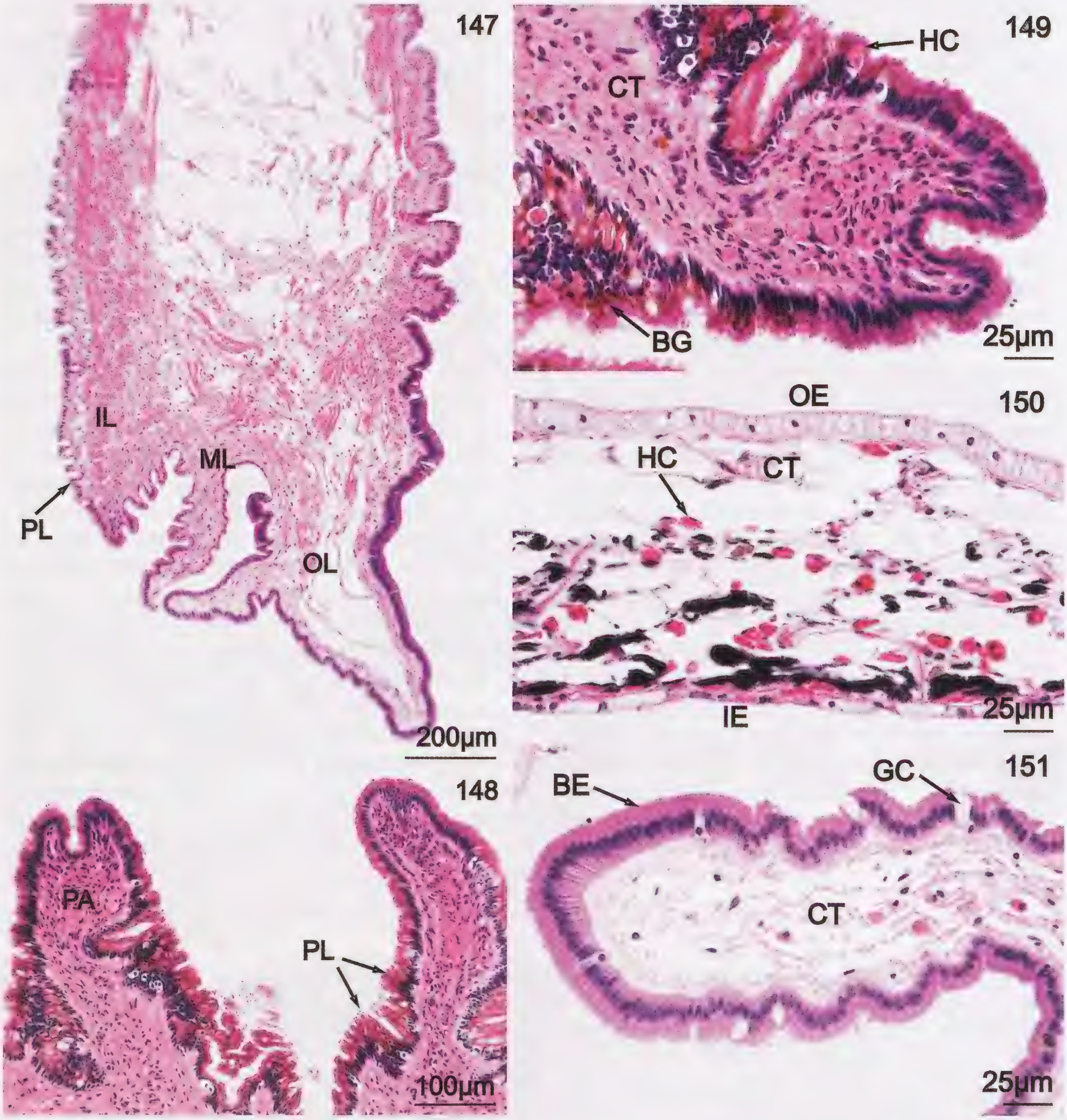

FIGS. 147–151. Posterior mantle edge, middle mantle, and mantle isthmus of *Fusconaia cerina*. FIG. 147: Transverse section of posterior mantle edge showing a forked outer lobe (OL), conical middle lobe (ML), and triangular inner lobe (IL) with distinct plications (PL); FIG. 148: Sagittal section of posterior mantle edge characterized by conical papillae (PA) and oblique plications (PL) along the surface; FIG. 149: Sagittal section of a papilla displaying brown intracellular granules (BG) of the columnar epithelium and wandering hemocytes (HC) interspersed among epithelial cells, and a subepithelium endowed with connective tissue fibers (CT); FIG. 150: Transverse section of middle mantle displaying columnar cells of outer epithelium (OE), squamous cells of inner epithelium (IE) and a fibrous subepithelial strata of connective tissue (CT), and hemocytes (HC); FIG. 151: Transverse section of mantle isthmus revealing a well-organized basophilic epithelium (BE), goblet cells (GC), and sinuous connective tissue fibers (CT).

portion of the foot, as seen in sagittal sections, is highly rugose and irregular (Fig. 177).

Histological sections of visceral mass reveal numerous horizontally to obliquely oriented bands of mesentery spanning the hemocoel (Fig. 178). Bundles of mesentery are characterized by a series of eosinophilic filaments with slender, basophilic nuclei. Sagittal sections of coelom reveal a preponderance of mesentery fascicles throughout the hemocoel (Fig. 179).

Labial Palps: Labial palps of *Fusconaia cerina* feature plicae along the inner surface and a smooth outer surface (Fig. 180). Plicae of the inner surface are bulbous at the distal margin and have two small epithelial folds along the stem. Ciliated columnar cells represent the main constituent of the inner palp epithelium and extend along the palp interior until the distal margin of each lip. Ciliated columnar cells of the labial palps have an eosinophilic cytoplasm, and an elliptical nucleus with no visible nucleolus (Fig. 181). The distal margin of the palp features prominent goblet cells as the tissue transitions to a flattened epithelium. Additionally, there appears to be two types of goblet cells, many have pale, white intracellular vesicles, while the second type features eosinophilic vesicles (Fig. 182). The outer surface of each palp features a flattened epithelium with teardrop-shaped columnar cells. Columnar cells have a minimal amount of cytoplasm with a slender, elliptical nucleus and no apparent nucleolus. Additionally, goblet cells are interspersed among columnar cells (Fig. 183). The subepithelium of the labial palps consists of eosinophilic fibers, a pale ground substance, and hemolymph.

Anterior Adductor and Anterior Pedal Retractors: Adductor muscle features large fascicles and conspicuous perimysium containing capillaries (Fig. 184). Myofibers of the anterior muscle group consists of spindle-shaped cells with cylindrical nuclei. Nuclei are cylindrical, pale and granular. Fascicles are well organized, and in sagittal sections, the musculature has a woven appearance. Myofibers of the anterior protractors have a dark eosinophilic composition, and the tissue features distinct fascicles (Fig. 185).

Oral Groove and Esophagus: The oral groove of *F. cerina* resembles a deep cavity located posteriorly to the anterior adductor. At the ventral entrance to the oral groove, there are two cylindrical extensions of tissue histologically resembling labial palp. The epithelium consists of teardrop-shaped columnar cells along the ventral surface and a pseudostratified, ciliated epithelium along the dorsal surface. The tip of each cylindrical extension of oral groove entrance consists of a preponderance of goblet cells. Subepithelium of the cylindrical extensions consists of muscle fibers and hemolymph sinuses (Fig. 186). Lateral to the cylindrical extensions, the walls of the oral groove curve dorsally and become vertically oriented. The curved portion of the oral groove wall is pleated, while the straight or vertically oriented extent of the walls consists of uniform line of ciliated columnar cells (Figs. 187, 188). Ciliated columnar cells of oral groove walls feature an eosinophilic cytoplasm and a homogenous, basophilic nucleus. The dorsal floor of the oral groove features ciliated plicae. Plicae of the dorsal aspect of the oral groove are histologically similar to the plications along the curved portion of the walls located at the ventral side of the organ.

The esophagus is an ovular tube characterized by deep sinuous folds extending into the

---

→

FIGS. 152–159. Outer demibranch, and inner demibranch of *Fusconaia cerina*. FIG. 152: Transverse section of inner gill showing characteristic cylindrical filaments (FI), and a septum (SE) uniting inner and outer lamella along the length of a water tube (WT); FIG. 153: Transverse section of inner gill lamella emphasizing the functional components including lateral cilia (LC), frontal lateral cilia (FL), frontal cilia (FC), skeletal rods (SR), hemolymph vessel (HV), ostium pore (OS), and corresponding water tube (WT); FIG. 154: Transverse section of the distal tip of an outer gill characterized by a convex distal margin (DM), derived from the fusion of filaments (FI); FIG. 155: Transverse section of the free distal margin (DM) of an inner ctenidium displaying a median ciliated groove (CG); FIG. 156: Transverse section of the free inner lamella (IL) of an inner gill showing its close proximity to the visceral mass (VM) and nephridium (NE); FIG. 157: Transverse section of the base of a gill displaying muscle fascicles (MU) in an anterior-posterio alignment, surrounded by a large mass of hemolymph (HE); FIG. 158: Transverse section of the base of a ctenidium revealing muscle fascicles (MU) and hemolymph (HE); FIG. 159: Transverse section of the base of an outer gill showing the union of the outer lamella (OL) and middle mantle (MA).

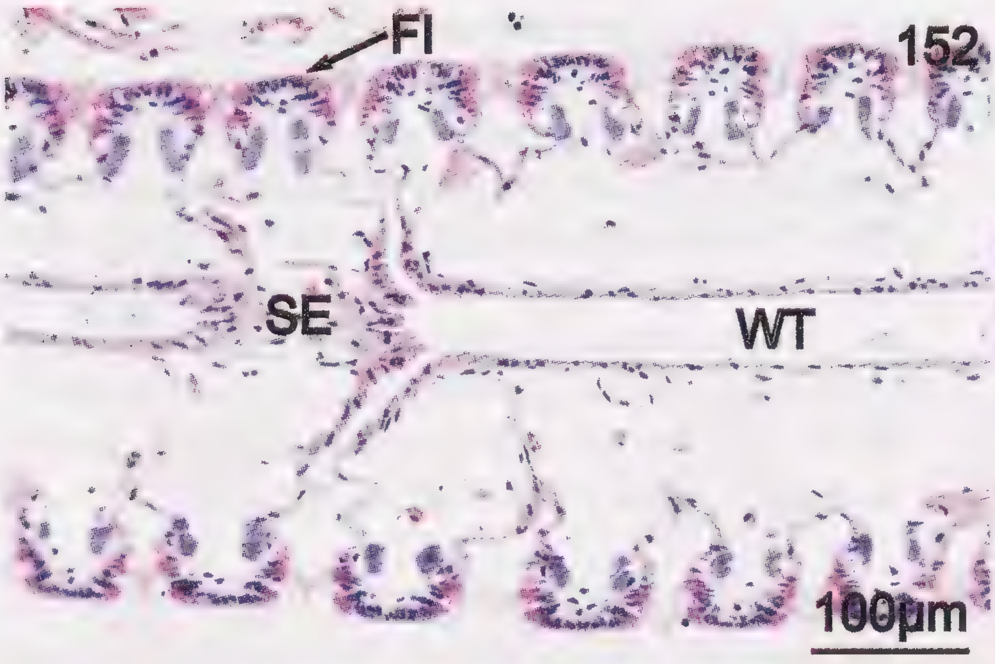
152
FI
SE
WT
100µm

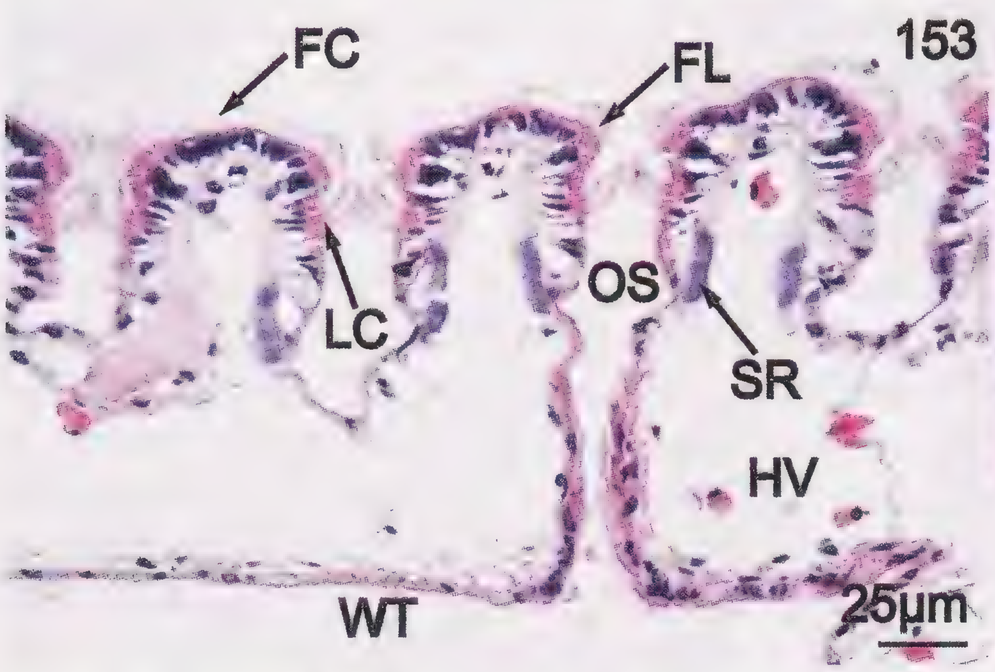
153
FC
FL
LC
OS
SR
HV
WT
25µm

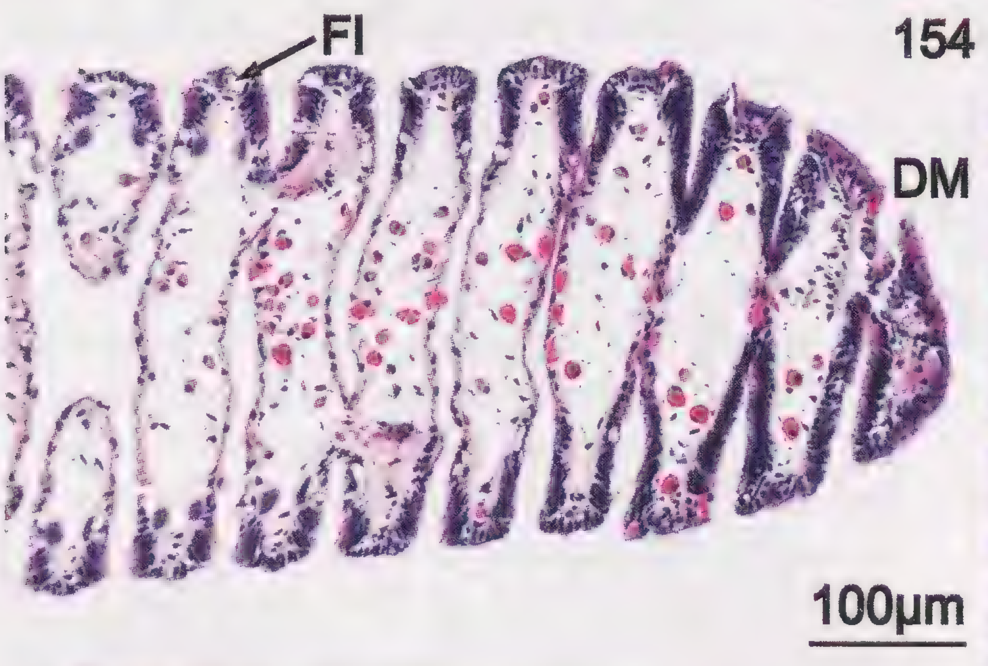
154
FI
DM
100µm

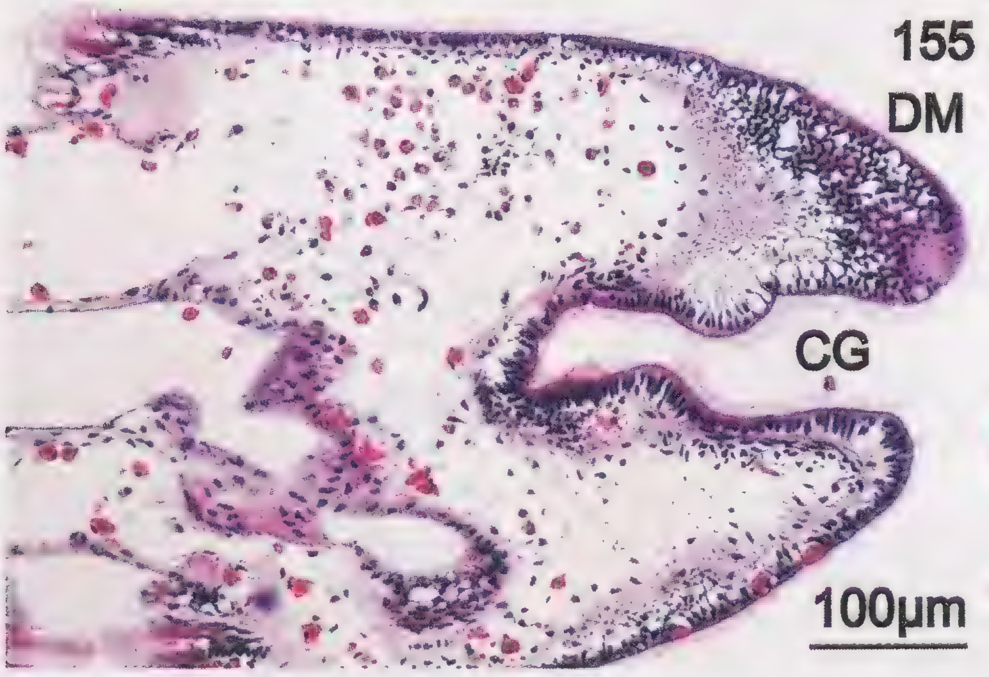
155
DM
CG
100µm

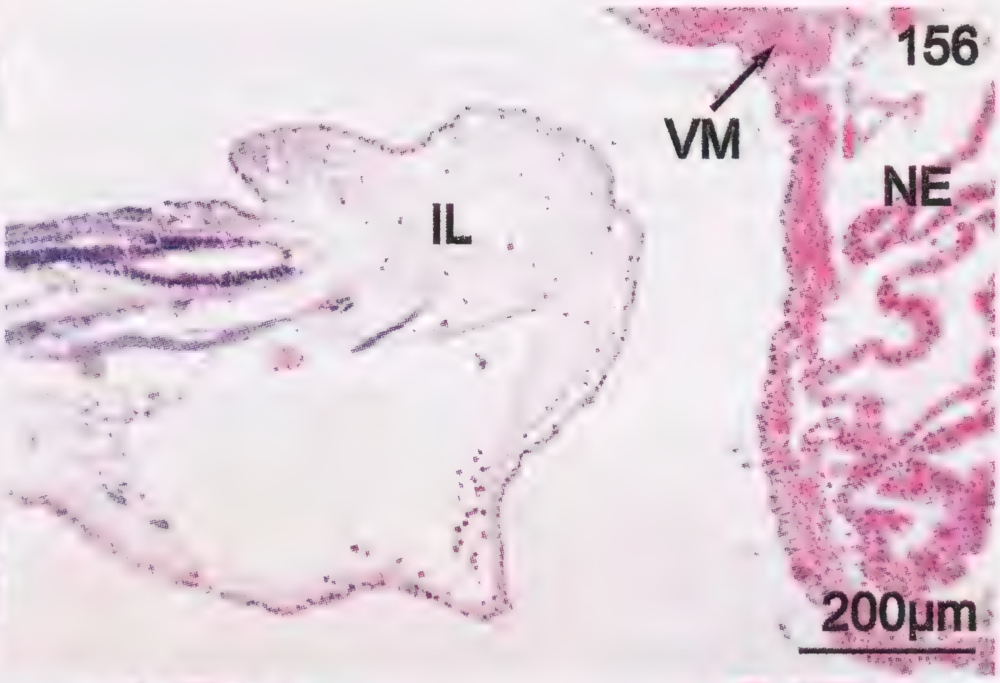
156
VM
NE
IL
200µm

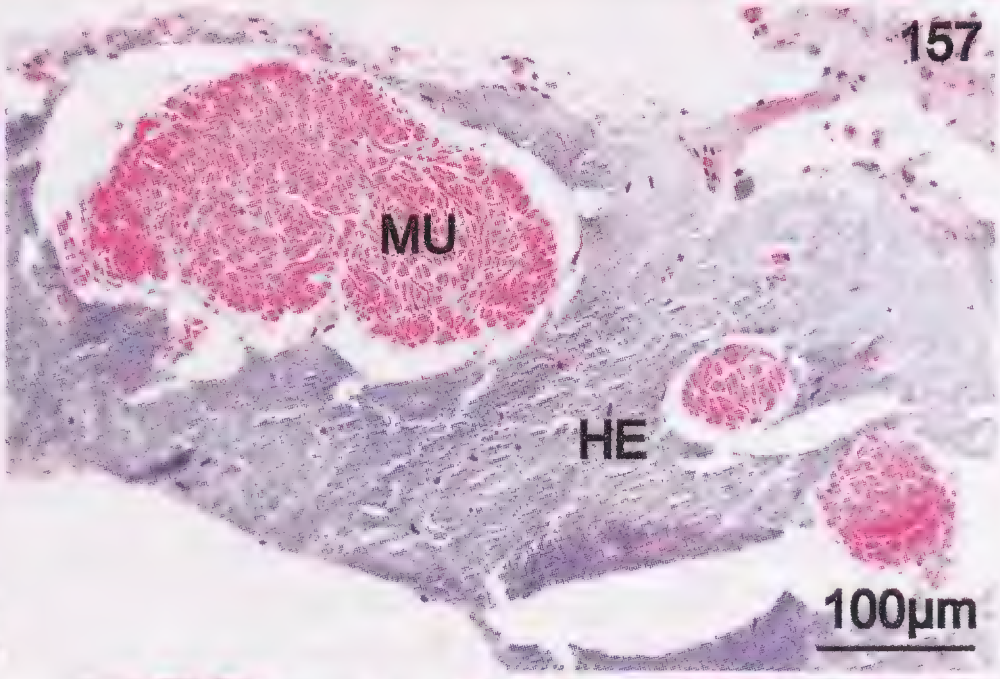
157
MU
HE
100µm

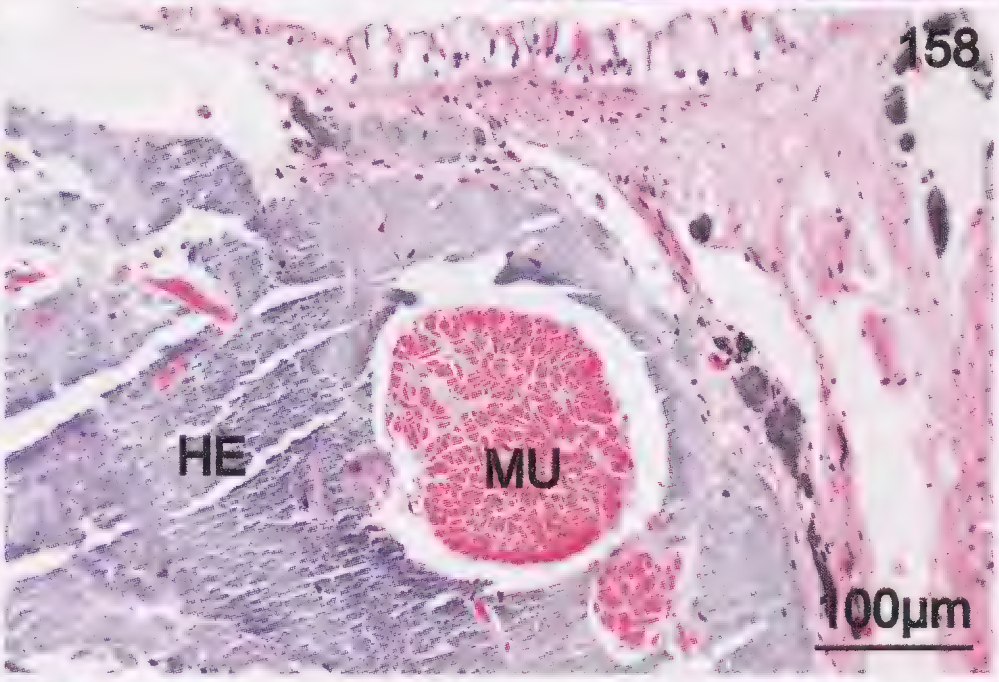
158
HE
MU
100µm

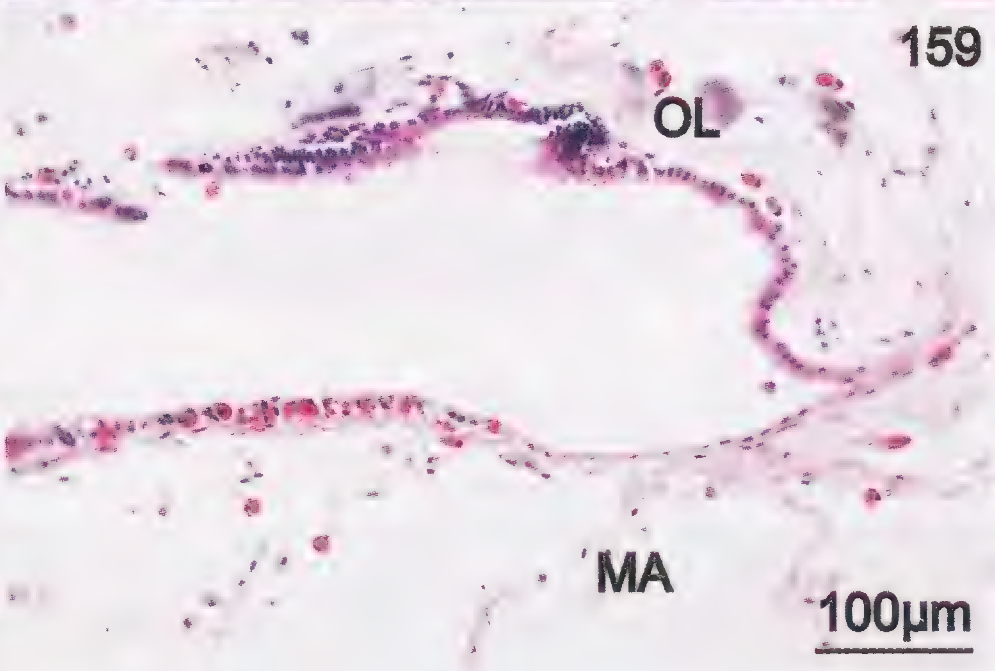
159
OL
MA
100µm

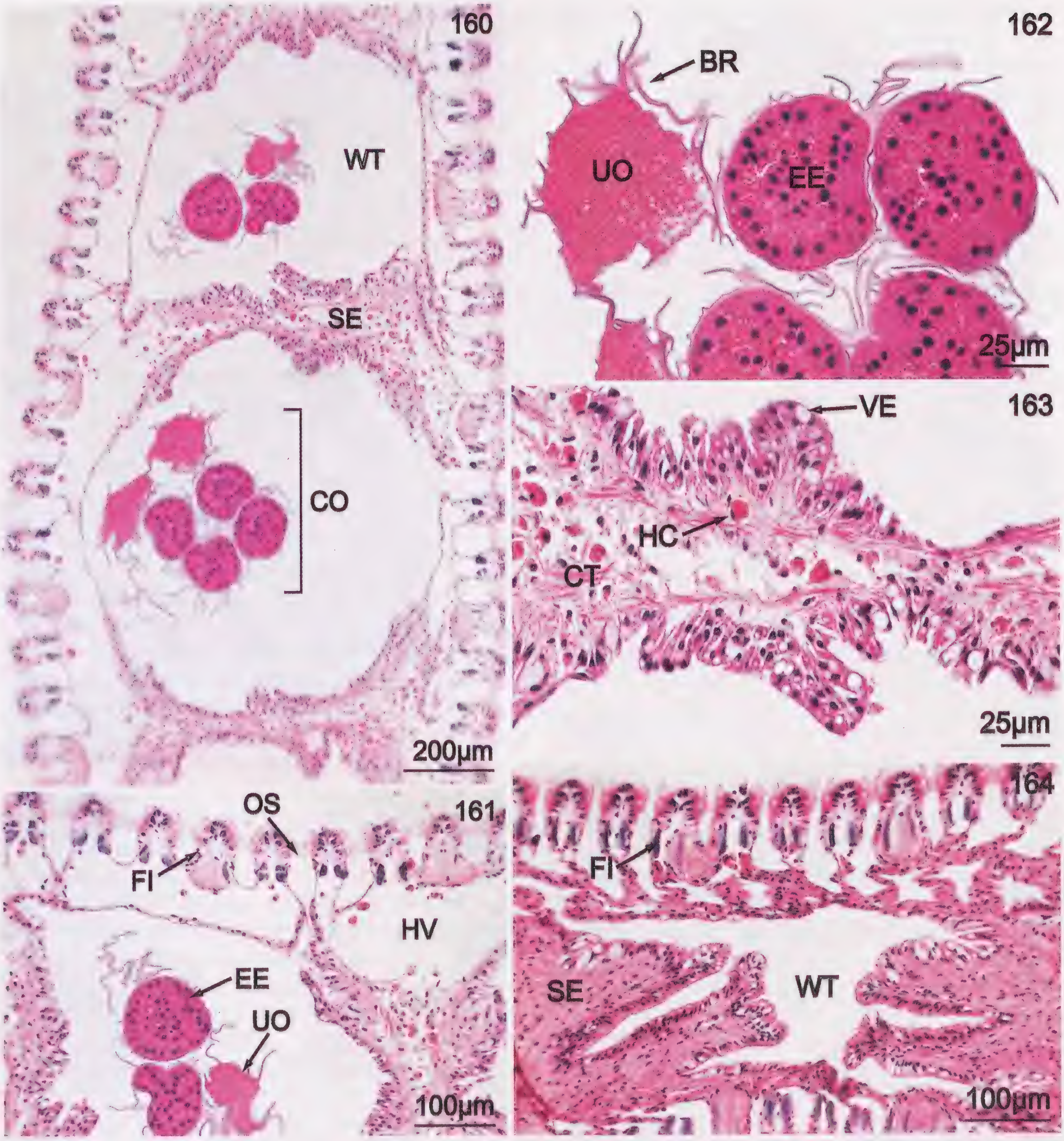

FIGS. 160–164. Marsupium, and conglutinates of *Fusconaia cerina*. FIG. 160: Transverse section of a marsupial ctenidium containing a conglutinate (CO), within a distended water tube (WT), supported by thickened septa (SE); FIG. 161: Transverse section of the lateral margin of a filled marsupium portraying filaments (FI), an ostium (OS), hemolymph vessels (HV), and a conglutinate consisting of early stage embryos (EE), and unfertilized ova (UO); FIG. 162: Transverse section of a marsupium portraying part of a conglutinate consisting of unfertilized ova (UO), early stage embryos (EE), both featuring basophilic apical branches (BR); FIG. 163: Transverse section of the marsupial septum consisting of a columnar epithelial cells with transparent vesicles (VE), and a subepithelium consisting of fibrous connective tissue (CT), and hemocytes (HC); FIG. 164: Transverse section of an empty marsupium illustrating how the histological composition of filaments (FI), water tube (WT) and septa (SE) exhibit minimal change long after conglutinates are shed.

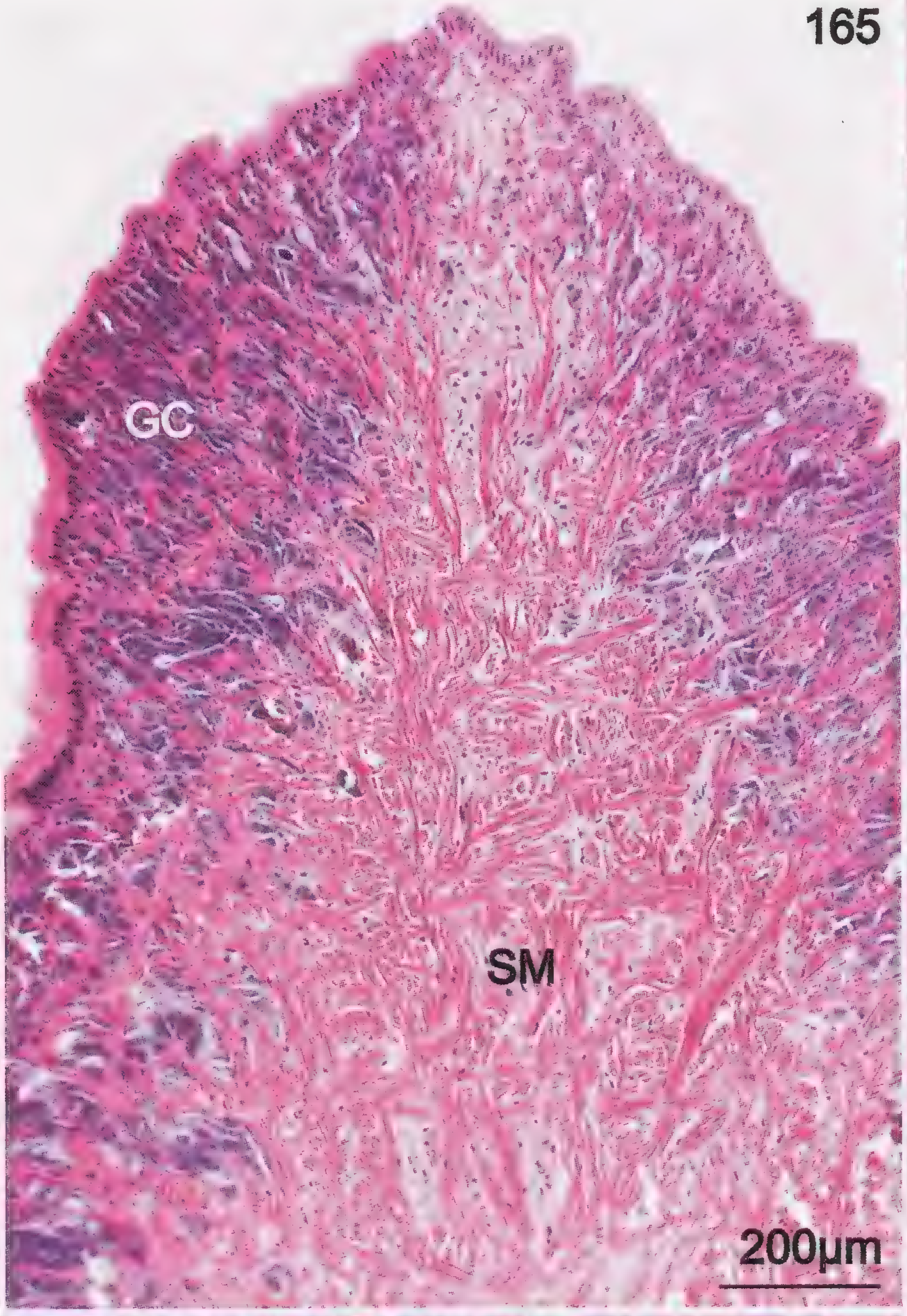
165
GC
SM
200µm

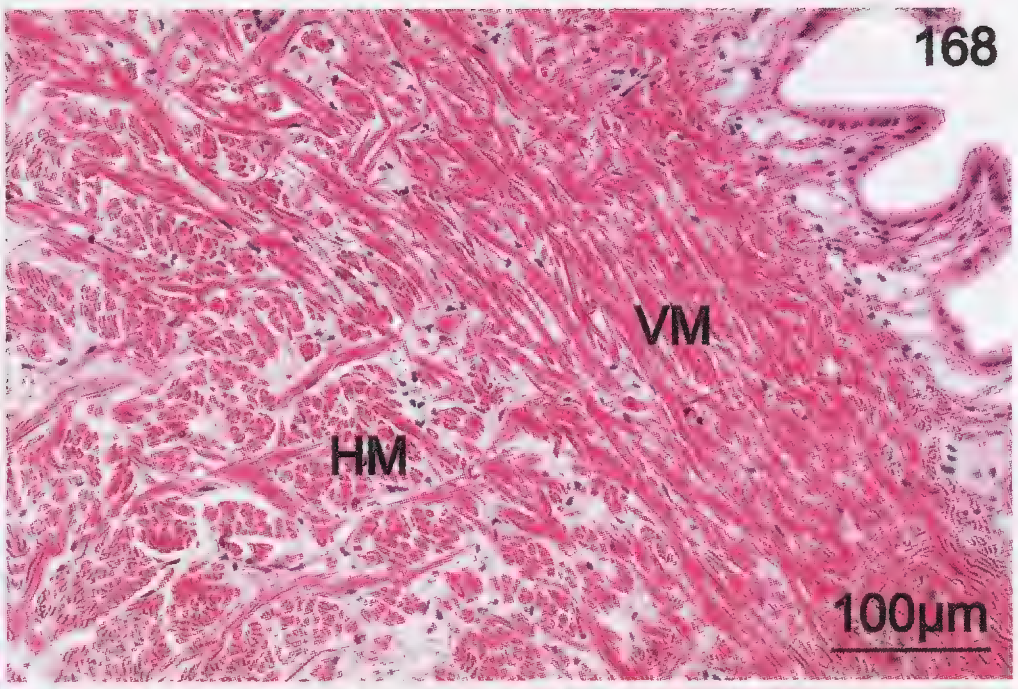
168
VM
HM
100µm

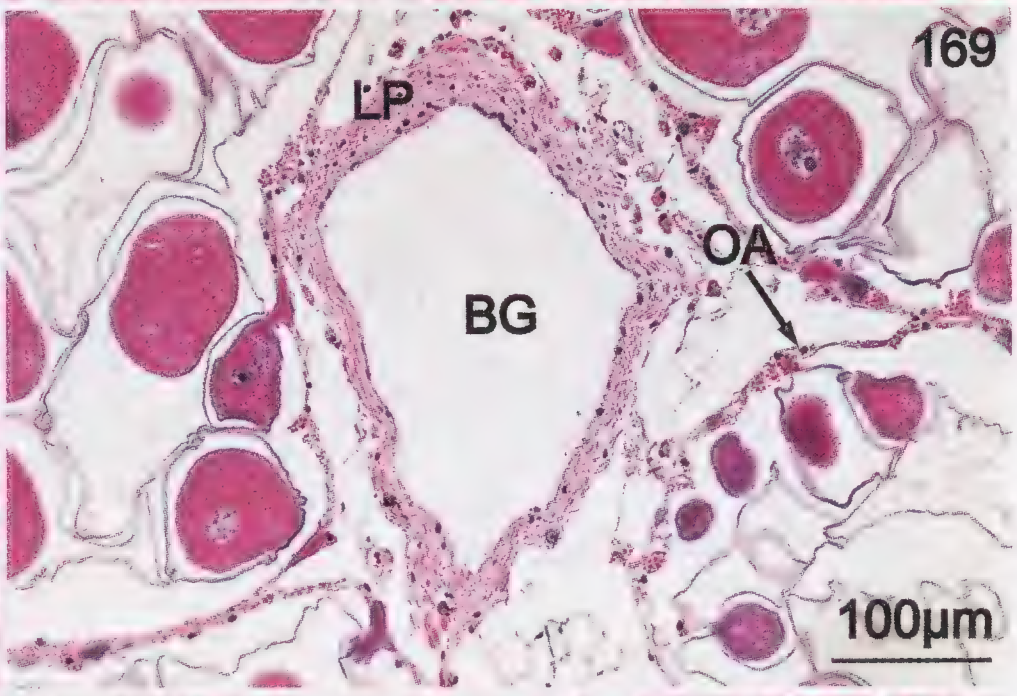
169
LP
OA
BG
100µm

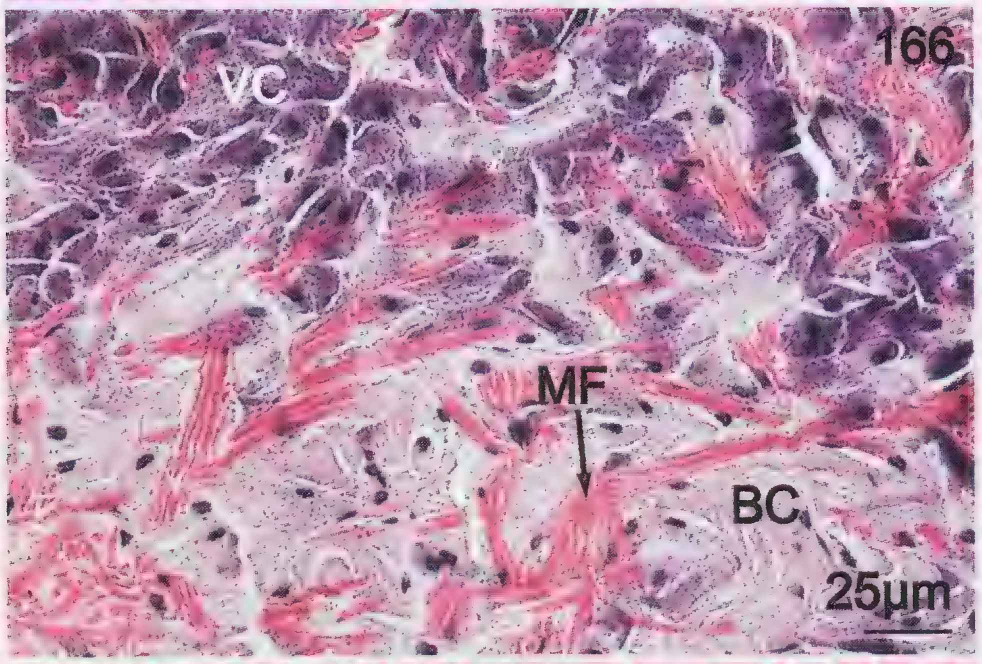
166
VC
MF
BC
25µm

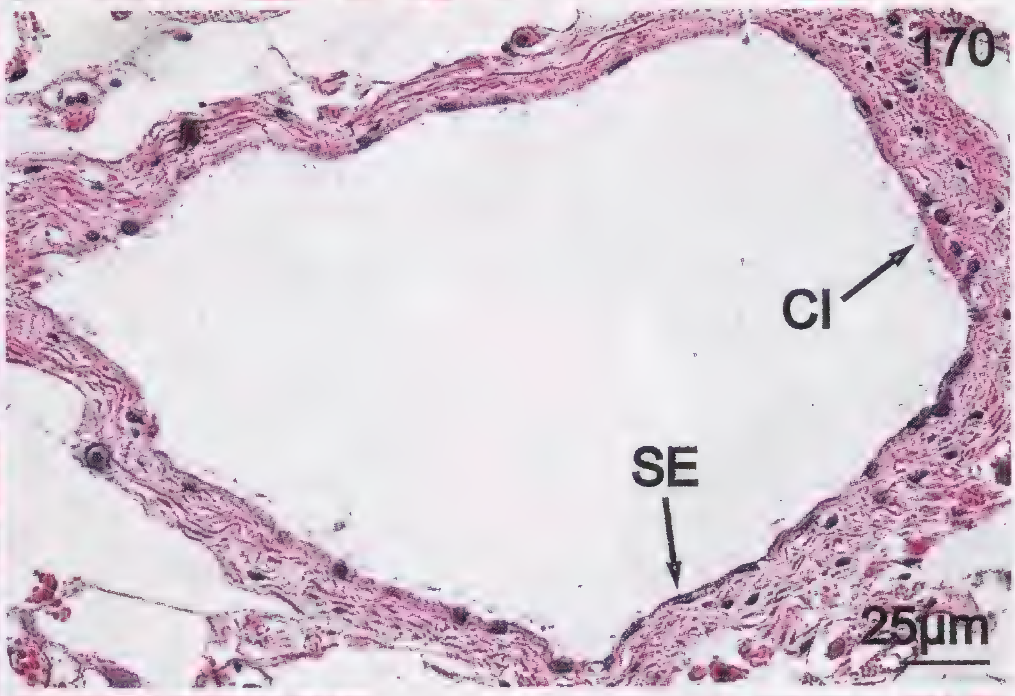
170
CI
SE
25µm

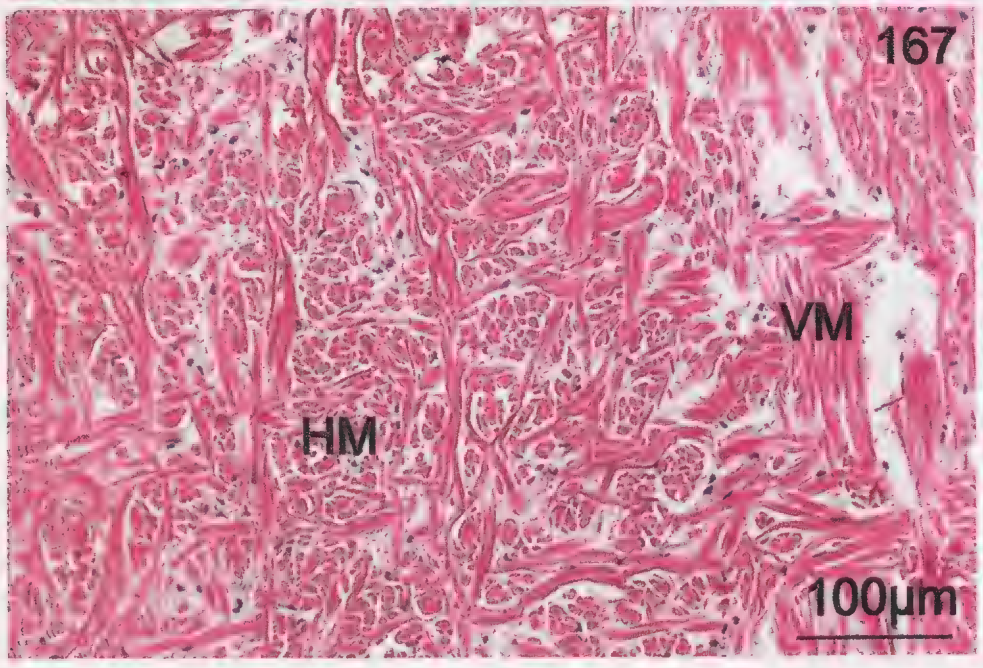
167
VM
HM
100µm

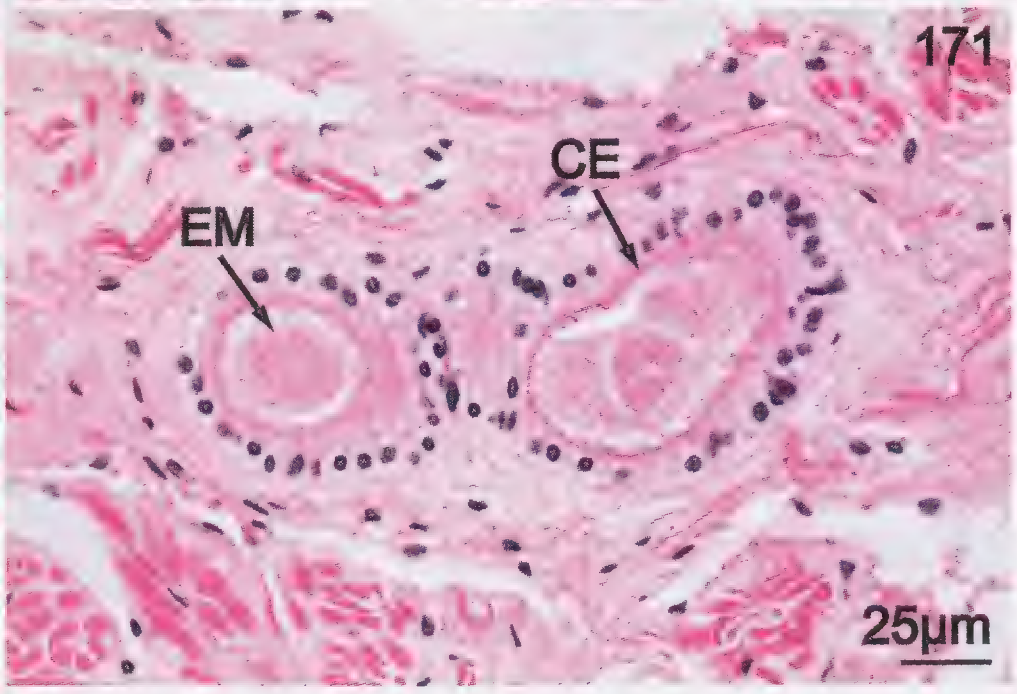
171
CE
EM
25µm

lumen from the dorsal and ventral surfaces (Fig. 189). The esophagus has a well-defined lamina propria consisting of loose connective tissue fibers and a pale ground substance. Esophageal epithelium consists of ciliated columnar cells arranged along tall, rectangular to “Y”-shaped plicae (Fig. 190).

Cellular Structure of the Alimentary Canal

Digestive Diverticulum: The esophagus enters the stomach on the left side of the body. The esophageal-stomach junction is characterized by a median typhlosole along the ventral surface of the esophagus. The typhlosole has a flattened, rectangular tip and a pleated stem. The ventral wall of the esophagus bends ventrally creating a rounded, sinistral fold of rounded plicae (Fig. 191). Rounded plicae feature ciliated columnar cells and such plicae are a repetitive feature of the stomach walls (Fig. 192). In contrast, the dorsal and lateral walls of the esophageal-stomach junction largely lack epithelial folds. Subepithelium of the stomach possesses a well-defined lamina propria.

Fusconaia cerina has primary, secondary and tertiary digestive tubules. The ciliated primary tubules feature thin, ciliated plicae extending to the midpoint of the lumen (Fig. 193). Ciliated columnar cells of primary digestive tubules are densely packed and teardrop-shaped. Additionally, cytoplasm of ciliated columnar cells lining the plicae has a strong eosinophilic characteristic (Fig. 194). Secondary tubules feature columnar cells with an eosinophilic and vesiculated cytoplasm and apical microvilli (Fig. 195). However, columnar cells of secondary tubules tend to curl or become teardrop-shaped at the junction of tertiary tubules. The morphology of secondary tubule cells creates the appearance of cycle-shaped valves extending into the lumen of tertiary tubules (Fig. 196). Tertiary tubules have a vesiculated and eosinophilic cytoplasm. The nuclei of tertiary tubule cells have a strongly basophilic, triangular region containing a spherical nucleus, typically with a distinct nucleolus (Fig. 197).

Stomach: The stomach is a dorsoventrally elongated chamber with ciliated plicae along the gastric walls and a large, forked typhlosole extending medially into the lumen from the sinistral wall (Fig. 198). The ventral epithelium has an eosinophilic cuticle or gastric shield along the sinistral portion of the stomach. The cuticle is relatively uniform across the surface, but may occasionally form a point as it may be whipped or pulled by ciliary action (Fig. 199). At a higher magnification, the cuticle appears gelatinous and layered with fine lines. The cuticle is attached directly to the cilia along the apical surface of the columnar epithelium. Columnar cells have an eosinophilic cytoplasm and an ovular nucleus with no visible nucleolus (Fig. 200). The medial portion of the ventral wall has a deep groove or furrow that is rectangular (Fig. 201). Dextral to the medial groove is a ciliated and plicated epithelium. Plicae are generally square-shaped, and they are similar in size (Fig. 202). The dorsal wall of the stomach has a series of tall, cylindrical plicae extending into the lumen. Plicae are ciliated and may also have a secretory function since the tissue appears to be bubbling (Fig. 203). A key characteristic of the stomach is the large, medially extending typhlosole located along the sinistral wall. The typhlosole has a forked epithelium with a gelatinous cuticle (Fig. 204).

←

FIGS. 165−171. Pedal musculature, and byssal gland of *Fusconaia cerina*. FIG. 165: Transverse section of the ventral tip of the foot displaying a median triangular ray of somatic musculature (SM), and a darkened subeptihelium of granulocytes (GC); FIG. 166: Transverse section of foot subepithelium characterized by irregular myofibers (MF), pale, blue granulocytes (BC), and violet cells (VC); FIG. 167: Transverse section of ventral foot musculature emphasizing bundles of horizontal myofibers (HM), and vertical myofibers (VM); FIG. 168: Transverse section of the foot portraying a distinct stratum of vertical foot musculature (VM) overlying layers of horizontal musculature (HM); FIG. 169: Transverse section of the byssal gland (BG) encircled by a lamina propria (LP) and surrounded by ovarian acini (OA); FIG. 170: Transverse section of the byssal gland emphasizing cilia (CI) and squamous epithelium (SE); FIG. 171: Sagittal section of the posterior portion of the foot emphasizing possible remnants of the byssal canal consisting of a ciliated epithelium (CE), enclosing an eosinophilic mass (EM).

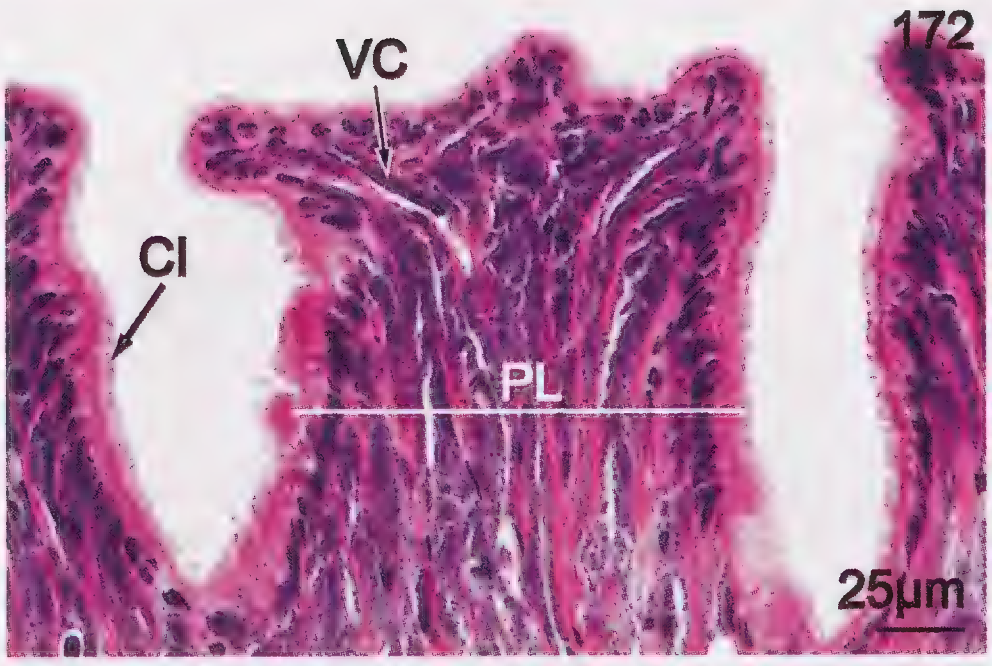
172
VC
CI
PL
25µm

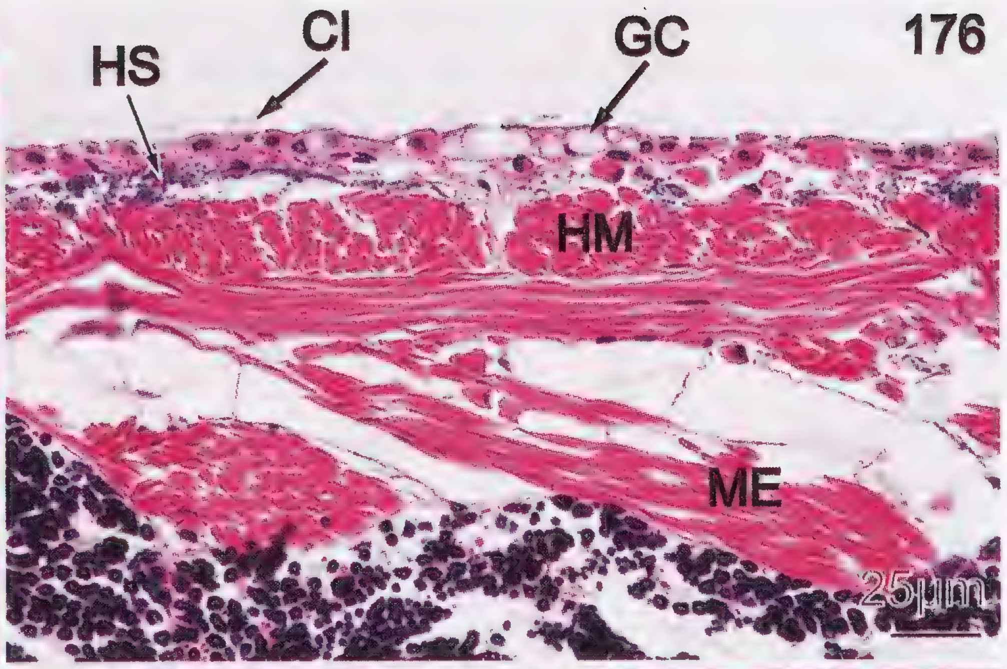
176
HS
CI
GC
HM
ME
25µm

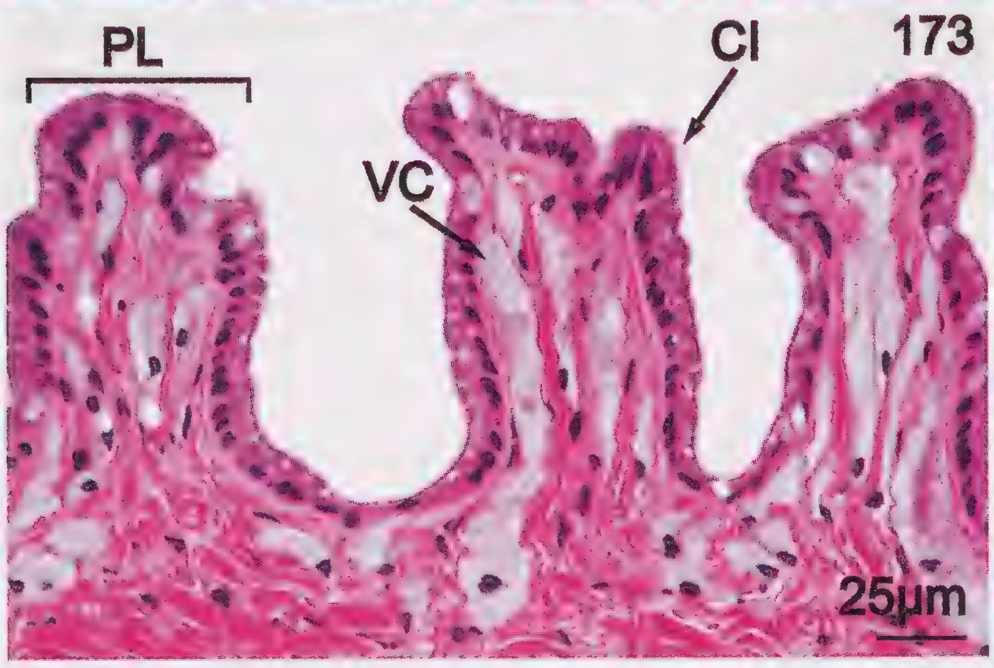
173
PL
CI
VC
25µm

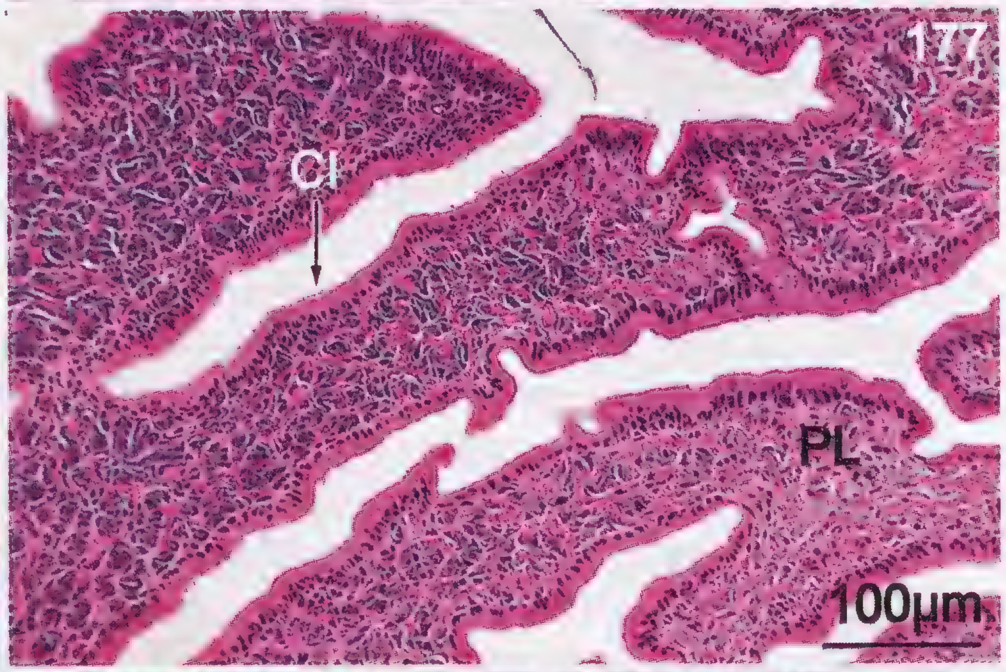
177
CI
PL
100µm

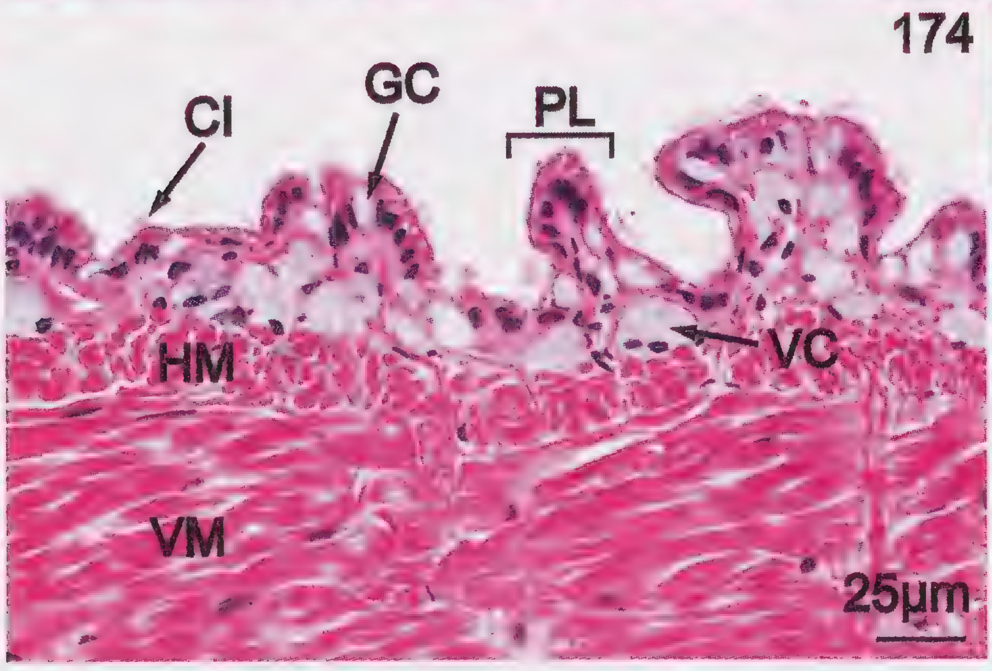
174
CI
GC
PL
HM
VC
VM
25µm

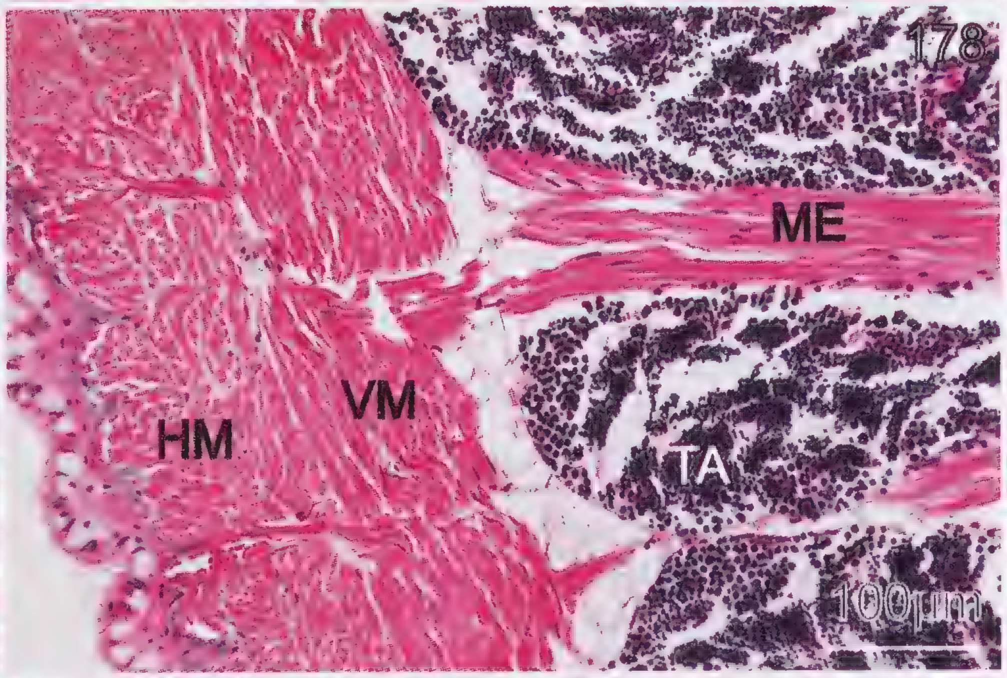
178
ME
HM
VM
TA
100µm

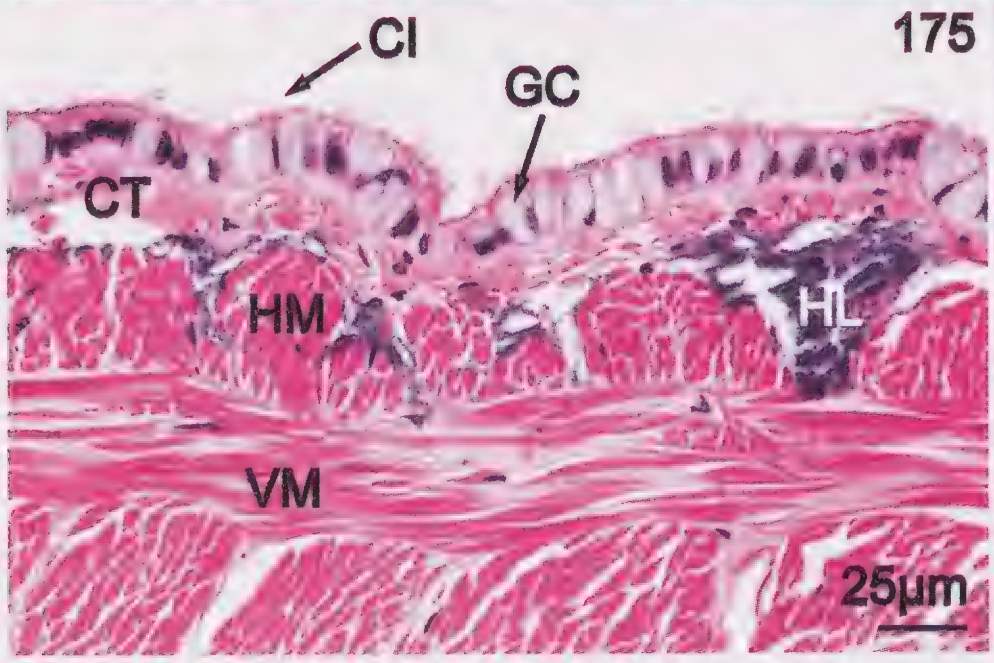
175
CI
GC
CT
HM
HL
VM
25µm

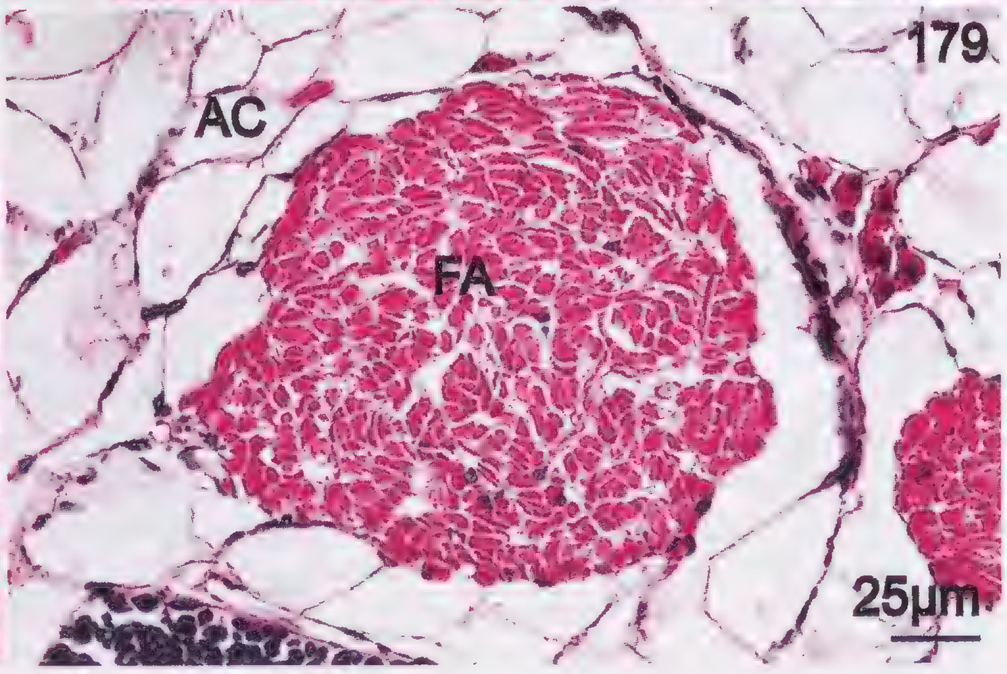
179
AC
FA
25µm

Crystalline Style Sac: The crystalline style sac begins as a ventral outpouching of the stomach. The style sac consists of a large spherical chamber or style sac and a horizontal stem canal or midgut (Fig. 205). The crystalline style is an eosinophilic rod within the style sac extending anterior to posterior throughout the length of the style sac. Style sac epithelium consists of three types of ciliated columnar cells, herein referred to as types one, two and three. Type one epithelium lines the majority of the style sac and is represented by dark-staining, eosinophilic columnar cells with straight cilia (Fig. 206). Type one columnar cells are brightly eosinophilic with a basally located nucleus and a distinct apical cell membrane. The midgut contains the second type of columnar epithelium. Type-two cells range in size from tall columnar cells along the dorsal and ventral surfaces to shorter columnar cells along the lateral aspect. Type two cells differ from type one epithelium because the cytoplasm has a pale staining characteristic and the cilia are wispy (Fig. 207). Type three epithelium is restricted to a small region of the ventral style sac wall representing a junction between epithelium type one and type two epithelium of the stem canal. Type three epithelium is pseudostratified consisting of thin, basophilic, ciliated columnar cells (Fig. 208). Crystalline style consists of a dense eosinophilic material that tends to form wrinkles during microtomy. The style appears to be layered with concentric, dark, granular lines. The central layers may contain small particulates and appear broken, with an irregular space surrounding such particulate matter (Fig. 209).

Intestine: The crystalline style sac extends posteriorly through the visceral mass, bends dorsally and represents the first intestinal limb. The walls of the first intestinal limb are pleated and deeply sinuous (Fig. 210). Subepithelium of first intestinal limb consists of a well-defined lamina propria supporting the plicae and becomes thinner around the straightened portions of the intestinal walls. Intestinal epithelium alternates between style sac epithelium types one, two and three and creates a heterogeneous luminal surface (Fig. 211).

Ventral to the crystalline style sac are a pair of elliptical ducts, which constitute the second and third intestinal limbs. In contrast to the sinuous epithelium comprising first intestinal limb, the second limb lacks deep epithelial folds (Figs. 212, 213). The ascending second intestinal limb consists of ciliated columnar cells with eosinophilic, granular vesicles. Cilia are thin and filamentous, similar to cilia of style sac type-three epithelium (Fig. 213). Transverse sections of second intestine reveal a generally flattened luminal surface, while sagittal sections portray the intestine as a tube with bends characterized by a small inclination. High magnification shows the intestinal epithelium has two types of columnar

---

←

FIGS. 172–179. Pedal integument, and mesentery of *Fusconaia cerina*. FIG. 172: Transverse section of pedal integument type 1, emphasizing rectangular plicae (PL), dense cilia (CI), and a large swath of violet cells (VC); FIG. 173: Transverse section of pedal integument type 2 characterized by thinner plicae (PL) with isolated patches of cilia (CI) and pale-staining violet cells (VC); FIG. 174: Transverse section of pedal integument type 3, displaying reduced, teardrop-shaped plicae (PL), cilia (CI), goblet cells (GC), violet cells (VC), horiztonal musculature (HM), and vertical musculature (VM); FIG. 175: Transverse section of pedal integument type 4, characterized by a flattened epithelium consisting of ciliated columnar cells (CI) and goblet cells (GC) overlying a subepithelium consisting of connective tissue (CT), hemolymph (HL), horitzontal muscle (HM) and vertical muscle (VM); FIG. 176: Transverse section of pedal integument type 5, featuring a flattened epithelium consisting of cilia (CI), goblet cells (GC), underlying hemolymph sinus (HS), horizontal musculature (HM), and mesentery (ME); FIG. 177: Sagittal section of pedal integument at the posterior margin of the foot, emphasizing cilia (CI) and plicae (PL); FIG. 178: Transverse section of the dorso-lateral aspect of the coelom illustrating testicular acini (TA), chords of mesentery (ME) spanning the coelomic cavity with linkage to the lateral vertical muscle (VM), and horizontal muscle (HM) strata; FIG. 179: Sagittal section through the posterior visceral mass revealing a mesenteric fascicle (FA) encircled by adipocytes (AC).

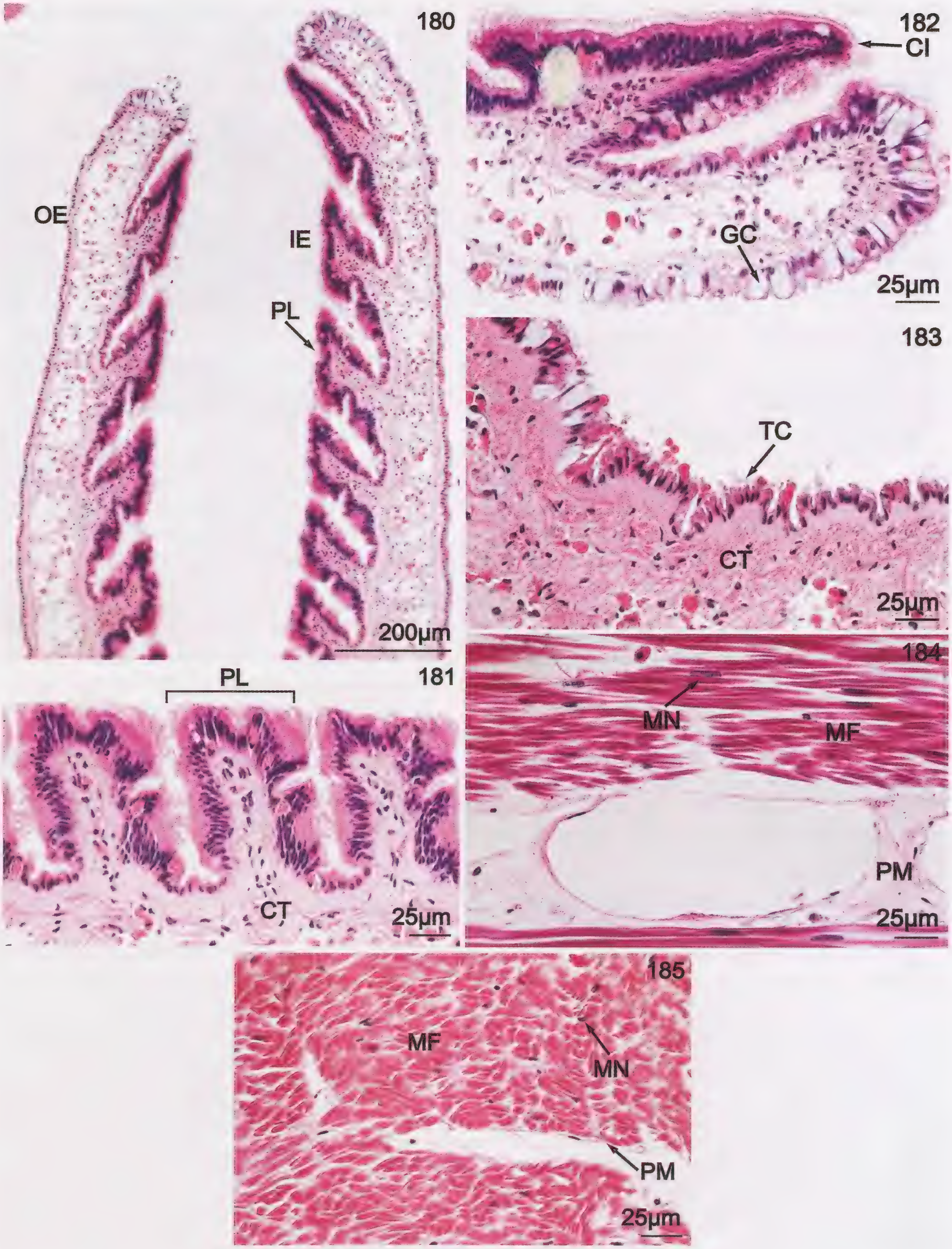

FIGS. 180–185. Labial palps, anterior pedal protractor, and anterior adductor of *Fusconaia cerina*. FIG. 180: Transverse section of labial palps revealing plicae (PL) along the inner epithelium (IE), and flattened outer epithelium (OE); FIG. 181: Transverse section of the inner palp epithelium featuring ciliated plicae (PL), and connective tissue fibers (CT) of the subepithelium; FIG. 182: Transverse section of distal palp margin showing cilia (CI) and goblet cells (GC); FIG. 183: Transverse section of outer epithelium emphasizing teardrop-shaped columnar cells (TC), and subepithelial connective tissue (CT); FIG. 184: Sagittal section of anterior adductor portraying myofibers (MF), myocyte nuclei (MN), and a pale eosinophilic perimysium (PM); FIG. 185: Transverse section of anterior pedal protractor illustrating densely packed myofibers (MF), scattered myocycte nuclei (MN) and perimysium (PM).

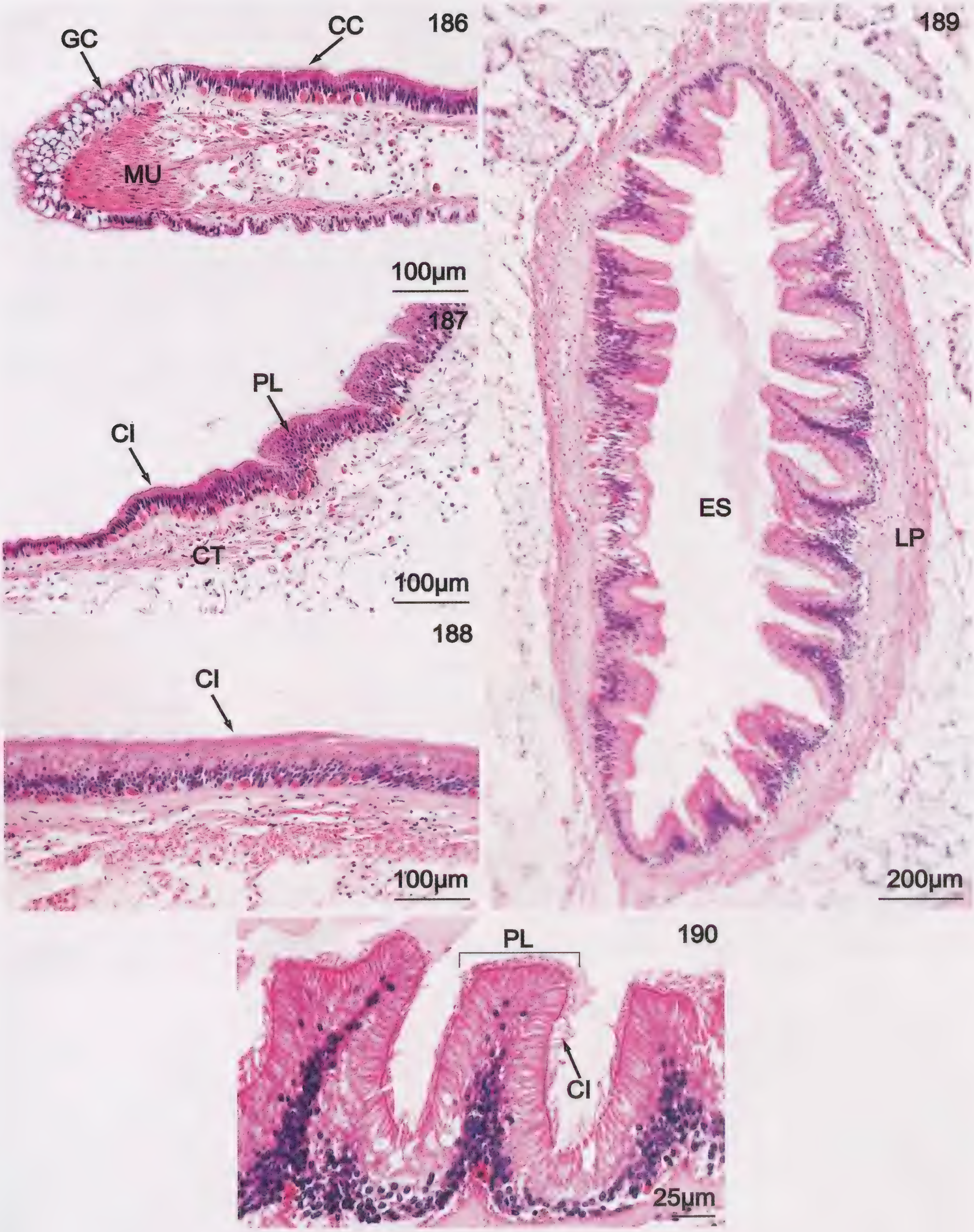

FIGS. 186–190. Oral groove, and esophagus of *Fusconaia cerina*. FIG. 186: Transverse section of the ventral portion of the oral groove featuring a muscular extension (MU) of ciliated columnar cells (CC), and goblet cells (GC); FIG. 187: Transverse section of ventral oral groove wall showing an extension of cilia (CI) along the surface of plicae (PL) and a subepithelium of connective tissue fibers (CT); FIG. 188: Transverse section of lateral oral groove epithelium emphasizing flattened columnar epithelial cells endowed with cilia (CI); FIG. 189: Transverse section of the dorsal aspect of anterior visceral mass portraying an ovoid esophagus (ES) with a distinct lamina propria (LP); FIG. 190: Transverse section of the esophagus revealing plicae (PL) and a densely ciliated epithelium (CI).

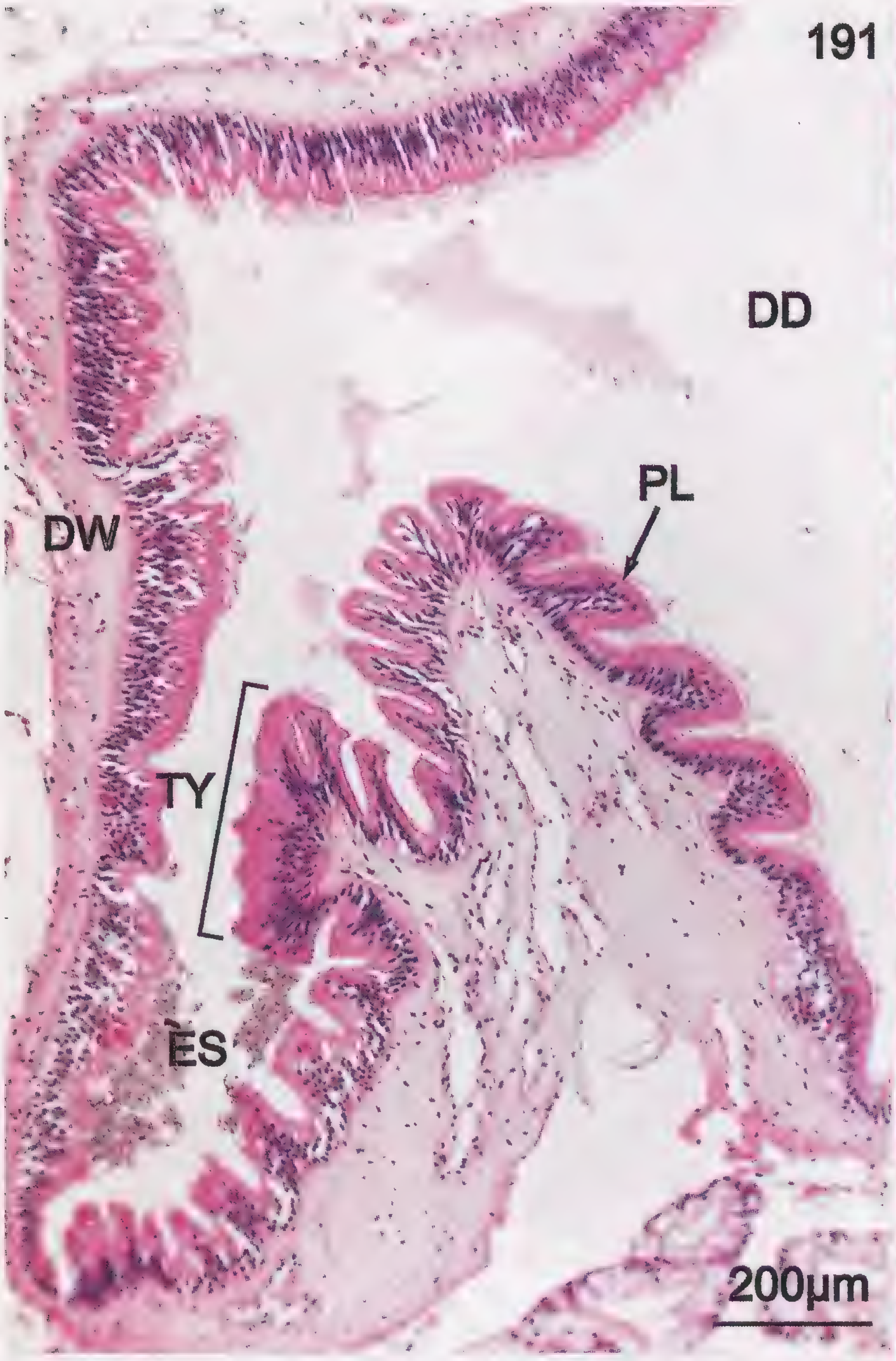
191
DD
DW
PL
TY
ES
200µm

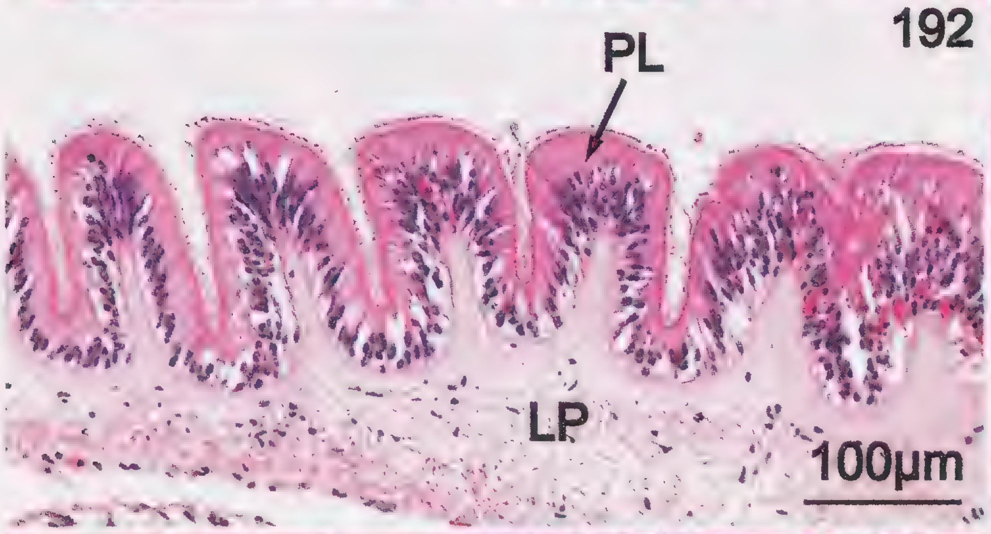
192
PL
LP
100µm

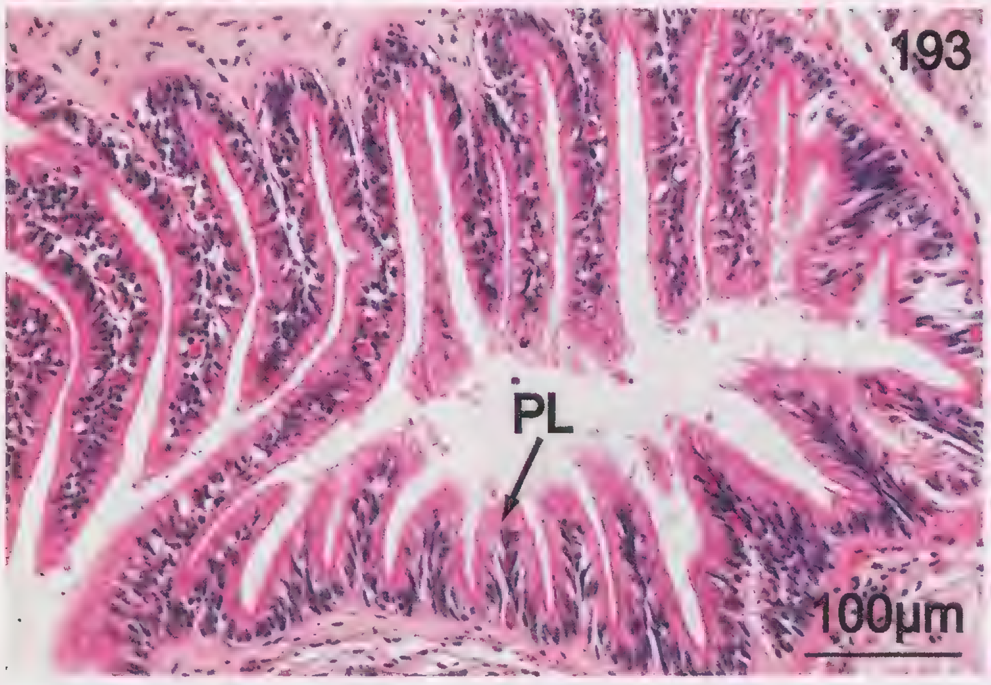
193
PL
100µm

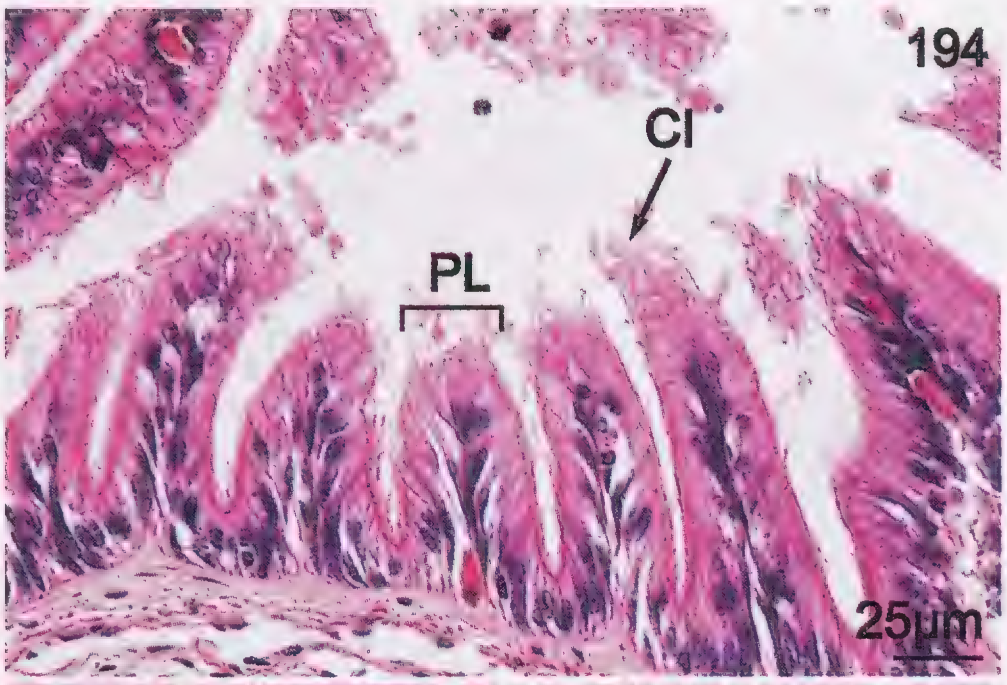
194
CI
PL
25µm

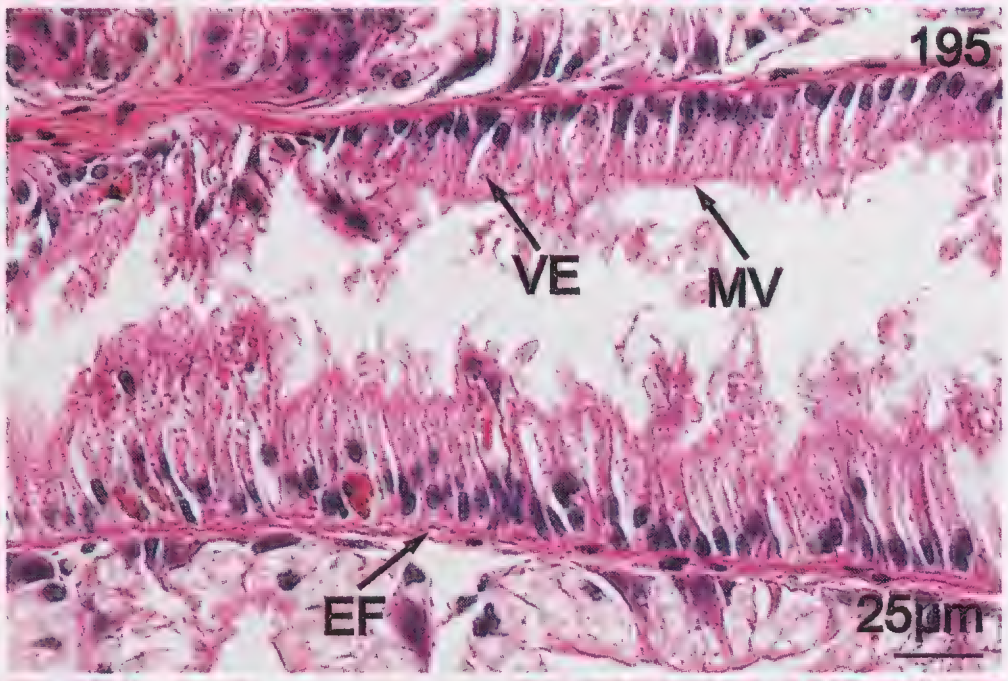
195
VE
MV
EF
25µm

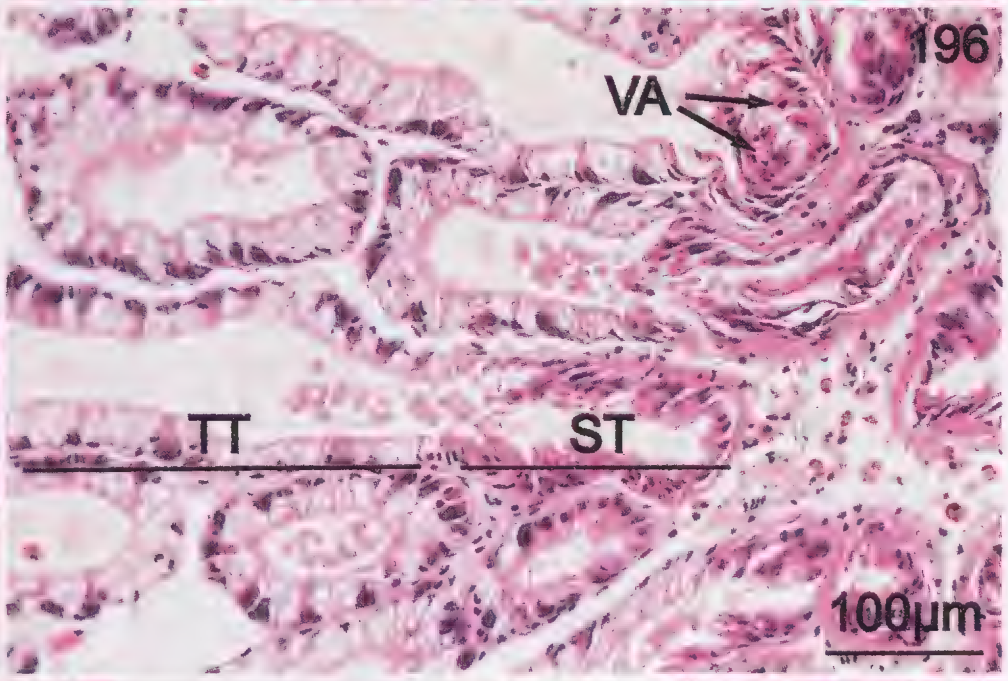
196
VA
TT
ST
100µm

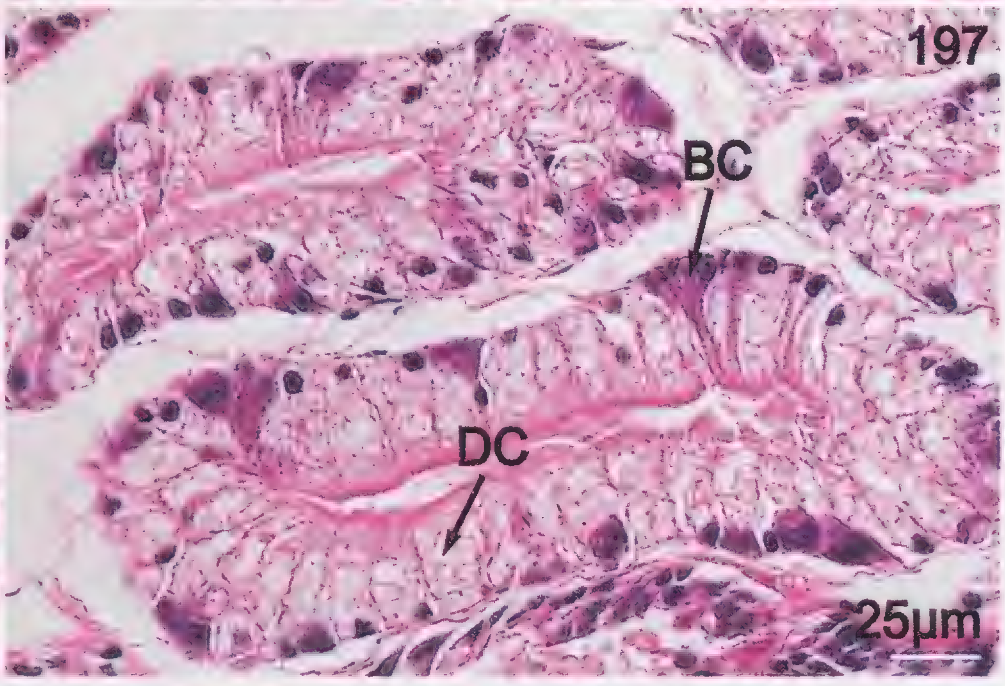
197
BC
DC
25µm

epithelium. There are ciliated columnar cells with eosinophilic intracellular granules, suggesting that these cells may have a secretory function (Fig. 214). The second columnar cell type has a homogenous eosinophilic cytoplasm that lacks intracellular granules (Fig. 215).

The fourth and fifth intestinal limbs are each characterized by a large typhlosole occupying a large proportion of the lumen. The typhlosole of the fourth intestinal limb extends ventrally into the lumen (Fig. 216). Ventral epithelium of the fourth intestinal limb is pleated around the lateral portion and smooth along the medial aspect. Epithelial cells of the ventral wall are ciliated and columnar with elliptical eosinophilic, granular inclusions (Fig. 217). Dorsal epithelium has a smooth surface, consisting of simple ciliated columnar cells (Fig. 218). Subepithelium of intestinal limb four is comprised of a distinct lamina propria containing a series of hemolymph sinuses. Lamina propria supporting dorsal epithelium is expansive, while marginal connective tissue of ventral epithelium is thin.

Fifth intestinal limb is analogous to intestinal limb four as the alimentary canal bends dorsally and continues along the hinge towards the posterior adductor. The typhlosole of the fifth intestinal limb projects dorsally from the visceral mass (Fig. 219). Ventral epithelium lining the typhlosole is pleated, with tall ciliated columnar cells (Fig. 220). Columnar cells of the dorsal epithelium are shorter than typhlosole cells. Dorsal epithelium is pleated around the lateral margins, but generally smooth in the median (Fig. 221). Unlike the fourth intestinal limb, dorsal epithelium lacks elliptical eosinophilic inclusions.

Cellular Structure of Cardiovascular System Tissues

Heart: The most prominent feature of the heart is the thickened, muscular ventricle surrounding the intestine (Fig. 222). The ventricle consists of an epicardium, and a thickened myocardium of irregular muscle fibers. Epicardial surface is sinuous with teardrop-shaped cells, some of which have a transparent apical vesicle (Fig. 223). Epicardium and myocardium feature red-staining hemocytes between epithelial cells of the epicardium and juxtaposed among myofibers. Cardiac myocytes are spindle-shaped, and form rectangular bands of musculature generally oriented anterior to posterior or dorsal to ventral (Fig. 224).

Auricles are thin-walled, tubular structures uniting the pericardial wall with the ventricle. Auricles are composed of an outer squamous epithelium, and inner myocardial fibers (Fig. 225). Each auricle has a ventral and a dorsal branch and the auricular branches may be closely apposed to the squamous pericardium. The heart has a pair of auriculoventricular valves, and each set of valves is located along the lateral margin of the ventricle at the auricular junction. Therefore, hemolymph flow is regulated as it travels from the auricles to the ventricle. Valves consist of an outer squamous epithelium covering the dark-staining myocardial and pale-staining connective tissue fibers (Fig. 226).

Arteries, Veins, Capillaries and Pericardial Gland: Throughout the body there are a series of hemolymph vessels resembling arteries, veins and capillaries based upon the overall

---

←

FIGS. 191–197. Digestive diverticulum of *Fusconaia cerina*. FIG. 191: Transverse section of the junction of esophagus (ES) and digestive diverticulum (DD) showing the position of plicae (PL) in relation to the typhlosole (TY) and the non-plicated dorsal wall (DW); FIG. 192: Transverse section of digestive diverticulum, ciliated plicae (PL) with a distinct lamina propria (LP); FIG. 193: Transverse section of digestive diverticulum portraying the deeply infolding plicae (PL) of a primary tubule; FIG. 194: Transverse section of a primary digestive diverticulum tubule illustrating cilia (CI) extending from conical plicae (PL); FIG. 195: Transverse section of secondary digestive diverticulum tubule emphasizing vesiculated epithelium (VE), apical microvilli (MV), and a thin subepithelium of eosinophilic connective tissue fibers (EF); FIG. 196: Transverse section of digestive diverticulum showing the valve-like (VA) appearance of the secondary tubules (ST) as they unite with tertiary tubules (TT); FIG. 197: Transverse section of tertiary digestive diverticulum tubules emphasizing the characteristic basophil cells (BC) and vesiculated digestive cells (DC).

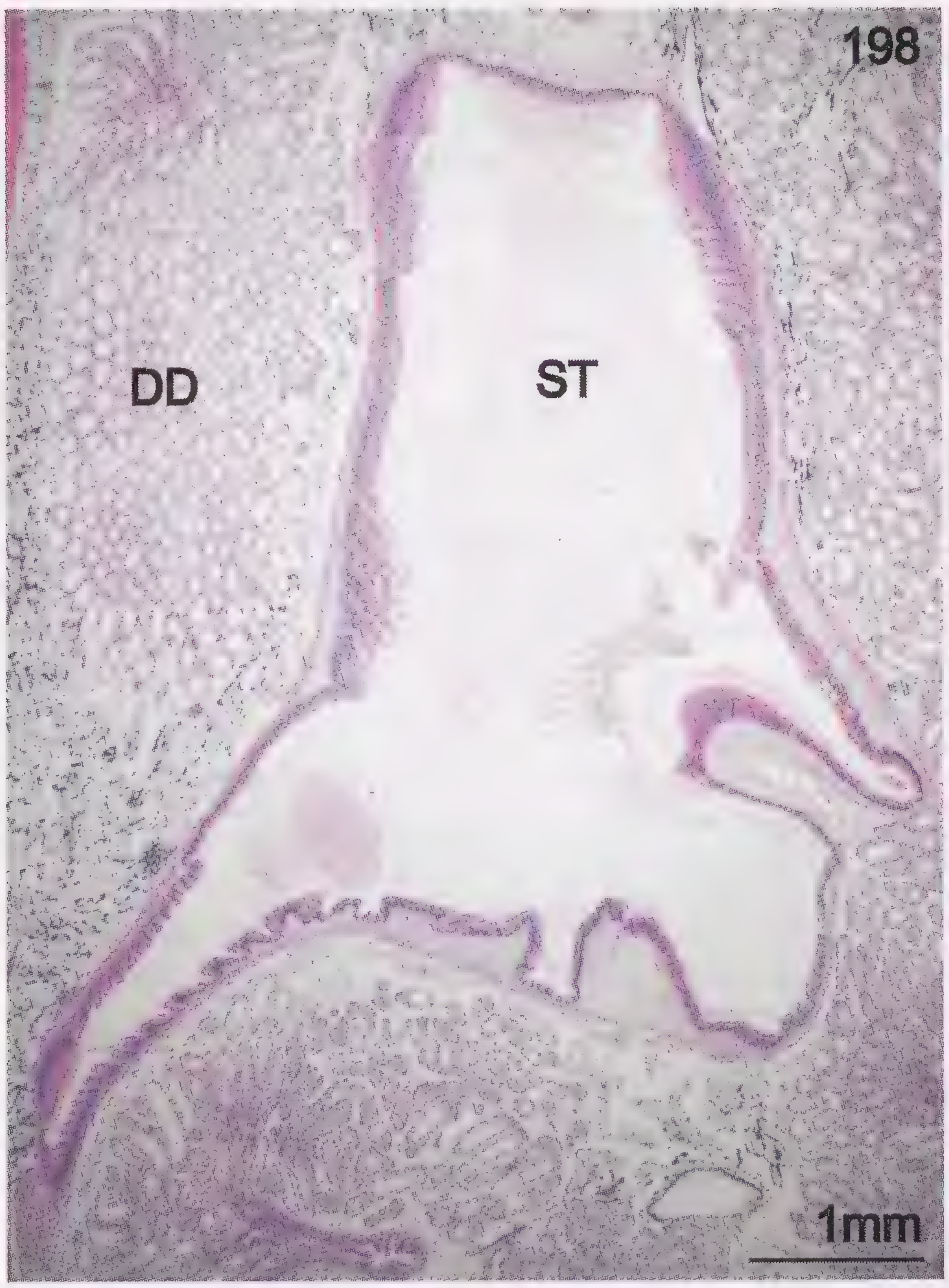
198

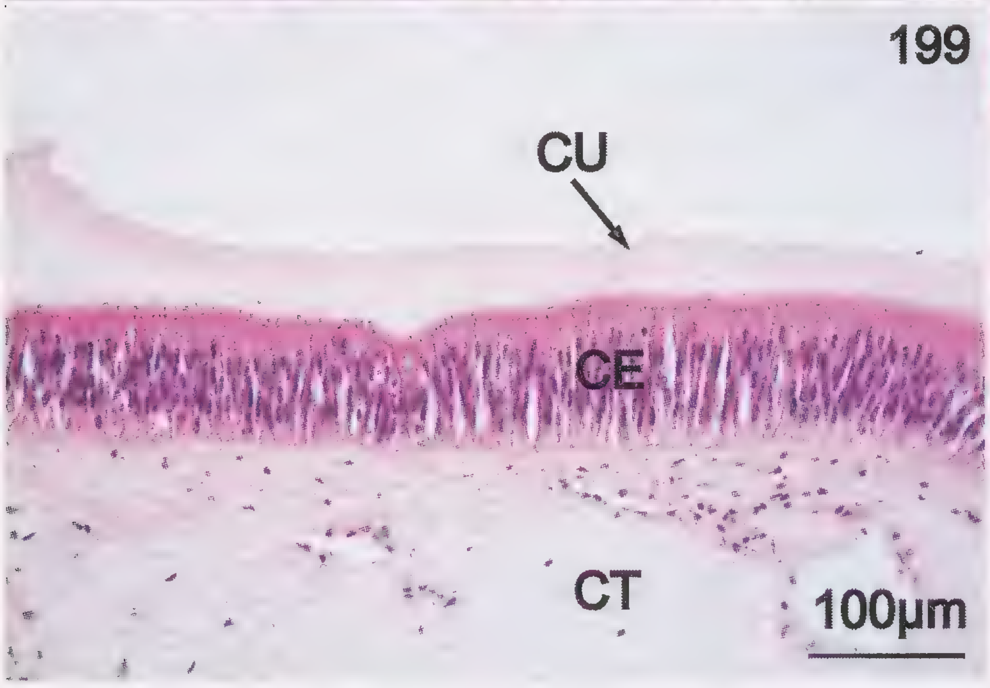
199

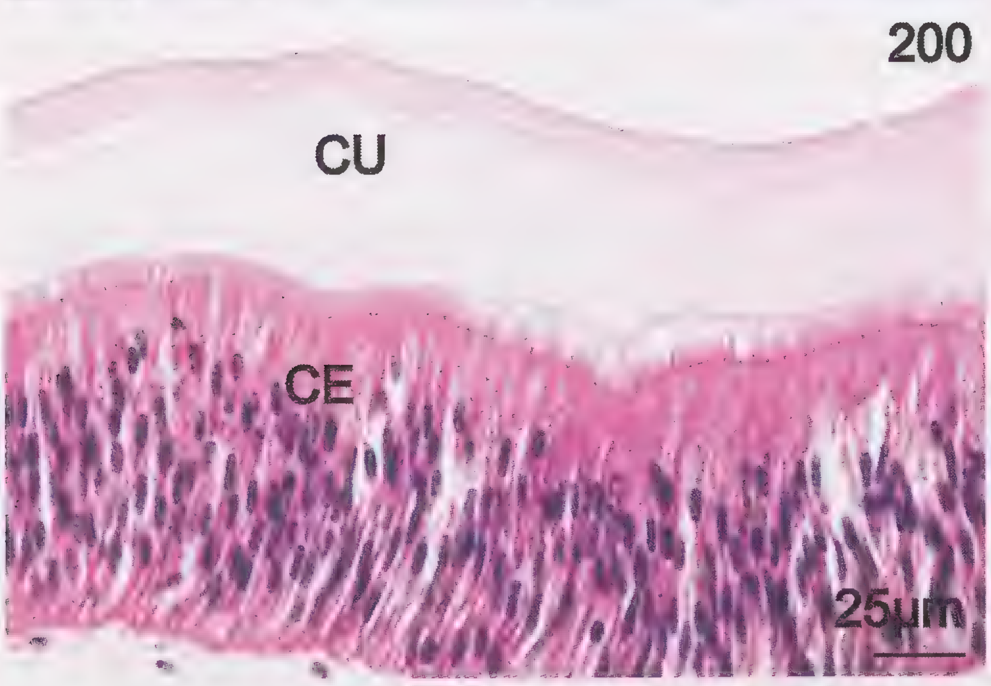
200

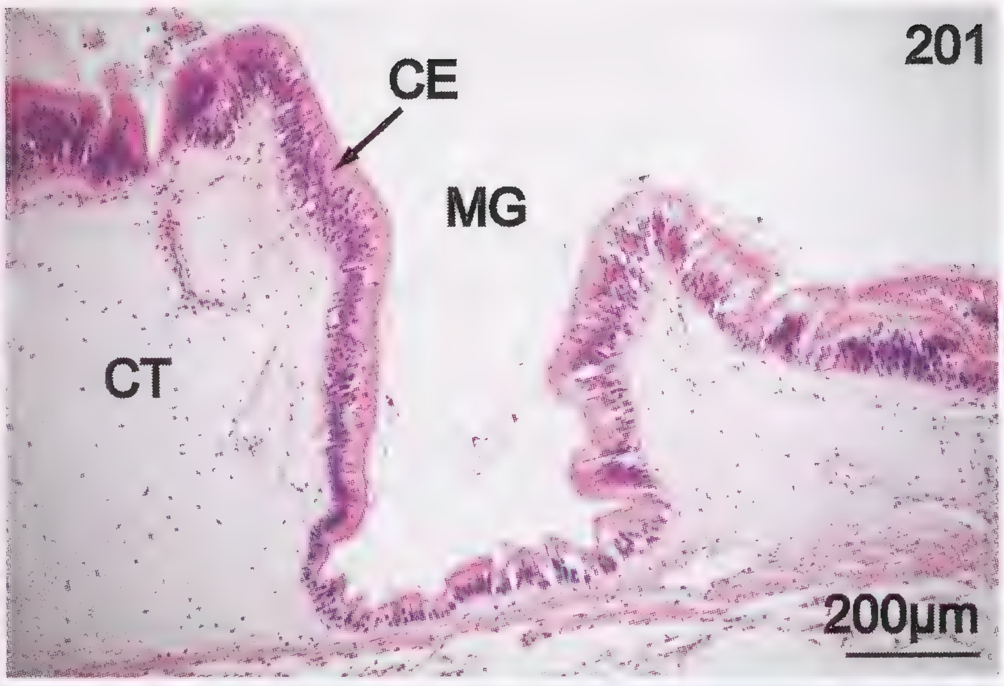
201

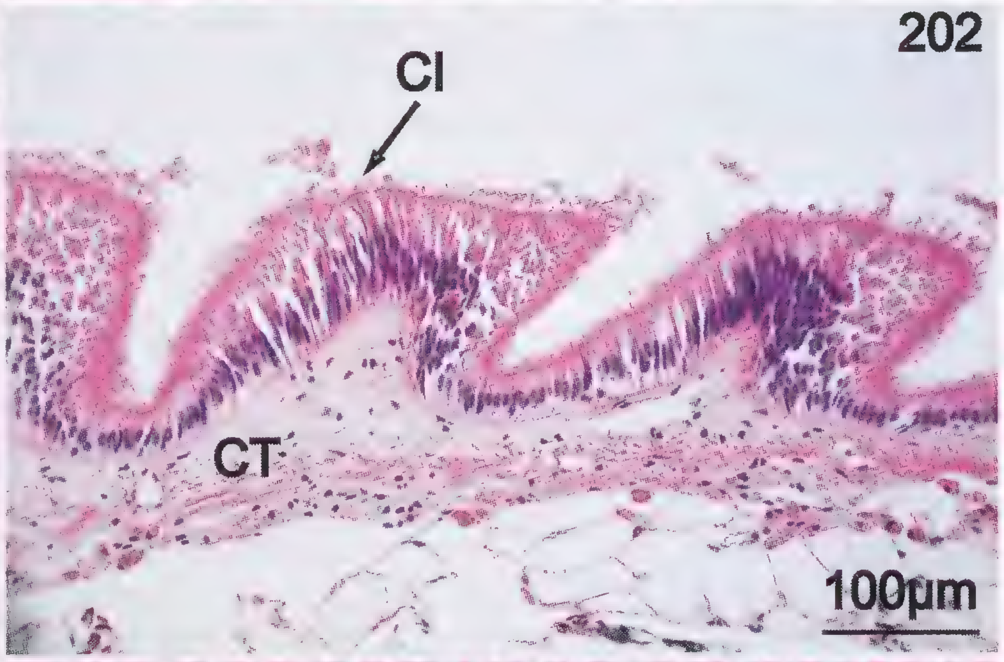
202

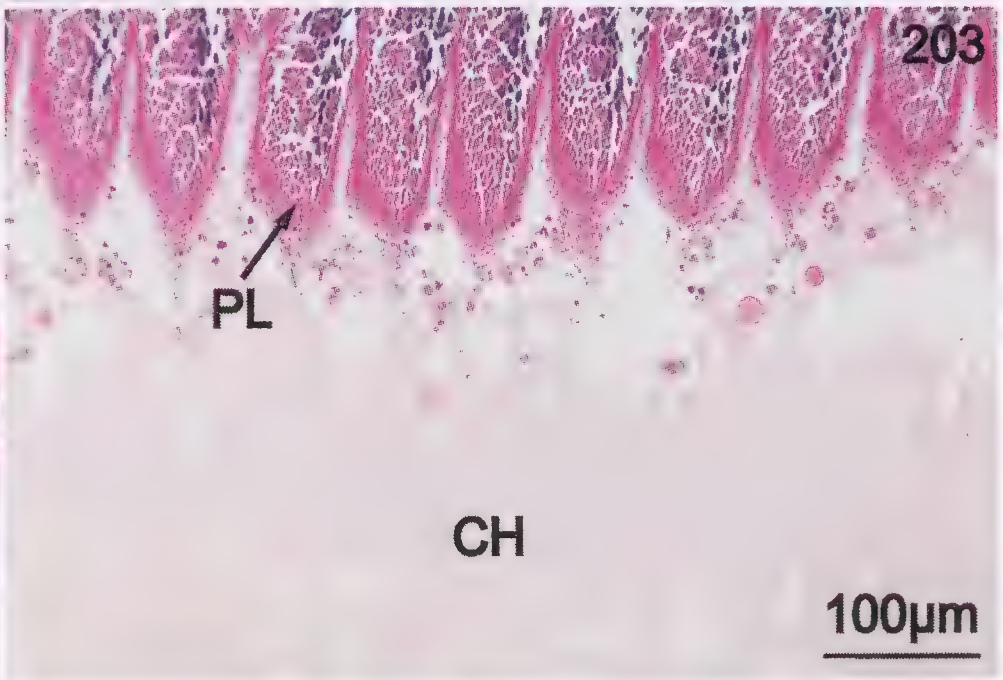
203

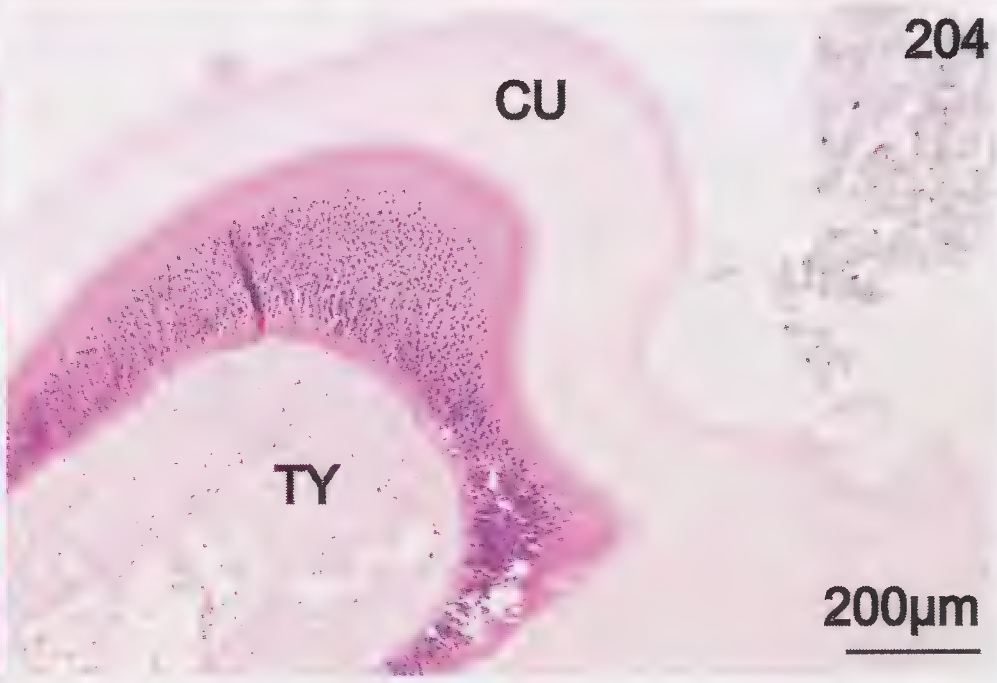
204

size of the tissue and its cellular constituents. Possible arteries consist of several layers of muscle encircling emarginated nuclei of endothelium. A good example of a potential artery is the medial hemolymph vessel located at the ventral margin of the hemocoel where it may regulate pedal circulation (Fig. 227). The muscular walls have a pale, eosinophilic ground substance with darker, red fibers interspersed throughout the arterial wall. Arteries and veins may be similar in size, but possible veins consist of a lesser-developed muscular wall encircling an endothelium (Fig. 228). Such vessels are abundant within the coelom, especially between the digestive diverticulum and gonad. Capillaries are small circular to ovular tubes consisting of endothelial cells surrounded by a delicate, loose connective tissue matrix. Capillaries are best observed within the perimysium of the adductors, pedal protractor, pedal retractors and mantle edge (Fig. 229). The pericardial gland is a large latticework of adipocyte-like cells surrounding the pericardial cavity. Hemocytes are typically present within the lumen and there are emarginated hemocytes that appear to be attached to the lumen or incorporated within a narrow space between emarginated pericardial gland cells (Fig. 230).

Cellular Structure of Renal System Tissues

Anterior Nephridium: Nephridium is located dorsally to ctenidia and visceral mass. Nephridium has a ventral, convoluted limb, while the dorsal limb has fewer epithelial folds extending into the lumen (Fig. 231). Anteriorly, ventral nephridium features numerous convoluted plicae restricting the lumen to a series of irregular, narrow spaces. Columnar cells of ventral epithelium have a vesiculated, eosinophilic cytoplasm. Ventral nephridial cells have a pale cytoplasm, but plicae appear mottled at a low magnification since wandering hemocytes are scattered throughout the plicated epithelium (Fig. 232). Hemocytes are distinguished from epithelial cells by a red-staining cytoplasm and a spherical nucleus. Subepithelium of nephridial plicae consists of connective tissue, endothelial cells and hemolymph. Plicae of the dorsal nephridium are more sparsely distributed and may be distinguished from ventral plicae in having a convoluted surface, whereas ventral nephridial plicae are smoother. Epithelium of dorsal plicae may be distinguished from ventral epithelium in having brown intracellular granules (Fig. 233). A characteristic feature of dorsal nephridium is the presence of teardrop-shaped columnar cells with a transparent apical vesicle. Teardrop cells are distributed along the lateral and dorsal surfaces of dorsal nephridium and contain brown intracellular granules (Fig. 234).

Anterior nephridium with its extensively folded luminal branches is located anterior to the heart and pericardium. Pericardium unites with the ventral nephridial limb at the anterior-posterior midpoint of the visceral mass. The most distinguishing feature of the anterior nephridium is the presence of the renopericardial canal and urethra (Figs. 235–237). The renopericardial canal is a pleated tubule derived from the pericardial cavity. The renopericardial canal is lined with narrow, rounded plicae containing ciliated columnar cells and elliptical goblet cells (Fig. 237). The renopericardial canal is adjacent to the urethra representing the excurrent aperture of the dorsal nephridium. Urethra

---

←

FIGS. 198–204. Stomach of *Fusconaia cerina*. FIG. 198: Transverse section through visceral mass showing the morphology of the stomach (ST) and surrounding digestive diverticulum (DD); FIG. 199: Transverse section of the dextral portion of the ventral stomach wall showing a cuticle (CU) attached to the columnar epithelium (CE) and the underlying connective tissue (CT) of the subepithelium; FIG. 200: Transverse section of the dextral portion of the ventral stomach wall revealing a layered cuticle (CU) along the surface of the columnar epithelium (CE); FIG. 201: Transverse section of the medial portion of the ventral stomach wall showing a columnar epithelium (CE), medial groove (MG), and underlying connective tissue (CT) of the subepithelium; FIG. 202: Transverse section of the sinistral portion of the ventral stomach wall revealing ciliated plicae (CI), and connective tissue (CT); FIG. 203: Transverse section of the dorsal stomach wall showing plicae (PL), and chyme (CH); FIG. 204: Transverse section of dextral stomach wall showing a rectangular and forked typhlosole (TY), with an attached cuticle (CU).

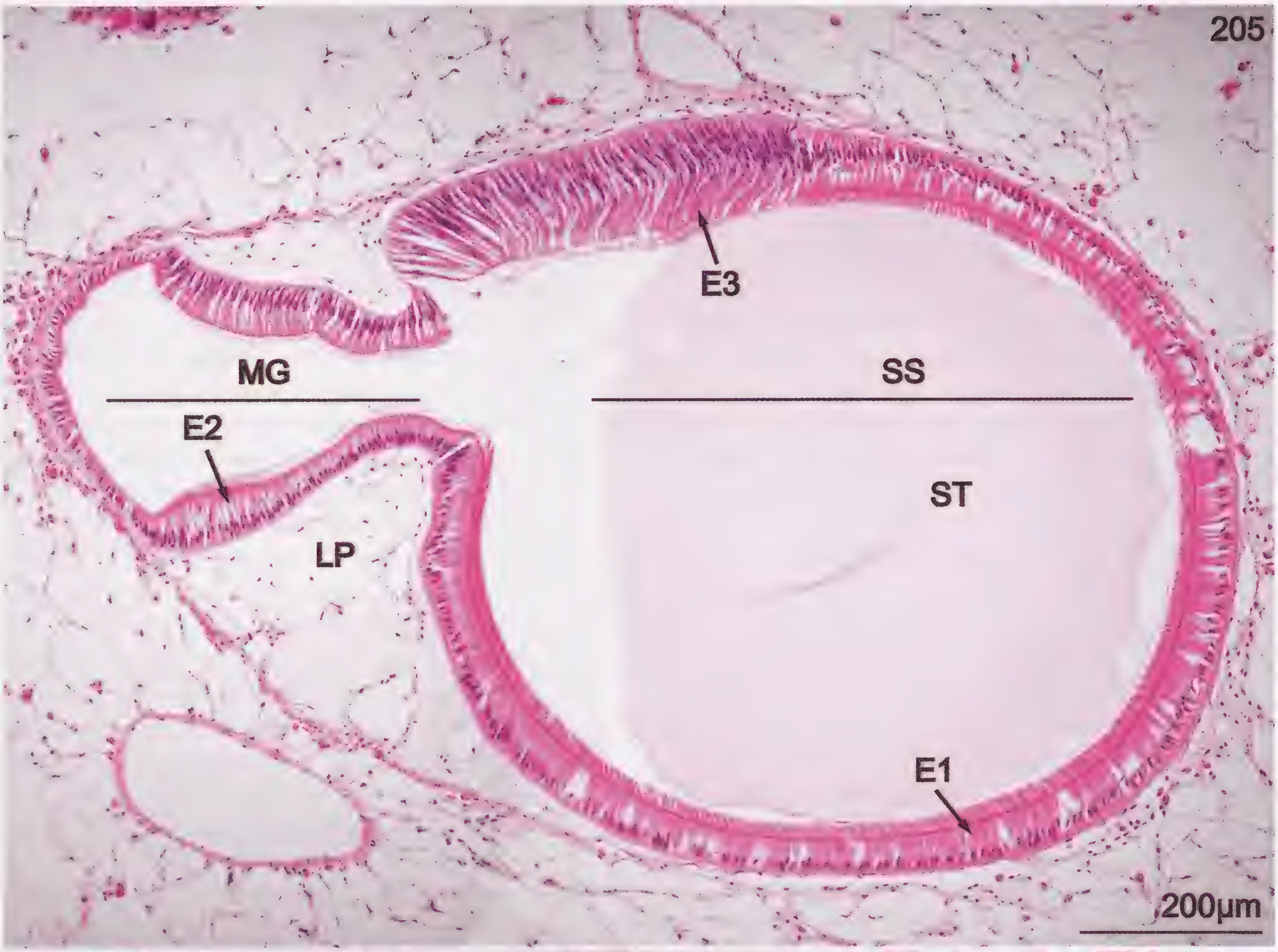
205

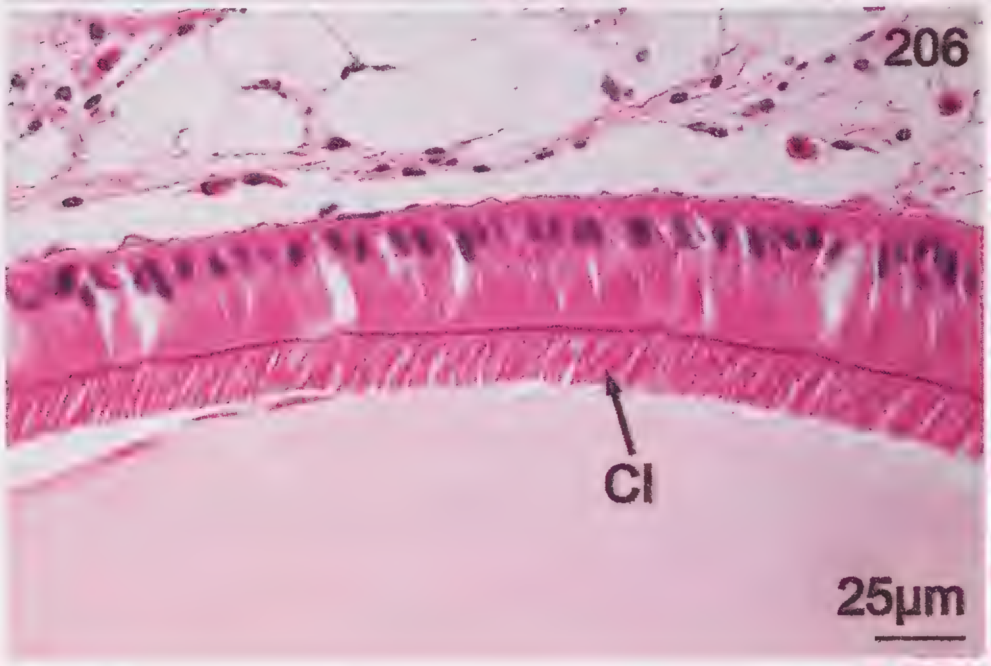
206

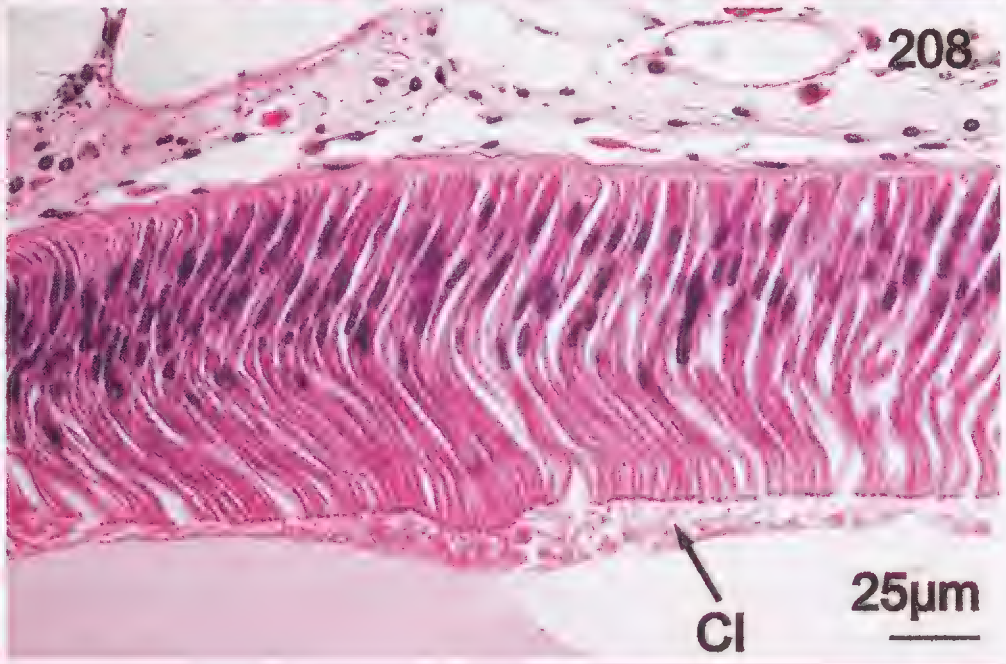
208

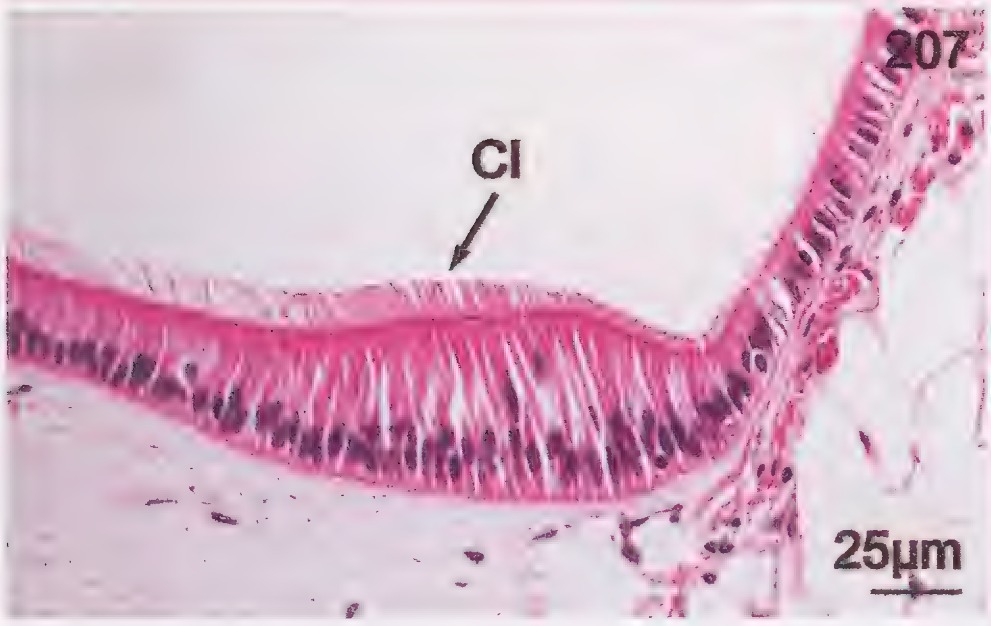
207

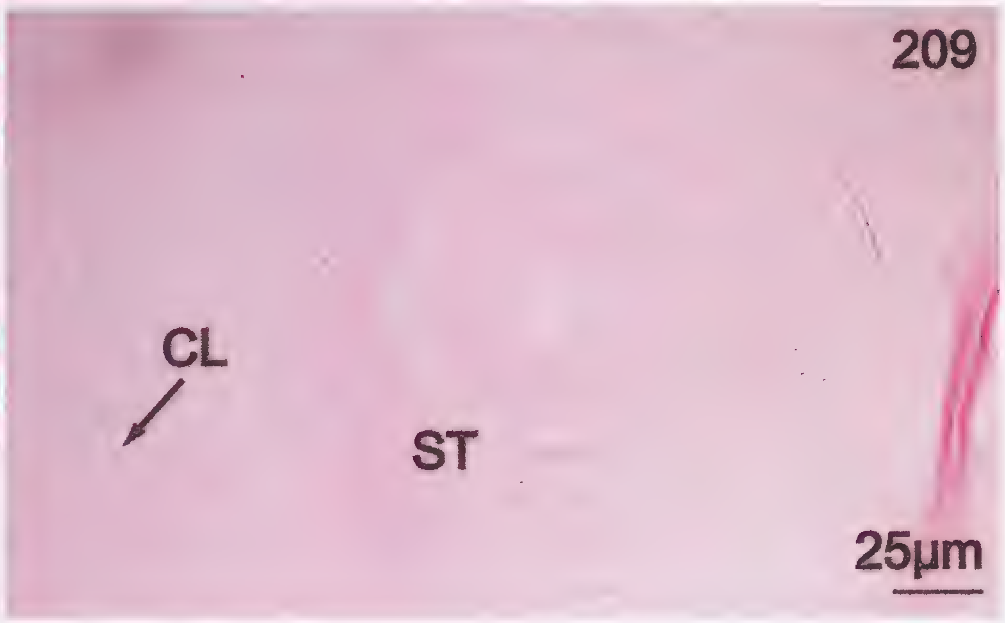
209

has a columnar epithelium with goblet cells lining the dorsal half of the tissue and a densely ciliated epithelium within the ventral half (Fig. 236). Goblet cells reappear along the ventral epithelium between the ctenidia and urethra. Some goblet cells in the urethra have eosinophilic contents.

Posterior Nephridium: Between the posterior terminus of the visceral mass and the posterior adductor, the nephridial branches become elongated and the lumen greatly expands (Fig. 238). Nephridial epithelium encircles the posterior pedal retractors, and nephridial branches resemble a series of stems and loops. Branches of posterior nephridium consist of columnar cells with pale, eosinophilic intracellular vesicles. The cell types of posterior nephridium appear morphologically similar to each other all around the organ. However, at high magnification, cells of the nephridial branches typically have an eosinophilic, wispy material at the apical surface (Fig. 239). Cells lining the walls of the posterior nephridium sometimes lack a wispy residue (Fig. 240). Additionally, the hemolymph vessels underlying columnar cells of epithelial branches are wider than in the anterior nephridium.

Posterior Adductor and Posterior Pedal Retractors: Posterior pedal retractors unite with the posterior margin of the visceral mass and extend ventrally into the foot. Transverse histological sections of the posterior region of *F. cerina* reveal groups of retractor fascicles with a distinct perimysium and endomysium (Fig. 241). Additionally there are thin, elliptical capillaries located between fascicles. Posterior adductor, as seen in a sagittal plane, consists of filamentous myofibers with an elliptical nucleus and a distinct nucleolus (Fig. 242). Myofilaments overlap and at high magnification and striations are not evident.

Cellular Structure of Nervous System Tissues

Pedal Ganglion, Cerebral Ganglia and Visceral Ganglion: The ganglia of *Fusconaia cerina* have similar cytological characteristics, and the description of the pedal ganglion is representative of the anterior and posterior ganglia. Pedal ganglion of *F. cerina* consists of a pair of vertically ovular lobes. Each lobe has a distinct outer cortex containing neuron cell bodies with axons extending into the inner medulla. Pedal ganglion has a distinct epineurium, dorsal and ventral fissures, with commissures uniting the two lobes (Fig. 243). Neuron cell bodies are polygonal, with a basophilic cytoplasm and a spherical, heterochromatic nucleus. Neurons have a homogenous cytoplasm and brown intracellular inclusions. Additionally, epineurium fibers appear granular and the tissue has a distinct filamentous appearance (Fig. 244). Axons are darkened and well defined as they extend from the neuron cell body into the medulla. Nerve fibers of pedal ganglion of *F. cerina* are distinctively filamentous (Figs. 245, 246). Glial cells of the medulla have a darkened, homogenous nucleus with a minimal amount of cytoplasm. Ganglionic roots are large bundles of axons extending dorsolaterally and ventral-laterally from each ganglionic lobe (Fig. 247).

Anterior ganglia are paired spherical masses located between the anterior adductor and labial palps (Fig. 248). The posterior ganglion is cylindrical, located anteriorly along the ventral surface of the adductor (Fig. 249). A horizontal band of connective tissue overlays the posterior ganglion and consists of fibrous tissue and hemolymph. Ventral to the hemolymph sinus is an apical layer of columnar cells and goblet cells (Fig. 250). The posterior ganglion extends into the base of the inner ctenidia and may appear as an ovular mass of nervous tissue at the base of the gill (Fig. 251).

←

FIGS. 205–209. Crystalline style sac of *Fusconaia cerina*. FIG. 205: Transverse section of the crystalline style sac showing the style sac (SS), style (ST), midgut (MG), style sac epitheium type 1 (E1), epithelium type 2 (E2), epithelium type 3 (E3), and underlying lamina propria (LP); FIG. 206: Transverse section of style sac showing the straightened cilia (Cl) of type one epithelium and the close proximity of cilia to the style (ST); FIG. 207: Transverse section of the midgut showing the slender cilia (Cl) of the columnar epithelium; FIG. 208: Transverse section of the style sac showing basophilic columnar cells of type-three epithelium and its apical cilia (Cl); FIG. 209: Transverse section of the crystalline style (ST) revealing darkened concentric layers (CL).

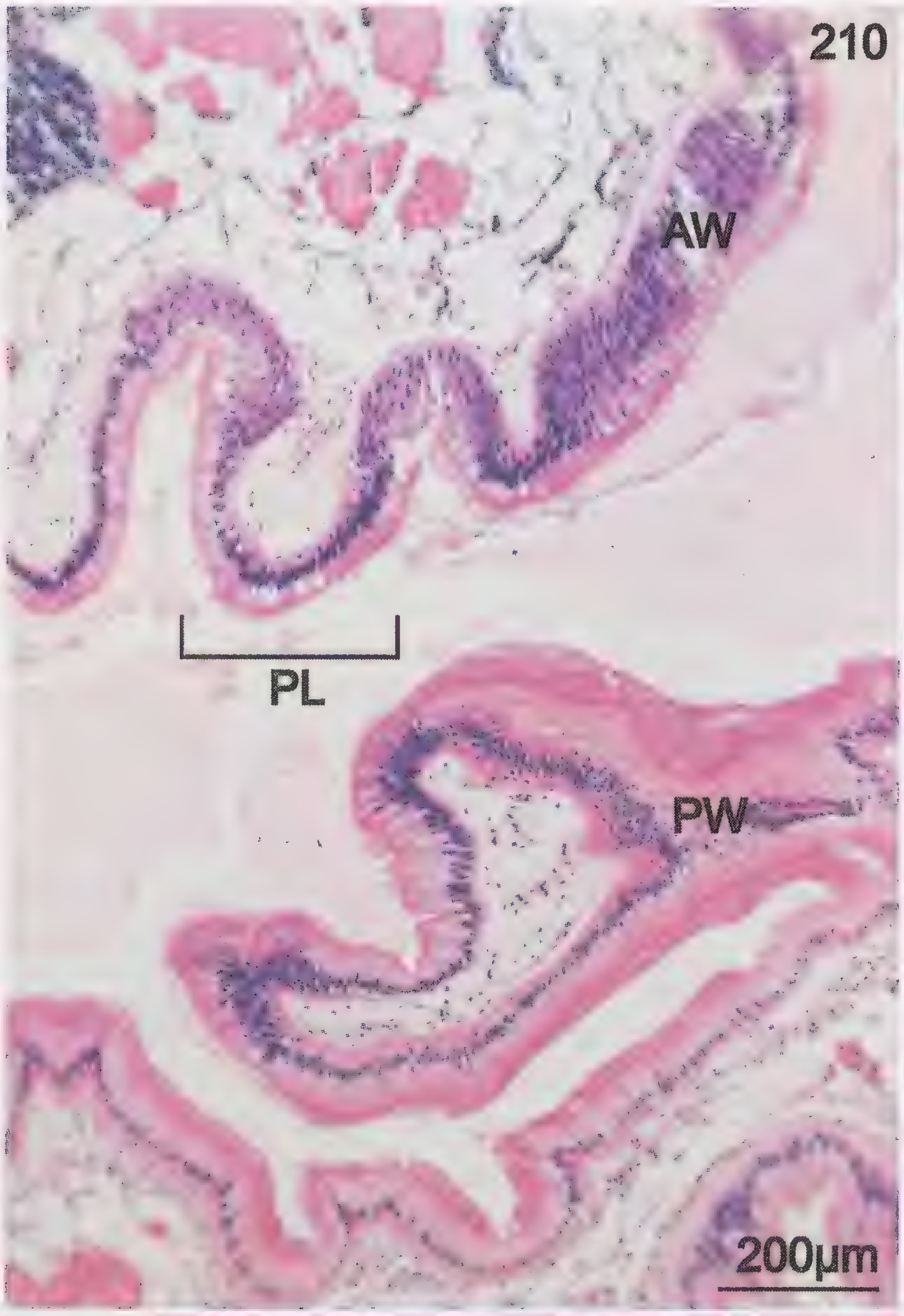
210

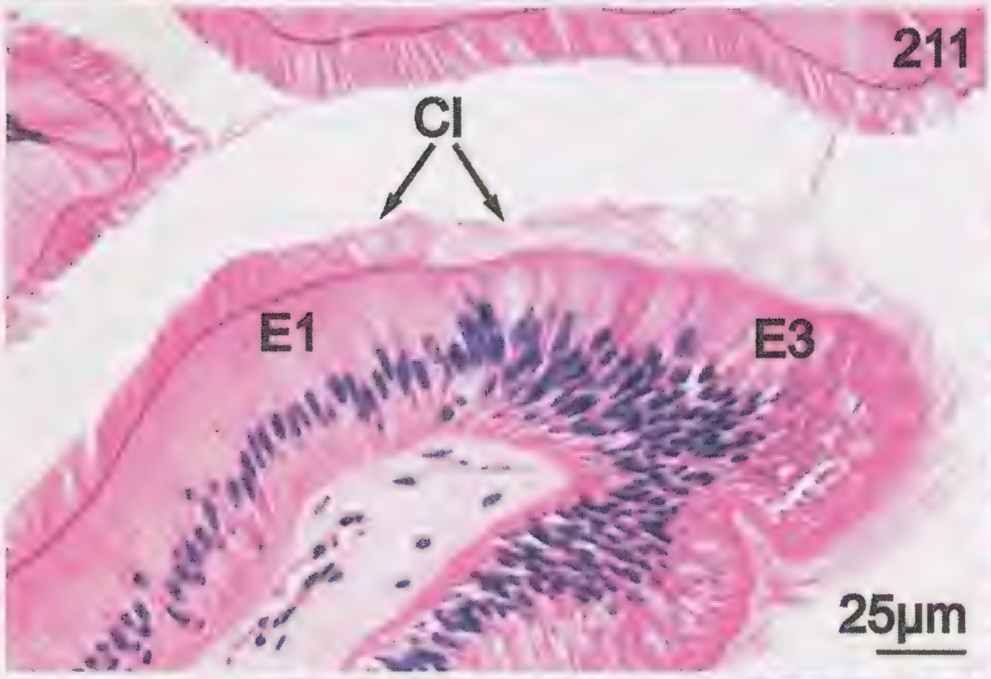
211

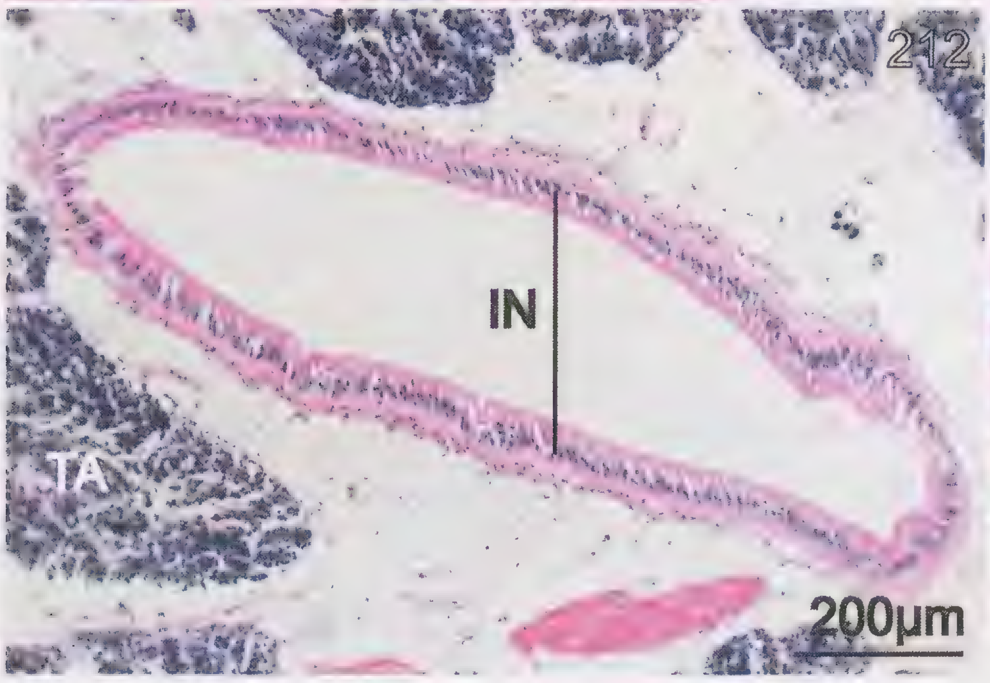
212

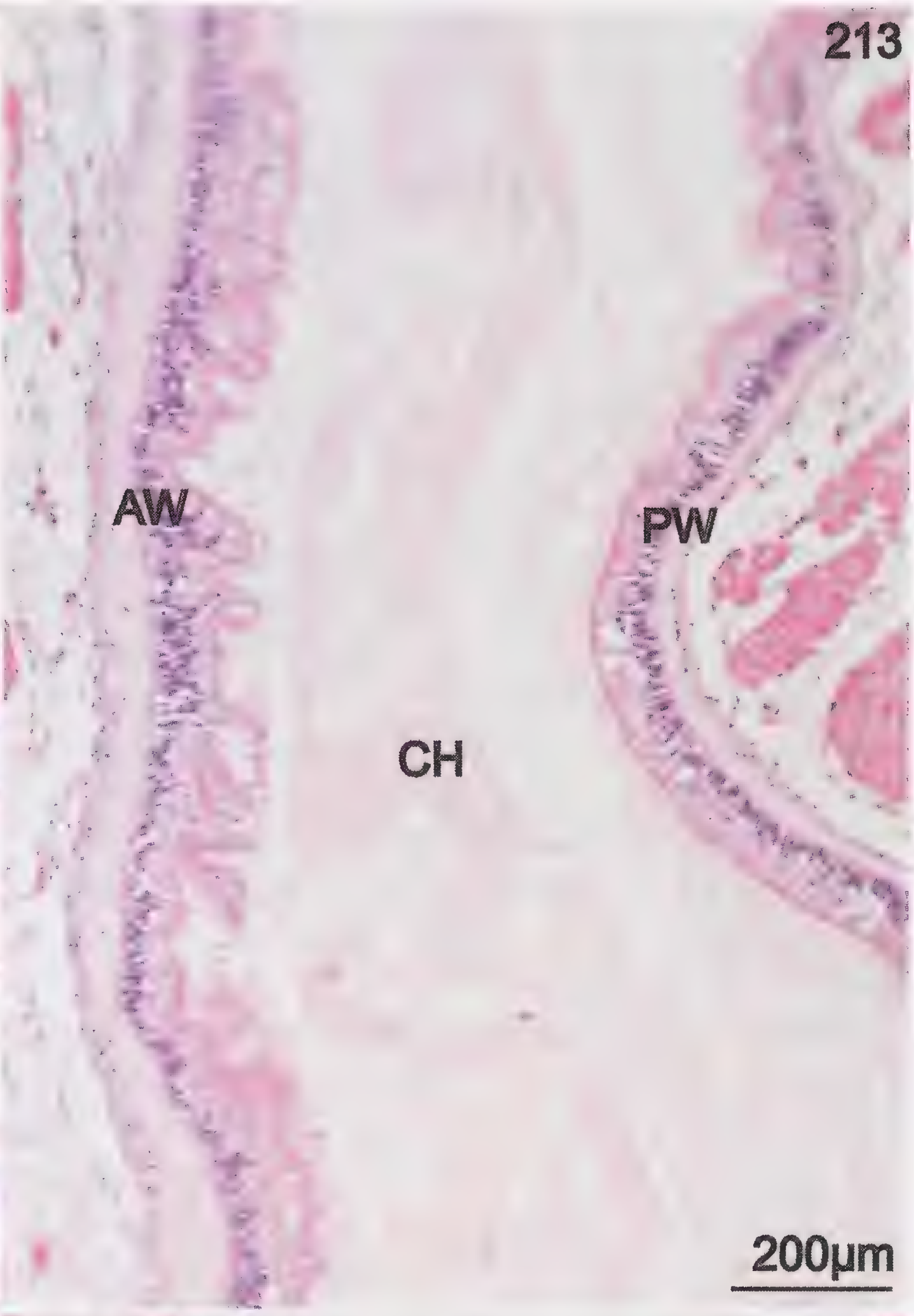
213

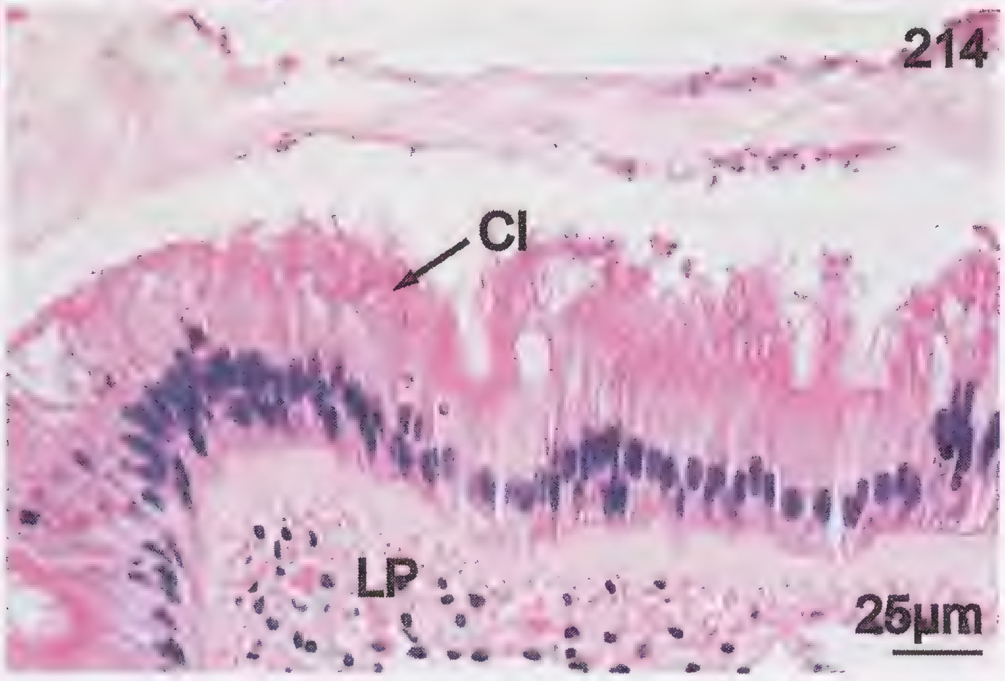
214

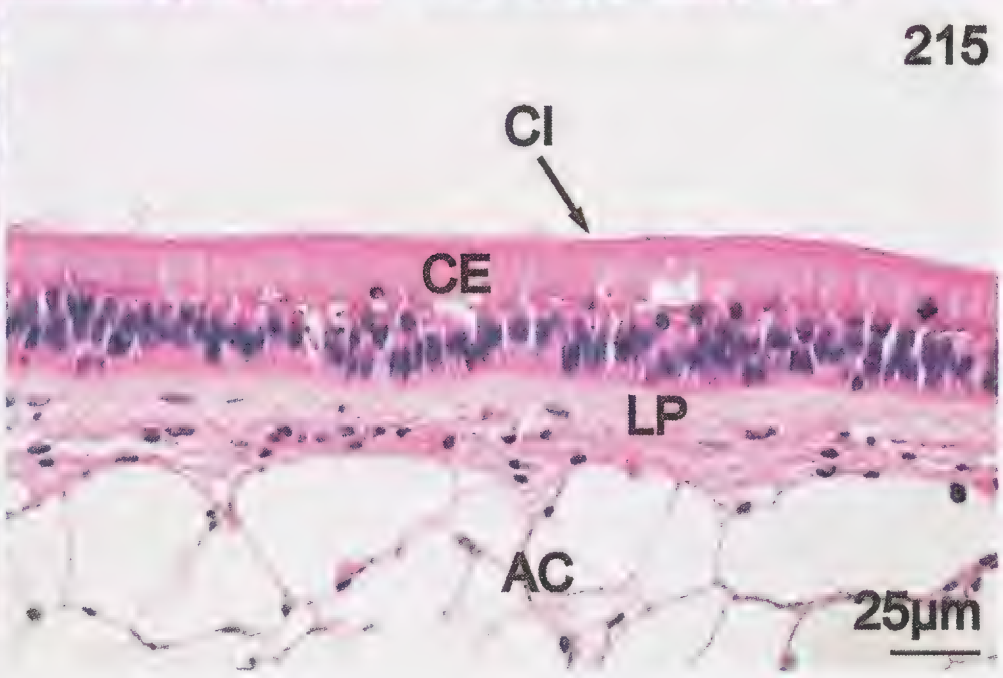
215

Nerves and Statocysts: Nerves are distributed throughout the visceral mass, foot, nephridium and mantle edge. Transverse sections of nerves reveal a thickened, eosinophilic epineurium encircling an irregular filamentous core of axons (Fig. 252). A sagittal view of a nerve illustrates how the tissue resembles a wavy band of filaments (Fig. 253). Additionally, there is a sinistral and dextral statocyst lateral to the pedal ganglion near the dorsal margin of the coelom. Statocysts appear stratified with ciliated columnar cells lining a spherical lumen (Fig. 254). Statocysts contain a spherical mass or statolith in the median of the lumen.

Cellular Structure of Reproductive System Tissues: Gonadal tissue consists of testicular and ovarian acini, ciliated gonadal ducts throughout the visceral mass, and a pair of ciliated gonadal pores located at the base of the visceral mass at the anterior end of the nephridium. Female and male *Fusconaia cerina* in the Cahaba River (Bibb, Shelby Co., Alabama) exhibit peak gametogenesis in May, and females may bear glochidia during June. Males and females collected in May 2011 exhibited peak gametogenesis, while considerably less gametogenesis was observed in individuals collected in August 2011. The luminal contents of stage 1 ovaries mainly consisted of an eosinophilic granular material with minimal input of oocytes (Fig. 255). Walls of stage 1 ovarian acini are lined with squamous cells with basophilic oocytes adhered to the luminal surface. Developing oocytes initially possess a violet cytoplasm and may appear to be attached to the acinus wall by a stem. Oocytes appear to grow and separate from the acinus wall. Separated oocytes have an irregular cell membrane, with a pale, basophilic margin. Immature oocytes feature a red, granular cytoplasm with a basophilic focus consisting of an irregular violet nuclear membrane and a spherical, black nucleolus (Fig. 256). Ovarian acini also produce a series of spherical, red, granular cells with a small basophilic nucleus. Given the small size and undifferentiated appearance, it is likely that the red cells are polar bodies. The lumen of stage 1 ovarian acini also appears to contain the remnants of polar bodies, considering the presence of an irregular, red, granular material and a series of nuclei lacking surrounding cytoplasm. Mature oocytes are enlarged and densely packed within the acinus (Fig. 257). Mature oocytes have a pale basophilic nucleus with a distinct nucleolus within a red, granular cytoplasm. Oocytes released from the acinus wall feature a pale, basophilic membrane surrounding the cell body. Developing oocytes are attached to the acinus wall via a basophilic stem.

Fusconaia cerina males predominantly exhibited stage 1 acini in August 2011. Stage 1 exhibited a preponderance of blackened single-celled spermatocytes and multicellular sperm morula (Fig. 258). Spermatozoa are present in some acini, but restricted to the center of the lumen. Primary spermatocytes are typically emarginated along the acinus wall and have a pale, basophilic cytoplasm. Violet spermatocytes appear to differentiate into sperm morula and cells of sperm morula become spermatozoa (Fig. 259). Additionally, stage 1 testicular acini contain a series of small eosinophilic granules, possibly representing remnants of degenerative spermatocytes or fluid. A high level of spermatogenesis was evident in stage 3 testicular acini in individuals collected in May 2011. Sperm morula as seen in stage 1 testes were less conspicuous within stage 3 testes. Violet spermatocytes along

---

←

FIGS. 210–215. First intestinal limb, second intestinal limbs of *Fusconaia cerina*. FIG. 210: Sagittal section of descending first intestinal limb emphasizing plicae (PL) along the anterior wall (AW) and posterior wall (PW); FIG. 211: Sagittal section of the posterior intestinal wall showing a junction between style sac epithelium types one (E1) and three (E3) with their respective, contrasting ciliated surfaces (CI); FIG. 212: Transverse section of the ventral portion of the coelom portraying a cylindrical portion of the third intestinal limb (IN) and adjacent testicular acini (TA); FIG. 213: Sagittal section through the second intestinal limb displaying sinuous anterior wall (AW), posterior wall (PW) and eosinophilic chyme (CH); FIG. 214: Sagittal section of second intestinal limb showing tall, thin columnar cells with cilia (CI) and eosinophilic vesicles overlying a fibrous lamina propria (LP); FIG. 215: Sagittal section of the third intestinal limb showing a homogenous columnar epithelium (CE), cilia (CI), and a thin lamina propria (LP) and underlying adipocytes (AC).

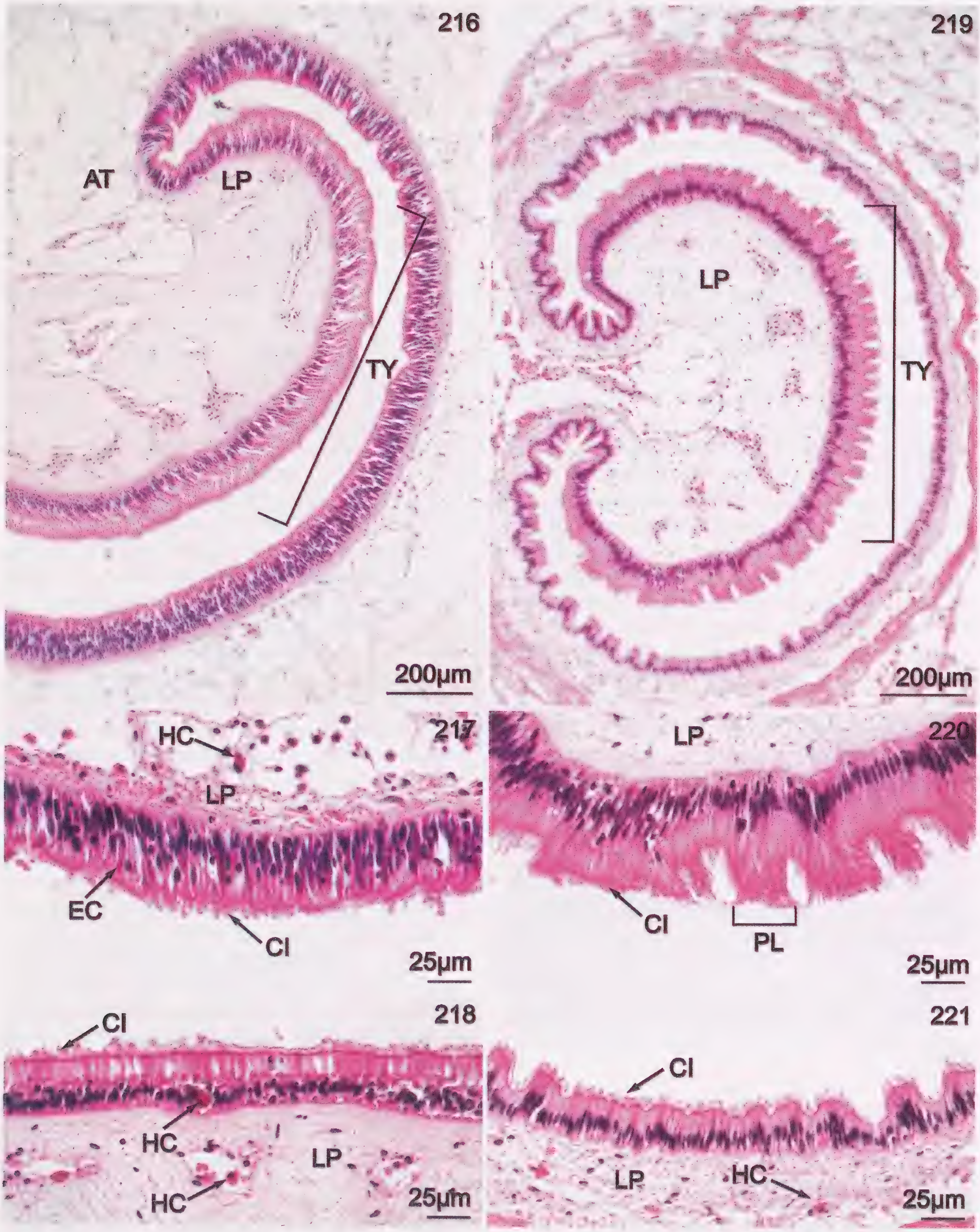

FIGS. 216−221. Fourth intestinal limb, and fifth intestinal limb of *Fusconaia cerina*. FIG. 216: Transverse section through the fourth intestinal limb emphasizing a large median typhlosole (TY), lamina propria (LP), and surrounding adipose tissue (AT); FIG. 217: Transverse section of the fourth intestinal limb showing eosinophilic columnar cells (EC) and cilia (CI) along the ventral wall, and a fibrous lamina propria (LP) and subepithelial hemocytes (HC); FIG. 218: Transverse section of fourth intestinal limb portraying the dense cilia (CI) of the typhlosole, hemocytes (HC) juxtaposed among epithelial cells as well as within sinuses of the lamina propria (LP); FIG. 219: Transverse section of the fifth intestinal limb showing a large median typhlosole (TY) with an expansive lamina propria (LP); FIG. 220: Transverse section of the dorsal epithelium surrounding the typhlosole consisting of ciliated columnar cells (CI), plicae (PL), and a distinct lamina propria (LP); FIG. 221: Transverse section of dorsal intestinal wall featuring cilia (CI), lamina propria (LP) and wandering hemocytes (HC).

the acinus wall appear to differentiate into darkened, spherical cells. Darkened testicular cells have such a small size that it is difficult to determine whether these cells represent clusters of spermatocytes or single-celled spermatocytes (Fig. 260).

Gonadal ducts of *Fusconaia cerina* consist of pale, eosinophilic, ciliated cells with an ovular nucleus. Spermatozoa were observed in the testicular ducts of stage 3 male *F. cerina* collected in May 2011 (Fig. 261). Gonadal ducts merge dorsally and extend along the lateral margins of the coelom to the base of the visceral mass. The gonadal pores of *F. cerina* feature a bulbous ventral ledge and a pleated, ciliated epithelium (Fig. 262).

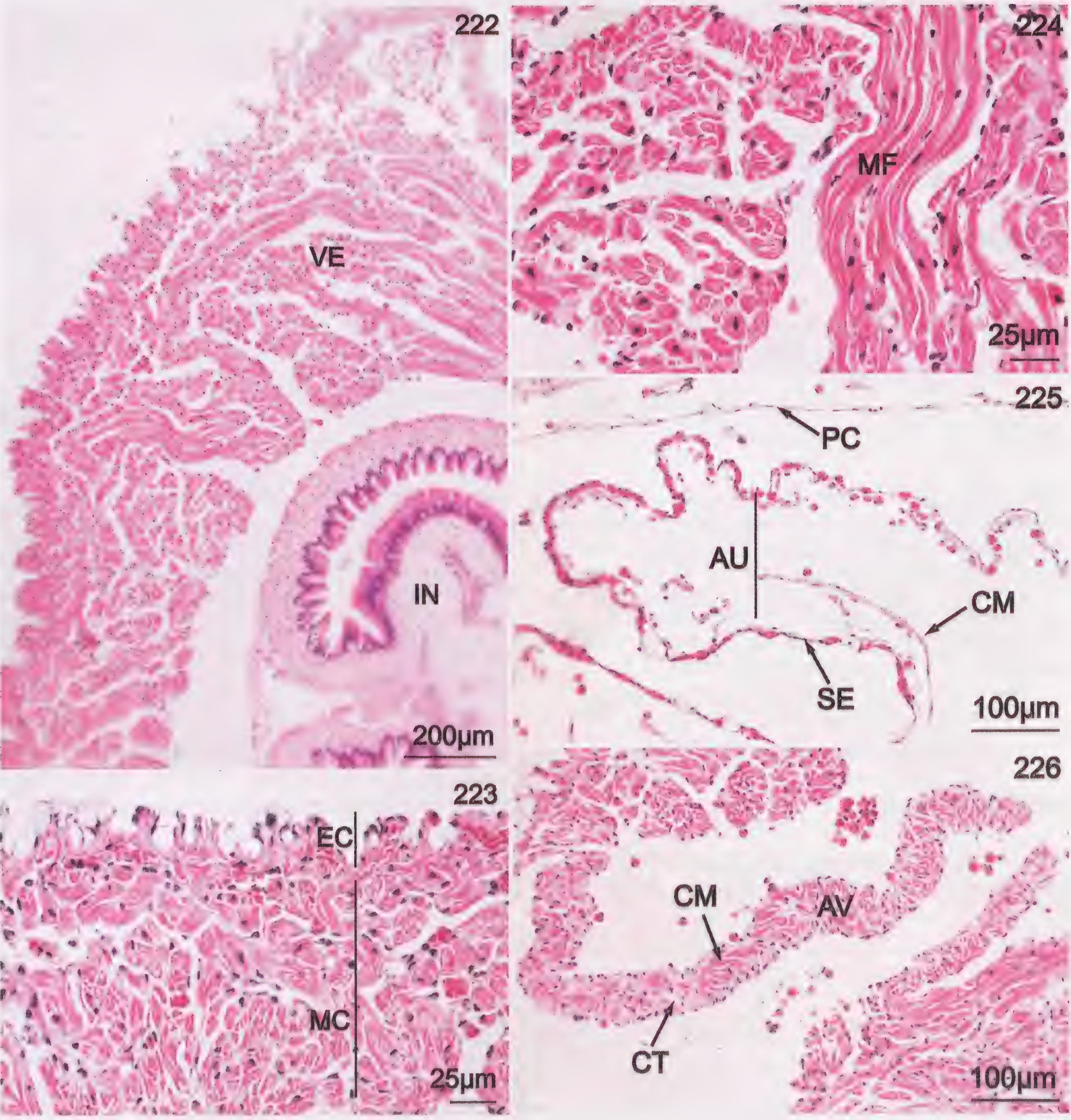

FIGS. 222–226. Heart, and pericardial cavity of *Fusconaia cerina*. FIG. 222: Transverse section through the dorsal portion of the visceral mass revealing branching myofibers of the ventricle (VE) surrounding the intestine (IN); FIG. 223: Transverse section of the ventricle revealing the epicardium (EC) and myocardium (MC); FIG. 224: Transverse section of the ventricle illustrating horizontal and verticle myofibers (MF); FIG. 225: Transverse section of the auricle (AU) emphasizing squamous epithelium (SE), cardiac muscle (CM), and adjacent pericardium (PC); FIG. 226: Transverse section of the ventricle focusing on an auriculoventricular valve (AV), endowed with connective tissue fibers (CT), and cardiac muscle (CM).

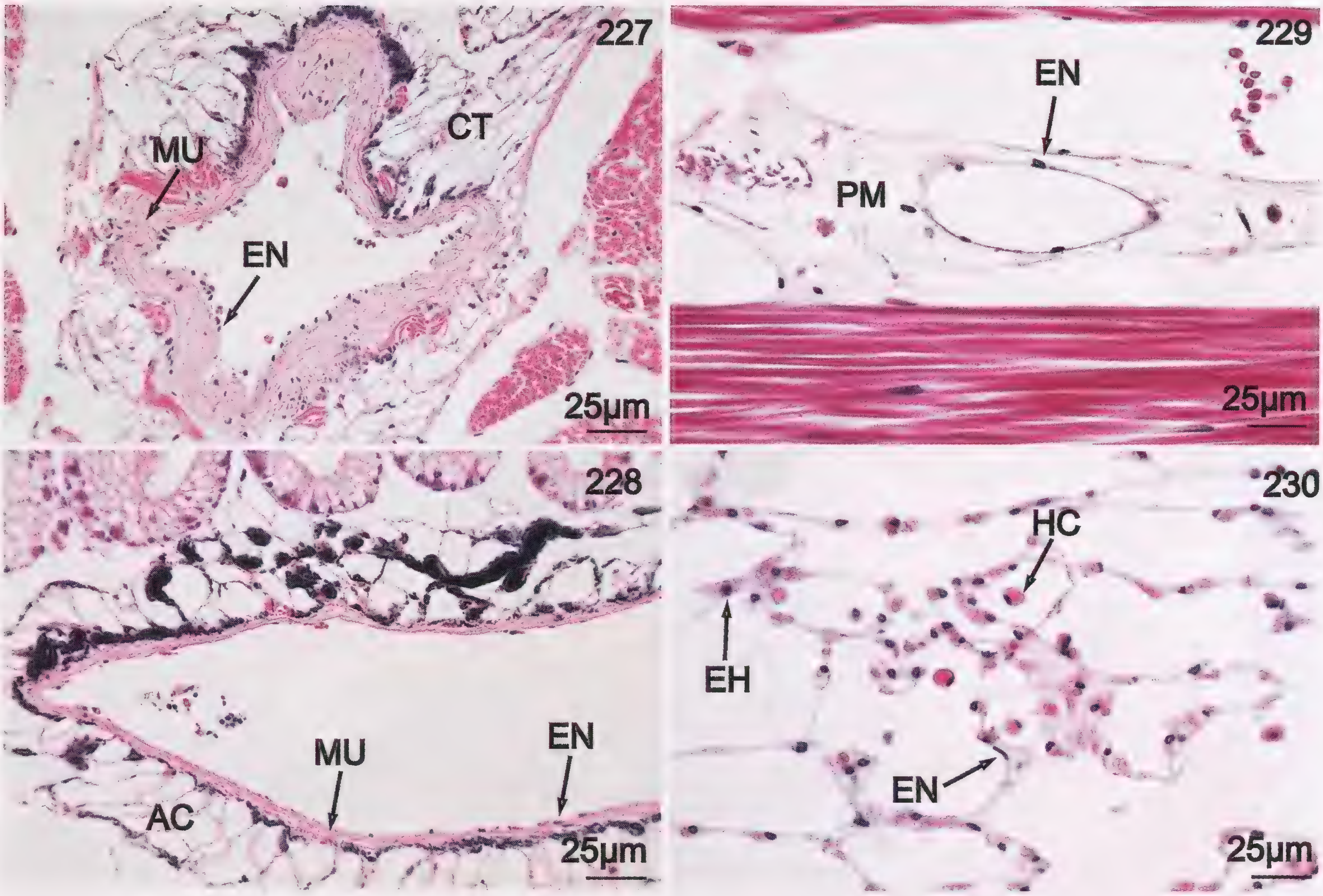

FIGS. 227–230. Hemolymph vessels of *Fusconaia cerina*. FIG. 227: Transverse section of the base of the foot showing a potential artery containing a thick muscular wall (MU), emarginated nuclei of endothelial cells (EN), and surrounding connective tissue (CT); FIG. 228: Transverse section of digestive diverticulum revealing a potential vein consisting of a thin muscular wall (MU), emarginated nuclei of endothelial cells (EN), and supporting adipocytes (AC); FIG. 229: Sagittal view of adductor muscle portraying a capillary and its endothelium (EN) within the perimysium (PM); FIG. 230: Transverse section of the pericardial gland displaying hemocytes (HC), emarginated hemocytes (EH), and emarginated nuclei (EN) of connective tissue cells.

Strophitus connasaugaensis

Shell Morphology

Valves of *Strophitus connasaugaensis* are elongated, and ovular to rhomboidal. The shell is characterized by a light-to-dark brown periostracum, and there may be thin to thick black lines along the posterior surface. The ventral margin of each valve is approximately double the length of the dorsal margin or hinge line. The ventral shell margin may be

---

→

FIGS. 231–237. Anterior nephridium of *Fusconaia cerina*. FIG. 231: Transverse section of anterior nephridium contrasting the convoluted ventral nephridium (VN), and relatively unbranched dorsal nephiridum (DN); FIG. 232: Transverse section of ventral nephridium portraying vesiculated columnar cells (VC), wandering hemocytes (HC) in the epithelium, and emarginated nuclei of endothelial cells (EN); FIG. 233: Transverse section of a dorsal nephridial limb emphasizing plicae (PL), brown, granular epithelial cells (BG), and hemocytes (HC); FIG. 234: Transverse section of dorsal nephridum displaying teardrop cells (TC) and underlying dense connective tissue (CT); FIG. 235: Transverse section of nephridium showing the ciliated renopericardial canal (RC) and adjacent urethra (UR); FIG. 236: Transverse section of nephrostome and urethra detailing cilia (CI), and goblet cells (GC); FIG. 237: Transverse section of urethra focusing on a dense layer of cilia (CI), and outer layer of goblet cells (GC).

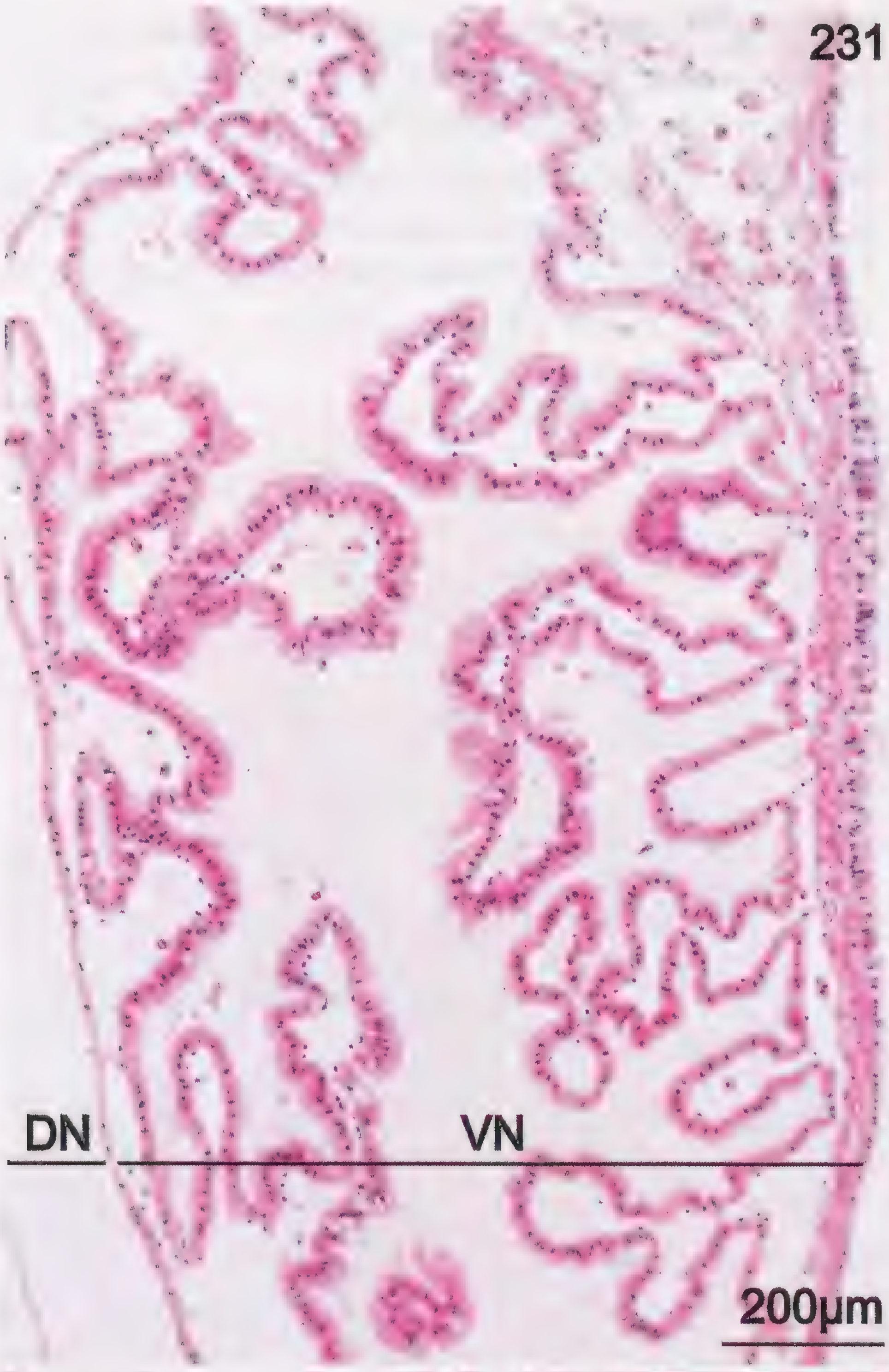
231
DN
VN
200µm

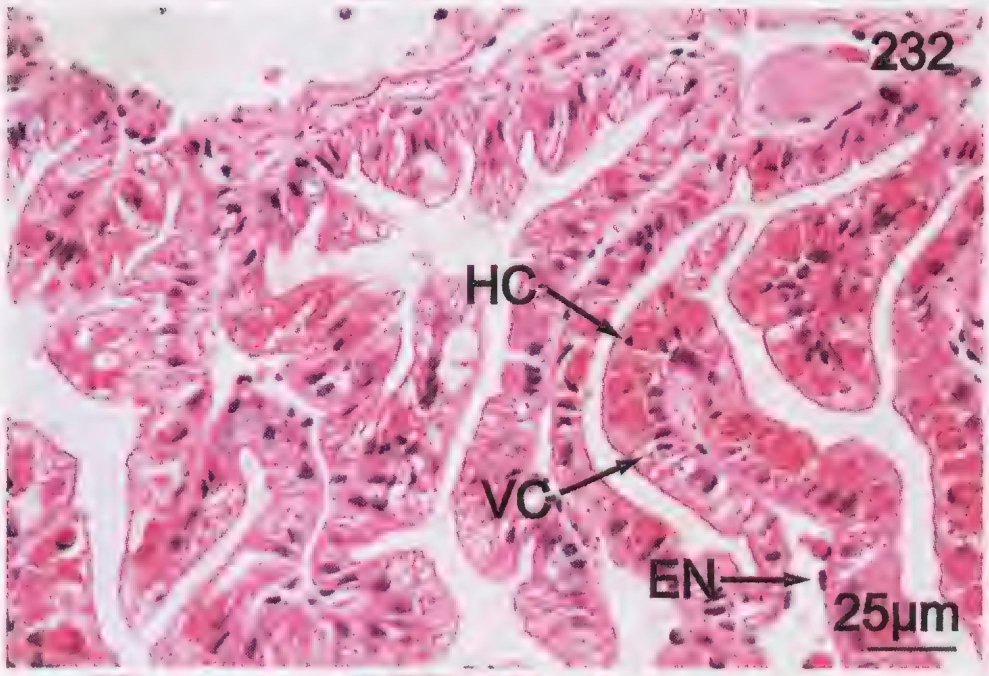
232
HC
VC
EN
25µm

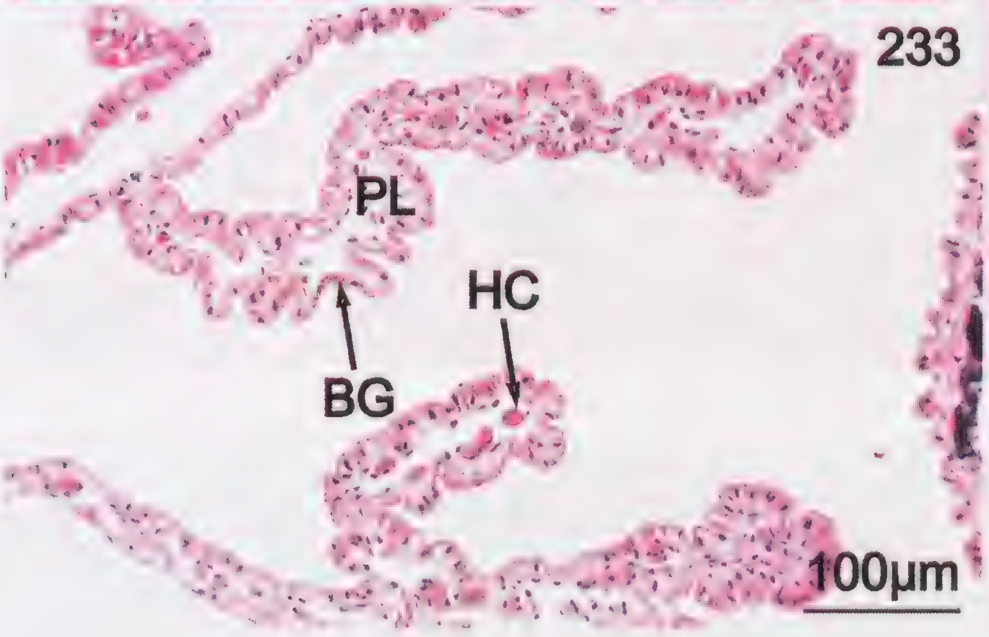
233
PL
BG
HC
100µm

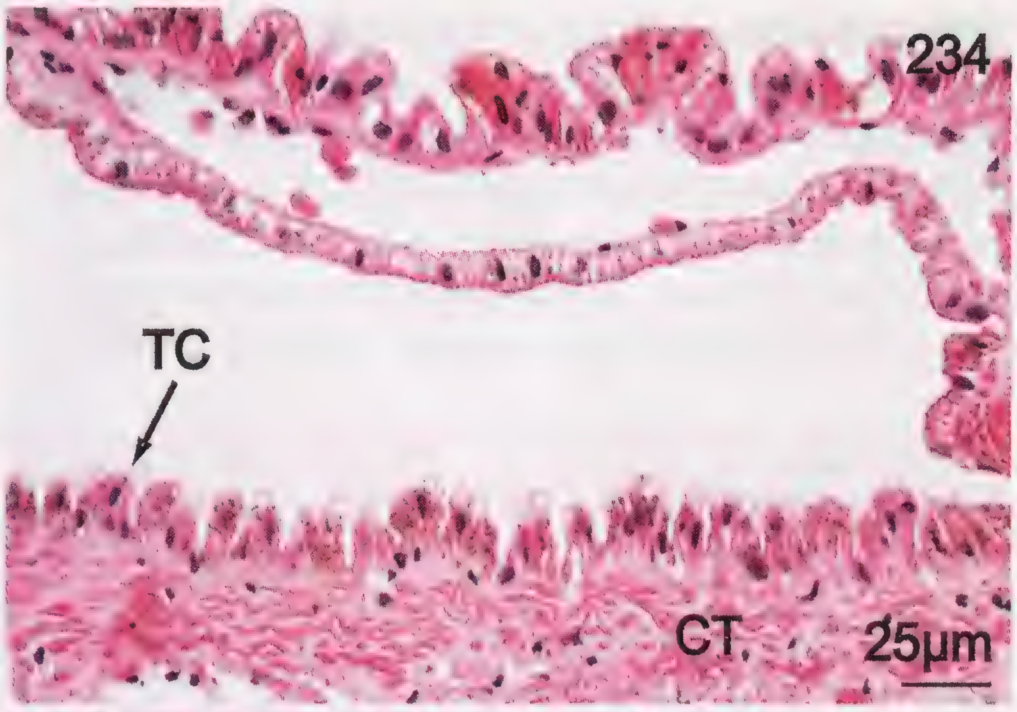
234
TC
CT
25µm

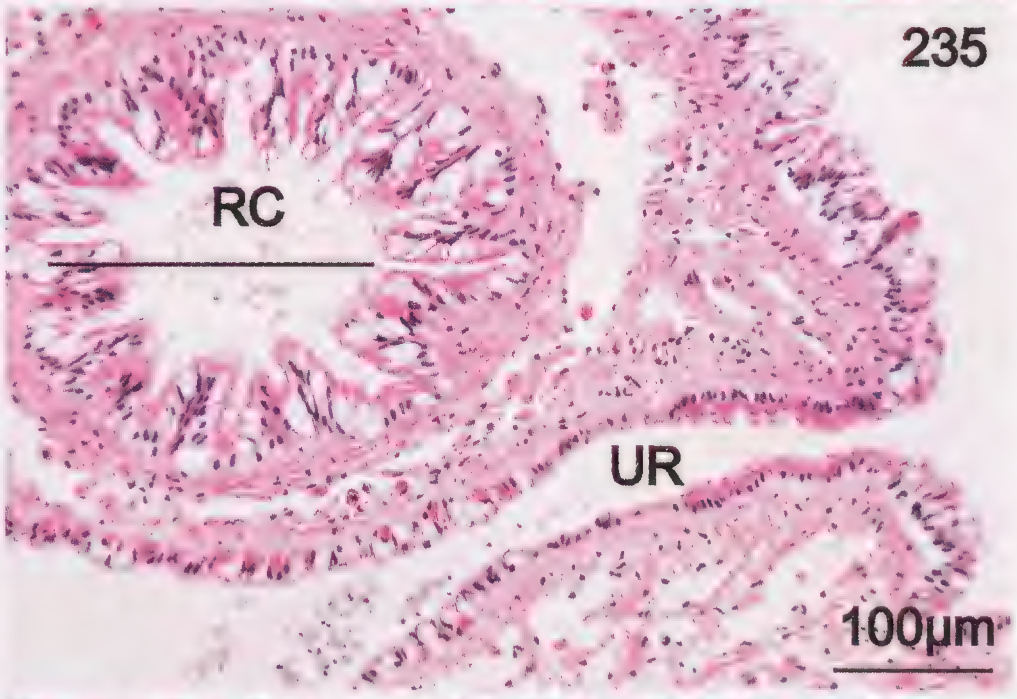
235
RC
UR
100µm

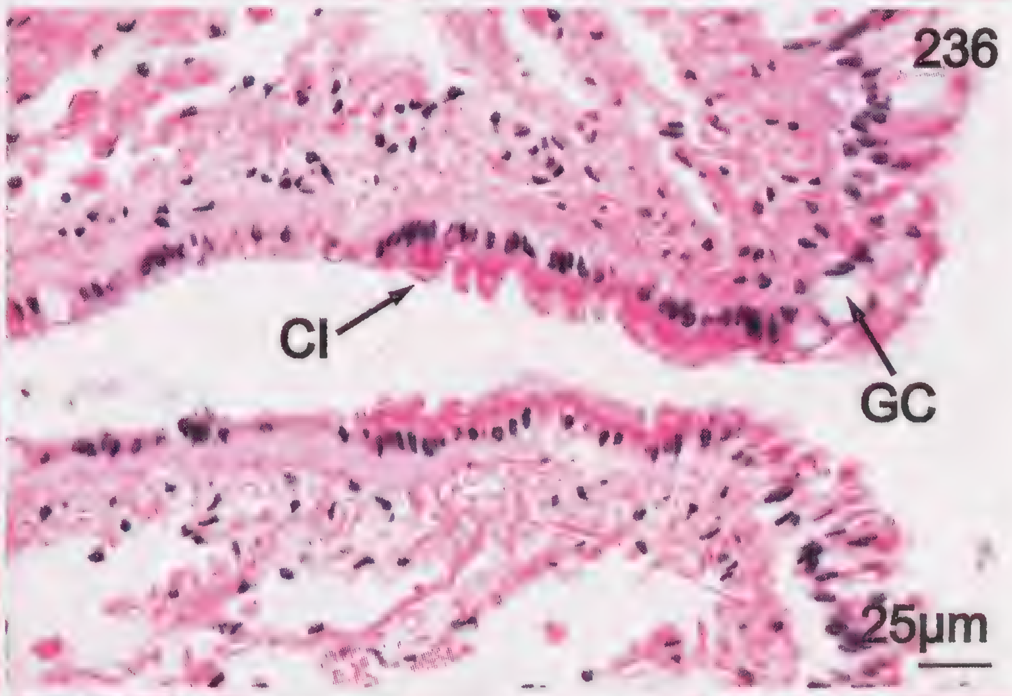
236
CI
GC
25µm

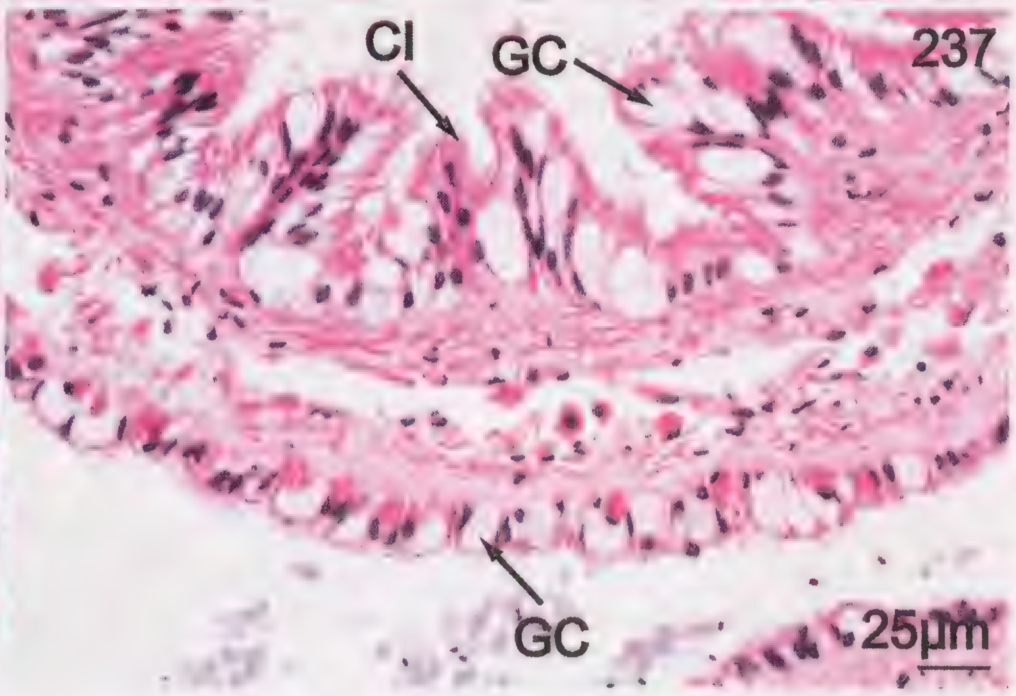
237
CI
GC
GC
25µm

straightened to slightly concave and the posterior margin may form a rounded point or be truncated with a short, flattened edge. Shell height from umbo to umbo may be moderately compressed to moderately inflated. The umbo extends obliquely towards the anterior shell, such that the anterior slope sharply curves dorsally. The posterior side of the shell may have a well-defined longitudinal crease or posterior ridge defining the shape and extent of the posterior slope. The posterior slope of *S. connasaugaensis* may be slightly flattened compared to the convex ventral surface (Figs. 263, 264) (Williams et al., 2008).

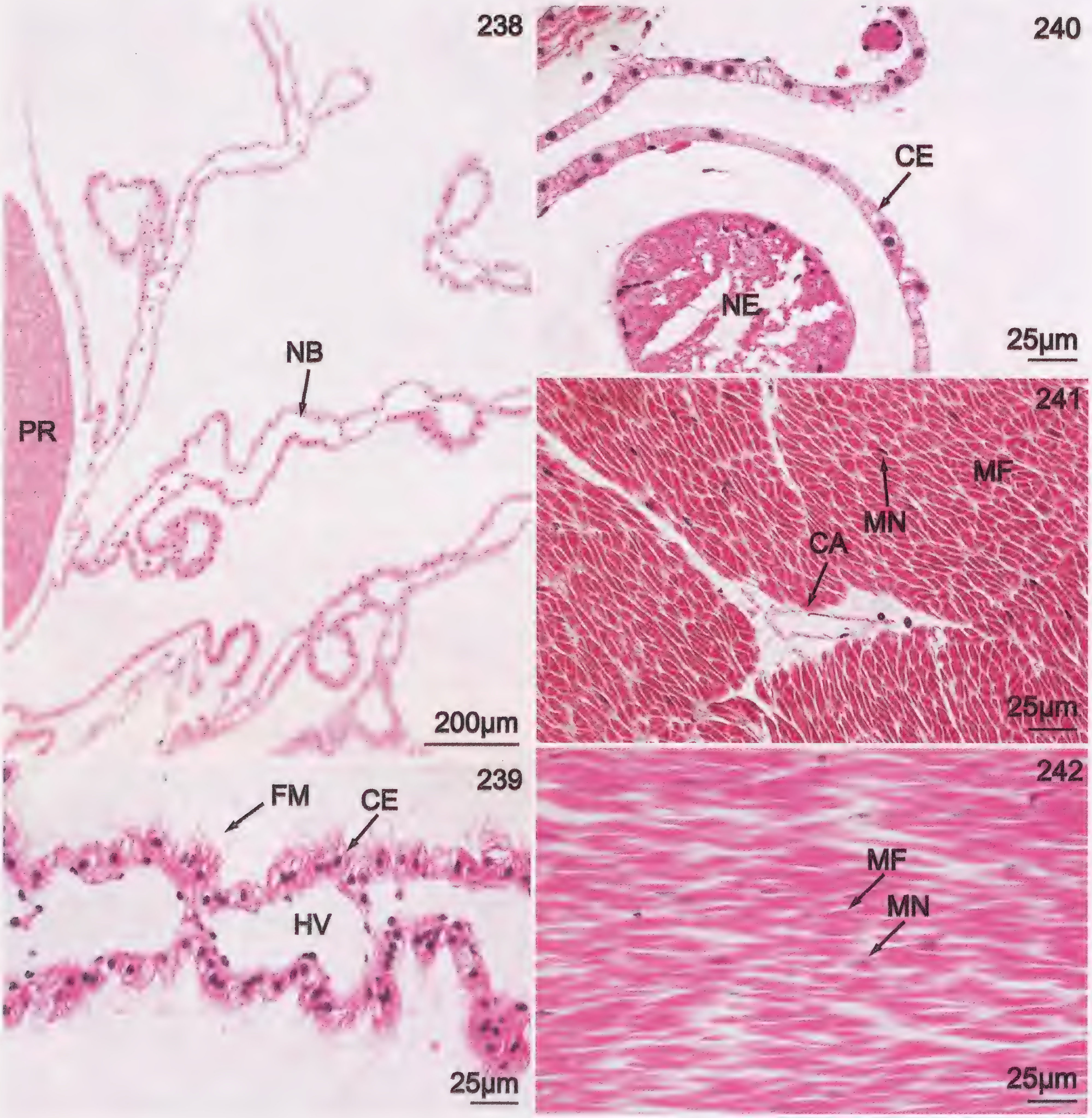

FIGS. 238–242. Posterior nephridium of *Fusconaia cerina*. FIG. 238: Transverse section of the posterior nephridium featuring nephridial branches (NB) and posterior pedal retractor (PR); FIG. 239: Transverse section of posterior nephridium detailing columnar epithelium (CE), and fibrous material (FM) of the apical surface, and underlying hemolymph vessels (HV); FIG. 240: Transverse section of posterior nephirdium consisting of a nerve fascicle (NE), and a smooth surfaced columnar epithelium (CE); FIG. 241: Transverse section of posterior retractor illustrating myofibers (MF), myocyte nuclei (MN), and a capillary (CA); FIG. 242: Sagittal view of posterior adductor portraying spindles of myofibers (MF) and cylindrical myocyte nuclei (MN).

The inside of the shell has a lustrous, silver nacre. The pallial line is a scar forming an incomplete ellipse around the ventral margin of the nacre between the anterior adductor scar and posterior adductor scar. The anterior adductor is a triangular depression between the anterior shell margin and interdentum. The posterior adductor scar is broad, ovular and flattened with a smaller, circular marking positioned anteriorly demarking the posterior pedal retractor scar. Pseudocardinal teeth are reduced to small, rounded triangular extensions of the shell at the anterior end of the

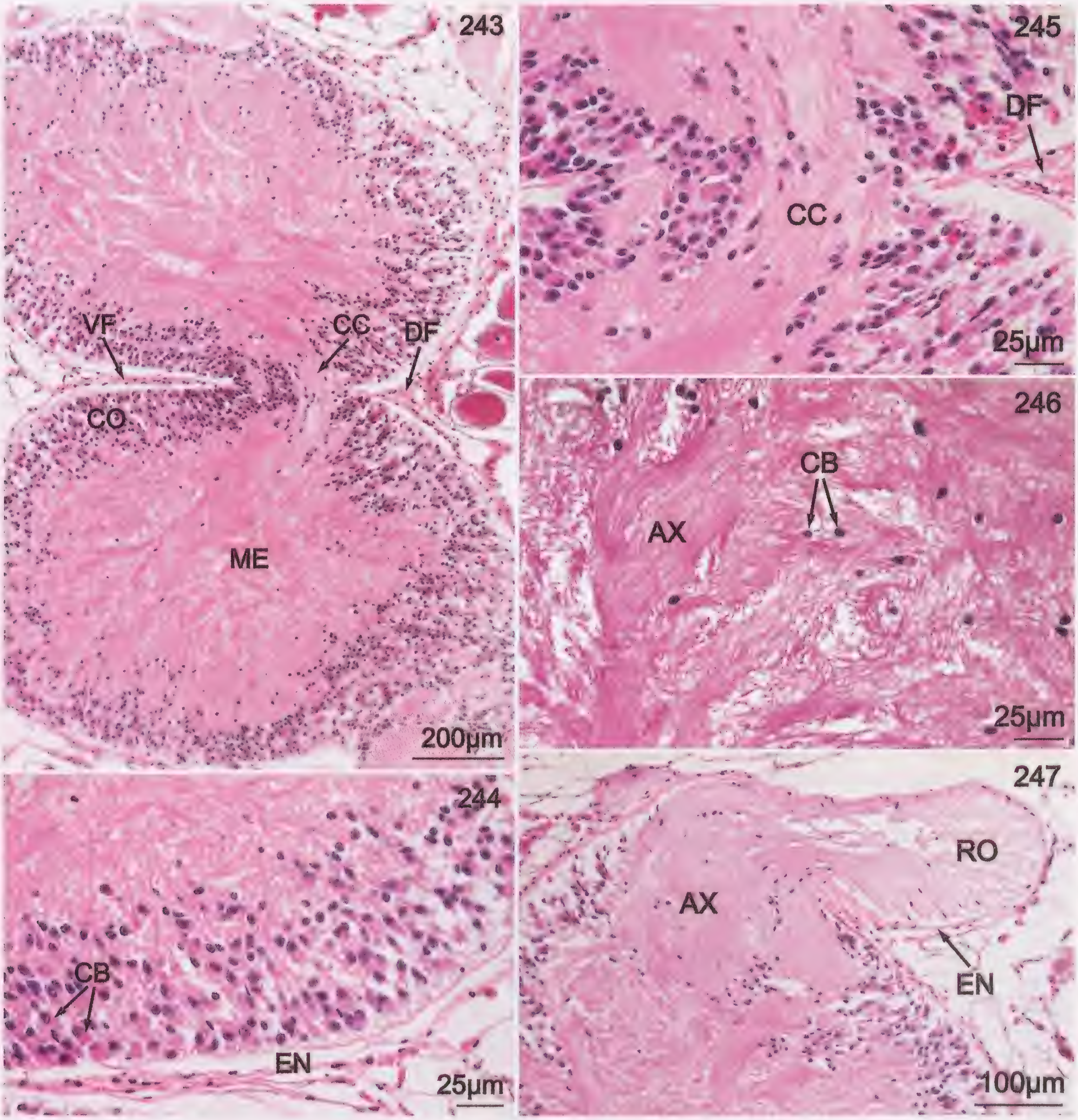

FIGS. 243–247. Pedal ganglion of *Fusconaia cerina*. FIG. 243: Transverse section of pedal ganglion portraying neural cortex (CO), inner medulla (ME), central commissures (CC), dorsal fissure (DF) and ventral fissure (VF); FIG. 244: Transverse section of pedal ganglion showing neuron cell bodies (CB), and fibrous epineurium (EN); FIG. 245: Transverse section of the median of the pedal ganglion showing central commissures (CC), and dorsal fissure (DF); FIG. 246: Transverse section of the pedal ganglion medulla emphasizing the irregular meshwork of axons (AX) and cell bodies (CB); FIG. 247: Transverse section of pedal ganglion revealing axons (AX) bundled within a root (RO) and surrounded by membranous connective tissue of the epineurium (EN).

hinge line between the interdentum and ligament. Lateral teeth are virtually absent and appear as low, rounded ridgeline ventral to the ligament. The umbo cavity is small, forming a narrow cavity that curves dorsally and anteriorly behind the interdentum (Figs. 265, 266) (Williams et al., 2008).

Gross Anatomical Features of the Mantle Cavity

The posterior aspect of the mantle edge forms a short, incomplete siphon when the sinistral and dextral mantle edges are cupped.

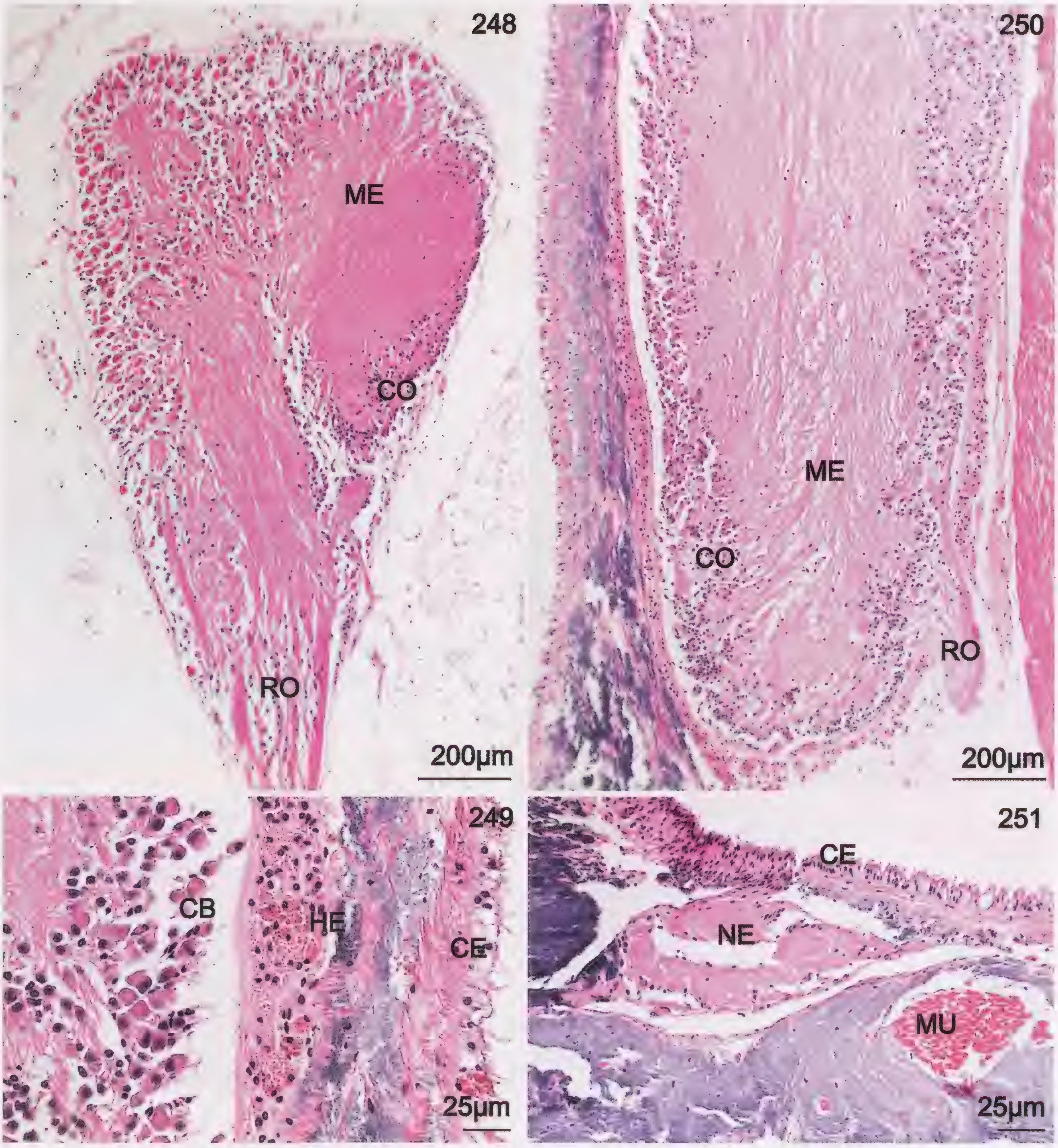

FIGS. 248–251. Anterior ganglion, and posterior ganglion of *Fusconaia cerina*. FIG. 248: Transverse section of anterior ganglion revealing the neural cortex (CO), neural medulla (ME) and a large nerve root (RO); FIG. 249: Transverse section of the ventral surface of the posterior ganglion revealing cell bodies (CB) of the neural cortex, and a thick layer of hemolymph (HE) between neural tissue and columnar epithelial cells (CE) facing the suprabranchial cavity; FIG. 250: Transverse section of posterior ganglion showing the neural cortex (CO), neural medulla (ME), and a nerve root (RO); FIG. 251: Transverse section of the base of the ctenidia showing an anterior nerve (NE) branch of the posterior ganglion juxtaposed with columnar epithelial cells (CE), and a muscle fascicle (MU).

The apertures of *S. connasaugaensis* are grey, uniformly pigmented externally, but with irregular transverse lines along the internal surface. When mantle edges are cupped, incurrent and excurrent apertures or openings are formed. The incurrent and excurrent apertures are not divided by a septum, but rather mantle tissue is curled medially and forms trapezoidal flaps that may meet medially or overlap. The incurrent aperture is papillose and papillae are uniramous. Papillae are reduced or absent along the excurrent aperture (Fig. 267).

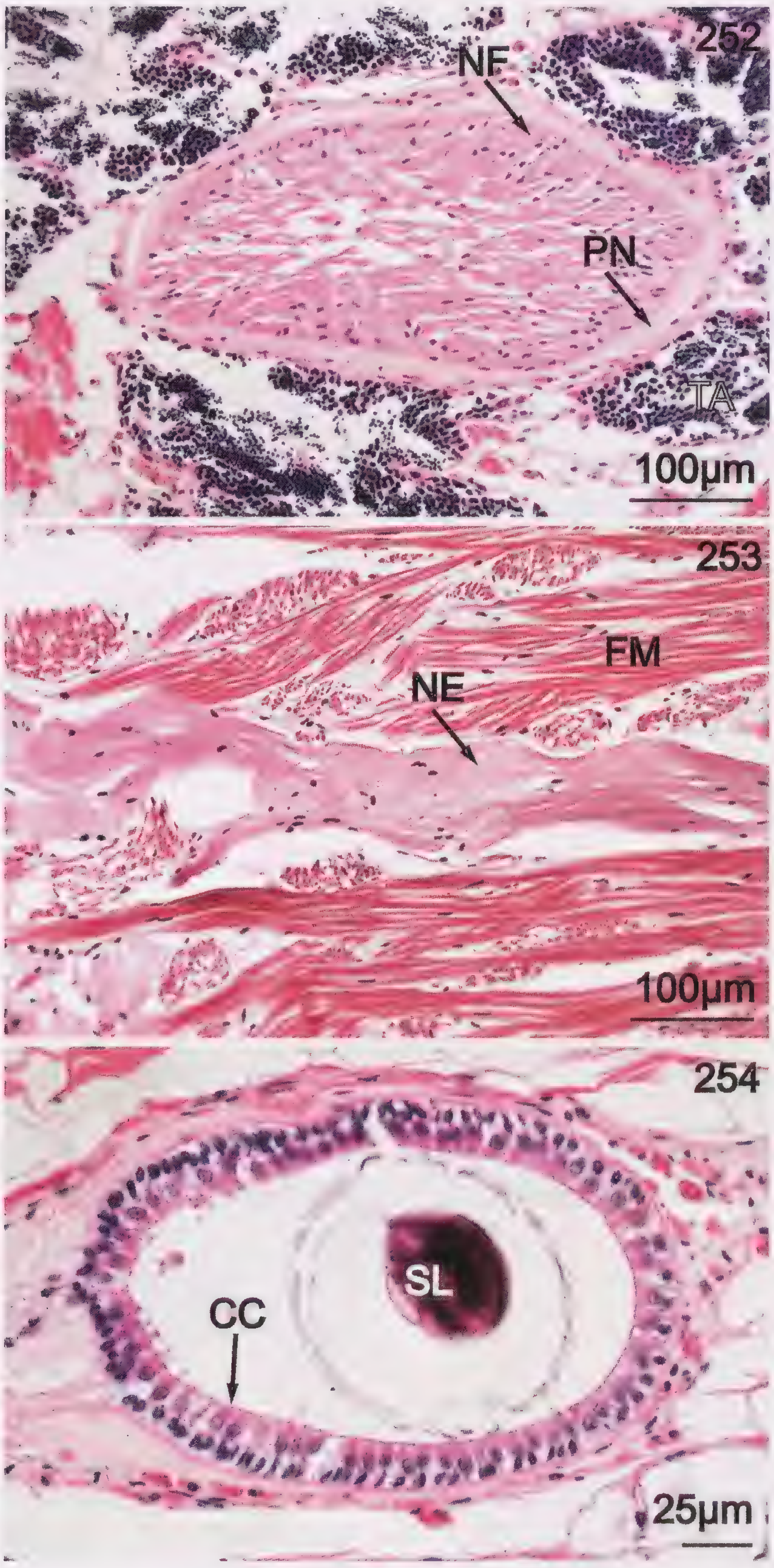

FIGS. 252–254. Nerves, and statocysts of *Fusconaia cerina*. FIG. 252: Transverse section gonad emphasizing a large nerve consisting of nerve fibers (NF) and a pale, eosinophilic perineurium (PN); FIG. 253: Transverse section of foot musculature (FM) detailing a nerve chord (NE) with filamentous axons; FIG. 254: Transverse section of a statocyst revealing stratification of columnar cells (CC) and the spherical, median statolith (SL).

The mantle edge is orange, flattened and pigmentation continues posteriorly to the blackened siphon, just posterior to the posterior adductor. The middle mantle is white and somewhat translucent, spanning the nacre. A translucent, trapezoidal keel of mantle tissue, the isthmus, extends dorsally into a cleft between the left and right halves of the shell. The ctenidia are paired, consisting of elongated inner and outer demibranchs (Fig. 268). Ovigerous females brood using the outer demibranchs and red lines of glochidia are present in marsupia of gravid females (Fig. 269). Removing the mantle and gill on one side exposes the foot and visceral mass. The foot of *S. connasaugaensis* is orange, forming a right triangle with a vertical anterior face and a posterior slope. The visceral mass is white and extends dorsally to the base of the ctenidia. Labial palps are translucent lips located anterolaterally between the foot and visceral mass. The anterior adductor is pale, white to orange, ovular in outline and oriented vertically between the anterior shell margin and foot. The posterior adductor is grossly identical to the anterior adductor, but is parallel with the posterior shell margin (Fig. 270).

Cellular Structure of the Mantle

Anterior Mantle Edge: Anterior mantle edge of *Strophitus connasaugaensis* is dorsoventrally compressed with outer, middle and inner lobes nearly equidistant from the base of the mantle edge (Fig. 271). The outer mantle lobe is generally flattened, except for a few trapezoidal plications along the ventral margin (Figs. 271–273), and pleated distal end (Figs. 271, 273). The outer lobe has a simple columnar epithelium, with deeply basophilic cells ventrally located along the medial half of the lobe. Outer lobe columnar cells feature an ovular, monochromatic nucleus, obliquely oriented in relation to the horizontal plane of the outer lobe, and the cytoplasm may contain a single, apical, transparent vesicle. In contrast, dorsal epithelium of the outer lobe is largely flattened and columnar cells characterizing dorsal epithelium have an eosinophilic cytoplasm, but are otherwise indistinguishable from ventral columnar cells (Figs. 272, 273). Dorsal epithelium of the outer lobe terminates at the small, cleft-like

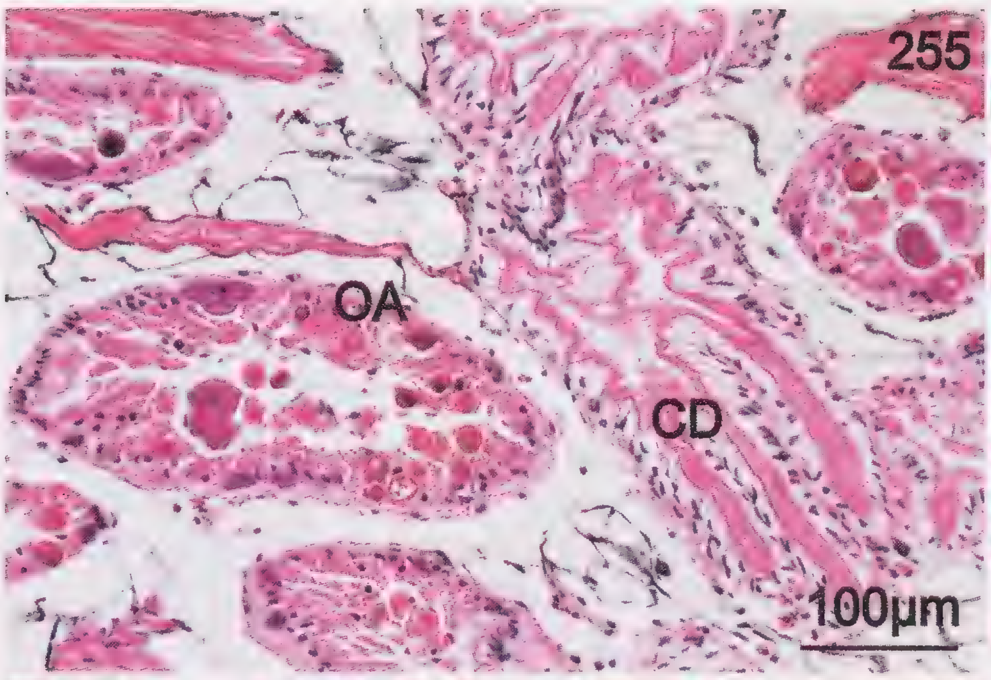
255

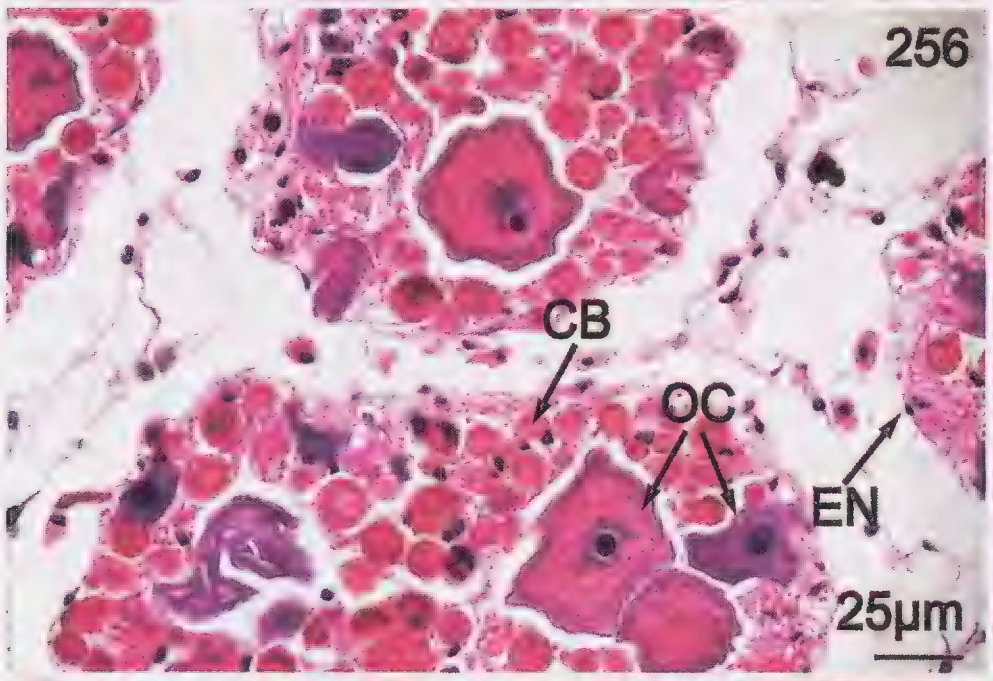
256

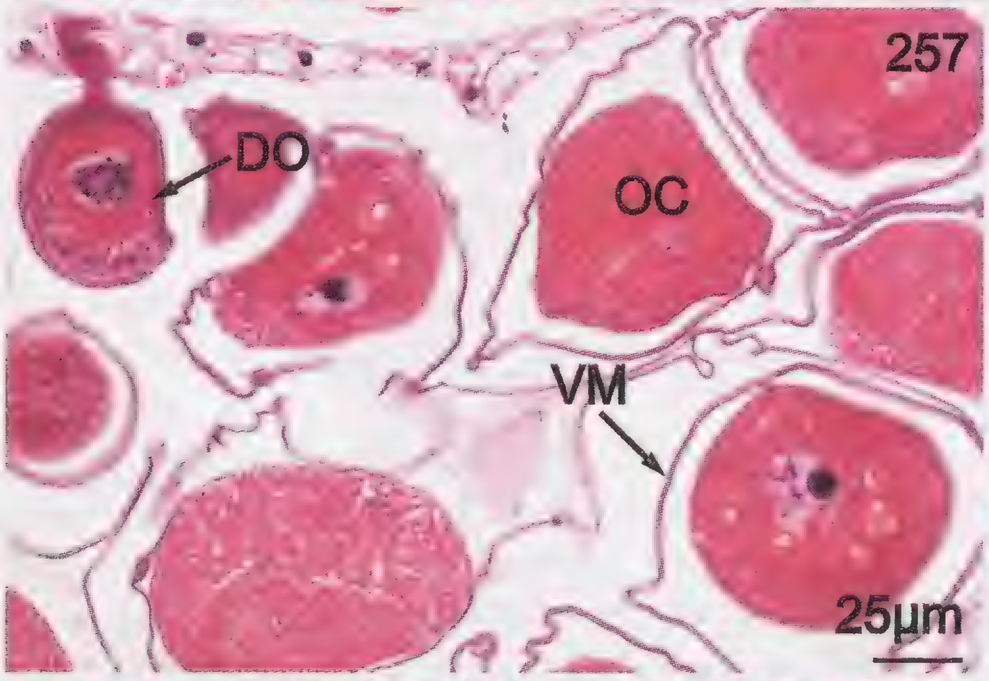
257

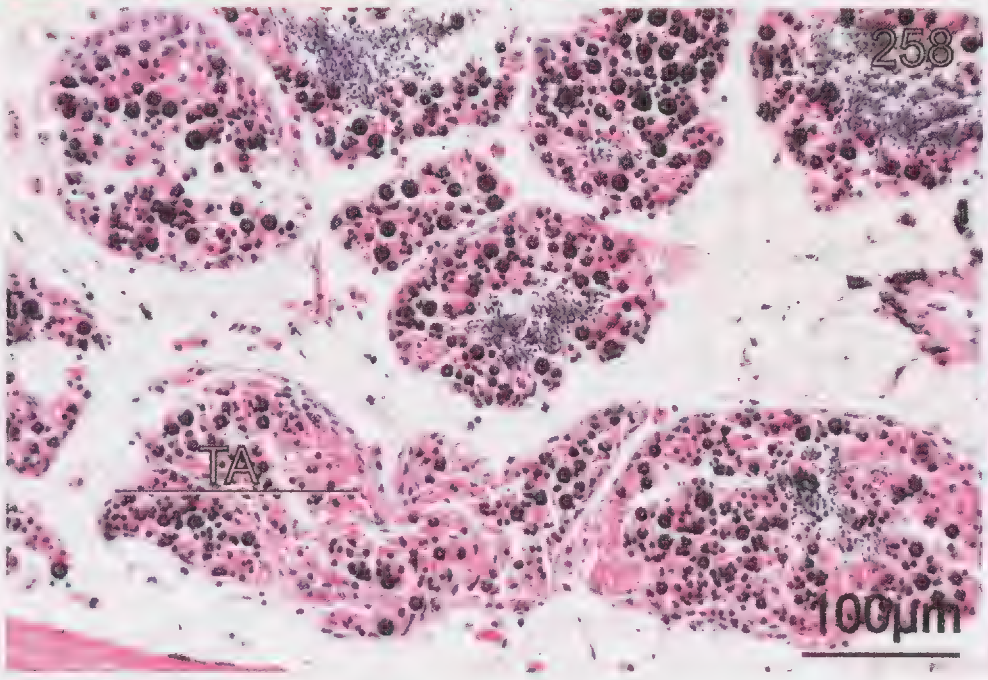
258

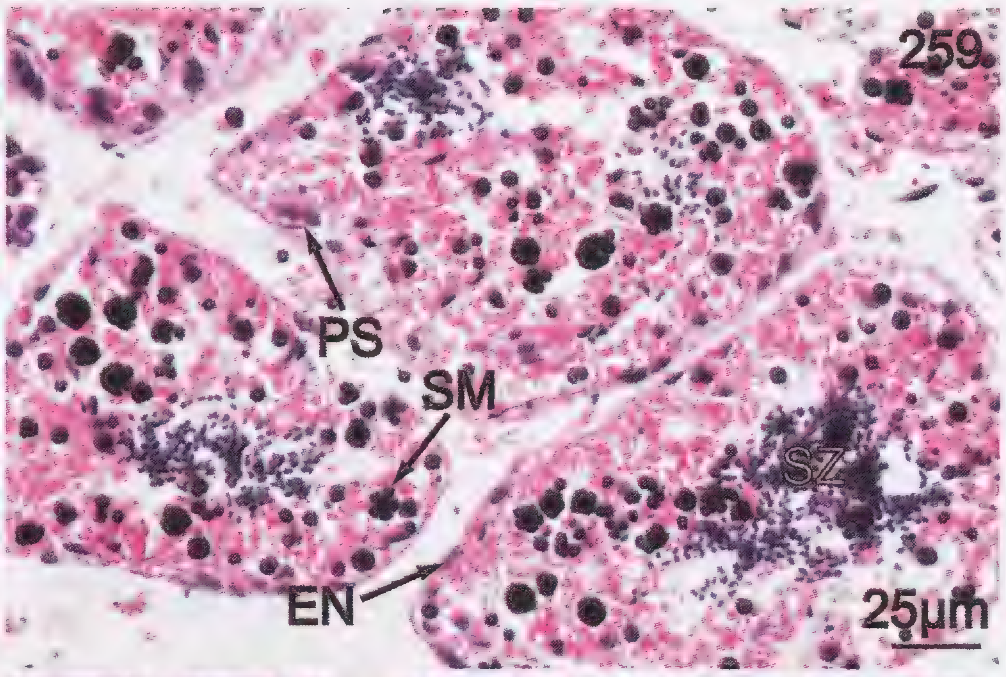
259

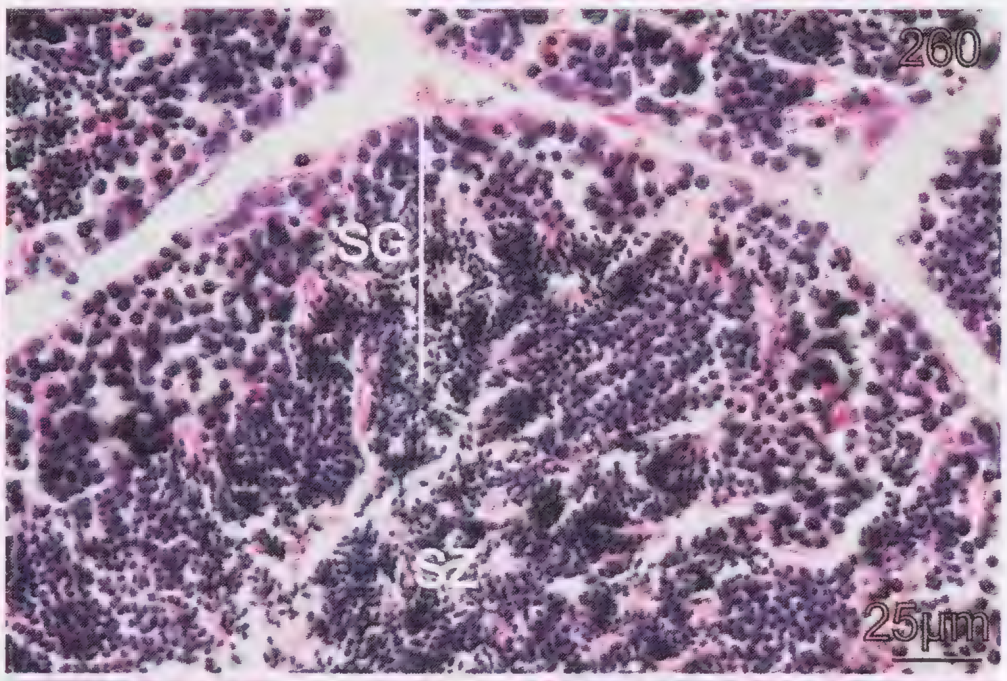
260

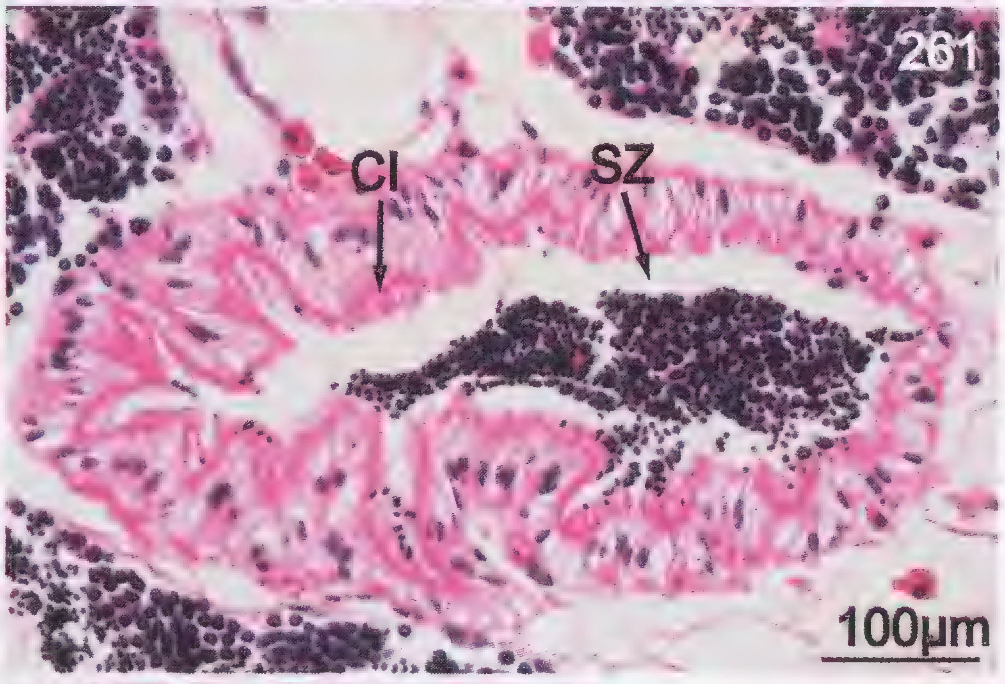
261

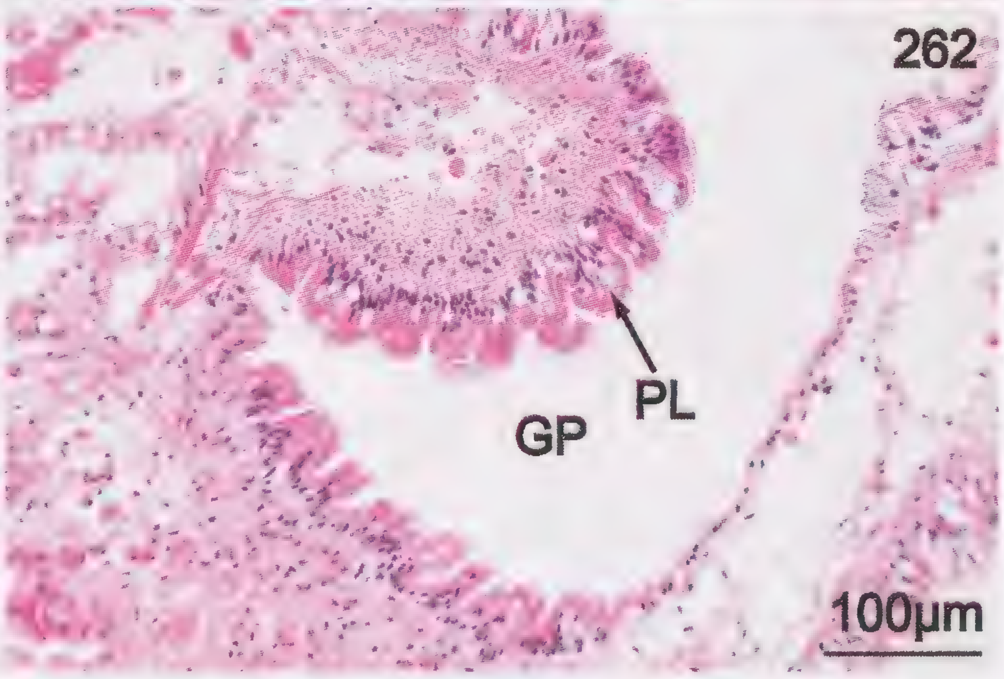
262

basal bulb and abruptly transitions to simple, squamous epithelium (Fig. 272). The middle lobe is flattened along the ventral surface, and pleated along the dorsal margin. Middle lobe cell types include a simple squamous epithelium along the ventral margin and a simple columnar epithelium lining the dorsal surface. Squamous cells of the ventral surface consist of an eosinophilic cytoplasm and a monochromatic nucleus. Secreted periostracum is sometimes observed in histological sections of outer and middle lobes, appearing as an eosinophilic filament, and may be closely apposed to the ventral surface. Columnar cells of the dorsal margin are eosinophilic with an ovular, monochromatic nucleus. Plications of the dorsal surface of the middle lobe give an irregularity to the spacing of columnar cells such that some cells appear more laterally compressed than others (Fig. 274). The inner mantle lobe is triangular with thin, teardrop-shaped plicae along the dorsal and ventral surfaces. Columnar cells of the inner lobe are indistinguishable from those of the dorsal surface of the middle lobe (Fig. 275). The dorsal bend to the middle lobe and the ventral bend to the inner lobe may represent fixation artifacts. Teardrop-shaped plicae with columnar epithelial cells extend medially towards the base of the mantle edge and are replaced by plicae endowed with goblet cells. Goblet cells may contain a single transparent vesicle or a series of vesicles, and goblet cell nuclei are ovular and emarginated (Fig. 276). Dorsal epithelium of anterior mantle edge is flattened, with a simple columnar epithelium, and the tissue maintains a flattened surface along the medial aspect of the tissue until the base of the outer mantle lobe. Columnar cells of dorsal mantle epithelium have a densely staining, basophilic cytoplasm and an ovular, monochromatic nucleus (Fig. 277).

Muscle tissue is a large constituent of the mantle edge (Fig. 271). The subepithelium of mantle lobes consists of linear tracts of muscle fibers. Myofibers are wavy and organized into dense bands in the outer and middle lobes (Figs. 272–274). Myofibers of the inner lobe are arranged in an irregular meshwork (Fig. 275). Other tissue components of the mantle edge include irregular sinuses containing blackened hemolymph, nerve fibers (Fig. 276), and blue to violet granular cells beneath the epithelium of the inner mantle lobe (Fig. 275).

Posterior Mantle Edge, Middle Mantle and Mantle Isthmus: Mantle lobe morphology differs from anterior mantle edge in several respects. The outer and middle lobes become a forked extension of mantle tissue, each lobe equidistant from its base. Inner mantle lobe is reduced in comparison to the outer and middle lobes. Outer and middle lobes each feature flattened ventral and dorsal epithelia, while epithelium surrounding the inner lobe is plicated. The distal tip of the outer lobe is rectangular and there is a single obliquely oriented crease near the dorsal margin. Inner mantle lobe is reduced and does not extend to the margins of the outer and middle lobes. The epithelium of the outer lobe and middle

---

←

FIGS. 255–262. Ovarian acini, testicular acini, and ciliated gonadal ducts of *Fusconaia cerina*. FIG. 255: Transverse section through the visceral mass of an adult female collected in August 2011 displaying stage 1 ovarian acini (OA), and ciliated gonadal ducts (CD); FIG. 256: Transverse section of the visceral mass of an adult female collected in August 2011 emphasizing immature oocytes (OC), cell bodies (CB), and emarginated nuclei (EN) of an acinus wall; FIG. 257: Transverse section of visceral mass of an adult female collected in May 2011 detailing developing oocytes (DO), enlarged mature oocytes (OC), and a surrounding vitelline membrane (VM); FIG. 258: Transverse section of the visceral mass of an adult male collected in August 2011 illustrating a series of stage 1 testicular acini (TA); FIG. 259: Transverse section of the visceral mass of an adult male collected in August 2011 emphasizing primary spermatocytes (PS), sperm morula (SM), spermatozoa (SZ), and emarginated nuclei (EN) of an acinus; FIG. 260: Transverse section of a stage 3 testicular acinus of a male collected in May 2011 detailing spermiogenesis (SG), and a large quantity of medially located spermatozoa (SZ); FIG. 261: Transverse section of the visceral mass of a stage 3 male collected in May 2011 illustrating the passage of spermatozoa (SZ) though a gonadal duct via the action of luminal cilia (CI); FIG. 262: Transverse section of the base of the visceral mass of a stage 3 male collected in May 2011 illustrating a gonadal pore (GP) with a pleated epithelial lining (PL).

lobe is flattened, while plicae extend along the inner lobe (Fig. 278). Papillae are conical extensions of the mantle edge along the narrow, posterior shell margin. Papillae are darkened, consisting of a simple columnar epithelium containing brown to black intracellular granules and an ovular, monochromatic nucleus. Subepithelium is fibrous and irregular, consisting of somatic musculature, hemolymph sinuses and nerve fibers. The epithelium and subepithelium of the papillae is wavy, giving the surface a folded texture with sharply defined crypts (Fig. 279). Darkened granules in posterior mantle edge are located in the

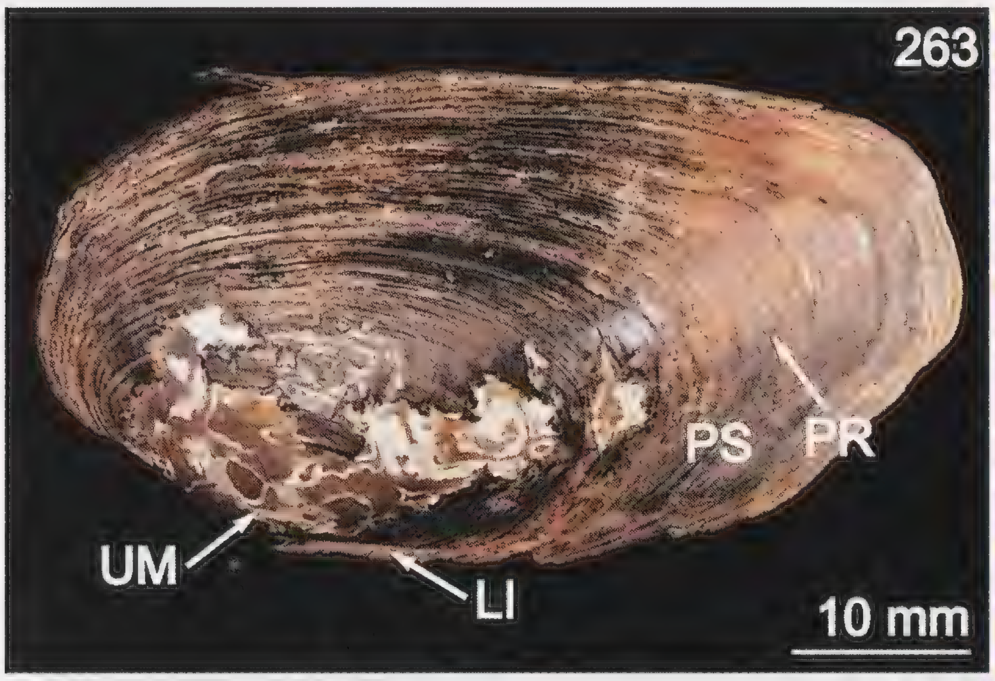

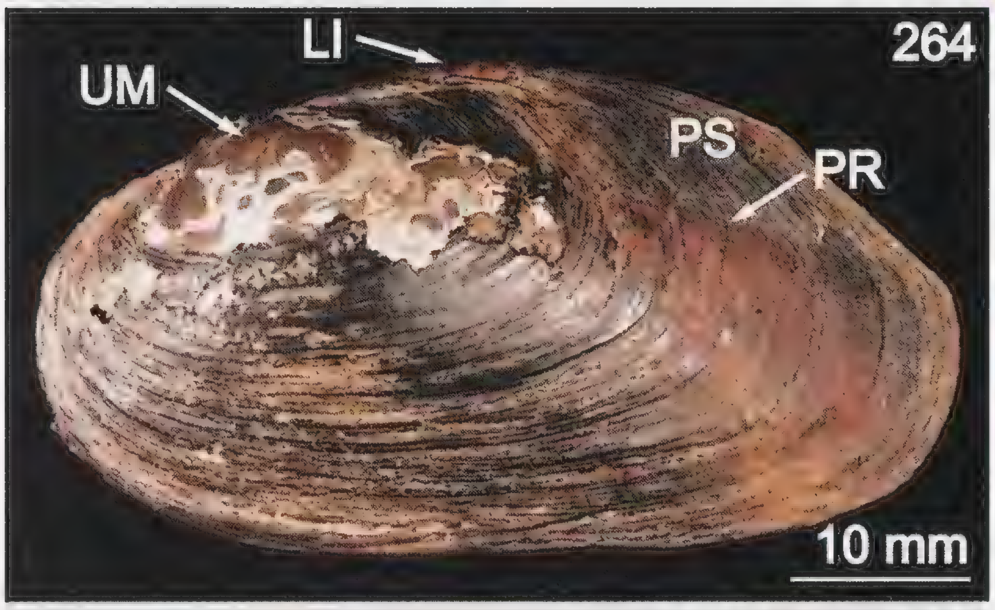

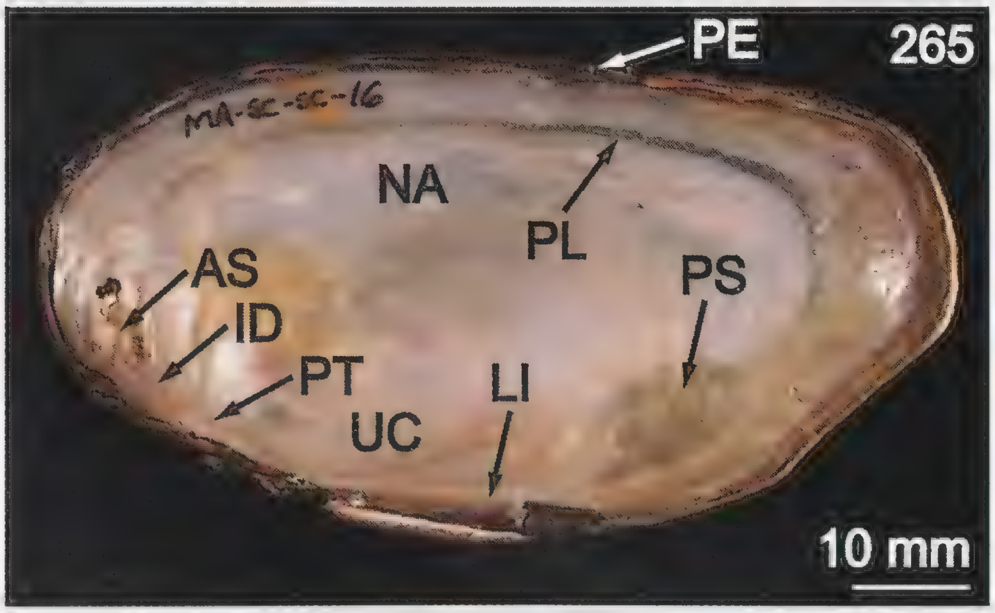

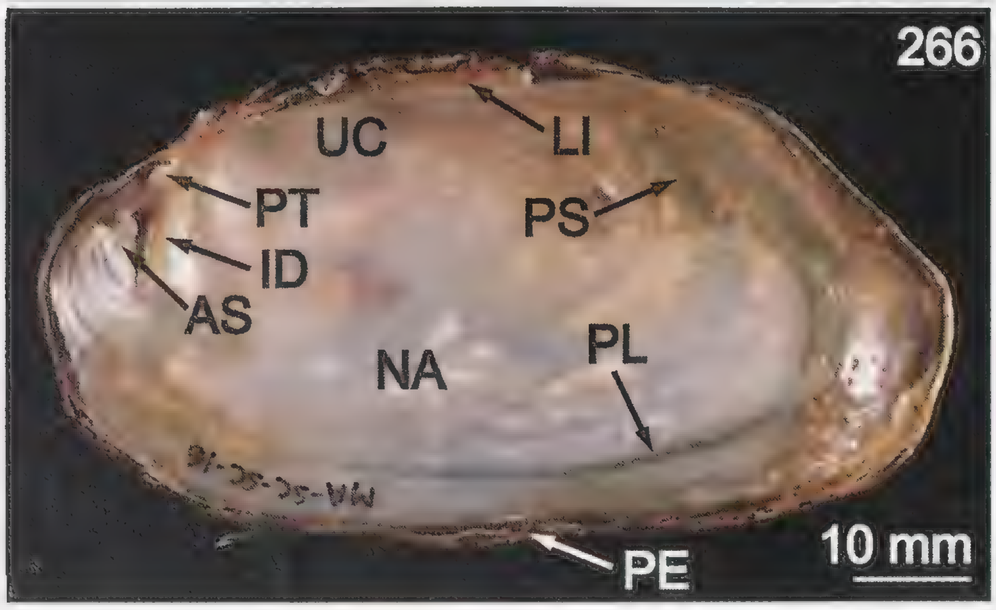

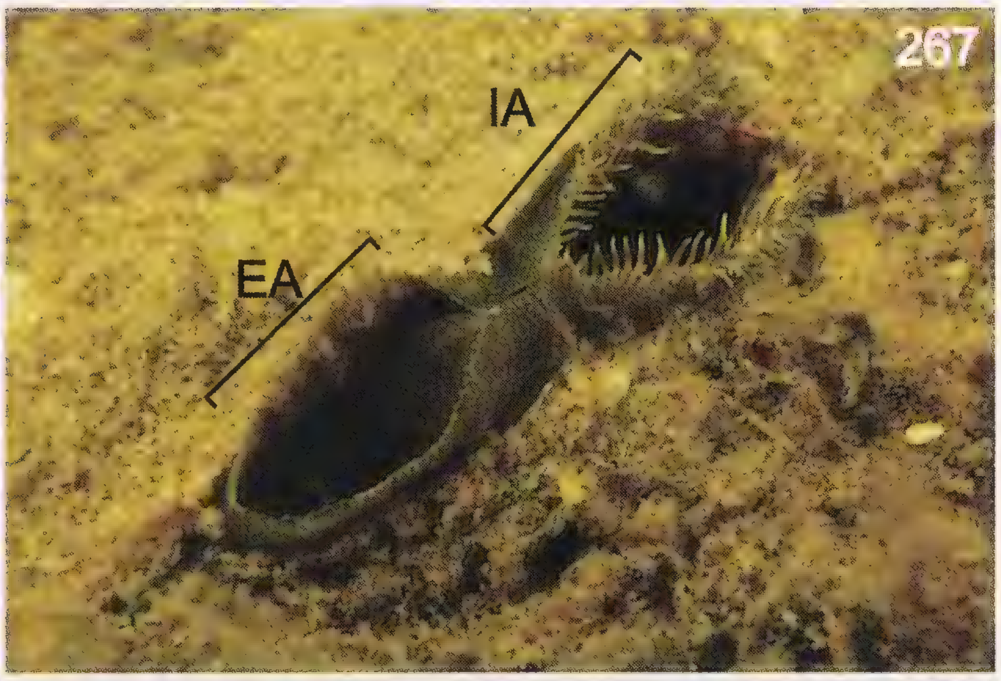

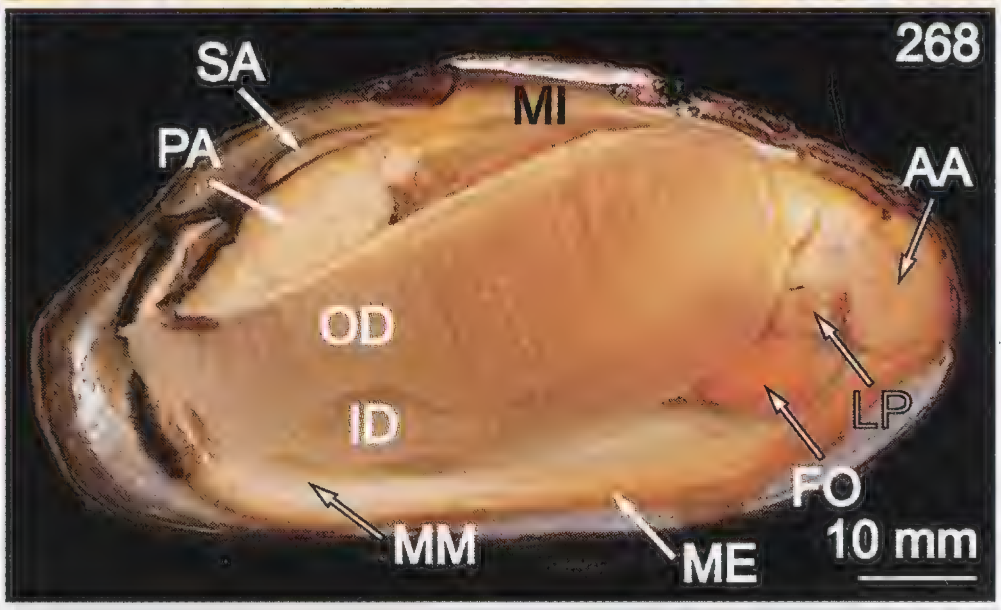

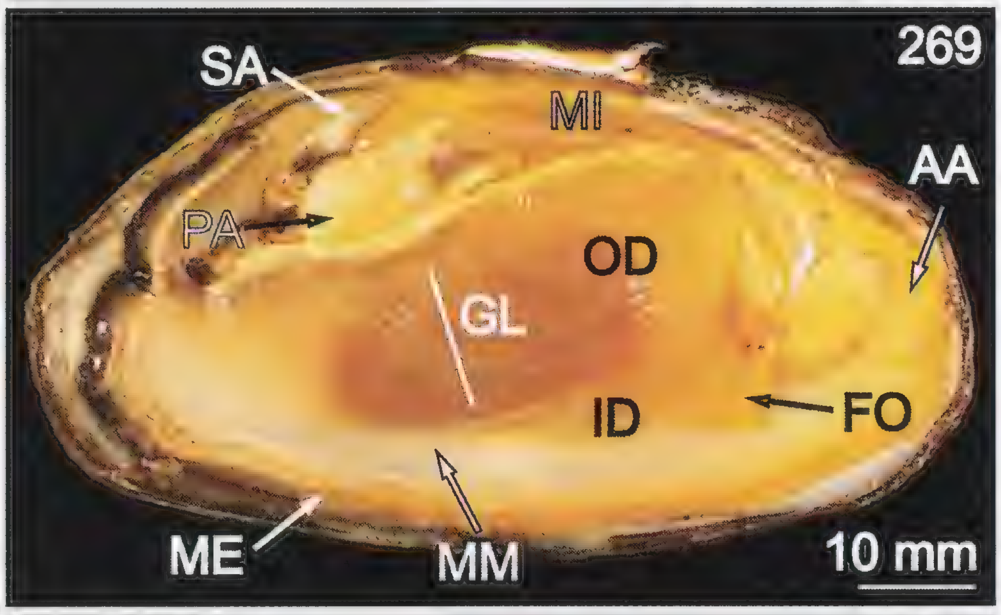

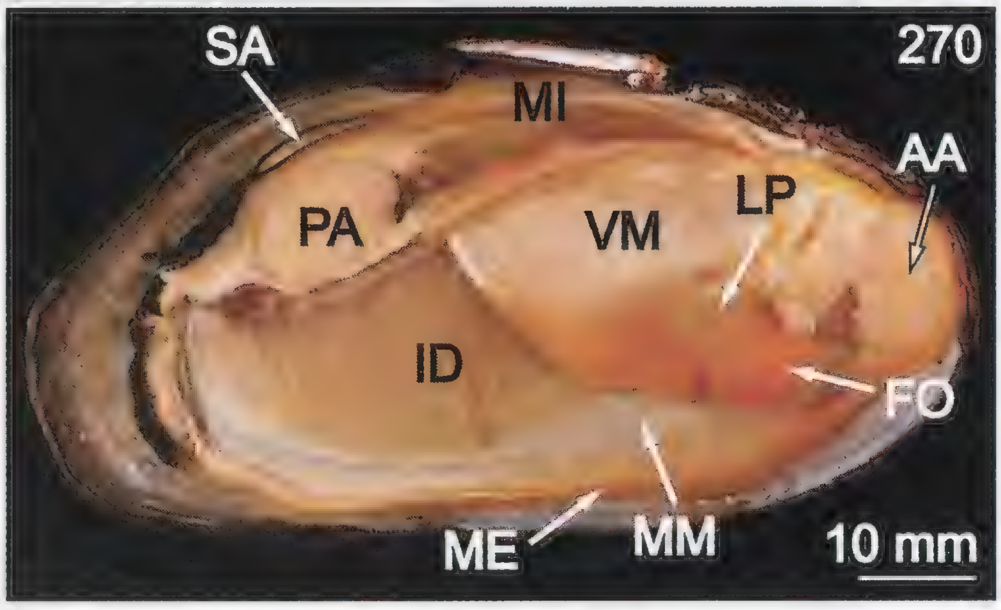

epithelium and subepithelial musculature, and the preponderance of granules conspicuously blackens the tissue (Fig. 280).

Middle mantle is a thin integument between mantle edge and visceral mass. An outer epithelium of columnar cells and goblet cells is adjacent to the nacre. Inner epithelium consists of cuboidal cells, and there is a fibrous subepithelium of connective tissue between the outer and inner epithelial layers. Connective tissue of the middle mantle consists of wavy fibers interspersed among hemocytes (Fig. 281).

The isthmus is a keel-like structure extending dorsally from the base of the visceral mass. Mantle isthmus originates anteriorly at the beginning of the digestive diverticulum and terminates posterior to the posterior adductor. Isthmus epithelium is simple columnar with isolated goblet cells and appears to have a flattened to irregular. Isthmus epithelial cells have a pale, eosinophilic cytoplasm and a monochromatic, ovular nucleus, but columnar cells along the dorsal margin are strongly basophilic. Mantle isthmus has a subepithelium consisting of connective tissue fibers and hemocytes (Fig. 282).

Cellular Structure of Gill

Non-Marsupial Demibranch: Gill demibranchs are non-plicate consisting of ascending and descending lamellae with a series of horizontally oriented filaments. Ascending and descending gill lamellae are joined by a regular arrangement of septa. Cylindrical, vertical water tubes are located between ascending and descending lamellae (Fig. 283). Branchial filaments are cylindrical with three groups of cilia (lateral, latero-frontal, and frontal) along the lateral and distal surfaces. Filaments are each supported by a pair of basophilic skeletal rods and a pale, eosinophilic matrix of connective tissue. The medial aspect of gill filaments consists of a simple squamous epithelium comprising hemolymph vessels. Groups of two or more ctenidial filaments are separated by horizontal pores or ostia. Water is admitted into the water tubes through a series of ostia distributed throughout the gill (Fig. 284). The structure of the inner and outer gills is functionally identical (except for marsupial demibranchs, see below) until the ventral margin. Outer demibranchs have a convex ventral margin (Fig. 285), and the ventral margin of an inner demibranch is furrowed to allow particles captured along the lateral surfaces to accumulate in the median (Fig. 286).

Inner demibranchs and outer demibranchs also differ in the way gill tissue is joined to connective tissue dorsally. Ascending lamellae of the inner demibranchs are united with the dorsolateral portion of the visceral mass until the anterior-posterior midline of the visceral mass near the gonopores. The ascending lamella of the inner gill becomes separated from the body at the anterior margin of the nephridium near the urethra (Fig. 287). Descending lamellae of the inner demibranchs

---

←

FIGS. 263–270. Shell morphology, and gross anatomical features of the mantle cavity of *Strophitus connasaugaensis*. FIG. 263: Lateral view of right valve showing the anteriorly directed umbo (UM), dorsally located ligament (LI), posterior slope (PS), and posterior ridge (PR); FIG. 264: Lateral view of left valve showing the anteriorly directed umbo (UM), dorsally located ligament (LI), posterior slope (PS), and a well-defined posterior ridge (PR); FIG. 265: Medial view of the right valve showing the leading edge of the periostracum (PE), nacre (NA), pallial line (PL), anterior adductor scar (AS), posterior adductor scar (PS), pseudocardinal tooth (PT), interdentum (ID), umbo cavity (UC), and ligament (LI); FIG. 266: Medial view of the left valve showing the leading edge of the periostracum (PE), nacre (NA), pallial line (PL), anterior adductor scar (AS), posterior adductor scar (PS), pseudocardinal tooth (PT), interdentum (ID), umbo cavity (UC), and ligament (LI). FIG. 267: Ventrolateral view of *Strophitus connasaugaensis* (ca. 80 mm shell length) buried in sand at Shoal Creek with its mantle cupped forming an incurrent aperture (IA) and excurrent aperture (EA); FIG. 268: Medial view of the mantle cavity with the right valve and right mantle removed to show the position of the mantle edge (ME), middle mantle (MM), foot (FO), anterior adductor (AA), labial palp (LP), inner demibranch (ID), outer demibranch (OD), posterior adductor (PA), mantle isthmus (MI), and supraanal aperture (SA); FIG. 269: Medial view of the mantle cavity with the right valve and right mantle removed to show the position of the mantle edge (ME), middle mantle (MM), foot (FO), anterior adductor (AA), inner demibranch (ID), outer demibranch (OD), glochidia (GL), posterior adductor (PA), mantle isthmus (MI), and supraanal aperture (SA); FIG. 270: Medial view of the mantle cavity with the right valve, right mantle, and right gills removed to show the position of the mantle edge (ME), middle mantle (MM), foot (FO), labial palp (LP), visceral mass (VM), anterior adductor (AA), left inner demibranch (ID), posterior adductor (PA), mantle isthmus (MI), and supraanal aperture (SA).

271

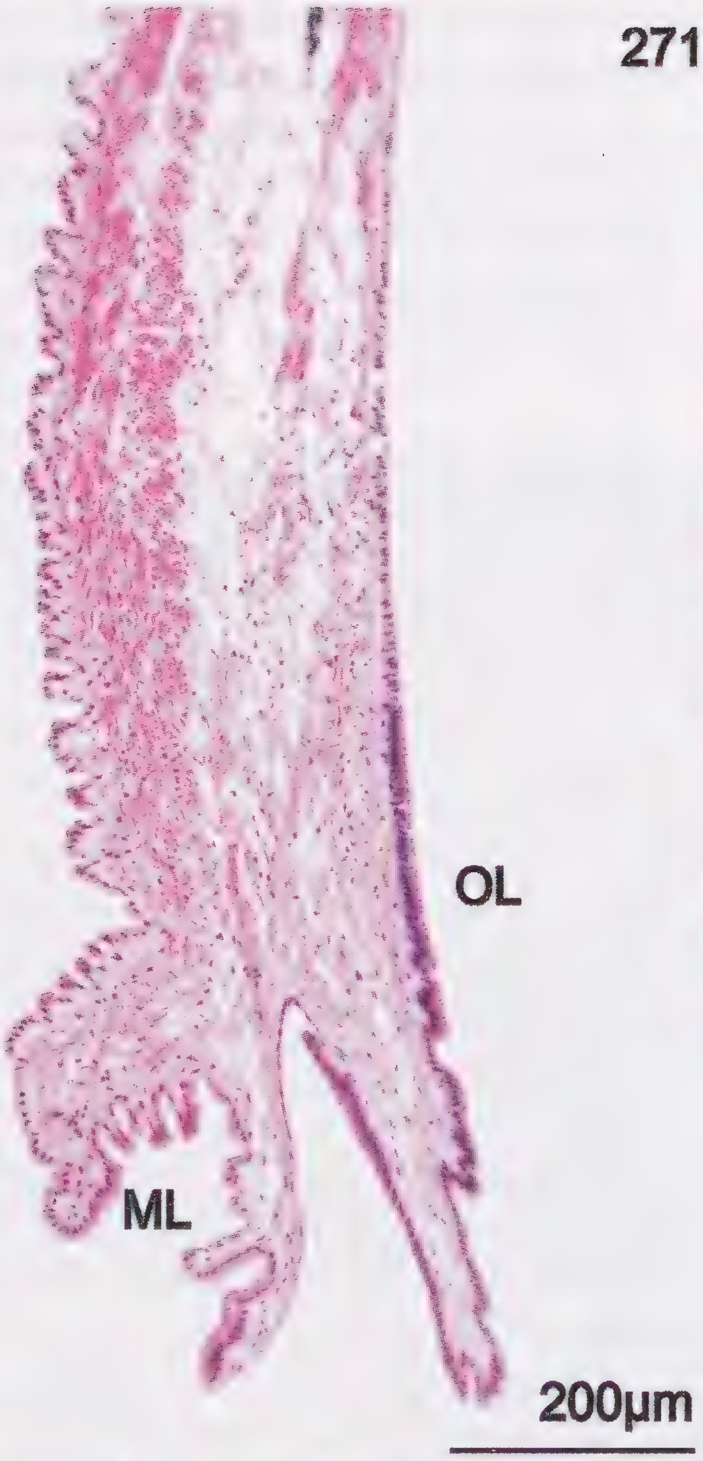

272

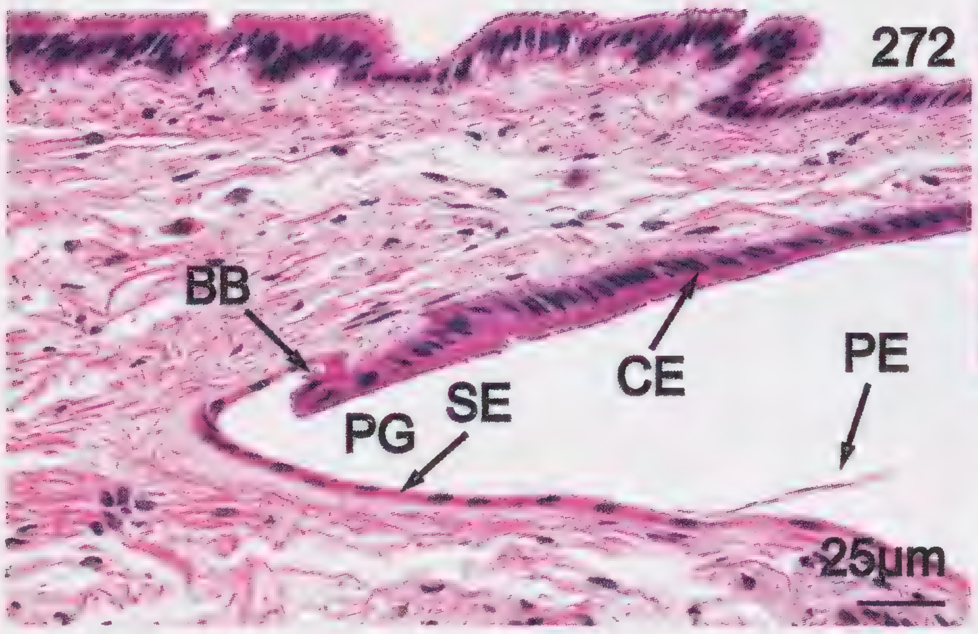

273

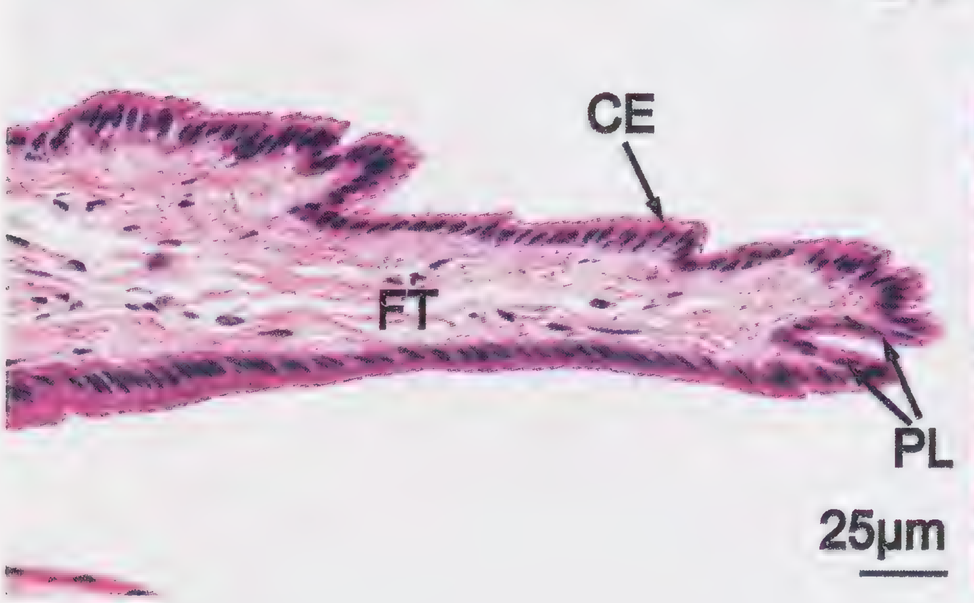

274

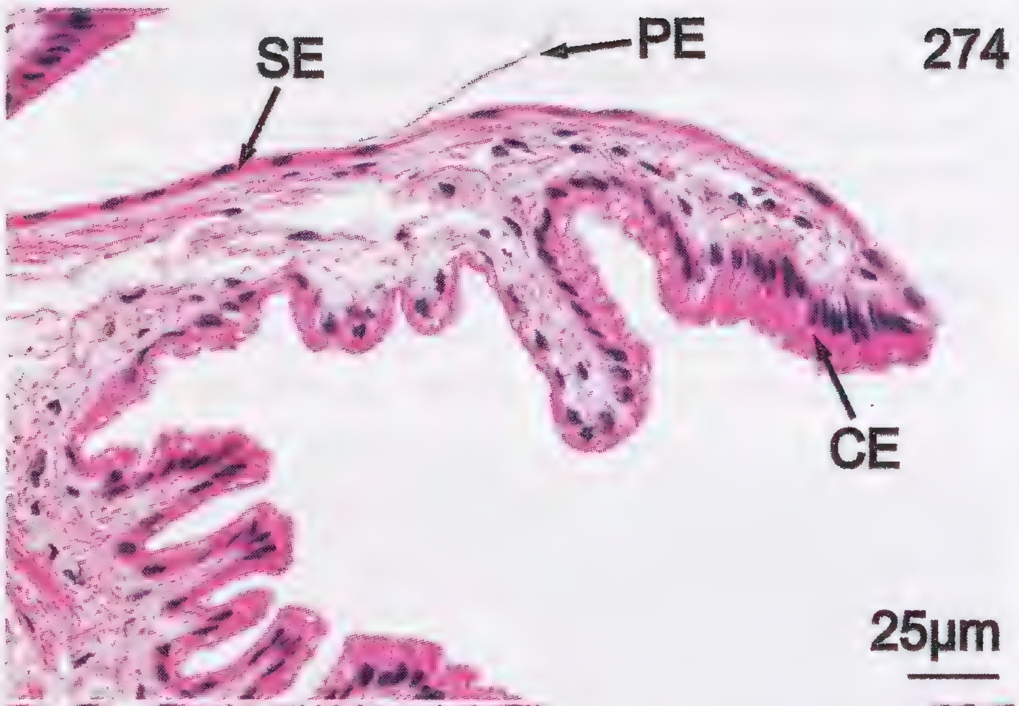

275

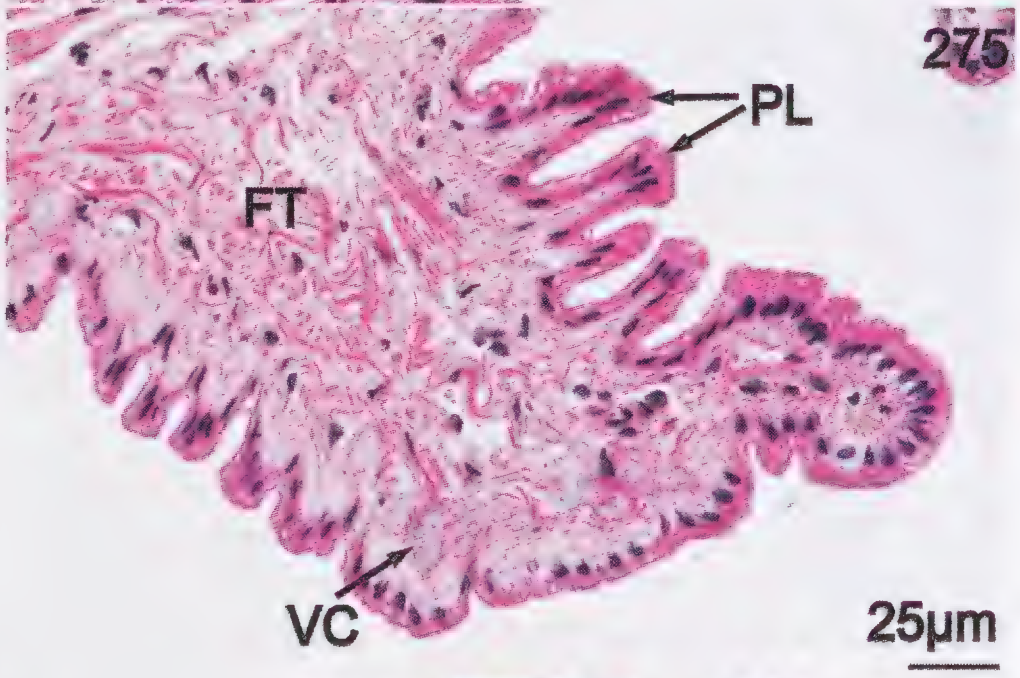

276

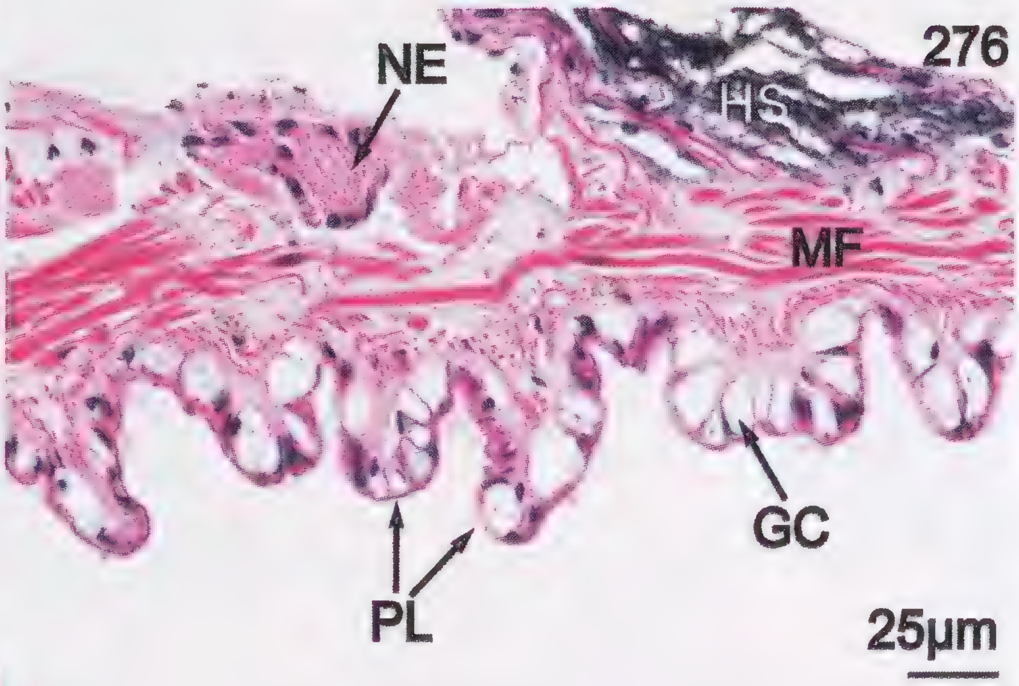

277

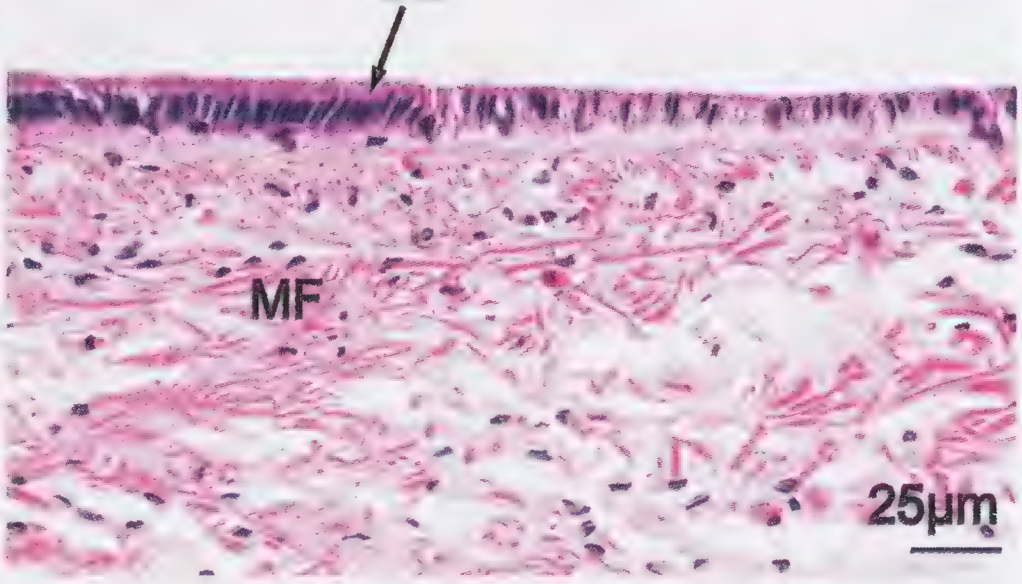

are connected to connective tissue located ventrally to the nephridia. At the dorsal end of the inner demibranch paired fascicles span the length of the gill (Fig. 288). Descending lamellae of the outer demibranchs are joined to the abdomen by connective tissue, and muscle fascicles are absent from the dorsal end of the outer demibranch (Fig. 289). Outer lamellae of outer demibranch joins a narrow region of connective tissue near the middle mantle (Fig. 290).

Marsupial Demibranch: Female *S. connasaugaensis* brood their glochidia larva in the outer demibranch, and virtually the whole gill is used for larval incubation (Fig. 291). A marsupial demibranch is expanded and includes a cylindrical mass of connective tissue, hemolymph and a sac containing glochidia. Overall, the marsupium of *S. connasaugaensis* is moderately enlarged. The ventral margin of the marsupium is convex and thickened with loose connective tissue and hemolymph (Fig. 292). Interbranchial septum consists of numerous spherical, goblet cells with a basophilic cytoplasm, and a vacuole containing pale, basophilic fibers (Fig. 293). Glochidia within a filled marsupium appear to be held together by strands of fibrous tissue, possibly representing a binding substance of a conglutinate of embryos. Glochidia are semicircular with a prominent, median adductor. Two tissue components are evident in regard to the valves; there is an eosinophilic, granular constituent and a basophilic material with a homogenous staining character (Fig. 294). Glochidia of *S. connasaugaensis* attach to fish skin and glochidial valves have spines along the ventral margin of the valves (Fig. 295). A collection of *S. connasaugaensis* from May 2011 presented an opportunity to study the outer gills of a female without glochidia. The marsupium was laterally expanded in comparison to the inner gill, and there was a medial core of connective tissue and hemolymph, which may represent a contracted placenta within the central water tube (Fig. 296).

Cellular Structure of Foot and Associated Tissues

Pedal Musculature and Byssal Gland: The ventral margin of the foot features a triangular array of overlapping muscle fibers in the median, subepithelial granulocytes and a highly folded integument (Fig. 297). Violet staining granulocytes are located directly beneath the pedal epithelium, while pale, blue-staining granulocytes are medial in respect to violet cells (Fig. 298). Foot muscle is composed of regions of irregular and regular muscle fibers. Musculature in the ventral region of the foot has a woven appearance, with fibers arranged into a vertical and horizontal plane (Fig. 299). The somatic muscle at the base of the foot is organized with distinct vertical and horizontal layers (Fig. 300). The base of the foot is broadly triangular, with an ovular byssal gland located medially at the ventral margin of the coelom, posterior to the pedal ganglion (Fig. 301). The byssal gland is supported by concentric connective tissue fibers and musculature. The lumen is lined with a simple, ciliated columnar epithelium with occasional, pale, basophilic goblet cells. Goblet

---

←

FIGS. 271−277. Anterior mantle edge of *Strophitus connasaugaensis*. FIG. 271: Transverse section of the mantle edge portraying the position of the outer lobe (OL), middle lobe (ML), and inner lobe (IL); FIG. 272: Transverse view of the base of the outer and inner mantle lobes showing columnar epithelium (CE) and basal bulb (BB) of the outer lobe, squamous epithelium (SE) of the middle lobe, periostracal groove (PG) and periostracum ribbon (PE); FIG. 273: Transverse section of the free distal tip of the outer mantle lobe featuring columnar epithelium (CE), plicae (PL), and fibrous tissue (FT) in the subepithelium; FIG. 274: Transverse section of the middle mantle lobe revealing squamous epithelium (SE) and periostracum (PE) along the ventral surface, and columnar epithelial cells (CE) of the dorsal surface; FIG. 275: Transverse section of the inner mantle lobe featuring narrow plicae (PL), violet cells (VC), and irregular fibrous tissue (FT); FIG. 276: Transverse section of the dorsal epithelium of the base of the mantle edge featuring plicae (PL), goblet cells (GC), and a subepithelium consisting of myofibers (MF), hemolymph sinuses (HS), and nerves (NE); FIG. 277: Transverse section of the base of the mantle edge revealing a deeply basophilic columnar epithelium (CE), and myofibers (MF) in the subepithelium.

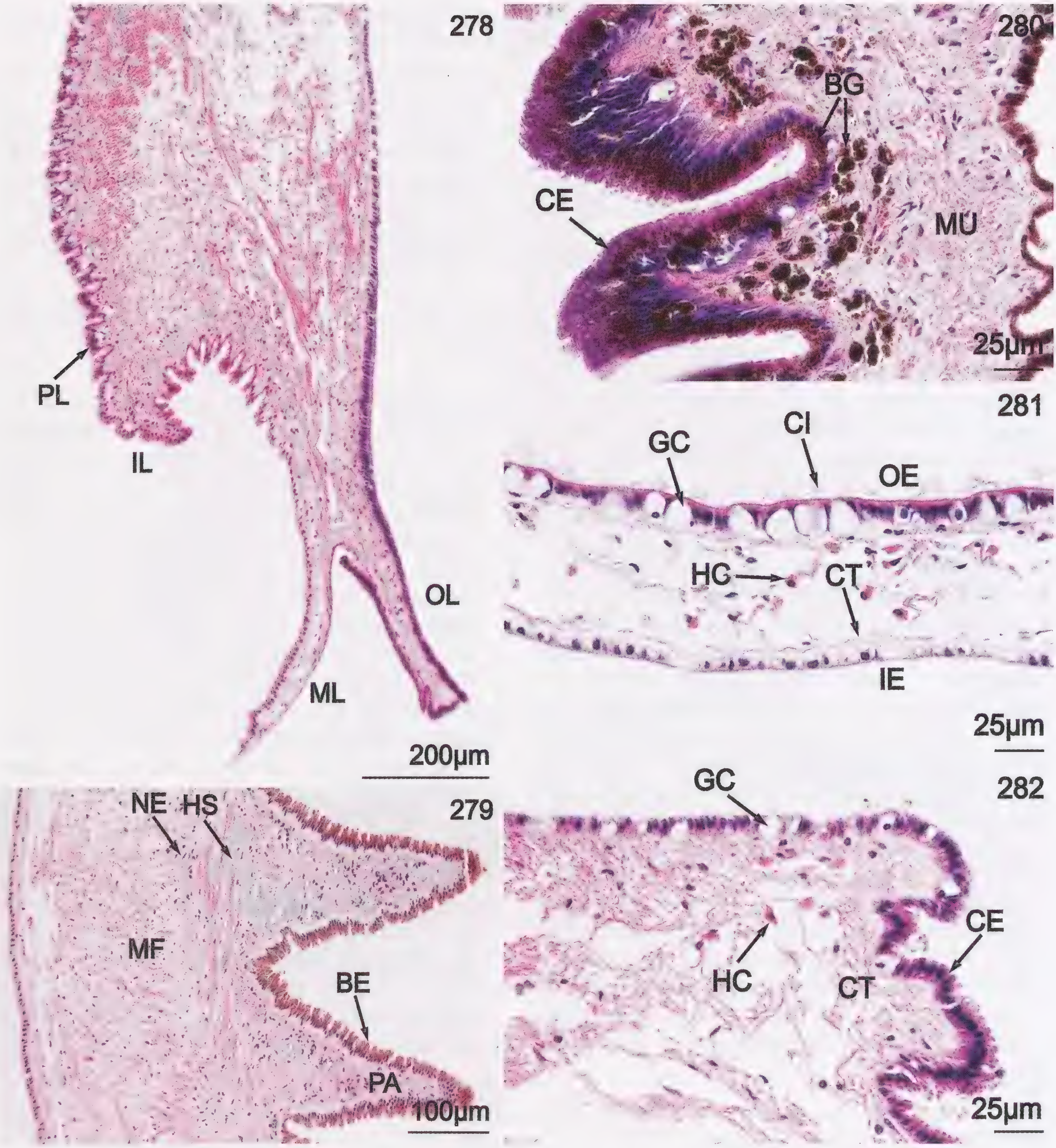

FIGS. 278–282. Posterior mantle edge, middle mantle, and mantle isthmus of *Strophitus connasaugaensis*. FIG. 278: Transverse section of posterior mantle edge revealing thin outer lobe (OL) and middle lobe (ML) and a triangular inner lobe (IL) featuring plicae (PL) along the dorsal and ventral surfaces; FIG. 279: Sagittal section of posterior mantle edge characterized by conical papillae (PA) with brown-pigmented epithelium (BE), and a subepithelium consisting of hemolymph sinuses (HS), nerves (NE) and myofibers (MF); FIG. 280: Sagittal section of posterior mantle edge emphasizing brown intracellular granules (BG) present in columnar epithelium (CE), and subepithelial musculature (MU); FIG. 281: Transverse section of middle mantle displaying a outer epithelium (OE) of columnar cells bearing cilia (CI), goblet cells (GC) inner epithelium (IE), connective tissue (CT), and hemocytes (HC); FIG. 282: Transverse section of mantle isthmus emphasizing columnar epithelium (CE), goblet cells (GC), and irregular connective tissue (CT) and hemocytes (HC) in the subepithelium.

cells are interspersed among columnar cells in the lumen, and the contents of goblet cells appear granular to wispy. Byssal gland goblet cells are similar in some respects to goblet cells of marsupial septa (see Fig. 293). The vestiges of the byssus is represented by a spherical, mass containing a pale to darkened eosinophilic material. The byssal mass occupies the center of the byssal gland lumen and is surrounded by an irregular, eosinophilic mass, likely constituting a fluid (Fig. 302). Vestiges of the byssal canal were not observed in histological sections of the foot.

Pedal Integument and Mesentery: There are five epithelium types surrounding the foot and visceral mass. From ventral to dorsal, the integument is initially pleated with deep folds, and the folds become shorter in height and narrower in width. In the first two regions, plicae are tall and thickened with subepithelial musculature. The first region possesses ciliated, columnar cells with a subepithelium consisting of irregular myofibers and violet granulocytes. Ciliated cells have an eosinophilic cytoplasm, similar to the coloration of the underlying muscle tissue, and cilia are short and nearly straight. Nuclei of type one epithelium are ovular and have a homogenous staining character (Fig. 303). Epithelial region two consists of tall plicae with a more conspicuous space between the folds. Columnar cells largely lack cilia and have an ovular, monochromatic nucleus. Numerous goblet cells are present and closely juxtaposed, giving the tissue the appearance of large, ovular to teardrop-shaped mucus pores. Subepithelial tissue of integument type two consists of horizontally arranged myofibers (Fig. 304). Plicae are noticeably reduced in height and width in region three. Cells in the second region have similar cytological characteristics as region one, however ciliated cells are sparsely distributed. The third integumentary region has two layers of musculature, including a horizontally and a vertically oriented layer (Fig. 305). Integument four consists of a squamous epithelium around rectangular folds of connective tissue. There is a prominent space between the epithelium and pedal musculature of region four. The space possibly represents a hemolymph sinus (Fig. 306). The fifth integumentary region of the foot is flattened, with squamous cells and goblet cells. Only a subtle waviness of the tissue layer is reminiscent of the plications further down the length of the foot. Musculature under the fifth epithelium is thinner and is separated from the overlying epithelium except for occasional fibrous, connective tissue linkages (Fig. 307). While the pedal integument is pleated, the folds occur in an irregular manner and sagittal sections reveal an irregular series of furrows (Fig. 308).

The sinistral and dextral halves of the visceral mass are joined by mesentery fascicles distributed throughout the coelom (Fig. 309). Fascicles are composed of eosinophilic fibrils with a pale to darkened cytoplasm, and fibrils are quadrangular to polygonal. Furthermore, there does not appear to be an obvious pattern of fibril arrangement within a fascicle, and the mesentery bundles are histologically identical to pedal muscle fibers (Fig. 310).

Labial Palps, Oral Groove and Esophagus: Labial palps of *S. connasaugaensis* have an inner surface lined with ciliated, rectangular plicae and a smooth outer surface (Fig. 311). Plicae of the inner palp surface are rectangular with a flattened dorsal margin and a pleated ventral surface. Ciliated columnar cells represent the main constituent of the inner palp epithelium and extend along the palp interior up to the distal margin of each lip. Ciliated cells of the inner palp surface have a pale, basophilic cytoplasm and an ovular, monochromatic nucleus. The surface of the epithelium is densely ciliated and cilia are wispy (Fig. 312). The free distal palp tip transitions from a pleated, ciliated epithelium to a non-ciliated mucosa characterized by ovular goblet cells (Fig. 313). The external palp surface is flattened, with non-ciliated cuboidal cells with a monochromatic nucleus (Fig. 314). Subepithelial tissue of the labial palp is composed of loose connective tissue and hemolymph sinuses.

Anterior Adductor and Anterior Pedal Retractors: Anterior adductor consists of bands of eosinophilic myofilaments longitudinally oriented across the viscera. Fibers are eosinophilic and typically appear wavy in histological sections. Myocytes have emarginated and

283

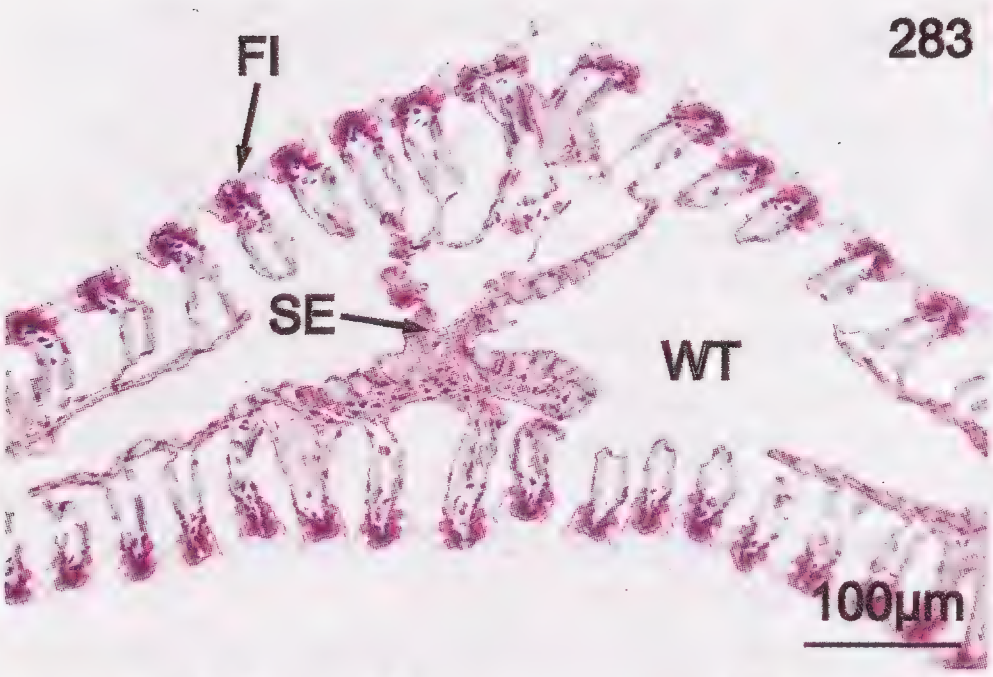

284

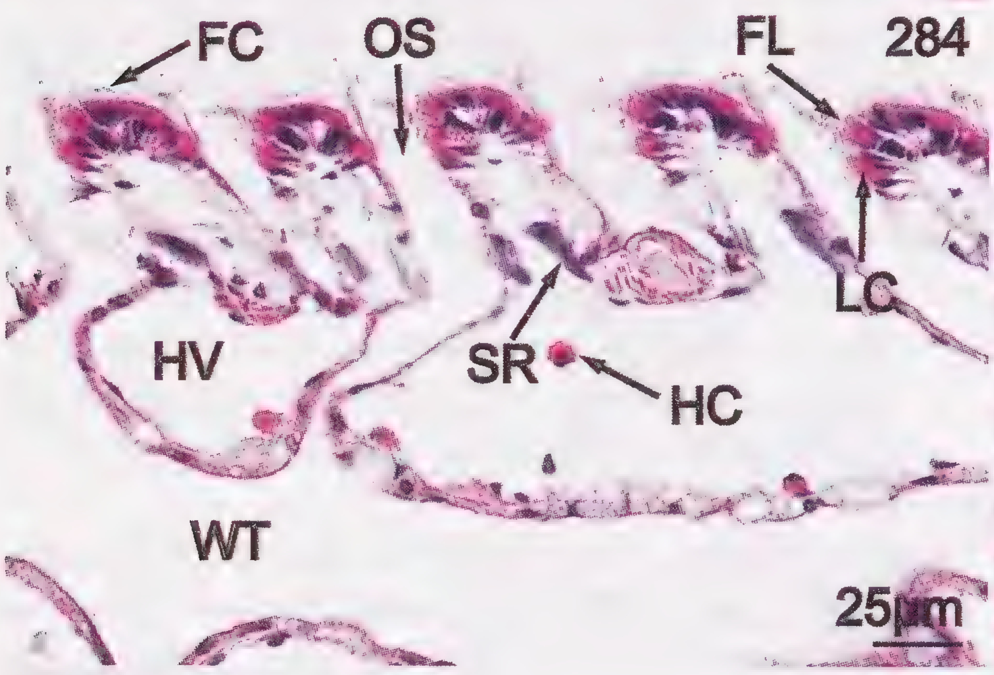

285

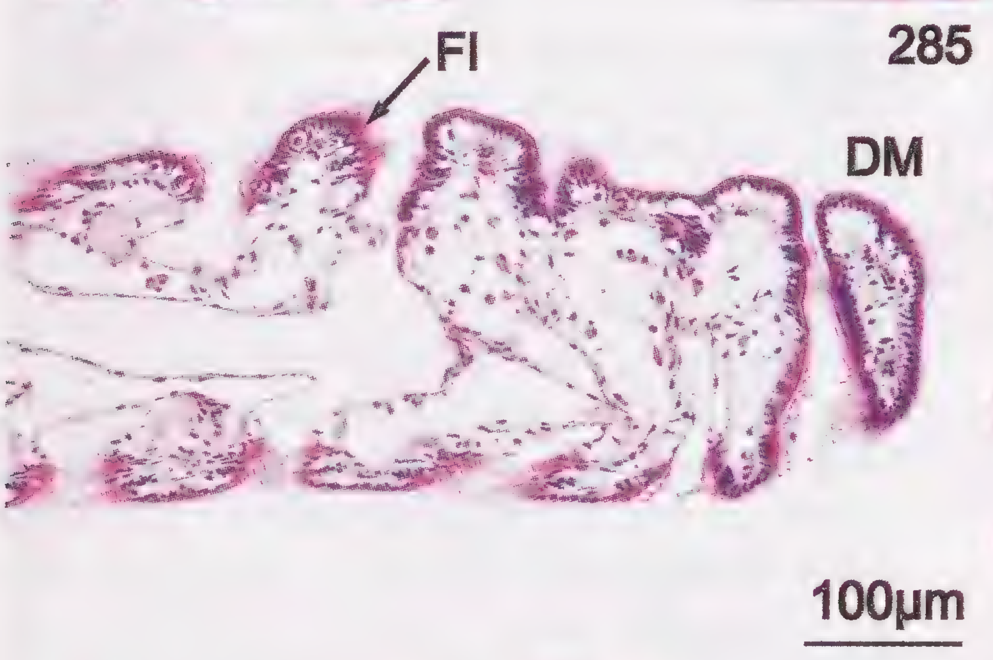

286

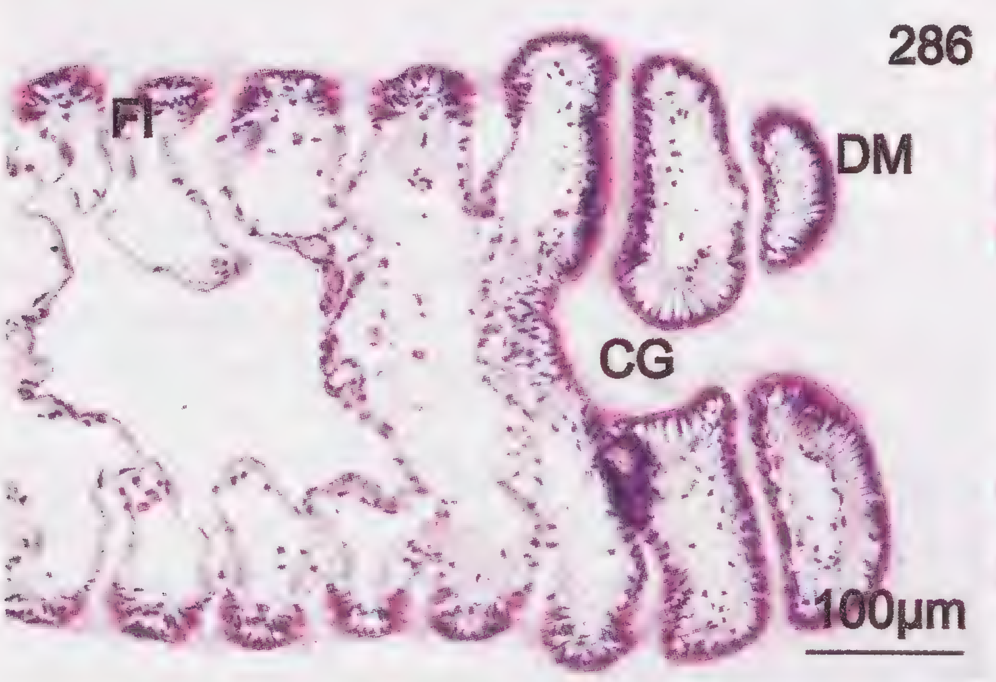

287

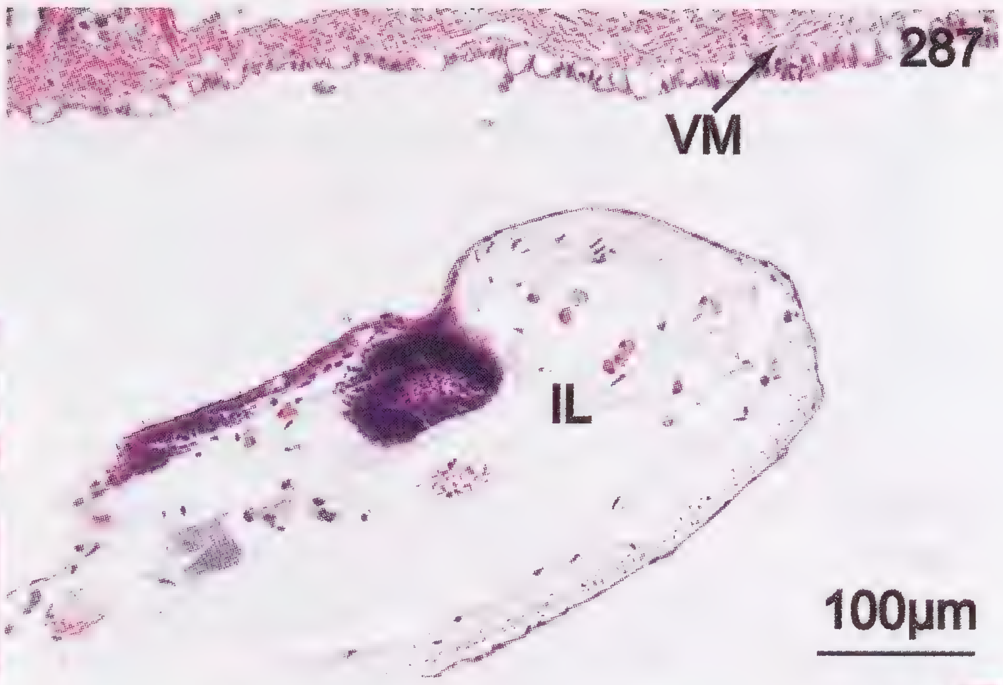

288

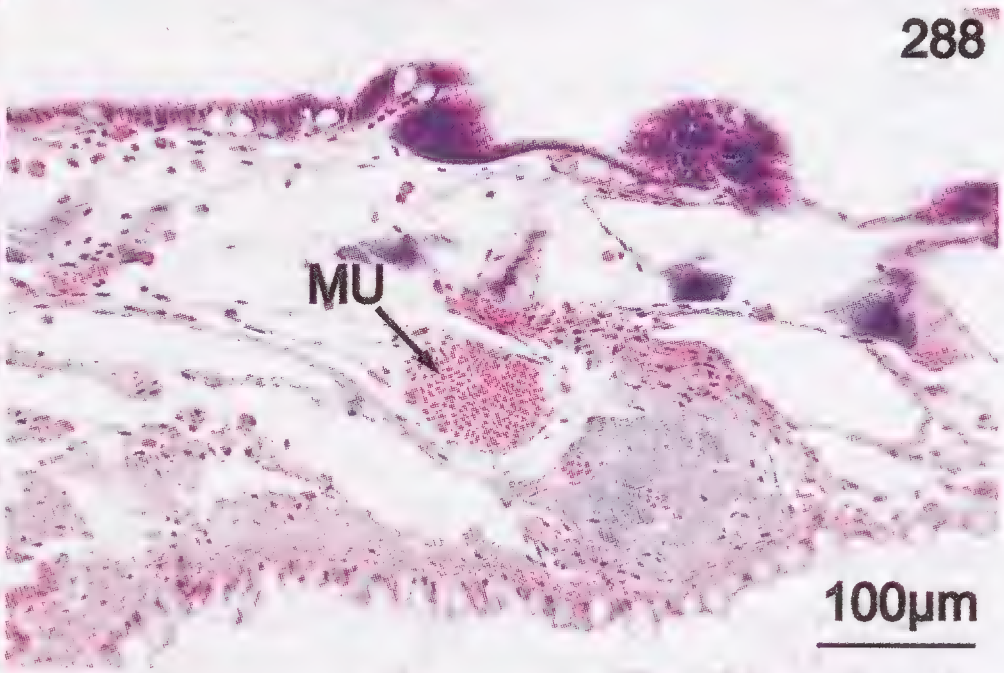

289

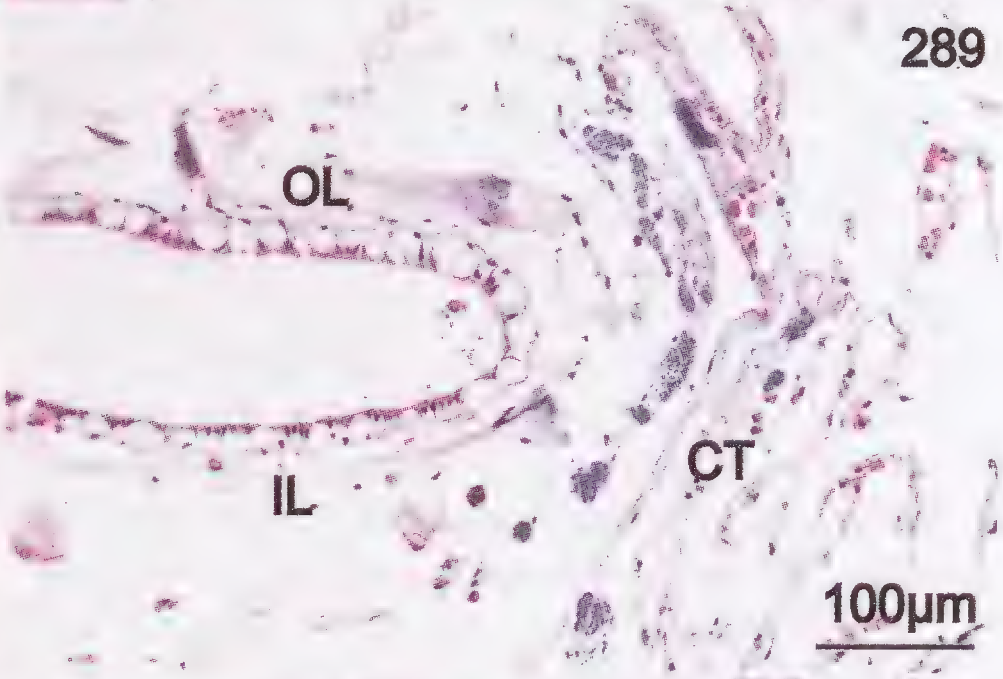

290

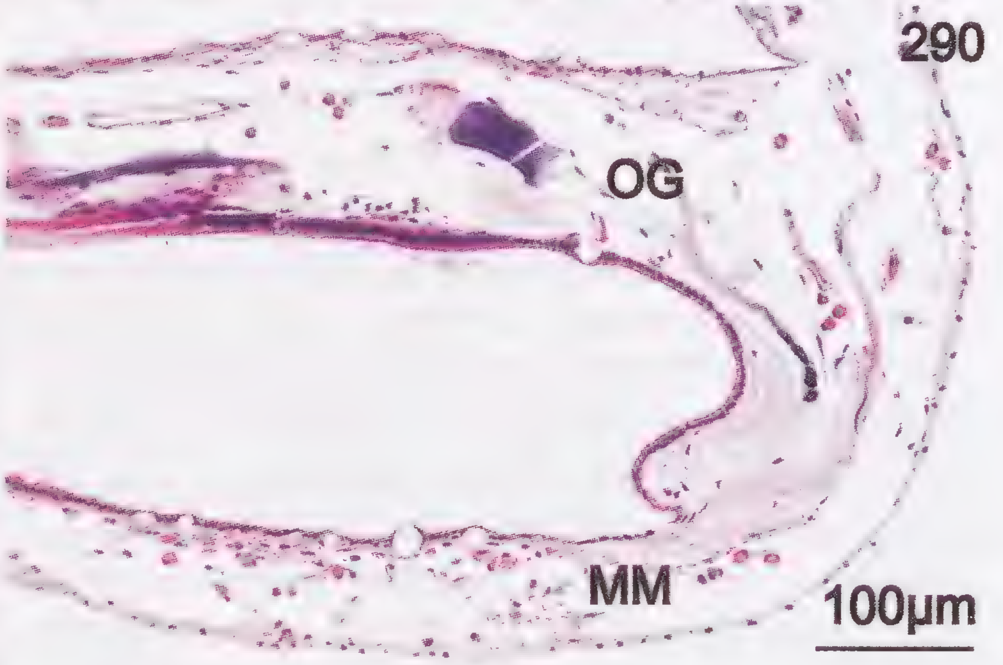

elongated nuclei with granular chromatin. Perimysium consists of thin wispy connective tissue fibers and form ellipsoid chambers that may contain hemolymph. Additionally, the underlying space of perimysium consists of black granules (Fig. 315). The anterior pedal retractors are located between the labial palps and mantle, and fascicles are arranged in a transverse orientation when the visceral mass is sectioned transversely. The epimysium, perimysium and endomysium are present, but these structures are delicate and thin (Fig. 316).

Oral Groove and Esophagus: Oral groove is a derivation of labial palp wrapping around the anterior visceral mass. In transverse sections of visceral mass, the oral groove appears as a large chamber posterior to the anterior adductor. The ventral wall of the oral groove resembles the distal margin of a labial palp. The ventral epithelium of the lip resembles the flattened epithelium along the outer surface of the palp, while the elongated, rectangular plicae appear to be a continuation of inner palp epithelium. Additionally, the plicae contain elliptical, basophilic goblet cells (Fig. 317). Note the similarity between the columnar epithelium of the oral groove ledge with the epithelia along the inner surfaces of the palps, located at the dorsal end of the palps (Fig. 311). The lateral walls of the oral groove consist of cuboidal cells bearing cilia, and a loose matrix of connective tissue fibers comprises the subepithelium (Fig. 318). The dorsal epithelium is flattened with ciliated columnar cells (Fig. 319).

The esophagus is a tubular continuation of the palps, since the walls feature, tall, rectangular plicae. The esophagus is ovular, with concentric connective tissue fibers forming a distinct lamina propria (Fig. 320). The esophagus is located at the base of the visceral mass, located between digestive gland tubules and the mantle isthmus. Ciliated, rectangular folds extend from the dorsal and ventral esophageal walls. Epithelial cells are pseudostratified and ciliated, with an eosinophilic cytoplasm and an elliptical, monochromatic nucleus. Cilia along the apical surface of esophageal cells are short and generally straight. The lumen of the esophagus may contain a shapeless, eosinophilic mass, which may represent mucus and ingested substances. Additionally, the esophageal epithelium is supported by concentric layers pink and red eosinophilic fibers, creating a heterogeneous lamina propria. The esophagus is lined with plicae featuring ciliated columnar cells, and there is a subtle, median furrow to the surface of each plication (Fig. 321).

Cellular Structure of the Alimentary Canal

Digestive Diverticulum: The esophagus opens dextrally into the digestive diverticulum and where there is a conspicuous “L”-shaped chamber. The walls of the vestibular chamber feature cylindrical plicae similar to the constituents of the esophageal-digestive diverticulum junction of *F. cerina*. The lumen of the vestibular chamber contains irregular patches of an eosinophilic fluid, possibly

←

FIGS. 283–290. Outer demibranch and inner demibranch of *Strophitus connasaugaensis*. FIG. 283: Transverse section of inner gill displaying horizontally oriented filaments (FI), a septum (SE) linking the inner and outer lamella, and a median water tube (WT); FIG. 284: Transverse section of the inner lamella of inner gill showing the main tissue components of gill including frontal cilia (FC), frontal-lateral cilia (FL), lateral cilia (LC), ostia (OS), hemolymph vessels (HV), hemocytes (HC) skeletal rods (SR), and a water tube (WT); FIG. 285: Transverse section of the distal tip of outer gill characterized by a rounded distal margin (DM), resembling merged branchial filaments (FI); FIG. 286: Transverse section of the distal margin (DM) of the inner gill characterized by a median ciliated groove (CG); FIG. 287: Transverse section of the inner lamella (IL) of the inner gill showing its separation from the base of the visceral mass (VM); FIG. 288: Transverse section of the base of the inner gill where muscle fascicles (MU) are aligned anterior to posterior; FIG. 289: Transverse section of the base of the gill showing the junction of the outer lamina of the inner gill (OL), and inner lamella of the outer gill (IL), and loose connective tissue; FIG. 290: Transverse section of the base of the gill showing the junction between the outer lamina of outer gill (OG) and middle mantle (MM).

291

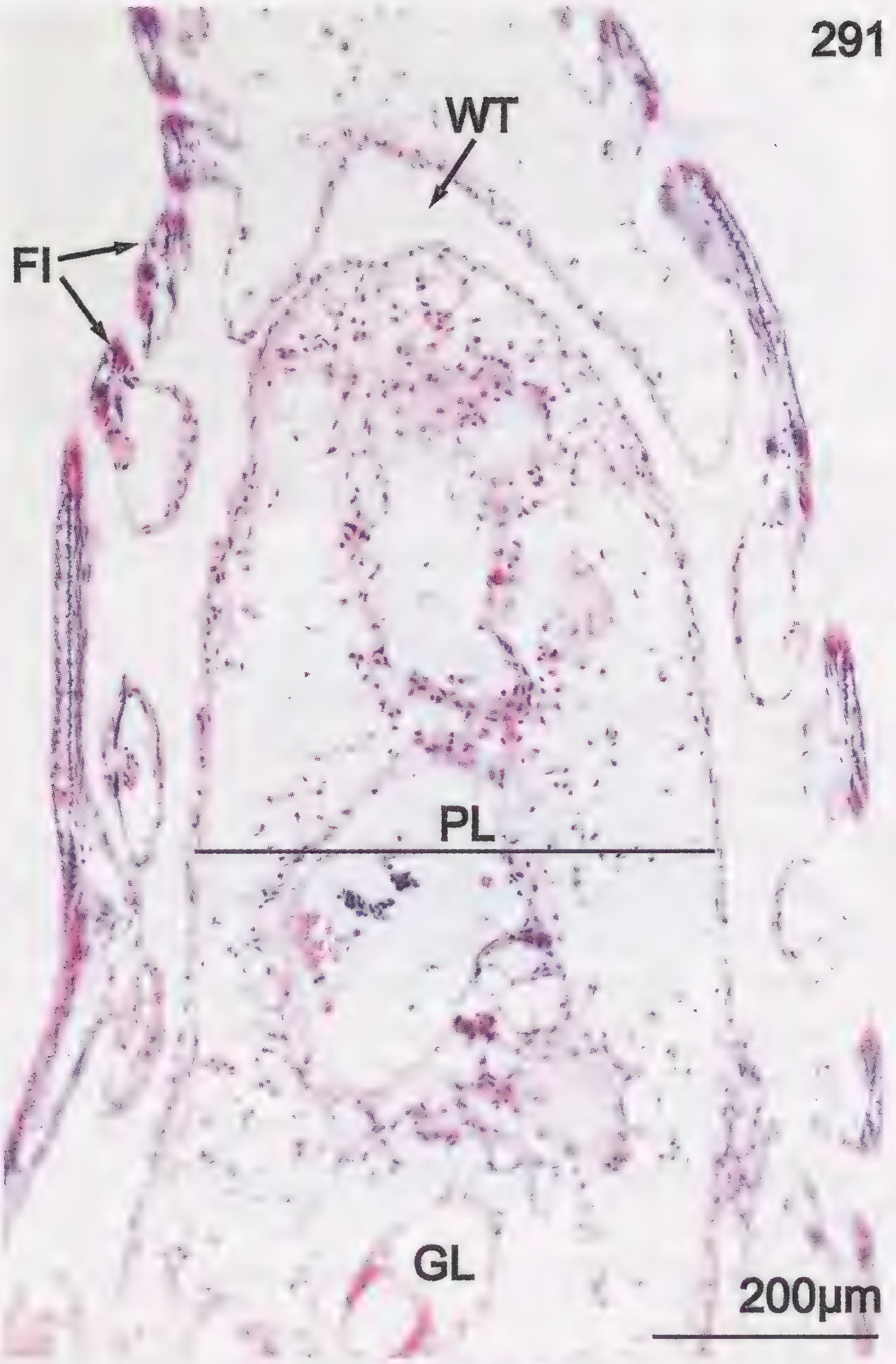

292

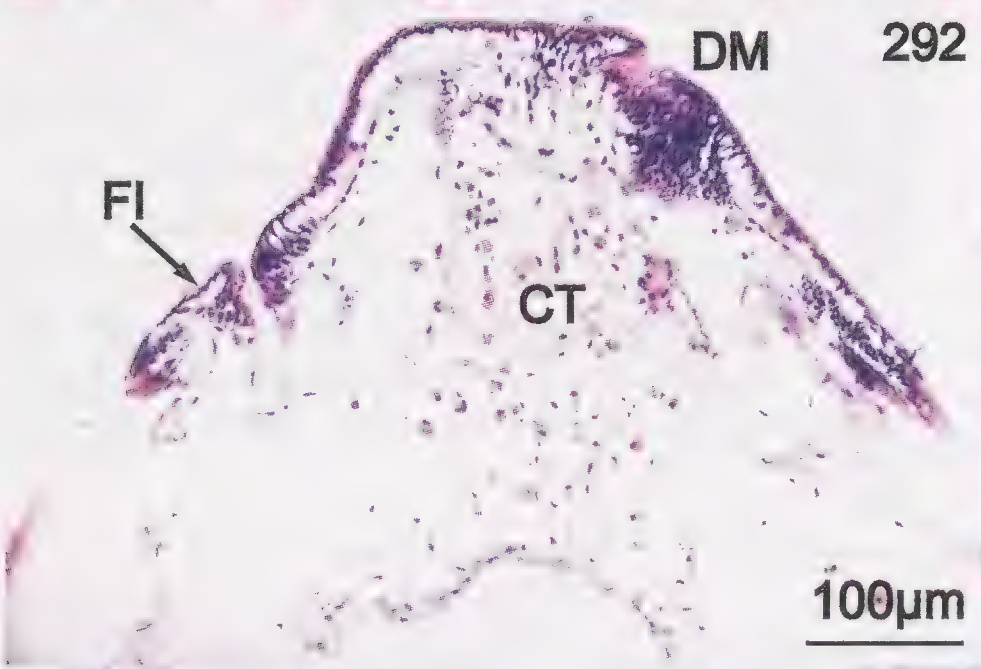

293

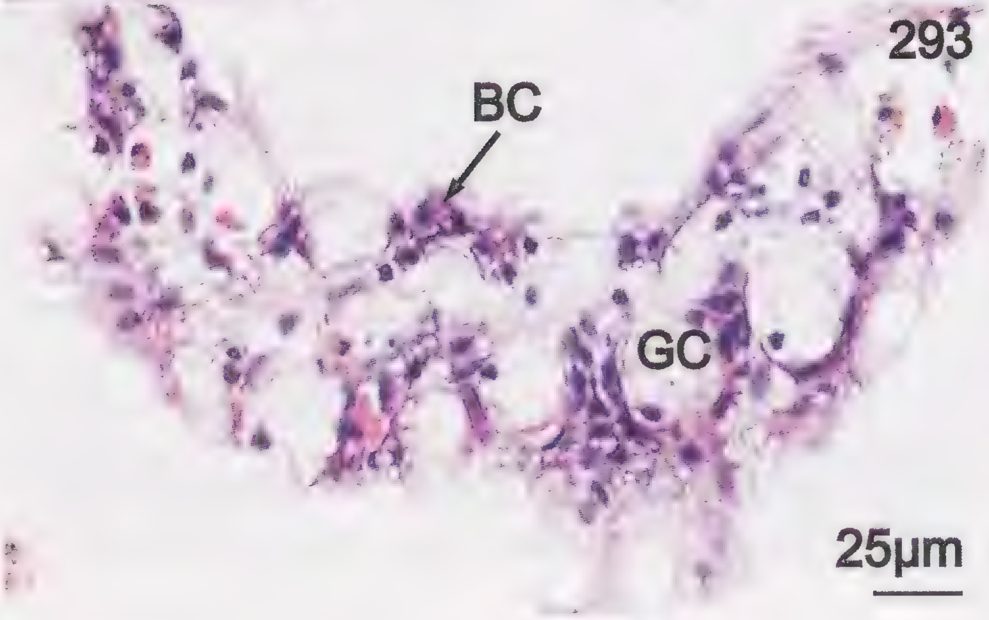

294

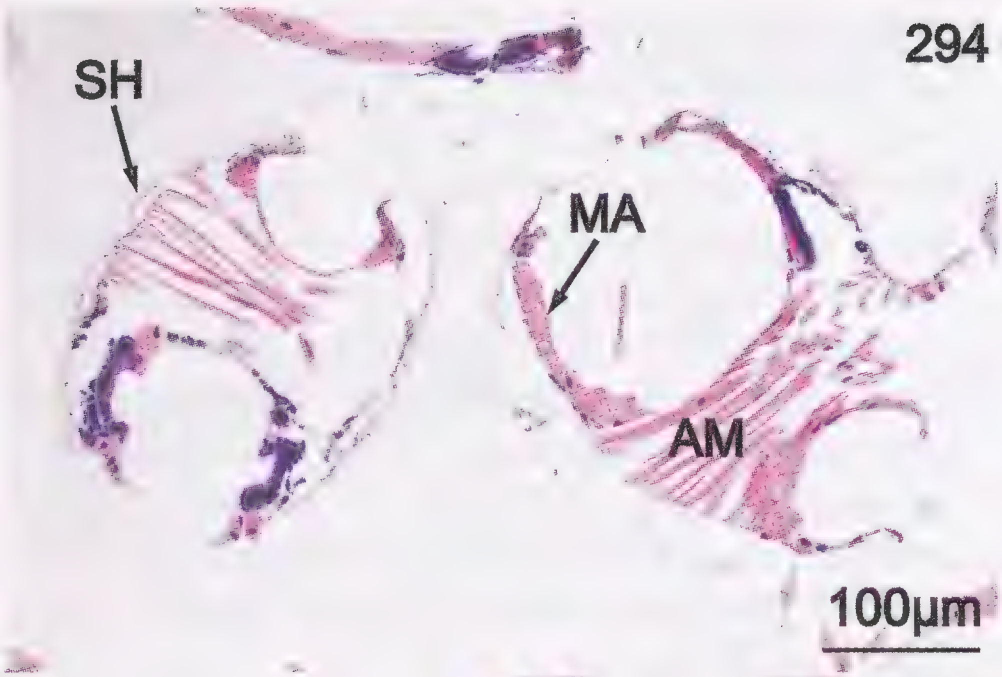

295

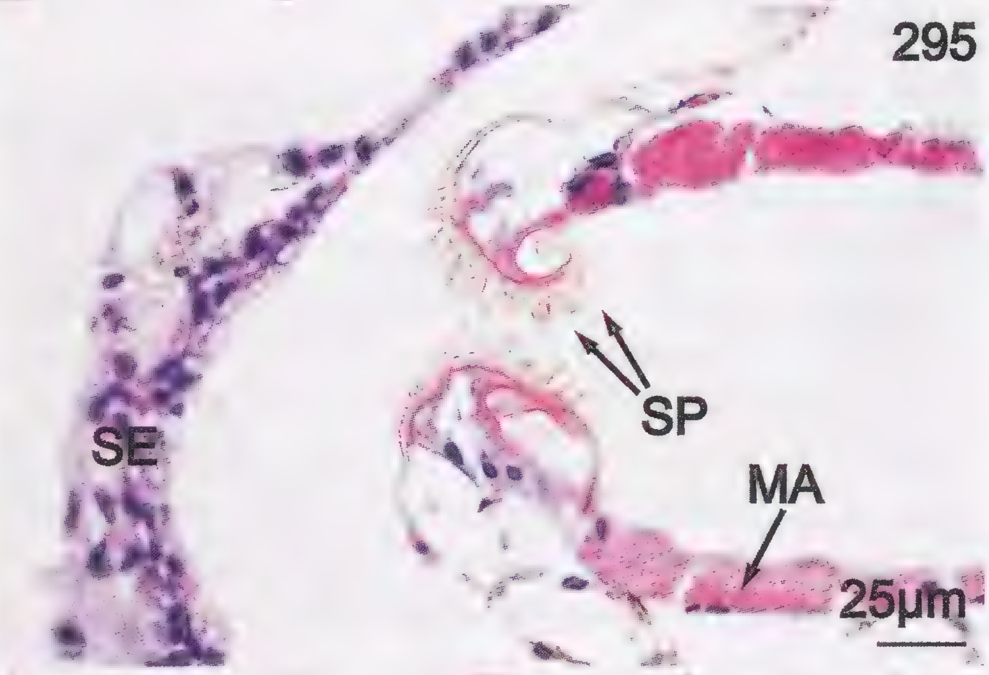

296

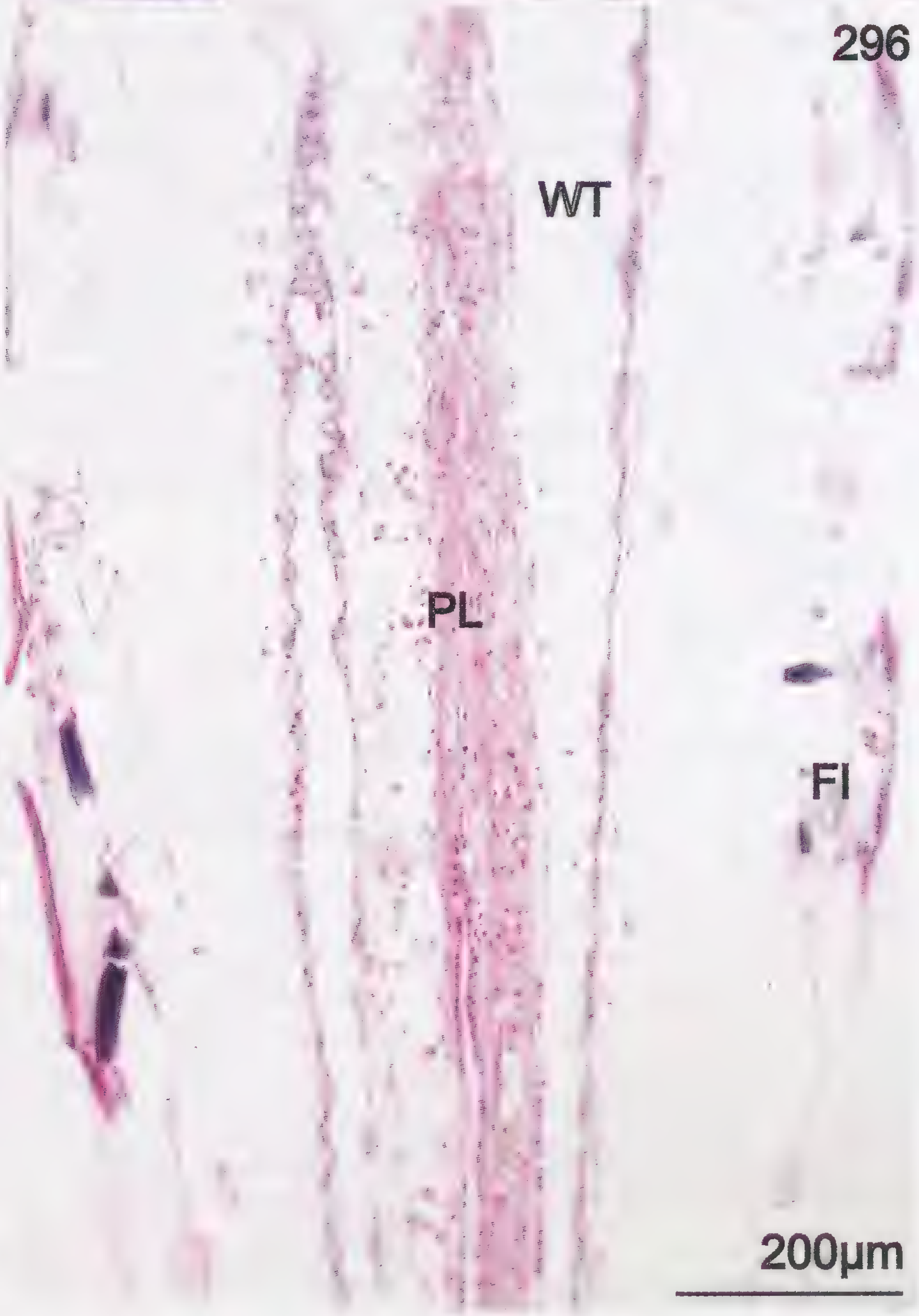

mucus (Fig. 322). Plicae of the vestibule are cylindrical and ciliated, and the subepithelium features a well-defined connective tissue support (Fig. 323). The cell types of the vestibule resemble digestive diverticulum type one epithelium. Cells are ciliated and columnar with a conspicuously eosinophilic cytoplasm and contain a granular nucleus with a small nucleolus. Plicae of type one tubules are flattened to rounded, and some plicae have a single, median furrow (Fig. 324). Secondary tubules have a homogenous, eosinophilic character and a minute brush border membrane (Fig. 325). Furthermore, type two tubules of *S. connasaugaensis* do not appear vesiculated (Fig. 326). Tertiary tubules of *S. connasaugaensis* consist of columnar digestive cells with an eosinophilic, vesiculated cytoplasm, and triangular, dark-staining basophil cells. A small, spherical nucleus may be located at the base of basophilic cells and the nucleus has a darker staining character than the surrounding cytoplasm (Fig. 326).

Stomach: The stomach is somewhat square-shaped, located between the digestive diverticulum and crystalline style sac. The gastric walls are pleated nearly on all sides, and there is a prominent typhlosole along the dextral wall (Fig. 327). The ventral wall has a distinctive cuticle (Fig. 328). The cuticle is attached to cilia of the columnar epithelium and it has linear fibers embedded within it. The cytoplasm of these columnar cells is pale, eosinophilic with brown intracellular granules. The nucleus is ovular and contains a distinct nucleolus (Fig. 329). The medial portion of the ventral gastric wall features a furrow and the cuticle is absent from the sinistral portion of the gastric epithelium (Fig. 330). The sinistral portion of the ventral stomach wall consists of a series of rounded, ciliated plicae (Fig. 331). The dorsal margin of the stomach features low, broadly rounded plicae with ciliated columnar cells (Fig. 332). The typhlosole also has a ciliated columnar epithelium, and the distal margin of the typhlosole is forked. Additionally, there is an eosinophilic cuticle surrounding the typhlosole, and it is dense such that microtomy dislodges it slightly from the apical surface of the epithelium (Fig. 333).

Crystalline Style Sac: The crystalline style sac is an ovular chamber spanning the length of the body from the stomach to the posterior margin of the visceral mass. The style is a pale, eosinophilic rod located sinistrally, within the circular aspect of the organ. Extending dextrally from the style sac is a horizontal chamber known as the midgut. The style sac consists of three different types of epithelium based on cell size, staining characteristics and cilium morphology (Fig. 334).

The style sac is lined with rectangular, eosinophilic columnar cells with thick, rigid cilia and a conspicuous cell membrane. Nuclei of type-one cells are ovular and contain a distinct nucleolus (Fig. 335). Type-two epithelium is located along the ventral surface of the midgut, dextral to the median fold. There are a series of short plicae along the dextral wall of the midgut and they are subtle in the anterior portion of the style sac, but become more prominent posteriorly. Columnar cells of type-two epithelium have a slightly more basophilic and vesiculated cytoplasm. Cilia of type-two epithelium are thinner than type-one cilia and appear correspondingly more flexible given their wispy appearance. Nuclei of type-two cells have an ovular nucleus and a median nucleolus (Fig. 336). Type-two epithelium represents the main constituent of the midgut

---

←

FIGS. 291–296. Marsupium, and glochidia of *Strophitus connasaugaenesis*. FIG. 291: Transverse section of a filled marsupium showing distended filaments (FI), water tube (WT), and a cylindrical placenta-like sac (PL) containing glochidia (GL); FIG. 292: Transverse section of the distal margin (DM) of a marsupium portraying distended filaments (FI) and loose connective tissue (CT); FIG. 293: Transverse section of a marsupial septum emphasizing basophilic cells (BC) between basophilic goblet cells (GC); FIG. 294: Transverse section of a marsupium emphasizing the shell (SH), mantle (MA), and adductor muscle (AM) of glochidia; FIG. 295: Transverse section of a marsupium near a septum (SE) emphasizing spines (SP) and mantle tissue (MA) at the ventral extent of glochidium valves; FIG. 296: Transverse section of an empty marsupium showing distended filaments (FI), water tube (WT), and a contracted placenta (PL).

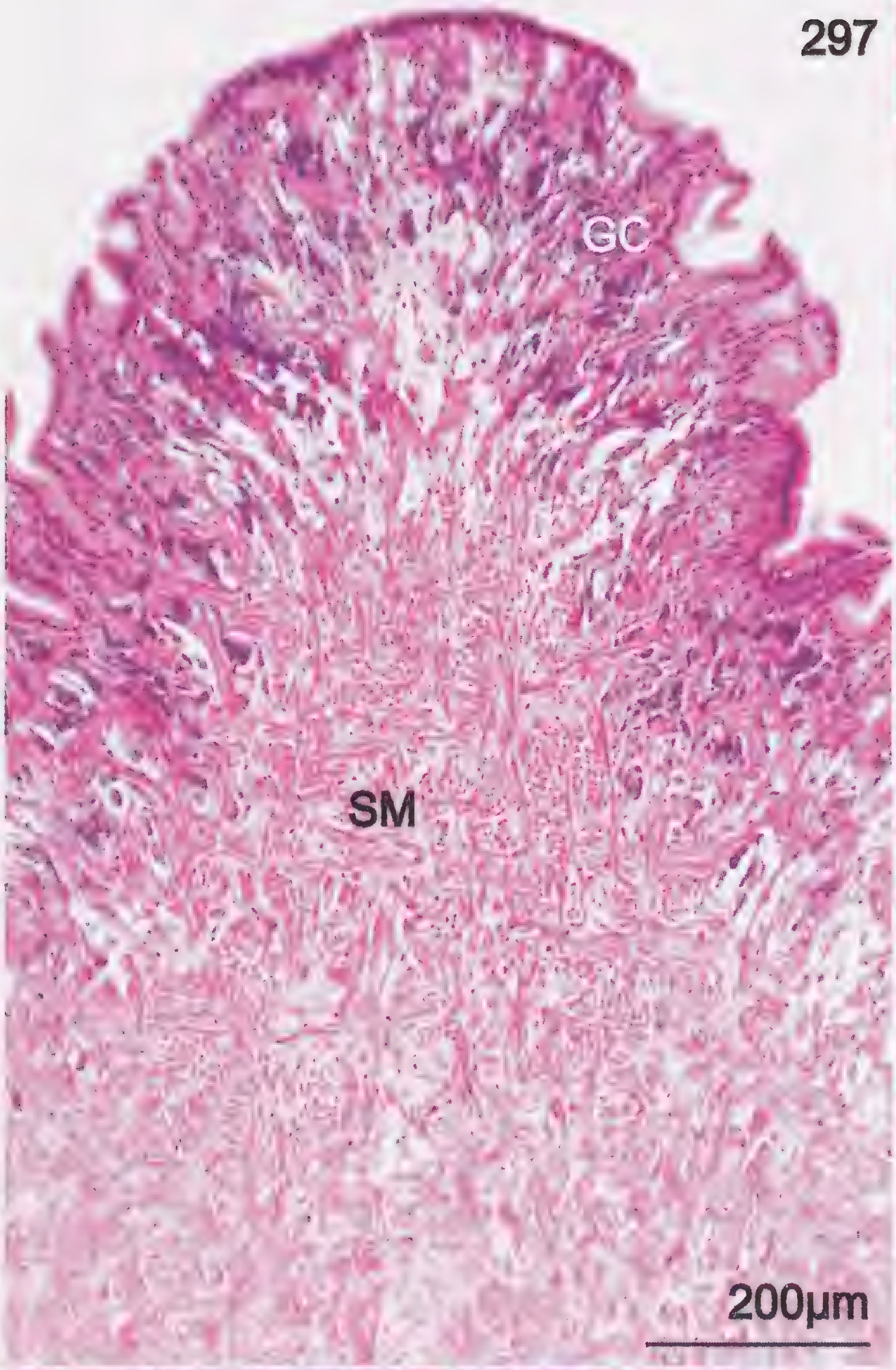
297

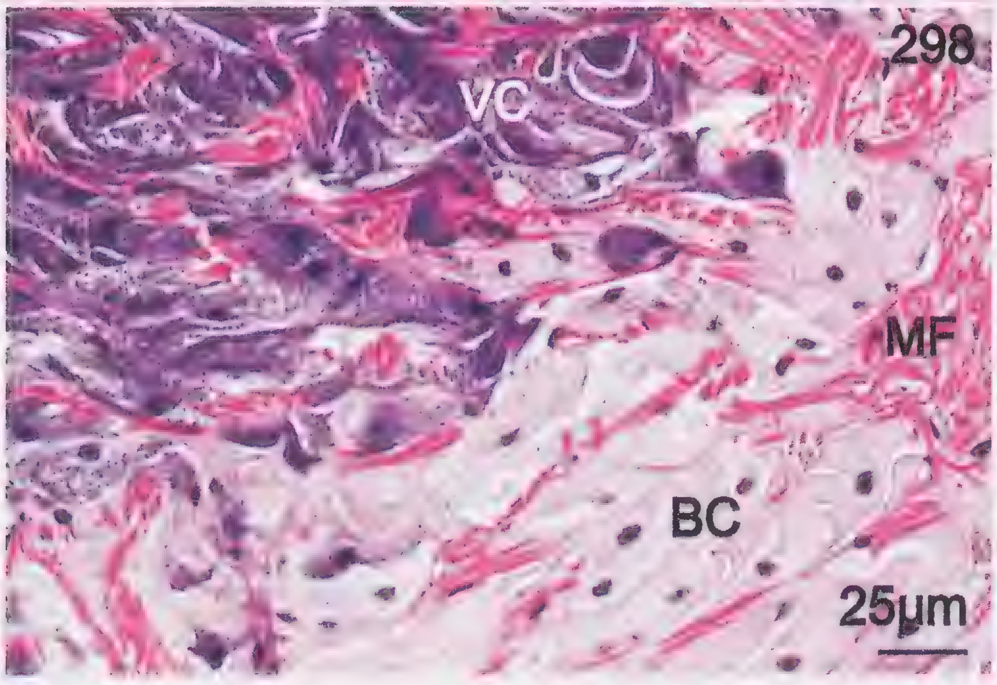
298

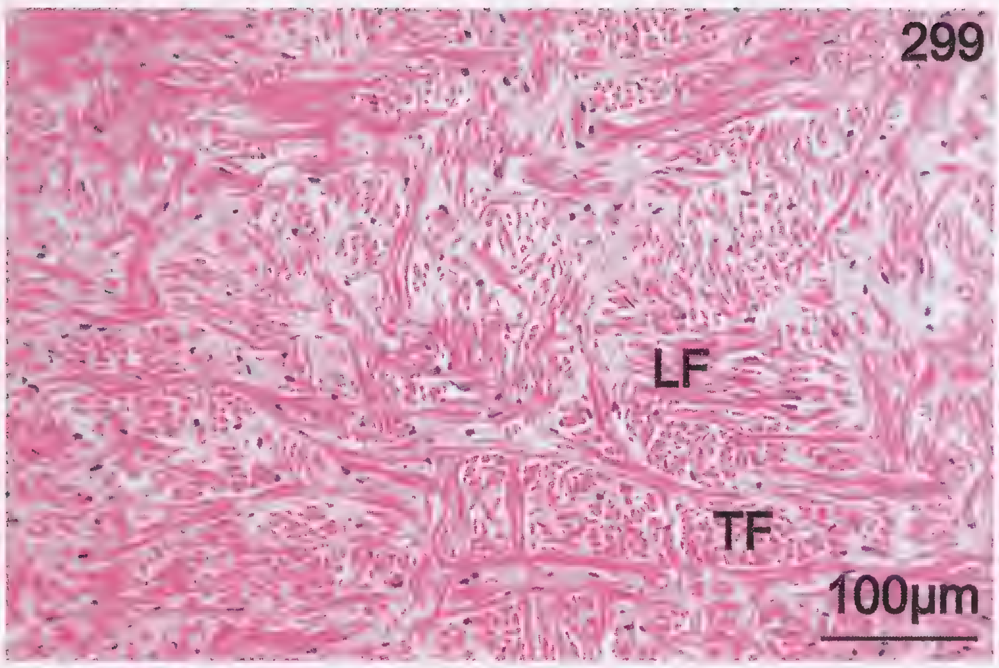
299

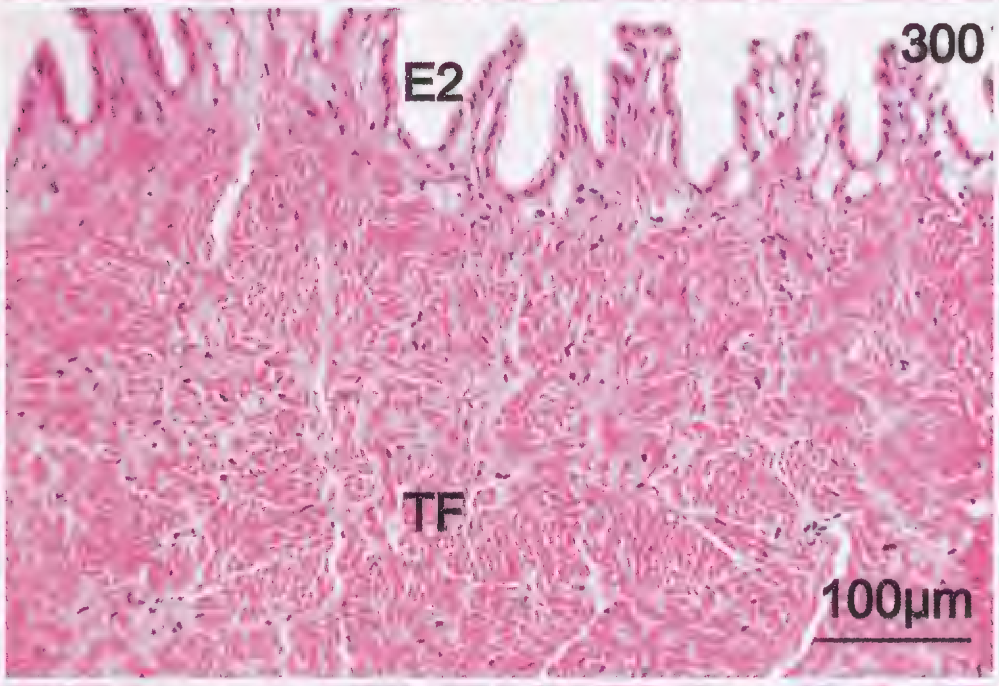
300

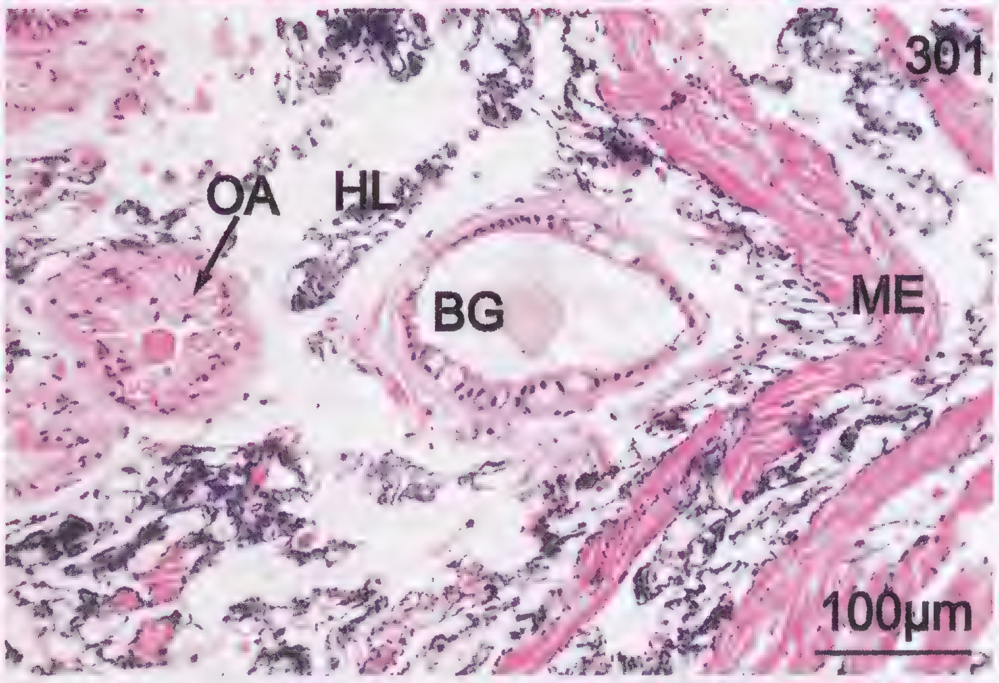
301

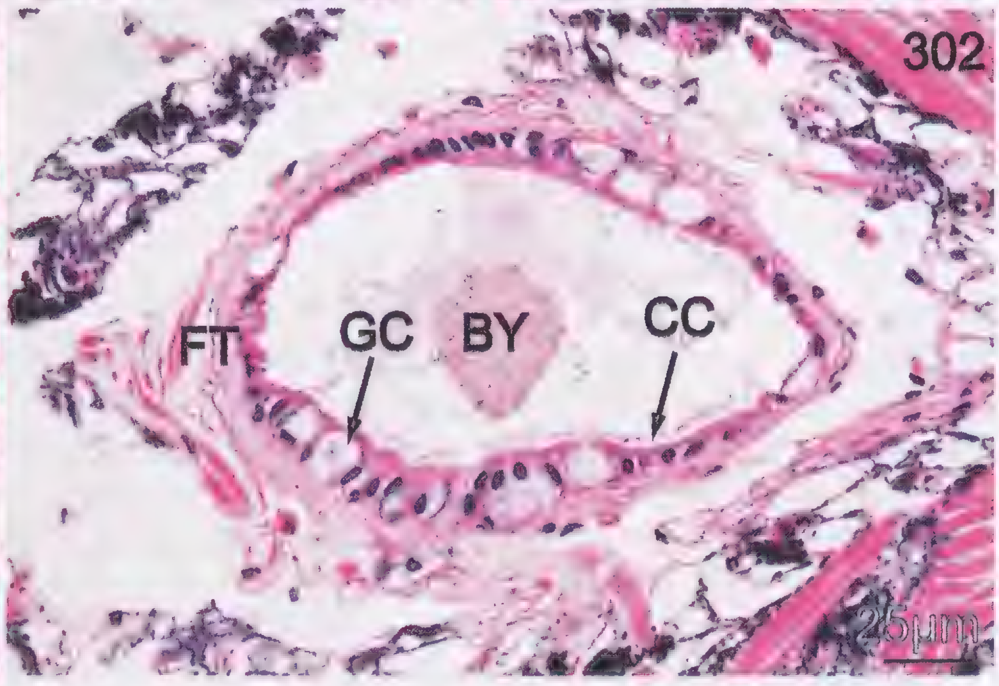
302

until the median, dorsal surface. Type-three epithelium comprises a distinct region of tall, thin, basophilic columnar cells with short cilia. Nuclei of type-three cells are elliptical, laterally compressed with a nucleolus (Fig. 337). The style consists of concentric layers of an eosinophilic, colloid material similar to the cuticular covering of the stomach (Fig. 338). The crystalline style sac is surrounded by loose connective tissue comprising a lamina propria (Fig. 334). Connective tissue is well developed around the folds, characterized by a lattice of thin fibers, a pale, eosinophilic ground substance, and spindle-shaped nuclei.

Intestine: The style sac represents the first limb of the intestine and it extends dorsally through the posterior visceral mass with an anteriorly directed curvature (Fig. 339). Sagittal sections of the posterior visceral mass reveal a complex epithelial structure at the posterior margin of the visceral mass. Style sac epithelium is consistent through the descending portion of its length, however each type of epithelium may be located on either the anterior or posterior intestinal wall, which creates a complex structure (Fig. 340).

Transverse sections of visceral mass reveal two limbs of the intestine ventral to the crystalline style sac in a sinistral and dextral position (Fig. 341). The sinistral limb comprises the ascending second intestinal limb, while the dextral limb represents the third, descending portion of the intestine. The second intestinal limb is characterized by tall and short plicae, and in a sagittal plane, the lumen has a slightly undulating appearance (Figs. 341, 342). There are two types of epithelium comprising the lining of the second intestinal limb. The first type of epithelium is located at the beginning of the second intestinal limb as it begins to bend along the posterior visceral margin. Type-one cells are columnar, with a pale, eosinophilic and vesiculated cytoplasm. Additionally, there are transparent bubbles located at the ciliated surface, possibly representing mucus secretions. Nuclei of type-one cells are ovular with a distinct nucleolus (Fig. 343). Secondly, there are ciliated columnar cells that are more widely distributed throughout the second and third intestinal limbs. Ciliated columnar cells are distinguished by a darker eosinophilic cytoplasm and the lack of vesicles. Nuclei of type-two epithelial cells are ovular and contain a distinct nucleolus (Fig. 344). The second intestinal limb travels anteriorly to the mid-point of the visceral mass and becomes the third intestinal limb when it bends to extend posteriorly. Epithelial tissue of the third intestinal limb is not different from the second intestinal limb. Connective tissue surrounding the second and third intestinal limbs is different from the supporting tissue surrounding the first intestinal limb. The tissue has a darker eosinophilic character, and nuclei are larger and more spherical than connective tissue surrounding the style sac.

The fourth limb of the intestine is characterized by a prominent, ventrally extending typhlosole. The typhlosole is a large extension of the dorsal intestinal wall consisting of pale, eosinophilic, columnar cells. The ventral wall of the fourth intestine is pleated with short, rounded to flattened plicae (Fig. 345). The ventral and dorsal epithelia are both ciliated with short cilia. Ventral epithelium consists of darkened, basophilic columnar cells. The nucleus of ventral epithelial cells is compressed and

---

←

FIGS. 297–302. Pedal musculature, and byssal gland of *Strophitus connasaugaensis*. FIG. 297: Transverse section of the ventral margin of the foot characterized by an inner core of somatic musculature (SM), and peripheral, basophilic granulocytes (GC); FIG. 298: Transverse section of pedal subepithelium characterized by myofibers (MF) pale, blue granulocytes (BC) in the median, and violet-staining granulocytes (VC) between the blue cells and the epithelium; FIG. 299: Transverse section of ventral pedal musculature featuring an irregular meshwork longitudinal fibers (LF), and transverse fibers (TF); FIG. 300: Transverse section of dorso-lateral foot musculature characterized by transverse myofibers (TF) and type-two pedal epithelium (E2); FIG. 301: Transverse section of the byssal gland (BG) showing its close proximity to ovarian acini (OA), hemolymph (HL), and mesentery (ME) characterizing the ventral margin of the coelom; FIG. 302: Transverse section of the byssal gland displaying ciliated columnar cells (CC), goblet cells (GC), byssus (BY) and an outer wrapping of fibrous tissue (FT).

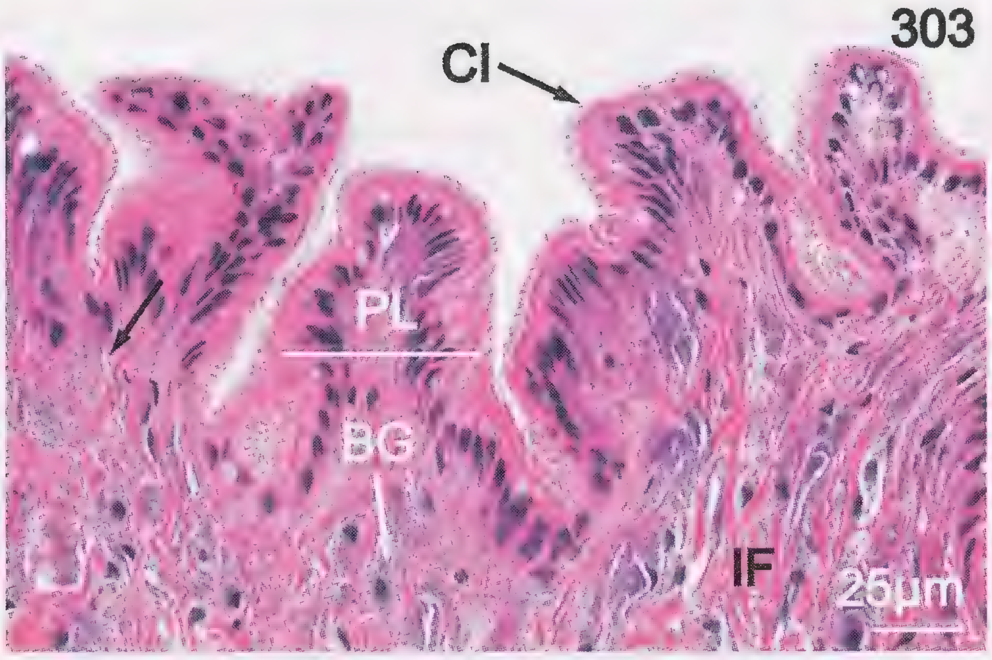
303

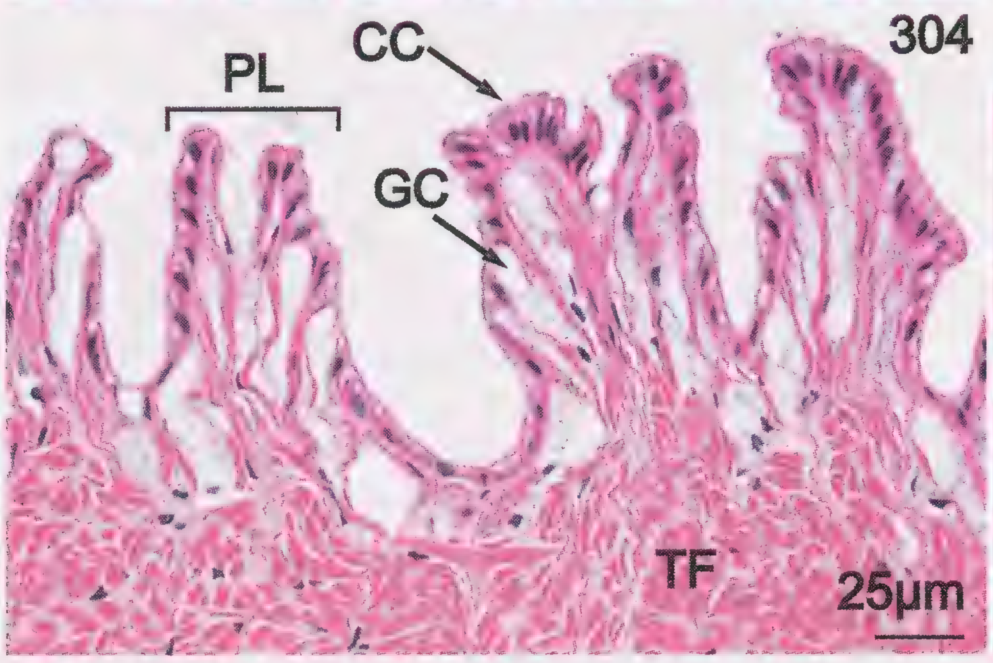
304

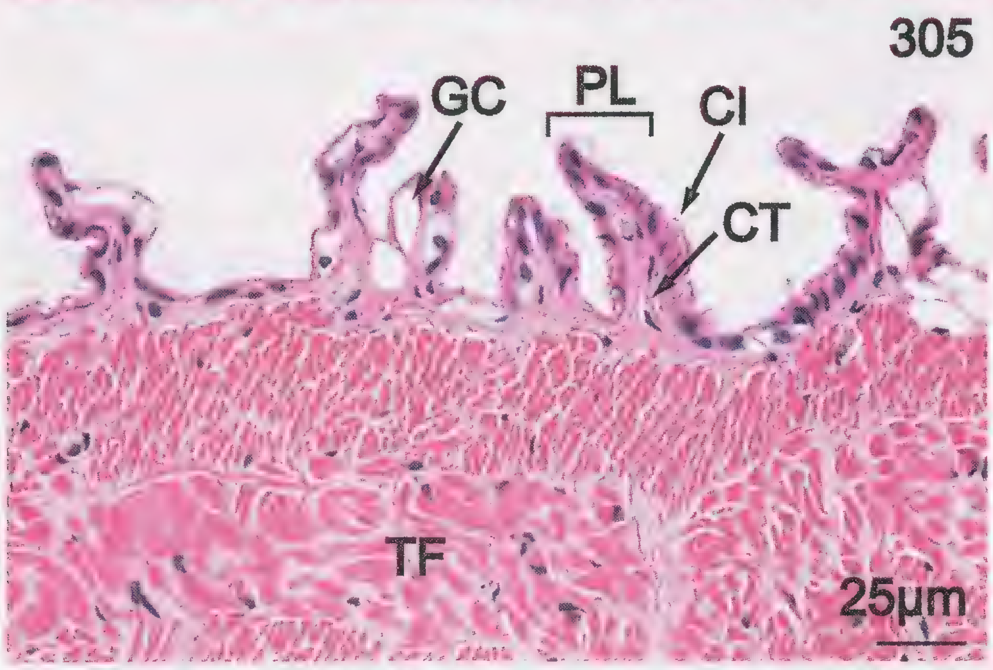
305

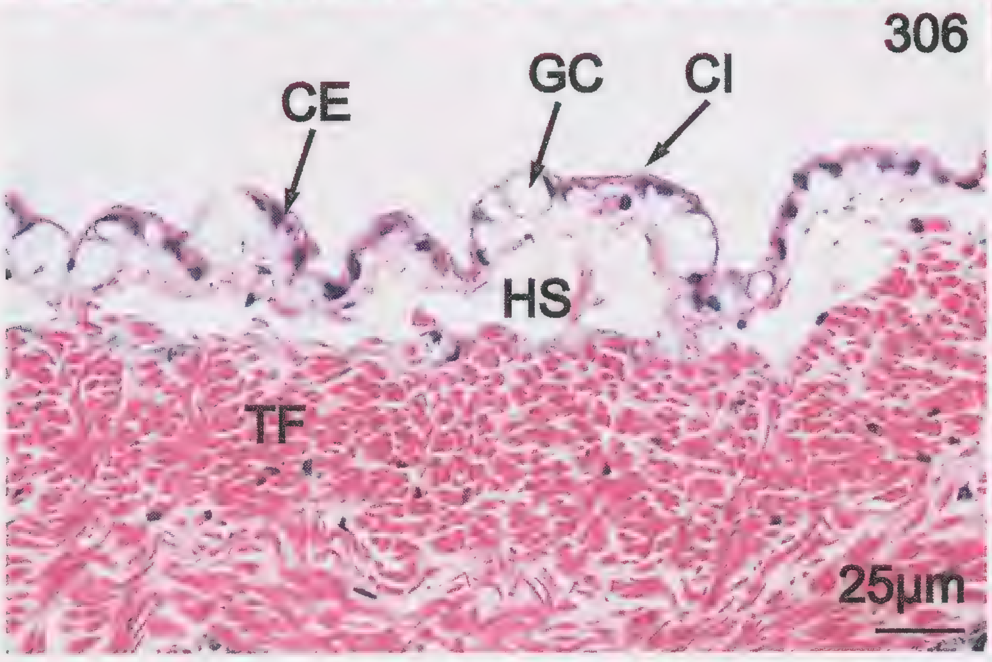
306

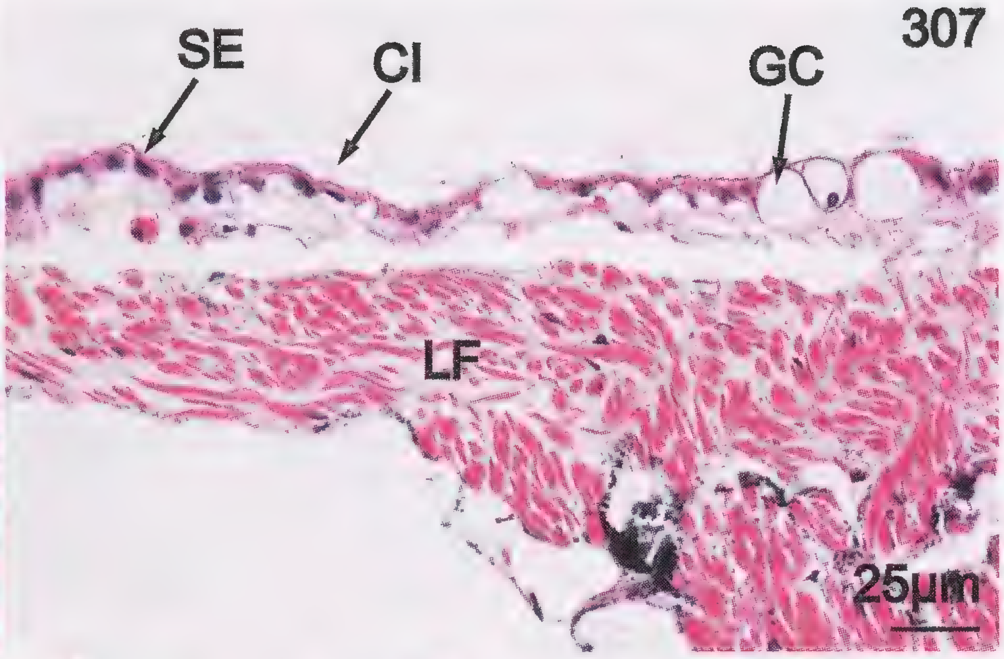
307

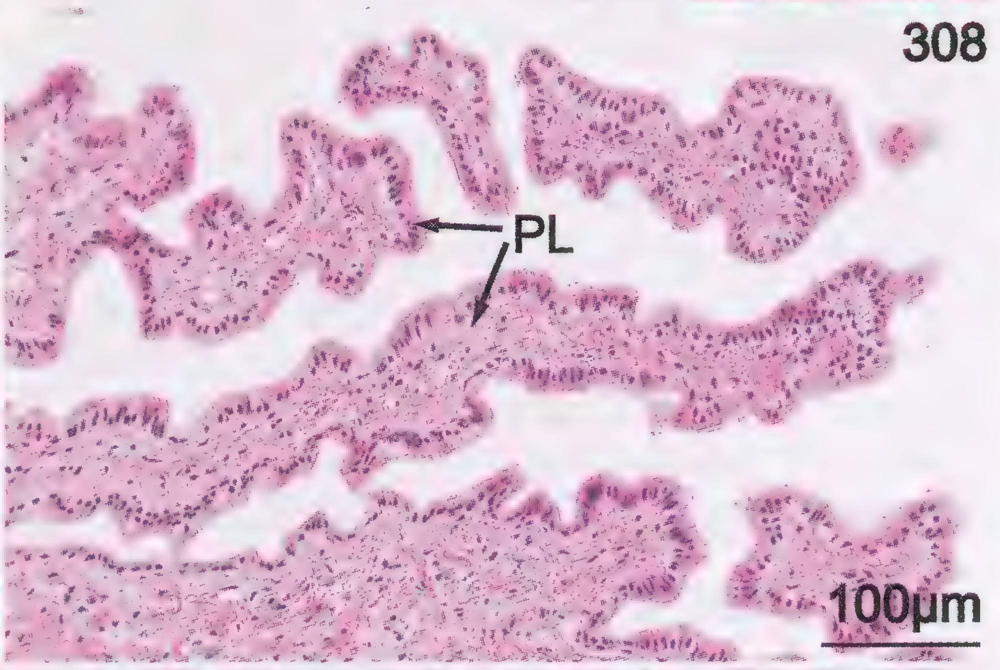
308

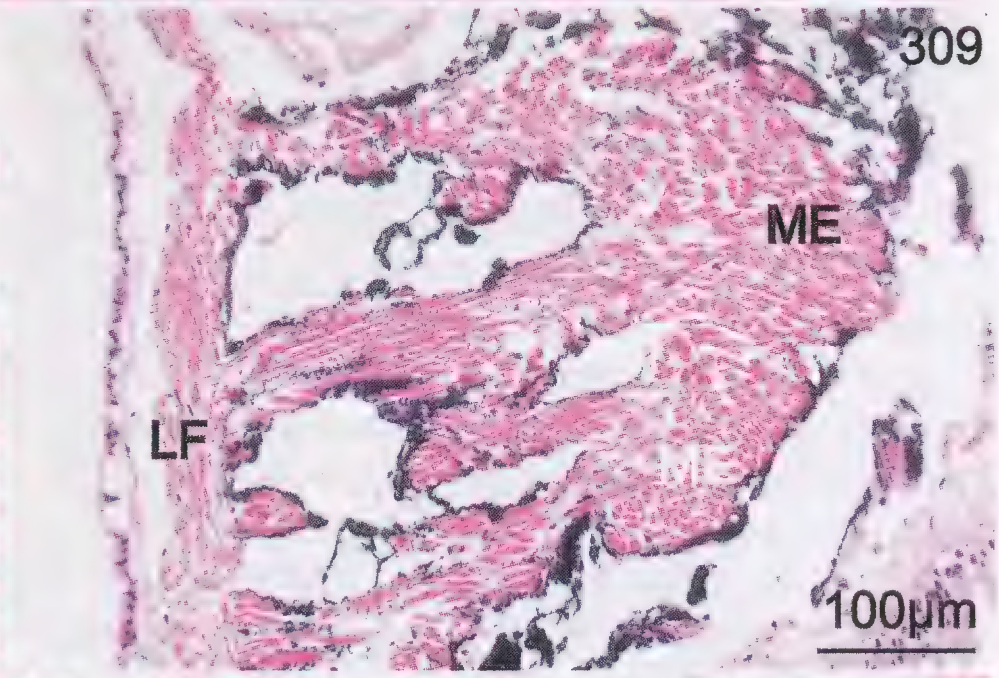
309

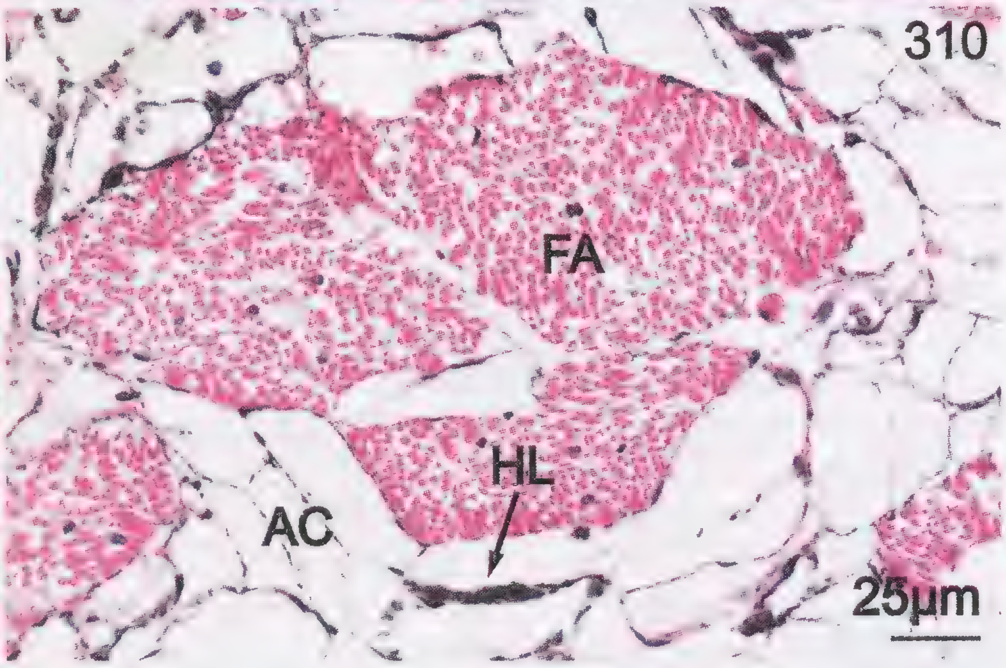
310

teardrop-shaped, and there is a slightly more eosinophilic granular region in the apical portion of the cell. Cytoplasm of ventral epithelial cells is thin and most conspicuous at the apical and lateral portions of plicae (Fig. 346). Nuclei of typhlosole columnar cells are ovular and contain a distinct nucleolus. Epithelial cells of the typhlosole are well defined in comparison to the darkened basophilic cells. Additionally, typhlosole epithelium contains isolated goblet cells. The nuclei of dorsal epithelial cells are ovular with a distinct nucleolus (Fig. 347). Connective tissue supporting the typhlosole consists of a latticework of loose connective tissue and spindle-shaped nuclei.

The fifth limb of the intestine is located medially and runs parallel to the hinge line. The intestine is enclosed within the heart, and there is a ring of cardiac muscle surrounding the anterior portion of the intestine. The most prominent feature of the fifth intestinal limb is the large typhlosole extending dorsally into the lumen, and the dorsal wall has numerous, narrow plicae (Fig. 348). Epithelium of the typhlosole is ciliated and columnar, with a pale, eosinophilic cytoplasm and an ovular nucleus with a distinct nucleolus (Fig. 349). Plications around the dorsal intestinal wall consist of pale, eosinophilic columnar cells bearing cilia. Columnar cells of dorsal and ventral epithelium of intestinal limb five bear a close resemblance to each other (Fig. 350). Connective tissue comprising lamina propria of the fifth intestinal limb consists of a lattice of fibers within a pale ground substance and spindle-shaped nuclei. However, there is a thin, darkened layer of fibrous tissue, possibly representing musculature, surrounding the intestine.

Cellular Structure of Cardiovascular System Tissues

Heart: The heart is located dorsally in relation to the visceral mass, and it begins at the anterior margin of the nephridium and terminates between the posterior margin of the visceral mass and posterior pedal retractors. Ventricular cardiac muscle begins as a thin wrapping around the intestine and progressively becomes thicker posteriorly. The ventricle is large, bulbous and medially located, while the auricles are thin, irregular extensions of cardiac tissue extending obliquely and medially into the ventricle from the lateral pericardium (Fig. 351). The ventricle consists of a thin epicardium and a thickened myocardium. Epicardium is a pale, eosinophilic, simple squamous epithelium enclosing the underlying myocardium and epicardium is highly irregular (Fig. 352). Myocardium consists of thick bands of myofibers oriented in a transverse and longitudinal plane. Cardiac myocytes have a dark, red, eosinophilic composition with spherical to ovular, monochromatic nuclei (Fig. 353). Auricles are thin, incorporate a small amount of cardiac muscle, and have an irregular epicardium. Auricles may be closely positioned to the pericardial sac, and pericardium is constructed

---

←

FIGS. 303–310. Pedal integument, and mesentery of *Strophitus connasaugaensis*. FIG. 303: Transverse section of pedal integument type-one, emphasizing tall irregular plicae (PL) with densely packed cilia (CI) overlying a subepithelium of irregular fibers (IF), and basophilic granulocytes (BG); FIG. 304: Transverse section of pedal integument type-two represented by tall plicae (PL), columnar cells (CC), goblet cells (GC), and transverse myofibers (TF); FIG. 305: Transverse section of pedal integument type-three, characterized by shorter, thinner plicae (PL) bearing goblet cells (GC), cilia (CI), and a distinct subepithelium of connective tissue (CT), and underlying strata of transverse myofibers (TF); FIG. 306: Transverse section of pedal integument type-four, characterized by a sinuous, but more flattened integument of cuboidal epithelium (CE), cilia (CI), goblet cells (GC), and a subepithelium of hemolymph sinues (HS), and transverse myofibers (TF); FIG. 307: Transverse section of pedal integument type-five, revealing the flattened squamous epithelium (SE), cilia (CI), goblet cells (GC), and longitudinal myofibers (LF); FIG. 308: Sagittal section of pedal integument featuring irregular plicae (PL) giving the integument a rugose structure; FIG. 309: Transverse section of the lateral coelomic margin emphasizing longitudinal myofibers (LF), and struts of musculature forming mesentery (ME); FIG. 310: Sagittal section through the coelom revealing a mesentery fascicle (FA) surrounded by adipocytes (AC), and hemolymph (HL).

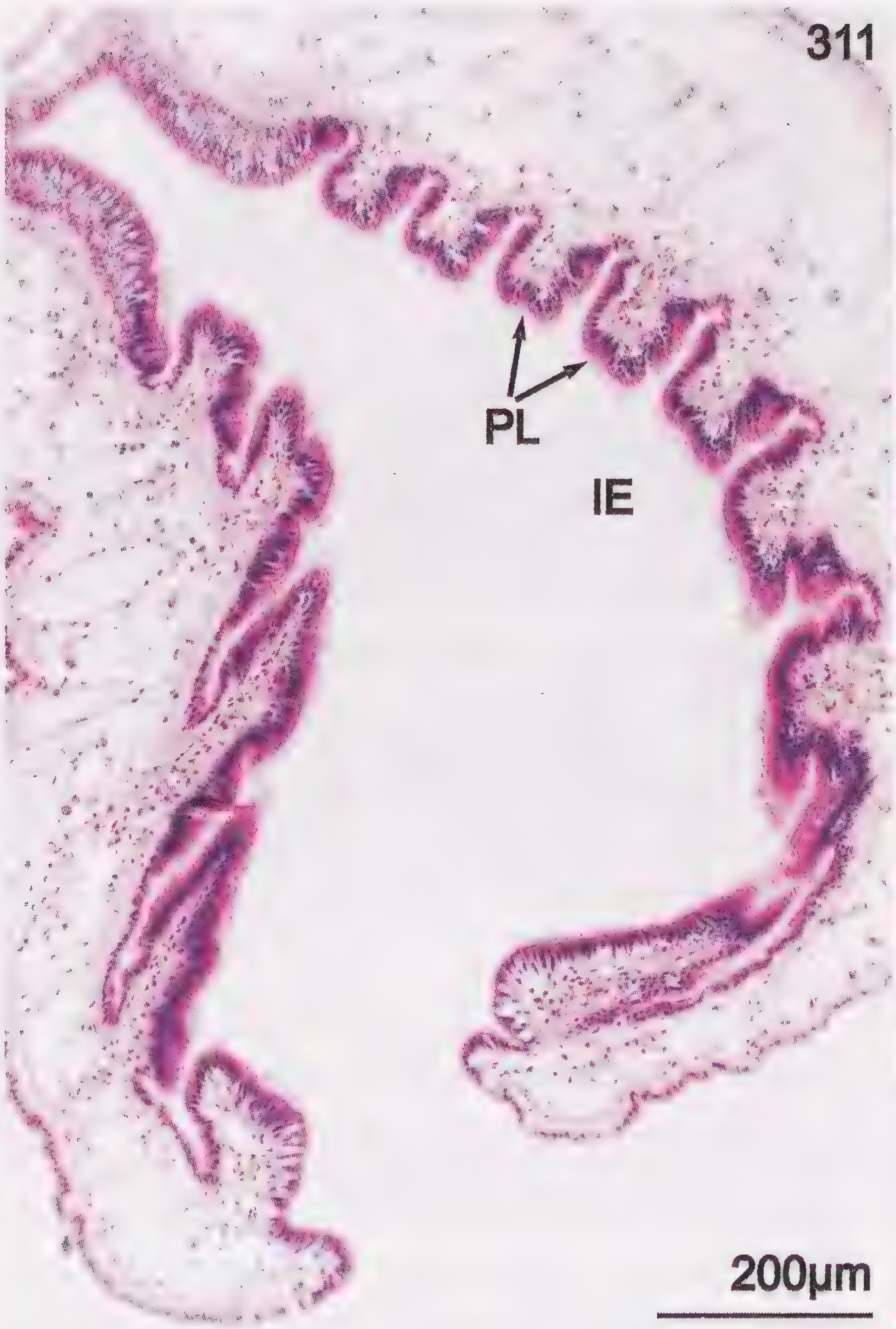
311

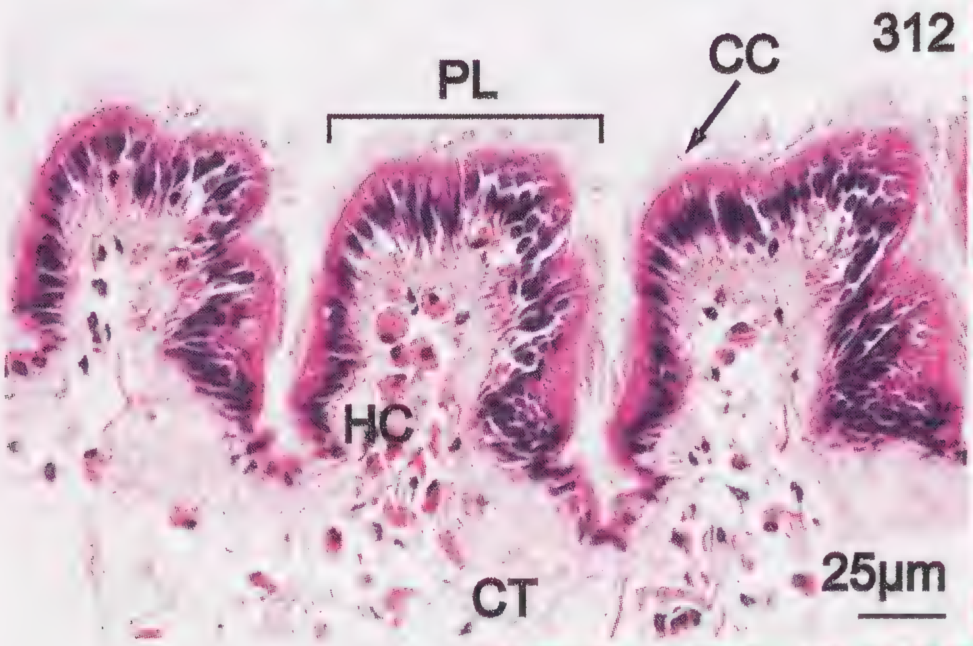
312

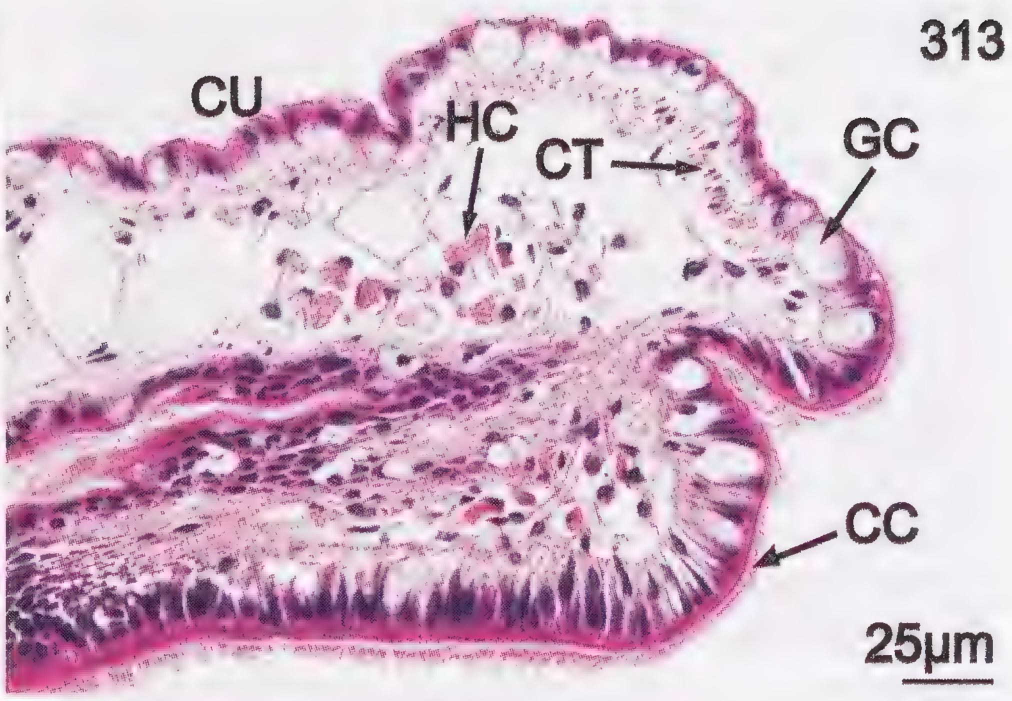
313

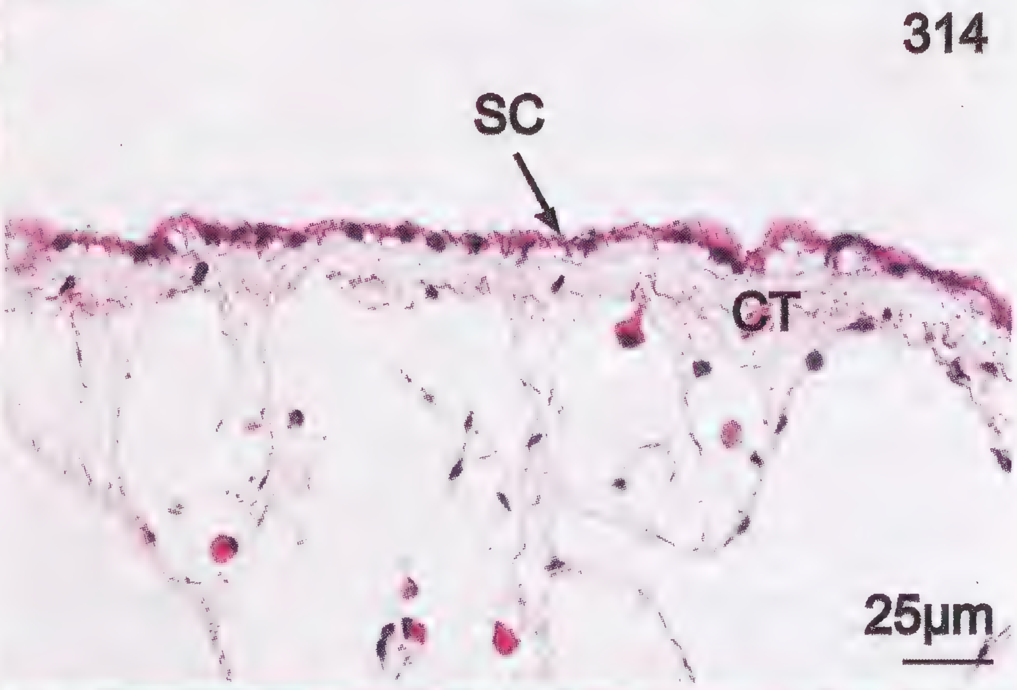
314

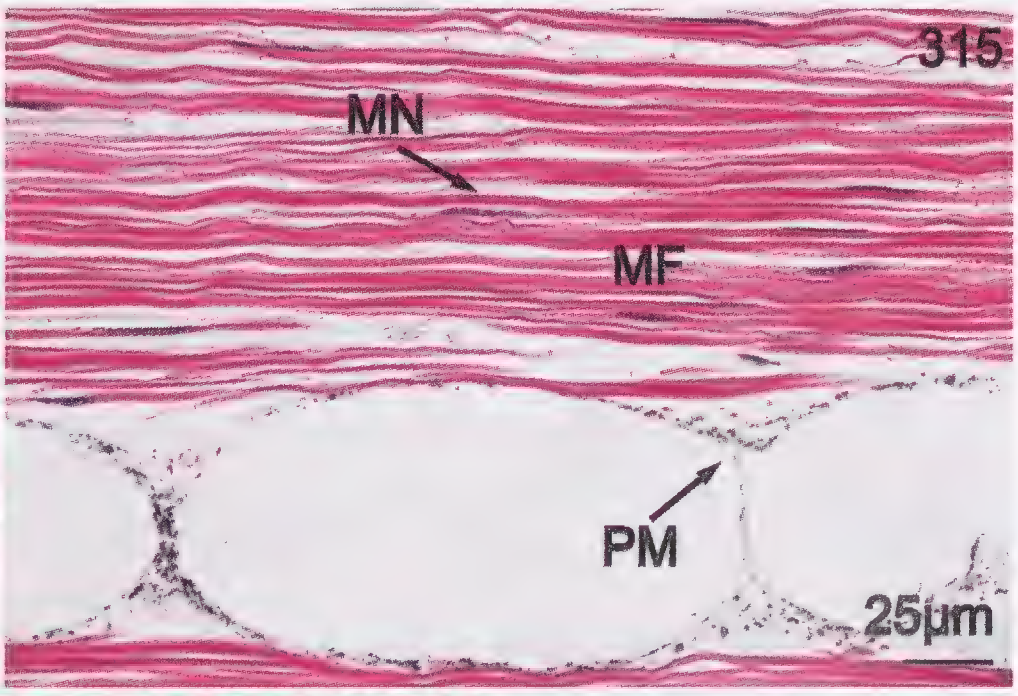
315

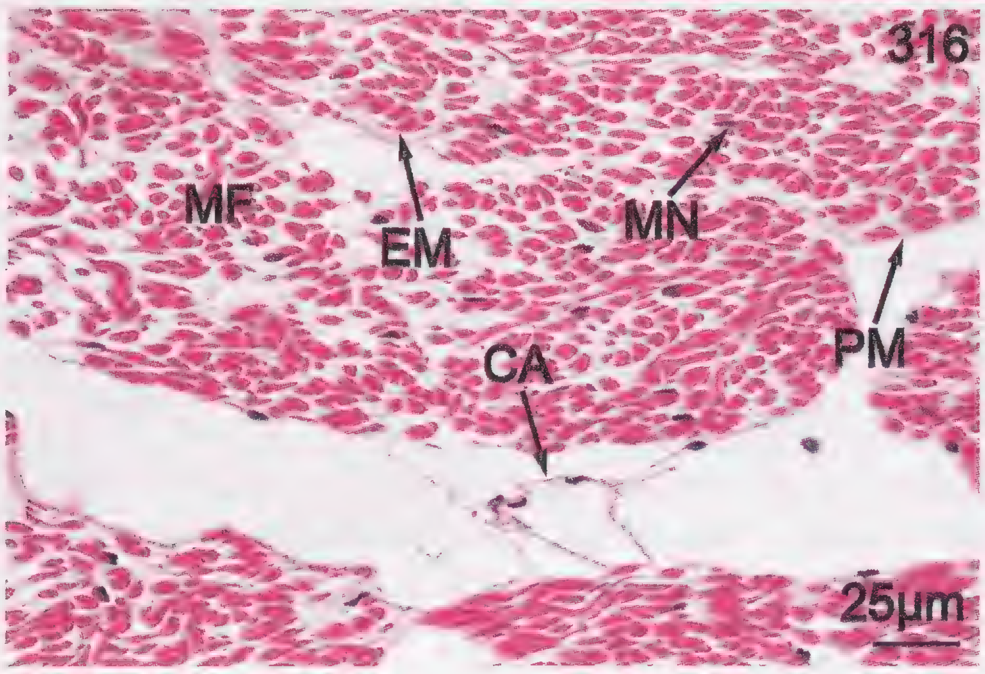
316

from squamous epithelial cells (Fig. 354). Hemolymph flow traveling into the ventricle is regulated on the sinistral and dextral sides of the ventricle by the auriculoventricular valves. The auriculoventricular valves are composed of squamous cells and cardiac muscle. Inner and outer valve surfaces feature squamous cells, and there is an inner layer of muscle tissue (Fig. 355).

Arteries, Veins, Capillaries and Pericardial Gland: Hemolymph is located throughout the viscera and mantle of *S. connasaugaensis*. Adipose tissue represents a significant portion of the connective tissue of the coelom and mantle, and there is a preponderance of black, ink-like granules located within the interstitial spaces of adipose tissue. Additionally, there are isolated hemocytes located within interstitial spaces of coelom and mantle (e.g., Figs. 281, 312, 357). However, the circulatory system has numerous circular to ovular tubes representing hemolymph vessels. Hemolymph vessels consisting of thickened musculature may comprise arteries (Fig. 356). Hemolymph vessels that incorporate less muscle tissue are potential veins and veins have a more irregular shape (Fig. 357). Capillaries are also apparent, especially within adductor muscle and mantle edge. Capillaries are characterized by a ring of squamous cells and correspondingly have a small diameter (Fig. 358).

The dorsal aspect of the visceral mass consists of an extensive fibrous tissue surrounding the pericardium. The fibrous tissue represents the pericardial gland and it is characterized by pale, eosinophilic fibers and hemocytes. Pericardial gland cells are irregularly oriented and possess an emarginated nucleus. Hemocytes are located freely within the lumen of the pericardial gland, and some hemocytes seem to adhere to the pericardial gland cells (Fig. 359).

Cellular Structure of Renal System Tissues

Anterior Nephridium: The nephridium is a large tubular organ located dorsally to the left and right of the visceral mass. Nephridium extends down the length of the body from the midpoint of the visceral mass to the posterior adductor. Nephridium consists of distinct ventral and dorsal limbs, and the morphology of each limb changes posterior to the visceral mass. At its anterior extent, the ventral nephridium has a convoluted epithelium, and the dorsal limb is a simple cavity underlying the ventral region (Fig. 360). Ventral nephridium features a simple columnar epithelium consisting of strongly eosinophilic, vesiculated cells. The surface of the ventral nephridial cells is smooth, seemingly lacking cilia or microvilli. Nuclei are spherical to ovular without a distinct nucleolus. The ventral limb has irregular branches of epithelial tissue extending into the nephridial lumen. The subepithelium of ventral nephridium consists of a pale, eosinophilic layer of squamous cells comprising the endothelium (Fig. 361). The dorsal nephridium consists of cuboidal cells with a pale, eosinophilic cytoplasm and a spherical, monochromatic nucleus. Dorsal nephridium has isolated regions of columnar cells containing a pallid median vesicle. Some vesiculated columnar cells are teardrop shaped with an apical vesicle (Fig. 362). Dorsal nephridium largely lacks branches, but a small number of reduced plicae are

←

FIGS. 311–316. Labial palps, anterior pedal protractor, and anterior adductor of *Strophitus connasaugaensis*. FIG. 311: Sagittal view of a labial palp portraying plicae (PL) constituting inner epithelium (IE), and the smooth outer epithelium; FIG. 312: Sagittal section of labial palps revealing plicae (PL), with ciliated columnar cells (CC), and subepithelial connective tissue (CT) and hemocytes (HC); FIG. 313: Sagittal section of the distal labial palp margin featuring the flattened outer epithelium of cuboidal cells (CU), goblet cells (GC), ciliated columnar cells (CC), hemocytes (HC) and subepithelial connective tissue (CT); FIG. 314: Sagittal section of outer palp surface highlighting squamous cells (SC), and subepithelial connective tissue (CT); FIG. 315: Sagittal section of anterior adductor showing longitudinal myofibers (MF), flattened myocyte nuclei (MN), and perimysium (PM); FIG. 316: Transverse section of anterior pedal retractor displaying thin perimysium (PM), endomysium (EM), polygonal myofibers (MF), myocyte nuclei (MN) and a capillary (CA) between adjacent fascicles.

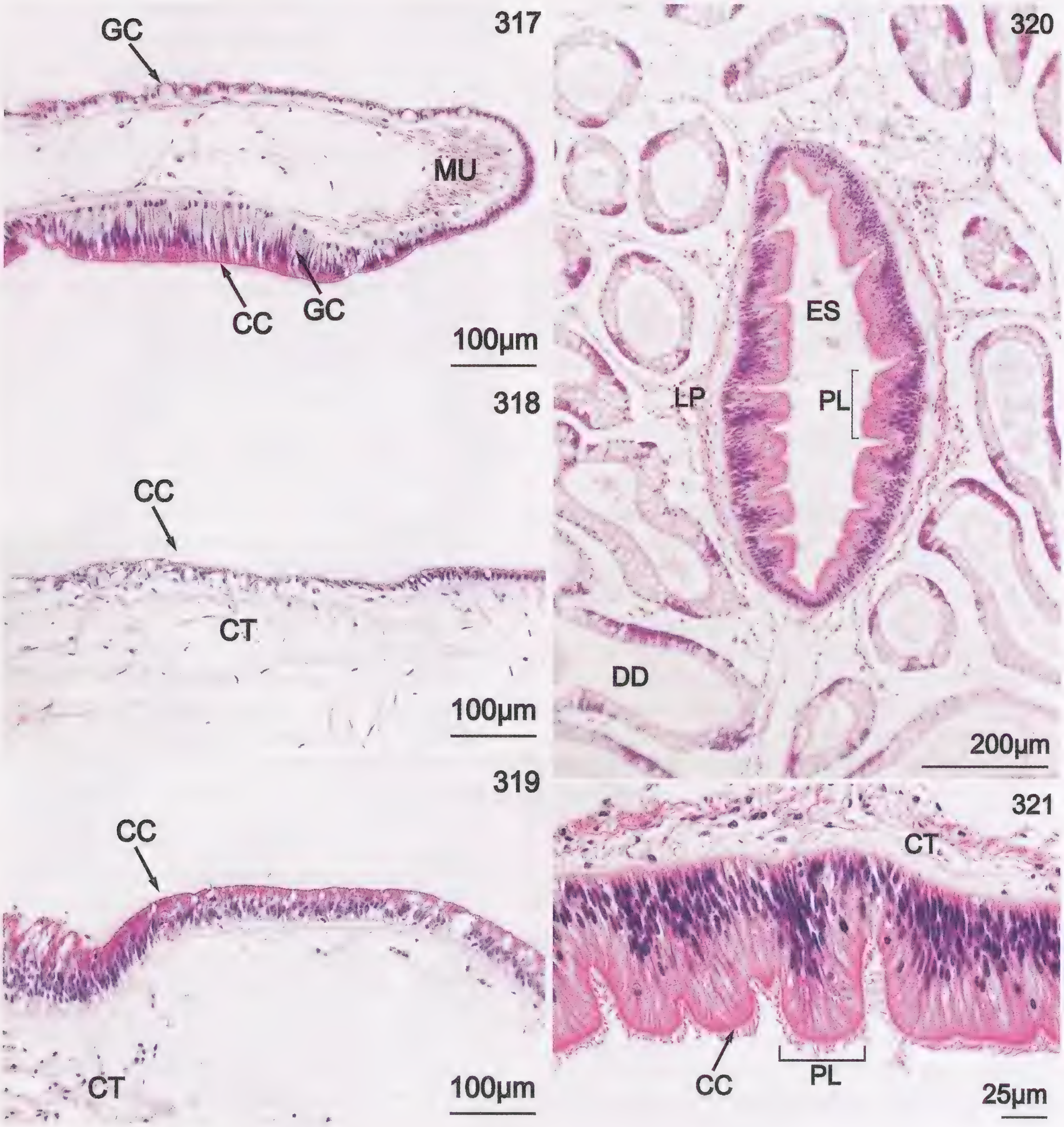

FIGS. 317–321. Oral groove, and esophagus of *Strophitus connasaugaensis*. FIG. 317: Transverse section of oral groove showing a cylindrical shelf consisting of musculature (MU), goblet cells (GC), and a ciliated columnar epithelium (CC); FIG. 318: Transverse section of the lateral oral groove wall displaying ciliated columnar cells (CC) and a subepithelium of loose connective tissue (CT); FIG. 319: Transverse section of the dorsal oral groove wall, displaying cilia (CI), and loose connective tissue (CT); FIG. 320: Transverse section through dorsal aspect of visceral mass showing the esophagus (ES) lined with plicae (PL), enclosed within a distinct lamina propria (LP), and surrounded by tubules of the digestive diverticulum (DD); FIG. 321: Transverse section of esophagus emphasizing plicae (PL) consisting of ciliated columnar cells (CC) supported by a dense matrix of fibrous connective tissue (CT).

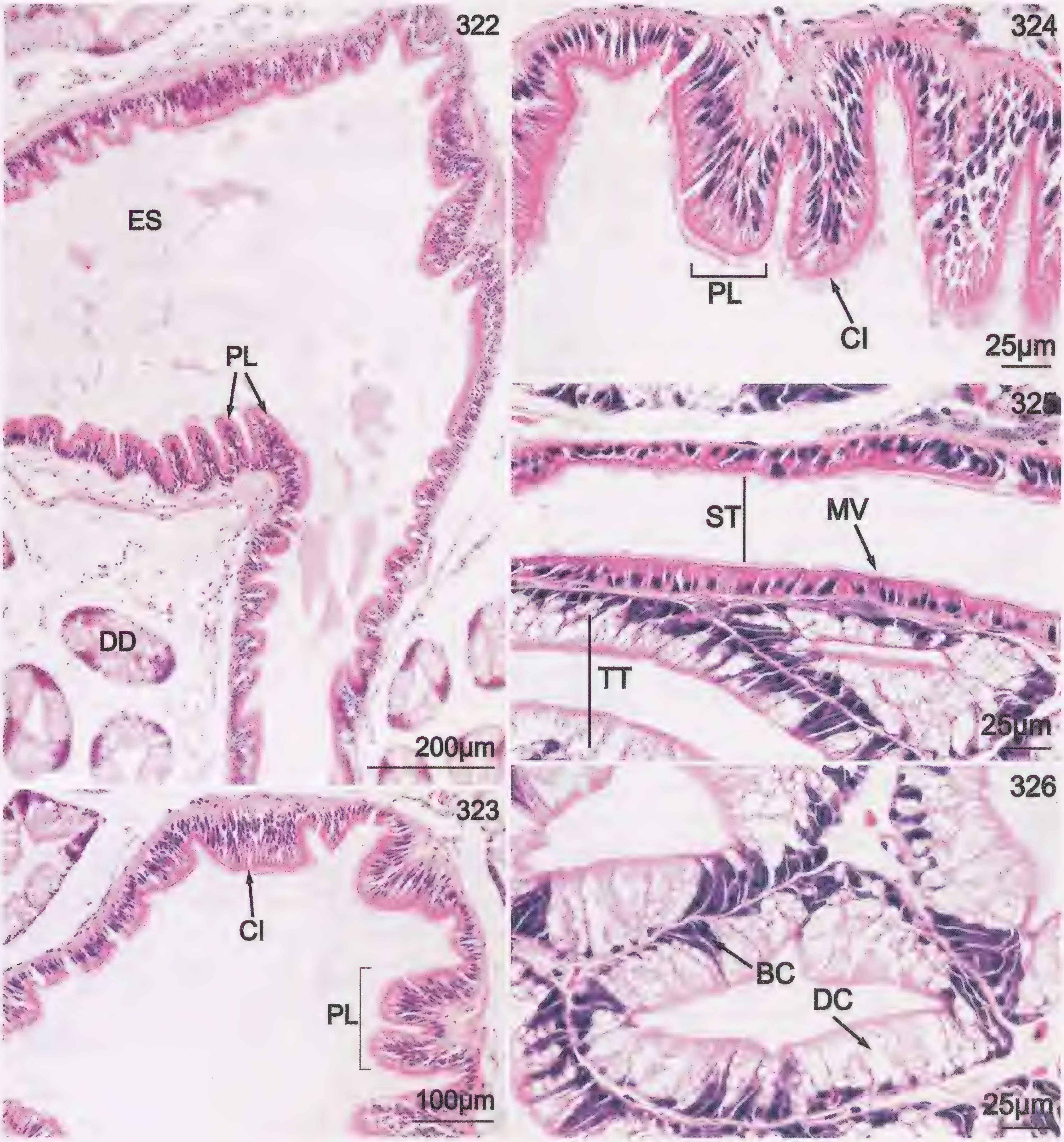

FIGS. 322–326. Digestive diverticulum of *Strophitus connasaugaensis*. FIG. 322: Transverse section of the junction between the esophagus (ES) and digestive diverticulum (DD) revealing a large vestibular chamber characterized by ciliated plicae (PL); FIG. 323: Transverse section of the junction between the esophagus and digestive diverticulum, emphasizing conical plicae (PL) bearing cilia (CI), and underlying lamina propria (LP); FIG. 324: Transverse section of digestive diverticulum portraying plicae (PL) and cilia (CI) of primary digestive tubules; FIG. 325: Transverse section of digestive diverticulum revealing the minute structure of microvilli (MV) of secondary tubules (ST) and the contrasting cellular features of tertiary tubules (TT); FIG. 326: Transverse section of the digestive diverticulum focusing on tertiary tubule structure including eosinophilic vesicles of digestive cells (DC), and violet-staining basophil cells (BC).

327

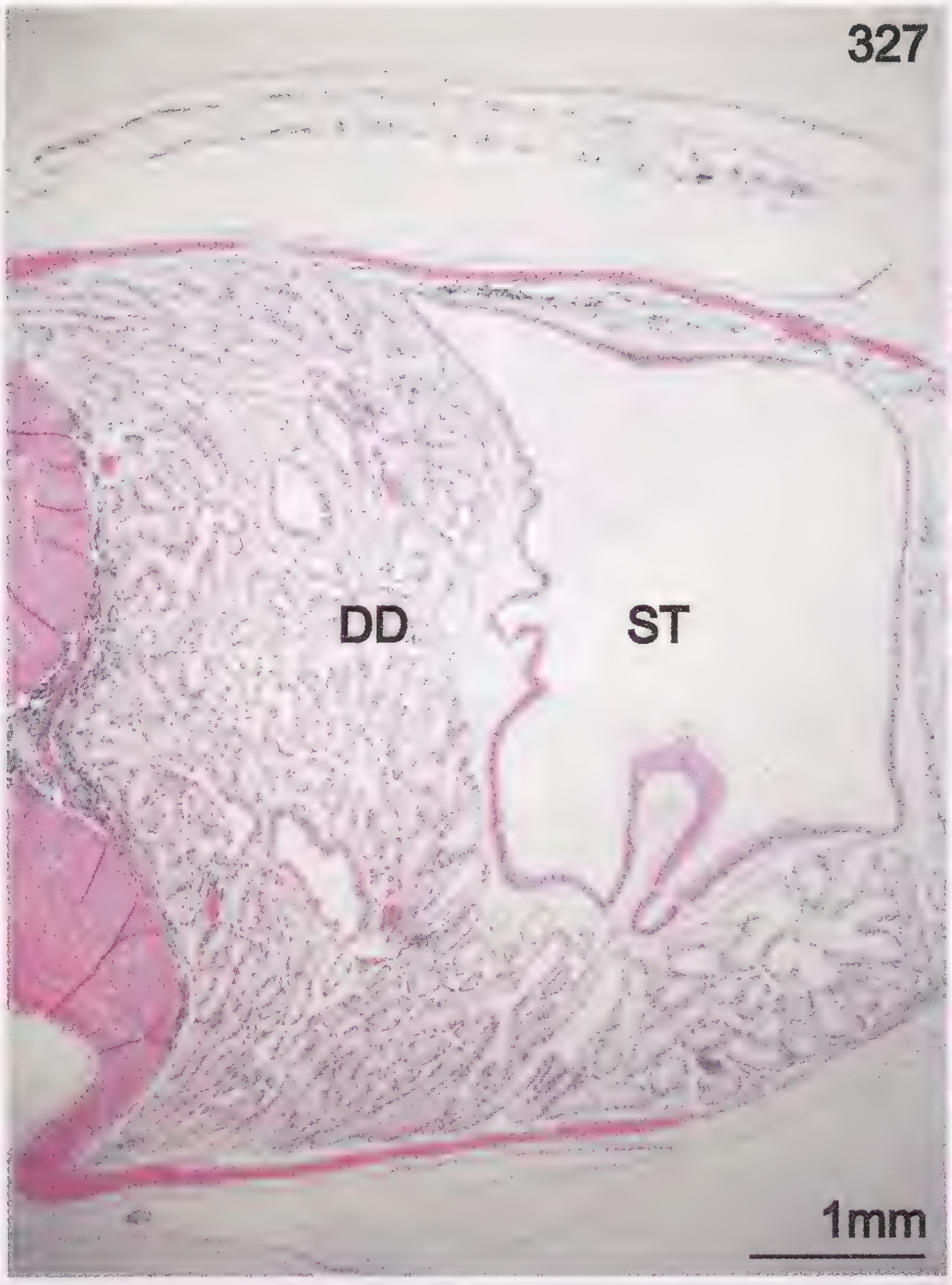

328

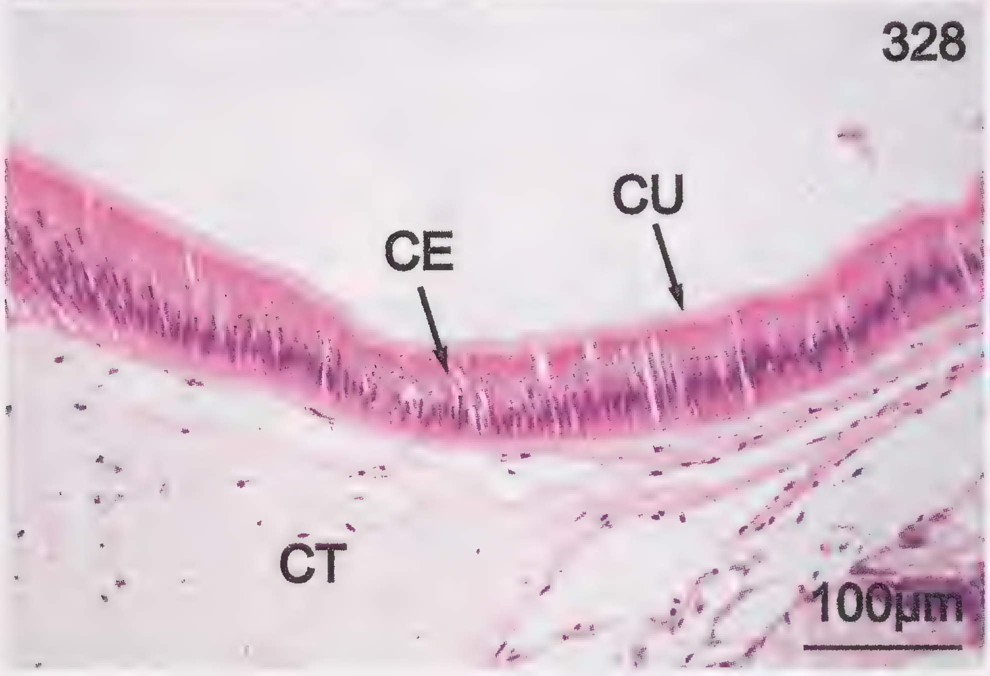

329

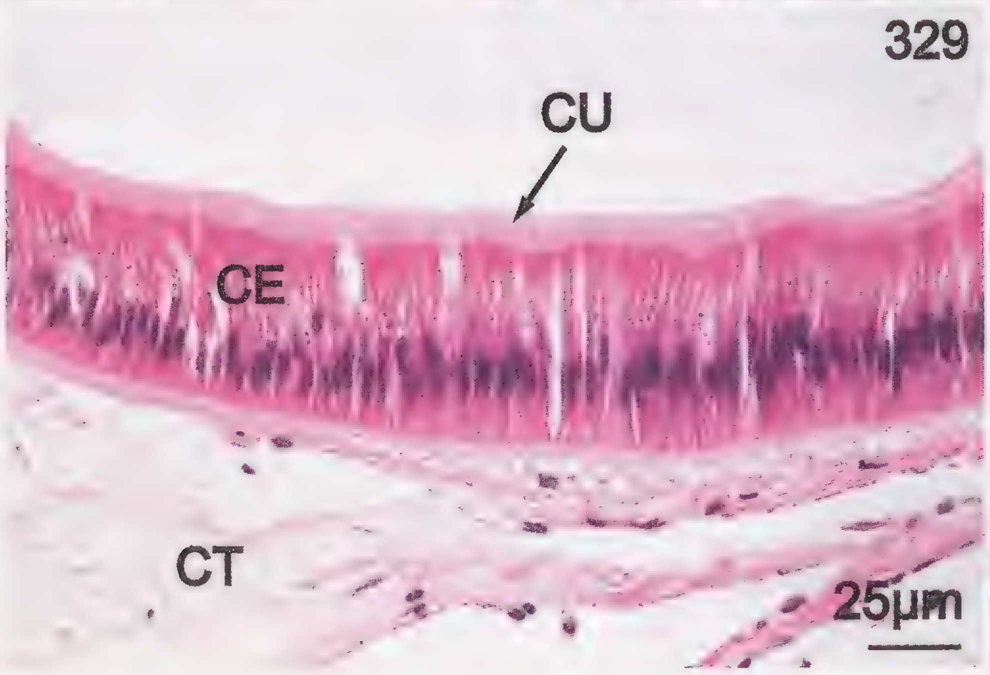

330

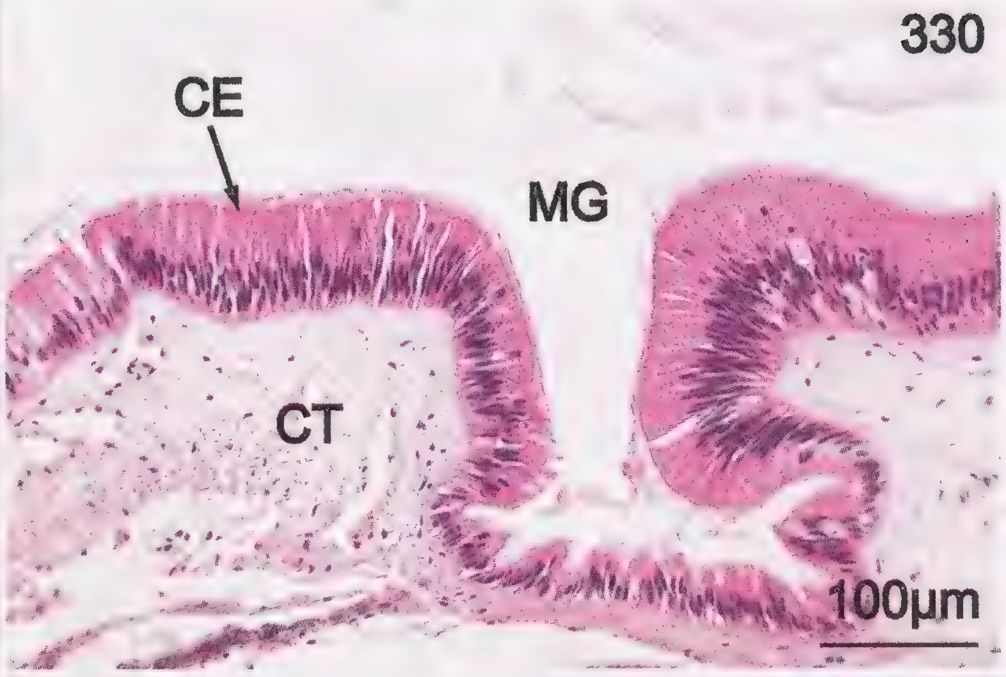

331

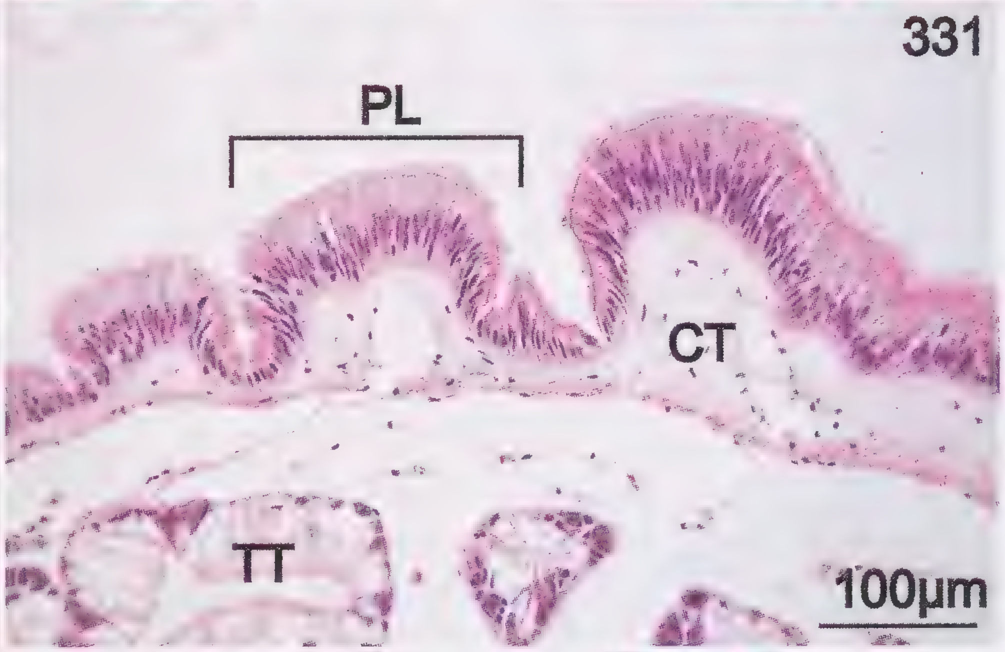

332

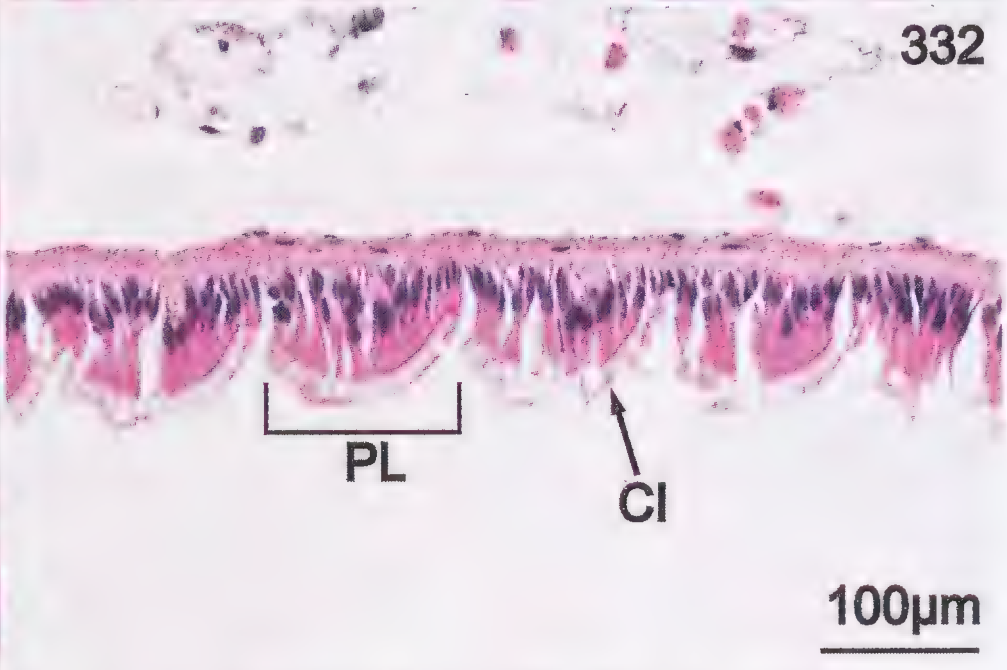

333

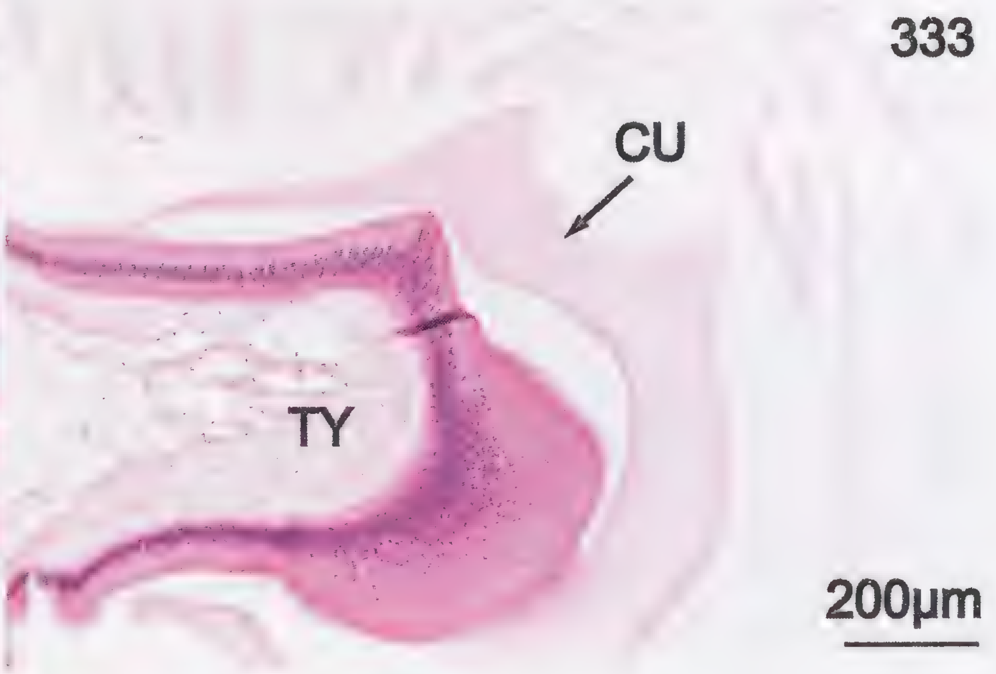

present (Fig. 363). Fluid from the pericardial cavity is flushed into the ventral nephridium through a ciliated duct or renopericardial canal at the anterior end of the nephridium. The renopericardial canal merges with ventral nephridium at the lateral margin of the ventral nephridium, but appears to be a circular duct at its midpoint. Transverse histological sections of the nephridium show a circular duct representing the midpoint of the renal-pericardial canal and the adjacent, laterally positioned urethra (Fig. 364). Epithelial tissue comprising the renopericardial canal features ciliated columnar cells, and goblet cells organized into conical plicae enclosed within a thickened circumferential lamina propria (Fig. 365). The histological composition of the urethra resembles the dorsal nephridial chamber until the distal-most portion near the communication between the nephridium and suprabranchial cavity. Darkened, basophilic columnar cells bearing cilia characterize the urethra of *S. connasaugaensis*. Cilia are short and densely distributed across the surface of the epithelium towards the distal end of the urethra (Fig. 366).

Posterior Nephridium: Nephridial branches expand, and the tissue becomes enlarged between the posterior margin of the visceral mass and posterior adductor. Nephridial epithelium is convoluted, consisting of epithelial folds with a repeating stem-loop configuration (Fig. 367). Posterior nephridial branches are spaced farther apart from each other than in the anterior nephridium. Epithelial cells are cuboidal to columnar with a pale eosinophilic and granular cytoplasm. Cytoplasm of nephridial cells may contain brown granules, while the apical surface of some cells has a filamentous, eosinophilic residue, possibly representing a secretion. Each half of a nephridial branch is united by filamentous, connective tissue septa. The medial portion of a nephridial branch constitutes a hemolymph vessel and emarginated nuclei of endothelial cells are present (Fig. 368). The ventral margin of the posterior nephridium features a pair of large nerves. Each nerve consists of an outer epineurium and an inner, granular focus of axons (Fig. 369).

Posterior Adductor and Posterior Pedal Retractors: Posterior pedal retractors are located within the nephridial septum, between the posterior adductor and visceral mass. Pedal retractors have a distinct epimysium surrounding a series of fascicles. Connective tissue of pedal retractors is delicate, especially the epimysium and perimysium. Endomysium consists of a pale, eosinophilic membranous material between myofibers. Myofibers are polygonal in a transverse orientation, and have a dark, eosinophilic cytoplasm (Fig. 370). The posterior adductor is located posterior to the retractors and is oriented longitudinally when mussels are transversely cut. Adductor myofibers are organized into large fascicles with a simple, squamous epimysium and a delicate, fibrous perimysium. Myofibers of the posterior adductor are long, eosinophilic filaments with elliptical, heterochromatic nuclei and a distinct nucleolus (Fig. 371). Perimysium is thin, membranous and contains a series of ellipsoid capillaries.

←

FIGS. 327–333. Stomach of *Strophitus connasaugaensis*. FIG. 327: Transverse section through visceral mass showing the morphology of the stomach (ST) and surrounding digestive diverticulum (DD); FIG. 328: Transverse section of the dextral portion of the ventral stomach wall showing a thin cuticle (CU) adhered to the columnar epithelium (CE) with fibrous underlying connective tissue (CT); FIG. 329: Transverse section of the dextral portion of the ventral stomach wall showing a dense cuticle (CU), vesiculated columnar epithelium (CE), and connective tissue (CT) of the subepithelium; FIG. 330: Transverse section of the medial portion of the ventral stomach wall showing a columnar epithelium (CE), medial groove (MG), and underlying connective tissue (CT) of the subepithelium; FIG. 331: Transverse section of the sinistral portion of the ventral stomach wall revealing broadly rounded plicae (PL), connective tissue (CT), and tertiary digestive tubules (TT); FIG. 332: Transverse section of the dorsal stomach wall showing short plicae (PL), and a dense mat of cilia (CI); FIG. 333; Transverse section of dextral stomach wall showing a rectangular and forked typhlosole (TY), with an attached cuticle (CU).

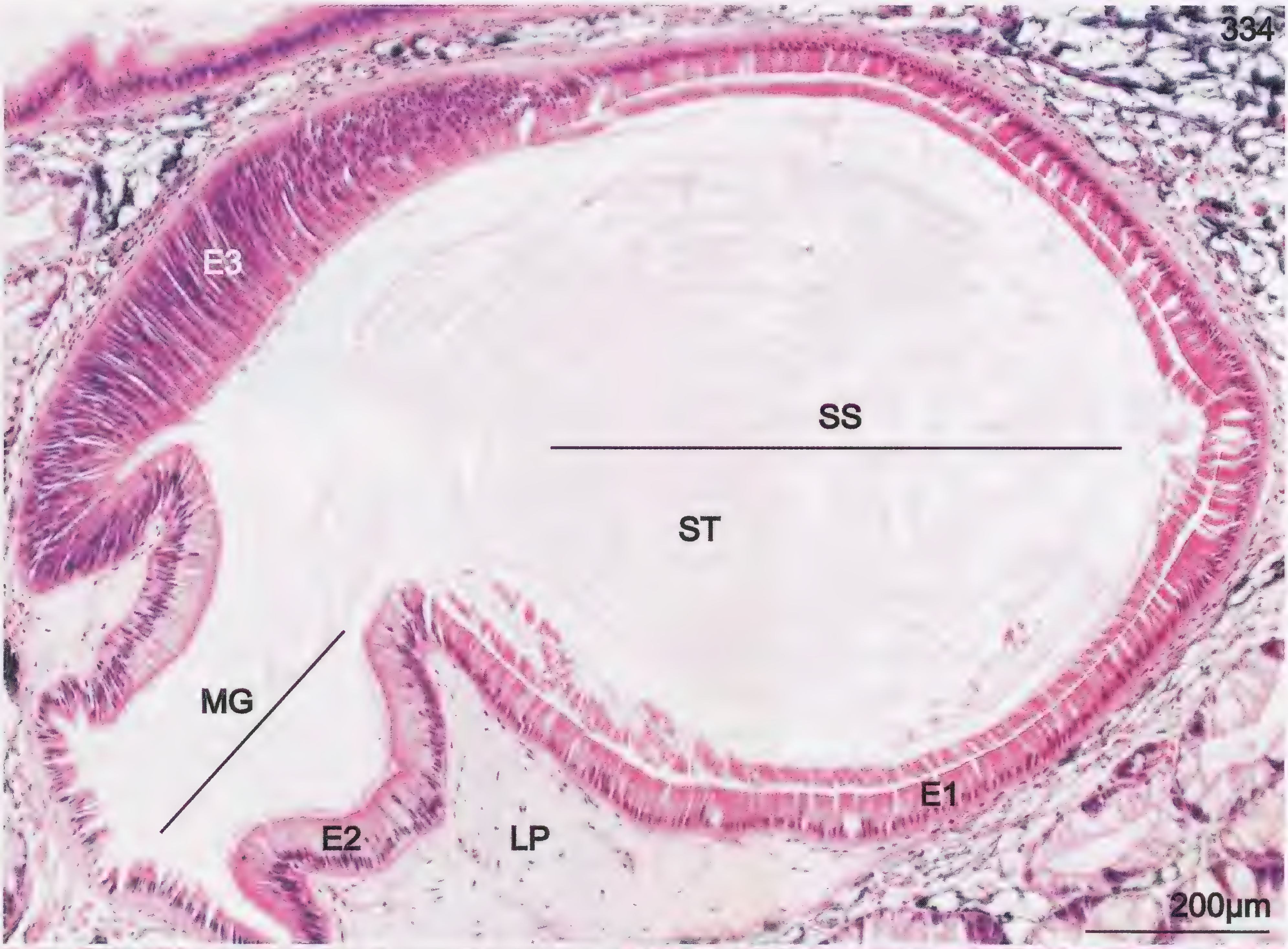
334
E3
SS
ST
MG
E1
E2
LP
200µm

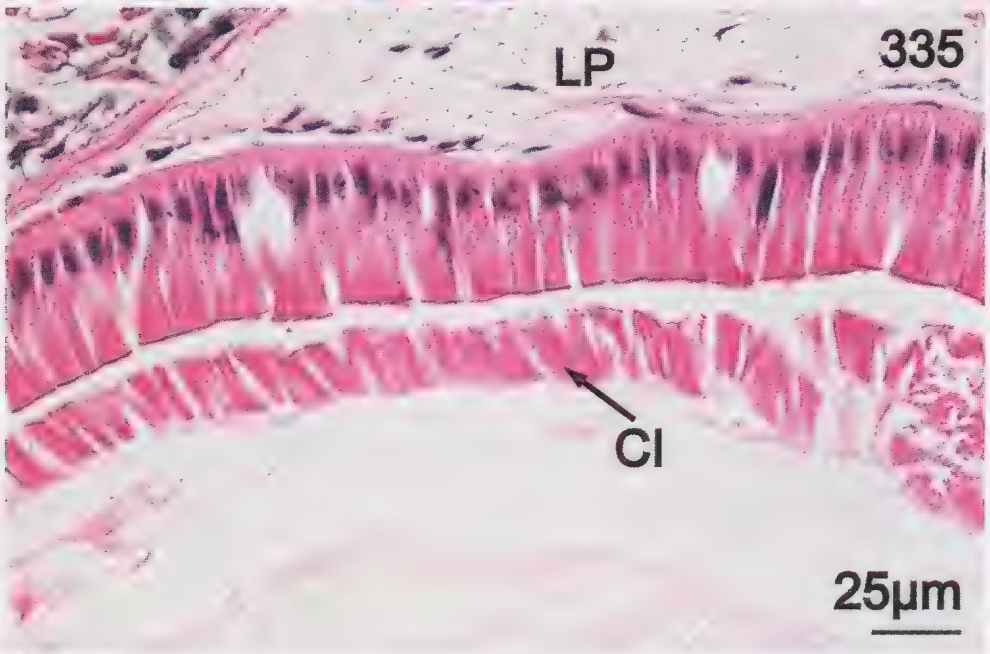
335
LP
CI
25µm

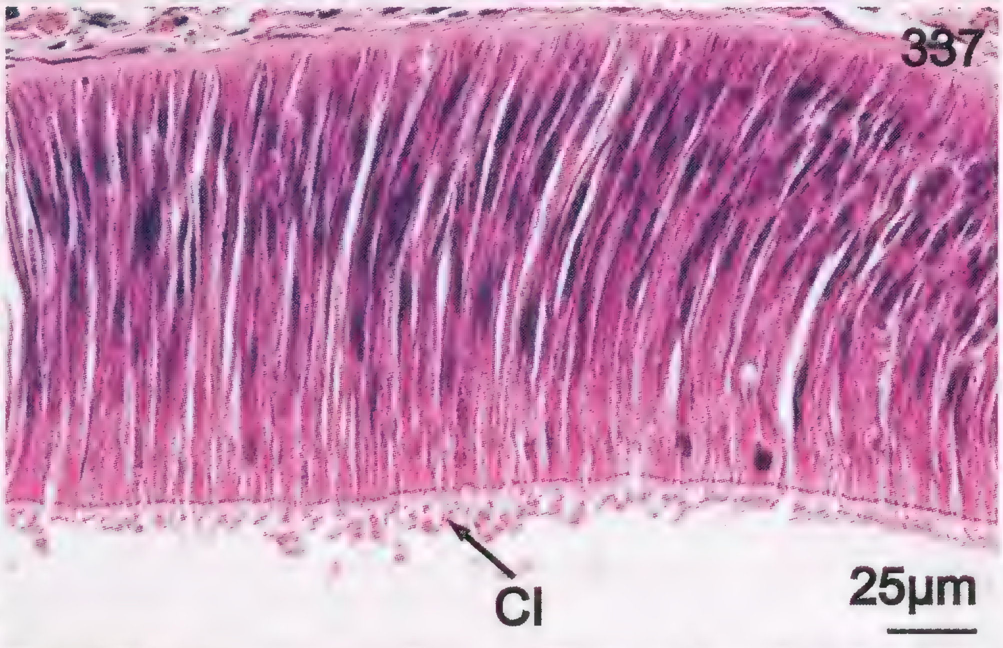
337
CI
25µm

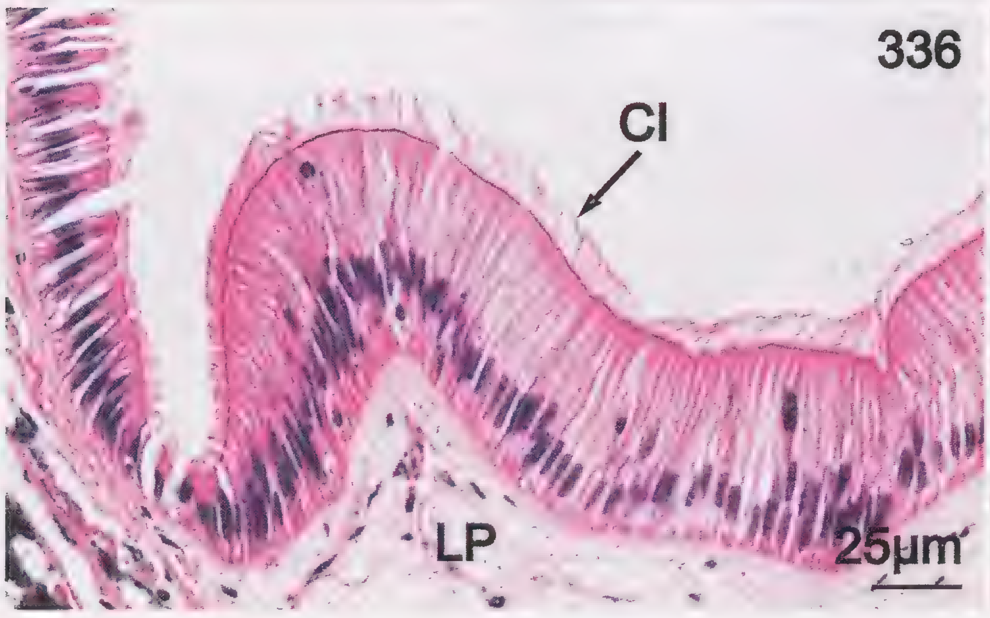
336
CI
LP
25µm

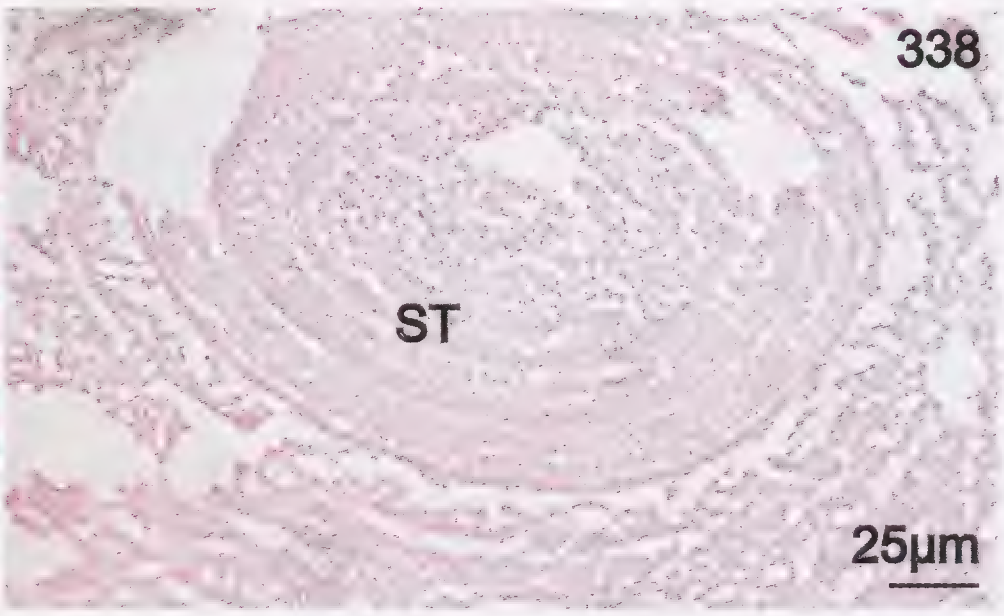
338
ST
25µm

Cellular Structure of Nervous System Tissues

Pedal Ganglion, Cerebral Ganglia and Visceral Ganglion: Nervous system of *S. connasaugaensis* consists of four ganglia, each with a series of nerve fibers extending throughout the body. A pair of cerebral ganglia is located anteriorly; each ganglion is positioned laterally along the body between the anterior adductor and labial palp. The third ganglion is referred to as the pedal ganglion since it is located at the ventral margin of the hemocoel between the digestive diverticulum and gonad, dorsal to the foot. Finally, the pleural ganglion is located on the ventral surface of the posterior adductor. Each ganglion has a distinct outer cortex of neuron cell bodies, and a fibrous inner medulla. Furthermore, there is not an obvious difference between the cellular characteristics of all ganglia, and therefore the foregoing description of the neural cortex and medulla of the pedal ganglion is representative of the anterior and posterior ganglia.

Pedal ganglion has two lobes, and each hemisphere is surrounded by a distinct epineurium and separated by a median fissure. Central commissures oriented horizontally represent communications between the hemispheres (Fig. 372). Neuron cell bodies in the cortex are conical to polygonal, with the apex extending towards the medulla neuron. Cell bodies have a pale, basophilic cytoplasm and a spherical nucleus, and a nucleolus may be observed in some cells (Fig. 373). Fissures separating the hemispheres are fibrous with a pale, eosinophilic character. The medulla has an irregular array of axons and isolated cell bodies. Commissures represent a continuation of the medulla, joining each ganglionic lobe by means of horizontal bundles of axons (Fig. 374). Cell bodies of the medulla have a spherical to spindle shaped nucleus and only a small amount of darkened, eosinophilic cytoplasm is visible (Fig. 375). Axons leave the hemispheres at lateral extensions of the medulla at dorsal and ventral margins of the hemispheres. Roots along the lateral margins of the pedal ganglion consist of large bundles of axons and supporting cells (Fig. 376). Nerves derived from the ventral aspect of each hemisphere extend ventrally through the pedal musculature. Pedal nerves from dorsal roots span the vertical length of the visceral mass.

The cerebral ganglia are spherical to ovular, located within connective tissue between the palp, anterior pedal retractor and adductor (Fig. 377). Nerves derived from these anterior ganglia extend into the anterior adductor, retractor, foot and mantle edge. The visceral ganglion is cylindrical, and closely applied to underlying myofibers of the posterior adductor. The ventral surface of the visceral ganglion consists of a thin layer of connective tissue and an epithelium represented by simple columnar cells and goblet cells. Additionally, columnar cells contain brown intracellular granules and the entire cytoplasm is darkened (Figs. 378, 379). The inner gill reunites with the body at the anterior margin of the posterior adductor. At ctenidial-adductor junction, ganglionic tissue extends ventrally into gill tissue (Fig. 380).

Nerves and Statocysts: Nerves may be distinguished from connective tissue by the pale eosinophilic membrane or perineurium, surrounding nerve fascicles. The perineurium

---

←

FIGS. 334–338. Crystalline style sac of *Strophitus connasaugaensis*. FIG. 334: Transverse section through the crystalline style sac showing the style sac (SS), style (ST), midgut (MG), epithelium type-one (E1), epithelium type-two (E2), epithelium type-three (E3), and the surrounding lamina propria (LP); FIG. 335: Transverse section of the crystalline style sac type-one epithelium, consisting of eosinophilic columnar cells bearing cilia (CI), and the lamina propria (LP); FIG. 336: Transverse section of style sac epithelium type-two, emphasizing eosinophilic and vesiculated columnar cells bearing cilia (CI) and the underlying lamina propria (LP); FIG. 337: Transverse section of style sac type-three epithelium featuring tall, basophilic columnar cells bearing cilia (CI); FIG. 338: Transverse section of the style (ST) showing concentric layers of an eosinophilic material.

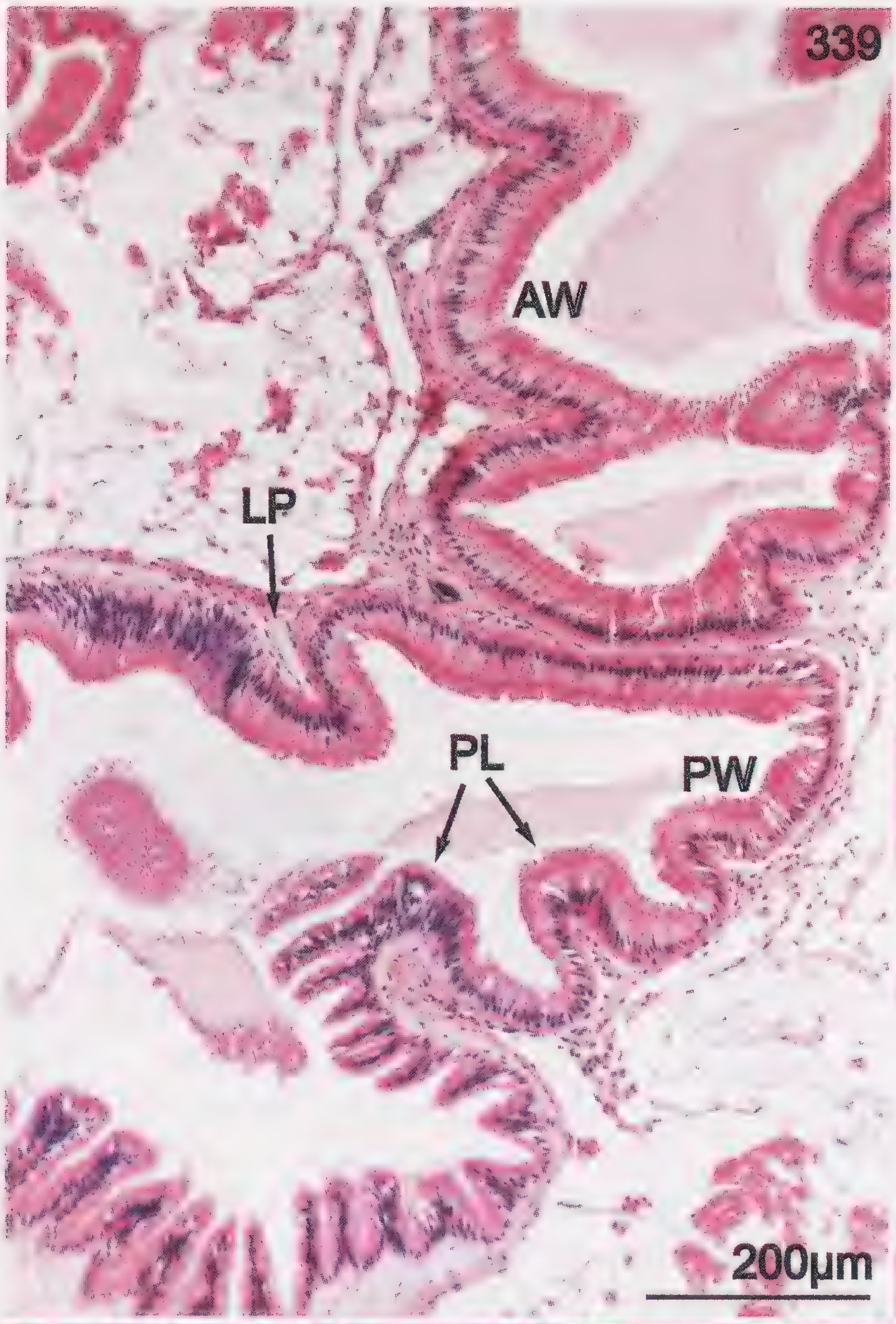
339
AW
LP
PL
PW
200µm

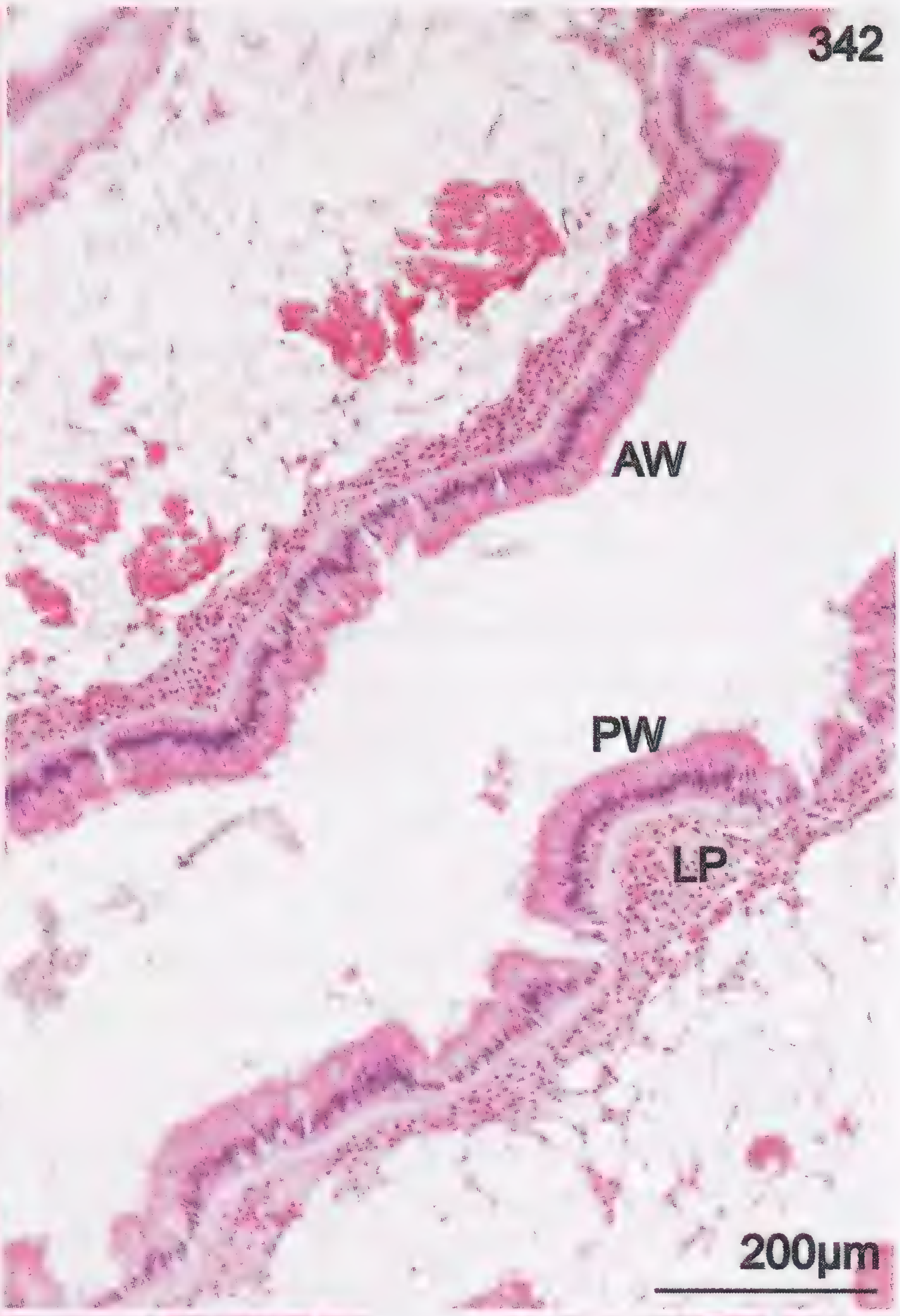
342
AW
PW
LP
200µm

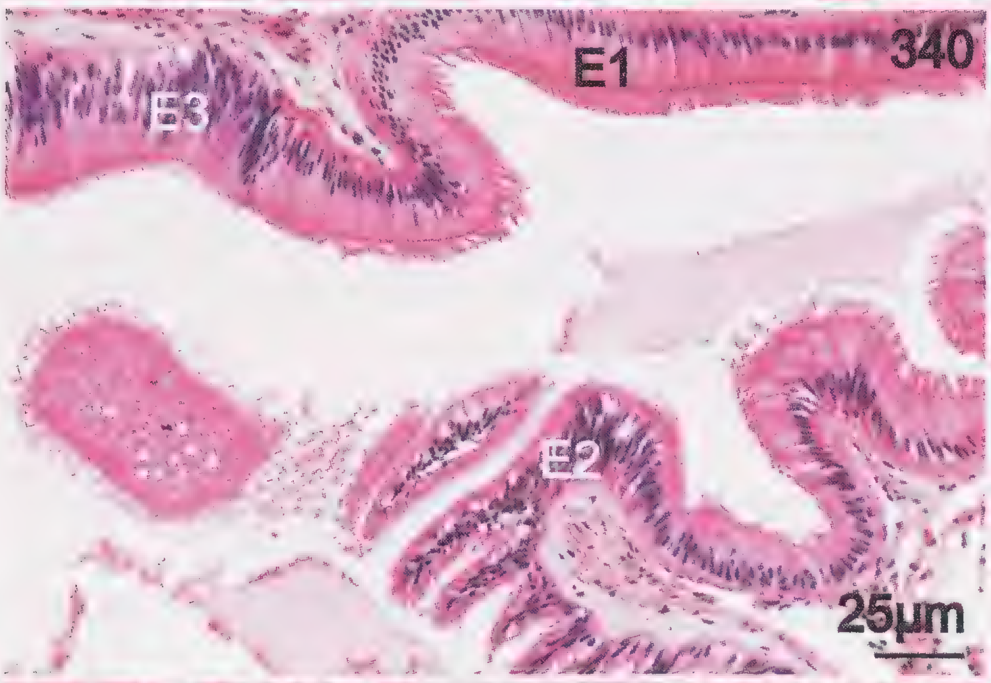
340
E3
E1
E2
25µm

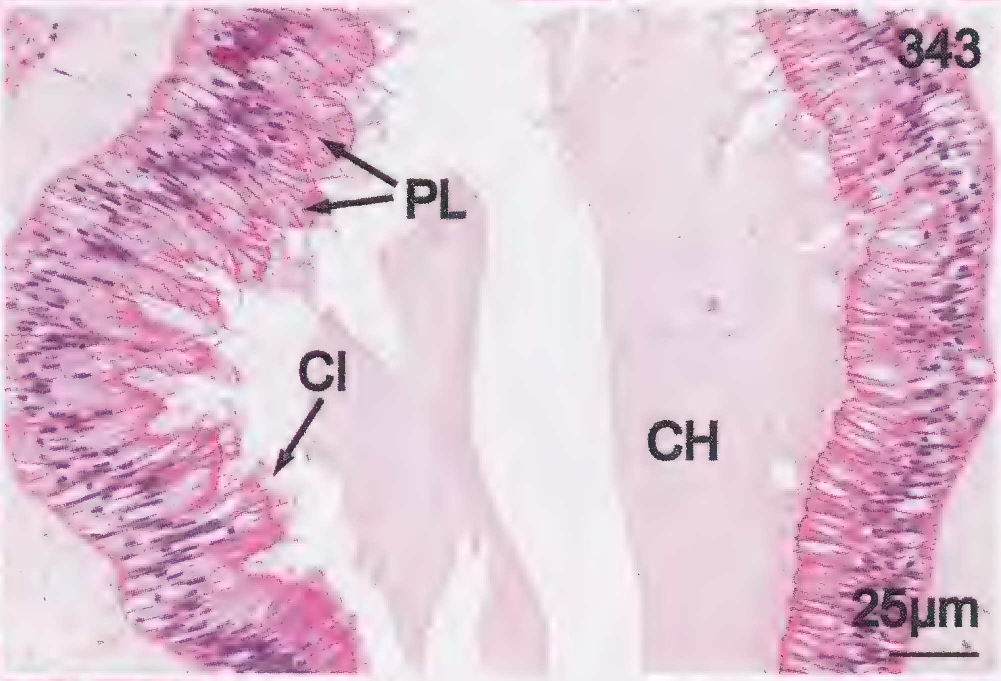
343
PL
CI
CH
25µm

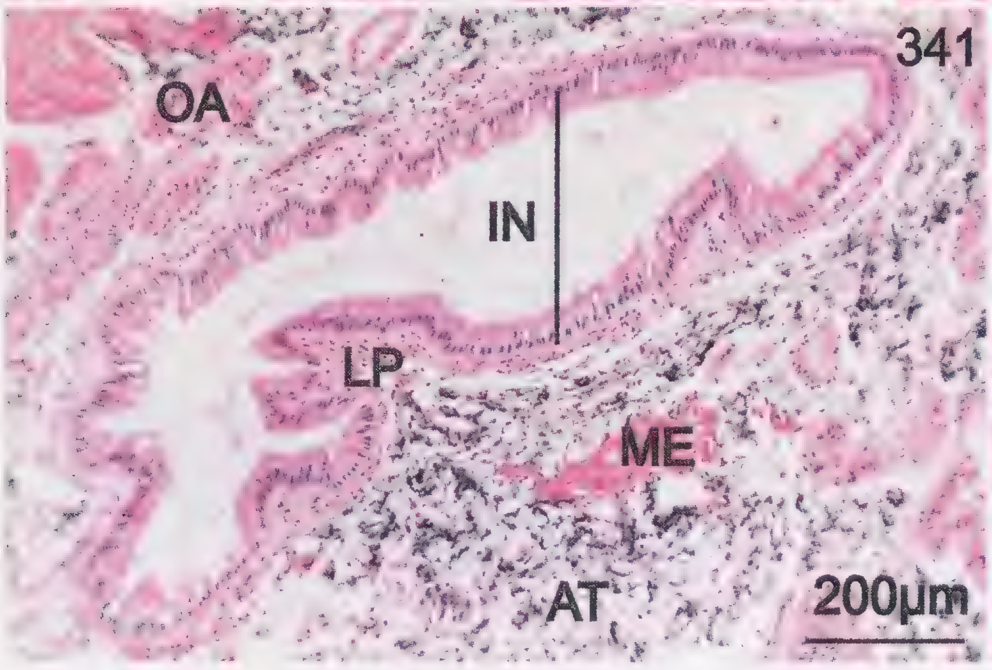
341
OA
IN
LP
ME
AT
200µm

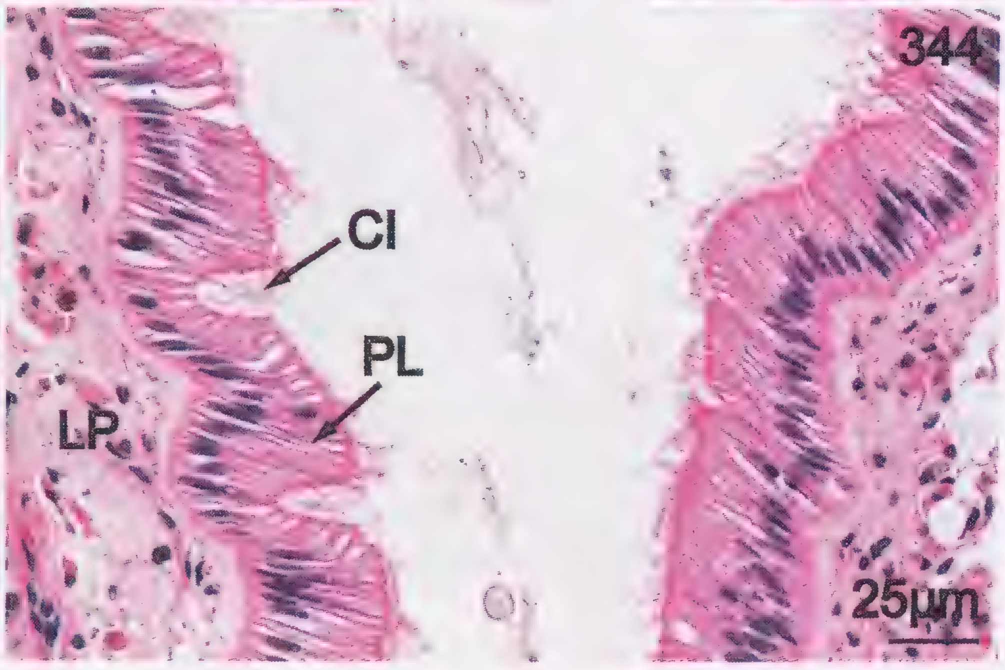
344
CI
PL
LP
25µm

is thickened with a homogenous staining character, while groups of axons have small, irregularly by polygonal spaces between each other. Transverse sections show how the contents of a bundle of nerves are irregular or vesiculated mass of fibers (Fig. 381). Longitudinal sections of nerves portray bundles of axons as sinuous ribbons of fine, eosinophilic fibers (Fig. 382). Additionally, nerves contain a series of nuclei; cylindrical to emarginated nuclei near the perineurium are possible Schwann cells. Spindle-shaped to polygonal nuclei medially located within a nerve appear to be neuron cell bodies. Nuclei of neuron cell bodies have a small perimeter of basophilic cytoplasm. Given the above, the smallness of nerve cells precludes definitive identification with hematoxylin and eosin-stained tissue sections.

Statocysts represent accessory structures of the nervous system associated with the pedal ganglion. A statocyst is an ovular capsule located at the ventral margin of the coelom, lateral to the pedal ganglion. Statocyst epithelium consists of ciliated columnar cells lining the lumen and a basal layer of cuboidal cells. Columnar cells of a statocyst have a pale eosinophilic cytoplasm and a spherical, basophilic nucleus containing a small nucleolus. The lumen of the statocyst contains a dark, spherical mass called the statolith. The statolith has a dark, violet character and may appear fragmented. A thickened, pale, eosinophilic capsule surrounds the statocyst and connective tissue becomes continuous with coelomic connective tissue associated with the pedal ganglion (Fig. 383).

Cellular Structure of Reproductive System Tissues

Ovarian and testicular tissues are organized into ovular acini. Ovarian and testicular acini exhibited a low-level of gametogenesis during May 2011 from individuals collected in Shoal Creek while peak gametogenesis was evident in one male and one female *S. connasaugaensis* collected from South Fork Terrapin Creek in August 2011. Ovarian acini characterized by depressed gametogenesis widely distributed amongst connective tissues and ciliated gonadal ducts (Fig. 384). Ovarian acini contained a large concentration of eosinophilic matter consisting of small, spherical granules and larger cells, possibly representing polar bodies. The eosinophilic granules may represent the remains of polar bodies and apoptotic oocytes. Oocytes were spherical to ovular, basophilic, with a distinct, spherical nucleus, and a series of transparent cytoplasmic vesicles. Some oocytes appeared to be free within the lumen or attached to the acinus wall by a pellicle (Fig. 385).

A higher level of gametogenesis was evident in August. Acini were enlarged with correspondingly enlarged mature oocytes. Mature oocytes typically exhibited a well-defined perimeter of eosinophilic granules and small irregular nuclei. Mature oocytes appear to begin as a small basophilic cell with a distinct nucleus and nucleolus. Oocytes are attached to the acinus wall by a pellicle and eventually separate from the wall when they reach a certain size. As oocytes mature, they become larger and eosinophilic cytoplasm becomes more prominent. Mature

---

←

FIGS. 339–344. First intestinal limb, and second intestinal limb of *Strophitus connasaugaensis*. FIG. 339: Sagittal section of the first, descending intestinal limb showing plicae (PL) along the anterior (AW) and posterior walls (PW), supported by lamina propria (LP); FIG. 340: Sagittal section of the first intestinal limb showing style sac epithelium type-one (E1), type-two (E2), and type-three (E3); FIG. 341: Transverse section through visceral mass revealing the second intestinal limb (IN), lamina propria (LP), mesentery (ME), adipose tissue (AT), and ovarian acini (OA); FIG. 342: Sagittal section of the ascending portion of the second intestinal limb showing the sinuous epithelium of the anterior (AW) and posterior walls (PW), and surrounding lamina propria (LP); FIG. 343: Sagittal section of the second intestinal limb focusing on plicae (PL), vesicular cells bearing cilia (CI), chyme (CH) in the lumen; FIG. 344: Sagittal section of the second intestinal limb showing rounded to flattened plicae (PL), bearing cilia (CI), supported by lamina propria (LP).

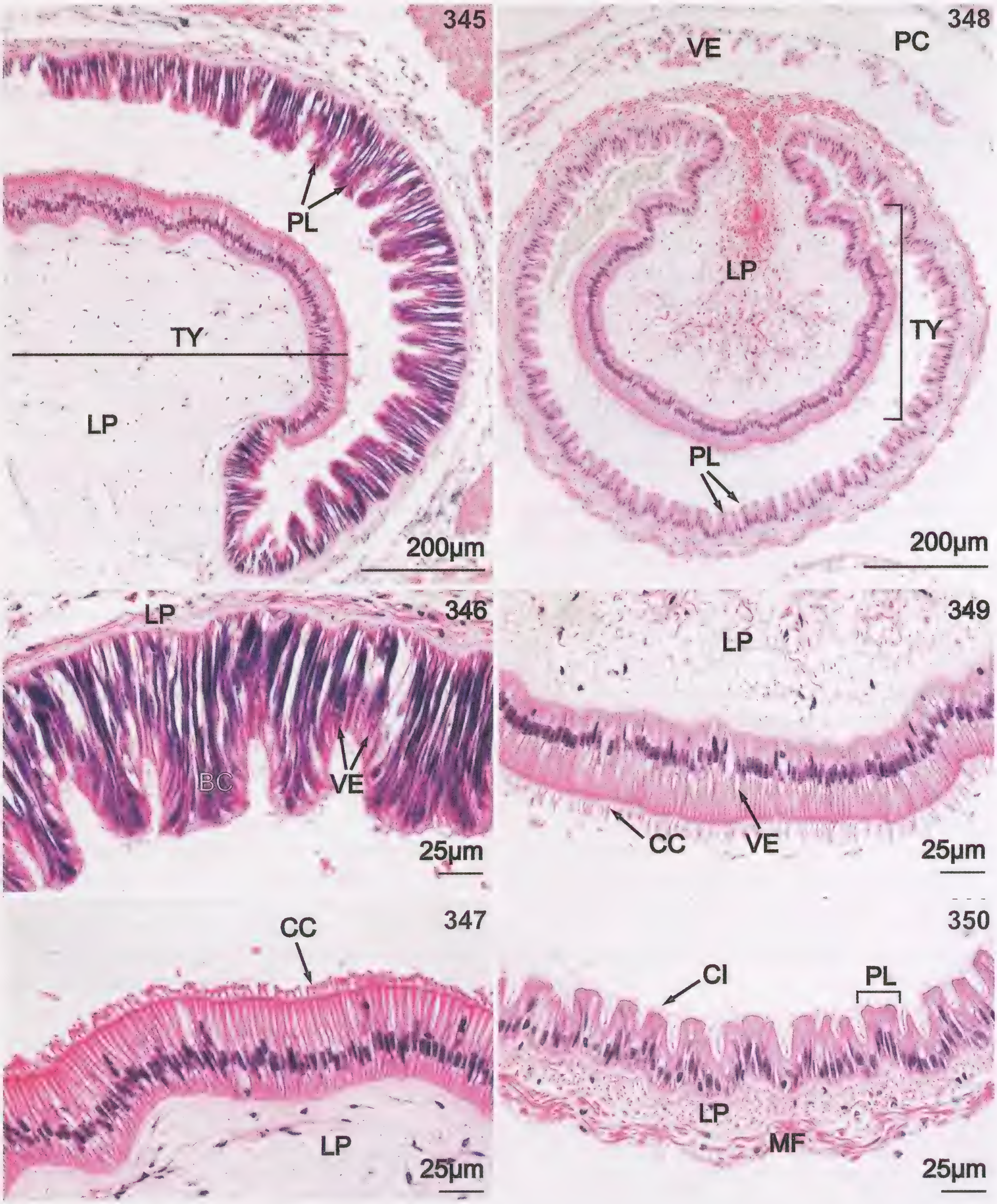

FIGS. 345–350. Fourth intestinal limb, and fifth intestinal limb of *Strophitus connasaugaensis*. FIG. 345: Transverse section of the fourth intestinal limb featuring a large, ventrally extending typhlosole (TY), with a correspondingly large lamina propria (LP), and plicae along the lateral-dorsal wall (PL); FIG. 346: Transverse section of ventral epithelium of the fourth intestinal limb focusing on basophilic cells (BC) containing vesicles (VE) and a thin lamina propria (LP); FIG. 347: Transverse section of dorsal epithelium of the fouth intestinal limb featuring ciliated columnar cells (CC), and the underlying lamina propria (LP); FIG. 348: Transverse section of the fifth intestinal limb revealing a large, dorsally extending typhlosole (TY), with an extensive lamina propria (LP), plications (PL) along the dorsal wall, and thin tissue layers comprising the ventricle (VE) and pericardium (PC); FIG. 349: Transverse section of the ventral epithelium of the typhlosole emphasizing ciliated columnar cells (CC), containing vesicles (VE), and extensive lamina propria (LP); FIG. 350: Transverse section of dorsal epithelium portraying conical plicae (PL), bearing cilia (CI), and underlying tissues including a thin lamina propria (LP) and rim of myofibers (MF).

oocytes of *S. connasaugaensis* have a red, granular cytoplasm and a pale, basophilic nucleus with dark patches of chromatin. The membrane of mature oocytes is irregular, with a pale staining character. However, the distal margin of the vitelline membrane appears to be more condensed and fibrous. Mature oocytes are greatly enlarged, occupying the majority of the lumen of the acinus (Fig. 386).

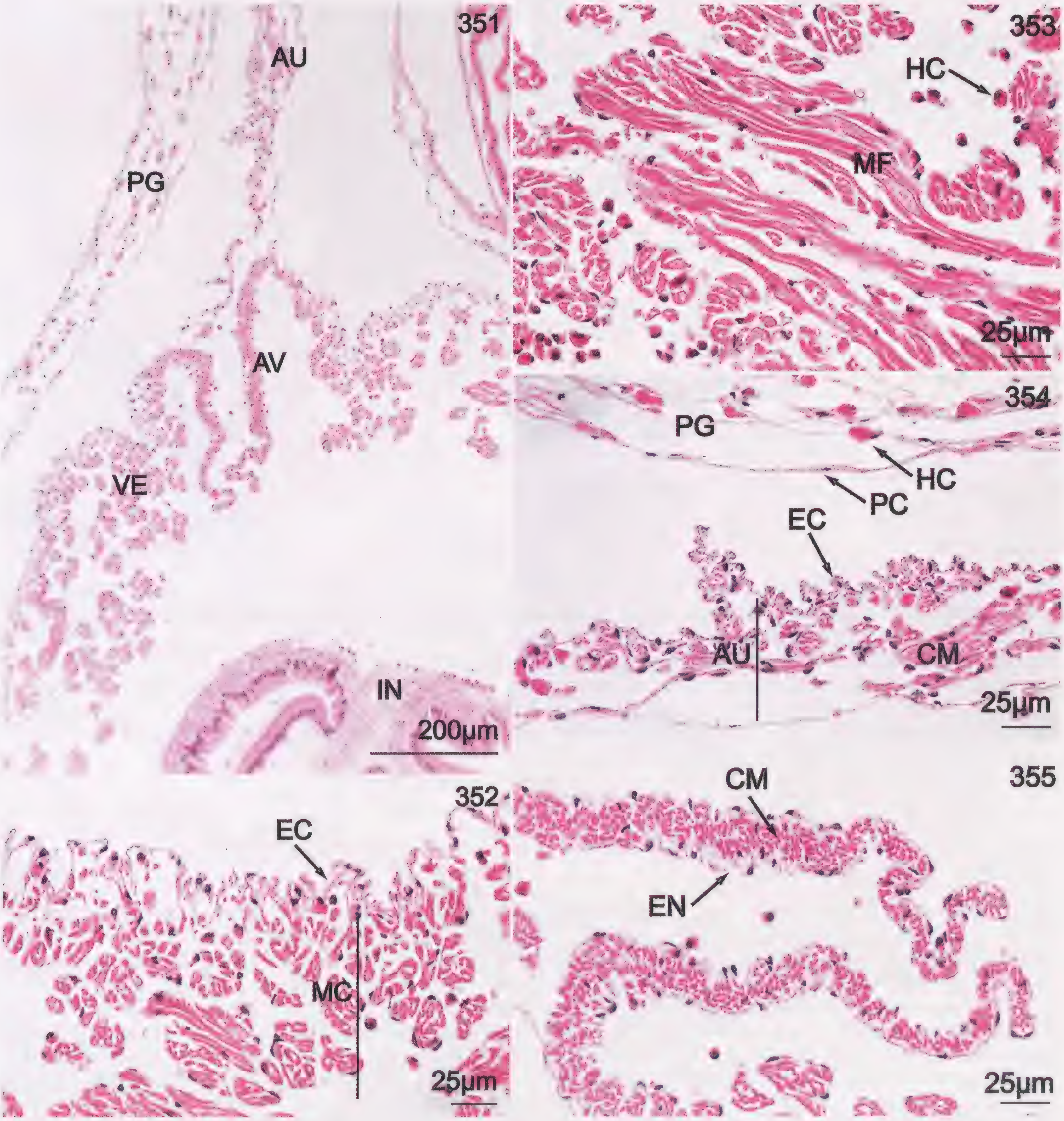

FIGS. 351–355. Heart, and pericardium of *Strophitus connasaugaensis*. FIG. 351: Transverse section the lateral portion of the heart showing the fifth intestinal limb (IN), ventricle (VE), auricle (AU), auriculoventircular valve (AV), and pericardial gland (PG); FIG. 352: Transverse section through the ventricle focusing on the thin epicardium (EC), and underlying myocardium (MC); FIG. 353: Transverse section of the ventricle emphasizing transverse and longitudinal myofibers (MF), and interspersed hemocytes (HC); FIG. 354: Transverse section of the auricle (AU) showing epicardium (EC), cardiac muscle (CM), pericardial sac (PC), hemocytes (HC), and pericardial gland (PG); FIG. 355: Transverse section of an auriculoventricular valve showing cardiac muscle (CM), enveloped by a thin endothelium (EN).

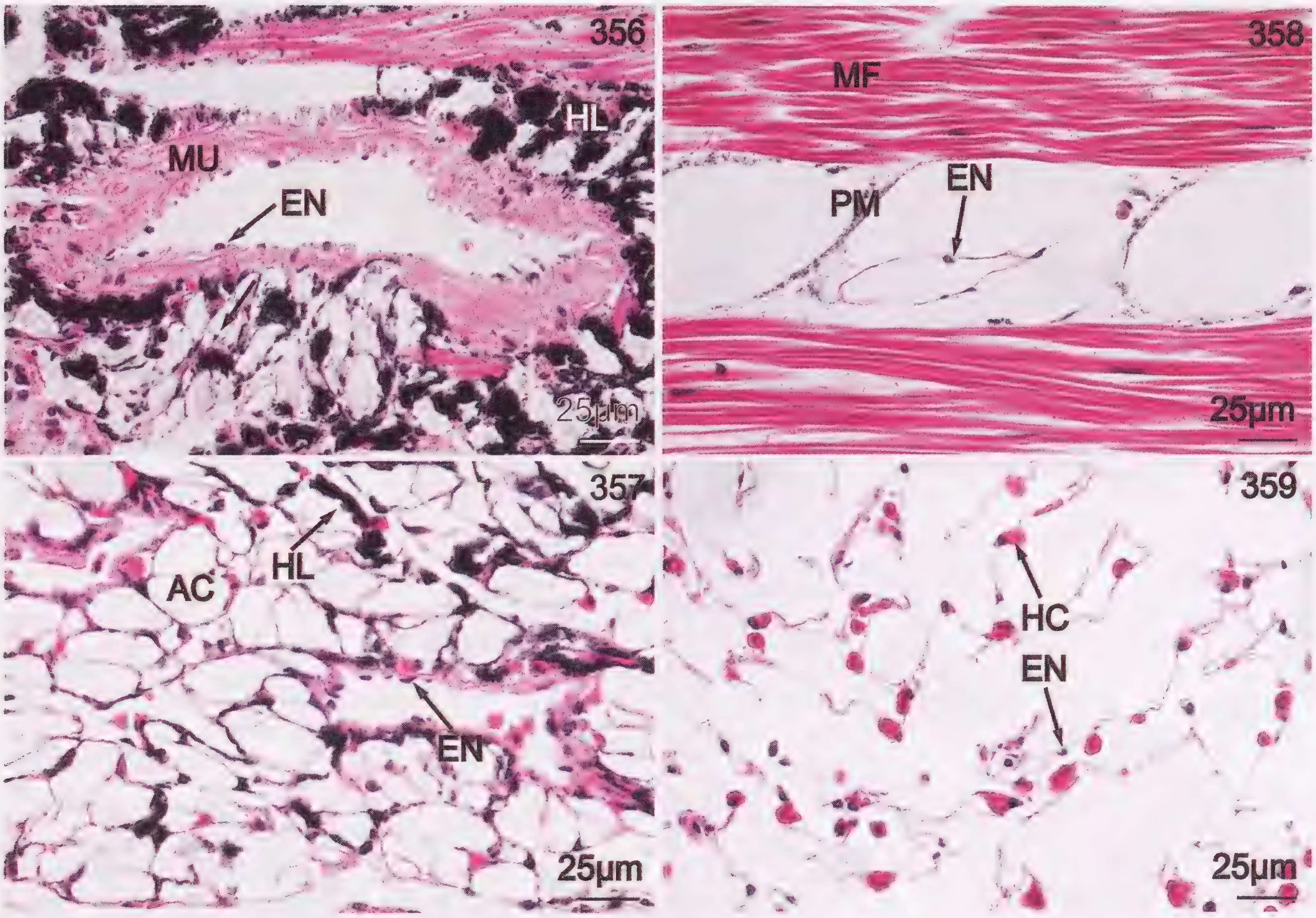

FIGS. 356–359. Hemolymph vessels, and pericardial gland of *Strophitus connasaugaensis*. FIG. 356: Transverse section of visceral mass showing a possible artery featuring an endothelium (EN), and thick muscular wrapping (MU), and surrounding pockets of hemolymph (HL); FIG. 357: Transverse section through the visceral mass featuring a possible vein demarcated by its endothelium (EN), and surrounded by adipocytes (AC) and pockets of hemolymph (HL); FIG. 358: Sagittal section through posterior adductor emphasizing longitudinal myofibers (MF), thin perimysium (PM), and a capillary consisting of endothelium (EN); FIG. 359: Transverse section of the pericardial gland showing emarginated nuclei of pericardial gland cells (EN), and hemocytes (HC).

→

FIGS. 360–366. Anterior nephridium of *Strophitus connasaugaensis.* FIG. 360: Transverse section of the dorsal aspect of the visceral mass (VM) showing the branched ventral nephridium (VN), dorsal nephridium (DN), pericardium (PC) and ventricle (VE); FIG. 361: Transverse section of the ventral nephirdium emphasizing the sinuous nephridial lumen (NL), eosinophilic intracellular granules (EG) of nephridial epithelium and subepithelial hemolymph vessels (HV), and endothelium (EN); FIG. 362: Transverse section of dorsal nephridium consisting of teardrop-shaped columnar cells (TC), an expansive nephridial lumen (NL), and adjacent hemolymph (HL) and ventral nephridium (VN); FIG. 363: Transverse section of ventral nephridium focusing on the flattened, columnar epithelium (CE) of the dorsal wall, short, rounded plicae (PL) along the ventral surface, and hemocytes (HC); FIG. 364: Transverse section of the lateral margin of the nephridium showing the ventral nephridial branches (VN), urethra (UR), ciliated renopericardial canal (RC), and hemolymph (HL); FIG. 365: Transverse section of the renopericardial canal featuring ciliated columnar cells (CC), goblet cells (GC), and an encircling lamina propria (LP); FIG. 366: Transverse section of the urethra showing basophilic columnar cells bearing cilia (CI), goblet cells (GC), and lamina propria (LP).

360

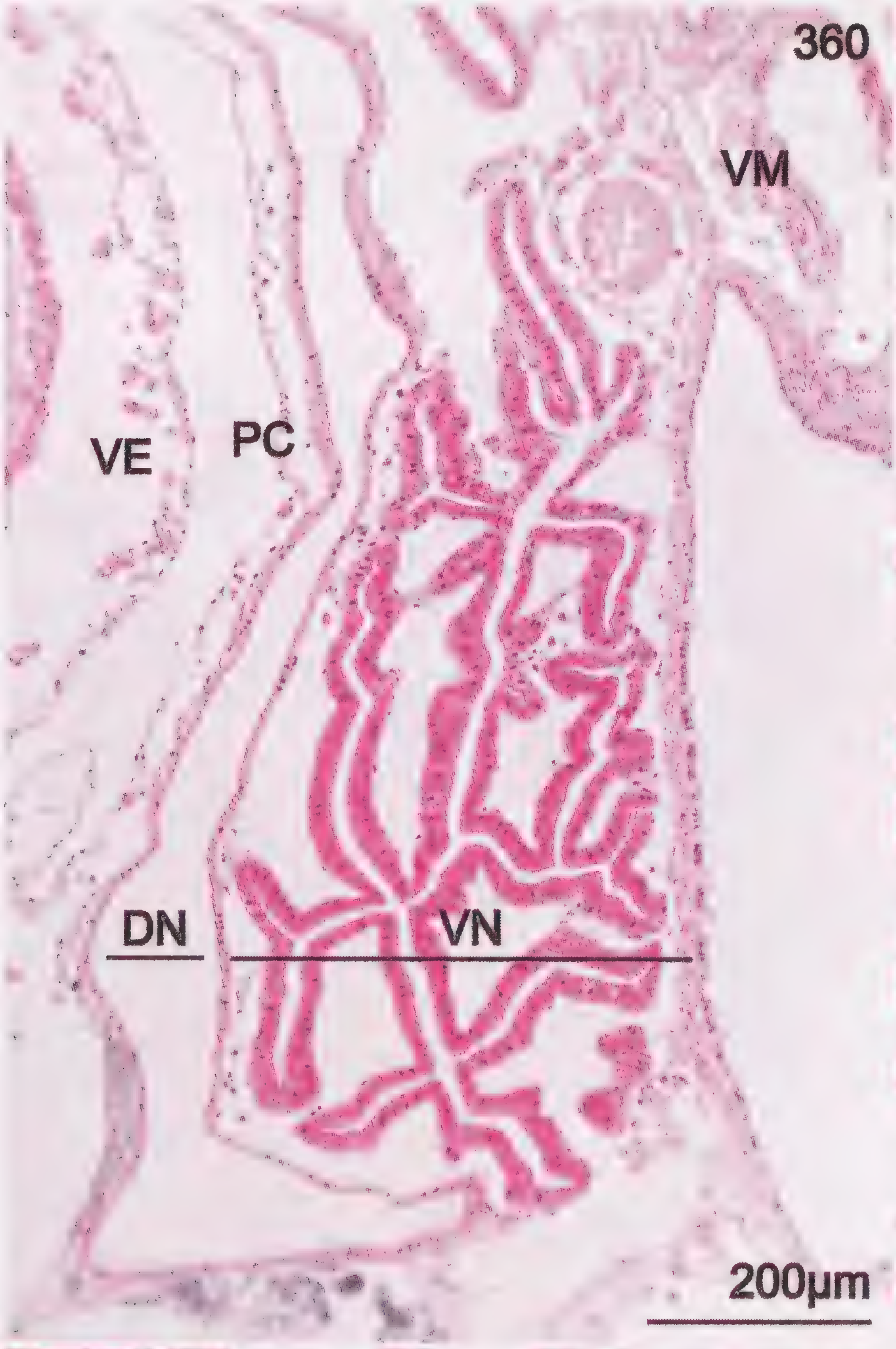

361

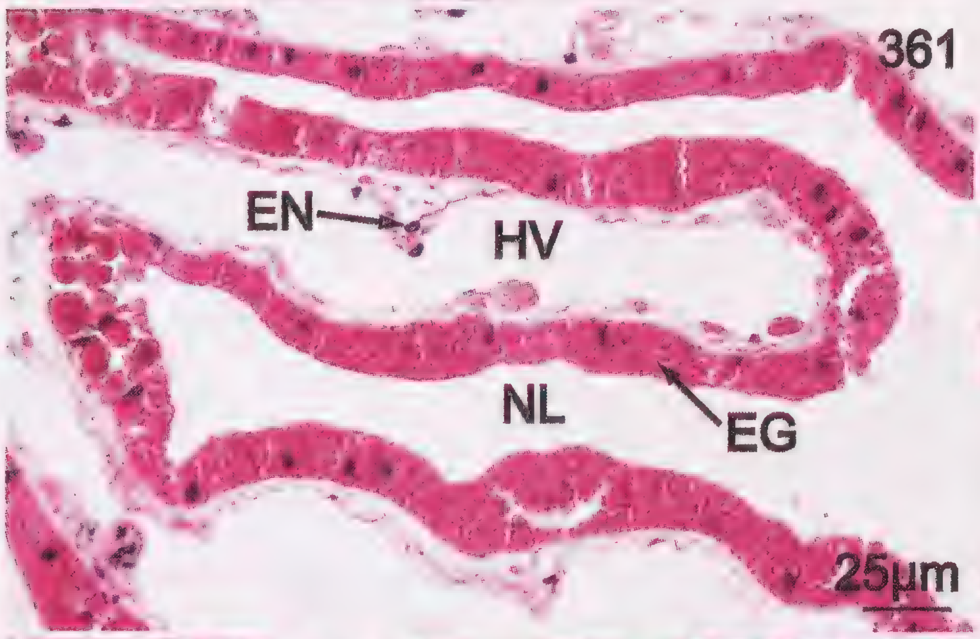

362

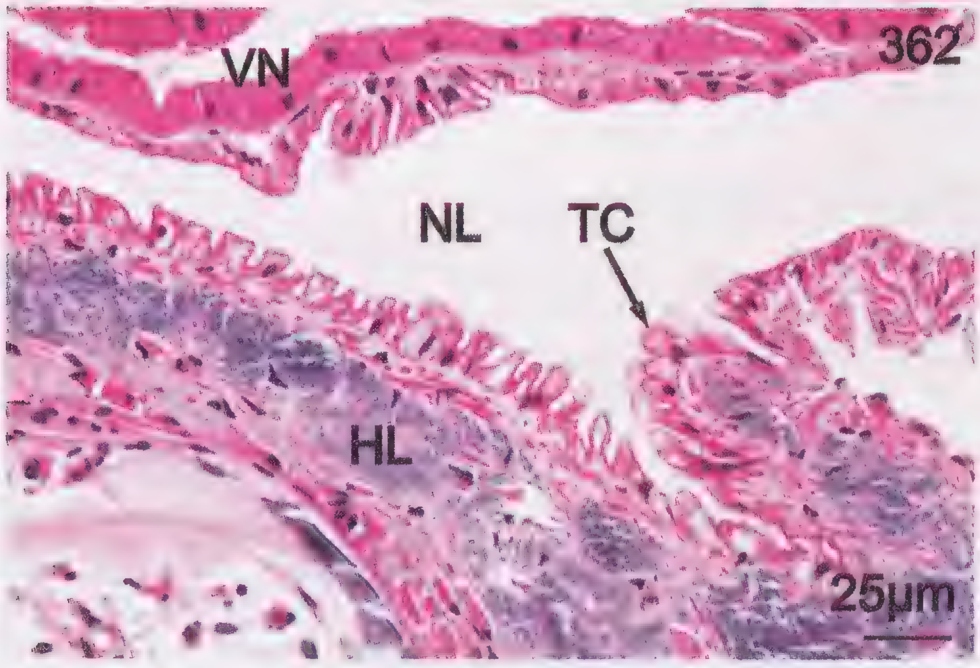

363

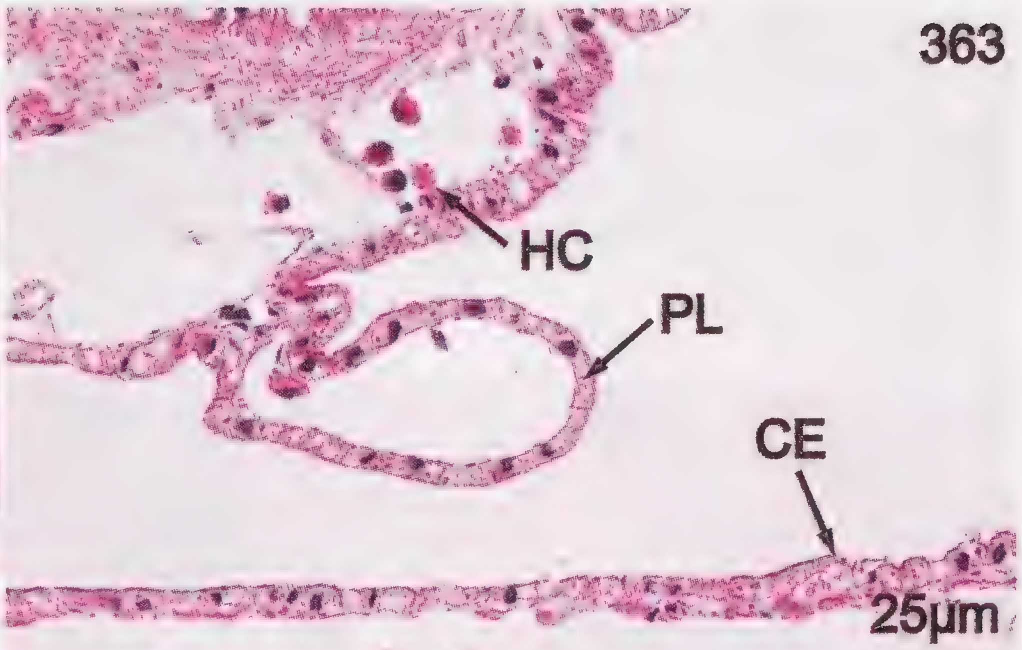

364

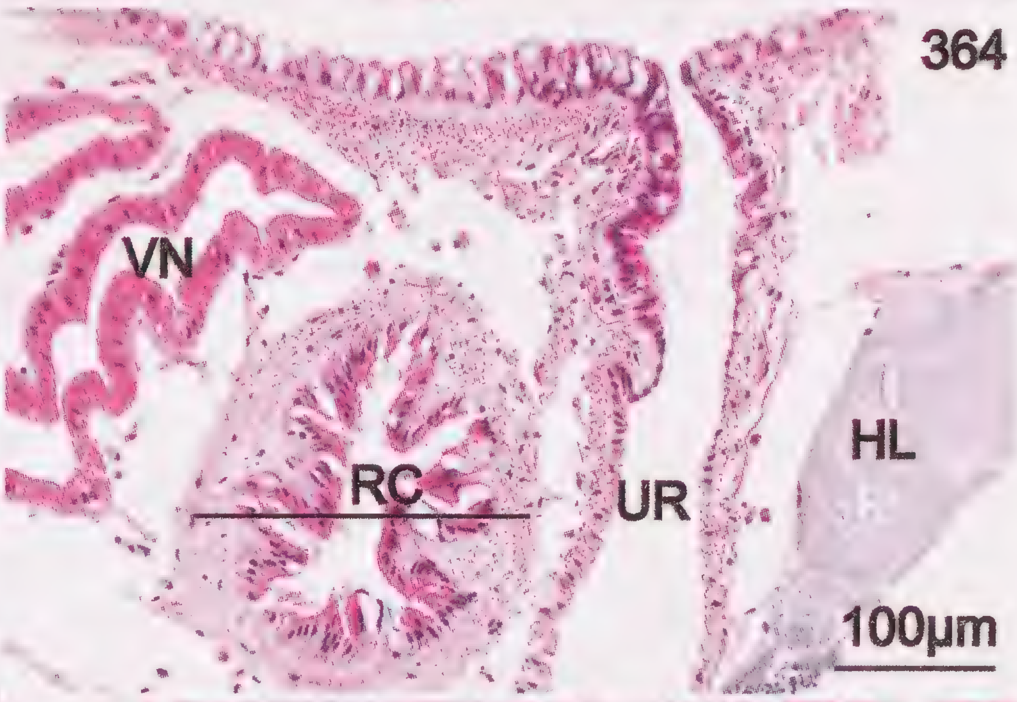

365

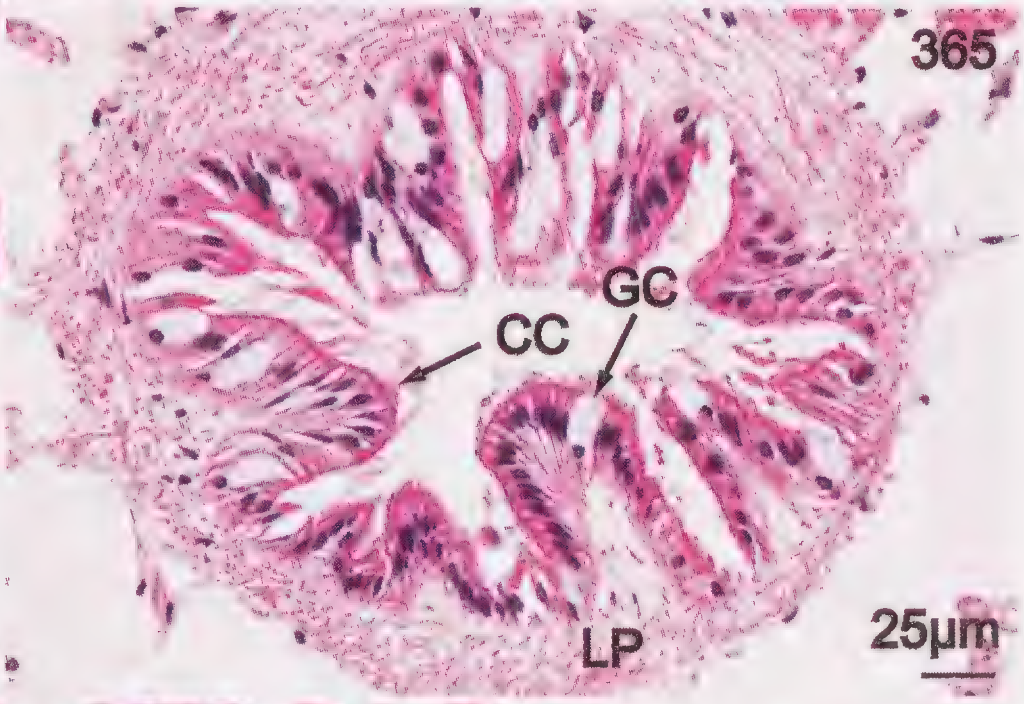

366

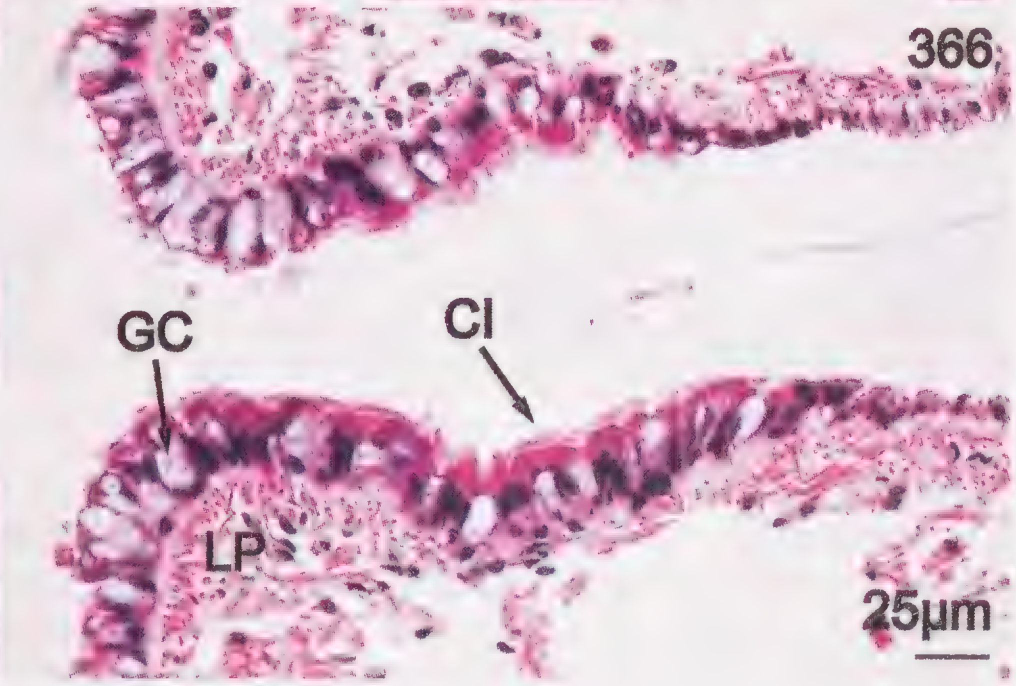

Stage 1 testicular acini are small and positioned within a matrix of adipocytes and ciliated ducts (Fig. 387). Low gametogenesis in testicular acini was characterized by the presence of sperm morula appearing as clusters of small, spherical cells. Spermatocytes undergo a cell division process resulting in a series of smaller, closely spaced cells. Spermatocytes of sperm morula appear to largely lack cytoplasm and consist of a darkened cell body. Small

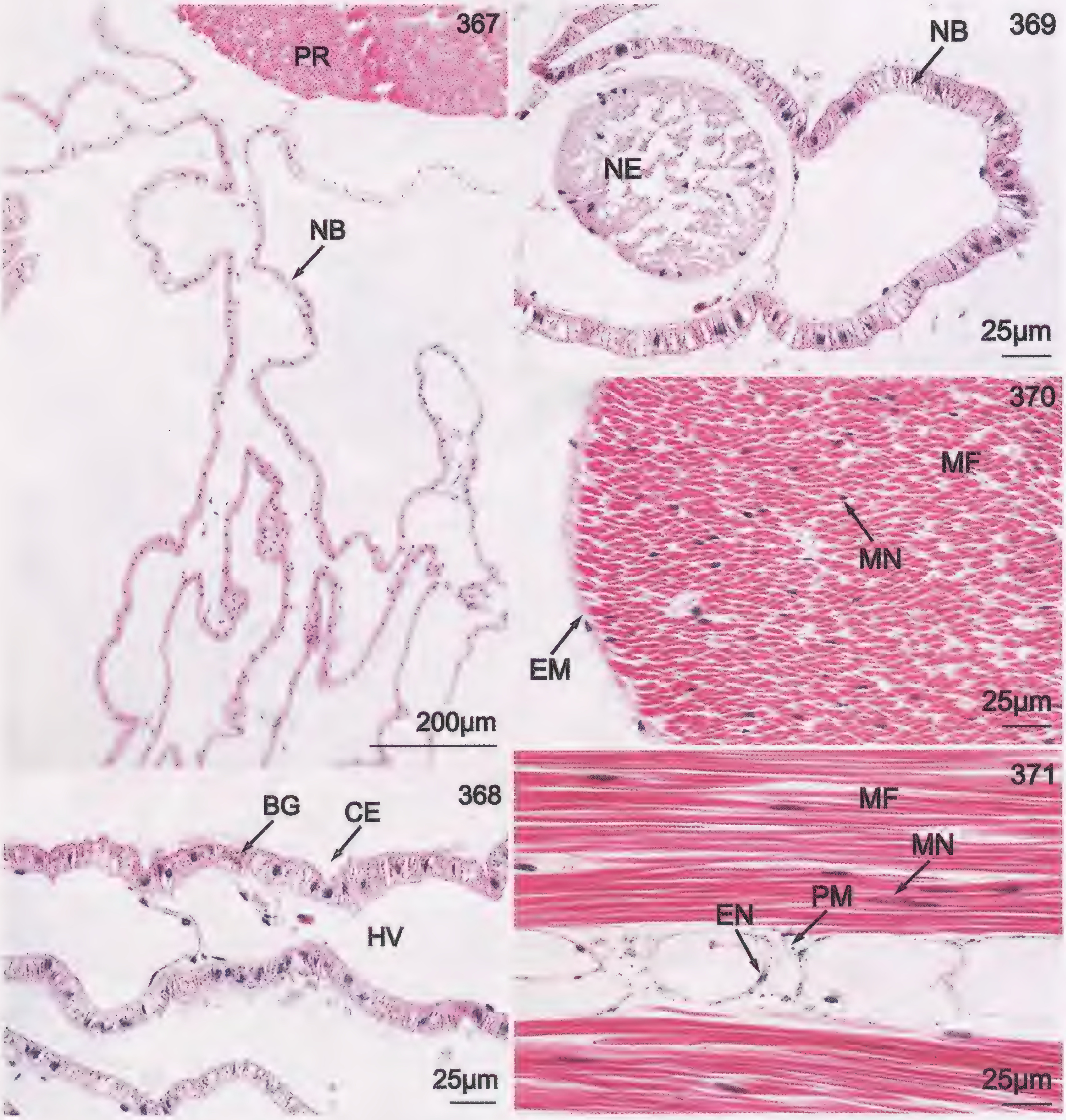

FIGS. 367–371. Posterior nephridium, posterior pedal retractor, and posterior adductor of *Strophitus connasaugaensis*. FIG. 367: Transverse section of posterior nephridium showing nephridial branches (NB) in relation to the posterior pedal retractor (PR); FIG. 368: Transverse section of nephridial branches showing a columnar epithelium (CE), brown intracellular granules (BG), and underlying hemolymph vessels (HV); FIG. 369: Transverse section of posterior nephridium revealing a short nephridial branch (NB), and a large transverse nerve (NE); FIG. 370: Transverse section of posterior retractor showing epimysium (EM), myocyte nuclei (MN), and myofibers (MF); FIG. 371: Sagittal section of posterior adductor showing linear myofiber (MF), elliptical myocyte nuclei (MN), perimysium (PM), and endothelium (EN) of capillaries.

eosinophilic granules are interspersed among sperm morula, possibly representing a fluid or the remains of broken down spermatocytes. A small quantity of spermatozoa may be present within the center of the acinus (Fig. 388).

Testicular acini in a male collected in August were conspicuously enlarged and distinguished by a plethora of spermatozoa. The luminal contents contain such a large quantity of actively dividing spermatocytes and spermatozoa that

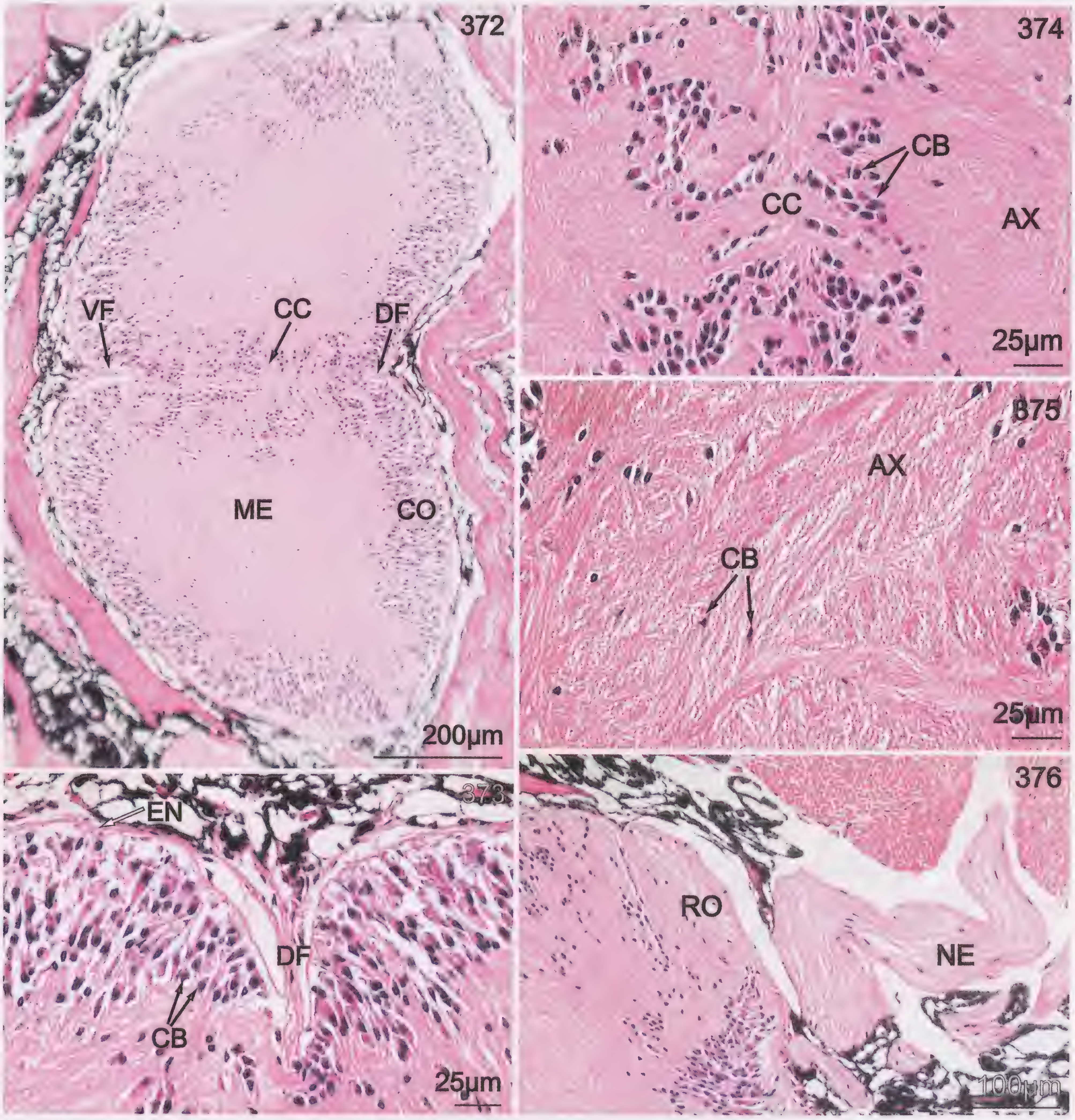

FIGS. 372–376. Pedal ganglion of *Strophitus connasaugaensis*. FIG. 372: Transverse section of the pedal ganglion showing the neural cortex (CO), medulla (ME), dorsal fissure (DF), ventral fissure (VF), and central commissures (CC); FIG. 373: Transverse section of pedal ganglion showing the epineurium (EN), dorsal fissure (DF), and neuron cell bodies (CB); FIG. 374: Transverse section of neural medulla showing axons (AX), neuron cell bodies (CB), and central commissures (CC); FIG. 375: Transverse section of the neural medulla showing axons (AX) and isolated cell bodies (CB); FIG. 376: Transverse section of pedal ganglion showing a nerve (NE) extending from a ventral root (RO).

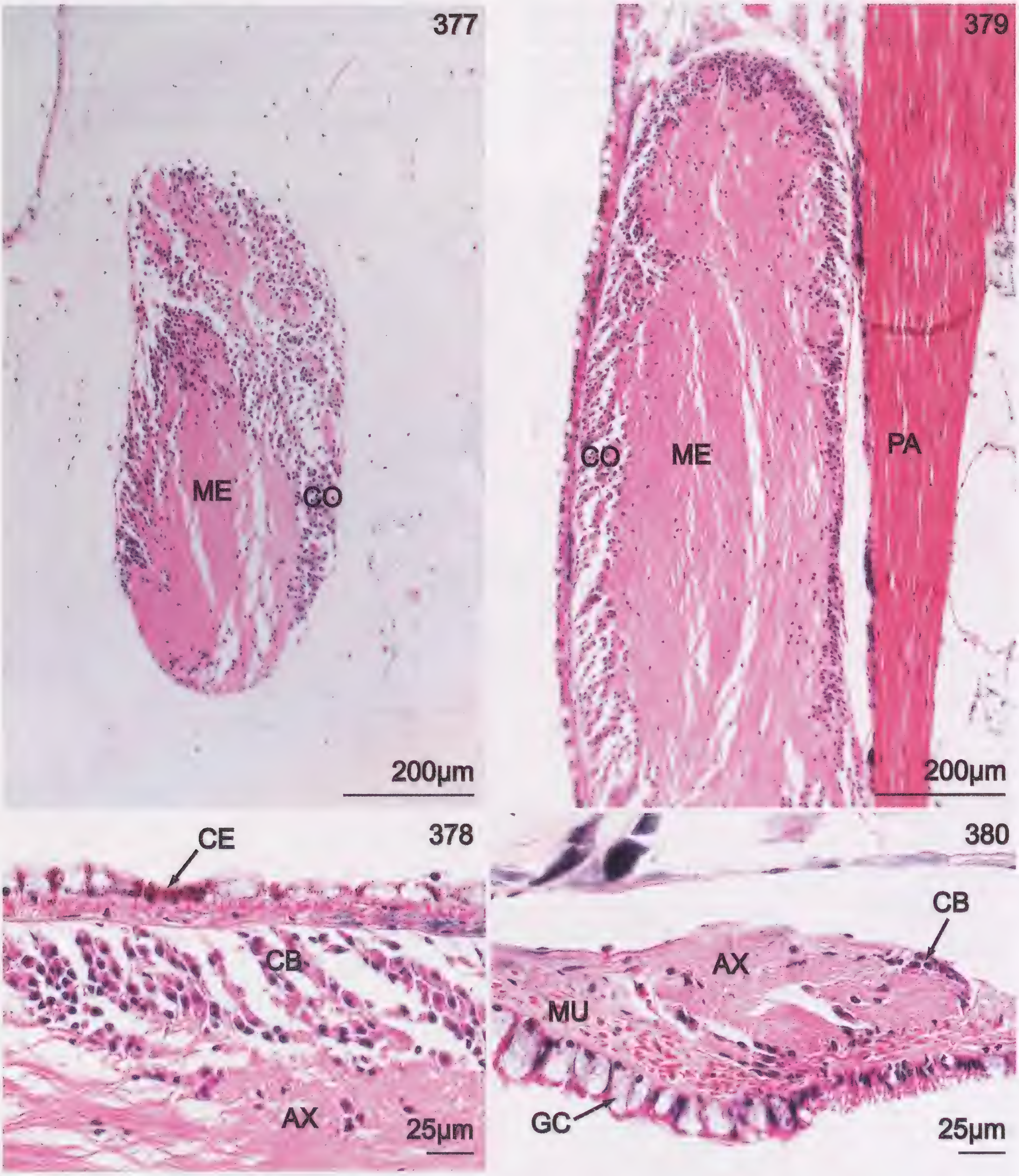

FIGS. 377–380. Cerebral ganglia, and visceral ganglion of *Strophitus connasaugaensis*. FIG. 377: Transverse section through cerebral ganglion showing neural cortex (CO), and medulla (ME); FIG. 378: Transverse section of visceral ganglion showing axons (AX), neuron cell bodies (CB), and a ventral layer of columnar epithelium (CE) containing brown intracellular granules; FIG. 379: Transverse section of visceral ganglion showing the cortex (CO), medulla (ME), and longitudinal myofibers of the posterior adductor (PA); FIG. 380: Transverse section of the base of the ctenidia near the posterior visceral mass showing goblet cells (GC), musculature (MU), and cell bodies (CB) and axons (AX) of a ventral extension of visceral ganglion.

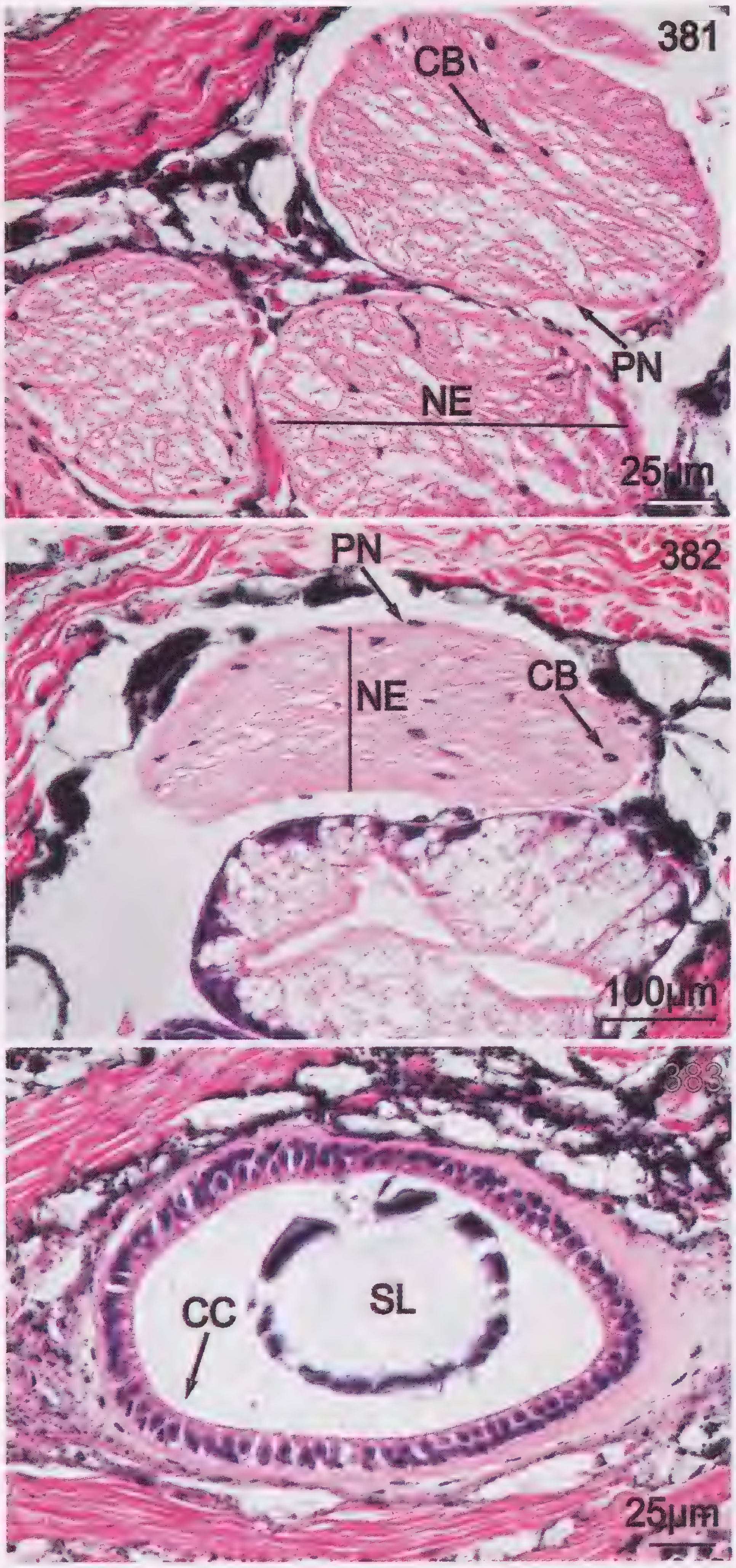

FIGS. 381–383. Nerves and statocysts of *Strophitus connasaugaensis*. FIG. 381: Transverse section through nerves (NE) extending from the pedal ganglion showing perineurium (PN), and cell bodies (CB); FIG. 382: Transverse section of visceral mass showing a longitudinally oriented nerve (NE) containing cell bodies (CB) and the outer perineurium (PN); FIG. 383: Transverse section of a statocyst showing ciliated columnar cells (CC) and the circular statolith (SL) in the lumen.

virtually the entire acinus is darkened. Dividing spermatocytes are spherical and have a pale basophilic character. Sperm morula are also present, but less abundant than in stage 1 testicular acini. As in stage 1 testicular acini, the small size and dark staining character of spermatocytes and sperm morula make observations of specific meiotic phases difficult (Fig. 389). When acini are mature, ciliated gonadal ducts carry sperm and ova from acini to the gonopores. Presently spermatozoa and mature ova were observed descending to the gonopores (Fig. 390). The gonopores are located at the dorsal end of the visceral mass, ventral and anterior to the nephridium. Gonopores appear C-shaped in histological sections, and the lining consists of ciliated columnar cells and goblet cells. Goblet cells are more numerous just outside of the gonopores (Fig. 391).

DISCUSSION

Overall, 13 tissues were structurally conserved between *V. nebulosa*, *F. cerina* and *S. connasaugaensis*, and there were 11 tissue types in which we observed interspecific morphological variation (Table 5). We have further summarized the morphological differences among these 11 tissue types in Tables 6–11. Given the above, we provide a detailed synthesis of the functional morphology of each tissue type. Noteworthy is that while there are many synoptical anatomical references for bivalves, few provide such details about how tissue morphology or cellular structure corresponds to bivalve physiology (Galtsoff, 1964; Yokley, 1968; Lasee, 1991; Norton & Jones, 1992; Eble, 2001; Grizel, 2003).

Tissue-Specific Conclusions

Mantle

Mantle of unionids has been described by various workers concerned with specific cells or functions of the mantle: Raßbach (1912; mantle edge and periostracum secretion in *Anodonta cygnea* (as *Anodonta cellensis*), Siebert (1913; cellular characteristics of mantle edge

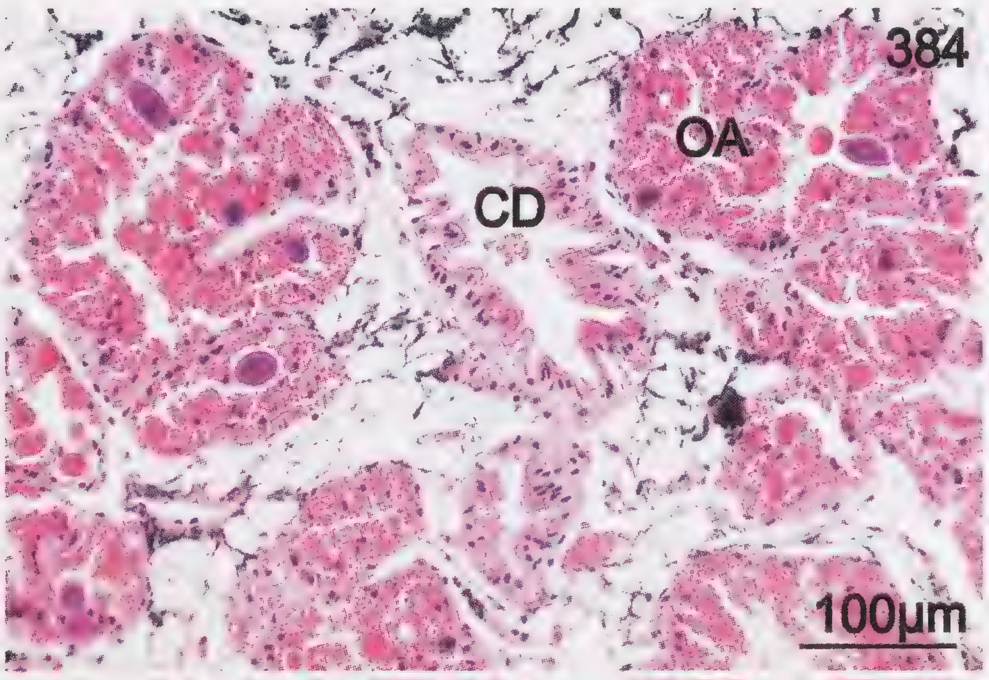
384
OA
CD
100µm

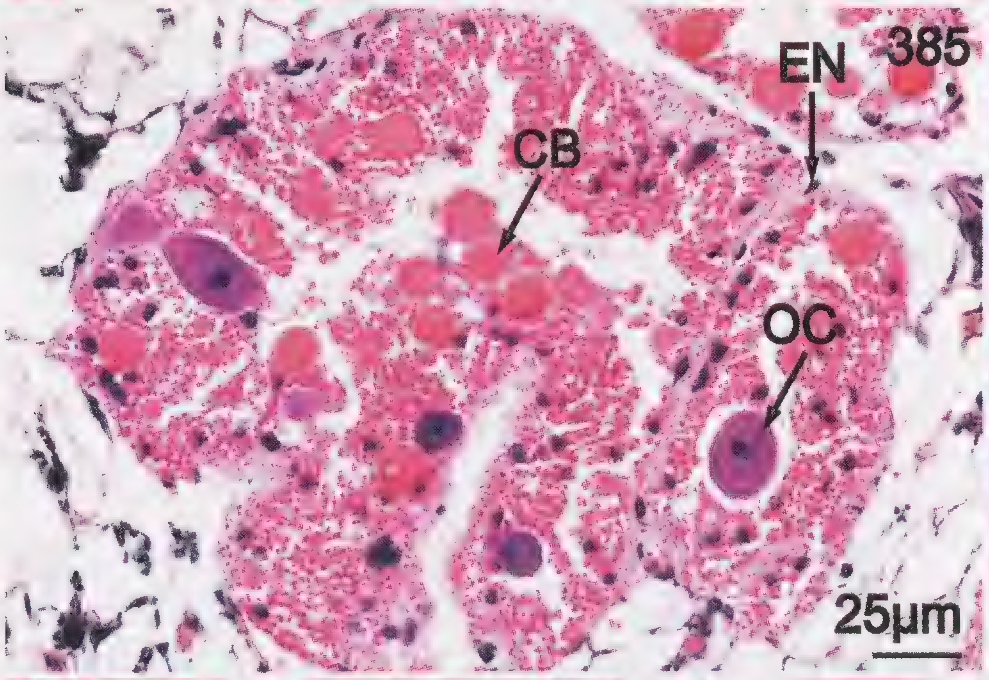
385
EN
CB
OC
25µm

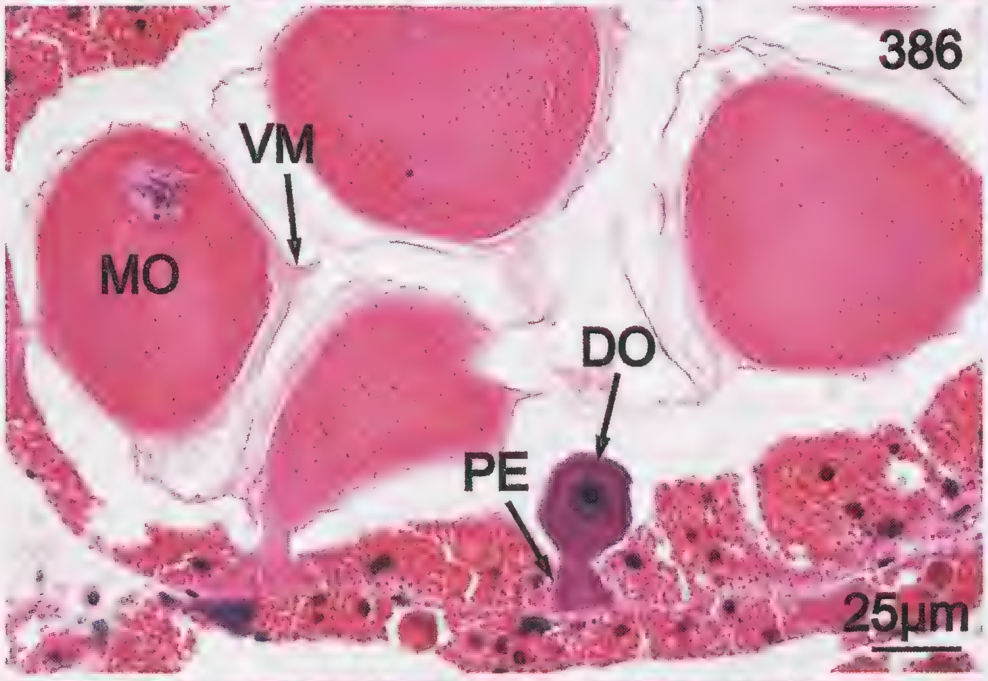
386
VM
MO
DO
PE
25µm

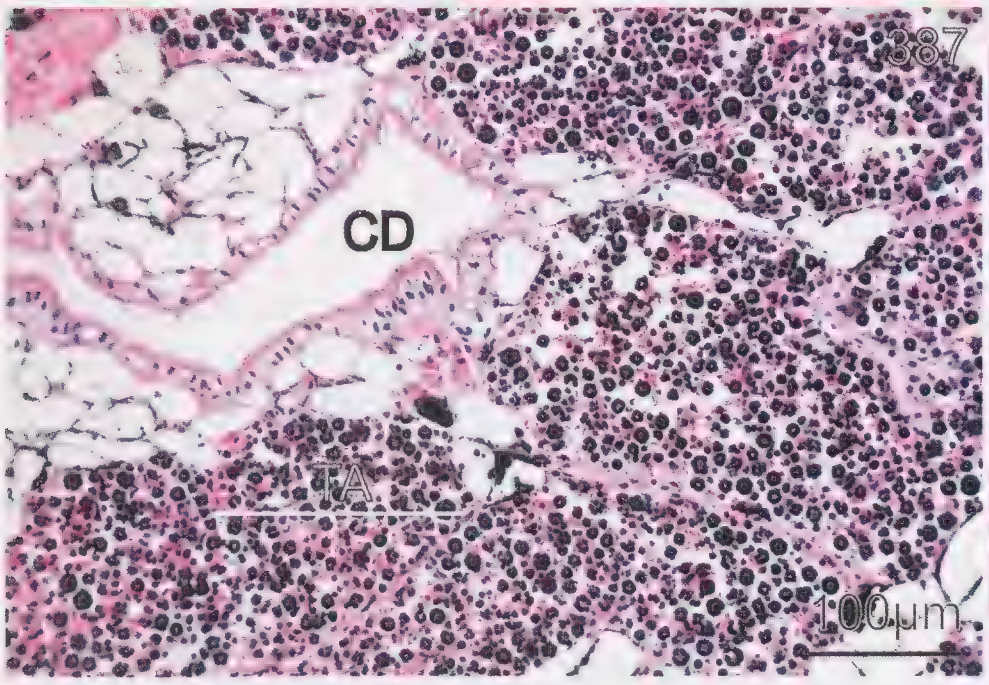
387
CD
TA
100µm

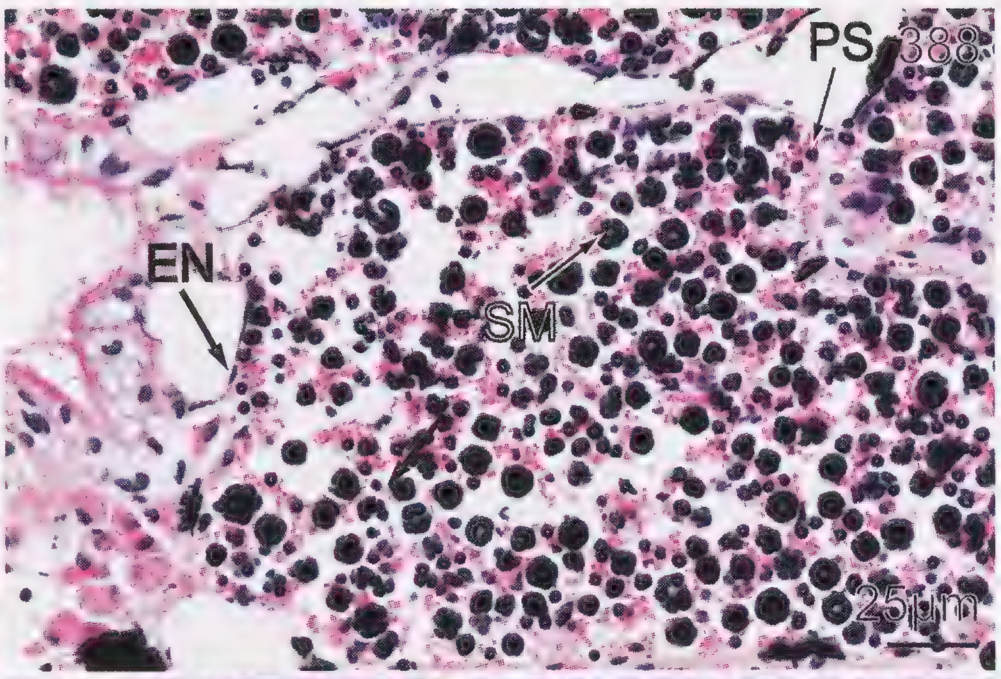
PS
388
EN
SM
25µm

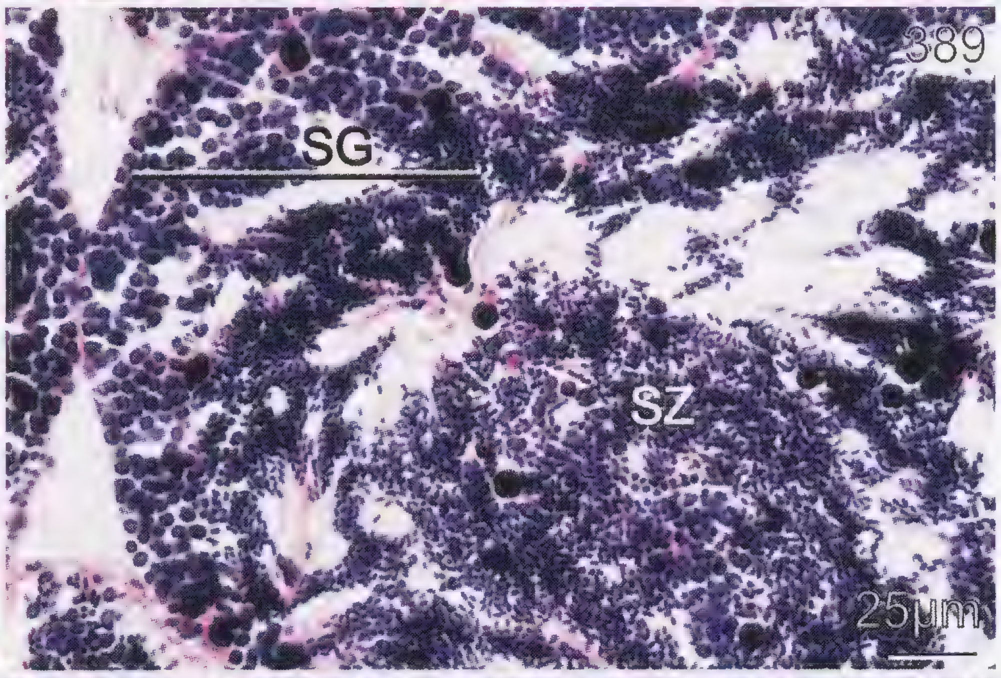
389
SG
SZ
25µm

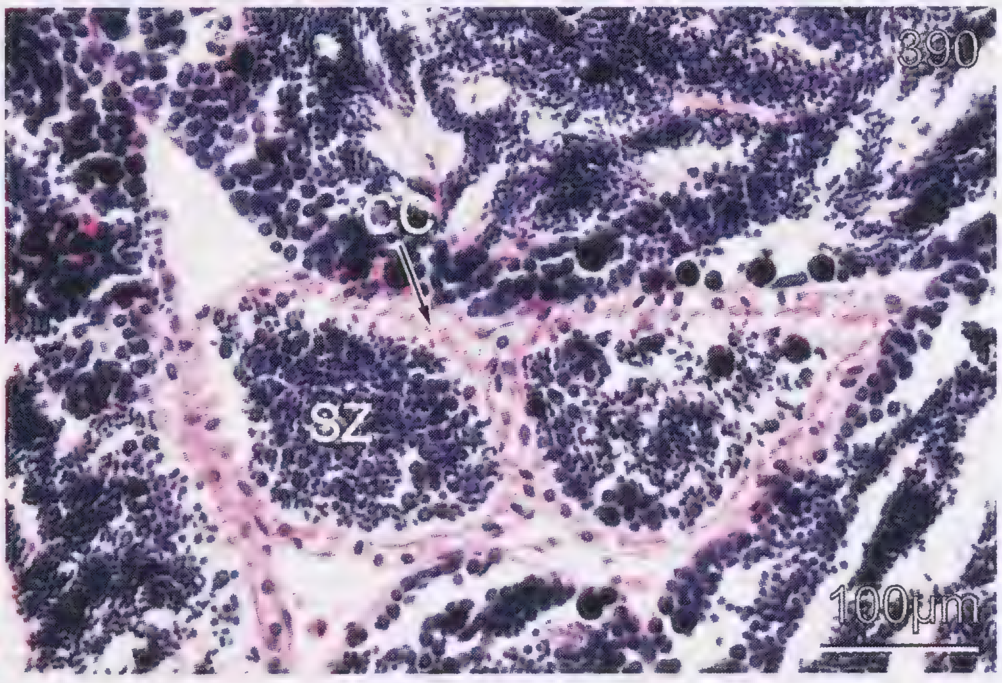
390
CC
SZ
100µm

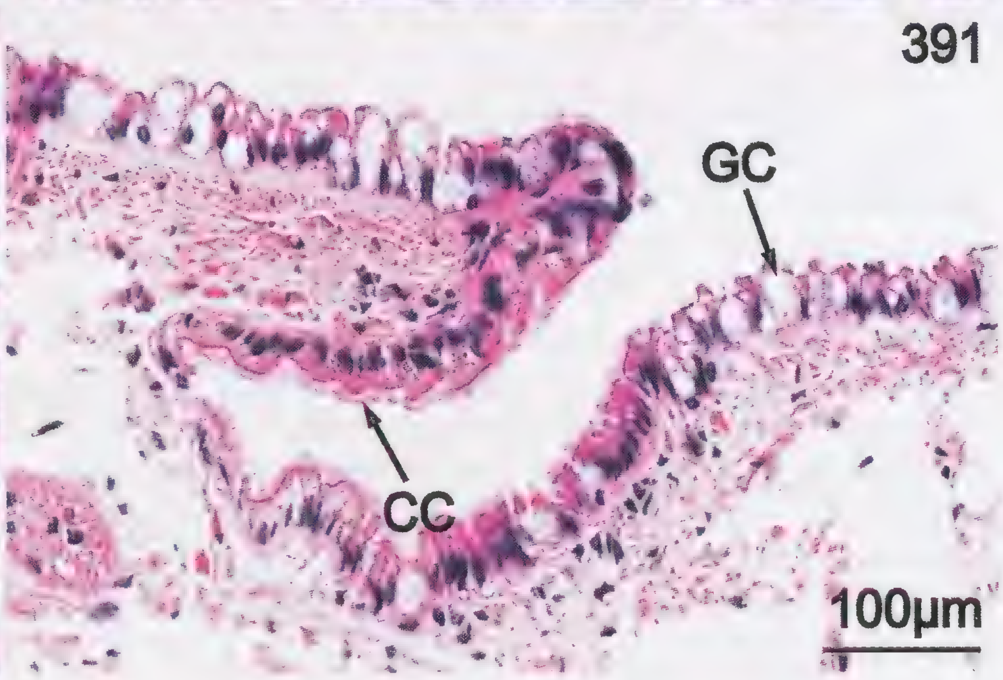
391
GC
CC
100µm

TABLE 5. List of structurally conserved and structurally distinct tissues of Alabama rainbow (*Villosa nebulosa*), Gulf pigtoe (*Fusconaia cerina*) and Alabama creekmussel (*Strophitus connasauagaensis*).

Structurally conserved	Structurally distinct
Middle mantle	Mantle edge
Mantle isthmus	Marsupium
Non-marsupial gill	Foot
Labial palp	Inner gill-connective tissue junction
Adductor/pedal retractor/protractor	Outer gill-connective tissue junction
Byssal gland	Digestive diverticulum
Esophagus	Stomach
Statocyst	Crystalline style sac
Intestinal limbs 4, 5	Intestinal limbs 2, 3
Pericardial gland	Ganglia
Heart	Ovarian acini
Nephridium	
Testicular acini	

in *Anodonta cellensis*), Brück (1914; muscle of mantle edge in *Anodonta cygnea* (as *Anodonta cellensis*), Yokley (1968; columnar epithelium of mantle edge surrounding three main lobes in *Pleurobema cordatum*), Smith (1988; morphology of mantle edge at junction of incurrent and excurrent apertures in *Margaritifera hembeli*), and Kovitvadhi et al. (2007; ultrastructure details of ontogeny of mantle in juvenile *Hyriopsis myersiana*).

The mantle edge secretes precursory shell material that later hardens. The following is a summary of the events that have been proposed for shell formation. The outer mantle lobe secretes a gelatinous, protein-based ribbon called periostracum. Periostracum is secreted from a crevice between the outer and middle mantle lobes called the periostracal groove (Figs. 10, 141, 272). The ribbon extends distally towards the mantle cavity, and wraps around the ventral surface of the outer lobe. As periostracum extends from the groove, columnar cells located between the periostracal groove and the tips of the outer and middle lobes may secrete filamentous substances (possibly proteins) that become incorporated into the extending ribbon (Petit et al., 1978, 1979). As the periostracum ribbon wraps around the outer lobe, it bends multiple times and begins to receive calcium-based

---

←

FIGS. 384−391. Ovarian acini, testicular acini, and ciliated gonadal ducts of *Strophitus connasaugaensis*. FIG. 384: Transverse section of visceral mass revealing stage 1 ovarian acini (OA) and adjacent ciliated gonadal duct (CD); FIG. 385: Transverse section of an ovarian acinus emphasizing emarginated nuclei (EN) constituting the acinus wall, developing oocytes (OC), and cell bodies (CB); FIG. 386: Transverse section of a stage 3 ovarian acinus showing a developing oocyte (DO) arising from a pellicle (PE), larger, mature oocytes (MO), and an irregular vitelline membrane (VM); FIG. 387: Transverse section of stage 1 testicular acini (TA), and an adjacent ciliated gonadal duct (CD); FIG. 388: Transverse section of an stage 1 testicular acinus revealing emarginated nuclei (EN) constituting the acinus wall, primary spermatocytes (PS), and sperm morula (SM); FIG. 389: Transverse section of a stage 3 testicular acinus showing prodigious spermatogenesis (SG), and spermatozoa (SZ) occupying the lumen; FIG. 390: Transverse section of a gonadal duct emphasizing ciliated columnar cells (CC), and preponderant spermatozoa (SZ) in the lumen; FIG. 391: Transverse section of a gonopore showing ciliated columnar cells (CC), and goblet cells (GC).

TABLE 6. Summary of structural differences in anterior mantle edge of Alabama rainbow (*Villosa nebulosa*), Gulf pigtoe (*Fusconaia cerina*) and Alabama creekmussel (*Strophitus connasaugaensis*).

	Anterior mantle edge		
Species	Outer lobe	Middle lobe	Inner lobe
Villosa nebulosa	Dorsoventrally compressed, tapering distally	Dorsoventrally compressed, tapering distally	Equilateral triangle, not extending past outer, middle lobes
	Ventral epithelium flattened	Ventral epithelium flattened	Presence of basophilic granulocytes
	Dorsal epithelium flattened with plicae along distal end of lobe	Dorsal epithelium flattened	
Fusconaia cerina	Branched and bulbous	Rounded distally	Compressed triangle, extending beyond outer and middle lobes
	Ventral epithelium with plicae	Ventral epithelium flattened	Absence of basophilic granulocytes
	Dorsal epithelium with plicae	Dorsal epithelium with plicae	
Strophitus connasaugaensis	Dorsoventrally compressed, tapering distally	Dorsoventrally compressed	Compressed triangle, not extending beyond outer and middle lobes
	Ventral epithelium flattened	Ventral epithelium flattened	Presence of basophilic granulocytes
	Dorsal epithelium with reduced, sparsely distributed plicae	Dorsal epithelium with irregular plicae	

crystals from the columnar epithelium located along the ventral surface of the outer mantle lobe (Petit et al., 1979).

Morphological differences in mantle lobe shape and epithelial topography were observed between *V. nebulosa*, *F. cerina*, and *S. connasaugaensis* at the anterior and posterior ends (Tables 6, 7). Potentially, the morphology of the mantle edge may correspond to shell geometry, thickness and or sculpture. *Villosa nebulosa* and *S. connasaugaensis* have an ovular shell of a moderate thickness and height (Figs. 1–4, 263–266). In contrast, the shell of *F. cerina* is circular to rhomboidal, considerably thicker and higher than the shells of *V. nebulosa* and *S. connasaugaensis* (Figs. 132–135) (also see Williams et al., 2008). The outer mantle lobe of *F. cerina* is branched and pleated, and the epithelium features numerous basophilic cells (Figs. 140–142). Given the high surface area of a branched mantle lobe with a pleated epithelium, the outer lobe of *F. cerina* may exhibit a high-level of protein production. In contrast, *V. nebulosa* and *S. connasaugaensis* both have a uniramous outer mantle lobe, and the epithelium features fewer plicae (Figs. 9–11, 271–273). Furthermore, plicae along the surface of the outer mantle lobe of these two species were shorter. Additionally, the columnar cells around the outer lobe of *F. cerina* appear to be taller (Figs. 140, 142) than outer lobe cells of *V. nebulosa* and *S. connasaugaensis* (Figs. 10, 11, 272, 273). Electron microscopy of the outer, and middle mantle lobes of *Amblema plicata* indicated additional substrate is added to the periostracum as it travels down the length of the mantle lobes (Petit et al., 1978). Although no secretions were observed between the outer and middle lobes of *V. nebulosa*, *F. cerina*, and *S. connasaugaensis*, the basophilic epithelium of the outer lobe may secrete additional substrate into the periostracum ribbon. The basophilic columnar epithelium located on the ventral surface of the outer mantle lobe is the site of nacre production (Figs. 9, 15, 140, 146, 271, 277). Considering the above, *F. cerina*

TABLE 7. Summary of structural differences in posterior mantle edge of Alabama rainbow (*Villosa nebulosa*), Gulf pigtoe (*Fusconaia cerina*) and Alabama creekmussel (*Strophitus connasaugaensis*).

	Posterior mantle edge			
Species	Outer lobe	Middle lobe	Inner lobe	Papillae
Villosa nebulosa	Dorsoventrally compressed, tapering distally, extending from an elongated base	Dorsoventrally compressed, tapering distally, extending from an elongated base	Bulbous, enlarged, extending to outer and middle lobes	Finely conical
	Ventral epithelium flattened	Ventral epithelium flattened	Epithelial cells with conspicuous black or brown, intracellular granules	
	Dorsal epithelium flattened	Dorsal epithelium flattened		
Fusconaia cerina	Outer lobe branched with two triangular lobes	Middle lobe straightened, not rounded distally	Triangular, compressed, not extending past outer, middle lobes	Subtriangular, branched
	Ventral epithelium flattened	Ventral epithelium flattened		
Strophitus connasaugaensis	Dorsoventrally compressed	Dorsoventrally compressed	Triangular, short, not extending beyond outer and middle lobes	Conical
	Flattened epithelium	Flattened epithelium		

may have a greater capacity to produce precursory shell material than either *V. nebulosa* or *S. connasaugaensis*, and this ability might explain why *F. cerina* has a thicker shell.

Although a mechanism for shell formation has been proposed for Unionidae, noteworthy is that shell formation has been studied from a limited range of species. Additionally, cellular structure of the mantle edge has been studied using different methods. Members of Unionidae are known for exhibiting a high degree of interspecific variation in shell geometry, height, thickness and sculpture (knobs, ridges or projections on the exterior surface) (Williams et al., 2008). From a sample of histological literature on mantle lobes of bivalves there is variation in the shape of the lobes, number plicae present, and size of plicae across different orders (Morton, 1987; Morrison, 1993; Eble, 2001; Colville & Lim, 2003). It seems likely that mantle lobe morphology is related to structural differences in bivalve shells, but this topic is understudied.

An additional consideration for shell formation should be mantle lobe musculature. The mantle edge is rich in somatic musculature, and myofibers extend into the mantle lobes. A recent theory regarding the formation of sculpture patterns on the shells of marine bivalves suggests muscle contractions may cause periostracum to build up unevenly. Extension, retraction and lateral movements of the mantle edge may cause periostracum to accumulate in such a way as to form shell ribs (Checa, 2002). The outer mantle lobe of *F. cerina* is branched and the flexure of one or more of these branches may allow periostracum to thicken.

The role of the triangular and pleated inner mantle lobe is indeterminate; the inner lobe plausibly can extend and retract given its highly muscular composition (Figs. 9, 13, 140, 144, 271, 275). Possibly the inner mantle lobe plays a role in initial settlement of juveniles considering the highly pleated surface and basophilic, subepithelial cells. Perhaps the mantle is glandular during the juvenile stage and produces an anchoring substance similar to a byssus. Pediveligers of *Ostrea edulis* have a glandular integument that secretes a cement to allow settlement (Cranfield, 1973a, b). Irregular, basophilic cells with a granular cytoplasm were located in the subepithelial tissue of the middle lobe and inner lobe of *V. nebulosa*, *F. cerina* and *S. connasaugaensis*. Such cells were also located in the subepithelium of the foot (see below). Possibly, these cells produce an adhesive substance needed for attachment to substrate, but ducts leading from the cell body to the apical surface of the mantle lobe epithelium were not observed. Therefore, the basophilic cells may be connected to ducts during an earlier life history stage. Beedham (1958) referred to the inner mantle lobe as the "sensory lobe," possibly because the inner lobe of scallops (*Pecten* spp.) is manifested as a series of tentacles that have a sensory function. However, axons observed in the lateral aspect of the mantle edge were not observed in the inner mantle lobe of *V. nebulosa*, *F. cerina* and *S. connasaugaensis* (e.g., Fig. 279). Furthermore, sensory cells such as ciliated olfactory receptors were not observed in histological sections of the inner lobe.

The base of the mantle edge between the pallial line and mantle lobes consists of adipose tissue and musculature. Adipocytes were observed in the subepithelial tissue of the base of the mantle edge (Figs. 14, 15, 140, 146, 271), and in the middle mantle and have been referred to as vesicular cells or Leydig cells. Leydig cells are located throughout the visceral mass and they may represent a source of energy in the form of glycogen (Colville & Lim, 2003). The dorsal surface of the mantle edge between the pallial line and the inner mantle lobe consists of a region of glandular plicae (Figs. 14, 145, 276). It is not certain what the true function of these structures is, but it seems likely that the plicae are associated with water currents that run parallel with the mantle cavity. The half-shell photographs of the mantle cavity of *V. nebulosa*, *F. cerina* and *S. connasaugaensis* show that the mantle edge lines up with the incurrent aperture (Figs. 6, 137, 268). Therefore, the plicae may be associated with water currents entering the mantle cavity, and the mucus produced by the extensive network of goblet cells may bind particles suspended in local water currents, and allow them to be collected by cilia along the gill filaments.

Papillae around the apertures were sectioned from *V. nebulosa*, *F. cerina* and *S. connasaugaensis* with the intent of revealing sensory receptor cells and associated nerves. While divisions of the pallial nerve extended from the base of the mantle edge to the main axis of each papilla, sensory neurons were not observed on epithelium surrounding each papilla (Figs. 17, 18, 148, 149, 279). Sensory receptor neurons have been described from mantle tentacles of *Lima hians* (Owen & McCrae, 1979) and from siphon papillae of *Eurytellina lineata* (as *Tellina lineata*) and *Macoma biota* (Vitonis et al., 2012). Owen & McCrae (1979) reported that there are three types of sensory receptors, two multi-ciliated receptors, and a third receptor featuring a single kinocilium surrounded by stereocilia. Ciliated receptors consist of types A, and B. Type A receptors consist of a dense tuft of 35–40 cilia distributed across 4−6 cells. Type B receptors have 17–20 cilia on the apical surface of one cell. Based on transmission, and scanning electron microscopy the authors were not able to determine whether the ciliated receptors respond to chemical or mechanical stimuli (Owen & McCrae, 1979). Vitonis et al. (2012) estimated that siphon papillae may contain as many as 10/100 μm^2 ciliated receptors while the epithelium facing the lumen has more sparsely distributed receptors (20/10,000 μm^2). Furthermore, papillae and lumenal epithelia have different types of ciliated receptors based on cilia density and cilium height. However, the status of ciliated receptors as either chemosensory or mechanoreceptory has yet to be determined.

Females of *Villosa* have a papillose mantle edge that functions as a lure to attract potential host fishes (Fig. 7; Haag et al., 1999; Williams et al., 2008). Species of *Lampsilis* and *Villosa* and have modified mantle flaps to attract host fishes (Ortmann 1910a; Haag & Warren, 1999; Haag et al., 1999; Williams et al., 2008). Kraemer (1967) observed a ganglion in the mantle edge of *Lampsilis ventricosa* (as *Lampsilis cardium*) and proposed that it may regulate mantle flap movements. However, no ganglia were observed in the mantle edge of gravid female *V. nebulosa*.

The middle mantle is a thin, delicate skin-like tissue and serves to exchange hemolymph between the mantle edge and viscera (Figs. 19, 143, 281). Illustrations of the mantle cavity of freshwater mussels suggest that there are a series of anterior to posterior currents along the surface of the middle mantle (Kellogg, 1915). Petit et al. (1978) observed ciliated cells along the inner surface of the middle mantle of *Am-*

blema plicata perplicata (as *Amblema plicata*). Herein, the presence of ciliated cells along the inner mantle surface can be confirmed from *V. nebulosa*, *F. cerina*, and *S. connasaugaensis*.

The darkened, basophilic columnar cells located at the dorsal margin of the isthmus may secrete periostracum (Figs. 20, 21, 144, 282). The ligament is composed of periostracum and represents a combined product from secretions of the isthmus and dorsal aspect of the mantle edge; mantle lobes produce the outer layer of the ligament while the inner layer is secreted by the isthmus (Beedham, 1958). Petit et al. (1978) observed thread-like secretions uniting the isthmus and ligament, and Beedham (1958) reported similar staining characteristics between columnar cells of the isthmus and outer mantle lobe.

Non-Marsupial Gill

Non-marsupial demibranchs in unionids have been described using light microscopy and SEM, to elucidate the functional morphology of the gill as both a feeding and respiratory organ: Posner (1875; histology of gill in *Anodonta anatina* and *Unio pictorum*), Peck (1877; cellular nature of gill in *Anodonta* sp.), Ridewood (1903; basic cellular structure of gill in *Anodonta cygnea, Monocondylaea* sp. (Unionidae), *Velesunio ambiguus* (as *Unio ambiguus*), *Unio pictorum* (Unionidae), and *Etheria elliptica* (as *Etheria plumbea*), *Pseudomulleria dalyi* (as *Mülleria dalyi*) (Etheriidae)), Ortmann (1911a, b; comparative morphology of inner and outer gills plus marsupial and non-marsupial gills of various unionids), Allen (1914; functional morphology of inner and outer gill plus ciliary currents for particle capture in *Pyganodon grandis* (as *Anodonta grandis*), *Potamilus alatus* (as *Lampsilis alatus*), *Lampsilis fasciola* (as *Lampsilis ligamentinus*), *Actinonaias ligamentina* (as *Lampsilis luteolus*), *Ligumia recta* (as *Lampsilis rectus*), *Ligumia subrostrata* (as *Lampsilis subrostratus*), *Fusconaia flava* (as *Quadrula rubiginosa*), *Elliptio dilatata* (as *Unio gibbosus*)), Atkins (1937; particle capture on gill in *Anodonta anatina*), Kellogg (1915; functional morphology of ctenidial currents in *Elliptio complanata* (as *Unio complanatus*)), Stasek (1963; ctenidial currents in *Anodonta californiensis*), Smith (1988; histology of fibrous tissue in gill of *Margaritifera hembeli*), Gardiner et al. (1991; SEM of ostium pores and water tubes in *Pyganodon grandis* (as *Anodonta grandis*), *and Ligumia subrostrata*), Kovitvadhi et al. (2007; ontogeny of gill in *Hyriopsis myersiana* (as *Hyriopsis* (*Limnoscapha*) *myersiana*).

Based on the above literature gill structure of *V. nebulosa*, *F. cerina* and *S. connasaugaensis* is similar to what has been reported previously on unionids. There was no apparent difference in the structure of gill filaments between each species studied herein (Figs. 22, 23, 152, 153, 283, 284). Galbraith et al. (2009) reported marginally significant differences in the density of cirral plates between *Actinonaias ligamentina*, *Amblema plicata*, *Fusconaia flava* and *Obliquaria reflexa* and intraspecific and interspecific variation in the number of cilia per cirrus. Considering the observations of Galbraith et al. (2009) were derived from SEM preparations of ctenidia, there may be differences in cirral plates and density of cilia between *V. nebulosa*, *F. cerina* and *S. connasaugaensis* at the ultrastructure level.

We observed interspecific morphological differences in fascicle structure located at the base of the inner and outer ctenidia (Table 8). The fascicles located at the base of the gill possibly represent supporting structures that allow attachment of gill filaments to dorsal connective tissue fibers near the nephridia. Alternatively, the fascicles may represent musculature that allows movement of the entire gill (Figs. 27, 28, 157, 158, 288). Longitudinal and transverse muscle groups in gill described may control water circulation by altering the diameter of ostia and water tubes. However, the description of musculature was based on myofibers that are incorporated into the water tubes (Gardiner et al., 1991). Given the above, it is uncertain whether transverse musculature located at the base of the gill would play a role in water circulation or if muscular contractions generated by this tissue would facilitate the transport of ova into marsupia.

Marsupial Gill

Early anatomical descriptions of unionid marsupial gill detailed gross anatomy and included illustrations of cells lining the gill, but later works focused on sexual dimorphism and reproductive biology of the structure and relationship with glochidia: Lefevre & Curtis (1910, illustrations of cells comprising the marsupial gill water tubes of *Pyganodon cataracta* (as *Anodonta cataracta*), *Alasmidonta marginata* (as *Alasmidonta truncata*) and *Lasmigona complanata* (as *Symphynota complanata*); see also Ortmann [1910b]), Ortmann (1911a, b; sexual

TABLE 8. Summary of structural differences in gill of Alabama rainbow (*Villosa nebulosa*), Gulf pigtoe (*Fusconaia cerina*) and Alabama creekmussel (*Strophitus connasaugaensis*).

	Gill		
Species	Outer gill base	Inner gill base	Marsupium
Villosa nebulosa	Two conspicuous fascicles spanning anterior-posterior	Two conspicuous fascicles spanning anterior-posterior	Water tube distension increases ventrally
			Water tubes thickened with fibrous tissue
			Small, ciliated plicae lining water tubes
			Glochidia enclosed in a thin membrane
Fusconaia cerina	Well developed fascicles between posterior third of visceral mass and posterior adductor	Reduced fascicles between posterior third of visceral mass and posterior adductor	Laterally distended, branchial width is the same dorsal to ventral
			Water tubes lined with squamous epithelium
			Septa with irregular, vesiculated plicae, plicae become tall in the median
			Glochidia and unfertilized ova linked together in conglutinate
Strophitus connasaugaensis	Reduced fascicles between posterior third of visceral mass and posterior adductor	Fascicles absent	Laterally distended, branchial width is the same dorsal to ventral
			Water tubes lined with squamous epithelium
			Septa with spherical, basophilic mucus cells
			Glochidia contained within a cylindircal placenta

dimorphism in ctenidia and variation in marsupial gill structure), Heard (1975, tri-partitic water tubes and associated morphological details observed in female *Anodonta californiensis*, *Utterbackia couperiana* (as *Anodonta couperiana*), *Strophitus connasaugaensis* (as *Anodonta hallenbeckii*), *Utterbackia imbecilis* (as *Anodonta imbecilis*), *Utterbackia peggyae* (as *Anodonta peggyae*) and *Anodonta nuttalliana* (as *Anodonta wahlamatensis*)), Silverman et al. (1983, 1985, 1987, 1989, calcium distribution, SEM, and TEM of gill in *Pyganodon grandis* (as *Anodonta grandis*), *Toxolasma texasiensis* (as *Carunculina texasensis*), *Elliptio crassidens* and *Ligumia subrostrata*), Kays et al. (1990, marsupial and non-marsupial gill structure, glochidial development, and calcium deposits in *Ligumia subrostrata* and anodontids), Tankersley & Dimock, Jr. (1992, SEM of sexual dimorphic ctenidia in *Pyganodon cataracta* (as *Anodonta cataracta*) and differences between marsupial and non-marsupial gill), Tankersley & Dimock, Jr. (1993, ciliary currents of gill of *Pyganodon cataracta*), Lima et al. (2006, primary water tube and relationship with glochidia of *Anodonta cygnea*).

We observed distinct differences in the morphology and cell types of the marsupium of *V. nebulosa*, *F. cerina*, and *S. connasaugaensis* (Table 8), and we feel the specific structural characteristics are a reflection of the dispersal strategy of each species. Species of *Villosa*, such as *V. nebulosa*, brood using the posterior portion of the outer gill. A marsupium of *V. nebulosa* is a grossly enlarged group of water tubes that become distended when filled with glochidia (Fig. 7) (Ortmann, 1911a). The walls of the water tubes are strengthened with connective tissue fibers to maintain a strong connection between the outer and inner faces of a marsupium as it expands to accommodate ova. The increasing diameter of the water tubes from dorsal to ventral may be reflective of the mechanism of glochidial release (Fig. 29). Glochidia are released from the ventral margin of a marsupium following the appropriate stimulus from a potential host fish (Fig. 30). Host fishes may approach a displaying mussel and bite or come into direct contact with flapping mantle tissue. Following a fish strike, a mussel may rapidly expel the contents of one or both marsupia (Haag et al., 1999).

The interbranchial septa and vertical water tube walls of the marsupia of *V. nebulosa* were lined with ciliated columnar cells (Figs. 31–37). Cilia may occur on the septa or along the walls of water tubes of non-marsupial gills but appeared to be localized near the ostia, most notably in *F. cerina* (Fig. 153). However, water currents through the vertical water tubes of unionid gills may be regulated by the muscular contractions of horizontal and vertical muscle fibers (Gardiner et al., 1991). The function of cilia within the marsupial chambers of *V. nebulosa* could serve to exchange oxygen rich and oxygen poor water currents (Figs. 32, 33). However, it is unclear if or how cilia inside of a marsupium function. Richard et al. (1991) demonstrated that water does not enter the water tubes of a marsupium in *Pyganodon grandis* (as *Anodonta grandis*), *Ligumia subrostrata* and *Toxolasma texasiensis* (as *Carunculina parva texasensis*) when filled with glochidia. Therefore, we may infer that cilia may be inactive in a filled marsupium or perhaps cilia aid in the delivery of calcium ions or nutrients to glochidia (Silverman et al., 1987; Schwartz & Dimock, Jr., 2001).

Glochidia contained within the marsupial water tubes were loosely organized within the lumen. Histological sections of the ventral margin of filled marsupia revealed the presence of a wispy, fibrous material possibly representing a sac that surrounds the entire mass of glochidia (Fig. 30). However, the contents of the gill of *V. nebulosa* were delicate, and the glochidia and embryos observed in the lumen of the water tube were often fragmented or displayed separation artifacts, making it difficult to study a membrane surrounding the mass of glochidia. Mature glochidia were mixed with early stage embryos judging by the presence of spherical clusters of undifferentiated cells (Fig. 34). Considering these observations were made from mussels collected in May and that spawning occurs during the late summer, these observations may indicate that not all fertilized ova mature into glochidia. Furthermore, there may be a limit to the total number of glochidia that could form from a set of fertilized ova. Glochidia of *V. nebulosa* have discoid valves that lack hooks along the ventral margin. Hookless glochidia are typically gill parasites that attach to the delicate gill lamellae of fishes. Based on laboratory infections, *V. nebulosa* is considered to be host specific and transform on species of *Micropterus* (Neves et al., 1985).

Species of *Fusconaia* incubate their larvae using all four gills and are therefore referred to as tetragenous brooders (Fuller, 1973). The marsupia of *F. cerina* are uniformly thickened dorsal to ventral, and virtually the entire gill becomes incorporated with glochidia. Like the marsupial gill of *V. nebulosa*, the water tubes are strengthened with fibrous tissue. Hookless glochidia of *Fusconaia* spp. are packaged into cylindrical masses called conglutinates (Fuller, 1973; Bruenderman & Neves, 1993; Haag & Warren, 2003). A single, mature conglutinate consists of layers of ova and each layer contains a linear arrangement of peach-colored glochidia, attached to red, unfertilized ova (Figs. 152, 154). Glochidia mature in a conglutinate while attached to unfertilized ova, and together, glochidia and unfertilized ova are released dorsally, through the suprabranchial cavity, as masses of conglutinates. Exactly how glochidia of *Fusconaia* spp. are transferred to a host fish is unknown, but possibly mature conglutinates, when released from a female mussel, are perceived as aquatic insect larvae and a fish strike may separate some glochidia from a conglutinate and attach to gill tissue of a potential host (Bruenderman & Neves, 1993; Haag & Warren, 2003). This seems plausible given that conglutinates consist of spherical bodies arranged into a cylindrical unit and appear segmented like insect larvae (DeWalt et al., 2010). Observations of released conglutinates of *F. cerina* indicated that conglutinates are buoyant, and cyprinids will closely approach (Haag & Warren, 2003). Laboratory infections have indicated that members of Cyprinidae may be suitable hosts for species of *Fusconaia*

(Bruenderman & Neves, 1993; Haag & Warren, 2003)

The structural features of the marsupia of *S. connasaugaensis* generally resembled marsupia of *F. cerina* (Figs. 160, 291). *Strophitus connasaugaensis* brood using the outer demibranchs and masses of glochidia may be contained within an entire demibranch. Species of *Strophitus* are generally believed to disperse glochidia within a matrix of mucus (Ortmann, 1911a; Lefevre & Curtis, 1912; Haag & Warren, 1997; Hove, 1995; Watters 2002). *Strophitus undulatus* may produce a gelatinous and cylindrical conglutinate (Ortmann, 1911a; Lefevre & Curtis, 1912; Watters, 2002). Haag & Warren (1997) reported that glochidia of *Strophitus subvexus* may be released within a copious mucus matrix that may indiscriminately entangle fish, however no specific details regarding the exact nature of the mucus was described. Furthermore, it may be implied from Haag & Warren (1997) that the mucus matrix of *Strophitus subvexus* conglutinates resembles a web of fibers similar to conglutinate of *Anodonta cygnea* and *Anodontoides ferussacianus*. Herein, we observed a placenta-like sac containing glochidia in gills of *S. connasaugaensis* (Fig. 291), and the core of placenta tissue appears to contract following the release of glochidia (Fig. 296). This cylindrical mass may represent a mold for the formation of a mucoid conglutinate similar to conglutinates described by Watters (2002). The interbranchial septa of the marsupium of *S. connasaugaensis* are distinctively basophilic, and the spherical cells containing wispy cytoplasmic figures may be responsible for the formation of a gel (Fig. 293). According to Watters (2002), the glochidia larva may be attached to the exterior of the conglutinate following its release into stream water and that osmotic pressure may drive internalized glochidia out of this gelatinous rod. Glochidia may become anchored to the exterior of the conglutinate by means of a filament extending from interior of the valves. Following the release of conglutinates from the gill, the opening and closing of glochidial valves may cause the whole conglutinate to move in a worm-like fashion and mimic a prey item of a host fish (Watters, 2002). Based on photographs of released conglutinates of *Strophitus undulatus*, it is possible that a fish might perceive conglutinates to be a worm (Barnhart, 2008). Glochidia of *Strophitus* spp. have hooks (Fig. 295), can attach to skin, and have proven to be host generalists capable of transforming off a phylogenetically broad spectrum of fish species in a laboratory setting (Watters, 2002). Glochidia of *S. undulatus* may transform on fish gill in a laboratory setting (Hove et al., 1997), but it is not certain where they typically attach in the wild. Lefevre & Curtis (1912) reported that some *Strophitus undulatus* (as *Strophitus edentulus*) larvae passed the glochidium stage while remaining within the mucoid conglutinate, since a small-number of newly transformed juveniles were observed and juveniles exhibited a protractible foot. Considering the above-mentioned adaptations for parasitism, the possibility that glochidia would forego the parasitic stage of their lifecycle and transform within the water tubes of its parent seems remote.

The conglutinates observed in demibranchs of *S. connasaugaensis* resembled a placenta with inner and outer walls of squamous epithelial cells and a subepithelium consisting of loose connective tissue and hemolymph (Fig. 291). Moreover, the placenta resembled a derivation of tissue from the interbranchial septum and water tube walls (Figs. 291, 296). Histological sections of the placenta revealed a loosely organized group of spinous glochidia, but it was indeterminate as to whether there was a gelatinous rod surrounding the glochidia and located within the placenta. However, the abundant, basophilic goblet cells along the dorsal and ventral surfaces of gill septa of *S. connasaugaensis* may extrude mucus into the lumen of the water tube and create a gelatinous rod prior to the release of a conglutinate (Fig. 293).

The possibility that glochidia receive nutrients by means of a placenta-like connection to the surrounding gill tissue has been suggested in Schwartz & Dimock, Jr. (2001). Herein, we have only observed a placenta-like structure in the marsupial gills of *S. connasaugaensis*. Conglutinates of *F. cerina* did not appear to be attached to the vertical walls of the water tube. Embryos and glochidia of *V. nebulosa* appeared to be enclosed within a sac, but the separation artifacts made it difficult to determine whether such a sac was united with the surrounding gill tissue. However, gill tissue was sectioned in a transverse orientation, and if the conglutinates of *F. cerina* or the sac encasing glochidia were attached to interbranchial septa, it may not be apparent from this orientation. Possibly, coronal sections through marsupia could provide insight into whether there is a connection between glochidia and gill tissue. Although no physical attachment of glochidia to gill tissue was observed, the abundance of goblet cells on the interbranchial septa of *F. cerina* and *S. connasaugaensis* could support the hypothesis that gill tissue somehow delivers nutrients to developing glochidia. Perhaps these cells secrete sugars derived from glycogen deposits in the septa.

Foot

The foot of unionids has been detailed by Brück (1914, pedal musculature in distinctive vertical and horizontal planes and the rugose pedal epithelium in *Anodonta cygnea* (as *Anodonta cellensis*), Yokley (1968; pedal musculature, extensive folds of pedal epithelium, with subepithelium comprised of basophilic cells in *Pleurobema cordatum*), Araujo et al. (2002; SEM showing dense mat of cilia covering the pedal integument in juvenile *Margaritifera auricularia*), Lasee (1991, used SEM and LM to show development of the foot in *Lampsilis cardium* (as *Lampsilis ventricosa*) [see also Lima et al. (2006)]), Kovitvadhi et al. (2007; SEM of pedal cilia on dorsal and ventral surface of foot in juvenile *Hyriopsis myersiana* (as *Hyriopsis* (*Limnoscapha*) *myersiana*).

Relative to the anatomical literature of foot, our observations dovetail with those of Brück (1914). The musculature in *V. nebulosa*, *F. cerina* and *S. connasaugaensis* consisted of dense, regular chords of muscle fibers that become irregular within the ventral tip (Figs. 36, 38, 165, 167, 297, 299). Whereas we describe the cellular structure of pedal musculature, Brück (1914) documented gross anatomy. Pedal musculature forms a median, triangular hemocoel that is likely filled with hemolymph and may be regulated by vasculature (Brand, 1972). Freshwater mussels burrow into sediment with the muscular foot, and the foot is a hydrostatic organ capable of great distension. For example, Trueman (1968) revealed that the foot of *Margaritifera margaritifera* can be flattened, and blade-like, and later expand ventrally and laterally, exhibiting a distended, spherical shape. The work of Brand (1972) indicated that distension of the foot is achieved by the rapid filling of pedal hemolymph sinuses with hemolymph. The irregular array of myofibers in the ventral tip of the foot may enable movement in many directions, and possibly maintains tensile strength when the foot is enlarged.

Secondly in regard to Brück (1914), we confirm that pedal epithelium of unionids is pleated. Overall there are conspicuous epithelial folds at the ventral margin of the foot and these folds became progressively shorter towards the gill-visceral mass junction (Table 9). The pedal epithelium of *V. nebulosa*, *F. cerina* and *S. connasaugaensis* is rugose with deep, irregular crypts along the surface of the integument around the ventral portion of the foot (types 1−3 epithelium). Considering that the foot may be used as an anchor, it seems that the high surface area created by the folded epithelium surrounding the foot would create a strong frictional force and allow a burrowing bivalve to remain embedded (Figs. 43–45, 172–174, 303–305). The plethora of mucus cells within pedal epithelium may create a lubricant that would minimize cutaneous damage from abrasion when the foot is inserted into fine sand. Based on histological sections of the three-unionid species, it seems that grooves around the foot were deeper on *F. cerina* than on *V. nebulosa* or *S. connasaugaensis*. This observation could be an indication of an adaptation exhibited by mussels in large rivers, such as the Cahaba River. Pedal grooves may enable mussels to stay firmly embedded in the substratum minimize the possibility of becoming dislodged by strong water currents. Likewise, plicae around the foot of *V. nebulosa* and *S. connasaugaensis* were shorter, and the small size of plicae may reflect adaptation to headwater streams, such as Terrapin Creek and Shoal Creek, where a smaller channel size would accommodate less water volume than a larger river such as the Cahaba. Since the historic ranges of *V. nebulosa*, *F. cerina* and *S. connasaugaensis* may have overlapped, perhaps there are differences in the depth of the pedal grooves that may reflect local adaptation (Williams et al., 2008).

The ventral-most region of the foot has a highly ciliated surface. Cilia may be present further down the vertical length of the foot and visceral mass, but ciliated cells were indistinct in epithelial regions 2–5. Juvenile unionids have minute gill buds and may employ pedal feeding during the weeks following transformation from the glochidium stage (Lasee, 1991; Yeager et al., 1994). During pedal feeding, particulate matter may be collected by a combination of foot scraping and ciliary action. Scanning electron microscopy of the foot of juvenile unionids has revealed a densely ciliated pedal surface (Lasee, 1991; Araujo et al., 2002; Lima et al., 2006).

Basophilic granulocytes were distributed within the subepithelium underlying pedal epi-

TABLE 9. Summary of structural differences in pedal epithelium of Alabama rainbow (*Villosa nebulosa*), Gulf pigtoe (*Fusconaia cerina*) and Alabama creekmussel (*Strophitus connasaugaensis*).

Species	Pedal epithelium				
	Type 1	Type 2	Type 3	Type 4	Type 5
Villosa nebulosa	Tall, irregular plicae	Medium-sized, irregular plicae	Short, irregular plicae	Epithelium plicated to papillose, folds becoming reduced	Epithelium papillose with teardrop-shaped columnar cells and convex squamous cells
	Violet basophilic granulocytes moderately abundant	Violet basophilic granulocytes sparsely distributed			
Fusconaia cerina	Tall, rectangular plicae	Tall, irregular plicae, may appear coalescing	Short, teardrop-shaped plicae, irregular shape	Columnar epithelium, epithelium is furrowed	Cuboidal epithelium, epithelium flattened
	Basophilic granulocytes very abundant	Basophilic granulocytes sparsely distributed			
Strophitus connasaugaensis	Tall, irregular, branched plicae	Tall, irregular, branched plicae	Short, thin, irregular plicae	Squamous epithelium, epithelium is furrowed	Squamous epithelium, epithelium flattened
	Basophilic granulocytes moderately abundant	Subepithelial glands, abundant			

thelium types one and two (Figs. 43, 44, 172, 173, 303, 304). The function of the granulocytes is unclear, possibly granulocytes are pigment cells associated with the orange coloration of foot and mantle edge of *V. nebulosa* and *S. connasaugaensis*. However, male and female *F. cerina* are somewhat pallid, and females develop a temporary red to orange pigmentation when gravid (Fig. 137; Bruenderman & Neves, 1993). *Fusconaia cerina* had a significantly high number of basophilic granulocytes such that histological sections of foot were conspicuously violet. Alternatively, granulocytes may produce mucus or an adhesive that may assist with settlement following the transition from glochidium to juvenile. Pediveligers of *Ostrea edulis* have exocrine cells that produce an adhesive enabling attachment to a hard substratum (Cranfield, 1973a, b). However, granulocytes observed in *V. nebulosa*, *F. cerina*, and *S. connasaugaensis* do not have distinct ducts communicating with the surface of the epithelium. A possible explanation for this may be that adhesive cells are only functional during the juvenile stage and ducts atrophy with age since larger mussels burrow into sediment (Trueman 1966, 1968). Lefevre & Curtis (1912) reported that juvenile mussels crawl by extending the foot, attaching to a substratum, and pulling the body forward while the foot is fully extended. Matteson (1948) observed crawling juvenile *Elliptio complanata* (as *Elliptio complanatus*) and reported that the foot appears to have an adhesive quality. If the basophilic granulocytes are part of a system of glands that secrete an adhesive substance on the surface of the foot, the preponderance of such cells in the foot of *F. cerina* may represent an adaptation to resist strong water currents. Since, fewer granulocytes were observed in the foot of *V. nebulosa* and *S. connasaugaensis*, this may reflect adaptation to smaller headwater streams (i.e., Terrapin Creek, and Shoal Creek) that would hold a smaller volume of water and may therefore be more stable than a larger river such as the Cahaba.

Byssal Gland

To our knowledge Smith (2000) is the only histological reference on byssal gland of unionids. Smith (2000) focused on byssal gland structure, formation, substrate affinity, morphology, and rigidity in *Elliptio complanata*, *Lampsilis radiata*, *Leptodea ochracea* and *Alasmidonta undulata*.

Juvenile unionids produce a single, translucent filament or byssus that allows small mussels to attach to a hard substratum (Kirtland, 1840; Lea, 1856; Smith, 2000). Spherical byssal glands were observed in adult *V. nebulosa*, *F. cerina* and *S. connasaugaensis*, and ciliated byssal canals were observed only in *V. nebulosa* and *F. cerina*. The histological structure of byssal glands and byssal canals observed herein indicate that the byssal gland becomes detached from the byssal canal with age and the byssal canal has largely disappeared in an adult. The histological differences in byssal gland cell types between *V. nebulosa*, *F. cerina*, and *S. connasaugaensis* may reflect variation in the composition of the byssus (Figs. 40, 41, 169, 170, 301, 302), but such differences are presently indeterminate. Smith (2000) observed a series of ducts leading into the byssal gland of juvenile *Elliptio complanata* and *Lampsilis radiata*. Such ducts were not observed in *V. nebulosa*, *F. cerina* and *S. connasaugaensis*, and the byssal gland of each species consisted of a spherical chamber with tightly associated columnar cells and a well-defined capsule of fibrous tissue. Whether or not byssal gland ducts are present in juveniles is indeterminate, and therefore there is a need to understand how a potentially non-glandular byssal gland and a more glandular byssal gland would functionally differ. For example, a glandular byssal gland may produce a stronger or larger filament extending from the foot. Smith (2000) proposed that unionids living in “low energy” environments lack a byssal gland; whereas, mussels in “high energy” environments have one. The present results show that representative species from three unionid lineages have a byssal gland. Secondly, Terrapin Creek and Shoal Creek may constitute low energy environments in comparison to the Cahaba River for reasons stated previously. Considering *V. nebulosa* and *S. connasaugaensis* were collected in small streams, and *F. cerina* was collected in a larger river, the “low energy-high energy” hypothesis, in terms of byssal glands, may be rejected.

Adductors, Pedal Retractors and Mesentery

In the treatise of the musculature of *Anodonta cygnea* (as *Anodonta cellensis*), Brück (1914) described the adductor, including details of myofiber organization, myocytes, perimysium and motor endplate nodes. Smith (1983) described columnar epithelial cells and fibrous tissue representing the mantle-shell junction of *Margaritifera margaritifera*.

Musculature of the foot, adductors, pedal retractor and mesentery fascicles all have similar cellular characteristics (Figs. 38, 50, 55, 56, 167, 179, 184, 185, 299, 309, 315, 316). Each type of fibrous tissue consists of long, filamentous cells with a dark, eosinophilic cytoplasm and a distinct, basophilic nucleus. Our observations differ from Brück (1914) in that we did not observe striations or a star-shaped pattern of chromatin within the nucleus of myocytes. Transverse sections through a whole mussel provide a longitudinal view of the adductors and pedal musculature. According to Morrison (1996), the adductor of *Crassostrea virginica* has translucent and opaque regions with the translucent portion representing the majority of the tissue volume. Translucent muscle has a fast contractile ability and consists of elongated, ribbons of myofibers approximately 3–4 µm thick. Opaque muscle fibers are round, 10–20 µm in diameter with a slow contractile ability (Morrison, 1996). Opaque and translucent muscle is best shown in Figures 6–8. However, the adductor muscles studied herein were sectioned such that myofibers were studied longitudinally. Possible differences between opaque and translucent muscle were not addressed herein.

Mesentery fascicles were observed throughout the visceral mass of *V. nebulosa*, *F. cerina* and *S. connasaugaensis*. These bands of fibrous tissue extend medially into the hemocoel from a layer of vertically oriented fibers along the inner surface of the hemocoel. The muscle fibers extending ventrally into the foot from the dorsal aspect of the visceral mass have similar staining characteristics to the mesentery based on hematoxylin and eosin-stained tissue sections (Figs. 49, 50, 178, 179, 309, 310). Considering that the mesentery fibers extend across the hemocoel, it seems their function is to hold the sinistral and dextral portions of the visceral mass together. Alternatively, if the mesentery fibers stained positively for muscle proteins using Masson's trichrome stain (Luna, 1968), possibly the fibrous bands could also serve to circulate hemolymph in the hemocoel.

Digestive System

Gutheil (1912) and Yokley (1968) previously comprised the most in depth treatments of the digestive system of unionids. Gutheil (1912) described all organs and cell types of the digestive tract of *Anodonta cygnea* (as *Anodonta cellensis*), and although the reference is useful towards understanding general morphological features, the illustrations of observed cell types may be inaccurate considering how much intracellular detail is depicted. For example, Gutheil (1912: figs. 22–24) shows cilia embedded deep into the cytoplasm, a series of distinct, and well-separated granules, and patches of chromatin that are linked together within the nucleus.

The digestive system consists of the labial palps, oral groove, esophagus, digestive diverticulum, stomach, crystalline style sac and intestine. Particles gathering in the ventral food groove of the inner gill travel anteriorly by means of ciliary action. The palps are positioned close to the anterior curvature of the inner demibranch such that food groove particles may be dispelled and captured by the palps. Particulate matter that does not get captured by the palps may travel dorsally and may be transported posteriorly towards the excurrent aperture by means of cilia. Cilia located on the middle mantle, and lateral portion of the foot may facilitate the departure of rejected particles (Kellogg, 1915).

Labial Palps and Oral Groove

Kellogg (1915) diagrammed the labial palps, including cylindrical folds of ciliated tissue along the inner surface of each lip, and functional morphology of cilia on palps in *Elliptio complanata* (as *Unio complanatus*). Yokley (1968) detailed the palps and esophagus of *Pleurobema cordatum*, and Colville & Lim (2003) detailed the labial palps in *Velesunio ambiguus* and *Hyridella depressa* with LM and SEM, respectively.

Herein, we have shown that the labial palps are a soft tissue with a complex structure. The description of unionid palps herein may be key to understanding how mussels discriminate between particles that should be accepted or rejected. Palps are muscular, endowed with large hemolymph sinuses and connective tissue, which supports prior observations of their pliable and contractile nature (Figs. 51, 180, 311) (Kellogg, 1915). Particles captured by the palps may travel anteriorly, perpendicular to the length of the plicae, become incorporated into a mucoid mass traveling to the esophagus (Kellogg, 1915). No cellular differences in the cellular structure of labial palps were observed between *V. nebulosa*, *F. cerina* and *S. connasaugaensis*. However, based on the

TABLE 10. Summary of structural differences in oral groove, and digestive diverticulum of Alabama rainbow (*Villosa nebulosa*), Gulf pigtoe (*Fusconaia cerina*) and Alabama creekmussel (*Strophitus connasaugaensis*).

			Digestive diverticulum tubules	
Species	Oral groove	Entrance to digestive diverticulum	Type 1	Type 2
Villosa nebulosa	Concave, tubular	Esophagus opens directly into sinistral and dextral tubules	Tubules with short, rounded plicae	Columnar cells rectangular, vesiculated, with microvilli Seamless transition between secondary and tertiary tubules
Fusconaia cerina	Deep cavity	Esophagus opens into a large sinistral chamber	Tubules with long, thin plicae	Tubules with teardrop-shaped columnar cells Abrupt transition between secondary and tertiary tubule cells, resembles valves
Strophitus connasaugaensis	Deep cavity	Esophagus opens into a large sinistral chamber	Short, thin, irregular plicae	Columnar cells rectangular, vesiculated, with microvilli Seamless transition between secondary and tertiary tubules

scanning electron microscopy observations of unionid gills by Galbraith et al. (2009), it seems that there could be interspecific differences in the density of these bristle-like structures. Also, considering the observations of ciliated sensory receptors on mantle tentacles (Owen & McCrae, 1979) and on siphons (Vitonis et al., 2012), there may be ciliated, sensory receptors on the free distal tips of the palps. Given that there are different types of ciliated receptors, the density of receptors, and their specific morphological features (e.g., number of cilia, height of cilia) may provide insights into particle selection at the labial palps. Presently, sensory receptors were not observed on the palps, but perhaps they would be located more readily with scanning electron microscopy and we would expect that there are sensory receptors located at the free distal margin of the palps, and along the surface of the inner palp epithelium, and that sensory receptors would be absent along the outer surface of each palp, since the functional component of the labial palps comprises the ridges and troughs of the inner epithelium.

The oral groove represents a continuation of the labial palps and transfers ingested particles to the esophagus. Variation in the size of the oral groove may be reflective of differences in the quantity of matter ingested by each species. The oral groove of *F. cerina* and *S. connasaugaensis* resembled a cavity (Figs. 186–188, 317–319), whereas the oral groove of *V. nebulosa* was a more narrow tube (Fig. 57). Seemingly, a broad cavity would accommodate a larger volume of particulate matter than the narrower, tubular oral groove of *V. nebulosa* (Table 10).

The esophagus connects the oral groove with the digestive diverticulum (Figs. 60, 189, 320). The esophageal lining consists of conical plicae bearing ciliated columnar cells, and the deep grooves between the plicae may allow separation of small and large-sized particles (Yokley, 1968). Given the abundant ciliated cells, and concentric layers of connective tissue surrounding the lumen, it seems that ingested matter is delivered into digestive diverticulum by means of ciliary action, and not peristalsis (e.g., Figs. 61, 190, 321).

The shape of the oral groove was similar between *S. connasaugaensis* and *F. cerina*. Additionally, the morphology of the lumen of the digestive diverticulum at the point of merger with the esophagus was similar between *S. connasaugaensis* and *F. cerina*. Such features are suggestive of a closer phylogenetic relationship to each other than to *V. nebulosa*. Additionally, the large oral groove and digestive gland entrance featured by both species possibly indicates that a larger quantity of particulate matter enters the digestive gland than in *V. nebulosa*. An alternative hypothesis could be that the rate at which particles move between the labial palps and the anterior portion of the digestive gland are different. If so, perhaps the expansive oral groove chamber and the anterior digestive gland chamber would cause particles to "bounce" around and not move efficiently within a better defined tube. Observations of fluorescent dye-labeled particles traveling across the gill filaments of *Mytilus edulis* and *Arca zebra* for example, suggests that ciliary action may not cause particles to move within a perfectly vertical or horizontal, linear direction (Ward et al., 1998).

Digestive Diverticulum

The cell types of the digestive diverticulum have been described from *Anodonta cygnea* (as *Anodonta cellensis*) by Gutheil (1912), *Anodonta anatina*, and *Unio tumidus* by Sumner (1966a, b), and *Pleurobema cordatum* by Yokley (1968). Feeding experiments conducted by Mansour & Zaki (1946) provided evidence that vesiculated cells of the digestive diverticulum of *Coelatura aegyptiaca* (as *Unio prasidens*) are specialized for intracellular digestion. Sumner (1966a, b) showed that there are two cell types in digestive tubules. Digestive cells are vesiculated columnar cells with an elaborate intracellular transport system involving vesicles that later fuse with lysosomes. Secondly, the conical, basophilic basiphil cells have an extensive rough endoplasmic reticulum and may therefore be specialized for protein synthesis and secretion. Therefore, it may be inferred from Sumner (1966a, b) that basiphil cells secrete lytic enzymes and perhaps these enzymes would digest algae and or bacteria, and the resulting chyme would be incorporated into digestive cells.

Our observations of digestive diverticulum of *V. nebulosa*, *F. cerina* and *S. connasaugaensis* support previous descriptions of digestive cells and basiphil cells from Sumner (1966a, b) and Yokley (1968). However, only scant details concerning primary and secondary tubules were presented in Yokley (1968). Digestive diverticulum is a large network of blind-ended tubules and constitutes one of the largest organs in a freshwater mussel. The openings of digestive tubules were mainly located between the esophagus and stomach (Figs. 62, 191, 322). A smaller subset of tubules communicated with the sinistral and dextral portions of the posteroventral aspect of the stomach. Together, there was no obvious histological difference between the anterior digestive diverticulum tubules and both the sinistral and dextral tubules leading into the posteroventral stomach chamber. Therefore, it would seem that each region of the digestive diverticulum is functionally identical. However, it is not clear why there is a separation of anterior and posterior digestive gland ducts. Seemingly these ducts take in particulate matter that escapes passage into the initial series of digestive gland ducts. A possible explanation for this could be that the anterior portion of the digestive gland could be filled to capacity, and an additional set of digestive ducts could handle excess food matter.

The key features of the digestive diverticulum that exhibited morphological variation include the primary and secondary tubules (Table 10). Based upon the tissue structure of *V. nebulosa*, *F. cerina* and *S. connasaugaensis*, it seems that ciliated primary tubules carry ingested particles down the length of a tubule, but it is not clear whether ingested matter travels into the secondary and tertiary portions of each tubule, since mussels were not fixed in the field and therefore, ingested matter that would normally be contained within the tubules was expelled. Some literature regarding ciliated digestive tubules suggests that cilia along the epithelial folds may create incurrent and excurrent pathways for particulate matter (Owen, 1955), but it is unclear whether cilia all around the lumen of primary tubules would create a synchronous ascending current and then later generate a synchronous descending current following a chemical change in the lumen. In contrast, Owen (1955) also stated that the subepithelium surrounding the digestive tubules contained myofibers that would create rhythmic contractions or peristalsis. Peristalsis seems unlikely considering the extensively developed ciliated epithelium, and although fibrous tissue was observed in the subepithelium of digestive tubules of *V. nebulosa*, *F. cerina*, and *S. connasaugaensis*, fibers more closely resembled thin, wispy connective tissue. Secondary tubules feature copious cytoplasmic vesicles, and microvilli, and the lumen may appear to be bubbling. Possibly secondary tubules produce mucus since tubule secretions were eosinophilic. Tertiary tubules constitute the longest and most conspicuous aspect of the organ. Given the affinity of hematoxylin to nucleic acids during hematoxylin and eosin staining, the conspicuously basophilic cytoplasm of basiphil cells may be an indication that these cells have an elaborate rough endoplasmic reticulum (Stevens, 1982). Additionally, the vacuolated cytoplasm of digestive cells would be an indication of a cell specialized for intracellular transport. Based on our observations herein, and the work of Sumner (1966a, b), it seems that particulate matter may be carried into the digestive diverticulum to be chemically broken down, possibly by enzymes secreted by basiphil cells (e.g., Fig. 326). Following digestion, the smaller endproducts may become incorporated into digestive cells via endocytosis. Additionally, considering the apical microvilli of secondary tubules, some absorption may occur in this region, although this tissue region is short (Figs. 65, 195, 325). Ciliary action in the primary tubules may transport some broken down particulate matter posteriorly into the stomach and some undigested matter into the stomach (Figs. 64, 194, 324). However, the digestive diverticulum literature presents competing hypotheses regarding possible functions of digestive tubules. Diverticulum cells may be absorptive considering observations India ink, iron or carmine particles in cytoplasm of tubule cells following experimental feeding trials (Yonge, 1926b; Owen, 1955). Furthermore, wet mounts or frozen sections of digestive tubules of recently collected animals contain green or brown intracellular pigments, while tubule cells appear colorless following a period of starvation (Mansour & Zaki, 1946). Alternatively, proteases, lipases, and enzymes capable of digesting carbohydrates have been isolated from digestive tubules of various marine bivalve species (Yonge, 1926b). Eble (1966) revealed the presence of acid phosphatase, alkaline phosphatases, and esterases on the apical surface of digestive tubules of *Crassostrea virginica* and reported that enzymes were most abundant during the summer and least abundant during the winter.

The long, finger-like plicae extending into the lumen of primary digestive gland tubules of *F. cerina* may be an indication that it feeds on algae or bacteria of a small size (Figs. 193, 194). The larger lumen of the primary tubules of *V. nebulosa* and *S. connasaugaensis* could represent adaptations for feeding on larger-sized particulate matter (Figs. 63, 64, 323, 324). Additionally, the long, slender plicae in the primary tubules of *F. cerina* may be indicative of foregut efficiency while the foregut of *V. nebulosa* and *S. connasaugaensis* is seemingly less efficient. Examinations of the second and third limbs of the intestine is needed (see below).

Stomach

Gutheil (1912), Purcheon (1958), Reid (1965), Dinamani (1967), Yokley (1968), Kat (1983) and Smith (1988) described general morphological characteristics of stomach, notably that the gastric walls have grooves and typhlosoles. Kat (1983) documented interspecific variation in stomach morphology based on a comparison of four species of *Lampsilis*. However, a pictorial representation of the morphology of the gastric lumen was not clearly presented in the above literature.

Our observations of the stomach of *V. nebulosa*, *F. cerina* and *S. connasaugaensis* support prior observations of rugose and ciliated gastric walls (Figs. 67, 70–72, 198, 201–203, 327, 330–332). Descriptions of the stomach of *Anodonta* have suggested that gastric grooves may transport particulate matter parallel to the grooves. Additionally, there may be circumferential currents that churn food matter (Purcheon, 1958; Dinamani, 1967). A cyclic arrangement of eosinophilic masses of fluid was observed in histological sections of the stomach of *V. nebulosa*, *F. cerina* and *S. connasaugaensis*. In addition to particle sorting, stomach epithelium may produce enzymes. For example, cellulase as well as dipeptidyl-aminopeptidase activity was detected in *Crassostrea gigas*, and N-acetylglycosaminidase was detected in *Pecten maximus* (Boucaurd-Camou & Henry, 2003). The histological sections of freshwater mussel stomachs herein provide some evidence of secretory activity in the stomach (e.g., Fig. 203). Eosinophilic, spherical vesicles were observed in close proximity to the stomach epithelium of each species.

Additionally, the stomach epithelium, especially along the ventral wall possesses an eosinophilic cuticle, referred to as the gastric shield (Figs. 69, 200, 329), and it may represent a dense form of mucus (Shaw & Battle, 1957, 1959; Norton & Jones, 1992; Boucaurd-Camou & Henry, 2003). Curiously, the gastric shield has been proposed to function along with the crystalline style as part of a grinding apparatus (Owen, 1955) (see below).

Although no significant morphological differences in stomach structure were observed between *V. nebulosa*, *F. cerina* and *S. connasaugaensis*, stomach structure is different across the various orders of Bivalvia (Purcheon, 1958; Dinamani, 1967). However, the authors did not propose any explanation as to what could be driving these differences.

Crystalline Style Sac

Mitra (1901) described how the crystalline style in *Anodonta* sp. was colloidal, and rod-shaped with a bulbous end and a tapered end. Gutheil (1912) showed that the style is ruffled at one end and may contain a fine granular material. Several authors have described the cellular structure of the style sac and commented on the functional morphology of the style (Gutheil, 1912; Nelson, 1925; Yokley, 1968; Lomte & Jadhav, 1980).

Based on our histological observations and the above literature, we recognize that the crystalline style sac represents the anterior aspect or first limb of the intestine. Particulate matter is routed through a long sinuous intestine following passage through the stomach. Histological sections of *V. nebulosa*, *F. cerina* and *S. connasaugaensis* reveal that the style sac consists of a circular chamber and a linear duct (Figs. 74, 205, 334). Based upon necropsies of freshwater mussels for the purpose of exploring metazoan parasites, the style is a long translucent rod that is soft and flexible. The style appears to be layered and particulate matter may become trapped within the concentric layers. The sectioning and staining characteristics of the gastric shield and style are similar, suggesting both structures have similar chemical composition. The rigid cilia in the style sac (Figs. 75, 206, 335) may cause the gelatinous rod to rotate causing loose food matter in the stomach to condense into a bolus such that it can efficiently travel through the intestine. Considering the above observations of the style and the fact that unionids are suspension feeders with a ciliated digestive tract, we feel that the crystalline style sac represents a churning mechanism. The elaborate mucosa constituting the gastric shield may represent mucus that coagulates a large, loosely organized volume of digested food matter entering the intestine from the expansive lumen of the stomach.

Given that the mussels were allowed to purge prior to being processed for histology, it is not clear whether condensed food matter traveling through the style sac passes through the spherical portion or the more linear midgut located laterally. However, we speculate that food matter would be directed into the midgut located laterally to the style. If not, the midgut would probably be non-existent or reduced similar to the morphology of the style sac of *Anadara broughtonii* (as *Anadara inflata*) described by Kato & Kubomura (1954). The style sac is depicted as ovular, and laterally expansive with a compressed or truncated midgut (Kato & Kubomura, 1954). The midgut of *V. nebulosa*, *F. cerina* and *S. connasaugaensis* features wispy cilia and goblet cells, but it was not clear whether any of the cells secrete enzymes. The narrow, basophilic cells comprising style sac epithelium type three seem specialized for protein synthesis. Kato & Kubomura (1954) suggested that the narrow, basophilic cells in the style sac produce a filamentous secretion, which may be an initial component of the style rod. Owen (1955) suggested that the style releases enzymes into the stomach, but provided no empirical evidence to support this idea. Boucaurd-Camou & Henry (2003) observed enzymes in sections of the style, but it was not clear what cells secrete enzymes or whether enzymes become incorporated into style rod layers from an anterior source.

Although it is recognized that the style creates sufficient suction to draw ingested material from the stomach into the intestine, there are a series of hypotheses regarding the function of the style that seem questionable. In the literature review regarding crystalline style function, Nelson (1918) indicated that several prior anatomical works on bivalves had proposed competing hypothesis for the function of the style. Among these hypotheses, Nelson (1918) indicated that the style extends into the stomach, and rotates in close proximity to the stomach wall such that it would pulverize food matter like a mortar and pestle. Yonge (1926a) proposed that the rotation of the style causes cilia located along the stomach wall, to fuse together and form the gastric shield. Other anatomical works on the digestive tract of bivalves suggest the style grinds against the gastric shield to pulverize particulate matter (Owen, 1955; Shaw & Battle, 1957; Galtsoff, 1964; Lomte & Jadhav, 1980; Boucaurd-Camou & Henry, 2003). Owen (1955: fig. 13) showed diagrammatically that the esophagus opens near the crystalline style sac such that the rotation of the style would create suction needed to draw particulate matter towards a rigid sorting area. Furthermore, the figure caption states that this mechanism is representative of what occurs in most species of Eulamellibranchia. Considering the above, the idea that the style is a grinding apparatus seems to have gained broad support, and the above information is summarized in books (Brusca & Brusca, 2002; Allaby, 2003).

The idea that the style rod is a grinding apparatus is questionable considering both the style and shield are soft. Nelson (1918) explained that the style is water soluble, and composed of mucus that is rolled up by ciliary action. Several others have pointed out that the style rod is soft and flexible (Owen, 1955; Lomte & Jadhav, 1980). A possible explanation for the grinding hypothesis could be that the style coagulates and becomes thickened when immersed in alcohol or boiling water (Nelson, 1918), and it would therefore appear to be a dense solid structure in a specimen preserved for anatomical study. Careful examination of Figures 74, 78, 205, 209, 334, and 338 provides evidence that the style may be a liquid or a soft, solid material. For example, creasing artifacts to the style indicate that the microtome knife had passed through a dense object. Secondly, the irregular composition of the style in Figures 334, 338 is evidence that the style may represent mucus that is being stirred. Concentric, semicircular rays were also observed in the stomach of all three species, but it seems likely that they represent a churning fluid (Figs. 67, 70, 73, 198, 204, 327, 333). Additionally, the gastric shield covers gastric epithelium in several locations including ventral surfaces where a pestle-like structure would never touch, and may support the hypothesis that it is an elaborate binding agent (Figs. 69, 73, 200, 204, 329, 333). Furthermore, if the style grinds particulate matter, it is unclear as to why grinding would occur between the stomach and intestine, especially considering the extensive digestive tubules located anterior to the stomach. It is also critical to point out that the illustration of the position of the crystalline style sac to the intestine and digestive diverticulum as depicted in Owen (1955) was proposed to be representative of many species of Eulamellibranchia. Based on serial sections of the digestive tract of *V. nebulosa*, *F. cerina* and *S. connasaugaensis*, the esophagus and digestive diverticulum are not located near the style sac and particles would not directly enter this structure from the esophagus. Nevertheless, the illustration in Owen (1955) appears in the more recent work of Boucaurd-Camou & Henry (2003) and appears to have been accepted at face value. Considering the significant morphological differences in the crystalline style sac and stomach across different bivalve orders (Kato & Kubomura, 1954; Purcheon, 1958; Dinamani, 1967).

Morphological differences in the style sac of *V. nebulosa*, *F. cerina* and *S. connasaugaensis* regard the shape of the midgut (Table 11), but the significance of such differences remains unclear given that mussels were allowed to purge prior to being processed for histology. At best we may infer that there are differences in how food matter is processed by this organ. We speculate that the shape or density of the bolus may be different or the rate at which food matter travels through the style sac is different.

Intestine

At present, there is limited information regarding the cellular structure of the intestine of freshwater mussels. Gutheil (1912) described morphological and cellular features of the intestine, namely that the intestine has a crescent shaped lumen with a typhlosole. Yokley (1968) described tall basophilic cells and mucus secreting cells in anterior aspect of intestine of *Pleurobema cordatum*.

Herein we describe five intestinal limbs from and including the crystalline style sac to the so-called “rectum” (Simpson, 1884), which constitutes a straight region of the alimentary canal running parallel with the hinge. We distinguish each intestinal limb based on the location within the viscera, orientation, morphology of the lumen, and cellular structure. The intestine of *V. nebulosa*, *F. cerina* and *S. connasaugaensis* is a long tubular organ that extends through the medial and posterior portions of the visceral mass. The intestine bends several times to form five regions or limbs. Based on histological sections of the digestive tract, the direction of the alimentary canal of *V. nebulosa*, *F. cerina* and *S. connasaugaensis* was generally identical and resembles the layout described from *Anodonta* spp. (Simpson, 1884; Gutheil, 1912).

TABLE 11. Summary of structural differences in crystalline style sac, intestine, pedal ganglion and ovarian acini of Alabama rainbow (*Villosa nebulosa*), Gulf pigtoe (*Fusconaia cerina*), and Alabama creekmussel (*Strophitus connasauagaensis*).

Species	Style sac	Intestinal limbs 2 and 3	Pedal ganglion	Ovarian acini
Villosa nebulosa	Midgut forked, epithelium continuous throughout midgut	Presence of numerous plicae, lumen is folded	Axons fine, filamentous	Mature ova with a thin vitelline membrane
			Surrounding connective tissue is fine	Abundance of fluid between vitelline membrane and ova
Fusconaia cerina	Midgut not forked, tall columnar cells along dorsal and ventral surfaces, short columnar cells along lateral margin	Plicae largely absent, lumen is flattened	Axons thickened, conspicuous	Mature ova with thickened vitelline membrane
			Surrounding connective tissue is thickened, conspicuous	Little or no fluid between vitelline membrane and ova
Strophitus connasaugaensis	Midgut with shallow fork, columnar cells along dorsal and ventral surfaces, short columnar cells along lateral margin	Presence of numerous plicae, lumen is folded	Axons fine, filamentous	Mature ova with a thin vitelline membrane
			Surrounding connective tissue is fine	Moderate quantitiy of fluid between vitelline membrane and ova

The crystalline style sac represents the first descending limb of the intestine (Figs. 79, 210, 339). The walls of the style sac feature numerous folds, and there was an eosinophilic mass typically associated with the ridges and troughs of the style sac walls. Since epithelial types 1−3 were sometimes seen on both the anterior and posterior walls of this intestinal limb, it seems that the style sac does not maintain its stem-loop configuration as it descends. Possibly, since style sac epithelium continues until the dorsal aspect of the visceral mass, circular mixing of food matter may continue to occur until the second intestinal limb. Even though the descending style sac appears to be significantly pleated, we think these folds are associated with mixing rather than absorption.

It is uncertain if absorption occurs in the crystalline style sac or if absorption begins in the second limb considering the bubbling observed in some areas and considering the conspicuous folding of the intestinal wall seen in *V. nebulosa* and *S. connasaugaensis* (Figs. 81, 82, 341, 342). In each species, the second and third intestinal limb featured numerous goblet cells and a dense, eosinophilic mass of chyme. In many areas, the ciliated cells along the intestinal wall appeared to be bubbling (Figs. 83, 214, 343), but it was not clear what these secretions might be. The second and third intestinal limbs appeared to have at least three cell types. The first cell type was ciliated with eosinophilic vesicles while the second cell type, lacked vesicles. Goblet cells represented the third cell type, but these cells were sparsely distributed. Although microvillar cells are typically associated with the intestinal epithelium of a vertebrate (Ross et al., 2003), there was not any indication of such cells in the intestine of each unionid species. This could mean that either the ciliated cells of the intestine have a significant capacity for absorption by themselves or microvilli were obscured from view.

The second and third intestinal limbs of *V. nebulosa* and *S. connasaugaensis* consisted of sinuous to deeply folded walls (Figs. 82, 344), but in *F. cerina*, the walls lacked folds or plicae (Figs. 212, 213; Table 11). A possible explanation for these differences could be that the deeply infolded walls of the ciliated digestive diverticulum tubules are more effective at delivering particles to cells that utilize intracellular digestion. A second explanation could be that *F. cerina* is taking in a greater volume of particulate matter than *V. nebulosa* or *S. connasaugaensis*.

The lumen of the fourth and fifth intestinal limbs was considerably larger than the lumen of the style sac, second and third intestinal limbs. In general, fourth and fifth intestinal limbs may have similar functions considering the morphological similarity of the typhlosole and surrounding intestinal wall (Figs. 85, 88, 216, 219, 345, 348). The primary distinction between the fourth and fifth intestinal limbs was the presence of granulocytes located along the ventral wall. Granulocytes reside in flattened plicae, have a teardrop-shape and contain eosinophilic to basophilic intracellular granules (Figs. 86, 217, 346). However, it is presently uncertain what the function of the granulocytes located within the plicae of the ventral wall of the fourth limb. There are two possible explanations, the strong staining character may be indicative of an apocrine cell that may produce enzymes or mucus. For example, aminopeptidase activity was detected in sections of the lower intestine of *Pecten maximus* (Boucaurd-Camou & Henry, 2003). Goblet cells observed in histological sections of *V. nebulosa*, *F. cerina* and *S. connasaugaensis* are located in many places throughout the body and may be transparent to eosinophilic to basophilic. Granular mucus cells were most frequently observed in the labial palps (Figs. 53, 182, 313). Alternatively, the granules observed in ventral epithelial cells of the fourth intestinal limb may represent intracellular bacteria. Symbiotic intracellular bacteria are known from species of marine bivalves (Lucinidae, Thyasiridae, Vesicomyidae, Mytilidae) that live in sulfur-rich environments. In many cases energy is derived from the oxidation of hydrogen sulfide by intracellular ctenidial bacteria (Cavanaugh et al., 2006). Intracellular bacteria are also known from the digestive tracts of herbivorous insects. Symbiotic bacteria inhabiting the digestive tract of such insects may allow insects to feed on diets that are rich in carbohydrates, but deficient in amino acids (Bauman et al., 2006). Transmission electron microscopy, bacterial stains such as Giemsa, or in situ hybridization using a universal bacterial DNA probe are needed to discern the nature of these granulocytes. Considering that the fourth and fifth intestinal limbs have a large typhlosole restricting the lumen and a perimeter of repeating plicae, it seems that absorption continues to occur. However, the morphological differences between the second, third, fourth and fifth limbs may be an indication that the absorptive processes occurring in each region are not identical. Scanning or transmission electron microscopy would provide a higher resolution images of the cell types characterizing each intestinal limb and could shed light on how or if absorption is different.

Histological sections of intestine sometimes revealed wandering hemocytes in the epithelium (e.g., Figs. 84, 218). Yokley (1968) observed wandering cells throughout the digestive tract and indicated that brown to green intracellular pigments may be evidence that these cells can engulf foreign bodies from digestive epithelium. Owen (1955) reported wandering cells in different places throughout the digestive tract. Owen (1955) suggested that hemocytes move into the digestive tract epithelium to engulf particles and that intracellular digestion by means of hemocytes is one of many ways in which bivalves derive nutrients from ingested matter. However, considering the sparse distribution of hemocytes in the epithelium of the intestine, it seems unlikely that phagocytic wandering cells would play a significant role in digestion. Alternatively, hemocytes may periodically move into the digestive epithelium to engulf invasive pathogens or repair local injuries.

Another curious matter regarding the function of the intestine stem from observations by Owen (1955) and Yokley (1968). Both authors reported that there are concentric bands of myofibers surrounding the intestine of bivalves. The supporting images in Owen (1955) are not informative about myofibers, and the micrographs appear to show dark-staining, thin filaments. Additionally, the micrographs of Sumner (1966a) do not show fibrous tissue between digestive ducts. Throughout the digestive tract of *V. nebulosa*, *F. cerina* and *S. connasaugaensis*, overlapping connective tissue fibers were typically observed supporting folded epithelial tissue (e.g., Figs. 70, 202, 336). In some cases, connective tissue appeared to be densely compacted around the intestine similar to a serosa. Owen (1955) and Yokley (1968) suggested that muscle tissue in the digestive tract of a bivalve would create peristalsis. However, this seems unlikely given that the epithelium of the alimentary canal of each unionid species has extensively ciliated with numerous folds or grooves along the walls. Secondly, the crystalline style rotates and delivers particulate matter into the intestine, and this seems like a logical alternative to peristalsis in a suspension-feeding animal that does not consume a large solid mass of food.

Considering the histological differences in oral groove, digestive diverticulum, style sac and intestine, it seems that *V. nebulosa*, *F. cerina* and *S. connasaugaensis* have different feeding strategies. Overall, the digestive tract of *V. nebulosa* and *S. connasaugaensis*, were most similar to each other, but different in comparison to *F. cerina.* It is difficult to speculate about how the feeding habits of each mussel could be different. Although *V. nebulosa* and *S. connasaugaensis* were collected in headwater streams, and *F. cerina* was obtained from a large river, the historic ranges of each species could have overlapped. Terrapin Creek and Shoal Creek may have less plankton biomass than the Cahaba considering that these areas have more shade. However, historically, *V. nebulosa* and *S. connasaugaensis* occurred in large rivers, such as the Cahaba, so it is likely that there is no relationship between the morphological features of the digestive tract of each species and available plankton (Williams et al., 2008). Histology of field fixed mussels could reveal whether quantity of ingested matter, or specific species of algae or bacteria, but this could be problematic considering that routine tissue preparation for paraffin embedding or electron microscopy removes water-soluble liquids (Sims et al., 1991). Therefore, we may end up with an incomplete picture of the dietary composition.

Cardiovascular System

The gross and histological features of the heart were described in Krug (1922; *Anodonta cygnea* (as *Anodonta cellensis*)), Motley (1932; *Tritogonia verrucosa*, *Amblema plicata* (as *Amblema peruviana*), *Lasmigona complanata* (as *Lasmagonia complanata*), *Elliptio crassidens*, *Fusconaia ebena*, *Actinonaias ligamentina* (as *Actinonaias carinata*), *Potamilus purpuratus* (as *Lampsilis purpurata*) and *Megalonaias nervosa* (as *Megalonaias gigantea*), Chaudhry & Narain (1972; *Lamellidens corrianus*), and Narain (1973, *Lamellidens corrianus*). An accessory pumping structure, the posterior aortic bulb, was described by Narain (1972; *Lamellidens corrianus*). Brand (1972) described the vascular structure of viscera, gill, and mantle of *Anodonta anatina*). Narain (1976) summarized knowledge about heart and cardiac output in unionids. Hemocytes were described in Dundee (1953; *Amblema plicata* (as *Amblema costata*), *Quadrula quadrula*, *Uniomerus tetralasmus*, *Tritogonia verrucosa*, *Toxolasma parvum* (as *Carunculina parva*), *Ligumia subrostrata*, *Potamilus alatus* (as *Proptera alata*), *Leptodea fragilis*, *Lasmigona complanata*, *Lampsilis teres* (as *Lampsilis fallaciosa*), and *Pyganodon grandis* (as *Anodonta grandis*)), and Burkhead et al. (2009; *Quadrula* sp.).

Our observations further support the notion of the histologically conserved nature of the auricles and ventricle among unionid species. The heart consists of a pair of laterally positioned auricles and a median muscular ventricle (e.g., Fig. 91). Overall cardiac structure of *V. nebulosa*, *F. cerina*, and *S. connasaugaensis* was very similar. Auricles and ventricle consisted of an epicardium of squamous cells, and a distinct myocardium of cardiac muscle. However, there was less investment of cardiac myofibers in the auricles than observed in the ventricle, possibly because the auricles are blood-receiving conduits that need to be distensible (Motley, 1932).

Andrews & Jennings (1993) reported that auricles of *Anodonta* sp. merge with the walls of the pericardium, and that fluid may leak out of the auricles into the surrounding pericardial gland. However, auricles of each mussel species studied herein extended freely into the pericardial cavity to merge with the ventricle at an oblique angle. Based on histological sections of three unionid species, it was not obvious whether the auricular epicardium would leak (Figs. 92, 223, 352). Examining the surface of the auricles of *V. nebulosa*, *F. cerina* and *S. connasaugaensis* may provide insight into whether there are gaps between epicardial cells that would be indicative of the passive transport of fluid into the surrounding pericardial cavity. Scanning electron microscopy of the heart of *Crassostrea gigas* has indicated that the ventricle and auricles each have a robust composition. Higher magnification images of the surface of the auricle and ventricle do not provide much information concerning the possibility of pores. Although *Crassostrea gigas* is a marine bivalve, the morphological features of the auricles and ventricles seem to be morphologically comparable to the heart of a unionid and may be an indication that fluid does not leak out of the heart (Grizel, 2003).

There is a pair of muscular, auriculoventricular valves separating each sinistral and dextral auricle (Figs. 95, 226, 355), from the ventricle, to maintain proper tidal rhythm (Motley, 1932). Cardiac myofibers in the ventricle are significantly developed, with numerous longitudinal and transversely oriented myofibers. Considering the extensive development of longitudinal and transverse myofibers in the ventricle (Figs. 92, 223, 353), the orientation of myofibers would seemingly cause the ventricle to contract in a circular, and linear (posterior-to-anterior) fashion to drive hemolymph into anterior, and posterior aortic vessels (Brand, 1972). Additionally, as in the heart of a vertebrate (Ross et al., 2003) cardiac myofibers were spaced apart to facilitate constant expansion and contraction of the organ, and to maintain a supply of oxygen to the myofibers. Additionally, myofibers contained brown, granular inclusions and it is uncertain what this material represents or how it relates to cardiac function (e.g., Fig. 224). Furthermore, intracellular inclusions were not observed in any other muscle tissue in *V. nebulosa*, *F. cerina* or *S. connasaugaensis*.

Herein we observed distinct vessels resembling arteries, veins and capillaries throughout the body, but it was sometimes difficult to distinguish between arteries and veins (e.g., Figs. 96, 97). Our observations support the work of Brand (1972), who revealed the presence of vasculature by injecting the heart of *Anodonta anatina* with rubber-latex and removing the soft surrounding tissues. Arteries in vertebrates have a dense wrapping of smooth muscle with a circular lumen. Veins typically have thinner walls with an irregular somewhat flattened lumen (Ross et al., 2003). The aorta for example, would have a thick muscular wall, but histological sections of the anterior and posterior aorta of mussels revealed a large, ovular lumen with a limited muscular wrapping. Thick musculature enclosed the lumen of arteries near the base of the foot, possibly to rapidly fill pedal hemolymph sinuses with hemolymph in order to facilitate expansion of the tissue (Trueman, 1966; Brand, 1972).

Andrews & Jennings (1993) suggested that there are a series of well-defined hemolymph vessels that converge at the base of the ctenidia, leading to the auricles. In transverse sections of the heart, a pale, violet, granular mass was observed at the base of the gill (e.g., Figs. 157, 158). Additionally, there was a network of loose connective tissue between the auricles and the gill. Well-defined hemolymph vessels leading from the base of the gills to the auricles were not observed. Possibly this region conveys hemolymph into the auricles in a diffuse manner considering the funnel-shaped configuration of unionid auricles.

Hemolymph consisted of distinct cellular and non-cellular components. Eosinophilic, granular hemocytes were observed throughout the viscera and mantle of *V. nebulosa*, *F. cerina* and *S. connasaugaensis* (e.g., Figs. 53, 86, 187, 196, 357, 363). Literature regarding hemocytes of unionids and marine bivalves suggests that there are distinct types of blood cells (Dundee, 1953). However, potential differences between hemocytes observed throughout the hemocoel and mantle are presently indeterminate. Hemolymph fluid appears in histological sections as a diffuse, black-pigmented material, throughout the body, typically within interstitial spaces (e.g., Figs. 18, 103, 150, 157, 341, 356). Considering that black granules were observed in the heart and interstitial spaces, it may represent plasma and interstitial fluid. Black granules may represent hematin, a pigmentation that occurs in blood-rich tissues when acidic formalin and hemoglobin react (Myers & McGavin, 2007). Clear examples demonstrating the appearance of hemolymph or interstitial fluid are lacking in the literature.

To our knowledge, the best micrograph of the pericardial gland of a bivalve appears in Norton & Jones (1992). The pericardial gland is a diffuse network of adipocyte-like cells located laterally and dorsally to the pericardial cavity (Figs. 99, 230, 359). Clearly this spongy tissue transmits hemolymph through the dorsum, and the high surface area of this tissue would be an indication that hemolymph travels slowly through this region. Prior studies on the pericardial gland have indicated that the pericardial gland plays a role in filtration (Morse, 1987; Andrews & Jennings, 1993). An additional possibility that bivalve researchers may have overlooked is hemopoesis. In an effort to understand the host-parasite relationship between the infective larval stages of trematodes (*Fasciola hepatica*) and snails *Galba truncatula* (as *Lymnaea truncatula*), Rondelaud & Barthe (1981) observed hemocyte proliferation between the nephridium and pericardium following experimental infection of snails with infective trematode larval stages (miracidium). Given the above we may phylogenetically infer that the pericardial gland could play a role in hemopoiesis, since we observed emarginated, eosinophilic cells resembling hemocytes along the surface of the adipocyte-like pericardial gland cells. However, in *V. nebulosa*, we sometimes observed brown or otherwise discolored hemocytes, and we speculate that these cells may be senescent. Therefore, we are uncertain of whether the pericardial gland is associated with hemopoiesis, hemocyte senescence or both.

Renal System

White (1942) documented the location and distribution of the nephridium and pericardial glands in species of Unionidae and Etheriidae and reviewed the literature regarding pericardial gland function. Myers & Franzen (1970) described cellular constituents and functional morphology of the nephridium and pericardial gland of *Quadrula nodulata*. Andrews & Jennings (1993) addressed functional morphology and cellular anatomy of auricles, ventricle, pericardial sac, pericardial glands, and renal-pericardial canal of *Anodonta cygnea*.

Many of the morphological features and cell types of the nephridium of *V. nebulosa*, *F. cerina* and *S. connasaugaensis* are consistent with the observations of Myers & Franzen (1970). However, the histological features of the nephridium of *V. nebulosa*, *F. cerina* and *S. connasaugaensis* reveal new insights into renal physiology of bivalves. Overall nephridial structure was different from anterior to posterior (Figs. 100, 107, 231, 238, 360, 367). The ventral nephridial limb is compressed anteriorly because it is located adjacent to the visceral mass. The lumen of the anterior portion of the ventral nephridial limb is restricted by the numerous infoldings. Given the extensive network of branched plicae, it seems that reabsorption occurs in the anterior portion of the ventral nephridium (Figs. 101, 232, 361). Plicae become more widely spaced apart posteriorly between the posterior margin of the visceral mass and posterior adductor, and the overall lumen of the nephridium expands possibly to accommodate a larger volume of fluid. Epithelial folds have a stem-loop structure and the cells have a pale-staining cytoplasm (Figs. 108, 239, 368). Therefore, the posterior portion of the nephridium may function similar to the thin loop of Henle in a vertebrate (Ross et al., 2003). Dorsal nephridium resembles a sac and contains a small number of short, thin plicae. Considering the absorptive nature of the ventral nephridial limb, the function of dorsal nephridium is thought to be analogous to a bladder (Myers & Franzen, 1970; Andrews & Jennings, 1993). The structure of the nephridium of *V. nebulosa*, *F. cerina* and *S. connasaugaensis* is similar to descriptions of unionid nephridia of *Pleurobema cordatum* and *Quadrula nodulata* (Yokley, 1968; Myers & Franzen, 1970).

Renal filtrate may be derived from hemolymph flowing through the pericardial gland. Podocytes are associated with the pericardial cavity and may be distinguished from other cells by the presence of branched cytoplasmic extensions of the basal part of the cell known as pedicels. Fluid derived from hemolymph may pass out of the pericardial gland and into the pericardial cavity (Meyhöfer et al., 1985; Morse, 1987). A more recent study indicated that podocytes of *A. cygnea* may be located anteriorly to the nephridium may allow passage of fluid into the renopericardial canal (Andrews & Jennings, 1993). A competing hypothesis regarding filtration suggests that fluid may pass through the pericardial wall from the pericardial gland (Yokley, 1968). Goblet cells located around the lumen of the renopericardial canal possibly secrete mucus into the renal lumen (Figs. 106, 237, 365), but the presence of mucigen has not been confirmed. Since these cells were located along the anterior wall of the pericardial sac, perhaps some of these cells represent podocytes. It is difficult to pinpoint exactly where podocytes occurred because there is no light microscopy reference point. Morse (1987), for example, illustrated two podocytes in a diagram portraying the path of fluid from the pericardial gland to the nephridium, but there is no information about the appearance of the surrounding tissue. Since podocytes were portrayed as teardrop-shaped columnar cells in Morse (1987), and since Andrews & Jennings (1993) stated that podocytes are located in the anterior region of the pericardial cavity, the columnar epithelium at the anterior portion of the pericardial sac at the entrance to the renopericardial canal may contain podocytes.

Ciliated cells in the renopericardial canal seemingly create the driving force needed to propel renal filtrate posteriorly through the nephridium. Cilia were conspicuous in the renopericardial canal (Figs. 106, 237, 365) and urethra (Figs. 107, 238, 366), but there were no obvious indications of cilia throughout the ventral and dorsal nephridial limbs. Fine, wispy structures were observed on the apical surface of cuboidal cells representing the stem-loop structures of the posterior nephridium (Figs. 108, 239, 368). However, it seemed that these filamentous structures were the remnants of a fluid. Given the limited amount of cilia in the nephridium and the extensive volume of tissue throughout the entire ventral and dorsal nephridial limbs, and that unionid exhibit low cardiovascular pressure (Brand, 1972), it would seem that passage of filtrate through the nephridium occurs at a slow rate.

The columnar epithelium of the ventral nephridial limb of *V. nebulosa*, *F. cerina* and *S. connasaugaensis* contained red to brown intracellular granules. Brown intracellular granules were most conspicuous in *V. nebulosa* (Fig. 98), and the red granules were most conspicuous in *S. connasaugaensis* (Fig. 361). In most cases, the granular material resembled wandering hemocytes. The brown granules may represent either senescent hemocytes or hemocytes with engulfed material. In either case, the eosin dye poorly presented itself and suggests some chemical change occurred in the cytoplasm of wandering cells. It is unclear why the epithelium of *S. connasaugaensis* would have such a strong eosinophilic and granular staining character. An alternative explanation for the intracellular granules in the ventral nephridium could be that the columnar cells are phagocytic or absorb substances from the nephridial lumen via microvilli to form concrements. Concrements may consist of lipofuscin granules, membrane remnants or other substances that would appear to be electron dense when the tissue is studied with transmission electron microscopy. Concrements may later be expelled into the lumen once the intracellular vacuole-lysosome system is filled to capacity (Morse, 1987).

Teardrop cells with an apical, transparent vesicle (Figs. 103, 234, 362) have been observed in unionids such as *Q. nodulata* (Myers & Franzen, 1970) as well as marine bivalves such as *C. virginica* (Galtsoff, 1964). Teardrop cells with apical vesicles located in the bladder and have been previously suggested to pinch off the apical vesicle. The vesicle may contain an anionic substance based on a positive staining reaction with Heidenhain's Azan Stain (Myers & Franzen, 1970). Possibly, this anionic substance is ammonia.

The cuboidal cells of the posterior nephridium (e.g., Figs. 109, 368), and especially dorsal nephridial cells (both, dorsal and ventral) contained brown intracellular granules (Figs. 102, 233, 234, 368). Possibly this substance represents more accumulations of waste products that have become internalized within renal epithelium. The observation of plicae in the dorsal nephridium is somewhat surprising considering the extensive infoldings of the anterior portion of the ventral limb. The plicae in the dorsal nephridium would suggest that reabsorption continues to occur at a low level once filtrate enters the dorsal nephridium, which is thought to represent a bladder (Myers & Franzen, 1970; Andrews & Jennings, 1993).

Nervous System

Splittstößer (1913) mapped nervous system of *Anodonta cygnea* (as *Anodonta cellensis*) and characterized gross morphological features of cerebral ganglia, pedal ganglia, visceral ganglia and statocysts. Motley (1943) stimulated the heart with electrical impulses and discerned that cardiac tissue is responsive to such stimulation; stimulation of cerebral and visceral ganglia did not depress heart rate, but instead caused contractions in the pedal musculature. Kraemer (1967), observed mantle flapping of *Lampsilis cardium* (as *Lampsilis ventricosa*) and explained how flapping was positively associated with light intensity. Additionally, he noted the presence of a ganglion near the mantle flap and a richer supply of axons in this area as compared to the siphon. Kraemer (1978) described the cellular structure of statocysts of *Lampsilis cardium* (as *Lampsilis ventricosa*). Yokley (1968) described the cerebral, pedal, and visceral ganglia from *Pleurobema cordatum*. Gross anatomy of visceral ganglion was described by *Margaritifera margaritifera*, *Margaritifera monodonta* (as *Cumberlandia monodonta*) (Smith, 1980) and *Margaritifera hembeli* (Smith, 1988).

Freshwater mussels have a decentralized nervous system consisting of a pair of anterior cerebral ganglia (Figs. 117, 248, 377), a bilobed pedal ganglion (Figs. 112, 243, 372) and visceral ganglion located posteriorly (Figs. 118, 250, 379). Each ganglion has a distinct cortex and medulla. Herein, we show that the cellular composition of each ganglion is similar. Furthermore, we observed subtle interspecific variation in the histological characteristics of the pedal ganglion of *F. cerina* as compared to *V. nebulosa* and *S. connasaugaensis*. The pedal ganglion of *F. cerina* had thickened axons and connective tissue surrounding each hemisphere (Figs. 244, 246; Table 11). It is unclear how the function of the pedal ganglion of *F. cerina* may differ from that of *V. nebulosa*, and *S. connasaugaensis* considering the later two species lacked thickened axons and connective tissue fibers (Figs. 112, 114, 372, 373). Each ganglion is associated with local tissue function and movement of musculature. Based upon experiments in which bodily regions are separated from the cerebral ganglion, it appears that the cerebral ganglion is required for complex motor functions. Moreover, ganglia are linked to each other and can work together to regulate tissue function. For example, the visceral ganglion enables shell closure, but opening requires signals from cerebral ganglia (Tauc, 1966). Prior work on the cellular anatomy of the bivalve nervous system has indicated that unipolar neurons are typically located in the cortex while bipolar and multipolar neurons tend to be located within the medulla (Tauc, 1966). However, cell bodies of the medulla in *V. nebulosa*, *F. cerina* and *S. connasaugaensis* were minute, making it difficult to determine whether some are neurons or glial cells.

The spherical statocysts located laterally to the pedal ganglion are associated with equilibrium. Statocysts are fluid-filled capsules containing a ciliated epithelium (Figs. 123, 254, 383). Sensation of equilibrium may be derived from neural impulses created following contact between the statolith and ciliated cells. The statolith had a dense consistency similar to the crystalline style since the statolith tended to wrinkle during microtomy. We speculate that the statolith is gelatinous and becomes rigid following routine histological preparation (also see Kraemer, 1978). Evidence of statocyst function is derived from experimental investigations in which impaired righting response was observed following mechanical damage to the statocyst or its associated nerve (Cragg & Nott, 1977). Our observations suggest that statocysts of unionids are histologically conserved.

Reproductive System

Reproductive tissues in freshwater mussels comprise ovarian and testicular acini, ciliated ducts that transfer ova and sperm dorsally to gonopores (Henley et al., 2007). Histology has been commonly used to determine spawning period for freshwater mussels (Van der Schalie & Van der Schalie, 1963; Yokley, 1972; Smith, 1978; Zale & Neves, 1982; Smith, 1988; Gordon & Smith, 1990; Jirka & Neves, 1992; Grande et al., 2001; Smith et al., 2003; Henley et al., 2007), and numerous authors have demonstrated seasonality of gametogenesis (Van der Schalie & Van der Schalie, 1963; Yokley, 1972; Zale & Neves, 1982; Smith, 1988; Gordon & Smith, 1990; Jirka & Neves, 1992; Grande et al., 2001; Smith et al., 2003; Henley et al., 2007).

Regarding the male anatomy, spermatocytes, spermatids and spermatozoa are minute such that only cellular shape and staining characteristics can be observed with light microscopy. Furthermore, differentiating early and late staged spermatocytes or spermatids and spermatozoa is difficult. Ovarian acini contain larger oocytes by comparison, with a distinct vitelline mass, and centrally located nucleus is typically seen in published micrographs. Spermatogenesis and morphology of nuclei and organelles of spermatocytes, spermatids and spermatozoa have been rendered from transmission electron microscopy studies (Heard, 1975; Healy, 1989; Peredo et al., 1990; Rocha & Azevedo, 1990). Seasonality of male gametogenesis is characterized by typical and atypical spermatogenesis. Typical spermatogenesis occurs during the summer when males are ready to spawn. Spermatozoa differentiate from spherical spermatocytes, and spermatocytes have chromosomes or granular chromatin. Atypical spermatogenesis occurs between the fall and spring and is distinguished by the presence of spermatocyte clusters called sperm morula given their resemblance to morula-stage embryos. Spermatocytes of sperm morula have a minimal amount of cytoplasm surrounding a nucleus with condensed chromatin (Heard, 1975). Male mussels disperse spermatozoa by packaging them into spherical masses resembling *Volvox* called spermatozeugmata. Spermatozeugmata were described from *Anodontoides ferussacianus* using light microscopy. Spermatozoa are spherical such that the acrosome was facing the median and the tail extended distally, allowing the entire mass to be propelled and steered by different groups of cells (Edgar, 1965). Waller & Lasee's (1997) SEM observations of spermatozoa and spermatozeugmata of *Truncilla truncata* revealed that a single spermatozeugmata had 8,000–9,000 spermatozoa (see also Edgar, 1965).

Regarding the female anatomy, Van der Schalie & Locke (1941) presented a detailed description of ova and was one of the first publications to specifically describe formation of sperm and ova with photomicrographs. Ova may have an irregular shape initially and maintain a connection to the acinus wall by means of a pellicle. During oogenesis, ova are surrounded by nurse cells, which may secrete a nutritive substance to become incorporated into a developing ovum. When ova reach maturity they are appreciably enlarged and contain a double nucleus (Beams & Sekhon, 1966). Ovarian acini contain degenerative or atretic cells between the fall and spring (Yokley, 1972). Herein we observed interspecific variation in vitelline. Micrographs in some comparative studies show interspecific variation in vitelline structure among at least some unionids (Van der Schalie, 1970; Yokley, 1972; Zale & Neves, 1982; Woody & Holland-Bartels, 1993) and margaritiferids (Gordon & Smith, 1990; Grande et al., 2001). Photomicrographs of the ova *Villosa nebulosa* reveal an irregular fluidic mass surrounding the vitelline, filling the lumen of the acini (Zale & Neves, 1982), while an irregular, linear membrane surrounded mature oocytes of *Margaritifera monodonta* (as *Cumberlandia monodonta*) (Gordon & Smith, 1990), *Margaritifera auricularia* (Margaritiferidae) (Grande et al., 2001), *Megalonaias nervosa* (Woody & Holland-Bartels, 1993), *Pleurobema cordatum* (Unionidae) (Yokley, 1972).

Histology of gametogenesis has potential as a biomarker of thermal stress. Heinricher & Layzer (1999) observed depressed gametogenesis in a population of *Megalonaias nervosa* below a dam on the Cumberland River as compared to individuals within Kentucky Lake. Mussels exhibited normal gametogenesis three years following transplantation.

Regarding hermaphroditism, histology of gonadal tissue has revealed that many freshwater mussel species exhibit different levels of hermaphroditism. However, the prevalence of this phenomenon in a population is low. Hermaphroditism may be characterized by the presence of both ovarian and testicular acini or the presence of one or more acini that produce both sperm and ova (Tepe, 1943 [in *Carunculina parva*]; Van der Schalie, 1970 [34 spp. of Unioninae, 20 of Anodontinae, 41 of Lampsilinae]; Heard, 1975 [in *Anodonta californiensis*, *Utterbackia couperiana* (as *Anodonta couperiana*), *Strophitus connasaugaensis* (as *Anodonta hallenbeckii*), *Utterbackia imbecilis* (as *Anodonta imbecilis*), *Utterbackia peggyae* (as *Anodonta peggyae*)]; and Heard, 1979 [in *Elliptio arctata*, *Elliptio jayensis* (as *Elliptio buckleyi*), *Elliptio complanata*, and *Elliptio icterina*]).

We observed seasonality of gametogenesis in *V. nebulosa*, *F. cerina* and *S. connasaugaensis*. Specifically, the peak spawning period for each species was different. The peak spawning period of *V. nebulosa* in Terrapin Creek was between late July and early August similar to the spawning time reported from Big Moccasin Creek, Virginia (Zale & Neves, 1982). Similarly, peak gametogenesis occurs in *S. connasaugaensis* between late July and early August. The spawning period of *F. cerina* in Cahaba River however occurs during May, similar to the spawning period of *Fusconaia cuneolus* in Clinch River, Virginia (Bruenderman & Neves, 1993). Acini expand to accommodate a small number of enlarged, mature oocytes in females (Figs. 126, 257, 386) and a large volume of spermatozoa in males (Figs. 129, 260, 389). Testicular (Figs. 128, 259, 388), and especially ovarian acini (Figs. 125, 256, 385) contained a preponderance of eosinophilic granules when gametogenesis was depressed. The small granules likely constitute fluid, however the larger granules in ovarian acini possibly represent a combination of polar bodies and degenerative oocytes considering the abundance of pycnotic nuclei within the lumen. Testicular acini also contained pycnotic nuclei to a lesser extent when gametogenesis was limited. Seemingly, gametogenesis occurs outside of the spawning season and that oocytes and spermatocytes breakdown prematurely. Specific seasonal cellular changes to acini were previously described from *Pleurobema cordatum* (Yokley, 1972).

Interspecific variation in the histological appearance of mature ova was pronounced owing to their great size (Table 11). However, it is difficult to determine the polarity of vitelline structure based on the available literature. For example, some comparative studies are inconsistent with the portrayal of each structure because photographs were taken at different orientations (Jirka & Neves, 1992; Henley et al., 2007). The vitelline membrane was the most distinctively different feature of oocytes (Figs. 126, 257, 386). The structure of oocytes of *V. nebulosa* correspond to the appearance of *V. nebulosa* oocytes that appear in Zale & Neves (1982), while the oocytes of *F. cerina* appear to be similar to oocytes of *Fusconaia flava* (Van der Schalie, 1970). Based upon histological sections of filled marsupia of *F. cerina*, it seems that the structure of vitelline membranes may be important for embryo packing. The vitelline membranes were irregular, filamentous extensions of ova, and ova appeared to be held together within a conglutinate by vitelline membranes (Figs. 160, 162). Therefore, the vitelline membranes of *F. cerina* may be adhesive and provide strength to a conglutinate. Histological sections of filled marsupia of *V. nebulosa* and *S. connasaugaensis* were derived from animals collected months after the spawning period, making it difficult to link structural characteristics of vitelline membranes to embryo packing (Figs. 30, 294). Differences in the thickness or composition of the vitelline membrane of bivalve ova are typically matched by corresponding adaptations of the spermatozoa. For example, the thickened ova of *Mytilus edulis*, may be fertilized by a spermatozoa that possess a large acrosome, which would be required to penetrate a thickened, gelatinous membrane (Morse & Zardus, 1997).

There were no obvious differences in the structure of spermatocytes or spermatozoa of each unionid species considering their minute size (Figs. 129, 260, 389). Spermatocytes and sperm morula of stage 1 testicular acini were loosely arranged, making it difficult to describe specific details of cellular progression from a spherical, single-celled spermatocyte to a spermatids and spermatozoa. Spermatogenesis in stage 1 and stage 3 acini was different. Stage 1 acini were characterized by “atypical” spermatogenesis consisting of copious sperm morula (Figs. 128, 259, 388) while stage 3 acini were characterized as exhibiting “typical” spermatogenesis (Figs. 129, 260, 389; Van der Schalie & Locke, 1941; Heard, 1975). Atypical and typical spermatogenesis may produce sperm cells that are identical based on light microscopy, but it is unclear whether there is a difference at the ultrastructure level. Considering the interspecific variation in oocyte structure, we speculate that spermatozoa of *V. nebulosa*, *F. cerina* and *S. connasaugaensis* would be structurally distinct from each other. Spermatozoa of marine bivalves can be highly species specific at the ultrastructure level and variation is associated with fertilization strategies. Differences are associated with external fertilization, fertilization in mantle cavity, and whether sperm are released freely or packaged into spermatophores (Morse & Zardus, 1997). Regarding reproductive biology of freshwater mussels, unionids are well known for their widely different dispersal strategies (Barnhart et al., 2008). Mussels are either short-term brooders (tachytictic), exhibiting gametogenesis during the early spring followed by the release of their glochidia shortly thereafter, or long-term brooders (bradytictic) spawning later in the summer and holding the glochidia within marsupia for weeks or months (Cummings & Graf, 2010). Potentially, variation in oocyte and spermatozoa morphology may correspond to dispersal strategies of *V. nebulosa*, *F. cerina* and *S. connasaugaensis*, or to differences in brooding.

ACKNOWLEDGEMENTS

We thank Paul Johnson (Alabama Department of Conservation and Natural Resources, [ADCNR], Marion, Alabama) for providing valuable comments on this work as it developed. We thank Andrew Austin, Stanton Belford, Carlos Ruiz and Triet Truong (all Aquatic Parasitology Laboratory, Department of Fisheries and Allied Aquacultures [FAA]) as well as P. Johnson and Thomas Tarpley (ADCNR) for helping collect mussels; Raquel Patella for producing some sections of *S. connasaugaensis*; Michael Miller (Department of Biological Sciences, Auburn University) as well as Cova Arias and James Stoeckel (both FAA]) for commenting on an earlier draft of this work comprising AM’s disseration; Pam Whaley (Ralph Brown Draughn Library, Document Delivery Department, Auburn University) for interlibrary loan help. We would also like to thank two anonymous reviewers for providing valuable comments that strengthened this manuscript. This is a contribution of the Southeastern Cooperative Fish Parasite and Disease Project (FAA) and was supported by research grants awarded to SAB from the National Science Foundation’s Division of Environmental Biology (Award nos. 1112729, 1051106, and 1048523) and the Alabama Agricultural Experiment Station’s HATCH program, which supported AM for the majority of his doctorate work represented herein. We also thank Cova Arias for providing some support to AM via a United States Department of Agriculture-Agriculture Research Service/ Auburn University Cooperative Agreement and CRIS Project No. 6420-32000-022-00D. The ADCNR provided seed monies to SAB in 2010 to formulate the initial concept for this work. We thank Dr. Richard Back, Interim Dean of the College of Liberal Arts and Sciences, SUNY Oswego, for helping to defray the cost of this publication.

LITERATURE CITED

AHLSTEDT, S. A. & J. J. JENKINSON, 1987, A mussel die-off in the Powell River, Virginia and Tennessee, in 1983. Pp. 21–28, in: R. J. Neves, ed., *Proceedings of the workshop on die-offs of freshwater mussels in the United States*, June 23−25, 1986, Davenport, Iowa. United States Fish and Wildlife Service, Upper Mississippi Conservation Committee, 166 pp.

ALLABY, M., 2003, *A dictionary of zoology*, 2nd ed. Oxford University Press, Oxford & New York, vi + 597 pp.

ALLEN, W. R., 1914, The food and feeding habits of freshwater mussels. *Biological Bulletin*, 27: 127–146.

ANDERSON, R. M., J. B. LAYZER & M. E. GORDON, 1991, Recent catastrophic decline of mussels (Bivalvia: Unionidae) in the Little South Fork Cumberland River, Kentucky. *Brimleyana*, 17: 1–8.

ANDREWS, E. B. & K. H. JENNINGS, 1993, The anatomical and ultrastructural basis of primary urine formation in bivalve mollusks. *Journal of Molluscan Studies*, 59: 223–257.

APPELTANS, W., P. BOUCHET, G. A. BOXSHALL, C. DE BOYER, N. J. DE VOOGD, D. P. GORDON, B. W. HOEKSEMA, T. HORTON, M. KENNEDY, J. MEES, G. C. B. POORE, G. READ, S. STÖHR, T. C. WALTER & M. J. COSTELLO, 2012, *World Register of Marine Species*. http://www.marinespecies.org. Last accessed 25 April 2013.

ARAUJO, R., N. CÁMARA & M. A. RAMOS, 2002, Glochidium metamorphosis in the endangered freshwater mussel *Margaritifera auricularia* (Spengler, 1793): a histological and scanning electron microscopy study. *Journal of Morphology*, 254: 259–265.

ATKINS, D., 1937, On the ciliary mechanisms and interrelationships of lamellibranchs. Part III: Types of lamellibranch gills and their food currents. *Quarterly Journal of Microscopical Science*, 79: 375–421.

ATKINSON, C. L., M. R. FIRST, A. P. COVICH, S. P. OPSAHI & S. W. GOLLADAY, 2011, Suspended material availability and filtration-biodeposition processes performed by a native and invasive bivalve species in streams. *Hydrobiologia*, 667: 191–204.

AVELAR, W. & A. CUNHA, 2009, The anatomy and functional morphology of *Diplodon rhombeus fontainianus* (Orbigny, 1835) (Mollusca Bivalvia, Hyriidae). *Brazilian Journal of Biology*, 69: 1153–1163.

BAKER, R. A., 1976, Tissue damage and leukocytic infiltration following attachment of the mite *Unionicola intermedia* to the gills of the bivalve mollusk *Anodonta anatina*. *Journal of Invertebrate Pathology*, 27: 371–376.

BANK, R., 2004, *Fauna Europaea: Gastropoda*. http://www.faunaeur.org. Last accessed 25 April 2013.

BARNHART, M. C., 2008, *Unio gallery*. http://unionid.missouristate.edu. Last accessed 28 September 2013.

BARNHART, M. C., W. R. HAAG & W. N. ROSTON, 2008, Adaptations to host infection and larval parasitism in Unionoida. *Journal of the North American Benthological Society*, 27: 370–394.

BAUER, G & K. WÄCHTLER, 2001, *Ecology and evolution of the freshwater mussels Unionoida*. Ecological Studies, Vol. 145. Springer-Verlag, Berlin, xxii + 394 pp.

BAUMANN, P., N. A. MORAN & L. BAUMANN, 2006, Bacteriocyte-associated endosymbionts of insects. Pp. 403–438, in: E. Rosenberg, E. Stackebrandt, F. Thompson, E. DeLong & S. Lory, eds., *The prokaryotes. A handbook on the biology of bacteria*. Vol. 1. *Symbiotic associations, biotechnology, applied microbiology*, 3rd ed. Springer Science + Business Media, New York, New York, 959 pp.

BEAMS, H. W. & S. S. SEKHON, 1966, Electron microscope studies on the oocyte of the freshwater mussel (*Anodonta*), with special reference to the stalk and mechanism of yolk deposition. *Journal of Morphology*, 119: 477−501.

BEEDHAM, G. E., 1958, Observations of the mantle of Lamellibranchia. *Quarterly Journal of Microscopical Science*, 99: 181–197.

BLODGETT, K. D. & R. E. SPARKS, 1987, Documentation of a mussel die-off in pools 14 and 15 of the upper Mississippi River. Pp. 76–90, in: R. J. Neves, ed., *Proceedings of the workshop on die-offs of freshwater mussels in the United States,* June 23−25, Davenport, Iowa. United States Fish and Wildlife Service, Upper Mississippi Conservation Committee, 166 pp.

BOUCAURD-CAMOU, E. & M. HENRY, 2003, The digestive system. Pp. 65–116, in: H. Grizel, ed., *Atlas d'histologie et de cytology des mollusques bivalves marins = An atlas of histology and cytology of marine bivalve molluscs*. Ifremer, Plouzané, France, 201 pp.

BRAND, A. R., 1972, The mechanism of blood circulation in *Anodonta anatina* (L.) (Bivalvia, Unionidae). *Journal of Experimental Biology*, 56: 361–379.

BROOKS, W. K., 1882, *Handbook of invertebrate zoology for laboratories and seaside work*. S. E. Cassino, Boston, Massachusetts, viii + 392 pp.

BRÜCK, A., 1914, Die Muskulatur von *Anodonta cellensis* Schröt: Ein Beitrag zur Anatomie und Histologie der Muskelfasern. *Zeitschrift für Wissenschaftliche Zoologie*, 110: 481–619.

BRUENDERMAN, S. A. & R. J. NEVES, 1993, Life history of the endangered fine-rayed pigtoe *Fusconaia cuneolus* (Bivalvia: Unionidae) in the Clinch River, Virginia. *American Malacological Bulletin*, 10: 83–91.

BRUSCA, R. C. & G. J. BRUSCA, 2002, *Invertebrates*, 2nd ed. Sinauer Associates, Sunderland, Massachussetts, xix + 936 pp.

BURCH, J. B., 1973, *Freshwater unionacean clams (Mollusca: Pelecypoda) of North America*. Biota of freshwater ecosystems, identification manual no. 11, United States Environmental Protection Agency, Washington, D.C., 176 pp.

BURKHEAD, M. J., S. LEAVELL, R. B. WEISS, K. KUEHNL, H. VALENTINE, G. T. WATTERS

& B. A. WOLFE, 2009, Analysis and cytologic characterization of hemocytes from freshwater mussels (*Quadrula* sp.). *Veterinary Clinical Pathology*, 38: 426–436.

CAVANAUGH, C., Z. P. MCKINESS, I. I. G. NEWTON & F. J. STEWART, 2006, Marine chemosynthetic symbioses. Pp. 475–507, in: E. Rosenberg, E. Stackebrandt, F. Thompson, E. DeLong & S. Lory, eds., *The prokaryotes. A handbook on the biology of bacteria*. Vol. 1. *Symbiotic associations, biotechnology, applied microbiology*, 3rd ed. Springer Science + Business Media, New York, New York, 959 pp.

CHAUDHRY, H. S. & A. S. NARAIN, 1972, Functional morphology of the heart of the freshwater mussel *Lamellidens corrianus*. *Zoologische Beiträge*, 18: 339–342.

CHECA, A. G., 2002, Fabricational morphology of oblique ribs in bivalves. *Journal of Morphology*, 254: 195–209.

CHITTICK, B., M. STOSKOPF, M. LAW, R. OVERSTREET & J. LEVINE, 2001, Evaluation of potential health risks to eastern elliptio (*Elliptio complanata*) (Mollusca: Bivalvia: Unionida: Unionidae) and implications for sympatric endangered freshwater mussel species. *Journal of Aquatic Ecosystem Stress and Recovery*, 9: 35–42.

COLVILLE, A. E. & R. P. LIM, 2003, Microscopic structure of the mantle and palps in the freshwater mussels *Velesunio ambiguous* and *Hyridella depressa* (Bivalvia: Hyriida). *Molluscan Research*, 23: 1–20.

CONRAD, T. A., 1834, *New freshwater shells of the United States, with coloured illustrations; and a monograph of the genus Anculotus of Say; also a synopsis of the American naiades*. J. Dobson, Philadelphia, Pennsylvania, 76 pp., 8 pls.

CONRAD, T. A., 1838, *Monography of the family Unionidae, or naiades of Lamarck, (fresh water bivalve shells) or North America, illustrated by figures drawn on stone from nature*. J. Dobson, Philadelphia, Pennslyvania, 11: 95–102, pls. 52–57.

COOKE, A. H., 1895, Molluscs. Pp. 1–459, in: S. F. Harmer & A. E. Shipley, eds., *The Cambridge Natural History*, Vol. 3. Macmillan and Co., New York, 535 pp.

COSGROVE, P., L. HASTIE & I. SIME, 2007, Recorded natural predation of freshwater pearl mussels *Margaritifera margaritifera* (L.) in Scotland. *Journal of Conchology*, 39: 469–472.

CRAGG, S. M. & J. A. NOTT, 1977, The ultrastructure of the statocysts in the pediveliger larvae of *Pecten maximus* (L.) (Bivalvia). *Journal of Experimental Marine Biology and Ecology*, 27: 23–36.

CRANFIELD, H. J., 1973a, A study of the morphology, ultrastructure, and histochemistry of the foot of the pediveliger of *Ostrea edulis*. *Marine Biology*, 22: 187–202.

CRANFIELD, H. J., 1973b, Observations on the function of the glands of the foot of the pediveliger of *Ostrea edulis* during settlement. *Marine Biology*, 22: 211–223.

CUMMINGS, K. S. & D. L. GRAF, 2010, Mollusca: Bivalvia, Pp 309–385, in: J. H. Thorp & A. P. Covich, eds., *Ecology and classification of North American freshwater invertebrates.* Elsevier, Amsterdam, 1,021 pp.

DEWALT, R. E., V. H. RESH & W. L. HILSENHOFF, 2010, Diversity and classification of insects and Collembola. Pp. 587–657, in: J. H. Thorp & A. P. Covich, eds. *Ecology and classification of North American freshwater invertebrates*, 3rd ed. Elsevier, Amsterdam, xiv + 1,021 pp.

DINAMANI, P., 1967, Variation in the stomach structure of the bivalvia. *Malacologia*, 5: 225–268.

DORLAND, W. A. N., 2007, *Dorland's medical dictionary*, 31st ed. Saunders, Philadelphia, Pennsylvania, 2,175 pp.

DUNDEE, D. S., 1953, Formed elements of the blood of certain fresh-water mussels. *Transactions of the American Microscopical Society*, 72: 254–264.

EBLE, A. F., 1966, Some observations on the seasonal distribution of selected enzymes in the American Oyster as revealed by enzyme histochemistry. *Proceedings of the National Shellfisheries Association*, 56: 37–42.

EBLE, A. F., 2001, Anatomy and histology of *Mercenaria mercenaria*. Pp. 117–220, in: J. N. Kraeuter & M. Castagna, eds., *Biology of the hard clam*. Elseveir, Amsterdam, xix + 751 pp.

EDGAR, A. L., 1965, Observations on the sperm of the pelecypod *Anodontoides ferussacianus*. *Transactions of the American Microscopical Society*, 84: 228–230.

FLEMING, W. J., T. P. AUGSPURGER & J. A. ALDERMAN, 1995, Freshwater mussel die-off attributed to anticholinesterase poisoning. *Environmental Toxicology and Chemistry*, 14: 877–879.

FRYER, G., 1961, The developmental history of *Mutela bourguignati* (Ancey) Bourguignet (Mollusca: Bivalvia). *Philosophical Transactions of the Royal Society of London*, 244B: 259–298.

FULLER, S. L. H., 1973, *Fusconaia masoni* (Conrad 1834) (Bivalvia: Unionacea) in the Atlantic drainage of the southeastern United States. *Malacological Review*, 6: 105–117.

FULLER, S. L. H., 1974, Clams and mussels (Mollusca: Bivalvia). Pp. 215–273, in: C. W. Hart, Jr. & S. L. H. Fuller, eds., *Pollution ecology of freshwater invertebrates.* Academic Press, New York, xiv + 389 pp.

GALBRAITH, H. S., S. E. FRAZIER, B. ALLISON & C. C. VAUGHN, 2009, Comparison of gill surface morphology across a guild of suspension-feeding unionid bivalves. *Journal of Molluscan Studies*, 75: 103–107.

GALTSOFF, P. S., 1964, The American oyster *Crassostrea virginica* Gmelin. *Fishery Bulletin of the Fish and Wildlife Service*, 64: 1–480.

GANGLOFF, M. M., J. D. WILLIAMS & J. W. FEMINELLA, 2006, A new species of freshwater mussel (Bivalvia: Unionidae), *Pleurobema athearni*, from the Coosa River drainage of Alabama, USA. *Zootaxa*, 1118: 43–56.

GARDINER, D. B., H. SILVERMAN & T. H. DIETZ, 1991, Musculature associated with the water canals in freshwater mussels and response to monoamines in vitro. *Biological Bulletin*, 180: 453–465.

GIRIBET, G. & W. WHEELER, 2002, On bivalve phylogeny: a high-level analysis of the Bivalvia (Mollusca) based on combined morphology and DNA sequence data. *Invertebrate Biology*, 121: 271–324.

GIROD, P., 1889, Manipulations de zoologie. Animaux vertébrés, animaux invertébrés. *Guide pour les travaux pratiques de dissection*, Tome 1. J. B. Baillière, Paris, France, 158 pp.

GORDON, M. E. & D. G. SMITH, 1990, Autumnal reproduction in *Cumberlandia monodonta* (Unionoidea: Margaritiferidae). *Transactions of the American Microscopical Society*, 109: 407–411.

GRAF, D. L. & K. S. CUMMINGS, 2006, Palaeoheterodont diversity (Mollusca: Trigonioida + Unionoida): what we know and what we wish we knew about freshwater mussel evolution. *Zoological Journal of the Linnean Society*, 148: 343–394.

GRAF, D. L. & K. S. CUMMINGS, 2007, Review of the systematics and global biodiversity of freshwater mussel species (Bivalvia: Unionoida). *Journal of Molluscan Studies*, 73: 291–314.

GRANDE, C., R. ARAUJO & M. A. RAMOS, 2001, The gonads of *Margaritifera auricularia* (Spengler, 1793) and *M. margaritifera* (Linnaeus, 1758) (Bivalvia: Unionoidea). *Journal of Molluscan Studies*, 67: 27–35.

GRIZEL, H., 2003, *Atlas d'histologie et de cytology des mollusques bivalves marins/An atlas of histology and cytology of marine bivalve molluscs*. Ifremer, Plouzané, France, 201 pp.

GRIZZLE, J. M. & C. J. BRUNNER, 2009, Infectious diseases of freshwater mussels and other freshwater bivalve mollusks. *Reviews in Fisheries Science*, 17: 425–467.

GUTHEIL, F., 1912, Über den Darmkanal und die Mitteldarmdruse von *Anodonta cellensis* Schröt. *Zeitschrift für Wissenschaftliche Zoologie*, 69: 444–538.

HAAG, W. R. & M. L. WARREN, JR. & M. SHILLINGSFORD, 1999, Host fishes and host-attracting behavior of *Lampsilis altilis* and *Villosa vibex* (Bivalvia: Unionidae). *American Midland Naturalist*, 141: 149–157.

HAAG, W. R. & M. L. WARREN, JR., 1997, Host fishes and reproductive biology of 6 freshwater mussel species from the Mobile Basin, USA. *Journal of the North American Benthological Society*, 16: 576–585.

HAAG, W. R. & M. L. WARREN, JR., 1999, Mantle displays of freshwater mussels elicit attacks from fish. *Freshwater Biology*, 42: 35–40.

HAAG, W. R. & M. L. WARREN, JR., 2003, Host fishes and infections strategies of freshwater mussels in large Mobile Basin streams, U.S.A. *Journal of the North American Benthological Society*, 22: 78–91.

HAAG, W. R., 2012, *North American freshwater mussels natural history, ecology, and conservation.* Cambridge University Press, Cambridge, xvi + 505 pp.

HAVLIK, M. E., 1987, Probable causes and considerations of the naiad mollusk die-off in the upper Mississippi River. Pp. 91–103, in: R. J. Neves, ed., *Proceedings of the workshop on die-offs of freshwater mussels in the United States*, June 23–25, 1986, Davenport, Iowa. United States Fish and Wildlife Service, Upper Mississippi Conservation Committee, 166 pp.

HEALY, J. M., 1989, Spermiogenesis and spermatozoa in the relict bivalve genus *Neotrigonia*: relevance to trigonioid relationships, particularly Unionoidea. *Marine Biology*, 103: 75–85.

HEARD, W. H., 1975, Sexuality and other aspects of reproduction in *Anodonta* (Pelecypoda: Unionidae). *Malacologia*, 15: 81–103.

HEARD, W. H., 1979, Hermaphroditism in *Elliptio* (Pelecypoda: Unionidae). *Malacologia*, 12: 21–28.

HEARD, W. H. & B. J. DOUGHERTY, 1980, Anatomical redescription of *Pleiodon* (*Cameronia*) *spekii* (Pelecypoda: Mutelidae: Pleiodoninae). *Malacological Review*, 13: 45–53.

HEINRICHER, J. R. & J. B. LAYZER, 1999, Reproduction by individuals of a nonreproducing population of *Megalonaias nervosa* (Mollusca: Unionidae) following translocation. *American Midland Naturalist*, 141: 140–148.

HENLEY, W. F., R. J. NEVES, T. CACECI & R. G. SAACKE, 2007, Anatomical descriptions and comparison of the reproductive tracts of *Utterbackia imbecillis* and *Villosa iris* (Bivalvia: Unionidae). *Invertebrate Reproduction and Development*, 50: 1–12.

HORNBACH, D. J., 2001, Macrohabitat factors influencing the distribution of naiads in the St. Croix River, Minnesota and Wisconsin, USA. Pp. 213–232, in: G. Bauer & K. Wächtler, eds., *Ecological Studies 145, Ecology and evolution of the freshwater mussels Unionoida*. Springer-Verlag, Berlin & Heidelberg, xxii + 394 pp.

HOVE, M. C., 1995, Early life history research on the squawfoot, *Strophitus undulatus*. *Triannual Unionid Report*, 7: 28–29.

HOVE, M. C., R. A. ENGELKING, M. E. PETELER, E. M. PETERSON, A. R. KAPUSCINSKI, L. A. SOVELL & E. R. EVERS, 1997, Suitable fish hosts for glochidia of four freshwater mussels. Pp. 21–25, in: K. Cummings, A. C. Buchanan, C. A. Mayer & T. J. Naimo, eds., *Conservation and management of freshwater mussels II: initiatives for the future.* Proceedings of a UMRCC Symposium, 16–18 October 1995, St. Lewis, Missouri. Upper Mississippi River Conservation Committee, Rock Island, Illinois, 293 pp.

HOWES, G. H., 1885, *An atlas of practical elementary biology*. Macmillan & Co., London, viii + 116 pp., 24 pls.

JIRKA, K. J. & R. J. NEVES, 1992, Reproductive biology of four species of freshwater mussels (Mollusca: Unionidae) in the New River, Virginia and West Virginia. *Journal of Freshwater Ecology*, 7: 35–44.

JONES, J. W. & R. J. NEVES, 2010, Descriptions of a new subspecies of freshwater mussels, *Epioblasma ahlstedti* and *Epioblasma florentina aureola* (Bivalvia: Unionidae), in the

Tennessee River drainage, USA. *The Nautilus*, 124: 77–92.

KAT, P. W., 1983, Morphological divergence, genetics, and speciation among *Lampsilis* (Bivalvia: Unionidae). *Journal of Molluscan Studies*, 49: 133–145.

KATO, K. & K. KUBOMURA, 1954, On the origins of the crystalline style of lamellibranchs. *The Science Reports of the Saitama University*, B3: 135–152.

KAYS, W. T., H. SILVERMAN & T. H. DIETZ, 1990, Water channels and water canals in the gill of the freshwater mussel, *Ligumia subrostrata*: ultrastructure and histochemistry. *The Journal of Experimental Zoology*, 254: 256–269.

KELLOGG, J. L., 1915, Ciliary mechanisms of lamellibranchs with descriptions of anatomy. *Journal of Morphology*, 26: 625–701.

KIRTLAND, J. P., 1840, Fragments of natural history. Number 1. Habits of naiades. *American Journal of Science and Arts*, 39: 164–168.

KOVITVADHI, S., U. KOVITVADHI, P. SAWANGWONG & J. MACHADO, 2007, Morphological development of the juvenile through to the adult in the freshwater pearl mussel, *Hyriopsis* (*Limnoscapha*) *myersiana*, under artificial culture. *Invertebrate Reproduction & Development*, 50: 207–218.

KRAEMER, L. R., 1967, The distribution of the posterior nerves in *Lampsilis ventricosa* (Barnes). *Bulletin of the American Malacological Union*, 1967: 42.

KRAEMER, L. R., 1978, Discovery of two kinds of statocysts in freshwater bivalve mollusks: some behavioral implications. *Bulletin of the American Malacological Union*, 1978: 24–28.

KRUG, C., 1922, Morphologie und Histologie des Herzens und Pericards von *Anodonta cellensis*. *Zeitschrift für Wissenschaftliche Zoologie*, 119: 155–246.

LASEE, B. A., 1991, *Histological and ultrastructural studies of larval and juvenile* Lampsilis *(Bivalvia) from the upper Mississippi River*. Dissertation, University of Iowa, Ames, Iowa, 146 pp.

LEA, I, 1856, Description of the byssus in the genus *Unio*. *Proceedings of the Academy of Natural Sciences of Philadelphia*, 8: 213–214.

LEA, I., 1858, Descriptions of seven new species of Margaritanae, and four new species of Anodontae. *Proceedings of the Academy of Natural Sciences of Philadelphia*, 10: 138–139.

LEFEVRE, G. & W. C. CURTIS, 1910, The marsupium of the Unionidae. *Biological Bulletin*, 89: 31–34.

LEFEVRE, G. & W. C. CURTIS, 1912, Studies on the reproduction and artificial propagation of freshwater mussels. *Bulletin of the Bureau of Fisheries*, 30: 107–201, plates 6–17.

LILLIE, F. R., 1895, The embryology of Unionidae. *Journal of Morphology*, 10: 1–100.

LILLIE, F. R., 1897, On the origin of the centers of the first cleavage spindle in *Unio complanata*. *Science*, 5: 389–390.

LILLIE, F. R., 1898, Centrosome and sphere in the egg of *Unio*. *Zoological Bulletin*, 1: 265–274.

LIMA, P., U. KOVITVADHI & J. MACHADO, 2006, In vitro culture of glochidia from the freshwater mussel *Anodonta cygnea*. *Invertebrate Biology*, 125: 34–44.

LOMTE, V. S. & M. L. JADHAV, 1980, A study on the crystalline style of the freshwater mussel, *Parreysia corrugata*. *Hydrobiologia*, 69: 175–178.

LUNA, L. G., 1968, *Manual of histologic staining methods of the Armed Forces Institute of Pathology*, 3rd ed. McGraw-Hill, New York, xii + 258 pp.

LYDEARD, C., R. H. COWIE, W. F. PONDER, A. E. BOGAN, P. BOUCHET, S. A. CLARK, K. S. CUMMINGS, T. J. FREST, O. GARGOMINY, G. G. HERBERT, R. HERSHLER, K. E. PEREZ, B. ROTH, M. SEDDON, E. E. STRONG & F. G. THOMPSON, 2004, The global decline of nonmarine mollusks. *Bioscience*, 54: 321–330.

MANSOUR, K. & F. G. ZAKI, 1946, The digestive diverticula of *Unio prasidens* as organs of secretion. *Proceedings of the Egyptian Academy of Sciences*, 2: 38–44.

MANSUR, M. C. D. & M. D.-G. O. DA SILVA, 1990, Compared morphology and microanatomy of *Bartlettia stefanensis* (Moricand, 1856) with *Anodontites tenebricosus* (Lea, 1834) (Bivalvia, Unionoida, Muteloidea). *Amazonia*, 11: 147–166.

MASTER, L. L., B. A. STEIN, L. S. KUTNER & G. A. HAMMERSON, 2000, Vanishing assets: Conservation status of U.S. species. Pp. 93–118, in: B. A. STEIN, L. S. KUTNER & J. S. ADAMS, eds., *Precious heritage: the status of biodiversity in the United States*. Oxford University Press, New York, xv + 399 pp.

MATTESON, M. R., 1948, Life history of *Elliptio complanatus* (Dillwyn, 1817). *American Midland Naturalist*, 40: 690–723.

McGREGOR, S. W. & J. T. GARNER, 2004, Results of qualitative sampling for protected mussel species at selected stations in the Cahaba River System, Alabama, 2005. *Geological Survey of Alabama Open-File Report, 0505, Tuscaloosa, Alabama*: 1–19.

MEYHÖFER, E., M. P. MORSE & W. E. ROBINSON, 1985, Podocytes in bivalve molluscs: Morphological evidence for ultrafiltration. *Comparative Physiology*, 156B: 151–161.

MITRA, S. R., 1901, The crystalline style of Lamellibranchia. *Quarterly Journal of Microscopical Science*, (N.S.), 44: 591–602, 1 pl.

MORRISON, C. M., 1993, Histology and cell ultrastructure of the mantle and mantle lobes of the eastern oyster, *Crassostrea virginica* (Gmelin). *American Malacological Bulletin*, 10: 1–24.

MORRISON, C. M., 1996, Adductor and mantle musculature. Pp. 169–183, in: V. S. KENNEDY, R. I. E. NEWELL & A. E. EBLE, eds., *The eastern oyster Crassostrea virginica*. Maryland Sea Grant College, College Park, Maryland, xvi + 734 pp.

MORSE, M. P., 1987, Comparative functional morphology of the bivalve excretory system. *American Zoologist*, 27: 737–746.

MORSE, M. P. & J. D. ZARDUS, 1997, Bivalvia. Pp. 7–118, in: F. W. HARRISON, ed., *Microscopic* *anatomy of invertebrates*, Vol. 6A: *Mollusca II*. Wiley-Liss, New York, xvi + 414 + 46 pp.

MORTON, B., 1987, The functional morphology of *Neotrigonia margaritacea* (Bivalvia: Trigoniacea), with a discussion of phylogenetic affinities. *Records of the Australian Museum*, 39: 339–354.

MOTLEY, H. L., 1932, Histology of the freshwater mussel heart with reference to its physiological reactions. *Journal of Morphology*, 54: 415–427.

MOTLEY, H. L., 1943, Physiological studies concerning the regulation of heartbeat in freshwater mussels. *Physiological Zoology*, 7: 62–84.

MYERS, P. R. & D. S. FRAZEN, 1970, Histological studies of the nephridium and pericardial lining of *Quadrula nodulata*. *The Nautilus*, 83: 139–144.

MYERS, R. K. & M. D. MCGAVIN, 2007, Cellular and tissue responses to injury. Pp. 3–63, in: M. D. McGavin & J. F. Zachary, eds., *Pathologic basis of veterinary disease*, 4th ed. Mosby, St. Louis, Missouri, xii + 1,476 pp.

NARAIN, A. S., 1972, On the posterior aortic bulb of the fresh water mussel, *Lamellidens corrianus*. *Indian Biologist*, 4: 81–83.

NARAIN, A. S., 1973, On the muscular apparatus of the heart of the fresh water mussel, *Lamellidens corrianus*. *Zoologische Beiträge*, 19: 157–161.

NARAIN, A. S., 1976, A review of the structure of the heart of mollusks, particularly bivalves, in relation to cardiac function. *Journal of Molluscan Studies*, 42: 46–62.

NELSON, T. C., 1918, On the origin, nature, and function of the crystalline style of lamellibranchs. *Journal of Morphology*, 31: 53–111.

NELSON, T. C., 1925, Recent contributions to the knowledge of the crystalline style of lamellibranchs. *Biological Bulletin*, 49: 86–99.

NEVES, R. J., 1987, *Proceedings of the workshop on die-offs of freshwater mussels in the United States*, June 23−25, 1986, Davenport, Iowa. United States Fish and Wildlife Service, Upper Mississippi Conservation Committee, 166 pp.

NEVES, R. J., L. R. WEAVER & A. V. ZALE, 1985, An evaluation of host suitability for glochidia of *Villosa vanuxemi* and *V. nebulosa* (Pelecypoda: Unionidae). *American Midland Naturalist*, 113: 13–19.

NEWTON, T. J. & W. G. COPE, 2007, Biomarker responses of unionid mussels to environmental contaminants. Pp. 257–284, in: J. L. Farris & J. H. Van Hassel, eds., *Freshwater bivalve ecotoxicology*. Boca Raton, Florida, 375 pp.

NORTON, J. H. & G. W. JONES, 1992, *The giant clam: an anatomical and histological atlas*. Australian Centre for International Agricultural Research, Canberra, Australia, 142 pp.

ORTMANN, A. E., 1910a, A new system of the Unionidae. *The Nautilus*, 23: 114–120.

ORTMANN, A. E., 1910b, The marsupium of Anodontinae. *Biological Bulletin*, 19: 217.

ORTMANN, A. E., 1911a, A monograph of the najads of Pennsylvania. *Memoirs of the Carnegie Museum*, 4: 279–347.

ORTMANN, A. E., 1911b, The anatomical structure of certain exotic naiades compared with that of the North American forms. *The Nautilus*, 24: 103–108, pls. 6–7; 114–120; 127–131.

ORTMANN, A. E., 1923a, Notes on the anatomy and taxonomy of certain Unioninae and Anodontinae from the Gulf drainage. *The Nautilus*, 36: 73–84, 129–132.

ORTMANN, A. E., 1923b, Notes on the anatomy and taxonomy of certain Lampsilinae from the Gulf drainage. *The Nautilus*, 37: 56–60.

ORTMANN, A. E., 1924, Notes on the anatomy and taxonomy of certain Lampsilinae from the Gulf drainage. *The Nautilus*, 37: 99–105, 137–144.

OWEN, G., 1955, Observations on the stomach and digestive diverticula of the Lamellibranchia. I. The Anisomyaria and Eulamellibranchia. *Quarterly Journal of Microscopical Science*, 96: 517–537.

OWEN, G. & J. M. McCRAE, 1979, Sensory cell/gland cell complexes associated with the pallial tentacles of the bivalve *Lima hians* (Gmelin), with a note on specialized cilia on the pallial curtains. *Transactions of the Royal Society of London*, 287B: 45–62.

PAIN, T. & F. R. WOODWARD, 1968, A monograph of the African bivalves of the genera *Brazzaea* Bourguiguat, *Mweruella* Haas, *Prisodontopsis* Tomlin and *Pseudospatha* Simpson. *Revue de Zoologie et de Botanique Africaines*, 77: 190–220.

PARMALEE, P. W. & A. E. BOGAN, 1998, *The freshwater mussels of Tennessee*. University of Tennessee Press, Knoxville, Tennessee, xii + 328 pp.

PAULEY, G. B., 1968, A disease of the freshwater mussel, *Margaritifera margaritifera*. *Journal of Invertebrate Pathology*, 12: 321–328.

PAULEY, G. B. & C. D. BECKER, 1968, *Aspidogaster conchicola* in mollusks of the Columbia River system with comments on the host's pathological response. *Journal of Parasitology*, 54: 917–920.

PECK, R. H., 1877, The minute structure of the gills of Lamellibranch Mollusca. *Quarterly Journal of Microscopical Science*, 17: 43–66, pl. 7.

PEREDO, S., O. GARRIDO & E. PARADA, 1990, Spermiogenesis and sperm ultrastructure in the freshwater mussel *Diplodon chilensis chilensis* (Mollusca: Bivalvia). *Invertebrate Reproduction and Development*, 17: 171–179.

PETIT, H., W. L. DAVIS & R. G. JONES, 1978, Morphological studies on the mantle of the fresh-water mussel *Amblema* (Unionidae): scanning electron microscopy. *Tissue & Cell*, 10: 619–627.

PETIT, H., W. L. DAVIS & R. G. JONES, 1979, Morphological studies on the periostracum of the fresh-water mussel *Amblema* (Unionidae): light microscopy, transmission electron microscopy, and scanning electron microscopy. *Tissue & Cell*, 11: 633–642.

POSNER, C., 1875, Ueber den Bau der Najadenkieme. *Archiv für Mikroskopische Anatomie*, 11: 517–560, plates 31, 32.

PURCHEON, R. D., 1958, The stomach in the Eulamellibranchia: Stomach Type IV. *Proceedings of the Zoological Society of London*, 131: 487–525.

RAßBACH, R., 1912, Beiträge zur Kenntis der Schale und Schalenregeneration von *Anodonta cellensis* Schröt. *Zeitschrift für Wissenschaftliche Zoologie*, 103: 363–448.

REID, R. G. B., 1965, The structure and function of the stomach in bivalve molluscs. *Journal of Zoology*, 147: 156–184.

RICHARD, P. E., T. H. DIETZ & H. SILVERMAN, 1991, Structure of the gill during reproduction in the unionids *Anodonta grandis*, *Ligumia subrostrata*, and *Carunculina parva texasensis*. *Canadian Journal of Zoology*, 69: 1744–1754.

RIDEWOOD, W. G., 1903, On the structure of gills of Lamellibranchia. *Philosophical Transactions of the Royal Society of London*, 195: 147–284.

ROCHA, E. & C. AZEVEDO, 1990, Ultrastructure study of the spermatogenesis of *Anodonta cygnea* L. (Bivalvia: Unionidae). *Invertebrate Reproduction and Development*, 18: 169–176.

RONDELAUD, D. & D. BARTHE, 1981, The development of the amoebocyte-producing organ in *Lymnaea truncatula* Müller infected by *Fasciola hepatica* L. *Zeitschrift für Parasitenkunde*, 65: 331–341.

ROSS, M. H., H. I. KAYE & W. PAWLINA, 2003, *Histology: a text and atlas*, 4th ed. Lippinicott Williams & Wilkins, Baltimore, Maryland, 864 pp.

SCHWARTZ, M. L. & R. V. DIMOCK, JR., 2001, Ultrastructural evidence for nutritional exchange between brooding unionid mussels and their glochidia larvae. *Invertebrate Biology*, 120: 227–236.

SHAW, B. L. & H. I. BATTLE, 1957, The gross and microscopic anatomy of the digestive tract of the oyster *Crassostrea virginica* (Gmelin). *Canadian Journal of Zoology*, 35: 325–347.

SHAW, B. L. & H. I. BATTLE, 1959, The chemical composition of the gastric shield of the oyster *Crassostrea virginica* (Gmelin). *Canadian Journal of Zoology*, 37: 214–215.

SIEBERT, W., 1913, Das Körperepithel von *Anodonta cellensis*. *Zeitschrift für Wissenschaftliche Zoologie*, 106: 449–525.

SILVERMAN, H., W. T. KAYS & T. H. DIETZ, 1987, Maternal calcium contribution to glochidial shells in freshwater mussels (Eulamellibranchia: Unionidae). *Journal of Experimental Zoology*, 242:137–146.

SILVERMAN, H., P. E. RICHARD, R. H. GODDARD & T. H. DIETZ, 1989, Intracellular formation of calcium concretions by phagocytic cells in freshwater mussels. *Canadian Journal of Zoology*, 67: 198–207.

SILVERMAN, H., W. L. STEFFENS & T. H. DIETZ, 1985, Calcium from extracellular concretions in the gills of freshwater unionid mussels is mobilized during reproduction. *Journal of Experimental Zoology*, 236: 137–147.

SILVERMAN, H., W. L. STEVENS & T. H. DIETZ, 1983, Calcium concentrations in the gills of a freshwater mussel serve as a calcium reservoir during periods of hypoxia. *Journal of Experimental Zoology*, 227: 177–189.

SIMPSON, C. T., 1884, Anatomy and physiology of *Anodonta fluviatilis*. *New York State Museum, Annual Report*, 35: 22–191.

SIMS, D. E., J. A. WESFALL, A. L. KIORPES & M. M. HORNE, 1991, Preservation of tracheal mucus by nonaqueous fixative. *Biotechnic and Histochemistry*, 66: 173–180.

SMITH, D. G., 1978, Biannual gametogenesis in *Margaritifera margaritifera* (L.) in notheastern North America. *Bulletin of the American Malacological Union*, 1978: 49–53.

SMITH, D. G., 1980, Anatomical studies on *Margaritifera margaritifera* and *Cumberlandia monodonta* (Mollusca: Pelecypoda: Margaritiferidae). *Zoological Journal of the Linnean Society*, 69: 257–270.

SMITH, D. G., 1983, On the so-called mantle muscle scars on shells of the margaritiferidae (Mollusca: Pelecypoda), with observations on mantle-shell attachment in the Unionoida and Trigonioida. *Zoologica Scripta*, 12: 67–71.

SMITH, D. G., 1988, Notes on the biology and morphology of *Margaritifera hembeli* (Conrad, 1838) (Unionacea: Margaritiferidae). *The Nautilus*, 102: 159–163.

SMITH, D. G., 2000, Investigations of the byssal gland in juvenile unionids. Pp. 103–107, in: R. A. Tankersley, ed., *Proceedings of the conservation, captive care and propagation of freshwater mussels symposium*, 1998, Columbus, Ohio. Part 1. Ohio Biological Survey, Ohio State University, Columbus, Ohio, 274 pp.

SMITH, D. G., B. K. LANG & M. E. GORDON, 2003, Gametogentic cycle, reproductive anatomy, and larval morphology of *Popenaias popeii* (Unionoida) from the Black River, New Mexico. *Southeastern Naturalist*, 48: 333–340.

SPLITTSTÖßER, P., 1913, Zur Morphologie des Nervensystems von *Anodonta cellensis* Schröt. *Zeitschrift für Wissenschaftliche Zoologie*, 104: 388–470.

STASEK, C. R., 1963, Synopsis and discussion of the associated of ctenidia and labial palps in the bivalve Mollusca. *The Veliger*, 6: 91–97.

STEVENS, A., 1982, The haematoxylins. Pp. 109–121, in: J. D. Bancroft & A. Stevens, eds., *Theory and practice of histological techniques*, 2nd ed. Churchill Livingstone, Edinburgh & New York, xiv + 662 pp.

STRAYER, D. L., 2008, *Freshwater mussel ecology: a multifactor approach to distribution and abundance*. University of California Press, Berkeley, ix + 204 pp.

SUMNER, A. T., 1966a, The cytology and histochemistry of the digestive-gland cells of some freshwater lamellibranchs. *Journal of the Royal Microscopical Society*, 85: 201–211.

SUMNER, A. T., 1966b, The fine structure of the digestive gland cells of *Anodonta*. *Journal of the Royal Microscopical Society*, 85: 417–423.

TANKERSLEY, R. A. & R. V. DIMOCK, JR., 1992, Quantitative analysis of the structure and function of the marsupial gills of the freshwater mussel *Anodonta cataracta*. *Biological Bulletin*, 182: 145–154.

TANKERSLEY, R. A. & R. V. DIMOCK, JR., 1993, Endoscopic visualization of the functional morphology of the unionid mussel *Pyganodon cataracta*. *Canadian Journal of Zoology*, 71: 811–819.

TASKINEN, J., T. MÄKELÄ & E. T. VALTONEN, 1997, Exploitation of *Anodonta piscinalis* (Bivalvia) by trematodes: parasite tactics and host longevity. *Annales Zoologici Fennici*, 34: 37–46.

TAUC, L., 1966, Physiology of the nervous system. Pp. 387–454, in: K. M. WILBUR & C. M. YONGE, eds., *Physiology of Mollusca*, Vol. II. Academic Press, New York, 645 pp.

TEPE, W. C., 1943, Hermaphorditism in *Carunculina parva*, a fresh water mussel. *American Midland Naturalist*, 29: 621–623.

TRUEMAN, E. R., 1966, Bivalve mollusks: fluid dynamics of burrowing. *Science*, 152: 523–525.

TRUEMAN, E. R., 1968, The locomotion of the freshwater clam *Margaritifera margaritifera* (Unionacea: Margaritiferidae). *Malacologia*, 6: 401–420.

VAN DER SCHALIE, H., 1970, Hermaphroditism among North American freshwater mussels. *Malacologia*, 10: 93–112.

VAN DER SCHALIE, H. & F. LOCKE, 1941, Hermaphroditism in *Anodonta grandis*, a fresh-water mussel. *Occasional Papers of the Museum of Zoology*, 432: 1–7, pls. 1–3.

VAN DER SCHALIE, H. & A. VAN DER SCHALIE, 1963, The distribution, ecology, and life history of the mussel, *Actinonaias ellipsiformis* (Conrad), in Michigan. *Occasional Papers of the Museum of Zoology University of Michigan*, 633: 1–17.

VAUGHN, C. C. & C. C. HAKENKAMP, 2001, The functional role of burrowing bivalves in freshwater ecosystems. *Freshwater Biology*, 46: 1431–1446.

VITONIS, J. E. V. V., C. P. ZANIRATTO, F. M. MACHADO & F. D. PASSOS, 2012, Comparative studies on the histology and ultrastructure of the siphons of two species of Tellinidae (Mollusca: Bivalvia) from Brasil. *Zoologia*, 29: 219–226.

WALLER, D. L. & B. A. LASEE, 1997, External morphology of spermatozoa and spermatozeugmata of the freshwater mussel *Truncilla truncata* (Mollusca: Bivalvia: Unionidae). *American Midland Naturalist*, 138: 220–223.

WARD, J. E., L. P. SANFORD, R. I. E. NEWELL & B. A. MACDONALD, 1998, A new explanation of particle capture in suspension-feeding molluscs. *Limnology and Oceanography*, 43: 741–752.

WATTERS, G. T., 2002, The kinetic conglutinate of the creeper freshwater mussel, *Strophitus undulatus* (Say, 1817). *Journal of Molluscan Studies*, 68: 155–158.

WATTERS, G. T., M. A. HOGGARTH & D. H. STANSBERY, 2009, *The freshwater mussels of Ohio*. Ohio State University of Press, Columbus, Ohio, xiii + 421 pp.

WHITE, R. M., 1942, The pericardial cavity and the pericardial gland of the Lamellibranchia. *Proceedings of the Malacological Society of London*, 25: 4–88.

WILLIAMS, J. D., A. E. BOGAN & J. T. GARNER, 2008, *Freshwater mussels of Alabama and the Mobile River Basin in Georgia, Mississippi and Tennessee*. University of Alabama Press, Tuscaloosa, Alabama, xv + 908 pp.

WILLIAMS, J. D., A. E. BOGAN & J. T. GARNER, 2009, A new species of freshwater mussel, *Anodonta hartfieldorum* (Bivalvia: Unionidae), from the Gulf Coastal Plain drainages of Alabama, Florida, Louisiana, and Mississippi, USA. *The Nautilus*, 123: 25–33.

WILLIAMS, J. D. & R. J. NEVES, 1995, Freshwater mussels: a neglected and declining aquatic resource. Pp. 177–179, in: E. T. LAROE, G. S. FARRIS, C. E. PUCKETT, P. D. DORAN & M. J. MAC, eds., *Our living resources: a report to the nation on the distribution, abundance, and health of U.S. plants, animals, and ecosystems*. U.S. Department of the Interior, National Biological Service, Washington, D.C., xi + 530 pp.

WOODY, C. A. & L. HOLLAND-BARTELS, 1993, Reproductive characteristics of a population of the washboard mussel *Megalonaias nervosa* (Rafinesque 1820) in the upper Mississippi River. *Journal of Freshwater Ecology*, 8: 57–66.

YEAGER, M. M., D. S. CHERRY & R. J. NEVES, 1994, Feeding and burrowing behaviors of juvenile rainbow mussels, *Villosa iris* (Bivalvia: Unionidae). *Journal of the North American Benthological Society*, 13: 217–222.

YOKLEY, P., JR., 1968, *A study of the anatomy of the naiad* Pleurobema cordatum *(Rafinesque, 1820) (Mollusca: Bivalvia: Unionoida)*. Dissertation, Ohio State University, Columbus, Ohio. 139 pp.

YOKLEY, P., JR., 1972, The life history of *Pleurobema cordatum* (Rafinesque 1820) (Bivalvia: Unionacea). *Malacologia*, 11: 351–364.

YONGE, C. M., 1926a, Structure and physiology of the organs of feeding and digestion in *Ostrea edulis*. *Journal of the Marine Biological Association of the United Kingdom*, 14: 295–396, pls. 1, 2.

YONGE, C. M., 1926b, The digestive diverticula in the lamellibranchs. *Transactions of the Royal Society*, 54: 703–717, 2 pls.

ZALE, A. V. & R. J. NEVES, 1982, Reproductive biology of four freshwater mussel species (Mollusca: Unionidae) in Virginia. *Freshwater Invertebrate Biology*, 1: 17–28.

ZHONG, L., T.-Y. XIAO, J. HUANG, L.-Y. DAI & X.-Y. LIU, 2011, Histopathological examination of bivalve mussel *Hyriopsis cumingii* Lea artificially infected by virus. *Acta Hydrobiologica Sinica*, 35: 666–671.

Revised ms. accepted October 6, 2013

RESEARCH NOTE

MALACOLOGIA, 2014, 57(1): 243

SINEANCYLUS, NOM. NOV.: A REPLACEMENT NAME FOR *ANANCYLUS* GUTIÉRREZ GREGORIC, 2012 (GASTROPODA, ANCYLIDAE)

Diego Eduardo Gutiérrez Gregoric

División Zoología Invertebrados, Museo de La Plata, Facultad de Ciencias Naturales y Museo, Universidad Nacional de La Plata, La Plata, Buenos Aires, Argentina and Consejo Nacional de Investigaciones Científicas y Técnicas (CONICET); dieguty@fcnym.unlp.edu.ar

Nestor Cazzaniga (Universidad Nacional del Sur, Argentina) and Philippe Bouchet (Museum National d'Histoire Naturelle, France) have kindly advised me of homonymy in the generic name *Anancylus* Gutiérrez Gregoric, 2012, proposed for an Ancylidae from Iguazú National Park, Argentina (Gutiérrez Gregoric, 2012: 109). The name is preoccupied by *Anancylus* Thomson, 1864 (Coleoptera, Cerambycidae) (Neave, 2005). Thus, in accordance with Articles 53.3 ("Homonyms in the genus group") and 60 ("Replacement of junior homonyms") of the *International Code of Zoological Nomenclature* (ICZN, 1999), I propose the replacement name *Sineancylus*, nom. nov.

Family Ancylidae
Rafinesque, 1815
Sineancylus, nom. nov.

Type Species

Anancylus rosanae Gutiérrez Gregoric, 2012.

Etymology

Sine (Latin) = without; *ancylus* (latinized Greek) = curved as a hook. Gender masculine.

Diagnosis

See Gutiérrez Gregoric (2012).

Sineancylus rosanae
(Gutiérrez Gregoric, 2012)
comb. nov.

Anancylus rosanae Gutiérrez Gregoric, 2012: 109; original description.

Type Material

Holotype (MLP 13219); paratypes (MLP 13220) housed at Museo de La Plata, Argentina.

Type Locality

Upper Iguazú River, Iguazú National Park, Misiones Province, Argentina.

Diagnosis

See Gutiérrez Gregoric (2012).

ACNOWLEDGEMENTS

I thank N. Cazzaniga and P. Bouchet for the information provided.

LITERATURE CITED

GUTIÉRREZ GREGORIC, D. E., 2012, *Anancylus rosanae* (Gastropoda: Pulmonata), new genera and new species from Iguazú National Park, Argentina. *Malacologia*, 55: 107–116.
ICZN, 1999, *International Code of Zoological Nomenclature*, 4th ed. International Trust for Zoological Nomenclature, London, 306 pp.
NEAVE, S. A., 2005, *Nomenclator Zoologicus*. A list of the names of the genera and subgenera in Zoology from the tenth edition on Linnaeus 1758 to the end of 2004. The Zoological Society of London, 10 vols. Available from www.ubio.org/NomenclatorZoologicus/ (Version 0.86).

Revised ms. accepted November 3, 2013

LETTER FROM THE EDITOR

MALACOLOGIA, 2014, 57(1): 247–248

A TRIBUTE TO DICK PETIT
1931–2013

On December 31, 2013 Richard Eugene Petit passed away, and with his passing the field of malacology lost a unique, highly valued colleague and contributor. He was one of those rare individuals who, as a successful businessman in insurance and real estate, turned an abundance of curiosity and energy into a parallel universe of fascination with shells, then shell books and subsequently delving ever deeper into the global malacological literature.

Charles Sturm remarked: "In 1965, he purchased a shell and book dealership, with which he would ultimately become the foremost used shell book dealer in the United States. Dick became an accomplished avocational paleontologist and malacologist. He was author or co-author of over 100 peer-reviewed publications on Recent and fossil mollusks, beginning in 1964 and continuing to the present. He was a recognized world expert on the gastropod family Cancellariidae."

But his truly unique passion was for nomenclature – determining when and where a taxon was first published. He learned early on that the encyclopedia of information for any species is based not only on the name of a species but also on the author and valid date of publication. His last published note on this all-consuming concern was published on the day he died, in the latest issue of *Malacologia*, 2013, 56(1/2): 357, Richard E. Petit & The Editors: "Literature citations: authors of taxa with date of publication should be mandatory."

Sturm further recognized that "Dick's knowledge of the malacological literature was legendary. He amassed one of the more significant private libraries and helped many others find the works they needed to prosecute their work. Dick also possessed an in-depth knowledge of the history of malacology. Many will remember some of his recent monographs on malacologists of the 19th Century, including Lovell Reeve, William Wood, and the Sowerby family. Many of us would have been proud to have produced any one of these monographs, let alone all of them and others."

And Dick was a real team player, a strong supporter of the American Malacological Society of which he was President (1987–1988), Secretary/Treasurer (1991–1993), and Honorary Life Member. For many years he served with me on the society's Endowment Committee. In 1990 he was awarded the Katherine Palmer Award by the Paleontological Research Institute, of which he was a Research Associate for 20 years (1982–2002). I will greatly miss his highly productive collaborative projects with like-minded colleagues, e.g. Eugene Coan, who is copy editor of Malacologia and affiliated with the Santa Barbara Museum of Natural History, Rüdiger Bieler of the Field Museum and Alan Kabat, a trained malacologist turned lawyer associated with the Museum of Comparative Zoology of Harvard University. I have listed below a sample of the works produced by this creative team. An in-depth review of Dick's life and publications is being prepared by others, so I do not provide an exhaustive list of his publications here.

I will deeply miss his constant willingness to review manuscripts and his strong guidance on matters of literature citations and taxonomic issues. He had such a deep fund of knowledge covering a wide swath of malacology. He was always willing to help researchers world-wide who asked him for help and assistance.

BIELER, R. & R. E. PETIT, 2011, Catalogue of Recent and fossil "worm-snail" taxa of the families Vermetidae, Siliquariidae, and Turritellidae (Mollusca: Caenogastropoda). *Zootaxa*, 2948: 1–103.

COAN, E. V. & R. E. PETIT, 2006, Replacement names and type material: examples from Hertlein and Strong (1940–1951) and Keen (1958). *The Nautilus*, 120(3): 112–115.

COAN, E. V. & R. E. PETIT, 2011, The publications and malacological taxa of William Wood (1774–1857). *Malacologia*, 54 (1/2): 1–56.

COAN, E. V., A. R. KABAT & R. E. PETIT, 2013, 2,400 years of malacology, 11th ed.: 1,092 pp. + 90 pp. [Annex 1 of Collations] + 65 pp. [Annex 2 of Collations Küster]. *The American Malacological Society Web*, http://www.malacological.org/epubs.html [10 previous editions by the same authors; the 14th edition has recently been posted, for the first time without Petit as an author].

KABAT, A. R. & R. E. PETIT, 2007, Glenn Robert Webb (1918–1999), his molluscan taxa, and his journal *Gastropodia* (1952–1994). *Zootaxa*, 1589: 1–21.

PETIT, R. E. & M. G. HARASEWYCH, 2005, Catalogue of the superfamily Cancellarioidea Forbes and Hanley, 1851 (Gastropoda: Prosobranchia), 2nd ed. *Zootaxa*, 1102: 1–161.

PETIT, R. E., 2009, George Brettingham Sowerby, I, II & III: their conchological publications and molluscan taxa. *Zootaxa*, 2189: 1–218.

PETIT, R. E., 2007, Lovell Augustus Reeve (1814–1865): malacological author and publisher. *Zootaxa*, 1648: 1–120.

PETIT, R. E. & E. V. COAN, 2008, The molluscan taxa made available in the Griffith & Pidgeon (1833–1834) edition of Cuvier, with notes on the editions of Cuvier and on Wood's *Index Testaceologicus*. *Malacologia*, 50(1/2): 219–264.

PETIT, R. E., 2012, John Edward Gray (1800–1875): his malacological publications and molluscan taxa. *Zootaxa*, 3214: 1–125.

PETIT, R. E. & A. N. VAN DER BIJL, 2012, P. P. Carpenter's 1857 "Mazatlan Catalogue". *Conchologia Ingrata*, 7: 1–7.

ACKNOWLEDGEMENTS

I thank Rüdiger Bieler, Eugene V. Coan and Alan Kabat for their comments on this tribute to Dick Petit. Sections in quotation marks were written and extracted from a short obituary provided by Charles Sturm. The photograph was kindly provided by Robert Robertson from his vast collection in his Rogues Gallery of Malacologists.

Geoge M. Davis, Editor

MALACOLOGIA, 2014, 57(1): 249–254

INDEX

Taxa in **bold** are new; pages in *italic* indicate figures of taxa.

Acropora 59
Actinonaias carinata 226
  ligamentina 211, 226
aegyptiaca, Coelatura 220
Alasmidonta marginata 211
  truncata 211
  undulata 217
alata, Proptera 226
alatus, Lampsilis 211
  Potamilus 211, 226
alii, Vermetus 18
ambiguus, Unio 211
  Velesunio 211, 218
Amblema costata 226
  peruviana 226
  plicata 208, 211, 226
  plicata perplicata 210–211
Ambleminae 99
ammonitiformis, Stoa 15
Anadara broughtonii 222
  inflata 222
Anancylus 243
  rosanae 243
anatina, Anodonta 101, 211, 220, 226, 227
Ancylidae 243
annulatus, Dendropoma 39
  Spiroglyphus 15, 35, 39
Anodonta 101, 211, 221–223, 226
  anatina 101, 211, 220, 226, 227
  californiensis 211, 212, 231
  cataracta 211, 212
  cellensis 205, 207, 215, 217, 218, 220, 226, 229
  couperiana 212, 231
  cygnea 101, 205, 207, 211, 212, 214, 215, 217, 218, 220, 226, 228, 229
  fluviatilis 101
  grandis 211–213, 226
  hallenbeckii 212, 231
  imbecilis 212, 231
  nuttalliana 212
  peggyae 212, 231
  wahlamatensis 212
Anodontinae 101, 231
Anodontoides ferussacianus 214, 230
Arca zebra 220
arctata, Elliptio 231
auricularia, Margaritifera 215, 231
australis, Posidonia 60
bahamensis, Novastoa 8, *50*, 55, *55*, *56*, 57, 59
batavia, Novastoa *50*, 59, *60–62*, *90*
bicarinata, Serpula 25, 26
biota, Macoma 210
Bivonia 15, 16, 86
  dragonella 19
  exserta 15, 86, *86*
  petraea 15, 32, 34
Brachidontes pharaonis 2
breigneti, Vermetus 16
broughtonii, Anadara 222
buckleyi, Elliptio 231

caboverdensis, Novastoa 8, *50*, 52, *53*, 54, *54*, 55, 62, 63, *90*
californiensis, Anodonta 211, 212, 231
Calyptraeoidea 10
Cancellariidae 247
Cancellarioidea 248
capitellum, Vasum 36
cardium, Lampsilis 101, 210, 215, 229
carinata, Actinonaias 226
Carunculina parva 226, 231
  parva texasensis 213
  texasensis 212
cataracta, Anodonta 211, 212
  Pyganodon 101, 211, 212
cellensis, Anodonta 205, 207, 215, 217, 218, 220, 226, 229
Ceraesignum 1, 8, 13, 14, *14*, 16, 20, 49, 63, 64, *64*, 87–89, 91
  maximum 8, 64, *64*, 65, *66*, *67*, 68, 71, 89–91, *90*
  robinsoncrusoei 8, 24, 64, *64*, 68, *69*, *70*, 71, 87, *90*
cerina, Fusconaia 99, 102–104, 136, 139, 141–143, *142–166*, 145, 147, 151, 161, 163, 165, *168–173*, 181, 205, 207–232
cerinus, Unio 102
Chama 29, 71
Coelatura aegyptiaca 220
complanata, Elliptio 211, 217, 218, 231
  Lasmagonia 226
  Lasmigona 211, 226
  Symphynota 211
complanatus, Elliptio 217
  Unio 211, 218
conica, Serpula 79
conicus, Vermetus 82
connasaugaensis, Margaritana 102
  Strophitus 99, 102, 103, 105, 166, *166*, *167*,

168, 171, *174–178*, 177, 179, *180–207*, 183, 189, 193, 197, 199, 205, *206*, *207*, 207–212, 214–232

corallinaceum, Dendropoma 45, 87

cordatum, Pleurobema 101, 207, 215, 220, 223, 228, 229, 231

corrianus, Lamellidens 226

corrodens, Dendropoma 2, *5*, 6, 7, 12, 14, 35, 39, 42, 89

  Dendropoma cf. *18*, 35, *37*, *38*, 39, *90*

  Dendropoma (*Dendropoma*) 35

  Spiroglyphus 35

  Vermetus 35, 39

  Vermetus (*Spiroglyphus*) *annulatus* var. 35

costata, Amblema 226

couperiana, Anodonta 212, 231

  Utterbackia 212, 231

crassidens, Elliptio 212, 226

Crassostrea gigas 221, 226

  virginica 218, 229

Crepidula fornicata 9, 10, *14*

cristatum, Dendropoma 34

  Dendropoma (*Novastoa*) 32

cristatus, Vermetus 32, 35

Cumberlandia monodonta 229, 231

cuneolus, Fusconaia 231

Cupolaconcha 1, *5*, 8, 12–14, *14*, 16, 20, 49, 64, 71–73, *73*, 76, 77, 82, 86–89, *90*, 91

  guana *5*, 8, *73*, 76, 79, *80*, *81*, 82, 89

  krypta 72, *73*, 76, 77, *78*, 79, 86

  maldivensis *73*, 84, *85*, 86

  meroclista 6, 8, 72, 73, *73*, *75*, *76*, 77, 79, 82, 83, 89

  sinaiensis *73*, 82, *83*, 86, 89

cygnea, Anodonta 101, 205, 207, 211, 212, 214, 215, 217, 218, 220, 226, 228, 229

Cyprinidae 213

dalyi, Mülleria 211

  Pseudomulleria 211

decussatus, Thylacodes cf. 9

Dendostrea frons 26, *26*, 79

Dendropoma 1–3, *5*, 6, 7, 13–20, *14*, *18*, *19*, 22, 23, 26, 31, 33, 34, 39, 41, 42, 45, 47, 49, 63, 68, 71–73, 77, 79, 82, 86–89, 91

  annulatus 39

  corallinaceum 45, 87

  corrodens 2, *5*, 6, 7, 12, 14, 35, 39, 42, 89

  corrodens cf. *18*, 35, *37*, *38*, 39, *90*

  cristatum 34

  (*Dendropoma*) 87

  (*Dendropoma*) *corrodens* 35

  (*Dendropoma*) *lituella* 20

  (*Dendropoma*) *maximum* 65

  (*Dendropoma*) *nebulosum* 25

  (*Dendropoma*) *platypus* 29

  expolitum *18*, 39, 42, 45, *46*, *47*, 48, *90*

  exsertum 86

  ghanaense 19, 87

  gregaria 39

  gregarium 2, 7, 12, *18*, *30*, 39, *40*, 41, *41*, 42, 76, 90, *90*

  howense *18*, 39, 42, *43*, *90*

  irregulare 25, *27*

  krypta 77

  lamellosa 49

  lituella *18*, 20, *20*, *21*, 22, 87, *90*

  marchadi 19, 54, 55

  maxima 65

  maximum 2, 65, 68, 87

  mejillonense 7, 12, *18*, 22–24, *22*, *24*, 71, 89, *90*

  mejillonensis 23

  meroclista 71–73, 77, 82, 87

  meroclistum 2, 71, 77

  nebulosum *5*, 7, 12, *18*, 22, 25–27, *26*, *27*, 57, 59, 89, *90*

  (*Novastoa*) 48, 87

  (*Novastoa*) *cristatum* 32

  (*Novastoa*) *irregulare* 35

  (*Novastoa*) *lamellosum* 49

  (*Novastoa*) *petraeum* 32

  petraeum 2, 3, 7, 15, 19, 32–34, 87, 89, 90

  petraeum cf. 12, *18*, 22, 32, *33*, 34, *34*, *90*

  platypus 2, 7, 12, *18*, 19, 22, 29, *30*, 31, *31*, 32, *90*

  psarocephalum 8, 12, 19, 39

  rhyssoconchum 7, 12, 19, 22, 90

  squamiferum 19

  tholia 43, 45, 87

  tholia cf. *18*, 39, 43, *44*, *90*

Dendropomatinae 2

Dendropominae 2

dentifera, Spiroglyphus annulatus var. 35

depressa, Hyridella 218

dilatata, Elliptio 211

dragonella, Bivonia 19

ebena, Fusconaia 226

edentulus, Strophitus 214

edulis, Mytilus 220, 232

  Ostrea 210, 217

elliptica, Etheria 211

Elliptio arctata 231

  buckleyi 231

  complanata 211, 217, 218, 231

  complanatus 217

  crassidens 212, 226

  dilatata 211

  icterina 231

  jayensis 231

Elliptovermetus 16, 87

Etheria elliptica 211
  plumbea 211
Etheriidae 99, 211, 228
Eualetes 1, 6, 9, 13
  tulipa 9, 18, 74
Eurytellina lineata 210
expolitum, Dendropoma *18*, 39, 42, 45, *46*, *47*, 48, *90*
exserta, Bivonia 15, 86, *86*
exsertum, Dendropoma 86

fallaciosa, Lampsilis 226
Fasciola hepatica 227
fasciola, Lampsilis 211
ferussacianus, Anodontoides 214, 230
Fissurella nodosa 36
flava, Fusconaia 211, 231
fluviatilis, Anodonta 101
fornicata, Crepidula 9, 10, *14*
fragilis, Leptodea 226
frons, Dendostrea 26, *26*, 79
Fusconaia 213
  cerina 99, 102–104, 136, 139, 141–143, *142–166*, 145, 147, 151, 161, 163, 165, *168–173*, 181, 205, 207–232
  cuneolus 231
  ebena 226
  flava 211, 231

Galba truncatula 104, 227
ghanaense, Dendropoma 19, 87
gibbosus, Unio 211
gigantea, Megalonaias 226
giganteum, Siphonium 65
giganteus, Vermetus 65
gigas, Crassostrea 221, 226
glomerata, Serpula 32
glomeratus, Spiroglyphus 32
  Vermetus 15, 32, 34
grandis, Anodonta 211–213, 226
  Pyganodon 211, 213, 226
gregaria, Dendropoma 39
gregarium, Dendropoma 2, 7, 12, *18*, *30*, 39, *40*, 41, *41*, 42, 76, 90, *90*
guana, Cupolaconcha *5*, 8, *73*, 76, 79, *80*, *81*, 82, 89

haemastoma, Stramonita *19*
Haliotis 21
hallenbeckii, Anodonta 212, 231
hembeli, Margaritifera 207, 211, 229
hepatica, Fasciola 227
hians, Lima 210
howense, Dendropoma *18*, 39, 42, *43*, *90*
howensis, Veristoa 16, 17, 42
Hyridella depressa 218

Hyriidae 99
Hyriopsis myersiana 207, 211, 215
  (*Limnoscapha*) *myersiana* 211, 215

icterina, Elliptio 231
imbecilis, Anodonta 212, 231
  Utterbackia 212, 231
inflata, Anadara 222
Iridinidae 99
irregulare, Dendropoma 25, *27*
  Dendropoma (*Novastoa*) 35
irregularis, Vermetus 25, 35, 39, 87

Janthinoidea 10
jayensis, Elliptio 231

krypta, Cupolaconcha 72, *73*, 76, 77, *78*, 79, 86
  Dendropoma 77

Lamellidens corrianus 226
lamellosa, Dendropoma 49
  Novastoa 49, *50–52*, 54, 87, 89, *90*
lamellosum, Dendropoma (*Novastoa*) 49
  Novastoa 49
  Siphonium 16, 48, 49
Lampsilinae 102, 231
Lampsilis 210, 221
  alatus 211
  cardium 101, 210, 215, 229
  fallaciosa 226
  fasciola 211
  ligamentinus 211
  luteolus 211
  purpurata 226
  radiata 217
  rectus 211
  subrostratus 211
  teres 226
  ventricosa 101, 210, 215, 229
Lasmagonia complanata 226
Lasmigona complanata 211, 226
Leptodea fragilis 226
  ochracea 217
ligamentina, Actinonaias 211, 226
ligamentinus, Lampsilis 211
Ligumia recta 211
  subrostrata 211–213, 226
Lima hians 210
lineata, Eurytellina 210
  Tellina 210
littorea, Littorina 9, 10, *14*
Littorina littorea 9, 10, *14*
Littorinoidea 10
lituella, Dendropoma *18*, 20, *20*, *21*, 22, 87, *90*
  Dendropoma (*Dendropoma*) 20
  Siphonium (*Dendropoma*) 1, 16, 17, 20

lituellus, Spiroglyphus 20
luchuana, Vermitoma 16
Lucinidae 225
luteolus, Lampsilis 211
Lymnaea truncatula 227

Macoma biota 210
Magilina 15
  serpuliformis 15
maldivensis, Cupolaconcha *73*, 84, *85*, 86
marchadi, Dendropoma 19, 54, 55
Margaritana connasaugaensis 102
Margaritifera auricularia 215, 231
  hembeli 207, 211, 229
  margaritifera 215, 218
  monodonta 229, 231
margaritifera, Margaritifera 215, 218
Margaritiferidae 99, 231
marginata, Alasmidonta 211
maxima, Dendropoma 65
  Serpula 63–65
maximum, Ceraesignum 8, 64, *64*, 65, *66*, *67*, 68, 71, 89, 90, *90*
  Dendropoma 2, 65, 68, 87
  Dendropoma (*Dendropoma*) 65
  Siphonium 65
maximus, Pecten 221, 225
Megalonaias gigantea 226
  nervosa 226, 231
mejillonense, Dendropoma 7, 12, *18*, 22–24, *22*, *24*, 71, 89, *90*
mejillonensis, Dendropoma 23
meroclista, Cupolaconcha 6, 8, 72, 73, *73*, *75*, *76*, 77, 79, 82, 83, 89
  Dendropoma 71–73, 77, 82, 87
meroclistum, Dendropoma 2, 71, 77
Micropterus 213
Monocondylaea 211
monodonta, Cumberlandia 229, 231
  Margaritifera 229, 231
montereyensis, Petaloconchus 9, 18
Mülleria dalyi 211
Mycetopodidae 99
myersiana, Hyriopsis 207, 211, 215
  Hyriopsis (*Limnoscapha*) 211, 215
Mytilidae 225
Mytilus 101
  edulis 220, 232

nebulosa, Serpula 25, 26
  Villosa 99, 102, 103, 105, *106–126*, 107, 111, 115, 117, 127, *128–141*, 131, 133, 135, 139–141, 205, 207–232
nebulosum, Dendropoma *5*, 7, 12, *18*, 22, 25–27, *26*, *27*, 57, 59, 89, *90*
  Dendropoma (*Dendropoma*) 25
  Siphonium 25
nebulosus, Spiroglyphus (*Novastoa*) 25
  Unio 102
  Vermetus (*Siphonium*) 25
nervosa, Megalonaias 226, 231
nodosa, Fissurella 36
nodulata, Quadrula 228, 229
novaehollandiae, Vermetus 65, 68
Novastoa 1, *5*, 8, 13, *14*, 16, 19, 20, 48, 49, *50*, 55, 64, 87–89, *90*, 91
  bahamensis 8, *50*, 55, *55*, *56*, 57, 59
  batavia *50*, 59, *60–62*, *90*
  caboverdensis 8, *50*, 52, *53*, 54, *54*, 55, 62, 63, *90*
  lamellosa 49, *50–52*, 54, 87, 89, *90*
  lamellosum 49
  pholetor *5*, 8, 26, *50*, 57, *58*, 59, 62, 63, *90*
nuttalliana, Anodonta 212

Obliquaria reflexa 211
ochracea, Leptodea 217
Ostrea edulis 210, 217

parva, Carunculina 226, 231
parvum, Toxolasma 226
Pecten 210
  maximus 221, 225
peggyae, Anodonta 212, 231
  Utterbackia 212, 231
perforans, Stoa 15
perplicata, Amblema plicata 210–211
personata, Vermetus conicus var. 79
peruviana, Amblema 226
Petaloconchus 1, 4, 6, 9, 13, 24, 72, 74, 87
  montereyensis 9, 18
  varians 3, 9
petraea, Bivonia 15, 32, 34
petraeum, Dendropoma 2, 3, 7, 15, 19, 32–34, 87, 89, 90
  Dendropoma cf. 12, *18*, 22, 32, *33*, 34, *34*, *90*
  Dendropoma (*Novastoa*) 32
pharaonis, Brachidontes 2
pholetor, Novastoa *5*, 8, 26, *50*, 57, *58*, 59, 62, 63, *90*
pictorum, Unio 211
Pinna *5*
platypus, Dendropoma 2, 7, 12, *18*, 19, 22, 29, *30*, 31, *31*, 32, *90*
  Dendropoma (*Dendropoma*) 29
  Siphonium 29
  Siphonium (*Stoa*) 29
Pleurobema cordatum 101, 207, 215, 220, 223, 228, 229, 231
plicata, Amblema 208, 211, 226
plumbea, Etheria 211

politus, Spiroglyphus 15
Posidonia australis 60
Potamilus alatus 211, 226
  purpuratus 226
prasidens, Unio 220
Proptera alata 226
psarocephalum, Dendropoma 8, 12, 19, 39
Pseudomulleria dalyi 211
purpurata, Lampsilis 226
purpuratus, Potamilus 226
Pyganodon cataracta 101, 211, 212
  grandis 211, 213, 226

Quadrula 226
  nodulata 228, 229
  quadrula 226
  rubiginosa 211
quadrula, Quadrula 226

radiata, Lampsilis 217
recta, Ligumia 211
rectus, Lampsilis 211
reflexa, Obliquaria 211
rhyssoconchum, Dendropoma 7, 12, 19, 22, 90
riisei, Serpulorbis 25, *27*
  Thylacodes 25
robinsoncrusoei, Ceraesignum 8, 24, 64, *64*, 68, *69*, *70*, 71, 87, *90*
rosanae, Anancylus 243
  Sineancylus 243
rubiginosa, Quadrula 211

Serpula 2
  bicarinata 25, 26
  conica 79
  glomerata 32
  maxima 63–65
  nebulosa 25, 26
Serpulidae 2
serpuliformis, Magilina 15
Serpulorbis 68, 72, 90
  riisei 25, *27*
Siliquariidae 248
sinaiensis, Cupolaconcha *73*, 82, *83*, 86, 89
Sineancylus 243
  rosanae 243
Siphonium 1, 15, 16, 26
  (*Dendropoma*) *lituella* 1, 16, 17, 20
  giganteum 65
  lamellosum 16, 48, 49
  maximum 65
  nebulosum 25
  platypus 29
  (*Stoa*) *platypus* 29
Spiroglyphus 15, 17
  annulatus 15, 35, 39
  annulatus var. *dentifera* 35
  annulatus var. *trochicola* 35
  corrodens 35
  glomeratus 32
  lituellus 20
  (*Novastoa*) *nebulosus* 25
  politus 15
  stramonitae 19, *19*
spiruliformis, Stoa 15
squamiferum, Dendropoma 19
squamigerus, Thylacodes 9, 12
Stoa 15, 17
  ammonitiformis 15
  perforans 15
  spiruliformis 15
Stramonita haemastoma *19*
stramonitae, Spiroglyphus 19, *19*
Stromboidea 10
Strombus 74, *75*
Strophitus 214
  connasaugaensis 99, 102, 103, 105, 166, *166*, *167*, 168, 171, *174–178*, 177, 179, *180–207*, 183, 189, 193, 197, 199, 205, *206*, *207*, 207–212, 214–232
  edentulus 214
  subvexus 214
  undulatus 214
subrostrata, Ligumia 211–213, 226
subrostratus, Lampsilis 211
subvexus, Strophitus 214
Symphynota complanata 211

Tellina lineata 210
teres, Lampsilis 226
tetralasmus, Uniomerus 226
texasensis, Carunculina 212
  Carunculina parva 213
texasiensis, Toxolasma 212, 213
tholia, Dendropoma 43, 45, 87
  Dendropoma cf. *18*, 39, 43, *44*, *90*
  Vermetus (*Dendropoma*) 43
Thyasiridae 225
Thylacodes 6, 9, 13, 64, 68, 72, 74
  decussatus cf. 9
  riisei 25
  squamigerus 9, 12
  variabilis 90
Thylaeodus 1, 6, 9, 12, 13
Toxolasma parvum 226
  texasiensis 212, 213
triquetrus, Vermetus 9
  Vermetus cf. 9
Tritogonia verrucosa 226
trochicola, Spiroglyphus annulatus var. 35
truncata, Alasmidonta 211
  Truncilla 230

truncatula, Galba 104, 227
  Lymnaea 227
Truncilla truncata 230
tulipa, Eualetes 9, 18, 74
tumidus, Unio 220
Turritellidae 248

undulata, Alasmidonta 217
undulatus, Strophitus 214
Unio ambiguus 211
  cerinus 102
  complanatus 211, 218
  gibbosus 211
  nebulosus 102
  pictorum 211
  prasidens 220
  tumidus 220
Uniomerus tetralasmus 226
Unionidae 99, 105, 211, 228, 231
Unioninae 99, 101, 104, 231
Utterbackia couperiana 212, 231
  imbecilis 212, 231
  peggyae 212, 231

variabilis, Thylacodes 90
varians, Petaloconchus 3, 9
Vasum capitellum 36
Velesunio ambiguus 211, 218
ventricosa, Lampsilis 101, 210, 215, 229
Veristoa 1, 16, 17
  howensis 16, 17, 42
Vermetidae 1–3, 6, 10, 15, 16, 86, 87, 89–91, 248
Vermetoidea 16
Vermetus 6, 9, 13, 15, 18, 72
  alii 18
  breigneti 16
  conicus 82
  conicus var. *personata* 79
  corrodens 35, 39
  cristatus 32, 35
  (*Dendropoma*) *tholia* 43
  giganteus 65
  glomeratus 15, 32, 34
  irregularis 25, 35, 39, 87
  novaehollandiae 65, 68
  (*Siphonium*) *nebulosus* 25
  (*Spiroglyphus*) *annulatus* var. *corrodens* 35
  triquetrus 9
  triquetrus cf. 9
Vermitoma 16
  luchuana 16
verrucosa, Tritogonia 226
Vesicomyidae 225
Villosa 106, 210, 212
  nebulosa 99, 102, 103, 105, *106–126*, 107, 111, 115, 117, 127, *128–141*, 131, 133, 135, 139–141, 205, 207–232
virginica, Crassostrea 218, 229

wahlamatensis, Anodonta 212

Xenophoroidea 10

zebra, Arca 220

Vol. 47, No. 1–2	20 July 2005
Vol. 48, No. 1–2	16 Feb. 2006
Vol. 49, No. 1	10 Nov. 2006
Vol. 49, No. 2	27 July 2007
Vol. 50, No. 1–2	9 June 2008
Vol. 51, No. 1	19 Mar. 2009
Vol. 51, No. 2	26 Aug. 2009
Vol. 52, No. 1	27 Jan. 2010
Vol. 52, No. 2	7 May 2010
Vol. 53, No. 1	19 Oct. 2010
Vol. 53, No. 2	8 Mar. 2011
Vol. 54, No. 1–2	25 Oct. 2011
Vol. 55, No. 1	17 Sep. 2012
Vol. 55, No. 2	28 Dec. 2012
Vol. 56, No. 1–2	31 Dec. 2013

MALACOLOGIA

INTERNATIONAL JOURNAL OF MALACOLOGY
Web: **http://malacologia.fmnh.org**

SUBSCRIPTION AND PAST ISSUE ORDER FORM

Name: ____

Address: ______________________________________

____

____

Personal rates:

Subscription (per volume)	
Regular	$75.00
Student discounted rate	$40.00
Single & past volumes	$75.00
Single & past issues	$38.00

Institutional and agency rates:

Subscription (per volume)	$105.00
Single & past volumes	$105.00
Single & past issues	$53.00

- Publication of MALACOLOGIA is irregular and may not coincide with the calendar year. Occasionally, more than one volume is published in the same year. Therefore, subscribers are invoiced by volume, not by year. Any changes in price will occur by volume, not by year.

- Each volume contains 2 numbers. Sometimes a volume is complete in one issue and sometimes each number is published separately.

- Subscriptions begin with the current volume. Current volume postage is included for subscribers having an American or Canadian mailing address. Subscribers requiring overseas shipment of the journal are charged an additional $16.00 per volume for a total of some 400 to 600 pages weighing up to 4 lbs.

- Single and past issues or volumes are available with the exception of volumes 17(1), 18, 28 and 37, which are out of print. Postage and handling for shipment to an American or a Canadian address is $13.00 per issue or volume. Shipment to an overseas address is $34.00 per issue or volume. Postage for orders weighing more than 4 lbs. will be determined by weight and destination.

- Prepayment is required. Postal money orders and checks (US $) must be drawn on American banks. VISA and MASTERCARD payments are accepted for an additional processing fee of $3.00 per volume. Electronic transfer of funds to a Malacologia bank account is also possible for an additional $10.00 fee.

Address: Malacologia
P.O. Box 385
Haddonfield, NJ 08033-0309
U.S.A.

fax: (856) 323-8794
e-mail: malacologia@comcast.net

MALACOLOGIA ADDRESSES

* * *

BUSINESS–SUBSCRIPTIONS

1ST CLASS MAIL INCLUDING AIR, CERTIFIED, REGISTERED, ETC.:

MALACOLOGIA
P.O. Box 385
Haddonfield, NJ 08033-0309
U.S.A.

e-mail: malacologia@comcast.net tel/fax: (856) 323-8794

MANUSCRIPTS

1ST CLASS MAIL INCLUDING AIR, CERTIFIED, REGISTERED, ETC.:

MALACOLOGIA
P.O. Box 1222
West Falmouth, MA 02574-1222
U.S.A.

e-mail: georgedavis99@hotmail.com tel/fax: (508) 457-0810

INSTRUCTIONS FOR AUTHORS

1. MALACOLOGIA publishes original research on the Mollusca that is of high quality and of broad international interest. Papers combining synthesis with innovation are particularly desired. While publishing symposia from time to time, MALACOLOGIA encourages submission of single manuscripts on diverse topics. Smaller papers of local geographical or systematic content, and of high quality and interest, may be accepted as 'Research Notes'. Nearly all branches of malacology are represented in the pages of MALACOLOGIA.
2. Manuscripts submitted for publication are received with the tacit understanding that they have not been submitted or published elsewhere in whole or in part.
3. Manuscripts must be in English, but may include an expanded abstract in a foreign language as well as the usual brief abstract in English. Both American and British spellings are allowed.
4. Unless indicated otherwise below, contributors should follow the recommendations in the Council of Science Editors (CSE) Scientific Style and Format manual, 7th ed., 2006.
5. Be brief.
6. Manuscripts must be prepared using Microsoft Word® (Windows-version), 12-pitch, Arial font, lines at 1.5 spaces throughout (including the references, tables and figure captions), no added spaces before or after paragraphs, text aligned left, ragged right. Tables, figure captions and figures are to be placed on separate pages at the end of the file. Make the hierarchy of headings within the text simple and consistent. Avoid internal page references.
7. Choose a running title (a shortened version of the main title) of fewer than 50 letters and spaces.
8. For full papers, provide a concise and informative abstract summarizing not only contents but also results. A separate summary is not wanted. Research Notes do not require an added abstract.
9. Supply between five and eight key (topic) words to go at the end of the Abstract for full-length papers.
10. Use the metric system throughout. Micron should be abbreviated µm.
11. Three types of illustrations are accepted: (A) line art figures (black-and-white drawings, diagrams), (B) gray-step figures ("black-and-white" photographs or gray-step drawings) and (C) color figures. Gray-step and color figs. should be saved with a resolution of 300 dpi; line art with 1200 dpi. Illustrations are printed either in one column or the full width of a page of the journal, so plan accordingly. The maximum size of a printed figure is 13.5 x 20.0 cm (preferably not as tall as this so that the caption does not have to be on the opposite page). The figure captions are not to be part of the figure.
12. Lines, letters, and numbers should be thick enough to allow reduction by 30% to 50%. Letters and numbers (Arial font) should be at least 2 mm (line art) or 3 mm (gray-step, color) high after reduction, but avoid letter sizes > 6 mm. In line drawings, the minimum line width of 0.2 mm is required (as measured by final size). Several drawings or photographs may be grouped together as plate.
13. All illustrations should be numbered sequentially and not as lettered sub-series. All figures must be cited in the text in the order in which they appear.
14. Scale lines are required for all none diagrammatic figures, and should be convenient lengths (e.g., "200 µm", not "163 µm"). Magnifications in captions are not acceptable. But object or specimen sizes in a caption are acceptable.
15. Be professional. Sloppy illustrations, labels, borders will not be accepted. If assistance is required of MALACOLOGIA's editorial staff, the author will be charged for the services rendered.
16. A caption should summarize what is shown in an illustration, and should not duplicate information given in the text. Each lettered abbreviation labeling an individual feature in a figure must either be explained in each caption (listed alphabetically), or be grouped in one alphabetic sequence after the Methods section. Use the latter method if many abbreviations are repeated on different figures.
17. Tables are to be used sparingly. All tables must be cited in the text in the order in which they appear. Tables should be composed using the table function of Word (and **not** tab-delimited text).
18. References cited in the text must appear in the Literature Cited section and vice versa.

Refer to a recent issue of MALACOLOGIA for bibliographic style, noting especially that serials are cited unabbreviated. Supply information on plates, etc., only if they are not included in the pagination.

19. In systematic papers, synonymies should not give complete citations but should relate by author, date and page to the Literature Cited section. All new type specimens must be deposited in museums where other scientists may study them. Likewise, MALACOLOGIA requires that voucher specimens upon which a paper is based be deposited in a museum where their identity can be verified.
20. For all papers dealing with molluscan species, each such species should include its author and date upon first appearance, with the correct use of parenthesis around an author in the case of a generic assignment other than the original combination. In all taxonomic papers dealing with one to a few species, the original description of each species should be represented in the Literature Cited. In other studies – physiological, ecological, etc. – involving one or a few species, the author should either cite the original description of the taxon/taxa involved or some other work showing its identity.
21. For electronic submission of manuscripts, send a **single manuscript file** (including manuscript text, tables, figure captions and figures) together with a cover letter to georgedavis99@hotmail.com. Contact the editor to determine the method of submission if the manuscript has a file sizes exceeding 5 MB.
22. Once the manuscript is accepted, high quality and full resolution graphic files have to be provided. Submit such graphics to the graphics editor (tom.wilke@allzool.bio.uni-giessen.de) as TIFF files. For other formats or any question regarding electronic submission of graphics, contact the graphics editor. Keep the individual file sizes below 5 MB (using the option "LZW compression" will greatly reduce the size of TIFF files).

REPRINTS AND PAGE COSTS

23. Reprints must be ordered from the Business Office at the time proof is returned to the copy editor. Later orders cannot be considered. When 100 or more reprints are ordered, an author will receive 25 additional copies free of charge.
24. PDF files of the paper for personal use are available with a purchase of reprints; free of charge for subscribers to Malacologia. Subscription must include current and two paid-for immediate past and/or future volumes.
25. Page costs must be paid prior to publication. Page cost recovery is required as follows.
    Regular subscribers:*
      Non-student: 10 pages free; U.S. $30.00 for each additional page (EAP)
      Student**: 15 pages free; U.S. $20.00 EAP
    Non-subscribers:
      Non-student: 8 pages free; U.S. $60.00 EAP
      Student**: 15 pages free; U.S. $30.00 EAP
    A reduction or elimination of page charges may be possible under certain circumstances by arrangement with the editor. A reduction of page charges may be negotiated for papers exceeding 30 pages.
26. Color figures must be paid-for by the author. Costs are U.S. $300 for the first color page in a paper and U.S. $150 for each subsequent color page.

SUBSCRIPTION PURCHASE

27. Effective with Vol. 57, subscription rates per volume are as follows:
      Personal: U.S. $75.00
      (Student discounted rate: U.S. $40.00)
      Institutional: U.S. $105.00
      Agency and Dealership: U.S. $105.00
    Current volume postage is included for shipment to an American or a Canadian address. Overseas postage is $16.00 per volume. Single and past volumes are available at subscription rates. Postage and handling is $13.00 per volume for shipment to an American or a Canadian address. Overseas postage is $34.00 per volume. Postage for orders weighing over 4 lbs. will be determined by weight.

* Regular subscribers are those who have paid-up subscriptions for the current volume and two immediate past and/or future volumes.

** Students must identify themselves at the time of manuscript submission and also provide the e-mail address of their advisor.

SMITHSONIAN LIBRARIES
3 9088 01816 2677

VOL. 57, NO. 1 MALACOLOGIA 2014

CONTENTS

FULL PAPERS

Rosemary E. Golding, Rüdiger Bieler, Timothy A. Rawlings & Timothy M. Collins
Deconstructing *Dendropoma*: A systematic revision of a world-wide worm-snail group, with descriptions of new genera (Caenogastropoda: Vermetidae) 1

Andrew McElwain & Stephen A. Bullard
Histological atlas of freshwater mussels (Bivalvia, Unionidae): *Villosa nebulosa* (Ambleminae: Lampsilini), *Fusconaia cerina* (Ambleminae: Pleurobemini) and *Strophitus connasaugaensis* (Unioninae: Anodontini) 99

RESEARCH NOTE

Diego Eduardo Gutiérrez Gregoric
Sineancylus, nom. nov.: A replacement name for *Anancylus* Gutiérrez Gregoric, 2012 (Gastropoda, Ancylidae) 243

LETTER FROM THE EDITOR

George M. Davis
A tribute to Dick Petit 1931–2013 247

INDEX 249

ALACOLOGIA

International Journal of Malacology

51
115X
2

57(2)

2014

MALACOLOGIA
http://malacologia.fmnh.org

One of the World's Leading Malacological Journals
Journal Impact Factor 0.977 (2013)

Founded in 1961

EDITOR-IN-CHIEF
GEORGE M. DAVIS

Editorial Office
Malacologia
P.O. Box 1222
West Falmouth, Massachusetts 02574, U.S.A.
georgedavis99@hotmail.com

Business & Subscription Office
Malacologia
P.O. Box 385
Haddonfield, New Jersey 08033, U.S.A.
malacologia@comcast.net

Copy Editor
EUGENE COAN
Santa Barbara Museum of Natural History
Santa Barbara, California, U.S.A.
genecoan@gmail.com

Associate Editor
JOHN B.BURCH
University of Michigan
Ann Arbor, Michigan, U.S.A.
jbburch@umich.edu

Managing Editor
CARYL HESTERMAN
Haddon Heights, New Jersey, U.S.A.
malacologia@comcast.net

Composition Editor
CLAUDIA WILKE
Giessen, Germany
claudiawilke@hotmail.com

Graphics Editor
THOMAS WILKE
Justus Liebig University
Giessen, Germany
tom.wilke@allzool.bio.uni-giessen.de

MALACOLOGIA is published by the INSTITUTE OF MALACOLOGY

Board of Directors - U.S.A.:

President

DIARMAID Ó FOIGHIL
University of Michigan, Ann Arbor

Vice President

ELLEN STRONG
National Museum of Natural History, Washington D.C.

Secretary and Treasurer

GEORGE M. DAVIS
West Falmouth, Massachusetts

Members

RÜDIGER BIELER
Field Museum, Chicago, Illinois

JOHN B. BURCH
University of Michigan, Ann Arbor

CAROLE S. HICKMAN
University of California, Berkeley

ALAN KOHN
University of Washington, Seattle

PAULA M. MIKKELSEN
Paleontological Research Institution, Ithaca, New York

Copyright © 2014 by the Institute of Malacology
ISSN: 0076-2997 (Print)
ISSN: 2168-9075 (Online)

J. A. ALLEN
Marine Biological Station
Millport, United Kingdom

T. ASAMI
Shinshu University
Matsumo, Japan

T. BACKELJAU
University of Antwerp
Antwerp, Belgium

B. BAUR
Universität Basel
Basel, Switzerland

D. BLAIR
James Cook University
Townsville, Australia

P. BOUCHET
Muséum National d'Histoire Naturelle
Paris, France

R. A. D. CAMERON
University of Sheffield
Sheffield, United Kingdom

J. G. CARTER
University of North Carolina
Chapel Hill, North Carolina, U.S.A.

R. CIPRIANI
California State University
Fullerton, California, U.S.A.

T. COLLINS
Florida International University
Miami, Florida, U.S.A.

R. H. COWIE
University of Hawaii
Honolulu, Hawaii, U.S.A.

G. CUEZZO
Universidad Nacional de Tucumán
Tucumán, Argentina

B. DAYRAT
University of California
Merced, California, U.S.A.

B. DEGNAN
University of Queensland
Brisbane, Australia

D. J. EERNISSE
California State University Fullerton
Fullerton, California, U.S.A.

D. GEIGER
Santa Barbara Museum of Natural History
Santa Barbara, California, U.S.A.

G. GIRIBET
Harvard University
Cambridge, Massachusetts, U.S.A.

E. GITTENBERGER
Naturalis Biodiversity Center
Leiden, The Netherlands

F. GIUSTI
Università di Siena
Siena, Italy

M. GLAUBRECHT
Museum of Natural History Berlin
Berlin, Germany

D. GRAF
University of Wisconsin
Stevens Point, Wisconsin, U.S.A.

E. HARPER
University of Cambridge
Cambridge, United Kingdom

G. HASZPRUNAR
Zoologische Staatssammlung München
München, Germany

K. HAYES
University of Hawaii
Honolulu, Hawaii, U.S.A.

K. E. HOAGLAND
Independent Consultant
Falmouth, Massachusetts, U.S.A.

M. HORSAK
Masaryk University
Drno, Czech Republic

C. ITUARTE
Museo Argentino de Ciencias Naturales
Buenos Aires, Argentina

M. S. JOHNSON
University of Western Australia
Crawley, Australia

SMITHSONIAN
JUL 08 2015
LIBRARIES

G. KAMENEV
Institute of Marine Biology
Vladivostok, Russia

Y. KANTOR
Russian Academy of Sciences
Moscow, Russia

F. KOEHLER
Australian Museum
Sydney, Australia

T. KONDO
Osaka Kyoiku University
Osaka, Japan

K. A. LUTAENKO
Institute of Marine Biology
Vladivostok, Russia

C. LYDEARD
Western Illinois University
Macomb, Illinois, U.S.A.

BRUCE A. MARSHALL
Museum of New Zealand Te Papa Tongarewa
Wellington, New Zealand

J. NEKOLA
University of New Mexico
Albuquerque, New Mexico, U.S.A

T. OKUTANI
Tokyo University of Fisheries
Tokyo, Japan

L. PAGE
University of Victoria
Victoria, BC, Canada

G. PAULEY
Florida Museum of Natural History
Gainesville, Florida, U.S.A.

R. PIPE
The Marine Biological Association
Plymouth, United Kingdom

W. F. PONDER
Australian Museum
Sydney, Australia

T. RAWLINGS
Cape Breton University
Nova Scotia, Canada

T. SASAKI
University Museum, University of Tokyo
Tokyo, Japan

L. R. L. SIMONE
Museu de Zoologia da Universidade
de São Paulo, Brazil

P. TATTERSFIELD
Tideswell, Buxton
United Kingdom

C. THIRIOT
University Pierre et Marie Curie
Paris, France

S. TILLIER
Muséum National d'Histoire Naturelle
Paris, France

Á. VALDÉS
California State Polytechnic University
Pomona, California, U.S.A.

J. VOIGHT
Field Museum Natural History
Chicago, Illinois, U.S.A.

A. WARÉN
Museum of Natural History
Stockholm, Sweden

M. WU
Hebei University
Hebei, China

ELECTRONIC ACCESS TO *MALACOLOGIA*

Malacologia is available on line, with volumes 1 (1962) to 48 (2006) freely accessible via the *Biodiversity Heritage Library* (BHL; a consortium of natural history and botanical libraries that cooperate to digitize and make accessible the legacy literature of biodiversity held in their collections), and most recent numbers obtainable from *BioOne*, a global not-for-profit collaboration of scientific publishers and libraries:
BHL (www.biodiversitylibrary.org): *Malacologia* grants open access to electronic copies of all pre-2007 volumes, which can be read and downloaded at http://www.biodiversitylibrary.org/bibliography/12920.

BHL
Biodiversity Heritage Library

BioOne (www.bioone.org): *Malacologia* is part of the BioOne.2 collection of scientific journals. Access is available to institutions and consortia holding BioOne subscriptions (see the BioOne web site for details). In addition, subscribers to the *Malacologia* print edition are given access to this journal on BioOne. To be granted such individual access, contact the subscription office at malacologia@comcast.net.

BioOne™ RESEARCH EVOLVED

ANNOUNCEMENT

The J Frances Allen Institute of Malacology Outstanding Student Publication Award

The Board of Directors of the Institute of Malacology, publisher of the academic journal *Malacologia*, is pleased to announce the creation of the J Frances Allen Institute of Malacology Outstanding Publication Award. This cash award of $500 will be presented for an outstanding paper published in *Malacologia* by a student, with the timing dependent on the superior quality of the student paper as judged by a committee of the IM Board. There is no formal application or deadline. A student submitting a manuscript must be sole or senior author of the paper, and should indicate that the paper being submitted stems from Master's or Ph.D. research to confirm his or her eligibility for the award. The Allen Publication Award was established in 2011 to honor J Frances "Jady" Allen, who provided indispensable help and guidance in establishing the journal *Malacologia*, first published in 1962.

ANNOUNCING THE J FRANCES ALLEN INSTITUTE OF MALACOLOGY OUTSTANDING STUDENT PUBLICATION AWARD FOR 2013

The Board of Directors of the Institute of Malacology, publisher of Malacologia, is pleased to announce that doctoral student Catharina Clewing has been selected as the 2013 recipient of the **J. Frances Allen Institute of Malacology Outstanding Publication Award** for the paper "Molecular phylogeny and biogeography of a high mountain bivalve fauna: the Sphaeriidae of the Tibetan Plateau" published in *Malacologia* 56(1/2). Catharina is the second recipient of this award. Her manuscript was selected from among ten outstanding entries published in *Malacologia* during the 2013 calendar year. The selection committee was comprised of three members from the Institute of Malacology Board of Directors, plus four additional members from the Editorial Board.

Any sole- or senior-authored publication by an undergraduate or graduate student was eligible for consideration. Selection criteria included originality, study design, methods, quality of prose and figures, and potential impact of the publication. The award is made when at least seven full length student papers have been published since the last awardee was selected. The award includes $500 U.S.

Catharina Clewing
Animal Ecology and Systematic
Justus Liebig University
Heinrich-Buff-Ring 26-32 (IFZ)
D-35392 Giessen, Germany

Catharina finished her diploma thesis at the Justus Liebig University, Giessen, in 2011 entitled "Establishment of microsatellite analyses for *Oncomelania hupensis robertsoni* (Gastropoda, Rissooidea) – intermediate host for the human blood fluke". Currently, she is a Ph.D. student in the Animal Ecology and Systematics group of Professor Thomas Wilke (supervised by Dr. Christian Albrecht) at the Justus Liebig University. Her doctoral research concerns the biodiversity and evolution of freshwater mollusks on the high-elevation Tibetan Plateau and its surrounding regions.

Diarmaid Ȯ Foighil

President
Institute of Malacology

MALACOLOGIA, 2014, 57(2): 255–277

TWO NEW SPECIES OF THE GENUS *SILICULA* (BIVALVIA: SILICULIDAE) FROM THE NORTHWESTERN PACIFIC, WITH NOTES ON *SILICULA SANDERSI* (BERNARD, 1989) AND *PROPELEDA SOYOMARUAE* (OKUTANI, 1962)

Gennady M. Kamenev

A.V. Zhirmunsky Institute of Marine Biology of the Far Eastern Branch of the Russian Academy of Sciences, Palchevskogo Stn. 17, Vladivostok 690041, Russia; gennady.kamenev@mail.ru

ABSTRACT

Two new species, ***Silicula beringiana*** and ***S. okutanii***, are described from the northwestern Pacific. These species have an elongate shell with extended and tapered posterior end, differing from each other in form and proportions. ***Silicula beringiana*** was found in the Bering Sea, Kamtchatky Strait, and near the southeastern coast of Kamchatka (Pacific Ocean) at 489–4,984 m depth. ***Silicula okutanii*** was found in the Pacific Ocean at a latitude of the northern part of Japan at 5,219–5,352 m depth. *Silicula sandersi* (Bernard, 1989) and *Propeleda soyomaruae* (Okutani, 1962) were re-examined. Based on comparison with the description, pictures and photos of the type species of *Silicula* Jeffreys, 1879, *Lamellileda* Cotton, 1930, *Poroleda* Hutton, 1893, and *Propeleda* Iredale, 1924, the following combinations are suggested: *Lamellileda sandersi* Bernard, 1989, and *L. soyomaruae* (Okutani, 1962).

Key words: *Silicula*, bivalve mollusks, systematics, morphology, distribution, Pacific Ocean.

INTRODUCTION

Allen & Sanders (1973) placed the genus *Silicula* Jeffreys, 1879, in the family Siliculidae, which they erected following the investigation of deep-water Protobranchia of the Atlantic Ocean. Earlier, the genus *Silicula* comprised three species: *Silicula fragilis* Jeffreys, 1879, *Silicula patagonica* (Dall, 1908), and *Silicula rouchi* Lamy, 1910. Allen & Sanders (1973) described two new species – *Silicula filatovae* Allen & Sanders, 1973, and *Silicula mcalesteri* Allen & Sanders, 1973 – and examined, in great detail, the shell morphology and anatomy of all species of the genus *Silicula*, except *S. patagonica*, which was described from a single valve with a destroyed beak (Dall, 1908). Later, Bernard (1989) described one more species *Silicula alleni* Bernard, 1989. In the same work, he described the species *Lamellileda sandersi* Bernard, 1989, which Coan et al. (2000) referred to the genus *Silicula.* Thus, the genus *Silicula* currently contains seven species that were recorded in the bathyal and abyssal zones of different regions of the Atlantic and Pacific oceans. However, despite the wide distribution of Siliculidae representatives in the World Ocean, collections of *Silicula* species in most cases consist of a small number of specimens. In the Pacific Ocean, the siliculids *S. patagonica, S. alleni,* and *S. sandersi* were found only at the coast of America, and all Pacific species were described from a minimal amount material – *S. patagonica* from one valve, *S. alleni* and *S. sandersi* from one specimen each.

Following the examination of extensive original material of bivalves collected during the period from 1950 to 2012 in the bathyal and abyssal zones of different regions of the northwestern Pacific, two new species of *Silicula* were discovered. One was recorded in the bathyal and abyssal of the deep-sea basin of the Bering Sea and the other in an abyssal plain of the northwestern Pacific. Thus, the new representatives of the genus *Silicula* were first recorded in the western Pacific Ocean. The present paper mainly focuses on the description of these new species.

MATERIALS AND METHODS

Material Studied

In this study, I used the material collected by expeditions of IO RAS in the bathyal and abyssal zones of the Bering Sea (R/V "Vityaz", cruise 5, August 5–October 5, 1950; R/V "Vityaz", cruise 8, September 14–October 28, 1951; R/V "Akademik Mstislav Keldysh", cruise 22, July 25–October 27, 1990) and in the abyssal zone of the northern Pacific (R/V "Vityaz", cruise 45, April 23–July 10, 1969; R/V "Akademik Mstislav Keldysh", cruise 22, July 25–October 27, 1990), as well as by the German-Russian deep-sea expedition KuramBio (Kurile Kamchatka Biodiversity Study) in the abyssal zone of the northwestern Pacific (R/V "Sonne", cruise 223, July 21–September 7, 2012). The material of *Silicula* species collected by the IO RAS was fixed and stored in 70% ethanol in the IO RAS. The material collected by the KuramBio expedition was fixed in pre-cooled 96% ethanol and stored in the IMB.

The following were used for the comparison purposes: the type material of *P. soyomaruae* (holotype NSMT Mo 62762, paratype NSMT 49827), photos of type and other materials of *S. mcalesteri* (holotype MCZ 271974, paratype MCZ 361654, photos by A. J. Baldinger from MCZ website), *S. filatovae* (holotype MCZ 271977, paratype MCZ 361653, photos by A. J. Baldinger from MCZ website, "President and Fellows of Harvard College"), *S. alleni* (holotype LACM 2344, photos by L. T. Groves and P. Valentich-Scott), *S. sandersi* (holotype LACM 2348, photos by L. T. Groves and P. Valentich-Scott), *S. patagonica* (holotype USNM 96914, photos from USNM website ("Information provided with the permission of the National Museum of Natural History, Smithsonian Institution, 10th and Constitution Ave. N.W., Washington, D.C. 20560-0193 (http://www.nmnh.si.edu/)"), *S. fragilis* (NMW, image numbers: M011725, M011726, M011727, from Marine Bivalve Shells of the British Isles website (Oliver et al., 2010)), and *S. rouchi* (USNM 870326, photos from USNM website ("Information provided with the permission of the National Museum of Natural History, Smithsonian Institution, 10th and Constitution Ave., N.W., Washington, D.C. 20560-0193 (http://www.nmnh.si.edu/)"); photos of 2 specimens by D. G. Zelaya).

Shell Measurements

Figure 1 shows the shell morphology measurements. Shell length (L), anterior end length (A), height (H) and width (W) were measured for shells. The ratios of these parameters to shell length (A/L, H/L, W/L, respectively) were determined. Shell measurements were made using a caliper and an ocular micrometer with an accuracy of 0.1 mm.

Methods

The statistical analysis was performed based on the calculated indices (A/L, H/L, W/L) which are less susceptible to change compared with other measured parameters using Data Analysis Module of MS Excel 97-2003. All indices for pairs of shells of *Silicula* species were compared using the Student (T) parametric test and one-way analysis of variance (ANOVA). Throughout this study, statistical significance was defined as $P < 0.05$.

For scanning electron microscopy, shells were cleaned of traces of soft tissues and periostracum in diluted commercial bleach, washed in distilled water, and dried. They were then mounted to aluminium stubs using an adhesive tape and coated with gold for examination with an EVO 40XVP.

Gross anatomy was observed on preserved live-taken specimens. For anatomical studies, several specimens of species from the Bering Sea and two specimens with broken shell of species from the Pacific Ocean were dissected in 70% ethanol and drawn schematically.

Abbreviations

The following institutional abbreviations are used in the paper:

IMB – A.V. Zhirmunsky Institute of Marine Biology, Far Eastern Branch of the Russian Academy of Sciences, Vladivostok
IO RAS – P. P. Shirshov Institute of Oceanology, Russian Academy of Sciences, Moscow

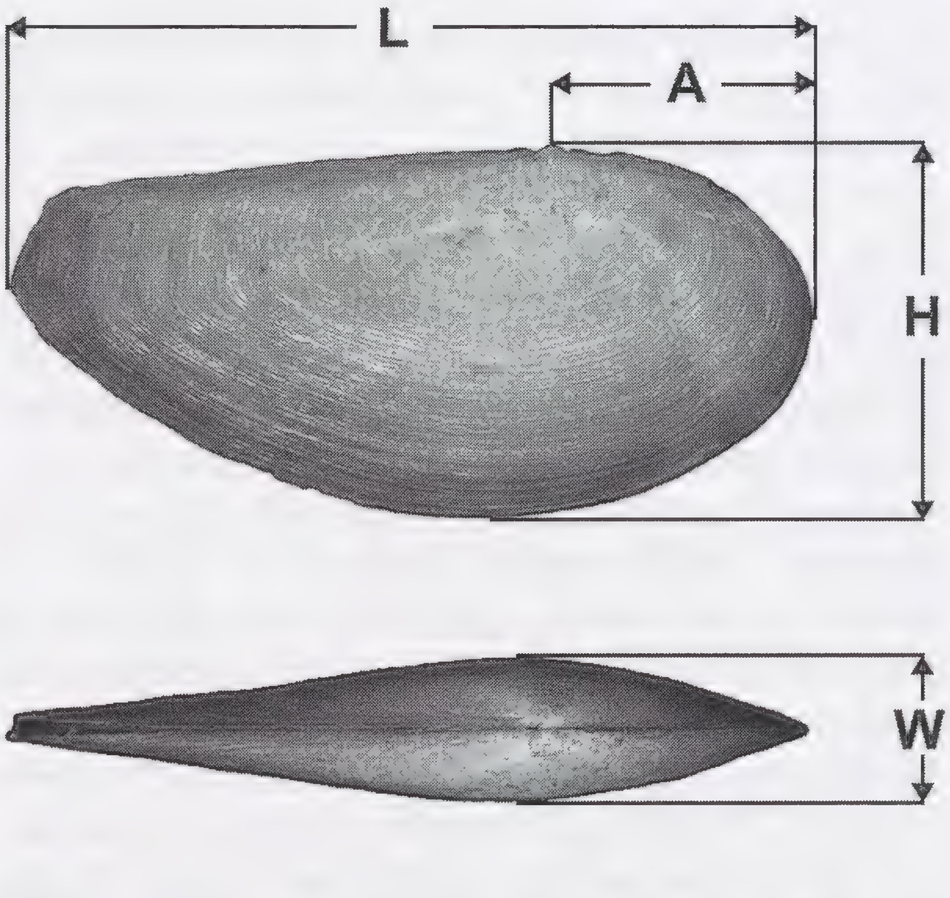

FIG. 1. Placement of shell measurements: L – shell length; H – height; A – anterior end length; W – width.

TABLE 1. Main differentiating characters of genera *Silicula*, *Poroleda*, *Propeleda* and *Lamellileda*.

Characters	*Silicula* Jeffreys, 1879	*Poroleda* Hutton, 1893	*Propeleda* Iredale, 1924	*Lamellileda* Cotton, 1930
Shell	Elongate, inequilateral, longer posteriorly, sometimes rostrate	Very elongate, low, very inequilateral, extended posteriorly, rostrate	Elongate, inequilateral, longer posteriorly, rostrate	Very elongate, low, very inequilateral, extended posteriorly, rostrate
Posterodorsal Shell Margin	Straight, sometimes slightly convex or concave	Slightly concave	Strongly concave, sometimes straight	Slightly concave
Anterior Teeth	Long, lamellate, almost parallel to anterodorsal shell margin	V-shaped	Numerous, V-shaped, sometimes a few lamellate near beak	Short, subequal, lamellate, horizontal
Posterior Teeth	Very long, lamellate, almost parallel to posterodorsal shell margin	Short, lamellate, oblique to posterodorsal shell margin	Numerous, V-shaped and a few lamellate near beak	Long, lamellate, oblique to posterodorsal shell margin
References	Allen & Sanders, 1973; Heinberg, 1989; Coan et al., 2000	Hedley, 1905, 1915; Heinberg, 1989	Hedley, 1915; Nijssen-Meyer, 1972; Heinberg, 1989	Cotton, 1930; Ludbrook, 1961; Heinberg, 1989

LACM – Natural History Museum of Los Angeles County, Los Angeles
MCZ – Museum of Comparative Zoology, Harvard University, Cambridge
MIMB – Museum of the Institute of Marine Biology, Vladivostok
NMW – National Museums & Galleries of Wales, Cardiff
NSMT – National Museum of Nature and Science, Tsukuba
USNM – United States National Museum of Natural History, Smithsonian Institute, Washington, D.C.
ZMMU – Zoological Museum of Moscow University, Moscow

SYSTEMATICS

Family Siliculidae Allen & Sanders, 1973

Genus *Silicula* Jeffreys, 1879

Type Species – *Silicula fragilis* Jeffreys, 1879

Diagnosis

Shell small (< 20 mm), very thin, fragile, often translucent, very compressed, elongate, inequilateral, longer posteriorly, sometimes abruptly and somewhat squarely truncated, with anterior and posterior ends gaping. Surface with very weak, dense, shiny, commarginal ribs, often with widely spaced and weak, radial rays of short and very dense riblets. Beaks very small, not prominent, prosogyrate. Lunule and escutcheon absent. Periostracum thin, adherent. Hinge plate very narrow, weak. Teeth long, lamellate, almost parallel to posterior shell margin, partially overlapping each other, anteriorly and posteriorly increasing in length, divided into anterior (up to 6 teeth) and posterior (up to 8 teeth) sets. Anterior teeth shorter than posterior. Ligament internal, elongate, opisthodetic, posteroventrally directed. Resilifer deep, elongate, oblique, posterior to beaks. Pallial line with shallow pallial sinus of same shape and size in both valves. Pallial sinus not confluent with pallial line.

Remarks

The genus *Silicula* is most close in terms of the hinge structure to the genera *Lamellileda* Cotton, 1930, and *Poroleda* Hutton, 1893 (Figs. 2–12). Like *Silicula*, species of *Lamellileda* and *Poroleda* have long and lamellate teeth (Hedley, 1905; Cotton, 1930, Ludbrook, 1961) (Table 1). This has hampered the identification of generic status of species that occur in different regions of the World Ocean and have lamellate teeth in the hinge (Heinberg, 1989). In the northern Pacific, such species are *Silicula sandersi* (Bernard, 1989) and *Propeleda soyomaruae* (Okutani, 1962) (Figs. 13–24).

Huber (2010) suggested that Bernard (1989) originally correctly placed *S. sandersi* in *Lamellileda*. *Silicula sandersi* was described from one specimen from the abyssal plain (5,180 m depth) of the northeastern Pacific. In contrast to other species of the genus *Silicula*, this species has a much more extended posteriorly and more rostrate shell; more than 10 relatively short posterior hinge teeth, becoming posteriorly shorter and oblique relative to the posterodorsal shell margin; more than 5 short subequal anterior teeth located horizontally and

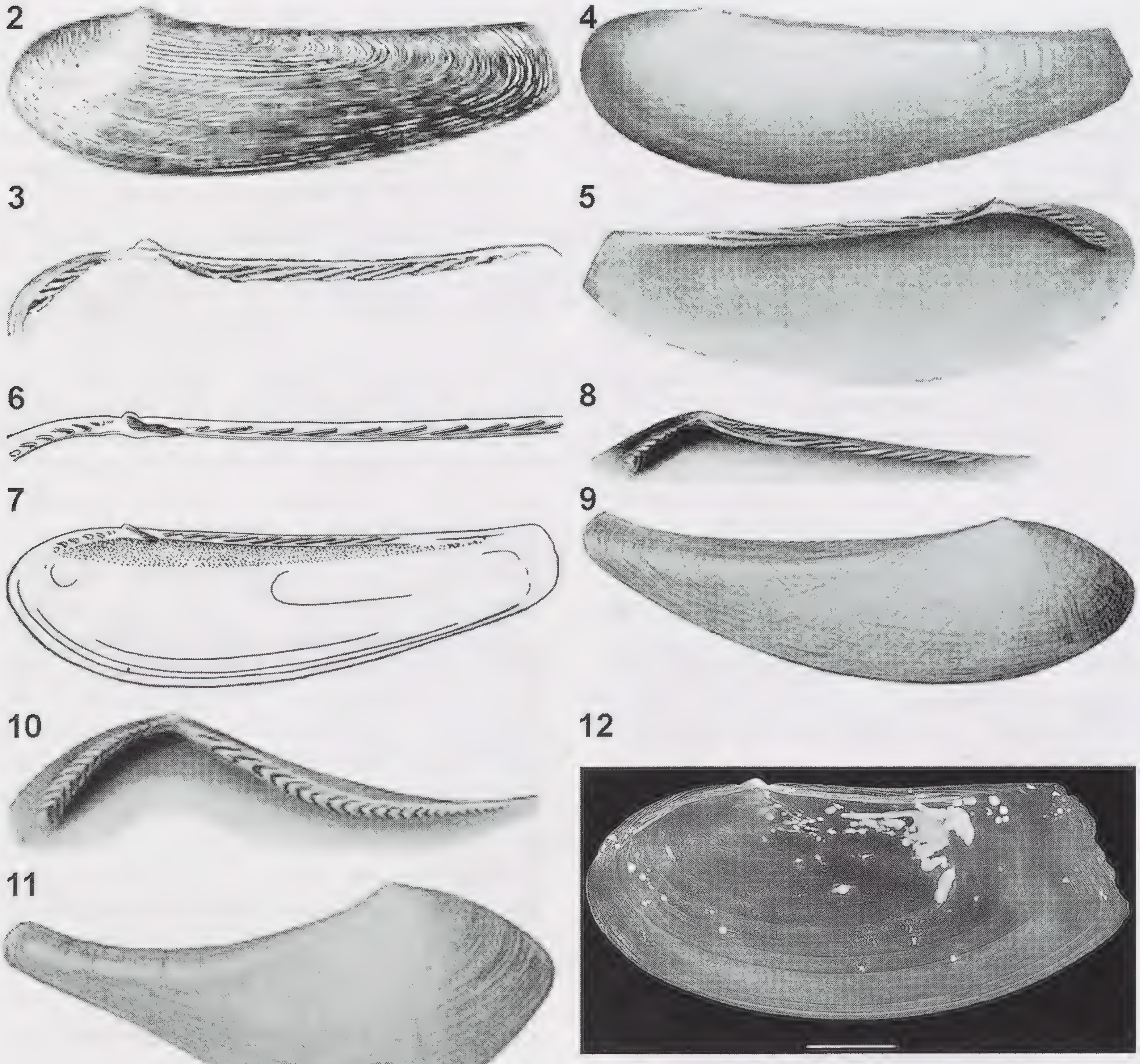

FIGS. 2–12. Species of genera *Lamellileda*, *Poroleda*, *Propeleda*, and *Silicula*. FIGS. 2, 3: *Lamellileda typica* Cotton, 1930 (type species of *Lamellileda*), holotype, shell length 11.2 mm (from Cotton, 1930); FIGS. 4, 5: *Lamellileda tatei* (Hedley, 1904), holotype, shell length 11.7 mm (from Ludbrook, 1961); FIGS. 6, 7: *Poroleda lanceolata* (Hutton, 1885) (type species of *Poroleda*), shell length 13.8 mm (from Hedley, 1905); FIGS. 8, 9: *Poroleda spathula* Hedley, 1915, holotype, shell length 14.0 mm (from Hedley, 1915); FIGS. 10, 11: *Propeleda ensicula* (Angas, 1877) (type species of *Propeleda*), shell length 11.0 mm (from Hedley, 1915); FIG. 12: *Silicula fragilis* Jeffrey, 1879 (type species of *Silicula*) (NMW, image number M011725, from Marine Bivalve Shells of the British Isles web site (Oliver et al., 2010)). Scale bar = 1 mm.

parallel to each other; a broad thickening of the hinge plate under the beak, in which an oblique resilifer is located (Bernard, 1989; Coan et al., 2000; Figs. 13–16). These peculiarities of the shell morphology and the hinge structure of *S. sandersi* correspond much more to the diagnosis of the genus *Lamellileda* (Cotton, 1930; Ludbrook, 1961; Heinberg, 1989; Table 1). The type species of this genus, *Lamellileda typica* Cotton, 1930, has analogous proportions of the shell, numerous relatively short lamellate posterior teeth becoming posteriorly shorter and oblique to the dorsal shell margin, and short lamellate horizontal anterior teeth not parallel to the anterodorsal shell margin (Cotton, 1930) (Figs. 2, 3). Therefore, I share the Huber's

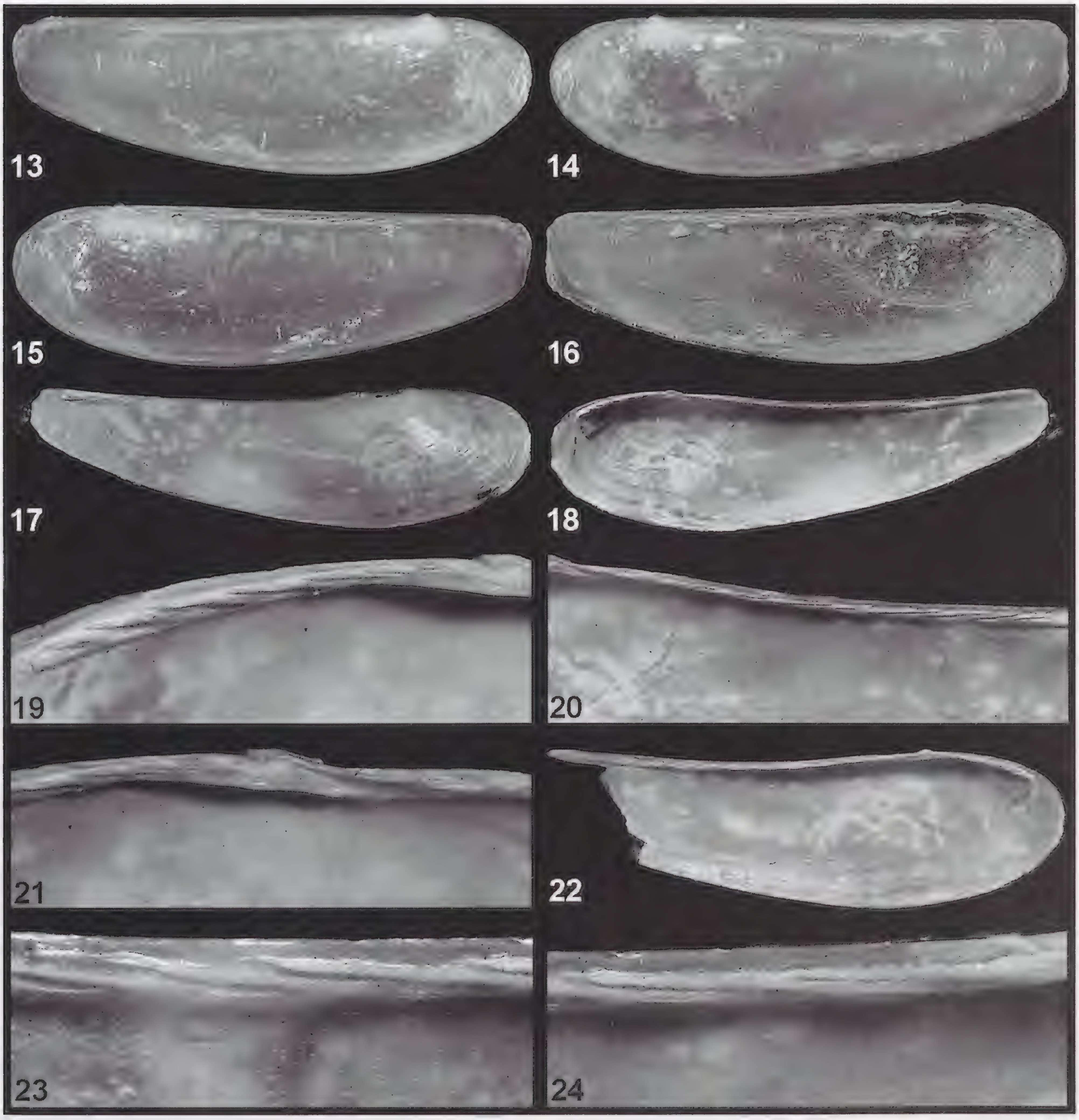

FIGS. 13–24. *Silicula sandersi* (Bernard, 1989) and *Propeleda soyomaruae* (Okutani, 1962). FIGS. 13–16: *S. sandersi*, holotype (LACM 2348), exterior and interior views of right and left valves, shell length 11.2 mm (photos by L. T. Groves and P. Valentich Scott); FIGS. 17–24: *P. soyomaruae*. FIGS: 17–21: Holotype (NSMT Mo 62762), exterior and interior views of right valve, anterior and posterior sets of teeth, resilifer, shell length 20.0 mm; FIGS. 22–24: Paratype (NSMT Mo 49827), exterior view of left valve, posterior teeth, length of shell fragment 18.0 mm.

(2010) viewpoint that Bernard (1989) correctly referred *S. sandersi* to *Lamellileda* and exclude this species from comparative analysis with other species of the genus *Silicula*.

Bernard (1989) remarked that *L. sandersi* is most close to *P. soyomaruae*. Okutani (1962) described *P. soyomaruae* from only one specimen found in the northwestern Pacific at the coast of Japan at a depth of 730–760 m. He originally placed this species in the genus *Poroleda* Hutton, 1893, with the type species *Poroleda lanceolata* (Hutton, 1885), which has numerous oblique lamellate teeth in the posterior set and V-shaped teeth in the anterior (Hedley, 1905; Heinberg, 1989; Table 1; Figs. 6–9). Later, Okutani (2000) transferred this species to the genus *Propeleda* Iredale, 1924, with the type species *Propeleda ensicula* (Angas, 1877) (Iredale, 1924). However, *P. ensicula* has V-shaped posterior and anterior teeth and only a few lamellate posterior teeth closest to beak (Angas, 1877; Hedley, 1915; Nijssen-Meyer, 1972; Heinberg, 1989; Figs. 10, 11). In contrast to *P. ensicula*, both anterior and posterior teeth in *P. soyomaruae* are lamellate (Figs. 17–24). The proximal posterior teeth are the longest and almost parallel to the posterodorsal shell margin, while posterior distal teeth are shorter and located diagonally across the hinge plate. The anterior teeth are subequal in length, horizontal, parallel to each other, the hinge plate under the beak is markedly thickened to harbor an oblique resilifer directed posteroventrally. Thus, the shell shape and proportions and the hinge structure of *P. soyomaruae* are very similar to those of *L. typica*, but not *P. ensicula*. Therefore, Huber (2010) referred *P. soyomaruae* to the genus *Lamellileda*. I agree with the Huber's (2010) opinion that *P. soyomaruae* should be recognized as a species of *Lamellileda*. Taking into account the marked differences in the shell shape and proportions, as well as in the habitat depth, it can be suggested with a high degree of probability that *Lamellileda soyomaruae* (Okutani, 1962) and *L. sandersi* are different species, though the differences in the shell morphology may be due to the age variation, because the holotype of *L. soyomaruae* is 20.0 mm long, while the holotype of *L. sandersi* is 11.2 mm long (Okutani, 1962; Bernard, 1989). *Lamellileda soyomaruae* is much closer in shell morphology and habitat depth to *L. typica*. However, further investigations of the type and additional material are needed to make valid conclusions about the relationships of these species.

Silicula beringiana
Kamenev, n. sp.
(Figs. 25–70, 72, Table 2)

Type Material and Locality

Holotype (ZMMU Ld-3052), Bering Island, Commander Islands, Bering Sea (55°36.1'N, 167°23.04'E–55°35'N, 167°24.5'E), 4,294–4,200 m, Sigsbee trawl, Coll. L. I. Moskalev, 05-VIII-1990 (R/V "Akademik Mstislav Keldysh", cruise 22, stn. 2316); paratypes (40) (ZMMU Ld-3053 (30 paratypes), MIMB 28313 (10 paratypes)) from holotype locality; paratypes (20) (MIMB 28314), Bering Island, Commander Islands, Bering Sea (55°13.2'N, 167°29.07'E–55°12.02'N, 167°26.7'E), 3,957–3,978 m, Sigsbee trawl, Coll. L. I. Moskalev, 31-VII-1990 (R/V "Akademik Mstislav Keldysh", cruise 22, stn. 2309).

Other Material Examined

960 specimens (IO RAN) from holotype locality; 71 specimens (IO RAN), Bering Island, Commander Islands, Bering Sea (55°13.2'N, 167°29.07'E–55°12.02N, 167°26.7'E), 3,957–3,978 m, Sigsbee trawl, Coll. L.I. Moskalev, 31-VII-1990 (R/V "Akademik Mstislav Keldysh", cruise 22, stn. 2309); one damaged specimen (IO RAN), Bering Island, Commander Islands, Bering Sea (55°23.8'N, 167°15.52'E), 489 m, manned submersible "Mir-II", Coll. L.I. Moskalev, 7-VIII-1990 (R/V "Akademik Mstislav Keldysh", cruise 22, stn. 2320); two damaged specimens (IO RAN), Bering Island, Commander Islands, Bering Sea (55°22.3'N, 167°18.8'E–55°21.8'N, 167°18'E), 1,490–1,554 m, dredge, Coll. L. I. Moskalev, 8-VIII-1990 (R/V "Akademik Mstislav Keldysh", cruise 22, stn. 2321); one damaged specimen (IO RAN), Bering Island, Commander Islands, Bering Sea (55°32.2'N, 167°16.76'E–55°31.37'N, 167°16.2'E), 3,446–3,313 m, dredge, Coll. L. I. Moskalev, 7-VIII-1990 (R/V "Akademik Mstislav Keldysh", cruise 22, stn. 2318); 4 damaged specimens (IO RAN), Bering Sea (57°03'N, 168°30'E), 3,875 m, Sigsbee trawl, 25-IX-1950 (R/V "Vityaz", cruise 5, stn. 618); 5 specimens (IO RAN), Kamchatsky Strait, Bering Sea (55°52'N, 164°08'E), 4,382 m, Sigsbee trawl, 17-IX-1950 (R/V "Vityaz", cruise 5, stn. 524); one damaged specimen (IO RAN), Kamchatsky Strait, Bering Sea (55°39'N, 164°31'E), 4,811 m, Okean grab,

28-IX-1951 (R/V "Vityaz", cruise 8, stn. 956a); one specimen (IO RAN), southeastern Kamchatka, Pacific Ocean (53°05.4'N, 161°55.2'E–53°20.7'N, 161°56.1'E), 4,890–4,984 m, Sigsbee trawl, Coll. L.I. Moskalev, 10-VIII-1990 (R/V "Akademik Mstislav Keldysh", cruise 22, stn. 2323). Total of 1,046 specimens.

Description

Exterior: Shell small (to 14.7 mm), elongate (H/L = 0.486 ± 0.003), equivalve, inequilateral, gaping anteriorly and posteriorly, flattened (W/L = 0.204 ± 0.003), thin, fragile, translucent in young specimens (L < 9 mm). Surface with very thin, dense, commarginal ribs, well defined along the ventral margin and sparse radial rays formed by densely spaced short concentric riblets most expressed at the anterior shell end. Periostracum thin, adherent, yellow-green. Beaks small, very low, slightly prominent above dorsal shell margin, rounded, prosogyrate, anterior to midline (A/L = 0.347 ± 0.002). Anterior shell end rounded, angular. Posterior shell end extended, tapered, truncated, with long, week flexure and shallow sulcus extending from beaks to posterior shell margin. Dorsal shell margin anterior to posterior and to beaks forming very small concavities. Anterodorsal shell margin strongly convex, often forming a smooth angle, rather sharply descending, and almost straight in lower portion. Anterior shell margin rounded, often forming a weak rounded angle. Posterodorsal shell margin straight, sometimes slightly convex or concave, form-

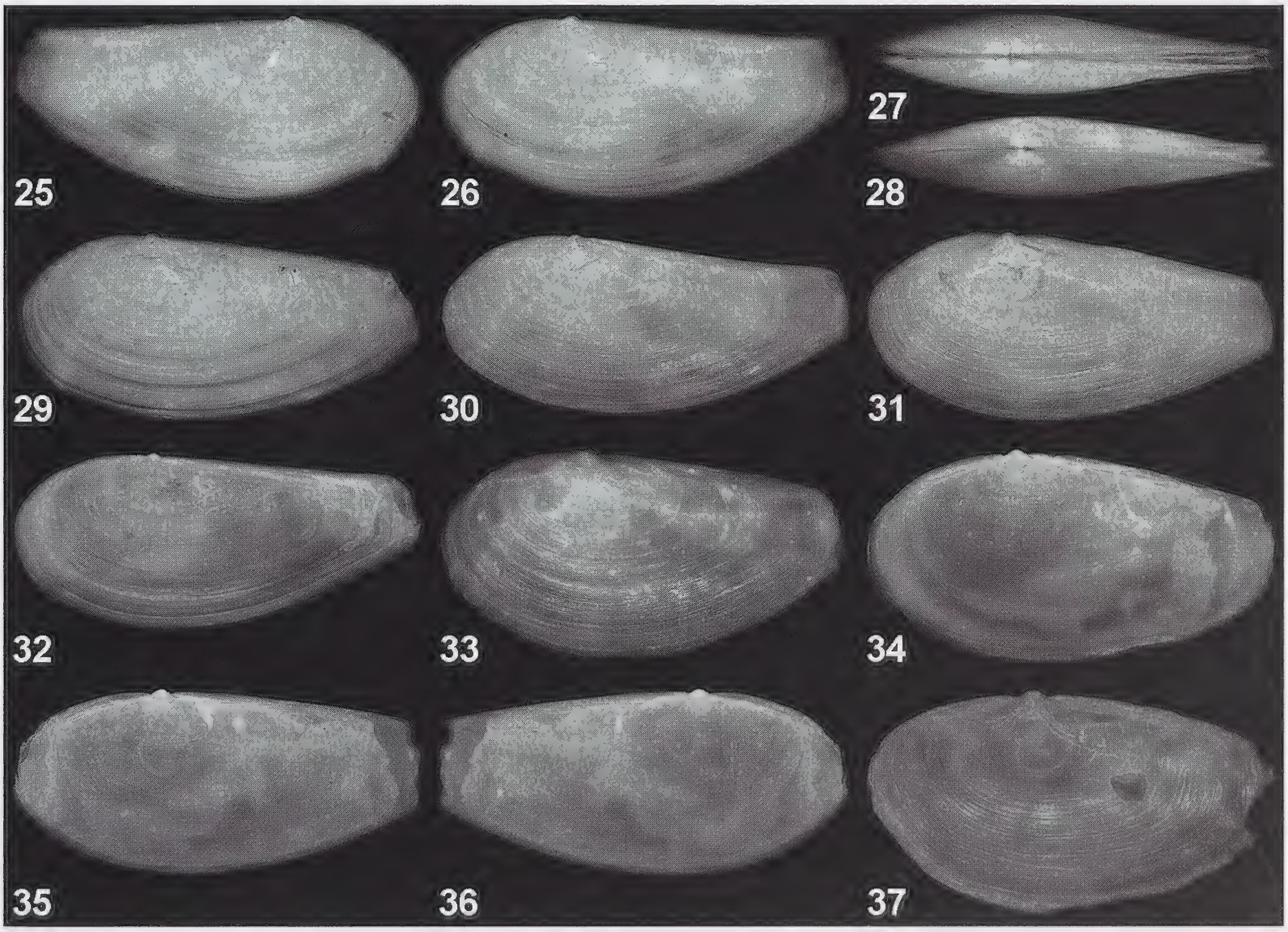

FIGS. 25–37. ***Silicula beringiana*** Kamenev, n. sp. FIGS. 25–27: Holotype (ZMMU Ld-3052), exterior and dorsal views of both valves, shell length 13.7 mm; FIGS. 28–37: Shells of different age specimens. FIG. 28: Paratype (ZMMU Ld-3053), dorsal view of both valves, shell length 11.0 mm; FIG. 29: Paratype (ZMMU Ld-3053), shell length 14.7 mm; FIG. 30: Specimen from holotype locality, shell length 14.2 mm; FIG. 31: Paratype (ZMMU Ld-3053), shell length 12.6 mm; FIG. 32: Paratype (ZMMU Ld-3053), shell length 13.5 mm; FIG. 33: Paratype (ZMMU Ld-3053), shell length 10.9 mm; FIG. 34: Paratype (ZMMU Ld-3053), shell length 7.8 mm; FIGS. 35, 36: Paratype (ZMMU Ld-3053), exterior view of left and right valves, shell length 8.7 mm; FIG. 37: Specimen from holotype locality, shell length 4.3 mm.

TABLE 2. ***Silicula beringiana*** Kamenev, n. sp. Shell measurements (mm), indices and summary statistics of characters, n = 65, size range of shells used 5.0 to 14.7 mm; L – shell length; H – height; W – width; A – anterior end length.

Depository	L	H	A	W	H/L	A/L	W/L
Holotype ZMMU Ld-3052	13.7	6.2	4.3	2.7	0.453	0.314	0.197
Paratype ZMMU Ld-3053	14.7	6.6	5.0	3.4	0.449	0.340	0.231
Paratype ZMMU Ld-3053	13.3	6.2	4.9	2.4	0.466	0.368	0.180
Paratype ZMMU Ld-3053	12.8	6.0	4.5	2.3	0.469	0.352	0.180
Paratype ZMMU Ld-3053	12.3	6.1	4.2	2.5	0.496	0.341	0.203
Paratype ZMMU Ld-3053	12.6	6.0	3.9	2.6	0.476	0.310	0.206
Paratype ZMMU Ld-3053	12.3	6.0	4.1	2.5	0.488	0.333	0.203
Paratype ZMMU Ld-3053	12.0	6.0	4.0	2.4	0.500	0.333	0.200
Paratype ZMMU Ld-3053	11.4	5.8	4.0	2.3	0.509	0.351	0.202
Paratype ZMMU Ld-3053	9.9	5.1	3.5	2.0	0.515	0.354	0.202
Paratype ZMMU Ld-3053	8.5	4.0	3.0	1.6	0.471	0.353	0.188
Paratype ZMMU Ld-3053	8.0	3.9	2.7	1.6	0.488	0.338	0.200
Paratype ZMMU Ld-3053	7.8	4.0	2.7	1.8	0.512	0.346	0.231
Paratype ZMMU Ld-3053	7.3	3.7	2.7	1.7	0.507	0.370	0.233
Paratype ZMMU Ld-3053	6.5	3.3	2.4	1.3	0.508	0.369	0.200
Paratype ZMMU Ld-3053	5.6	2.9	2.2	1.0	0.518	0.393	0.179
Statistics	L	H	A	W	H/L	A/L	W/L
Mean	-	-	-	-	0.486	0.347	0.204
SE	-	-	-	-	0.003	0.002	0.003
SD	-	-	-	-	0.023	0.020	0.020
Min	-	-	-	-	0.440	0.304	0.155
Max	-	-	-	-	0.533	0.393	0.243

ing a distinct, weakly rounded obtuse angle at transition to posterior shell margin. Posterior shell margin short, straight or slightly convex, vertical or directed slightly posterior, forming a distinct, weakly rounded angle at transition to ventral shell margin. Ventral shell margin gently curved. Prodissoconch small (length 190–207 µm), D-shaped, distinctly marked, with net-like, cellular sculpture.

Interior: Hinge plate narrow, long, slightly curved. Teeth divided into anterior and posterior sets by small, edentulous gap of hinge plate with resilifer. Internal ligament opisthodetic, well developed, large, elongate, oblique, posterior to beaks. Resilifer elongate, narrow, oblique, extending posteriorly (somewhat into shell) from beak to almost end of first posterior tooth. In adult specimens (L > 9 mm) anterior teeth set of 5 teeth, posterior one 5–6. Anterior teeth narrow, long, overlapping each other, almost parallel to anterodorsal shell margin, becoming longer towards anterior shell margin, except last short tooth. First anterior tooth slightly concave, thinnest, low, arising from dorsal margin of hinge plate under beak; teeth 2–4 much longer, highest, slightly convex, arising from ventral margin of hinge plate; tooth 5 short, weakly expressed, lowest, positioned almost entirely under tooth 4. Posterior teeth narrow, longer than anterior teeth, overlapping each other, almost parallel to posterodorsal shell margin, becoming longer towards posterior shell margin, except last short tooth. First posterior tooth concave, thinnest, low, located above resilifer, arising from dorsal margin of hinge plate under beak. Second tooth 2–2.5 times longer than first, slightly concave, arising from hinge plate above resulifer and partially forming posterodorsal margin of resilifer. Third tooth straight, arising from ventral margin of hinge plate at posterior resilifer end. Teeth 4–5 straight, longest, arising from ventral margin of hinge plate. Sixth tooth short, weakly expressed, low, positioned almost entirely under tooth 5, present only in largest specimens. Adductors scars weakly visible, unequal; anterior adductor scar larger than posterior. Anterior adductor scar slightly elongated, almost vertically extended, positioned under anterior end of hinge plate. Posterior adductor scar slightly elongated, oblique, positioned under posterior end of hinge plate. Pallial line extending beyond posterior adductor scar, forming distinct shallow pallial sinus not confluent with pallial line; sinus apex not extending beyond anterior margin of posterior adductor scar.

Anatomy: Mantle very thin, except thickened ventral margin. Exhalant siphon long. Adductor muscles slightly oval, oblique; anterior muscle larger than posterior, more vertically extended. Food large, with a large anterior toe and a small posterior heel; toe with numerous papillae of varying size. Posterior pairs of pedal retractors large, wide, passing anterior to posterior adductor muscle. Three anterior pairs of pedal retractor muscles narrow, long, passing between anterior adductor muscle and stomach. Gills long, narrow, almost horizontal, extending from ventral side of stomach to ventral side of posterior adductor muscle; gill filaments short. Palps very long, with about 40 ridges, almost parallel to ventral shell margin, positioned close to ventral shell margin. Palp proboscides

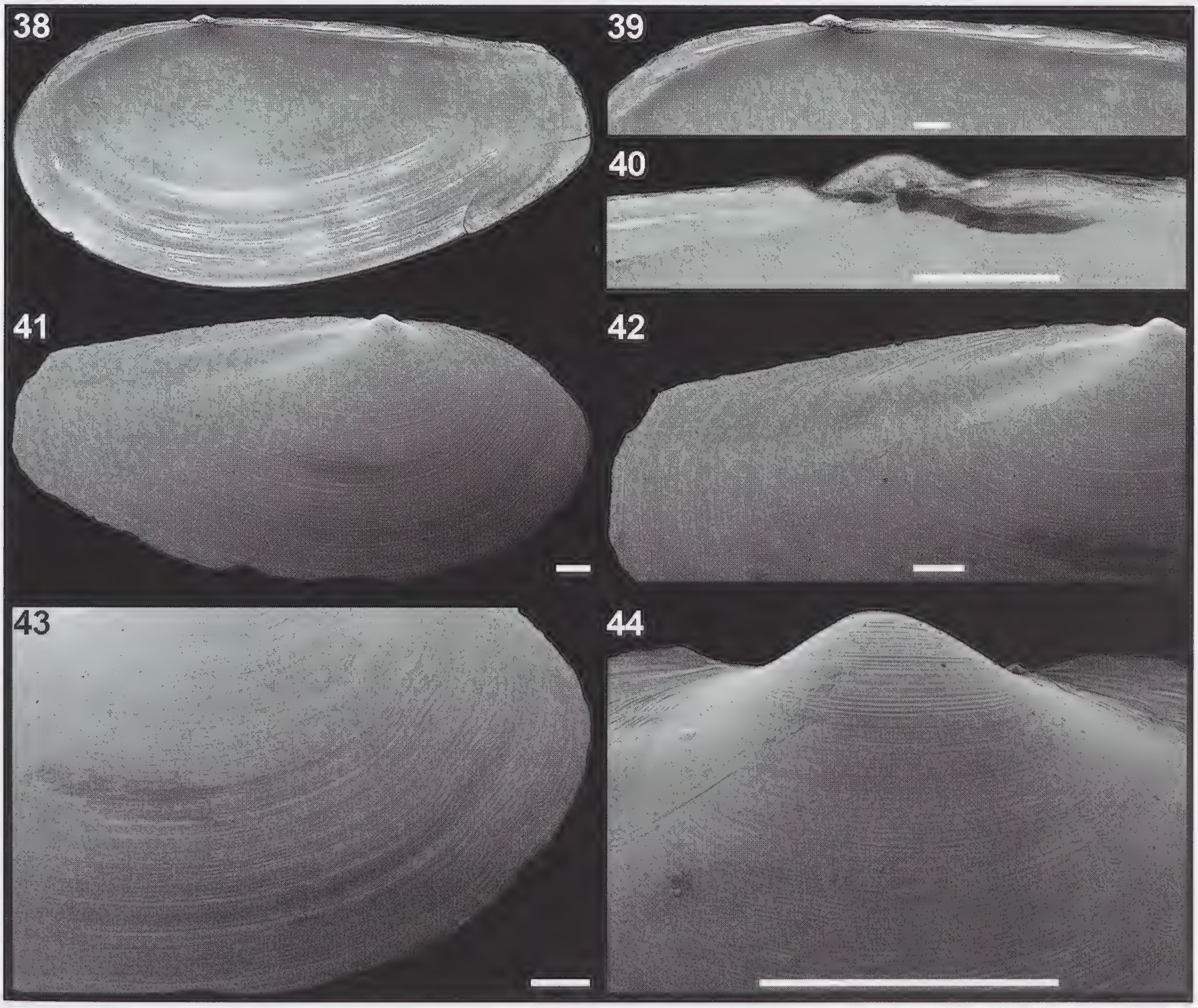

FIGS. 38–44. ***Silicula beringiana*** Kamenev, n. sp. FIGS. 38–40: Interior view, hinge plate, and internal ligament of right valve of specimen from holotype locality, shell length 11.4 mm; FIGS. 41–44: Exterior view, sulcus of posterior shell end, sculpture of anterior shell end, beak of right valve of specimen from holotype locality. Scale bars = 500 μm.

relatively short in contacted state. Mouth in central part of mantle cavity. Oesophagus long, displaced to right side of body, passing behind anterior adductor muscle and along anterodorsal shell margin forming a large uniformly rounded bend. Stomach large, oval, lying under beak along dorsoventral axis. Combined style sac and midgut leaving stomach at posteroventral border, directed almost vertical, passing into foot; midgut usually with one or two small bends. Hindgut penetrating deep into foot heel, forming a short loop into ventral part of heel, turning dorsally, slightly curving behind style sac and passing in right side of body. In right side of body hindgut sharply bending backward, turning forward and passing under beak into left side of body. In left side of body hindgut forming a large loop and passing under the beak backward into right side of body. Here hindgut forming a large (about two times diameter of loop in left side) oval loop corresponding to shape and size of stomach, turning posteriorly under and passing along posterodorsal shell margin above posterior adductor muscle to anus. Digestive diverticula surrounding anterior adductor muscle, oesophagus, stomach, partially labial palps and gills, reaching posterior pedal retractors.

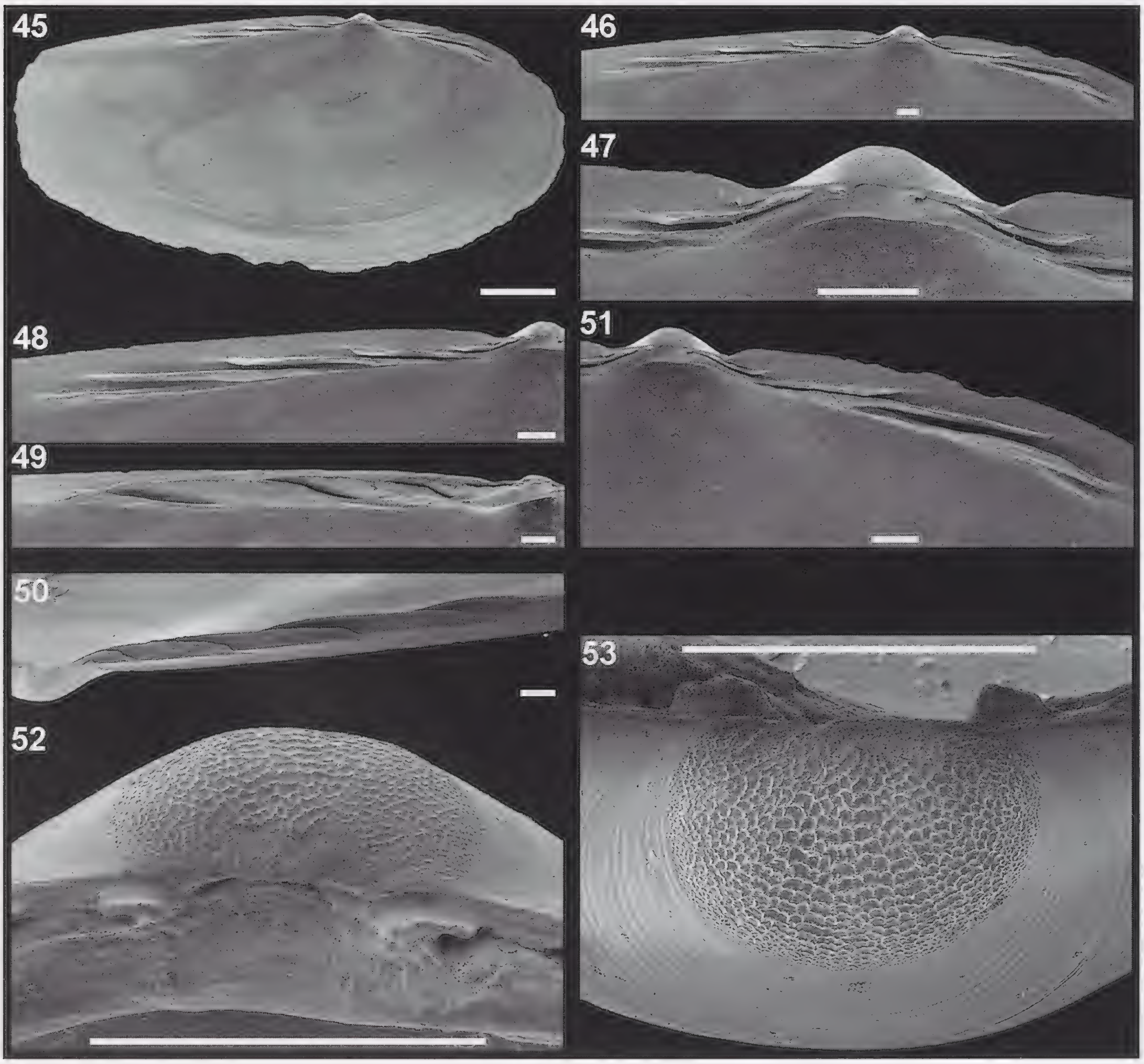

FIGS. 45–53. ***Silicula beringiana*** Kamenev, n.sp. Left valve of specimen from holotype locality. FIGS. 45–47: Interior view, hinge plate, and resilifer; FIGS. 48–51: Posterior (ventral and dorsal views) and anterior sets of teeth; FIGS. 52, 53: Prodissoconch. Scale bars: Fig. 45 = 1 mm, Figs. 46–53 = 200 µm.

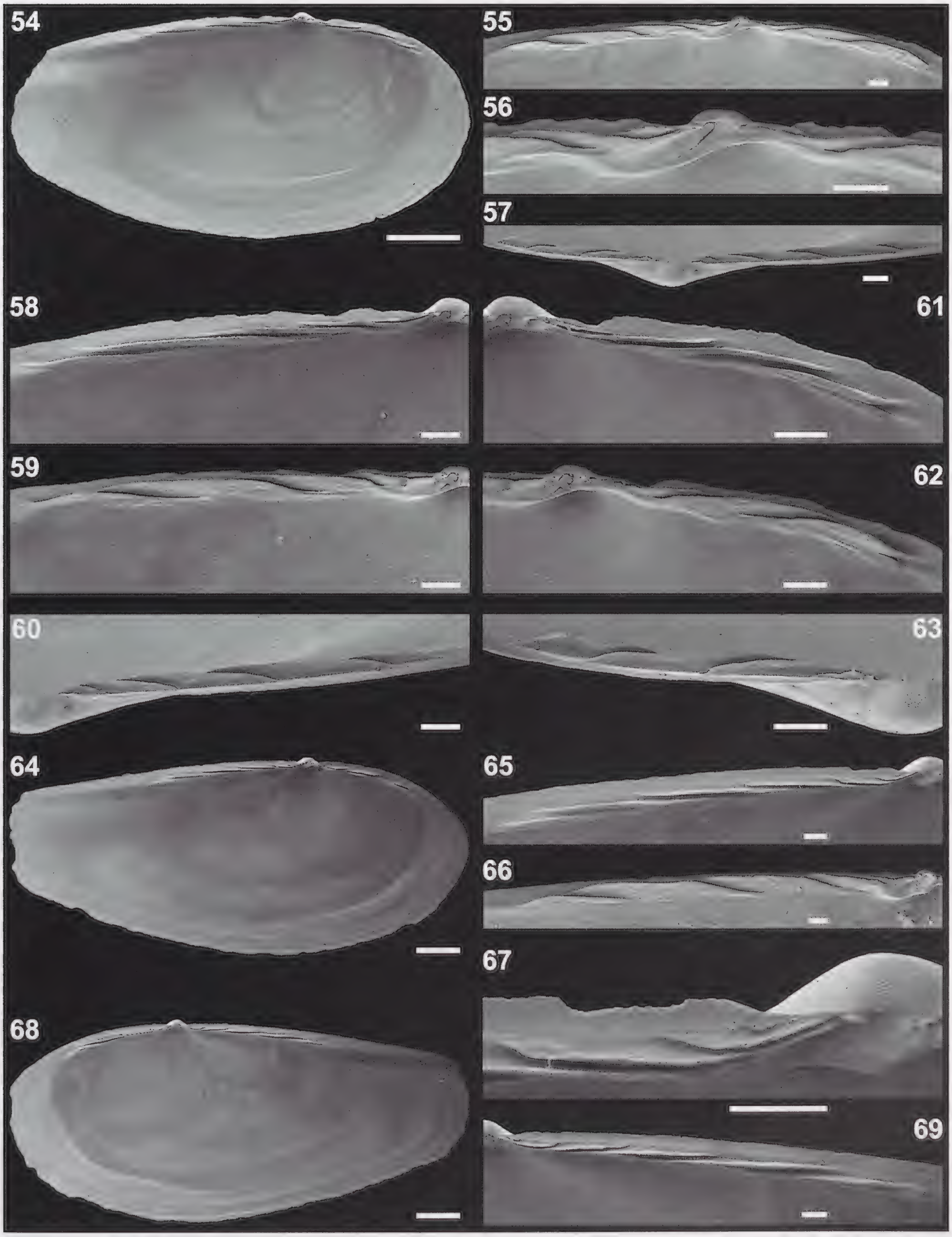

FIGS. 54–69. ***Silicula beringiana*** Kamenev, n. sp. FIGS. 54–63: Interior morphology of left valve of young specimen from holotype locality; FIGS: 54–57: Internal view of valve, ventral view of hinge plate and resilifer, dorsal view of hinge plate; FIGS. 58–60: Posterior (ventral and dorsal views) set of teeth; FIGS. 61–63: Anterior (ventral and dorsal views) set of teeth; FIGS. 64–69: Interior morphology of left and right valves of adult specimen from holotype locality. FIGS. 64–67: Internal view, posterior teeth, ventral view of posterior teeth, resilifer of left valve; FIGS. 68, 69: Internal view and posterior teeth of right valve. Scale bars: Figs. 54, 64, 68 = 1 mm, Figs. 55–63, 65–67, 69 = 200 μm.

Variability

Silicula beringiana exhibits large individual and age variations in shell shape and proportions. In young specimens (L < 8 mm), the shell is higher (H/L > 0.5), the beaks are positioned closer to the middle of the shell (A/L > 0.36) and the posterior shell margin is directed vertically down. In specimens larger than 8 mm, the shell is relatively more elongate, the beaks are more displaced anteriorly, the rostrum is narrower, often slightly curved upward, thus making the posterodorsal margin concave, the posterior shell margin is oblique, directed posteriorly. In adult specimens (L > 8 mm), the shell height and width vary markedly (H/L = 0.444–0.521; W/L = 0.155–0.243), the posterodorsal shell margin may be straight or concave. The hindgut in the right side of the body also varies in size. The length of the gut loop in the right side is about 2 times usually greater than in the left but sometimes the loops in both sides of the body are about the same length.

70

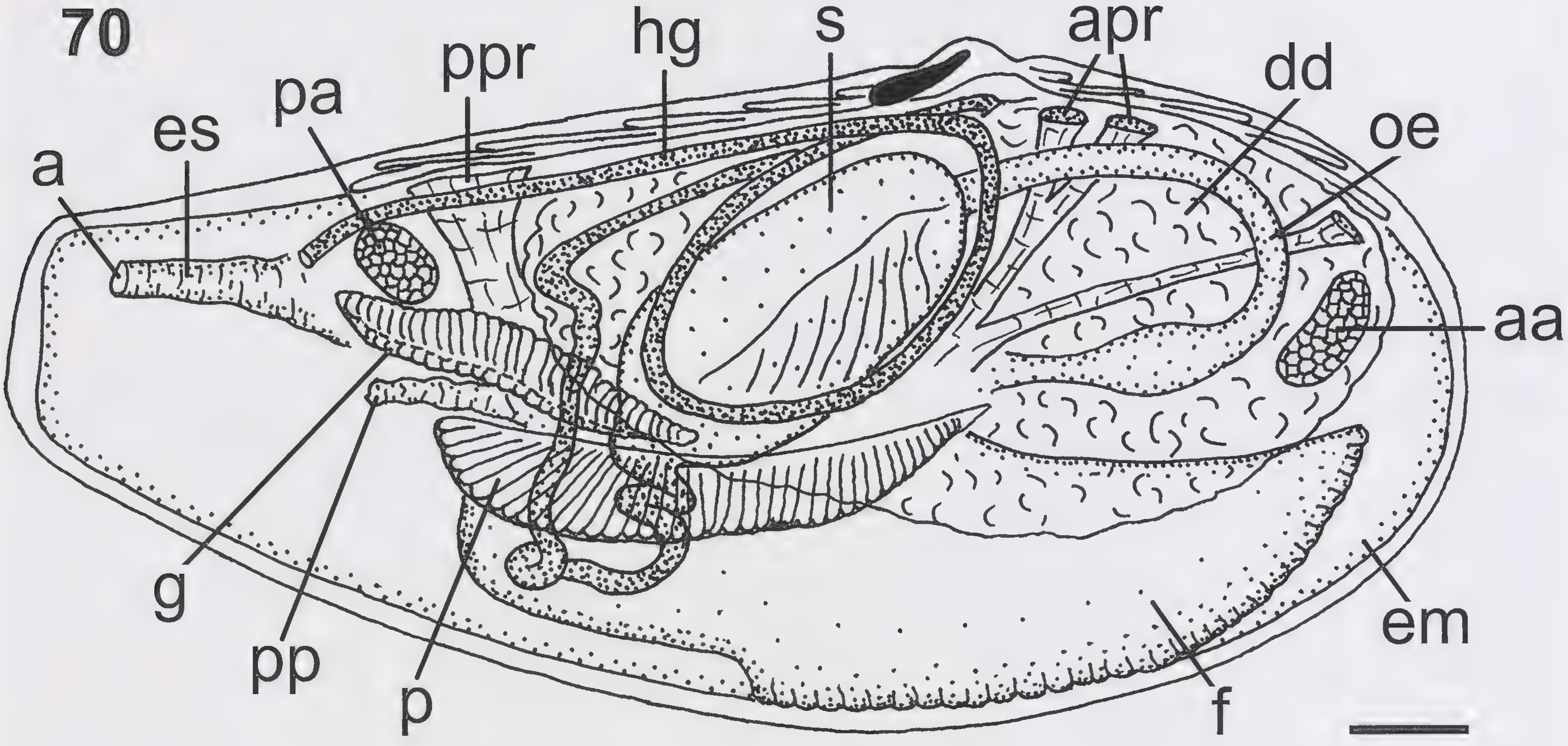

71

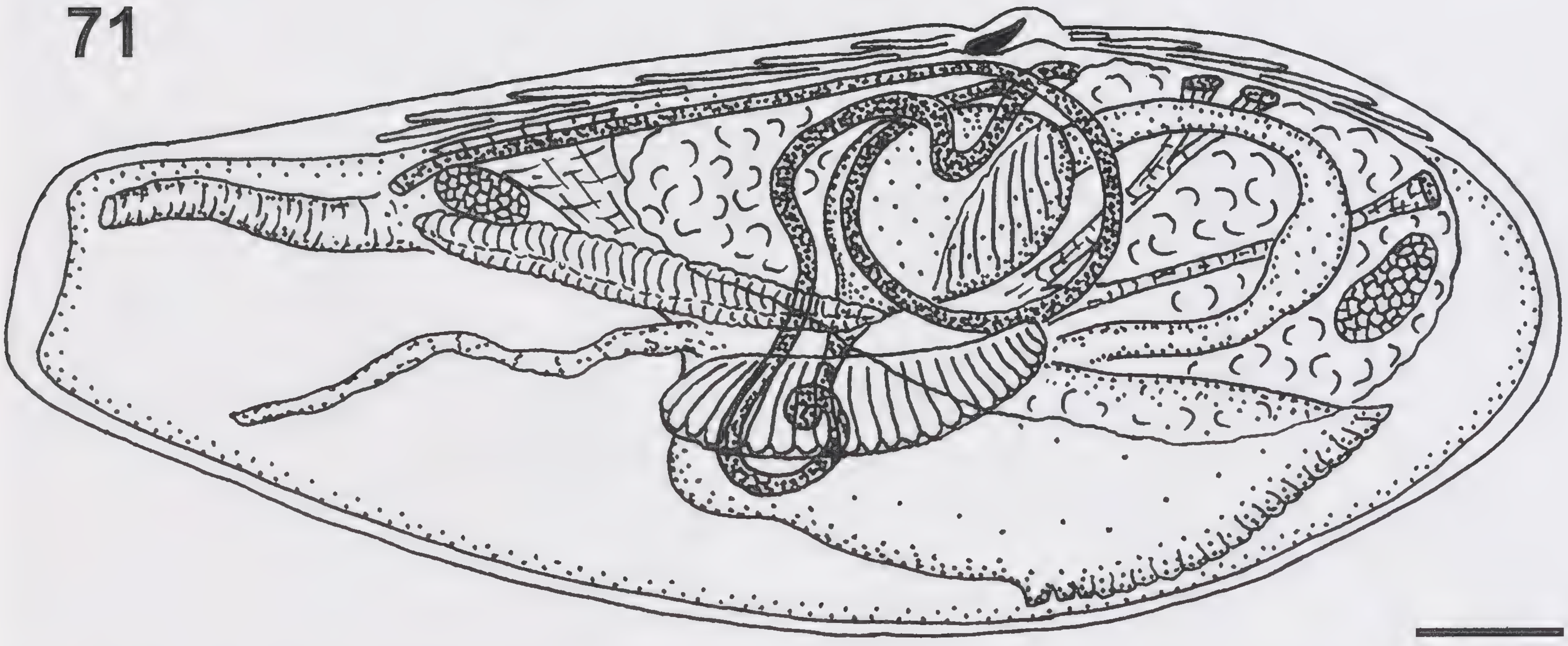

FIGS. 70, 71. ***Silicula beringiana*** Kamenev, n. sp., and ***Silicula okutanii*** Kamenev, n. sp. Internal morphology as seen from right side with right shell, mantle, and parth of the body removed. FIG. 70: ***Silicula beringiana*** Kamenev, n. sp.; FIG. 71: ***Silicula okutanii*** Kamenev, n. sp. Scale bars = 1 mm. Abbreviations: a, anus; aa, anterior adductor muscle; apr, anterior pedal retractors; dd, digestive diverticula; em, edge of mantle; es, exhalant siphon; f, foot; g, gill; hg, hindgut; oe, oesophagus; p, palp; pa, posterior adductor muscle; pp, palp proboscis; ppr, posterior pedal retractor; s, stomach.

72

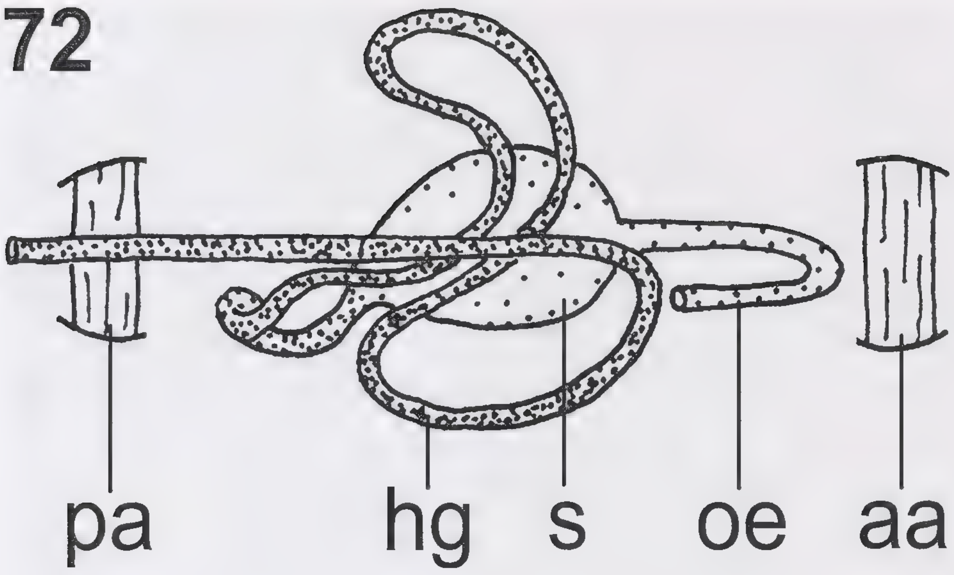

FIG. 72. Diagram of gut of ***Silicula beringiana*** and ***Silicula okutanii*** as seen from dorsal side. Abreviations: aa, anterior adductor muscle; h, hindgut; oe, oesophagus; pa, posterior adductor muscle; s, stomach.

Distribution and Habitat (Fig. 73)

This species was recorded in the Bering Sea (Commander Basin) at a depth from 489 m (55°23.8'N, 167°15.52'E) to 4,294 m (55°36.1'N, 167°23.04'E); in Kamchatsky Strait, Bering Sea, at 4,382 m (55°52'N, 164°08'E) to 4,811 m (55°39'N, 164°31'E); off southeastern Kamchatka, Pacific Ocean, at 4,890–4,984 m (53°05.4'N, 161°55.2'E–53°20.7'N, 161°56.1'E).

Comparisons

Silicula beringiana is easily distinguished from *S. fragilis*, *S. filatovae*, *S. rouchi* and *S. alleni* in having a highly elongated shell with the posterior end produced like a rostrum and

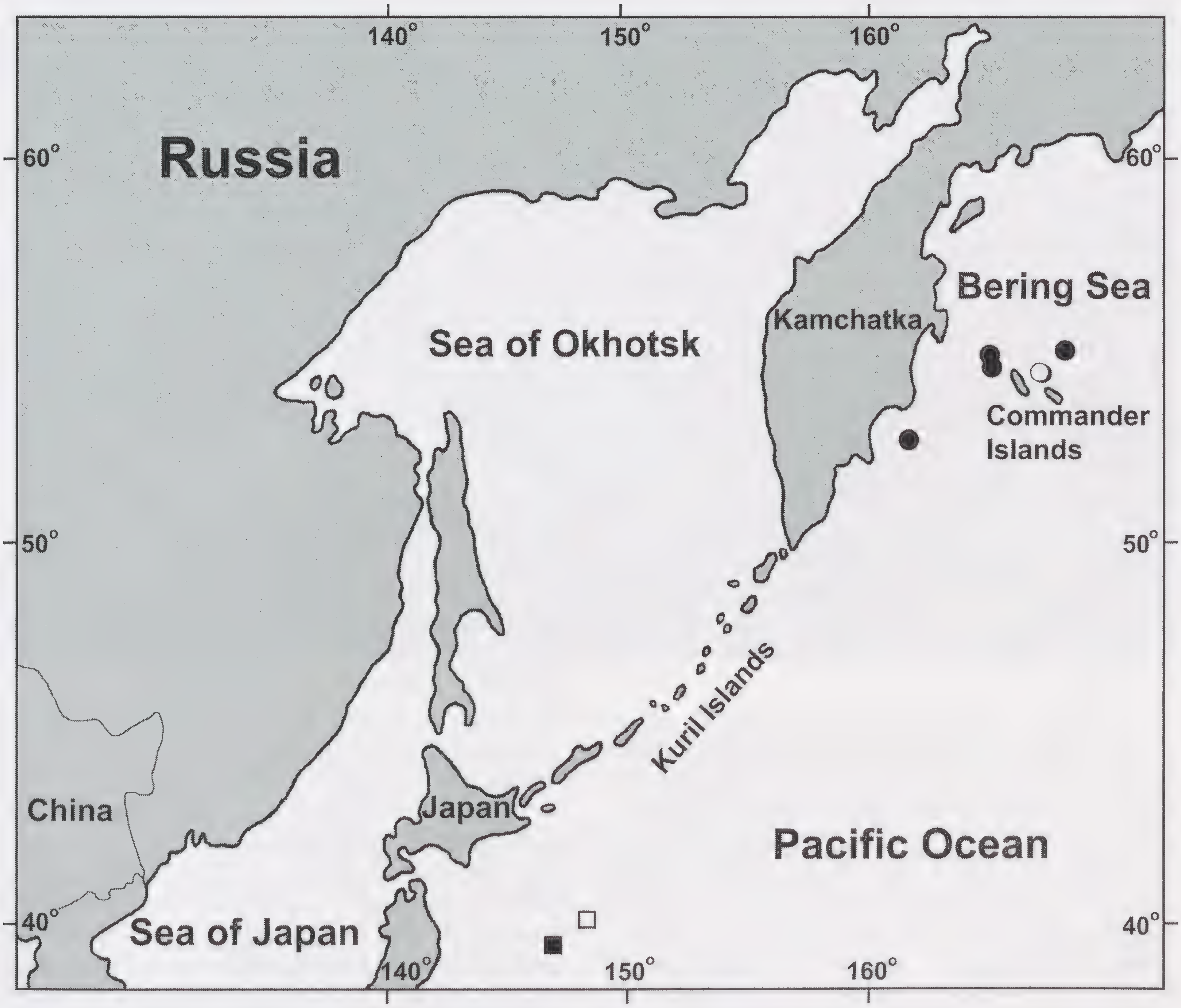

FIG. 73. Distribution of ***Silicula beringiana*** and ***Silicula okutanii***. ● ***S. beringiana*** (○ type locality), ■ ***S. okutanii*** (□ type locality).

truncated (Figs. 74–85, Table 3). According to shell shape and proportions, this species is most close to *S. patagonica* and *S. mcalesteri*, which have an elongate shell with a produced and truncated posterior end. Adult specimens of ***S. beringiana*** well differ from *S. mcalesteri* in having a more flattened ($W/L_{S.\ mcalesteri} = 0.27$; $W/L_{S.\ beringiana} = 0.204$) (Allen & Sanders, 1973), nontransparent, thicker shell with the beaks less displaced anteriorly, a more rounded anterior end and a straight or concave posterodorsal margin, no more than 6 instead of 8 posterior teeth in the hinge, a far smaller prodissoconch, and two large loops of the gut in both sides of the body but not one loop only in the right side (Figs. 86–88).

A fairly complete comparison of ***S. beringiana*** and *S. patagonica* is hindered because the holotype of *S. patagonica* is represented merely by one damaged valve 8.4 mm long (Dall, 1908; Fig. 89, 90). Judging from the position of the inner pit, which is under the beak (Dall, 1908), the beak of *S. patagonica* is much more displaced anteriorly compared to ***S. beringiana***. In the figure and photo of the valves of *S. patagonica* with a shell length of 9.8 and 8 mm provided in works of Dell (1990) and Villarroel & Stuardo (1998), the position of the beaks nearly corresponds to that in ***S. beringiana***. However, large specimens of ***S. beringiana*** (larger than 9 mm), unlike *S. patagonica*, have a more elongate shell with a narrow and truncated posterior end and a straight or concave posterodorsal margin (Table 3).

Etymology

The species name “beringiana” derives from the name of the Bering Sea, where almost entire material of this species was collected.

Remarks

Allen & Sanders (1973) noted that in contrast to the close genera *Poroleda* and *Propeleda*, representatives of the genus *Silicula* have a slightly convex or straight, but not concave posterodorsal shell margin. Nevertheless, adult specimens of ***S. beringiana***, *S. fragilis* and *S. rouchi* often have a slightly concave posterodorsal shell margin (Figs. 74–79). Therefore, I think that the lack of concavity in the posterodorsal shell margin is an erroneous distinctive character of the genus *Silicula*.

Allen & Sanders (1973) showed that the shell of *Silicula* species investigated by them elongates as it grows. This elongation is largely posterior growth of the shell. Similarly, shell shape and proportions in ***S. beringiana*** change as its shell grows. In juvenile specimens, the shell is less elongate and the beaks are located closer to the middle of the shell. As the shell size increases, the posterior shell end elongates, the rostrum becomes narrower, slightly curves upwards, and the beaks, correspondingly, are displaced anteriorly.

Due to the transparent shell of *S. filatovae* and *S. mcalesteri,* Allen & Sanders (1973) were able to determine the degree of development of the gonad through the shell. Specimens of ***S. beringiana*** larger than 9 mm have an opaque shell. Therefore, the shells of specimens of varying size from stations 2309 and 2316 were opened for the study of the gonads. However, it was not possible to determine the sex in all the specimens because the gonads were immature.

Silicula beringiana was found at depths of 489–4,984 m. At present, this is the largest depth range for *Silicula* species. *S. patagonica*, *S. rouchi* and *S. mcalesteri* were only recorded in the shelf and bathyal zones at depths of 135 to 1,153 m (Dall, 1908; Lamy, 1910, 1911; Dell, 1964, 1990; Allen & Sanders, 1973; Egorova, 1982; Villarroel & Stuardo, 1998; D. G. Zelaya, personal communication). *Silicula fragilis* was found from the lower bathyal to abyssal zone (1,493–4,402 m), *S. alleni* (3650 m) and *S. filatovae* (3,826–5,042 m) in the abyssal zone (Allen & Sanders, 1973; Bernard, 1989).

Almost all specimens of ***S. beringiana*** were discovered in the deep-sea basin of the Bering Sea and in the deep-water Kamchatsky Strait connecting the Bering Sea and the Pacific Ocean. Only one specimen of this species was found in the Pacific Ocean to the south of the Kamchatsky Strait. However, 5 strongly damaged specimens of siliculids that closely resemble ***S. beringiana*** were taken at a depth of 4,180 m in the Pacific Ocean south of Unimak Island (53°25’0N, 163°23’0W, Aleutian Islands, U.S.A.). It is therefore very likely that further studies will reveal ***S. beringiana*** in other regions of the North Pacific.

At stations 2316 and 2309 (R/V “Akademik Mstislav Keldysh”, cruise 22), conducted at maximum depths (3,957–4,294 m) of the Bering Sea, ***S. beringiana*** was found in very large numbers. This species comprised more than 50% of the total number of all bivalve specimens in the sample. Therefore, it can be stated that ***S. beringiana*** is one of the dominant species of bivalves at maximum depths of the deep-water basin of the Bering Sea.

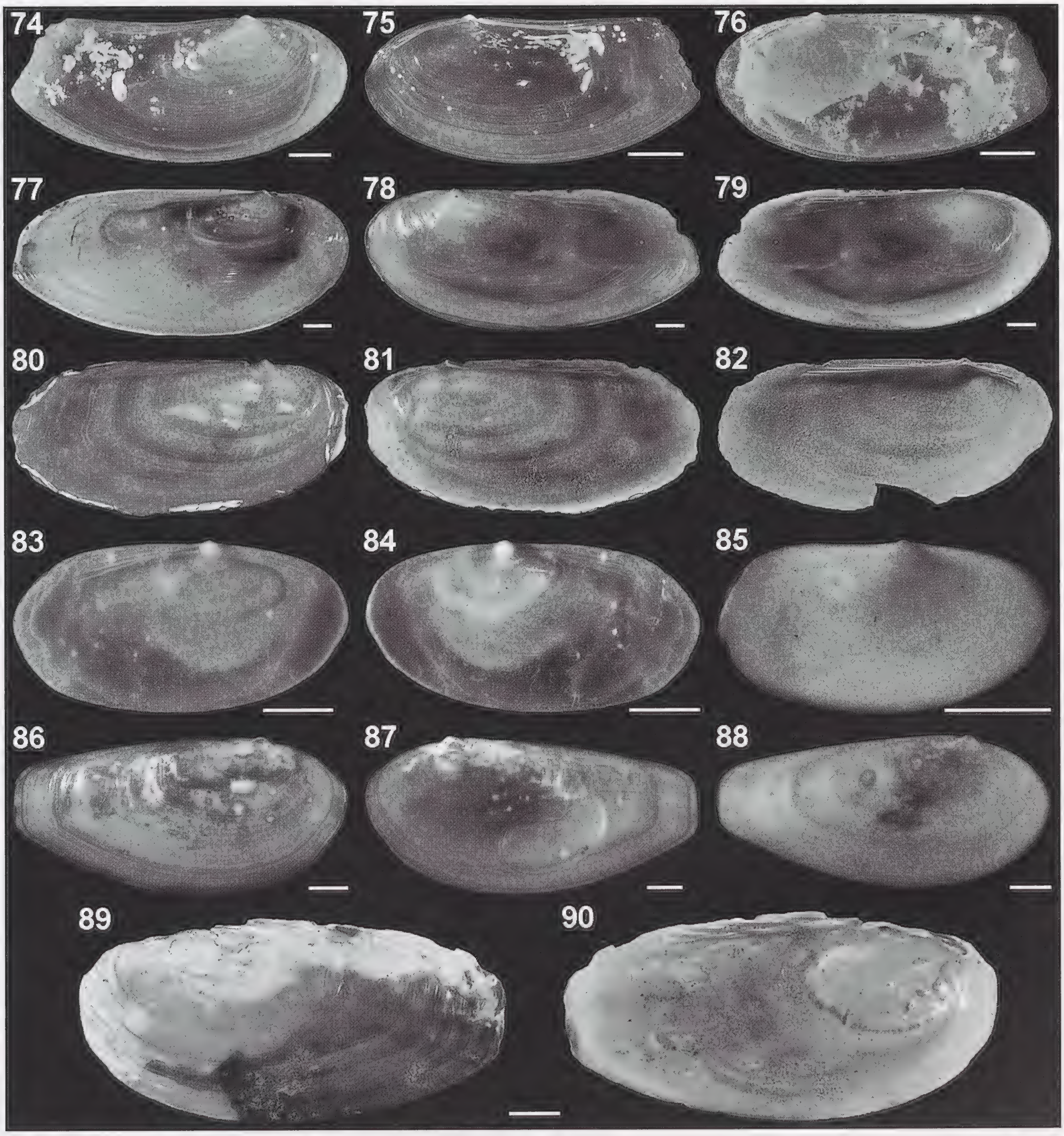

FIGS. 74–90. Species of the genus *Silicula*. FIGS. 74–76: *Silicula fragilis*, exterior view of right valve (NWM, image number M011727), interior view of right valve (NWM, image number M011725), exterior view of left valve (NWM, image number M011726). Photos from Marine Bivalve Shells of the British Isles web site (Oliver et al., 2010); FIGS. 77–79: *Silicula rouchi*, interior view of right valve (photo by D. G. Zelaya), exterior and interior views of left valve (USNM 870326). Photos from USNM Web site, "Information provided with the permission of the National Museum of Natural History, Smithsonian Institution, 10th and Constitution Ave. N.W., Washington, DC 20560-0193 (http://www.nmnh.si.edu/)"; FIGS. 80–82: *Silicula alleni*, holotype (LACM 2344), exterior and interior views of right valve, interior view of left valve, shell length 8.6 mm. Photos by L. T. Groves and P. Valentich-Scott; FIGS. 83–85: *Silicula filatovae*. FIGS. 83, 84: Holotype (MCZ 271977); FIG. 85: Paratype (MCZ 361653). Photos by A. J. Baldinger from MCZ Web site, "President and Fellows of Harvard Colledge"; FIGS. 86–88: *Silicula mcalesteri*. FIGS. 86, 87: Holotype (MCZ 271974); FIG. 88: Paratype (MCZ 361654). Photos by A. J. Baldinger from MCZ Web site, "President and Fellows of Harvard Colledge"; FIGS. 89, 90: *Silicula patagonica*, holotype (USNM 96914). Photos from USNM Web site, "Information provided with the permission of the National Museum of Natural History, Smithsonian Institution, 10th and Constitution Ave. N.W., Washington, DC 20560-0193 (http://www.nmnh.si.edu/)". Scale bars = 1 mm.

TABLE 3. Main differentiating characters of *Silicula* species. L – shell length; H – height; W – valve width; A – anterior end length.

Characters	*Silicula fragilis*	*Silicula patagonica*	*Silicula rouchi*	*Silicula alleni*	*Silicula filatovae*	*Silicula mcalesteri*	***Silicula beringiana***	***Silicula okutanii***
Max. Shell Length	8.0 mm	9.8 mm	14.5 mm	8.6 mm	5.2 mm	11.4 mm	14.7 mm	11.8 mm
Shell (H/L)	Opaque, elongate rectangular, high (0.436–0.634)	Opaque, elongate, tapering pasteriorly, low	Semi-transparent, elongate irregular oval, high (0.479)	Semi-transparent, elongate oval, high (0.465)	Transparent, elongate oval, high (0.491–0.559)	Semi-transparent, elongate, tapering pasteriorly, low (0.43–0.48)	Opaque, elongate, tapering pasteriorly, high (0.444–0.533)	Transparent, very elongate, tapering pasteriorly, very low (0.397–0.444)
Valves (W/L)	Very flattened (0.16)	No data	Very flattened (0.17)	Flattened (0.244)	Very flattened (0.17)	Flattened (0.27)	Flattened (0.204)	Very flattened (0.165)
Position of Beaks (A/L)	Strongly anterior	Strongly anterior	Strongly anterior	Strongly anterior	Slightly anterior	Strongly anterior	Strongly anterior (0.347)	Strongly anterior (0.296)
Posterior Shell End	Broad, obliquely truncated	Narrow, not truncated	Broad, slightly truncated	Broad, rounded, not truncated	Broad, rounded, not truncated	Narrow, truncated	Narrow, truncated	Narrow, truncated
Posterodorsal Shell Margin	Straight or concave	Slightly convex	Straight or slightly concave	Straight	Slightly convex	Slightly convex	Straight or concave	Straight or slightly convex
Prodisoconch (mμ)	Small, 200	No data	No data	No data	Middle, 290–310	Large, 580	Small, 190–207	Small, 190–207
Teeth	Parallel to dorsal shell margin, arise from ventral edge of hinge plate; posterior teeth very long	Almost parallel to dorsal shell margin, arise from ventral edge of hinge plate; posterior teeth long	Parallel to dorsal shell margin; posterior teeth very long, arise from ventral edge of hinge plate, anterior teeth diverge from dorsal shell margin	Parallel to dorsal shell margin, arise from ventral edge of hinge plate; posterior teeth very long	Almost parallel to dorsal shell margin, diverge from dorsal shell margin; posterior teeth very long	Almost parallel to dorsal shell margin, arise from ventral edge of hinge plate; posterior teeth long	Almost parallel to dorsal shell margin, arise from ventral edge of hinge plate; posterior teeth long	Almost parallel to dorsal shell margin, arise from ventral edge of hinge plate; posterior teeth very long
Max. No. of Anterior and Posterior Teeth	4 and 5	No data	5 and 7	No data	3 and 4	5 and 8	5 and 6	6 and 7
Gut Loops	Two loops on both sides of body	No data	One loop on right side of body	No data	One loop on right side of body	One loop on right side of body	Two loops on both sides of body	Two loops on both sides of body
References	Allen & Sanders, 1973; Oliver et al., 2010	Dall, 1908; Allen & Sanders, 1973; Dell, 1990; Villarroel & Stuardo, 1998	Lamy, 1911; Allen & Sanders, 1973; Egorova, 1982; Dell, 1990; Hain, 1990; Villarroel & Stuardo, 1998	Bernard, 1989; Coan et al., 2000	Allen & Sanders, 1973	Allen & Sanders, 1973		

Silicula okutanii
Kamenev, n. sp.
(Figs. 71, 91–119, Table 4)

Type Material and Locality

Holotype (MIMB 28315), Pacific Ocean (40°13.33'N, 148°6.48'E–40°12.53'N, 148°5.76'E), 5,348–5,347 m, Agassiz trawl, Coll. G. M. Kamenev, 30-VIII-2012 (R/V "Sonne", cruise 223, stn. 11-10); paratypes (3) (MIMB 28316), Pacific Ocean (40°13.10'N, 148°6.45'E–40°12.10'N, 148°5.53'E), 5,351–5,348 m, epibenthic sledge, Coll. G. M. Kamenev, 31-VIII-2012 (R/V "Sonne", cruise 223, stn. 11-12).

Other Material Examined

Two specimens from holotype locality; 8 specimens (MIMB 28317), Pacific Ocean (39°43.80'N, 147°10.16'E–39°42.49'N, 147°9.37'E), 5,224–5,215 m, epibenthic sledge, Coll. G. M. Kamenev, 1-IX-2012 (R/V "Sonne", cruise 223, stn. 12-4); 2 specimens (MIMB 28318), Pacific Ocean (39°43.47'N, 147°10.11'E–39°42.54'N, 147°9.51'E), 5,229–5,217 m, Agassiz trawl, Coll. G. M. Kamenev, 1-IX-2012 (R/V "Sonne", cruise 223, stn. 12-5); 2 specimens (MIMB 28319), Pacific Ocean (39°43.43'N, 147°9.98'E), 5,243 m, boxcorer, Coll. G. M. Kamenev, 31-VIII-2012 (R/V "Sonne", cruise 223, stn. 12-2). Total of 18 specimens.

TABLE 4. ***Silicula okutanii*** Kamenev, sp. nov. Shell measurements (mm), indices and summary statistics of characters, n = 17, size range of shells used 7.1 to 11.8 mm: L – shell length; H – height; W – width; A – anterior end length.

Depository	L	H	A	W	H/L	A/L	W/L
Holotype MIMB 28315	11.7	4.8	3.4	2.2	0.410	0.291	0.188
Paratype MIMB 28316	11.6	4.7	3.4	1.8	0.405	0.293	0.155
Paratype MIMB 28316	11.1	4.5	3.2	1.8	0.405	0.288	0.162
Paratype MIMB 28316	8.1	3.6	2.5	1.3	0.444	0.309	0.160
MIMB 28317	11.8	4.9	3.5	2.0	0.415	0.297	0.169
MIMB 28317	10.8	4.5	3.3	1.6	0.417	0.306	0.148
MIMB 28317	10.3	4.2	3.0	1.5	0.408	0.291	0.146
MIMB 28317	9.6	4.0	2.8	1.5	0.417	0.292	0.156
MIMB 28317	9.6	3.9	2.8	1.6	0.406	0.292	0.167
MIMB 28317	8.9	3.7	2.6	1.4	0.416	0.292	0.157
MIMB 28317	8.8	3.5	2.6	1.4	0.398	0.295	0.159
MIMB 28317	8.5	3.6	2.6	1.3	0.424	0.306	0.153
MIMB 28319	8.5	3.5	2.5	1.3	0.412	0.294	0.153
MIMB 28319	8.1	3.4	2.4	1.6	0.420	0.296	0.198
MIMB 28320	8.0	3.4	2.4	1.6	0.425	0.300	0.200
MIMB 28320	7.8	3.1	2.3	1.4	0.397	0.295	0.179
MIMB 28318	7.1	3.0	2.1	1.1	0.423	0.296	0.155
Statistics	L	H	A	W	H/L	A/L	W/L
Mean	-	-	-	-	0.414	0.296	0.165
SE	-	-	-	-	0.003	0.001	0.004
SD	-	-	-	-	0.011	0.006	0.017
Min	-	-	-	-	0.397	0.288	0.146
Max	-	-	-	-	0.444	0.309	0.200

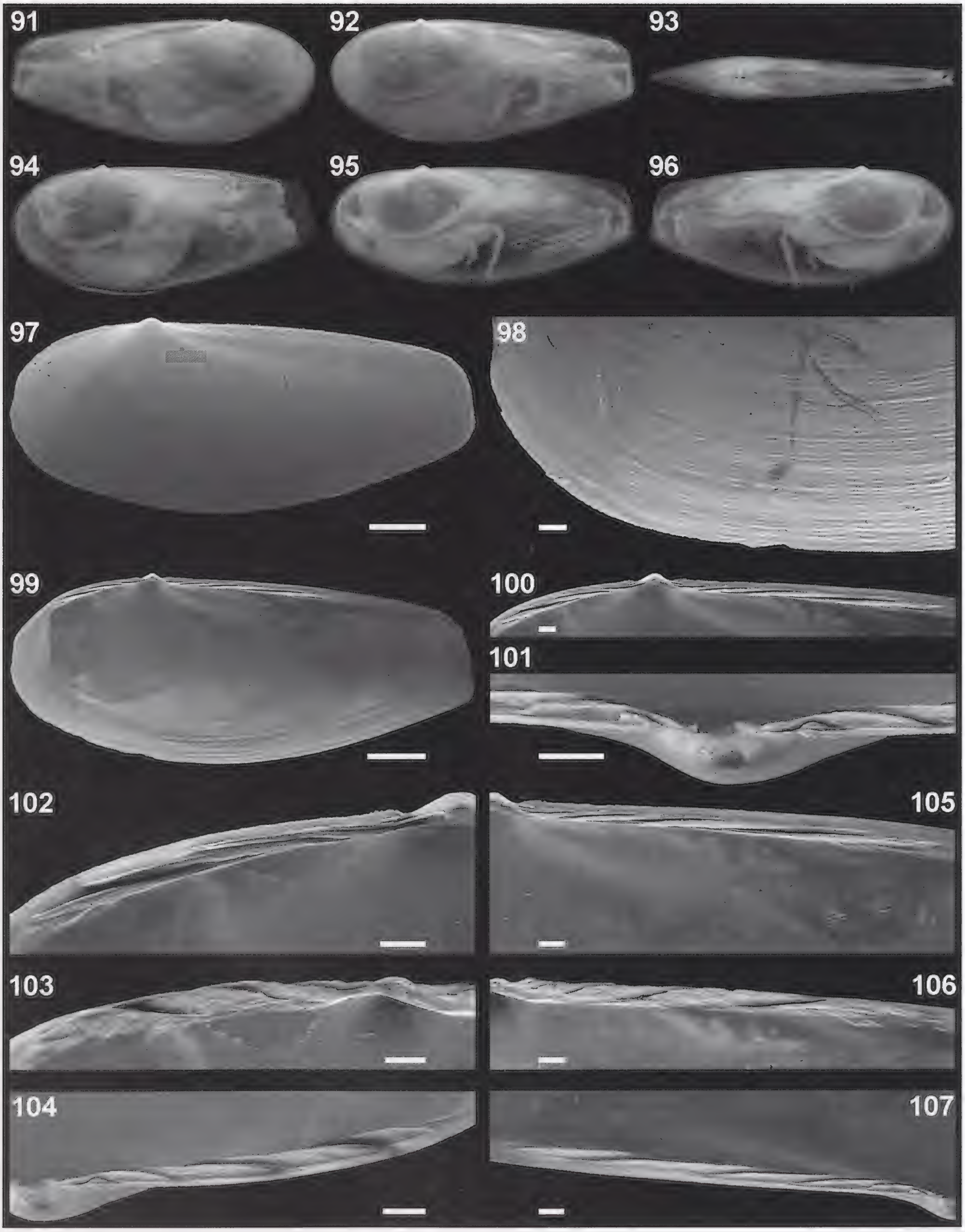

FIGS. 91–107. ***Silicula okutanii*** Kamenev, n. sp. FIGS. 91–93: Holotype (MIMB 28315), exterior and dorsal views of both valves, shell length 11.7 mm; FIGS. 94–107: Shells of different age specimens. FIG. 94: Exterior view of left valve of specimen (MIMB 28320) from holotype locality, shell length 8.0 mm; FIG. 95–107. Specimen (MIMB 28320) from holotype locality, shell length 7.8 mm. FIGS. 95, 96: Exterior view of left and right valves; FIGS. 97–99: Exterior and interior views of left valve; FIGS. 100–107: Hinge plate, dorsal view of beak, anterior (ventral and dorsal views) and posterior (ventral and dorsal views) sets of teeth. Scale bars: Figs. 97, 99 = 1 mm, Figs. 98, 100–107 = 200 μm.

Description

Exterior: Shell small (to 11.8 mm), very elongate (H/L = 0.414 ± 0.003), equivalve, strongly inequilateral, gaping anteriorly and posteriorly, very flattened (W/L = 0.165 ± 0.004), very thin, fragile, transparent. Surface with very thin, dense, commarginal ribs, best defined along ventral margin and sparse radial rays formed by densely spaced short concentric riblets most expressed at anterior shell end. Periostracum thin, adherent, yellow-green. Beaks small, very low, slightly prominent above dorsal shell margin, rounded, prosogyrate, strongly anterior to midline (A/L = 0.296 ± 0.001). Anterior shell end smoothly rounded. Posterior shell end very extended, tapered, truncated, with long, very week flexure and shallow sulcus extending from beaks to posterior shell margin. Dorsal shell margin anterior to posterior to beaks forming very small concavities. Anterodorsal shell margin slightly convex, almost horizontal, smoothly transitioning to anterior shell margin. Anterior shell margin smoothly rounded. Posterodorsal shell margin slightly convex, forming a distinct, rounded obtuse angle at transition to posterior shell margin. Posterior shell margin short, straight or slightly convex, directed slightly posterior, forming a distinct, weakly rounded angle at transition to ventral shell margin. Ventral shell margin gently curved. Prodissoconch small (length 193–227 μm), D-shaped, distinctly marked, with net-like, cellular sculpture.

Interior: Hinge plate narrow, long, slightly curved. Teeth divided into anterior and posterior sets by small, edentulous gap of hinge plate with resilifer. Internal ligament opisthodetic, well developed, large, elongate, extending posteriorly from beaks. Resilifer elongate, narrow, oblique, directed posteriorly (somewhat into shell) from beaks to almost end of first posterior tooth. Anterior teeth set of 5–6 teeth, posterior one 6–7. Anterior teeth narrow, long, overlapping each other, almost parallel to anterodorsal shell margin, becoming longer towards anterior shell margin, except very short last tooth in largest specimens. First anterior tooth slightly concave, low, thinnest, arising from dorsal margin of hinge plate under beak; teeth 2–5 by far longer, highest, straight or slightly convex; tooth 6 shortest and lowest, weakly expressed, located almost entirely under tooth 5. Second tooth, like first tooth, arising from dorsal margin of hinge plate under beak. Teeth 3–6 arising from ventral margin of hinge plate. Posterior teeth narrow, longer than anterior teeth, overlapping each other, parallel to posterodorsal shell margin, almost horizontal, becoming longer towards posterior shell margin, except last short tooth. First posterior tooth slightly concave, thinnest, low, located under resilifer, arising from dorsal margin of hinge plate under beak. Second tooth 2–2.5 times longer than first tooth, slightly concave, arising from dorsal margin of hinge plate under beak, partially forming posterodorsal margin of resilifer. Tooth 3 straight, extending from ventral margin of hinge plate at posterior resilifer end. Teeth 4–6 straight, longest, arising from ventral margin of hinge plate. Tooth 7 straight, short, weakly expressed, low, almost entirely located under tooth 6, present only in largest specimens. Adductors scars weakly visible, unequal; anterior adductor scar larger than posterior. Anterior adductor scar slightly elongated, almost vertically extended, located under anterior end of hinge plate. Posterior adductor scar highly elongated, almost horizontally extended, located under posterior end of hinge plate. Pallial line extending beyond posterior adductor scar, forming a very shallow pallial sinus, not confluent with pallial line; sinus apex reaching to middle of ventral margin of posterior adductor scar.

Anatomy: Internal morphology similar to that of ***S. beringiana***. Mantle very thin, except thickened ventral margin. Exhalant siphon very long. Both adductor muscles oval, elongated; anterior muscle larger than posterior, oblique, directed anterodorsally; posterior muscle extending almost horizontally. Foot large, with a large anterior toe and a small posterior heel; toe with numerous papillae of varying size. Posterior pairs of pedal retractors large, wide, passing anterior to posterior adductor muscle. Three anterior pairs of pedal retractor muscles narrow, long, running between anterior adductor muscle and stomach. Gills long, narrow, almost horizontal, extending from ventral side of stomach to ventral side of posterior adductor muscle; gill filaments short. Palps short, with 20 palp ridges, almost parallel to ventral shell margin, occupying central part of mantle cavity. Palp proboscides very long in contracted state. Mouth located in central part of mantle cavity. Oesophagus long, displaced to right side of body, passing posterior to anterior adductor scar and along anterodorsal shell margin, forming a large uniformly rounded bend. Stomach large, globular, lying in space under beaks, along dorsoventral axis. Combined style sac and midgut leaving stomach at posteroventral border, passing ventrally into foot. Hindgut penetrating deep into foot heel, forming a short loop, turning dorsally, passing posterior to style sac in right side of body. In right side of body hindgut forming a broad and smooth curve posterodorsally, then sharply curving ventrally, passing under beaks into left side of body. In left side of body, hindgut forming a rounded loop, passing under beaks backward to right side of body. Here hindgut forming a large rounded loop corresponding to stomach size, turning posteriorly under beak and passing along posterodorsal shell margin above posterior adductor muscle to anus. Digestive diverticula surrounding anterior adductor muscle, oesophagus, stomach, partially labial palps and gills.

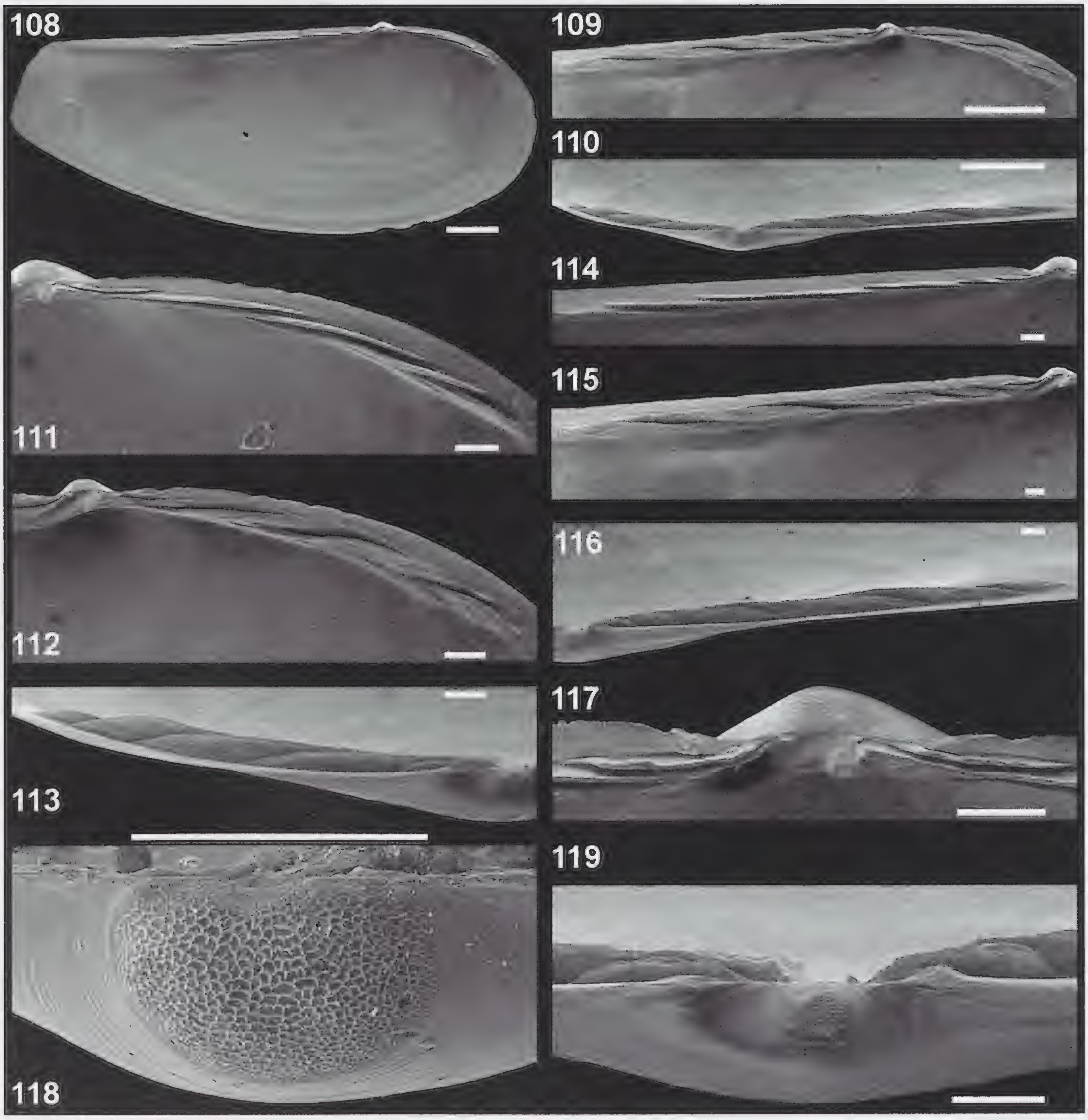

FIGS. 108–119. ***Silicula okutanii*** Kamenev, n. sp. Interior morphology of left valve of adult specimen (MIMB 28317), Pacific Ocean (39°43.80'N, 147°10.16'E–39°42.49'N, 147°9.37'E), 5,224–5,215 m. FIGS: 108–110: Internal view of valve, ventral and dorsal views of hinge plate; FIGS. 111–113: Anterior (ventral and dorsal views) set of teeth; FIGS. 114–116: Posterior (ventral and dorsal views) set of teeth; FIGS: 117–119: Resilifer, prodissoconch, dorsal view of beak. Scale bars: Figs. 108–110 = 1 mm, Figs. 111–119 = 200 μm.

TABLE 5. Results of comparison by pairs of mean values (T-test) and variances (ANOVA) of indices of the shells of ***Silicula beringiana*** and ***Silicula okutanii***: L – shell length; A – anterior end length; H – height; W – width; P – probability that index values in ***S. beringiana*** and ***S. okutanii*** are drawn from the same population; n – number of valves of compared species, respectively; * – significant difference.

Indices	T-test		ANOVA		
	T	P	F	T	n
A/L*	17.67	< 0.001	104.66	A/L*	17.67
H/L*	17.89	< 0.001	149.43	H/L*	17.89
W/L*	8.27	< 0.001	54.22	W/L*	8.27

Variability

The shell shape and proportions of ***S. okutanii*** little changes with age. In most of young specimens (L < 9 mm), the shell is slightly higher (H/L = 0.412–0.444) with beaks less displaced anteriorly (A/L = 0.294–0.309), compared to specimens with a shell length more than 10 mm (H/L = 0.405–0.417; A/L = 0.288–0.306). However, some young specimens had the same shell proportions as in adult specimens. Specimens with a length less than 7 mm were lacking in the examined material. It is possible that more distinct differences in shell shape may be found between juvenile and adult specimens. Adult specimens show slight variations of shell height, relative position of beaks, and the degree of convexity of the posterodorsal shell margin (sometimes almost straight).

Distribution and Habitat (Fig. 73)

This species was recorded in the northwestern Pacific at a latitude of the northern part of Japan at 5,219–5,352 m depth (bottom temperature 1.6°C, salinity 34.7‰).

Comparisons

Like ***S. beringiana***, ***S. okutanii*** is readily distinguished from *S. fragilis*, *S. filatovae*, *S. rouchi* and *S. alleni* in having a strongly elongate shell with its posterior end extended in the form of a rostrum and truncated (Figs. 74–85). ***Silicula okutanii*** is most close in shell shape and proportions to *S. patagonica*, *S. mcalesteri* and ***S. beringiana***, which also have elongate shells with extended and truncated posterior end (Figs. 25–69, 86–90). However, in contrast to these three species, ***S. okutanii*** has a markedly lower and elongate shell with more extended and tapering posterior end (Table 3). Furthermore, ***S. okutanii*** differs from *S. mcalesteri* in having a thinner and more flattened shell (W/L$_{\textit{S. mcalesteri}}$ = 0.27; W/L$_{\textit{S. okutanii}}$ = 0.165) with more rounded and more extended anterior end, much smaller prodissoconch, fewer posterior teeth in the hinge, almost horizontal position of the posterior adductor muscle, the presence of large intestinal loops in both sides of the body, but not one loop in the right side (Allen & Sanders, 1973). Compared to *S. patagonica*, the shell of *S.* ***okutanii,*** in addition to the differences in shape and proportions, is thinner, translucent and the apex of the pallial sinus does not project beyond posterior adductor scar.

Silicula okutanii is most close to ***S. beringiana***, from which it differs in its more flattened and elongate shell with more extended posterior end and more rounded anterior end. Mean values and variances of the indices characterizing the position of beaks (A/L), the relative height (H/L) and width (W/L) in ***S. okutanii*** were significantly different from the mean values and variances of the same indices of ***S. beringiana*** (Table 5). Besides, unlike *S.* ***beringiana***, ***S. okutanii*** has a thinner, semitransparent shell with slightly convex posterodorsal margin, relatively longer posterior teeth of the hinge, almost horizontally located posterior adductor muscle, less deep pallial sinus, fewer palp ridges.

Etymology

The species name honors Professor, Dr. T. Okutani, a noted malacologist who made a great contribution to the study of the molluscan fauna of the northwestern Pacific.

Remarks

Like most species of the genus *Silicula*, the posterior shell end of ***S. okutanii*** becomes longer as it grows, and the beaks are thus displaced anteriorly. In contrast to ***S. beringiana***, ***S. okutanii*** has a transparent shell through which the body is well visible. However, I failed to determine the sex in all examined specimens of this species as they showed no sign of gonadal development.

Silicula okutanii is an abyssal species. This is the most deep water species of the genus *Silicula.* All specimens of ***S. okutanii*** were recorded in all samples collected with the different sampling gear at the two southernmost stations of the KuramBio expedition conducted at the coast of Japan at depth greater than 5,200 m. Most often, there were several specimens in a sample. Thus, ***S. okutanii***, while not forming the mass aggregations of ***S. beringiana*** in the abyssal of the Bering Sea is, nevertheless, a fairly common, though not numerous species of the deep-sea macrobenthos fauna. Interestingly, ***S. okutanii*** was not found at the other 10 stations of the KuramBio expedition conducted to the north of Japan (up to the latitude of the northern Kuril Islands) at 4,859–5,780 m depths. It is possible that in the northwestern Pacific at latitudes north of Japan this species either may be rarer or may not occur whatsoever.

ACKNOWLEDGMENTS

I am very grateful to Drs. A. V. Gebruk, E. M. Krylova, T. N. Molodtsova and all collaborators of Laboratory of Ocean Bottom Fauna (IO RAS), as well as to Dr. H. Saito (NSMT) for arrangement of my work with the bivalve mollusk collections at the IO RAS and NSMT and great help during this work; to Dr. M. V. Malyutina (MIMB) and Prof. Dr. A. Brandt (Zoological Institute and Zoological Museum, Hamburg) for invitation and arrangement of my work in the German-Russian deep-sea expedition KuramBio (R/V "Sonne") as well as all scientific stuff of the expedition and the ship crew for help during expedition; to Drs. E. V. Coan (Department of Invertebrate Zoology, California Academy of Sciences, San Francisco), E. M. Krylova, D. G. Zelaya (Departamento de Biodiversidad y Biologia Experimental, Facultad de Ciencias Exactas y Naturales, Universidad de Buenos Aires, Buenos Aires), Mr. P. Valentich-Scott (Santa Barbara Museum of Natural History, Santa Barbara) for the sending copies of scientific papers necessary for this work; to Drs. L. T. Groves (LACM), D. G. Zelaya, P. Valentich-Scott, A. J. Baldinger (MCZ) for sending photos of *Silicula* species; to Dr. A. M. Holmes (NMW) for help during this work; to Ms. T. N. Koznova (IMB) for help with translating the manuscript into English; to Dr. G. M. Davis (George Washington University, Washington, D.C.) for help in the publication of manuscript; to two anonymous reviewers for comments on the manuscript.

This research was supported by the Russian Foundation for Basic Research (grants no. 11-04-00328-a and no. 14-04-00872-a).

LITERATURE CITED

ANGAS, G. F., 1877, Description of one genus and twenty-five species of marine shells from New South Wales. *Proceedings of the Zoological Society of London*, 45: 171–177.

ALLEN, J. A. & H. L. SANDERS, 1973, Studies on deep-sea Protobranchia (Bivalvia); the families Siliculidae and Lametilidae. *Bulletin of the Museum Comparative Zoology*, 145: 263–310.

BERNARD, F. R., 1989, Six new species of the Order Septibranchia (Bivalvia) from the Northeastern Pacific Ocean. *Venus*, 48: 61–66.

COAN, E. V., P. V. SCOTT & F. R. BERNARD, 2000, *Bivalve seashells of western North America. Marine bivalve mollusks from Arctic Alaska to Baja California.* Santa Barbara Museum of Natural History, Santa Barbara, California, viii + 764 pp.

COTTON, B. C., 1930, Pelecypoda of the "Flindersian" region, southern Australia. No. 1. *Records of the South Australian Museum*, 4: 223–240.

DALL, W. H., 1908, The Mollusca and the Brachiopoda. *Bulletin of the Museum of Comparative Zoology*, 43: 205–487.

DELL, R. K., 1964, Antarctic and Subantarctic Mollusca: Amphineura, Scaphopoda and Bivalvia. *Discovery Reports*, 33: 93–250.

DELL, R. K., 1990, Antarctic Mollusca with special reference to the fauna of the Ross Sea. *Bulletin of the Royal Society of New Zealand*, 27: 1–311.

EGOROVA, E. N., 1982, Mollusks of the Davis Sea. Biological results of the Soviet Antarctic expeditions, 7. *Explorations of the fauna of the seas*, 26(34): 1–143 [in Russian].

HAIN, S., 1990, *The benthic seashells (Gastropoda and Bivalvia) of the Weddell Sea, Antarctica. Berichte zur Polarforschung*, 70: 121 pp.

HEDLEY, C., 1905, Results of dredging on the continental shelf of New Zealand. *Transactions and Proceedings of the Royal Society of New Zealand*, 38: 68–76.

HEDLEY, C., 1915, Studies on Australian Mollusca. Part XII. *The Proceedings of the Linnean Society of New South Wales*, 39: 695–755.

HEINBERG, C., 1989, Bivalves from the white chalk (Maastrichtian) of Denmark, IV: Nuculoida. *Bulletin of the Geological Society of Denmark*, 37: 227–236.

HUBER, M., 2010, *Compendium of bivalves. A full-color guide to 3'300 of the world's marine bivalves. A status on Bivalvia after 250 years of research.* ConchBooks, Hackenheim, 901 pp.

HUTTON, F. W., 1885, Descriptions of new Tertiary shells. Part I. *Transactions of the New Zealand Institute*, 17(Geology): 313–332, pl. 18.

HUTTON, F. W., 1893, The Pliocene Mollusca of New Zealand. *Linnean Society of New South Wales, Macleary Memorial Volume*: 35–92, pls. 6–9.

IREDALE, T., 1924, Results from Roy Bell's molluscan collections. *Proceedings of the Linnean Society of New South Wales*, 49: 179–278.

JEFFREYS, J. G., 1879, On the Mollusca procured during the *Lightning* and *Porcupine* expeditions. II. *Proceedings of the Zoological Society of London*, for 1879(3): 553–588.

LAMY, E., 1910, Mission dans l'Antarctique dirigée par le Dr. Jacqnes Liouville. Pélécypodes. *Bulletin du Museum National d'Historie Naturelle, Paris*, 16: 388–394.

LAMY, E., 1911, Gastropodes, prosobranches, dcaphopodes et pélécypodes. Deuxiéme Expedition Antarctique Francais (1908–1910) commandée par le Jean Charcot. *Sciences Naturelles: Documents Scientifiques*: 1–31.

LUDBROOK, N. H., 1961, Revision of the Tate molluscan types: Pelecypoda – Nuculidae and Nuculanidae. *Transacations of the Royal Society of South Australia*, 85: 55–65.

NIJSSEN-MEYER, J., 1972, *Propeleda platessa* (Dall, 1890), a nut clam new for the coastal waters of Surinam (Pelecypoda, Nuculanidae). *Zoologische Mededelingen*, 47: 449–456.

OKUTANI, T., 1962, Report on the archibenthal and abyssal lamellibranchiate Mollusca mainly collected from Sagami Bay and adjacent waters by the R.V. *Soyou-Maru* during the years 1955–1960. *Bulletin of the Tokai Regional Fisheries Research Laboratory*, 32: 1–40.

OKUTANI, T., ed., 2000, *Marine mollusks in Japan.* Tokai University Press, Tokyo, 1,175 pp.

OLIVER, P. G., A. M. HOLMES, I. J. KILLEEN & J. A. TURNER, 2010, *Marine bivalve shells of the British Isles* (Mollusca: Bivalvia). Amgueddfa Cymru – National Museum Wales. Available online at http://naturalhistory.museumwales.ac.uk/britishbivalves.

VILLARROEL, M. & J. STUARDO, 1998, Protobranchia (Mollusca: Bivalvia) Chilenos recientes y algunos fósiles. *Malacologia*, 40: 113–229.

Revised ms. accepted January 14, 2014

MALACOLOGIA, 2014, 57(2): 279–293

PANOPEA ABBREVIATA (BIVALVIA: HIATELLIDAE) IN THE SOUTHWESTERN ATLANTIC OCEAN, TAXONOMIC REVISION AND ANATOMY

Javier H. Signorelli* & José E. F. Alfaya

Biología y Manejo de Recursos Acuáticos, LARBIM – CENPAT – CONICET,
Bvd. Brown 2915, U9120ACD, Puerto Madryn, Chubut, Argentina

ABSTRACT

The taxonomy and anatomy of the southwestern Atlantic geoduck, *Panopea abbreviata* Valenciennes, 1839, are revised. Materials from several institutions, as well as new living specimens collected from the coast of Argentina were studied. Type materials of all related nominal species are illustrated. The shell morphology, shell ultrastructure, hinge, ligament and mantle cavity organs are described. The symbiotic relationship with the nemertean *Malacobdella arrokeana*, attached to host mantle tissues, is mentioned. *Panopea abbreviata* is abundant in the gulfs of northern Patagonia. It occurs in the subtidal zone from 8 to 25 meters deep, deeply buried in the sediment. It has a large thick shell, shortener at the posterior end, with exposed siphons covered by a dark brownish periostracum; a hinge plate characterized by a single cardinal tooth in each valve; and shell ultrastructure with three layers: an outer layer of nearly vertical and composite prisms, a middle, true homogeneous layer, and an inner layer of alternating sublayers of fine complex crossed lamellar and irregular simple prisms. The fused mantle is only interrupted in the pedal gape. Ctenidia and labial palps association belongs to the Category III and ctenidia type C(1). *Panopea antarctica* is its only synonym. The fossil taxa *Panopea truncata*, *P. inferior*, *P. hauthali*, *P. coquimbensis* and *P. guayacanensis* are excluded from the synonymy.

Key words: *Panopea*, Argentina, taxonomy, anatomy, Hiatellidae.

INTRODUCTION

The suprageneric arrangement of the family Hiatellidae Gray, 1824, was revised by Carter et al. (2011), in which the new Order Hiatellida was introduced to group the superfamilies Edmondioidea W. King, 1850, and Hiatelloidea J. Gray, 1824. Other phylogenetic analyses confirm the relationship of Hiatellidae with the Solenidae and Pharidae (Solenoidea) as a sister group, and excludes it from the Myoida (Adamkewicz et al., 1997; Taylor et al., 2007, among others).

Nine genus-level names were included as valid in the Hiatellidae by Keen (1969). *Degrangia* Cossmann & Peyrot, 1909, and *Panomya* Gray, 1857, were considered subgenera of *Panopea* by Keen. However, they have since been regarded as valid genera (Yonge, 1971; Vaught, 1989; Huber, 2010).

The genus *Panopea* was introduced by Ménard de la Groye (1807). An historical review of this genus was carried out by Dall (1912). He reviewed the previous illustrations of this genus from Aldrovandus in 1606 to Ménard de la Groye in 1807, who finally gave the name of *Panopea aldrovandi* to the Mediterranean species. Dall (1912) mentioned that *Panope*, published in a separate "Mémoire", should be accepted instead *Panopea*, published in the *Annales du Muséum d'Histoire Naturelle*. This taxonomic issue was submitted to the International Commission on Zoological Nomenclature by Vokes & Cox (1961), and almost 25 years after their proposal, the ICZN ruled the correct name to be *Panopea* (ICZN, 1986; Opinion 1414).

Other members of this genus have been studied in different parts of the world. In the northeast Pacific Ocean, several aspects of the biology of *P. generosa*, such as, functional morphology, ecology, morphometry, aquaculture and taxonomic reviews have been carried out (Bower & Blackbourn, 2003; Feldman et al., 2004; Fisher et al., 2008; Goodwin & Pease, 1991; Rocha Olivares et al., 2010; Marshall et al., 2012; Leyva-Valencia et al., 2012). In some publications, the name *P. abrupta* (Conrad, 1849) was considered as valid, with *P. generosa* regarded as a junior synonym. However, Vadopalas et al. (2010) recognized the Recent *P. generosa* as valid and excluded it from the synonymy of Conrad's fossil species. Arambula-Pujol et al. (2008) studied the reproductive biology of *Panopea globosa* (Dall, 1898) in the Gulf of California. The functional morphology of several species of this family was studied by Yonge (1971).

---

*Corresponding author: javierhsignorelli@gmail.com

Along the southwestern Atlantic Ocean, the family Hiatellidae is represented by about 14 species (Carcelles, 1944; Carcelles & Williamson, 1951; Castellanos, 1970; Abbott & Dance, 1986; Scarabino, 2003; Rios, 2009), but only one species of *Panopea* is commonly cited. The geoduck *Panopea abbreviata* (Valenciennes, 1839) is an endemic species well represented all along the Argentine coast (Carcelles, 1944; Carcelles & Williamson, 1951; Castellanos, 1970). It was mentioned by Bernard (1983) as occurring in the Pliocene and as the senior synonym of several species described from the fossil record of Chile and Argentina.

In recent years, this species has been studied as a possible target of artisanal fisheries in north Patagonia (Ciocco et al., 2001; Morsán & Ciocco, 2004; Narvarte & Filippo, 2007; Morsán et al., 2010). The reproductive cycle of *P. abbreviata* was studied by Van der Molen et al. (2007) and Zaidman et al. (2012). The development of these fisheries allowed the study of biological interactions between the geoduck and other organisms. The most studied has been the presence of the symbiotic nemertean *Malacobdella arrokeana* Ivanov, Bigatti, Penchaszadeh & Norenburg, 2002, in its mantle cavity (Ivanov et al., 2002; Martorelli et al., 2003; Vázquez et al., 2009, 2010; Teso et al., 2006; Alfaya et al., 2013). In addition, a new species of flat worm (Platyhelminthes) living in the intestine of *P. abbreviata* was recently described (Brusa et al., 2011). During an ongoing study of genetics, population structure and reproduction of the nemertean *Malacobdella arrokeana* the taxonomic revision and anatomical description of *Panopea abbreviata* was carried out. In addition, the type material of related nominal species was illustrated.

MATERIALS AND METHODS

Living specimens were collected by scuba diving at 20 m from San José gulf (42°24'11"S, 64°17'10"W) (Fig. 1). The microstructure of the valves was analyzed with a scanning electron microscope (JEOL JSM-6460LV, Aluar S.A). The outer shell layer was revealed at posterior shell margin radial section, the middle layer just exterior to the pallial line and the inner layer in the umbonal region. All shell sections were polished with 500 grit sandpaper followed by 1,000 grit sandpaper, then etched the surfaces with 2% hydrochloric for 40 seconds. All type material and additional specimens studied are deposited in the following institutions: Centro Nacional Patagónico (CNP-Inv), Museo Argentino de Ciencias Naturales "Bernardino Rivadavia" (MACN-In), Buenos Aires; Museo de la Plata (MLP); Museúm National d'Histoire Naturelle (MNHN), Paris; Rio Grande do Sul; Museu de Zoologia da Universidade de São Paulo (MZUSP) and the National Museum of Natural History, Smithsonian Institution (USNM), Washington D.C., United States.

Morphological Abbreviations

a	anus
aa	ascendant arm
aam	anterior adductor muscle
cs	ctenidial septum
ct	cardinal tooth
da	descendent arm
dd	digestive diverticula
es	excurrent siphons
fs	fibrous sublayer
f	foot
fg	food groove
g	gonad
hd	hindgut
id	inner demibranch
ilp	inner labial palp
is	incurrent siphon
la	left auricle
lc	left caecum
ls	lamellar sublayer
m	mouth
mc	mantle cavity
md	midgut
od	outer demibranch
olp	outer labial palp
pam	posterior adductor muscle
pa	papillae
p	periostracum
pn	pseudonymphal ridge
r	rectum
ra	right auricle
sa	supporting axis
sae	supraaxial extension
sps	siphonal pallial septum
st	stomach
t	tentacle
v	ventricle

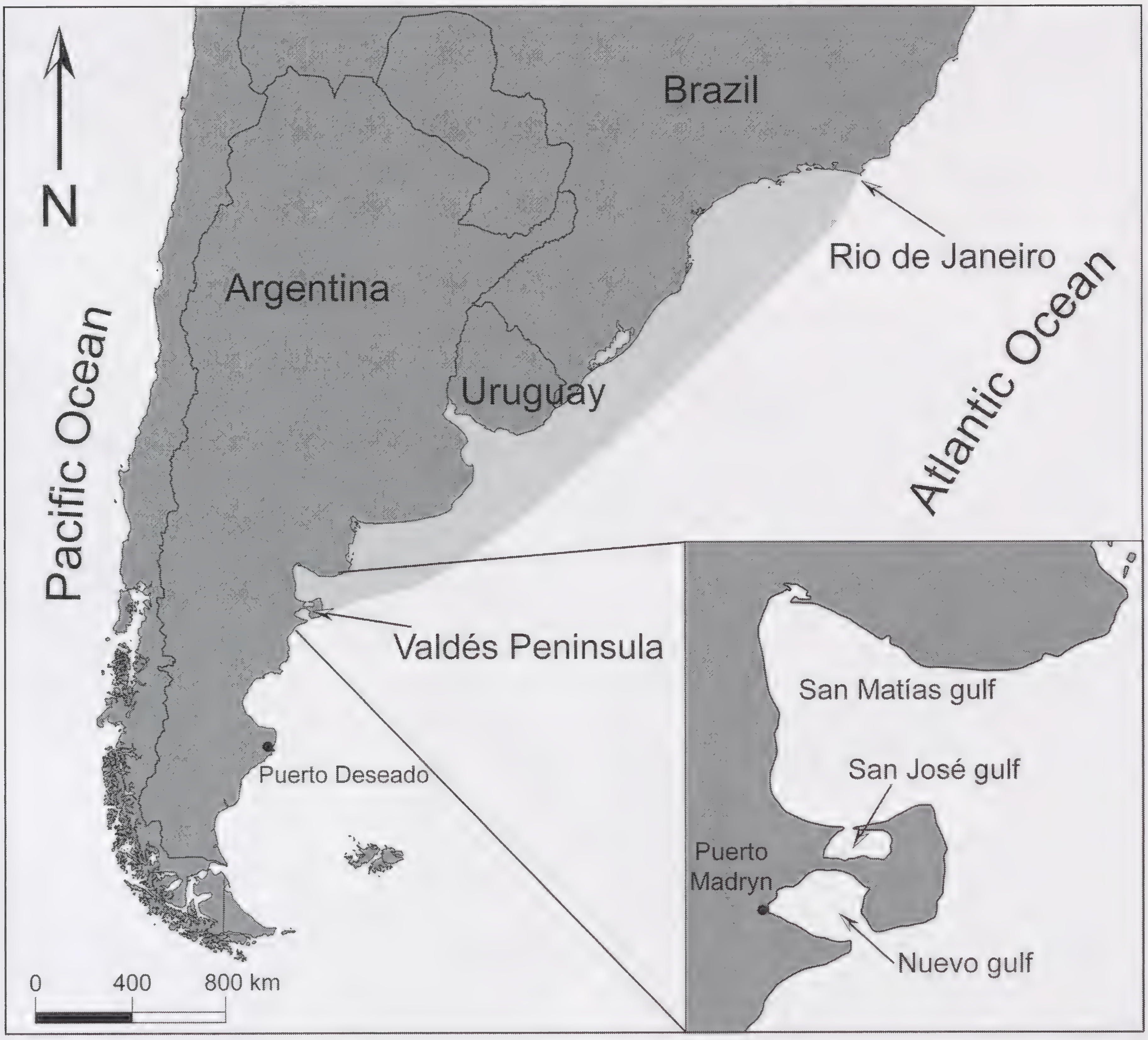

FIG. 1. Distribution map of *Panopea abbreviata* with a detail of collecting localities.

SYSTEMATIC RESULTS

Order Hiatellida Carter, 2011
Superfamily Hiatelloidea J. Gray, 1824
Family Hiatellidae J. Gray, 1824
Subfamily Panopeinae
Bronn, 1862

Genus Panopea Ménard de la Groye, 1807 (p. 135)

[= *Glycimeris* Lamarck, 1799; type species: *Mya glycimeris Born, 1778*, by tautonymy (suppressed for the purposes of the Principle of Priority by the ICZN, 1986; Opinion 1414); *Panope* Ménard de la Groye, 1807 (*nom. null.*); *Panodea* Oken, 1817 (*nom. null.*); *Panopaea* Lamarck, 1818 (*nom. null.*); *Myopsis* Agassiz 1840; type species: *Mya mandibula* J. Sowerby, 1813, by the subsequent designation of Cox, 1964; *Heteromya* Mayer-Eymar 1884; type species: *Panopea* (*Heteromya*) *lessepsi* Mayer-Eymar, 1884, by monotypy; *Capistrocardia* Tate, 1887; type species: *Capistrocardia fragilis* Tate, 1887, by original designation].

Type species: *Panopea aldrovandi* Ménard de la Groye, 1807 (= *Mya glycimeris* Born, 1778), by subsequent designation of Children, 1822. Pliocene-Recent, Europe.

Remarks

Panopea aldrovandi Ménard de la Groye, 1807 (= *Mya glycimeris* Born, 1778) is regarded as having been fixed as the type species of the genus by the subsequent designation of Children (1822: 84). A few years prior, Fleming (1818) designated as type *Mya glycimeris* Born, 1778, a designation that was accepted by Winckworth (1929) and later by Keen (1969).

However, the ICZN (1986, Opinion 1414) concluded that Fleming's identification was invalid because *Mya glycimeris* Born was not originally included in *Panopea*.

Panopea abbreviata
Valenciennes, 1839
(Figs. 2–9)

Panopea abbreviata Valenciennes, 1839: 18, pl. 6, fig. 1a, b; Valenciennes, 1843: pl. 9, fig.1; Lamy, 1925: 276; Castellanos, 1970: 265; Rios, 1975: 253, pl. 80, fig. 1213; 1994: 294, pl. 100, fig. 1433; 2009: 589, fig. 1628; Scarabino, 1977: 214; Lasta et al., 1998: 130, fig. 5d; Scarabino, 2003: 240; Scarabino et al., 2006: 164.

Panopaea abbrebiata (Valenciennes) – d'Orbigny, 1846: 509; Woodward, 1854: 220; Woodward, 1856: 378; Mayer-Eymar, 1870: 68; Woodward, 1870: 87; G. B. Sowerby II, 1873: pl. 6, fig. 10; Clessin, 1895: 50, pl. 18, fig. 3.

Panopaea antarctica Gould, 1850: 214; 1852: 386; 1862: 74; H. Adams & A. Adams, 1856: 350.

Glycimeris abbreviata (Valenciennes) – H. Adams & A. Adams, 1856: 350; Tryon, 1868: 60.

Panope abbreviata (Valenciennes) – Carcelles, 1944: 294, pl. 14, fig. 114; Carcelles & Williamson, 1951: 346; Barattini & Ureta, 1961: 183; Figueiras & Sicardi, 1970: 409.

Type Material: *Panopea abbreviata* Valenciennes, 1839, MNHN 25707, two syntypes (Figs. 2–7); *Panopea antarctica* Gould, 1850, USNM 17515, holotype (Figs. 8, 9).

Type Locality: Mouth of Rio Negro, Patagonia, Argentina.

Other Material Examined: Brazil – Niterói, Rio de Janeiro (MZUSP 106418, collected in 1969); São Sebastião, Barra Velha (MZUSP 189720130); Santa Catarina, Cabo Santa Marta (MZUSP 20131, 137 m depth); Santa Catarina Laguna (MZUSP 32714, 110–130 m depth, collected in 2000). Uruguay – Montevideo (MACN 15187); 85 miles southeast from Puerto La Paloma (MACN 16634). Argentina – Mar Chiquita (MLP 2565); Mar del Plata (MACN 377, 9361, 16688, 10309, 9361-38, 10229, 9154-8, 19162, 9379-14, 29560, 15781; MLP 1879, 2087, 2421, 4889); Puerto Quequén (MACN 21071, 416); Bahía San Blas (MACN 20232); Mouth of Río Negro (MACN 20649); San Antonio Oeste (MACN 9379-12, 13345, 13135, 9151-12, 9379-13; MLP 2706; MZUSP 13134); San Matías gulf (MACN 21277); San José gulf (MACN 9175-24; MLP 2744, 13203); Puerto Pirámides, Nuevo gulf (MACN 26442); Punta Norte, Valdez peninsula (MACN 11492); Punta Ninfas, Nuevo gulf (USNM 869774).

Distribution

From Rio de Janeiro, Brazil, to Nuevo Gulf, Chubut Province, Argentina.

Diagnosis

Shell thick, rounded, large, up to 15 cm, gaping widely at both ends, elongated but posteriorly shortened, inflated; external ligament strong; periostracum dark brownish; ultrastructure outer prismatic, middle homogeneous and inner complex crossed lamellar (CCL) layers; cardinal tooth sharp, erect.

Description

Shell: Thick, large, up to 15 cm length, externally white, surface smooth with irregular growth lines, covered by a thin, yellowish-green periostracum; umbo slightly inflated, prosogyrate; lunule and escutcheon not defined; antero-posteriorly elongated, but shortened at posterior end, anteriorly rounded, ventral margin rounded and usually eroded; widely gaping at both ends; all exposed siphons and tissues covered by dark brownish periostracum (Fig. 18); internally white, pallial line separated from ventral edge of shell about 1.5 cm, pallial sinus U-shaped, higher than deep; adductor muscle scar clearly visible, the anterior larger; nymphal ridge very prominent at posterior side of hinge; external ligament strong, quasiparivincular, wide, dark brown, opisthodetic, on strong pseudonymph, with fibrous sublayers attached to dorsal and lateral surfaces of pseudonymph and covered by the lamellar sublayer (Figs. 10–13); hinge plate characterized by sharp, erect single cardinal tooth in each valve, fitting into corresponding socket in other valve (Figs. 14–17); ultrastructure of the shell with three layers (Figs. 23–28): an outer layer of nearly vertical and composite prisms (Figs. 24, 25), a middle true homogeneous layer of rounded units (Fig. 26) and a complex crossed lamellar inner layer with intercalations of irregular simple prisms (Figs. 27, 28).

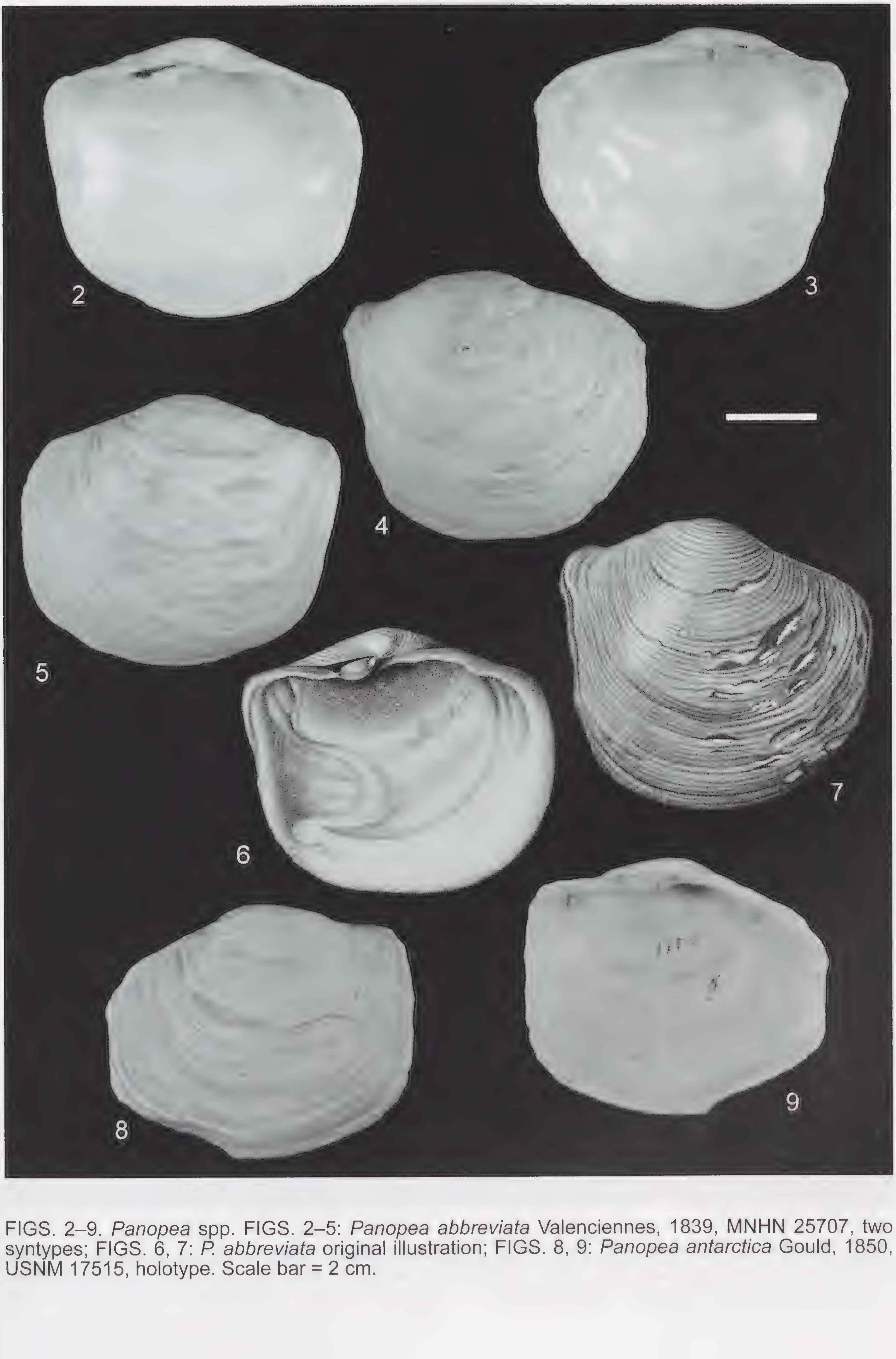

FIGS. 2–9. *Panopea* spp. FIGS. 2–5: *Panopea abbreviata* Valenciennes, 1839, MNHN 25707, two syntypes; FIGS. 6, 7: *P. abbreviata* original illustration; FIGS. 8, 9: *Panopea antarctica* Gould, 1850, USNM 17515, holotype. Scale bar = 2 cm.

Mantle Cavity Organs: The mantle fusion is only interrupted at the pedal gape, which is anteriorly positioned. Inside the large mantle cavity, two pairs of labial palps surround the mouth, the inner one longer than wider (Figs. 19, 33); the association of ctenidia and labial palps is Category III of Stasek (1963), wherein the ventral tips of the anterior filaments of the inner demibranch are not inserted into the distal oral groove. However, the anteroventral margin of the inner demibranch is fused to the inner palp lamella. The ctenidia surround the visceral mass laterally (Figs. 29, 30); they belong to type C (1) of Atkins (1937), characterized by an outer demibranch with a distinct supra-axial extension and food groove only present in the inner demibranch (Fig. 31), the outer demibranch less deep than the inner. Frontal currents at

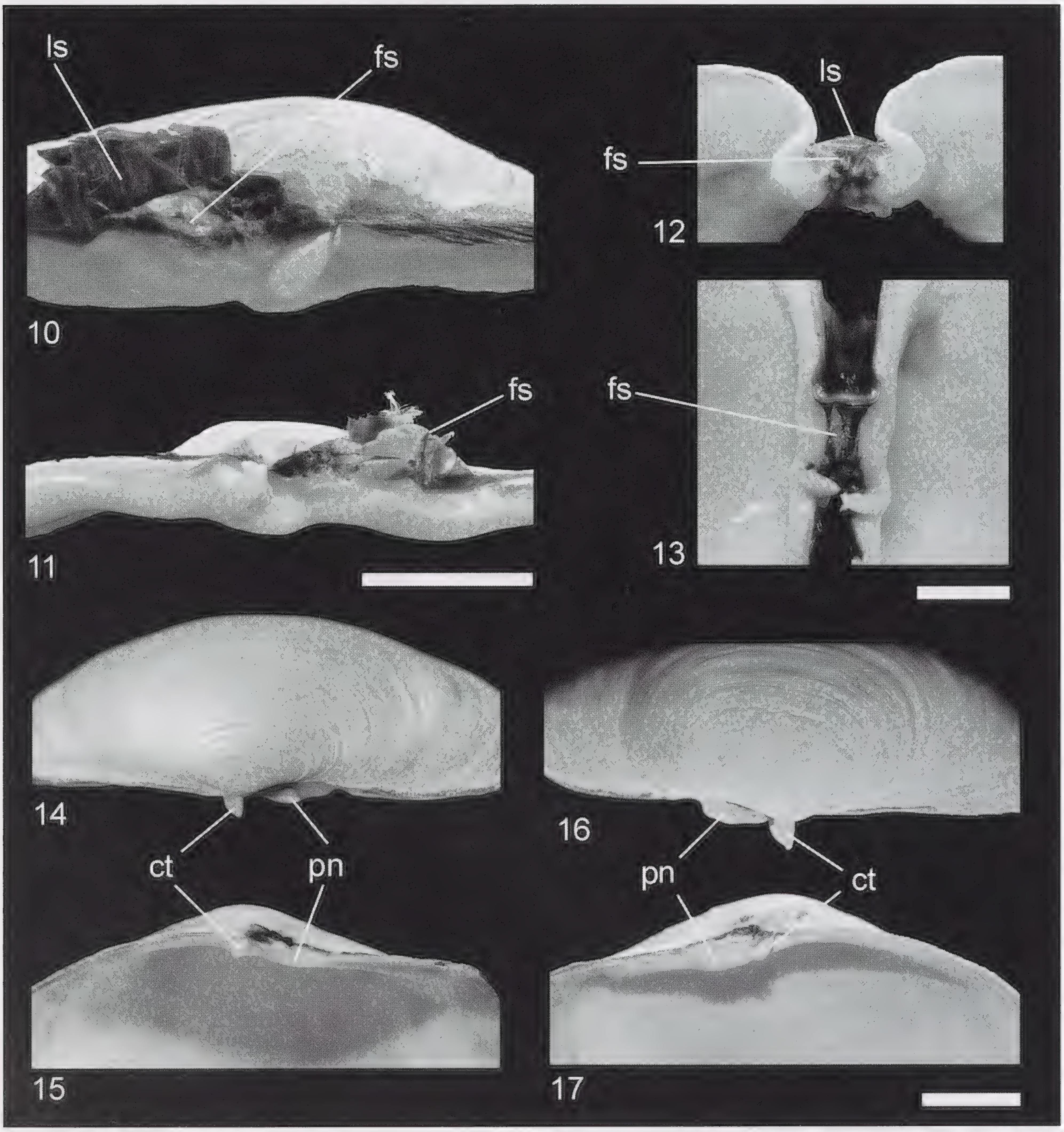

FIGS. 10–17. *Panopea abbreviata*. FIGS. 10–13: External ligament showing fibrous sublayers attached to dorsal and lateral surfaces of pseudonymph covered by lamellar sublayer. Scale bar = 1 cm; FIGS. 14, 15: Right hinge; FIGS. 16, 17: Left hinge.

both sides of inner demibranch go to the food groove. The oral current is observed along the groove as well as between the bases of the two demibranchs on each side of the body. In the outer demibranch, particles are carried ventrally on the ascending lamella and dorsally on the descending lamella (Fig. 31). Ctenidial septum with two rows of perforations that separate the suprabranchial and infrabranchial chambers (Fig. 32). It is placed posterodorsal to the visceral mass, and behind it is positioned the base of the siphons. A short, anteriorly directed, rudimentary foot is present at the anterior side of the body (Figs. 29, 30). The adductor muscles are large, the anterior slightly larger than the posterior (Fig. 19); siphons large, hypertrophied, about two times shell length, completely covered, together with all pallial surfaces, with

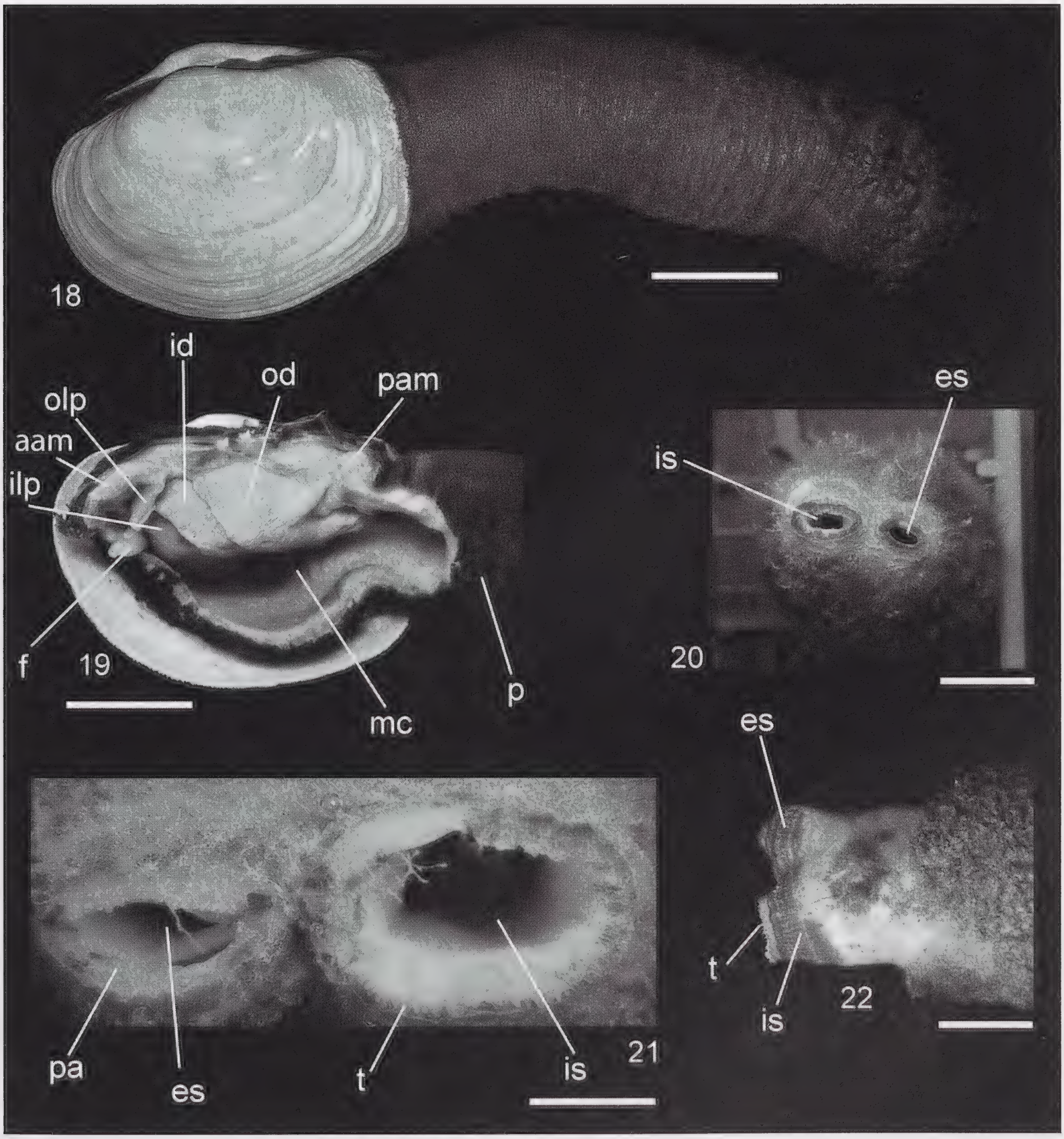

FIGS. 18–22. *Panopea abbreviata.* FIG. 18: General aspect. Scale bar = 4 cm; FIG. 19: Mantle cavity organs. Scale bar = 4 cm; FIGS. 20–22: Excurrent and incurrent siphons with papillae and short tentacles along the aperture respectively. Scale bar Figs. 20, 22 = 1cm, Fig. 21 = 5 mm.

a thick, wrinkled, dark brownish periostracum, near the aperture with symbiotic red algae (Figs. 20–22); with small papillae along aperture ring in the excurrent siphon; and with short, irregular tentacles surrounding the apertures in the incurrent siphon (Figs. 20–22); it belongs to type C of Yonge (1957, 1982) formed by fusion of all surfaces of the inner and middle mantle folds (*sensu* Yonge, 1982; Carter et al., 2012), evidenced by the posterior position of the periostracal groove encircling both siphonal apertures; siphonal pallial septum strong separating the incurrent and excurrent channels by the fused left and right mantle tissue (Fig. 34). Alimentary canal with a mouth followed by a short esophagus that enters the stomach anterodorsally (Figs. 37, 38). The style sac and the midgut are combined leaving the stomach ventrally (Fig. 37); the coiled intestine passes backward through the right side of the visceral

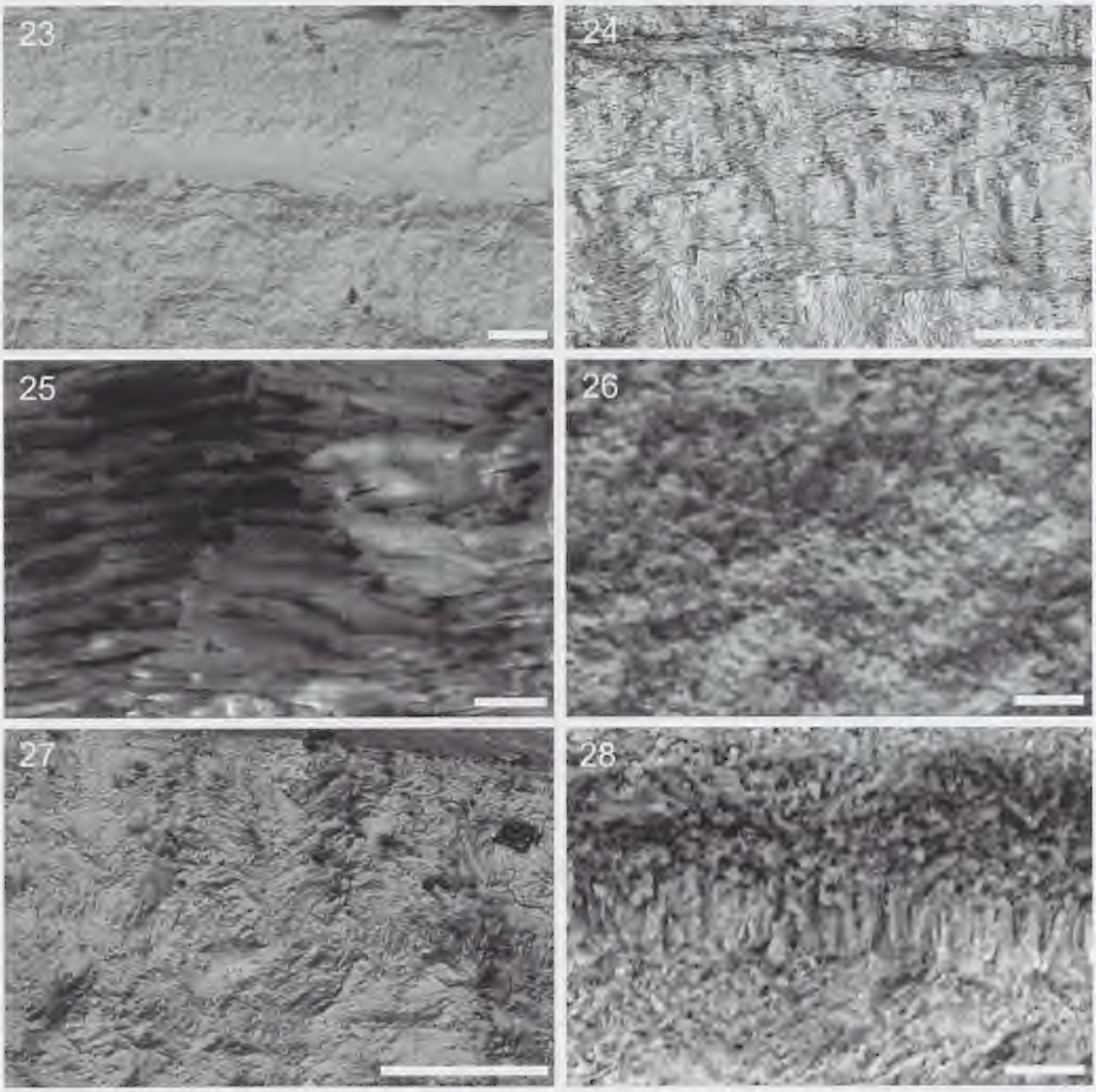

FIGS. 23–28. Shell ultrastructure. FIG. 23: Three layers. Scale bar = 100 µm; FIGS. 24, 25: Detail of vertical and composite prisms of outer layer. Scale bar = 100 µm and 5 µm respectively; FIG. 26: Middle true homogeneous layer. Scale bar = 10 µm; FIG. 27: Complex crossed lamellar inner layer. Scale bar = 100 µm; FIG. 28: Detail of intercalations of irregular simple prisms in the inner layer. Scale bar = 10 µm.

mass ascending to the pericardial cavity as the hindgut, then it passes through the heart to end in the rectum and posteriorly in the anus. The stomach of *P. abbreviata* belongs to Type IVa *sensu* Purchon (1987, 1990) and Carter et al. (2012). The major typhlosole is curved to the left in an incomplete spiral; it goes together with the intestinal groove to its anterior end passing towards the left caecum (Fig. 37). Circulatory system pumped by a muscular heart that surrounds the hindgut-rectum placed in a posterodorsal position between visceral mass and posterior adductor muscle in the pericardial cavity, with two inflated auricles, dorsally positioned and one ventral ventricle (Figs. 35, 36).

Symbiosis with Malacobdella arrokeana: The symbiotic relationship between *P. abbreviata*

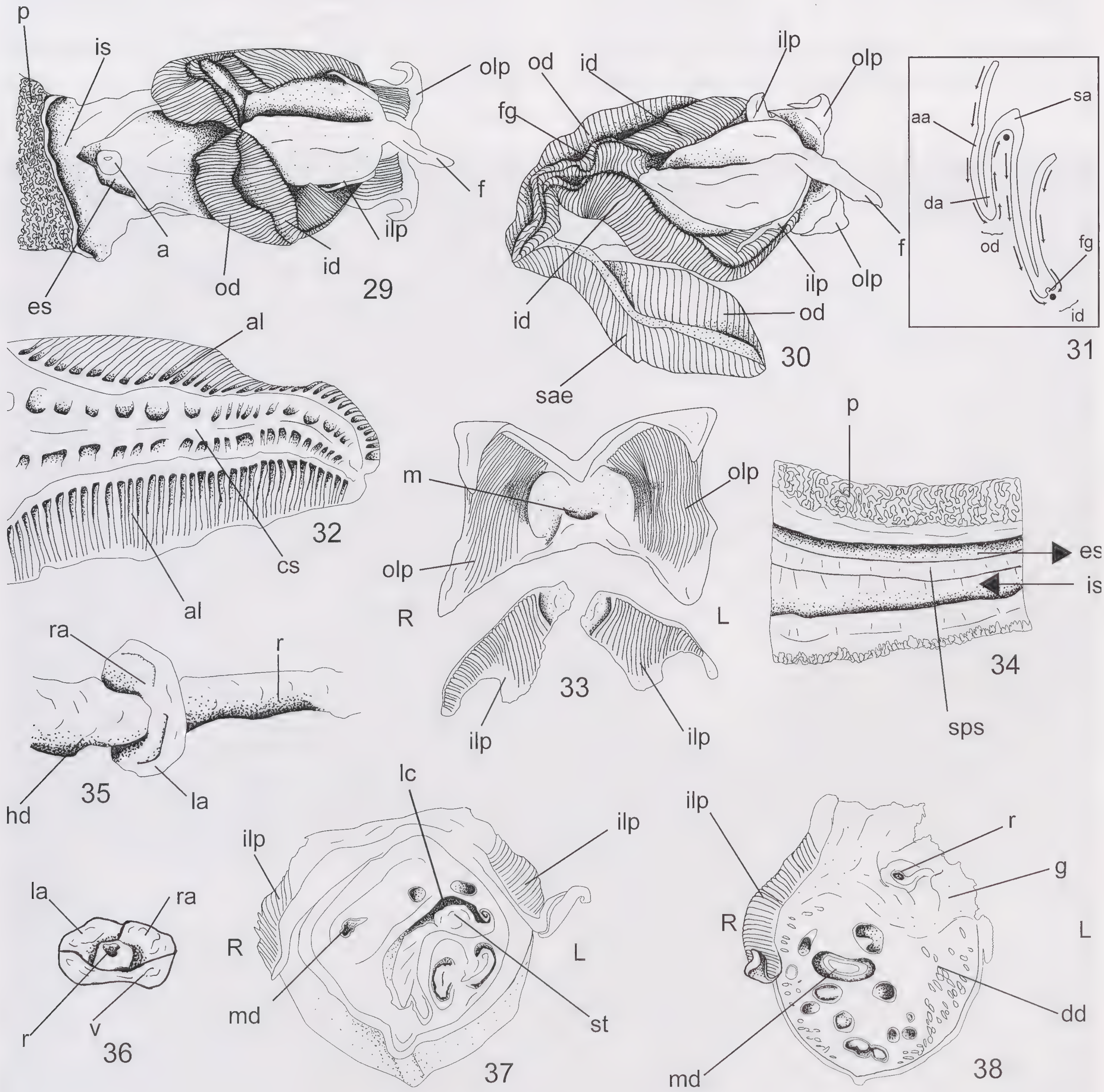

FIGS. 29–38. Anatomy of *Panopea abbreviata*. FIGS. 29, 30: General aspect showing a sectioned outer demibranch and anus aperture; FIG. 31: Diagrammatic transverse section showing the form of the ctenidia and frontal currents direction (from Atkins, 1837); FIG. 32: Ctenidial septum with two rows of perforations; FIG. 33: outer and inner labial palps; FIG. 34: Siphonal pallial septum strong separating the incurrent and excurrent channels; FIGS. 35, 36: Heart with two auricles and one ventricle surrounding the hindgut; FIGS. 37, 38: Transversal section of visceral mass showing digestive system.

and the nemertean *M. arrokeana* has been widely studied (Ivanov et al., 2002; Vazquez et al., 2009; Alfaya et al., 2013). These authors found that almost all collected specimens of *Panopea* (99.4%) were inhabited by the nemertean, which has host specificity, being found only in *P. abbreviata. Malacobdella arrokeana*, which lives attached by its terminal sucker, is the only member of the genus reported in the southern Atlantic Ocean (Ivanov et al., 2002). The association allows *M. arrokeana* to obtain food and shelter during its development inside *P. abbreviata*. Immature nemerteans were observed living attached to the gills laminae. After its development, the nemertean moves and attaches to the mantle cavity by its terminal sucker. The main food sources for both species are diatoms and small crustaceans.

Habitat

Panopea abbreviata has been collected from 8 to 25 meters, deeply buried, up to 40 cm in sand and mud substrata rich in organic matter. It is usually recorded with such other clams as *Ensis macha, Leukoma antiqua* and *Retrotapes exalbidus.*

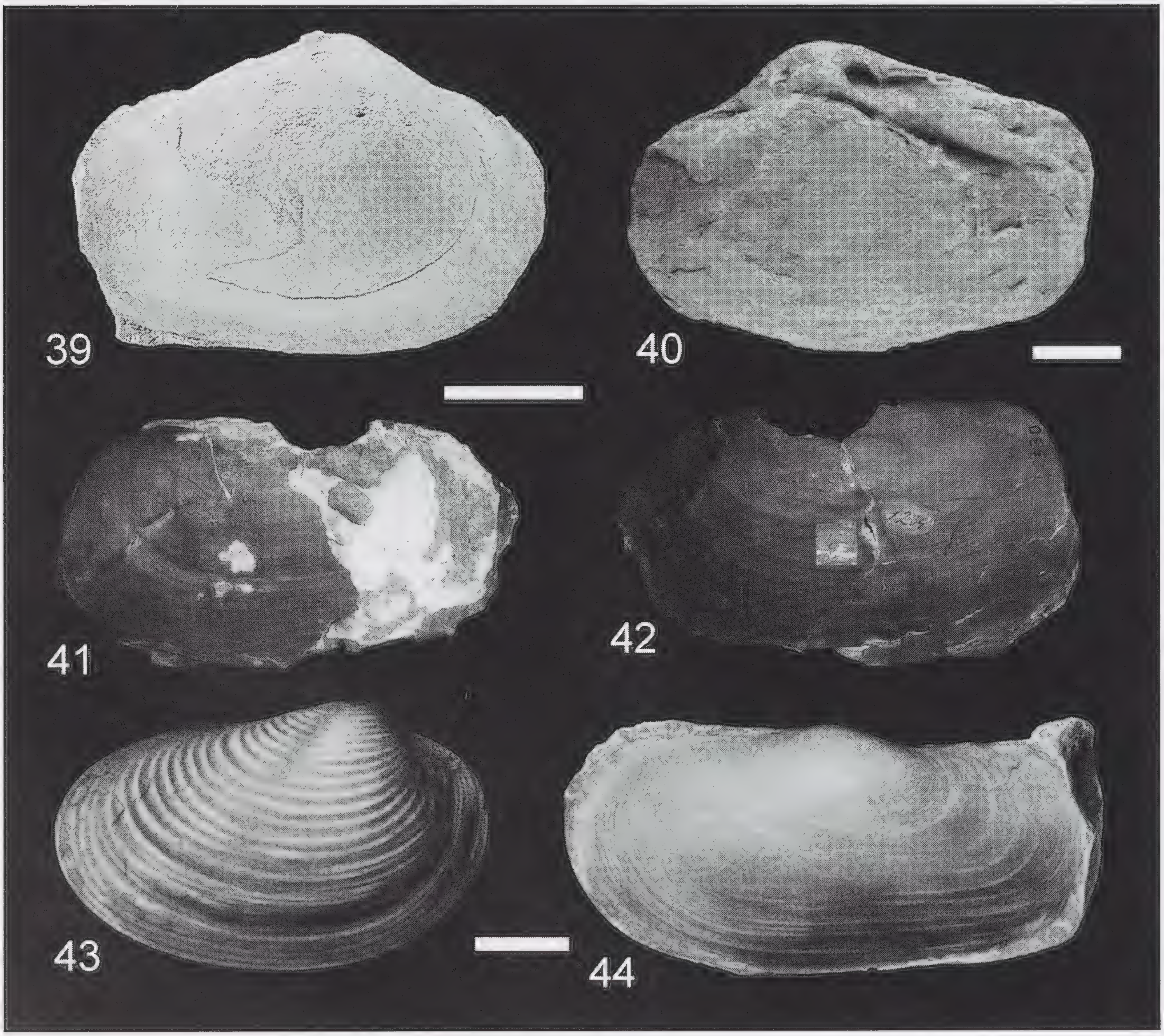

FIGS. 39–44. South American fossil taxa of *Panopea*. FIG. 39: *Panopea coquimbensis* d'Orbigny, 1843, MNHN 13626, syntypes; FIG. 40: *Panopea guayacanensis* Philippi, 1887, MNHNC-Pi 247, holotype; FIGS. 41, 42: *Panopaea truncata* Borchert, 1901, MACN-Pi 2530, holotype; FIG. 43: *Panopaea inferior* Wilckens, 1907, original illustration; FIG. 44: *Panopaea hauthali* Wilckens, 1907, original illustration. Scale bar: Figs. 39, 41, 42 = 1 cm; Fig. 40 = 3 cm; Figs. 43, 44 = 2 cm.

Remarks

Type material examination revealed morphological differences between related nominal species that allow us to update the taxonomic status of *P. abbreviata*. *Panopea coquimbensis* d'Orbigny, 1843 (p. 126, pl. 15. figs. 7, 8), described from Tertiary sands around Coquimbo, in northern Chile was incorrectly synonymized with *P. abbreviata* by Bernard (1983). Study of the syntypes deposited at MNHN, represented by internal molds, shows a more elongate shell with a siphonal gap folding outwards more defined and with a pallial sinus V-shaped (Fig. 39). Herm (1969) synonymized *Panopea guayacanensis* Philippi, 1887 (p. 167, pl. 34, fig. 2) from Guayacan, Chile with d´Orbigny's species. Griffin & Nielsen (2008), after an examination of type material of both nominal species, confirmed the synonymy proposed by Herm. *Panopea guayacanensis*, described from Tertiary deposits of Guayacan, was also considered a junior synonym of *P. abbreviata* by Bernard (1983). The type material of Philippi species coincides with d´Orbigny species and clearly differs from the type material of Valenciennes (Fig. 40). *Panopaea truncata* Borchert, 1901 (p. 212, pl. 9, figs. 1, 2), described from Paraná Formation, was also synonymized in the literature (Bernard, 1983). The type material, as well as the original illustration, revealed that Borchert species must be excluded from the synonymy of *P. abbreviata* (Fig. 41, 42). *Panopea truncata* shows a more elongate, rectangular shell, with a straight ventral edge. However, its articulated valves do not allow the study of the hinge. In addition, del Río (1994) considered it to be a junior synonym of *P. regularis* (Ortmann, 1900). *Panopaea inferior* (p. 47, pl. 9, fig. 2) and *P. hauthali* (p. 49, pl. 9, fig. 3), both described by Wilckens (1907), were incorrectly cited as synonyms of *P. abbreviata* by Bernard (1983). The first was described from deposits exposed in Cerro Cazador, Sierra de los Baguales and Cancha Carrera in Santa Cruz Province, and the second from Sierra de los Baguales only. The characters observed in the original illustrations of Wilckens clearly differ with those of *P. abbreviata* (Fig. 43, 44 respectively). The type material of both species was not found in the collection of Freiburg, and they probably did not survive to the Second World War (Sven Nielsen, pers. comm.).

DISCUSSION

From six nominal species synonymized in the literature, only the recent *P. antarctica* Gould, 1850, can be considered a junior synonym of the Valenciennes species. The others are fossils names described along southern Patagonia of Argentina and Chile. The stratigraphic range of Miocene-Recent mentioned by Aguirre & Farinati (1999) is incorrect. The Recent geoduck was never mentioned in various revisions of the fossil mollusks in the Miocene of Argentina (Ihering, 1907; Martínez & del Río, 2002; del Río, 1992, 1994, 2002, 2004, Griffin, 1991, among others). This is a Quaternary-Recent species, well represented in north patagonian gulfs. The material examined shows a well defined distribution from Rio de Janeiro to Peninsula Valdés. Some lots were found in examined malacological collections from localities beyond this southern limit of distribution. The examination of those materials (MACN 17734; MZUSP 13138) revealed the presence of *Panopea aff. abbreviata* in Puerto Deseado, Santa Cruz Province, Argentina. After field work that included the localities of Bahía Camarones, Bahía Bustamante, Caleta Sara, Comodoro Rivadavia (Chubut Province), Punta Buque and Puerto Deseado (Santa Cruz Province), living specimens of *P. abbreviata* were not found. Within this context, the distribution mentioned by Carcelles & Williamson (1951) and Castellanos (1970) is at least uncertain in the southern localities from Península Valdés to Puerto Deseado, as suggested by Alfaya et al. (2013).

The anatomy of this species is similar to other members of the genus. The mantle cavity organs observed by Yonge (1971) and Bower & Blackbourn (2003) for the Pacific species *P. generosa* are similar to those in *P. abbreviata*. The examined morphology of the stomach of *P. abbreviata* agrees with that observed by Narchi (1973) and Purchon (1958) in *Hiatella solida* and *H. arctica* respectively. The shell morphology allows us to differentiate the valid American species of the genus. Additional morphological revisions of other species of the genus are necessary to understand the conservative morphology of this group of bivalves. *Panopea abbreviata* Valenciennes, 1839, constitutes together with *Panopea bitruncata* (Conrad, 1872), the two Recent western Atlantic species of the genus.

ACKNOWLEDGMENTS

Special thanks to Virginie Heros and A. Robin (MNHN), Alejandro Tablado (MACN), Cristina Damborenea (MLP), David Rubilar and Christian Salazar (MNHNC), Paula Spotorno (MORG) and Ellen Strong and Yolanda Villacampa (USNM) for their assistance in the revision of the type material and additional examined specimens. Special thanks to Leandro Pérez and Sven Nielsen for the images provided for this work and to Leticia Mercante for her comments on the early version of the manuscript. Many thanks to Eugene Coan and Joseph Carter for their considerable suggestions and to Jaime Groizard (Aluar S.A.) for their assistance in SEM images. To "Idea Wild" for contributing with a 60-mm Nikkor micro lens. JHS and JEFA acknowledge CONICET of Argentina. This work was partially supported by the following projects: PICT-R01869 and PICT-0323 of Agencia Nacional de Promoción Científica y Tecnológica, Argentina and the Agencia Española de Cooperación Internacional y Desarrollo (AECID: A/023484/09 and A/032441/10).

LITERATURE CITED

ABBOTT, R. T. & S. P. DANCE, 1986, *Compendium of seashells*, revised ed. American Malacologists, Melbourne, Florida, USA, ix + 411 pp.

ADAMKEWICZ, S. L., M. G. HARASEWYCH, J. BLAKE, D. SAUFDEK & C. J. BULT, 1997, A molecular phylogeny of the bivalve mollusks. *Molecular Biology and Evolution*, 14: 619–629.

ADAMS, H. & A. ADAMS, 1856 [1853–1858], *The genera of Recent Mollusca, arranged according to their organization*. Van Voorst, London, 2 vols. Vol. 1: xl + 484 pp.; Vol. 2: 1–604.

AGUIRRE, M. L. & E. A. FARINATI, 1999, Paleobiogeografía de las faunas de moluscos marinos del Neógeno y Cuaternario del Atlántico Sudoccidental. *Revista de la Sociedad Geológica de España*, 12(1): 93–112.

ALFAYA, J. E. F., G. BIGATTI & A. MACHORDOM, 2013, Mitochondrial and nuclear markers reveal a lack of genetic structure in the entocommensal nemertean *Malacobdella arrokeana* in the Patagonian gulfs. *Helgoland Marine Research*, 67(2): 407–412.

ARAMBULA-PUJOL, E. M., A. R. GARCÍA-JUÁREZ, E. ALCÁNTARA-RAZO & E. ARAGÓN-NORIEGA, 2008, Aspectos de biología reproductiva de la almeja de sifón *Panopea globosa* (Dall 1898) en el Golfo de California. *Hidrobiológica*, 18(2): 89–98.

ATKINS, D., 1937, On the ciliary mechanisms and interrelationships of Lamellibranchia. *Quarterly Journal of the Microscopical Science*, (n.s.), 79(3): 375–421.

BARATTINI, L. P. & E. H. URETA, 1961 ["1960"], La fauna de las costas del este (invertebrados). *Publicaciones de Divulgación Científica, Museo "Dámaso Antonio Larrañaga"*, Montevideo, Uruguay, 108 pp.

BERNARD, F. R., 1983, Catalogue of the living Bivalvia of the eastern Pacific Ocean: Bering Strait to Cape Horn. *Canadian Special Publication of Fisheries and Aquatic Sciences*, 61: 1–102.

BORCHERT, A., 1901, Die Molluskenfauna und das Alter der Parana-Stufe. In: G. Steimann, ed., Beitrage zur Geologie und Palaeontologie von Südamerika. *Neues Jahrbuch für Mineralogie, Geologie und Paläontologie*, 14: 171–245.

BOWER, S. M. & J. BLACKBOURN, 2003, *Geoduck clam* (*Panopea abrupta*): *Anatomy, histology, development, pathology, parasites and symbionts*, URL: http://www.pac.dfo-mpo.gc.ca/science/species-especes/shellfish-coquillages/geopath/index-eng.htm

BRUSA, F., N. VÁZQUEZ & F. CREMONTE, 2011, *Paravortex panopea* n. sp. (Platyhelminthes: Rhabdocoela) on clams from the northern Patagonian coast, Argentina: pathogeny and specificity. *Helminthologia*, 48(2): 94–100.

CARCELLES, A., 1944, Catálogo de los moluscos marinos de Puerto Quequen. *Revista del Museo de La Plata, 3 - Seccion Zoologia*: 233–309.

CARCELLES, A. & S. WILLIAMSON, 1951, Catálogo de los moluscos marinos de la provincia magallánica. *Revista del Instituto Nacional de Investigación de las Ciencias Naturales, 2 Ciencias Zoológicas*: 225–383.

CARTER, J. G. & D. C. CAMPBELL, with contributions by C. R. Altaba, L. C. Anderson, R. Araujo, A. Beu, A. S. Biakov, A. Bogan, M. Campbell, C. Jin-Hua, J. Cope, G. Delvene, H. Dijkstra, F. Zong-Jie, V. Gavrilova, I. Goncharova, A. Guzhov, P. Harries, J. H. Hartman, W. R. Hoeh, J. Hylleberg, J. Bao-Yu, P. Johnston, L. Kirkendale, K. Kleemann, J. Koppka, J. Kříž, D. Machado, N. Malchus, O. Mandic, A. Márquez-Aliaga, J. Masse, P. U. Middelfart, S. Mitchell, L. A. Nevesskaja, S. Özer, J. Pojeta, jr., I. V. Polubotko, J. M. Pons, S. Popov, T. Sánchez, A. F. Sartori, R. W. Scott, I. I. Sey, S. Jin-Geng, J. H. Signorelli, V. V. Silantiev, P. W. Skelton, T. Steuber, J. B. Waterhouse, G. L. Wingard & T. Yancey, 2011, A synoptical classification of the Bivalvia (Mollusca). *Paleontological Contributions*, 4: 1–47.

CARTER, J., P. HARRIES, N. MALCHUS, A. F. SARTORI, L. C. ANDERSON, R. BIELER, A. E. BOGAN, E. V. COAN, J. C. W. COPE, S. M. CRAGG, J. M. GARCÍA-MARCH, J. HYLLEBERG, P. KELLEY, K. KLEEMANN, J. KŘÍŽ, C. MCROBERTS, P. MIKKELSEN, J. POJETA, jr., I. TËMKIN, T. YANCEY & A. ZIERITZ, 2012, Illustrated glossary of the Bivalvia. *Treatise Online: Treatise on Invertebrate Paleontology*, Part N, Revised, Vol. 1(31): 1–211.

CASTELLANOS, Z. J. A. D., 1970, Catálogo de los moluscos marinos bonaerenses. *Anales de la Comision de Investigaciones Cientificas de la Provincia de Buenos Aires*, 8: 9–365.

CHILDREN, J. G., 1822, Lamarck's genera of shells translated from French by J. G. Children, with plates from original drawings, by Miss Anna Children. *Quarterly Journal of Science, Literature and Arts*, 14(27): 64–86.

CIOCCO, N., I. ELÍAS, J. M. ORENSANZ, A. PARMA, P. CICCARONE, G. SARSA, A. SERDÁ, P. OROQUIETA & M. PIÑEIRO, 2001, Explotación de la almeja *Panopea* (*Panopea abbreviata*) en Chubut Consideraciones para su Manejo. *Documento Técnico No 1 Comisión Técnica DGIMPC-CENPAT-APAPM*, 1: 18 pp.

CLESSIN, S., 1895 [1893–1895], Mollusca Dimyaria. Gastrochaenacea, Gastrochaenaceen. Die Familie Gastrochaenidae. Systematisches Conchylien-Cabinet von Martini und Chemintz, 2nd ed., Bauer & Raspe, Nürnberg. 11(4a): 1–58, pls. 1–21 [pls. 1–3 (1893); pp. 1–24, pls. 4–9 (1894); pp. 25–57 + [1], pls. 10–21 (1895)].

DALL, W. H., 1912, Note on the genus *Panope*, Menard. *Proceedings of the Malacological Society of London*, 10: 34–35.

DEL RÍO, C. J., 1992, Middle Miocene bivalves of the Puerto Madryn Formation, Valdés Peninsula, Chubut Province, Argentina (Nuculidae – Pectinidae). Part 1. *Paleontographica,* 225A: 1–57.

DEL RÍO, C. J., 1994, Middle Miocene bivalves of the Puerto Madryn Formation, Valdés Peninsula, Chubut Province, Argentina (Lucinidae – Pholadidae). Part 2. *Palaeontographica*, 231A: 93–132.

DEL RÍO, C. J., 2002, Moluscos del Terciario Marino. In: *XV Congreso Geológico Argentino*. Geología y Recursos Naturales de Santa Cruz; M. J. Haller, ed., *Relatorio*, II–9: 1–22.

DEL RÍO, C. J., 2004, Tertiary marine molluscan assemblages of eastern Patagonia (Argentina): a biostraatigraphic analysis. *Journal of Paleontology*, 78: 1097–1122.

FELDMAN, K., B. VADOPALAS, D. ARMSTRONG, C. FRIEDMAN, R. HILBORN, K. NAISH, J. M. ORENSANZ, J. VALERO, J. RUESINK, A. SUHRBIER, A. CHRISTY, D. CHENEY & J. DAVIS, 2004, *Comprehensive literature review and synopsis of issues relating to geoduck (Panopea abrupta) ecology and aquaculture production.* Washington State Department of Natural Resources, 134 pp.

FIGUEIRAS, A. & O. E. SICARDI, 1970, Catálogo de los moluscos marinos del Uruguay parte 4. *Comunicaciones de la Sociedad Malacologica del Uruguay*, 2: 407–421.

FISHER, J., M. MEADERS, S. LUCHESSA & K. MUELLER, 2008, *A supplemental analysis of the environmental concerns associated with intertidal geoduck clam aquaculture: effects on wild geoduck genetics, potential for toxin re-suspension and effects on soft-sediment associated communities.* ENVIRON Seattle, 40 pp.

FLEMING, J., 1818 [1818–1819], Conchology. Pp. 284–316, in: Volume third of: *Supplement to the fourth, fifth, and sixth editions of the Encyclopaedia Britannica [1815–1824]. With preliminary dissertations on the history of the sciences. Illustrated by engravings.* Archibald Constable & Company, Edinburgh; Hurst, Robinson & Company, London [article signed "Q. Q."].

GOODWIN, C. L. & B. C. PEASE, 1991, Geoduck, *Panopea abrupta* (Conrad, 1849), size, density, and quality as related to various environmental parameters in Pudget Sound, Washington. *Journal of Shellfish Research*, 10: 65–77.

GOULD, A. A., 1850, Shells from the United States Exploring Expedition. *Proceedings of the Boston Society Natural History*, 3: 214–218.

GOULD, A. A., 1852–1861, Atlas. Mollusca and shells. In: *United States Exploring Expedition. During the years 1838, 1839, 1840, 1041, 1842. Under the command of Charles Wilkes, U.S.N.*, Vol. 12). C. Sherman & Son, Philadelphia, xv+ 510 pp.; 16 pp., 52 pls.

GOULD, A. A., 1862, *Otia conchologica: descriptions of shells and mollusks, from 1839 to 1862.* Gould & Lincoln, Boston, 256 pp.

GRIFFIN, M., 1991, Eocene Bivalves from the Rio Turbio Formation, southwestern Patagonia (Argentina). *Journal of Paleontology*, 65: 119–146.

GRIFFIN, M. & S. NIELSEN, 2008, A revision of the type specimens of Tertiary molluscs from Chile and Argentina described by Orbigny (1843), Sowerby (1846) and Hupé (1854). *Journal of Systematic Paleontology*, 6(3): 251–316.

HERM, D., 1969, Marines Pliozän und Pleistozän in Nord- und Mittel-Chile unter besonderer Berücksichtigung der Entwicklung der Mollusken-Faunen. *Zitteliana,* 2: 1–159.

HUBER, M., 2010, *Compendium of bivalves.* Hackenheim, Germany, 901 pp.

ICZN, 1986, Opinion 1414. *Panopea* Menard de la Groye, 1807 (Mollusca, Bivalvia): conserved. *Bulletin of Zoological Nomenclature*, 43(3): 258–261.

IHERING, H. V., 1907, Les mollusques fossiles du Tertiaire et du Cretace Superieur de l'Argentine. *Anales del Museo Nacional de Buenos Aires*, Serie III: 1–611.

IVANOV, V. A., G. BIGATTI, P. PENCHASZADEH & J. L. NORENBURG, 2002, *Malacobdella arrokeana* (Nemertea: Bdellonemertea), a new species of a nemertean from southwestern Atlantic Ocean entocommensal in *Panopea abbreviata* (Bivalvia, Heterodonta, Hiatellidae) in Argentina. *Proceedings of the Biological Society of Washington*, 115: 359–367.

KEEN, A. M., 1969, Superfamily Hiatellacea Gray, 1824. Pp. N700–N702, in: R. C. MOORE, ed., *Treatise on Invertebrate Paleontology*. Part N: Mollusca 6, Bivalvia. Geological Society of America & University of Kansas Press, Boulder, Colorado & Lawrence, Kansas.

LAMY, E., 1925, Révision des Saxicavidae vivants du Muséum National d'Histoire Naturelle de Paris. *Journal de Conchyliologie (Paris)*, 68(4): 261–283.

LASTA, M. L., N. F. CIOCCO, C. BREMEC & A. ROUX, 1998, Bivalve and gastropod molluscs. The Argentine Sea and its fisheries resources. Molluscs of interest for fisheries. *Culture and reproductive strategies of bivalves and echinoids*, 2: 115–142.

LEYVA-VALENCIA, I., S. ÁLVAREZ-CASTAÑEDA TICUL, D. LLUCH-COTA, S. GONZÁLEZ PE-

LÁEZ, S. PÉREZ-VALENCIA, B. VADOPALAS, S. RAMÍREZ-PÉREZ & P. HERNÁNDEZ CRUZ, 2012, Shell shape differences between two species and phenotypic variation among *P. globosa* at different sites using two geometric morphometrics approaches. *Malacologia*, 55(1): 1–13.

MARSHALL, R., R. S. MCKINLEY & C. M.PEARCE, 2012, Effect of temperature on gonad development of the Pacific geoduck clam (*Panopea generosa* Gould, 1850). *Aquaculture*, 338–341: 264–273.

MARTÍNEZ, S. & C. DEL RÍO, 2002, Las provincias malacológicas Miocenas y Recientes del Atlántico sudoccidental. *Anales de Biología*, 24: 121–130.

MARTORELLI S. R., N. CIOCCO & M. BAZTERRICA, 2003, *Nuevos aportes a la morfología y distribución de* Malacobdella arrokeana *(Nemertini: Malacobdellidae) un endocomensal del geoduck del sur* Panopea abbreviata *(Valenciennes, 1839)*. Segundo Congreso Virtual de Acuicultura. Zaragoza, España, pp. 399–419.

MAYER-EYMAR, K. W., 1870, Catalogue systématique et descriptif des fossiles qui se trouvent au Musée Fédéral de Zürich, 4e cahier. Mollusques de la famille des Panopéides. *Vierteljahrsschrift der Naturforschenden Gesellschaft in Zürich*, 15: 31–82.

MÉNARD DE LA GROYE, M., 1807, Mémoire sur un nouveau genre de coquille de la famille des solénoides. *Annales du Muséum d'Histoire Naturelle,* 9: 131–139.

MORSÁN, E. & N. CIOCCO, 2004, Age and growth model for the southern geoduck, *Panopea abbreviata*, off Puerto Lobos (Patagonia, Argentina). *Fisheries Research*, 69(3): 343–348.

MORSÁN, E., P. ZAIDMAN, M. OCAMPOS-REINALDO & N. CIOCCO, 2010, population structure, distribution and harvesting of southern geoduck, *Panopea abbreviata*, in San Matías Gulf (Patagonia, Argentina). *Scientia Marina*, 74: 763–772.

NARCHI, W., 1973, On the functional morphology of *Hiatella solida* (Hiatellidae: Bivalvia). *Marine Biology*, 19: 332–337.

NARVARTE, M., R. GONZÁLEZ & P. FILIPPO, 2007, Artisanal mollusk fisheries in San Matías Gulf (Patagonia, Argentina): an appraisal of the factors contributing to unsustainability. *Fisheries Research*, 87 (1): 68–76.

ORBIGNY, A. D. d', 1843–1844, *Voyage dans l'Amérique méridionale ... exécuté pendant les années 1826, 1827, 1828, 1829, 1830, 1831, 1832, et 1833,* Vol. 3(4) [Paléontologie.]: 188 pp., 22 pls. [in Atlas]. Paris (Bertrand) & Strasbourg (Levrault).

ORBIGNY, A. D. d', 1846 [1835–1847], *Voyage dans l'Amérique méridionale (Le Bresil, La Republique Orientale de L'Uruguay, La Republique Argentine, La Patagonie, La Republique du Chili, La Republique de Bolivia, La Republique du Perou) exécuté pendant les années 1826, 1827, 1828, 1829, 1830, 1831, 1832 et 1833*, Vol. 3(4), *Paléontologie*. Pitois-Levrault, Ve. Levrault, Paris & Strasbourg.

ORTMANN, A. E., 1900, Synopsis of the collections of invertebrate fossils made by Princeton expedition to southern Patagonia. *American Journal of Science* (Ser. 4), 10: 368–381.

PHILIPPI, R. A., 1887, Die Tertiären und Quartären Versteinerungen Chiles. F. A. Brockhaus, Leipzig, 266 pp., 58 pls.

PURCHON, R. D., 1958, The stomach in the Eulamellibranchia; stomach type IV. *Proceedings of the Zoological Society of London*, 131(4):487–525.

PURCHON, R. D., 1987, The stomach in the Bivalvia. *Royal Society of London, Philosophical Transactions (series B, Biological Sciences),* 316(1177): 183–276.

PURCHON, R. D., 1990, Stomach structure, classification and evolution of the Bivalvia. Pp. 73–82, in: B. MORTON, ed., *The Bivalvia – Proceedings of a Memorial Symposium in Honour of Sir Charles Maurice Yonge (1899–1986)*, Edinburgh, 1986. Hong Kong University Press, Hong Kong, viii + 355 pp.

RIOS, E.C., 1975, *Brazilian marine mollusks iconography*. Rio Grande, 331 pp.

RIOS, E.C., 1994, *Seashells of Brazil*. Editora da Fundaçao Universidade do Rio Grande, Rio Grande, 368 pp.

RIOS, E. C., 2009, *Compendium of Brazilian sea shells*. Rio Grande, R. S., Brazil, 676 pp.

ROCHA OLIVARES, A., L. CALDERON AGUILERA, E. ARAGÓN NORIEGA, N. SAAVEDRA SOTELO & V. M. MORENO RIVERA, 2010, Genetic and morphological variation of northeast Pacific *Panopea* clams: evolutionary implications. *Journal of Shellfish Research,* 29: 327–335.

SCARABINO, V., 1977, Moluscos del Golfo San Matías (Provincia de Rio Negro, Republica Argentina. Inventario y Claves para su identificación. *Comunicaciones de la Sociedad Malacológica del Uruguay*, 4: 177–285.

SCARABINO, F., 2003, Lista sistemática de los bivalvia marinos y estuarinos de Uruguay. *Comunicaciones de la Sociedad Malacologica del Uruguay,* 8: 229–259.

SCARABINO, F., J. C. ZAFFARONI, C. CLAVIJO, A. CARRANZA & M. NIN, 2006, Bivalvos marinos y estuarinos de la costa Uruguaya: faunística, distribución, taxonomía y conservación. Pp. 157–169, in: R. MENAFRA, L. RODRÍGUEZ-GALLEGO, F. SCARABINO & D. CONDE, eds., *Bases para la conservación y el manejo de la costa uruguaya.* Vida Silvestre Uruguay, Montevideo, xx pp.

SOWERBY, G. B., II, 1873, Monograph of the genus *Panopaea*. Vol. 19: 6 pls., in: L. A. REEVE & G. B. SOWERBY, II, eds., 1843–1878, *Conchologia Iconica, or Illustrations of the shells of molluscous animals.* L. Reeve & Co., London, 20 vols. [unnumbered pages are captions for the plates].

STASEK, C. R., 1963, Synopsis and discussion of the association of ctenidia and labial palps in the bivalved Mollusca. *The Veliger*, 6: 91–97.

TAYLOR, J. D., S. WILLIAMS, E. GLOVER & O. DYAK, 2007, A molecular phylogeny of heterodont bivalves (Mollusca: Bivalvia: Heterodonta):

new analyses of 18S and 28S rRNA genes. *Zoologica Scripta*, 36: 587–606.

TESO, S. V., G. BIGATTI, M. C. BAZTERRICA, N. CIOCCO & P. PENCHASZADEH, 2006, The reproductive cycle of the entocommensal nemertean *Malacobdella arrokeana* and its symbiosis with the geoduck *Panopea abbreviata. Invertebrate Biology*, 125: 314–324.

TRYON, G. W., JR., 1869, Catalogue of the families Saxicavidae, Myidae and Corbulidae. *American Journal of Conchology,* 4(5) [Appendix]: 57–68.

VADOPALAS, B., T. W. PIETSCH & C. S. FRIEDMAN, 2010, The proper name for the geoduck: resurrection of *Panopea generosa* Gould, 1850, from the synonymy of *Panopea abrupta* (Conrad, 1849) (Bivalvia: Myoida: Hiatellidae). *Malacologia*, 52(1): 169–173.

VALENCIENNES, A., 1839, Description de l'animal de la panopée Australe, et recherches sur les autres espèces vivants ou fossiles de ce genre. *Archives du Muséum National d'Histoire Naturelle*, 1: 1–38.

VALENCIENNES, A., 1843, *Panopaea*. Panopée Ménard de la Groye. In: J. C. CHENU, 1842, 1843, 1846, ed., *Illustrations conchyliologiques ou description et figures de toutes les coquilles connues vivantes et fossiles, classées suivant le système Lamarck modifié d'après les progres de la science, et comprenant les genres nouveaux et les espèces récemment découvertes*. Franck, Paris, 4 Vols., 215 pp., 482 pls.

VAN DER MOLEN, S., M. KROECK & N. CIOCCO, 2007, Reproductive cycle of the southern geoduck clam, *Panopea abbreviata* (Bivalvia: Hiatellidae), in north Patagonia, Argentina. *Invertebrate Reproduction and Development*, 50(2): 75–84.

VAUGHT, K. C., 1989, *A classification of the living Mollusca*. American Malacologists, Melbourne, Florida, xii + 195 pp.

VÁZQUEZ, N., G. BIGATTI, C. ITUARTE & F. CREMONTE, 2009, Attachment of the nemertean *Malacobdella arrokeana* to the mantle of the geoduck *Panopea abbreviata* and survival outside the host. *Journal of Shellfish Research*, 28: 759–761.

VÁZQUEZ, N., F. RODRÍGUEZ, C. ITUARTE, J. KLAICH & F.CREMONTE, 2010, Host-parasite relationship of the geoduck *Panopea abbreviata* and the green alga *Coccomyxa parasitica* in the Argentinean Patagonian coast. *Journal of Invertebrate Pathology*, 105: 254–260.

VOKES, H. E. & L. R. COX, 1961, Proposal to validate the generic name *Panopea* Ménard de la Groye, 1807 (Mollusca: Bivalvia) under the Plenary Powers, together with certain related proposals. *Bulletin of Zoological Nomenclature*, 18: 184–188.

WILCKENS, O., 1907, Die Lamellibranchiaten, Gastropoden, etc., der oberen Kreide Südpatagoniens. *Berichte der Naturforschenden Gesellschaft zu Freiburg im Breisgau*, 50: 97–166.

WINCKWORTH, R., 1929, The genotypes selected by Fleming in 1818 and 1822. *Proceedings of the Malacological Society of London*, 18: 224–229.

WOODWARD, S. P., 1851, 1854, 1856, *A manual of the Mollusca; or, rudimentary treatise of Recent and fossil shells.* J. Weale, London, xvi + 486 pp., 24 pls., 1 map [published in parts and reissued in 1856 in one vol.].

WOODWARD, S. P., 1870, *Manuel de conchyliologie, ou histoire naturelle des mollusques vivants et fossiles* [French translation of Woodward, 1866, the 2nd edition of *A manual of the Mollusca*... With appendix by Aloïs Humbert.]. F. Savy, Paris, iii + 657 p., 23 pls., 1 map.

YONGE, C. M., 1957, Mantle fusion in the lamellibranchia. *Pubblicazione Stazzione Zoologica di Napoli*, 29: 151–171.

YONGE, C. M., 1982, Mantle margins with a revision of siphonal types in the Bivaliva. *Journal of Molluscan Studies*, 48: 102–103.

YONGE, C. M., 1971, On functional morphology and adaptative radiation in the bivalve superfamily Saxicavacea (*Hiatella* (= Saxicava), *Saxicavella*, *Panomya*, *Panope*, *Cyrtodaria*). *Malacologia*, 11 (1): 1–44.

YONGE, C. M., 1982, Mantle margins with a revision of siphonal types in Bivalvia. *Journal of Molluscan Studies*, 48(1):102–103.

ZAIDMAN, P. C., M. A. KROECK, E. M. OEHRENS KISSNER & E. MORSÁN, 2012, Reproductive pattern of southern geoduck, *Panopea abbreviata*, at El Sótano (San Matías Gulf, Patagonia, Argentina). *Marine Biology Research*, 8 (2): 172–181.

Revised ms. accepted March 16, 2014

MALACOLOGIA, 2014, 57(2): 295–307

HABITAT USE AND MOVEMENT PATTERNS OF THE ENDANGERED LAND SNAIL *THERSITES MITCHELLAE* (COX, 1864) (CAMAENIDAE)

Jonathan Parkyn[1*], Lyndon Brooks[2] & David Newell[1]

ABSTRACT

Thersites mitchellae (Cox, 1864) (Camaenidae) is a regionally endemic Australian land snail that is critically endangered under the Commonwealth *Environment Protection and Biodiversity Conservation Act* 1999 (EPBC Act). We studied its habitat use and movement patterns. Knowledge of habitat use is relevant to the conservation of the species, and knowledge of movements is relevant to the interpretation of the results of capture-recapture studies and occupancy-based habitat models. We provide quantitative data of nightly distances travelled, the probability of moving on a night, retreat site selection, overnight substrate use and activity. A total of 636 location positions for 11 snails was recorded on 12 nights over an 18-day period. Nocturnal movements measured at approximately 2-hour intervals showed that the mean nightly movement was 457.8 cm. The maximum nightly movement by an individual was 1,575 cm, and the maximum nightly displacement was 1,270 cm. Over the study period, the maximum movement from capture was 74.45 m, and the maximum displacement was 31.80 m. The results show that the probability of moving on a night, and the nightly distance moved once active both increase with increasing humidity up to a maximum and then decline. Whilst individuals did not return to the same retreat site location with any reliability, there is evidence of active and frequent selection of particular retreat site types within selected habitats. Snails most frequently selected sedge retreat in rainforest (66.7%) and in paperbark wetland (59.3%), and despite the scarcity of sedge in palm forest, it was the most frequented retreat site group overall (42.5%). Snails selected palm frond retreats most frequently in the palm forest (66.7%), and coarse woody debris (CWD) was selected in all habitats (17.9%) and most frequently in the palm forest (27.8%). Statistical analysis revealed significant variation among individuals in their relative use of retreat site types, and significant association between the selection of retreat site types and the initial habitat in which the individuals were located.

Key words: Camaenidae, *Thersites*, land snail, radio-telemetry.

INTRODUCTION

Molluscs are recognized as being among the most imperiled group of invertebrates on the planet and are over represented in modern extinction rate records (Lydeard et al., 2004; Régnier et al., 2009). Extinctions of molluscs and other invertebrates are generally overlooked because most scientific effort is applied to vertebrates and to taxa with greater economic importance. Terrestrial species appear to be particularly at risk, as it is within this group that the greatest documented losses seem to have occurred. Despite this, few detailed ecological studies have been conducted on those species recognized as being at risk of extinction (Parkyn & Newell, 2013). Information pertaining to habitat use may provide insights into habitat attributes that are critical to survival and assist in determining the suitability (or otherwise) of snail sampling techniques.

Land snail activity (Bailey, 1981; Attia, 2004) is influenced by the condition of an individual snail (Minoretti et al., 2011), species requirements and climatic factors (Bailey, 1975; Cameron, 1992). The daily cycles of feeding and movement (Bailey, 1989a) and the effects of temperature and humidity on movement have usually been investigated under laboratory conditions (Abdel-Rehim, 1983) and are likely to differ in the natural environment (Staikou et al., 1989; Baur & Baur, 1993). However, there are substantial problems in obtaining useful data on land snails in natural populations that

---

[1]School of Environment, Science and Engineering, Southern Cross University, P.O. Box 157, Lismore, NSW 2480 Australia
[2]Marine Ecology Research Centre, Southern Cross University, P.O. Box 157, Lismore, NSW 2480 Australia
*Corresponding author: jonathan.parkyn@scu.edu.au

include both spatial sampling and detection. A systematic, quantitative approach is required to identify small-scale habitat use, and the environmental variables that may influence the spatial distribution and population size of land snails.

Sophisticated techniques in capture-mark-recapture (CMR) (Pollock, 1982; Kendall & Nichols, 1995; Kendall et al., 1997; Kendall, 1999) and occupancy frameworks (MacKenzie et al., 2003) are available to estimate population parameters such as abundance and probability of survival, and probability of site occupancy. Together, these models take detection probability into account and allow for the inclusion of sampling, habitat and individual animal covariates. However, these techniques detect, but do not account for, temporary emigration. In fact, snails may be temporarily absent from the study site, or on site but unavailable for capture due to cryptic behaviour in complex habitat.

Radio-telemetry can provide a history of detailed movements that is not possible with CMR and occupancy studies, and theoretically allows 100% detection rates. The technique can also be used to locate individuals that would otherwise be temporarily unavailable for capture. Radio-telemetry has previously been used for investigating land snail movement (Auffenberg, 1982; Bailey, 1989b; Tomiyama & Nakane, 1993), but the weight and dimensions of transmitters in these studies may have influenced snail behaviour. Recent technical advances have resulted in miniaturization of transmitters and provide an acceptable transmitter/body weight ratio for monitoring land snails.

Thersites mitchellae (Cox, 1864) (Camaenidae) is a regionally endemic Australian land snail that has declined in distribution and abundance due to clearing of much of its former habitat for coastal development. The species occurs in the South Eastern Queensland (SEQ) interim Biogeographic Region for Australia (IBRA) in northeastern New South Wales (NSW) and is listed as endangered under the NSW *Threatened Species Conservation Act* 1995 (TSC Act), and critically endangered under the Commonwealth *Environment Protection and Biodiversity Conservation Act* 1999 (EPBC Act). This was the first species for which a critical habitat determination was made under the TSC Act (National Parks & Wildlife Service, 2001a), yet there appears to be no published information regarding the autecology of this species. The species is believed to shelter in cryptic habitats, such as under leaf litter and inside palm frond stems (Cox, 1864; National Parks & Wildlife Service, 2001b) and is most obvious on humid nights (Andrade et al., 2011). Detection probability likely varies due to the size of individuals, spatially due to site-specific habitat characteristics and as a result of changing climatic conditions.

The aim of the present study is to investigate habitat use and movement that is relevant to the conservation of *T. mitchellae* in order to inform survey and population assessment. The potential for using radio-telemetry to augment capture-mark-recapture studies and occupancy-based habitat models is considered.

METHODS

Study Area

The study area was located in New South Wales, Australia (28°40’45”S, 153°36’44”E) and is typical of coastal lowland habitat where *T. mitchellae* has been historically recorded. The three-hectare site consists of *Melaleuca quinquenervia* dominated wetland interspersed with areas of littoral rainforest, and *Archontophoenix cunninghamiana* palm forest. The site is adjacent to a natural creek and other boundaries are encroached by urban development.

Snail Collection

Four snails were collected from across each of three different habitats at the study site 24 hours prior to the commencement of tracking. Only individuals with a minimum shell diameter of 3 cm were selected, but the sample included individuals that could be classified as juvenile or adult by the presence or absence of an umbilicus. These were kept in the laboratory for 24 hours in order to attach transmitters before releasing to their original locations. Individuals were released at their point of collection on 1 November 2011 and monitored for up to 18 nights.

Radio-Telemetry

We used single stage transmitters (Titley Scientific, Australia) with a weight of 0.4 g. We attached the transmitters to the shell with tan coloured micropore tape (Fig. 1). The technique provided an adequate temporary attachment that minimised adhesive residue and potential shell damage upon removal. The tan colour also reduced the risk of increased visibility and

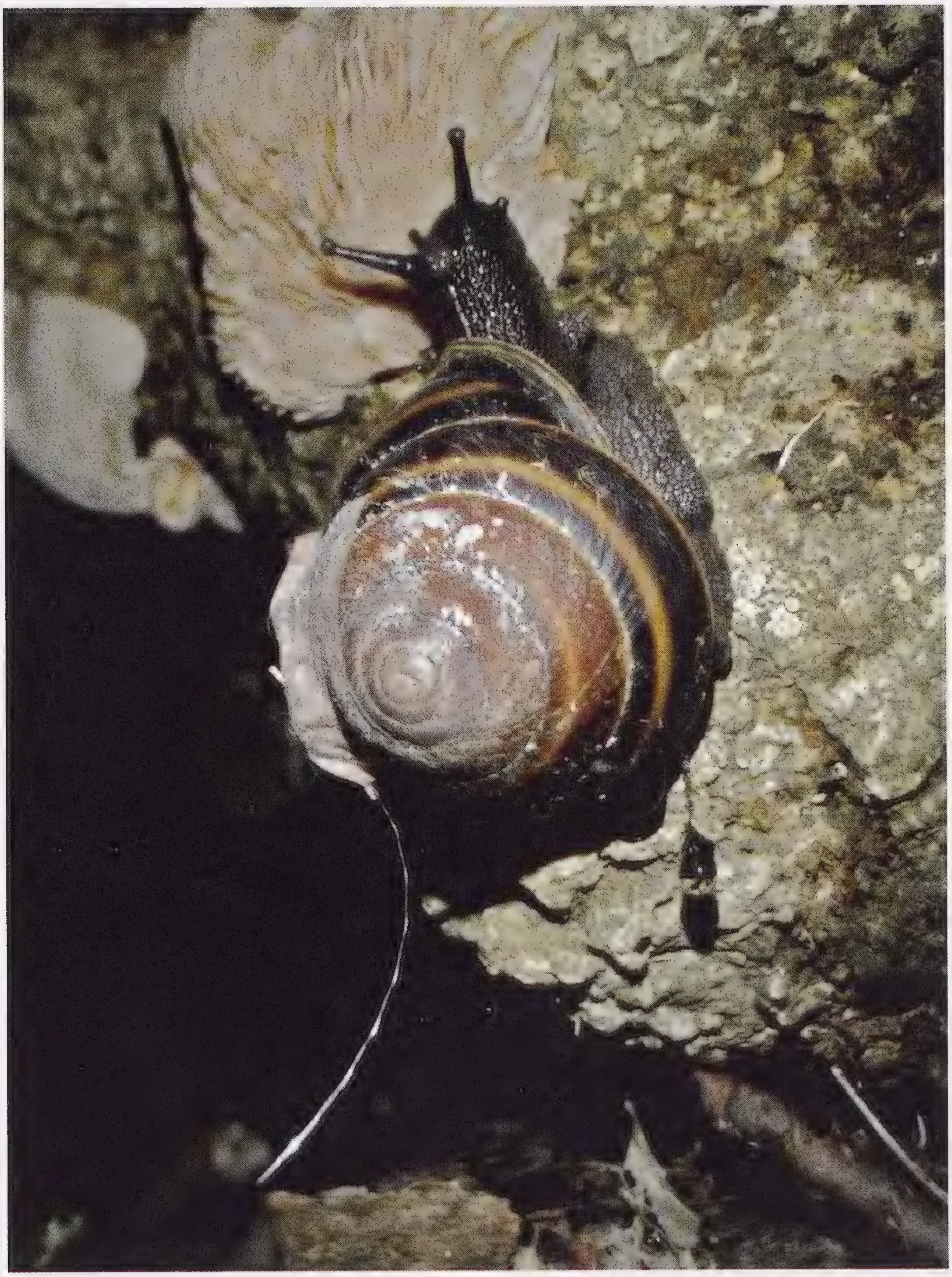

FIG. 1. Transmitter attached to *Thersites mitchellae* shell with tan-coloured micropore tape.

hence the likelihood of predation. This method also ensured that transmitters would fall off after a few weeks in the event of transmitter failure. The total weight of the transmitter and tape was less than 4% of the weight of the smallest tracked snail.

Study Design

Commencing at dusk, snails were located at approximately two-hour intervals to obtain six location positions per snail per night, with the last observation on each snail made around dawn when individuals had ceased nocturnal activity. At each position, we measured the bearing and straight-line distance travelled (cm) from the previous position, and from the initial capture/release point. We also recorded the substrate upon which snails were found (palm frond, coarse woody debris (CWD), tree, leaf, sedge, boardwalk) at each position, their activity (travelling, eating, resting), and selection of diurnal retreat site at dawn (sedge, palm frond, CWD, leaf litter, tree). The climatic conditions (temperature, humidity, occurrence of rain) at ground level were recorded for each individual on all occasions.

Data Analysis

We report between night's analyses, including total nightly distances travelled and the probability of moving, along with selection of diurnal retreat sites. We also report within night's analyses, including substrate selection and activity. Because some transmitters failed during the course of the study, we report the number of nights on which each snail was observed prior to transmitter failure, and its weight (g), size and maturity status (adult, juvenile). For each night, we provide the minimum, maximum and mean temperature and humidity, and occurrence of rain.

Nightly Distances Travelled

The data for the analysis included the total distances moved by each snail on each night on which it was recorded, the maturity status and weight of each snail, and the mean temperature (°C) and mean humidity (% RH) of each night. Three models were fitted to the nightly distance travelled data; the first used all the data including zero movements, the second used only whether a snail moved or not on a night, and the third used the distances travelled with zero movements excluded.

Model 1. Nightly Distances Travelled Using All Data: A linear mixed effects model was fitted to the nightly distances with random variables "snail" and "night within snail" (Pinheiro & Bates, 2000; SPSS V19.0). Fixed effects were assessed for the maturity status and weight of the snail, the mean temperature and mean humidity, and the square of the mean humidity of the night. The mean humidity variable was centered by subtracting the total mean over nights (81.2%) from the nightly means prior to analysis. A model that included all these main effects was initially fitted. *F*-tests (with adjusted degrees of freedom) (McLean & Sanders, 1988) were used to assess their significance. Non-significant effects were sequentially removed in descending order of the size of their *p*-values until a final model that included only significant ($p < 0.05$) effects were obtained. Estimates were obtained by the maximum likelihood (ML) method. The distribution of nightly movements was right-skewed and zero-inflated due to the nights when some snails did not move. The residuals from the final model were assessed for skew and zero-inflation to assess the assumption of normally distributed residuals. The distribution of residuals was reasonably symmetric with no obvious inflation, and with106 residuals from the model, the Central Limit Theorem allows confidence in the assumption of a normally distributed sampling distribution. A further model, employing an alternative functional form, was fitted to assess the appropriateness of the functional form in the final model.

Model 2. Probability of Moving on a Night: The data for the analyses included whether each snail moved from its retreat or not on each night on which it was observed, the maturity status and weight of each snail, and the mean temperature and mean humidity of each night. A mixed effects logistic regression model was fitted to the binary response with random variables "snail" and "night within snail" (Goldstein, 1995; MLwiN V2.24). Fixed effects were assessed for the maturity status and weight of the snail, the mean temperature and mean humidity, and the square of the mean humidity of the night. The mean humidity variable was centered by subtracting the total mean over nights (81.2%) from the nightly data prior to analysis. A model that included all these main effects was initially fitted. Wald *z*-tests (Goldstein, 1995, z = estimate/SE) were used to assess their significance. Non-significant effects were sequentially removed in descending order of the size of their *p*-values until a final model that included only significant ($p < 0.05$) effects was obtained. The Markov Chain Monte Carlo (MCMC) method (Rasbash et al., 2009) with 5,000 iterations burn-in and a 50,000 iterations monitoring chain was employed to obtain estimates for the final model.

Model 3. Nightly Distances Travelled Using Data with Non-Movements Excluded: This model and the modeling process were as for Model 1 but used only the data on non-zero movements.

We attempted to accommodate both snail and initial habitat effects using a multi-level (snail, observation within snail), multinomial (retreat site group) mixed effects model, but there were insufficient data to estimate the effect of initial habitat on the probability of retreat site group selection, and convergence was not reached. This was because no snails

TABLE 1. The number of nights observed from 1st–18th November 2011, maturity, weight, and descriptive statistics for nightly movement by snail. Zero indicates the number of nights with no movement.

				Nightly Movement (cm)				
Snail	Nights	Maturity	Weight (g)	Min.	Max.	Mean	*SD*	Zero
1	1–12	juvenile	10.6	0.0	988.0	240.4	298.3	3
2	1–4	adult	22.3	185.0	1123.0	549.5	423.0	0
3	1–12	adult	14.5	0.0	1236.0	472.5	405.6	2
4	1–8	juvenile	10.4	0.0	726.0	250.0	311.9	4
5	1–11	adult	18.1	265.0	1105.0	632.5	302.9	0
6	1–12	adult	15.8	0.0	1015.0	291.0	328.1	3
7	1–8	adult	19.3	403.0	1575.0	930.6	488.2	0
8	1–12	adult	24.2	0.0	805.0	396.7	247.0	2
9	1–4	juvenile	17.2	369.0	1012.0	718.3	266.3	0
10	1–12	adult	26.2	0.0	569.0	300.0	213.2	2
11	1–11	juvenile	15.9	0.0	982.0	604.0	304.1	1

initially found in palm forest habitat selected sedge retreat, and no snails initially found in paperbark wetland habitat selected tree retreat, despite these features being present.

Descriptive Data for Retreat Site Selection

Habitats within the fragment of vegetation were classed into three groups: *Archontophoenix cunninghamiana* palm forest (palm forest), littoral rainforest (rainforest), and *Melaleuca quinquenervia*-dominated wetland (paperbark wetland). The diurnal retreat sites were classified into five groups: sedge, palm frond (on the ground), coarse woody debris (CWD), leaf litter and tree. We report the frequencies of co-occurrence of initial habitat and retreat site group. The variation among snails in retreat site selection was examined prior to testing the association between initial habitats and retreat sites using Fisher's Exact Test (MCMC method with 100,000 iterations).

Nocturnal Substrate Selection and Activity and Model Selection

Substrate was classed into six groups: palm frond, CWD, tree, leaf, sedge and boardwalk. Activity was classed into three groups: travelling, eating and resting. We report the frequencies of co-occurrence of substrates selected and activity groups. The variation among snails in substrate selection and activity profiles was examined prior to testing the association between the selected substrates and the activities observed on them using Fisher's Exact Test (MCMC method with 100,000 iterations).

RESULTS

Descriptives

A total of 636 location positions for 11 snails were recorded on 12 nights over an 18-day period (Table 1). (There were no data for one of the twelve 12 due to transmitter failure on the first night.) Five snails were tracked over 12 nights, and two snails over 11, 8, and 4 nights each. Radio-tracked snails ranged from 10.4 g to 26.2 g with a mean weight of 17.6 g (*SD* = 5.1). Size (shell diameter) ranged from 33–41 mm with a mean diameter of 38 mm (*SD* = 2.4), and included juvenile (*n* = 5) and adult (*n* = 7) snails. Over the study period, observed temperature ranged from 13.1°C to 23.7°C (mean, 18.6°C; *SD* = 4.5) and observed humidity ranged from 59.5% RH to 100% RH (mean, 81.8% RH; *SD* = 8.9). Rain was observed on nights 4 and 8.

Nightly Distances Travelled

Nocturnal movements measured at approximately 2-hourly intervals showed that the mean nightly movement was 457.8 cm. The maximum nightly movement by an individual was 1,575 cm (*SD* = 369.6). The maximum nightly displacement was 1,270 cm (mean, 302 cm; *SD*

TABLE 2. Model 1: Results of tests of the fixed and random effects in the final model for nightly distances travelled using all data.

Fixed Effects	*F*	*df*	*p*
Mean Humidity[1]	4.543	1, 99.07	0.036
Mean Humidity Squared[1]	9.089	1, 95.89	0.003
Random Effects	Wald Z		*p*
Snail	1.651		0.099
Night within Snail (Residual)	6.844		< 0.001

[1] Mean humidity centred at 81.2%.

= 425.8). Over the study period the maximum movement from capture was 74.45 m, and the maximum displacement was 31.80 m. The number of nights observed for each snail from 1 to 18 November 2011, maturity, weight, and descriptive statistics for nightly movement are reported in Table 1.

Model 1. Nightly Distances Travelled Using All Data: Results of tests of the fixed and random effects in the final model are reported in Table 2. Only a quadratic function of mean nightly humidity remained as a significant effect after systematic elimination of non-significant ($p > 0.05$) fixed effects. While the random variation among snails was not significant ($p < 0.05$), this effect was retained in the model to adjust standard errors for the fixed effects. Estimated fixed and random effects are reported with their standard errors in Table 3. The model-predicted values of mean nightly distance moved by mean nightly humidity are plotted in Figure 2.

To assess the appropriateness of the quadratic functional form, models were fitted using maximum nightly humidity rather than mean nightly humidity and a logarithmic function of the humidity variable (humidity + log.humidity) rather than a quadratic function with very little effect on the substantive results. In particular, maxima for mean nightly movement were reached at about the same nightly humidity levels (mean or maximum), and all models showed a distinct decline in mean movement beyond those points. Rain was observed on the two nights with the greatest mean humidity (> 85%), with heavy rain being observed on the night with mean humidity 90.9% and light rain being observed on the night with mean humidity at 88.1%.

Model 2. Probability of Moving: Model 1 was built on data that included zero nightly movements. To assess the effect of the probability that nightly movement was zero on the results for model 1, a binary logistic mixed effects model was fitted to the moved/not moved data. Among the effects for maturity status and weight of the snail, the mean temperature and mean maximum humidity, and the square of the mean humidity of the night, only a quadratic function of the mean nightly humidity was statistically significant. The logit scale estimates were: intercept $\beta = 2.452$, $SE = 0.535$, $p < 0.0001$; mean humidity $\beta = 0.0924$, $SE = 0.0492$, $p = 0.060$; mean humidity squared $\beta = 0.0228$, $SE = 0.0091$, $p = 0.013$. The logit scale estimates were transformed to the probability scale and the probabilities of moving were calculated for the

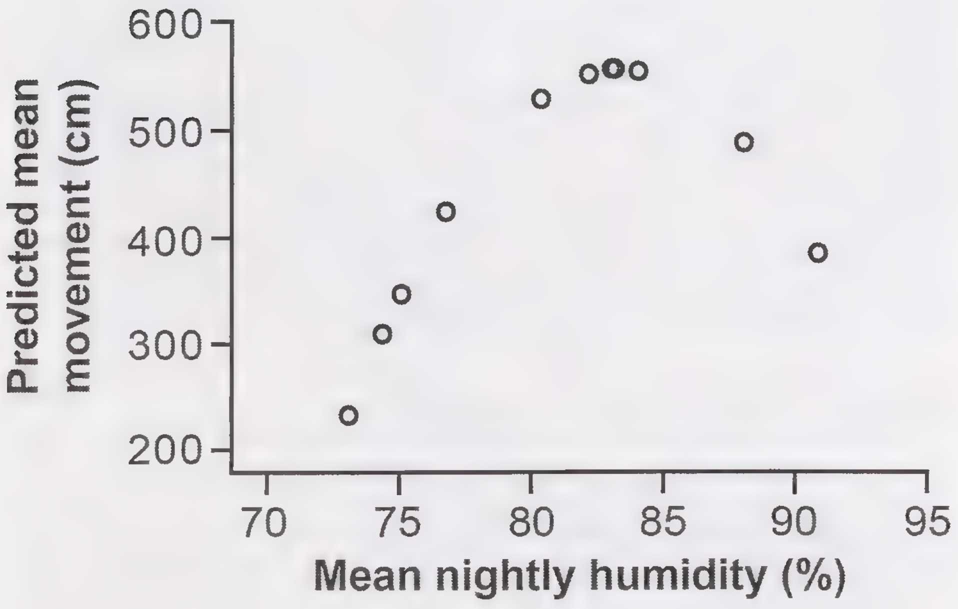

FIG. 2. Model-predicted values (Model 1) of mean nightly distance moved by mean nightly humidity.

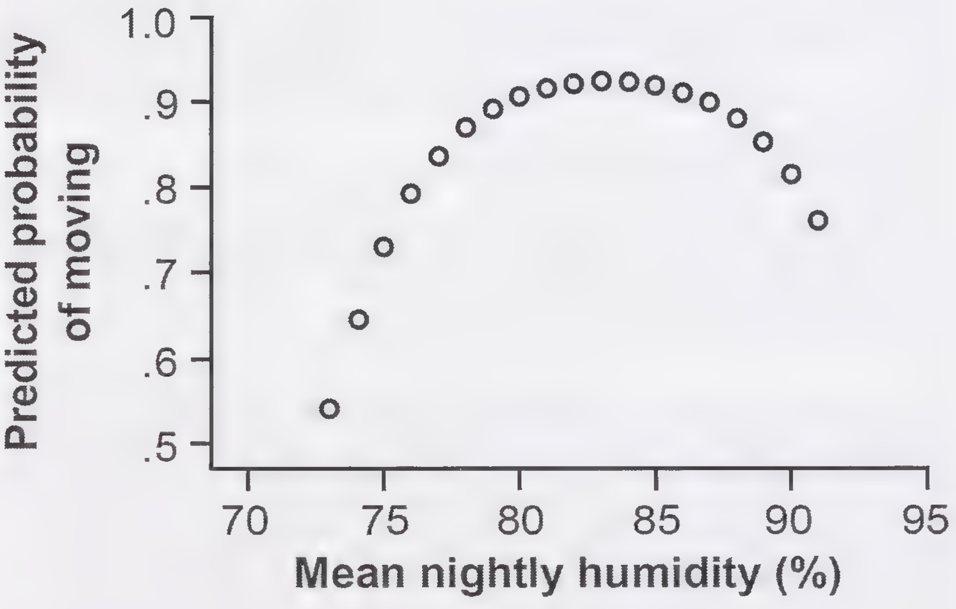

FIG. 3. Model-predicted values (Model 2) of probabilities of moving by mean nightly humidity.

TABLE 3. Model 1: Estimated fixed and random effects for nightly distances travelled using all data.

Fixed Effects (Beta)	Estimate	SE	L95%CI	U95%CI
Intercept	541.59	64.56	403.63	679.55
Mean Humidity[1]	13.45	6.31	0.93	25.97
Mean Humidity Squared[1]	-3.05	1.01	-5.06	-1.04
Random Effects (Variance)	Estimate	SE	L95%CI	U95%CI
Snail	27745.97	16804.63	8465.66	90936.61
Night within Snail (Residual)	96217.53	13977.59	72376.82	127911.29

[1] Mean humidity centered at 81.2%.

range of mean nightly humidity in the data. These values are plotted in Fig. 3.

Model 3. Nightly Distances Travelled Using Data with Non-Movements Excluded: Model 1 was built on data that included zero nightly movements. To assess the effect of the predictor variables on the non-zero distances travelled, a model was built as for model 1 but with the zero movement data removed (*N* = 88). While the coefficients of the quadratic function of humidity did not reach the $p < 0.05$ level of significance (humidity $p = 0.158$, humidity squared $p = 0.081$), a plot of the predicted values by mean nightly humidity (Fig. 4) followed a very similar form to the plots of the predicted probability of movement and predicted nightly mean distance moved (all data including zero movements).

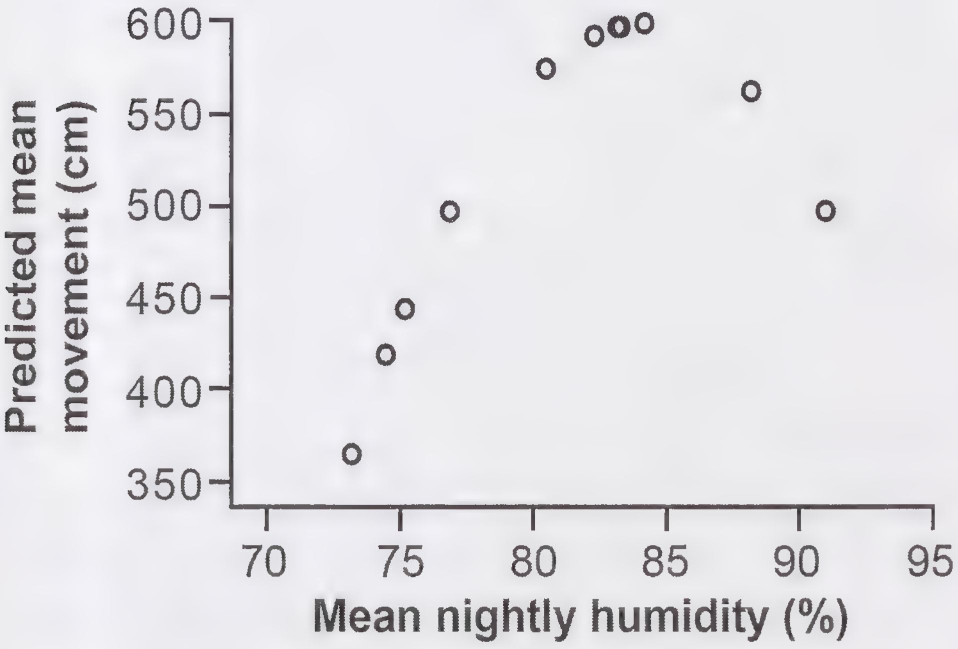

FIG. 4. Model-predicted values (Model 3) of all non-zero mean nightly distance moved by mean nightly humidity.

Retreat Site Selection

A total of 106 retreat sites were recorded for 11 snails. Snails most frequently selected sedge retreat in rainforest (66.7%) and in paperbark wetland (59.3%), and despite the scarcity of sedge in palm forest it was the most frequented retreat site group overall (42.5%). Snails selected palm frond retreats most frequently in the palm forest (66.7%), and CWD was selected in all habitats (17.9%) and most frequently in the palm forest (27.8%). Leaf litter (5.7%) and trees (3.8%) were infrequently selected overall. The frequencies of co-occurrence of initial/release habitat (palm forest, rainforest, wetland) and retreat sites (tree, leaf litter, CWD, palm forest, sedge) selected by snails are reported in Table 4.

There was a significant association between the initial habitats where snails were found and their relative use of the five retreat site groups (Fisher's Exact Test, Monte-Carlo 100,000 iterations, $p = < 0.001$). There was, however, significant variation among individuals in their relative use of the retreat site groups (Fisher's Exact Test, Monte-Carlo 100,000 iterations, $p = < 0.001$) that may not be fully accounted for by the differences in their initial habitats. Consequently, the *p*-value for the test of association between initial habitat and retreat site group may be too small and some caution is warranted in interpreting the effect shown in Table 4.

Nocturnal Habitats and Activity

Snails were only active at night, and a total of 408 temporal positions were recorded for

TABLE 4. The frequencies of co-occurrence of initial/release habitat and retreat sites selected by snails (CWD = coarse woody debris).

Initial/ Release Habitat		Retreat Site					
		Tree	Leaf Litter	CWD	Palm Frond	Sedge	Total
Palm Forest	Count	1	1	10	24	0	36
	%	2.8%	2.8%	27.8%	66.7%	0%	100%
Rainforest	Count	3	4	4	3	29	43
	%	7.0%	9.3%	9.3%	7.0%	67.4%	100%
Paperbark	Count	0	1	5	5	16	27
	%	0%	3.7%	18.5%	18.5%	59.3%	100%
Total	Count	4	6	19	32	45	106
	%	3.8%	5.7%	17.9%	30.2%	42.5%	100%

the 11 snails during which their activity and substrate use was recorded. There were 13 instances when snails were located but were not observable inside rotting tree stumps (CWD). The frequencies of co-occurrence of substrate group and activity type are reported in Table 5.

There was a significant association between the substrate groups where snails were found and the activity types observed (Fisher's Exact Test, Monte-Carlo 100,000 iterations, $p = < 0.001$). However, there was significant variation among individuals in their relative use of the six substrate groups (Fisher's Exact Test, Monte-Carlo 100,000 iterations, $p = < 0.001$) and the variation among individuals in their relative allocation of time to activity types did not reach the conventional $\alpha \leq 0.05$ level of significance (Fisher's Exact Test, Monte-Carlo 100,000 iterations, $p = 0.096$). This analysis does not accommodate both snail and substrate group effects on activity type and the *p*-value for the test of association of the substrate groups where snails were found and the activity types observed there may be too small and some caution is warranted in interpreting the effect shown in Table 5.

Periods of Inactivity

On seventeen occasions we observed that snails were not active at night. Seven of the 11 snails recorded zero-nightly movement on at least one occasion, and remained at their retreat site for up to four days. We noticed that snail number 6 seemed to have actively made a nest within moist bark litter at the base of a broad-leaved paperbark tree. The snail remained at the location for three consecutive nights. After the snail had left the retreat site, a clutch of 54 white, ovoid eggs (Ø ≈ 5 mm) were observed (Fig. 5). A portion of the substrate and 17 eggs (mean Ø 4.95 ± 0.09 *SE*) were transferred to the laboratory for observation. All snails hatched within 28 days and hatchlings consumed their own egg shells. Two days later the snails had climbed the litter and attached themselves to the underside of the uppermost

TABLE 5. Summary of snail's substrate use and activity (traveling, eating, resting).

Substrate		Traveling	Eating	Resting	Total
Frond	Count	53	16	18	87
	%	60.9	18.4	20.7	100
Deadwood	Count	25	57	7	89
	%	28.1	64.0	7.9	100
Tree	Count	3	1	3	7
	%	42.9	14.3	42.9	100
Leaf	Count	17	1	6	24
	%	70.8	4.2	25.0	100
Shrub	Count	93	47	14	154
	%	60.4	30.5	9.1	100
Boardwalk	Count	23	4	20	47
	%	48.9	8.5	42.6	100
Total	Count	214	126	68	408
	%	52.5	30.9	16.7	100

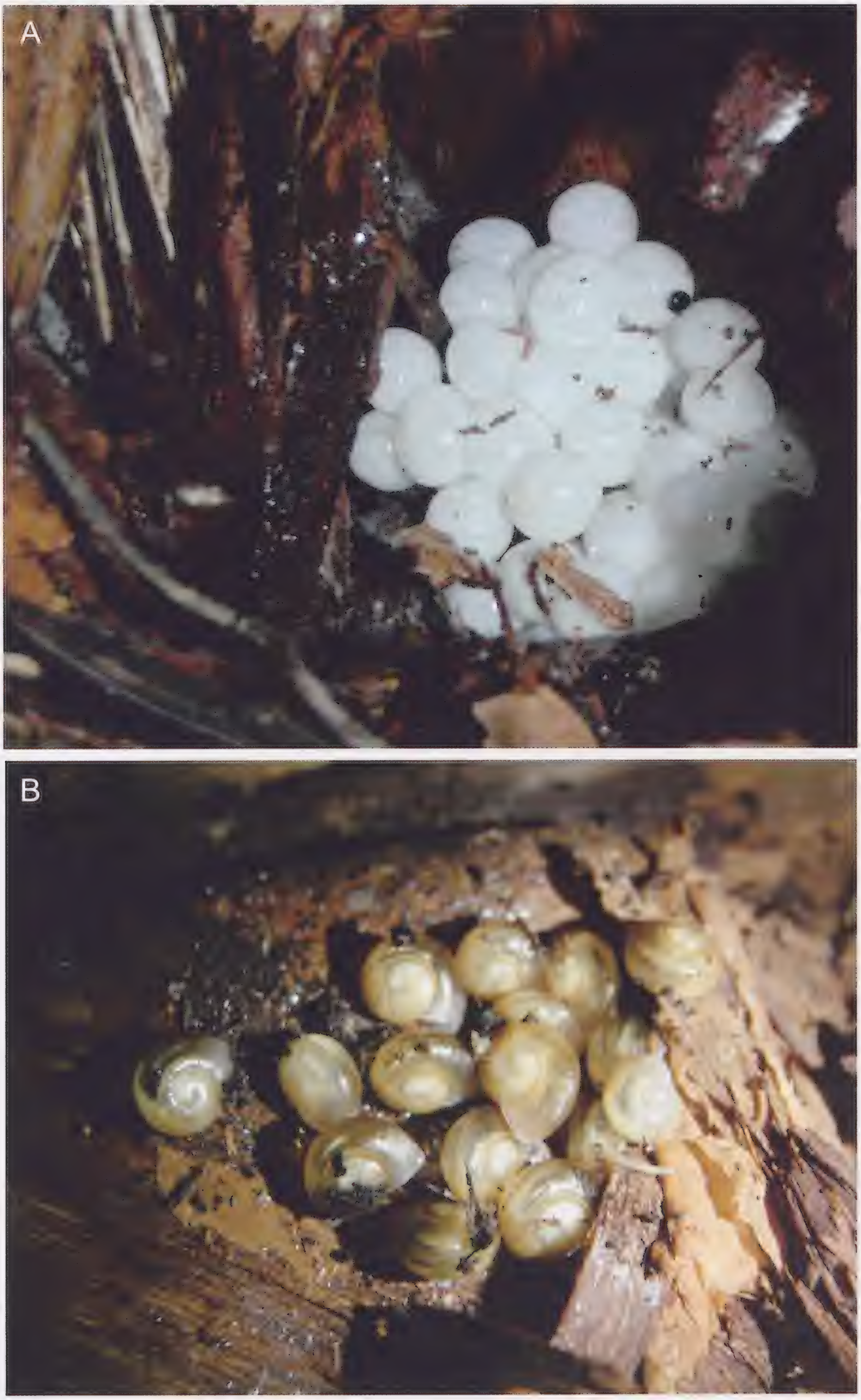

FIG. 5. *Thersites mitchellae*. (A): Clutch of 54 white ovoid eggs (Ø ≈ 5 mm); (B): One month later, a cluster of *T. mitchellae* attached to the underside of bark litter.

bark debris (Fig. 6). After seven days the snails (mean Ø 6 mm ± 0.07 *SE*) dispersed throughout the substrate. Four months after the initial egg stage (February 13), all 17 snails (mean Ø 8.1 mm ± 0.09 *SE*; mean weight 0.2 g ± 0.01 *SE*) were returned to their original habitat.

DISCUSSION

This study provides new information on habitat use and movement that can be used to inform survey and population assessment relevant to the conservation of *T. mitchellae*. The results support the usefulness of radio-telemetry to augment capture-mark-recapture studies and occupancy-based habitat models.

Thersites mitchellae is known from a small number of sites between the Richmond and Tweed rivers along the coastal flood plain of northeastern New South Wales. This coastal plain continues to be subjected to development pressure and protection of all remaining populations is desirable.

Most of these sites are small habitat fragments that are considered marginal, and were previously thought to be represented by three or fewer specimens (National Parks and Wildlife Service, 2001b). However, the results from this study show that *T. mitchellae* can be extremely cryptic and difficult to detect during surveys.

We have provided information regarding diurnal sites used and thus the areas upon which habitat searches should focus. Snails were most frequently found to shelter within sedges (42.5% of all retreats used) and inside frond litter in palm forest (66.7%), with CWD selected in all habitats (17.9%). The presence of sedge (*Gahnia clarkei*), palm frond litter and CWD are thus critical components of *T. mitchellae* habitat at our study site. Small, discrete habitat patches within the fragment range in size from approximately 100 m^2 to 1000 m^2 and are sufficiently close for individual snails to travel between patches. Given that the site is typical of *T. mitchellae* habitat, we believe our results have broader implications across the narrow range of this species.

Movements

The results from our study demonstrate that *T. mitchellae* is capable of relatively long-range movements within suitable habitat under favourable climatic conditions. One individual was displaced over 30 m from its initial capture location and moved approximately 75 m over the 18 days of our study. This suggests that snails may be capable of colonising new habitat patches if appropriate connectivity is available between habitats, and this has important implications for future attempts to restore habitat for this critically endangered land snail.

The duration of feeding, traveling and activity of *Limax pseudoflavus* Boettger, 1881 (= *Limax ecarinatus*) (Limacidea), was recorded by Ford & Cook (1994) using time-lapse cinematography. They observed that periods of activity were interspersed with rest. While we did not constantly monitor individuals over the course of a night we provide information that is indicative of the activity levels of individual snails based on six two-hourly samples. We determined that about half (52.5%) of nightly activity was spent travelling between resources, and about a third (31%) was feeding. The function of resting is associated with contact rehydration (Prior, 1985). Our findings are similar to those of Bailey (1989a) on the behaviour of *Cantareus aspersus* Müller 1774 (= *Helix aspersa*) (Helicidae), whereby snails exhibited two to three rest intervals per night accounting for 17% of the total recorded activity. We observed resting prior to retreat on all nights and this could be a rehydration strategy to minimise evaporative loss during daytime sheltering.

With conventional searching, detection probabilities are expected to be less than one, but radio-telemetry allowed us to locate snails that were out of sight. Out of 408 location positions during periods of snail activity, there were 13 instances (3.2%) when a snail was located but not observable. On all of these occasions, snails had crawled inside CWD, specifically, rotting tree stumps. All snails could be observed in sedge and on other substrates after being located with radio-telemetry, but due to their natural camouflage they would probably have often been overlooked without the implementation of this technique.

Humidity

The probability of movement and thus the likelihood that individuals will be encountered during a survey was strongly influenced by humidity.

Previous studies (Abdel-Rehim, 1983; Tomiyama & Nakane, 1993; Murphy, 2002) have demonstrated a positive relationship between movement and humidity in land snails. The results presented here support this association and demonstrate that the probability of moving on a night, and the nightly distance moved once active, both increase with increasing humidity. The range of temperature was relatively small during the investigation period of 18 days. Thus, the available data do not allow any assessment of a potential temperature effect. The decrease in predicted mean movement on nights of highest mean humidity correlate with two rainfall events, but it is unclear whether the decrease in movement is a behavioral response to rainfall per se or to very high humidity levels. The limited number of rainfall events constrains our ability to distinguish between these alternatives.

Biotic Effects, Homing Behavior and Retreat Sites

While land snail activity is initiated by a circadian component (Attia, 2004) and influenced by climatic factors (Bailey, 1975), the extent of movements can also be determined by the nutritional (Croll & Chase, 1977), reproductive (Baur, 1988; Baker, 1991) and osmotic status of an individual (Cook, 2001). On 17 occasions we observed that snails were not active on suitably humid nights. Seven of the 11 snails recorded zero-nightly movement on at least one occasion, and remained at their retreat site for up to four days. On one of these occasions we observed an egg laying site. Minoretti et al. (2011) found that mating and reproductive success in *Arianta arbustorum* (Linnaeus, 1758) (Helicidae) are mainly determined by the activity of individual snails. It is unlikely that the distances travelled by *T. mitchellae* per night might show considerable seasonal variation due to a peak phase of reproduction, as the species occurs in a subtropical climate. Copulation has been observed throughout the year (J. Parkyn, unpublished data), and it is likely that individuals will achieve multiple mating successes. It is clear that successive nightly movement of snails is not independent, and that the probability of movement is also dependent on an individual's requirements. In the present study, there were insufficient sequential data to allow the fitting of a Markov model to estimate the probability of moving on a night as a consequence of previous night's activity.

Homing behaviour has been demonstrated in laboratory experiments (Bailey, 1989b), but in a natural environment with numerous potential retreat sites, it is more likely that snails are nomadic within their preferred habitat (Staikou et al., 1989; Baur & Baur, 1993). Our results indicate that while individuals did not return to the same retreat site location with any reliability, there is evidence of active and frequent selection of particular retreat site types within selected habitats. Statistical analysis revealed significant variation among individuals in their relative use of retreat site types. Further, we found significant association between the selection of retreat site types and the initial habitat in which the individuals were located.

We found that *T. mitchellae* preferred sedge (*Gahnia clarkei*) retreat sites in the rainforest and wetland, and Bangalow palm (*Archontophoenix cunninghamiana*) fronds in the palm forest. Sedge is a tall tussock-forming perennial in which snails retreated and attached upside-down to the stalk. The plant provides insulation for the snails and protection from birds during the day. In palm forest, sedge was scarce and most often snails retreated inside palm frond stems. The preference for this retreat may also be due to microclimatic stability, and protection from noisy pittas (*Pitta versicolor*) and brushturkeys (*Alectura lathami*). The frond litter provides numerous potential retreat sites with a hard substrate for the upside-down attachment that we observed.

Only one snail remained wholly within the rainforest for the duration of the study. All others initially found in the rainforest or wetland habitat, moved back and forth between the adjacent wetland and rainforest habitat. No snails that were initially found in the palm forest moved entirely out of the habitat. Prior to this study, the foraging and retreat sites of *T. mitchellae* were unknown, though it was suggested that a well-developed leaf litter layer may be a key habitat component (Cox, 1864; National Parks & Wildlife Service, 2001b). When active at night, snails travelled over leaf litter, but rarely sheltered under leaves. Snails most frequently travelled on sedge as the long, lower leaves formed an extensive ground cover. Here, the leaf surface was grazed for biofilm. Adult *T. mitchellae* are probably ground dwelling (National Parks & Wildlife Service, 2001a), and we found that snails were unlikely to travel on, or retreat up trees unless to escape localised flooding.

Coarse wood debris (CWD) has been shown to be an important factor for populations of forest-associated snails (Müller et al., 2005; Kappes et al., 2009). Similarly, our results show that snails selected CWD for retreat sites in all habitats and it was the substrate most frequently selected for feeding. The diet of land snails can differ between different habitats and may be influenced by the quantity and accessibility of food in each habitat (Williamson & Cameron, 1976; Iglesias & Castillejo, 1999); we also observed snails feeding in each of the three habitats and on all substrates. Further experiments on the dietary composition of *T. mitchellae* from different habitats would provide new insights into food preferences and habitat selection.

Management Implications

Within typical general habitat of *T. mitchellae* we have identified two important areas: (1) the ecotone between the wetland and rainforest, and (2) palm forest. *Therisites mitchellae* showed a clear preference for sedge as diurnal retreat sites in forest and wetland, and frond litter in the palm forest. Coarse woody debris is likely to be an important resource for *T. mitchellae*, and may provide a more complex role in habitat quality. Our findings have relevance to guidelines for survey, and recovery planning for *T. mitchellae.* The discovery of frequent use of particular retreat site types within selected habitats can assist in field assessment including provision of recommendations to avoid or minimise impacts to these habitats, and guide proposals for planting and embellishment of habitat for restoration.

The species exhibits nomadic behaviour and an ability to travel relatively large distances at night. Linking areas of existing remnant vegetation and other habitat with revegetation to increase retreat sites and foraging substrate would assist recolonization of adjacent habitat patches. Our results show that the probability of moving on a night, and the nightly distance moved once active both increase to a maximum with increasing humidity. These results only partly correspond with current guidelines for survey (National Parks & Wildlife Service, 2001b) that suggest searching leaf litter and loose bark on tree trunks during the day, and undertaking nocturnal surveys during warm, wet weather. Our use of radio-telemetry demonstrates that the inability to capture a live snail during a survey is not conclusive evidence of its absence from the location. Snails may not be active even in suitable habitat under favourable conditions, and active snails may be inaccessible in cryptic habitats.

ACKNOWLEDGEMENTS

We thank Dr. John Stanisic and Dr. Alison Specht for constructive discussions and advice; John Parché for providing access to the site; Dr. Mark Kingston for administering a Tweed Shire Council Biodiversity Grant; and Dr. Mandy Reid, Dr. Frank Köhler and an anonymous reviewer for their valuable comments on the manuscript. Jonathan Parkyn is supported by an Australian Postgraduate Award from the Commonwealth Government. Work was conducted under scientific licence (S12832) from the NSW National Parks and Wildlife Service.

LITERATURE CITED

ABDEL-REHIM, A. H., 1983, The effects of temperature and humidity on the nocturnal activity of different shell colour morphs of the land snail *Arianta arbustorum*. *Biological Journal of the Linnaean Society*, 20: 385–395.

ANDRADE, L., A. KLOOTWIJK, J. PARKYN & A. SPECHT, 2011, Initial observations of a population of Mitchell's rainforest snail *Thersites mitchellae* (Cox, 1864), *Australian Zoologist*, 35: 590–598.

ATTIA, J., 2004, Behavioural rhythms of land snails in the field. *Biological Rhythm Research*, 35: 35–41.

AUFFENBERG, K., 1982, Bio-electronic techniques for the study of molluscan activity. *Malacological Review*, 15: 137–138.

BAILEY, S. E. R., 1975, The seasonal and daily locomotor activity in the snail *Helix aspersa* Müller, and their relationship to environmental variables. *Journal of Molluscan Studies*, 41: 415–428.

BAILEY, S. E. R., 1981, Circannual and circadian rhythms in the snail *Helix aspersa* Müller and the photoperiodic control of annual activity and reproduction. *Journal of Comparative Physiology*, 142: 89–94.

BAILEY, S. E. R., 1989a, Daily cycles of feeding and locomotion in *Helix aspersa*. *Haliotis*, 19: 23–31.

BAILEY, S. R., 1989b, Foraging behaviour of terrestrial gastropods: integrating field and laboratory studies. *Journal of Molluscan Studies*, 55: 263–272.

BAKER, G., 1991, Production of eggs and young snails by adult *Theba pisana* (Müller) and *Cernuella virgata* (Da Costa) (Mollusca, Helicidae) in laboratory cultures and field populations. *Australian Journal of Zoology*, 39: 673–679.

BAUR, B., 1988, Repeated mating and female fecundity in the simultaneously hermaphroditic land snail *Arianta arbustorum*. *International Journal of Invertebrate Reproduction and Development*, 14: 197–204.

BAUR, A. & B. BAUR, 1993, Daily movement patterns and dispersal in the land snail *Arianta arbustorum*. *Malacologia*, 35: 89–98.

CAMERON, R. A. D., 1992, Land snail faunas of the Napier and Oscar ranges, Western Australia; diversity, distribution and speciation. *Biological Journal of the Linnean Society*, 45: 271–286.

COOK, A., 2001, *Behavioural ecology: on doing the right thing, in the right place at the right time.* CABI Publishing, Oxon, 558 pp.

COX, J. C., 1864, *Catalogue of Australian land shells*. John Alex Engel, Sydney, 46 pp.

CROLL, R. P. & R. CHASE, 1977, A long-term memory for food odors in the land snail, *Achatina fulica*. *Behavioral Biology*, 19: 261–268.

FORD, D. J. G. & A. COOK, 1994, The modulation of rhythmic behaviour in the pulmonate slug *Limax pseudoflavus* by season and photoperiod. *Journal of Zoology*, 232: 419–434.

GOLDSTEIN, H., 1995, *Multilevel statistical models*. Halstead Press, London, xiv + 178 pp.

IGLESIAS, J. & J. CASTILLEJO, 1999, Field observations on feeding of the land snail *Helix aspersa* Müller. *Journal of Molluscan Studies*, 65: 411–423.

KAPPES, H., M. JABIN, J. KULFAN, P. ZACH & W. TOPP, 2009, Spatial patterns of litter-dwelling taxa in relation to the amounts of coarse woody debris in European temperate deciduous forests. *Forest Ecology and Management*, 257: 1255–1260.

KENDALL, W. L., 1999, Robustness of closed capture-recapture methods to violations of the closure assumption. *Ecology*, 80: 2517–2525.

KENDALL, W. L. & J. D. NICHOLS, 1995, On the use of secondary capture-recapture samples to estimate temporary emigration and breeding proportions. *Journal of Applied Statistics*, 22: 751–762.

KENDALL, W. L., J. D. NICHOLS & J. E. HINES, 1997, Estimating temporary emigration using capture-recapture data with Pollock's robust design. *Ecology*, 78: 563–578.

LYDEARD, C., R. H. COWIE, W. F. PONDER, A. E. BOGAN, P. BOUCHET, S. A. CLARK, K. S. CUMMINGS, T. J. FREST, O. GARGOMINY, D. G. HERBERT, R. HERSHLER, K. E. PEREZ, B. ROTH, M. SEDDON, E. E. STRONG & F. G. THOMPSON, 2004, The global decline of nonmarine mollusks. *Bioscience*, 54: 321–330.

MacKENZIE, D. I., J. D. NICHOLS, J. E. HINES, M. G. KNUTSON & A. B. FRANKLIN, 2003, Estimating site occupancy, colonization, and local extinction when a species is detected imperfectly. *Ecology*, 84: 2200–2207.

McLEAN, R. A. & W. L. SANDERS, 1988, *Approximating degrees of freedom for standard errors in mixed linear models. Proceedings of the statistical computing section*. American Statistical Association, New Orleans, pp. 50–59.

MINORETTI, N., D. SCHMERA, S. KUPFERNAGEL, S. ZSCHOKKE, G. F. J. ARMBRUSTER, K. BEESE, A. BAUR & B. BAUR, 2011, Determinants of female and male reproductive success in a simultaneous hermaphrodite land snail. *Animal Behaviour*, 82, 707–715.

MÜLLER, J., C. STRÄTZ & T. HOTHORN, 2005, Habitat factors for land snails in European beech forests with a special focus on coarse woody debris. *European Journal of Forest Research*, 124: 233–242.

MURPHY, M. J., 2002, Observations on the behaviour of the Australian land snail *Hedleyella falconeri* (Gray, 1834) (Pulmonata Caryodidae) using the spool-and-line tracking technique. *Molluscan Research*, 22: 149–164.

NATIONAL PARKS & WILDLIFE SERVICE, 2001a, 11 December 2012, *Declaration of critical habitat for Mitchell's rainforest snail* (Thersites mitchellae) *in Stotts Island Nature Reserve.* Available online at http://www.environment.nsw.gov.au/resources/nature/thersitesS47CriticalHabitatFinal.pdf.

NATIONAL PARKS & WILDLIFE SERVICE, 2001b, 11 December 2012, *Mitchell's Rainforest Snail* Thersites mitchellae *recovery plan*. Available online at http://www.environment.gov.au/system/files/resources/c5ea7c55-808c-4b01-8a28-c04260f76e8d/files/t-mitchellae.pdf.

PARKYN, J. & D. NEWELL, 2013, Australian land snails: a review of ecological research and conservation approaches. *Molluscan Research*, 33: 116–129.

PINHEIRO, J. C. & D. M. BATES, 2000, Mixed-effects models in S and S-PLUS. *Statistics and computing series*. Springer-Verlag, New York, xvi + 528 pp.

POLLOCK, K. H., 1982, A capture-recapture design robust to unequal probability of capture. *Journal of Wildlife Management*, 46: 757–760.

PRIOR, D. J., 1985, Water regulatory behaviour in terrestrial gastropods. *Biological Reviews*, 60: 403–424.

RASHBASH, J., F. STEELE, W. J. BROWNE & H. GOLDSTEIN, 2009, *A user's guide to MLwiN* (*Version 2.10*). University of Bristol, Centre for Multilevel Modelling, xviii + 296 pp.

RÉGNIER, C., B. FONTAINE & P. BOUCHET, 2009, Not knowing, not recording, not listing: numerous unnoticed mollusk extinctions. *Conservation Biology*, 23: 1214–1221.

STAIKOU, A., M. LAZARIDOU-DIMITRIADOU & M. KATTOULAS, 1989, Behavioural patterns of the edible snail *Helix lucorum* L. in the different seasons of the year in the field. *Haliotis*, 19: 129–136.

TOMIYAMA, K. & M. NAKANE, 1993, Dispersal patterns of the giant African snail, *Achatina fulica* (Ferussac) (Stylommatophora: Achatinidae), equipped with a radio-transmitter. *Journal of Molluscan Studies*, 59: 315–322.

WILLIAMSON, P. & R. A. D. CAMERON, 1976, Natural diet of the landsnail *Cepaea nemoralis*. *Oikos*, 27: 483–500.

Revised ms. accepted May 7, 2014

MALACOLOGIA, 2014, 57(2): 309–317

A NEW GENERIC PLACEMENT FOR "*CALLIOSTOMA*" *BLAKEI* CLENCH & AGUAYO, 1938 (GASTROPODA: TROCHOIDEA)

Marina Güller[1]* & Diego G. Zelaya[2]

ABSTRACT

"Calliostoma" blakei Clench & Aguayo, 1938, described from Río Negro Province, Argentina, appears in the literature either under the genera *Calliostoma*, *Photinula* (Calliostomatidae) or as a member of the Umboniinae (Trochidae). The study of live-collected specimens allows to revise its generic placement.The species is characterized by a bipectinate ctenidium with short afferent membrane, isolated appendices in the left side of the neck, and the rachidian and the first lateral teeth reduced to their base. This set of characters, not present in any other trochoid, leads us to propose the new genus *Carolesia* for this species.

Key words: Gastropoda, Trochoidea, *Carolesia*, southwestern Atlantic.

INTRODUCTION

The Trochoidea is one of the most diversified gastropod superfamilies, with a large number of genera and species (Hickman & McLean, 1990). Traditional classification within the group has been based upon shell characters alone (e.g., Carcelles, 1945; Clench & Turner, 1960; McLean, 1964, 1970; Quinn, 1992a, b; Nascimento de Barros, 2010). Hickman & McLean (1990) recognized the plasticity and convergent nature of the shell morphology in the group, suggesting the combination of this information with anatomical characters from such structures as the ctenidium, radula, epipodial elements, snout and foot. On the basis of this information, they recognized two formal families (Turbinidae and Trochidae), and a third "provisional" and paraphyletic (Skeneidae) group. However, a number of subsequent molecular studies showed some inconsistencies between morphological / anatomical and molecular characters, mainly arising in the fact that both Trochidae and Turbinidae [in Hickman & McLean's (1990) sense], appear as polyphyletic (Geiger & Thacker, 2005; Williams & Ozawa, 2006; Kano, 2008; Williams et al., 2008, 2010). This resulted in the splitting of these taxa into up to eight families (Williams, 2012). Despite the numerous contributions and new findings that have been published in the recent years on the global Trochoidea, the diversity and taxonomy of the species of this group occurring in Argentinean waters remain obscure. The only exceptions are the genera *Calliostoma* Swainson, 1840, and *Margarella* Thiele, 1893, revised by Clench & Turner (1960) and Castellanos & Fernández (1976), and Zelaya (2004), respectively.

Clench & Aguayo (1938) described "*Calliostoma*" *blakei* from off Cape Bermeja, Río Negro Province, Argentina. Clench & Turner (1960), although with doubts, placed it in *Photinula* Adams & Adams, 1854, also a member of the the Calliostomatidae. This generic placement was followed in the subsequent literature (Figueiras & Sicardi, 1970, 1980; Scarabino, 1977; Castellanos, 1982; Ageitos de Castellanos & Landoni, 1989; Rios, 1994; Rosenberg, 2013). However, the radula of "*Photinula*" *blakei* (figured by Calvo, 1987: fig. 30) clearly differs from that of *Photinula caerulescens* (King, 1832), the type species of the genus (figured by McLean, 2012: fig. 7). Quinn (1992a) stated that the correct placement of "*Photinula*" *blakei* is among the Lirulariinae (= Umboniinae, Trochidae; Williams et al., 2010), and Aguirre & Farinati (2000) tentatively listed the species under *Tegula* (*Agathistoma*), but without any argument for this proposed placement.

The objective of this contribution is to provide a new generic placement for "*Calliostoma*" *blakei*, and to discuss the familial affinities of this species.

[1]División Invertebrados, Museo Argentino de Ciencias Naturales "Bernardino Rivadavia", Av. Ángel Gallardo 470 (C1405DJR), Ciudad Autónoma de Buenos Aires, Argentina
[2]Departamento Biodiversidad y Biología Experimental, Facultad de Ciencias Exactas y Naturales, Universidad de Buenos Aires, Ciudad Universitaria, Pabellón 2, 4° piso (C1428EHA), Ciudad Autónoma de Buenos Aires, Argentina
*Corresponding author: mguller@macn.gov.ar

MATERIALS AND METHODS

This study is based on living specimens collected in the Golfo San Matías, Río Negro Province, Argentina. Samples were hand-collected from the intertidal zone during the lowest low tides, by diving in the shallow subtidal, and with a 2 mm mesh-size net at greater depths. Information of living animals was obtained and documented from specimens maintained in aquaria. Specimens for anatomy were relaxed in magnesium chloride and fixed in 10% sea-water formalin. The gross anatomy and radulae were studied with ten specimens from different sites and depths. Radulae were removed by dissection, cleaned by rinsing in a sodium hypochlorite solution and mounted for scanning electron microscopy (SEM); soft parts were hexamethyldisilazane prepared for SEM. Voucher specimens were deposited in the collection of the Museo Argentino de Ciencias Naturales "Bernardino Rivadavia" (MACN), Buenos Aires. This collection was also studied in search for additional information on the distribution of the species. The number of specimens (spec.) and shells (s.) for each lot is indicated in the material examined section. The terminology used throughout the text follows Hickman & McLean (1990). The ratio height/width is refered to as H/W. For comparative purposes live-collected specimens of *Tegula patagonica* d'Orbigny, 1835, were also studied. *Tegula* Lesson, 1832, is here used in a broad sense, including some species formerly assigned by different authors to the (sub)genera *Chlorostoma* Swainson, 1840, and *Agathistoma* Olsson & Harbison, 1953. This is due to the uncertainties concerning the distinctive characters for these (sub)genera, the consequently differing opinions on the usage of these names, and the lack of a recent world-wide revision on the (sub)generic placement of most species of this / these group(s).

SYSTEMATICS

Carolesia, new genus

Type species: Calliostoma (*Calliostoma*) *blakei* Clench & Aguayo, 1938.

Distinctive Characters: Shell solid, with low spiral sculpture. Columella with moderately to well-developed basal denticle and a depression beneath it. Left side of the neck with a triangular, flattened projection at the anteriormost part, and two or three smooth, tentaculiform processes posteriorly. Ctenidium bipectinate, with short afferent membrane. Radula with rachidian and first lateral teeth reduced to rectangular, wider than high, basal plates; remaining laterals narrower, with well-developed shaft and cusp. First marginal with well developed shaft and cusp, and inner projection at the base.

Ethymology: The new genus is named after Carole S. Hickman, in recognition for her contributions to the understanding of Trochoidea.

Comparisons: The shell of *Carolesia* closely resembles that of *Tegula mariana* Dall, 1919 (figured by Hickman & McLean, 1990: fig. 35E). *Tegula* (as defined by Hickman & McLean, 1990) and *Carolesia* share the presence of a bipectinate ctenidium, with a short afferent membrane and four pairs of epipodial tentacles. However, *Tegula* strikingly differs from *Carolesia* in having: (1) a smooth or digitated longitudinal and continuous fringe, extending all along the left side of the neck (i.e., from the posterior part of the left eye stalk to the base of the first epipodial tentacle) (Hickman & McLean, 1990; Collado, 2008), while in *Carolesia* the left side of the neck shows discontinuos elements: a short, triangular, flat, anterior projecton, followed by two or three smooth tentaculiform processes; (2) all five lateral teeth narrow, similar, and with well-developed cusps, while in *Carolesia*, the first laterals differ from the other laterals in being widened and in lacking of distinct cusp.

Carolesia blakei
(Clench & Aguayo, 1938)
new combination
Figs. 1–23

Calliostoma (*Calliostoma*) *blakei* Clench & Aguayo, 1938: 376, pl. 28, fig. 6.

Photinula blakei: Figueiras & Sicardi, 1970: 31, pl. 8, fig. 115; Scarabino, 1977: 181, pl. 2, fig. 15; Figueiras & Sicardi, 1980: 184 [listed only]; Calvo, 1987: 65, fig. 30; Ageitos de Castellanos & Landoni, 1989: 23, pl. 4, fig. 2; Rios, 1994: 35, pl. 10, fig. 103.

Photinula blackei [sic]: Castellanos, 1982: 42 [listed only].

Tegula (*Agathistoma*)? *blakei*: Aguirre & Farinati, 2000: 256, pl. 2, figs. 16, 17.

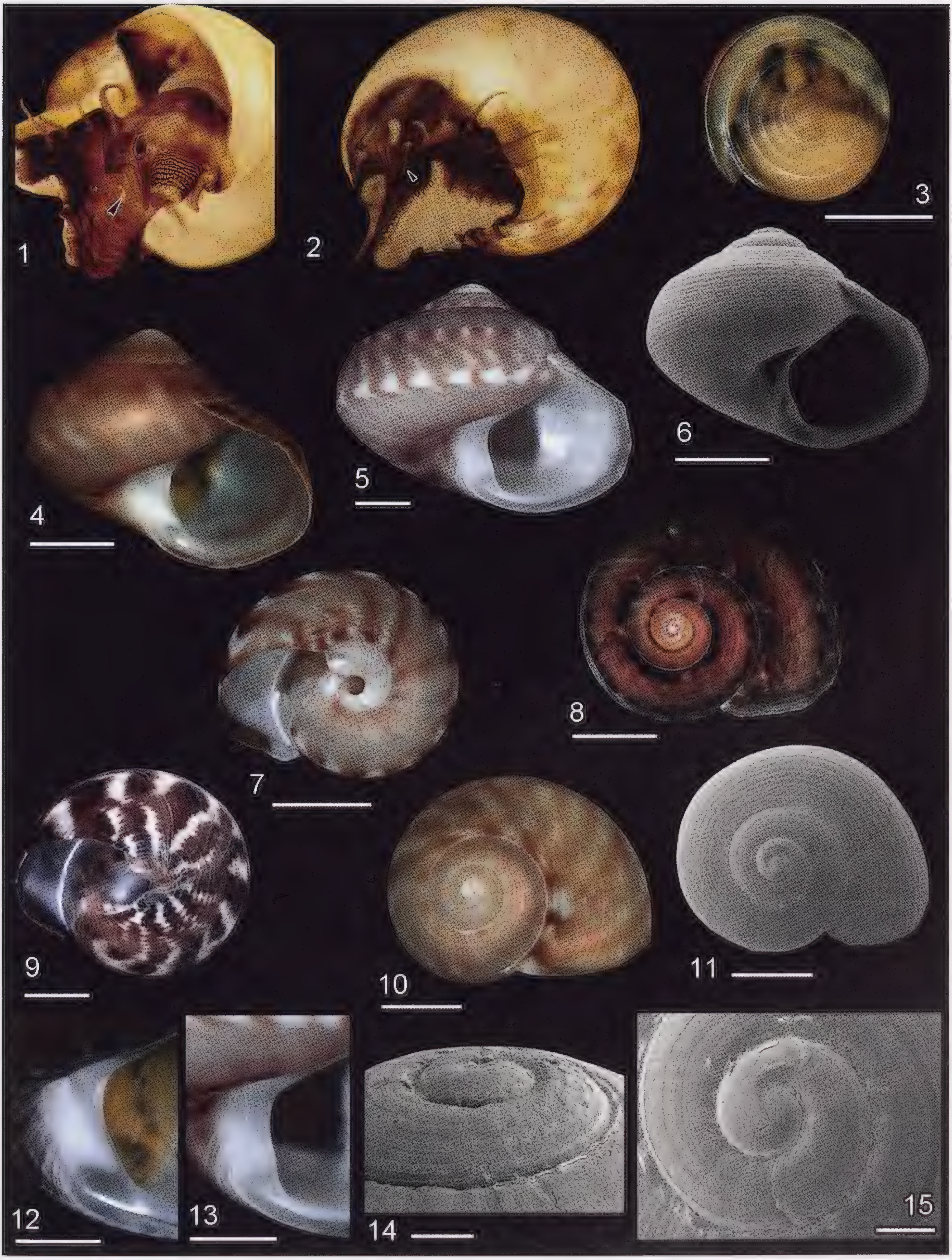

FIGS. 1–15. *Carolesia blakei*. FIGS. 1, 2: Living specimens (arrowhead showing the lateral papillae); FIG. 3: Operculum; FIGS. 4–15: Shell. FIGS. 4–6: Apertural view; FIGS. 7, 9: Umbilical view; FIGS. 8, 10, 11: Apical view; FIGS. 12, 13: Detail of columella; FIGS. 14, 15: Protoconch. FIG. 14: Lateral view; FIG. 15: Apical view. Figs. 1, 2: Specimen from El Buque, MACN-In 3946; Figs. 3–15: Specimens from Las Grutas. Figs. 3, 5, 8, 10, 12, 13: MACN-In 39455; Fig. 4: MACN-In 39459; Figs. 6, 14: MACN-In 39464; Fig. 7: MACN-In 39458; Fig. 9: MACN-In 39462; Figs. 11, 15: MACN-In 39463. Scale bars: Figs. 3–5, 10, 12, 13 = 1 mm; Figs. 6, 11 = 500 µm; Figs. 7–9 = 2 mm; Figs. 14, 15 = 100 µm.

Type Material: Holotype and 50 paratypes at Museum of Comparative Zoology, Harvard; [n?] Paratypes at Museum Poey, Havana (*fide* Clench & Aguayo, 1938).

Type locality: off Cape Bermeja, Argentina (41°17'S), 17 fathoms [31 m].

Material Examined: Uruguay: 34°40'00"S, 53°59'30"W, Rocha, 30 m (MACN-In 15359: 47 s.); [34°40'S, 54°10'W], Cabo Santa María (MACN-In 15289: 3 s.). Argentina: [38°22'S, 57°30'W], Mar del Plata, Buenos Aires (MACN-In 8731: 1 s.); [38°22'S, 57°30'W], Mar del Plata, Buenos Aires (MACN-In 8587-2: 1 s.); [38°22'S, 57°30'W], Mar del Plata, Buenos Aires, 33–37 m (MACN-In 8727: 1 s.); [38°22'S, 57°30'W], Mar del Plata, Buenos Aires (MACN-In 8729: 3 s.); [38°22'S, 57°30'W], Mar del Plata, Buenos Aires (MACN-In 14344: 7 s.); [38°22'S, 57°30'W], Mar del Plata, Buenos Aires (MACN-In 16539: 7 s.); [38°17'S, 57°29'W], Mar del Plata, Buenos Aires (MACN-In 8728: 6 s.); [38°22'S, 57°30'W], Mar del Plata, Buenos Aires (MACN-In 8655: 156 spec., 2 s.); [38°22'S, 57°30'W], Mar del Plata, Buenos Aires (MACN-In 8730: 3 s.); [38°22'S, 57°30'W], Mar del Plata, Buenos Aires (MACN-In 8726: 8 s.); [38°22'S, 57°30'W], Mar del Plata, Buenos Aires (MACN-In 29452: 3 s.); [38°35'S, 58°41'W], Puerto Quequén, Buenos Aires, 18 m (MACN-In 19545: 1 s.); [38°37'S, 57°32'W], Punta Mogotes, Buenos Aires, 39 m (MACN-In 8629: 15 s.); [38°37'S, 57°32'W], Punta Mogotes, Buenos Aires (MACN-In 8653-2: 5 s.); 38°40'S, 56°00'W, Buenos Aires, 93 m (MACN-In 8725-1: 2 spec.); Golfo San Matías, Río Negro (MACN-In 21299: 8 s.); [40°51'S, 65°3'W], San Antonio Oeste, Río Negro (MACN-In 23695: 2 s.); 40°25'47.4"S, 65°25'14.1"W, Las Grutas, 8 m (MACN-In 39455: 16 spec., 3 s.); 40°25'47.4"S, 65°30'01.2"W, Las Grutas, 8 m (MACN-In 39456: 2 spec.); 40°29'35.2"S, 65°31'44.7"W, Las Grutas, 6 m (MACN-In 39457: 8 spec., 62 s.); 40°29'46.2"S, 65°28'20.1"W, Las Grutas, 10–11 m (MACN-In 39458: 11 spec., 1 s.); 40°30'16.2"S, 65°27'29.6"W, Las Grutas, 10 m (MACN-In 39459: 8 spec., 1s.); 40°32'00.6"S, 65°47'29.5"W, El Buque, intertidal (MACN-In 39460: 14 spec., 18 s.; MACN-In 39461: 24 spec., 10 s.); 40°49'56.6"S, 65°05'16.2"W, Las Grutas, 7 m (MACN-In 39462: 28 spec., 27 s.); 40°50'12.8"S, 65°04'42.2"W, Las Grutas, 10 m (MACN-In 39463: 37 spec., 48 s.); 40°50'35.5"S, 65°04'43.7"W, Las Grutas, 12 m (MACN-In 39464: 2 spec., 5 s.); 41°58'22.8"S, 65°03'28.6"W, Puerto Lobos, 16.5 m (MACN-In 39465: 6 s.); 41°58'31.7"S, 65°03'38.6"W, Puerto Lobos, 13 m (MACN-In 39466: 1 s.); 42°15'25"S, 62°54'53"W–42°14'15"S, 62°59'42"W, 60 m (MACN-In 39467: 1 spec., 5 s.).

Known Distribution: Rio Grande do Sul, Brazil (Rios, 1994) to Golfo San Matías, Argentina. Living specimens: lower intertidal to 93 m.

Description

Shell: small (up to 9.7 mm wide), trochoid, of up to 5 whorls, solid. Spire moderately elevated (H / W = 0.84 ± 0.05, n= 22) (Figs. 4–6). Protoconch of one whorl, about 200 µm wide, with one or two spiral threads at peripheral margin; raised from teleoconch (Figs. 14, 15). Spire whorls obliquely straight, slightly angulated or evenly convex; separated by well-marked suture (Figs. 4–6, 10, 11, 14). Last whorl usually biangulated in larger specimens, sometimes evenly rounded (Figs. 4–6). In the first case, adapical area straight or concave. Base convex. Umbilicus open, deep in small specimens; partially to fully closed by columellar callus in larger specimens; umbilical area sunken (Figs. 7, 9). Shell surface sculptured with low spiral cords and microscopic granules between cords (Fig. 15). First ¾ teleoconch whorl with 3–4 spiral cords, narrower than interspaces; intercalated thread-like cords appear, gradually increasing their width on subsequent whorls. Last whorl (in larger specimens) with 17–29 cords between suture and lower angulation; base with 17–25 low cords as wide as or wider than interspaces (Figs. 4–11). Growth disruptions frequent along the shell (Fig. 11). Outer shell surface shiny in living specimens. Color highly variable, even among specimens from the same site (Figs. 4, 5, 7–10): brown, reddish-brown, tan, greenish-brown to whitish; uniform, variegated or spirally banded; in last case, frequently alternating dark and light stains. These bands usually wider near suture, at periphery of last whorl, and sometimes in umbilical area (Figs. 5, 7, 9). Sometimes this pattern also present in intermediate areas, resulting in irregular axial bands along spire and radial bands on base (Figs. 5, 9).

Aperture: large, obliquely ovate; aperture lip finely crenulated by external sculpture; peristome interrupted (Figs. 4–6). Collumella solid, arched, widening towards base, with moderately to well-developed denticle, and depression beneath (Figs. 12, 13). Inner shell surface nacreous.

Operculum: corneous, circular, multispiral, with slightly expanded growing edge (Fig. 3); deeply retractable into shell.

Radula (Figs. 21–23): rhipidoglossate, bilaterally symmetrical, regularly arched. Rachidian tooth reduced to ovate, wider than high basal plate, without cutting edge; with deep depression at anterior front (Fig. 22); anterior margin thickened; secondary attachment membrane absent. Five unequal lateral teeth. First (innermost) laterals wider than high, resembling rachidian tooth in outline, also lacking distinct cutting edge (Figs. 21–22). Remaining four laterals on each side gradually narrowing their overlapping bases, increasing size and serrations of cutting edges outwards (Fig. 21). First marginal with well developed shaft and cusp, and inner projection at the base; cusp similar to other inner marginals (Fig. 23). Remaining marginal teeth (up to 49 according to this study; 60 *fide* Calvo, 1987) long, narrow; cusps elongate, strongly serrated on both sides; well-developed compressional ridge in midregion (Fig. 23). Marginal teeth gradually decreasing in size and robustness outwards. Jaws well developed, with elongate, juxtaposed, rod-like scales in anterior area (Fig. 20).

Anatomy: Snout short, broad, somewhat tapering, with short papillae and slit ventral lip (Figs. 1, 16, 17). Cephalic lappets extremely small, wide, lobed (Figs. 1, 2, 16, 17). Cephalic tentacles elongate, cylindrical, micropapillate (Figs. 17, 19). Eye stalks short, right one stout, left one widely expanded forming posterior flap (Fig. 17). Right neck lobe formed by wide, simple fringe, extending from eye stalk to first epipodial tentacle; left side of the neck with a short, triangular, flat projection immediately behind the eye stalk, separated from two (sometimes three) smooth, posterior tentaculiform processes (Figs. 2, 16). Posterior process sometimes bifurcated. Below neck, two or three conspicuous papillae on each side (Figs. 1, 2, 16, 18). Four pairs of narrow, micropapillate epipodial tentacles, with conspicuous epipodial sense organs at their bases (Figs. 1, 2, 16); sometimes one additional epipodial tentacle on left side. Foot anteriorly rounded. Animal dark brown to black; snout sometimes with fine, irregular, transverse lines (Figs. 1, 2). Ctenidium bipectinate, with short afferent membrane and long free tip.

Remarks: The shells of *Carolesia blakei* resemble small specimens of *Tegula patagonica* (Fig. 27), and the two are found living together.

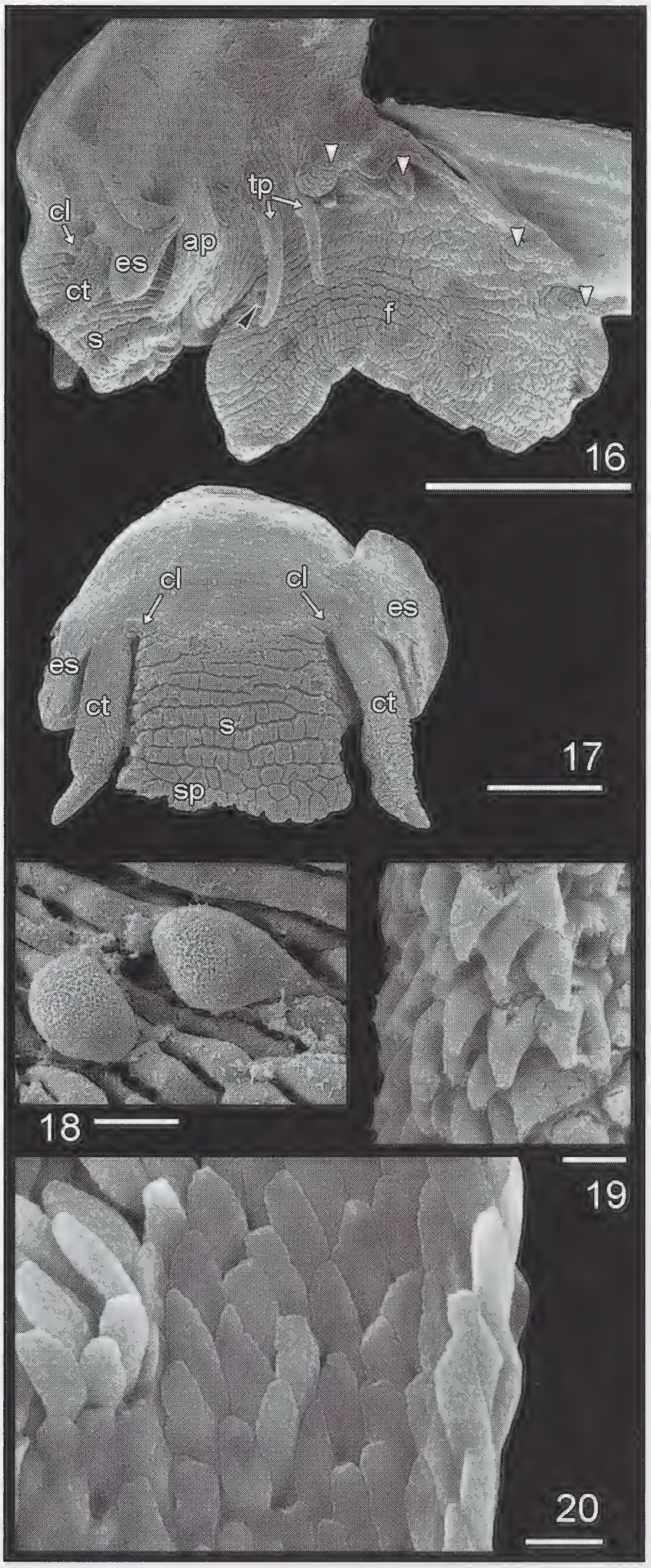

FIGS. 16–20. *Carolesia blakei*, anatomy. FIG. 16: Left side view of an HMDS specimen (black arrowhead showing lateral papillae, see Fig. 18); FIG. 17: Detail of head; FIG. 18: Detail of lateral papillae; FIG. 19: Detail of cephalic tentacle's micropapillae; FIG. 20: Detail of jaw. Figs. 16, 18: Specimens from Las Grutas, MACN-In 39455; Figs. 17, 19, 20: Specimens from El Buque, MACN-In 39461. Scale bars: Fig. 16 = 1 mm; Fig. 17 = 500 µm; Fig. 18 = 50 µm; Fig. 19 = 20 µm; Fig. 20 = 5 µm. Abbreviations: ap = anterior projection; cl = cephalic lappet; ct = cephalic tentacle; es = eye stalk; f = foot; s = snout; sp = snout papillae; tp = tentaculiform processes; white arrowhead = epipodial tentacle (see epipodial sense organ below).

The latter may be differentiated by having a higher spire with more evenly convex whorls; the protoconch sunken, partially covered by the first teleoconch whorl (Figs. 30, 31); stronger spiral cords; and uniform dark-color. The larger specimens of *T. patagonica* are consistently stouter, show irregular granules or scales, have the last whorl evenly curved (not angulated), and reach a greater size (~ 21 mm wide) (Figs. 28, 29). Additionally, in *T. patagonica* the columellar denticle(s) project(s) towards the umbilicus (which may be open, partially or entirely covered), and the outer lip may be smooth or conspicuously denticulated. Anatomically, the main difference between these species is found on the left side of the neck, which in *T. patagonica* shows a longitudinal fringe, either evenly smooth or with one or two digitations at the posterior part (Collado, 2008: fig. 2E; pers. obs.), while in *C. blakei* there is a short, triangular flat projection at the anterior part separated from two or three smooth tentaculiform projections. The radula of *T. patagonica* (Figs. 24–26), like other species of *Tegula* (*s.l.*), shows an additional difference with that of *C. blakei* (see below).

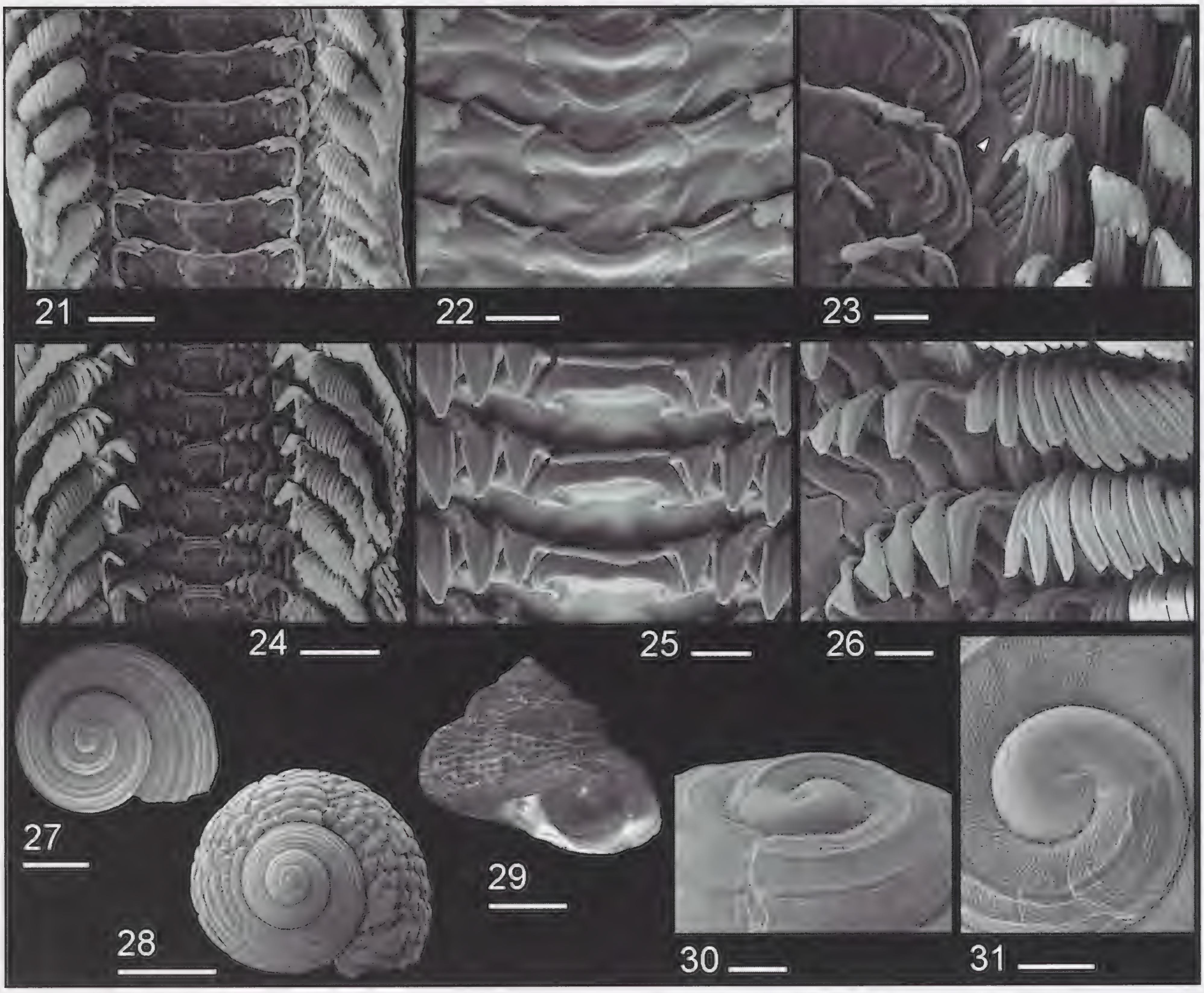

FIGS. 21–31. *Carolesia blakei* and *Tegula patagonica.* FIGS. 21–23: *Carolesia blakei*, radula; FIG. 21: Full radula width; FIG. 22: Detail of central field (rachidian and innermost lateral) tilt, showing the depression at anterior front of rachidian; FIG. 23: Detail of outer laterals and inner marginal teeth (arrowhead showing first marginal tooth). FIGS. 24–31: *Tegula patagonica*; FIGS. 24–26: Radula; FIG. 24: Full radular width; FIG. 25: Detail of central field, tilt radula; FIG. 26: Detail of lateral and marginal teeth; FIGS. 27–31: Shell; FIGS. 27, 28: Apical view; FIG. 29: Apertural view; FIG. 30: Protoconch, lateral view; FIG. 31: Protoconch, apical view. Figs. 21, 22, 24–26, 28, 30, 31: Specimens from Las Grutas; Figs. 27, 29: Specimens from Puerto Lobos; Figs. 21, 22: MACN-In 39455; Fig. 23: MACN-In 39467; Figs. 24–26: MACN-In 39471 (intertidal); Figs. 27, 29: MACN-In 39469 (21 m); Fig. 28: MACN-In 39470 (9 m); Figs. 30, 31: MACN-In 39468 (6 m). Scale bars: Figs. 21, 25, 26 = 50 µm; Figs. 22, 23 = 20 µm; Fig. 24 = 200 µm; Fig. 27 = 500 µm; Fig. 28 = 2 mm; Fig. 29 = 5 mm; Figs. 30, 31 = 100 µm.

In the original description of *Carolesia blakei*, Clench & Aguayo (1938) compared this species with *Calliostoma coppingeri* (Smith, 1880), pointing out as main differences in the latter the presence of beaded cords, a closed umbilicus, and the lack of a columellar denticle. The radula of *Calliostoma coppingeri* (figured by Clench & Turner, 1960: pl. 4, fig. 4) confirms the correct generic placement of that species under *Calliostoma*, and the distinction with that of *Carolesia*.

DISCUSSION

Carolesia blakei had been previously assigned to the calliostomatid genera *Calliostoma* and *Photinula*. However, both the ctenidium and radula morphology precludes the inclusion of this species under these genera: calliostomatids (as currently defined) have extremely narrow, flexible rachidian and lateral teeth, all with elongate, finely serrated tapering cusps; and the ctenidium with a long afferent membrane. In addition members of *Calliostoma* and *Photinula* possess a pseudoproboscis, which is absent in *Carolesia*. Furthermore, *Calliostoma* shows a characteristic protoconch with reticulate ("honey-comb" or "hexagonal spaces") pattern (Hickman & McLean, 1990; Marshall, 1995), clearly distinct from the condition present in *Carolesia blakei*.

Quinn (1992a) stated that according to "characters of the animal and radula ... [*Carolesia blakei*] should be assigned to the Lirulariinae Hickman & McLean, 1990 (Quinn, in preparation)", although the manuscript he mentioned was never subsequently published. On the basis of molecular evidence, Lirulariinae is currently regarded as a synonym of Umboniinae (Williams et al., 2010). Members of this subfamily show the rachidian and lateral teeth reduced to basal plates, with shafts and cusps extremely reduced or, more often, absent; and with bases either completely separated or only slightly overlapping (Hickman & McLean, 1990; Herbert, 1992). On the contrary, in *Carolesia blakei* the reduction of the central field involves only the rachidian and innermost lateral teeth, while the remaining laterals have well-developed shafts and cusps, and the laterals show interlocking bases. Other characters reported for Umboniinae are the presence of a monopectinate or bipectinate ctenidium with long afferent membrane, the foot with a bifid propodium, and the snout with long papillae ("processes") (Hickman & McLean, 1990; Herbert, 1992). None of these characters are present in *Carolesia blakei*.

Carolesia blakei shows a number of similarities with the Tegulidae [as defined by Williams, 2012; corresponding to Hickman & McLean's (1990) Tegulinae]. Among such similarities are the presence of a ctenidium with short afferent membrane, the snout with a shallowly-slit ventral lip, the anterior end of the foot broadly rounded, and the radula with the base of laterals complexly interlocking and the marginals with compressional ridges. *Carolesia blakei* also shows an operculum with slightly expanded growing edge, which is a typical tegulid character (McLean, pers. com.). Another shared character is the presence of a denticle at the base of columella, although this character was reported by Hickman & McLean (1990) as present in other trochoideans. As mentioned above, the shell of *Carolesia blakei* closely resembles that of *Tegula mariana* (from northwest America), although several studies proved that shells in Trochoidea appear as plastic characters, frequently showing convergence among distantly related groups (Hickman & McLean, 1990). Aguirre & Farinati (2000), in fact, tentatively referred this species under *Tegula*. Despite the overall similarities above mentioned, *Carolesia blakei* differs from the current concept of Tegulidae by lacking the "rolled" anterior margin of the rachidian tooth, by having very distinctive (wide) innermost laterals, without shaft and cusp, and by the laterals that gradually become narrower outwards. In addition, the left neck lobe of tegulids is a wide longitudinal fringe, either smooth or with digitiform projections (Hickman & McLean, 1990; Collado, 2008; Collado et al., 2012), whereas the left side of the neck in *Carolesia blakei* shows isolated projections: a flat anterior projection and two tentaculiform posterior processes.

The unique combination of shell, anatomical and radular characters present in *Carolesia blakei* leads us to propose a new genus to include this species. The distinctive characters used here to define *Carolesia* were not previously reported for any other species thus far anatomically investigated. This study highlights once again the importance of considering anatomical characters in addition to shell morphology, for a proper classification of trochoids. *Carolesia* is here tentatively located under Tegulidae, although the above-mentioned differences with other members of this family should not be diminished. These differences suggests that *Carolesia* may even belong to a new (sub)family, but we prefer to avoid introducing a new family-group name considering the high instability of trochoidean classification at this time.

AKNOWLEDGEMENTS

The authors express their gratitude to Alejandro Tablado for providing access to the collection of the MACN. Carole Hickman, Daniel Geiger, Bruce Marshall, James McLean, and an anonymous reviewer provided valuable criticisms that greatly improved this paper. This study was partially funded by PICT 2011-2182. Authors are members of the Consejo Nacional de Investigaciones Científicas y Técnicas (CONICET), Argentina.

LITERATURE CITED

ADAMS, H. & A. ADAMS, 1854, *The genera of Recent Mollusca; arranged according to their organization*. John van Voorst, London, vol. 1: 257–484, vol. 3: pls. 33–72.

AGEITOS De CASTELLANOS, Z. J. & N. A. LANDONI, 1989, Catálogo descriptivo de la malacofauna marina magallánica 3. Trochidae y Turbinidae (Archigastropoda).*Comisión de Investigaciones Científicas de la Provincia de Buenos Aires (CIC)*: 3–40.

AGUIRRE, M. L. & E. A. FARINATI, 2000, Moluscos del Cuaternario marino de la Argentina. *Boletín de la Academia Nacional de Ciencias*, 64: 235–333.

CALVO, I. S., 1987, *Rádulas de gastropodes marinhos brasileiros*. Fundação Universidade do Rio Grande, Rio Grande, 201 pp.

CARCELLES, A. R., 1945, Las especies actuales de *Tegula* en la República Argentina. *Physis*, 20(55): 31–40.

CASTELLANOS, Z. A. De, 1982, Los moluscos de las campañas del "Shinkai Maru". *Neotropica*, 28(79): 41–46.

CASTELLANOS, Z. A. De & D. FERNÁNDEZ, 1976, Los géneros *Calliostoma* y *Neocalliostoma* del Mar Argentino con especial referencia al área subantártica. *Revista del Museo de La Plata*, 12: 135–156.

CLENCH, W. J. & C. G. AGUAYO, 1938, Notes and descriptions of new species of *Calliostoma*, *Gaza* and *Columbarium* (Mollusca); obtained by the Harvard-Habana Expedition off the coast of Cuba. *Memorias de la Sociedad Cubana de Historia Natural*, 12: 375–384, pl. 328.

CLENCH, W. J. & R. D. TURNER, 1960, The genus *Calliostoma* in the western Atlantic. *Johnsonia*, 4: 1–80.

COLLADO, G. A., 2008, Significancia taxonómica del complejo epipodial en especies sudamericanas del género *Tegula* Lesson, 1832 (Mollusca: Vetigastropoda). *Amici Molluscarum*, 16: 14–19.

COLLADO, G. A., M. A. MÉNDEZ, D. I. BROWN & J. PÉREZ-SCHULTHEISS, 2012, Phylogenetic analyses and redescription of *Tegula ignota* (Mollusca: Vetigastropoda). *Journal of the Marine Biological Association of the United Kingdom*, 92: 1151–1159.

DALL, W. H., 1919, Descriptions of new species of Mollusca from the North Pacific Ocean in the collection of the United States National Museum. *Proceedings of the United States National Museum*, 56: 293–371.

FIGUEIRAS, A. & O. E. SICARDI, 1970, Catálogo de los moluscos marinos del Uruguay, parte V. *Comunicaciones Sociedad Malacológica del Uruguay*, 3(19): 25–35.

FIGUEIRAS, A. & O. E. SICARDI, 1980, Catálogo de los moluscos marinos del Uruguay. Parte X: Revisión actualizada de los moluscos marinos del Uruguay con descripción de las especies agregadas. Sección II: Gastropoda–Cephalopoda y bibliografía consultada. *Comunicaciones de la Sociedad Malacologica del Uruguay*, 5(38): 179–277.

GEIGER, D. L. & C. E. THACKER, 2005, Molecular phylogeny of Vetigastropoda reveals non-monophyletic Scissurellidae, Trochoidea, and Fissurelloidea. *Molluscan Research*, 25: 47–55.

HERBERT, D. G., 1992, Revision of the Umboniinae (Mollusca: Prosobranchia: Trochidae) in southern Africa and Mozambique. *Annals of the National Museum*, 33: 379–459.

HICKMAN, C. S. & J. H. MCLEAN, 1990, *Systematic revision and suprageneric classification of trochacean gastropods. Natural History Museum of Los Angeles County, Science Series*, 35: vi + 169 pp.

KANO, Y., 2008, Vetigastropod phylogeny and a new concept of Seguenzioidea: independent evolution of copulatory organs in the deep-sea habitats. *Zoologica Scripta*, 37: 1–21.

KING, P., 1832, Description of the Cirripedia, Conchifera and Mollusca in a collection formed by the officers of HMS Adventure and Beagle employed between the years 1826 and 1830 in surveying the southern coast of South America including the Strait of Magalhaens and the coast of Tierra del Fuego. *Zoological Journal*, 5: 332–349.

LESSON, R. P., 1832–1835?, *Illustrations de zoologie, ou, Recueil de figures d'animaux peintes d'après nature*. Bertrand, Paris, 60 pls.

MARSHALL, B. A., 1995, Calliostomatidae (Gastropoda: Trochoidea) from New Caledonia, the Loyalty Islands, and the northern Lord Howe Rise. Résults des Campagnes Murstom, vol. 14, N° 5. *Mémoires du Museum National d'Histoire Naturelle*, 167: 381–458.

McLEAN, J. H., 1964, New species of Recent and fossil West American aspidobranch gastropods. *The Veliger*, 7: 129–133.

McLEAN, J. H., 1970, New species of tropical Eastern Pacific Gastropoda. *Malacological Review*, 2: 115–130.

McLEAN, J. H., 2012, Detrital feeding in *Xeniostoma inexpectans*, new genus, new species, and new subfamily Xeniostomatinae of Calliostomatidae (Gastropoda: Vetigastropoda), hosted by hexactinellid sponges of the Aleutian Islands, Alaska. *The Nautilus*, 126: 89–97.

NASCIMENTO DE BARROS, J. C., 2010, Trochidae from the continental slope of northeast Brazil, with the description of a new species. *Revista Nordestina de Zoologia*, 4: 54–72.

OLSSON, A. A. & A. HARBISON, 1953, Pliocene Mollusca of southern Florida with special reference to those from North Saint Petersburg. *Monographs of the Academy of Natural Sciences of Philadelphia* 8: v + 1–457, 465 pls.

ORBIGNY, A. D. d', 1835 [1834–1847], *Voyage dans l'Amérique Méridionale.* Bertrand & Strasbourg, Levraul, Paris, 5(3) [Mollusques]: xliii + 758 pp., 85 pls. [in Atlas].

QUINN, J. F., Jr., 1992a, New species of *Calliostoma* Swainson, 1840 (Gastropoda: Trochidae), and notes on some poorly known species from the western Atlantic Ocean. *The Nautilus*, 106: 77–114.

QUINN, J. F., Jr., 1992b, New species of *Solariella* (Gastropoda: Trochidae) from the Western Atlantic Ocean. *The Nautilus*, 106: 50–54.

RIOS, E. C., 1994, *Seashells of Brazil*, 2nd ed. Fundação Ciudade do Rio Grande: Fundação Universidade do Rio Grande, 368 pp., 113 pls.

ROSENBERG, G., 2013, *Photinula blakei* (Clench & Aguayo, 1938). Accessed through: World Register of Marine Species at http://www.marinespecies.org/aphia.php?p=taxdetails&id=533295 (2013-07-03).

SCARABINO, V., 1977, Moluscos del Golfo San Matías (Provincia de Río Negro, República Argentina). Inventario y claves para su identificación. *Comunicaciones de la Sociedad Malacológica del Uruguay* 4(31–32): I + 177–285.

SMITH, E. A., 1880, Descriptions of five new species of shells from Uruguay. *Annals and Magazine of Natural History 5,* 6(34): 319–322.

SWAINSON, W., 1840, *A treatise on malacology; or the natural classification of shells and shell-fish.* Longman, Orme, Brown, Green & *Longmans* & *Taylor*, *London*, 419 *pp.*

THIELE, J., 1893, *Das Gebiss der Schnecken zur Begründung einer natürlichen Classification.* Untersucht von Professor Dr. F. H. Troschel, fortgesetzt von Dr. J. Thiele. R. Stricker, Berlin, vol. 2, part 8: pp. 337–409, plates 29–32.

WILLIAMS, S. T., 2012, Advances in molecular systematics of the vetigastropod superfamily Trochoidea. *Zoologica Scripta*, 41: 571–595.

WILLIAMS, S. T., K. M. DONALD, H. G. SPENCER & T. NAKANO, 2010, Molecular systematics of the marine gastropod families Trochidae and Calliostomatidae (Mollusca: Superfamily Trochoidea). *Molecular Phylogenetics and Evolution*, 54: 783–809.

WILLIAMS, S. T. & T. OZAWA, 2006, Molecular phylogeny suggests polyphyly of both the turban shells (family Turbinidae) and the superfamily Trochoidea (Mollusca: Vetigastropoda). *Molecular Phylogenetics and Evolution*, 39: 33–51.

WILLIAMS, S. T., S. KARUBE & T. OZAWA, 2008, Molecular systematics of Vetigastropoda: Trochidae, Turbinidae and Trochoidea redefined. *Zoologica Scripta*, 37: 483–506.

ZELAYA, D. G., 2004, The genus *Margarella* Thiele, 1893 (Gastropoda: Trochidae) in the southwestern Atlantic Ocean. *The Nautilus*, 118: 112–120.

Revised ms. accepted 16 November 2013

MALACOLOGIA, 2014, 57(2): 319–327

NUPTIAL GIFTS IN *POMACEA CANALICULATA* (AMPULLARIIDAE, CAENOGASTROPODA): EXPERIMENTAL AND FIELD EVIDENCE ABOUT THEIR FUNCTION

Silvana Burela[1,2*] & Pablo Rafael Martín[1,2]

ABSTRACT

Pomacea canaliculata is a South American apple snail that shows a multiple mating behavior. The copulations are frequent and long lasting, and consequently the males have to face strong sperm competition. The outer gland at the base of the penis sheath secrets drops of mucus that females eat during copulation. These mucus drops are nuptial gifts, and the occurrence of them is the only known instance of this behavior in molluscs. We investigated three possible functions of the gift-giving behavior in *P. canaliculata* based on three hypotheses: prowler deterrence, male mating effort and paternal investment. We also quantified the frequency of nuptial gifts in two populations of *P. canaliculata* and its possible role in male competition. We found no aversive reaction neither in females nor in males, but females were attracted to the mucus secretion. The consumption of artificial nuptial gifts (homogenates of the outer sheath gland) had no effect on the copulation duration nor on the total number of eggs and egg masses laid by females. In the field, the frequency of nuptial gifts was almost ten times greater in the population with the highest density of snails, indicating a much higher rate of production of nuptial gifts. The proportion of couples with both nuptial gifts and a prowler males attached was significantly higher than expected by chance in the population with the highest population density. Even though our results give no support for the three hypothesized functions for the nuptial gifts in *P. canaliculata*, this study revealed a possible different role in male competition: the enticement of the female to remain in copulation when the other males are trying to gain access.

Key words: apple snail, copulation, male competition, paternal investment, mating effort.

INTRODUCTION

Pomacea canaliculata (Lamarck, 1819) is a South American snail in the Ampullariidae. It is well known as crop pest and listed among 100 of the "World's Worst Invasive Alien Species" (Lowe et al., 2000). It exhibits a multiple-mating behaviour with frequent (2–3 times per week) and long lasting copulations (12–18 hours) (Albrecht et al., 1996; Burela & Martín, 2011). The sperm provided by a male tends to be replaced by the following ones (Yusa, 2004, 2007). The number of viable eggs that a female can lay after a single copulation is positively related to copulation duration (Burela & Martín, 2011). Males have a bipartite copulatory apparatus consisting of a slender penis that runs along an open channel of the penial sheath (Gamarra-Luques et al., 2006; Giraud-Billoud et al., 2013). The penial sheath presents a conspicuous outer sheath gland (OSG) that during copulation secrets mucus drops eaten by the female (Fig. 1; Burela & Martín, 2007, 2009). Andrews (1964) observed the mucus drops but not their ingestion by the female and hypothesized that their function was to repel prowler males during copulation, although this remained untested until now.

Lewis & South (2012) defined nuptial gifts (NGs) as "...materials beyond the obligatory gametes that are transferred from one sex to another during courtship or mating" and if eaten by the females they can be considered as oral NGs (Gwynne, 2008). The behaviour observed in *P. canaliculata* is so far the only reported case of oral NG-giving or nuptial feeding in molluscs

[1]Laboratorio de Ecología, Departamento de Biología, Bioquímica y Farmacia, Universidad Nacional del Sur, San Juan 670 (8000), Bahía Blanca, Argentina
[2]Consejo Nacional de Investigaciones Científicas y Técnicas (CONICET), Ciudad Autónoma de Buenos Aires, Av. Rivadavia 1917, Argentina
*Corresponding author: silvana.burela@gmail.com

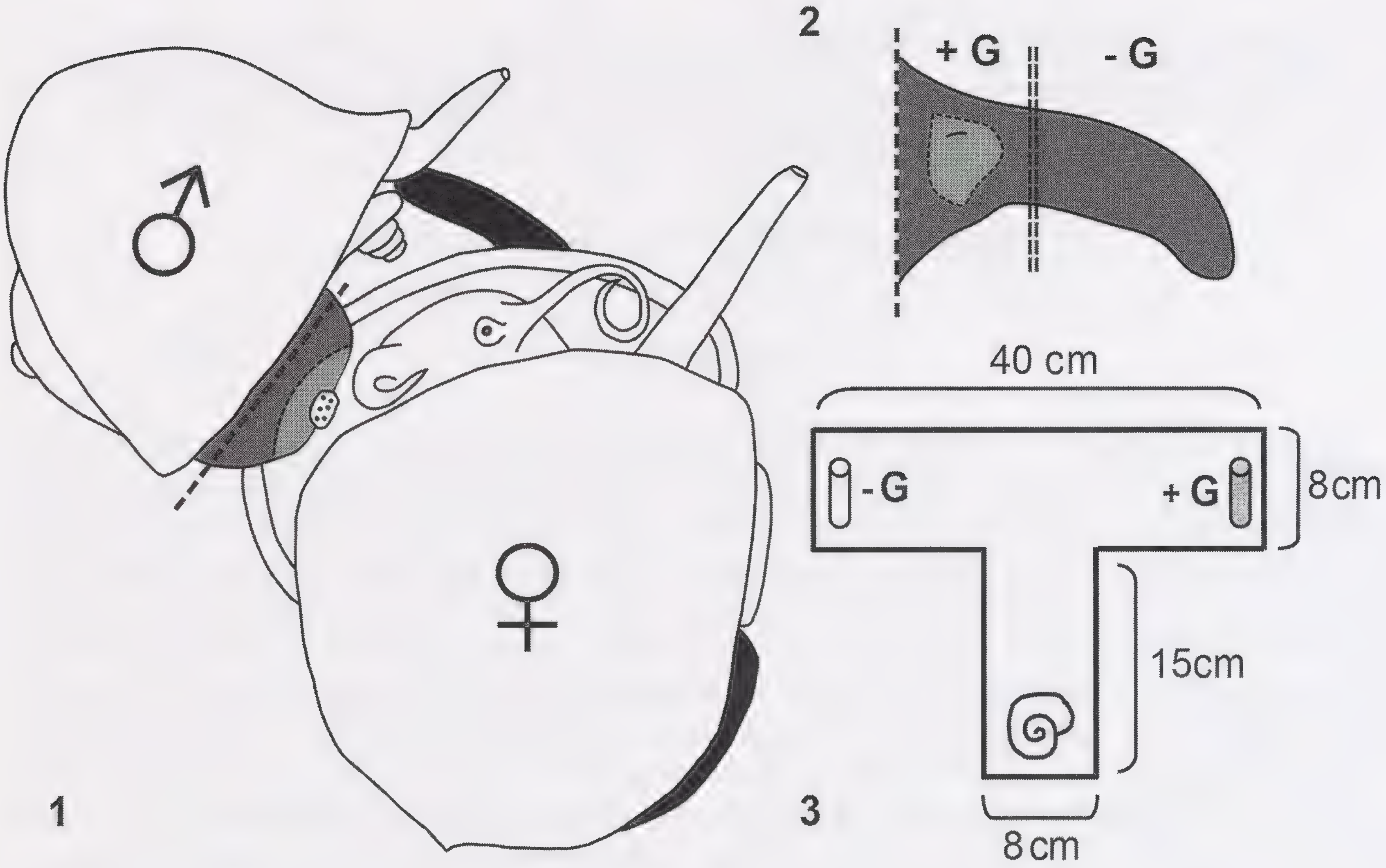

FIGS. 1–3. *Pomacea canaliculata.* FIG. 1: Scheme of a copulating pair of *P. canaliculata*; FIG. 2: Scheme of the penis sheath (dorsal view); FIG. 3: Scheme of the T-maze employed in the aversion-attraction experiment. Shells and soft parts are in white; opercula in solid black, penis sheath in dark grey, outer sheath gland (OSG) in light gray and nuptial gift (NG) in dotted white. Dashed lines indicate the incision made to sever the penis sheath from the mantle edge and the double dashed line indicates the cut executed to separate the portion of the penis sheath containing the OSG (+G) from the rest of it (-G).

(Burela & Martín, 2007). Most observations on NGs are derived from laboratory experiments, with the exception of several studies on insects (Svensson et al., 1990).

The functions of NGs have been explained under two non-mutually exclusive hypotheses (Vahed, 1998). The paternal investment hypothesis states that NGs increase the fitness or the number of offspring fathered by the gift-giving male. The male mating effort hypothesis states that the NGs attract the females to facilitate copulation or entice the females to remain in copulation for long periods, thus increasing the sperm transference and reducing the chance of sperm competition by other males. Another form of male mating effort is to give direct benefits to the females (e.g., nutritional) that increase their reproductive output after copulation. Among insects there are examples that illustrate these hypotheses: males that can manipulate the copulation duration with the size of the NG (Svensson et al., 1990) or can increase the egg production of females which consume the male's salivary secretion during copulation (Engqvist, 2007).

Within this evolutionary context we may expect similar functions of oral NGs in *P. canaliculata*. To test this we addressed three questions regarding the function of the male secretion during copulation. (1) Does it act as a repellent or attractant for males or females? (2) Does it serve as an enticement for females to remain in copulation for a longer period? (3) Does it improve the female reproductive output in the short term? Finally, we quantified the occurrence of NGs in the field and its relationship with competition among males.

METHODS

Experimental Approach

To control the release and the frequency of the NGs in the laboratory, we tested several approaches without success (e.g., cauterization of the OSG pore and adhesion of mechanical barriers to the shell to impede the consumption of NGs). For some trials, we needed large amounts of NG but obtaining the required quantities of naturally released NG was unpractical, because the males release no more than four drops during 13.31 (± 3.5 h) of copulation (Burela & Martín, 2007).

To mimic the effects of OSG secretion, we used tissue macerates obtained from the OSG portion of the penis sheath (Fig. 2). From each penis sheath, the portion with the OSG (+G) was dissected; an equivalent piece of sheath without the OSG was obtained (-G, Fig. 2) to be used as control of aversive reactions to conspecific's hemolympha (Aizaki & Yusa, 2010; Ichinose, 2002).

Aversion-Attraction Experiment

To test the aversive or attractive effects of the mucus secretion, we employed the tissue from the penis sheath of 20 males larger than 35 mm of shell length (SL, measured from the apex to the farthest extreme of the aperture) collected in the field (Pigüé-Venado Channel, 37°09'59"S, 62°40'28"W, Buenos Aires Province). The males were killed by submersion in a bath of water with cubs of ice at -20°C, and their penis sheaths were dissected. The +G and -G portions of the penis sheaths were pooled and macerated separately with an electric microblender for five min. Each macerate was diluted with deionised water to obtain a suspension of 0.05 g tissue/ml. Doses of 1 ml of both suspensions were placed in Eppendorf tubes and frozen at -20°C.

The aversion-attraction trials were conducted in two T-mazes of polystyrene foam that were coated with a polyethylene film before each trial in order to avoid any trace left by the previous experimental snail. The T-mazes were filled with tap water at 25°C. The experimental snails (50 females and 50 males larger than 42 mm SL, sexed by observation of the shape of the shell aperture and of the operculum; Estebenet et al., 2006) were collected from the same population in Pigüé-Venado Channel. Males and females were maintained in separate collective tanks at 25°C and fed with lettuce *ad libitum*. We observed simultaneously a male and a female, each one in a different T-maze. Snails were positioned at the base of the T-maze (Fig. 3) and frozen +G or -G Eppendorf tubes were randomly placed at the opposite arms of the T-maze. The experimental snails were observed for 30 min after they became active (moving the operculum, extending the tentacles, crawling, etc.) and their behaviour and choice of the arms (-G or +G) were registered. Choice data were analyzed with Chi-square tests.

Copulation Duration Experiment

To evaluate if the NGs prolong the copulation duration, we conducted an experiment with 40 females (mean SL = 43.95 ± 3.56 mm) and 40 males (mean SL = 41.44 ± 2.34 mm) collected in the Pigüé-Venado Channel. To mimic the NGs, the females were fed during copulation with artificial nuptial gifts (ANG): the same +G or -G suspensions described for the previous experiment that in order to facilitate the feeding were jellified with commercial red jelly (Royal ®), placed in plastic canulae and stored at -20°C.

The females and males were randomly paired in 3 L aquaria filled with tap water at 25°C. The treatments were applied randomly to copulating pairs (n = 29), and the females were fed with ANG that came out from the tip of the canula with the help of a syringe. Two hours after copulation began, one group of females (n = 10) was fed with (+G) ANG and another one (n = 10) with doses of (-G) ANG; every 30 min the females were fed with a dose of their respective treatment until the copulation ended. A third group of copulating pairs (n = 9) was used as a control of the ANG method, in which females were not fed with ANG but, in order to equate with the rest of the treatments, empty canula were submerged every 30 min. The copulation durations were recorded and analyzed with a one-way Kruskal-Wallis test.

Female Reproductive Output Experiment

An experiment with four different ANG treatments was conducted in order to study a possible effect of the oral NG on the female reproductive output. Thirty-seven females (SL = 47.74 ± 4.10 mm) were collected from Pigüé-Venado Channel in the middle of the reproductive season (February; Estebenet & Martín, 2002), so we assumed that they all have already copulated. They were acclimatized during one week in individual 3 L aquaria with tap water and kept under controlled conditions of light (14 h light) and temperature (25 ± 2°C).

After acclimatization females were randomly assigned to different ANG feeding treatments (in addition to lettuce *ad libitum*): (1) no ANG (controls), (2) females that were fed with 1 ml of suspension (-G) ANG, (3) females that were fed with 1 ml of suspension (+G) ANG; (4) females that were fed with 3 ml of suspension (+G) ANG. The ANGs were dosed in Eppendorf tubes in the same way as for the aversion-attraction experiment; the ANGs were provided in a single dose at the beginning of the experiment (day 0). The females were kept isolated in the same aquaria for 25 days and fed with lettuce *ad libitum*. The egg masses laid on the aquarium walls were gently separated and submersed in water until the individual eggs separated to count the number of eggs. The total number of eggs and egg masses per female were analyzed with one-way Kruskal-Wallis tests.

Nuptial Gifts in the Field

Field observations of occurrence of NGs in mating pairs were registered in two natural populations with contrasting abundances of *P. canaliculata*: El Huáscar stream (36°55'50"S, 61°35'48"W, Buenos Aires Province) during one day (December 27, 2011) and Piedras Moras Reservoir (32°10'23"S, 64°14'57"W, Córdoba Province) during a complete reproductive season (one day per month, from October 2011 to March 2012). Both water bodies have transparent water (which is odd for *P. canaliculata* habitats; Martín et al., 2001) that allowed us a good view of mating pairs on the bottom; the gentle slopes also allowed their easy capture by wading. This permitted the rapid examination of the mating couples to check for the presence of NG near the pore of the OSG before the snails retract deep into their shells. For each of the collected mating pairs, we recorded the presence of NG, the sizes (SL) of each male and female, and the presence of prowler males firmly attached to the shell of one of the mates; we also recorded whether or not the penis sheath of the prowler was inside the pallial cavity of either member of the mating pair.

Due to the great differences in abundance in the two locations, different methods were used to estimate the density of *P. canaliculata*. In the denser population, it was estimated by counting the number of snails in ten quadrates (96 x 48 cm) deployed along the shore (Saveanu & Martín, 2013), and in the less dense population by counting the snails collected along a wading path at least 32 m-long and 3.0 m-wide (assuming a maximum visual detection distance of 1.5 m on each side of the path) in each sampling date. The association of prowler males and the presence of NGs in copulating pairs was analyzed using X^2-tests. The sizes of copulating males were compared with those of prowler males using a paired t-test.

RESULTS

Aversion-Attraction Experiment

Seventy-one out of 100 tested snails chose an arm of the T-maze with no significant difference in the behaviour between sexes (X^2_1 = 1.47, P = 0.306; Fig. 4). However, the number of females that entered the (+G) arm was significantly higher than the number that entered in the (-G) arm, while the males showed no deviations from the expected by random crawling. Five out of 26 females that chose the (+G) arm inserted the mouth inside the Eppendorf tube and fed on its content; none of the males or the females that entered in to the (-G) arm did this.

Copulation Duration Experiment

Despite slightly shorter copulation durations in the treatment (+G), there were no significant differences among the two treatments with ANG or the control without them (X^2_2 = 5.226, P = 0.073; Fig. 5).

Female Reproductive Output Experiment

The total number of eggs laid was highest for females fed with three doses of (+G), but it was the lowest for those fed only 1 dose of (+G) (Fig. 6). There were no significant differences among the treatments in the total number of eggs (X^2_3 = 1.151, P = 0.765) and egg masses (X^2_3 =1.410, P = 0.703).

Nuptial Gifts in the Field

Both NGs (Fig. 7) and prowler males (Fig. 8) were observed in mating pairs from the two populations. The estimated densities were six times higher in El Huáscar stream than in Piedras Moras Reservoir (Fig. 9). In Piedras Moras Reservoir, 156 mating couples were observed, but only four couples (2.56%) had NGs; prowler males were found in only three mating couples (1.92%), so the data from this population were not analyzed further. In El Huáscar stream, 63 of 269 mating couples (23.42%) had NGs on the OSG and 44 of 269 (16.36%) had a prowler male; one couple had two prowler males. No female was found in prowler position. The frequency of mating couples with both NG and a prowler male was higher than expected by chance (X^2_1 = 4.914,

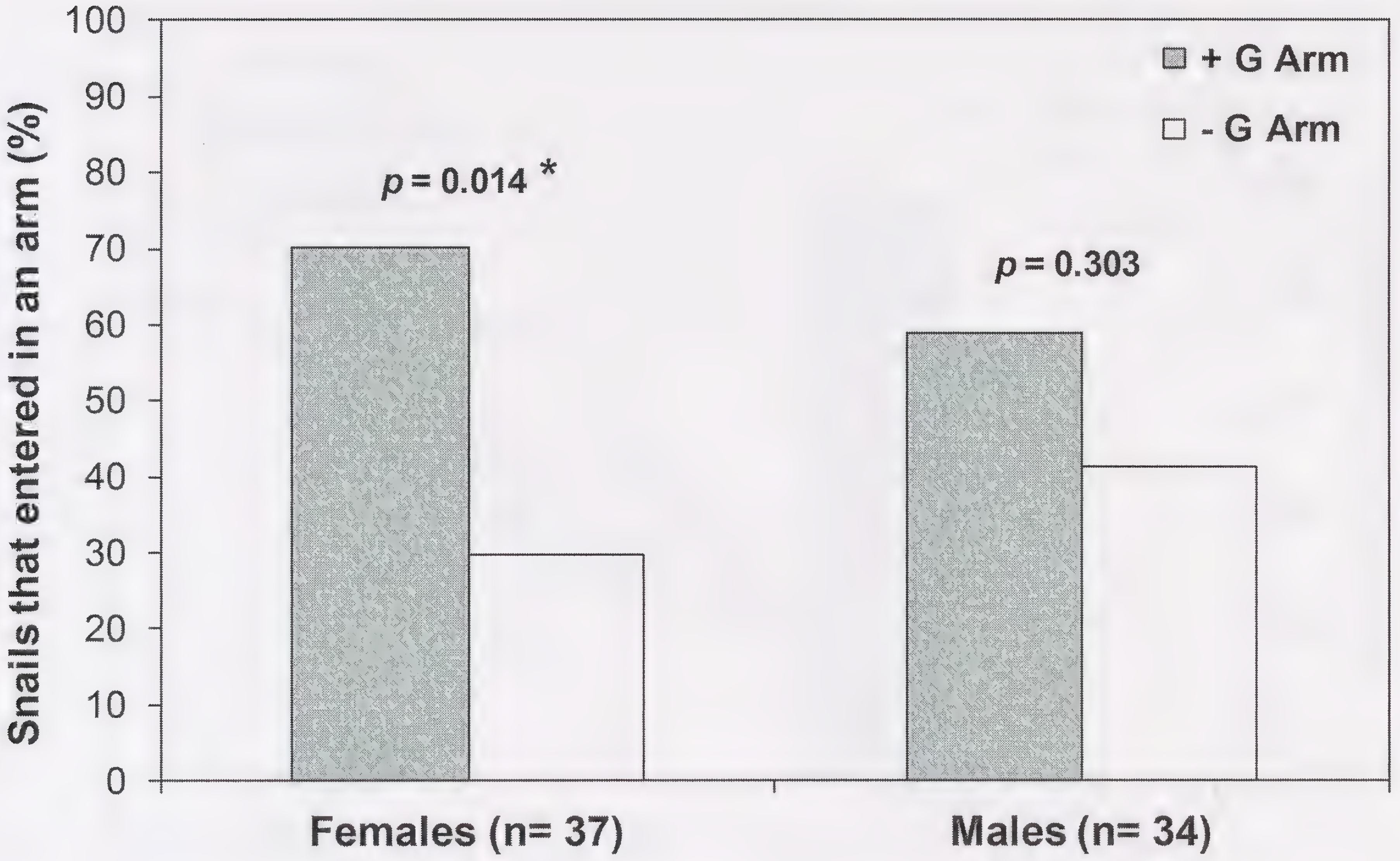

FIG. 4. Percentage of females and males that entered in the arms (+G) and (-G) in the T-maze experiment of aversion-attraction.

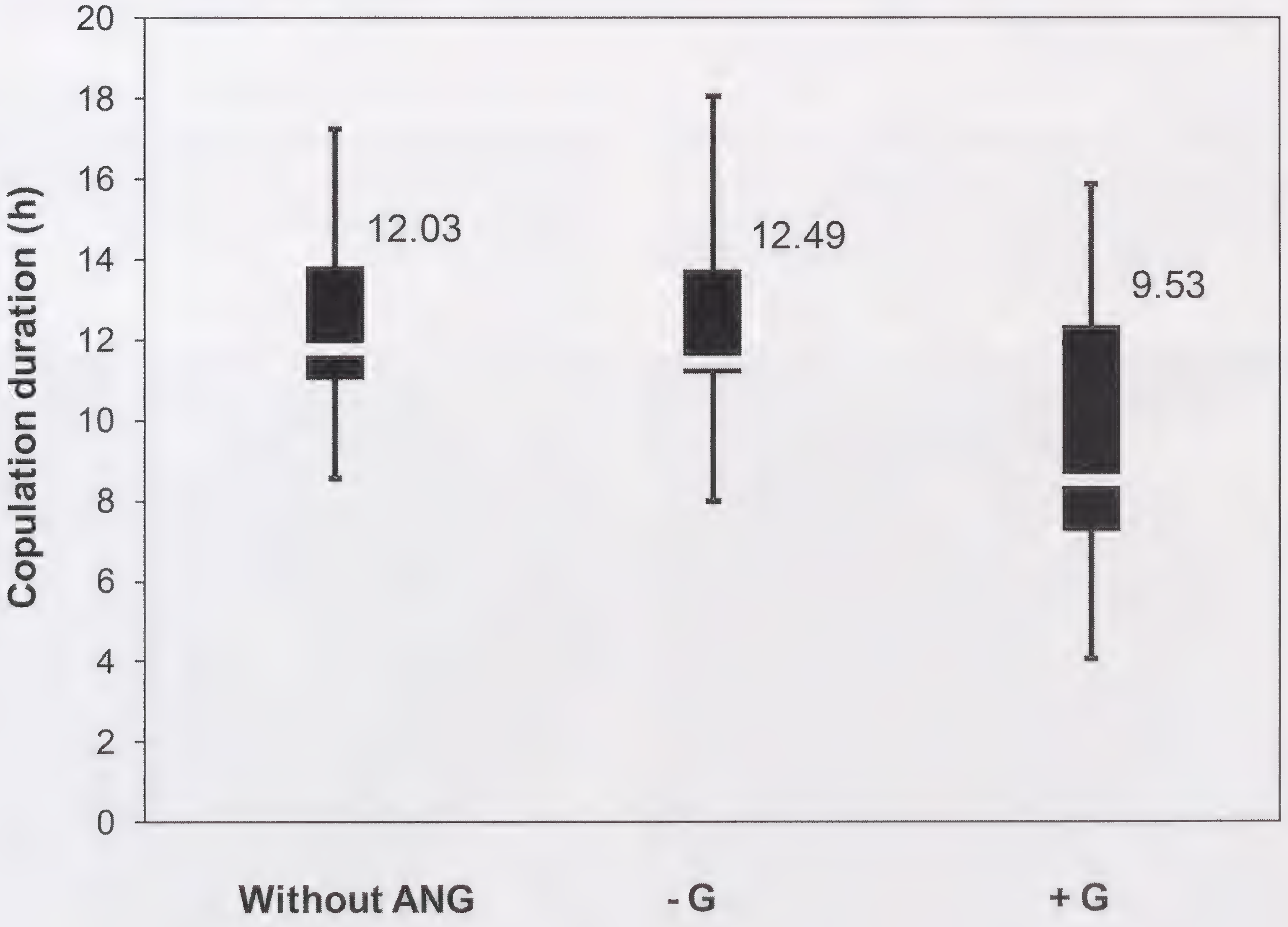

FIG. 5. Copulation durations in the experiment with ANG. Boxes and bars indicate quartiles and extreme values (maximum and minimum) respectively. White lines indicate the median and numbers indicate the mean values.

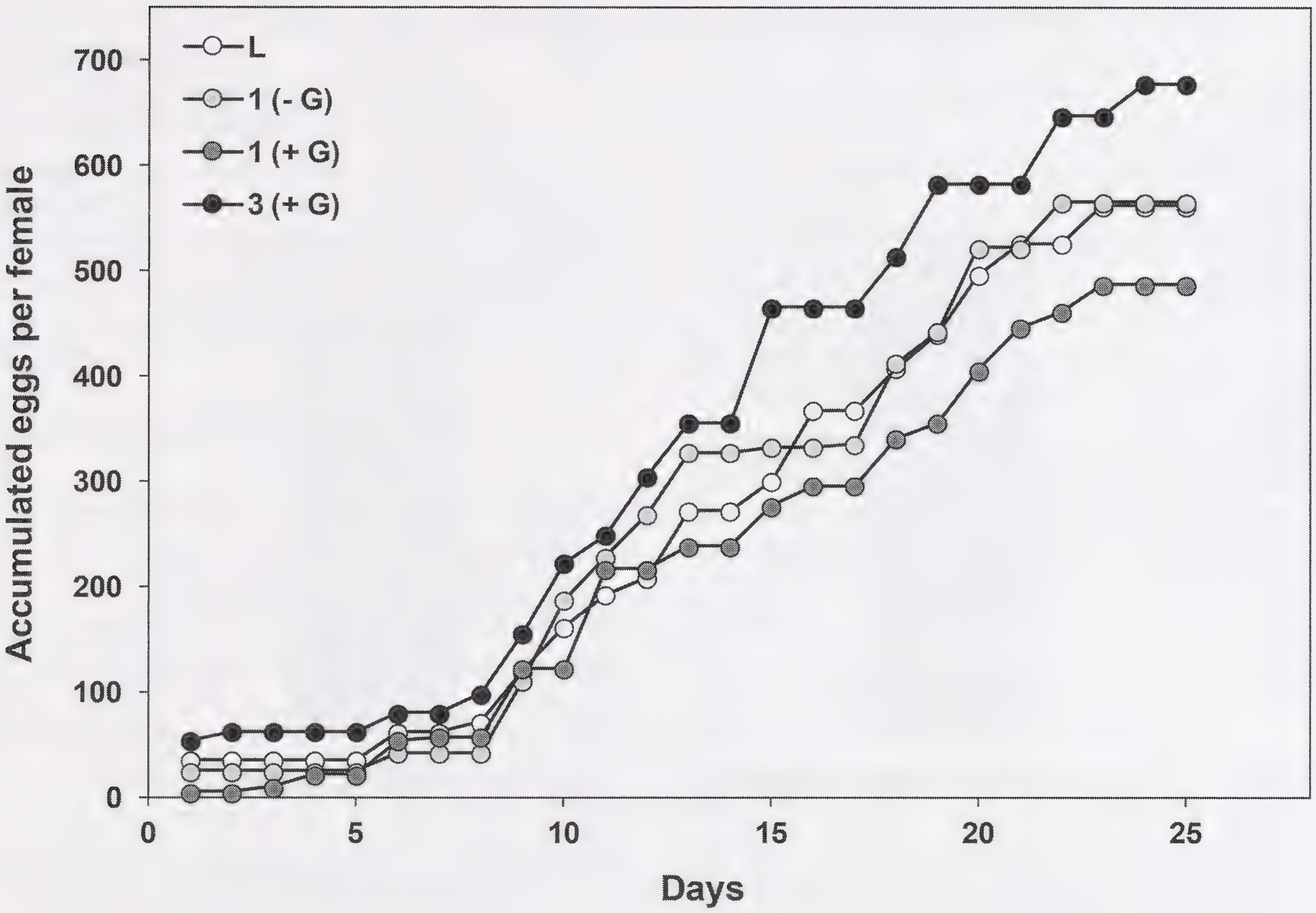

FIG. 6. Cumulative number of eggs per female during a period of 25 days for the different treatments: L = lettuce only, 1(+G) = 1ml of +G suspension, 1(-G) = 1 ml of -G suspension, 3(+G) = 3ml of +G suspension).

P = 0.025). The penis sheath of the prowler was inserted in the pallial cavity of one of the mating snails in 31.82% of the cases; in 78.57% of these cases, it was inserted in the pallial cavity of the copulating male. The mean SL of prowler males was significantly smaller than that of the copulating males (*t* = 3.009, *P* = 0.004, n = 44).

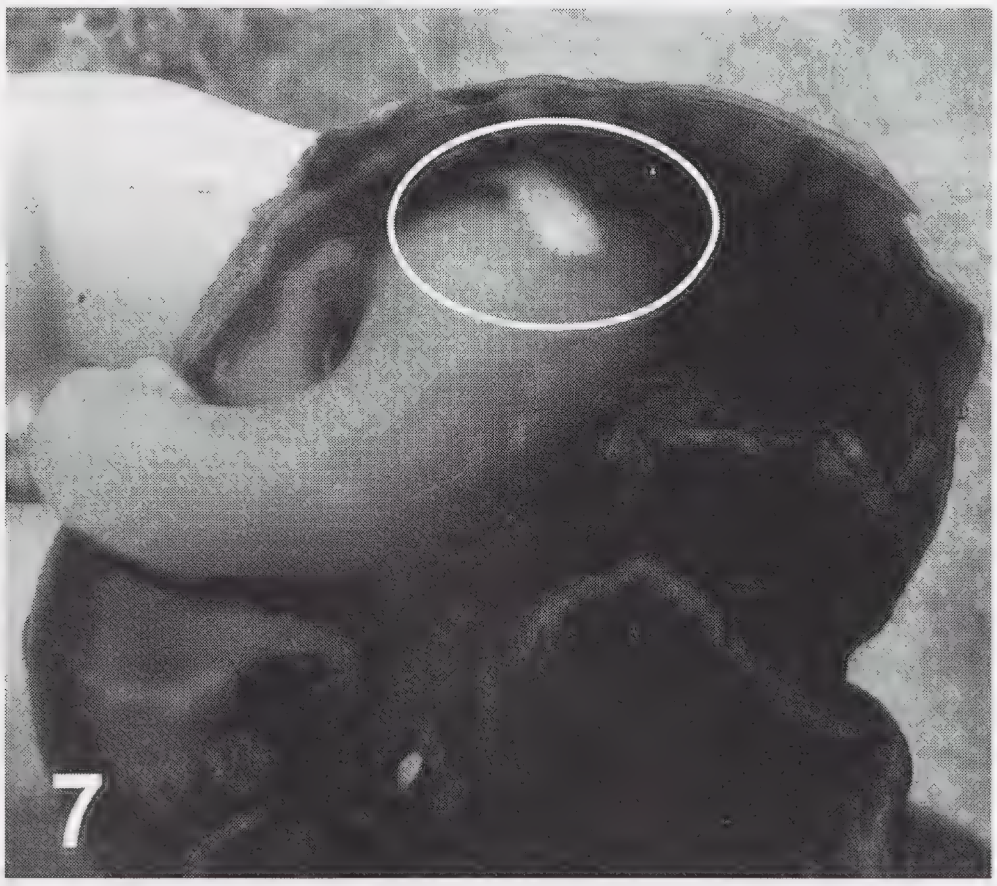

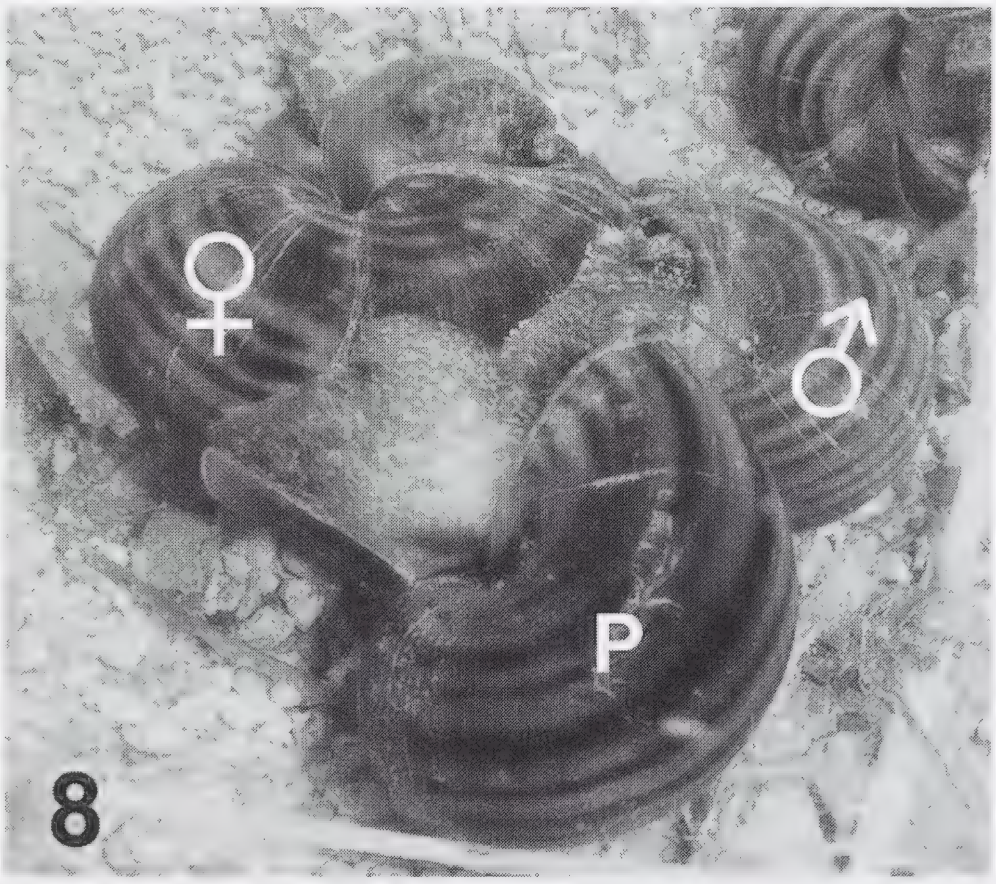

FIGS. 7, 8. Copulating pairs of *Pomacea canaliculata* in the field. FIG. 7: *P. canaliculata* male with a mucus secretion drop on his penis sheath (ellipse), after being separated from the female in copulation, from El Huáscar stream; FIG. 8: Mating couple (♀ and ♂) from El Huáscar stream with a prowler male (P) attached to the female shell.

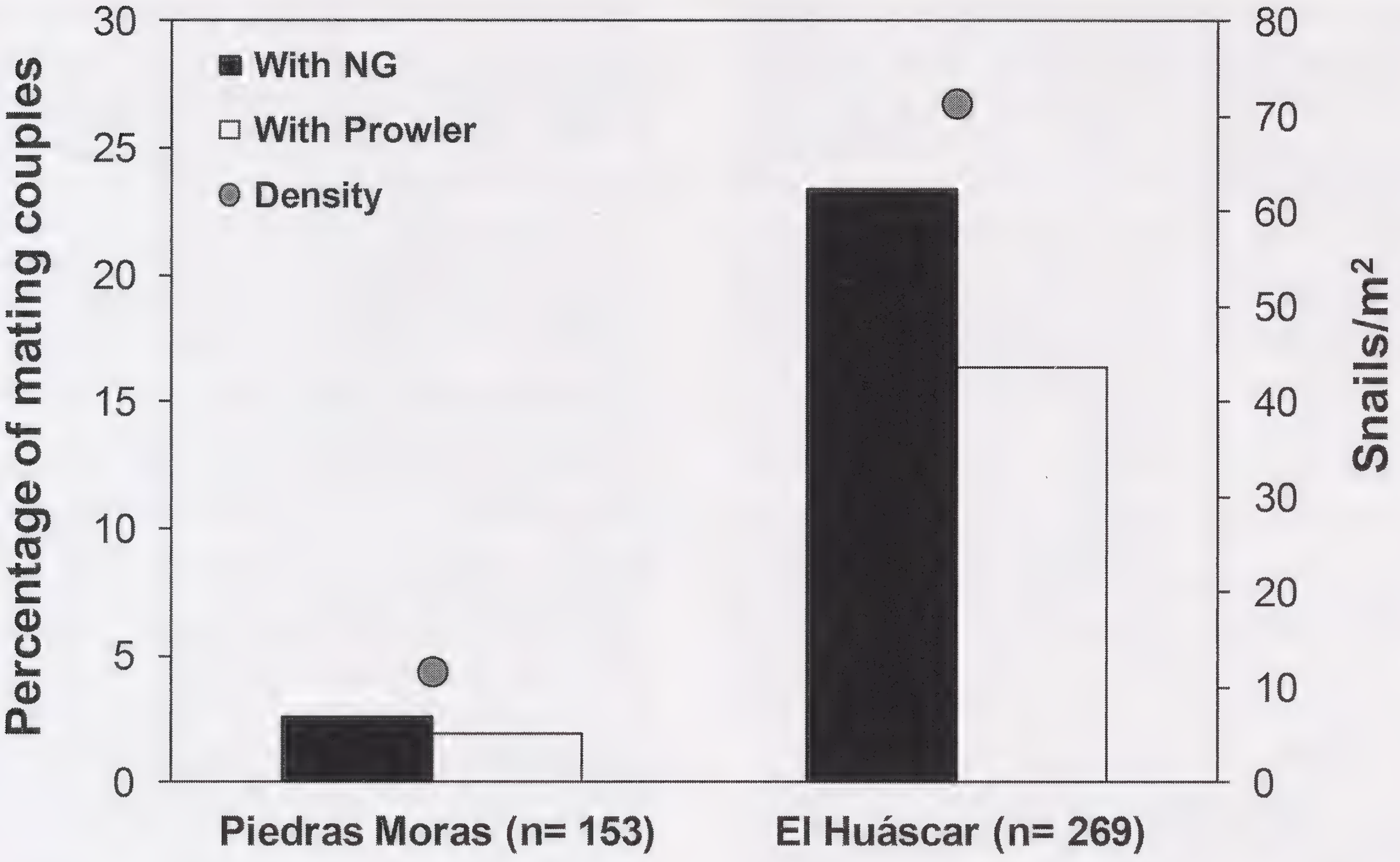

FIG. 9. Percentage of mating couples with prowler males and NG registered in Piedras Moras reservoir and El Huáscar stream.

DISCUSSION

No aversive reactions were observed in the trials with penis sheath suspensions in spite of the fact that *P. canaliculata* snails usually display alarm responses to chemical cues released from injured conspecifics (e.g., Aizaki & Yusa, 2010; Ichinose, 2002). *Pomacea canaliculata* snails are attracted by water-borne odours from aquatic plants and conspecifics from short distances (Estebenet, 1995; Takeichi et al., 2007). Tests for aversive-attractive effects demonstrated that the males were indifferent to the presence of NGs. Moreover, the copulating males of *P. canaliculata* frequently produce NGs even if other males are not present in the same aquarium (Burela & Martín, 2007), so the repellent effect on prowler males suggested by Andrews (1964) seems not to be a plausible function. In fact, in the field, prowler males were associated more frequently to couples in which males were releasing NGs than to those without them.

Conversely, *P. canaliculata* females are strongly attracted to the mucus secretion of the OSG even when it is not offered within a sexual context during the experiment. Possibly, the attractive effect is due to phagostimulant substances in the mucus, as occurs in some species of insects in which males produce NGs rich in free aminoacids (i.e., candymaker hypothesis; Warwick et al., 2009).

In some snails, the transfer of bioactive substances like allohormones during courtship or copulation can manipulate physiologically the female's reproductive output, influencing the numbers of deposited eggs or affecting the re-mating rate (Koene, 2005; Koene & ter Maat, 2001). However, in *P. canaliculata* the total number of eggs and egg masses laid by the females of different treatments was practically the same in the short term, therefore not supporting the paternal investment hypothesis. Perhaps, the *ad libitum* feeding of females could have masked the differences in the oviposition among treatments if the paternal investment is relevant only under trophic deprivation. However, the amount of material transferred (one to four NG of 9 mm^3; Burela & Martín, 2007) is very small relative to the volume of eggs per egg mass produced during the experiment (9.9 ± 0.2 mm^3 per egg times 101.0 ± 6.8 eggs per egg mass, Albrecht et al., 1996), which points against a direct trophic significance of NGs. Although empirically more difficult to test, it is possible that the NG-giving males can increase the number of eggs that they fertilize and thus achieve a greater genetic representation in the progeny (Gwynne, 2008; Vahed, 1998).

For the NGs to function as a paternal investment, the benefits to the progeny must appear before the sperm of a subsequent mate begins to fertilize the ova. In *P. canaliculata* females, the replacement of the sperm of the first mate by the sperm belonging to the second mate occurs on average within the first 3.6 egg masses and during the first 19.8 days (Yusa, 2004). The frequent copulation of *P. canaliculata* relative to egg mass laying (2.9 vs. 1.4 times a week; Albrecht et al., 1996) probably does not favour the evolution of such paternal investment. However, the minimum time needed for sperm replacement could be in turn modified by the consumption of NGs, which could reduce the re-mating rate in some insects (Gwynne, 2008). The lack of evidence of direct benefits of consuming the NG in *P. canaliculata* is coincident with recent studies that provide little support to the beneficial effects of NGs in females and give more strength to the negative or manipulative effects of the male donations, reducing the female re-mating rate even below its optimum (Engqvist, 2007; Gwynne, 2008).

The consumption of ANGs had no effect on the copulation duration of *P. canaliculata* couples relative to those that received no ANGs. As it was not possible to impede the spontaneous release of NGs and their ingestion, NG probably occurred in all treatments. Perhaps the addition of ANG had no additive effect on copulation duration due to the fact that the males already attained their optimum duration with their own NGs. In decorated crickets, the males produce NGs large enough to reach a complete sperm transfer from the spermatophore to the female spermatheca (Sakaluk, 1984).

Except for the T-maze experiment, the doses of macerated penis sheath tissues were jellified and coloured in order to achieve a better administration. The processing of penis sheath tissues perhaps diminished or cancelled the putative manipulative effect (possibly allohormonal, *sensu* Koene & ter Maat, 2002) of the mucus secretion in the copulation duration experiment (e.g., Benke et al., 2010), but this seems less plausible for the supposed nutritional effects in the reproductive output experiment (e.g., Gwynne, 2008).

The production of NGs in the field is reported here for the first time in two natural populations of *P. canaliculata*. Laboratory observations (Burela & Martín, 2007, 2009) on the interval between the start of release of NGs and their consumption (ca. 30 seconds), the frequency of NGs per copulation (maximum four) and the copulation duration (mean 12.8 h) indicate that NGs are detectable only during a very short part of the duration of the copulation (ca. 0.25%). Hence the frequency of detection of NG in the field is probably an underestimation of the proportion of snails that produce them; even under continuous observation in the lab, NGs were observed only in 19.91% of the mating couples that reached the insemination phase (Burela & Martín, 2009). On the other hand, the frequency of snails with NGs in the field is probably positively correlated to the rate of NGs production. The frequency of NGs was almost ten times higher in the population with the highest density of snails (El Huáscar stream), indicating a much higher rate of production of NGs. The proportion of couples with prowler males was also higher in El Huáscar stream, and moreover, the proportion of couples with both NGs and prowler males attached was significantly higher than expected by chance in the population with the highest population density.

The evidence gathered here supports a possible role of NGs in the male-to-male competition for ova. NGs are a common in the long copulations of *P. canaliculata* (Burela & Martín, 2007, 2009), and they are released even in the absence of other males. However, the copulating males that perceive a male competitor or risk of male competition probably deliver more NGs during copulation to entice the female to remain in copulation through a sensory exploitation (discussed below). Perhaps, a non NG-giving copulating male cannot achieve its optimal sperm transference if the interference of a competitor male prompts the female to disengage prematurely. Thus, a good NG-giving male would have a competitive advantage to face male competition, but this explanation needs to be tested in the future.

The present results provided little support for the hitherto tested functional explanations of the gift-giving behaviour in *P. canaliculata*. However, the explanations related to the increase in copulation duration and reproductive output cannot be absolutely discarded with our experimental approach using ANGs, as we could not impede natural NGs. Until now, the paradoxical association of NG production with prowler males and the female attraction to the mucus secretion are the only clues to the significance of this behaviour in *P. canaliculata*.

ACKNOWLEDGEMENTS

We wish to thank to Daniela Miloch, Nicolás Cecchetto, Lucía Saveanu and Juan Francisco Tellarini by their assistance with field work. This work was funded by grants from CONICET (Consejo Nacional de Investigaciones Científicas y Técnicas, PIP 112 200901 00473) and UNS (Universidad Nacional del Sur, PGI 24/B185 and PGI 24B/144). S. B. and P. R. M. are researchers in CONICET.

LITERATURE CITED

AIZAKI, K. & Y. YUSA, 2010, Learned predator recognition in a freshwater snail, *Pomacea canaliculata*. *Malacologia*, 52: 21–29.

ALBRECHT, E., N. B. CARREÑO & A. CASTRO-VÁZQUEZ, 1996, A quantitative study of copulation and spawning in the South American apple-snail *Pomacea canaliculata* Lamarck (Prosobranchia, Ampullariidae). *The Veliger*, 39: 142–147.

ANDREWS, E. B., 1964, The functional anatomy and histology of the reproductive system of some pilid gastropod molluscs. *Proceedings of the Malacological Society of London*, 36: 121–140.

BENKE, M., H. REISE, K. MONTAGNE-WAJER & J. M. KOENE, 2010, Cutaneous application of an accessory-gland secretion after sperm exchange in a terrestrial slug (Mollusca: Pulmonata). *Zoology*, 113: 118–124.

BURELA, S. & P. R. MARTÍN, 2007, Nuptial feeding in the freshwater snail *Pomacea canaliculata* (Gastropoda: Ampullariidae). *Malacologia*, 49: 465–470.

BURELA, S. & P. R. MARTÍN, 2009, Sequential pathways in the mating behavior of the apple snail *Pomacea canaliculata* (Caenogastropoda: Ampullariidae). *Malacologia*, 51: 157–164.

BURELA, S. & P. R. MARTÍN, 2011, Evolutionary and functional significance of lengthy copulations in a promiscuous apple snail, *Pomacea canaliculata* (Caenogastropoda: Ampullariidae). *Journal of Molluscan Studies*, 77: 54–64.

ENGQVIST, L., 2007, Nuptial gift consumption influences female remating in a scorpionfly: male or female control of mating rate? *Evolutionary Ecology*, 21: 49–61.

ESTEBENET, A. L., 1995, Food and feeding in *Pomacea canaliculata* (Gastropoda: Ampullariidae). *The Veliger*, 38: 277–283.

ESTEBENET, A. L. & P. R. MARTÍN, 2002, *Pomacea canaliculata* (Gastropoda: Ampullariidae): life-history traits and their plasticity. *Biocell*, 26: 83.

ESTEBENET, A. L., P. R. MARTÍN & S. BURELA, 2006, Conchological variation in *Pomacea canaliculata* and other South American Ampullariidae (Caenogastropoda, Architaenioglossa). *Biocell*, 30: 329–335.

GAMARRA-LUQUES, C., B. C. WINIK, I. A. VEGA, E. A. ALBRECHT, N. M. CATALAN & A. CASTRO-VÁZQUEZ, 2006, An integrative view to structure, function, ontogeny and phylogenetical significance of the male genital system in *Pomacea canaliculata* (Caenogastropoda, Ampullariidae). *Biocell* (Mendoza), 30: 345–357.

GIRAUD-BILLOUD, M., C. GAMARRA-LUQUES & A. CASTRO-VAZQUEZ, 2013, Functional anatomy of male copulatory organs of *Pomacea canaliculata* (Caenogastropoda, Ampullariidae). *Zoomorphology*: 1–15.

GWYNNE, D. T., 2008, Sexual conflict over a gifts in insects. *Annual Review of Entomology*, 53: 83–101.

ICHINOSE, K., 2002, Influence of age and body size on alarm responses in a freshwater snail *Pomacea canaliculata*. *Journal of Chemical Ecology*, 28: 2017–2028.

KOENE, J. M., 2005, Allohormones and sensory traps: fundamental difference between hermaphrodites and gonochorists? *Invertebrate Reproduction and Development*, 48: 101–107.

KOENE, J. M. & A. TER MAAT, 2001, "Allohormones": a class of bioactive subtances favoured by sexual selection. *Journal of Comparative Physiology A*, 187: 323–326.

KOENE, J. M. & A. TER MAAT, 2002, The distinction between pheromones and allohormones. *Journal of Comparative Physiology A: Neuroethology, Sensory, Neural, and Behavioral Physiology*, 188: 163–164.

LEWIS, S. & A. SOUTH, 2012, The evolution of animal nuptial gifts. *Advances in the Study of Behavior*, 44: 53–97.

LOWE, S., M. BROWNE, S. BOUDJELAS & M. DE POORTER. 2000, *100 of the world's worst invasive alien species: a selection from the global invasive species database*. Invasive Species Specialist Group Auckland, New Zealand,

MARTÍN, P. R., A. L. ESTEBENET & N. J. CAZZANIGA, 2001, Factors affecting the distribution of *Pomacea canaliculata* (Gastropoda: Ampullariidae) along its southernmost natural limit. *Malacologia*, 43: 13–23.

SAKALUK, K. S., 1984, Male crickets feed females to ensure complete sperm transfer. *Science*, 223: 609–610.

SAVEANU, L. & P. R. MARTÍN, 2013, Pedal surface collecting as an alternative feeding mechanism of the invasive apple snail *Pomacea canaliculata* (Caenogastropoda: Ampullariidae). *Journal of Molluscan Studies*, 79: 11–18.

SVENSSON, B. O. G., E. PETERSSON & M. FRISK, 1990, Nuptial gift size prolongs copulation duration in the dance fly *Empis borealis*. *Ecological Entomology*, 15: 225–229.

TAKEICHI, M., Y. HIRAI & Y. YUSA, 2007, A waterborne sex pheromone and trail following in the apple snail, *Pomacea canaliculata*. *Journal of Molluscan Studies*, 73: 275–278.

VAHED, K., 1998, The function of nuptial feeding in insects: a review of empirical studies. *Biological Reviews*, 73: 43–78.

WARWICK, S., K. VAHED, D. RAUBENHEIMER & S. J. SIMPSON, 2009, Free amino acids as phagostimulants in cricket nuptial gifts: support for the 'Candymaker' hypothesis. *Biology Letters*, 5: 194–196.

YUSA, Y., 2004, Inheritance of colour polymorphism and the pattern of sperm competition in the apple snail *Pomacea canaliculata* (Gastropoda: Ampullariidae) *Journal of Molluscan Studies*, 70: 43–48.

YUSA, Y., 2007, Nuclear sex-determining genes cause large sex-ratio variation in the apple snail *Pomacea canaliculata*. *Genetics*, 175: 179–184.

Revised ms. accepted October 11, 2013

MALACOLOGIA, 2014, 57(2): 329–339

ULTRASTRUCTURE OF THE SPERMATOGENIC PROCESS IN THE PENSHELL *ATRINA MAURA* (BIVALVIA: PINNIDAE)

Marian Alejandra Camacho-Mondragón[1], Bertha Patricia Ceballos-Vázquez[1],
Esther Uría Galicia[2] , Edgar Oliver López Villegas[2] & Marcial Arellano-Martínez[1*]

ABSTRACT

The ultrastructural features of the spermatogenic development and mature spermatozoa morphology of *Atrina maura* were investigated through transmission electron microscopy. The testis displays a diffuse tubular structure in which gametes develop within a concentric arrangement according to the degree of development. Within the tubules also appear Sertoli cells, which contain a large amount of lipid droplets and glycogen granules in the cytoplasm, suggesting a nutritive role in the first spermatogenesis stage (spermatogonia). Four gamete maturation stages co-occurred in the same individual: spermatogonia (4–8 μm), spermatocytes (3–4 μm) (including primary and secondary), spermatids (2.5 μm) and spermatozoa (~ 2 μm head length). The proacrosomal vesicle and flagellum occur only until the first stages of spermiogenesis, contrasting with the early formation of both structures in spermatogonia and spermatocytes in other bivalves. In *A. maura,* the material in the acrosomal vesicle of mature spermatozoa shows a characteristic electron density pattern, which seems to be an exclusive taxonomic feature of the family Pinnidae. However, *A. maura* displayed only four mitochondria in the midpiece, contrasting with five in all other species in this family.

Key words: acrosomal complex, Sertoli cells, spermatic ultrastructure, Pteriomorphia, taxonomic implications.

INTRODUCTION

Atrina maura (G. B. Sowerby I, 1835) is one of the edible bivalve species of economic importance in Mexico. Its distribution range stretches from Baja California Sur, Mexico (including the Gulf of California) to Peru (Coan & Valentich-Scott, 2012). It has been recognized as an abundant natural resource along temperate and tropical Mexican Pacific coasts for several decades (Vélez-Barajas & Fajardo-León, 1996; Ahumada-Sempoal et al., 2002). But recently, Baja California Sur fishers have witnessed a marked decline in the abundance of this species in several harvesting areas, although government officials have not reported this decline. Derived from this situation, several research institutions have made various attempts to produce *A. maura* seed in the laboratory. However, a number of unsolved questions remain about the reproductive biology of the species, and there is no standardized culture methodology to date (Reynoso-Granados et al., 1996; Cardoza-Velasco & Maeda-Martínez, 1997; Lora-Vilchis et al., 2004).

A number of investigations have been conducted previously on the reproductive features of *A. maura*, including gonad development, maturation and the reproductive cycle (Rodríguez-Jaramillo et al., 2001; Enríquez-Diaz et al., 2003; Ángel-Pérez et al., 2007; Ángel-Dapa et al., 2010; Camacho-Mondragón et al., 2012). However, these investigations have focused on histology using light microscopy and paraffin-embedded sections, leading to a limited interpretation of the cytological characteristics due to the intrinsically low resolution of this technique. Studies on spermatic ultrastructure have proven to be a useful source of information about additional features for taxonomic and phylogenetic analyses in bivalves (Franzen, 1983; Hodgson et al., 1990;

[1]Instituto Politécnico Nacional, Centro Interdisciplinario de Ciencias Marinas. Av. Instituto Politécnico Nacional s/n, Col. Playa Palo de Santa Rita. C.P. 23096. La Paz, Baja California Sur, México
[2]Instituto Politécnico Nacional, Escuela Nacional de Ciencias Biológicas, Unidad Profesional Lázaro Cárdenas. Prolongación Manuel Carpio y Plan de Ayala s/n, Col. Santo Tomás C.P. 11340 Delegación Miguel Hidalgo, Distrito Federal, México
*Corresponding author: marellam@ipn.mx

Healy, 1996; Kafanov & Drozdov, 1998; Healy et al., 2000). Similarly, these studies constitute the framework for carrying out more specialized work, that is, molecular analysis and for gamete characterization at the cell level, as accomplished in vertebrate species (Com et al., 2003). Moreover, ultrastructural descriptions serve as an initial model from which studies comparing abnormalities caused by contaminants or diseases may derive (Yurchenko & Vaschenko, 2010).

To date, there are no published studies on the ultrastructure of spermatogenesis to supplement the morphological descriptions of the gametes for *A. maura*, which would advance the basic understanding of the reproductive biology of this species. Furthermore, there is little information on spermatic ultrastructure for the Pinnidae family (subclass Pteriomorphia), which comprises only two genera: *Pinna* and *Atrina* (Gaulejac de et al., 1995; Healy et al., 2000; Kang et al., 2012). The only published works on this family refer to *Pinna nobilis* (Linnaeus, 1758) (Gaulejac de et al., 1995) and describe all the spermatogenesis stages; however, the characterization of the most important organelles, that is, the acrosomal complex, require further investigation. As regards the genus *Atrina,* the ultrastructure of spermatozoa has been investigated in detail for *Atrina vexillum* (Born, 1778) (Healy et al., 2000) and *Atrina pectinata* (Linnaeus, 1767) (Kang et al., 2012); in the latter, cell differentiation during spermatogenesis has also been analyzed.

The present study describes the ultrastructural features of spermatogenesis in *A. maura* and emphasizes the morphological characteristics of spermatozoa that are considered taxonomically and phylogenetically relevant, allowing interspecific comparisons while providing information on the general spermatozoa pattern in the family Pinnidae.

MATERIALS AND METHODS

Atrina maura males (> 12 cm shell length) were collected in the Ensenada de La Paz, Baja California Sur, Mexico, which are considered as adults based on the size at first maturity of this particular species in the same area (Camacho-Mondragón et al., 2012). Gonads of these specimens were dissected; 5-mm samples were obtained and fixed in 2.5% glutaraldehyde (Electron Microscopy Sciences) for six h; afterwards, five 10-min washes were done using Sorensen's phosphate buffer. Post-fixation was performed with 1% osmium tetroxide for one h followed by buffer washes as described above. Then samples were dehydrated with a series of alcohols of increasing concentration (70% to 100%). Tissue samples were infiltrated in a propylene oxide solution and epoxy resin for three h and then, embedded in EPON 812 resin. Ultra thin 70-nm sections were obtained using an ultramicrotome, and these were stained with uranyl acetate and lead citrate. Finally, sections were examined in a Jeol-100SX (60000 V) transmission electron microscope and micrographs from different portions of the gonad were obtained.

To characterize spermatogenesis, gametes in different development stages were selected, and a number of morphological parameters commonly used for comparative purposes were measured. In spermatogonia, spermatocytes (primary and secondary) and spermatids, the total and nucleus diameter were measured. In the mature spermatozoa, acrosome length (linear distance from the posterior edge of the acrosome to the posterior edge of the nuclear invagination), nucleus length (linear distance from the posterior edge of the invagination to the anterior edge of the midpiece) and nucleus width (at its widest point) were measured.

RESULTS

The male gonad of *A. maura* comprises blind tubules in which gametes are aligned along the inner wall. Spermatogenesis follows a concentric arrangement; from the inner wall towards the lumen, all gamete development stages co-occur in a single individual, including spermatogonia, primary and secondary spermatocytes, spermatids and spermatozoa. Cells of any given stage are arranged in clusters, and spermatozoa agglomerate toward the tubule center with flagella directed towards the lumen.

Spermatogonia

Spermatogonia are located along the inner wall of tubules, arranged in 2 or 3 cell rows. In the first layer, spermatogonia either are occasionally in contact or separated by cytoplasm projections of Sertoli cells. Spermatogonia measure 4 to 8 μm and have irregular edges. The nucleus measures 2 to 5 μm, with a heterogeneous chromatin arrangement, and contains one or two nucleoli (Fig. 1). The cytoplasm includes numerous mitochondria, Golgi apparatus and occasional dense aggregates (Fig. 2).

Spermatocytes

Primary spermatocytes measure 3–4 μm; the nucleus is similar in shape to that of the spermatogonia, but shows early signs of chromatin condensation. The cytoplasm is reduced, and thus the nucleus: cytoplasm ratio increases. The cytoplasm contains the same organelles as spermatogonia. Spermatocytes develop cytoplasmic projections devoid of organelles. Cell edges are irregular (Fig. 3).

Secondary spermatocytes are rarely observed, probably due to the rapid onset of the second meiotic division (Fig. 4). These cells

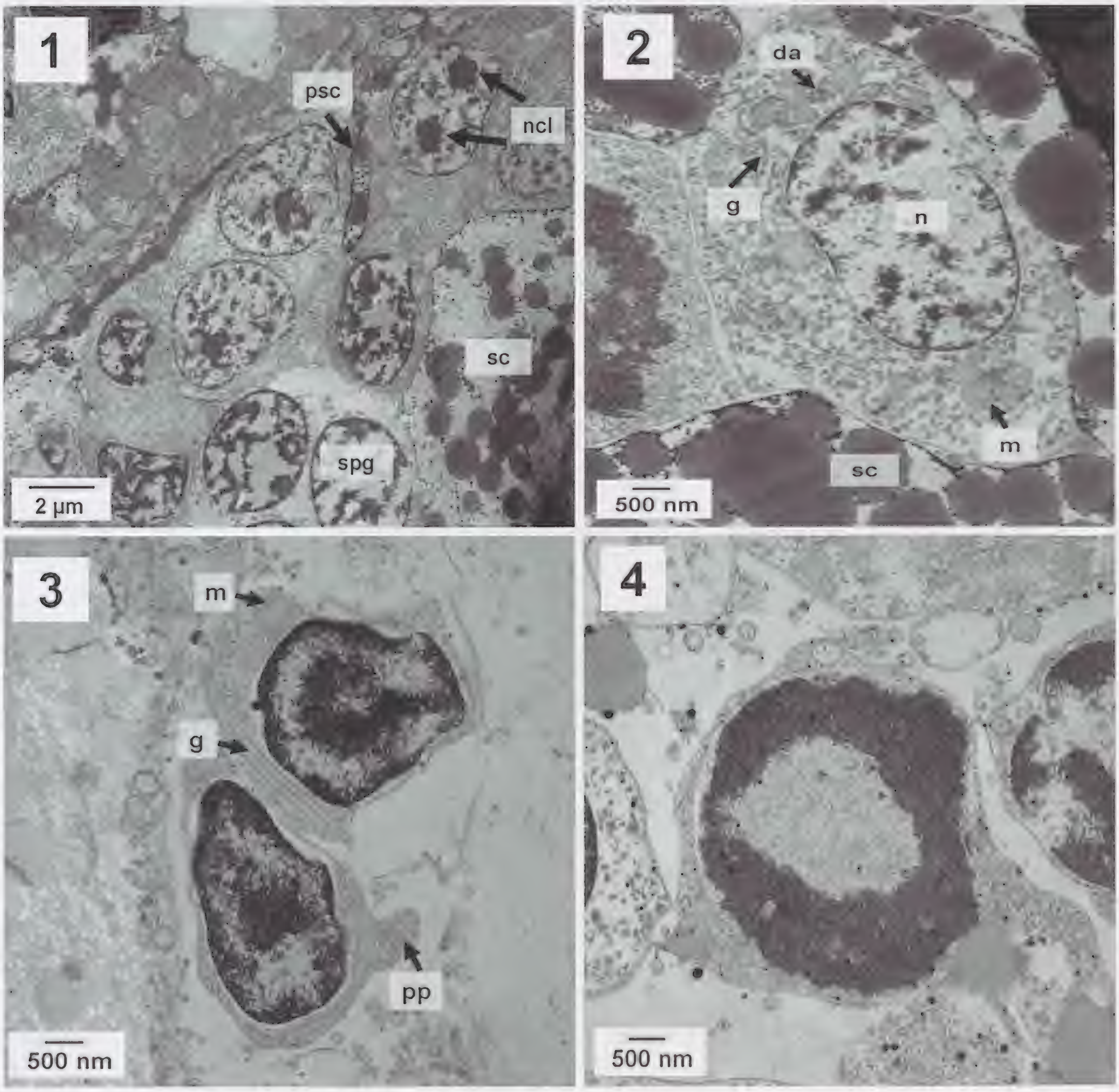

FIGS. 1–4. Transmission electron micrographs of spermatogonia and spermatocytes in *Atrina maura* males. FIG. 1: Espermatogonia (spg) in bands separated by pseudopodia-like projections (psc) of Sertoli cell (sc); the nucleus may display one or two nucleoli (ncl); FIG. 2: Spermatogonia surrounded by Sertoli cell (sc), the nucleus (n) is voluminous, g: Golgi apparatus, m: mitochondria, da: dense aggregates; FIG. 3: Primary spermatocyte showing early chromatin condensation, g: Golgi apparatus, m: mitochondria, pp: pseudopodia-like cytoplasm projection; FIG. 4: Secondary spermatocyte showing heterochromatin condensation (dark area) in the nucleus towards the periphery.

are irregularly shaped and are dimensionally similar to primary spermatocytes. The nucleus is spherical and heterochromatin is condensed towards the periphery. The cytoplasm is reduced and mitochondria are the most abundant and visible organelles.

Spermatids

Spermiogenesis (spermatid differentiation) starts with spherical cells measuring 2.5 μm in diameter and that have a round nucleus with scattered marginal heterochromatin (Fig. 5).

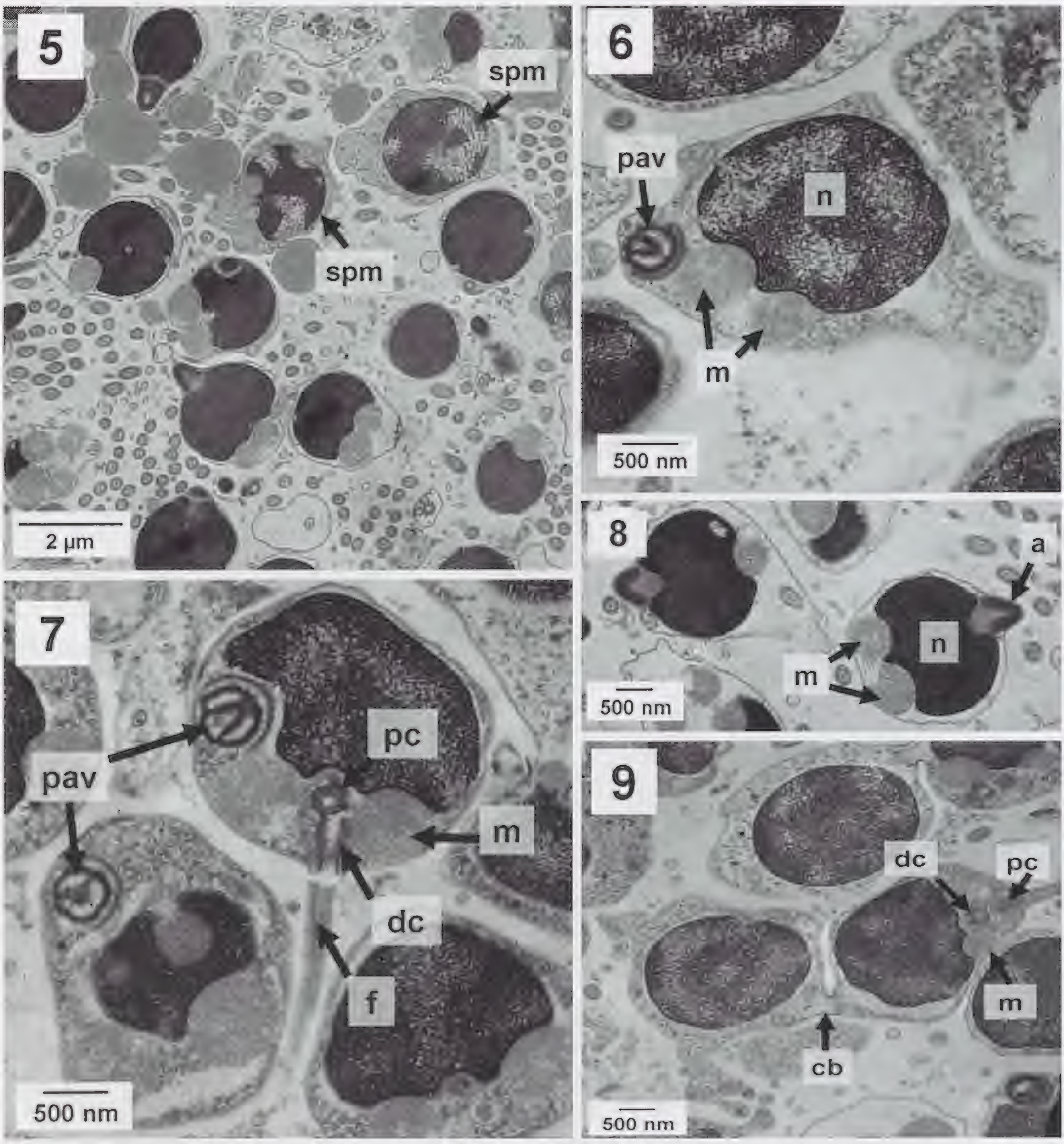

FIGS. 5–9. Transmission electron micrographs of spermatids in *Atrina maura* males. FIG. 5: Spermatids (spm) in early development stages; FIG. 6: Spermatids in advanced development stages; nucleus (n); mitochondria (m); proacrosomal vesicle (pav); FIG. 7: Mature spermatids. The proacrosomal vesicle is observed at different positions in its migration towards the cell apex; distal centriole (dc); proacrosomal vesicle (pav), flagellum (f); proximal centriole (pc), mitochondria (m); FIG. 8: Mature spermatids, acrosome (a), mitochondria (m); FIG. 9: Mature spermatids. Note the cell bridge (cb); distal centriole (dc); proximal centriole (pc), mitochondria (m).

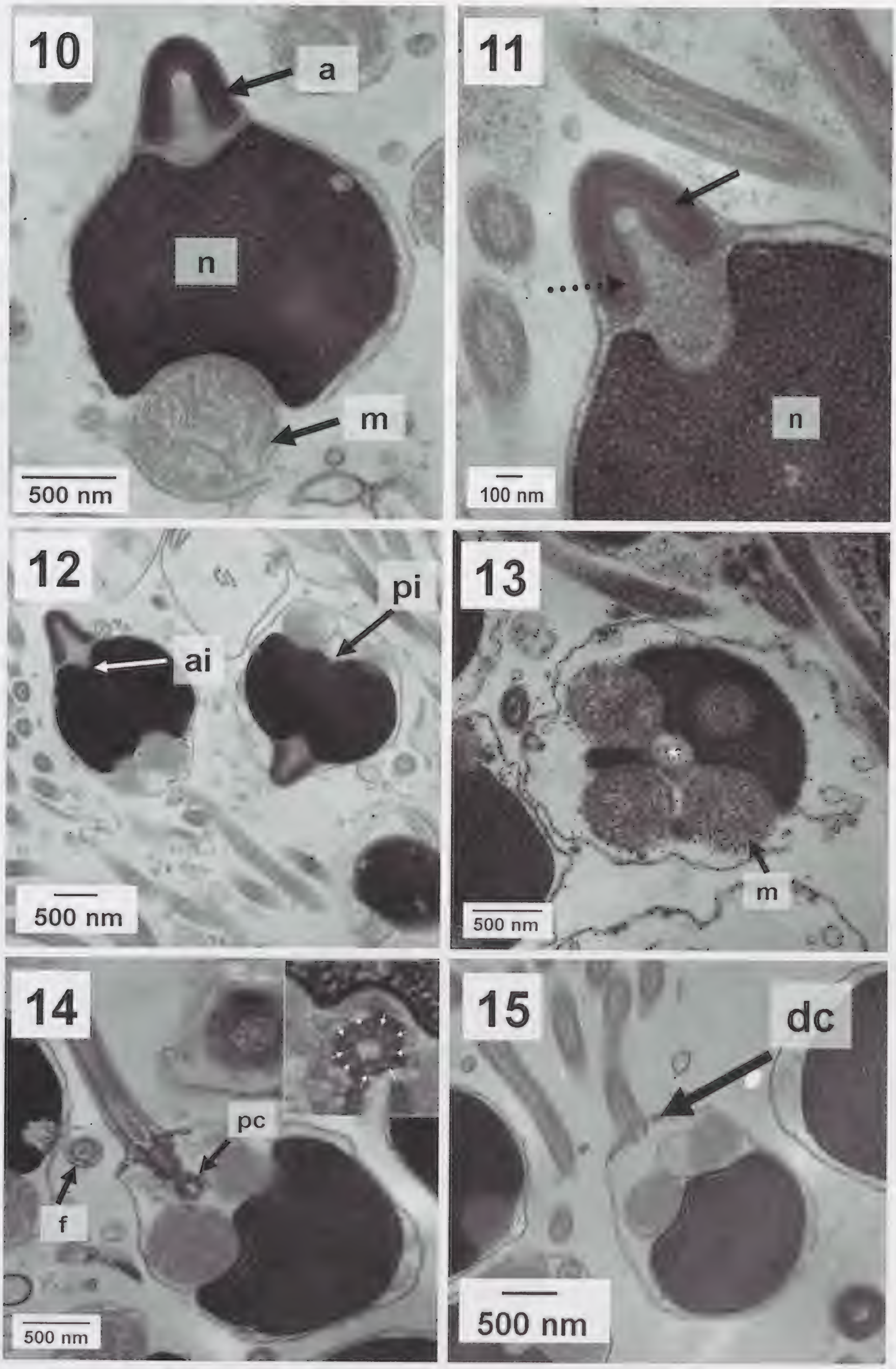

FIGS. 10–15. Transmission electron micrographs of mature sperm in *Atrina maura* males. FIG. 10: The condensed nucleus is observed; acrosome (a), nucleus (n), mitochondria (m); FIG. 11: Detail of the acrosome that shows one electron-dense region (solid arrow) and one electron-translucent region (dotted arrow), nucleus (n); FIG. 12: The nucleus shows two invaginations: anterior invagination (ai) and posterior invagination (pi); FIG. 13: Posterior view of the midpiece with four mitochondria (m) surrounding the distal centriole (*); FIG. 14: The box shows the nine microtubule triplets in the proximal centriole (pc). Flagellum cross section (f) showing the internal 9 + 2 microtubular structure; FIG. 15: The distal centriole (dc) constitute the flagellum base.

The amount of cytoplasm decreases and several clusters of mitochondria are observed. As development progresses, the nucleus becomes smaller, and chromatin becomes scattered in irregular clumps. In this stage, spermatids display four voluminous mitochondria that congregate at the posterior side of the nucleus. A proacrosomal vesicle appears in the same zone, which shows a characteristic "V"-shaped arrangement of electron-dense material to the center (Fig. 6). The cytoplasm displays two centrioles in orthogonal position exhibiting the typical nine triplets of microtubules. The flagellum is produced by the distal centriole, the closest to the plasma membrane (Fig. 7).

Mature spermatids are characterized by the condensation of nuclear material that begins at the periphery. The proacrosomal vesicle migrates from the bottom to the apex of the cell (Fig. 7) and becomes conical, being invaginated and less electron-dense at the periphery (Fig. 8). Spherical mitochondria are located at the base of the nucleus and surround the centrioles. The Golgi apparatus is commonly not observed. Spermatids may be connected by intracellular bridges that link the bottom of one cell with the apex of another (Fig. 9).

In summary, spermiogenesis involves the progressive condensation of chromatin from the periphery to the center, coupled with the reduction of the nucleus size; the formation of a proacrosomal vesicle at the base of cells and its migration to the apex, where it becomes the acrosome; the fusion of small mitochondria into four mitochondrial spheres arranged around centrioles; the production of the flagellum by the distal centriole; the reduction of cytoplasm into a very thin layer and the loss of the Golgi apparatus.

Spermatozoa

Mature spermatozoa has a conical head measuring ~ 2 μm from the acrosome tip to the back of the midpiece. The nearly spherical nucleus is fully condensed and measures ~ 1.4 μm long by ~ 1.6 μm wide (Fig. 10). A small conical acrosome (~ 0.7 μm, including subacrosomal material), without an axial rod, is located to the front. The acrosome is invaginated in the posterior end. It appears to be composed of two different materials, one electron-dense outer region shaped as a thin elliptical line and an electron-translucent inner region. The subacrosomal space contains granular material (Fig. 11).

The nucleus shows two invaginations: one to the front, adjacent to the acromosome, containing moderately dense granular material, and the other to the back, where the proximal

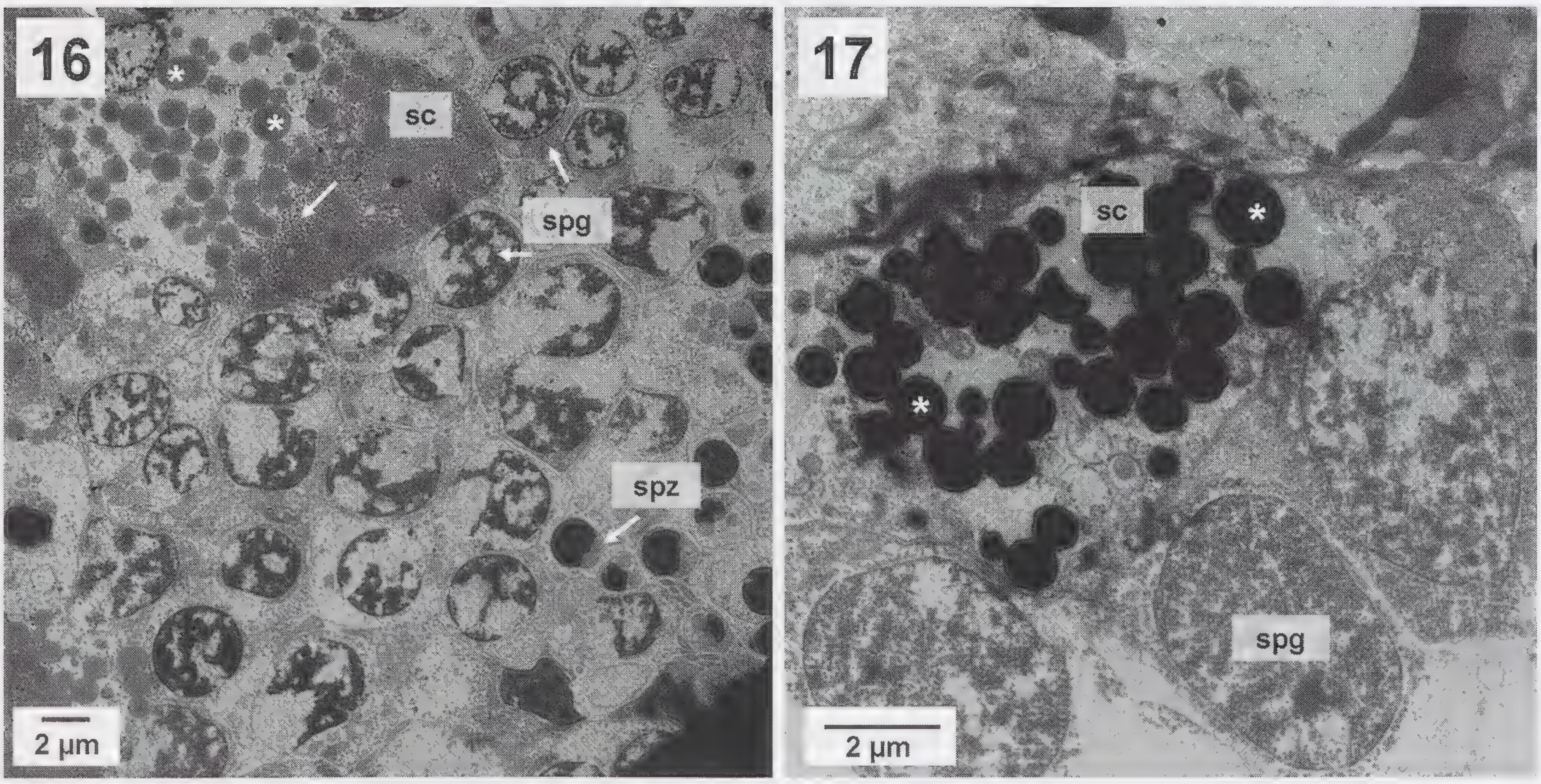

FIGS. 16, 17. Transmission electron micrographs of Sertoli cells in *Atrina maura* males. FIG. 16: One Sertoli cell (sc) is observed adjacent to the first spermatogonia (spg) row. The Sertoli cell content includes lipid droplets (*) and small glycogen granules (arrow); FIG. 17: Detail of one Sertoli cell in contact with three spermatogonia.

centriole is located (Fig. 12). At the base of the nucleus, mitochondria are located near the nucleus membrane. Up to four spherical mitochondria measuring 0.5 µm in diameter were observed surrounding the diplosoma, which constitutes the midpiece (Fig. 13). The proximal centriole is located at the posterior invagination of the nucleus perpendicular to the axoneme and shows a configuration of nine microtubule triplets (Fig. 14). The distal centriole constitutes the basal body of the flagellum (Fig. 15), which displays the typical 9 + 2 structure of inner microtubules (nine peripheral microtubules surrounding a central pair) (Fig. 14). The spermatozoa cytoplasm is highly reduced, so that the nucleus : cytoplasm ratio is high in these cells.

Sertoli Cells

Inside the tubules large irregular-shaped somatic cells known as Sertoli cells can be found. The cytoplasm of these cells contains a large number of lipid droplets and small dispersed glycogen particles (~ 0.5µm) (Figs. 16, 17). No membrane-enclosed organelles were observed in the cytoplasm of these cells.

DISCUSSION

The general spermatogenesis process in *A. maura* is similar to that of other bivalves (Thielley et al., 1993; Gaulejac de et al., 1995; Chung et al., 2007). In any one specimen, gametes in all development stages were observed displaying the concentric distribution that characterizes the male gonad of this species (Camacho-Mondragón et al., 2012). However, the different cell types were not observed with the same frequency. Specifically, secondary spermatocytes were rarely observed; this condition has been reported previously for other bivalves and is attributed to the rapid cell division rate, which is difficult to distinguish histologically using light microscopy (Sastry, 1979).

The major changes in cell morphology during the spermatogenesis of *A. maura* occur in the spermatid stage, including the condensation of nuclear chromatin, the mitochondrial fusion and acrosome formation. As in *P. nobilis* and *A. pectinata,* also members of the family Pinnidae (Gaulejac de et al., 1995; Kang et al., 2012), in *A. maura* the proacrosomal vesicle and the flagellum appear until the early spermiogenesis stages, in contrast to bivalve species such other as *Barbatia obliquata* (W. Wood, 1828) and *B. foliata* (Forsskål in Nieburh, 1775) (Arcidae), *Brachidontes semistriatus* (Krauss, 1848) (Mytilidae), *Arcuatula capensis* (Krauss, 1848) (Mytilidae), *Bathymodiolus childressi* Gustafson, Turner, Lutz & Vrijenhoek, 1998 (Mytilidae) and *Tivela polita* (G. B. Sowerby II, 1851) (Veneridae), all of which show an early formation of both structures in spermatogonia and spermatocytes (Reunov & Hodgson, 1994; Eckelbarger & Young, 1999). In *A. maura*, the acrosome is formed at the posterior end of the spermatid and subsequently migrates to the anterior end, as in other bivalves (Erkan & Sousa, 2002; Chung et al., 2007). When this migration is completed, the acrosome shows an outer apical region that is more electron dense and homogeneous relative to the electron-translucent inner region. This difference in electron density across the acrosome has been observed in *Perna perna* (Linnaeus, 1758) (Bernard & Hodgson, 1985), *Pinctada margaritifera* (Linnaeus, 1758) (Thielley et al., 1993), *Chama macerophylla* Gmelin, 1791, and *Spisula solidisima* (Dillwyn, 1817) (Hylander & Summers, 1977); this may be due to the various functions of the acrosome during fertilization (Popham, 1974). There is evidence that the electron-dense region is involved in the binding of spermatozoa to the microvilli on the oocyte surface, releasing lysines during the acrosome reaction (Hylander & Summers, 1977), maybe arylsulphatase and acid phosphatase as stated by Pipe & Da Silveira (1989) for *Mytilus edulis* Linnaeus, 1758. Whereas, the electron-translucent region might result from the crystalline alignment of enzymes involved in fertilization (Friend & Fawcett, 1974).

Numerous studies have demonstrated that all bivalves have “primitive” spermatozoa (Franzen, 1956) or aqua sperm (Rouse & Jamieson, 1987), typical of animals that release their gametes to the surrounding aquatic environment. Rouse & Jamieson (1987) recognize two aqua-sperm categories: (1) ect-aquasperm: spermatozoa that, at least potentially, fertilizes oocytes in the surrounding water, (2) ent-aquasperm: spermatozoa released to water but that is subsequently attracted by an incoming current to the mantle cavity where fertilization takes place. In the case of *A. maura,* the spermatozoa displays the basic structural plan, presumably suitable for swimming (ect-aquasperm), with an acrosomal complex, a condensed spheroidal nucleus, a midpiece consisting of four mitochondria surrounding the two centrioles and a flagellum with a 9 + 2 microtubular configuration.

The morphology of the midpiece in *A. maura* is similar to the one reported for several bivalves (Popham, 1979): four mitochondria are apparent, similar to the spermatozoa of other members of the order Pterioidea (Healy, 1989). These giant mitochondria likely result from the fusion of small preexisting ones, as reported for other bivalves (Longo & Dornfeld, 1967; Bernard & Hodgson, 1985; Hodgson & Bernard, 1986). Their position around the flagellum suggests that they may be involved in the energy supply for spermatozoa mobility and metabolism.

The shape of the nucleus, which is basically the mature spermatozoa head, varies from one mollusk species to another. In the case of the "primitive" bivalve sperm, the nucleus shape may be either ovoid, conical or spherical (Popham, 1979). *A. maura*'s spermatozoa has a spherical nucleus that exhibits a granular pattern of chromatin condensation during spermiogenesis, similar to other bivalves with nearly spherical spermatozoa nuclei (Maxwell, 1983).

Unlike spermatozoids from other mollusks (e.g., gastropods), bivalve spermatozoids possesses a limited number of available features for taxonomic or phylogenetic purposes. Traits which provide relevant information include the shape and inner structure of the acrosomal vesicle, and the spatial relationship between this vesicle and the nuclear apex (Healy et al., 2000). The nucleus of spermatozoids in *A. maura* has an anterior invagination under the acrosomal vesicle that contains a substance of unknown nature which is not organized in an axial rod (or perforatorium); the same is observed in *A. vexillum* and apparently represents the primitive bivalve condition (Popham, 1979). Moreover, the absence of an axial rod and the presence of a small acrosomal vesicle (~ 0.7 µm) in *A. maura* may be associated with functional aspects and be related to the thickness of the vitelline membrane. In the family Mytilidae, for example, there is a well-defined axial rod and a long acrosomal vesicle (2 µm), and both traits are attributed to the fact that in this family oocytes have a thicker membrane (Healy et al., 2000).

The ultrastructural details of the *A. maura* spermatozoa observed in this study essentially agree with those reported for other members of the family Pinnidae, such as *P. nobilis* (Gaulejac de et al., 1995), *A. vexillum* (Healy et al., 2000) and *A. pectinata* (Kang et al., 2012), but also contribute additional information regarding the acrosomal vesicle profile and substructure. These allow the identification of significant morphological differences and similarities between species in the family. Four important features were detected in *A. maura*: (1) the acrosomal vesicle is conical and larger (length ~ 0.7µm) than that reported for *A. vexillum* (~ 0.4 µm) and *A. pectinata* (~ 0.5 µm), deeply invaginated at the base and containing material differentiated in a highly electron-dense anterior layer forming a thin elliptical line (which might correspond to the radiated plates in *A. vexillum*) and a less electron-dense posterior layer. This particular arrangement of electron-dense material (in a thin elliptical line) in the acrosomal vesicle was also detected in *A. vexillum* (Healy et al., 2000) and *A. pectinata* (Kang et al., 2012), but not in other species of the families Pteriidae, Ostreidae, Mytilidae and Arcidae (Healy et al., 2000), so this feature could be used for taxonomic analyses at the family level; (2) the subacrosomal material is highly granular and, although it fills the nuclear depression, does not spread to the upper limit of the vesicle invagination as in *A. vexillum*; (3) the nucleus is small (~ 1.4 µm) compared with the large nuclei (2–10 µm) reported for *A. vexillum* and species of other families such as Arcidae and Glycymeridae (Healy et al., 2000). It also displays a granular texture and a remarkable anterior invagination; (4) mitochondria are spherical and are associated with the centriole pair in the three species; however, *A. maura* presents four in contrast with five commonly observed in *P. nobilis*, *A. vexillum* and *A. pectinata*. Healy (1995) reported that the number of mitochondria in the spermatozoa midpiece is a trait that is widely used in taxonomic analyses, since it tends to be stable at the family or superfamily level. Recently, has been reported that the families Arcidae, Mytilidae, Pteriidae and Pinnidae of the subclass Pteriomorphia all have spermatozoids with five mitochondria (Healy et al., 2000; Kang et al., 2012). However, it is accepted that the number of mitochondria in the midpiece may vary to some extent between species in the same family (Healy et al., 2000). Sometimes, this trait may display slight variations even within a single species (Healy, 1995), although *A. maura* always displayed four mitochondria.

On the other hand, the use of electron microscopy techniques has allowed us to unveil the details regarding the evolution of various cell categories and the presence of specific somatic cells that accompany the development of bivalve gametes (Avendaño & Le Pennec, 1998). In *A. maura*, the presence and relative abundance (in accordance with the gonad ripening) of adipogranular cells in the male gonad was reported by Camacho-Mondragón et al. (2012) using only the paraffin histological technique coupled with Sudan black staining to demonstrate the lipid content. The present investigation could not confirm the existence of these cells, but instead revealed the presence of Sertoli cells inside the tubules.

The arrangement of Sertoli cells in the male gonad of *A. maura* could not be described in detail previously due to the intrinsic limitations of light microscopy. The higher resolution of the present study revealed that Sertoli cells only surround spermatogonia, that is, any interaction of Sertolli cells with any other gamete type in a more advanced developing stage was not observed. This finding reinforces the hypothesis of the active role of Sertoli cells in nutrition during the early stages of spermatic development, as observed in other bivalve species (Pipe, 1987; Mathieu & Lubet, 1993; Eckelbarger & Young, 1999). The cytoplasm of Sertolli cells includes a number of biomolecules, such as protein, glycogen and lipid granules, all of which are transferred to gametes through pinocytosis to support the metabolic reactions required in this stage (Herlin-Houtteville & Lubet, 1975; Pipe, 1987).

ACKNOWLEDGMENTS

This research was funded by projects Multidisciplinary SIP 1535 and CONACYT-909000. Camacho-Mondragón, M.A. is a fellow student of PIFI (IPN) and CONACYT, the results presented here are part of her PhD thesis. B.P. Ceballos-Vázquez and M. Arellano-Martínez received grants from SIBE (COFAA), EDI (IPN), and SNI-CONACYT. The authors wish to acknowledge Richard Pipe for his useful comments on previous version of the manuscript. We thank María Elena Sánchez-Salazar, M. Sc. for her editorial contribution to the English manuscript.

LITERATURE CITED

AHUMADA-SEMPOAL, M. A., S. J. SERRANO-GUZMÁN & N. RUIZ-GARCÍA, 2002, Abundancia, estructura poblacional y crecimiento de *Atrina maura* (Bivalvia: Pinnidae) en una laguna costera tropical del Pacífico mexicano. *Revista de Biología Tropical*, 50: 1091–1100.

ÁNGEL-DAPA, M. A., C. RODRÍGUEZ-JARAMILLO, C. J. CÁCERES-MARTÍNEZ & P. E. SAUCEDO, 2010, Changes in lipid content of oocytes of the penshell *Atrina maura* as a criterion of gamete development and quality: a study of histochemistry and digital image analysis. *Journal of Shellfish Research*, 29: 407–413.

ÁNGEL-PÉREZ, C., S. J. SERRANO-GUZMÁN & M. A. AHUMADA-SEMPOAL, 2007, Ciclo reproductivo del molusco *Atrina maura* (Pterioidea: Pinnidae) en un sistema lagunar costero, al sur del Pacífico tropical mexicano. *Revista de Biología Tropical*, 55: 839–852.

AVENDAÑO, M. & M. LE PENNEC, 1998, Presencia de células auxiliares en la gametogénesis del ostión del norte, *Argopecten purpuratus* (Lamarck, 1819), (Mollusca, Bivalvia, Pectinidae). *Estudios Oceanológicos*, 17: 13–16.

BERNARD, R. T. F. & A. N. HODGSON, 1985, The fine structure of the sperm and spermatid differentiation in the brown mussel *Perna perna*. *South African Journal of Zoology*, 20: 5–9.

CAMACHO-MONDRAGÓN, M. A., M. ARELLANO-MARTÍNEZ & B. P. CEBALLOS-VÁZQUEZ, 2012, Particular features of gonadal maturation and size at first maturity in *Atrina maura* (Bivalvia: Pinnidae). *Scientia Marina*, 76: 539–548.

CARDOZA-VELASCO, F. & A. MAEDA-MARTÍNEZ, 1997, An approach to aquacultural production of the penshell *Atrina maura* Sowerby, 1835 (Bivalvia: Pinnidae) in northwest Mexico. *Journal of Shellfish Research*, 16: 311.

CHUNG, E., E. KIM & G. M. PARK, 2007, Spermatogenesis and sexual maturation in male *Mactra chinensis* (Bivalvia: Mactridae) of Korea. *Integrative Biosciences*, 11: 227–234.

COAN, E. V. & P. H. VALENTICH-SCOTT, 2012, Bivalve seashells of tropical west America. Marine bivalve mollusks from Baja California to northern Perú. Santa Barbara, California. *Santa Barbara Museum of Natural History, Monographs 6*: 1,258 pp.

COM, E., B. EVRARD, P. ROEPSTORFF, F. AUBRY & C. PINEAU, 2003, New insinghts into the rat spermatogonial proteome. *Molecular & Cellular Proteomics*, 2: 248–261.

ECKELBARGER, K. J. & C. M. YOUNG, 1999, Ultrastructure of gametogenesis in a chemosynthetic mytilid bivalve (*Bathymodiolus childressi*) from a bathyal, methane seep environment (northern Gulf of Mexico). *Marine Biology*, 135: 635–646.

ENRÍQUEZ-DÍAZ, M., C. CÁCERES-MARTÍNEZ, J. CHÁVEZ-VILLALBA, G. LE PENNEC & M. LE PENNEC, 2003, Gametogensesis of *Atrina maura* (Bivalvia: Pinnidae) under artificial conditions. *Invertebrate Reproduction & Development*, 43: 151–161.

ERKAN, M. & M. SOUSA, 2002, Fine structural study of the spermatogenetic cycle in *Pitar rudis* and *Chamelea gallina* (Mollusca, Bivalvia, Veneridae). *Tissue & Cell*, 34: 262–272.

FRANZEN, A., 1956, On spermiogenesis, morphology of the spermatozoon, and biology of fertilization among invertebrates. *Zoologiska Bidrag från Uppsala*, 31: 355–82.

FRANZEN, A., 1983, Ultrastructural studies of spermatozoa in three bivalve species with notes on evolution of elongated sperm nucleus in primitive spermatozoa. *Gamete Research*, 7: 199–214.

FRIEND, D. S. & D. W. FAWCETT, 1974, Membrane differentiation in freeze-fractured mammalian sperm. *Journal of Cell Biology*, 63: 641–664.

GAULEJAC DE, B., M. HENRY & N. VICENTE, 1995, An ultrastructural study of gametogenesis of the marine bivalve *Pinna nobilis* (Linnaeus 1758). II. Spermatogenesis. *Journal of Molluscan Studies*, 61: 393–403.

HEALY, J. M., 1989, Spermiogenesis and spermatozoa in the relict bivalve genus *Neotrigonia*: relevance to trigonioid relationships, particularly Unionoidea. *Marine Biology*, 103: 75–85.

HEALY, J. M., 1995, Sperm ultrastructure in in the marine bivalve families Carditidae and Crassatellidae and its bearing on unification of the Crasssatelloidea with the Carditoidea. *Zoological Science*, 24: 21–28.

HEALY, J. M., 1996, Molluscan sperm ultrastructure: correlation with taxonomic units within the Gastropoda, Cephalopoda, and Bivalvia. Pp. 99–113, in: J. Taylor, ed.,*Origin and evolutionary radiation of the Mollusca*. Oxford University Press, London, U.K., xiv + 392 pp.

HEALY, J. M., J. L. KEYS & L. Y. M. DADDOW, 2000, Comparative sperm ultrastructure in pteriomorphian bivalves with special reference to phylogenetic and taxonomic implications. Pp. 169–190, in: E. M. Harper, J. D. Taylor & J. A. Crame, eds.,*The evolutionary biology of the Bivalvia*. Special Publications Geological Society, London, UK, vii + 494 pp.

HERLIN-HOUTTEVILLE, P. & P. E. LUBET, 1975, The sexuality of pelecypod molluscs. Pp. 179–187, in: R. Reinboth, ed., *Intersexuality in the animal kingdom*. Springer-Verlag, Berlin, Heidelberg, New York, xiii + 449 pp.

HODGSON, A. N. & R. T. F. BERNARD, 1986, Ultrastructure of the sperm and spermatogenesis of three species of Mytilidae (Mollusca, Bivalvia). *Gamete Research*, 15: 123–135.

HODGSON, A. N., R. T. F. BERNARD & G. VAN DER HORST, 1990, Comparative spermatology of three species of *Donax* (Bivalvia) from South Africa. *Journal of Molluscan Studies*, 56: 257–265.

HYLANDER, B. L. & R. G. SUMMERS, 1977, An ultrastructural analysis of the gametes and early fertilization in two bivalves molluscs, *Chama macerophylla* and *Spisula solidissima* with special reference to gamete binding. *Cell and Tissue Research*, 182: 469–489.

KAFANOV, A. I. & A. L. DROZDOV, 1998, Comparative sperm morphology and phylogenetic classification of recent Mytiloidea (Bivalvia). *Malacologia*, 39: 129–139.

KANG, H. W., E. Y. CHUNG, J. H. KIM, J. S. CHUNG & K. Y. LEE, 2012, Germ cell differentiations during spermatogenesis and taxonomic values of mature sperm morphology of *Atrina* (*Servatrina*) *pectinata* (Bivalvia, Pteriomorphia, Pinnidae). *Development and Reproduction*, 16: 19–29.

LONGO, F. G. & E. J. DORNFELD, 1967, The fine structure of spermatid differentiation in the mussel, *Mytilus edulis*. *Journal of Ultrastructure Research*, 20: 462–480.

LORA-VILCHIS, M. C., E. RUIZ-VELASCO-CRUZ & T. REYNOSO-GRANADOS, 2004, Evaluation of five microalgae diets for juvenile pen shells *Atrina maura*. *Journal of the World Aquaculture Society*, 35: 232–236.

MATHIEU, M. & P. LUBET, 1993, Storage tissue metabolism and reproduction in marine bivalves - a brief review. *Invertebrate Reproduction & Development*, 23:123–129.

MAXWELL, W. L., 1983, Mollusca. Pp. 275–239, in: K. G. Adiyodi & R. G. Adiyodi, eds., *Reproductive biology of the invertebrates, Vol. 2: Spermatogenesis and sperm function*. John Wiley & Sons, Chichester, xiii + 718 pp.

PIPE, R. K., 1987, Ultrastructural and cytochemical study on interactions between nutrient storage cells and gametogenesis in the mussel *Mytilus edulis*. *Marine Biology*, 96: 519–528.

PIPE, R. K. & H. M. C. DA SILVEIRA, 1989, Arylsulphatase and acid phosphatase activity associated with developing and ripe spermatozoa of the mussel *Mytilus edulis*. *Histochemical Journal*, 21: 23–32.

POPHAM, J. D., 1974, The acrosome reaction in the sperm of the shipworm *Bankia australis* Caiman (Bivalvia, Mollusca). *Cell and Tissue Research*, 151: 93–101.

POPHAM, J. D., 1979, Comparative spermatozoon morphology and bivalve phylogeny. *Malacological Review*, 12: 1–20.

REUNOV, A. A. & A. N. HODGSON, 1994, Ultrastructure of the spermatozoa of five species of South African bivalves (Mollusca), and an examination of early spermatogenesis. *Journal of Morphology*, 219: 275–283.

REYNOSO-GRANADOS, T., A. N. MAEDA-MARTÍNEZ, F. CARDOZA-VELASCO & P. MONSLAVO-SPENCER, 1996, Cultivo de Hacha. Pp. 545–550, in: M. Casas-Valdez & G. Ponce-Díaz, eds., *Estudio del potencial pesquero y acuícola de Baja California Sur, Vol. 2.* SEMARNAT, Mexico, iv + 685 pp.

RODRÍGUEZ-JARAMILLO, C., A. N. MAEDA-MARTÍNEZ, M. E. VALDEZ, T. REYNOSO, P. MONSALVO-SPENCER, D. PRADO-ANCONA, F. CARDOZA-VELASCO, M. ROBLES-MUNGARAY & M. T. SICARD, 2001, The effect of temperature on the reproductive maturity of the penshell *Atrina maura* (Sowerby, 1835) (Bivalvia: Pinnidae). *Journal of Shellfish Research*, 20: 39–47.

ROUSE, G. W. & B. G. M. JAMIESON, 1987, An ultrastructural study of the spermatozoa of the polychaetes *Eurythoe complanata* (Amphinomidae), *Clymenella* sp. and *Micromaldane* sp. (Maldanidae), with definition of sperm types in relation to reproductive biology. *Journal of Submicroscopic Cytology*, 19: 573–584.

SASTRY, A. N., 1979, Pelecypoda (excluding Ostreidae). Pp. 113–292, in: A. C. GIESE & J. S. PEARSE, eds., *Reproduction of marine invertebrates, Vol. 5. Molluscs: pelecypods and lesser classes*. Academic Press, New York, viii + 369 pp.

SOWERBY, G. B., I., 1835, [... the previously undescribed species of shells contained in the collection of Mr. Cuming]. *Proceedings of the Zoological Society of London*, for 1835[3], (30): 84–85.

THIELLEY, M., M. WEPPE & C. HERBAUT, 1993, Ultrastructural study of gametogenesis in the French Polynesian black pearl oyster *Pinctada margaritifera* (Mollusca, Bivalvia), I-spermatogenesis. *Journal of Shellfish Research*, 12: 41–47.

VÉLEZ-BARAJAS, J. & M. FAJARDO-LEÓN, 1996, Pesquería de hacha. Pp. 101–111, in: M. CASAS-VALDEZ & G. PONCE-DÍAZ, eds., *Estudio del potencial pesquero y acuícola de Baja California Sur, Vol. 1*. SEMARNAT, Mexico, xx + 317 pp.

YURCHENKO, O. & M. A. VASCHENKO, 2010, Morphology of spermatogenic and accessory cells in the mussel *Modiolus kurilensis* under environmental pollution. *Marine Environmental Research*, 70: 171–180.

Revised ms. accepted November 9, 2013

MALACOLOGIA, 2014, 57(2): 341–351

EGG CANNIBALISM IN *POMACEA CANALICULATA* (CAENOGASTROPODA: AMPULLARIIDAE) FROM THE SOUTHERN PAMPAS: AN ALTERNATIVE TROPHIC STRATEGY?

Lucía Saveanu & Pablo R. Martín*

Departamento de Biología, Bioquímica y Farmacia, Universidad Nacional del Sur,
San Juan 670, 8000, Bahía Blanca, Argentina

ABSTRACT

Pomacea canaliculata is a freshwater gastropod native to southern South America and is listed among the world's 100 worst invaders. Diverse food sources can be exploited by this apple snail, including snails with gelatinous and subaquatic egg masses. Records of ingestion of their own egg masses (egg cannibalism), which are aerial and calcareous, have only been anecdotal in *P. canaliculata.* Our aims were to study egg cannibalism in a natural population and also under laboratory conditions. In a stream population from the southern Pampas, we recorded *P. canaliculata* attacking their own fresh egg masses, which had been naturally submerged by an increase in water level. In addition, when we artificially submerged fresh and old egg masses in a field experiment, we observed several snails readily attacking both. In the laboratory, we also observed the capture by pedal surface collecting of floating remains of egg masses. In laboratory trials, juveniles fed on eggs reached larger sizes than starved snails but smaller than those fed on lettuce; adult snails also eat eggs, but their growth rates were not affected by the food regime. *Pomacea canaliculata* eggs present defensive and anti-nutritive compounds that apparently dissuade almost all potential predators, but this snail did not appear to be negatively affected when feeds on its own eggs. The ingestion of egg remains and submerged egg masses is probably more frequent than previously considered in *P. canaliculata*, which may take advantage of using these alternative food resources when others are scarce.

Key words: apple snail, invader, intraspecific predation, feeding, growth, pedal surface collecting.

INTRODUCTION

Pomacea canaliculata (Lamarck, 1822) is a South American apple snail (family Ampullariidae) naturally distributed from Paraguay and southern Brazil southwards to southern Buenos Aires Province, Argentina (Martín et al., 2001; Hayes et al., 2012), and it is the only freshwater snail listed among the 100 worst invaders worldwide (Lowe et al., 2000). This species and its congeners inhabit lentic and lotic waterbodies in tropical to warm temperate regions and have invaded several countries around the world, causing important ecological changes in natural wetlands and economic losses in aquatic agricultural systems (Horgan et al., 2014). A noticeable feature of *Pomacea* species is the reproductive strategy of depositing masses of eggs with calcareous eggshells above the water level on exposed stems, leaves or stones (Heras et al., 1998; Pizani et al., 2005). Underwater predation has been suggested as one of the main selective pressures driving the evolution of the aerial egg masses in apple snails (Snyder & Snyder, 1971; Turner, 1998; Tiecher et al., 2014).

Due to the voracious consumption of macrophytes by apple snails, they are mainly regarded as macrophytophagous, and this habit has been the most intensely studied in ampullariids (e.g., Cowie, 2002; Tamburi & Martín, 2009; Morrison & Hay, 2011b). However, apple snails are able to use different feeding mechanisms to consume a wide spectrum of vegetal and animal resources (Cazzaniga & Estebenet, 1984; Aditya & Raut, 2001; Wood et al., 2006; Kwong et al., 2009; Saveanu & Martín, 2013), including the subaquatic egg masses of other freshwater snails (e.g., Cedeño-Leon & Thomas, 1983; Cazzaniga, 1990; Aditya & Raut, 2001, 2002; Kwong et al., 2009).

---

*Corresponding author: pmartin@criba.edu.ar

Intraspecific predation or cannibalism is a widespread habit that had received little attention up until a few decades ago (Fox, 1975; Polis, 1981). Cannibalism is mainly known in larger individuals that prey on smaller ones or on unprotected life-cycle phases (molting individuals, newborn or eggs). Egg cannibalism has been recorded in almost all groups of oviparous animals (Polis, 1981), probably because egg contents and embryos are highly nutritious, easy to capture and seldom toxic (Orians & Janzen, 1974). However, the eggs of *Pomacea canaliculata* and its congeners are very peculiar in that they present aposematic coloration, they contain different defensive compounds (Heras et al., 2008; Dreon et al., 2010, 2013; Frassa et al., 2010), and they almost lack natural predators (Snyder & Snyder, 1971; Yusa, 2001). All records of egg cannibalism in apple snails have come from the laboratory and are mostly anecdotal (Alonso & Ageitos de Castellanos, 1949; Cazzaniga & Estebenet, 1984; Tiecher et al., 2014), but only one study addressed experimentally the topic (Horn et al., 2008). Although their own eggs cannot be the staple trophic resource for any animal population, egg cannibalism may represent an alternative strategy at the individual level when other resources are scarce or absent. For instance, hatchlings of *Arianta arbustorum* (Linnaeus, 1758) (Helicidae) only cannibalize conspecific eggs, irrespective of their relatedness, and those that do so increase their chances of reaching maturity (Baur, 1994).

The aims of the present study are to describe and quantify the occurrence of egg cannibalism in *P. canaliculata* in a stream population in the southern Pampas. We also performed laboratory trials to study the consumption of eggs and egg remains and to determine the effect of this alternative food source on growth rates of juveniles and adults of *P. canaliculata*.

MATERIALS AND METHODS

Field Observations

During a study of the daily rhythms of pedal surface collecting in a Southern Pampas population of *Pomacea canaliculata* (El Huáscar stream; 36°55’50”S, 61°35’48”W), we performed systematic observations of surface and subsurface activities on ten floating quadrats (96 x 48 cm, at 10–30 cm from the shore, along 30 m of the stream) during 27 h (nine observation periods of one hour every three hours); in each observation period two operators recorded the activities in each quadrat (during 1 minute and 45 seconds every 20 minutes; Saveanu & Martín, 2013) three times. On 8 December 2011 at 8:30 AM (ART) we detected a 5 cm increase in water level relative to the previous observation period and the natural submergence of many egg masses deposited on stems of shore plants. During that and subsequent observation periods, we recorded the presence of apple snails on the submerged egg masses, making radular and jaws movements on them (Fig. 1).

El Huáscar stream (20–25 m wide and 0.2–0.3 m deep) presents a slow current, fairly transparent water and gently sloping banks that allowed us to make observations without disturbing the snails’ activities. Water temperature was 25.2 ± 4.4°C. *Eleocharis bonariensis* was the predominant plant and their stems were used by *P. canaliculata* as substratum for the egg masses. Other snail species present in the stream were *Chilina parchappii* (d’Orbigny, 1835) (Chilinidae), *Biomphalaria peregrina* (d’Orbigny, 1835) (Planorbidae) and *Physa acuta* (Draparnaud, 1805) (Physidae).

Experimental Field Observations

An experiment was performed in El Huáscar stream on 28 December 2011, to quantify the occurrence of egg cannibalism and to test for the effect of egg mass freshness. Egg masses from *P. canaliculata* were obtained in the surroundings of the study site by cutting the stems of *Eleocharis bonariensis* on which they were laid.

An egg mass was considered fresh when the egg shells and the mucus surrounding them were still soft and moist, indicating that it had been laid during the night before the observation (Turner, 1998; Pizani et al., 2005); an egg mass was considered old (one to seven days old) when the mucus was dry and the egg shell had become hardened but there was no visual evidence of consumption of the pink perivitelline fluid by the embryos (Heras et al., 1998). A fresh and an old egg mass were deployed on the stream bottom near each of the ten quadrats of the pedal surface collecting study.

Observations started one hour after the deployment of egg masses and followed the

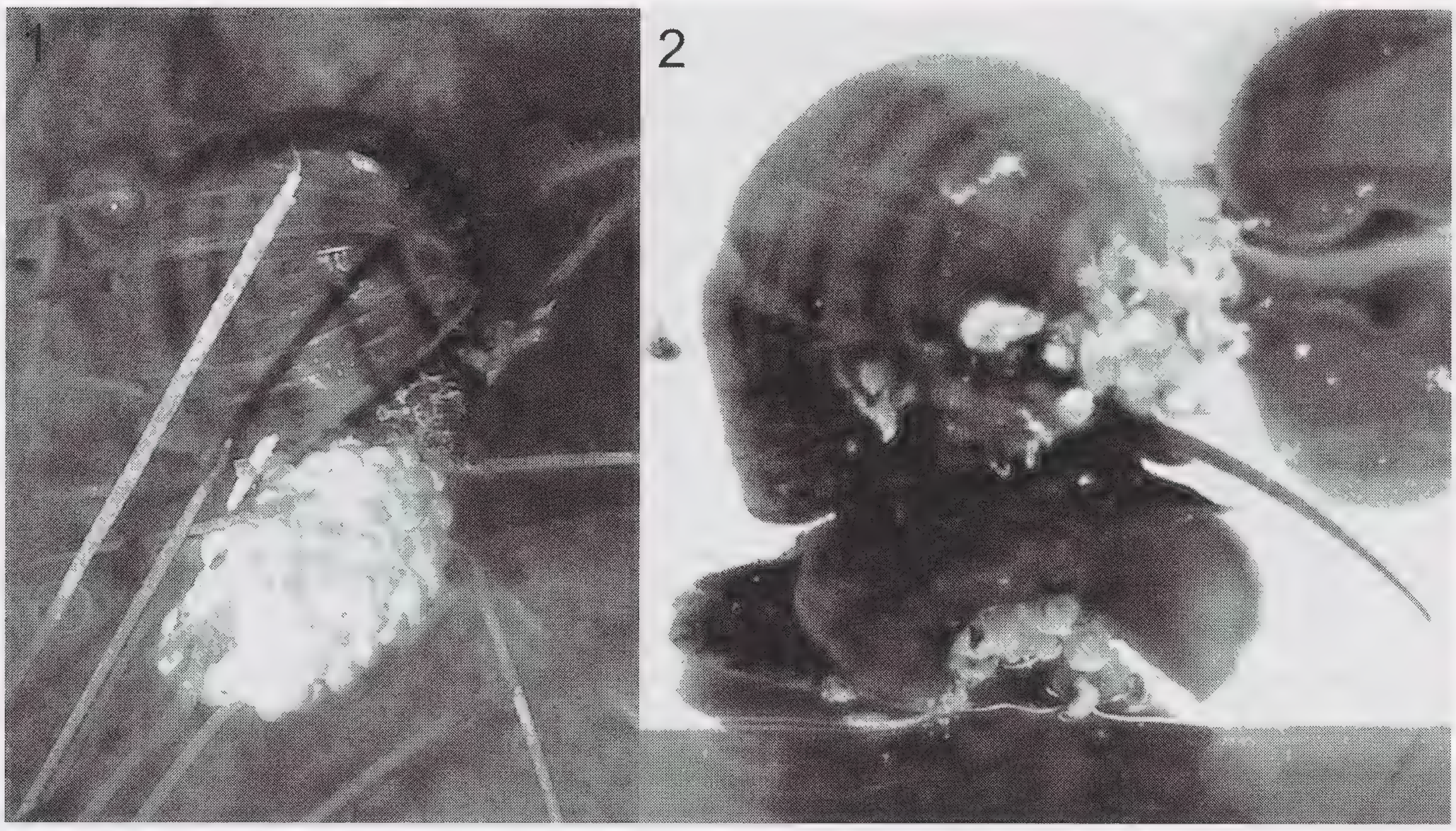

FIGS. 1, 2. *Pomacea canaliculata* feeding on its own eggs. FIG. 1: Adult of *Pomacea canaliculata* attacking an egg mass deposited on *Eleocharis bonariensis* in El Huáscar stream; FIG. 2: Adult of *Pomacea canaliculata* capturing *Pomacea canaliculata* eggs by pedal surface collecting.

same time schedule used for the pedal surface collecting study (Saveanu & Martín, 2013). During three observation periods, the percentage of egg masses of each type attacked was recorded and compared with Fisher's exact test. At the end of the 27 h of observation, the apple snails below each quadrat were handpicked. The intensity of egg mass attack during each observation period was estimated as the average number of snails observed in each egg mass divided by the number of snails picked up below that quadrat. Pairwise comparisons (t-test) were performed to compare the intensity of the attack between fresh and old egg masses at the 8:30 AM ART and 11:30 AM ART observation periods.

Feeding on Floating Eggs in the Laboratory

Snails, maintained without food for 24 h, were randomly chosen from a laboratory stock and placed in a glass aquarium at 25°C under natural illumination complemented with artificial light on March 2012. One or ten snails (shell length (SL) 10–50 mm, measured from the apex to the farthest point of the aperture) were put in 12 L and 24 L aquaria, respectively. Remains of hatched egg masses (non-developed pink eggs in clumps or isolated, egg shells and dry hatchlings; Fig. 2) were scattered gently onto the surface. Direct capture by mouth or by pedal surface collecting (Saveanu & Martín, 2013) and subsequent ingestion were recorded for two hours.

Egg Cannibalism and Growth Rates in the Laboratory

Juvenile and adult snails were fed under three different regimes: no food (0), only eggs (E) and only lettuce (L) to study the effects of egg cannibalism on the growth rates of *P. canaliculata*.

Adults and egg masses of *P. canaliculata* were collected in El Huáscar stream on 9 February 2012. Twenty egg masses (one to seven days old according to their colour, hardness and dryness) were frozen at -18°C in the laboratory. Adults and hatchlings (obtained from six egg masses) were maintained in $CaCO_3$-saturated tap water at 25 ± 2°C, under a photoperiod of 12:12 h, and fed fresh lettuce *ad libitum*. Aquaria were cleaned and the water changed once a week. Thirty hatchlings were reared individually in 200 mL aquaria for two months until they reached a shell length between 14 and 17 mm (juveniles); thirty adults (34–50 mm SL) were maintained in three collective 20 L aquaria for four months.

The experimental regimes were applied to the juveniles and adults for four weeks in individual 3 L glass aquaria under the same conditions as before, with the exception that no $CaCO_3$ was added to the water. Each aquarium had a grid (1.0 mm mesh size) on the bottom to avoid coprophagy. Egg masses were provided in small pieces (10 to 20 eggs). Known amounts of lettuce (drained hydrated weight) and eggs (fresh weight) were provided in excess of consumption for the experimental snails in L regime and in E regime, respectively.

Every Friday, the aquarium was cleaned and water changed and at the same time the shell length (SL, mm) and live weight (LW, g, weighed after the snail had crawled onto a dry plastic surface) were recorded.

Specific growth rates of SL and LW (SLR, $mm.mm^{-1}\cdot day^{-1}$ and LWR, $g\cdot g^{-1}\cdot day^{-1}$) were calculated on a weekly basis, as the difference between the final and initial values, divided by the initial value. At the end of each experiment, snails were sacrificed by immersion in water at 100°C and frozen at -18°C for later dissection. The body was extracted from the shell and was dried at 70°C for 48 h, to obtain the body dry weight (BDW, g). The shell and operculum were weighed after 48 h at 70°C to obtain shell dry weight (SDW, g).

At the end of each week, egg remains were collected with a sieve, drained and weighed, to obtain the weight of the consumed eggs; to consider hydration effects the weight of eggs was corrected by a factor obtained from the fresh and drained weight of similar amounts of eggs after a week of submergence in control aquaria without any snails (n = 8). Daily specific ingestion rates (SIR, $g\cdot g^{-1}\cdot day^{-1}$) were estimated as the weight of consumed eggs divided by LW of each week.

As the four week experiments were not performed simultaneously for juvenile and adult snails they were analyzed separately. Pairwise comparisons (t-test) between the initial and final SL and LW were performed between the three regimes (L, E and 0). The specific growth rates (SLR and LWR) and final measurements (SL, LW, BDW and SDW) were compared using ANOVAs; least significant difference (LSD) tests were performed to locate the differences between regimes. Some variables were transformed after the rejection of Levene's test of homoscedasticity ($p < 0.05$); when the no transformation was applicable or effective, Kruskal-Wallis tests were performed followed by t-test for unequal variances between pairs of means.

RESULTS

Field Observations

After the water level rise at 8:30 AM ART, we recorded the submergence of some egg masses. In one out of ten quadrats, we observed one apple snail attacking a submerged egg mass. In the following observation (11:30 AM ART), the same egg mass was observed being attacked by up to four apple snails simultaneously, and in another quadrat an egg mass was also attacked by up to two apple snails. At 2:30 PM ART observation, five and one apple snails, respectively, were observed attacking the same egg masses. The two attacked egg masses were fresh, laid early the same night. One of the egg masses was only partially submerged, and part of the snails' shell and cephalopodium frequently emerged during the attacks (Fig. 1).

Experimental Field Observations

During our observations apple snails of various sizes (25 to 45 mm) were observed attacking the egg masses, mainly fresh ones, within one hour of their submergence. During the first and second observation periods, fresh egg masses were attacked more frequently than the old ones (Fig. 3), although without any significant differences (Fisher's exact test, 8.30 h, $p = 0.370$ and 11.30 h, $p = 0.474$). The fresh egg masses showed signs of disintegration during the first and second observation periods. In the last observation period (2:30 PM ART), nine out of the ten fresh egg masses had almost completely disappeared (just a few scattered eggs remained in two of them), and very few snails were detected on the old egg masses (Fig. 4). No significant differences were found between the intensity of egg mass attack on fresh and old egg masses at 08.30 and 11.30 h AM ART (paired t-tests, $t_9 = 1.938$, $p = 0.085$ and $t_9 = 0.853$, $p = 0.416$, respectively). The number of snails simultaneously attacking an egg mass ranged from one to six; no attacks were observed by any other snail or fish species. During the 27 h of observation, between 0.13 and 2.60 snails per quadrat were recorded shredding or scraping vegetal material and between 0.00 and 1.13 snails per quadrat were observed performing pedal surface collecting.

3

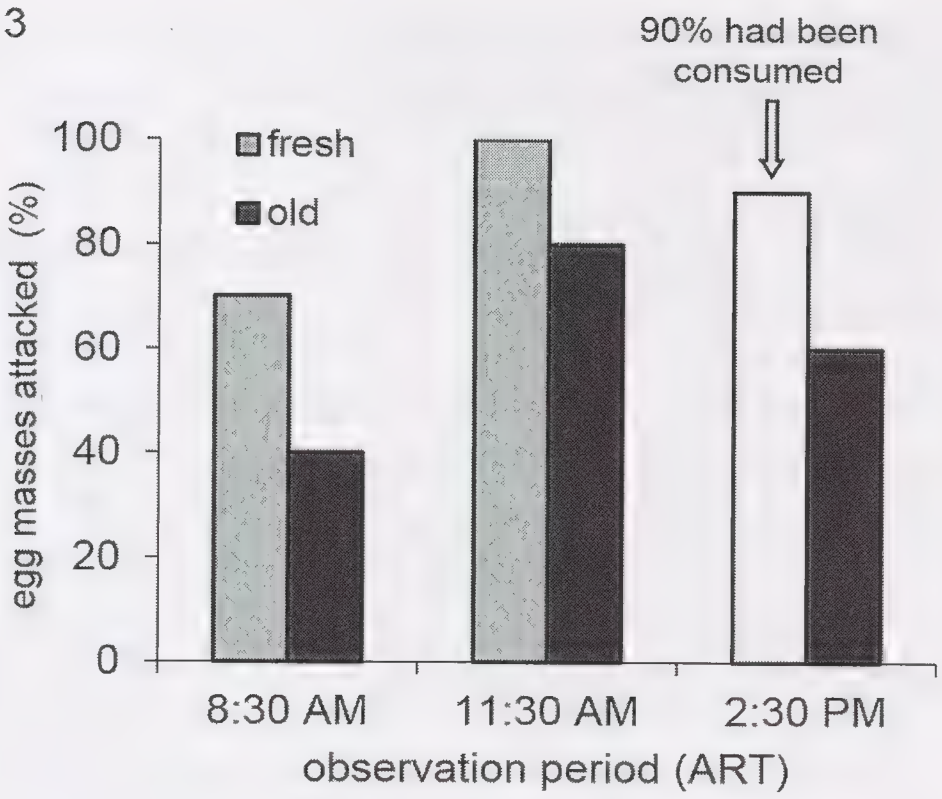

4

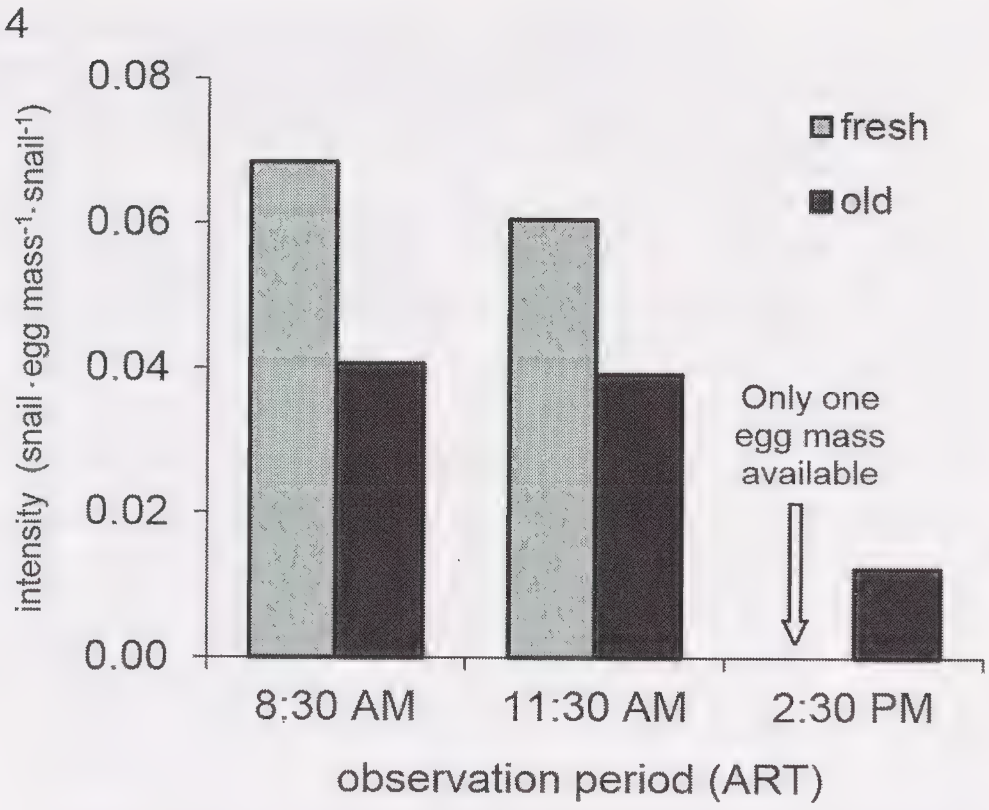

FIGS. 3, 4. Cannibalistic attacks on *Pomacea canaliculata* egg masses in El Huáscar stream in each observation period. FIG. 3: Percentage of egg masses attacked; FIG. 4: Means of attack intensity (number of snails attacking each egg mass divided by snail density in each quadrat).

Feeding on Floating Egg Mass Remains in the Laboratory

A few minutes after the snails were placed on the bottom of the aquarium, they became active and crawled up to the water surface, formed funnels with their forefeet and started to collect material from the surface (pedal surface collecting; Fig. 2). The captured material (unhatched eggs, egg shells and dry hatchlings) formed a mass with mucus within the funnels and then the snails put their mouths into the funnels and ingested it, using their jaws and radulae. The snails also ingested the egg mass remains without forming any pedal funnels, when they directly contacted the material on reaching the water surface. The snails were observed for a week after the trial and no harmful effects or deaths were recorded.

5

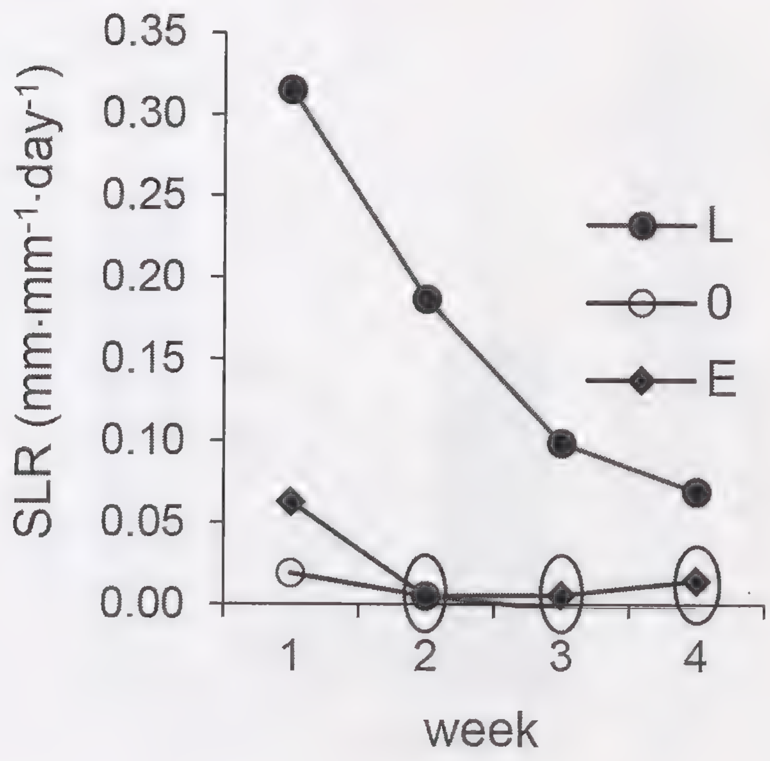

6

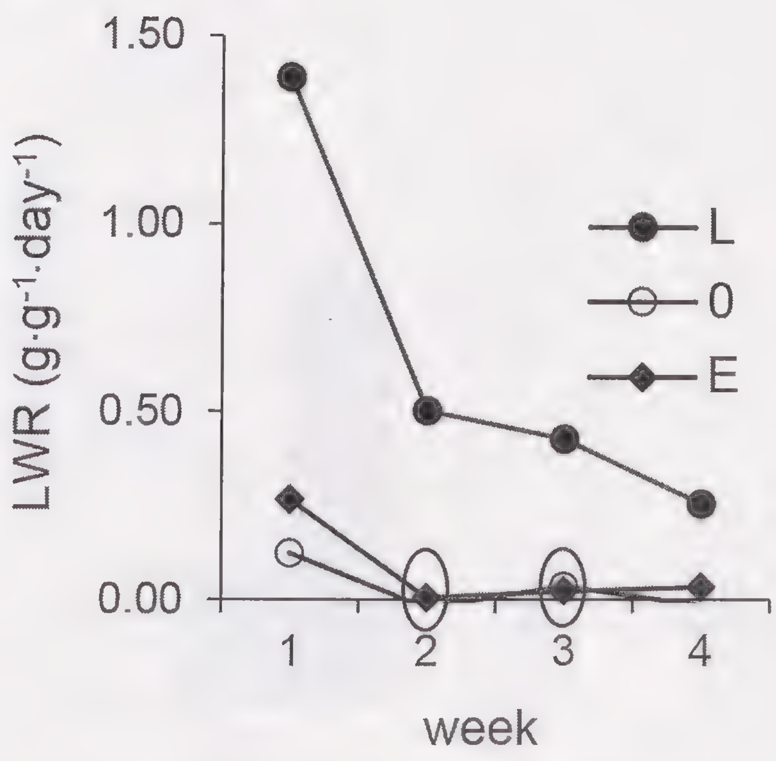

FIGS. 5, 6. Means of daily growth rates along the experiment for juveniles of *Pomacea canaliculata* under three different food regimes: L: lettuce; 0: no food; E: eggs. Means inside the ellipses were not significantly different (t-test for unequal variances, $p < 0.05$). FIG. 5: Shell length rate (SLR); FIG. 6: Live weight rate (LWR).

TABLE 1. Summary of Kruskal-Wallis results for shell length (SLR) and live weight (LWR) growth rates along the experiment for juveniles of *Pomacea canaliculata* under three different food regimes.

	SLR ($mm{\cdot}mm^{-1}{\cdot}day^{-1}$)		LWR ($g{\cdot}g^{-1}{\cdot}day^{-1}$)	
Week	X^2	p	X^2	p
1	$X^2_2 = 22.826$	$p < 0.001$	$X^2_2 = 25.306$	$p < 0.001$
2	$X^2_2 = 20.179$	$p < 0.001$	$X^2_2 = 20.020$	$p < 0.001$
3	$X^2_2 = 20.132$	$p < 0.001$	$X^2_2 = 19.676$	$p < 0.001$
4	$X^2_2 = 20.359$	$p < 0.001$	$X^2_2 = 20.921$	$p < 0.001$

Egg Cannibalism and Growth Rates in the Laboratory

None of the snails died during the experiment. No significant differences in initial LW and SL of the juvenile snails assigned to the different food regimes were found (one-way ANOVAs, $F_{2,27} = 1.285$, $p = 0.293$ and $F_{2,27} = 1.082$, $p = 0.353$, respectively). The juvenile snails under the three food regimes, including those starved, grew significantly in SL and LW after four weeks (paired t-tests, $p < 0.01$). Daily SLR and LWR

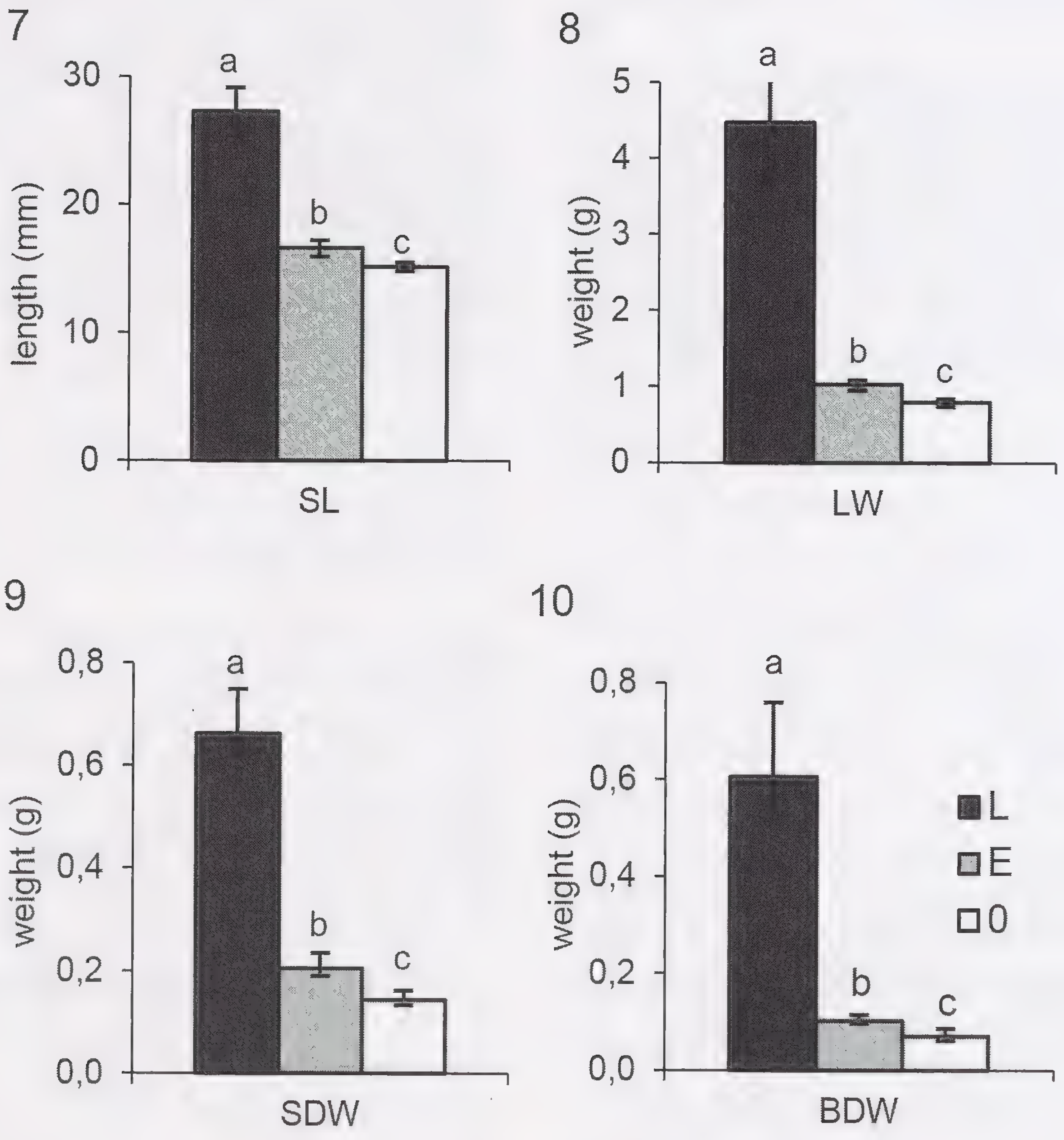

FIGS. 7–10. Back-transformed means (± 95% CI) of final sizes for juveniles of *Pomacea canaliculata* under three food regimes: lettuce (L), eggs (E), no food (0). Different letters indicate significant differences between means (LSD test, $p < 0.05$). FIG. 7: Shell length (SL); FIG. 8: Live weight (LW); FIG. 9: Shell dry weight (SDW); FIG. 10: Body dry weight (BDW). SL and LW were reciprocally-transformed and SDW and BDW were $\log_{10}$-transformed.

were significantly different under the three food regimes (Table 1); during the first week, juveniles feeding on eggs grew two and four times faster, in LW and SL, respectively, compared with unfed snails but less than those feeding on lettuce. In the following weeks, no differences were found between juveniles feeding on eggs and those starved, exception made of LWR in the last week (Figs. 5, 6). After four weeks the final SL and LW showed that the juveniles fed on eggs were significantly larger and heavier (9% and 29%, respectively) than the starved snails, although smaller than those fed on lettuce ($F_{2,27}$ = 308.782, $p < 0.001$ and $F_{2,27}$ = 333.617, $p < 0.001$, respectively; Figs. 7, 8). Both SDW and BDW showed the same pattern with the same significant differences ($F_{2,27}$ = 685.084, $p < 0.001$ and $F_{2,27}$ = 611.119, $p < 0.001$, respectively, Figs. 9, 10), although the relative differences with starved snails were greater (43% and 46%, respectively).

For adult snails there were marginal differences in initial LW and SL among the snails assigned to the different treatments (one-way ANOVA, $F_{2,27}$ = 3.319, p = 0.051 and $F_{2,27}$ = 3.161, p = 0.058, respectively); those assigned to the L regime were larger and heavier than those assigned to the E regime (unprotected LSD test, $p < 0.05$).

The adults fed with lettuce grew significantly after four weeks but only in LW (paired t-tests, p = 0.035); the adults under the other food regimes did not grow either in SL or in LW (paired t-tests, $p > 0.200$). However, the final SL and LW showed significant differences between different regimes ($F_{2,27}$ = 3.677, p = 0.039 and $F_{2,27}$ = 4.618, p = 0.019, respectively) with the same pattern observed in initial SL and LW values. No significant effect of the food regime was observed for SDW and BDW ($F_{2,27}$ = 0.795, p = 0.462 and $F_{2,27}$ = 2.961, p = 0.069, respectively).

The daily specific ingestion rates of eggs (SIR, $g \cdot g^{-1} \cdot d^{-1}$) were higher for juveniles than for adult snails (Figs. 11, 12). For juvenile snails, an increase in SIR was apparent from the first to the fourth week; the estimated SIR was not significantly different from zero for the first two weeks (probably due to some negative values obtained when the absolute amount of eggs ingested was very small). On the other hand, SIR was significantly higher than zero during the third and fourth weeks (t-tests, n = 10, $p < 0.009$ and $p < 0.007$, respectively). For adult snails, the pattern was not clear, with the estimated SIR being significantly different from zero only at the second and third weeks (t-tests, n = 10, $p < 0.030$ and $p < 0.007$, respectively).

11

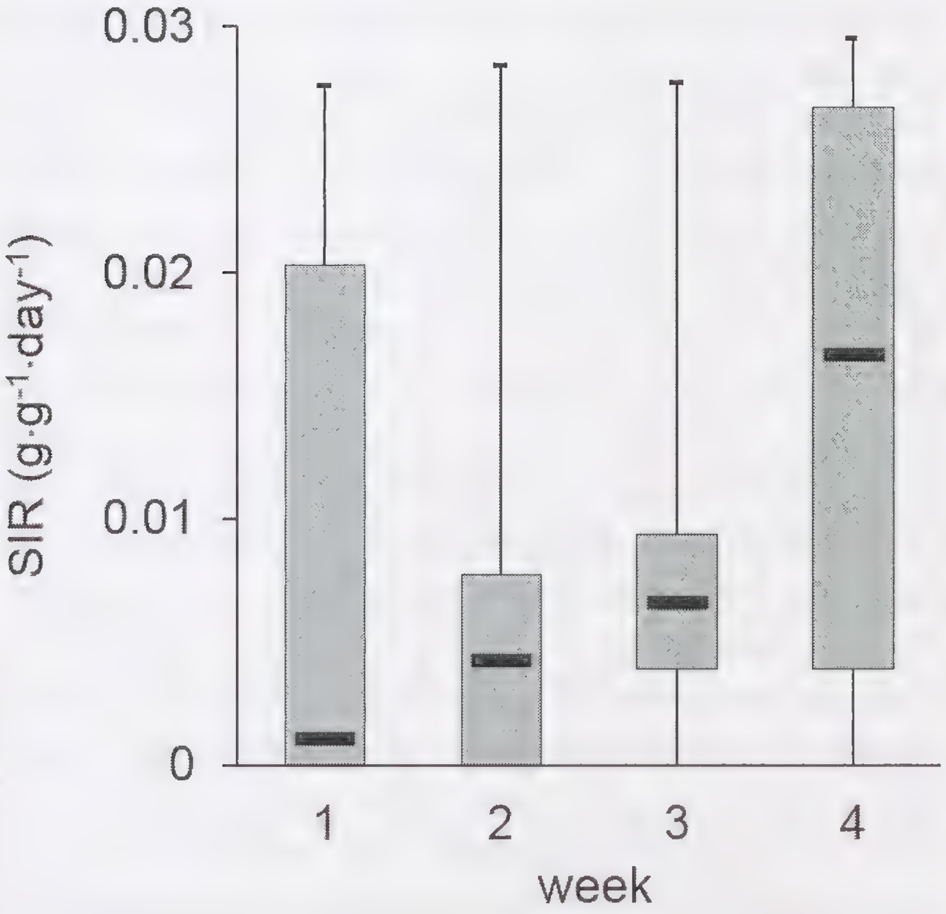

12

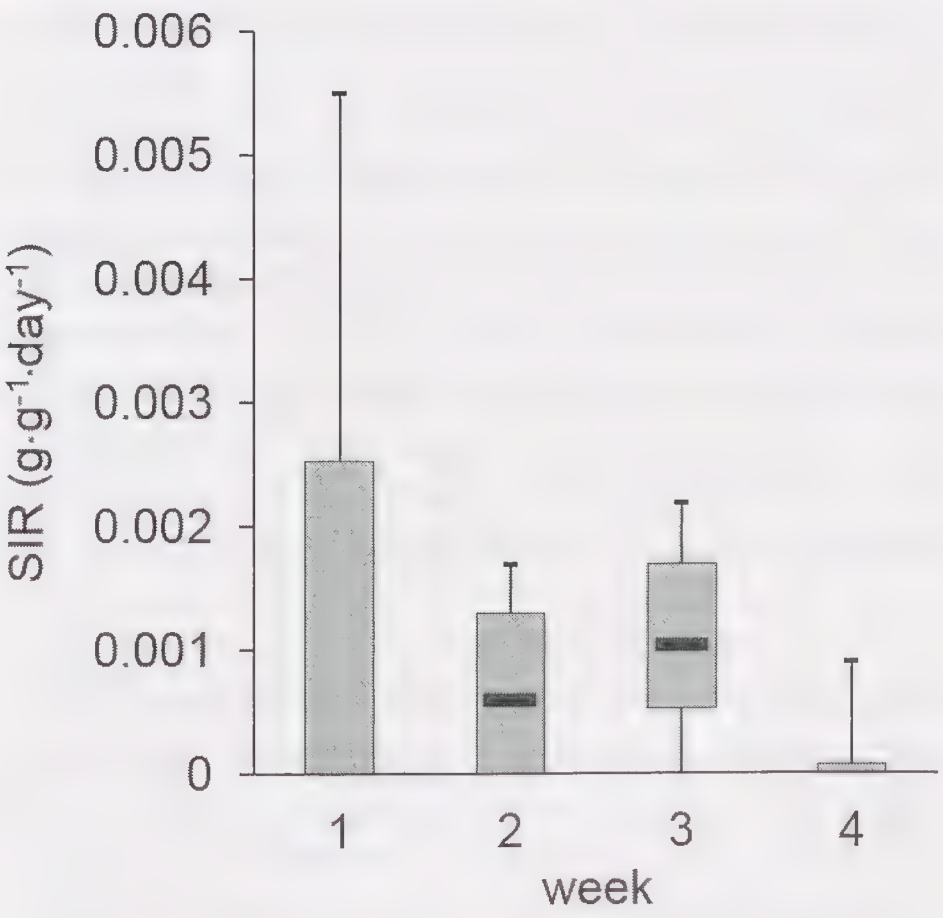

FIGS. 11, 12. Box-and-whiskers plot (black line: median; grey box: interquartile range; bar: extreme values) for daily specific ingestion rates of eggs (SIR, $g \cdot g^{-1} \cdot d^{-1}$) of *Pomacea canaliculata* along the experiment. FIG. 11: Juveniles; FIG. 12: Adults.

DISCUSSION

The observation of attacks of *Pomacea canaliculata* snails on conspecific egg masses naturally submerged in the field was recorded for the first time. Artificially submerged egg masses were also readily attacked and the fresh ones were mostly disintegrated in the course of a few hours by the feeding attempts of several snails. These attacks were recorded even when vegetal material was available and snails were detected feeding on it.

Predation of eggs of other freshwater snails is probably not uncommon behaviour in apple snails (e.g., Cedeño-Leon & Thomas, 1983; Cazzaniga & Estebenet, 1984; Cazzaniga, 1990) including *Pomacea* species (Aditya & Raut, 2001, 2002). In particular, *P. canaliculata* devoured the egg masses of five different species of freshwater snails in laboratory experiments (Kwong et al., 2009). In all these studies, the egg masses were gelatinous and subaquatic.

Egg cannibalism is apparently common in *Asolene pulchella* (Anton, 1838), an apple snail that lays gelatinous egg masses underwater (Tiecher et al., 2014). On the other hand, it seems to be rare in apple snails that lay aerial egg masses with calcareous eggshells. Egg cannibalism in aquaria was reported for *Pomacea maculata* (Perry, 1810) (Alonso & Castellanos, 1949) and *P. canaliculata*, as noted by Cazzaniga & Estebenet (1984) although it is not clear if it occurred above or under water. We have also observed egg masses partially devoured above water in small aquaria with only one female or a couple of *P. canaliculata* (pers. obs.). Females of *Pomacea* get out of the water to lay eggs 1.4 times a week on average (Albrecht et al., 1996) The above-water attack on egg masses seems to be infrequent, since the probability of an encounter with an egg mass depends on the female getting out of the water in the same place as previously used by herself or by another female.

In our experimental field observations, submerged egg masses were not attacked by any other snail species or fish (mostly *Jennynsia multidentata*) present in the stream. Neither did we observe any attacks from terrestrial animals on *P. canaliculata* egg masses above the waterline. The conspicuously coloured aerial egg masses of *Pomacea* spp. are seldom attacked by predators, which has been attributed to their unpalatability and aposematic colour (Snyder & Snyder, 1971; Dreon et al., 2010, 2013; Frassa et al., 2010). Fire ants and some terrestrial snails are some of the few animals that have been observed feeding on *Pomacea* eggs (Yusa, 2001; Ng & Tan, 2011). On the contrary, *P. canaliculata* attacked readily and persistently its own egg masses in our laboratory and field experiments, even when other food sources are present; Horn et al. (2008) also mentioned cannibalism of submerged egg masses of *P. maculata* in the presence of lettuce.

Turner (1998) found little evidence of underwater predation (including cannibalism) for experimentally submerged egg masses of *P. paludosa* in two Florida lakes. Our field evidence indicates that egg cannibalism is probably not as infrequent in natural populations of *P. canaliculata* in the southern Pampas. Cannibalism of egg masses depends critically on water level fluctuations wide enough to submerge them, events that occur frequently but quite unpredictably in lotic waterbodies in the area (Pizani et al., 2005). In addition to water fluctuations, heavy rains, winds and birds may tumble the egg masses or bend their substrates down to the water level. These situations are probably more common in watercourses like El Huáscar stream, where practically the only substratum available for egg laying is a very tiny sedge (*Eleocharis bonariensis*) with thin flexible stems no more than 15 cm tall.

The capture of floating remains of hatched egg masses by pedal surface collecting constitutes an alternative mechanism that may be more frequent than direct attacks on submersed egg masses and hence may predispose the snails to attack them whenever possible. Pedal surface collecting is apparently common in *P. canaliculata* though more intense during the night, which probably accounts for the lack of field reports of this behaviour (Saveanu & Martín, 2013). The need to ventilate the lung compels the snails to reach the water surface every 20 minutes at 25°C (Seuffert & Martín, 2009, 2010), which increases the probability of detecting the presence of floating food items.

Egg cannibalism only had a significant effect on the growth of juvenile snails although adult snails also fed on eggs. Juvenile snails with eggs as the only food item grew more than starved ones, but significantly less than those fed with lettuce *ad libitum*, indicating that eggs could serve as an alternative trophic resource although of poor nutritive quality. This is odd, as eggs and embryos are usually considered as highly nutritious and energetic food items (Orians & Janzen, 1974). Probably the explanation of this pattern lies in the anti-nutritive and neurotoxic properties of the perivitelline proteins present in the eggs of *P. canaliculata* (Dreon et al., 2010, 2013; Frassa et al., 2010). Even though the consequences on size and biomass remained through the duration of the experiment, the positive effect of egg cannibalism on growth rate relative to starved snails was mostly significant for the first week. The increase in the egg ingestion rate of juveniles during the experiment was probably due to the increase in the time that they remained without any alternative food but the increased ingestion was apparently balanced by lower assimilation. However, further work is needed to confirm this.

The specific ingestion rates of eggs were around eight times higher for juveniles than for adult *P. canaliculata* but this is probably due to an ontogenetic decrease in the specific feeding rate already described for shredding and scraping of plant material (Tamburi & Martín, 2009), and pedal surface collecting of floating particulate material (Saveanu & Martín, 2013). The specific ingestion rates of eggs resulted around 100 times lower than those obtained with lettuce for snails of comparable size (Tamburi & Martín, 2009) Defensive secondary compounds and high dry matter contents reduce the feeding rate of *P. canaliculata* on macrophytes (Qiu et al., 2009, 2011; Wong et al., 2010; Morrison & Hay, 2011a).

Continued submergence of the egg masses of *Pomacea* spp. detrimentally affects hatching and developmental rates, although they are able to withstand up to two weeks of submergence without a total failure (Turner, 1998; Pizani et al., 2005; Horn et al., 2008; Wang et al., 2012). However, egg cannibalism can change this situation dramatically. Horn et al. (2008) attributed a 99% reduction in hatchling survival to egg cannibalism observed for experimentally submerged egg masses of *P. maculata* in aquaria with one adult snail and presence of lettuce. In our field experiment, nine out of ten fresh egg masses disintegrated after seven hours under the simultaneous attack of several (up to six) snails. In the absence of cannibalistic snails in the laboratory, fresh egg masses of *P. canaliculata* lost their integrity more slowly and more infrequently (nine out of 21 disintegrated spontaneously after submergence periods of at least a day; Pizani et al., 2005). Even if the eggs are not eaten or destroyed by radular movements or chewing, the loose eggs sink to the bottom or are swept by currents and they would not become exposed to the air if the water level decreased, so they are completely non-viable (Pizani et al., 2005).

Turner et al. (2007) demonstrated that intraguild egg predation in freshwater snails with subaquatic egg masses may play an important role in the competitive outcome among them. As mentioned above, egg cannibalism was not common in the Florida apple snail, *P. paludosa*, as observed by Turner (1998). However, some wetlands in Florida have been invaded by *P. canaliculata* and *P. maculata* (Rawlings, 2007; Morrison & Hay, 2011b; EDDMapS, 2013), and so the possibility of interspecific egg predation among these apple snails exists. The evidence gathered indicates that such interactions would be strongly asymmetric for the native snail and detrimental to its hatching rate. The same effects would probably appear on the egg masses of *Pila* spp., which are laid very close to the waterline (Bahl, 1928; Cowie, 2002), since both *Pomacea* species have invaded their native wetlands in Southeast Asia.

Egg cannibalism or at least the ingestion of unhatched eggs and egg remains is probably more common in *P. canaliculata* than previously thought. The attack on egg masses depends mostly on their submergence, but the egg remains and unhatched eggs that naturally fall into the water are trophic items that are probably available during most of the reproductive season and for some time afterwards. Whenever *P. canaliculata* snails found egg masses or egg remains, they feed readily on them and, at least the juveniles, benefit in the short term when other trophic resources are absent. This benefit seems to decline with time, but its effects may be long lasting in habitats that are poor in trophic resources. Apple snails seem to be relatively immune to the defensive compounds that deter feeding by most animals on these complex eggs, and during periods of food shortage they may take advantage from energy previously captured by other members of the population.

Negative density-dependent effects have been reported in laboratory and field populations of *P. canaliculata* and may be responsible of regulation of population size and density (Cazzaniga & Estebenet, 1988; Tanaka et al., 1999; Yoshida et al., 2013). Competition trough food limitation has been seen as the main mechanism underlying these effects (Yoshida et al., 2013), although the very wide trophic spectrum and the different feeding mechanisms would diminish the competitive interactions.

On the other hand, egg cannibalism may also play a role in negative density dependence of *P. canaliculata*, as suggested for other snails (Baur, 1988). At high densities, many of the temporarily submersed egg masses of *P. canaliculata*, which would otherwise endure submersion, may be lost with negative consequences on recruitment (Horn et al., 2008). Even though in the long term cannibalism cannot be the trophic basis for any animal population, it nevertheless may have important consequences on population dynamics.

ACKNOWLEDGEMENTS

This study was funded with grants from CONICET (Consejo Nacional de Investigaciones Científicas y Técnicas, PIP 112 200901 00473) and UNS (Universidad Nacional del Sur, PGI 24B/185). L. S. is a doctoral fellow in CONICET. P. R. M. is a researcher in CONICET. We wish to thank two anonymous reviewers.

LITERATURE CITED

ADITYA, G. & S. K. RAUT, 2001, Food of the snail, *Pomacea bridgesi*, introduced in India. *Current Science*, 80: 919–921.

ADITYA, G. & S. K. RAUT, 2002, Destruction of *Indoplanorbis exustus* (Planorbidae) eggs by *Pomacea bridgesi* (Ampullariidae). *Molluscan Research*, 22: 87–90.

ALBRECHT, E. A., N. B. CARREÑO & A. CASTRO-VAZQUEZ, 1996, A quantitative study of copulation and spawning in the South American apple-snail *Pomacea canaliculata* Lamarck (Prosobranchia, Ampullariidae). *The Veliger*, 39: 142–147.

ALONSO, A. S. & Z. J. AGEITOS DE CASTELLANOS, 1949, Algunos datos sobre alimentación de las ampularias. *Notas del Museo de La Plata*, 14(*Zoología*, 115): 31–34, 4 láminas.

BAHL, K. N., 1928, On the reproductive processes and development of *Pila globosa* (Swainson). Part I, Copulation and oviposition. *Memoirs of the Indian Museum*, 9: 1–11.

BAUR, B., 1988, Population regulation in the land snail *Arianta arbustorum*: density effects on adult size, clutch size and incidence of egg cannibalism. *Oecologia*, 77(3): 390–394.

BAUR, B., 1994, Inter-population differences in propensity for egg cannibalism in hatchlings of the land snail *Arianta arbustorum*. *Animal Behaviour*, 48(4): 851–860.

CAZZANIGA, N. J., 1990, Predation of *Pomacea canaliculata* (Ampullariidae) on adult *Biomphalaria peregrina* (Planorbidae). *Annals of Tropical Medicine and Parasitology*, 84: 97–100.

CAZZANIGA, N. J. & A. L. ESTEBENET, 1984, Revisión y notas sobre los hábitos alimentarios de los Ampullariidae (Gastropoda). *Historia Natural*, 4: 213–224.

CAZZANIGA, N. J. & A. L. ESTEBENET, 1988, The effect of crowding on breeding *Pomacea canaliculata* (Gastropoda, Ampullariidae). *Comparative Physiology and Ecology*, 13: 89–96.

CEDEÑO-LEÓN, A. & J. D. THOMAS, 1983, The predatory behaviour of *Marisa cornuarietis* on eggs and neonates of *Biomphalaria glabrata*, the snail host of *Schistosoma mansoni*. *Malacologia*, 24: 289–297.

COWIE, R. H., 2002, Apple snails (Ampullariidae) as agricultural pests: their biology, impacts and management. Pp. 145–192, in: G. M. BAKER, ed., *Molluscs as crop pests,* CABI Publishing, Wallingford, New Zealand, 576 pp.

DREON, M. S., S. ITUARTE & H. HERAS, 2010, The role of the proteinase inhibitor ovorubin in Apple Snail eggs resembles plant embryo defense against predation. *PLoS ONE*, 5 (12): e15059, doi: 10.1371/journal.pone.0015059.

DREON, M. S., M. V. FRASSA, M. CEOLÍN, S. ITUARTE, J.-W. QIU, J. SUN, P.E. FERNÁNDEZ & H. HERAS, 2013, Novel animal defenses against predation: a snail egg neurotoxin combining lectin and pore-forming chains that resembles plant defense and bacteria attack toxins. *PLoS ONE*, 8 (5): e63782, doi: 10.1371/journal.pone.0063782.

EDDMapS, 2013, Early Detection & Distribution Mapping System. The University of Georgia - Center for Invasive Species and Ecosystem Health. Available online at http://www.eddmaps.org/distribution/point.cfm?id=2409900; last accessed June 26, 2013.

FOX, L. R., 1975, Cannibalism in natural populations. *Annual Review of Ecology and Systematics*, 6: 87–106.

FRASSA, M. V., M. CEOLÍN, M. S. DREON & H. HERAS, 2010, Structure and stability of the neurotoxin PV2 from the eggs of the apple snail *Pomacea canaliculata*. *Biochimica et Biophysica Acta*, 1804(7): 1492–1499.

HAYES, K. A., R. H. COWIE, S. C. THIENGO & E. E. STRONG, 2012, Comparing apples with apples: clarifying the identities of two highly invasive Neotropical Ampullariidae (Caenogastropoda). *Zoological Journal of the Linnean Society*, 166: 723–753.

HERAS, H., C. F. GARIN & R. J. POLLERO, 1998, Biochemical composition and energy sources during embryo development and in early juveniles of the snail *Pomacea canaliculata* (Mollusca: Gastropoda). *Journal of Experimental Zoology*, 280(6): 375–383.

HERAS, H., M. V. FRASSA, P. E. FERNÁNDEZ, C. M. GALOSI, E. J. GIMENO & M. S. DREON, 2008, First egg protein with a neurotoxic effect on mice. *Toxicon*, 52(3): 481–488.

HORGAN, F. G., A. M. STUART & E. P. KUDAVIDANAGE, 2014, Impact of invasive apple snails on the functioning and services of natural and managed wetlands. *Acta Oecologica*, 54: 90–100.

HORN, K. C., S. D. JOHNSON, K. M. BOLES, A. M. EVAN SIEMANN & C. A. GABLER, 2008, Factors affecting hatching success of golden apple snail eggs: effects of water immersion and cannibalism. *Wetlands*, 28(2): 544–549.

KWONG, K. L., R. K. Y. CHAN & J. W. QIU, 2009, The potential of the invasive snail *Pomacea canaliculata* as a predator of various life-stages of five species of freshwater snails. *Malacologia*, 51: 343-356.

LOWE, S., M. BROWNE, S. BOUDJELAS & M. DE POORTER, 2000, *100 of the World's worst invasive alien species*. The Invasive Species Specialist Group, IUCN, Auckland.

MARTÍN, P. R., A. L. ESTEBENET & N. J. CAZZANIGA, 2001, Factors affecting the distribution of *Pomacea canaliculata* (Gastropoda: Ampullariidae) along its southernmost natural limit. *Malacologia*, 43: 13–23.

MORRISON, W. E. & M. E. HAY, 2011a, Induced chemical defenses in a freshwater macrophyte suppress herbivore fitness and the growth of associated microbes. *Oecologia*, 165: 427–436.

MORRISON, W. E. & M. E. HAY, 2011b, Feeding and growth of native, invasive and non-invasive alien apple snails (Ampullariidae) in the United States: Invasives eat more and grow more. *Biological Invasions*, 13(4): 945–955.

NG, T. H. & S. K. TAN, 2011, Observations of land snails feeding on the eggs of *Pomacea canaliculata* (Lamarck, 1822) (Mollusca: Gastropoda). *Nature in Singapore*, 4: 79–83.

ORIANS, G. H. & D. H. JANZEN, 1974, Why are embryos so tasty? *The American Naturalist*, 108(963): 581–592.

PIZANI, N. V., A. L. ESTEBENET & P. R. MARTÍN, 2005, Effects of submersion and aerial exposure on clutches and hatchlings of *Pomacea canaliculata* (Gastropoda: Ampullariidae). *American Malacological Bulletin*, 20(1–2): 55–63.

POLIS, G. A., 1981, The evolution and dynamics of intraspecific predation. *Annual Review of Ecology, Evolution and Systematics*, 12: 225–251.

QIU, J. W. & K. L. KWONG, 2009, Effects of macrophytes on feeding and life-history traits of the invasive apple snail *Pomacea canaliculata*. *Freshwater Biology*, 54: 1720–1730.

QIU, J.-W., M. T. CHAN, K. L. KWONG & J. SUN, 2011, Consumption, survival and growth in the invasive freshwater snail *Pomacea canaliculata*: Does food freshness matter? *Journal of Molluscan Studies*, 77(2): 189–195.

RAWLINGS, T. A., K. A. HAYES, R. H. COWIE & T. M. COLLINS, 2007, The identity, distribution, and impacts of non-native apple snails in the continental United States. *BMC Evolutionary Biology*, 7: 97–111.

SAVEANU, L. & P. R. MARTÍN, 2013, Pedal surface collecting as an alternative feeding mechanism of the invasive apple snail *Pomacea canaliculata* (Caenogastropoda: Ampullariidae). *Journal of Molluscan Studies*, 79(1): 11–18.

SEUFFERT, M. E. & P. R. MARTÍN, 2009, Influence of temperature, size and sex on aerial respiration of *Pomacea canaliculata* (Gastropoda: Ampullariidae) from Southern Pampas, Argentina. *Malacologia*, 51(1): 191–200.

SEUFFERT, M. E. & P. R. MARTÍN, 2010, Dependence on aerial respiration and its influence on microdistribution in the invasive freshwater snail *Pomacea canaliculata* (Caenogastropoda, Ampullariidae). *Biological Invasions*, 12: 1695–1708.

SNYDER, N. F. R. & H. A. SNYDER, 1971, Defenses of the Florida apple snail *Pomacea paludosa*. *Behaviour*, 40(3–4): 175–215.

TAMBURI, N. E. & P. R. MARTÍN, 2009, Feeding rates and food conversion efficiencies of the apple snail *Pomacea canaliculata* (Caenogastropoda: Ampullariidae). *Malacologia*, 51: 221–232.

TANAKA, K., T. WATANABE, H. HIGUCHI, K. MIYAMOTO, Y. YUSA, T. KIYONAGA, H. KIYOTA, Y. SUZUKI & T. WADA, 1999, Density-dependent growth and reproduction of the apple snail, *Pomacea canaliculata*: a density manipulation experiment in a paddy field. *Researches on Population Ecology*, 41(3): 253–262.

TIECHER, M. J., S. BURELA & P. R. MARTÍN, 2014, Mating behavior, egg laying, and embryonic development in the South American apple snail *Asolene pulchella* (Ampullariidae, Caenogastropoda). *Invertebrate Reproduction & Development*, 58(1): 13–22.

TURNER, R. L., 1998, Effects of submergence on embryonic survival and developmental rate of the Florida applesnail, *Pomacea paludosa*: implications for egg predation and marsh management. *Florida Scientist*, 61:118–129.

TURNER, A. M., R. R. TURNER & S. R. RAY, 2007, Competition and intraguild egg predation among freshwater snails: re-examining the mechanism of interspecific interactions. *Oikos*, 116: 1895–1903.

WANG, Z., J. TAN, L. TAN, J. LIU & L. ZHONG, 2012, Control the egg hatchling process of *Pomacea canaliculata* (Lamarck) by water spraying and submersion. *Acta Ecologica Sinica*, 32: 184–188.

WONG, P. K., Y. LIANG, N. Y. LIU & J.-W. QIU, 2010, Palatability of macrophytes to the invasive freshwater snail *Pomacea canaliculata*: differential effects of multiple plant traits. *Freshwater Biology*, 55: 2023–2031.

WOOD, T. S., P. ANURAKPONGSATORN, R. CHAICHANA, J. MAHUJCHARIYAWONG & T. SATAPANAJARU, 2006, Heavy predation on freshwater bryozoans by the golden apple snail, *Pomacea canaliculata* Lamarck, 1822 (Ampullariidae). *The Natural History Journal of Chulalongkorn University*, 6(1): 31–36.

YOSHIDA, K., K. HOSHIKAWA, T. WADA & Y. YUSA, 2013, Patterns of density dependence in growth, reproduction and survival in the invasive freshwater snail *Pomacea canaliculata* in Japanese rice fields. *Freshwater Biology*, 58: 2065–2073.

YUSA, Y., 2001, Predation on eggs of the apple snail *Pomacea canaliculata* (Gastropoda: Ampullariidae) by the fire ant *Solenopsis geminata*. *Journal of Molluscan Studies*, 67: 275–279.

Revised ms. accepted January 2, 2014

MALACOLOGIA, 2014, 57(2): 353–364

GROWTH AND LONGEVITY OF THE „LIVING FOSSIL“ *CONGERIA KUSCERI* (BIVALVIA: DREISSENIDAE) FROM THE SUBTERRANEAN DINARIC KARST OF CROATIA

Sanja Puljas[1*], Melita Peharda[2], Brian Morton[3],
Nives Štambuk Giljanović[4] & Ivana Jurić[2]

ABSTRACT

The present study analyzed growth and longevity of the endemic cave dwelling bivalve *Congeria kusceri* obtained from the pit Jama u Predolcu, Croatia. A water temperature of 13–14°C constituted the lower limit for shell growth of *C. kusceri*. Obtained data also indicated that enhanced calcium uptake by *C. kusceri* during its summer growth and reproductive phases coincided with a decrease in alkalinity of the pit water. An analysis of shell growth rings in *C. kusceri* has identified an impressive longevity of 53 years. Calculations of growth rate suggested maximum theoretical shell lengths (L_∞) of 16.7 mm for males and 18.7 mm for females and a growth constant of 0.04 year^{-1} for both sexes. *Congeria kusceri* can, however, grow to a shell length of > 24 mm, suggesting that longevity of this species could be greater than that identified in this study. The obtained results add to our understanding of how colonisation and continued and successful occupation of a subterranean freshwater habitat has been achieved.

Key words: Cave-dwelling bivalve, age, longevity, life-history trait.

INTRODUCTION

The amount of energy allocated to growth is a fundamental feature of an organism's life history evolution and diversification (Haag & Rypel, 2010). Bivalves are one of the most diverse group of animals and offer a rich variety of lifestyles, adaptations to specific environmental conditions and corresponding aging strategies (Abele et al., 2009). According to Philipp & Abele (2010), bivalves have vastly differing maximum life spans ranging from 1 to hundreds of years. The wide variations in age and growth of bivalves show that they employ a diverse array of life history strategies requiring different conservation and management approaches (Haag & Rypel, 2010).

Congeria kusceri Bole, 1962, is of especial conservation importance since it is representative of the only known genus of subterranean, troglobiotc, bivalves and occurs only in the underground lakes, rivers and pits of the Dinaric karst (Morton et al., 1998). *Congeria kusceri* is an endemic Tertiary relic, with most other congeners, save for two other newly described species *Congeria jalzici*. Morton & Bilandžija, 2013, and *Congeria mulaomerovici* Morton & Bilandžija, 2013, identified by Bilandžija et al. (2013), having become extinct by the end of the Miocene (Morton et al., 1998). Accordingly, *C. kusceri* is regarded as a "living fossil". *Congeria kusceri* possesses a unique life history trait including a reproductive strategy characterized by early larval brooding in the ctenidia and secondary juvenile brooding in mantle pouches (Morton & Puljas, 2013). It was suggested by Morton et al. (1998) that such a novel life history trait is related specifically to decadal length longevity. All the evidence to date, therefore, points to the possession by *C. kusceri* of an unique suite of characteristics that not only adapt it to life in the subterranean Dinaric karst, but which are wholly different from the thin-shelled, short lived (< 4 years), opportunistic, non-brooding, planktotrophically dispersed, representatives of related dreissenid genera, that is, *Dreissena* van Beneden, 1835, and *Mytilopsis* Conrad, 1857 (Morton, 1969, 1989).

---

[1] Department of Biology, Faculty of Science, University of Split, Teslina 12/III, 21000 Split, Croatia
[2] Institute of Oceanography and Fisheries, Šetalište Ivana Meštrovića 63, 21000 Split, Croatia
[3] School of Biological Sciences, The Univerity of Hong Kong, Hong Kong SAR, PR China
[4] Institute for Public Health, Split, University of Split Medical School, Vukovarska 46, 21000 Split, Croatia
*Corresponding author: spuljas@pmfst.hr

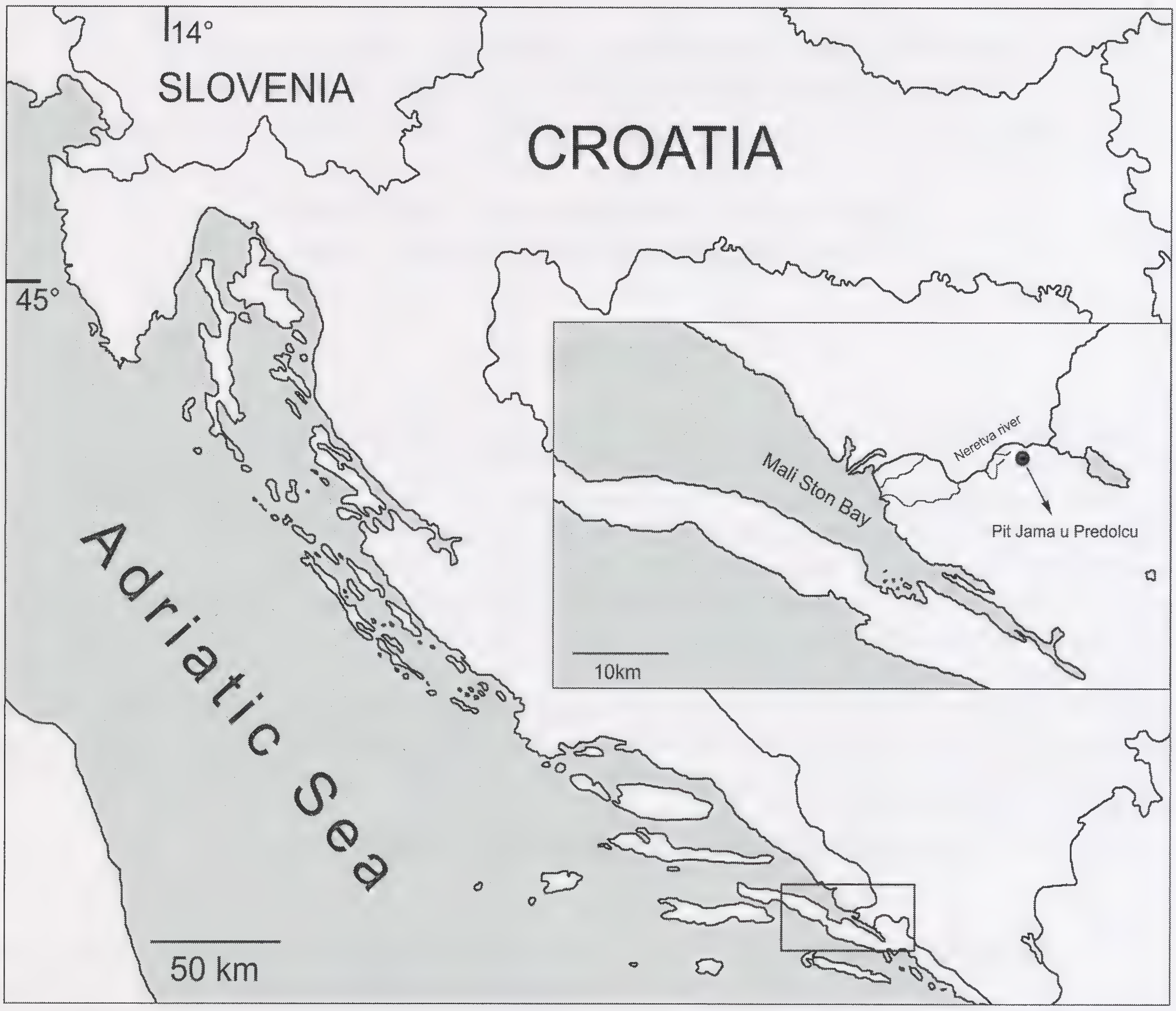

FIG. 1. Map of Croatia showing the location of the study site.

In contrast to the large volume of literature engendered as a result of the opportunistic and invasive characters of *Dreissena* and *Mytilopsis*, this study identifies all of the significant, but still meagre, research that has been undertaken on *Congeria*. In particular, because of their large population sizes, all four of the above species of *Dreissena* and *Mytilopsis* have been studied extensively to reveal growth phases and longevities – indicating opportunistic and short life history traits for them all. Conversely, *C. kusceri* occurs as scattered individuals and clusters in remote subterranean habitats. As noted above, Morton et al. (1998) undertook a study of shell microstructure and estimated the age attained by *C. kusceri*. That study was, however, of necessity, limited by the availability of but a few specimens. In 2009, the Croatian Ministry of Environment and Nature Protection, Zagreb, gave permission for the authors to collect, monthly, a larger number of individuals of *C. kusceri* from a readily accessible pit near Metković, Croatia. One of the aims of that study was to examine the reproductive strategy of *C. kusceri* (Morton & Puljas, 2013). A second component of the study, which is objective of this research and paper, was to obtain: (i), a better picture of the growth phases of *C. kusceri* in the pit and (ii), obtain an estimate, through etched and acetate peel replicas of sections through the shells, of the longevity of this remarkable species.

METHODS

Samples of the stygobiotic bivalve *C. kusceri* were collected monthly from the pit Jama u Predolcu (Fig. 1), from January to December 2009, to study the reproductive and life history strategies of this protected species (Puljas, 2012; Morton & Puljas, 2013). In addition, measurements of abiotic parameters including pH, water temperature, dissolved oxygen,

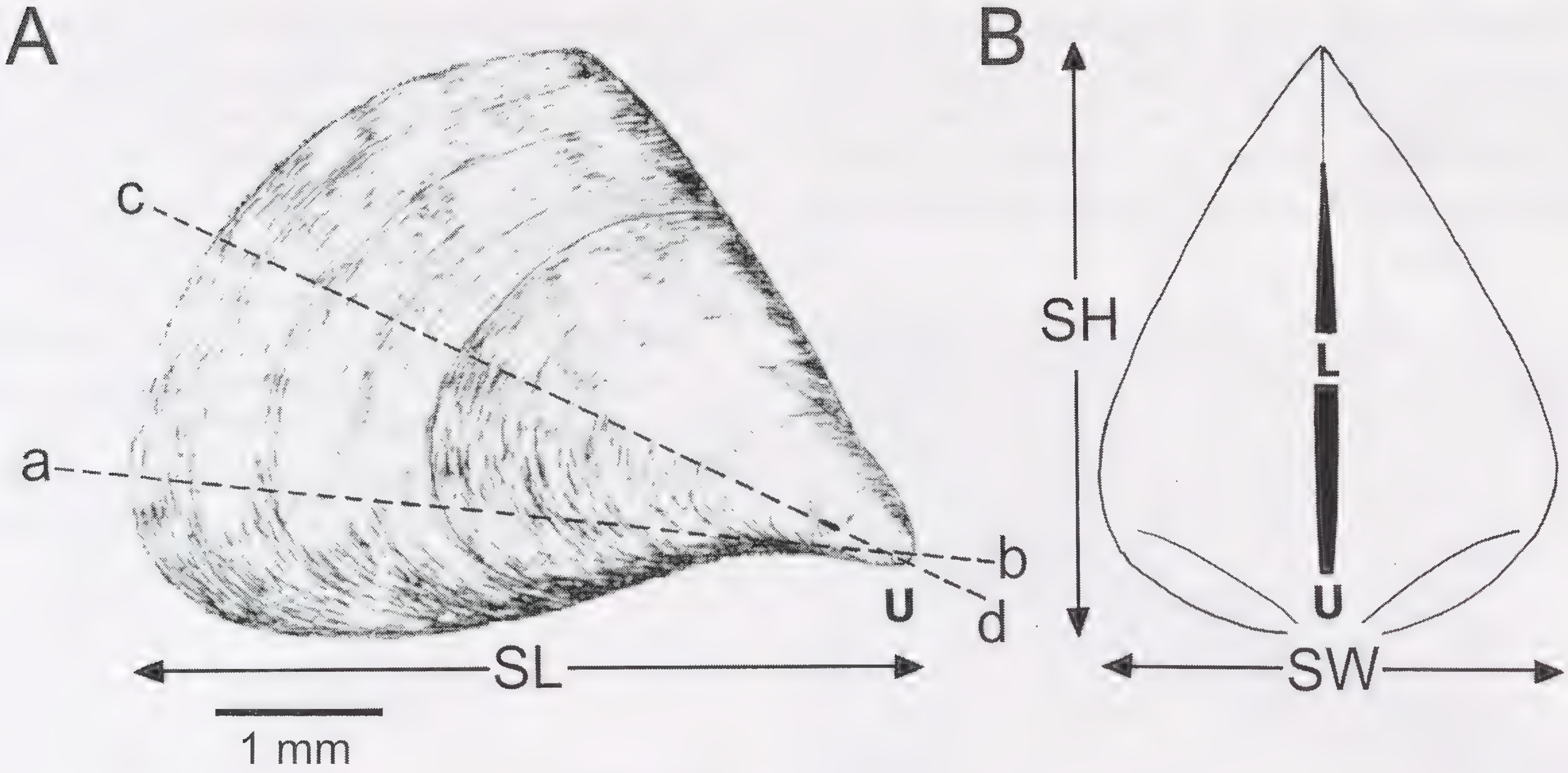

FIG. 2. *Congeria kusceri.* The shell of an individual as seen from (A): Right side showing the directions of the sections made for acetate peel replicas (a-b; c-d) and shell length (SL); (B): The same individual seen from the anterior aspect showing shell height (SH) and shell width (SW). (U = umbones; L = ligament).

dissolved carbon dioxide, nitrate, phosphate, chloride, sulphate, degree of hardness and alkalinity (all following the procedures identified in American Public Health Association [APHA],1995) were made on each sampling occasion. This dataset, described in Puljas (2012: 256, table 2) was subjected to t-tests in order to compare the means of nine hydrological parameters obtained for two periods: (1), the six non-growing and non-brooding (November–April) and (2), six growing and brooding (May–October) phases. pH was not analyzed because it did not vary throughout the year, presumably because of karst buffering. Prior to analysis, the data were tested for homogeneity of variance using Levene's test.

The shells of the collected *C. kusceri* individuals, subsequent to the removal of the internal tissues for the above reproductive study, were cleaned of epibionts and left to air dry. Information on shell morphometrics, including shell length (from the umbones to the posterior shell margin, Fig. 2A: SL and a–b), shell height (dorso-ventral axis, Fig. 2B: SH) and shell width (left to right across the valves, Fig. 2B: SW) were obtained for each individual to the nearest 0.1 mm using Vernier callipers.

The archived left shell valves from 40 smaller individuals (2–4 shells month^{-1}) of *C. kusceri*, ranging in shell length from 6.0–11.0 mm, were used for marginal growth increment analysis (MGI). Dried shell valves were embedded in epofix resin (Struers), sectioned from the umbo to the posterior shell margin (Fig. 2A: a–b), ground, polished, washed in detergent, air-dried and etched in 0.01 M HCl for 20 minutes. After washing in water and air-drying, acetate peel replicas were prepared (Richardson, 2001). Replicas mounted on glass slides were observed under an Axio Zeiss Imager M1 microscope, and photographed with an AxioCamera (MRc5). The distance between the last clearly visible growth line (Figs. 3A, 3B, arrow) and the shell margin was measured using the Axio-Vision Rel 4.8 program.

Acetate peel replicas of a further 50 individuals of *C. kusceri* collected during 2009, with shell lengths ranging from 7.5–17.0 mm, were prepared following the same procedure. Analyzed individuals were selected on the basis of shell length and sex, obtained in the earlier reproductive studies (Puljas, 2012; Morton & Puljas, 2013), to determine differences in growth rates (if any) with respect to sex. Two experienced readers counted independently the numbers of growth lines in the umbonal region of each peel (Fig. 3C). Prior to this analysis, the ages of ten randomly selected shells were estimated from the growth rings in the umbonal region and those in the prismatic shell layer. The obtained numbers were identical, indicating that age can be estimated from both areas.

Length-at-age data obtained for the *C. kusceri* shells were fitted to the von Bertalanffy growth function $L_t = L_\infty(1–e^{-k\ (t-to)})$, where L_t is the shell length at time t, L_∞ is the asymptotic maximum length, k is a growth constant and t_o is the length at time zero (von Bertalanffy, 1938). The FiSAT II software package version 1.2.2 was used for data analysis. A growth performance index ($\varnothing' = \log k + 2\log L_\infty$) was applied to the obtained dataset for comparison of growth parameters with those obtained in other studies (Sparre & Venema, 1998).

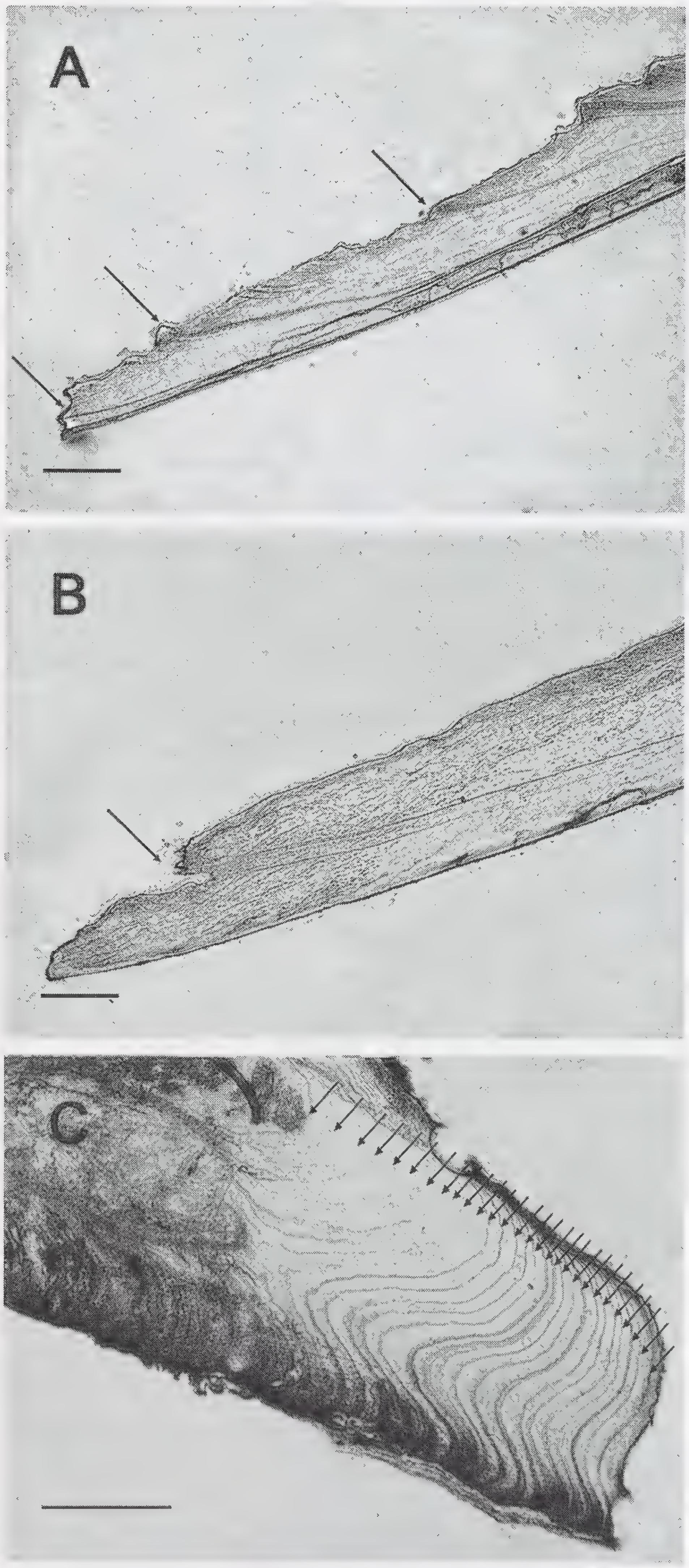

FIG. 3. *Congeria kusceri.* (A–B): Photomicrographs of acetate peel replicas of sections through shell margin used for the study of marginal increment analysis; (C): Photomicrograph of acetate peel replicas of sections through the umbonal region. Positions of growth lines are indicated by arrows. Scale bar = 100 µm.

ANCOVA was used for testing differences in shell length with respect to sex to ascertain any sexual dimorphism, with shell width as a covariate, and for testing differences in the age structure of individuals with respect to sex and with shell length as a covariate.

RESULTS

Hydrology

Ranges obtained for the nine hydrological parameters were as follows: pH (7.0), water temperature (12.5–17.50°C), dissolved oxygen (DO = 1.30–11.65 mg L^{-1}), dissolved carbon dioxide (DCO_2 = 0.5–4.2 mg L^{-1}), nitrate (NO_3 = 0.22–0.65 mg L^{-1}), phosphate ($PO^{3-}{}_4$ = 0.02–0.10 mg L^{-1}), chloride (Cl = 16–110 mg L^{-1}), sulphate (SO_4 = 10–56 mg L^{-1}), degree of hardness (dH = 11.4–16.2) and alkalinity (156–267 mg $CaCO_3$ L^{-1}). Of the nine hydrological parameters tested, however, only differences in temperature ($t = 4.929$, $p < 0.001$) and alkalinity ($t = 3.702$, $p = 0.004$) of the six non-growth and non-brooding and six growth and brooding months were highly significant.

The analyzed dataset thus suggests: (i), there is a threshold water temperature of ~13–14°C, from May to October (in 2009), above which both growth and reproduction by *C. kusceri* take place, and (ii), during the summer period of growth and reproduction, alkalinity values within the pit water were reduced significantly, from 208–267 mg $CaCO_3$ L^{-1} in the latter period to 156–176 mg $CaCO_3$ L^{-1} in the former.

Comparison of the growth line formation results with environmental water quality parameters showed that water temperature rose from 13°C to 17.5°C in May and decreased from 17°C to 14°C in October. As described above, the difference in temperature means for these two 6-month periods were statistically significant. The decrease in alkalinity from 219 to 173 mg $CaCO_3$ L^{-1} in May and increase from 156 to 241 mg $CaCO_3$ L^{-1} in October could also be correlated with the duration of the growth season (Fig. 4) and were again statistically significant.

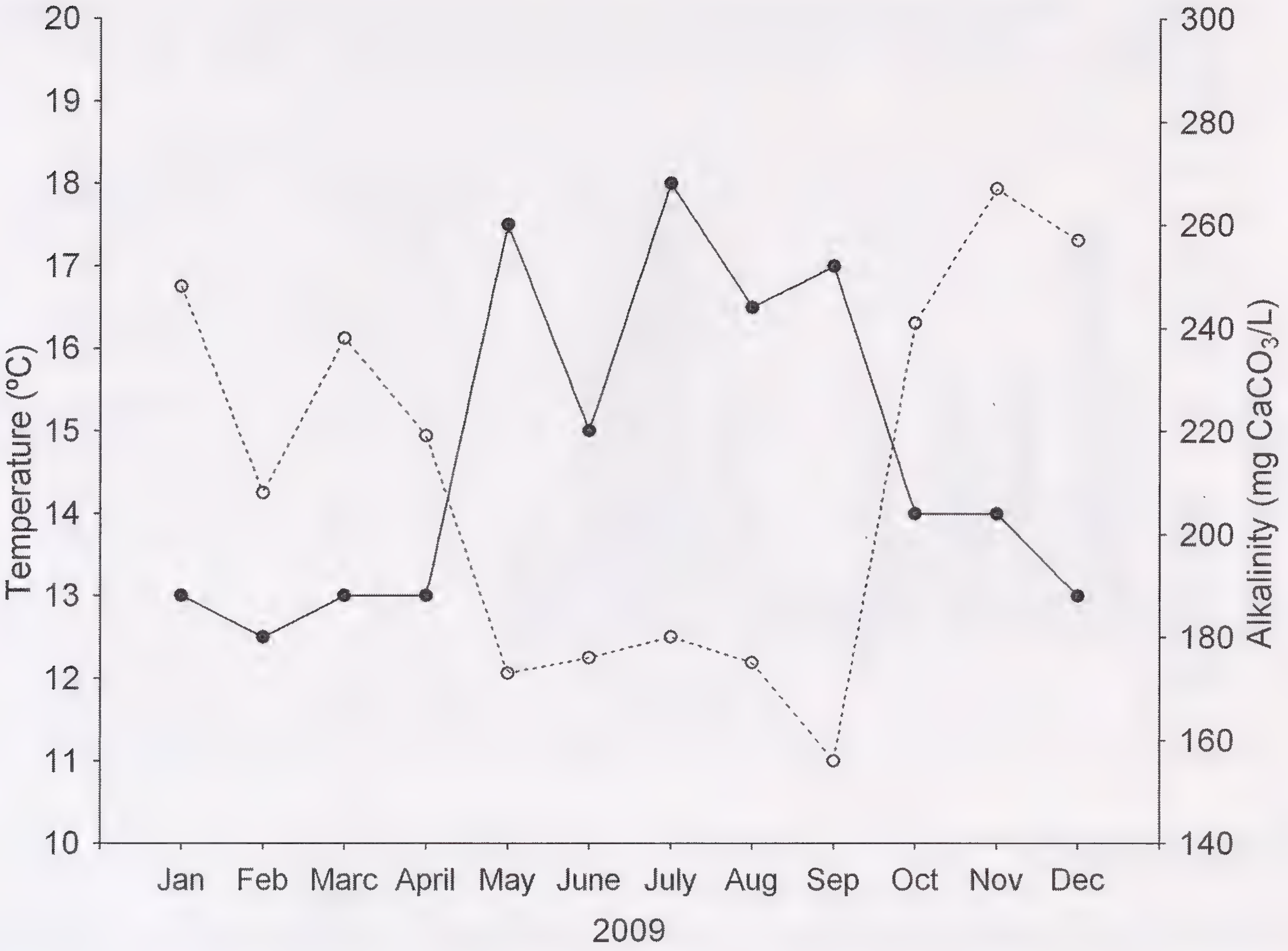

FIG. 4. Temperature (closed circles, solid line), and alkalinity (open circles, dashed line) variations in the pit Jama u Predolcu.

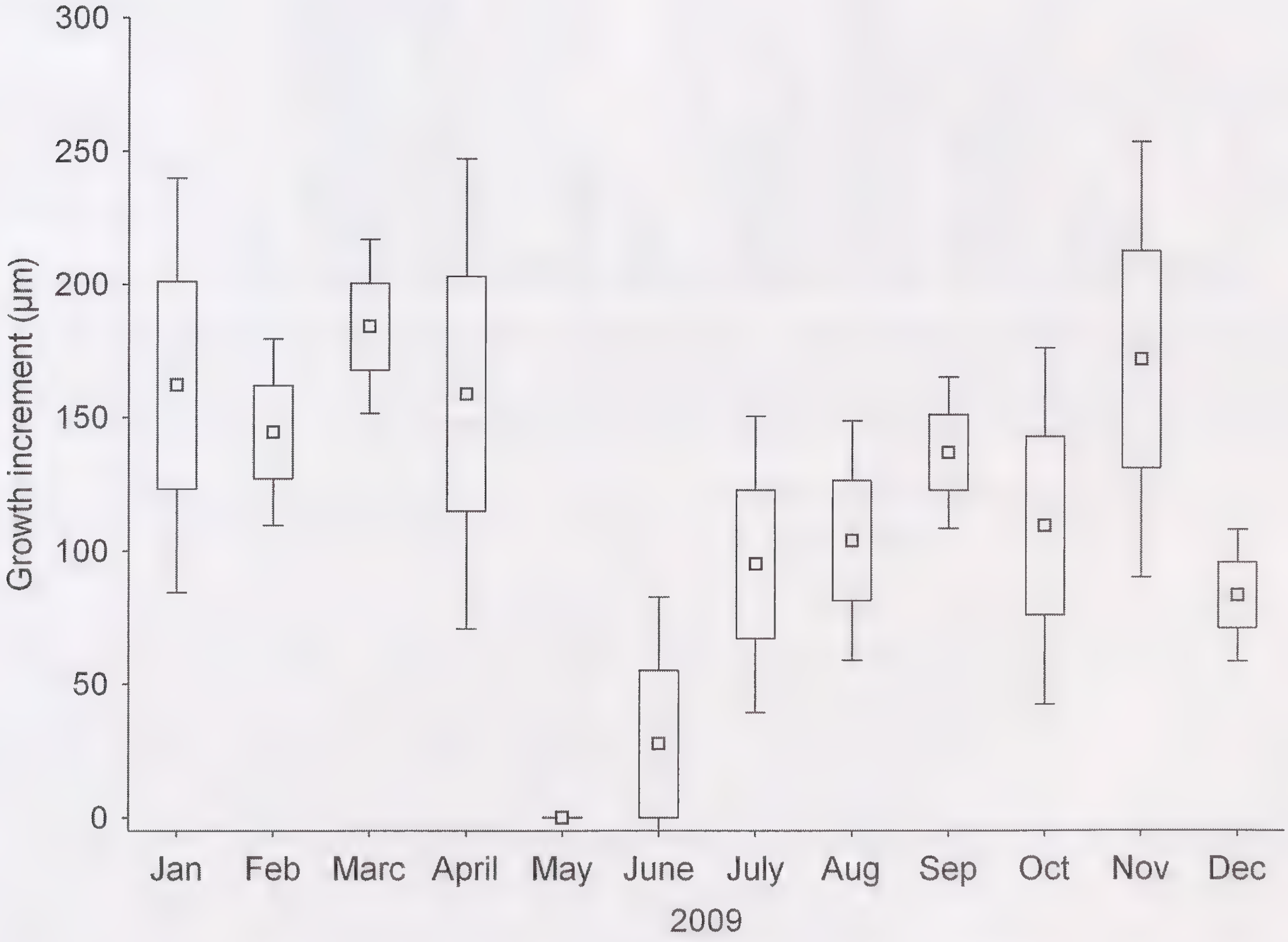

FIG. 5. *Congeria kusceri*. Seasonal variations in the distance between the last growth line and the shell margin of individuals collected monthly from the pit Jama u Predolcu. Values are presented as means, standard errors (box) and standard deviations (WHISKER).

TABLE 1. Morphometric data obtained for *Congeria kusceri* from the pit Jama u Predolcu during 2009. Values are presented as means ± standard deviations (minimum-maximum).

	n	Shell length (mm)	Shell height (mm)	Shell width (mm)
Males	46	11.0 ± 2.7 (6.6–15.4)	6.3 ± 1.4 (3.7–8.5)	6.7 ± 1.8 (4.0–9.2)
Females	41	11.6 ± 3.4 (6.0–17.0)	6.8 ± 1.9 (4.0–11.6)	6.9 ± 1.9 (3.7–10.0)
Hermaphrodites	2	10.0 ± 1.4 (9.0–11.0)	6.3 ± 1.8 (5.0–7.5)	5.9 ± 1.6 (4.8–7.0)
Undifferentiated	1	7.2	4.2	4.0
Total	90	11.2 ± 3.0 (6.0–17.0)	6.5 ± 1.6 (3.7–11.6)	6.8 ± 1.8 (3.7–10.0)

Morphometric Analysis

The morphometric data obtained for the three measured shell axes of *C. kusceri* with respect to sex, are summarized in Table 1. Shell lengths of males (n = 46) ranged from 6.6 mm to 15.4 mm, with a mean (± SD) of 11.0 ± 2.7 mm, whereas females (n = 41) ranged from 6.0 mm to 17.0 mm, with a mean (± SD) of 11.6 ± 3.4 mm. ANCOVA showed that there was no significant difference in shell length of animals with respect to sex ($F_{1.86} = 1.52$, $p = 0.216$), that is, *C. kusceri is* not sexually dimorphic.

Growth Increments

Results of the marginal increment analysis suggested that *C. kusceri* deposits one growth line annually. Growth lines were present either at the shell margin or close to it for individuals collected in May and June 2009, whereas for a period of five months after June, the distance between the last growth line and the shell margin generally increased (Fig. 5).

Of the 90 individuals of *C. kusceri* examined in this study, age was estimated for 80 of them. Due to the heteromyarian shell form of the *C. kusceri* shell, it was not always pos-

TABLE 2. *Congeria kusceri*. Comparison of the estimated von Bertalanffy growth parameters for the total sample of all individuals obtained from the pit Jama u Predolcu during 2009 with respect to sex. Values are presented as means ± standard deviations (minimum-maximum). L_∞ asymptotic length; k, growth constant; t_0, initial condition parameter; r^2, coefficient of determination; ø', growth performance index.

	n	Shell length (mm)	Age (years)	L_∞ (mm)	k ($year^{-1}$)	t_0 (year)	r^2	Ø'
Males	44	11.1 ± 2.7 (6.6–15.4)	27.3 ± 12.7 (11–53)	16.7	0.04	-3.69	0.924	1.05
Females	35	12.1 ± 3.4 (6.5–17.0)	28.4 ± 12.9 (9–51)	18.7	0.04	-2.31	0.912	1.14
Hermaphrodites	1	11.0	26					
Total	80	11.5 ± 3.0 (6.5–17.0)	27.8 ± 12.7 (9–53)	18.2	0.03	-3.96	0.908	1.01

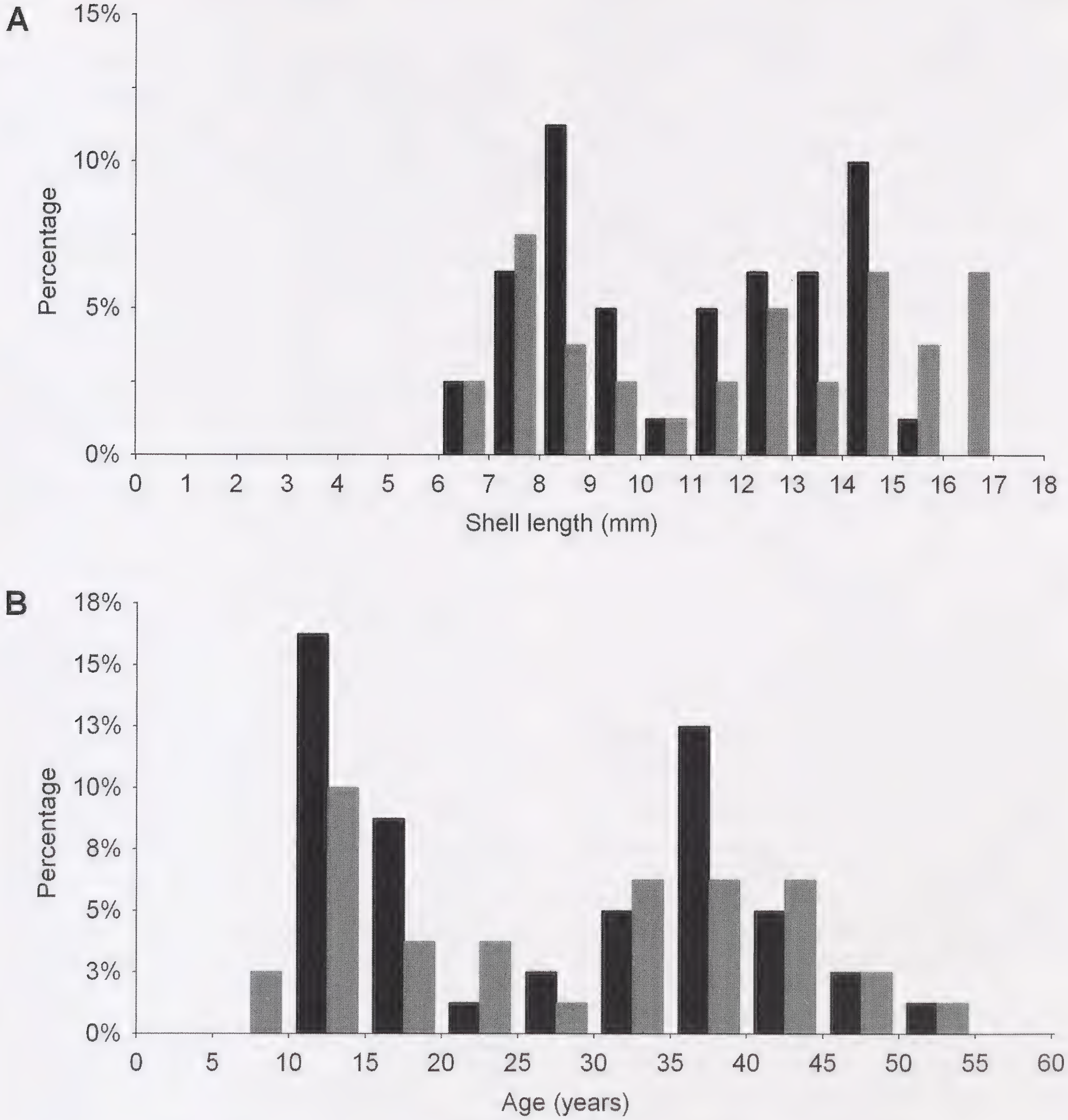

FIG. 6. *Congeria kusceri.* (A): Shell length; (B): Age distribution of male (black) and female (grey) individuals used in this age analysis study.

sible to prepare acetate peel replicas along the maximum growth axis, that is, from the umbones to the postero-ventral margin of the shell valve (Fig. 2A: a, b), as used for marginal growth increment analysis and ageing (Fig. 2A: c, d). This was particularly problematic for ten smaller individuals used for marginal growth analysis, and it was thus not possible to estimate their ages. Shell length and age structure data obtained for the *C. kusceri* individuals used in the age analysis component of this study are presented in Figure 6. The population growth curve data generated for *C. kusceri* from the length-at-age data are shown in Table 2 and illustrated in Figure 7. Analysis using ANCOVA showed that there was a statistically significant difference in the age structure of individuals with respect to sex when shell length was used as the covariate ($F_{1.78} = 4.07$, $p = 0.047$).

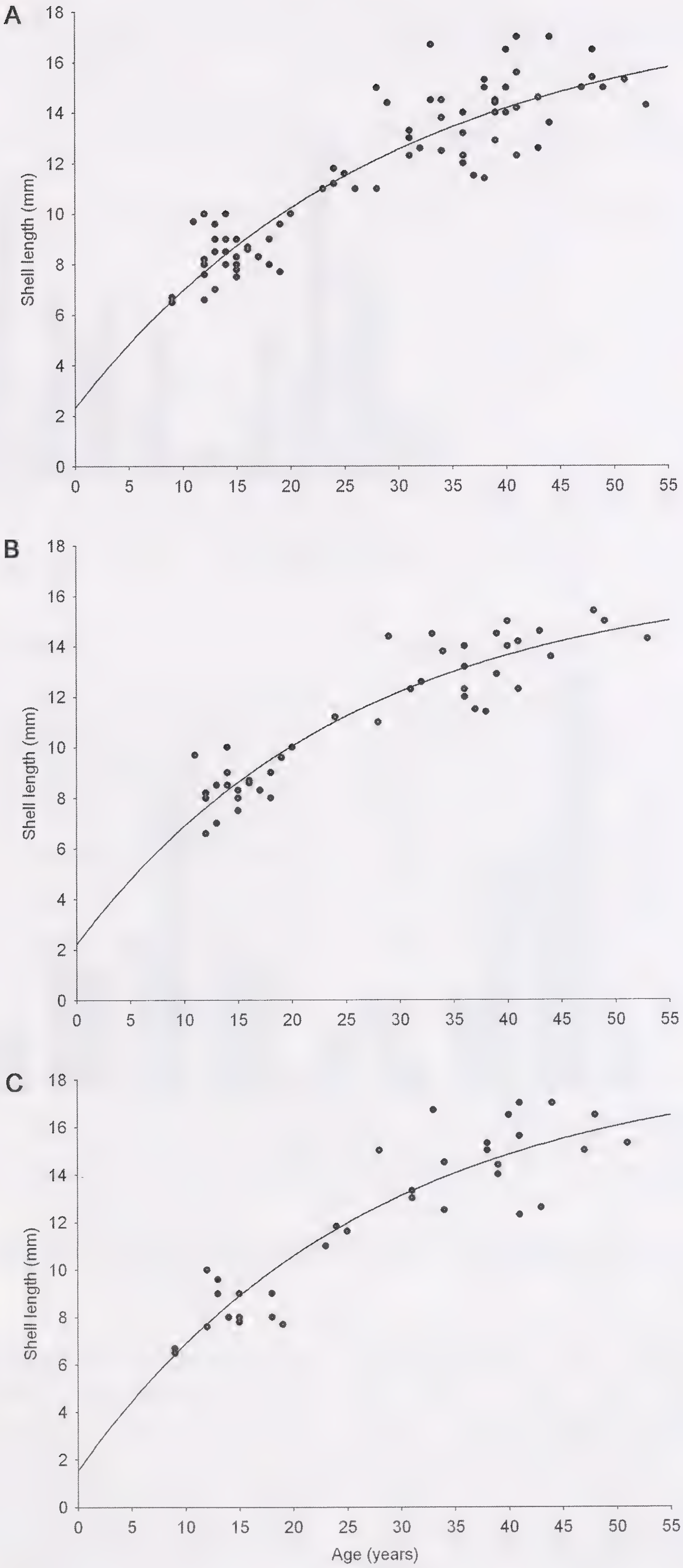

FIG. 7. *Congeria kusceri.* Von Bertalanffy growth curves for (A): The total sample; (B): Males; (C): Female individuals. Collected during 2009.

DISCUSSION

Karatayev et al. (2006) noted that in temperate regions, shell growth by *Dreissena polymorpha* (Pallas, 1771) ceases in winter and resumes each spring after an increase in water temperature. Results of our study identify the same growth pattern for *C. kusceri*, despite its occupation of subterranean waters. That is, the annual pattern of growth line formation in *C. kusceri* coincided with an increase in water temperature, which occurs in the pit Jama u Predolcu from May to June. A water temperature of 13–14°C has been identified as the lower limit for both the initiation and cessation of shell growth and the reproductive maturity of *C. kusceri*, since the annual pattern of growth ring formation coincides with the spawning period (Morton & Puljas, 2013). It can thus be concluded that an increasing temperature is the main regulator of shell growth in *C. kusceri* but it is also the primary factor triggering and co-ordinating reproductive timing (Puljas, 2012). It has been further demonstrated that the annual pattern of growth expressed by *C. kusceri* is related to variations in alkalinity. Several studies have recorded that increases in alkalinity and a high requirement for calcium may be associated with growth in *D. polymorpha* (Ramcharan et al., 1992; Vinogradov et al., 1992; Barbiero et al., 2006). Our data indicate that calcium uptake by *C. kusceri* coincides with a decrease in the alkalinity of the pit water. This observation, however, needs physiological elaboration as well as investigation of other factors that might be responsible for such a decrease in alkalinity.

Unlike *D. polymorpha* and *C. kusceri*, growth of *Mytilopsis leucophaeata* (Conrad, 1831) oscillated each year and comprised a single phase of major growth from late spring until summer, followed by a second period of minor growth in autumn and winter (Verween et al., 2010).

A statistical analysis of the expression of sexuality exhibited by 280 individuals of *C. kusceri* collected monthly from the pit, during 2009, suggested a slight sexual dimorphism (Puljas, 2012). According to that study, females were statistically significantly larger than males, although observed shell lengths of the former (5.3–17.0 mm) were relatively similar to those of the latter (4.0–15.4 mm). The differences between males and females in terms of age structure calculated in this study have been shown to differ with respect to shell length, the males being somewhat smaller than females, as previously concluded by Puljas (2012).

This study shows that the population of *C. kusceri* in the Jama u Predolcu pit is characterized by an impressive longevity of 53 years. The oldest individual was a male of 14.3 mm shell length, which compares well with the longevity estimate obtained by Morton et al. (1998) for an age of between 30 to 40 years for *C. kusceri* at ~ 17 mm shell length. Calculations of growth rate obtained from this study suggested a maximum theoretical shell length (L_∞) of 16.7 mm for males and 18.7 mm for females. Morton et al. (1998), however, identified *C. kusceri* individuals with shell lengths ranging from 9 to 24 mm. The longevity of this species is, therefore, greater than that identified in this study and such individuals will be much older than the 53 years assigned to the individuals reported upon herein.

Obtained estimates of the growth constant (k) for *C. kusceri* are relatively low for both sexes (0.04 year^{-1}) and similar to k-values obtained for other long-lived bivalves, such as the freshwater unionids *Margaritifera margaritifera* Linnaeus, 1758 (k = 0.023–0.075 year^{-1}; Hastie et al., 2000) and *Megalonaias nervosa* (Rafinesque, 1820) (k = 0.04–0.092 year^{-1}; Christian et al., 2000; Haag & Rypel, 2010) and some marine bivalves such as *Arctica islandica* Linnaeus, 1767 (k = 0.02–0.06 year^{-1}; Kilada et al., 2007) and *Glycymeris glycymeris* (Linnaeus, 1758) (k = 0.11 and 0.13 year^{-1}; Savina, 2004). Such values are characteristic of slow-growing and long-lived species (Beverton & Holt, 1959).

In accordance with the rate-of-living/free radical theory of ageing, sedentary bivalve molluscs are some of the longest living animals (Abele et al., 2009; 2010; Buttemer et al., 2010). An age of ~ 200 years was recently documented for *G. glycymeris* by Reynolds (2011) while Wanamaker et al. (2008) has identified individuals of *A. islandica* that were estimated to be ~ 400 years old. Both of these latter species occur in subtidal marine habitats and are relatively large, that is, a shell length of ~ 9 cm for *G. glycymeris* (Reynolds, 2011) and ~ 12.5 cm for *A. islandica* (Morton, 2011). Although these bivalves are often referred to as "large", they are nowhere near as large as giant clams, for example, the 'small' giant clam *Tridacna maxima* Röding, 1798, which lives for only ~ 30 years (Romanek, 1987). It thus seems that adult size probably has little or no relationship with longevity, at least in the sea, and that other features of a species' biology can better explain the phenomenon of bivalve extreme longevity investigated only relatively recently.

But what is the situation in freshwater bivalve species? In comparison with other representatives of the Dreissenidae, *C. kusceri* has significantly smaller shell length values but greatly expanded longevity. In England, for example, *D. polymorpha* can attain a shell length of 50 mm and live for five years, although a general longevity of 3.5 years is normal (Morton, 1969). Similarly, maximum shell lengths of 22 mm (Verween et al., 2010) and 25.2 mm (Kennedy, 2011), and a longevity of between 2 to 4 years has been recorded for *M. leucophaeata* (Verween et al., 2010), while the equivalent figures for its congeneric, *M. sallei*, are 29 mm and < 2 years (in Hong Kong) (Morton, 1989).

Also in Hong Kong, the freshwater unionid *Sinanodonta woodiana* (Lea, 1834) attains a maximum theoretical shell length of ~162 mm and has a life span of ~ 12 years (Dudgeon & Morton, 1983). This compares well with life span estimates of between 10 to 15 years for unionids in the River Thames in England (Negus, 1966). But some unionids can reach impressive longevities, such as *Margaritifera margaritifera*, which can reach an age of 100–200 years (Bauer, 1992; Ziuganov et al., 2000; Haag & Rypel, 2010) and *Elliptio complanata* (Lightfoot, 1786) and *Lampsilis siliquoidea* (Barnes, 1823) both with longevities of > 150 years (Anthony et al., 2001). Further, Helama & Valovirta (2008) considered that, in Finland, if not anthropogenically disturbed, *M. margaritifera* may reach super-centenarian ages with the oldest perhaps attaining > 200 years. In Japan, the congeneric *Margaritifera laevis* Haas, 1910 attains shell lengths of between 111 to 133 mm and lives for between 36 to 67 years (Awakura & Sugiwaka, 1988; Akiyama & Iwakuma, 2009).

The longevity values obtained for the marine and freshwater species identified above can, in some instances, indicate an extremely slow growth rate. Among the Dreissenidae, *C. kusceri* is the only species that displays such an extreme longevity, presumably because of its underground habitat and adaptations that uniquely fit it and, possibly, its congeners (Bilandžija et al., 2013) for such a troglodytic life style. Furthermore, achieving a shell length of less than half that of its short-lived cousins *Dreissena* and *Mytilopsis*, *C. kusceri* too must have an extremely slow growth rate in comparison to their fast ones. According to Culver (1982), nearly all cave organisms for which any data are available show either some or all of the following characteristics: delayed reproduction, low fecundity, larger eggs and increased longevity. Such features are commonly associated with K-selection (Pianka, 1970) and, as discussed herein and by Morton & Puljas (2013), *C. kusceri* would seem to fit such a definition, in contrast to its opportunistic, *r*-selected, confamilial cousins *Dreissena* and *Mytilopsis*.

But what attributes does *C. kusceri* possess that allow it to live for so long? Certainly, there is a general absence of molluscivorous predators in its highly subterranean environment but, perhaps, just as importantly, Morton & Puljas (2013) have demonstrated that the species exhibits a low fecundity, highly specialized larval brooding resulting in only "occasional" low-level recruitments, retrieval by resorption of unfertilized gametes, and no loss of reproductive abilities with age. That is, by adapting to, in evolutionary terms, over the last 22–23 million years (Bilandžija et al., 2013), and optimizing the constraints imposed by occupation of a subterranean habitat on the individual, the species has survived by reducing the effects and consequences of physiological ageing thereby nullifying reproductive senescence (Morton & Puljas, 2013). The recent discovery of an unique 'flock' of subterranean species of *Congeria* (Bilandžija et al., 2013), of which *C. kusceri* is but one, has thrown new light on how colonization and continued and successful occupation of such a freshwater habitat has been achieved, adding further complexity to an ongoing story of amazing vicariant evolution.

ACKNOWLEDGEMENTS

The authors are grateful to the Croatian Ministry of Environment and Nature Protection, Zagreb, for permission to collect the specimens of *Congeria kusceri* herein described and discussed.

LITERATURE CITED

ABELE, D., T. BREY & E. PHILIPP, 2009, Bivalve models of aging and the determination of molluscan lifespans. *Experimental Gerontology*, 44: 307–315.

ABELE, D., M. KRUPPE, E. PHILIPP & T. BREY, 2010, Mantle cavity water oxygen partial pressure ($P0_2$) in marine molluscs aligns with lifestyle. *Canadian Journal of Fisheries and Aquatic Sciences*, 67: 977–986.

AKIYAMA, Y. B. & T. IWAKUMA, 2009, Growth parameters of endangered freshwater pearl mussel (*Margaritifera laevis*, Unionoida). *Archiv für Hydrobiologie*, 175: 295–305.

AMERICAN PUBLIC HEALTH ASSOCIATION, 1995, Standard methods for the examination of water and wastewater. 19th Edition. American Public Health Association, Washington, DC, U.S.A., 1100 pp.

ANTHONY, J. L., D. H. KESLER, W. L. DOWNING & J. A. DOWNING, 2001, Length-specific growth rates in freshwater mussels (Bivalvia: Unionidae): extreme longevity or generalized growth cessation?*Freshwater Biology*, 46: 1349–1359.

AWAKURA, T. & K. SUGIWAKA, 1988, Age and growth of freshwater pearl mussel, *Margaritifera laevis*. *Fish and Water*, 25: 41–44.

BARBIERO, R. P., M. L. TUCHMAN & E. S. SCOTT MILLARD, 2006, Post-dreissenid increases in transparency during summer stratification in the offshore waters of Lake Ontario: is a reduction in whiting events the cause? *Journal of Great Lakes Research*, 32: 131–141.

BAUER, G., 1992, Variation in the life span and size of the freshwater pearl mussel. *Journal of Animal Ecology*, 61: 425–436.

BEVERTON, R. J. H. & S. J. HOLT, 1959, A review of the lifespans and mortality rates of fish in nature, and their relation to growth and other physiological characteristics. Pp. 142–180, in: G. E. W. WOLSTENHOLME & M. O'CONNOR, eds., *CIBA Foundation Colloquia on Ageing: the lifespan of animals*, Vol. 5. J. & A. Churchill Ltd., London, 324 pp.

BILANDŽIJA, H., B. MORTON, M. PODNAR & H. ĆETKOVIĆ, 2013, Evolutionary history of relict *Congeria* (Bivalvia: Dreissenidae): unearthing the subterranean biodiversity of the Dinaric Karst. *Frontiers in Zoology*, 10: 5 (1–17).

BUTTEMER, W. A., D. ABELE & D. COSTANTINI, 2010, From bivalves to birds: oxidative stress and longevity. *Functional Ecology*, 24: 971–983.

CULVER, D. C., 1982, *Cave life – evolution and ecology*. Harvard University Press, Cambridge, Massachusetts, 189 pp.

CHRISTIAN, A. D., C. L. DAVIDSON, W. R. POSEY, P. J. RUST, J. L. FARRIS, J. L. HARRIS & G. L. HARP, 2000, Growth curves of four species of commercially valuable freshwater mussels (Bivalvia: Unionidae) in Arkansas. *Journal of the Arkansas Academy of Science*, 54: 41–50.

DUDGEON, D. & B. MORTON, 1983, The population structure and sexual strategy of *Anodonta woodiana* (Bivalvia: Unionacea) in Plover Cove Reservoir, Hong Kong. *Journal of Zoology, London*, 201: 161–183.

HAAG, W. R. & A. L. RYPEL, 2010, Growth and longevity in freshwater mussels: evolutionary and conservation implications. *Biological Reviews*, 86: 225–247.

HASTIE, L. C., M. R. YOUNG & P. J. BOON, 2000, Growth characteristics of freshwater pearl mussels, *Margaritifera margaritifera* (L.). *Freshwater Biology*, 43: 243–256.

HELAMA, S. & I. VALOVIRTA, 2008, The oldest recorded animal in Finland: ontogenetic age and growth in *Margaritifera margaritifera* (L. 1758) based on internal shell increments. *Memoranda Societatis pro Fauna et Flora Fennica*, 84: 20–30.

KARATAYEV, A. Y., L. E. BURLAKOVA & D. K. PADILLA, 2006, Growth rate and longevity of *Dreissena polymorpha* (Pallas): a review and recommendations for future study. *Journal of Shellfish Research*, 25: 23–32.

KENNEDY, V. S., 2011, Biology of the uncommon dreissenid bivalve *Mytilopsis leucophaeata* (Conrad, 1831) in central Chesapeake Bay. *Journal of Molluscan Studies*, 77: 154–164.

KILADA, R. W., S. E. CAMPANA & D. RODDICK, 2007, Validated age, growth, and mortality estimates of the ocean quahog (*Arctica islandica*) in the western Atlantic. *ICES Journal of Marine Science*, 64: 31–38.

MORTON, B., 1969, Studies on the biology of *Dreissena polymorpha* Pall. (III). Population dynamics. *Proceedings of the Malacological Society of London*, 38: 471–482.

MORTON, B., 1989, Life history characteristics and sexual strategy of *Mytilopsis sallei* (Bivalvia: Dreissenacea), introduced into Hong Kong. *Journal of Zoology, London*, 219: 469–485.

MORTON, B., 2011, The biology and functional morphology of *Arctica islandica* (Bivalvia: Arcticidae): a gerontophilic living fossil. *Marine Biology Research*, 7: 540–553.

MORTON, B. & S. PULJAS, 2013, Life history strategy, with ctenidial and mantle larval brooding, of the troglodytic "living fossil" *Congeria kusceri* (Bivalvia: Dreissenidae) from the subterranean Dinaric karst of Croatia. *Biological Journal of the Linnean Society*, DOI: 10.1111/j.1095-8312.2012.02020.x

MORTON, B., F. VELKOVRH & B. SKET, 1998, Biology and anatomy of the "living fossil" *Congeria kusceri* (Bivalvia: Dreissenidae) from subterranean rivers and caves in the Dinaric karst of the former Yugoslavia. *Journal of Zoology, London*, 245: 147–174.

NEGUS, C. L., 1966, A quantitative study of growth and production of unionid mussels in the river Thames at Reading. *Journal of Animal Ecology*, 35: 513–532.

PHILIPP, E. E. R. & D. ABELE, 2010, Masters of longevity: lessons from long-lived bivalves – a mini-review. *Gerontology*, 56: 55–65.

PIANKA, E. R., 1970, On *r*- and K selection. *American Naturalist*, 104: 595–597.

PULJAS, S., 2012, The reproductive cycle of the living fossil *Congeria kusceri* (Bivalvia: Dreissenidae) from the pit Jama u Predolcu (Metković, Croatia). Pp. 251–261, in: I. Lučić & J. Mulaomerović, eds., *Proceedings of International Scientific Symposium "Man and Karst" 13th–16th October 2011, Bijakovići – Međugorje, B&H.* Faculty of Social Sciences dr. Milenko Brkić, Bijakovići – Međugorje and Centre for Karst and Speleology, Sarajevo, Bosnia, 283 pp.

RAMCHARAN, C. W., D. K. PADILLA & S. I. DODSON, 1992, Models to predict potential occurrence and density of the zebra mussel, *Dreissena polymorpha. Canadian Journal of Fisheries and Aquatic Sciences*, 49: 2611–2620.

REYNOLDS, D. J., 2011, *Establishing multi-bivalve species sclerochronology*. PhD Thesis, Bangor University, School of Ocean Science, 146 pp.

RICHARDSON, C. A., 2001, Molluscs as archives of environmental change. *Oceanography and Marine Biology: an Annual Review*, 39: 103–164.

ROMANEK, C. S., D. S. JONES, D. F. WILLIAM, D. E. KRANTZ & R. RADTKE, 1987, Stable isotopic investigation of physiological and environmental changes recorded in shell carbonate from the giant clam *Tridacna maxima. Marine Biology*, 94: 385–393.

SAVINA, M., 2004, *Modélisation écologique des populations de palourdes roses (Paphia rhomboïdes) et d'amandes de mer (Glycymeris glycymeris) en Manche.* PhD Thesis, Université d'Aix-Marseille II., 205 pp.

SPARRE, P. & S. C. VENEMA, 1998, *Introduction to tropical fish stock assessment.* Manual, FAO Fisheries Technical Paper 306/1, Rev. 2, Rome, 376 pp.

VERWEEN, A., M. VINCX & S. DEGRAER, 2010, *Mytilopsis leucophaeata*: The brackish water equivalent of *Dreissena polymorpha*? Pp. 29–44, in: G. van der Velde, S. Rajagopal & A. bij de Vaate, eds., *The zebra mussel in Europe.* Backhuys Publishers, Leiden, the Netherlands, 490 pp.

VINOGRADOV, G. A., N. F. SMIRNOVA, V. A. SOKOLOV & A. A. BUZNITSKY, 1992, Influence of chemical composition of the water on the mollusk *Dreissena polymorpha*. Pp. 283–294, in: T. Nalepa & D. Schloesser, eds., *Zebra mussels: biology, impacts, and control*. Lewis Publishers, Boca Raton, Florida, 832 pp.

VON BERTALANFFY, L., 1938, A quantitative theory of organic growth. *Human Biology*, 10: 181–213.

WANAMAKER, JR. A. D., J. HEINEMEIER, J. D. SCOURSE, C. A. RICHARDSON, P. G. BUTLER, J. EIRÍKSSON & K. L. KNUDSEN, 2008, Very long-lived molluscs confirm 17th century AD tephra-based radiocarbon reservoir ages for North Icelandic shelf waters. *Radiocarbon*, 50: 399–412.

ZIUGANOV, V., E. SAN MIFUEL, R. J. NEVES, A. LONGA, C. FERNÁNDEZ, R. AMARO, V. BELETSKA, E. POPOVITCH, S. KALIUZHIN & T. JOHNSON, 2000, Life span variation of the freshwater pearl shell: a model species for testing longevity mecahnisms in animals. *Ambio*, 29: 102–105.

Revised ms. accepted January 13, 2014

MALACOLOGIA, 2014, 57(2): 365–376

CALCIUM DETECTION AND OTHER CELLULAR STUDIES IN THE ESOPHAGUS AND CROP OF THE MARINE SLUG *AGLAJA TRICOLORATA* (EUOPISTHOBRANCHIA, CEPHALASPIDEA)

Alexandre Lobo-da-Cunha[1,2*], Joana Pereira-Sousa[2], Elsa Oliveira[1], Ângela Alves[1],
Fernanda Guimarães[3] & Gonçalo Calado[4]

ABSTRACT

To obtain more data about the digestive system of cephalaspideans, the esophagus and crop of *Aglaja tricolorata* were investigated using light and electron microscopy. In this cephalaspidean, the low epithelial cells of the anterior esophagus have a border of microvilli covered by a cuticle formed by acid polysaccharides. The esophageal pouches at the hind region of the anterior esophagus contain subepithelial secretory cells filled with electron-dense vesicles rich in neutral polysaccharides and proteins. A ciliated epithelium covers the base of the esophageal pouches. In the crop, the tall columnar epithelium is covered by a cuticle and forms many deep invaginations. The cuticle on the surface of the epithelium contains acid polysaccharides, but the material filling the lumen of the epithelial invaginations consists of neutral polysaccharides and proteins. Epithelial cells of the crop have a border of short microvilli and many mitochondria; lysosome-like bodies and some lipid droplets are present in the apical region. The elongated nucleus, numerous deep cell membrane invaginations and several hemidesmosomes are located at the basal region. Secretory cells are absent in the crop. Numerous large vacuolar cells are present in the connective tissue of the crop. With the pyroantimonate method, calcium was detected in the peripheral vesicles and central vacuole of these cells. WDS X-ray Intensity maps obtained by EPMA (Electron microprobe) confirmed the presence of calcium. This result supports the relationship between the vacuolar cells of aglajids and the calcium cells of pulmonate gastropods. In the posterior esophagus, epithelial cells are similar to the epithelial cells of the crop and secretory cells are also absent.

Keywords: Aglajidae, digestive tract, Gastropoda, histochemistry, microscopy, calcium cells, microanalysis.

INTRODUCTION

Currently, opisthobranch research is largely devoted to molecular phylogenetic studies (Klussmann-Kolb et al., 2008; Malaquias et al., 2009; Dinapoli & Klussmann-Kolb, 2010; Jörger et al., 2010; Wägele et al., 2014). As a consequence, the taxonomy has been profoundly revised and the clade Euopisthobranchia was recently created to include the Tylodinoidea (or Umbraculoidea), Cephalaspidea, Runcinacea, Anaspidea (or Aplysiomorpha) and Pteropoda (Jörger et al., 2010; Wägele et al., 2014). On the other hand, the digestive system of these gastropods has received much less attention in recent years and is far from being fully investigated. The clade Cephalaspidea has a worldwide distribution and it is the largest within the Euopisthobranchia, comprising more than 800 species of marine slugs and bubble snails (Wägele, 2004). However, for most species just gross anatomy data are available, but in order to understand the evolution of the digestive system in cephalaspideans more detailed information must be obtained from species belonging to different families/clades. The family Aglajidae consists of carnivorous marine slugs that feed on other opisthobranchs, polychaetes, nemerteans and flat worms, although the specific diet of *Aglaja tricolorata* is still unknown (Gosliner, 1980; Rudman & Willan, 1998). The digestive system of aglajids includes a bulbous

[1]Institute of Biomedical Sciences Abel Salazar (ICBAS), University of Porto, 4050-313 Porto, Portugal
[2]Interdisciplinary Centre of Marine and Environmental Research (CIIMAR/CIMAR), 4050-123 Porto, Portugal
[3]LNEG, 4466-956 S. Mamede de Infesta, Portugal
[4]Lusophone University of Humanities and Technologies, 1749-024 Lisbon, Portugal
*Corresponding author: alcunha@icbas.up.pt

or tubular muscular buccal bulb that can be eversible in some species to grasp the prey, but the radula is present only in *Odontoglaja* (Gosliner, 1980; Rudman & Willan, 1998). The muscular gizzard with three hard plates, which is considered a synapomorphy of the cephalaspideans (Mikkelsen, 1996), is absent in aglajids (Rudman, 1974; Gosliner, 1980). At least in most aglajids, the prey is swallowed whole and slowly digested within the crop by a fluid containing enzymes secreted by the digestive gland (Rudman, 1972). Subsequently, a nutrient rich fluid proceeds to the stomach embedded in the digestive gland and linked to it by ducts. Endocytosis of nutritive particles and lysosomal digestion take place in the digestive cells of the digestive gland (Rudman, 1972), but also seems to occur in the esophagus and crop of cephalaspideans (Lobo-da-Cunha et al., 2010a, 2010b, 2011), as in other gastropods (Walker, 1972; Bourne et al., 1991; Lobo-da-Cunha & Batista-Pinto, 2005).

Recently, the first histochemical and ultrastructural studies of digestive organs of aglajids were published, revealing formally unknown aspects (Lobo-da-Cunha et al., 2009, 2011). However, additional species must be investigated in order to obtain a more comprehensive perspective of the digestive system in this family. The vacuolar cells found in the connective tissue of the crop in *Philinopsis depicta* are of special interest. The morphology of these cells suggests a relationship with the calcium cells of pulmonates (Lobo-da-Cunha et al., 2011), and to explore this hypothesis calcium detection methods were applied in the study of the crop of *Aglaja tricolorata*.

MATERIAL & METHODS

Morphology

Several specimens of *Aglaja tricolorata* Renier, 1807, about 4 cm in length were captured in the Arade Estuary on the south coast of Portugal. For light microscopy, the esophagus and crop were fixed in Bouin's solution for 24 h, dehydrated with ethanol and embedded in paraffin. Tissue sections were stained with hematoxylin and eosin, or with Masson's trichrome. Small pieces of these organs (no more than 1 mm^3) were fixed for about 2 h at 4°C in fixative containing 2.5% glutaraldehyde and 4% formaldehyde (obtained from hydrolysis of paraformaldehyde) diluted with 0.4 M cacodylate buffer pH 7.4 (final buffer concentration 0.28 M). After washing in buffer, tissue fragments were post-fixed with 2% OsO_4 buffered with cacodylate, dehydrated in ethanol and embedded in Epon. Semithin sections for light microscopy were stained with methylene blue and azure II. Ultrathin sections for transmission electron microscopy were stained with uranyl acetate and lead citrate, before being observed in a JEOL 100CXII transmission electron microscope operated at 60 kV.

Histochemistry

The tetrazonium coupling reaction for protein detection, PAS reaction for polysaccharides, and alcian blue staining for acid polysaccharide detection were applied to deparaffinised sections of esophagus and crop fixed with Bouin's solution (Ganter & Jollès, 1970). The same techniques were used in semithin sections (2 µm) of Epon embedded pieces, but for alcian blue staining the embedding medium was removed by treatment of the sections with a saturated solution of NaOH in ethanol for 10 min (Lane & Europa, 1965).

Tetrazonium Coupling Reaction – Sections were treated for 10 min with a freshly prepared 0.2% solution of fast blue salt B in veronal-acetate buffer pH 9.2, washed and treated for 15 min with a saturated solution of β-naphthol in veronal-acetate buffer pH 9.2.

PAS – Sections were treated with 1% periodic acid for 10 min, washed and stained with Schiff's reagent for 15 min. In control sections the oxidation with periodic acid was omitted.

Alcian Blue – Sections were stained with a 0.5% solution of alcian blue diluted in 3% acetic acid at pH 2.5 for detection of carboxylated polysaccharides and in an HCl solution with pH 1.0 for detection of sulphated polysaccharides.

Calcium Detection

Crop fragments no bigger than 1 mm^3 were fixed with 2.5% glutaraldehyde and 4% formaldehyde (obtained from hydrolysis of paraformaldehyde) diluted in 0.2 M phosphate buffer pH 7.4 containing 1% sucrose, for 12 h at 4°C (adapted from Probst, 1986). For fixation of control fragments, 10 mM of EGTA were added to this fixative. After washing in phosphate buffer for at least 2 h, tissue fragments were post-fixed for 2 h at 4°C with an unbuffered solution containing 2% OsO_4 and 2% potassium pyroantimonate, dehydrated in ethanol and embedded in Epon (Wick & Hepler, 1982). Ultrathin sections were stained for 10 min with uranyl acetate. To confirm the presence of calcium in the electron-dense deposits, ultrathin sections were treated for 30 min at 60°C with a 10 mM solution of EGTA. To prepare this solution the pH was raised to 9–10 with NaOH, and after dissolution of EGTA the pH was lowered to 7.2 with HCl (Probst, 1986). For controls, ultrathin sections were incubated under the same conditions with water at pH 7.2. Additionally, 4 μm thick semithin sections mounted on squares of aluminum foil were carbon coated to provide a conductive layer on the surface and prevent charging. A JEOL JXA 8500-F microprobe was used to detect the presence of Ca and its spatial distribution. X-Ray Intensity maps were obtained by WDS spectrometers equipped with a PETH crystal for Ca (Kα) line and PETJ crystal for Sb (Lα) line.

RESULTS

Anatomy, Histology and Histochemistry

The anterior part of the digestive tract of *A. tricolorata* includes a muscular buccal bulb, a short anterior esophagus connected to the crop, followed by the posterior esophagus (Fig. 1). In the observed animals, the crop was empty or contained unrecognizable food remains.

At the connection between the anterior esophagus and the crop, depressions on the digestive tract wall form the esophageal pouches (Figs. 2, 3). Eosinophilic subepithelial secretory cells are present around the esophageal pouches, on their lateral walls and base, but were not observed in the remaining part of the anterior esophagus (Figs. 2, 3). These cells are filled with secretory vesicles that are not stained by alcian blue (Fig. 4), but strongly stained by PAS and tetrazonium coupling reaction (Figs. 5–7). The apical region of these cells crosses the epithelium and their nuclei are located in the basal region that is inserted in the connective tissue (Fig. 7). The low epithelium of the anterior esophagus and lateral walls of the pouches are covered by a cuticle stained by alcian blue (Fig. 4), but not by PAS or tetrazonium coupling reaction (Figs. 5, 6). The bases of the esophageal pouches are covered by a ciliated epithelium without cuticle, but secretory cells of the same type are present (Fig. 7).

The tall columnar epithelium of the crop forms many deep, branched invaginations, but secretory cells are absent (Figs. 8, 9). The crop epithelium is covered by a cuticle strongly stained by hematoxylin, and the lumen of the epithelial invaginations is also stained by hematoxylin (Fig. 9). On the surface of the epithelium the cuticle is not stained by the tetrazonium coupling reaction, but a positive reaction is detected in the lumen of the epithelial invaginations (Fig. 10). Conversely, the cuticle on the surface of the epithelium is stained by alcian blue, but acid polysaccharides are not detected in the lumen

→

FIGS. 1–12. Anatomy, histology and histochemistry. FIG.1: Anatomy of the digestive system. bb – buccal bulb, sg – salivary glands, ae – anterior esophagus, cr – crop, pe – posterior esophagus, dg – digestive gland; FIG. 2: Esophageal pouch (arrow) at the transition zone between the anterior esophagus (ae) and the crop (cr). Eosinophilic secretory cells (arrowheads) are present in this zone. Section stained with haematoxylin and eosin; FIG. 3: Semithin section of an esophageal pouch. Secretory cells are found at the base (arrow) and in the lateral walls of the pouch (arrowheads); FIG. 4: The cuticle covering the epithelium of the esophageal pouches is stained by Alcian blue (arrowheads), but the secretory cells (sc) are not stained; FIG. 5: The secretory cells of the esophageal pouches (sc) are strongly PAS positive, but the cuticle (arrowhead) is unstained; FIG. 6: The cuticle of the esophageal pouches (arrowhead) is not stained by the tretrazonium coupling reaction, but the secretory cells (sc) are strongly stained; FIG. 7: Secretory cell (sc) at the base of an esophageal pouch stained by the tetrazonium coupling reaction. The nucleus (nu) is located in the basal region of the cell that is embedded in the connective tissue, and the apical region crosses the ciliated epithelium (asterisk); FIG. 8: Section of the crop stained with Masson´s trichrome, showing the epithelium (arrows) and several vacuolar cells in the connective tissue (arrowheads); FIG. 9: Section of the crop stained with hematoxylin and eosin. The epithelium forms deep invaginations (arrows) and is covered by a cuticle that stains with hematoxylin (arrowheads). Several vacuolar cells (asterisks) are visible in the connective tissue; FIG. 10: The cuticle of the crop (arrowhead) is not stained by the tetrazonium coupling reaction, but the lumen of the epithelial invaginations shows positive reaction (arrows); FIG. 11: The cuticle of the crop (arrowheads) is stained by alcian blue, but the lumena of the epithelial invaginations are not (arrows); FIG. 12: In the crop, the cuticle (arrowheads) and the lumena of the epithelial invaginations (arrows) are both strongly PAS positive.

1

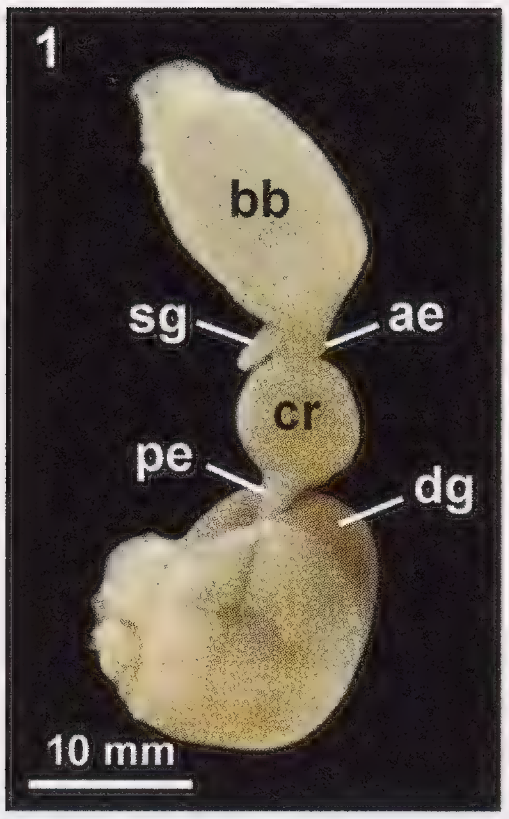

2

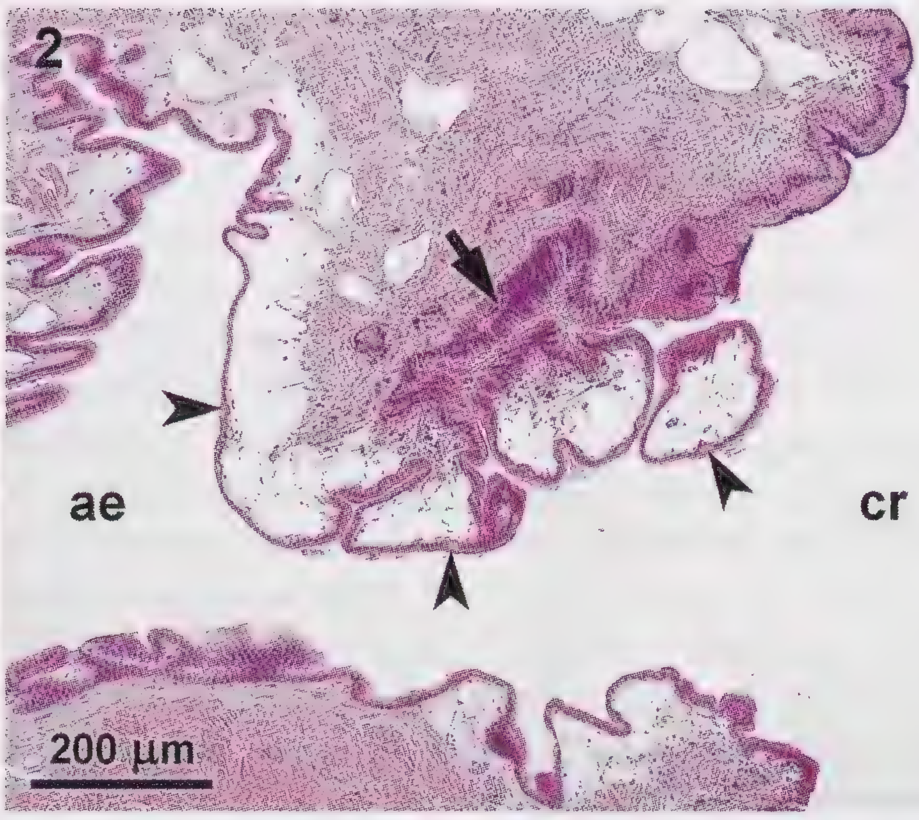

3

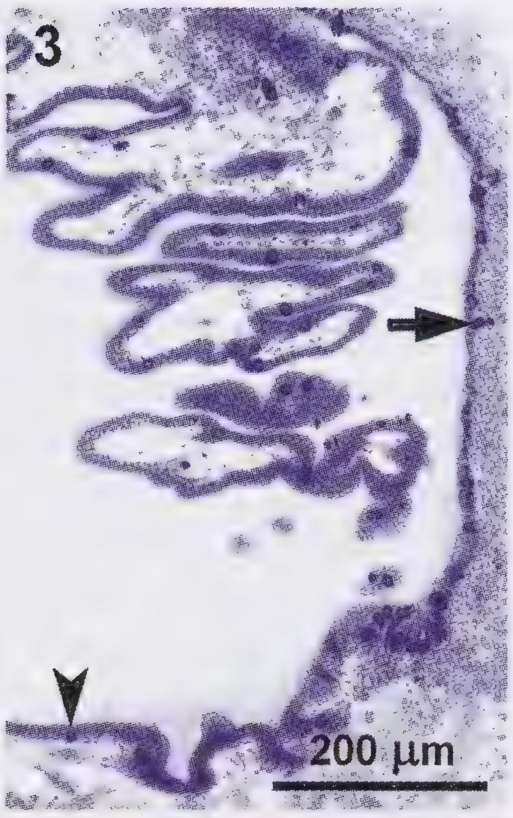

4

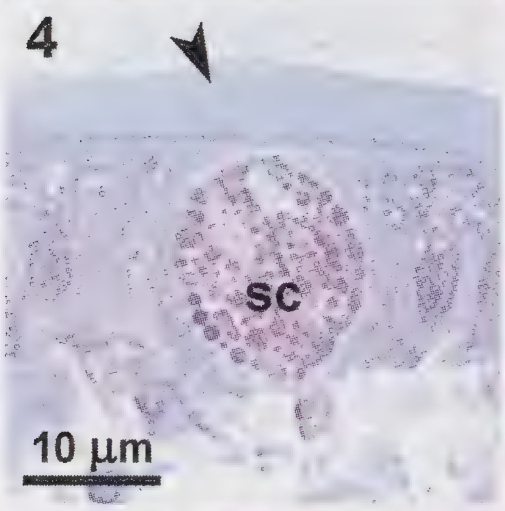

5

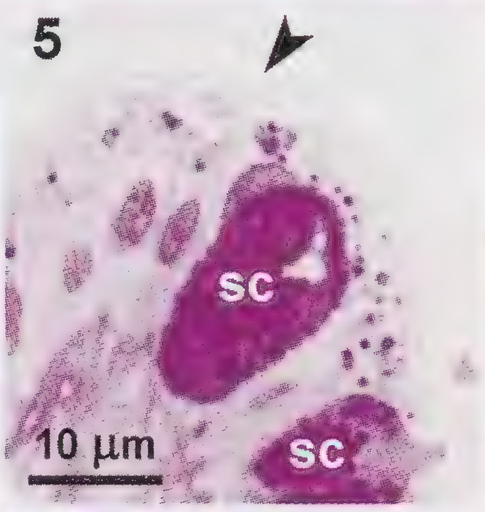

6

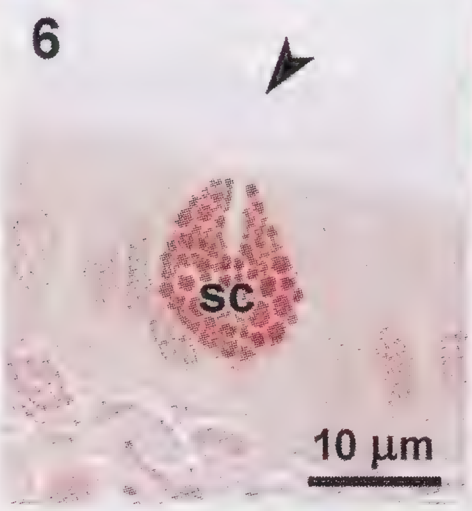

7

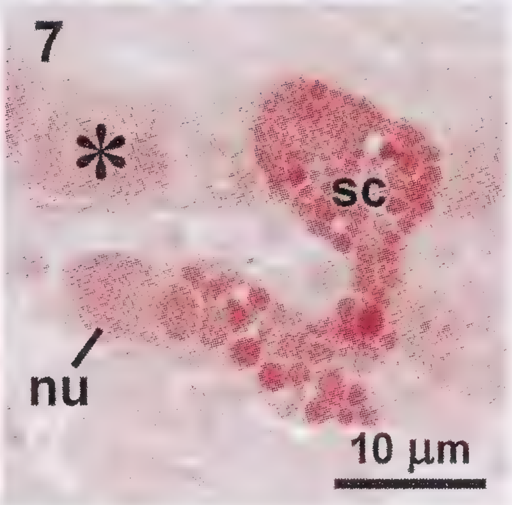

8

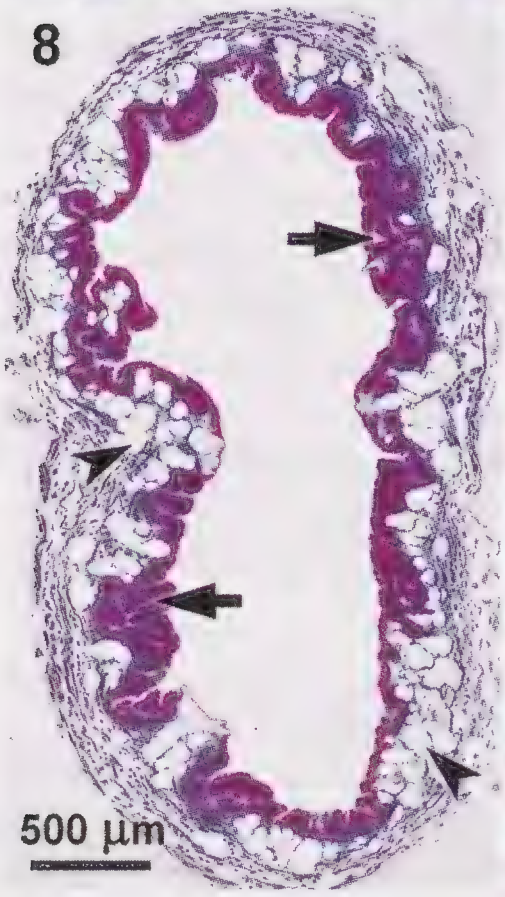

9

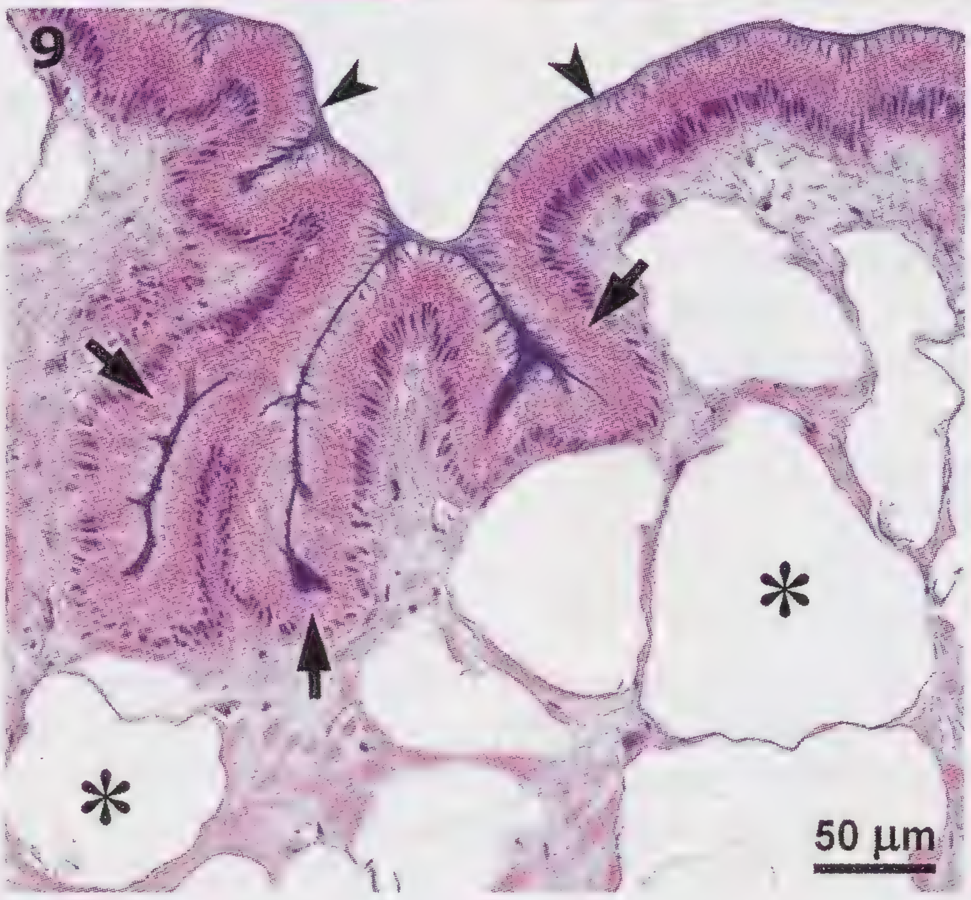

10

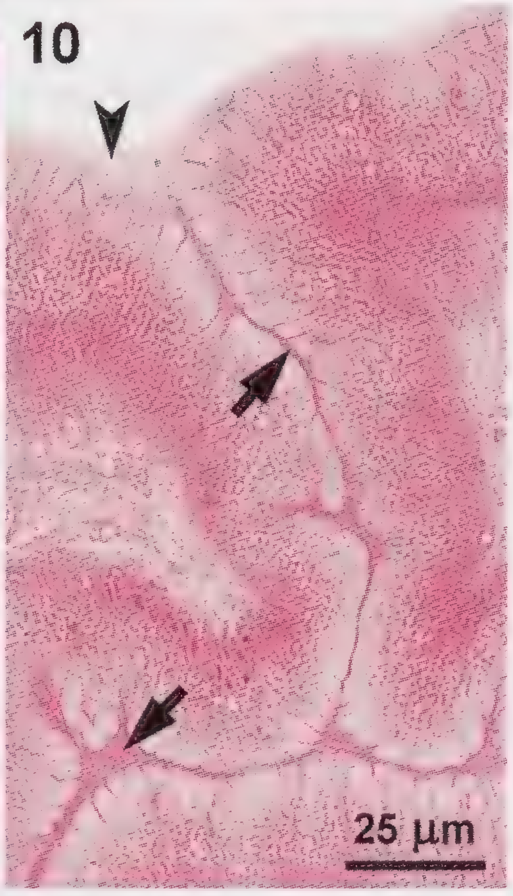

11

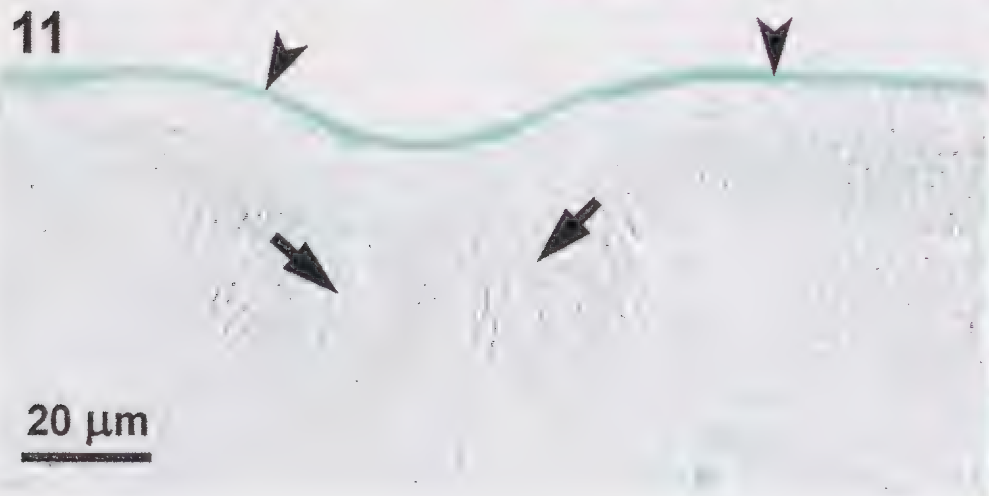

12

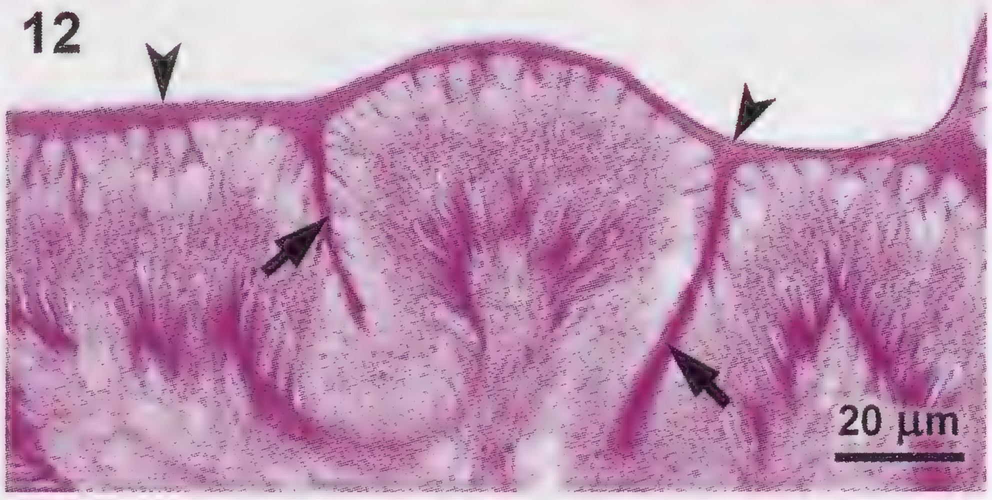

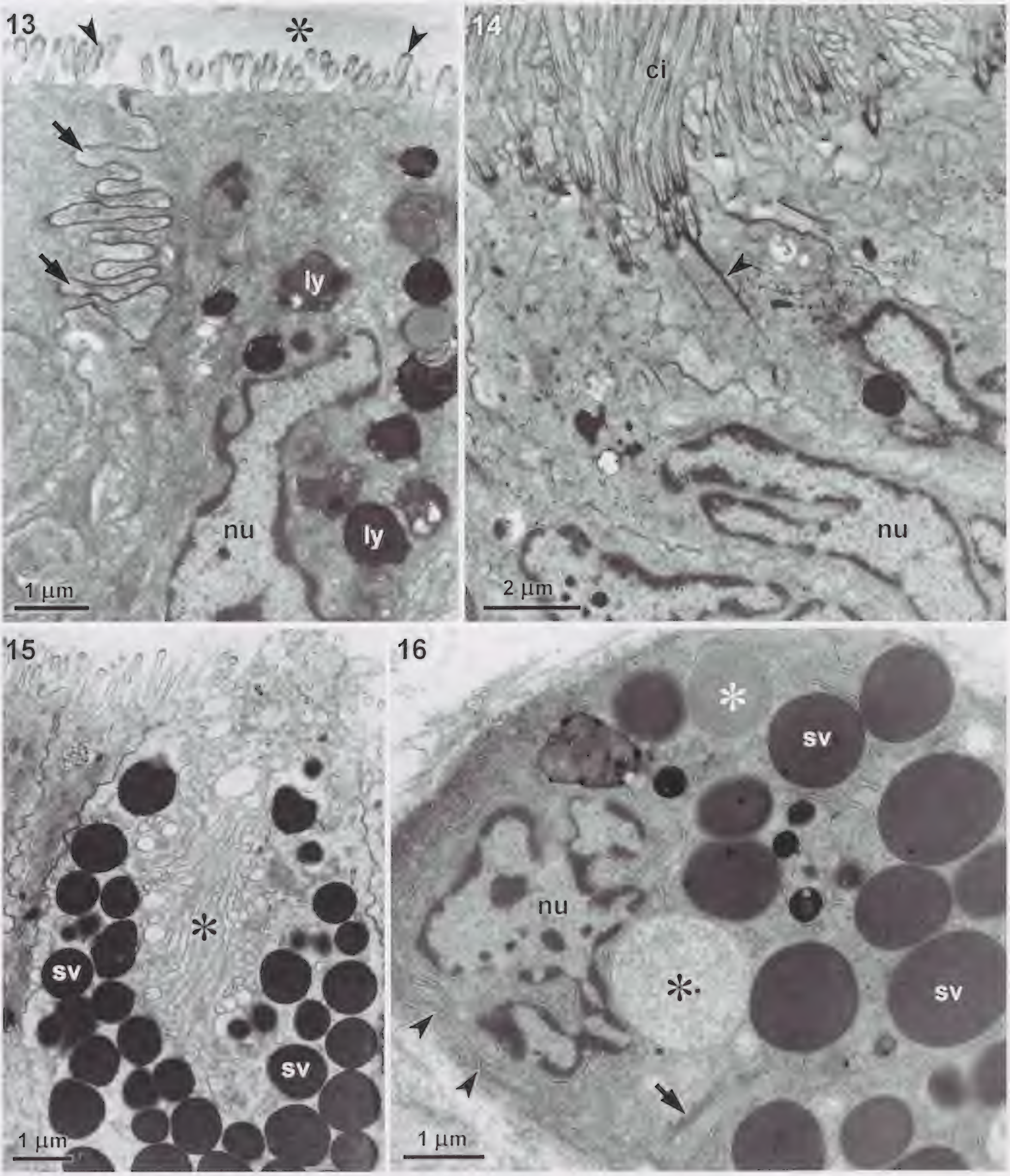

FIGS. 13–16. Ultrastructure of the anterior esophagus cells. FIG. 13: Epithelial cells from the lateral walls of an esophageal pouch showing the cuticle (asterisk), microvilli (arrowheads), interdigitations between cells (arrows), lysosome-like bodies (ly) and the nucleus (nu); FIG. 14: Epithelial cells densely covered by cilia (ci) at the base of an esophageal pouch. Ciliar roots (arrowhead) and nuclei (nu) are also visible; FIG. 15: The depression at the apex of the secretory cells is filled with microvilli (asterisk), and electron-dense secretory vesicles (sv) are abundant in the cytoplasm; FIG. 16: The basal region of the secretory cells contains the nucleus (nu), rough endoplasmic reticulum cisternae (arrowheads), Golgi stacks (arrow) and numerous secretory vesicles (sv) some of them still immature (asterisks).

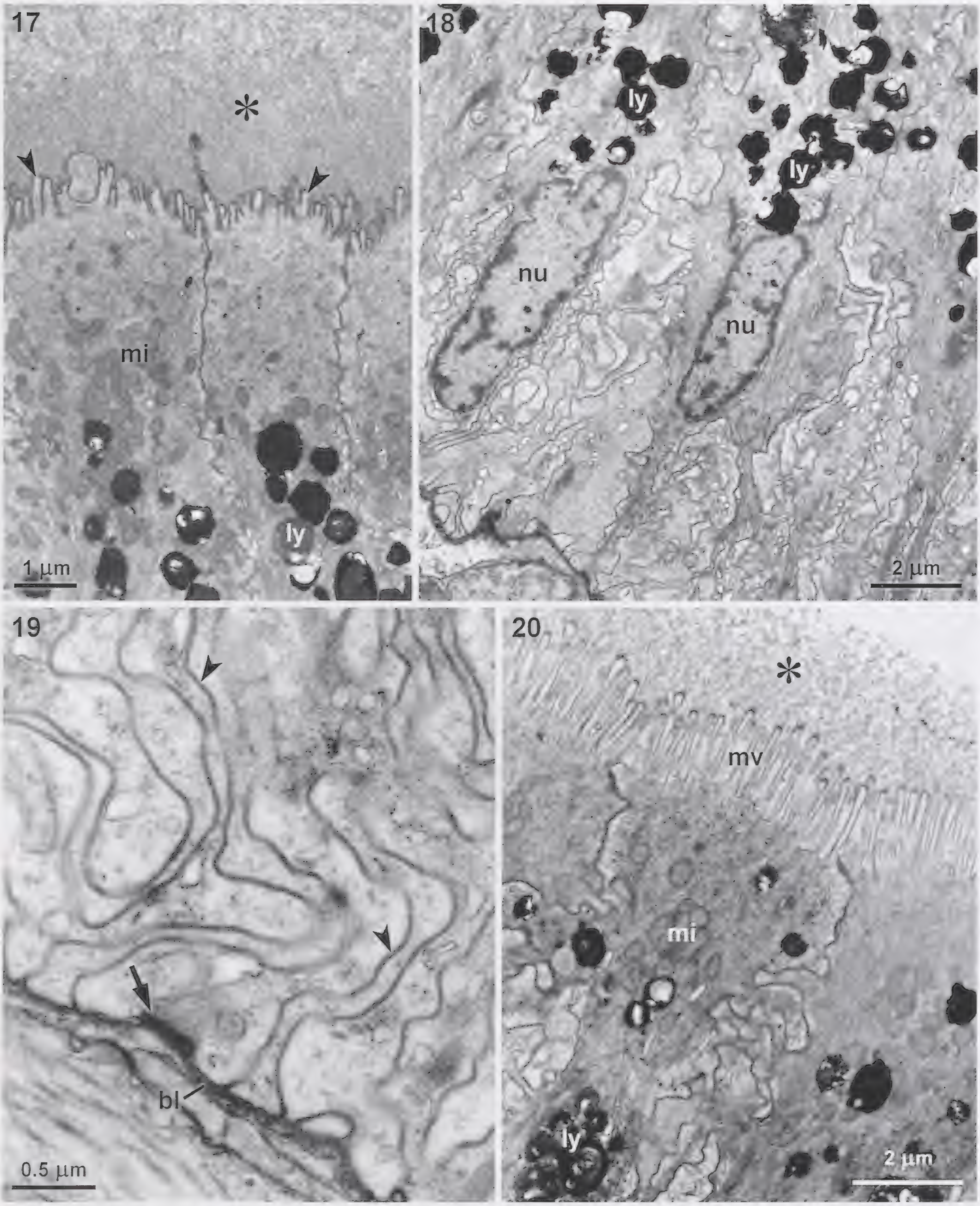

FIGS. 17–20. Ultrastructure of the crop and posterior esophagus cells. FIG. 17: Crop epithelial cells possess a border of microvilli (arrowheads) covered by a thick cuticle (asterisk). Many mitochondria (mi) and several lysosomal-like bodies (ly) are visible in the supranuclear region; FIG. 18: Nuclei (nu) at the basal region of crop epithelial cells; FIG: 19. Cell membrane invaginations (arrowheads) are abundant in the basal region of crop epithelial cells. A hemidesmosome (arrow) attached to a bundle of intermediate filaments is also visible. bl – basal lamina; FIG. 20: Apical region of the epithelial cells from the posterior esophagus showing the cuticle (asterisk), microvilli (mv), mitochondria (mi) and lysosome-like bodies (ly).

of the epithelial invaginations (Fig. 11). PAS positive material was detected both on the surface of the epithelium and in the invaginations (Fig. 12). In the connective tissue of the crop many very large vacuolar cells are present, mostly near the epithelium, being surrounded by muscle cells (Figs. 8, 9).

Ultrastructure and Microanalysis

In the anterior esophagus and lateral walls of the esophageal pouches the epithelial cells have a border of short microvilli covered by a thin cuticle. These cells contain several lysosome-like structures and many interdigita-

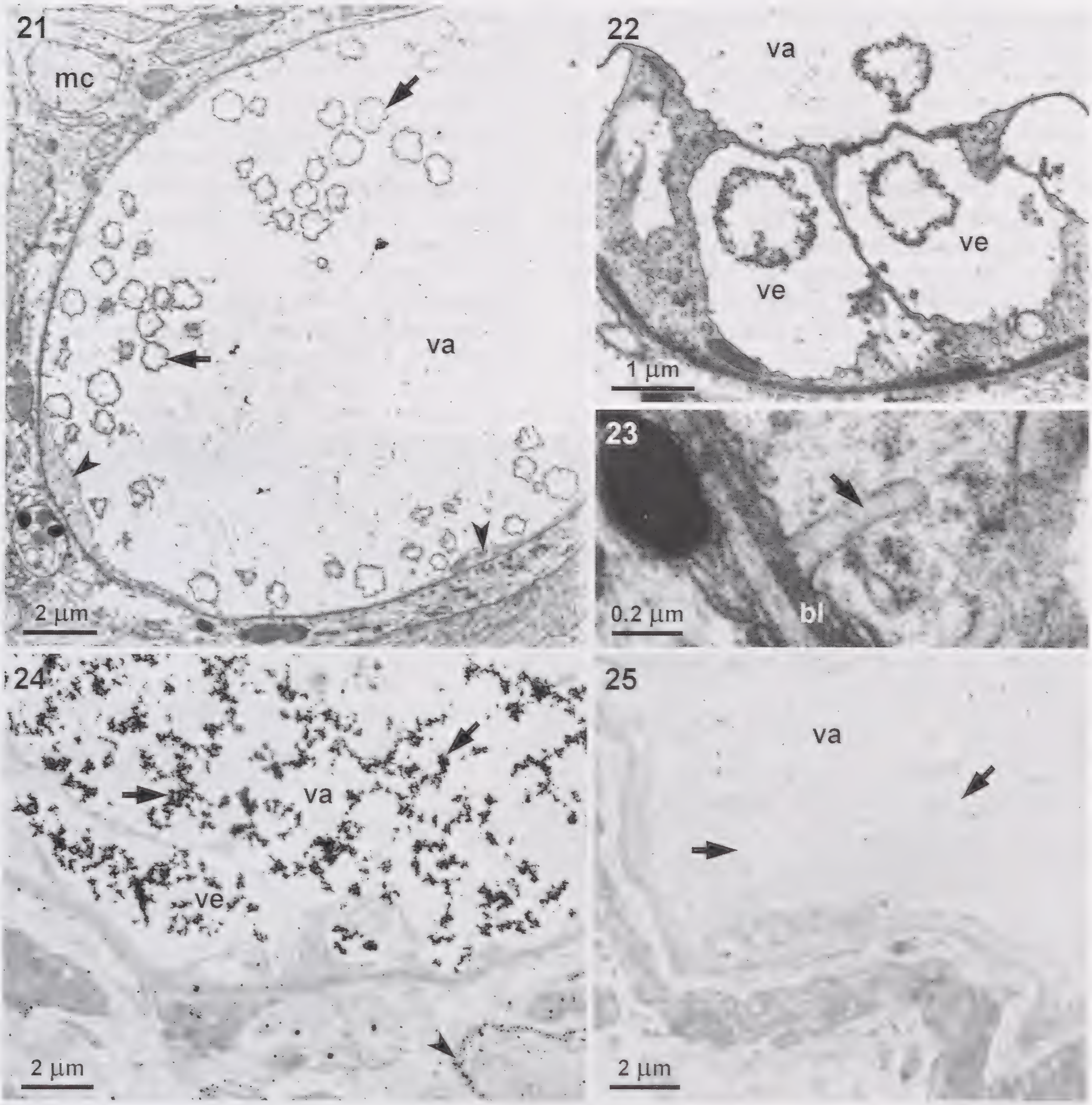

FIGS. 21–25. Ultrastructure and calcium detection in vacuolar cells. FIG. 21: Vacuolar cell with a thin peripheral cytoplasmic layer (arrowheads) and several structures with ring-shaped cross-section (arrows) inside the vacuole (va); FIG. 22: Structures with ring-shaped cross-section are also present within vesicles (ve) in the peripheral cytoplasm of the vacuolar cells; FIG. 23: Tubular cell membrane invagination (arrow) in a vacuolar cell. A thick basal lamina (bl) surrounds these cells; FIG. 24: Calcium detection with pyroantimonate in a vacuolar cell. Electron-dense deposits (arrows) are noticeable in the vacuole (va) and in vesicles (ve). Other cell types contain much lower amounts of electron-dense antimonate deposits (arrowhead); FIG. 25: Electron-dense antimonate deposits were removed from ultrathin sections after treatment with 10 mM EGTA for 30 min at 60°C, leaving clear spots in the epoxy resin (arrows).

tions connect neighboring cells (Fig. 13). At the base of the esophageal pouches, epithelial cells possess a border of cilia and the cuticle is absent (Fig. 14). The secretory cells of the esophageal pouches contain a large number of electron-dense vesicles, attaining a diameter of 1.5 µm. The apical region of these cells forms a depression that is full of microvilli (Fig. 15). The basal region, which is inserted into the connective tissue, contains endoplasmic reticulum cisternae around the nucleus and a few Golgi stacks are also present nearby (Fig. 16).

Epithelial cells of the crop have a border of short microvilli covered by a thick cuticle. Additionally, in the apical region these cells contain many mitochondria, lysosome-like bodies and some lipid droplets (Fig. 17). The elongated nucleus is basally located and numerous deep cell membrane invaginations are formed in the basal region (Figs. 18, 19). Several hemidesmosomes attached to bundles of intermediate filaments were observed on the basal membrane (Fig. 19). In the posterior esophagus, epithelial cells are similar to the epithelial cells of the crop (Fig. 20), and secretory cells are not present.

The vacuolar cells of the crop connective tissue are characterized by a very thin layer of cytoplasm surrounding a huge vacuole that occupies most of the cell volume. Several structures showing a ring-shape when viewed in cross-section were found inside the vacuole and also within vesicles located in the peripheral cytoplasm (Figs. 21, 22). Tubular cell membrane invaginations are another trait of these cells (Fig. 23). Calcium detection with potassium pyroantimonate revealed that these cells contain significant amounts of calcium. A large quantity of electron-dense antimonate deposits were observed in the central vacuole and in vesicles (Fig. 24), although some vacuolar cells contained more deposits than others. Small electron-dense deposits were also visible in other cell types, including muscle cells. Addition of EGTA during fixation of control fragments

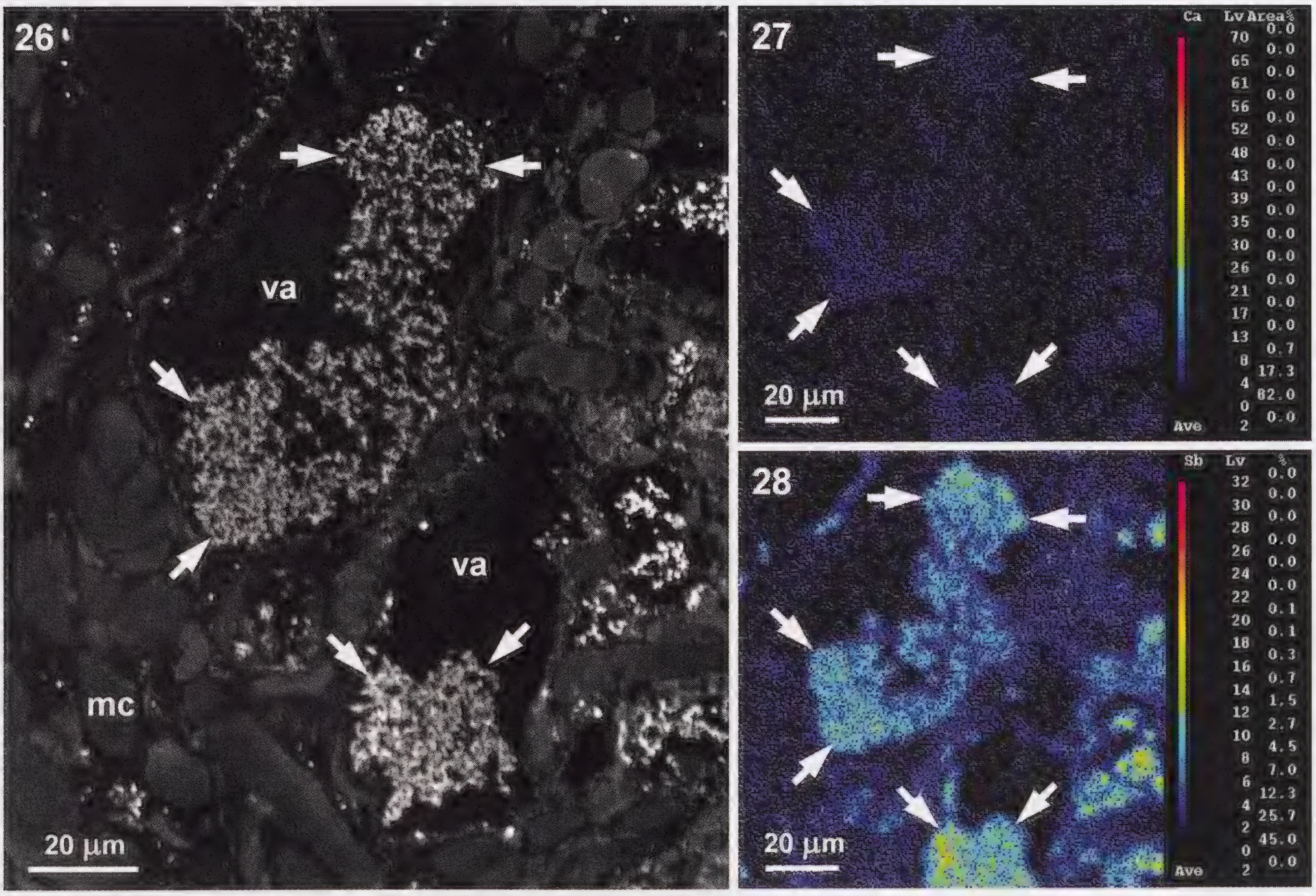

FIGS. 26–28. Microanalysis in vacuolar cells. FIG. 26: Backscattered electron image of a semithin section showing extensive antimonate deposits (arrows) in vacuolar cells (va). mc – muscle cells; FIG. 27: Intensity X-ray distribution map of calcium in the same semithin section. Calcium is more abundant in the areas corresponding to the antimonate deposits in vacuolar cells (arrows); FIG. 28: Intensity X-ray distribution map of antimony shows that the areas with higher amounts of antimony (arrows) correspond to the areas with higher amounts of calcium.

TABLE 1. Summary of main features of the esophagus and crop of *A. tricolorata* and *P. depicta*.

Species	Anterior esophagus	Crop histology			Histology of the posterior esophagus
		Epithelium	Secretory cells	Vacuolar cells	
A. tricolorata	Short, with esophageal pouches	Invaginations	Absent	Present	Identical to crop, but with ridges instead of invaginations
P. depicta	Absent	Ridges	Present	Present	Identical to crop

was not sufficient to prevent the formation of electron-dense deposits. However, the antimonate deposits were completely removed from ultrathin sections treated with 10 mM EGTA for 30 min at 60°C (Fig. 25), confirming the presence of calcium. The electron-dense deposits were not affected in water-incubated ultrathin sections. Additionally, 4 µm thick semithin sections were analyzed with an electron microprobe equipped with WDS detectors. Vacuolar cells containing electron-dense deposits were clearly visible in backscattered electron images obtained with the microprobe (Fig. 26). Although low amounts of calcium were detected (Fig. 27), the distribution of this element in the sections correlates well with the distribution of antimony (Fig. 28), corroborating the presence of calcium in the antimonate electron-dense deposits.

DISCUSSION

Among aglajids, histochemical and ultrastructural data on the esophagus and crop are available only for *A. tricolorata* (present article) and *Philinopsis depicta* (Lobo-da-Cunha et al., 2011). A comparison between these species reveals substantial differences, but also similarities in the digestive tract (Table 1). Contrary to what happens in *A. tricolorata*, in *P. depicta* an anterior esophagus is not noticeable between the buccal bulb and the crop (Lobo-da-Cunha et al., 2011). In *P. depicta*, the crop wall forms many ridges and two large folds (Lobo-da-Cunha et al., 2011). However, in *A. tricolorata* instead of ridges the crop presents numerous deep and branched invaginations, which are a different way to obtain an enlargement of the epithelial surface and enhance absorption of substances from the lumen. Another difference between these species is the presence of mucus-secreting cells in the crop epithelium of *P. depicta* and its absence in *A. tricolorata*. Moreover, the secretory cells found in the esophageal pouches and surrounding areas of the anterior esophagus of *A. tricolorata* secrete proteins associated with neutral polysaccharides, whereas the crop secretory cells of *P. depicta* secrete acid polysaccharides (Lobo-da-Cunha et al., 2011). Among all of these differences, the presence of many vacuolar cells in the connective tissue of the crop wall in both species seems to have a special significance. The presence of these peculiar cells in such large numbers in the two genera of aglajids that have been studied by transmission electron microscopy suggests that this could be a special trait of the crop of aglajids. So far, similar cells have not been reported in the digestive tract of other euopisthobranchs (Lobo-da-Cunha & Batista-Pinto, 2005; Lobo-da-Cunha et al., 2010a, 2010b).

The vacuolar cells of the crop connective tissue have the same main features in *A. tricolorata* and *P. depicta*, which are the large vacuole occupying most of the cell volume and the tubular cell membrane invaginations. However, in *A. tricolorata* the central vacuole and peripheral vesicles contain structures with a ring-shaped cross-section that were not observed in the vacuolar cells of *P. depicta* (Lobo-da-Cunha et al., 2011). Previously, it was suggested that these vacuolar cells could be related to the calcium cells of pulmonate gastropods (Lobo-da-Cunha et al., 2011), which could be a specific and modified type of rhogocyte according to Haszprunar (1996). In pulmonate gastropods, calcium cells reach a large diameter and contain large vacuoles loaded with concretions mainly consisting of calcium carbonate deposited on an organic matrix (Sminia et al., 1977; Luchtel et al., 1997). These cells can contain a single vacuole surrounded by a very thin layer of cytoplasm, with a peripheral nucleus (Richardot & Wautier, 1972; Sminia et al., 1977), resembling the vacuolar cells of aglajids. The typical calcium concretions of mollusks present a multilayered concentric pattern, but in calcium cells of *Lymnaea stagnalis* some of these formations show a simpler structure consisting on a single electron-dense layer (Sminia et al., 1977), closely resembling the structures with a ring-shaped cross-section found in *A. tricolorata* vacuolar cells. The pyroantimonate method revealed the presence of calcium in vacuolar cells of *A. tricolorata*, supporting the relationship with the calcium cells of pulmonates. However, the electron-dense antimonate deposits are scattered all over the central vacuole and vesicles, but not associated with the ring-shaped formations. Control with the calcium chelator EGTA added during fixation might not be effective in preventing the formation of electron-dense deposits containing calcium (Probst, 1986). For this reason, incubation of ultrathin sections with EGTA was used to confirm the presence of calcium. This last procedure specifically removes calcium causing the dissolution of the electron-dense deposits (Wick & Hepler, 1982; Probst, 1986), as reported in the vacuolar cells of *A. tricolorata*. An additional confirmation of the presence of calcium in the antimonate deposits was obtained with WDS X-Ray mapping of the cells. Experiments with the freshwater pulmonate *L. stagnalis* under acidosis conditions suggest that calcium cells can be a source of ions for pH buffering (Sminia et al., 1977), and that is a possible function for the connective tissue vacuolar cells in the crop of aglajids.

In *A. tricolorata*, a cuticular layer covers the epithelium of the esophagus and crop. However, the histochemical analysis shows that these cuticles have differences in composition. In the anterior esophagus the cuticle contains acid polysaccharides that are not PAS reactive, whereas the cuticle covering the crop epithelium contains acid polysaccharides and is stained by PAS reaction. More significant are the histochemical differences between the cuticle on the surface of crop epithelium and the material filling the lumen of crop epithelial invaginations. Both contain PAS reactive polysaccharides, but acid polysaccharides are only detected in the cuticle covering the surface of the epithelium in direct contact with the lumen. On the other hand, proteins that are reactive to the tetrazonium coupling reaction are found in the lumen of the invaginations but not on the surface of the crop epithelium. Acid polysaccharides were also detected in the extracellular material covering the crop epithelium of *P. depicta*, but in this species the epithelium does not form invaginations (Lobo-da-Cunha et al., 2011). However, it seems that the extracellular materials covering these epithelia can be crossed by substances that are collected by epithelial cells. In gastropods, esophageal and crop epithelial cells typically possess several lysosomes in the cytoplasm above the nucleus (Bush, 1989; Leal-Zanchet, 2002; Lobo-da-Cunha & Batista-Pinto, 2005; Lobo-da-Cunha et al., 2010a), which seem to be involved in the intracellular digestion of substances collected by endocytosis (Boer & Kits, 1990; Bourne et al., 1991), and the abundance of lysosome-like bodies in the crop epithelium of *A. tricolorata* suggests a similar activity. Additionally, the numerous deep cell membrane invaginations in the basal region of crop epithelial cells in *A. tricolorata* are a sign of intense transport activity, also reported in other gastropods (Payne & Crisp, 1989). All these aspects indicate that the crop epithelium performs an important physiological role.

Hemidesmosomes are frequent in the crop epithelium of *A. triclorata* and *P.depicta* (Lobo-da-Cunha et al., 2011). These cell junctions reinforce the adhesion between epithelial cells and the underlying connective tissue (Bairati & Gioria, 2008) and might be particularly important in the crop of aglajids that is subjected to substantial distention when filled with food (Lobo-da-Cunha et al., 2011).

In cephalaspideans with gizzard, a dilated crop is not present, and the gizzard divides the esophagus into anterior and posterior regions (Lobo-da-Cunha et al., 2010a, 2010b). Aglajids have lost the gizzard and acquired a dilated crop. Considering that in *A. tricolorata* and *P. depicta* the crop and the posterior esophagus present very similar histological and ultrastructural aspects, and given that in *A. tricolorata* the anterior esophagus is substantially different from the crop, according to available data, it seems that the crop of aglajids was originated as a dilated region of the posterior esophagus.

The anatomical and functional characteristics of the buccal bulb have been considered the most significant features of the digestive tract for distinction among aglajid genera (Rudman, 1974; Gosliner, 1980). However, detailed information on the digestive system of aglajids and other cephalaspideans is still scarce. In most taxonomic articles, the digestive system is very briefly described, but the new studies on the esophagus and crop of *P. depicta* (Lobo-da-Cunha et al., 2011) and *A. tricolorata* have revealed substantially different aspects that should be investigated in other species to evaluate potential taxonomic relevance.

ACKNOWLEDGEMENTS

The authors thank Mr João Carvalheiro and Miss Joana Carvalheiro for the reproduction of photomicrographs. This work was partially supported by ICBAS-UP and by the European Regional Development Fund (ERDF) through the COMPETE – Operational Competitiveness Programme and national funds through FCT – Foundation for Science and Technology, under the project PEst-C/MAR/LA0015/2011.

LITERATURE CITED

BAIRATI, A. & M. GIORIA, 2008, An ultrastructural study of cell junctions and the cytoskeleton in epithelial cells of the molluscan integument. *Journal of Morphology*, 269: 319–331.

BOER, H. H. & K. S. KITS, 1990, Histochemical and ultrastructural study of the alimentary tract of the freshwater snail *Lymnaea stagnalis*. *Journal of Morphology*, 205: 97–111.

BOURNE, N. B., G. W. JONES & I. D. BOWEN, 1991, Endocytosis in the crop of the slug, *Deroceras reticulatum* (Müller) and the effects of the ingested molluscicides, metaldehyde and methiocarb. *Journal of Molluscan Studies*, 57: 71–80.

BUSH, M. S., 1989, The ultrastructure and function of the esophagus of *Patella vulgata* Linnaeus. *Journal of Molluscan Studies*, 55: 111–124.

DINAPOLI, A. & A. KLUSSMANN-KOLB, 2010, The long way to diversity – Phylogeny and evolution of the Heterobranchia (Mollusca: Gastropoda). *Molecular Phylogenetics and Evolution*, 55: 60–76.

GANTER, P. & G. JOLLÈS, 1970, *Histochimie normal et pathologique*. Gauthier-Villars, Paris, 2 vols.

GOSLINER, T. M., 1980, Systematics and phylogeny of the Aglajidae (Opisthobranchia: Mollusca). *Zoological Journal of the Linnean Society*, 68: 325–360.

HASZPRUNAR, G., 1996, The molluscan rhogocyte (pore-cell, blasenzelle, cellule nucale), and its significance for ideas on nephridial evolution. *Journal of Molluscan Studies*, 62: 185–211.

JÖRGER, K. M., I. STÖGER, Y. KANO, H. FUKUDA, T. KNEBELSBERGER & M. SCHRÖDL, 2010, On the origin of Acochlidia and other enigmatic euthyneuran gastropods, with implications for the systematics of Heterobranchia. *BMC Evolutionary Biology*, 10(323): 1–20.

KLUSSMANN-KOLB, A., A. DINAPOLI, K. KUHN, B. STREIT & C. ALBRECHT, 2008, From sea to land and beyond – New insights into the evolution of euthyneuran Gastropods (Mollusca). *BMC Evolutionary Biology*, 8(57): 1–16.

LANE, B. P. & D. L. EUROPA, 1965, Differential staining of ultrathin sections of Epon-embedded tissues for light microscopy. *Journal of Histochemistry and Cytochemistry*, 13: 579–582.

LEAL-ZANCHET, A. M., 2002, Ultrastructure of the supporting cells and secretory cells of the alimentary canal of the slugs, *Lehmannia marginata* and *Boettgerilla pallens* (Pulmonata: Stylommatophora: Limacoidea). *Malacologia*, 44: 223–239.

LOBO-DA-CUNHA, A. & C. BATISTA-PINTO, 2005, Light and electron microscopy studies of the esophagus and crop epithelium in *Aplysia depilans* (Mollusca, Opisthobranchia). *Tissue & Cell*, 37: 447–456.

LOBO-DA-CUNHA, A., I. FERREIRA, R. COELHO & G. CALADO, 2009, Light and electron microscopy study of the salivary glands of the carnivorous opisthobranch *Philinopsis depicta* (Mollusca, Gastropoda). *Tissue & Cell*, 41: 367–375.

LOBO-DA-CUNHA, A., E. OLIVEIRA, A. ALVES, R. COELHO & G. CALADO, 2010a, Light and electron microscopic study of the anterior esophagus of *Bulla striata* (Mollusca, Opisthobranchia). *Acta Zoologica*, 91: 125–138.

LOBO-DA-CUNHA, A., E. OLIVEIRA, I. FERREIRA, R. COELHO & G. CALADO, 2010b, Histochemical and ultrastructural characterisation of the posterior esophagus of *Bulla striata* (Mollusca, Opisthobranchia). *Microscopy and Microanalysis*, 16: 688–698.

LOBO-DA-CUNHA, A., T. SANTOS, E. OLIVEIRA, A. ALVES, R. COELHO & G. CALADO, 2011, Microscopical study of the crop and oesophagus of the carnivorous opisthobranch *Philinopsis depicta* (Cephalaspidea, Aglajidae). *Journal of Molluscan Studies*, 77: 322–331.

LUCHTEL, D. L., A. W. MARTIN, I. DEYRUP-OLSEN & H. H. BOER, 1997, Gastropoda: Pulmonata. Pp. 459–718, in: F. W. HARRISON & A. J. KOHN, eds., *Microscopic anatomy of invertebrates*, Vols. 6A–B [Mollusca II]. Wiley-Liss, New York, 828 pp.

MALAQUIAS, M. A. E., J. M. DODDS, P. BOUCHET & D. G. REID, 2009, A molecular phylogeny of the Cephalaspidea *sensu lato* (Gastropoda: Euthyneura): Architectibranchia redefined and Runcinacea reinstated. *Zoologica Scripta*, 38: 23–41.

MIKKELSEN, P. M., 1996, The evolutionary relationships of Cephalaspidea s. l. (Gastropoda: Opisthobranchia): a phylogenetic analysis. *Malacologia*, 37: 375–442.

PAYNE, C. M. & M. CRISP, 1989, Ultrastructure and histochemistry of the posterior esophagus of *Nassarius reticulatus* (Linnaeus). *Journal of Molluscan Studies*, 55: 313–321.

PROBST, W., 1986, Ultrastructural localization of calcium in the CNS of vertebrates. *Histochemistry*, 85: 231–239.

RICHARDOT, M. & J. WAUTIER, 1972, Les cellules à calcium du conjonctif de *Ferrissia wautieri* (Moll. Ancylidae). Description, minéralogie et variation saisonnières. *Zeitschrift für Zellforschung*, 134: 227–243.

RUDMAN, W. B., 1972, Structure and functioning of the gut in the Bullomorpha (Opisthobranchia). Part 4. Aglajidae. *Journal of Natural History*, 6: 547–560.

RUDMAN, W. B., 1974, A comparison of *Chelidonura*, *Navanax* and *Aglaja* with other genera of the Aglajidae (Opisthobranchia: Gastropoda). *Zoological Journal of the Linnean Society*, 54: 185–212.

RUDMAN, W. B. & R. C. WILLAN, 1998, Opisthobranchia. Pp. 915–1035, in: P. L. Beesley, G. J. B. Ross & A. Wells, eds., *Fauna of Australia. The southern synthesis, Vol. 5. Mollusca.* CSIRO Publishing, Melbourne, xv + 1234 pp.

SMINIA, T., N. D. DE WITH, J. L. BOS, M. E. VAN NIEUWMEGEN, M. P. WITTER & J. WONDERGEM, 1977, Structure and function of the calcium cells of the freshwater pulmonate snail *Lymnaea stagnalis. Netherlands Journal of Zoology*, 27: 195–208.

WÄGELE, H., 2004, Potential key characters in Opisthobranchia (Gastropoda, Mollusca) enhancing adaptive radiation. *Organism Diversity and Evolution*, 4: 175–188.

WÄGELE, H., A. KLUSSMANN-KOLB, E. VERBEEK & M. SCHRÖDLE, 2014, Flashback and foreshadowing – a review of the taxon Opisthobranchia. *Organisms Diversity and Evolution*, 14: 133–149.

WALKER, G., 1972, The digestive system of the slug, *Agriolimax reticulatus* (Müller): experiments on phagocytosis and nutrient absorption. *Proceedings of the Malacological Society of London*, 40: 33–43.

WICK, S. M. & P. K. HEPLER, 1982, Selective localization of intracellular Ca^{2+} with potassium antimonate. *Journal of Histochemistry and Cytochemistry*, 30: 1190–1204.

Revised ms. accepted October 7, 2013

MALACOLOGIA, 2014, 57(2): 377–397

CHROMOSOMAL CHARACTERISTICS OF NORTH AMERICAN AND OTHER NAIADES (BIVALVIA: UNIONIDA)

John J. Jenkinson

305 Revere Ave., Clinton, Tennessee 37716, U.S.A.; jjjenkinson@hotmail.com

ABSTRACT

This project was conducted to determine if chromosomal characteristics can provide information useful in systematics of the naiades (Bivalvia: Unionida). A field-compatible slide preparation technique was perfected to the point that a few chromosome spreads could be expected from most processed animals. Chromosome slides were prepared from 250 naiades collected in ten of the east-central and southeastern United States, the western state of Oregon, and Manitoba Province, Canada.

The 65 species of North American naiades for which chromosome numbers were determined during this project (64 members of the family Unionidae and one member of the family Margaritiferidae) all have a diploid number of 38 chromosomes. This number is identical to reported diploid numbers for the 11 European and seven of the eight Asian unionid and margaritiferid species that have been studied, strongly suggesting that 38 is the diploid number present in the largely Northern Hemisphere superfamily Unionoidea. In the other unionid superfamily, the Etherioidea, the three Australian and one South American hyriid naiades that have been studied all have 34 diploid chromosomes, while the single studied African iridinid species has 20 chromosomes. If this difference in chromosome numbers is substantiated as more, especially Southern Hemisphere species are studied, this straight-forward morphologic character could become important in recognizing distinctions between high-level groups of naiades.

An analysis of chromosomal morphology focused on two metrics: Arm Ratio (r) and Relative Length (RL). When considered together, these two virtually independent metrics sort the chromosomes into similar-size and similar-shape groups that can facilitate comparisons between species. Analysis of the suggested karyotypes for these two metrics and the detailed karyotypes of their interaction demonstrates the similarity of two species in the same naiad genus and the substantial dissimilarity of two species in different naiad tribes. Analysis of the r and RL metrics for ten species and an all-inclusive composite demonstrates that karyotypic data can recognize similarities and differences among naiad species that correspond with results from other morphologic and genetic character sets.

Key words: Bivalvia, Unionida, naiad, chromosome, karyotype, relative length.

INTRODUCTION

All of the approximately 900 species of large bivalve mollusks that occur in freshwater habitats around the world are considered members of the order Unionida (Graf & Cummings, 2006). A variety of English common names have been used when considering all of these species as a group (freshwater mussels, clams, unionids, etc.); I prefer to use "naiad," (plural: naiades) because – as it is used by Simpson (1896), Ortmann (1921), and others – naiad is the only broadly inclusive term for all of the members of this order that is not burdened by any taxonomic bias or inaccuracy. Fossil evidence suggests that the naiades have existed in freshwater habitats since Paleozoic time (Giribet, 2008). The combination of their large size, often obvious presence in freshwater habitats, world-wide distribution, and long geologic history have made the naiades interesting to a long list of naturalists, malacologists and evolutionary biologists (e.g., Say, 1817; Baker, 1928; Fuller, 1974; Haag, 2012). Over the years, researchers have used a variety of shell, anatomical, developmental and genetic characteristics to suggest evolutionary and taxonomic relationships among various groups of naiades (e.g., Lea, 1870; Simpson, 1896; Ortmann, 1921; Davis & Fuller, 1981; Graf & Cummings, 2007). To date, however, no authors have used counts of the chromosomes or other chromosomal characteristics in their studies of naiad relationships.

Apparently, Lillie (1901) was the first to publish a count of the chromosomes present in any naiad. In his extensive study of naiad eggs and their development, Lillie saw many sectioned chromosome spreads and reported that *Unio complanata* (= *Elliptio complanatus*) has 16 haploid [= 32 diploid] chromosomes (Lillie, 1901). Both Menzel (1968) and Patterson (1969) found it difficult to make accurate counts of the chromosomes from sectioned material and chose not to include counts based on sectioned material in their lists of molluscan chromosome numbers. That precedent is followed in this paper.

In their monograph on naiades in Australia, McMichael & Hiscock (1958) included a paragraph indicating that *Alathyria pertexta*, *Velesunio ambiguus* and *Velesunio legrandi* all have 34 diploid chromosomes. Patterson (1969) tabulated many previous reports of mollusk chromosome numbers, listing 1,100 chromosome counts for species of gastropods, two for cephalopods, and 22 for pelecypods. None of the bivalve chromosome numbers cited by Patterson were for naiades. Van Griethuysen et al. (1969) described 38 diploid chromosomes for two European naiad species, and Nadamitsu & Kanai (1975, 1978) reported 38 diploid chromosomes for three Japanese naiades. A preliminary report on this project (Jenkinson, 1976) indicated that 15 North American naiad species all have 38 diploid chromosomes.

In more recent years, Nakamura (1985) accumulated published chromosome data on the molluscan classes Bivalvia, Polyplacophora and Cephalopoda. His list includes chromosome numbers for 125 bivalve species, including seven naiad species beyond the 15 reported by Jenkinson (1976). Park & Burch (1995) reported chromosome numbers for two additional North American naiades and recognized chromosome numbers for seven Korean species studied by Park & Kwon (1991). Thiriot-Quiévreux published compilations of recent chromosome counts for aquatic organisms (Thiriot-Quiévreux, 1994), bivalves (Thiriot-Quiévreux, 2002) and gastropods (Thiriot-Quiévreux, 2003). By 2002, her bivalve list included 66 species, four of which were naiades: two from Europe, one from Africa and one from China (Thiriot-Quiévreux, 2002). In their review of bivalve chromosomal banding studies, Leitão & Chaves (2008) listed chromosome numbers for 48 additional species, including two naiades: one from Europe and one from Asia. Table 1 presents a summary of published chromosome numbers for the order Unionida, aggrading records from a variety of sources.

The pattern indicated early on by the extensive work on gastropods and more sparse work on the other classes suggested that mollusks show a remarkable degree of conservation in chromosome number (Patterson, 1969; Murray, 1975). Based on more extensive and more recent data, Thiriot-Quiévreux (2002: 197) observed that: “This pattern remains ... but this review shows that, as more species are examined, the range of chromosome numbers increases.” Information on chromosome numbers accumulated by various authors (many tabulated in Thiriot-Quiévreux, 2002; and Leitão & Chaves, 2008) indicates that bivalve diploid numbers range between 12 and 213, with complete uniformity in the Osterida (all 20), an extremely wide range in the Venerida (from 20 to 213), and more modest ranges in the other orders. The most common diploid chromosome number found within the Bivalvia is 38, present in 40% of the species examined so far. As indicated in Table 1, 38 is the typical chromosome number within the Unionida. The only exceptions reported so far are three species from Australia (all 34), two from Egypt (one 20 and one 28), one from Chile (34), and one from Thailand (37).

This project was conducted to determine if chromosomal characteristics of North American naiades could be examined as a routine procedure and if the study of these characteristics could provide information useful in naiad systematics. Much of the original research presented here is taken from a dissertation I completed and defended in 1983 (Jenkinson, 1983). At that time, I was deeply involved in the first of a series of large projects for my post-graduate employer and, although an oral summary of this work was presented at the 1983 American Malacological Union meeting (Jenkinson, 1984), the body of this work has remained unpublished until now. Recently, it has come to my attention that the few people who remember this project believe it demonstrated that chromosomal characteristics would not help clarify evolutionary and taxonomic relationships among the naiades. The work I conducted 30 years ago convinced me of just the opposite; it showed me that chromosomal characteristics offer a new perspective on how

TABLE 1. Published chromosome numbers for the Order Unionida. Some of these entries are included in the reviews by Nakamura (1985), Park & Burch (1995), Thiriot-Quiévreux (2002) and Leitão & Chaves (2008). The suprageneric groupings follow Graf & Cummings (2007). Most author and date entries come from the cited references; others come from Graf & Cummings (2007) and Simpson (1900).

Species	Diploid No.	Location	References
Superfamily Etherioidea			
Family Hyriidae			
Alathyria pertexta Iredale, 1934	34	E Australia	McMichael & Hiscock, 1958
Diplodon chilensis (Gray, 1828)	34	Villarrica Lake, Chile	Jara-Seguel et al., 2000
Velesunio ambiguus (Philippi, 1847)	34	SE Australia	McMichael & Hiscock, 1958
Velesunio legrandi (Petterd, 1889)	34	Tazmania	McMichael & Hiscock, 1958
Family Iridinidae			
Mutela rostrata (Rang, 1835)	20	Egypt	Ebied, 1998
Superfamily Unionioidea			
Family Margaritiferidae			
Margaritifera laevis (Hass, 1910)	38	Hiroshima Prefecture, Japan	Nadamitsu & Kanai, 1975
Margaritifera margaritifera form *falcata* (Gould, 1850)	38	Willamette River, Oregon	Jenkinson, 1976
Family Unionidae			
Africa			
Unio elongatulus Pfeiffer, 1825	28	Egypt	Ebied, 1998
Asia			
Anodonta arcaeformis flavotincta von Martens, 1905	38	Korea	Park & Kwon, 1991
Anodonta woodiana (Lea, 1834)	38	Korea	Park et al., 1988; Park & Kwon, 1991
Anodonta woodiana elliptica Heude, 1878	38	China	Shi, 1980
Anodonta woodiana pacifica Heude, 1878	38	China	Wen et al., 2009
Cristaria plicata (Leach,1815)	38	China	Shi, 1980
Hyriopsis cumingii (Lea, 1852)	38	China	Shi, 1980; Wang et al., 2000
Inversidens japonensis (Lea, 1859)	38	Iwakuni, Japan	Nadamitsu & Kanai, 1978
Lamprotula gottschei (von Martens, 1894)	38	Korea	Park & Kwon, 1991
Lanceolaria acrorrhyncha (von Martens, 1894)	38	Korea	Park & Kwon, 1991
Pseudodon obovalis omiensis (von Heimburg, 1884)	38	Miyoshi, Japan	Nadamitsu & Kanai, 1978
Solenia khwaegnoiensis Panha & Deein, 2003	"37"	Khwae Noi River, Thailand	Deein et al., 2003
Unio douglasiae (Griffith & Pidgeon, 1834)	38	Korea	Park & Kwon, 1991

(continues)

(continued)

Species	Diploid No.	Location	References
Unio douglasiae sinuolatus von Martens, 1905	38	Korea	Park & Kwon, 1991
Sorenia triangularis (Heude, 1885)	38	Korea	Park & Kwon, 1991
Europe			
Anodonta anatina (Linnaeus, 1758)	38	Damien Lake, Netherlands; Wulpinskie Lake, Poland	van Griethuysen et al., 1969; Woznicki & Jankun, 2004
Anodonta cygnea (Linnaeus, 1758)	38	Lagoa de Mira, Portugal; Ukraine	Carrilho et al., 2008; Melnychenko & Yanovich, 2004
Anodonta stagnalis (Gmelin in Linnaeus, 1758)	38	Ukraine	Melnychenko & Yanovich, 2004
Anodonta woodiana (Lea, 1834)	38	Konin Lakes, Poland	Woznicki, 2004
Anodonta zellensis Model, 1945	38	Ukraine	Melnychenko & Yanovich, 2004
Colletopterum piscinale (Drouet, 1881)	38	Ukraine	Melnychenko & Yanovich, 2004
Colletopterum ponderosum Bourguignat, 1880	38	Ukraine	Melnychenko & Yanovich, 2004
Pseudanodonta complanata (Rossmaessler, 1835)	38	Ukraine	Melnychenko & Yanovich, 2004
Unio conus Spengler, 1793	38	Ukraine	Melnychenko, 2000
Unio elongatulus Pfeiffer, 1825	38	Brenta River, Italy	Vitturi et al., 1982
Unio pictorum (Linnaeus, 1758)	38	Damien Lake, Netherlands; Ukraine	van Griethuysen et al., 1969; Melnychenko, 2000
North America			
Alasmidonta arcula (Lea, 1838)	38	Ohoopee River, Georgia	Jenkinson, 1976
Alasmidonta marginata Say, 1818	38	Big Darby Creek, Ohio	Jenkinson, 1976
Anodontoides ferussacianus (Lea, 1834)	38	Buffalo Creek, Ohio; Michigan	Jenkinson, 1976; Park & Burch, 1995
Elliptio complanata (Lightfoot, 1786)	38	Michigan	Park & Burch, 1995
Epioblasma triquetra (Rafinesque, 1820)	38	Michigan	Park & Burch, 1995
Gonidea angulata (Lea, 1838)	38	Willamette River, Oregon	Jenkinson, 1976
Lampsilis radiata luteola (Lamarck, 1819)	38	Big Darby Creek, Ohio	Jenkinson, 1976
Lasmigona costata (Rafinesque, 1820)	38	Big Darby Creek, Ohio	Jenkinson, 1976
Potamilus alatus (Say, 1817)	38	Buck Creek, Kentucky	Jenkinson, 1976
Ptychobranchus fasciolaris (Rafinesque, 1820)	38	Big Darby Creek, Ohio; Michigan	Jenkinson, 1976; Park & Burch, 1995
Pyganodon [as *Anodonta*] *grandis* (Say, 1829)	38	Michigan, Colorado; Buffalo Creek, Ohio	Park & Burch, 1995; Jenkinson, 1976
Quadrula quadrula (Rafinesque, 1820)	38	Big Darby Creek, Ohio	Jenkinson, 1976
Toxolasma lividus Rafinesque, 1831	38	Buck Creek, Kentucky	Jenkinson, 1976
Tritogonia verrucosa (Rafinesque, 1820)	38	Big Darby Creek, Ohio	Jenkinson, 1976
Villosa iris iris (Lea, 1829)	38	Big Darby Creek, Ohio	Jenkinson, 1976
Villosa lienosa (Conrad, 1834)	38	Buffalo Creek, Ohio	Jenkinson, 1976

closely various groups of naiades are, and are not, related to each other.

When I started to consider publishing this research, I had no desire to reexamine all of the slides and chromosome spreads, or to reanalyze all of the data that had been generated thirty years ago. I did, however, recognize the need to update the identifications of the species that had been included in my work. All of the naiades and other bivalves examined as part of this project had been deposited at the Ohio State University Museum of Biological Diversity (OSUM) and, over the years, had been catalogued into that bivalve collection. During 2011, Dr. G. Thomas Watters, curator of the OSUM bivalve collection, provided the updated identifications for the specimens used in this paper. In my 1983 dissertation, the concluding analysis used chromosomal characteristics to compare and contrast the relationships proposed in several published taxonomic groupings of naiad genera. Present-day workers are in the midst of using genetic characteristics to reexamine relationships among the naiades. One recent publication (Graf & Cummings, 2007) proposes a new classification of this group based on an integration of morphologic, anatomical and genetic characteristics, but does not include any chromosomal characters. Rather than repeat the strictly academic (and now, incomplete) analysis included in my dissertation, this paper concludes with a new analysis using chromosomal characteristics to look at relationships among species from some of the naiad groupings proposed by Graf & Cummings (2007).

METHODS

Ideally, for chromosomal information to be used as a common and versatile tool in naiad identification and taxonomy, the preparation methods ought to meet a number of procedural and use criteria. In the field, it would be most useful if chromosome preparation techniques could provide information from specimens collected at any time throughout the year and be simple enough to interfere very little with other stream-side activities. In the laboratory, it would be best if chromosome preparations could provide readily retrievable, independent information about the specimens from which they were taken; be permanent, reusable records; be adaptable enough to be reanalyzed when new comparison techniques are discovered; and, ideally, be usable on specimens already housed in a research collection.

Obviously, this set of goals is not likely to be completely met by any technique. All techniques require some commitment of time and expertise, and none proposed so far are usable on preserved animals. Some chromosome preparation techniques do not attempt to produce permanent or widely usable slides. In fact, the aceto-orcein squash technique once used in most non-mammalian chromosome work (La Cour, 1941) produces pre-stained, temporary slides that are difficult to transport or to convert into more-permanent preparations.

Slide Preparation Technique

At the beginning of this project, it became apparent that the most detailed chromosome comparisons then being conducted were the largely mammalian studies of various types of chromosome banding patterns. Examination of the procedures used to produce banded chromosomes showed that many of them involved a relatively simple basic process, produced unstained permanent slides, and appeared to be adaptable to molluscan subjects. Arrighi & Hsu (1974) describe the basic steps in this process, essentially as follows:

- if the number of mitoses is low, treat cell preparations or tissues with a metaphase arresting agent.
- treat the cell preparation with a hypotonic solution.
- fix cells in 1 glacial acetic acid: 3 methanol.
- place cells on a microscope slide and either air-dry or flame-dry.

The development of a technique for naiad specimens started with these basic steps and resulted in the following procedure which, although not totally satisfactory, generally yields some chromosome spreads from most specimens:

- sever both adductor muscles at their insertion on one valve of the shell, pull the mantle loose from that valve and open the living naiad.
- remove all of the labial palp and/or part of a non-gravid gill from one side of the animal.
- cut each tissue sample into 5–10 mm pieces and place them in demineralized, double distilled water for 30 minutes.
- remove the tissue samples from the water, accept any water that will come off easily on a paper towel, then flood the samples with freshly-mixed 1 glacial acetic acid: 3 absolute methanol fixative.

- change the fixative twice during 30–45 minutes.
- gently swab a piece of tissue over most of a labeled, clean, dry microscope slide.
- dry the slide by waving it in the air, blowing on it, or by heating it gently high over an alcohol lamp.

The slides are permanent at this point and can be stored for staining at some later time:

- for unbanded, stained chromosomes, heat the slides at 60°C for one hour, stain them in 1% Giemsa blood stain for 5–7 minutes, rinse under the tap, and allow to dry.
- mount stained slides with an oversize coverslip using Permount or some other permanent mounting medium.

The modifications from the mammalian process included in this naiad chromosome procedure were derived from a series of trial-and-error and more specific experiments on a fairly large number of naiad specimens. The bases for these modifications are discussed in the following paragraphs.

Tissue Choice: Considerable early effort was invested in determining which naiad tissue would provide the highest number of chromosome spreads and the lowest amount of cellular or environmental debris on the slides. Tissues or structural areas examined at one time or another included: un-modified mantle, anterior free edge of the mantle, siphonal area of the mantle, labial palps, non-gravid gill, foot, gonad, kidney, and developing embryos. The edges of the mantle and the foot were apparently too firm to release many cells when swabbed onto slides. Gonadal and kidney tissues were so soft that globs of material came off on the slides and individual nuclei or chromosome spreads were obscured by this debris. Developing embryos were observed and the preparations of chromosome slides were attempted only on two occasions, both of which yielded some chromosome spreads; however, this source of chromosomal material is so rarely available that it was abandoned as a routine option.

The relative usefulness of the three remaining tissues (un-modified mantle, labial palps and non-gravid gill) were compared in the process of gathering chromosome spreads from a number of naiades. Un-modified mantle tissue gave some spreads; however, it often deposited a good deal of debris on the slides. Both labial palp and non-gravid gill material routinely produced clean slides but labial palp preparations almost always yielded more chromosome spreads than non-gravid gill (average from 13 pairs of comparisons: palp – 12.8 spreads per slide, non-gravid gill – 5.0 spreads per slide).

Pretreatment: Most chromosome preparation techniques include one or more pretreatment steps to accumulate the mitotic figures (Arrighi & Hsu, 1974; Chambers, 1982). Several experiments with Velban (vinblastine sulphate), one of the mitotic arresting agents then in common usage, failed to show any increase in spread number but did seem to cause the chromosomes to contract. A single experiment with phytohemaglutanin, a mitotic inducer, also failed to increase the number of spreads.

Recent studies describe ways to improve the number of chromosome spreads on slides that were not available when the laboratory work on this project was being conducted. Cornet (1993, 1995) cultured somatic cells of the marine mussel *Mytilus edulis* in vitro for a few days and substantially increased the number of mitotic figures observed on chromosomal slides. The adaptation of this culture technique for use with freshwater bivalves would eliminate the possibility of making slides in the field; however, it would improve the likelihood of gathering chromosomal data from each animal that was processed. This technique also seems to have the potential for collecting chromosomal data by taking tissue samples from – instead of sacrificing – live naiades, a change that would be especially important when working with protected species.

In another study, Woznicki & Jankun (2004) improved the mitotic index on slides from the unionid *Anodonta anatina* by injecting a cell proliferation stimulator (0.05 ml of 0.4% cobalt chloride) 60 hours before beginning other steps in the slide-making process. They also increased the mitotic index while reducing chromosomal contraction in *A. anatina* by quantifying the volume of the arresting agent that they used (from 0.5 to 1.0 ml of 0.1% colchicine solution, depending on size of the animal) before taking their tissue samples. Had any of these techniques been available in the late 1970s, they might have made a considerable difference in the results of this project.

Hypotonic Treatment: Typical hypotonic treatments for vertebrate animals are dilutions of 1% sodium citrate (Arrighi & Hsu, 1974). Although a number of dilutions of this material were tried, no recognizable chromosome spreads were observed until demineralized double distilled water was used alone as the hypotonic treatment. With regard to the treatment time, tissue samples of one animal were fixed after 0, 10, 20, 30, 40, 50 and 60 minutes in demineralized double distilled water. Although the number of chromosome spreads continued to increase with treatment time, the edges of individual chromosomes became increasingly fuzzy in treatments longer than 30 minutes.

Transition into Fixative: For some time after this technique should have become standardized, variations continued to occur in the size of interphase nuclei and, apparently, in the number of chromosome figures. Careful monitoring indicated that water on the tissue samples when they were flooded with fixative reduced the size of nuclei on the resulting slides. This problem was overcome by touching the tissue samples to dry paper towels as they came out of the hypotonic treatment before placing them in a dry vial where they were flooded with the fixative.

Fixation: No substantial change was made in the composition of the fixative or the length of fixation time because experimental results indicated that some fixation was required but that long fixation time did not change the number of chromosome spreads observed on slides. In one case, chromosome spreads were observed on slides made 32 days after the tissue samples were fixed. Similar tests using tissue samples that had been in fixative for one and two years failed to produce spreads or even recognizable cell nuclei.

Slide-Making Technique: Experimentation with this aspect of the procedure was concerned with how to get cells on the slides and how best to dry the liquid preparations. Several tests were run “dabbing” or “swabbing” tissue samples onto dry or wet slides. The best technique involved lightly rubbing the tissue sample over the surface of a dry slide, making sure to keep the sample wet with fixative. Three types of drying techniques were tested (air-drying, fanning, and warming) without determining obvious differences. The use of a standardized warming technique may help improve some staining results.

Staining (*Unbanded*): All staining of these chromosome preparations included the use of a stock solution of Giemsa blood stain (150 g Giemsa stain, 10 ml glycerin and 10 ml methanol in 1 l of water). Experimental results suggested that three factors are involved in staining intensity: stain concentration, staining time, and the initial dryness of the slides. Slides more than four days old that had been heated at 50–60°C for one hour stained well during 5–7 minutes in a 1–2% stock solution of Giemsa stain. Slides less than four days old, with or without the heat treatment, generally took stain more slowly, but some areas were overstained. Very old slides (3 to 15 months) varied considerably in their acceptance of stain regardless of the one hour heat treatment; however, 5–7 minutes in 1–2% stain was most likely to yield acceptable results.

Staining (*Banded*): During the laboratory part of this project, a number of experiments were conducted using various vertebrate banding techniques to see if banding could be demonstrated on these naiad slides. Some techniques produced a few weakly banded naiad spreads; however, the banded chromosomes were not sufficiently clear to be considered usable, and the few banded spreads on any one slide differed from each other so much that ways to improve the staining technique were not apparent. No banded naiad chromosome spreads were photographed and studied as part of this project.

Identification and Deposition of Specimens

After the various tissue samples had been removed and processed for chromosomal use, the remaining soft parts of each specimen were preserved in 70% ethanol. Identification of each specimen was made using shell and soft part characteristics and, for nearly all specimens, was verified or corrected by Dr. David H. Stansbery, then curator of the OSUM bivalve collection. All specimens from which chromosome slides were made were deposited and cataloged into the OSUM collection. In 2011, Dr. G. Thomas Watters, present curator of the OSUM bivalve collection, confirmed or provided updated identifications for these specimens. The cataloged specimens retain the “JJJ” numbers used during this project, as well as a label notation that chromosome slides had been prepared from them.

Location and Analysis of Chromosome Spreads

After the slides were stained, chromosome spreads were located by conducting a complete scan of the area under a 20 x 50 mm cover slip using a 200x lens combination on an Olympus phase contrast microscope. Well-separated spreads that included indications of centromeres or arms were photographed using a Pentax Spotomatic camera mounted on the Olympus phase contrast microscope with a built-in light source. All photographs were taken on Kodak High Contrast Copy Film at 1500x, at between one and four seconds for well-stained spreads, or at 15 or 30 seconds for lightly-stained spreads enhanced with a green filter. All usable negatives were printed to the same scale to simplify comparisons between spreads. Individual chromosomes on the photographs were outlined and, when possible, the centromeres were located while comparing the photograph to the actual spread magnified to 1500x through the microscope.

Digital calipers were used to measure the outlined chromosomes on the photographs. Generally, the longer arm on each end of the chromosome was measured from the centromere to the tip. When the chromatid arm or the centromere could not be distinguished, the greatest length of the arm or of the entire chromosome was measured. All measurements for arms or entire chromosomes were recorded at the nearest 0.05 mm. Two metrics were calculated for each chromosome: Arm Ratio (r) and Relative Length (RL).

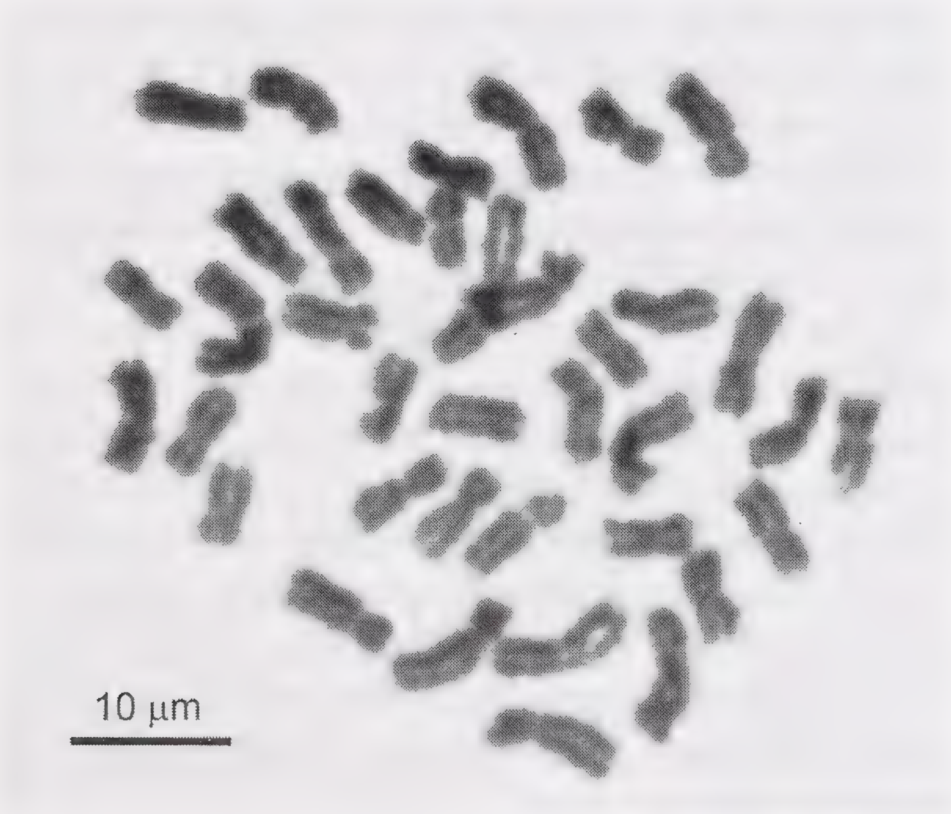

FIG. 1. A good quality spread of the 38 chromosomes from the labial palp of the North American naiad *Villosa trabalis*.

RESULTS AND DISCUSSION

During this project, 250 naiades representing approximately 75 species were used as sources of chromosomal material. These animals were collected between August 1975, and May 1978, from ten of the east-central and southeastern United States, the western state of Oregon, and Manitoba Province, Canada. They yielded chromosome counts for 65 species in 34 presently-recognized naiad genera. Overall, of the 771 spreads that were counted, 502 (65%) included 38 chromosomes (Fig. 1). Five or more chromosome counts were obtained from 42 of these species, and 38 was the clear modal number for each of them. Two-hundred-five superior quality chromosome spreads were photographed, 125 of them (representing 39 species in 24 genera) were measured, and the 87 measured spreads that included exactly 38 chromosomes were analyzed. Table 2 presents a species-by-species summary of the chromosome counts and analysis results that were generated during this project.

Chromosome Number

The information presented in Table 2 indicates that 38 is the modal number of diploid chromosomes found during this study of North American naiades. Figure 2 reinforces this assertion by tallying the numbers of chromosomes observed in all of the 771 countable spreads encountered during this project. The clear mode of these counts at 38 (65% of the total), accompanied by the sharply skewed distribution pattern, strongly suggests that 38 is the typical chromosome number present in these naiades. The 257 counts that were lower than 38 (33% of the total) most likely consist of spreads where some chromosomes landed on top of others or where chromosomes were washed away when the cell membranes ruptured during slide preparation. The 14 counts higher than 38 (2%) probably include some separated chromatids, the results of atypical cell divisions, and – more much more rarely on these slides – chromosomes that had floated in from other spreads.

On an individual basis, each of the 42 species represented by five or more counts had a modal number of 38 chromosomes (Table 2). In addition, among the 23 species represented by between one and four counts, the strongest

TABLE 2. Chromosome numbers and suggested karyotypes for North American naiades determined during this study. The suprageneric groupings and most author and date entries follow Graf & Cummings (2007).

					Suggested Karyotypes	
Species	Source	Chromosome Counts	No. of 38s	Spreads Analyzed	Arm Ratio (r)	Relative Length (RL)
Family Margaritiferidae						
Margaritifera falcata (Gould, 1850)	Willamette River, Oregon	11	8	1		
Family Unionidae						
Subfamily Unioninae						
Tribe Anodontini						
Alasmidonta arcula (Lea, 1838)	Ohoopee River, Georgia	5	3			
Alasmidonta marginata Say, 1818	Big Darby Creek, Ohio	20	13	3	10m, 7sm, 2st	2(0–4), 13(4–6), 4(6–8)
Anodonta imbecillis (Say, 1829)	Lake Erie, Ohio	6	4			
Anodonta oregonensis Lea, 1838	Devils Lake, Oregon	3	3			
Anodontoides ferussacianus (Lea, 1834)	Buffalo Creek, Ohio	36	21	2	8m, 8sm, 3st	2(0–4), 13(4–6), 4(6–8)
Arcidens confragosus (Say, 1829)	Green River, Kentucky	1	1			
Lasmigona complanata (Barnes, 1823)	Big Darby Creek, Ohio	7	3	1		
Lasmigona costata (Rafinesque, 1820)	Big Darby Creek, Ohio	42	29	6	9m, 7sm, 3st	3(0–4), 12(4–6), 4(6–8)
Pseudanodonta radiatus radiatus (Conrad, 1834)	Cane Creek, Alabama	8	3			
Pseudanodonta undulatus (Say, 1817)	Big Darby Creek, Ohio	13	11			
Pyganodon grandis grandis (Say, 1829)	Buffalo Creek, Ohio	40	22	6	11m, 6sm, 2st	1(0–4), 13(4–6), 4(6–8), 1(>8)
Subfamily Ambleminae						
Tribe Amblemini						
Amblema plicata plicata (Say, 1817)	Lake Erie, Ohio	19	11			
Tribe Lampsilini						
Actinonaias ligamentina carinata (Barnes, 1823)	Green River, Kentucky	21	15	4	10m, 7sm, 2st	3(0–4), 12(4–6), 3(6–8), 1(>8)
Ellipsaria lineolata (Rafinesque, 1820)	Green River, Kentucky	1	1			
Epioblasma torulosa rangiana (Lea, 1838)	Big Darby Creek, Ohio	7	5			

(continues)

(continued)

Species	Source	Chromo-some Counts	No. of 38s	Spreads Analyzed	Suggested Karyotypes	
					Arm Ratio (r)	Relative Length (RL)
Hamiota australis (Simpson, 1900)	Burnt Corn Creek, Alabama	5	2			
Hamiota subangulata (Lea, 1840)	Uchee Creek, Alabama	5	2			
Lampsilis cardium Rafinesque, 1820	Buffalo Creek, Ohio	27	13	1		
Lampsilis fasciola Rafinesque, 1820	Buck Creek, Kentucky	4	3	1		
Lampsilis higginsi (Lea, 1857)	Mississippi River, Wisconsin	2	1			
Lampsilis ornata (Conrad, 1835)	Uphapee Creek, Alabama	1	1			
Lampsilis radiata luteola (Lamarck, 1819)	Big Darby Creek, Ohio	15	13	1		
Lampsilis teres (Rafinesque, 1820)	Uphapee Creek, Alabama	2	1			
Lemiox rimosus (Rafinesque, 1831)	Duck River, Tennessee	4	3	1		
Leptodea fragilis (Rafinesque, 1820)	Lake Erie, Ohio	28	13	3	9m, 8sm, 2st	2(0–4), 11(4–6), 5(6–8), 1(>8)
Ligumia nasuta (Say, 1817)	Lake Erie, Ohio	18	15	4	10m, 7sm, 2st	2(0–4), 13(4–6), 3(6–8), 1(>8)
Ligumia recta (Lamarck, 1819)	Lake Erie, Ohio	10	10	2	11m, 6sm, 2st	2(0–4), 12(4–6), 4(6–8), 1(>8)
Medionidus conradicus (Lea, 1834)	Copper Creek, Virginia	4	2	1		
Medionidus penicillatus (Lea, 1857)	Whitewater Creek, Georgia	2	1			
Obovaria olivaria (Rafinesque, 1820)	Mississippi River, Wisconsin	16	9	1		
Obovaria subrotunda (Rafinesque, 1820)	Buck Creek, Kentucky	20	13	6	10m, 6sm, 3st	2(0–4), 13(4–6), 4(6–8)
Potamilus alatus (Say, 1817)	Buck Creek, Kentucky	15	10	2	11m, 7sm, 1st	2(0–4), 12(4–6), 4(6–8), 1(>8)
Ptychobranchus fasciolaris (Rafinesque, 1820)	Big Darby Creek, Ohio	43	31	4	8m, 10sm, 1st	2(0–4), 12(4–6), 4(6–8), 1(>8)
Ptychobranchus subtentum (Say, 1825)	Clinch River, Tennessee	3	2			
Toxolasma lividus Rafinesque, 1831	Buck Creek, Kentucky	5	3	1		
Toxolasma parvum (Barnes, 1823)	Lake Erie, Ohio	24	17	2	13m, 6sm	2(0–4), 12(4–6), 5(6–8)
Villosa iris iris (Lea, 1829)	Big Darby Creek, Ohio	25	14	6	11m, 6sm, 2st	1(0–4), 14(4–6), 3(6–8), 1(>8)
Villosa lienosa (Conrad, 1834)	Buffalo Creek, Ohio	16	9	1		
Villosa nebulosa (Conrad, 1834)	Pitmann Creek, Kentucky	1	1			
Villosa taeniata punctata (Lea, 1865)	Buck Creek, Kentucky	27	21	7	11m, 6sm, 2st	3(0–4), 12(4–6), 3(6–8), 1(>8)
Villosa trabalis (Conrad, 1834)	Buck Creek, Kentucky	71	46	8	11m, 6sm, 2st	1(0–4), 13(4–6), 4(6–8), 1(>8)

(continues)

(continued)

Species	Source	Chromo-some Counts	No. of 38s	Spreads Analyzed	Suggested Karyotypes	
					Arm Ratio (r)	Relative Length (RL)
Villosa vibex (Conrad, 1834)	Uphapee Creek, Alabama	5	4			
Tribe Pleurobemini						
Cyclonaias tuberculata (Rafinesque, 1820)	Duck River, Tennessee	2	1			
Elliptio arca (Conrad, 1834)	Uchee Creek, Alabama	2	1			
Elliptio crassidens (Lamarck, 1819)	Green River, Kentucky	1	1	1		
Elliptio dariensis (Lea, 1842)	Ohoopee River, Georgia	13	8			
Elliptio dilatatus (Rafinesque, 1820)	Little Darby Creek, Ohio	5	5	2	12m, 6sm, 1st	3(0–4), 12(4–6), 3(6–8), 1(>8)
Elliptio pullata (Lea, 1856)	Cane Creek, Alabama	2	1			
Pleurobema oviforme (Conrad, 1834)	Duck River, Tennessee	1	1			
Pleurobema pyriforme (Lea, 1857)	Uchee Creek, Alabama	4	2			
Pleurobema rubrum (Rafinesque, 1820)	Duck River, Tennessee	5	5	4	13m, 6sm	2(0-4), 14(4-6), 2(6-8), 1(>8)
Pleurobema sintoxia (Rafinesque, 1820)	Green River, Kentucky	2	1			
Pleuronaia barnesiana (Lea, 1838)	Duck River, Tennessee	11	6			
Pleuronaia cuneolus (Lea, 1840)	Clinch River, Tennessee	1	1			
Pleuronaia dolabelloides (Lea, 1840)	Duck River, Tennessee	7	4			
Pleuronaia flava (Rafinesque, 1820)	Lake Erie, Ohio	11	9			
Uniomerus carolinianus (Bosc, 1801)	Whitewater Creek, Georgia	1	1			
Uniomerus declivus (Say, 1831)	Cane Creek, Alabama	5	5			
Tribe Quadrulini						
Megalonaias nervosa (Rafinesque, 1820)	Whitewater Creek, Georgia	1	1			
Quadrula infucata (Conrad, 1834)	Uchee Creek, Alabama	4	1			
Quadrula pustulosa (Lea, 1831)	Lake Erie, Ohio	6	4	1		
Quadrula quadrula (Rafinesque, 1820)	Big Darby Creek, Ohio	19	12			
Tritogonia verrucosa (Rafinesque, 1820)	Big Darby Creek, Ohio	6	3	1		
Tribe Gonideini						
Gonidea angulata (Lea, 1838)	Willamette River, Oregon	24	16	3	6m, 11sm, 2st	3(0–4), 12(4–6), 4(6–8)

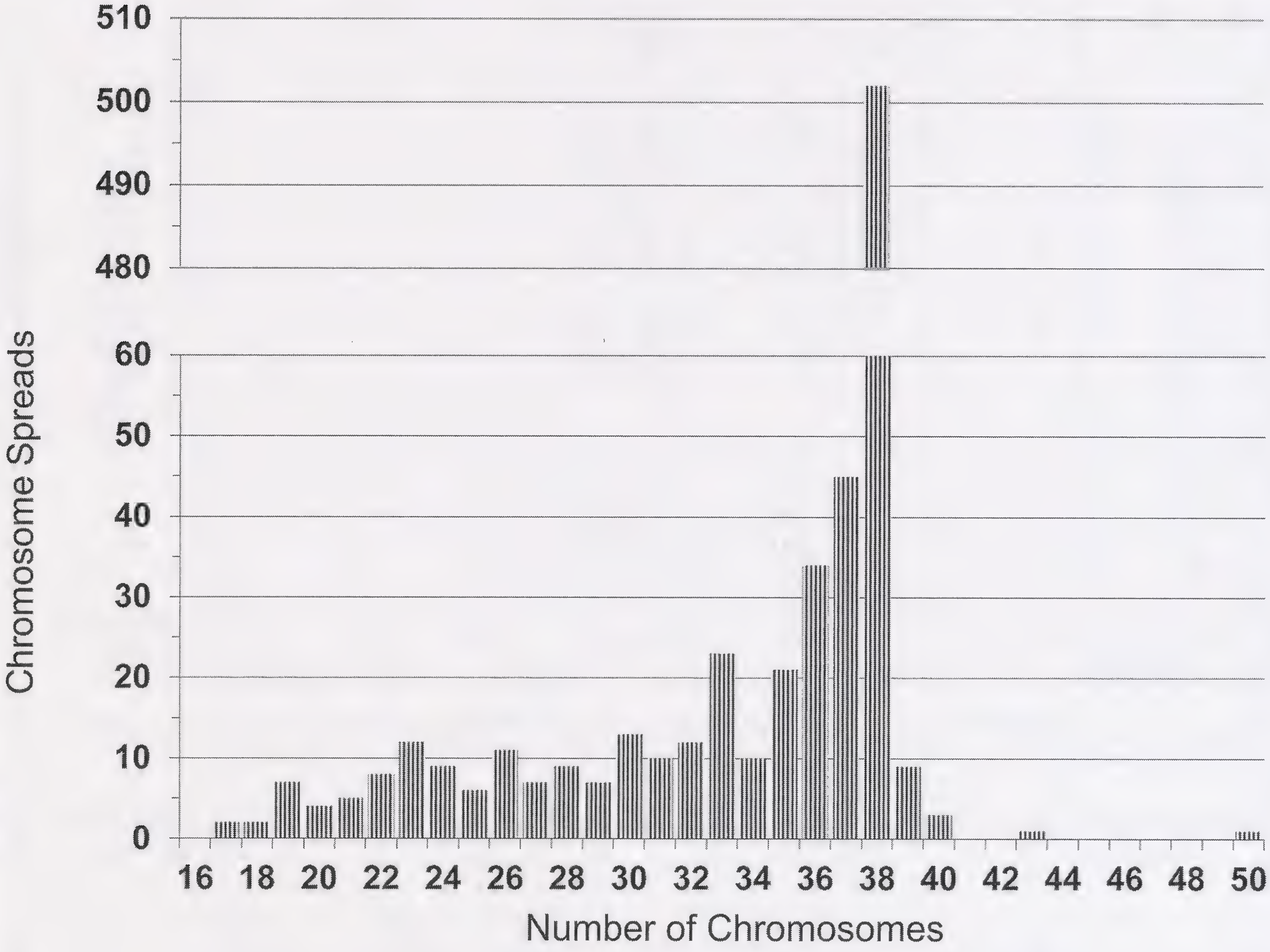

FIG. 2. The numbers of naiad chromosomes observed in the 773 spreads counted during this project. The 502 counts with the modal number (38) make up 64.9% of the total.

suggestion of a modal number other than 38 was for *Quadrula infucata* (four counts: 31–1, 36–2, 38–1). These results reinforce the conclusion that 38 is the diploid chromosome number for all 65 naiad species that were studied, including *Quadrula infucata*.

The conclusion that all 65 North American naiad species examined during this study have 38 chromosomes adds substantial new information to the compilation of published naiad chromosomal numbers presented in Table 1. Considered together, Tables 1 and 2 indicate that the 67 species of North American naiades that have been examined [15 reported in Jenkinson (1976), two added by Park & Burch (1995) and 50 first reported here] all have 38 chromosomes. These North American species are considered members of two naiad families: Unionidae and Margaritiferidae (Graf & Cummings, 2007). Similarly, all 11 naiad species studied in Europe (all in Unionidae) and 14 of the 15 naiades studied in Asia (both Margaritiferidae and Unionidae) also have 38 chromosomes. [The 15th Asian species, *Solenia khwaegnoiensis*, was reported to have 37 diploid chromosomes; however, the haploid number was still listed as 19 (Deein et al., 2003).] The one unionid species studied so far in Africa (*Unio elongatulus*) is reported to have 28 chromosomes (Ebied, 1998); however, an Italian study of what was identified as the same species is reported to have 38 chromosomes (Vitturi et al., 1982). With the possible exceptions of *Solenia khwaegnoiensis* and African *Unio elongatulus*, 38 is the diploid chromosome number known for all of the unionid and margaritiferid species that have been studied. All of these species occur in the Northern Hemisphere, and all of them are considered members of the superfamily Unionoidea (Graf & Cummings, 2007).

The five remaining naiad species listed in Table 1 are all considered members of the superfamily Etherioidea (Graf & Cummings, 2007). Four of these species (*Alathyria pertexta*, *Diplodon chilensis*, *Velesunio ambiguus* and *Velesunio legrandi* – all in the family Hyriidae) have 34 chromosomes, and the fifth (*Mutela rostrata* in the family Iridinidae) has 20 chromosomes. As indicated in Table 1, three of the hyriid species occur in Australia and Tazmania, while the fourth (*Diplodon chilensis*) is found in Chile. The iridinid species occurs in Egypt. Obviously, the chromosome numbers of these five mostly Southern Hemisphere etherioid species are different from those of the much larger number of Northern Hemisphere unionoids.

In their broad-spectrum cladistic analysis of relationships within the bivalve subclass Palaeoheterodonta, Graf & Cummings (2006) conclude that the order Unionoida is monophyletic and can be represented by eight morphologic synapomorphies: four characters associated with gill morphology, and four associated with life history and reproductive characters. Their analysis also indicates this order can be divided into two superfamilies (Etherioidea and Unionoidea); however, few morphological characters align with the distinctions indicated by the DNA data. The chromosome numbers reported so far for the naiades suggest a clear distinction between the 38 present in both the Margaritiferidae and the Unionidae of the Northern Hemisphere (the Unionoidea) and different numbers (34 for the Hyriidae and 20 for at least one iridinid from Africa) in the Etherioidea of the Southern Hemisphere. If this difference in chromosome numbers is substantiated as more, especially Southern Hemisphere naiades are studied, this straight-forward morphologic character could become important in recognizing distinctions between high-level groups of naiades.

Supernumerary Chromosomes

The chromosome slides from three animals studied during this project include a chromosomal feature not indicated in Table 2. One slide each of *Leptodea fragilis*, *Obovaria olivaria*, and *Pyganodon g. grandis* contained a few spreads that included a small "dot" chromosome. Single dots were present in six of 14 spreads (43%) noted on the *P. g. grandis* slide, four of 21 spreads (19%) on the *L. fragilis* slide, and one of 14 spreads (7%) on the *O. olivaria* slide. The dot in two measured *P. g. grandis* spreads comprised 0.64 and 0.81% of the total complement length, less than half the length of the next smallest chromosome (Fig. 3). No centromere was observed on any of the dots.

The dot chromosomes on these naiad slides appear to fit the general description of supernumerary or "B" chromosomes (Jones & Houben, 2003; Palestis et al., 2010). As a group, supernumeraries are small chromosomes that occur infrequently in species and individuals, and appear to act essentially as chromosomal parasites. Supernumerary chromosomes have been found in fungi, plants and animals; may or may not contain active genetic material that can affect phenotypes; may deviate from normal duplication and separation patterns during cell division (nondisjunction); and may occur in a variety of numbers within the cells of an organism (Camacho et al., 2000).

Patterson (1969) cited a few cases of supernumerary chromosomes in gastropods but none in other mollusks. Some of the cases, Patterson presented appear to be similar to the rare occurrence, non-uniform pattern found during this project. Other cases, however, seem more likely to have been various types of disruptions of the normal chromosome complement. The first published description of supernumerary chromosomes in bivalves was in a report by Insua & Thiriot-Quiévreux (1992). Leitão et al. (2008) used banding techniques to identify the supernumeraries they found in the marine bivalve *Cerastoderma edule* as fragments of the normal chromosomes and suggested that fissions in the normal chromosomes might have been caused by environmental pollution.

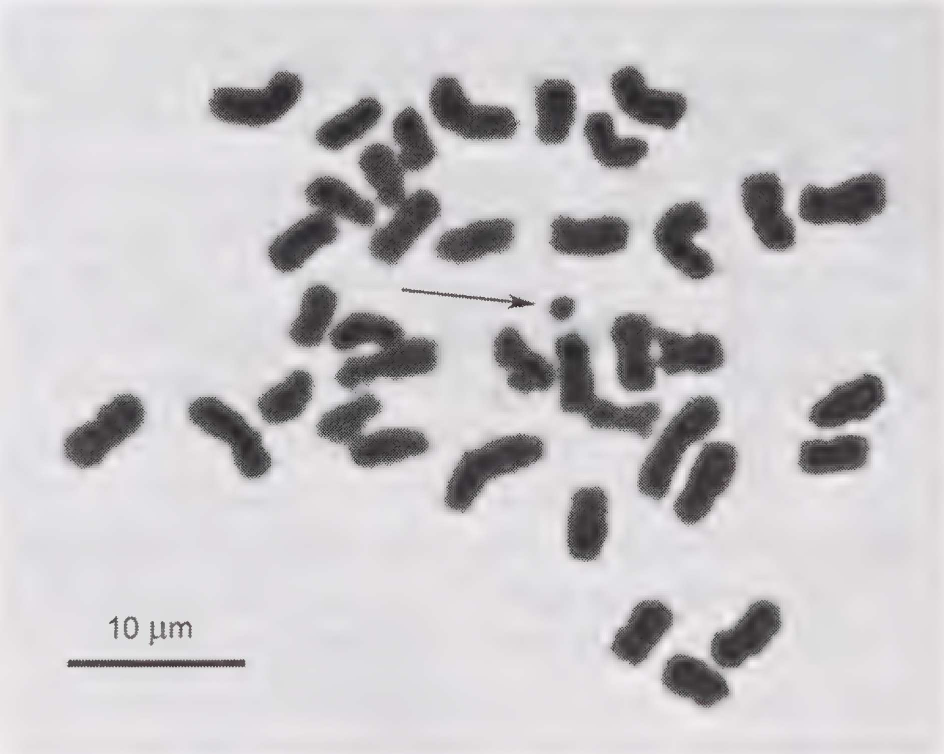

FIG. 3. A chromosome spread from the labial palp of *Pyganodon grandis grandis* including 38 normal chromosomes and (at arrow) one supernumerary chromosome.

Chromosome Morphology

The number of chromosomes is not the only chromosomal characteristic that might be useful in identifying relationships among naiad species, genera, and higher taxa. In many animal and plant groups, variations in the relative lengths of the chromosomes and in the location of the centromere on each chromosome – the karyotype of an individual, population, or species – provide quantifiable features that can be analyzed and compared. In recent years, karyotypic analyses have become much more common than simple lists of chromosome numbers and are supplying more useful data than was previously thought available from chromosomal work (Takagi & Sasaki, 1974; Bogart, 1973; Melnychenko & Yanovich, 2004). Karyotypic studies on mollusks were begun by Burch (1962) and Patterson (1965), and continue to increase in sophistication and application (e.g., Babrakzai et al., 1976; Nakamura, 1985; Thiriot-Quiévreux, 2002).

In most analyses, the chromosomes within a spread are sorted into groups based on the position of the centromere. Typically, the length of the longer arm of a chromosome is divided by the length of the shorter arm and the result is presented as the Arm Ratio (r) (Thiriot-Quiévreux, 2002).

Another useful chromosomal metric, Relative Length (RL), is calculated by dividing the length of each chromosome (long arm plus short arm) by one-half the length of all the chromosomes in the spread, then multiplying the result by 100 to convert it into a percentage of the haploid length (Petkevičiūtė et al., 2007). Apparently, RL is nearly always presented with reference to the haploid length because this metric was first used in regard to human chromosomes and, in order to avoid differences in RL values between the sexes, the female haploid (autosome) complement was used as its basis (Chu & Giles, 1959).

The r and RL metrics are virtually independent of each other. The r value describes the relative location of the centromere without regard to the overall length of any chromosome. The RL value compares the total length of one chromosome to the aggregate length of all chromosomes in the spread without regard to the location of any centromere. These metrics are virtually independent of each other because obscured folding along the length of a chromosome and other measurement errors will affect the values of both r and RL.

It is also important to realize that both r and RL are continuous variables. The stabilization in Arm Ratio terminology proposed by Levan et al. (1964) includes a clear description of the range of possible locations of the centromere (from 1.00 to well above 7.00), along with the authors' logic for the mathematical break points between the metacentric (m; r = 1.00–1.70), submetacentric (sm; r = 1.71–3.00), subtelocentric (st; r = 3.01–7.0) and acrocentric [= telocentric] (t; r > 7.00) segments they established.

No comparable separation of RL values into consistent segments is likely to be widely applicable because of the wide range in chromosome numbers (and, therefore, the relative lengths of the individual chromosomes) among animal and plant species. Early in this project, the break points between segments of the RL spectrum were arbitrarily set at 2% intervals of the haploid length; however, so few data points fell below 2% or above 10% that the outlying intervals were combined to produce the 0–4.0%, 4.01–6.0%, 6.01–8.0%, and > 8.0% RL segments used in this analysis.

With regard to the r metric, most the chromosomes in the 87 measured 38-chromosome spreads included in this study have centromeres located near the center (53% are metacentric), followed in abundance by submetacentrics (36%), subtelocentrics (11%) and telocentrics (0.2%). The virtual absence of telocentric chromosomes indicates there is little or no value in comparing "fundamental numbers" among these karyotypes. The concept of counting all of the arms of the chromosomes in a spread was proposed by Matthey (1949) and has been used to describe situations in which several single-armed (telocentric) chromosomes exist in some species while fewer telocentrics occur in others. This absence of telocentrics, when combined with the uniform 38 diploid chromosome number present in these species produces a fundamental number of 76 for all of the karyotypes analyzed during this study.

With regard to the RL data, most of these chromosomes (67%) occur in the 4–6% range, about the average length expected for spreads including 38 chromosomes (100%/19 haploid chromosomes = 5.3 RL). Approximately 11% (in the 0–4% range) are shorter than average, 19% (in the 6–8 RL range) are slightly longer than average, and 3% (in the > 8 RL range) are substantially longer than average. Many recent karyotypic papers include RL values as part of the description of the chromosomes being examined (e.g., Pasantes et al., 1990; Insua et al., 1994; González-Tizón et al., 2000; Iqbal et al., 2008); however, I could not find any previous study that has sorted the RL data into segments and used it as an analytical tool.

Measurement Error

The comparisons of naiad karyotypes presented below are based solely on measurement data and the analyses of the r and RL metrics assume that whatever errors might be included in the measurements were not large enough to materially affect the results. The validation of this assumption requires an examination of measurement error.

A review of the measurement data indicated that naiad species within the genus *Villosa* have two pairs of distinctive subtelocentric chromosomes, typically in the 4–6 RL size range that could be studied to determine the margin of error in their measurement. The four chromosomes with the largest r values in each of the 22 *Villosa* spreads available for this comparison were sorted into pairs based solely on their RL values. Mean and standard deviation values were calculated for the short arms, long arms, and for the full lengths of each chromosome pair (Table 3). If the means of these RL measurements are taken to represent the actual (relative) lengths of the chromosome segments, and the standard deviations are taken to estimate the total effects of inconsistencies in outlining, locating the centromeres, and measuring them, then the Coefficient of Variation (100s/x) based on all of the pairs included in each test is an estimate of the error in these measurements (Steel & Torrie, 1960). The data presented in Table 3 indicate that error was greatest (15 and 13%) for the short arms of these two chromosome pairs and approximately half of that (6 to 8%) for the long arms and for the total lengths. The average error value based on the four arm measurement tests was 10.9%.

TABLE 3. Relative lengths of two pairs of subtelocentric chromosomes in 22 measured spreads from four species in the genus *Villosa*. The Coefficient of Variation (CV) was calculated by dividing 100 times the Standard Deviation (SD) by the Mean.

Segment	n	Mean	SD	CV
Longer RL Pair				
Short Arms	44	4.03	0.63	15.63
Long Arms	44	15.39	0.97	6.33
Total Length	44	19.42	1.33	6.85
Shorter RL Pair				
Short Arms	44	3.32	0.45	13.40
Long Arms	44	12.83	1.07	8.32
Total Length	44	16.15	1.28	7.93

Future projects involving the measurement of naiad chromosomes are likely to avoid at least this high a level of measurement error. Recent chromosomal studies, such as Martinez-Lage et al. (1996) and Skuza et al. (2009), cover this aspect of the work simply by identifying the computer programs they ran to take the measurements.

Karyotype Analysis

As indicated in Table 2, 125 high quality chromosome spreads (representing 39 species in 24 genera) were measured and analyzed during this project. Unfortunately, 38 of these spreads had fewer (29 spreads, 27%) or more (9 spreads, 3%) than exactly 38 chromosomes. With the exclusion of these "imperfect" spreads, the following analysis includes 87 38-chromosome spreads representing 31 species in 21 genera.

Because r and RL are virtually independent metrics, analyzing them together makes it possible to sort the sizes and shapes of chromosomes from a spread or a species in a more detailed way than is possible by examining either metric alone. Sorting the number of chromosomes that plot in each of the four r segments into whichever of the four RL segments they also represent divides the data into as many as 16 unique size/shape categories.

Eighteen species included in this study were each represented by two or more measured 38-chromosome spreads. For this analysis, the r and RL metric data from the spreads of each species were averaged together to identify the most likely even (diploid) number of chromosomes within each of the 16 possible r/RL categories that would add up to the most likely r and RL segment totals and to the overall total of 38 chromosomes. Both the r and RL segment values of the suggested karyotypes for these 18 species are presented in Table 2. Following the approach typically used for Arm Ratio karyotypes (e.g., Nakamura, 1985; Leitão et al., 1999a) and for Relative Lengths when they are listed (e.g., Park & Burch, 1995; Carrilho et al., 2008), the suggested karyotypes in Table 2 are presented using haploid numbers.

Tables 4 and 5 present some of the results of this analysis. In both of these tables, the four r metric segments form the rows, and the four RL segments form the columns. The totals for the r segments are presented along the right side and the RL segment totals are presented along the bottom. In Table 4, the upper left number in each cell and for each segment total is the most likely even (diploid) number of chromosomes that plot within both that r and RL segment based on the eight 38-chromosome spreads of *Villosa trabalis* that were measured during this study. The lower right value in each cell and total is the comparable chromosome number based on the seven 38-chromosome spreads of *Villosa taeniata punctata* that were included. These two species are typically placed in the same naiad genus (Parmalee & Bogan, 1998; Graf & Cummings, 2007).

As indicated in the right-hand column of Table 4, the suggested r karyotypes of these two species are identical to each other; however, the bottom row indicates that their suggested RL karyotypes differ in three of the four RL segments. The detailed karyotypes (16 interior table cells) indicate that *V. t. punctata* has four chromosomes (two pairs) more than *V. trabalis* that plot in the m(0–4) cell and two fewer chromosomes (one pair) that plot in both the m(4–6) and m(6–8) cells. The most parsimonious set of chromosomal modifications that could produce this difference in these karyotypes would involve the deletion (or, conversely, the duplication) of part of the lengths of two different chromosome pairs (two separate chromosomal modifications), neither of which was sufficient to move them from the metacentric to the submetacentric segment of the r metric. In general, changes in RL values indicate additions or deletions in overall chromosome length (duplications, deletions, etc.), while changes in r values indicate relocations in the position of the centromeres (inversions, translocations, etc.).

TABLE 4. Comparison of the detailed karyotypes of *Villosa trabalis* (upper left numbers in each cell) and *Villosa taeniata punctata* (lower right numbers). These two species have identical suggested Arm Ratio karyotypes (right column totals) but they differ in 3 of the 4 suggested Relative Length karyotype categories (bottom row totals) and in three 3 of the 16 detailed karyotype cells [m(0–4), m(4–6), and m(6–8)].

		Relative Length (RL)				
		0–4	4–6	6–8	> 8	r Totals
Arm Ratio (r)	m	2 **6**	14 **12**	4 **2**	2 **2**	22 **22**
	sm	0 **0**	8 **8**	4 **4**	0 **0**	12 **12**
	st	0 **0**	4 **4**	0 **0**	0 **0**	4 **4**
	t	0 **0**	0 **0**	0 **0**	0 **0**	0 **0**
	RL Totals	2 **6**	26 **24**	8 **6**	2 **2**	38 **38**

Table 5 presents a similar comparison between *Villosa trabalis* (upper left, based on eight measured spreads) and *Lasmigona costata* (lower right, based on six measured spreads), two species that are generally considered to be in different naiad subfamilies or tribes (Vokes, 1980; Graf & Cummings, 2007). The suggested r (right column totals) and RL (bottom row totals) karyotypes for these species differ from each other in six of the eight metric segments (all but telocentrics and 6–8 RL). The detailed karyotypes of these species differ from each other in all eight of the cells

TABLE 5. Comparison of the detailed karyotypes of *Villosa trabalis* (upper left numbers in each cell) and *Lasmigona costata* (lower right numbers). The suggested Arm Ratio (right column totals) and Relative Length (bottom row totals) karyotypes for these species differ from each other in 6 of the 8 categories (all but telocentrics and RL 6–8). Similarly, the detailed karyotypes of these species differ from each other in all 8 of the cells where naiad chromosomes usually plot [m(0–4), m(4–6), m(6–8), m(> 8), sm(0–4), sm(4–6), sm(6–8), and st(4–6)].

		Relative Length (RL)				
		0–4	4–6	6–8	> 8	r Totals
Arm Ratio (r)	m	2 **4**	14 **8**	4 **6**	2 **0**	22 **18**
	sm	0 **2**	8 **10**	4 **2**	0 **0**	12 **14**
	st	0 **0**	4 **6**	0 **0**	0 **0**	4 **6**
	t	0 **0**	0 **0**	0 **0**	0 **0**	0 **0**
	RL Totals	2 **6**	26 **24**	8 **8**	2 **0**	38 **38**

where these naiad chromosomes usually plot [m(0–4), m(4–6), m(6–8), m(> 8), sm(0–4), sm(4–6), sm(6–8), and st(4–6)]. Assuming that each 2-chromosome difference (either increases or decreases, but not both) in the detailed karyotypes represent one chromosomal modification, *Villosa trabalis* and *Lasmigona costata* differ from each other by at least five separate duplications, deletions, translocations or other changes in the morphology of their chromosomes. This number of differences is large enough that several possible sets of chromosomal modifications are equally likely to have produced the detailed karyotypes that were observed.

Table 6 expands this species-by-species comparison to include the ten species that are each represented by four or more measured 38-chromosome spreads in addition to a composite karyotype derived from all 87 measured 38-chromosome spreads included in this analysis. The third column in Table 6 indicates the number of cells in which the detailed karyotype value for each species differs from the composite, and the succeeding columns indicate the number of cells in which pairs of species have either more or fewer chromosomes in a cell than the composite. Highlighted values in Table 6 indicate sets of species that share pairs of cells in which their detailed karyotype values differ from the composite in complementary ways (one cell with +2 and the other with -2 chromosomes different from the composite). Single values in the species-by-species part of Table 6 are assumed to represent random occurrences of the same difference from the composite. Larger numbers of occurrences that are not highlighted represent situations in which both species differ from the composite in the same way in those cells (both species are either higher or lower than the composite in both cells) or where one of the occurrences is committed to a different, multi-species relationship.

The relationships identified in Table 6 are illustrated on Figure 4. The concentric circles on this figure represent the number of chromosomal modifications by which the species and the composite differ from each other. Straight lines indicate the identified (solid) and alternative (dashed) connections between species and the composite. For example, *Ligumia nasuta* and *Ptychobranchus fasciolaris* share one pair of differences from the composite [an inversion that relocates a pair of chromosomes

TABLE 6. Apparent relationships among the detailed karyotypes of the 10 naiad species and the 87-spread composite included in this analysis. The species are arranged here in descending order based on the number of measured spreads they represent. The meaningful relationships (highlighted cells) are illustrated on Figure 4.

			Number of Shared Differences from Composite								
Species	No. of Spreads	Differences from Composite	*V. trabalis*	*V. t. punctata*	*L. costata*	*O. subrotunda*	*P. g. grandis*	*V. iris*	*A. l. carinata*	*L. nasuta*	*P. rubrum*
Villosa trabalis	8	2	*								
Villosa t. punctata	7	4	1	*							
Lasmignona costata	6	8	0	1	*						
Obovaria subrotunda	6	4	1	2	3	*					
Pyganodon g. grandis	6	2	0	0	2	0	*				
Villosa iris	6	2	1	0	1	0	1	*			
Actinonaias l. carinata	4	4	1	3	2	2	0	0	*		
Ligumia nasuta	4	4	0	1	3	1	1	1	1	*	
Pleurobema rubrum	4	10	2	2	2	1	1	2	3	0	*
Ptychobranchus fasciolaris	4	6	0	0	1	0	0	0	2	2	2

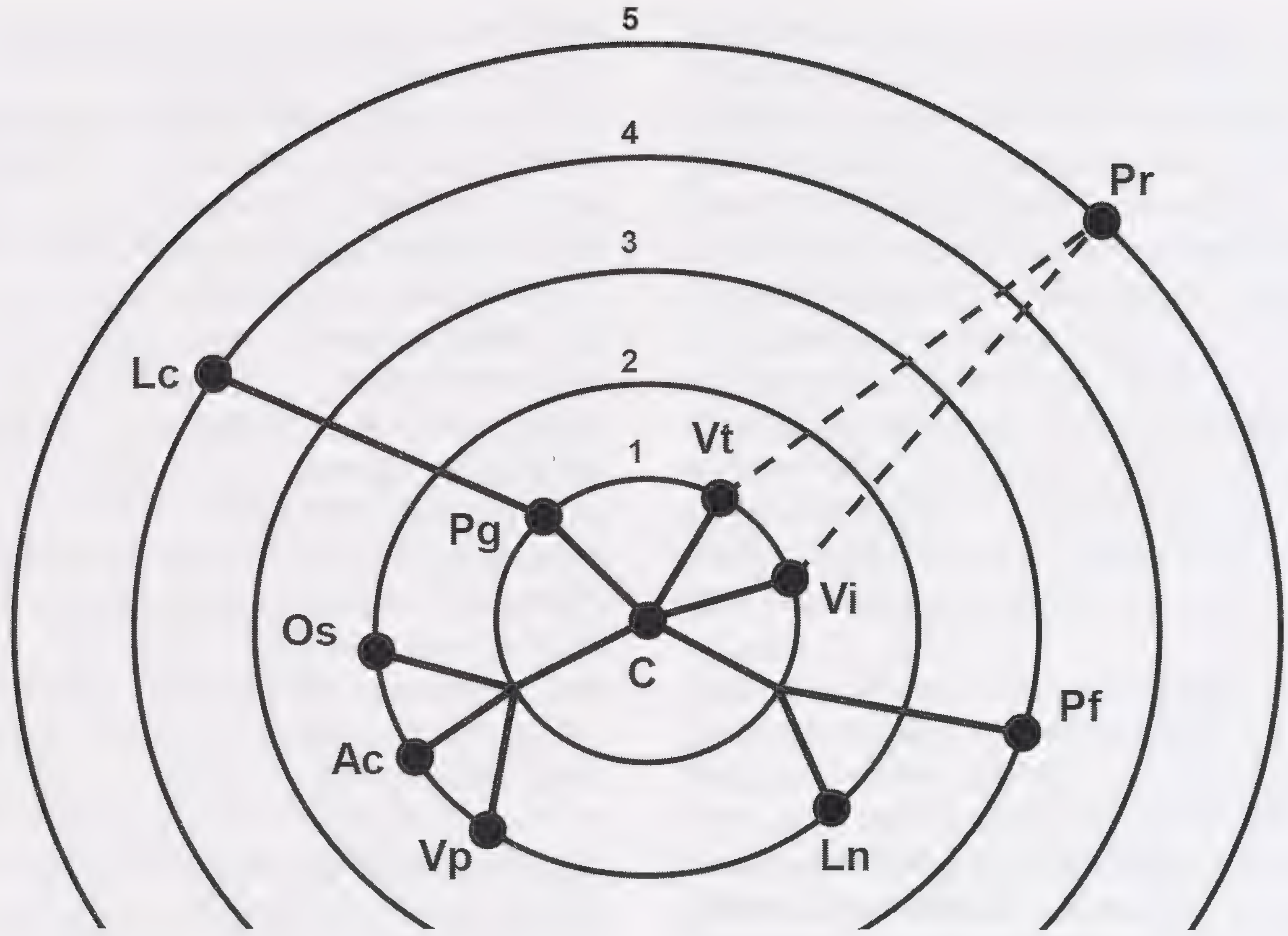

FIG. 4. Apparent relationships among the detailed karyotypes of 10 naiad species and a composite based on all 87 38-chromosome spreads included in this analysis. Each ring on this figure represents one chromosomal modification from the adjacent ring or the center. Abbreviations: Ac – *Actinonaias l. carinata*, C – Composite of all 87 spreads, Lc – *Lasmigona costata*, Ln – *Ligumia nasuta*, Os – *Obovaria subrotunda*, Pf – *Ptychobranchus fasciolaris*, Pg – *Pyganodon g. grandis*, Pr – *Pleurobma rubrum*, Vi – *Villosa iris*, Vp – *Villosa taenaita punctata*, and Vt – *Villosa trabalis.*

from m(4–6) to sm(4–6)], then *Ligumia nasuta* exhibits one more modification, while *Ptychobranchus fasciolaris* exhibits two different modifications away from the composite. Similarly, *Obovaria subrotunda*, *Actinonaias ligamentina carinata* and *Villosa taeniata punctata* all share one modification from the composite [a deletion that relocates one pair of chromosomes from sm(4–6) to m(0–4)], then each of them exhibits an additional, different modification from the composite.

As indicated in Table 6 and illustrated on Figure 4, *Pleurobema rubrum* differs from the composite by five chromosomal modifications. One of those modifications also occurs in *Villosa trabalis* while another occurs in *Villosa iris*; however, those two *Villosa* species do not share any difference from the composite. As a result, Figure 4 indicates that either *Villosa trabalis* or *Villosa iris* could be part of the sequence of modifications separating the karyotype of *Pleurobema rubrum* from the composite.

The overall image conveyed by Figure 4 is that most of these ten species form a fairly tight cluster around the center (the composite), while two species are clear outliers. Examination of Table 2 indicates that most of the 87 spreads that contributed to the composite (56 spreads, 64% of the total) are from species typically considered in the subfamily or tribe Lampsilini (Vokes, 1980; Graf & Cummings, 2007). Given the large number of lampsiline spreads included in the composite, it is not surprising that most of the seven lampsiline species included in this analysis plot near the center on Figure 4, and that the single pleurobemine species (*Pleurobema rubrum*) and one of the two anodontine species (*Lasmigona costata*) plot so far from the center. What may be more interesting is the fact that *Pyganodon g. grandis*, typically considered an anodontine species (Vokes, 1980; Graf & Cummings, 2007), plots just one chromosomal modification away from this lampsiline-dominated composite. This figure also suggests that *Ptychobranchus fasciolaris* has a more divergent karyotype than the other lampsiline species included in this analysis.

While the possible karyotypic relationships presented in Figure 4 may be interesting to some, the long-term value of this analysis is more likely to be associated with the process instead of these specific results. The ten species included in this analysis are each represented by between four and eight measured chromosome spreads and, as indicated above, the margin of error associated with the measurement of these chromosomes is about 11%. In spite of its small sample sizes and relatively large error component, this analysis does associate most of the species thought to be members of the same naiad tribe, and does segregate out two of the three species thought to be members of different tribes. In other words, even this small and relatively noisy analysis of these two chromosomal metrics, when considered together, is able to demonstrate similarities and differences among naiad species that correspond with results from other sets of morphological and genetic characteristics. This conclusion suggests that the potential benefits of exploring this entirely new set of naiad morphological characteristics is likely to justify the effort necessary to improve the quality of the chromosomal measurements, increase the number of measured spreads per species, and augment the number of species that can be included.

ACKNOWLEDGEMENTS

Three people were instrumental in bringing this nearly forgotten research to print. Nathan Johnson showed graduate student enthusiasm in this work and encouraged me to publish it. Tom Watters spent too much of his valuable time confirming or updating the identifications of the naiades included in this paper. And, an anonymous reviewer clearly familiar with bivalve chromosomes provided both encouragement for the publication of this work and suggestions for condensing earlier drafts into its present form.

LITERATURE CITED

ARRIGHI, F. & T. HSU, 1974, Staining constitutive heterochromatin and Giemsa crossbands of mammalian chromosomes. *Human Chromosome Methodology*, 59–71.

BABRAKZAI, N., W. MILLER & S. SAMSAM, 1976, Procedures and methods in molluscan cytology and cytogenetics. *Bulletin of the American Malacological Union*, 1976: 57–63.

BAKER, F. C., 1928, The fresh water mollusca of Wisconsin Part II. Pelecypoda. *Bulletin of the Wisconsin Geological and Natural History Survey*, 70: 495 pp.

BOGART, J., 1973, Evolution of anuran karyotypes. Pp. 337–349, in: J. Vail, ed., *Evolutionary biology of the anurans: contemporary research on major problems*. University of Missouri Press, Columbia, 470 pp.

BURCH, J., 1962, Cytotaxonomic studies of freshwater limpets (Gastropoda: Basommatophora). I. The European lake limpet, *Acroloxus lacustris*. *Malacologia*, 1(1): 55–72.

CAMACHO, J., T. SHARBEL & L. BEUKEBOOM, 2000, B-chromosome evolution. *Philosophical Transactions of the Royal Society London, B*, 355: 163–178.

CARRIHO, J., A. LEITÄO, C. VICENTE & I. MALHEIRO, 2008, Cytogenetics of *Anodonta cygnea* (Mollusca: Bivalvia) as possible indicator of environmental adversity. *Estuarine, Coastal and Shelf Science*, 80(2): 303–306.

CHAMBERS, S., 1982, Chromosomal evidence for parallel evolution of shell sculpture pattern in *Goniobasis*. *Evolution*, 36(1): 113–120.

CORNET, M., 1993, A short-term culture method for chromosome preparation from somatic tissues of adult mussel (*Mytilus edulis*). *Cellular and Molecular Life Sciences*, 49(1): 87–90.

CORNET, M., 1995, A study of some factors affecting the efficiency of *in vitro* mussel tissue culture for chromosome preparation. *Cytobios*, 84: 7–12.

CHU, E. & N. GILES, 1959, Human chromosome complements in normal somatic cells in culture. *American Journal of Human Genetics*, 11(1): 63.

DAVIS, G. M. & S. L. H. FULLER, 1981, Genetic relationships among Recent Unionacea (Bivalvia) of North America. *Malacologia*, 20(2): 217–253.

DEEIN, G., Y. UNAKORNSAWAT, P. RATTANADAENG, C. SUTCHARIT, B. KONG-IM & S. PANHA, 2003, A new species of *Solenaia* from Thailand (Bivalvia: Unionidae: Ambleminae). *Natural History Journal of Chulalongkorn University,* 3(2): 53–58.

EBIED, A., 1998, Karyological studies on three Egyptian freshwater species of order Eulamellibranchiata (Bivalvia: Mollusca). *Cytologia*, 63: 17–26.

FULLER, S. L. H., 1974, Clams and mussels (Mollusca:Bivalvia). Pp. 215–273, in: C. W. Hart, Jr. & S. L. H. Fuller, eds., *Pollution ecology of freshwater invertebrates.* Academic Press, New York & London, 359 pp.

GIRIBET, G., 2008, Bivalvia. Pp. 105–141, in: W. F. Ponder & D. R. Lindberg, eds., *Phylogeny and evolution of the Mollusca.* University of California Press, Berkeley, xi + 469 pp.

GONZÁLEZ-TIZÓN, A., A. MARTINEZ-LAGE, I. REGO, J. AUSIO & J. MÉNDEZ, 2000, DNA contents, karyotypes, and chromosomal location of 18S-5.8S-28S ribosomal loci in some species of bivalve molluscs from the Pacific Canadian coast. *Genome*, 43: 1065–1072.

GRAF, D. & K. CUMMINGS, 2006, Palaeoheterodont diversity (Mollusca: Trigonioida + Unionoida): what we know and what we wish we knew about freshwater mussel evolution.

Zoological Journal of the Linnean Society, 148: 343–394.

GRAF, D. & K. CUMMINGS, 2007, Review of the systematics and global diversity of freshwater mussel species (Bivalvia: Unionoida). *Journal of Molluscan Studies*, 73: 291–314.

HAAG, R. W., 2012, *North American freshwater mussels: natural history, ecology, and conservation.* Cambridge University Press, 505 pp.

INSUA, A., J. LABAT & C. THIRIOT-QUIÉVREUX, 1994, Comparative analysis of karyotypes and nucleolar organizer regions in different populations of *Mytilus trossulus*, *Mytilus edulis*, and *Mytilus galloprovincialis*. *Journal of Molluscan Studies*, 60: 359–370.

INSUA, A. & C. THIRIOT-QUIÉVREUX, 1992, Karyotypes of *Cerastoderma edule*, *Venerupis pullastra,* and *Venerupis rhomboides* (Bivalvia, Veneroida). *Aquatic Living Resources*, 5(1): 1–18.

IQBAL, A., M. KHAN & U. GOSWAMI, 2008, Cytogenetic studies in green mussel, *Perna viridis* (Mytiloida: Pterimorphia) from west coast of India. *Marine Biology*, 153: 987–993.

JARA-SEGUEL, P., S. PEREDO, C. PALMA-ROJAS, E. PARADA & G. LARA, 2000, Quantitative karyotype of *Diplodon chilensis* (Gray, 1828) (Bivalvia: Hyriidae). *Gayana* (Concepción), 64(2): [6 pp.].

JENKINSON, J., 1976, Chromosome numbers of some North American naiades. *Bulletin of the American Malacological Union*, 1976: 16–17.

JENKINSON, J., 1983, *Mitotic and chromosomal characteristics in the North American naiades (Bivalvia: Unionacea).* Ph.D. Dissertation, The Ohio State University, Columbus, Ohio, 226 pp.

JENKINSON, J., 1984, An analysis of naiad chromosomal morphology (Bivalvia: Unionacea). *American Malacological Bulletin*, 2: 86–87.

JONES, N. & A. HOUBEN, 2003, B chromosomes in plants: escapees from the A chromosome genome? *Trends in Plant Science*, 8(9): 417–423.

LA COUR, L., 1941, Acetic-orcein: a new stain-fixative for chromosomes. *Stain Technology*, 16(4): 169–174.

LEA, I., 1870, *A synopsis of the family Unionidae*, 4th ed. Henry C. Lea, Philadelphia, Pennsylvania, 184 pp.

LEITÃO, A., P. BOUDRY, J.-P. LABAT & C. THIRIOT-QUIÉVREUX, 1999a, Comparative karyological study of cupped oysters. *Malacologia,* 41(1): 175–186.

LEITÃO, A. & R. CHAVES, 2008, Banding for chromosomal identification in bivalves: a 20-year history. *Dynamic Biochemistry, Process Biotechnology and Molecular Biology*, 2 (Special Issue 1): 44–49.

LEITÃO, A., R. CHAVES, S. JOAQUIM, D. MATIAS, F. RUANO & H. GUEDES-PINTO, 2008, Supernumerary chromosomes on southern European populations of the cockle *Cerastoderma edule*: Consequence of environmental pollution? *Estuarine, Coastal and Shelf Science*, 79(1): 152–156.

LEVAN, A., K. FREDGA & A. SANDBERG, 1964, Nomenclature for centromeric position on chromosomes. *Hereditas*, 52(2): 201–220.

LILLIE, F., 1901, The organization of the egg of *Unio*, based on a study of its maturation, fertilization, and cleavage. *Journal of Morphology*, 17(2): 227–292.

MARTINEZ-LAGE, A., A. GONZÁLEZ-TIZÓN & J. MÉNDEZ, 1996, Characterization of different chromatin types in *Mytilus galloprovincialis* L. after C-banding, fluorochrome and restriction endonuclease treatments. *Heredity*, 72: 242–242.

MATTHEY, R., 1949, *Les chromosomes des vertébrés*. Rouge, Lausanne, 356 pp.

McMICHAEL, D. & I. HISCOCK, 1958, A monograph of the freshwater mussels (Mollusca: Pelecypoda) of the Australian Region. *Australian Journal of Marine and Freshwater Research*, 9(3): 372–508.

MELNYCHENKO, R., 2000, The comparative analysis of two species of the genus *Unio* (Mollusca: Bivalvia: Unionidae). *Vestnik Zoologii*, Kiev, 134: 85–88 [in Russian].

MELNYCHENKO, R. & L. YANOVICH, 2004, Karyotypes and reproductive cycles of Anodontinae (Mollusca: Unionidae) of the Ukrainian fauna. Pp. 99–101, in: *Abstracts of the conference "Mollusks of the northeastern Asia and northern Pacific: biodiversity, ecology, biogeography, and faunal history."* Vladivostok.

MENZEL, R., 1968, Chromosome number in nine families of marine pelecypod mollusks. *The Nautilus*, 82(2): 45–50, 53–58.

MURRAY, J., 1975, The genetics of the Mollusca. Pp. 3–31, in: *Handbook of genetics, Volume 3, Invertebrates of genetic interest.* Plenum Press, New York, 874 pp.

NAKAMURA, H., 1985, A review of molluscan cytogenetic information based on the CISMOCH – Computerized index system for molluscan chromosomes: Bivalvia, Polyplacophora, and Cephalopoda. *Venus*, *The Japanese Journal of Malacology*, 44(3): 193–225.

NADAMITSU, S. & T. KANAI, 1975, Chromosomes of the freshwater pearl-mussel *Margaritifera laevis* (Haas). *Bulletin of Hiroshima Women's University*, 10: 1–3.

NADAMITSU, S. & T. KANAI, 1978, On the chromosomes of three species in two families of freshwater Bivalvia. *Bulletin of Hiroshima Women's University*, 13: 1–5.

ORTMANN, A. E., 1921, South American naiades: a contribution to the knowledge of the freshwater mussels of South America, *Memoirs of the Carnegie Museum*, 8: 451–670.

PALESTIS, B., J. CABRERO, R. TRIVERS & J. CAMACHO, 2010, Prevalence of B chromosomes in Orthoptera is associated with shape and number of A chromosomes. *Genetica*, 138(11–12): 1181–1189.

PARK, G. & J. BURCH, 1995, Karyotype analysis of six species of North American freshwater mussels (Bivlavia: Unionidae). *Malacological Review*, 28: 43–61.

PARK, G. & O. KWON, 1991, Chromosome study of seven species of Unionidae (Bivalvia: Palaeoheterodonta) in Korea. *Korean Journal of Malacology*, 7: 12–29.

PARK, G., J. LEE, H. SONG, J. PARK & O. KWON, 1988, Cytological studies of *Anodonta* (*Sianodonta*) *woodiana* (Paleoheterodonta: Unionidae) in Korea. *Korean Journal of Malacology*, 7: 12–29.

PARMALEE, P. & A. BOGAN, 1998, *The freshwater mussels of Tennessee*. University of Tennessee Press, Knoxville, 328 pp.

PASANTES, J., M. MARTINEZ-EXPÓSITO, A. MARTINEZ-LAGE & J. MÉNDEZ, 1990, Chromosomes of Galician mussels. *Journal of Molluscan Studies*, 56: 123–126.

PATTERSON, C., 1965, The chromosomes of *Tulotoma angulata* (Streptoneura: Viviparidae). *Malacologia*, 2(2): 259–265.

PATTERSON, C., 1969, Chromosomes of molluscs. *Proceedings of the Second Symposium on Mollusca. Part II. Marine Biology Association of India*, 2: 635–686.

PETKEVIČIŪTĖ, R., G. STANEVIČIŪTĖ, V. STUNŽENAS, T. LEE & D. Ó FOIGHIL, 2007, Pronounced karyological divergence of the North American congeners *Sphaerium rhomboideum* and *S. occidentale* (Bivalvia: Verenoida: Sphaeriidae). *Journal of Molluscan Studies*, 73(4): 315–321.

SAY, T., 1817, Conchology. W. Nicholson, ed., *The first American edition of the British encyclopedia; or Dictionary of arts and sciences, comprising an accurate and popular view of the present improved state of human knowledge.* Samuel A. Mitchell & Horace Ames, Philadelphia, Pennsylvania, [no pagination].

SHI, A., 1980, Some investigations of the chromosomes of three species of freshwater shells. *Journal of Sichuan University* (*Natural Science*), 4, 018.

SIMPSON, C. T., 1896, The classification and geographical distribution of the pearly fresh-water mussels. *Proceedings of the United States National Museum,* 18: 295–343.

SIMPSON, C. T., 1900, Synopsis of the naiades, or pearly freshwater mussels. *Proceedings of the U.S. National Museum*, 22(1205): 501–1044.

SKUZA, L., A. LABECKA & J. DOMAGALA, 2009, Cytogenetic and morphological chacterization of *Corbicula fluminalis* (O.F. Miller 1774) (Bivalvia: Veneroida: Corbiculidae): Taxonomic status assessment of a freshwater clam. *Folia Biologica* (Krakow), 57(3–4): 177–185.

STEEL, R. & J. TORRIE, 1960, *Principles and procedures of statistics*. McGraw-Hill Book Company. Inc., New York, 481 pp.

TAKAGI, N. & M. SASAKI, 1974, A phylogenetic study of bird karyotypes. *Chromosoma*, 46(1): 91–120.

THIRIOT-QUIÉVREUX, C., 1992, Karyotype of *Lasaea australis*, a brooding bivalve species. *Australian Journal of Marine and Freshwater Research*, 43: 403–408.

THIRIOT-QUIÉVREUX, C., 1994, Advances in cytogenetics of aquatic organisms. Pp. 369–388, in: A. R. Beaumont, ed., *Genetics and evolution of aquatic organisms.* Chapman and Hall, 539 pp.

THIRIOT-QUIÉVREUX, C., 2002, Review of the literature on bivalve cytogenetics in the last ten years. *Cahiers de Biologie Marine*, 43: 17–26.

THIRIOT-QUIÉVREUX, C., 2003, Advances in chromosomal studies of gastropod molluscs. *Journal of Molluscan Studies*, 69: 187–201.

VAN GRIETHUYSEN, G., B. KIATU & L. BUTOT, 1969, The chromosomes of *Anodonta anatina* (Linnaeus 1758) and *Unio pictorum* (L. 1758) (Mollusca: Bivalvia: Unionidae). *Basteria*, 33(1–4): 51–56.

VITTURI, R., M. RASOTTO & N. FARINELLA-FERRUZZA, 1982, The chromosomes of 16 molluscan species. *Bullettino di Zoologia*, 49: 61–71.

VOKES, H., 1980, *Genera of the Bivalvia: a systematic and bibliographic catalogue* (*revised and updated*). Paleontological Research Institution, Ithaca, New York, 307 pp.

WANG, X., Y. WANG, A. SHI & X. WANG, 2000, Research on chromosomes of *Hyriopsis cumingi*. *Sichuan Daxue Xuebo* (*Journal of Sichuan University*), 37: 252–256.

WEN, H., R. GU & G. XU, 2009, Karyotypes on round mussel (*Anodonta woodiana pacifica*). *Journal of Zhejiang Ocean University* (*Natural Science*), 2, 010.

WOZNICKI, P., 2004, Chromosomes of the Chinese mussel *Anodonta woodiana* (Lea, 1834) (Bivalvia: Unionidae) from the heated Konin Lakes system in Poland. *Malacologia,* 46(1): 205–209.

WOZNICKI, P. & M. JANKUN, 2004, Chromosome study of *Anodonta anatina* (L., 1758) (Bivalvia: Unionidae). *Folia Biologica* (Kakow), 52(3–4): 171–174.

Revised ms. accepted March 17, 2014

RESEARCH NOTE

MALACOLOGIA, 2014, 57(2): 401–408

THE TAXONOMY, DISTRIBUTION AND INTRODUCTION HISTORY OF THE EARLIEST REPORTED ALIEN FRESHWATER MOLLUSC IN SINGAPORE – *SINOTAIA GUANGDUNGENSIS* (GASTROPODA: VIVIPARIDAE)

Ting Hui Ng[1,2*], Siong Kiat Tan[3] & Darren C. J. Yeo[1,2]

INTRODUCTION

Freshwater fauna introductions in Singapore have been relatively well documented (Yeo & Chia, 2010), but the origins of many alien species, such as freshwater molluscs are unconfirmed (Tan et al., 2012). Among the known introduced molluscs, the South American *Pomacea canaliculata* is perhaps the most notorious owing to it being a widespread and major agriculture pest (Joshi & Sebastian, 2006). However, *P. canaliculata* is a relatively recent introduction to Singapore (since 1980s; Tan et al., 2012) compared to *Sinotaia guangdungensis* (Kobelt, 1906) (Viviparidae), which was first recorded in the 1950s (as *Vivipara polyzonata* by Johnson, 1957), making it the earliest reported introduced freshwater mollusc here.

The taxonomy of *Sinotaia guangdungensis* has been confusing, resulting in the species being referred to by different names. Following Johnson (1973), the species has been known in Singapore as *Angulyagra polyzonata* (and subsequently as *Taia polyzonata* in Clements et al., 2006; Tan et al., 2012); however, the name *Taia polyzonata* appears to have been used almost exclusively in Singapore and neighbouring Malaysia (e.g., Palmieri et al., 1980; Sengupta et al., 2009; Tan et al., 2012). Shea (1994) re-identified the species in Singapore as *Bellamya heudei guangdungensis*, by differentiating it from *Angulyagra polyzonata*, and although Shea's correction was noted by Chan (1997), this name has been overlooked in Singapore to date.

Sinotaia guangdungensis is rarely documented in its native region in southern China (Shea, 1994) and little else is known about the species. Therefore, an account based on specimens collected in Singapore can contribute to informing and guiding future efforts to resolve the taxonomic and biogeographic confusion associated with this species and with the Viviparidae in general. Additionally, a record of its introduction history can also be useful in elucidating freshwater biological introductions to Singapore. In this research note, we review the taxonomy of *Sinotaia guangdungensis*, its current distribution in Singapore, as well as its known distribution within its invaded range, and the likely origins of the introduced population. Records from the Zoological Reference Collection (ZRC) of the Lee Kong Chian Natural History Museum (formerly Raffles Museum of Biodiversity Research), National University of Singapore; published literature; and unpublished data were consulted. Singapore material was also compared to photographs of type material from Senckenberg Forschungsinstitut und Naturmuseum, Frankfurt, Germany, and the Naturhistorisches Museum Wien, Austria.

SPECIES ACCOUNT

Family Vivipariidae Gray, 1847
Genus *Sinotaia* Haas, 1939

Type species: *Paludina quadrata* Benson, 1842 (type locality: Chusan, China).

Sinotaia guangdungensis
(Kobelt, 1906)
(Fig. 1)

Vivipara (*quadrata* var.) *heudei* var. *guangdungensis* Kobelt, 1906: 124–125, pl. 21, figs. 12, 14.

Dactylochalamys quangdugensis [sic] – Prashad, 1928: 169.

---

[1]Department of Biological Sciences, National University of Singapore, 14 Science Drive 4, Singapore 117543, Republic of Singapore

[2]NUS Environmental Research Institute, National University of Singapore, 5A Engineering Drive 1, #02-01, Singapore 117411, Republic of Singapore

[3]Lee Kong Chian Natural History Museum, Department of Biological Sciences National University of Singapore, 6 Science Drive 2, Singapore 117546, Republic of Singapore

*Corresponding author: ng.tinghui@nus.edu.sg

Vivipara polyzonata – Yen, 1939: 37, pl. 3, figs. 14, 15 [*non* Frauenfeld, 1862].
Angulyagra quangdungensis – Yen, 1943: 128.
Sinotaia polyzonata – Zilch, 1955: 77 [*non* Frauenfeld, 1862].
Vivipara polyzonatus – Johnson, 1957: 65 [*non* Frauenfeld, 1862].
Taia polyzonata – Johnson, 1973: 120, 122; Palmieri et al., 1980: 40; Ng, 1991: 125; Chan, 1996: 184–185, fig. 2; 1997: 35; Maassen, 2001: 44; Clements et al., 2006: 144; Tan & Woo, 2010: 26; Yeo & Chia, 2010: 32; Tan et al., 2012: 133 [*non* Frauenfeld, 1862].
Sinotaia quadrata guangdungensis – Brandt, 1974: 30.
Viviparus polyzonata – Ng et al., 1993: 20 [*non* Frauenfeld, 1862].
Bellamya heudei guangdungensis – Shea, 1994: 3–11.

Material Examined

Singapore: Jurong Road, 11 ½ miles: ZRC1989.118; ZRC1989.1181–1989.1183, 20 Jul. 1960. Kian Teck Road: ZRC1989.1184–1989.1185, 23 Jun. 1961. Potong Pasir: ZRC1989.1186–1989.1190, 27 Jun. 1962. Buona Vista, pond: ZRC1989.1191–1989.1202, 20 Nov. 1957; ZRC1989.1220–1989.1231, 11 Nov. 1958; MacRitchie, Sungei Whampoa:

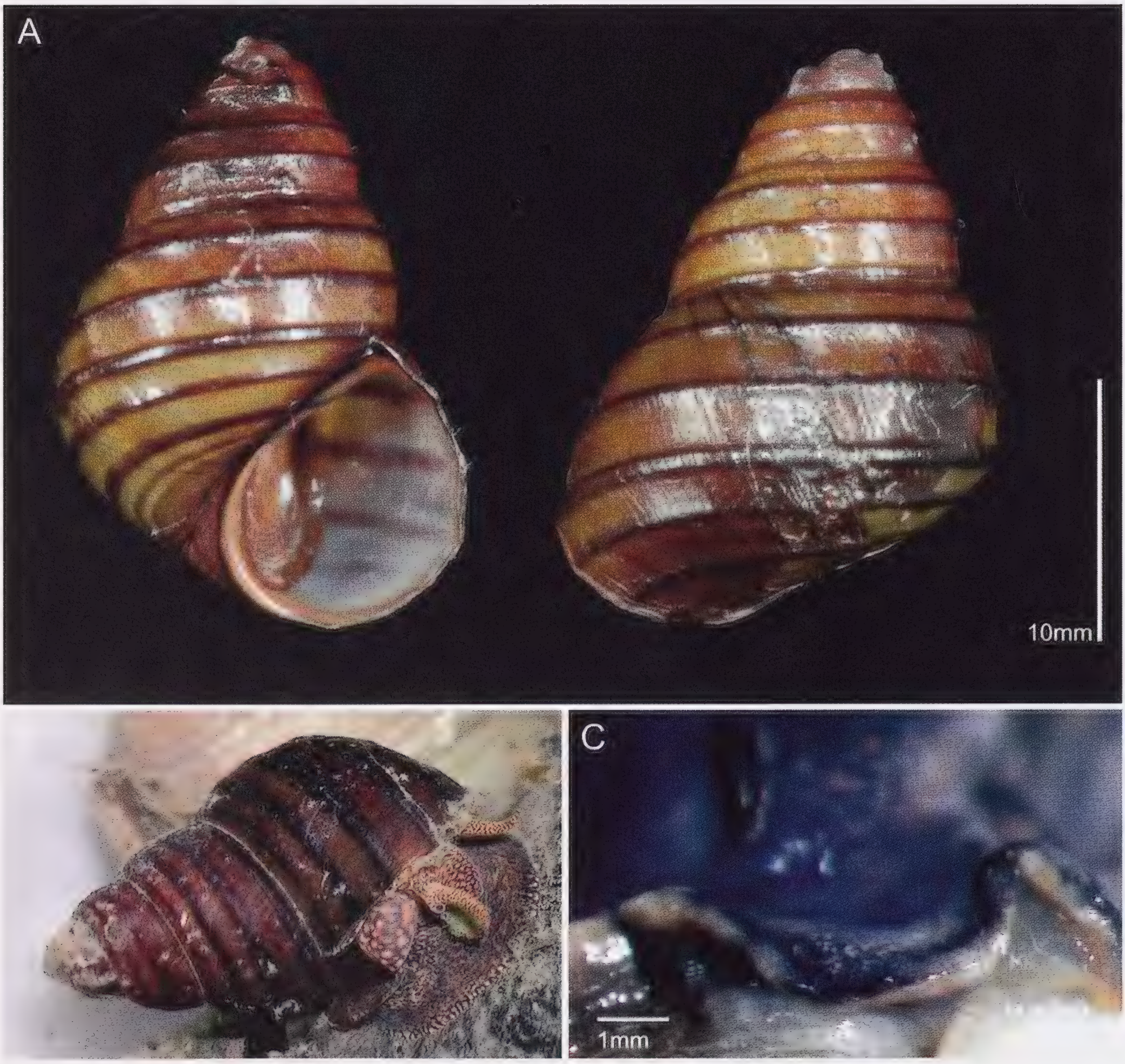

FIG. 1. *Sinotaia guangdungensis* from Singapore. (A): A specimen from Jurong Lake; (B): A live specimen from Lower Seletar Reservoir; (C): Mantle edge of a specimen from Sungei Seletar. Photographs by Ting Hui Ng (A & C) and Siong Kiat Tan (B).

ZRC1989.1203–1989.1209, 16 May 1962. University of Malaya, Botany Department tank: ZRC1989.1210–1989.1219, 25 May 1968. Jurong Road, pond: ZRC1989.1232–1989.1253, 23 May 1962; ZRC1989.1254–1989.1261, 21 May 1962; ZRC1989.1262–1989.1280, 23 May 1963. Potong Pasir, pond: ZRC1989.1281–1989.1307, ZRC1989.1332–1989.1339, 2 Jul. 1962. Sungei Whampoa: ZRC1989.1308–1989.1331, ZRC1989.1344–1989.1826. Seletar Reservoir (currently known as Upper Seletar Reservoir): ZRC1989.1340–1989.1343, 4 Feb. 1981; ZRC1990.868–1990.872, 11 Mar. 1990; ZRC1999.1398, 1 Feb. 1999; ZRC.MOL.21–22, 4 Jun. 2002. Vaughan Road, pond: ZRC1989.1837–1989.1841, 27 Jun. 1963. Holland Road: ZRC1989.1942–1989.1943. Lower Peirce Reservoir: ZRC1990.738–1990.829, 29 Nov. 1990; ZRC.MOL.19, 8 Aug. 2002. Jurong Lake: ZRC1991.19290–1990.19308, 16 Apr. 1991; ZRC.MOL.20, 11 Jul. 2002. Nee Soon Road: ZRC1995.672, 10 Jun. 1995. Lower Seletar Reservoir: ZRC.MOL.18, 24 May. 2002; ZRC.MOL.2931, 19 Feb. 2009. Kranji Reservoir: ZRC.MOL.17, 7 Jul. 2002. Unknown localities: ZRC1989.1827–1989.1834; ZRC1989.1835–1989.1836; ZRC1989.1842–1989.1865.

Description

Shell ovately conic, spire turreted, base rounded, usually less than 25 mm in shell height, thin but solid; shell colour yellowish green to light greenish brown, spiral ribs reddish brown to dark brown, aperture and parietal callus white to orange; whorls 6–7, slightly convex in profile, suture slightly impressed, body whorl round in profile without prominent angle at periphery, space between ribs slightly concave, ribs usually 3 above periphery and spire whorls, usually much weaker after the first rib below the periphery; aperture subovate, columella thickened and reflected over the umbilical area, umbilicus absent, parietal wall usually callused.

Geographic Distribution

Sinotaia guangdungensis appears to originate from Guangdong and Guangxi provinces in southern China, and from Hong Kong (Shea, 1994). It has been introduced to Australia, Malaysia and Singapore (Shea, 1994; Chan, 1997; Tan et al., 2012).

TAXONOMY AND NOMENCLATURE

Vivipara guangdungensis was described by Kobelt (1906: 124–125, pl. 21, fig. 12) as an unusual form of *Vivipara heudei*, itself described as a variety of *Paludina quadrata* Benson, 1842, by Dautzenberg & Fischer (1905), from Guangdong ("Guangdung") province in China (Fig. 2). Confusion over the identity and validity of *Vivipara guangdungensis* seems to have started when Yen (1939) mistakenly synonymised this species with *Vivipara polyzonata* Frauenfeld, 1862 (Yen, 1939; Brandt, 1974; Shea, 1994; Fig. 3). Although Yen (1943) subsequently restored both as separate species, Zilch (1955) appears to have overlooked Yen's publication and maintained the synonymy in his catalogue of the viviparid type material in the Senckenberg Naturmuseum. The type material of *V. polyzonata*, however, is composed of two species (see Fig. 3; Shea, 1994) and may continue to confound future taxonomic studies if not resolved. As also noted by Shea (1994: 8), at least two of the paralectotypes (NHMW68038) are actually *Vivipara guangdungensis* (Fig. 3).

Prashad (1928: 169) disagreed with Kobelt (1906) that *Vivipara quangdugensis* [sic] was related to *Vivipara quadratus* var. *heudei,* and instead suggested that it was a distinct species of the genus *Dactylochlamys* Rao, 1925 [*non* Lauterborn, 1901]. Rao (1925) established the genus *Dactylochlamys* for *Paludina oxytropis* Benson, 1836, and described it as having prominent "finger shaped processes" along the mantle edge, a feature missing from the species discussed here (Fig. 1C). However, *Dactylochlamys* was a preoccupied name, and so Rao (1931: 301) subsequently proposed *Angulyagra* as a replacement. We concur with Prashad (1928) that *guangdungensis* represents a species distinct from *heudei*, but follow Brandt (1974) in assigning it to the genus *Sinotaia* Haas, 1939. The description for the genus *Sinotaia* agrees well with the species: "…characterized by the narrow, rather thick shell with an expanded columellar thickening, mostly blackish towards its outer margin, and by the indication or strong development of keels on the upper, middle, and lower part of the whorls" (Haas, 1939: 96).

The species in Singapore was apparently first identified by the prominent malacologist R. Tucker Abbott as *Vivipara polyzonata* Fraunfeld; but this identification was doubted by D. S. Johnson owing to the mistaken belief that *V. polyzonata* was a Mediterranean species

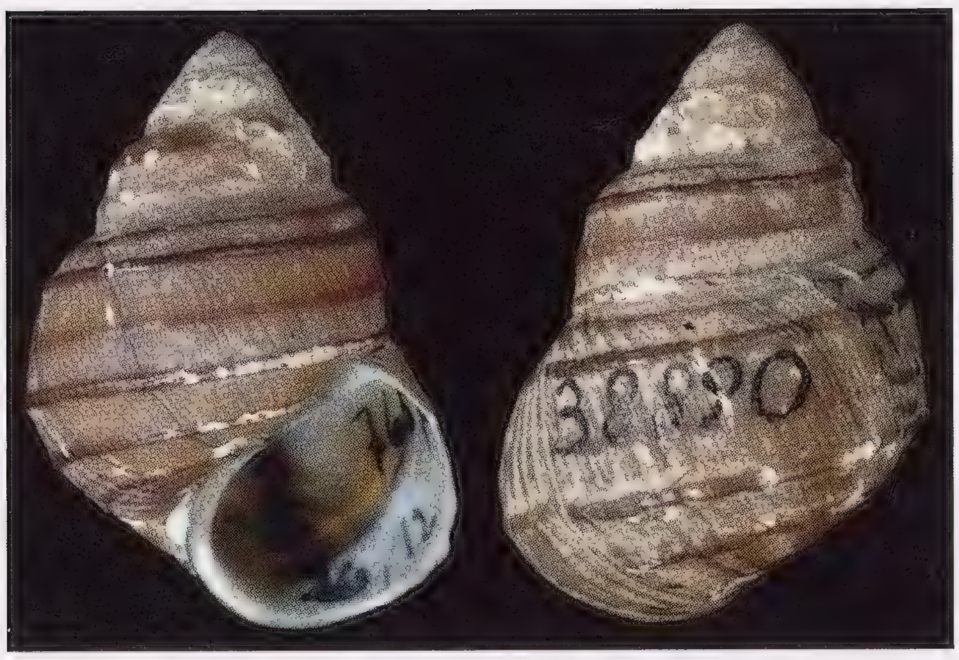

FIG. 2. *Vivipara guangdungensis* Kobelt, 1906, holotype (SMF38890), Canton, China. Photographs by Eike Neubert; courtesy of Ronald Janssen, Mollusc Section, Senckenberg Forschungsinstitut und Naturmuseum Frankfurt, Germany.

(Johnson, unpublished manuscript). Nonetheless, Johnson continued to apply the names *Vivipara polyzonata*, and *Taia polyzonata* (e.g., Johnson, 1957, 1973), and the name *Taia polyzonata* continued to be used in Singapore up to now (Tan & Woo, 2010). Shea (1994) was the first to correctly identify the species found in Singapore as *Sinotaia guangdungensis* (as *Bellamya heudei guangdungensis*), and detailed its taxonomic history. All material from Singapore that we examined, and verifiable records in the literature conform to the descriptions and conchological characteristics of the holotype of *Sinotaia guangdungensis* (Fig. 2; Kobelt, 1906; Shea, 1994), and no *Angulyagra polyzonata* was located. It is therefore very likely that all previous Singapore records of *Angulyagra polyzonata* – alternatively represented in the literature as *Vivipara polyzonatus*, *Viviparus polyzonata*, and *Taia polyzonata* – are misidentifications (see synonymy for *Sinotaia guangdungensis*).

DISTRIBUTION AND HABITATS IN SINGAPORE

In the early reports of *Sinotaia guangdungensis* in Singapore, it was found to be common in fish breeding ponds (as *Vivipara polyzonatus* in Johnson, 1957; as *Taia polyzonata* in Johnson,

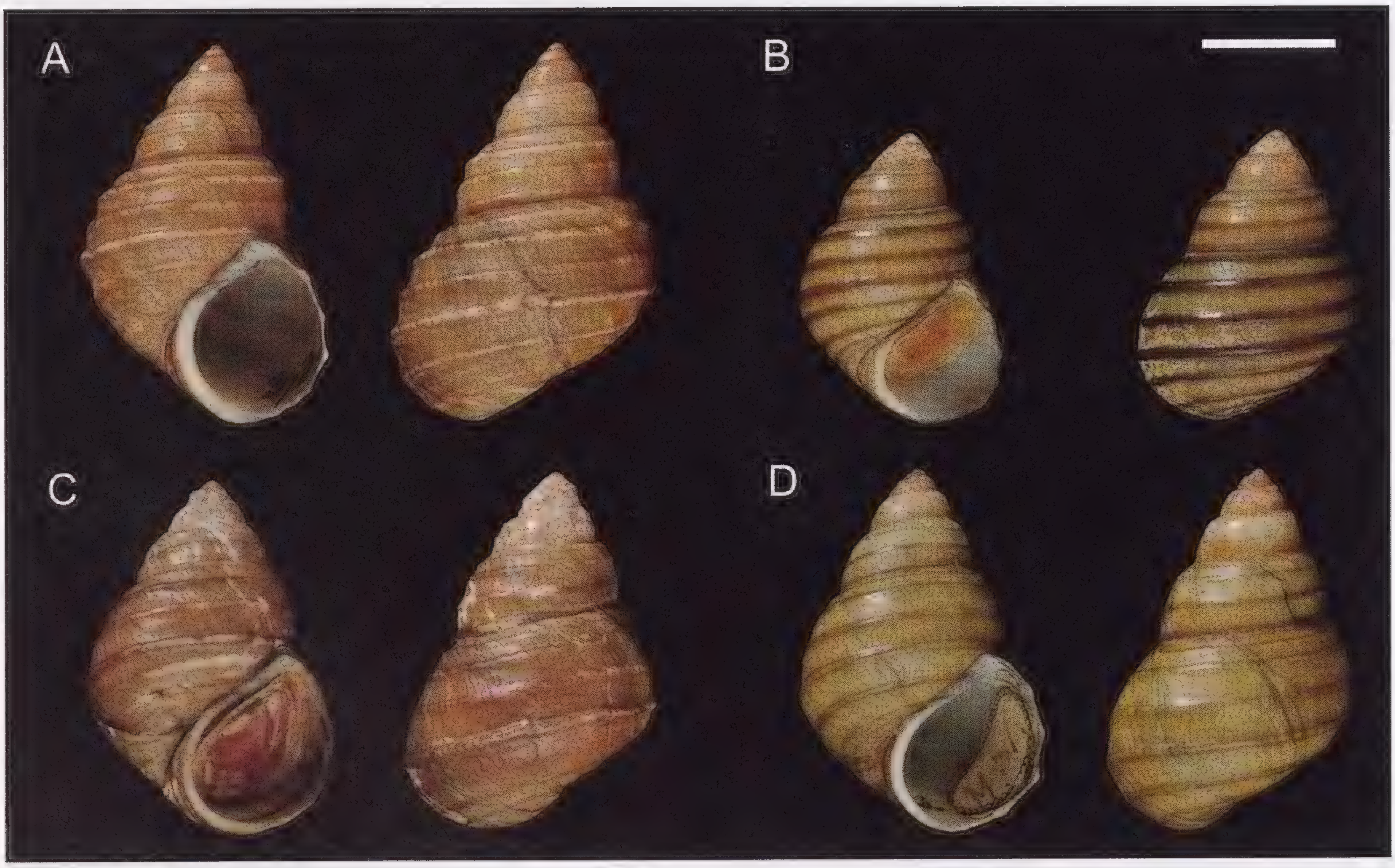

FIG. 3. Types of *Vivipara polyzonata* Frauenfeld, 1862. (A): Lectotype (NHMW68037), designated by Yen (1939); (B–D): Paralectotypes (NHMW68038) [B, D = *Sinotaia guangdungensis*], (B) locality marked as "China?", (C, D) accompanied by multiple labels with no clearly identified locality information. Photographs by Alice Schumacher; courtesy of Anita Eschner, Collection Mollusca, Naturhistorisches Museum Wien, Austria. Scale bar = 10mm.

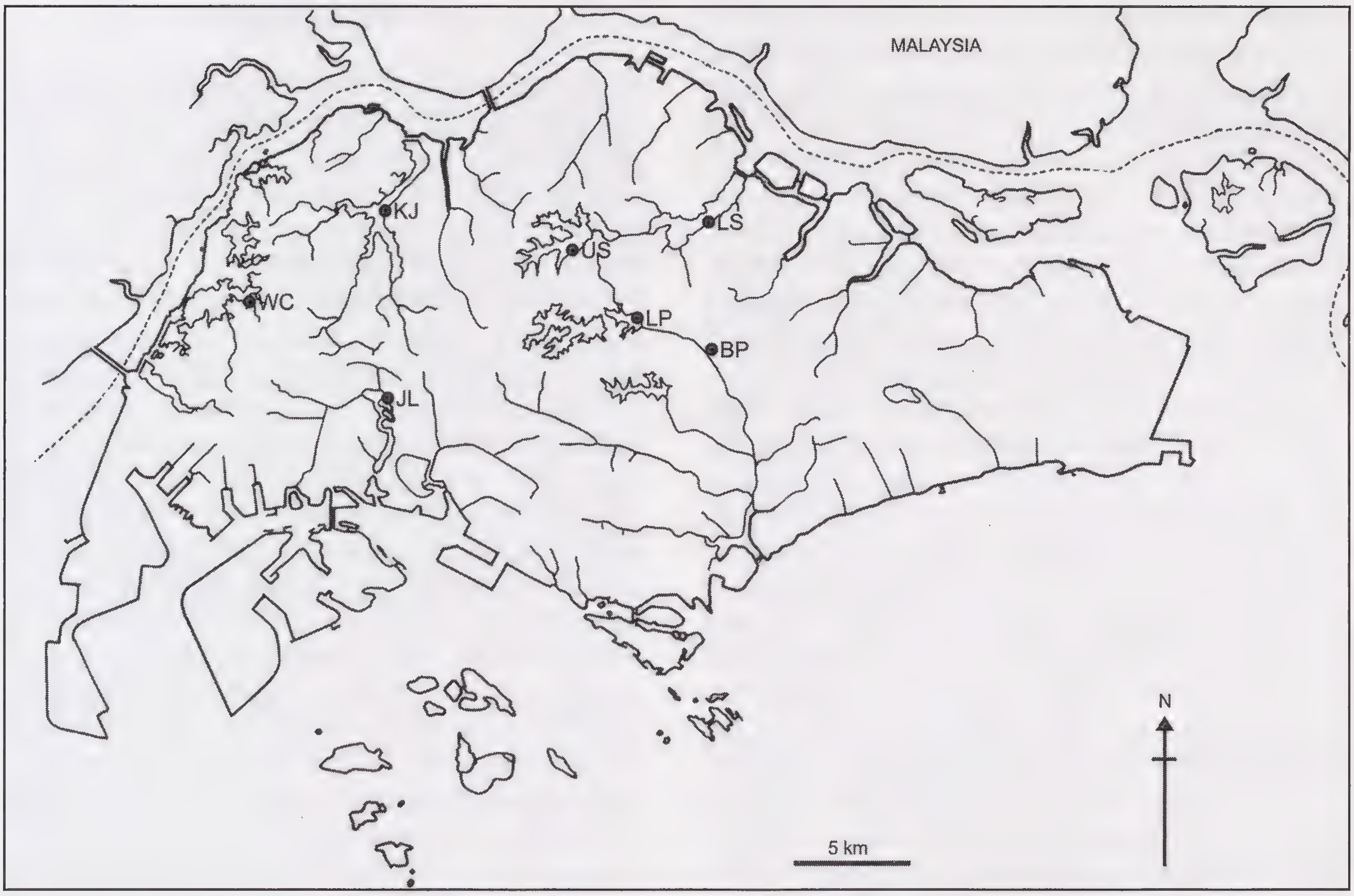

FIG. 4. Current distribution of *Sinotaia guangdungensis* in Singapore. JL (Jurong Lake and tributaries), KJ (Kranji Reservoir and tributaries), LP (Lower Peirce Reservoir), LS (Lower Seletar Reservoir and tributaries), WC (Western Catchment Reservoirs: Tengeh, Poyan, Murai, Sarimbun), US (Upper Seletar Reservoir), BP (Bishan Park canal).

1973). Established populations were recorded from such ponds around the island (Buona Vista, Jurong Road, Potong Pasir), and also from canals and ditches (Sungei Whampoa, Lorong Buang Kok) (Ponniah, 1962; Johnson, unpublished manuscript). There is a gap in published records of the species in the 1970s and 1980s, after Johnson – who had led much of the research on freshwater invertebrates at the then University of Singapore – passed away in 1972 (Harding, 1974). Collections of freshwater molluscs mainly resumed in the 1990s.

By the 1990s, most of the fishponds had disappeared, and other types of artificial freshwater habitats had become more dominant, with most of Singapore's rivers being impounded in the 1970s and 1980s to create reservoirs throughout the island (Yeo et al., 2010). Freshwater molluscs soon established in these reservoirs, including *Sinotaia guangdungensis*, which was found in five reservoirs by the early 2000s – Upper Seletar, Lower Seletar, Lower Peirce, Kranji, and Jurong Lake (Fig. 4; Ng, 1991; Clements et al., 2006; Tan et al., 2012). The species is now also established in four more reservoirs in the Western Catchment area of Singapore, and in various waterways connected to reservoirs, for example, Sungei Jurong (connected to Jurong Lake), Sungei Seletar (Lower Seletar), and the main stream in Bishan Park (Lower Peirce) (T. H. N., pers. obs.). Although widespread, *Sinotaia guangdungensis* seems to avoid hard-bottomed concrete canals, unlike common molluscs like *Pomacea canaliculata* (S. K. T. & T. H. N., pers. obs.).

INTRODUCTION HISTORY

As *Sinotaia guangdungensis* was initially established in fishponds, the species may have been introduced together with the freshwater fish used to stock these ponds (Johnson, unpublished). Various carp species (e.g., *Ctenopharyngodon idella*, *Hypophthalmichthys nobilis*) were imported from Guangdong province in China, and cultivated in ponds across Singapore since the early 1900s (Herre, 1937; Burdon, 1950). In China, the carp fry were collected from around villages and transported to ports in Guangdong province, from which they were subsequently transported to Singapore in tubs containing water from their nursery ponds (Britwistle, 1931b). This is likely to have resulted in accidental transfer of other fish species (Alfred, 1966), and even molluscs. The ponds in Singapore were ideal habitats for freshwater molluscs as the water was fertilised to enhance the growth of algae for the fish (Britwistle, 1931a: 376).

While *Sinotaia guangdungensis* was well established in Singapore by the mid-20th century, it did not appear to have been found in neighbouring Peninsular Malaysia at the time (Johnson, 1957; 1973). A record of *Taia polyzonata* in Malaysia by Palmieri et al. (1980) was unverified, as identifications were said to have followed Brandt (1974), who did not include a description of this species. However, in 1995, its presence in Malaysia was confirmed by S. Y. Chan, an amateur malacologist familiar with species from Singapore, and verified to be the same species as the one in Singapore (Chan, 1997). The snail could have been introduced to Malaysia with fish from China, which were transported using similar methods as imports to Singapore (Lin, 1949; Acosta & Gupta, 2005).

To date, *Sinotaia guangdungensis* has also been introduced to Australia. It was first recorded in New South Wales in 1939, and subsequently in the late 1970s, but populations appear to have declined by the early 1990s (Shea, 1994). Since the late 19th century, fish introductions have been common in southeastern Australia, where early settlers stocked water bodies with European carp and other imported fish, including some from Singapore (Koehn et al., 2000). It is possible that *Sinotaia guangdungensis* may have also been introduced to Australia with such shipments of fish, either from China or even from Singapore. Accidental introductions are complex and usually difficult to resolve (van Leeuwen et al., 2013). A recently established population of the congeneric *Sinotaia quadrata* (Benson, 1842) in Argentina was also likely to have been accidentally introduced (Ovando & Cuezzo, 2012). Nonetheless, further work to compare the population genetics of native and introduced *Sinotaia guangdungensis* may help explain the routes of introduction (Ficetola et al., 2008; Hayes et al., 2008).

CONCLUSION

The introduced viviparid species with a spirally ribbed shell in Singapore that has been referred to in the literature as *Vivipara polyzonatus*, *Viviparus polyzonata* and *Taia polyzonata*, is now more appropriately called *Sinotaia guangdungensis* (Kobelt, 1906). While it has been established in Singapore for more than half a century, *Sinotaia guangdungensis* has not caused any discernible impacts in the natural environment, perhaps owing to its distribution being restricted to artificial or more modified habitats. Molecular and ecological studies of *Sinotaia guangdungensis* in Singapore are needed to identify introduction routes, and potential traits or environmental factors that have enabled it to establish so successfully here. Further study of the populations here would not only provide valuable insight into the mechanisms through which freshwater molluscs have been introduced and established in Singapore's novel freshwater habitats (e.g., reservoirs), but may also aid in the management of these habitats.

ACKNOWLEDGEMENTS

We thank Hui Kheng Lua (Raffles Museum of Biodiversity Research, National University of Singapore), Anita Eschner (Natural History Museum Vienna), and Ronald Janssen (Senckenberg Forschungsinstitut und Naturmuseum Frankfurt) for assistance in accessing museum collections and providing photographs of type specimens, and the Natural History Museum, London, for providing access to the unpublished work of D. S. Johnson. Support and permission from the Public Utilities Board for some of the recent surveys is gratefully acknowledged. We would also like to thank Martyn Low for providing some literature and comments on the manuscript, and Alvin Lok, Heok Hee Ng, Yen-Ling Lee, and members of the Freshwater and Invasion Biology Laboratory for assistance in collecting specimens. We acknowledge the financial support from the National Research Foundation and the Economic Development Board (SPORE, COY-15-EWI-RCFSA/N197-1), and NUS grant number R-154-000-465-133.

LITERATURE CITED

ACOSTA, B. O. & M. V. GUPTA, 2005, The status of introduced carp species in Asia. Pp. 121–137, in: D. J. PENMAN, M. V. GUPTA & M. M. DEY, eds., *Carp genetic resources for aquaculture in Asia. WorldFish Center Technical Report 65*. WorldFish Center, Penang, 152 pp.

ALFRED, E. R., 1966, The fresh-water fishes of Singapore. *Zoologische Verhandelingen*, 78: 68.

BENSON, W. H., 1836, Descriptive catalogue of a collection of land and fresh-water shells, chiefly contained in the Museum of the Asiatic Society. Part 2. – Fluviatile shells. *Journal of the Asiatic Society of Bengal*, 5: 741–750.

BENSON, W. H., 1842, 5. Mollusca in Dr. Cantor, on the flora and fauna of Chusan. *The Annals and Magazine of Natural History, including Zoology, Botany and Geology*, 9: 486–490.

BIRTWISTLE, W., 1931a, Rearing of carp in ponds. *The Malayan Agricultural Journal*, 19(8): 372–383.

BIRTWISTLE, W., 1931b, Transport of carp fry from China. *The Malayan Agricultural Journal*, 19(10): 490–493.

BRANDT, R. A. M., 1974, The non-marine aquatic Mollusca of Thailand. *Archiv für Molluskenkunde*, 105: i–iv + 1–423.

BURDON, T. W., 1950, The pond cultivation of fish in the colony of Singapore. Pp. 130–142, in: D. W. LE MARE, ed., *Report of the Fisheries Department, Malaya 1949*. Fisheries Department, Malaya.

CHAN, S. Y., 1996, Some freshwater gastropods of Singapore. *Of Sea and Shore*, 18: 184–187.

CHAN, S. Y., 1997, Non marine mollusks from Selangor, West Malaysia, with a comparison note on introduced species. *Club Conchylia Informationen*, 29: 35–46.

CLEMENTS, R., L. P. KOH, T. M. LEE, R. MEIER & D. LI, 2006, Importance of reservoirs for the conservation of freshwater molluscs in a tropical urban landscape. *Biological Conservation*, 128: 136–146.

DAUTZENBERG, P. & H. FISCHER, 1905, Liste des mollusques recoltes par M. le Capitaine de Fregate Blaise au Tonkin, et description d'especes nouvelles. *Journal de Conchyliologie*, 53: 85–233.

FICETOLA, G. F., A. BONIN & C. MIAUD, 2008, Population genetics reveals origin and number of founders in a biological invasion. *Molecular Ecology*, 17: 773–782.

FRAUENFELD, G. R. VON, 1862, Zusammenstellung der Arten der Gattung *Vivipara* Lmk. in der kaiserlichen Sammlung. *Verhandlungen der Kaiserlich-Königlichen Zoologisch-Botanischen Gesellschaft in Wien*, 12: 1161–1170.

GRAY, J. E., 1847, A list of the genera of Recent Mollusca, their synonyms and types. *Proceedings of the Zoological Society of London*, 15: 129–219.

HAAS, F., 1939, Malacological notes. *Zoological Series of Field Museum of Natural History*, 24: 93–103.

HARDING, J. P., 1974, Notes and news: Professor D. S. Johnson, 1924–1972. *Crustaceana*, 27: 103–107.

HAYES, K. A., R. C. JOSHI, S. C. THIENGO & R. H. COWIE, 2008, Out of South America: multiple origins of non-native apple snails in Asia. *Diversity and Distributions* 14: 701–712.

HERRE, A. W. C. T., 1937, A contribution to the ichthyology of the Malay Peninsula. *Bulletin of the Raffles Museum*, 13: 5–75.

JOHNSON, D. S., 1957, A survey of Malayan freshwater life. *The Malayan Nature Journal*, 12: 57–65.

JOHNSON, D. S., 1973, Freshwater life. Pp. 103–127, in: S. H. CHUANG, ed., *Animal life and nature in Singapore*. Singapore University Press, Singapore, 340 pp.

JOSHI, R. C. & L. S. SEBASTIAN, eds., 2006, *Global advances in ecology and management of golden apple snails*. Philippine Rice Research Institute, Neuva Ecija, 588 pp.

KOBELT, W., 1906, Die Gattung *Paludina* Lam. Neue Folge. *Martini und Chemnitz System Conchylien Cabinet* 1, 21a: 97–128.

KOEHN, J. D., A. BRUMLEY & P. C. GEHRKE, 2000, *Managing the impacts of carp.* Australian Government Bureau of Rural Sciences, Canberra, 249 pp.

LAUTERBORN, R., 1901, Die "sapropelische" Lebewelt. *Zoologischer Anzeiger*, 24: 50.

LIN, S. Y., 1949, Notes on the fish fry industry of China. *Proceedings of the Indo-Pacific Fisheries Council*, 1: 65–71.

MAASSEN, W. J. M., 2001, A preliminary checklist of the non-marine mollusks of Malaysia: "A hand list". *De Kreukel*, Extra Ed.: 1–155.

NG, P. K. L., ed., 1991, *Freshwater life in Singapore*. Science Centre Singapore, Singapore, 158 pp.

NG, P. K. L., L. M. CHOU & T. J. LAM, 1993, The status and impact of introduced freshwater animals in Singapore. *Biological Conservation*, 64: 29–24.

OVANDO, X. M. C. & M. G. CUEZZO, 2012, Discovery of an established population of a non-native species of Viviparidae (Caenogastropoda) in Argentina. *Molluscan Research*, 32: 121–131.

PALMIERI, M., J. PALMEIRI & J. SULLIVAN, 1980, A chemical analysis of the habitat of nine commonly occurring Malaysia freshwater snails. *The Malayan Nature Journal*, 34: 1–7.

PONNIAH, A. J., 1962, *Studies on some non-marine aquatic gastropods of Singapore island, with a note on five species collected from Malacca*. Unpublished B.Sc. (Hons.) Thesis, University of Singapore, Singapore, 58 pp.

PRASHAD, B., 1928, Recent and fossil Viviparidae. A study in distribution, evolution and palaeogeography. *Memoirs of the Indian Museum*, 8: 153–252.

RAO, H. S., 1925, On the comparative anatomy of Oriental Viviparidae. *Records of the Indian Museum*, 27: 129–135.

RAO, H. S., 1931, *Angulyagra oxytropis* (Benson) nom. nov. – a correction. *Records of the Indian Museum*, 33: 301.

SENGUPTA, M. E., T. K. KRISTENSEN, H. MADSEN & A. JØRGENSEN, 2009, Molecular phylogenetic investigations of the Viviparidae (Gastropoda: Caenogastropoda) in the lakes of the Rift Valley area of Africa. *Molecular Phylogenetics and Evolution*, 52: 797–805.

SHEA, M., 1994, The Chinese viviparid snail *Bellamya heudei guangdungensis* (Kobelt, 1906) in Australia (Prosobranchia: Viviparidae). *Molluscan Research*, 15: 3–11.

TAN, S. K., S. Y. CHAN & G. R. CLEMENTS, 2012, *A guide to snails and other non-marine mollucs of Singapore*. Science Centre Singapore, Singapore, 176 pp.

TAN, S. K. & H. P. M. WOO, 2010, *A preliminary checklist of the molluscs of Singapore.* Raffles Museum of Biodiversity Research, Singapore, 78 pp.

VAN LEEUWEN, C. H. A., N. HUIG, G. VAN DER VELDE, T. A. VAN ALEN, C. A. M. WAGEMAKER, C. D. H. SHERMAN, M. KLAASSEN & J. FIGUEROLA, 2013, How did this snail get here? Several dispersal vectors inferred for an aquatic invasive species. *Freshwater Biology*, 58: 89–99.

YEN, T. C., 1939, Die Chinesischen Land- und Süsswasser-Gastropoden des Natur-Museums Senckenberg. *Abhandlungen der Senckenbergischen Naturforschenden Gesellschaft*, 444: 1–233.

YEN, T. C., 1943, A preliminary revision of the recent species of Chinese Viviparidae. *The Nautilus*, 56: 124–130.

YEO, D. C. J. & C. S. W. CHIA, 2010, Introduced species in Singapore: an overview. *COSMOS*, 6: 23–37.

YEO, D. C. J., L. K. WANG & K. K. P. LIM, eds., 2010, *Private lives: an exposé of Singapore's freshwaters*. Raffles Museum of Biodiversity Research, Singapore, 259 pp.

ZILCH, A., 1955, Die Typen und Typoide des Natur-Museums Senckenberg, 14: Mollusca, Viviparidae. *Archiv für Molluskenkunde*, 64: 1–41.

Revised ms. accepted November 20, 2013

MALACOLOGIA, 2014, 57(2): 409–414

INDEX

Taxa in **bold** are new; pages in *italic* indicate figures of taxa.

abbrebiata, Panopaea 282
abbreviata, Glycimeris 282
  Panope 282
  Panopea 279, 280, *281*, 282, *283–285*, 287–289, *287*
abrupta, Panopea 279
acrorrhyncha, Lanceolaria 379
Actinonaias ligamentina carinata 385, 393, 394, *394*
acuta, Physa 342
Agathistoma 310
Aglaja tricolorata 365–367, 373–375
Aglajidae 365
Alasmidonta arcula 380, 385
  marginata 380, 385
Alathyria pertexta 378, 379, 389
alatus, Potamilus 380, 386
aldrovandi, Panopea 279, 281
alleni, Silicula 255, 256, 267, 268, *269*, 270, 275
ambiguus, Velesunio 378, 379, 389
Amblema plicata plicata 385
Ambleminae 385
Ampullariidae 319, 341
Anaspidea 365
anatina, Anodonta 380, 382
angulata, Gonidea 380, 387
Angulyagra 403
  guangdungensis 402, 403
  heudei 403
  polyzonata 401, 404
Anodonta anatina 380, 382
  arcaeformis flavotincta 379
  cygnea 380
  grandis, 380
  imbecillis 385
  oregonensis 385
  stagnalis 380
  woodiana 379 380
  woodiana elliptica 379
  woodiana pacifica 379
  zellensis 380
Anodontoides ferussacianus 380, 385
antarctica, Panopaea 282
  Panopea 279, 282, *283*, 289
antiqua, Leukoma 288
arbustorum, Arianta 305, 342
arca, Elliptio 387
Arcidae 335, 336
Arcidens confragosus 385
Arctica islandica 361
arctica, Hiatella 289
Arcuatula capensis 335
arcula, Alasmidonta 380, 385
Arianta arbustorum 305, 342
arrokeana, Malacobdella 279, 280, 287, 288
Asolene pulchella 348
aspersa, Helix 304
asperses, Cantareus 304
Atrina 330
  maura 329, 330, *331–334*, 335–337
  pectinata 330, 335, 336
  vexillum 330, 336
australis, Hamiota 386

Barbatia foliata 335
  obliquata 335
barnesiana, Pleuronaia 387
Bathymodiolus childressi 335
Bellamya heudei guangdungensis 401, 402, 404
beringiana, Silicula 255, 260, *261*, 262, *263–267*, 266–268, 270, 273, 275, 276
Biomphalaria peregrina 342
bitruncata, Panopea 289
blackei, Photinula 310
blakei, Calliostoma 309
  Calliostoma (*Calliostoma*) 310
  Carolesia 310, *311*, *313*, 313–315, *314*
  Photinula 309, 310
  Tegula (*Agathistoma*) 310
bonariensis, Eleocharis 342, 348
Brachidontes semistriatus 335

caerulescens, Photinula 309
Calliostoma 309, 315
  blakei 309
  (*Calliostoma*) *blakei* 310
  coppingeri 315
Calliostomatidae 309
Camaenidae 295, 296
canaliculata, Pomacea 319, 320, *320*, 322, *324*, 325, 326, 341–343, *343*, *345–347*, 346, 348–350, 401, 405
Cantareus aspersus 304
capensis, Arcuatula 335
Capistrocardia 281
  fragilis 281
cardium, Lampsilis 386
carinata, Actinonaias ligamentina 385, 393, 394, *394*

Carolesia 309, 310, 315
  blakei 310, *311*, *313*, 313–315, *314*
carolinianus, Uniomerus 387
Cephalaspidea 365
Cerastoderma edule 389
Chama macerophylla 335
childressi, Bathymodiolus 335
chilensis, Diplodon 379, 389
Chilina parchappii 342
Chilinidae 342
Chlorostoma 310
Colletopterum piscinale 380
  ponderosum 380
complanata, Elliptio 362, 380
  Lasmigona 385
  Pseudanodonta 380
  Unio 378
complanatus, Elliptio 378
confragosus, Arcidens 385
Congeria 354, 362
  jalzici 353
  kusceri 353–356, *355–357*, 358, 359, *359*, *360*, 361, 362
  mulaomerovici 353
conradicus, Medionidus 386
conus, Unio 380
coppingeri, Calliostoma 315
coquimbensis, Panopea 279, *288*, 289
costata, Lasmigona 380, 385, 392–394, *394*
crassidens, Elliptio 387
Cristaria plicata 379
cumingii, Hyriopsis 379
cuneolus, Pleuronaia 387
Cyclonaias tuberculata 387
cygnea, Anodonta 380

Dactylochalamys 403
  quangdugensis 401
dariensis, Elliptio 387
declivus, Uniomerus 387
Degrangia 279
depicta, Philinopsis 366, 373–375
dilatatus, Elliptio 387
Diplodon chilensis 379, 389
dolabelloides, Pleuronaia 387
douglasiae, Unio 379
Dreissena 353, 354, 362
  polymorpha 359, 361, 362
Dreissenidae 353, 361, 362

ecarinatus, Limax 304
Edmondioidea 279
edule, Cerastoderma 389
edulis, Mytilus 335, 382
Eleocharis bonariensis 342, 348
Ellipsaria lineolata 385
elliptica, Anodonta woodiana 379
Elliptio arca 387
  complanata 362, 380
  complanatus 378
  crassidens 387
  dariensis 387
  dilatatus 387
  pullata 387
elongatulus, Unio 379, 380, 388
ensicula, Propeleda *258*, 260
Ensis macha 288
Epioblasma torulosa rangiana 385
  triquetra 380
Etherioidea 377, 379, 388, 389
exalbidus, Retrotapes 288

falcata, Margaritifera 379, 385
fasciola, Lampsilis 386
fasciolaris, Ptychobranchus 380, 386, 393, 394, *394*
ferussacianus, Anodontoides 380, 385
filatovae, Silicula 255, 256, 267, 268, *269*, 270, 275
flava, Pleuronaia 387
flavotincta, Anodonta arcaeformis 379
foliata, Barbatia 335
fragilis, Capistrocardia 281
  Leptodea 386, 389
  Silicula 255–257, *258*, 267, 268, *269*, 270, 275

generosa, Panopea 279, 280, 289
globosa, Panopea 280
Glycimeris 281
  abbreviata 282
glycimeris, Mya 281, 282
Glycymeridae 336
Glycymeris glycymeris 361
glycymeris, Glycymeris 361
Gonidea angulata 380, 387
gottschei, Lamprotula 379
grandis, Anodonta 380
  Pyganodon 380
  Pyganodon grandis 385, 389, *389*, 393, 394, *394*
guangdungensis, Angulyagra 402, 403
  Bellamya heudei 401, 402, 404
  Dactylochalamys 401
  Sinotaia 401, *402*, 403–406, *404*, *405*
  Sinotaia quadrata 402
  Vivipara 403, *404*
  Vivipara (*quadrata* var.) *heudei* var. 401
guayacanensis, Panopea 279, *288*, 289

Hamiota australis 386
  subangulata 386
hauthali, Panopaea *288*, 289
  Panopea 279

Helicidae 304, 305, 342
Helix aspersa 304
Heteromya 281
heudei, Angulyagra 403
  Vivipara 403
  Vivipara quadratus var. 403
Hiatella arctica 289
  solida 289
Hiatellidae 279–281
Hiatelloidea 279, 281
higginsi, Lampsilis 386
Hyriidae 379, 389
Hyriopsis cumingii 379

imbecillis, Anodonta 385
inferior, Panopaea *288*, 289
  Panopea 279
infucata, Quadrula 387, 388
Inversidens japonensis 379
Iridinidae 379, 389
iris, Villosa 393, 394, *394*
  Villosa iris 380, 386
islandica, Arctica 361

jalzici, Congeria 353
japonensis, Inversidens 379
Jennynsia multidentata 348

khwaegnoiensis, Solenia 379, 388
kusceri, Congeria 353–356, *355–357*, 358, 359, *359*, *360*, 361, 362

laevis, Margaritifera 362, 379
Lamellileda 255, 257–260, *258*
  sandersi 255, 260
  soyomaruae 255, 260
  tatei *258*
  typica *258*, 259, 260
Lamprotula gottschei 379
Lampsilis cardium 386
  fasciola 386
  higginsi 386
  ornata 386
  radiata luteola 380, 386
  siliquoidea 362
  teres 386
Lanceolaria acrorrhyncha 379
lanceolata, Poroleda *258*, 260
Lasmigona complanata 385
  costata 380, 385, 392–394, *394*
legrandi, Velesunio 378, 379, 389
Lemiox rimosus 386
Leptodea fragilis 386, 389
lessepsi, Panopea (*Heteromya*) 281
leucophaeata, Mytilopsis 361, 362
Leukoma antiqua 288
lienosa, Villosa 380, 386
Ligumia nasuta 386, 393, 394, *394*
  recta 386
Limacidea 304
Limax ecarinatus 304
  pseudoflavus 304
lineolata, Ellipsaria 385
Lirulariinae 309, 315
lividus, Toxolasma 380, 386
luteola, Lampsilis radiata 380, 386
Lymnaea stagnalis 374

macerophylla, Chama 335
macha, Ensis 288
maculata, Pomacea 348, 349
Malacobdella arrokeana 279, 280, 287, 288
mandibula, Mya 281
Margarella 309
Margaritifera falcata 379, 385
  laevis 362, 379
  margaritifera 361, 362
margaritifera, Margaritifera 361, 362
  Pinctada 335
Margaritiferidae 377, 379, 385, 388, 389
marginata, Alasmidonta 380, 385
mariana, Tegula 310, 315
maura, Atrina 329, 330, *331–334*, 335–337
maxima, Tridacna 361
mcalesteri, Silicula 255, 256, 268, *269*, 270, 275
Medionidus conradicus 386
  penicillatus 386
Megalonaias nervosa 361, 387
mitchellae, Thersites 295, 296, *297*, *303*, 304–306
mulaomerovici, Congeria 353
multidentata, Jennynsia 348
Mutela rostrata 379, 389
Mya glycimeris 281, 282
  mandibula 281
Myoida 279
Myopsis 281
Mytilidae 335, 336
Mytilopsis 353, 354, 362
  leucophaeata 361, 362
  sallei 362
Mytilus edulis 335, 382

nasuta, Ligumia 386, 393, 394, *394*
nebulosa, Villosa 386
nervosa, Megalonaias 361, 387
nobilis, Pinna 330, 335, 336

obliquata, Barbatia 335
Obovaria olivaria 386, 389
  subrotunda 386, 393, 394, *394*

Odontoglaja 366
okutanii, Silicula 255, *266*, *267*, 270, 271, *272*, *274*, 275, 276
olivaria, Obovaria 386, 389
omiensis, Pseudodon obovalis 379
oregonensis, Anodonta 385
ornata, Lampsilis 386
Ostreidae 336
oviforme, Pleurobema 387
oxytropis, Paludina 403

pacifica, Anodonta woodiana 379
Paludina oxytropis 403
  quadrata 401, 403
paludosa, Pomacea 348, 349
Panodea 281
Panomya 279
Panopaea 281
  abbrebiata 282
  antarctica 282
  hauthali *288*, 289
  inferior *288*, 289
  truncata *288*, 289
Panope 279, 281
  abbreviata 282
Panopea 279–282, *283*, 288, *288*
  abbreviata 279, 280, *281*, 282, *283–285*, 287–289, *287*
  abrupta 279
  aldrovandi 279, 281
  antarctica 279, 282, *283*,
  bitruncata 289
  coquimbensis 279, *288*, 289
  generosa 279, 280, 289
  globosa 280
  guayacanensis 279, *288*, 289
  hauthali 279
  (*Heteromya*) *lessepsi* 281
  inferior 279
  regularis 289
  truncata 279
Panopeinae 281
parchappii, Chilina 342
parvum, Toxolasma 386
patagonica, Silicula 255, 256, 268, *269*, 270, 275
  Tegula 310, 313, 314, *314*
pectinata, Atrina 330, 335, 336
penicillatus, Medionidus 386
peregrina, Biomphalaria 342
Perna perna 335
perna, Perna 335
pertexta, Alathyria 378, 379, 389
Pharidae 279
Philinopsis depicta 366, 373–375
Photinula 309, 315
  blackei 310
  blakei 309, 310
  caerulescens 309
Physa acuta 342
Physidae 342
pictorum, Unio 380
Pila 349
Pinctada margaritifera 335
Pinna 330
  nobilis 330, 335, 336
Pinnidae 329, 330, 335, 336
piscinale, Colletopterum 380
Planorbidae 342
Pleurobema oviforme 387
  pyriforme 387
  rubrum 387, 393, 394, *394*
  sintoxia 387
Pleuronaia barnesiana 387
  cuneolus 387
  dolabelloides 387
  flava 387
plicata, Amblema plicata 385
  Cristaria 379
polita, Tivela 335
polymorpha, Dreissena 359, 361, 362
polyzonata, Angulyagra 401, 404
  Sinotaia 402
  Taia 401, 402, 404, 406
  Vivipara 401–404, *404*
  Viviparus 402, 404, 406
polyzonatus, Vivipara 402, 404, 406
Pomacea 341, 348, 349
  canaliculata 319, 320, *320*, 322, *324*, 325, 326, 341–343, *343*, *345–347*, 346, 348–350, 401, 405
  maculata 348, 349
  paludosa 348, 349
ponderosum, Colletopterum 380
Poroleda 255, 257, *258*, 260, 268
  lanceolata *258*, 260
  spathula *258*
Potamilus alatus 380, 386
Propeleda 255, 257, *258*, 260, 268
  ensicula *258*, 260
  soyomaruae 255, 256, 258, *259*, 260
Pseudanodonta complanata 380
  radiatus radiatus 385
  undulatus 385
Pseudodon obovalis omiensis 379
pseudoflavus, Limax 304
Pteriidae 336
Pterioidea 336
Ptychobranchus fasciolaris 380, 386, 393, 394, *394*
  subtentum 386
pulchella, Asolene 348
pullata, Elliptio 387
punctata, Villosa taeniata 386, 392–394, *394*

pustulosa, Quadrula 387
Pyganodon grandis 380
  grandis grandis 385, 389, *389*, 393, 394, *394*
pyriforme, Pleurobema 387

quadrata, Paludina 401, 403
  Sinotaia 406
Quadrula infucata 387, 388
  pustulosa 387
  quadrula 380, 387
quadrula, Quadrula 380, 387

radiatus, Pseudanodonta radiatus 385
rangiana, Epioblasma torulosa 385
recta, Ligumia 386
regularis, Panopea 289
Retrotapes exalbidus 288
rimosus, Lemiox 386
rostrata, Mutela 379, 389
rouchi, Silicula 255, 256, 267, 268, *269*, 270, 275
rubrum, Pleurobema 387, 393, 394, *394*
Runcinacea 365

sallei, Mytilopsis 362
sandersi, Lamellileda 255, 260
  Silicula 255, 256, 258–260, *259*
semistriatus, Brachidontes 335
Silicula 255–258, *258*, 260, 268, *269*, 270, 275
  alleni 255, 256, 267, 268, *269*, 270, 275
  beringiana 255, 260, *261*, 262, *263–267*, 266–268, 270, 273, 275, 276
  filatovae 255, 256, 267, 268, *269*, 270, 275
  fragilis 255–257, *258*, 267, 268, *269*, 270, 275
  mcalesteri 255, 256, 268, *269*, 270, 275
  okutanii 255, *266*, *267*, 270, 271, *272*, *274*, 275, 276
  patagonica 255, 256, 268, *269*, 270, 275
  rouchi 255, 256, 267, 268, *269*, 270, 275
  sandersi 255, 256, 258–260, *259*
Siliculidae 255
siliquoidea, Lampsilis 362
Sinanodonta woodiana 362
Sinotaia 401, 403
  guangdungensis 401, *402*, 403–406, *404*, *405*
  polyzonata 402
  quadrata 406
  quadrata guangdungensis 402
sintoxia, Pleurobema 387
sinuolatus, Unio douglasiae 380
Skeneidae 309
Solenia khwaegnoiensis 379, 388
Solenidae 279
Solenoidea 279
solida, Hiatella 289
solidisima, Spisula 335
Sorenia triangularis 380
soyomaruae, Lamellileda 255, 260
  Propeleda 255, 256, 258, *259*, 260
spathula, Poroleda 258
Spisula solidisima 335
stagnalis, Anodonta 380
  Lymnaea 374
subangulata, Hamiota 386
subrotunda, Obovaria 386, 393, 394, *394*
subtentum, Ptychobranchus 386

Taia polyzonata 401, 402, 404, 406
tatei, Lamellileda 258
Tegula 310, 314, 315
  (*Agathistoma*) 309
  (*Agathistoma*) *blakei* 310
  mariana 310, 315
  patagonica 310, 313, 314, *314*
Tegulidae 315
Tegulinae 315
teres, Lampsilis 386
Thersites 295
  mitchellae 295, 296, *297*, *303*, 304–306
Tivela polita 335
Toxolasma lividus 380, 386
  parvum 386
trabalis, Villosa 384, 386, 392–394, *394*
triangularis, Sorenia 380
tricolorata, Aglaja 365–367, 373–375
Tridacna maxima 361
triquetra, Epioblasma 380
Tritogonia verrucosa 380, 387
Trochidae 309
Trochoidea 309, 315
truncata, Panopaea 288, 289
  Panopea 279
tuberculata, Cyclonaias 387
Turbinidae 309
Tylodinoidea 365
typica, Lamellileda 258, 259, 260

Umboniinae 309, 315
Umbraculoidea 365
undulatus, Pseudanodonta 385
Unio complanata 378
  conus 380
  douglasiae 379
  douglasiae sinuolatus 380
  elongatulus 379, 380, 388
  pictorum 380
Uniomerus carolinianus 387
  declivus 387

Unionidae 377, 379, 385, 388, 389
Unioninae 385
Unionioidea 379
Unionoidea 377, 388, 389

Velesunio ambiguus 378, 379, 389
  legrandi 378, 379, 389
Veneridae 335
verrucosa, Tritogonia 380, 387
vexillum, Atrina 330, 336
vibex, Villosa 387
Villosa 391, 394
  iris 393, 394, *394*
  iris iris 380, 386
  lienosa 380, 386
  nebulosa 386
  taeniata punctata 386, 392–394, *394*
  trabalis *384*, 386, 392–394, *394*
  vibex 387
Vivipara guangdungensis 403, *404*
  heudei 403
  polyzonata 401–404, *404*
  polyzonatus 402, 404, 406
  (*quadrata* var.) *heudei* var. *guangdungensis* 401
  quadratus var. *heudei* 403
Viviparidae 401
Vivipariidae 401
Viviparus polyzonata 402, 404, 406

woodiana, Anodonta 379, 380
  Sinanodonta 362

zellensis, Anodonta 380

PUBLICATION DATES

Vol. 48, No. 1–2	16 Feb. 2006
Vol. 49, No. 1	10 Nov. 2006
Vol. 49, No. 2	27 July 2007
Vol. 50, No. 1–2	9 June 2008
Vol. 51, No. 1	19 Mar. 2009
Vol. 51, No. 2	26 Aug. 2009
Vol. 52, No. 1	27 Jan. 2010
Vol. 52, No. 2	7 May 2010
Vol. 53, No. 1	19 Oct. 2010
Vol. 53, No. 2	8 Mar. 2011
Vol. 54, No. 1–2	25 Oct. 2011
Vol. 55, No. 1	17 Sep. 2012
Vol. 55, No. 2	28 Dec. 2012
Vol. 56, No. 1–2	31 Dec. 2013
Vol. 57, No. 1	26 June 2014

INSTRUCTIONS FOR AUTHORS

1. MALACOLOGIA publishes original research on the Mollusca that is of high quality and of broad international interest. Papers combining synthesis with innovation are particularly desired. While publishing symposia from time to time, MALACOLOGIA encourages submission of single manuscripts on diverse topics. Smaller papers of local geographical or systematic content, and of high quality and interest, may be accepted as 'Research Notes'. Nearly all branches of malacology are represented in the pages of MALACOLOGIA.
2. Manuscripts submitted for publication are received with the tacit understanding that they have not been submitted or published elsewhere in whole or in part.
3. Manuscripts must be in English, but may include an expanded abstract in a foreign language as well as the usual brief abstract in English. Both American and British spellings are allowed.
4. Unless indicated otherwise below, contributors should follow the recommendations in the Council of Science Editors (CSE) Scientific Style and Format manual, 7th ed., 2006.
5. Be brief.
6. Manuscripts must be prepared using Microsoft Word® (Windows-version), 12-pitch, Arial font, lines at 1.5 spaces throughout (including the references, tables and figure captions), no added spaces before or after paragraphs, text aligned left, ragged right. Tables, figure captions and figures are to be placed on separate pages at the end of the file. Make the hierarchy of headings within the text simple and consistent. Avoid internal page references.
7. Choose a running title (a shortened version of the main title) of fewer than 50 letters and spaces.
8. For full papers, provide a concise and informative abstract summarizing not only contents but also results. A separate summary is not wanted. Research Notes do not require an added abstract.
9. Supply between five and eight key (topic) words to go at the end of the Abstract for full-length papers.
10. Use the metric system throughout. Micron should be abbreviated μm.
11. Three types of illustrations are accepted: (A) line art figures (black-and-white drawings, diagrams), (B) gray-step figures ("black-and-white" photographs or gray-step drawings) and (C) color figures. Gray-step and color figs. should be saved with a resolution of 300 dpi; line art with 1200 dpi. Illustrations are printed either in one column or the full width of a page of the journal, so plan accordingly. The maximum size of a printed figure is 13.5 x 20.0 cm (preferably not as tall as this so that the caption does not have to be on the opposite page). The figure captions are not to be part of the figure.
12. Lines, letters, and numbers should be thick enough to allow reduction by 30% to 50%. Letters and numbers (Arial font) should be at least 2 mm (line art) or 3 mm (gray-step, color) high after reduction, but avoid letter sizes > 6 mm. In line drawings, the minimum line width of 0.2 mm is required (as measured by final size). Several drawings or photographs may be grouped together as plate.
13. All illustrations should be numbered sequentially and not as lettered sub-series. All figures must be cited in the text in the order in which they appear.
14. Scale lines are required for all none diagrammatic figures, and should be convenient lengths (e.g., "200 μm", not "163 μm"). Magnifications in captions are not acceptable. But object or specimen sizes in a caption are acceptable.
15. Be professional. Sloppy illustrations, labels, borders will not be accepted. If assistance is required of MALACOLOGIA's editorial staff, the author will be charged for the services rendered.
16. A caption should summarize what is shown in an illustration, and should not duplicate information given in the text. Each lettered abbreviation labeling an individual feature in a figure must either be explained in each caption (listed alphabetically), or be grouped in one alphabetic sequence after the Methods section. Use the latter method if many abbreviations are repeated on different figures.
17. Tables are to be used sparingly. All tables must be cited in the text in the order in which they appear. Tables should be composed using the table function of Word (and **not** tab-delimited text).
18. References cited in the text must appear in the Literature Cited section and vice versa.

Refer to a recent issue of MALACOLOGIA for bibliographic style, noting especially that serials are cited unabbreviated. Supply information on plates, etc., only if they are not included in the pagination.

19. In systematic papers, synonymies should not give complete citations but should relate by author, date and page to the Literature Cited section. All new type specimens must be deposited in museums where other scientists may study them. Likewise, MALACOLOGIA requires that voucher specimens upon which a paper is based be deposited in a museum where their identity can be verified.
20. For all papers dealing with molluscan species, each such species should include its author and date upon first appearance, with the correct use of parenthesis around an author in the case of a generic assignment other than the original combination. In all taxonomic papers dealing with one to a few species, the original description of each species should be represented in the Literature Cited. In other studies – physiological, ecological, etc. – involving one or a few species, the author should either cite the original description of the taxon/taxa involved or some other work showing its identity.
21. For electronic submission of manuscripts, send a **single manuscript file** (including manuscript text, tables, figure captions and figures) together with a cover letter to georgedavis99@hotmail.com. Contact the editor to determine the method of submission if the manuscript has a file sizes exceeding 5 MB.
22. Once the manuscript is accepted, high quality and full resolution graphic files have to be provided. Submit such graphics to the graphics editor (tom.wilke@allzool.bio.uni-giessen.de) as TIFF files. For other formats or any question regarding electronic submission of graphics, contact the graphics editor. Keep the individual file sizes below 5 MB (using the option "LZW compression" will greatly reduce the size of TIFF files).

REPRINTS AND PAGE COSTS

23. Reprints must be ordered from the Business Office at the time proof is returned to the copy editor. Later orders cannot be considered. When 100 or more reprints are ordered, an author will receive 25 additional copies free of charge.
24. PDF files of the paper for personal use are available with a purchase of reprints; free of charge for subscribers to Malacologia. Subscription must include current and two paid-for immediate past and/or future volumes.
25. Page costs must be paid prior to publication. Page cost recovery is required as follows.
    Regular subscribers:*
    - Non-student: 10 pages free; U.S. $30.00 for each additional page (EAP)
    - Student**: 15 pages free; U.S. $20.00 EAP

    Non-subscribers:
    - Non-student: 8 pages free; U.S. $60.00 EAP
    - Student**: 15 pages free; U.S. $30.00 EAP

    A reduction or elimination of page charges may be possible under certain circumstances by arrangement with the editor. A reduction of page charges may be negotiated for papers exceeding 30 pages.
26. Color figures must be paid-for by the author. Costs are U.S. $300 for the first color page in a paper and U.S. $150 for each subsequent color page.

SUBSCRIPTION PURCHASE

27. Effective with Vol. 57, subscription rates per volume are as follows:
    - Personal: U.S. $75.00
    - (Student discounted rate: U.S. $40.00)
    - Institutional: U.S. $105.00
    - Agency and Dealership: U.S. $105.00

    Current volume postage is included for shipment to an American or a Canadian address. Overseas postage is $16.00 per volume. Single and past volumes are available at subscription rates. Postage and handling is $13.00 per volume for shipment to an American or a Canadian address. Overseas postage is $34.00 per volume. Postage for orders weighing over 4 lbs. will be determined by weight.

* Regular subscribers are those who have paid-up subscriptions for the current volume and two immediate past and/or future volumes.

** Students must identify themselves at the time of manuscript submission and also provide the e-mail address of their advisor.

SMITHSONIAN LIBRARIES
3 9088 01815 9368

VOL. 57, NO. 2 MALACOLOGIA 2014

CONTENTS

FULL PAPERS

Gennady M. Kamenev
Two new species of the genus *Silicula* (Bivalvia: Siliculidae) from the northwestern Pacific, with notes on *Silicula sandersi* (Bernard, 1989) and *Propeleda soyomaruae* (Okutani, 1962) 255

Javier H. Signorelli & José E. F. Alfaya
Panopea abbreviata (Bivalvia: Hiatellidae) in the southwestern Atlantic Ocean, taxonomic revision and anatomy 279

Jonathan Parkyn, Lyndon Brooks & David Newell
Habitat use and movement patterns of the endangered land snail *Thersites mitchellae* (Cox, 1864) (Camaenidae) 295

Marina Güller & Diego G. Zelaya
A new generic placement for "*Calliostoma*" *blakei* Clench & Aguayo, 1938 (Gastropoda: Trochoidea) 309

Silvana Burela & Pablo Rafael Martín
Nuptial gifts in *Pomacea canaliculata* (Ampullariidae, Caenogastropoda): Experimental and field evidence about their function 319

Marian Alejandra Camacho-Mondragón, Bertha Patricia Ceballos-Vázquez, Esther Uría Galicia, Edgar Oliver López Villegas & Marcial Arellano-Martínez
Ultrastructure of the spermatogenic process in the penshell *Atrina maura* (Bivalvia: Pinnidae) 329

Lucía Saveanu & Pablo R. Martín
Egg cannibalism in *Pomacea canaliculata* (Caenogastropoda: Ampullariidae) from the southern Pampas: An alternative trophic strategy? 341

Sanja Puljas, Melita Peharda, Brian Morton, Nives Štambuk Giljanović & Ivana Jurić
Growth and longevity of the „living fossil" *Congeria kusceri* (Bivalvia: Dreissenidae) from the subterranean Dinaric karst of Croatia 353

Alexandre Lobo-da-Cunha, Joana Pereira-Sousa, Elsa Oliveira, Ângela Alves Fernanda Guimarães & Gonçalo Calado
Calcium detection and other cellular studies in the esophagus and crop of the marine slug *Aglaja tricolorata* (Euopisthobranchia, Cephalaspidea) 365

John J. Jenkinson
Chromosomal characteristics of North American and other Naiades (Bivalvia: Unionida) 377

RESEARCH NOTE

Ting Hui Ng, Siong Kiat Tan & Darren C. J. Yeo
The taxonomy, distribution and introduction history of the earliest reported alien freshwater mollusc in Singapore – *Sinotaia guangdungensis* (Gastropoda: Viviparidae) 401

INDEX 409

ALACOLOGIA

International Journal of Malacology

)1
15X
2

. 58(1–2)

2015

MALACOLOGIA
http://malacologia.fmnh.org

One of the World's Leading Malacological Journals
Journal Impact Factor 0.977 (2013)

Founded in 1961

EDITOR-IN-CHIEF
GEORGE M. DAVIS

Editorial Office
Malacologia
P.O. Box 1222
West Falmouth, Massachusetts 02574, U.S.A.
georgedavis99@hotmail.com

Business & Subscription Office
Malacologia
P.O. Box 385
Haddonfield, New Jersey 08033, U.S.A.
malacologia@comcast.net

Copy Editor
EUGENE COAN
Santa Barbara Museum of Natural History
Santa Barbara, California, U.S.A.
genecoan@gmail.com

Associate Editor
JOHN B.BURCH
University of Michigan
Ann Arbor, Michigan, U.S.A.
jbburch@umich.edu

Managing Editor
CARYL HESTERMAN
Haddon Heights, New Jersey, U.S.A.
malacologia@comcast.net

Composition Editor
CLAUDIA WILKE
Giessen, Germany
claudiawilke@hotmail.com

Graphics Editor
THOMAS WILKE
Justus Liebig University
Giessen, Germany
tom.wilke@allzool.bio.uni-giessen.de

MALACOLOGIA is published by the INSTITUTE OF MALACOLOGY
Board of Directors - U.S.A.:

President

DIARMAID Ó FOIGHIL
University of Michigan, Ann Arbor

Vice President

ELLEN STRONG
National Museum of Natural History, Washington D.C.

Secretary and Treasurer

GEORGE M. DAVIS
West Falmouth, Massachusetts

Members

RÜDIGER BIELER
Field Museum, Chicago, Illinois

JOHN B. BURCH
University of Michigan, Ann Arbor

CAROLE S. HICKMAN
University of California, Berkeley

ALAN KOHN
University of Washington, Seattle

PAULA M. MIKKELSEN
Paleontological Research Institution, Ithaca, New York

Copyright © 2015 by the Institute of Malacology
ISSN: 0076-2997 (Print)
ISSN: 2168-9075 (Online)

J. A. ALLEN
Marine Biological Station
Millport, United Kingdom

T. ASAMI
Shinshu University
Matsumo, Japan

T. BACKELJAU
University of Antwerp
Antwerp, Belgium

B. BAUR
Universität Basel
Basel, Switzerland

D. BLAIR
James Cook University
Townsville, Australia

P. BOUCHET
Muséum National d'Histoire Naturelle
Paris, France

R. A. D. CAMERON
University of Sheffield
Sheffield, United Kingdom

J. G. CARTER
University of North Carolina
Chapel Hill, North Carolina, U.S.A.

R. CIPRIANI
California State University
Fullerton, California, U.S.A.

T. COLLINS
Florida International University
Miami, Florida, U.S.A.

R. H. COWIE
University of Hawaii
Honolulu, Hawaii, U.S.A.

G. CUEZZO
Universidad Nacional de Tucumán
Tucumán, Argentina

B. DAYRAT
University of California
Merced, California, U.S.A.

B. DEGNAN
University of Queensland
Brisbane, Australia

D. J. EERNISSE
California State University Fullerton
Fullerton, California, U.S.A.

D. GEIGER
Santa Barbara Museum of Natural History
Santa Barbara, California, U.S.A.

G. GIRIBET
Harvard University
Cambridge, Massachusetts, U.S.A.

E. GITTENBERGER
Naturalis Biodiversity Center
Leiden, The Netherlands

F. GIUSTI
Università di Siena
Siena, Italy

M. GLAUBRECHT
Museum of Natural History Berlin
Berlin, Germany

D. GRAF
University of Wisconsin
Stevens Point, Wisconsin, U.S.A.

E. HARPER
University of Cambridge
Cambridge, United Kingdom

G. HASZPRUNAR
Zoologische Staatssammlung München
München, Germany

K. HAYES
University of Hawaii
Honolulu, Hawaii, U.S.A.

K. E. HOAGLAND
Independent Consultant
Falmouth, Massachusetts, U.S.A.

M. HORSAK
Masaryk University
Drno, Czech Republic

C. ITUARTE
Museo Argentino de Ciencias Naturales
Buenos Aires, Argentina

M. S. JOHNSON
University of Western Australia
Crawley, Australia

SMITHSONIAN
JUL 08 2015

G. KAMENEV
Institute of Marine Biology
Vladivostok, Russia

Y. KANTOR
Russian Academy of Sciences
Moscow, Russia

F. KOEHLER
Australian Museum
Sydney, Australia

T. KONDO
Osaka Kyoiku University
Osaka, Japan

K. A. LUTAENKO
Institute of Marine Biology
Vladivostok, Russia

C. LYDEARD
Western Illinois University
Macomb, Illinois, U.S.A.

B. A. MARSHALL
Museum of New Zealand Te Papa Tongarewa
Wellington, New Zealand

J. NEKOLA
University of New Mexico
Albuquerque, New Mexico, U.S.A

T. OKUTANI
Tokyo University of Fisheries
Tokyo, Japan

L. PAGE
University of Victoria
Victoria, BC, Canada

G. PAULEY
Florida Museum of Natural History
Gainesville, Florida, U.S.A.

R. PIPE
The Marine Biological Association
Plymouth, United Kingdom

W. F. PONDER
Australian Museum
Sydney, Australia

T. RAWLINGS
Cape Breton University
Nova Scotia, Canada

T. SASAKI
University Museum, University of Tokyo
Tokyo, Japan

L. R. L. SIMONE
Museu de Zoologia da Universidade
de São Paulo, Brazil

P. TATTERSFIELD
Tideswell, Buxton
United Kingdom

C. THIRIOT
University Pierre et Marie Curie
Paris, France

S. TILLIER
Muséum National d'Histoire Naturelle
Paris, France

Á. VALDÉS
California State Polytechnic University
Pomona, California, U.S.A.

J. VOIGHT
Field Museum Natural History
Chicago, Illinois, U.S.A.

A. WARÉN
Museum of Natural History
Stockholm, Sweden

M. WU
Hebei University
Hebei, China

ELECTRONIC ACCESS TO *MALACOLOGIA*

Malacologia is available on line, with volumes 1 (1962) to 48 (2006) freely accessible via the *Biodiversity Heritage Library* (BHL; a consortium of natural history and botanical libraries that cooperate to digitize and make accessible the legacy literature of biodiversity held in their collections), and most recent numbers obtainable from *BioOne*, a global not-for-profit collaboration of scientific publishers and libraries:
BHL (www.biodiversitylibrary.org): *Malacologia* grants open access to electronic copies of all pre-2007 volumes, which can be read and downloaded at http://www.biodiversitylibrary.org/bibliography/12920.

BHL
Biodiversity Heritage Library

BioOne (www.bioone.org): *Malacologia* is part of the BioOne.2 collection of scientific journals. Access is available to institutions and consortia holding BioOne subscriptions (see the BioOne web site for details). In addition, subscribers to the *Malacologia* print edition are given access to this journal on BioOne. To be granted such individual access, contact the subscription office at malacologia@comcast.net.

BioOne™ RESEARCH EVOLVED

ANNOUNCEMENT

The J Frances Allen Institute of Malacology Outstanding Student Publication Award

The Board of Directors of the Institute of Malacology, publisher of the academic journal *Malacologia*, is pleased to announce the creation of the J Frances Allen Institute of Malacology Outstanding Publication Award. This cash award of $500 will be presented for an outstanding paper published in *Malacologia* by a student, with the timing dependent on the superior quality of the student paper as judged by a committee of the IM Board. There is no formal application or deadline. A student submitting a manuscript must be sole or senior author of the paper, and should indicate that the paper being submitted stems from Master's or Ph.D. research to confirm his or her eligibility for the award. The Allen Publication Award was established in 2011 to honor J Frances "Jady" Allen, who provided indispensable help and guidance in establishing the journal *Malacologia*, first published in 1962.

MALACOLOGIA, 2015, 58(1–2): 1–127

COMPARATIVE ANATOMY OF SELECTED MARINE BIVALVES FROM THE FLORIDA KEYS, WITH NOTES ON BRAZILIAN CONGENERS (MOLLUSCA: BIVALVIA)

Luiz Ricardo L. Simone[1], Paula M. Mikkelsen[2] & Rüdiger Bieler[3*]

ABSTRACT

To broaden the anatomical knowledge of marine bivalves, detailed gross anatomical studies of 20 species from the Florida Keys are presented, representing 19 families: *Solemya occidentalis* Deshayes, 1857 (Solemyidae), *Propeleda carpenteri* (Dall, 1881) (Nuculanidae), *Arcopsis adamsi* (Dall, 1886) (Noetiidae), *Limopsis* aff. *cristata* Jeffreys, 1876 (Limopsidae), *Brachidontes exustus* (Linnaeus, 1758) (Mytilidae), *Isognomon alatus* (Gmelin, 1791) (Isognomonidae), *Hyotissa mcgintyi* (Harry, 1985) and *H. hyotis* (Linnaeus, 1758) (Gryphaeidae), *Pinna carnea* Gmelin, 1791 (Pinnidae), *Spondylus americanus* Hermann, 1781 (Spondylidae), *Plicatula gibbosa* Lamarck, 1801 (Plicatulidae), *Anomia simplex* d'Orbigny, 1853 (Anomiidae), *Carditamera floridana* Conrad, 1838 (Carditidae), *Entodesma beana* (d'Orbigny, 1853) (Lyonsiidae), *Codakia orbicularis* (Linnaeus, 1758) (Lucinidae), *Chama macerophylla* Gmelin, 1791 (Chamidae), *Lamychaena hians* (Gmelin, 1791) (Gastrochaenidae), *Polymesoda floridana* (Conrad, 1846) (Cyrenidae), *Laevicardium serratum* (Linnaeus, 1758) (Cardiidae) and *Scissula similis* (J. Sowerby, 1806) (Tellinidae). These taxa represent various clades of the class Bivalvia and interface with broader regional and phylogenetic studies (e.g., the Bivalve Tree of Life, http://www.bivatol.org, and Bivalves-in-Time-and-Space, http://www.bivatol.org/bits), in which many serve as exemplar species in different contexts. These descriptions provide the most complete anatomical descriptions yet presented for all species, most especially for *Solemya occidentalis, Limopsis* aff. *cristata, Hyotissa mcgintyi, H. hyotis, Carditamera floridana, Entodesma beana, Chama macerophylla* and *Polymesoda floridana*, for which no or only minimal anatomical information has been previously published. This work presents the first anatomical description of any species of *Scissula*, based on *S. similis*. Two controversial characters – the promyal passages (in *Hyotissa* spp., in *Anomia simplex* noted here for the first time, and in *Crassostrea* reported in the literature) and the various kinds of posterior apertures and siphons present in the species examined and across the Bivalvia – emphasize the need for further comparative study to confirm homologies. Conspecificity of Brazilian material with that from the North American coast is clarified for all species, resulting in nine species being removed from Brazilian checklists (*S. occidentalis, B. exustus, I. alatus, P. carnea, C. floridana, C. macerophylla, L. hians, L. serratum,* and *S. similis*). Pertinent anatomical characters are summarized in a data matrix, and an analysis is provided to demonstrate the utility and resolving power of such characters (but from this limited taxon sampling is not intended to provide a revised phylogenetic hypothesis of bivalve relationships); data for three additional species from Florida, published earlier, are included in the analysis and discussion.

Key words: characters, morphology, phylogeny, western Atlantic.

INTRODUCTION

Marine bivalves are among the most familiar invertebrates, to lay people and scientists alike. They include some of the easiest species to collect and study, but knowledge about them often is limited to their shells. In some cases, only a single species per family has been anatomically studied and has become the *de facto* representative of a much larger clade, resulting

---

[1]Museu de Zoologia da Universidade de São Paulo, Cx. Postal 42494, 04218-970, São Paulo, SP, Brazil.
[2]Paleontological Research Institution, 1259 Trumansburg Road, and Department of Earth and Atmospheric Sciences, Cornell University, Ithaca, New York 14850, U.S.A.
[3]Field Museum of Natural History, 1400 South Lake Shore Drive, Chicago, Illinois 60605-2496, U.S.A.
*Corresponding author: rbieler@fieldmuseum.org

in assumptions of uniformity and anatomical "types" across entire superfamilies. Not all of these serve particularly well as representatives of their larger groups, because some were chosen for their particularly interesting (unusual and perhaps apomorphic) morphological features (Bieler & Mikkelsen, 2006). In other groups, "bauplan" concepts of bivalve families are based on chimeric descriptions compiled from partial desciptions of several species (as discussed by Bieler et al., 2013). Attempting to broaden the anatomical knowledge of marine bivalves by offering detailed descriptions of exemplar species (*sensu* Prendini, 2001), the current paper presents detailed anatomical studies of 20 species, representing 19 families, from the Florida Keys; data for three additional species (adding two additional families) from the Florida Keys, published earlier and illustrating the same character systems (Simone & Chichvarkhin, 2004; Simone & Dougherty, 2004; Simone & Gonçalves, 2006), are included in the discussion. These taxa represent various clades of the class Bivalvia and interface with broader regional (Bieler & Mikkelsen, 2004; Mikkelsen & Bieler, 2007) and phylogenetic studies (e.g., the Bivalve Tree of Life project, http://www.bivatol.org; and the Bivalves-in-Time-and-Space project, http://www.bivatol.org/bits), in which many serve as exemplar species in a different context (e.g., Sharma et al., 2012; Bieler et al., 2014). Several of these dissections formed the basis for diagrammatic anatomical drawings ("transparent clams") presented by Mikkelsen & Bieler (2007). Two members of Gryphaeidae were included because prior data (Harry, 1985) indicated substantive anatomical differences between them. In many cases, the Florida Keys populations – and in some instances the very specimens investigated herein – were the sources for previous and ongoing molecular studies by various authors, which are referenced herein. Most of these species have been considered, based on shell characters, to have distributional ranges extending to the southwestern Atlantic; comparisons are made herein with presumed conspecifics in Brazil to support or refute these claims. To aid comparative study and to demonstrate the utility and resolving power of fine-anatomical characters, a data matrix and associated phylogenetic analysis are provided (but from this limited taxon sampling is not intended to provide a revised phylogenetic hypothesis of bivalve relationships).

MATERIALS AND METHODS

The species were investigated in the context of a National Science Foundation Partnerships in Enhancing Expertise in Taxonomy (NSF-PEET) project focusing on Bivalvia. Living specimens were collected in the Florida Keys as part of the Florida Keys Molluscan Biodiversity Program (e.g., Bieler & Mikkelsen, 2004), during an NSF-PEET-supported workshop (Mikkelsen & Bieler, 2004), and supplemented by fieldwork for the Bivalve Tree of Life project (http://www.bivatol.org) (Table 1).

Most specimens were cold-relaxed by refrigeration, fixed in 5% formalin, preserved in 70% ethanol, and dissected under a stereomicroscope while immersed in preservative; some additional material was fixed in Bouin's solution or directly in ethanol. Material examined sections refer mainly to material used in anatomical studies ("specimens"); additional conchological material ("shells") was examined particularly in cases of rarer species and to establish distributional ranges, especially within Brazil. Digital photographs of most dissection steps were produced for reference and some of these are included herein. All line drawings were produced with the aid of a camera lucida and are in most cases renditions based on multiple dissections (in these cases, no individual specimen is identified in the figure captions). Anatomical measurements and ratios were obtained from selected specimens, typically those dissected. All colors described are those in preserved specimens unless otherwise noted. Additional information on many of the dissected specimens at the Field Museum of Natural History (FMNH) can be found at the museum's online collections website (via www.fieldmuseum.org).

The family-level arrangement follows the recent classification presented by Bieler et al. (2010); the species-level treatments follow those of Mikkelsen & Bieler (2007). Several species names treated herein were placed in synonymy of unused older names by Huber (2010) in violation of the current ICZN (1999) *Code*; we are maintaining prevailing usage, with details discussed under each entry. Synonymy/chresonymy listings are restricted to the original descriptions of the valid name, a few relevant synonyms in recent use (especially those applied to the Florida Keys and Brazilian faunas), plus references to previous anatomical descriptions. Because recent molecular studies (e.g., Lee & Ó Foighil, 2004; Marko & Moran,

TABLE 1. Florida Keys (Monroe County, Florida) station data for material examined. nmi, nautical miles; nr, not recorded.

Station no.	Locality	Depth	Date
FK-028	Key Largo, 25°10.5’N, 80°22.8’W	0.5–1 m	07/iii/1996
FK-037	Spanish Harbor Keys, “Horseshoe” site (formerly West Summerland Key, now Scout Key), 24°39.3’N, 81°18.2’W	0.5–1 m	11/iii/1996
FK-045	Indian Key Fill, 24°53.2’N, 80°40.3’W	0.5–1 m	20/ix/1996
FK-047	off Ramrod Key, 24°35.8’N, 81°27.2’W	4.6 m	21/ix/1996
FK-048	American Shoals, 24°31.4’N, 81°31.3’W	4.6 m	21/ix/1996
FK-055	Upper Matecumbe Key, 24°54.2’N, 80°38.4’W	2.0 m	24/ix/1996
FK-056	Ohio Key, 24°40.4’N, 81°14.7’W	< 0.5 m	26/ix/1996
FK-083	N of Rebecca Shoal, between Marquesas Keys and Dry Tortugas, 24°44.9’N, 82°36.1’W to 24°44.4’N, 82°37.4’W	28.9 m	22/iv/1997
FK-117	Key Vaca, channel W of Stirrup Key, 24°44.2’N, 81º02.9’N	4.6 m	14/vii/1997
FK-128	Rachel Shoal, off Marathon, 24°45.0’N, 81°05.0’W	1–5 m	25/vii/1997
FK-138	Sister Creek, Boot Key, 24°41.9’N, 81°05.4’W to 24°41.9’N, 81°05.5’W	1.8–3.6 m	10/viii/1997
FK-139	E of Bethel Bank, 24°44.0’N, 81°07.6’W	2 m	10/viii/1997
FK-141	E of Bethel Bank, 24°43.9’N, 81°07.6’W	1 m	12/viii/1997
FK-145	Grassy Key Bank, 24°47.2’N, 80°57.7’W	1 m	20/viii/1997
FK-148	Grassy Key Bank, 24°47.2’N, 80°57.6’W	nr	22/viii/1997
FK-154	Cocoanut Key, 24°44.7’N, 81°14.0’W	1 m	25/viii/1997
FK-188	Blackwater Sound, 25°08.8’N, 80°25.3’W	1.8 m	14/x/1998
FK-195	off Key Largo, between Key Largo Dry Rocks and Cannon Patch, 25°07.2’N, 80°19.1’W	1.5–1.8 m	03/iv/1999
FK-202	Molasses Reef, 25°00.5’N, 80°22.6’W	7.3 m	08/iv/1999
FK-206	French Reef, 25°02.1’N, 80°21.1’W	8.5 m	11/iv/1999
FK-219	Mud Key Channel (bayside of Big Coppitt Key area), 24°40.5’N, 81°41.7’W	3.3–4.0 m	19/iv/1999
FK-223	Big Coppitt Key, 24°36.0’N, 81°39.0’W	< 0.5 m	19/iv/1999
FK-226	Saddlebunch Harbor, 24°35.2’N, 81°37.9’W	0.3 m	20/iv/1999
FK-235	Long Key, 24°51.0’N, 80°57.8’W	0.2–0.5 m	02/viii/1999
FK-239	SE of Lignum Vitae Key, 24°53.7’N, 80°41.2’W	0.3–0.6 m	03/viii/1999
FK-244	Spanish Harbor Keys, “Horseshoe” site (formerly West Summerland Key, now Scout Key), 24°39.3’N, 81°18.2’W	7 m	05/viii/1999
FK-257	Bahia Honda Key, 24°43.8’N, 81°16.5’W to 24°43.8’N, 81°16.6’W	4 m	09/viii/1999
FK-260	Looe Key coral reef, oceanside of Ramrod Key, 24°32.8’N, 81°24.8’W	7.3–7.6 m	10/viii/1999
FK-287	Spanish Harbor Keys, “Horseshoe” site (formerly West Summerland Key, now Scout Key), 24°39.3’N, 81°18.2’W	< 1 m	09/iv/2000
FK-351	Looe Key back reef, 24°32.9’N, 81°24.4’W	0.9–2.1 m	08/vii/2000
FK-352	Spanish Harbor Keys, “Horseshoe” site (formerly West Summerland Key, now Scout Key), 24°39.3’N, 81°18.2’W	0–1.5 m	08/vii/2000
FK-503	off Sand Key, 24°21.4’N, 81°53.4’W	196 m	25/vii/2001
FK-504	off Sand Key, 24°20.7’N, 81°53.5’W	209 m	25/vii/2001

(continues)

(continued)

Station no.	Locality	Depth	Date
FK-629	Spanish Harbor Keys, "Horseshoe" site (formerly West Summerland Key, now Scout Key), 24°39.3'N, 81°18.2'W	0–1 m	21–26/vii/2002
FK-649	Sprigger Bank, off Conch Keys, 24°54.7'N, 80°56.2'W	1 m	22/vii/2002
FK-650	wreck of "Thunderbolt," *ca.* 6 nmi S of Marathon, Key Vaca, 24°39.7'N, 80°57.8'W	29.0–36.6 m	27/vii/2002
FK-717	wreck of "Thunderbolt," *ca.* 6 nmi S of Marathon, Key Vaca, 24°39.7'N, 80°57.8'W	29.0–36.6 m	27/vii/2002
FK-760	Ramrod Key, near blind end of side canal S of Saint Martin Lane, 24°39.4'N, 81°24.3'W	< 0.5 m	11/vii/2006
FK-786	Ramrod Key, near S end of Breezeswept Beach Estate canal system, 24°39.1'N, 81°24.4'W	< 0.3 m	18/v/2007
FK-787	Ramrod Key, near NE end of Breezeswept Beach Estate canal system, 24°39.7'N, 81°24.3'W	< 0.3 m	18/v/2007
FK-908	wreck of the "Adolphus Busch," W of Looe Key reef, 24°31.8'N, 81°27.7'W	31.7 m	26/viii/2009
FK-991	wreck of the "Adolphus Busch," W of Looe Key reef, 24°31.8'N, 81°27.7'W	27–28 m	30/xi/2011
RB-1582	Indian Key Fill, 24°53.2'N, 80°40.3'W	0.5–1 m	29/vii/1992

2009) have demonstrated that the bivalve clade diversity in the western Atlantic is much greater than previously assumed, the descriptions herein apply to the Florida Keys morphs unless specifically noted. Geographical ranges are discussed with reference to Turgeon et al. (2009). Remarks sections include reference to all known anatomical and functional morphological treatments of the species and/or its congeners or close relatives. In cases of composite drawings based on multiple specimens, no scale bar or dimension is provided with the figure.

Anatomical descriptions to the level of detail provided here supply valuable data in their own right, but are more powerful if the utility of such characters can be demonstrated in a phylogenetic context. To that end, a data matrix was constructed (Table 2) and a parsimony analysis was performed (1000 RAS/TBR swapping/10 trees kept per replication) using TNT 1.1 (Goloboff et al., 2008) and further explored with WinClada 1.00.08 (Nixon, 2002). Outgroups were *Paradentalium disparile* (d'Orbigny, 1853) (Scaphopoda) and *Neopilina galatheae* Lemche, 1957 (Monoplacophora); coding for these taxa was derived from the literature (Simone, 2009, and Lemche & Wingstrand, 1959, respectively). Three species in two additional families [Arcidae: *Barbatia cancellaria* (Lamarck, 1819); Mytilidae: *Lithophaga aristata* (Dillwyn, 1817); Donacidae: *Donax variabilis* Say, 1822] also from Florida, and studied by the first author and colleagues under identical methods and illustrating the same character systems (Simone & Chichvarkhin, 2004; Simone & Gonçalves, 2006; and Simone & Dougherty, 2004, respectively), were also included. Simone & Gonçalves (2006) had treated the mytilid species as *Myoforceps aristatus*; herein were are following Kleemann & Maestrati (2012) who considered *Myoforceps* P. Fischer, 1886, a junior synonym of *Leioselenus* Carpenter, 1856, and placed the latter as a subgenus of *Lithophaga* Röding, 1798. The results of this analysis are intended to provide coding suggestions for future investigations and illustrate the resolving power of the selected characters, but not for inferring fundamental bivalve relationships.

Abbreviations used in the text include: A, area; D, diameter; H, height; L, length; LV, left valve; n/a, not applicable (in the data matrix); RV, right valve; SD, shell diameter; SH, shell (dorsoventral) height; SL, shell (anteroposterior) length; ST, shell thickness, SV, shell internal volume; SW, shell (latero-lateral) inflation; T, thickness; V, volume; VA, valve area; W, width. Other cited museum repositories include the American Museum of Natural History, New York (AMNH), Museu de Zoologia da Universidade de São Paulo, Brazil (MZSP), and the National Museum of Natural History, Washington, D.C. (USNM).

TABLE 2. Data matrix. The two *Hyotissa* spp. described here are coded identically, therefore, only one entry represents both species in the matrix. N = not applicable.

	000000000	1111111111	2222222222	3333333333	4444444444	5555555555	6666666666	7777777777	8
	123456789	0123456789	0123456789	0123456789	0123456789	0123456789	0123456789	0123456789	0
Paradentalium	000NNNNN1	NNNNN0000?	?N0NN0N00N	10NNNN000N	NNNNNNNNNN	NNNNNNNN00	N0N0000000	N000000000	N
Neopilina	000NNNNN?	NNNNN0000?	?N0NN1?00N	00NNNN000N	0NNNNNNNNN	NNNNN00N00	N0N0000000	N100000000	N
Anomia	0010N00N0	12N1100010	0011011000	0000NN110N	1N01100110	10001?0010	11N0011111	0201100011	1
Arcopsis	0111000N1	1000100010	1011110000	0000NN110N	1N01100100	0000001010	0110011111	0001000011	1
Barbatia	0111000N1	1000100010	1011110000	0000NN110N	1N01100100	0000001010	0110011111	0001000011	1
Brachidontes	0011?00N0	1110100011	?011010110	0010NN110N	1N01100100	0111000110	0101011111	0001020011	1
Carditamera	0011100N1	1010100011	?010010110	0010NN1110	1N01011100	010?000010	0110011111	0001001011	1
Chama	1011?00N1	00101000?1	?00NN11011	1010001110	1011011100	000?010110	0110011111	0001001011	1
Codakia	0011100N1	1100100011	?00NN11011	0010NN1111	1??10?1111	100?000010	0110011100	N001001011	1
Donax	001110111	1000100010	010NN11011	0011101111	1N11011110	0001000010	0110011111	0210001111	1
Entodesma	0010N10N0	1110100011	?010011111	1111111110	1N010111?0	010?010010	0100011111	1001001111	1
Hyotissa	1010N00N1	N2N111?1?1	?00NN11110	0000NN1110	1001001111	111?110110	11N0111111	10011000??	?
Isognomon	0010?00N0	12N1100010	0010011100	0000NN110N	1101100100	0100000110	11N0011110	N001000011	1
Laevicardium	001110101	1010100010	000NN11011	0010001110	1011011110	1101000010	0110111101	1101011111	1
Lamychaena	0010N0111	1110100010	0011010011	1111111110	1001001110	111?010010	0110011110	N001101111	1
Limopsis	0111000N1	1100100010	1010010000	0000NN110N	1N01100100	0000000010	0110011110	N001100011	1
Lithophaga	0010N00N1	1110100011	?010010010	0011NN110N	1N01100100	0011010110	0101011?00	N001010011	1
Pinna	0010N00N0	1101100011	?010011110	0010NN110N	1101100100	011?000110	1101011111	0001100011	1
Plicatula	1011?10N1	N2N111?1?1	?00NN11100	0000NN110N	1N01100100	0000000011	11N0011110	N0011000?1	1
Polymesoda	001110101	1000100010	000NN10011	0011001111	1011011111	1001000010	0110011111	1001001111	1
Propeleda	0011000N0	0000001000	000NN00000	0011NN100N	0NN00NN0NN	NNN0000010	0100010000	N000000000	0
Scissula	001110111	1000100010	010NN11011	1011101111	1N11011100	010?000010	0100011111	0010001111	1
Solemya	0010N00N0	0000001000	000NN00000	1010NN000N	0NN0?NN0NN	NNN0000010	0100000000	NN00000000	0
Spondylus	2011?10N1	N2N11001?1	?00NN11000	0000NN110N	1N01100100	0000000011	11N0011111	0001100011	1

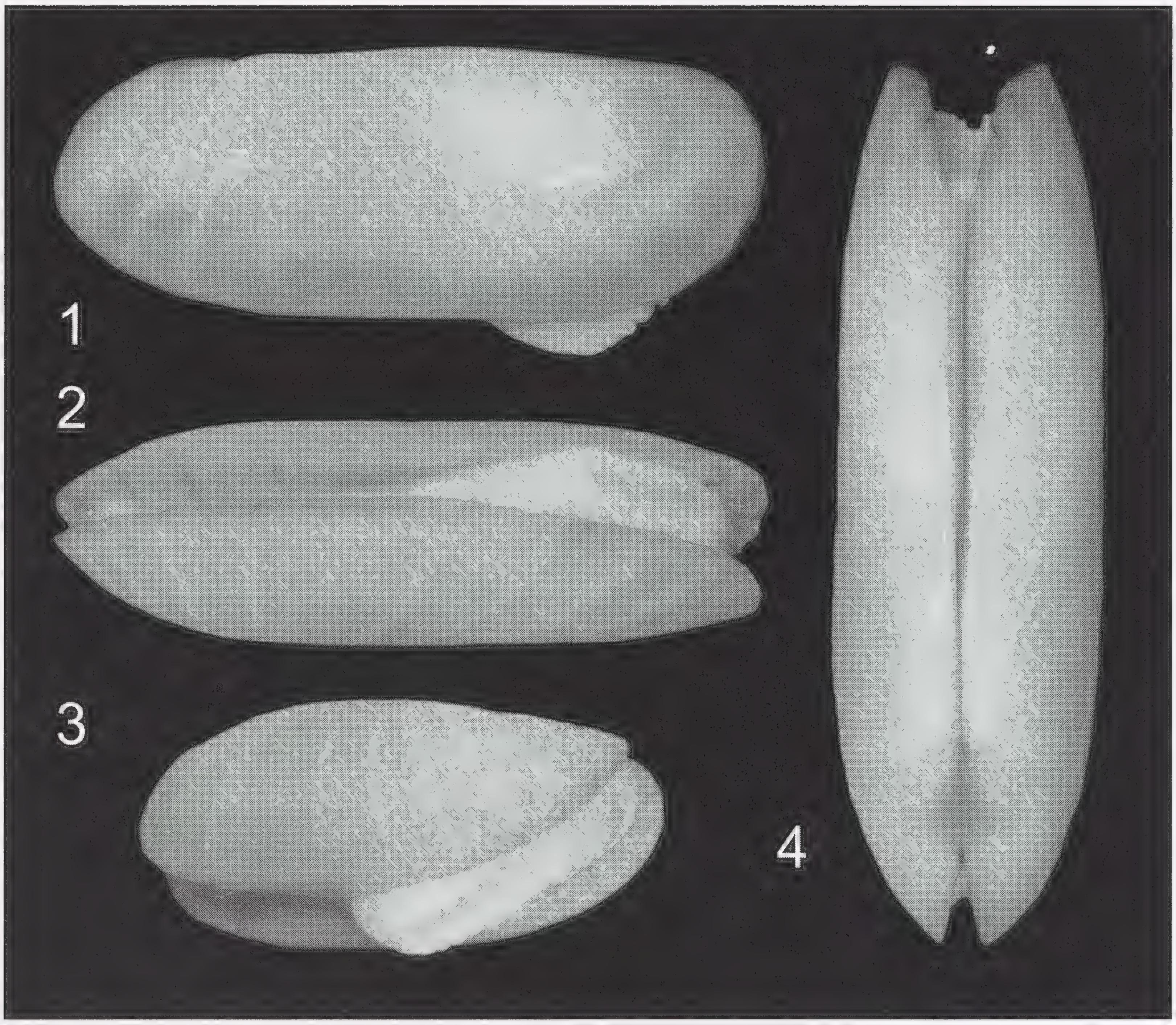

FIGS. 1–4. *Solemya occidentalis*, shell morphology, intact specimen, AMNH 298933, 6.1 mm L. FIG. 1: Right view; FIG. 2: Ventral and slightly left view; FIG. 3: Posteroventral and slightly right view; FIG. 4: Dorsal view.

ANATOMICAL DESCRIPTIONS

Family Solemyidae
Gray, 1840

Solemya occidentalis
Deshayes, 1857
Figs. 1–13

Synonymy/Chresonymy

Solemya occidentalis Deshayes, 1857: 139 [Type locality: Antilles].
Solemya (Petrasma) occidentalis – Abbott, 1974: 420, fig. 4955.
Solemya occidentalis – Bieler & Mikkelsen, 2004: 520; Mikkelsen & Bieler, 2007: 30–31, 5 figs.; Simone, 2009: 405 ff.

Description

Shell (Figs. 1–4): Thin, translucent, fragile, slightly rectangular; SL ≈ 6 mm in material examined ≈ 2.5 SH. Anterior and posterior ends rounded, subequal. Periostracum thin, translucent, glossy, yellow to beige-brown, with 10–15 radial, pale-beige bands, slightly more concentrated posteriorly (Fig. 1), less pigmented close to umbones; ca. 25% extending beyond calcareous portion of shell (Figs. 2, 3), attaching to ventral connection between mantle lobes. Umbones at posterior quarter of SL, not protruding, flattened. Pair of oblique, very shallow, narrow furrows running anteriorly to umbones along posteroventral region (Fig. 4) for ca. 12% SL. Ligament simple, posterior, becoming abruptly wider posterior to umbones; L ≈ 17% SH (Fig. 4). Hinge plate edentulous. Inner surface white, non-nacreous. Scars of adductor muscles subequal (posterior scar slightly smaller), each in A ≈ 15% VA (calcareous portion); anterior adductor muscle scar close to dorsal edge, just posterior of anterior quarter of SL; posterior adductor muscle scar very near posterior shell margin. Pallial line

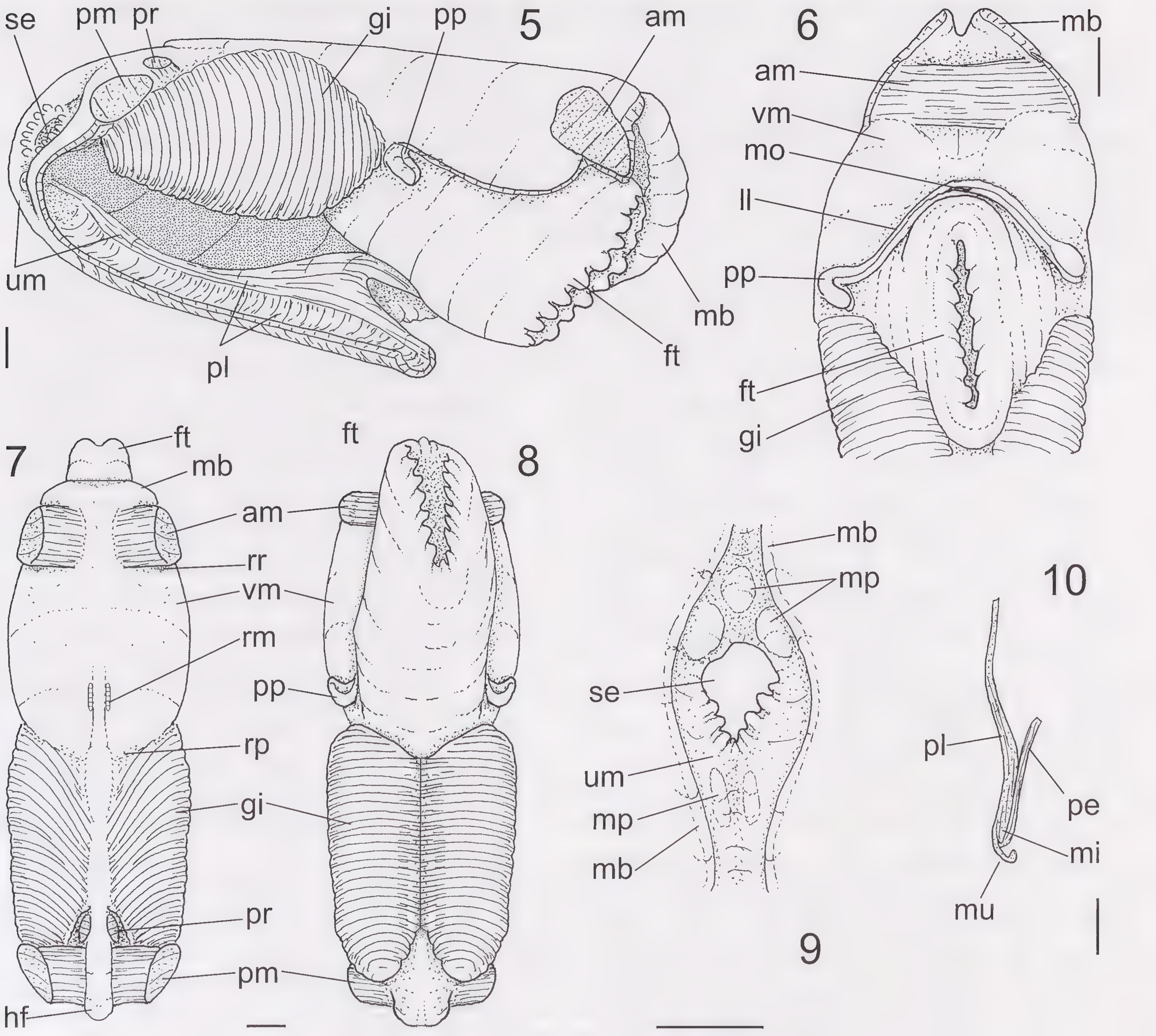

FIGS. 5–10. *Solemya occidentalis*, anatomy. FIG. 5: Intact right view, shell and part of right mantle lobe removed; FIG. 6: Detail of anterior region, ventral view, both mantle lobes mostly removed, foot (ft) deflected posteriorly to show buccal region; FIG. 7: Specimen with shell and mantle lobes removed, dorsal view; FIG. 8: Same, ventral view; FIG. 9: Detail of excurrent siphon (se), posterior view; FIG. 10: Mantle border, cross section in posteroventral quadrant. Scale bars = 0.5 mm. Abbreviations: am, anterior adductor muscle; ft, foot; gi, gill; hf, hinge fold of mantle; ll, labial lips preceding mouth; mb, mantle border; mi, mantle border inner fold; mo, mouth; mp, mantle papillae; mu, mantle border outer fold; pe, periostracum; pl, pallial muscles; pm, posterior adductor muscle; pp, labial palp; pr, posterior pedal retractor muscle; rm, middle pedal retractor muscle; rp, midposterior pedal retractor muscle; rr, pedal protractor muscle; se, excurrent aperture; um, fusion between left and right mantle lobes; vm, visceral mass.

simple, thick, between middle and ventral thirds of SH.

Main muscle system (Figs. 5, 7, 11): Muscle positions as described for scars above. Anterior adductor muscle (Fig. 5: *am*) oval in cross section (longer axis parallel to shell margin); A ≈ 15% VA. Posterior adductor muscle (Fig. 5: *pm*) similar to *am*, slightly more rounded in cross section; A ≈ 75% of *am* A. Pedal protractor muscle inconspicuous, immersed in anterior visceral integument, originating surrounding ventral edge of *am*, running immersed in anteroventral wall of visceral mass, diminishing along dorsal foot base. Paired anterior pedal retractor muscles (Fig. 11: *rr*) narrow, long, originating just dorsal and posterior to *am*, in A ≈ 6% of *am* A, running posteroventrally with uniform W, in L ≈ 16% SL, inserting splaying across wall between visceral mass and anterodorsal foot base. Paired middle pedal retractor muscles (Fig. 11: *rm*) broad, thick, originating in umbonal

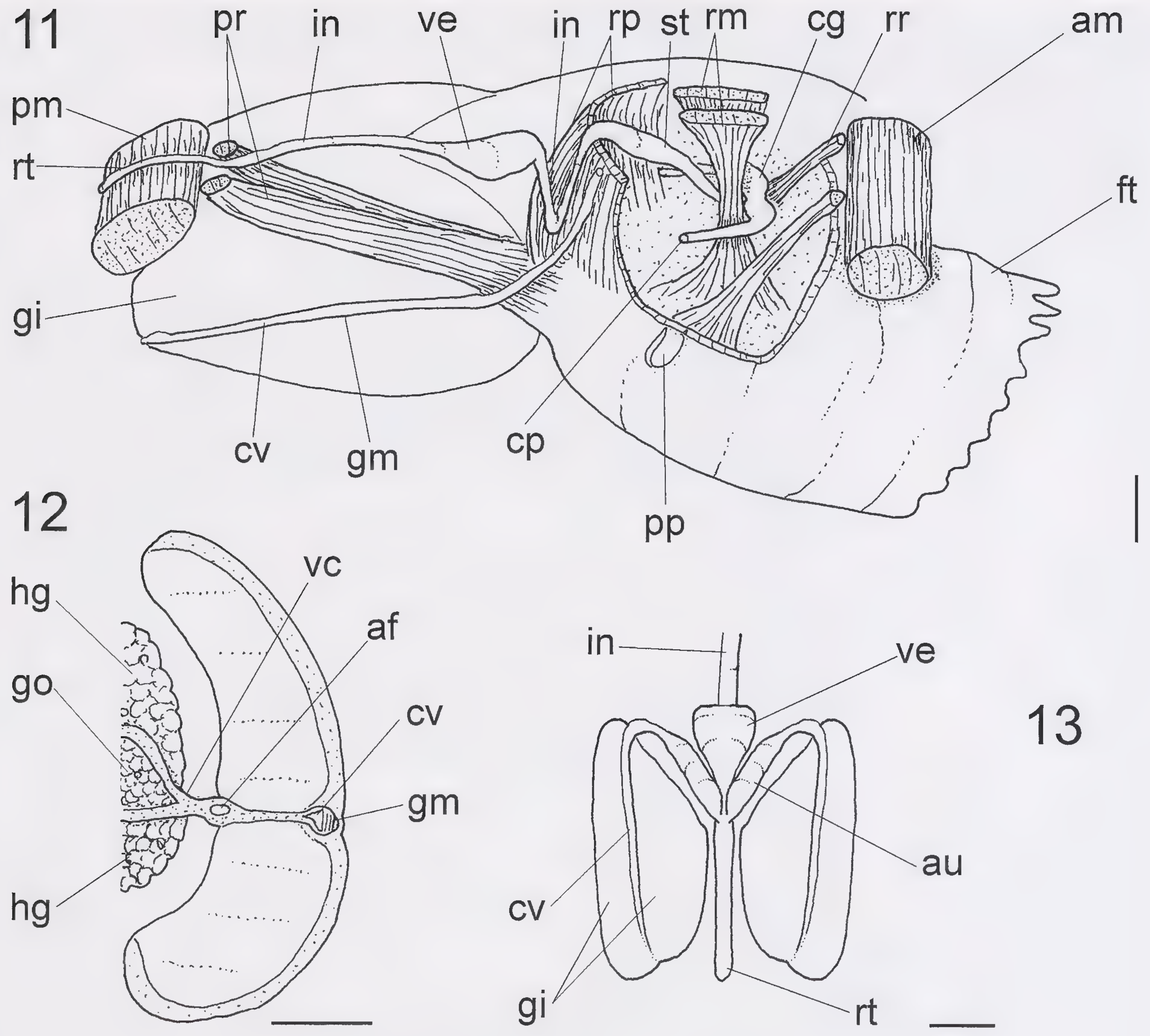

FIGS. 11–13. *Solemya occidentalis*, anatomy. FIG. 11: Foot (ft), main musculature, digestive system, and part of nervous system *in situ*, right and slightly dorsal view, topologies of some adjacent structures shown; FIG. 12: Right gill, cross section in its midregion, with adjacent portion of visceral mass also shown; FIG. 13: Pericardial structures, dorsal view, topologies of some adjacent structures also shown. Scale bars = 0.5 mm. Abbreviations: af, afferent gill vessel; am, anterior adductor muscle; au, auricle; cg, cerebropleural ganglion; cp, cerebrovisceral connective; cv, ctenidial (efferent) vessel; ft, foot; gi, gill; gm, gill retractor muscle; go, gonad; hg, hypobranchial gland; in, intestine; pm, posterior adductor muscle; pp, labial palp; pr, posterior pedal retractor muscle; rm, middle pedal retractor muscle; rp, midposterior pedal retractor muscle; rr, pedal protractor muscle; rt, rectum; st, stomach; vc, visceral mass gill connection; ve, ventricle.

cavity close to midline, in L ≈ 3 W, running ventrally, narrowing gradually, inserting just internal to insertion of *rr*. Midposterior pedal retractor muscle (Fig. 11: *rp*) as single muscular layer covering posterior wall of visceral mass anterior to pericardium, originating in wide, transverse horseshoe shape (concavity anterior) between umbones and posterior end; anteriorly thicker, directed internally; remaining ca. 50% W, performing arc, running ventrally separating renopericardial structures from gonad, inserting along posteroventral walls of foot. Paired posterior pedal retractor muscles (Fig. 11: *pr*) long, thick, originating just posterodorsal to *pm*, in A ≈ 16% of *pm* A; each slightly elongating anteroposteriorly (L ≈ 1.5 W), running anteroventrally for ca. 50% SL, of uniform W; inserting covering insertion of *rp* in posteroventral foot base. Pallial muscles as described below.

Foot (Figs. 2, 3, 5, 6, 8, 11: *ft*): Directed anteroventrally, cylindrical; V ≈ 33% SV, L (retracted) = 33–50% SL. Foot distal tip white in living animal, umbrella-like, with thinner, undulating edges with short, stubby papillae, expanding distally to ca. 2 times foot base W. Byssal groove and byssus absent.

Mantle (Figs. 3, 5, 9, 10): Mantle lobes (Fig. 5: *mb*) in A ≈ 125% VA (calcified portion); overlapping portion folding internally in retracted position (Fig. 3). Edges of mantle lobes broadly fused, thickly muscular. Pedal aperture anterior; L ≈ 33% SL. Anterodorsal mantle edge smooth, without tentacles. Excurrent aperture (Figs. 5, 9: *se*) at midlevel of posterior border, of D ≈ 12% of pedal aperture D; edges simple, with ca. 7 papillae flanking ventral half along edges (Fig. 9); 3 larger dorsal papillae, each in L ≈ 50% of excurrent aperture L, equidistantly dorsal to *se*; 2 pairs of dorsoventrally elongated papillae (L ≈ 3 W) at some distance ventral to *se*. Pallial muscles (Fig. 5: *pl*) mostly perpendicularly disposed, each T ≈ 2 ST, inserting into thick pallial line between middle and ventral thirds of calcareous shell; ca. 66% of mantle containing pallial muscles covered only by periostracum (Fig. 3). Pallial longitudinal muscle running along ventral pallial fusion (Fig. 5) from pedal aperture to *se*, T slightly > ST, comprised dorsally by oblique muscles and ventrally by pallial tissue. Mantle edges beyond calcareous shell (Fig. 10) with 2 folds; outer fold T ≈ ST, H ≈ 4T, with periostracum attaching to inner surface; inner fold T ≈ 2 outer fold T, mostly attaching to periostracum (Fig. 10). Adoral sense organs and tubular mantle glands not observed.

Pallial cavity (Figs. 5, 6, 8, 12): In A ≈ 75% VA, V > 50% SV. Paired labial palps (Figs. 5, 6, 8: *pp*) small, just anterior to anterior ends of gills; free portion L ≈ 1.5H ≈ 10% SH. *Pp* inner surface smooth. *Pp* connected by long pair of lips (Fig. 6: *ll*); W ≈ SW. Palp pouch not observed. Gills bipectinate, in posterior half of SV, large; L ≈ 50% SL ≈ 75% SH. Dorsal gill filament L ≈ 1.5 ventral filament L (Fig. 12); ventral filaments with pointed tips positioned vertically. Gill filaments with skeletal rods at external edges; rod W ≈ 33% of filament W (Fig. 12). Gill central; horizontal axis with efferent gill vessel externally, afferent gill vessel internally. Gill longitudinal muscle (Fig. 12: *gm*) along outer efferent gill vessel. Suprabranchial chamber small, compressed by *pr*, *am*, *pm*, and kidneys.

Visceral mass (Figs. 7, 11, 12): Central in dorsal half, compressed by shell muscles; V ≈ 25% SV. Anterior half reflecting over dorsal surface of foot. Region anterior to *rp* mostly filled by pale cream gonad. Region posterior to *rp* mostly filled by renopericardial structures, with pericardium dorsal, kidneys ventral, subequal; renopericardial structures V ≈ 12% of visceral mass V. Hypobranchial gland (Fig. 12: *hg*) whitish-translucent, covering ventral and dorsal surfaces of visceral mass portion adjacent to gills; V ≈ 50% of visceral mass V.

Circulatory and excretory systems (Fig. 13): In triangular space between *rp* and *pr*, V ≈ 12% of visceral mass V. Pericardium oval, dorsoventrally compressed; L ≈ 70% SW. Paired auricles (*au*) lateral, positioned horizontally and obliquely (medial region more posterior) at midpericardial region, connecting anterior end of gill efferent vessel with posterior ventricle. Ventricle (*ve*) oval, tapering posteriorly, surrounding 80% of intestinal loop traversing pericardium; V = au V ≈ 20% of pericardial V. Kidneys (*ki*) solid, white, filling ventral pericardium and dorsal surface of *pr*.

Digestive system (Fig. 11): *Pp* as described above. Mouth very small, central between *pp*, compressed between foot and anterior visceral mass. Esophagus (*es*) filiform, running between *rm*, gradually running posterodorsally, progressively expanding to form stomach without obvious demarcation. Stomach (*st*) very small, in L ≈ 6% SL ≈ 3 W; inner surface smooth, simple (lacking sorting areas, gastric shield, etc.), with 2 ducts to digestive diverticula in anterior third of gastric lateral walls. Digestive diverticula (*dd*) small, intermingling with gonad. Intestine (*in*) filiform, with single loop posterior to *rp*, along median plane, crossing dorsal edge of *rp*, running almost directly along midline at edge of hinge plate, passing between origins of *pr* and along dorsal and posterior surfaces of *pm*. Anus (*an*) simple, sessile, at midlevel of posterior surface of *pm*.

Reproductive system: Gonad in visceral mass as described above. Genital duct, pore, and other details not observed.

Nervous system (Fig. 11): Paired cerebropleural ganglia (*cg*) as a single, curved mass anterior to midportion of *es*, surrounding midlevel of *rp*; T ≈ 10% of *am* T (in wider anterior region). Cerebrovisceral connectives (*cp*) running laterally and posteriorly through gonad, in dorsal *rp*, through dorsal muscular posterior wall of visceral mass, then between gill bases and dorsal *pr*. Visceral ganglia (*vg*) as single transverse mass, slightly wider than preceding connective, small (V ≈ 20% of *cg* V), at midlevel of dorsal third of *pr*. Pedal ganglia not observed.

Material Examined

USA, Florida Keys, AMNH 298933, 9 specimens (sta. FK-219; 1 dissected: 6.1 mm L, 2.8 mm H, 2.0 mm W).

Distribution

Stated by Turgeon et al. (2009) to range from South Florida to Louisiana and the offshore banks of the northwestern Gulf of Mexico, and the West Indies. Reported from Colombia by Diaz & Puyana (1994). Previously claimed to range to Brazil (e.g., Rios, 1985: 207; 1994: 224; 2009: 459), but all studied Brazilian material was shown to belong to a species with different anatomical characters (e.g., much longer labial palps) and has been described as the new species *Solemya notialis* Simone, 2009.

Remarks

This is the first full anatomical description of *Solemya occidentalis*. All species of *Solemya* that have been studied have an obligatory host-specific association with intracellular, sufur-oxidizing, chemautotrophic symbionts (Krueger & Cavanaugh, 1997). The degree of anatomical specialization (reduction) differs, however, and ranges from having small functional digestive systems as in the present species, *S. velum* Say, 1822, and *S. togata* (Poli, 1791) (the latter two studied by Yonge, 1939, with *S. togata* also investigated by Stempell, 1899) to a complete absence of gut and mouth in *S. reidi* Bernard, 1980 (Reid, 1980). Such extreme cases of reduction led some authors (Huber 2010: 90) to state that members of this family generally have no digestive tract. Krueger et al. (1996) studied the sulfur-oxidizing chemautotrophic bacterial symbionts in the gills of the present species from specimens collected in Belize. They were found to be a proteobacterial species distinct from those described from other *Solemya* species, with its closet known relative being the symbiont of *S. velum*, also from the western Atlantic. The bacteriocytes were found nearest to the cilitated edge of the gill.

The presence of sulfur-oxidizing symbionts allows *Solemya* to remain completely buried without the advantage of posterior siphons to maintain contact with the water column. Although a posterior excurrent aperture is present, the functional incurrent aperture [indicated only by a tentaculate mantle edge in *S. togata* by Yonge, 1939; tentacles not seen here] is anterior, as in other Protobranchia. Yonge (1939) observed *S. togata* buried below 1–2 cm of sediment, without any indication of an opening to the surface. The symbionts facilitate this lifestyle by providing sustinence in a hypoxic environment. The unique periostracum (described by Beedham & Owen, 1965) and shell form of *Solemya* species allow them to cleanse sediment particles from the mantle cavity through rapid muscular pumping movements (which when unburied often manifest in what has been called "swimming").

Adoral (or cephalic) sense organs were reported by Stempell (1899) in *Solemya togata*, but were not observed here. Tubular mantle glands, reported by Beedham & Owen (1965: 413) and apparently unique to *Solemya*, were not observed here.

Data for this species, based on the present Florida Keys material, were employed in the comparative morphological study of Scaphopoda and protobranch bivalves by Simone (2009).

Family Nuculanidae
H. Adams & A. Adams, 1858 [1854]

Propeleda carpenteri
(Dall, 1881)
Figs. 14–27

Synonymy/Chresonymy

Leda carpenteri Dall, 1881: 125 [Type locality: Barbados and *Blake* stations 5, 9, and 21 in the western Caribbean].

Nuculana carpenteri – Abbott, 1974: 414, fig. 4851.

Propeleda carpenteri – Allen & Sanders, 1996: 125–127, figs. 39–42; Bieler & Mikkelsen, 2004: 517; Mikkelsen & Bieler, 2007: 38–39, 5 figs.

Propeleda carpentieri [*sic*] – Simone, 2009: 405 ff.

Description

Shell (Figs. 14–17): Claviform, whitish-translucent, compressed laterally; SL ≈ 8 mm in material examined ≈ 2 SH ≈ 4 SW. External surface glossy, lacking sculpture except for delicate commarginal growth lines (Figs. 14, 15). Umbones small, weakly protruding, between anterior and middle thirds of hinge line, very close (Fig. 16). Anterior end rounded, narrowing gradually medially and posteriorly, weakly curving dorsally; posterior end narrow, slightly truncated. Inner surface smooth, glossy, non-nacreous. Hinge plate (Fig. 17: *hi*) curving from umbones, convex anterior to umbo, concave posterior to umbo, in RV mostly constituted by teeth, in LV by sockets; anterior to umbo with ca. 12 teeth/sockets,

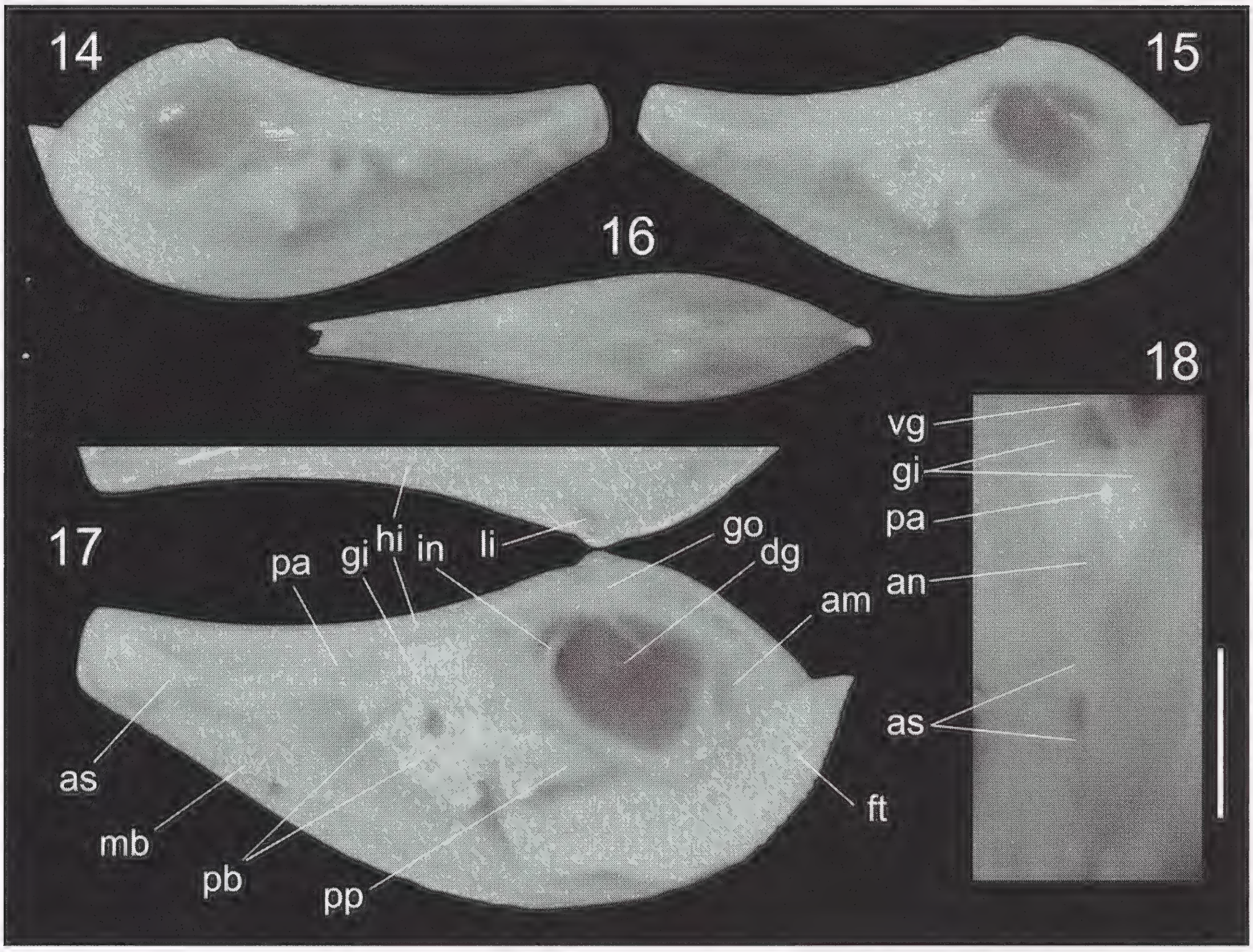

FIGS. 14–18. *Propeleda carpenteri*, shell morphology, FMNH 302085, 7.7 mm L. FIG. 14: Intact left view; FIG. 15: Intact right view; FIG. 16: Intact dorsal view; FIG. 17: Intact right view, RV removed, deflected upward and partially shown, right mantle lobe partially removed; FIG. 18: Anatomy, posterior region of pallial cavity, ventral view, mantle lobes partially deflected. Scale bar = 1 mm. Abbreviations: am, anterior adductor muscle; an, anus; as, anal siphon; dg, digestive diverticula; ft, foot; gi, gill; go, gonad; hi, hinge; in, intestine; li, ligament; mb, mantle border; pa, pedal aperture of fused mantle border; pb, palp proboscides; pp, labial palp; vg, visceral ganglia.

successively narrower and smaller toward umbones; posterior to umbo with ca. 18 teeth/sockets, also successively narrower and smaller toward umbones; teeth abruptly ending on posterior third of dorsal shell surface. Hinge teeth flat, relatively tall, with weakly concave ventral surfaces, perpendicular to shell margin at anterior and posterior ends, becoming gradually oblique closer to umbo. Ligament (Fig. 17: *li*) subumbonal, small, with a narrow external component, thicker internal component curving posteriorly. Muscle scars weakly impressed.

Main muscle system (Figs. 17, 19, 25): Anterior adductor muscle (Figs. 17, 19, 25: *am*) at anterior end of hinge plate, elliptical in cross section, anterodorsally at some distance from shell margin; A ≈ 5% VA, H ≈ 1.5 L. Posterior adductor muscle (Figs. 17, 19, 25: *pm*) approximately midway between umbo and posterior end, close to and at level of posterior end of *hi*; A ≈ *am* A, L ≈ 3H. Paired pedal protractor muscles (Fig. 25: *rr*) small, narrow, originating ventral to *am*, running ventromedially attached to inner surface of integument, gradually splaying after distance ≈ 50% of *am* L across anterodorsal foot. Paired anteromedial pedal retractor muscles (Fig. 25: *ra*) long, slender, originating close to midline dorsal to *am*, in A = 5% of *am* A, running ventrally through visceral glands, close to midline, splaying insertion just posterior to that of *rr*. Paired anterolateral pedal retractor muscles (Fig. 25: *rl*) long, slender, originating dorsolaterally to but separate from *am*, in A = 10% of *am* A, running posteroventrally through visceral glands at distance = 33% SL, splaying insertion close to midline of foot base. Paired middle pedal retractor muscles (Fig. 25: *rm*) thick, originating in anteropos-

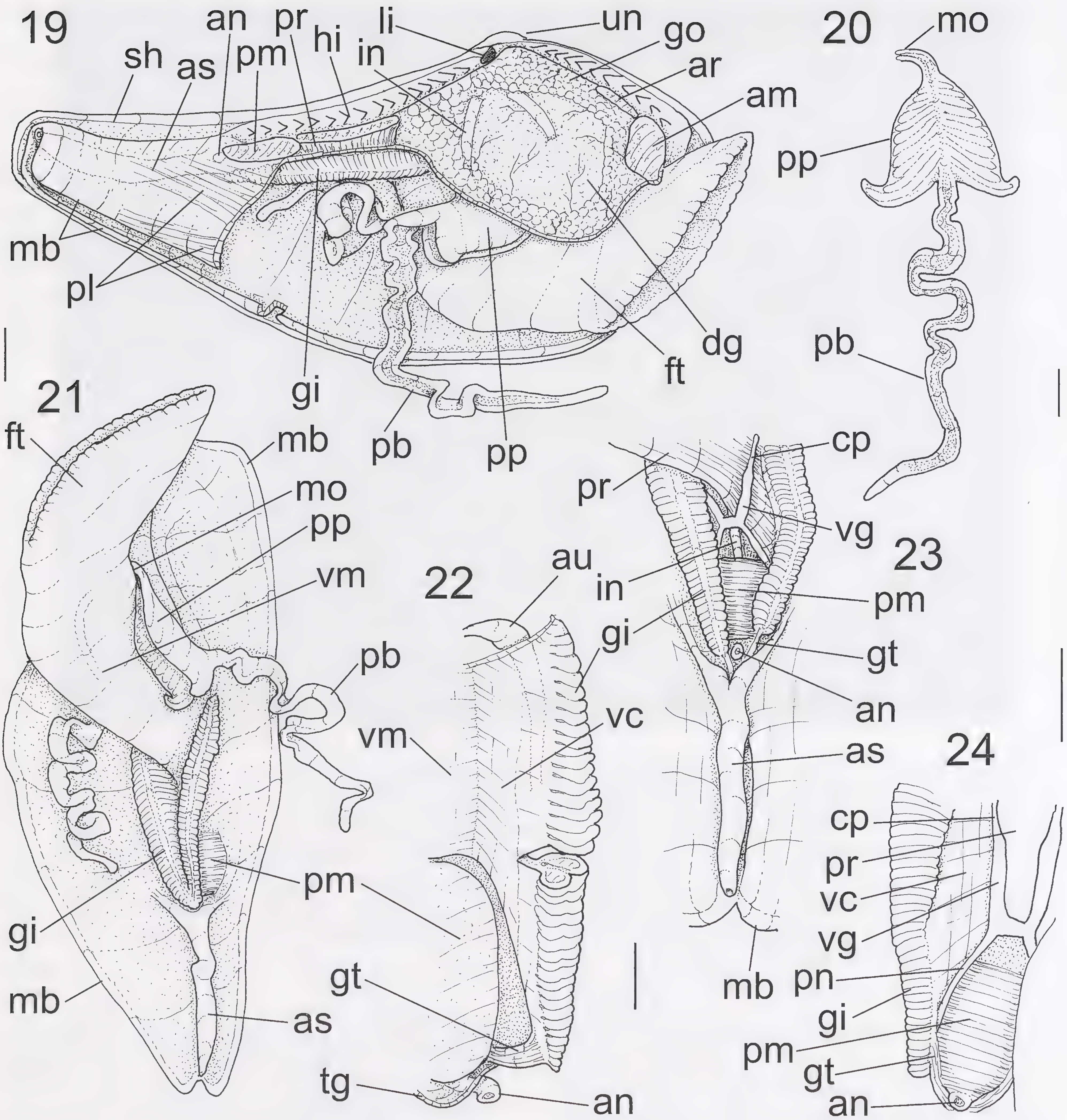

FIGS. 19–24. *Propeleda carpenteri*, anatomy. FIG. 19: Intact right view, RV and part of left mantle lobe removed; FIG. 20: Isolated right labial palp, both hemipalps deflected, palp proboscis (pb) extended, inner surface exposed; FIG. 21: Intact ventral and slightly left view, both mantle lobes deflected; FIG. 22: Posterior region of pallial cavity, ventral view, detail of left gill and adjacent structures, pericardial ventral wall partially removed, some gill filaments removed at midlevel of gill, gill partially deflected; FIG. 23: Posterior region of pallial cavity, ventral view, both gills partially deflected to show suprabranchial chamber; FIG. 24: Same, detail of visceral ganglion (vg) region. Scale bars = 0.5 mm. Abbreviations: am, anterior adductor muscle; an, anus; ar, anterior pedal retractor muscle; as, anal siphon; au, auricle; cp, cerebrovisceral connective; dg, digestive diverticula; ft, foot; gi, gill; go, gonad; gt, gill suspensory stalk; hi, hinge; in, intestine; li, ligament; mb, mantle border; mo, mouth; pb, palp proboscis; pl, pallial muscles; pm, posterior adductor muscle; pn, pallial nerve from visceral ganglion; pp, labial palp; pr, posterior pedal retractor muscle; sh, shell; tg, integument; un, umbo; vc, visceral mass gill connection; vg, visceral ganglia; vm, visceral mass.

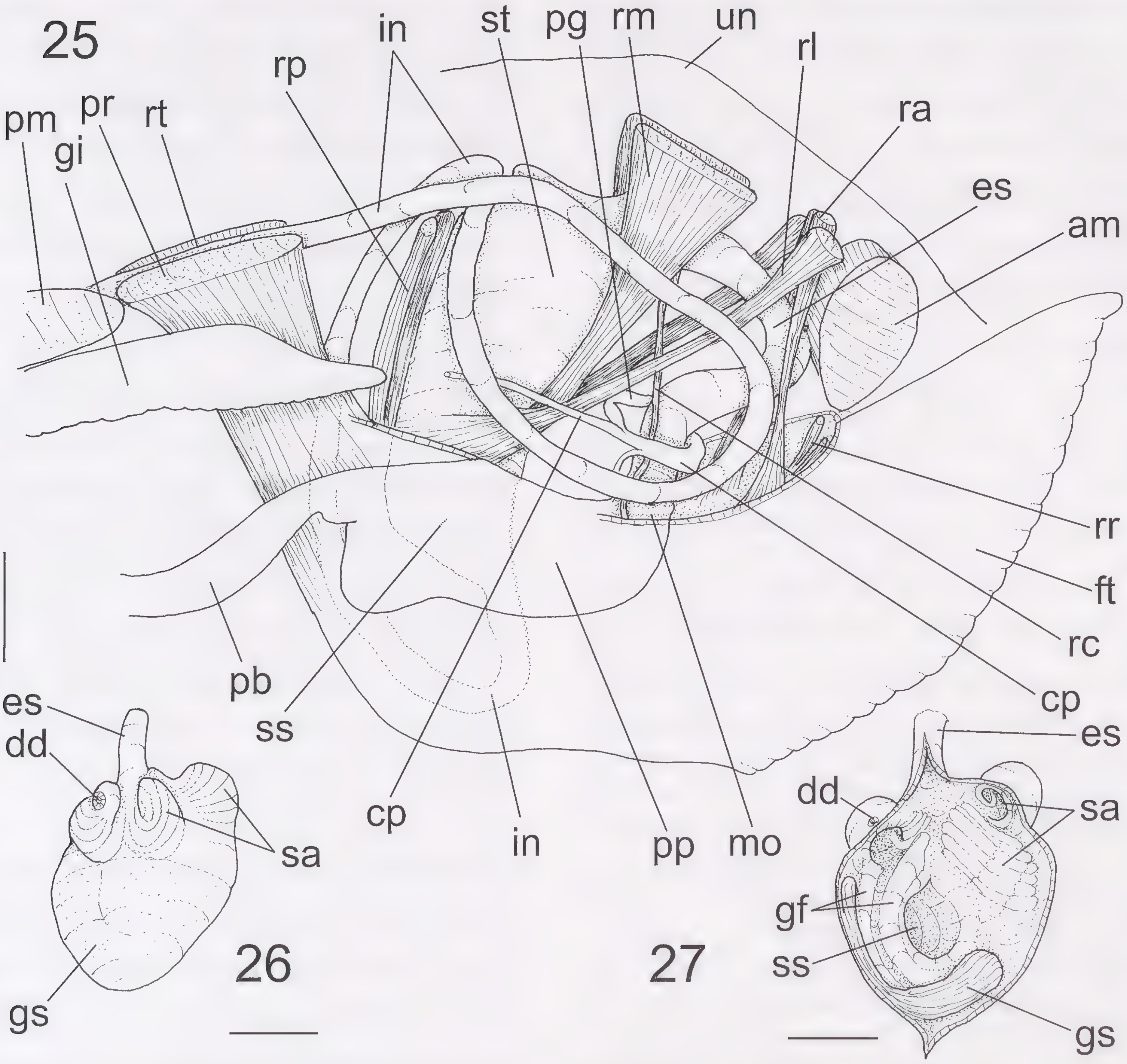

FIGS. 25–27. *Propeleda carpenteri*, anatomy. FIG. 25: Visceral and pedal structures *in situ*, right view, ventral region of style sac (ss) and intestine (in) represented by dotted lines; FIG. 26: Stomach, dorsal view; FIG. 27: Same, opened longitudinally along dorsal wall, inner surface exposed. Scale bars = 0.5 mm. Abbreviations: am, anterior adductor muscle; cp, cerebrovisceral connective; dd, ducts to digestive diverticula; es, esophagus; ft, foot; gf, gastric fold; gi, gill; gs, gastric shield; in, intestine; mo, mouth; pb, palp proboscis; pg, pedal ganglion; pm, posterior adductor muscle; pp, labial palp; pr, posterior pedal retractor muscle; ra, anteromedial pedal retractor muscle; rc, accessory middle pedal retractor muscle; rl, anterolateral pedal retractor muscle; rm, middle pedal retractor muscle; rp, midposterior pedal retractor muscle; rr, pedal protractor muscle; rt, rectum; sa, gastric sorting area; ss, style sac; un, umbo.

teriorly long narrow area of umbonal cavity (L ≈ 5W), close to midline, in L = *am* L, running ventrally and weakly posteriorly, narrowing abruptly through visceral glands, at distance = 33% SL, inserting in midregion of foot base just medial to insertion of *rl*. Paired accessory central pedal retractor muscles (Fig. 25: *rc*) very narrow, thin, originating approximately midway between origins of central pedal retractors, in A = 5% of central pedal retractors A, running ventrally close to midline, surrounding digestive system, through visceral glands at distance = 33% SL, passing through nerve ring, inserting along midanterior foot base, more ventrally and more anterior than those of main central retractors. Paired midposterior pedal retractor muscles (Fig. 25: *rp*) slender, originating in lateral area midway between umbo and *pm*, in A = 5% of *pm* A, running ventrally through gonad approaching from midline, along ca. 33% SL; inserting into posterior foot base.

Paired posterior pedal retractor muscles (Fig. 25: *pr*) thick, broad, originating just anterior to *pm*, close to midline, in L = of *pm* L ≈ 5 W; running ventrally covering posterior wall of visceral mass along ca. 33% SL, inserting splaying across posterior foot base.

Foot (Figs. 17, 19, 21, 25): Distally relatively thin, umbrella-like, with anteroventral concavity; V ≈ 25% SV. Edges with series of low, broad, uniform folds; solid medially and basally, compressed laterally. Byssus and byssal gland absent.

Mantle (Figs. 17–19, 21, 23): Mantle edges (Figs. 17, 19: *mb*) thin, with single fold. Mantle lobes totally unfused except along dorsal edge. Anteroposterior paired pallial muscles (Fig. 19: *pl*) well-developed along posterior half of mantle lobes, separated into dorsal and ventral bundles. Excurrent (anal) siphon (Figs. 17, 18, 21, 23: *as*) long, originating as concavity just posterior to *pm*, with pair of lateral, muscular roots running along mantle on both sides of gills (Fig. 23); remaining regions of *as* thin-walled, translucent, tubular, running freely posteriorly between *pm* and posterior end of shell; distal end of *as* with weakly narrow aperture, at level of posterodorsal mantle edge. Incurrent siphon absent.

Pallial cavity (Figs. 17–24): In A ≈ 66% VA. Labial palps (Figs. 17, 19–21: *pp*) large, in A ≈ 2 gill A, midventral to lateral visceral mass, at anterior foot base. Hemipalps triangular, with ventral edges slightly rounded and inner surface covered by transverse folds; each broad with rounded ventral end, close to *pp* ventral edge. Palp proboscides (Figs. 19–21: *pb*) narrow, flat, long (L ≈ 3 remaining *pp* L); inner surface smooth, concave; edges thick; *pb* originating on *pp* posteroventral corners, weakly curving ventrally and anteriorly, irregularly coiled in retracted position, narrowing gradually distally; distal end rounded, preceded by region narrower than remaining *pb*; dorsal tip unclear in dissected material, fading into furrow uniting hemipalps. *Pp* inner folds parallel to posterior edge, decreasing in L gradually toward anterior, terminating near lips. Palp pouch absent. Gills (Figs. 17, 19, 21–24: *gi*) small, in V ≈ 10% of pallial cavity V, L ≈ 30% SL ≈ 10W; mid-dorsal just ventral to *pr* and adductor muscles. Gill base a long, flattened membrane, in L = *gi* L, decreasing abruptly near *gi* (mainly at posterior edge), originating from posterior visceral mass (mainly in *pr*); posterior edge of this membrane surrounding *pm* ventral surface. Gill suspensory stalk (Fig. 22: *gt*) connecting posterior end of *gi*, in L ≈ 10% of stalk L, originating from anteroventral surface of *pm*, on both sides of anus. *Gi* with ca. 30 bipectinate filaments, alternating along flattened longitudinal axis; efferent vessel running in base; afferent vessel running close to distal edge of axis. Each filament rounded, with edges weakly thicker, decreasing gradually in size posteriorly. Posterodistal end of *gi* pointed, fitting inside base of *as* (Fig. 23).

Visceral mass (Figs. 17, 19, 25–27): Laterally compressed, subcircular; V ≈ 66% of visceral-mass-plus-foot V. Walls relatively thin, translucent, thicker closer to foot. Gonad pale cream, at periphery surrounding anterior, dorsal, ventral, and posterior digestive diverticula. Digestive diverticula greenish-brown, central, seen by translucency on midlateral surfaces. Intestinal loops (Fig. 25: *in*) simple, visible at some points on lateral surface of visceral mass. Stomach (Figs. 25–27: *st*) posterior, close to *pr*; V ≈ 33% of visceral mass V. *Pr* and digestive system passing through visceral glands.

Circulatory and excretory systems (Fig. 22): Pericardium and kidneys each greatly compressed near posterior visceral mass, just anterior to *pr*. Auricles (*au*) paired, relatively small, at anterior base of *gi*, as continuation of efferent gill vessel, connecting laterally to small ventricle (*ve*) surrounding *in* passing through pericardium. Kidneys not observed in detail.

Digestive system (Figs. 18, 20–27): *Pp* as described above. Mouth (Figs. 20, 21: *mo*) flanked by pair of tall lips as continuation of *pp*; inner surface smooth; located between foot and ventral surface of visceral mass, far from *am*. Esophagus (Fig. 25: *es*) in L ≈ *pp* L, broad, sinuous, with smooth inner surface, running anterodorsally from posterior surface of *am*, there broadly curved, passing between *rm*, close to their origins; W ≈ 16% of *am* W. *St* as described above, posterior, close to *pr*; V ≈ 33% of visceral mass V. Pair of low gastric projections (Fig. 26) on dorsal surface, close to *es* opening; each projection with longitudinal, low folds forming sorting area (Fig. 27: *sa*) running divergently as short spirals. Left projection with duct to digestive diverticula (Figs. 26, 27: *dd*) at tip. Right projection as spiral blind sac; other *sa* with transverse folds on right anteroventral gastric surface, ventral to right dorsal projection; subelliptical; A ≈ 25% of inner gastric surface A. Pair of gastric folds (Fig. 27: *gf*) running close along left-ventral inner gastric surface, flanking conjoined style sac-intestinal opening; anterior end of median fold tall, rounded; anterior end of lateral fold surrounding aperture of left dorsal projection; posterior ends of folds low, close to mid-gastric shield. Gastric shield (*gs*) on left posterodorsal inner surface; A ≈ 25% of inner gastric surface A. Style sac (*ss*) and *in* conjoined, separated by narrow, low pair of longitudinal folds running along anterior surface. Intestine (Fig. 25: *in*) diverging from *ss* abruptly, close to posteroventral foot, narrowly curving posteriorly, then dorsally, running between *pr* to umbonal cavity; there and close to origin of *rp* with relatively simple loop on right, abruptly curving ventrally and to right, flanking right wall of visceral mass; this portion performing wide loop almost as large as visceral mass, returning to umbonal cavity, passing at right of preceding loop, then passing through pericardium and between origins of *pr*. Rectum very narrow, running along midline on dorsal and posterior surfaces of *pm*. Anus (Figs. 18, 22–24: *an*) on posterior, slightly ventral surface of *pm*; edges thickened.

Nervous system (Figs. 18, 23–25): Nerve ring [formed of cerebropleural (*cg*) and pedal (*pg*) ganglia and connectives] surrounding anterior *es*, just posterior to *mo*, at midventral visceral mass surface. Pedal ganglia (*pg*) adjacent, forming posterior nerve ring, their connection to remaining ganglia with another pair of nerves, narrower one running ventrally, another very broad, running posteriorly to visceral ganglia (as connective). Visceral ganglia (Figs. 18, 23, 24: *vg*) narrow, between *pr* and *pm*, in L ≈ 3 W; visceral connective almost as thick as *vg*, in T ≈ 50% L, giving rise to pair of posterior nerves.

Material Examined

USA, Florida Keys, FMNH 302085, 1 specimen (sta. FK-504; dissected: 7.7 mm L, 3.7 mm H, 1.8 mm W).

Distribution

Stated by Turgeon et al. (2009) to range from Florida to Campeche Bank, Mexico, as well as the West Indies. It is not known from Brazil.

Remarks

The shell, foot, musculature, siphons, and gut of *Propeleda carpenteri* were briefly described by Allen & Sanders (1996). Our material differs in having the siphons incompletely fused, and fewer gill filaments (17); the small "anterior mantle sense organ" (Heath, 1937; Yonge, 1939; Allen & Sanders, 1996) was not observed. Data for this species, based on the present Florida Keys material, were employed in the comparative morphological study of Scaphopoda and protobranch bivalves by Simone (2009, as *P. carpentieri* [*sic*]).

Family Noetiidae
Stewart, 1930

Arcopsis adamsi
(Dall, 1886)
Figs. 28–45

Synonymy/Chresonymy

Arca adamsi Dall, 1886: 243 [credited to "Shuttleworth"; type locality: off Havana, Cuba, in 80 fms and *Blake* sta. 220, "near Santa Lucia," in 116 fms].

Arcopsis adamsi – Abbott, 1974: 425, fig. 4998; Oliver & Järnegren, 2004: 327 ff., figs. 1–35; Bieler & Mikkelsen, 2004: 516; Mikkelsen & Bieler, 2007: 58–59, 6 figs.; Rios, 1994: 232–233, pl. 80, fig. 1147; 2009: 476–477, fig.; Sharma et al., 2012: table 1.

Description

Shell (Figs. 28–34): Subrectangular, inflated, white to pale beige or pale brown; SL ≈ 15 mm in material examined ≈ 2 SH, typically SW > SH (Figs. 28–30). Periostracum hirsute, thin, more evident at margins (Fig. 31). Anterior and posterior margins of similar L or posterior end with low, blunt, ventral angle (Figs. 28, 29). Ventral margin horizontal to weakly concave. Dorsal margin (between umbones) horizontal along ca. 80% SL (e.g., Figs. 30, 33). Umbones central to weakly anterior, typically elevated ca. 25% SH beyond hinge plate. Cardinal area separating umbones at distance = 12% SW. Sculpture of subequal reticulated cords (Figs. 28) or with commarginal or radial cords slightly larger; interspace W = cord W; ca. 20–30 radial cords, increasing with SL, more widely spaced on posterior slope. Commarginal sculpture sometimes forming low scales or strong undulations. Ligament along hinge plate restricted to narrow space between valves, producing narrow brown lozenge covering cardinal

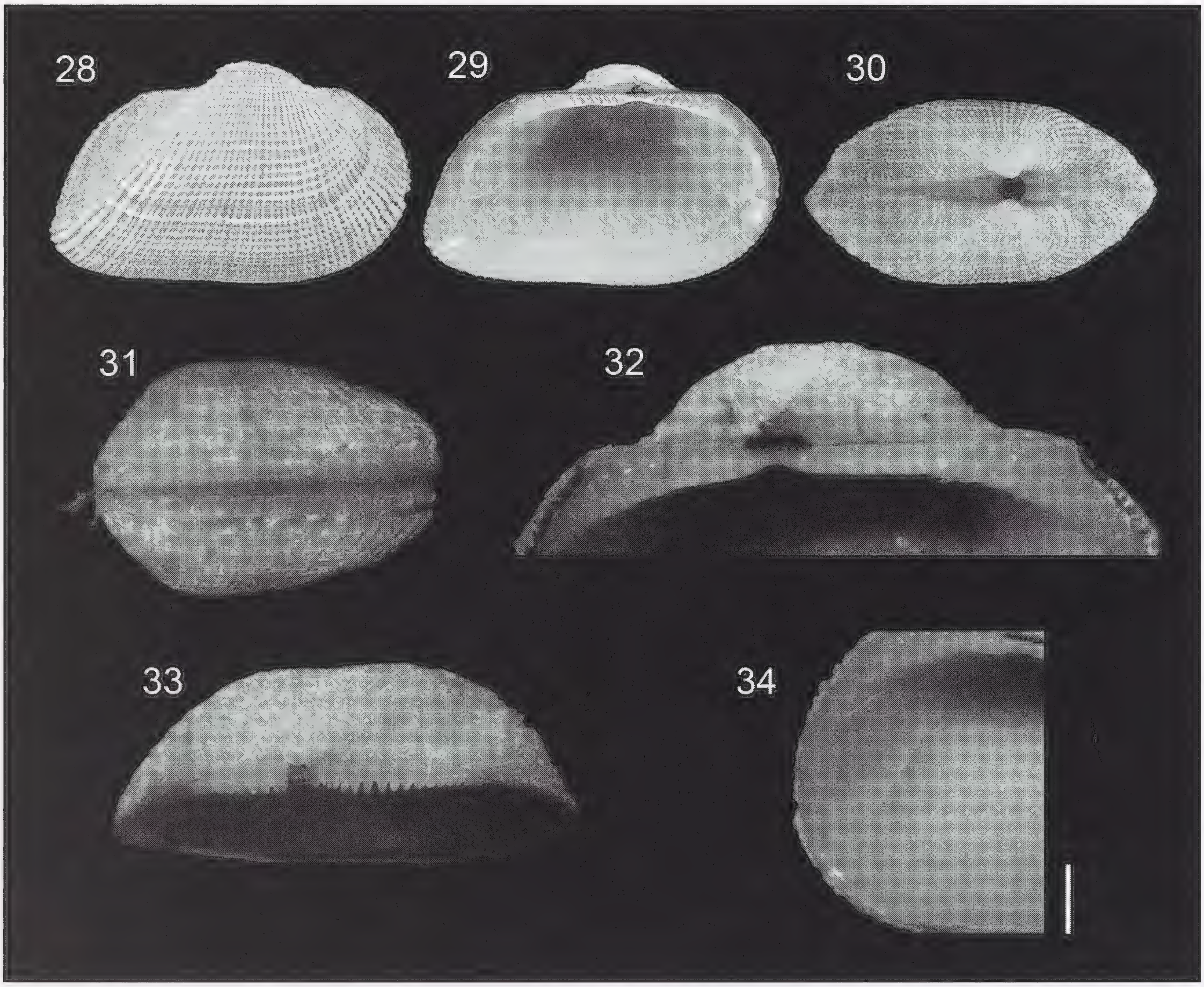

FIGS. 28–34. *Arcopsis adamsi*, shell morphology. FIGS. 28, 29. FMNH 94728, 12.3 mm L. FIG. 28: RV, exterior view; FIG. 29: LV, interior view; FIG. 30: FMNH 295591, 12.4 mm L, dorsal view. FIGS. 31, 32: MZSP 77946, 13.3 mm L. FIG. 31: Ventral view; FIG. 32: RV, detail of hinge region; FIG. 33: MZSP 36170, 13.4 mm L, RV, dorsal and lightly left view showing profile of hinge; FIG. 34: MZSP 28313, 11.9 mm L, RV, interior view, detail of anterior region showing elevated adductor scar. Scale bar = 1 mm.

area subumbonally (Figs. 30, 32, 33) at ca. 11% of hinge L. Hinge plate (Figs. 29, 32, 33) with 5–10 anterior and 9–17 posterior teeth, separated by smooth, narrower, subumbonal area in L ≈ 5% of hinge plate L. Hinge teeth oblique; anterior teeth slanting anterior to posterior, posterior teeth contrarily. Anterior and posterior tooth series each with larger teeth at center, decreasing in size at ends (Fig. 33). Inner surface glossy, white, non-nacreous. Muscle scars isomyarian (Fig. 29) or with posterior scar slightly larger; each scar A ≈ 10% of inner VA. Adductor scars in most cases on elevated platforms (Fig. 34), with edges projecting, sometimes barbed, including projections oriented toward umbonal cavities corresponding to previous muscle positions during ontogeny.

Main muscle system (Figs. 35, 36, 43, 44): Anterior adductor muscle (Figs. 35, 36, 43: *am*) elliptical, at mid-anterior shell margin and short distance posterior; A ≈ 33% SH ≈ 10% SL; with 2 differently colored ("catch" and "quick") portions, but without obvious division. Posterior adductor muscle (Figs. 35, 36, 43: *pm*) similar to *am* in form, in A = *pm* A, mid- to slightly dorsal to posterior margin, at short distance anterior to it; anterior third of *pm* differently colored than remainder (i.e., "catch" and "quick"). Anterior paired pedal protractor muscles (Figs. 36, 43: *rr*) narrow, originating widely but thinly at midventral edge of *am*, surrounding *am* ventral edge; running posteriorly, attaching to inner surface of integument; inserting splaying into anterior foot base. Paired anterior pedal retractor muscles (Figs.

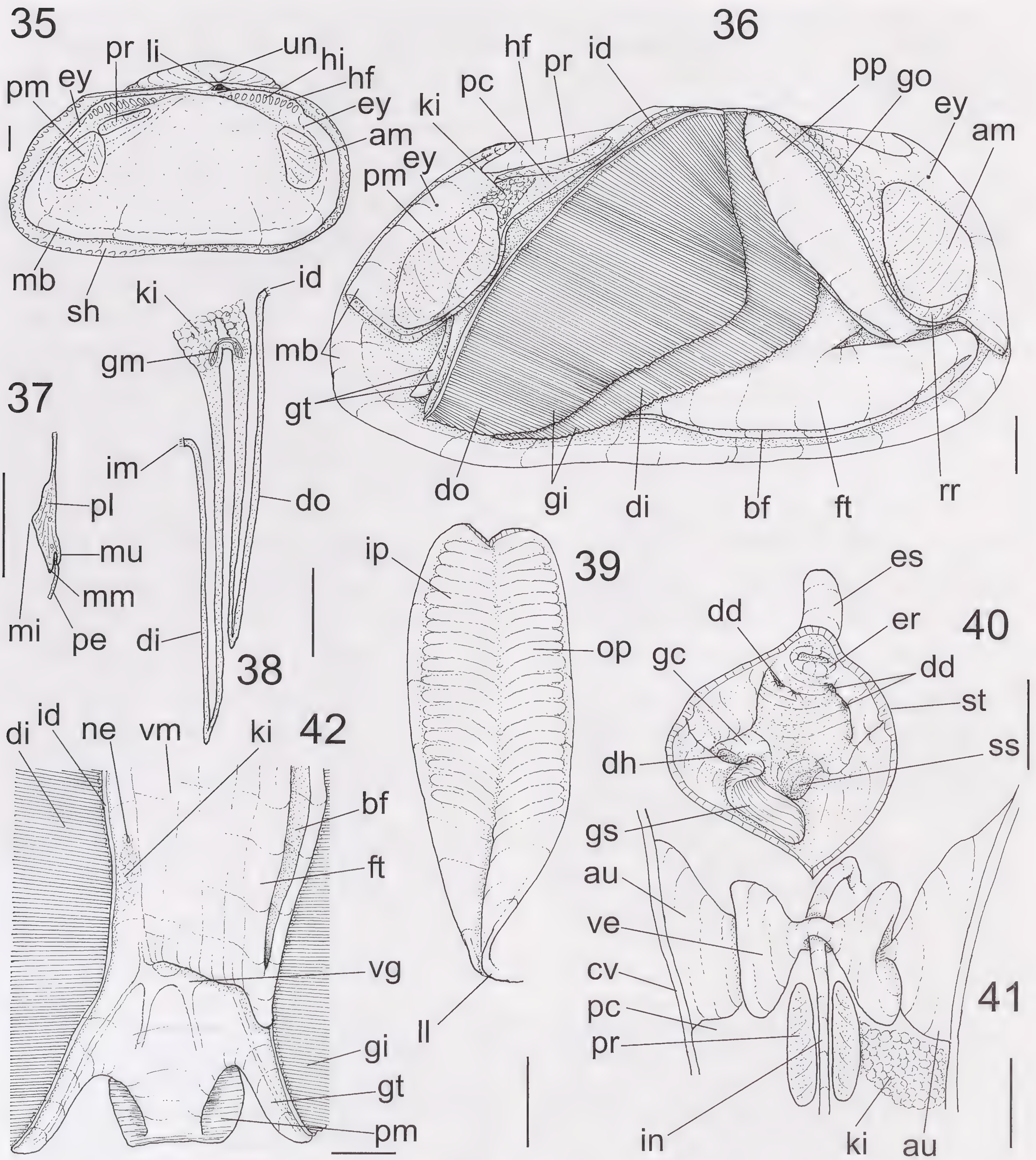

FIGS. 35–42. *Arcopsis adamsi*, anatomy. FIG. 35: Intact right view, RV removed; FIG. 36: Same, most of right mantle lobe removed, some visceral structures seen by transparency; FIG. 37: Mantle border, cross section at midregion of ventral edge; FIG. 38: Right gill, cross section at midregion; FIG. 39: Right labial palp, right view, outer hemipalp (op) deflected to show inner surface; FIG. 40: Stomach, opened by longitudinal cut of its dorsal wall, inner surface exposed, wall not shown; FIG. 41: Pericardial organs, dorsal view, topologies of some adjacent structures also shown; FIG. 42: Detail of posterior region, ventral and slightly right view, both gills deflected. Scale bars = 1 mm. Abbreviations: am, anterior adductor muscle; au, auricle; bf, byssal furrow; cv, ctenidial (efferent) vessel; dd, ducts to digestive diverticula; dh, dorsal hood; di, inner demibranch; do, outer demibranch; er, esophageal rim; es, esophagus; ey, pallial eye; ft, foot; gc, gastric central pad; gi, gill; gm, gill retractor muscle; go, gonad; gs, gastric shield; gt, gill suspensory stalk; hf, hinge fold of mantle; hi, hinge; id, insertion of outer demibranch in mantle; im, insertion of inner demibranch in visceral mass; in, intestine; ip, inner hemipalp; ki, kidney; li, ligament; ll, labial lips preceding mouth; mb, mantle border; mi, mantle border inner fold; mm, mantle border middle fold; mu, mantle border outer fold; ne, nephropore; op, outer hemipalp; pc, pericardium; pe, periostracum; pl, pallial muscle; pm, posterior adductor muscle; pp, labial palp; pr, posterior pedal retractor muscle; rr, pedal protractor muscle; sh, shell; ss, style sac; st, stomach; un, umbo; ve, ventricle; vg, visceral ganglia; vm, visceral mass.

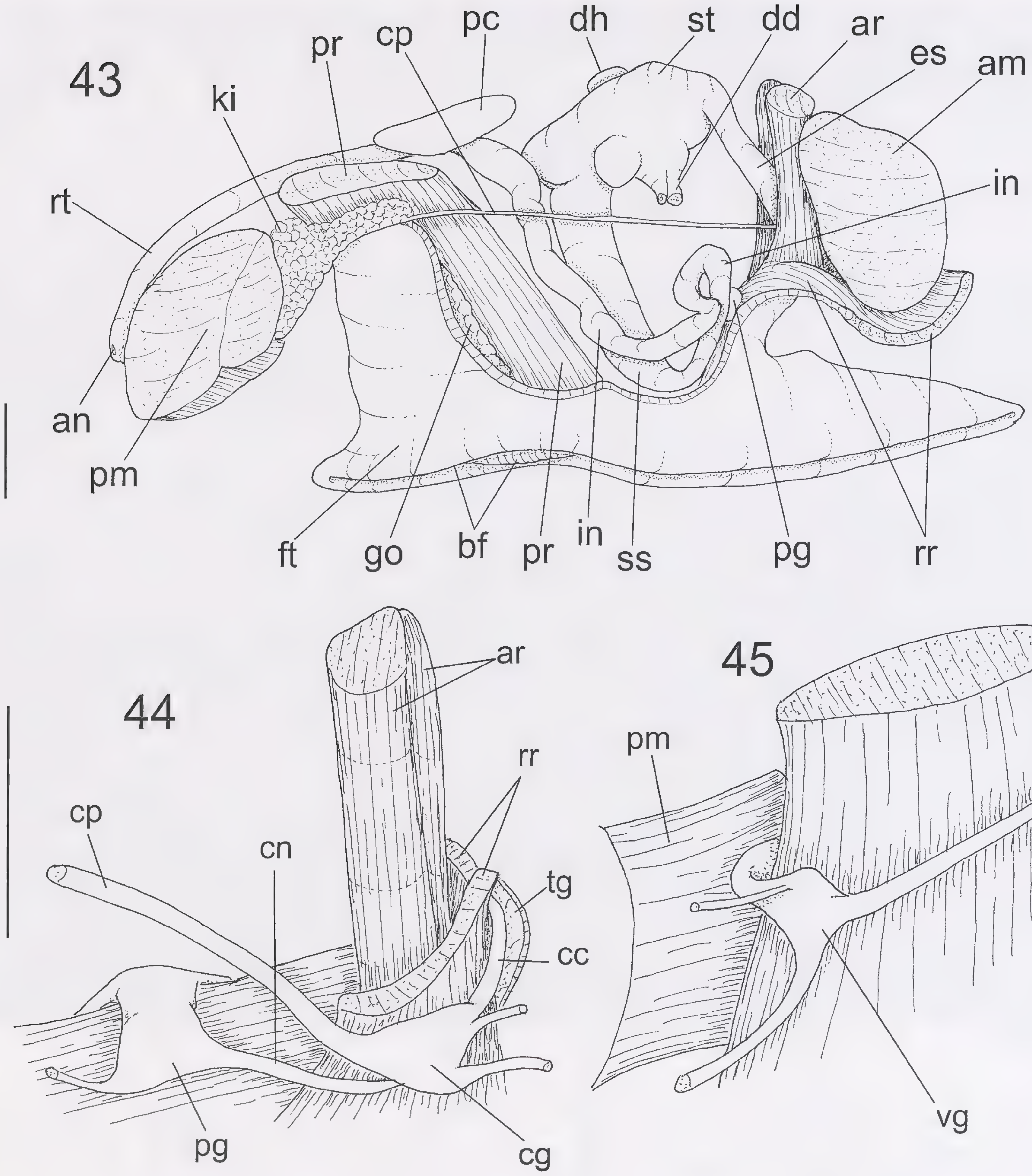

FIGS. 43–45. *Arcopsis adamsi*, anatomy. FIG. 43: Foot, main musculature, and digestive system shown *in situ*, right view, topologies of other structures (e.g., kidney, nervous system, and posterior lobe of gonad) also shown; FIG. 44: Region of cerebropleural (cg) and pedal (pe) ganglia, right and slightly dorsal view, adjacent muscles also shown; FIG. 45: Region of visceral ganglion (vg), right view. Scale bars = 1 mm. Abbreviations: am, anterior adductor muscle; an, anus; ar, anterior pedal retractor muscle; bf, byssal furrow; cc, cerebral commissure; cg, cerebropleural ganglion; cn, cerebropedal connective; cp, cerebrovisceral connective; dd, ducts to digestive diverticula; dh, dorsal hood; es, esophagus; ft, foot; go, gonad; in, intestine; ki, kidney; pc, pericardium; pg, pedal ganglion; pm, posterior adductor muscle; pr, posterior pedal retractor muscle; rr, pedal protractor muscle; rt, rectum; ss, style sac; st, stomach; tg, integument; vg, visceral ganglia.

43, 44: *ar*; obscured by umbonal organs in Fig. 36) thick, originating in small area just posterodorsal to *am*, running ventrally close to midline, inserting into anterior foot. Paired posterior pedal retractor muscles (Figs. 36, 43: *pr*) very large, thick, in V ≈ 33% of visceral mass V, originating in umbonal cavity just anterior to *pm*, extending anteriorly along *pm* L, running ventrally and anteriorly closely attached to *pm* (except in narrow dorsal area along midline), inserting along middle and posterior foot. Visceral wall of visceral cavity thickly muscular, serving as base for foot. Transverse visceral muscle narrow, slender, originating in integument just anterior to *pm*, running anteriorly through visceral glands, inserting into integument just posterior to midposterior edge of *am*. Paired gill muscles (Fig. 38: *gm*) running along ventral surface of ctenidial vein, between demibranchs.

Foot (Figs. 36, 43: *ft*): Broad, long. Byssal furrow (Fig. 43: *bf*) deep, broad, running along entire ventral surface to *ft* tip, becoming weakly broader midposteriorly. Byssus not observed, but *ft* with ca. 5 large, central, flattened, oblique convexities (similar to those in Arcidae), restricted to anterior half (posterior half smooth). Byssal furrow broader in living animal, used as crawling sole.

Mantle (Figs. 35–37): Pale cream-colored. Edge of each mantle lobe (Figs. 35, 36: *mb*) free except dorsally, thick, in most cases with 2 folds (Fig. 37); folds simple, lacking appendages. Outer fold thin, short. Middle fold thicker, taller than outer fold. Inner fold absent or marked by low T running at some distance from mantle edge. Remaining areas of mantle very thin, translucent. Siphons absent. Two pairs of pallial eyes (Figs. 35, 36: *ey*) on each side of the mantle edge hinge portion, located in midregion between junction of mantle lobes and adjacent adductor muscles. Each *ey* pair at same relative position anteriorly and posteriorly. Each *ey* minute, spherical, black; posterior pair duplicated in some specimens.

Pallial cavity (Figs. 36, 38, 39): Surrounding 75% of animal, except at narrow area anterior to *pm*. Labial palps (Fig. 36: *pp*) contouring anterior edge of pallial cavity, just posterior to *am*, surrounding anterior edges of gills. *Pp* dorsoventrally very long (L ≈ 4W); dorsal end rounded, otherwise of uniform W. *Pp* outer surfaces smooth, inner surfaces with similar special arrangement of folds on outer and inner hemipalps (Fig. 39); folds on dorsal half of each *pp* transverse, perpendicular to posterior *pp* edge, gradually becoming weakly oblique. *Pp* ventral connection (Fig. 39: *ll*) narrow. Inner smooth area contouring entire posterior edge of *pp* and entire ventral connection between *pp* (Fig. 39). Gill large, filibranch, with numerous, narrow, uniform filaments, with inner demibranch (*di*) conspicuously broader than outer (*do*); V ≈ 75% of pallial cavity V. Anterior two-thirds of gill L attached by tissue connections to visceral mass; outer basal edge of *do* and inner basal edge of *di* attached, respectively, to mantle and visceral mass, via cilia (Fig. 38: *id, im*). Posterior third of each gill attached dorsally to long, muscular, mobile suspensory stalk (Fig. 36: *gt*). *Gt* originating side-by-side from ventral surface of *pm*, relatively broad, tapering posterodistally, at which point outer basal edge of *do* and inner basal edge of *di* attach, respectively, to mantle and to counterpart, via cilia.

Visceral mass (Figs. 36, 43): Broad, thick, with posterior third entirely filled by *pr* and remainder filled by visceral organs. Gonad yellowish, mostly surrounding digestive system and diverticula, also filling space between *pr* and integument. Digestive diverticula brownish green, surrounding stomach, below umbonal cavity.

Circulatory and excretory systems (Figs. 36, 41–43): Pericardium (Fig. 41: *pc*) relatively small, just anterior to origin of *pr*, in umbonal cavity. Auricles (*au*) originating at mid-ctenidial vein, giving rise to short anterior and long (L = 50% of gill L) posterior portions of ctenidial vein. Each *au* connecting to expansion of ventricle (*ve*) (“ventricular pouches” of Heath, 1941) at midregion of broad outer surface, gradually tapering and inserting into *ve*. *Ve* narrow, surrounding intestine. Kidneys (Figs. 36, 43: *ki*) mostly solid, brown, along posterior half of inner edge of gill insertion in visceral mass, gradually broadening, crossing dorsal to gill in visceral mass. Nephrostomes (Fig. 42: *ne*) as small slits on anterior extremity of each *ki*.

Digestive system (Figs. 40, 43): *Pp* as described above. Mouth at anterior end of ventral connections between *pp*. Esophagus (Figs. 40, 43: *es*) running close to posterior surface of *am*, along almost entire L, relatively narrow, with smooth inner surface. Stomach (Figs. 40, 43: *st*) transverse at mid-visceral mass, dorsally roughly spherical and horizontal, abruptly curving ventrally, gradually narrowing, then continuing as style sac (*ss*). Gastric inner surface (Fig. 40) separated from *es* surface by narrow, low rim, surrounding entire *es* aperture. Broad, deep, concave sorting area immediately posterior to rim, bearing several uniform, transverse (anteroposterior) folds. Two pairs of ducts to digestive diverticula (Fig. 43: *dd*), each between sorting area folds, 2 on each side. Gastric central pad transverse on midventral surface, as posterior limit of previous sorting area; central pad with longitudinal (left to right), low, uniform folds, tall anterior and right borders; posterior border surrounding intestinal opening; broad fold at right edge of central pad, with right end appearing abruptly close to intestinal opening, left end penetrating dorsal hood (*dh*). Relatively deep furrow originating from aperture of *dh*, running dorsally along gastric surface, diminishing into right side of intestine (*in*). Paired typhlosoles inconspicuous. Gastric shield (*gs*) at midposterodorsal inner surface. *Dh* low, at mid- to left sides of gastric dorsal surface. *Dd* as described above. *In* narrow (Fig. 43), of uniform W, as continuation of *ss*, curving anteriorly, performing strong, short loop anteriorly at some distance from right surface of *ss*, then running posterodorsally, close to *ss*, to *pc*, turning horizontally though *ve* and narrowly between *pr*. Rectum exposed in excurrent chamber (although covered by integument), running over posterodorsal surface of *pm*. Anal papilla (Fig. 43: *an*) simple, rounded, on ventral *pm*.

Reproductive system: Gonad as described above, with aperture inside *ki*.

Nervous system (Figs. 42, 44, 45): Paired cerebropleural ganglia (Fig. 44: *cg*) between *ar* and posteroventral *am*; each subtriangular, in A ≈ 25% of *es* D; cerebral commissure (Fig. 44: *cc*) in L ≈ 2 single *cg* L. Paired pedal ganglia (Fig. 44: *pg*) adjacent on anteroventral surface of visceral mass, at base of anterior *rr*; each V = single *cg* V; pedal commissure L ≈ single *pg* W. Paired visceral ganglia (Figs. 42, 45: *vg*) at base of gill projections, adjacent, close to midline; each V = single *cg* V. Broad nerve running along gill projection axis. Abdominal sense organs not observed.

Material Examined

USA, Florida Keys, FMNH 295595, 11 specimens (sta. FK-037); FMNH 295591, 9 specimens (sta. FK-244); Pigeon Key, 24°42.2’N, 81°09.3’W, MZSP 36170, 4 specimens (1 dissected: 13.4 mm L); Key West, FMNH 94728, 2 specimens.

BRAZIL, Fernando de Noronha Archipelago, Porto beach, 03°50’05.1”S, 32°24’04.1”W, 1–2 m, MZSP 49070, 16 specimens (30/iv/2005; 1 dissected: 11.3 mm L). Ceará, Paracuru, Pedra Rachada beach, 3°23’58”S, 39°00’45”W, MZSP 36433, 3 specimens (date not recorded). Pernambuco, Cabo, Gaibu beach, 08°19’25”S, 34°57’03”W, MZSP 36064, 18 specimens (22/vii/2001). Bahia, Alcobaça, close to Recife da Escalada, 17°33’S, 39°06’W, 5–10 m, MZSP 34072, 16 specimens (vii/2001). Rio de Janeiro, Arraial do Cabo, Forno beach, 22°57’58.5”S, 42°00’41.2”W, 6 m, MZSP 49327, 4 specimens (IMP sta. 3, 18/iii/2005). São Paulo, Ubatuba, I.O. Base, MZSP 19724, 51 specimens (19/iv/1968; 3 dissected: #1: 16.6 mm L, 10.1 mm H, 9.8 mm W; #2: 14.6 mm L, 9.5 mm H, 9.5 mm W; #3 not measured); Ilha Bela, off Ilha das Cabras, 23°49’46.9”S, 45°23’21.4”W, 3 m, MZSP 77946, 30 specimens (12/v/1990; 2 dissected: #1: 13.3 mm L, 8.8 mm H, 8.7 mm W; #2 not measured); Alcatrazes Island, Porto dos Faroleiros, 24°06’S, 45°42’W, 5 m, MZSP 28313, 32 specimens (01/xii/1996; 2 dissected: #1: 11.9 mm L, 8.0 mm H, 7.4 mm W; #2 not measured).

Distribution

Stated by Turgeon et al. (2009) to range from North Carolina to Quintana Roo (Mexico), the Gulf of Mexico, West Indies and Caribbean to Brazil; also in Bermuda. Occurence to Santa Catarina, Brazil, is here confirmed.

Remarks

This description agrees in most respects with that presented by Heath (1941) for *Arcopsis adamsi* and *A. solida* (G. B. Sowerby I, 1833) from Florida and the Gulf of California, respectively. Abdominal sense organs, although reportedly present near the anus (Heath, 1941; Oliver & Järnegren, 2004: 334, as “each in the form of a simple dome”), were “unusually indistinct” (not detectable) in gross dissection. Small gland-like structures near the visceral ganglia were noted during this study but were not verified through histology as abdominal sense organs. Oliver & Järnegren (2004) studied Florida Keys populations of *A. adamsi* and noted abdominal sense organs and quick/catch portions of the anterior adductor muscle, neither of which were noticed here; all other features discerned from their gross dissections on living specimens agree with those presented here.

Oliver & Järnegren’s (2004) case study of *Arcopsis adamsi* in the Keys documented and discussed differences in shell sculpture, periostracum, and haemoglobin content between supratidal, sublittoral, and offshore specimens of this species. Our dissected material from the Spanish Harbor Keys (now Scout Key) is from their sublittoral sampling site. Sharma et al. (2012) studied nuclear protein-coding genes from the same Scout Key sample. The Brazilian material came from comparable sites and no substantive morphological differences between it and the Keys material was noticed. Atlantic-Panamanian material was included in a molecular study of geminate species pairs across the isthmus by Marko (2002), with a comparison to eastern Pacific *A. solida*.

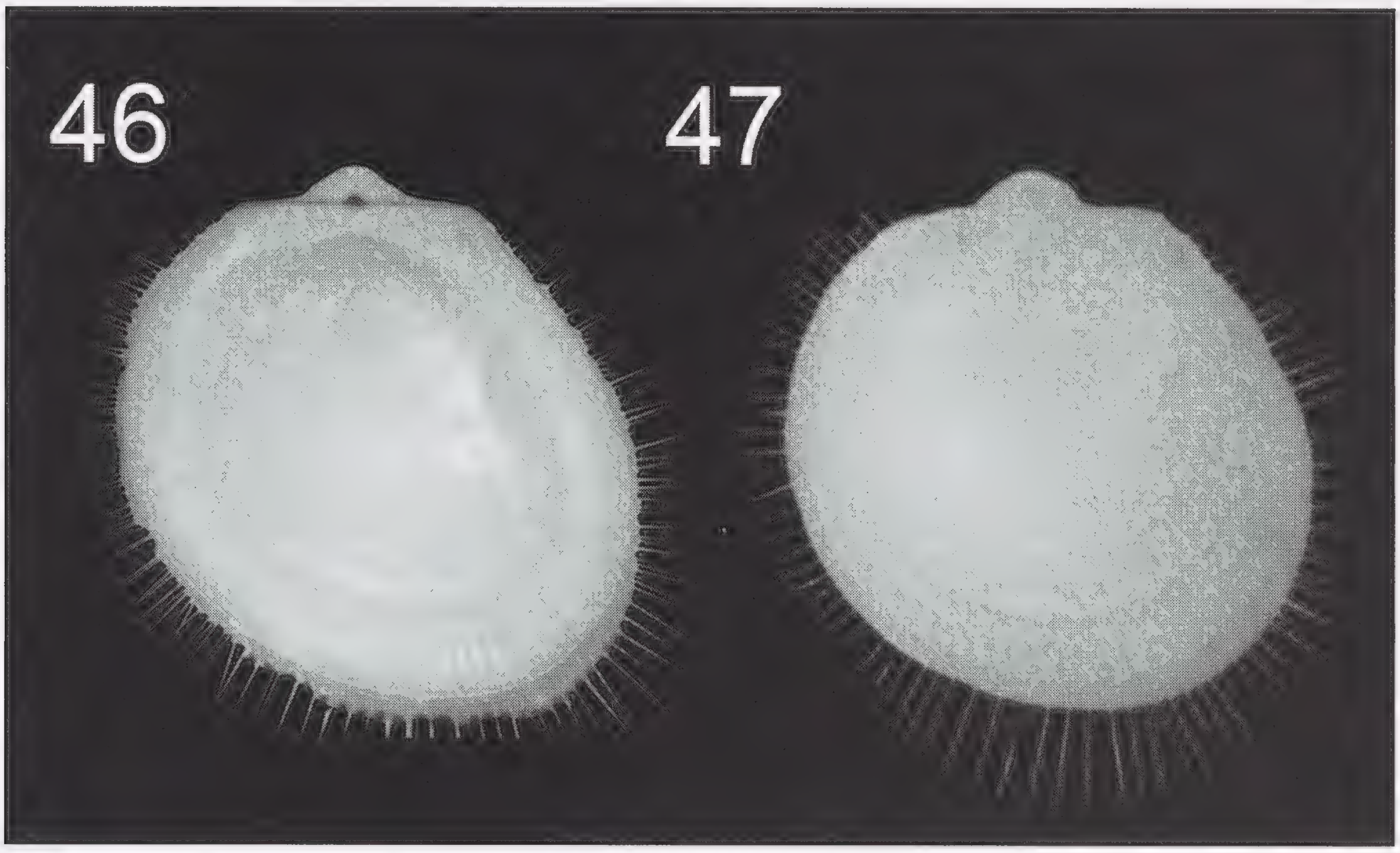

FIGS. 46, 47. *Limopsis* aff. *cristata,* shell morphology, FMNH 302084. FIG. 46: RV interior view, 5.2 mm H; FIG. 47: Intact left view, 4.0 mm H.

Family Limopsidae
Dall, 1895

Limopsis aff. *cristata*
Jeffreys, 1876
Figs. 46–54

Synonymy/Chresonymy

?*Limopsis cristata* Jeffreys, 1876: 434–435, 1879a, pl. 46, fig. 8 [from the Valorous Expedition, sta. 13, 690 fms, and several others off the coast of Ireland, from the Bay of Biscay, and the North Sea; type locality not designated according to Warén (1980: 42), but near-simultaneously given as "West of Ireland. Porcupine (1869), station 13, 1263 m" by Oliver & Allen (1980) who refer to "Type. *Limopsis cristata* Jeffreys 1876. Location: British Museum (Natural History)"].

?*Limopsis cristata* – Abbott, 1974: 425, fig. 5000; Oliver & Allen, 1980: 99–105, figs. 21–25; Oliver, 1981: 83.

Limopsis cristata – Bieler & Mikkelsen, 2004: 514; Mikkelsen & Bieler, 2007: 68–69, 6 figs.

Description

Shell (Figs. 46, 47): Circular (Fig. 47) to oblique (Fig. 46), pale cream-colored to beige; SL ≈ 5 mm in material examined ≈ SW ≈ 80% SH, SW = 60–70% SH. Periostracum beige, hirsute, velvet-like, with long, flexible, spine-like projections aligned with radial sculpture, extending beyond shell margins to 20–30% SH, entirely surrounding shell margin (except hinge area). Umbones central, rounded, weakly protruding, extending 5–7% SH dorsal to hinge plate; umbones separation W = 10% SW. Sculpture of 30–40 uniform radial ribs, slightly closer anteriorly; interspace W = 2–3 rib W; commarginal undulations and growth lines weakly developed. Ligament pale brown, narrowly along dorsal hinge margins, and short lozenge-shaped portion ventral to umbones, of median maximum L ≈ 10% of hinge plate L. Hinge plate horizontal, central on dorsal margin; L ≈ 40% SL. Hinge plate H = 5% (centrally) to 10% (laterally) SH. Hinge teeth oblique, 5–6 anterior and 6–7 posterior to umbo, increasing in size from umbo to ends. Inner surface glossy, white, translucent, non-nacreous; margin denticulate; muscle scars shallowly impressed. Scar of anterior adductor muscle (*am*) oval, just ventral to anterior end of hinge plate; L ≈ 15% SL (posterior of anterior border), A ≈ 3% VA. Scar of posterior adductor muscle (*pm*) elliptical, in A ≈ 5 *am* A, positioned more ventrally (ca. 40% SH ventral to hinge plate), separated from shell posterior margin by ca. 10% SL. Pallial line simple, located 15–20% SH away from margin.

Main muscle system (Figs. 48, 49, 52, 53): Adductor muscle positions and sizes as

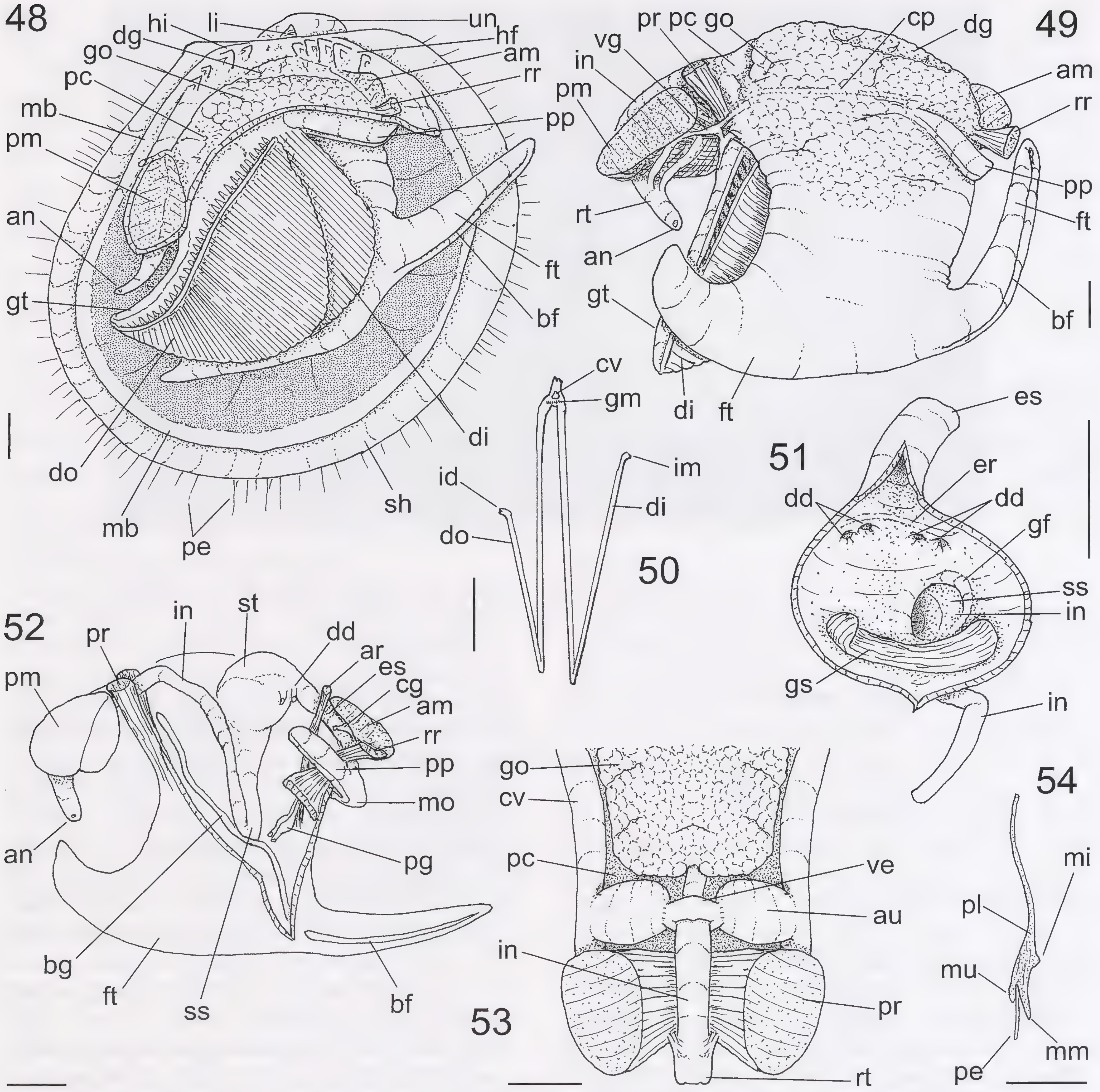

FIGS. 48–54. *Limopsis* aff. *cristata,* anatomy, FMNH 302084. FIG. 48: Intact right view, RV and part of right mantle lobe removed; FIG. 49: Same, mantle and right pallial structures mostly removed; FIG. 50: Gill, cross section through midregion; FIG. 51: Stomach, dorsal view, opened longitudinally, adjacent portion of intestine also shown; FIG. 52: Digestive system and main musculature *in situ*, right view, topologies of some adjacent structures also shown; FIG. 53: Visceral mass, dorsal view, detail of posterior region preceding posterior adductor muscle, dorsal layer of mantle and integument removed; FIG. 54: Mantle border, cross section at midlevel of ventral edge. Scale bars = 0.5 mm. Abbreviations: am, anterior adductor muscle; an, anus; ar, anterior pedal retractor muscle; au, auricle; bf, byssal furrow; bg, byssal gland; cg, cerebropleural ganglion; cp, cerebrovisceral connective; cv, ctenidial (efferent) vessel; dd, ducts to digestive diverticula; dg, digestive diverticula; di, inner demibranch; do, outer demibranch; er, esophageal rim; es, esophagus; ft, foot; gf, gastric fold; gm, gill retractor muscle; go, gonad; gs, gastric shield; gt, gill suspensory stalk; hf, hinge fold of mantle; hi, hinge; id, insertion of outer demibranch in mantle; im, insertion of inner demibranch in visceral mass; in, intestineli, ligament; mb, mantle border; mi, mantle border inner fold; mm, mantle border middle fold; mo, mouth; mu, mantle border outer fold; pc, pericardium; pe, periostracum; pg, pedal ganglion; pl, pallial muscle; pm, posterior adductor muscle; pp, labial palp; pr, posterior pedal retractor muscle; rr, pedal protractor muscle; rt, rectum; sh, shell; ss, style sac; st, stomach; un, umbo; ve, ventricle; vg, visceral ganglia.

described above. Posterior adductor muscle (Figs. 48, 49, 52: *pm*) clearly divided into 2 ("catch" and "quick") portions along dorsoventral line; posterior A ≈ 2 anterior A. Paired pedal protractor muscles (Figs. 48, 49, 52: *rr*) originating at posteroventral edge of anterior adductor muscle (*am*), in A = 6% of *am* A; running posteriorly immersed in integument, crossing anterior palp base, gradually becoming thinner and splaying across anterior foot base. Paired anterior pedal retractor muscles (Fig. 52: *ar*) originating just dorsal to *am*, in A = 5% of *am* A, running narrowly ventrally and slightly posterior along distance ≈ 50% SH, surrounding esophagus and anterior wall of visceral mass, inserting along anterior wall of foot base, internal to those of *rr*. Paired posterior pedal retractor muscles (Figs. 49, 52, 53: *pr*) A ≈ 3–4 *ar*, originating just dorsal to *pm*, running ventrally and slightly anterior along discance ≈ 50% SL, splaying across posterior foot base.

Foot (Figs. 48, 49, 52): A ≈ 25% VA, inverted T-shaped, with anterior "toe" 3–4 times longer than posterior "heel"; central portion of foot W ≈ 33% SL ≈ 80% SV. Byssal furrow (Figs. 48, 49, 52: *bf*) deep, running along entire ventral side of anterior "toe." Byssal gland (Fig. 52: *bg*) long, slender, narrow, of uniform W, L ≈ visceral mass L, originating at posterior end of *bf*, rounded distally, pale brown. Byssus not observed.

Mantle (Figs. 48, 54): Simple, white; edges of lobes totally free. Inner mantle edge (Fig. 54) low, slightly displaced internally; middle fold thin, T ≈ ST; outer fold similar to middle fold, but ca. 50% H.

Pallial cavity (Figs. 48, 49, 50, 52): A ≈ 70% VA, excepting dorsal, visceral, arched region. Labial palps (Figs. 48, 49, 52: *pp*) oblique, in anterodorsal quadrant of pallial cavity, L ≈ 4 H, totally attached to visceral mass on anterior edge; A ≈ 2% VA. Hemipalps symmetrical, weakly narrowing dorsally; dorsal end surrounding anterior end of inner demibranch, along ca. 20% of *pp* L. *Pp* inner surface entirely smooth, lacking visible folds. Connection between *pp* W ≈ ventral *pp* W, surrounding anterodorsal foot base. Gill (Figs. 48, 50: *di, do*) A ≈ 25% VA, semicircular, obliquely and centrally placed. Outer demibranch (*do*) W ≈ inner demibranch (*di*) W, but *do* L ≈ 85% of *di* L, ending at some distance from anterior end of *di*. Gill suspensory stalk (Figs. 48, 49: *gt*) L ≈ 50% of gill L, originating at midanterior side of *pm*, at junction with visceral mass. Gill filaments simple, lacking inner reinforcements, food grooves, and tissue connections with other filaments or with neighboring structures (Fig. 50). Almost entire posterior half of gill attached to counterpart via cilia, along *gt* (Figs. 48, 49).

Visceral mass (Figs. 49, 52): V ≈ 20% SV. Digestive system mostly central; V ≈ 16% of visceral mass V. Digestive diverticula pale greenish brown, anterodorsal; V ≈ 25% of inner visceral mass V. Gonad cream-colored, filling remaining inner visceral space and laterally around digestive diverticula. Byssal gland as described above.

Circulatory and excretory systems (Figs. 48, 49, 53): Renopericardial structures V ≈ 10% of visceral mass V, just anterior to insertion of paired *pr* (Figs. 48, 49, 53: *pc*), triangular; H ≈ 2 L. Auricles (*au*) simple, connecting to midlevel of ctenidial veins, almost vertical, running weakly laterally; each *au* V ≈ 33% of pericardial inner V. Ventricle (*ve*) central, short, connecting to *au* midlaterally. Kidneys very small, solid, white, in V ≈ 16% of pericardial V between posteroventral surface of pericardium and anterior surface of *pm*. Nephropores simple, small, at anterior ends of kidneys.

Digestive system (Figs. 48, 49, 51–53): *Pp* as described above. Esophagus (Figs. 51, 52: *es*) L ≈ 2 *am* L ≈ 25% of *am* W; midregion running in contact with *am*; inner surface smooth; rim simple, mostly ventral and lateral (Fig. 51: *er*). Stomach (Fig. 52: *st*) main chamber spherical, in subumbonal cavity, lacking any detectable projections. Two pairs of ducts to digestive diverticula (Fig. 52: *dd*) just ventral to *es* opening. Gastric inner surface (Fig. 51) mostly smooth, lacking detectable folds or glands; gastric fold (Fig. 51: *gf*) surrounding right side of conjoined style sac-intestinal opening, becoming typhlosoles near posterior end. Gastric shield (Fig. 51: *gs*) on posterodorsal surface; A ≈ 16% of inner gastric surface A. Style sac (*ss*) and intestine (*in*) totally fused; *ss* L ≈ 1.5 gastric main chamber L, tapering gradually ventrally; low typhlosoles internally separating it from intestine. *In* (Figs. 51–53) separating from *ss* at ventral end, performing abrupt 180° curve to run dorsally, arching gradually posteriorly, passing horizontally through pericardium and between insertions of *pr* (Fig. 53); *in* of uniform W (W slightly > 50% of *es* W). Anus (Figs. 48, 49, 52: *an*) preceded by long, siphon-like stalk, with pair of folds as reinforcements running along ventral side of *pm*.

Reproductive system (Figs. 48, 49, 53): Gonad (*go*) as described above; connection with kidney not observed.

Nervous system (Figs. 50, 51): Paired cerebropleural ganglia (Fig. 52: *cg*) at midlevel of posterior surface of *am*; each *cg* D ≈ 33% of *es* D, placed very laterally. Cerebral commissure slender, almost as long as *am* W. Paired pedal ganglia (Fig. 52: *pg*) elliptical, very adjacent, separated from *cg* by L = 50% of visceral mass-foot H; each *pg* V = single *cg* V. Paired visceral ganglia (Fig. 49: *vg*) oval, anterior to *pm*, each *vg* V ≈ 1.5 single *cg* V; visceral commissure L ≈ 50% of single *vg* L. Cerebrovisceral commissure relatively thick, running almost horizontally through gonad.

Material Examined

USA, Florida Keys, FMNH 302084, 2 specimens (sta. FK-503; dissected: #1: 5.0 mm L, 5.2 mm H; #2: 4.2 mm L, 4.0 mm H).

Distribution

Limopsis cristata was stated by Turgeon et al. (2009) to range from Massachussetts to the Dry Tortugas and off Texas in the Gulf of Mexico. The form here studied (see Remarks) is known so far only from comparatively shallow waters off Florida.

Remarks

Limopsis cristata belongs to the limopsiform functional group, "morphological class V" proposed by Oliver (1981). Features of this group include an adult byssus, a long anterior foot ("toe"), oblique shell form, unequal adductor muscles, and weak sculpture, with stiff periostracal spines (for anchoring), denticulate interior shell margins, a thick (muscular) gill suspensory stalk, and a separate byssal retractor element in the pedal retractor muscle. This species is endobyssate, producing multiple byssal threads and burrowing only shallowly according to Oliver & Allen (1980) and Oliver (1981). However, no attached epifauna were noted in the present material to confirm this.

Four subspecies of *Limopsis cristata* were distinguished by Oliver & Allen (1980), all from much deeper water ranges. None of these nominal subspecies (subsequently raised to specific level by Oliver, 1981) were recorded from the Florida Keys. The present material conforms most closely in shell shape and size to *L. intermedia* Oliver & Allen, 1980, which occurs off of Suriname, South America, in depths exceeding 1,400 m. However, it is closest to *L. lanceolata* Oliver & Allen, 1980, in periostracal appearance; that species is described from off of Angola, southwestern Africa, and depths beyond 1,000 m.

The anatomical description here differs substantially from that provided for *Limopsis cristata* by Oliver & Allen (1980) in the following: The mantle edge was described as thickened and folded posteriorly; this was not noticed in the present material. The outer demibranchs of the ctenidia have a dorsally reflected portion in adults; this was not seen here. The labial palps have 6–7 well-developed ridges; no ridges are present in Florida Keys specimens. The esophagus invariably has 4 internal ridges; no ridges are present here. It is possible that this material represents a heretofore undescribed species. No comparable material is known from Brazil.

Family Mytilidae Rafinesque, 1815

Brachidontes exustus (Linnaeus, 1758) species complex

Figs. 55–71

Synonymy/Chresonymy

Mytilus exustus Linnaeus, 1758: 705 [Type locality: Jamaica].

Brachidontes (Hormomya) exustus – Abbott, 1974: 429, fig. 5044, pl. 20, fig. 2044.

Brachidontes exustus – Bieler & Mikkelsen, 2004: 516; Lee & Ó Foighil, 2004: 3527 ff., figs.; Lee & Ó Foighil, 2005: 2139 ff., figs. 1–7; Mikkelsen & Bieler, 2007: 78–80, 5 figs.; Bennett et al., 2011: 63 ff., figs. 1–14.

Description

Shell (Figs. 55–58): Thin, mytiliform, often expanding dorsally, with umbones at extreme anterior end and fine divaricating radial ribs, yellow to dark brown; SL ≈ 11 mm in material examined. Periostracum not persistent. Interior thinly nacreous, with muscle scars barely evident; margin denticulate. Hinge at extreme anterior end, with 1–4 small teeth;

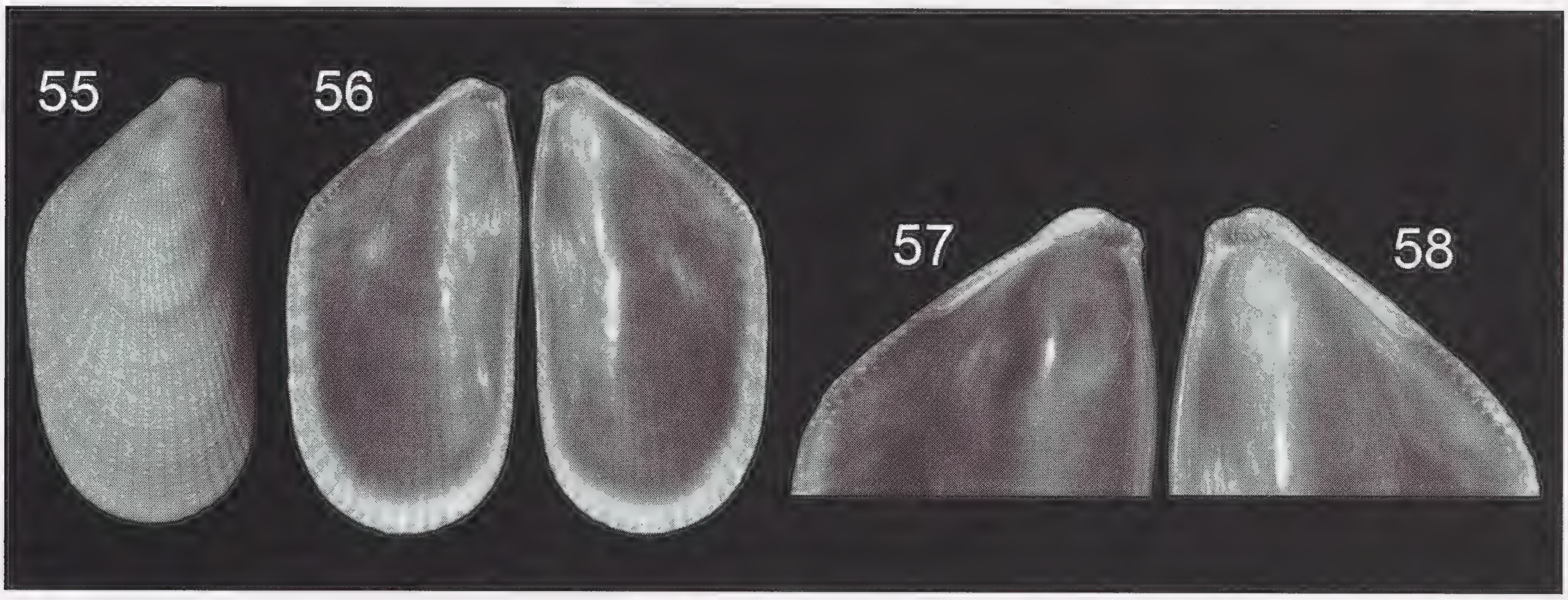

FIGS. 55–58. *Brachidontes exustus*, shell morphology, FMNH 295632, 11.3 mm L. FIG. 55: RV, exterior view; FIG. 56: Both valves, interior view; FIG. 57: LV, detail of hinge; FIG. 58: Same, RV.

ligament running along dorsal margin for ca. 50% SL; ca. 10 pairs of denticles along dorsal edge just posterior to ligament; denticle field L = ligament L.

Main muscle system (Figs. 59–61, 64, 67): Anterior adductor muscle (Figs. 59–61, 64: *am*) dorsoventrally compressed, thin, attaching to shell anteroventrally, close to shell margin; L ≈ 8 H = 10% SL, H ≈ 6% SH. Posterior adductor muscle (Figs. 59–62, 64, 67: *pm*) roughly circular in cross section, in A = 3% VA, in posterodorsal quadrant, close to shell margin. Paired anterior pedal retractor muscles (Figs. 59, 60: *ar*) very narrow, slender, originating on anterodorsal shell surface at level of umbo, in A = 10% of *pm* A, running posteriorly, attaching to integument, inserting into anterior foot base. Paired posterior pedal retractor muscles (Figs. 59–61, 67: *pr*) broad, thick, originating anterior of *pm*, in A ≈ *pm* A, L ≈ 1.5 *pm* L; running close anteroventrally, narrowing abruptly, inserting into posterior foot base. Accessory paired pallial muscles (Fig. 64: *ma*) narrow, thin, originating supraumbonally, running directly posteriorly, inserting in outer palp base.

Foot (Figs. 59, 61, 64: *ft*): Long, slender, stalk-like; V = 2 *pm* V. Byssal furrow (Fig. 61: *bf*) narrow, deep, running along ventral *ft* surface, from posterior end to near distal tip. *Ft* distal tip thicker than preceding areas, broadly pointed, with dorsal surface slightly planar, ventral surface abruptly ascending. Byssus (Fig. 61: *by*) of narrow, separated fibers, mostly originating at *bf* posterior end.

Mantle (Figs. 59, 60, 62): With 3 folds, free except for narrow separation (Figs. 59, 60, 62: *um*) between incurrent (*si*) and excurrent apertures (*se*). Outer and middle folds of mantle edge smooth, thin, simple; middle fold slightly thicker than outer fold. Periostracum produced between middle and outer folds. Inner fold broad, thick, at some distance from other folds, thicker posteriorly preceding *se*, bearing ca. 8 pairs of papillae (Fig. 62: *mp*); each papilla stubby, with rounded tip; interspace W = papilla W; papillae initiating at posteroventral quadrant, ending at mantle fusion. Mantle fusion separating *si* and *se* ("branchial septum" of Avelar & Narchi, 1984) broad, constituted only by inner fold; pair of flattened flaps on each side of fusion, originating on lateral surface, projecting inward, with rounded tips. *Se* simple, rounded (Fig. 62); A = *pm* A. Thick layer of pallial muscle fibers connecting mantle folds and pallial line of shell; another thin layer of sparse muscle fibers posteriorly, just posterior to thick portion of pallial muscles. Remaining mantle thin, translucent, except for portion presenting gonad (see below).

Pallial cavity (Figs. 59, 61, 63–65): V ≈ 66% SV, surrounding visceral region (anterior and dorsal). Labial palps (Figs. 61, 64: *pp*, 63) relatively small, long, sinuous, with pointed distal ends, smooth outer surfaces; inner surfaces possessing transverse, uniform folds successively increasing from distal end toward base, with smooth edge surrounding folds, ventral portion narrow; dorsal portion broader, almost as broad as folded area; inner hemipalps slightly smaller than outer hemipalps; inner folds abruptly ending at some distance from mouth. Gills (Figs. 59:

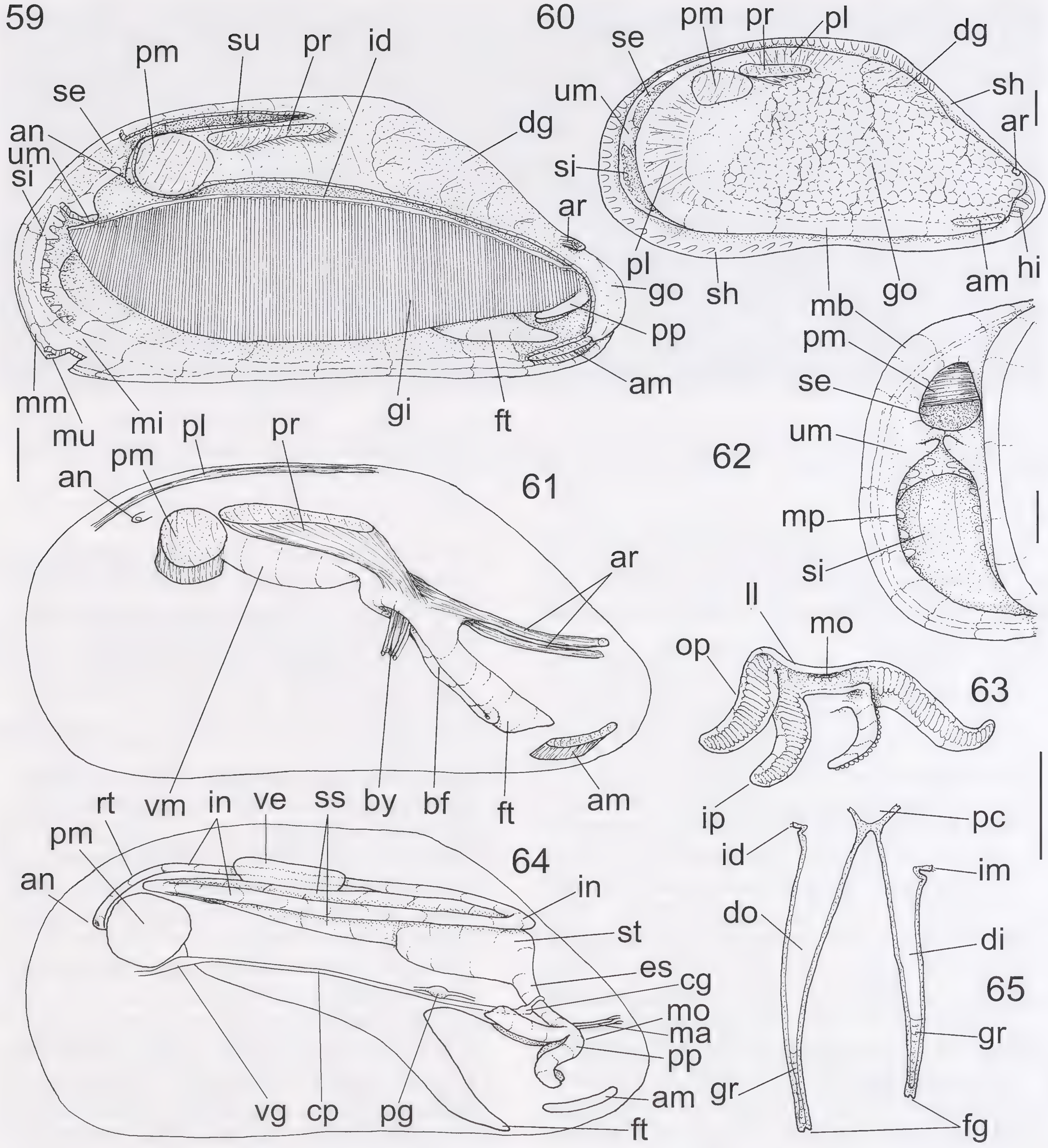

FIGS. 59–65. *Brachidontes exustus*, anatomy. FIG. 59. Intact animal, right view, shell and part of right mantle lobe extracted; FIG. 60: Same, only RV removed; FIG. 61: Main musculature and foot *in situ*, topologies of some adjacent structures also shown; FIG. 62: Posterior region, posterior to slightly right view, valves removed; FIG. 63: Detail of labial palps, anterior to slightly ventral view; FIG. 64: Digestive and nervous systems *in situ*, topologies of some adjacent structures also shown; FIG. 65: Right gill, cross section in midregion. Scale bars = 1 mm. Abbreviations: am, anterior adductor muscle; an, anus; ar, anterior pedal retractor muscle; bf, byssal furrow; by, byssus; cg, cerebropleural ganglion; cp, cerebrovisceral connective; dg, digestive diverticula; di, inner demibranch; do, outer demibranch; es, esophagus; fg, food groove; ft, foot; gi, gill; go, gonad; gr, gill transverse septum in suprabranchial chamber; hi, hinge; id, insertion of outer demibranch in mantle; im, insertion of inner demibranch in visceral mass; in, intestine; ip, inner hemipalp; ll, labial lips preceding mouth; ma, auxiliary pallial muscle; mb, mantle border; mi, mantle border inner fold; mm, mantle border middle fold; mo, mouth; mp, mantle papillae; mu, mantle border outer fold; op, outer hemipalp; pc, pericardium; pg, pedal ganglion; pl, pallial muscles; pm, posterior adductor muscle; pp, labial palp; pr, posterior pedal retractor muscle; rt, rectum; se, excurrent aperture; sh, shell; si, incurrent aperture; ss, style sac; st, stomach; su, supra-anal chamber of suprabranchial pallial cavity; um, fusion between left and right mantle lobes; ve, ventricle; vg, visceral ganglia; vm, visceral mass.

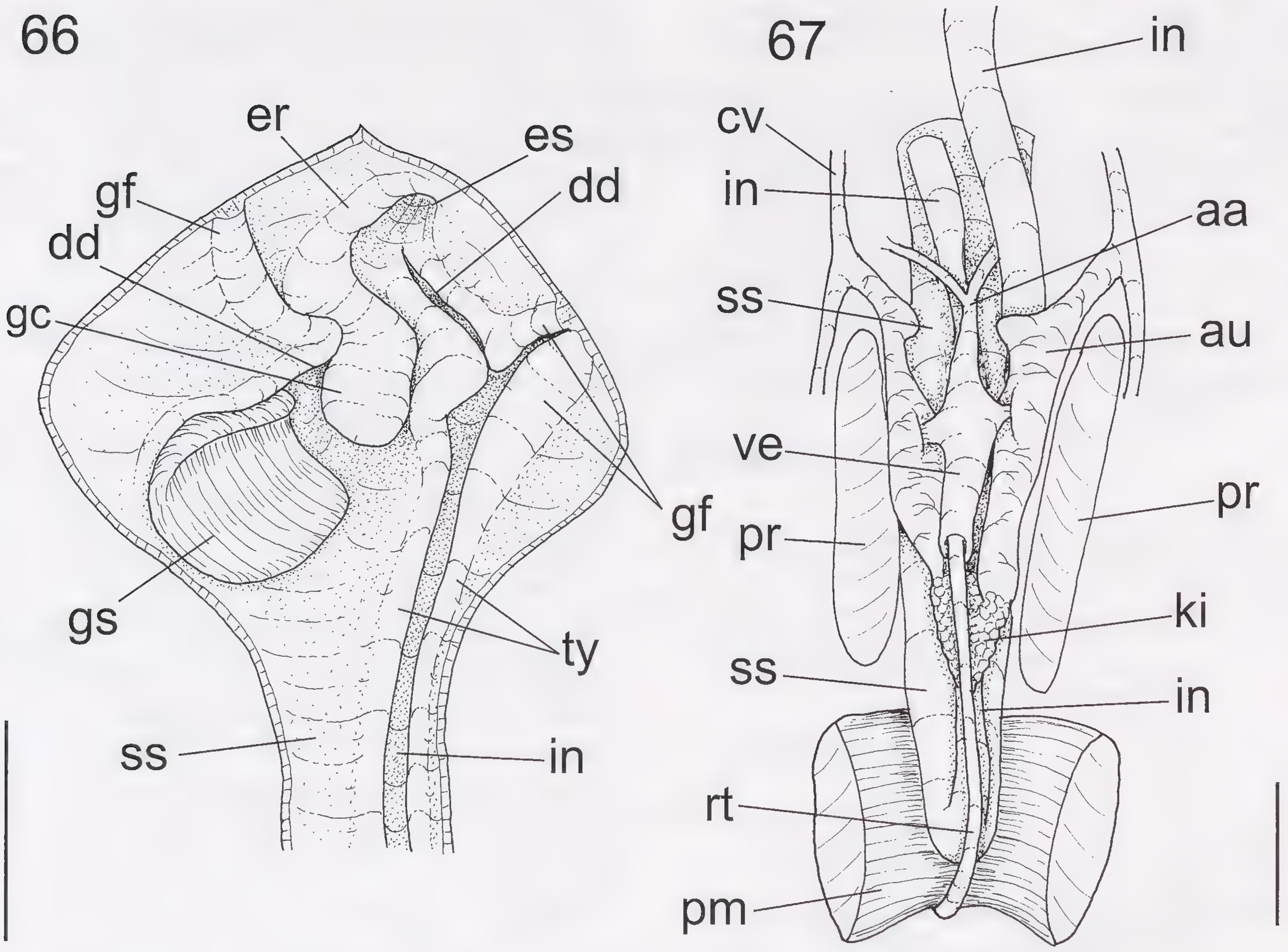

FIGS. 66, 67. *Brachidontes exustus*, anatomy. FIG. 66: Stomach, dorsal view, dorsal wall opened longitudinally, inner surface exposed; FIG. 67: Pericardial region, dorsal view, dorsal region of mantle and pericardium removed, some adjacent structures only partially shown. Scale bars = 1 mm. Abbreviations: aa, anterior aorta; au, auricle; cv, ctenidial (efferent) vessel; dd, ducts to digestive diverticula; er, esophageal rim; es, esophagus; gc, gastric central pad; gf, gastric fold; gs, gastric shield; in, intestine; ki, kidney; pm, posterior adductor muscle; pr, posterior pedal retractor muscle; rt, rectum; ss, style sac; ty, typhlosole; ve, ventricle.

gi, 65) with numerous, subequal, narrow, thin filaments; inner (*di*) and outer demibranchs (*do*) subequal, broader between middle and posterior thirds, gradually narrowing toward each end; anterior ends rounded; posterior ends broadly pointed. Outer edge of *do* and inner edge of *di* connected, respectively, to mantle and visceral mass, by cilia; ciliary edge preceded by strong fold; *di* connection more ventral than that of *do*. Each gill filament with connective membrane in ventral third of each demibranch. Food groove (Fig. 65: *fg*) shallow, on ventral edge of each demibranch. Posterior 20% of each gill suspended by weakly muscular, narrow stalks, originating on ventral surface of *pm*; stalks inserting between demibranchs, insertion of outer connection of *do* and inner connection of *di* in this posterior region, respectively, to mantle and to counterpart. Posterior gill separating functionally, but not anatomically, infrabranchial chamber from suprabranchial chamber, by union of mantle lobes.

Visceral mass (Figs. 60, 61, 64): Relatively reduced, anterodorsal; V ≈ 33% SV. Inner V compressed by muscles. Stomach (Fig. 64: *st*) central, posterior to umbones and running posteriorly, limited to dorsalmost SV, surrounded by beige digestive diverticula. Gonad (Fig. 60: *go*) filling remaining V, including portion between *pr*, bulging ventrally, extending into mantle, anterodorsal, encroaching ventrally to close to mantle border.

Circulatory and excretory systems (Figs. 64, 67): Pericardium (*pc*) dorsoventrally compressed between *pr*, posterior *st*, and mid-dorsal shell margin (Fig. 67); V ≈ 20% of visceral mass V. Auricles (Fig. 67: *au*) anteroposteriorly elongate, running parallel to inner edges of *pr*, connecting with midportion of anterior ends of ctenidial veins, surrounding anterior origin of *pr*. Ctenidial vein narrow, including at insertion with *au*; blood flow in both halves of ctenidial vein running toward *au* (thus flowing posteriorly in anterior ctenidial vein, anteriorly in posterior ctenidial vein). *Au*

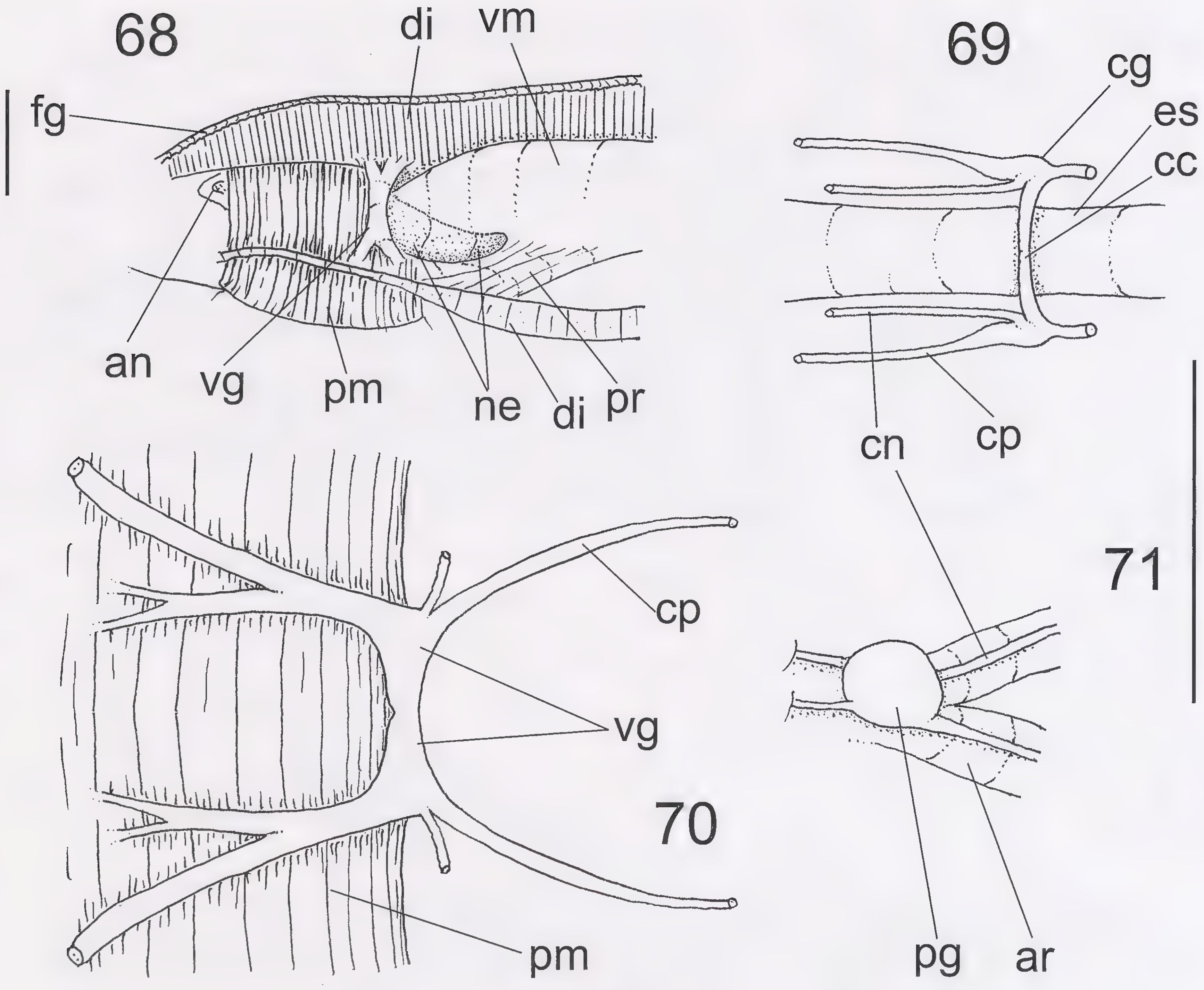

FIGS. 68–71. *Brachidontes exustus*, anatomy. FIG. 68. Visceral mass, ventral-slightly right view, detail of its posterior region, right gill deflected, left gill extracted; FIG. 69: Cerebropleural ganglia (cg) and adjacent esophagus (es), dorsal view; FIG. 70: Visceral ganglia (vg) and adjacent structures, ventral view; FIG. 71: Pedal ganglia (pe), ventral-slightly right view, some adjacent strucutures also shown. Scale bars = 1 mm. Abbreviations: an, anus; ar, anterior pedal retractor muscle; cc, cerebral commissure; cg, cerebropleural ganglion; cn, cerebropedal connective; cp, cerebrovisceral connective; di, inner demibranch; es, esophagus; fg, food groove; ne, nephropore; pg, pedal ganglion; pm, posterior adductor muscle; pr, posterior pedal retractor muscle; vg, visceral ganglia; vm, visceral mass.

connections with mid-ventricle, posterior to bulging median portions. Ventricle (Figs. 64, 67: *ve*) relatively small, surrounding intestine as it traverses *pc*; *ve* connection with *au* narrow, midlateral. Anterior aorta dorsal, branching close to origin; posterior aorta ventral, very narrow. Kidneys (Fig. 67: *ki*) very small (V ≈ 12% of pericardial V), whitish, solid, at posterior end of *pc* between posterior ends of *au* and at posterior origin of *pr*. Nephropores widely open; aperture A = 70% of *pm* L, L ≈ 2 W, located just anterior to *pm*.

Digestive system (Figs. 64, 66, 68): *Pp* as described above. Anterior and posterior lips of mouth (Fig. 64: *mo*) relatively tall, thin, with smooth inner surfaces. Esophagus (Figs. 64, 66: *es*) broad, in L = *pm* L, running far posteriorly from *am* and umbones; inserting into *st* anteroventrally; inner surface smooth. Stomach (Figs. 64, 66) V ≈ 33% of visceral mass V, running anteroposteriorly, broader anteriorly, gradually narrowing posteriorly, with bulging anterior portion. Gastric inner surface (Fig. 66) with broad, transverse *es* rim, restricted to dorsal surface, with right end fading, left end connecting to central pad. Central pad low, elliptical, longer anteroposteriorly; anterior end fusing with *es* rim, remaining edges rounded. Ventral surface of *es* opening bearing pair of broad, relatively tall folds, beginning just anterior to *es* rim level; left fold surrounding right edge of central pad, becoming broader, narrowing within short distance beyond posterior level of central pad, running into conjoined style sac-intestine as left typhlosole; right fold running parallel to left fold to broader region, abruptly twisting perpendicularly toward right, crossing dorsal gastric wall transversely, then on left gastric side abruptly twisting perpendicularly at level between *es* rim and central pad, running posteriorly, surrounding left edge of gastric shield. Ducts to digestive diverticula in 3–4 pairs between anterior portions of ventral folds just anterior to *es* opening, and between left edge of central pad and perpendicular twist of dorsal transverse fold. Digestive diverticula location as described above. Gastric shield A ≈ 20% of gastric inner A, on posterodorsal and slightly left surface. Right typhlosole beginning abruptly and broadly in divergence between ventral folds anterior to *es* rim, running posteriorly parallel and close to left typhlosole, becoming gradually narrower. Conjoined style sac-intestine (Figs. 64, 66: *ss, in*) originating as posterior gastric continuation, lacking obvious separation with *st*. *Ss* separated internally from *in* by pair of typhlosoles, running along ventral and slightly right surface of *ss*; each running posteriorly, passing through origins of *pr*, ventral to *pc*, reaching dorsal surface of *pm*, posterior to *ki* (Figs. 64, 67). At this posterior level, both typhlosoles fading; *in* abruptly twisting ca. 180°, running anteriorly along right dorsal surface of *ss* to anterior *st*. At this level, *in* making wide curve surrounding anterodorsal *st*, running posteriorly, initially on left side of *st*, gradually closer to midline, becoming very narrow close to *pc*, beyond *pc* on dorsal surface of *ss*, then on posterodorsal surface of *pm*. Anus (Figs. 64, 68: *an*) simple, sessile, on posteroventral *pm*, at some distance from *se*.

Reproductive system: No difference in color found between males and females in preserved material (although frequently noted in living specimens in family). *Go* distinct in encroaching mantle, expanding as thin flaps immersed in mantle beyond normal position inside visceral mass, reaching close to mantle edge in mature specimens.

Nervous system (Figs. 68–71): Cerebropleural ganglia (Fig. 69: *cg*) at mid-level between *mo* and *st*, one on each side of *es*; each ganglion small (A ≈ 12% of *es* D), elliptical. Cerebral commissure (Fig. 69: *cc*) long (L = es W); W ≈ 3 single *cg* W. Pair of connectives and a single anterior nerve running posteriorly from each *cg*. Paired pedal ganglia (Fig. 71: *pg*) forming single spherical mass at mid-level between *mo* and *ft* base; *pg* mass V ≈ 5 single *cg* V; 2 pairs of pedal connectives, one on each side, each inserting ventrally into *pg* mass. Paired visceral ganglia (Figs. 68, 70: *vg*) located just anterior to *pm*; each triangular, in W ≈ 2 L, V ≈ 5 single *cg* V; pedal and cerebrovisceral connectives inserting anterolaterally (Fig. 70); pedal connective W ≈ 50% of cerebrovisceral connective W; thick pair of posterior nerves attaching to *pm*, bifurcating after distance = single *vg* W. Abdominal sense organs not observed.

Material Examined

USA, Florida Keys, FMNH 295632, 40+ specimens (sta. FK-028; 2 dissected: #1: 11.3 mm L, 5.7 mm H, 4.5 mm W; #2: 10.3 mm L, 5.2 mm H, 4.8 mm W).

Distribution

Stated by Turgeon et al. (2009) to range from North Carolina to the Gulf of Mexico, Cuba, and West Indies to Uruguay. It apparently does not occur in Brazil (see Remarks).

Remarks

The anatomy of *Brachidontes exustus* agrees in most major aspects with that of *B. solisianus* (d'Orbigny, 1846) from Brazil as described by Avelar & Narchi (1984). However, two major differences were recorded: (1) the posterior pedal retractor muscle in the present species appears as a single muscle mass, whereas that of *B. solisianus* is comprised of four distinct, closely adjacent muscles; and (2) a "multilobate appendix" opening into the posterolateral wall of the stomach of *B. solisianus* was not observed in *B. exustus*.

Molecular analyses using nuclear and mitochondrial genes have recognized that the morphospecies *Brachidontes exustus* is a species complex containing at least five molecular taxonomic units, with each of these having been assigned informal names based on core geographic distribution: Antilles, Atlantic, Bahamas, Gulf and western Caribbean (Lee & Ó Foighil, 2005). All except the western Caribbean of these unnamed cryptic species are known to occur in the Florida Keys (Lee & Ó Foighil, 2004), often with two species micro-sympatric at a given site. Species-level distinction of these by morphology alone has not yet been achieved. A study of *Brachidontes* specimens from different wave exposures in the Florida Keys (Bennett & Willan, 2003) concluded that the observed morphological differences were the result of phenotypic plasticity, but the study was conducted before the presence of multiple cryptic species in the region was known and the observed morphological variation might well be a combination of genotypic constraints and phenotypic plasticity. A recent study by Bennett et al. (2011) has taken a closer look, by DNA barcoding, at specimens from seawall and mangrove substrata on Long Key and found them to belong to the Antillean and Gulf clades, respectively. The specimens in the present study were collected in *Caulerpa* (green algae) on mangrove roots in Lake Surprise, a brackish (salinity ca. 24 ppt), landlocked tidal lake in Key Largo. This population was not analysed by any of the above three studies.

The species *Brachidontes muelleri* (Dunker, 1875), described from Desterro, Santa Catarina, southern Brazil, has been considered as a synonym of *B. exustus* (e.g., Rios, 1994: 236; 2009: 482; often misspelled "*mulleri*"). In a parallel study on Brazilian mytilids, no specimens with similar morphological characters to Floridian specimens were found; therefore, *B. muelleri* is here removed from the *B. exustus* synonymy. An ongoing study of "*B. exustus*" from Ilha do Mel, Paraná state, Brazil, using cytochrome c oxidase subunit I (COI) sequences (Wadleigh et al., 2012), suggests that a sixth species be recognized in the species complex; it is unclear whether this material is equivalent to so-called *B. muelleri*.

Family Isognomonidae
Woodring, 1925 [1828]

Isognomon alatus
(Gmelin, 1791)
Figs. 72–82

Synonymy/Chresonymy

Ostrea alata Gmelin, 1791: 3339 [Type locality: Oceano americano = American Ocean].

Isognomon alatus – Abbott, 1974: 441, pl. 20, fig. 5124; Domaneschi & Martins, 2002: 621–624, fig. 9C; Bieler & Mikkelsen, 2004: 514; Tëmkin, 2006: 262, figs. 1A, 8A, 9B, 13A, 14A, 17C; Mikkelsen & Bieler, 2007: 98–99, 5 figs.; Wilk & Bieler, 2009: 1 ff., figs. 1–10.

Description

Shell (Figs. 72, 73): Quadrangular to oval, greenish pale brown or beige, with radial, narrow, irregular, dark brown spots, more evident close to margins; SL ≈ 20–60 mm in material examined, typically SW = SL, SW ≈ 0.1 SL (greatly compressed). Byssal notch narrow, in RV. Sculpture of series of low, thin, narrow, undulated, commarginal scales; generally irregularly lamellate close to shell margin; scales typically arranged in radial rows. Inner surface smooth; nacreous A = 66% VA, close to hinge, iridescent whitish-

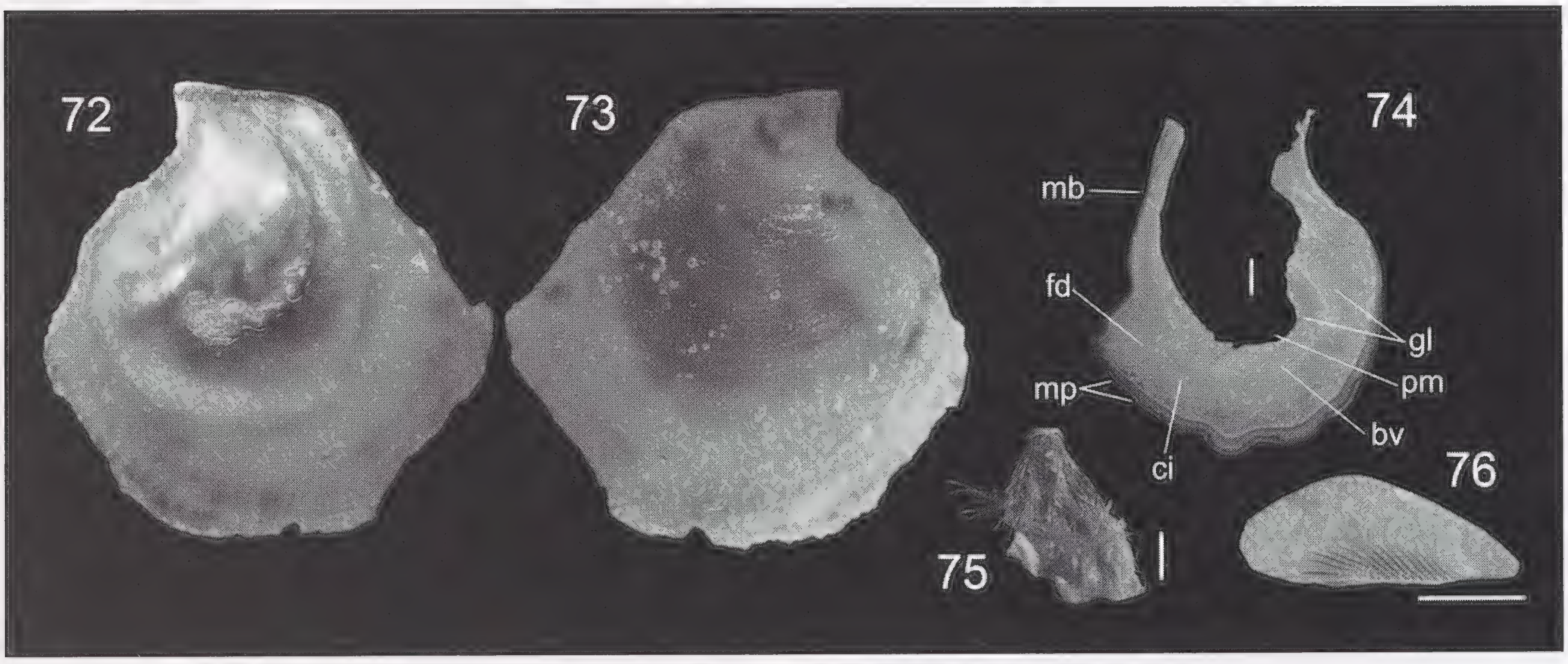

FIGS. 72–76. *Isognomon alatus*. FIGS. 72, 73: Shell morphology, RV, FMNH 295559, 64.4 mm L. FIG. 72: Interior view; FIG. 73: Outer view. FIGS. 74–76: Anatomy. FIG. 74: Left mantle lobe, interior view; FIG. 75: Byssus, right view, its base in foot also shown; FIG. 76: Posterior pedal retractor muscle, cross section along its midregion, note dark spots corresponding to byssal gland. Scale bars = 5 mm. Abbreviations: bv, "blood" vessel; ci, ciliary connection of gill; fd, fold; gl, glands; mb, mantle border; mp, mantle papillae; pm, posterior adductor muscle.

violet; remaining third along shell margin opaque, translucent, of same color as outer shell surface. Umbones low, terminal. Hinge line almost horizontal; ligament internal, with 6–8 resilia set in resilifers; each resilifer of regular L, of irregular W and disposition, more closely spaced anteriorly. Hinge plate with small subequal teeth near umbones, more evident in juveniles. Muscle scar in central nacreous portion, shallow, elliptical, in V ≈ 12% of inner VA; 66% of scar closest to hinge area comprising posterior pedal retractor muscle (*pr*); remaining third narrowly crescent-shaped, comprising posterior adductor muscle (*pm*). Scars of anterior pedal retractor muscles (*ar*) small, circular, in A ≈ 5% of *pm* A, close to hinge plate, between middle and posterior thirds.

Main muscle system (Fig. 77): Anterior adductor muscle absent. *Pm* central, crescent-shaped, with thicker anteroventral end, rounded, posterodorsal end tapering to point; W ≈ 50% SW, H ≈ 20% SH. Paired *ar* narrow, originating close to hinge plate, between middle and posterior thirds, running posteriorly close to ventral integument of visceral mass, inserting along anterior foot base. Paired anterior auxiliary pedal retractor muscles (*ap*) short, very narrow, in L ≈ 20% of *ar* L, originating in umbonal cavity at distance = that between origin of *ar* and hinge plate; running posteromedially, inserting partly in middle of *ar*, partly in adjacent foot base. Paired *pr* acting as byssal retractors, very thick, broad, originating in wide, elliptical area just anterior to *pm*, closer to ventral end, in L ≈ 50% of *pm* L, running anteroventrally, narrowing abruptly, inserting on middle and posterior foot base, just dorsal to byssal furrow.

Foot (Figs. 75–77): Small, appendix-like, slender, narrowing gradually, with distal end broadly pointed; typically pigmented by dark brown, irregular, coalescent spots. Byssal furrow (Fig. 77: *bf*) deep, running along ventral surface and midline, unpigmented, very wide posteriorly, surrounding byssus; very shallow furrow also running along dorsal surface, diminishing close to foot base. Byssus (Figs. 75, 77: *by*) broad, thick, consisting of greenish-iridescent flattened strips connecting soon after exiting foot; dorsal to this, separating and organizing in uniform arrangement of 10–12 pairs of long strips, inserting along *pr*, close to their internal surface (Figs. 76, 77). Hollow, flattened chamber between strips immersing in *pr*; W = strip W (Fig. 76).

Mantle (Figs. 74, 77, 79): Mantle border dark brown, paler near edge; outer fold thin, short, simple, weakly pigmented (Fig. 79). Periostracum attaching to inner surface of outer fold. Middle fold weakly taller and thicker than outer fold, with series of long, slender papillae (Figs. 74, 79: *mp*) mostly inserting subterminally along inner surface; distal papillar tips sharply pointed; interspace W = 3 W. Inner fold T and H each ≈ 2 middle fold H; edge with series of papillae, inserting terminally, with remaining characters similar to those of middle fold. Inner mantle fold forming pallial veil. Papillae of middle and inner folds longer in posteroventral half, gradually decreasing dorsally to mantle lobe fusion at hinge area. Low, narrow, transverse fold (Figs. 74, 77: *fd*) at distal end of gill between dorsal and posterior regions; broad ciliary strip running anteriorly from fold, surrounding mantle border. Pallial muscles narrow, thin, radiating from border to near *pm*. Two pairs of pallial glands (Fig. 74: *gl*) orange, visible as thickened mantle; one pair anterior, broad, W ≈ distance between *pm* and mantle edge; second pair narrow, surrounding *pm* and short distance beyond, with well-developed vessel (Fig. 74: *bv*) surrounding outer edge.

Pallial cavity (Figs. 74, 77, 80, 82): A ≈ 66% VA, totally surrounding visceral mass except dorsally adjacent to hinge; very narrow in this region; laterally compressed. Labial palps (Figs. 77: *pp*, 80) L ≈ 16% of gill L, W ≈ 50% of gill W; each hemipalp elliptical. Anterior ends of demibranchs inserting into short portion between posterodorsal ends of hemipalps (Fig. 80). *Pp* posterior ends taller, with low projections; posterior edge weakly concave, preceded by short smooth inner region, then as series of low, narrow folds perpendicular to dorsal border (Fig. 80); each fold with rounded ventral end, located near *pp* ventral edge, with narrow smooth inner border; dorsal ends of folds diminishing into dorsal furrow. Folds covering ca. 75% of *pp* L, diminishing subtly into remaining anterior region, with smooth inner surface preceding mouth, with thick walls (Fig. 80: *ll*), apparently glandular, yellowish, friable. Latter thicker region gradually decreasing preceding mouth. Gills (Fig. 77: *gi*) narrow; L ≈ 1.5 visceral mass L. Short anterior base connecting to visceral mass for distance ≈ 25% of gill L, remaining free, sustained by very long, muscular suspensory stalk (Fig. 77: *gt*). Gills dark brown in distal third.

77

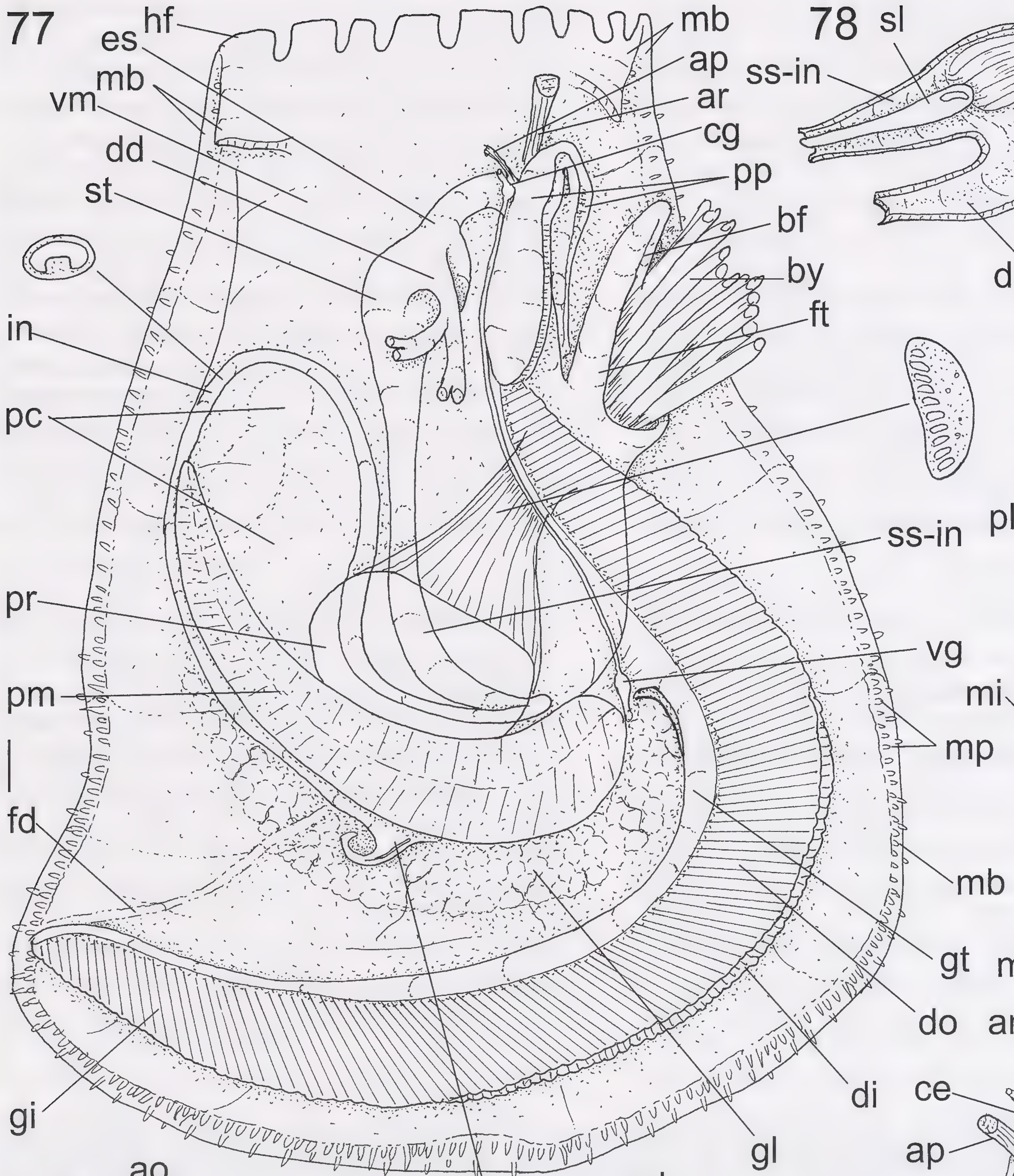

78

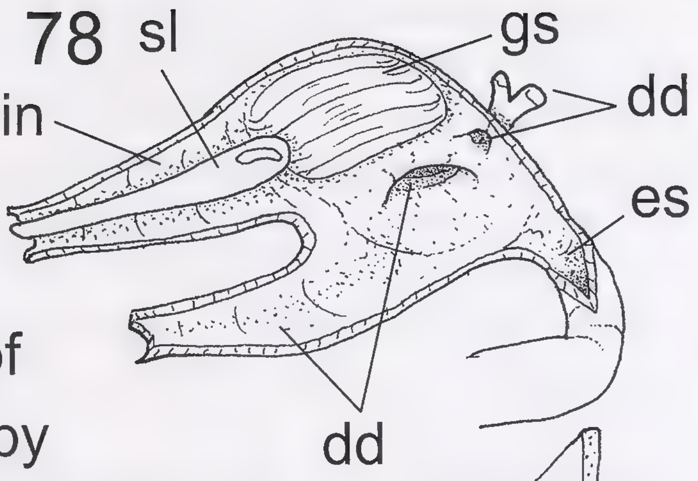

79

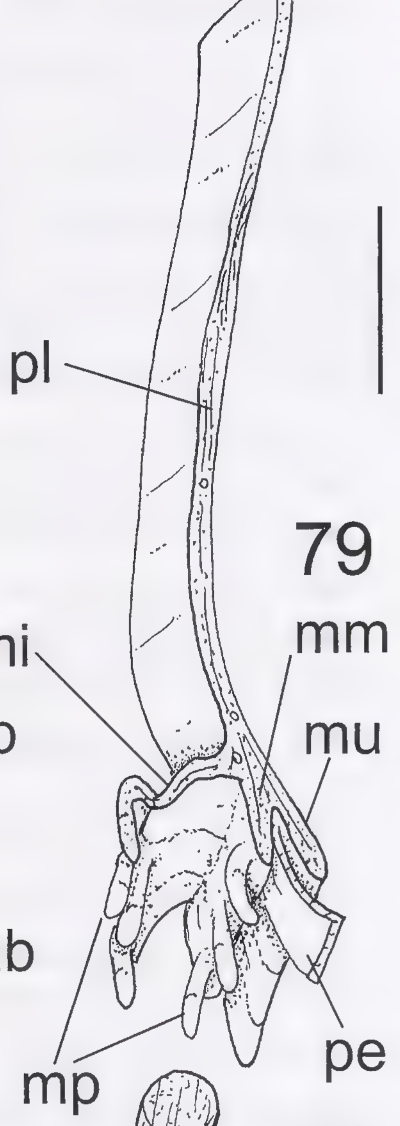

80

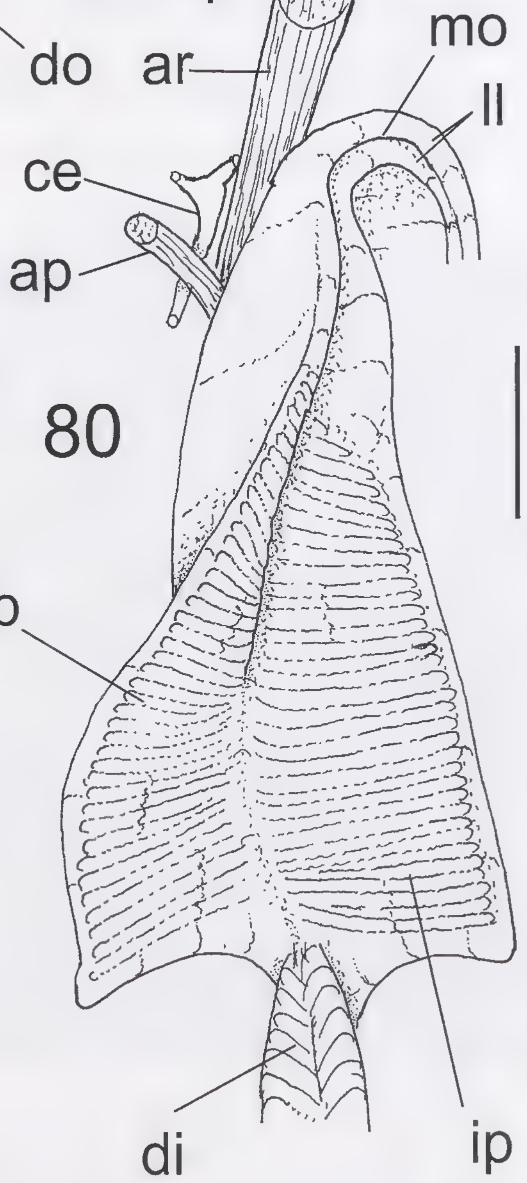

81

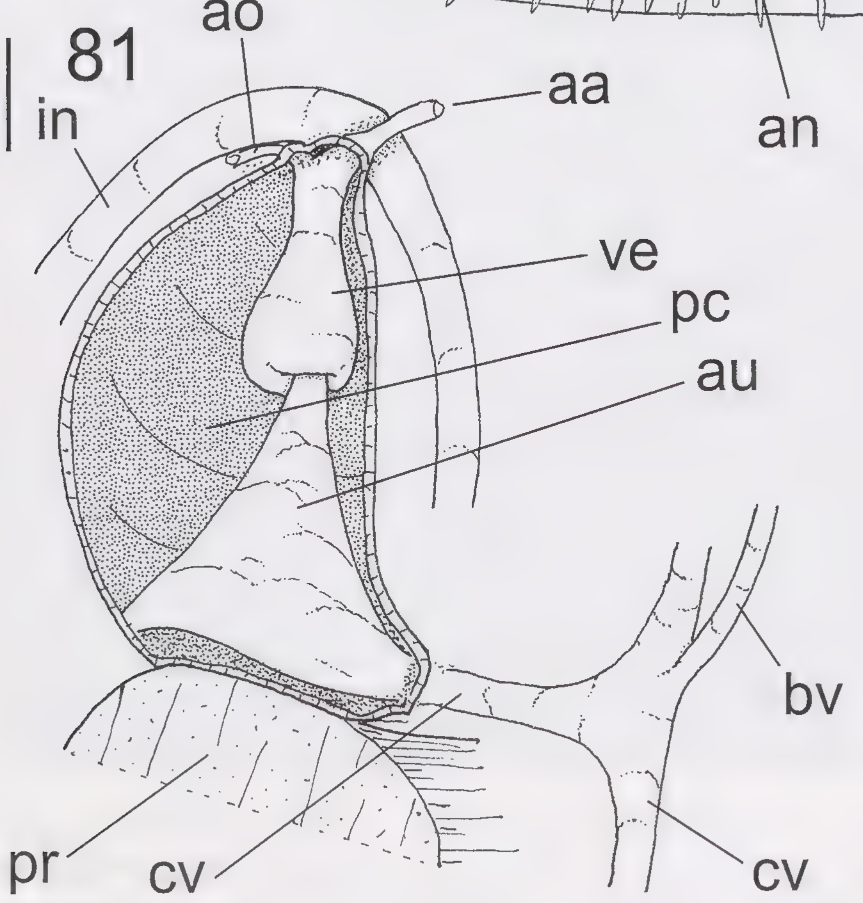

82

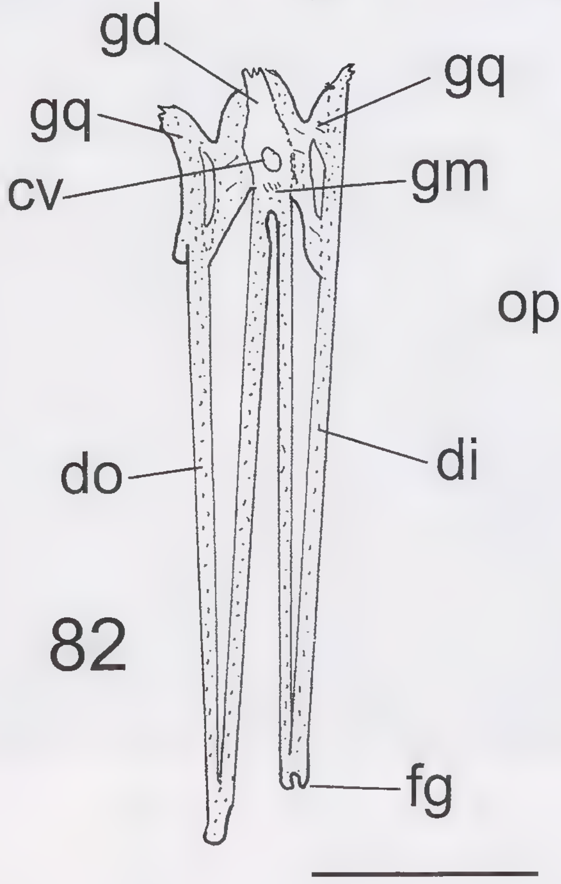

Demibranchs subequal (Figs. 77, 80: *do, di*). Food grooves (Fig. 82: *fg*) shallow, along ventral edge of each *di*. Each gill filament very narrow, connecting to neighboring filaments by regular ciliary bridges. Transverse septum (Fig. 82: *gq*) every 8–10 filaments, restricted to dorsal demibranch; each pair of septa connecting to *gt*, with short portion protruding dorsally, opposing connection to free portion of gill filament only at one dorsal and one ventral point; septa W ≈ 20% of gill W, wider and taller toward anterior. *Do* connecting to mantle; *di* connecting to visceral mass anteriorly or to counterpart by cilia (Fig. 74: *ci*) along relatively wide bands.

Visceral mass (Figs. 77, 81): Restricted to space between hinge area and *pm*, laterally compressed, mostly filled by yellowish gonad. Digestive diverticula surrounding stomach midanteriorly, of same color as gonad; V ≈ 25% of visceral mass V. Posteroventrally greatly compressed by paired *pr*, with portion passing between them, bulging posterior to foot base. Pericardium (*pc*) posterodorsal, just anterior to dorsal half of *pm*, attaching directly to posterodorsal half of *pm*; V ≈ 20% of visceral mass V.

Circulatory and excretory systems (Fig. 81): Pericardium (*pc*) as described above. Paired connections between ctenidial vein and auricles (*au*) narrow, long, surrounding anterior edge of *pr*, inserting into *au* at posterolateral ends. Narrow pallial vessel inserting just anterior and external to connection of *au* and ctenidial vein, coming from anterior mantle. Paired *au* totally fused externally, internally bearing several irregular transverse septa, apparently separating *au* lumens, each with subtriangular, posterior region, wide, curving (with ventral concavity), abruptly narrowing to ventricle connection. Ventricle (*ve*) small, anterior to *au*, internally with few transverse, irregular septa, connecting to *au* apparently with common aperture, protected by low internal, thin-walled, bicuspid valve, surrounding intestine, with main part dorsal. Common aorta very short, anterior to *ve*, contacting intestinal portion crossing anterior end of *pc*; anterior aorta (*aa*) running dorsally at right of this portion of intestine; posterior aorta (*ao*) W ≈ 4 times narrower than *aa* W, running posteriorly, ventral to intestine. Kidneys inconspicuous, very small, surrounding anteroventral insertions of *pr*.

Digestive system (Figs. 77, 78, 81): *Pp* as described above. Lips tall, thinner than preceding posterior regions. Esophagus (Figs. 77, 78: *es*) broad, short, curving posterodorsally; L ≈ 33% of *pp* L. Stomach (Fig. 77: *st*) oval; gastric chamber only slightly shorter and wider than *pp*. Large duct to digestive diverticula on right-anterior side, curving posteroventrally; inner gastric surface with longitudinal, broad folds; similar, slightly smaller duct on opposing (left) side, usually with another small duct just anterior to it. Gastric inner surface mostly smooth (Fig. 78). Gastric shield (Fig. 78: *gs*) thin, in anterodorsal gastric chamber. Conjoined style sac-intestine (Figs. 77, 78: *ss-in*) weakly separated by pair of very low,

←

FIGS. 77–82. *Isognomon alatus*, anatomy. FIG. 77: Intact right view, RV and most of right mantle lobe removed, digestive system shown *in situ* as though visceral mass is transparent; cross sections of indicated levels of intestine (in) and posterior pedal retractor muscle (pr) also shown; FIG. 78: Stomach, right view, mostly opened longitudinally, including style sac (*ss-in*) and one duct to the digestive diverticula (dd); FIG. 79: Mantle border, section at midlevel of ventral region; FIG. 80: Right labial palp and some adjacent structures, right and slightly ventral view, outer hemipalp (op) deflected; FIG. 81: Pericardial region, right view, right region of pericardium removed; FIG. 82: Gill, cross section at midregion. Scale bars = 2 mm. Abbreviations: aa, anterior aorta; an, anus; ao, posterior aorta; ap, auxiliary pedal retractor muscle; ar, anterior pedal retractor muscle; au, auricle; bf, byssal furrow; bv, "blood" vessel; by, byssus; ce, cerebral ganglion; cv, ctenidial (efferent) vessel; dd, ducts to digestive diverticula; di, inner demibranch; do, outer demibranch; es, esophagus; fd, fold; fg, food groove; ft, foot; gd, gill suspensory rod; gi, gill; gl, gland; gm, gill retractor muscle; gq, gill transverse reinforcement in suprabranchial chamber; gs, gastric shield; gt, gill suspensory stalk; hf, hinge fold of mantle; in, intestine; ip, inner hemipalp; ll, labial lips preceding mouth; mb, mantle border; mi, mantle border inner fold; mm, mantle border middle fold; mo, mouth; mp, mantle papillae; mu, mantle border outer fold; op, outer hemipalp; pc, pericardium; pe, periostracum; pl, pallial muscle(s); pm, posterior adductor muscle; pp, labial palp; pr, posterior pedal retractor muscle; sl, crystalline style; ss-in, conjoined style sac-intestine; st, stomach; ve, ventricle; vg, visceral ganglia; vm, visceral mass.

longitudinal folds, running posteriorly, forming wide curve ventrally to ventral end of *pm*. Intestine (Fig. 77: *in*) becoming free from *ss* posteroventrally, abruptly curving almost 360°, running initially left of distal *ss*, then surrounding posterior surface of *pm*, posterior surface of *pc*, performing wide, sigmoid loop. *In* running posteriorly after crossing dorsal surface of *pc* (Fig. 81), exiting to dorsal pallial cavity, running along midline attaching to posterior surface of *pm*; inner surface mostly smooth, except for broad, tall typhlosole, in W ≈ 25% of intestinal W, running along entire L, on face of *pm*; typhlosole narrower at mid-*in*, wider in region running in pallial cavity; ending abruptly close to anus. Anus (Fig. 77: *an*) broad, with long, posterior anal papilla projecting from dorsal edge; anal papilla with flattened, sharply pointed distal end.

Nervous system (Fig. 77): Paired cerebropleural ganglia (*cg*) small, in lateral region just posterior to mouth, close to *ap*. Cerebropleural commissure long, slender, crossing anterior to *es* opening. Pedal ganglia not observed. Visceral ganglia (*vg*) V ≈ 3 *cg* V, at ventral end on surface of *pm*, just anterior to *gt* origin; ganglia adjacent, close to midline; connective with *cg* running along ventral surface of visceral mass, contacting integument and foot base. Abdominal sense organs not observed.

Material Examined

USA, Florida Keys, FMNH 295559, 4 specimens (sta. FK-223; 3 dissected: #1: 64.4 mm L, 65.0 mm H, 9.0 mm W; #2: 59.0 mm L, 67.0 mm H, 10.7 mm W; #3: 21.0 mm L, 22.5 mm H, 4.4 mm W); FMNH 311673–311687, 230 specimens (sta. FK-760); FMNH 311812–311813, 2 specimens (sta. FK-786); FMNH 311814–311815, 2 specimens (sta. FK-787). The material of Domaneschi & Martins (2002: 621) from Florida and the Caribbean was also examined.

Distribution

Stated by Turgeon et al. (2009) to range from Florida to Campeche Bank, northern South America to Brazil, the West Indies and Bermuda. *Isognomon alatus* has been reported from the Brazilian coast (Rios, 1994: 241). However, although specimens and further data about this record were intensely searched, no confirmation was obtained. Because the single species of the genus confirmed on the Brazilian coast is the invasive *I. bicolor* (C. B. Adams, 1845), the Brazilian reports have been removed from the synonymy herein as most probably refering to *I. bicolor*; Domaneschi & Martins (2002) also could not confirm previous records of *I. alatus* or *I. radiatus* (Anton, 1838).

Remarks

Shell morphology of *Isognomon alatus* was investigated by Domaneschi & Martins (2002) specifically for comparison with Brazilian specimens of *I. bicolor*; specimens from Florida, including several populations in the Florida Keys, were used in that study. The anatomy of *I. alatus* presented here agrees in most respects with that of the much more elongated species *I. isognomon* (Linnaeus,1758) figured (but not extensively discussed) by Yonge (1968: fig. 8). The most complete earlier anatomical investigation was by Pelseneer (1911) for *I. perna* (Linnaeus, 1767) and *I. isognomum* (Linnaeus, 1758). The latter study, despite its very brief description, included figures of the gross anatomy, with details of the musculature, gills, labial palps, and digestive tract, which agree with the observations presented here. The one exception is the relationship to the heart and intestine, described by Pelseneer (1911) and Yonge (1968) with the intestine passing through the heart. Specimens studied here could be interpreted as such, but the main portion of the ventricle is ventral to the intestine, with weak, smaller portions of the ventricle passing up and around the intestine. The same condition occurs in members of the genus *Crassostrea* (Ostreidae; L. Simone, unpubl. data), which is traditionally described as the intestine not passing through the heart. The sharply pointed distal end of the intestine was called “triangular anal funnel” by Tëmkin (2006: fig. 17C).

Various aspects of the biology of *Isognomon alatus* have been studied. Wilk & Bieler (2009) explored the ecophenotypic variation of this species across a tidal microhabitat gradient, based on specimens from Ramrod Key that were also included in the present study. Material from the same location was analysed in the morphological study by Tëmkin (2006), and specimens from the same and/or other Lower Florida Keys locations were used in the molecular analyses by Campbell et al. (1998) and Ó Foighil & Taylor (2000). Chromosome karyotypes of this species were studied by Wada (1978), based on specimens from Biscayne Bay, Florida (just north of the Florida Keys), and by Rodríguez et al. (1983) based on material from Veracruz, Mexico (with a diploid [2n] number = 28). Veracruz specimens were also used in the study of chromosomal rearrangements (meiotic behavior) of *I. alatus* by Rodríguez-Romero et al. (1991). Specimens from Panama were investigated in a study of spermatozoan ultrastructural morphology by Introíni et al. (2009). Siung (1980) investigated its potential as a commercial species in Jamaica.

Family Gryphaeidae
Vyalov, 1936

Hyotissa mcgintyi
(Harry, 1985)
Figs. 83–94

Synonymy/Chresonymy

Le Bajet – Adanson, 1757: pl. 14, fig. 4. See also Fischer-Piette (1942: 295, pl. 12, fig. 2).

Mytilus roseus Gmelin, 1791: 3362 (based on Adanson's Le Bajet; see above). A forgotten name reinstated by Huber (2010: 616) under violation of Art. 23.9 and 23.11 of the ICZN (1999) *Code*. Prevailing usage of *Hyotissa mcgintyi* is here maintained; see Remarks.

Ostrea (Ostrea) thomasi McLean, 1941: 7, pl. 3, figs. 1, 2, pl. 4, figs. 1, 2 [Type locality: off Palm Beach, Florida] (non *Ostrea sellaeformis* var. *thomasi* "Conrad" Glenn, 1904).

Pycnodonte (Hyotissa) hyotis – Abbott, 1974: 457 [non *Mytilus hyotis* Linnaeus, 1758; see below].

Parahyotissa (Parahyotissa) mcgintyi Harry, 1985: 130 [replacement name for *O. thomasi* McLean, 1941, non Glenn, 1904].

Pycnodonte hiotis [sic] – Rios, 2009: 498, fig.

Parahyotissa macgintyi [sic] – Ardovini & Cossignani, 2004: 49.

Hyotissa mcgintyi – Kirkendale et al., 2004: 309 ff., fig. 2 [first record in the Florida Keys]; Bieler et al., 2004: 150–151, figs 1–2; Bieler & Mikkelsen, 2004: 513; Mikkelsen & Bieler, 2007: 114–117, 5 figs.

Parahyotissa rosea – Huber, 2010: 615.

Description

Shell (Figs. 83–85): Rounded or D-shaped, reddish, thick; maximum SD ≈ 50 mm in material examined. Inner layer with vesicular structure most apparent marginally as foam-like or spongy, especially under magnification. LV cementing to and assuming shape of hard substrata; RV smaller, more planar. Outer surface highly irregular, covered by minute concavities; sometimes radially pleated. Valve margins undulating or irregularly plicated. Hinge plate edentulous; L ≈ 60% SD. Vermiculate chomata on shell margin on either side of ligament. Ligament occupying entire dorsal hinge plate, thicker in central third. Inner surface glossy white. Adductor muscle scar rounded, subcentral, slightly posterodorsal; A ≈ 7% of inner VA.

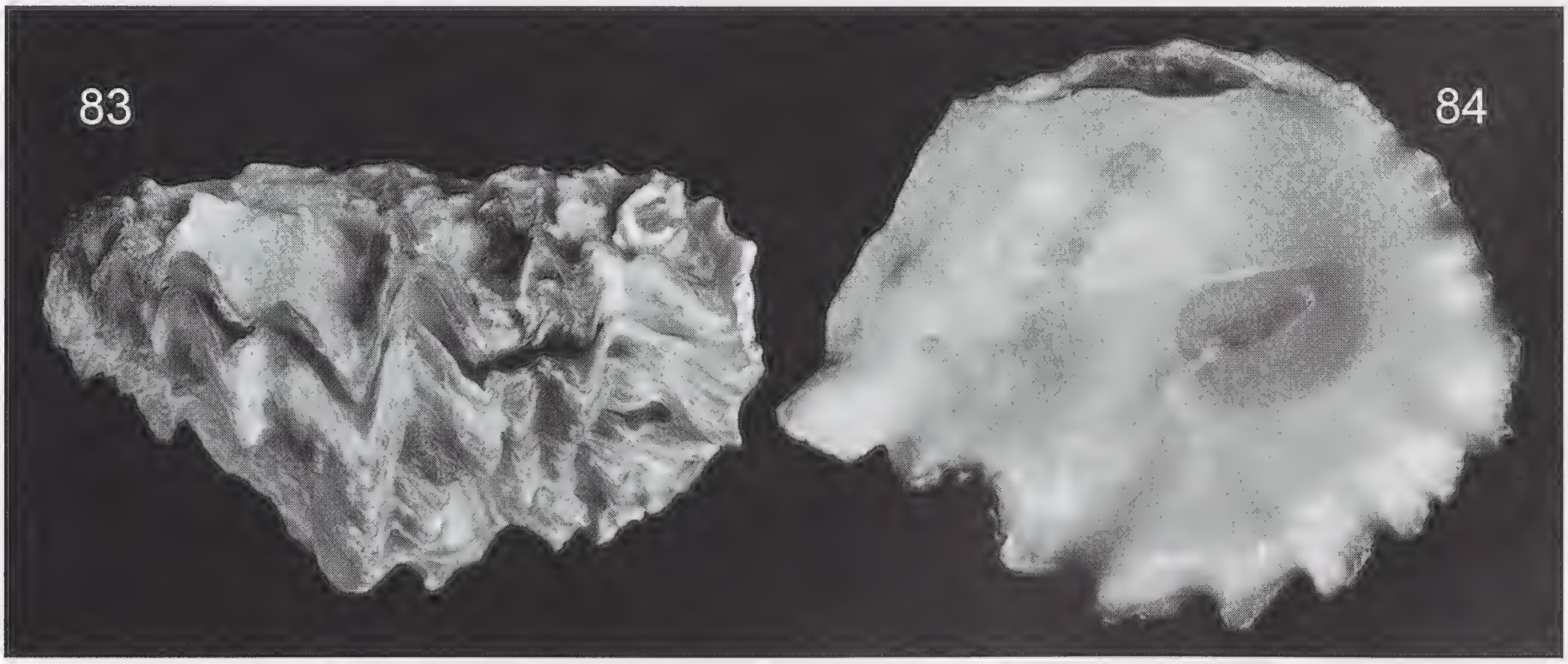

FIGS. 83, 84. *Hyotissa mcgintyi*, shell morphology, FMNH 302069, 69 mm maximum D. FIG. 83: Articulated specimen, ventral view showing zigzag shell margin; FIG. 84: RV, interior view.

Main muscle system (Figs. 85, 88): Anterior adductor and pedal retractor muscles absent. Posterior adductor muscle (*pm*) very large, at approximate midpoint of posterior third of animal, clearly with 2 ("catch" and "quick") portions of subequal A; anteriorly oval; posteriorly crescent-shaped (with concavity anterior); A ≈ 20% VA.

Foot: Absent.

Mantle (Figs. 86, 90, 94): Mantle lobes almost totally free except for relatively narrow dorsal region adjacent to hinge area, and another very short area separating incurrent and excurrent apertures, composed of inner fold (Fig. 94: *um*). Outer fold of mantle edge thin, smooth, simple. Periostracum separating outer and middle folds. Middle fold T ≈ 2 outer fold T, H ≈ outer fold H, bearing series of papillae at edge (most of H ≈ 2 fold base H); each papilla slender, relatively tall, pointed, with interspace = 3 papilla W; papillar size and interspaces weakly variable. Inner fold L and T = middle fold L and T, bearing series of very small papillae, with interspaces = 3 papilla W. Remaining areas of mantle inner surface almost totally covered by small papillae (Fig. 86), distributed randomly, variable in size, more concentrated in regions preceding edges and anteriorly preceding palps; narrow band lacking papillae at some distance from mantle edge (mostly probably a rejection tract); each papilla with whitish beige base and brown-stained tip. Pallial muscles relatively thick, originating at pallial line in inner edge of above-described smooth area. Pigmented papillae covering most structures of pallial cavity, including suprabranchial chamber, *pm*, and inner (dorsal) surface of gill.

Pallial cavity (Figs. 85, 87, 88, 91, 92, 94): On left side overlaying most of body surface, except *pm* and narrow visceral region close to hinge area. Visceral mass extending farther dorsally on right side, filling space between *pm* and hinge area. Infrabranchial chamber ventral to *pm* and visceral mass. Single right promyal passage (Fig. 88: *po*) as suprabranchial chamber passing through visceral mass on left, passing anteriorly to *pm*, and on both sides ventral to *pm*, also with region = *pm* L toward posterior. Labial palp (*pp*) L ≈ 14% of gill L, covering anterior end of gill (Fig. 87). Outer hemipalps connected, covering anterior ends of demibranchs, with longer region at level of inner demibranch.

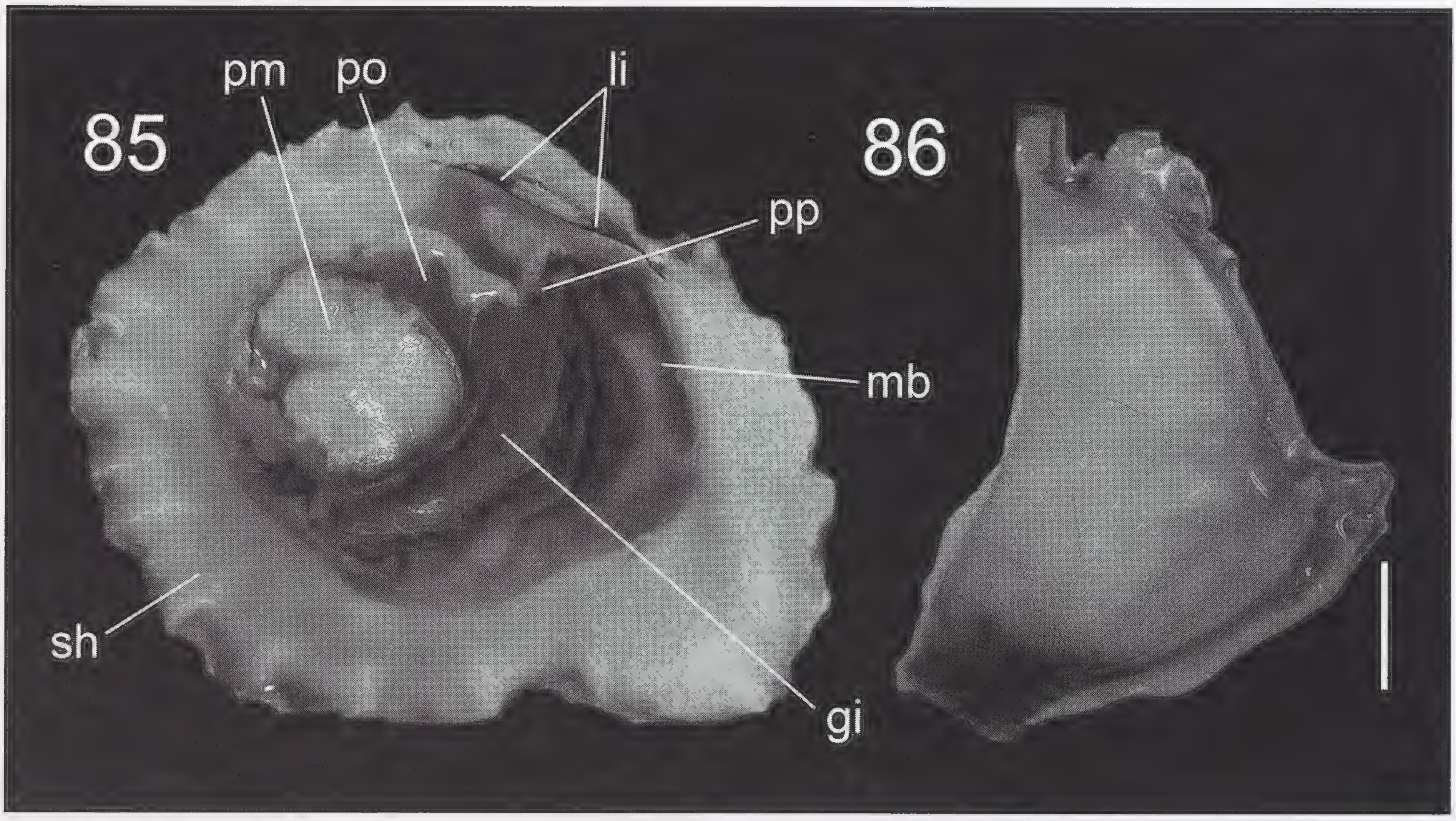

FIGS. 85, 86. *Hyotissa mcgintyi*, anatomy, FMNH 302069, 50 mm maximum D. FIG. 85: Intact right view, RV and mantle lobe removed; FIG. 86: Right mantle lobe, interior view, showing infrabranchial chamber, mantle edge, papillar cover (pigmented dots), and some pallial nerves. Scale bar = 10 mm. Abbreviations: gi, gill; li, ligament; mb, mantle border; pm, posterior adductor muscle; po, promyal passage of suprabranchial cavity; pp, labial palp; sh, shell.

Inner surface of each outer hemipalp with series of arched, uniform, narrow folds, starting between demibranchs, running ventrally, arching medially; before midline, inner folds abruptly ending at same level, with smooth area uniting outer hemipalps in A = 66% of folded area A, Another narrow smooth area at posterolateral ends of each hemipalp, broadly attaching to mantle at level posterior to anterior end of outer demibranch (*do*); taller region of each outer hemipalp bearing short, projecting, flattened flap. Inner hemipalp A ≈ 66% of outer hemipalp A, along midline from approximately same level of posterior end of outer hemipalp, adjacent only to inner surface of inner demibranch (*di*), posteriorly taller, decreasing gradually anteriorly; inner surface with transverse folds perpendicular to longitudinal body axis, ending ventrally close to ventral edge, with narrow ventral smooth inner edge. Remaining folds similar to those of outer hemipalps; folds ending approximately at same level as those of outer hemipalp, with smooth area preceding mouth. Gill A ≈ 66% of infrabranchial chamber A ≈ infrabranchial chamber L. Each demibranch subequal in size (Fig. 85); *di* with anterior end slightly more anterior than that of *do* (Fig. 87). Ventral demibranch edges narrow, each bearing shallow food groove; dorsally wide, with ascending and descending portions well-separated at base. Transverse inner septa (Figs. 88, 91: *gr*) uniting portions of each demibranch, between every 10–15 filaments; septa of all 4 demibranchs aligning transversely (Figs. 92, 94). Each septum connecting entire inner (dorsal) edge of filament, from ventral to dorsal ends, leaving suprabranchial chamber free; septum gradually becoming broader from ventral to dorsal, accompanying gill enlargement. Suprabranchial chamber totally covered by papillae similar to those on inner surfaces of mantle lobes, including surfaces of *pm* and visceral mass, and inner (dorsal) surface of gills and septa. Ctenidial vessels running along central connections between gills, also between connections of demibranchs (Fig. 91: *bv*). Tissue connections between gills along midline and between gills and mantle. Gill filaments connecting to neighboring filaments by transverse, narrow tissue connections. Anterior half of gills connecting to ventral surface of visceral mass; posterior half of gills supported by 3 suspensory stalks (Fig. 94: *do, di*), one at center along union between gills, remaining 2 connecting to union of demibranchs of each gill. Origins of all 3 suspensory stalks on anteroventral surface of *pm* (leaving ventral surface free), slightly more posterior toward right. Posterior half of gills connecting via tissue to adjacent mantle along lateral edges, to mantle connection separating incurrent (*si*) and excurrent (*se*) apertures (Fig. 94: *um*).

Visceral mass (Figs. 85, 89, 92, 93): Filling entire space immediately ventral to umbones and hinge area; becoming narrower and restricted on right side after distance = 14% SH, keeping *po* anterior to *pm*, with space at right = W as suprabranchial chamber (Fig. 85). Stomach (Figs. 89: *st*; 93) filling anterodorsal region, immediately and entirely surrounded by greenish brown digestive diverticula. Gonad surrounding digestive diverticula and filling remaining subumbonal region plus short space in visceral mass at left of suprabranchial chamber, anterior to *pm* (Fig. 92). Pericardium anterodorsal to suprabranchial chamber; V ≈ 12% of visceral mass V.

Circulatory and excretory systems (Fig. 92): Pericardium relatively small, in dorsal region of visceral mass anterior to suprabranchial chamber, anterior to *pm*. Auricles (*au*) lobed, beige, V ≈ 25% of pericardial V; other characters of heart similar to that of *Hyotissa hyotis* (see below). Kidney (*ki*) internally hollow, compressed between remaining visceral mass and anterior surface of *pm*, filling left region adjacent to suprabranchial chamber; *ki* lobe V < 50% of inner *ki* V, restricted to ventral and left sides, bearing longitudinal, irregular folds, with dichotomies posteriorly, splaying across *pm* anterior surface.

Digestive system (Figs. 87, 89, 93, 94): *Pp* as described above. Mouth (Fig. 87: *mo*) transverse, surrounded only by smooth areas; posterior lip H ≈ 66% of anterior lip H. Esophagus (Figs. 89, 93: *es*) short, broad, in L = 33% of *pp* L; inner surface covered by longitudinal, narrow, low folds well-separated. Stomach (Figs. 89: *st*; 93) oval; L and W ≈ 3 *es* L and W. Dorsal hood (Figs. 89, 93: *dh*) L ≈ 2 *st* L ≈ 50% of *st* W, originating on anterior-right surface of *st*, just posterior to *es* opening, running left, immersed in visceral glands. Opening of conjoined style sac-intestine (Figs. 89, 93: *ss, in*) marked by abrupt constriction of posterior *st*, running posteriorly, weakly curving ventrally; L = *st* L. Gastric inner surface (Fig. 93) with *es* folds abruptly ending in ventral, tall, broad gastric fold, running left along ventral surface

87

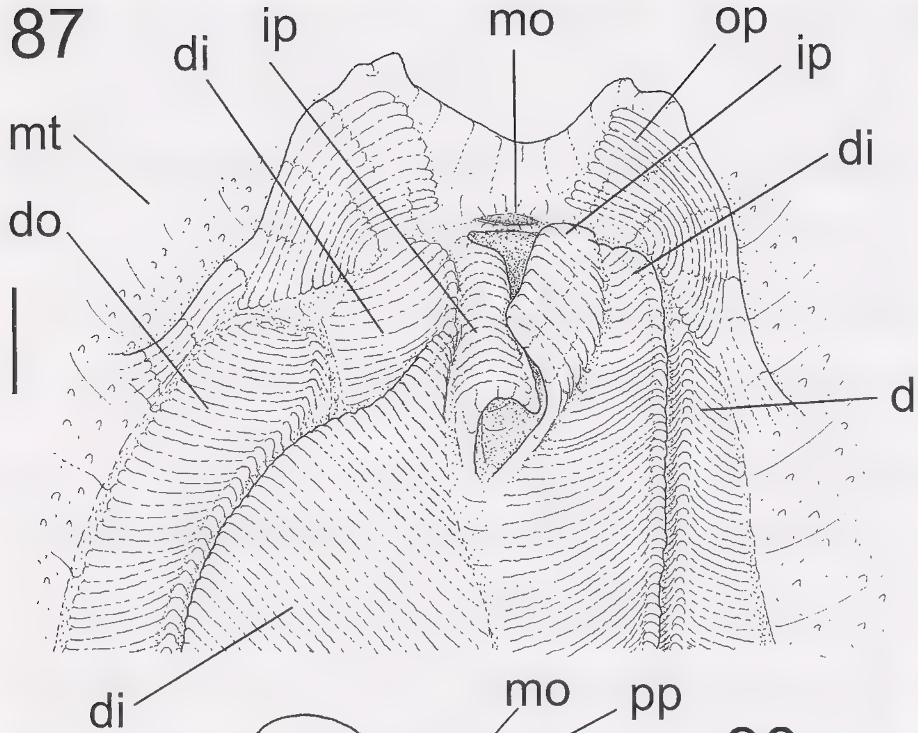

88

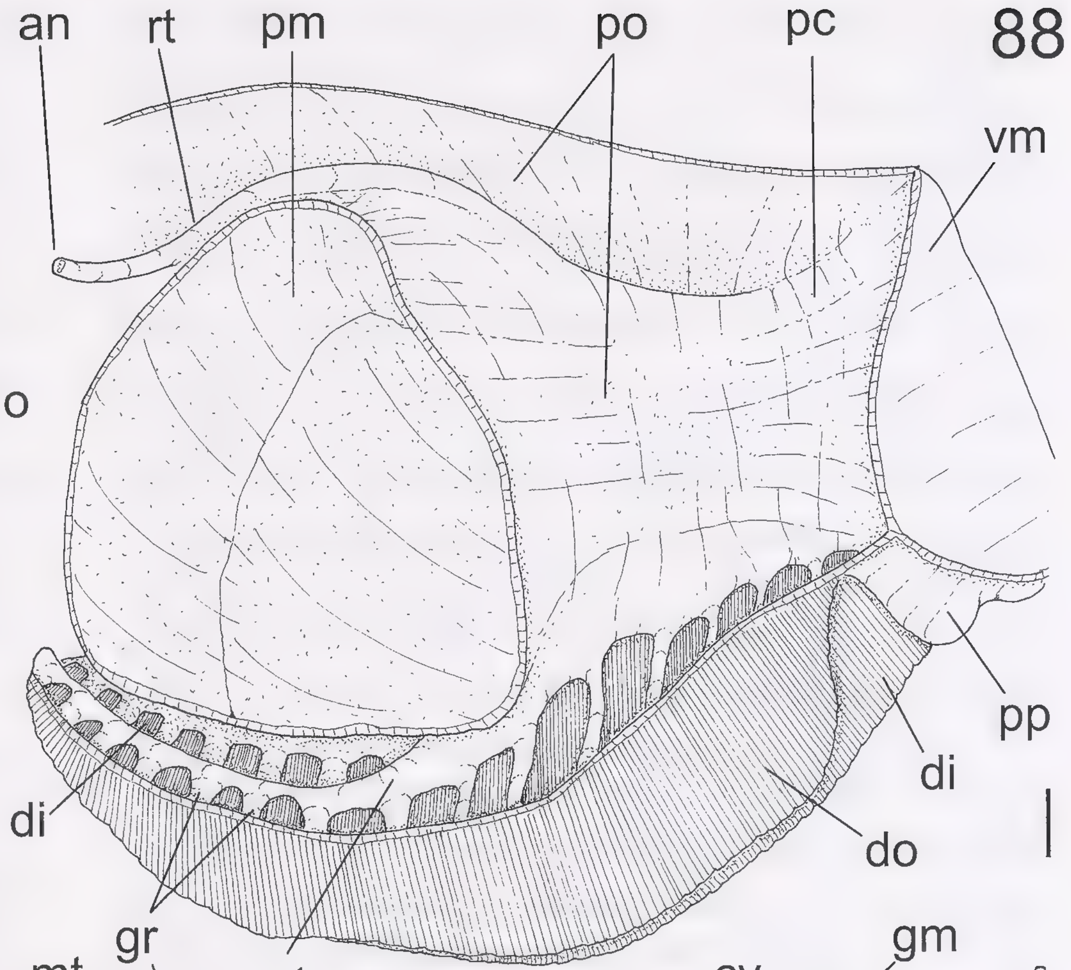

89

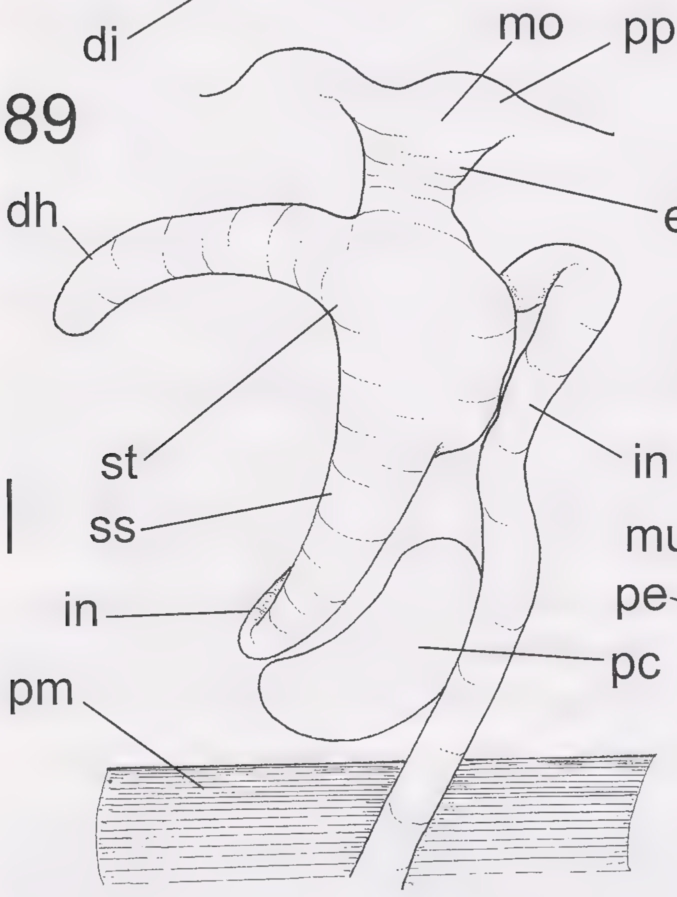

90

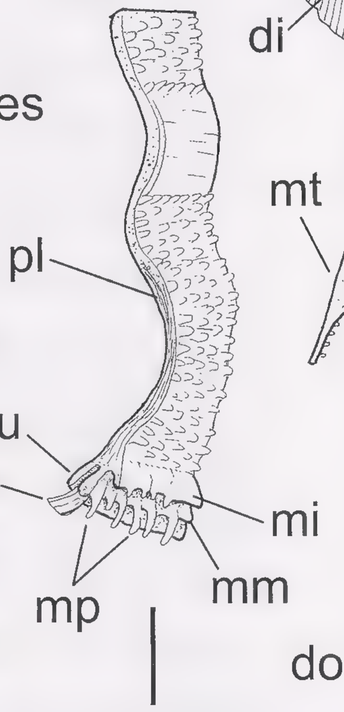

91

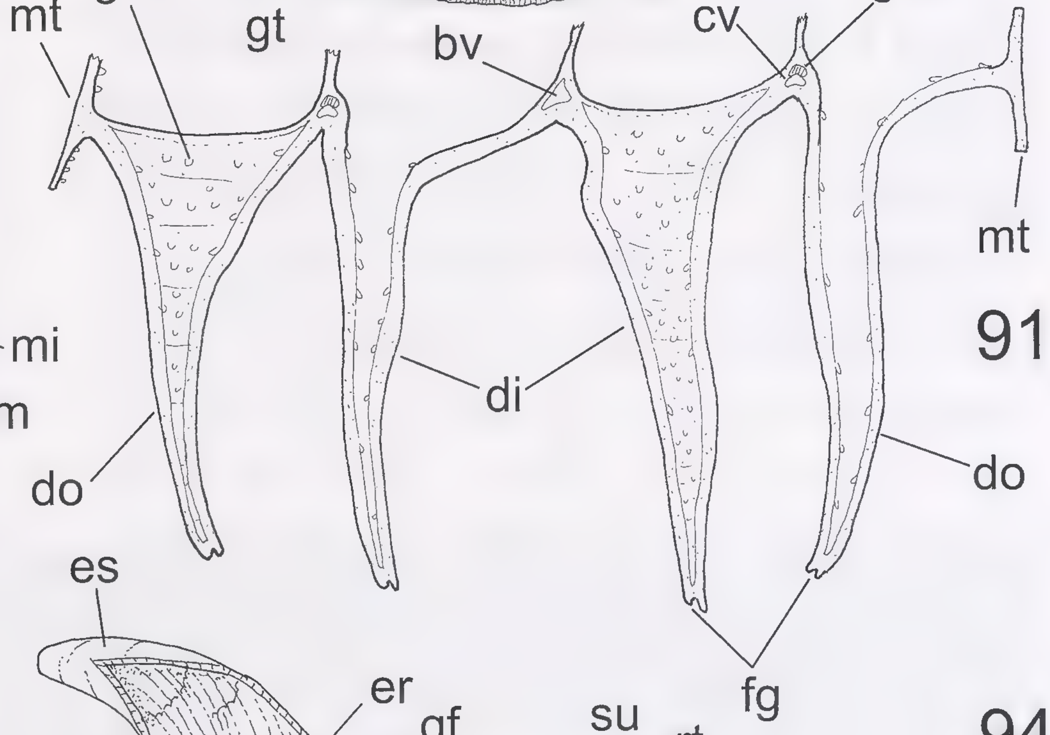

92

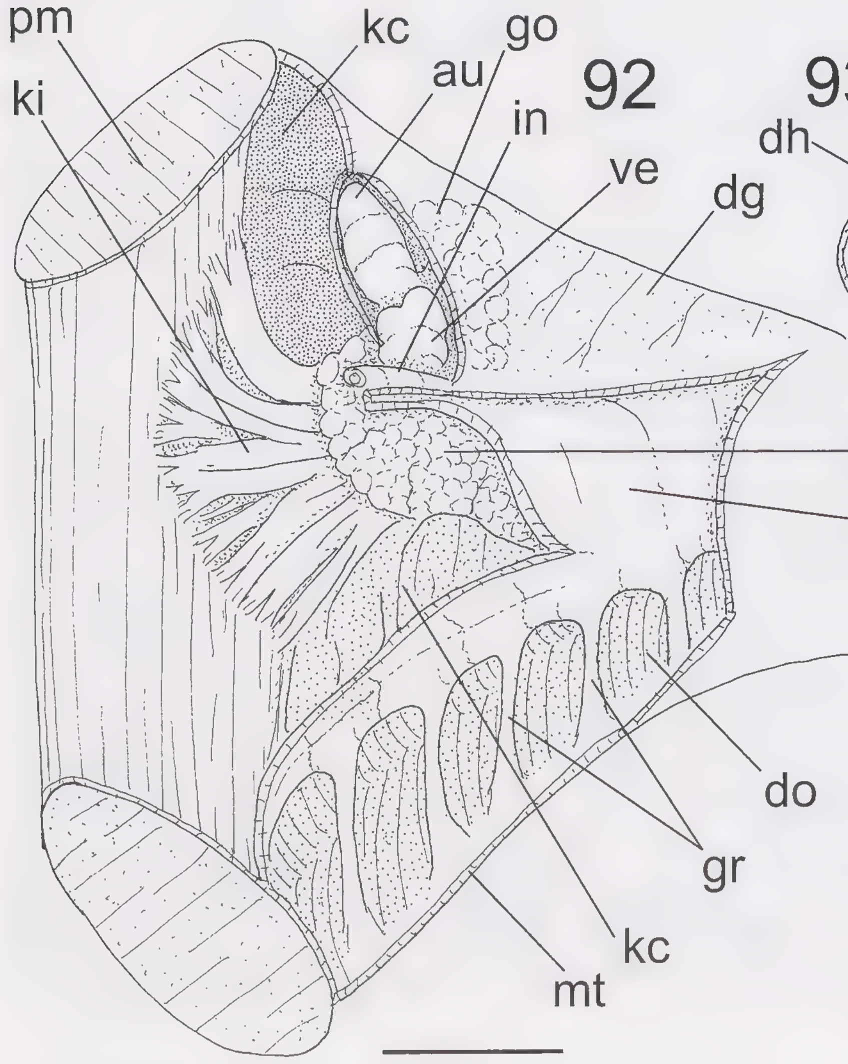

93

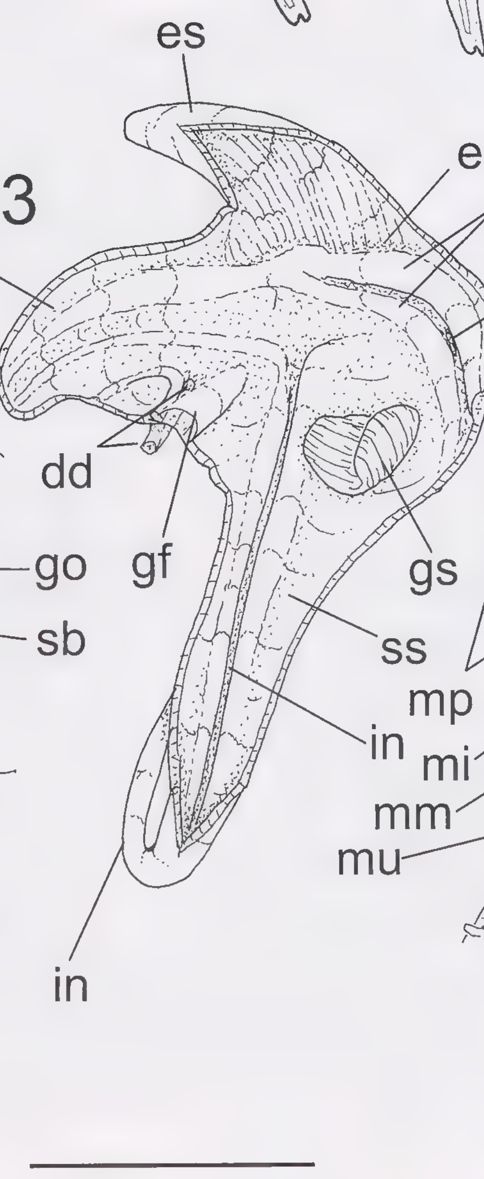

94

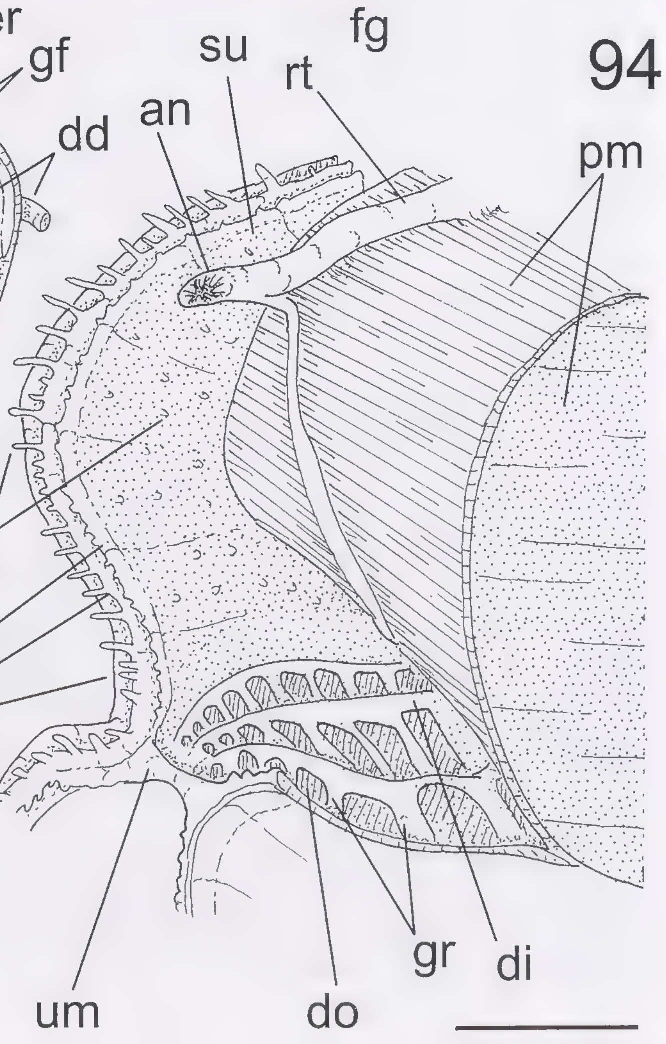

of *dh*, decreasing at distal end of *dh*; also running toward right as pair of parallel folds, initially close, with anterior branch surrounding right gastric inner surface transversely, crossing dorsal surface, ending on opposite (left) side; posterior branch surrounding right edge of gastric shield (*gs*), diminishing into posterior *st*; another gastric fold in W ≈ 50% W of previous fold W, running parallel and just posterior to ventral surface of *dh* main fold, anteriorly surrounding end of anterior branch of main gastric fold, curving perpendicularly posteriorly, running along *ss* as minor typhlosole; major typhlosole originating gradually on left edge of *gs*, running posteriorly next to minor typhlosole. Typhlosoles separating *in* (ventral) from *ss* (dorsal) (Fig. 93). *Gs* on posterior-right inner gastric surface (Fig. 93); A ≈ 16% of inner gastric surface A. Ducts to digestive diverticula (Fig. 93: *dd*) between branches of right region of main gastric fold; *dd* as described above. *In* curving abruptly posterior to *ss* (Figs. 89, 93), running anteriorly close to *ss* to anterior-right region of *st*, making another ample loop in this region slightly away from gastric outer surface, then running posteriorly, obliquely, and sinuously from right side to closer to midline, at level of *pm*. Anus (Fig. 88: *an*) preceded by long, detached (siphoned) portion of rectum, originating on posterior surface of *pm*, closer to left side; edge bearing few small folds on inner surface.

Reproductive system: Gonad as described above; genital aperture not observed.

Nervous system: Not examined.

Material Examined

USA, Florida Keys, FMNH 302069, 3 specimens (sta. FK-650; dissected: #1: 69 mm L, 55 mm H, 40 mm W; #2: 50 mm L, 39 mm H, 18 mm W; #3: 26 mm L, 25 mm H, 14 mm W); FMNH 317471, 3 shells (FK-260); FMNH 326538, 5 specimens (sta. FK-908/Bivatol-275); FMNH 333754, 6 specimens (sta. FK-991/Bivatol-450).

BRAZIL, Bahia, off Alcobaça, 10–15 m, MZSP 69725, 1 shell (iv/2002).

Distribution

Stated by Turgeon et al. (2009) to range from North Carolina to Texas, the Gulf of Mexico, Cuba, the tropical western Atlantic and the tropical eastern Pacific. A range to Bahia, Brazil, is here confirmed.

Remarks

Harry (1985) introduced the genus *Parahyotissa* with this species as the type species, distinguished from *Hyotissa* (type species *H. hyotis* – see below) by the promyal passage open only on the right side in *Parahyotissa* (here confirmed), and open on both sides in *Hyotissa*;

←

FIGS. 87–94. *Hyotissa mcgintyi*, anatomy. FIG. 87: Labial palps and adjacent region of gill and mantle, ventral view, hemipalps deflected to show inner surface; FIG. 88: Suprabranchial chamber, lateral to right view, right mantle lobe removed, note promyal passage (po) anterior to adductor muscle (restricted to right side); FIG. 89: Digestive system *in situ*, dorsal view, topologies of some adjacent structures also shown; FIG. 90: Cross section of midportion of mantle lobe, in region close to mantle border; FIG. 91: Cross section through gills in midregion (anterior to adductor muscle); FIG. 92: Posterior region of visceral mass, dorsal view, left region of pericardium, renal membrane, and part of right mantle lobe removed, showing inner renal structures and part of suprabranchial chamber anterior to adductor muscle; FIG. 93: Stomach, dorsal view, opened longitudinally; FIG. 94: Anal region of mantle cavity, right and slightly posterior view, right mantle lobe partially removed. Scale bars = 2 mm (FIGS. 88–91); 5 mm (FIGS. 92–94). Abbreviations: an, anus; au, auricle; bv, "blood" vessel; cv, ctenidial (efferent) vessel; dd, ducts to digestive diverticula; dg, digestive diverticula; dh, dorsal hood; di, inner demibranch; do, outer demibranch; er, esophageal rim; es, esophagus; fg, food grooves; gf, gastric fold; gm, gill retractor muscle; go, gonad; gr, gill transverse septum in suprabranchial chamber; gs, gastric shield; gt, gill suspensory stalk; in, intestine; ip, inner hemipalp; kc, renal chamber; ki, kidney; mi, mantle border inner fold; mm, mantle border middle fold; mo, mouth; mp, mantle papillae; mt, mantle; mu, mantle border outer fold; op, outer hemipalp; pc, pericardium; pe, periostracum; pl, pallial muscles; pm, posterior adductor muscle; po, promyal passage of suprabranchial cavity; pp, labial palp; rt, rectum; sb, suprabranchial chamber; ss, style sac; st, stomach; su, supra-anal chamber of suprabranchial pallial cavity; um, fusion between left and right mantle lobes; vm, visceral mass.

The subsequent synonymy of *Parahyotissa* with *Hyotissa* is based on a molecular phylogeny advocated by Kirkendale et al. (2004); the material used in the molecular study is from the the same site ("Thunderbolt" wreck, off Key Vaca) as the material here dissected. See also remarks under *H. hyotis*. No material from Brazil was available for dissection.

Hyotissa mcgintyi is assumed to have amphi-atlantic distribution (e.g., Harry, 1985; Carriker & Gaffney, 1996; Ardovini & Cossignani, 2004); unfortunately no anatomical or molecular data are available for eastern Atlantic specimens. Huber (2010: 614) synonymized this nominal species under *Parahyotissa rosea* (Gmelin, 1791), based on *Mytilus roseus* Gmelin, 1791, described from West Africa (not be confused with *Ostrea rosea* Gmelin, 1791, of the same work). As Huber's action appears to be in violation of ICZN (1999) Articles 23.9 and 23.11 (we have not located any prior post-1899 usage of *Mytilus roseus* as a valid name, whereas the name *H. mcgintyi* has been used frequently enough to fulfill the conditions of Art. 23.9.1.2) we are maintaining prevailing usage herein.

Hyotissa hyotis
(Linnaeus, 1758)
Figs. 95–104

Synonymy/Chresonymy

Mytilus hyotis Linnaeus, 1758: 704 [Type locality: "Pelagi Gorgoniis" = in the Gorgonia corals of the sea].

Hyotissa hyotis – Harry, 1985: 128–131; Sevilla-H. et al., 1998: 25–32, figs. 1–2; Bieler et al., 2004: 149–159, figs. 3–4; Mikkelsen & Bieler, 2007: 118, 4 figs.

Description

Morphology similar to that of *Hyotissa mcgintyi,* except as noted here.

Shell (Figs. 95–97): Purplish black to magenta to violet-brown, with irregular sculpture of pleated ribs bearing hollow spines; maximum SL ≈ 180 mm in material examined. Interior bluish or yellowish white with black or brown stains; valve margins near ligament with both vermiculate and lath chomata.

Main muscle system (Fig. 101): Posterior adductor muscle (*pm*) more posterior, close to posterior mantle edge.

Mantle (Figs. 100, 101, 103): Middle and inner folds of mantle edge dark brown, almost black, including connection between lobes (Fig. 100: *um*); separating excurrent (*se*) and incurrent (*si*) apertures. Three mantle border folds of subequal T and H, except for slightly thinner outer fold. Middle fold bearing series of papillae (Fig. 103: *mp*) along edge, most in L < 50% of remaining region of fold H; with 3 rows of papillae covering distal region of inner surface of fold to edge. Inner fold (Fig. 103: *mi*) bearing series of short, broad, dense papillae. Remaining areas of mantle inner surface lacking papillae, bearing only few bulging hemolymph sinuses in region close to mantle border folds. Promyal passage (Fig. 101: *po*) widely open on right side, narrow on left.

Pallial cavity (Figs. 98, 101): Suprabranchial chamber lacking papillae. Labial palps (Fig. 98: *op, ip*) with proportionally more internal folds.

Visceral mass (Fig. 99): Anteroposteriorly longer. Gonad (*go*) pale cream-colored, surrounding greenish-beige digestive diverticula

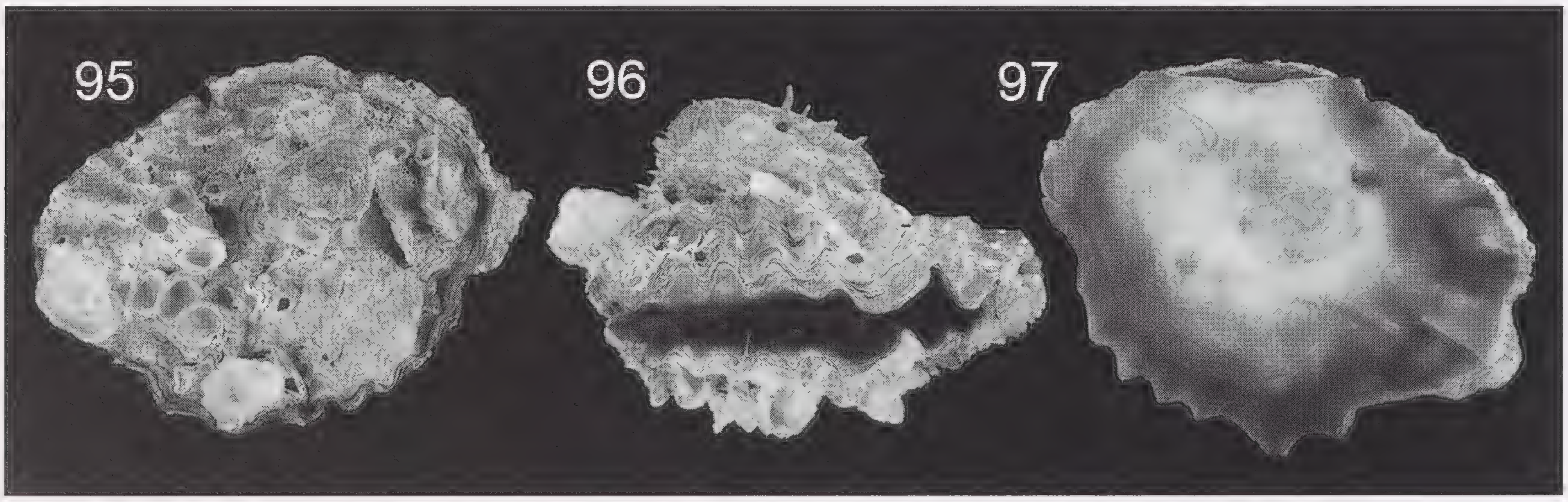

FIGS. 95–97. *Hyotissa hyotis*, shell morphology, FMNH 302010, 178.0 mm L. FIG. 95: RV, exterior view; FIG. 96: Articulated specimen, ventral view showing zigzag shell margins; FIG. 97: RV, interior view.

and remaining subumbonal region; with large space in visceral mass to left of suprabranchial chamber, anterior to *pm*. Connective tissue brown, surrounding most of digestive system, isolating it from surrounding *go*.

Circulatory and excretory systems (Figs. 99, 101): Pericardium (Fig. 101: *pc*) in V ≈ 25% of visceral mass V, highly asymmetrical; right side A ≈ 2 left side A. Ctenidial veins running along connection between demibranchs of each gill, connecting with T-shaped branch of ctenidial vein (Fig. 101: *cv*) running perpendicularly, originating between middle and anterior thirds of gill, running dorsally along ca. 50% of visceral H, bearing internal longitudinal, narrow, low folds. Ctenidial vein connecting to ventral end of auricle (*au*), marked by abrupt change in ST and color. *Au* multilobed (Fig. 99); right *au* V ≈ 130% of left *au* V, placed more dorsally; walls thickly glandular, dark brown; *au* lobes covering most of pericardial posterior half, surrounding ventricle (*ve*). *Ve* thickly muscular, pyriform (Fig. 99); L ≈ 80% of *pc* L, V ≈ 50% of *pc* V. *Ve-au* connections narrow, with unpigmented ducts at center of posterior *ve* slope; L and W ≈ 20% of *ve* L and W.

Digestive system (Figs. 101, 102, 104): Inner surface of esophagus (*es*) covered by series of regular, broad, low, transverse folds, adjacent, abruptly ending in ventral gastric fold (Fig. 104); without distinct rim. Dorsal hood (Figs. 102, 104: *dh*) in V ≈ 12% of stomach V; inner surface with transverse folds. Gastric inner surface with pair of ventral, transverse folds (Fig. 104: *gf*) just posterior of *es* opening; aperture of *dh* between these folds; pair of narrow folds originating from right side of

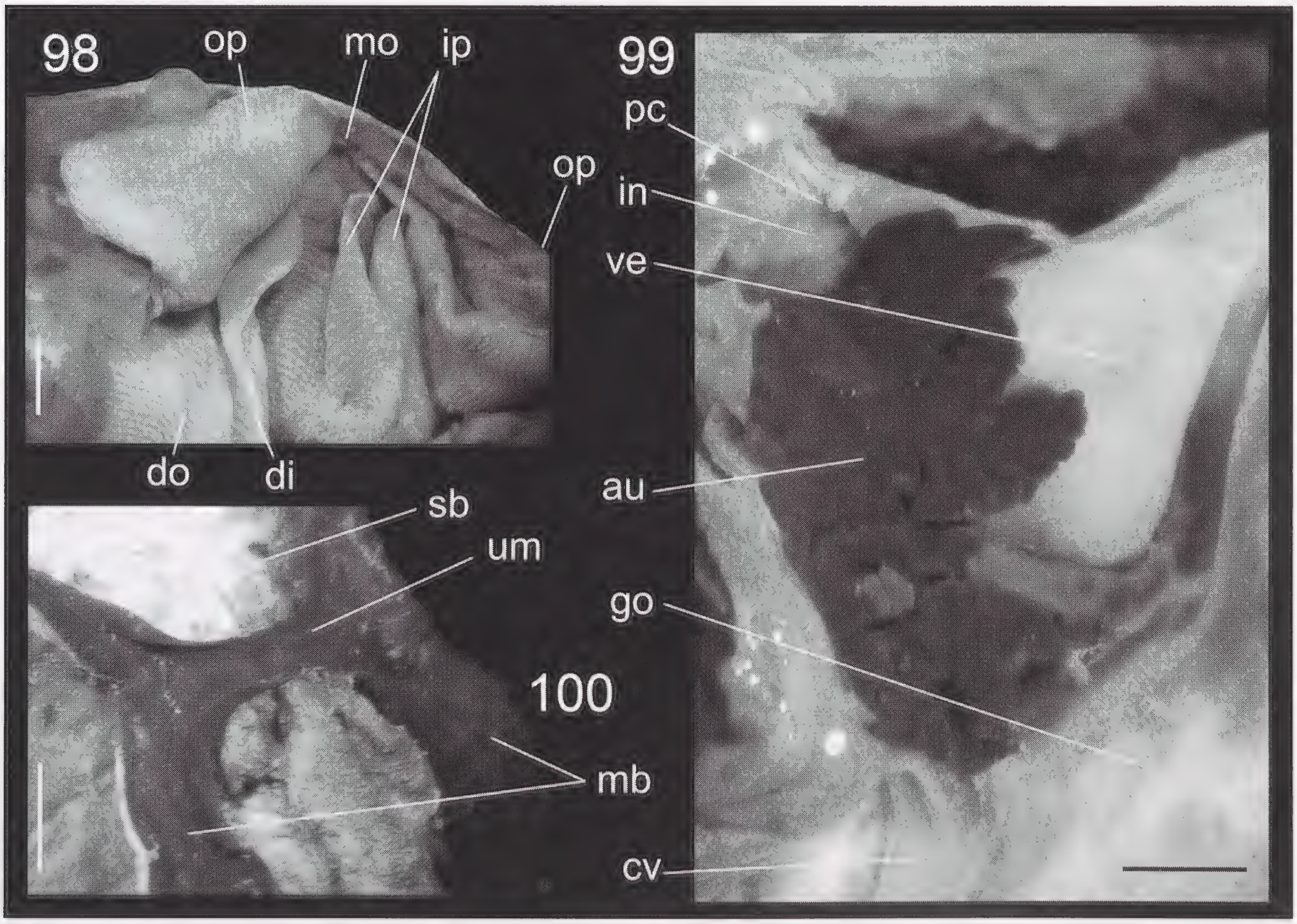

FIGS. 98–100. *Hyotissa hyotis*, anatomy, FMNH 302067. FIG. 98: Pallial cavity, ventral view, detail of anterior region, outer hemipalp (op) partially deflected; FIG. 99: Pericardial region, right view, right wall of pericardium removed, ctenidial vein (cv) opened longitudinally, including adjacent portion of auricle (au); FIG. 100: Mantle border, posterior view, detail of region between incurrent and excurrent flows. Scale bars = 5 mm (FIG. 98); 2 mm (FIGS. 99, 100). Abbreviations: au, auricle; cv, ctenidial (efferent) vessel; di, inner demibranch; do, outer demibranch; go, gonad; in, intestine; ip, inner hemipalp; mb, mantle border; mo, mouth; op, outer hemipalp; pc, pericardium; sb, suprabranchial chamber; um, fusion between left and right mantle lobes; ve, ventricle.

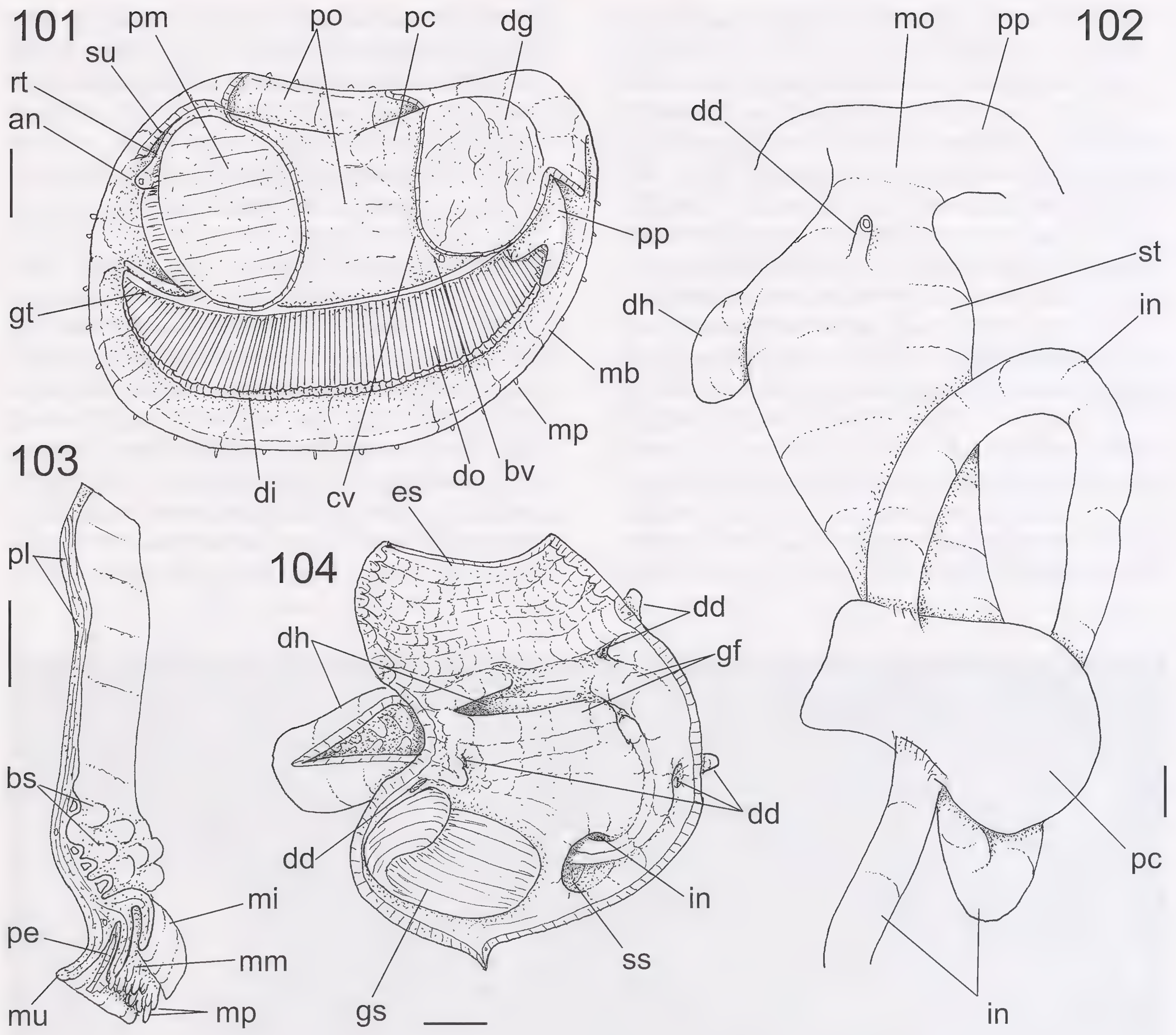

FIGS. 101–104. *Hyotissa hyotis*, anatomy. FIG. 101: Intact right view, RV and part of left mantle lobe removed; FIG. 102: Digestive system *in situ*, dorsal view, topologies of some adjacent structures also shown; FIG. 103: Mantle edge, cross section at midventral region; FIG. 104: Stomach, dorsal view, opened longitudinally, dorsal hood (dh) also opened longitudinally. Scale bars = 10 mm (FIG. 101), 2 mm (FIGS. 102–104). an, anus; bs, hemolymph ("blood") sinus; bv, "blood" vessel; cv, ctenidial (efferent) vessel; dd, ducts to digestive diverticula; dg, digestive diverticula; dh, dorsal hood; di, inner demibranch; do, outer demibranch; es, esophagus; gf, gastric fold; gs, gastric shield; gt, gill suspensory stalk; in, intestine; mb, mantle border; mi, mantle border inner fold; mm, mantle border middle fold; mo, mouth; mp, mantle papillae; mu, mantle border outer fold; pc, pericardium; pe, periostracum; pl, pallial muscles; pm, posterior adductor muscle; po, promyal passage of suprabranchial cavity; pp, labial palp; rt, rectum; ss, style sac; st, stomach; su, supra-anal chamber of suprabranchial pallial cavity.

transverse folds, running posteriorly, penetrating conjoined style sac-intestinal opening; 2 pairs of ducts to digestive diverticula (Figs. 102, 104: *dd*) at midventral region of main gastric chamber, just posterior to *dh* and to origin of longitudinal gastric folds; left pair of ducts to *dd* separated by sharp, narrow fold. Gastric shield (Fig. 104: *gs*) on posterior-left side; A ≈ 25% of gastric inner surface A. Intestinal loops running more dorsally along dorsal wall of stomach-style sac. Anus (Fig. 101: *an*) preceded by short stalk; W ≈ 20% of *pm* W.

Material Examined

USA, Florida Keys, FMNH 302010, 1 specimen [sta. FK-717; dissected: 180 mm L, 145 mm H, ca. 48 mm W (without fouling organisms)].

Distribution

An Indo-Pacific species recently introduced to Florida. This species is not known from Brazil.

Remarks

The discovery of this specimen, and hence the confirmed presence of this introduced Indo-Pacific species in South Florida, led to the tracking of this potentially invasive species by the Florida Fish and Wildlife Commission in its Exotic Species Database. Tissue samples from this Florida Keys specimen were used in the molecular analyses of Bieler et al. (2004) and Tëmkin (2010).

This work provides the most complete anatomical descriptions of the two examined species of *Hyotissa* to date. They have similar anatomical features; however, a set of differences, detected here, facilitates the species-level distinction. The most readily perceived is the near-black mantle edges of *H. hyotis* (Fig. 100), in contrast to the pale beige or cream-colored ones of *H. mcgintyi* (Fig. 86). Another distinct feature is the greater development of pallial papillae in *H. mcgintyi*, covering the entire mantle lobes (Fig. 86), and some pallial structures, such as the surface of the posterior adductor muscle and the dorsal surface of the gills; this is not found in *H. hyotis*, in which these structures are smooth. Adult size appears to be another distinction, with *H. hyotis* typically reaching 3–4 times the size of *H. mcgintyi*. The extraordinary size and complexity of the auricles of *H. hyotis*, including the dark brown color, is less developed in *H. mcgintyi*. In the digestive system, *H. hyotis* has a shorter dorsal hood (Fig. 102) and anal papilla (Fig. 101), both of which are very long in *H. mcgintyi* (Figs. 89, 94); the inner organization of the stomach is also different (compare Figs. 93 and 104); the intestine of *H. hyotis* runs more dorsally than that of *H. mcgintyi* (Figs. 89, 102). On the other hand, the two species share some interesting and unusual features, such as the right promyal passage (Figs. 88, 101: *po*), the lobed auricles (Fig. 99), and the eulamellibranch gills with well-developed sequential septa reinforcing the filaments (Fig. 91: *gr*). The existence of a narrower left promyal passage in *H. hyotis* – a feature that led Harry (1985) to distinguish between the two genera *Hyotissa* and *Parahyotissa* (the latter with only the right passage) – was here confirmed (see comments above, under *H. mcgintyi*).

Family Pinnidae
Leach, 1819

Pinna carnea
Gmelin, 1791
Figs. 105–118

Synonymy/Chresonymy

Pinna carnea Gmelin, 1791: 3365 [Type locality originally unspecified; designated as Guantánamo Bay, Cuba, by Turner & Rosewater 1958: 308.

Pinna carnea – Winckworth, 1929: 291; Turner & Rosewater, 1958: 306–310, pl. 149, pl. 150, figs. 1, 2, pl. 151, pl. 157; Abbott, 1974: 437–438, fig. 5108; Bieler & Mikkelsen, 2004: 519; Mikkelsen & Bieler, 2007: 120–122, 6 figs.; Sharma et al., 2012: table 1.

Description

Shell (Figs. 105, 106): Elongated triangular, fragile, translucent, beige to pale pinkish brown to orange; SL ≈ 135 mm in material examined. Anteriorly slightly cylindrical, sharply pointed, gradually increasing posteriorly, becoming laterally compressed (SH ≈ 3 SW). Maximum (posterior) SH between middle and posterior thirds ≈ 50% SL. Dorsal margin horizontal; ventral margin horizontal to weakly concave, lacking obvious pedal/byssal gape; posterior margin convex, with sharp edge and sometimes 4–6 short posterior projections corresponding to sculpture. Sculpture of 5–7 wide, uniformly distributed, longitudinal ridges; interspace W = ridge W; ridges slightly taller and narrower anteriorly; subcentral pair of ridges forming weak lateral carina at widest margin of shell, gradually diminishing posteriorly. Periostracum not evident. Hinge plate edentulous, with narrow external ligament connecting valves along entire dorsal shell margin. Inner surface glossy, translucent; muscle scars shallow; nacre very thin, restricted to anterior third; posteriorly with shallow longitudinal furrows corresponding to external radial sculpture. Scar of anterior adductor muscle (*am*) very close to anterior end, elliptical; A ≈ 0.5% SA. Posterior muscle scar oval, comprising posterior adductor muscle (*pm*; posterior half) and posterior pedal retractor muscle (*pr*; anterior half), located between middle and posterior thirds of SA, close to hinge plate; A ≈ 7% SA. Paired scars of pallial muscles concentrated ventral and anterior to *pr* scars, in A ≈ 10%

of *pm* A, at posterior end of shallow longitudinal furrows starting at anterior end, running posteriorly at midlevel, dividing nacre into 2 subequal dorsal and ventral portions.

Main muscle system (Figs. 109, 111, 113, 115): Proportions and positions of adductor muscles as described above; *pm* W ≈ 2 *am* W. Paired anterior pedal retractor muscles (Figs. 109, 111: *rr*) very narrow, slender, originating just posterodorsal to *am*, in A = 6% of *am* A, running horizontally and directly posteriorly at distance = 33% SL, in roof of anterior portion of pallial cavity, splaying across anterior side of foot base. Paired *pr* (Figs. 109, 113) several times larger than *rr*, originating just anterior to *pm*, in semicircular A = *pm* A; running anteriorly and slightly ventrally along ca. 33% SL, diminishing in W by ca. 33% along L toward insertion, inserting along middle and posterior foot base, just dorsal to byssal gland. Byssal gland running internally along this pair of muscles as described below. Paired dorsal pallial retractor muscles (Figs. 109, 113: *lm*) narrow, slender (in origin and size = *rr*), originating at midpoint of hinge plate, running posteriorly close to midline; after distance ≈ 50% SL, splaying across dorsal mantle border. Paired ventral pallial retractor muscles (Figs. 113, 115: *vpm*) as concentration of pallial muscles, in V and W ≈ 2 *rr* V and W, originating just ventral to origin of *pr*, running directly posteriorly along ca. 33% SL, flanking ventral edges of origins of *pr* and *pm*, then gradually splaying along midposterior mantle edge, mainly in region of mantle fusion. Paired cardinal muscles (Fig. 109: *ca*) small, short, conical, originating at ca. 8% SL posterior to origins of longitudinal hinge muscles, just dorsal to heart, directed dorsally, separated by distance = 16% SW, splaying around adjacent regions ventral to their origins.

Foot (Figs. 107: *ft*, 109, 111, 115): Divided into 2 regions; anterior slender, projecting; posterior

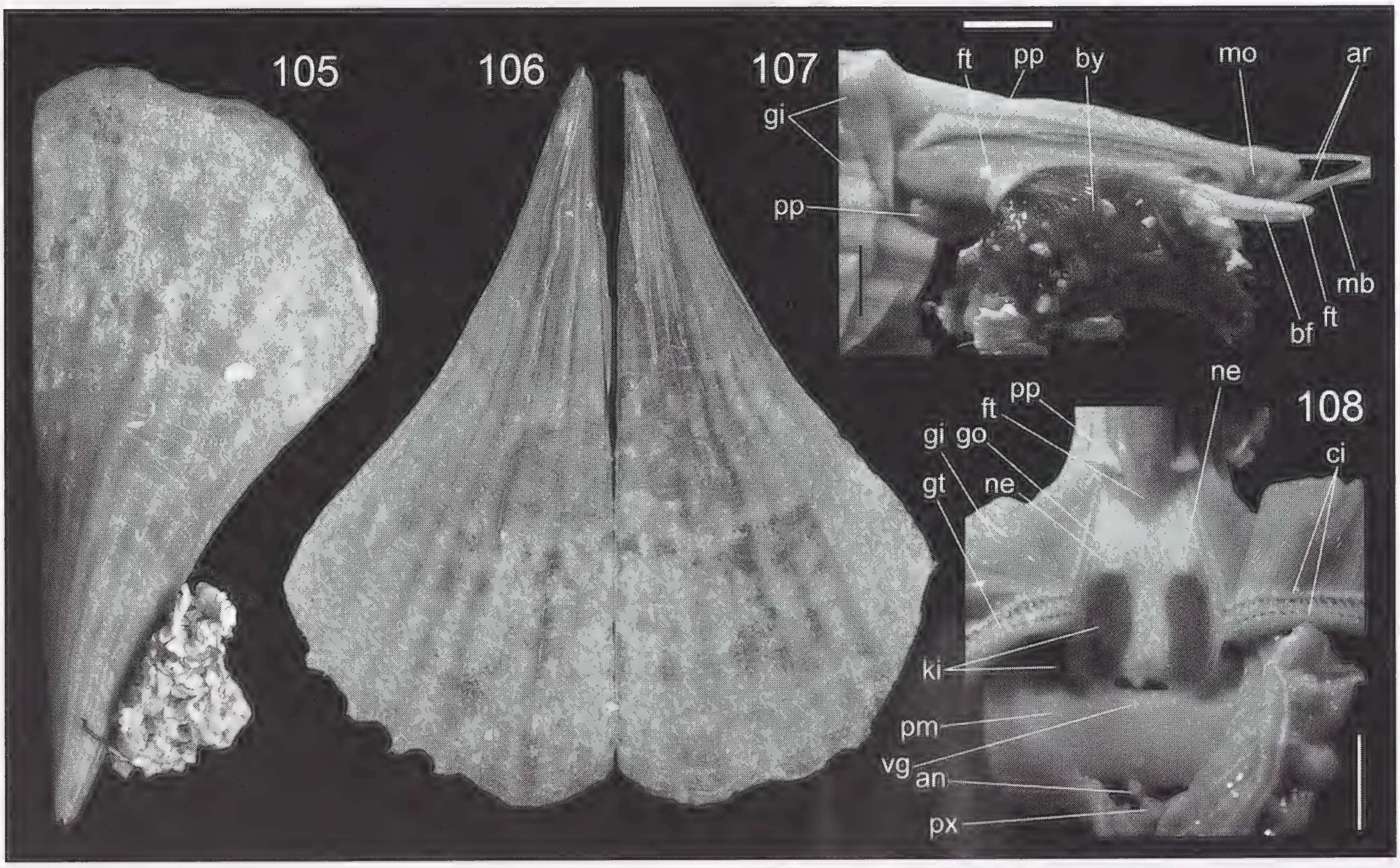

FIGS. 105–108. *Pinna carnea.* FIGS. 105, 106: Shell morphology, FMNH 295746, 138.0 mm L. FIG. 105: Shell, left view, position in life with byssus attached to sediment particles; FIG. 106: Interior view, both valves; FIGS. 107, 108: Anatomy. FIG. 107: Foot and adjacent structures, right and slightly ventral view, most of mantle removed; FIG. 108: Detail of posterior region of visceral mass, ventral view, both gills and left mantle lobe deflected, right mantle lobe removed. Scale bars = 5 mm (FIGS. 107, 108). Abbreviations: an, anus; ar, anterior pedal retractor muscle; bf, byssal furrow; by, byssus; ci, ciliary connection of gill; ft, foot; gi, gill; go, gonad; gt, gill suspensory stalk; ki, kidney; mb, mantle border; mo, mouth; ne, nephropore; pm, posterior adductor muscle; pp, labial palp; px, pallial organ; vg, visceral ganglia.

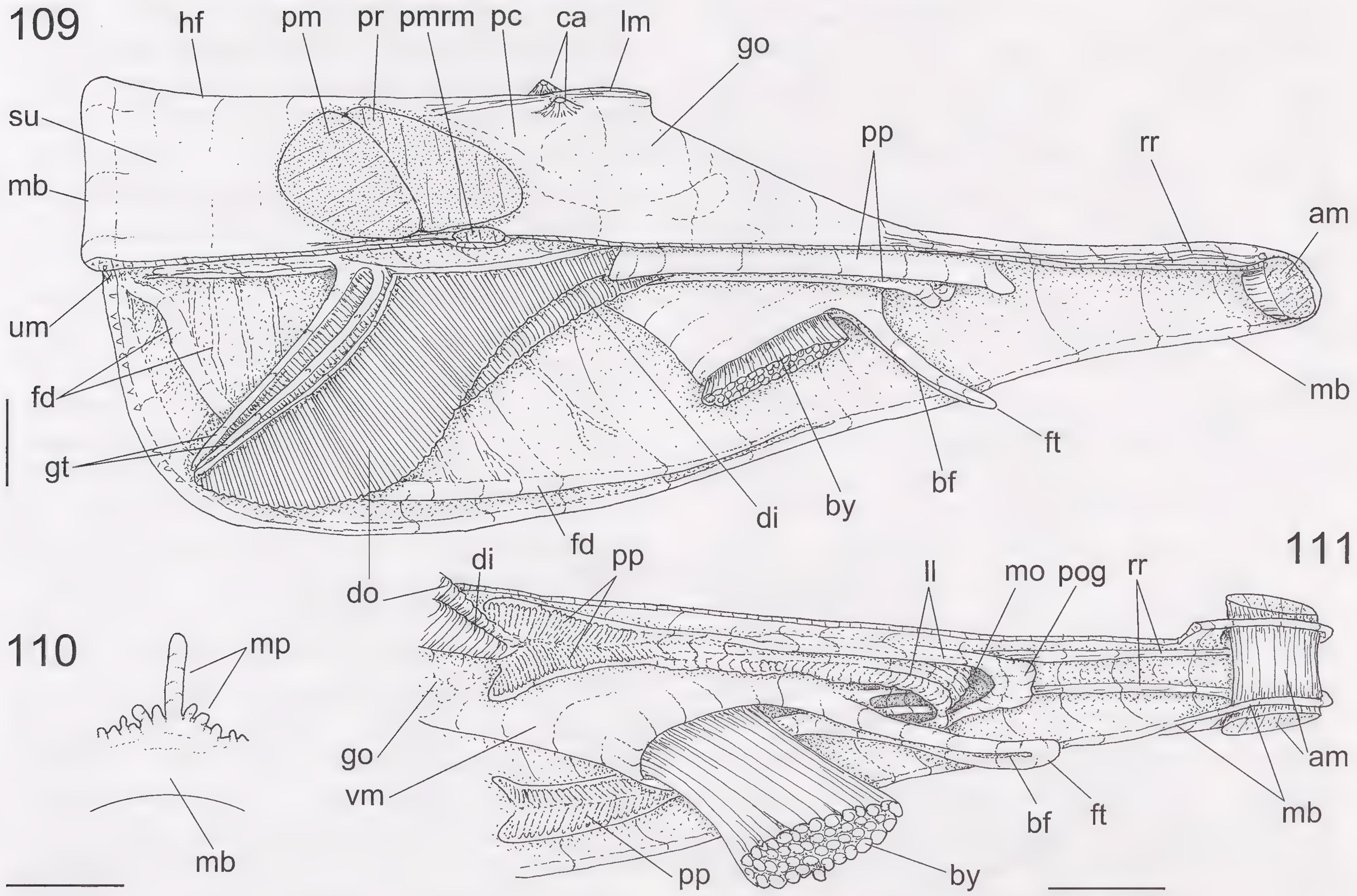

FIGS. 109–111. *Pinna carnea*, anatomy. FIG. 109: Intact right view, shell and part of right mantle lobe removed, posterior half of gills displaced from their more dorsal position; FIG. 110: Mantle border, detail of papillar arrangement of inner fold; FIG. 111: Detail of anterior region, ventral and slightly right view, part of right mantle lobe removed. Scale bars = 5 mm (FIGS. 109, 111); 1 mm (FIG. 110). Abbreviations: am, anterior adductor muscle; bf, byssal furrow; by, byssus; ca, cardinal muscle; di, inner demibranch; do, outer demibranch; fd, fold; ft, foot; go, gonad; gt, gill suspensory stalk; hf, hinge fold of mantle; ll, labial lips preceding mouth; lm, dorsal pallial retractor muscles; mb, mantle border; mo, mouth; mp, mantle papillae; pc, pericardium; pm, posterior adductor muscle; pmrm, posterior mantle retractor muscle; pog, preoral gland; pp, labial palp; pr, posterior pedal retractor muscle; rr, pedal protractor muscle; su, supra-anal chamber of suprabranchial pallial cavity; um, fusion between left and right mantle lobes; vm, visceral mass.

surrounding byssal base. Projecting portion L ≈ 16% SL, L = 8–9 W; distal tip bluntly pointed; byssal furrow running along most of ventral surface; anterior end subterminal. Basal portion (Fig. 107) with relatively thin, translucent walls surrounding byssal base, approximately as long as projecting portion. Byssus (Figs. 107, 109, 111: *by*) composed of large number of separated threads, pale brown, iridescent; each thread in L ≈ SH in material examined. Byssal gland as pair of bands running along central *pr* (Fig. 115) in their anterior, then gradually running medially, protruding inside visceral mass beyond these muscles, making long loop (Fig. 115: *bg*) in L ≈ *pr* L.

Mantle (Figs. 109, 110, 113, 114): Translucent, except bearing brown, sparse, coalescent spots at posterior edges. Mantle edges totally free, except for short portion in posterior region separating infra- and suprabranchial chambers (Fig. 113: *um*); this fusion forming horizontal platform in L ≈ 70% of *pm* L. Anterior border of platform horizontal; posterior border concave, with pair of lateral expansions extending narrowly along lateral walls toward posterior (Fig. 113). Posterior half of mantle lobes with several, well-developed transverse folds (Figs. 109, 114: *fd*) and pair of longitudinal folds running parallel to mantle edge, forming characteristic pinnid waste canal, gradually appearing at midlevel of shell, close to mantle edge, gradually separating from mantle edge, becoming ca. 20% SH away from mantle edge in posteroventral quadrant, then gradually approaching mantle edge, inserting into mantle fusion; this longitudinal fold T-shaped in cross section (Fig. 114: *fd*). Outer fold of mantle edge simple; T

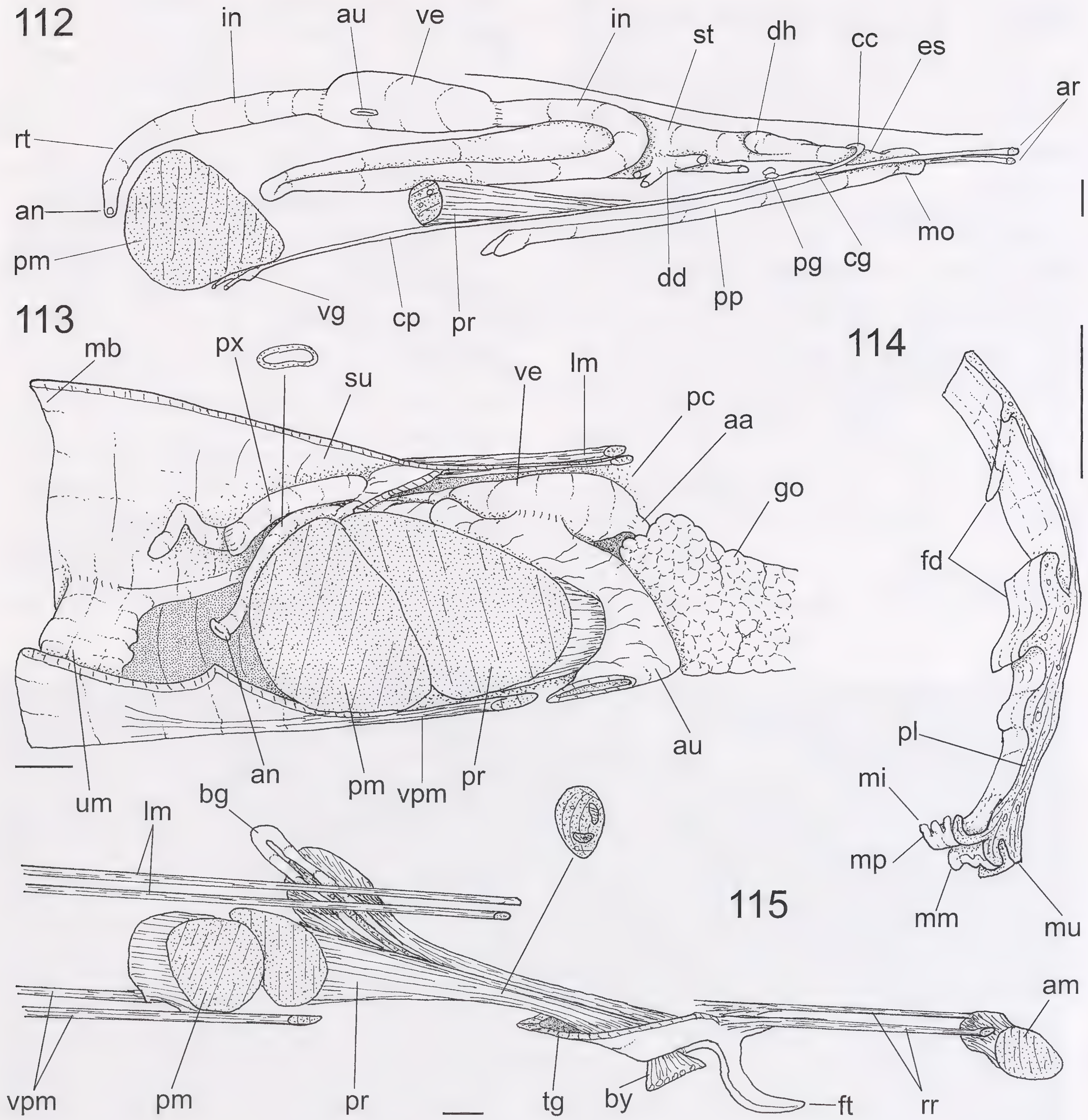

FIGS. 112–115. *Pinna carnea*, anatomy. FIG. 112: Digestive and nervous systems *in situ*, right view, topologies of some adjacent structures also shown; FIG. 113: Detail of posterior region, right view, right wall of pericardium removed, right mantle lobe longitudinally sectioned and deflected upward, detail of indicated region of rectum also shown; FIG. 114: Mantle edge, cross section of portion between ventral and posterior regions; FIG. 115: Foot and main musculature *in situ*, right view, cross section at indicated level of posterior pedal retractor muscle (pr) also shown. Scale bars = 2 mm. Abbreviations: aa, anterior aorta; am, anterior adductor muscle; an, anus; ar, anterior pedal retractor muscle; au, auricle; bg, byssal gland; by, byssus; cc, cerebral commissure; cg, cerebropleural ganglion; cp, cerebrovisceral connective; dd, ducts to digestive diverticula; dh, dorsal hood; es, esophagus; fd, folds; ft, foot; go, gonad; in, intestine; lm, dorsal pallial retractor muscles; mb, mantle border; mi, mantle border inner fold; mm, mantle border middle fold; mo, mouth; mp, mantle papillae; mu, mantle border outer fold; pc, pericardium; pg, pedal ganglion; pl, pallial muscles; pm, posterior adductor muscle; pp, labial palp; pr, posterior pedal retractor muscle; px, pallial organ; rr, pedal protractor muscle; rt, rectum; st, stomach; su, supra-anal chamber of suprabranchial pallial cavity; tg, integument; um, fusion between left and right mantle lobes; ve, ventricle; vg, visceral ganglia; vpm, ventral pallial retractor muscles.

≈ 2 ST, H ≈ 2 T. Middle mantle fold similar to outer fold, except with undulating edge; inner fold slightly taller and thinner than outer fold, forming pallial veil, bearing series of papillae at edge; papillae becoming larger and more complex from anterior to posterior; in posteroventral region (i.e., incurrent aperture) papillae arranged successively in pattern of each tall papilla (in L ≈ inner fold L) flanked by successively smaller papillae (in L ≈ 33% of tall papilla L; Fig. 110). Several pallial muscles mainly in posterior pallial lobes, not distinctly in pairs, mostly thick.

Pallial cavity (Figs. 107–109, 111, 113, 118): In V ≈ 85% SV, except in mid-dorsal visceral area. Anterior third narrow, bearing only *rr* on roof and *am* anteriorly. Posterior quarter of pallial cavity (posterior to *pm*; Fig. 113) mostly empty. Labial palps (Fig. 109: *pp*) very elongated anteroposteriorly, located horizontally between anterior and posterior thirds; L ≈ 16 H. Each hemipalp mostly symmetrical in middle and posterior regions (Fig. 111), with posterior ends bordering anterior end of gill along ca. 8% of *pp* L. *Pp* posterior third with 20–25 oblique, almost perpendicular folds, each with rounded ventral end, leaving smooth ventral margin of H ≈ 12% of *pp* H; ends of dorsal folds diminishing; folds adjacent, diminishing from posterior to anterior. Middle and anterior thirds of *pp* lacking inner folds, flanking wide, thick-walled furrow (oral groove); walls of inner hemipalp thicker than those of outer hemipalp, with multifolded, broad distal edge (Figs. 107, 111: *ll*), surrounding posterior lip of mouth; edges of outer hemipalps simpler and thinner than those of inner hemipalps, at anterior region of mouth (Figs. 107, 111: *mo*) with thick, broad gland-like thickening in V ≈ 50% of *am* V, with concave anterior and posterior margins. Gills large, in A ≈ 20% VA, L ≈ 50% SL, almost entirely in posterior half; anterior and posterior ends narrow, widening gradually at midregion to W ≈ 33% SH. Each gill anterior half attaching to visceral mass; posterior half free, connecting to ventral side of *pm* by long, slender gill suspensory stalk (Fig. 109: *gt*). *Gt* originating from posteroventral visceral mass, anterior to *pm* (Fig. 108). Each inner demibranch connecting via ciliary strip to visceral mass in anterior half, and to counterpart in posterior half. Outer demibranchs also connecting via ciliary strips to mantle lobes; in posterior half, strips on top of longitudinal folds, ending posteriorly on mantle union platform (Fig. 113: *um*), running longitudinally between middle and dorsal thirds of body. Demibranchs subequal, except in anterior half with outer demibranchs slightly narrower. Gill transverse reinforcements (Fig. 118: *gq*) at dorsal ends of each demibranch, as narrow transverse septa in H ≈ 4% of filament H, maintaining both branches of each filament in position; another reinforcement just dorsal to food groove on each demibranch, in W ≈ 33% of dorsal reinforcement W; another 2–3 transverse, filiform reinforcements sparsely placed along demibranchs. Gill filaments attaching by longitudinal series of narrow tissue bridges; interval between successive longitudinal bridges = 2–3 filament W. Food groove (Fig. 118: *fg*) at distal edge of each demibranch, narrow, deep; H ≈ 8% of filament H. Pallial organ (= mantle gland of Winckworth, 1929; Fig. 113: *px*) long, slender, originating in integument of anterior wall of supra-anal chamber just dorsal to rectum, projecting posteriorly along ca. 16% SL, in L ≈ 15 W; fold entirely surrounding division between middle and distal thirds, orange except for pale beige region close to distal tip; distal tip bluntly conical.

Visceral mass (Figs. 108, 112): Mostly compressed in central third of body, just anterior to *pm*; posteroventral region greatly compressed by paired *pr*; V ≈ 16% of visceral mass V. Digestive system longitudinal along central region; V ≈ 33% of visceral mass V. Renopericardial structures surrounding *pr*, wider in dorsal region of *pr*, along ca. 50% of visceral mass L and ca. 20% of visceral mass V. Digestive diverticula grayish beige, in anterior region along ca. 20% of visceral mass V. Gonad (Fig. 108, 112: *go*) cream-colored, filling remaining visceral regions, including ventral side of *pr*.

Circulatory and excretory systems (Figs. 108, 112–113): Location and size of renopericardial structures as described above. Pericardium greatly compressed by paired *pr*, surrounding *pr* just distal to origins. Auricles (*au*) dorsoventrally elongated, with thin, translucent walls, with narrow connection to ctenidial veins at midregion, running dorsally closely surrounding *rr*; blind sac posterior to connection to ventricle in L ≈ 25% of *au* L. Ventricle (Fig. 112: *ve*) at some distance from *pm*, in L = *pm* L; connections to *au* at lateral midregion, with intestine (Fig.112: *in*) passing

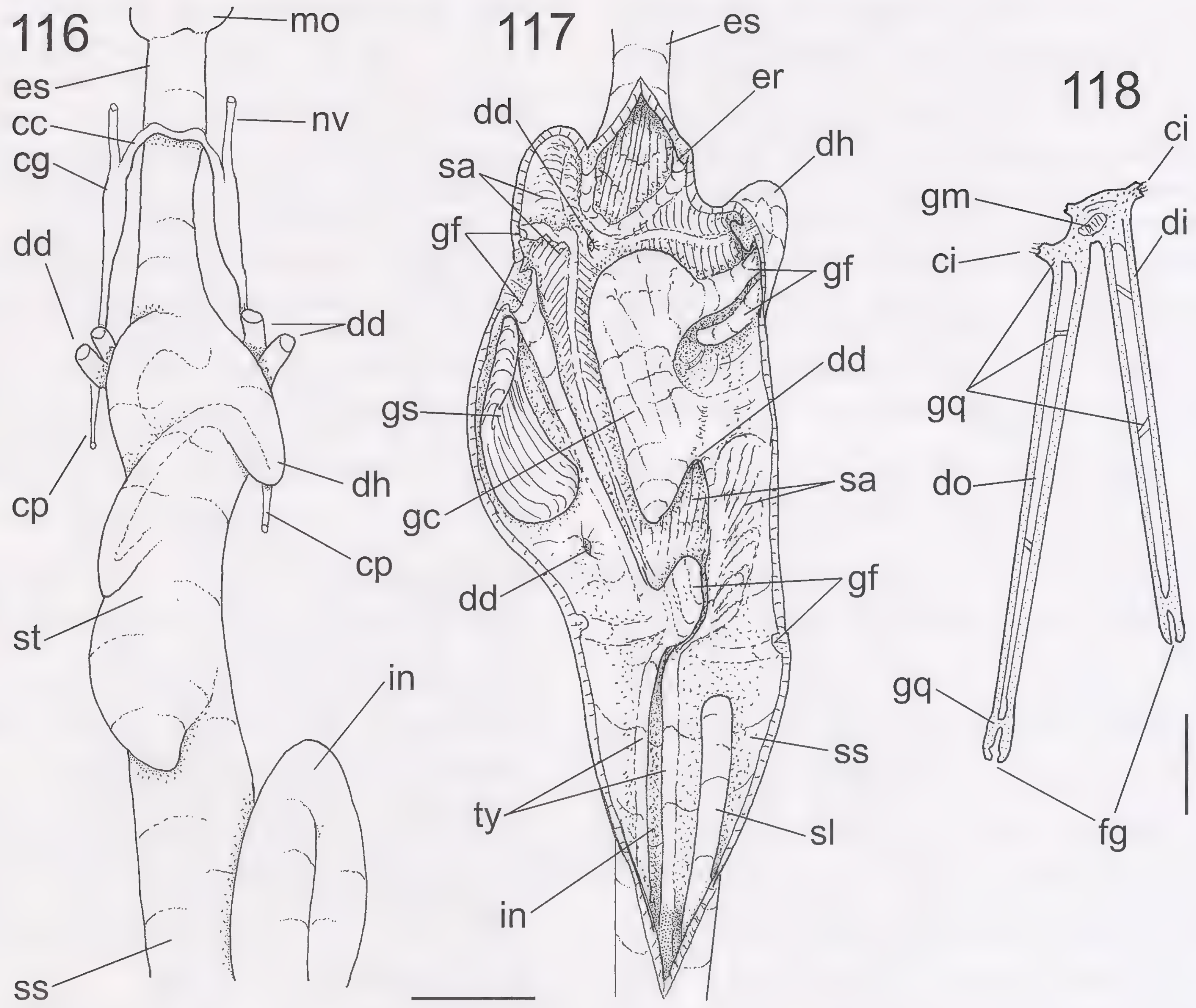

FIGS. 116–118. *Pinna carnea*, anatomy. FIG. 116: Anterior digestive system, dorsal view, anterior region of nervous system also shown *in situ*; FIG. 117: Stomach, dorsal view, opened longitudinally along midline; FIG. 118: Gill, cross section at midlevel. Scale bars = 2 mm. Abbreviations: cc, cerebral commissure; cg, cerebropleural ganglion; ci, ciliary connection of gill; cp, cerebrovisceral connective; dd, ducts to digestive diverticula; dh, dorsal hood; di, inner demibranch; do, outer demibranch; er, esophageal rim; es, esophagus; fg, food grooves; gc, gastric central pad; gf, gastric folds; gm, gill retractor muscle; gq, gill transverse reinforcement in suprabranchial chamber; gs, gastric shield; in, intestine; mo, mouth; nv, nerve; sa, gastric sorting area; sl, crystalline style; ss, style sac; st, stomach; ty, typhlosole.

through *ve*. Kidneys (Fig. 108: *ki*) brown, in ventral renopericardial area, just posterior to *pm*, solid, in V ≈ 12% of renopericardial V; each *ki* L ≈ 3 W, separated by distance = W. Nephropore (Fig. 108: *ne*) small, with sphincter, just anterior to *ki*, in ventral surface of visceral mass.

Digestive system (Figs. 107, 108, 111–113, 116, 117): *Pp* as described above. *Mo* relatively wide, preceded by glands in both lips (as described above) and series of transverse folds (Figs. 107, 111). Unpaired preoral gland (= pallial gland of Yonge, 1953a; glande prébuccal of Pelseneer, 1911; Fig. 111: *pog*) bulbous, anterior to *mo*. Esophagus (*es*) short, in L ≈ 70% of *am* L, W ≈ 33% of *am* W; inner surface bearing 8–10 narrow longitudinal folds (Fig. 117). *Es* rim (Fig. 117: *er*) simple, transverse fold surrounding entire *es* opening. Stomach (Figs. 116: *st*; 117) main chamber elliptical; L ≈ 3 H ≈ 16% of visceral mass L, H ≈ 33% of adjacent visceral mass H. Ducts to digestive diverticula at midlevel of ventral *st*. Dorsal hood (Figs. 116–119: *dh*) projecting at right posterior; V ≈ 25% of main gastric chamber V. Gastric dorsal surface with 3 additional low projections on left, corresponding to inner folds and cavities. Gastric inner surface (Fig. 117) complex. Gastric central pad (Fig. 117: *gc*) oval, midventral, in A ≈ 25% of inner gastric surface A; fold connecting to anterior-right corner of central pad running longitudinally in *dh*. Another gastric fold connecting to posterior-right edge of *gc*, surrounding right duct to digestive diverticula. Gastric shield (Fig. 117: *gs*) almost as large as *gc*, on posterodorsal inner gastric surface; furrow in left side between *gc* and *gs*, bearing tall fold dorsally, continuing as sigmoid furrow including right duct to digestive diverticula (anteriorly), passing posteriorly between another flattened posterior fold (similar to, but A ≈ 25% of *gc* A) and elliptical right-posterior sorting area (Fig. 117: *sa*). Left furrow as continuation from *dh*, bearing longitudinally 2 *sa* separated by narrow, central fold, mainly visible in anterior region of gastric ventral surface. Another *sa* divided by low, narrow fold in right side, just posterior to *es* rim, running to ventral side of *dh*. Left duct to digestive diverticula simple, at same level as right duct. Left gastric furrow continuing between typhlosoles (Fig. 117: *ty*) separating *in* from style sac (*ss*). Transverse fold separating gastric main chamber from conjoined *ss-in* opening. *Ss* L ≈ 50% of visceral mass L, tapering gradually, running horizontally posteriorly, totally fusing with *in*, with relatively low and narrow *ty* separating *in* from *ss*. *In* making single loop beyond *ss*, initiated by abrupt 180° loop, running along right side of *ss* and, at level of main gastric chamber, performing another wide curve, crossing from ventral to dorsal, then running along midline below hinge plate, posteriorly along ca. 50% visceral mass L. Rectum surrounding midregion of posterodorsal surface of *pm*, mostly exposed in pallial cavity (Fig. 113), lacking inner folds. Anus (Figs. 108, 113: *an*) with wide, blunt edges projecting away from *pm* surface, preceded by detached, siphon-like stalk in L ≈ 20% of rectum L.

Reproductive system: Gonad as described above; connection to *ki* not observed.

Nervous system (Figs. 108, 112, 116): Paired cerebropleural ganglia (Fig. 112, 116: *cg*) on either side of *es*; each *cg* elongated, in L ≈ 2 W, W = 33% of *es* D. Cerebral commissure in L ≈ single *cg* W. Paired pedal ganglia (Fig. 112: *pg*) posterior to *cg*; each elliptical, adjacent; V ≈ 33% of single *cg* V. Paired visceral ganglia (Fig. 108, 112: *vg*) on anteroventral surface of *pm*; each elliptical; V ≈ single *cg* V. Visceral commissure long; L = single *vg* W. Abdominal sense organs not observed.

Material Examined

USA, Florida Keys, FMNH 295720, 1 juvenile specimen (sta. FK-047); FMNH 295719, 1 specimen (sta. FK-195; dissected: 134.0 mm L, 56.0 mm H, 16.5 mm W); FMNH 295746, 1 specimen (sta. FK-351; dissected: 138.0 mm L, 63.5 mm H, 20.5 mm W).

Distribution

Stated by Turgeon et al. (2009) to range from southeastern Florida, Quintana Roo (Mexico), the Gulf of Mexico, Cuba, the Caribbean, Brazil, and Bermuda. *Pinna carnea* has been reported to occur on the Brazilian coast (e.g., Rios, 1994: 242; 2009: 494). However, Brazilian specimens differ in conchological and anatomical features from the Floridian species. This indicates a separate and potentially unnamed species in Brazil and Brazilian records therefore are not included in this account.

Remarks

For other details of the shell of *Pinna carnea*, see Mikkelsen & Bieler (2007: 120). Its anatomy reported here agrees with those presented for Pinnidae in general by Turner & Rosewater (1958), for *Atrina fragilis* (Pennant, 1777) by Winckworth (1929), and for *P. carnea* by Yonge (1953a), with the following exceptions. The present material is less heavily sculptured (5–7 longitudinal ridges here; 8–12 reported by Turner & Rosewater, 1958); this is likely a factor of size, our specimens (135 mm L) being only ca. 50% maximum adult L (288 mm L). Organs of Will (pigmented glandular spots on the middle and inner mantle folds in members of Pinnidae) were not observed. Paired cardinal muscles were recorded just dorsal to the heart; these are not connected to any other pallial muscles and have not been previously recorded in Pinnidae.

Yonge (1953a) described the functional morphology of *Pinna carnea* from Bermuda, based on both living and preserved specimens (with histology), including additional notes on behavior, ontogeny, physiology, and evolution of the family.

Several studies have concentrated on aspects of the biology of this species. Narváez et al. (2000) investigated abundance and growth of juveniles in Venezuela to investigate aquaculture potential. Tëmkin's (2010) molecular phylogeny of pearl oysters and their relatives included *Pinna carnea* from West Summerland Key (now Scout Key) in the Florida Keys. Sharma et al. (2012) studied protein-coding genes from a population in Beaufort, North Carolina.

Family Spondylidae Gray, 1826

Spondylus americanus Hermann, 1781
Figs. 119–135

Synonymy/Chresonymy

Spondylus americanus Hermann, 1781: 51 [Type locality: Santo Domingo]; Yonge, 1973: 177–188, figs. 2, 5, 9–11; Abbott, 1974: 450, pl. 21, fig. 5221; Rios, 1994: 250, pl. 86, fig. 1224; Viana & Rocha-Barreira, 2007: 815–819, figs. 1–4; Bieler & Mikkelsen, 2004: 520; Mikkelsen & Bieler, 2007: 154–155, 5 figs.; Rios, 2009: 508–509, fig.

Description

Shell (Figs. 119, 120): Highly variable, thick, varying from white, yellow, orange, red, brown, to combination; SL ≈ 80 mm in material examined, SH = 1–2 SL. Valves highly asymmetrical; RV larger, cementing to and assuming shape of hard substratum, with tall, triangular auricles; free LV more planar. Sculpture most evident on LV and detached portion of RV, composed of 20–30 radial threads; interspace W = thread W; normal arrangement of smaller and larger threads intercalated, with smaller thread W ≈ 50% of larger thread W. Spines and long scales typically occurring along threads, directed externally and to periphery; disposition regular, aligning commarginally; spines of larger threads typically larger than those of smaller threads; spines variable, absent in some specimens. Outer shell surface opaque, delicately irregular. Ligament (Fig. 120: *li*) along entire horizontal dorsal hinge plate, centrally occupying 70–80% SL, with triangular expansion at midregion, along ca. 10% SL, running along auricles of each valve, dividing them into 2 equal portions. Internal component of *li* extending at midregion of hinge plate along ca. 6% SH. Hinge plate occupying 70–80% SL and ca. 6% SH, symmetrical from internal component of *li*. RV with wide medial tooth and lateral socket on each side of *li*, each in L ≈ 15% of hinge plate L; LV with medial socket and wide lateral tooth on each side of *li*; tooth with tip wider than base; tip bluntly bifid. Inner surface glossy white, except same color as external surface at valve margin (Fig. 120), colored band H ≈ 7% SH at midventral edge, gradually diminishing toward hinge. Inner surface mostly smooth, except close to margin; latter with uniform denticles corresponding to external sculpture. Strong scar of adductor muscle subcentral, slightly posterodorsal; A ≈ 30% of inner VA.

Main muscle system (Figs. 120, 124, 125): Anterior adductor muscle absent. Posterior adductor muscle (*pm*) very large, circular in cross section, subcentral, slightly posterodorsal, in A ≈ 25% of inner VA, divided into 2 semicircular, subequal ("catch" and "quick") portions. No other well-developed muscles except T of visceral wall serving as pedal protractor muscles, thicker anteriorly, forming 2 lateral, anterior, dorsoventral folds (Fig. 124: *rr*).

Foot (Figs. 124, 125: *ft*): Well-developed, anteroventral, in form of wide bell, with relatively thick muscular walls and deep concavity; V ≈ 10% SV ≈ 50% of visceral mass portion ventral to *pm*. Outer surface smooth, pigmented by sparse, dark brown spots. Inner surface white, covered by uniform, low radial folds, originating in small, central, smooth area; each fold separated from others by narrow furrow and mostly dichotomizing at midlevel. Pair of deeper, wider furrows running, respectively, anteriorly and posteriorly. Byssus and byssal gland absent.

Mantle (Figs. 126–128): Mantle edge thickened, with 3 well-developed folds, mostly pigmented dark brown (rarely pale beige), with coalescent, broad, whitish spots, subcircular in some areas. Outer mantle fold thin (T ≈ 33% ST, H ≈ 2 T), simple, white. Periostracum separating outer and middle folds. Middle fold T ≈ 3 outer fold T, bearing large, tall papillae and eyes in following arrangement (Figs. 126, 127): outer row of small, slender, pointed papillae; inner row of larger, taller papillae, fewer in number than smaller papillae of outer row; one eye between every one or 2 papillae. Each eye (Figs. 127, 128: *ey*) on short eyestalk, containing large lens and dark retina contacting and covering basal and lateral sides of lens; cornea thin, occupying central tip; cornea surrounded by black integument. Ocular nerve thick, running from retina toward base of eyestalk, then as 8–10 nerves running radially along mantle lobes (Fig. 121: *nv*). Inner mantle fold very wide (W ≈ 20% SH), directed internally as pallial veil, contacting inner fold of opposing mantle lobe, especially high midventrally. Mantle muscles thick, originating at pallial line at some distance from shell margin, inserting along 3 folds, mostly in inner fold. Remaining mantle thin, translucent from pallial line to *pm*, bearing several iridescent, radial pallial nerves.

Pallial cavity (Figs. 123, 124, 133): In V ≈ 33% of body V, especially broader ventrally and anteriorly. Labial palps (Figs. 123, 124: *pp*) dorsoventrally long, anteroposteriorly short; region between hemipalps attaching along anterior border of pallial cavity. Anterior ends of demibranchs ending between dorsal ends of hemipalps. Dorsal ends of hemipalps partially fused and situated as anterior cover of

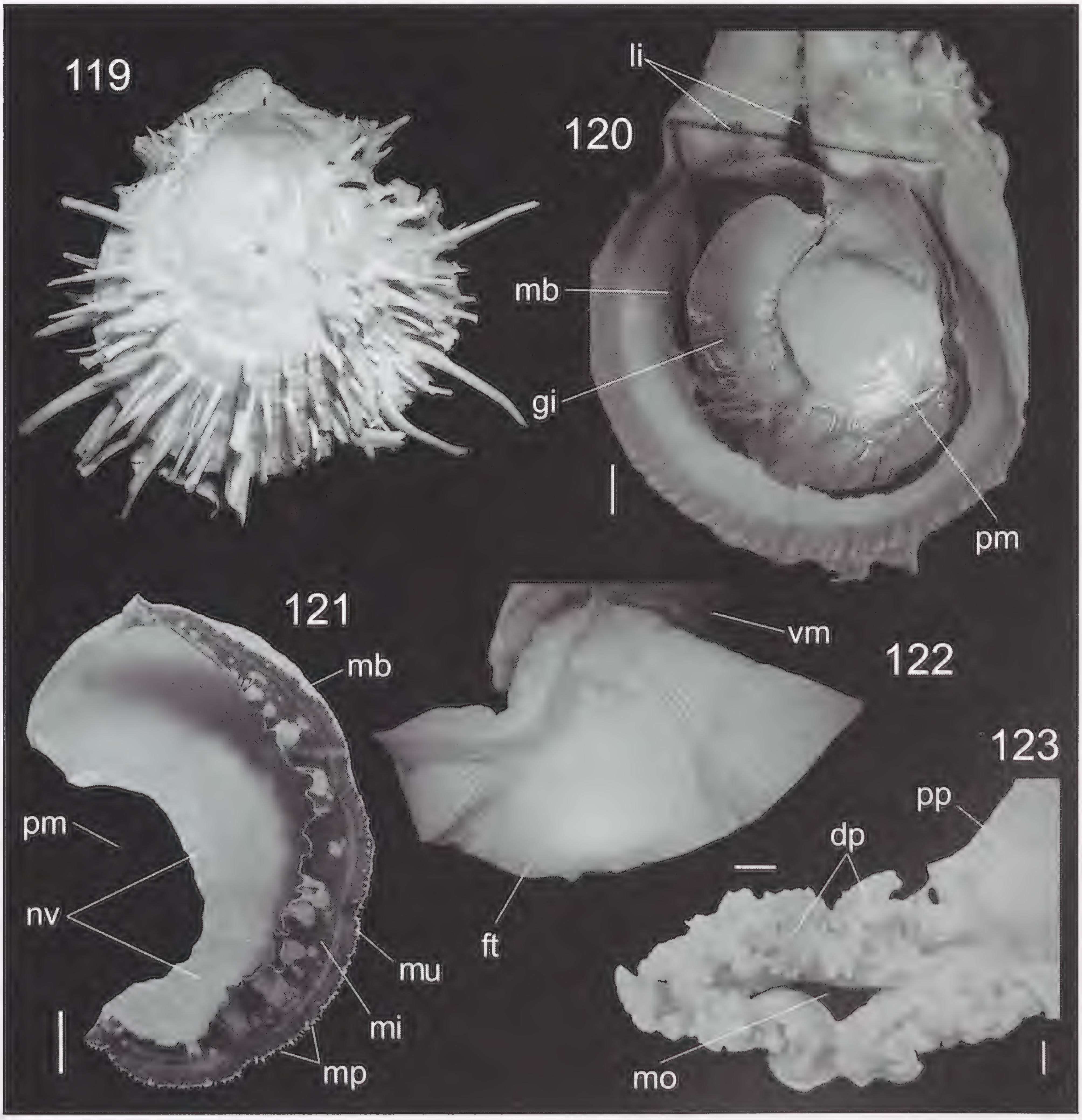

FIGS. 119–123. *Spondylus americanus.* FIG. 119: Shell morphology, articulated specimen, right view, FMNH 177515, 84.9 mm L. FIGS. 120–123: Anatomy, FMNH 302068, 98.0 mm maximum D; FIG. 120: Intact left view, LV and part of left mantle lobe removed; FIG. 121: Left mantle lobe, interior view; FIG. 122: Foot, opened longitudinally, exposing inner (ventral) surface; FIG. 123: Buccal region, ventral view, adjacent part of left labial palp (pp) also shown. Scale bars = 10 mm. dp, dentritic projection of lips and labial palps; ft, foot; gi, gill; li, ligament; mb, mantle border; mi, mantle border inner fold; mo, mouth; mp, mantle papillae; mu, mantle border outer fold; nv, nerves; pm, posterior adductor muscle; pp, labial palp; vm, visceral mass.

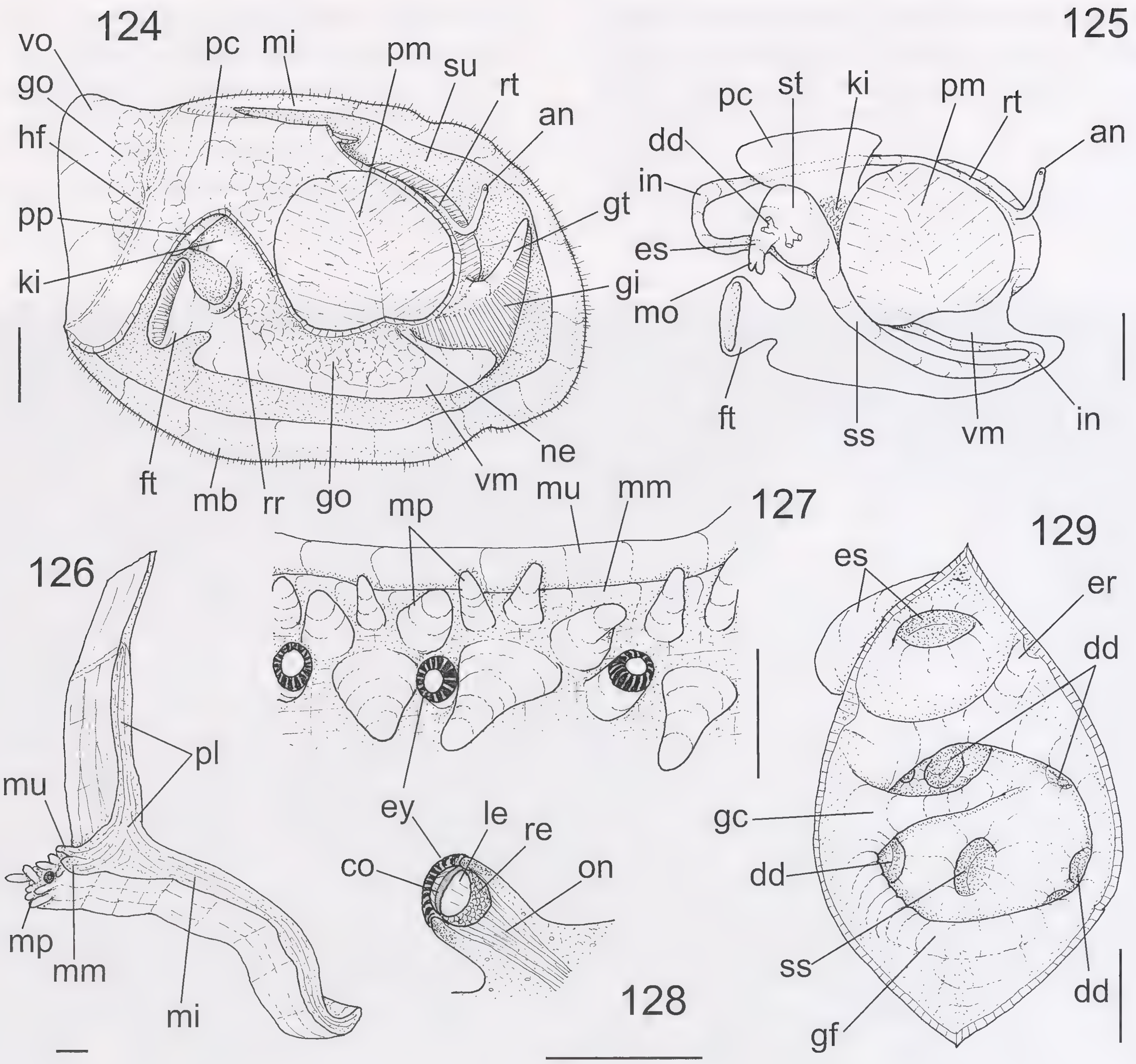

FIGS. 124–129. *Spondylus americanus*, anatomy. FIG. 124: Left overview, shell and part of left mantle lobe removed; FIG. 125: Same, digestive system *in situ*, topologies of some adjacent structures also shown; FIG. 126: Mantle border, cross section at midventral region; FIG. 127: Same, detail of outer and middle folds, ventral view; FIG. 128: Pallial eye, sectioned longitudinally; FIG. 129: Stomach, dorsal view, dorsal wall sectioned longitudinally and deflected. Scale bars = 10 mm (FIGS. 124, 125); 1 mm (FIGS. 126–129). Abbreviations: co, cornea; dd, ducts to digestive diverticula; er, esophageal rim; es, esophagus; ey, pallial eye; ft, foot; gc, gastric central pad; gf, gastric fold; gi, gill; go, gonad; gt, gill suspensory stalk; hf, hinge fold of mantle; in, intestine; ki, kidney; le, lens; mb, mantle border; mi, mantle border inner fold; mm, mantle border middle fold; mo, mouth; mp, mantle papillae; mu, mantle border outer fold; ne, nephropore; on, optical nerve; pc, pericardium; pl, pallial muscles; pm, posterior adductor muscle; pp, labial palp; re, retina; rr, pedal protractor muscle; rt, rectum; ss, style sac; st, stomach; su, supra-anal chamber of suprabranchial pallial cavity; vm, visceral mass; vo, mantle portion occupying umbonal cavity (in fixed valve only).

gill. Inner surfaces of hemipalps similar (Fig. 133), each with ca. 25 transverse folds, alternating on each hemipalp. Posterior end of each fold rounded, with narrow smooth area preceding *pp* edge; posterior half of each fold slightly narrower than anterior half (gradually transitioning); anterior end gradually diminishing, with smooth furrow separating hemipalps. Inner surfaces of hemipalps abruptly changing ventrally (Figs. 123, 133), becoming longitudinal (perpendicular in relation to preceding folds), their distal ends curving toward *pp* edge, becoming tall and successively branching "lips," each with dendritic projections (Figs. 123, 133: *dp*) protruding into flaps on inner surface of *pp* surrounding

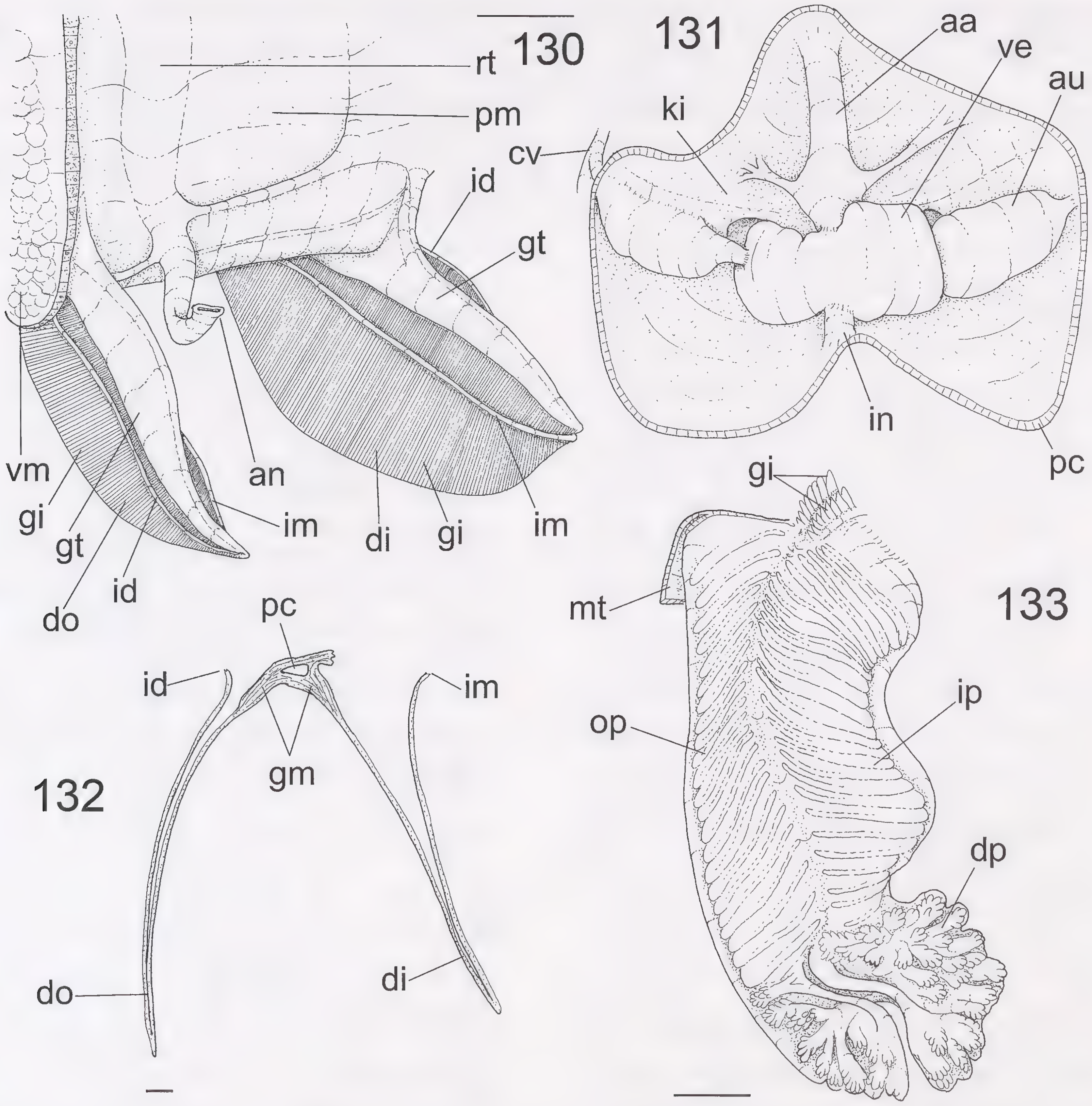

FIGS. 130–133. *Spondylus americanus*, anatomy. FIG. 130: Pallial cavity, detail of region posterior to posterior adductor muscle (pm), with gill deflected and mantle lobes removed; FIG. 131: Pericardial structures, dorsal view, dorsal region of pericardium removed; FIG. 132: Left gill, cross section in midregion; FIG. 133: Left labial palp, right-lateral view, outer hemipalp (op) deflected to show inner surface, short portion of adjacent region of gill (gi) and mantle (mt) also shown. Scale bars = 2 mm. Abbreviations: aa, anterior aorta; an, anus; au, auricle; cv, ctenidial (efferent) vessel; di, inner demibranch; do, outer demibranch; dp, dentritic projection of lips and labial palps; gi, gill; gm, gill retractor muscle; gt, gill suspensory stalk; id, insertion of outer demibranch in mantle; im, insertion of inner demibranch in visceral mass; in, intestine; ip, inner hemipalp; ki, kidney; mt, mantle; op, outer hemipalp; pc, pericardium; pm, posterior adductor muscle; rt, rectum; ve, ventricle; vm, visceral mass.

mouth. Smooth membrane as continuation of outer surface of *pp* surrounding dendritic external surface, little beyond them.

Gills (Fig. 130: *gi*): Surrounding ventral surface of *pm*; L = SL, V ≈ 70% of pallial cavity V. *Gi* filaments free (i.e., filibranch) and free from neighboring structures (mantle and visceral mass), connecting to latter by cilia. Each filament (Fig. 132) very narrow, long, without food grooves; ventral third of each demibranch descending and ascending lamellae connected; remaining part of lamellae free. Ctenidial vein running along *gi* base between demibranchs, surrounded by thin longitudinal muscle (Fig. 132); transverse muscle present ventral to it, also running in basal portion of each demibranch. Posterior projections of *gi* supported by suspensory stalk (Fig. 130: *gt*); each *gt* weakly muscular, laterally compressed, dorsoventrally tall; base of each *gt*

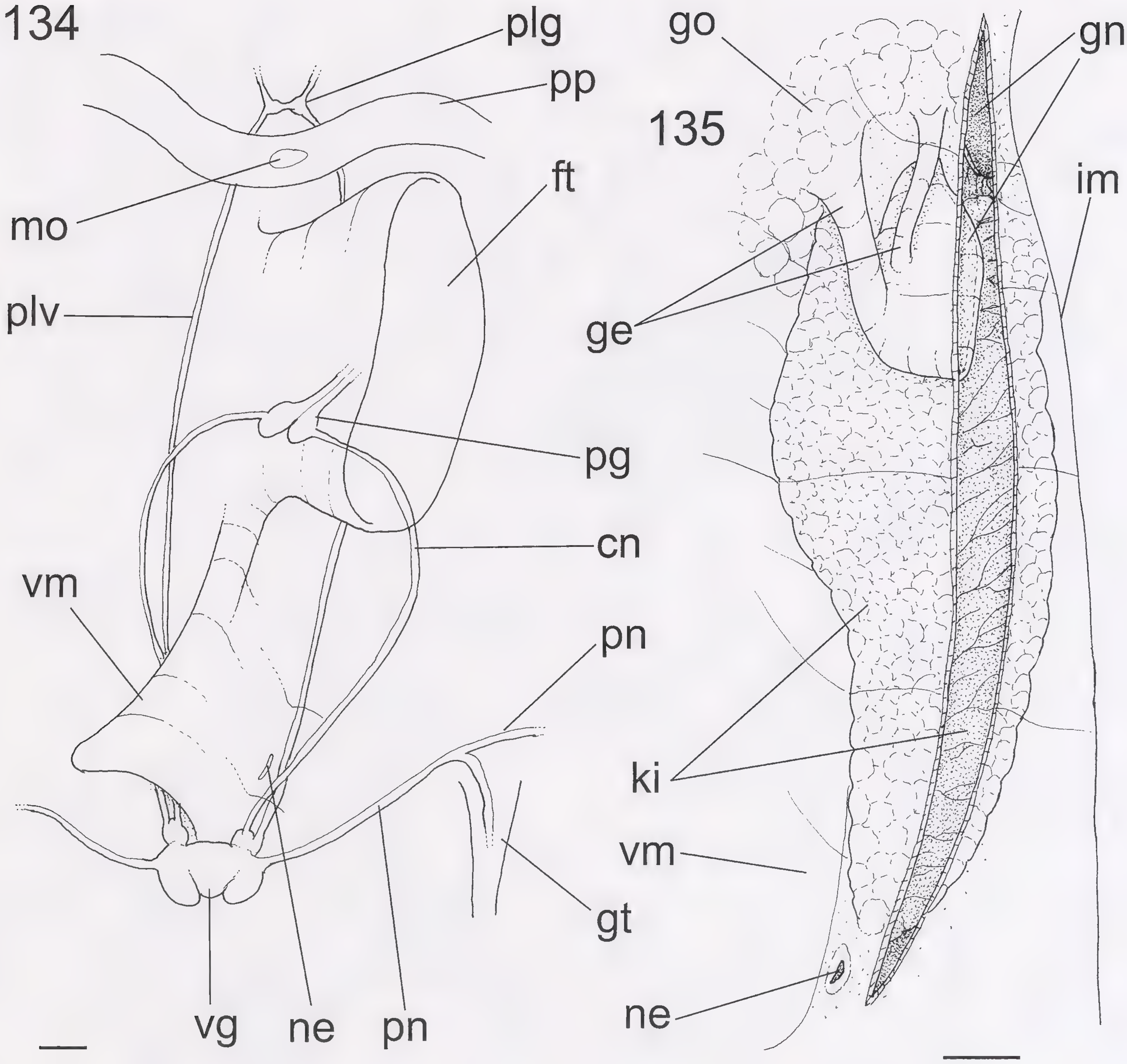

FIGS. 134, 135. *Spondylus americanus*, anatomy. FIG. 134: Nervous system *in situ*, ventral view, topologies of adjacent structures also shown, foot (ft) slightly deflected to left (at right in figure) and posterior region of visceral mass (vm) to right (at left in figure); FIG. 135: Left kidney and terminal reproductive structures, ventral view, topologies of adjacent structures also shown; ventral renal wall sectioned longitudinally; some inner structures exposed or seen by transparency. Scale bars = 1 mm. Abbreviations: cn, cerebropedal connective; ft, foot; ge, genital ducts; gn, genital chamber; go, gonad; gt, gill suspensory stalk; im, insertion of inner demibranch in visceral mass; ki, kidney; mo, mouth; ne, nephropore; pg, pedal ganglion; plg, anterior (?pleural) ganglion; plv, pleurovisceral (?) connective; pn, pallial nerve from visceral ganglion; pp, labial palp; vg, visceral ganglia; vm, visceral mass.

originating at ventral *pm*, gradually tapering posteriorly; distal tip pointed; L ≈ 25% of *gi* L. Inner demibranchs connecting by cilia along midline in posterior third of L.

Visceral mass (Figs. 124, 125, 129) asymmetrical anterodorsally, accompanying asymmetry of umbonal region of shell valves; right portion taller and longer than left; taller portion very variable, mostly filled with connective tissue, ventrally compressed, extending posterior to *ft* and ventral to *pm*, protruding posteriorly as "heel" slightly beyond *pm*. Stomach (Figs. 125: *st*; 129) mid-dorsal. Digestive diverticula greenish-brown, covering *st* almost totally and slightly beyond. Gonad cream-colored, covering digestive diverticula and extending dorsally into both umbonal regions, ventrally in compressed ventral region posterior to *ft*, and lateroposteriorly contacting *pm*. Pericardium just anterior to *pm*, compressed anteriorly by gonad.

Circulatory and excretory systems (Figs. 125, 131, 134, 135): Pericardium (Fig. 125: *pc*) anteroposteriorly short, laterally broad; W ≈

pm W, V ≈ 20% of visceral mass V (including adductor). Ventricle (*ve*) massive, in central region, surrounding intestine crossing *pc*, with central portion narrower than lateral portions. *Ve* connection with auricles (*au*) narrow, in central region of lateral walls. *Au* lateral, each as large as *ve*; anterior surface of each connecting to pericardial wall; lateral end connecting to ctenidial vein. Anterior aorta broad, dichotomizing after short distance, running along surface of adjacent anterior portion of gonad, dorsal to intestine. Posterior aorta narrow, running ventral to intestine. Ctenidial vein narrow along entire L, connecting with *au* by short vein of same D between anterior and middle thirds of *gi*, just anterior to *pm*. Kidney (*ki*) brown, extending ventral to *pc* to posteroventral *pm*, posterodorsal to *ft*, mostly solid, containing tall transverse folds, coalescent and branching. Ventral wall of *ki* separating it from pallial cavity, thin, translucent, detached from renal tissue. Nephropore (Figs. 134, 135: *ne*) small, at posterior end of renal chamber, at level of posteroventral *pm*. Genital structures bulging into posterior *ki* as described below.

Digestive system (Figs. 123, 125, 129, 130, 133): *Pp* as described above. Mouth wide, located deep among dendritic lips of *pp* (Figs. 123, 133: *dp*). Esophagus (*es*) broad, conic, short (L ≈ 33% of *pp* L); inner surface smooth; inserting into stomach (*st*) anteroventrally. Gastric main chamber occupying ca. 33% of visceral portion anterior to *pm*, close to latter. Gastric inner surface (Fig. 129) with 3 transverse, mostly ventral, tall folds; anterior one close to *es* opening; middle one close to anterior fold; posterior one close to posterior end of *st*; relatively deep concavity between each successive ventral fold; anterior and posterior folds connecting by longitudinal, low, right fold; another tall longitudinal connection on left side uniting middle and posterior folds (Fig. 129: *gf*), with transverse furrow as sorting area. Ducts to digestive diverticula (Fig. 129: *dd*) relatively wide; one pair in concavity between anterior and middle ventral folds; another 3 ducts in ventral edge of longitudinal fold connecting anterior and posterior folds; another large duct in ventral edge of longitudinal fold uniting middle and posterior ventral folds. Gastric shield (*gs*) between posterior ventral fold and posterior end of *st*. Intestine (*in*) and style sac (*ss*) broadly conjoined, originating at midregion of concavity between middle and posterior ventral folds; opening relatively broad (W ≈ 33% of *st* W), running posteroventrally, narrowing gradually to end of ventral, compressed region of visceral mass at posterior level of *pm*; *in* abruptly twisting in this region, running anterodorsally to *ss*, crossing to right of conjoined *ss-in* opening at right-ventral *st*; *in* running anteriorly beyond *st*, making wide loop dorsally, then running posteriorly, crossing *pc* and dorsal surface of *pm*, gradually running closer to LV. Anus (Fig. 130: *an*) simple, dorsoventrally compressed, preceded by long, free stalk, originating on left third of *pm* posterior surface; stalk base with pair of transverse folds, each originating from base of *gt*; right fold slightly more dorsal than left.

Reproductive system (Fig. 135): Gonad as described above, separated into 2 pairs of lobes; dorsal pair with terminal hollow chamber in anterior end of *ki*, in anteroventral visceral mass; this chamber separated from *ki* by membrane, latter abruptly becoming tube-like (*ge*) at midventral surface; tube running posteriorly, opening at midventral region of other prerenal chamber. Ventral lobes without obvious terminal chambers, but also with terminal tube (*ge*) in W ≈ 2 dorsal lobe W; terminal tube inserting into prerenal chamber in medial edge. Each prerenal chamber with thin walls, dorsoventrally compressed, in A = 16% of *ki* A; ventral surface attaching to walls separating renal and pallial chambers, also covering tube of dorsal gonadal lobes; dorsal surface free in renal chamber; anteroventral region of renal lobe bulging; aperture wide. Gametes apparently traversing these tubes and prerenal chamber, exiting at nephropores after crossing entire renal L.

Nervous system (Fig. 134): Paired anterior (pleural?; see Remarks) ganglia (*plg*) spherical, small (A ≈ 33% of *es* D), adjacent, close to midline, just anterior to mouth; commissure L ≈ 50% of single *plg* L. Paired pedal ganglia (*pg*) each in V ≈ 2 single *plg* V, adjacent in posterodorsal region of visceral surface of *ft*; each *pg* with large anterior nerve running through pedal musculature. Paired visceral ganglia (*vg*) very large, just posterior to junction of visceral mass with ventral surface of *pm*, each in V = 6–7 single *plg* V. *Vg* forming 5-lobed structure; central lobe largest, with 2 lateral lobes, each in V ≈ 50% of central lobe V, and 2 posterior lobes (cerebral ganglia?), each in V ≈ 25% of central lobe V, bulging at anterior surface of this ganglionic mass, slightly away from midline. Pleurovisceral

(?; see Remarks) connectives (*plv*) running through visceral glands, close to integument, surrounding *ft* base, joining with lateral region of posterior *vg* lobes. Cerebropedal connectives (*cn*) in T ≈ pleurovisceral connectives T, running ventral to latter, inserting medially into posterior visceral lobes. Thick pair of nerves inserting into lateral surface of *vg*, between posterior and lateral lobes, with 2 branches each, one innervating gill stalks, other mantle border. Pallial eyes as described above. Abdominal sense organs not observed.

Material Examined

USA, Florida Keys, FMNH 302065, 302066, 302068, 4 specimens [sta. FK-717; 2 dissected: #1: ca. 86 mm L, 103 mm H, 45 mm W (without spines); #2: ca. 80 mm L,118 mm H, 46 mm W; Garden Key, Dry Tortugas, FMNH 177515 (84.9 mm L); FMNH 295736, 1 specimen (= *S. ambiguus*) (sta. FK-048; dissected: ca. 67 mm L, 45 mm H, 41 mm W).

BRAZIL. Pernambuco. Fernando de Noronha Archipelago, Conceição beach, 3°50'22.3"S, 32°24'55.8"W, 10 m, MZSP 31402, 1 specimen (vii/1999; dissected: 77.5 mm L, 72.2 mm H, 45.4 mm W). Bahia. Salvador; Itapuã beach, 12°57'13"S, 38°21'43"W, 2 m, MZSP 28437, 1 specimen (27/xi/1997; dissected, not measured). Espírito Santo. Off Guarapari, 45 m, MZSP 70127, 1 specimen (in lobster net, vi/2006), MZSP 37381, 2 specimens, 1 shell (vi/2003; dissected, not measured). Rio de Janeiro. Conceição beach, 23°12'03.1"S, 44°37'36.8"W, 4 m, MZSP 55737, 2 specimens (09/xii/2005; dissected, not measured), MZSP 55739, 2 specimens (09/xii/2005; dissected, not measured); Ilha Comprida, 23°11'23.8"S, 44°37'23.9"W, MZSP 55693, 1 specimen (09/xii/2005; dissected, not measured); Lula beach, 23°11'38.5"S, 44°38'06.5"W, MZSP 55812, 1 specimen (10/xii/2005; dissected, not measured), 23°11'47.4"S, 44°37'44.1"W, MZSP 58953, 1 specimen (12/i/2006; dissected, not measured), Restaurante beach, 23°11'39.0"S, 44°37'32.2"W, 3 m, MZSP 55775, 1 specimen (10/xii/2005; dissected, not measured), Catimbau beach, 23°11'26.4"S, 44°37'25.5"W, 10 m, MZSP 55945, 2 specimens (10/xii/2005; dissected, #1: 77.5 mm L, 69.0 mm H, 48.0 mm W; #2: 62.0 mm L, 64.0 mm H, 41.3 mm W), MZSP 55944, 2 specimens (10/xii/2005; dissected, not measured); Ilha Grande; Imbuacica Is., MZSP 79343, 2 specimens (20/viii/2006; dissected, not measured), Freguesia do Sul beach, MZSP 23079, 1 specimen, 1 shell (24/vii/1966; dissected, not measured), Parcel do Aleijado, MZSP 23080, 1 specimen (18/vii/1966; dissected, not measured). São Paulo. Queimada Grande Is., 24°28'57"S, 46°40'41"W, 8–25 m, MZSP 35664, 2 specimens (28/vi/2002; dissected, not measured).

Distribution

Stated by Turgeon et al. (2009) to range from North Carolina to Quintana Roo (Mexico), the Gulf of Mexico outer banks, Brazil, and Bermuda. Its occurrence in Brazil to São Paulo is here confirmed.

Remarks

The anatomy described here agrees in all aspects with previous studies of spondylid anatomy (Dakin, 1928a, b, based mostly on Mediterranean *Spondylus gaederopus* Linnaeus, 1758; Yonge, 1973, based on *S. americanus* from Jamaica), including verifying two unusual features of the spondylid nervous system: (1) the very large visceral ganglionic complex (similar to that found in Pectinidae), and (2) the pedal ganglia joined via connectives with the latter (unique to Spondylidae). Watson (1930b) and Yonge (1973) postulated that the greater part of the cerebropleural ganglia are actually part of the visceral ganglionic complex (here as the two anterior bulges on the mass), evidenced by their connection with the pedal ganglia; if so, the anterior ganglia reported here are merely remnants, possibly only of the pleural ganglia. Further details of the pallial eyes of *S. americanus*, based on specimens from Brazil, were provided by Viana & Rocha-Barreira (2007).

This species shows a high degree of shell variation, due to phenotypic plasticity, incrustation, and moulding with the hard substratum. Logan (1974) explored the functional morphology of this species in Bermuda, identifying five main modes of life, ranging from cementation on exposed deep reef walls to lying free in sediment pockets after having been dislodged from its substratum. In the Florida Keys, and elsewhere off both coasts of Florida, *Spondylus americanus* occurs in deeper water, on hard substrata (including shipwrecks) from ca. 25–30 m. It is replaced in shallower water by *S. ambiguus* Chenu, 1844 (in 1843–1845; previously known as *S. ictericus* Reeve, 1856, a synonym *teste* Lamprell, 2006; Finet

& Lamprell, 2008), a morphospecies with brick-red shells (see Mikkelsen & Bieler, 2007: 156–157). [Both nominal species (*S. ictericus*, *S. ambiguus*) were recently synonymized under *S. tenuis* Schreibers, 1793, by Huber (2010: 628). Because the question of whether Schreibers' work can be accepted as binominal appears to be unresolved (see also Cox, 1929), we are using the name *S. ambiguus* herein]. In other parts of the western Atlantic, including Brazil and Bermuda, *S. americanus* also occurs in shallow water. *Spondylus ambiguus* is also stated to occur in Brazil (Rios, 1994: 250, as *S. ictericus*), but no comparable anatomical differences were found by LRS in a study of extensive material that would justify a separation into two morphospecies within the Brazilian fauna. The *S. americanus* specimens from Florida and Brazil showed no anatomical differences. However, because the shells of *S. americanus* and *S. ambiguus* are clearly separable in Florida populations, we refrain from formally synonymizing the two species and await future molecular studies.

Family Plicatulidae
Gray, 1854

Plicatula gibbosa
Lamarck, 1801
Figs. 136–147

Synonymy/Chresonymy

Plicatula gibbosa Lamarck, 1801: 132 [no locality given]; Yonge, 1973: 188–197, figs. 14–23; Abbott, 1974: 450, fig. 5216, pl. 20, fig. 5216; Bieler & Mikkelsen, 2004: 519; Mikkelsen & Bieler, 2007: 158–159, 5 figs.

Description

Shell (Figs. 136–138): Oval to subtriangular, irregular, typically thick, white to brown, homogeneous to spotted; SL ≈ 9 mm in material examined. RV totally or partially cementing to hard substratum, fitting into surfaces even if irregular; periumbonally attaching to substratum in partially attached specimens. RV typically slightly more distorted and more concave than LV. Outer surface opaque, covered by pores, with 3–5 wide, irregular, radial undulations/plicae, producing undulating ventral and posterior margins (Figs. 137, 138). Hinge plate of RV with medial pair of strong, symmetrical, divergent teeth, with corresponding medial sockets in LV; tooth L = 10–16% SH. Ligament central, between teeth. Inner surface smooth, translucent, glossy. Scar of adductor muscle circular, at mid-SH between middle and posterior thirds of SL; A ≈ 7% of inner VA.

Main muscle system (Figs. 138, 139): Anterior adductor muscle absent. Posterior adductor muscle (*pm*) location and proportions as described above, clearly possessing 2 ("catch" and "quick") portions; anterior A ≈ 40% of *pm* A. Pedal muscles absent.

Foot: Absent.

Mantle (Figs. 139, 147): Mantle lobes thin, translucent except at relatively thick borders; lobes free except for dorsal hinge fold; H = 33% SH. Pallial muscles connecting to pallial line, at distance from shell margin = 25–33% SH. Outer fold of mantle lobe (Fig. 147: *mu*) thin, simple; T ≈ 33% ST, H ≈ 3 T. Middle fold (Fig. 147: *mm*) in T and H = 2 outer fold T and H; papillae gradually appearing along entire posterior half of edge; each papilla L ≈ W, at edges of fold, slightly internal; interspace W = 2–3 papilla W; longer papillae alternating with shorter papillae; shorter papilla L ≈ 50% of longer papilla L. Inner mantle fold (Fig. 147: *mi*) of similar proportions to middle fold, except forming narrow pallial veil and having fewer and smaller papillae.

Pallial cavity (Figs. 138, 139, 142, 143, 145): In V ≈ 75% of inner SV, except visceral mass from hinge area to midlevel of valves; cavity surrounding ventral, posterior, and dorsal sides of visceral mass. Labial palp A ≈ 2% VA ≈ 25% SL ventral to hinge plate. Palps (*pp*) covering anterior end of gills, extending ca. 12% SL anterior to gills. Hemipalps similarly shaped (Figs. 142, 143) as 2 successive layers of bent flaps, in L ≈ 2 H, narrowing gradually from anterodorsal to posterior. Outer hemipalps widely fused anteriorly; dendritic projection (Figs. 142, 143: *dp*) with 3 papillae at ventral edge, located midway between outer hemipalps, in H = 20% of *pp* H; base slightly narrower than tip. Inner hemipalps widely connecting anteriorly, almost as tall as same regions of outer hemipalps, lacking dendritic projection. *Pp* inner surface with 5–7 wide transverse folds, successively shorter from anterior to posterior; each fold with rounded ventral end, leaving smooth ventral edge in W ≈ 12% of *pp* W; interspace W = 50% of fold W; dorsal ends of folds connecting to dorsal furrow.

Gills (*gi*): Not plicated, linear, lying along ca. 70% SL, in H ≈ 25% SH in wider (anterior and middle) portions; anterior ends rounded; posterior ends tapering gradually. Gill suspensory stalks (Figs. 138, 139: *gt*) inserting into posteroventral *pm*; base almost as wide as *pm*, gradually tapering to bluntly pointed tip; extending along (posterior) 50% of *gi*. *Gi* filaments connecting to one another and to adjacent structures only via cilia; each ascending lamella L ≈ 50% of descending lamella L (Fig. 145); distal tip of these shorter lamellae bent laterally preceding ciliary connection (Fig. 145: *id, im*). Anterior ends of *gi* inserting between hemipalps along ca. 20% of posterior region (Figs. 142, 143).

Visceral mass (Figs. 138–140, 144): Along relatively narrow horizontal band between hinge area and *pm*; V ≈ 16% SV, L ≈ 2 H. Digestive system along central region; V ≈ 50% of visceral mass V. Digestive diverticula greenish-cream, surrounding stomach; V ≈ 12% of visceral mass V. Gonad greenish-cream, with clearly visible acini on nodular surface, filling entire remaining visceral mass V, including umbones. Renopericardial structures rectangular in section; V ≈ 16% of visceral mass V just anterior to *pm* (Fig. 144).

Circulatory and excretory systems (Figs. 144, 145): Size and location of renopericardial structures as described above. Ctenidial veins (Fig. 145: *cv*) running along central region of dorsal *gi* connections, with perpendicular component between anterior and middle thirds, wider ventrally than dorsally, along 50% of visceral mass H, connecting with ventral ends of auricles. Auricles (*au*) subtriangular, attaching to posterolateral sides of pericardium (*pc*). Posterior wall of *au* bearing white, gland-like, middle protuberances in L ≈ 25% of posterior wall T. Ventricle (*ve*) surrounding intestine as it traverses *pc*; L ≈ 20% of *pc* L. *Ve* connection to *au* on posteroventral sides. Kidneys (*ki*) white, solid; V ≈ 10% of *pc* V on ventral side. Nephropores minute, on anterior ends of *ki*.

Digestive system (Figs. 139–141, 146): *Pp* as described above. Esophagus (*es*) running dorsoventrally along ca. 70% of *pm* L, and similar distance ventral to hinge area; W ≈ 25% of *pm* W. Stomach (*st*) conical, slightly perpendicular to *es*; main chamber L ≈ 2 *es* L. Gastric inner surface with narrow, transverse *es* rim (Fig. 146: *er*); sorting area (*sa*) just dorsal to *es* opening, with wide, transverse, low folds. Gastric shield (*gs*) posterodoral; A ≈ 20% of inner gastric surface A. Paired ducts to digestive diverticula (*dd*) ventral and at some distance from *es* opening, at ends of horseshoe-shaped furrow (with posterior concavity in L ≈ 25% of main gastric chamber L); wide groove running longitudinally at right, edges gradually increasing in H, forming pair of typhlosoles (*ty*). Intestine (*in*) and style sac (*ss*) totally fused, separated only by pair of *ty*. *Ss* tapering gradually posteroventrally to ventral side of *pm*; L ≈ main gastric chamber L. *In* making 180° loop just posterior to *ss*,

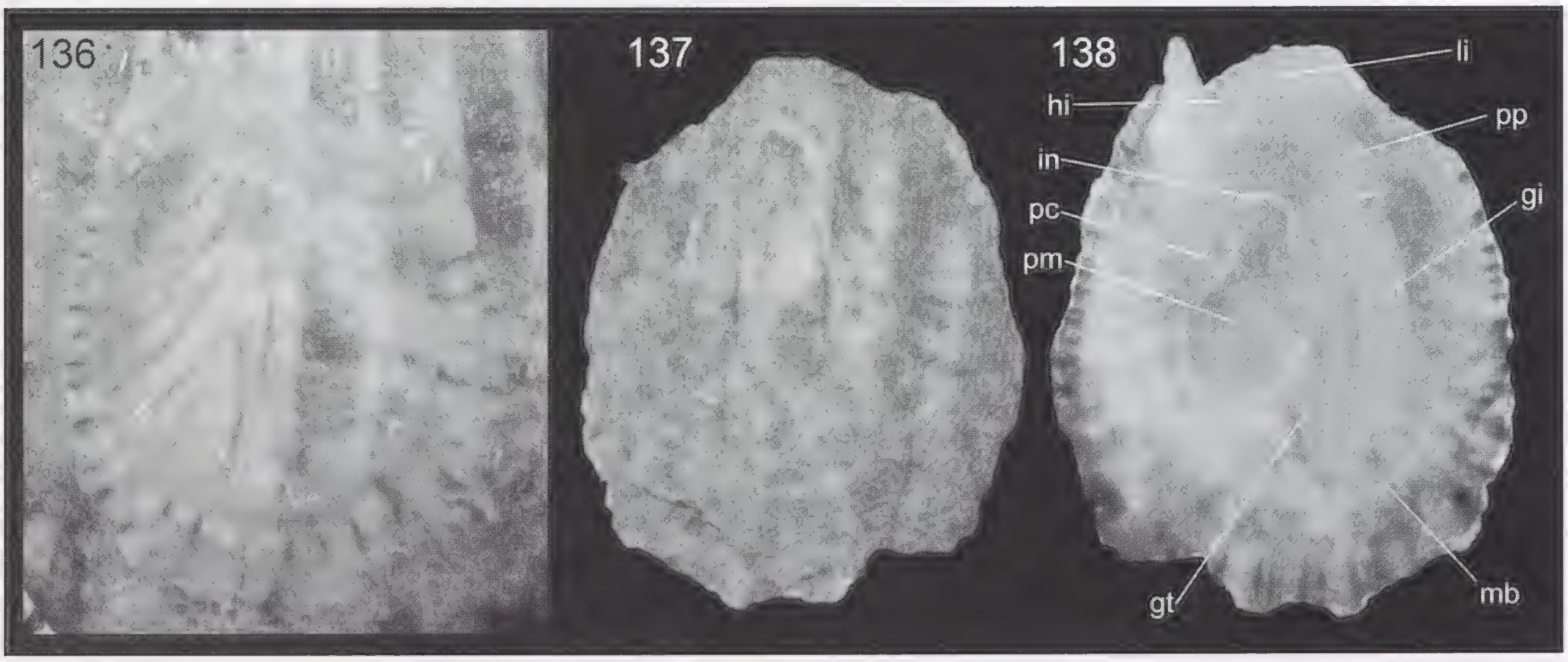

FIGS. 136–138. *Plicatula gibbosa,* shell morphology and anatomy, AMNH 298913, 8.9 mm L. FIG. 136: LV attached to shell of another bivalve, interior view; FIG. 137: RV, outer view; FIG. 138: Intact right view, RV and part of right mantle lobe removed. Abbreviations: gi, gill; gt, gill suspensory stalk; hi, hinge; in, intestine; li, ligament; mb, mantle border; pc, pericardium; pm, posterior adductor muscle; pp, labial palp.

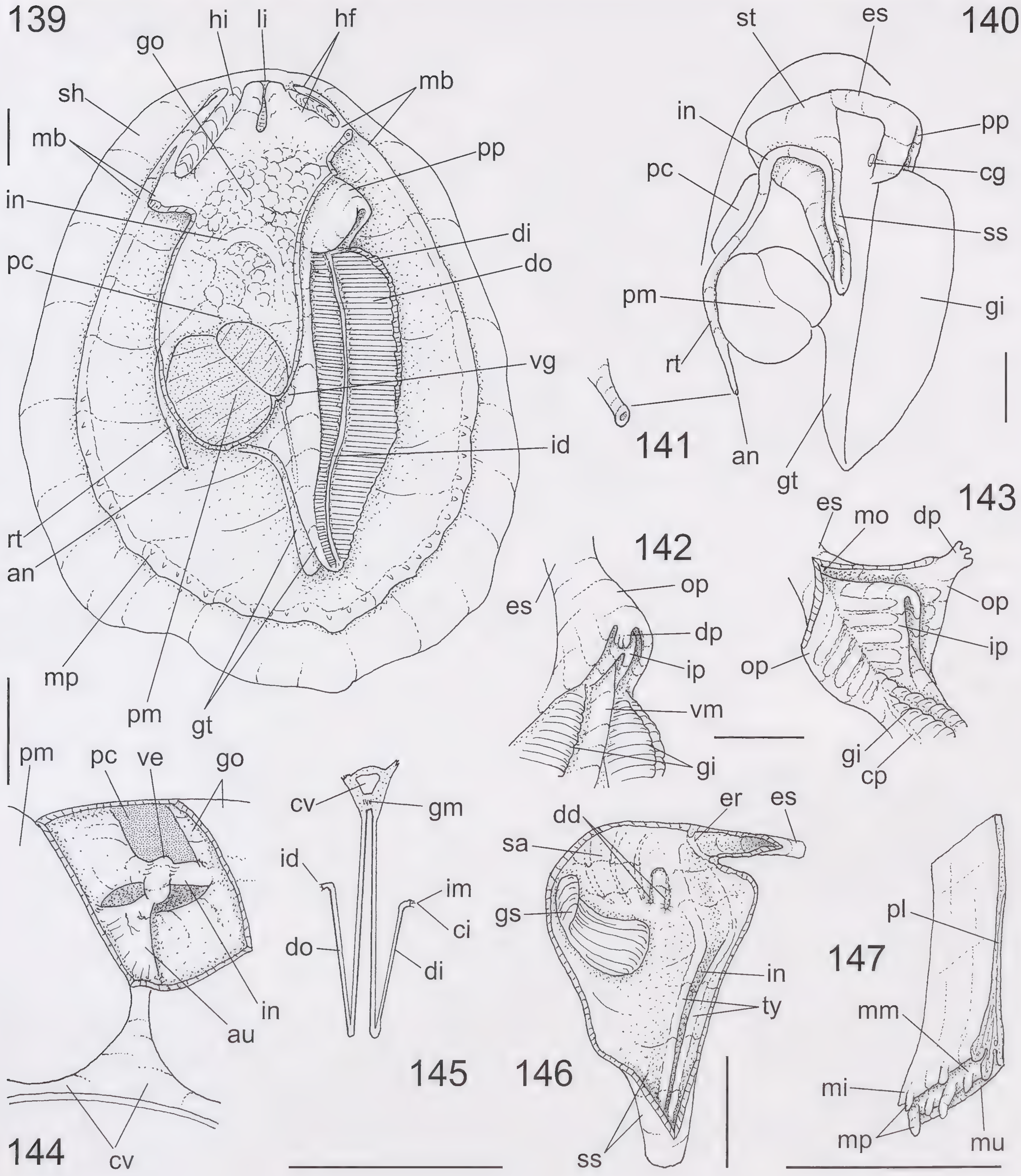

FIGS. 139–147. *Plicatula gibbosa*, anatomy. FIG. 139: Intact right view, RV and part of right mantle lobe removed; FIG. 140: Digestive system, right view, topologies of some adjacent structures also shown; FIG. 141: Detail of anus (an), right and slightly posterior view; FIG. 142: Labial palps, anterior and slightly right view, adjacent portion of gills (gi) and visceral mass (vm) also shown; FIG. 143: Same, outer hemipalp (op) sectioned along midline, right outer hemipalp deflected; FIG. 144: Pericardial region, right view, right pericardial wall removed, adjacent region of ctenidial vein (cv) also shown; FIG. 145: Gill, cross section in midregion; FIG. 146: Stomach, right view, sectioned longitudinally along dorsal region; FIG. 147: Mantle edge, cross section from midregion of posterior side. Scale bars = 1 mm. Abbreviations: an, anus; au, auricle; cg, cerebropleural ganglion; ci, ciliary connection of gill; cp, cerebrovisceral connective; cv, ctenidial (efferent) vessel; dd, ducts to digestive diverticula; di, inner demibranch; do, outer demibranch; dp, dentritic projection of lips and labial palps; er, esophageal rim; es, esophagus; gi, gill; gm, gill retractor muscle; go, gonad; gs, gastric shield; gt, gill suspensory stalk; hf, hinge fold of mantle; hi, hinge; id, insertion of outer demibranch in mantle; im, insertion of inner demibranch in visceral mass; in, intestine; ip, inner hemipalp; li, ligament; mb, mantle border; mi, mantle border inner fold; mm, mantle border middle fold; mo, mouth; mp, mantle papillae; mu, mantle border outer fold; op, outer hemipalp; pc, pericardium; pl, pallial muscles; pm, posterior adductor muscle; pp, labial palp; rt, rectum; sa, gastric sorting area; sh, shell; ss, style sac; st, stomach; ty, typhlosole; ve, ventricle; vg, visceral ganglia; vm, visceral mass.

then performing wide, sinuous loop, running to right of *ss* and gastric main chamber, and along midline; total *in* L ≈ SL. Anus (Figs. 139–141: *an*) with blunt, weakly expanded edges, preceded by long portion of rectum detached from *pm*; L ≈ 50% of *pm* L.

Reproductive system: Gonad as described above; genital aperture on *ki* not observed in detail.

Nervous system (Figs. 139, 140): Paired cerebropleural ganglia (Fig. 140: *cg*) elliptical, located laterally close to posterior third of *pp*; D ≈ 16% of *es* D. Cerebral commissure long, narrow. Pedal ganglia not observed. Paired visceral ganglia (Fig. 139: *vg*) elliptical, on middle of *pm* ventral side, very close; V ≈ 1.5 *cg* V. Abdominal sense organs not observed.

Material Examined

USA, Florida Keys, AMNH 298913, 1 specimen (sta. FK-083; dissected: 8.9 mm L, 11.2 mm H).

Distribution

Stated by Turgeon et al. (2009) to range from North Carolina to Quintana Roo (Mexico), the Gulf of Mexico outer banks, the West Indies, Brazil and Bermuda.

Remarks

These anatomical results agree with those on *Plicatula australis* Lamarck, 1819, by Watson (1930a) and on *P. gibbosa* from Jamaica reported by Yonge (1973). There are many shell specimen records from Brazil, but no anatomical material was available for dissection.

Family Anomiidae
Rafinesque, 1815

Anomia simplex
d'Orbigny, 1853
Figs. 148–165

Synonymy/Chresonymy

Anomia acontes J. E. Gray, 1850: 17 [Type locality: Jamaica]. A forgotten name reinstated by Huber (2010: 616) under violation of Art. 23.9 and 23.11 of the ICZN (1999) *Code*. Prevailing usage of *Anomia simplex* is here maintained; see Remarks.

Anomia simplex d'Orbigny, 1853: 367, pl. 28, figs. 31–33 [Type locality: Martinique, Cuba]. *Nomen protectum*.

Anomia simplex – Abbott, 1974: 451–452, fig. 5232, pl. 20, fig. 5232; Fuller et al., 1989: 83–94, figs. 1–26; Bieler & Mikkelsen, 2004: 510; Mikkelsen & Bieler, 2007: 162–163, 6 figs.

Anomia ephippium – Rios, 1994: 251 pl. 86, fig. 1227; 2009: 510, fig. (*non* Linnaeus, 1758; see Remarks).

Description

Shell (Figs. 148–150, 154–156): Oval to circular, fragile, translucent, iridescent whitish to pale beige, orange, or brown, laterally very compressed; SL ≈ 15–20 mm in material examined, maximum SW ≈ 12% SD. Both valves (mainly RV) conforming to shape of substratum. LV simple, weakly convex; outer surface opaque smooth (Fig. 148) to glossy (Fig. 154); inner surface glossy, thinly iridescent; muscle scars restricted to infraumbonal region (Fig. 150), in A ≈ 16% of inner VA, W ≈ 2 L. Scar of posterior adductor muscle (*pm*) circular, in A ≈ 12% of total scar A, on posteroventral side of each valve. Scars of split posterior pedal retractor muscle anterior and dorsal to adductor scar, inserting on LV only; one portion subequal in size and form to adductor scar, anterior to adductor scar; other portion (= byssal retractor of authors) circular, dorsal to posterior adductor scar; A = 2 *pm* scar A. Scar of anterior pedal retractor muscle (left only) in umbonal cavity, elongated; A ≈ 25% of *pm* scar A. RV with unclosed byssal orifice close to umbo, surrounding byssal portion of foot; A ≈ 6% of LV A. Posterodorsal region of RV including hinge plate on thickened crurum; *pm* scar midway between orifice and posterior margin of valve (Fig. 155). Periostracum not evident. Hinge plate edentulous, composed only of dorsoventrally elongated internal ligament (L ≈ 5 W ≈ 20% SW) on resilifer, preceded by thick, peduncular portion of RV (Fig. 156) and single concavity in LV (Fig. 150).

Main muscle system (Figs. 151–153, 157, 162): Anterior adductor muscle absent. *Pm* relatively small (Figs. 157, 162), approximately central on each valve, in A ≈ 5% VA; comprised of 2 ("catch" and "quick") portions, one (darker) centrally, extending posteriorly, other (paler) surrounding lateral and anterior regions. Anterior pedal retractor muscle (Figs.

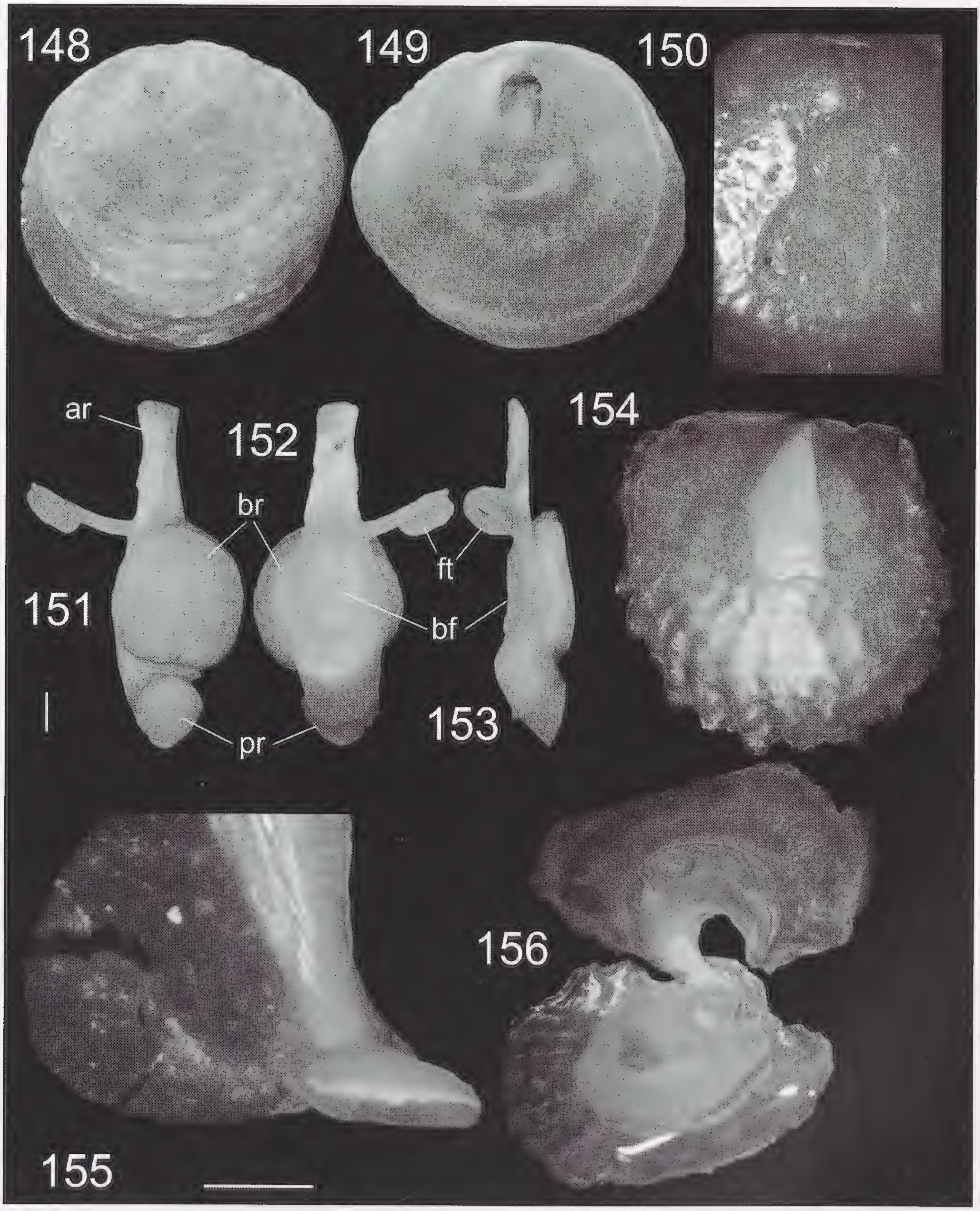

FIGS. 148–156. *Anomia simplex*, shell morphology. FIGS. 148–150: AMNH 298953, 23.6 mm maximum D. FIG. 148: Left view; FIG. 149: Right view; FIG. 150: LV, interior view, detail of subumbonal region with muscular scars. FIGS. 151–153: Same specimen as in Fig. 148, isolated foot and adjacent musculature, left, right, and ventral views respectively. FIG. 151: Left view; FIG. 152: Right view; FIG. 153: Ventral view; FIG. 154: MZSP 23067, 19.5 mm D, left view. FIGS. 155, 156: MZSP 26345, 24.0 mm D. FIG. 155: Detail of hinge of RV; FIG. 156: Ventral view, RV deflected upward. Scale bars = 1 mm (FIGS. 151–153, 155). Abbreviations: ar, anterior pedal retractor muscle; bf, byssal furrow; br, byssal retractor muscle (derived from posterior pedal retractor muscle); ft, foot; pr, posterior pedal retractor muscle.

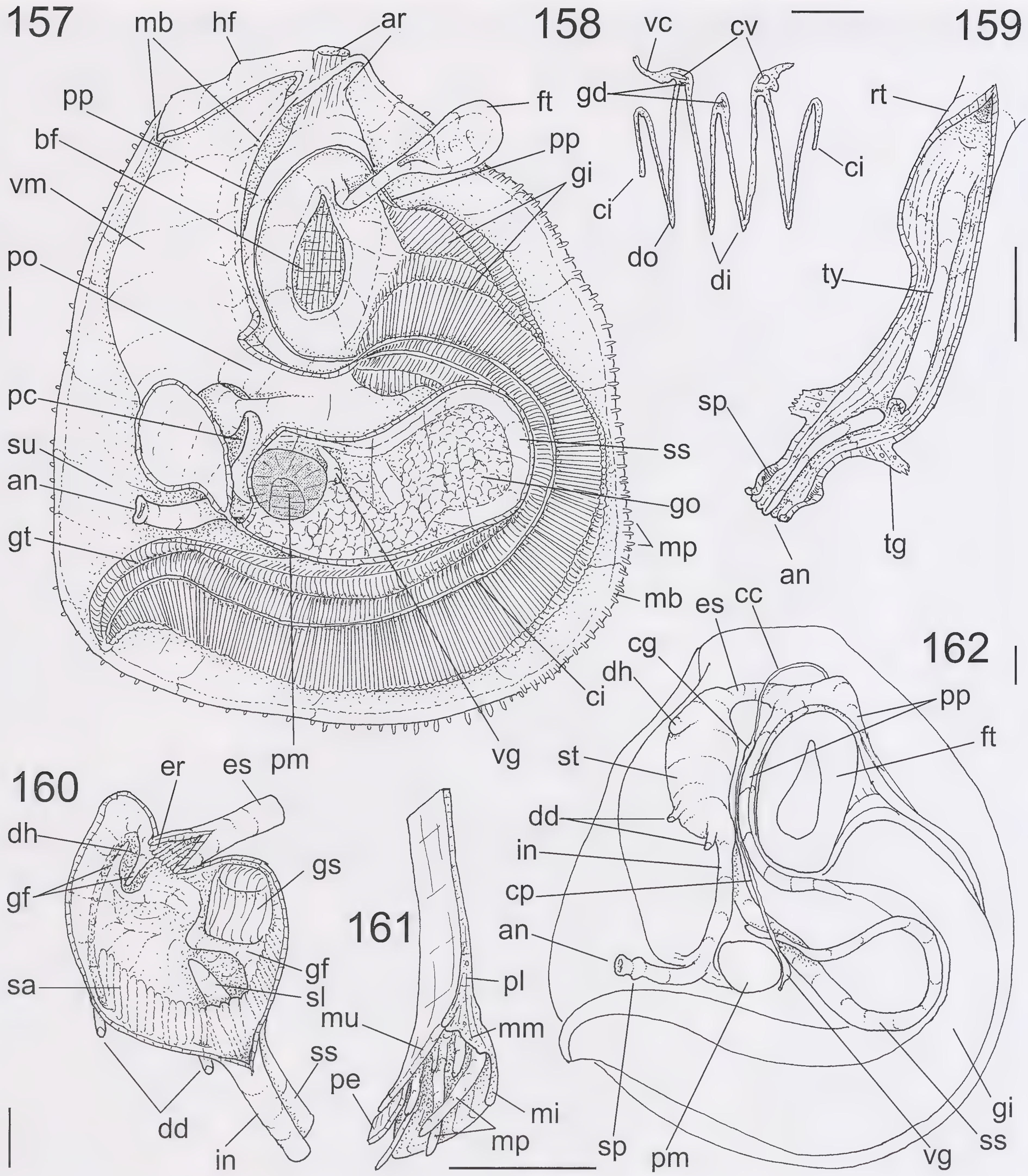

FIGS. 157–162. *Anomia simplex*, anatomy. FIG. 157: Intact right view, RV and part of right mantle lobe removed; FIG. 158: Gills, cross section in midregion; FIG. 159: Rectum and anus, dorsal view, both longitudinally opened, typhlosole (ty) sectioned in distal third to show its profile; FIG. 160: Stomach, dorsal view, sectioned dorsally with inner surface exposed; FIG. 161: Mantle border, a portion extracted from the midventral region, with a portion of the periostracum still attached; FIG. 162: Intact right view, digestive system and nervous system *in situ*, topologies of some adjacent structures also shown. Scale bars = 1 mm. Abbreviations: an, anus; ar, anterior pedal retractor muscle; bf, byssal furrow; cc, cerebral commissure; cg, cerebropleural ganglion; ci, ciliary connection of gill; cp, cerebrovisceral connective; cv, ctenidial (efferent) vessel; dd, ducts to digestive diverticula; dh, dorsal hood; di, inner demibranch; do, outer demibranch; er, esophageal rim; es, esophagus; ft, foot; gf, gastric fold; gi, gill; go, gonad; gs, gastric shield; gt, gill suspensory stalk; hf, hinge fold of mantle; in, intestine; mb, mantle border; mi, mantle border inner fold; mm, mantle border middle fold; mp, mantle papillae; mu, mantle border outer fold; pc, pericardium; pe, periostracum; pl, pallial muscles; pm, posterior adductor muscle; po, promyal passage of suprabranchial cavity; pp, labial palp; rt, rectum; sa, gastric sorting area; sl, crystalline style; sp, sphincter; ss, style sac; st, stomach; su, supra-anal chamber of suprabranchial pallial cavity; tg, integument; ty, typhlosole; vc, visceral mass gill connection; vg, visceral ganglia; vm, visceral mass.

151–153, 157: *ar*) single (left), originating in umbonal cavity of LV, in A = 50% of ligament A, relatively long dorsoventrally; running directly posteriorly for distance = 25% SL, through wide portion of mantle tissue, laterally compressed, becoming slightly wider posteriorly; inserting along anterior byssal furrow in base of main pedal retractor muscle (origin in RV indicating probable homology with left anterior pedal retractor of more typical bivalves, with right anterior pedal retractor here lost). Posterior pedal retractor muscle single (left, *pr*), divided into 2 bundles. Anterior branch directly to left of byssal furrow (Figs. 151, 152: *br*), originating on left surface of byssus, running short distance toward left, inserting at midanterior LV, in A = 3 pm A, approximately midway between *pm* and hinge area. Posterior branch originating in posterior byssal furrow, running posteriorly and to left, surrounding posterior surface of anterior branch, gradually running away from anterior branch (Figs. 151, 152: *pr*), inserting into LV just posterior to anterior branch, at some distance from it; insertion area between *pm* and anterior branch, displaced ventrally, slightly smaller than that of *pm*. Right posterior pedal retractor muscle absent.

Foot (Figs. 151–153, 157: *ft*): Consisting of a thin, free shaft plus a massive, plug-like portion that produces calcified byssus. Pedal musculature as described above, with anterior projection in left *ar* (Fig. 157), and cylindrical, massive portion possessing both branches of *pr*. Byssal furrow (Figs. 152, 157: *bf*) wide, shallow, rimmed by thin walls, slightly smaller than insertion of anterior branch of *pr*. Both left pedal retractors originating from furrow, in anteroposterior alignment. *Ft* shaft just anterior to *bf*, turning right-anteriorly, in L = *ar* L; basal 66% comprising long, slender, cylindrical stalk; terminal third compressed, in W ≈ 3 basal stalk W; right surface concave, bearing byssal gland. Byssus solid, short, cylindrical, calcareous.

Mantle (Figs. 157, 161): Mantle lobes asymmetrical, thin, translucent, possessing whitish, coalescent spots. Left mantle lobe simple, as inner mold of generally compressed valve. Right mantle lobe forming arch surrounding byssal foramen to region close to hinge plate, maintaining narrow gap between foramen and hinge plate. Mantle edge with 3 folds (Fig. 161). Outer fold thin, smooth, simple, typically connecting to periostracum (*pe*) on inner surface. Middle fold with long, slender papillae except in region surrounding byssal foramen in right lobe. Papillae of middle fold organized in 3 layers; outer layer of short, aligned papillae; other 2 layers internal to outer layer, each with 3–4 times longer papillae; each papilla tall, slender; interspace W = 2–3 papilla W; papilla L not uniform, with longer and shorter papillae alternating; longer papilla L ≈ 5% SL, shorter papilla L ≈ 25–33% of longer papilla L. Inner fold smooth, simple, forming pallial veil; W and T ≈ 2 outer fold W and T. Pallial muscles well developed, as radial, iridescent, mostly dichotomous fibers between edge of muscle area and mantle edge.

Pallial cavity (Figs. 157, 158, 162, 163): Surrounding entire visceral mass, except dorsally; V ≈ 50% SV. Promyal passage (Fig. 157: *po*) only on right side, connecting suprabranchial chamber with posterodorsal region, from anterior end of right gill, passing between *pm* and *ft*. Paired labial palps (Figs. 157, 162: *pp*) asymmetrical, long, surrounding midregion of byssal base of *ft*; left *pp* more ventral than right, connecting by oral groove on anterodorsal side of byssal base of *ft*. Hemipalps subequal, with smooth inner surfaces; inner folds inconspicuous. Gills (Fig. 162: *gi*) widely curved, in L ≈ SL ≈ 8 T; anterior third asymmetrical, with left *gi* more anterodorsal; middle and posterior thirds symmetrical, narrow, long. Inner demibranch of right *gi* connecting to right and left *pp* (Fig. 157); both demibranchs of left *gi* connecting to left *pp*. Inner (*di*) and outer (*do*) demibranchs similarly shaped. *Gi* suspensory stalk (Figs. 157, 163: *gt*) lying along 50% of *gi* L, narrow, weakly muscular. *Gi* filaments attaching to one another and to visceral mass and mantle via cilial connections; right and left *gi* uniting posterior to visceral mass via tissue connections. *Do* with additional ventral prolongation along outer-dorsal edge of ascending branch (Fig. 158).

Visceral mass (Figs. 157, 162): Strongly laterally compressed, more concentrated on left side, in dorsal and posterior regions around *ft*; V ≈ 25% SV. Stomach and remaining digestive system central; remaining mostly filled by pale cream-colored gonad. Pericardial region just posterior to *pm*; digestive diverticula greenish beige, anterior, surrounding stomach.

Circulatory and excretory systems (Figs. 157, 163): Pericardium (Fig. 157: *pc*) irregular, just posterior to *pm*, in V = 10–12% of visceral mass V; auricles and ventricle not detected in any dissected specimen. Kidneys (Fig. 163: *ki*) solid, whitish, on both sides of pos-

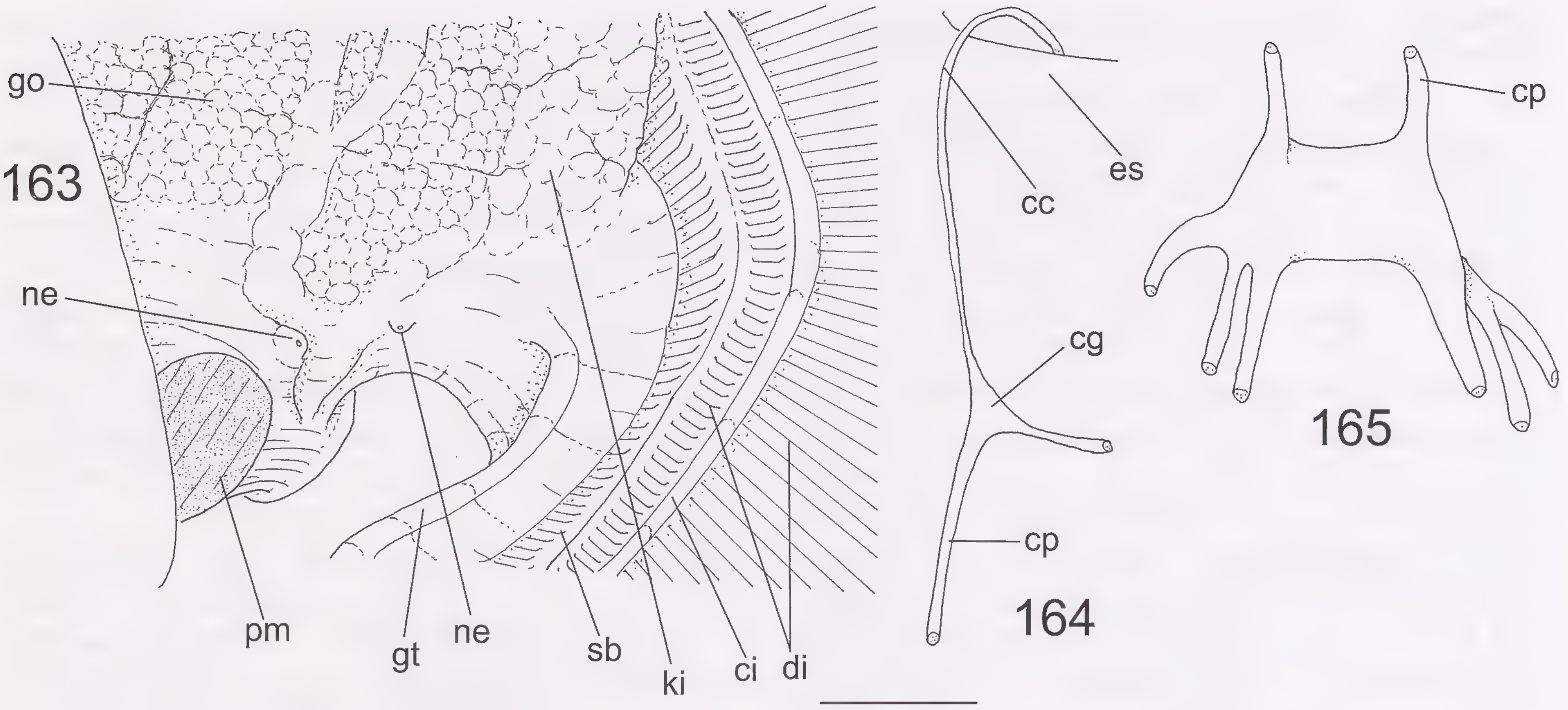

FIGS. 163–165. *Anomia simplex*, anatomy. FIG. 163: Detail of posterior region of visceral mass, ventral-slightly right view, both gills deflected and only partially shown; FIG. 164: Right cerebropleural ganglion (cg) *in situ*, right view; FIG. 165: Visceral ganglia, ventral view. Scale bars = 0.5 mm. cc, cerebral commissure; cg, cerebropleural ganglion; ci, ciliary connection of gill; cp, cerebrovisceral connective; di, inner demibranch; es, esophagus; go, gonad; gt, gill suspensory stalk; ki, kidney; ne, nephropore; pm, posterior adductor muscle; sb, suprabranchial chamber.

teroventral visceral mass, at base of each *gt*. Nephropores (Fig. 163: *ne*) as small papillae on both sides of *pm*, on internal surfaces of *gt* bases.

Digestive system (Figs. 157, 159, 160, 162): *Pp* as described above. Esophagus (*es*) located ca. 16% SH below umbones; L ≈ *pm* L, W ≈ 33% of *pm* W. *Es* inner surface bearing 8–10 longitudinal, narrow, uniform folds. Stomach (*st*) elliptical; L ≈ 2 W, V ≈ 20% of visceral mass V. Dorsal hood (*dh*) in posterior-right region; A ≈ 12% of inner gastric surface A. Two pairs of ducts to digestive diverticula, simple, on posterodorsal gastric surface. Gastric inner surface (Fig. 160) with low *es* rim (*er*); *dh* preceded by pair of triangular adjacent folds, pointing in opposite directions. Gastric shield (*gs*) right-dorsal; A ≈ 16% of gastric inner surface A. Large sorting area (*sa*) lying along posterodorsal gastric surface, with uniform, transverse, low folds; *sa* separating (on posterior-right side) intestinal (*in*) and style sac (*ss*) origins; transverse, tall, wide, arched fold separating *gs* from style sac opening. *Ss* totally separated from *in* (Fig. 157), narrow, very long, only slightly shorter than SH; making wide loop in posteroventral visceral mass, gradually passing from left to right side, weakly protruding into suprabranchial chamber; most regions W ≈ 16% of main gastric chamber W, narrowing gradually distally to pointed tip just anterior to *pm*. *In* short (L ≈ 50% of visceral mass L), at right of *ss* opening, running almost directly posteroventrally, in W ≈ *ss* W; ca. 33% of *in* L exposed in pallial cavity as anal stalk. *In* inner surface almost entirely with longitudinal typhlosole (Fig. 159: *ty*); *ty* tall, relatively thin, arching; remaining *in* inner surface with longitudinal, narrow, uniform folds. *In* passing anterior to (not through) *pc*. Anus preceded by relatively long free stalk; edges fringed; subterminal sphincter (Fig. 159: *sp*) very evident.

Reproductive system (Fig. 163): Not observed in detail. Gonad filling most of visceral mass; genital ducts opening inside posteroventral *ki*.

Nervous system (Figs. 162, 164, 165): Cerebropleural ganglia (*cg*) simple, triangular, well separated, connecting by long, narrow commissure (Fig. 164: *cc*) in L ≈ 5 *es* D; right *cg* more posterior than left; *cg* A ≈ 16% of *es* D. Pedal ganglia not observed. Each visceral ganglion (*vg*) in V ≈ 5 single cg V, on anteroventral surface of *pm*; broadly connected, with no visible commissure (Figs. 157, 165); weakly asymmetrical, with posterior nerves of left *vg* slightly more dorsal than those of right. Abdominal sense organs not observed.

Material Examined

USA, Florida Keys, Florida Keys, MZSP 36126, 1 specimen (sta. FK-649); AMNH 298953, 3 specimens (sta. FK-352; 1 dissected, 23.6 mm maximum D); FMNH 301413, 1 specimen (FK-629; dissected: 29 mm L, 30 mm H, 9 mm W); FMNH 314534, 1 specimen (FK-287; dissected: 35.6 mm L, 29.2 mm H, 7.4 mm W).

BRAZIL, Rio de Janeiro, Buzios, Ferradura beach, MZSP 48466, 1 specimen (19/iii/2005; dissected, not measured); Arraial do Cabo, Porcos Island, 22°57'53.5"S, 41°59'47.7"W, 8 m (18/iii/2005; dissected, not measured); Ilha Grande, Pau-Paulo beach, MZSP 45890, 1 specimen (22/vii/1966; dissected, not measured); Paraty, Mantinelo Island, 23°11'15.6"S, 44°39'33.1"W, 3 m, MZSP 83252, 3 specimens (26/i/2007; dissected, not measured). São Paulo, Anchieta Island (IO Bentos), Sul beach, MZSP 23065, 15 specimens, MZSP 23064, 6 specimens, (26/ii/1963; dissected, not measured), MZSP 23063, 3 specimens (28/ii/1963; dissected, not measured); Ubatuba, MZSP 26345, 2 specimens (1 dissected: 24.0 mm D, 22.2 mm H, 8.3 mm W); Enseada das Palmas (IO Bentos), MZSP 23067, 5 specimens (13/ii/1963; 2 dissected: #1: 19.5 mm L, 19.1 mm H, 4.1 mm W; #2: 14.9 mm L, 9.9 mm H, 3.1 mm W), MZSP 23068, 6 specimens (02/iii/1962; dissected, not measured), Andorinhas beach (IO Bentos), 1 m, MZSP 23058, 1 specimen (23/i/1962; dissected, not measured), MZSP 23060, 1 specimen (12/vii/1962; dissected, not measured), MZSP 23066, 1 specimen (24/ii/1962; dissected, not measured), MZSP 23059, 1 specimen (23/i/1962; dissected, not measured), Boqueirão (IO Bentos), 20 m, MZSP 23061, 1 specimen (19/vii/1961; dissected, not measured), 32 m, MZSP 23062, 1 specimen (14/vii/1962; dissected, not measured), Ponta do Navio, MZSP 23069, 1 specimen (IO Bentos, 03/vii/1962; dissected, not measured); Ilha Bela, Garapucaia beach, MZSP 45921, 2 specimens (04/iii/1967; dissected, not measured); Santos, Lage de Santos, 24°17'23"S, 46°11'57"W, 31–32 m, MZSP 26285, 1 specimen (IO sta. 16, 23/iii/1961; dissected, not measured).

Distribution

Stated by Turgeon et al. (2009) to range from Massachussetts to Yucatan, the Gulf of Mexico outer banks, Cuba, Brazil, and Bermuda. Range in Brazil to São Paulo is here confirmed.

Remarks

For other details of the shell, see Mikkelsen & Bieler (2007: 162). The anatomy of *Anomia* (as reported here in agreement with earlier authors) is extremely asymmetrical with some organs (e.g., pedal retractor muscle, adductor muscle, gonad; Yonge, 1980) represented only or mainly on one side. Yonge (1977) compared the anatomy of *Anomia* (including New England *A. simplex*) to other members of the family and superfamily, and pointed out that *Anomia* is distinct from other genera in Anomioidea in having a split posterior pedal retractor muscle, which results in three central muscle scars on the left valve. The foot is rotated, with a small free portion (used primarily for cleaning; Yonge, 1977; Prezant, 1984) and a bulbous portion that produces the calcified byssus rotated strongly to the right so that the byssus passes through the hole in the right valve. The labial palps literally wrap around the byssal portion of the foot, and the anterior portions of the demibranchs are asymmetrical in their association with the palps. Yonge (1977) wrote that three demibranchs are associated with the left palp, and only one demibranch with the right palp; this study confirmed this, however, each palp receives two demibranchs in *A. ephippium* Linnaeus, 1758 (S. Staubach, pers. comm., June 2012). Because there are no food grooves on the gills of *Anomia*, examinations of ciliary currents are needed to confirm these associations. According to Pelseneer (1911), the anomiid heart consists of a ventricle only, without auricles or a surrounding pericardium; Yonge (1977) indicated that the pericardium is absent and auricles are present and asymmetrical. A pericardium (ventricle?) was detected in these dissections but did not contain typical heart chambers; clearly the anomiid heart requires further investigation across the family. Purchon (1957) reported five ducts to the digestive diverticula in *A. ephippium*; only two were found here, but each duct branches soon after leaving the stomach, so this feature could be easily misinterpreted, or could vary among species. The visceral ganglia are on the anterior surface of the posterior adductor muscle, rather than the posterior surface as is true for most bivalves (Yonge, 1977).

Most striking as as a result of this study is the presence of an apparent right promyal passage in *Anomia simplex*, similar to that characteristic of members of Gryphaeidae, not before recorded in Anomiidae.

Until recently, d'Orbigny's description of *Anomia simplex* was dated as 1842 but is now interpreted as having been published much later, between 1851 and 1853 (e.g., Mikkelsen & Bieler, 2007: 413; who adopted a 1853 date). *Anomia acontes* Gray, 1850, is an available older name. However, the name *A. simplex* d'Orbigny, 1853, has been in prevailing usage, with more than 25 usages in the last 50 years. By contrast, the name *A. acontes* apparently had not been used as valid since 1899 until Huber (2010: 616) reinstated it, thereby violating Art. 23.9 of the ICZN (1999) *Code*. Prevailing usage of *A. simplex* is here maintained.

Some authors have considered *Anomia simplex* a synonym of eastern Atlantic/ Mediterranean *A. ephippium* Linnaeus, 1758, whereas others (e.g., Huber, 2011: 616) reported morphological differences. Additional research is needed.

Other studies of *Anomia simplex* from a variety of western Atlantic localities have included larval development and metamorphosis (Loosanoff, 1961; Loosanoff et al., 1966; reared from plankton from Long Island Sound), cardiac physiology (Navez, 1936, from Woods Hole, Masschussetts), and formation and mineralogy of the calcified byssus (Prezant, 1984, from Sanibel Island, Florida).

No morphological difference was found between Floridian and Brazilian specimens.

Family Carditidae
Férussac, 1822

Carditamera floridana
Conrad, 1838
Figs. 166–177

Synonymy/Chresonymy

Carditamera floridana Conrad, 1838: 30 [Florida].

Carditamera floridana – Abbott, 1974: 476, pl. 21, fig. 5478; Bieler & Mikkelsen, 2004: 511; Mikkelsen & Bieler, 2007: 176–177, 5 figs.

Description

Shell (Figs. 166–169): Elongate quadrate, with strong, nodose radial ribs, solid, whitish gray with small bars of chestnut brown arranged concentrically on ribs, with gray periostracum; SL ≈ 6–18 mm in material examined. Lunule small, oblique, deeply indented; escutcheon obscure. Interior non-nacreous, white, with small light brown patches above subequal adductor muscle scars.

Main muscle system (Figs. 170, 171, 173, 176): Anterior adductor muscle (*am*) in anteroventral quadrant, close to shell margin; outline elongate semicircular, weakly oblique; anterior edge convex; posterior edge weakly concave; H = 25% SH, L ≈ 10% SL. Posterior adductor muscle (*pm*) in posterodorsal quadrant, close to shell margin; outline more elliptical than *am*; *pm* A slightly > *am* A. Each adductor muscle dividing into differently colored ("catch" and "quick") portions. Pallial muscles (Fig. 170: *pl*) thin, radial, connecting in continuous line uniting adductor muscles surrounding at some distance from ventral and posterior shell margins. Paired anterior pedal retractor muscles (Figs. 170, 171: *ar*) narrow, slender, originating in dorsal *am* A = 10% *am* A, separated from *am*; converging running posteroventrally, with anterior halves separated, then splaying across lateral walls of foot base. Paired posterior pedal retractor muscles (Figs. 170, 171, 173: *pr*) in T = 3–4 *ar* T; originating just posterior and dorsal to *pm* in A = 10% of *pm* A; running anteroventrally adjacent, forming posterior wall of visceral mass; inserting into posterior foot base. No other muscles (e.g., pedal protractors) detected.

Foot (Figs. 171, 176: *ft*): Small (V ≈ 2 *am* V), narrow, blunt. Base broad, narrowing over short distance to rounded tip. Byssal furrow restricted to posterior half of ventral side, deep, surrounded by whitish byssal gland. Byssus with few, very narrow, thin threads.

Mantle (Figs. 170, 171, 173): Border of each mantle lobe mostly separated; fusion present only (1) anteriorly, adjacent to *am*, (2) dorsally and posteriorly, adjacent to *pm*, and (3) separating incurrent (*si*) and excurrent (*se*) apertures (Fig. 171). Mantle edge with 3 folds; outer and middle folds similar, simple, low, flattened, thin, separated by periostracal groove; inner fold thicker, taller, mostly simple, bearing series of short, simple, stubby papillae on posterior third, just inside *se*, with ca. 15 pairs of papillae becoming slightly taller and closer toward separation. *Se* bordered by tall flap as short "siphon," formed by inner mantle fold, with additional pair of projections in ventral region (Fig. 173) close to ventral fusion. Pair of transverse folds narrow, low, running posteroventrally from ventral *pm*, ending at junction of *si* and *se*, dividing infrabranchial and suprabranchial chambers (Fig. 173: *id*); gill attaching by cilia just ventral to fold.

Pallial cavity (Figs. 171, 172, 174, 175): Occupying lateral areas; V = 80% SV. Labial palps (*pp*) relatively small (A ≈ 10% of gill A), triangular; outer hemipalp with smooth outer surface; inner surface of each hemipalp bearing 8–10 transverse-oblique folds (Fig. 175), with dorsal fold longer, gradually decreasing and abruptly diminishing at some distance from mouth; smooth, narrow canal separating hemipalps; smooth area separating folds from *pp* edge; folds of uniform W, with rounded distal ends, proximal ends fading. Gill V ≈ 66% of pallial cavity V. Outer demibranch (*do*) triangular, smaller than inner demibranch (*di*), with broader region approximately halfway between posterior and middle thirds; gradually decreasing anterior and posterior to ventral edge; anterior end sharply pointed, posterior to that of *di*; posterior end rounded, at same level as end of *di*. Posterior *di* similar to that of *do*; middle and anterior portions of approximately same W as anterior end, becoming attached entirely to visceral wall via cilia. Gills composed of uniform slender filaments, connecting by regular longitudinal tissue bridges forming reticular net; longitudinal bridge W ≈ filament W. Both walls of each demibranch connecting internally by sparse transverse tissue shafts (Fig. 172: *gq*), mainly distributed in ventral half of each gill. Anterior half of each demibranch connecting to visceral mass or mantle (for *di* and *do*, respectively) by tissue connections; each posterior half (posterior to *pm*) attaching to mantle or counterpart (in case of *do* or *di*, respectively) by cilia, easily detachable during dissection. *Do* attachment just ventral to fold as described above. Main branchial axis sustaining gill between *di* and *do*, in visceral portion bearing pericardium

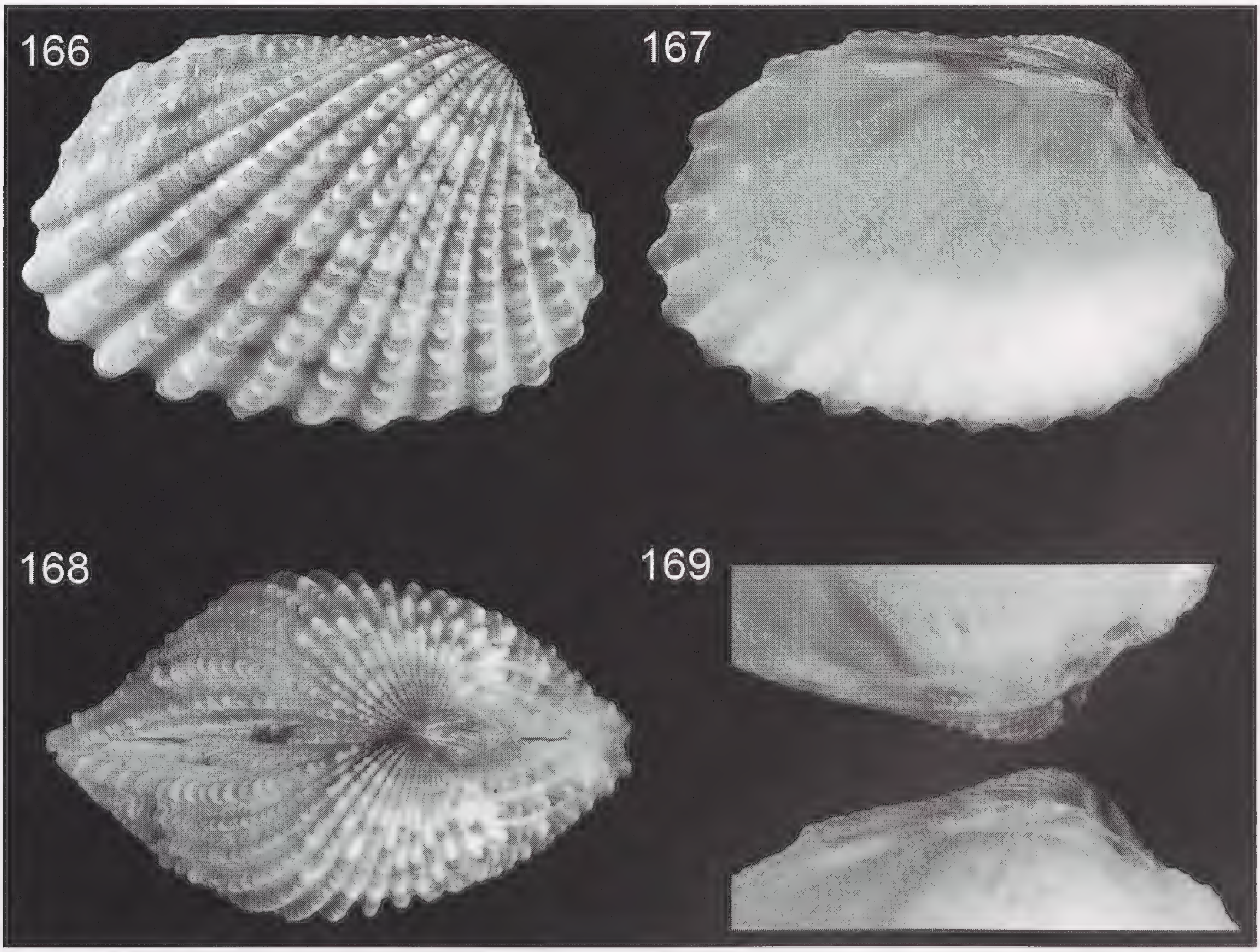

FIGS. 166–169. *Carditamera floridana*, shell morphology, FMNH 311591, 18.1 mm L. FIG. 166: RV, exterior view; FIG. 167: RV, interior view; FIG. 168: Articulated specimen, dorsal view; FIG. 169: Detail of hinge.

and kidney, in region posterior to *pm* weakly thick, nonmuscular. Gill ventral edges simple on *do*; *di* bearing narrow food groove (Fig. 172: *fg*).

Visceral mass (Figs. 176, 177): Conspicuously bilobed dorsally by separation of umbones; A ≈ 25% of lateral A of intact body. Stomach restricted to right lobe. Digestive diverticula mostly distributed anteriorly, surrounding stomach and filling entire left dorsal lobe. Gonad whitish, mostly in posterior and ventral regions of visceral mass, surrounding posterior digestive system and diverticula.

Circulatory and excretory systems (Figs. 176, 177): Dorsal just posterior to stomach and umbones; V ≈ 12% of visceral mass V. Pericardium (Fig. 176: *pc*) flattened. Auricles (*au*)

170

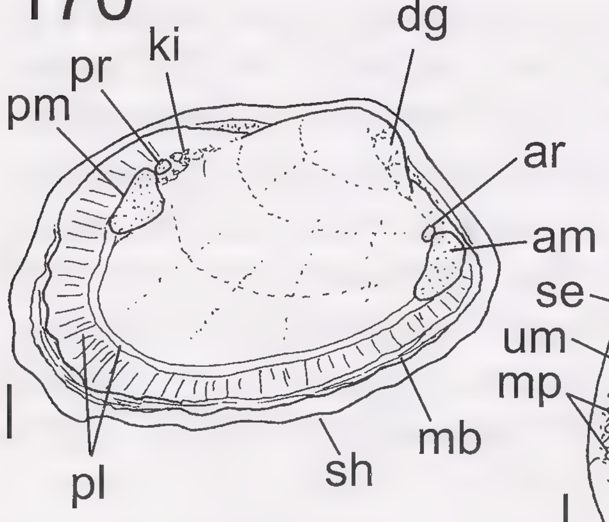

171

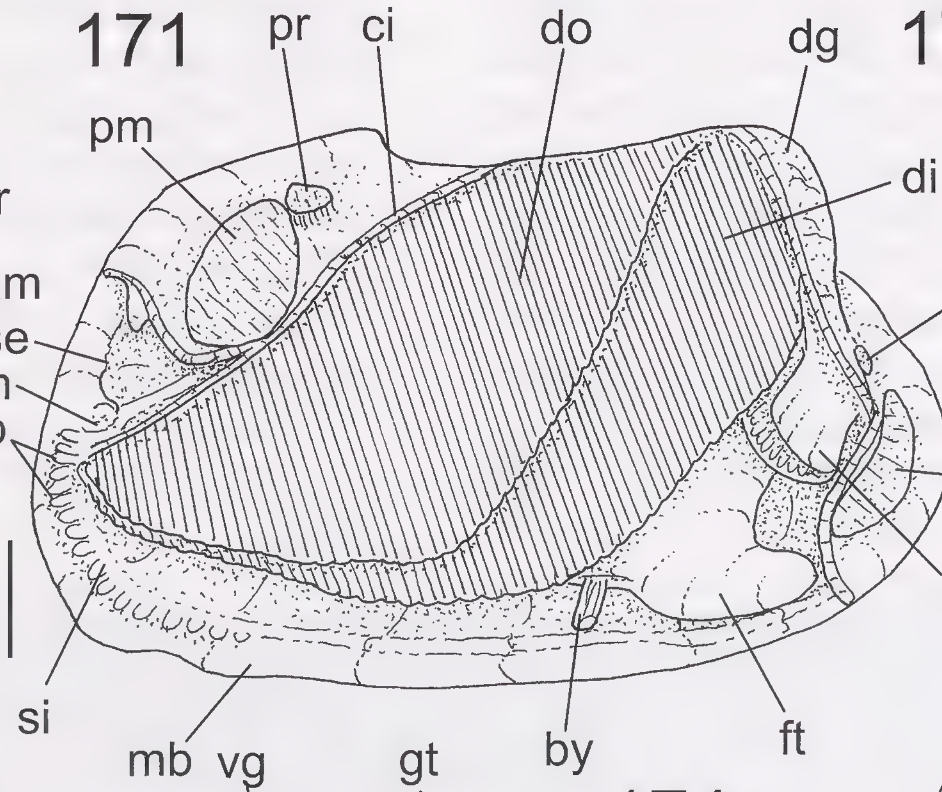

172

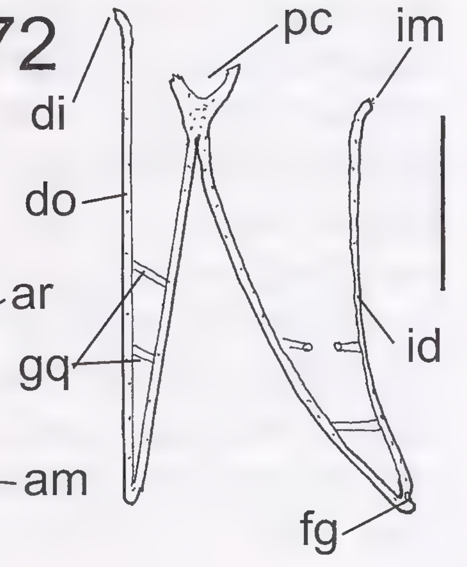

173

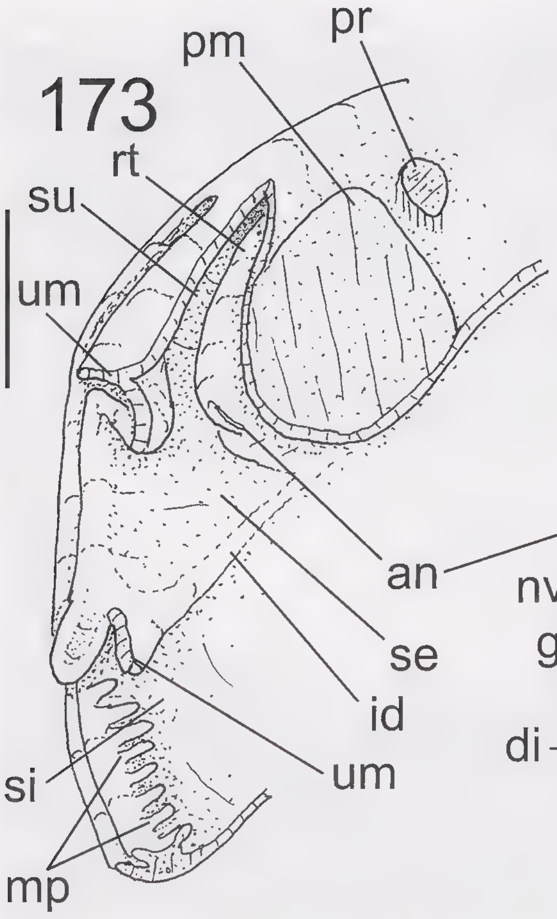

174

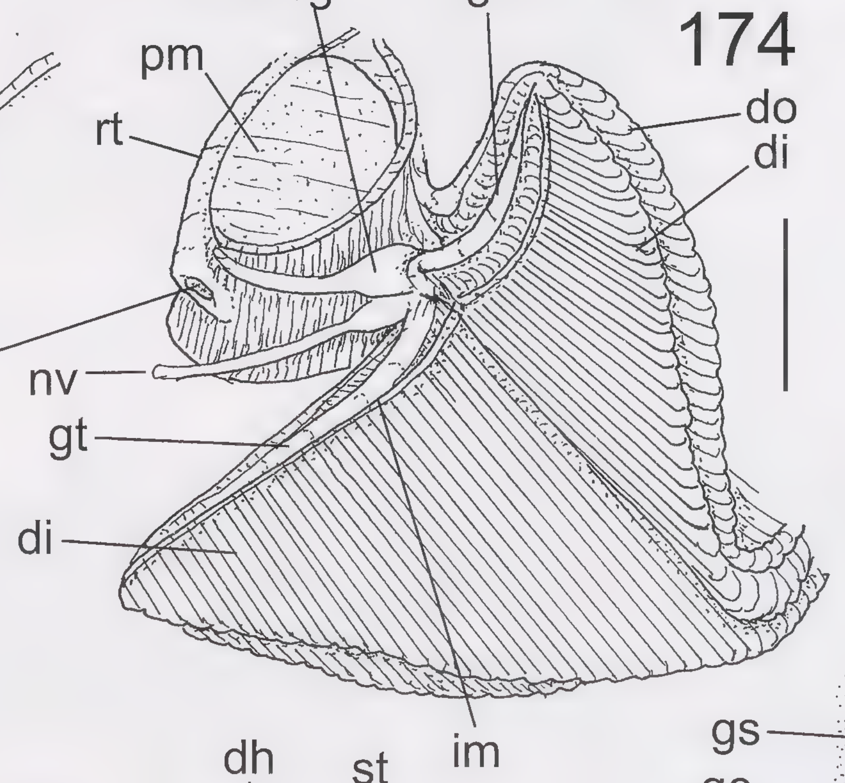

175

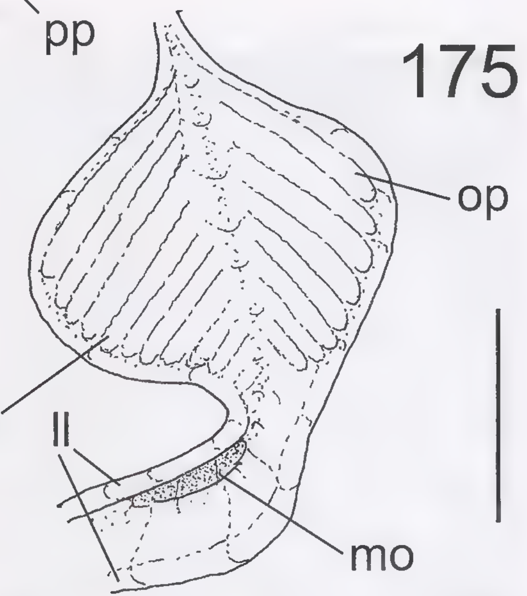

176

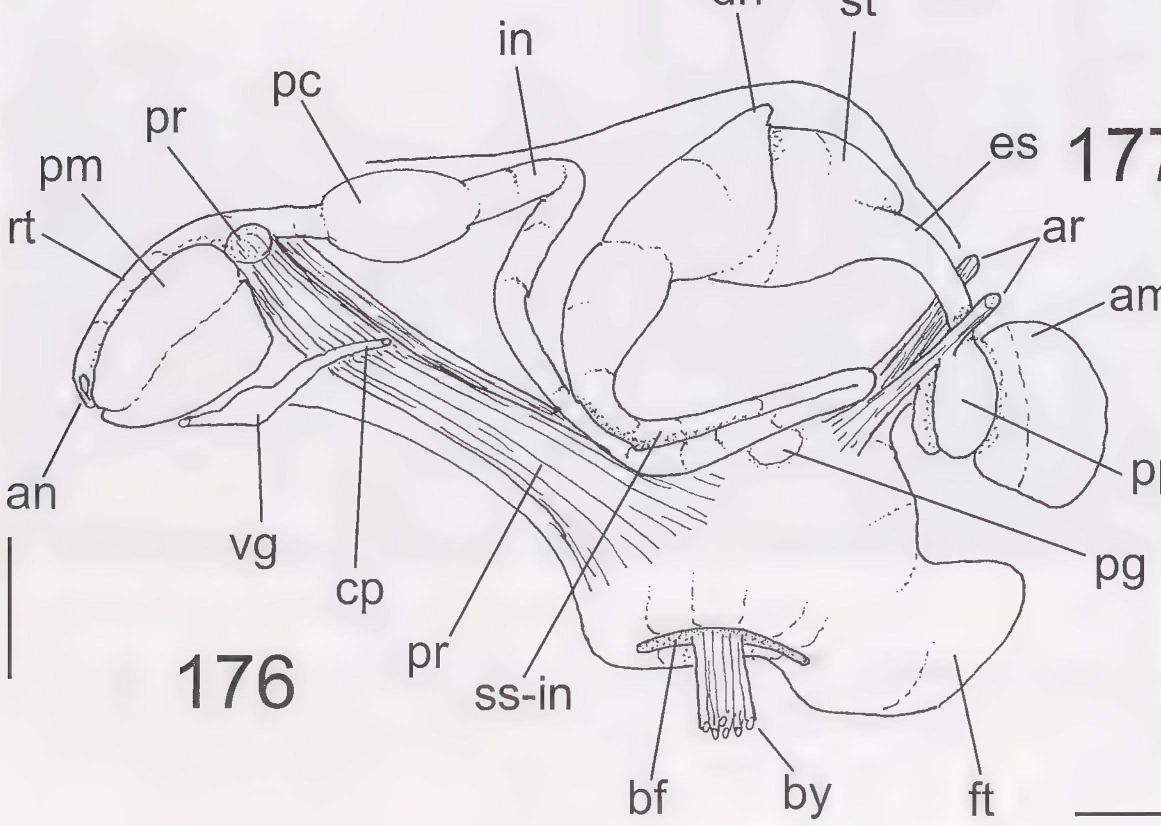

177

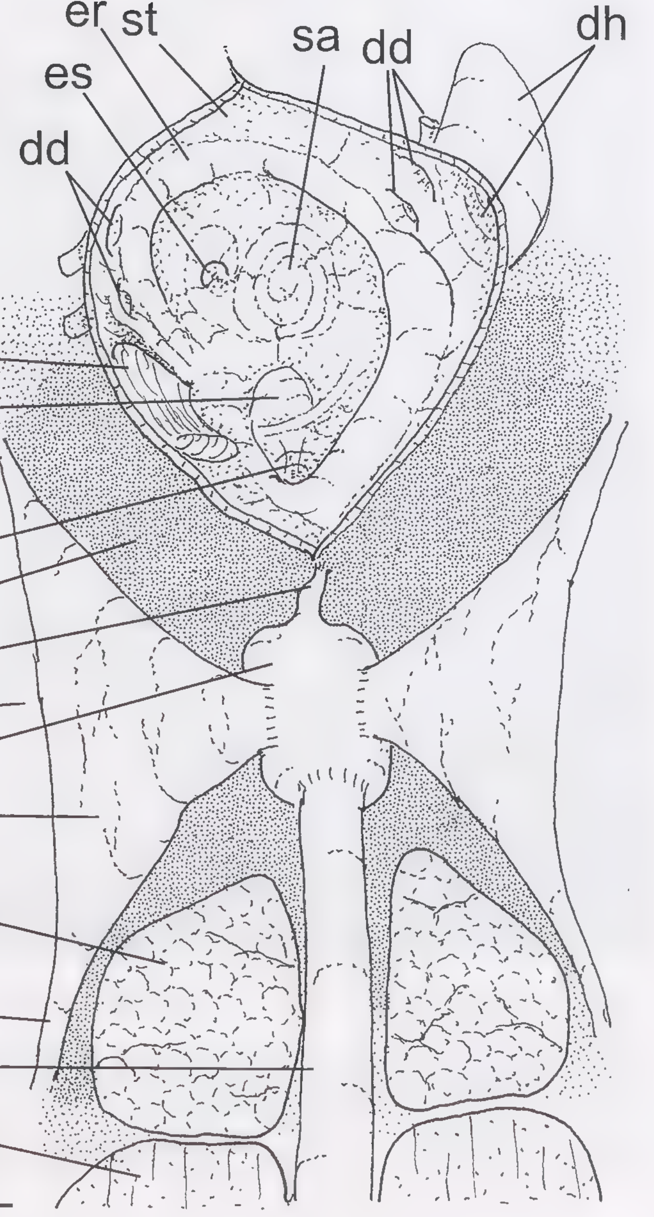

triangular, connecting directly to gills at level approximately halfway between their middle and anterior thirds; ca. 25% of anterior and 50% of posterior gill drainage accomplished by narrow vessels inserting into *au* extremities. Ventricle (*ve*) surrounding intestine; connections with *au* mid-lateral. Anterior aorta dorsal, on intestine; posterior aorta ventral. Kidney (*ki*) solid, beige to pale brown, filling 50% of *pc* V, just posterior to *pc*, compressed by anterior surface of *pm*.

Digestive system (Figs. 173–177): *Pp* as described above. Mouth (Fig. 175: *mo*) preceded by tall paired lips, with smooth inner surfaces. *Mo* and anterior esophagus just posterior to and separated from *am*. Esophagus (*es*) broad, in L = *am* D, opening into anteroventral stomach. Stomach (*st*) broad, massive (V ≈ 20% of visceral mass V), filling right side only of visceral mass beneath umbones. Dorsal hood (*dh*) small, short, on mid-dorsal gastric surface, turning to right. Gastric inner surface (Fig. 177) with wide *es* aperture on anterior ventral surface, with spiral sorting area (*sa*) or typhlosole immediately to right; *sa* A = *es* aperture D ≈ 16% of ventral inner gastric surface A. *Es* rim (Fig. 177: *er*) as broad fold surrounding *es* aperture and spiral *sa* entirely, at some distance from them; left branch of fold becoming broader and lower in posterior region, surrounding anterior-left intestinal-style sac (*in-ss*) aperture; right branch of fold running posteriorly along dorsal gastric wall, fading gradually; central pad small, low, just anterior to intestinal aperture and at left end of *er*; central pad (Fig. 177: *gc*) posteriorly low, except for narrow secondary fold, running to anterior-right, separating *in* aperture from *st*. Gastric shield (Fig. 177: *gs*) thin, on posterodorsal inner gastric surface, at level of conjoined *ss-in* opening. Two pairs of ducts to digestive diverticula (Fig. 177: *dd*), each close to dorsal edge of *er*, on left side parallel to it, on right side perpendicular to it. *Dh* inner surface smooth; aperture close to right pair of *dd* apertures. *In* and *ss* totally fused, opening broadly into posteroventral *st*, gradually narrowing. *In* curving ventrally then anteriorly, running along pedal musculature, close to anterior end of visceral mass, abruptly twisting 180°, running parallel, close to, and to right of preceding loop, near *ss*; running dorsally and slightly anteriorly to posterodorsal *st*; twisting almost 90°, running posteriorly, crossing through *ve*, between *pr* origins and posterodorsal surface of *pm*. Anus (Figs. 173, 174: *an*) simple, rounded, on posteroventral *pm*.

Reproductive system: Gonad as described above; no dimorphism observed. Genital apertures as small slits bearing sphincters, just anteroventral to nephropores.

Nervous system (Figs. 174, 176): Cerebropleural ganglia (*cg*) at intersection of *am*, *pp*, and *ar*; A ≈ 12% of *es* D. Paired pedal ganglia (Fig. 174: *pg*) at mid-visceral mass, close to insertion of *ar*; V ≈ 3 *cg* V. Paired visceral ganglia (Fig. 174: *vg*) at mid-*pm*, at bases of gill posterior stalks; V ≈ 1.5 *pg* V.

←

FIGS. 170–177. *Carditamera floridana*, anatomy. FIG. 170: Intact right view, RV removed; FIG. 171: Same, part of right mantle lobe removed; FIG. 172: Gill, cross section at midregion; FIG. 173: Pallial cavity, right view, detail of posterior region, right mantle lobe partially removed, supra-anal chamber longitudinally opened, gills removed; FIG. 174: Posterior region of gills (di, do) and posterior adductor muscle (pm), right view, right gill partially deflected, integument covering ventral region of adductor muscle removed; FIG. 175: Right labial palp, right view, outer hemipalp (op) deflected, topology of inner demibranch (id) indicated; FIG. 176: Foot (ft), main musculature, digestive system, and part of nervous system *in situ*, right view, topologies of some other structures also shown; FIG. 177: Region posterior to umbones, dorsal view, stomach (st) opened longitudinally to show inner surface, dorsal integument removed. Scale bars = 1 mm. Abbreviations: aa, anterior aorta; am, anterior adductor muscle; an, anus; ar, anterior pedal retractor muscle; au, auricle; bf, byssal furrow; by, byssus; cp, cerebrovisceral connective; cv, ctenidial (efferent) vessel; dd, ducts to digestive diverticula; dg, digestive diverticula; dh, dorsal hood; di, inner demibranch; do, outer demibranch; er, esophageal rim; es, esophagus; fg, food groove; ft, foot; gc, gastric central pad; gi, gill; gq, gill transverse reinforcement in suprabranchial chamber; gs, gastric shield; gt, gill suspensory stalk; id, insertion of outer demibranch in mantle; im, insertion of inner demibranch in visceral mass; in, intestine; ip, inner hemipalp; ki, kidney; ll, labial lips preceding mouth; mb, mantle border; mo, mouth; mp, mantle papillae; nv, nerve; op, outer hemipalp; pc, pericardium; pg, pedal ganglion; pl, pallial muscles; pm, posterior adductor muscle; pp, labial palp; pr, posterior pedal retractor muscle; rt, rectum; sa, gastric sorting area; se, excurrent aperture; sh, shell; si, incurrent aperture; ss-in, conjoined style sac-intestine; st, stomach; su, supra-anal chamber of suprabranchial pallial cavity; um, fusion between left and right mantle lobes; ve, ventricle; vg, visceral ganglia.

Material Examined

USA, Florida Keys, FMNH 288866, 5 specimens (sta. FK-188; dissected, not measured); FMNH 288861, 14 specimens (RB-1582; 2 dissected: #1: 7.9 mm L, 5.5 mm W, 4.1mm H; #2: 9.1 mm L, 6.6 mm W, 5.4mm H); FMNH 288830, 1 specimen (sta. FK-045); FMNH 295639, 1 specimen (sta. FK-145); FMNH 288865, 2 specimens (sta. FK-055; 1 dissected; 8.2 mm L, 5.8 mm H, 4.7 mm W). Spanish Harbor Keys, "Horseshoe" site (formerly West Summerland Key, now Scout Key), FMNH 288864, 1 specimen (sta. RB unnumb., 26/iii/1989; dissected; 6.2 mm L, 4.6 mm H, 3.5 mm W); FMNH 311591, 7 shells (sta. FK-629); FMNH 288849, 6 specimens (sta. FK-045; 2 dissected, not measured, shells destroyed).

Distribution

Stated by Turgeon et al. (2009) to range from south Florida to Quintana Roo, Mexico. *Carditamera floridana* has been reported from the Brazilian coast to Uruguay (e.g., Rios, 1994: 258; 2009: 524). However, significant differences have been found between samples from Florida and Brazil, which suggest specific separation. The shells of the Floridian specimens are larger, more darkly pigmented, and longer. A distributional gap also exists between the southern Caribbean and Espirito Santo, Brazil. For these reasons, the Brazilian reports of *C. floridana* are assumed to represent a separate species; they have not been included here, and require further studies to resolve.

Remarks

The anatomy of *Carditamera floridana* here presented agrees with earlier descriptions of those of other members of the family across a wide variety of genera and species, including *Cyclocardia ventricosa* (Gould, 1850), *Glans carpenteri* (Lamy, 1922), *Beguina semiorbiculata* (Linnaeus, 1758), *Cardita variegata* Bruguière, 1792 (all by Yonge, 1969; *B. semiorbiculata* also by Purchon, 1958), *Cardites ovalis* (Reeve, 1843) (by Pelseneer, 1911), *Cardites antiquatus* (Linnaeus, 1758), and *Cyclocardia velutina* (E. A. Smith, 1881) (both by Kaspar, 1913, the former as *Cardita sulcata* Bruguière, 1792). Purchon (1958) described a similar stomach structure in *B. semiorbiculata*. Variances across the group were noted by Pelseneer (1911) and Kaspar (1913) who found that the ventricle can be pierced to a varying extent by the intestine, and that an anal papilla can be present or absent at the end of the rectum. The spiral typhlosole has variously been described as a caecum, extending out of the stomach proper (Pelseneer, 1911), or as a structure on the stomach wall (Purchon, 1958; this study). The number of ducts from the stomach to the digestive diverticula also apparently varies (8 in *B. semiorbiculata*, Purchon, 1958; 4 in this study).

Harvey (1995) studied the reproductive biology of *Carditamera floridana* from the northern Gulf of Mexico coast in Bay County, Florida. Material from western Florida (Manatee County) was used in molecular studies of bivalves by Campbell (2000) and subsequent authors (e.g., Harper et al., 2006).

Family Lyonsiidae
P. Fischer, 1887

Entodesma beana
(d'Orbigny, 1853)
Figs. 178–191

Synonymy/Chresonymy

?*Osteodesma brasiliensis* "Couthouy, MS." – Gould, 1850: 218 [Type locality: Rio de Janeiro, Brazil]. See Remarks.
Lyonsia beana d'Orbigny, 1853: 225, pl. 25, figs. 26–28 [Type locality: Antilles].
Lyonsia (Philippina) beana – Abbott, 1974: 555, fig. 6082.
Entodesma beana – Prezant, 1981c: 65–66, fig. 13; Rios, 1994: 301, pl. 103, fig. 1472; Bieler & Mikkelsen, 2004: 515; Mikkelsen & Bieler, 2007: 192–193, 5 figs.

Description

Shell (Figs. 178–180): Translucent beige, weakly iridescent, fragile, gaping posteriorly, inequivalve, with LV typically broader; SL ≈ 13 mm in material examined ≈ 2 SH, SW ≈ 70% SH. Umbones low, subterminal, anterior. Outer surface smooth, except for growth lines and undulations; posteriorly typically distorted by nestling habit (Figs. 178, 179). Periostracum translucent, yellowish, extending beyond calcareous edges of shell. Anterior margin L ≈ 33% of posterior margin L; dorsal margin almost horizontal; ventral margin horizontal to convex. Hinge plate edentulous. Ligament internal, posterior to umbones at distance ≈ 14% SL. Calcareous lithodesma elongated (Fig. 180); L ≈ 50% of ligament L. Inner surface nacreous, smooth. Scar of anterior adductor muscle (*am*) in anteroventral quadrant, close to margin; H ≈ 3 L, A ≈ 2% of inner VA. Scar of posterior adductor muscle (*pm*) rounded, in posterodorsal area close to dorsal margin, at distance = 25% SL anterior to posterior margin; A ≈ 3 *am* scar A.

Main muscle system (Figs. 181, 185, 187, 188): Proportions and location of adductor muscles as described above. *Am* away from visceral structures (Fig. 187); V ≈ 5% SV. *Pm* opposite *am* at some distance from siphonal base (see above; Fig. 187). Anterior pedal retractor muscles (Fig. 187: *ar*) originating on posterodorsal side of *am*, running posteroventrally for distance = 25% SL, widening weakly, splaying across anterior foot base; A = 10% of *am* A. Paired posterior pedal retractor muscles (Figs. 187, 188: *pr*) originating on anterodorsal *pm*, abruptly decreasing over short distance from origin, running anteroventrally for distance = 33% SL, splaying across posterior foot base; A = 12% of *pm* A. Pedal protractor muscles not detected.

Foot (Figs. 181, 187): Small, narrowing abruptly ventrally; base on ventral surface of visceral mass; L ≈ 25% SL. Remaining 75% of foot as long stalk, with pointed tip. Byssal furrow running along ca. 80% of posteroventral side, ending at some distance from distal tip. Byssus simple, narrow, comprised of single thread in present material, attaching to posterior end of foot.

Mantle (Figs. 181, 185): Outer fold of mantle edges small, free; middle folds almost entirely fused. Anterior (pedal) aperture close to *am* (distance ≈ 10% SL); minute posterior (= fourth pallial) aperture approximately midway between *am* and posterior shell margin; A ≈ 25% of anterior aperture A. Incurrent (*si*) and excurrent (*se*) siphons mostly fused, composed of outer fold of mantle edge; periostracum covering most of outer siphonal surfaces; shallow grooves separating siphons along mid-siphonal L; siphons separating ca. 20% from distal ends into 2 similar branches, each with subterminal fold surrounded by papillae (Fig. 181: *mp*); papillae sparse along distal portions of siphons, excluding terminal rim of *se*. Siphons with uniformly muscular

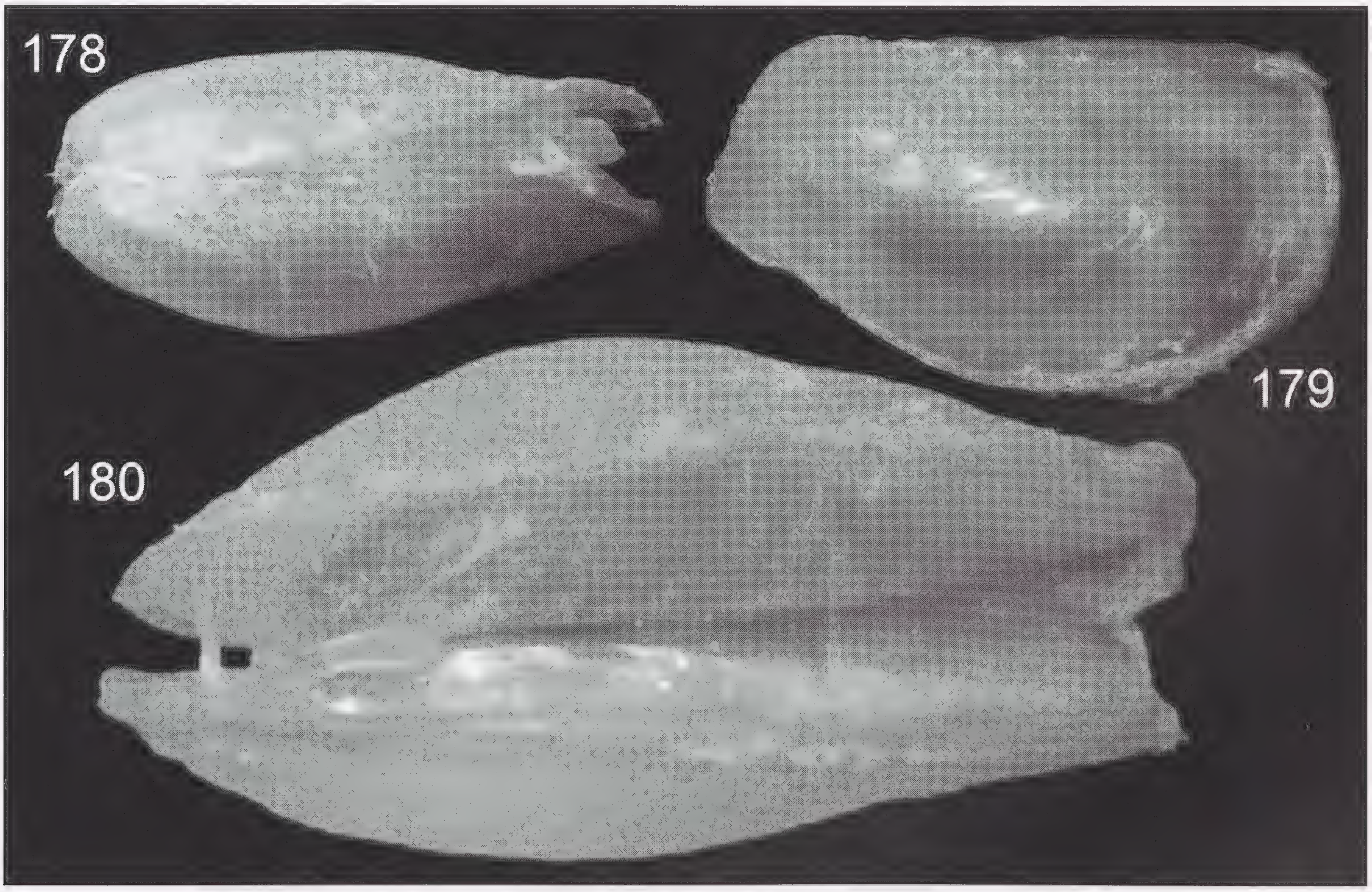

FIGS. 178–180. *Entodesma beana*, shell morphology, FMNH 295556, 13.0 mm L. FIG. 178: Dorsal view; FIG. 179: Left view; FIG. 180: Ventral view with partially opened valves, portions of adductor muscles still attached.

Central pad curved, surrounding left and anterior edges of conjoined *in*-style sac (*ss*) opening; A ≈ 20% of inner gastric surface A. Dorsal hood (Fig. 190: *dh*) aperture simple, in left-dorsal region at left end of transverse gastric fold. Conjoined *in-ss* opening in posteroventral region. Gastric shield (Fig. 190: *gs*) in posterodorsal region and slightly to left; A ≈ 20% of inner gastric surface A. Another sorting area with longitudinal folds along dorsal inner gastric surface; A ≈ 50% of ventral sorting area A. *In* and *ss* entirely interconnected, weakly separated by pair of low folds; *ss* L ≈ gastric main chamber L. *In* forming two short loops just anterior to end of *ss*, then crossing right surface of *ss* from anteroventral to posterodorsal (Fig. 187). *In* running horizontally, then posteriorly in region preceding *pc*. Anus (Figs. 185, 187: *an*) simple, papilla-like, with short siphon.

181

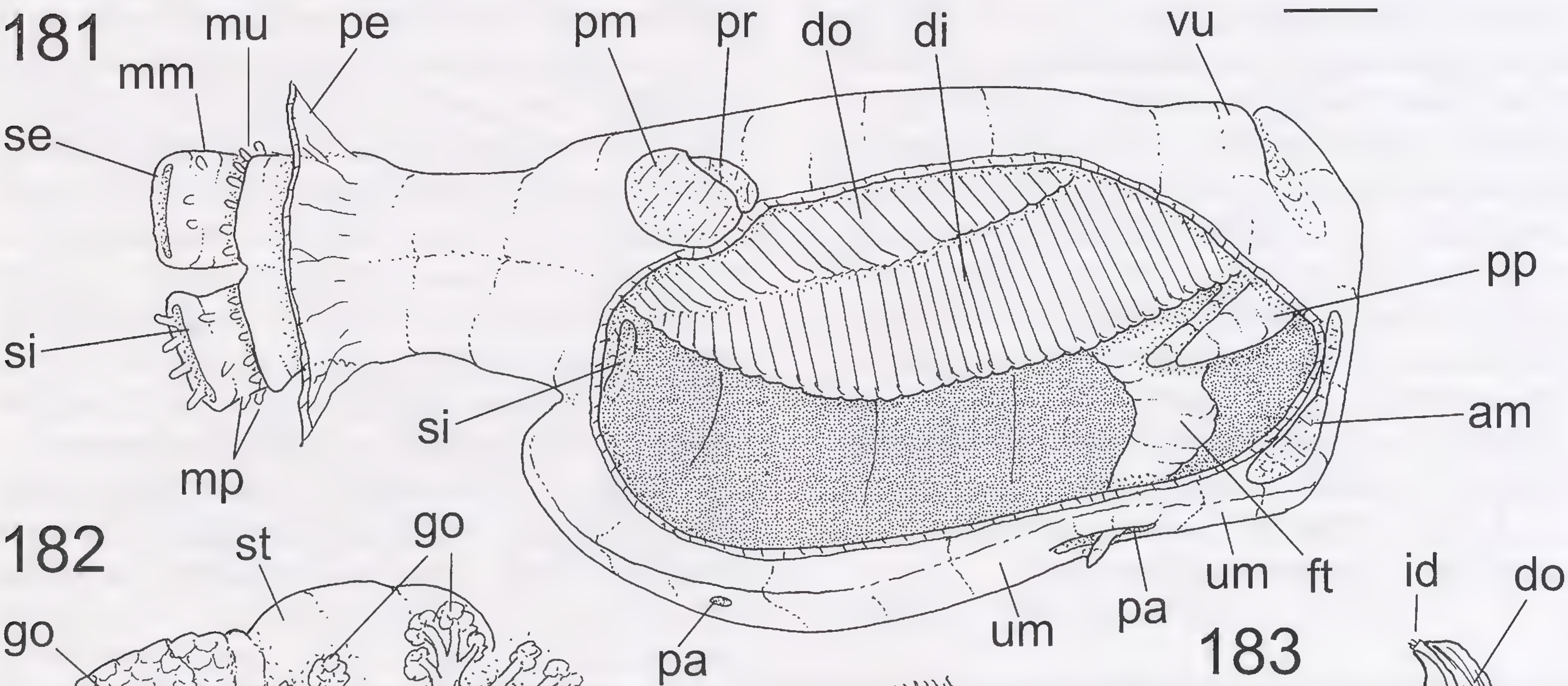

182

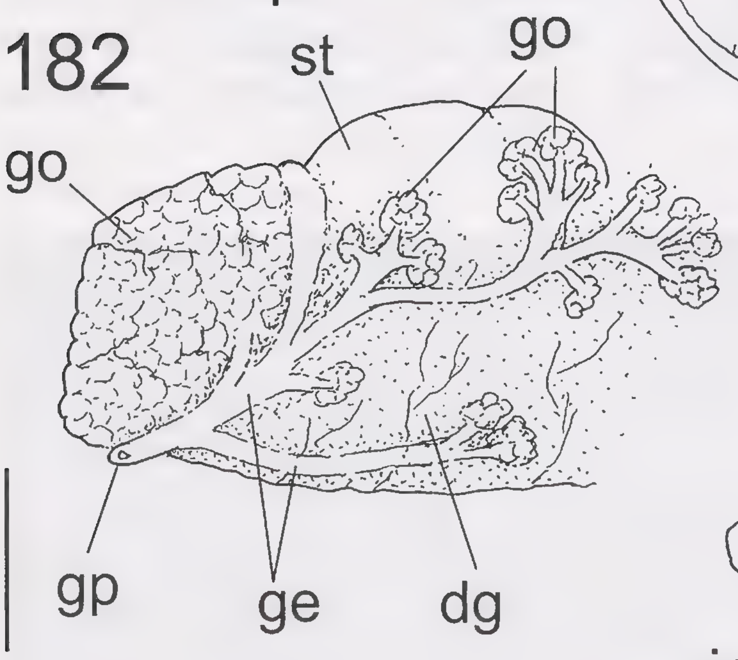

183

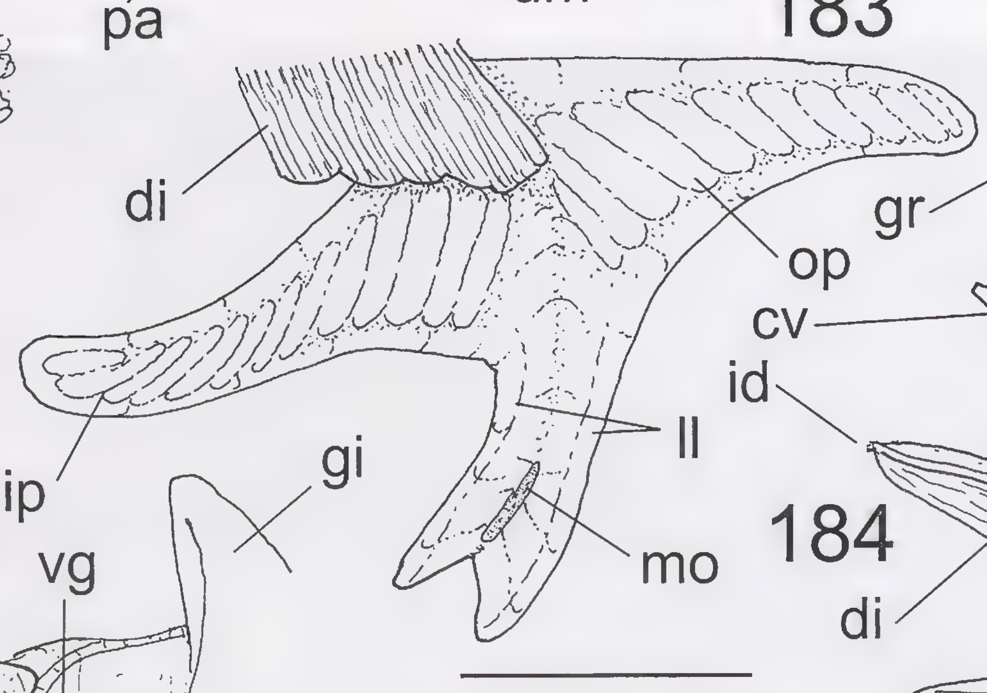

184

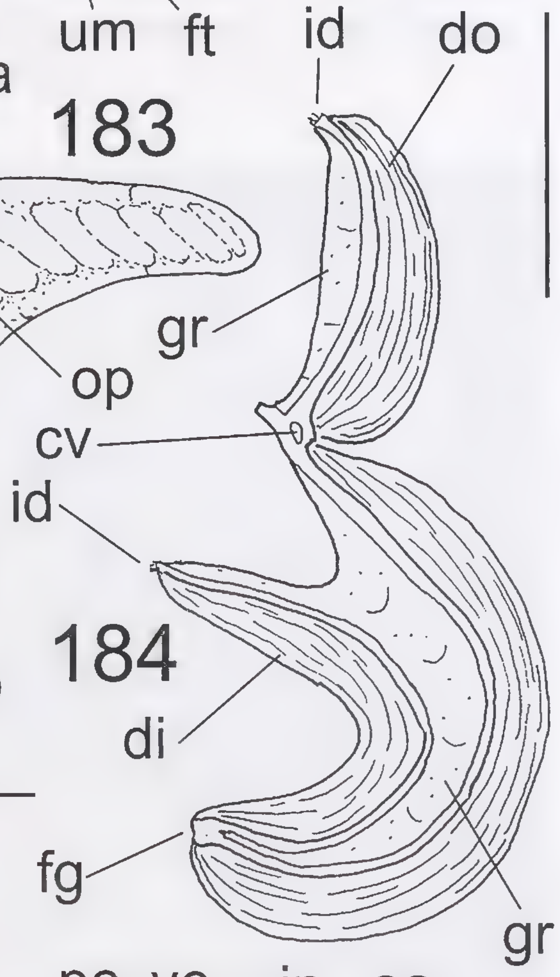

185

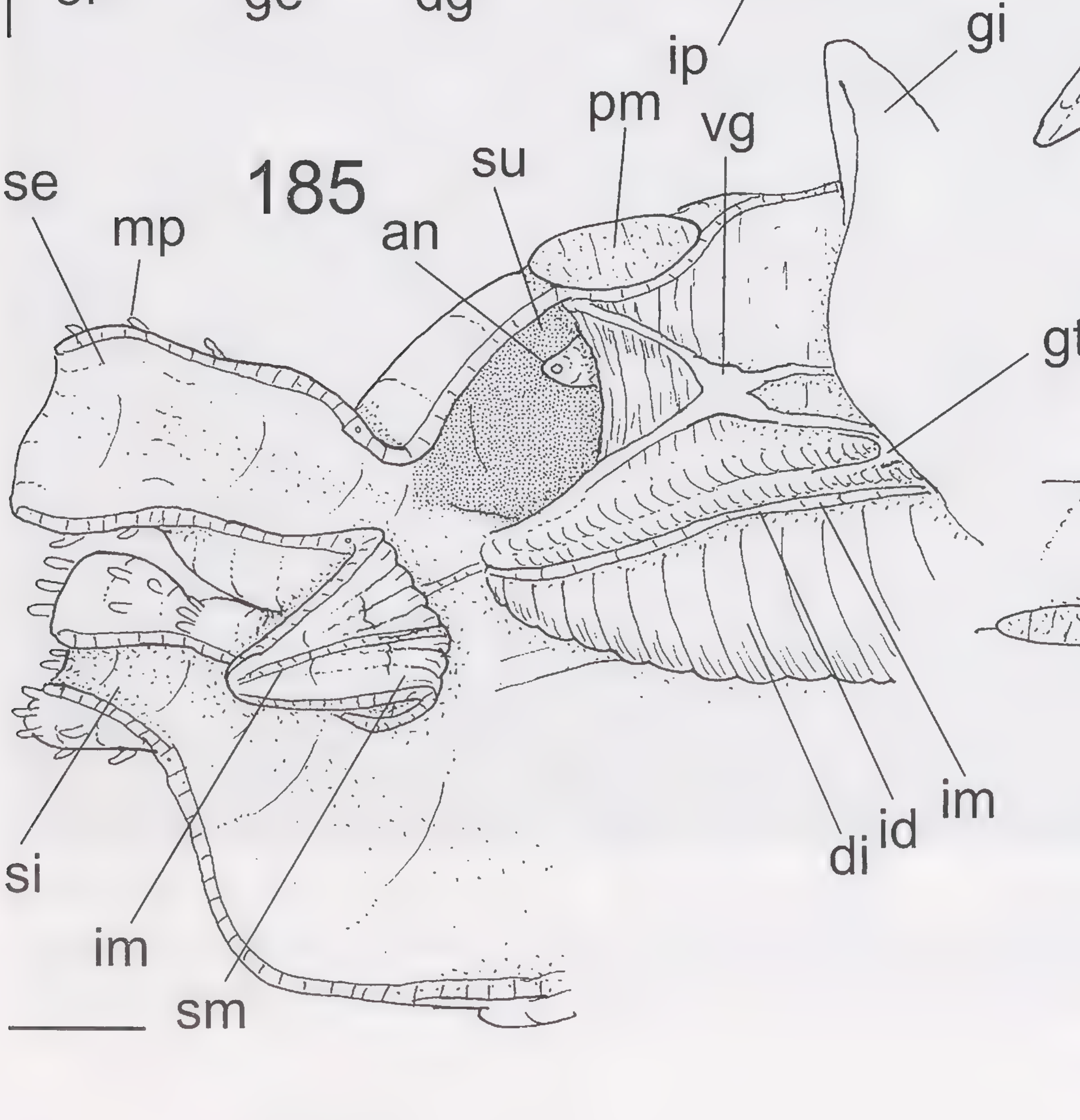

186

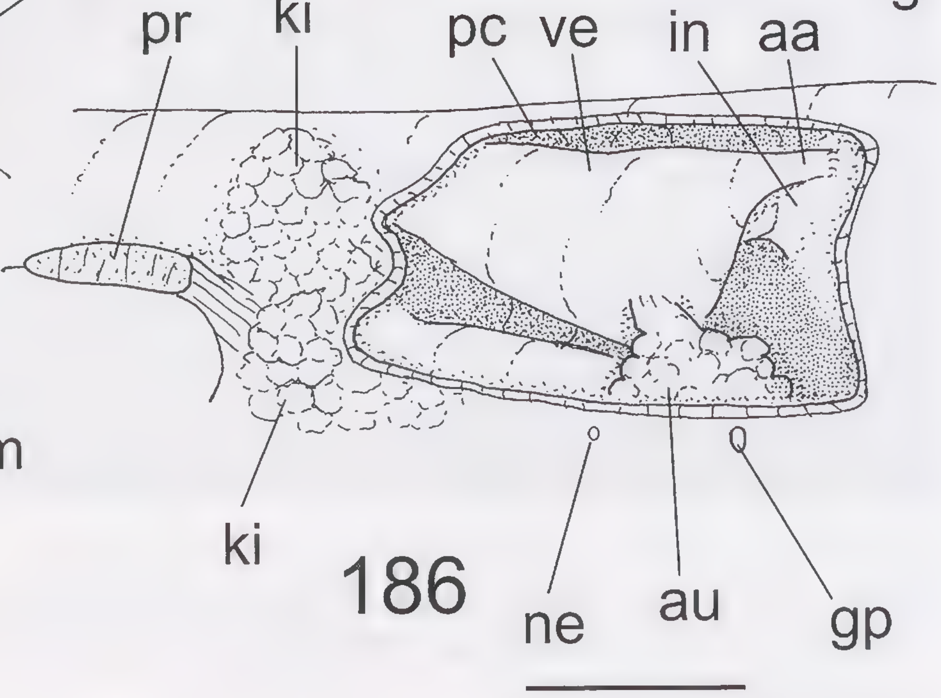

walls; all muscles originating in wide vertical arc ventral to *pm* (Fig. 185: *sm*). Siphonal inner surface smooth, simple.

Pallial cavity (Figs. 181, 183–185): In V ≈ 80% SV plus most of lateral regions, except area on dorsal side = 20% SH. Labial palps (*pp*) in A ≈ 10% of gill A; with hemipalps of similar shape, tapering posteriorly; L ≈ 3 H. *Pp* inner surfaces (Fig. 183) each composed of 10–15 wide, transverse folds, adjacent and at some distance from edges, leaving smooth space surrounding folds; folds and smooth edges becoming wider toward base; ends of folds rounded, similarly shaped; inner demibranch (*di*) inserting between dorsal halves of hemipalps. Smooth groove between hemipalps, running toward mouth. Palps separated by distance = *pp* L. Lips (Fig. 183: *ll*) simple, smooth, low. Gills large, restricted to dorsal half of pallial cavity; A ≈ 60% VA, L ≈ SL. Each outer demibranch (Fig. 184: *do*) comprised of single lamella, entirely dorsal to *di*; A ≈ 50% of *di* A. *Di* with subequal ascending and descending lamellae, with transverse septa every 10–15 filaments, vertically aligned (Fig. 184: *gr*), producing strong transverse folds in each demibranch. Anterior fifth of each gill composed only of *di*. Food groove shallow, running along ventral edge of *do* (Fig. 184: *fg*). Gill filaments connecting by longitudinal bridges of tissue, separated by distance = 3–4 filament W; bridge W = filament W. *Do* and *di* connecting to neighboring structures by ciliary strips.

Visceral mass (Fig. 187): Dorsal; V ≈ 25% SV. Stomach (*st*) located vertically in central region; V ≈ 20% of visceral mass V. Digestive diverticula greenish white, mostly anterior to *st*; V ≈ 20% of visceral mass V. Gonad yellowish white, filling remaining visceral mass V. Pericardium (*pc*) triangular, along posterior region; V ≈ 25% of visceral mass V.

Circulatory and excretory systems (Figs. 186, 188): Paired auricles (*au*) with lobed walls, connecting to gills between their middle and posterior thirds, along ca. 12% of gill L, in anterolateral pericardium (*pc*); V ≈ 12% of pericardial V. *Au* connections to ventricle (*ve*) preceded by smooth, unlobed, narrow region. *Ve* encircling intestine along most of L within *pc*. Kidneys greenish white, filling ventrolateral *pc*; V ≈ 50% of renopericardial V. Paired urinary ducts (Fig. 188: *kd*) running along entire dorsal kidney surface, white, opening at nephropore. Nephropores as small, low papillae, located posterior to *pm* at distance = *pm* L.

Digestive system (Figs. 185, 187, 189, 190): *Pp* as described above. Mouth close to dorsal edge of *am*. Esophagus (*es*) running posterodorsally at distance = 33% SH, forming wide arc; W = 12% *am* W. *Es* inserting terminally in anterior gastric wall, with low, multifolded *es* rim (Fig. 190: *er*). Stomach (*st*) vertically disposed; gastric main chamber oval (Fig. 189); V ≈ 12% of visceral mass V. Dorsal hood (Figs. 189, 190: *dh*) in L ≈ gastric main chamber L, W ≈ 50% *es* W. Gastric inner surface (Fig. 190) with strong transverse fold on ventral surface between *es* and intestinal (*in*) openings; posterior edge of transverse fold laterally flanking ducts to digestive diverticula (Fig. 190: *dd*); wide ventral sorting area covering ca. 20% of inner gastric surface.

←

FIGS. 181–186. *Entodesma beana*, anatomy. FIG. 181: Intact right view, right mantle lobe partially removed; FIG. 182: Visceral mass, right view, detail of posterior region, integument removed to show genital ducts (ge); FIG. 183: Right labial palp, right view, outer hemipalp (op) deflected, portion of adjacent region of inner demibranch (di) shown; FIG. 184: Gill, cross section in midregion showing several filaments that comprise a gill fold; FIG. 185: Siphons (se, si) and adjacent region of visceral mass, ventral-slightly right view, siphons opened longitudinally, right pedal retractor muscles deflected, right gill deflected and only topologically shown; FIG. 186: Visceral mass, posterodorsal region, most of right side of pericardium removed. Scale bars = 1 mm. Abbreviations: aa, anterior aorta; am, anterior adductor muscle; an, anus; au, auricle; cv, ctenidial (efferent) vessel; dg, digestive diverticula; di, inner demibranch; do, outer demibranch; fg, food groove; ft, foot; ge, genital ducts; gi, gill; go, gonad; gp, genital pore; gr, gill transverse septum in suprabranchial chamber; gt, gill suspensory stalk; id, insertion of outer demibranch in mantle; im, insertion of inner demibranch in visceral mass; in, intestine; ip, inner hemipalp; ki, kidney; ll, labial lips preceding mouth; mm, mantle border middle fold; mo, mouth; mp, mantle papillae; mu, mantle border outer fold; ne, nephropore; op, outer hemipalp; pa, pedal aperture of fused mantle border; pc, pericardium; pe, periostracum; pm, posterior adductor muscle; pp, labial palp; pr, posterior pedal retractor muscle; se, excurrent siphon; si, incurrent siphon (and internal opening); sm, siphonal retractor muscle; st, stomach; su, supra-anal chamber of suprabranchial pallial cavity; um, fusion between left and right mantle lobes; ve, ventricle; vg, visceral ganglia; vu, visceral portion inside umbonal cavity.

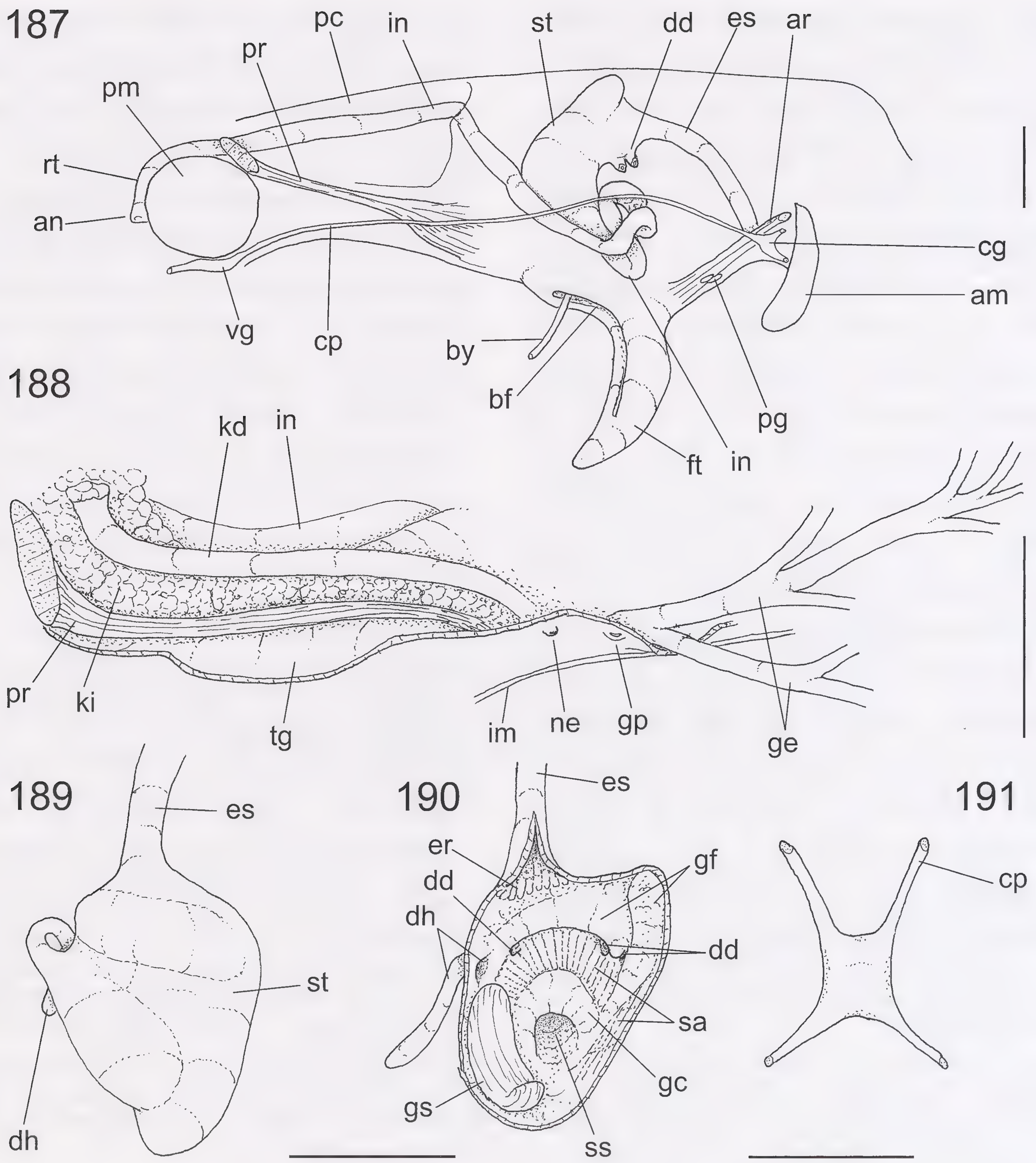

FIGS. 187–191. *Entodesma beana*, anatomy. FIG. 187: Digestive system, main musculature, and nervous system *in situ*, right view, topologies of some adjacent structures also shown; FIG. 188: Ventral region of visceral mass, right view, integument and visceral glands partially removed; FIG. 189: Stomach, dorsal view; FIG. 190: Same, longitudinally opened, inner surface exposed; FIG. 191: Visceral ganglia, ventral view. Scale bars = 1 mm. Abbreviations: am, anterior adductor muscle; an, anus; ar, anterior pedal retractor muscle; bf, byssal furrow; by, byssus; cg, cerebropleural ganglion; cp, cerebrovisceral connective; dd, ducts to digestive diverticula; dh, dorsal hood; er, esophageal rim; es, esophagus; ft, foot; gc, gastric central pad; ge, genital ducts; gf, gastric fold; gp, genital pore; gs, gastric shield; im, insertion of inner demibranch in visceral mass; in, intestine; kd, renal-urinary duct; ki, kidney; ne, nephropore; pc, pericardium; pg, pedal ganglion; pm, posterior adductor muscle; pr, posterior pedal retractor muscle; rt, rectum; sa, gastric sorting area; ss, style sac; st, stomach; tg, integument; vg, visceral ganglia.

Reproductive system (Figs. 182, 188): Gonad (in part described above) composed of posterior main region and several other portions along anterior visceral regions, connecting by branching ducts (Fig. 182), with symmetrical sides. Genital ducts converging posteriorly to genital pore, forming tubular genital chamber preceding pore (Fig. 188: *ge*). *Gp* small, located anterior to nephropore at distance = 50% of *pm* L.

Nervous system (Figs. 187, 191): Cerebropleural ganglia (Fig. 187: *cg*) lateral, near origins of *ar*, *am*, and *pp* base; L = *es* D. Cerebral commissure almost as long as *am* W. Paired pedal ganglia (Fig. 187: *pg*) elliptical, adjacent, approximately midway between *cg* and pedal tip; L ≈ 25% of *cg* L. Paired visceral ganglia (Fig. 187: *vg*) slightly larger than *cg*, on ventral surface of *pm*, broadly connected (Fig. 191). Cerebrovisceral connectives (Fig. 187: *cp*) running almost directly through visceral mass.

Material Examined

USA, Florida Keys, FMNH 295556, 1 specimen (sta. FK-138; dissected: 13.0 mm L, 7.4 mm H, 6.2 mm W).

Distribution

Stated by Turgeon et al. (2009) to range from North Carolina to Gulf of Mexico, Cuba, West Indies, Brazil, and Bermuda. *Entodesma brasiliensis*, orginally described from Rio de Janeiro as *Osteodesma brasiliensis* "Couthouy, MS." Gould, 1850, has been synonymized with this species (e.g., Prezant, 1981c; Rios, 1994: 301; 2009: 602; sometimes misspelled *braziliensis*). No anatomical material from Brazil was available for this study, so the question of species identity could not be investigated.

Remarks

The description here is in agreement with that of *Entodesma saxicola* (Baird, 1863) [now a synonym of *E. navicula* (A. Adams & Reeve, 1850)] as described by Yonge (1952, 1976) and Morgan & Allen (1976), with that of *Mytilimeria nuttallii* Conrad, 1837, described by Yonge (1952a, 1976), and with that of *Lyonsia californica* Conrad, 1837, described by Narchi (1968). Ultrastructural characters of the shell and periostracum of *Entodesma beana* were described by Prezant (1981b; from USNM specimens) in comparison with other species in the family Lyonsiidae; this material agrees with those data as far as they were observed here in gross examination. No byssal notch or embayment in the ventral edge of the shell, as was seen in some *E. saxicola* specimens, was noted in *E. beana*. For other details of the shell of *E. beana*, see Mikkelsen & Bieler (2007: 192).

Morgan & Allen (1976) described a somewhat different muscle configuration associated with the foot and byssus. Here we observed anterior and posterior pedal retractor muscles only. Morton & Allen labeled what we call posterior pedal retractor muscles as posterior byssal retractors. They considered posterior pedal retractors as atrophied/absent. Anteriorly, they described both anterior pedal and byssal retractor muscles. Yonge's (1952a: 441) description is in agreement with our interpretation of only one set of muscles, but he labeled them slightly differently as "small anterior and posterior pedal retractors, or, more accurately, byssal muscles."

The mantle of *Entodesma beana* is bright orange in life (Mikkelsen & Bieler, 2007: 192). Prezant (1981a) described the arenophilic (sand-adhering) glands of the mantle of *E. beana* from Puerto Rico, using general histology and histochemical procedures. These glands secrete onto the surface of the periostracum and thus allow the attachment of adhering particles from the environment. Morton (1987) described the same for *E. saxicola* and *E. inflata* (Conrad, 1837) from the western U.S. using similar techniques. Such observations were beyond the scope of this work, however, the periostracum of specimens studied here did have some sand grains attached.

The siphons of *Entodesma beana* are here interpreted as long, mostly fused, and invested partly by the gill (as in *Lamychaena hians*), with short free portions at the tips. This is in conflict with the interpretation by Mikkelsen & Bieler (2007: 193), which described (based on these same dissections) short, free siphons at the posterior end of an extended mantle cavity. In the absence of well-developed siphonal retractor muscles (as in *Lamychaena hians*) to mark the base of the siphons, the relative length and degree of fusion in the siphons of *Entodesma beana* remains controversial.

The labial palps of *Entodesma saxicola* are unridged dorsally (Morgan & Allen, 1976: fig. 4A), a condition claimed to be unusual for bivalves, but not seen here. Yonge (1952a) described *E. saxicola* as an hermaphrodite with separate ovaries and testes; we noted two separate portions of the gonad in *E. beana*, a posterior main region and other anterior portions – possibly (but unverified) representing male and female gonads.

Family Lucinidae
J. Fleming, 1828

Codakia orbicularis
(Linnaeus, 1758)
Figs. 192–210

Synonymy/Chresonymy

Venus orbicularis Linnaeus, 1758: 688 [Type locality: "Habitat intra Tropicos," within the tropics].

Codakia (Codakia) orbicularis – Abbott, 1974: 459, pl. 22, fig. 5297.

Codakia orbicularis – Allen, 1958: 427, 429–430, 432, 436, 442–443, 451, 471, 475, 479, figs. 3, 5b, 9b, 13, 29, 40a, 48d, pl. 18, fig. 58; Rios, 1994: 253, pl. 87, fig. 1237; 2009: 514, fig.; Taylor & Glover, 2000: 214, figs. 7a, 8; Bieler & Mikkelsen, 2004: 515; Mikkelsen & Bieler, 2007: 228–230, 6 figs.; Taylor et al., 2011: 19 ff. (DNA).

Description

Shell (Figs. 192–196): Rounded, laterally compressed, opaque, pale cream-colored to yellowish; SL ≈ 35–60 mm L in material examined. Sculpture of ca. 50 wide radial and narrow commarginal threads, equally predominant; threads and interspaces of weakly uniform W. Inner surface glossy, uniformly irregular, whitish or yellowish. Anterior adductor muscle (*am*) scar W ≈ posterior adductor muscle (*pm*) scar W ≈ 2 *pm* H; A ≈ 5% of inner VA (Figs. 193, 194). Pallial line somewhat wide, connecting to each adductor scar at outer dorsal edge (instead of ventral, as is usual in most other bivalves), more clearly evident at *am* scar. Hinge plate (Figs. 195, 196) occupying ca. 50% SW (Figs. 193, 194), including 3 cardinal teeth in LV, 2 in RV. Ligament (Figs. 193–196) external, in posterior half of hinge plate.

Main muscle system (Figs. 197, 200–202, 205): *Am* dorsoventrally elongated (H > 50% SH), anteroposteriorly slender (L < 12% SL) (Figs. 197, 200–202); distance between anterior edge and shell margin = *am* W, with ventral end slightly more posterior than dorsal end; connecting to visceral mass only posterodorsally (25% H); remaining 75% of posterior surface exposed in pallial cavity. *Pm* only slightly broader than *am* (Figs. 200–202, 205), in H ≈ 50% *am* H; remaining attributes similar to those of *am*. Dorsal end of each adductor muscle at approximately same horizontal level, close to hinge plate; each adductor muscle composed of subequal, differently colored ("catch" and "quick") portions. Paired anterior pedal retractor muscles (Figs. 200–202: *ar*) wide, thick, originating just posterior and dorsal to *am*, running posteroventrally close to midline, adjacent, splaying across anterior foot base; A = 16% of *am* A. Paired posterior pedal retractor muscles (Figs. 200–202: *pr*) in W and T > *ar* W and T, originating just anterior to *pm*, running anteroventrally, splaying across posterior foot base; A = 50% of *pm* A; H ≈ 2 anteroposterior W. Pedal protractors absent.

Foot (Figs. 200–202): Simple, conical, laterally compressed, with pointed tip; A ≈ 10% VA. Byssal groove and byssus absent.

Mantle (Figs.197, 198, 200, 203, 204): Mantle border relatively thick, not pigmented. Mantle lobes free except at posterior region adjacent to incurrent (*si*) and excurrent (*se*) apertures (Fig. 204). Outer fold simple, relatively thick (Fig. 203). Middle fold thinner than outer fold, but of similar H; distal edge undulating; distal portions of undulations weakly projecting, becoming papilla-like posteriorly, surrounding apertures (Figs. 200, 204). Inner fold thick,

---

→

FIGS. 192–199. *Codakia orbicularis.* FIGS. 192–196: Shell morphology, FMNH 295647, 50 mm L. FIG. 192: RV outer view; FIG. 193: LV interior view; FIG. 194: RV interior view; FIG. 195: Detail of hinge and adjacent area of RV, ligament (li) sectioned longitudinally; FIG. 196: Same, LV. FIGS. 197–199: Anatomy. FIG. 197: Detail of anteroventral region of pallial cavity, right mantle lobe, interior view, left mantle lobe extracted, showing pallial gills (sg) and adjacent structures; FIG. 198: Detail of posterior region of visceral mass, left view, gill removed, horizontal section from genital pore toward anterior, inner chamber exposed; FIG. 199: Anterior region of body, anterior view, anterior adductor muscle removed, both anterior pedal retractor muscles deflected. Scales bars = 5 mm (FIGS. 193–197); 0.5 mm (FIGS. 198, 199). Abbreviations: am, anterior adductor muscle; ar, anterior pedal retractor muscle; cg, cerebropleural ganglion; es, esophagus; ft, foot; gi, gill; gn, genital chamber; gp, genital pore; im, insertion of inner demibranch in visceral mass; li, ligament; mb, mantle border; ne, nephropore; pe, periostracum; pp, labial palp; sg, secondary (pallial) gills.

low, running internally at some distance from other 2 folds. Another fold running close to inner edge of inner fold, with inner constitution glandular (Fig. 203: *gl*); H ≈ inner fold H, W = 2 inner fold W. Secondary (pallial or mantle) gills (Figs. 197, 200: *sg*) on inner surface of each mantle lobe ventral to *am*, composed of 5–6 horizontal folds in L ≈ *am* L, parallel to anteroventral mantle border, from close to mantle border to ventral end of *am*; second-

192

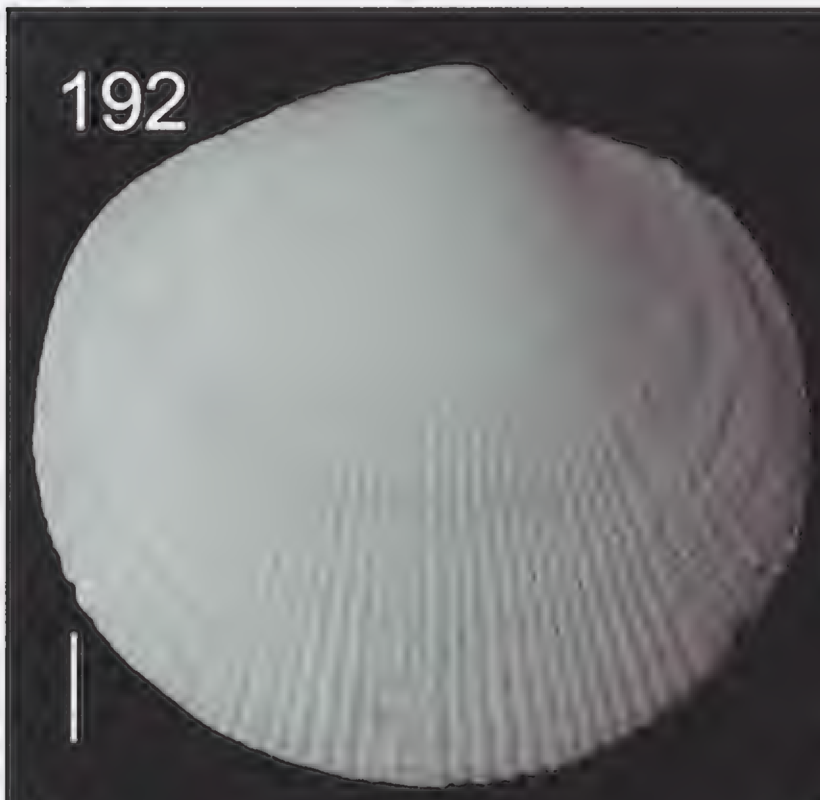

193 194

195 196

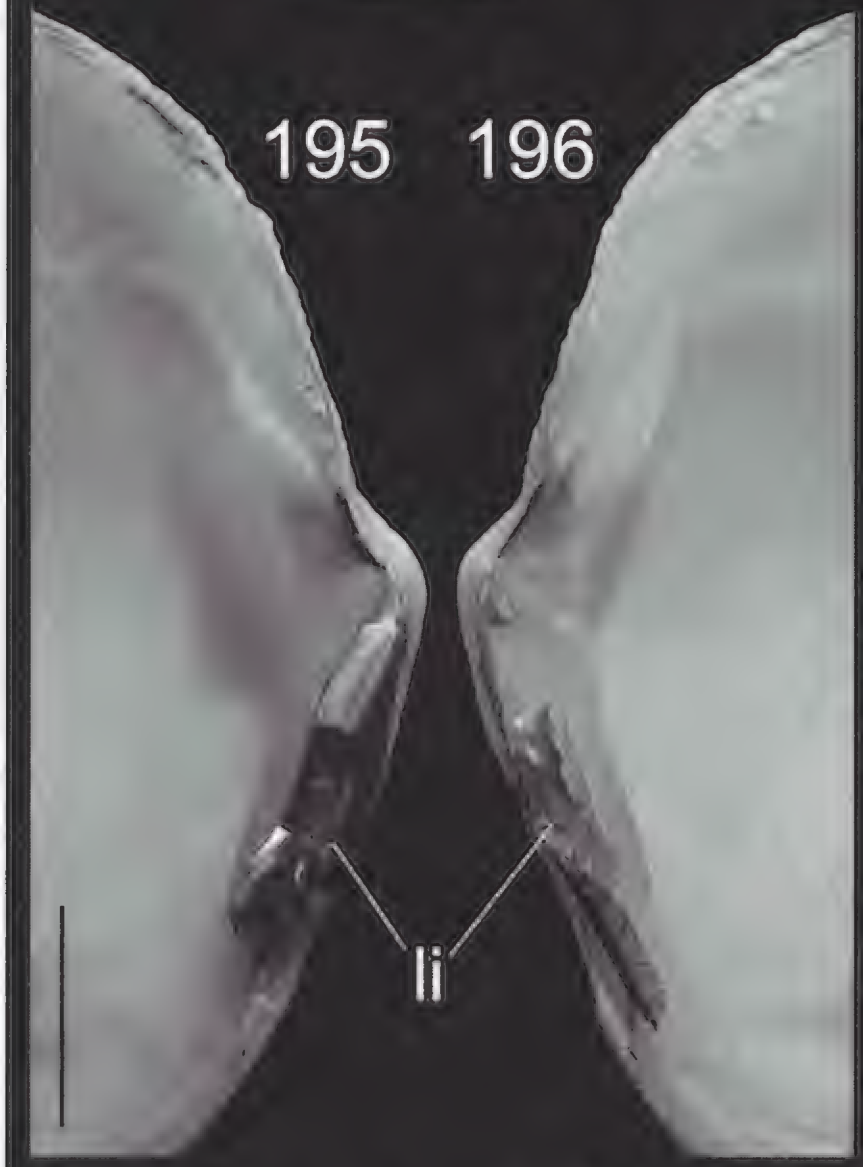

197

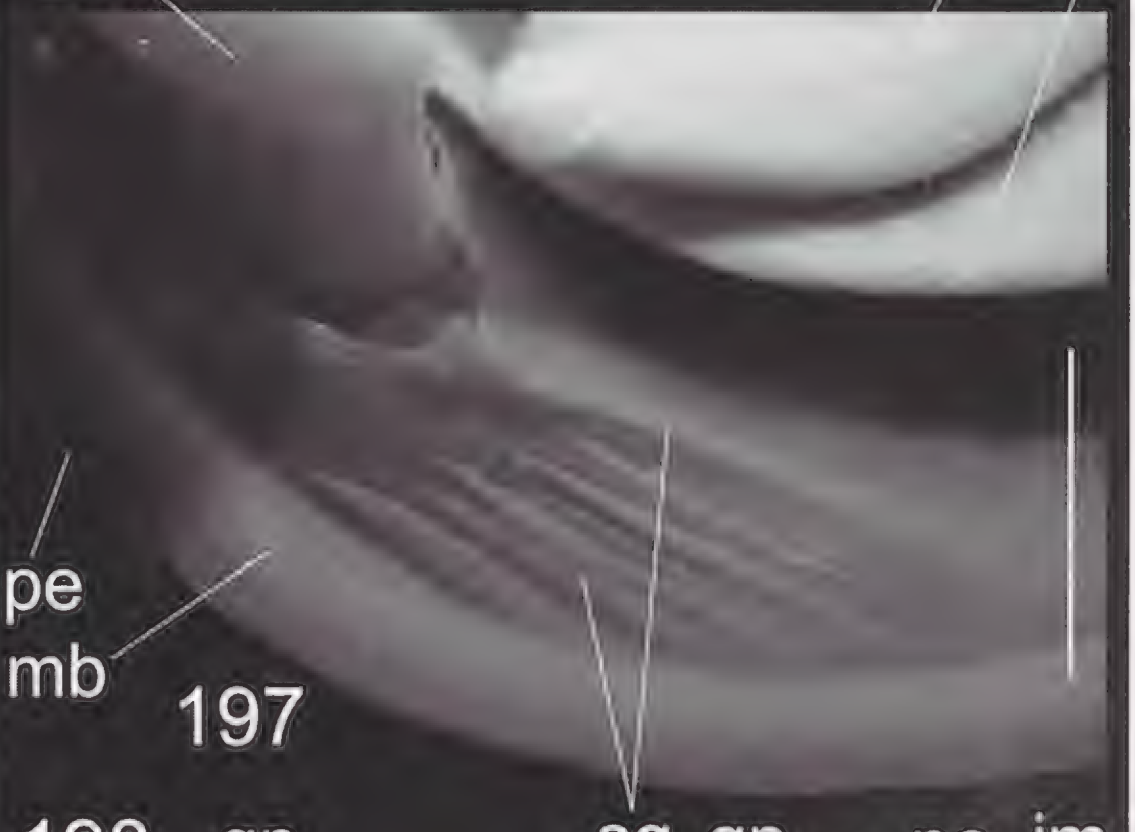

198

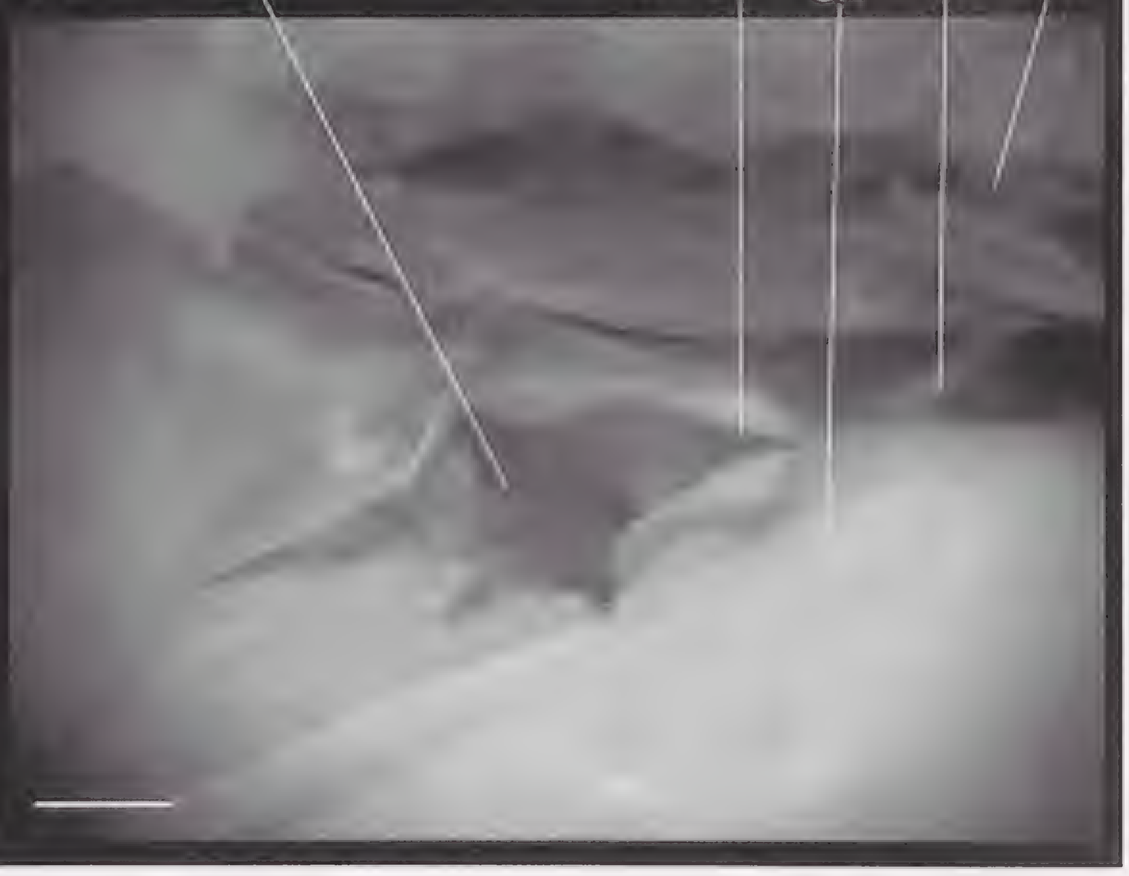

199

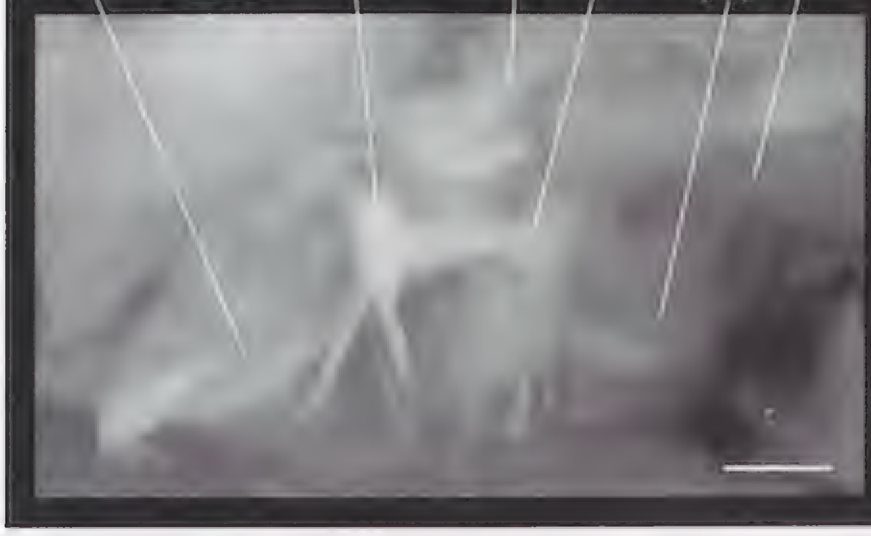

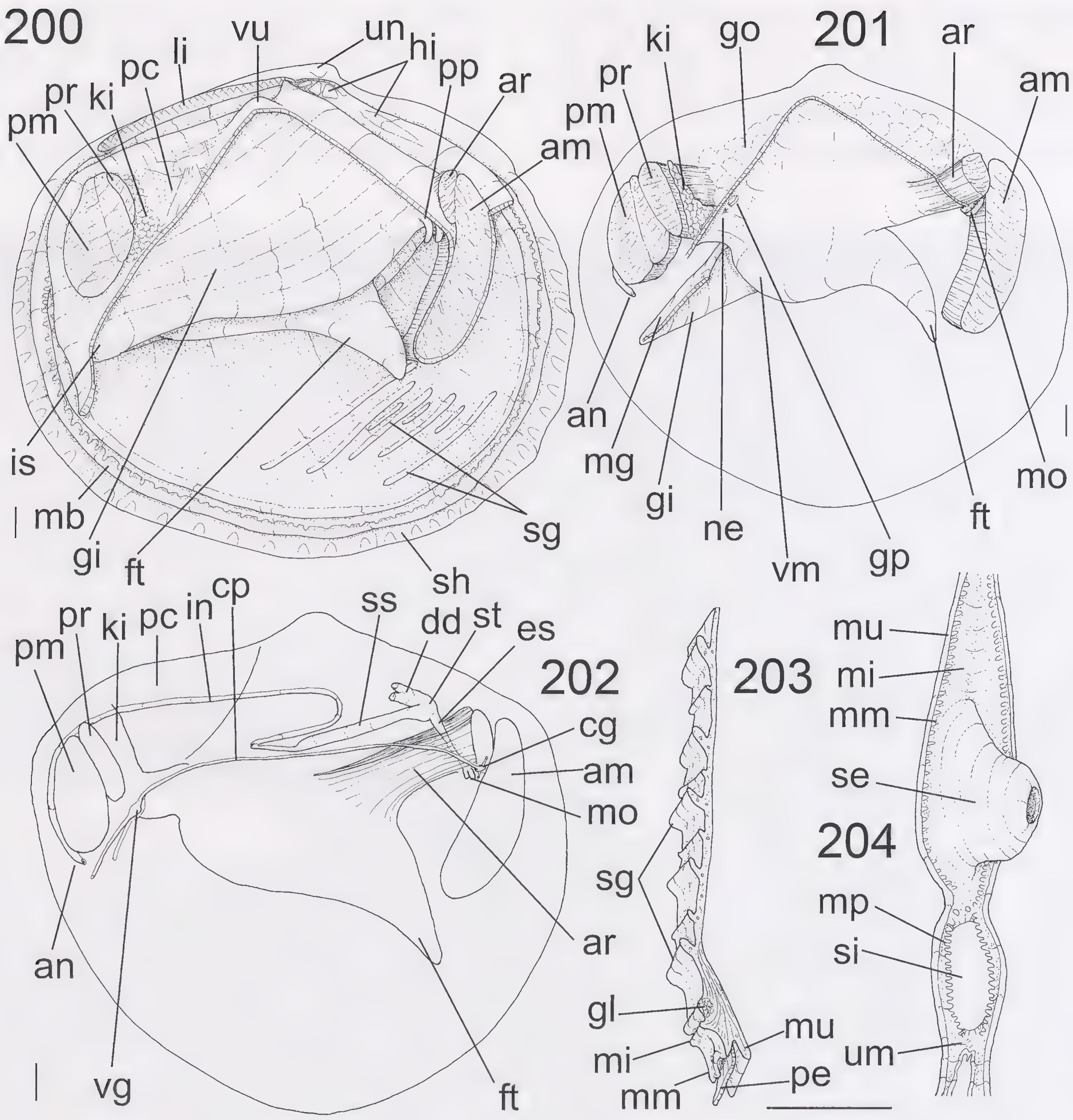

FIGS. 200–204. *Codakia orbicularis*, anatomy. FIG. 200: Intact specimen, right view, RV and part of mantle lobe removed; FIG. 201: Same, showing main musculature, visceral mass, and foot *in situ*, right gill removed; FIG. 202: Same, showing digestive system and nervous system *in situ*, topologies of main structures also shown; FIG. 203: Cross section of middle to anterior region of mantle, through secondary gill and mantle border; FIG. 204: Posterior apertural region, posterior and slightly left view. Scale bars = 1 mm. Abbreviations: am, anterior adductor muscle; an, anus; ar, anterior pedal retractor muscle; cg, cerebropleural ganglion; cp, cerebrovisceral connective; dd, ducts to digestive diverticula; es, esophagus; ft, foot; gi, gill; gl, gland; go, gonad; gp, genital pore; hi, hinge; in, intestine; is, siphonal septum; ki, kidney; li, ligament; mb, mantle border; mg, membrane uniting inner demibranchs in region posterior to visceral mass; mi, mantle border inner fold; mm, mantle border middle fold; mo, mouth; mp, mantle papillae; mu, mantle border outer fold; ne, nephropore; pc, pericardium; pe, periostracum; pm, posterior adductor muscle; pp, labial palp; pr, posterior pedal retractor muscle; se, excurrent aperture; sg, secondary (pallial) gills; sh, shell; si, incurrent aperture; ss, style sac; st, stomach; um, fusion between left and right mantle lobes; un, umbo; vg, visceral ganglia; vm, visceral mass; vu, visceral portion inside umbonal cavity.

ary folds present mainly in larger specimens between main folds; L and H ≈ 50% of main fold L and H; dorsalmost fold largest (ca. 50% longer than remaining folds), anteriorly inserting at midregion ("knot" of Allen, 1958; Taylor & Glover, 2000) of another fold surrounding auricle, broadly connecting to ctenidial vein, but separating from it by thin transverse septum; anterior and posterior ends of auricles connecting terminally to ctenidial vein. *Si* comprised only of inner fold. Short connection between inner folds of both mantle lobes just

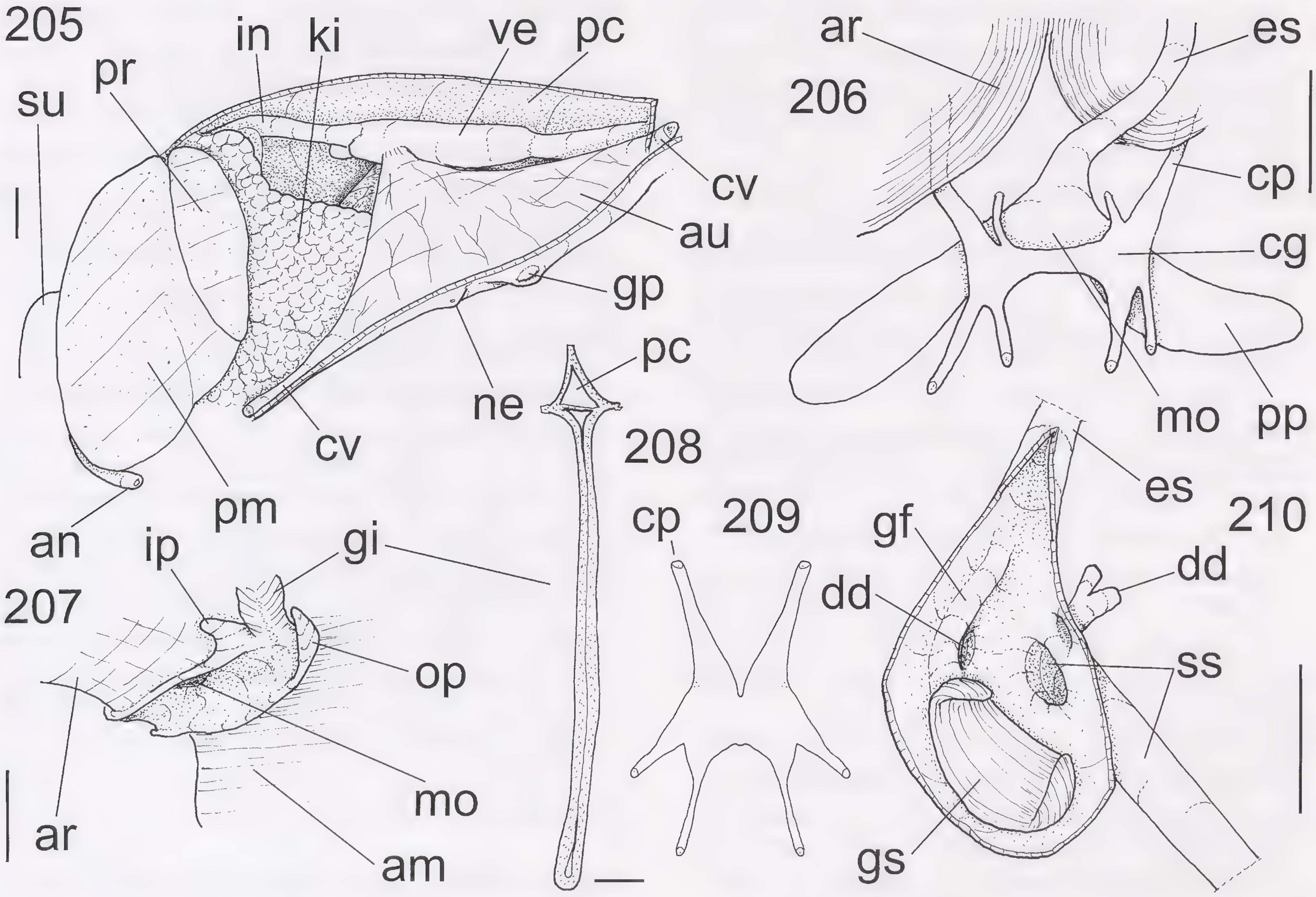

FIGS. 205–210. *Codakia orbicularis*, anatomy. FIG. 205: Pericardium and adjacent structures, right view, left wall of pericardium and gill removed; FIG. 206: Anterior region of body, anterior view, anterior adductor muscle removed, both anterior pedal retractor muscles deflected, esophagus and ganglia *in situ*; FIG. 207: Labial palps and adjacent region, right and slightly ventral view; FIG. 208: Gill, cross section of midportion; FIG. 209: Visceral ganglia, ventral view; FIG. 210: Stomach, dorsal view, sectioned longitudinally to expose inner surface. Scale bars = 1 mm. Abbreviations: am, anterior adductor muscle; an, anus; ar, anterior pedal retractor muscle; au, auricle; cg, cerebropleural ganglion; cp, cerebrovisceral connective; cv, ctenidial (efferent) vessel; dd, ducts to digestive diverticula; es, esophagus; gf, gastric fold; gi, gill; gp, genital pore; gs, gastric shield; in, intestine; ip, inner hemipalp; ki, kidney; mo, mouth; ne, nephropore; op, outer hemipalp; pc, pericardium; pm, posterior adductor muscle; pp, labial palp; pr, posterior pedal retractor muscle; ss, style sac; su, supra-anal chamber of suprabranchial pallial cavity; ve, ventricle.

ventral to *si*. Inner folds broadly connected, forming deep supra-anal chamber near *se*. *Se* conical (Fig. 204); L = 6–10 inner fold L; distal tip simple, lacking papillae. Transverse septum separating infra- and suprabranchial chambers as posterior extensions of gill.

Pallial cavity (Figs. 200–202, 206–208): Spacious except for oblique *am*; A ≈ 85% VA. Labial palps (Figs. 200–202: *pp*), minute, between origins of *ar* and *am*, just anterior to ends of gills. Hemipalps similar, with smooth inner surfaces, in form of small, triangular, lateral expansions of lips (Figs. 206, 207); with wide smooth area between ventral and dorsal lips. Gills each consisting of a single (inner) thickened demibranch (Fig. 208); surface uniform, weakly folded longitudinally; ventral edge almost horizontal; dorsal edge forming triangle fully connecting to mantle and visceral mass. Ascending and descending branches of each filament subequal, very thick due to presence of symbiotic bacteria. Gill filaments connecting by wide tissue bridges; connecting by thin, translucent transverse septum posterior to foot (Fig. 201: *mg*), surrounding posterior surface of foot, leaving foot free. Outer and posterior regions of gill with tissue connections to transverse mantle septum separating infra- and suprabranchial chambers.

Visceral mass (Figs. 202, 205): Greatly compressed dorsally, close to hinge plate; A ≈ 20% VA. Digestive diverticula greenish brown, mostly anterior, clustering around stomach. Gonad greenish beige, filling most of remaining inner space, with hollow chamber preceding genital pore. Pericardial structures posterior, just anterior to *pr* origins; V ≈ 16% of visceral mass V.

Circulatory and excretory systems (Figs. 198, 201, 205): Pericardial cavity triangular, just anterior to *pr* origin; ventral surface separated by tall elevation of visceral glands and kidney; V = 20% of visceral mass V. Auricles (*au*) triangular, one on each side; *au* connections to ventricle (*ve*) mid-lateral, narrow. *Ve* surrounding slightly > 50% of intestine passing through pericardium (*pc*). Kidney (Fig. 205: *ki*) flat, solid, in posterior region of ventral elevation bulging inside *pc*. Nephropores (Figs. 198, 201, 205: *ne*) very small, at central level of *au*, posterior to and separated from genital near (but not attaching to) ventral *am*; dorsalmost fold with tall, triangular projection projecting inward at posterior end (Fig. 198).

Digestive system (Figs. 199, 202, 206, 210): *Pp* as described above. Smooth area between *pp* and mouth = 2 single *pp* A. Esophagus (Figs. 199, 206: *es*) running directly posterodorsally almost perpendicular to longitudinal axis of body between *ar*; slightly longer than *ar* W; inner surface smooth. Stomach (*st*) small (W ≈ 2 *es* W); *es* opening anteroventral, without rim; pair of relatively large ducts to digestive diverticula on each side of anterodorsal region. Gastric inner surface (Fig. 210) mostly smooth, lacking obvious folded sorting areas; low, broad longitudinal fold separating ducts to digestive diverticula, one at level of *es* opening, another at anterior edge of gastric shield. Gastric shield (*gs*) in posterodorsal region of *st*; A ≈ 33% of inner gastric surface A. Conjoined style sac-intestine (Fig. 210: *ss, in*) originating in posteroventral *st*, in D > opening of ducts to digestive diverticula D; running posteriorly and weakly ventrally immersed in digestive diverticula and gonad. *Ss* lacking any apparent inner separation from *in*; inner surface yellowish iridescent; *ss-in* W weakly > *es* W; L ≈ 1.5 *es* L. *In* becoming free from *ss* after abrupt decrease in D, becoming very narrow, continuing posteriorly for distance = 25% of *ss* L, then curving abruptly anteriorly, running immersed in gonad dorsally to preceding branch. *In* making wide, gradual curve, then running directly posteriorly along midline; passing through *pc*, between insertions of *pr* and along dorsal and posterior surfaces of *pm*. Anus very small, preceded by very short stalk, on ventral surface of *pm*.

Reproductive system (Figs. 198, 201, 205): Gonad as described above, clearly branching, forming digitiform acini. Genital pore slit-like, forming low, broad, bulging papilla surrounded by sphincter, at some distance anterior and ventral to nephrostome, on base of visceral mass. Wide, hollow, irregular chamber just internal to genital pore, communicating with pore on other side (Fig. 198: *gn*).

Nervous system (Figs. 199, 202, 206, 209): Cerebropleural ganglia (Figs. 199, 206: *cg*) of moderate size, adjacent, close to posterior surface of *am*, just between ventral region of *ar* origin and adjacent *am*, close to midline; A ≈ *es* D. Cerebral commissure short, broad; L ≈ single *cg* W. Pedal ganglia minute. Cerebrovisceral connectives (Fig. 202: *cp*) running through visceral glands, close to integument; anterior region running through tissue of *ar* basal region. Visceral ganglia (Fig. 209: *vg*) adjacent, close to midline, anterior of *pm*, ventral to *pr* origins; V ≈ *cg* V.

Material Examined

USA, Florida Keys, FMNH 295647, 2 specimens (sta. FK-139; 2 dissected: #1: 50.0 mm L, 45.5 mm H, 20.0 mm W; #2: 35.0 mm L, 31.8 mm H, 14.0 mm W); FMNH 295648, 1 juvenile specimen (sta. FK-154; dissected: 18.0 mm L, 15.8 mm H, 6.5 mm W); FMNH 295646, 1 specimen (sta. FK-239; dissected: 50.1 mm L, 45.6 H, 22.4 mm W).

VENEZUELA, Isla Margarita, Portlamar, off Margabela Hotel, 10°57'12.42"N, 63°50'35.70"W, 2 m, MZSP 57414, 2 specimens (29/i/1996; dissected, not measured). BRAZIL, Fernando de Noronha Archipelago, Ressureta beach, 03°49'S, 32°23'W, 3 m, MZSP 48859, 2 specimens (02/v/2005). Atol das Rocas, 3°51'54.11"S, 33°46'48.03"W, MZSP 45570, 1 specimen (vii/1995). Alagoas, Maceió, Sete Coqueiros beach, MZSP 22920, 1 specimen (19/ix/1970). Bahia, Itapuã beach, 12°57'08.78"S, 38°20'26.88"W, 2 m, MZSP 28432, 1 specimen (23–27/ii/1997; dissected: 62.0 mm L, 55.7 mm H, 30.0 mm W).

Distribution

Stated by Turgeon et al. (2009) to range from the Gulf of Mexico, Cuba, Central America, the West Indies, Brazil and Bermuda. Also present from North Carolina to the Florida Keys (Mikkelsen & Bieler, 2007). Range in Brazil to Bahia is here confirmed.

Remarks

For other details of the shell, see Mikkelsen & Bieler (2007: 228). The gross anatomy reported here agrees with that in previous reports (Allen, 1958, specimens from Jamaica, the Bahamas, and the Florida Keys; Taylor & Glover, 2000, specimens from Islamorada, Upper Florida Keys) except in the following. The excurrent aperture has been called a "siphon" (e.g., Allen, 1958; Taylor & Glover, 2000), but the animal does not have concentrated siphonal retractor muscles *sensu* Tellinidae and Veneridae. The apertural papillae surround the base of the projecting tube, rather than at the tip, as would be expected of a true siphon. Furthermore, its eversibility into the suprabranchial chamber has been called a unique retraction method among bivalves (Allen, 1958: fig. 14); these three observations provide ample justification for avoiding the term "siphon" for this structure and the term "aperture" is preferred here. Clearly, the homologies of so-called siphons across the Bivalvia are in need of in-depth investigation.

The palps, reported as "smooth" here from gross dissection, each have vestigial folds according to Allen (1958). The simplified stomach includes three apertures to the digestive diverticula according to Allen (1958: 471, "the third aperture is a much reduced right caecum"), although only two were noted in this study; these are apparently the major right and left caeca into which several ducts open. The end of the hindgut and anus can apparently either be sessile (Mikkelsen & Bieler, 2007) or with a short stalk (herein). The pedal ganglia were called "very large" throughout the superfamily Lucinoidea by Allen (1958: 479) but are considered minute here. Brazilian material was found to be morphologically indistinguishable.

A large body of literature exists that deals with the biology of this species, with special focus on the gills and sulfur-oxidizing bacterial gill symbionts (e.g., Allen, 1958; Frenkiel & Mouëza, 1995; Gros et al., 1998, 2003), reproduction, development, and sperm ultrastructure (e.g., Alatalo et al., 1984; Gros et al., 1997; Mouëza & Frenkiel, 1995) . Florida Keys specimens of this species were used in the study of reproductive biology by Bigatti et al. (2004), the functional anatomical work by Taylor & Glover (2000), and the molecular analyses by Taylor et al. (2007, 2011). The cited study by Alatalo et al. (1984) involved specimens from Key Biscayne near Miami, Florida.

Family Chamidae
Lamarck, 1809

Chama macerophylla
Gmelin, 1791
Figs. 211–225

Synonymy/Chresonymy

Chama macerophylla Gmelin, 1791: 3304 [Type locality: Oceano Americano = American Ocean].

Chama macerophylla – Abbott, 1974: 466, pl. 21, fig. 5384; Campbell et al., 2004: 395–396, figs. 2D–F, 3A; Bieler & Mikkelsen, 2004: 512; Mikkelsen & Bieler, 2007: 250–251, 5 figs.

Description

Shell (Figs. 211–214, 216, 217): Rounded, thick, varying from yellow, white, red, brown, to combination of colors; SL ≈ 40 mm in material examined. Valves strongly asymmetrical (Figs. 211–213), LV cementing to hard substratum, with lateral surface almost planar or assuming irregularities of substratum; outer surface irregular, opaque; portion not attaching to substratum bearing commarginal, low, wide, irregular scales (Figs. 213, 214). Umbonal region protruding, weakly spiral (Fig. 213). RV lid-like (Fig. 211); outer surface irregularly smooth or bearing irregular, low to tall (taller near shell margin), wide commarginal scales; A ≈ 33% LV A. Inner surface of both valves smooth, opaque, whitish, showing external color at margins (Figs. 212, 213). Ligament external, posterior to umbones, thickened at midpoint of hinge plate (Figs. 212, 216). Hinge plate of LV (Fig. 217) broad, tall (L ≈ 33% SL), with central, wide, oblique furrow (Fig. 217: 3) in W ≈ 12% of hinge plate W, directed anterodorsally, narrowing and curving, dorsally encircling broad, low cardinal tooth (Fig. 217: 4), with 3–4 shallow, narrow, secondary furrows parallel to main furrow; another tooth (Fig. 217: 6) immediately anterior to latter tooth, in L ≈ 25% of latter tooth L, slightly more protruding; posterior end of central furrow (Fig. 217: 3) flanked by long, oblique, tall, narrow cardinal tooth (Fig. 217: 2) in W ≈ furrow W; another low posterior tooth (Fig. 217: 1) at some distance posteriorly, preceded by smooth region. Hinge plate of RV (Fig. 212) bearing teeth and sockets corresponding to those of LV, e.g., curved central cardinal tooth in LV corresponding to curved furrow in RV. Anterior and posterior adductor muscle scars large, subequal, elliptical, weakly elongating dorsoventrally, slightly elevated off valve inner surface. Pallial line simple, uniting ventral ends of adductor muscle scars, close and parallel to ventral shell margin.

Main muscle system (Figs. 218, 219, 222): Anterior adductor muscle (*am*) transversly elliptical to semicircular (with posterior surface less rounded), longer dorsoventrally than anteroposteriorly, very close to shell margin (separated only by mantle border) in anteroventral quadrant of valve, in A ≈ 16% VA; anterior surface several times shorter than posterior surface, subtriangular in cross section, with differently colored ("catch" and "quick") portions; larger region forming anterior and ventral surfaces; smaller region forming posterior surface; posterior surface totally exposed in pallial cavity. Posterior adductor muscle (*pm*) similar to *am*, except slightly longer dorsoventrally and more elliptical, in posterodorsal quadrant of valve. Each adductor muscle triangular in dorsal view (Fig. 222), with external ends much shorter than internal sides. Pedal retractors inconspicuous, immersed in integument. Paired gill muscles

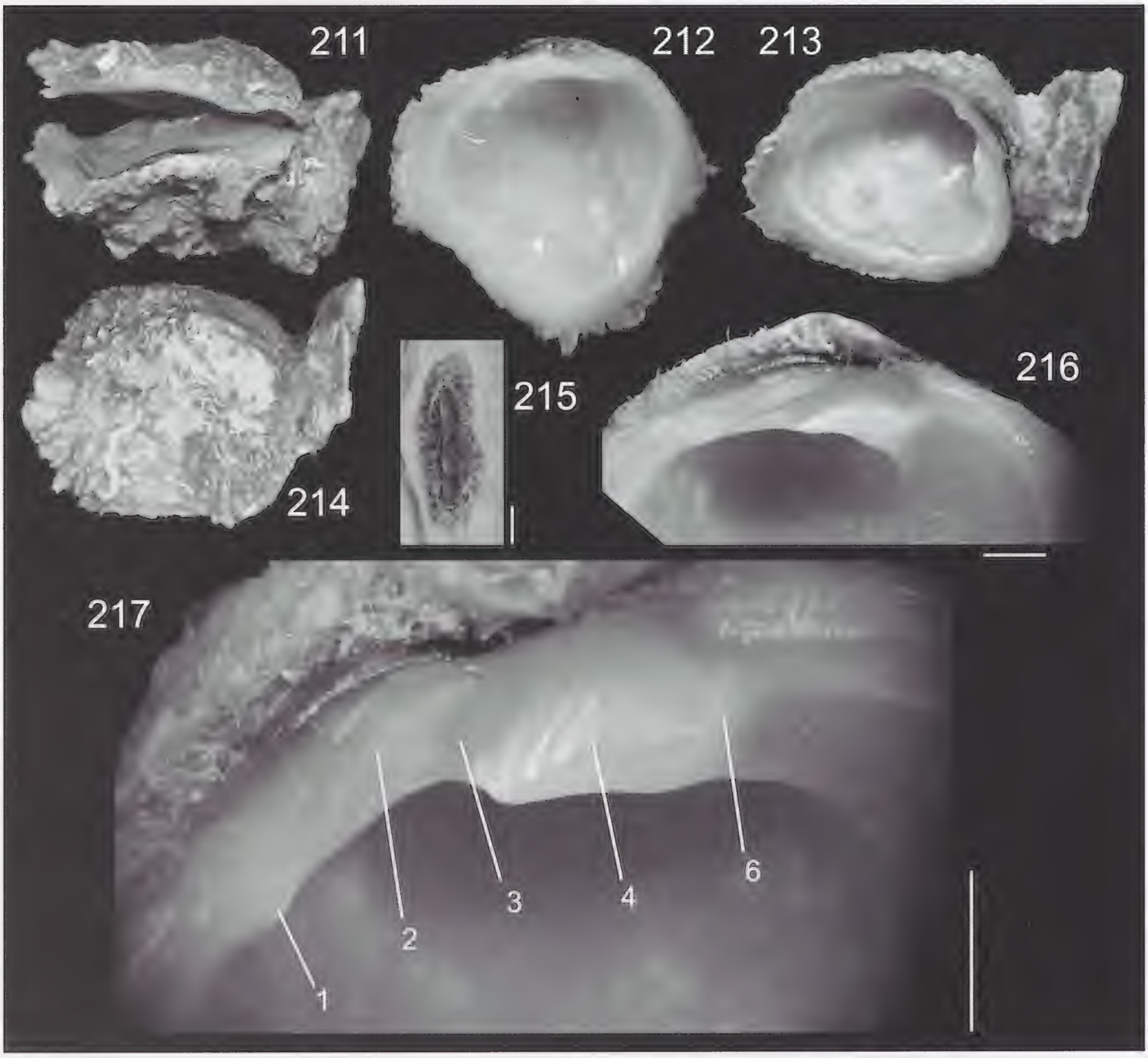

FIGS. 211–217. *Chama macerophylla*, shell morphology and anatomy, FMNH 295681, 32 mm maximum D. FIG. 211: Ventral view, valves partially opened; FIG. 212: RV interior view; FIG. 213: LV interior view, with part of attached substratum at right; FIG. 214: Intact right view; FIG. 215: Detail of incurrent aperture, posterior view; FIGS. 216, 217: LV, detail of hinge (for explanation of numbers, see text). Scale bars = 2 mm.

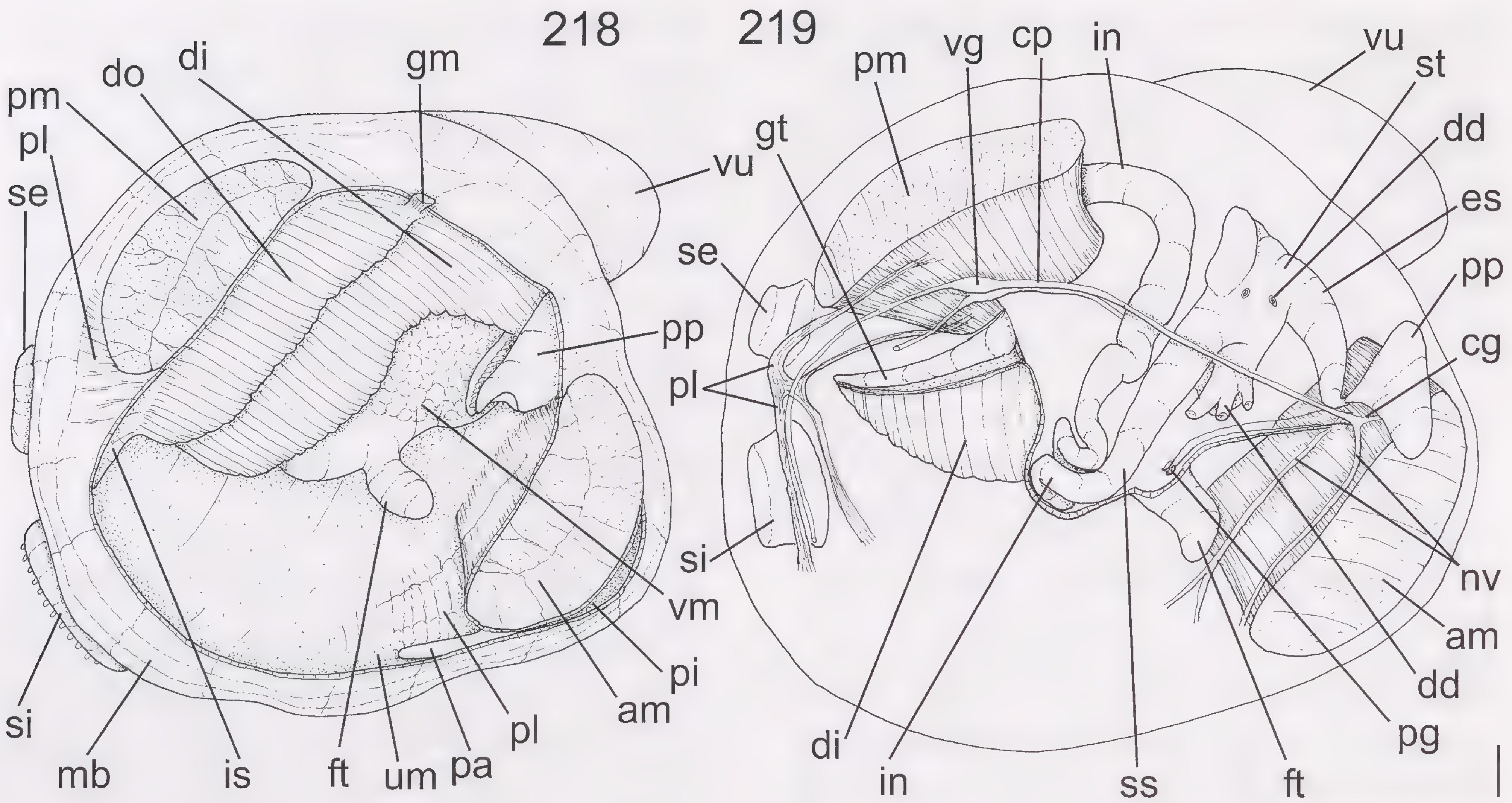

FIGS. 218, 219. *Chama macerophylla*, anatomy. FIG. 218: Intact right view, shell removed, right mantle lobe partially removed (except mantle border and visceral portions); FIG. 219: Same, main muscles, digestive system, and nervous system *in situ*. Scale bar = 2 mm. Abbreviations: am, anterior adductor muscle; cg, cerebropleural ganglion; cp, cerebrovisceral connective; dd, ducts to digestive diverticula; di, inner demibranch; do, outer demibranch; es, esophagus; ft, foot; gm, gill retractor muscle; gt, gill suspensory stalk; in, intestine; is, siphonal septum; mb, mantle border; nv, nerve; pa, pedal aperture of fused mantle border; pg, pedal ganglion; pi, pallial chamber; pl, pallial muscles; pm, posterior adductor muscle; pp, labial palp; se, excurrent aperture; si, incurrent aperture; ss, style sac; st, stomach; um, fusion between left and right mantle lobes; vg, visceral ganglia; vm, visceral mass; vu, visceral portion inside umbonal cavity.

well developed (Fig. 218: *gm*), originating at mid-umbonal cavity, running between demibranchs, initially somewhat thick, gradually becoming thinner anteriorly. Arrangement of pallial muscles as described below.

Foot (Figs. 218, 219): Small (A ≈ 10% of *am* A), simple, anteroposteriorly weakly broad, laterally compressed; W somewhat uniform along L; distal tip rounded. Byssal groove and byssus absent.

Mantle (Figs. 215, 218–220): Mantle border thick, broad. Inner fold mostly fused with counterpart except at posterior and pedal apertures, latter spanning from ventral *am* to just posterior. Outer folds simple, somewhat thickened, smooth; with inner surface attaching to periostracum (Fig. 220). Middle fold at some distance from outer fold, thin; left middle fold simple, smooth, not pigmented; right middle fold bearing series of small, simple papillae along distal edge, with interpapillar space W = 3 papillae W; similarly fashioned papillae distributed along area between inner surface of right middle fold and base of middle fold (Fig. 220: *mp*); this papillated surface also with small, dark brown, coalescent spots. Posterior apertures similar, bearing short invaginable tubes ("siphons"), with minute, dark brown, coalescent spots, more concentrated distally (Fig. 215). Edge of incurrent aperture (Figs. 218, 219: *si*) bearing series of small, whitish papillae, distributed somewhat uniformly; interspace W = papilla W. Similarly fashioned papillae distributed randomly and sparsely on outer and inner surfaces, more concentrated ventrally. Excurrent aperture (*se*) similar to *si*, except lacking papillae. Pallial muscles (Fig. 219: *pl*) with special arrangement between posterior apertures, with pair of narrow, slender muscles originating at midregion ventral to *pm*, running attached to mantle posteroventrally, parallel to posteroventral edge of *pm*; another similar pair of muscles originating on posteroventral mantle border, running posteriorly around mantle border; both pairs of muscles fusing between posterior apertures in a thick X-shape.

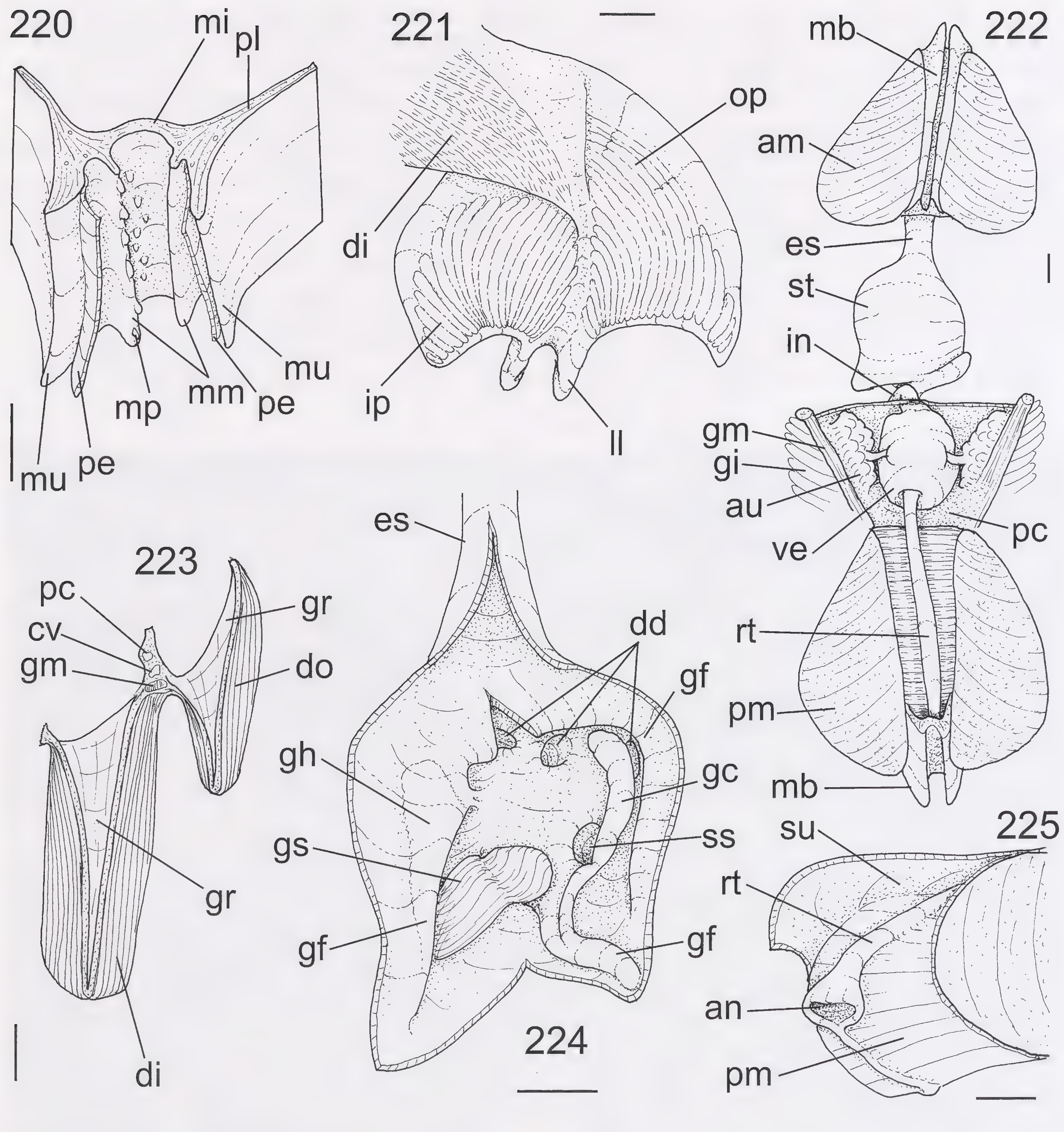

FIGS. 220–225. *Chama macerophylla*, anatomy. FIG. 220: Mantle border, detail of midventral region, ventral and slightly anterior view, right mantle lobe at left; FIG. 221: Right labial palp and adjacent portion of gill, both hemipalps deflected to show inner surface; FIG. 222: Intact dorsal view to show adductor muscles, midportion of digestive system (*in situ*), and pericardial structures, dorsal mantle and glands removed; FIG. 223: Right gill, cross section of midportion in region of transverse septum and some filaments anterior to it; FIG. 224: Stomach, dorsal view, dorsal wall opened longitudinally; FIG. 225: Anal region of pallial cavity, right and slightly posterior view, right edge of supra-anal chamber sectioned and deflected. Scale bars = 1 mm. Abbreviations: am, anterior adductor muscle; an, anus; au, auricle; cv, ctenidial (efferent) vessel; di, inner demibranch; do, outer demibranch; es, esophagus; gc, gastric central pad; gf, gastric fold; gh, gastric chamber; gi, gill; gm, gill retractor muscle; gr, gill transverse septum in suprabranchial chamber; gs, gastric shield; in, intestine; ip, inner hemipalp; ll, labial lips preceding mouth; mb, mantle border; mi, mantle border inner fold; mm, mantle border middle fold; mp, mantle papillae; mu, mantle border outer fold; op, outer hemipalp; pc, pericardium; pe, periostracum; pl, pallial muscles; pm, posterior adductor muscle; rt, rectum; ss, style sac; st, stomach; su, supra-anal chamber of suprabranchial pallial cavity; ve, ventricle.

Remaining *pl* radiating from pallial line and from outer edge of *am* (Fig. 218: *pl*). Mantle with well-developed posterior septum (Fig. 218: *is*; "diaphragm" of Mikkelsen & Bieler, 2007) separating infra- and suprabranchial chambers, broader in posterior region (as continuation of gill axis), becoming thinner in lateral regions along mantle surface; gill attaching to *is* via cilia.

Pallial cavity (Figs. 218, 219, 221, 223): Restricted by mantle fusion and *am*; A ≈ 33% of RV A. Each hemipalp (Fig. 218: *pp*) weakly triangular, with convex dorsal edge, concave ventral edge; A ≈ 33% of *am* A. Gill fitting between hemipalps for ca. 50% of *pp* L (Fig. 221), flanked by smooth region. Hemipalps with similar outlines (Fig. 221), but different arrangements of inner folds; outer hemipalp with folds mostly parallel to dorsal edge; inner hemipalp with folds somewhat perpendicular to dorsal edge. Inner folds narrow, adjacent, with ventral ends rounded, close to *pp* ventral edge, leaving narrow smooth area; dorsal ends also rounded, far from *pp* dorsal edge, leaving smooth area in W = 25% of *pp* W. Inner folds of each hemipalp decreasing gradually toward each end, abruptly ending preceding lips. Inner surface of lips smooth. Gills (Fig. 218: *di, do*) covering little beyond visceral mass, disposed obliquely, almost dorsoventrally vertical; A ≈ 33% of pallial cavity A. *Do* smaller (H slightly > 50% of *di* H; Fig. 223), inserting dorsal to *di* insertion at posterodorsal border of pallial cavity; anterior origin far from that of *di* and *pp* (distance = 1.5 W); posterior end almost at same level as that of *di*, on septum (Fig. 218: *is*). *Do* ascending lamellae each in L ≈ 2 descending lamella L (Fig. 223), with cilial connections to visceral mass and *is*. *Di* broader at anterior origin, with portion inserting between *pp*; abruptly decreasing in W posteriorly; outer branch inserting just dorsal to ventral edge of *do*, weakly longer than inner branch. Inner branch of *di* with cilial connection to visceral mass or counterpart (posterior to visceral mass). Transverse septa (Fig. 223: *gr*) on inner surface of each demibranch, aligning in all 4 demibranchs at intervals of 15–20 filaments; each *gr* attaching to entire inner edge of adjacent filament, becoming gradually broader dorsally; dorsal edge shallowly concave; *gr* producing greatly folded appearance of demibranchs. Gill axis running along each demibranch, composed of thick gill muscle (described above) ventrally, and 2 successive vessels. Gill suspensory stalk (Fig. 219: *gt*) inserting at center of *pm* ventral surface, weakly muscular, supporting posterior third of gill.

Visceral mass (Figs. 213, 218, 219, 222): Strongly asymmetrical because of valve asymmetry, with left side taller, wider, fitting inside larger umbonal cavity (Figs. 213, 218, 219: *vu*); A ≈ 33% of RV A. Asymmetry mostly expressed by translucent, whitish connective tissue; interior structures somewhat symmetrical. Middle and ventral regions somewhat rounded, flat, with anterodorsal, greenish beige digestive diverticula surrounding stomach. Gonad beige, surrounding digestive diverticula and mid-visceral mass. Visceral mass almost entirely filled posteroventrally by terminal region of style sac and adjacent intestinal loops, attaching only to small dorsal area of *am* and ca. 50% of *pm*.

Circulatory and excretory systems (Fig. 222): Pericardium (*pc*) in posterior half of posterior region between adductor muscles, attaching to dorsal *pm*. Auricles (*au*) each running along dorsal ctenidial vein, with outer surface lobed and apparently glandular; connections with ventricle (*ve*) in midlateral region, preceded by narrow duct. *Ve* wide, surrounding entire intestine passing through *pc*. Kidneys not observed.

Digestive system (Figs. 219, 222, 224, 225): *Pp* as described above. Mouth between middle and dorsal thirds of *am* posterior surface. Esophagus (*es*) initially narrow, becoming gradually broader posterodorsally; inner surface smooth, joining anterodorsal side of stomach. Stomach (*st*) broad, between umbonal regions, on midline. Gastric posterior surface with pair of lateral, irregular, asymmetrical projections (Fig. 222); left projection (dorsal hood) pointed, directed posterolaterally; right projection blunt, directed laterally and weakly anteriorly. Gastric inner surface (Fig. 224) mostly smooth, lacking obvious sorting areas and *es* rim; tall, transverse fold just ventral to *es* opening, running horizontally along both lateral surfaces; left branch of fold with short portion connecting to gastric ventral surface near *es* opening at left-posterior; remaining posterior region of fold encircling somewhat deep, blind-ending, flattened chamber (Fig. 224: *gf*); right branch of fold with edge running free, decreasing gradually posteriorly; anterior region of fold covering 4 wide ducts to digestive diverticula (2 each side), transversely aligned; gastric central pad anteroposteriorly long, somewhat narrow, on ventral inner gastric surface close to right branch of horizontal fold, with anterior end rounded, covering rightmost duct to digestive diverticula, narrowing gradually posteriorly, connecting to right side of another gastric fold running longitudinally in posterior-right *st* projection; latter fold with another anterior branch near central pad posterior end surrounding right-anterior edge of gastric shield. Gastric shield (Fig. 224: *gs*) thin, in posterior-left quadrant of ventral inner gastric surface; A ≈ 20% of inner gastric surface A. Opening of conjoined style sac-intestine (*ss-in*) at midlevel of central pad, covered by left edge; D slightly larger than ducts to digestive diverticula. *Ss* and *in* totally fused, separated only by pair of low, longitudinal folds. *Ss* ending in posteroventral quadrant of visceral mass; L = 3 *st* L ≈ 33% of (straightened) *in* L. *In* somewhat wide, performing 3 short loops in posterior region near *ss*, then running weakly and sinuously dorsally parallel to *ss*, gradually widening, curving anteriorly at some distance anterior to *pm*, passing through *pc* and along median dorsal surface of *pm*. Rectum mostly exposed (covered by integument) in supra-anal pallial chamber (Fig. 225). Anus (Fig. 225: *an*) abruptly broadened bell-like, with wide aperture; narrow, low fold continuing posterodistal margin of *an*, running along median ventral surface of *pm*, diminishing gradually.

Nervous system (Fig. 219): Cerebropleural ganglia (*cg*) located laterally between mouth and posterodorsal *am* insertion; A ≈ 20% of *es* D. Cerebral commissure wide, slender. Pedal ganglia (*pg*) in anterior border of foot base, adjacent, very close to midline; A ≈ 33% of *cg* A. Cerebropedal connective extremely slender. Visceral ganglia (*vg*) at midregion of *pm*, adjacent, close to midline. Cerebrovisceral connective (*cp*) thick, running through visceral mass glands. Pair of thick nerves originating from anterior side of *vg*, running anteroventrally, passing *si* on each side.

Material Examined

USA, Florida Keys, FMNH 295681, 2 specimens (sta. FK-117; 2 dissected, #1: 38.0 mm L, 32.7 mm H, 21.2 mm W; #2: 46.0 mm L, 36.7 mm H, 25.5 mm W); FMNH 295685, 1 specimen (sta. FK-202); FMNH 295682, 1 specimen (sta. FK-260).

Distribution

Stated by Turgeon et al. (2009) to range from North Carolina to Brazil, the Gulf of Mexico, Puerto Rico, and the West Indies. *Chama macerophylla* is a known introduced species in the Pacific Ocean (e.g., Eldredge & Smith, 2001: Hawaii; Paulay, 2003: Guam). It has been reported from the Brazilian coast (e.g., Rios, 1994: 260; 2009: 526); however, no specimens from that region have been found with similar morphological features. For this reason, Brazilian reports of this species have been excluded from the treatment herein pending further studies.

Remarks

Although the specimens studied here were consistently attached to the substratum by the LV, Campbell et al. (2004) showed that some species in this family can attach by either valve, unlike members of other families, e.g., Ostreidae, which are consistently cemented by the LV (Yonge, 1953b). The hinge teeth labeled 2 and 4 in Fig. 217 are those referred to as the two cardinal teeth by other authors; the tooth labeled 1 is the posterior lateral tooth. For this and other details of the shell, see Yonge (1967), Campbell et al. (2004), and Mikkelsen & Bieler (2007: 250).

Anatomically, this description agrees with previous descriptions (Yonge, 1967, for *Chama pellucida* Broderip, 1835, and *C. exogyra* Conrad, 1837, based in part on earlier publications) except in two features. The "gill muscles" described here (alternately called pedal elevator muscles; e.g., Mikkelsen & Bieler, 2007) passed into the visceral mass in Yonge's (1967) description, but none was found during this study. Also, no food groove was seen on either demibranch, although an "exceptionally deep and narrow" groove on the edge of the inner demibranch was noted by Yonge (1967: 50). Similar to the condition in *Laevicardium serratum*, the incurrent and excurrent apertures can bear tube-like extensions, called "siphons" or "siphonal tubes" by Yonge (1967), but the animal does not have concentrated siphonal retractor muscles. The tubes apparently retract via invagination. The term "aperture" for each of these openings is preferred here.

The nepionic shell of this species was studied by Ferreira & Xavier (1981). The monographic treatment by Campbell et al. (2004) included material from the Florida Keys. An ultrastructural study of gametes by Hylander & Summers (1977) was based on specimens from Bermuda.

Family Gastrochaenidae
Gray, 1840

Lamychaena hians
(Gmelin, 1791)
Figs. 226–245

Synonymy/Chresonymy

Pholas hians Gmelin, 1791: 3217 [Type locality: "ad insulas Americae mediae oppositas"; opposite side of Mesoamerican islands].

Gastrochaena (Rocellaria) hians – Abbott, 1974: 540, fig. 6015.

Gastrochaena (Gastrochaena) hians: Carter, 1978: 1 ff., figs. 3–5, 8, 10C, 16.

Gastrochaena hians – Valentich-Scott & Dinesen, 2004: 351–352, figs. 28–30; Bieler & Mikkelsen, 2004: 513.

Lamychaena hians – Mikkelsen & Bieler, 2007: 268–270, 7 figs.

Description

Shell (Figs. 226–230, 232): Pale beige to white, thin, fragile; SL ≈ 15 mm in material exam-

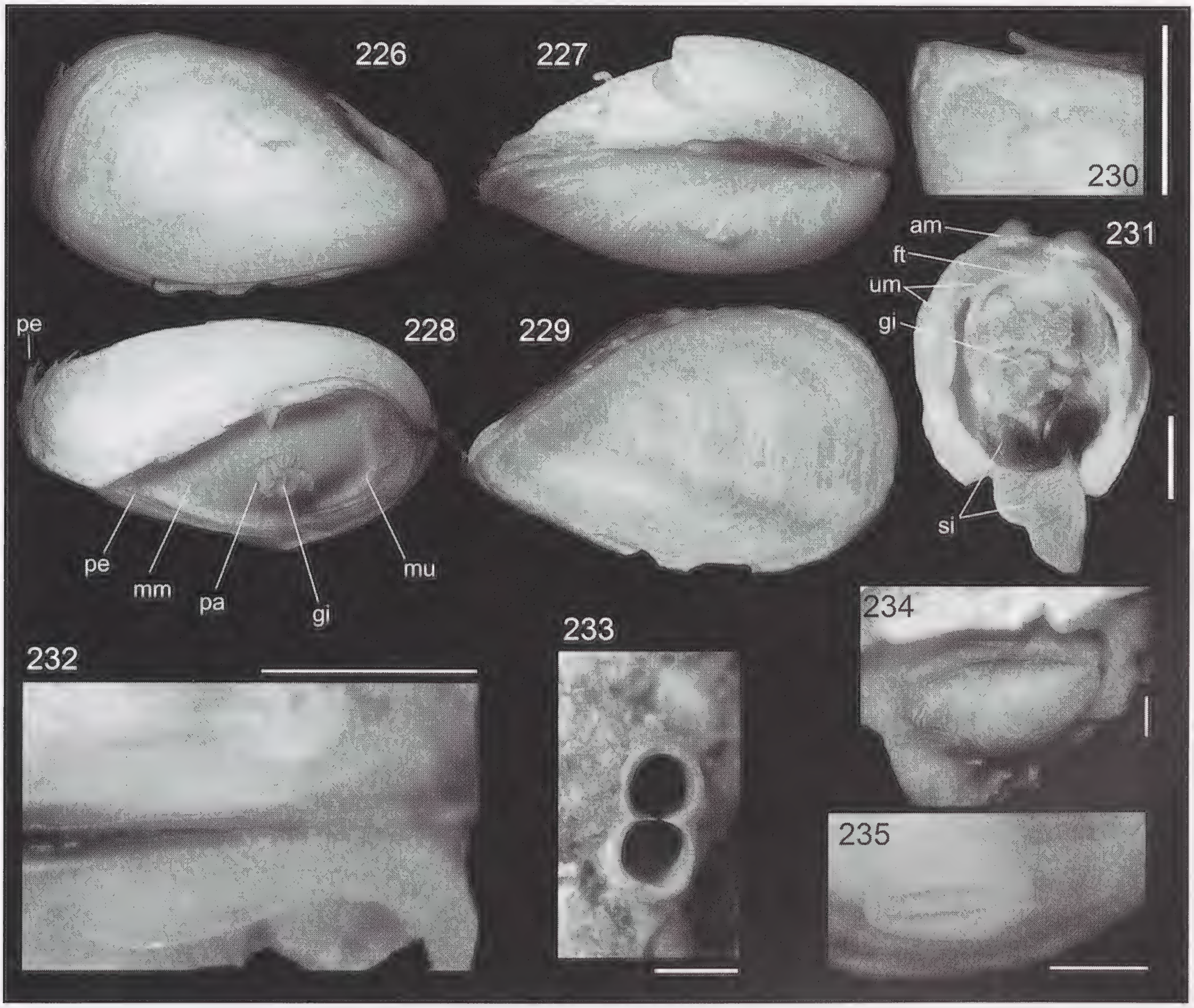

FIGS. 226–235. *Lamychaena hians*, shell and burrow morphology, FMNH 295554, 16.6 mm L. FIG. 226: Intact right view; FIG. 227: Intact dorsal view (LV damaged); FIG. 228: Intact ventral and slightly right view; FIG. 229: RV interior view; FIG. 230: Same, detail of umbonal region; FIG. 231: Contracted specimen, ventral view, shell removed, fusion of both mantle lobes sectioned longitudinally and deflected, note gills and intensely infolded siphons; FIG. 232: Hinge, inner-ventral view, both valves partially deflected; FIGS. 233–235: FMNH 295554, 15 mm L.; FIG. 233: Outer "chimneys" of burrow; FIG. 234: Specimen inside its burrow (partially opened); FIG. 235: Foot region, ventral and slightly right view. Scale bars = 5 mm. Abbreviations: am, anterior adductor muscle; ft, foot; gi, gill; mm, mantle border middle fold; mu, mantle border outer fold; pa, pedal aperture of fused mantle border; pe, periostracum; si, incurrent siphon; um, fusion between left and right mantle lobes.

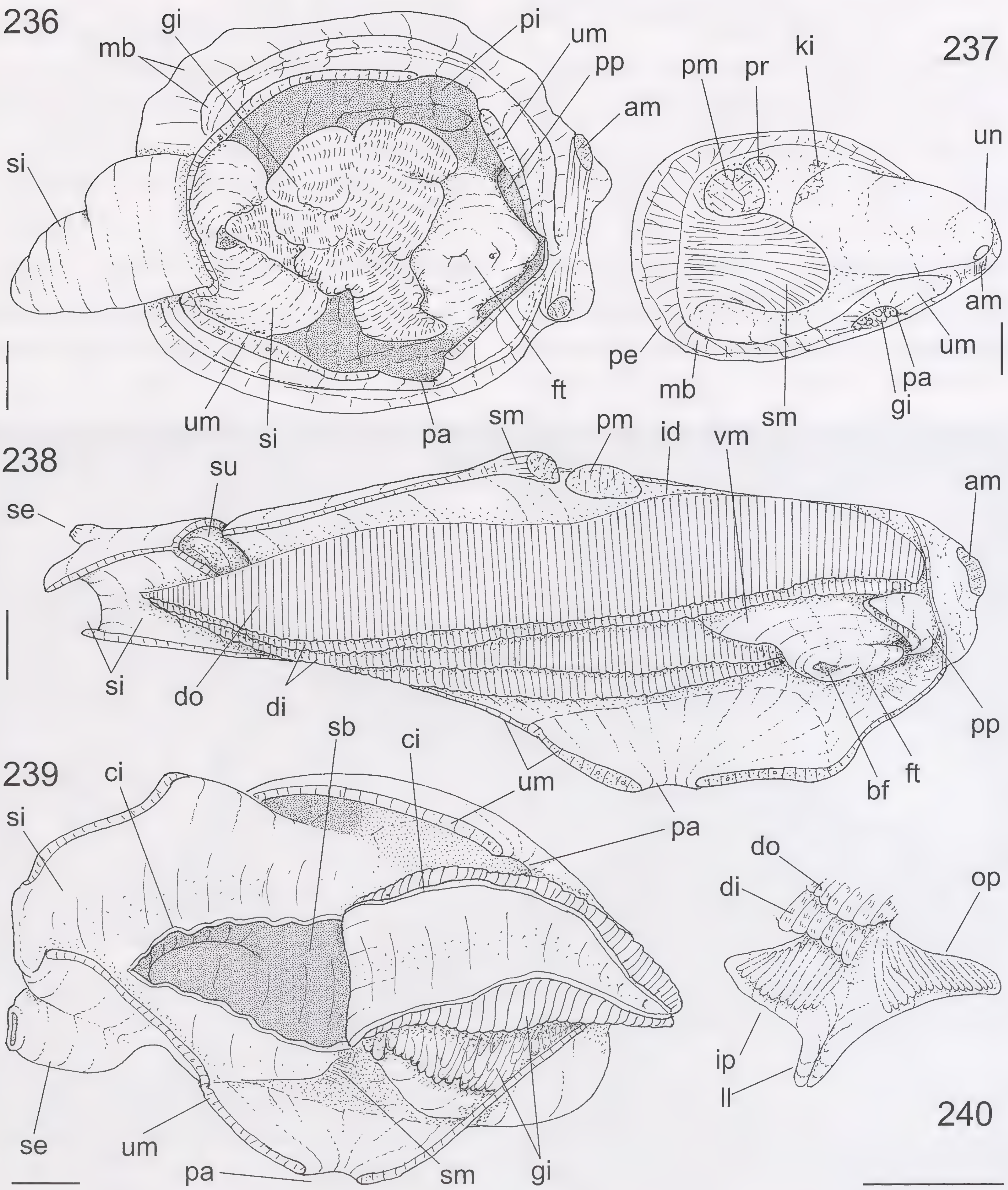

FIGS. 236–240. *Lamychaena hians*, anatomy, FMNH 295554. FIG. 236: Contracted specimen, ventral view, shell removed, fusion of both mantle lobes sectioned longitudinally and deflected, gills and retracted siphons intensely infolded; FIG. 237: Same, intact right view; FIG. 238: Intact right view with re-extended siphons, right mantle lobe partially removed, cross section of excurrent siphon, right siphonal retractor muscle deflected upward; FIG. 239: Intact ventral view, both mantle lobes sectioned longitudinally, gill partially removed from ciliary connection with siphons and deflected to right; FIG. 240: Right labial palps, right view, outer hemipalp deflected, adjacent portion of gill also shown. Scale bars = 2 mm. Abbreviations: am, anterior adductor muscle; bf, byssal furrow; ci, ciliary connection of gill; di, inner demibranch; do, outer demibranch; ft, foot; gi, gill; id, insertion of outer demibranch in mantle; ip, inner hemipalp; ki, kidney; ll, labial lips preceding mouth; mb, mantle border; op, outer hemipalp; pa, pedal aperture of fused mantle border; pe, periostracum; pi, pallial chamber; pm, posterior adductor muscle; pp, labial palp; pr, posterior pedal retractor muscle; sb, suprabranchial chamber; se, excurrent siphon; si, incurrent siphon; sm, siphonal retractor muscle; su, supra-anal chamber of suprabranchial pallial cavity; um, fusion between left and right mantle lobes; un, umbonal region; vm, visceral mass.

ined ≈ 2 SH, SW ≈ SH. Anterior A ≈ 50% of posterior A; H increasing gradually along L. Periostracum pale brown, thin, translucent, mostly only close to shell margins. Umbones terminal, adjacent, weakly curving dorsally. Sculpture lacking, except well-marked growth lines. Ventral pedal gape (Fig. 228) very wide, almost as wide as SW anteriorly, gradually narrowing posteriorly along ca. 80% SL; anterior edges of pedal gape rounded; posterior end pointed. Ligament external, extending from umbones posteriorly to ca. 70% of dorsal edge (Figs. 226, 227, 229); middle and posterior thirds broader, bulging externally. Hinge plate edentulous (Figs. 229, 230), with pair of subequal horizontal myophores (Figs. 230, 232) extending externally from median edges for distance ≈ 12% SW, from umbonal cavity posteriorly for distance ≈ 25% SL; each myophore slightly narrower between anterior and middle thirds. Inner surface smooth, glossy, white. Muscle scars very shallow. Heteromyarian; scar of anterior adductor muscle (*am*) at level of umbones, close to ventral margin; L ≈ 2 H, A ≈ 5% of valve inner surface A. Scar of posterior adductor muscle (*pm*) rounded, located at ca. 20% SL anterior of posterior margin, close to dorsal margin; V ≈ 8 *am* V. Pallial line running close to ventral margin, with deep pallial sinus in L = 50% SL.

Burrow in soft calcareous substrata lined by calcareous tube ending at entrance in figure-eight-shaped "chimney" (Fig. 233).

Main muscle system (Figs. 236–238, 241, 243): Proportions and location of adductor muscles as described above; both muscles very thick; W ≈ 60% of broadest SW (Fig. 236). Paired pedal protractor muscles (Fig. 241: *rr*) narrow, slender, originating just dorsal to *am*, running posteroventrally attached to anterior integument, splaying across anterior foot base; A = 6% of *am* A. Paired anterior pedal retractor muscles (Fig. 241: *ar*) originating dorsally and more medial to *am*, running almost vertically posteroventrally, splaying across median anterior foot base; A = *am* A, separated from *am* by distance = 80% of *am* W. Paired posterior pedal retractor muscles (Fig. 241: *pr*) originating just dorsal and medial to *pm* (Fig. 243), running anteriorly and gradually ventrally for distance = 70% SL, splaying across middle and posterior foot base; A = 25% of *pm* A. Paired siphonal retractor muscles (Figs. 237, 242: *sm*) relatively thick, running along siphons to arched pallial sinus; L ≈ 50% SL, H ≈ 70% SH.

Foot (Figs. 231, 235, 238, 241: *ft*): Relatively small, dorsoventrally compressed; L = 25% SL, W = 25% SW. Anterior half ("pedal organ" of Carter, 1978) compressed, rectangular, projecting anteriorly. Small, shallow orifice (Fig. 241: *fo*) at intersection of 2 *ft* portions. Byssus short, solidly calcified.

Mantle (Figs. 228, 231, 236–239): Edges of mantle lobes mostly fused. Pedal aperture (Fig. 237: *pa*) rounded, at midregion of shell pedal gape; L ≈ 12% SL. Fusion based on inner fold, thick, muscular; ventral region corresponding to pedal gape and surrounding pedal aperture, particularly thicker, planar (Figs. 238, 239). Excurrent (*se*) and incurrent (*si*) siphons pigmented brown externally, mostly fused, forming cylinder, except short portion preceding distal tips; separated by horizontal, incomplete septum (Figs. 238, 239), filled by dorsal surface of gills along ca. 70% L; siphonal L = 1–2 SL; completely retracted inside shell by several infoldings (Figs. 231, 236). Siphonal distal tips as pair of simple openings, lacking papillae; *si* opening D ≈ 2 *se* opening D.

Pallial cavity (Figs. 231, 236, 238–240, 244): Extending into siphons; V ≈ 70% SV. Labial palps (*pp*) inside umbonal cavity, close to *am*; A = 10% VA. Hemipalps symmetrical, triangular, with bluntly pointed distal tips. Each hemipalp inner surface with 10–12 transverse folds (Fig. 240); each fold weakly oblique, with ventral ends slightly broader and rounded; dorsal ends narrow, gradually diminishing; narrow smooth edge entirely surrounding folds; ventral region H ≈ 16% of hemipalp H. Inner demibranch (*di*) attaching to dorsal half of furrow between hemipalps. Smooth space L (between hemipalps) = 20% *pp* L. Lips smooth between *pp*; W ≈ 33% SW. Gill inner (*di*) and outer (*do*) demibranchs subequal; W somewhat uniform along their L, with anterior end rounded, attaching to anterior wall; posteriorly gradually diminishing to pointed end; L ≈ 2 SL ≈ 50% SH. Gills separating most of *si* and *se*, attaching to septum that divides siphons by ciliary strips (Figs. 239, 244: *ci*). Gills intensely folded and detached from siphons in retracted condition (Figs. 231, 236: *gi*; 239). Gill filaments connecting by well-developed horizontal tissue bridges in W ≈ filament W, successively and longitudinally positioned at interval W = of 4–5 filament W; with tissue connections between demibranchs and between gills (Fig. 244). Transverse septa (Fig. 244: *gr*) successively filling suprabranchial space of some

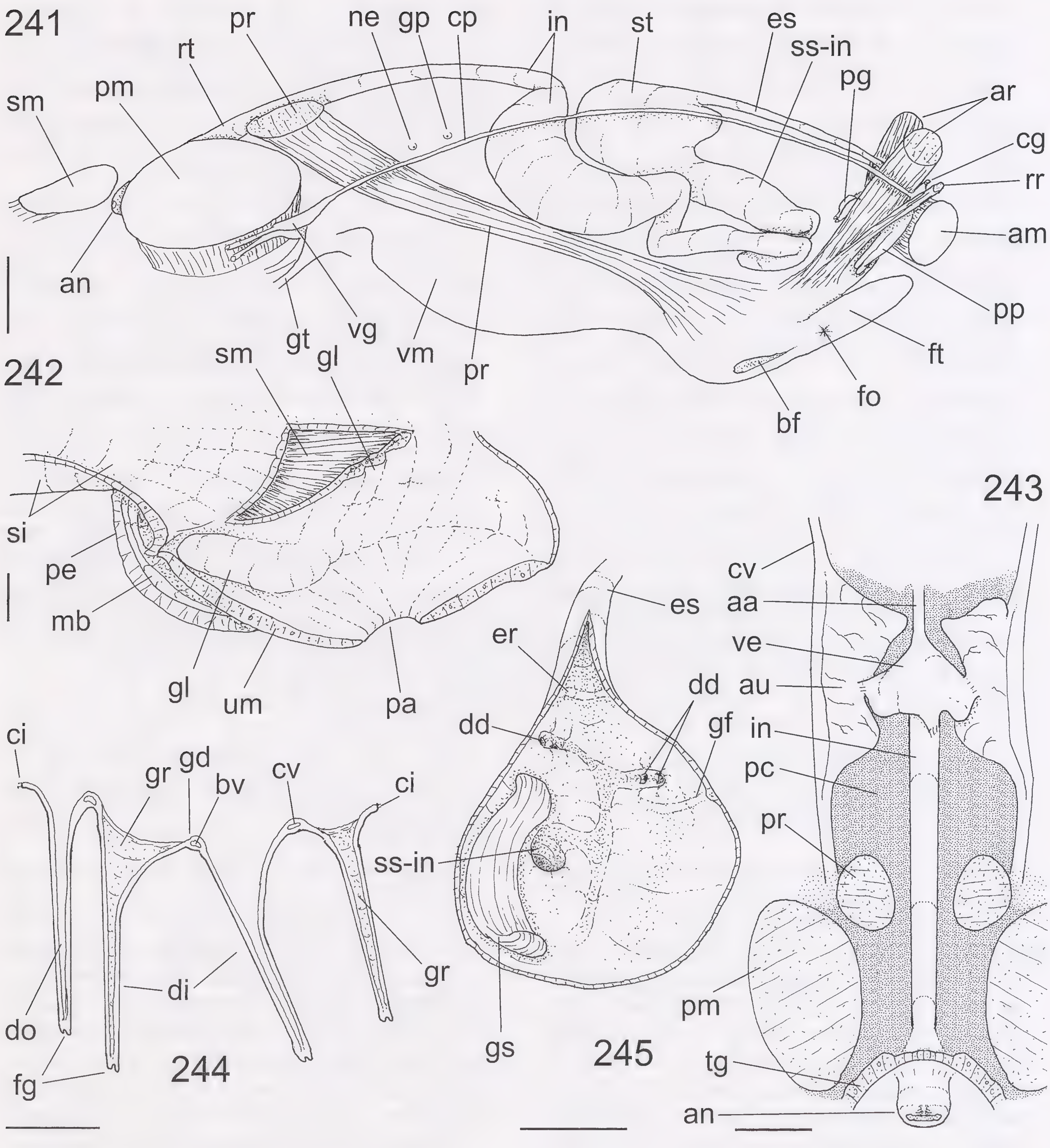

FIGS. 241–245. *Lamychaena hians*, anatomy. FIG. 241: Main muscles, digestive system, and nervous system *in situ*, right view, topologies of some adjacent structures also shown; FIG. 242: Left mantle lobe, inner-right view, a portion of inner layer removed to show siphonal musculature; FIG. 243: Pericardial region, dorsal view, dorsal pericardial wall removed; FIG. 244: Gill, cross section at midregion; FIG. 245: Stomach, dorsal view, sectioned longitudinally. Scale bars = 1 mm. Abbreviations: aa, anterior aorta; am, anterior adductor muscle; an, anus; ar, anterior pedal retractor muscle; au, auricle; bf, byssal furrow; bv, "blood" vessel; cg, cerebropleural ganglion; ci, ciliary connection of gill; cp, cerebrovisceral connective; cv, ctenidial (efferent) vessel; dd, ducts to digestive diverticula; di, inner demibranch; do, outer demibranch; er, esophageal rim; es, esophagus; fg, food grooves; fo, foot orifice; ft, foot; gd, gill suspensory rod; gf, gastric fold; gl, gland; gp, genital pore; gr, gill transverse septum in suprabranchial chamber; gs, gastric shield; gt, gill suspensory stalk; in, intestine; mb, mantle border; ne, nephropore; pa, pedal aperture of fused mantle border; pc, pericardium; pe, periostracum; pg, pedal ganglion; pm, posterior adductor muscle; pp, labial palp; pr, posterior pedal retractor muscle; rr, pedal protractor muscle; rt, rectum; si, incurrent siphon; sm, siphonal retractor muscle; ss-in, conjoined style sac-intestine; st, stomach; tg, integument; um, fusion between left and right mantle lobes; ve, ventricle; vg, visceral ganglia; vm, visceral mass.

filaments, at intervals of 10–15 filaments, between *di* and *do*, as well as between gills (*di* septa aligning with *do* septa of other gill and vice versa); each *gr* very thin, translucent, smooth. Food grooves (Fig. 244: *fg*) shallow, on ventral edge of each demibranch. Ctenidial veins (Fig. 244: *bv*) between demibranchs of each gill and between demibranchs in middle and posterior regions.

Visceral mass (Fig. 241): Stomach and intestine located vertically at midregion; V ≈ 20% of inner SV. Digestive diverticula whitish, surrounding stomach and part of anterior region; V ≈ 12% of visceral mss V. Gonad filling remaining visceral space, white, bulging posteroventrally to *pr*. Pericardial structures just anterior to *pr*; V ≈ 12% of visceral mass V.

Circulatory and excretory systems (Figs. 241, 243): Pericardium (*pc*) compressed dorsally. Auricles (*au*) pale brown, connecting to gills over ca. 12% of distance between anterior and middle thirds; remaining ctenidial veins simple; *au* walls relatively thick, apparently glandular. Ventricle (*ve*) white, connecting laterally to each *au* at midregion; V ≈ 25% of *pc* V. Kidneys white, solid; V ≈ *pc* V. Nephropores (Fig. 241: *ne*) close to *pr*.

Digestive system (Figs. 241, 243, 245): *Pp* as described above. Mouth close to posterodorsal surface of *am*. Esophagus (*es*) narrow, long (L ≈ 33% of distance between *am* and *pm*), running almost horizontally along dorsal visceral mass, inserting on anterodorsal side of stomach (*st*). Gastric main chamber rounded, midway between adductor muscles, close to dorsal wall; D ≈ 70% of *es* L. Gastric inner surface with low, narrow, transverse *es* rim (Fig. 245: *er*); two pairs of ducts to digestive diverticula (Fig. 245: *dd*) posterolateral at some distance from *er*; right pair of ducts slightly more posterior; both pairs of ducts aligning transversely, as ends of ventral, transverse furrow; another longitudinal furrow connecting to midregion of transverse furrow, running to posterior *st*; another short furrow connecting to midlevel of longitudinal furrow, running toward left, entering conjoined style sac-intestinal opening (Fig. 245: *ss, in*). Gastric shield (Fig. 245: *gs*) posterodorsal; A ≈ 20% of gastric inner surface A. *Ss* entirely fusing with adjacent *in*, running directly anteriorly and slightly ventrally; L = *st* D. *In* ≈ 1.5 times distance between adductor muscles, making narrow loops just anterior and to left of end of *ss*, then making smooth loops posterodorsally along ventral side of *st* and *ss*. Midportion of *in* widened, almost as wide as *st*; L ≈ 25% of *in* L; wider region then narrowing and making wide curve along midline almost as long as 50% of distance between adductor muscles. Rectum running along posterodorsal surface of *pm*. Anus (Fig. 243: *an*) simple, on posterior side of *pm*, with short siphon-like terminus; small dark spot in anal dorsal region.

Reproductive system: Gonad as described above. Genital duct not detected except for pair of short, tubular genital chambers preceding pores. Genital pores posterior to *ne*, at distance = distance between *ne* and *pr*.

Nervous system (Fig. 241): Cerebropleural ganglia (*cg*) at intersection of *rr*, *ar*, and *pp* bases, in L = 10% of *am* D; ganglia separated by long commissure. Paired pedal ganglia (*pg*) close to midline, adjacent, separated from *cg* by adjacent region of *ar*; V ≈ *cg* V. Cerebrovisceral connective (*cp*) running in wide arch through visceral glands. Visceral ganglia (*vg*) on anteroventral side of *pm*, adjacent; L ≈ 2 H, each ganglion L ≈ 2 single *cg* L.

Material Examined

USA, Florida Keys, FMNH 295554, 2 specimens (sta. FK-206; 2 dissected: #1: 16.6 mm L, 9.0 mm H, 9.1 mm W; #2: 15.0 mm L).

Distribution

Stated by Turgeon et al. (2009) to range from North Carolina to Quintana Roo (Mexico), Gulf of Mexico offshore banks, Cuba, Brazil, and Bermuda. *Lamychaena hians* reportedly occurs on the Brazilian coastline (e.g., Rios, 1994: 293; 2009: 587, as *Gastrochaena*). However, no specimens from that region have been found as part of this study with matching shell and anatomical characters. The conclusion is that Brazil has a similar, but separate and possibly unnamed, species. For this reason, Brazil has been excluded from the range of *L. hians*.

Remarks

For other details of the shell, see Mikkelsen & Bieler (2007: 268). Carter (1978) described certain aspects of the morphology (shell, mantle, siphons, ctenidia, labial palps, foot, muscles, and gut contents) of *Lamychaena hians* (as *Gastrochaena*) and several other gastrochaenids based on live-dissected specimens from Soldier Key, Florida (in Biscayne Bay, Miami area). In most aspects, Carter's description closely matches that given here. In other respects, there are differences, some of which clearly benefitted from observations being taken from living (rather than preserved) specimens. (1) The myophores were found to be unequal by Carter (1978: 24), with the left one slightly larger than the right at a surface area ratio of 1.43:1; the myophores in our material were subequal. (2) The lateral mantle walls were described as "glandular and ... superficially irregularly folded" (Carter, 1978: 16); this was not observed in the present material but could refer to the pallial gland as interpreted herein. (3) The excurrent siphon bears a cone-shaped annular membrane at its tip, not noted here. (4) The tip of each siphon bears a single row of tentacles or papillae; Florida Keys specimens lacked papillae entirely. (5) Carter (1978: 22) noted the extreme heteromyarian nature of gastrochaenids, finding *L. hians* to have the greatest ratio of posterior to anterior adductor cross-sectional area (12.1, compared to ca. 8 reported here); other aspects of the musculature were as reported here. (6) A distinct "accessory adductor muscle," formed by the posteroventral pallial muscles, was noted by Carter (1978: 24); this was not noted in Florida Keys specimens, although it could possibly refer to the dorsal retractors of the siphons. Valentich-Scott & Dinesen (2004) largely agreed with Carter's (1978) description, from material from a bayside locality (although immediately adjacent to an inlet, thus quite oceanic in character) in the middle Florida Keys. These anatomical differences could reflect a cryptic species pair in the Florida Keys – one fully oceanic on coral reefs (this study) and one in shallow-water bays (Biscayne Bay, Carter, 1978; bayside of West Summerland (now Scout) Key, Valentich-Scott & Dinesen, 2004).

This species creates calcareous-lined burrows in living and dead coral and other limestone substrata (Carter, 1978; Valentich-Scott & Dinesen, 2004: 352 [based on Keys material]; this study).

Family Cyrenidae
Gray, 1840
[= Corbiculidae Gray, 1847]

Polymesoda floridana
(Conrad, 1846)
Figs. 246–266

Synonymy/Chresonymy

Cyrena floridana Conrad, 1846: 23, pl. 1, fig. 1 [Type locality: Tampa Bay, Florida].

Cyclas maritima d'Orbigny, 1853: 280, pl. 26, figs. 47–50 [Type localty: Cuba].

Polymesoda (Pseudocyrena) maritima – Abbott, 1974: 521, fig. 5851.

Polymesoda maritima – Bieler & Mikkelsen, 2004: 512.

Polymesoda floridana – Mikkelsen & Bieler, 2007: 284–285, 7 figs.

Description

Shell (Figs. 246–250): Oval, brown to beige to purple in commarginal bands (Figs. 246, 248); SL ≈ 20 mm in material examined, SH ≈ 80% SL, SW ≈ 50% SL. Anterior margin rounded; posterior margin bluntly pointed. Umbones central to between middle and anterior thirds, protruding ca. 10% SH, bluntly pointed, adjacent. Sculpture absent, except for commarginal undulations mainly on anterior and posterior regions; outer surface smooth, glossy, with growth lines. Periostracum thin, beige, velvet-like, more visible close to shell margins. Ligament just posterior to umbones; L ≈ 20% SL ≈ 5 W. Hinge plate arched, central, barely symmetrical; L ≈ 80% SL. Two pairs of divergent cardinal teeth; wider ventral region A ≈ 8% of central hinge plate A (Figs. 247, 249); each tooth with median longitudinal furrow, almost dividing it into 2 equal parts (Fig. 250); RV with more anterior tooth. Third cardinal tooth in RV just anterior to umbones, somewhat horizontal, dorsal; L ≈ sum of other cardinal teeth L (Fig. 250). Two pairs of lateral teeth almost symmetrical; anterior tooth slightly closer to umbo than posterior tooth; teeth of RV (Fig. 247) more ventral than those of LV; posterior lateral tooth L ≈ 33% of hinge plate L, anterior tooth L ≈ 60% of posterior lateral tooth L. Inner shell surface opaque, mostly purple; muscle scars shallowly impressed. Scar of anterior adductor muscle (*am*) weakly arching (concavity posterior), just anteroventral to anterior lateral tooth, at approximate mid-SH; A ≈ 1.5% VA. Scar of posterior adductor muscle (*pm*) elliptical, slightly larger than *am* scar, at approximately same level and same relation to lateral tooth, except being slightly more distant from posterior margin. Pallial line running ca. 15% SH away from ventral shell margin. Pallial sinus shallow (Fig. 247); L ≈ 8% SL.

Main muscle system (Figs. 251, 255, 263): Size and position of adductor muscles as described above; each adductor W ≈ 75% of maximum SW. Paired pedal protractor muscles (Fig. 255: *rr*) immersing in integument of anterior visceral mass and foot base, originating posterior to *am* at distance = 6% SL, at midlevel of *am*, running ventrally and slightly posterior, inserting splaying across anterior foot base; A ≈ 4% of *am* A. Paired anterior pedal retractor muscles (Figs. 251, 255, 263: *ar*) slender, originating just dorsal to *am*; A = 8% of *am* A; running ventrally, gradually approaching midline, along ca. 50% SH, inserting into anterior foot base, covered externally by *rr*. Paired posterior pedal retractor muscles (Fig. 255: *pr*) slender, originating near and dorsal to *pm*; A = 10% of *pm* A, L ≈ 2 W; running posteriorly and slightly ventrally at distance = 33% SL, of uniform L except in anterior third, splaying gradually, inserting along posterior foot base and posterior walls of visceral mass.

Foot (Fig. 251): Axe-like, anteroventral; V ≈ 16% SV. Solid portion relatively narrow; V = 33% of foot V. Anterior end somewhat bluntly pointed; posterior end rounded. Byssal groove and byssus absent.

Mantle (Figs. 251–253): Edges of mantle lobes free except dorsally (L ≈ 75% SL) and at posterior siphonal area (L ≈ 33% SL). Free mantle edges each with 3 folds (Fig. 253), all short, subequal, in H and T = 50% of shell H and T, except outer fold, which is ca. 2 times thicker

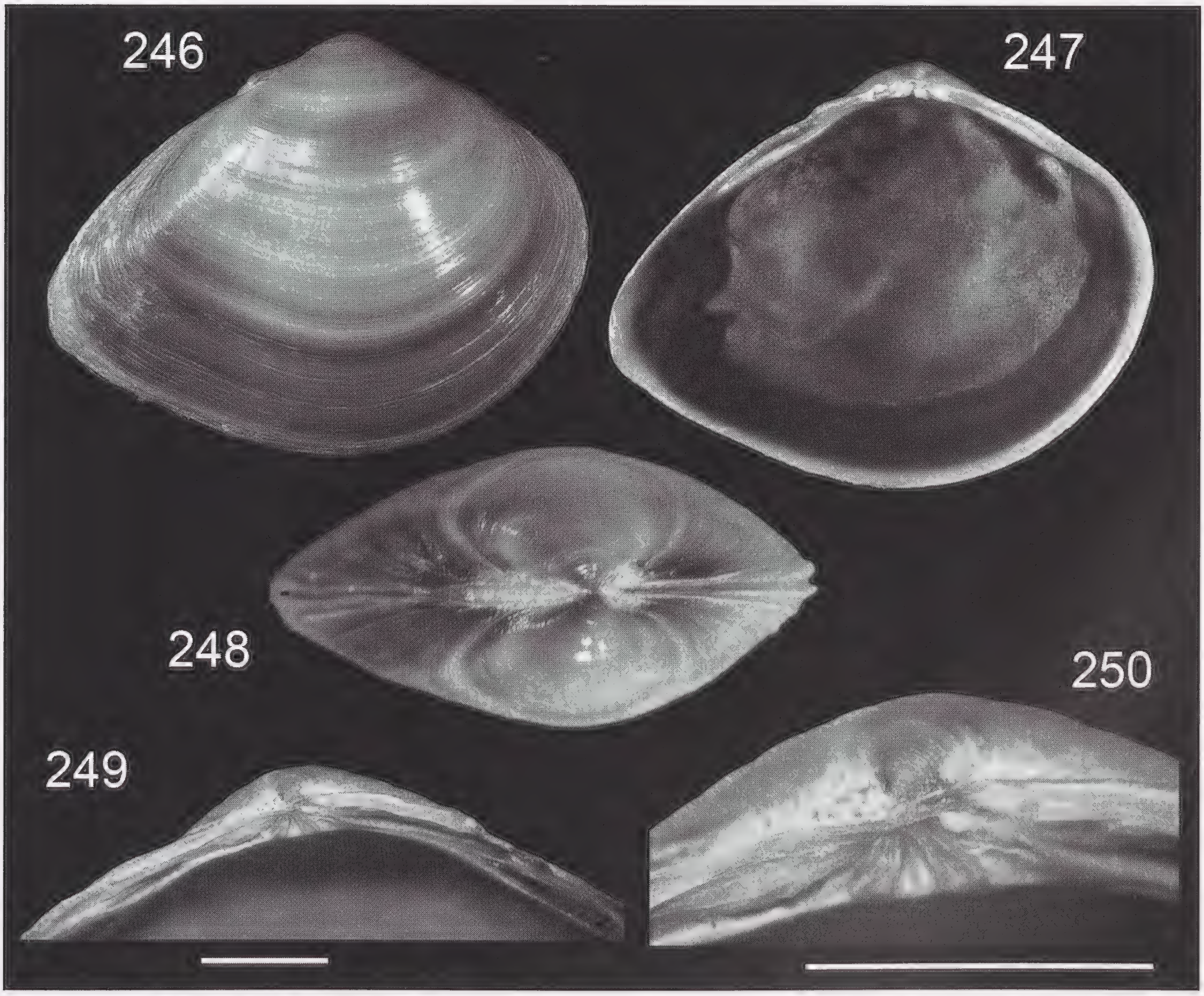

FIGS. 246–250. *Polymesoda floridana,* shell morphology, FMNH 288869, 27.0 mm L. FIG. 246: Intact left view; FIG. 247: RV interior view; FIG. 248: Intact dorsal view; FIG. 249: RV, detail of hinge, inner-left view; FIG. 250: Same, detail of cardinal teeth. Scale bars = 5 mm.

due to collar vessel. Pallial muscle relatively thick (T ≈ ST). Excurrent (*se*) and incurrent (*si*) siphons (Fig. 252) entirely separated; L ≈ 10% SL, *si* W ≈ 2 *se* W. Distal edge of *se* smooth; that of *si* with series of small papillae internally, approximate arrangement of longer papillae intercalating with shorter papillae; shorter papilla L ≈ 50% of longer papilla L. Two pairs of siphonal retractor muscles (Fig. 252: *sm*) subequal; dorsal pair L ≈ 6% SL, originating just ventral to *pm*, splaying gradually posteriorly between siphons, with

251

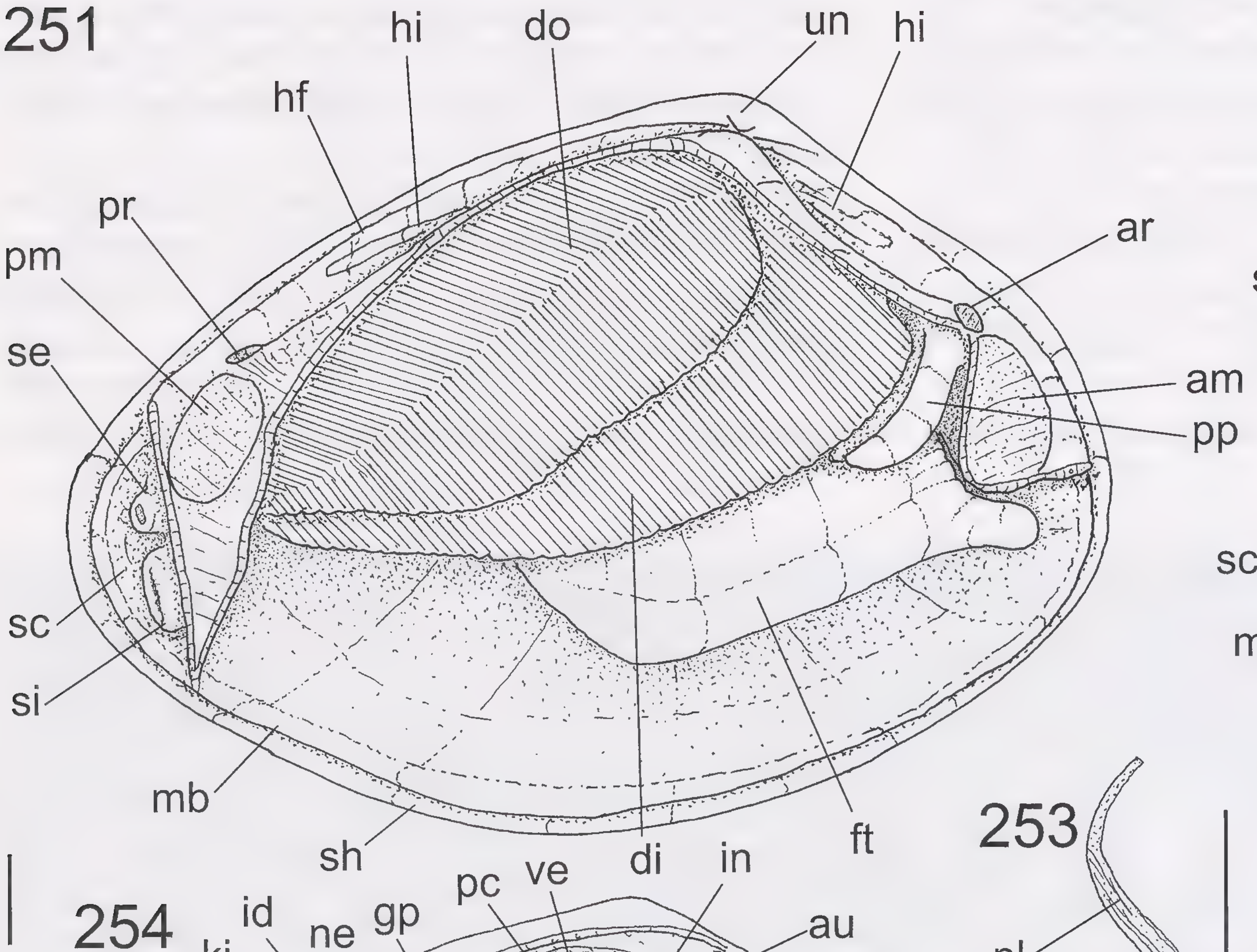

252

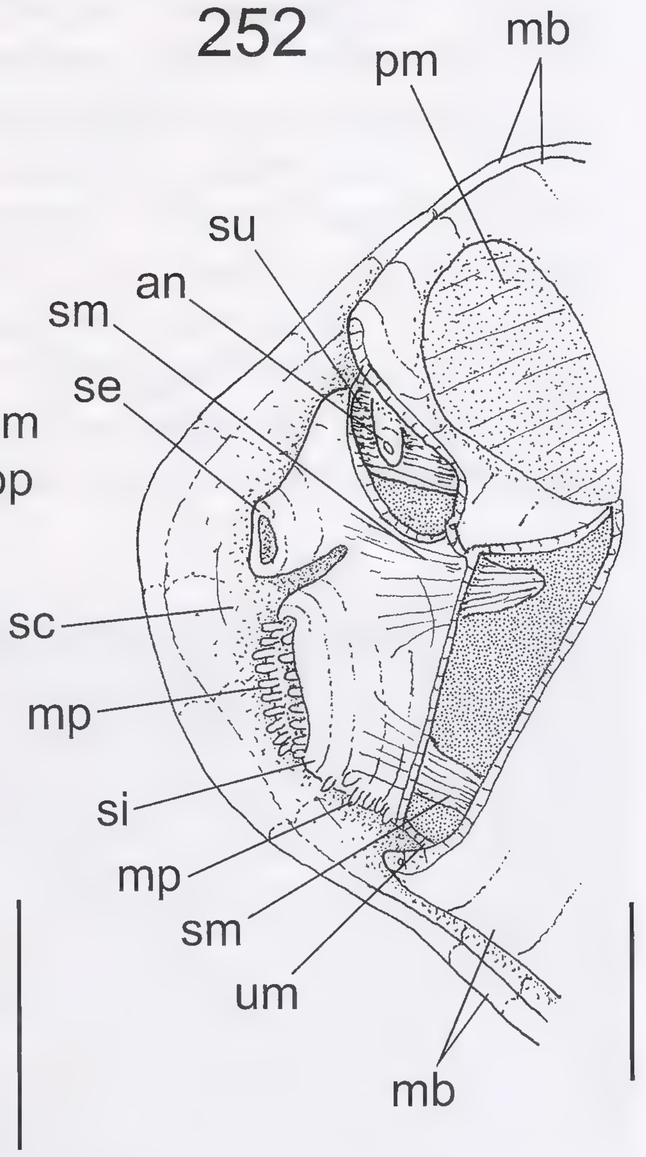

253

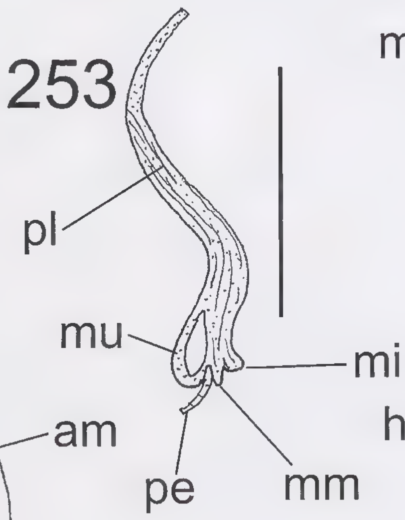

254

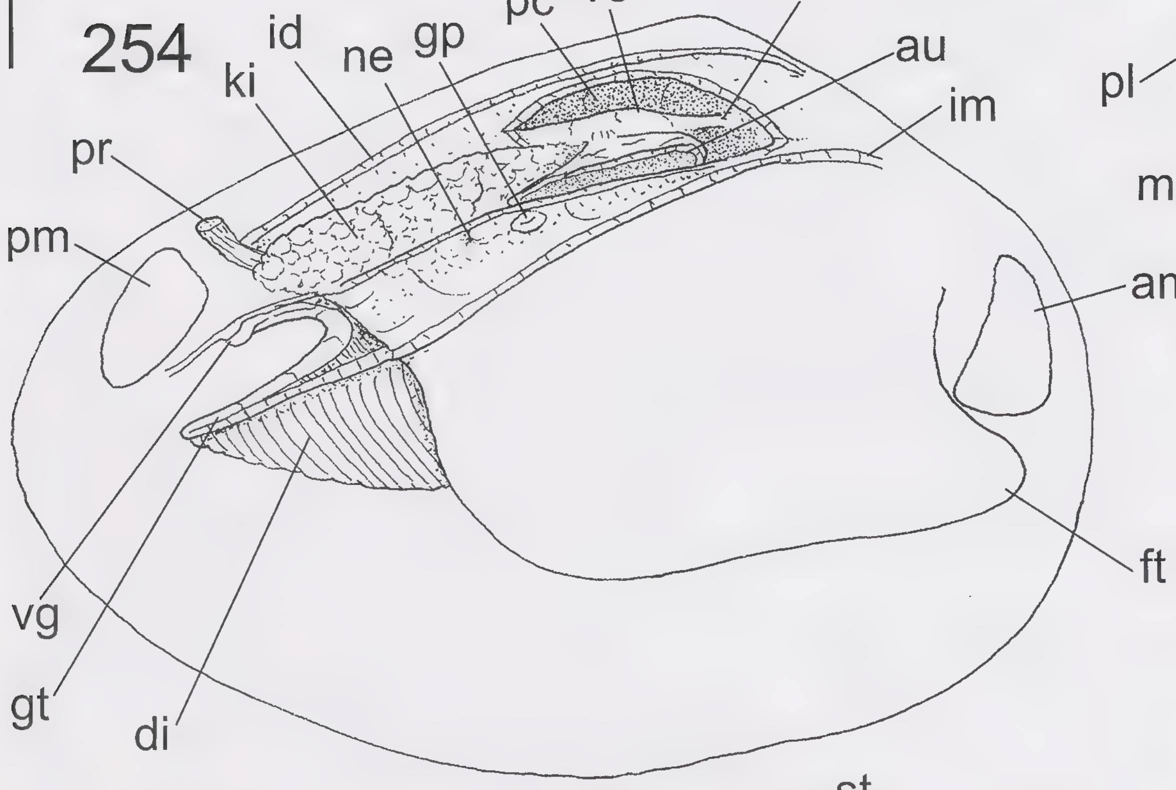

255

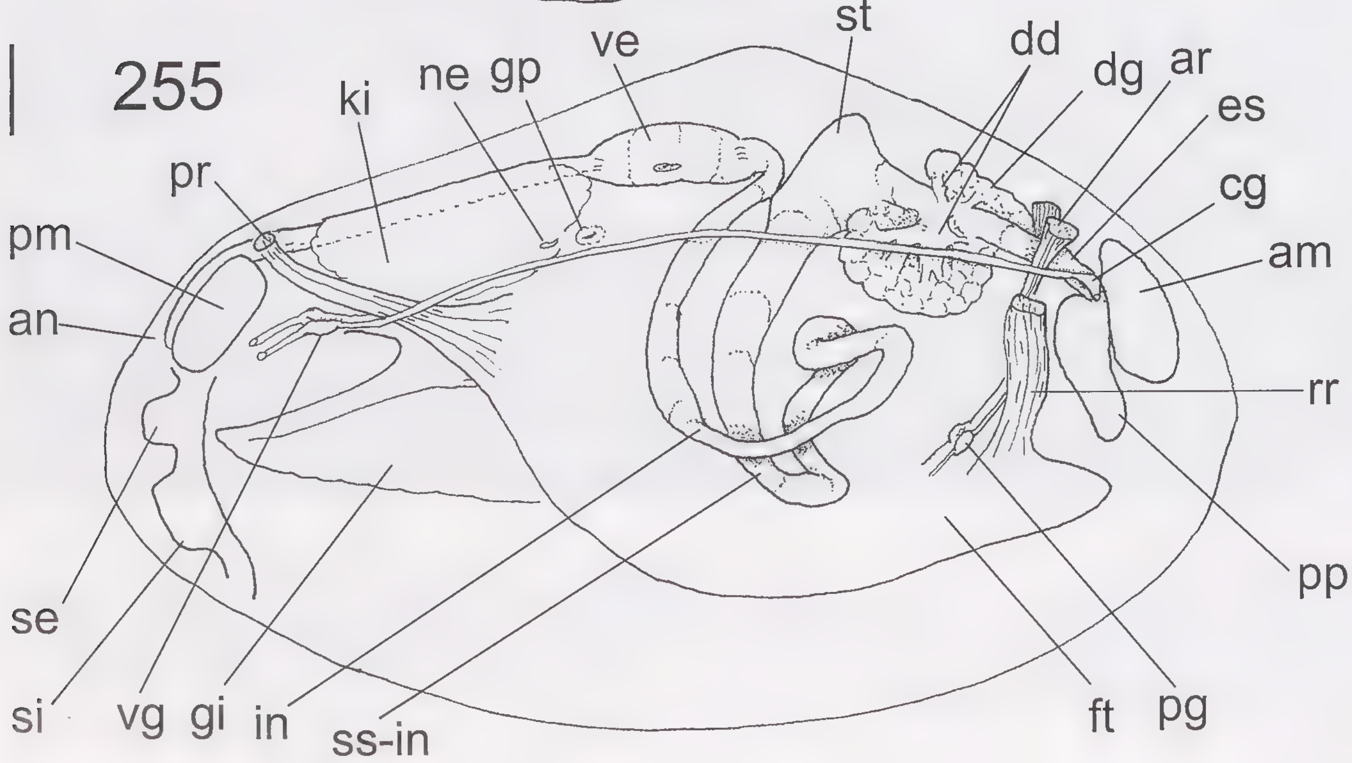

256

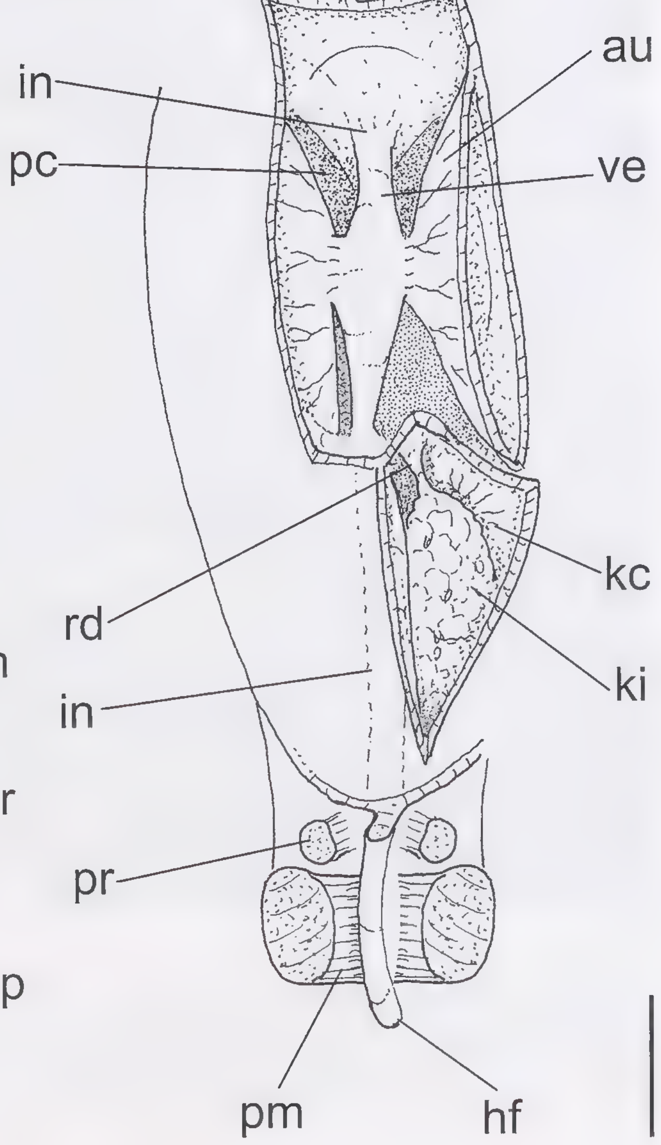

ca. 50% of muscle fibers allocated to each siphon; ventral pair originating along same vertical line as dorsal pair, close to ventral edge, running posteriorly and dorsally, splaying across ventral side of *si*. Fusion of mantle lobes beginning at posterior 15% of ventral edge, forming siphonal chamber (Figs. 251, 252: *sc*); V ≈ 10% SV.

Pallial cavity (Figs. 251, 254, 257, 266): Dorsally occupied by very narrow visceral mass; A ≈ 90% VA, V ≈ 80% SV. Labial palps (Fig. 251: *pp*) just posterior to *am*, originating at posterodorsal edge of *am*. Hemipalps symmetrical, each one subtriangular; A ≈ 1.5% VA, wider (anterior) region L ≈ 50% of total L. *Pp* inner surface (Fig. 257) with 20–25 transverse folds; distal folds shorter, more oblique; ventral ends of folds rounded, dorsal ends gradually diminishing; uniformly smooth edges surrounding entire *pp* free borders; W ≈ 3 single fold W. Smooth region preceding oral furrow between hemipalps (Fig. 257); L ≈ 20% of *pp* L. Gills mid-dorsal (Fig. 251); A ≈ 33% VA, L ≈ 80% SL, H ≈ 55% SH. Demibranchs very different (Fig. 266). Outer demibranch (*do*) more dorsal, with 2 subequal regions; A ≈ 80% of inner demibranch A; ventral region with descending and ascending lamellae, covering most of dorsal half of inner demibranch; dorsal region composed only of ascending lamella, covering outer surface of dorsal visceral surface exposed in pallial cavity; outer tissue connection of *do* with dorsal edge of pallial cavity. Inner demibranch (Figs. 251, 266: *di*) with subequal descending and ascending lamellae; ventral region extending beyond ventral edge of *do* along ca. 2 times ventral region of *do*; tissue connection to visceral mass and to counterpart in posterior quarter of gill L (Fig. 254). Anterior edge of *do* rounded, ca. 50% free; anterior edge of *di* attaching to anterior edge of pallial cavity at ca. 75% H, remaining 25% free ventrally. Posterior ends of demibranchs bluntly pointed, at same level ventral to *pm*. Gills suspensory stalks (Fig. 254: *gt*) originating on anteroposterior side of *pm*, weakly muscular, arching ventrally along ca. 25% of posterior gill L. Food groove on ventral edge of *di*.

Visceral mass (Figs. 254–256): Digestive system lying mostly vertically in central region; V ≈ 20% of visceral mass V. Digestive diverticula greenish-beige, restricted to anterodorsal region, composed of small, rounded, multi-branched acini; V ≈ 20% of visceral mass V. Gonad filling remaining visceral space, cream-colored, with uniform surface. Renopericardial structures dorsal from posterior umbonal cavity to posterior surface of *pm*; V ≈ 25% of visceral mass V.

Circulatory and excretory systems (Figs. 254–256, 258): Pericardial size and position as described above, filling anterior half of renopericardial V. Auricles (Fig. 254: *au*) broadly connecting to central region of ctenidial vein, along ca. 25% of gill L; auricular connections to ventricle (*ve*) at center of ventricular lateral walls. Kidneys (Fig. 258: *ki*) greenish pale brown, mostly solid, of relatively complex organization, with 3 narrow, longitudinal, subequal, hollow chambers. Pair of dorsal chambers subcylindrical, surrounded by blind-sac of relatively thick, glandular walls, with 4–5 longitudinal folds, lying along both sides of intestine (posterior to portion running through

←

FIGS. 251–256. *Polymesoda floridana*, anatomy. FIG. 251: Intact right view, RV and part of right mantle lobe removed; FIG. 252: Same, detail of siphonal region, with part of adjacent portion of mantle lobe removed; FIG. 253: Mantle edge, cross section in midventral region; FIG. 254: Dorsal region of visceral mass, right view, superficial structures removed, topologies of other structures also shown; FIG. 255: Main musculature, digestive system, and nervous system *in situ*, right view, topologies of other structures also shown; FIG. 256: Renopericardial structures, dorsal view, part of dorsal wall of pericardium removed, right kidney sectioned longitudinally and right wall deflected. Scale bars = 2 mm. Abbreviations: am, anterior adductor muscle; an, anus; ar, anterior pedal retractor muscle; au, auricle; cg, cerebropleural ganglion; dd, ducts to digestive diverticula; dg, digestive diverticula; di, inner demibranch; do, outer demibranch; es, esophagus; ft, foot; gi, gill; gp, genital pore; gt, gill suspensory stalk; hf, hinge fold of mantle; hi, hinge; id, insertion of outer demibranch in mantle; im, insertion of inner demibranch in visceral mass; in, intestine; kc, renal chamber; ki, kidney; mb, mantle border; mi, mantle border inner fold; mm, mantle border middle fold; mp, mantle papillae; mu, mantle border outer fold; ne, nephropore; pc, pericardium; pe, periostracum; pg, pedal ganglion; pl, pallial muscles; pm, posterior adductor muscle; pp, labial palp; pr, posterior pedal retractor muscle; rd, renopericardial duct; rr, pedal protractor muscle; sc, siphonal chamber; se, excurrent siphon; sh, shell; si, incurrent siphon; sm, siphonal retractor muscle; ss-in, conjoined style sac-intestine; st, stomach; su, supra-anal chamber of suprabranchial pallial cavity; um, fusion between left and right mantle lobes; un, umbo; ve, ventricle; vg, visceral ganglia.

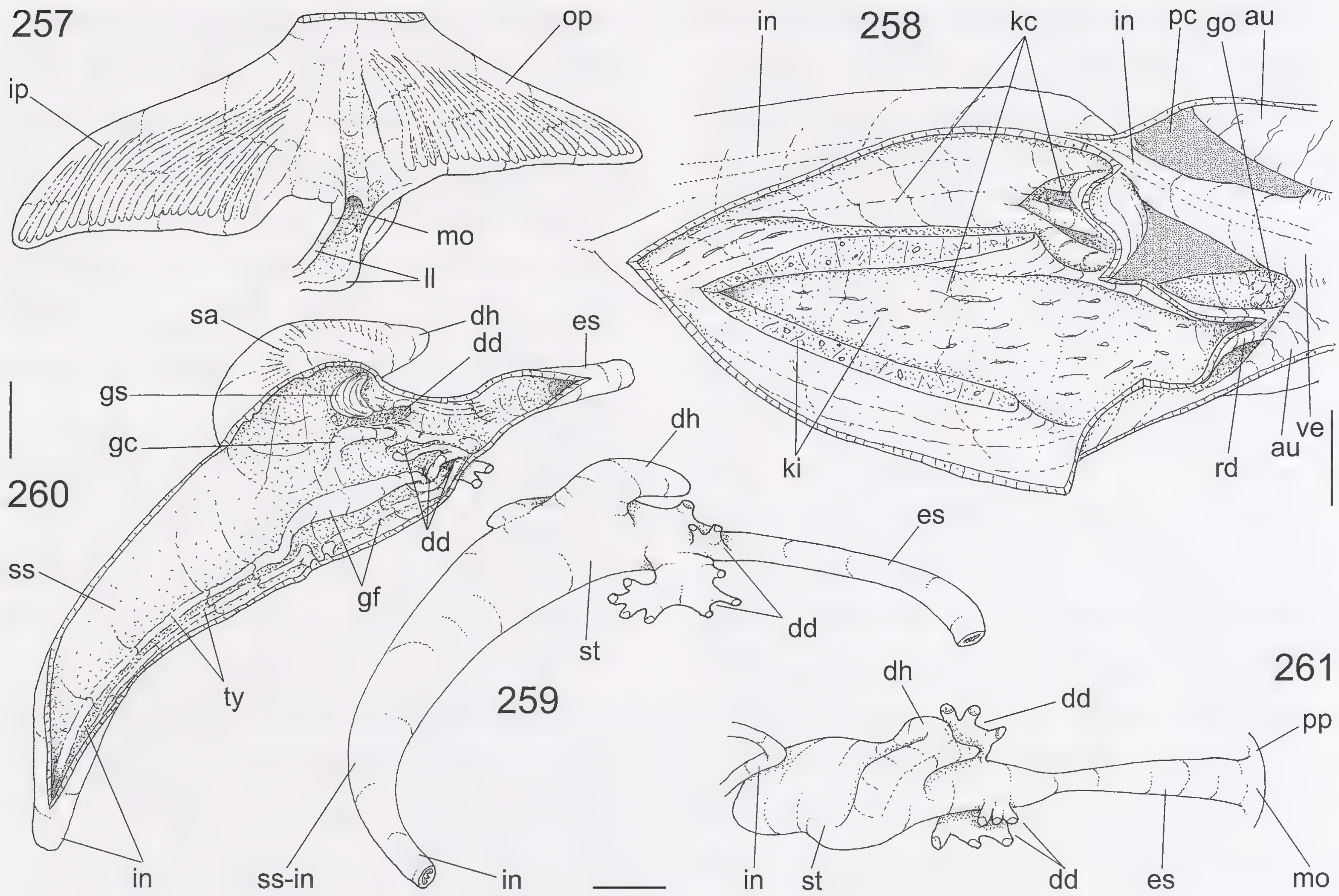

FIGS. 257–261. *Polymesoda floridana*, anatomy. FIG. 257: Right labial palp, right view, outer hemipalp deflected; FIG. 258: Right kidney, dorsal and slightly right view, right portions longitudinally sectioned and partly deflected to posterior region of pericardium; FIG. 259: Isolated digestive system, right view; FIG. 260: Stomach, sectioned longitudinally; FIG. 261: Unopened stomach, dorsal view. Scale bars = 1 mm. Abbreviations: au, auricle; dd, ducts to digestive diverticula; dh, dorsal hood; es, esophagus; gc, gastric central pad; gf, gastric fold; go, gonad; gs, gastric shield; in, intestine; ip, inner hemipalp; kc, renal chamber; ki, kidney; ll, labial lips preceding mouth; mo, mouth; op, outer hemipalp; pc, pericardium; pp, labial palp; rd, renopericardial duct; sa, gastric sorting area; ss, style sac; ss-in, conjoined style sac-intestine; st, stomach; ty, typhlosole; ve, ventricle.

pericardium); aperture on anteroventral side. Two remaining pairs of chambers flattened, separated by transverse, thick flap of renal tissue, opening widely anteriorly. Anterior aperture of these 3 pairs of chambers with content flowing directly to renopericardial duct (Fig. 258: *rd*), lying ventral to *au*, and in part receiving vessels from visceral mass; anterior chambers with nephropores (Figs. 254, 255: *ne*) on ventral sides.

Digestive system (Figs. 252, 255, 257, 259–261): *Pp* as described above. Mouth wide, preceded by relatively tall lips (Fig. 257: *ll*) with smooth inner surfaces. Esophagus (*es*) running almost directly posterodorsally, with only anterior end close to midlevel of posterior surface of anterior adductor muscle, remaining running through digestive diverticula; L ≈ 20% SL ≈ 10 W. *Es* inner surface mostly smooth (Fig. 260), except for 3–4 low, narrow longitudinal folds at left side of *es* opening in stomach. Stomach main chamber in L ≈ *es* L ≈ 2 W; dorsal inner gastric surface irregular, with oblique, dorsal fold H and L ≈ 33% of *es* L; anterior-left end of dorsal fold comprising relatively long dorsal hood (Figs. 259, 261: *dh*). Ducts to digestive diverticula (Figs. 259, 261: *dd*) composed of pair of wide, ventrolateral projections originating just anterior to *es* opening; L ≈ 25% of *es* L ≈ 2 *es* W; other additional, smaller (25–33% size of larger) ducts to *dd* just dorsal to larger ducts. Gastric inner surface mostly smooth; sorting area (Fig. 260: *sa*) composed of short transverse folds running along dorsal surface of *dh* and part of dorsal wall; *sa* A ≈ 16% of main gastric chamber surface A. Gastric central pad (Fig. 260: *gc*) simple; L ≈ 3 W, A ≈ 12% of midventral inner gastric surface A. Ducts to *dd* on both sides of *gc* anterior end; gastric shield

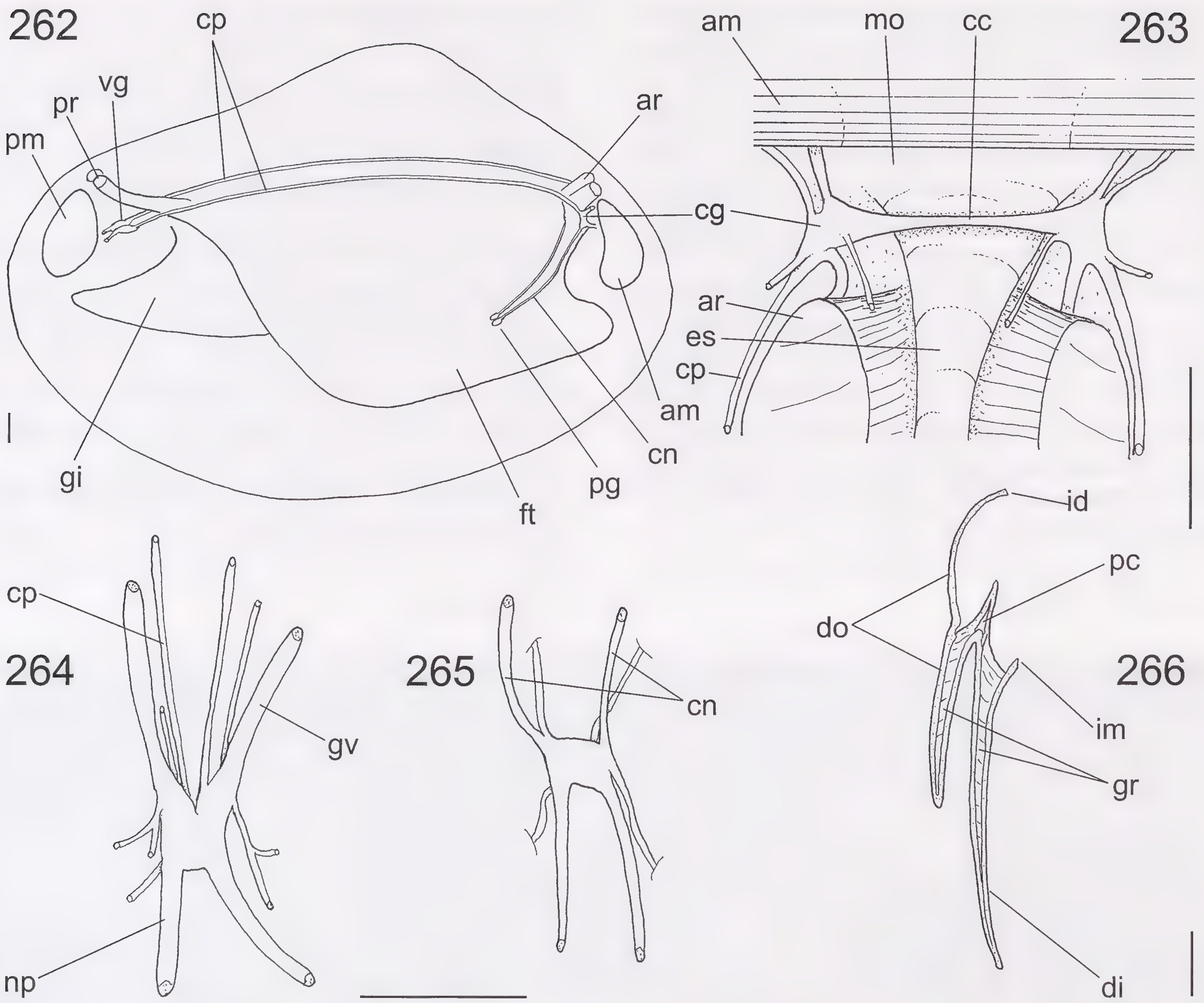

FIGS. 262–266. *Polymesoda floridana*, anatomy. FIG. 262: Nervous system *in situ*, right and slightly dorsal view, topologies of some structures also shown; FIG. 263: Region of cerebropleural ganglia, dorsal view, dorsal integument removed; FIG. 264: Visceral ganglia, ventral view; FIG. 265: Pedal ganglia, posterior view; FIG. 266: Gill, cross section along midregion. Scale bars = 1 mm. Abbreviations: am, anterior adductor muscle; ar, anterior pedal retractor muscle; cc, cerebral commissure; cg, cerebropleural ganglion; cn, cerebropedal connective; cp, cerebrovisceral connective; di, inner demibranch; do, outer demibranch; es, esophagus; ft, foot; gi, gill; gr, gill transverse septum in suprabranchial chamber; gv, gill nerve; id, insertion of outer demibranch in mantle; im, insertion of inner demibranch in visceral mass; mo, mouth; np, nerve to posterior adductor muscle; pc, pericardium; pg, pedal ganglion; pm, posterior adductor muscle; pr, posterior pedal retractor muscle; vg, visceral ganglia.

(Fig. 260: *gs*) in ventral region of origin of *dh*; A ≈ 16% of main chamber surface A. Small, narrow, longitudinal folds between ducts to *dd*; another larger longitudinal, ventral fold running posteriorly from right-ventral duct to *dd*, continuing as typhlosole (*ty*); another longitudinal fold, ca. 3 times narrower, lying to right of larger fold, with perpendicular curve at level of intestinal opening, running along *dh* dorsal wall. *Dh* V ≈ 25% of main gastric chamber V; *sa* (described above) flanked by pair of folds; posterior fold making perpendicular curve into conjoined style sac-intestinal opening, becoming *ty*. Style sac (*ss*) totally fused with intestine, separated only by pair of typhlosoles (Fig. 260: *ty*); L ≈ 1.5 gastric main chamber L, W ≈ 50% of gastric main chamber W. Intestine (Fig. 255: *in*), after separating from *ss* performing short loops anterior to *ss*, then crossing to right of *ss* ventral end, performing wide curve dorsal to anterior side of pericardium, in this region abruptly running posteriorly along midline; *in* L ≈ 2 SL. Anus (Fig. 252: *an*) simple, sessile, at mid-posterior surface of *pm*.

Reproductive system (Figs. 254, 255): Gonad as described above. Genital duct not detected, except for pair of short, tubular genital chambers preceding pores. Paired genital apertures (*gp*) papilla-like, posterior to *ne* at distance = 50% of *pm* W.

Nervous system (Figs. 262–265): Paired cerebropleural ganglia (Figs. 262, 263: *cg*; 265) just posterior to mouth; each subtriangular; L ≈ *es* D. Cerebral commissure L ≈ 2 single *cg* L. Paired pedal ganglia (Fig. 262: *pg*) broadly fused, on dorsal, inner wall of foot, at distance from *cg* ≈ 20% SL; each subquadrate; V ≈ 50% of single *cg* V. Paired visceral ganglia (Fig. 262: *vg*) at midlevel of anterior surface of *pm*; each subelliptical; anterior halves of ganglia nearly entirely fused; V ≈ *cg* V. Paired cerebrovisceral connectives (Figs. 263, 264: *cp*) in L ≈ 85% SL.

Material Examined

USA, Florida Keys, FMNH 288869, 100+ specimens (sta. FK-056; 3 dissected, #1 not measured; #2: 19.0 mm L, 13.1 mm H, 8.6 mm W; #3: 22.0 mm L, 16.1 mm H, 10.0 mm W).

Distribution

Stated by Turgeon et al. (2009; as *Polymesoda maritima*) to range from Florida to Quintana Roo (Mexico), Cuba, the Bahamas, and Dominican Republic. It is not known from Brazil.

Remarks

For other details of the shell, see Mikkelsen & Bieler (2007: 284). Morton (1976) described the anatomy of *Geloina erosa* (Solander in Ellis & Solander, 1786) [as *Polymesoda* (*Geloina*)] from Southeast Asia; van der Schalie (1933) provided brief notes and figures on the anatomy of *P. caroliniana* (Bosc, 1802). These two descriptions agree in all major respects with the present species.

Until recently, d'Orbigny's description of *Cyclas maritima* was dated as 1842 but is now interpreted as having been published much later, between 1851 and 1853 (e.g., Mikkelsen & Bieler, 2007: 413; who adopted the 1853 date), giving the name *Cyrena floridana* priority.

Family Cardiidae
Lamarck, 1809

Laevicardium serratum
(Linnaeus, 1758)
Figs. 267–283

Synonymy/Chresonymy

Cardium serratum Linnaeus, 1758: 680 [Type locality given as Mediterranean, but in error; see Remarks].

Cardium oviputamen Reeve, 1844: sp. 36, pl. 7, fig. 36.

Laevicardium laevigatum – Clench & Smith, 1944: 22–25, pl. 12, figs. 1, 2, 5 [figs. 3, 4 seem to belong to the similar *L. pristis* (Bory de Saint-Vincent, 1827)]; Abbott, 1974: 485–486, pl. 22, fig. 5572; Bieler & Mikkelsen, 2004: 511 [non *Cardium laevigatum* Linnaeus, 1758; see Remarks].

Laevicardium serratum – Mikkelsen & Bieler, 2007: 288–290, 5 figs.

Description

Shell (Figs. 267–271, 273, 274): White to yellow, elliptical, weakly oblique anteroposteriorly; posteriorly with abrupt slope, weakly convex; anterior and ventral margins forming semicircular arch; SL ≈ 30 mm in material examined ≈ 80% SH ≈ SH in very large (50 mm) specimens, maximum SW ≈ 75% SL (Fig. 268). Umbones (Figs. 273, 274) close to midline, rounded, weakly protruding ca. 5% SH dorsal to hinge plate. Periostracum pale brown, thin, mostly abraded at umbones. Outer surface smooth, glossy, lacking sculpture except for growth lines and radial striae in some areas. Ligament (Fig. 268) external, bulging just posterior to umbones along 25% SL. Hinge plate (Figs. 269, 270) highly arched; T of edges ≈ 3% SH, L ≈ 60% SL. Two cardinal teeth in each valve (subequal in LV, one tooth much larger than other in RV); total W ≈ 15% of hinge plate L. Two pairs of equidistant, symmetrical lateral teeth (Figs. 269–271), each weakly broader than midportion of hinge plate; L ≈ 25% of hinge plate L. Inner surface (Fig. 274) glossy, yellowish, often with purple hinge plate and purple stain anteriorly, sculptured by radial striae more visible closer to margins, producing weak riblets, larger anteroventrally. Muscle scars very shallow. Scar of anterior adductor muscle (*am*) oval, close to anterior margin, just ventral to hinge plate; A ≈ 4% of inner VA. Scar of posterior adductor muscle (*pm*) elliptical, at same level as *am* scar; A ≈ 50% of *am* scar A. Indentation in pallial line shallow, displacing toward anterior ca. 20% SL.

Main muscle system (Figs. 275, 276, 278): Proportions and positions of adductor muscles as described above; W of each adductor muscle = 60% of maximum SW. Paired pedal protractor muscles (Fig. 278: *rr*) minute, originating in ventral region of *am*; A = 3% of *am* A; running posteriorly for distance = 50% of *am* L, through anteroventral palps, splaying in adjacent integument across anterior visceral mass. Paired anterior pedal retractor muscles (Figs. 275, 276, 278: *ar*) originating in dorsal region of *am* at distance = 20% of *am* L; A = 10% of *am* A; running ventrally and slightly posterior, becoming wider and thinner, for distance = *am* L, splaying across anterior and lateral foot base. Paired posterior pedal retractor muscles (Figs. 275, 276, 278: *pr*) each in V ≈ 50% *ar* V, originating dorsal to *pm*, for distance toward anterodorsal = 70% of *pm* L; running anteroventrally for distance ≈ 2 *pm* L, splaying across posterior foot base.

Foot (Figs. 275, 276, 278): At base of visceral mass; L (foot plus visceral mass) ≈ 1.5 SH ≈ 25% SL. Basal and middle thirds cylindrical; distal third tapering gradually to pointed tip. Well-developed transverse muscles (Fig. 278: *tm*) vertically aligning at midlevel of anterior foot base. Retraction into shell typically accomplished by perpendicular bending toward anterior at foot base. Byssus absent.

Mantle (Figs. 272, 275, 276, 279): Anterior and ventral mantle edges free; posterior and dorsal edges fused. Free mantle edges composed of 3 folds (Fig. 279); outer and middle folds short (L = 50% ST); periostracum between these 2 folds; inner fold L and T = 5–8

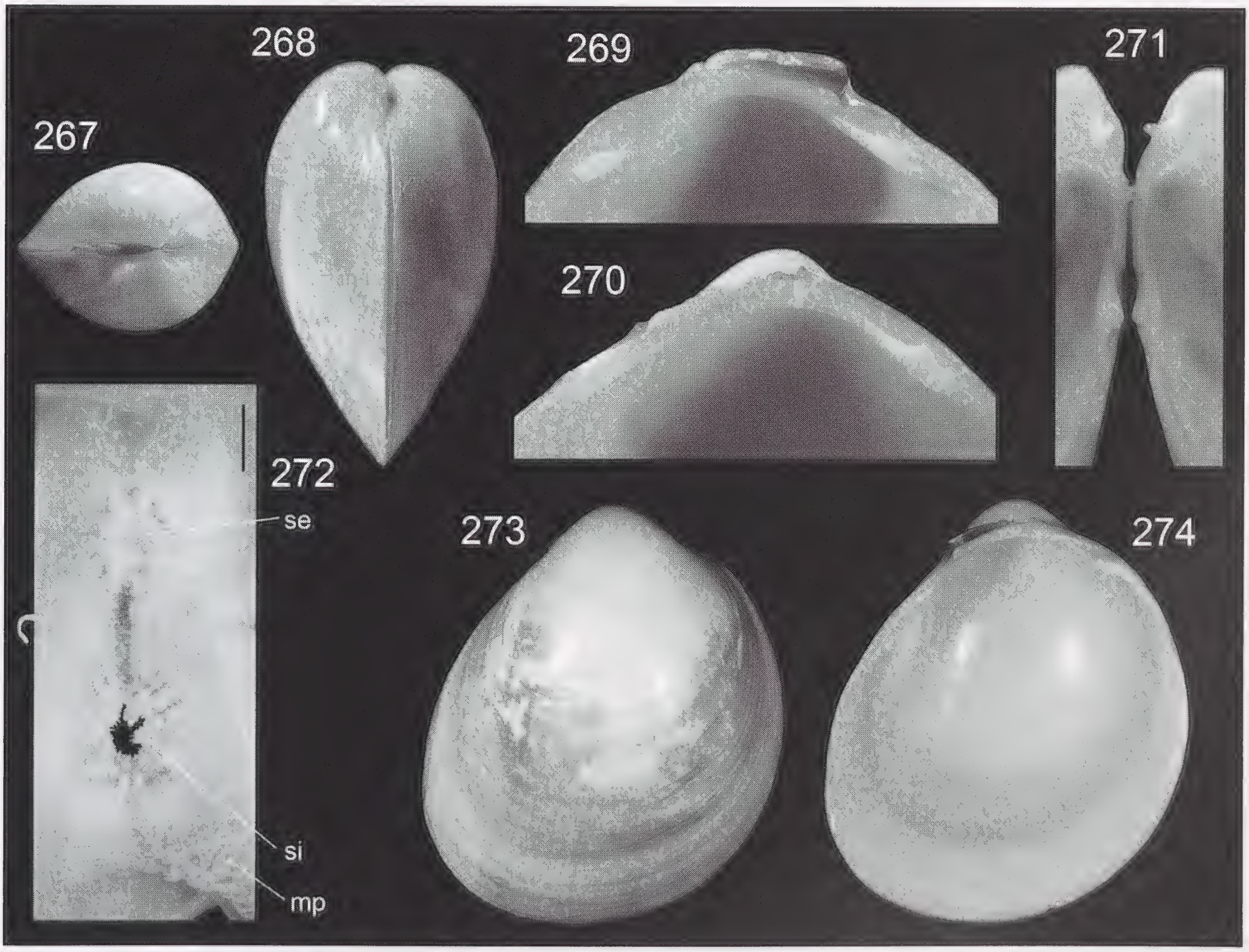

FIGS. 267–274. *Laevicardium serratum*, shell morphology and anatomy. FIGS. 267–272, FMNH 295693, 29.7 mm L. FIG. 267: Intact dorsal view; FIG. 268: Posterior view; FIG. 269: RV, detail of hinge; FIG. 270: Same, LV; FIG. 271: Hinge, interior view, with valves connected, weakly deflected; FIG. 272: Mantle and posterior apertural area, posterior view. Scale bar = 2 mm. FIGS. 273, 274: FMNH 227405, 31.1 mm L. FIG. 273: LV, interior view; FIG. 274: RV, interior view. Abbreviations: mp, mantle papillae; se, excurrent aperture; si, incurrent aperture.

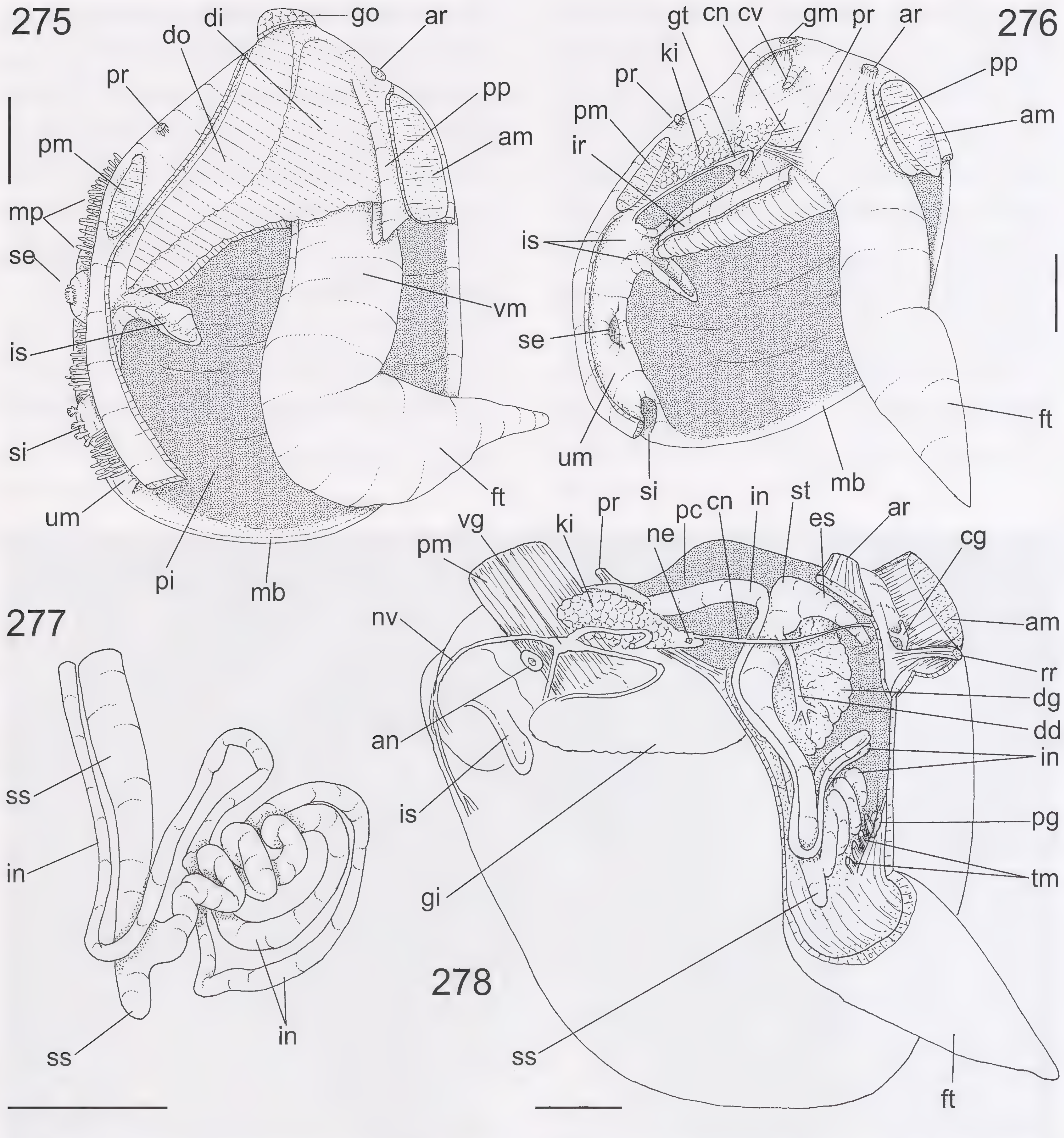

FIGS. 275–278. *Laevicardium serratum*, anatomy. FIG. 275: Intact right view, RV and part of right mantle lobe removed; FIG. 276: Same, right gill removed, posterior apertural area slightly deflected to expose inner surface; FIG. 277: Style sac and intestine *in situ*, right view; FIG. 278: Visceral structures, right view, posterior region somewhat deflected and in ventral view, topologies of some adjacent structures also shown. Scale bars = 5 mm. Abbreviations: am, anterior adductor muscle; an, anus; ar, anterior pedal retractor muscle; cg, cerebropleural ganglion; cn, cerebropedal connective; cv, ctenidial (efferent) vessel; dd, ducts to digestive diverticula; dg, digestive diverticula; di, inner demibranch; do, outer demibranch; es, esophagus; ft, foot; gi, gill; gm, gill retractor muscle; go, gonad; gt, gill suspensory stalk; in, intestine; ir, membrane connecting both inner demibranchs; is, siphonal septum; ki, kidney; mb, mantle border; mp, mantle papillae; ne, nephropore; nv, nerve; pc, pericardium; pi, pallial chamber; pm, posterior adductor muscle; pp, labial palp; pr, posterior pedal retractor muscle; rr, pedal protractor muscle; se, excurrent aperture; si, incurrent aperture; ss, style sac; st, stomach; tm, transverse muscles into visceral cavity; um, fusion between left and right mantle lobes; vg, visceral ganglia; vm, visceral mass.

outer and middle fold L and T. Pallial muscles in unfused edges T ≈ 2 ST. Posterior siphonal area with inner folds broadly fused; W = 33% SW; ventral fusion beginning in arched fold in posteroventral region. Outer surface almost entirely covered by tall, slender papillae (Figs. 272, 275: *mp*); lateral papillae longer (L ≈ 75% of fusion W), those closer to midline of L ≈ 33% of remaining papilla L. Incurrent and excurrent apertures (Figs. 272, 275: *si, se*) tube-like, subequal; *si* slightly larger. Both apertures entirely covered on outer surface by pallial papillae, similar to those in neighboring regions, except in being more complex, each possessing several small branches along L. Inner surface of mantle edge fusion smooth, with long, solid, tongue-like siphonal septum (Figs. 275, 276: *is*) at midlevel separating supra- and infrabranchial chambers, projecting anteriorly for distance = 20% SL, concave dorsally, bluntly pointed distally, with no obvious connection to gills.

Pallial cavity (Figs. 275, 276, 280, 283): In V ≈ 70% SV; ventral 66% providing chamber for foot movement. Labial palps (*pp*) in L ≈ 8 H, weakly arching (with concavities posterior); ventral region L ≈ 8% SL, narrowing gradually dorsally along distance slightly longer than *am* H; dorsal half narrow, of similar W (≈ 20% of ventral palp W) along entire L. Hemipalps (Fig. 283) surrounding both sides of inner demibranch anteroventral edges, symmetrical, with each ventral inner surface with 12–15 transverse to slightly oblique folds; each fold gradually increasing medially, with ventral end rounded, dorsal end diminishing; folds relatively wide, low, adjacent; smooth edge W = 20% of *pp* W, uniformly surrounding ventral and dorsal halves of *pp* borders. Dorsal half of *pp* with anterior edge attaching to that of inner demibranch (Fig. 283: *di*). Gills (Figs. 275, 276: *di, do*; 280) subtriangular, in dorsal half of pallial cavity, closely surrounding visceral mass; L ≈ SL, anterior region H ≈ 33% SH; narrowing gradually posteriorly and ventrally to pointed posterior end. Demibranchs strongly asymmetrical; *do* A ≈ 50% of di A, placed more dorsally than *di*. Gill filaments attaching by longitudinal, tissue bridges almost as numerous as filaments. Transverse septa (Fig. 280: *gr*) in suprabranchial chamber at intervals of ca. 20 filaments; all 4 demibranchs possessing transversally aligned septa, producing intense folding of gill surfaces. Connection of *do* with mantle-visceral mass junction ciliary (Fig. 280: *ci*); connection of *di* with anterior pallial cavity border (inclusive between both hemipalps) composed of tissue. Inner branch of *di* free of connections in anterior third, surrounding foot base; middle and posterior thirds connecting to horizontal tissue membrane (Figs. 276, 280: *ir*), medially uniting both gills. Gill suspensory stalks (Figs. 276: *gt*) between anterior and middle thirds of gill dorsal surface, originating on visceral mass ventral surface. Food groove (Fig. 280: *fg*) on ventral edge of each *di*.

Visceral mass (Figs. 276, 278): With 2 almost perpendicular regions; dorsal region in umbonal cavity and posterior, bearing renopericardial structures; ventral region inside foot base, in V ≈ 66% of visceral mass V, bearing most of digestive system and gonad. Digestive diverticula brown, mainly in anterior and middle thirds of visceral mass; gonad pale-beige to cream-colored, mainly filling ventral half of visceral portion inside foot base and lateral regions of remaining visceral regions. Renopericardial structures (posterior) V ≈ 66% of dorsal visceral mass V.

Circulatory and excretory systems (Figs. 276, 278, 280, 282): Pericardium filling nearly entire space between *ar* and *pr*, and ca. 16% SH behind umbones. Auricles (*au*) triangular, very wide, attaching to almost entire pericardial lateral walls; walls thin, translucent; connection to ctenidial vein (Figs. 276, 280, 282: *cv*) at anterior end as pair of vessels situated almost perpendicularly, running between demibranchs. Ventricle (*ve*) elliptical, in L ≈ 60% of pericardial L, with *au* connections at midregion. Aortic bulb absent. Kidneys dark beige, along ventral pericardial wall, from midregion of visceral mass ventral surface to anterior surface of *pm*, in V ≈ 33% of pericardial V; conical, hollow renal chamber in posteroventral pericardium (Fig. 282: *kc*), in V ≈ 33% of renal V; remainder of kidneys solid. Nephropores (Fig. 278: *ne*) at anterior end of kidneys.

Digestive system (Figs. 277, 278, 281, 282): *Pp* as described above. Mouth preceded by short, smooth portion between *pp*, close to posteroventral surface of *am*. Esophagus (*es*) broadening gradually, running obliquely posterodorsally away from *am*; L ≈ *am* H. *Es* inner surface smooth; rim on inner gastric wall inconspicuous (Fig. 281). Stomach (*st*) dorsoventrally elongated, running from pre-

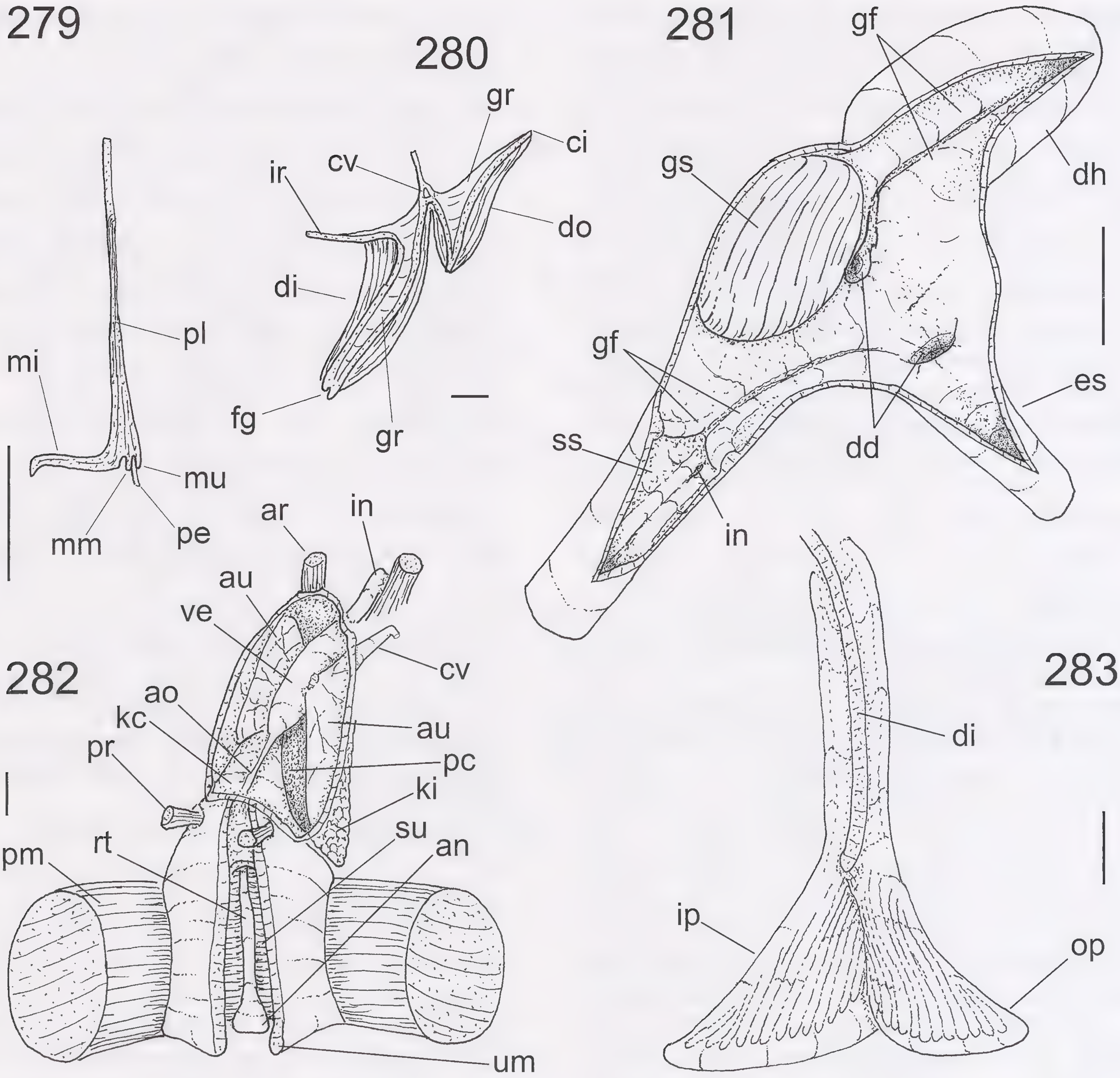

FIGS. 279–283. *Laevicardium serratum*, anatomy. FIG. 279: Mantle, cross section at midventral edge; FIG. 280: Gill, cross section at midportion, showing filaments comprising a fold; FIG. 281: Stomach, dorsal view, partially opened longitudinally; FIG. 282: Visceral mass, detail of posterior region, dorsal view (anteriormost region in slightly right view), with dorsal piece of mantle and pericardium removed; FIG. 283: Right labial palp, right view, outer hemipalp deflected, showing attachment of inner demibranch. Scale bars = 1 mm. Abbreviations: an, anus; ao, posterior aorta; ar, anterior pedal retractor muscle; au, auricle; ci, ciliary connection of gill; cv, ctenidial (efferent) vessel; dd, ducts to digestive diverticula; dh, dorsal hood; di, inner demibranch; do, outer demibranch; es, esophagus; fg, food groove; gf, gastric fold; gr, gill transverse septum in suprabranchial chamber; gs, gastric shield; in, intestine; ip, inner hemipalp; ir, membrane connecting both inner demibranchs; kc, renal chamber; ki, kidney; i, mantle border inner fold; mm, mantle border middle fold; mu, mantle border outer fold; op, outer hemipalp; pc, pericardium; pe, periostracum; pl, pallial muscles; pm, posterior adductor muscle; pr, posterior pedal retractor muscle; rt, rectum; ss, style sac; su, supra-anal chamber of suprabranchial pallial cavity; um, fusion between left and right mantle lobes; ve, ventricle.

umbonal region to ventral end of visceral cavity inside foot base, close to posterior pedal walls; V ≈ 20% of visceral mass V. Gastric main chamber in dorsal quarter, with conjoined style sac-intestine comprising ventral 75%. Dorsal hood (*dh*) almost as long as and in W ca. 50% that of gastric main chamber, on dorsal-left inside gastric surface, running anteroventrally. Inner gastric surface smooth, except for pair of wide, longitudinal, ventral folds (Fig. 281: *gf*). Ducts to digestive diverticula (Fig. 281: *dd*) in anteroventral region of *st*; left duct as posterior end of furrow of both folds of *dh*; right duct just anteroventral to *es* opening. Furrow shallow, narrow, running ventrally from right duct to *dd* toward conjoined style sac-intestinal opening, gradually differentiating into fold (Fig. 281: *gf*) surrounding opening; typhlosoles separating intestine from style sac running on ventral inner gastric surface, initiating perpendicularly from fold surrounding their origins. Style sac (*ss*) in L ≈ 50% SH, mostly fused with intestine, separated by typhlosoles; sorting portion L = 16% of *ss* L, bulging ventrally beyond separation of intestine from *ss*. Intestine (Fig. 277: *in*) of uniform, narrow W, proximally in complex set of loops, then flanking posterior gastric surface, bending perpendicularly posteriorly in subumbonal region, finally traversing through pericardium and *ve*. Rectum mostly exposed in narrow supra-anal chamber (Fig. 282: *su*) along *pm* W. Anus (Figs. 278, 282: *an*) sessile, expanding bell-like, with thickened edges, turning ventrally.

Reproductive system: Gonad as described above, composed of several acinar branches, connecting along very narrow pair of genital ducts, on both sides of visceral portion inside foot base, in posterior half of this visceral region to pair of simple genital pores, near and anterior to *ne*. Pores preceded by pair of short, tubular genital chambers.

Nervous system (Fig. 278): Paired cerebropleural ganglia (*cg*) very lateral, between *am* and origins of *rr*; cerebral commissure almost as wide as *am*; D = 3% of *am* D. Paired pedal ganglia (*pg*) almost as large as *cg*, closely adjacent, in anteroventral end of visceral cavity inside foot base; distance from *cg* = 40% SH. Paired visceral ganglia (*vg*) V ≈ 2 *cg* V, adjacent on anteroventral surface of *pm*, broadly connected, with no obvious commissure. Cerebrovisceral connective (*cn*) running along digestive system, through visceral glands. Each *vg* with two pairs of large nerves inserting into anterior and posterior ends; anterior nerves running along *gt*; posterior nerves running along posterior apertures and union of mantle lobes.

Material Examined

USA, Florida Keys, FMNH 295693, 1 specimen (sta. FK-148; dissected: 29.7 mm L, 34.8 mm H, 20.3 mm W); FMNH 295695, 1 specimen (sta. FK-141; dissected: 27.4 mm L, 30.0 mm H, 17.5 mm W); Marathon, Key Vaca, FMNH 227405, many specimens (1 dissected: 31.1 mm L); Missouri Key, FMNH 288815, 1 specimen (08/i/1986, dissected: 29.2 mm L, 25.9 mm H, 17.1 mm W).

Distribution

Stated by Turgeon et al. (2009; as *Laevicardium laevigatum*) to range from North Carolina, Gulf of Mexico, Cuba, Honduras, West Indies, Brazil and Bermuda. Rios (1994: 264; 2009: 534) used *L. brasilianum* (Lamarck, 1819) as the senior name for this species thought to occur from Florida to Brazil. New morphological study reveals *L. brasilianum* to be distinct and its anatomy will be described elsewhere; true *L. serratum* is not known to occur in Brazil. Known from Colombia (ter Poorten, in lit., May 2012). Records from Venezuela (Clench & Smith, 1944) have not been verified.

Remarks

This species has been referred to by several names such as *Cardium serratum* Linnaeus, 1758, *C. oviputamen* Reeve, 1844, and most commonly *Laevicardium laevigatum* (Linnaeus, 1758). However, Vidal (1999: 327) examined the syntypes of *Cardium laevigatum* Linnaeus, 1758, from which he designated a lectotype that he considered synonymous with *Fulvia papyracea* (Bruguière, 1789), an Indo-Pacific species (see ter Poorten 2009: pl. 12, fig. 3 for a figure of the lectotype). In the same work, Vidal (1999: 327) established a lectotype for *C. serratum* Linnaeus, 1758, establishing it as the valid name for the Floridian and Caribbean *L. laevigatum* of authors. *Cardium brasilianum* Lamarck, 1819 (= *Cardium lamarckii* d'Orbigny, 1846; *non Cardium lamarckii* Reeve, 1845) is considered by some authors (e.g., Clench & Smith, 1944; Rosenberg, 2009) a synonym of *Laevicardium serratum* (and of *L. laevigatum* of authors), but see Distribution (above).

For other details of the shell, see Mikkelsen & Bieler (2007: 288). Similar to the condition in *Codakia orbicularis*, the tubular incurrent and excurrent apertures of *Laevicardium serratum* have been called "siphons" (e.g., Schneider, 1992), but the animal does not have concentrated siphonal retractor muscles. The method of siphonal retraction has not been described for this species. Although the pallial line exhibits a very shallow indentation in the siphonal area, this is not homologous with the pallial sinus of species with siphonal retractor muscles. The term "aperture" for each of these openings is preferred here. The derived tridacnine cardiids, which embed themselves in coral reefs, do have siphons with siphonal retractor muscles (Yonge, 1981), although the latter are configured in a continuous pallial band and do not leave a recognizeable pallial sinus *per se* on the inner shell surface.

The pedal muscle configuration described here (no pedal elevator muscles, paired anterior and posterior pedal retractor muscles, paired pedal protractor muscles) differs from published accounts; Mikkelsen & Bieler (2007) reported (for the family, based on multiple published works) paired pedal elevator muscles, paired anterior and posterior pedal retractor muscles, and no pedal protractor muscles. The siphonal septum separating supra- and infrabranchial chambers was not found to be connected to the gills, contrary to the condition reported by Mikkelsen & Bieler (2007).

Schneider (1995) included *Laevicardium serratum* (as *L. laevigatum*) in his phylogenetic analysis based on shell and anatomical characters of Recent and fossil species. Lateral and ventral ridges on the foot were coded as moderate, and were found to be a possible synapomorphy for the family; neither was noted during this study, perhaps because the study was based on preserved rather than living material. Complex eyes (with lens, retina, pigmented subepithelial cells, etc.) were coded as present on the distal tips of some of the posterior ("siphonal") tentacles, but were not recorded here, likely because of their microscopic nature.

Penchaszadeh & Salaya (1983) investigated reproduction and gonadal changes of this species in Venezuela (as *Laevicardium laevigatum*; possibly also involving sympatric *L. pristis*). Stanley (1970; 157, as *L. laevigatum*) provided interesting observations regarding life habit, including burrowing, jumping, and swimming behaviors based on specimens from Biscayne Bay (near Miami, Florida).

Family Tellinidae
Blainville, 1814

Scissula similis
(J. Sowerby, 1806)
Figs. 284–300

Synonymy/Chresonymy

Tellina similis J. Sowerby, 1806: 29, pl. 75 [Type locality: Brighton, England; in error].

Tellina (Scissula) similis – Boss, 1968: 328–331, pl. 160, figs. 1, 2; Abbott, 1974: 503, pl. 23, fig. 5696.

Scissula similis – Bieler & Mikkelsen, 2004: 522; Mikkelsen & Bieler, 2007: 322–323, 6 figs.; Sharma et al., 2012: table 1.

Description

Shell (Figs. 284–291): Relatively thin, weakly translucent; SL ≈ 13 mm in material examined, SH ≈ 63% SL (subelliptical), SW ≈ 25% SL (laterally compressed). Valves slightly asymmetrical, with RV slightly less convex (flatter) than LV; whitish to pale pink, with sparse, pink radial markings. Umbones bluntly pointed, low, approximately at mid-valve or somewhat posterior, protruding dorsally ca. 3% SH. Anterior margin amply rounded, continuous with anterior edge of umbo. Ventral margin weakly convex. Posterior margin similar, L ≈ 90% of anterior margin L, with gentle posteroventral slope (Figs. 284, 285). Transition between posterior and ventral margins marked by bluntly pointed margin, more weakly rounded than umbones. Sculpture uniformly commarginal, with low striae on posterior slope (Fig. 290), with 6 or 7 striae per mm. Very delicate oblique striae (scissulations) covering anterior and midregions, at ca. 45° in relation to longitudinal axis, abruptly ceasing on posterior slope (Fig. 290); scissulations subequally spaced, more uniform than commarginal undulations; furrows between scissulations = 20% of scissulation W. Inner surface (Figs. 286, 287) whitish, glossy. Cardinal teeth restricted infraumbonally (Figs. 288, 289, 291), consisting of 2 divergent teeth per valve. Anterior lateral teeth in LV; posterior lateral tooth only in RV (Fig. 286), anteroposteriorly elongated, in L ≈ 9% SL, with increasing platform covering adjacent hinge plate of LV; posterior, wider region L ≈ 30% L, running parallel and close to dorsal shell margin. Ligament extending from umbones posteriorly along 15% SL. Muscle scars shallow (Figs. 286, 287). Scar of anterior adductor muscle (*am*) elliptical, dorsoventrally elongated, with pointed dorsal end, in A ≈ 5% of inner VA, close to anterodorsal margin. Scar of posterior adductor muscle (*pm*) in L ≈ 80% of *am* scar L, at same horizontal level, between middle and posterior thirds of distance between umbones and posterior margin. Pallial sinus (Figs. 286, 287) deep, forming arch in A ≈ 60% VA, running close to, but at some distance from, *am* scar. Double scars of cruciform muscle (Fig. 287) ventral to pallial line, parallel to mantle edge, directly below of anterior edge of *pm*.

Main muscle system (Figs. 292, 295, 299): *Am* elliptical in cross section, dorsoventrally elongated (L ≈ 1.5 W), oblique, in size and position as described for scars above. *Pm* barely oval in cross section, in size and position as described for scars above. Paired pedal protractor muscles (Fig. 299: *rr*) anteroposterior; origins dividing *am* transversely, with *am* almost at center (weakly displaced dorsally in relation to midlevel of *am*; Fig. 292), cuneiform, in A ≈ 10% of *am* A, running horizontally and posteriorly, splaying

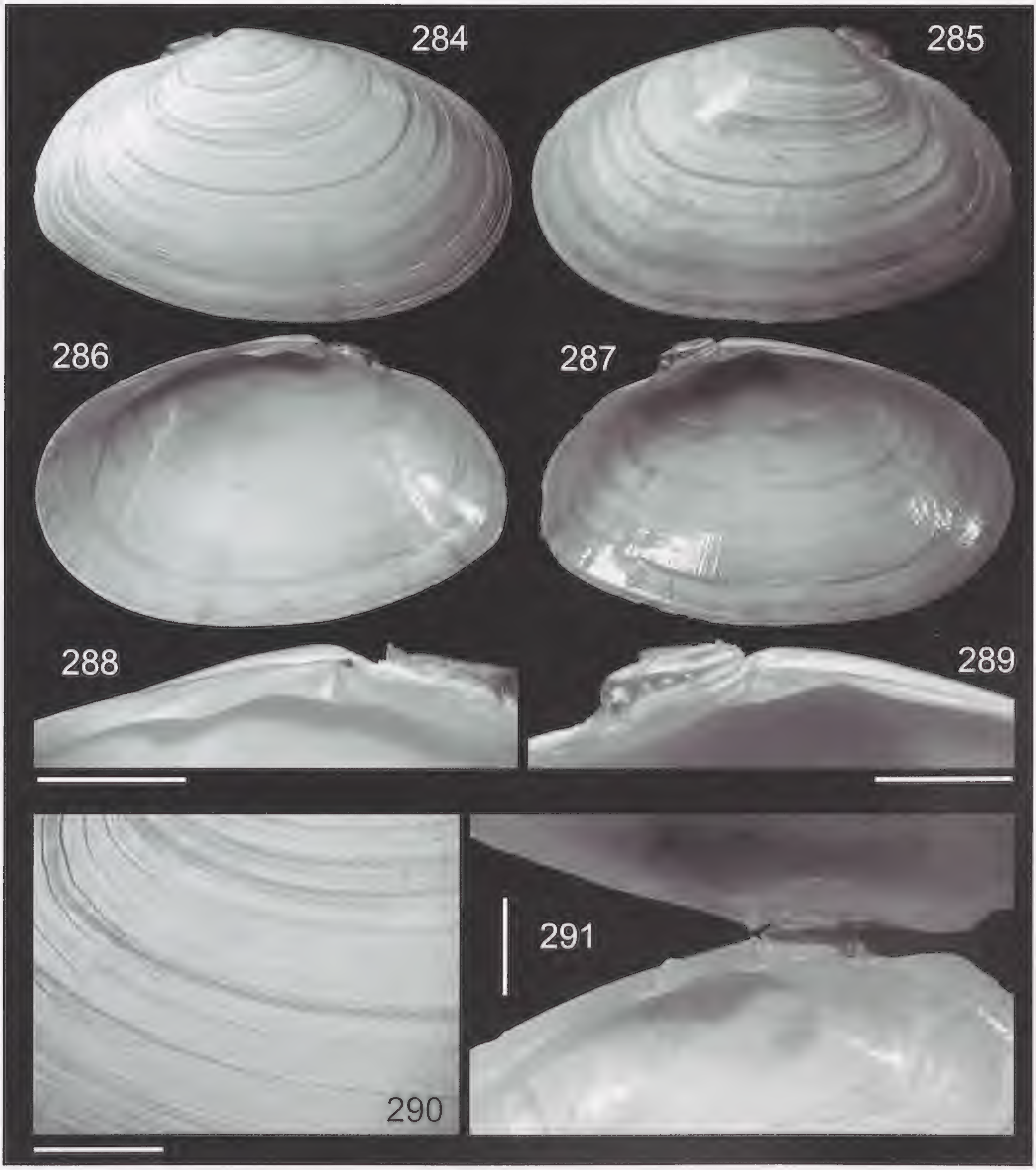

FIGS. 284–291. *Scissula similis*, shell morphology, FMNH 295740, 13.2 mm L. FIG. 284: RV, outer view; FIG. 285: LV, outer view; FIG. 286: RV, Interior view; FIG. 287: LV, interior view; FIG. 288: RV, detail of hinge; FIG. 289: LV, same; FIG. 290: RV, detail of sculpture in posteroventral quadrant; FIG. 291: Detail of hinge with valves still attached, ventral view, valves somewhat deflected. Scale bars = 2 mm.

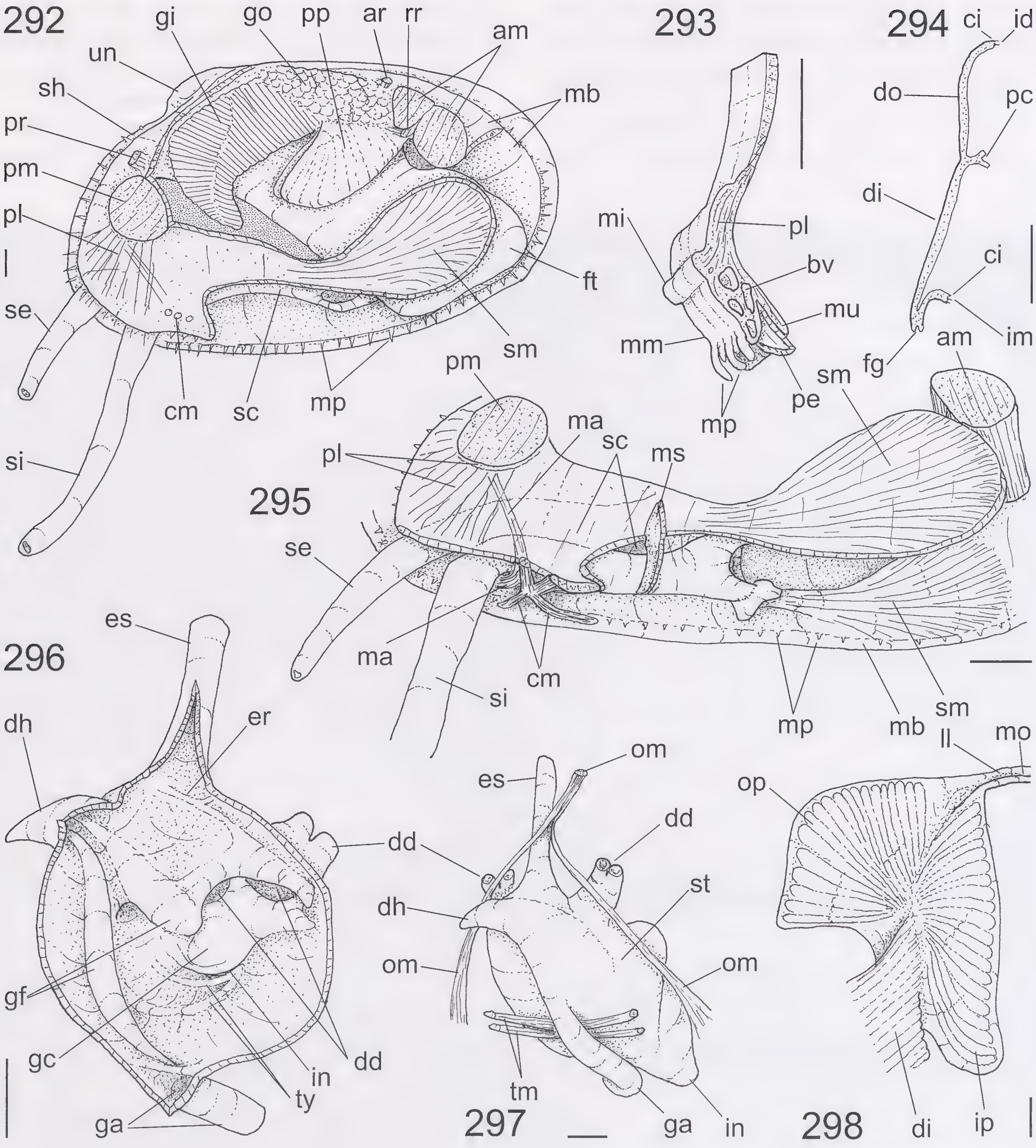

FIGS. 292–298. *Scissula similis*, anatomy. FIG. 292: Intact right view, RV and part of right mantle lobe removed, siphonal retractor muscles *in situ*; FIG. 293: Mantle border, cross section at midregion; FIG. 294: Gill, cross section at midregion; FIG. 295: Posteroventral region of pallial cavity, ventral and right view, showing siphonal musculature and some adjacent structures; FIG. 296: Stomach, dorsal view, opened longitudinally to show inner surface; FIG. 297: Stomach, dorsal view, some adjacent visceral muscles also shown; FIG. 298: Right labial palp, ventral view, outer hemipalp deflected, adjacent portion of gill also shown. Scale bars = 0.5 mm. Abbreviations: am, anterior adductor muscle; ar, anterior pedal retractor muscle; bv, "blood" vessel; ci, ciliary connection of gill; cm, cruciform muscle; dd, ducts to digestive diverticula; dh, dorsal hood; di, inner demibranch; do, outer demibranch; er, esophageal rim; es, esophagus; fg, food groove; ft, foot; ga, gastric dorsal appendix; gc, gastric central pad; gf, gastric fold; gi, gill; go, gonad; id, insertion of outer demibranch in mantle; im, insertion of inner demibranch in visceral mass; in, intestine; ip, inner hemipalp; ll, labial lips preceding mouth; ma, auxiliary pallial muscle; mb, mantle border; mi, mantle border inner fold; mm, mantle border middle fold; mo, mouth; mp, mantle papillae; ms, siphonal chamber membrane; mu, mantle border outer fold; om, oblique visceral muscle; op, outer hemipalp; pc, pericardium; pe, periostracum; pl, pallial muscles; pm, posterior adductor muscle; pp, labial palp; pr, posterior pedal retractor muscle; rr, pedal protractor muscle; sc, siphonal chamber; se, excurrent siphon; sh, shell; si, incurrent siphon; sm, siphonal retractor muscle; st, stomach; tm, transverse muscles into visceral cavity; ty, typhlosole; un, umbo.

across middle and ventral lateral walls of visceral mass, with some fibers also inserting along intersection of hemipalps. Paired anterior pedal retractor muscles (Fig. 299: *ar*) dorsoventral, slightly posterior, much thicker than *rr*, originating just dorsal and slightly posterior to *am*, in A = 6% of *am* A, running ventrally along ca. 33% SH, splaying across anterior surface of visceral mass and foot base, becoming thicker, bulging inside visceral cavity. Paired posterior pedal retractor muscles (Fig. 299: *pr*) in W ≈ 1.5 *ar* W, originating just dorsal and anterior to *pm*, in A = 12% of *pm* A, running anteroventrally, initially at some distance, gradually becoming closer and running attached into integument along ca. 50% SL, splaying across posteroventral foot base, weakly bulging inside visceral cavity. Paired siphonal retractor muscles (Figs. 292, 295: *sm*) originating in pallial sinus, with fibers directed commarginally toward lateral intersection of incurrent and excurrent siphons (*si, se*), then running along siphons, splaying across their walls in thin longitudinal layer. Cruciform muscle (Fig. 295: *cm*) L slightly shorter than *pm* L, close to ventral shell margin slightly anterior to level of *pm*; anterior branches more oblique, in L ≈ 2 posterior branch L; posterior branches each with conspicuous basal transverse furrow on dorsal surface. Several well-developed radial pallial muscles (Figs. 292, 295: *pl*) in lateral walls of siphonal chamber, slightly thicker and shorter dorsally, originating in narrow space surrounding ventral edge of *pm* (Fig. 295). Differentiated pallial muscle (Fig. 295: *ma*) running obliquely and more internally from radial *pl*, originating on each side of posteroventral edge of *pm*, running anteroventrally, surrounding base of *si* slightly dorsal to *cm*.

Foot (Figs. 292, 299): Flat; retracted V ≈ 33% SV; tip bluntly pointed. Byssal groove and byssus absent.

Mantle (Figs. 292, 293, 295): Mantle edges unpigmented, with 3 folds (Fig. 293). Outer fold flat, in T ≈ 50% ST; periostracum attaching to inner surface of outer fold; middle fold H = outer fold H, T ≈ 2 outer fold T; inner fold W ≈ middle fold W, H ≈ 50% of middle fold H, displaced internally at distance ≈ 2 outer fold H. Distal half of mantle edge relatively thick due to 3 or 4 blood vessels (Fig. 293: *bv*). Mantle edges mostly free, except close to siphonal chamber (Fig. 295). Middle fold with small, uniformly distributed papillae (Fig. 293), alternating longer and shorter; longer papilla L ≈ middle fold H = 3 W; shorter papilla L ≈ 50% of longer papilla H. Incurrent and excurrent siphons (Figs. 292, 295: *se, si*) totally separate, except at base; *si* somewhat longer than *se*. Inner surfaces of siphons simple, smooth. Siphonal tips simple, lacking papillae. Siphonal chamber (Fig. 295: *ms*) composed of inner mantle fold, thin, translucent, in V ≈ 25% SV; each siphon totally retractable inside chamber in 2 or 3 successive bends. Two posterior apertures: posterior siphonal aperture and posterodorsal branchial aperture (covered by gill; gill connecting to membrane by cilia). Pallial and *cm* muscles as described above. Mantle inner folds fusing septum-like along posterior surface of anterior branches of *cm* (Fig. 295).

Pallial cavity (Figs. 292, 294, 298): In A = 80% VA, excluding both adductor muscles and narrow portion of visceral mass extending from *am* to umbonal region. Labial palps (Fig. 292: *pp*) relatively large, subtriangular; hemipalp A ≈ 12% VA; inner hemipalp somewhat larger than outer. Intersection of hemipalps attached to visceral mass at anterodorsal edge, at distance from anterior valve margin = 33% SH. Outer surface of *pp* slightly folded; inner surface (Fig. 298) with ca. 15 transverse folds, ending at some distance from border producing smooth edge; with small, smooth area in A = 10% of *pp* A, in posterodorsal quadrant; another smooth area, of similar size, preceding lips. Each *pp* fold with rounded ventral end, gradually diminishing close to intersection of hemipalps; posterior folds slightly wider than anterior folds. *Pp* with rounded distal ends, in L ≈ 1.5 H, narrowing anteriorly. Gill in A ≈ 120% *pp* A, L ≈ 50% SL, H ≈ 20% SH in anterior region, gradually narrowing posteriorly, curving ventrally. Outer demibranch (Fig. 294: *do*) upturned, dorsal to inner demibranch (*di*); anterior end sharply pointed; *do* L ≈ 75% of *di* L; middle portion W ≈ 50% of gill W, gradually decreasing posteriorly and abruptly decreasing anteriorly; with single lamella covering adjacent region of visceral mass and pericardium, with dorsal edge connecting by row of cilia surrounding dorsal edge of pallial cavity (Fig. 294: *ci*); ventral edge connecting to *di*, ctenidial vein, and auricle; posterior third connecting laterally to anterodorsal wall of siphonal chamber aperture. *Di* (Fig. 294) ventral to *do*, comprising entire gill in anterior third, with descending and ascending lamellae covering visceral mass; descending lamella A ≈ 12%

of ascending lamella A; outer tissue connection with *do* and pericardial structures; inner cilial connection with visceral mass, running ventral to and near outer connection; food groove at ventral edge of *di*; posterior half of each *di* connecting medially by tissue with counterpart.

Visceral mass (Figs. 292, 297, 299): Laterally compressed, longer dorsoventrally, subtriangular; V ≈ 66% of total visceral-foot mass V. Anterior and posterior walls relatively compressed by *ar* and *pr*. Anterodorsal third filled by greenish-brown digestive diverticula, in V ≈ 25% of visceral mass V; remaining filled by pale cream-colored gonad. Stomach-style sac disposed vertically along midportion of visceral mass; V ≈ 33% of visceral mass V. Paired longitudinal visceral muscles (Fig. 297: *om*) running along anterodorsal surface of stomach, originating in anterior hinge plate just posterior to *am*, running posteriorly, initially adjacent, gradually separating and surrounding gastric main chamber, through gonad and digestive diverticula, finally splaying across posterolateral integument.

Circulatory and excretory systems (Fig. 299): Pericardium near dorsal visceral mass, extending from umbonal cavity to posterodorsal surface of *pm*; L = 2 H, V ≈ 20% of visceral mass V. Paired auricles (*au*) connecting to middle third of gill; walls thin, translucent. Ventricle (*ve*) surrounding ca. 80% of intestine traversing pericardium, with midlateral connection to *au*. Kidneys (*ki*) pale beige, solid, elongated, in posteroventral quarter of pericardium, externally surrounding both *pr* to posterior surface of *pm*. Nephropores (*ne*) at anterior ends of *ki*.

Digestive system (Figs. 296–299): *Pp* as described above. Mouth with relatively thin lips (Fig. 298); internally smooth, lacking folds. Esophagus (*es*) long, narrow (W ≈ 20% of *am* W), with anterior end contacting posterior end of *am*, running broadly curving posterodorsally at distance = 20% SL, immersed in digestive diverticula; inner surface smooth. Stomach (*st*) main chamber oval, anteroposteriorly elongated, ventral to umbones, in L ≈ 50% of visceral mass L = 25% of visceral mass H; paired ducts to digestive diverticula anteroventral, on each side of *es* opening; both ducts directed anteriorly. Glandular appendix (Figs. 296, 297, 299: *ga*) originating in right-posterior quadrant of gastric dorsal surface, relatively narrow, long, in W ≈ 12% of main gastric chamber W, L ≈ 10 W, with distal end tightly curving to left; paired transverse visceral muscles (Fig. 297: *tm*) crossing between *ga* base and adjacent main gastric chamber. Dorsal hood (Figs. 296, 297: *dh*) protruding to left on anterodorsal gastric surface; V ≈ 12% of main gastric chamber V. Gastric inner surface (Fig. 296) mostly smooth, with no obvious sorting area. Gastric shield (*gs*) thin, translucent, covering left-dorsal side, with anterior expansions to *dh* and to left duct to digestive diverticula; A ≈ 25% of inner gastric surface A. Central pad (Fig. 296: *gc*) in midventral gastric region, in A ≈ 20% of gastric A, with 3 anterior folds surrounding relatively wide chambers originating ducts to digestive diverticula (Fig. 296: *dd*); pair of dorsal, longitudinal, wide folds (Fig. 296: *gf*) running posteriorly from left-ventral surface of *dh*; right fold increasing, bulging dorsally to central pad; left fold increasing slightly less than right fold, running over longer distance to *ga* opening; paired typhlosoles (Fig. 296: *ty*) small; ventral folds just posterior to central pad, running to conjoined style sac-intestinal opening. Style sac (*ss*) dorsoventral, fusing with intestine, narrowing gradually to ventral end of visceral mass. Intestine (*in*) narrow, becoming free from *ss* at distal end, then making several short loops, more concentrated at midlevel of *st* (Fig. 299); total *in* L ≈ SL. Anus (Fig. 299: *an*) simple, sessile, on ventral surface of *pm*.

Reproductive system (Fig. 299): Gonad as described above. Paired genital ducts receiving branches from several gonadal acini along L in posterior visceral mass, forming short, tubular genital chambers in region preceding pores. Genital pore (*gp*) simple, near and anterior to nephropore.

Nervous system (Figs. 299, 300): Paired cerebropleural ganglia (Fig. 299: *cg*) in A ≈ 50% of *es* D, each very lateral, between *rr* and posterodorsal end of *am*, protected by thin layer of pallial membrane; cerebral commissure long, almost as long as *am* W. Paired pedal ganglia (Fig. 299: *pg*) elliptical, in V ≈ 1.5 cg V, closely adjacent, approximately midway between *cg* and ventral end of visceral cavity. Cerebropedal connective (Fig. 299: *cn*) very narrow, running though *ar*. Paired visceral ganglia (Fig. 299: *vg*) adjacent at midregion of anterior surface of *pm* (Fig. 299), in V ≈ 2 single *cg* V, L ≈ 1.5 W, with 2 pairs of larger anterior nerves forming additional pair of posterolateral ganglia. Cerebrovisceral connective (Fig. 299: *cp*) long; T = 2 *cn* T.

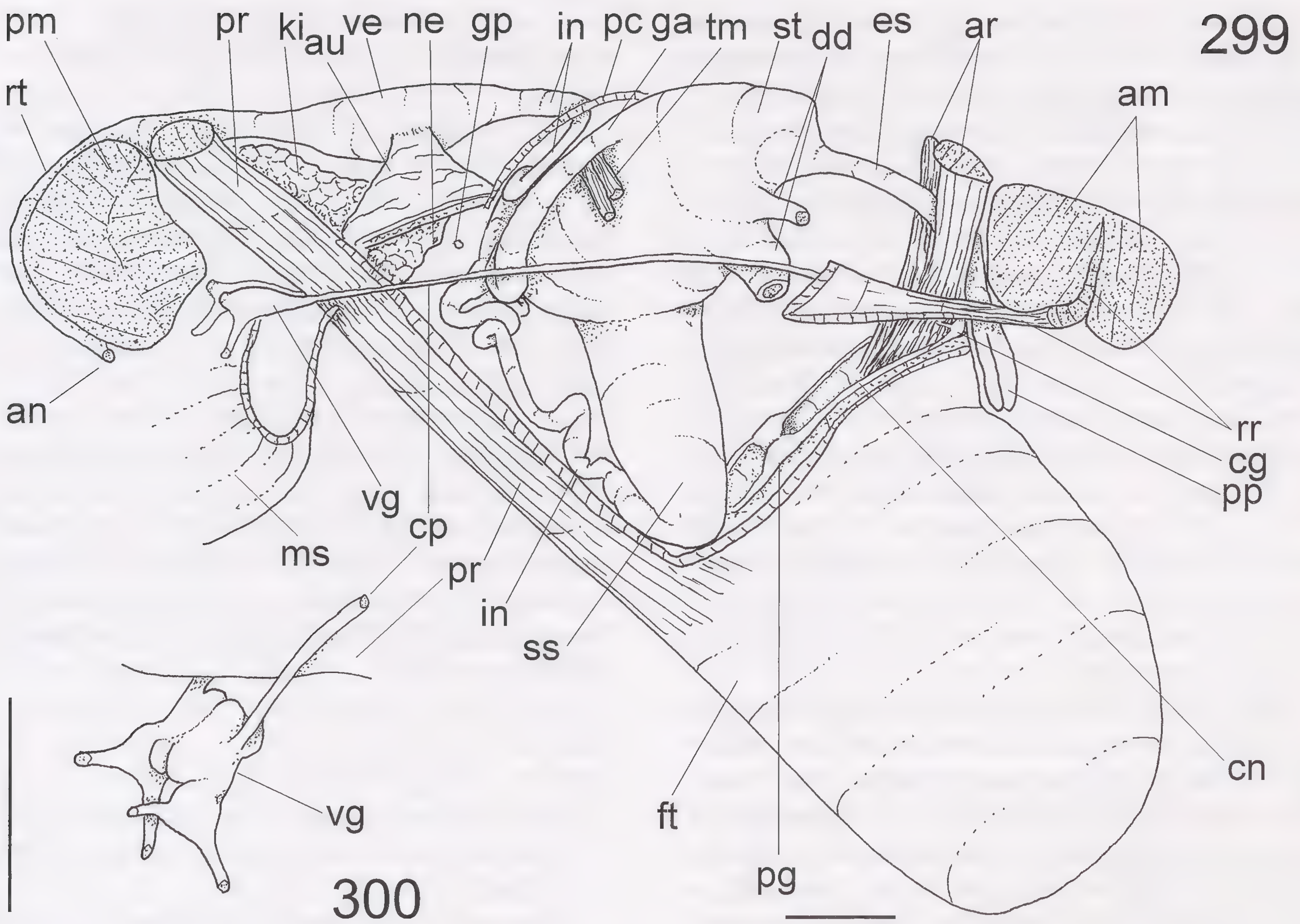

FIGS. 299, 300: *Scissula similis*, anatomy. FIG. 299: Digestive system, nervous system, and main musculature *in situ*, right view, topologies of other adjacent structures also shown; FIG. 300: Visceral ganglia, right and slightly dorsal view. Scale bars = 1 mm. Abbreviations: am, anterior adductor muscle; an, anus; ar, anterior pedal retractor muscle; au, auricle; ca, cardinal muscle; cn, cerebropedal connective; cp, cerebrovisceral connective; dd, ducts to digestive diverticula; es, esophagus; ft, foot; ga, gastric dorsal appendix; gp, genital pore; in, intestine; ki, kidney; ms, siphonal chamber membrane; ne, nephropore; pc, pericardium; pm, posterior adductor muscle; pp, labial palp; pr, posterior pedal retractor muscle; rr, pedal protractor muscle; rt, rectum; ss, style sac; st, stomach; tm, transverse muscles into visceral cavity; ve, ventricle; vg, visceral ganglia.

Material Examined

USA, Florida Keys, FMNH 295740, 1 specimen (sta. FK-235; dissected: 13.2 mm L, 8.2 mm H, 8.8 mm W); FMNH 295742, 2 specimens (sta. FK-226; 1 dissected: 13.0 mm L, 7.5 mm H, 3.3 mm W); FMNH 295739, 1 specimen (sta. FK-257); FMNH 295738, 1 specimen (sta. FK-128; dissected: 12.2 mm L, 7.6 mm H, 3.2 mm W).

Distribution

Stated by Turgeon et al. (2009) to range from east Florida to Quintana Roo (Mexico), Cuba, the West Indies to Brazil, and Bermuda. Brazil is here removed from its recognized range; no conspecific specimens have been located from that region.

Remarks

Boss (1968) summarized the conchological characters of *Scissula* (then a subgenus of *Tellina*) and *S. similis*. These descriptions agree with that presented here for the present species. For other details of the shell, see Mikkelsen & Bieler (2007: 322).

The soft anatomy of *Scissula similis* has not been previously studied; this study also represents the most thorough description of the anatomy of any species of *Scissula* to date, although that differs little from those of other genera of Tellinidae. Yonge (1949) described the functional anatomy of *Angulus tenuis* (Da Costa, 1778) from Great Britain in comparison with other tellinoideans. He described the tips of the incurrent and excurrent siphons each with "six blunt lobes" in lieu of tentacles; these were not noted here. The intestine of *A. tenuis* terminates in a freely hanging portion on the posteroventral surface of the posterior adductor muscle; that of *S. similis* is sessile. The sensory organs associated with the cruciform muscle, noted by Yonge as externally indicated by a slit at the base of each posterior branch, were here seen as a "conspicuous basal transverse furrow" on each, although they were not confirmed as sensory organs. Other than these few discrepancies, the anatomy of *S. similis* here compares favorably with Yonge's description of *A. tenuis.* Compared to *Phyllodina persica* (Dall & Simpson, 1901) from Brazil, *S. similis* differs in having a wider division of the anterior adductor muscle by the anterior foot retractors, less-developed transverse muscles in the visceral mass, a proportionally larger stomach, and more complex visceral ganglia (Marques & Simone, 2013).

Boss (1967) summarized tellinid anatomy based on the work of numerous earlier authors on a variety of species and genera. The characteristic siphonal organ and paired parasiphonal organs, mentioned by Boss as known in several species of *Tellina*, require microdissection or histology and were not seen during this study. Otherwise, this description agrees with that presented here for the present species.

Gilbert (1978) described the digestive morphologies and diets of *Acorylus gouldii* (Hanley, 1846), *Scissula candeana* (d'Orbigny, 1853), and *Angulus sybariticus* (Dall, 1881) from Bermuda. The major anatomical difference between these three species (then all in *Tellina*, now representing three genera) was in the morphology of the labial palps. Those of *S. candeana* were distinct in having posterior palp ridges with prominent adoral shelves and ciliated grooves; these details were not seen in this study, which was limited to gross dissection.

Barón & Ciocco (1997, 1998; also Ciocco & Barón, 1998) described the anatomy (gross and histological) in detail of *Tellina petitiana* d'Orbigny, 1846, from Argentina. These descriptions agree in all respects with the present species. The especially large visceral ganglia described here can be explained by Barón & Ciocco's (1998) interpretation of these as visceropallial ganglia (i.e., fused visceral and pallial ganglia), noting that in *Macoma* (studied by Lammens, 1969), the visceral ganglia are fused and the pallial ganglia are unfused; these authors called the "additional pair of posterolateral ganglia" seen here perivisceral ganglia.

Sharma et al. (2012) studied protein-coding genes from a Florida Keys population sampled at Crane Key Shoal, between Sawyer and West Content Keys.

CHARACTER ANALYSIS
CHARACTER DESCRIPTIONS

The following 80 characters encountered during the anatomical investigations presented here were coded to detect patterns of character evolution. These include 18 characters of the gills (nos. 37–54), 17 of the digestive system (nos. 58–74), 14 of the foot (including byssus) and main musculature (nos. 11–24), 12 of the mantle border (nos. 25–36), 10 of the shell (including hinge and ligament, nos. 1–10), and 3 characters each of the renopericardial (nos. 55–57), reproductive (nos. 75–77), and nervous systems (nos. 78–80). The data matrix is presented in Table 2. In the following section, consistency and retention indices resulting from the character analysis (below) are included for each character.

Shell

1. Shell cemented to hard substratum: 0 = not cemented; 1 = LV attached; 2 = RV attached. (CI = 50; RI = 0)
   The most basal form of bivalve is generally believed to be adapted for digging in an infaunal environment (Harper et al., 2000; Giribet & Wheeler, 2002). Modifications included in the taxa examined here include attachment to hard substrata by a noncalcified byssus (e.g., *Barbatia*) and cementation to hard substratum (e.g., *Hyotissa*). Details of the bivalve cementing process were discussed by Yonge (1979) and Harper (1992). *Anomia simplex* is cemented, but by a calcified byssus rather than by a shell valve, so it is coded here as n/a.
2. Periostracum: 0 = not hirsute; 1 = hirsute. (CI = 100; RI = 100)
   The periostracum is potentially informative for comparative analyses, however, its presence and extent varies among specimens for various reasons. The most interesting in the present assemblage are the hirsute periostraca present in *Arcopsis, Barbatia,* and *Limopsis*. Another modification is the extension of the periostracum beyond the calcified portion of the shell in *Solemya* (Figs. 2, 3; see also Beedham & Owen, 1965).
3. Two valves connected by hinge and adductor muscle(s): 0 = absent; 1 = present. (CI = 100; RI = 100)
   This character serves to differentiate the ingroup bivalves from the outgroup taxa.
4. Adult hinge teeth: 0 = absent; 1 = present. (CI = 25; RI = 57)

5. Adult hinge teeth: 0 = taxodont (many subequal teeth in tooth row); 1 = heterodont (umbonal cardinal teeth with or without lateral teeth. (CI = 100; RI = 100)
These hinge types are here coded for adult forms; other types of hinges are found in the respective larvae (see, e.g., Fuller et al., 1989, on *Anomia simplex*).
6. Ligament type: 0 = external; 1 = with internal component. (CI = 50; RI = 50)
The ligament is an exclusive feature of bivalves. Most are external, extending along part or all of the hinge plate, but in some taxa (e.g., *Spondylus*), are positioned both internally and externally. Comparative analysis of this structure, which connects the two shell valves and is formed by the hinge fold of the mantle (e.g., Fig. 35: *hf*), are found in the literature (Owen, 1959; Yonge, 1977; Yonge & Morton, 1980; Starobogatov, 1992; Thomas et al., 2000). Ligaments have also been categorized according to position relative to the umbones (i.e., amphidetic or opisthodetic; Yonge, 1978, 1982; Waller, 1990), and ligamental microstructure (i.e., simple, duplivincular, alivincular, transverse, or parivincular; Carter, 1990).
7. Pallial sinus: 0 = absent; 1 = present. (CI = 50; RI = 75)
8. Pallial sinus: 0 = shallow (< 50% SL); 1 = deep (50% or more of SL). (CI = 50; RI = 0)
The pallial sinus is a modification of the pallial line, created by the attachment of concentrated siphonal retractor muscles to the shell. Its depth is related to the length of the siphons; typically, a deeper pallial sinus is indicative of longer siphons. Here, depth of the pallial sinus is expressed relative to total shell length.
9. Nacre: 0 = present; 1 = absent. (CI = 20; RI = 33; for tree 2: CI = 17; RI = 17)
The presence of nacre in monoplacophorans (including *Neopilina*) has been widely debated (e.g., Checa et al., 2009). It is here coded as "?"
10. Separation of posterior pedal retractor muscle scar in relation to that of posterior adductor muscle: 0 = clearly separate; 1 = continuous. (CI = 100; RI = 100)

Foot and Main Musculature

11. Adductor muscles: 0 = isomyarian (anterior and posterior adductors subequal); 1 = heteromyarian (anterior and posterior adductors unequal); 2 = monomyarian (adult lacking anterior adductor). (CI = 33; RI = 60)
The paired adductor muscles have long been recognized as a synapomorphy of the Bivalvia; these muscles are primitively subequal. The presence and size of the adductor muscles have been used in other comparative studies (Yonge, 1953b; Gilmour, 1990; Giribet & Wheeler, 2002).
12. Anterior adductor muscle insertion: 0 = distant from shell margin (≈ 16% SL); 1 = close to shell margin (≈ 8% SL). (CI = 33; RI = 67)
13. Posterior adductor muscle location: 0 = close to posterior shell margin; 1 = central. (CI = 100; RI = 100)
14. Adductor muscle structure: 0 = simple; 1 = with visible quick and slow components. (CI = 100; RI = 100)
15. Adult foot: 0 = present; 1 = absent. (CI = 50; RI = 0)
16. Foot type: 0 = without umbrella-like extension at distal end; 1 = with umbrella-like extension at distal end. (CI = 100; RI = 100; for tree 2: CI = 50; RI = 0)
The foot is typically used for burrowing in bivalves, but is reduced in some sessile taxa. However, loss of the foot in sessile bivalves is not an absolute rule; *Spondylus americanus* and *Chama macerophylla* (Figs. 124 and 218, respectively), both cemented species, each have a distinguishable foot. A foot has been shown to be present in the larval stages of some sessile bivalves, notably the ostreoideans (Harry, 1985), which includes *Hyotissa*, and the pectinoidean *Plicatula,* both of which lack the foot entirely as adults. Species that are attached by a byssus as adults generally retain a small foot, presumably for the main purpose of producing the byssus. The typical digging foot of bivalves only appears in the autobranchs. The protobranchs (here represented by *Solemya occidentalis* and *Propeleda carpenteri*) have a distal region close to the tip of the foot (sometimes called an anterior enlargement) that looks like an umbrella and assists in anchoring the bivalve. Scaphopods also have such a structure, and it has been regarded as either homologous in the two classes (Steiner, 1992; Salvini-Plawén & Steiner, 1996; Giribet & Wheeler, 2002; Simone, 2009) or merely convergent (Waller, 1998).
17. Pedal retractor muscles: 0 = present; 1 = absent. (CI = 50; RI = 50)
18. Number of pedal retractor muscle pairs: 0 = > 2; 1 = 2. (CI = 100; RI = 100)
Pedal retractor muscles can be absent in some sessile, foot-reduced taxa (e.g., *Hyo-*

tissa, Spondylus). *Chama macerophylla* has inconspicuous pedal retractor muscles embedded in integument, and is coded here as "?"

19. Pedal protractor muscles: 0 = present; 1 = absent. (CI = 20; RI = 56)
20. Shape at shell insertion of pedal protractor muscles: 0 = rounded; 1 = appressed to ventral anterior adductor muscle. (CI = 100; RI = 100)
21. Cruciform muscle: 0 = absent; 1 = present. (CI = 100; RI = 100)
    The presence of a cruciform muscle is exclusive to the tellinoideans (e.g., *Scissula, Donax*). It is associated with the presence of two shell valves (Mikkelsen & Bieler, 2007), and is therefore coded as n/a for the outgroups.
22. Adult byssus: 0 = absent; 1 = present. (CI = 20; RI = 60)
    The byssus presumably developed as a larval feature and is lost during ontogenetic development in most bivalves; it is maintained in the adult form of several bivalve clades (Waller, 1998). Most of the species that possess an adult byssus live on hard substrata; *Pinna carnea*, examined here, attaches to solid particles buried in its soft-sediment habitat. Associated with the presence of a byssus is a noticeable byssal shell gape found in some pteriomorph and arcoid bivalves (Waller, 1998; Giribet & Wheeler, 2002).
23. Form of adult byssus: 0 = separated threads; 1 = solid bundle. (CI = 25; RI = 25)
24. Inner longitudinal fold along posterior region of byssal furrow: 0 = absent; 1 = present. (CI = 100; RI = 100)

Mantle Border

25. Mantle border folds: 0 = 2; 1 = 3. (CI = 50; RI = 50)
26. Papillae on middle fold: 0 = absent; 1 = present. (CI = 25; RI = 67)
27. Papillae on inner fold: 0 = absent; 1 = present. (CI = 20; RI = 33)
    Exposed to the environment, the mantle edges bear several kinds of receptors that transmit mechanical, photoreceptive, or chemical stimuli to the nervous system. The presence of papillae, or small tentacles, on the mantle border folds has been analyzed in several comparative studies (Waller, 1978, 1998; Gilmour, 1963, 1967; Giribet & Wheeler, 2002). Photoreceptors can be developed into eyes, as in *Spondylus americanus* (Figs. 127, 128; see also Dakin, 1928a, b).
28. Mantle fusion separating incurrent and excurrent water flow: 0 = absent; 1 = present. (CI = 50; RI = 90)
29. Ventral mantle fusion forming incurrent aperture: 0 = absent; 1 = present. (CI = 100; RI = 100)
30. Ventral mantle border fusion: 0 = absent; 1 = present. (CI = 20; RI = 20)
31. Anterior mantle fusion: 0 = absent; 1 = present. (CI = 100; RI = 100)
32. Dorsal mantle fusion forming excurrent aperture (and supra-anal chamber): 0 = absent; 1 = present. Outgroups are coded n/a due to differing dorsal-ventral orientation. (CI = 50; RI = 86)
    The degree of mantle fusion varies widely in bivalves. The most common type occurs in the region between the incurrent and excurrent apertures, which typically includes attachment to the posterior end of the gills. In such cases, water currents necessarily must pass through the gill, presumably increasing the efficiency of feeding. The mantle border can be further fused ventral to the incurrent aperture. A still greater degree of fusion along the ventral mantle border is present in *Solemya*, *Entodesma*, *Chama*, and *Lamychaena*; ventral mantle fusion is present in scaphopods according to Salvini-Plawen & Steiner (1996). The fusion extends anteriorly to the pedal gape in *Entodesma* and *Lamychaena*; the protobranch *Solemya* also has a broad fusion between the two mantle lobes, which appears to be convergent. This assumption can be corroborated through examination of the various muscles of the mantle border (Fig. 5: *pl*; see also Morse, 1913; Owen, 1961), compared to those of autobranchs with equal degrees of mantle fusion (e.g., Figs. 181, 237).
33. Siphons: 0 = absent; 1 = present. (CI = 25; RI = 50)
34. Siphons: 0 = short, extending little beyond mantle border; 1 = long, > 50% SL. (CI = 50; RI = 50)
35. Siphonal fusion: 0 = absent (siphons separate); 1 = siphons largely fused. (CI = 100; RI = 100)
    Another important feature of the mantle border is the differentiation of siphons. Short posterior tubes that extend only slightly beyond the mantle border, but that are not accompanied by concentrated

siphonal retractor muscles, are found in *Codakia*, *Chama,* and *Laevicardium*; these are coded here as "siphons absent." True siphons (accompanied by siphonal retractor muscles that impress a pallial sinus onto the shell's interior) are short in *Polymesoda*, or long in *Entodesma*, *Lamychaena*, *Donax*, and *Scissula*, permitting the animal to bury deeply in the sediment. The incurrent siphon can be either separate from the excurrent siphon (*Polymesoda*, *Donax*, and *Scissula*), or the two can be fused (*Entodesma* and *Lamychaena*; see Remarks under *E. beana* for a discussion of varying interpretations). Fused siphons are constituted mainly by the outer fold of mantle edge; periostracum typically surrounds the outer surface of this type of siphon when protruded. Unfused siphons are constituted mainly by the inner folds of mantle border; in such cases, the outer and middle folds of mantle border are maintained surrounding the posterior region of the shell, forming a siphonal chamber (e.g., Fig. 295). A posterior, siphon-like projection is found in the protobranch *Propeleda* (Figs. 21, 23: *as*); this structure (here coded as a true siphon) could be an autapomorphic adaptation for exteriorizing fecal matter from the more medially placed anus. The homologies of siphons and other posterior tube-like structures across the Bivalvia are in need of further investigation.

36. Incurrent water flow anterior: 0 = present; 1 = absent. (CI = 50; RI = 50)
Anterior incurrent flow has been previously considered as primitive (Yonge, 1939, 1957; Saleuddin, 1965; Giribet & Wheeler, 2002), with several exceptions, e.g., lucinids (Allen, 1958) and galeommatoideans (Popham, 1940; Yonge, 1952b).

Gills

37. Gill size: 0 = < 33% of visceral area; 1 = > 66% of visceral area. (CI = 100; RI = 100)
The typical protobranch gill occupies less than one-third of the valve area, whereas those of autobranchs occupy more than two-thirds. An exception is *Solemya*, which has relatively large gills supporting symbiotic bacteria (Gustafson & Reid, 1986; Reid & Brand, 1987). Additional discussion of protobranch gills is found in the literature (e.g., Yonge, 1939; Allen & Sanders, 1973; Waller, 1998; Simone, 2009).
38. Connections between gill filaments: 0 = ciliary; 1 = tissue bridges. (CI = 50; RI = 89)
39. Tissue connections between gill filaments: 0 = narrow, forming a reticulate structure; 1 = broad. (CI = 50; RI = 67)
Another potentially informative gill character is the presence of connections between filaments, i.e., interfilamental junctions. In basal taxa, as well as in other molluscan classes, interfilamental junctions are purely ciliary. However, in some bivalve taxa, they are formed of narrow tissue bridges, forming a reticulate structure (e.g., in *Hyotissa, Lamychaena*), or by broad bridges (e.g., in *Codakia*, *Scissula*).
40. Gills comprised of demibranchs: 0 = absent; 1 = present. (CI = 100; RI = 100)
One pair of demibranchs (ciliated gills composed of two flattened lamellae) per side is characteristic of autobranchs (Atkins, 1937). Demibranchs are absent in the outgroups (*Paradentalium* coded n/a due to the absence of gills) and the protobranchs *Propeleda* and *Solemya*.
41. Transverse septa: 0 = in entire filament; 1= only in filament base. (CI = 50; RI = 0)
Besides interfilamental junctions, each of the two demibranchs (outer and inner) can possess transverse septa, also known as interlamellar junctions. These septa can occur all along the filaments (e.g., in *Hyotissa*, *Chama*) or only at the bases of the filaments (e.g., in *Isognomon*, *Pinna*).
42. Demibranch size: 0 = subequal; 1= outer demibranch shorter than inner demibranch. (CI = 50; RI = 75)
Typically, the two demibranchs of autobranchs are subequal (e.g., Fig. 91), but in some cases, the outer demibranch is smaller and more dorsal (e.g., Fig. 294). *Codakia* is here coded "?" because only a single demibranch is present (Fig. 208) and hosts symbiotic bacteria (Glover & Taylor, 2001).
43. Main point of attachment of gill suspensory stalk: 0 = visceral mass; 1 = posterior adductor muscle. (CI = 100; RI = 100)
44. Structure of gill suspensory stalk: 0 = membranous; 1 = muscular. (CI = 33; RI = 78)
The posterior region of the gill, extending beyond the visceral mass, is supported by a suspensory stalk or membrane. This structure is more highly developed in those taxa that have free gills, in which the gills are weakly attached to neighboring structures (e.g., in *Isognomon*, *Pinna*). These gills

are more mobile, and can be retracted into more internal regions of the pallial cavity. In such cases, the suspensory stalks are strong and muscular (e.g., Figs. 36, 77: *gt*). On the other hand, in taxa that possess gills more strongly attached to neighboring structures, i.e., to mantle lobes laterally and to the visceral mass and their counterparts medially (e.g., in *Chama*, *Scissula*), the suspensory stalks are thinner and less muscular (e.g., Figs. 157, 254: *gt*); these gills do not have the same capacity for retraction.

45. Bases of demibranchs: 0 = at approximately the same level; 1 = outer demibranch originating in dorsal region. (CI = 50; RI = 80)
46. Gill connection to anterior edge of pallial cavity: 0 = ciliary; 1 = tissue. (CI = 50; RI = 89)
47. Afferent gill vessel: 0 = distinct, paralleling efferent gill vessel; 1 = inconspicuous. (CI = 100; RI = 100)
48. Inner demibranch connection to visceral sac: 0 = ciliary; 1 = tissue. (CI = 25; RI = 50)
49. Outer demibranch connection to mantle: 0 = ciliary; 1 = tissue. (CI = 33; RI = 0)
50. Inner demibranch connection to its counterpart in region posterior to visceral sac: 0 = ciliary; 1 = tissue. (CI = 20; RI = 20)
51. Food groove on ventral edge of inner demibranch: 0 = absent; 1 = present. (CI = 20; RI = 50)
52. Food groove on ventral edge of outer demibranch: 0 = absent; 1 = present. (CI = 33; RI = 50)

Food grooves are modifications of the demibranchs' ventral edges for carrying filtered food particles to the palps via ciliary currents. In some cases, there are food grooves in other locations on the gills, for example, in the dorsal region between the outer and inner demibranchs or between the demibranchs and neighboring structures (i.e., mantle); these cases cannot always be detected anatomically and are best confirmed via live examination (Yonge, 1969). The same approach is necessary to investigate the variety and activity of branchial cilia; these potential characters have been applied in several comparative analyses in Bivalvia (Owen, 1966, 1978; Atkins, 1938; Giribet & Wheeler, 2002).

53. Branchial/siphonal septum: 0 = absent; 1 = present. (CI = 100; RI = 100)
54. Promyal passage in anterior region of posterior adductor muscle: 0 = absent; 1 = present. (CI = 50; RI = 0)

The promyal passage is an anatomical "shortcut" for the water current from the midregion of the gills to the dorsal region of animal's body (Figs. 88, 101, 157: *po*). It lies anterior to the posterior adductor muscle, and is only present in the right side of the visceral mass in *Hyotissa mcgintyi* and, here reported for the first time, on the left side in *Anomia simplex* (Figs. 88, 101, 157: *po*). The presence of a narrower left promyal passage, in addition to a wider one on the right, was here confirmed for *H. hyotis*. A corresponding set of promyal passages (smaller left, larger right) were reported in the ostreid genus *Crassostrea* Sacco, 1897 by Galtsoff (1964: 71), but not confimed by Harry (1985: 125), who found this channel present only on the right side in Crassostreinae. The homologies and comparative functional anatomy of these passages has not yet been investigated.

Renopericardial System

55. Auricles: 0 = simple; 1 = lobed. (CI = 25; RI = 25)

A multilobed auricle (e.g., Fig. 99) is found in some species (e.g., *Hyotissa*, *Entodesma*), and could be an adaptation for increasing the contact of the auricular wall with the hemolymph inside the pericardium. The glandular inner surface possibly assists in the metabolism of the hemolymph, mainly passing through the auricular wall to the pericardial cavity.

56. Lateral expansions of ventricle as accessory auricles: 0 = absent; 1 = present. (CI = 100; RI = 100)
57. Auricle connection to ctenidial vein: 0 = wide; 1 = via narrow vessel. (CI = 33; RI = 60)

In several bivalves, a wide connection of the auricles with the ctenidial veins, which lie between the demibranchs of each gill, is present (e.g., Fig. 299). In bivalves that possess a pericardium far removed from the gill, a long, narrow portion of each auricle is detectable on each side of the visceral mass, typically just anterior to the posterior adductor muscle, in the form of a vessel (e.g., Fig. 113). This condition was found here in *Brachidontes, Chama, Hyotissa, Isognomon, Lithophaga*, and *Pinna*. The condition of the heart in *Anomia simplex* (Fig. 157: pc) and in all other anomiids (Yonge, 1977) is controversial (see Remarks under *A. simplex*) and requires further comparative study.

Digestive System

58. Paired labial palps: 0 = absent; 1 = present. (CI = 100; RI = 100)
    In most groups of protobranchs (see, e.g., *Propeleda*), the labial palps are proportionally larger and more lateral than in the autobranchs, and possess palp proboscides, which have been regarded as plesiomorphic within Bivalvia (Waller, 1998). In protobranchs except members of Solemyoidea (most of which possess minute labial palps and palp proboscides; Yonge, 1939; but see also Morse, 1913), the palp probocides are used to collect particles directly from the surrounding sediment for transport to the labial palps. In the autobranchs, palp proboscides are absent and the much smaller, more anterior labial palps provide a sorting function for food particles.
59. Palp dendritic projections (arborescent lips): 0 = absent; 1 = present. (CI = 100; RI = 100)
60. Hemipalp symmetry: 0 = flattened and symmetrical; 1 = asymmetrical, forming an anterior cover to gill. (CI = 100; RI = 100)
    The labial palps typically consist of an outer and inner flattened, symmetrical hemipalp on each side. Asymmetrical hemipalps, covering the anterior end of the gill, are found in some taxa (e.g., *Isognomon*, *Pinna*). In most bivalves, the labial palps are situated on the ventrolateral region of the visceral mass. Other taxa (e.g., *Arcopsis*, *Spondylus*) possess elongated labial palps running along the anterior edge of the pallial cavity. Dendritic palp projections are found in some pectinoideans (e.g., *Spondylus*, *Plicatula*).
61. Odontophore and radular apparatus: 0 = present; 1 = absent. (CI = 100; RI = 100)
    This character serves to differentiate the ingroup bivalves from the outgroup taxa.
62. Mouth distance from anterior adductor muscle: 0 = distant; 1 = in close proximity. (CI = 25; RI = 50)
63. Stomach shape: 0 = subspherical; 1 = anteroposteriorly elongate, compressed dorsally. (CI = 50; RI = 50)
    The typical form of the main chamber of the bivalve stomach, located in the central region of the visceral mass, is subspherical. In *Brachidontes*, *Lithophaga*, and *Pinna*, however, it is anteroposteriorly elongated and laterally compressed in the dorsal region of the smaller visceral mass (Figs. 61, 112).
64. Gastric left expansion: 0 = absent; 1 = present. (CI = 50; RI = 0)
65. Complex sorting areas and folds in stomach: 0 = absent; 1 = present. (CI = 50; RI = 50)
    In the absence of the radular apparatus, bivalve stomachs are typically complex, functioning to sort food particles already presorted by the gills and palps, and to grind and begin digestive action with the crystalline style; the stomachs of anomalodesmatans (e.g., *Entodesma*) are considered secondarily simplified. Comparative studies of the features of bivalve stomachs were the main work of Purchon (e.g., 1956, 1987), and are widely used. Most of the gastric characters here discussed are in accordance with these studies, however, the categories of stomach types I through V (Purchon 1956, 1957, 1958, 1960, 1987; Reid, 1965; Dinamani, 1967) are not employed here. Gastric complexity is most evident on the inner surface, typically including sorting areas and various folds. These are notably absent in *Solemya*; reduction of digestive system complexity has been regarded as apomorphic for the Solenomyoidea by some authors (e.g., Waller, 1998).
66. Gastric central pad: 0 = absent; 1 = present. (CI = 100; RI = 100)
67. Paired typhlosoles running from stomach ventral surface to intestine/style sac: 0 = absent; 1 = present. (CI = 100; RI = 100)
68. Esophageal rim: 0 = absent; 1 = present. (CI = 25; RI = 50)
69. Dorsal hood: 0 = absent; 1 = present. (CI = 14; RI = 33).
70. Dorsal hood length: 0 = short; 1 = long (≈ gastric main chamber length). (CI = 50; RI = 67).
71. Style sac fusion with intestine: 0 = totally fused; 1 = with a short portion free from intestine; 2 = totally free. (CI = 50; RI = 0)
    The style sac, which builds and rotates the enzyme-laden crystalline style, is a remarkable character of most bivalves and some gastropods; it is absent here only in *Solemya occidentalis*. In this analysis, the style sac is completely separate from the intestine in *Anomia simplex* (Fig. 162) and *Donax variabilis*, is partially separated, i.e., has a short portion free from the intestine in *Laevicardium serratum* (Fig. 277; also in the outgroup *Neopilina*), or is totally conjoined with the intestine (in all other species examined here; e.g., Fig. 146). No

detailed study of these various states has so far been produced.

72. Gastric posterodorsal glandular diverticulum (AKA caecum or appendix): 0 = absent; 1 = present. (CI = 100; RI = 100)
73. Intestinal loops: 0 = 3–4; 1 = 1–2. (CI = 50; RI = 80).
74. Rectal attachment: 0 = directly attached to adjacent area (sessile); 1 = with a stalk (siphoned). (CI = 25; RI = 50)

Reproductive System

75. Gonad: 0 = restricted to visceral mass; 1 = extending into mantle. (CI = 50; RI = 50)
76. Genital and renal apertures: 0 = combined; 1 = separate. (CI = 100; RI = 100)
    The genital aperture is typically inside the renal sac, with gametes being released via the nephropore. The genital aperture is separate from the nephrophore in heterodonts (i.e., *Carditamera*, *Codakia*).
77. Tubular genital chamber preceding each genital pore: 0 = absent; 1 = present. (CI = 50; RI = 83)
    This character is present in *Donax variabilis*, although it was not so noted by Simone & Dougherty (2004).

Nervous System

78. Pedal ganglia position relative to cerebral ganglia: 0 = close; 1 = displaced ventrally. (CI = 100; RI = 100)
79. Circumesophageal nerve loop: 0 = present; 1 = absent. (CI = 100; RI = 100)
80. Visceral ganglia position relative to posterior adductor muscle: 0 = anterior; 1 = ventral (CI = 100; RI = 100)
    The nervous system is circumesophageal, as in gastropods, in the protobranchs *Solemya* and *Propeleda* (Figs. 11 and 25, respectively). In the remaining bivalves examined here, it is less concentrated, with cerebropleural ganglia close to the anterior adductor muscle, pedal ganglia displaced ventrally, and visceral ganglia displaced posteriorly to lie near the posterior adductor muscle. Possibly because of the functional importance of the posterior area of bivalves – the region at which greatest interaction with the environment occurs – the visceral ganglia are typically the largest pair. Pedal ganglia were not observed in *Plicatula* and *Hyotissa*; the foot is absent in both of these taxa.

ANALYSIS AND DISCUSSION

Analysis of the data matrix in Table 2 resulted in two equally parsimonious trees, both of which are shown in Fig. 301. The trees are generally well resolved. The topologies are discussed here for purposes of character analysis alone; it would be inappropriate as a class-wide phylogenetic analysis based on the present taxon sampling, which was not designed for that purpose. The results reveal character states that are informative at various levels.

Of the 80 characters analyzed, ten are from the shell and the remaining 70 are from soft anatomy. Gills provided the greatest number of codable characters, followed by the digestive system, foot and muscles, and mantle. Other systems (renopericardial, reproductive, and nervous) supplied small numbers of characters. Thirty-one characters (38.7% of the total) were nonhomoplastic, yielding consistency and retention indices of 100%. These characters are spread across the coded morphological systems – shell (4), muscles (6), foot (1), mantle (3), gills (5), renopericardial system (1), digestive system (7), reproductive system (1), and nervous system (3) – indicating that all organ systems have potential utility in supporting tree structure. The digestive system, particularly labial palps and the stomach, yielded the greatest number of nonhomoplastic characters in this particular study.

The topology of the two equally parsimonious trees (Fig. 301) differ only in the relative positions of the two protobranch taxa, *Propeleda* and *Solemya*. Optimizing the foot type (char. 16) as a synapomorphy of the protobranchs supports monophyly for this group (Fig. 301, "Tree 1"), whereas char. 36 (water flow direction) and char. 65 (complexity of stomach) unite *Propeleda* with the Autobranchia (indicated by "A"; Fig. 301, inset "Tree 2").

Three nonhomoplastic characters are informative only at the level of Bivalvia (i.e., separating bivalves from the outgroups [two valves connected by a hinge and adductor muscles present (char. 3); paired labial palps present (char. 58); and odontophore/radula absent (char. 61)]. These characters were intentionally included in the analysis to support this separation.

Ten of the remaining nonhomoplastic characters separate the protobranchs from rest of bivalves at node A in Tree 1: pedal retractor muscles numbering two (char. 18); gill size comprising > 66% of visceral area (char. 37); gills comprised of demibranchs (char. 40);

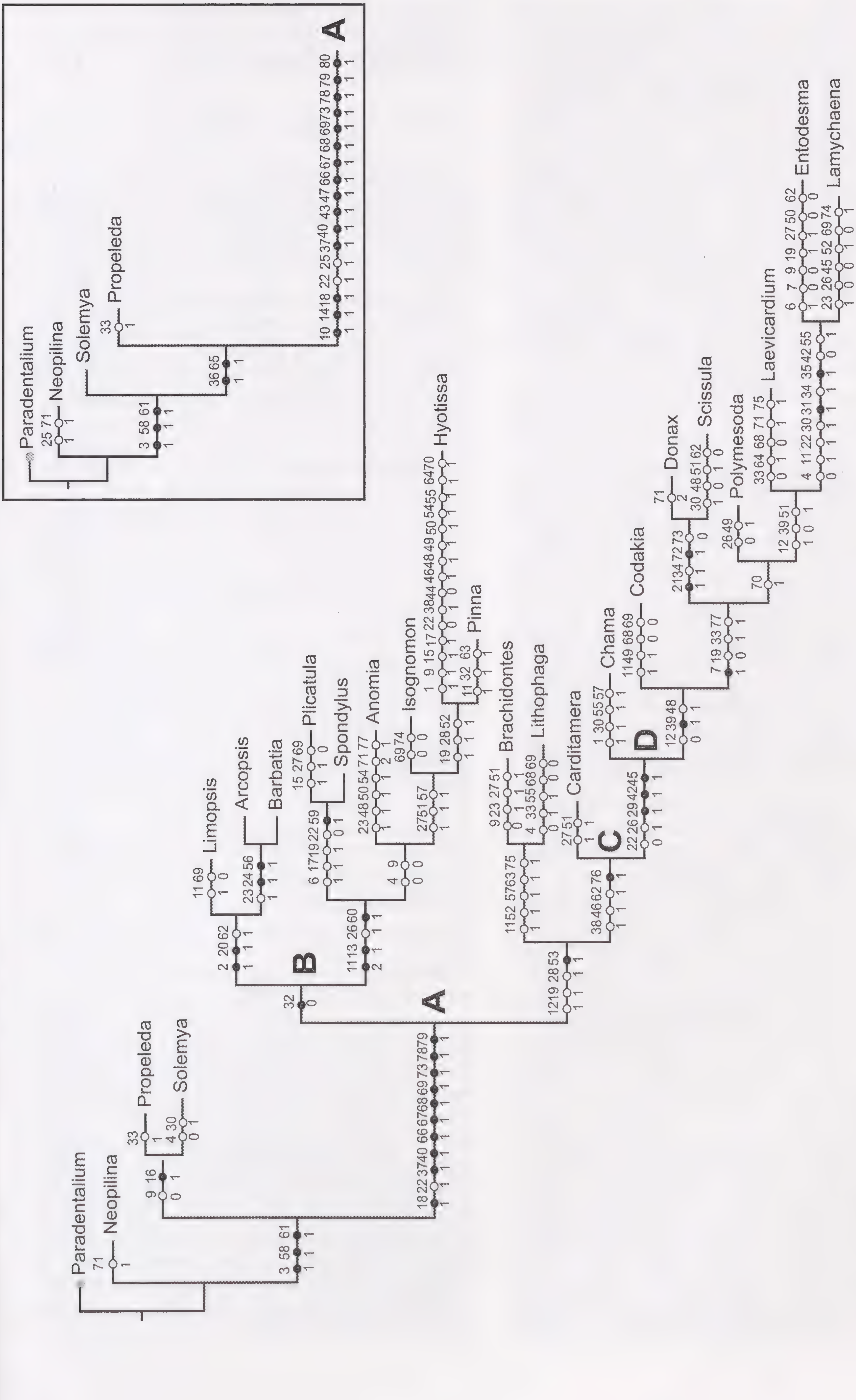

FIG. 301. The two most parsimonious trees from analysis of the data matrix in Table 2, length = 186, CI = 44; RI = 66. "Tree 1" shown in entirety; base of "Tree 2" shown in inset (remainder of tree at node A same as in "Tree 1"). See discussion for explanation of nodes. Character numbers in support of each branch appear above each hashmark; character states for characters at that branch are below each hashmark. Black hashmarks indicate nonhomoplastic characters; white hashmarks show homoplasy. These results are intended to explore the utility of characters in phylogenetic analyses, not as a hypothesis of bivalve evolution.

gastric central pad present (char. 66); paired typhlosoles from stomach ventral surface to intestine/style sac (char. 67); esophageal rim present (char. 68); dorsal hood present (char. 69); intestinal loops present (char. 73); pedal ganglia displaced ventrally in relation to the cerebral ganglia (char. 78); and circumesophageal nerve loop absent (char. 79). Assuming Protobranchia paraphyly (Tree 2), an additional set of nonhomoplastic characters supports the autobranch branch (node A), including the separation of posterior muscle scars (char. 10); adductor muscle structure (char. 14); the position of the main point of attachment of the gill suspensory stalk (char. 43); and the condition of the afferent gill vessel (char. 47).

The autobranchs (Fig. 301, node A) form two large clades in the tree, which roughly correspond to the current concepts of bivalve classification (e.g., Bieler et al., 2010, 2014) that separate Pteriomorphia (node B) and Heteroconchia (node C). However, the Mytilidae clade (*Brachidontes*, *Lithophaga*), a group clearly belonging to Pteriomorphia, is here sister to Heteroconchia. Support for this is provided by the shared presence of a branchial/siphonal septum (char. 53). The node leading to Heteroconchia (node C), here including Archiheterodonta (*Carditamera*) and Euheterodonta (remaining taxa including *Chama*, node D), has nonhomoplastic character support in char. 76 (separate genital and renal apertures). Within the latter group, the tellinoideans (*Donax*, *Scissula*) are well supported by the presence of a cruciform muscle (char. 21) and a gastric posterodorsal glandular diverticulum (char. 72).

Only *Entodesma*, interestingly one of the most extensively supported taxa in the resulting trees), is fundamentally misplaced when compared to most recent class-wide morphological and molecular analyses. Although it here (Fig. 301) clusters with the gastrochaenid *Lamychaena* deep within the euheterodonts, it is actually a member of the Anomalodesmata, whose position in the bivalve tree was recently investigated based on multiple genetic markers (Sharma et al., 2012) and morphological characters (sperm ultrastructure; e.g., Healy et al., 2008) not employed herein. Based on total evidence analyses (Bieler et al., 2014), anomalodesmatans are now considered a sister taxon to Imparidentia (herein represented by all euheterodonts except *Lamychaena*).

Overall, despite limited taxon selection and a high degree of character homoplasy, the chosen anatomical characters from a variety of bivalve organ systems produced a remarkably strong phylogenetic signal that can resolve bivalve clades at various levels.

ACKNOWLEDGMENTS

Major funding for this work was provided by U.S. National Science Foundation Partnerships in Enhancing Expertise in Taxonomy (PEET) award DEB-9978119 to RB and PMM (http://fieldmuseum.org/explore/peet-bivalves) for LRS's postdoctoral appointment at the Field Museum of Natural History (FMNH) and the 2002 International Marine Bivalve Workshop in the Florida Keys. Most of the fieldwork in the Florida Keys that resulted in these collections was also supported by the Comer Science & Education Foundation and the FMNH Zoology Department Marshall Field Fund. Research on exemplar species in the Bivalve Tree-of-Life (http://www.bivatol.org) and Bivalves-in-Time-and-Space (http://www.bivatol/bits) projects was supported by U.S. National Science Foundation awards DEB-0732854 and DEB-0918982 to RB and PMM. We are grateful to the late Richard E. Petit (North Myrtle Beach, South Carolina) for access to literature, to Sid Staubach (FMNH) for review of gill and labial palp descriptions and discussion, Liz Harper (University of Cambridge, UK) for review of Lyonsiidae and Chamidae descriptions, Ellen Strong (USNM) for review of digestive system discussion, John Taylor (The Natural History Museum, London) for review of Lucinidae descriptions, John Zardus (The Citadel, Charleston, South Carolina) for review of protobranch descriptions, and Jan Johan ter Poorten (Amsterdam, The Netherlands; and Research Associate, FMNH) for review of Cardiidae descriptions. BivAToL project illustrator Lisa Kanellos assisted with final image arrangements; Janeen Jones (FMNH) helped with specimen management. Collecting in the protected waters of the Florida Keys was permitted under Florida Keys National Marine Sanctuary Research Permits FKNMS 1998-080 to 2009-024, FKNMS educational event permit (FKNMS-2002-079), Florida Department of Environmental Protection (FDEP 5-02-43, for Long Key and Bahia Honda State Parks), and U.S. Fish & Wildlife Service Special Use Permit 41580-2010-20 (and earlier issues of these permits) for work in the National Wildlife Refuges. Four reviewers of earlier drafts are thanked for their input.

LITERATURE CITED

ABBOTT, R. T., 1974, *American Seashells, 2nd ed.* Van Nostrand Reinhold Company, New York, 663 pp., 24 pls.

ADAMS, A. & L. A. REEVE, 1848–1850, Mollusca. Pp. x + 87 pp., 24 pls., in: A. ADAMS, ed., *The zoology of the voyage of H. M. S. Samarang, under the command of Captain Sir Edward Belcher, during the years 1843–1846*. London.

ADAMS, C. B., 1845, Specierum novarum conchyliorum, in Jamaica repertorum, synopsis. *Proceedings of the Boston Society of Natural History*, 2: 1–17.

ADANSON, M., 1757, *Histoire naturelle du Sénégal. Coquillages*. Claude-Jean-Baptiste Bauche, Paris, [xcvi] + 275 + [1] pp., 19 pls.

ALATALO, P., C. J. BERG & C. N. D'ASARO, 1984, Reproduction and development in the lucinid clam *Codakia orbicularis* (Linné, 1758). *Bulletin of Marine Science*, 34(3): 424–434.

ALLEN, J. A., 1958, On the basic form and adaptations to habitat in the Lucinacea (Eulamellibranchia). *Philosophical Transactions of the Royal Society of London, Series B, Biological Sciences*, 241(684): 421–484, pl. 18.

ALLEN, J. A. & H. L. SANDERS, 1973, Studies on deep-sea Protobranchia (Bivalvia); the families Siliculidae and Lametilidae. *Bulletin of the Museum of Comparative Zoology*, 145(6): 263–309.

ALLEN, J. A. & H. L. SANDERS, 1996, Studies on the deep-Sea Protobranchia (Bivalvia): the family Neiloneillidae and the family Nuculanidae. *Bulletin of the Natural History Museum of London (Zoology)*, 62: 101–132.

ANTON, H. E., 1838, *Verzeichniss der Conchylien welche sich in der Sammlung von Herrmann Eduard Anton befinden.* Eduard Anton, Halle, xvi + 110 [title page dated 1839; true date 9 October 1838 *fide* p. 110 therein].

ARDOVINI, R. & T. COSSIGNANI, 2004, *West African seashells (including Azores, Madeira and Canary Is.)*. L'Informatore Piceno, Ancona, 319 pp.

ATKINS, D., 1937, On the ciliary mechanisms and interrelationships of Lamellibranchs: Part III: Types of lamellibranch gills and their food currents. *Quarterly Journal of Microscopical Science*, 79(315): 375–421.

ATKINS, D., 1938, On the ciliary mechanisms and interrelationships of lamellibranchs. VII. Latero-frontal cilia of the gill filaments and their phylogenetic value. *Quarterly Journal of Microscopical Science*, 80: 346–430.

AVELAR, W. E. P. & W. NARCHI, 1984, Functional anatomy of *Brachidontes solisianus* (Orbigny, 1846) (Bivalvia: Mytilidae). *Boletim de Zoologia, Universidade de São Paulo*, 8: 215–237.

BAIRD, W., 1863, Description of some new species of shells, collected at Vancouver Island and in British Columbia by J. K. Lord, Esq., naturalist to the British North-American Boundary Commission, in the years 1858–1862. *Proceedings of the Zoological Society of London*, for 1863(1): 66–70.

BARÓN, P. J. & N. F. CIOCCO, 1997, Anatomía de la almeja *Tellina petitiana* d'Orbigny, 1846. I. Organización general, valvas, manto, sifones, aductores, pie y branquias (Bivalvia, Tellinidae). *Revista de Biología Marina y Oceanografía*, 32(2): 95–110.

BARÓN, P. J. & N. F. CIOCCO, 1998, Anatomía de la almeja *Tellina petitiana* d'Orbigny, 1846. III. Sistema nervioso y gónada (Bivalvia, Tellinidae). *Revista de Biología Marina y Oceanografía*, 33(1): 139–154.

BEEDHAM, G. E. & G. OWEN, 1965, The mantle and shell of *Solemya parkinsoni* (Protobranchia: Bivalvia). *Proceedings of the Zoological Society of London*, 145(3): 405–430.

BENNETT, K. F., A. J. REED & R. A. LUTZ, 2011, DNA barcoding reveals *Brachidontes* (Bivalvia: Mytilidae from two ecologically distinct intertidal habitat on Long Key, Florida Keys, are cryptic species, not ecotypes. *The Nautilus*, 125(2) 63–71.

BENNETT, K. F. & R. C. WILLAN, 2003, Phenotypic plasticity of *Brachidontes* mussels from differing shorelines and habitats in the Florida Keys. *Program and Abstracts, American Malacological Society 69th Annual Meeting, Ann Arbor, Michigan, June 25–29, 2003*: 4.

BERNARD, F. R., 1980, A new *Solemya* s. str. from the northeastern Pacific (Bivalvia: Cryptodonta). *Venus*, 39(1): 17–23.

BIELER, R., J. G. CARTER & E. V. COAN, 2010, Classification of bivalve families. Pp. 113–133, in: P. BOUCHET & J.-P. ROCROI, Nomenclator of bivalve families. *Malacologia*, 52(2): 1–184.

BIELER, R. & P. M. MIKKELSEN, 2004, Marine bivalves of the Florida Keys: a qualitative faunal analysis based on original collections, museum holdings and literature data. *Malacologia*, 46(2): 503–544.

BIELER, R. & P. M. MIKKELSEN, 2006, Bivalvia – a look at the branches. *Zoological Journal of the Linnean Society*, 148(3): 223–235.

BIELER, R., P. M. MIKKELSEN, T. M. COLLINS, E. A. GLOVER, V. L. GONZÁLEZ, D. L. GRAF, E. M. HARPER, J. HEALY, G. Y. KAWAUCHI, P. P. SHARMA, S. STAUBACH, E. E. STRONG, J. D. TAYLOR, I. TËMKIN, J. D. ZARDUS, S. CLARK, A. GUZMÁN, E. MCINTYRE, P. SHARP & G. GIRIBET, 2014, Investigating the Bivalve Tree of Life – an exemplar-based approach combining molecular and novel morphological characters. *Invertebrate Systematics*, 28: 32–115.

BIELER, R., P. M. MIKKELSEN & G. GIRIBET, 2013, Bivalvia – a discussion of known unknowns. *American Malacological Bulletin*, 31(1): 123–133.

BIELER, R., P. M. MIKKELSEN, T. LEE & D. Ó FOIGHIL, 2004, Discovery of the Indo-Pacific oyster *Hyotissa hyotis* (Linnaeus, 1758) in the Florida Keys (Bivalvia: Gryphaeidae). *Molluscan Research*, 24(3): 149–159.

BIGATTI, G., M. PEHARDA & J. D. TAYLOR, 2004, Size at first maturity, oocyte envelopes and external morphology of sperm in three species of Lucinidae (Mollusca: Bivalvia) from Florida Keys, U.S.A. *Malacologia*, 46(2): 417–426.

BOSC, L. A. G., 1801, *Histoire naturelle des coquilles, contenant leur description, les moeurs des animaux qui les habitent et leurs usages. Avec figures dessinées d'après nature*. Tome III. Deterville, Paris, 292 pp., pls. 16–28.

BOSC, L. A. G., 1802, Histoire naturelle des coquilles, contenant leur description, les moeurs des animaux qui les habitant et leurs usages: avec figures dessinées d'aprés nature (coquilles 2), vol. 56. Pp. 1–330, in: G. L. L. Buffon, *Histoire naturelle de Buffon, classée par ordres, genres et espèces, d'après le systéme de Linné, avec les charactères génériques et la nomenclature Linnéenne*. Imprimerie de Crapelet, Paris.

BOSS, K. J., 1966, The subfamily Tellininae in the western Atlantic. The genus *Tellina*. *Johnsonia*, 4(45): 217–272.

BOSS, K. J., 1968, The subfamily Tellininae in the western Atlantic. The genera *Tellina* (part II) and *Tellidora*. *Johnsonia*, 4(46): 273–344.

BRODERIP, W. J., 1835, Description of some species of *Chama*. *Proceedings of the Zoological Society of London*, 2: 148–151.

BROWNING, M. R. & B. L. MONROE, JR., 1991, Clarifications and corrections of the dates of issue of some publications containing descriptions of North American birds. *Archives of Natural History*, 18(3): 381–405.

BRUGUIÈRE, J. G., 1789–1792, *Encyclopédie méthodique. Histoire naturelle de vers*. Paris. Vol. 1(1): 1–344 (1789); Vol. 1(2): 345–758 (1792).

CAMPBELL, D. C., 2000, Molecular evidence on the evolution of the Bivalvia. Pp. 31–46, in: E. M. Harper, J. D. Taylor & J. A. Crame, eds., *The evolutionary biology of the Bivalvia*. Geological Society of London Special Publication 177: vii + 494 pp.

CAMPBELL, D. C., K. J. HOEKSTRA & J. G. CARTER, 1998, 18S ribosomal DNA and evolutionary relationships within the Bivalvia. Pp. 75–85, in: P. A. Johnston, P. & J. W. Haggart, eds., *Bivalves: an eon of evolution – Paleobiological Studies Honoring Norman D. Newell*. University of Calgary Press, Calgary, Canada, xiv + 461 pp.

CAMPBELL, M. R., G. STEINER, L. CAMPBELL & H. DREYER, 2004, Recent Chamidae (Bivalvia) from the western Atlantic Ocean. *Malacologia*, 46(2): 381–415.

CARRIKER, M. R. & P. M. Gaffney, 1996, A catalogue of selected species of living oysters (Ostreacea) of the world. Pp. 1–18, in: V. S. Kennedy, R. I. E. Newell & A. F. Eble, eds., *The eastern oyster Crassostrea virginica*. Maryland Sea Grant College, College Park, xvi + 734 pp.

CARTER, J. G., 1978, Ecology and evolution of the Gastrochaenacea (Mollusca, Bivalvia) with notes on the evolution of the endolithic habitat. *Peabody Museum of Natural History, Yale University, Bulletin*, 41: 92 pp.

CARTER, J. G., 1990, Evolutionary significance of shell microstructure in the Palaeotaxodonta, Pteriomorphia and Isofilibranchia (Bivalvia: Mollusca). Pp. 135–296, in: J. G. Carter, ed., *Skeletal biomineralization: patterns, processes and evolutionary trends, Vol. 1*. Van Nostrand Reinhold, New York, xvii + 832 pp.

CHECA, A. G., J. RAMÍREZ-RICO, A. GONZÁLEZ-SEGURA & A. SÁNCHEZ-NAVAS, 2009, Nacre and false nacre (foliated aragonite) in extant monoplacophorans (= Tryblidiida: Mollusca). *Naturwissenschaften*, 96: 111–122.

CHENU, J. C., 1843–1845, *Spondylus. Illustrations conchyliologiques ou description et figures de toutes les coquilles connues vivante et fossiles*. A. Francke, Paris [pp. 1–9 (1845); pls. 1–2, 6–10, 16–18, 20 (1843); pls. 3–4, 11–15, 19, 21–30 (1844); pls. 31–32 (1845)].

CIOCCO, N. F. & P. J. BARÓN, 1998, Anatomía de la almeja *Tellina petitiana* d'Orbigny, 1846. II. Sistema digestivo, corazón, riñones, cavidad y glándulas pericárdicas (Bivalvia, Tellinidae). *Revista de Biología Marina y Oceanografía*, 33(1): 73–87.

CLENCH, W. J. & L. C. SMITH, 1944, The family Cardiidae in the western Atlantic. *Johnsonia*, 1(13): 1–32.

CONRAD, T. A., 1837, Descriptions of new marine shells from Upper California, collected by Thomas Nuttall, Esq. *Journal of the Academy of Natural Sciences*, 7(2): 227–268, pls. 17–20.

CONRAD, T. A., 1838, *Fossils of the Tertiary formations of the United States. Illustrated by figures drawn from nature*. J. Dobson, Philadelphia, 1: i–xvi, 1–32 p., pls. 1–17.

CONRAD, T. A., 1846, Descriptions of new species of fossil and Recent shells and corals. *Proceedings of the Academy of Natural Sciences of Philadelphia*, 3(1): 19–27, pl. 1.

COX, L. R., 1929, On the varietal names for *Spondylus* in K. Schreibers' Versuch einer vollständigen Conchylienkenntnis (1793). *Proceedings of the Malacological Society of London*, 18(5): 251–254.

DA COSTA, E. M., 1778, *Historia Naturalis Testaceorum Britanniae, or the British Conchology; containing the descriptions and other particulars of natural history of the shells of Great Britain and Ireland: illustrated with figures*. The author, London, xii + 254 pp., 17 pls.

DAKIN, W. J., 1928a, The anatomy and phylogeny of *Spondylus*, with a particular reference to the lamellibranch nervous system. *Proceedings of the Royal Society of London, series B, Containing Papers of a Biological Character*, 103(725): 337–354.

DAKIN, W. J., 1928b, The eyes of *Pecten, Spondylus, Amussium*, and allied lamellibranchs, with a short discussion on their evolution. *Proceedings of the Royal Society of London, series B, Containing Papers of a Biological Character*, 103(725): 355–365.

DALL, W. H., 1881, Reports on the results of dredging, under the supervision of Alexander Agassiz, in the Gulf of Mexico, and in the Caribbean Sea, 1877–79, by the U. S. Coast Survey Steamer "Blake," Lieut.-Commander C. D. Sigsbee, U. S. N., and Commander J. R Bartlett, U. S. N., commanding. XV. Preliminary report on the Mollusca. *Bulletin of the Museum of Comparative Zoology at Harvard College*, 9(2): 33–144.

DALL, W. H., 1886, Report on the results of dredging, under the supervision of Alexander Agassiz, in the Gulf of Mexico (1877–78) and in the Caribbean Sea (1879–80), by the U. S. Coast Survey Steamer “Blake,” Lieut.-Commander C. D. Sigsbee, U. S. N., and Commander J. R Bartlett, U. S. N., commanding. XXIX. Report on the Mollusca. Part I. Brachiopoda and Pelecypoda. *Bulletin of the Museum of Comparative Zoology at Harvard College*, 12: 171–318, pls. 1–9.

DESHAYES, G. P., 1857, Note sur différents mollusques de la Guadeloupe, envoyés par M. Schramm. *Journal de Conchyliologie*, 7: 137–143.

DIAZ MERLANO, J. M. & M. PUYANA HEGEDUS, 1994, *Moluscos del Caribe Colombiano. Un catálogo ilustrado.* Colciencias y Fundación Natura Colombia, Santafe de Bogota, 291 pp, 78 pls.

DINAMANI, P., 1967, Variation in the stomach structure of the Bivalvia. *Malacologia*, 5(2): 225–268.

DOMANESCHI, O. & C. M. MARTINS, 2002, *Isognomon bicolor* (C. B. Adams) (Bivalvia, Isognomonidae): primeiro registro para o Brasil, redescrição da espécie e considerações sobre a ocorrência e distribuição de *Isognomon* na costa brasileira. *Revista Brasileira de Zoologia*, 19(2): 611–627.

DUNKER, W., 1875, Ueber Conchylien von Desterro, Provinz Sta. Catharina, Brasilien. *Jahrbücher der Deutschen Malakozoologischen Gesellschaft*, 2: 240–254.

ELDREDGE, L. G. & C. M. SMITH, 2001, A guidebook of introduced marine species in Hawai’i. *Bishop Museum Technical Report*, 21: i–vi, 1–60.

ELLIS, J. & D. SOLANDER, 1786, *The natural history of many curious and uncommon zoophytes.* Benjamin White & Son, London, 208 pp.

EVENHUIS, N. L. & R. H. COWIE, 1995, Bibliography. Pp. 205–235, in: R. H. COWIE, N. L. EVENHUIS & C. C. CHRISTENSEN, *Catalog of the native land and freshwater molluscs of Hawaii.* Backhuys Publishers, Leiden, 248 pp.

FERREIRA, S. C. & S. Z. XAVIER, 1981, Notas sobre a ontogenia da familia Chamidae (Mollusca – Bivalvia). *Boletim do Museo Nacional (Rio de Janeiro), n.s. Geologia*, 38: 1–6, 1 pl.

FINET, Y. & K. L. LAMPRELL, 2008, The Spondylidae in the historical collections of the Muséum d’Histoire Naturelle, Geneva, with revision of the species described by Lamarck and by Chenu, and notes on nomenclature (Bivalvia: Pectinoidea: Spondylidae). *Archiv für Molluskenkunde*, 137(1): 1–73, incl. 30 pls.

FISCHER-PIETTE, E., 1942, Les mollusques d’Adanson. *Journal de Conchyliologie*, 85, 101–366, pls. 1–16 [title page includes: “avec la collaboration de P.-H. Fischer, L. Germain et P. Pallary”].

FRENKIEL, L. & M. MOUËZA, 1995, Gill ultrastructure and symbiotic bacteria in *Codakia orbicularis* (Bivalvia: Lucinidae). *Zoomorphology*, 115: 51–61.

FULLER, S. C., R. A. LUTZ & Y. P. HU, 1989, Bilateral asymmetry in the shell morphology and microsculpture of early ontogenetic stages of *Anomia simplex*. *Biological Bulletin*, 177: 83–95.

GALTSOFF, P. S., 1964, The American oyster *Crassostrea virginica* (Gmelin, 1791). *Bulletin of Fishery and Wildlife Service*, 64: 21–82.

GILBERT, M. A., 1978, Aspects of feeding in three species of *Tellina* (Tellinidae: Bivalvia) from Tuckertown Bay, Bermuda. *Bulletin of the American Malacological Union*, for 1977: 56–60.

GILMOUR, T. H. J., 1963, A note on the tentacles of *Lima hians* (Gmelin) (Bivalvia). *Proceedings of the Malacological Society of London*, 35(2–3): 81–85.

GILMOUR, T. H. J., 1967, The defensive adaptations of *Lima hians* (Mollusca, Bivalvia). *Journal of the Marine Biological Association of the United Kingdom*, 47: 209–221.

GILMOUR, T. H. J., 1990, The adaptive significance of foot reversal in the Limoida. Pp. 249–263, in: B. MORTON, ed., *The Bivalvia, Proceedings of a memorial symposium in honour of Sir Charles Maurice Yonge (1899–1986), Edinburgh, 1986.* Hong Kong University Press, Hong Kong, 364 pp.

GIRIBET, G. & W. C. WHEELER, 2002, On bivalve phylogeny: a high-level analysis of the Bivalvia (Mollusca) based on combined morphology and DNA sequence data. *Invertebrate Biology*, 121(4): 271–324.

GLENN, L. C., 1904, Systematic paleontology of the Miocene deposits of Maryland: Pelecypoda. Pp. 274–402, pls. 65–108, in: W. B. CLARK, ed., *Maryland Geological Survey, Miocene, vol. 1.* Johns Hopkins Press, Baltimore, Maryland, clv + 543 pp.

GLOVER, E. A. & J. D. TAYLOR, 2001, Systematic revision of Australian and Indo-Pacific Lucinidae (Mollusca: Bivalvia): *Pillucina*, *Wallucina* and descriptions of two new genera and four new species. *Records of the Australian Museum*, 53: 263–292.

GMELIN, J. F., 1791, *Caroli a Linné Systema Naturae per regna tria naturae, secundum classes, ordines, genera, species cum characteribus, differentiis, synonymis, locis. Editio decima tertia, aucta, reformata.* G. E. Beer, Lipsiae [Leipzig], 1(6): 3021–3910.

GOLOBOFF, P. A., J. S. FARRIS & K. C. NIXON, 2008, TNT, a free program for phylogenetic analysis. *Cladistics*, 24: 774–786.

GOULD, A. A., 1850, Shells collected by the United States Exploring Expedition under the command of Charles Wilkes. *Proceedings of the Boston Society of Natural History*, 3: 214–219 [here only cited the part that was issued in May 1850; for full compilation see Johnson, 1964].

GRAY, J. E., 1850, On the species of Anomiadae. *Proceedings of the Zoological Society of London*, for 1849, 17(197): 113–124, pl. 4.

GROS, O., L. FRENKIEL & M. MOUËZA, 1997, Embryonic, larval, and post-larval development in the symbiotic clam *Codakia orbicularis* (Bivalvia: Lucinidae). *Invertebrate Biology*, 116(2): 86–101.

GROS, O., L. FRENKIEL & M. MOUËZA, 1998, Gill filament differentiation and experimental colonization by symbiotic bacteria in aposymbiotic juveniles of *Codakia orbicularis* (Bivalvia: Lucinidae). *Invertebrate Reproduction and Development*, 34: 219–231.

GROS, O., M. LIBERGE & H. FELBECK, 2003, Interspecific infection of aposymbiotic juveniles of *Codakia orbicularis* by various tropical lucinid gill-endosymbionts. *Marine Biology*, 142(1): 57–66.

GUSTAFSON, R. G. & R. G. B. REID, 1986, Development of the pericalymma larva of *Solemya reidi* (Bivalvia: Cryptodonta: Solemyidae) as revealed by light and electron microscopy. *Marine Biology*, 93: 411–427.

HANLEY, S., 1846, Monograph of the genus *Tellina*. In: G. B. Sowerby II, ed., *Thesaurus conchyliorum; or, monographs of genera of shells*, 1(6): 2–21–336, pls. 56–66.

HARPER, E. M., 1992, Post-larval cementation in the Ostreidae and its implications for other cementing bivalves. *Journal of Molluscan Studies*, 58(1): 37–47.

HARPER, E. M., H. DREYER & G. STEINER, 2006, Reconstructing the Anomalodesmata (Mollusca: Bivalvia): morphology and molecules. *Zoological Journal of the Linnean Society*, 148(3): 395–420.

HARPER, E. M., J. D. TAYLOR & J. A. CRAME, 2000, Unravelling the evolutionary biology of the Bivalvia: a multidisciplinary approach. Pp. 1–9, in: E. M. Harper, J. D. Taylor & J. A. Crame, eds., *The evolutionary biology of the Bivalvia*. Geological Society of London Special Publication, 177: vii + 494 pp.

HARRY, H. W., 1985, Synopsis of the supraspecific classification of living oysters (Bivalvia: Gryphaeidae and Ostreidae). *The Veliger*, 28: 121–158.

HARVEY, M. C., 1995, *Reproduction in* Carditamera floridana *(Conrad) (Bivalvia: Carditidae).* Unpublished MSc thesis, Florida State University, College of Arts and Sciences, Tallahassee, x + 79 pp.

HEALY, J. M., R. BIELER & P. M. MIKKELSEN, 2008, Spermatozoa of the Anomalodesmata (Bivalvia, Mollusca) with special reference to relationships within the group. *Acta Zoologica*, 88(4): 339–350.

HEATH, H., 1937, The anatomy of some protobranch mollusks. *Mémoires du Musée Royal d'Histoire Naturelle de Belgique*, ser. 2, 10:1–26, pls. 1–10.

HEATH, H., 1941, The anatomy of the pelecypod family Arcidae. *Transactions of the American Philosophical Society*, 31(5): 287–319, pls. 1–22.

HERMANN, J., 1781, Erster Brief über einige Conchylien an den Herausgeber. *Der Naturforscher*, 16: 50–56, pl. 2.

HUBER, M., 2010, *Compendium of bivalves*. ConchBooks, Hackenheim, Germany, 901 pp.

HYLANDER, B. L. & R. G. SUMMERS, 1977, An ultrastructure analysis of the gametes and early fertilization in two bivalve mollusks, *Chama macerophylla* and *Spisula solidissima* with special reference to gamete binding. *Cell and Tissue Research*, 182: 469–489.

[ICZN] INTERNATIONAL COMMISSION ON ZOOLOGICAL NOMENCLATURE, 1999, *International Code of Zoological Nomenclature, 4th ed.* I.T.Z.N., London, xxix + 306 pp.

INTROÍNI, G. O., C. A. MAGALHÃES, H. FORTUNATO & S. M. RECCO-PIMENTEL, 2009, Comparison of the spermatozoan morphology of *Isognomon bicolor* and *Isognomon alatus* (Mollusca, Bivalvia, Isognomonidae). *Tissue and Cell*, 41(1): 67–74.

JEFFREYS, J. G., 1876, New and peculiar Mollusca of the *Pecten*, *Mytilus*, and *Arca* families procured in the 'Valarous' Expedition. *The Annals and Magazine of Natural History*, (4)18: 424–436.

JOHNSON, R. I., 1964, The Recent Mollusca of Augustus Addison Gould. Illustrations of the types described by Gould with a bibliography and catalog of his species. *United States National Museum Bulletin*, 239, 1–182, pls. 1–45.

KASPAR, J., 1913, Beiträge zur Kenntnis der Familie der Eryciniden und Carditiden. *Zoologische Jahrbücher, Supplement 13, Fauna Chilensis*, 4(4): 545–625.

KIRKENDALE, L., T. LEE, P. BAKER & D. Ó FOIGHIL, 2004, Oysters of the Conch Republic (Florida Keys); a molecular phylogenetic study of *Parahyotissa mcgintyi*, *Teskeyostrea weberi* and *Ostreola equestris*. *Malacologia*, 46: 309–326.

KLEEMANN, K. & P. MAESTRATI, 2012, Pacific *Lithophaga* (Bivalvia, Mytilidae) from recent French expeditions with the description of two new species. *Bollettino Malacologico*, 48(2): 73–102.

KRUEGER, D. M. & C. M. CAVANAUGH, 1997, Phylogenetic diversity of bacterial symbionts of *Solemya* hosts based on comparative sequence analysis of 16S rRNA genes. *Applied and Environmental Microbiology*, 63: 91–98.

KRUEGER, D. M., N. DUBILIER & C. M. CAVANAUGH, 1996, Chemoautotrophic symbiosis in the tropical clam *Solemya occidentalis* (Bivalvia: Protobranchia): ultrastructural and phylogenetic analysis. *Marine Biology*, 126: 55–64.

LAMARCK, J. B., 1801, *Système des animaux sans vertèbres, ou Tableau général des classes, des ordres, et des genres de ces animaux.* Author & Deterville, Paris, 432 pp.

LAMARCK, J. B., 1819, *Histoire naturelle des animaux sans vertèbres*. Paris, 6(1): vi + 343 pp.

LAMMENS, J. J., 1969, The morphology of the central nervous system of *Macoma balthica* (L.). *Netherlands Journal of Zoology*, 19(1): 105–127.

LAMPRELL, K., 2006, *Spiny oysters: a revison of the living* Spondylus *species of the world.* Privately published: Jean Lamprell, Brisbane, 119 pp.

LAMY, E., 1922, Révision des Carditacea vivants du Muséum d'Histoire Naturelle de Paris. *Journal de Conchyliologie*, 66[(4)20](3): 218–276, pl. 7.

LEE, T. & D. Ó FOIGHIL, 2004, Hidden Floridian biodiversity: mitochondrial and nuclear gene trees reveal four cryptic species within the scorched mussel, *Brachidontes exustus*, species complex. *Molecular Ecology*, 13(11): 3527–3542 [erratum published in 2005, vol. 14(7): 2245].

LEE, T. & D. Ó FOIGHIL, 2005, Placing the Floridian marine genetic disjunction into a regional evolutionary context using the scorched mussel, *Brachidontes exustus*, species complex. *Evolution*, 59: 2139–2158.

LEMCHE, H. & K. G. WINGSTRAND, 1959, The anatomy of *Neopilina galatheae* Lemche, 1957 (Mollusca, Tryblidiacea). *Galathea Report*, 3: 9–73.

LINNAEUS, C., 1758*, Systema naturae per regna tria naturae. Editio decima, reformata*. Vol. 1, Regnum animale. Stockholm, 824 pp.

LINNAEUS, C., 1767, *Systema naturae per regna tria naturae. Editio duodecimo reformata.* Stockholm, 1(2), 533–1327.

LOGAN, A., 1974, Morphology and life habits of the Recent cementing bivalve *Spondylus americanus* Hermann from the Bermuda platform. *Bulletin of Marine Science*, 24(3): 568–594.

LOOSANOFF, V. L., 1961, Partial metamorphosis in *Anomia simplex*. *Science*, 133(3470): 2070–2071.

LOOSANOFF, V. L., H. C. DAVIS & P. E. CHANLEY, 1966, Dimensions and shapes of larvae of some marine bivalve mollusks. *Malacologia*, 4(2): 351–435.

MARQUES, R. C. & L. R. L. SIMONE, 2013, Anatomy of *Phyllodina persica* (Bivalvia: Tellinidae), and its first occurrence in southeastern Brazilian waters. *Papéis Avulsos de Zoologia*, 53(9): 115–127.

MARKO, P. B., 2002, Fossil calibration of molecular clocks and the divergence times of geminate species pairs separated by the Isthmus of Panama. *Molecular Biology and Evolution*, 19(11): 2005–2021.

MARKO, P. B. & A. L. MORAN, 2009, Out of sight, out of mind: high cryptic diversity obscures the identities and histories of geminate species in the marine bivalve subgenus *Acar. Journal of Biogeography*, 36(10): 1861–1880.

McLEAN, R. A., 1939, The Cardiidae of the western Atlantic. *Memorias Sociedad Cubana de Historia Naturale*, 13(3): 157–173, pls. 3–26.

McLEAN, R. A., 1941, The oysters of the western Atlantic. *Notula Naturae*, 67: 1–14.

MIKKELSEN, P. M. & R. BIELER, 2004, International Marine Bivalve Workshop 2002: introduction and summary. *Malacologia*, 46(2): 241–248.

MIKKELSEN, P. M. & R. BIELER, 2007, *Seashells of southern Florida – Living marine mollusks of the Florida Keys and adjacent regions: bivalves*. Princeton University Press, Princeton, New Jersey. x + 503 pp. [copyright date 2008, but issued in Nov. 2007].

MORGAN, R. E. & J. A. ALLEN, 1976, On the functional morphology and adaptations of *Entodesma saxicola* (Bivalvia: Anomalodesmacea). *Malacologia*, 15(2): 233–240.

MORSE, E. S., 1913, Observations on living *Solenomya. The Biological Bulletin*, 25(4): 261–281.

MORTON, B. S., 1976, The biology and functional morphology of the Southeast Asian mangrove bivalve, *Polymesoda (Geloina) erosa* (Solander, 1786) (Bivalvia: Corbiculidae). *Canadian Journal of Zoology*, 54(4): 482–500.

MORTON, B. S., 1987, The mantle margin and radial mantle glands of *Entodesma saxicola* and *E. inflata* (Bivalvia: Anomalodesmata: Lyonsiidae). *Journal of Molluscan Studies*, 53(2): 139–151.

MOUËZA, M. & L. FRENKIEL, 1995, Ultrastructural study of the spermatozoon in a tropical lucinid bivalve: *Codakia orbicularis* L. *Invertebrate Reproduction and Development*, 27: 205–211.

NARCHI, W., 1968, The functional morphology of *Lyonsia californica* Conrad, 1837 (Bivalvia). *The Veliger*, 10(4): 305–313.

NARVÁEZ, N., C. LODEIROS, L. FREITES, M. NUÑEZ, D. PICO, & A. PRIETO, 2000, Abundancia de juveniles y crecimiento de *Pinna carnea* (Mytiloida: Pinnacea) en cultivo suspendido. *Revista de Biologia Tropical*, 48(4): 785–797.

NAVEZ, A. E., 1936, Observations sur le rythme cardiaque d'*Anomia simplex* (d'Orbigny) (Lamellibranchiae). *Mémoires du Musée Royal d'Histoire Naturelle de Belgique*, (2) 3: 701–737.

NIXON, K. C., 2002, *WinClada ver. 1.00.08*. Software published by the author, Ithaca, New York.

Ó FOIGHIL, D. O. & D. J. TAYLOR, 2000, Evolution of parental care and ovulation behavior in oysters. *Molecular Phylogenetics and Evolution*, 15(2): 301–313.

OLIVER, P. G., 1981, The functional morphology and evolution of Recent Limopsidae (Bivalvia, Arcoidea). *Malacologia*, 21(1–2): 61–93.

OLIVER, P. G. & J. A. ALLEN, 1980, The functional and adaptive morphology of the deep-sea species of the family Limopsidae (Bivalvia: Arcoida) from the Atlantic. *Philosophical Transactions of the Royal Society of London, Series B, Biological Sciences*, 291(1045): 77–125.

OLIVER, P. G. & J. JÄRNEGREN, 2004, How reliable is morphology based species taxonomy in the Bivalvia? A case study on *Arcopsis adamsi* (Bivalvia: Arcoidea) from the Florida Keys. *Malacologia*, 46(2): 327–338.

ORBIGNY, A. d', 1839, *Voyage dans l'Amérique Méridionale*. P. Bertrand, Paris, Vol. 5, pt. 3, Mollusques [pls. 54, 60–63 (1839); pp. 425–472 (1841) [dates *teste* EVENHUIS & COWIE, 1995: 220–221].

ORBIGNY, A. d', 1841–1853, Mollusques. In: R. SAGRA, *Histoire physique, politique, et naturelle de l'Ile de Cuba.* 2 vols. and atlas. [Issued as of 1853, but published in parts earlier, as follows: French edition, 1: 1–264 (1841); 2: 1–112, pts. 1–7 (1842); 113–380, pts. 8–24 (by 1853; exact dates to be clarified). The Spanish edition, with title page dated 1845, was translated from and published after the French edition.]

ORBIGNY, A. d', 1834–1847, *Voyage dans l'Amérique Méridionale* [...] Exécuté Pendant lea Années 1826, [...] 1833. Volume 5(3), Mollusques, pp. 1–48, 73–128, pls. 1–2, 9–13, 15–16, 56 [1834]; pp. 49–72, 129–176, pls. 3–8, 17–23, 25, 55 [1835]; pp. 177–184, pls. 14, 24, 26–28, 30–32, 34, 35, 37, 58 [1836]; pls. 33, 36 [1836?]; pp. 185–376, pls. 29, 38–52, 57 [1837]; pls. 54, 59–66, 68, 69 [1839]; pp. 377–424, pls. 53, 67, 70, 71 [1840]; pp. 425–488, pls. 72–76, 80 [1841]; pls. 83, 85 [1842]; pl. 84 [1842?]; pp. 529–600 [1845]; pp. 489–528, 601–728 [1846]; pp. 729–758 [1847?]; pls. 77–79, 81, 82 [1847]. P. Bertrand, Paris [dates *teste* Sherborn & Griffin, 1934; Browning & Monroe, 1991].

OWEN, G., 1959, The ligament and the digestive system in the taxodont bivalves. *Proceedings of the Malacological Society of London*, 33(5): 215–223.

OWEN, G., 1961, A note on the habits and nutrition of *Solemya parkinsoni* (Protobranchia: Bivalvia). *Quarterly Journal of Microscopical Science*, 102(1): 15–21, 2 pls.

OWEN, G., 1966, Feeding. Pp. 1–51, in: K. M. Wilbur & C. M. Yonge, eds., *Physiology of Mollusca, Vol. 2*. Academic Press, New York, xiii + 645 pp.

OWEN, G., 1978, Classification and the bivalve gill. *Philosophical Transactions of the Royal Society of London, Series B, Biological Sciences*, 284(1001): 377–385.

PAULAY, G., 2003, Marine Bivalvia (Mollusca) of Guam. *Micronesica*, 35–36: 218–243.

PELSENEER, P., 1911, Les Lamellibranches de l'Expédition du Siboga. Partie Anatomique. In: M. Weber, ed., *Siboga-Expeditie, Utkomsten op zoologisch, botanisch, oceanographisch en geologisch Gebied, verzameld in de Oost-Indië 1899–1900, aan boord H. M. Siboga onder commando van Luitenant ter zee 1e kl. G. F. Tydeman*, 53ª. E. J. Brill, Leiden, 125 + [ii] pp., 26 pls.

PENCHASZADEH, P. E. & J. J. SALAYA, 1983, Reproduction and gonadal changes in *Laevicardium laevigatum* (Mollusca: Bivalvia: Cardiidae) of Golfo Triste, Venezuela. *The Veliger*, 25(4): 343–346, 2 pls.

PENNANT, T., 1777, *The British zoology, 4th ed., Vol. 4, Crustacea, Mollusca, Testacea*. White, London, 154 pp., 93 pls.

POLI, G. S., 1791, *Testacea utriusque Siciliae eorumque historia et anatome*. Regio Typographeio, Parma, [6] + x + 90 + 50 + lxxiii p., frontispiece, pls. 1–8.

POPHAM, M. L., 1940, The mantle cavity of some of the Erycinidae, Montacutidae and Galeommatidae with special reference to the ciliary mechanisms. *Journal of the Marine Biological Association of the United Kingdom*, 24(2): 549–587.

PRENDINI, L., 2001, Species or supraspecific taxa as terminals in cladistic analysis? Groundplans versus exemplars revisited. *Systematic Biology*, 50: 290–300.

PREZANT, R. S., 1981a, The arenophilic radial mantle glands of the Lyonsiidae (Bivalvia: Anomalodesmata) with notes on lyonsiid evolution. *Malacologia*, 20(2): 267–289.

PREZANT, R. S., 1981b, Comparative shell ultrastructure of lyonsiid bivalves. *The Veliger*, 23(4): 289–299, 12 pls.

PREZANT, R. S., 1981c, Taxonomic re-evaluation of the bivalve family Lyonsiidae. *The Nautilus*, 95(2): 58–72.

PREZANT, R. S., 1984, Functional microstructure and mineralogy of the byssal complex of *Anomia simplex* Orbigny (Bivalvia: Anomiidae). *American Malacological Bulletin*, 2: 41–50.

PURCHON, R. D., 1956, The stomach in the Protobranchia and Septibranchia (Lamellibranchia). *Proceedings of the Zoological Society of London*, 127(4): 511–525.

PURCHON, R. D., 1957, The stomach in the Filibranchia and Pseudolamellibranchia. *Proceedings of the Zoological Society of London*, 129: 27–60.

PURCHON, R. D., 1958, The stomach in the Eulamellibranchia; stomach type IV. *Proceedings of the Zoological Society of London*, 131(4): 487–525.

PURCHON, R. D., 1960, The stomach in the Eulamellibranchia; stomach types IV and V. *Proceedings of the Zoological Society of London*, 135(3): 431–489.

PURCHON, R. D., 1987, The stomach in the Bivalvia. *Philosophical Transactions of the Royal Society of London, Series B, Biological Sciences*, 316(1177): 183–276.

REEVE, L., 1843, Monograph of the genus *Cardita*. *Conchologia Iconica: or, Illustrations of the shells of molluscous animals*, 1: pls. 1–9.

REEVE, L. A., 1844–1845, Monograph of the genus *Cardium*. *Conchologia Iconica: or, illustrations of the shells of molluscous animals*, 2: pls. 1–4 (Oct. 1844); 5–8 (Nov. 1844); 9–12 (Dec. 1844); 13–16 (Jan. 1845); 17–22 (Mar. 1845).

REEVE, L. A., 1856, Monograph of the genus *Spondylus*. *Conchologia Iconica: or, illustrations of the shells of molluscous animals*, 9: pls. 1–4 (Jan. 1856); 5–8 (Feb. 1856); 9–14 (May 1856); 15–18 (Jun. 1856).

REID, R. G. B., 1965, The structure and function of the stomach in bivalve molluscs. *Journal of Zoology*, 147: 156–184.

REID, R. G. B., 1980, Aspects of the biology of a gutless species of *Solemya* (Bivalvia: Protobranchia). *Canadian Journal of Zoology*, 58(3): 386–393.

REID, R. G. B. & D. G. BRAND, 1987, Observations on Australian Solemyidae. *Journal of the Malacological Society of Australia*, 8: 41–50.

RIOS, E. de C., 1985, *Seashells of Brazil*. Fundação Cidade do Rio Grande, Fundação Universidade do Rio Grande, Museu Oceanográfico, Rio Grande, 329 pp., 102 pls.

RIOS, E. de C., 1994, *Seashells of Brazil, 2nd ed.* Museu Oceanográfico, Rio Grande, Brazil, 368 pp., 113 pls.

RIOS, E. de C., 2009, *Compendium of Brazilian sea shells*. Universidade Federal do Rio Grande, Rio Grande, viii + 668 pp.

RODRÍGUEZ-ROMERO, F., M. GASCA-MONTES-DE-OCA & J. DE-LA-ROSA-VÉLEZ, 1991, Meiotic behaviour during pachytene and diakinesis of *Isognomon alatus* (Molusca [*sic*]—Isognomonidae) from Veracruz, Mexico. *Ciencias Marinas*, 17(1): 73–78.

RODRÍGUEZ, F., A. LAGUARDA & A. GARCÍA-CUBAS, 1983, The karyotype of *Isognomon alatus*. *Canadian Journal of Genetics and Cytology*, 25: 85–87.

ROSENBERG, G., 2009, *Malacolog 4.1.1: a database of western Atlantic marine Mollusca*. WWW database (version 4.1.1), http://www.malacolog.org.

SALEUDDIN, A. S. M., 1965, The mode of life and functional anatomy of *Astarte* spp. (Eulamellibranchia). *Proceedings of the Malacological Society of London*, 36(4): 229–257.

SALVINI-PLAWEN, L. V. & G. STEINER, 1996, Synapomorphies and plesiomorphies in higher classification of Mollusca. Pp. 29–51, in: J. Taylor, ed., *Origin and evolutionary radiation of the Mollusca*. Oxford University Press, Oxford, UK, xv + 392 pp.

SAY, T., 1822, An account of some of the marine shells of the United States. *Academy of Natural Sciences of Philadelphia*, 2(2): 221–224, 225–248, 257–276, 302–320, 321–325.

SCHNEIDER, J. A., 1992, Preliminary cladistic analysis of the bivalve family Cardiidae. *American Malacological Bulletin*, 9(2): 145–155.

SCHNEIDER, J. A., 1995, Phylogeny of the Cardiidae (Mollusca: Bivalvia): Protocardiinae, Laevicardiinae, Lahilliinae, Tulongoncardiinae subfam. n. and Pleuriocardiinae subfam. n. *Zoologica Scripta*, 24(4): 321–346.

SCHREIBERS, K., 1793, *Versuch einer vollständigen Conchylienkenntniss nach Linnes System*. J. Elden v. Kurzbeck, Vienna, Vol. 1: [12] + [1]–446 + [1] p. errata.

SEVILLA-H., M. L., F. GARCÍA-D. & E. URIA-G., 1998, Datos anatómicos de *Hyotissa hyotis* (Linnaeus, 1758), Ostreacea: Gryphaeidae. *Anales de la Escuela Nacional de Ciencias Biológicas*, 43(1–4): 25–32.

SHARMA, P. P., V. L. GONZALEZ, G. Y. KAWAUCHI, S. C. ANDRADE, A. GUZMAN, T. M. COLLINS, E. A. GLOVER, E. M. HARPER, J. M. HEALY, P. M. MIKKELSEN, J. D. TAYLOR, R. BIELER & G. GIRIBET, 2012, Phylogenetic analysis of four nuclear protein-encoding genes largely corroborates the traditional classification of Bivalvia (Mollusca). *Molecular Phylogenetics and Evolution*, 65(1): 64–74. http://www.sciencedirect.com/science/article/pii/S1055790312002035

SHERBORN, C. D. & F. J. GRIFFIN, 1934, On the dates of publication of the natural history portions of Alcide d'Orbigny's 'Voyage Amérique Méridionale.' *Annals and Magazine of Natural History, series 10*, 13(73): 130–134.

SIMONE, L. R. L., 2009, Comparative morphology among representatives of main taxa of Scaphopoda and basal protobranch Bivalvia (Mollusca). *Papéis Avulsos de Zoologia*, 49(32): 405–457.

SIMONE, L. R. L. & A. CHICHVARKHIN, 2004, Comparative morphological study of four species of *Barbatia* occurring on the southern Florida coast (Arcoidea, Arcidae). *Malacologia*, 46(2, Bivalve studies in the Florida Keys, R. Bieler & P. M. Mikkelsen, eds.): 355–379.

SIMONE, L. R. L. & J. R. DOUGHERTY, 2004, Anatomy and systematics of northwestern Atlantic *Donax* (Bivalvia, Veneroidea, Donacidae). *Malacologia*, 46(2): 459–472.

SIMONE, L. R. L. & E. P. GONÇALVES, 2006, Anatomical study on *Myoforceps aristatus*, an invasive boring bivalve in S. E. Brazilian coast (Mytilidae). *Papéis Avulsos de Zoologia*, 46(6): 57–65.

SIUNG, A. M., 1980, Studies on the biology of *Isognomon alatus* Gmelin (Bivalvia: Isognomonidae) with notes on its potential as a commercial species. *Bulletin of Marine Science*, 30(1): 90–101.

SMITH, E. A., 1881, Account of the zoological collection made during the survey of H. M. S. "Alert" in the Straits of Magellan and on the coast of Patagonia, IV: Mollusca and Molluscoida. *Proceedings of the Zoological Society of London,* 1881(1): 22–44.

SOWERBY I, G. B., 1833, [Characters of new species of shells from the collection formed by Mr. Cuming on the western coast of South America, and among the islands of the South Pacific Ocean.] *Proceedings of the Zoological Society of London*, 1833: 16–22.

SOWERBY, J., 1806, *The British miscellany, or coloured figures of new, rare, or little known animal subjects; many not before ascertained to be inhabitants of the British Isles; and chiefly in the possession of the author, James Sowerby, 2 vols.* R. Taylor & Co., London, vi + 136 pp., 76 pls.

STANLEY, S. M., 1970, Relation of shell form to life habits in the Bivalvia. *Geological Society of America, Memoir*, 125: 296 pp.

STAROBOGATOV, Y. I., 1992, Morphological basis for phylogeny and classification of Bivalvia. *Ruthenica*, 2: 1–25.

STEINER, G., 1992, Phylogeny and classification of Scaphopoda. *Journal of Molluscan Studies*, 58: 385–400.

STEMPELL, W., 1899, Zur Anatomie von *Solemya togata* Poli. *Zoologische Jahrbücher, Abtheilung für Anatomie und Ontogenie der Thiere*, 13: 89–170, pls. 8–10.

TAYLOR, J. D. & E. A. GLOVER, 2000, Functional anatomy, chemosymbiosis and evolution of the Lucinidae. Pp. 207–225, in: E. M. Harper, J. D. Taylor & J. A. Crame, eds., *The evolutionary biology of the Bivalvia*. Geological Society of London Special Publication 177, vii + 494 pp.

TAYLOR, J. D., E. A. GLOVER, L. SMITH, P. DYAL & S. T. WILLIAMS, 2011, Molecular phylogeny and classification of the chemosymbiotic bivalve family Lucinidae (Mollusca: Bivalvia). *Zoological Journal of the Linnean Society*, 163: 15–49.

TAYLOR, J. D., S. T. WILLIAMS, E. A. GLOVER & P. DYAL, 2007, A molecular phylogeny of heterodont bivalves (Mollusca: Bivalvia: Heterodonta): new analyses of 18S and 28S rRNA genes. *Zoologica Scripta*, 36(6): 587–606.

TËMKIN, I., 2006, Morphological perspective on the classification and evolution of Recent Pterioidea (Mollusca: Bivalvia). *Zoological Journal of the Linnean Society*, 148(3): 253–312.

TËMKIN, I., 2010, Molecular phylogeny of pearl oysters and their relatives (Mollusca, Bivalvia, Pterioidea). *BMC Evolutionary Biology*, 10(342): 28 pp.

TER POORTEN, J. J., 2009, The Cardiidae of the Panglao Marine Biodiversity Project 2004 and the Panglao 2005 Deep-Sea Cruise with descriptions of four new species (Bivalvia). *Vita Malacologica*, 8: 9–96.

THOMAS, R. D. K., A. MADZVAMUSE, P. K. MAINI & A. J. WATHEN, 2000, Growth patterns of noetiid ligaments: implications of developmental models for the origin of an evolutionary novelty among arcoid bivalves. Pp. 279–289, in: E. M. Harper, J. D. Taylor & J. A. Crame, eds., *The evolutionary biology of the Bivalvia*. Geological Society of London Special Publication 177, vii + 494 pp.

TURGEON, D. D., W. G. LYONS, P. MIKKELSEN, G. ROSENBERG & F. MORETZSOHN, 2009, Bivalvia (Mollusca) of the Gulf of Mexico. Pp. 711–744, in: D. L. Felder & D. K. Camp, eds., *Gulf of Mexico – origin, waters, and biota, Volume 1, Biodiversity*. Texas A & M University Press, College Station, Texas, xxi + 1393 pp.

TURNER, R. D. & J. ROSEWATER, 1958, The family Pinnidae in the western Atlantic. *Johnsonia*, 3(38): 285–326.

VALENTICH-SCOTT, P. & G. E. DINESEN, 2004, Rock and coral boring Bivalvia (Mollusca) off the Middle Florida Keys, U.S.A. *Malacologia*, 46(2): 339–354.

VAN DER SCHALIE, H., 1933, Notes on the brackish water bivalve, *Polymesoda caroliniana* (Bosc). *Occasional Papers of the Museum of Zoology, University of Michigan*, 11(258): 1–8, pl. 1.

VIANA, M. G. & C. A. ROCHA-BARREIRA, 2007, The sensorial structures of *Spondylus americanus* Hermann, 1781 (Mollusca: Bivalvia, Spondylidae). *Brazilian Archives of Biology and Technology*, 50(5): 815–819.

VIDAL, J., 1999, Taxonomic review of the elongated cockles: genera *Trachycardium, Vasticardium* and *Acrosterigma* (Mollusca, Cardiidae). *Zoosystema*, 21(2): 259–335.

WADA, K., 1978, Chromosome karyotypes of three bivalves: the oysters, *Isognomon alatus* and *Pinctada imbricata*, and the bay scallop, *Argopecten irradians irradians*. *Biological Bulletin*, 155: 235–245.

WADLEIGH, J. K., T. M. ABSHER & K. F. BENNETT, 2012, A sixth species within the scorched mussel (*Brachidontes exustus*) cryptic species complex (abstract). *Program and Abstracts, American Malacological Society 78th Annual Meeting, Cherry Hill, New Jersey, 16–21 June, 2012*: 117.

WALLER, T. R., 1978, Morphology, morphoclines and a new classification of the Pteriomorpha (Mollusca: Bivalvia). *Philosophical Transactions of the Royal Society of London, Series B, Biological Sciences*, 284(1001): 345–365.

WALLER, T. R., 1990, The evolution of ligament systems in the Bivalvia. Pp. 49–71, in: B. Morton, ed., *The Bivalvia—Proceedings of a Memorial Symposium in Honour of Sir Charles Maurice Yonge, Edinburgh, 1986*. Hong Kong University Press, Hong Kong, viii + 355 pp.

WALLER, T. R., 1998, Origin of the molluscan class Bivalvia and a phylogeny of major groups. Pp. 1–47, in: P. A. Johnston & J. W. Haggart, eds., *Bivalves: an eon of evolution*. University of Calgary Press, Calgary, Canada, xiv + 461 pp.

WARÉN, A., 1980, Marine Mollusca described by John Gwyn Jeffreys, with the location of the type material. *Conchological Society of Great Britain and Ireland Special Publication*, 1: 1–60, pls. 1–8.

WATSON, H., 1930a, On the anatomy and affinities of *Plicatula*. *Proceedings of the Malacological Society of London*, 19(1): 25–31, pl. 5.

WATSON, H., 1930b, On the central nervous system of *Spondylus* and what happens to a headless mollusc's brain. *Proceedings of the Malacological Society of London*, 19(1): 31–36.

WILK, J. & R. BIELER, 2009, Ecophenotypic variation in the flat tree oyster, *Isognomon alatus* (Bivalvia: Isognomonidae), across a tidal microhabitat gradient. *Marine Biology Research*, 5(2):155–163.

WINCKWORTH, R., 1929, Marine Mollusca from south India and Ceylon. III: *Pinna*. With an index to the Recent species of *Pinna*. *Proceedings of the Malacological Society of London*, 18(6): 276–297.

YONGE, C. M., 1939, The protobranchiate Mollusca; a functional interpretation of their structure and evolution. *Philosophical Transactions of the Royal Society of London, Series B, Biological Sciences*, 230: 79–147.

YONGE, C. M., 1949, On the structure and adaptations of the Tellinacea, deposit-feeding Eulamellibranchia. *Philosophical Transactions of the Royal Society of London, Series B, Biological Sciences*, 234(609): 29–76.

YONGE, C. M., 1952a, Studies on Pacific coast mollusks. V. Structure and adaptation in *Entodesma saxicola* (Baird) and *Mytilimeria nuttallii* Conrad with a discussion on evolution within the family Lyonsiidae (Eulamellibranchia). *University of California Publications in Zoology*, 55(10): 439–450.

YONGE, C. M., 1952b, Studies on Pacific coast mollusks. VI. A note on *Kellia laperousii* (Deshayes). *University of California Publications in Zoology*, 55(11): 451–454.

YONGE, C. M., 1953a, Form and habit in *Pinna carnea* Gmelin. *Philosophical Transactions of the Royal Society of London, Series B, Biological Sciences*, 237(648): 335–374.

YONGE, C. M., 1953b, The monomyarian condition in the Lamellibranchia. *Transactions of the Royal Society of Edinburgh*, 42(2): 443–478.

YONGE, C. M., 1957, Mantle fusion in the Lamellibranchia. *Pubblicazioni della Stazione Zoologica di Napoli*, 29: 151–171.

YONGE, C. M., 1967, Form, habit and evolution in the Chamidae (Bivalvia) with reference to conditions in the rudists (Hippuritacea). *Philosophical Transactions of the Royal Society of London, Series B, Biological Sciences*, 252(775): 49–105.

YONGE, C. M., 1968, Form and habit in species of *Malleus* (including the "hammer oysters") with comparative observations on *Isognomon isognomon*. *The Biological Bulletin*, 135(2): 378–405.

YONGE, C. M., 1969, Functional morphology and evolution within the Carditacea (Bivalvia). *Proceedings of the Malacological Society of London*, 38(6): 493–527.

YONGE, C. M., 1973, Functional morphology with particular reference to hinge and ligament in *Spondylus* and *Plicatula* and a discussion on relations within the superfamily Pectinacea (Mollusca: Bivalvia). *Philosophical Transactions of the Royal Society of London, Series B, Biological Sciences*, 267(883): 173–208.

YONGE, C. M., 1976, Primary and secondary ligaments with the lithodesma in the Lyonsiidae (Bivalvia: Pandoracea). *Journal of Molluscan Studies*, 42(3): 395–408.

YONGE, C. M., 1977, Form and evolution in the Anomiacea (Mollusca: Bivalvia) – *Pododesmus*, *Anomia*, *Patro*, *Enigmonia* (Anomiidae): *Placunanomia*, *Placuna* (Placunidae fam. nov.). *Philosophical Transactions of the Royal Society of London, Series B, Biological Sciences*, 276(950): 453–523.

YONGE, C. M., 1978, Significance of the ligament in the classification of the Bivalvia. *Philosophical Transactions of the Royal Society of London, Series B, Biological Sciences*, 284(1001): 375.

YONGE, C. M., 1979, Cementation in bivalves. Pp. 83–106, in: S. van der Spoel, A. C. van Bruggen & J. Lever, eds., *Pathways in malacology*. Bohn, Scheltema & Holkema, Utrecht, 295 pp.

YONGE, C. M., 1980, On *Patro australis* with comparisons of structure throughout the Anomiidae (Bivalvia). *Malacologia*, 20(1): 143–151.

YONGE, C. M., 1981, Functional morphology and evolution in the Tridacnidae (Mollusca: Bivalvia: Cardiacea). *Records of the Australian Museum*, 33(17): 735–777.

YONGE, C. M., 1982, Ligamental structure in Mactracea and Myacea (Mollusca: Bivalvia). *Journal of the Marine Biological Association of the United Kingdom*, 62(1): 171–186.

YONGE, C. M. & B. MORTON, 1980, Ligament and lithodesma in the Pandoracea and the Poromyacea with a discussion on evolutionary history in the Anomalodesmata (Mollusca: Bivalvia). *Journal of Zoology*, 191(2): 263–292.

Revised ms. accepted July 12, 2014

MALACOLOGIA, 2015, 58(1–2): 129–145

GROWTH AND BODY WEIGHT VARIABILITY OF THE INVASIVE MUSSEL *LIMNOPERNA FORTUNEI* (MYTILIDAE) ACROSS HABITAT AND SEASON

Nicolás Bonel[1,2*] & Julio Lorda[3,4]

ABSTRACT

The freshwater mussel *Limnoperna fortunei* is adapted to colonize a wide range of aquatic environments, and its ability to contend with environmental stress through phenotypic plasticity has allowed this species to successfully colonize and become established in new regions. Only limited information is currently available on the wide intraspecific variability of this species in response to environmental heterogeneity. Here, we tested the hypotheses that (1) growth and body weight of mussels from a highly polluted environment differed from those from a less polluted habitat, and (2) growth parameters estimated in this study differed from those reported for other invaded ecosystems. We conducted controlled field experiments in two study sites with differing levels of pollution. To compare our results to those reported elsewhere, we considered growth data from studies performed in different locations. We found that mussels from the more polluted habitat showed lower shell growth and body weight than those from the less polluted environment. We also observed differences in the growth performances of the golden mussel between our estimates and those from other invaded habitats. Our findings provide useful information to better understand the striking intraspecific variability of this species in response to stressful conditions. Knowledge on the phenotypic plasticity of *L. fortunei* is essential for predicting and managing this species.

Key words: invasive species, freshwater bivalve, golden mussel, population dynamics, growth model, weight, water pollution.

INTRODUCTION

Understanding the temporal and spatial variability of invasive species' populations is essential for accurate predictive power and effective management of these populations. Traits common to invasive species include *r*-selected life histories, such as use of pioneer habit, short generation time, high fecundity and high growth rates. In addition, through phenotypic plasticity – adaptation to environmental stress – and high tolerance to environmental heterogeneity, non-native species are able to colonize and successfully establish in new areas (Sakai et al., 2001).

One successful invader, the freshwater golden mussel, *Limnoperna fortunei* (Dunker, 1857) is a bivalve native to Southeast Asia that has been introduced into other regions of Asia and South America over the last few decades (Pastorino et al., 1993). In general, the available information on *L. fortunei* includes its geographic distribution, ecologic interactions, reproductive activity, ecological and economic impacts, and some aspects of its population dynamics (summarized in Boltovoskoy et al., 2009). However, most of the biological and ecological studies of *L. fortunei* have been restricted to specific locations, and therefore the performance of *L. fortunei* among different habitats is unknown (Boltovskoy et al., 2009). Recently, Bonel et al. (2013) found spatial differences in density and growth. They observed that these biological parameters were lower in a more polluted environment, but the growth data obtained from settlement plates in that study was better described by a linear model and did not account for the effect of seasonality on growth.

The life history of an organism implies the allocation of its resources among maintenance,

---

[1] Laboratorio de Zoología de Invertebrados I - Departamento de Biología, Bioquímica y Farmacia, Universidad Nacional del Sur, San Juan No. 670, B8000ICN Bahía Blanca, Buenos Aires, Argentina.
[2] CONICET (Consejo Nacional de Investigaciones Científicas y Técnicas).
[3] Department of Ecology, Evolution, and Marine Biology, University of California, Santa Barbara, California 93106, U.S.A.
[4] Tijuana River National Estuarine Research Reserve, 301 Caspian Way Imperial Beach, California 91932, U.S.A.
*Corresponding author: nbonel@criba.edu.ar

growth, and reproduction, which changes over time with age and/or season (Harvey & Vincent, 1990; Chase & Bailey, 1999) and across geography within different habitats. The growth of *L. fortunei* has been independently estimated for populations established in different habitats in the Neotropical Region and in Asia (Boltovskoy & Cataldo, 1999; Maroñas et al., 2003; dos Santos et al., 2008; Belz et al., 2010; Darrigran et al., 2011; Nakano et al., 2011; Bonel et al., 2013). In bivalves, the magnitude of weight variability over season has been used to estimate fecundity, allocation of resources to reproduction (Hilbish, 1986), and as a general index of physiological condition (Nalepa et al., 1995). Sylvester et al. (2007) estimated the weight-to-length relationship for individuals of *L. fortunei* collected from a single sampling point in the Parana River in South America. However, studies analyzing the spatial and temporal changes in body weight are still inchoate or nil for the golden mussel.

In this paper we address the question of how individual growth and body weight of *L. fortunei* varies in response to environmental heterogeneity and season. Based on data obtained from controlled field experiments in two study sites with differing levels of pollution, we ask whether the high levels of water pollution decrease growth and body weight of *L. fortunei* despite its high tolerance to environmental stress. We also tested the hypothesis that the growth parameters estimated here differed from the corresponding data for mussels established in other habitats worldwide as evidence of the high phenotypic plasticity of *L. fortunei* to environmental heterogeneity. Except for Nakano et al. (2011), the sites referred in those studies we compared do not provide environmental information (Boltovskoy & Cataldo, 1999; Maroñas et al., 2003; dos Santos et al., 2008; Belz et al., 2010; Darrigran et al., 2011). We therefore assume that they are environmentally different from our study sites because they belong to different river systems at different latitudes. Comparative studies are essential in the field of invasion ecology because non-indigenous species' populations and their impacts are not homogeneous in space or time (Boltovskoy et al., 2009). Within the context of global change, the comparative approach of this study will be of great value for understanding the ecology and evolutionary biology of the golden mussel.

METHODS

Study Sites

To perform this study, we selected two water bodies from the Río de la Plata basin, Argentina. The first site was in the Coronda River, a secondary course of the Paraná River (31°41'26.88"S, 60°44'34.08"W). The second site was the Santiago River (34°51'5.76"S, 57°53'29.76"W) located 350 km southeast of the first sampling point. Environmental conditions for the two river systems are fully described in a previous study where the Santiago River is defined as the more polluted environment of the two sites (Bonel et al., 2013).

Sampling Procedure

To study the individual growth and body weight of *Limnoperna fortunei*, we conducted controlled field experiments by following cohorts of mussels placed in cages deployed at the Santiago River and the Coronda River starting in March 2007. The cages had tetrahedral shape (edge: 45 cm, height: 42 cm, basis: 30 cm) in order to diminish resistance to water current. The internal volume of each cage was approximately 12,700 cm^3. Each cage was lined with 1 mm plastic mesh screen to prevent small mussels from escaping and to avoid predation from crabs and fish while allowing water circulation through the cage. However, the cages also allowed entrance of *L. fortunei* larvae. The efficiency of the cage design was tested in a previous study (Darrigran et al., 2011).

First, we collected juveniles of *L. fortunei* from both study sites. Then, we measured the total length (*L*; maximum anteroposterior axis) of all individuals to the nearest 0.01 mm with digital Mitutoyo calipers. In the Coronda River we deployed two cages with 397 and 427 individuals per cage. The average (± SD) shell-length within each cage was 4.27 ± 0.82 and 4.12 ± 0.84 mm; respectively. In the Santiago River we placed three cages with 457, 410, and 452 juveniles per cage with an average (± SD) shell-length of 4.41 ± 0.63, 4.23 ± 0.57, and 4.14 ± 0.67 mm; respectively. Cages were suspended one meter in depth in the rivers and were spaced ten meters apart within the same river. We considered all experimental mussels to be within the same cohort, given their similarity in shell-length (Lévêque, 1971; Vakily, 1992). Mussels attached readily to the interior of the cages, including the plastic mesh, and were usually found in clumps.

Monthly, we randomly subsampled mussels without replacement in both rivers. In the Coronda River we collected an average (± SD) of 21 ± 5 individuals per cage from April 2007 through October 2007. However, when recruitment was observed in December 2007, the average number of individuals subsampled from that month through December 2008 was 184 ± 100. In the Santiago River, we collected 23 ± 5 individuals from May 2007 through September 2007 prior to recruitment, and 337 ± 260 from November 2007 through April 2009 after recruitment.

Size-Structure, Cohort Analysis, and Shell Morphometric Ratios

We measured the shell-length of all individuals collected from each cage. The size-class interval for length-frequency distributions was calculated by means of the Sturges's method previously described by Bonel et al. (2013). To identify cohorts by means of the length-frequency distributions we pooled shell-length data from each replicate and applied the Bhattacharya's method available in FISAT II software (Version 1.2.0, FAO-ICLARM Fish Assessment Tools; Gayanilo et al., 2002). To confirm each component normal distributions from the modal progression analysis, we used the NORMSEP method also available in the FISAT II software (Pauly & Caddy, 1985).

As noted above the mesh screen of cages allowed water circulation as well as entrance of larvae of *L. fortunei*. Bonel et al. (2013) observed that high mussel density yields individuals with more elongated shells, that is, higher length-to-width ratio. Changes in shell morphometry of enclosed mussels could occur due to possible effects of high density or environmental heterogeneity. Thus, it would be likely to find elongated or flattened – length-to-width ratio – mussels in more densely populated cages. Therefore, in those individuals with shell length larger than 3 mm, we additionally measured height and width to compare morphometric ratios between the linear shell dimensions length-to-width (L/W), length-to-height (L/H), and height-to-width (H/W). We transformed the ratios to arc-sine square roots to meet normality and homoscedastic conditions, and we used two-tail *t*-tests to make comparisons between the groups.

Individual Growth

Growth curves were represented by a modified von Bertalanffy growth function (VBGF) with seasonal oscillations, according to Pauly & Gaschütz (1979), Hoenig & Choudary Hanumara (1982), and Somers (1988):

$$L_t = L_\infty \left(1 - exp^{-K\,[(t - t0) + T1 - T2]}\right)$$

$$T_1 = C \sin\left(2\pi\,(t - t_s)\right) / 2\pi$$

$$T_2 = C \sin\left(2\pi\,(t_0 - t_s)\right) / 2\pi$$

where L_t is the predicted length at age t; L_∞ is the asymptotic length, K is the growth constant of dimension time^{-1} (year^{-1} in most seasonally oscillating growth curves) expressing the rate at which L_∞ is approached; t_0 is the theoretical 'age' the mussel have at length zero; C expresses the relative amplitude of the seasonal oscillation and varies between 0 and 1 (0 indicating lack of summer-winter differences in growth); and t_s is the starting point of the oscillation. For visualization, we define the period when growth is slowest as a fraction of the year called the Winter Point (WP = t_s + 0.5). The parameters of the function were estimated by the modeling method available in JMP statistical software (v9.0 SAS Institute) which uses the iterative non-linear Gauss-Newton algorithm. Preliminary results of the oscillating VBGF failed to estimate the asymptotic shell-length (L_∞). Therefore, we used the maximum shell-length (L_{max}) observed in caged conditions at the Coronda and Santiago rivers (L_{max} = 25.22 and 26.17 mm, respectively) to calculate the asymptotic shell-length following the equation suggested by Taylor (1958):

$$L_{max} / 0.95 = L_\infty$$

The asymptotic shell-length obtained for the Coronda River was L_∞ = 26.55 mm while for the Santiago mussels was L_∞ = 27.55 mm. These values were fixed when we performed a second fit. We used the sum of the squares from the *F*-test to compare growth models fitted to cohorts with similar t_0 from each study site. A non-significant *F* statistic indicates that a single growth curve is sufficient to describe the populations being compared (Blanchard & Feder, 2000; Bonel et al., 2013). As t_0 is the theoretical 'age' the mussel have at length zero, we could define t_{max} as the theoretical 'age' the mussel reaches its maximum length (L_{max}). Since L_{max} is dependently related to a maximum point in time (years), we therefore assume that L_{max}

implicates t_{max} ($L_{max} \Rightarrow t_{max}$). Thus, we could approximately express theoretical longevity of a mussel cohort (in years) as:

$$\text{longevity} = t_{max} - t_0$$

We calculated the daily growth rate (GR) for each mussel by dividing the increase in length during each growth interval by the number of days elapsed (Borrero & Hilbish, 1988). To analyze and compare temporal variation of growth rates between sites, we performed a two-way ANOVA and post-hoc Tukey HSD to test for differences among seasons and sites.

To compare growth in terms of length, we used the growth-performance index, phi prime (ϕ') defined by Pauly & Munro (1984) as:

$$\phi' = 2\log_{10} L_\infty + \log_{10} K$$

This criterion was chosen because the negative correlation between growth parameters (K and L_∞) invalidated comparisons based on individual parameters (Vakily, 1992; Ramón et al., 2007). We calculated the growth-performance index using the Growth Performance Indices application available in FISAT II software (Gayanilo et al., 2002), and we performed a *t*-test to compare the indices between the two populations studied here. Alternatively, in order to compare our results to those obtained in other studies we had to calculate growth-performance indices (ϕ') from growth parameters provided in ecological studies of *L. fortunei* that used the von Bertalanffy growth function (Boltovskoy & Cataldo, 1999; Maroñas et al., 2003; Belz et al., 2010). By means of one-sample *t*-test, we tested whether the average growth-performance indices estimated here, and for each study site, differed significantly from those calculated from K and L_∞ reported in published studies.

Body Weight

To analyze and compare body weight between individuals from each site, we used a subsample of individuals collected from cages from the Coronda River (n = 706) and the Santiago River (n = 1,275) following the length-frequency distribution obtained previously for each date and site.

Previous experiments indicated that the weight of individuals lower than 5 mm shell-length was too small for accurate weight measurements, so they were excluded from the analysis. With a scouring pad, we removed byssal threads, sediment, and epibiota before weighing and measuring the organic content of the mussel. We dried individual mussels in porcelain crucibles for 48 hours at 60°C, weighed the mussels with a digital scale (precision, 0.1 mg), ashed the mussels for two hours in a muffle furnace at 500°C, and then reweighed them (Nalepa et al., 1995). Weight values were grouped into size class intervals constructed from length measurements of subsampled mussels.

We analyzed the relationship between ash-free dry weight (AFDW) and length with the allometric equation:

$$\text{AFDW} = a\text{Length}^b$$

where a is the intersect and b the allometric coefficient (or slope) of the equation. The allometric regressions were calculated separately for the two populations from the Coronda and Santiago rivers. The parameters of the allometric function were estimated by the modeling method in JMP statistical software (v9.0 SAS Institute) previously described. The correspondence of the allometric curves fitted to different groups was then tested through the use of the sum of the squares from the *F*-test explained in the *individual growth* methods section. To analyze the effect of spatial variation, we performed an ANCOVA with AFDW as the dependent variable, length as a covariate, and sites as factors. Shell-length and AFDW data were natural-log transformed to obtain linear relationship and to meet the assumptions of normality and homoscedasticity.

Alternatively, we defined the corresponding season (i.e., summer, autumn, winter, and spring) based on the sampling date, and we compared seasonal variation of the average AFDW between sites using two-way ANOVA and post-hoc Tukey HSD to test for differences among seasons and sites. To analyze the relationship between daily growth rates and AFDW of each cohort from each study site, we used nonparametric Spearman's rank correlation test.

RESULTS

Size-Structure, Cohort Analysis, and Shell Morphometric Ratios

We constructed length-frequency distributions based on the length values of 4,870 mussels from the Coronda River from March 2007 through December 2008 (Fig. 1). Polymodal

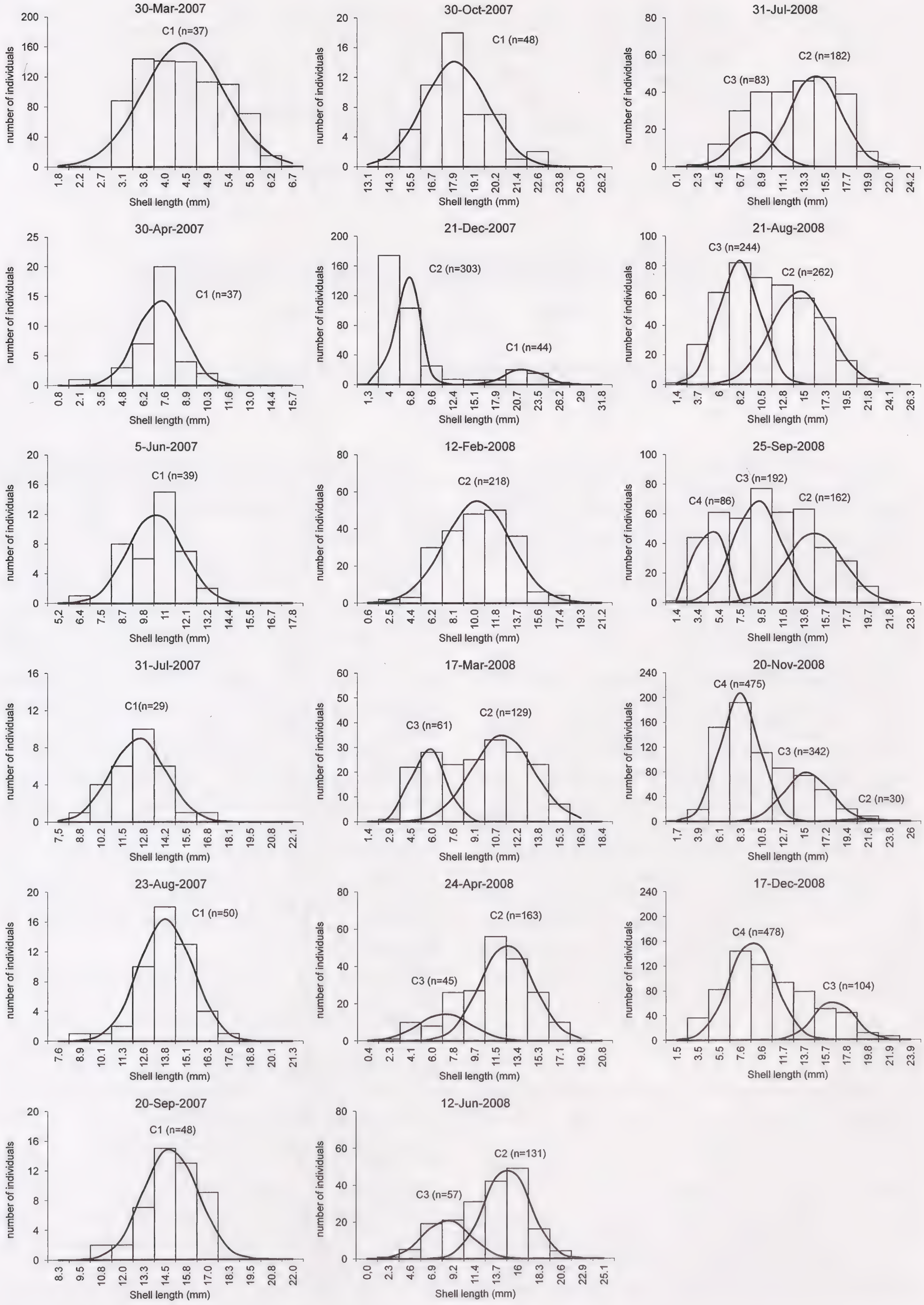

FIG. 1. Length-frequency distribution of *Limnoperna fortunei* from the Coronda River from March 2007 through December 2008; *C*, cohort; *n*, number of mussels from each cohort.

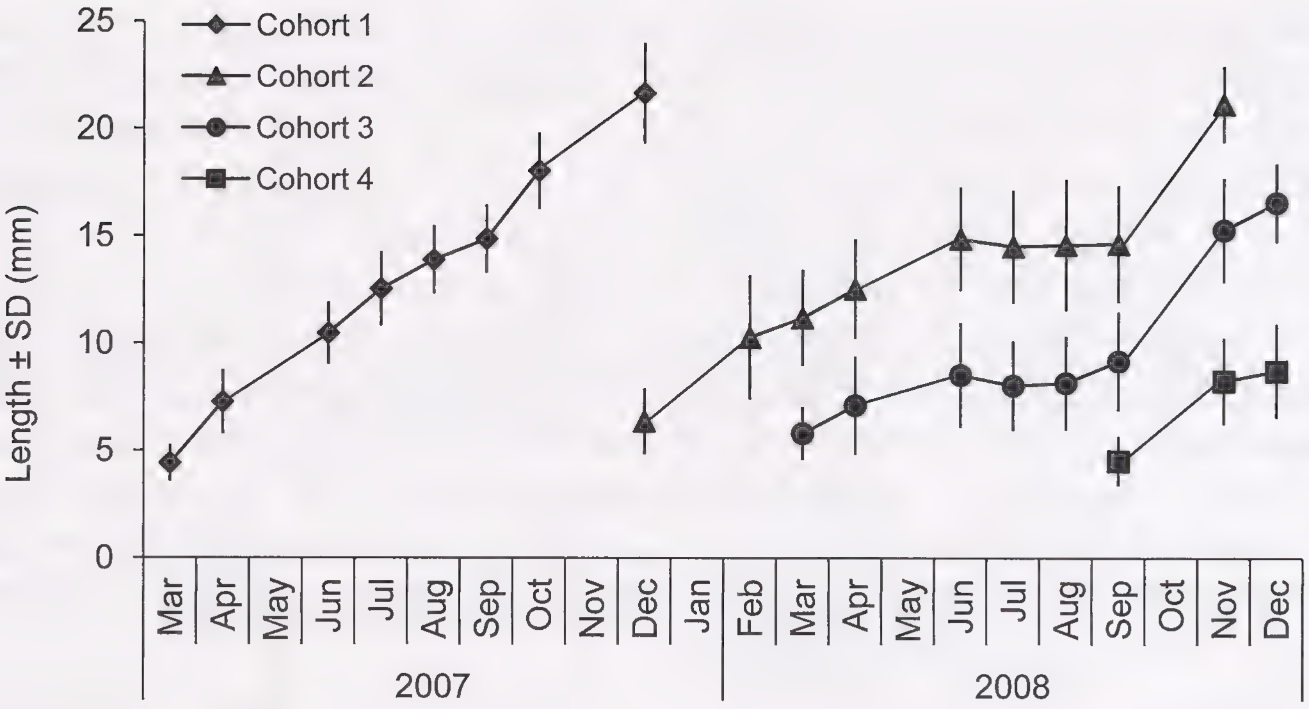

FIG. 2. Cohorts identified from length-frequency distributions. *SD*, standard deviation.

decomposition identified four cohorts throughout the study period (Fig. 2). In the Santiago River, we constructed the length-frequency distributions using 13,582 mussels sampled from March 2007 through April 2009 (Fig. 3) and we identified five cohorts (Fig. 4).

We also measured the height and width of 3,941 individuals from the Coronda and 12,162 from the Santiago Rivers. The measurements on the mussels from the Coronda River had shells of length 1.35 ± 0.06 and 2.55 ± 0.02 times greater than the height and the width, respectively; while the mussels from the Santiago River showed that the shell length was 1.35 ± 0.03 and 2.27 ± 0.19 times greater than the height and the width, respectively. We found that mussels from cages in the Coronda River showed higher length-to-height (L/H: $t_{(35)} = -1.945$, $P = 0.0297$) and length-to-width (L/W: $t_{(35)} = -1.857$, $P = 0.0358$) ratios than those from the Santiago River, but we found no significant differences in height-to-width ratio (H/W: $t_{(35)} = -0.284$, $P = 0.3890$) between the rivers.

Individual Growth

Seasonally oscillating VBGF growth model yielded a high degree of goodness of fit for cohort 1, 2, and 3 from the Coronda River, and for cohort 1 to cohort 4 from the Santiago River (Table 1, Fig. 5). In contrast, cohort 4 from the Coronda River and cohort 5 from the Santiago River were excluded from the analysis because they were only constituted by three modal components that prevented us from appropriately fit the seasonal growth model.

The average growth performance index (ϕ') for mussels from the Coronda River (3.04 ± 0.16 SD, range: 2.93 to 3.23) was higher than Santiago River mussels (2.77 ± 0.18 SD, range: from 2.57 to 2.99) ($t_{(5)} = -2.077$, $P = 0.0464$). In contrast, the theoretical longevity for mussels sampled from the Santiago River was higher than those from the Coronda River ($t_{(5)} = 2.080$, $P = 0.0460$; Table 1 and 2). We analyzed this spatial difference in growth comparing those cohorts that showed similar values of t_0 (Table 1, Fig. 6). Consistent with the estimations of growth performance index, the *F*-test of the sum of squares between the seasonal growth model fitted to cohort 2 from the Coronda River and cohort 3 from the Santiago River gave significant differences ($F_{(2,20)} = 28.960$, $P < 0.001$) as well as the comparison between cohort 3 from the Coronda River and cohort 4 from the Santiago River ($F_{(2,16)} = 249.606$, $P < 0.001$).

The two-way ANOVA used to analyze temporal variation on growth rates showed no significant interaction between sites and seasons ($F_{(3,68)} = 1.355$, $P = 0.2639$); therefore, we removed the effect of interaction from the final analysis. The ANOVA showed significant differences between sites ($F_{(1,71)} = 6.536$, $P = 0.0127$) and between seasons ($F_{(3,71)} = 10.084$, $P < 0.0001$). In average, growth rate was 1.5 times higher in the Coronda River compared to the Santiago River (Table 2). In both sites, the lowest growth rate occurred during winter. The peak of growth in the Coronda River was in spring and about four times the growth during winter. In the

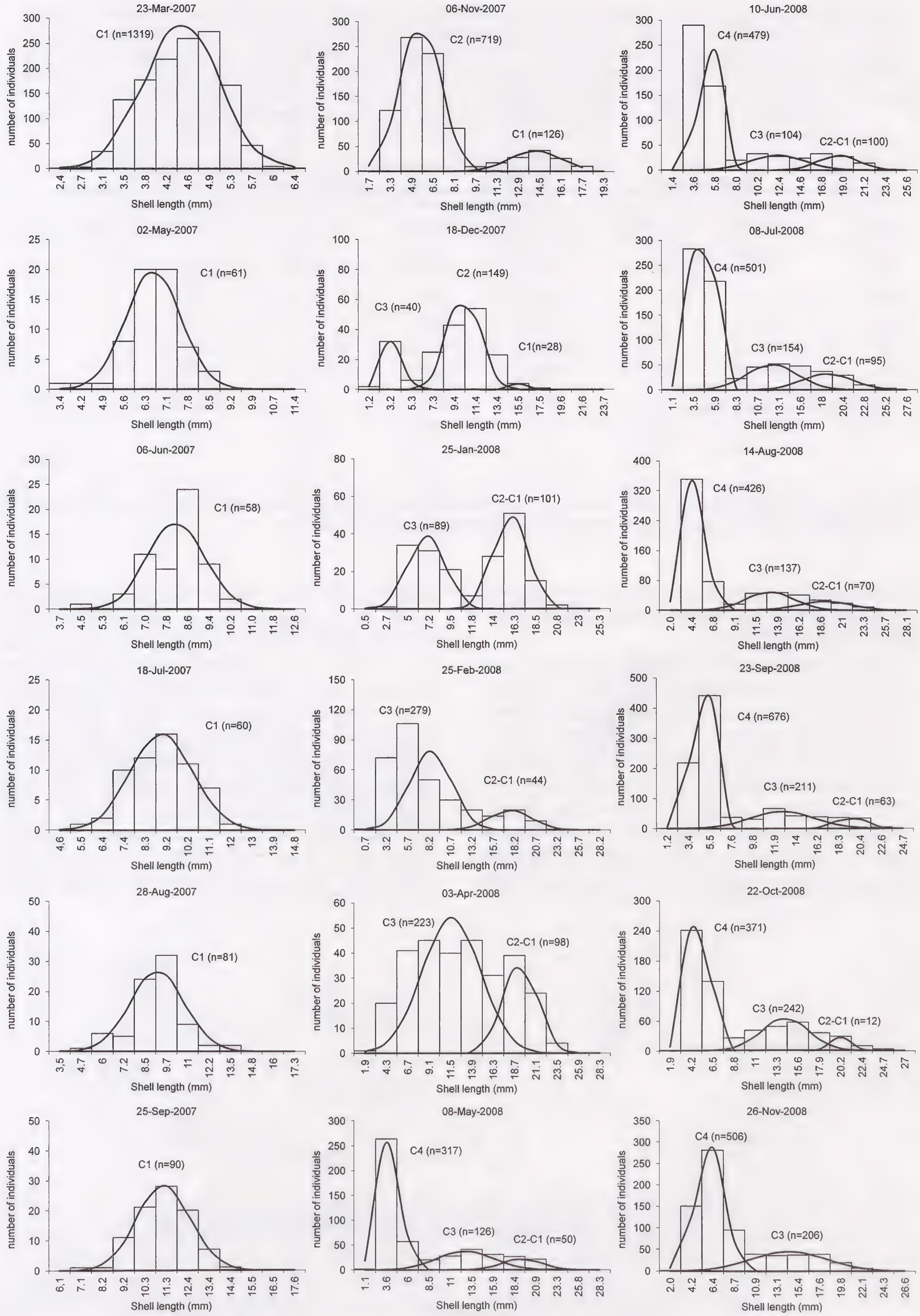
23-Mar-2007
C1 (n=1319)
number of individuals
0 50 100 150 200 250 300
2.4 2.7 3.1 3.5 3.8 4.2 4.6 4.9 5.3 5.7 6 6.4
Shell length (mm)
06-Nov-2007
C2 (n=719)
C1 (n=126)
number of individuals
0 50 100 150 200 250 300
1.7 3.3 4.9 6.5 8.1 9.7 11.3 12.9 14.5 16.1 17.7 19.3
Shell length (mm)
10-Jun-2008
C4 (n=479)
C3 (n=104)
C2-C1 (n=100)
number of individuals
0 50 100 150 200 250 300
1.4 3.6 5.8 8.0 10.2 12.4 14.6 16.8 19.0 21.2 23.4 25.6
Shell length (mm)
02-May-2007
C1 (n=61)
number of individuals
0 5 10 15 20 25
3.4 4.2 4.9 5.6 6.3 7.1 7.8 8.5 9.2 9.9 10.7 11.4
Shell length (mm)
18-Dec-2007
C3 (n=40)
C2 (n=149)
C1(n=28)
number of individuals
0 20 40 60 80 100
1.2 3.2 5.3 7.3 9.4 11.4 13.4 15.5 17.5 19.6 21.6 23.7
Shell length (mm)
08-Jul-2008
C4 (n=501)
C3 (n=154)
C2-C1 (n=95)
number of individuals
0 50 100 150 200 250 300
1.1 3.5 5.9 8.3 10.7 13.1 15.6 18 20.4 22.8 25.2 27.6
Shell length (mm)
06-Jun-2007
C1 (n=58)
number of individuals
0 5 10 15 20 25 30
3.7 4.5 5.3 6.1 7.0 7.8 8.6 9.4 10.2 11.0 11.8 12.6
Shell length (mm)
25-Jan-2008
C3 (n=89)
C2-C1 (n=101)
number of individuals
0 20 40 60 80
0.5 2.7 5 7.2 9.5 11.8 14 16.3 18.5 20.8 23 25.3
Shell length (mm)
14-Aug-2008
C4 (n=426)
C3 (n=137)
C2-C1 (n=70)
number of individuals
0 80 160 240 320 400
2.0 4.4 6.8 9.1 11.5 13.9 16.2 18.6 21 23.3 25.7 28.1
Shell length (mm)
18-Jul-2007
C1 (n=60)
number of individuals
0 5 10 15 20 25
4.6 5.5 6.4 7.4 8.3 9.2 10.2 11.1 12 13 13.9 14.8
Shell length (mm)
25-Feb-2008
C3 (n=279)
C2-C1 (n=44)
number of individuals
0 30 60 90 120 150
0.7 3.2 5.7 8.2 10.7 13.2 15.7 18.2 20.7 23.2 25.7 28.2
Shell length (mm)
23-Sep-2008
C4 (n=676)
C3 (n=211)
C2-C1 (n=63)
number of individuals
0 100 200 300 400 500
1.2 3.4 5.5 7.6 9.8 11.9 14 16.2 18.3 20.4 22.6 24.7
Shell length (mm)
28-Aug-2007
C1 (n=81)
number of individuals
0 10 20 30 40 50
3.5 4.7 6 7.2 8.5 9.7 11 12.2 13.5 14.8 16 17.3
Shell length (mm)
03-Apr-2008
C3 (n=223)
C2-C1 (n=98)
number of individuals
0 10 20 30 40 50 60
1.9 4.3 6.7 9.1 11.5 13.9 16.3 18.7 21.1 23.5 25.9 28.3
Shell length (mm)
22-Oct-2008
C4 (n=371)
C3 (n=242)
C2-C1 (n=12)
number of individuals
0 60 120 180 240 300
1.9 4.2 6.5 8.8 11 13.3 15.6 17.9 20.2 22.4 24.7 27
Shell length (mm)
25-Sep-2007
C1 (n=90)
number of individuals
0 10 20 30 40 50
6.1 7.1 8.2 9.2 10.3 11.3 12.4 13.4 14.4 15.5 16.5 17.6
Shell length (mm)
08-May-2008
C4 (n=317)
C3 (n=126)
C2-C1 (n=50)
number of individuals
0 50 100 150 200 250 300
1.1 3.6 6 8.5 11 13.5 15.9 18.4 20.9 23.3 25.8 28.3
Shell length (mm)
26-Nov-2008
C4 (n=506)
C3 (n=206)
number of individuals
0 50 100 150 200 250 300 350
2.0 4.2 6.4 8.7 10.9 13.1 15.4 17.6 19.8 22.1 24.3 26.6
Shell length (mm)

(continues)

(continued)

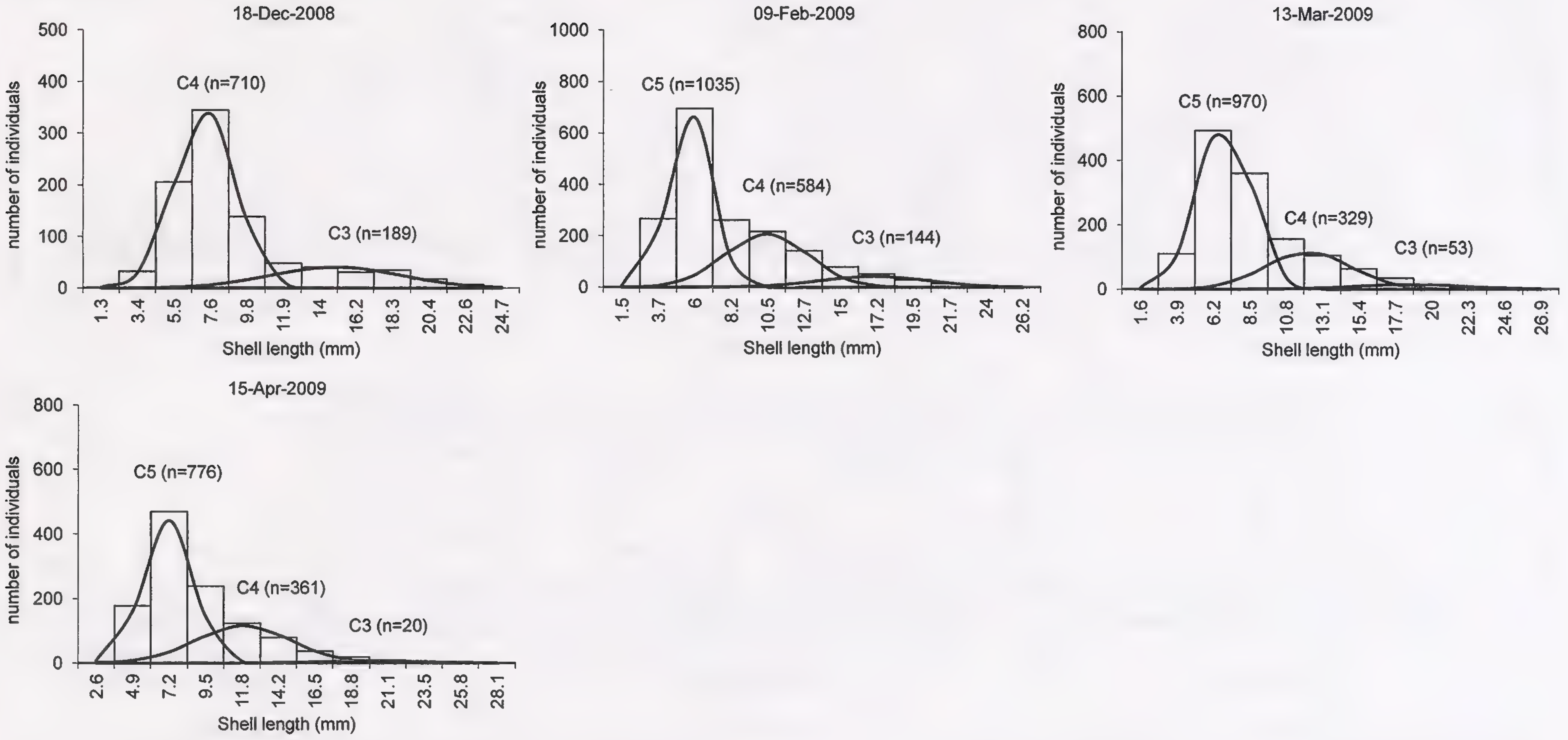

FIG. 3. Length-frequency distribution of *Limnoperna fortunei* from the Santiago River from March 2007 through April 2009; *C*, cohorts; *n*, number of mussels from each cohort.

Santiago River, growth peaked during summer and was about six times greater than winter growth (Fig. 7).

Growth-performance indices (ϕ') calculated from growth parameters provided in other works that used the von Bertalanffy growth function are summarized in Table 2 along with the shell growth rates reported in different studies carried out in the species' area of origin and other locations where the golden mussel has been introduced. The average growth-performance index of mussels from the Coronda River was significantly higher than the Bagliardi Beach, Argentina (one-tailed $t_{(2)}$ = 3.984, P = 0.0288), it was not different from the Paraná de las Palmas, Argentina (one-tailed $t_{(2)}$ = -0.524, P = 0.3262), and it was lower than the index from the Bela Vista Reservoir, Brazil (one-tailed $t_{(2)}$ = -5.137, P = 0.0179). In contrast, the average growth-performance index of mussels from the Santiago River was significantly lower than the index from Paraná de las Palmas (one-tailed $t_{(3)}$ = -3.666, P = 0.0176) and the Bela Vista Reservoir (one-tailed $t_{(3)}$ = -8.667, P = 0.0016) but was not different from the growth-performance index

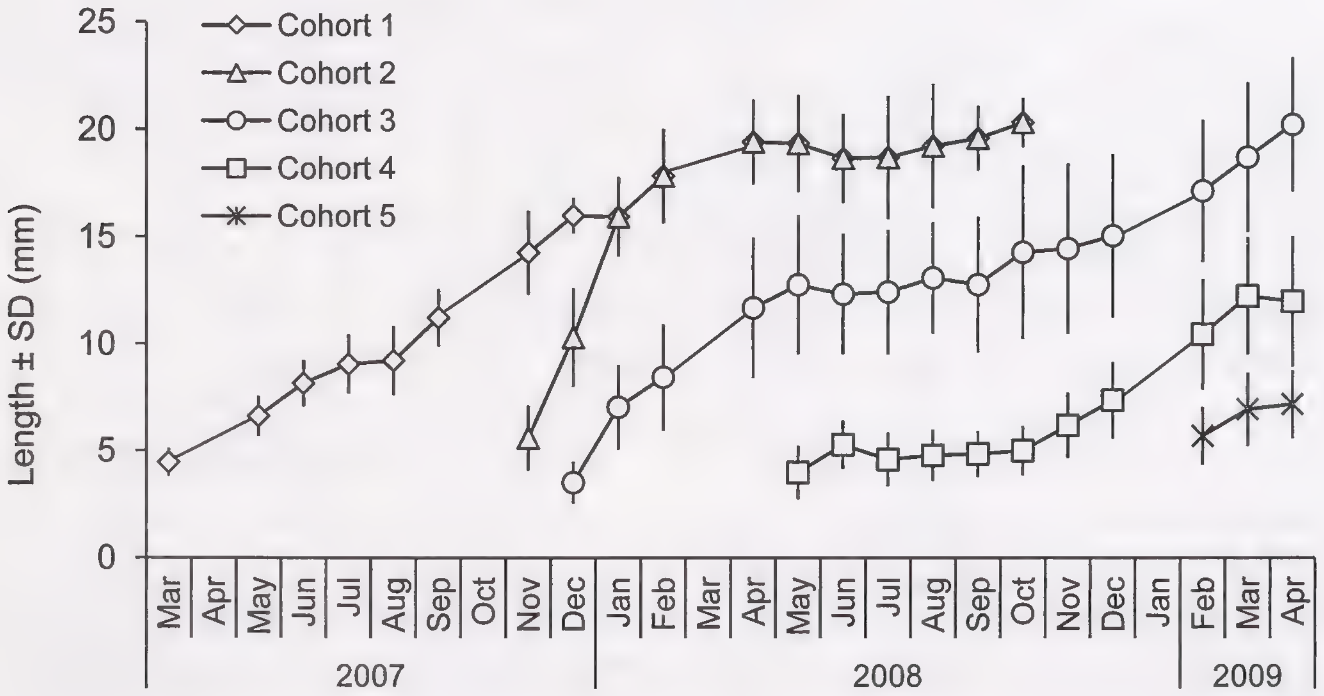

FIG. 4. Cohorts identified from length-frequency distributions. *SD*, standard deviation.

TABLE 1. Seasonally oscillating von Bertalanffy growth function parameters of cohorts of two populations of *Limnoperna fortunei* from contrasting aquatic environments (the Coronda and Santiago rivers) from the Río de la Plata basin. L_∞ is asymptotic length (mm), K is the growth constant (year^{-1}), t_0 is age at zero length (fraction of the year), C is the oscillation amplitude parameter, WP is the winter point, and ϕ' is the growth performance index. The coefficient of determination for nonlinear regressions estimated according to Brey (2001) is denoted with R^2, and the number of data points is denoted with n.

	Coronda River			Santiago River			
Parameters	Cohort 1	Cohort 2	Cohort 3	Cohort 1	Cohort 2	Cohort 3	Cohort 4
L_∞	26.55	26.55	26.55	27.55	27.55	27.55	27.55
K	2.42	1.22	1.28	0.83	1.31	0.68	0.49
t_0	0.18 (Summer)	0.85 (Spring)	1.08 (Summer)	-0.01 (Spring)	0.73 (Winter)	0.81 (Spring)	1.14 (Summer)
C	0.610	0.777	1.000	0.552	1.000	1.000	1.000
WP	2.50	1.39	1.47	2.40	1.47	0.57	0.98
ϕ'	3.23	2.93	2.96	2.80	2.99	2.71	2.57
Longevity	1.3	2.6	2.4	3.5	2.3	4.2	6.4
R^2	0.997	0.916	0.974	0.981	0.978	0.988	0.979
n	8	9	8	17	11	15	11

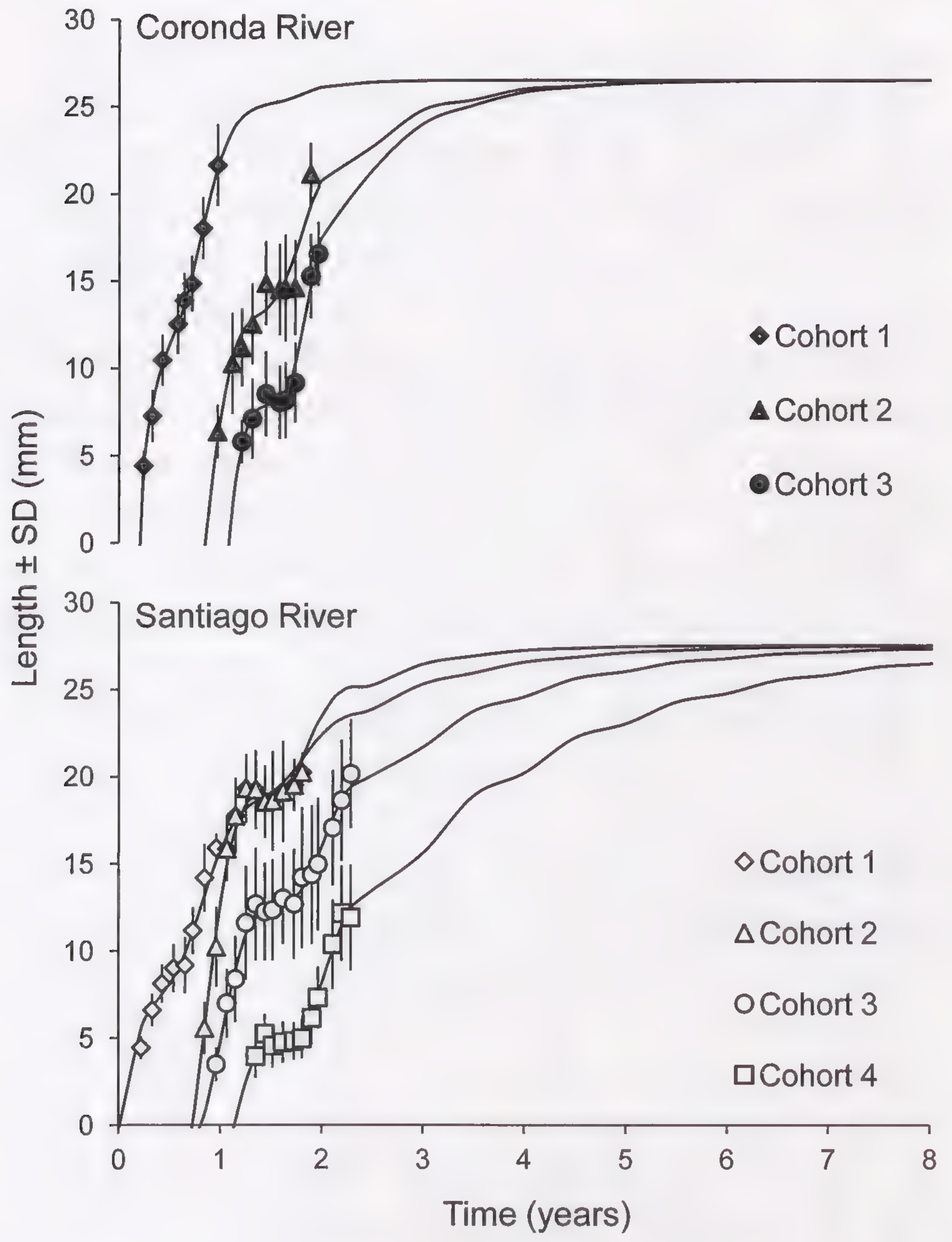

FIG. 5. Seasonally oscillating von Bertalanffy growth curve fitted to each cohort of the two populations of *Limnoperna fortunei* from the Coronda and Santiago rivers. Time is calculated as fractions of the year starting from 1 January 2007. *SD*, standard deviation.

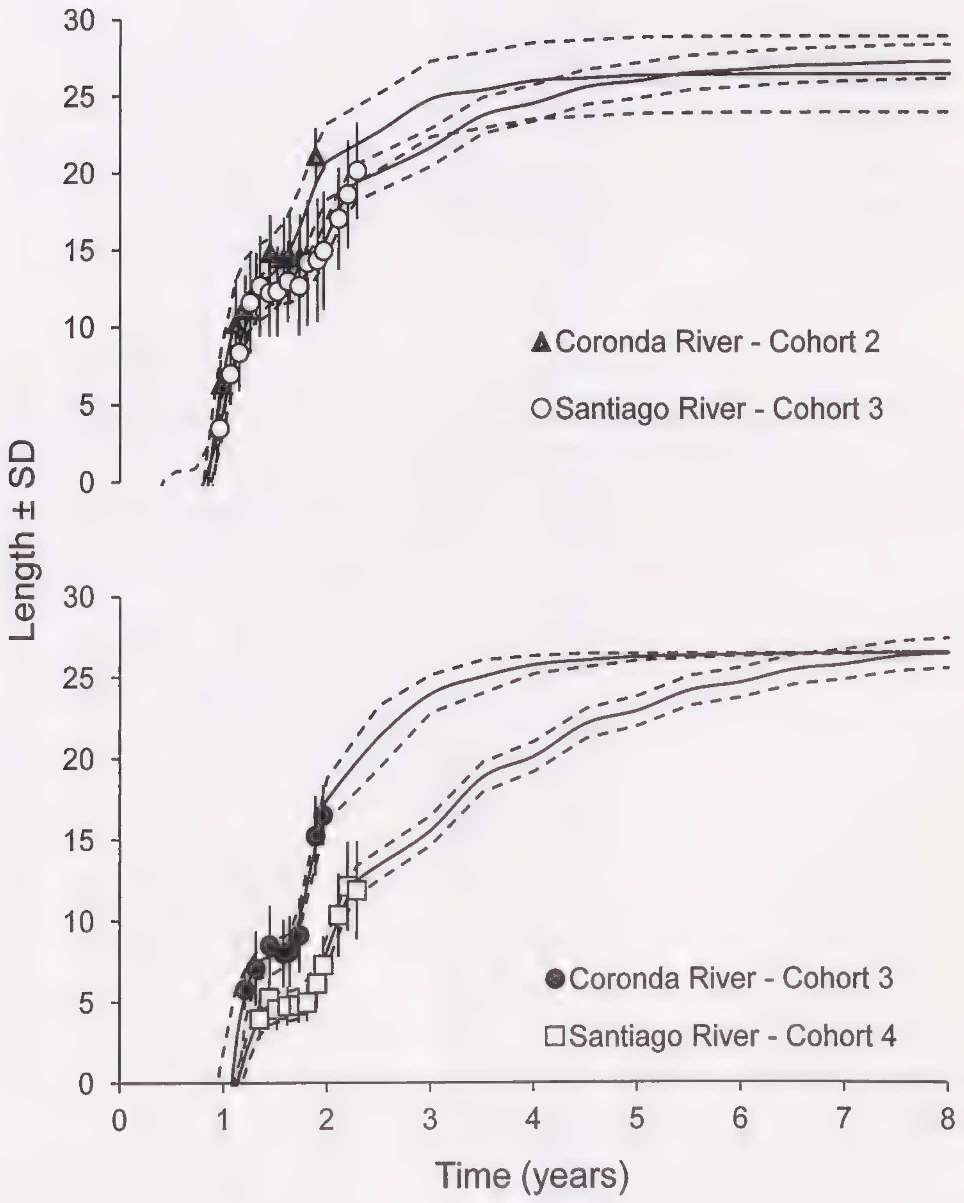

FIG. 6. Seasonally oscillating von Bertalanffy growth curve fitted to cohorts from both populations of *Limnoperna fortunei* with similar t_0 from the Coronda and Santiago rivers. Time is calculated as fractions of the year starting from 1 January 2007. Dotted lines indicate confidence limits of predictive model.

TABLE 2. Growth data (mean ± SD) from different populations of *Limnoperna fortunei*. *SGVBF*, Seasonally oscillating von Bertalanffy growth function; *VBGF*, Standard von Bertalanffy growth function; *SGR*, Shell growth rate indicated by the coefficient (*b*) of the linear growth model (y = *a* + *b*x) or estimated as the difference between the initial and the final shell length divided by the number of days elapsed; *ND*, No data available. Abbreviations are indicated in Table 1. (*Study in native distribution range, otherwise from invasive distribution.)

Country	Study Site	Growth Model	SGR (mm day^{-1})	L_∞ (mm)	*K* (year^{-1})	C	ϕ'	Longevity	Reference
Argentina	Paraná de las Palmas	SGVBF	ND	35.00	1	1	3.09	3	Boltovskoy & Cataldo (1999)
	Bagliardi Beach	VBGF	ND	36.00	0.35 ± 0.02	ND	2.66 ± 0.03	3.5	Maroñas et al. (2003)
	Coronda River	Linear	0.056 ± 0.012	ND	ND	ND	ND	ND	Bonel et al. (2013)
	Santiago River	Linear	0.031 ± 0.007	ND	ND	ND	ND	ND	Bonel et al. (2013)
	Coronda River	SGVBF	0.045 ± 0.036	26.55	1.64 ± 0.67	0.80 ± 0.20	3.04 ± 0.16	2.1 ± 0.7	This paper
	Santiago River	SGVBF	0.030 ± 0.035	27.55	0.83 ± 0.35	0.89 ± 0.22	2.77 ± 0.18	4.1 ± 1.7	This paper
Brazil	Guaíba Lake	ND	0.041 ± 0.011	ND	ND	ND	ND	ND	dos Santos et al. (2008)
	Bela Vista Reservoir	VBGF	ND	38.00	2.36 ± 0.41	ND	3.53 ± 0.07	3.1	Belz et al. (2010)
Japan	Uji River	ND	0.048 ± 0.007	ND	ND	ND	ND	2	Iwasaki & Uryu (1998)
	Lake Biwa-Yodo River system	ND	0.041	ND	ND	ND	ND	2	Magara et al. (2001)
China*	Lake Ohshio	ND	0.026	ND	ND	ND	ND	ND	Nakano et al. (2011)
	Plover Cove	ND	0.057 ± 0.010	ND	ND	ND	ND	2	Morton (1977)

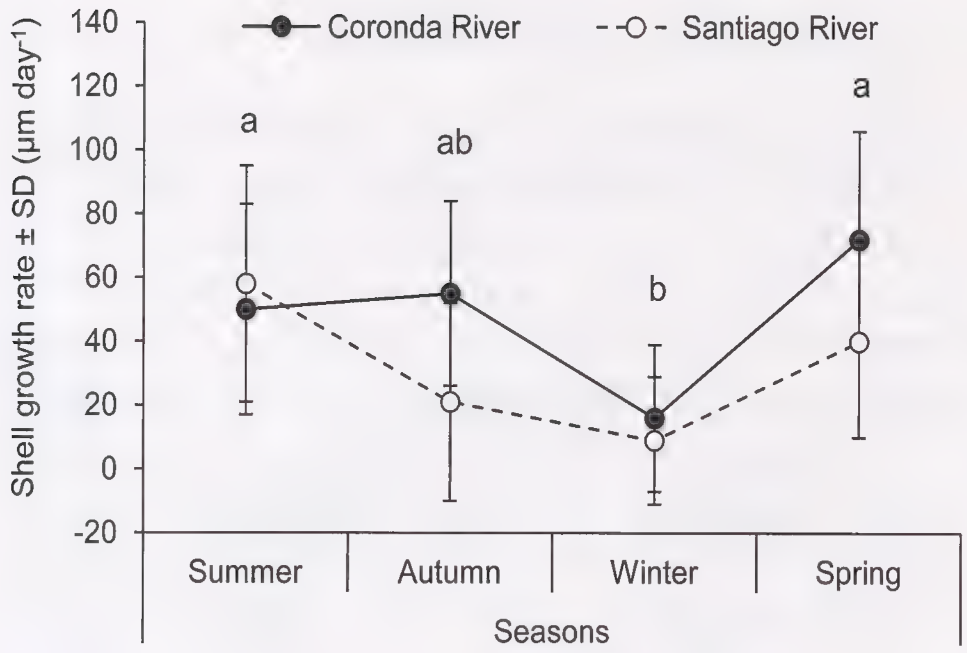

FIG. 7. Results of two-way ANOVA and Tukey HSD test for seasonal variation of growth rate (GR). Different letters (a-b) indicate significant differences of GR between seasons. *SD*, standard deviation.

from the Bagliardi Beach (one-tailed $t_{(3)}$ = 1.222, P = 0.8455).

Body Weight

We found significant differences in the weight-to-length relationship between individuals from both study sites ($F_{(2,21)}$ = 3.467, P = 0.0105). The allometric regressions indicated a negative allometry for mussels from the Coronda River (b = 1.995; Fig. 8A) and the Santiago River (b = 1.686; Fig. 8A). In both allometric models, we observed an increase in the standard deviation of AFDW in mussels with length greater than 13 mm (Fig. 8A). The ANCOVA we used to explain the spatial differences of weight showed a significant interaction between length and sites ($F_{(1,19)}$ = 8.807, P = 0.0079; Fig. 8B). The significant interaction between site and length means that the slopes of the relationship between length and AFDW has different slopes for the different sites with the AFDW being greater at the Coronda River compared to the Santiago River, as mussels get bigger, but the opposite in small mussels (Fig. 8B).

The two-way ANOVA used to explain seasonal variation of AFDW between sites and seasons showed significant differences between seasons ($F_{(3,29)}$ = 5.215, P = 0.0053) but no significant differences between sites ($F_{(1,29)}$ = 0.4967, P = 0.4866) nor were there significant interactions of both variables ($F_{(3,29)}$ = 0.8408, P = 0.4826). In both sites, the highest weight was observed during spring, and it was about two to six times the weight in the summer and autumn (Fig. 9). Growth rate of shell and AFDW of each cohort in both sites were uncoupled; these variables showed no significant correlation between them (Fig. 10).

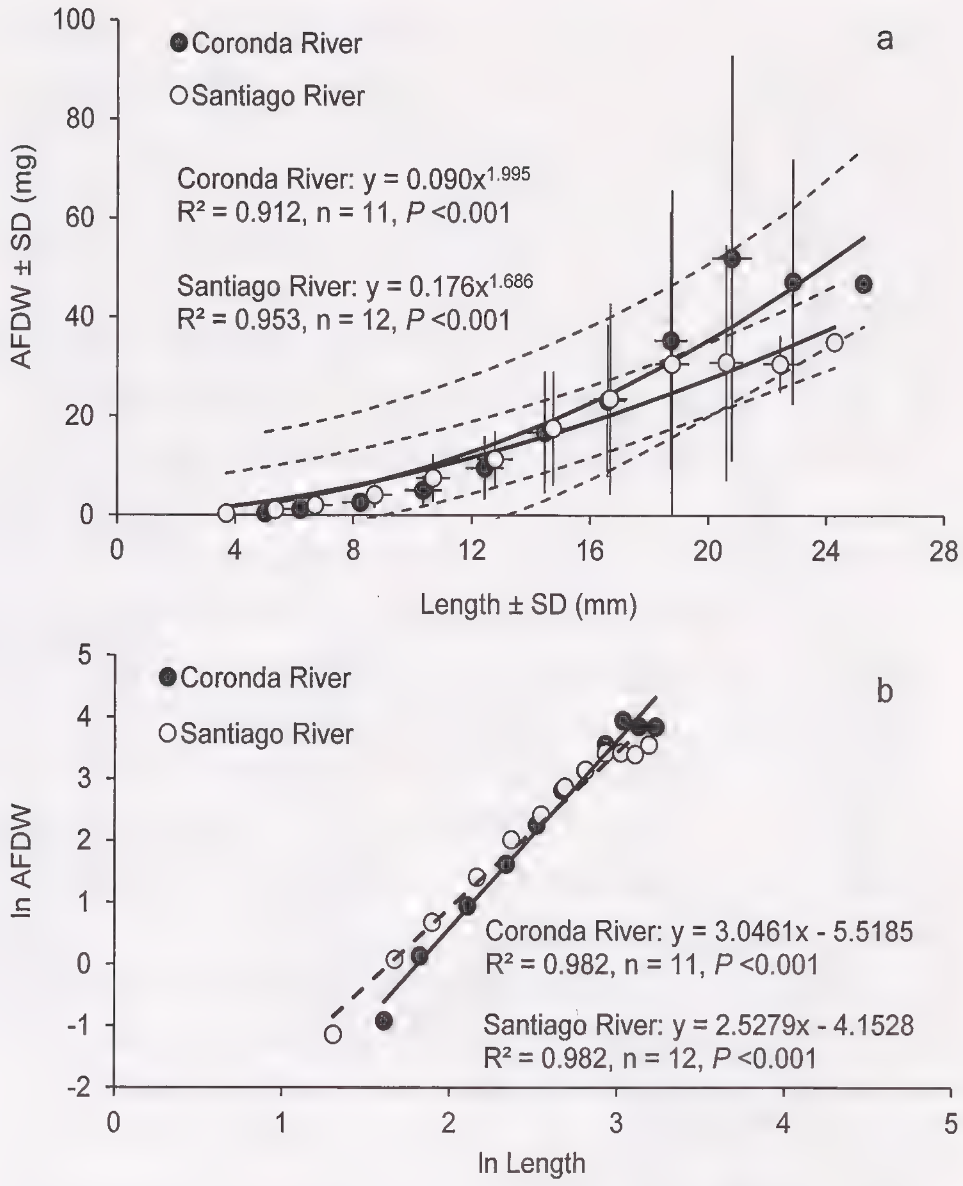

FIG. 8. Allometric relationships. A) Allometric relationships (AFDW = a Length ^{b}) between shell length and ash-free-dry-weight (AFDW); B) Allometric relationships (ln AFDW = a + b ln Length) between ln-transformed parameters. *SD*, standard deviation. Dotted lines indicate confidence limits of predictive model.

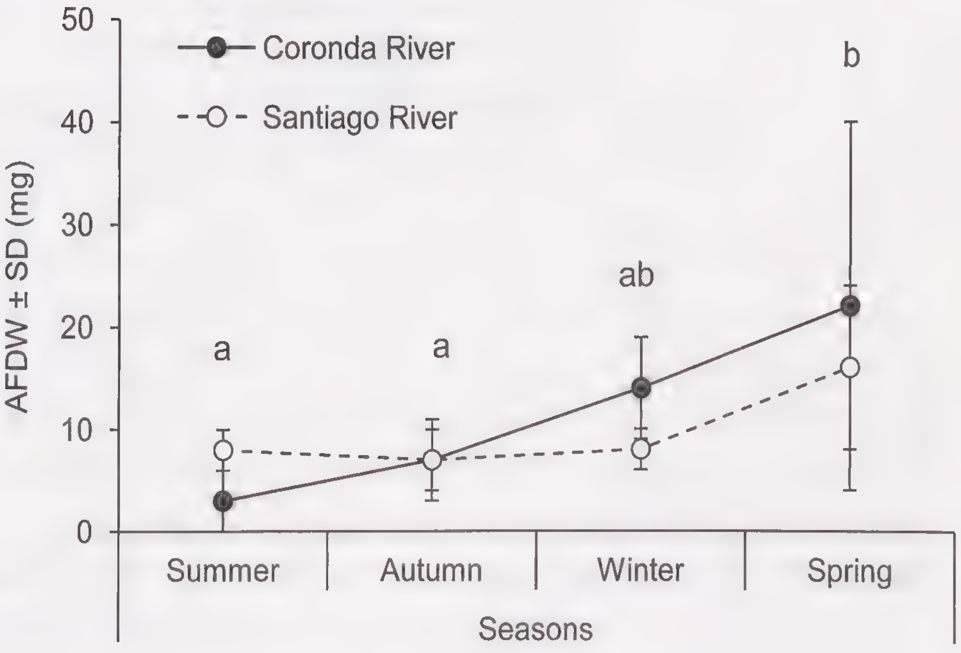

FIG. 9. Results of two-way ANOVA and Tukey HSD test for seasonal variation of ash-free-dry-weight (AFDW). Different letters (a-b) indicate significant differences of AFDW between seasons. *SD*, standard deviation.

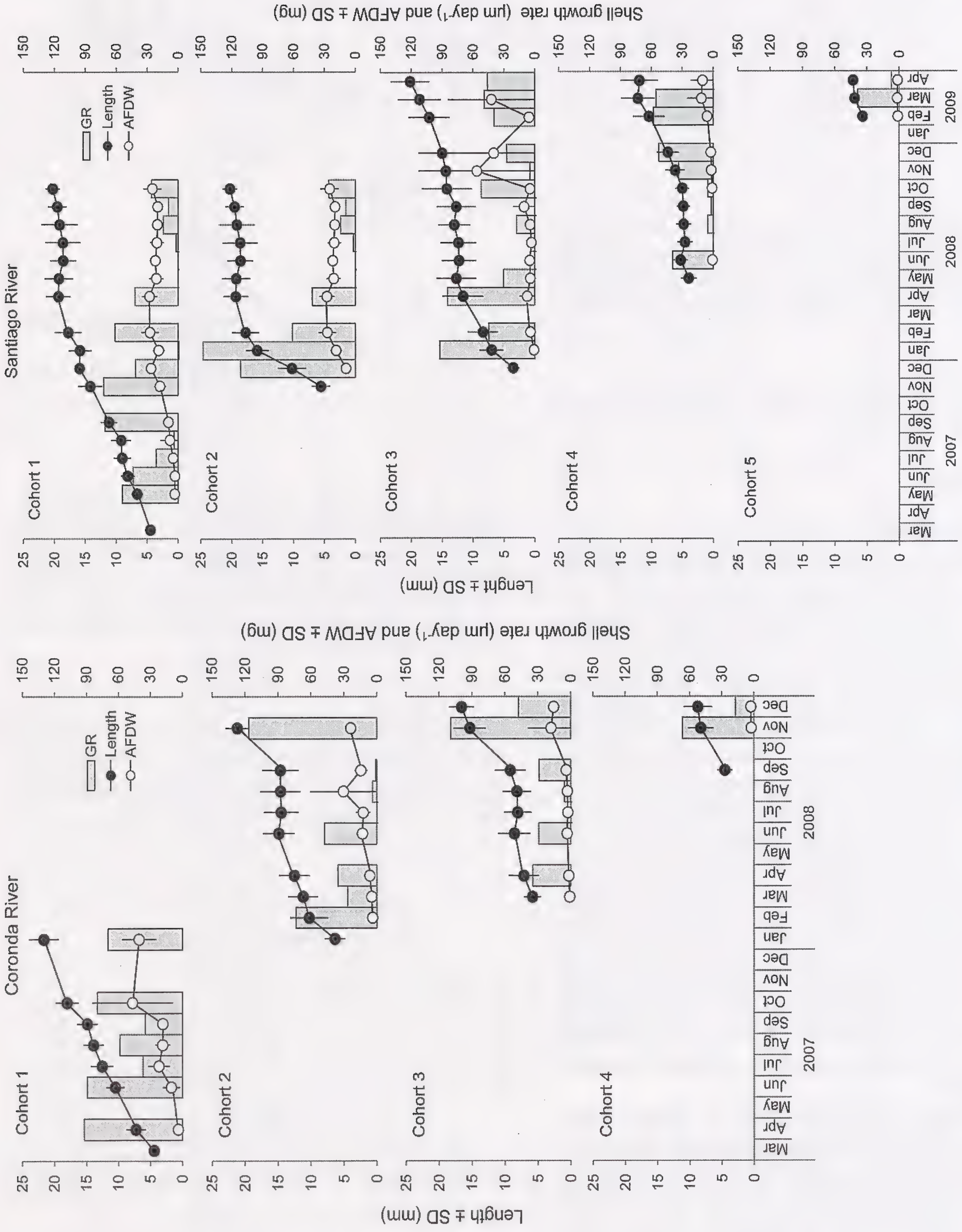

FIG. 10. Growth rate of shell length (GR) and ash-free-dry-weight (AFDW) plotted against shell length (L) increment of each cohort throughout the experimental period at each study site. *SD*, standard deviation.

DISCUSSION

The present work has documented for the first time the effects of environmental variability and seasonality on the individual growth and body weight of *Limnoperna fortunei*. We found evidence supporting our predictions that the individual growth and weight of *L. fortunei* were both lower in the more polluted habitat. The comparative approach of this work revealed differences between the growth-performance indices estimated here and those calculated from ecological studies in other ecosystems. We also found the first evidence of temporal variation in shell growth and body weight in both mussel populations. We observed the lowest shell growth rates in winter while the mussel weight became the highest in the spring.

In previous work, Bonel et al. (2013) found that individuals of *L. fortunei* established in highly polluted environments showed a decrease in growth, but the authors indicated that the linearized model was the best one to explain growth on the basis of their data. Therefore, they did not account for the effect of seasonality on growth. In contrast, we found significant evidence of temporal variation in growth, both within and among populations. The average amplitude of the seasonal oscillation for both study sites obtained from the seasonalized von Bertalanffy growth function indicated a high variation in growth between summer and winter (Table 2). This result was consistent with seasonal differences in growth rates, which values were significantly lower during the winter and four to six times higher during the spring and summer in both aquatic environments.

Although we observed similar seasonal patterns in growth between the two populations, we also found spatial differences. When cohorts with similar values of t_0 were compared, we observed that the growth in the Santiago River was significantly lower. In fact, mussels from the more polluted environment showed, on average, lower growth-performance indices than individuals from the less polluted habitat. As opposed to the Coronda River, the Santiago River is subjected to sewage input from large and small coastal cities, industrial waste discharge, and spills of oil and other materials associated with maritime transport and shipyard activities (cf. Bonel et al., 2013). Bivalves exposed to habitats that are heavily polluted tend to bioaccumulate inorganic and organic contaminants and can respond to stress by exhibiting poor growth and a decline in body weight that can, in turn, negatively affect reproduction (Widdows & Donkin, 1992; Stirling & Okumus, 1994; Alfaro et al., 2008). Our results support and extend the conclusion provided by Bonel et al. (2013) that the high level of pollution in the Santiago River decreased the growth of *L. fortunei.*

Mollusks including bivalves tend to exhibit negative density-dependent growth (Alunno-Bruscia et al., 2000). In these experiments, we did not estimate the density inside the cages and even though we placed a known initial number of mussels inside the cages, densities increased throughout the experiment due to recruitment of larvae produced inside and/or outside the cages. Thus, the negative effect of pollution on the growth of *L. fortunei* might be confounded with negative density-dependent effects. Bonel et al. (2013) found that at high densities these mussels became more elongated – that is, they exhibited higher length-to-width ratios than mussels at the lower densities. Therefore, if density within the cages had become high enough to negatively affect growth, we might have expected to see also an effect on mussel morphology. On the basis of the number of individuals sampled, the abundance of mussels within the cages in the Santiago River appeared to be higher. As indirect evidence of density-dependent effects, we therefore would have expected that the individuals from that site would have been characterized by higher morphometric shell ratios than the mussels from the Coronda. Instead, we found that individuals from the Coronda River showed higher morphometric ratios than those from the Santiago River. According to size-structure, the number of individuals sampled in the Santiago River consisted of a high percentage of small individuals (69% with shell-length = 5.85 ± 1.43 mm), whereas in the Coronda River that size class (shell-length = 5.92 ± 1.24 mm) represented only 28% of the total of individuals collected (Figs. 1 and 3). We thus believe that the density within cages in the Santiago River was not the primary cause affecting mussel growth because the population density pressure caused by small individuals appeared to not be significant to even affect shell morphometrics. Instead, we favor the interpretation that the higher levels of pollution in the Santiago River was the more influential condition exerting the physiologic stress on the mussels that significantly decreased their growth. Nevertheless, we are aware that our data might be insufficient to support this hypothesis firmly. In order to understand the density-dependent effects upon the biology of *L. fortunei*, future laboratory and field studies are needed.

Previous to the present work no study had compared the growth between different locations where *L. fortunei* had become established. We found that, on average, individuals from the more polluted environment showed a lower growth-performance index than mussels from the less polluted habitat. In addition, the average growth-performance index that we estimated from Boltovskoy & Cataldo (1999) was higher than that from the Santiago River but showed no difference from the one from the Coronda River. In contrast, the index from Maroñas et al. (2003) was lower than the one from the Coronda River and showed no differences in the average value from that of the Santiago River. So far, we have compared growth-performance indices estimated for mussels living in a temperate climate, but the index estimated from a study in a subtropical area (Belz et al., 2010) was significantly higher than the average indices obtained in the present work. The spatial differences in growth-performance indices found in this study emphasize the high variability of growth in response to environmental heterogeneity. Nevertheless, the comparative results between our data and the indices from Maroñas et al. (2003) and Belz et al. (2010) should be regarded with caution. The growth parameters (L_∞ and K) in those two studies were estimated by means of the standard von Bertalanffy growth function instead of the seasonalized version used by us and in the work of Boltovskoy & Cataldo (1999). According to Pauly (1990), growth models that do not explicitly consider seasonal oscillations fail to capture an essential aspect of the growth process. We believe that the growth-performance indices that we estimated by means of parameters from these studies may be under- or overestimated, so that the differences we found could be biased.

In this study, we found that the weight-to-length relationships showed a strong negative allometry for mussels from the Coronda and Santiago rivers but that the allometric coefficient was significantly lower for mussels from the Santiago River. A negative allometric exponent indicates that mussels grew relatively slower in mass than in length (Alunno-Bruscia et al., 2001). In addition, the weight-to-length relationship in mollusks provides a measure of the relative condition or nutritional state of the population (Nalepa et al., 1995). Thus, mussels from a more polluted environment would grow significantly slower in mass versus length than mussels from a less polluted site, reflecting a diminished physiological condition in response to the higher levels of pollution.

The relationship between length and weight and the significant interaction between the covariate (length) and the factor (sites) (Fig. 8B) might be a result of Santiago's mussels allocating more energy for reproduction early on in response to the stressful environmental conditions (Petes et al., 2007) in the Santiago River. Many organisms exhibit early spawning in response to stress (Petes et al., 2007, 2008). In fact, we observed a recruitment event that occurred during the winter period in the Santiago River (cohort 2) but it was absent in the Coronda River. We believe that the physiological stress caused by higher levels of pollution in the Santiago River might have induced those mussels to allocate energy from growth into reproduction and caused that earlier spawning in winter. This hypothesis agrees with the fact that small individuals in the Santiago River showed higher weight than those in the Coronda River, though this relationship changed when individuals became larger. Organisms continually adjust physiological processes and energy allocation in response to varying environmental conditions in order to minimize negative effects on growth, reproduction, and survival (Stoeckmann & Garton, 2001). The hypothesis of energy allocation from growth into reproduction as an adaptive response to stress of the Santiago River's mussels could also explain the difference in growth between the two populations, with the Coronda River's mussels growing faster compared to Santiago River's mussels.

We observed that weight of both populations of *L. fortunei* was significantly higher in spring and lower in summer and autumn. Annual weight variation is commonly the result of cyclical periods of gamete production and release (van Ekrom Schurink & Griffiths, 1993; Steffani & Branch, 2003). As temperatures increase, spawning is initiated and weight loss occurs throughout the summer months until a minimum weight occurs in late summer to early autumn (Nalepa et al., 1995). Observations on spawning in field populations provide the most reliable evidence of the natural process, but the same conclusions can also be inferred from the appearance of larvae in plankton or the recruitment of juvenile mussels into populations (Seed & Suchanek, 1992). The highest peaks of larval densities and recruitment of *L. fortunei* occurring from late spring through the beginning of autumn in the Coronda and Santiago rivers (Bonel et al., 2013) are consistent with the seasonal changes of body weight observed in this study.

In the present work, we found no correlation between the seasonal patterns of shell and weight growth. In general, shell growth occurs regularly – though at different rates in temperate climates – while weight fluctuates widely with respect to the size at which mussels attain maturity, as a result of cyclical periods of gamete production and release (van Ekrom Schurink & Griffiths, 1993). We observed that weight was highly variable in mussels greater than 13 mm in shell-length (Fig. 10), probably because of the full or partial gamete release that occurred during spring and summer. The highest larval densities reported by Bonel et al. (2013) during those seasons would support our observations. Nevertheless, an apparent decline in weight could also be a result of the rapid change in the covariate, shell length (Hilbish, 1986). According to Palmer (1981), this situation reflects a strategy to increase the habitable volume of shells in anticipation of future soft-tissue growth. Therefore, shell morphology alone may not be a sufficient indicator of the condition of the population (Chase & Bailey, 1999).

In conclusion, our findings demonstrate for the first time how environmental stress and seasonality affect individual growth and body weight of *L. fortunei*, both within and among populations. Different studies concluded that the golden mussel tolerates a wide range of environmental conditions (Ricciardi, 1998; Karatayev et al., 2007; Oliveira et al., 2010), but the lower growth and body weight observed in the mussels from the more polluted sites in this study might be a consequence of diminished physiological condition. Our results confirm and extend the spatial differences in density, shell allometry and growth reported previously by Bonel et al. (2013) and help in our understanding of the influence of environmental heterogeneity on the biological and ecological processes of *L. fortunei*. In the face of the predicted increase in stressful environmental conditions brought about by climate change, future laboratory and field studies are needed to garner a better comprehension of the adaptive responses of this worldwide invasive species to multiple stressors over space and time.

ACKNOWLEDGEMENTS

We thank the anonymous referees for their critical review of the manuscript and constructive suggestions. NB was supported by a CONICET fellowship to carry out this research. NB thanks Dr. G. A. Darrigran (Staff researcher, CONICET) for introducing him to this invasive species. NB is also grateful to Dr. N. J. Cazzaniga (Staff researcher, CIC) for his support and to Dr. C. Ituarte (Staff researcher, CONICET) for providing helpful suggestions on early stages of this manuscript. The authors express their gratitude to S. Teck and D. F. Haggerty for their comments and edits on the manuscript, and to the La Plata Port Consortium Management (La Plata city) and the Amphibious Engineer Battalion (Santo Tomé city, Santa Fe province) for providing access to the restricted area where the study was carried out.

LITERATURE CITED

ALFARO, A. C., S. C. WEBB & C. BARNABY, 2008, Variability of growth, health, and population turnover within mussel beds of *Perna canaliculus* in northern New Zealand. *Marine Biology Research*, 4: 376–383.

ALUNNO-BRUSCIA, M., P. S. PETRAITIS, E. BOURGET & M. FRECHETTE, 2000, Body size-density relationship for *Mytilus edulis* in an experimental food-regulated situation. *Oikos*, 90: 28–42.

ALUNNO-BRUSCIA, M., E. BOURGET & M. FRÉCHETTE, 2001, Shell allometry and length-mass-density relationship for *Mytilus edulis* in an experimental food-regulated situation. *Marine Ecology Progress Series*, 219: 177–188.

BELZ, C. E., G. DARRIGRAN, N. BONEL & O. S. MÄDDER NETTO, 2010, Density, recruitment, and shell growth of *Limnoperna fortunei* (Mytilidae), an invasive mussel in tropical South America. *Journal of Freshwater Ecology*, 25: 227–234.

BREY, T., 2001, *Population dynamics in benthic invertebrates*. A virtual handbook. Version 01.2. http://www.thomas-brey.de/science/virtualhandbook

BOLTOVSKOY, D. & D. H. CATALDO, 1999, Population dynamics of *Limnoperna fortunei*, an invasive fouling mollusc, in the lower Parana River (Argentina). *Biofouling*, 14: 255–263.

BOLTOVSKOY, D., F. SYLVESTER, A. OTAEGUI, V. LEITES & D. H. CATALDO, 2009, Environmental modulation of reproductive activity of the invasive mussel *Limnoperna fortunei*: implications for antifouling strategies. *Austral Ecology*, 34: 719–730.

BONEL, N., C. SOLARI & J. LORDA, 2013, Differences in density, shell allometry, and growth between two populations of *Limnoperna fortunei* (Mytilidae) from the Río de La Plata basin, Argentina. *Malacologia,* 56: 43–58.

BORRERO, F. J. & T. J. HILBISH, 1988, Temporal variation in shell and soft tissue growth of the mussel *Geukensia demissa*. *Marine Ecology Progress Series*, 42: 9–15.

CHASE, M. E. & R. C. BAILEY, 1999, The ecology of the zebra mussel (*Dreissena polymorpha*) in the lower Great Lakes of North America: I. Populations dynamics and growth. *Journal of Great Lakes Research*, 25: 107–121.

DARRIGRAN, G., N. BONEL, D. COLAUTTI & N. J. CAZZANIGA, 2011, An alternative method to assess individual growth of the golden mussel (*Limnoperna fortunei*) in the wild. *Journal of Freshwater Ecology*, 26: 527–535.

DOS SANTOS, C. P., M. C. MANSUR & N. L. WÜRDIG, 2008, Variações no comprimento dos indivíduos de uma população de mexhilão dourado, *Limnoperna fortunei* (Molusca: Bivalvia: Mytilidae), ao longo do ano, na Praia do Veludo, Lago Guaíba, Rio Grande do Sul, Brasil. *Revista Brasileira de Zoologia*, 25: 389–396.

DUNKER, W., 1857, Mytilacea nova collectionis Cumingianae. *Proceedings of the Zoological Society of London*, 24: 358–366.

GAYANILO, F. C., P. SPARRE & D. PAULY, 2002, FAO-ICLARM Stock Assessment Tools (FiSAT). Software version 1.2.0. FAO. Roma.

HARVEY, M. & B. VINCENT, 1990, Density, size distribution, energy allocation and seasonal variations in shell and soft tissue growth at two tidal levels of a *Macoma balthica* (L.) population. *Journal of Experimental Marine Biology and Ecology*, 142: 151–168.

HILBISH, T. J., 1986, Growth trajectories of shell and soft tissue in bivalves: seasonal variation in *Mytilus edulis* L. *Journal of Experimental Marine Biology and Ecology*, 96: 103–113.

HOENIG, N. & R. CHOUDARY HANUMARA, 1982, A statistical study of seasonal growth models for fishes. *Technical Reports, Department of Computer Science and Statistics,* University of Rhode Island, Kingston, USA, 91 pp.

IWASAKI, K. & Y. URYU, 1998, Life cycle of a freshwater mytilid mussel, *Limnoperna fortunei,* in Uji River, Kyoto. *Venus*, 57: 105–113.

KARATAYEV, A. Y., D. BOLTOVSKOY, D. K. PADILLA & L. E. BURLAKOVA, 2007, The invasive bivalves *Dresissena polymorpha* and *Limnoperna fortunei*: parallels, contrasts, potential spread and invasions impacts. *Journal of Shellfish Research*, 26: 205–213.

LÉVÊQUE, C., 1971, Équation de von Bertalanffy et croissance des mollusques benthiques de Lac Tchad. Cahiers O.R.S.T.O.M., Série Hydrobiologie, 5: 263–283.

MAROÑAS, M., G. DARRIGRAN, E. SENDRA & G. BRECKON, 2003, Shell growth of the golden mussel, *Limnoperna fortunei* (Dunker, 1857) (Mytilidae), from a Neotropical temperate locality. *Hydrobiologia,* 495: 41–45.

MAGARA, Y., Y. MATSUI, Y. GOTO & A. YUASA, 2001, Invasion of the non-indigenous nuisance mussel, *Limnoperna fortunei*, into water supply facilities in Japan. *Journal of Water Supply: Research and Technology-AQUA*, 50: 13-24.

MORTON, B., 1977, The population dynamics of *Limnoperna fortunei* (Dunker, 1857) (Bivalvia: Mytilacea) in Plover Cove reservoir, Hong Kong. *Malacologia*, 16: 165–182.

NAKANO, D., T. KOBAYASHI, N. ENDO & I. SAKAGUCHI, 2011, Growth rate and settlement of *Limnoperna fortunei* in a temperate reservoir. *Journal of Molluscan Studies*, 77: 142–148.

NALEPA, T. F., J. A. WOJCIK, D. L. FANSLOW & G. A. LANG, 1995, Initial colonization of the zebra mussel (*Dresissena polymorha*) in Saginaw Bay, Lake Huron: population recruitment, density, and size structure. *Journal of Great Lakes Research*, 21: 417–434.

OLIVEIRA, M. D., S. K. HAMILTON & C. M. JACOBI, 2010, Forecasting the expansion of the invasive golden mussel *Limnoperna fortunei* in Brazilian and North American rivers based on its occurrence in the Paraguay River and Pantanal wetland of Brazil. *Aquatic Invasions*, 5: 59–73.

PALMER, A. R., 1981, Do carbonate skeletons limit the rate of body growth? *Nature*, 292: 15–152.

PASTORINO, G., G. DARRIGRAN, S. M. MARTIN & L. LUNASCHI, 1993, *Limnoperna fortunei* (Dunker, 1857) (Mytilidae), nuevo invasor en aguas del Río de la Plata. *Neotropica*, 39: 34.

PAULY, D., 1990, Length-converted catch curves and the seasonal growth of fishes. *Fishbyte*, 8: 33–38.

PAULY, D. & J. F. CADDY, 1985, A modification of Bhattacharya's method for analysis of mixtures of normal distributions. *Fisheries Circular*, 781: 1–16.

PAULY, D. & G. GASCHÜTZ, 1979, A simple method for fitting oscillating length growth data, with a program for pocket calculator. *International Council for the Exploration of the Seas, Council Meeting Demersal Fish Committee*, G: 24: 26 pp.

PAULY, D. & J. L. MUNRO, 1984, Once more on the comparison of growth in fish and invertebrates. *Fishbyte* ICLARM, 2(1): 21 pp.

PETES, L. E., G. D. MURPHY & B. A. MENGE, 2007, Environmental stress decreases survival, Experimental Marine growth, and reproduction in New Zealand mussels. *Journal of Biology and Ecology*, 11: 151–162.

PETES, L. E., M. E. MOUCHKA, R. H. MILSTON-CLEMENTS, T. S. MOMODA & B. A. MENGE, 2008, Effects of environmental stress on intertidal mussels and their sea star predators. *Oecologia*, 156: 671–680.

RAMÓN, M., M. FERNÁNDEZ & E. GALIMANY, 2007, Development of mussel (*Mytilus* galloprovincialis) seed from two different origins in a semi-enclosed Mediterranean Bay (N.E. Spain). *Aquaculture*, 264: 148–159.

RICCIARDI, A., 1998, Global range expansion of the Asian mussel *Limnoperna fortunei* (Mytilidae): another fouling threat to freshwater systems. *Biofouling*, 13: 97–106.

SAKAI, A. K., F. W. ALLENDORF, J. S. HOLT, D. M. LODGE, J. MOLOFSKY, K. A. WITH, S. BAUGHMAN, R. J. CABIN, J. E. COHEN, N. C. ELLSTRAND, D. E. MCCAULEY, P. O'NEIL, I. M. PARKER, J. N. THOMPSON & S. G. WELLER, 2001, The population biology of invasive species. *Annual Review of Ecology and Systematics*, 32: 305–332.

SEED, R. & T. H. SUCHANEK, 1992, Population and community ecology of *Mytilus*. Pp. 87–169, in: E. GOSLING, ed., *The mussel Mytilus: ecology, physiology, genetics and culture. Development in Aquaculture and Fisheries Science*. Elsevier, Amsterdam, 590 pp.

SOMERS, I. F., 1988, On a seasonally oscillation growth function. *Fishbyte*, 6: 8–11.

STEFFANI, C. N. & G. M. BRANCH, 2003, Growth rate, condition, and shell shape of *Mytilus galloprovincialis*: responses to wave exposure. *Marine Ecology Progress Series*, 246: 197–209.

STIRLING, H. P. & I. OKUMUS 1994. Growth, mortality and shell morphology of cultivated mussel (*Mytilus edulis*) stock cross-planted between two Scotish sea Lochs. *Marine Biology*, 119: 115–123.

STOECKMANN, A. M. & D. W. GARTON, 2001, Flexible energy allocation in zebra mussels (*Dreissena polymorpha*) in response to different environmental conditions. *Journal of the North American Benthological Society*, 20: 486–500.

SYLVESTER, F., D. BOLTOVSKOY & D. H. CATALDO, 2007, Fast response of freshwater consumers to a new trophic resource: predation on the recently introduced Asian bivalve *Limnoperna fortunei* in the lower Paraná River, South America. *Austral Ecology*, 32: 403–415.

TAYLOR, C. C., 1958, Cod growth and temperature. *Journal du Conseil International pour l'Exploration de la Mer*, 23: 366–370.

VAKILY, J. M., 1992, Determination and comparison of bivalve growth, with emphasis on Thailand and other tropical areas. *ICLARM Technical Reports*, 36: 125 pp.

VAN EKROM SCHURINK, C. & C. L. GRIFFITHS, 1993, Factors affecting relative rates of growth in four South African mussel species. *Aquaculture*, 109: 257–273.

WIDDOWS, J. & P. DONKIN, 1992, Mussels and environmental contaminants: Bioacumulation and physiological aspects. Pp. 383–424, in: E. GOSLING, ed., *The mussel Mytilus: ecology, physiology, genetics and culture. Development in Aquaculture and Fisheries Science*. Elsevier, Amsterdam, 590 pp.

Revised ms. accepted July 7, 2014

MALACOLOGIA, 2015, 58(1–2): 147–155

A NEW SPECIES OF *LEPTOCHITON* (POLYPLACOPHORA: LEPTOCHITONIDAE) FROM THE SOUTHWESTERN ATLANTIC

Marina Güller[1]*, María G. Liuzzi[1] & Diego G. Zelaya[2]

ABSTRACT

Leptochiton sanmatiensis, new species, is described from shallow-waters of Argentina. The species is characterized by having a quincuncial arrangement of tegmental granules on head valve, lateral areas of intermediate valves and postmucronal area of tail valve, and a longitudinal arrangement of these structures on the central areas of intermediate valves; each granule having a macraesthete and four micraesthetes. In addition, the new species has pectinated dorsal scales, with 14–21 ridges; a low number of ctenidia (up to six on each side in the largest specimens); and the second lateral tooth with three denticles in the cusp. The species lives on small gravel and shells.

Key words: Lepidopleurida, Lepidopleurina, Argentina, Polyplacophora, diversity.

INTRODUCTION

The most important morphological features currently used to define the Order Lepidopleurida include the usual absence of insertion plates or if present, the absence of slits, and the merobranchial adanal gill arrangement (Kaas & Van Belle, 1985; Sirenko, 2006; Sigwart, 2009; Sigwart et al., 2013, 2014). Sigwart et al. (2014) also added the Schwabe organ as a synapomorphy of the order. Included in Lepidopleurida is *Leptochiton* Gray, 1847, a specious, non-monophyletic genus (Sigwart, 2009; Sigwart et al., 2011) with about 100 valid extant, small-sized species, characterized by slit-less brittle valves and finely granulose tegmentum (Gray, 1847; Kaas & Van Belle, 1985; Sirenko & Schwabe, 2011).

Three valid species of this genus are currently accepted from the southwestern Atlantic: *Leptochiton kerguelensis* Haddon, 1886, *L. medinae* (Plate, 1899) and *L. darioi* (Righi, 1973b). Two other species, *L. pagenstecheri* Pfeffer (in von Martens & Pfeffer), 1886, described from South Georgia, and *L. agesilaus* (Dall, 1919), described from the Magellan Strait, are currently regarded as synonyms of *L. kerguelensis* and *L. medinae*, respectively (Thiele, 1906, 1908; Kaas & Van Belle, 1985). Thiele (1893) identified one specimen collected at Tuesday Bay, Magellan Strait, as *Lophyropsis imitatrix* Smith, although this record was subsequently reassigned by the same author (Thiele, 1908) to *L. medinae*.

In the course of studying the diversity of mollusks from the San Matías Gulf, we found a species of *Leptochiton* that did not fit any published description. The aim of this contribution is to describe this species and to compare it with other species of this genus present in the area.

MATERIAL AND METHODS

Benthic samples were collected by diving with a hand-trawl of 2 mm mesh-size net. Living mollusks were sorted from the sediment under a stereoscopic microscope, photographed alive, fixed in 5% sea-water formalin and preserved in 70% ethanol.

The 16 largest specimens of *Leptochiton* n. sp. were measured according to the following criteria: length (L): refers to the maximum distance between the anteriormost part of the head valve and the posteriormost part of the tail valve; and width (W): refers to the maximum distance perpendicular to L, of valve IV. None of these measurements included the girdle. The mean value and standard deviation (SD) for the W/L ratio were calculated. Height and width of valves IV, in anterior view, were

---

[1]Museo Argentino de Ciencias Naturales “Bernardino Rivadavia”, Av. Ángel Gallardo 470 (C1405DJR), Buenos Aires, Argentina.

[2]Departamento Biodiversidad y Biología Experimental, Facultad de Ciencias Exactas y Naturales - UBA, Ciudad Universitaria, Pab. 2, Lab. 31 (C1428EHA), Buenos Aires, Argentina.

*Corresponding author: mguller@macn.gov.ar

measured in five specimens following Kaas & Van Belle's (1985) criterion to obtain the dorsal elevation H/W.

Six whole specimens were dehydrated in an ascending ethanol series (from 70% to 100%), treated with hexamethyldisilazane and air-dried, coated with gold-palladium (40–60%) and photographed with a Phillips XL-30 scanning electron microscope (SEM). The radula of five specimens was dissected and treated with a 5% sodium hypochlorite solution under stereoscopic microscope until completely clean, and subsequently studied with SEM. Isolated valves, scales and spicules were obtained by digestion of the girdle in the same way. Measurements of isolated scales and spines were obtained from SEM photographs.

To confirm the adulthood condition of the largest individuals examined, histological sections of three Bouin's fixed specimens (about 4 mm length) were performed. For this, specimens were dehydrated in ethanol, embedded in Historesin® Leica™, sectioned at 3.5 µm thick, with a Leica RM2255 motorized microtome, and stained with hematoxilin-eosin.

The studied material is deposited at the Invertebrates Collection of the Museo Argentino de Ciencias Naturales "Bernardino Rivadavia" (MACN-In), Buenos Aires. Number of specimens (s.) for each lot is indicated in the material examined section. The MACN-In collection was also searched for additional specimens.

Information on other species of *Leptochiton* described from the area comes from their original descriptions and illustrations; the examination of photographs of the syntype of *L. kerguelensis*, housed at The Natural History Museum, United Kingdom (NHMUK 1889.11.9.4); the photograph of the paratype (wrongly referred to as holotype in the text) of *L. darioi*, provided by Dornellas & Simone (2011); and the photographs of the lectotype of *L. medinae* provided by Schwabe & Sellanes (2010); as well as from the complementary information provided by Leloup (1956), Kaas & Van Belle (1985) and Schwabe & Sellanes (2010). Morphological and anatomical characters of other species of *Leptochiton* in the discussion are mainly based on their original descriptions and their re-descriptions by Kaas & Van Belle (1985, 1990). A lot of *L. medinae* from the Beagle Channel (MACN-In 39659) was examined for comparative purposes, to determine the number of ctenidia of small-sized specimens of this species.

SYSTEMATICS

Order Lepidopleurida Thiele, 1909
Suborder Lepidopleurina Thiele, 1909
Family Leptochitonidae Dall, 1889
Genus *Leptochiton* Gray, 1847

Type species: *Chiton cinereus* Linnaeus, 1767, sensu Montagu, 1803 (*non* Linnaeus) (SD Gray, 1847); = *Chiton asellus* Gmelin, 1791. Europe.

Leptochiton sanmatiensis
Güller, Liuzzi & Zelaya, n. sp.
(Figs. 1–37)

Type Locality

Las Grutas, San Matías Gulf, Río Negro Province, Argentina (40º56'27.2''S 65º07'58.2"W), 10–11 m.

Type Material

Holotype (2.6 mm L, 1.6 mm W, 0.58 mm H, partially curved) (MACN-In 39660) and 5 paratypes from the type locality (5 paratypes MACN-In 39661.

Other Material Examined

San Matías Gulf: Las Grutas: 40°25'47.4"S, 65°25'14.1"W, 8 m (MACN-In 39662: 2 s.); 40°50'12.8"S, 65°04'42.2"W, 10 m (MACN-In 39663: 2 s.); 40°50'35.5"S, 65°04'43.7"W, 12 m (MACN-In 39664: 1 s.); 40°54'00.0"S, 65°06'43.1"W, 6 m (MACN-In 39665: 2 s.); 40°54'08.3"S, 65°06'28.0"W, 9 m (MACN-In 39666: 1 s.); 40°55'17.4"S, 65°08'07.6"W, 7–8 m (MACN-In 39667: 3 s.); 40°56'26.6"S, 65°07'59.1"W, 9 m (MACN-In 39668: 2 s.); 40°56'49.0"S, 65°07'36.2"W, 5 m (MACN-In 39669: 2 s.); 40°57'29.4"S, 65°05'59.6"W, 20 m (MACN-In 39670: 74 s.).

Playas Doradas: 41°39'03.1"S, 65°00'38.3"W, 12–14 m (MACN-In 39671: 7 s.); 41°40'17.8"S, 65°00'27.8"W, 16 m (MACN-In 39672: 14 s.); 41°40'48.3"S, 65°00'46.1"W, 12 m (MACN-In 39673: 1 s.); 41°40'49.1"S, 65°00'46.5"W, 12 m (MACN-In 39674: 2 s.).

Puerto Lobos: 41°58'03.9"S, 65°03'27.6"W, 15–18 m (MACN-In 39675: 13 s.); 41°58'22.8"S, 65°03'28.6"W, 16.5 m (MACN-In 39676: 38 s.); 41°58'31.7"S, 65°03'38.6"W, 13 m (MACN-In 39677: 14 s.); 41°59'0.4"S, 65°03'34.2"W, 15 m (MACN-In 39678: 25 s.); 41°59'48.5"S,

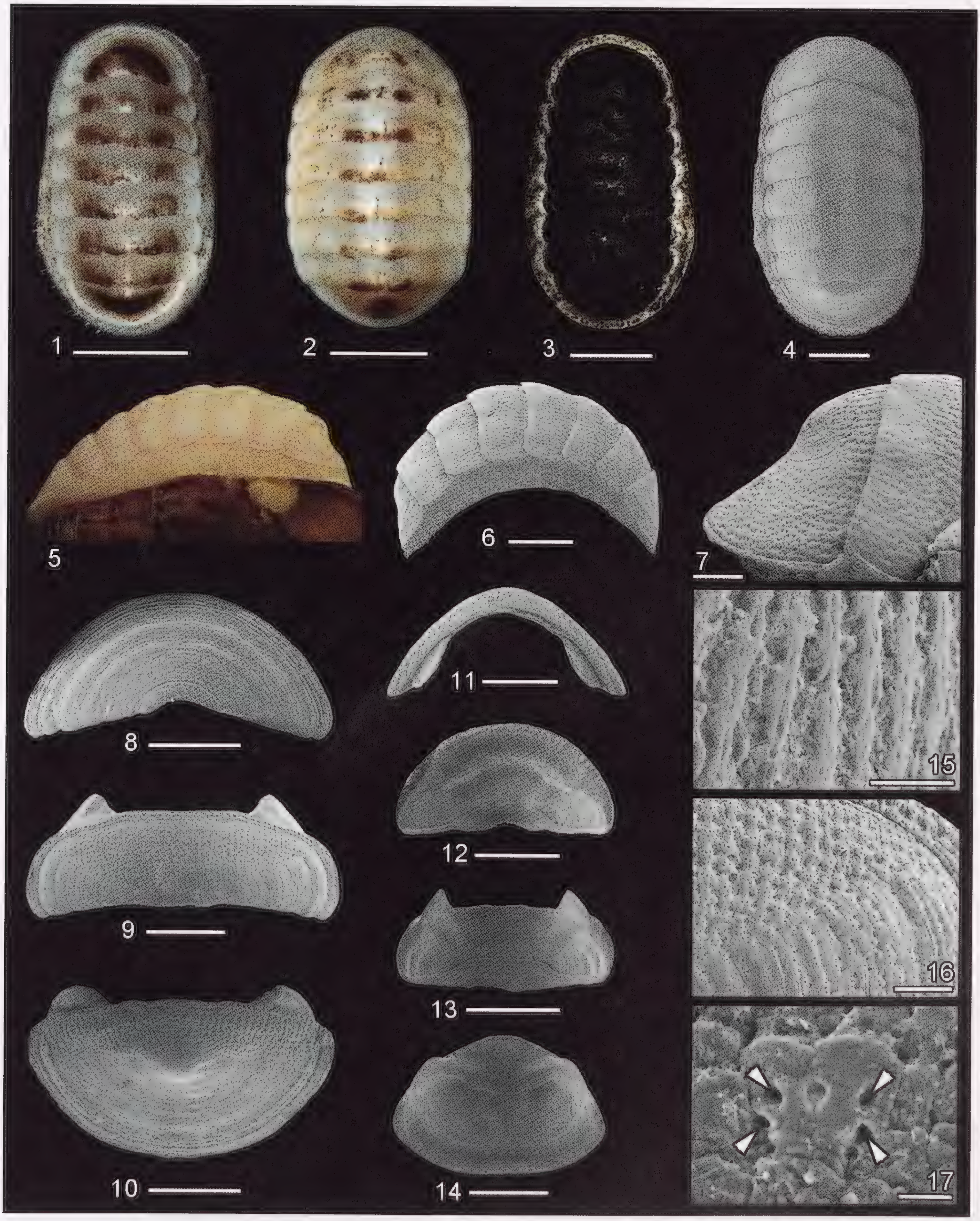

FIGS. 1–17. ***Leptochiton sanmatiensis***, n. sp. FIGS. 1–4: Dorsal views. FIGS. 5, 6: Lateral views; FIG. 5: Living specimen; FIG. 6: Holotype; FIG. 7: Detail of tail valve, lateral view. FIGS. 8–10: Dorsal views of isolated valves. FIG. 8: Head valve; FIG. 9: Valve III; FIG. 10: Tail valve; FIG. 11: Anterior view of an intermediate valve. FIGS. 12–14: Ventral views of isolated valves. FIG. 12: Head valve; FIG. 13: Valve VII; FIG. 14: Tail valve. FIGS. 15–17: Detail of tegmentum. FIG. 15: Longitudinal rows of granules in central area of valve IV; FIG. 16: Central and lateral areas of valve III; FIG. 17: Detail of a granule and aesthetes (arrowheads showing micraesthetes). Figs. 1, 4: MACN-In 39676; Figs. 2, 3: MACN-In 39680; Fig. 5: Specimen from Las Grutas; Fig. 6: MACN-In 39660; Figs. 7, 15: MACN-IN 39665; Figs. 8–11, 13, 14, 16, 17: MACN-In 39670; Fig. 12: MACN-In 39672. Scale bars: Figs. 1–3 = 1 mm, Figs. 4, 6, 8–14 = 500 μm, Fig. 7 = 200 μm, Fig. 15 = 50 μm, Fig. 16 = 100 μm, Fig. 17 = 10 μm.

65°03’32.3”W, 11.5 m (MACN-In 39679: 1 s.); 42°00’07”S, 65°03’20.8”W, 21 m (MACN-In 39680: 10 s.).

Buenos Aires coast: off Mar del Plata, 38°14’55.68”S, 57°01’41.16”W, 55–60 m (MACN-In 38200: 2 s.).

Habitat

On small gravel or shells, associated to coarse sand, gravel, mud or hard bottoms, from 5 to 60 m deep.

Etymology

The species name refers to San Matías Gulf, from which most of the studied material comes.

Diagnosis

Tegmentum sculptured with granules arranged in quincunx on head valve, lateral areas of intermediate valves and postmucronal area of tail valve, and longitudinally on central areas of intermediate valves and antemucronal area of tail valve. Each granule with a megalaesthete and four micraesthetes. Dorsal girdle scales imbricated, each with 14–21 ridges. With up to six pairs of ctenidia. Second lateral tooth with three denticles in the cusp.

Description

Exterior Morphology: Animal small (max. L observed = 5.7 mm), elongate-ovate (W/L = 0.49 ± 0.04), delicate (Figs. 1–4). Valves thin, rather elevated (dorsal elevation up to 0.48), lacking insertion plates (Figs. 5, 6, 11–14). Tegmentum and girdle white-yellowish, frequently stained with brown deposits, which give a darker appearance (Figs. 1–3, 5).

Tegmentum with low, coarse, irregular granules and faint, thin striae radiating from the apex, only visible under high magnification (Figs. 7–10, 15–17). Each granule containing a central megalaesthete and four micraesthetes: two of them flanking the megalaesthete, and the other two at the base of the granule, scarcely visible in dorsal view (Fig. 17). Granules more evident towards the growing margins of valves, hardly visible on eroded specimens. Valves with well-marked growth lines forming step-like disruptions, less pronounced on central areas of intermediate valves (Figs. 8–10).

Head valve more than semicircular; posterior margin widely V-shaped (Fig. 8); tegmentum with granules arranged in quincunx. Intermediate valves subrectangular (Fig. 9), anterior margins straight, slightly convex or sinuous; valve II sometimes with widely convex anterior margin. Central area sculptured with 37–47 rows of granules joined by coarse longitudinal cords; adjacent rows joined by lateral projections of granules (Figs. 15, 16). Lateral areas somewhat raised; granules arranged in quincunx (Fig. 16). Tail valve subovate, similar in size to head valve. Anterior margin almost straight. Mucro prominent, anteromedial (Fig. 10). Antemucronal area with about 40 longitudinal rows of granules joined as in the central areas of intermediate valves; postmucronal slope concave, with granules arranged in quincunx (Fig. 7).

Articulamentum frequently mimicking outer step-like growth disruptions, more evident underneath lateral areas of intermediate valves (Fig. 13). Apophyses of intermediate valves triangular, with rounded tips, markedly asymmetrical, with inner margin about 2/3 the length of outer; widely separated (Figs. 9, 13). Apophyses of tail valve trapezoidal, symmetric, with rounded margins (Fig. 10).

Girdle of about 200 μm in diameter (in fixed specimens) bearing irregularly imbricated scales, and spicules (Figs. 21, 22). Dorsal scales bent (Fig. 23), usually wider than longer (30–45 μm wide x 20–40 μm long; Figs. 24–26), longer at valve margins; base wide, ovate, smooth; distal part pectinated with 14–21 strong, narrow longitudinal ribs which sometimes form pairs; interspaces as wide as ribs or somewhat narrower (Figs. 24–26). Bunches of up to four intersegmental spicules present between all valves (Fig. 21); spicules elongated (about 50 μm x 7 μm), rounded at the tip, smooth or faintly longitudinally striated. Marginal scales-spicules cylindrical, elongated (about 50 μm x 10 μm), distally pointed, sculptured with strong longitudinal ridges, separated by wide interspaces (Figs. 22, 28, 29). Marginal spicules smooth or faintly striated, needle-like (about 50 μm x 7 μm), with rounded tip and narrow stalk (Figs. 22, 27). Ventral scales flat, subrectangular to ovate (50–65 μm x 45–50 μm), with rounded to bluntly pointed distal tip, increasing in size outwards; imbricated, radially arranged; ventral side of scales faintly longitudinally striated (Figs. 22, 30); dorsal side with 3–4 short but stout, longitudinal ridges at tip (Fig. 31).

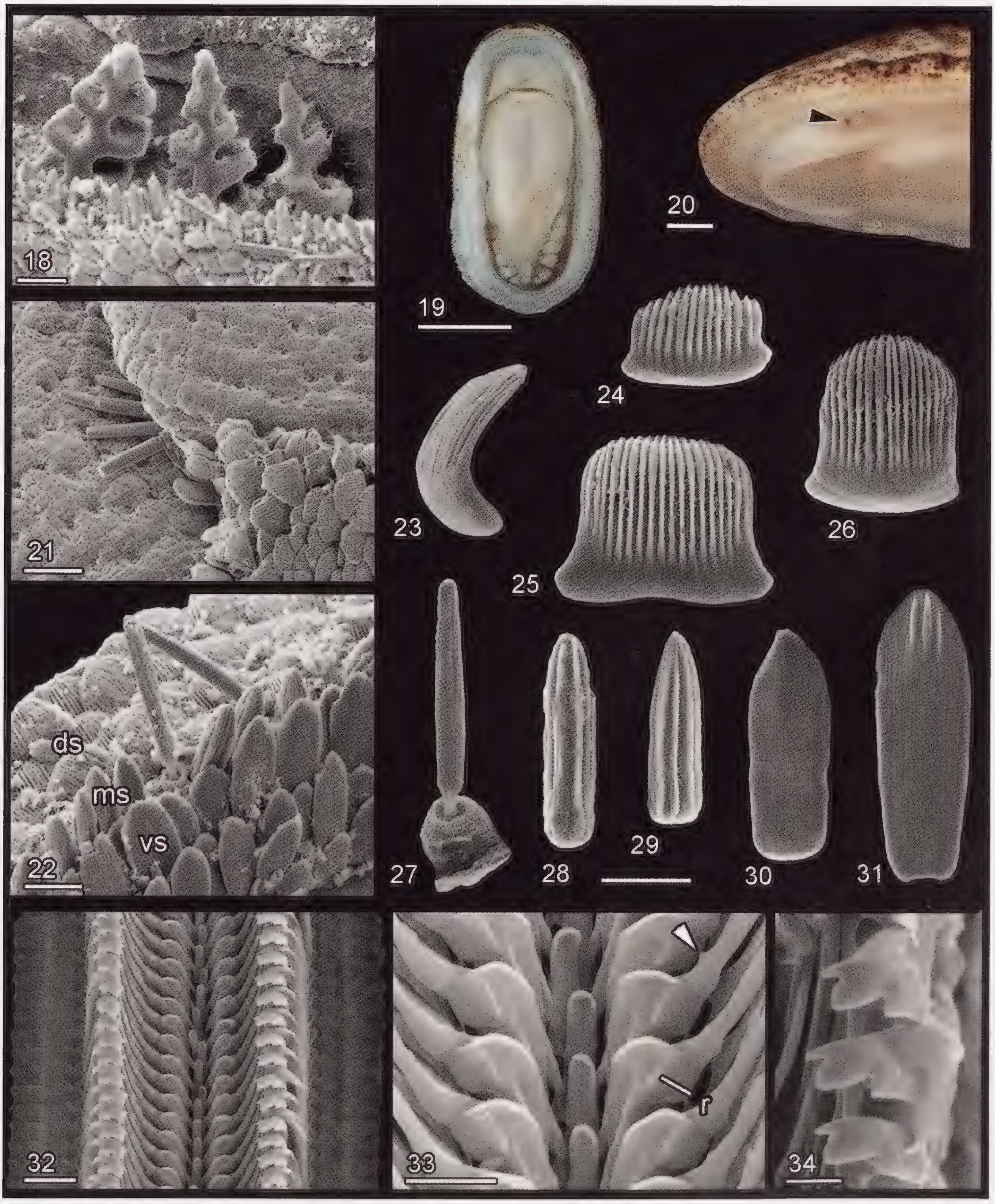

FIGS. 18–34. ***Leptochiton sanmatiensis***, n. sp. FIG. 18: Detail of the three anteriormost left side ctenidia of a hexamethylized specimen; FIG. 19: Specimen in ventral view. FIG. 20: Anterior part of a specimen showing Schwabe organ (arrowhead); FIGS. 21–31: Details of scales and spicules. FIG. 21: Intersegmental spicules between valves V and VI; FIG. 22: Dorsal scales, marginal scales-spicules and ventral scales; FIGS. 23–26: Dorsal scales; FIG. 23: Lateral view; FIGS. 24–26: Dorsal view; FIG. 27: Marginal spicule; FIGS. 28, 29: Marginal scales-spicules; FIGS. 30, 31: Ventral scales; FIG. 30: Ventral view; FIG. 31: Dorsal view. FIGS. 32–34: Radula. FIG. 32: Full radular width; FIG. 33: Detail of central and first lateral tooth (arrowhead pointing the knob on the shaft of second lateral tooth); FIG. 34: Detail of cusps of second lateral teeth. Figs. 18, 19, 22, 25, 28, 30–34: MACN-In 39670; Fig. 20: MACN-In 39680; Fig. 21: MACN-In 39665; Figs. 23, 24, 26, 29: MACN-In 39672; Fig. 27: MACN-In 39676. References: ds = dorsal scales; ms = marginal scales-spicules; r = ridge or thickening; vs = ventral scales. Scale bars: Figs. 18, 21 = 50 μm, Fig. 19 = 1 mm, Fig. 20 = 200 μm, Figs. 22, 23–31 (common scale), 32 = 20 μm, Fig. 33 = 10 μm, Fig. 34 = 5 μm.

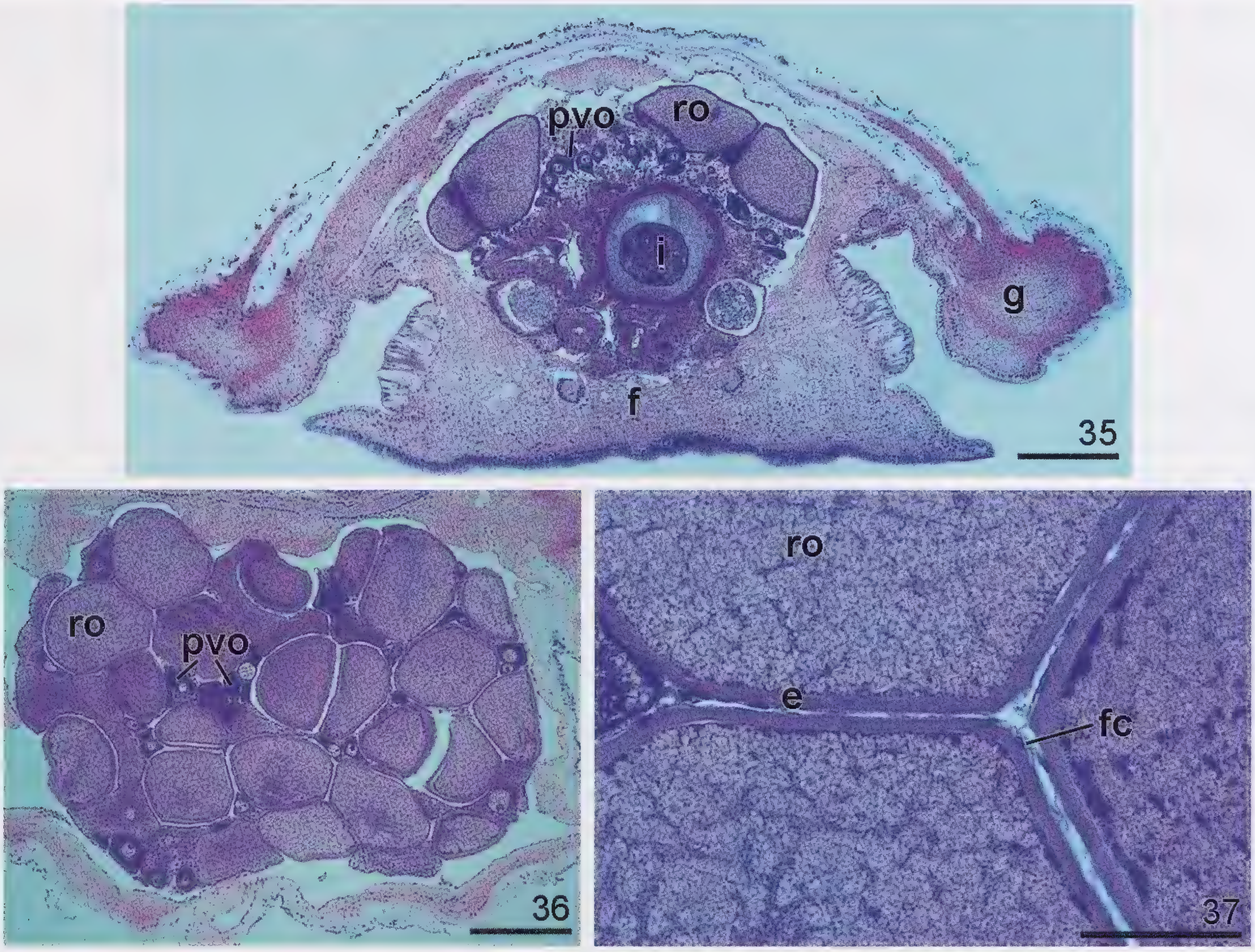

FIGS. 35–37. ***Leptochiton sanmatiensis***, n. sp., histological sections. FIG. 35: Transverse section of whole specimen showing several oocytes in advanced stage of vitellogenesis; FIG. 36: Frontal section of a dorsal portion of the gonad showing oocytes in advanced stage of vitellogenesis; FIG. 37: Detail of ripe oocytes showing the egg hull. References: e = egg hull; f = foot; fc = follicle cell; g = girdle; I = intestine; pvo = previtellogenic oocyte; ro = ripe oocyte. Scale bars: Fig. 35 = 100 µm, Fig. 36 = 200 µm, Fig. 37 = 50 µm.

Anatomy: Gill merobranchial; with up to six ctenidia on each side, extending from beneath valve VI to anus (Fig. 19). Ctenidia increasing in size posteriorly (Figs. 18, 19), except for the rearmost, which is the smallest, located close to the anus. Mouth lappets large, covering a concentrated dot of brownish pigment on each side (the Schwabe organ) (Fig. 20). Out of the three histologically processed specimens, two were females and one male. Transverse sections of female gonads showed two clearly separated cohorts of gametes: one, towards the periphery, formed by late vitellogenic and ripe oocytes, and a second, at the gonad base, with crowded primary and previtellogenic oocytes which likely enter the vitellogenesis after the spawning of the former cohort (Figs. 35, 36). Ripe oocytes (about 200 µm diameter), polygonal in shape due to the compression within the gonad, showed a well-developed smooth egg hull and surrounding follicular epithelium (Figs. 36, 37). The gonad of male specimen showed already mature sperm. This degree of gonad development confirms the adulthood condition at 4 mm length.

Radula: Central tooth narrow, elongate, rectangular, enlarged at the base; cutting edge smooth, rounded (Figs. 32, 33). First lateral tooth larger than central tooth, hardly cusped, with strong ridge or thickening at the base (Figs. 32, 33). Second lateral tooth with narrow, elongated shaft bearing irregular knobs (Figs. 32, 33), and three denticles in the cusp, the central, the largest (Figs. 32, 34). Fifth lateral ("major uncinal") tooth elongated, slightly curved, with lanceolate cusp. Second ("middle") marginal tooth rhomboidal, smaller than the third ("outer") marginal tooth, which is elongated, wider than high (Fig. 32).

DISCUSSION

In the general arrangement of tegmental granules, the presence of multistriated dorsal scales and the tricuspid second lateral tooth, ***Leptochiton sanmatiensis***, n. sp., resembles *L. muelleri* Sirenko & Schwabe, 2011, from Sri Lanka, *L. compostellanum* Carmona Zalvide & Urgorri, 1999, from the Iberian Peninsula, and *L. cimicoides* (Monterosato, 1879) from Italy. *Leptochiton compostellanum*, however, has a smaller tail valve than head valve, more numerous longitudinal rows of granules on the central areas of intermediate valves (52–63 *vs.* 37–47 in ***L. sanmatiensis***, n. sp.), pointed dorsal scales, and the fifth lateral tooth shorter than the second lateral. *Leptochiton cimicoides* has a smaller tail valve with a postmedian mucro, stronger tegmentum sculpture, longer intersegmental spicules (100 µm *vs.* 50 µm) and the central tooth pinched in the middle and distally widened. In *Leptochiton muelleri* the tail valve is shorter and has a narrow antemucronal area, the sculpture is more prominent, the dorsal scales have less ribs (8–10 *vs.* 14–21 in ***L. sanmatiensis***, n. sp.), and the needle-like spicules are much longer (210 µm).

Leptochiton sanmatiensis, n. sp., also shares with the Japanese species *L. latidens* (Bergenhayn, 1933) and *L. habei* Saito, 1997, the Australian *L. badius* (Hedley & Hull, 1909), and with the Iberian *L. gascognensis* Kaas & Van Belle, 1985, the arrangement of granules and the presence of multistriated dorsal scales. However, *L. latidens* and *L. habei* clearly differ in the morphology of the second lateral tooth (tricuspid in ***L. sanmatiensis***, n. sp., unicuspid in *L. latidens* and bicuspid in *L. habei*). Furthermore, *L. latidens* has sharply pointed marginal spicules, very long intersegmental spicules (360 µm), a narrow first lateral tooth with a wing-like projection, and 9–10 ctenidia on each side. *Leptochiton habei* reaches a larger size, has elongated dorsal scales (50 µm x 20 µm), with fewer (8–12) ribs, 7 aesthetes per granule (*vs.* 5 in ***L. sanmatiensis***, n. sp.), flat and longer marginal scales (100 µm long), and lacks needle-like spicules. *Leptochiton badius* is somewhat less elevated than ***L. sanmatiensis***, n. sp. (dorsal elevation: 0.33 *vs.* 0.48), has a more pronounced sculpture, a straight postmucronal slope, the longitudinal rows of granules on the central areas of intermediate valves slightly curved on the pleural area and converging posteriorly, near the outer sides, and the marginal spicules (100 µm long) and needle-like spicules (about 150 µm long) longer than those of ***L. sanmatiensis***, n. sp. According to the original description, *L. gascognensis* is highly elevated (dorsal elevation *ca.* 0.55), has trapezoidal intermediate valves and a small, triangular tail valve. In addition, its marginal scales-spicules are bent, the needle-like spicules are scattered among dorsal scales, and most girdle elements are longer than in ***L. sanmatiensis***, n. sp. (dorsal needle-like spicules: 192 µm, intersegmental spines: 216 µm, marginal scales-spicules: 85–90 µm, ventral scales: 88 µm).

Comparing with the other *Leptochiton* species currently known from the southwestern Atlantic, ***L. sanmatiensis***, n. sp., may be clearly distinguished by the presence of shorter and wider dorsal scales, sculptured with a greater number of ribs (14–21 in ***L. sanmatiensis***, n. sp., *vs.* 3–4 in *L. darioi*; 4–6 in *L. kerguelensis*; and 6 in *L. medinae*). Furthermore, ***L. sanmatiensis***, n. sp., has a lower number of ctenidia on each side compared to similar-sized specimens (6 ctenidia in specimens of ***L. sanmatiensis***, n. sp., of about 5.5 mm long *vs.* 8–9 in *L. medinae* about 5.0 mm long, 8–10 in *L. darioi* 3.6 to 4.2 mm long and 8–10 in *L. kerguelensis* of about 5 mm long). The quincuncial arrangement of the granules on the head valve, lateral areas of intermediate valves and postmucronal area of tail valve of ***L. sanmatiensis***, n. sp., clearly differs from that of *L. medinae* (including its synonym, *L. agesilaus*) and *L. darioi*, where granules are arranged in radial rows (or comarginally in the case of postmucronal area of *L. darioi*), and resembles the pattern present in *L. kerguelensis*. However, the latter species (as well as *L. pagenstecheri*) lacks the longitudinal rows of granules in the central area of intermediate valves, and antemucronal area of posterior valves, which characterize ***L. sanmatiensis***, n. sp. Moreover, in *L. kerguelensis* each granule has only a single aesthete (megalasthete), while in ***L. sanmatiensis***, n. sp., granules show a megalaesthete and four micraesthetes. Like *Leptochiton darioi*, ***L. sanmatiensis***, n. sp., has a tricuspid second lateral, while this tooth is bicuspid in *L. kerguelensis* and *L. medinae*. Furthermore, insertion plates on the terminal valves are mentioned in the original description of *L. darioi*, which are absent in ***L. sanmatiensis***, n. sp.

At present, currently available information suggests that ***Leptochiton sanmatiensis***, n. sp., is allopatric with the three other *Leptochiton* species reported for the southwestern Atlantic:

L. darioi is thus far only known from Brazil, between São Paulo and Rio de Janeiro (although Rios (1994) reported it up to Espírito Santo); *L. kerguelensis* and *L. medinae* occur in southern Argentina and the southeastern Pacific, the former also occurring in sub-Antarctic and Antarctic waters (Kaas & Van Belle, 1985). The northernmost confirmed record of *L. medinae* in the Southwestern Atlantic comes from Villarino, Golfo San José (MACN-In 37534); that of *L. kerguelensis* is from Malvinas/Falkland Islands (Dell, 1964; Sirenko, 2006). Dell (1964) reported *L. kerguelensis* from *RRS William Scoresby* station 583, wrongly georeferentiating it as "38°22'S, 73°41'W", although this station actually comes from 53°39'S, 70°54.5'W, Magellan Strait (Anonymous, 1949). Righi (1973a) assigned to *Leptochiton kerguelensis* (as *Lepidopleurus*) "one rolled and partially fragmented specimen" from Baía da Ilha Grande, Rio de Janeiro, Brazil. However, Kaas & Van Belle (1985), based on the short, multistriate girdle scales figured by Righi (1973a: fig. 1), noted that this record is a misidentification. In fact, these girdle elements appear similar to those described herein for ***L. sanmatiensis***, n. sp., *Leptochiton kerguelensis* was also reported from Gough Island by Dell (1964), but taking into account the great isolation of this site, the record requires revision.

AKNOWLEDGEMENTS

The authors are grateful to Cristián Ituarte (MACN) for allowing us to reproduce the photographs of the histological sections he obtained and his comments on the oogenesis and gonad anatomy. The authors also wish to express their gratitude to Alejandro Tablado for providing access to the Invertebrates Collection of MACN, and to Juan López Gappa for his valuable comments on an early version of the manuscript. Authors are members of the Consejo Nacional de Investigaciones Científicas y Técnicas (CONICET). This study was partially funded by PICT 2011-2182 to Diego G. Zelaya and D4541-12 (CONICET) to María G. Liuzzi.

LITERATURE CITED

ANONYMOUS, 1949, Station List, R.R.S. 'William Scoresby', 1931-1938. *Discovery Reports*, 25: 143–280.

BERGENHAYN, J. R. M., 1933, Die Loricaten von Prof. Dr. Sixten Bocks Expedition nach Japan und den Bonin-Inseln 1914. *Kungliga Svenska Vetenskaps Akademiens Handlingar*, 12: 1–58, figs. 1–17, pls.1–3.

CARMONA ZALVIDE, P. & V. URGORRI, 1999, Description of two new species of Mollusca Polyplacophora from the Iberian Atlantic coast: *Leptochiton* (*L.*) *gascognensis* Kaas and Van Belle, 1985 and *L* (*L.*) *compostellanum* sp. nov. *Iberus*, 17: 97–107.

DALL, W. H., 1889, Report on the results of dredging, under the supervision of Alexander Agassiz, in the Gulf of Mexico (1877–78) and in the Caribbean Sea (1879–80), by the U. S. coast survey steamer "Blake", Lieutenant-Commander C. D. Sigsbee, U. S. N., and Commander J. R. Bartlett, U. S. N., commanding, 29, Report on the Mollusca. Part 2, Gastropoda and Scaphopoda. *Bulletin of the Museum of Comparative Zoology, Harvard University*, 18: 1–492, pls. 10–40.

DALL, W. H., 1919, Descriptions of new species of chitons from the Pacific coast of America. *Proceedings of the United Stated National Museum*, 55: 499–516.

DELL, R. K., 1964, Antarctic and sub-Antarctic Mollusca: Amphineura, Scaphopoda and Bivalvia. *Discovery Reports,* 33: 93–250, pls. 2–7.

DORNELLAS, A. P. S. & L. R. L. SIMONE, 2011, Annotated list of type specimens of mollusks deposited in Museu de Zoologia da Universidade de São Paulo, Brazil. *Arquivos de Zoologia*, 42: 1–81.

GMELIN, J. F., 1791, Vermes. *Caroli a Linné Systema Naturae*, Editio Decima Tertia, Aucta Reformata. Tome 1, Pars 6 (Vermes). G. E. Beer, Lipsiae [Leipzig], pp. 3021–3910.

GRAY, J. E., 1847, Additional observations on chitones. *Proceedings of the Zoological Society of London*, 15: 126–127.

HADDON, A. C., 1886, Report on the Polyplacophora collected by H.M.S. Challenger during the years 1873–76. In: *Report on the Scientific Results of the Voyage of H.M.S. Challenger*, Zoology, 15: 1–50, pls. 1–3.

HEDLEY, C. & A. F. B. HULL, 1909, Descriptions of new and notes on other Australian Polyplacophora. *Records of the Australian Museum*, 7: 260–266, pls. 73–74.

KAAS, P. & R. A. VAN BELLE, 1985, *Monograph of living chitons (Mollusca: Polyplacophora). Vol. 1, Order Neoloricata: Lepidopleurina*. Brill, J. E., Leiden, 240 pp.

KAAS, P. & R. A. VAN BELLE, 1990, *Monograph of living chitons* (*Mollusca: Polyplacophora*). *Vol. 4, Suborder Ischnochitonina: Ischnochitonidae: Ischnochitoninae* (*continued*). *Additions to vols 1, 2 and 3.* Brill, J. E., Leiden, 298 pp.

LELOUP, E., 1956, Polyplacophora. *Reports of the Lund University Chile Expedition 1948–49. 27. Acta Universitatis Lundensis*, Avd. 2, Bd. 52, 15: 1–93.

MARTENS, E. VON & G. PFEFFER, 1886, Die Mollusken von Süd-Georgien, nach der Ausbeute der Deutschen Station 1882–83. *Jahrbuch der Hamburgischen wissenschaftlichen Anstalten*, 3: 63–135.

MONTAGU, G., 1803, *Testacea Britannica, or natural history of British shells, marine, land and the fresh-water, including the most minute: systematically arranged and embellished with figures.* Romsey, London, XXXVII + 606 pp., 16 pls.

MONTEROSATO, T. A. DI, 1879, Monografia dei chitonidi del Mediterraneo. *Giornale di Scienze Naturali ed Economiche*, 14: 1–23.

PLATE, L. H., 1899, Die Anatomie und Phylogenie der Chitonen. Fauna Chilensis II, Heft 1. *Zoologische Jahrbücher,* Suppl. 4: 15–216.

RIGHI, G., 1973a, Moluscos da Baía da Ilha Grande, Rio de Janeiro, Brasil. II. Polyplacophora. *Papéis Avulsos de Zoologia*, 26: 237–245.

RIGHI, G., 1973b, Adições aos Polyplacophora brasileiros (Mollusca). *Papéis Avulsos de Zoologia*, 26: 259–273.

RIOS, E., 1994, *Seashells of Brazil.* Editora da FURG, Rio Grande, 368 pp., 113 pls.

SAITO, H., 1997, Deep-sea chiton fauna of Suruga Bay (Mollusca: Polyplacophora) with descriptions of six new species. *National Science Museum Monographs*, 12: 31–58, pls. 1, 2.

SCHWABE, E. & J. SELLANES, 2010, Revision of Chilean bathyal chitons (Mollusca: Polyplacophora) associated with cold-seeps, including description of a new species of *Leptochiton* (Leptochitonidae). *Organisms Diversity & Evolution*, 10: 31–55.

SIGWART, J. D., 2009, Morphological cladistic analysis as a model for character evaluation in primitive living chitons (Polyplacophora, Lepidopleurina). *American Malacological Bulletin*, 27: 95–104.

SIGWART, J. D., E. SCHWABE, H. SAITO, S. SAMADI & G. GIRIBET, 2011, Evolution in the deep sea: a combined analysis of the earliest diverging living chitons (Mollusca: Polyplacophora: Lepidopleurida). *Invertebrate Systematics*, 24: 560–572.

SIGWART, J. D., I. STOEGER, T. KNEBELSBERGER & E. SCHWABE, 2013, Chiton phylogeny (Mollusca: Polyplacophora) and the placement of the enigmatic species *Choriplax grayi* (H. Adams & Angas). *Invertebrate Systematics*, 27: 603–621.

SIGWART, J. D., L. H. SUMMER-ROONEY, E. SCHWABE, M. HEß, G. P. BRENNAN & M. SCHÖDL, 2014, A new sensory organ in "primitive" molluscs (Polyplacophora: Lepidopleurida), and its context in the nervous system of chitons. *Frontiers in Zoology*, 11: 7.

SIRENKO, B., 2006, New outlook on the system of chitons (Mollusca: Polyplacophora). *Venus*, 65: 27–49.

SIRENKO, B. & E. SCHWABE, 2011, Description of a minute new chiton (Mollusca, Polyplacophora) from Sri Lanka. *Ruthenica*, 21: 113–121.

THIELE, J., 1893, *Das Gebiss der Schnecken, zur Begründung einer Natürlichen Classification.* Nicolai, Berlin, pp. 337–409, pls. 29–32.

THIELE, J., 1906, Ueber die Chitonen der deutschen Tiefsee-Expedition. *Wissenschaftliche Ergebnisse der Deutschen Tiefsee-Expedition*, 9: 325–336.

THIELE, J., 1908, Die Antarktischen und Subantarktischen Chitonen. *Deutsche Südpolar Expedition 1901–1903*, 10. Band, Zoologie, Teil 2: 9–23, pl. 1.

THIELE, J., 1909, Revision des Systems der Chitonen. II. *Zoologica. Original-Abhandlungen aus dem Gesamtgebiete der Zoologie*, 22: 71–132, pls. 7–10.

Revised ms. accepted August 13, 2014

MALACOLOGIA, 2015, 58(1–2): 157–165

MORPHOLOGY AND CYCLIC ACTIVITY OF THE DIGESTIVE GLAND OF *ZIDONA DUFRESNEI* (CAENOGASTROPODA: VOLUTIDAE)

Mariel Ojeda[1*], Florencia Arrighetti[2] & Juliana Giménez[1,3]

ABSTRACT

Zidona dufresnei is a carnivorous snail that plays an important role in the trophic web as a top predator. It is a threatened species due to high levels of fisheries exploitation. In this study, we describe the morphology of the digestive gland of *Z. dufresnei* from Mar del Plata, Argentina, and discuss the function and the cycle of activity of the different cell types. Histological analysis reveals two types of tubules: type 1 tubules composed of digestive and basophilic cells and type 2 tubules lined by basophilic cells only. Pyramidal basophilic cells contain lipofuscin and a large amount of rough endoplasmic reticulum, which suggests that these cells are responsible for the secretion of digestive enzymes that initiate the extracellular digestion of the food. Columnar digestive cells exhibit large membrane-bound vesicles that contain proteoglycans, neutral glycosaminoglycans and small amounts of lipid and lipofuscin. The presence in digestive cells of many endocytic vesicles and residual lysosomal bodies, as evidenced by the presence of lipofuscin pigments in the apical region, indicate that digestion is completed intracellularly within these cells. The digestive cells are subject to cyclical changes involving four phases: initial, digestion, fragmentation, and disintegration stages.

Key words: Gastropoda, carnivorous snail, digestive cells, basophilic cells, South Atlantic Ocean.

INTRODUCTION

Zidona dufresnei (Donovan, 1823) is a large carnivorous neogastropod endemic to the south-western Atlantic Ocean, inhabiting the region from Rio de Janeiro, Brazil (22°S), to Patagonian waters, San Matías Gulf, Argentina (42°S) (Kaiser, 1977). Reproductive aspects, population dynamics, growth and mortality were studied in *Z. dufresnei* (Giménez & Penchaszadeh, 2002, 2003; Giménez et al., 2004, 2008), but a detailed study on the anatomy, histology and ultrastructure of the digestive system of *Z. dufresnei* is missing. In recent years *Z. dufresnei* became a valuable resource in Argentina and is likely to be seriously endangered by high levels of exploitation (Giménez et al., 2005; Torroglosa & Giménez, 2010).

Most studies of the histology of the molluscan digestive gland have been conducted on bivalves (Owen, 1970; Thompson et al., 1974; Logan et al., 2008) and herbivorous microphagous gastropods (Merdsoy & Farley, 1973; Boghen & Farley, 1974; Reader, 1976; Wigham, 1976; Nelson & Morton, 1979; Taïeb & Vicente, 1999; Lobo-da-Cunha, 1999, 2000; Taïeb, 2001; Baqueiro Cárdenas et al., 2007; Gros et al., 2009; Volland & Gros, 2012). However, a study by Dimitriadis & Andrews (2000) on the neogastropod *Nucella lapillus* (Linnaeus, 1758) has provided the only report of the functional morphology of the digestive gland of a carnivorous caenogastropod.

The main objective of this study is to describe the structure and function of cells of the digestive gland in the carnivorous snail *Z. dufresnei.* We used histochemical tests and ultrastructural analysis to identify the function of the various cell types and their cycles of activity, in order to compare and contrast the digestive glands of herbivorous grazers and predatory carnivores within the Caenogastropoda.

---

[1] Biología de Invertebrados Marinos. Departamento de Biodiversidad y Biología Experimental. FCEyN, Universidad de Buenos Aires, Cdad. Univ., C1428EGA, Buenos Aires, Argentina.
[2] Malacología y Ecosistemas Costeros. Museo Argentino de Ciencias Naturales. CONICET. Buenos Aires, Argentina.
[3] IBBEA, CONICET - UBA, Buenos Aires, Argentina.
*Corresponding author: mojeda@bg.fcen.uba.ar

MATERIALS AND METHODS

A total of 152 adults specimens of *Z. dufresnei* were collected from October 2008 to December 2009 by bottom trawling in Mar del Plata (38°20'S, 57°37'W) at depths of 40 to 60 m. For histological analysis of the digestive gland, individuals were removed from the shell and small pieces of the digestive gland of each were fixed in Carnoy solution for 1 h, 10% formaldehyde for 12 h, and Bouin's solution for 12 h, and then were subsequently stored in 70% alcohol. Tissues were dehydrated using an ascending series of ethanol concentrations and then embedded in resin (Leica Historesin). Sections were cut at 5 μm with an electronic microtome (Leica), stained with hematoxylin and eosin, and observed under a light microscope.

All the samples collected were used for histochemical studies. The following methods were performed and modified for resin: periodic acid Schiff (PAS) for neutral glycosaminoglycans, Alcian Blue (pH 2.5) for proteoglycan (AMPS), Sudan Black for neutral lipids and phospholipids, Von Kossa method for calcium, Schmorl test for lipofuscin and Best´s carmine for glycogen. Sections of positive and negative controls were made for all histochemical studies.

For electron microscopical analysis, small pieces of tissue form 7 individuals were fixed for 3 h at 4°C in 2.5% glutaraldehyde in phosphate buffer (pH 7.4) and washed in the same buffer. Subsequently, these tissues were placed in a 1% solution of osmium tetroxide in 0.1 M sodium phosphate buffer for 1.5 h, again buffer-rinsed, ethanol-dehydrated, and embedded in araldite resin. Ultrathin sections were cut using either a Reichert or an LKB IV ultramicrotome and stained with uranyl acetate and lead citrate. Sections were examined and photographed using Zeiss EM 109T, Hitachi 300 and Jeol 1010 transmission electron microscopes operated at 75 to 80 kV.

RESULTS

The digestive gland of *Z. dufresnei* was situated in the distal portion of the coiled visceral hump close to the gonad. It was an array of blind-ending tubules interconnected with large ducts opening into the stomach. Tubules and ducts were surrounded by connective tissue, muscle fibres, and blood vessels, and had different appearances based on histological sections (Fig. 1). Whatever the month in which the animals were collected, the digestive gland showed the same histological features.

Histochemical Tests

The results of histochemical tests on resin sections are summarized in Table 1. Ducts were characterized by the presence of one type of ciliated, columnar epithelial cells with a basal nucleus (Figs. 2–5). The apical region contained vesicles that reacted positively to the PAS test, showing the presence of neutral glycosaminoglycans (Fig. 2). Lipid vesicles were evidenced by the Sudan Black technique (Fig. 4) and Schmorl reactions showed the presence of lipofuscin (Fig. 5). Secretory cells were interspersed with ciliated cells and stained intensely with the PAS (Fig. 2) and AMPS test (Fig. 3). The lumens of the ducts were usually

TABLE 1. Histochemical test in the *Zidona dufresnei* digestive gland.

	Duct cells		Tubule cells			
	Columnar cells	Secretory cells	Digestive cells			Basophilic cells
			apical	media	basal	
PAS	+	+++	+++	+++	+	-
Alcian Blue pH 2.5	-	+++	+++	+	-	-
Sudan Black	++	-	+++	+	+	+
Schmorl	+	-	+++	-	-	+++
Von Kossa	-	-	-	-	-	-
Best's carmin	-	-	-	-	-	-

filled with an amorphous substance histochemically similar to the contents of the columnar ciliated cells (Figs. 1–5).

In relation to the characteristics of the cells, two types of digestive tubules were observed (Fig. 6): type 1 tubules were lined by digestive and basophilic cells (Fig. 6) while the type 2 tubules contained only clumps of basophilic cells (Fig. 6). The most abundant cell type was the narrow, closely packed columnar digestive cell, which contained a basal nucleus and a variety of membrane-bound vesicles in the cytoplasm (Fig. 7). Granules of neutral glycosaminoglycans (PAS-positive) were frequently observed occupying a large portion of the digestive cells, although sometimes they were restricted to the basal and medial region (Fig. 7). The apical region, and, to a lesser extent, the middle region of the cell, contained vesicles that reacted positively to the AMPS test for proteoglycan

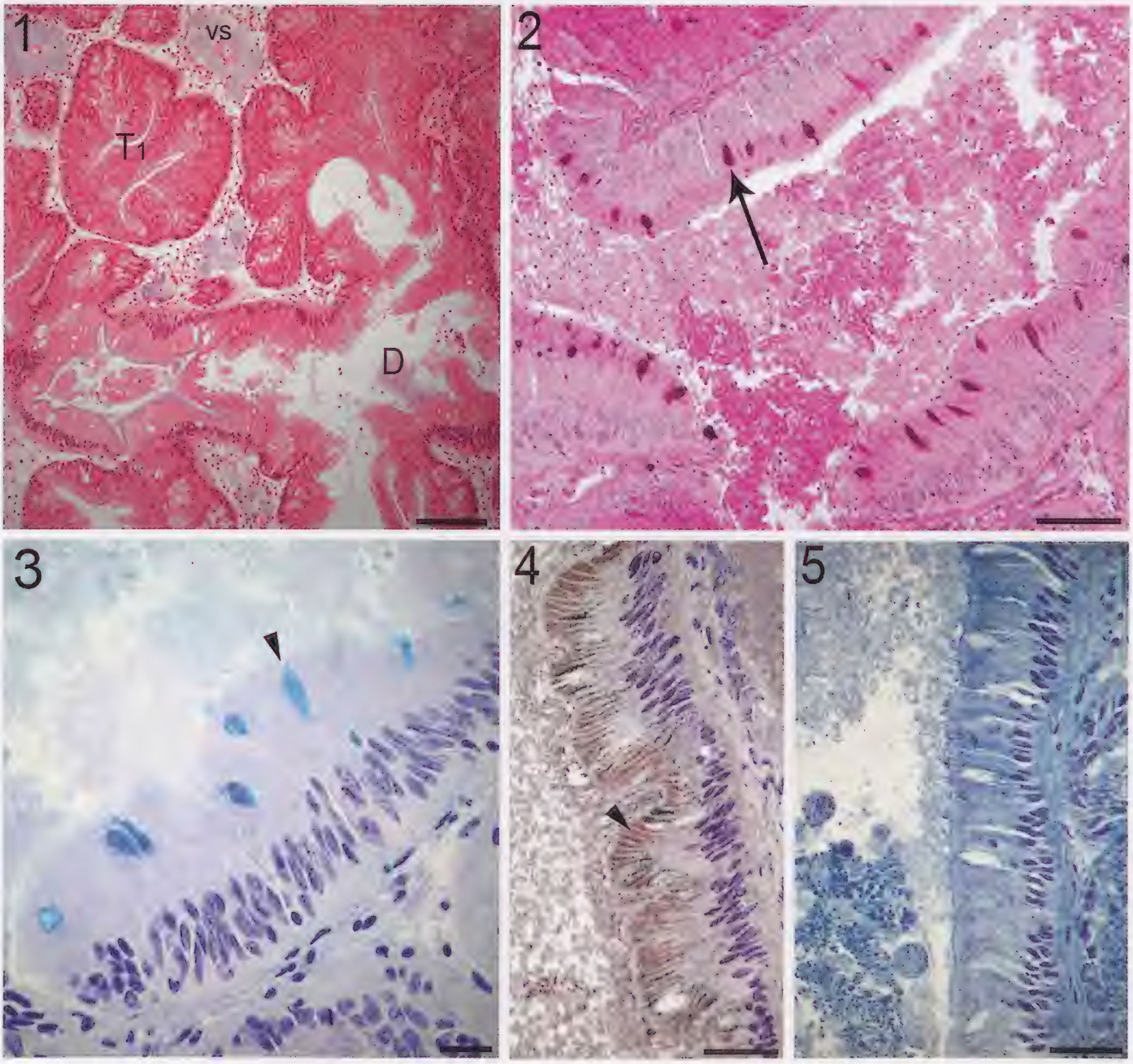

FIGS. 1–5. Histology of *Zidona dufresnei*. FIG. 1: General view of a portion of the digestive gland of *Zidona dufresnei* comprising sections of the ducts (D) and tubules type 1 (T_1), note blood vessel (vs); FIG. 2: Transversal section of a duct with PAS test, a pronounced neutral glycosaminoglycans accumulation is evident in the secretory cells (arrow); FIG. 3: Transversal section of a duct with AMPS test, proteoglycans are accumulated in secretory cells (arrowhead); FIG. 4: Sudan Black technique reveals an accumulation of lipidic vesicles in the apical region of the columnar cells (arrowhead); FIG. 5: Presence of lipofuscin revealed by Schmorl technique. Scale bars: Fig. 1 = 100 µm; Figs. 2, 4, 5 = 50 µm; Fig. 3 = 20 µm.

(Fig. 8), to the Schmorl test for lipofuscin (Fig. 9) and to the Sudan Black technique (Figs. 10, 11). Von Kossa tested positive on some diffuse vascular tissue but not on the digestive cells. There was no positive reaction of the cells with the glycogen reagent Best's carmine.

The pyramidal-shaped basophilic cells were located in crypts of the tubules. The cytoplasm of this cell type contained small vacuoles which reacted negatively to all tests except for the Schmorl reaction for lipofucsin (Fig. 10).

Ultrastructure

The apical surface of the digestive cells was ciliated and bore microvilli (Figs. 12–14). A series of membrane-bound vesicles was present in the cytoplasm (Figs. 12, 13, 15). Pinocytotic vesicles appeared at the base of the microvilli (Fig. 13, inset) followed by vesicles with different contents and electron densities. Type V_1 vesicles were electron transparent (Fig. 12) and of various sizes. Vesicles of type V_2 were frequently found in the mid-region of the cell; they were large and contained granular or fibrillar material of moderate electron density (Fig. 15). Some of these vesicles exhibited an electron-transparent space separating contents and membrane. From the mid-region toward the basal region of the cytoplasm, vesicles containing dense material (type V_3 vesicles) were observed (Fig. 12).

The nucleus in the basophilic cells was situated in the basal region (Figs. 16, 17) and a highly developed rough endoplasmic reticulum, free ribosomes, and abundant secretory granules occupied the cytoplasm (Fig. 17, inset). The secretory granules contained a homogenous electron-dense material (Fig. 17).

Cycle of Activity

Epithelial digestive cells of type 1 tubules displayed four distinct morphological phases,

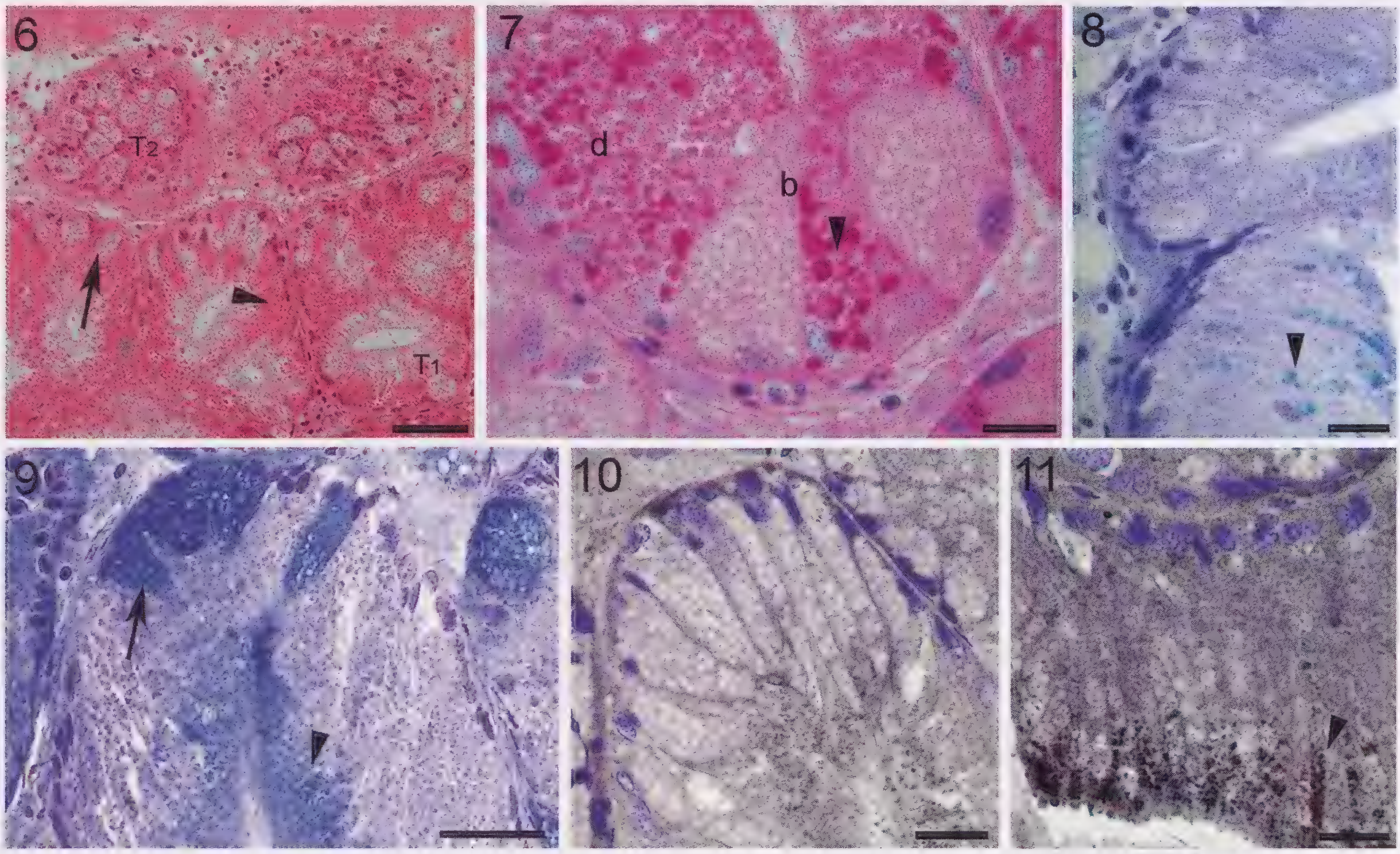

FIGS. 6–11. Histology of the tubules of the digestive gland of *Zidona dufresnei*. FIG. 6: Digestive tubules of type 1 (T_1) are lined by basophilic (arrow) and digestive cells (arrowhead) and tubule of type 2 (T_2) are lined by basophilic cells; FIG. 7: Presence of neutral glycosaminoglycans granules (arrowhead) in the basal and medial region of digestive cells (d) by PAS technique. Note the absence of neutral glycosaminoglycans in the cytoplasm of the basophilic cell (b); FIG. 8: AMPS test showing proteoglycan in the apical and medial region of the digestive cells (arrowhead); FIG. 9: Lipofuscin inclusions in the apical and medial region of digestive cells by Schmorl technique (arrowhead) and in the entire cytoplasm of the basophilic cells (arrow); FIG. 10: Basophilic cells showing the negative reaction to the Sudan Black technique; FIG. 11: Phospholipids and neutral lipids, as evidenced by the Sudan Black technique in the middle and apical region of the digestive cells (arrowhead). Scale bars: Fig. 6 = 50 µm; Figs. 7, 8 = 20 µm; Figs. 9–11 = 50 µm.

but intermediate stages between these four were commonly found:

Stage 1. Tubules 1 and 2 were present and the digestive cells were characterized by a homogeneous cytoplasm without granules (Fig. 18).

Stage 2. The digestive cells were characterized by the presence of granules (Fig. 19) in their cytoplasm.

Stage 3. In this stage, the apical region of digestive cells was rounded and the brush border was not observed. The lumen of the tubules

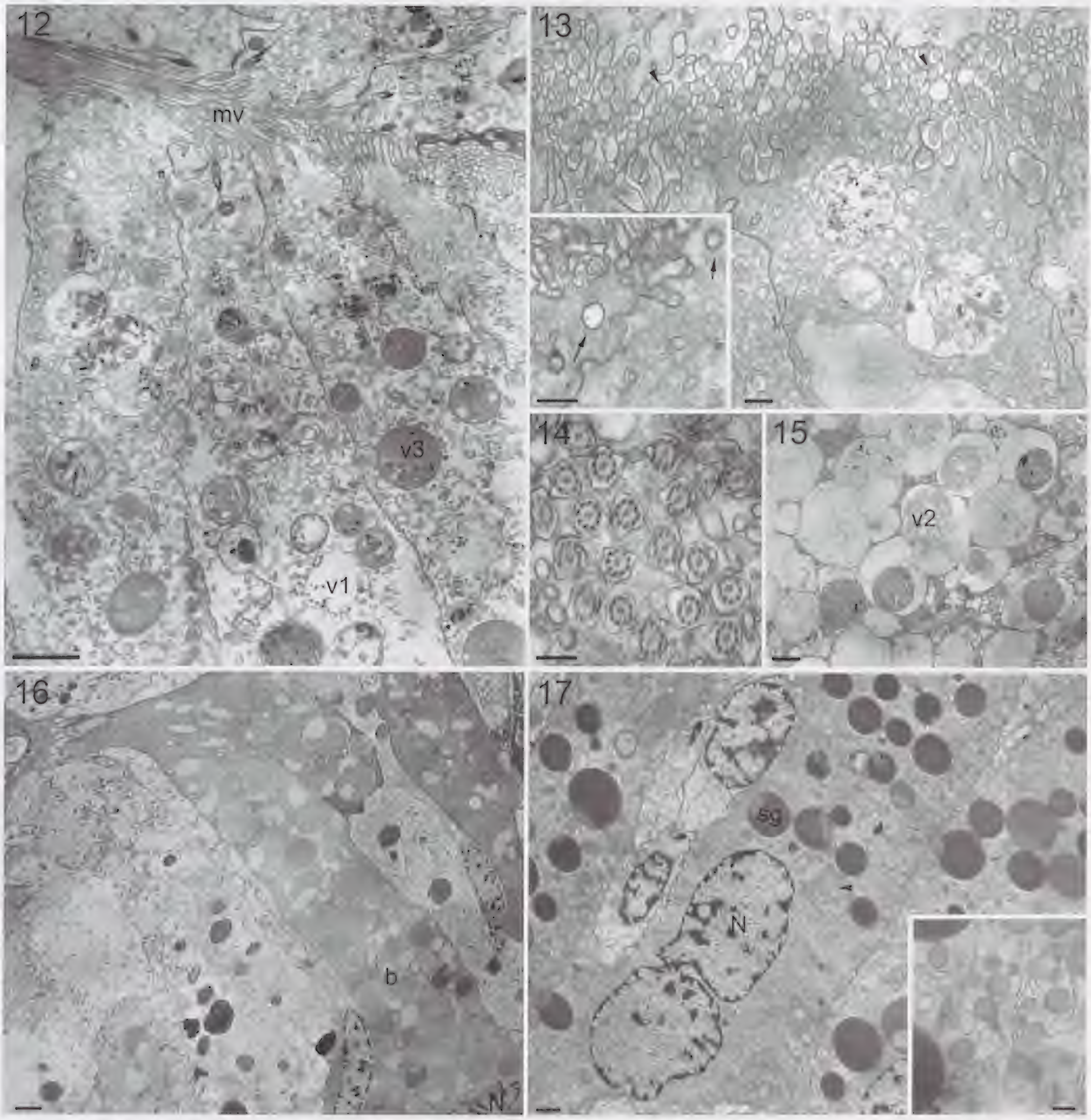

FIGS. 12–17. Ultrastructural aspect of the digestive and basophilic cells of the digestive gland of *Zidona dufresnei*. FIG. 12: General view of the apical surface of the digestive cell showing the presence of microvilli (mv) and different type of vesicles (V_1 and V_3); FIG. 13: General view showing the presence of the cilias (arrowhead). Inset, pinocytotic vesicles in the apex of a digestive cell (arrow); FIG. 14: Detail of the transversal section of the cilias; FIG. 15: Detail of the vesicles (V_2) present in the cytoplasm of a digestive cells; FIG. 16: General view of a basophilic cell (b); FIG. 17: Detail of a basophilic cell showing the cytoplasm full of secretory granules (sg) and rough endoplasmic reticulum (arrowhead). Note the presence of the nucleus (N) in the basal region. Inset, Detail of the well-developed rough endoplasmic reticulum in the cytoplasm of a basophilic cell. Scale bars: Figs. 12, 13 = 1 µm; Fig. 13, inset = 0.2 µm; Fig. 14 = 0.2 µm; Fig. 15 = 1 µm; Figs. 16, 17 = 2 µm; Fig. 17, inset = 1 µm.

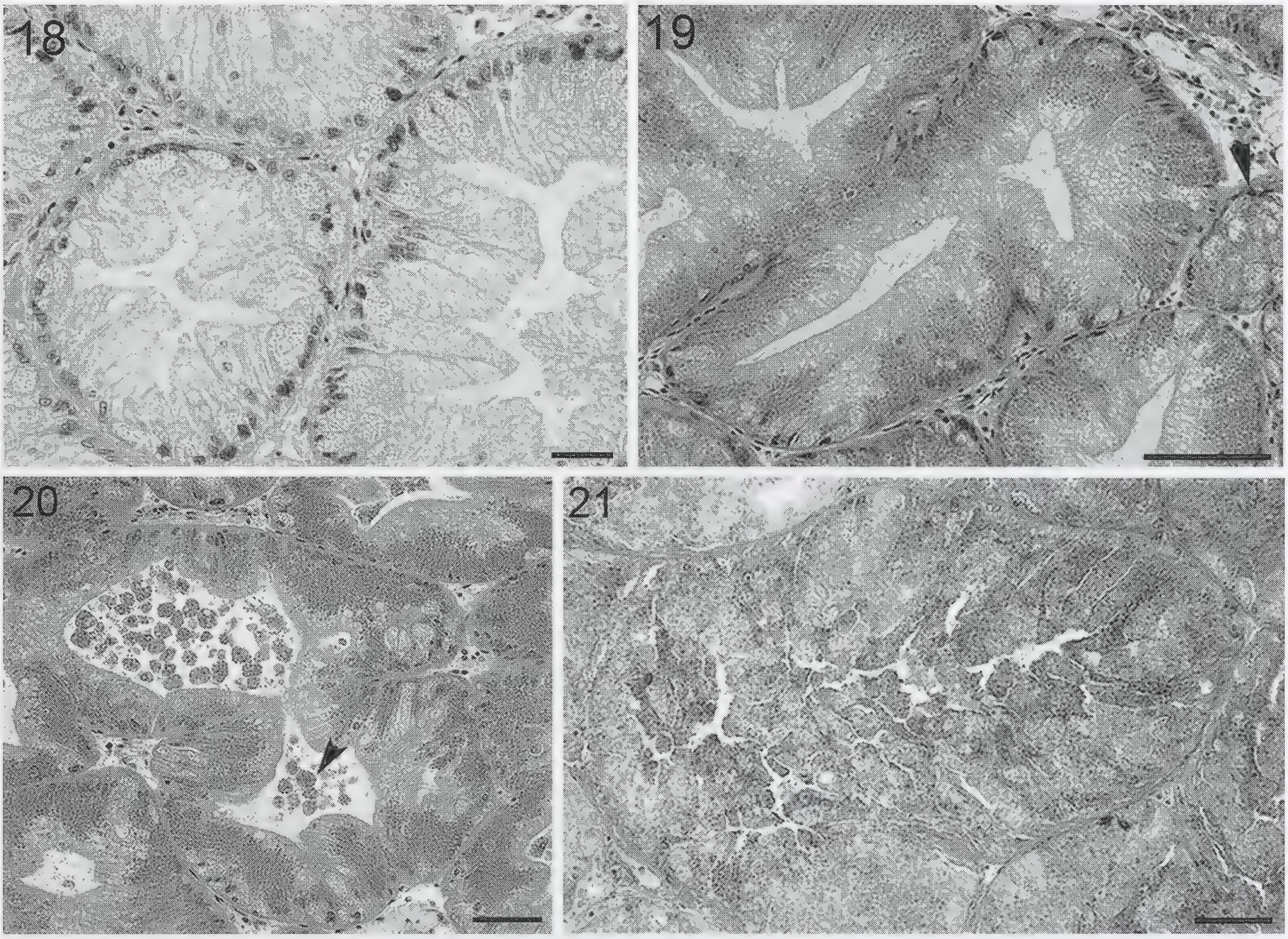

FIGS. 18–21. Cycle of activity in the type 1 tubules of the digestive gland of *Zidona dufresnei*. FIG. 18: Digestive cells in the initial stage, with an homogeneous cytoplasm; FIG. 19: Digestive cells in digestive stage, containing numerous granules in the cytoplasm. Note the presence of type 2 tubule (arrowhead); FIG. 20: Digestive cells in fragmentation stage with fragmentation spherules (arrowhead) in the lumen of the digestive tubule; FIG. 21: Disintegration of the epithelium. Scale bars: Figs. 18, 20, 21 = 50 µm; Fig. 19 = 100 µm.

was characterized by the presence of some fragmentation spherules (Fig. 20). Vesicles present in the digestive cells were histochemically similar to the spherules, in that they reacted positively to the AMPS and PAS tests.

Stage 4. The cytoplasm of the digestive cells seemed to be breaking off from the rest of the cell, and the cellular limits were not defined (Fig. 21). The apical region of the digestive cells reacted positively to the PAS test.

DISCUSSION

The general aspect of the digestive gland of *Z. dufresnei* is similar to that found in other gastropod species, although it appeared to be more complex than the digestive gland of microphagous (Wigham, 1976), herbivorous (Owen, 1958; Merdsoy & Farley, 1973) or other carnivorous gastropods (Dimitriadis & Andrews, 2000). The digestive gland of *Z. dufresnei* consisted of a single digestive duct that connected the stomach to the digestive tubules. The epithelium of the digestive tubules was composed of columnar ciliated cells with neutral glycosaminoglycans and lipids in their cytoplasm. Positioned among these cells were the secretory cells with their cytoplasm composed of neutral glycosaminoglycans and proteoglycans. The glycosaminoglycans of both cells, columnar and secretory, were likely responsible for the lubrication of the lumina surface of the digestive tract and seemed to be related to the flow of secretion along the duct caused by ciliary beating. Also, beating of duct cilia probably carried fine food particles from the stomach into the digestive gland tubules.

The tubules of the digestive gland of *Z. dufresnei* shared some characteristics with the digestive tubules in *Aplysia punctata* (Cuvier, 1803) (Taïeb & Vicente, 1999; Taïeb, 2001) and *Strombus gigas* (Linnaeus, 1758) (Gros et al., 2009) in that two different type of digestive tubules with different cell types were present. In *Z. dufresnei*, tubules of type 1 were formed by an epithelium containing two cell types: digestive and basophilic cells, as in most other gastropods that have been studied (Morton, 1955; Merdsoy & Farley, 1973; Reader, 1976; Wigham, 1976; Nelson & Morton, 1979; Dimitriadis & Andrews, 2000; Baqueiro Cárdenas et al., 2007; Gros et al., 2009; Volland et al., 2012). The type 2 tubules of *Z. dufresnei* are exclusively composed of basophilic cells and different stages are not observed in these cells as in *A. punctata* (Taïeb, 2001).

In some species, digestive cells can collect relatively large food particles by phagocytosis, but in others extracellular digestion occurs and only dissolved substances are captured by small endocytic vesicles (Merdsoy & Farley, 1973; Boghen & Farley, 1974; Lobo-da-Cunha, 2000). Many endocytic vesicles were observed in the apical border of *Z. dufresnei* digestive cells. Basal to this area, there is a zone full of vesicles, morphological and histochemically different.

Type 1 vesicles (V_1) are electron-lucent structures limited by a single membrane and containing only a small amount of material. These vesicles could be formed by the fusion of endocytic vesicles, as was observed in other mollusc species (Owen, 1970; Boghen & Farley, 1974; Lobo-da-Cunha, 2000; Taïeb, 2001). The second type of vesicle (V_2) resembled the heterolysosomes (or phagosomes, or digestive vacuoles, or green granules) reported in other molluscs; these are structures produced by the fusion of endocytic vesicles and enzyme-rich vesicles such as lysosomes (Owen, 1970; Pal, 1972; Dimitriadis & Andrews, 2000). Continuous intracellular digestion results in the accumulation of residual bodies (here called V_3 vesicles). These residual bodies correspond to the granules stained positively with Alcian blue. These "blue granules" are composed of proteoglycan and seemed similar to the large residual bodies described in other molluscan digestive cells (Dimitriadis et al., 2004; Lobo-Da-Cunha, 2000; Taïeb, 2001). Such residual bodies could be secretory products as they were found concentrated in the apical surface of the cell and also in the lumen of the digestive ducts. But some remained in the cytoplasm, becoming lipofuscin granules that stained positively with Schmorl technique. The remnants of undigested material were extruded to the lumen of the digestive gland together with the apical cytoplasm of the cell; the same process has been observed in *Aplysia depilans* (Gmelin, 1791) (Lobo-da-Cunha, 2000) and *Nucella lapillus* (Dimitriadis & Andrews, 2000).

In *N. lapillus* a third cell type full of secretory granules is present in the tubules of the digestive gland epithelium (Dimitriadis & Andrews, 2000). The main function of these small cells was the lubrication and protection of the tubule surface, a function that is analogous to that of secretory cells found in the digestive ducts of the *Z. dufresnei* digestive gland.

The morphology of basophilic cells (also named crypt cells, excretory cells, or secretory cells) found in the digestive tubules of *Z. dufresnei* is similar to the basophilic cells described for other molluscs species (Owen, 1970, 1973; Pal, 1971; Merdsoy & Farley, 1973; Boghen & Farley, 1974; Mathers et al., 1979; Nelson & Morton, 1979; Henry et al., 1991; Lobo-da-Cunha, 1999; Baqueiro Cárdenas et al., 2007; Gros et al., 2009; Volland & Gros, 2012). In *A. punctata*, similar cells containing dense granules of calcium salts, named calcium cells, were found (Taïeb & Vicente, 1999). These cells were not observed in the digestive gland of *Z. dufresnei*. Basophilic cells have a pyramidal shape, large amount of rough endoplasmic reticulum and secretion granules. Some studies reported a positive cytochemical detection for ß-glucuronidase and arylsulphatase in the secretory granules of the basophilic cells (Pipe, 1986; Cajaraville et al., 1995; Lobo-da-Cunha, 1999; Dimitriadis et al., 2004), which enhances the hypothesis concerning the production and secretion of lysosomal enzymes. The presence of a large amount of lipofuscin, an insoluble pigment that is accumulated in lysosome-like structures, in the basophilic cells of *Z. dufresnei* is consistent with this hypothesis. According to this, basophilic cells seem to be responsible for the secretion of digestive enzymes that undertake the extracellular digestion of the food. This statement is supported by the ultrastructural observation of the rough endoplasmic reticulum in the basophilic cells.

Little is known about the cycle of activity present in the tubules of the digestive gland in gastropods. Digestive phases linked to environmental factors such as the tidal cycle have been described in some bivalves (Benninger & Le Pennec, 2006) and gastropods (Merdsoy & Farley, 1973; Boghen & Farley, 1974; Nelson & Morton, 1979). The digestive gland of *Z. dufresnei* has a dynamic state in its morphology, in which most tubules are at the same stage. A cycle of activity is observed in type 1 tubules involving changes in the composition and morphology in digestive cells. During the first stage, here called initial stage, no digestive activity was observed. The absorption of food material is presumed to take place in the tubules at this stage as was demonstrated in numerous experiments with marker substances (Owen, 1955; Mathers et al., 1979). In the second stage, called the digestion stage, the absorption is less important, and intracellular digestion takes place in digestive cells within the large mid-region vesicles. The end-products of this process are accumulated in residual bodies; this was also observed in *Maoricrypta monoxyla* (Lesson, 1831) (Nelson & Morton, 1979). In stage 3, called fragmentation, the fragmentation spherules observed in the lumen are formed by "nipping off" the apical portion of the digestive cells. The next stage is the disintegration of the epithelium. The new tubules could be formed either by reformation of existing tubules or by disassociation of clumps of basophilic cells, forming type 2 tubules, as has been described for other molluscs (Owen, 1970; Nelson & Morton, 1979; Beninger & Le Pennec, 2006).This is supported by the prevalence of type 2 tubules during the breakdown and disintegration stage.

The duration of a complete digestive cycle was studied in some bivalves and it may range from 12 to 24 hours duration to accommodate feeding during each twelve hour tidal cycle (Mathers et al., 1979). The duration of a complete digestive cycle of a single tubule of *Z. dufresnei* is still not known and some feeding and starvation experiments are necessary to correlate feeding activity and digestive functions with localized variations of environment. Complementary information is necessary for the better understanding of the structure and precise function of the cells, specifically through the use of immunocytochemistry.

Further comparative studies including physiology and functional assessment will be considered to understand the role of the principal cell components of the digestive glands related to the feeding habits of the marine gastropods.

ACKNOWLEDGMENTS

Studies have been conducted in accordance with institutional and national guidelines concerning the use of animals in research and the sampling. We are grateful to Jennifer Antonides and an anonymous reviewer for improving the English version of this manuscript. This work was partially supported by CONICET PIP 0253 and UBACyT X 273.

LITERATURE CITED

BAQUEIRO CÁRDENAS, E., L. FRENKIEL, A. Z. ZÁRATE & D. ALDANA ARANDA, 2007, Coccidian (Apicoplexa) parasite infecting *Strombus gigas* Linné, 1758 digestive gland. *Journal of Shellfish Research*, 26: 319–321.

BENINGER, P. G. & M. LE PENNEC, 2006, Structure and function in scallops. Pp. 123–227, in: S. E. Shumway & G. J. Parsons, eds., *Scallops: biology, ecology and aquaculture.* Elsevier, Amsterdam, 1,460 pp.

BOGHEN, A. & J. FARLEY, 1974, Phasic activity in the digestive gland cells of the intertidal prosobranch, *Littorina saxatilis* (Olivi) and its relations to the tidal cycle. *Proceedings of the Malacological Society of London*, 41: 41–56.

CAJARAVILLE, M. P., Y. ROBLEDO, M. ETXEBERRIA & I. MARIGOMEZ, 1995, Cellular biomarkers as useful tools in the biological monitoring of environmental pollution: Molluscan digestive lysosomes. Pp. 29–55, in: M. P. Cajaraville, ed., *Cell Biology in Environmental Toxicology*. University of the Basque Country Press Service, Bilbao, 299 pp.

DIMITRIADIS, V. K. & E. B. ANDREWS, 2000, Ultrastructural and cytochemical study of the digestive gland cells of the marine prosobranch mollusc *Nucella lapillus* (L.) in relation to function. *Malacologia*, 42: 103–112.

DIMITRIADIS, V. K., G. P. DOMOUHTSIDOU & M. P. CAJARAVILLE, 2004, Cytochemical and histochemical aspects of the digestive gland cells of the mussel *Mytilus galloprovincialis* (L.) in relation to function. *Journal of Molecular Histology*, 35: 501–509.

DONOVAN, E., 1823 [1822–1826], *Naturalists' Repository*, vol. 2: pl. 61.

GIMÉNEZ, J., T. BREY, A. MACKENSEN & P. E PENCHASZADEH, 2004, Age, growth and mortality of the prosobranch snail *Zidona dufresnei* (Donovan, 1823) in the Mar del Plata area, SW Atlantic Ocean. *Marine Biology*, 145: 707–712.

GIMÉNEZ, J., J. M. HEALY, G. HERMIDA, F. LO NOSTRO & P. E. PENCHASZADEH, 2008, Ultrastructure and potential taxonomic importance of euspermatozoa and paraspermatozoa in the volutid gastropods *Zidona dufresnei* and *Provocator mirabilis* (Caenogastropoda, Mollusca). *Zoomorphology*, 127: 161–173.

GIMÉNEZ, J., M. LASTA, G. BIGATTI & P. E. PENCHASZADEH, 2005, Exploitation of the volute *Zidona dufresnei* in argentine waters, Southwestern Atlantic Ocean. *Journal of Shellfish Research*, 24: 1135–1140.

GIMÉNEZ, J. & P. E. PENCHASZADEH, 2002, Reproductive cycle of *Zidona dufresnei* (Caenogastropoda: Volutidae) from the southwestern Atlantic Ocean. *Marine Biology*, 140: 755–761.

GIMÉNEZ, J. & P. E. PENCHASZADEH, 2003, Size at first sexual maturity in *Zidona dufresnei* (Caenogastropoda: Volutidae) of the southwestern Atlantic Ocean (Mar del Plata, Argentina). *Journal of the Marine Biological Association of the United Kingdom*, 83: 293–296.

GROS, O., L. FRENKIEL & D. ALDANA ARANDA, 2009, Structural analysis of the digestive gland of the queen conch *Strombus gigas* Linnaeus, 1758 and its intracellular parasites. *Journal of Molluscan Studies*, 75: 59–68.

HENRY, M., E. BOUCAUD-CAMOU & Y. LEFORT, 1991, Functional microanatomy of the digestive gland of the scallop *Pecten maximus* (L.). *Aquatic Living Resources*, 4: 191–202.

KAISER, P., 1977, Beiträge zur Kenntnis der Voluten (Mollusca) in argentinisch brasilianischen Gewässern (mit der Beschreibung zweier neuer Arten). *Mitteilungen aus dem Hamburgischen Zoologischen Museum und Institut*, 74S: 11–26.

LOBO-DA-CUNHA, A., 1999, Ultrastructural and cytochemical aspects of the basophilic cells in the hepatopancreas of *Aplysia depilans* (Mollusca, Opisthobranchia). *Tissue & Cell*, 31: 8–16.

LOBO-DA-CUNHA, A., 2000, The digestive cells of the hepatopancreas in *Aplysia depilans* (Mollusca, Opisthobranchia): ultrastructural and cytochemical study. *Tissue & Cell*, 32: 49–57.

LOGAN, C. R., M. B. EVANS, M. E. WARD, J. L. SCOTT, R. B. CARNEGIE & C. L. VAN DOVER, 2008, Comparative ultrastructure of digestive diverticulae in bathymodiolin mussels discovery of an unknown spherical inclusion (six) in digestive cells of a seep mussel. *Journal of Shellfish Research*, 27: 97–105.

MATHERS, N. F., T. SMITH & N. COLINS, 1979, Monophasic and diphasic digestive cycles in *Venerupis decussata* and *Chlamys varia*. *Journal of Molluscan Studies*, 45: 68–81.

MERDSOY, B. & J. FARLEY, 1973, Phasic activity in the digestive gland cells of the marine prosobranch gastropod, *Littorina littorea* (L.). *Proceedings of the Malacological Society London*, 40: 473–482.

MORTON, J. E., 1955, The functional morphology of the British Ellobiidae (Gastropoda, Pulmonata) with special reference to the digestive and reproductive systems. *Philosophical Transactions of the Royal Society of London (B)*, 239: 86–160.

NELSON, L. & J. E. MORTON, 1979, Cyclic activity and epithelial renewal in the digestive gland tubules of the marine prosobranch *Maoricrypta monoxyla* (Lesson). *Journal of Molluscan Studies*, 45: 262–283.

OWEN, G., 1955, Observations on the stomach and digestive diverticula of the Lamellibranchia. I. The Anisomyaria and Eulamellibranchia. *Quarterly Journal of Microscopical Science*, 96: 517–537.

OWEN, G., 1958, Observations on the stomach and digestive gland of *Scutus breviculus* (Blainville) *Proceedings of the Malacological Society of London*, 33: 103–114.

OWEN, G., 1970, The fine structure of the digestive tubules of the marine bivalve *Cardium edule*. *Philosophical Transactions of the Royal Society of London (B)*, 258: 245–260.

OWEN, G., 1973, The fine structure and histochemistry of the digestive diverticula of the protobranchiate bivalve *Nucula sulcata*. *Philosophical Transactions of the Royal Society of London (B)*, 183: 249–264.

PAL, P., 1971, The fine structure of the digestive tubules of *Mya arenaria* L. I. Basiphil cell. *Proceedings of the Malacological Society of London*, 39: 303–309.

PAL, S. G., 1972, The fine structure of the digestive tubules of *Mya arenaria* L. II. Digestive cell. *Proceedings of the Malacological Society of London*, 40: 161–170.

PIPE, R. K., 1986, Light and electron microscopic localization of ß-glucuronidase activity in the stomach and digestive gland of the marine gastropod *Littorina littorea*. *Histochemical Journal*, 18: 175–186.

READER, T. A. J., 1976, Studies on the ultrastructure, histochemistry and cytochemistry of the uninfected digestive gland of *Bithynia tentaculata* (Mollusca: Gastropoda) and on the ultrastructure of this host organ in snails infected with larval digeneans. *Parasitology Research*, 30: 11–30.

TAÏEB, N., 2001, Distribution of digestive tubules and fine structure of digestive cells of *Aplysia punctata* (Cuvier, 1803). *Journal of Molluscan Studies*, 67: 169–182.

TAÏEB, N. & N. VICENTE, 1999, Histochemistry and ultraestructure of the crypt cells in the digestive gland of *Aplysia punctata* (Cuvier, 1803). *Journal of Molluscan Studies*, 65: 385–398.

THOMPSON, R. J., N. A. RATCLIFFE & B. L. BAYNE, 1974, Effects of starvation on structure and function in the digestive gland of the mussel (*Mytilus edulis* L.). *Journal of the Marine Biological Association of the United Kingdom*, 54: 699–712.

TORROGLOSA, M. E. & J. GIMÉNEZ, 2010, Temporal variation in the size at maturity of the snail *Zidona dufresnei* from the Southwestern Atlantic Ocean after ten years of fishery exploitation. *Aquatic Biology*, 11: 163–167.

VOLLAND, J.-M. & O. GROS, 2012, Cytochemical investigation of the digestive gland of two strombidae species (*Strombus gigas* and *Strombus pugilis*) in relation to the nutrition. *Microscopy Research and Technique*, 75: 1353–1360.

VOLLAND, J.-M., J.-P. LECHAIRE, G. FREBOURG, D. ALDANA ARANDA, G. RAMDINE & O. GROS, 2012, Insight of EDX analysis and EFTEM: Are spherocrystals located in strombidae digestive gland implied in detoxification of trace metals? *Microscopy Research and Technique*, 75: 425–432.

WIGHAM, G. D., 1976, Feeding and digestion in the marine prosobranch *Rissoa parva* (Da Costa). *Journal of Molluscan Studies*, 42: 74–94.

Revised ms. accepted October 2, 2014

MALACOLOGIA, 2015, 58(1–2): 167–177

SPATIAL AND TEMPORAL PATTERN IN LENGTH-MASS REGRESSIONS OF FRESHWATER GASTROPODS IN NEVADA SPRING ECOSYSTEMS

Knut Mehler[1]*, Kumud Acharya[1] & Donald W. Sada[2]

ABSTRACT

We developed length-mass regressions for 16 aquatic gastropods collected from 27 springs in Nevada, United States. The relationship between shell length and body mass for all species was best described by fitting a power function. The mean value of the exponent *b* (2.40 ± 0.39) was lower than reported for other aquatic gastropods, particularly for smaller genera, such as *Pyrgulopsis* and *Tryonia*. Length-mass regressions of gastropods showed intraspecific variation, as well as spatiotemporal variation among the same species. Certain habitat characteristics, especially water temperature, may play a key role in determining growth rates and ultimately length-mass regressions in this study. Although the power term *b* showed high variability when the same species (*Melanoides tuberculata*, *Pyrgulopsis lockensis*, and *Pyrgulopsis turbatrix*) were collected from different springs, the power term was similar when the same species (*Pyrgulopsis marcida*) was collected from the same spring during different seasons and years. Therefore, we suggest that published equations should be used with caution and only when habitat characteristics and length ranges are similar compared to those in the literature.

Key words: gastropods, length-mass regressions, power term, spring ecosystems, Nevada.

INTRODUCTION

Aquatic gastropods are ubiquitous and inhabit many spring-related water bodies scattered throughout the southwestern United States (Hershler, 1994; Hershler & Sada, 2002; Unmack & Minckley, 2008). It has been recognized that the disconnection of springs from other water bodies after the Pleistocene era and their long-term isolation have led to habitat fragmentation and, in turn, to distinct gastropod population distributions, population genetics and speciation (Hershler, 1994). Particularly for species belonging to *Pyrgulopsis* (Hydrobiidae), local endemism is common, and many species are restricted to a single spring, spring complex or drainage system (Hershler, 1984, 1998). Their presence indicates the long-term, stable conditions of certain habitat characteristics and that many gastropods have evolved in isolation over time (Frest & Johannes, 1995; Sada & Vineyard, 2002).

Assessing the importance of those aquatic gastropods in energy and nutrient transfer between trophic levels, as well as nutrient recycling, requires information about their biomass (Benke et al., 1999; Hall et al., 2003; Silva et al., 2010). However, determining biomass, particularly of small gastropods (e.g. *Pyrgulopsis* and *Tryonia*) by direct measurement is often difficult and time consuming. Furthermore, in many cases the direct measurement of dry mass is often hindered by an incomplete specimen, either because soft tissue is partly digested from chemical preservation or from passing through the digestive systems of predators so that only the shell is left behind (Hódar, 1997).

A widely accepted tool for estimating biomass, growth rates and/or secondary production of benthic invertebrates in ecological studies is length-mass regression (Benke et al., 1999; Gruner, 2003; Becker et al., 2009). By using the power function $DM = aL^b$, dry mass can be derived as a power of the linear dimension of an organism, where DM is the dry mass (in mg), L is the body length (for this study, shell length in mm), and a and b are constants (Benke et al., 1999). The power function can also be expressed in a linearized form as: $\log_{10} DM = \log_{10}a + (b \times \log_{10} L)$. The term b describes how

---

[1]Desert Research Institute, Division of Hydrologic Science, 755 E. Flamingo Rd., Las Vegas, Nevada 89119, U.S.A.
[2]Desert Research Institute, Division of Hydrologic Science 2215 Raggio Parkway, Reno Nevada 89512, U.S.A.
*Corresponding author: knut.mehler@dri.edu

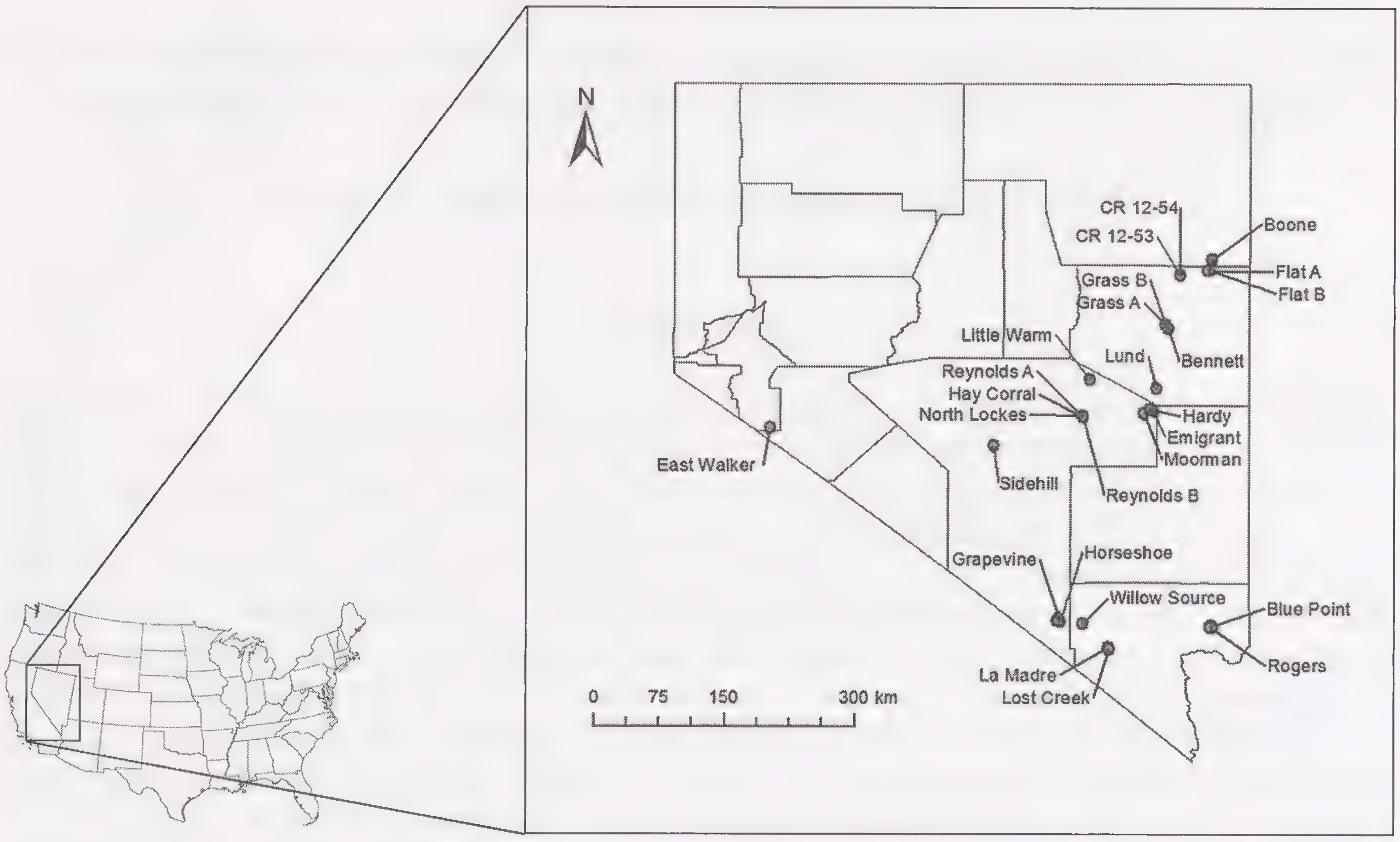

FIG. 1. Map of Nevada indicating the sampling locations.

body proportions change with increasing size during ontogeny (Hirst, 2012). A value close to 3 indicates isometric enlargement (i.e., the body proportions remain constant during growth), whereas a value less than 3 implies a relative increase in elongation (Hirst, 2012). Information about changes in body shape during ontogeny is essential for predicting further biological and ecological consequences. For example, Glazier (2010) showed that metabolic-rate scaling is related to changes in body shape during ontogeny and that even closely related species can exhibit significant variation in respiration scaling.

The advantage of estimating dry mass (DM) using length-mass regressions is that they not only provide rapid measurements, but also allow the biomass of already extinct spring gastropod populations to be reconstructed using preserved shells. Although length-mass regressions have been applied to many terrestrial and aquatic invertebrates, there are only few studies that have analyzed length-mass relationships for spring-dwelling gastropods (e.g., Elkarmi & Ismail, 2007). The long-term adaption of most of the spring-dwelling gastropods makes them the ideal subjects for studying the link between long-term, stable conditions and length-mass relationships in crenic food webs. Moreover, when springs are persistent, they are generally more stable than lotic and lentic systems because they are not exposed to seasonal variability in water chemistry, temperature, and discharge (McCabe, 1998). These characteristics suggest that the processes that determine growth rates and consequently the intraspecific length-to-mass scaling of spring-dwelling gastropods during ontogeny might be trenchantly different from gastropods that inhabit lentic and lotic ecosystems. The overall objective of this study was to develop length-mass regressions from spring-dwelling gastropods to predict DM from the shell lengths of the major gastropod species in spring ecosystems along a temperature gradient in Nevada. The occurrence of the same species in multiple springs during different seasons allowed us to test the spatial and temporal effects on length-mass relationships (i.e., variations in the *b* value).

MATERIALS AND METHODS

Study Sites

Twenty-seven springs were selected according to the historical and recent occurrences of spring-dwelling gastropods (Fig. 1). The springs are situated in the Great Basin Province in southern and central Nevada and range from 469 m to 2,002 m in elevation. The springs are widely separated by vast areas with little or no evidence of groundwater discharge. The springs themselves have nearly constant discharge and probably represent points or zones of principal discharge from large regional flow systems. The Cenozoic sand and gravel deposits of the overlying basin-fill aquifer readily yield water to springs and wells, which are the major water supply for agricultural, livestock, and municipal use (Harrill & Prudic, 1998; Welch et al., 2008). Groundwater quality in this region is characterized by low dissolved oxygen and low nitrate concentration (2.5 mg/L and < 1 mg/L, respectively) and a high total dissolved solids concentration (410 mg/ L on average) (Berndt et al., 2005). Springs fed by local aquifers usually have cooler temperatures because the water stays in the ground for shorter periods of time. The temperature in the study region ranges from -11°C to -2°C in the winter and 18°C to 27°C in the summer, which is typical of the Great Basin Desert. Annual precipitation varies greatly between valley locations, ranging from 20 cm to 38 cm annually (Hershey et al., 2007).

Biological Sampling

A total of 1,451 gastropods belonging to three families (Hydrobiidae, Physidae, and Thiaridae) and 16 species were collected in April 2010, May 2012, and June 2012 by either washing substrates (rocks, wood, macrophytes) or sifting fine sediments with a 250 μm sieve. Gastropods were put in filtered spring water for one hour to ensure that they emptied their guts. Water temperature was recorded at each site during collection using an YSI-model 650 MDS temperature-oxygen meter. A one-liter water sample was collected from each spring for nitrate-nitrogen (NO_3-N), soluble reactive phosphorus (SRP), and chlorophyll *a* (Chl *a*) analysis.

Gastropods from each spring were identified by gastropod expert Donald W. Sada of the Desert Research Institute in Reno, Nevada, based on shell characteristics and penial morphology (for details see Hershler, 1998) and by using collections of preserved gastropod of all the populations in their original description sampled in this study (Sada, 2008; Hershler & Sada, 1987, 2001, 2002). The species identification has also been verified by Robert Hershler of the Smithsonian Institution in Washington, D.C.

In the laboratory, undamaged gastropods were dried at 50°C for 72 h until the weight was constant. To obtain DM, gastropods were weighed individually to the nearest 0.01 mg on a Mettler Toledo New Classic MS balance. Body length (BL) was expressed as the maximum shell length (the distance between the tip of the apex and the edge of the bottom lip) and was measured with calipers to the nearest 0.01 mm. Water samples from each spring were analyzed for NO_3-N and SRP at the Desert Research Institute's Water Analysis Laboratory (Reno, Nevada) using standard EPA methods (U.S. Environmental Protection Agency, 1979). We determined Chl *a* for each spring spectrophotometrically by measuring the absorbance of algae pigments from a known volume of water. The Chl *a* concentration (μg/L) was used to represent the primary producer's biomass (i.e., food availability).

Statistics

The power function $M = aL^b$ was applied exclusively to all taxa because this function yielded the highest coefficient of determination (r^2). Analysis of covariance (ANCOVA) was used to test for differences in the slope of the length-mass regression equations among all gastropod species. We used the most abundant species found at multiple springs during different years and seasons – *Melanoides tuberculata* (Müller, 1774), *Pyrgulopsis lockensis* Hershler, 1998, *Pyrgulopsis turbatrix* Herschler, 1998, *Pyrgulopsis marcida* Herschler, 1998, and *Physa acuta* (Draparnaud, 1805); see Table 1 for the spring names where each species was collected – to test for differences in the length-mass regressions. The ANCOVA was used when (i) the same species were sampled from different springs (*Melanoides tuberculata*, *Pyrgulopsis lockensis*, *Pyrgulopsis turbatrix*, and *Physa acuta*) and (ii) the same gastropod species were sampled from the same spring during different years and seasons (*Pyrgulopsis marcida*). In this case, the "site" was the categorical variable, "body length" was the regressor variable (*x*), and body mass was the response variable. Univariate linear regressions were used to test for any correlations between physicochemical variables. All statistical analyses were done in SAS (version 8.2; SAS Institute, Cary, North Carolina).

TABLE 1. The length-mass regression equations for gastropod species found in twenty-seven springs based on shell length. All equations were calculated using the power function: DM = aL^b, where DM is dry mass, L is body length (shell length in this study), and a and b are constants. Range BL = range body length in mm, range DM = range dry mass (including shells) in mg, r^2 = coefficient of determination, n = number of individuals used to calculate the regression equation. Physicochemical variables are given for each of the springs (Temp. = water temperature, NO_3-N = nitrate concentration, SRP = soluble reactive phosphorus concentration, Chl a = chlorophyll a concentration).

Taxon	Spring Name	Temp. (in °C)	NO_3-N (in mg/L)	SRP (in mg/L)	Chl *a* (in µg/L)	*a*	*b*	Range BL (in Mm)	Range DM (in mg)	r^2	n
Melanoides tuberculata	Moorman[c]	36.2	0.034	0.004	26.2	0.02	3.01	21.39–32.57	211.86–724.53	0.94	9
M. tuberculata	Blue Point[b]	30	0.217	0.004	14.9	0.04	2.78	10.44–15.05	27.21–86.01	0.95	15
M. tuberculata	Rogers[b]	20.9	0.264	0.003	32	0.04	2.83	9.11–30.02	21.81–599.26	0.99	13
M. tuberculata	Little Warm[a]	31.6	0.01	0.21	n/a	0.05	2.65	8.50–23.40	14.53–182.73	0.98	11
Pyrgulopsis carinata	Little Warm[a]	31.6	0.01	0.21	n/a	0.22	2.59	1.70–2.50	0.73–2.39	0.71	23
P. cruciglans	Flat A 12-58[c]	14.4	1.77	0.334	7.7	0.15	2.56	1.22–2.06	0.19–0.49	0.83	43
P. cruciglans	Flat B 12-59[c]	15.2	1.67	0.016	8.4	0.14	2.84	1.22–2.38	0.31–1.96	0.91	43
P. cruciglans	Boone Springs[a]	16.6	n/a	n/a	n/a	0.18	2.17	1.27–1.97	0.29–0.86	0.78	54
P. gibba	East Walker[a]	n/a	n/a	n/a	n/a	0.17	2.32	1.25–2.72	0.23–1.54	0.84	77
P. gracilis	Emigrant[a]	19.4	0.75	0.13	n/a	0.31	2.13	1.60–2.40	0.81–2.09	0.74	47
P. isolata	Sidehill[b]	19.9	0.6	0.03	18.4	0.20	2.25	1.18–2.25	0.20–1.47	0.83	43
P. lockensis	Reynolds A[c]	36.2	0.014	0.086	47.6	0.20	2.61	0.94–1.89	0.15–1.12	0.91	41
P. lockensis	Reynolds B[c]	36.2	0.016	0.018	55.9	0.19	2.68	0.92–1.94	0.09–1.01	0.87	42
P. lockensis	North Lockes[c]	35.2	0.015	0.002	54.2	0.23	2.50	1.02–2.00	0.19–1.22	0.86	43
P. lockensis	Hay Corral[c]	34.2	0.004	0.028	39.5	0.33	1.74	1.18–1.98	0.35–1.22	0.62	91
P. marcida	Hardy[a]	13.9	0.99	0.49	n/a	0.26	2.15	1.84–3.26	0.76–3.22	0.86	42
P. marcida	Hardy[c]	13.9	1.06	0.027	24.3	0.20	2.18	1.30–2.79	0.24–1.86	0.81	78

(continues)

(continued)

Taxon	Spring Name	Temp. (in °C)	NO_3-N (in mg/L)	SRP (in mg/L)	Chl *a* (in µg/L)	*a*	*b*	Range BL (in Mm)	Range DM (in mg)	r^2	n
P. marcida	Emigrant[a]	19.4	0.75	0.13	n/a	0.29	2.06	1.40–2.60	0.54–1.97	0.78	57
P. merriami	Lund[a]	19.3	n/a	n/a	n/a	0.21	2.71	1.40–3.18	0.52–5.83	0.94	72
P. merriami	Moorman[c]	36.2	0.034	0.004	26.2	0.28	3.05	1.06–2.26	0.27–2.91	0.93	41
P. sathos	Emigrant[a]	19.4	0.75	0.13	n/a	0.50	1.49	1.80–3.20	1.24–2.88	0.75	22
P. serrata	Cold[c]	10.9	0.55	0.038	7.2	0.20	2.38	0.99–2.85	0.13–2.13	0.94	41
P. serrata	CR 12-53[c]	14.2	0.007	0.065	3.2	0.21	2.23	1.34–2.72	0.42–1.93	0.91	44
P. serrata	CR 12-54[c]	11.9	0.337	0.29	4.3	0.15	2.60	1.36–2.46	0.28–1.76	0.85	41
P. sulcata	Grass A[c]	20.6	0.57	0.012	n/a	0.12	2.55	1.78–3.37	0.52–2.58	0.95	14
P. planulata	Grass B[c]	19	0.51	0.138	8.3	0.22	3.16	0.82–1.39	0.13–0.60	0.81	41
P. turbatrix	Horseshoe[b]	18.5	1.14	0.018	18.3	0.12	2.41	1.63–3.46	0.39–2.14	0.88	101
P. turbatrix	Grapevine[b]	19.9	0.281	0.01	4	0.13	2.35	1.02–2.86	0.08–1.75	0.91	45
P. turbatrix	Willow Source[b]	11.2	0.249	0.014	9.2	0.20	2.15	1.31–3.05	0.33–2.21	0.87	46
P. turbatrix	La Madre[b]	n/a	n/a	n/a	n/a	0.12	2.97	1.32–2.75	0.24–1.93	0.91	43
Physa acuta	CR 12-53[c]	14.2	0.007	0.065	3.2	0.14	2.24	3.37–8.95	2.01–18.62	0.98	13
P. acuta	Bennett[c]	14.8	0.48	0.033	23.8	0.11	2.40	6.33–2.87	8.60–22.34	0.85	16
P. acuta	Lost Creek[b]	15.2	0.212	0.016	n/a	0.07	2.67	1.89–4.59	0.38–5.01	0.93	24
Tryonia porrecta	Blue Point[b]	30	0.217	0.004	14.9	0.09	2.44	1.43–2.56	0.13–1.05	0.78	42
T. sp.	Little Warm[a]	31.6	0.01	0.21	n/a	0.36	1.54	2.70–5.40	1.47–5.16	0.77	33

[a] sampled in April 2010, [b] sampled in May 2012, [c] sampled in June 2012

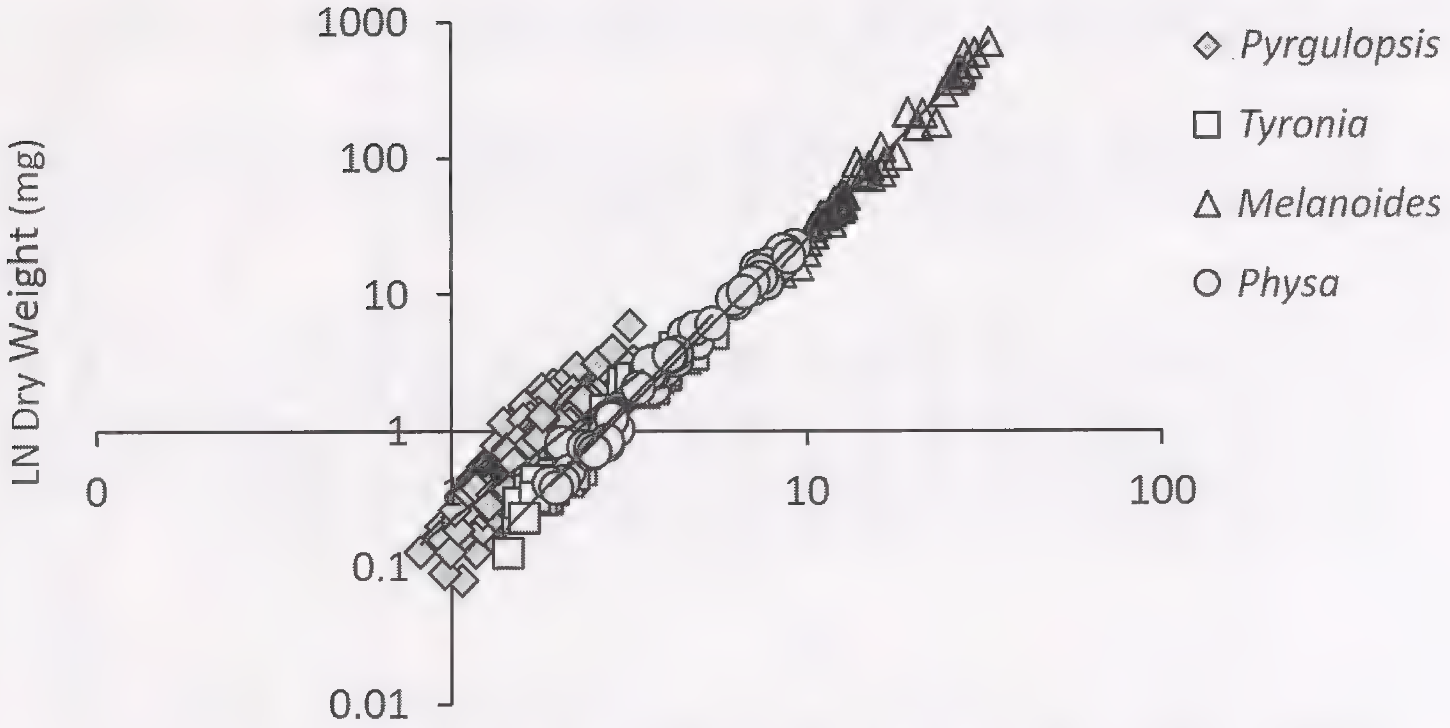

FIG. 2. Comparison of composite length-mass regressions for four gastropod genera (*Pyrgulopsis*, *Tryonia*, *Melanoides*, and *Physa*) based on shell length (mm) and dry mass (mg, including shell).

RESULTS

The 27 springs exhibited a wide range of physicochemical characteristics. The water temperature ranged from 10.9°C to 36°C and NO_3-N and SRP ranged from 0.004 mg/L to 1.77 mg/L and 0.002 mg/L to 0.49 mg/L, respectively (Table 1). Although there was a significant negative correlation between temperature and NO_3-N ($r^2 = 0.32$, $p = 0.0008$), there was no correlation between temperature and SRP ($r^2 = 0.04$, $p = 0.266$) or SRP and NO_3-N ($r^2 = 0.08$, $p = 0.119$). However, there was a significant positive correlation between temperature and Chl *a* ($r^2 = 0.57$, $p < 0.001$).

Body length ($p < 0.001$) significantly predicted DM for all taxa, which was shown by high coefficients of determination (range: 0.65–0.99) (Table 1). On average, the power term *b* was 2.45 ± 0.39 when all gastropods were pooled together. There was a significant difference in the length-mass regressions between the four gastropod genera (ANCOVA, $p < 0.001$, Fig. 2). Thiaridae (*Melanoides tuberculata*) had the highest mean *b* values (2.82 ± 0.15), whereas *Tryonia* (*Tryonia spp.*) had the lowest mean *b* values (1.99 ± 0.64). The shell lengths of the *Tryonia* genera collected from two springs were significantly different (ANOVA, $p < 0.001$). This caused a much higher mean *b* value in Figure 1 ($b = 2.69$) when individuals from the two springs were pooled in the length-mass regression. The mean *b* values of *Pyrgulopsis* and *Physa* were 2.04 ± 0.37 and 2.58 ± 0.22, respectively.

The length-mass regressions for four genera (*M. tuberculata*, *P. lockensis*, *P. turbatrix*, and *P. acuta*) collected from different springs during different seasons are presented in Figure 3. The power term *b* was similar (range: 2.50–2.68) among *P. lockensis* collected in summer from springs that are located close together, but not for the *P. lockensis* sampled from Hay Corral Spring, which had a much lower power term *b* ($b = 1.74$, Fig. 3a). There was a significant effect of BL × site interaction ($p < 0.001$), indicating that the slopes of length-mass regressions of *P. lockensis* were different between the four sites. We also found a significant effect of BL ($p < 0.001$) and an effect of site ($p < 0.001$), which were most likely due to the very small power term of 1.74 for individuals collected from Hay Corral Spring. There was a significant effect of BL ($p < 0.001$) and site ($p < 0.001$) on the slope of the length-mass regression of *M. tuberculata* ($p < 0.001$, Fig. 3b). However, there was no effect of site × BL interaction ($p = 0.4043$), indicating that the slopes of the length-mass regressions were not significantly different among the four sites. The *b* values of *P. acuta* sampled in different springs showed some variation, but the effect of site × BL interaction was only marginally significant ($p = 0.055$), indicating that the slope of regressions between the three springs are only slightly different (Fig. 3c). There was a significant effect of BL ($p < 0.001$), but no effect of site ($p = 0.349$). A large range in the power term *b*, from 2.15–2.91, was found for the *P. turbatrix* collected from four springs that are located far apart (Fig. 3d). There was a significant

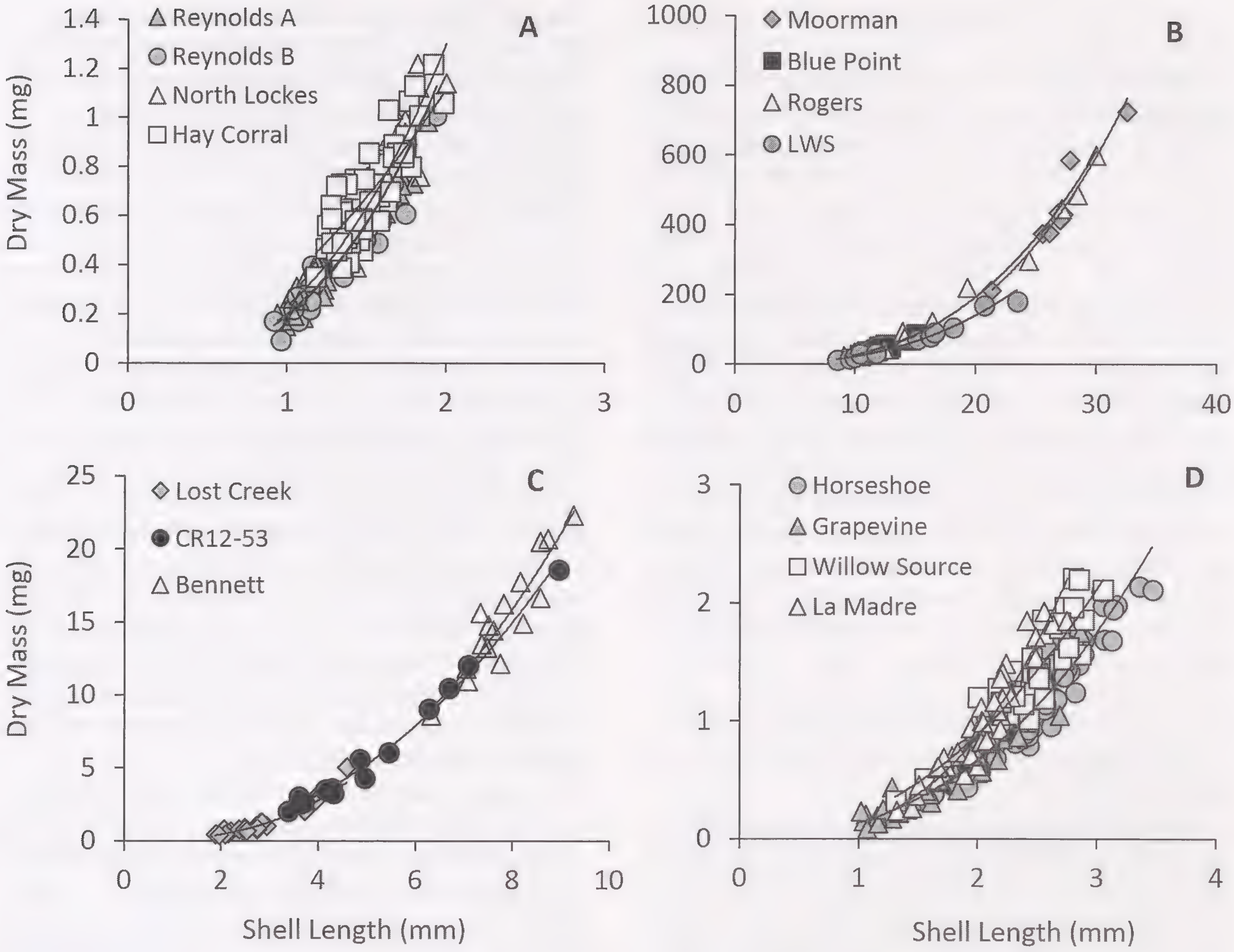

FIG. 3. Length-mass relationships for *Pyrgulopsis lockensis*. A: Power term *b* values for Reynolds A 2.61, Reynolds B 2.68, North Lockes 2.50, and Hay Corral 1.71, *Melanoides tuberculata*; B: Power term *b* values for Moorman 3.01, Blue Point 2.78, Rogers 2.83, and LWS 2.65, *Physa acuta*; C: Power term *b* values for Lost Creek 2.67, CR12-53 2.24, and Bennett 2.40, and *Pyrgulopsis turbatrix*; D: Power term *b* values for Grapevine 2.35, Horseshoe 2.41, La Madre 2.91, and Willow Source 2.51).

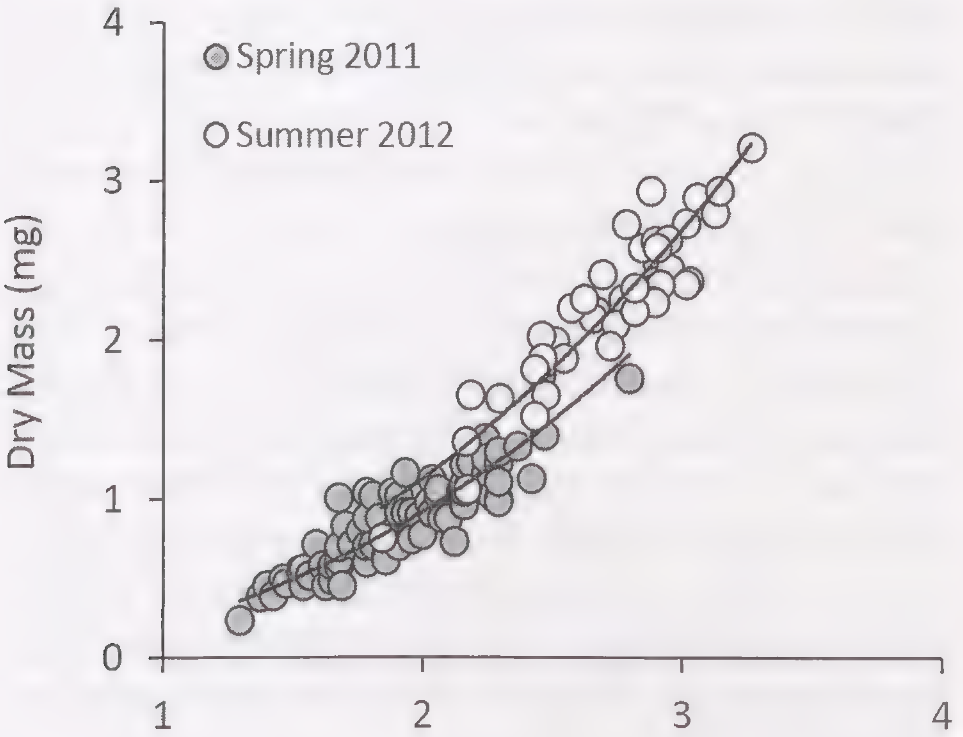

FIG. 4. Length-mass relationships for *Pyrgulopsis marcida* collected from Hardy Springs in two different seasons and years (power term *b* values for spring 2011: 2.15, and summer 2012: 2.18).

effect of BL ($p < 0.001$), an effect of site ($p < 0.001$), and a significant site × BL interaction ($p = 0.0037$), indicating that the slopes of the length-mass regressions of *P. turbatrix* were different between the four sites.

Individuals belonging to *P. marcida* were collected from the same spring (Hardy Springs) during different seasons and years (April 2011 and June 2012). The power terms *b* were 2.14 and 2.17, respectively, even though individuals sampled in summer 2012 had a significantly larger BL compared to individuals sampled in spring 2011 (t-test, $p < 0.001$; Fig. 4). Site had a marginally significant effect ($p = 0.0457$). However, BL × site interaction had no effect on the slope of the length-mass regression of *P. marcida* ($p = 0.1997$), indicating that the slopes of length-mass regressions were similar between seasons.

DISCUSSION

Body length was a good predictor of DM of aquatic gastropods. In accordance with other studies, the relationship between gastropods' linear body dimension and dry mass was best explained using a power function over the exponential model (e.g., Rosemond et al., 1993; Benke et al., 1999; McKinney et al., 2004). The mean of the power term *b* was lower than 3 (2.44 ± 0.37) for all genera combined, indicating an elongation in shape during ontogeny in our gastropods (Hirst, 2012). Our data suggest that long-term adaption of gastropods to a certain spring ecosystem might affect length-mass relationships. First, when the same species was sampled from different springs, they showed significant variation in the power term *b*. Second, when the same species was sampled from the same spring during different years and seasons, they only showed slight variations in the power term *b*. Several explanations-which are not necessarily exclusive-that may explain these patterns in length-mass regressions are proposed here.

Most of the *Pyrgulopsis* and *Tryonia* genera are tightly linked to running water close to spring sources (Hershler, 1998). Therefore, *Pyrgulopsis* might increase their body length more rapidly than their body diameter during ontogeny and become proportionately narrower to withstand the higher flow velocities around the spring head. In contrast, *b* values of *M. tuberculata* were around 3. This exotic mollusk prefers slow-flowing or standing water bodies (de Kock, 2009), which is probably one reason for the isometric enlargement. Unfortunately, we did not measure flow velocities in our study springs. Therefore, this assumption needs to be tested further by recording flow velocities and/or shear stress at sites where gastropods are being collected.

Temperature is a key component that regulates fundamental biological processes, such as growth rates and body size (Angiletta et al., 2003; Woods et al., 2003). Previous studies on *Pyrgulopsis bruneauensis* showed an intimate relationship between temperature and growth rates (Mladenka & Minshall, 2001). Elkarmi & Ismail (2007) also reported differences in shell length between two *M. tuberculata* populations collected from hot springs and freshwater pools that differed in temperature. In our study, *M. tuberculata* were collected from springs ranging in water temperatures from 20.9°C to 36.2°C, which most likely caused differences in growth and age. In contrast to *Melanoides*, the slopes for *Physa* sampled from multiple springs during different seasons did not vary significantly. Although those springs varied widely in NO_3-N and Chl *a*, water temperature only varied by 0.4°C and 1°C, respectively. Therefore, it seems that water temperature is one of the most important variables affecting length-mass regressions of gastropods in this study. Water temperature has also been shown to affect gastropod shell plasticity and body mass, which consequently affects length-mass regressions. Trussel (2000) showed that phenotypic plasticity (i.e., the differences in shell morphology and body mass of *Littorina obtusata*) were in parts related to water temperature. We did not separate shells from soft tissue in our study. However, using an ash-free dry mass (dried material ashed at 550°C and reweighed) instead of the dry mass including the shell would have improved the detection of differences in shell morphology when calculating the soft-tissue-to-shell-mass ratio in same-sized individuals.

Contrary to the findings of Silva et al. (2010), growth rates of *Melanoides* in our study seem to be lower according to the power term *b*. This may be related to differences in food abundance and quality. The interaction of low food quantity and high population density has been shown to affect the shell length of *Mytilus edulis* (Alunno-Bruscia et al., 2001). To represent food quantity, we used the Chl a concentration, which was found to vary widely among our springs (3.3–55.9 µg/L) and was positively related to temperature. This is interesting because we expected a mutualistic effect of higher-temperature-related growth rates accompanied by higher food quantity. Furthermore, spring-dwelling gastropods such as *Pyrgulopsis* and *Melanoides* can reach densities of > 1,000 individuals/m^2 and > 1,500 individuals/m^2, respectively, in some of our springs (Hershler, 1998; Mehler, unpublished data). However, these high densities and the potential for greater food competition might have offset the favorable conditions of warm temperature and abundant food. Therefore, gastropods in those springs might increase in body length faster than they gain weight, ultimately causing *b* values to be < 3 due to the relative elongation in shape during ontogeny.

In contrast to the *Pyrgulopsis* species collected from different springs, the power term *b* of *P. marcida* collected from Hardy Springs during different seasons and years was not significantly different. This indicates that growth rates between seasons and years are similar. When springs are persistent, they are generally more stable than lakes and streams because they are not exposed to seasonal variability in water chemistry, temperature, and discharge (McCabe, 1998; Cantonati et al., 2006). Therefore, we assume that growth rates of *P. marcida* are similar between seasons and years in long-term stable springs. We assume that growth variations within the same species are most likely caused by differences in the physical and chemical habitat characteristics. This is consistent with several other studies on benthic invertebrates and emphasizes the need to be cautious when using regressions for the same taxa from different regions (Meyer, 1989; Wenzel et al., 1990; Burgherr & Meyer, 1997). Moreover, an issue we want to address is the error that arises due to the potential misidentification of some of the gastropod species in this study. Gastropods belonging to the genera of *Melanoides* and *Physa* are very difficult to identify because of potentially different clonal lineages and a lack of shell characters, respectively (Samadi et al., 1999; Taylor, 2003). Therefore, it is possible that differences in growth rates and consequently the power term *b* might be the result of different clonal lineages and/or species.

Although there are several factors that affect the mass-length regressions of gastropods, we recommend considering water temperature in particular because of the tight interrelation of temperature, metabolic rates, and population growth (Savage et al., 2004). In accordance with other studies, collecting the full range of size cohorts can be as important to interpreting the power term *b* as sampling the same gastropod species in different geographic regions (Becker et al., 2009).

In conclusion, this study is one of the first to describe length-mass relationships for populations of gastropods from a wide range of spring ecosystems in Nevada. Our data can be used in further studies to determine growth rates, biomass, and the secondary production of aquatic gastropods. However, length-mass regressions obtained for gastropods in a specific area are not generally transferable to other geographical regions, so particular emphasis should be given to the correct identification of species. Therefore, we recommend that the published length-mass regression should only be applied after a thorough review of habitat characteristics and observed length ranges. To better understand variations of length-mass regressions even within the same species, further studies are necessary to determine which site-specific characteristics are most important in affecting growth and body size.

ACKNOWLEDGEMENTS

This study was funded by the EPA/Nevada Natural Heritage Program (EPA/ST NV NNHP-WETLAND PROGRAM 12821). The authors thank Christopher Rosamond from the Desert Research Institute in Reno for help with field sampling. We are also grateful to Mary Miller from the Desert Research Institute's Water Analysis Laboratory in Reno for nutrient analyses of water samples. We also thank Nicole Damon for editing and her valuable comments on the manuscript.

LITERATURE CITED

ALUNNO-BRUSCIA, M., E. BOURGET & M. FRÉCHETTE, 2001, Shell allometry and length-mass-density relationship for *Mytilus edulis* in an experimental food-regulated situation. *Marine Ecology Progress Series*, 219: 177–188.

ANGILLETTA, M. J., JR. & A. E. DUNHAM, 2003, The temperature-size rule in ectotherms: simple evolutionary explanations may not be general. *The American Naturalist*, 162: 332–342.

BECKER, B., M. S. MORETTI & M. CALLISTO, 2009, Length-dry mass relationships for a typical shredder in Brazilian stream (Trichoptera: *Calamoceratidae*). *Aquatic Insects*, 31: 227–234.

BENKE, A. C., A. D. HURYN, L. A. SMOCK & J. B. WALLACE, 1999, Length-mass relationships for freshwater macroinvertebrates in North America with particular reference to the southeastern United States. *Journal of the North American Benthological Society*, 18: 308–343.

BERNDT, M. P., B. G. KATZ, B. D. LINDSEY, A. F. ARDIS & K. A. SKACH, 2005, Comparison of water chemistry in spring and well samples from selected carbonate aquifers in the United States. Pp. 74–81, in: E. L. KUNIANSKY, ed., U.S. Geological Survey Karst Interest Group Proceedings, Rapid City, South Dakota, September 12–15, 2005. *U.S. Geological Survey Scientific 1 Investigations Report*, 2005: 5160.

BURGHERR, P. & E. I. MEYER, 1997, Regression analysis of linear body dimensions vs. dry mass in stream macroinvertebrates. *Archiv für Hydrobiologie*, 139: 101–112.

CANTONATI, M., R. GERECKE & E. BERTUZZI, 2006, Springs of the Alps-sensitive ecosystems to environmental change: from biodiversity assessments to long-term studies. *Hydrobiologia*, 562: 59–96.

DE KOCK, K. N. & C. T. WOLMARANS, 2009, Distribution and habitats of *Melanoides tuberculata* (Müller, 1774) and *M. victoriae* (Dohrn, 1865) (Mollusca: Prosobranchia: Thiaridae) in South Africa. *Water SA*, 35: 713–720.

DRAPARNAUD, J., 1805, *Histoire naturele des molusques terrestres et fluviatiles de la France*. Louis Colas, Paris, France, 614 pp.

ELKARMI, A. Z. & N. S. ISMAIL, 2007, Growth models and shell morphometrics of two populations of *Melanoides tuberculata* (Thiaridae) living in hot springs and freshwater pools. *Journal of Limnology*, 66: 90–96.

FREST, T. J. & E. J. JOHANNES, 1995, *Interior Columbia Basin mollusk species of special concern. Final report: Interior Columbia Basin Ecosystem Management Project*, No. 43-0E00-4-9112. Walla Walla, Washington, 274 pp.

GLAZIER, D. S., 2010, A unifying explanation for diverse metabolic scaling in animals and plants. *Biological Reviews*, 85: 111–138.

GRUNER, D. S., 2003, Regressions of length and width to predict arthropod biomass in the Hawaiian Islands. *Pacific Science*, 57: 325–336.

HALL, R. O., J. L. TANK & M. F. DYBDAHL, 2003, Exotic snails dominate carbon and nitrogen cycling in a highly productive stream. *Frontiers in Ecology and the Environment*, 1: 408–411.

HARRILL, J. R. & D. E. PRUDIC, 1998, Aquifer systems in the Great Basin region of Nevada, Utah, and adjacent States – a summary report. *U. S. Geological Survey Professional Paper*, 1409–13 A: 66 pp.

HERSHEY, R. L., V. M. HEILWEIL, P. GARDNER, B. F. LYLES, S. EARMAN, J. M. THOMAS & K. W. LUNDMARK, 2007, Ground-water chemistry interpretations supporting the Basin and Range Regional Carbonate-rock Aquifer System (BARCAS) Study, eastern Nevada and western Utah. *DHS Publication*, 41230.

HERSHLER, R., 1984, The freshwater snails (Gastropoda: Rissoacea) of the Cuatro Cienga Basin: Systematic relationships and ecology of a unique fauna. *Journal of the Arizona Nevada Academy of Science*, 19: 61–76.

HERSHLER, R., 1994, A review of the North American freshwater snail genus *Pyrgulopsis* (Hydrobiidae). *Smithsonian Contributions to Zoology*, 554: 1–115.

HERSHLER, R., 1998, A systematic review of the hydrobiid snail (Gastropoda: *Rissooidea*) of the Great Basin, western United States. Part I. Genus *Pyrgulopsis*. *The Veliger*, 41: 1–132.

HERSHLER, R. D. & W. SADA, 1987, Springsnails (Gastropoda:Hydrobiidae) of Ash Meadows, Amargosa basin, California and Nevada. *Proceedings of the Biological Society of Washington*, 100: 776-843.

HERSHLER, R. & D. W. SADA, 2001, A new species of hydrobiid snail of the genus *Pyrgulopsis* from northwestern Nevada. *The Veliger*, 43: 367–375.

HERSHLER, R. & D.W. SADA, 2002, Biogeography of Great Basin freshwater snails of the genus *Pyrgulopsis*. Pp. 255–276, in: R. HERSHLER, D. B. MADSEN & D. R. CURREY, eds., *Great Basin aquatic systems history*. Smithsonian Contributions to Earth Sciences, 33: 405 pp.

HIRST, A. G., 2012, Intraspecific scaling of mass to length in pelagic animals: Ontogenetic shape change and its implications. *Limnology and Oceanography*, 57: 1579–1590.

HÓDAR, J. A., 1997, The use of regression equations for estimation of prey length and biomass in diet studies of insectivore vertebrates. *Miscelania Zoologica*, 202: 1–10.

McCABE, D. J., 1998, Biological communities in springbrooks. Pp. 221–228, in: L. BOTOSANEAU, ed., *Studies in crenobiology. The biology of springs and springbrooks.* Backhuys Publishers, Leiden, The Netherlands, 261pp.

McKINNEY, R. A., S. N. GLATT & R. S. WILLIAMS, 2004, Allometric length-weight relationships for benthic prey of aquatic wildlife in coastal marine habitats. *Wildlife Biology*, 10: 241–249.

MEYER, E., 1989, The relationship between body length parameters and dry mass in running water invertebrates. *Archiv für Hydrobiologie*, 117: 191–203.

MLADENKA, G. C. & G. WAYNE MINSHALL, 2001, Variation in the life history and abundance of three populations of bruneau hot springsnails (*Pyrgulopsis bruneauensis*). *Western North American Naturalist*, 61: 204–212.

MÜLLER, O. F., 1774 [1773–1774], *Vermium terrestrium et fluviatilium, seu animalium infusoriorum, helminthicorum et testaceorum, non marinorum, succincta historia*, ... Heineck & Faber, Havniae & Lipsiae, 2 vols. [1, [xxx] + 135 pp. (1773); 72 + [viii] pp. (1774); 2, xxxvi + 214 + [x] (1774)].

ROSEMOND, A. D., P. J. MULHOLLAND & J. W. ELWOOD, 1993, Top-down and bottom-up control of stream periphyton: effects of nutrients and herbivores. *Ecology*, 74: 1264–1280.

SADA, D. W., 2008, Synecology of a springsnail (Prosobranchia: Family Hydrobiidae) assemblage in a western U.S. thermal spring province. *The Veliger*, 50: 59–71.

SADA, D. W. & G. L. VINEYARD, 2002. Anthropogenic changes in biogeography of the Great Basin aquatic biota. Pp. 277–293, in: R. HERSHLER, D. B. MADSEN & D. R. CURREY, eds., *Great Basin aquatic systems history*. Smithsonian Contributions of the Earth Science, 33: 405 pp.

SAMADI, S., J. MAVÁREZ, J.-P. POINTIER, B. DELAY & P. JARNE, 1999, Microsatellite and morphological analysis of population structure in the parthenogenetic freshwater snail *Melanoides tuberculata*: insights into the creation of clonal variability. *Molecular Ecology,* 8: 1141–1153.

SAVAGE, V. M., J. F. GILLOOLY, J. H. BROWN, G. B. WEST & E. L. CHARNOV, 2004, Effects of body size and temperature on population growth. *The American Naturalist*, 163: 429–441.

SILVA, E. C., J. MOLOZZI & M. CALLISTO, 2010, Size-mass relationships of *Melanoides tuberculatus* (Thiaridae: Gastropoda) in a eutrophic reservoir. *Zoologia*, 27: 691–695.

TAYLOR, D. W., 2003, Introduction to Physidae (Gastropoda: Hygrophila); biogeography, classification, morphology. *Revista de Biologia Tropical*, 51: 1–287.

TRUSSELL, G. C., 2000, Phenotypic clines, plasticity, and morphological trade-offs in an intertidal snail. *Evolutionary Ecology Research*, 2: 803–822.

UNMACK, P. J. & W. L. MINCKLEY, 2008, The demise of desert springs. Pp. 11–34, in: L. E. Stevens & V. J. Meretsky, eds., *Aridland springs in North America*. University of Arizona Press, 432 pp.

U.S. ENVIRONMENTAL PROTECTION AGENCY, 1979, *Methods for chemical analysis of water and wastes*. USEPA, Cincinnati, Ohio, 491 pp.

WELCH, A. H., D. J. BRIGHT & L. A. KNOCHENMUS, 2008, Water Resources of the Basin and Range Carbonate-rock Aquifer Systems, White Pine County, Nevada, and Adjacent areas of Nevada and Utah. *U.S. Geological Survey Scientific Investigations Report*, 2007-5261: 96 pp.

WENZEL, E., E. MEYER & J. SCHWOERBEL, 1990, Morphology and biomass determination of dominant mayfly larvae (Ephemeroptera) in running waters. *Archiv für Hydrobiologie*, 118: 31–46.

WOODS, H. A., W. MAKINO, J. B. COTNER, S. E. HOBBIE, J. F. HARRISON, K. ACHARYA & J. J. ELSER, 2003, Temperature and the chemical composition of poikilothermic organisms. *Functional Ecology*, 17: 237–245.

Revised ms. accepted October 21, 2014

MALACOLOGIA, 2015, 58(1–2): 179–224

THE MOLLUSCAN TAXA OF A. W. GRABAU & S. G. KING (1928) AND THEIR TYPES

Eugene V. Coan[1], Konstantin A. Lutaenko[2], Junlong Zhang[3*] & Qimeng Sun[3,4]

ABSTRACT

The 46 names of species of marine bivalves and gastropods made available by Grabau & King in 1928 are discussed. Probable or possible type material for all but 13 of these taxa has been located in the Institute of Oceanology, Chinese Academy of Sciences. Of these taxa, nine are regarded as valid, the rest being junior synonyms. The valid taxa are: *Verilarca interplicata*, *Collisella peitaihoensis*, *Rissoina barbara, Rissoina bureri, Epitonium scalare minor, Gradatiscala gradata pygmaea, Nassarius gregarius, Terebra bellanodosa* and *Mangelia dobsoni*, all Grabau & King, 1928. Brief biographies of Amadeus William Grabau (1870–1946) and Chinese malacologist Sohtsu Gee King (1886–1949) are provided.

Key words: China, taxonomy, malacological history, A. W. Grabau, S. G. King.

INTRODUCTION

The first scientific reports on the marine mollusks of China were published by western malacologists in the first half of the 19th century, although economically important mollusks were treated in Chinese encyclopedias and manuals on the culture of bivalves as early as the Ming Dynasty (Bernard et al., 1993). National taxonomic and faunal studies in China started in the 1950s, and the collected material is now mostly housed in the Institute of Oceanology, Chinese Academy of Sciences (formerly, Academia Sinica), Qingdao. However, several important studies on mollusks were done before the World War II, among them those by A. W. Grabau, S. G. King, Chi Ping, Teng-Chien Yen and Tchang Si [Zhang Xi].

The German-American geologist and paleontologist Professor Amadeus William Grabau (1870–1946) and the Chinese malacologist Sohtsu Gee King (1886–1949) were two important early researchers on the Mollusca in China. During 1927–1928, they published *Shells of Peitaiho* in the *China Journal of Science and Arts* in seven parts with five chapters (Grabau & King 1927a–c, 1928a–d). These articles were then compiled into a small handbook Grabau & King (1928e), presumably after the last article had appeared in July. Still later in 1928, they greatly revised the book and published a second edition, divided into ten chapters and with the addition of many text-figures and photographs (Grabau & King 1928f). The new species and varieties of the first papers, as well as some additional new taxa, were redescribed and illustrated in the second edition. The new taxa all date from 1928, because the 1927 parts of this series were devoted to general descriptions of the Mollusca. (Grabau also published two short papers about shells while in China – Grabau, 1927, 1928.)

Amadeus W. Grabau made many contributions to science. He was born on January 9, 1870, in the village of Cedarburg, Wisconsin, where his father was a Lutheran pastor. His college education was at the Massachusetts Institute of Technology, where he studied geology, mineralogy and physical geography. He was influenced by, among others, by Alpheus Hyatt, the Chief Director of the Museum of the Boston Society of Natural History and the Curator of Paleontology of the Museum of Comparative Zoology at Harvard University (Ting, 1931; Wang, 1931; Thomas, 1946; Manzur, 2004). After obtaining a doctorate from Harvard

---

[1] Research Associate, Santa Barbara Museum of Natural History, 2559 Puesta del Sol Road, Santa Barbara, California 94306-2640, U.S.A.

[2] A. V. Zhirmunsky Institute of Marine Biology, Far East Branch of the Russian Academy of Sciences, Palchevsky Street 17, Vladivostok 690041, Russia.

[3] Department of Marine Organism Taxonomy and Phylogeny, Institute of Oceanology, Chinese Academy of Sciences, 7 Nanhai Rd., Qingdao 266071, China.

[4] University of Chinese Academy of Sciences, No.19A Yuquan Road, Beijing, 100049, China.

*Corresponding author: zhangjl@qdio.ac.cn

in 1900, he served as Adjunct Professor at Columbia University in 1902–1905, and then Professor there until 1918. His main research interests were stratigraphy and paleontology (Sun, 1947).

In 1920, Grabau moved to China and became Professor of Paleontology at the National University of Peking and Chief Paleontologist of the Geological Survey of China (Sun, 1947). At that time, he began to issue paleontological monographs – *Palaeontologia Sinica* – and participated in the organization of the Geological Society of China, the Paleontological Society of China and the Peking Society of Natural History. Altogether, he published some 291 papers and books (Sun, 1947).

Grabau's collaborator Sohtsu Gee King was another pioneer of the Chinese malacology. In addition to the Peitaiho book, he and Chi Ping published a series of reports on the gastropods of Hong Kong (King & Ping, 1931a, b, 1933, 1936) along with several other papers (King, 1926; King & Ping, 1935). Sohtsu G. King [also spelled as "Sho-Tsu G. King", or "Chin Shao-Chi"] was born at Nanziung, Chekiang [= Nanxun, Zhejiang Province] in 1886. He went to England in 1902, where he studied at King's College [probably that in London], specializing in electric engineering. He returned to China in 1905 and organized the electric department in the technical school of the Board of Commerce at Peking [= Beijing]. Later, he was appointed a member of the Board of Communications, and joined the Nanyang College as the head of the Chemistry Department. In 1911, he rejoined the Ministry of Communications. In 1911, King went to Hankow [= Hankou, Hubei Province] as managing director of a real estate and trading company, and in 1916 he went to Peking to engage in business. He was recognized as "the first conchologist of this country" [China] (Anonymous, 1936a). He was on the Board of Trustees of the China Foundation, dedicated to the promotion of science, for over ten years from the 1930s to the 1940s (Yang, 1991).

In the second edition of the *Shells of Peitaiho* (Grabau & King, 1828f), Sohtsu G. King is also identified as the President of the Peking Society of Natural History, Honorary Secretary and Curator of the Peking Laboratory of Natural History, and, additionally, a member of the Malacological Society of London and the Conchological Society of Great Britain and Ireland. He was also known as Vice-President of the Peking Rotary Club and Vice-President of the Peiping Institute of Fine Arts (Anonymous, 1936a). A note in *Nature* (Anonymous, 1936b) said that King, "the Chinese conchologist and banker," had given a valuable collection of malacological literature to the Science Society of China Library in Shanghai, and that this collection was started some 20 years earlier when he was studying conchology with Prof. Grabau of Peking University. The Council of the Society decided that a special room was to be used to house the collection under the name "Sohtsu G. King Library of Conchology," which was a part of Mingfu Library. The Science Society Library is now the Huangpu District Mingfu Library, but after the founding of the People's Republic of China, the early volumes were moved into the Shanghai Library, where some of the original King volumes can now be identified by stamps and labels (Fig. 1).

For a long time, the location of the type material of Grabau & King's new species and varieties was unknown, and some of their names have been taken as junior synonyms of other taxa, in many cases based on guess work because of the poor original illustrations. Several years ago, one of us (Lutaenko) had suggested that the Grabau-King collection might be housed in the Marine Biological Museum, Chinese Academy of Sciences (MBM CAS), Qingdao, and drew the attention of Coan to the problem that the first papers and first edition of the *Shells of Peitaiho* were not often cited in the literature. During their work on taxonomic study of molluscan collections in the MBM CAS, Zhang and Sun found a number of shells labeled as "Grabau-King Laboratory of Natural History, Peking, China." We believe that these shells are the materials of Grabau & King from their study of marine mollusks of Peitaiho.

These shells were previously located in the Fan Memorial Institute of Biology (= Fan Institute of Biology), Beijing (now Institute of Zoology, Chinese Academy of Science), and are now housed in the MBM CAS. According to a label found with these shells, they may have been originally donated by Sohtsu G. King (Fig. 2). On August 1, 1950, when the Qingdao Marine Biology Laboratory, the predecessor of Institute of Oceanology, Chinese Academy of Sciences (IOCAS), was founded, Professor Zhang Xi, Qi Zhongyan, Liu Ruiyu, Li Jiemin and Ma Xiutong came to Qingdao and brought some marine collections that may have included the shells of Grabau & King.

The Peitaiho region, which is now known as Beidaihe, is located west of Qinhuangdao City,

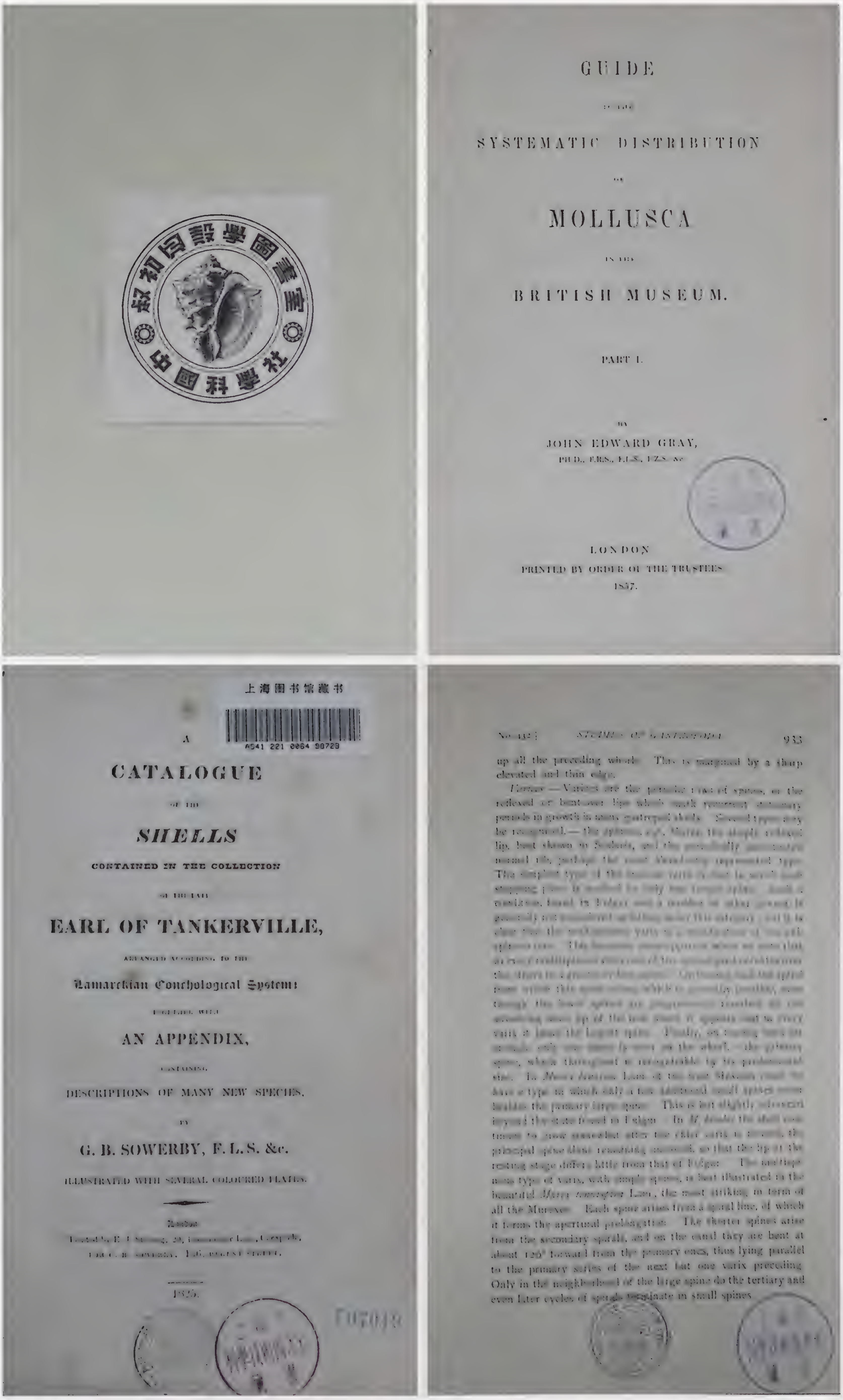

叔和貝殼學圖書室
中國科學社
上海图书馆藏书
A541 221 0264 98728

GUIDE

TO THE

SYSTEMATIC DISTRIBUTION

OF

MOLLUSCA

IN THE

BRITISH MUSEUM.

PART I.

BY

JOHN EDWARD GRAY,

PH.D., F.R.S., F.L.S., F.Z.S. &c.

LONDON

PRINTED BY ORDER OF THE TRUSTEES

1857.

A

CATALOGUE

OF THE

SHELLS

CONTAINED IN THE COLLECTION

OF THE LATE

EARL OF TANKERVILLE,

ARRANGED ACCORDING TO THE

Lamarckian Conchological System:

TOGETHER WITH

AN APPENDIX,

CONTAINING

DESCRIPTIONS OF MANY NEW SPECIES,

BY

G. B. SOWERBY, F. L. S. &c.

ILLUSTRATED WITH SEVERAL COLOURED PLATES.

1825.

FIG. 1. Book stamps from the Sohtsu G. King Library of Conchology on volumes now in the Shanghai Library.

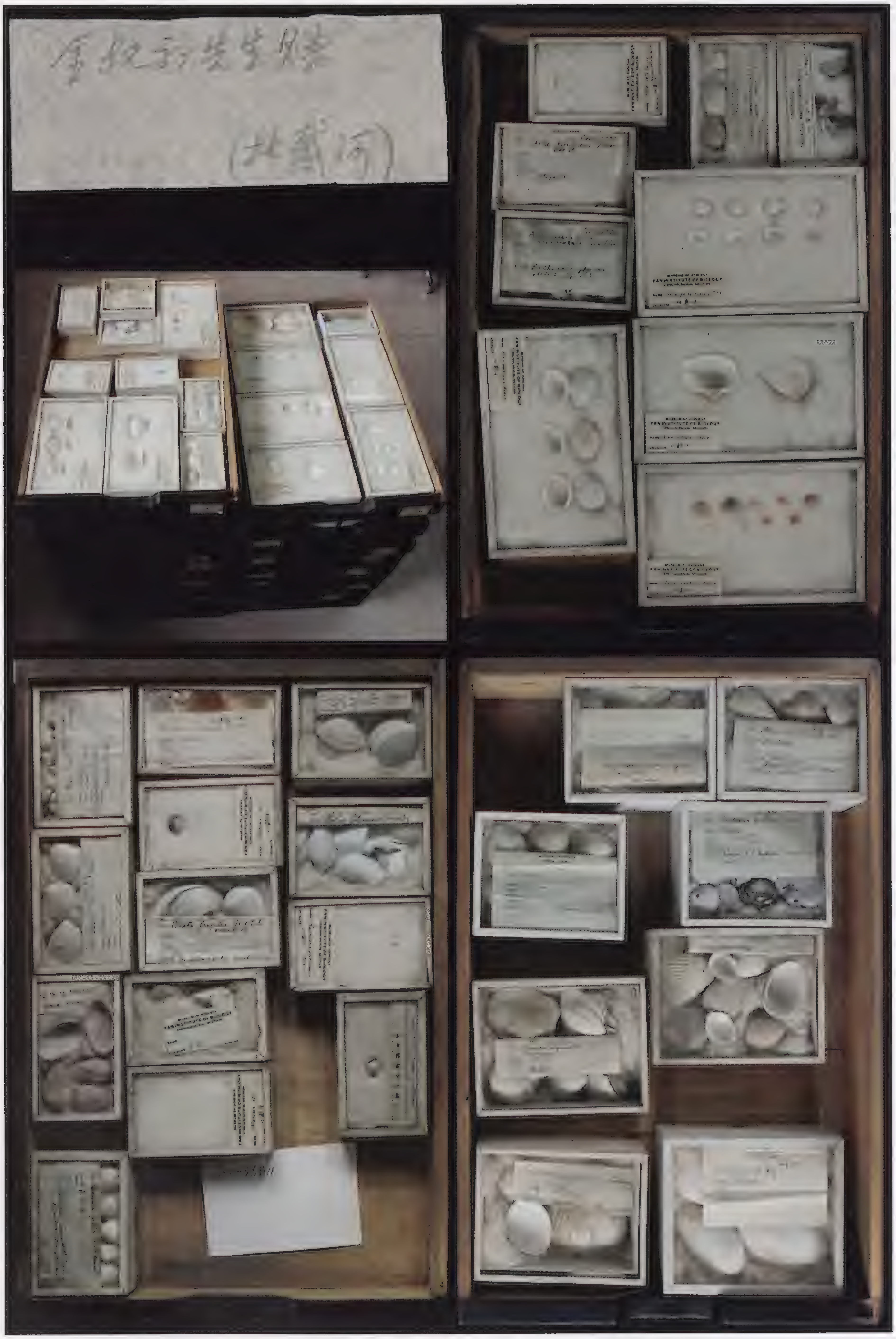

FIG. 2. Photographs of materials in the MBM CAS. The Chinese characters in the label in the upper left reads “Donated by Sohtsu G. King” and “(Beidaihe)” from top to bottom.

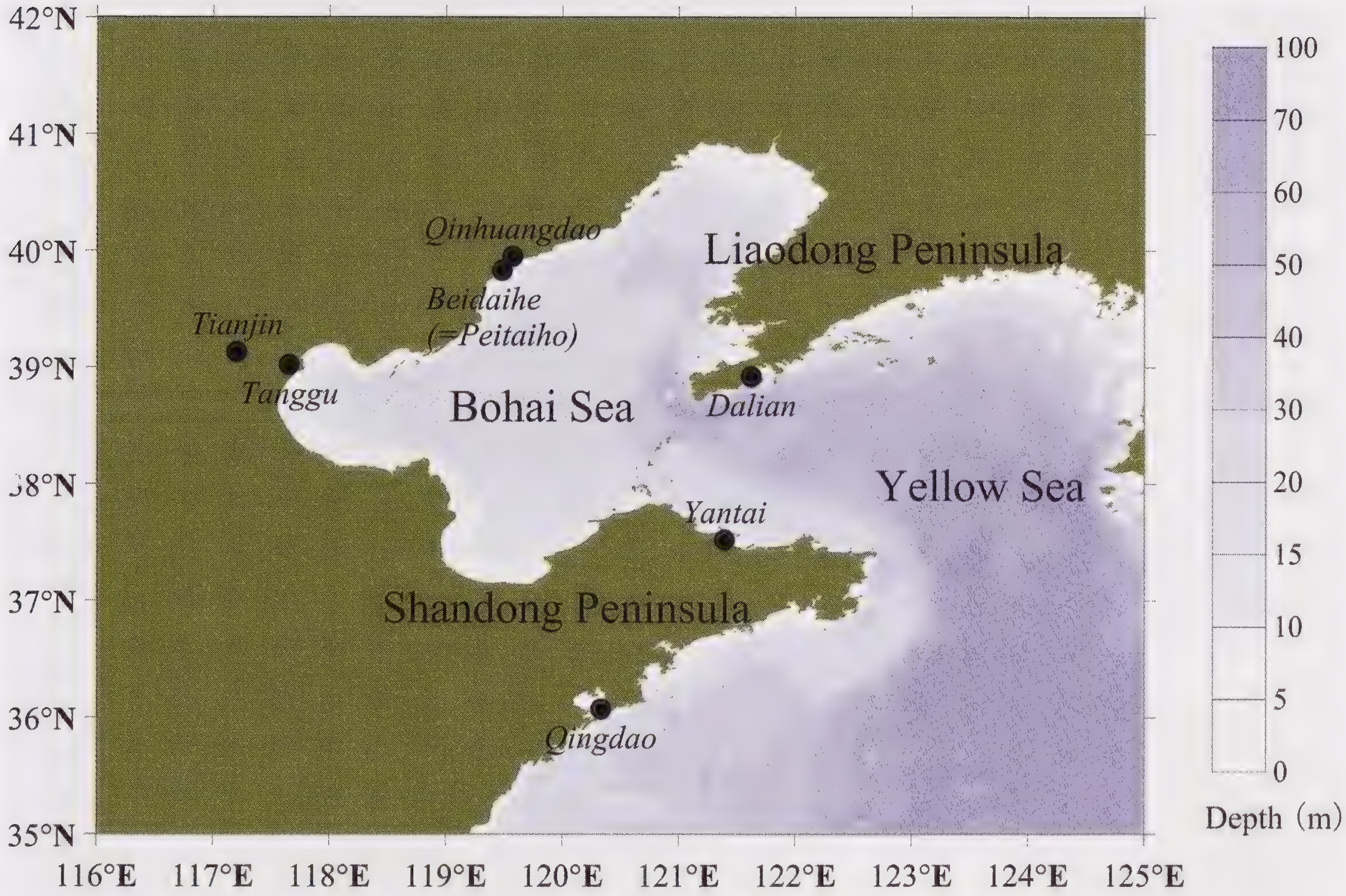

FIG. 3. Map showing Beidaihe [Peitaiho] on the Bohai Sea.

Hebei Province, and is a well-known summer resort (Fig. 3). The Beidaihe district is located on the coast of China's Bohai Sea. It has an area of about 70 km^2 and a coastline of about 22 km in length. The beach consists of fine yellow sand some 100 meters wide. Grabau & King (1928f) also mentioned another geographical name, Pechili Bay, an old name of the Bohai Sea – until the early 20th century, Bohai Sea was often called the Gulf of Pechihli or Pechili. The Bohai Sea, now also known as Bohai Gulf, Bohai, or Bo Hai, is the innermost part of the Yellow Sea on the coast of northeastern and northern China (Fig. 3). Most of the shells collected by Grabau & King cannot be found there now because of habitat loss due to construction of tourist and industrial facilities, decreased water quality and overfishing.

We here list the taxa made available by Grabau & King, and we figure the type material that has been located in the collection of the MBM CAS, Qingdao. We also comment on the present taxonomic status of the species. The type material of bivalve mollusks described by other Chinese malacologists after World War I and stored in the same museum was recently reviewed by Lutaenko & Xu (2008).

MATERIAL AND METHODS

All examined specimens are dry shells in boxes at the Marine Biological Museum, Chinese Academy of Sciences (abbreviated MBM), in Qingdao, China. For each registered lot number, specimen quantity, collection locality, collector and collection date as on labels are recorded, except for some lots that lack this information.

The specimens labeled "Grabau-King Laboratory of Natural History" were taken as syntypes herein, except a specimen of *Arca* (*Barbatia*) *interplicata* Grabau & King, 1928, which was labeled as the holotype. Other specimens labeled only as "Museum of Zoology, Fan Institute of Biology, Conchological Section" deposited with these presumed types are also likely to be Grabau & King materials, but there is insufficient evidence to regard them as type material.

In the course of the review of this material, additional unpublished manuscript names by Grabau & King were noted on museum labels, but these are not mentioned here so as not to create additional confusion.

It should be noted that Grabau & King followed the old tradition of assigning female gender to varietal names, regardless of generic combination, and we have retained the original spellings with the initial entries.

The sources of the suggested synonymies are indicated. Those not indicated as being by other workers are new herein.

Abbreviations

MBM CAS – Marine Biological Museum, Chinese Academy of Sciences, IOCAS, Qingdao, China
IOCAS – Institute of Oceanology, Chinese Academy of Sciences, Qingdao, China
MZFIBCS – Museum of Zoology, Fan Institute of Biology, Conchological Section, Beijing, China
GKLNH – Grabau-King Laboratory of Natural History, Peking [Beijing], China
pv – paired valves
lv – left valve
rv – right valve
L – length
H – height
W – width

SYSTEMATICS

Class Bivalvia Linnaeus, 1758
Family Arcidae Lamarck, 1809

Arca (*Scapharca*) *peitaihoensis* Grabau & King, 1928

Figure 4A–D

Scapharca peitaihoensis Grabau & King, 1928a: 35; 1928e: 29; 1928f: 65, 159, 254, pl. 1, fig. 6.

Material Examined

MBM280616 (ex MZFIBCS, 5 lv, 3 rv), Peitaiho.

Modern Status

Synonym of *Arca kagoshimensis* (Tokunaga, 1906).

Remarks

This has been listed as a possible synonym of *Anadara kagoshimensis* (Tokunaga, 1906) (Higo et al., 1999: 425), or as a synonym of *Anadara gubernaculum* (Reeve, 1844) (Huber, 2010: 136, 586).

We do not agree that *Arca* (*Scapharca*) *peitaihoensis* Grabau & King, 1928, is a juvenile *Anadara gubernaculum* (Reeve, 1844). The syntype of *Anadara gubernaculum* (Reeve, 1844) (Lamprell & Healy 1998: 58, sp. 87) is triangular and this species usually has 30 ribs (not 45 ribs, as per Huber, 2010), whereas the Grabau & King specimens have oval shells, many dense, thin ribs and inflated umbones.

Arca kagoshimensis Tokunaga, 1906, has been listed as a synonym of what was widely known as *Anadara subcrenata* (Lischke, 1869) by Habe (1951, 1965) and Noda (1966: 119). Bernard et al. (1993) noted that *Arca subcrenata* Lischke, 1869, is preoccupied (*non Arca subcrenata* Michelotti, 1861). Although they proposed the replacement name *Scapharca sativa* Bernard, Cai & Morton, 1993, they also listed *Scapharca kagoshimensis* (Tokunaga, 1906) as a synonym. Thus, *A. kagoshimensis* is the first available name for this species (Tsuchida & Kurozumi, 1993: 8, pl. 2, fig. 3; Evseev & Lutaenko, 1998: 26–28). It should be noted that Lischke (1869) printed another name in the caption to pl. 9 of his volume subsequent to the journal article that first made the name available – *Arca nodoso crenata* [sic], but he noted in the second volume "On the panel, this kind of mistake of the printer '*Arca-nodoso crenata*' was stated" (Lischke, 1871: 144), thus indicating that it was merely a subsequent misspelling and is therefore unavailable (ICZN *Code* Art. 33.3).

Anadara peitaihoensis is also close to *Anadara* (*Scapharca*) *cornea* (Reeve, 1844), which is rarely figured in northeast Asian literature and has often been misinterpreted. Habe (1965: 79–80, pl. 2, figs. 3, 4) differentiated the Japanese form and said that *A. cornea* is closely related to *A. subcrenata* but has fewer radial ribs (27–30) (29 in Reeve's original description). It is strange that Grabau & King (1928f: 157, pl. 1, fig. 2) clearly described in detail and figured true adult *"Arca* (*Anomalocardia*) *subcrenata* Lischke" of 34–44 mm (maximum 56 mm) as being "by far the most common species on these beaches" (Grabau & King, 1928f: 157) but did not compare it with their *A. peitaihoensis.*

That said, there are many unresolved taxonomic difficulties with inaequivalve anadarines in Asian waters (particularly the "*Anadara inaequivalvis*" complex) (Huber, 2010; Lutaenko & Volvenko, 2013), and correct names of a number of species remain to be resolved.

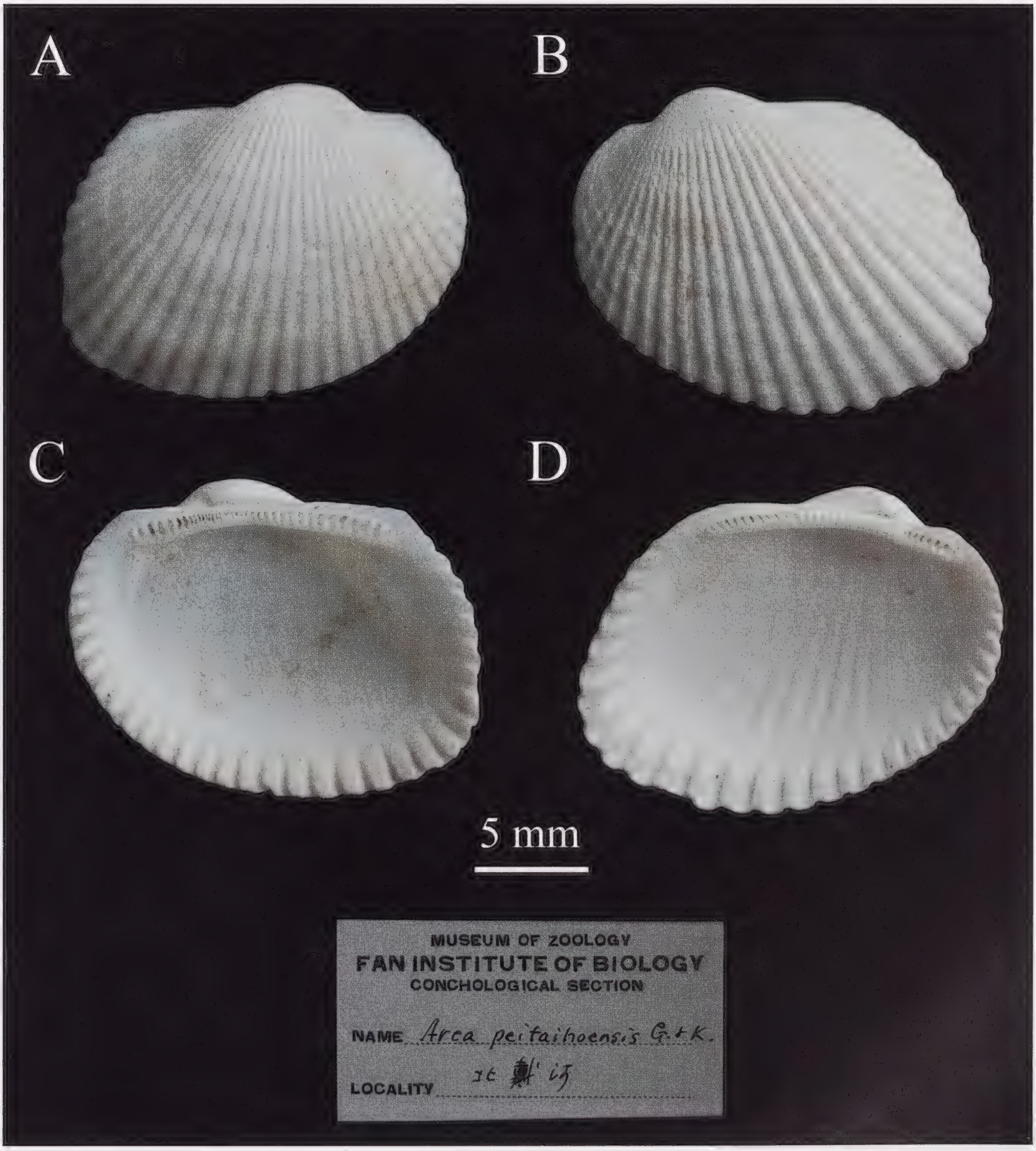

MUSEUM OF ZOOLOGY
FAN INSTITUTE OF BIOLOGY
CONCHOLOGICAL SECTION
NAME *Arca peitaihoensis* G.+K.
LOCALITY 北戴河

FIG. 4A–D. *Arca* (*Scapharca*) *peitaihoensis* Grabau & King. MBM280616, length = 18.84 mm.

Arca obtusa var. *duplicostata* Grabau & King, 1928 Figure 5A–D

Arca obtusa [Reeve, 1844] var. *duplicostata* Grabau & King, 1928a: 35; 1928e: 30; 1928f: 67, 159–160, 254, pl. 1, fig. 7.

Material Examined

Syntypes, MBM280617 (ex GKLNH, 4 lv, 9 rv), no collection information; MBM280627 (ex MZFIBCS, 3 rv), Beidaihe.

Modern Status

Synonym of *Mesocibota bistrigata* (Dunker, 1866).

Remarks

While placed in different genera by Bernard et al. (1993: 23) (*Nipponarca*), Xu (1997: 21) (*Barbatia*) and Huber (2010: 132, 562) (*Mesocibota*), it has been widely accepted as a synonym of Dunker's *bistrigata*, the exception being Higo et al. (1999: 422), who synonymized it with *Barbatia* (*Savignyarca*) *virescens* (Reeve, 1844). Lamprell & Healy (1998) synonymyzed *Barbatia signata* (Dunker, 1868) with *B. bistrigata* and *Nipponarca adamsiana* (Dunker, 1866) (although a syntype of *N. adamsiana* from the collection of the Natural History Museum in London figured by them (1969241, China, Cuming coll.) is different from those figured by Scott (1994: pl. 2, fig. A). The relationships among the genera (or subgenera) of *Barbatia*, including *Nipponarca* Habe, 1951, *Hawaiarca* Dall et al., 1938, and *Mesocibota* Iredale, 1939, are much in need of revision.

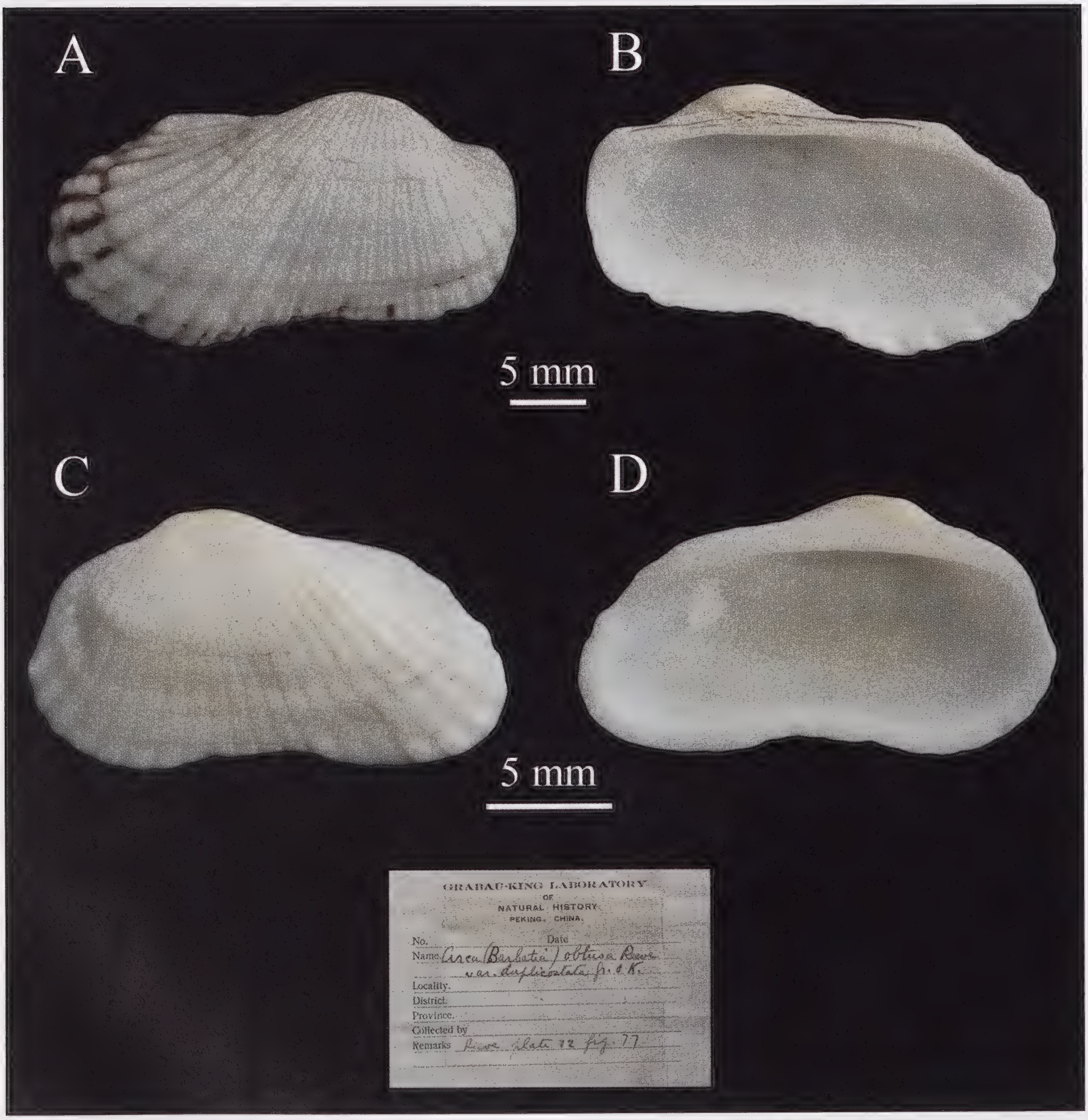

GRABAU-KING LABORATORY
OF
NATURAL HISTORY
PEKING, CHINA.

No. Date
Name *Arca (Barbatia) obtusa Reeve*
var. duplicostata Gr. & K.
Locality.
District.
Province.
Collected by
Remarks *Reeve plate 72 fig. 77*

FIG. 5A–D. *Arca obtusa* var. *duplicostata* Grabau & King. A, B: MBM280617, syntype, length = 30.1 mm; C, D: MBM280627, length = 14.1 mm.

Arca (*Barbatia*) *interplicata*
Grabau & King, 1928
Figure 6A, B

Barbatia interplicata Grabau & King, 1928a: 35; 1928e: 29–30; 1928f: 66–67, 161–162, 254, pl. 1, fig. 9.

Material Examined

"Holotype", MBM280618 (ex GKLNH, 1 lv), no collection information. The original description indicated that there was only a single specimen.

Modern Status

Verilarca (*Verilarca*) *interplicata* (Grabau & King, 1928).

Remarks

Bernard et al. (1993: 26) listed this species both as a synonym of *Striarca symmetrica* (Reeve, 1844) and as *Verilarca interplicata* (Grabau & King, 1928) (Bernard et al., 1993: 27). Qi (2004: 222, pl. 116C) and Xu & Zhang (2008: 41) listed it as valid as *Arcopsis interplicata* (Grabau & King, 1928), and Huber (2010: 146) regarded it as a valid species as *Verilarca* (*Verilarca*) *interplicata* (Grabau & King, 1928).

Family Ostreidae Rafinesque, 1815

Ostrea chemnitzi var. *elongata*
Grabau & King, 1928
Figure 7A–F

Ostrea chemnitzi [Hanley, 1846] var. *elongata* Grabau & King, 1928a: 31; 1928e: 26; 1928f: 58, 164, 256, pl. 2, fig. 14, *non Ostrea elongata* Born, 1778.

Material Examined

Lectotype (here designated), MBM229012 (ex GKLNH, 1 pv), Peitaiho, July 1925 (Dimension: lv = 21.7 mm × 15.9 mm, rv =

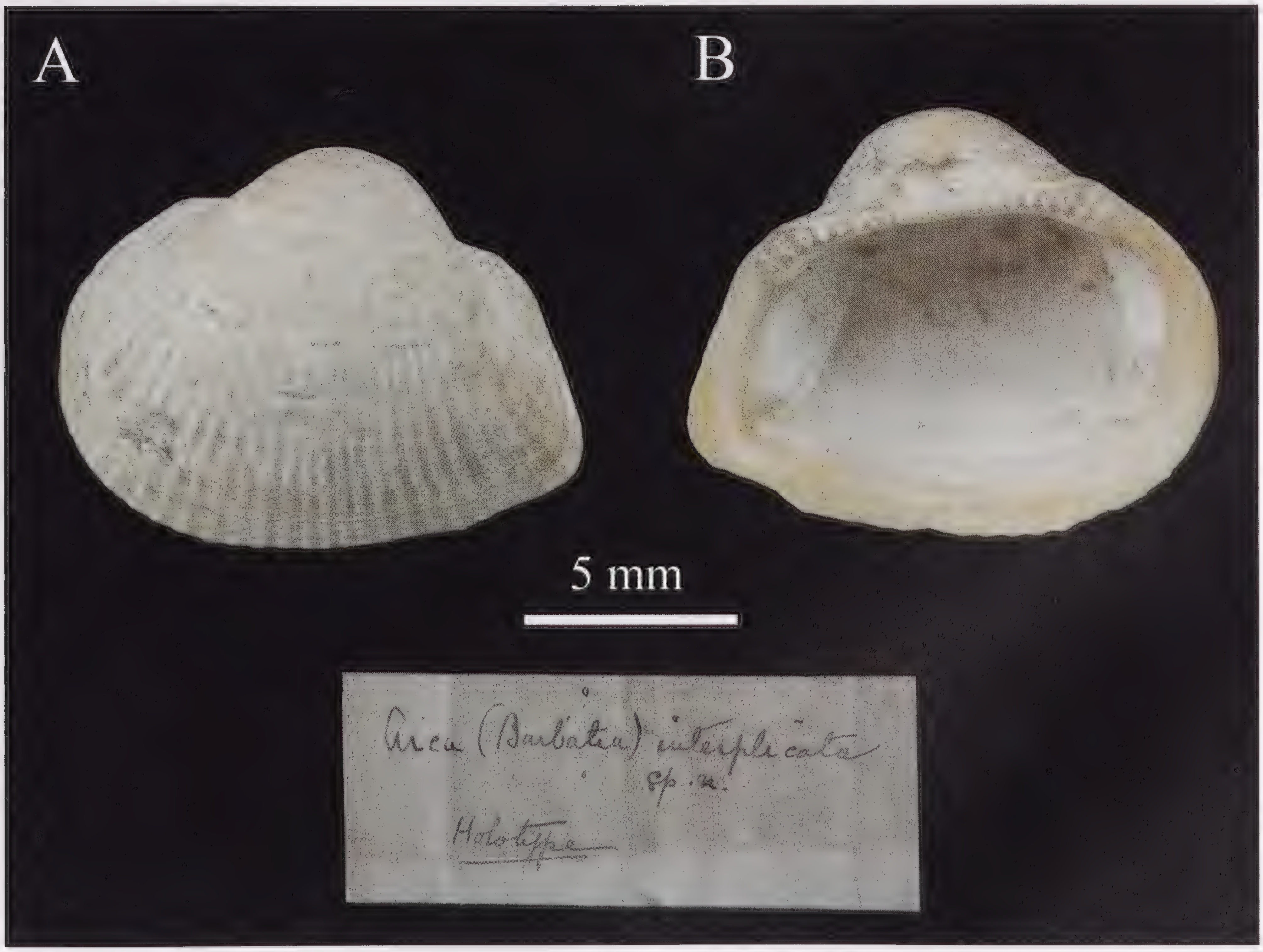

FIG. 6A, B. *Arca* (*Barbatia*) *interplicata* Grabau & King. MBM280618, holotype, length = 12.1 mm.

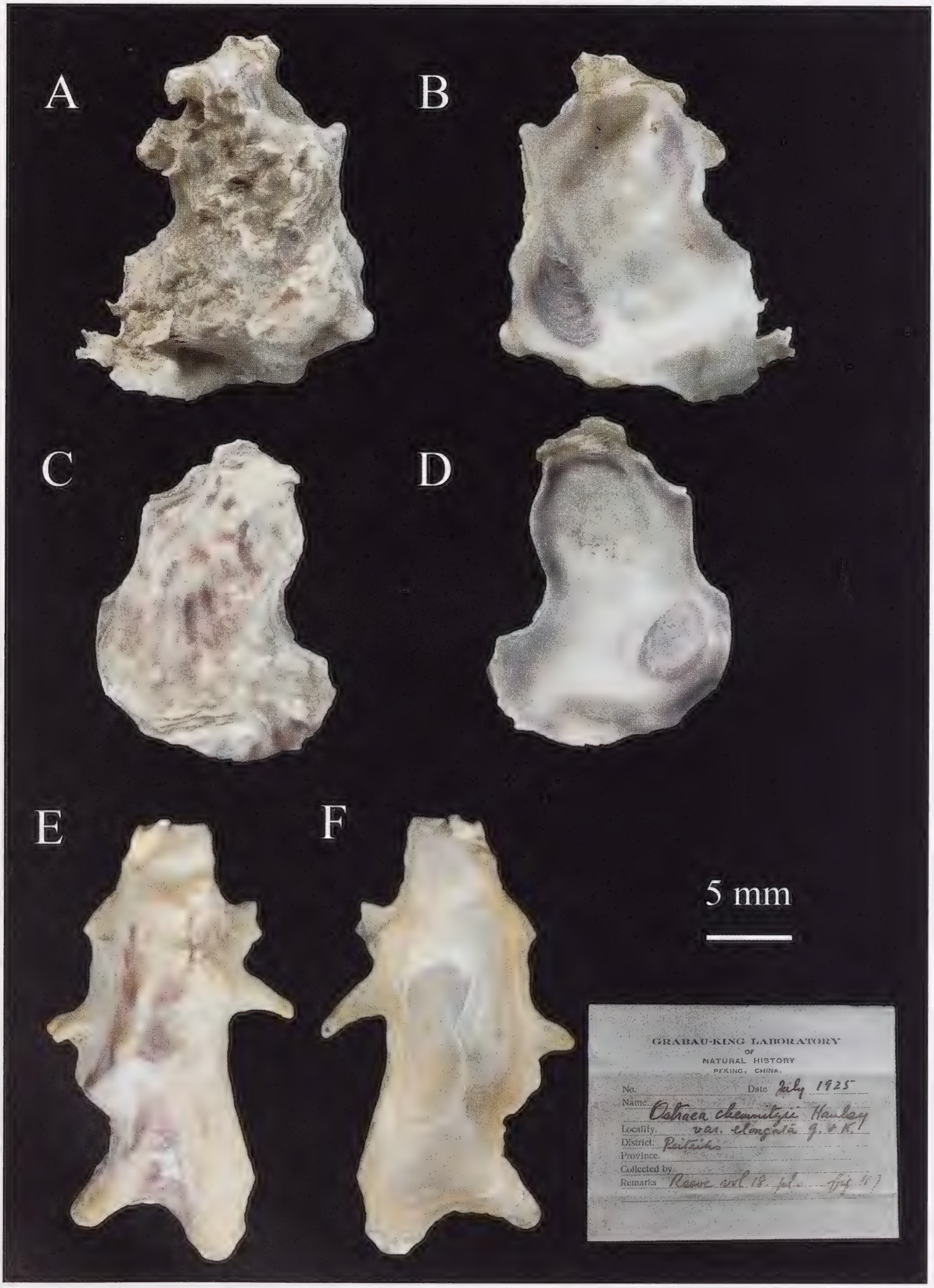

GRABAU-KING LABORATORY
OF
NATURAL HISTORY
PEKING, CHINA.

No.
Date July 1925
Name. Ostraea chemnitzii Hanley
Locality. var. elongata G. & K.
District. Peitaiho
Province.
Collected by
Remarks Reeve vol 18. pl. fig. 5)

FIG. 7A–F. *Ostrea chemnitzi* var. *elongata* Grabau & King. A–D: MBM229012, lectotype. A, B: length = 21.7 mm; C, D: length = 18.7 mm; E–F: MBM260724, paralectotype, length = 25.8 mm.

18.7 mm × 14.0 mm, width of pv = 7.0 mm); paralectotypes, MBM260724 (ex GKLNH, 6 pv, 4 lv, 14 rv), Peitaiho, July 1925.

Modern Status

Synonym of *Crassostrea gigas* (Thunberg, 1793).

Remarks

The type material of this junior homonym included specimens of both *Crassostrea gigas* (Thunberg, 1793) and of *Talonostrea talonata* Li & Qi, 1994. This species has also been regarded as a synonym of *Parahyotissa chemnitzii* (Hanley, 1846) (Higo et al., 1999: 438), or of *Talonostrea talonata* Li & Qi, 1994 (Inaba et al., 2004: 21–22). One label in the box with the type material was written (by Lou Tze-Kong) as *Ostrea* (*Crassostrea*) *pes-tigris* Hanley, and Tchang & Lou (1956) took it as a synonym of *Ostrea* (*Crassostrea*) *pestigris* (Hanley, 1845). But Li & Qi (1994) thought it was not Hanley's species and described it as *Talonostrea talonata* Li & Qi, 1994. We do not agree with Bernard et al. (1993: 47) that it is a synonym of *Pretostrea rosacea* (Deshayes, 1836). Indeed, the specimens of Grabau & King were of two different species, *Crassostrea gigas* (Thunberg, 1793) (Fig. 5A–D) and *Talonostrea talonata* Li & Qi, 1994 (Fig. 5E, F), and our lectotype now settles its status as a synonym of *C. gigas*, thereby maximizing nomenclaural stability.

Ostrea gigas var. *tientsiensis*
Grabau & King, 1928

Ostrea gigas [Thunberg, 1793] var. *tientsiensis* Grabau & King, 1928a: 32; 1928e: 26; 1928f: 59.

Material Examined

Not found.

Modern Status

Probably a synonym of *Crassostrea gigas* (Thunberg, 1793).

Remarks

We think it may be *Crassostrea gigas*, only longer and thicker than most specimens. It may have been based on a subfossil specimens, because this species once lived in estuary of the ancient Huang-Ho (Yellow River), half way between Tientsin (Tianjin) and the Taku Bar (Tanggu).

Family Anomiidae Rafinesque, 1815

Anomia nipponensis var. *obsoletocostata*
Grabau & King, 1928
Figure 8A–F

Anomia nipponensis [Yokoyama, 1920] var. *obsoleto-costata* Grabau & King, 1928f: 165–166, 256, pl. 2, fig. 16a, b.

Material Examined

Syntypes, MBM280620 (ex GKLNH, 11 lv), Peitaiho, July 1925; MBM280621 (ex MZFIBCS, 4 lv), Yindao (now Hondao, Qingdao).

Modern Status

Synonym of *Anomia chinensis* Philippi, 1849.

Remarks

It is not yet certain whether there is more than one species of *Anomia* on the coast of China. Assuming that there is only one, then *Anomia nipponensis* var. *obsoletocostata* Grabau & King, 1928, *A. cuticula* Grabau & King, 1928, and *A. plana* Grabau & King, 1928, are all synonyms of the oldest available name, *Anomia chinensis* Philippi, 1849. Some authors have also recognized *Anomia cytaeum* Gray, 1850, such as Huber (2010: 188, 617), with the Grabau & King taxa variously synonymized. Until additional morphological and genetic studies are done, these issues cannot be resolved.

Anomia cuticula
Grabau & King, 1928
Figure 9A–D

Anomia cuticulum Grabau & King, 1928b: 97; 1928e: 38; 1928f: 85, 166 [on the latter page as *Anomia* "*outicula*", and corrected on errata sheet], 256, pl. 2, fig. 17.

Material Examined

Syntypes, MBM280622 (ex GKLNH, 8 lv), Peitaiho, July 1925.

Modern Status

Synonym of *Anomia chinensis* Philippi, 1849.

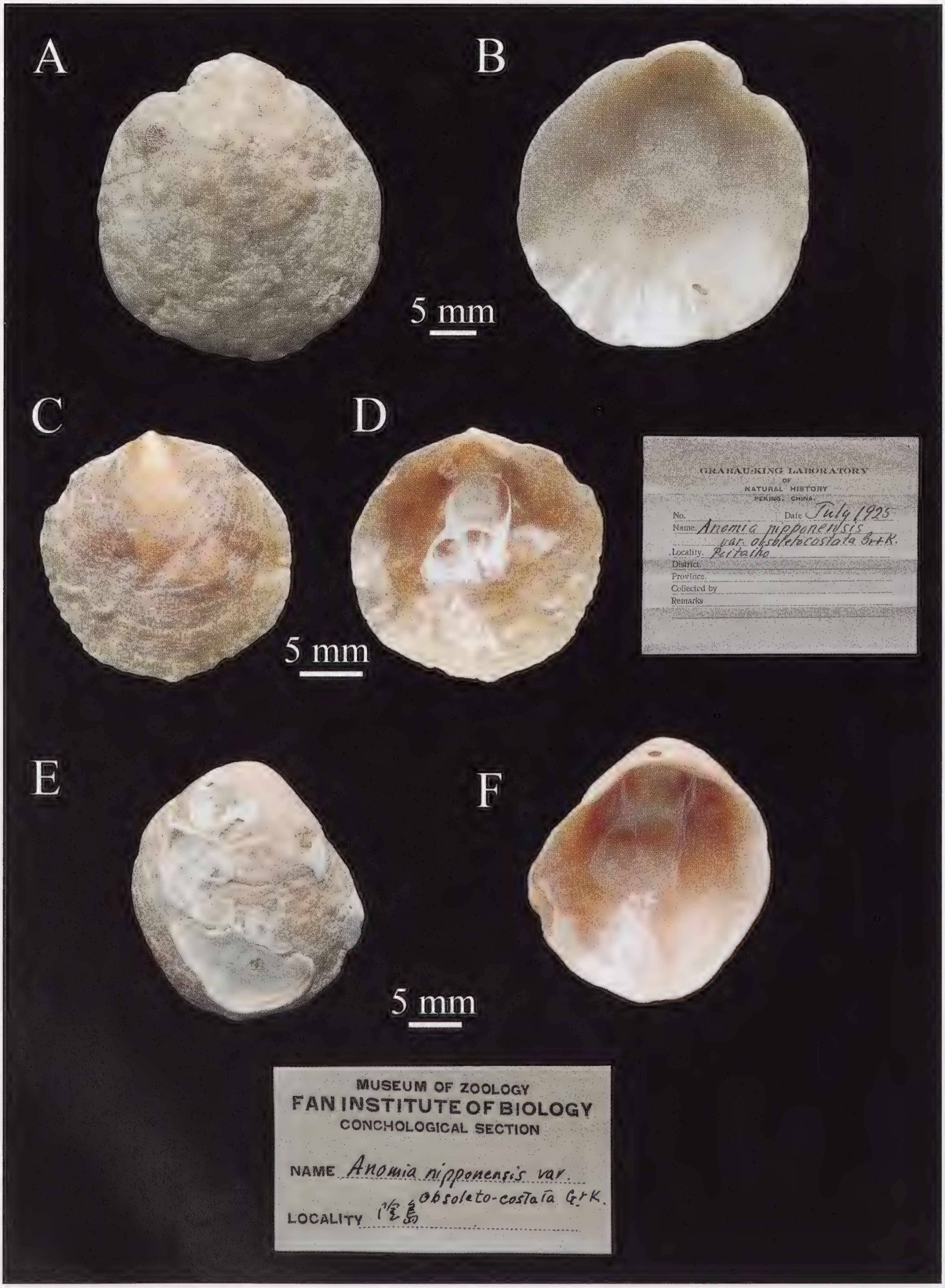

GRABAU-KING LABORATORY
OF
NATURAL HISTORY
PEKING, CHINA.

No.
Date July 1925
Name. Anomia nipponensis var. obsoletocostata Gr+K.
Locality. Peitaiho
District.
Province.
Collected by
Remarks

MUSEUM OF ZOOLOGY
FAN INSTITUTE OF BIOLOGY
CONCHOLOGICAL SECTION

NAME Anomia nipponensis var. obsoleto-costata Gr+K.
LOCALITY [illegible]島

FIG. 8A–F. *Anomia nipponensis* var. *obsoletocostata* Grabau & King. MBM280620, syntype. A, B: length = 30.5 mm; C, D: length = 19.6 mm; MBM280621, length = 22.4 mm.

Remarks

See Remarks under previous species.

Anomia plana
Grabau & King, 1928

Anomia plana Grabau & King, 1928b: 97; 1928e: 38; 1928f: 166, 256, pl. 2, fig. 18a, b.

Material Examined
Not found.

Modern Status
Synonym of *Anomia chinensis* Philippi, 1849.

Remarks

See Remarks above.

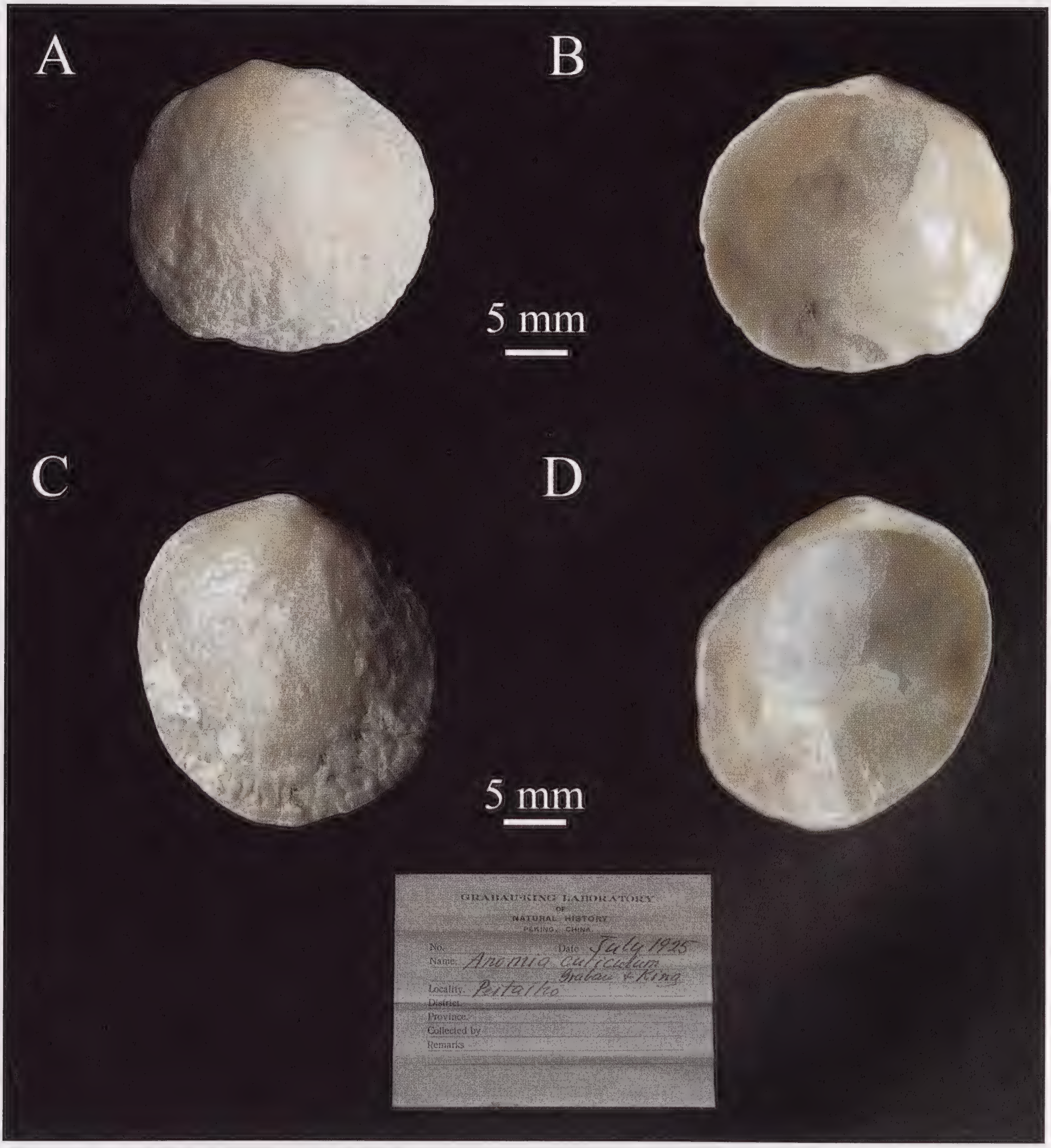

GRABAU-KING LABORATORY
OF
NATURAL HISTORY
PEKING, CHINA

No.
Date July 1925
Name Anomia cuticulum Grabau & King
Locality Peitaiho
District
Province
Collected by
Remarks

FIG. 9A–D. *Anomia cuticulum* Grabau & King. MBM280622, syntype. A, B: length = 24.2 mm; C, D: length = 23.3 mm.

Family Pectinidae Rafinesque, 1815

Pecten teilhardi
Grabau & King, 1928
Figure 10A, B

Pecten teilhardi Grabau & King, 1928b: 98–99; 1928e: 39; 1928f: 87–88, 168, 258, pl. 3, fig. 21a, b.

Material Examined
MBM280624 (ex MZFIBCS, 1 lv), Beidaihe.

Modern Status
Synonym of *Volachlamys hirasei* (Bavay, 1904).

Remarks

Wang (1990, 2002) regarded this species as a synonym of *Volachlamys hirasei* (Bavay, 1904), as did Raines & Poppe (2006: 328–330, 340, 354, pl. 287, figs. 1–7) and Huber (2010: 203, 625).

Chlamys solaris var. *peitaihoensis*
Grabau & King, 1928
Figure 11A–D

Chlamys solaris [Born, 1778] var. *peitaihoensis* Grabau & King, 1928b: 98; 1928e: 38; 1928f: 86, 168, not figured.

Material Examined
Syntypes, MBM280625 (ex GKLNH, 1 rv, 1 lv; labeled "*Pecten solaris* Born var. *peitaihoensis* Grabau & King"), Peitaiho, July 1925.

Modern Status
Synonym of *Volachlamys hirasei* (Bavay, 1904) (H. K. Dijkstra, pers. commun., 29 Nov. 2013).

Remarks

Although this species was not figured, it is clear from the description and syntypes that it is *Volachlamys hirasei* (Bavay, 1904).

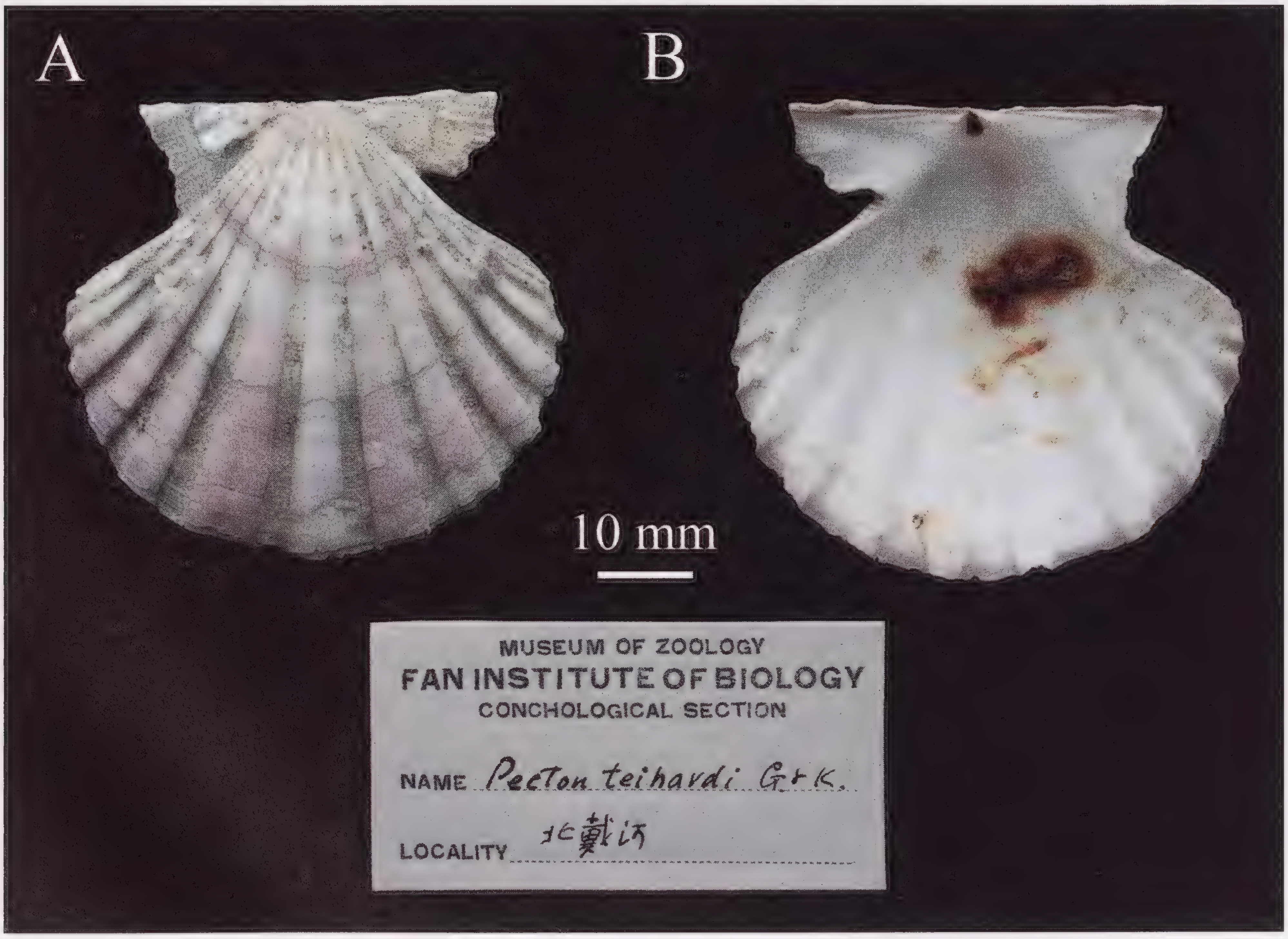

MUSEUM OF ZOOLOGY
FAN INSTITUTE OF BIOLOGY
CONCHOLOGICAL SECTION

NAME Pecton teihardi G+K.
LOCALITY 北戴河

FIG. 10A, B. *Pecten teilhardi* Grabau & King. MBM280624, length = 51.9 mm.

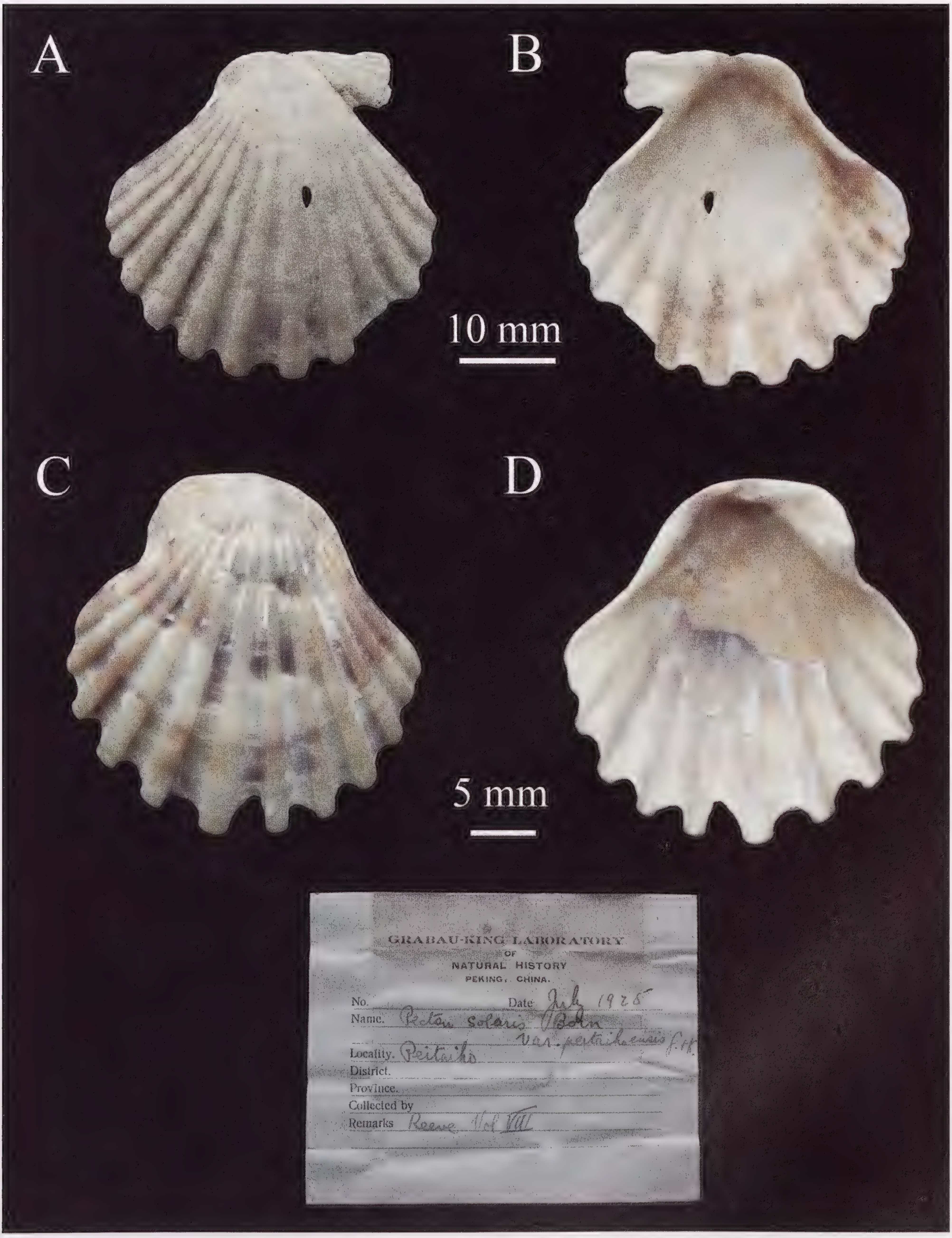

GRABAU-KING LABORATORY
OF
NATURAL HISTORY
PEKING, CHINA.

No. Date July 1925
Name. Pecten solaris Born
var. peitaihoensis f. H.
Locality. Peitaiho
District.
Province.
Collected by
Remarks Reeve Vol VIII

FIG. 11A–D. *Chlamys solaris* var. *peitaihoensis* Grabau & King. MBM280625, syntype. A, B: length = 33.9 mm; C, D: length = 26.6 mm.

Family Limidae Rafinesque, 1815

Lima angulata var. *minor* Grabau & King, 1928

Lima angulata [G. B. Sowerby II, 1843] var. *minor* Grabau & King, 1928b: 99; 1928e: 39; 1928f: 88, 169, 258, pl. 3, fig. 22.

Material Examined
Not found.

Modern Status
Most likely a synonym of *Limaria hakodatensis* (Tokunaga, 1906).

Remarks

This species has been variously treated, but unfortunately the type material cannot be found. Bernard et al. (1993: 44) treated it as a distinct species, *Promantellum minor* (Grabau & King, 1928), while Higo et al. (1999: 438) listed it as *Notolimea minor* (Grabau & King, 1928). However, most authors have listed it as a synonym of *Limaria hakodatensis* (Tokunaga, 1906) (Xu, 1997: 77; Wang, 2002: 308–309; Huber, 2010: 637).

Additionally, the taxonomy of Asian species of *Limaria* remains unstable. *Lima hakodatensis* was synonymized with *Limaria* (*Limaria*) *basi-*

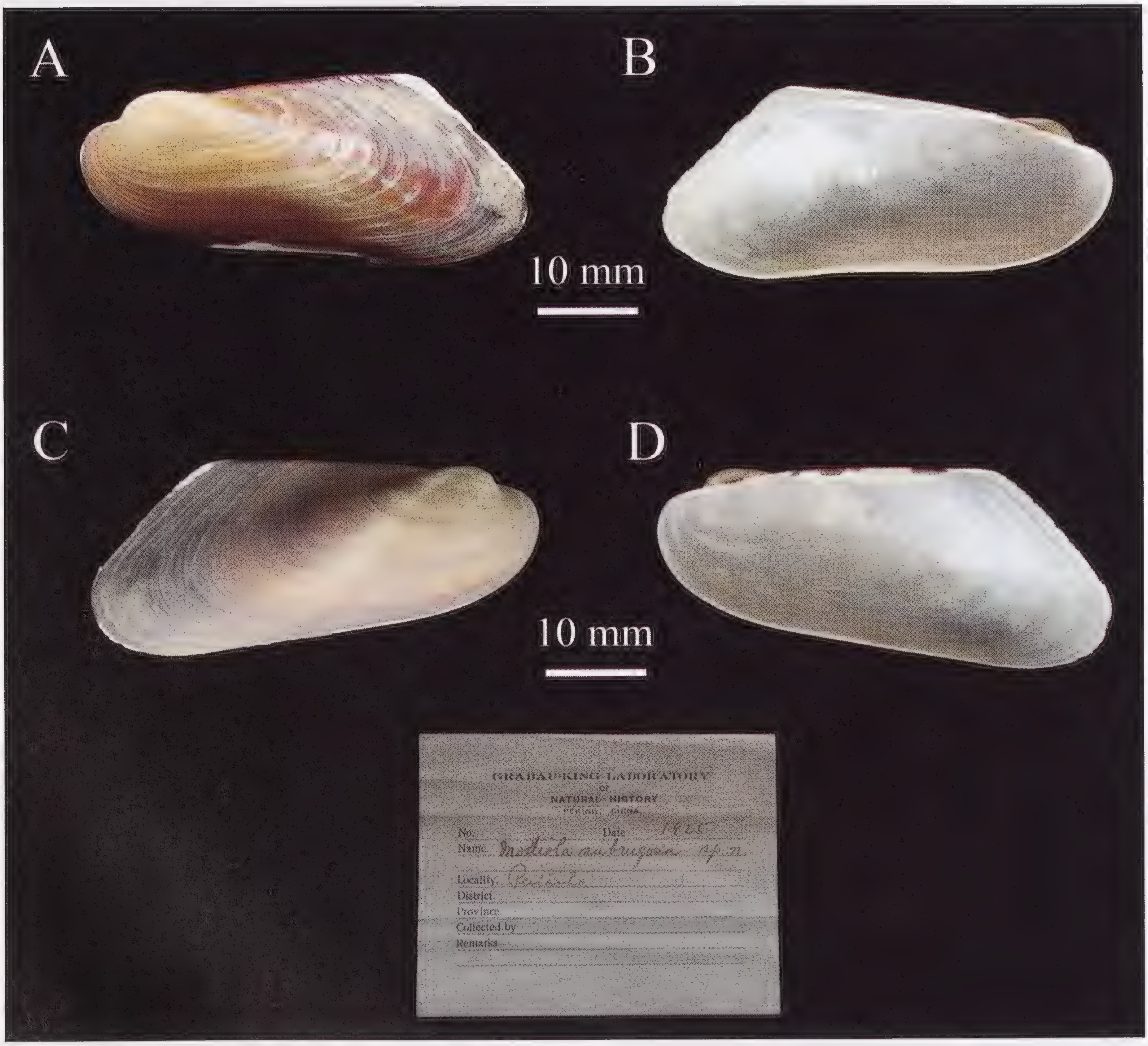

GRABAU-KING LABORATORY
OF
NATURAL HISTORY
PEKING, CHINA
No. Date 1925
Name Modiola subrugosa sp. n.
Locality Peitaiho
District
Province
Collected by
Remarks

FIG. 12A–D. *Modiola subrugosa* Grabau & King. MBM266848, syntype. A, B: length = 44.6 mm; C, D: length = 47.3 mm.

lanica (A. Adams & Reeve, 1850) (Bernard et al., 1993: 43) or with *Limaria* (*Limaria*) *orientalis* (A. Adams & Reeve, 1850) (Choe et al., 1994: 76; Higo et al., 1999: 436). Kuroda et al. (1971: 586–587; 375) and Habe (1977: 103) first considered *L. hakodatensis* as a distinct species; but later, Habe (1981: 78) synonymized it with *L. orientalis.* The type materials of *L. orientalis* and *L. basilanica* were figured by Higo et al. (2001: 154, as B365 & B364).

Family Mytilidae Rafinesque, 1815

Modiola subrugosa
Grabau & King, 1928
Figure 12A–D

Modiola subrugosa Grabau & King, 1928: 97; 1928e: 37; 1928f: 83, 170–171, 260, pl. 4, fig. 24.

Material Examined

Syntype, MBM266848 (ex GKLNH, 1 pv, 7 lv, 4 rv), Peitaiho, July 1925.

Modern Status

Synonym of *Jolya rhomboidea* (Reeve, 1857) (Huber, 2010: 125, 556), or of *Modiolus* (*Modiolusia*) *elongatus* (Swainson, 1821) (Wang, 1997: 186–188; Higo et al., 1999: 415).

Remarks

Earlier, Bernard et al. (1993: 32) placed this as a synonym of *Modiolus nitidus* (Reeve, 1857). Huber (2010) stated that *Modiola subrugosa* Grabau & King, 1928, and the species identified as *Modiolus* (*Modiolusia*) *elongatus* (Swainson, 1821) in China were actually *Jolya rhomboidea* (Reeve, 1857), so this fundamental issue needs to be resolved before Grabau & King's species can be correctly synonymized.

Modiola aquarius
Grabau & King, 1928

Modiola aquarius Grabau & King, 1928: 97; 1928e: 37; 1928f: 83–84, 171–172, 260, pl. 4, fig. 25a, b.

Material Examined

Not found.

Modern Status

Synonym of *Arcuatula senhousia* (Benson in Cantor, 1842) (Scarlato, 1981: 242; Bernard et al., 1993; 35, as *Musculista*; Huber, 2010: 112, pers. commun., 16 Dec. 2013). The genus *Arcuatula* Lamy, 1919, *ex* Jousseaume ms, is now regarded as a senior synonym of *Musculista* Yamamoto & Habe, 1958.

Family Veneridae Rafinesque, 1815

Venus jidoensis [sic; = *jedoensis*] var. *alta*
Grabau & King, 1928
Figure 13A–D

Venus jidoensis [sic; = *jedoensis* Lischke, 1874] var. *alta* Grabau & King, 1928f: 176, 262, pl. 5, fig. 33, *non Venus alta* G. B. Sowerby II, 1853.

Material Examined

Syntype, MBM280626 (ex GKLNH, 1 pv, 1 rv), Peitaiho.

Modern Status

Synonym of *Leukoma* [or *Protothaca*] *jedoensis* (Lischke, 1874) (Huber, 2010: Excel file on CD).

Rupellaria pechiliensis
Grabau & King, 1928
Figure 14A–F

Rupellaria pechiliensis Grabau & King, 1928f: 94–95, 179–180, 262, pl. 5, fig. 36.

Material Examined

Syntype, MBM280628 (ex GKLNH, 2 pv, 1 lv, 3 rv), Peitaiho, Grabau, 1922; MBM280629 (ex MZFIBCS, 1 rv), Beidaihe.

Modern Status

Synonym of *Irus mitis* (Deshayes, 1854) (Huber, 2010: 750).

Remarks

While some authors have considered this to be a synonym of *Rupellaria fabagella* (Lamarck, 1818) (Bernard et al., 1993: 87; Higo et al., 1999: 513), the type material shows that it is instead a junior synonym of *Irus mitis* (Deshayes, 1854).

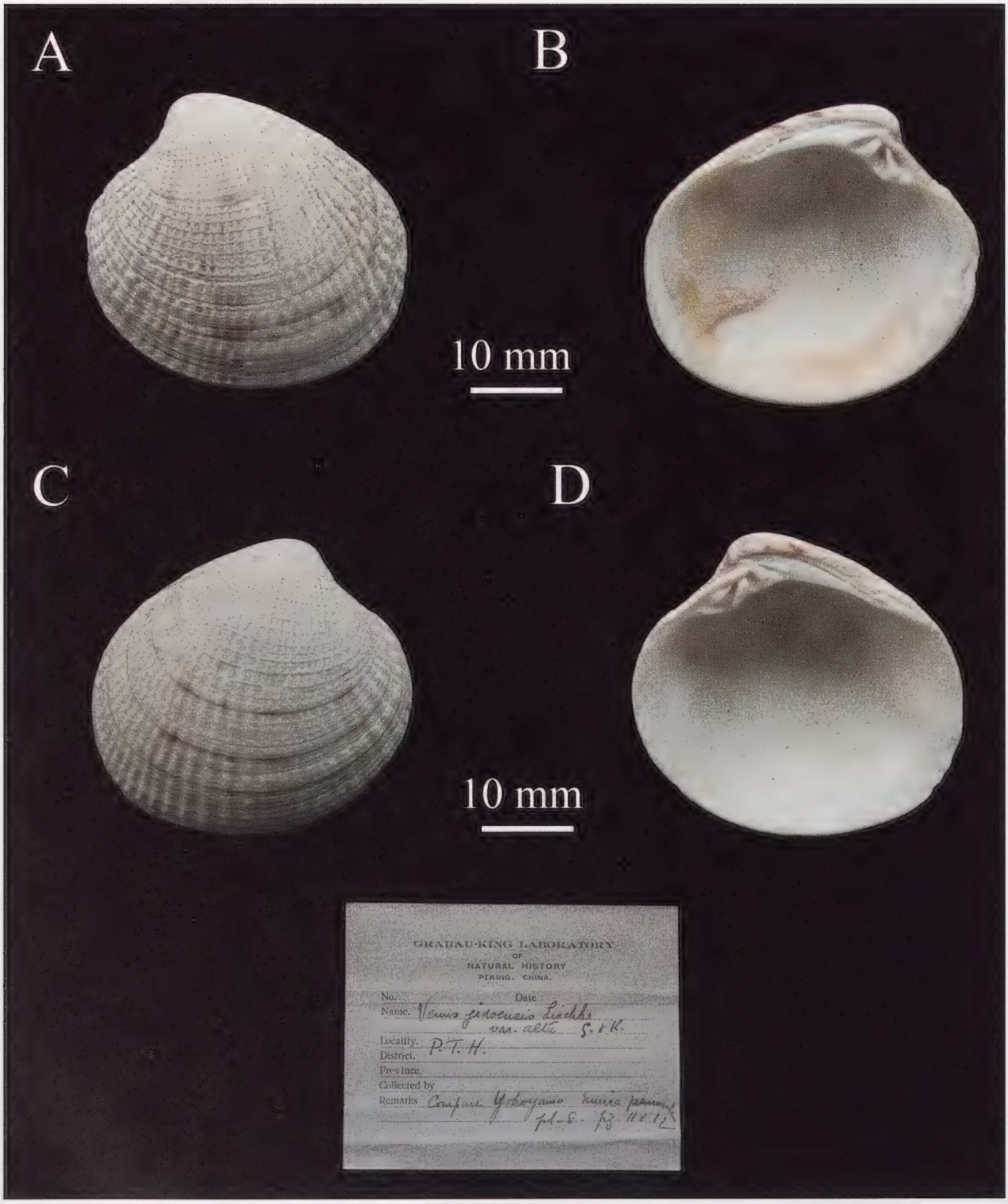

GRABAU-KING LABORATORY
OF
NATURAL HISTORY
PEKING. CHINA.

No. Date

Name. Venus jidoensis Lischke
var. alta G. & K.

Locality. P.T.H.

District.

Province.

Collected by

Remarks Compare Yokoyama Venus pennata
pl. 8. fig 11 & 12

FIG. 13A–D. *Venus jidoensis* (sic; = *jedoensis*) var. *alta* Grabau & King. MBM280626, syntype, length = 35.1 mm.

→

FIG. 14A–F. *Rupellaria pechiliensis* Grabau & King. MBM280628, syntype. A–D: length = 12.4 mm; MBM280629; E, F: length = 7.7 mm.

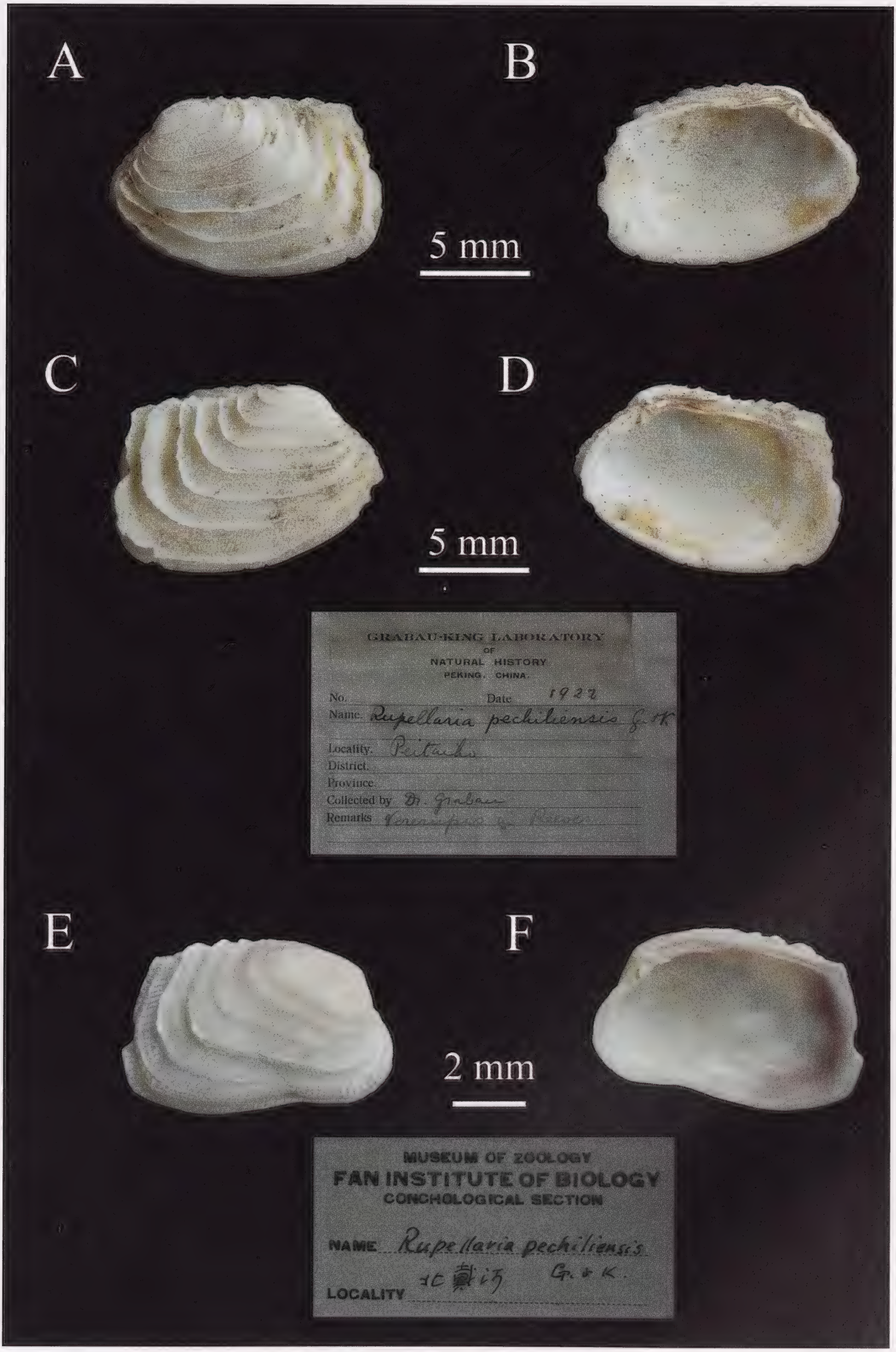

GRABAU-KING LABORATORY
OF
NATURAL HISTORY
PEKING, CHINA.

No. Date 1922
Name. Rupellaria pechiliensis G. & K.
Locality. Peitaiho
District.
Province.
Collected by Dr. Grabau
Remarks Venerupis [illegible] Reeve

MUSEUM OF ZOOLOGY
FAN INSTITUTE OF BIOLOGY
CONCHOLOGICAL SECTION

NAME Rupellaria pechiliensis
G. & K.
LOCALITY 北戴河

Family Tellinidae Blainville, 1814

Tellina (*Tellinides*) *planissima* var. *peitaihoensis*
Grabau & King, 1928
Figure 15A–H

Tellina (*Tellinides*) *planissima* [Anton, 1838] var. *peitaihoensis* Grabau & King, 1928b: 99; 1928e: 39; 1928f: 89, 180–181, 262, pl. 5, fig. 37.

Material Examined
Syntype, MBM280630 (ex GKLNH, 30 pv, 68 rv, 63 lv), Peitaiho, lab staff of GKLNH, July 1925; syntype, MBM280633 (ex GKLNH, 28 pv, 15 rv, 19 lv), Peitaiho, July 1925.

Modern Status
Most likely a synonym of *Tellina* (s.l.) *pumila* Hanley, 1844 (Huber, pers. commun., May 10, 2014).

Remarks

This species has been treated in various ways. It has been treated as a distinct species, *Fabulina* (*Moerella*) *peitaihoensis* (Grabau & King, 1928) (Oyama, 1973: 114, pl. 53, figs. 3, 9), a synonym of *Moerella rutila* (Dunker,1860) (Scarlato, 1965: 84; Bernard et al., 1993: 93; Xu, 1997: 165; Higo et al., 1999: 487; T. Haga, pers. commun., July 2014), or a synonym of *Tellinides ovalis* G. B. Sowerby I, 1825 (Bernard et al., 1993: 90, a second entry for the same taxon).

Family Semelidae Stoliczka, 1870 [1825]

Tellina murrayi
Grabau & King, 1928

Tellina murrayi Grabau & King, 1928f: 90, 182–183, 266, pl. 7, fig. 41, *non* E. A. Smith, 1885. Renamed *Tellina murrayana* Salisbury, 1934: 85.

Material examined
Not found.

Modern Status
Possibly a distinct species of *Abra*, *Abra murrayana* (Salisbury, 1934) (M. Huber, pers. commun., 20 Dec. 2013), or a synonym of *Abra lunella* (Gould, 1861) (Haga, pers. commun., July 2014).

Remarks

Because *murrayi* was preoccupied by *Tellina murrayi* E. A. Smith, 1885, Salisbury (1934) renamed it as *Tellina murrayana*. It has been regarded as *Macoma murrayi* Grabau & King (Scarlato, 1965: 78, pl. 6, fig. 8; Xu, 1997: 168; Qi, 2004: 283, pl. 155A), and as a synonym of *Macoma incongrua* (Martens, 1865) (Bernard et al., 1993: 94; Xu & Zhang, 2008: 187; Higo et al., 1999: 489). However, the shell shape and prominent beaks are inconsistent with those of *Macoma*, and the small size is indicative of an *Abra*.

Family Donacidae Fleming, 1828

Tellina trigonoides
Grabau & King, 1928

Tellina trigonoides Grabau & King, 1928b: 100; 1928e: 40; 1928f: 90–91, 183, 266, pl. 7, fig. 42.

Material examined
Not found.

Modern Status
Synonym of *Donax kiusiuensis* Pilsbry, 1901 (Scarlato, 1965: 45–46; Bernard et al., 1993: 100; Xu, 1997: 151; Higo et al., 1999: 497).

Family Solenidae Lamarck, 1809

Solen corneus var. *pechiliensis*
Grabau & King, 1928
Figure 16A–D

Solen corneus [Lamarck, 1818] var. *pechiliensis* Grabau & King, 1928b: 95; 1928e: 35; 1928f: 79, 186, 264, pl. 6, fig. 47a, b.

Material Examined
Syntypes, MBM280631 (ex GKLNH, 6 rv, 5 lv).

Modern Status
Synonym of *Solen strictus* Gould, 1861 (Xu, 1997: 187; Higo et al., 1999: 481; Xu & Zhang, 2008: 213).

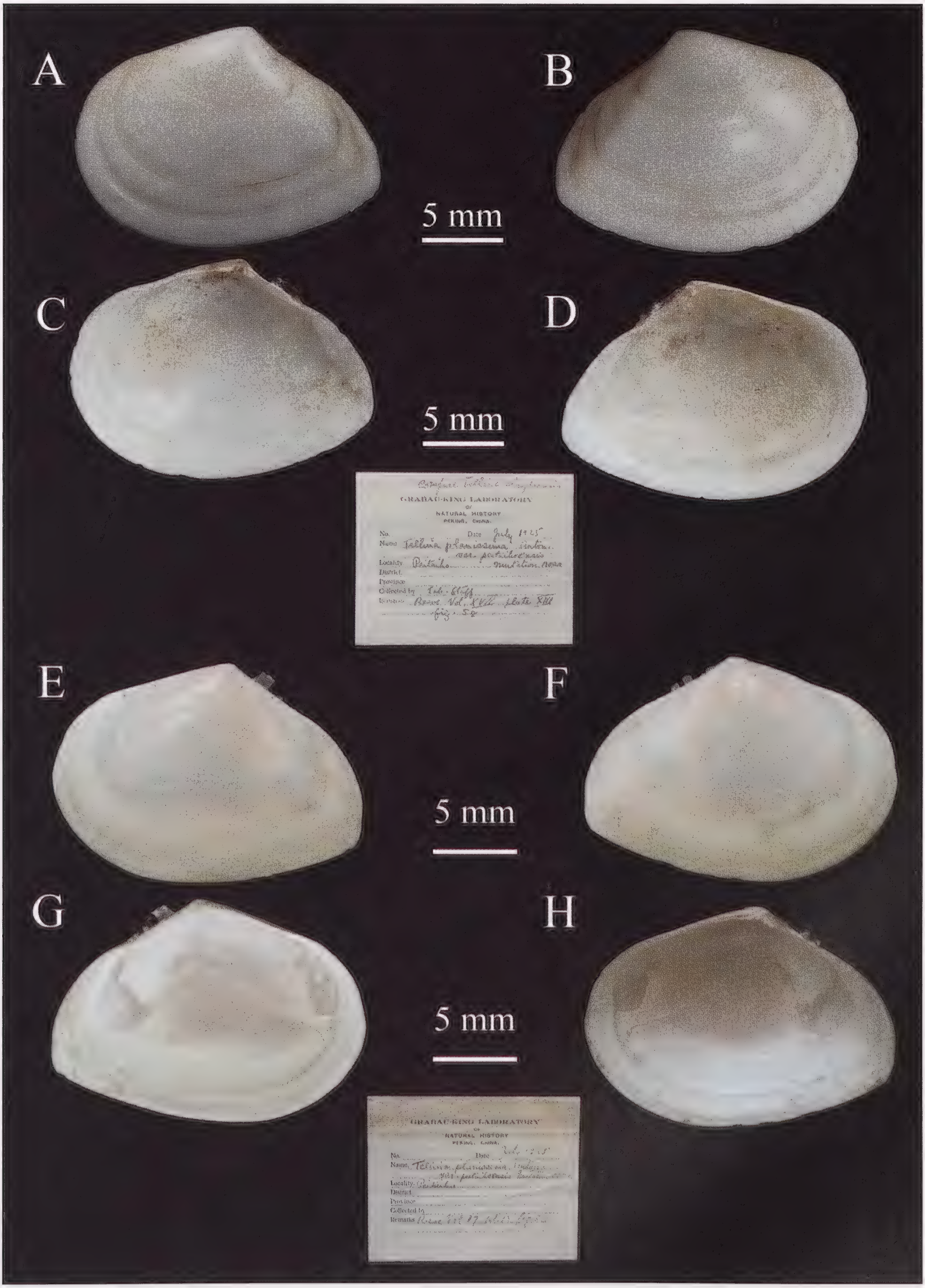

FIG. 15A–H. *Tellina* (*Tellinides*) *planissima* var. *peitaihoensis* Grabau & King. A–D: MBM280630, syntype, length = 18.9 mm; E, F: MBM280633, length = 18.7 mm.

Remarks

Tchang & Hwang (1964) thought this species was a synonym of *Solen gouldii* Conrad, 1867. However, *Solen gouldii* Conrad, 1867, is now regarded as a synonym of *Solen strictus* Gould, 1861. Bernard et al. (1993: 101) took this species and *Solen strictus* Gould, 1861, to be synonyms of *Solen corneus* Lamarck, 1818. However, the latter is a tropical species that occurs in Malaysia, Indonesia, Philippines, Thailand and Vietnam. Indeed, Cosel (2002: 329) noted that the name *S. corneus* was applied in error to *S. strictus* by several authors including Grabau & King; *S. strictus* is much longer and more slender than *S. corneus*, with a more rounded posterior margin, and the shell may have a brownish hue, whereas *S. corneus* is white (Cosel, 2002).

Family Mactridae Lamarck, 1809

Trigonella quadrangularis var. *ventricosa*
Grabau & King, 1928
Figure 17A–D

Trigonella quadrangularis [Reeve, 1854] var. *ventricosa* Grabau & King, 1928a: 39; 1928e: 34; 1928f: 76, 190, 264, pl. 6, fig. 53.

Material Examined

Syntypes, MBM280632 (ex GKLNH, 3 rv, 4 lv), Peitaiho, July 1925.

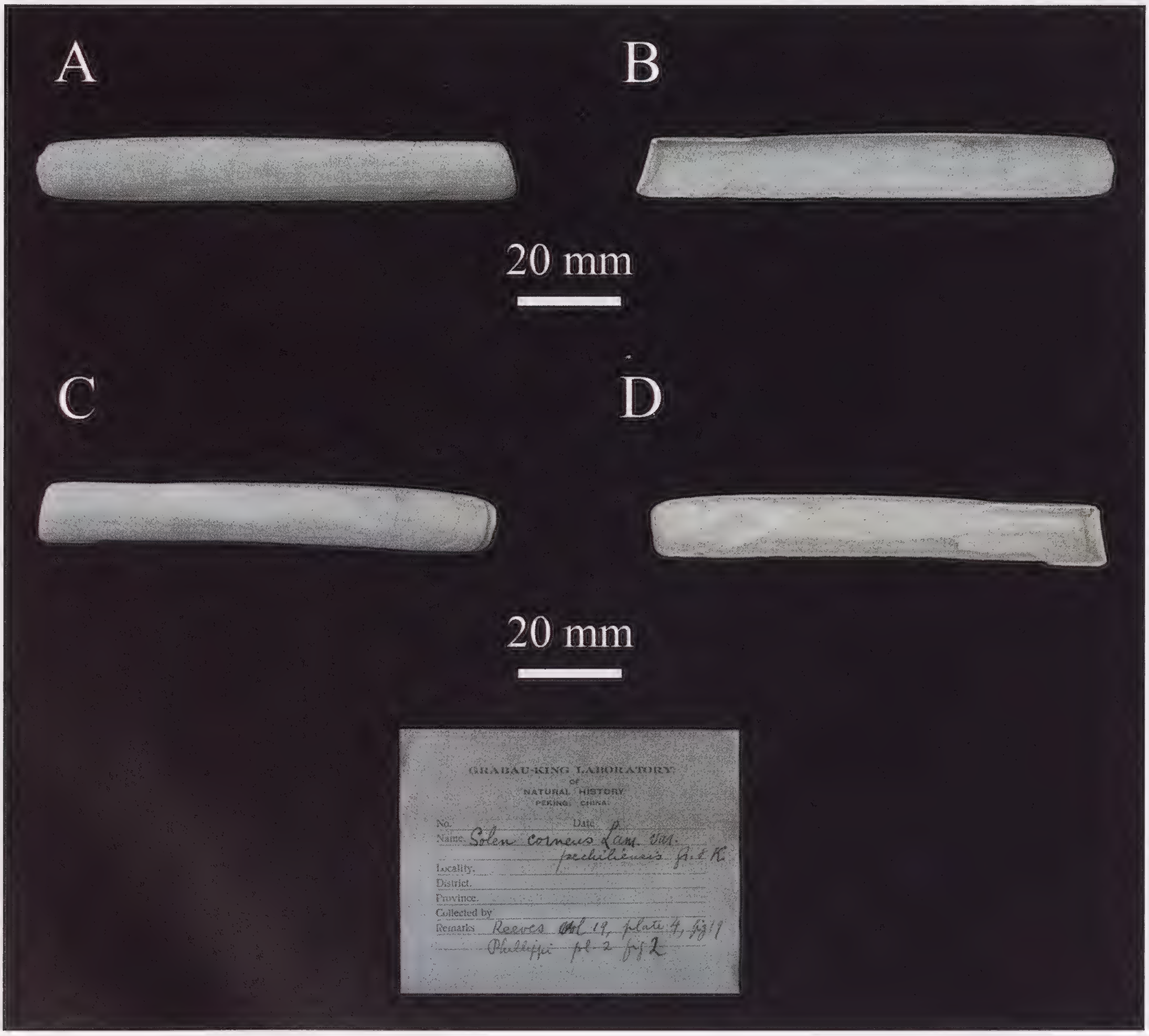

GRABAU-KING LABORATORY
OF
NATURAL HISTORY
PEKING, CHINA

No. Date
Name. Solen corneus Lam. var. pechiliensis G. & K.
Locality.
District.
Province.
Collected by
Remarks Reeves Vol 19, plate 4, fig 11
Philippi pl 2 fig 2

FIG. 16A–D. *Solen corneus* var. *pechiliensis* Grabau & King. MBM280631, syntype. A, B: length = 91.7 mm; C, D: length = 87.4 mm.

Modern Status

Synonym of *Mactra quadrangularis* Reeve, 1854 (Bernard et al., 1993: 104; Higo et al., 1999: 476, as "*Mactra* (*Mactra*) *veneriformis* Reeve, 1854, *ex* Deshayes ms, *non* W. Wood, 1828"; Huber, 2010: Excel file on CD).

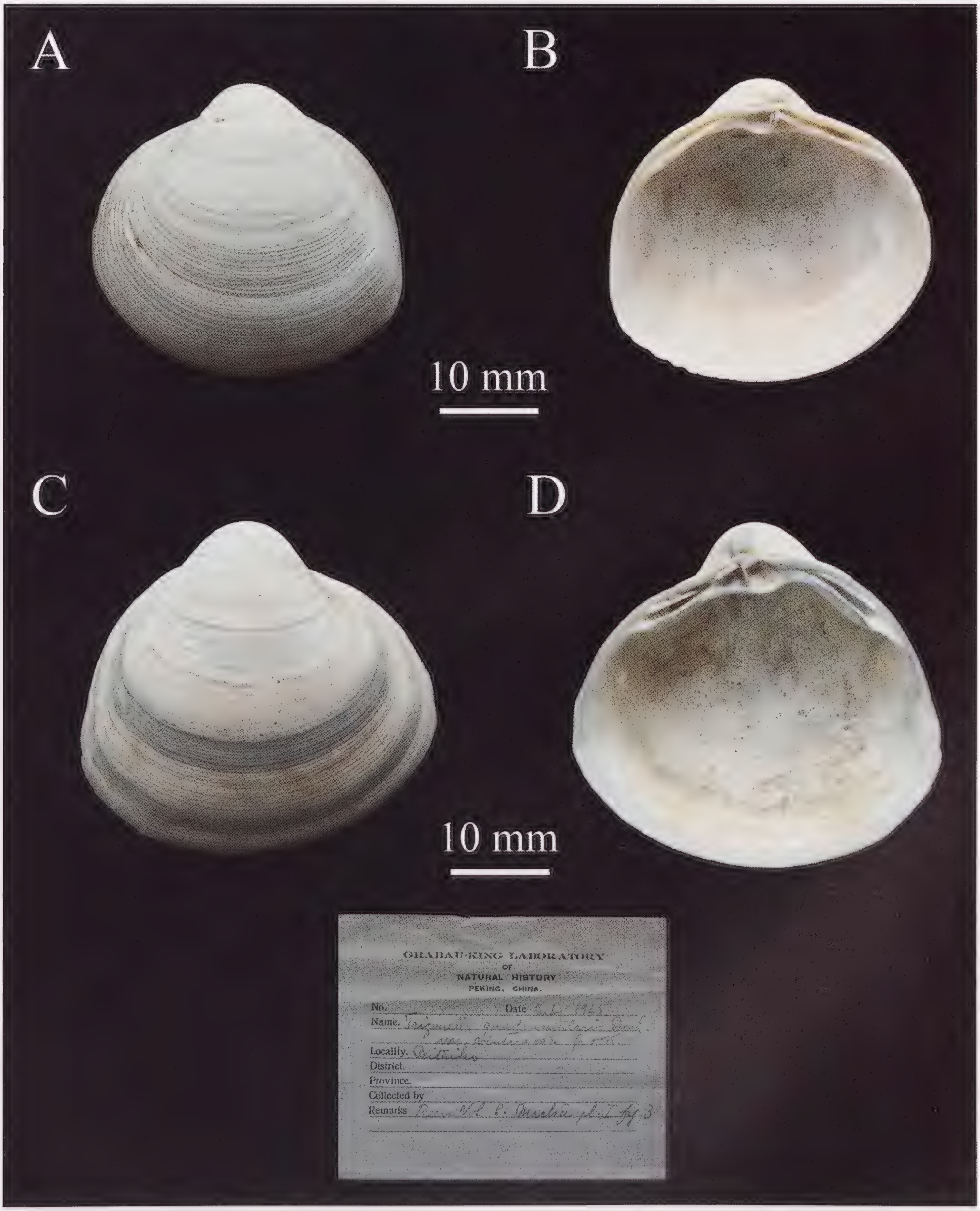

FIG. 17A–D. *Trigonella quadrangularis* var. *ventricosa* Grabau & King. MBM280632, syntype. A, B: length = 30.6 mm; C, D: length = 41.7 mm.

Raeta fragilis
Grabau & King, 1928
Figure 18A–D

Rhaeta [sic; pro *Raeta*] *fragilis* Grabau & King, 1928b: 94; 1928e: 34; 1928f: 190–192, 266, pl. 7, fig. 54.

Material Examined

Syntypes, MBM280634 (ex GKLNH, 1 rv, 1 lv).

Modern Status

Synonym of *Raeta pellicula* (Reeve, 1854) (Bernard et al., 1993: 106; Xu, 1997: 145; Higo et al., 1999: 479; Xu & Zhang, 2008: 165; Huber, 2010: Excel file on CD).

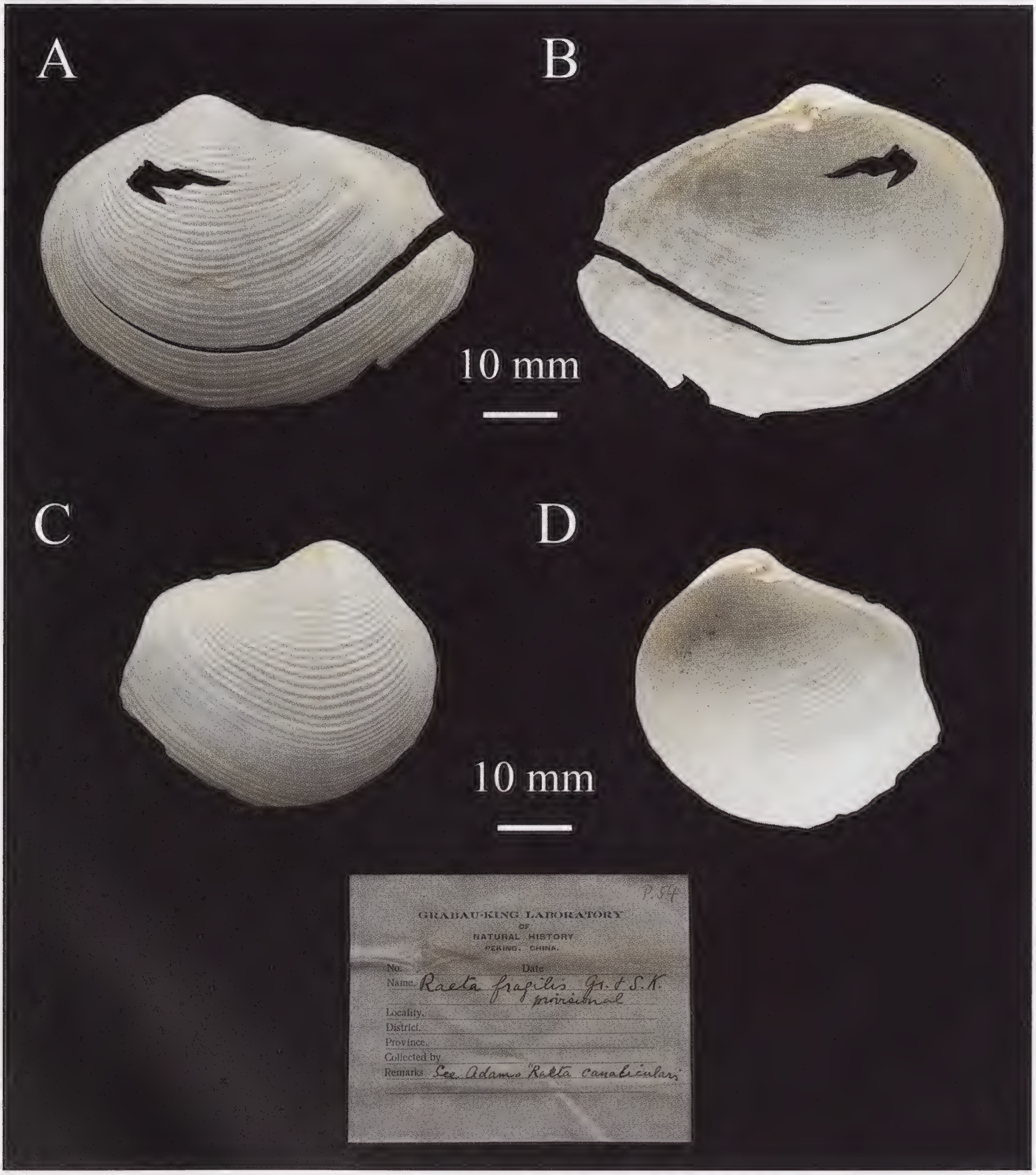

P.54

GRABAU-KING LABORATORY
OF
NATURAL HISTORY
PEKING, CHINA.

No.
Date
Name. Raeta fragilis Gr. & S.K. provisional
Locality.
District.
Province.
Collected by
Remarks See Adams "Raeta canalicularis"

FIG. 18A–D. *Raeta fragilis* Grabau & King. MBM280634, syntype. A, B: length = 56.1 mm; C, D: length = 41.4 mm.

Family Laternulidae Hedley, 1918 [1840]

Anatina pechiliensis
Grabau & King, 1928
Figure 19A–D

Anatina pechiliensis Grabau & King, 1928a: 36–37; 1928e: 31; 1928f: 70, 193–194, 266, pl. 7, fig. 58.

Material Examined

Syntypes, MBM280635 (ex GKLNH, 9 pv, 1 rv, 1 lv), Peitaiho, July 1925.

Modern Status

Synonym of *Laternula marilina* (Reeve, 1863) (Bernard et al., 1993: 116; Xu, 1997: 256–257; Higo et al., 1999: 523; Xu & Zhang, 2008: 277) or of *Laternula liautaudi* (Mittre, 1844) (Huber, 2010: 523, and pers. commun.).

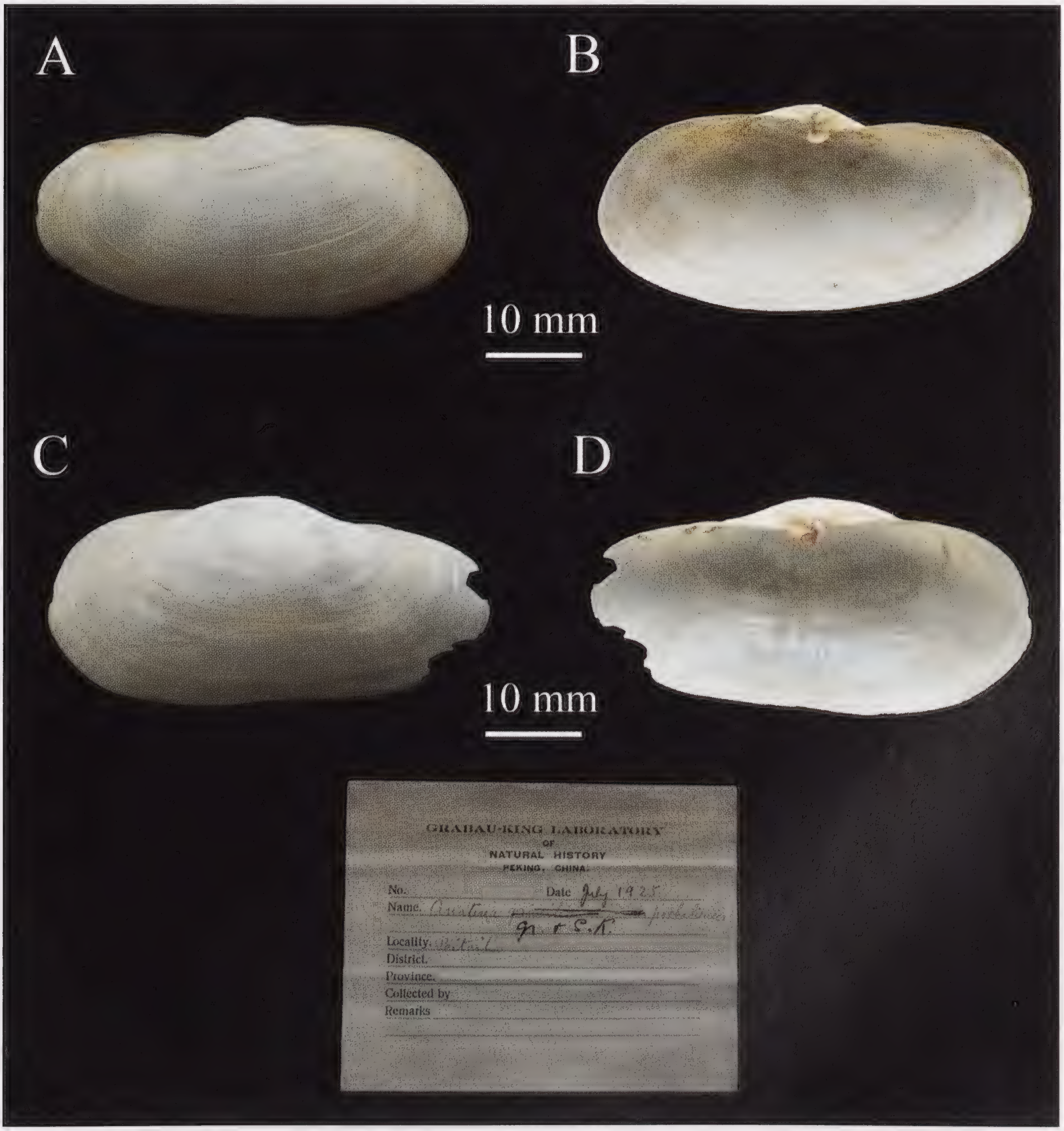

GRABAU-KING LABORATORY
OF
NATURAL HISTORY
PEKING, CHINA.

No.
Date July 1925
Name. Anatina [illegible] pechiliensis
Gr. & K.
Locality. Peitaih.
District.
Province.
Collected by
Remarks

FIG. 19A–D. *Anatina pechiliensis* Grabau & King. MBM280635, syntype. A, B: length = 43.5 mm; C, D: length = 44.7 mm.

Class Gastropoda Cuvier, 1795
Family Acmaeidae Forbes, 1850

Acmaea peitaihoensis Grabau & King, 1928 & *Acmaea kolarovai* Grabau & King, 1928
Figure 20A–D

Acmaea peitaihoensis Grabau & King, 1928d: 39; 1928e: 61.
Acmaea kolarovai Grabau & King, 1928f: 143–144, 235, 278, pl. 11, fig. 114.

Material Examined

Syntypes, MBM229002 (ex GKLNH, 38 shells), Peitaiho, July 1925; syntypes, MBM229003 (ex GKLNH, 24 shells), July 1925, labeled "*Patella peitahoensis* Grabau & King".

Modern Status

A distinct species, *Collisella peitaihoensis* (Grabau & King, 1928) (Qi, 2004: 14, pl. 6F).

Remarks

The description of *Acmaea peitaihoensis* (Grabau & King, 1928d: 39) is identical to that of *Acmaea kolarovai* (Grabau & King, 1928f: p. 143–144), the latter named in honor of Dr. F. N. Kolarova, and the authors evidently changed their minds about the name. *Acmaea peitaihoensis* Grabau & King, 1928, has priority, and *Acmaea kolarovai* Grabau & King, 1928, is thus a junior synonym. Placed in various genera by authors (Zhao et al., 1982: 20–21, pl. 2, fig. 2, pl. 3, fig. 3, as *Patelloida*; Qi et al., 1989: 21, text-fig. 24, as *Acmaea*).

Family Patellidae Rafinesque, 1815

Acmaea testudinalis Müller, var. *minor* Grabau & King, 1928
Figure 21A–C

Acmaea testudinalis [Müller, 1776] var. *minor* Grabau & King, 1928d: 39; 1928e: 61–62, not preoccupied by *Acmaea testudinalis var. minor* Verkrüzen, 1881, which is a *nom. nud.* [from Newfoundland]; 1928f: 144, 235–236, 278, pl. 11, figs. 115a, b, c.

Material Examined

We did not find any specimens labeled *Acmaea testudinalis* Müller, var. *minor* Grabau & King, 1928, but we found a lot with label of "*Acmaea testudinaria* Grabau & King" (Fig. 21A–C, MBM280639, ex GKLNH, 71 shells, Peitaiho, July 1925) [*non Patella testudinaria* Linnaeus, 1758], the specimens in which closely resemble the original figures of *Acmaea testudinalis* Müller, var. *minor* (Grabau & King, 1928f: pl. 11, figs. 115a–c.), and might be the syntypes.

Modern Status

Synonym of *Patelloida pygmaea* (Dunker, 1860).

Family Trochidae Rafinesque, 1815

Trochus (*Livona*) *ephebocostalis* Grabau & King, 1928
Figure 22A–D

Trochus ephebicostalis Grabau & King, 1928d: 35; 1928e: 57; 1928f: 134, 237–238. 278, pl. 11, fig. 118 [as "*Trochus* (*Livona*) *ephebocostalis*"; corrected on errata sheet].

Material Examined

Syntypes, MBM280641 (ex GKLNH, 17 shells), Peitaiho, July 1925; MBM229005 (ex MZFIBCS, 1 shell), Beidaihe [= Peitaiho].

Modern Status

Synonym of *Chlorostoma rustica* (Gmelin, 1791) (Qi et al., 1989: 26, pl. 4, fig. 11).

Monodonta trochiformis Grabau & King, 1928
Figure 23A, B

Monodonta trochiformis Grabau & King, 1928d: 34; 1928e: 57; 1928f: 133, 238, 278, pl. 11, fig. 119.

Material Examined

Syntypes, MBM280640 (ex GKLNH, 80 shells), Peitaiho, July 1925.

Modern Status

Synonym of *Monodonta labio* Linnaeus, 1758 (Qi et al., 1989: 25, pl. 1, fig. 4).

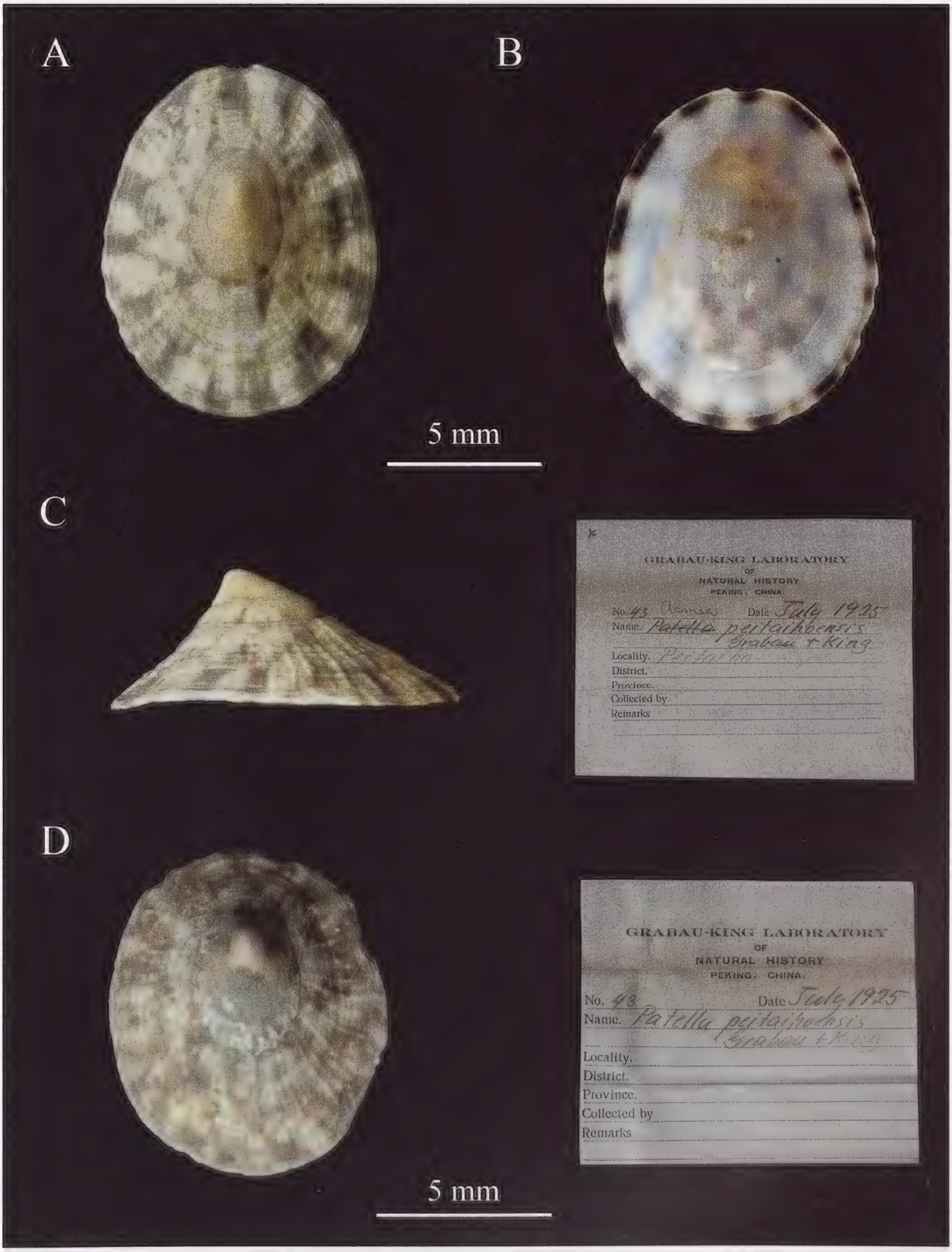

GRABAU-KING LABORATORY
OF
NATURAL HISTORY
PEKING, CHINA.
No. 43 Acmaea Date July 1925
Name. Patella peitaihoensis Grabau + King
Locality. Peitaiho
District.
Province.
Collected by
Remarks

GRABAU-KING LABORATORY
OF
NATURAL HISTORY
PEKING, CHINA.
No. 48 Date July 1925
Name. Patella peitaihoensis Grabau + King
Locality.
District.
Province.
Collected by
Remarks

FIG. 20A–C. *Acmaea peitaihoensis* Grabau & King. MBM229002, syntype, length = 11.4 mm; D: *Patella peitahoensis* Grabau & King, 1928. MBM229003, syntype, length = 9.5 mm.

Remarks

Oyama (1973: 14, pl. 1, fig. 23a, b) thought that this might be a distinct species or a subspecies of *Monodonta labio*, but he still listed it as synonym of *Monodonta glabratum* and *Monodonta labio.* We agree with Qi et al. (1989) that this species is actually the Indo-Pacific widely distributed *Monodonta labio.*

Family Littorinidae Children, 1834

Littorina heterospiralis
Grabau & King, 1928
Figure 24A, B

Littorina heterospiralis Grabau & King, 1928f: 230–231, 274, pl. 10, fig. 104.

Material Examined
Syntypes, MBM280647 (ex GKLNH, 14 shells), Peitaiho, July 1925.

Modern Status
Synonym of *Littorina brevicula* (Philippi, 1844) (Qi et al., 1998: 28–29, text-fig. 27; Higo et al., 1999: 90).

Remarks

Qi et al. (1998), Reid (1996) and Higo et al. (1999) all agreed that this species is a synonym of *Littorina brevicula* (Philippi, 1844).

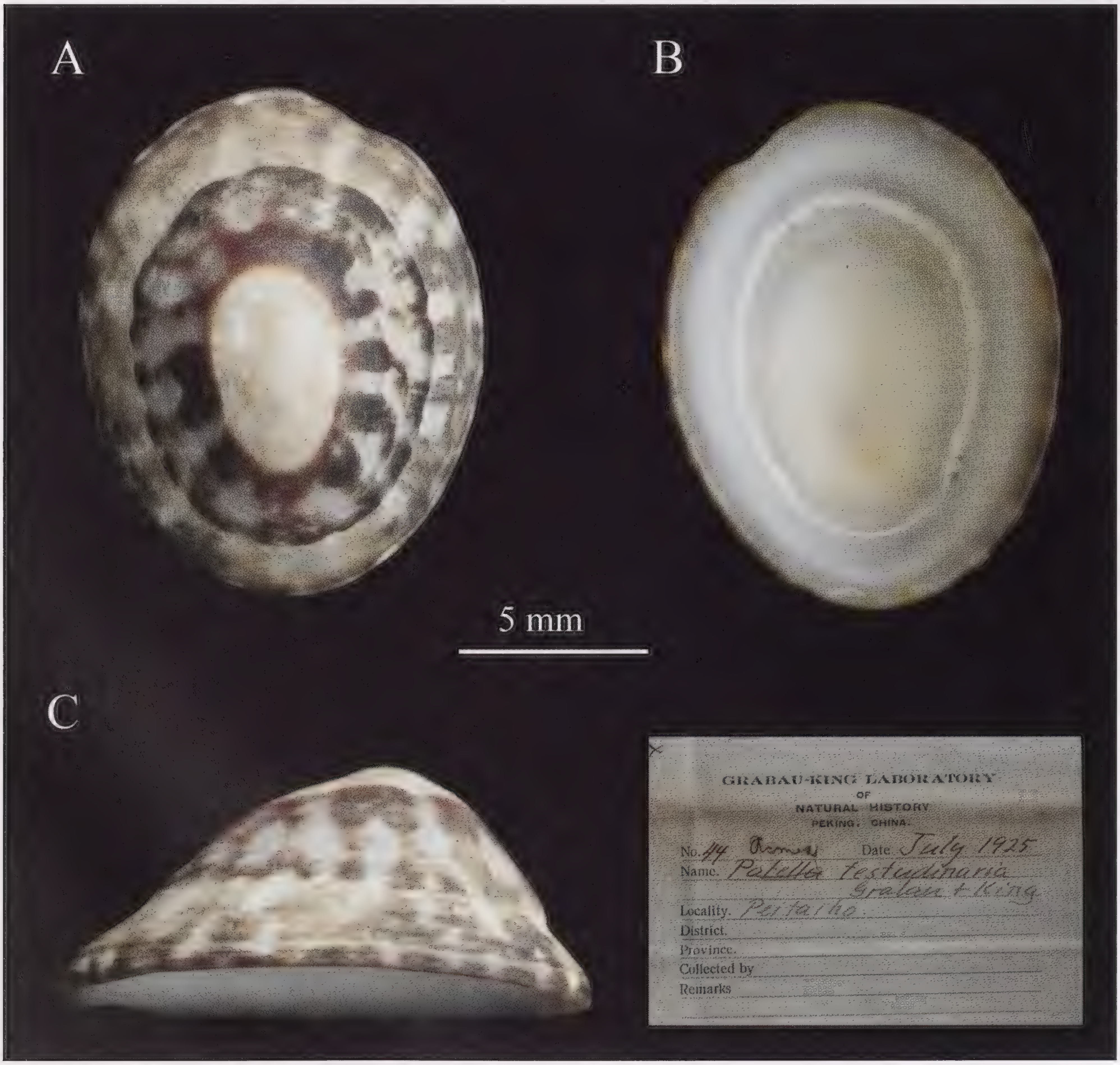

GRABAU-KING LABORATORY
OF
NATURAL HISTORY
PEKING, CHINA.
No. 44 [illegible] Date July 1925
Name. Patella testudinaria Grabau + King
Locality. Peitaiho
District.
Province.
Collected by
Remarks

FIG. 21A–C. *Acmaea testudinaria* Grabau & King. MBM280639, length= 13.9 mm.

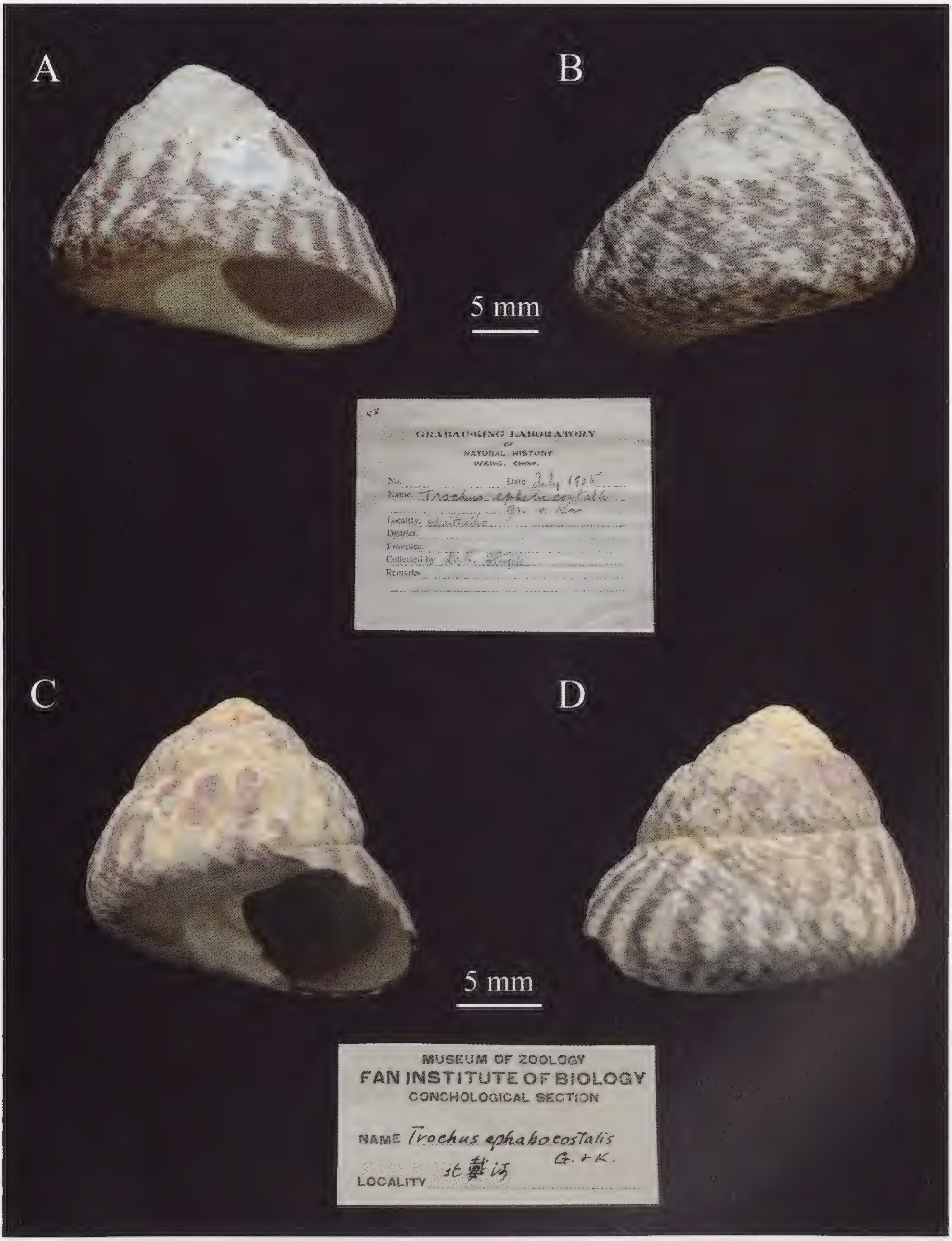

××

GRABAU-KING LABORATORY
OF
NATURAL HISTORY
PEKING, CHINA.

No. Date July 1925
Name Trochus ephebecostalis
Gr. & K.
Locality Peitaiho
District
Province
Collected by [illegible]
Remarks

MUSEUM OF ZOOLOGY
FAN INSTITUTE OF BIOLOGY
CONCHOLOGICAL SECTION

NAME Trochus ephabocostalis
G. & K.
LOCALITY 北戴河

FIG. 22A–D. *Trochus* (*Livona*) *ephebocostalis* Grabau & King. A, B: MBM280641, syntype, length = 21.9 mm; C, D: MBM229005, length = 16.9 mm.

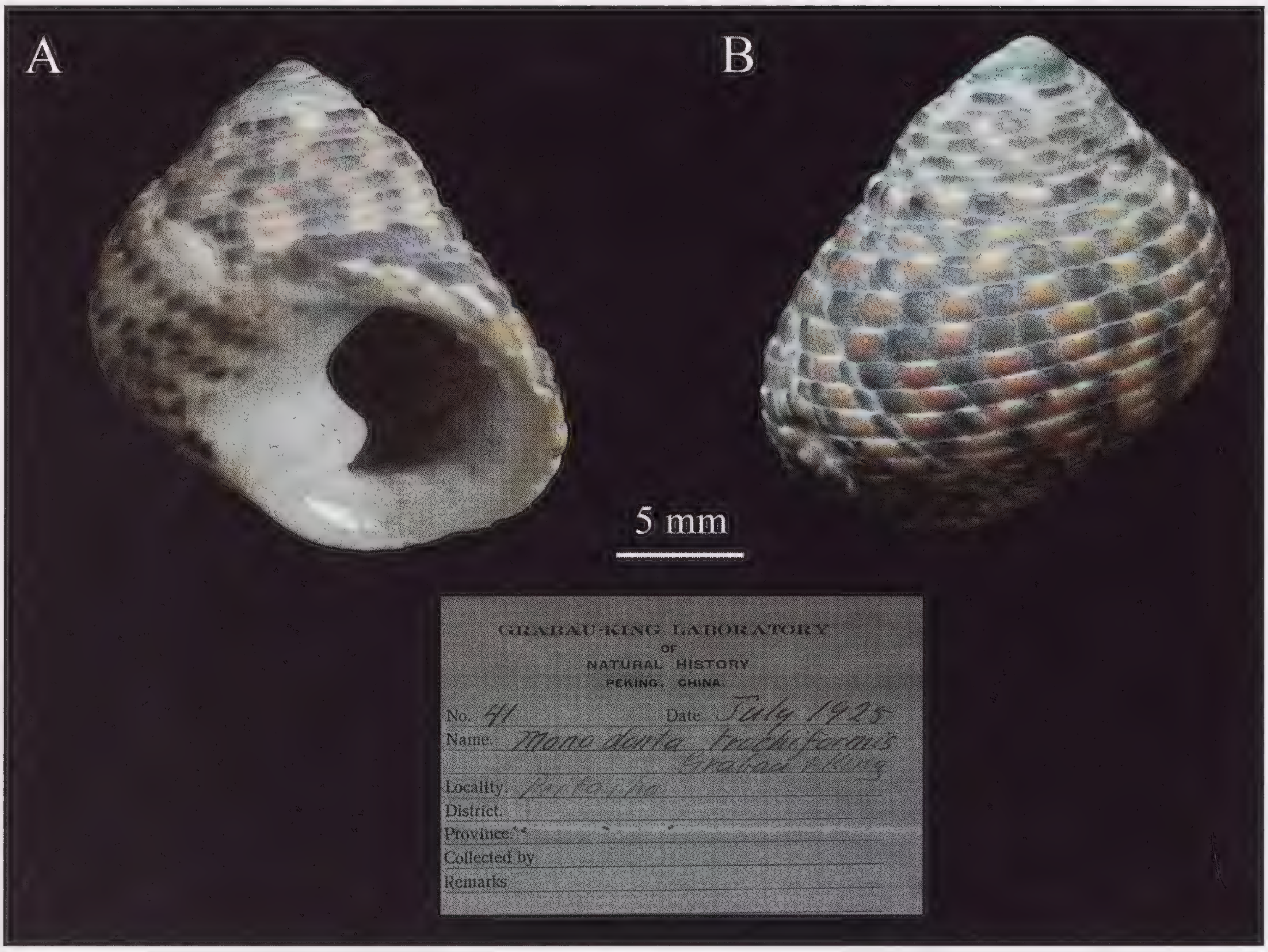

GRABAU-KING LABORATORY
OF
NATURAL HISTORY
PEKING, CHINA.

No. 41 Date July 1925
Name. Mono donta trochiformis Grabau & King
Locality. Peitaiho
District.
Province.
Collected by
Remarks

FIG. 23A, B. *Monodonta trochiformis* Grabau & King. MBM280640, syntype, length = 19.0 mm.

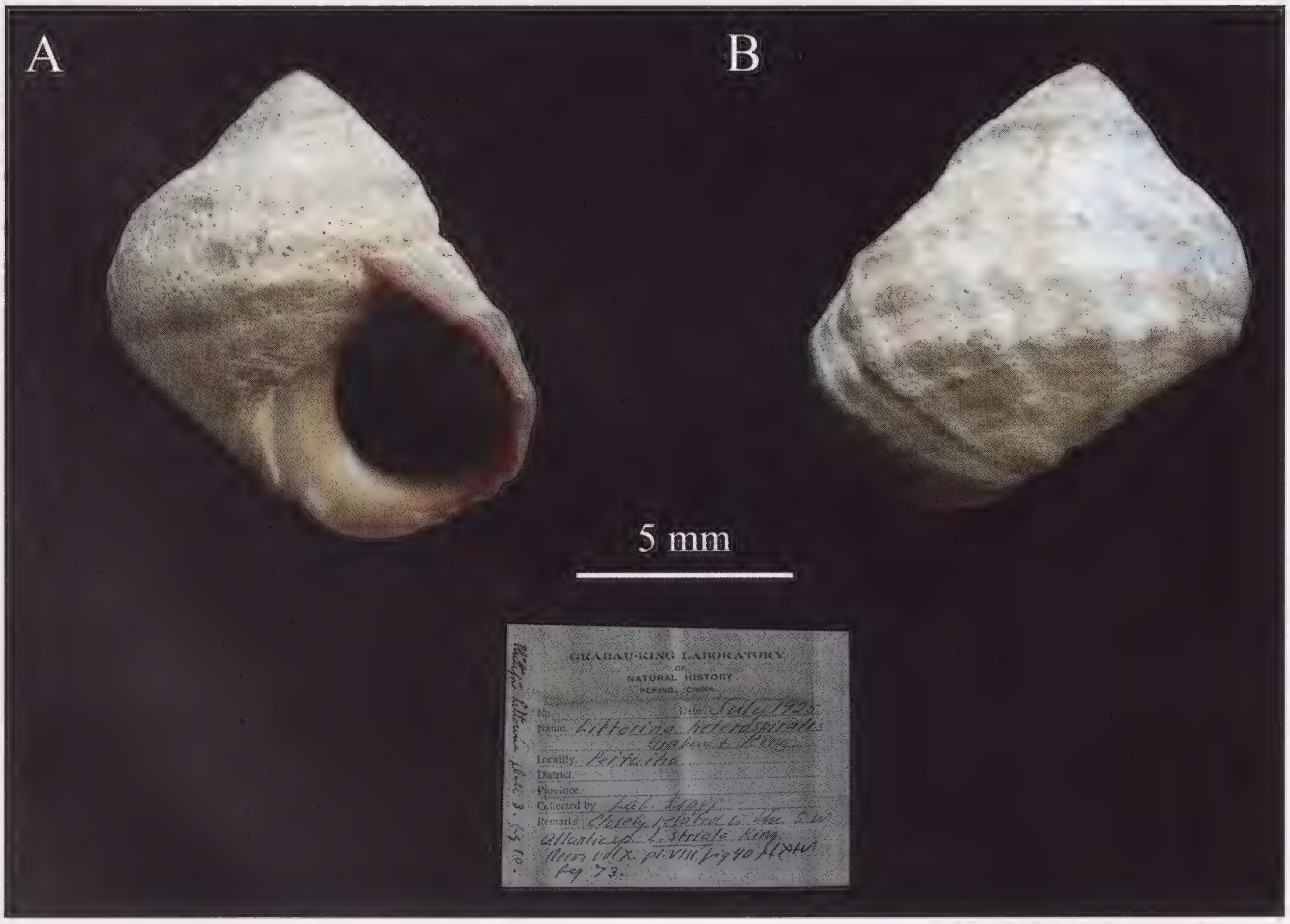

Philippi Littorina plate 3, fig 10.

GRABAU-KING LABORATORY
OF
NATURAL HISTORY
PEKING, CHINA.

No. Date July 1925
Name. Littorina heterospiralis Grabau & King
Locality. Peitaiho
District.
Province.
Collected by Lab. Staff
Remarks. Closely related to the [illegible] atlantic sp. L. striata King [illegible] vol X. pl. VIII fig 40 pl. XIV fig 73.

FIG. 24A, B. *Littorina heterospiralis* Grabau & King. MBM280647, syntype, length = 10.7 mm.

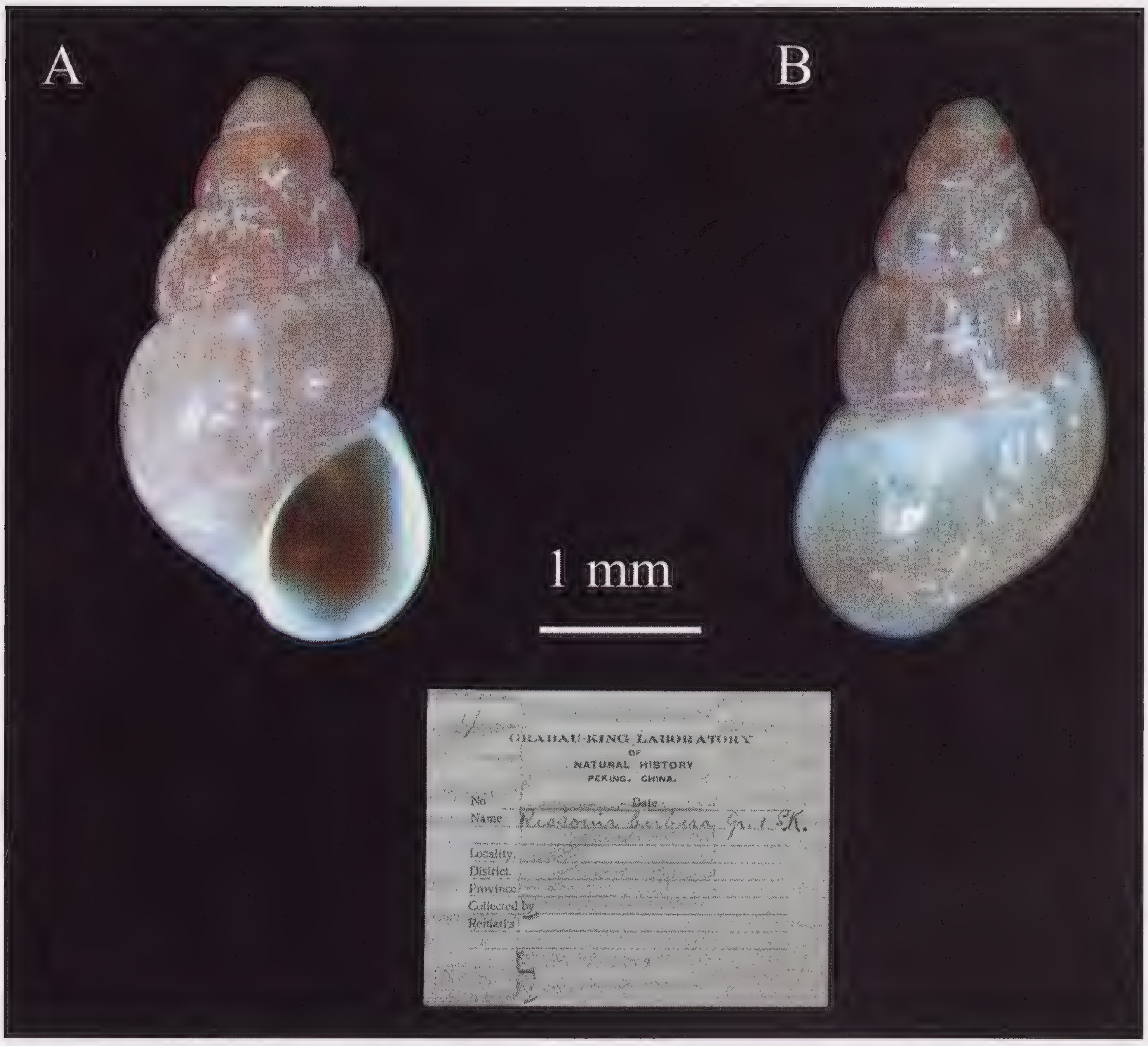

GRABAU-KING LABORATORY
OF
NATURAL HISTORY
PEKING, CHINA.
No Date
Name Rissoina barbara G. & K.
Locality
District
Province
Collected by
Remarks

FIG. 25A, B. *Rissoina barbara* Grabau & King. MBM280646, syntype, length = 2.76 mm.

Family Rissoidae Gray, 1847

Rissoina barbara
Grabau & King, 1928
Figure 25A, B

Rissoina barbara Grabau & King, 1928d: 34; 1928e: 57; 1928f: 132–133, 230–231, 275, pl. 10, fig. 105.

Material Examined
Syntypes, MBM280646 (ex GKLNH, 80 shells), no collection information.

Modern Status
Rissoina barbara Grabau & King, 1928, or possibly a synonym of *Alvania concinna* (A. Adams, 1861) (T. Haga, pers. commun., July 2014).

Rissoina dunedini
Grabau & King, 1928
Figure 26A, B

Rissoina dunedini Grabau & King, 1928d: 34; 1928e: 57; 1928f: 133 [as "*R. dunedoni*"; corrected on errata sheet], 231, 275, pl. 10, fig. 106.

Material Examined
Syntypes, MBM280645 (ex GKLNH, 6 shells), no collection information.

Modern Status
Synonym of *Barleeia angustata* (Pilsbry, 1901) (T. Haga, pers. commun., July 2014; S. Zhang, pers. commun., October 2014).

Remarks

Regarded by Zhao et al. (1982: 31–32, pl. 4, fig. 2) as a distinct species.

Rissoina nelsoni
Grabau & King, 1928
Figure 27A, B

Rissoina nelsoni Grabau & King, 1928d: 34; 1928e: 57; 1928f: 231, 275, pl. 10, fig. 107.

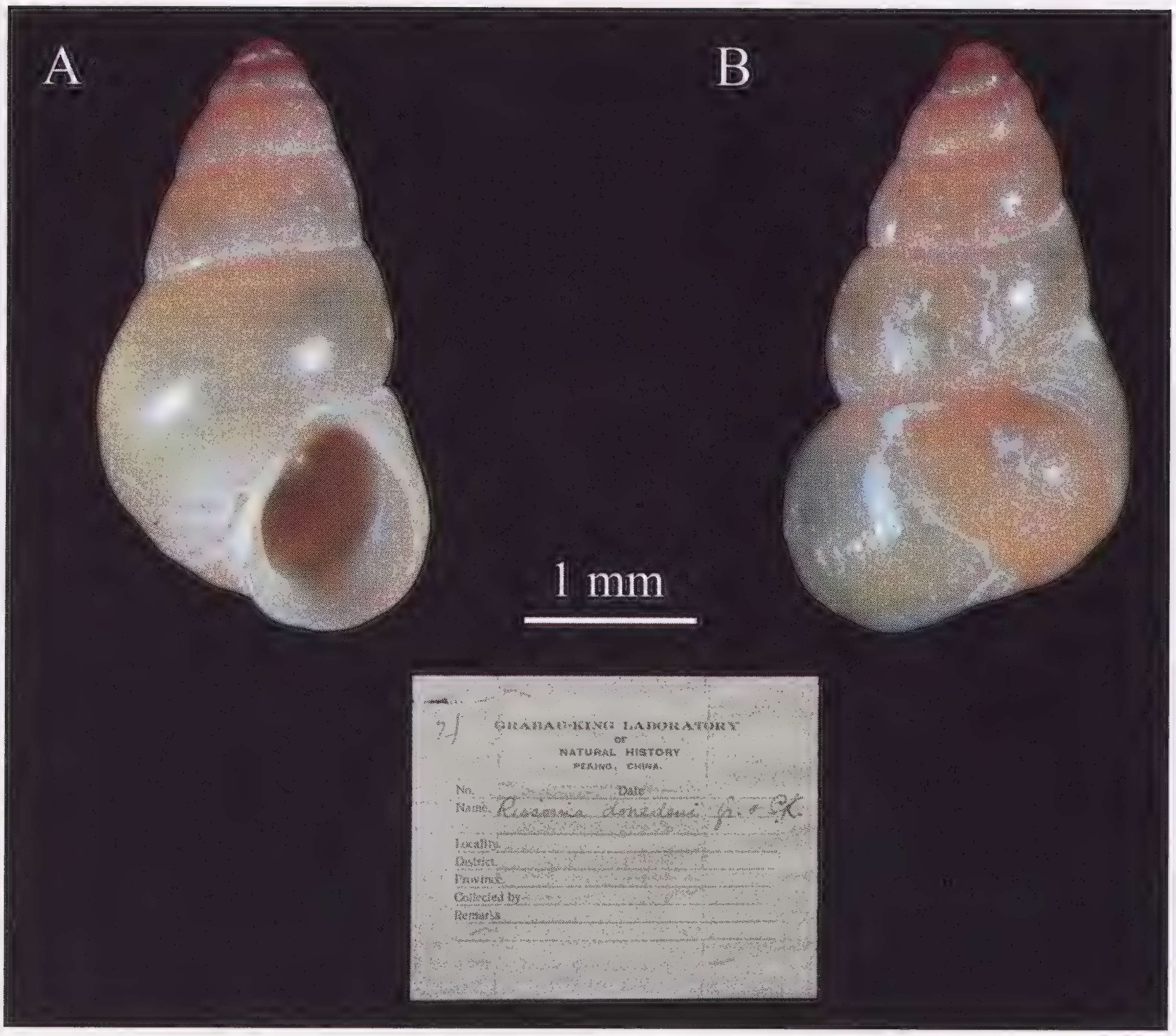

71
GRABAU-KING LABORATORY
OF
NATURAL HISTORY
PEKING, CHINA.
No. Date
Name *Rissoina dunedini sp. n. G.K.*
Locality
District
Province
Collected by
Remarks

FIG. 26A, B. *Rissoina dunedini* Grabau & King. MBM280645, syntype, length = 2.40 mm.

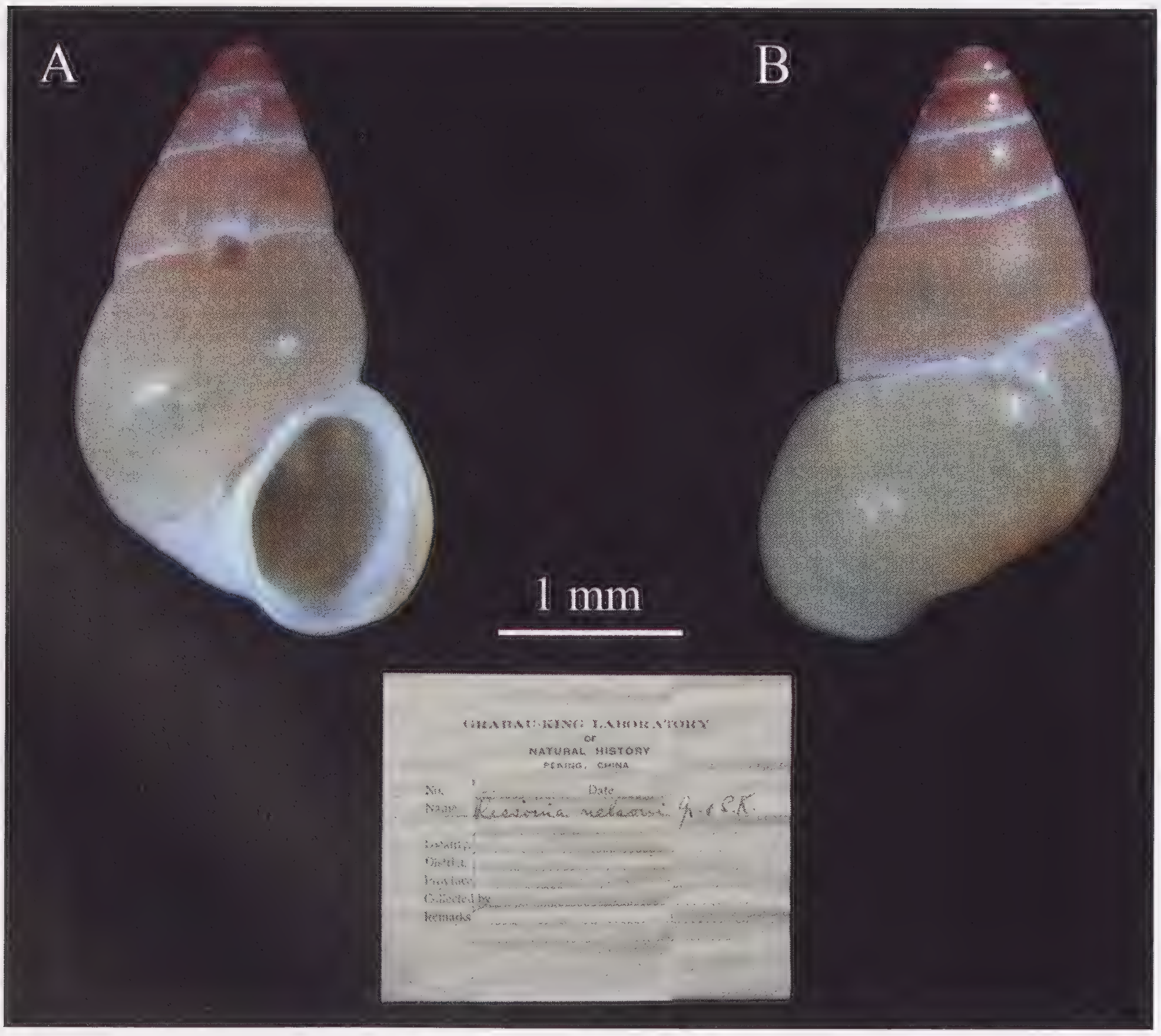

GRABAU-KING LABORATORY
OF
NATURAL HISTORY
PEKING, CHINA
No. Date
Name *Rissoina nelsoni sp. n. G.K.*
Locality
District
Province
Collected by
Remarks

FIG. 27A, B. *Rissoina nelsoni* Grabau & King. MBM280644, syntype, length = 2.20 mm.

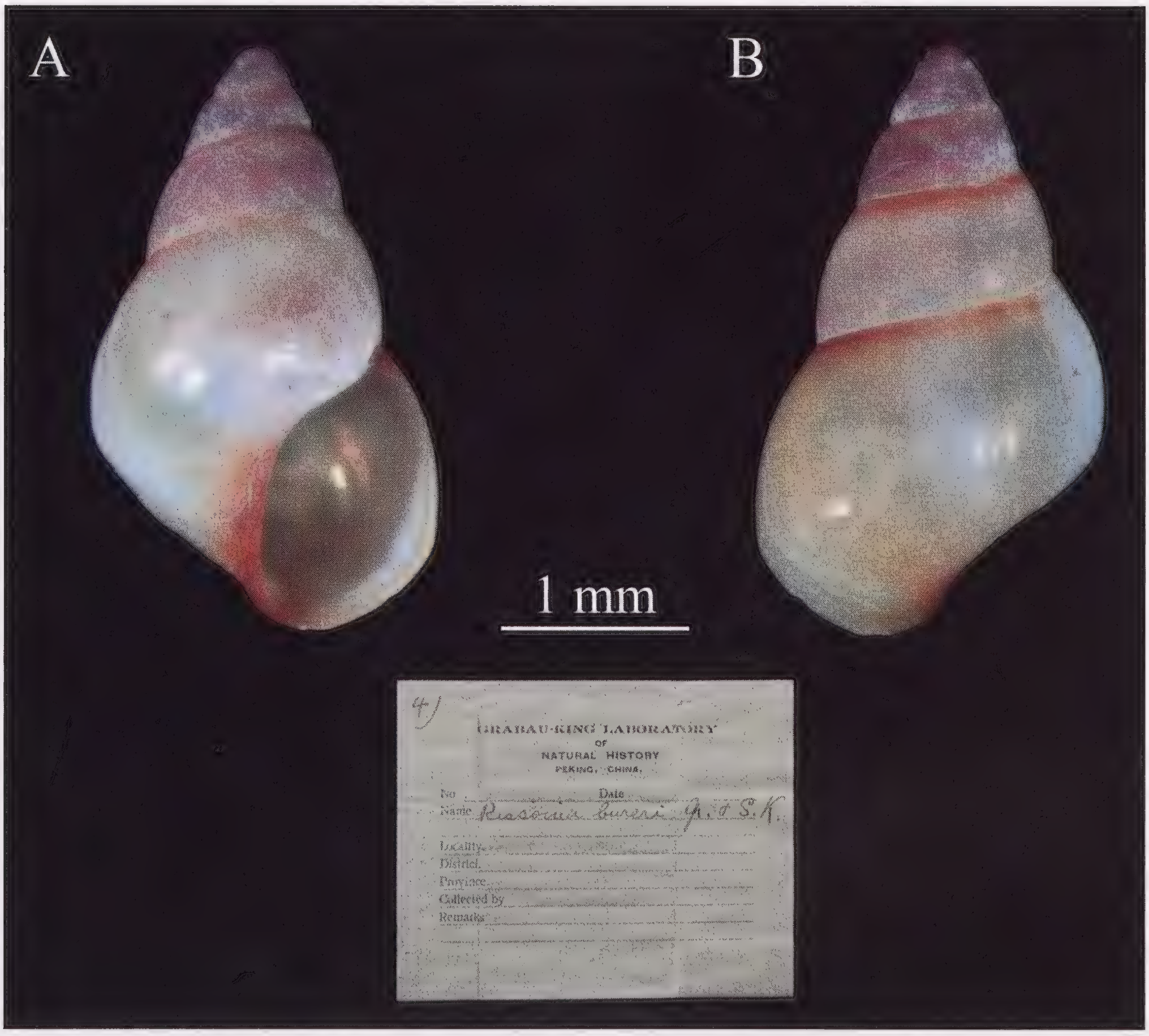

FIG. 28A, B. *Rissoina bureri* Grabau & King. MBM280643, syntype, length = 2.74 mm.

Material Examined

Syntypes, MBM280644 (ex GKLNH, 13 shells), no collection information.

Modern Status

Synonym of *Barleeia angustata* (Pilsbry, 1901) (T. Haga, pers. commun., July 2014; S. Zhang, pers. commun., October 2014).

Rissoina bureri
Grabau & King, 1928
Figure 28A, B

Rissoina bureri Grabau & King, 1928d: 34; 1928e: 57; 1928f: 133, 231–232, 275, pl. 10, fig. 108.

Material Examined

Syntypes, MBM280643 (ex GKLNH, 4 shells), no collection information.

Modern Status

Rissoina bureri Grabau & King, 1928 (Zhao et al., 1982: 32, pl. 4, fig. 1; Qi et al., 1989: 34, text-figs. 32 & 33; Qi, 2004: 36, pl. 15H).

Family Calyptraeidae Lamarck, 1809

Crepidula ostraeiformis
Grabau & King, 1928
Figure 29A, B

Crepidula ostraeiformis Grabau & King, 1928d: 38; 1928e: 61; 1928f: 142–143, 232, 275, pl. 10, fig. 109.

Material Examined

Syntypes, MBM229001 (ex GKLNH, 27 shells), no collection information.

Modern Status
Synonym of *Siphopatella walshi* (Reeve, 1859) (syn. nov. herein).

Family Eulimidae Philippi, 1853

Eulima bilineata
Grabau & King, 1928
Figure 30A, B

Eulema [sic; pro *Eulima*] *bilineata* Grabau & King, 1928d: 36, *non* Alder, 1848, *non* A. Adams & Reeve, 1850; 1928e: 59; 1928f: 138, 215, 270, pl. 9, fig. 81.

Material Examined
Syntypes, MBM280650 (ex GKLNH, 3 shells), Peitaiho.

Modern Status
Qi et al. (1989: 43, text-fig. 36) listed it as a synonym of *Eulima bifascialis* (A. Adams, 1863). However, it seems to be both a junior homonym and a synonym of *Eulima bilineata* A. Adams & Reeve, 1850. However, the latter itself requires a replacement name, best done in the context of a comprehensive review of this genus.

Family Epitoniidae Berry, 1910 [1812]

Epitonium (*Scalaria*) *pretiosa* var. *minor*
Grabau & King, 1928
Figure 31A, B

Scalaria pretiosa [Lamarck, 1816] *minor* Grabau & King, 1928d: 35; 1928e: 58; 1928f:

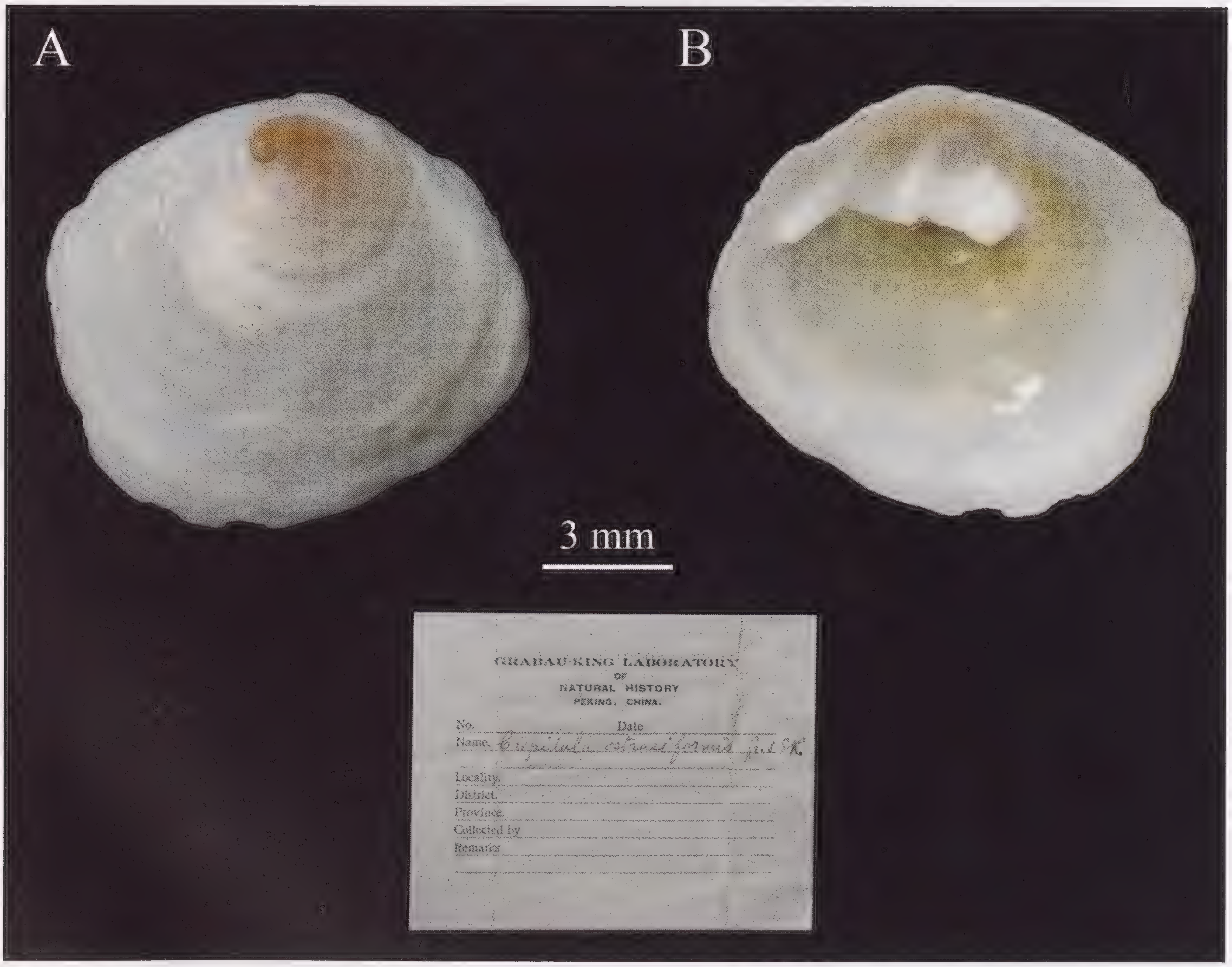

FIG. 29A, B. *Crepidula ostraeiformis* Grabau & King. MBM229001, syntype, length = 10.0 mm, width = 11.1 mm.

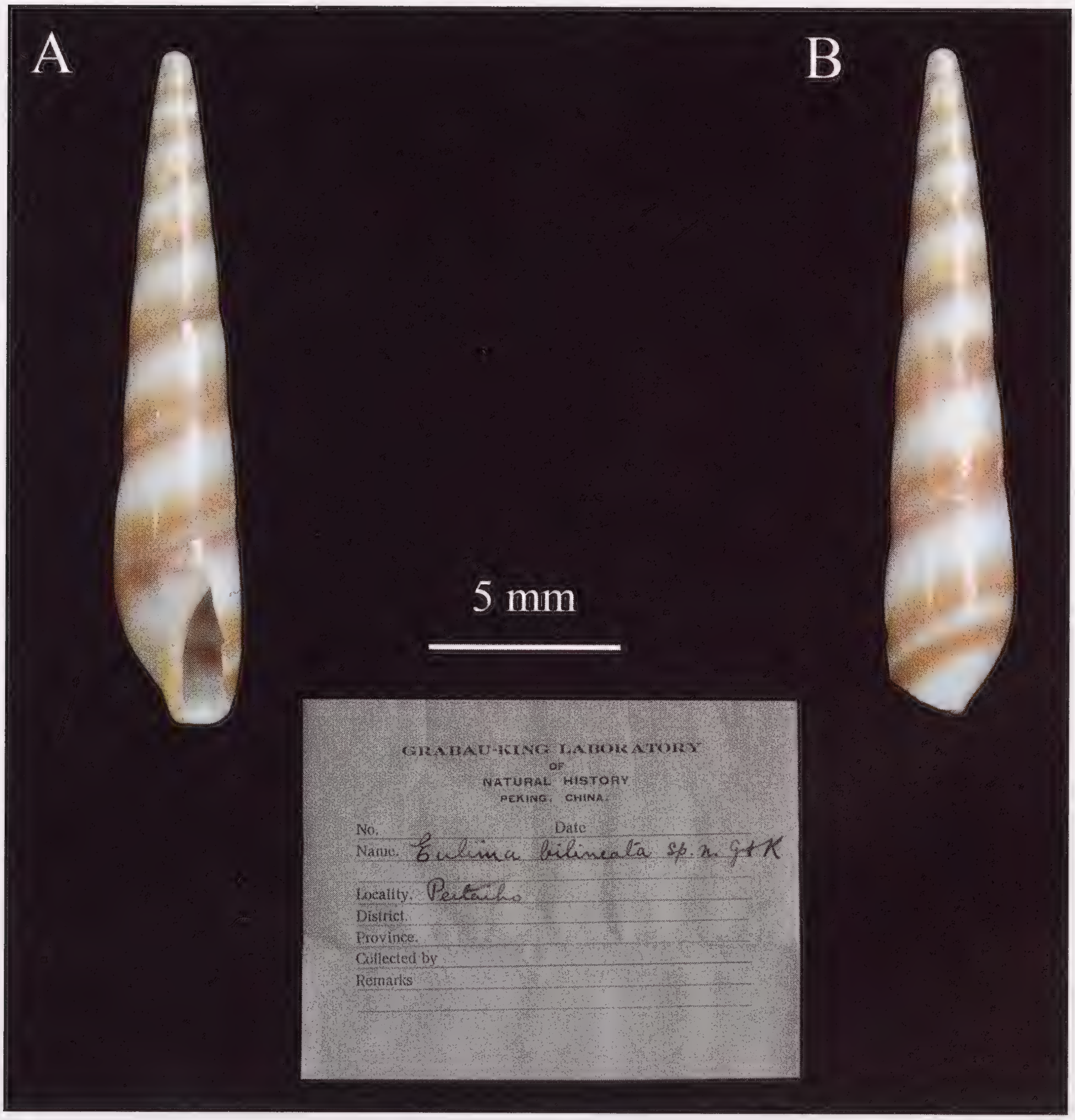

GRABAU-KING LABORATORY
OF
NATURAL HISTORY
PEKING, CHINA.
No. Date
Name. Eulima bilineata sp. n. G&K
Locality. Peitaiho
District.
Province.
Collected by
Remarks

FIG. 30A, B. *Eulima bilineata* Grabau & King. MBM280650, syntype, length = 10.6 mm.

135–136, 226–227, 274, pl. 10, fig. 98 [as *Epitonium* (*Scalaria*)].

Material Examined
Syntypes, MBM280648 (ex GKLNH, 7 shells), Peitaiho, July 1925.

Modern Status
Epitonium scalare minor Garbau & King, 1928 (Qi et al., 1989: 80, pl. 5, fig. 3; Qi, 2004: 131, pl. 78C).

Epitonium (*Scalaria*) *gradata* var. *pygmaea* Grabau & King, 1928

Scalaria gradata [G. B. Sowerby II, 1844, ex Hinds ms] *pygmaea* Grabau & King, 1928d: 36; 1928e: 58–59; 1928f: 137, 227–228, 274, pl. 10, fig. 100 [as *Epitonium* (*Scalaria*)].

Material Examined
Not found.

Modern Status
Gradatiscala gradata pygmaea (Grabau & King, 1928) (Qi et al., 1989: 81–82, pl. 5, fig. 13; Qi, 2004: 132, fig. 78I).

Epitonium (*Scalaria*) *subtilis* var. *laevis* Grabau & King, 1928

Scalaria subtilis [G. B. Sowerby II, 1844] *oevis* Grabau & King, 1928d: 36; 1928e: 59; 1928f: 137, 228, 274, pl. 10, fig. 101a, b [as *Epito-*

nium (*Scalaria*) *subtilis laevis* throughout]. It is clear from the original account that the spelling "*oevis*" was a typographical error – "but in the present variety, this crenulation is scarcely marked", and it was so corrected in their last account.

Material Examined

Not found.

Modern Status

Synonym of *Acrilla acuminata* (G. B. Sowerby II, 1844) (Qi et al., 1989: 85, pl. 5, fig. 20).

Family Muricidae Rafinesque, 1815

Rapana pechiliensis
Grabau & King, 1928
Figure 32A–D

Rapana pechiliensis Grabau & King, 1928c: 324; 1928e: 46; 1928f: 202, 268, pl. 8, fig. 62.

Material Examined

MBM258933 (ex MZFIBCS, 1 shell), Yantai and Beidaihe [= Peitaiho]. MBM258597 (MBM-CAS, 1 shell) collected on December 8, 1952, Tsingtao [Qingdao], identified by Tchang.

Modern Status

Synonym of *Rapana venosa* (Valenciennes, 1846) (Zhao et al. 1982: 55–56, pl. 6, fig. 9, pl. 2, fig. 34; Qi et al., 1989: 55–56, pl. 2, fig. 6).

Remarks

This name was listed by many authors, including Yen (1936: 243–244, pl. 22, fig. 55), Tchang et al. (1955: 19, pl. 4, fig. 1–3, text-fig. 15), Higo et al. (1999: 215) and Okutani (2000: 399) as a subspecies of *Rapana venosa* (Valenciennes, 1946). Zhang (1980) studied the distribution, ecology and morphology of this species and concluded that Grabau & King's taxon was a synonym of *Rapana venosa*. This was confirmed by quantitative study of Yang et al. (2006).

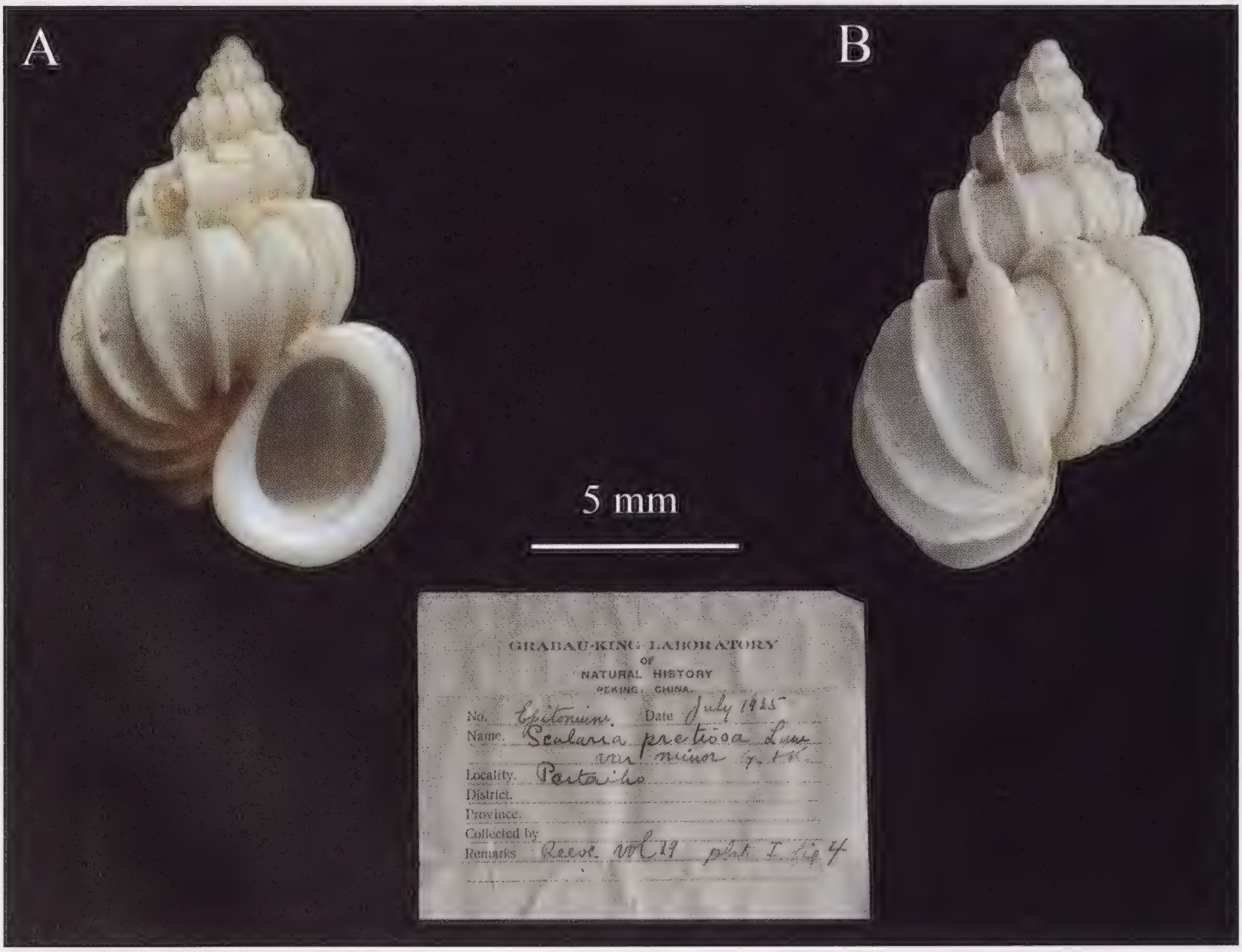

GRABAU-KING LABORATORY
OF
NATURAL HISTORY
PEKING, CHINA.
No. Epitonium. Date July 1915
Name. Scalaria pretiosa Lam
var minor G. & K.
Locality. Peitaiho
District.
Province.
Collected by
Remarks Reeve vol 19 plt. I fig 4

FIG. 31A, B. *Epitonium* (*Scalaria*) *pretiosa* var. *minor* Grabau & King. MBM280648, syntype, length = 12.8 mm.

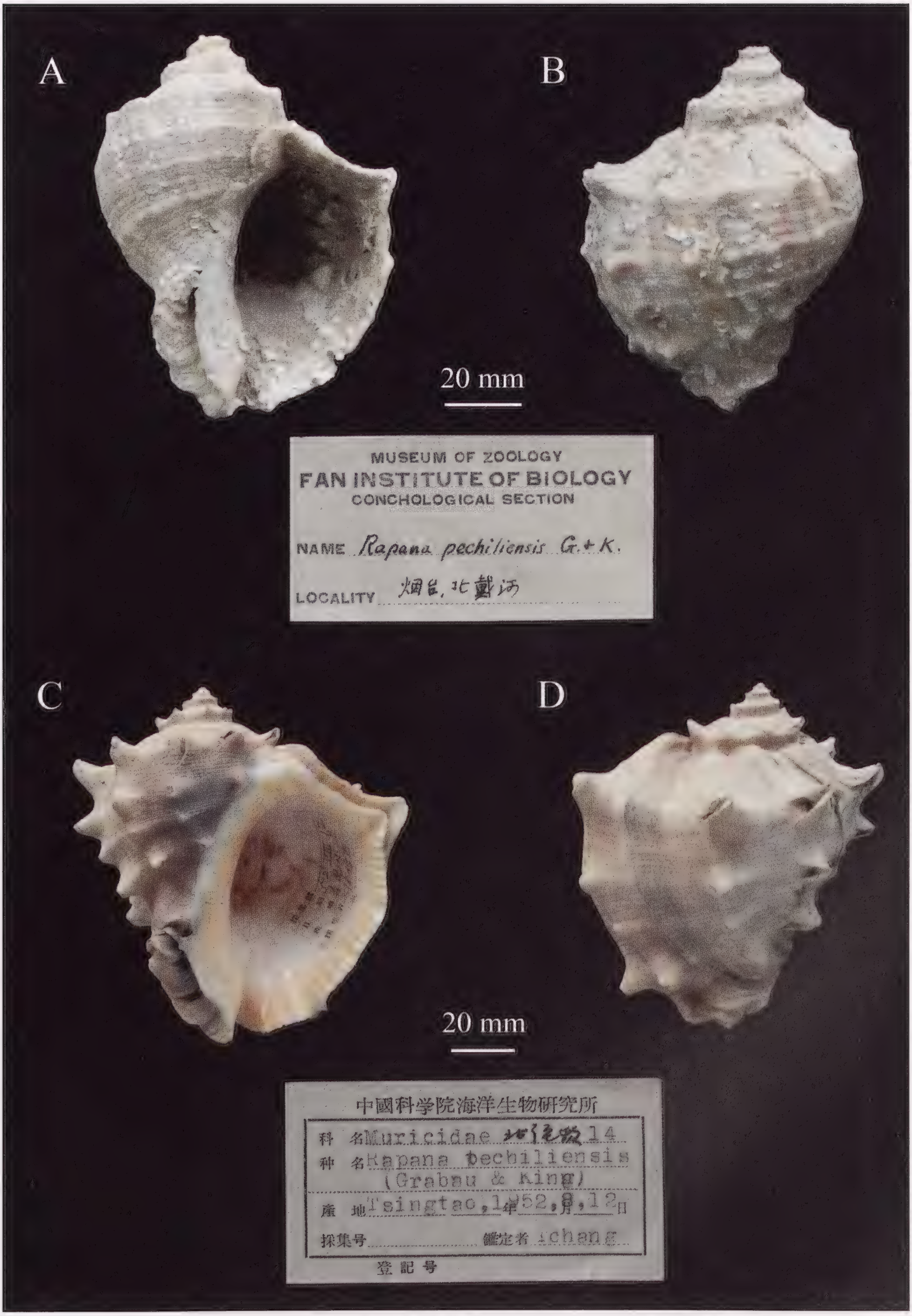

MUSEUM OF ZOOLOGY
FAN INSTITUTE OF BIOLOGY
CONCHOLOGICAL SECTION

NAME *Rapana pechiliensis G.+K.*
LOCALITY 烟台, 北戴河

中國科学院海洋生物研究所
科 名 Muricidae [illegible] 14
种 名 Rapana pechiliensis (Grabau & King)
產 地 Tsingtao, 1952 年 8 月 12 日
採集号 鑑定者 Tchang
登記号

FIG. 32A–D. *Rapana pechiliensis* Grabau & King. A, B: MBM258933, length = 87.7 mm; C, D: MBM258597, length = 105.5 mm.

Purpura alveolata var. *pechiliensis* Grabau & King, 1928
Figure 33A, B

Purpura alveclata [sic; *alveolata* Reeve, 1846] var. *pechiliensis* Grabau & King, 1928c: 325; 1928e: 47; 1928f: 108–109, 203, 268, pl. 8, fig. 64.

Material Examined
Syntypes, MBM258837 (ex GKLNH, 9 shells), Peitaiho, July 1925.

Modern Status
Synonym of *Thais clavigera* (Küster, 1860) (Qi et al., 1989: 56–57, pl. 1, fig. 5).

Purpura bronni Dunker var. *suppressa* Grabau & King, 1928
Figure 34A–D

Purpura bronni [Dunker, 1860] var. *suppressa* Grabau & King, 1928c: 325; 1928e: 47; 1928f: 108.
Purpura bronii [sic] [Dunker, 1860] var. *suppressa* Grabau & King, 1928f: 204, 268, pl. 8, fig. 66.

Material Examined
Syntypes, MBM280653 (ex GKLNH, 4 shells), no collection information.

Modern Status
Synonym of *Thais luteostoma* (Holten, 1803) (Qi et al., 1989: 57, pl. 8, fig. 7).

Remarks

Earlier authors merely repeated the original combination but in a different genus, *Thais bronni suppressa* (Grabau & King) (Yen, 1936: 238–239, pl. 21, figs. 52, 52a; Zhao et al., 1982: 58, pl. 4, fig. 5).

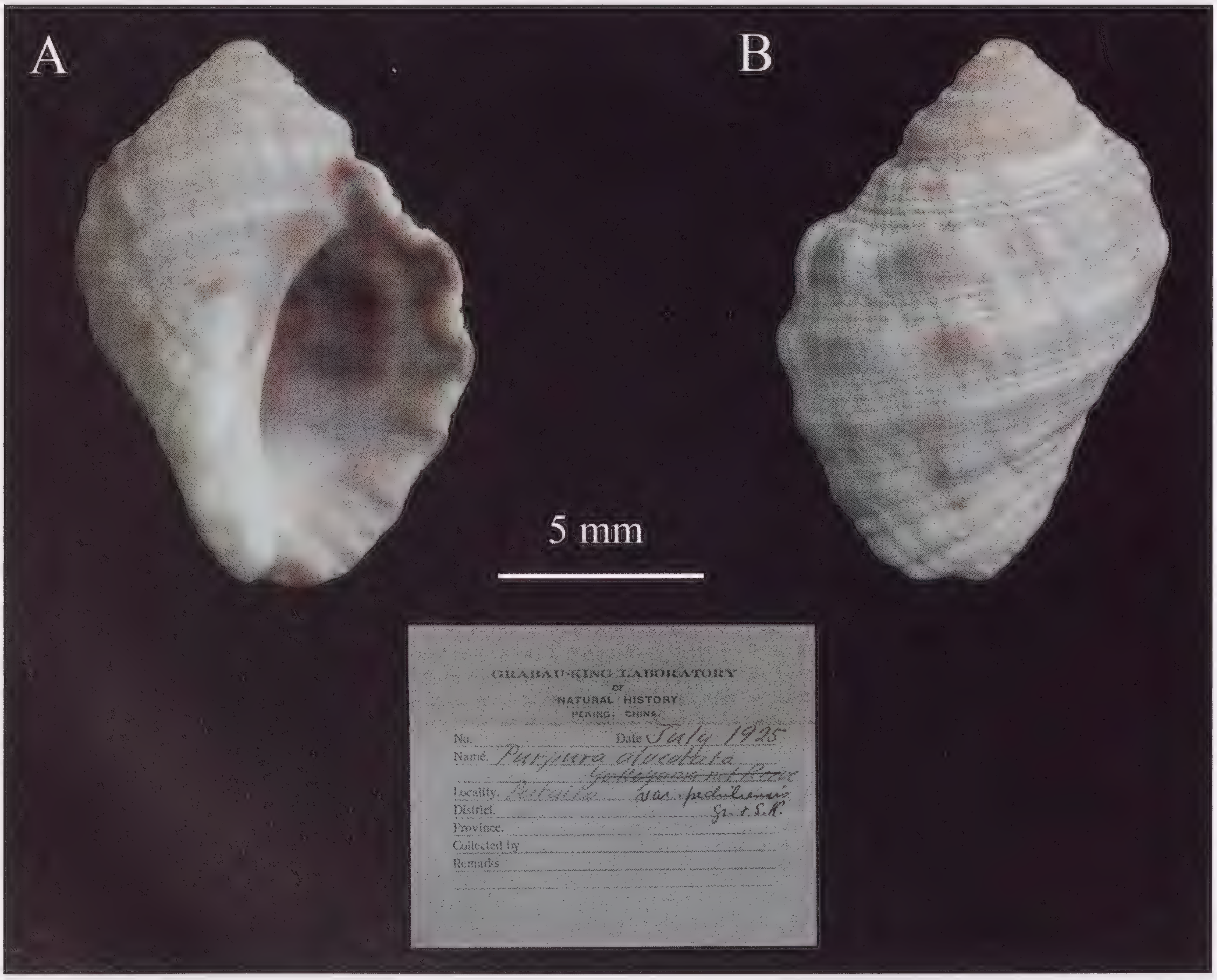

GRABAU-KING LABORATORY
OF
NATURAL HISTORY
PEKING, CHINA.

No. Date July 1925
Name. Purpura alveolata
~~[illegible]~~
Locality. Peitaiho var. pechiliensis
District. Gr. & S.K.
Province.
Collected by
Remarks

FIG. 33A, B. *Purpura alveolata* var. *pechiliensis* Grabau & King. MBM258837, syntype, length = 20.4 mm.

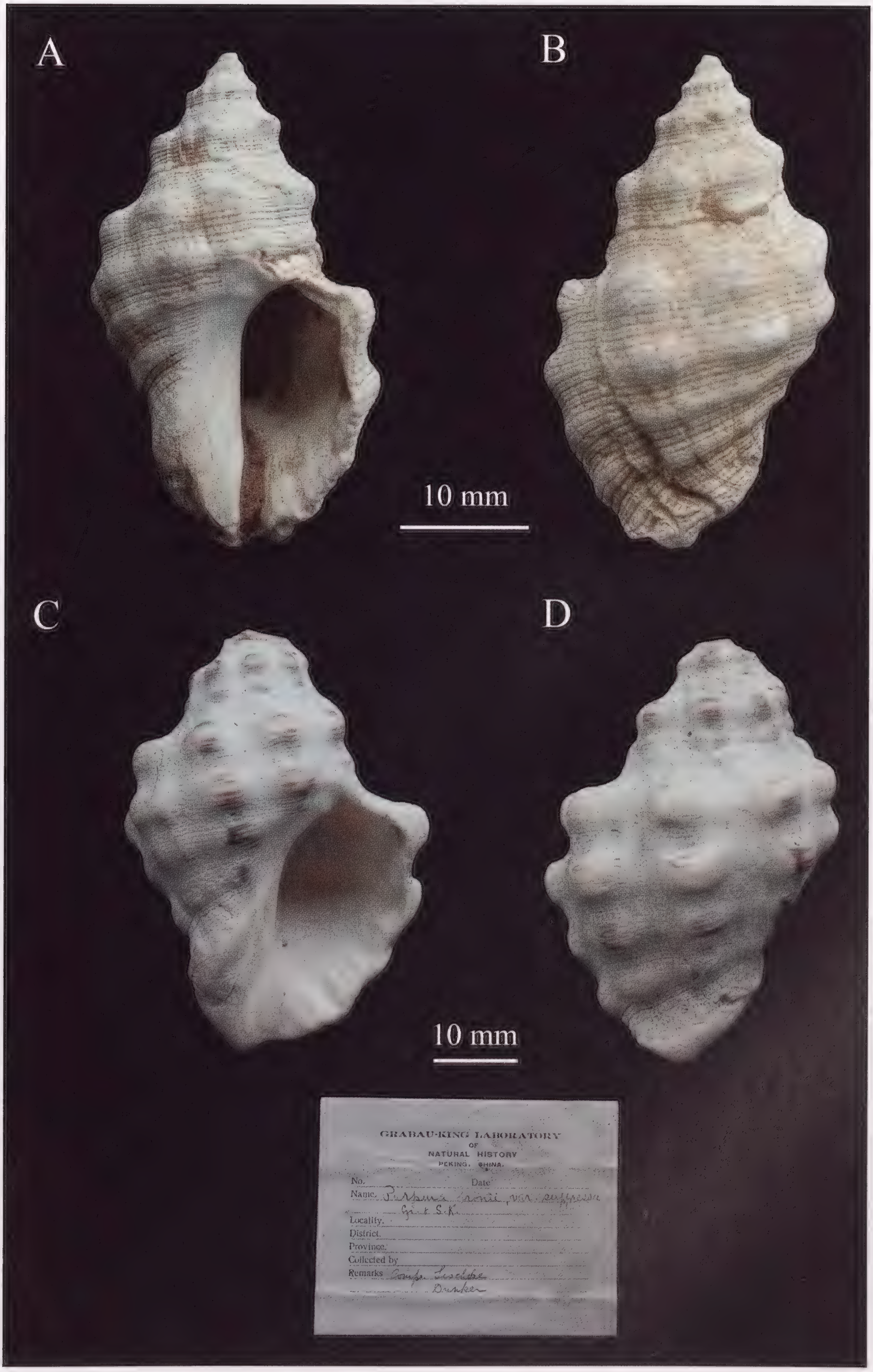

GRABAU-KING LABORATORY
OF
NATURAL HISTORY
PEKING, CHINA.

No. Date
Name. Purpura bronii, var. suppressa
Gr. + S.K.
Locality.
District.
Province.
Collected by
Remarks Comp. Lischke
Dunker

FIG. 34A–D. *Purpura bronni* var. *suppressa* Grabau & King. MBM280653, syntype, length = 47.1 mm.

Purpura altispiralis
Grabau & King, 1928
Figure 35A, B

Purpura altispiralis Grabau & King, 1928c: 326; 1928e: 47–48; 1928f: 110, 204–205, 268, pl. 8, fig. 67.

Material Examined
Syntypes, MBM258524 (ex GKLNH, 44 shells), Peitaiho.

Modern Status
Synonym of *Thais clavigera* (Küster, 1860) (Qi et al., 1989: 56–57, pl. 1, fig. 5).

Family Nassariidae Iredale, 1916 [1835]

Nassa gregaria
Grabau & King, 1928

Nassa gregaria Grabau & King, 1928c: 328; 1928e: 50; 1928f: 115, 207, 268, pl. 8, fig. 71.

Material Examined
Not found.

Modern Status
Nassarius gregarius (Grabau & King, 1928).

Remarks

Cernohorsky (1984: 176–178, pl. 37, figs. 1–14) regarded this species as a synonym of *Nassarius* (*Hima*) *pauper* (Gould, 1850). On the other hand, Qi et al. (1989: 70, pl. 7, fig. 2) and Qi (2004: 99, pl. 59J) thought this species was valid. Kool & Dekker (2006: 63) examined the synonyms of *Nassarius* (*Hima*) *pauper* (Gould, 1850) and also regarded *Nassarius gregarius* (Grabau & King, 1928) as a distinct species.

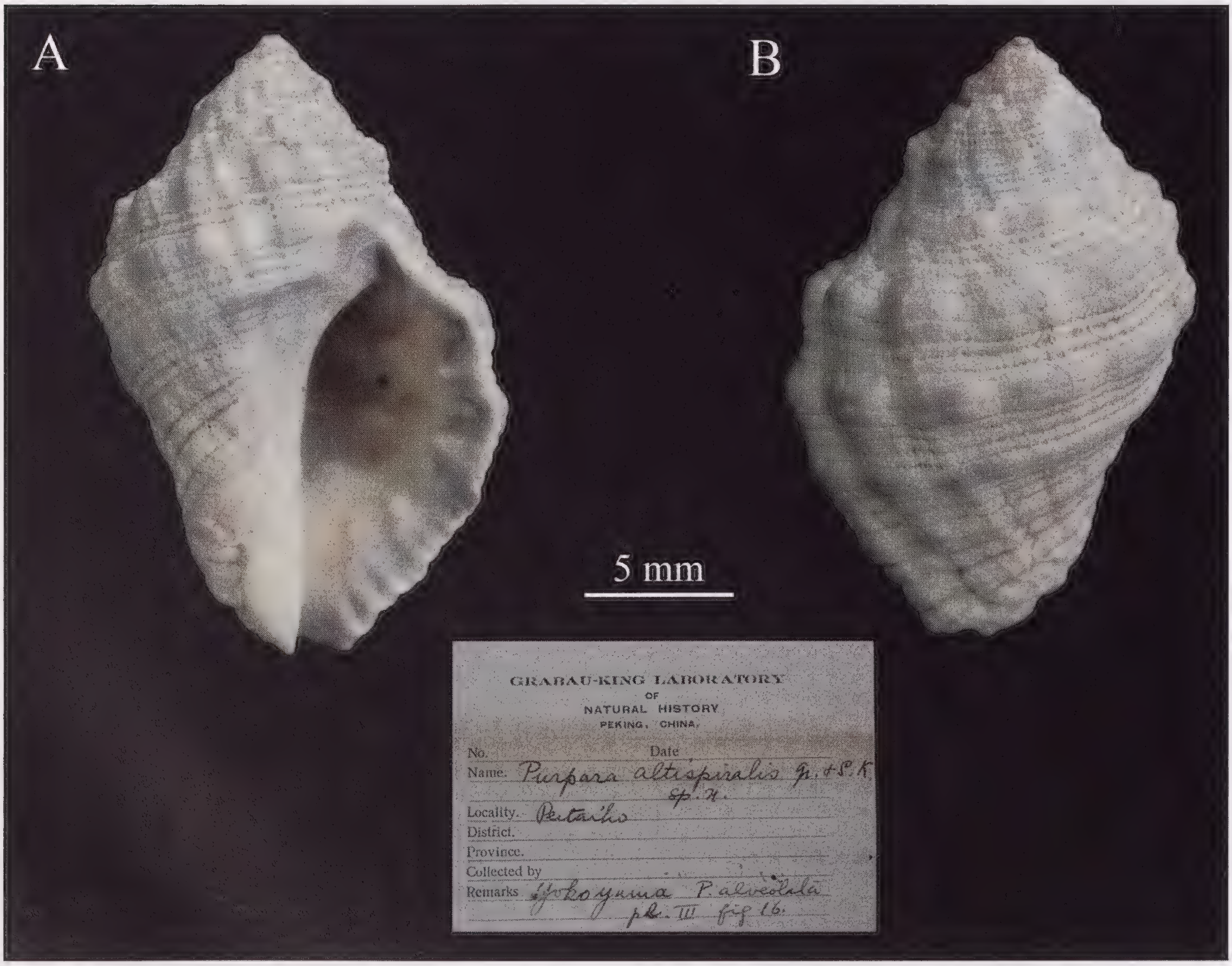

GRABAU-KING LABORATORY
OF
NATURAL HISTORY
PEKING, CHINA.

No. Date
Name. Purpara altispiralis Gr. & S.K sp. n.
Locality. Peitaiho
District.
Province.
Collected by
Remarks Yokoyama P. alveolata pl. III fig 16.

FIG. 35A, B. *Purpura altispiralis* Grabau & King. MBM258524, syntype, length = 20.4 mm.

Family Terebridae Mörch, 1852

Terebra bellanodosa
Grabau & King, 1928
Figure 36A, B

Terebra "*ballanodosa*" [error pro "*bellanodosa*"] Grabau & King, 1928c: 330; 1928e: 51–52; 1928f: 119, 214, 270, pl. 9, fig. 80, as *T. bellanodosa* [Terebridae]. It is clear from the original account – "This is the beautifully noded *Terebra*" – that the spelling "*balla*" was intended to be "*bella*", and it was so corrected in the 1928f treatment.

Material Examined

Syntypes, MBM280652 (ex GKLNH, 12 shells), Peitaiho, July 1925.

Modern Status

Regarded by Bratcher & Cernohorsky (1987: 229) as a *nomen dubium*, it instead seems to be a distinct species, *Terebra bellanodosa* Grabau & King, 1928 (Zhao et al., 1982: 71, pl. 2, fig. 29; Qi et al., 1989: 79, pl. 8, fig. 10; Qi, 2004: 129, pl. 77I & text-fig. 29). Other material of the same species in the MBM collection has an additional Grabau & King ms name.

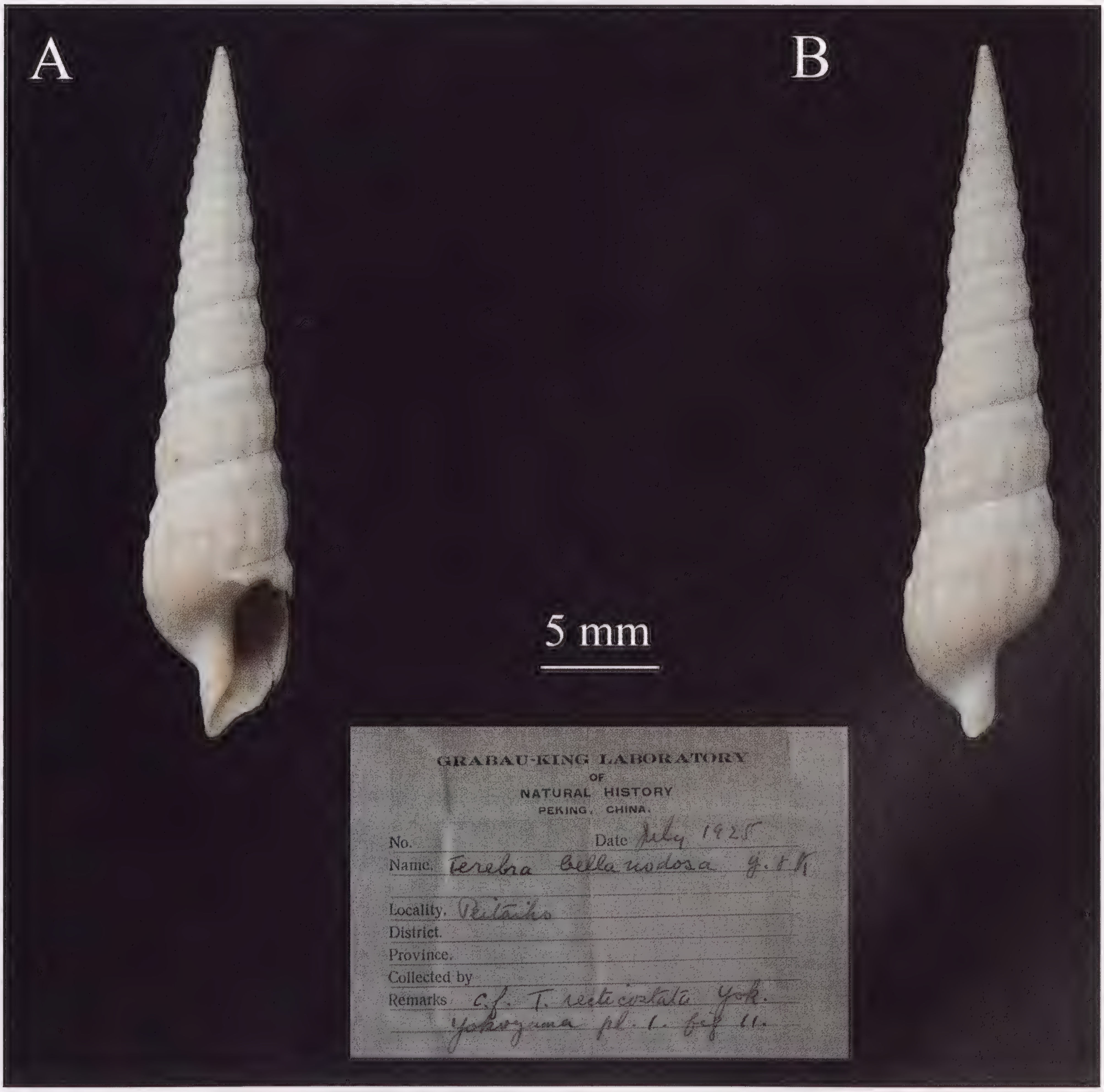

GRABAU-KING LABORATORY
OF
NATURAL HISTORY
PEKING, CHINA.

No. Date July 1925
Name. Terebra bellanodosa G. & K
Locality. Peitaiho
District.
Province.
Collected by
Remarks c.f. T. recticostata Yok.
Yokoyama pl. 1. fig 11.

FIG. 36A, B. *Terebra bellanodosa* Grabau & King. MBM280652, syntype, length = 29.7 mm.

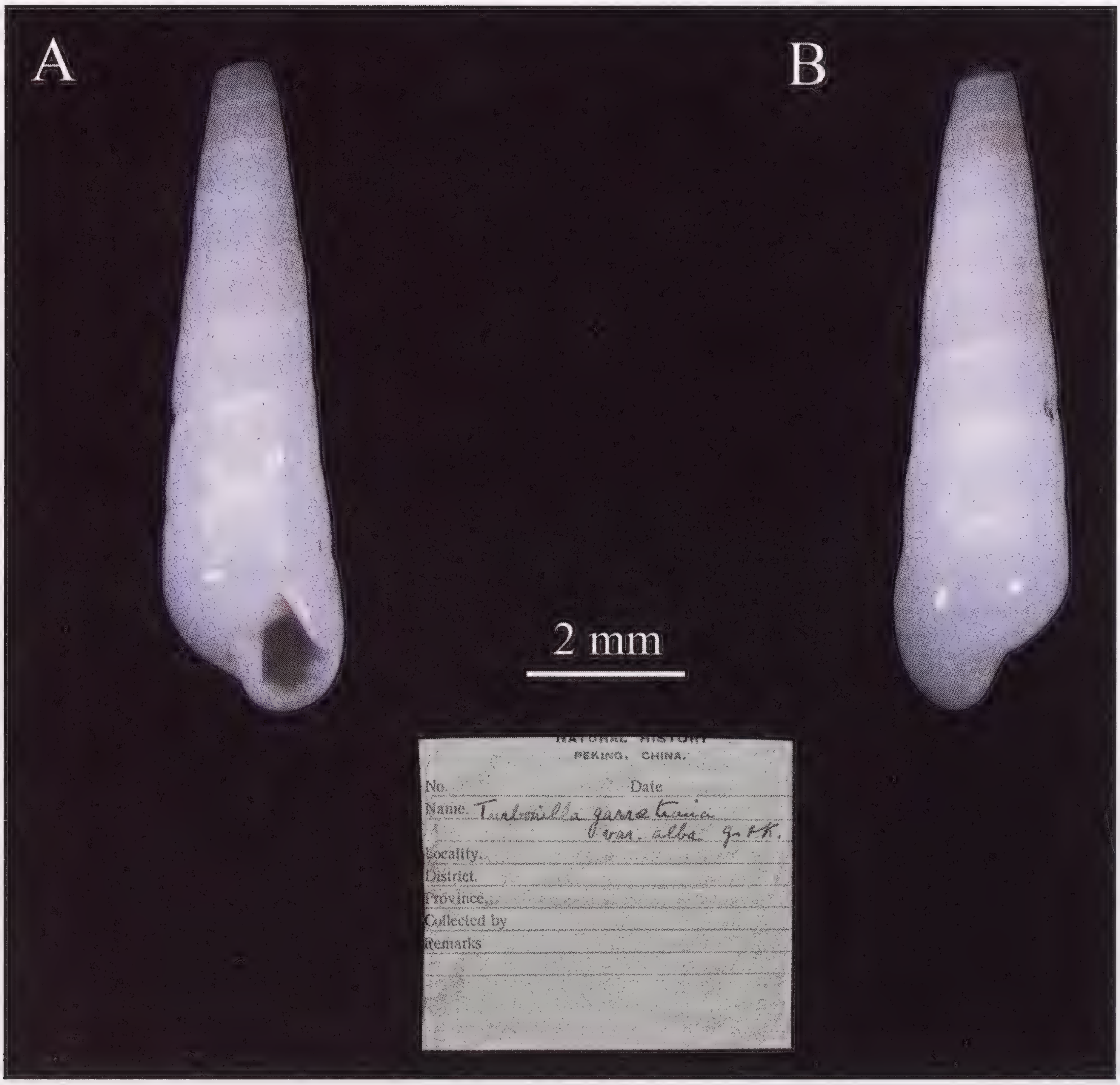

FIG. 37A, B. *Turbonilla garrettiana* var. *alba* Grabau & King. MBM280649, syntype, length = 9.3 mm.

Family Mangeliidae P. Fischer, 1883

Mangelia dobsoni Grabau & King, 1928

Mangelia dobsoni Grabau & King, 1928d: 32; 1928e: 55; 1928f: 126, 220, 270, pl. 9, fig. 91.

Material Examined

Not found.

Modern Status

Mangelia dobsoni Grabau & King, 1928.

Remarks

Qi et al. (1989: 75–76) mentioned that *M. costulata* illustrated by Grabau & King (1928f: pl. 9, fig. 90) was not Dunker's (1860) species. However, the figure of *M. dobsoni* (Grabau & King, 1928f: pl. 9, fig. 91) was remarkably similar to the real *M. costulata* (Dunker, 1860).

Family Pyramidellidae Gray, 1840

Turbonilla garrettiana var. *alba* Grabau & King, 1928
Figure 37A, B

Turbonilla garrettiana [Dall & Bartsch, 1906] *alba* Grabau & King, 1928d: 37; 1928e: 59–60; 1928f: 139, 217, 270, pl. 9, fig. 85.

Material Examined

Syntypes, MBM280649 (ex GKLNH, 21 shells), no collection information.

Modern Status

Nomen dubium; probably a *Mormula* and unrelated to *Turbonilla* (*Chemnitzia*) *garrettiana* (pers. commun., P. I. LaFollette, 10 May 2014).

Family Siphonariidae Gray, 1827

Siphonaria alterniplicata
Grabau & King, 1928
Figure 38A, B

Siphonalia [sic; pro *Siphonaria*] *alterniplata* Grabau & King, 1928d: 39; 1928e: 62; 1928f: 145, 237, 278, pl. 11, fig. 117a–c.

Material Examined

Syntypes, MBM280642 (ex GKLNH, 72 shells), Peitaiho, July 1925.

Modern Status

Synonym of *Siphonaria japonica* (Donovan, 1834) (Qi et al., 1989: 143–144, text-fig. 110).

ACKNOWLEDGEMENTS

This work was supported by the National Natural Science Foundation of China under Grant No. 41306159 and IOCAS funding under Grant No. 2012IO060104. We also thank Markus Huber, Henk K. Dijkstra, Patrick I. LaFollette, and Suping Zhang for their help. Paul Valentich-Scott made some editorial suggestions on an earlier draft, and reviewers Alan R. Kabat, Rüdiger Bieler and Takuma Haga made many useful comments. Andreia Salvador of The Natural History Museum in London kindly supplied images of two A. Adams type specimens for comparisons.

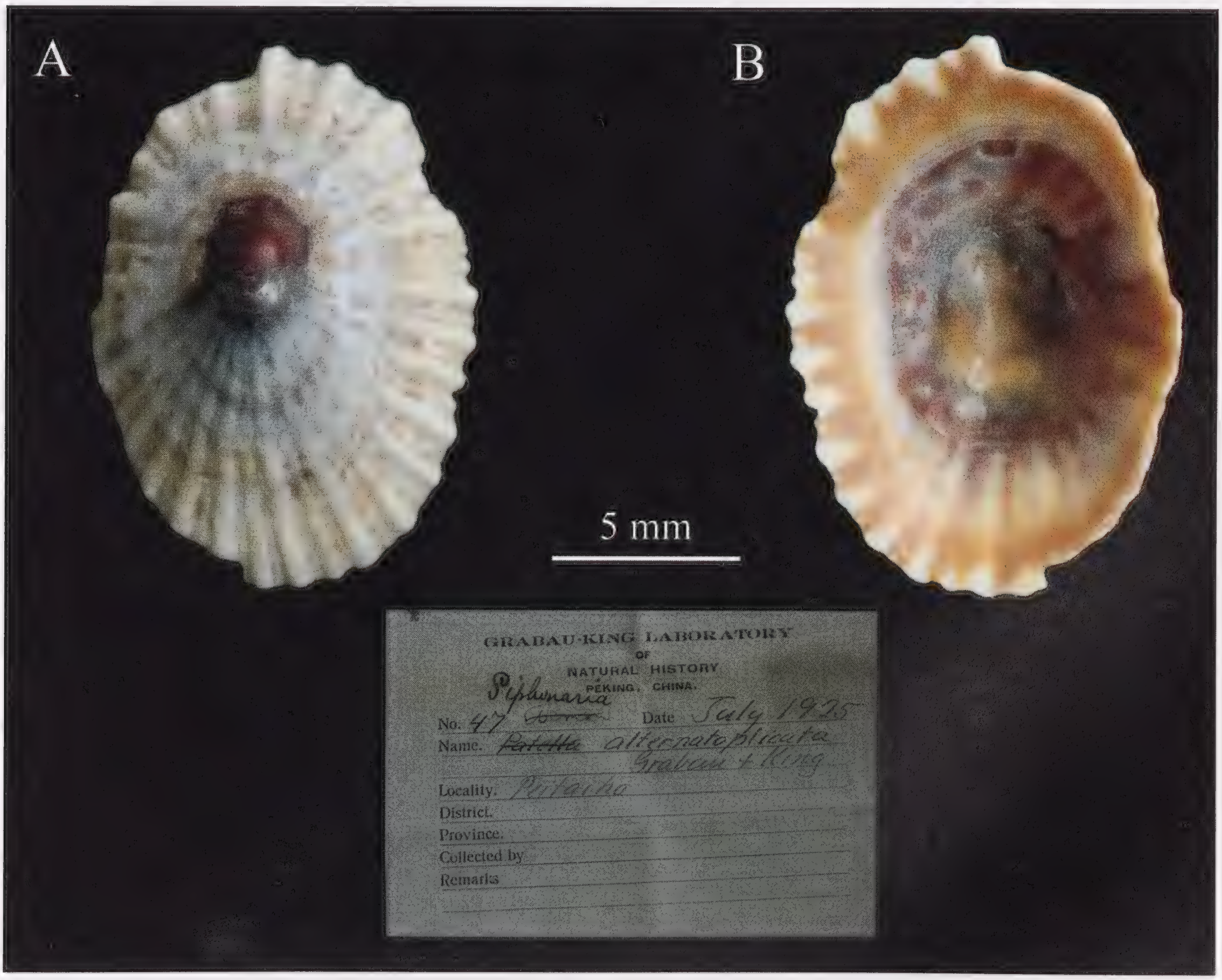

GRABAU-KING LABORATORY
OF
NATURAL HISTORY
PEKING, CHINA.
Siphonaria
No. 47 Date July 1925
Name. ~~Patella~~ alternatoplicata
Grabau & King
Locality. Peitaiho
District.
Province.
Collected by
Remarks

FIG. 38A, B. *Siphonaria alterniplicata* Grabau & King. MBM280642, syntype, length = 14.2 mm.

LITERATURE CITED

ANONYMOUS, 1936a, *Who's who in China: biographies of Chinese leaders*, 5th ed. Shanghai, The China Weekly Review, 315 pp.

ANONYMOUS, 1936b. Library of conchology. *Nature*, 138(3481): 110.

ANTON, H. E., 1838, *Verzeichniss der Conchylien welch sich in der Sammlung von H. E. Anton befinden*. Anton, Halle, xiv + 110 pp.

BERNARD, F. R., Y.-Y. CAI & B. MORTON, 1993, *Catalogue of the living marine bivalve molluscs of China*. Hong Kong University Press, Hong Kong, 146 pp.

BORN, I., 1778, *Index rerum naturalium Musei Cesarei Vindobonensis, pars I. Testacea*. Vendobonae, Krausiana, [xliii] + 458 + [80] + [2] pp., 1 pl.

BRATCHER, T. & W. O. CERNOHORSKY, 1987, *Living terebras of the world. A monograph of the recent Terebridae of the world*. American Malacologists, Melbourne, Florida & Burlington, Massachusetts, 240 pp.

CERNOHORSKY, W. O., 1984, Systematics of the family Nassariidae (Mollusca: Gastropoda). *Bulletin of the Auckland Institute and Museum*, 14: 1–356.

CHOE, B. L., W. KIM, J. R. LEE & S. H. YOON, 1994, Pteriomorphia (Mollusca: Bivalvia) from Ullung Island, Korea. *Korean Journal of Systematic Zoology*, 10(1): 61–83.

COSEL, R. VON, 2002, Seven new species of *Solen* (Bivalvia: Solenidae) from the tropical western Pacific, with remarks on other species. Pp. 301–341, pls. 31–38, in: M. FALKNER, K. GROH & C. D. SPEIGHT, eds., *Collectanea Malacologica. Festschrift für Gerhard Falkner*. Conchbooks, Friedrich-Held-Gesellschaft, Hackenheim & München, 10 + 547 pp. + 48 pls.

DALL, W. H. & P. BARTSCH, 1906, Notes on Japanese, Indo-Pacific, and American Pyramidellidae. *Proceedings of the United States National Museum*, 30(1452): 321–369, pls. 17–26.

DUNKER, W., 1860, Neue japanische Mollusken. *Malakologische Blätter*, 6(4): 221–240.

EVSEEV, G. A. & K. A. LUTAENKO, 1998, Bivalves of the subfamily Anadarinae (Arcidae) from Vietnam. *Malacological Review*, Suppl. 7: 1–37.

GRABAU, A. W., 1927, Shells of the China coast. *Bulletin of the Peking Society of Natural History*, 1(4): xliv–xlvii.

GRABAU, A. W., 1928, The significance of the so-called ornamental characters in the molluscan shell. *Bulletin of the Peking Society of Natural History*, 2(4): xxvii–xxxvi.

GRABAU, A. W. & S. G. KING, 1927a, Shells of Peitaiho. Chapter I. Introduction. *The China Journal of Science and Arts*, 6 (4): 189–197 (April).

GRABAU, A. W. & S. G. KING, 1927b, Shells of Peitaiho. Chapter II. Types of shells and shell-like structures found at Peitaiho. *The China Journal of Science and Arts*, 6(5): 252–255 (May).

GRABAU, A. W. & S. G. KING, 1927c, Shells of Peitaiho. Chapter III. Chief Characters of the Molluscan Shell. *The China Journal of Science and Arts*, 6 (6): 318–330 (June).

GRABAU, A. W. & S. B. KING, 1928a, Shells of Peitaiho. Chapter IV. Common bivalve or pelecypod shells of the Peitaiho beaches. *The China Journal of Science and Arts*, 8(1): 30–39 (January).

GRABAU, A. W. & S. B. KING, 1928b, Shells of Peitaiho. Chapter IV. Continued. *The China Journal of Science and Arts*, 8(2): 94–102 (February).

GRABAU, A. W. & S. G. KING, 1928c, Shells of Peitaiho. Chapter V. Common univalves or gastropods of the Peitaiho beaches. *The China Journal of Science and Arts*, 8(6): 320–332 (June).

GRABAU, A. W. & S. G. KING, 1928d, Shells of Peitaiho. Chapter V. Continued. *The China Journal of Science and Arts*, 9(1): 31–41 (July).

GRABAU, A. W. & S. G. KING, 1928e, *Shells of Peitaiho*. Compiled and reprinted as Peking Society of Natural History Educational Handbooks 2: 64 pp (presumably later than July).

GRABAU, A. W. & S. G. KING, 1928f, *Shells of Peitaiho*, 2nd ed. Peking Society of Natural History, Hand-Book No. 2: vi + 279 + [1 – Errata] pp., 11 pls. (presumably later than July 1928 and later than 1928e).

GRAY, J. E., 1850, On the species of Anomiadae. *Proceedings of the Zoological Society of London*, for 1849[17](197): 113–124, pl. 4.

HABE, T., 1951, *Genera of Japanese shells*. Pelecypoda. No. 1: [ii] + 96 pp.

HABE, T., 1965, The arcid subfamily Anadarinae in Japan and its adjacent areas (Mollusca). *Bulletin of the National Science Museum*, Tokyo, 8(1): 71–85, 3 pls.

HABE, T., 1977, *Systematics of Mollusca in Japan. Bivalvia and Scaphopoda*. Hokuryukan, Tokyo, xiii+ 372 + [4] pp., 72 pls. [in Japanese].

HABE, T., 1981, Bivalvia. In: A catalogue of molluscs of Wakayama Prefecture, the Province of Kii. I. Bivalvia, Scaphopoda and Cephalopoda. *Publications of the Seto Marine Biological Laboratory, Special Publication Series*, 7, N 1: 25–222.

HANLEY, S. C. T., 1846, A description of new species of *Ostreae*, in the collection of H. Cuming, Esq. *Proceedings of the Zoological Society of London*, for 1845[13](152): 105–107.

HIGO, S., P. CALLOMON & Y. GOTO, 1999. *Catalogue and bibliography of the marine shell-bearing Mollusca of Japan. Gastropoda. Bivalvia. Polyplacophora. Scaphopoda*. Elle Scientific Publications, Osaka, 749 pp.

HIGO, S., P. CALLOMON & Y. GOTO, 2001, *Catalogue and bibliography of the marine shell-bearing Mollusca of Japan. Gastropoda, Bivalvia, Polyplacophora, Scaphopoda: type figures*. Elle Scientific Publications, Osaka, 208 pp.

HUBER, M., 2010, *Compendium of bivalves*. ConchBooks, Hackenheim, Germay, 901 pp. + CD with searchable version of chapter 6 and Excel file.

INABA, A., K. TORIGOE & Y. OTANI, 2004, Oysters of the world. Part 2. Systematic descriptions of Recent oysters. *Nishinomiya Shell Museum, Bulletin*, 3: 63 + 10 pp., 13 pls.

KING, S. G., 1926, Notes on the fossils [sic] shells of the Sanmen Series. *Bulletin of the Geological Society of China*, 5(1–2): 157–160 (March).

KING, S. G. & C. PING, 1931a, The molluscan shells of Hong Kong. Part I. *The Hong Kong Naturalist*, 2(1): 9–29 (February).

KING, S. G. & C. PING, 1931b, The molluscan shells of Hong Kong. Part II. *The Hong Kong Naturalist*, 2(4): 265–286 (November).

KING, S. G. & C. PING, 1933, The molluscan shells of Hong Kong. Part III. *The Hong Kong Naturalist*, 4(2): 90–105 (December).

KING, S. G. & C. PING, 1935, Notes on a new *Dentalium* from Peitaiho. *The Chinese Journal of Zoology*, 1: 103–106 (May).

KING, S. G. & C. PING, 1936, The molluscan shells of Hong Kong. Part IV. *The Hong Kong Naturalist*, 7(2): 123–137 (June).

KOOL, H. H. & H. DEKKER, 2006, Review of the *Nassarius pauper* (Gould, 1850) complex (Gastropoda: Nassariidae). Part 1, with the description of four new species from the Indo-West-Pacific. *Visaya*, 1(6): 54–75.

KURODA, T., T. HABE & K. OYAMA, 1971, *The sea shells of Sagami Bay collected by His Majesty the Emperor of Japan.* Maruzen, Tokyo, xiv + 741 pp. [Japanese] + 489 pp. [English] + 51 pp. [Index], 121 pls.

LAMARCK, [J. B. P. A. DE M.] DE, 1816, Liste des objets représentés dans les planches de cette livraison. Part 23. In: *Tableau encyclopédie et méthodique des trois regnes de la nature.* Paris, 16 pp.

LAMARCK, J. B. P. A. DE M. DE, 1818, *Histoire naturelle des animaux sans vertébres, ...* 5. Deterville & chez l'auteur, Paris, Verdière, 612 pp.

LAMPRELL, K. & J. HEALY, 1998, *Bivalves of Australia*, Vol. 2. Backhuys Publishers, Leiden, 288 pp.

LI, X.-X. & Z.-Y. QI, 1994, Studies on the comparative anatomy, systematic classification and evolution of Chinese oysters. *Studia Marina Sinica*, 35: 143–178 [Chinese with English abstract].

LISCHKE, C. E., 1869–1874, *Japanische Meeres-Conchylien. Ein Beitrag zur Kenntniss der Mollusken Japan's, mit besonderer Rücksicht auf die geographische Verbreitung derselben.* Fischer, Cassel [1: 192 pp., 14 pls., 1869; 2: 184 pp., 14 pls., 1871; 3: 123 pp., 9 pls., 1874].

LUTAENKO, K. A. & I. E. VOLVENKO, 2013, On the fauna of bivalve mollusks of Hong Kong (South China Sea). *Bulletin of the Russian Far East Malacological Society*, 17: 79–141 [in Russian with English abstract].

LUTAENKO, K. A. & F.-S. XU, 2008, A catalogue of types of bivalve mollusks in the Marine Biological Museum, Chinese Academy of Sciences (Qingdao). *Bulletin of the Russian Far East Malacological Society*, 12: 42–70.

MANZUR, A., 2004, *A romance in natural history. The lives and works of Amadeus Grabau and Mary Antin.* Garret, Syracuse, New York, viii + 484 pp.

MÜLLER, O. F., 1776, *Zoologiae Danicae prodromus, seu animalium Daniae et Norvegiae indigenarum characteres, nomina, et synonyma imprimis popularium.* Hallageriis, Havniae, xxxii + 274 pp.

NODA, H., 1966, The Cenozoic Arcidae of Japan. *Science Reports of the Tohoku University*, Second Series (Geology), 38(1): 1–163.

OKUTANI, T., ed., 2000, *Marine mollusks in Japan.* Tokai University Press, Tokyo, Japan, xlviii + 1175 pp., incl. 542 pls.

OYAMA, K., 1973, Revision of Matajiro Yokoyama's type Mollusca from the Tertiary and Quaternary of the Kanto area. *Palaeontological Society of Japan, Special Papers*, 17: 148 pp., 57 pls.

QI, Z.-Y., ed., 2004, *Seashells of China.* China Ocean Press, Beijing, China, viii + 418 pp., 193 pls.

QI, Z.-Y., X.-T. MA, Z.-R. WANG, G.-Y. LIN, F.-S. XU, Z.-Z. DONG, F.-L. LI & D.-H. LV, 1989, Mollusca of Huanghai and Bohai. China Agricultural Press, Beijing, xiv + 309 pp., 13 pls. [in Chinese].

RAINES, B. K. & G. T. POPPE, 2006, *The family Pectinidae.* In: G. T. POPPE & K. GROH, eds., *A conchological iconography.* Conchbooks, Hackenheim, Germany, 402 pp., 320 pls.

REEVE, L.A., 1843–1844, Monograph of the genus *Arca.* In: L. A. REEVE, ed., *Conchologia iconica; or, illustrations of the shells of molluscous animals*, 2: 17 pls. + unpaginated pages with text. [pls. 1, 2, December 1843; pls. 3, 4, January 1844; pls. 5–8, February; pls. 9–12, March; pls. 13, 14, April; pls. 15, 16, May; pl. 17, June].

REEVE, L. A., 1846, Monograph of the genus *Purpura.* In: L. A. REEVE, ed., *Conchologia iconica; or, illustrations of the shells of molluscous animals*, 3: 13 pls. [pls. 2, 3, July 1846; 4–8, Aug. 1846; 9–12, Sept. 1846; 1, 13, Oct. 1846].

REEVE, L. A., 1854, Monograph of the genus *Mactra.* In: L. A. REEVE, ed., *Conchologia iconica; or, illustrations of the shells of molluscous animals*, 8: 21 pls. + unpaginated pages with text [pls. 2–5, March; 1, 6–14, April; 15–21, May].

REID, D. G., 1996, *Systematics and evolution of Littorina.* The Ray Society, London, 463 pp.

SALISBURY, A. E., 1934, On the nomenclature of Tellinidae, with descriptions of new species and some remarks on distribution. *Proceedings of the Malacological Society of London*, 21(2): 74–91.

SCARLATO, O. A., 1965, Bivalve species of superfamily Tellinacea in the China seas. *Studia Marina Sinica*, 8: 27–114, 13 pls. [in Chinese with Russian abstract].

SCARLATO, O. A., 1981, *Dvustvorchatye molliuski umerennykh shirot zapadnoi chasti Tikhogo Okeana* [*Bivalve mollusks of the temperate latitudes of the western part of the Pacific Ocean*]. Akademiia Nauk SSSR, Zoologicheskii Institut, Opredeliteli po Faune SSSR, 126: 480 pp., 64 pls.

SCOTT, P. H., 1994, Bivalve molluscs from the southeastern waters of Hong Kong. Pp. 55–100, in: B. Morton, ed., *The malacofauna of Hong Kong and southern China III: Proceedings of the Third International Workshop on the Malacofauna of Hong Kong and Southern China, Hong Kong, 13 April–1 May 1992*. Hong Kong University Press, Hong Kong, xxii + 504 pp.

SOWERBY, G. B., II, 1843, Monograph of the genus *Lima*. In: G. B. Sowerby II, ed., *Thesaurus conchyliorum; or, monographs of genera of shells,* 1(3): 83–88, pls. 21, 22.

SOWERBY, G. B., II, 1844a, Monograph of the genus *Scalaria*. In: G. B. Sowerby II, ed., *Thesaurus conchyliorum; or, monographs of genera of shells*, 1(4): 83bis–108bis, pls. 32–35.

SOWERBY, G. B., II, 1844b, Continuation of Mr. G. G. Sowerby's description of *Scalaria*. *Proceedings of the Zoological Society of London,* for 1844[12](131–132): 26–31.

SUN, Y.-C., 1947, Professor Amadeus William Grabau. Biographical note. *Bulletin of the Geological Society of China*, 27: 1–26.

TCHANG, S. & H.-M. HWANG, 1964, On the Chinese species of Solenidae. *Acta Zoologica Sinica*, 16(2): 193–206 [in Chinese with English abstract].

TCHANG, S. & T.-K. LOU, 1956, A study on Chinese oysters. *Acta Zoologica Sinica*, 8(1): 65–94 [in Chinese with English abstract].

TCHANG, S., Z.-Y. QI & J.-M. LI, 1955, *Economic marine Mollusca in North China Sea*. Science Press, Beijing, iii + 98 pp., 35 pls. [in Chinese].

THOMAS, H. D., 1946, Prof. Amadeus W. Grabau. *Nature*, 158(4003): 89–90.

THUNBERG, C. P., 1793, Tekning och beskrifning på en stor ostronsort ifrån Japan. *Kongliga Svenska Vetenskaps-Akademiens, Handlingar*, 14(2): 140–142, pl. 6.

TING, V. K., 1931, Biographical note. *Bulletin of the Geological Society of China*, 10: iii–xviii.

TSUCHIDA, E. & T. KUROZUMI, 1993, Fauna of marine mollusks of the sea around Otsuchi Bay, Iwate Prefecture (4) Bivalvia – 1. *Otsuchi Marine Research Center Reports*, 19: 1–30.

WANG, C.-Y., 1931, A reminiscence. *Bulletin of the Geological Society of China*, 10(1): 19–20.

WANG, Z.-R., 1990, A study on species of the family Pectinidae I. Genera *Volachlamys* and *Annachlamys* off the China coasts. *Transactions of the Chinese Society of Malacology*, 3: 13–18 [in Chinese with English abstract].

WANG, Z.-R., 1997, *Fauna Sinica, Mollusca, Bivalvia, Mytiloida*. Science Press, Beijing, vi + 268 pp., 4 pls. [in Chinese].

WANG, Z.-R., 2002, *Fauna Sinica, Mollusca, Bivalvia, Pteriina*. Science Press, Beijing, x + 374 pp. [in Chinese].

YANG, J.-M., X.-D. ZHENG, Q. LI, R.-C. WANG, Z.-L. SONG & B.-C. YOU, 2006, Quantitative study on phenotypic genetic diversity of *Rapana venosa* in China's coastal waters. *Oceanologia et Limnologia Sinica*, 37 (5): 385–392 [in Chinese with abstract in English].

YANG, T.-H., 1991, Patronage of science: the China Foundation for the Promotion of Education and Culture. *Academia Sinica, Institute of Modern History*, Monograph Series 65: [online version].

YEN, T. C., 1936, The marine Gastropoda of Shantung Peninsula. *Contributions from the Institute of Zoology National Academy of Peiping*, 3(5): 165–255.

YOKOYAMA, M., 1920, Fossils from the Miura Peninsula and its immediate north. *Tokyo,* [*Imperial*] *University, College of Science, Journal*, 39(6): 1–193, 20 pls.

XU, F.-S., 1997, *Bivalve Mollusca of China seas*. Science Press, Beijing, xxiv + 333 pp. [in Chinese].

XU, F.-S. & S.-P. ZHANG, 2008, *An illustrated Bivalvia Mollusca fauna of China Seas*. Science Press, Beijing, China, viii + 336 pp. [in Chinese].

ZHANG, F.-S., 1980, Studies on the species of Muricidae of the China coasts. III. *Rapana*. *Studia. Marina Sinica*, 16: 113–123 [in Chinese with English abstract].

ZHAO, R.-Y., J.-M. CHENG & D.-D. ZHAO, 1982, *Fauna of marine mollusks in Dalian Province*. China Ocean Press, Beijing, vii + 167 pp., 21 pls. [in Chinese].

Revised ms. accepted October 19, 2014

MALACOLOGIA, 2015, 58(1–2): 225–232

COMPARATIVE CYTOGENETIC STUDY IN FOUR ALOPIINAE DOOR SNAILS (GASTROPODA, CLAUSILIIDAE)

Agnese Petraccioli[1*], Teresa Capriglione[1], Mariastella Colomba[2], Paolo Crovato[3], Gaetano Odierna[1], Ignazio Sparacio[4] & Nicola Maio[1]

ABSTRACT

A cytogenetic study was carried out by means of standard and NOR-FISH staining methods on the chromosomes of four Alopiinae door snails, two species of the Delimini tribe (*Siciliaria paestana* and *Papillifera bidens*) and two species of Medorini tribe (*Leucostigma candidescens* and *Medora* sp.). The two Delimini species and *Medora* sp. showed similar karyotypes, concerning the number of chromosomes, 2n = 62, and the first metacentric pair of chromosomes clearly bigger than the other pairs, but differed in the number of the telocentric pairs: none in *P. bidens*, four in *S. paestana* and, even, 21 in *Medora* sp. *Leucostigma candidescens* had 2n = 48, all biarmed chromosomes. Loci of NORs were on a single medium small chromosome pair in all the four studied species. The obtained results evidence a relevant degree of intergeneric karyotypic diversity in Alopiinae, concerning both chromosome number and/or shape. The data allow us to make a hypothesis on the evolutionary chromosome trends for this door snail subfamily.

Key words: chromosome diversification, karyotype, NOR-FISH banding, Alopiinae, Clausiliidae.

INTRODUCTION

Alopiinae is a subfamily of the pulmonate land snails of the family Clausiliidae, known as door snails, because of the peculiar closing apparatus, which derives from their sinistrorsal, turriculate shell. The subfamily Alopiinae is particularly rich in species, comprising more than 360 living species distributed along the perimediterranean regions and in northern and southeastern Europe (Nordsieck, 2007; Uit de Weerd & Gittenberger, 2013). Nordsieck (2007), in his accurate and exhaustive systematic revision of Clausiliidae, based on shell and genital characters, recognizes Alopiinae as a monophyletic assemblage, with the about 360 species subdivided in five tribes (Alopiini, Cochlodinini, Delimini, Medorini and Montenegrini). The molecular phylogenetic analysis of Clausiliidae by Uit de Weerd & Gittenberger (2013) is in agreement with the morphological systematic revision of the family proposed by Nordsieck (2013a). Concerning Alopiinae, it retrieves monophyletic, as well as various tribes, including Delimini and Medorini (Nordsieck, 2013a). However, many taxonomic, systematic and phylogenetic questions are not clearly defined. In this context, useful information can be gathered from other studies, such as chromosome analysis. In fact, the recognition of the main changes in karyotype composition of a given lineage may be helpful in understanding its evolutionary history. For example, the utility and efficiency of cytogenetic studies in exploring chiton taxa diversity has been recently shown, (Odierna et al., 2008; Petraccioli et al., 2012), highlighting the main evolutionary events of the karyotype diversification in two different taxa.

The present paper shows the results of a chromosomal study performed with standard and NOR-FISH staining methods on two species of Delimini, *Siciliaria paestana* (Philippi, 1836) and *Papillifera bidens* (Linnaeus, 1758) and two of Medorini. The two Delimini species belong to the *Siciliaria* group (Nordsieck, 2013b), considered monophyletic also in molecular phylogenetic studies (Uit de Weerd & Gittenberger, 2013). The two Medorini species analyzed were *Leucostigma candidescens* (Rossmässler, 1835) and specimens of genus

---

[1]Dipartimento di Biologia, Università di Napoli Federico II, Via Cinthia, 21- 80126 Naples, Italy.
[2]Università di Urbino "Carlo Bo", Dipartimento di Scienze Biomolecolari, via Maggetti, 22 (loc. Sasso) - 61029 Urbino (PU), Italy.
[3]Via S. Liborio, 1 - 80134 Napoli, Italy.
[4]Via E. Notarbartolo, 54 int. 13 - 90145 Palermo, Italy.
*Corresponding author: petra.ag@gmail.com

Medora, here designed as *Medora* sp., because the anatomical and molecular characters of the samples collected were similar but not perfectively matching with those of *M. italiana* (Küster, 1847), studied so far (Giusti, 1967, 1971; Giusti et al., 1986, Giusti & Manganelli, 1992; Reitano et al., 2007; Nordsieck, 2009, 2012; Colomba et al., 2012).

Alopiinae and Clausiliidae chromosomal data are scarce (for details, see Park, 2007) and mainly referred to the number of the chromosomes. Only one karyotype of the Phaedusinae species, *Euphaedusa fusaniana* (2n = 58, all biarmed chromosomes) was described (Park, 2007). The data available for Alopiinae concern *Herilla bosniensis* and *Cochlodina laminata*, both with 2n = 48 (Thaler, 1963; Rainer, 1967), *Delima itala* and *P. bidens*, with tentatively 2n = 60 (Rainer, 1967). So far, no data were available for localization of NORs in Clausiliidae.

MATERIALS AND METHODS

We studied four specimens of *Medora* sp. and four specimens of *S. paestana* from Monti Alburni (Salerno), six of *P. bidens* from Aversa (Caserta) and five specimens of *L. candidescens* from Cusano Mutri (Benevento).

Chromosomes were prepared from gonads as described by Petraccioli et al. (2012). In brief, from each individual the gonads were removed and incubated for two hours in one ml of calf serum, inactivated at 56°C for 30 min in a solution containing 50 µl of colcemid at 10 µg/ml. The gonads were incubated for 30 min in hypotonic solution (KCl 0.075 M + sodium citrate 0.5%, 1:1) and fixed for 15 min in methanol: acetic acid, 3:1. Cell dissociations of gonads were made on a sieve and chromosomes were prepared for dropping on the slides 25 µl of the obtained cell suspensions.

Standard chromosome staining was performed by incubating chromosomes in DAPI at 0.5 µg/ml. After detection of metaphase plates with an epifluorescent microscope (Leica DM) equipped with a digital camera, the images were transformed in gray. For karyotyping, five metaphase plates of each species were used, which were also employed to get chromosome morphometric parameters, centromeric index (CI) and relative length (RL) according to Levan et al. (1964).

NOR-FISH staining was performed as described by Petraccioli et al. (2012) using as a probe the biotinaled 18S rRNA gene sequence units of the pectinid *Adamussium colbecki*. Slides were aged for one day at room temperature and then two hours at 60°C; after that, slides were incubated for 30 min in RNase at 100 µg/ml in Tris-HCl 10 mM at pH 6.5, dehydrated in ethanol 50, 70, 90 and 100% and air dried. Chromosomes and probe were denatured for 3 min at 72°C in hybridization mixture (10 ng/ml biotinylated 16 dUTP probe + 0.1 mg/ml shared *E.coli* DNA in 2 x SSC with 50% formamide). Hybridization was carried out at 40°C for 20 h. Washes were performed in 1 x SSC at 72°C for 5 min and at RT for 2 min. Probe detection was performed by monoclonal anti-biotin (Sigma cod. B7653) diluted 1:500 in PTB (1 ml PTB = 5 µl of Tween 20% + 0.01 g of Dry milk in 1 ml of PBS 0.2 M). After one hour, slides were washed in 1 x PBS and incubated for 30 min in FITC conjugated anti-anti-biotin antibodies (Sigma cod. F9137) diluted 1:50 in PTB. Chromosomes were washed in 1 x PBS, counterstained with 5 µg/ml propidium iodide (PI) in 1 x PBS for 15 min at RT and then mounted with antifade (DABCO, Sigma). The hybridization signals were detected and recorded under an epifluorescent microscope (Leica DM) equipped with a digital camera.

RESULTS

Diakinetic meiotic bivalents and gonadic metaphase plates were successfully obtained from at least one individual of each studied species. Cytogenetic analysis showed that *Medora* sp., *S. paestana* and *P. bidens* had 31 bivalents and 62 chromosomes (Fig. 1). In the three karyotypes, only the first chromosome pair was clearly recognizable, shaped as a large metacentric, much bigger than the others (Fig. 1). Besides, the karyotype of three species differed in the number of biarmed and uniarmed elements. *Medora* sp. had a karyotype with ten biarmed pairs [8 metacentric (M), one submetacentric (SM) and one subtelocentric (ST)] and 21 pairs of telocentric (T) chromosomes (fundamental number, FN = 82) (Fig. 1, Table 1). In the karyotype of *S. paestana,* the number of biarmed chromosome pairs was 27 (25M, 2SM), and four pairs were telocentric, FN = 116) (Fig. 1, Table 1); instead all the chromosomes of *P. bidens* were biarmed (28M, 3SM), FN = 124 (Fig. 1, Table 1). Differently from the above three species, *L. candidescens* displayed a karyotype with 2n = 48 chromosomes, all biarmed and progressively decreasing in length (22M, 2SM) FN = 96 (Fig. 1, Table 1).

In metaphase plates of the four studied species, NOR-FISH showed hybridization signals only on one small sized chromosome pair, while their relative nuclei showed two signals (Fig. 2A) or one signal, due to NORs tendency to join in a one nuclear domain (Fig. 2B, C, D).

Noteworthy, in the 25 scored diakinesis figures in each of the four studied specimens of *S. paestana*, some of them, namely, 2, 3, 3 and 4 for specimen (in total 12%), presented a medium small sized achiasmatic bivalent with a gap on each of subterminal regions (Fig. 1).

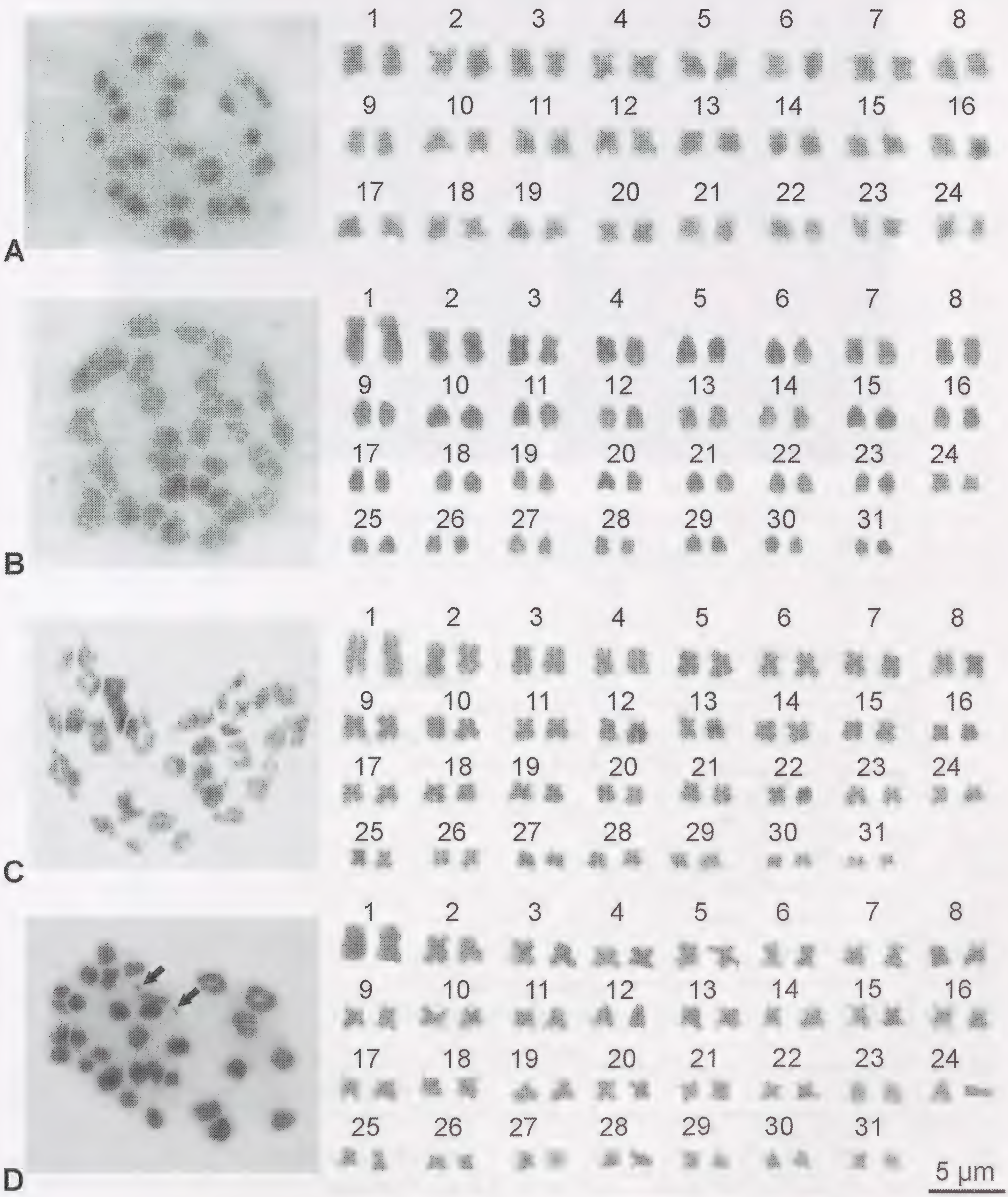

FIG.1. Diakinetic meiotic plates (on the left) and karyotypes (on the right). A: *L. candidescens*; B: *Medora* sp.; C: *P. bidens*; D: *S. paestana*. The micrometer bar applies to all images. The arrows point to the gaps on the subteminal regions of an achiasmatic bivalent of *S. paestana*.

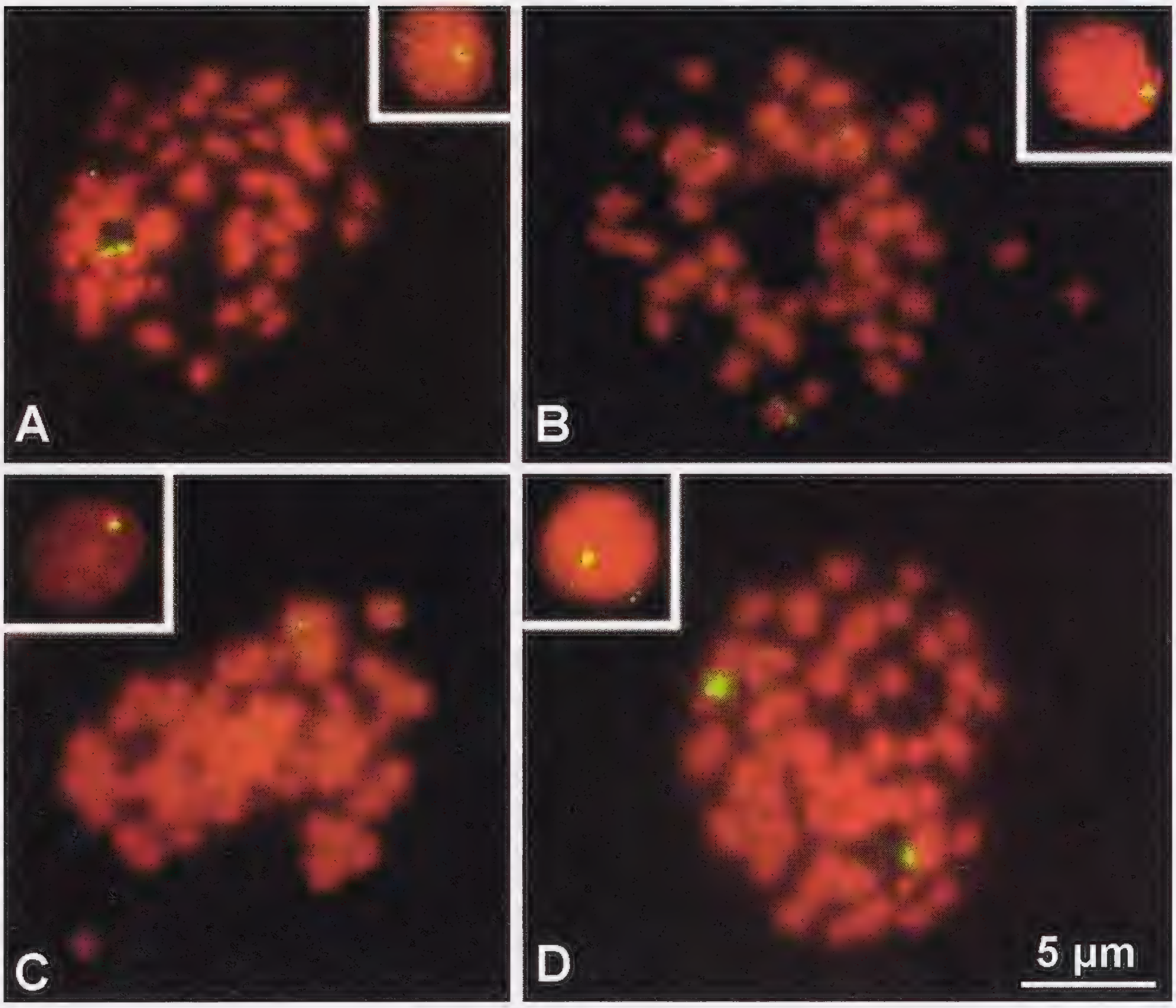

FIG. 2. NOR-FISH on partial chromosome metaphase plates, with a relative nucleus in the insert. A: *L. candidescens*; B: *Medora* sp.; C: *P. bidens*; D: *S. paestana*, in the inserts, the relative nucleus. The micrometer bar applies to all images.

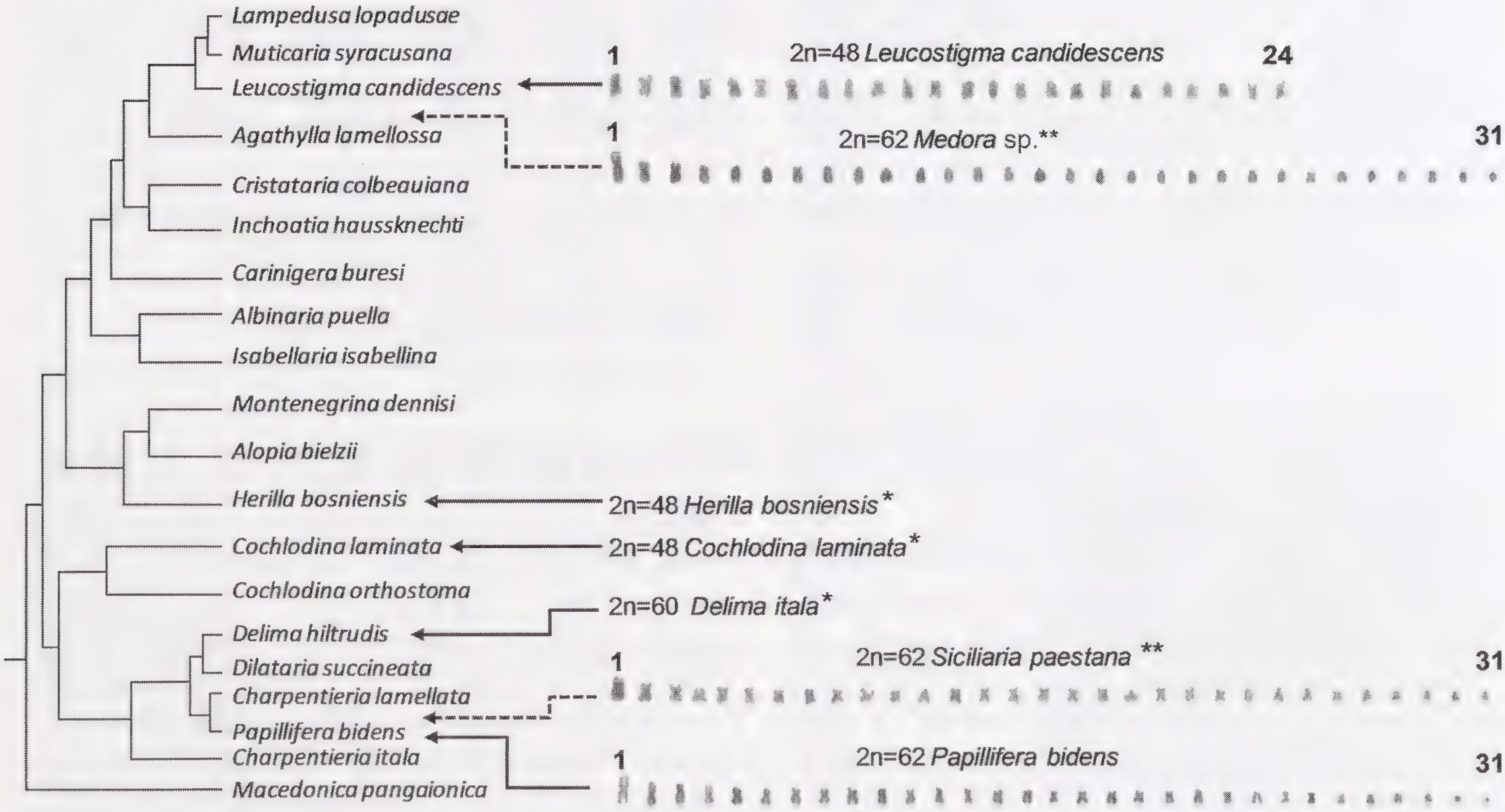

FIG. 3. Phylogenetic tree of Alopiinae redrawn from the Clausiliidae tree by Uit de Weerd & Gittenberger (2013) with superimposed the so far known karyological data of Alopiinae. (* data by Thaler (1963) and Rainer (1967); ** see text, for the phylogenetic positions on the tree of *S. paestana* and *Medora* sp.).

DISCUSSION

The karyotype of *Medora* sp. (2n = 62; FN = 82) with a straight prevalence of telocentric elements (21 pairs) is quite unusual among both gastropods and bivalves (Thiriot-Quiévreux, 2002, 2003), whose karyotypes, as a rule, include all or almost all biarmed (meta- and/or submeta- centric) chromosomes. The other three investigated Alopiinae species do not deviate from this general rule, possessing a karyotype with all biarmed chromosomes (*P. bidens* and *L. candidescens*) or almost all biarmed elements (*S. paestana*). In Alopiinae, additional karyological data concern the chromosome number of two species only, namely

TABLE 1. Morphometric parameters of chromosomes of the studied Alopiinae species. R.L. = Relative length; C.I. = Centromeric index; C.S = Chromosome shape (M= metacentric; SM = Submetacentric; ST = Subtelocentric and T = Telocentric).

	L. candidescens			*Medora* sp.			*P. bidens*			*S. paestana*		
Chr. Nr.	R.L.	C.I.	C.S.	R.L.	C.I.	C.S.	R.L.	C.I.	C.S.	R.L.	C.I.	C.S.
1	5.1	44.1	M	7.3	40.2	M	7.9	46.4	M	7.1	40.8	M
2	5.0	43.2	M	4.8	43.2	M	5.3	43.2	M	4.8	44.4	M
3	4.9	45.6	M	4.5	45.1	M	4.4	39.1	M	4.3	44.9	M
4	4.9	40.2	M	4.2	40.3	M	4.2	40.3	M	4.2	41.0	M
5	4.8	42.8	M	4.1	0	T	4.0	44.5	M	4.1	39.9	M
6	4.8	46.6	M	4.1	0	T	3.9	42.7	M	3.7	45.1	M
7	4.5	44.3	M	3.9	32.3	SM	3.7	45.0	M	3.7	43.2	M
8	4.3	45.9	M	3.7	42.8	M	3.6	44.3	M	3.6	34.5	SM
9	4.3	44.7	M	3.6	0	T	3.5	39.9	M	3.6	40.1	M
10	4.3	43.6	M	3.5	0	T	3.5	45.0	M	3.3	43.3	M
11	4.2	43.8	M	3.4	0	T	3.4	42.5	M	3.3	43.7	M
12	4.1	41.9	M	3.3	0	T	3.4	31.4	SM	3.3	0	T
13	4.1	43.6	M	3.3	44.6	M	3.3	39.8	M	3.3	42.5	M
14	4.0	42.9	M	3.2	16.9	ST	3.3	40.7	M	3.2	44.4	M
15	3.9	44.4	M	3.1	0	T	3.3	43.0	M	3.2	41.5	M
16	3.9	45.1	M	2.9	0	T	3.2	44.5	M	3.2	42.6	M
17	3.9	45.0	M	2.8	0	T	2.9	43.1	M	3.2	44.1	M
18	3.9	40.8	M	2.8	0	T	2.9	42.9	M	3.1	43.5	M
19	3.8	31.1	SM	2.7	0	T	2.9	44.8	M	3.1	31.2	SM
20	3.8	42.7	M	2.7	0	T	2.7	43.7	M	3.1	42.8	M
21	3.5	42.0	M	2.6	0	T	2.7	42.0	M	2.9	39.8	M
22	3.5	32.3	SM	2.6	0	T	2.6	43.7	M	2.8	43.0	M
23	3.4	40.8	M	2.6	0	T	2.6	32.5	SM	2.8	0	T
24	3.1	46.2	M	2.6	41.9	M	2.4	46.5	M	2.8	0	T
25				2.5	0	T	2.3	43.8	M	2.5	41.6	M
26				2.4	0	T	2.3	42.9	M	2.2	43.0	M
27				2.4	0	T	2.0	42.5	M	2.2	44.8	M
28				2.3	42.5	M	2.0	43.0	M	2.1	45.2	M
29				2.2	0	T	2.0	30.5	SM	2.1	42.7	M
30				2.0	0	T	1.8	42.2	M	2.0	0	T
31				1.9	0	T	1.6	43.3	M	1.7	41.7	M

H. bosniensis (Thaler, 1963) and *C. laminata* (Thaler, 1963; Rainer, 1967). The comparison of karyological data with the phylogentic tree proposed by Uit de Weerd & Gittenberger (2013), provides useful information (Fig. 3; note that the phyletic positions of *Medora* sp. and *S. paestana* is on the basis of evidence of phylogenetic tree by Uit de Weerd et al. (2004)). Each of the two main clades includes species both with 2n = 48 and 2n = 62, suggesting that chromosome rearrangements affecting the number of elements occurred independently in the two main clades. However, the karyotypes of the two Delimini, *P. bidens* and *S. paestana*, differ in showing a diverse number of telocentric elements, none in the former species and four pairs in *S. paestana.* The differences between the two karyotypes probably originated by four events of inversion or, as recently evidenced in mammals from comparative genome analysis (Stanyon & Bigoni, 2010; Rocchi et al., 2012), of centromere repositioning. In Medorini, in addition to the rearrangements of the chromosome number, also events of inversion (or centromere repositioning) have to be considered. In fact, seven fusions (or fissions) and eight inversions occur for the transition between the karyotypes of *Medora* sp. (2n = 62; NF = 80) and *L. candidescens* (2n = 48; NF = 96). Unfortunately, karyological data are not sufficient to surely assess the polarity of the rearrangements which operated during Alopiinae species diversification. In this context, the results of NORs are unhelpful. Comparable data of NORs in Pulmonata are scarce (see reference in Thiriot-Quiévreux, 2003), while, so far, those ones obtained by FISH with rDNA probes, concern two Helicidae (Vitturi et al., 2005), and four slugs (Vitturi et al., 2004; Colomba et al., 2009). In those FISH evidence, loci of NORs were observed either on a single or multiple chromosome pairs, which are considered, respectively, a primitive and derivate character in several taxa, including molluscs (Thiriot-Quiévreux, 2002, 2003; Wang & Guo, 2004; Colomba et al., 2009; Petraccioli et al., 2012).Then the four investigated Alopiinae species, possessing NORs on a single chromosome pair, display the plesiomorphic (ancestral) condition.

In other 2n = 62 Pulmonata species, for example, some arionid slug species, the first chromosome pair is not distinctively bigger than the other pairs (Patrão et al., 2013). Conversely, in *Medora* sp., *S. paestana* and *P. bidens* the chromosomes of the first pair are distinctively larger than ones of the other pairs. The chromosomal similarities of the three Alopiinae species, namely 2n = 62 with the first pair distinctively bigger than the other pairs, are intriguing and candidate as plesiomorphic, because showed by species of either main clades of Alopiinae.

Our chromosomal data show a relevant degree of intergeneric karyotypic diversity in Alopiinae concerning both number and/or shape of chromosomes. Probably, the process of karyological diversification still is ongoing in this group of door snails, as suggested by the presence of gaps on chromosomes of *S. paestana*. Indeed, this door snail species shows high frequency of gaps on the subterminal regions of an achiasmatic medium small bivalent. Chromosome gaps represent hot spots for recombination (Yunis & Soreng, 1984; Glover & Stein, 1988) and their expression can be induced by genomic or environmental stress (Durkin & Glover, 2007). In *S. paestana*, we consider improbable a possible involvement of environment, because the studied samples came from a pristine areas in the Cilento, Vallo di Diano and Alburni National Park. So, the presence of two fragile sites on a medium small bivalent of *S. paestana* suggests a propensity of this chromosome pair to structural rearrangements.

ACKNOWLEDGMENTS

This research was funded with the support of the Cilento, Vallo di Diano and Alburni National Park (CVANP). Authors wish to thank: the authorities of the National Park of the Cilento, Vallo di Diano and Alburni, in particular: Amilcare Troiano (President), Corrado Matera (Vice-President), Angelo De Vita (Director) and Laura De Riso (Technical area) for collaboration as well as advising on technical and administrative aspects. We want to thank Camillo Pignataro and Nicola Auricchio (respectively Scientific Director and President of Fondazione I.RI.DI.A. – Museo Naturalistico) and Antonietta Mordente (Banca Monte Pruno, Credito Cooperativo di Roscigno e Laurino) for scientific and administrative cooperation. Furthermore, we thank Pasquale and Pietro Cappelli (Ottati, Salerno).

LITERATURE CITED

COLOMBA, M. S., R. VITTURI, M. RAMPIN, A. LANNINO, A. TARAVELLA & A. LIBERTINI, 2009, Comparative cytogenetic analysis of three Stylommatophoran slugs (Mollusca, Pulmonata). *Malacologia*, 51: 173–179.

COLOMBA, M. S., F. LIBERTO, A. REITANO, W. RENDA, G. POCATERRA, A. GREGORINI & I. SPARACIO, 2012, Molecular studies on the genus *Medora* H. et A. Adams, 1855 from Italy (Gastropoda Pulmonata Clausiliidae). *Biodiversity Journal*, 3: 571–582.

DURKIN, S. G. & T. W. GLOVER, 2007, Chromosome fragile sites. *Annual Review of Genetics*, 41: 169–192.

GIUSTI, F., 1967, Notulae Malacologicae I. Sulla sistematica e distribuzione del genere *Medora* M. et A. Adams nell'Italia appenninica. *Archivio Botanico e Biogeografico Italiano*, 43: 406–424.

GIUSTI, F., 1971, Notulae malacologicae XVI. I molluschi terrestri e di acqua dolce viventi sul massiccio dei Monti Reatini (Appennino Centrale). *Lavori della Società italiana di Biogeografia* (N.S.), 2: 423–576.

GIUSTI, F., C. GRAPPELLI, G. MANGANELLI, R. FONDI & L. BULLINI, 1986, An attempt of natural classification of the genus *Medora* in Italy and Yugoslavia, on the basis of conchological, anatomical and allozymic characters (Pulmonata: Clausiliidae). *Lavori Società italiana di Malacolologia*, 22/1984: 259–362.

GIUSTI, F. & G. MANGANELLI, 1992, The problem of the species in malacology after clear evidence of the limits of morphological systematics. Pp. 153–172, in: E. GITTENBERGER & J. GOUD, eds., *Proceedings of 9th International Malacological Congress Edinburgh, 31 August–6 September 1986*. Unitas Malacologica, Leiden, 414 pp.

GLOVER, T. W. & C. K. STEIN, 1988, Chromosome breakage and recombination at fragile sites. *American Journal of Human Genetics*, 43: 265–273.

KÜSTER, H. C., 1847 [1844–1862], Die Schliessschnecken und die verwandten Gattungen (*Clausilia*, *Balea*, *Cylindrella*, *Megaspira*.), mit Beiträgen von Dr. Philippi. In Abbildungen nach der Natur mit Beschreibungen. *Systematisches Conchylien-Cabinet*, 1(14): 355 pp., 38 pls. Nürnberg.

LEVAN, A., K. FREDGA & A. A. SANDBERG, 1964, Nomenclature for centromeric position on chromosomes. *Hereditas*, 52: 201–220.

LINNAEUS, C., 1758, *Systema naturae per regna tria naturae ... editio decima, reformata, Vol. 1. Animalia*. L. Salvii, Stockholm, 824 + iii pp.

NORDSIECK, H., 2007, *Worldwide door snails (Clausiliidae) Recent and fossil*. ConchBooks Press, Hackenheim, 214 pp.

NORDSIECK, H., 2009, Ergänzung der Revision der Gattung *Medora* H. & A. ADAMS, mit Beschreibung neuer Taxa (Gastropoda, Stylommatophora, Clausiliidae, Alopiinae). *Conchylia*, 40: 2–11.

NORDSIECK, H., 2012, Ergänzung der Revision der Gattung *Medora* H. & A. ADAMS: Die *Medora*-Arten Italiens (Gastropoda, Stylommatophora, Clausiliidae, Alopiinae), mit Beschreibung einer neuen Unterart von *Medora dalmatina* Rossmässler. *Conchylia*, 42: 75–81.

NORDSIECK, H., 2013a, Comment on Uit de Weerd & Gittenberger (2013): Phylogeny of Clausiliidae. http://www.hnords.de/535642a125135e10d/535642a211106da02/index.html.

NORDSIECK, H., 2013b, Delimini (Gastropoda, Pulmonata, Clausiliidae) from Apennine Italy, with the description of three new subspecies from Calabria. *Conchylia,* 44: 3–14.

ODIERNA, G., G. APREA, M. BARUCCA, M. A. BISCOTTI, T. CAPRIGLIONE & E. OLMO, 2008, Karyology of the Antarctic chiton *Nuttallochiton mirandus* (Thiele, 1906) (Mollusca: Polyplacophora) with some considerations on chromosome evolution in chitons. *Chromosome Research,* 16: 899–906.

PARK, G. M., 2007, Cytological study of *Euphaedusa fusaniana* (Stylommataphora: Clausiliidae) of Korea. *Korean Journal of Malacology*, 23: 59–63.

PATRÃO, C., J. TEIXEIRA DE SOUSA, K. JORDAENS, T. BACKELJAU, R. CASTILHO & A. LEITÃO, 2013, *Geomalacus* and *Letourneuxia* (Mollusca Pulmonata): a cytogenetic assessment. *Malacologia*, 56: 333–338.

PETRACCIOLI, A., N. MAIO & G. ODIERNA, 2012, Chromosomes of *Lepidochitona caprearum* (Scacchi, 1836) (Polyplacophora, Acanthochitonina, Tonicellidae) provide insights into *Acanthochitonina* karyological evolution. *Comparative Cytogenetics*, 6: 397–407.

PHILIPPI, R. A., 1836, *Enumeratio molluscorum Siciliae cum viventium tum in tellure Tertiaria fossilium quae in itinere suo observavit*, vol. 1. Schroppi, Berolini [Berlin], xiv + 268 pp., 12 pls.

RAINER, M., 1967, Cromosomenuntersuchungen an Gastropoden (Stylommatophora). *Malacologia*, 5: 341–373.

REITANO, A., F. LIBERTO & I. SPARACIO, 2007, Nuovi dati su Molluschi terrestri e dulciacquicoli di Sicilia. 1° Contributo (Gastropoda Prosobranchia Neotaenioglossa; Gastropoda Pulmonata Basommatophora, Stylommatophora). *Il Naturalista Siciliano*, 31: 311–330.

ROCCHI, M., N. ARCHIDIACONO, W. SCHEMPP, O. CAPOZZI & R. STANYON, 2012, Centromerere positioning in mammals. *Heredity*, 108: 59–67.

ROSSMÄSSLER, E. A., 1835 [1835–1837], *Iconographie der Land- und Süsswasser-Mollusken, mit vorzüglicher Berücksichtigung der Europäischen noch nicht abgebildeten Arten*, vol. 1: vi + 132 + 26 + 33 + 27 + 70 pp., 30 pls.

STANYON, R. & F. BIGONI, 2010, Primate chromosome evolution: with reference to marker order and Neocentromeres. *Russian Journal of Genetics*, 46: 1087–1093.

THALER, E., 1963, Beiträge zur Cytologie der Clausiliidae (Gastropoda, Pulmonata. Stlommatophora). *Österreichische Akademie der Wissenschaften*, 24: 1–19.

THIRIOT-QUIÉVREUX, C., 2002, Review of the literature on bivalve cytogenetics in the last ten years. *Cahiers de Biologie Marine*, 43: 17–26.

THIRIOT-QUIÉVREUX, C., 2003, Advances in chromosomal studies of gastropod molluscs. *Journal of Molluscan Studies*, 69: 187–201.

UIT DE WEERD, D. R., W. H. PIEL & E. GITTENBERGER, 2004, Widespread polyphyly among Alopiinae snail genera: when phylogeny mirrors biogeography more closely than morphology. *Molecular Phylogenetics and Evolution*, 33: 533–548.

UIT DE WEERD, D. R. & E. GITTENBERGER, 2013, Phylogeny of the land snail family Clausiliidae (Gastropoda: Pulmonata). *Molecular Phylogenetics and Evolution*, 67: 201–216.

VITTURI, R., L. SINEO, N. VOLPE, A. LANNINO & M. S. COLOMBA, 2004, Repetitive DNAs in the slug *Milax nigricans*: association of ribosomal (18S–28S and 5S rDNA) and (TTAGGG) *n* telomeric sequences) in the slug *M. nigricans* (Mollusca: Gastropoda: Pulmonata). *Micron*, 35: 255–260.

VITTURI, R., A. LIBERTINI, L. SINEO, I. PARACIO, A. LANNINO, A. GREGORINI & M. S. COLOMBA, 2005, Cytogenetics of the land snails *Cantareus aspersus* and *C. mazzullii* (Mollusca: Gastropoda: Pulmonata). *Micron*, 36: 351–357.

WANG, Y. & X. GUO, 2004, Chromosomal rearrangement in Pectinidae revealed by rRNA loci and implications for bivalve evolution. *Biological Bulletin*, 207: 247–256.

YUNIS, J. J. & A. L. SORENG, 1984, Constitutive fragile sites and cancer. *Science*, 226: 1199–1204.

Revised ms. accepted October 21, 2014

MALACOLOGIA, 2015, 58(1–2): 233–243

THERMAL BIOLOGY OF THE SOUTH AMERICAN APPLE SNAIL *ASOLENE PLATAE* (CAENOGASTROPODA: AMPULLARIIDAE)

María J. Tiecher, María E. Seuffert & Pablo R. Martín*

Laboratorio de Ecología, INBIOSUR (Universidad Nacional del Sur-CONICET)
San Juan 670, 8000, Bahía Blanca, Argentina.

ABSTRACT

Asolene platae is a freshwater snail of the Ampullariidae native from La Plata River basin in South America. Water temperature has an overwhelming influence on the biology of apple snails, though there are no systematic studies related to the thermal biology of this species. The effect of temperature on the activity, growth and mortality of *A. platae* was studied through laboratory experiments using constant temperatures of 15, 20, 25, 30 and 35°C. The lower threshold and cumulative degree-days for the embryonic development were estimated under fluctuating temperature. Water temperature had a significant effect on the activity of *A. platae*, being almost null at 15°C, reaching its maximum in the range 25–30°C and decreasing above 30°C. Regardless of temperature, snails remained resting nearly half of the time, exhibiting less activity than other apple snails across similar temperatures. Mortality was higher for hatchlings than for adults at all temperatures with the exception of 35°C, which resulted in high levels of mortality for both groups. Growth of hatchlings was significantly affected by temperature, being highest between 25 and 35°C. The lower temperature threshold for the embryonic development was around 16°C and the cumulative degree-days to complete development were estimated between 107.5 and 120.5°C.d. The optimum temperature for *A. platae* would be 25–30°C. Temperatures of 35°C and above would be harmful, while temperatures below 20°C resulted in rapid decreasing in activity and slower growth rates. The information about the thermal requirements of *A. platae* will be useful optimizing rearing conditions and developing predictive models of the potential distribution of *A. platae* in scenarios where it is introduced outside of its native range.

Key words: temperature, growth, mortality, activity, embryonic development; degree-days, threshold.

INTRODUCTION

Ampullariids or apple snails are recognized worldwide as successful invaders, especially *Pomacea* spp. that became serious pests of aquatic crops (Cowie, 2002; Hayes et al., 2008), promoters of ecosystemic changes in natural wetlands (Carlsson et al., 2004, Fang et al., 2010; Horgan et al., 2014) and vectors of parasitic diseases (Lv et al., 2009). For these reasons, *Pomacea* has been the target of most research on ampullariids and hence a vast knowledge of its species is available, whereas little is known about the biology and ecology of other apple snail genera like *Asolene*.

Water temperature has an overwhelming influence on most aspects of the biology of ampullariids, including activity levels, aerial respiration, growth rate, development, reproduction and survival (e.g., Freiburg & Hazelwood, 1977; Albrecht et al., 1999; Estebenet & Martín, 2002; Aufderheide et al., 2006; Gettys et al., 2008; Seuffert & Martín, 2009; Seuffert et al., 2010, 2012). However, there are no systematic studies to date related to the thermal biology of the genus *Asolene*. The information about the thermal limits of ectotherms in general and aquatic snails in particular would be necessary to understand and predict changes in distribution ranges and abundances in native and invaded areas in the face of global climatic changes (Tomanek, 2008; Madeira et al., 2012; Fordham et al., 2013).

Asolene platae (Maton, 1811) is an apple snail native from La Plata River basin, whose range extends from Bolivia to northern Buenos Aires province, Argentina (Cowie & Thiengo, 2003). Recently, this species has been considered a senior synonym of *Asolene pulchella* (Maton,

---

*Corresponding author: pmartin@criba.edu.ar

1838) on the basis of their genetic, anatomical and conchological similarity (Hayes et al., 2009a; Leon et al., 2014). The embryonic development of *A. platae* has been determined under a controlled temperature of 25 ± 2°C, extending for 10.8 days on average (range: 8–16 days; Tiecher et al., 2014). However, the temperature below which embryonic development stops, known as lower temperature threshold (Seuffert et al., 2012), is so far unknown. As temperature increases above the lower threshold, the duration of embryonic development will decrease. However, the combination of temperature above the lower threshold and time required to hatch remains generally constant (Zalom et al., 1983; Seuffert et al., 2012). The estimation of this physiological time (measured in cumulative degree-days) and the lower threshold are essential to estimate the duration of embryonic development in thermally fluctuating environments, since a bigger difference between temperature and the lower threshold implies an earlier accumulation of the required degree-days and hence a faster developmental rate. Among apple snails, these parameters are only known so far for species of *Pomacea* that have aerial egg masses and calcareous eggshells (Seuffert et al., 2012) but not for genera possessing gelatinous and subaquatic egg masses such as *Asolene* (Hayes et al., 2009b).

A series of experiments were designed to study the effect of temperature on the activity of *A. platae* and the relation with some aspects of its life cycle, such as growth and mortality. Additionally, we estimated the lower threshold and cumulative degree-days for embryonic development. These results provide insights into the fundamental biology of ampullariids and contribute to our understanding of the factors influencing its distribution. These data are also informative for developing predictive models of successful establishment and spread of this species if introduced outside of its native range, and which are critical for assessment of invasion potential by regulatory agencies (e.g., EFSA, 2013, 2014). Furthermore, the results of this study and those on thermal requirements of other ampullariids are useful for optimizing culturing conditions for research and aquaculture projects (Seuffert & Martín, 2013).

MATERIALS AND METHODS

Origin and Maintenance of Snails

The snails used in this study were descendants of a pool originally obtained from Regatas pond (Ciudad Autónoma de Buenos Aires, Argentina; 34°33'S, 58°26'W). They were raised in 20 L collective aquaria with $CaCO_3$ saturated tap water, kept in a room at 25 ± 2°C under a 14:10 h (light/dark) photoperiod. The snails were fed with fresh lettuce *ad libitum* and the aquaria were cleaned and renewed weekly. Before each trial, snail shell length (SL, from the apex to the extreme opposite lip of the aperture) was measured with a Vernier caliper to the nearest 0.1 mm.

The laboratory experiments were performed in 10.8 L glass aquaria (20 cm-wide, 27 cm-long and 30 cm-deep). Water temperatures (T) were kept constant with electric thermostats located at the bottom of each aquarium to reduce thermal stratification. The aquaria were provided with a 1 cm sand layer to allow the snails to bury themselves. The snails were provided with fresh lettuce as entire leaves and also fragmented in floating particles, allowing pedal surface collecting (Saveanu & Martín, 2013). The aquaria were not provided with artificial aeration.

Experiment 1: Effect of Constant Temperatures on Activity

The water temperatures used in this experiment were: 15, 20, 25, 30 and 35°C and for each temperature three snails (SL: 11.1–31.3 mm) were randomly chosen from the general pool. Before the observation period, the snails were acclimated to the target temperature for 48 h. After, they were observed at five minute intervals for over three hours with all treatments run concurrently. At the end of each observation period snails were evaluated to see if they were dead or alive by checking on the heartbeat through the translucent shell or by stimulating them with a probe; in some cases, it was obvious because of the putrefaction state. For each treatment five replicated aquaria were used and each snail was used only once.

During the observation period, the instantaneous activity or state of each snail was recorded and classified as: feeding (F, considering both shredding and pedal surface collecting), crawling (C), ventilating the lung (V, during which it was also registered the number of pumping movements; Seuffert & Martín, 2009), resting (R, on the bottom or clinging to the sides of the aquarium with the foot extended) and inactive (I, with the head and foot fully or partially retracted inside the shell, either lying on the bottom or buried in the sand).

On the basis of the total records during the 3 h observation period, the percentage of time spent in the different activities per aquarium was calculated as:

$$\frac{\text{number of records for each activity}}{(\text{number of snails per aquarium} * \text{total number of observations})} \times 100$$

Experiment 2: Effect of Constant Temperatures on Mortality of Adult Snails and on Mortality and Growth of Hatchlings

The water temperatures used were as in experiment 1. To analyze the effect of temperature on the mortality of adult snails, five snails (SL: 14.8–31.5 mm) were randomly assigned to each temperature. During a 25 day trial period, aquaria were checked every two to three days to determine if snails were alive or dead. Five replicated aquaria were used for each temperature.

To analyze the effect of temperature on the mortality and growth of hatchlings, one week-old hatchlings were reared in tap water in 500 ml plastic bottles containers held inside 10.8 L aquaria containing water maintained at one of the following temperatures: 15, 20, 25, 30 and 35°C. During 20 days the number of dead hatchlings was counted every three days. The five temperatures were replicated three times and the total number of hatchlings per container varied according availability at the start of each trial, but were the same for all five temperatures (31, 21 or 19 for each of the replicates).

At the end of the trials, the mortality (percentage of dead snails or hatchlings) was calculated for each temperature. A scaled digital photograph was taken of ten randomly chosen surviving hatchlings to determine their shell lengths.

Experiment 3: Threshold Temperature and Degree-days Requirement for Embryonic Development

The egg masses used in this experiment were laid in 2.8 L aquaria by snails reared under the general conditions described previously. Females were allowed to copulate each week to ensure that sperm reserves were not depleted. Due to the lack of external sexual dimorphism, females were recognized while they were laying eggs in a collective aquaria or when an egg mass was found in an individual aquaria where a putative female was isolated after being mounted by a male (Tiecher et al., 2014). Egg masses were incubated in 7 cm diameter dishes filled with 2 cm of tap water in a room with variable temperature which was recorded hourly with a Hobo® data-logger (T_h, °C). Water temperature in the dishes followed closely the air temperature but with a delay of approximately one hour. The egg masses were checked daily to record the appearance of the first hatchling. The counting of hatchlings continued until the last egg hatched and the remaining eggs were counted to estimate egg mass viability. The duration of embryonic development (d, days) was calculated as the number of days elapsed between the date of egg laying and the date of first hatching.

Following the results with *Pomacea canaliculata* (Lamarck, 1822) reported by Seuffert et al. (2012), the lower temperature threshold (T_L) for embryonic development was estimated by three different methods: the least standard deviation from the mean observed number of days (SD-day), the coefficient of variation in days (CV-day) and the linear regression coefficient method (REG). The different threshold temperatures were estimated using the equations developed by Yang et al. (1995) based on these methods.

The degree-days (DD, °C.d) for the embryonic development were calculated on the basis of hourly records of temperature by computing the degree-hours and summing over the 24-h period. Degree-hours were calculated as the difference between the recorded hourly mean temperature (T_h) and the lower threshold (T_L):

$$DD = \Sigma\ (T_h - T_L)$$

The cumulative DD were estimated by summing the daily DD over the specific period of development of each egg mass (Seuffert et al., 2012). To estimate the possible error due to the use of air temperatures instead of water temperatures we mimicked the smaller variation of the latter using the moving average of the last ten hourly records of air temperature and estimated T_L and the cumulative DD again.

Statistical Analysis

The effect of temperature on the snails' activity and mortality was investigated through one-way ANOVAs. If homogeneity of variances was rejected by Levene's test, the dependent variable was arcsine square root transformed and re-analyzed. Means were compared with LSD post hoc test. Differences in hatchlings' size among treatments were analyzed with nested ANOVAs, with the three replicates (bottles) being the nested random factor and water temperature the main fixed factor.

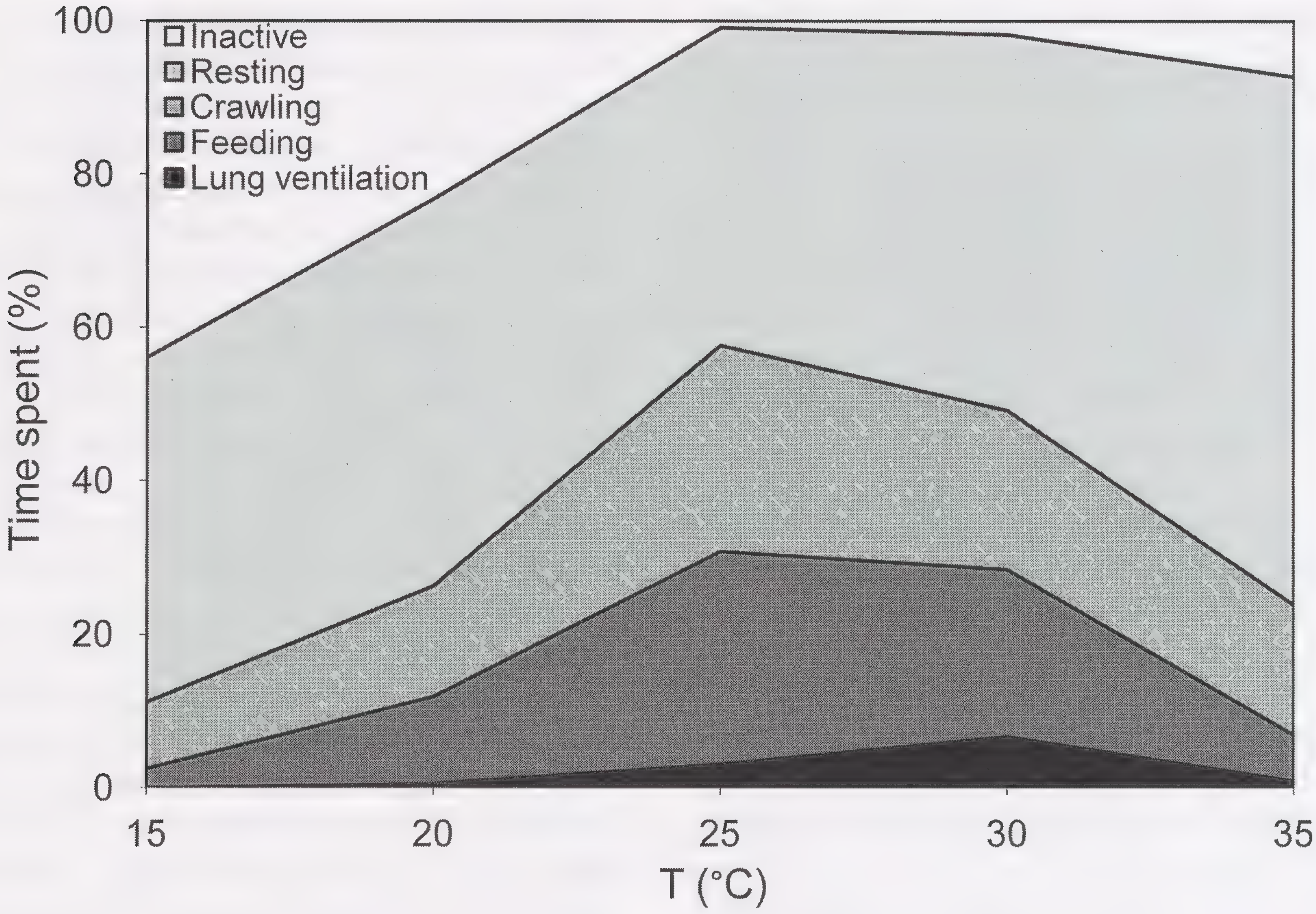

FIG. 1. Time spent (%) in different activities by *A. platae* at different constant temperatures (T).

RESULTS

Experiment 1: Effect of Constant Temperatures on Activity

Snails spent nearly half of the total time resting with the foot extended regardless of temperature (range: 41.4–68.8%; Fig. 1), without significant differences among treatments (Table 1). The percentage of time that the snails were inactive (fully or partially retracted) decreased significantly with temperature (Table 1); the mean percentage recorded at 15°C (44%) was significantly higher than the means at 25, 30 and 35°C (Fig. 2), temperatures with very low levels of inactivity (between 0.9 and 7.3%). The time spent ventilating the lung increased significantly with temperature (Table 1), from zero at 15°C to a maximum of 6.7% at 30°C (Fig. 3). The mean frequency of pumping movements per ventilation event was seven and ranged between 1 and 18. The time spent feeding increased significantly with temperature from 2.5% at 15°C to a maximum of 28% at 25°C, and then decreased significantly from 25 to 35°C (Table 1; Fig. 4). In contrast, the percentage of time spent crawling was not affected by temperature (Table 1).

At 15 and 20°C the snails were found buried in the sand with a mean frequency of 17.3 and 16.8%, respectively, and at higher temperatures (25, 30 and 35°C) burying was almost null (< 1% of total time). During the duration of this experiment, no snails were observed mating and no eggs were laid.

Experiment 2: Effect of Constant Temperatures on Mortality of Adult Snails and on Mortality and Growth of Hatchlings

Temperature had a significant effect on the mortality of adult snails ($F_{4,10} = 4.67$, $p = 0.022$), reaching a maximum of 60% at 35°C (Fig. 5). This mean was significantly higher than the mean mortalities recorded at the other temperatures (LSD test, $p < 0.05$) that were quite

TABLE 1. Summary of one-way ANOVAs for activity variables of *A. platae* at different constant temperatures. Dependent variables: time spent inactive (I), ventilating the lung (V), feeding (F), crawling (C) and resting (R); I and V were arcsine square root transformed before the analysis.

	I	V	F	C	R
$F_{4,20}$	5.335	3.765	8.139	1.410	1.304
p	0.004	0.019	< 0.001	0.267	0.302

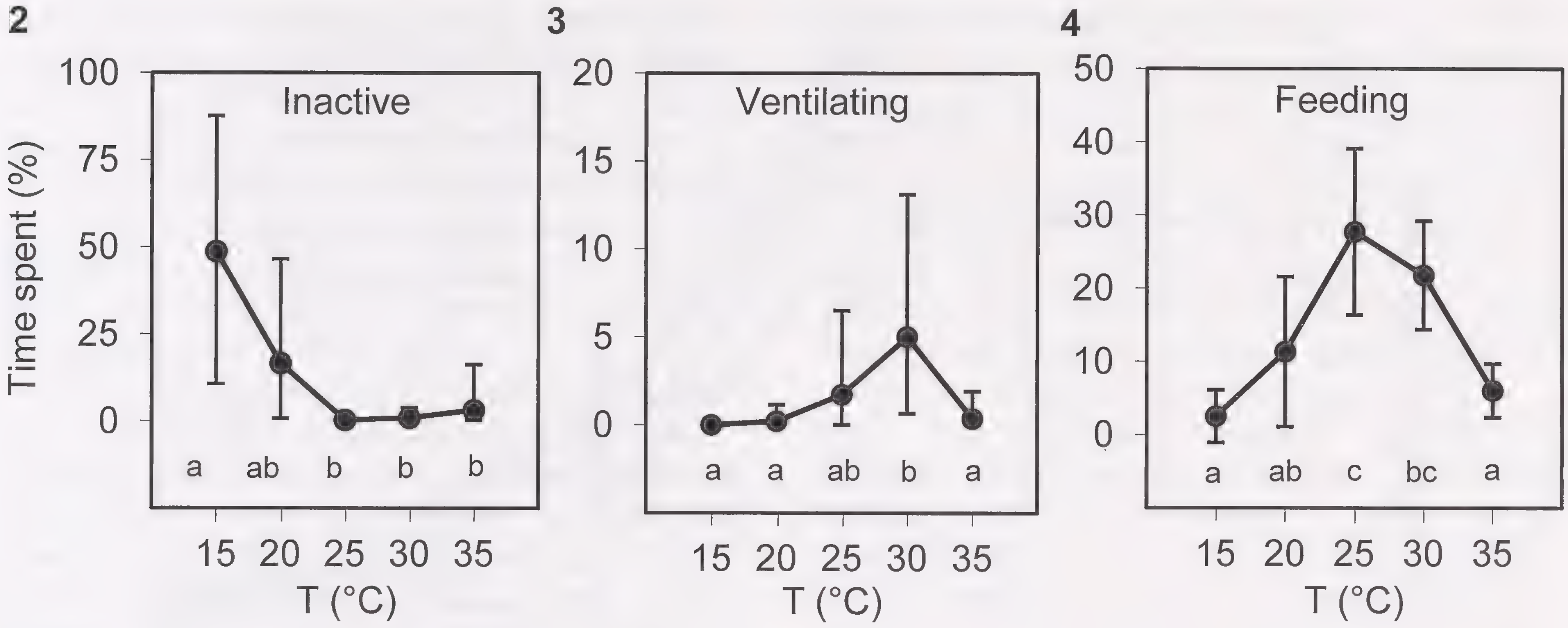

FIGS. 2–4. Means ± confidence interval (95%) of time spent in different activities by *A. platae* at different constant temperatures (T); different letters indicate significantly different means after LSD test (y-axis are in different scales). FIG. 2: Inactive; FIG. 3: Ventilating the lung; FIG. 4: Feeding; for the first two variables back-transformed values are shown.

low (6–20%). The mortality of hatchlings was not significantly affected by temperature ($F_{4, 10}$ = 3.00, $p = 0.072$) despite being higher at 35°C with a mean mortality of 60% as with adults. For all the other temperatures, mortality was 2.0 to 6.6 times higher for hatchlings than for adults.

The mean size of hatchlings after 20 days was significantly affected by temperature ($F_{4, 135}$ = 13.774, $p < 0.001$) while the nested factor (replicated bottles) was not significant ($F_{10, 135}$ = 0.895, $p = 0.539$). The minimum size was recorded at 15°C (mean = 2.42 mm; Fig. 6), being significantly lower than the sizes recorded at all the other temperatures (LSD test, $p <$ 0.05). The biggest size was obtained at 30°C, being 48.7% higher than the minimum and significantly bigger than the size recorded at 20°C but not significantly different from those of 25° or 35°C.

Experiment 3: Threshold Temperature and Degree-days Requirement for Embryonic Development

A total of 84 egg masses were used in this experiment. The mean viability of egg masses

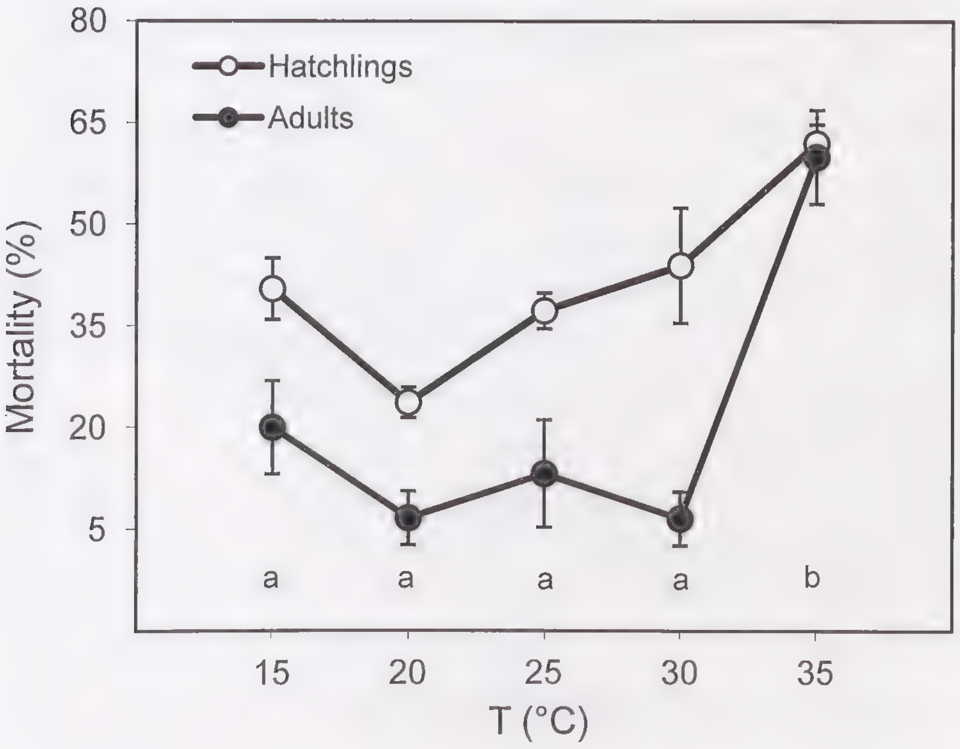

FIG. 5. Means ± confidence interval (95%) of the mortality (percentage of dead snails) of adults and hatchlings of *A. platae* at different constant temperatures (T); different letters indicate significantly different means for adults after LSD test.

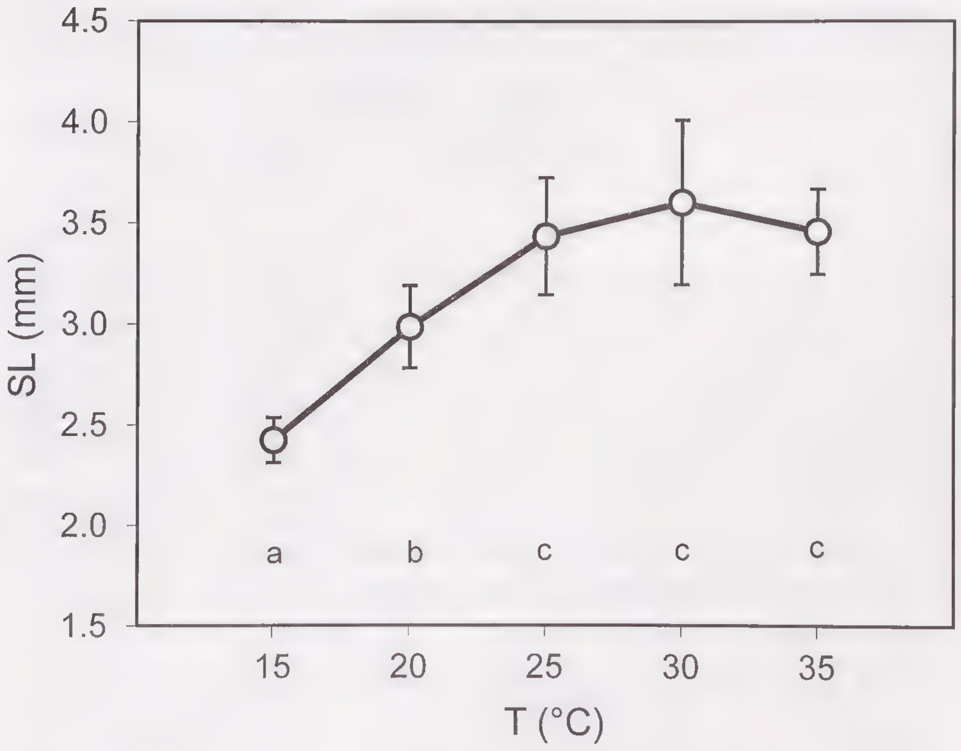

FIG. 6. Means ± confidence interval (95%) of shell length (SL) of hatchlings of *A. platae* attained after 20 days at different constant temperatures (T); different letters indicate significantly different means after LSD test.

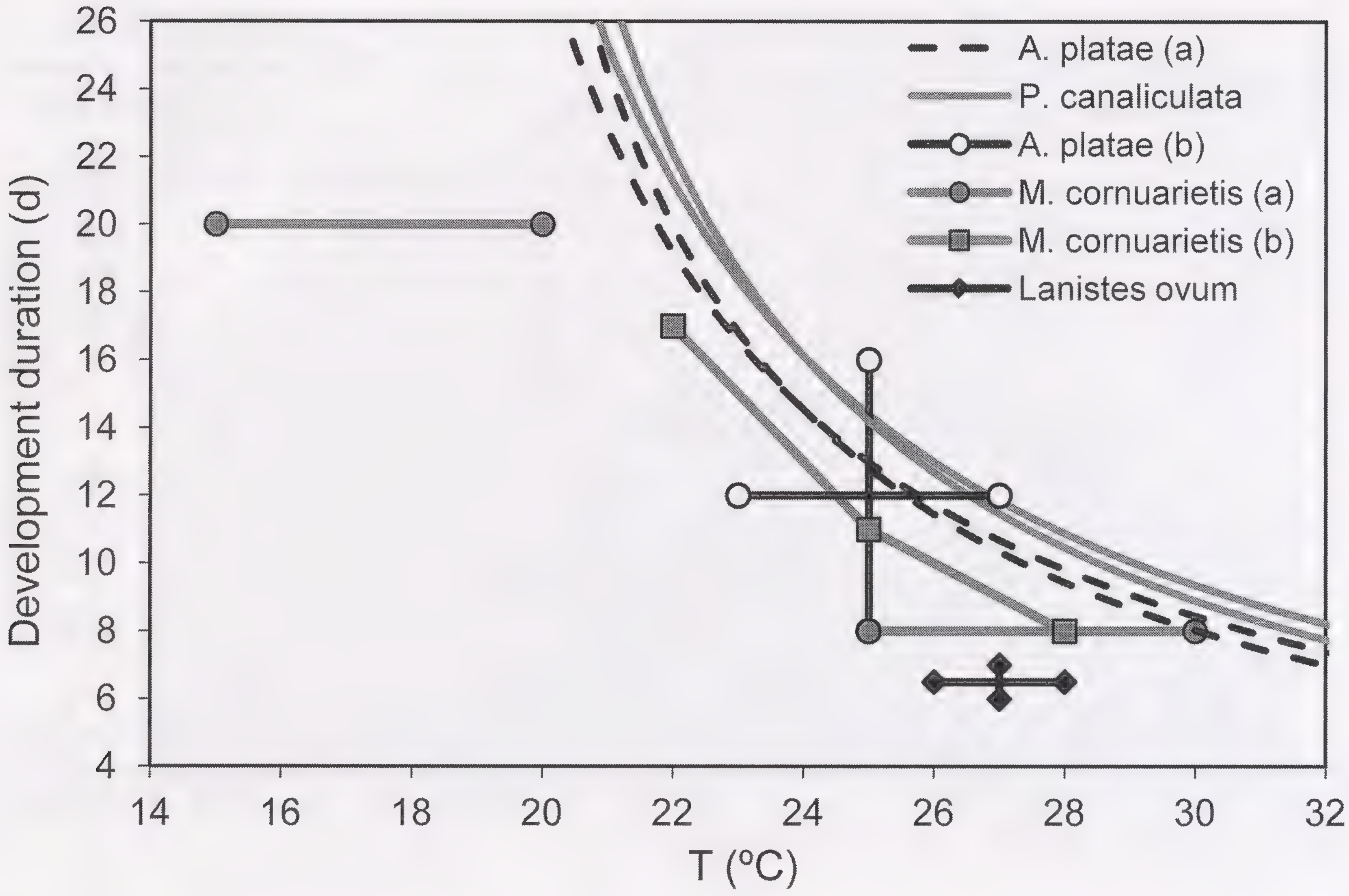

FIG. 7. Duration of embryonic development of *A. platae* at different temperatures (T) [a: calculated with the extreme estimations obtained in this paper (Table 2); b: reported by Tiecher et al. (2014)], durations of two other species with subaquatic egg masses [*Marisa cornuarietis* (a: Demian & Yousif, 1973, b: Aufderheide et al., 2006) and *Lanistes ovum* (Heiler et al., 2007)] and those obtained for aerial egg masses of *Pomacea canaliculata* with the same methods used here (bars indicates ranges of temperatures and/or durations).

(100 * number of live hatchlings / total number of eggs) was 57.8% and fluctuated between 1.1 and 100%. For the estimations of thresholds and degree-days we decided to use the data obtained from egg masses with viabilities greater than 10%, leaving a total of 77 egg masses. The duration of embryonic development (d) varied from a minimum of 9 days to a maximum of 26 days (mean ± SD = 14.57 ± 3.18 d). The estimations of the lower temperature threshold for the embryonic development of *A. platae* varied between 15.7°C and 16.6°C according to the method used (Table 2), and the corresponding mean cumulative DD estimations ranged between 107.6°C.d and 120.7°C.d. The cumulative DD of each egg mass was not related to the mean temperature to which it was exposed during development ($F_{1,75} = 0.029$, $p = 0.864$, estimated slope ± SD = -0.51 ± 2.97) indicating that degree days were constant within the temperature range to which the eggs were exposed (19–28°C). The estimations obtained using the moving average of water temperatures (whose greater delay reduced the variation in 4.5%) were only 1.5% higher and 2.4% lesser at most for the lower threshold and cumulative degree-day estimations, respectively.

TABLE 2. Threshold temperatures (°C) and cumulative degree-days (DD; °C.d) for the embryonic development of *A. platae*. Threshold temperatures were estimated by different methods: the least standard deviation in days (SD-day), the coefficient of variation in days (CV-day) and the linear regression coefficient method (REG); the values for the cumulative DD are mean ± SD.

Method	Threshold	Cumulative DD
SD-days	16.1	114.9 ± 23.4
CV- days	15.7	120.7 ± 24.5
REG	16.6	107.6 ± 21.9

DISCUSSION

Water temperature had a significant effect on the general level of activity of *Asolene platae*. Regardless of temperature, snails remained resting attached to the substratum nearly half of the time. At 15°C snails were inactive (i.e., fully or partially retracted) the other 44% of time; only during 1% of the time snails were found crawling or feeding. The general level of activity of *A. platae* reached its maximum in the range 25–30°C, and the time that the snails spent buried was almost null above 25°C. Above 30°C activity began to decrease, increasing the percentage of time resting.

The level of inactivity at 15°C comprised nearly half of the total observation time. In a study of the thermal biology of *P. canaliculata*, it was reported that although the time inactive was lower at 15°C (25%) it steeply increased to 98% at 10°C (Seuffert et al., 2010). These results suggest that *A. platae* will also be inactive at 10°C. On the other hand, *A. platae* snails spent nearly half of the time resting, with the foot extended but motionless, regardless of water temperature. Based on the scarce information available, *A. plate* is apparently a slow growing (MJT, unpublished results) species, much less mobile than *P. canaliculata* which spends only 26% of the time on average resting between 15 and 30°C (Seuffert et al., 2010).

The time spent feeding increased significantly with temperature, reaching its maximum at 25–30°C and decreasing at 35°C. This increase in feeding corresponded with the decrease of inactivity above 20°C and not to a decrease in resting time as it was reported for *P. canaliculata* (Seuffert et al., 2010). Feeding in this species was maximum at 25°C and began to decrease with higher temperatures. The level of feeding of *Pomacea maculata* Perry, 1810, was minimum at 15°C and reached its maximum at 30°C (Gettys et al., 2008). For ectothermic animals, this increase seems to be essential to fulfill the energetic demands of an increased metabolism. The decrease in feeding recorded at 35°C may indicate that temperatures above 30°C begin to be suboptimal and even harmful for *A. platae* in the midterm, since growth decreases and mortality reaches its maximum at 35°C.

The amount of time that *A. platae* individuals spent crawling (average 17.5%) was not affected by temperature. A similar result was reported for *P. canaliculata*, which spent almost the same proportion of time crawling (20.2%) regardless of temperature variation (Seuffert et al., 2010). As it was previously proposed, a plausible explanation is that the snails can crawl faster with increasing temperature. In consequence, they do not spend additional time to move between different places to perform their routine activities.

Ampullariids have both a functional gill and a lung and are considered as amphibious snails (Andrews, 1965; Berthold, 1991; Seuffert & Martín, 2009). The maximum level of lung ventilation in *A. platae* was recorded at 30°C, probably related to an increase in metabolic rate (Åkerlund, 1969; Freiburg & Hazelwood, 1977) and to the fact that the levels of dissolved oxygen decrease with increasing temperatures, since the aquaria were not artificially aerated. With increasing levels of hypoxia, the significance of aerial respiration increases, becoming a complementary mechanism to branchial intake of oxygen (Seuffert & Martín, 2010). Whereas *P. canaliculata* breathes air between 15 and 35°C, irrespective of water aeration (Seuffert & Martín, 2009), *A. platae* ventilates the lung only between 25 and 35°C in non-aerated water. This indicates a lower degree of dependence on aerial respiration in *A. platae*, which is correlated with the smaller size of its siphon (Seuffert & Martín, 2009) and the late development of its lung (Tiecher et al., 2014). The number of pumping movements per ventilation event varied greatly among replicates and showed no relation to temperature. Similarly, no effect of temperature was detected on the number of pumping movements of *P. canaliculata* (Seuffert & Martín, 2009).

Mortality was higher for hatchlings than for adults at all temperatures with the exception of 35°C, which resulted in high levels of mortality for both groups. Temperature significantly affected the mortality of *A. platae* adults but no differences were detected with the mortality of hatchlings. By contrast, an effect of temperature on the mortality rate of hatchlings was reported for *Marisa cornuarietis* (Linnaeus, 1758) and *P. canaliculata* (Selck et al., 2006; Seuffert & Martín, 2013). The influence of temperature on the mortality rates of *A. platae* hatchlings was probably masked by their high intrinsic mortality rates (MJT, unpublished data), since the survivorship curves of *A. platae* generally conform to Type III (Deevey, 1947). A different pattern has been reported for *P. canaliculata* (survivorship curves Type I; Estebenet & Martín, 2002), which evidences a very low intrinsic mortality of hatchlings and juvenile snails (Estebenet & Cazzaniga, 1992, 1998), even when exposed to extreme temperatures (only 20% after ten weeks of exposure at 35°C; Seuffert & Martín, 2013).

The shell length of hatchlings attained after 20 days was significantly affected by temperature, being highest at 25, 30 and 35°C. The smaller snails were obtained in the treatment of 15°C. Similarly, the maximum shell length of *P. canaliculata* hatchlings after ten weeks was recorded between 25 and 35°C, being significantly higher than the sizes attained with 15 and 20°C (Seuffert & Martín, 2013). Hatchlings of *P. maculata* reared at 15°C did not grow at all and at 35°C grew significantly less than at 20–30°C (Gettys et al., 2008). The growth rate of *M. cornuarietis* (Linnaeus, 1758) juveniles significantly decreased with temperature from 28°C to 22°C (Aufderheide et al., 2006; Selck et al., 2006). Based on this information we conclude that the optimum temperature range for growth varies a little among these South American ampullariids, but for all of them temperatures below 20°C will result in a stunted growth.

The risks of predation, severe hypoxia or prolonged air exposure of subaquatic egg masses (McMahon, 1983; Turner et al., 2007; Tiecher et al., 2014) increase with the duration of development for most oviparous snails inhabiting freshwater habitats, which are highly variable and unpredictable as compared with marine ones. Temperature and oxygen are the main environmental drivers of the duration of development although the effects of temperature may be contradictory, increasing mitotic rates but also reducing oxygen concentrations in water. The analyses of this trait would be important to understand the selective pressures that aquatic snails faced during colonization of inland waters from the sea or terrestrial habitats (McMahon, 1983; Dillon, 2000) and also the evolution of aerial egg masses in some lineages (Hayes et al., 2009b).

The duration of embryonic development of *A. platae* predicted by our degree-day models at different temperatures was compared to the durations previously reported for this species and for other species of ampullariids with subaquatic egg masses and also to the duration estimated for the aerial egg masses of *P. canaliculata* using the same methods (Fig. 7). Due to the small size and flat shape of the dishes used for the incubation of egg masses, the effect of using air temperature instead of water temperature in our present estimations was smaller than the effect of the three different calculation methods. The durations reported by Tiecher et al. (2014) for egg masses incubated under controlled temperature (25 ± 2°C) in the same laboratory and deposited by snails from the same pool as the present study showed a wide variation but the mean duration (10.8 days) agrees with the predictions from our degree-day models. The lower temperature threshold for the embryonic development of *A. platae* is around 16°C, coinciding with the values of 15.7–16.2°C estimated for *P. canaliculata*. The cumulative degree-days estimated for *A. platae* ranged between 107.5 and 120.5°C.d, being also very close to those obtained for *P. canaliculata* (120.7–132.2°C.d.; Seuffert et al., 2012; Fig. 7). On the other hand, up to 1400°C.d have been estimated for acroloxid limpets inhabiting a high latitude lake (Shirokaya & Röpstorf, 2003).

The duration of development in the temperature range of 25–30°C for *M. cornuarietis* (Demian & Yousif, 1973), whose subaquatic egg masses are similar to those of *A. platae* (Tiecher et al., 2014), are quite coincident with our estimations. In contrast, the duration of 20 days reported for *M. cornuarietis* in the range of 15–20°C is much shorter than that predicted by our model as temperature approaches the lower threshold (30 days below 20°C). Even though it is a different species, it seems odd that development occurs at such low temperatures, given the tropical origin of the snails used in that study (Puerto Rico). Demian & Yousif (1973) only mentioned the extreme temperatures recorded (15–20°C) so the actual temperature regime under which the eggs developed is unknown. In another study, *M. cornuarietis* eggs took eight days at 28°C and 17 days at 22°C to hatch (Aufderheide et al., 2006), which is consistent with the reports for this species in the range 25–30°C and only two to three days shorter than our estimates for *A. platae*. In contrast, the only report to date of the development of an Old World ampullariid with subaquatic egg masses (*Lanistes ovum* Peters, 1845) indicates that it requires 6–7 days at 26–28°C (Heiler et al., 2007), which is faster than the development for *A. platae* and *M. cornuarietis* at similar temperatures. Perhaps this is related to the fact that the eggs of *L. ovum* are disposed in a single layer and hence there is a reduced chance of competition for oxygen within the gelatinous egg mass, which usually delays hatching (Moran & Woods, 2007; Lardies & Fernández, 2002). On the other hand, the cleidoic eggs of *P. canaliculata* develop at all temperatures at a slightly lower rate (Seuffert et al., 2012) than the aquatic eggs of *A. platae* studied here. However, the difference may not be significant when taking into account the high inter- and intra-egg mass variation in the duration of development in *A. platae* (Tiecher et al., 2014) and the consequently high standard deviations in the degree-days estimations (Table 2).

Considering the overall results found in this study, we conclude that the optimum temperature for *A. platae* populations would be the range 25–30°C. These temperatures were the optimum for the performing of this species' routine activities. Temperatures of 35°C and above would be harmful for the snails since not only the levels of activity dropped above 30°C but also mortality rates were higher. On the other hand, at temperatures of 20°C and below the level of general activity rapidly decreased and the snails grew at a slower rate. *Asolene platae* exhibits a wide range of thermal tolerance, similar to that of *P. canaliculata* from Encadenadas del Oeste basin (Seuffert et al., 2010). However, the lower activity levels at low temperatures and the higher mortalities at high temperatures probably explains the narrower latitudinal range on *A. platae* (25 to 35°S; Castellanos & Fernández, 1976) as compared to *P. canaliculata* (20 to 38°S; Hayes et al., 2012).

Even though *A. platae* is not regarded as an invasive species, it is entering in the aquarium pet trade and thus there are chances of dispersal to other regions of America and other continents by this mean in the future (Smith, 2006). Specimens are being obtained from natural populations within the natural range of *A. platae* (Lower Paraná river and the southern shore of La Plata river) and offered as Zebra Apple Snails in pet shops and in aquarist web pages (PRM; personal observations).

Temperature has been considered the main determinant of establishment in models predicting the spread of *Pomacea* spp. (e.g., Lv et al., 2009; Byers et al., 2013; EFSA, 2013). Based only on the thermal regime, the potential range of distribution of *A. platae* in the possible scenario of an introduction would be less extensive than the currently invaded regions with *Pomacea* spp. (southern and eastern Asia, southern USA, Pacific Islands and Spain; Rawlings et al., 2007; Hayes et al., 2008; López et al., 2010), nevertheless it could include many temperate and subtropical regions around the world. However, other factors like predation, competition and feeding need to be considered when developing predictive models of the success of its establishment outside of its native range. Knowing the potential range of distribution of *A. platae* would be useful for detecting and controlling incipient invasions of these apple snails.

ACKNOWLEDGMENTS

This work was funded with grants by CONICET ("Consejo Nacional de Investigaciones Científicas y Técnicas", PIP 112 200901 00473), UNS ("Universidad Nacional del Sur", PGI 24/B185) and ANPCyT ("Agencia Nacional de Promoción Científica y Tecnológica, PICT 2012-1956). MES and PRM are researchers in CONICET.

LITERATURE CITED

ÅKERLUND, G., 1969, Oxygen consumption of the ampullariid snail *Marisa cornuarietis* L. in relation to body weight and temperature. *Oikos*, 20(2): 529–533.

ALBRECHT, E. A., N. B. CARREÑO & A. CASTRO-VAZQUEZ, 1999, A quantitative study of environmental factors influencing the seasonal onset of reproductive behaviour in the South American apple-snail *Pomacea canaliculata* (Gastropoda: Ampullariidae). *Journal of Molluscan Studies*, 65: 241–250.

ANDREWS, E. B., 1965, The functional anatomy of the mantle cavity, kidney and blood system of some pilids gastropods (Prosobranchia). *Journal of Zoology*, 146: 70–94.

AUFDERHEIDE, J., R. WARBRITTON, N. POUNDS, S. FILE-EMPERADOR, C. STAPLES, N. CASPERS & V. FORBES, 2006, Effects of husbandry parameters on the life-history traits of the apple snail, *Marisa cornuarietis*: effects of temperature, photoperiod, and population density. *Invertebrate Biology*, 125(1): 9–20.

BERTHOLD, T., 1991, Vergleichende Anatomie, Phylogenie und Historische Biogeographie der Ampullariidae (Mollusca: Gastropoda). *Abhandlungen des Naturwissenschaftlichen Vereins in Hamburg Series*, (NF), 29: 1–256.

BYERS, J. E., W. G. McDOWELL, S. R. DODD, R. S. HAYNIE, L. M. PINTOR & S. B. WILDE, 2013, Climate and pH predict the potential range of the invasive apple snail (*Pomacea insularum*) in the southeastern United States. *PLoS One*, 8: e56812.

CARLSSON, N. O., C. BRÖNMARK & L. A. HANSON, 2004, Invading herbivory: the golden apple snail alters ecosystem functioning in Asian wetlands. *Ecology*, 85(6): 1575–1580.

CASTELLANOS, Z. J. A. & D. FERNÁNDEZ, 1976, Gastropoda Ampullariidae. Pp. 1–33, in: R. A. RINGUELET, ed., *Fauna de agua dulce de la República Argentina*, FECIC, Buenos Aires.

COWIE, R. H., 2002, Apple snails (Ampullariidae) as agricultural pests: their biology, impacts and management. Pp. 145–192, in: G. M. BARKER, ed., *Molluscs as crop pests*. CABI Publishing, Wallingford, New Zealand, 468 pp.

COWIE, R. H. & S. C. THIENGO, 2003, The apple snails of the Americas (Mollusca: Gastropoda: Ampullariidae: *Asolene, Felipponea, Marisa,* *Pomacea, Pomella*): a nomenclatural and type catalog. *Malacologia*, 45(1): 41–100.

DEEVEY, E. S., 1947, Life tables for natural populations of animals. *Quarterly Review of Biology*, 22: 283–314.

DEMIAN, E. & F. YOUSIF, 1973, Embryonic development and organogenesis in the snail *Marisa cornuarietis* (Mesogastropoda: Ampullariidae). *Malacologia*, 12(1): 123–150.

DILLON, R. T., 2000, *The ecology of freshwater molluscs*. Cambridge University Press, 509 pp.

EFSA [European Food Safety Authority, Panel on Plant Health], 2013, Scientific Opinion on the assessment of the potential establishment of the apple snail in the EU. *EFSA Journal 2013*, 11(12): 3487, 49 pp.

EFSA [European Food Safety Authority, Panel on Plant Health], 2014, Scientific Opinion on the environmental risk assessment of the apple snail for the EU. *EFSA Journal 2014*, 12(4): 3641, 97 pp.

ESTEBENET, A. L. & N. J. CAZZANIGA, 1992, Growth and demography of *Pomacea canaliculata* (Gastropoda: Ampullariidae) under laboratory conditions. *Malacological Review*, 25: 1–12.

ESTEBENET, A. L. & N. J. CAZZANIGA, 1998, Sex related differential growth in *Pomacea canaliculata* (Gastropoda: Ampullariidae). *Journal of Molluscan Studies*, 64: 119–123.

ESTEBENET, A. L. & P. R. MARTÍN, 2002, *Pomacea canaliculata* (Gastropoda: Ampullariidae): Life-history traits and their plasticity. *Biocell*, 26: 83–89.

FANG, L., P. K. WONG, L. LIN, C. LAN & J. W. QIU, 2010, Impact of invasive apple snails in Hong Kong on wetland macrophytes, nutrients, phytoplankton and filamentous algae. *Freshwater Biology*, 55: 1191–1204.

FORDHAM, D. A., C. MELLIN, B. D. RUSSELL, R. H. AKÇAKAYA, C. J. A. BRADSHAW, M. E. AIELLO-LAMMENS, J. M. CALEY, S. D. CONNELL, S. MAYFIELD, S. A. SHEPHERD & B. W. BROOK, 2013, Population dynamics can be more important than physiological limits for determining range shifts under climate change. *Global Change Biology*, 19 (10): 3224–3237.

FREIBURG, M. W. & D. H. HAZELWOOD, 1977, Oxygen consumption of two amphibious snails: *Pomacea paludosa* and *Marisa cornuarietis* (Prosobranchia: Ampullariidae). *Malacologia*, 16: 541–548.

GETTYS, L. A., W. T. HALLER, C. R. MUDGE & T. J. KOSCHNICK, 2008, Effect of temperature and feeding preference on submerged plants by the island apple snail, *Pomacea insularum* (d'Orbigny, 1839) (Ampullariidae). *The Veliger*, 50: 248–254.

HAYES, K. A., R. H. COWIE, A. JØRGENSEN, R. SCHULTHEIß, C. ALBRECHT & S. C. THIENGO, 2009b, Molluscan models in evolutionary biology: apple snails (Gastropoda: Ampullariidae) as a system for addressing fundamental questions. *American Malacological Bulletin*, 27: 47–58.

HAYES, K. A., R. H. COWIE & S. C. THIENGO, 2009a. A global phylogeny of apple snails: Gondwanan origin, generic relationships, and the influence of outgroup choice (Caenogastropoda: Ampullariidae) *Biological Journal of the Linnean Society*, 98, 61–76.

HAYES, K. A., R. H. COWIE, S. C. THIENGO & E. E. STRONG, 2012, Comparing apples with apples: clarifying the identities of two highly invasive Neotropical Ampullariidae (Caenogastropoda). *Zoological Journal of the Linnean Society,* 166: 723–753.

HAYES, K. A., R. C. JOSHI, S. C. THIENGO & R. H. COWIE, 2008, Out of South America: multiple origins of non-native apple snails in Asia. *Diversity and Distributions*, 14: 701–712.

HEILER, K. C. M., R. SCHULTHEIß, T. GEERTZ & C. ALBRECHT, 2007, Caught in the act: insights into the sex life of *Lanistes ovum* (Gastopoda: Ampullariidae). *Antwerp: World Congress of Malacology*, *Abstracts*, p. 94.

HORGAN, F. G., A. M. STUART & E. P. KUDAVIDANAGE, 2014, Impact of invasive apple snails on the functioning and services of natural and managed wetlands. *Acta Oecologica*, 54: 90–100.

LARDIES, M. A. & M. FERNÁNDEZ, 2002, Effect of oxygen availability in determining clutch size in *Acanthia monodon. Marine Ecology Progress Series*, 239: 139–146.

LEON, J. A., K. A. HAYES & R. H. COWIE, 2014, Ampullariidae revisionary systematics: claryifying the taxanomic status of *Asolene platae* (Maton, 1811) and *Asolene pulchella* (Anton, 1838). *Mollusca 2014. The meeting of the Americas* (Abstracts), Mexico City, Mexico, 119–120.

LÓPEZ, M. A., C. R. ALTABA, K. B. ANDREE & V. LÓPEZ, 2010, First invasive apple snails in Europe. *Tentacle*, 18: 26–28.

LV, S., Y. ZHANG, H. X. LIU, L. HU, K. YANG, P. STEINMANN, Z. CHEN, L. Y. WANG, J. UTZINGER & X. N. ZHOU, 2009, Invasive Snails and an Emerging Infectious Disease: Results from the First National Survey on *Angiostrongylus cantonensis* in China. *PLoS Neglected Tropical Disease* 3(2): e368. doi:10.1371/journal.pntd.0000368.

MADEIRA, D., L. NARCISO, H. N. CABRAL & C. VINAGRE, 2012, Thermal tolerance and potential impacts of climate change on coastal and estuarine organisms. *Journal of Sea Research*, 70: 32–41.

MATON, W. G., 1811, Description of seven new species of Testacea. *Transactions of the Linnean Society of London*, 10: 325–332, pl. 2.

McMAHON, R. F., 1983, Physiological ecology of freshwater pulmonates. Pp. 359–430, in: W. D. RUSSELL-HUNTER, ed., *The Mollusca VI, Ecology.* Academic Press, New York, 697 pp.

MORAN, A. L. & H. A. WOODS, 2007, Oxygen in egg masses: interactive effects of temperature, age, and egg-mass morphology on oxygen supply to embryos. *The Journal of Experimental Biology*, 210: 722–731.

RAWLINGS, T. A., K. A. HAYES, R. H. COWIE & T. M. COLLINS, 2007, The identity, distribution, and impacts of non-native apple snails in the continental United States. *BMC Evolutionary Biology*, 7: 97.

SAVEANU, L. & P. R. MARTÍN, 2013, Pedal surface collecting as an alternative feeding mechanism of the invasive apple snail *Pomacea canaliculata* (Caenogastropoda: Ampullariidae). *Journal of Molluscan Studies*, 79: 11–18.

SELCK, H., J. AUFDERHEIDE, N. POUNDS, C. STAPLES, N. CASPERS & V. FORBES, 2006, Effects of food type, feeding frequency, and temperature on juvenile survival and growth of *Marisa cornuarietis* (Mollusca: Gastropoda). *Invertebrate Biology*, 125(2): 106–116.

SEUFFERT, M. E. & P. R. MARTÍN, 2009, Influence of temperature, size and sex on aerial respiration of on *Pomacea canaliculata* (Gastropoda: Ampullariidae) from southern Pampas, Argentina. *Malacologia*, 51: 191–200.

SEUFFERT, M. E. & P. R. MARTÍN, 2010, Dependence on aerial respiration and its influence on microdistribution in the invasive freshwater snail *Pomacea canaliculata* (Caenogastropoda, Ampullariidae). *Biological Invasions*, 12: 1695–1708.

SEUFFERT, M. E. & P. R. MARTÍN, 2013, Juvenile growth and survival of the apple snail *Pomacea canaliculata* (Caenogastropoda: Ampullariidae) reared at different constant temperatures. *SpringerPlus*, 2: 312.

SEUFFERT, M. E., S. BURELA & P. R. MARTÍN, 2010, Influence of water temperature on the activity of the freshwater snail *Pomacea canaliculata* (Caenogastropoda: Ampullariidae) at its southernmost limit (Southern Pampas, Argentina). *Jounal of Thermal Biology*, 35: 77–84.

SEUFFERT, M. E., L. SAVEANU & P. R. MARTÍN, 2012, Threshold temperatures and degree-day estimates for embryonic development of the invasive apple snail *Pomacea canaliculata* (Caenogastropoda: Ampullariidae). *Malacologia*, 55(2): 209–217.

SHIROKAYA, A. A. & P. RÖPSTORF, 2003, Morphology of syncapsules and the duration of embryogeny of Baikalian endemic limpets (Gastropoda, Pulmonata, Acroloxidae). *Berliner Paläobiologische Abhandlungen*, 4: 183–192.

SMITH, J. W., 2006, Ampullariidae pathways. Pp. 113–120, in: R. C. JOSHI & L. S. SEBASTIAN, eds., *Global advances in ecology and management of golden apple snails*. Philippine Rice Research Institute, Nueva Ecija, Philippines, 600 pp.

TIECHER, M. J., S. BURELA & P. R. MARTÍN, 2014, Mating behavior, egg laying, and embryonic development in the South American apple snail *Asolene pulchella* (Ampullariidae, Caenogastropoda). *Invertebrate Reproduction & Development*, 58(1): 13–22.

TOMANEK, L., 2008, The importance of physiological limits in determining biogeographical range shifts due to global climate change: the heat shock response. *Physiological and Biochemical Zoology*, 81(6): 709–717.

TURNER, A. M., R. R. TURNER & S. R. RAY, 2007, Competition and intraguild egg predation among freshwater snails: re-examining the mechanism of interspecific interactions *Oikos*, 116(11): 1895–1903.

YANG, S., J. LOGAN & D. L. COFFEY, 1995, Mathematical formulae for calculating the base temperature for growing degree days. *Agricultural and Forest Meteorology*, 74: 61–74.

ZALOM, F. G., P. B. GOODELL, L. T. WILSON, W. W. BARNETT & W. J. BENTLEY, 1983, *Degreedays: the calculation and use of heat units in pest management*. Leaflet 21373. Division of Agriculture and Natural Resources, University of California, Davis, California, U.S.A., 10 pp.

Revised ms. accepted November 5, 2014

MALACOLOGIA, 2015, 58(1–2): 245–302

INSIGHTS FROM AN INTEGRATED VIEW OF THE BIOLOGY OF APPLE SNAILS (CAENOGASTROPODA: AMPULLARIIDAE)

Kenneth A. Hayes[1,2,3*], Romi L. Burks[4], Alfredo Castro-Vazquez[5], Philip C. Darby[6], Horacio Heras[7], Pablo R. Martín[8], Jian-Wen Qiu[9], Silvana C. Thiengo[10], Israel A. Vega[5,11], Takashi Wada[12], Yoichi Yusa[13], Silvana Burela[8], M. Pilar Cadierno[7], Juan A. Cueto[5], Federico A. Dellagnola[5], Marcos S. Dreon[7,14], M. Victoria Frassa[7], Maximiliano Giraud-Billoud[5], Martín S. Godoy[5], Santiago Ituarte[7], Eduardo Koch[5], Keiichiro Matsukura[2,12], M. Yanina Pasquevich[7], Cristian Rodriguez[5], Lucía Saveanu[8], María E. Seuffert[8], Ellen E. Strong[3], Jin Sun[9], Nicolás E. Tamburi[8], María J. Tiecher[8], Richard L. Turner[15], Patricia L. Valentine-Darby[16] & Robert H. Cowie[2]

ABSTRACT

Apple snails (Ampullariidae) are among the largest and most ecologically important freshwater snails. The introduction of multiple species has reinvigorated the field and spurred a burgeoning body of research since the early 1990s, particularly regarding two species introduced to Asian wetlands and elsewhere, where they have become serious agricultural pests. This review places these recent advances in the context of previous work, across diverse fields ranging from phylogenetics and biogeography through ecology and developmental biology, and the more applied areas of environmental health and human disease. The review does not deal with the role of ampullariids as pests, nor their control and management, as this has been substantially reviewed elsewhere. Despite this large and diverse body of research, significant gaps in knowledge of these important snails remain, particularly in a comparative framework. The great majority of the work to date concerns a single species, *Pomacea canaliculata*, which we see as having the potential to become a model organism in a wide range of fields. However, additional comparative data are essential for understanding this diverse and potentially informative group. With the rapid advances in genomic technologies, many questions, seemingly intractable two decades ago, can be addressed, and ampullariids will provide valuable insights to our understanding across diverse fields in integrative biology.

Key words: behavior, benthic macroinvertebrates, development, dormancy, ecology, evolution, freshwater, Gastropoda, immune system, invasive species, parasitology, reproduction, symbiosis.

[1] Department of Biology, Howard University, 415 College St., Washington, DC. 20059, U.S.A.
[2] Pacific Biosciences Research Center, University of Hawaii, 3050 Maile Way, Gilmore 408, Honolulu, Hawaii 96822, U.S.A.
[3] Smithsonian Institution, National Museum of Natural History, P.O. Box 37012, MRC 163, Washington, D.C. 20013-7012, U.S.A.
[4] Department of Biology, Southwestern University, 1001 East University Avenue, Georgetown, Texas 78626, U.S.A.
[5] Instituto de Fisiología (FCM-UNCuyo) and Laboratorio de Fisiología (IHEM-CONICET), Casilla de Correo 33, 5500 Mendoza, Argentina.
[6] Department of Biology, University of West Florida, 11000 University Parkway, Pensacola, Florida 32514, U.S.A.
[7] Instituto de Investigaciones Bioquímicas de La Plata (INIBIOLP, CONICET, Universidad Nacional de La Plata), Facultad de Ciencias Médicas, 60 y 120, 1900 La Plata, Argentina.
[8] Laboratorio de Ecología, INBIOSUR (Universidad Nacional del Sur-CONICET), Bahía Blanca, Argentina.
[9] Department of Biology, Hong Kong Baptist University, 224 Waterloo Road, Kowloon, Hong Kong.
[10] Laboratório de Malacologia, Instituto Oswaldo Cruz/Fiocruz, Av. Brasil 4365, 21040-900 Rio de Janeiro, RJ, Brasil.
[11] Área de Biología, Facultad de Ciencias Exactas y Naturales, Universidad Nacional de Cuyo, Mendoza, Argentina.
[12] NARO Kyushu Okinawa Agricultural Research Center, Suya 2421, Koshi, Kumamoto 861-1192, Japan.
[13] Faculty of Science, Nara Women's University, Kitauoya-nishi, Nara 630-8506, Japan.
[14] Comisión de Investigaciones Científicas (CIC), La Plata, Argentina.
[15] Biological Sciences Department, Florida Institute of Technology, 150 W. University Blvd., Melbourne, Florida 32901, U.S.A.
[16] The Pomacea Project, Inc., Pensacola, Florida, U.S.A.
* Corresponding author: kenneth.hayes@howard.edu

TABLE OF CONTENTS

ABSTRACT 245
TABLE OF CONTENTS 246
INTRODUCTION 246
CLASSIFICATION, DIVERSITY AND TAXONOMY 248
  Classification 248
  Diversity and Taxonomy 248
PHYLOGENETICS AND BIOGEOGRAPHY 249
  Phylogenetics 249
    Morphological 249
    Molecular 249
  Biogeography 251
SHELL MORPHOLOGY 251
  Shell Size and Thickness 251
  Shell Shape and Ontogeny 251
  Shell Banding 252
  Operculum 253
REPRODUCTIVE MORPHOLOGY 253
  Male Reproductive System 253
    Testis and Sperm 253
    Male Tract and Sperm Transfer 254
  Female Reproductive System 254
    Ovary 254
    Female Tract 255
DEVELOPMENT 256
  Initial Stages of Development 256
  Cardiac, Respiratory and Renal Organogenesis 256
  Digestive Tract 257
  Post-hatching Reproductive Development 257
LIFE HISTORY 258
  Life Cycle and Reproductive Seasonality 258
  Life History Variation 258
REPRODUCTIVE BEHAVIOR 259
  Mating 259
  Egg Laying 260
SEX RATIO, SEX DETERMINATION AND KARYOLOGY 261
HABITATS AND DETERMINANTS OF DISTRIBUTION 262
  Habitats 262
  Determinants of Distribution 263
AMPHIBIOUSNESS 263
DORMANCY 264
  Aestivation 265
  Hibernation and Cold Hardiness 266
FOOD, FEEDING AND DIGESTION 267
  Phytophagy and Preferences 267
  Intraspecific Variation in Feeding and Assimilation 268
  Feeding on Other Animals 268
  Digestion 269
PREDATORS AND PREDATOR AVOIDANCE 269
  Predators 269
  Predator Avoidance 270
EGG PROTEINS: STRUCTURE AND ROLE IN DEFENSE 270
  Perivitellin Structure and Synthesis 271
  Perivitellin Functions 271
  Evolutionary and Ecological Implications of Egg Defenses 272
SYMBIOTIC ASSOCIATIONS 273
  Epibiotic Organisms 273
  Endosymbiotic Animals 273
  Endosymbiotic Protists and Bacteria 275
  Intracellular Pigmented Corpuscles in the Midgut Gland 275
IMMUNE DEFENSES 276
  Ampullariid Hemocytes 276
  Hemocyte-producing Organs and/or Immune Barriers 276
ENVIRONMENTAL HEALTH AND POLLUTION 277
  Accumulation of Pollutants 277
  Toxicity of Pollutants to Apple Snails 278
  Mechanisms of Toxicity 278
HUMAN HEALTH CONCERNS 279
  Angiostrongyliasis 279
  Cercarial Dermatitis 280
  Echinostomiasis 280
CONCLUSION AND FUTURE RESEARCH OPPORTUNITIES 281
ACKNOWLEDGEMENTS 282
LITERATURE CITED 282

INTRODUCTION

Apple snails (Ampullariidae) are freshwater and amphibious snails predominantly distributed throughout the humid tropics and subtropics of Africa, the Americas and Asia (Berthold, 1991), where they often constitute a major portion of the native freshwater molluscan fauna (Fig. 1). They are commonly referred to as apple snails because of their large, round shells and include the largest of all freshwater snails. The family belongs to the Caenogastropoda, a large and diverse clade containing roughly 60% of living Gastropoda (Ponder et al., 2008).

Increasing interest in apple snail research has been driven in part by the introduction of several species as aquarium pets or food to many locations around the world, where they frequently have become major agricultural and

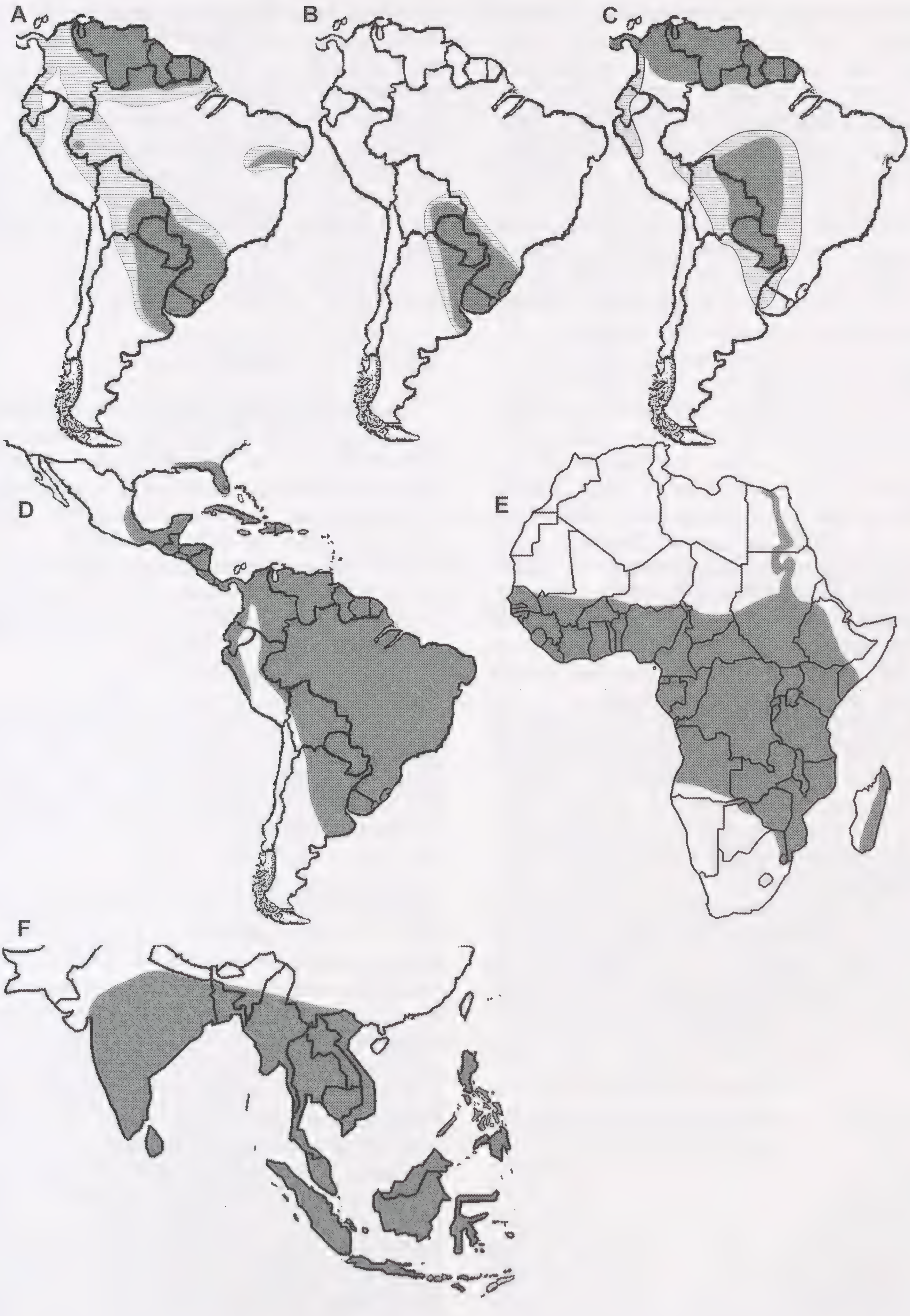

FIG. 1. Known (shaded grey) and probable (hashed) native distributions of *Asolene* (A), *Felipponea* (B), *Marisa* (C), *Pomacea* (D), *Lanistes* and *Pila* in Africa (E), and *Pila* in Asia (F). *Afropomus* and *Lanistes* are restricted to western Africa in Sierra Leone and Liberia, and the genus *Forbesopomus* is known only from a single location in the Philippines. Known distributions of New World taxa determined from literature and historical and recent collection data. Probable distributions estimated based on habitat suitability. Distributions for *Lanistes* and *Pila* based primarily on historical and recent collections.

environmental pests (Cowie, 2002; Joshi & Sebastian, 2006; Cowie & Hayes, 2012). This interest has been further fueled by questions surrounding the origin of several novel anatomical and behavioral characteristics, some associated with the transition from aquatic to terrestrial habitats (Hayes et al., 2009a). Addressing these questions in an integrative framework may provide insights fundamental to understanding the evolutionary biology of snails and freshwater taxa more generally (Hayes et al., 2009a), and has the potential to elevate apple snails to a valuable model system.

Cowie (2002) reviewed what was then known of apple snail biology, focusing on their ecology and behavior, impacts as pests and approaches to managing them. At the time of that review, the true identity of the pest species was not well understood, but this has since been clarified (Rawlings et al., 2007; Hayes et al., 2008, 2012; Tran et al., 2008). Since then, there has been a burgeoning of studies, primarily by South American, Asian and North American authors, focused mainly on the pest species *Pomacea canaliculata* (Lamarck, 1822) and *Pomacea maculata* Perry, 1810. The present review provides an update and extension of Cowie (2002) and focuses on studies on fundamental biology and applied topics in human health and ecotoxicology undertaken in the intervening years, as well as on topics not covered in that review, but excluding pest management, which has been covered extensively by Joshi & Sebastian (2006).

Much of the review focuses inevitably on species of *Pomacea*, most notably *Pomacea canaliculata*. However, various species of *Pila* are also frequently mentioned. To avoid confusion, we only abbreviate *Pomacea* to "*P.*", always spelling out *Pila* in full.

CLASSIFICATION, DIVERSITY AND TAXONOMY

Classification

Ampullariids are basal members of the Caenogastropoda. The family Ampullariidae Gray, 1824 (junior synonym: Pilidae – Cowie, 1997; ICZN, 1999), is in the superfamily Ampullarioidea within the informal group Architaenioglossa, which also includes the Cyclophoroidea and Viviparoidea (Bouchet & Rocroi, 2005). The Architaenioglossa has been resolved as paraphyletic in higher-order analyses using both molecular and morphological data (e.g., Harasewych et al., 1998; Colgan et al., 2003, 2007; Ponder et al., 2008). The Campaniloidea also may be closely related. Although marine ancestry of the architaenioglossan taxa is assumed by most, relationships among the four superfamilies and the resolution of the base of the Caenogastropoda remain unresolved (Ponder & Lindberg, 1997; McArthur & Harasewych, 2003; Strong, 2003; Simone, 2004; Colgan et al., 2003, 2007; Jørgensen et al., 2008; Ponder et al., 2008; Hayes et al., 2009b).

Diversity and Taxonomy

There are ten genera with approximately 120 species currently considered valid within the Ampullariidae. One of these genera, *Pseudoceratodes* (African, fossil only), is included in the family only tentatively (Berthold, 1991). The great majority of the remaining species are referred to just three genera (Table 1): *Pila* (*Ampullaria* and *Ampullarius* are junior synonyms – Cowie, 1997; ICZN, 1999), *Lanistes* and *Pomacea*. The remaining six genera each contain only one or a few species (Table 1).

Ampullariid taxonomy has relied almost exclusively on shell morphology. However, it has been extremely confused because of the gross morphological similarity within major groups accompanied by considerable intra-specific variation. Consequently, species boundaries have been very difficult to assess based solely on conchology. Berthold (1991) published very detailed descriptions not only of the shells but also of the soft anatomy of a selection of 36 species spanning the family. This work remains the most detailed analysis of ampullariid morphology to date, although the anatomy of *Pomacea canaliculata* and *P. maculata* has recently been redescribed in detail by Hayes et al. (2012), with significant modification to the interpretations of Berthold (1991). Additional anatomical information has been provided for *Pomacea diffusa* Blume, 1957, *P. figulina* (Spix in Wagner, 1827), *P. glauca* (Linnaeus, 1758), *P. lineata* (Spix in Wagner, 1827), *P. scalaris* (d'Orbigny, 1835) and *P. sordida* (Swainson, 1823) by Thiengo et al. (2011). Hayes et al. (2012) also synonymized the genus *Pomella* (which contained three valid species; Cowie & Thiengo, 2003) with *Pomacea*. In addition, these authors treated a number of species as synonyms of *P. canaliculata*, and others, including *P. insularum* (d'Orbigny, 1835), as synonyms of *P. maculata*. In the latter case, be-

TABLE 1. Numbers of nomenclaturally available species-group names and numbers of taxa of Ampullariidae (excluding fossil taxa).

Genus	Distribution	Currently valid species[1]	Estimated actual species diversity[2]	Subspecies, varieties, etc.[1]	Synonyms[1]
Afropomus	Africa	1	1	1	-
Asolene	South America	8	8	2	14
Felipponea	South America	3	3	-	-
Forbesopomus	Asia	1	1	-	-
Lanistes	Africa	43	20	16	34
Marisa	South America	2	3	-	6
Pila	Africa and Asia	29	30	16	84
Pomacea	South, Central and North America	96	50	22	112
Saulea	Africa	1	1	-	-
Total		186	117	57	250

[1] For the New World, from Cowie & Thiengo (2003), and taking into account changes subsequent to that publication, as tabulated by Cowie (in preparation); and for the Old World, Cowie (in preparation). Homonyms considered by Cowie & Thiengo (2003) and Cowie (in preparation) to represent taxonomically valid species and infraspecific taxa are counted as such.
[2] From Berthold (1991), Hayes & Cowie (unpublished).

cause Hayes et al. (2012) designated the same specimen as the neotype of *P. maculata* and as the lectotype of *P. insularum*, these become objective synonyms and the name *insularum* d'Orbigny, 1835, is no longer valid.

PHYLOGENETICS AND BIOGEOGRAPHY

Phylogenetics

Morphological

The first morphological phylogenetic analyses of ampullariids were those of Berthold (1991), who included conchological and anatomical characters, as well as characters of the eggs and reproductive behavior (i.e., deposition of egg masses above or below the water surface). The analyses were criticized by Bieler (1993) owing to Berthold's use of Hennigian argumentation without formal presentation of a character state matrix; when Bieler (1993) re-analyzed the data, a tree that differed in certain fundamental aspects resulted, most notably in the relative positions of *Saulea* and *Afropomus* and in the monophyly/paraphyly of *Pomacea* (Hayes et al., 2009b). A more recent and extensive character set (Simone, 2004) included only ten species, all from the New World, and produced a unique arrangement with *Felipponea* and *Asolene* nested within a paraphyletic *Pomacea*, and *Marisa* as sister to this assemblage.

Molecular

Jørgensen et al. (2008) published the first major molecular phylogeny of Ampullariidae, with a focus on African species and only three New World and four Asian species. Their five-locus analysis of 21 species recovered Old and New World taxa as non-monophyletic groups. Using a similar suite of markers (COI, 16S, H3, 18S and elongation factor 1 alpha instead of 28S), Hayes et al. (2009b) analyzed 40 species representing nine ampullariid genera and potential outgroups that included five viviparids, the only extant campanilid, and a cyclophorid. Their results contradicted those of Jørgensen et al. (2008) and showed that the Old and New World ampullariids are indeed reciprocally monophyletic. However, although four Old World genera (*Afropomus*, *Saulea*, *Pila, Lanistes*) were recovered as monophyletic, only *Asolene* was monophyletic among the five New World genera represented by more than a single species, with *Marisa* paraphyletic and *Pomella* (now a junior synonym of *Pomacea*: Hayes et al., 2012), nested within the polyphyletic *Pomacea* (Fig. 2).

Consistent with Jørgensen et al. (2008), *Lanistes* and *Pila* were robustly supported as reciprocally monophyletic sister clades, a relationship not supported by the morphological analyses (Berthold, 1991; Bieler, 1993). A monophyletic *Pila* consisted of two strongly-supported sister clades, one Asian and one African. *Saulea* was not supported as the sister taxon to New World ampullariids (Jørgensen et al., 2008), but was recovered as the basal member of the Old World ampullariids, consistent with the reanalysis of Berthold's (1991) data by Bieler (1993). The genus *Forbesopomus* has not been included in any phylogenetic analysis. Hayes et al. (2009b) demonstrated the importance of outgroup choice for inferring relationships among ampullariid genera, and for understanding evolutionary patterns within the group broadly. The remaining uncertainty regarding family-level relationships among basal caenogastropods is an area ripe for research incorporating additional anatomical and genomic data.

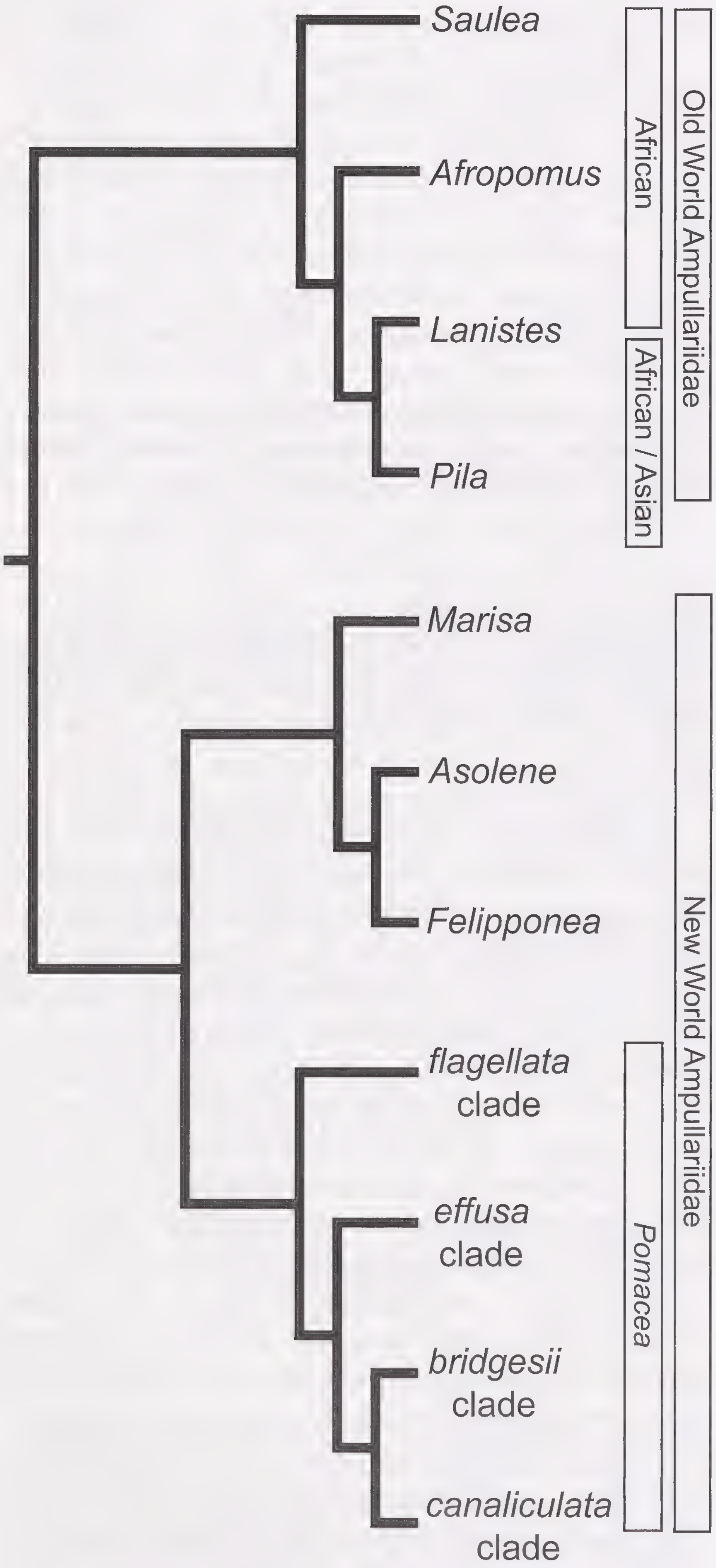

FIG. 2. Phylogenetic tree showing generic relationships within Ampullariidae and among major clades within the New World genus *Pomacea*. Redrawn from Hayes et al. (2009b) and Hayes (2009).

In early 2003, 20 years after the initial release of NCBI's (National Center for Biotechnology Information) GenBank sequence database, there were only nine ampullariid sequences, including three mitochondrial and six nuclear ribosomal, from individuals representing four *Pomacea* spp. and *Marisa cornuarietis* (Linnaeus, 1758). As of May 2014, a little more than a decade later, ampullariid sequence data on GenBank included 1,050 entries representing all extant genera except *Forbesopomus*. The majority of these (69%) are mitochondrial gene fragments (e.g., COI, 16S) commonly used in phylogenetic and phylogeographic analyses (e.g., Rawlings et al., 2007; Jørgensen et al., 2008; Hayes et al., 2008, 2009b; Bian et al., 2013) representing 54 species.

The advent of next-generation sequencing techniques has made feasible the generation of large amounts of genomic data, such as transcriptomes from whole organisms or from different organs and cost effective. Sun et al. (2012a) have made a significant step forward by conducting a *de novo* assembly of the transcriptome of *P. canaliculata*. They reported the identification of 128,436 unigenes with an average length of 419 bp and listed a number of genomic resources that may be useful for ecological and physiological studies including 2,439 unigenes with transposable elements, 3,196 microsatellites and 15,412 single-nucleotide polymorphisms. However, much of these data are not available on public databases and remain uncharacterized without an annotated expressed sequence tag database and comparative data from other closely related taxa. More recently, Sun et al. (2013) have made further advances through identification of 1,040 proteins from *Pomacea canaliculata*, among which more than 50 were differentially expressed under active and a estivating conditions. These efforts, combined with those of a number of ongoing genomic research projects, will soon yield vast amounts of data that will provide broad insights into the evolution and ecology of ampullariids.

Biogeography

Ampullariids probably originated from Gondwanan lineages that inhabited what is now Africa (Hayes et al., 2009b). Although fossil records are scarce (e.g., Prashad, 1925a; Pilsbry & Bequaert, 1927; Fischer, 1963; Boss & Parodiz, 1977; Martín & De Francesco, 2006), the Gondwanan origin is supported in part by the distribution of the two most basal genera in the family, *Saulea* and *Afropomus*, in current day Sierra Leone and Liberia on the African west coast, and the presence in Africa of two remaining Old World genera *Lanistes* and *Pila*. New World taxa (*Felipponea*, *Asolene*, *Marisa* and *Pomacea*) evolved in South and Central America after the South American continent split from Africa in the early Cretaceous (Hayes et al., 2009b).

The estimated timing of the split between the African and Asian clades of *Pila* occurred after the separation of Madagascar and India from Africa (Hayes et al., 2009b), which does not support the Out-of-India dispersal hypothesis (McKenna, 1973) that has been suggested to account for many Asian biotic elements with Gondwannan origins. Thus, if *Pila* originated in Africa (Berthold, 1991), instead of rafting on the Indian land mass, it may have reached Asia via North Africa and the Middle East. Alternatively, *Pila* originated in Asia from an unknown ancestor, subsequently dispersing into Africa. The finding of a 160 Mya ampullariid operculum in China (Wang, 1984) is more consistent with this latter hypothesis. This pattern of sister clades in Africa and Asia is seen in other groups (e.g., Bossuyt & Milinkovitch, 2001; Rutschmann et al., 2004; Sparks, 2004), but additional sampling of Asian and African lineages and the incorporation of biogeographic, anatomical and molecular data are necessary to evaluate the various hypotheses above (Hayes et al., 2009b).

SHELL MORPHOLOGY

Until recently, gross shell morphology of ampullariids has been the main feature on which their taxonomy has been based and is therefore well characterized (Fig. 3). Here we focus on recent advances in understanding and quantifying various aspects of shell morphology and variation, previously reviewed by Estebenet et al. (2006) for South American species.

Shell Size and Thickness

Apple snails range greatly in size and include the largest freshwater snails, with the shell of *P. maculata* capable of reaching 17 cm in maximum dimension (Cowie et al., 2006). In contrast, adults of *P. curumim* Simone, 2004, rarely grow larger than the size of *P. urceus* (Müller, 1774) hatchlings (10.5 mm on average; Burky, 1974; Simone, 2004). Shells range from very thick and porcelain-like (e.g., *Asolene* spp., *Felipponea* spp.) to much thinner (e.g., certain populations of *Pomacea*), and in *P. papyracea* (Spix in Wagner, 1827) they are almost devoid of calcium carbonate, with a very high relative content of organic matter and a thick periostracum (Berthold, 1989; Brown, 1994; Perera & Walls, 1996; Hayes, 2009). Shell thickness is highly variable within some species of *Pomacea*, increasing with calcium content and pH of the water (Glass & Darby, 2009) and decreasing with growth rate (Estebenet & Martín, 2003; Estebenet et al., 2006). Release of lactic acid generated by anaerobic metabolism during aestivation corrodes calcium carbonate and reduces the shell weight of *Pila globosa* (Swainson, 1822) by 5.25% after five months (Haniffa, 1978). The shells of males tend to be thicker than those of females in *P. canaliculata*, probably because of the investment of calcium in the egg shells and perivitelline fluid (Cazzaniga, 1990; Estebenet & Martín, 2003; Tamburi & Martín, 2012) or perhaps because of their lower growth rates (Estebenet et al., 2006; Tamburi & Martín, 2012).

Shell Shape and Ontogeny

Most apple snails are globose in shape and dextrally coiled, with the notable exception of species of *Marisa*, which are planispiral, and species of *Lanistes*, which are dextral but hyperstrophic and thus outwardly appear sinistral (Fig. 3). Although the globose *bauplan* places a general constraint on shell shape, some species express many variations on this theme, resulting in significant confusion for their shell-based taxonomy. In *P. canaliculata*, the inter-population variation has both a genetic and an environmental basis (Estebenet & Martín, 2003). Sexual dimorphism is also well known in *P. canaliculata*. The shell of female *P. canaliculata* is relatively more globose and with a broader body whorl than that of males (Tamburi & Martín, 2012); this dimorphism is not affected by growth rate, while the relative aperture width increases with growth rate in both sexes. Hanning (1979) showed sexual dimorphism in some populations of *P. paludosa* (Say, 1829). The shell of *P. canaliculata* has been studied recently using geometric morphometrics (Tabugo et al., 2010; Torres et al., 2011; Moneva et al., 2012; Tamburi & Martín, 2013) to disentangle the relationship between size and shape. Both sexes exhibit static allometry (i.e., adults at the same stage of maturity but of different sizes have different shapes); spire height decreases with size in both sexes, whereas aperture and body whorl size increase with size in males and females, respectively (Tamburi & Martín, 2013).

Changes in shape through ontogeny have only been studied by Estebenet (1998) in *P. canaliculata* and Youens & Burks (2008) in *P. maculata*. In the former, many dimensions of the shell show slightly allometric growth relative to shell length and hence shell shape changes gradually during ontogeny. However, there is a clear change in growth pattern in the operculum and aperture of males (Estebenet et al., 2006).

Shell Banding

Many species exhibit a pattern of dark spiral bands that varies considerably both within and among species. Some species consistently lack bands, for example *Pomacea scalaris* (d'Orbigny, 1835), *P. papyracea*, *P. curumin* and *Pila virescens* (Deshayes, in Bory de Saint Vincent, 1824) [*Pila polita* (Deshayes, 1830) is an objective junior synonym of *Pila virescens*; Cowie & Héros, 2012] (Keawjam, 1986; Simone, 2004). Unbanded individuals also often appear in normally banded species, for example *M. cornuarietis*, *P. canaliculata*, *Pila pesmei* (Morlet, 1889) and *Pila gracilis* (Lea, 1856) (Keawjam, 1986; Dillon, 2002; Estebenet et al., 2006). At least in *P. canaliculata*, the bands are not in the periostracum, but are the result of pigments produced by specialized cells in the

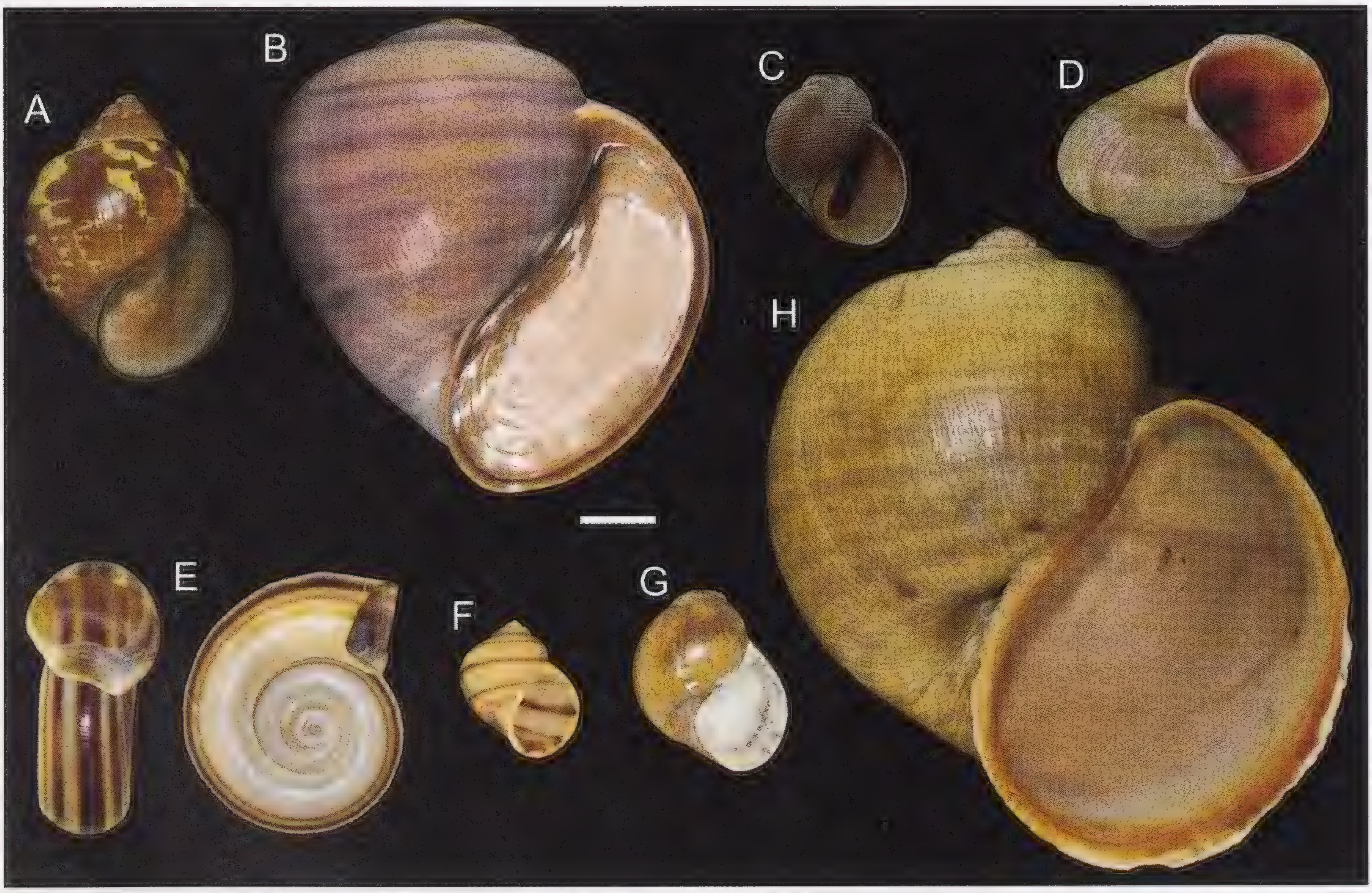

FIG. 3. Type species of extant Ampullariidae genera (except *Forbesopomus*) showing the diversity of shell morphology in the family. A: *Saulea vitrea*; B: *Pila ampullacea*; C: *Afropomus balanoidea*; D: *Lanistes carinatus*; E: *Marisa cornuarietis*; F: *Asolene platae*; G: *Felipponea neritiniformis*; H: *Pomacea maculata*. Scale bar = 1 cm; Photos: Hayes; except B: J.-P. Pointier and D: Muséum National d'Histoire Naturelle, Paris.

mantle margin and deposited in the outer layer of the shell (Estebenet et al., 2006). Banding seems to be controlled by simple Mendelian inheritance, with the unbanded condition recessive (Dillon, 2002; Yusa, 2004a). However, the environment may also influence the expression of banding, with bands often appearing, disappearing or changing in intensity coincident with strong growth lines (Estebenet et al., 2006). *Saulea vitrea* (Born, 1778) exhibits a quite different banding pattern, with highly variable coaxial zigzag brown and yellow bands, or may lack bands entirely (Brown, 1994).

Operculum

A calcified operculum is present only in the genus *Pila*, with all other ampullariids possessing a proteinaceous, horny operculum. The adult operculum of *Pomacea maculata* is thicker and more rigid than that of *P. canaliculata* or *Asolene* spp. (Bachmann, 1960; Hayes et al., 2012). In contrast to *P. maculata,* the flexible edge of the operculum in *P. canaliculata* enables it to seal the shell hermetically, but is not as effective for this purpose in larger *P. maculata* with much thicker operculae (Bachman, 1960; Yoshida et al., 2014). However, even in cases in which it does form a substantial seal, some water is still lost during aestivation (Little, 1968; Giraud-Billoud et al., 2011). In *P. canaliculata*, the operculum of hatchlings and juveniles of both sexes is concave (Estebenet et al., 2006; Gamarra-Luques et al., 2013). The female operculum remains concave throughout life, but becomes convex toward the posterior margin in males as the animal grows (Estebenet et al., 2006). This change in shape of the male operculum starts when shell length reaches 15–20 mm (Gamarra-Luques et al., 2013).

REPRODUCTIVE MORPHOLOGY

Rather than describing the complete internal anatomy of ampullariids in detail, which has been covered elsewhere (e.g., Hylton Scott, 1958; Andrews, 1964; Berthold, 1991; Catalán et al., 2002; Hayes et al., 2012; Gamarra-Luques et al., 2013), this section summarizes key recent advances in the understanding of the structure and function of the reproductive system. This system deserves special attention, as reproductive biology has significance for understanding biogeographical patterns, invasion biology and possibly the evolution of the amphibious habit seen in most ampullariids. The majority of studies have focused on *P. canaliculata,* and unless otherwise indicated, descriptions refer to this species.

Male Reproductive System

Testis and Sperm

The male gonad is a sponge-like mass of interconnected tubules that are delimited by a continuous layer of Sertoli cells (= tubular somatic cells) (Gamarra-Luques et al., 2006) that are flattened rather than columnar, as in other caenogastropods (Buckland-Nicks & Chia, 1986). The large ovoid nuclei of Sertoli cells contain one or more conspicuous nucleoli (Gamarra-Luques et al., 2006) and deep invaginations (Winik et al., 2009), and are polyploid, with 4 to 64 times the haploid nuclear DNA content (Cueto et al., 2006). The Sertoli cell cytoplasm contains abundant smooth endoplasmic reticulum and multilamellar bodies (Winik et al., 1994) made up of circularly arranged membranes. No interstitial epithelioid cells similar to the androgen-secreting interstitial cells of vertebrates have been observed (Gamarra-Luques et al., 2006).

The spermatogenic epithelium is arranged in nests of germinal cells at the same developmental stage. However, development is markedly asynchronous among contiguous nests (Gamarra-Luques et al., 2006), assuring continuous sperm production during the breeding season. This may be correlated with the repeated copulations (two to three per week) observed in reproductively active snails (Albrecht et al., 1996) and may contribute to the rapid growth of invasive populations.

As in many caenogastropods, the testis of *P. canaliculata* produces fertile sperm (“eupyrene sperm” or “eusperm”), as well as infertile “apyrene” and “oligopyrene” parasperm that lose all or part of their chromatin during spermiogenesis, respectively. Among ampullariids, parasperm have also been reported in *P. maculata* (Sachwatkin, 1920) and *Asolene pulchella* (Anton, 1838) (Tiecher et al., 2014). Eupyrene sperm in *P. canaliculata* result from a typical spermatogenic process and are of the basic monoflagellate “introsperm” type (Rouse & Jamieson, 1987; Catalán et al., 1997). While eusperm are only able to produce erratic lateral movements in testicular squashes, the highly motile fusiform parasperm, lacking chromatin and resembling those of other gastropods, are propelled by three to five flagellae (Buckland-

Nicks, 1998; Hodgson, 1999; Winik et al., 2001). They are produced at an apparently lower rate than eusperm (Winik et al., 2001).

Pomacea canaliculata also produces monoflagellate oligopyrene parasperm that are unique among known gastropod sperm. They are similar to the externally fertilizing "ectaquasperm" (Rouse & Jamieson, 1987) found in the Radiata and many Bilateria and may be produced by a truncation of euspermiogenesis, during which an ephemeral acrosome is formed at the anterior cell pole, by loss of contact with Sertoli cell projections (Buckland-Nicks & Scheltema, 1995; Winik et al., 2009).

The functional role of parasperm, particularly in the context of sperm competition and paternity assurance, is a matter of speculation (Buckland-Nicks, 1998; Till-Bottraud et al., 2005). In *P. canaliculata*, mating with a second male displaces sperm deposited by a previous one (Yusa, 2004a), and both eusperm and parasperm from the second male are likely to participate in displacing rival sperm.

Male Tract and Sperm Transfer

Sperm produced in the testis are transported to the tip of the penis along a path that comprises two distinct segments: (1) gonoduct derivatives, that is, vas deferens, seminal vesicle, prostate and genital papilla; and (2) mantle edge derivatives, that is, the copulatory apparatus, which is uniquely derived in the family, and varies among and sometimes within genera and hence is of considerable taxonomic utility (Berthold, 1991; Hayes et al., 2012).

As there is no direct connection between the genital papilla at the anterior end of the prostate, and the copulatory apparatus, sperm are deposited in a "sperm pit" (Andrews, 1964; Berthold, 1989) at the base of the copulatory apparatus, and from there are drawn, presumably through muscular contraction, into the spermiduct that extends the length of the penial complex. The copulatory apparatus is composed of a penial sheath and a penis (or a penial complex) in all studied species (Berthold, 1989). The penial sheath is short and nonglandular in *Afropomus*, *Saulea* and *Lanistes* (Berthold, 1989; Hayes, 2009), larger but "delicate" in *Pila* (Prashad, 1925b; Andrews, 1964) and stout and muscular in *Marisa* and *Pomacea* (Hylton Scott, 1958; Andrews, 1964; Berthold, 1989; Schulte-Oehlmann et al., 1994; Hayes et al., 2012; Giraud-Billoud et al., 2013a).

When present, there is considerable diversity among species in the number, structure and placement of penial sheath glands. An "outer gland" embedded at the sheath's base in *Pila*, *Marisa* and *Pomacea* extrudes quantities of a mucous secretion through an anterior duct during copulation, a "nuptial gift" eaten by the female, at least in *P. canaliculata* (Burela & Martín, 2007, 2014). There may also be one or more superficial glands lined with irregularly textured epithelia on the right margin of the penial sheath groove, which differ among genera and species (Hayes, 2009). They have been given different names by different authors reflecting conflicting interpretations about the number and homology of these glands (Table 2).

In their studies of the copulatory apparatus of *P. canaliculata*, Giraud-Billoud et al. (2013a) observed branched microvilli at the surface of the distal gland, which at the nanoscale level increase adhesion of this gland when inserted into the female's mantle cavity during copulation. A secretion composed of coarse protein granules may also play a role in enhancing adhesion, as suggested by Andrews (1964).

The penial complex comprises a muscular penial bulb (absent in Old World taxa) and a long penis that contains an open (Old World) or a closed (New World) spermiduct (Berthold, 1991). When at rest, the slender penis is enclosed in the penial pouch, which has an opening through which the penis passes to lie within the groove of the penial sheath (Hayes et al., 2012; Giraud-Billoud et al., 2013a). In *Pomacea* species the muscular penial bulb may also play a role in pumping fluid within the hemolymphatic spaces of the penis to deploy it from its resting coiled position (Giraud-Billoud et al., 2013a). However, the lack of the penial bulb in Old World taxa leaves the question of sperm transfer and penis deployment incompletely answered with regard to ampullariid functional morphology.

Female Reproductive System

Ovary

The ovary forms a layer of arborescent tubules beneath the mantle epithelium (Thiengo, 1987, 1989; Thiengo et al., 1993). The tubules are lined by the germinal epithelium, composed of Sertoli cells and oogenic cells (i.e., oogonia and previtellogenic and vitellogenic oocytes; Martín, 1986). Even though vitellogenic oocytes exhibit ultrastructural indications of active protein synthesis and endocytosis of tubular fluid (Winik & Castro-Vazquez, 2015), they never attain the massive accumulation of

TABLE 2. Presence or absence of penial sheath glands in some ampullariid species, and proposed equivalence of names by various authors. The works of Sachawatkin (1920), Hägler (1925), Prashad (1925c), Hylton Scott (1958) and Andrews (1964) are not included, because they referred to these glands collectively as "sheath glands", "superficial glands" or "marginal glands.

Gland	I	II	III	IV
Pila globosa (Swainson, 1822)	outer[1]	absent[1]	absent[1]	distal[1]
Marisa cornuarietis (Linnaeus, 1758)	outer[1]	absent[1,4]	proximal[1]	distal[1]
	gland 3[4]		gland 2[4]	gland 1[4]
Pomacea canaliculata (Lamarck, 1822)	outer[1,2]	absent[1,2,7]	proximal[1, 2]	distal[1,2]
	ventral basal[3]		medial[3]	apical[7]
Pomacea maculata Perry, 1810	ventral basal[3]	basal[3]	absent[3]	apical[3]
Pomacea figulina (Spix in Wagner, 1827)[a]	basal outer[5]	absent[5]	inner median[5]	apical[5]
Pomacea sordida (Swainson, 1823)	basal outer[6]	absent[6]	inner median[6]	apical[6]
Pomacea urceus (Müller, 1774)	outer[1]	absent[1]	proximal[1]	distal[1]

[1]Berthold (1989), [2]Giraud-Billoud et al. (2013a), [3]Hayes et al. (2012), [4]Schulte-Oehlmann et al. (1994), [5]Thiengo (1987), [6]Thiengo (1989), [7]Thiengo et al. (1993), [a]misidentified as *Pomacea lineata* by Thiengo (1987).

vitelline material observed in other caenogastropods (e.g., Cledón et al., 2005; Averbuj et al., 2010). This difference may be explained by the observation of periodic oocyte formation and gonadal evacuation in those studies but that occur continuously during the breeding season in *P. canaliculata* (Albrecht et al., 1996). Another correlate of the meager provisioning of oocytes is that developing embryos must rely mostly on perivitelline fluid for nutrition (Heras et al., 1998) (see Egg Proteins: Structure and Role in Defense).

Female Tract

The visceral oviduct ("renal" oviduct of many authors, at least in part) derives from the visceral section of primordial gonoduct and is homologous with the vas deferens in males (Gamarra Luques et al., 2013). It is also a slender tube, lined by a ciliated epithelium, that runs along the columellar axis to join the seminal receptacle, which is a complex structure at least in *Marisa* (Schulte-Oehlmann et al., 1994) and *Pomacea* (Andrews, 1964; Catalán et al., 2002; Hayes et al., 2012). The seminal receptacle is the site for sperm storage and fertilization (Hylton Scott, 1958; Andrews, 1964), and the sperm stored in the seminal receptacle may remain fertile for up to 140 days after copulation (Estebenet & Cazzaniga, 1993; Albrecht et al., 1996; Estebenet & Martín, 2002).

The more distal sections of the female tract of *P. canaliculata* (the albumen and capsule glands) are derivatives of the female pallial gonoduct (Gamarra-Luques et al., 2013) and are referred to collectively as the "pallial oviduct" (Catalán et al., 2002, 2006; Simone, 2004; Hayes et al., 2012) or primarily in the older literature as the "uterus" or "uterine gland" (Blainville, 1822; Sachwatkin, 1920; Hägler, 1923; Hylton Scott, 1958; Catalán de Canelada & Moreno, 1984; Giraud-Billoud et al., 2013a). The pallial oviduct of *Pomacea*, with its chambered seminal receptacle, branching albumen gland and coiled capsule gland, all embedded in a spongy mass of parenchymal tissue, is one of the most complex among the caenogastropods. Accordingly, understanding its structure and function is a field of active research and many aspects remain unresolved.

The seminal receptacle and the albumen and capsule gland ducts are connected in series in at least *Pila* (Keawjam, 1987), *Marisa* (Schulte-Oehlmann et al., 1994) and *Pomacea* (Berthold, 1991; Hayes et al., 2012), as in most caenogastropods (e.g., Hyman, 1967; Fretter & Graham, 1994). Nonetheless, descriptions by several authors (Catalán de Canelada & Moreno, 1984; Catalán et al., 2002) have suggested that the albumen and capsule glands are not connected in series in *Pomacea*, requiring that the fertilized oocytes receive a perivitelline quota at the junction of the albumen and capsule ducts in *P. canaliculata* (Andrews, 1964; Catalán et al., 2002, 2006). However, Hayes et al. (2012) have hypothesized that, like other caenogastropods, the fertilized oocytes enter the albumen gland ("albumen gland diverticula" or "albumen duct" of other authors) and traverse its entire periphery via a ciliated tract while being coated with albumen. As in other caenogastropods (Ponder & Lindberg, 1997; Strong, 2003; Ponder et al., 2008), the bursa copulatrix has been considered as a place to receive sperm during copulation before transferring them into the seminal receptacle (Andrews, 1964; Hayes et al., 2012), although others (Giraud-Billoud et al., 2013a) have hypothesized that the bursa is an organ for sperm resorption and phagocytosis, that is, analogous to the "ingesting glands" of higher caenogastropods (Ponder & Lindberg, 1997). The structural relationships among these complex ducts still require further research, as do functional aspects, for example whether and how sperm are resorbed and how the egg envelopes are provided.

DEVELOPMENT

The field of ampullariid development has recently experienced a revival but can be traced back to Semper's (1862) monograph on *Pila virescens* (as *Ampullaria polita*). Subsequent work during the 20th century treated a few species but has never been comprehensively reviewed. Future integrated studies of morphology, gene expression and proteomics may shed light on the mechanisms by which aspects of ampullariid development are controlled.

Initial Stages of Development

The eggs of ampullariids are fertilized internally and develop externally in calcareous or non-calcareous eggs, deposited in clutches or in gelatinous masses respectively, on submerged vegetation, rocks or other firm substrates (Hayes et al., 2009a, 2012; Burks et al., 2010; Tiecher et al., 2014). The eggs of some species contain pigmented proteins collectively referred to as perivitellins, the colors of which range from white to vivid pink, orange and green, which play diverse functions in the developing embryo (see Egg Laying under Reproductive Behavior and Egg Proteins, for details; Heras et al., 2007; Dreon et al., 2008, 2013; Hayes et al., 2009a).

Eggs exhibit distinct animal and vegetal poles before the first cleavage in *Pila globosa*, *Pomacea canaliculata* and *Marisa cornuarietis* (see Ranjah, 1942; Hylton Scott, 1934; Demian & Yousif, 1973a, respectively). Gastrulation is the result of invagination (emboly) in *Pila globosa* and *P. canaliculata*, but is epibolic in *M. cornuarietis* according to Ranjah (1942), Hylton Scott (1958) and Demian & Yousif (1973a), respectively; both of these patterns of gastrulation occur in other caenogastropods (e.g., Hyman, 1967).

Like other gastropods lacking a planktonic larval phase, the prototroch in *Pila globosa*, *P. canaliculata* and *M. cornuarietis* does not develop into a full velum (Brooks & McGlone, 1908; Hylton Scott, 1934; Ranjah, 1942; Demian & Yousif, 1973a, 1975; Koch et al., 2009). The rudiment of the mantle cavity forms at an early stage in *Pila globosa* according to Ranjah (1942) and in *P. canaliculata* (see Brooks & McGlone, 1908; Fernando, 1931; Hylton Scott, 1934; Koch et al., 2009) as an ectodermal depression close to the anus and immediately beneath the pericardial rudiments. It seems to occur later in *M. cornuarietis* according to Demian & Yousif (1973a). In all cases, the growing shell gland engulfs the primitive mantle cavity and turns to the left and front during anopedal flexure and torsion.

A protein-expression approach has been applied for the first time to the development of a gastropod in a study of *P. canaliculata* eggs at stages when most of the organs are formed (Sun et al., 2010). Of the 125 most abundant proteins, 65 were identified and associated with 11 types of cellular functions or pathways. Of these 65, 63% were related to either metabolism (11%), energy (11%), protein fate (29%) or to proteins with binding functions or cofactor requirements (12%).

Cardiac, Respiratory and Renal Organogenesis

The pericardium (and thus the heart) develops in the mesoderm dorsal to the gut as either a single or a double rudiment (Fernando, 1931; Ranjah, 1942; Demian & Yousif, 1973b). The ctenidium develops in the mantle cavity, but Demian & Yousif (1973c) traced it back to an ectodermal thickening on the right, posterior side of the embryo in *M. cornuarietis*. The lung develops later during intracapsular development as an outgrowth of the mantle cavity's roof (between the ctenidium and the osphradium) in *Pila globosa*, *P. canaliculata* and *M. cornuarietis* (Brooks & McGlone, 1908; Hylton Scott, 1934, 1958; Ranjah, 1942; Demian & Yousif, 1973c, d; Koch et al., 2009). The lung of *Asolene pul-*

chella develops in the same location but only after hatching (Tiecher et al., 2014).

In *Pila globosa*, *P. canaliculata* and *M. cornuarietis*, the rudiment of the post-torsional left kidney develops as an outgrowth of the primitive pericardium and connects with the rudiment of the ureter, which itself is an ectodermal outgrowth of the primitive mantle cavity (Fernando, 1931; Ranjah, 1942; Demian & Yousif, 1973d). The embryonic kidney and ureter become the posterior and anterior kidney chambers of the adult, respectively. The latter opens to the rear of the mantle cavity and communicates with the posterior kidney through a small opening; the posterior kidney is connected to the pericardium via the reno-pericardial duct.

The gonadal sector of the gonoduct in *Pila globosa* originates from a thickening of the pericardial cavity (Ranjah, 1942). The embryonic, post-torsional right kidney, which would give rise to the visceral (or renal) sector of the gonoduct, has also been reported in *Pila globosa* (Ranjah, 1942) and *P. maculata* [as *Ampullaria* (*Pila*) *gigas* Spix in Wagner, 1827] (Fernando, 1931), but has not been found in *P. canaliculata* (see Hylton Scott, 1934; Koch et al., 2009) and *M. cornuarietis* (see Demian & Yousif, 1973b, d).

Digestive Tract

The cells lining the archenteron, or primitive gut, are large and yellowish in *Pila globosa* and *M. cornuarietis* according to Ranjah (1942) and Demian & Yousif (1973d), respectively. In *P. canaliculata*, they are colorless until the stomodaeum connects with the archenteron and the perivitelline fluid starts to be ingested (Koch et al., 2009), at which point they become reddish-pink and increase in size (that is, "giant cells"; Koch et al., 2009). *Pomacea canaliculata* embryos rely heavily on the pink-reddish perivitelline fluid for their nutrition (Heras et al., 1998), rather than the limited amount of yolk invested in the oocytes (Winik & Castro-Vazquez, 2015).

As development proceeds, the foregut, midgut and hindgut become clearly differentiated (Hylton Scott, 1934; Ranjah, 1942; Demian & Yousif, 1973c; Koch et al., 2009). In *Pila globosa*, *P. canaliculata* and *M. cornuarietis*, the foregut gives rise to the pharyngeal bulb with the radula and to the esophagus with the salivary glands and crop. The midgut gives rise to the three-chambered stomach (vestibule, gizzard, style sac) and the midgut gland. The hindgut gives rise to the intestine. The midgut gland develops as two lobes (anterior and posterior), but even though the anterior lobe is initially larger it disappears with development and only the posterior lobe persists into adulthood (Ranjah, 1942; Demian & Yousif, 1973a; Koch et al., 2009). The detailed origin and putative functions of the cells lining the midgut lobes and forming the midgut alveoli have been described in varying degrees of detail in *M. cornuarietis* by Lutfy & Demian (1967) and Demian & Yousif (1973a) and in *P. canaliculata* by Koch et al. (2006, 2009), appearing similar in the two species.

Post-Hatching Reproductive Development

At hatching, the primordial gonoduct of *P. canaliculata* is formed by interconnected cell cords contained within the posterior wall of the mantle cavity. It takes about ten days (by which time the juveniles have reached 5 mm in shell height) for these cords to develop into a sexually undifferentiated primordial gonoduct. At about the same time, the primordium of the copulatory apparatus appears near the inner right mantle edge and will develop either into the full copulatory apparatus of adult males or the rudimentary apparatus of adult females (Gamarra-Luques et al., 2013). The occurrence of this copulatory rudiment has also been reported in adult females of other *Pomacea* species (Thiengo, 1987, 1989; Thiengo et al., 1993) and of *M. cornuarietis* (see Schulte-Oehlmann et al., 1995), but is not attributed to masculinizing pollutants often associated with this phenomenon in other gastropods. Although sometimes apparently lacking (Liu et al., 2006), this rudimentary copulatory apparatus in females can continue to grow after sexual maturity, even in the absence of masculinizing pollutants (Gamarra-Luques et al., 2013; see Environmental Health and Pollution).

In *P. canaliculata*, the gonad is sexually differentiated in 10 mm juveniles, but the pallial section of the gonoduct remains undifferentiated and the copulatory rudiment is similar in both sexes. In 15 mm juveniles (30 days old), the pallial gonoduct has differentiated in both sexes, and includes all the components that will be present in the adults. Copulation takes place once snails reach 20 mm (40 days old), but no eggs are laid, which may be related to the inability of males to fertilize females (oviposition may be directly related to fertilization as most deposited eggs are fertile in *P. canaliculata*) or to the inability of females to provide egg envelopes. The snails appear reproductively mature at 25 mm as their copulations result in the deposition of fertile eggs, and their anatomical and histological features are those of adults (Gamarra-Luques et al., 2013).

LIFE HISTORY

Life Cycle and Reproductive Seasonality

Published estimates of longevity in apple snails range from one to four years in *Pomacea* spp., three years or more in *Marisa cornuarietis* and *Pila* spp., and up to ten years in *Lanistes nyassianus* Dohrn, 1865 (reviewed by Cowie, 2002).

At the southernmost extreme of its native range, in Argentina, *P. canaliculata* may remain inactive for several months due to low winter temperatures (Seuffert et al., 2010) and usually has three to four annual reproductive periods (Estebenet & Cazzaniga, 1993; Estebenet & Martín, 2002; Martín & Burela, personal observations). A one- to two-year life span, similar to that observed in laboratory populations reared at 25°C (Estebenet & Cazzaniga, 1993; Estebenet & Martín, 2002; Martín & Estebenet, 2002), may be expected in warmer, subtropical and tropical areas where winter temperatures are not low enough for the snails to become inactive. In their introduced range of more temperate southern Japan, high winter mortality means that the proportion of snails that survive two summers is low (Yoshida et al., 2009). However, a water temperature of 18°C seems to be adequate to trigger reproductive activity in overwintering *P. canaliculata* (Albrecht et al., 1999), and reproductive activity still proceeds if temperature is lowered from 25°C to 18°C (Albrecht et al., 2005). In Hong Kong, with minimum water temperatures of 16°C, the recruitment period extends up to ten months (Kwong et al., 2010). Photoperiod is not important for initiating and continuing reproduction, because the shortest winter day length (10 h) for the southernmost populations sufficed, given adequate temperatures (Albrecht et al., 1999, 2005). At the other extreme, *P. canaliculata* reared since hatching under constant illumination, matured, copulated and laid eggs normally (Estebenet & Martín, 2002; Martín & Estebenet, 2002).

Also in temperate Argentina, adult *P. scalaris* and *Asolene platae* (Maton, 1811) were present throughout the year (although inactive during winter), and egg-laying and recruitment were observed from late spring to late summer (March) (Martín, 1984, 1993).

Whereas reproduction in temperate regions is more thermally regulated, in tropical regions it is much more related to water availability. Adults of the Indian *Pila globosa* remain dormant, buried in dry mud, for up to eight months during the dry season but begin to copulate and lay eggs as soon as the bottom sediments are covered by water at the start of the rainy season (Bahl, 1928; Raut, 1984). They attain maximum size at four years, but the life span is thought to be longer (Haniffa, 1980). *Pomacea urceus*, in tropical Venezuela, lives for 2.5–3.5 years and breeds during two to three seasons (Burky, 1974); most females attain maturity in their first year (Lum-Kong & Kenny, 1989). Adults begin to copulate just before the onset of the dry season, a decrease in water level being necessary for mating and egg-laying to begin (Ramnarine, 2003).

Pomacea paludosa in Florida has a short life span (1–1.5 years) and throughout much of its range, the majority of egg-laying occurs during spring/summer, followed by a post-reproductive die-off (Darby et al., 2003, 2008). In this case, both water temperature and depth are critical to oviposition and hatchling growth. Snails become inactive when temperatures drop below 13°C (Stevens et al., 2002), and relatively cool temperatures may delay oviposition in the spring (Hanning, 1979). The spring oviposition peak is associated with the dry season, which often culminates in a dry down (i.e., the water table falls below ground level) during which the snails become inactive (Darby et al., 2002, 2008), but, following summer rains, they re-initiate reproduction (O'Hare, 2010).

Thus, reproduction in ampullariids may occur if water is available and if temperatures are high, as during summer in temperate regions or throughout the year in many tropical and subtropical regions. In seasonally wet/dry tropical and subtropical regions, the reproductive cycle seems to be timed to allow hatchlings to reach a large enough size to survive the dry season, while in temperate regions, reproduction only occurs above a threshold temperature.

Life History Variation

Inter-population variation in many life history traits of *P. canaliculata* has both a genetic and an ecophenotypic basis. Although snails show differences in size at hatching, maturity and maximum size, often in response to different densities (Tanaka et al., 1999; Yoshida et al., 2009, 2013), such differences disappeared in snails reared under homogeneous laboratory conditions, indicating a strong environmental influence; slightly higher mortality, growth and oviposition rates in laboratory snails from unstable and unproductive habitats were attributable to genetic differences among source populations (Martín & Estebenet, 2002). The high environmental tolerance of *P. canaliculata* and its successful establishment in new environments may be associated with this high level of ecophenotypic plasticity (Estebenet & Martín, 2002).

The environmental factors involved are not fully understood. Population density and per capita food availability are probably important (Tanaka et al., 1999; Yoshida et al., 2009, 2013). For *P. canaliculata*, the relationship of food availability with size, age at maturity and reproductive performance differ between males and females (Estebenet & Martín, 2002; Estoy et al., 2002a, b; Tamburi & Martín, 2009a, 2011). When food availability is lower than optimum, the reproductive strategy of females is to delay maturation and the onset of reproduction (Estoy et al., 2002b; Tamburi & Martín, 2009a). With reductions in food availability, the mean number of eggs laid during the first reproductive month decreased, although without a significant decrease in the number of clutches or egg size (Estoy et al., 2002b; Tamburi & Martín, 2011). The size of *P. canaliculata* eggs does not differ relative to food availability (Albrecht et al., 2005; Tamburi & Martín, 2011) or among populations (Estebenet & Cazzaniga, 1993). The survival rates of *P. canaliculata* offspring under starvation actually increase if the mothers are faced with chronic food restrictions (Tamburi & Martín, 2011).

On the other hand, *P. canaliculata* males mature at the same age irrespective of food availability. Growth rates, and hence maturation sizes, are strongly negatively affected by reduced food availability (Tamburi & Martín, 2009a), but there is no apparent negative effect on reproductive success (Estoy et al., 2002a; Burela & Martín, 2011; Tamburi & Martín, 2011).

In laboratory studies of *P. canaliculata*, mortality rate was not affected by food availability, up to a point. Most snails completed their life cycle with food available 30–100% of the time (Estoy et al., 2002a) and with 20–100% of the *ad libitum* daily consumption (Tamburi & Martín, 2009a). In addition, male growth rate was not reduced with the onset of copulatory activity, while that of females decreased at the start of reproduction (Tamburi & Martín, 2009a, 2011). This decrease was also observed in isolated cohorts of *P. canaliculata* females that were not allowed to reproduce (Estebenet & Cazzaniga, 1998) and is probably caused by the decrease in ingestion rates and food conversion efficiencies as snails grow (Tamburi & Martín, 2009b).

Food quality may also be important because *P. canaliculata* prefers to consume plant species on which it achieves higher growth rates, and despite its broad food preferences avoids certain plants (Estebenet, 1995; Estebenet & Martín, 2002; Lach et al., 2000; Morrison & Hay, 2011a). Therefore, even among highly productive habitats, life history variation in *P. canaliculata* could result from differences in availability of preferred food. Interspecific differences in the nutritional value and chemical and physical defenses of plants are correlated with changes in growth, oviposition and mortality rates (Qiu & Kwong, 2009).

Life history traits, such as number of eggs, age at maturity in females, size at maturity in males and offspring endurance, are highly plastic and influenced by food availability in the environment. This adjustment to different food availabilities allows other traits (that is, egg laying rate, maturation size in females and maturation age in males) to remain unchanged or conserved, probably because these are subject to the strongest selection pressures (Whitman & Agrawal, 2009). *Pomacea canaliculata* exhibits the same sexually dimorphic reproductive patterns and the same combination of canalized and plastic traits between native (Tamburi & Martín, 2009a, 2011) and introduced (Estoy et al., 2002a, b) populations, indicating that this strategy in the non-native range is neither the product of founder effects nor of anthropogenic selective pressures, but an adaptive strategy evolved in its native environment.

REPRODUCTIVE BEHAVIOR

Mating

Mating behaviour has been studied in several ampullariids, mostly in the laboratory but in a few cases in the field (Bahl, 1928; Nono & Mane, 1931; Demian & Ibrahim, 1971; Hanning, 1979; Guimarães, 1981a, b; Berthold, 1989, 1991; Faraco et al., 2002; Heiler et al., 2007; Tiecher et al., 2014), although thoroughly only in *Pomacea canaliculata* (Andrews, 1964; Albrecht et al., 1996; Burela & Martín, 2007, 2009, 2011, 2014). All descriptions of copulation agree on a basic pattern. Copulation and sperm transfer occur under water, during which the male's foot adheres to the right side of the body whorl of the female while gripping the rim of her shell with the penis sheath. The penis is guided by the penial sheath to the vaginal opening, and from there it passes along the central channel of the capsule gland towards the proximity of the seminal receptacle (Giraud-Billoud et al., 2013a).

There is great inter- and intra-specific variation in length of copulation in apple snails, ranging from an average of 38 min to as long as 20 h (Burela & Martín, 2011). The lengthy copulations may be attributed to the complexity of the male and female reproductive anatomy, to the high fecundity of the females, to the existence of mate guarding behavior, or some combination of these (Burela & Martín, 2011).

In *P. canaliculata*, copulation may occur during the day or night, with females able to continue to move about freely. Both males and females mate frequently with different partners (Albrecht et al., 1996; Burela & Martín, 2011; Liu et al., 2012), and mating can be distinguished into four distinct phases: precourtship, courtship, copulation and post copulation (Burela & Martín, 2009). The precourtship phase, contact with tentacles, palps, feet or snouts, lasts a few seconds. The courtship phase frequently begins with the male circling the female shell but often ends prior to the copulation phase, with the female swinging her shell to dislodge the male. The insertion of the penis sheath into the mantle during the initiation of the copulation phase frequently elicits swinging and withdrawal-wrestling behavior in the female, interrupting the copulation in many cases (Nono & Mane, 1931; Hanning, 1979). This rejection indicates a possible underlying mate choice mechanism in females (Burela & Martín, 2009). Copulation may last 13 h on average, and can extend up to almost 20 h, with most of this time seemingly devoted to the transfer of eusperm (Burela & Martín, 2011). During copulation the male often secretes a nuptial gift from the outer basal sheath gland. Females feed on this gift, which is probably a mechanism for enticing females to remain in copula (Burela & Martín, 2011, 2014). Postcopulation has only been observed in a few cases, and may last as long as 1 h, during which the male remains mounted on the female's shell with its sheath retracted into the mantle, a behavior explained as possible mate guarding (Burela & Martín, 2011).

Egg Laying

The majority of species, those in *Pomacea* and *Pila*, deposit calcareous eggs out of water. Most *Pomacea* species lay them well above the water line on stems of emergent plants, trunks of riparian trees, rocks and other hard structures, such as bridge supports, and *Pila* deposit them on vegetation at the water line or directly on the soil surface at the margin of the water (Hurdle, 1973; Hanning, 1979; Turner, 1996; Cowie, 2002; Hayes et al., 2009a; Burks et al., 2010; Kyle et al., 2013). Some *Pila* species dig a depression in the mud near the shore in which to deposit their eggs (Bahl, 1928; Cowie, 2002). *Pomacea paludosa* in Florida exhibits preferences for certain plant species on which to lay its eggs, perhaps related in part to the ability of larger stems to support a mature female (Turner, 1996).

Oviposition usually occurs during the night or early morning, probably to reduce the risk of predation by terrestrial animals and the heat and desiccation stress on females and eggs, which take time to harden (Schnorbach, 1995; Albrecht et al., 1996; Estebenet & Martín, 2002). Oviposition may last up to several hours and occurs with the right side of the foot forming a longitudinal groove that conducts the eggs from the vagina to the substrate at intervals that depend on species (Bahl, 1928; Bachman, 1960; Andrews, 1964; Hanning, 1979; Albrecht et al., 1996; Estebenet & Martín, 2003). Among species, the average number of eggs per egg mass is inversely related to egg size (Turner & McCabe, 1990; Cowie, 2002; Martín & Estebenet, 2002; Barnes et al., 2008; Burks et al., 2010; Kyle et al., 2013).

Aerial egg laying may have evolved to avoid the predation or cannibalism that submerged egg masses suffer (Turner, 1998; Cowie, 2002; Horn et al., 2008; Saveanu & Martín, 2014), but it incurs diverse costs. There may also be a cost of producing the calcium coating of the eggs, resulting in a trade off between production of progeny and maternal defense, inasmuch as shells of female *P. canaliculata* tend to be thinner than those of males (see Shell Morphology).

A notable exception among *Pomacea* species to this normal egg laying strategy is the behavior of *P. urceus*, which adopts a strategy apparently unique among ampullariids. These snails bury themselves in the drying mud at the beginning of the dry season to aestivate, prior to which females lay their eggs within their shells, between the aperture and the operculum (Burky et al., 1972; Burky, 1974; Lum-Kong & Kenny, 1989). Development takes place during the dry season and the females release some of their own body water at intervals to cool themselves and their progeny (Burky et al., 1972), which are very sensitive to desiccation (Ramnarine, 2003). The hatchlings emerge as the wet season begins.

All other species of apple snails for which information is available, that is, in the genera *Afropomus*, *Asolene*, *Felipponea*, *Lanistes*, *Marisa* and *Saulea*, deposit non-calcareous eggs in a gelatinous matrix under water (Hayes et al., 2009a; Thiengo et al., 2011). The process is similar to that described for *P. canaliculata*. Deposition of gelatinous packages of three to four eggs usually occurs during the night or early morning on submerged plant stems or leaves in a process that can last 1–3 h (*M. cornuarietis* – Demian & Ibrahim, 1971; Schulte-Oehlmann et al., 1994; *Asolene pulchella* – Tiecher et al., 2014).

SEX RATIO, SEX DETERMINATION AND KARYOLOGY

The sex ratio in wild (introduced) populations of *Pomacea canaliculata* in Japan is 0.5 overall but highly variable among egg masses (Yusa & Suzuki, 2003; Yusa, 2004b). Chromosomes have been studied in species of *Lanistes*, *Pila*, *Pomacea* and *Marisa* and there appear to be no dimorphic sex chromosomes (Table 3),

TABLE 3. Ampullariid chromosomes. Unless otherwise indicated, numbers refer to the haploid complement.

Species	Haploid number	Chromosome groups[1]				Reference
		m	sm	st	t	
Lanistes bolteniana (Deshayes & Milne Edwards, 1838)[2]	14	-	-	-	-	Lutfy & Demian, 1965
Lanistes bolteniana (Deshayes & Milne Edwards, 1838)[2]	13	8	0	2	3	Yaseen et al., 1991
Pila ovata (Olivier, 1804)	14	-	-	-	-	Lutfy & Demian, 1965
Pila virens (Lamarck, 1822)	14	-	-	-	-	Choudhury & Pandit, 1997
Pila globosa (Swainson, 1822)	14	9	5	0	0	Choudhury & Pandit, 1997
Pomacea canaliculata (Lamarck, 1822)[3]	14	20* 19*	6* 7**	2* 2**	0* 0**	von Brand et al., 1990
Pomacea canaliculata (Lamarck, 1822)[4]	14	11	3	0	0	Mercado-Laczkó & Lopretto, 1998
Pomacea sp.[5]	14	9	4	1	0	Kawano et al., 1990
Pomacea flagellata (Say, 1829)	13	9	4	0	0	Diupotex-Chong et al., 2007
Pomacea patula catemacensis (Baker, 1922)	13	9	4	0	0	Diupotex-Chong et al., 2004
Marisa cornuarietis (Linnaeus, 1758)	14	-	-	-	-	Lutfy & Demian, 1965

Dashes indicate no information reported.

[1] Abbreviations: m, metacentric; sm, submetacentric; st, subtelocentric; t, telocentric.

[2] Incorrectly referred to as "*bolteni*".

[3] Animals introduced in Japan. One star indicates the diploid complement in females, two stars that in males.

[4] Animals from the native range (Buenos Aires).

[5] Animals from São Paulo, Brasil.

with the possible exception of *P. canaliculata* (perhaps misidentified *P. maculata*) (von Brandt et al., 1990). Instead, sex in *P. canaliculata* is determined by a small number of nuclear genes, inherited from both parents (Yusa, 2006a, 2007a, b).

The haploid complement seems to be n = 14, with n = 13 only reported for *P. flagellata* (Say, 1829) and *P. patula catemacensis* (Baker, 1922), two taxa from Mexico, and the African *Lanistes bolteniana* (Deshayes & Milne Edwards, 1838), though there are conflicting reports for this species (Table 3). Metacentric chromosomes are predominant in all species (8–11 chromosomes/pairs), followed by submetacentric ones (3–5 chromosomes/pairs, with the exception of the *L. bolteniana* of Yaseen et al., 1991). Subtelocentric or telocentric chromosomes are absent in most species (Table 3).

With the single exception of *P. patula catemacensis*, in which rather long chromosomes have been observed (Diupotex-Chong et al., 2004, 2007), ampullariid chromosomes are much contracted in metaphase, so that measurement error may explain some of the differences summarized above.

HABITATS AND DETERMINANTS OF DISTRIBUTION

There is no information concerning the ecological determinants of the distributions of the Neotropical genera *Marisa*, *Asolene* and *Felipponea*, nor a quantitative description of their preferred habitats. Similarly, data on Old World taxa are almost lacking.

Habitats

Most reports of ampullariid habitats are qualitative descriptions, with only a few quantitative studies (Ichinose et al., 2000; Ito, 2002; Karunaratne et al., 2006; Seuffert & Martín, 2010, 2013a). Apple snails inhabit a wide variety of habitats, but are generally found in shallow, slow-moving or stagnant waters, including waterbodies that dry seasonally (e.g., Brown, 1994; Turner, 1994, Ichinose et al., 2000; Darby et al., 2002; Karatayev et al., 2009; Burlakova et al., 2010; Kwong et al., 2010). Nearly all Old World taxa have been reported from ditches, creeks, small rivers and streams, lakes, pools, reservoirs, swamps, monsoon canals and areas generally associated with shallow, slowly flowing waters, macrophytes, muddy bottoms and shade (McCullough, 1964; Ndifon & Ukoli, 1989; Brown, 1994; Omudu & Iyough, 2005; Clements et al., 2006).

A few Old World ampullariids seem adapted to live in flowing waters (Prashad, 1925b; Starmühlner, 1979; Keawjam, 1986; Brown, 1994), and some species of *Lanistes* can occur to depths of 27–82 m (Louda & McKaye, 1982; Brown, 1994). Similarly, species of *Felipponea* and some species of *Pomacea* inhabit faster flowing waters, including those in the highlands of the northern Andes and rivers associated with rocky substrates (Dall, 1904; Faraco et al., 2002; Scarabino, 2004; Corrao et al., 2006; Hayes, 2009).

Pomacea canaliculata is most often considered a lentic species (Hylton Scott, 1958; Castellanos & Fernández, 1976) although in its native range it is found in both lotic and lentic environments (Martín et al., 2001; Martínez & Rojas, 2004; Martín & De Francesco, 2006; Martello et al., 2006). In both habitat types, it is generally found near the margins, associated with macrophytes, slow currents and shallow depths (Lanzer & Schafer, 1985; Ichinose et al., 2000; Kwong et al., 2010; Maltchik et al., 2010; Seuffert & Martín, 2010, 2013a). Although *P. canaliculata* is not commonly found in fast flowing environments, it is able to resist current velocities that are among the highest recorded in streams in the Argentinian Pampas (1.61 $m.s^{-1}$; Seuffert & Martín, 2012, 2013a).

Pomacea species are more abundant in the shallow marginal areas rich in vegetation in diverse habitat types (Guimarães, 1981b; Karatayev et al., 2009; Burks et al., 2010; Burlakova et al., 2010; Pomacea Project, 2013). They require emergent surfaces including plants for laying eggs above the waterline and, in some cases, for climbing to the water's surface for respiration (Turner, 1996), and prefer marshes with low to moderate density of emergent plant stems over lily-pad dominated habitats (Karunaratne et al., 2006). In some cases, species of *Pomacea* exhibit preferences for specific vegetation types (Bryan, 1990; Kyle et al., 2011). For example, in the Everglades of Florida, the greatest concentrations of egg clutches occur along the ecotone created by sawgrass and wet prairie or slough habitat (Darby et al., 1999). For all these species, the association with microhabitats close to the margins or with emergent vegetation is probably due not only to availability of adequate substrates for oviposition but also to a combination of factors including predator avoidance, food availability and the need for frequent lung ventilation (Seuffert & Martín, 2010).

Determinants of Distribution

In general, ampullariids are typically regarded as freshwater snails that do not live in brackish waters (Lanzer & Schafer, 1985; Cowie, 2002; Hamli et al., 2013). Factors determining the distribution of *P. canaliculata* across different waterbodies have been investigated both in its native range (Southern Pampas; Martín et al., 2001; Seuffert & Martín, 2013a) and in a non-native region (Hong Kong; Kwong et al., 2008). These two regions have contrasting climates and topographies, semi-arid to arid plains and subtropical humid hilly terrains, respectively. These studies indicate that *P. canaliculata* distributions are determined by a combination of physicochemical (salinity, alkalinity) and geographic (mountains) barriers in conjunction with stochastic patterns of extinction-colonization events related to local variability of climatic and hydrological conditions (Martín et al., 2001; Martín & De Francesco, 2006; Seuffert & Martín, 2013a). However, in the non-native range this species can be found in sub-optimal habitats, indicating that it can at least survive in these habitats for a period of time (Kwong et al., 2008).

Low calcium availability and low pH (< 6.5) limit the growth of *P. paludosa* in Florida and lead to thinner, more eroded and more fragile shells (Glass & Darby, 2009), probably restricting its distribution (Hurdle, 1973; Glass & Darby, 2009). In the southeastern USA, the models of Byers et al. (2013) show that a pH of < 5.5 probably precludes invasion by *P. maculata*. Nevertheless, in Cuba, *P. paludosa* seems to be more tolerant than pulmonates of the acidic waters in most reservoirs as it is the only snail present, although in none of them is the pH less than 6.0 (Perera & Yong, 1984). In Nigeria, the abundance of *Lanistes libycus* (Morelet, 1849) shows no significant correlation with any physicochemical variable (Owojori et al., 2006).

Temperature limits the range of many ampullariids as it is a key determinant of their activity thresholds (Stevens et al., 2002; Heiler et al., 2008; Seuffert et al., 2010), growth (Estebenet & Cazzaniga, 1992; Seuffert & Martín, 2013b), reproduction (Estebenet & Martín, 2002; Albrecht et al., 1999, 2005), development (Seuffert et al., 2012) and survival (Matsukura & Wada, 2007; Wada & Matsukura, 2007; Matsukura et al., 2009a; Seuffert & Martín, 2013b). Temperature has therefore been used, among other climatic factors, to predict the potential spread of both *P. canaliculata* (Baker, 1998; Zhou et al., 2003; Kwong et al., 2008; Lv et al., 2009a, 2011; EFSA, 2013) and *P. maculata* (Byers et al., 2013) in their non-native ranges. Ecological niche modeling, combining such climatic models with developmental rates at different temperatures, could be used to predict the isotherms limiting the expansion of ampullariids to higher latitudes, both in their native and non-native ranges (e.g., Lv et al., 2011). At the southernmost limit of its native range *P. canaliculata* is occasionally exposed to temperatures near 0°C (Seuffert et al., 2010). However, it cannot tolerate freezing (Matsukura et al., 2009a), suggesting that the isotherm limiting its southern expansion may be close to its actual southernmost extent (37–38°S; Martín et al., 2001; Seuffert et al., 2010). The northern limit of *P. canaliculata*, in its non-native range, is 36°N in Japan (Ito, 2002) and around 31°N in China (Lv et al., 2011). For *P. maculata* in Europe it is between 40 and 41°N, in the Ebro Delta in Spain (López et al., 2010; Anonymous, 2011); this may also be the limit for *P. canaliculata* as it may also be present in the Ebro Delta.

AMPHIBIOUSNESS

Ampullariids are unique among freshwater snails in possessing both a fully functional lung for aerial respiration and a gill for aquatic breathing (Andrews, 1965; Berthold, 1989, 1991). The possession of a lung allows many apple snail species to dwell in habitats with poorly oxygenated waters or that frequently dry out (Darby et al., 2002, 2003, 2008; Yusa et al., 2006b; Seuffert & Martín, 2009). The long siphon of some species allows ventilation of the lung without the snail completely surfacing (Prashad, 1925c; McClary, 1964; Andrews, 1965; Berthold, 1991). Juvenile *P. canaliculata* begin aerial respiration within three hours of hatching, and lung ventilation frequency increases with shell size (Seuffert & Martín, 2009). In contrast, Burky & Burky (1977) showed that lung ventilation frequency decreases with body size in *P. urceus*, perhaps related to metabolic depression in the adults during aestivation. The number of pumping movements per lung ventilation increases with snail size in both species (McClary, 1964;

Burky & Burky, 1977; Seuffert & Martín, 2009), probably because of an increase in the volume of the respiratory dead space in the lung and siphon (Seuffert & Martín, 2009).

While they are primarily aquatic, ampullariids display varying degrees of amphibiousness that range from greater (*Asolene*, *Felipponea*, *Marisa*, *Lanistes*, and presumably *Afropomus* and *Saulea*) to lesser (*Pomacea*, *Pila*) reliance on water for the completion of their life cycle (Hayes et al., 2009a). The shift from aquatic to amphibious habits, including aerial oviposition, was probably a key innovation that may have facilitated, at least in part, the diversification and spread of *Pila* and *Pomacea* (Hayes et al., 2009a).The cleidoic eggs of most *Pomacea* species are adapted to exposure to extreme conditions and have developed a physiological dependence on aerial incubation such that they will not develop completely if submerged (Turner, 1998; Pizani et al., 2005; Horn et al., 2008). The deposition of cleidoic eggs above water by *Pomacea* and *Pila* and the observation that most *Pila virescens* die if covered totally by water indicate that they are truly amphibious (Andrews, 1965; Keawjam, 1986; Berthold, 1989, 1991; Cowie, 2002; Hayes, 2009; Hayes et al., 2009a; Seuffert & Martín, 2010). However, the eggs of some *Pila* spp. (deposited in pits dug in the ground or at the bases of plants) and *P. urceus* (incubated within the mother's shell) depend on deposition in humid microenvironments, and the embryos are highly susceptible to desiccation (Bahl, 1928; Ramnarine, 2003). In contrast, the other genera, with their gelatinous eggs deposited under water, are linked to aquatic habitats from hatching to maturity (Hayes et al., 2009a).

In *Pomacea* species, males and females do not differ in lung ventilation frequency nor in oxygen consumption rates (Freiburg & Hazelwood, 1977; Santos & Mendes, 1981; Seuffert & Martín, 2009). However, when access to the water surface for aerial respiration was restricted, females of *P. canaliculata* died or became comatose more frequently than males, which may be a consequence of decreased efficiency of water flow over the gill in females due to the bulging of the albumen gland into the mantle cavity (Seuffert & Martín, 2010). A reduced lung and a more aquatic mode of life with no air breathing has been suggested for species of *Lanistes* that occur at deeper depths (Berthold, 1990). However, Bandel (1998) reported that these snails always had air in the lung, even when found 500 m from the shoreline and 6 m deep, apparently a result of their ability to capture air bubbles released by aquatic vegetation in the mantle cavity.

DORMANCY

The fluctuating and highly variable habitats of many ampullariids have influenced the evolution of many aspects of their behavior and physiology, including those underlying aestivation, hibernation and seasonal reproduction. These processes may be entrained by largely predictable changes (e.g., annual changes in photoperiod and mean temperature) but also to less predictable changes (e.g., occasional temperature fluctuations, droughts, rains or floods).

Many ampullariids become dormant in response to drought and/or cold temperatures (d'Orbigny, 1847; Lal & Saxena, 1952; Meenakshi, 1956, 1964; Oya et al., 1987; Yusa et al., 2006b; Seuffert et al., 2010). Although aestivation is most commonly thought of as a response to high temperatures, it is here defined as when dormancy is induced by lack of water caused by natural or anthropogenic lowering of the water below ground level (e.g., Lal & Saxena, 1952; Little, 1968; Watanabe et al., 2000). Defined as such, aestivation may occur in either winter or summer (e.g., d'Orbigny, 1847; Wada & Matsukura, 2007). Hibernation in ampullariids is here defined as dormancy when the ambient temperature becomes low. However, the snails do not enter a deep lethargic state that persists during the entire cold season but show a rather quick response to instantaneous temperature changes, being able to reactivate as soon as conditions are favorable (Seuffert et al., 2010).

Burrowing and closing the shell with the operculum are common apple snail behaviors associated with dormancy. Closing the operculum during dormancy may minimize exposure to the environment, conserve body water (during aestivation) and protect the snail from predators (Meenakshi, 1956, 1957; Coles, 1968; Stevens et al., 2002; Seuffert et al., 2010). Burrowing may occur at the onset of either aestivation or hibernation and may vary diurnally during summer, with maxima around noon and minima around midnight (Oya et al., 1987; Wada & Yoshida, 2000). High water temperatures (35–40°C) increased adult male burrowing behavior, but had no effect on females and juveniles. Lower temperatures (< 10°C) led to increased proportions of snails buried (Wada & Yoshida, 2000; Stevens et al., 2002).

Aestivation

Ampullariids can tolerate prolonged drying of their shallow freshwater habitats (Lal & Saxena, 1952; Meenakshi, 1956, 1964; Little, 1968; Wada & Yoshida, 2000; Yusa et al., 2006b), and dormancy seems to be a contingent event precipitated by the dry down of their habitats. Although some species switch to anaerobic respiration at some stage during dry-down events, the capacity for aerial gas exchange is particularly significant during such events, when the snails burrow in the mud (Meenakshi, 1956, 1964; Burky et al., 1972; Thomas & Agard, 1992). The behavior displayed during experimental induction of aestivation and arousal from it are similar in *P. lineata* and *P. canaliculata*, but the process of entering aestivation takes 2–4 times longer in *P. lineata* (Little, 1968; Giraud-Billoud et al., 2011). Only in *P. urceus* is this dry dormancy thought to be an obligatory part of the life cycle, as drying conditions are a cue for the onset of reproduction (Ramnarine, 2003; see Life History).

Mortality during aestivation in *Pomacea* species may be affected by duration, water conditions and body size (Little, 1968; Burky et al., 1972; Fan et al., 2000; Darby et al., 2003; Giraud-Billoud et al., 2011). Species differences seem particularly evident in mortality as a function of aestivation duration, but detailed comparisons are difficult, because most reports are of extreme survival times rather than changes in mortality rate over time (Cowie, 2002; Giraud-Billoud et al., 2011). Percent body mass loss during aestivation may be critical for survival. In *P. canaliculata*, a ~50% loss of body mass was accompanied by a relatively low mortality rate and appeared mostly related to water loss (Giraud-Billoud et al., 2011). Mortality rates were similar in both laboratory and semi-field conditions (Yusa et al., 2006b; Giraud-Billoud et al., 2011). A similar figure for body mass loss was reported for *P. lineata* by Little (1968), but Meenakshi (1964) reported only a 5% loss in *Pila globosa*.

Water loss may be limited by rising solute concentrations and hence the osmolality of body fluids. Urea and both uric and lactic acids are accumulated during water deprivation in several ampullariids (see Giraud-Billoud et al., 2011, for references) and may help to retain water, as in other gastropods (Withers et al., 1996). However, the actual increase in osmolality during aestivation in *P. lineata* was lower than expected on the basis of water loss alone (Little, 1968). In fact, deposition of uric acid in urate tissues may reduce osmolality by removing this purine from circulation (Giraud-Billoud et al., 2011).

Reduction in metabolic rate is also important for long-term survival during aestivation and/or hibernation because the greater the reduction in metabolic rate, the longer a fixed nutritional reserve can sustain basal metabolism (Storey, 2002). Reduction of oxygen consumption (Burky et al., 1972) and eventual shifting to anaerobic metabolism (in some species) may thus occur during aestivation. Both *Pila globosa* and *P. urceus* accumulate lactic acid during aestivation, according to Meenakshi (1956) and Burky et al. (1972), respectively, indicating such a shift.

A physiologically significant challenge that limits survival after dormancy is tissue reoxygenation during arousal (Hermes-Lima et al., 1998), which is more sudden after aestivation (and hence, more challenging) than after hibernation. The damaging effects of tissue reoxygenation may be worse than those of the preceding hypoxia (Hermes-Lima et al., 1998). Pulmonates have evolved a variety of enzymatic mechanisms that allow them to endure oxyradical production during tissue reoxygenation (Hermes-Lima et al., 1998; Hermes-Lima & Zenteno-Savin, 2002; Ramos-Vasconcelos et al., 2005), and recently enzymatic and non-enzymatic antioxidant defense mechanisms have been characterized during the activity-aestivation cyle in *P. canaliculata* (Giraud-Billoud et al., 2011, 2013b). Nothing else is known of the process of reoxygenation following dormancy in ampullariids, and this is an area where additional ecophysiological research may provide crucial insights.

In *P. canaliculata* there is an array of tissues containing intracellular urate crystalloids, which exhibit a sequential process of formation and lysis, suggesting active turnover of uric acid (Giraud-Billoud et al., 2008). Urate tissues begin to differentiate several days before hatching (Koch et al., 2009). Although such tissues have not been reported in other ampullariids, uric acid accumulates during aestivation in both *Pila globosa* and *Pila virens* (Lamarck, 1822) (Meenakshi, 1964; Reddy et al., 1974; Chaturvedi & Agarwal, 1981). Uric acid concentration increases in soft tissues of *P. canaliculata* during aestivation, and drops after arousal.

Also the concentration of allantoin, a urate oxidation product, increases in kidney and foot tissue after arousal, indicating that uric acid is used as a significant antioxidant defense in the activity-aestivation cycle (Giraud-Billoud et al., 2011, 2013b). Reduced glutathione also seems to participate as an antioxidant in the activity-aestivation cycle. Furthermore, changes in the expression of molecular chaperones (Hsc 70, Hsp 70s, Hsp 90) indicate they may participate in protecting the proteome during aestivation and arousal (Giraud-Billoud et al., 2013b).

Sun et al. (2013) quantified and compared 701 proteins isolated from *P. canaliculata* during the activity-aestivation cycle, revealing 53 proteins that were differentially regulated during the cycle. Proteins known to be critical for translation, duplication and energy production were all down-regulated during aestivation, probably because the snails need to conserve resources during aestivation and therefore become hypometabolic. Likewise, hydrocarbon digesting enzymes were down-regulated. Proteins related to lipid metabolism were up-regulated, which is consistent with the use of lipids as an energy source during fasting. In the context of enzymatic and non-enzymatic protection against oxidative damage, catalase and a small heat shock protein (sHsp) were up-regulated during aestivation (Sun et al., 2013). Also, two proteins participating in uric acid synthesis were up-regulated, which is in agreement with the central role of this purine as an antioxidant during the activity-aestivation cycle (Giraud-Billoud et al., 2011, 2013b).

The accumulation of uric acid in both active and aestivating ampullariids may also serve other functions (Athawale & Reddy, 2002; Vega et al., 2007; Giraud-Billoud et al., 2011). Ampullariids may be confronted with drastic environmental changes during which the availability and demand for combined nitrogen may change, and a nitrogen store in the form of uric acid may be adaptive. The reuse of nitrogen contained in uric acid requires its oxidation to allantoin, and then conversion to smaller molecules that can enter the pathways for amino acid and nucleic acid synthesis (Nelson & Cox, 2004). Uric acid oxidation may occur non-enzymatically (acting as an oxyradical scavenger) or may be catalyzed by urate oxidase. Urate oxidase activity has been found in the midgut gland, foot, lung and gut of *P. canaliculata* (Giraud-Billoud et al., 2011) and in several symbiotic gut bacteria (Koch et al., 2014). However, the incorporation of uric acid nitrogen into protein and nucleic acids has not been demonstrated directly in ampullariids.

Hibernation and Cold Hardiness

Hibernation in ampullariids has not received as much attention as aestivation, perhaps because most ampullariid species live in tropical or subtropical regions. However, *P. canaliculata* occurs widely in temperate zones of Argentina, as far south as 38°S (Albrecht, 1998; Martín et al., 2001), and invasive populations in Japan also reach similar latitudes (approx. 36°N), withstanding cold temperatures and freezing conditions (Oya et al., 1987; Ito, 2002).

During the coldest months in temperate climates, the snails hibernate lying on the bottom or burying in the mud (Seuffert et al., 2010), but the physiological changes during the activity-hibernation cycle have not been studied. Instead, recent work on *P. canaliculata* has been focused on the related subject of cold hardiness. In invaded areas of temperate Japan, snails increase their cold tolerance before the onset of winter (Wada & Matsukura, 2007; Matsukura et al., 2008). The gradually decreasing temperature in autumn is the main environmental cue to enhance cold tolerance (Matsukura & Wada, 2007). Dry conditions enhance cold tolerance, but photoperiod has no clear effect. After winter, cold tolerance of overwintered snails decreases (Matsukura et al., 2009b).

Cold-tolerant snails in winter accumulate glycerol and possibly glucose in their bodies while glycogen concentration decreases (Matsukura et al., 2008). Among other low-molecular-weight compounds, glutamine and carnosine concentrations increased while phenylalanine decreased. These compunds may be acting as cryoprotectants, as they do in insects (Lee, 1991; Storey & Storey, 1997), preventing protein denaturation and membrane damage (Michaud et al., 2008; Sjursen & Somme, 2000). However, glycerol concentration in the snails was much lower than in many insects, and no differences in supercooling points were observed in snails with or without cold tolerance (Lee, 1991; Matsukura et al., 2008, 2009a).

Death of *P. canaliculata* may occur at temperatures as high as 10°C, well above the temperature (ca. -7°C) at which the snails freeze (Wada & Matsukura, 2007; Matsukura & Wada, 2007; Matsukura et al., 2009b). The mechanism of lethal injury by chilling in the absence of freezing is not well understood, and so the actual function of glycerol in *P. canaliculata* is unknown.

Cold tolerance appears to have evolved in ampullariids well before they became invasive species (Seuffert et al., 2010), as populations of *P. canaliculata* established in the Philippines have never experienced cold temperatures in the three decades since their introduction, yet individuals are able to enhance their cold tolerance (Wada & Matsukura, 2011). Similar responses are noted with snails from northern Argentina (Yoshida et al., 2014). *Pomacea canaliculata* may not have successfully colonized these temperate areas without some ability to adapt to cold conditions (Ito, 2002; Yoshida et al., 2009), and juveniles of *P. canaliculata* are more tolerant to both cold and desiccation than those of *P. maculata* (Yoshida et al., 2014). (Unfortunately, the specimens identified by Yoshida et al. (2014) as *P. maculata* are almost certainly a much more narrowly distributed species, which would lead to considerably different interpretations of their data; Hayes, unpublished.). Linkage of cold tolerance with desiccation tolerance is found in both temperate and tropical snails: cold-tolerant snails survive longer after desiccation exposure than cold-intolerant snails (Wada & Matsukura, 2011). There are often similarities in the mechanisms underlying adaptation to cold and desiccation, notably accumulation of metabolites including polyols and sugars, and adjustments of water content and habitat choice (Ring & Danks, 1994; Michaud et al., 2008). Because the most important abiotic stress on snails in the tropics seems to be drought, this linkage may contribute to retention of the ability to adapt to cold.

FOOD, FEEDING AND DIGESTION

Feeding has been a major focus of recent ampullariid research. In contrast to the majority of freshwater caenogastropods, which tend to be phytophagous, omnivorous or deposit feeders (Dillon, 2000; Strong et al., 2008), many ampullariids are generalists and capable of feeding on a variety of items such as biofilms, periphyton, floating, submerged and emergent macrophytes, living animals and animal carrion (Cowie, 2002).

Phytophagy and Preferences

Macrophytes, periphyton and plant detritus are the main food items for ampullariids (Fellerhoff, 2002; Shuford et al., 2005; Kwong et al., 2010). Some species can detect macrophytes from a distance (Estebenet, 1995). While they generally are not known as major pests in their native ranges (Cazzaniga, 2006), *P. maculata and P. canaliculata* cause major damage to wetland agriculture, notably to rice, taro and semi-aquatic vegetables, in their invaded ranges (Joshi & Sebastian, 2006). *Pomacea* species also have direct grazing effects on macrophytes in non-agricultural wetlands (Carlsson & Lacoursière, 2005; Burlakova et al., 2009; Wong et al., 2009; Fang et al., 2010) and indirect effects on wetland water quality and ecosystem processes (Carlsson et al., 2004a).

Given the substantial impact of grazing by *Pomacea* species on macrophyte diversity and ecosystem processes, several laboratory studies have examined their feeding on macrophytes: *P. canaliculata* in Argentina (Estebenet, 1995), Hawaii (Lach et al., 2000) and Hong Kong (Qiu & Kwong, 2009; Fang et al., 2010; Wong et al., 2010), and *P. maculata* in the U.S.A. in Georgia (Morrison & Hay, 2011a), Texas (Boland et al., 2008; Burlakova et al., 2009; Burks et al., 2011) and Florida (Baker et al., 2010). These studies show that although these species will feed on a diversity of plant species, they do exhibit preferences among them. Snails feeding on their preferred macrophyte species exhibit higher growth rates than snails that have access only to unpalatable food; these snails feed very little, have a low survivorship and grow little.

Other species seem to prefer periphyton, metaphyton (floating mats of detached benthic algae) or floating algae (Rich, 1990; Browder et al., 1994; Sharfstein & Steinman, 2001; Shuford et al., 2005; Morrison & Hay, 2011a). Some species are capable of feeding by pedal surface collecting (McClary, 1964; Cazzaniga & Estebenet, 1984; Saveanu & Martín, 2013), in which particles on the water surface are collected by ciliary action of the foot sole and periodically ingested. Periphyton is a major food source of *P. paludosa* but vascular plant material may also be important (Rich, 1990) and this species feeds readily on *Chara* sp. (muskgrass) and *Najas marina* (spiny naiad) in the field (Hurdle, 1973).

Food preference in herbivores is affected by several characteristics of the plants (Lodge, 1991). Physical defenses include external and internal structures that deter grazing (e.g., spines, hairs, tough leaves, cellulose, lignin). Studies of physical defenses against grazing by ampullariids have used toughness (Qiu & Kwong, 2009) and dry matter content (DMC), with snail feeding rate in both *P. canaliculata* and *P. maculata* negatively correlated with DMC (Burlakova et al., 2009; Wong et al., 2010).

Plant secondary metabolites (e.g., phenolics, alkaloids, terpenes, wax) that are toxic or that interfere with digestion affect food preference in generalist herbivores (Lodge, 1991; Burks et al., 2006). The leaves of *Myriophyllum* spp. contain high levels of phenolic compounds (Burks & Lodge, 2002). Incorporating an extract of *Myriophyllum* spp. into reconstituted but otherwise palatable food reduces the feeding rate of *P. canaliculata* and *P. maculata*, and, when fed on *Myriophyllum aquaticum* alone, *P. canaliculata* do not grow or reproduce (Boland et al., 2008; Qiu & Kwong, 2009; Wong et al., 2010). Non-phenolic secondary plant metabolites may also be involved in defense against ampullariids. For instance, *Alternanthera philoxeroides* containing low phenolic content and a medium level of DMC was not palatable to *P. canaliculata*, and an *A. philoxeroides* extract greatly reduced its feeding rate (Wong et al., 2010). *Pomacea canaliculata* will use both fresh and decaying macrophyte leaves as long as they contain adequate levels of nutrients and low levels of phenolics (Qiu et al., 2011). Ampullariid grazing can also induce the production of unidentified defense chemicals (Morrison & Hay, 2011b).

Preferences also reflect the nutritional value of the plants, with snails preferring to feed on plants with higher nitrogen, phosphorous and chlorophyll content than those that are more easily digested but with lower amounts of nutritionally important compounds (Grantham et al., 1993; Sharfstein & Steinman, 2001; Wong et al., 2010). Similarly, growth rate and egg production were positively correlated with phosphorus and nitrogen content, respectively (Qiu & Kwong, 2009).

Intraspecific Variation in Feeding and Assimilation

Specific ingestion rates (weight:weight) decrease inversely with snail size (Haniffa & Pandian, 1974; Haniffa, 1980; Boland et al., 2008; Burlakova et al., 2009; Tamburi & Martín, 2009a). This has been related to an allometric decrease in the gut cross-sectional area relative to the biomass that must be nourished as body size increases (Tamburi & Martín, 2009b) and is probably coupled to an ontogenetic decrease in metabolic rate. Similarly, gender differences in ecophysiological performance can be substantial in some species. For instance, the specific ingestion rate in *P. canaliculata* is 50% higher in females than males of the same size (Tamburi & Martín, 2009a), perhaps related to the smaller mid-gut gland of males (61–72% the size of that of females) (Koch et al., 2006), which may restrict the amount of food that can be processed per unit time. Growth rates in male *P. canaliculata* are lower than in females, probably also as a consequence of their smaller mid-gut glands, which in turn results in lower food assimilation (Tamburi & Martín, 2009b). These findings, in combination with a tendency to mature later (Tamburi & Martín, 2009b), may explain the common pattern of females growing to be larger than males (Estebenet & Martín, 2002, 2003; Estebenet et al., 2006). This size difference was also seen in *M. cornuarietis* by Demian & Ibrahim (1972), *P. urceus* by Burky (1974) and Lum-Kong & Kenny (1989), *P. paludosa* by Hanning (1979) and *Pila* spp. by Keawjam (1987), although the possibility of different ingestion rates or growth efficiencies has not been investigated in these species.

In *P. canaliculata* some studies have shown that young snails are microphagous, changing to macrophytophagy when reaching 15 mm shell height (Halwart, 1994; Schnorbach, 1995). However, Carlsson & Brönmark (2006) found no ontogenetic changes in diet in this species, although they did indicate that small snails had higher specific grazing rates, interpreted as higher competitive abilities. Also, hatchlings will survive and grow when fed only fresh vascular plants in the laboratory (e.g., Estebenet & Cazzaniga, 1992, 1998; Estebenet, 1995; Tamburi & Martín, 2009b; Qiu & Kwong, 2009). Furthermore, the relative preference for different macrophytic plants does not change with age (Estebenet, 1995), although large and small snails may feed on different parts of the same plant (Carlsson & Brönmark, 2006). In *Pila globosa*, the relative weight of the radula is inversely related to body weight, which was suggested as the cause of declining feeding rates as the snails grow (Haniffa & Pandian, 1974).

Feeding on Other Animals

Some ampullariids will prey on the eggs, juveniles and adults of various other snail species (Demian & Lutfy, 1965a, b, 1966; Cedeño-León

& Thomas, 1983; Cazzaniga, 1990; Aditya & Raut, 2002; Anto et al., 2005; Wong et al., 2009). For this reason, they have been proposed as biocontrol agents against other snail species that are intermediate hosts of human parasites (e.g., Pointier et al., 1988, 1991) as well as against invasive plants, although such approaches can have serious non-target impacts and have been criticized (Cowie, 2001). In Asia, the invasion of *P. canaliculata* may have caused a delay in reproduction and a longer recruitment period in *Radix plicatulus* (Benson, 1842), perhaps in response to high juvenile mortality from apple snail predation (Lam, 1994). *Pomacea canaliculata* has also been suggested as causing the decline of *Pila* species, but whether this occurred through predation or competition remains unclear (Acosta & Pullin, 1991; Halwart, 1994). Apple snails will even consume conspecific eggs (Horn et al., 2008; Tiecher et al., 2014; Saveanu & Martín, 2014), hatchlings and juveniles (Yusa et al., 2006a).

Ampullariids may prey on other small animals, such as freshwater oligochaetes (Aditya & Raut, 2001) and bryozoans (Wood et al., 2005, 2006), as well as eggs of fish (Phillips et al., 2010) and amphibians (Karraker & Dudgeon, 2014). They will also feed on many kinds of carrion, for example, dead frogs (Cowie & Hayes, personal observation) and fish (Qiu, personal observation).

It is not known whether some species are capable of detecting their animal prey at distance. However, their large size and a crawling speed that is faster than their prey allow them to search a large area and thus enhance their prey encounter rate; the predation rate varies with the species and life stage of the predator and the size, shape, and shell crushing resistance of the prey (Kwong et al., 2009). Consumption rates vary widely among and within species (Cedeño-León & Thomas, 1983; Cazzaniga, 1990; Aditya & Raut, 2002; Anto et al., 2005; Kwong et al., 2009).

Digestion

Polysaccharides, including cellulose and hemicellulose (the major components of plant cell walls) and starch (a cytoplasmic component), are universally present in the diet of ampullariids. The ability of *P. canaliculata* to digest cellulose (Vega et al., 2006) has recently been confirmed by cloning and expression of two endogenous cellulases (Imjongjirak et al., 2008). Another cellulase produced by an endosymbiotic *Bacillus* has been reported in a species that is probably also *P. canaliculata* (Zhang et al., 2007). Hemicellulose can be hydrolized by endo-1,4-β-D-xylanase, which has been purified from soft tissue extracts of *P. canaliculata* (Yamaura et al., 1997), and starch can be hydrolyzed by an amylase found in the midgut gland (Sun et al., 2013). Carbohydrate residues can be released from macromolecules by several enzymes (α-and β-mannosidase, β-N-acetylglucosaminidase, β-galactosidase and α-fucosidase; Hirata et al., 1996, 1998a–c).

Several proteases have been reported in *P. canaliculata*, including one produced by the salivary glands and two in the intestine; one associated with C and K morphotypes of an endosymbiont released from midgut gland cells, is ubiquitous in the digestive tract (Godoy et al., 2013) (see Symbiotic Associations).

PREDATORS AND PREDATOR AVOIDANCE

Predators

The best-known natural enemies of apple snails throughout much of their natural range in North, South and Central America include limpkins (*Aramus guarauna*) and snail kites (*Rostrhamus sociabilis*), for which apple snails are the almost exclusive food source (Snyder & Snyder, 1969; Snyder & Kale, 1983; Tanaka et al., 2006; Mapelli & Kittlein, 2011; Bergmann et al., 2013). Predation presents a strong selective pressure on shell color and shell size of Central American *Pomacea flagellata* (Reed & Janzen, 1999), and is likely to have similar effects on other apple snail species, including *P. paludosa* (Darby et al., 2007; Cattau et al., 2010). In Florida, although the snail kite's natural prey is *P. paludosa*, since the introduction of *P. maculata* (Rawlings et al., 2007), this non-native species has become a common prey, despite the kites' difficulty in handling the largest individuals (Darby et al., 2007; Cattau et al., 2010; Pomacea Project, 2013).

In their native range, apple snails are also eaten by caimans (Alligatoridae) (Halwart, 1994; Laporta-Ferreira & Salomão, 2004) caiman lizards (*Dracaena* spp., Teiidae) (Perera & Walls, 1996) and a wide range of avian and aquatic predators that target all size classes. These include more generalist avian predators such as boat-tailed grackles (*Quiscalus major*) and white ibis (*Eudocimus albus*), aquatic predators such as redear sunfish (*Lepomis microlophus*), turtles (*Trionyx ferox*, *Trachemys scripta elegans*, *Sternotherus* spp., *Kinosternon* spp.) and alligators (*Alligator mississippiensis*) (reviewed in Pomacea Project, 2013; Burks, unpubl. dat.).

Yusa (2006b) provided a relatively comprehensive but non-exhaustive list of known predators of invasive apple snails in Asia, including 46 species in 16 orders. This list, together with additional predators noted by other authors indicates apple snails are on the menu for a wide array of insects, crustaceans, fish, reptiles, leeches, birds and mammals (Yusa et al., 2000; Yusa, 2001; Ichinose et al., 2002; Carlsson et al., 2004b; Wong et al., 2009; Sawangproh & Poonswad, 2010).

The relatively small size of many *Pomacea* hatchlings (e.g., *P. canaliculata* shell height < 3 mm; Hayes et al., 2012) and their relatively thin shells allow them to be readily consumed. An additional suite of predators target juvenile apple snails in their native range including crayfish (*Procambarus* sp.) and aquatic insects (water bugs, *Belostoma* sp.; dragonfly naiads, *Coryphaeschna ingens*; and diving beetles, *Dytiscus marginalis*) (Snyder & Snyder, 1971). However, in general, apple snails become decreasingly vulnerable to predation with size, and after reaching 20 mm, relatively few predators in the non-native range in Asia can prey on them. The effectiveness of carp, tilapia, ducks and turtles has been evaluated in the field in the context of biological control (Yusa, 2006b; Yoshie & Yusa, 2008, and references therein). Each of them acts fairly well as a biocontrol agent, although their use may have negative impacts on other aquatic animals and plants (Yoshie & Yusa, 2008; Wong et al., 2009).

Direct comparisons of predation pressures on native snails and introduced *Pomacea* have been few, but two species of rats both prefer *P. canaliculata* over native *Semisulcospira libertina* (Gould, 1859) or *Radix quadrasi* (Möllendorff, 1898), respectively (Yusa et al., 2000; Joshi et al., 2006). In the laboratory, common carp readily consume *P. canaliculata* while rejecting the thicker-shelled *Sinotaia quadrata* (Benson, 1842) (Kwong et al., 2009). In Japan, while apple snails rapidly multiply in rice fields and other shallow wetlands with few predators (Yusa, 2006b), predators seem to effectively control their populations in canals, creeks and rivers (Yusa, 2006b; Yusa et al., 2006a) in an apparent example of biotic resistance to an invasive species (Yamanishi et al., 2012).

Predator Avoidance

In addition to the fact that the largest *Pomacea* individuals are not readily preyed upon, these species exhibit two major predator avoidance strategies: chemical defenses during the egg/hatchling stages (see Egg Proteins: Structure and Role in Defense) and predator avoidance behaviors.

The presumably aposematic color of *Pomacea* eggs is due to pigmented proteins that advertise the presence of neurotoxins, antinutrivitve proteins and digestive inhibitors at least in *P. canaliculata* (Heras et al., 2008; Dreon et al., 2010, 2013). Eggs of various *Pomacea* species have been reported as being ingested by a few species, including ants, Hemiptera and Orthoptera, but only the fire ant *Solenopsis geminata* is known to consume them significantly (Yusa, 2001, 2006a). Other observations of birds (Guimarães, 1981b), fish, a frog and a millipede (Snyder & Snyder, 1971), a land snail (Ng & Tan, 2011) and turtles (Burks, unpublished) all require additional study to ascertain whether they represented anything more than accidental ingestion or ingestion only under captive experimental conditions. Whether other apple snail eggs deposited above water but lacking pigmentation (i.e., *Pila* spp.) or laid under water possess such protections is not known.

Ampullariids avoid predators by crawling out of the water, situating themselves near the water surface, burying themselves in the mud, and falling from substrates on which they were crawling (Snyder & Snyder, 1971; Ichinose, 2002; Ichinose et al., 2003; Carlsson et al., 2004b; Aizaki & Yusa, 2009, 2010). In *P. canaliculata*, these behavioral repertoires are size-dependent: hatchlings tend to crawl out of the water; juveniles mainly bury themselves or use near-surface habitats; larger snails are less responsive (Ichinose, 2002). These behaviors are in part innate, but can be learned in some instances when exposed to novel predators (Aizaki & Yusa, 2010) and may be predator specific (Ueshima & Yusa, 2014). These diverse strategies have surely played a role in their success in the native range and probably also enhance invasiveness.

EGG PROTEINS: STRUCTURE AND ROLE IN DEFENSE

The main components of the egg vitellus (lipids, proteins, carbohydrates) are incorporated during vitellogenesis into primary oocytes to serve mainly as energetic and structural sources for the developing embryo. Most gastropods, however, contain a limited amount of vitellus, and instead, egg reserves are accumulated surrounding the fertilized oocyte as a perivitelline fluid (De Jong-Brink et al., 1983).

The successful strategy of laying eggs above water results in a variety of selective challenges as the eggs are exposed to stressful environmental conditions that may affect embryonic development and survival of offspring (Przeslawski, 2004). Ampullariids have evolved to handle these challenges through the production of several egg proteins found in the perivitelline fluid, referred to as perivitellins. Although the eggs of many snail species face intense predation pressure, those of *P. canaliculata* have very few predators (Yusa, 2001) (see Predators and Predator Avoidance) because of a suite of chemical defenses provided by the perivitellins. These defenses are advertised by the conspicuous color of the eggs (Heras et al., 2007).

At the biochemical level, the eggs of at least some *Pomacea* species possess a unique group of perivitellins, which are multifunctional complexes functioning in storage, predator defense and protection from the environment (e.g., Dreon et al., 2008, 2013). In spite of the central role of perivitellins in reproduction and development, there is little information on their structural features in invertebrates. Studies in molluscs are limited essentially to the perivitellins of *Pomacea*, mostly in *P. canaliculata* but also *P. scalaris* and *P. maculata* (Ituarte et al., 2012; Pasquevich et al., 2014).

Perivitellin Structure and Synthesis

Two major perivitellins, now known as PcOvo and PcPV2, have been characterized from the perivitelline fluid of *P. canaliculata* (Cheesman, 1958; Garín et al., 1996; Dreon et al., 2004a, 2010, 2013; Ituarte et al., 2010; Sun et al., 2012b). Both perivitellins are multimeric proteins with remarkabe thermal stability up to 100°C and 60°C, respectively, and over a wide range of pH (Dreon et al., 2008; Frassa et al., 2010). They are highly resistant to the combined action of pepsin and trypsin proteases, and PcOvo has proteinase inhibitor activity (Norden, 1972; Dreon et al., 2010).

The perivitelline fluid of *P. scalaris* contains two major perivitellins, of which only the pigmented one, PsSC, which is structurally similar to PcOvo, has been characterized (Ituarte et al., 2008, 2012). The perivitelline fluid of *P. maculata* is also similar, with two major perivitellins, PmPV1 and PmPV2 (Pasquevich et al., 2014). PcOvo, PsSC and PmPV1 act as carriers of antioxidant carotenoid cofactors, notably astaxanthin, which are extremely labile in solution but are not degraded when bound to the perivitellins (Ituarte et al., 2008; Pasquevich et al., 2014). PcOvo and PsSC also carry phosphate groups attached to serine residues that may serve as a phosphorous reserve for the embryo, as do other egg proteins (Ituarte et al., 2010).

Synthesis of PcOvo and PcPV2 occurs in the albumen gland with no circulating perivitellin precursors in the hemolymph (Dreon et al., 2002, 2003). Analysis of the albumen gland transcriptome indicated that other components of the perivitelline fluid, as well as these perivitellins, are also exclusively synthesized in the albumen gland (Sun et al., 2012b). In the parenchymal mass of this gland, albumen secretory cells and labyrinth cells are involved in the synthesis of perivitelline fluid, but only the albumen secretory cells are involved in PcOvo and PcPV2 synthesis, with both proteins packed into the same secretory granules, together with galactogen (Catalán et al., 2006).

Perivitellin Functions

Analysis of the perivitellin sequences of *P. canaliculata*, based on the Kyoto Encyclopedia of Genes and Genomes (KEGG), classified the 59 sequenced proteins into “unknown” (34), “environmental information processing” (10), “metabolism” (7), “organismal systems” (2), “cellular processes” (3), and “others” (3). Among the “environmental information processing” cluster, nine proteins are related to innate immunity (Sun et al., 2012b). These results indicate that maternal investment in *P. canaliculata* eggs is complex.

In *P. canaliculata* PcOvo and PcPV2 are storage proteins that provide energetic and structural precursors for the embryos, since they are consumed during development (Heras et al., 1998). The different glycosylation patterns of these two perivitellins probably allow the differential uptake and protein targeting observed during embryogenesis (Heras et al., 1998). In addition, PcOvo carries and stabilizes astaxanthin within the perivitelline fluid and when embryos take up PcOvo (Heras et al., 1998), this potent antioxidant carotenoid can be incorporated into their cytoplasmic membranes for protection, while providing the pink-reddish color of the eggs (Dreon et al., 2004b). PcOvo also helps eggs cope with the harsh above-water conditions. First, the saccharide moiety of PcOvo, together with the high levels of galactogen in the perivitellline fluid (Heras et al., 1998), prevents egg desiccation. Second, the pigmented perivitellins may also protect the embryos against solar radiation, acting as filters (Dreon et al., 2004b).

PcPV2 is a potent neurotoxin (Heras et al., 2008). Each of the four dimeric units of PcPV2 consists of a carbohydrate-binding protein (probably the targeting module) attached to a pore-forming subunit (probably the toxic moiety). Due to their high pH stability and protease resistance, the dimers are able to reach the intestine while still biologically active and to bind to enterocytes, eventually reaching the circulatory system. PcPV2 is the first proteinaceous egg neurotoxin reported, and bears structural resemblance to botulinic and ricin heterodimeric toxins, the so called "AB toxins" previously only known in bacteria and plants (Dreon et al., 2013). However, as PcPV2 is rather slow-acting (at least in mice) it seems unlikely that it could by itself account for the extremely low levels of predation. Some sort of synergy occurs with PcOvo, which rapidly decreases rat growth when administered orally, probably involving both the inhibition of trypsin activity (antidigestive role) and resistance of the protein to digestion by gut enzymes (antinutritive role), thereby limiting the predator's capacity to digest egg nutrients (Dreon et al., 2010).

PcOvo and PcPV2 are also present in the midgut gland of new *P. canaliculata* hatchlings. In the laboratory, goldfish (*Carassina gibelio*) will not eat new hatchlings after they sample them (Yusa, personal observations). Similar observations have been made on eggs of *P. paludosa* (Snyder & Snyder, 1971; Romer, 1972). Also, the albumen gland cytosol of *P. canaliculata* is lethal to mice after intraperitoneal administration (Cadierno, Dreon & Heras, unpublished). The toxicity seems to be due to the presence of an active PcPV2 neurotoxin as the mice showed similar signs to those exhibited by mice that had been administered purified PcPV2 (Cadierno, Dreon & Heras, unpublished). It is possible that toxic perivitellins together with still unknown compounds present in the albumen gland of adult *Pomacea* females may explain why some predators avoid eating the gland while consuming the rest of the body, as for example rats and crows in the non-native range and the snail kite and limpkins in the native range (Yusa et al., 2000; Heras, personal observations; Yusa, personal observations).

In *P. scalaris*, apart from its assumed nutritive role, PsSC acts as a carotenoid carrier, giving pigmentation to the eggs and supplying the embryos with antioxidant molecules, as does PcOvo (Ituarte et al., 2008). However, unlike PcOvo, this perivitellin is a carbohydrate binding protein, which agglutinates erythrocytes, showing a high specificity for galactosamine and glucosamine containing glycans (Ituarte et al., 2012). Carbohydrate binding proteins may have an immune function, agglutinating bacteria or other pathogens. However, given that PcSC is resistant to pH changes and gastrointestinal digestion, it may also have an antipredator function; there are multiple examples of a similar function in plants, in which lectins from seeds protect the embryos (Peumans & Van Damme, 1995). Although *P. scalaris* eggs do not possess an active PcPV2-like toxin, and the perivitelline fluid seems non-toxic to mice (Ituarte, personal observations), predation on these eggs has not been reported.

Evolutionary and Ecological Implications of Egg Defenses

Pomacea canaliculata is the first animal known to deter predation with a combination of antinutritive, antidigestive and neurotoxic compounds, a widespread defensive strategy in plants. Among predator avoidance tactics, conspicuous coloration advertises antipredator defense across many taxa. However, *P. canaliculata* eggs are unusual in that PcOvo not only provides the warning signal but also participates in the biochemical defense. Another unusual aspect is that the defensive molecules are at the same time storage proteins that are later consumed by embryos and hatchlings (Heras et al., 1998), making synthesis particularly cost-effective. Also, as the toxins are proteins, females do not need to ingest toxic prey to endow the eggs with chemical defenses, a common practice in other organisms. The multiple functions of these egg proteins are summarized in Figure 4.

Considering that aerial eggs with conspicuous coloration are frequent across the Ampullariidae, biochemical defenses similar to those of *P. canaliculata* are probably more widespread in the genus, providing a potentially important

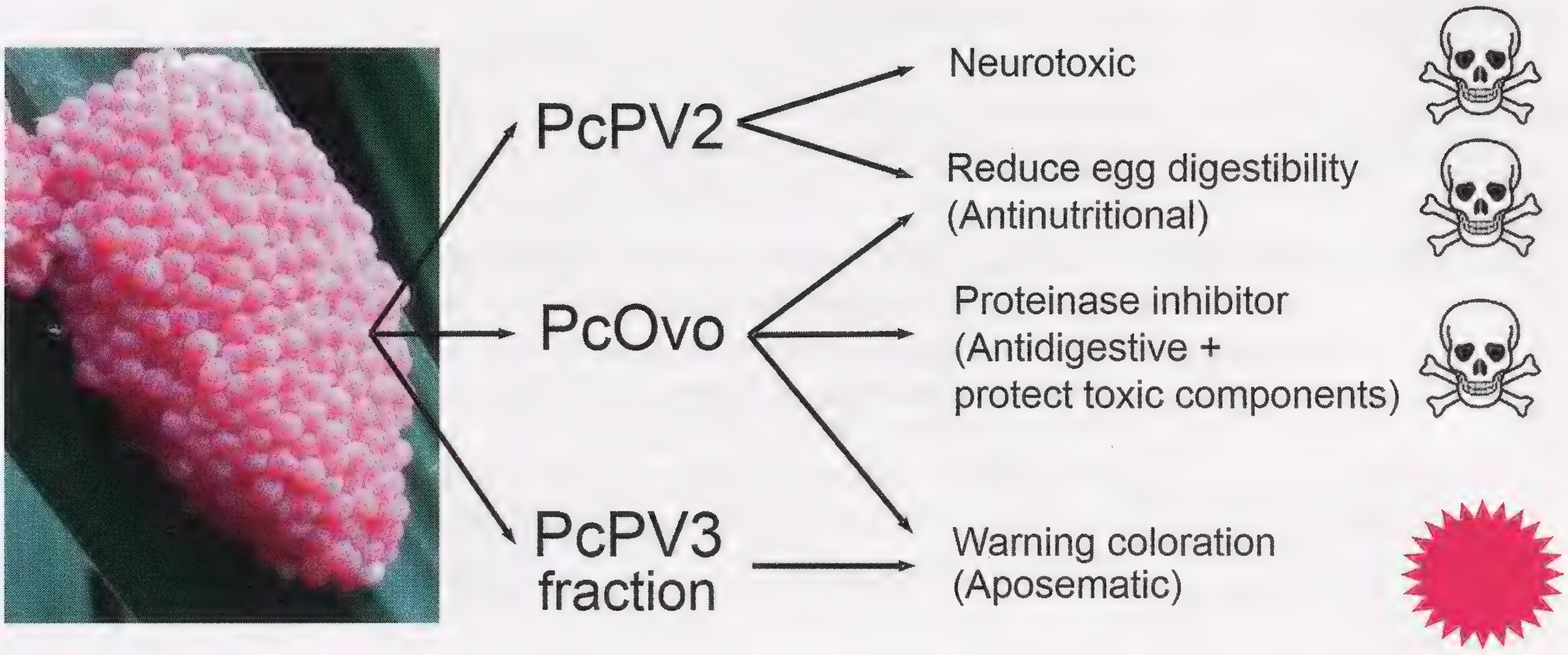

FIG. 4. The multiple roles of egg proteins in *Pomacea canaliculata*.

model for the study of the evolution of aposematism and defense using perivitellins (Heras et al., 2007; Dreon et al., 2010).

SYMBIOTIC ASSOCIATIONS

Ampullariids have established an amazing variety of symbiotic associations, but like much of the other information for apple snails, knowledge of these symbioses comes primarily from studies of *P. canaliculata*.

Epibiotic Organisms

The periostracum of relatively large and slowly moving snails like apple snails provides a potential surface for the attachment of many aquatic organisms. Di Persia & Radici de Cura (1973) described diverse assemblages of epibionts including filamentous cyanobacteria, chlorophytes and chrysophytes, and sessile ciliates, with a diverse assemblage of motile organisms living within this algal mat, including euglenophytes, ciliates, rotifers, annelids and dipteran larvae. Additional epibionts recorded on apple snails include the colonial sessile peritrich *Epistylis plicatilis* (Vega et al., 2006; Utz, 2007), the ectoproct *Hyalinella vaihiriae* (see Cazzaniga, 1988) and naidid oligochaetes in the umbilicus (Gorni & Alves, 2006).

Endosymbiotic Animals

Numerous animal taxa have been reported in the mantle cavity, hemocoel or connective tissue as symbionts of various ampullariids (Table 4). Leeches are the most frequently reported annelids in the mantle cavity. All life stages of *Helobdella ampullariae* (juveniles, adults and adults with both cocoons and broods) were found inside *P. canaliculata* but never free in the habitat (Damborenea & Gullo, 1996). The abundance of *H. ampullariae* on *P. canaliculata* increases with host size, with up to 65 in the largest snails. Transmission of the symbiont seems to occur during copulation (Damborenea & Gullo, 1996). Adult brooders and juveniles of *H. ampullariae* were also found in autumn and winter, while the four other Hirudinea species were only found during the spring and summer (Damborenea & Gullo, 1996).

Although the two cyclopoid copepods (Table 4) are found in the hemocoel, *Ozmana huarpium* is more common in the mantle cavity (63–65% of mature forms), where it occurs mainly in the ctenidium (in both sexes) and in the penial sheath groove in males. Female *O. huarpium* are more frequent than males in the mantle cavity, and mature females bearing egg sacs seem to be the infecting stage, and to be transmitted by copulation (Gamarra-Luques et al., 2004). Cyclopoid copepods are primarily marine species, but two of the ten recognized families are associated exclusively with freshwater hosts: the Lernaeidae with freshwater fish and the Ozmanidae with ampullariids (Ho, 1994; Boxshall & Strong, 2006).

Trematodes and nematodes occur in the mantle cavity, hemocoel and connective tissue of various organs or the gut lumen of ampullariids (Table 4; see Human Health Concerns). In addition, Keawjam et al. (1993) reported meta-

TABLE 4. Animal endosymbionts of Ampullariidae.

Symbiont	Host ampullariid species	References
Turbellaria		
Temnocephala iheringi[1,2]	*Pomacea canaliculata* (Lamarck, 1822) *Pomacea haustrum* (Reeve, 1856) *Pomacea lineata* (Spix in Wagner, 1827) *Pomacea megastoma* (Sowerby, 1825) *Asolene platae* (Maton, 1811)	Damborenea, 1996; Damborenea & Cannon, 2001; Martín et al., 2005
T. haswelli	*Pomacea canaliculata* (Lamarck, 1822)	Seixas et al., 2010a
T. rochensis	*Pomacea canaliculata* (Lamarck, 1822)	Seixas et al., 2010b
T. lamothei	*Pomacea megastoma* (Sowerby, 1825)	Damborenea & Brusa, 2008
Hirudinea		
Helobdella ampullariae[1]	*Pomacea canaliculata* (Lamarck, 1822) *Pomacea megastoma* (Sowerby, 1825) *Pomacea maculata* Perry, 1810	Ringuelet, 1945, 1985; Damborenea & Gullo, 1996
H. triserialis	*Pomacea canaliculata* (Lamarck, 1822)	Damborenea & Gullo, 1996
H. simplex	*Pomacea canaliculata* (Lamarck, 1822)	Damborenea & Gullo, 1996
H. adiastola	*Pomacea canaliculata* (Lamarck, 1822)	Damborenea & Gullo, 1996
Gloiobdella michaelseni	*Pomacea canaliculata* (Lamarck, 1822)	Damborenea & Gullo, 1996
Acari		
Unionicola (*Ampullariatax*) *ampullariae*[1]	*Pomacea canaliculata* (Lamarck, 1822) *Pomacea maculata* Perry, 1810	Di Persia & Radici de Cura, 1973
Copepoda		
Ozmana haemophila[3]	*Pomacea maculata* Perry, 1810	Ho & Thatcher, 1989
O. huarpium[1,3]	*Pomacea canaliculata* (Lamarck, 1822)	Gamarra-Luques et al., 2004
Trematoda		
Cercaria pomaceae	*Pomacea paludosa* (Say, 1829)	Hanning & Leedom, 1978; Leedom & Short, 1981
Schistosomatidae	*Pomacea canaliculata* (Lamarck, 1822) *Pomacea figulina* (Spix in Wagner, 1827) *Pomacea lineata* (Spix in Wagner, 1827) *Pomacea maculata* Perry, 1810	Ostrowski de Nuñez, 1979; Digiani & Ostrowski de Nuñez, 2000; Damborenea et al., 2006; Thiengo, unpublished
Echinostoma spp.	*Pila scutata* (Mousson, 1848) *Pila* spp. *Pomacea canaliculata* (Lamarck, 1822)	Graczyk & Fried, 1998; Weerachai et al., 2011
Echinostoma parcespinosum	*Pomacea canaliculata* (Lamarck, 1822)	Martorelli, 1987
Dietziella egregia	*Pomacea canaliculata* (Lamarck, 1822)	Digiani & Ostrowski de Núñez, 2000
Catadiscus pomaceae	*Pomacea canaliculata* (Lamarck, 1822)	Hamann, 1992
Rotifera		
Bdelloidea	*Pomacea canaliculata* (Lamarck, 1822)	Vega et al., 2006
Nematoda		
Angiostrongylus cantonensis	*Pomacea canaliculata* (Lamarck, 1822)	Lv et al., 2008, 2009a, b, 2011

(continues)

(continued)

Symbiont	Host ampullariid species	References
	Pomacea lineata (Spix in Wagner, 1827)	Thiengo et al., 2010
	Pomacea maculata Perry, 1810	Teem et al., 2013
	Pomacea paludosa (Say, 1829)[4]	Wallace & Rosen, 1969
	Lanistes carinatus (Olivier, 1804)	Ibrahim, 2007
	Pila ampullacea (Linnaeus, 1758)	Punyagupta, 1965
	Pila virescens (Deshayes, in Bory de Saint Vincent, 1824)[5]	Tesana et al., 2009
	Pila pesmei (Morlet, 1889)	Tesana et al., 2009
	Pila gracilis (Lea, 1856)	Tesana et al., 2009
	Pila scutata (Mousson, 1848)	Tesana et al., 2009

[1] Detected in mantle cavity.
[2] Detected in lung.
[3] Detected in hemocoel.
[4] Perhaps incorrectly identified, as *P. paludosa* is not otherwise known from Hawaii (Cowie et al., 2007).
[5] Reported as *Pila polita*, which is an objective junior synonym of *P. virescens* (Cowie & Héros, 2012).

cercariae of three trematodes (an amphistome, a distome and an echinostome) in introduced *P. canaliculata* in Thailand.

Endosymbiotic Protists and Bacteria

Among protists, two species of large ciliates have been found in the gut of *P. canaliculata* (Gascón, 1975). Numerous coccoid or rod-like heterotrophic bacteria occur in the gut of ampullariids but almost no attempt has been made to identify them or to explore their functions, such as cellulose digestion (Vega et al., 2005). Several endoglucanases have been isolated from *Pomacea* "*insularus*" (probably *P. canaliculata* or perhaps *P. maculata*) (Yamaura & Matsumoto, 1993; Yamaura et al., 1997; Li et al., 2005), which were probably of bacterial origin. Specifically, a cellulase is secreted by a *Bacillus* strain (Zhang et al., 2007) (see Digestion), and bacteria in the genera *Pseudomonas*, *Enterobacter*, *Citrobacter* and *Lactoccocus* degrade uric acid (Koch et al., 2014).

Intracellular Pigmented Corpuscles in the Midgut Gland

At least some ampullariids bear two types of intracellular pigmented corpuscles (named C and K corpuscles) in the midgut gland that are eliminated in the feces and for which a symbiotic nature has been proposed. These include the Neotropical *Pomacea canaliculata*, *P. maculata*, *P. scalaris*, *Marisa cornuarietis*, *Asolene pulchella* and *A. spixii* (d'Orbigny, 1838) (Castro-Vazquez et al., 2002; Vega et al., 2006; Takebayashi, 2013) and the Asian *Pila virens* (Meenakshi, 1955; Devi et al., 1981) and *Pila scutata* (Mousson, 1848) (as *conica* Wood, 1828, a junior synonym of *scutata*; Ng et al., 2014) introduced in Hawaii (Takebayashi, 2013).

Among all the symbiotic associations summarized here, this is the only one that appears to be obligate for the host, as the symbionts are present in all individuals of all studied populations (Vega et al., 2006). Both morphotypes together account for 8–11% of the midgut gland mass (Vega et al., 2005). Because they have a plasma membrane and thick, electron dense wall, but lack a nucleus (Koch et al., 2006), they have been considered as prokaryotes. Even though axenic cultures of these corpuscles have not been obtained (Koch, 2008), morphotype C may persist for at least 3 years in aquarium sediments that had contained fecal droppings of *P. canaliculata*, while morphotype K tends to disappear with time (Koch et al., 2006).

Morphotypes C and K occur respectively in columnar and pyramidal cells of the midgut gland tubular alveoli (Koch et al., 2006). These cells originate in the midgut gland before hatching, before pigmented corpuscles can be recognized, and have been described in both *Marisa cornuarietis* by Demian & Yousif (1973b) and *P. canaliculata* by Koch et al. (2009) (see Development: Digestive Tract). Pyramidal cells have large nuclei and conspicuous nucleoli, and are polyploid, with a nuclear DNA content ranging from 4 to 16 C (Cueto et al., 2006). This large DNA endowment is correlated with great development of the rough endoplasmic reticulum (Koch et al., 2006, 2009), which may contribute to the secretion of the multiple lamellae of K corpuscles (Koch et al., 2006).

Both C and K corpuscles contain chlorophyll-like pigments identified as steryl pheophorbides (Vega et al., 2012b). However, because the shell filters out most photosynthetically active radiation (Dellagnola, 2010) and the pheophorbides are not suitable for light harvesting, their significance is not clear. They may be interpreted as evolutionary remnants in a formerly photosynthetic organism that has been strongly modified by endosymbiosis in darkness.

IMMUNE DEFENSES

Molluscs, as all invertebrates so far investigated, possess defense mechanisms analogous to those of the innate immune system of vertebrates that are based mainly on cellular responses and on circulating and fixed lectins (Ottaviani, 2006, 2011). They serve a variety of functions, such as recognition and phagocytosis of invaders (Bayne, 1983), capsule formation around parasites (e.g., Yousif et al., 1980; Lv et al., 2009b), hemostasis, wound healing, shell formation and repair (Franchini & Ottaviani, 2000) and storage/transport of nutrients (e.g., Travers et al., 2008). Hemocytes have also been involved in stress response through the release of vertebrate-like endocrine molecules (Ottaviani et al., 1991).

Development of *in vitro* culture systems for ampullariid hemocytes may be critical for understanding many aspects of their biology. However, a culture system has only been reported for *P. canaliculata* (see Cueto et al., 2013); it uses a medium mimicking the physicochemical and chemical characteristics of the snail's internal milieu (Cueto et al., 2011).

Ampullariid Hemocytes

Substantial information has been gathered regarding hemocyte structure and function in the ampullariids *Pila globosa* (see Mahilini & Rajendran, 2008) and *P. canaliculata* (Shozawa & Suto, 1990; Cueto et al., 2007, 2013, submitted; Ray et al., 2012; Accorsi et al., 2013). Recent authors (Mahilini & Rajendran, 2008; Ray et al., 2012; Accorsi et al., 2013) have used various names for the different kinds of hemocytes, but in an attempt to standardize the nomenclature, Cueto et al. (submitted) adopted the classical terminology of Cheng (1975), recognizing three types: agranulocytes, hyalinocytes and granulocytes.

Agranulocytes constitute 28% of circulating cells in *P. canaliculata* according to Cueto et al. (2013) and are likely to include circulating blasts (Ray et al., 2012; Accorsi et al., 2013), though this hypothesis needs testing. Hyalinocytes are larger cells with membrane-bound granules of moderate electron density and may be lysosomes (Cueto et al., submitted). Approximately one quarter of circulating hyalinocytes show phagocytic activity and may participate in circulation and storage of glycogen (Cueto et al., 2013). Granulocytes are about the size of hyalinocytes but show no evidence of phagocytosis. They contain conspicuous eosinophilic granules that are membrane-bound, large and rod-shaped and show a high electron density. These granules merge and form even larger ones when granulocytes are exposed to microbes and may degranulate in a kind of "compound exocytosis" (Pickett & Edwardson, 2006). Degranulation of granulocytes has been linked to the release of lysozyme and other bactericidal hydrolases in other molluscs (e.g., Ottaviani, 1991).

Hemocyte-Producing Organs and/or Immune Barriers

Many authors have reported that gastropod hemocytes are generated in the circulation (Sminia, 1981; Monteil & Matricon-Gondran, 1991; van der Knaap et al., 1993; Souza & Andrade, 2006). However, "amoebocyte-producing organs" have also been reported in the pericardial wall of some heterobranchs (Lie et al., 1975; Rondelaud & Barthe, 1982; Jeong et al., 1983; Ruellan & Rondelaud, 1992) and in the roof of the lung of *M. cornuarietis* (see Yousif et al., 1980). No such organs have been found in *P. canaliculata*, although spheroidal hemocyte aggregates, similar to those formed *in vitro* (Cueto et al., 2013), were found in the lung following injection of yeast cells into the visceral hump (Rodriguez et al., 2012), suggesting a role of the hemocytes in fighting infection. Also, large hemocyte islets occupy the hemocoelic spaces in the kidney of *P. canaliculata* (Cueto, 2011; Giraud-Billoud et al., 2013b; Cueto et al., submitted), and it is possible that

TABLE 5. Mean metal concentrations (mg/kg dry weight) in the soft tissues of apple snails reported in previous studies. (Dashes indicate no data available.)

Species and tissue	Cu	Cd	Pb	Zn	Location	Reference
Pila ovata (viscera)	2.0–5.8	-	-	23.6–45.0	Southern Nigeria	Ezemonye et al., 2006
'*Pila ovum*'[1]	24.6	1.0	4.8	-	Southwestern Nigeria	Adewunmi et al., 1996
Lanistes libycus	48.2	0.8	5.42	-	Southwestern Nigeria	Adewunmi et al., 1996
Pomacea canaliculata (head-foot)	32–90	0.4–2.5	5–32	70–240	Guangdong, China	Deng et al., 2008
Pomacea canaliculata (viscera)	60–170	5–29	160–620	3000–6400	Guangdong, China	Deng et al., 2008
Pomacea paludosa	23.9–732	-	-	-	Florida, USA	Frakes et al., 2008
Pomacea paludosa (foot)	44–145	-	-	-	Florida, USA	Hoang et al., 2008
Pomacea paludosa (viscera)	75–229	-	-	-	Florida, USA	Hoang et al., 2008

[1] Misnamed; could be either *Lanistes ovum* Troschel, 1845 or *Pila ovata*.

they function as a hemocyte-producing organ. Also, hemocyte spheroids are formed in these islets after the injection of yeast cells in the foot (Rodriguez et al., 2012), demonstrating the reactivity of the islets to an immune challenge. The presumptive hemopoietic role of the lung roof and the kidney in ampullariids needs to be further explored, but their role as immune barriers against intruders seems clear.

ENVIRONMENTAL HEALTH AND POLLUTION

This review has focused thus far on the basic biology of ampullariids. However, there are important applied issues, notably their role as major agricultural pests, environmental pests, vectors of human disease and in ecotoxicology. Their role as crop pests, primarily of rice in Asia but also of taro and other crops in Asia and elsewhere, has been thoroughly reviewed elsewhere (Cowie, 2002; Joshi & Sebastian, 2006), and the limited understanding of their importance as environmental pests has been covered in the present review. However, their role in ecotoxicological research has been extensive in the last two decades but has not been reviewed. Also, important work regarding their role as human parasitic disease vectors has appeared since the review of Hollingsworth & Cowie (2006). Therefore these topics are reviewed briefly.

Accumulation of Pollutants

Several reports, notably from Nigeria, China and Florida, of heavy metal concentrations have shown that apple snails have the potential to accumulate high concentrations of these elements in their tissues, especially the viscera (Table 5). Thus they have the potential to affect animals at higher trophic levels, including humans. The high tissue concentrations of lead and zinc reported in *P. canaliculata* from a lead/zinc mine in southern China were probably due to accumulation and detoxification through binding to proteins or ligands, as in *Lymnaea stagnalis* (Linnaeus, 1758) (Desouky, 2006), rather than contamination by sediment. In some cases, there is a positive correlation between tissue burden and environmental concentration of toxicants, such that these ampullariids may serve as bioindicators of environmental pollution.

Vega et al. (2012b) determined the bioconcentration factors (BCFs) for a range of elements in tissues, eggs and midgut gland endosymbionts of *P. canaliculata*. The highest BCF was exhibited by barium (Ba) in all studied tissues, including the pallial oviduct, as well as the eggs, which showed the lowest BCFs for the other elements, suggesting the existence of a barrier protecting the eggs from most metal pollutants. Other tissues exhibited a range of BCFs for other elements. The BCFs for barium were extremely high in the intracellular endosymbionts (C and K morphotypes) and other more toxic pollutants (e.g., uranium, mercury, arsenic, bromine) were also heavily concentrated. The endosymbionts are released in the snail's feces so may serve a detoxification function.

The accumulation of metal pollutants by ampullariids and their endosymbionts indicates the potential harm of using these snails as soil fertilizers or animal food (Halwart, 1994; Vega et al., 2012a). Also, ampullariids are considered a delicacy in some parts of the world (Diupotex-Chong et al., 2004; Eamsobhana et al., 2010; Lv et al., 2011), and industrial development in such areas may transform these traditional foods into hazardous ones. In Florida, *P. paludosa* have high tissue concentrations of copper, accumulated primarily via the diet, related to high levels in the sediment due to the use of copper-based fungicides in citrus plantations, which is thus a serious concern for the Everglades snail kite (Rogevich et al., 2008).

Toxicity of Pollutants to Apple Snails

Apple snail toxicity assays for metals and organic pesticides appear very sensitive (Sawasdee & Köhler, 2009), and apple snails may therefore have potential as toxicity test organisms. However, their responses to different pollutants are complex and not broadly understood. For example, the toxicity of copper, to which *Pomacea* spp. are especially sensitive (Cazzaniga, 1981; Sun, 2013), may depend on a number of factors, including animal age and such water quality parameters as pH and dissolved oxygen concentration (Rogevich et al., 2008; Sun, 2013). In adult *P. canaliculata*, there are also complex feeding and growth rate relationships to exposure time and copper concentration (Peña & Pocsidio, 2007). Few studies have investigated the detailed responses to toxins. However, in sublethal toxicity tests on *M. cornuarietis* embryos, in which copper and nickel were more toxic than other metals, there were significant delays in formation of tentacles and eyes; and various concentrations of zinc, palladium, nickel and lithium also reduced heart rate or resulted in a delay in hatching (Sawasdee & Köhler, 2009, 2010). Toxicity assays have also been conducted using organic pesticides, including Diclobenil, Diuron and Simizina (Cazzaniga, 1981) and Paraquat (Melo et al., 2000). The effects of Atrazine and Imidacloprid on hatching rate of embryos have been investigated, with the former much more toxic (Sawasdee & Köhler, 2009). However, it is even more difficult to draw broad conclusions about the effects of such pesticides, not only because only very few studies have been undertaken on the immense diversity of pesticides in use but also because of lack of methodological standardization and a focus on either lethal or specific sublethal effects in different studies.

Mechanisms of Toxicity

The above studies have evaluated both lethal and non-lethal toxicity, mostly driven by the need for control of pest apple snails and environmental monitoring, but little is known about the mechanisms actually causing the toxicity. For example, several hypotheses have been proposed to explain the endocrine disrupting effects of organotins on female snails, although none appears exclusive (Oehlmann et al., 2007). The masculinizing compound tributyltin (TBT) induces lipid and fatty acid accumulation in female *M. cornuarietis* according to Janer et al. (2007), just as organotin compounds induce adipogenesis in vertebrates through interaction with retinoid X receptor (RXR) and peroxisome proliferator-activated γ receptor (Grün et al., 2006). In the neogastropod *Thais clavigera* (Küster, 1860), TBT also binds to RXR with high affinity (Nishikawa et al., 2004). In addition, TBT has spermicidal action, targeting the seminal receptacle (Giraud-Billoud et al., 2013c).

As well as effects on survival of juveniles and adults, endocrine disrupting effects have been reported in females exposed to several environmental contaminants, including TBT and TPT (triphenyltin), at different ages from hatching to adulthood (Schulte-Oehlmann et al., 1995, 2000; Tillmann et al., 2001). However, during development, different physiological control mechanisms may be acting at different times, each potentially generating different responses to pollutants. Because masculinizing substances act on the copulatory rudiment that is normally present in juvenile and adult female apple snails (e.g., Schulte-Oehlmann et al., 2000) and because this rudiment continues to grow even after females reach sexual maturity (Gamarra-Luques et al., 2013), studies of female masculinization ("imposex") in ampullariids should consider age at exposure (Giraud-Billoud et al., 2013c).

The endocrine disrupting effects of bisphenol A are less clear than those of masculinizing pollutants. Bisphenol A has estrogenic effects on many aquatic invertebrates (Kang et al., 2007). In *M. cornuarietis* females, exposure at low concentrations resulted in formation of additional female organs, enlarged accessory sex glands, malformations of the pallial oviduct, enhanced egg and clutch production, and increased female mortality (Oehlmann et al., 2000, 2006). However, these studies were criticized for flaws in experimental design, analysis and interpretation (Staples et al., 2002; Dietrich et al., 2006). Subsequent studies exposing *M. cornuarietis* at higher concentrations detected no effect on eggs/female/month, percentage of eggs hatching successfully and time to hatching (Forbes et al., 2007a, b) and showed that a major part of the variability in such traits was simply individual differences (Forbes et al., 2008).

Sun (2013) examined the responses of the proteome of juvenile *P. canaliculata* after exposure to copper and cadmium. Eleven differentially expressed proteins were identified that function in many vital cellular functions, such as antioxidation, energy metabolism, detoxification, signaling transduction and cytoskeleton disruption. Although some of these functions are non-specific stress responses (i.e., antioxidation and energy metabolism), others may serve as biomarkers of exposure as they may be related to metal toxicity pathways.

HUMAN HEALTH CONCERNS

At least three human diseases are caused by transmission of parasites from ampullariids: angiostrongyliasis or rat lungworm disease caused by the nematode *Angiostrongylus cantonensis*, cercarial dermatitis or swimmer's itch caused by schistosome cercariae, and echinostomiasis caused by species in the trematode genus *Echinostoma*. The following brief review updates that of Hollingsworth & Cowie (2006).

Angiostrongyliasis

Infection by *A. cantonensis*, the rat lungworm, is the most common cause of eosinophilic meningitis worldwide (Graeff-Teixeira et al., 2009; Cowie, 2013a). It is an acute disease, with mild infections spontaneously resolving in a few weeks, but heavier infections sometimes entailing serious sequelae, although rarely death (Dorta-Contreras et al., 2009; Graeff-Teixeira et al., 2009; Cowie, 2013a; Murphy & Johnson, 2013). Widely and probably naturally occurring in much of Southeast Asia, this zoonosis is by far the most serious disease transmitted by ampullariids. It has been considered an emerging disease, as its geographical range has been expanding rapidly in recent years (Lv et al., 2011; Cowie, 2013a; Morassutti et al., 2014), and it has now been reported from over 30 countries (Wang et al., 2008; Cowie, 2013b; Kim et al., 2014). As development of the larvae depends on the temperature of their intermediate snail hosts, for example, *P. canaliculata* (Lv et al., 2006), global climate change may lead to further range expansion (Lv et al., 2011). However, with the exception of the many cases in parts of Asia, most reports are not associated with ampullariids.

The life cycle of *A. cantonensis* (Graeff-Teixeira et al., 2009; Cowie, 2013b) involves rats as definitive hosts and numerous species of terrestrial and freshwater gastropods as intermediate hosts (Kim et al., 2014), including a number of ampullariid species (Table 6). Humans become infected mainly through ingestion of raw or undercooked snails (as well as crabs or other paratenic hosts) (Cowie, 2013c). Deliberate ingestion is the primary route of infection in parts of Asia. In southern China, where non-native *P. canaliculata* is widespread, the number of cases of angiostrongyliasis has been increasing, with most cases directly related to the deliberate consumption of introduced *P. canaliculata*, which is currently considered the main cause of the spread of the disease in China (Lv et al., 2008, 2009a, b, 2011; Yang et al., 2013). *Pomacea canaliculata* is also a major source of infection in Taiwan (Tsai et al., 2013). Similarly, in Thailand, native *Pila* spp. are widely eaten and the main source of infection (Eamsobhana et al., 2010). Inadvertent ingestion of infected snails associated with vegetables, green salads, fresh vegetable juice and other produce is also an important avenue of infection (Lv, 2009a; Cowie, 2013c), but ingestion of larvae on produce contaminated with snail slime, drinking of contaminated water, or via breaks in the skin have not been demonstrated and ampullariids have not been implicated in these infection pathways (Hollingsworth & Cowie, 2006; Cowie, 2013c).

TABLE 6. Known ampullariid hosts of *Angiostrongylus cantonensis*. Data from Kim et al. (2014). (*Experimental infection only.)

Species	Location
Lanistes carinatus (Olivier, 1804)	Egypt
Marisa cornuarietis (Linnaeus, 1758)*	
Pila ampullacea (Linnaeus, 1758)	Thailand
Pila angelica (Annandale, 1920)*	
Pila gracilis (Lea, 1856)	Thailand
Pila pesmei (Morlet, 1889)	Thailand
Pila scutata (Mousson, 1848)	Indonesia, Malaysia, Thailand
Pila turbinis (Lea, 1856)	Thailand
Pila virescens (Deshayes, in Bory de Saint Vincent, 1824) [as *polita* Deshayes, 1830]	China, Thailand
Pomacea canaliculata (Lamarck, 1822)	China, Hawaii, Okinawa (Japan), Taiwan
Pomacea lineata (Spix in Wagner, 1827)	Brazil
Pomacea maculata Perry, 1810	China, Louisiana (USA)
Pomacea paludosa (Say, 1829)	Cuba, Hawaii (possible misidentification)

According to published reports, abdominal angiostrongyliasis caused by the closely related *Angiostrongylus costaricensis*, primarily in South and Central America (Rodriguez et al., 2008), is not associated with ampullariids.

Cercarial Dermatitis

Various trematode parasites of birds and mammals use freshwater snails as intermediate hosts (Brown, 1994; Muller, 2002). Transmission is achieved by swimming larvae, that is, the miracidia and cercariae that are infective to the intermediate and definitive hosts, respectively (Muller, 2002). Species of the genus *Schistosoma* are by far the most important trematodes from a medical viewpoint as they cause schistosomiasis that affects millions of people in tropical regions (Muller, 2002). Various species of other genera of Schistosomatidae may cause cercarial dermatitis or swimmer's itch in humans, in which the cercariae penetrate the skin but do not develop further (Muller, 2002; Burke & Tester, 2002). Among ampullariids, only *P. paludosa* has been definitively demonstrated as a vector, and only of cercarial dermatitis, in Florida (Hanning & Leedom, 1978). In Brazil, although there is no record of cercarial dermatitis associated with species of *Pomacea*, schistosomatid cercariae have been detected in *P. lineata* and *P. maculata* by Mattos et al. (2013) and in *P. figulina* by Thiengo (unpublished).

Echinostomiasis

Human echinostomiasis is a food-borne, zoonotic parasitosis attributed to various species of digenean trematodes, many of which are transmitted by freshwater snails. This zoonosis, endemic in Southeast and eastern Asia, causes intestinal problems involving severe diarrhea and abdominal pain, eosinophilia, edema and hepatomegaly (Eveland & Haseeb, 2003; Graczyk & Fried, 1998). The life cycle of *Echinostoma* spp. involves birds and small mammals as definitive hosts, and snails, clams, and fishes as first and second intermediate hosts. Humans become infected through the ingestion of raw or undercooked intermediate hosts infected with the metacercariae of the parasite.

Eating raw or undercooked *Pila luzonica* (Reeve, 1856) (probably a synonym of *Pila scutata*) has been considered the main route of transmission in the Philippines (Graczyk & Fried, 1998), though it is also possible that because of the difficulty non-experts have in distinguishing ampullariid species, *P. canaliculata*, which is now widely distributed in the Philippines (Hayes et al., 2008), is involved. In Thailand, *Pila* spp. and *P. canaliculata* (and perhaps *P. maculata*, with which *P. canaliculata* has frequently been confused; Hayes et al., 2008, 2012) have been identified as intermediate hosts of *Echinostoma* spp. (Weerachai et al., 2011). The high incidence of the disease in northern Thailand (Graczyk & Fried, 1998) and other parts of Asia is probably also a result of consuming raw apple snails, as for angiostrongyliasis (Eamsobhana et al., 2010).

CONCLUSION AND FUTURE RESEARCH OPPORTUNITIES

The large amount of information that has been gathered makes the Ampullariidae one of the more intensively studied families of Gastropoda. However, nearly all studies have focused on a single species, *P. canaliculata*, and have done so in a non-comparative context, limiting their general applicability for understanding the biology of the family as a whole. These two issues suggest the need for (1) comparative data for other species to provide insight into the evolution, ecology and biology of Ampullariidae broadly, and (2) information on particular areas of the biology of *P. canaliculata*, particularly (but not exclusively) genomics, which would support the development of this species, and perhaps other apple snails, as "emerging model organisms" in physiology, development and ecology (in the sense of Behringer et al., 2008). The significance of the family as a model for studies in evolutionary and invasion biology in particular has already been discussed by Hayes et al. (2009a). Additional priorities for future ampullariid research, in no particular order, are:

- Integrative eco-physiological and comparative genomic studies aimed at understanding the evolution of the family as a whole and the novel behavioral, biochemical, anatomical and physiological traits that may have driven diversification and transitions among habitats.
- Comparative behavioral studies to reveal patterns across genera and within the family that may have played a role in ecological adaptation and speciation.
- Proteomic and biochemical studies of perivitellins and associated egg proteins to explore their origins, functions and ecological and evolutionary roles in diversification.
- Functional anatomical studies of male and female reproductive systems, particularly as they relate to evolution and ecology of amphibious traits and behavior.
- Phylogenetics, systematics and biogeography of Old World Ampullariidae.
- Integrative studies exploring the role of behavior, sexual selection and trophic ecology in the invasive and evolutionary success of the family.
- Studies integrating population genomics and captive rearing to better understand the role of hybridization in the native and non-native ranges of ampullariids.
- Comparative evolutionary-developmental studies.
- Ampullariid medical malacology, particularly at the interface of disease ecology and invasion biology.
- Ecosystem services provided by ampullariids, particulary in the context of conservation.

In all studies on ampullariid evolution and ecology, there is a need for a deeper and broader comparative investigation into the degree of dependence on aquatic and terrestrial resources for all species and the processes that have driven adaptations (Hayes et al., 2009a). For example, the shift to aerial oviposition in some groups was probably a key event in ampullariid evolution (Hayes et al., 2009a). Apple snail eggs provide an exceptional model to study the evolution of biochemical and physiological adaptations, which may have profound implications for addressing questions of ecology and evolution (Dreon et al., 2013).

Among predator avoidance tactics, the egg defenses of *P. canaliculata* open new perspectives on the study of aposematism (Dreon et al., 2010). Further studies on perivitellins of other ampullariids, particularly of below-water egg laying species, will reveal if this peculiar group of proteins is an acquisition exclusive to the aerial egg laying ampullariids.

There is therefore a clear need for more comparative work on the factors that shaped the evolution of amphibious traits. This will allow a better understanding of the successful reproductive strategy of *Pomacea* species and the selective pressures that have driven these acquisitions. Ampullariids and their close relatives offer a unique and potentially powerful system for addressing the physiological and behavioral ramifications of the transition from aquatic to terrestrial modes of life.

Additional specific areas of need and opportunity include the basic documenting of species diversity, especially in Africa and Asia, considerable progress having already been made in this regard in South America (Hayes et al., 2009b), and the resulting understanding of evolutionary patterns has provided the necessary framework for interpreting many of the studies discussed herein. There remains much more that could be learned regarding detailed aspects of life-history and its variation, even of the most well understood species (*P. canaliculata* and to a lesser extent *P. maculata*), which in a comparative framework could enlighten fundamental ideas about the evolution of life histories. Much basic ecology remains to be discovered, including how such abiotic factors as water level, temperature and quality influence apple snail behavior. Population dynamics, including the impacts of predation, has barely been addressed. Finally, there remain fascinating questions arising from the invasion of apple snails into new regions, which can be considered a natural experiment in evolution and ecology (Hayes et al., 2009a).

ACKNOWLEDGEMENTS

The idea for this review originated at the 4th International Workshop on the Biology of Ampullariidae (POMACEA 2010), San Miguel de Tucumán, Argentina (November 16–20, 2010), organized by Horacio Heras, María Gabriela Cuezzo and the late Beatriz C. Winik. Writing the review was supported by grants from: the U.S. National Science Foundation to R. H. Cowie, K. A. Hayes, S. C. Thiengo and E. E. Strong (DEB-0949061) and R. L. Burks, K. A. Hayes and R. H. Cowie (OISE-1130694); the Universidad Nacional del Sur to P. R. Martín (PGI 24B/185); CONICET, Argentina to P. R. Martín (PIP 112 200901 00473), A. Castro-Vazquez (PIP 112 201101 00052) and I. A. Vega (2012-2014); ANPCyT, Argentina to P. R. Martín (PICT 2012-1956), A. Castro-Vazquez (PICT 2013-1190) and H. Heras (PICT 2011-1428, PICT 2008-1865); the Universidad Nacional de la Plata (N-684) to H. Heras; and the Universidad Nacional de Cuyo to I. A. Vega, M. Giraud-Billoud and A. Castro-Vazquez.

LITERATURE CITED

ACCORSI, A., L. BUCCI, M. DE EGUILEOR, E. OTTAVIANI & D. MALAGOLI, 2013, Comparative analysis of circulating hemocytes of the freshwater snail *Pomacea canaliculata*. *Fish & Shellfish Immunology*, 34: 1260–1268.

ACOSTA, B. O. & R. S. V. PULLIN, 1991, *Environmental impact of the golden snail (*Pomacea *sp.) on rice farming systems in the Philippines*. Freshwater Aquaculture Center, Central Luzon State University, Munoz, Nueva Ecija; ICLARM, Manila, vi + 34 pp.

ADEWUNMI, C. O., W. BECKER, O. KUEHNAST, F. OLUWOLE & G. DÖRFLER, 1996, Accumulation of copper, lead and cadmium in freshwater snails in southwestern Nigeria. *Science of the Total Environment*, 193: 69–73.

ADITYA, G. & S. K. RAUT, 2001, Food of the snail, *Pomacea bridgesi*, introduced in India. *Current Science*, 80: 919–921.

ADITYA, G. & S. K. RAUT, 2002, Destruction of *Indoplanorbis exustus* (Planorbidae) eggs by *Pomacea bridgesi* (Ampullariidae). *Molluscan Research*, 22: 87–90.

AIZAKI, K. & Y. YUSA, 2009, Field observations of the alarm response to crushed conspecifics in the freshwater snail *Pomacea canaliculata*: effects of habitat, vegetation, and body size. *Journal of Ethology*, 27: 175–180.

AIZAKI, K. & Y. YUSA, 2010, Learned predator response in a freshwater snail, *Pomacea canaliculata*. *Malacologia*, 52: 21–29.

ALBRECHT, E., 1998, *Control de la estacionalidad reproductiva en el gastrópodo* Pomacea canaliculata *(Prosobranchia, Ampullariidae)*. Ph.D. thesis, Universidad Nacional de Cuyo, Mendoza, 148 pp.

ALBRECHT, E., N. CARREÑO & A. CASTRO-VAZQUEZ, 1996, A quantitative study of copulation and spawning in the South American applesnail, *Pomacea canaliculata* (Prosobranchia: Ampullariidae). *The Veliger*, 39: 142–147.

ALBRECHT, E., N. CARRENO & A. CASTRO-VAZQUEZ, 1999, A quantitative study of environmental factors influencing the seasonal onset of reproductive behaviour in the South American apple-snail *Pomacea canaliculata* (Gastropoda: Ampullariidae). *Journal of Molluscan Studies*, 65: 241–250.

ALBRECHT, E. A., E. KOCH, N. B. CARREÑO & A. CASTRO-VAZQUEZ, 2005, Control of the seasonal arrest of copulation and spawning in the apple snail *Pomacea canaliculata* (Prosobranchia: Ampullariidae): differential effects of food availability, water temperature, and day length. *The Veliger*, 47: 169–174.

ANDREWS, E. B., 1964, The functional anatomy and histology of the reproductive system of some pilid gastropod molluscs. *Proceedings of the Malacological Society of London*, 36: 121–140.

ANDREWS, E. B., 1965, The functional anatomy of the mantle cavity, kidney and blood system of some pilid gastropods (Prosobranchia). *Journal of Zoology*, 146: 70–94.

ANNANDALE, N., 1920, The apple-snails of Siam. *Journal of the Natural History Society of Siam*, 4(1): 1–24.

ANONYMOUS, 2011, *Pest risk analysis on the introduction of Pomacea insularum (d'Orbigny, 1835) into the EU*. Ministerio de Medio Ambiente y Medio Rural y Marino, Spain, 45 pp.

ANTO, F., K. BOSOMPEM, J. KPIKPI, M. ADJIK & D. EDOH, 2005, Experimental control of *Biomphalaria pfeifferi*, the intermediate host of

Schistosoma mansoni, by the ampullariid snail *Lanistes varicus*. *Annals of Tropical Medicine and Parasitology*, 99: 203–209.

ANTON, H. E., 1838, *Verzeichniss der Conchylien welche sich in der Sammlung von Hermann Eduard Anton befinden*. Eduard Anton, Halle, xvi + 110 pp.

ATHAWALE, M. & S. REDDY, 2002, Storage excretion in the Indian apple snail, *Pila globosa* (Swainson), during aestivation. *Indian Journal of Experimental Biology*, 40: 1304–1306.

AVERBUJ, A., G. BIGATTI & P. E. PENCHASZADEH, 2010, Gametogenic cycle and size at first maturity of the Patagonic edible snail *Buccinanops cochlidium* from Argentina. *Marine Biology*, 157: 2229–2240.

BACHMANN, A., 1960, Apuntes para una hidrobiología argentina. II. *Ampullaria insularum* Orb. y *A. canaliculata* Lam. (Moll. Prosobr., Ampullaridae). Observaciones biológicas y ecológicas. *Actas y Trabajos del Primer Congreso Sudamericano de Zoología*, 1: 19–26.

BAHL, K. N., 1928, On the reproductive processes and development of *Pila globosa* (Swainson). Part I, Copulation and oviposition. *Memoirs of the Indian Museum*, 9: 1–11.

BAKER, G. H., 1998, The golden apple snail, *Pomacea canaliculata* (Lamarck) (Mollusca: Ampullariidae), a potential invader of fresh water habitats in Australia. Pp. 21–26, in: M. P. Zalucki, R. A. I. Drew & G. G. White, eds., *Pest management – future challenges. Proceedings of the sixth Australasian applied entomological research conference. Brisbane, Australia. 29 September–2nd October 1998*, Volume 2. University of Queensland, Brisbane.

BAKER, H. B., 1922, The Mollusca collected by the University of Michigan − Walker expedition in southern Vera Cruz, Mexico. I. *Occasional Papers of the Museum of Zoology, University of Michigan*, 106: 1–95.

BAKER, P., F. ZIMMANCK & S. M. BAKER, 2010, Feeding rates of an introduced freshwater gastropod *Pomacea insularum* on native and nonindigenous aquatic plants in Florida. *Journal of Molluscan Studies*, 76: 138–143.

BANDEL, K., 1998, Evolutionary history of East African fresh water gastropods interpreted from the fauna of Lake Tanganyika and Lake Malawi. *Zentralblatt für Geologie und Paläontologie*, 1: 233–292.

BARNES, M. A., R. K. FORDHAM & R. L. BURKS, 2008, Fecundity of the exotic applesnail, *Pomacea insularum*. *Journal of the North American Benthological Society*, 27: 738–745.

BAYNE, C. J., 1983, Molluscan immunobiology. Pp. 407–486, in: A. Saleuddin & K. Wilbur, eds., *The Mollusca. Volume 5: Physiology, Part 2*. Academic Press, New York, 500 pp.

BEHRINGER, R. R., M. K. LEVINE, N. PATEL & N. SINHA, 2008, *Emerging model organisms: a laboratory manual, volume 1*. Cold Spring Harbor Laboratory Press, New York, 592 pp.

BENSON, W. H., 1842, Mollusca. *Annals and Magazine of Natural History*, 9: 486–490.

BERGMANN, F. B., H. L. C. AMARAL, D. P. PINTO, C. C. CHIVITTZ & A. M. TOZETTI, 2013, Foraging activity of the snail kite, *Rostrhamus sociabilis* (Aves: Accipitridae) in wetlands of southern Brazil. *Brazilian Journal of Biology*, 73: 245–252.

BERTHOLD, T., 1989, Comparative conchology and functional morphology of the copulatory organ of the Ampullariidae (Gastropoda, Monotocardia) and their bearing upon phylogeny and palaeontology. *Abhandlungen des Naturwissenschaftlichen Vereins in Hamburg*, (NF)28: 141–164.

BERTHOLD, T., 1990, Phylogenetic relationships, adaptations and biogeographic origin of the Ampullariidae (Mollusca, Gastropoda) endemic to Lake Malawi, Africa. *Verhandlungen des Naturwissenschaftlichen Vereins Hamburg*, (NF)31/32: 47–84.

BERTHOLD, T., 1991, Vergleichende Anatomie, Phylogenie und historische Biogeographie der Ampullariidae (Mollusca, Gastropoda). *Abhandlungen des Naturwissenschaftlichen Vereins in Hamburg*, (NF)29: 1–256.

BIAN, Q.-Q., X.-Y Li, Y.-Q. Fang, Y.-Q. Jia & X.-D. Mu, 2013, Molecular identification of *Pomacea canaliculata* and *P. insularum* from rice paddy in different origins in China using mitochondrial adenosine triphosphate subunit 6 gene. *Mitochondrial DNA*, doi:10.3109/19401736.2013.830302

BIELER, R., 1993, Ampullariid phylogeny – book review and cladistic re-analysis. *The Veliger*, 36: 291–299.

BLAINVILLE, H. M. D. de, 1822, Note sur l'organisation de l'animal de l'Ampullaire. *Journal de Physique, de Chimie et d'Histoire Naturelle*, 95: 459–464.

BLUME, W., 1957, Eine bis heute unbekannte Interart von *Pomacea bridgesi* Rve. *Opuscula Zoologica*, 1: 1–2.

BOLAND, B. B., M. MEERHOFF, C. FOSALBA, N. MAZZEO, M. A. BARNES & R. L. BURKS, 2008, Juvenile snails, adult appetites: contrasting resource consumption between two species of applesnails (*Pomacea*). *Journal of Molluscan Studies*, 74: 47–54.

BORN, I. von, 1778, *Index rerum naturalium Musei Caesarei Vindobonensis. Pars Ima Testacea. Verzeichniß der natürlichen Seltenheiten des k. k. Naturalien Cabinets zu Wien. Erster Theil. Schalthiere*. J. P. Kraus, Vindobonae [= Vienna], xlii + 458 + [82] p., 1 pl.

BORY DE SAINT-VINCENT [J. B. G. M.], ed., 1824, *Dictionnaire classique d'histoire naturelle*. Planches. Cinquième livraison. Rey et Gravier, Baudouin Frères, Paris.

BOSS, K. J. & J. J. PARODIZ, 1977, Paleospecies of Neotropical ampullariids and notes on other fossil non-marine South American gastropods. *Annals of Carnegie Museum*, 46: 107–127.

BOSSUYT, F. & M. MILINKOVITCH, 2001, Amphibians as indicators of early Tertiary 'out-of-India' dispersal of vertebrates. *Science*, 292: 93–95.

BOUCHET, P. & J.-P. ROCROI, 2005, Classification and nomenclator of gastropod families. *Malacologia*, 47: 1–397

BOXSHALL, G. A. & E. E. STRONG, 2006, An extraordinary shift in life habit within a genus of cyclopid copepods in Lake Tanganyika. *Zoological Journal of the Linnean Society*, 146: 275–286.

BROOKS, W. & B. McGLONE, 1908, The origin of the lung of *Ampullaria*. *Carnegie Institution of Washington Publication*, 102: 95–104.

BROWDER, J. A., P. J. GLEASON & D. R. SWIFT, 1994, Periphyton in the Everglades: spatial variation, environmental correlates, and ecological implications. Pp. 379–418, in: J. Ogden & S. Davis, eds., *Everglades, the ecosystem and its restoration*. St. Lucie Press, Delray Beach, Florida, 860 pp.

BRYAN, D. C., 1990, Apple snail densities at Alexander Springs, Lake County, and observations on snail ecology. *Florida Scientist*, 53 (Suppl. 1): 13.

BROWN, D. S., 1994, *Freshwater snails of Africa and their medical importance*, 2nd ed.Taylor & Francis, London, x +608 + [1] pp.

BUCKLAND-NICKS, J., 1998, Prosobranch parasperm: sterile germ cells that promote paternity? *Micron*, 29: 267–280.

BUCKLAND-NICKS, J. & F. S. CHIA, 1986, Fine structure of Sertoli cells in three marine snails with a discussion on the functional morphology of Sertoli cells in general. *Cell and Tissue Research*, 245: 305–313.

BUCKLAND-NICKS, J. & A. SCHELTEMA, 1995, Was internal fertilization an innovation of early Bilateria? Evidence from sperm structure of a mollusc. *Proceedings of the Royal Society of London B, Biological Sciences*, 261: 11–18.

BURELA, S. & P. R. MARTÍN, 2007, Nuptial feeding in the freshwater snail *Pomacea canaliculata* (Gastropoda: Ampullariidae). *Malacologia*, 49: 465–470.

BURELA, S. & P. R. MARTÍN, 2009, Sequential pathways in the mating behavior of the apple snail *Pomacea canaliculata* (Caenogastropoda: Ampullariidae). *Malacologia*, 51: 157–164.

BURELA, S. & P. R. MARTÍN, 2011, Evolutionary and functional significance of lengthy copulations in a promiscuous apple snail, *Pomacea canaliculata* (Caenogastropoda: Ampullariidae). *Journal of Molluscan Studies*, 77: 54–64.

BURELA, S. & P. R. MARTÍN, 2014, Nuptial gifts in *Pomacea canaliculata* (Ampullariidae, Caenogastropoda): experimental and field evidence about their function. *Malacologia*, 57(2): 319–327.

BURKE, W. A. & P. A. TESTER, 2002, Skin problems related to noninfectious coastal microorganisms. *Dermatologic Therapy*, 15: 10–17.

BURKS, R. L., S. A. HENSLEY & C. H. KYLE, 2011, Quite the appetite: juvenile island apple snails (*Pomacea insularum*) survive consuming only exotic invasive plants. *Journal of Molluscan Studies*, 77: 423–428.

BURKS, R. L., C. H. KYLE & M. K. TRAWICK, 2010, Pink eggs and snails: field oviposition patterns of an invasive snail, *Pomacea insularum*, indicate a preference for an invasive macrophyte. *Hydrobiologia*, 646: 243–251.

BURKS, R. L. & D. M. LODGE, 2002, Cued in: advances and opportunities in freshwater chemical ecology. *Journal of Chemical Ecology*, 28: 1901–1917.

BURKS, R. L., G. MULDERIJ, E. GROSS, I. JONES, L. JACOBSEN, E. VAN DONK & E. JEPPESEN, 2006, Center stage: the crucial role of macrophytes in regulating trophic interactions in shallow lake wetlands. Pp. 37–59, in: R. Bobbink, B. Beltman, J. T. A. Verhoeven & D. F. Whigham, eds., *Wetlands: functioning, biodiversity conservation, and restoration*. Springer-Verlag, Berlin and Heidelberg, xxv + 315 pp.

BURKY, A. J., 1974, Growth and biomass production of an amphibious snail, *Pomacea urceus* (Muller) [sic], from the Venezuelan savannah. *Journal of Molluscan Studies*, 41: 127–143.

BURKY, K. A. & A. J. BURKY, 1977, Buoyancy changes as related to respiroatory behavior in an amphibious snail, *Pomacea urceus* (Müller), from Venezuela. *The Nautilus*, 91: 97–104.

BURKY, A. J., J. PACHECO & E. PEREYRA, 1972, Temperature, water, and respiratory regimes of an amphibious snail, *Pomacea urceus* (Müller), from the Venezuelan savannah. *Biological Bulletin*, 143: 304–316.

BURLAKOVA, L. E., A. Y. KARATAYEV, D. K. PADILLA, L. D. CARTWRIGHT & D. N. HOLLAS, 2009, Wetland restoration and invasive species: apple snail (*Pomacea insularum*) feeding on native and invasive aquatic plants. *Restoration Ecology*, 17: 433–440.

BURLAKOVA, L. E., D. K. PADILLA, A. Y. KARATAYEV, D. N. HOLLAS, L. D. CARTWRIGHT & K. D. NICHOL, 2010, Differences in population dynamics and potential impacts of a freshwater invader driven by temporal habitat stability. *Biological Invasions*, 12: 927–941.

BYERS, J. E., W. G. McDOWELL, S. R. DODD, R. S. HAYNIE, L. M. PINTOR & S. B. WILDE, 2013, Climate and pH predict the potential range of the invasive apple snail (*Pomacea insularum*) in the southeastern United States. *PLoS One*, 8: e56812.

CARLSSON, N. O. L. & C. BRÖNMARK, 2006, Size-dependent effects of an invasive herbivorous snail (*Pomacea canaliculata*) on macrophytes and periphyton in Asian wetlands. *Freshwater Biology*, 51: 695–704.

CARLSSON, N. O. L., C. BRÖNMARK & L.-A. HANSSON, 2004a, Invading herbivory: the golden apple snail alters ecosystem functioning in Asian wetlands. *Ecology*, 85: 1575–1580.

CARLSSON, N. [O. L.], Å. KESTRUP, M. MÅRTENSSON & P. NYSTRÖM, 2004b, Lethal and non-lethal effects of multiple indigenous predators on the invasive golden apple snail (*Pomacea canaliculata*). *Freshwater Biology*, 49: 1269–1279.

CARLSSON, N. O. L. & J. O. LACOURSIÈRE, 2005, Herbivory on aquatic vascular plants by the introduced golden apple snail (*Pomacea canaliculata*) in Lao PDR. *Biological Invasions*, 7: 233–241.

CASTELLANOS, Z. J. A. & D. FERNANDEZ, 1976, Gastropoda Ampullariidae. Pp. 1–33, in: R. A. Ringuelet, ed., *Fauna de agua dulce de la República Argentina*. FECIC, Buenos Aires.

CASTRO-VAZQUEZ, A., E. A. ALBRECHT, I. A. VEGA, E. KOCH & C. GAMARRA-LUQUES, 2002, Pigmented corpuscles in the midgut gland of *Pomacea canaliculata* and other Neotropical apple-snails (Prosobranchia, Ampullariidae): a possible symbiotic association. *Biocell*, 26: 101–109.

CATALÁN, M., M. S. DREON, H. HERAS, R. J. POLLERO, S. N. FERNÁNDEZ & B. WINIK, 2006, Pallial oviduct of *Pomacea canaliculata* (Gastropoda): ultrastructural studies of the parenchymal cellular types involved in the metabolism of perivitellins. *Cell and Tissue Research*, 324: 523–533.

CATALÁN, N. M. Y., S. N. FERNANDEZ & B. C. WINIK, 2002, Oviductal structure and provision of egg envelops in the apple snail *Pomacea canaliculata* (Gastropoda, Prosobranchia, Ampullariidae). *Biocell*, 26: 91–100.

CATALÁN, M., C. SCHLICK DE SANTOLAYA & B. WINIK, 1997, Ultrastructural study of eupyrene spermatozoon in the pond snail *Ampullaria canaliculata* (Gastropoda, Prosobranchia). *Biocell*, 21: 175–185.

CATALÁN DE CANELADA, N. M. Y. & A. MORENO, 1984, Descripción del tracto intrauterino en el gasterópodo *Ampullaria canaliculata*. *Neotropica*, 30: 153–160.

CATTAU, C. E., J. MARTIN & W. M. KITCHENS, 2010, Effects of an exotic prey species on a native specialist: example of trhe snail kite. *Biological Conservation*, 143: 513–520.

CAZZANIGA, N. J., 1981, Evaluación preliminar de un gasterópodo para el control de malezas acuáticas sumergidas. Pp. 131–166, in: *CIC, II Reunión sobre Malezas Subacuáticas en Canales de Desagüe de CORFO, La Plata, Buenos Aires*.

CAZZANIGA, N. J., 1988, *Hyalinella vahiriae* (Ectoprocta) en la Provincia de San Juan. *Revista de la Asociación de Ciencias Naturales del Litoral*, 19: 205–208.

CAZZANIGA, N. J., 1990, Predation of *Pomacea canaliculata* (Ampullariidae) on adult *Biomphalaria peregrina* (Planorbidae). *Annals of Tropical Medicine and Parasitology*, 48: 97–100.

CAZZANIGA, N., 2006, *Pomacea canaliculata*: harmless and useless in its natural realm (Argentina). Pp. 37–60, in: R. C. JOSHI & L. C. SEBASTIAN, eds., *Global advances in ecology and management of golden apple snails*. Philippine Rice Research Institute, Muñoz, Nueva Ecija, Philippines, x + 588 pp.

CAZZANIGA, N. J. & A. L. ESTEBENET, 1984, Revisión y notas sombre los hábitos alimentarios de los Ampullariidae (Gastropoda). *Historia Natural*, 4: 213–224.

CEDEÑO-LEÓN, A. & J. D. THOMAS, 1983, The predatory behaviour of *Marisa cornuarietis* on eggs and neonates of *Biomphalaria glabrata*, the snail host of *Schistosoma mansoni*. *Malacologia*, 24: 289–297.

CHATURVEDI, M. & R. AGARWAL, 1981, Comparative study of storage pattern and site of synthesis of uric acid in the snails *Viviparus bengalensis* (Lamarck) and *Pila globosa* (Swainson), during active and dormant periods. *Indian Journal of Experimental Biology*, 19: 130–134.

CHEESMAN, D. F., 1958, Ovorubin, a chromoprotein from the eggs of the gastropod mollusc *Pomacea canaliculata*. *Proceedings of the Royal Society of London B, Biological Sciences*, 149: 571–587.

CHENG, T. C., 1975, Functional morphology and biochemistry of molluscan phagocytes. *Annals of the New York Academy of Sciences*, 266: 343–379.

CHOUDHURY, R. & R. PANDIT, 1997, Chromosomes of three prosobranch gastropods from Viviparidae, Pilidae and Cyclophoridae (Order: Mesogastropoda) *Caryologia*, 50: 303–315.

CLEDÓN, M., W. ARNTZ & P. E. PENCHASZADEH, 2005, Gonadal cycle in *Adelomelon brasiliana* (Neogastropoda: Volutidae) population of Buenos Aires province, Argentina. *Marine Biology*, 147: 439–445.

CLEMENTS, R., L. P. KOH, T. M. LEE, R. MEIER & D. LI, 2006, Importance of reservoirs for the conservation of freshwater molluscs in a tropical urban landscape. *Biological Conservation*, 128: 136–146.

COLES, G. C., 1968, The termination of aestivation in the large fresh-water snail *Pila ovata* (Ampulariidae) [sic] - I. Changes in oxygen uptake. *Comparative Biochemistry and Physiology*, 25: 517–522.

COLGAN, D. J., W. F. PONDER, E. BEACHAM & J. M. MACARANAS, 2003, Gastropod phylogeny based on six segments from four genes representing coding or non-coding and mitochondrial or nucelar DNA. *Molluscan Research*, 23: 123–148.

COLGAN, D. J., W. F. PONDER, E. BEACHAM & J. MACARANAS, 2007, Molecular phylogenetics of Caenogastropoda (Gastropoda: Mollusca). *Molecular Phylogenetics and Evolution*, 42: 717–737.

CORRAO, N. M., P. C. DARBY & C. M. POMORY, 2006, Nitrate impacts on the Florida apple snail, *Pomacea paludosa*. *Hydrobiologia*, 568: 135–143.

COWIE, R. H., 1997, *Pila* Röding, 1798 and *Pomacea* Perry, 1810 (Mollusca, Gastropoda): proposed placement on the Official List, and Ampullariidae Gray, 1824: proposed confirmation as the nomenclaturally valid synonym of Pilidae Preston, 1915. *Bulletin of Zoological Nomenclature*, 54: 83–88.

COWIE, R. H., 2001, Can snails ever be effective and safe biocontrol agents? *International Journal of Pest Management*, 47(1): 23–40.

COWIE, R. H., 2002, Apple snails (Ampullariidae) as agricultural pests: their biology, impacts and management. Pp. 145–192, in: G. M. BARKER, ed., *Molluscs as crop pests*. CABI, Wallingford, xii + 400 pp.

COWIE, R. H., ed., 2013a, Eosinophilic meningitis caused by *Angiostrongylus cantonensis*, the rat lungworm: biology, distribution, epidemiology, detection, diagnosis, treatment, and management. *Hawai'i Journal of Medicine and Public Health*, 72 (Suppl. 2): 1–88.

COWIE, R. H., 2013b, Biology, systematics, life cycle, and distribution of *Angiostrongylus cantonensis*, the cause of rat lungworm disease. *Hawai'i Journal of Medicine and Public Health*, 72 (Suppl. 2): 6–9.

COWIE, R. H., 2013c, Pathways for transmission of angiostrongyliasis and the risk of disease associated with them. *Hawai'i Journal of Medicine and Public Health*, 72 (Suppl. 2): 70–74.

COWIE, R. H. & K. A. HAYES, 2012, Apple snails. Pp. 207–221, in: R. A. Francis, ed., *A handbook of global freshwater invasive species*. Earthscan, London, xxiv + 460 pp.

COWIE, R. H., K. A. HAYES & S. C. THIENGO, 2006, What are apple snails? Confused taxonomy and some preliminary resolution. Pp. 3–23, in: R. C. Joshi & L. C. Sebastian, eds., *Global advances in ecology and management of golden apple snails*. Philippine Rice Research Institute, Muñoz, Nueva Ecija, Philippines, x + 588 pp.

COWIE, R. H., K. A. HAYES, C. T. TRAN & P. LEVIN, 2007, Distribution of the invasive apple snail *Pomacea canaliculata* (Lamarck) in the Hawaiian Islands (Gastropoda: Ampullariidae). *Bishop Museum Occasional Papers*, 96: 48–51.

COWIE, R. H. & V. HÉROS, 2012, Annotated catalogue of the types of Ampullariidae (Mollusca: Gastropoda) in the Muséum National d'Histoire Naturelle, Paris, with lectotype designations. *Zoosystema*, 34: 793–824.

COWIE, R. H. & S. C. THIENGO, 2003, The apple snails of the Americas (Mollusca: Gastropoda: Ampullariidae: *Asolene*, *Felipponea*, *Marisa*, *Pomacea*, *Pomella*): a nomenclatural and type catalog. *Malacologia*, 45: 41–100.

CUETO, J. A., 2011, Pomacea canaliculata *(Architaenioglossa, Ampullariidae): la hemolinfa y sus células*. Ph.D. thesis, Universidad Nacional de Cuyo, Mendoza, 126 pp.

CUETO, J. A., T. FOGAL & A. CASTRO-VAZQUEZ, 2007, Ultrastructural characterization of circulating hemocytes of *Pomacea canaliculata*. *Biocell*, 32: 103.

CUETO, J. A., M. GIRAUD-BILLOUD, I. A. VEGA & A. CASTRO-VAZQUEZ, 2011, Haemolymph plasma constituents of the invasive snail *Pomacea canaliculata* (Caenogastropoda, Architaenioglossa, Ampullariidae). *Molluscan Research*, 31: 57–60.

CUETO, J. A., C. RODRIGUEZ, I. A. VEGA & A. CASTRO-VAZQUEZ, submitted, Immune defenses of the apple snail *Pomacea canaliculata* (Architaenioglossa, Ampullariidae): hemocytes and organ barriers. *PLoS ONE*.

CUETO, J. A., I. A. VEGA & A. CASTRO-VAZQUEZ, 2013, Multicellular spheroid formation and evolutionary conserved behaviors of apple snail hemocytes in culture. *Fish & Shellfish Immunology*, 34: 443–453.

CUETO, J. A., I. A. VEGA, E. KOCH & A. CASTRO-VAZQUEZ, 2006, Poliploidía en células que contienen a un endocianobionte de la glándula digestiva de Pomacea canaliculata (Caenogastropoda, Ampullariidae). *Journal of Basic and Applied Genetics*, 17 (Suppl. 2): 111.

DALL, W. H., 1904, Notes on the genus *Ampullaria*. *Journal of Conchology*, 11: 51–55.

DAMBORENEA, M. C., 1996, Patrones de distribución y abundancia de *Temnocephala iheringi* (Platyhelminthes, Temnocephalidae) en una población de *Pomacea canaliculata* (Mollusca Ampullariidae). *Gayana, Zoología*, 60: 1–12.

DAMBORENEA, [M.] C. & F. BRUSA, 2008, A new species of *Temnocephala* (Platyhelminthes, Temnocephalida) commensal of *Pomella megastoma* (Mollusca, Ampullariidae) from Misiones, Argentina. *Revista Mexicana de Biodiversidad*, 79: 1S–7S.

DAMBORENEA, [M.] C., F. BRUSA & A. PAOLA, 2006, Variation in worm assemblages associated with *Pomacea canaliculata* (Caenogastropoda, Ampullariidae) in sites near the Río de la Plata estuary, Argentina. *Biocell*, 30: 457–468.

DAMBORENEA, M. C. & L. R. G. CANNON, 2001, On neotropical *Temnocephala* (Platyhelminthes). *Journal of Natural History*, 35: 1103–1118.

DAMBORENEA, M. C. & B. S. GULLO, 1996, Hirudíneos asociados a la cavidad paleal de *Pomacea canaliculata* (Lamarck, 1822) (Gastropoda: Ampullariidae) del balneario Bagliardi, Rio de la Plata, Argentina. *Neotropica*, 42: 97–101.

DARBY, P. C., R. E. BENNETTS, J. D. CROOP, P. L. VALENTINE-DARBY & W. M. KITCHENS, 1999, A comparison of sampling techniques for quantifying abundance of the Florida apple snail (*Pomacea paludosa* Say). *Journal of Molluscan Studies*, 65: 195–208.

DARBY, P. C., R. E. BENNETTS, S. J. MILLER & H. F. PERCIVAL, 2002, Movements of Florida apple snails in relation to water levels and drying events. *Wetlands*, 22: 489–498.

DARBY, P. C., R. E. BENNETTS & H. F. PERCIVAL, 2008, Dry down impacts on apple snail (*Pomacea paludosa*) demography: implications for wetland water management. *Wetlands*, 28: 204–214.

DARBY, P. C., D. J. MELLOW & M. L. WATFORD, 2007, Food-handling difficulties for snail kites capturing non-native apple snails. *Florida Field Naturalist*, 35: 79–85.

DARBY, P., P. VALENTINE-DARBY & H. PERCIVAL, 2003, Dry season survival in a Florida apple snail (*Pomacea paludosa* Say) population. *Malacologia*, 45: 179–184.

DE JONG-BRINK, M., H. H. BOER J. & JOOSSE, 1983, Mollusca. Pp. 297–355, in: K. G. Adiyodi & R. G. Adiyodi, eds., *Reproductive biology of invertebrates, Vol. 1: Oogenesis, oviposition, oosorption*. John Wiley & Sons, New York, 770 pp.

DELLAGNOLA, F. A., 2010, *Una simbiosis procariota-molusco: contribuciones funcionales y taxonómicas*. Tesis de Licenciatura. Instituto de Ciencias Básicas, Universidad Nacional de Cuyo, Mendoza, Argentina, 52 pp.

DEMIAN, E. S. & A. M. IBRAHIM, 1971, The eggs masses, egg laying and mating behavior of the snail *Marisa cornuarietis* (L.). *Bulletin of the Zoological Society of Egypt*, 23: 1–12.

DEMIAN, E. & A. M. IBRAHIM, 1972, Sexual dimorphism and sex ratio in the snail *Marisa cornuarietis* (L). *Bulletin of the Zoological Society of Egypt*, 24: 52–63.

DEMIAN, E. S. & R. G. LUTFY, 1965a, Predatory activity of *Marisa cornuarietis* against *Bulinus* (*Bulinus*) *truncatus*, the transmitter of urinary schistosomiasis. *Annals of Tropical Medicine and Parasitology*, 59: 331–336.

DEMIAN, E. S. & R. G. LUTFY, 1965b, Predatory activity of *Marisa cornuarietis* against *Biomphalaria alexandrina* under laboratory conditions. *Annals of Tropical Medicine and Parasitology*, 59: 337–339.

DEMIAN, E. S. & R. G. LUTFY, 1966, Factors affecting the predation of *Marisa cornuarietis* on *Bulinus* (*B.*) *truncatus*, *Biomphalaria alexandrina* and *Lymnaea caillaudi*. *Oikos*, 17: 212–230.

DEMIAN, E. S. & F. YOUSIF, 1973a, Embryonic development and organogenesis in the snail *Marisa cornuarietis* (Mesogastropoda, Ampullariidae). II. Development of the alimentary system. *Malacologia*, 12: 151–174.

DEMIAN, E. S. & F. YOUSIF, 1973b, Embryonic development and organogenesis in the snail *Marisa cornuarietis* (Mesogastropoda: Ampullariidae). III. Development of the circulatory and renal systems. *Malacologia*, 12: 175–194.

DEMIAN, E. S. & F. YOUSIF, 1973c, Embryonic development and organogenesis in the snail *Marisa cornuarietis* (Mesogastropoda: Ampullariidae). IV. Development of the shell gland, mantle and respiratory organs. *Malacologia*, 12: 195–211.

DEMIAN, E. S. & F. YOUSIF, 1973d, Embryonic development and organogenesis in the snail *Marisa cornuarietis* (Mesogastropoda: Ampullariidae). I. General outlines of development. *Malacologia*, 12: 123–150.

DEMIAN, E. S. & F. YOUSIF, 1975, Embryonic development and organogenesis in the snail *Marisa cornuarietis* (Mesogastropoda: Ampullariidae). V. Development of the nervous system. *Malacologia*, 15: 29–42.

DENG, P. Y., W. S. SHU, C. Y. LAN & W. LIU, 2008, Metal contamination in the sediment, pondweed, and snails of a stream receiving effluent from a lead/zinc mine in southern China. *Bulletin of Environmental Contamination and Toxicology*, 81: 69–74.

DESHAYES, G. P., 1830 [1830–1832], *Encyclopédie méthodique. Histoire naturelle des vers.* Tome second. Agasse, Paris, 1,152 pp.

DESHAYES, G. P. & H. MILNE EDWARDS, 1838, *Histoire naturelle des animaux sans vertèbres...* Deuxième édition, Tome huitième. J. B. Baillière, Paris, 660 pp.

DESOUKY, M. M. A., 2006, Tissue distribution and subcellular localization of trace metals in the pond snail *Lymnaea stagnalis* with special reference to the role of lysosomal granules in metal sequestration. *Aquatic Toxicology*, 77: 143–152.

DEVI, C. U., K. H. RAO & K. SHYAMASUNDARI, 1981, Observations on the histology and cytochemistry of the digestive gland in *Pila virens* (Lamarck) (Mollusca: Gastropoda). *Proceedings of the Indian Academy of Sciences (Animal Sciences)*, 90: 307–314.

DIETRICH, D. R., E. O'BRIEN, S. HOFFMANN, P. BALAGUER, J.-C. NICOLAS, W. SEINEN & M. DEPLEDGE, 2006, Effects of BPA in snails. *Environmental Health Perspectives*, 114: A340–A341.

DIGIANI, M. & M. OSTROWSKI DE NÚÑEZ, 2000, Estudios preliminares sobre el ciclo biológico de *Dietziella egregia* (Dietz, 1909) (Digenea: Echinostomatidae) en la provincia de Buenos Aires. P. 366, in: *III Congreso Argentino de Parasitología, 1–4 Noviembre 2000, Mar del Plata.*

DILLON, R. T., Jr., 2000, *The ecology of freshwater molluscs.* Cambridge University Press, Cambridge, UK, xii + 509 pp.

DILLON, R. T., Jr., 2002, The inheritance of *golden*, a shell color variant of *Marisa cornuarietis*. *Malacological Review* 31/32: 155–157.

DI PERSIA, D. & M. RADICI DE CURA, 1973, Algunas consideraciones acerca de los organismos epibiontes desarrollados sobre Ampullariidae. *Physis*, 32: 309–319.

DIUPOTEX-CHONG, M., N. CAZZANIGA, A. HERNÁNDEZ-SANTOYO & J. BETANCOURT-RULE, 2004, Karyotype description of *Pomacea patula catemacensis* (Caenogastropoda, Ampullariidae), with an assessment of the taxonomic status of *Pomacea patula*. *Biocell*, 28: 279–285.

DIUPOTEX-CHONG, M., N. CAZZANIGA & M. URIBE-ALCOCER, 2007, Karyological and electrophoretic differences between *Pomacea flagellata* and *P. patula catemacensis* (Caenogastropoda: Ampullariidae). *Biocell*, 31: 365–373.

DOHRN, H., 1865, List of the land and freshwater shells of the Zambesi and Lake Nyassa, Eastern tropical Africa, collected by John Kirk, M.D., F.L.S., &c. *Proceedings of the Zoological Society of London* 1865: 231–234.

DORTA-CONTRERAS, A. J., M. E. MAGRANER-TARRAU & E. SÁNCHEZ-ZULUETA, 2009, Angiostrongyliasis in the Americas. *Emerging Infectious Diseases*, 15: 991.

DRAPARNAUD J.-P.-R., 1805, *Histoire naturelle des mollusques terrestres et fluviatiles de la France, ouvrage posthume.* Louis Colas, Paris.

DREON, M. S., M. V. FRASSA, M. CEOLIN, S. ITUARTE, J.-W. QIU, J. SUN, P. E. FERNÁNDEZ & H. HERAS, 2013, Novel animal defenses against predation: a snail egg neurotoxin combining lectin and pore-forming chains that resembles plant defense and bacteria attack toxins. *PLoS One*, 8(5): e63782.

DREON, M. S., H. HERAS & R. J. POLLERO, 2003, Metabolism of ovorubin, the major egg lipoprotein from the apple snail. *Molecular and Cellular Biochemistry*, 243: 9–14.

DREON, M. S., H. HERAS & R. J. POLLERO, 2004a, Characterization of the major egg glycolipoproteins from the perivitellin fluid of the apple snail *Pomacea canaliculata*. *Molecular Reproduction and Development*, 68: 359–364.

DREON, M. S., S. ITUARTE, M. CEOLIN & H. HERAS, 2008, Global shape and pH stability of ovorubin, an oligomeric protein from the eggs of *Pomacea canaliculata*. *FEBS Journal*, 275(4522): 4530.

DREON, M. S., S. ITUARTE & H. HERAS, 2010, The Role of the Proteinase Inhibitor Ovorubin in Apple Snail Eggs Resembles Plant Embryo Defense against Predation. *PLoS One*, 5(12): e15059.

DREON, M. S., S. LAVARÍAS, C. F. GARÍN, H. HERAS & R. J. POLLERO, 2002, Synthesis, distribution, and levels of an egg lipoprotein from the apple snail *Pomacea canaliculata* (Mollusca: Gastropoda). *Journal of Experimental Zoology*, 292: 323–330.

DREON, M. S., G. SCHINELLA, H. HERAS & R. J. POLLERO, 2004b, Antioxidant defense system in the apple snail eggs, the role of ovorubin. *Archives of Biochemistry and Biophysics*, 422: 1–8.

EAMSOBHANA, P., A. YOOLEK & H.-S. YONG, 2010, Effect of Thai 'koi-hoi' food flavoring on the viability and infectivity of the third-stage larvae of *Angiostrongylus cantonensis* (Nematoda: Angiostrongylidae). *Acta Tropica*, 113: 245–247.

EFSA [European Food Safety Authority, Panel on Plant Health], 2013, Assessment of the potential establishment of the apple snail in the EU. *EFSA Journal 2013*, 11(12): 3487, 50 pp.

ESTEBENET, A. L., 1995, Food and feeding in *Pomacea canaliculata* (Gastropoda: Ampullariidae). *The Veliger*, 38: 277–283.

ESTEBENET, A. L., 1998, Allometric growth and insight on sexual dimorphism in *Pomacea canaliculata* (Gastropoda: Ampullariidae). *Malacologia*, 39: 207–213.

ESTEBENET, A. L. & N. J. CAZZANIGA, 1992, Growth and demography of *Pomacea canaliculata* (Gastropoda: Ampullariidae) under laboratory conditions. *Malacological Review*, 25:1–12.

ESTEBENET, A. L. & N. J. CAZZANIGA, 1993, Egg variability and the reproductive strategy of *Pomacea canaliculata* (Gastropoda: Ampullariidae). *Apex*, 8: 129–138.

ESTEBENET, A. L. & N. J. CAZZANIGA, 1998, Sex-related differential growth in *Pomacea canaliculata* (Gastropoda: Ampullaridae). *Journal of Molluscan Studies*, 64: 119–123.

ESTEBENET, A. L. & P. R. MARTÍN, 2002, *Pomacea canaliculata* (Gastropoda: Ampullariidae): life-history traits and their plasticity. *Biocell*, 26: 83–89.

ESTEBENET, A. L. & P. R. MARTÍN, 2003, Shell interpopulation variation and its origin in *Pomacea canaliculata* (Gastropoda: Ampullariidae) from southern Pampas, Argentina. *Journal of Molluscan Studies*, 69: 301–310.

ESTEBENET, A. L., P. R. MARTÍN & S. BURELA, 2006, Conchological variation in *Pomacea canaliculata* and other South American Ampullariidae (Caenogastropoda, Architaenioglossa). *Biocell*, 30: 329–335.

ESTOY, G. F. Jr., Y. YUSA, T. WADA, H. SAKURAI & K. TSUCHIDA, 2002a, Size and age at first copulation and spawning of the apple snail, *Pomacea canaliculata* (Gastropoda: Ampullariidae). *Applied Entomology and Zoology*, 37: 199–205.

ESTOY, G. F. Jr., Y. YUSA, T. WADA, H. SAKURAI & K. TSUCHIDA, 2002b, Effects of food availability and age on the reproductive effort of the apple snail, *Pomacea canaliculata* (Lamarck) (Gastropoda: Ampullariidae). *Applied Entomology and Zoology*, 37: 543–550.

EVELAND, L. K. & M. A. HASEEB, 2003, *Echinostoma* species. Pp. 571–579, in: M. D. Miliotis & J. W. Bier, eds., *International handbook of foodborne pathogens*. Marcel Dekker, Inc., New York and Basel, [vi] +xi + [i] + 839 pp.

EZEMONYE, L., V. ENOBAKHARE & I. ILECHIE, 2006, Bioaccumulation of heavy metals (Cu, Zn, Fe) in freshwater snail (*Pila ovata*; Oliver [*sic*] 1804) from Ikpoba River of Southern Nigeria. *Journal of Aquatic Sciences*, 21: 23–28.

FAN, P., C. WU, C. YEN & P. HUANG, 2000, Survival of Pomacea species out of water kept in 25°C laboratory condition. *Bulletin of Malacology, Taiwan, ROC*, 24: 1–6.

FANG, L., P. K. WONG, L. LIN, C. LAN & J.-W. QIU, 2010, Impact of invasive apple snails in Hong Kong on wetland macrophytes, nutrients, phytoplankton and filamentous algae. *Freshwater Biology*, 55: 1191–1204.

FARACO, F., I. L. VEITENHEIMER-MENDES & E. BORGES, 2002, *Felipponea neritiformis* (Gastropoda, Ampullariidae): concha, rádula, complexo peniano e primeiras observações sobre comportamento reprodutivo. *Biociências*, 10: 65–78.

FELLERHOFF, C., 2002. Feeding and growth of apple snail *Pomacea lineata* [sic] in the Pantanal wetland, Brazil – a stable isotope approach. *Isotopes in Environmental and Health Studies*, 38: 227–243.

FERNANDO, W., 1931, The development of the kidney in *Ampullaria* (*Pila*) *gigas*. *Proceedings of the Zoological Society of London*, 62: 745–750.

FISCHER, J.-C., 1963, Les gastéropodes du "continental intercalaire" du Sahara. In: D. Mongin ongin & J.-C. Fischer, Les mollusques du "continental intercalaire" (Mésozoïque) du Sahara central. *Mémoires de la Société Géologique de France* (Nouvelle Série), 42(96): 41–49, pls. 7–8.

FORBES, V. E., J. AUFDERHEIDE, R. WARBRITTON, N. VAN DER HOEVEN & N. CASPERS, 2007a, Does bisphenol A induce superfeminization in *Marisa cornuarietis*? Part II: toxicity test results and requirements for statistical power analyses. *Ecotoxicology and Environmental Safety*, 66: 319–325.

FORBES, V. E., H. SELCK, A. PALMQVIST, J. AUFDERHEIDE, R. WARBRITTON, N. POUNDS, R. THOMPSON, N. VAN DER HOEVEN & N. CASPERS, 2007b, Does bisphenol A induce superfeminization in *Marisa cornuarietis*? Part I: intra- and inter-laboratory variability in test endpoints. *Ecotoxicology and Environmental Safety*, 66: 309–318.

FORBES, V. E., R. WARBRITTON, J. AUFDERHEIDE, N. VAN DER HOEVEN & N. CASPERS, 2008, Effects of bisphenol A on fecundity, egg hatchability, and juvenile growth of *Marisa cornuarietis*. *Environmental Toxicology and Chemistry*, 27: 2332–2340.

FRAKES, R. A., T. A. BARGAR & E. A. BOUGHNER, 2008, Sediment copper bioavailability to freshwater snails in South Florida: risk implications for the Everglade snail kite (*Rostrhamus sociabilis* plumbeus). *Ecotoxicology*, 17: 598–604.

FRANCHINI, A. & E. OTTAVIANI, 2000, Repair of molluscan tissue injury: role of PDGF and TGF-b1. *Tissue and Cell*, 32: 312–321.

FRASSA, M. V., M. CEOLÍN, M. S. DREON & H. HERAS, 2010, Structure and stability of the neurotoxin PV2 from the eggs of the apple snail *Pomacea canaliculata*. *Biochimica et Biophysica Acta – Proteins and Proteomics*, 1804: 1492–1499.

FREIBURG, M. W. & D. H. HAZELWOOD, 1977, Oxygen consumption of two amphibious snails: *Pomacea paludosa* and *Marisa cornuarietis* (Prosobranchia: Ampullariidae). *Malacologia*, 16: 541–548.

FRETTER, V. & A. GRAHAM, 1994, *British prosobranch molluscs: their functional anatomy and ecology*. Ray Society, London, xix + 820 pp.

GAMARRA-LUQUES, C., M. GIRAUD-BILLOUD & A. CASTRO-VAZQUEZ, 2013, Reproductive organogenesis in the apple snail *Pomacea canaliculata* (Lamarck, 1822), with reference to the effects of xenobiotics. *Journal of Molluscan Studies*, 79: 147–162.

GAMARRA-LUQUES, C., I. A. VEGA, E. KOCH & A. CASTRO-VAZQUEZ, 2004, Intrahost distribution and transmission of a new species of cyclopoid copepod endosymbiotic to a freshwater snail, *Pomacea canaliculata* (Caenogastropoda, Ampullariidae), from Argentina. *Biocell*, 28: 155–164.

GAMARRA-LUQUES, C., B. C. WINIK, I. A. VEGA, E. A. ALBRECHT, N. M. CATALÁN & A. CASTRO-VAZQUEZ, 2006, An integrative view to structure, function, ontogeny and phylogenetical significance of the male genital system in *Pomacea canaliculata* (Caenogastropoda, Ampullariidae). *Biocell*, 30: 345–357.

GARÍN, C. F., H. HERAS & R. J. POLLERO, 1996, Lipoproteins of the egg perivitellin fluid of *Pomacea canaliculata* snails (Mollusca: Gastropoda). *Journal of Experimental Zoology*, 276: 307–314.

GASCÓN, A., 1975, Dos ciliados del género *Parasicuophora* parásitos de *Pomacea canaliculata*. *Revista de Biología del Uruguay*, 3: 111–125.

GIRAUD-BILLOUD, M., M. ABUD, J. CUETO, I. VEGA & A. CASTRO-VAZQUEZ, 2011, Uric acid deposits and estivation in the invasive apple-snail, *Pomacea canaliculata*. *Comparative Biochemistry and Physiology, A*, 158: 506–512.

GIRAUD-BILLOUD, M., C. GAMARRA-LUQUES & A. CASTRO-VAZQUEZ, 2013a, Functional anatomy of male copulatory organs of *Pomacea canaliculata* (Caenogastropoda, Ampullariidae). *Zoomorphology*, 132: 129–143.

GIRAUD-BILLOUD, M., E. KOCH, I. A. VEGA, C. GAMARRA-LUQUES & A. CASTRO-VAZQUEZ, 2008, Urate cells and tissues in the South American apple-snail *Pomacea canaliculata*. *Journal of Molluscan Studies*, 74: 259–266.

GIRAUD-BILLOUD, M., I. A. VEGA, M. E. RINALDI TOSI, M. A. ABUD, M. L. CALDERÓN & A. CASTRO-VAZQUEZ, 2013b, Antioxidant and molecular chaperone defenses during estivation and arousal in the South American apple-snail *Pomacea canaliculata*. *Journal of Experimental Biology*, 216: 614–622.

GIRAUD-BILLOUD, M., I. A. VEGA, R. G. WUILLOUD, M. E. CLEMENT & A. CASTRO-VAZQUEZ, 2013c, Imposex and novel mechanisms of reproductive failure induced by tributyltin (TBT) in the freshwater snail *Pomacea canaliculata*. *Environmental Toxicology and Chemistry*, 32: 2365–2371.

GLASS, N. H. & P. C. DARBY, 2009, The effect of calcium and pH on Florida apple snail, *Pomacea paludosa* (Gastropoda: Ampullariidae), shell growth and crush weight. *Aquatic Ecology*, 43: 1085–1093.

GODOY, M. S., A. CASTRO-VAZQUEZ & I. A. VEGA, 2013, Endosymbiotic and host proteases in the digestive tract of the invasive snail *Pomacea canaliculata*: diversity, origin and characterization. *PLoS One*, 8: e66689.

GORNI, G. R. & R. G. ALVES, 2006, Naididae (Annelida, Oligochaeta) associated with *Pomacea bridgesii* (Reeve)(Gastropoda, Ampullaridae). *Revista Brasileira de Zoologia*, 23: 1059–1061.

GOULD, A. A., 1859, Descriptions of new species of shells. *Proceedings of the Boston Society of Natural History*, 7: 40–45.

GRACZYK, T. K. & B. FRIED, 1998, Echinostomiasis: a common but forgotten food-borne disease. *American Journal of Tropical Medicine and Hygiene*, 58: 501–504.

GRAEFF-TEIXEIRA, C., A. C. A. SILVA & K. YOSHIMURA, 2009, Update on eosinophilic meningoencephalitis and its clinical relevance. *Clinical Microbiology Reviews*, 22: 322–348.

GRANTHAM, Ö., D. L. MOORHEAD & M. R. WILLIG, 1993, Feeding preference of an aquatic gastropod, *Marisa cornuarietis*: effects of pre-exposure. *Journal of the North American Benthological Society*, 12: 431–437.

GRÜN, F., H. WATANABE, Z. ZAMANIAN, L. MAEDA, K. ARIMA, R. CHUBACHA, D. M. GARDINER, J. KANNO, T. IGUCHI & B. BLUMBERG, 2006, Endocrine disrupting organotin compounds are potent inducers of adipogenesis in vertebrates. *Molecular Endocrinology*, 20: 2141–2155.

GUIMARÃES, C. T., 1981a, Algumas observações de laboratória sobre biologia e ecologia de *Pomacea haustrum* (Reeve, 1856). *Memorias do Instituto Oswaldo Cruz*, 76: 33–46.

GUIMARÃES, C. T., 1981b, Algumas observações de campo sobre biologia e ecologia de *Pomacea haustrum* (Reeve, 1856) (Mollusca, Pilidae). *Memórias do Instituto Oswaldo Cruz*, 76: 343–351.

HÄGLER, K., 1923, Anatomie von *Pachylabra* (*Ampullaria*) *cinerea* Reeve: I. Teil. Mit Einschluss einer kurzen Besprechung der wichstigen Literatur über die Ampullariidae. *Acta Zoologica*, 4: 313–424.

HALWART, M., 1994, The golden apple snail *Pomacea canaliculata* in Asian rice farming systems: present impact and future threat. *International Journal of Pest Management*, 40: 199–206.

HAMLI, H., M. H. IDRIS, M. K. ABU HENA, S. K. WONG & A. ARSHAD, 2013, Checklist and habitat descriptions of edible gastropods from Sarawak, Malaysia. *Journal of Fisheries and Aquatic Science*, 8: 412–418.

HAMANN, M. I., 1992, *Catadiscus pomaceae* sp. n. (Trematoda, Paramphistomidae) from *Pomacea canaliculata* (Lamarck, 1801 [sic]) (Prosobranchia, Ampullariidae). *Memórias do Instituto Oswaldo Cruz*, 87: 9–14.

HANIFFA, M. A., 1978, Energy loss in an aestivating population of the tropical snail *Pila Globosa. Hydrobiologia*, 61: 169–182.

HANIFFA, M. A., 1980, Studies on life span, growth increments and energy budget of the freshwater snail *Pila globosa* (Swainson) in an artificial pond. *Proceedings of the Indian Academy of Sciences* (*Animal Sciences*), 89: 275–286.

HANIFFA, M. A. & T. T. PANDIAN, 1974, Effects of body weight on feeding and radula size in the freshwater snail *Pila globosa*. *The Veliger*, 16: 415–418.

HANNING, G. W., 1979, *Aspects of reproduction in* Pomacea paludosa *(Mesogastropoda: Pilidae)*. MS thesis, Florida State University, Tallahassee, Florida, U.S.A.

HANNING, G. W. & W. S. LEEDOM, 1978, Schistosome dermatitis from *Pomacea paludosa* (Say) (Prosobranchia: Pilidae). *The Nautilus*, 92: 105–106.

HARASEWYCH, M. G., S. L. ADAMKEWICZ, M. PLASSMEYER & P. M. GILLEVET, 1998, Phylogenetic relationships of the lower Caenogastropoda (Mollusca, Gastropoda, Architaenioglossa, Campaniloidea, Cerithiodea) as determined by partial 18S rDNA sequences. *Zoologica Scripta*, 27: 361–372.

HAYES, K. A., 2009, *Evolution, molecular systematics and invasion biology of Ampullariidae*. Ph.D. Dissertation, University of Hawaii, Honolulu.

HAYES, K. A., R. H. COWIE, A. JØRGENSEN, R. SCHULTHEIß, C. ALBRECHT & S. C. THIENGO, 2009a, Molluscan models in evolutionary biology: apple snails (Gastropoda: Ampullariidae) as a system for addressing fundamental questions. *American Malacological Bulletin*, 27: 47–58.

HAYES, K. A., R. H. COWIE & S. C. THIENGO, 2009b, A global phylogeny of apple snails: Gondwanan origin, generic relationships and the influence of outgroup choice (Caenogastropoda: Ampullariidae). *Biological Journal of the Linnean Society*, 98: 61–76.

HAYES, K. A., R. H. COWIE, S. C. THIENGO & E. E. STRONG, 2012, Comparing apples with apples: clarifying the identities of two highly invasive Neotropical Ampullariidae (Caenogastropoda). *Zoological Journal of the Linnean Society*, 166: 723–753.

HAYES, K. A., R. C. JOSHI, S. C. THIENGO & R. H. COWIE, 2008, Out of South America: multiple origins of non native apple snails in Asia. *Diversity and Distributions*, 14: 701–712.

HEILER, K. C. M., R. SCHULTHEIß, T. GEERTZ & C. ALBRECHT, 2007, Caught in the act: Insights into the sex life of *Lanistes ovum* (Gastopoda: Ampullariidae). P. 94, in: K. JORDAENS, N. VAN HOUTTE, J. VAN GOETHEM & T. BACKELJAU, eds., *World Congress of Malacology. Antwerp, Belgium, 15–20 July 2007*. Abstracts, Unitas Malacologica, Antwerp, lxxix + 298 pp.

HEILER, K. C. M., P. V. VON OHEIMB, K. EKSCHMITT & C. ALBRECHT, 2008, Studies on the temperature dependence of activity and on the diurnal activity rhythm of the invasive *Pomacea canaliculata* (Gastropoda: Ampullariidae). *Mollusca*, 26: 73–81.

HERAS, H., M. S. DREON, S. ITUARTE & R. J. POLLERO, 2007, Egg carotenoproteins in neotropical Ampullariidae (Gastropoda: Arquitaenioglossa). *Comparative Biochemistry and Physiology C*, 146: 158–167.

HERAS, H., M. V. FRASSA, P. E. FERNÁNDEZ, C. M. GALOSI, E. J. GIMENO & M. S. DREON, 2008, First egg protein with a neurotoxic effect on mice. *Toxicon*, 52: 481–488.

HERAS, H., C. F. GARÍN & R. J. POLLERO, 1998, Biochemical composition and energy sources during embryo development and in early juveniles of the snail *Pomacea canaliculata* (Mollusca: Gastropoda). *Journal of Experimental Zoology*, 280: 375–383.

HERMES-LIMA, M., J. STOREY & K. STOREY, 1998, Antioxidant defenses and metabolic depression. The hypothesis of preparation for oxidative stress in land snails. *Comparative Biochemistry and Physiology B*, 120: 437–448.

HERMES-LIMA, M. & T. ZENTENO-SAVIN, 2002, Animal response to drastic changes in oxygen availability and physiological oxidative stress. *Comparative Biochemistry and Physiology C*, 133: 537–556.

HIRATA, K., Y. ASO & M. ISHIGURO, 1998a, Purification and some properties of β-mannosidase, β-N-acetylglucosaminidase, and β-galactosidase from apple snails (*Pomacea canaliculata*). *Journal of the Faculty of Agriculture, Kyushu University*, 42: 463–472.

HIRATA, K., Y. ASO & M. ISHIGURO, 1998b, Properties of α-mannosidase partially purified from the apple snail, *Pomacea canaliculata. Bioscience, Biotechnology, and Biochemistry*, 62: 2242–2245.

HIRATA, K., Y. ASO, S. YASUDA & M. ISHIGURO, 1998c, Purification of *Pomacea canaliculata* α-fucosidase isoforms with different thermostabilities. *Bioscience, Biotechnology, and Biochemistry*, 62: 807–810.

HIRATA, K., Y. NAKAHARA, Y. KIMURA & G. FUNATSU, 1996, Purification and some properties of a β-xylosidase and an α-fucosidase from apple snails (*Pomacea canaliculata*).

Bioscience, Biotechnology, and Biochemistry, 59: 249–254.

HO, J. S., 1994, Origin and evolution of the parasitic cyclopoid copepods. *International Journal for Parasitology*, 24: 1293–1300.

HO, J. S. & V. E. THATCHER, 1989, A new family of cyclopoid copepods (Ozmanidae) parasitic in the hemocoel of a snail from the Brazilian Amazon. *Journal of Natural History*, 23: 903–911.

HOANG, T. C., E. C. ROGEVICH, G. M. RAND & R. A. FRAKES, 2008, Copper uptake and depuration by juvenile and adult Florida apple snails (*Pomacea paludosa*). *Ecotoxicology*, 17: 605–615.

HODGSON, A. N., 1999, Paraspermatozoa. Pp. 656–668, in: E. Knobil & J. D. Neill, eds., *Encyclopedia of Reproduction, Vol. 3.* Academic Press, San Diego, California, U.S.A., xxvi + 1072 pp.

HOLLINGSWORTH, R. C. & R. H. COWIE, 2006, Apple snails as disease vectors. Pp. 121–132, in: R. Joshi & L. S. Sebastian, eds., *Global advances in ecology and management of golden apple snails.* Philippine Rice Research Institute, Muñoz, Nueva Ecija, Philippines, x + 588 pp.

HORN, K. C., S. D. JOHNSON, K. M. BOLES, A. MOORE, E. SIEMANN & C. A. GABLER, 2008, Factors affecting hatching success of golden apple snail eggs: effects of water immersion and cannibalism. *Wetlands*, 28: 544–549.

HURDLE, M. T., 1973, Life history studies and habitat requirements of the apple snail at Lake Woodruff National Wildlife Refuge. *Proceedings of the Twenty-seventh Annual Conference. Southeastern Association of Game and Fish Commissioners*, 27: 215–224.

HYLTON SCOTT, M. I., 1934, Sobre el desarrollo embrionario de *Ampullaria canaliculata. Revista del Museo de La Plata*, 34: 373–385.

HYLTON SCOTT, M. I., 1958, Estudio morfológico y taxonómico de los ampulláridos de la República Argentina. *Revista del Museo Argentino de Ciencias Naturales 'Bernardino Rivadavia'*, 3: 233–333.

HYMAN, L., 1967, *The invertebrates, Vol. 6: Mollusca I.* McGraw-Hill, New York, 792 pp.

IBRAHIM, M. M., 2007, Prevalence and intensity of *Angiostrongylus cantonensis* in freshwater snails in relation to some ecological and biological factors. *Parasite*, 14: 61–70.

ICHINOSE, K., 2002, Influence of age and body size on alarm responses in a freshwater snail *Pomacea canaliculata. Journal of Chemical Ecology*, 28: 2017–2028.

ICHINOSE, K., M. TOCHIHARA, T. WADA, N. SUGUIURA & Y. YUSA, 2002, Influence of common carp on apple snail in a rice field evaluated by a predator-prey logistic model. *International Journal of Pest Management*, 48: 133–138.

ICHINOSE, K., T. WADA, Y. YUSA & T. KUBOTA, 2000, Influence of habitat differences brought about by environmental changes on the densities of adults and eggs of *Pomacea canaliculata. Proceedings of the Association for Plant Protection of Kyushu*, 46: 78–84.

ICHINOSE, K., Y. YUSA & K. YOSHIDA, 2003, Alarm response of hatchlings of the apple snail, *Pomacea canaliculata* (Gastropoda: Ampullariidae), to aqueous extracts of other individuals. *Ecological Research*, 18: 213–219.

ICZN [International Commission on Zoological Nomenclature], 1999, Opinion 1913. *Pila* Röding, 1798 and *Pomacea* Perry, 1810 (Mollusca, Gastropoda): placed on the Official List, and Ampullariidae Gray, 1824: confirmed as the nomenclaturally valid synonym of Pilidae Preston, 1915. *Bulletin of Zoological Nomenclature*, 56: 74–76.

IMJONGJIRAK, C., P. AMPARYUP & S. SITTIPRANEED, 2008, Cloning, genomic organization and expression of two glycosyl hydrolase family 10 (GHF10) genes from golden apple snail (*Pomacea canaliculata*). *DNA Sequence*, 19: 224–236.

ITO, K., 2002, Environmental factors influencing overwintering success of the golden apple snail, *Pomacea canaliculata* (Gastropoda: Ampullariidae), in the northernmost population of Japan. *Applied Entomology and Zoology*, 37: 655–661.

ITUARTE, S., M. S. DREON, M. CEOLIN & H. HERAS, 2012, Agglutinating activity and structural characterization of scalarin, the major egg protein of the snail *Pomacea scalaris* (d'Orbigny, 1832). *PLoS One*, 7(11): e50115.

ITUARTE, S., M. S. DREON, M. Y. PASQUEVICH, P. E. FERNANDEZ & H. HERAS, 2010, Carbohydrates and glycoforms of the major egg perivitellins from *Pomacea* apple snails (Architaenioglossa: Ampullariidae). *Comparative Biochemistry and Physiology B*, 157: 66–72.

ITUARTE, S., M. S. DREON, R. J. POLLERO & H. HERAS, 2008, Isolation and partial characterization of a new lipo-glyco-carotenoprotein from *Pomacea scalaris* (Gastropoda: Ampullariidae). *Molecular Reproduction and Development*, 75: 1441–1448.

JANER, G., J. C. NAVARRO & C. PORTE, 2007, Exposure to TBT increases accumulation of lipids and alters fatty acid homeostasis in the ramshorn snail *Marisa cornuarietis. Comparative Biochemistry and Physiology C*, 146: 368–374.

JEONG, K. H., K. J. LIE & D. HEYNEMAN, 1983, The ultrastructure of the amoebocyte-producing organ in *Biomphalaria glabrata. Developmental and Comparative Immunology*, 7: 217–228.

JØRGENSEN, A., T. K. KRISTENSEN & H. MADSEN, 2008, A molecular phylogeny of apple snails (Gastropoda, Caenogastropoda, Ampullariidae) with an emphasis on African species. *Zoologica Scripta*, 37: 245–252.

JOSHI, R. C., E. C. MARTIN, T. WADA & L. S. SEBASTIAN, 2006, Role of golden apple snails in organic rice cultivation and weed management. Pp. 483–488, in: R. C. Joshi & L. S. Sebastian, eds., *Global advances in ecology and management of golden apple snails.* Philippine Rice Research Institute, Muñoz, Nueva Ecija, Philippines, x + 588 pp.

JOSHI, R. C. & L. A. SEBASTIAN, eds., 2006, *Global advances in ecology and management of golden apple snails.* Philippine Rice Research Institute, Muñoz, Nueva Ecija, Philippines, x + 588 pp.

KANG, J.-H., D. ASAI & Y. KATAYAMA, 2007, Bisphenol A in the aquatic environment and its endocrine-disruptive effects on aquatic organisms. *Critical Reviews in Toxicology*, 37: 607–625.

KARATAYEV, A. Y., L. E. BURLAKOVA, V. A. KARATAYEV & D. K. PADILLA, 2009, Introduction, distribution, spread, and impacts of exotic freshwater gastropods in Texas. *Hydrobiologia*, 619: 181–194.

KARRAKER, N. E. & D. DUDGEON, 2014, Invasive apple snails (*Pomacea canaliculata*) are predators of amphibians in south China. *Biological Invasions*, 16: 1785–1789.

KARUNARATNE, L. B., P. C. DARBY & R. E. BENNETTS, 2006, The effects of wetland habitat structure on Florida apple snail density. *Wetlands*, 26: 1143–1150.

KAWANO, T., L. SIMÖES & F. CORREA, 1990, Chromosomes of *Pomacea* sp. (Perry, 1811) (Mesogastropoda, Mollusca). *Revista Brasileira de Genética*, 13: 675–685.

KEAWJAM, R. S., 1986, The apple snails of Thailand: distribution, habitats and shell morphology. *Malacological Review*, 19: 61–81.

KEAWJAM, R. S., 1987, The apple snails of Thailand: aspects of comparative anatomy. *Malacological Review*, 20: 69–89.

KEAWJAM, R. S., P. POONSWAD, E. S. UPATHAM & S. BANPAVICHIT, 1993, Natural parasitic infection of the golden apple snail, *Pomacea canaliculata*. *Southeast Asian Journal of Tropical Medicine and Public Health*, 24: 170–177.

KIM, J. R., K. A. HAYES, N. W. YEUNG & R. H. COWIE, 2014, Diverse gastropod hosts of *Angiostrongylus cantonensis*, the rat lungworm, globally and with a focus on the Hawaiian Islands. *PLoS ONE*, 9(5): e940969.

KOCH, E., 2008, *Transmisión de un endocianobionte de* Pomacea canaliculata *(Caenogastropoda, Ampullariidae): dónde, cuándo y cómo*. Ph.D. Thesis, Universidad Nacional de Cuyo, Mendoza.

KOCH, E., M. LOZADA, H. DIONISI & A. CASTRO-VAZQUEZ, 2014, Uric acid-degrading bacteria in the gut of the apple snail *Pomacea canaliculata* and their possible symbiotic significance. *Symbiosis*, 63: 149−155.

KOCH, E., I. A. VEGA, E. A. ALBRECHT, H. ORTEGA & A. CASTRO-VAZQUEZ, 2006, A light and electron microscopic study of pigmented corpuscles in the midgut gland and feces of *Pomacea canaliculata* (Caenogastropoda: Ampullariidae). *The Veliger*, 48: 17–25.

KOCH, E., B. WINIK & A. CASTRO-VAZQUEZ, 2009, Development beyond the gastrula stage and digestive organogenesis in the apple-snail *Pomacea canaliculata* (Architaenioglossa, Ampullariidae). *Biocell*, 33: 49–65.

KÜSTER, H. C., 1860 [1843–1860], Die Gattungen *Buccinum*, *Purpura*, *Concholepas* und *Monoceros*. In: H. C. Küster, ed., *Systematisches Conchylien-Cabinet von Martini und Chemnitz*. Dritten Bandes erste Abteilung. Erster Theil. Bauer & Raspe, Nurnberg, 229 pp., 43 pls.

KWONG, K.-L., R. K. Y. CHAN & J.-W. QIU, 2009, The potential of the invasive snail *Pomacea canaliculata* as a predator of various life-stages of five species of freshwater snails. *Malacologia*, 51: 343–356.

KWONG, K. L., D. DUDGEON, P. K. WONG & J.-W. QIU, 2010, Secondary production and diet of an invasive snail in freshwater wetlands: implications for resource utilization and competition. *Biological Invasions*, 12: 1153–1164.

KWONG, K.-L., P.-K. WONG, S. S. S. LAU & J.-W. QIU, 2008, Determinants of the distribution of apple snails in Hong Kong two decades after their initial invasion. *Malacologia*, 50: 293–302.

KYLE, C. H., A. W. KROPF & R. L. BURKS, 2011, Prime waterfront real estate: apple snails choose wild taro for oviposition sites. *Current Zoology*, 57: 630−641.

KYLE, C. H., A. L. PLANTZ, T. SHELTON & R. L. BURKS, 2013, Count your eggs before they invade: identifying and quantifying egg clutches of two invasive apple snail species (*Pomacea*). *PLoS ONE*, 8(10): e77736.

LACH, L., D. K. BRITTON, R. J. RUNDELL & R. H. COWIE, 2000, Food preference and reproductive plasticity in an invasive freshwater snail. *Biological Invasions*, 2: 279–288.

LAL, M. B. & B. B. SAXENA, 1952, Uricotelism in the common Indian apple-snail, *Pila globosa* (Swainson). *Nature*, 170: 1024.

LAM, P. K. S., 1994, Intraspecific life-history variation in *Radix plicatulus* (Gastropoda: Pulmonata: Lymnaeidae). *Journal of Zoology*, 232: 435–446.

LAMARCK, [J. B. P. A. de M.] de, 1822, *Histoire naturelle des animaux sans vertèbres...*, Tome sixième, 2me partie. L'auteur, Paris, 232 pp.

LANZER, R. M. & A. SCHAFER, 1985, Padrões de distribuição de moluscos dulceaquícolas nas lagoas costeiras do Sul do Brasil. *Revista Brasileira de Biologia*, 45: 535–545.

LAPORTA-FERREIRA, I. L. & M. G. SALOMÃO, 2004, Reptilian predators of terrestrial gastropods. Pp. 427–481, in: G. M. Barker, ed., *Natural enemies of terrestrial molluscs.* CABI, Wallingford, x + 644 pp.

LEA, I., 1856, Description of thirteen new species of exotic Peristomata. *Proceedings of the Academy of Natural Sciences of Philadelphia*, 8: 109–111.

LEE, R. E., Jr., 1991, Principles of insect low temperature tolerance. Pp. 131–148, in: R. E. Lee, Jr. & D. L. Denlinger, eds., *Insects at low temperature*. Chapman & Hall, New York, x + 513 pp.

LEEDOM, W. S. & R. B. SHORT, 1981, *Cercaria pomaceae* sp. n., a dermatitis-producing schistosome cercaria from *Pomacea paludosa*, the Florida apple snail. *Journal of Parasitology*, 67: 257–261.

LI, Y. H., R. GUO, Q. Y. YIN, M. DING, S. L. ZHANG, G. J. XU & F. K. ZHAO, 2005, Purification and characterization of two endo-beta-1,4-glucanases from Mollusca, *Ampullaria crossean* [sic]. *Acta Biochimica et Biophysica Sinica*, 37: 702–708.

LIE, K. J., D. HEYNEMAN & P. YAU, 1975, The origin of amoebocytes in *Biomphalaria glabrata*. *Journal of Parasitology*, 63: 574–576.

LINNAEUS, C., 1758, *Systema naturae per regna tria naturae, secundum classes, ordines, genera, species, cum caracteribus, differentiis, synonymis, locis.* Tomus I. Editio decima, reformata. L. Salvii, Holmiae [= Stockholm], 824 + iii pp.

LITTLE, C., 1968, Aestivation and ionic regulation in two species of *Pomacea* (Gastropoda, Prosobranchia). *Journal of Experimental Biology*, 48: 569–585.

LIU, J., Y. HE, J. TAN, C. XU, L. ZHONG, Z. WANG & Q. LIAO, 2012, Characteristics of *Pomacea canaliculata* reproduction under natural conditions. *Chinese Journal of Applied Ecology*, 23: 559–565.

LIU, W.-H., Y.-W. CHIU, D.-J. HUANG, M.-Y. LIU, C.-C. LEE & L.-L. LIU, 2006, Imposex in the golden apple snail *Pomacea canaliculata* in Taiwan. *Science of the Total Environment*, 371: 138–143.

LODGE, D. M., 1991, Herbivory on freshwater macrophytes. *Aquatic Botany*, 41: 195–224.

LÓPEZ, M. A., C. R. ALTABA, K. B. ANDREE & V. LÓPEZ, 2010, First invasion of the apple snail *Pomacea insularum* in Europe. *Tentacle*, 18: 26–28.

LOUDA, S. M. & K. R. McKAYE, 1982, Diurnal movements in populations of the prosobranch *Lanistes nyassanus* at Cape Maclear, Lake Malawi, Africa. *Malacologia*, 23: 13–21.

LUM-KONG, A. & J. S. KENNY, 1989, The reproductive biology of the ampullariid snail *Pomacea urceus* (Müller). *Journal of Molluscan Studies*, 55: 53–65.

LUTFY, R. G. & E. S. DEMIAN, 1965, Studies on the chromosome numbers in the Ampullariidae (Gastropoda, Prosobranchiata). *Proceedings of the Egyptian Academy of Sciences*, 18: 34–49.

LUTFY, R. G. & E. S. DEMIAN, 1967, The histology of the alimentary system of *Marisa cornuarietis* (Mesogastropoda: Ampullariidae). *Malacologia*, 5: 375–422.

LV, S., Y. ZHANG, H.-X. LIU, L. HU, K. YANG, STEINMANN, Z. CHEN, L.-Y. WANG, J. UTZINGER & X.-N. ZHOU, 2009a, Invasive snails and an emerging infectious disease: results from the first national survey on *Angiostrongylus cantonensis* in China. *PLoS Neglected Tropical Diseases*, 3: e368.

LV, S., Y. ZHANG, H. LIU, C. ZHANG, P. STEINMANN, X. ZHOU & J. UTZINGER, 2009b, *Angiostrongylus cantonensis*: morphological and behavioral investigation within the freshwater snail *Pomacea canaliculata*. *Parasitology Research*, 104: 1351–1359.

LV, S., Y. ZHANG, P. STEINMANN & X.-N. ZHOU, 2008, Emerging angiostrongyliasis in mainland China. *Emerging Infectious Diseases*, 14: 161–164.

LV, S., Y. ZHANG, P. STEINMANN, G.-J. YANG, K. YANG, X.-N. ZHOU & J. UTZINGER, 2011. The emergence of angiostrongyliasis in the People's Republic of China: the interplay between invasive snails, climate change and transmission dynamics. *Freshwater Biology*, 56: 717–734.

LV, S., X.-N. ZHOU, Y. ZHANG, H.-X. LIU, D. ZHU, W.-G. YIN, P. STEINMANN, X.-H. WANG & T.-W. JIA, 2006, The effect of temperature on the development of *Angiostrongylus cantonensis* (Chen 1935) in *Pomacea canaliculata* (Lamarck 1822). *Parasitology Research*, 99: 583–587.

MAHILINI, H. & A. RAJENDRAN, 2008, Categorization of hemocytes of three gastropod species *Trachea vittata* (Muller) [sic], *Pila globosa* (Swainson) and *Indoplanorbis exustus* (Dehays) [sic]. *Journal of Invertebrate Pathology*, 97: 20–26.

MALTCHIK, L., C. STENERT, C. B. KOTZIAN & D. PEREIRA, 2010, Responses of freshwater molluscs to environmental factors in southern Brazil wetlands. *Brazilian Journal of Biology*, 70: 473–482.

MAPELLI, F. J. & M. J. KITTLEIN, 2011, Prey selection by the snail kite (*Rostrhamus sociabilis*) in permanent and temporary wetlands of central Argentina. *Ornitologia Neotropical*, 22: 281–293.

MARTELLO, A. R., C. B. KOTZIAN & M. G. SIMÕES, 2006, Quantitative fidelity of recent freshwater mollusk assemblages from the Touro Passo River, Rio Grande do Sul, Brazil. *Iheringia Série Zoologia*, 96: 453–465.

MARTÍN, P. R. & C. G. DE FRANCESCO, 2006, Fossil record of *Pomacea* (Caenogastropoda: Ampullariidae) in Argentina and its paleoenvironmental implications. *Biocell*, 30: 337–343.

MARTÍN, P. R. & A. L. ESTEBENET, 2002, Interpopulation variation of life-history traits in *Pomacea canaliculata* (Gastropoda: Ampullariidae) in southwestern Buenos Aires Province, Argentina. *Malacologia*, 44: 153–163.

MARTÍN, P. R., A. ESTEBENET & S. BURELA, 2005, Factors affecting the distribution and abundance of the commensal *Temnocephala iheringi* (Platyhelminthes: Temnocephalidae) among the southernmost populations of the apple snail *Pomacea canaliculata* (Mollusca: Ampullariidae). *Hydrobiologia*, 545: 45–53.

MARTÍN, P. R., A. ESTEBENET & N. CAZZANIGA, 2001, Factors affecting the distribution of *Pomacea canaliculata* (Gastropoda: Ampullariidae) along its southernmost natural limit. *Malacologia*, 43: 13–24.

MARTÍN, S. M., 1984, Estudio del complejo penial de *Asolene platae* (Maton) (Mollusca Gasteropoda). *Neotropica*. 30: 107–110.

MARTÍN, S. M., 1986, Ciclo reproductivo de *Ampullaria canaliculata* (Gastropoda: Ampullariidae) en el área rioplatense. *Neotropica*, 32: 171–181.

MARTÍN, S. M., 1993, Características poblacionales de *Ampullaria scalaris* d'Orbigny, 1835 (Mollusca, Gastropoda, Ampullariidae) en las Canteras de Los Talas (Berisso, Buenos Aires). *Studies on Neotropical Fauna and Environment*, 28: 223–231.

MARTINEZ, S. & A. ROJAS, 2004, Quaternary continental molluscs from northern Uruguay: distribution and paleoecology. *Quaternary International*, 114: 123–128.

MARTORELLI, S., 1987, Estudios parasitológicos en biotopos lénticos de la República Argentina. IV. El ciclo biológico de *Echinostoma parcespinosum* Lutz, 1924 (Digenea) parásito de *Rallus maculatus maculatus* y *Rallus sanguinolentus sanguinolentus* (Aves: Rallidae). *Revista del Museo de La Plata*, *Zoología* (Nueva Serie), 14: 48–59.

MATON, W. G., 1811, Description of seven new species of Testacea. *The Transactions of the Linnean Society of London*, 10: 325–332, pl. 24.

MATSUKURA, K., H. TSUMUKI, Y. IZUMI & T. WADA, 2008, Changes in chemical components in the freshwater apple snail, *Pomacea canaliculata* (Gastropoda: Ampullariidae), in relation to the development of its cold hardiness. *Cryobiology*, 56: 131–137.

MATSUKURA, K., H. TSUMUKI, Y. IZUMI & T. WADA, 2009a, Physiological response to low temperature in the freshwater apple snail, *Pomacea canaliculata* (Gastropoda: Ampullariidae). *Journal of Experimental Biology*, 212: 2558–2563.

MATSUKURA, K., H. TSUMUKI, Y. IZUMI & T. WADA, 2009b, Temperature and water availability affect decrease of cold hardiness in the apple snail, *Pomacea canaliculata*. *Malacologia*, 51: 263–269.

MATSUKURA, K. & T. WADA, 2007, Environmental factors affecting the increase of cold hardiness in the apple snail *Pomacea canaliculata* (Gastropoda: Ampullariidae). *Applied Entomology and Zoology*, 42: 533–539.

MATTOS, A. C., M. F. F. BOAVENTURA, M. A. FERNANDEZ & S. C. THIENGO, 2013, Larval trematodes in freshwater gastropods from Mato Grosso, Brazil: diversity and host-parasites relationships. *Biota Neotropica*, 13: 34–38.

McARTHUR, A. G. & M. G. HARASEWYCH, 2003, Molecular systematics of the major lineages of the Gastropoda. Pp. 140–160, in: C. Lydeard & D. R. Lindberg, eds., *Molecular systematics and phylogeography of mollusks*. Smithsonian Institution, Washington, D.C., xiii + [i] + 328 pp.

McCULLOUGH, F. S., 1964, Observations on bilha rziasis and the potential snail hosts in the Republic of the Congo (Brazzaville). *Bulletin of the World Health Organization*, 30: 375–388.

McCLARY, A., 1964, Surface inspiration and ciliary feeding in *Pomacea paludosa* (Prosobranchia: Mesogastropoda: Ampullariidae). *Malacologia*, 2: 87–104.

McKENNA, M. C., 1973, Sweepstakes, filters, corridors, Noah's Arks, and beached Viking funeral ships in palaeogeography. Pp. 295–308, in: D. H. Tarling & S. K. Runcorn, eds., *Implications of continental drift to the earth sciences*. Academic Press, London, 622 pp.

MEENAKSHI, V. R., 1955, The excretory spherioles in the digestive gland of *Pila virens*. *Journal of Animal Morphology and Physiology*, 3: 75–78.

MEENAKSHI, V. R., 1956, Physiology of hibernation of the apple-snail *Pila virens* (Lamarck). *Current Science*, 25: 321–322.

MEENAKSHI, V. R., 1957, Anaerobiosis in the south Indian apple-snail *Pila virens* (Lamarck) during aestivation. *Journal of the Zoological Society of India*, 9: 62–71.

MEENAKSHI, V. R., 1964, Aestivation in the Indian apple snail Pila—I. Adaptation in natural and experimental conditions. *Comparative Biochemistry and Physiology*, 11: 379–386.

MELO, L. E. L., R. A. COLER, T. WATANABE & J. F. BATALLA, 2000, Developing the gastropod *Pomacea lineata* (Spix, 1827) as a toxicity test organism. *Hydrobiologia*, 429: 73–78.

MERCADO-LACZKÓ, A. & E. LOPRETTO, 1998, Estudio cromosómico y cariotípico de *Pomacea canaliculata* (Lamarck, 1801) (Gastropoda: Ampullariidae). *Revista del Museo Argentino de Ciencias Naturales 'Bernardino Rivadavia', Hidrobiología*, 8: 15–20.

MICHAUD, M. R., J. B. BENOIT, G. LOPES-MARTINEZ, M. A. ELNITSKY, R. E. LEE, JR. & D. L. DENLINGER, 2008, Metabolomics reveals unique and shared metabolic changes in response to heat shock, freezing and desiccation in the Antarctic midge, *Belgica antarctica*. *Journal of Insect Physiology*, 54: 645–655.

MÖLLENDORFF, O. von, 1898, Zur Hochgebirgsfauna der Philippinen. *Nachrichtsblatt der Deutschen Malakozoologischen Gesellschaft*, 30: 5–12.

MONEVA, C. S. O., M. A. J. TORRES, T. WADA, R. JOSHI & C. G. DEMAYO, 2012, Relative warp and correlation analysis based on distances of the morphological shell shape patterns of *Pomacea canaliculata* Lamarck from Japan and Philippines. *International Journal of the Bioflux Society*, 4: 12–21.

MONTEIL, J. F. & M. MATRICON-GONDRAN, 1991, Hemocyte production in trematode-infected *Lymnaea truncatula*. *Parasitology Research*, 77: 491–497.

MORASSUTTI, A. L., S. C. THIENGO, M. FERNANDEZ, K. SAWANYAWISUTH & C. GRAEFF-TEIXEIRA, 2014, Eosinophilic meningitis caused by Angiostrongylus cantonensis: an emergent diseasse in Brazil. *Memórias do Instituto Oswaldo Cruz*, 109: 399–407.

MORELET, A., [1849], Testacea quædam Africæ occidentalis terrestria et fluviatilia. *Revue Zoologique, par la Société Cuvierienne*, 11(12) [1848]: 351–355.

MORLET, L., 1889, Catalogue des coquilles recueillies, par M. Pavie, dans le Cambodge et le Royaume de Siam et description d'espèces nouvelles. *Journal de Conchyliologie*, 37: 121–200, pls. 6–9.

MORRISON, W. E. & M. E. HAY, 2011a, Feeding and growth of native, invasive and non-invasive alien apple snails (Ampullariidae) in the United States: invasives eat more and grow more. *Biological Invasions*, 13: 945–955.

MORRISON, W. E. & M. E. HAY, 2011b, Induced chemical defenses in a freshwater macrophyte suppress herbivore fitness and the growth of associated microbes. *Oecologia*, 165: 427–436.

MOUSSON, A., [1849], Über die Land- und Süsswasser-Mollusken von Java. *Mittheilungen der Naturforschenden Gesellschaft in Zürich*, 1(3)(30) [1848]: 264–273.

MÜLLER, O. F., 1774, *Vermium terrestrum et fluviatilium, seu animalium infusoriorum, helminthicorum, et testaceorum, non marinorum, succincta historia. Volumen alterum.* Heineck & Faber, Havniae [= Copenhagen] & Lipsiae [= Leipzig].

MÜLLER, R., 2002, *Worms and human disease*, 2nd ed. CABI Publishing, Wallingford, ix + 300 pp.

MURPHY, G. S. & S. JOHNSON, 2013, Clinical aspects of eosinophilic meningitis and meningoencephalitis caused by *Angiostrongylus cantonensis*, the rat lungworm. *Hawai'i Journal of Medicine and Public Health*, 72 (Suppl. 2): 35–40.

NDIFON, G. T. & F. M. A. UKOLI, 1989, Ecology of freshwater snails in south-western Nigeria. I: Distribution and habitat preferences. *Hydrobiologia*, 171: 231–253.

NELSON, D. & M. COX, 2004, *Lehninger principles of biochemistry, 4th ed.* W. H. Freeman & Co, New York, 1119 + 17 pp.

NG, T. H. & S. K. TAN, 2011, Observations of land snails feeding on the eggs of *Pomacea canaliculata* (Lamarck, 1822) (Mollusca: Gastropoda). *Nature in Singapore*, 4: 79–83.

NG, T. H., S. K. TAN & M. E. Y. LOW, 2014, Singapore Mollusca: 7. The family Ampullariidae (Gastropoda: Caenogastropoda: Ampullarioidea). *Nature in Singapore*, 7: 31–47.

NISHIKAWA, J., S. MAMIYA, T. KANAYAMA, T. NISHIKAWA, F. SHIRAISHI & T. HORIGUCHI, 2004, Involvement of the retinoid X receptor in the development of imposex caused by organotins in gastropods. *Environmental Science and Technology*, 38: 6271–6276.

NONO, A. M. & A. M. MANE, 1931, Biology of cohol (*Ampullaria luzonica* Reeve) a common Philippine fresh-water snail. *The Phillipine Agriculturist*, 19: 675–695.

NORDEN, D. A., 1972, The inhibition of trypsin and some other proteases by ovorubin, a protein from the eggs of *Pomacea canaliculata*. *Comparative Biochemistry and Physiology B*, 42: 569–576.

OEHLMANN, J., U. SCHULTE-OEHLMANN, M. TILLMANN & B. MARKERT, 2000, Effects of endocrine disruptors on prosobranch snails (Mollusca: Gastropoda) in the laboratory. Part I: bisphenol A and octylphenol as xeno-estrogens. *Ecotoxicology*, 9: 383–397.

OEHLMANN, J., U. SCHULTE-OEHLMANN, J. BACHMANN, M. OETKEN, I. LUTZ, W. KLOAS & T. A. TERNES, 2006, Bisphenol A induces superfeminization in the ramshorn snail *Marisa cornuarietis*(Gastropoda: Prosobranchia) at environmentally relevant concentrations. *Environmental Health Perspectives*, 14 (Suppl. 1): 127–133.

OEHLMANN, J., P. DI BENEDETTO, M. TILLMANN, M. DUFT, M. OETKEN & U. SCHULTE-OEHLMANN, 2007, Endocrine discruption in prosobranch molluscs: evidence and ecological relevance. *Ecotoxicology*, 16: 29–43.

O'HARE, N. K., 2010, Florida apple snail (*Pomacea paludosa*) reproduction in restored and natural seasonal wetlands in Everglades National Park. *Wetlands*, 30: 1045–1052.

OLIVIER, G. A., 1804, *Voyage dans l'Empire Othoman, l'Egypte et la Perse, fait par ordre du Gouvernement, pendant les six premières années de la République.* 4to edition. Tome second. Henri Agasse, Paris, ii + 466 +[1] p.

OMUDU, E. A. & A. IYOUGH, 2005, Ecological studies of the gastropod fauna of some minor tributaries of river Benue in Makurdi, Nigeria. *Animal Research International*, 2: 306–310.

ORBIGNY, A. [D.] d', 1835, Synopsis terrestrium et fluviatilium molluscorum, in suo per Americam meridionalem itinere. *Magasin de Zoologie*, 5(61–62): 1–44.

ORBIGNY, A. [D.] d', 1838, 1847 [1834–1847], *Voyage dans l'Amérique Méridionale (le Brésil, la république orientale de l'Uruguay, la république Argentine, la Patagonie, la république du Chili, la république de Bolivia, la république du Pérou), exécuté pendant les années 1826, 1827, 1828, 1829, 1839, 1831, 1832 et 1833.* Tome cinquième. 3e partie: mollusques, 758 pp., 85 pls. P. Bertrand, Paris; V.e Levrault, Strasbourg.

OSTROWSKI DE NUÑEZ, M., 1979, Ungewöhnliche Xiphidiocercarie aus *Ampullaria canaliculata* nebst Bemerkungen über *Travtrema stenocotyle*. *Angewandte Parasitologie*, 20: 46–52.

OTTAVIANI, E., 1991, Tissue distribution and levels of natural and induced serum lysozyme immunoreactive molecules in a freshwater snail. *Tissue and Cell*, 23: 317–324.

OTTAVIANI, E., 2006, Molluscan immunorecognition. *Invertebrate Survival Journal*, 3: 50–63.

OTTAVIANI, E., 2011, Immunocyte: the invertebrate counterpart of the vertebrate macrophage. *Invertebrate Survival Journal*, 8: 1–4.

OTTAVIANI, E., A. COSSARIZZA, C. ORTOLANI, D. MONTI & C. FRANCESCHI, 1991, ACTH-like molecules in gastropod molluscs: a possible role in ancestral immune response and stress. *Proceedings of the Royal Society of London. Series B, Biological Sciences*, 245: 215–218.

OWOJORI, O. J., S. O. ASAOLU & I. E. OFOEZIE, 2006, Ecology of freshwater snails in Opa Reservoir and research farm ponds at Obafemi Awolowo University Ile-Ife, Nigeria. *Journal of Applied Sciences*, 6: 3004–3015.

OYA, S., Y. HIRAI & Y. MIYAHARA, 1987, Overwintering of the apple snail, *Pomacea canaliculata* Lamarck, in North Kyushu. *Japanese Journal of Applied Entomology and Zoology*, 31: 206–212.

PASQUEVICH, M. Y., M. S. DREON & H. HERAS, 2014, The major egg reserve protein from the invasive apple snail *Pomacea maculata* is a complex carotenoprotein related to those of *Pomacea canaliculata* and *Pomacea scalaris*. *Comparative Biochemistry and Physiology, Part B, Biochemistry and Molecular Biology*, 169: 63–71.

PEÑA, S. C. & G. N. POCSIDIO, 2007, Influence of copper on the feeding rate, growth and reproduction of the golden apple snail, *Pomacea canaliculata* Lamarck. *Bulletin of Environmental Contamination and Toxicology*, 79: 606–608.

PERERA, G. & J. G. WALLS, 1996, *Apple snails in the aquarium*. T.F.H. Publications, Neptune City, New Jersey, U.S.A., 121 pp.

PERERA, G. & M. YONG, 1984, The influence of some abiotic factors on the distribution of freshwater mollusks on the Isle of Youth (Isle of Pines), Cuba. *Walkerana*, 2: 131–139.

PERRY, G., 1810–1811, *Arcana; or the museum of natural history*. Stratford, London.

PEUMANS, W. J. & E. J. VAN DAMME, 1995, Lectins as plant defense proteins. *Plant Physiology*, 109: 347–352.

PHILLIPS, C. T., M. L. ALEXANDER & R. HOWARD, 2010, Consumption of eggs of the endangered fountain darter (*Etheostoma fonticola*) by native and nonnative snails. *The Southwestern Naturalist*, 55: 115–117.

PICKETT, J. A. & J. M. EDWARDSON, 2006, Compound exocytosis: mechanisms and functional significance. *Traffic*, 7: 109–116.

PILSBRY, H. A. & J. T. BEQUAERT, 1927, The aquatic mollusks of the Belgian Congo. With a geographical and ecological account of Congo malacology. *Bulletin of the American Museum of Natural History*, 53(2): 69–602, pls. 10–77.

PIZANI, N., A. L. ESTEBENET & P. R. MARTÍN, 2005, Effects of submersion and aerial exposure on clutches and hatchlings of *Pomacea canaliculata* (Gastropoda: Ampullariidae). *American Malacological Bulletin*, 20: 55–63.

POINTIER, J.-P., A. THÉRON & D. IMBERT-ESTABLET, 1988, Decline of a sylvatic focus of *Schistosoma mansoni* in Guadeloupe (French West Indies) following competitive displacement of the snail host *Biomphalaria glabrata* by *Ampullaria glauca*. *Oecologia*, 75: 38–43.

POINTIER, J.-P., A. THÉRON, D. IMBERT-ESTABLET & G. BOREL, 1991, Eradication of a sylvatic focus of *Schistosoma mansoni* using biological control by competitor snails. *Biological Control*, 1: 244–247.

POMACEA PROJECT, 2013, *Literature review of Florida apple snails and snail kites, and recommendations for their adaptive management*. Final report submitted to the National Park Service, Everglades National Park. The Pomacea Project, Inc., Pensacola, Florida. Available at http://www.pomaceaproject.org/.

PONDER, W. F., D. COLGAN, J. HEALY, A. NÜTZEL, L. R. L. SIMONE & E. E. STRONG, 2008, Caenogastropod phylogeny. Pp. 329–382. in: W. F. PONDER & D. R. LINDBERG, eds., *Phylogeny and evolution of the Mollusca*. University of California Press, Berkeley, xi + 269 pp.

PONDER, W. F. & D. R. LINDBERG, 1997, Towards a phylogeny of gastropod molluscs: an analysis using morphological characters. *Zoological Journal of the Linnean Society*, 119: 83–265.

PRASHAD, B., 1925a, On a fossil ampullariid from Poonch, Kashmir. *Records of the Geological Survey of India*, 56(3): 210–212, pl. 15.

PRASHAD, B., 1925b, Revision of the Indian Ampullariidae. *Memoirs of the Indian Museum*, 8: 69–89, pls. 13–15.

PRASHAD, B., 1925c, Anatomy of the common Indian apple-snail, *Pila globosa*. *Memoirs of the Indian Museum*, 8: 91–154.

PRZESLAWSKI, R., 2004, A review of the effects of environmental stress on embryonic development within intertidal gastropod egg masses. *Molluscan Research*, 24: 43–63.

PUNYAGUPTA, S., 1965, Eosinophilic meningoencephalitis in Thailand: summary of nine cases and observations on *Angiostrongylus cantonensis* as a causative agent and *Pila ampullacea* as a new intermediate host. *American Journal of Tropical Medicine and Hygiene*, 14: 370–374.

QIU, J.-W., M. T. CHAN, K. L. KWONG & J. SUN, 2011, Consumption, survival and growth in the invasive freshwater snail *Pomacea canaliculata*: does food freshness matter? *Journal of Molluscan Studies*, 77: 189–195.

QIU, J.-W. & K.-L. KWONG, 2009, Effects of macrophytes on feeding and life-history traits of the invasive apple snail *Pomacea canaliculata*. *Freshwater Biology*, 54: 1720–1730.

RAMNARINE, I. W., 2003, Induction of spawning and artificial incubation of eggs in the edible snail *Pomacea urceus* (Muller) [sic]. *Aquaculture*, 215: 163–166.

RAMOS-VASCONCELOS, G., L. CARDOSO & M. HERMES-LIMA, 2005, Seasonal modulation of free radical metabolism in estivating land snails *Helix aspersa*. *Comparative Biochemistry and Physiology C*, 140: 165–174.

RANJAH, A. R., 1942, The embryology of the Indian apple-snail *Pila globosa* (Swainson) (Mollusca, Gastropoda). *Records of the Indian Museum*, 44: 217–322.

RAUT, S., 1984, On the egg laying behaviour of the apple snail *Pila globosa* (Swainson) (Mollusca: Gastropoda). *Science and Culture*, 50: 198–199.

RAWLINGS, T. A., K. A. HAYES, R. H. COWIE & T. M. COLLINS, 2007, The identity, distribution, and impacts of non-native apple snails in the continental United States. *BMC Evolutionary Biology*, 7: 97 [14 pp.].

RAY, M., N. S. BHUNIA, A. S. BHUNIA & S. RAY, 2012, A comparative analyses [sic] of morphological variations, phagocytosis and generation of cytotoxic agents in flow cytometrically isolated hemocytes of Indian molluscs. *Fish & Shellfish Immunology*, 34: 244–253

REDDY, Y. S., P. V. RAO & K. S. SWAMI, 1974, Probable significance of urea and uric acid accumulation during aestivation in the gastropod, *Pila globosa* (Swainson). *Indian Journal of Experimental Biology*, 12: 454–456.

REED, W. L. & F. J. JANZEN, 1999, Natural selection by avian predators on size and colour of a freshwater snail (*Pornacea flagellata*). *Biological Journal of the Linnean Society*, 67: 331–342.

REEVE, L. [A.], 1856, Monograph of the genus *Ampullaria*. Pls. 1–28, in: L. [A.] REEVE, *Conchologia Iconica: or, illustrations of the shells of molluscous animals.* Vol. X. Lovell Reeve, London.

RICH, E. R., 1990, Observations on feeding by *Pomacea paludosa*. *Florida Scientist*, 53: 13.

RING, R. A. & H. V. DANKS, 1994, Desiccation and cryoprotection: overlapping adaptations. *CryoLetters*, 15: 181–190.

RINGUELET, R., 1945, Hirudíneos del Museo de La Plata. *Revista del Museo de La Plata (Nueva Serie) Zoología*, 4: 95–137.

RINGUELET, R., 1985, Annulata Hirudinea. *Fauna de agua dulce de la Republica Argentina*, 27: 1–321.

RODRIGUEZ, R., R. M. DEQUI, L. PERUZZO, P. M. MESQUITA, E. GARCIA & F. FORNARI, 2008, Abdominal angiostrongyliasis: report of two cases with different clinical presentations. *Revista do Instituto de Medicina Tropical de São Paulo*, 50: 339–341.

RODRIGUEZ, C., I. A. VEGA, J. A. CUETO & A. CASTRO-VAZQUEZ, 2012, Hemocyte spheroidal aggregates in the kidney and lung of the apple-snail (*Pomacea canaliculata*) after an immune challenge. *Biocell*, 36: A113.

ROGEVICH, E. C., T. C. HOANG & G. M. RAND, 2008, The effects of water quality and age on the acute toxicity of copper to the Florida apple snail, *Pomacea paludosa*. *Archives of Environmental Contamination and Toxicology*, 54: 690–696.

ROMER, A. J., Jr., 1972, *The aposomatic [sic] eggs of* Pomacea paludosa *(Say)*. MS thesis, University of South Florida, Tampa, vi + 44 p.

RONDELAUD, D. & D. BARTHE, 1982, Relationship of the amebocyte-producing organ with the generalized amoebocytic reaction in *Lymnaea truncatula* Müller infected by *Fasciola hepatica* L. *International Journal of Parasitology*, 68: 967–969.

ROUSE, G. W. & B. G. M. JAMIESON, 1987, An ultrastructural study of the spermatozoa of the polychaetes *Eurythoe complanata* (Amphinomidae), *Clymenella* sp. and *Micromaldane* sp. (Micromaldanidae), with definitions of sperm types in relation to reproductive biology. *Journal of Submicroscopical Cytology*, 19: 573–584.

RUELLAN, L. & D. RONDELAUD, 1992, Lamellar structure of the amoebocyte-producing tissue in *Lymnaea truncatula* infected with *Fasciola hepatica*. *Parasitology Research*, 78: 270–272.

RUTSCHMANN, F., T. ERIKSSON, J. SCHONENBERGER & E. CONTI, 2004, Did Crypteroniaceae really disperse out of India? Molecular dating evidence from rbcL, ndhF, and rp/16 intron sequences. *International Journal of Plant Science*, 164: S69–S83.

SACHWATKIN, V., 1920, Das Urogenitalsystem von *Ampullaria gigas* Spix. *Acta Zoologica*, 1: 67–130.

SANTOS, C. A. Z. & E. G. MENDES, 1981, Oxygen consumption of the amphibious snail *Pomacea lineata*; influence of weight, sex and environments. *Comparative Biochemistry and Physiology A*, 69: 595–598.

SAVEANU, L. & P. R. MARTÍN, 2013, Pedal surface collecting as an alternative feeding mechanism of the invasive apple snail *Pomacea canaliculata* (Caenogastropoda: Ampullariidae). *Journal of Molluscan Studies*, 79: 11–18.

SAVEANU, L. & P. R. MARTÍN, 2014, Egg cannibalism in *Pomacea canaliculata* (Caenogastropoda, Ampullariidae) from southern Pampas: an alternative trophic strategy? *Malacologia*, 57(2): in press.

SAWANGPROH, W. & P. POONSWAD, 2010, The population dynamics of *Pomacea canaliculata* (Lamarck, 1822) in relation to rice cultivation practice and seasons in Nakhon Pathom, Thailand. *Khon Kaen University Science Journal*, 38: 228–238.

SAWASDEE, B. & H.-R. KÖHLER, 2009, Embryo toxicity of pesticides and heavy metals to the ramshorn snail, *Marisa cornuarietis* (Prosobranchia). *Chemosphere*, 75: 1539–1547.

SAWASDEE, B. & H.-R. KÖHLER, 2010, Metal sensitivity of the embryonic development of the ramshorn snail *Marisa cornuarietis* (Prosobranchia). *Ecotoxicology*, 19: 1487–1495.

SAY, T., 1829, Descriptions of some new terrestrial and fluviatile shells of North America. *The Disseminator of Useful Knowledge* [New Harmony], 2: 229–230, 244–246, 259–261, 275–277, 291–293, 308–310, 323–325, 339–341, 355–356.

SCARABINO, F., 2004, Conservación de la malacofauna Uruguaya. *Comunicaciones de la Sociedad Malacológica del Uruguay*, 8: 267–273.

SCHNORBACH, H.-J., 1995, The golden apple snail (*Pomacea canaliculata* Lamarck), an increasingly important pest in rice, and methods of control with Bayluscid. *Pflanzenschutz-Nachrichten Bayer*, 48: 313–346.

SCHULTE-OEHLMANN, U., C. BETTIN, P. FIORONI, J. OEHLMANN & E. STROBEN, 1995, *Marisa cornuarietis* (Gastropoda, Prosobranchia): a potential TBT bioindicator for freshwater environments. *Ecotoxicology*, 4: 372–384.

SCHULTE-OEHLMANN, U., P. FIORONI, J. OEHLMANN & E. STROBEN, 1994, The genital system of *Marisa cornuarietis* (Gastropoda, Ampullariidae) – a morphological and histological analysis. *Zoologische Beiträge*, (N. F.), 36: 59–81.

SCHULTE-OEHLMANN, U., M. TILLMANN, B. MARKERT, J. OEHLMANN, B. WATERMANN & S. SCHERF, 2000, Effects of endocrine disruptors on prosobranch snails (Mollusca: Gastropoda) in the laboratory. Part II: triphenyltin as a xeno-androgen. *Ecotoxicology*, 9: 399–412.

SEIXAS, S. A., J. F. R. AMATO & S. B. AMATO, 2010a, First report of *Temnocephala haswelli* (Platyhelminthes: Temnocephalida) in *Pomacea canaliculata* (Mollusca: Ampullariidae) from Brazil: description update based on specimens from the state of Rio Grande do Sul, Brazil. *Zoologia*, 27: 455–464.

SEIXAS, S. A., J. F. R. AMATO & S. B. AMATO, 2010b, First report of *Temnocephala rochensis* (Platyhelminthes: Temnocephalida) from *Pomacea canaliculata* (Mollusca: Ampullariidae) outside Uruguay - description update based on specimens from the state of Rio Grande do Sul, Brazil. *Zoologia*, 27: 820–828.

SEMPER, C., 1862, *Entwickelungsgeschichte der* Ampullaria polita *Deshayes nebst Mittheilungen über die Entwickelungsgeschichte einiger an-*

dern Gastropoden aus den Tropen. C. van der Post Jr., Utrecht, 80 pp.

SEUFFERT, M. E., S. BURELA & P. R. MARTÍN, 2010, Influence of water temperature on the activity of the freshwater snail *Pomacea canaliculata* (Caenogastropoda: Ampullariidae) at its southernmost limit (Southern Pampas, Argentina). *Journal of Thermal Biology*, 35: 77–84.

SEUFFERT, M. E. & P. R. MARTÍN, 2009, Influence of temperature, size and sex on aerial respiration of *Pomacea canaliculata* (Gastropoda: Ampullariidae) from southern pampas, Argentina. *Malacologia*, 51: 191–200.

SEUFFERT, M. E. & P. R. MARTÍN, 2010, Dependence on aerial respiration and its influence on microdistribution in the invasive freshwater snail *Pomacea canaliculata* (Caenogastropoda, Ampullariidae). *Biological Invasions*, 12: 1695–1708.

SEUFFERT, M. E. & P. R. MARTÍN, 2012, A lentic dweller in lotic habitats: the behavior of the invasive South American apple snail *Pomacea canaliculata* in flowing water. *Aquatic Ecology*, 46: 129–142.

SEUFFERT, M. E. & P. R. MARTÍN, 2013a, Distribution of the apple snail *Pomacea canaliculata* in Pampean streams (Argentina) at different spatial scales. *Limnologica*, 43: 91–99.

SEUFFERT, M. E. & P. R. MARTÍN, 2013b, Juvenile growth and survival of the apple snail *Pomacea canaliculata* (Caenogastropoda: Ampullariidae) reared at different constant temperatures. *SpringerPlus*, 2: 312.

SEUFFERT, M. E., L. SAVEANU & P. R. MARTÍN, 2012, Threshold temperatures and degree-day estimates for embryonic development of the invasive apple snail *Pomacea canaliculata* (Caenogastropoda: Ampullariidae). *Malacologia*, 55: 209–217.

SHARFSTEIN, B. & A. D. STEINMAN, 2001, Growth and survival of the Florida apple snail (*Pomacea paludosa*) fed 3 naturally occurring macrophyte assemblages. *Journal of the North American Benthological Society*, 20: 84–95.

SHOZAWA, A. & C. SUTO, 1990, Hemocytes of *Pomacea canaliculata*: I. Reversible aggregation induced by Ca^{2+}. *Developmental and Comparative Immunology*, 14: 175–184.

SHUFORD, R. B. E., III, P. V. McCORMICK & J. MAGSON, 2005, Habitat related growth of juvenile Florida applesnails (*Pomacea paludosa*). *Florida Scientist*, 68: 11–19.

SIMONE, L. R. L., 2004, Comparative morphology and phylogeny of representatives of the superfamilies of Architaenioglossans and the Annulariidae (Mollusca, Caenogastropoda). *Arquivos do Museu Nacional, Rio de Janeiro*, 62: 387–504.

SJURSEN, H. & L. SOMME, 2000, Seasonal changes in tolerance to cold and desiccation in *Phauloppia* sp. (Acari, Oribatida) from Finse, Norway. *Journal of Insect Physiology*, 40: 1387–1396.

SMINIA, T., 1981, Gastropods. Pp. 191–232, in: N. A. Ratcliffe & A. Rowley, eds., *Invertebrate blood cells*. Academic Press, New York, 2 Vols.: lv + 1–[324] pp. (vol. 1), xlv + [325]–641 pp. (Vol. 2).

SNYDER, N. F. R. & H. W. KALE, II, 1983, Mollusk predation by snail kites in Colombia. *The Auk*, 100: 93–97.

SNYDER, N. F. R. & H. A. SNYDER, 1969, A comparative study of mollusc predation by limpkins, everglade kites, and boat-tailed grackles. *Living Bird*, 8: 177–223.

SNYDER, N. F. R. & H. A. SNYDER, 1971, Defenses of the Florida apple snail *Pomacea paludosa*. *Behaviour*, 40: 175–215, 4 pls.

SOUZA, S. D. S. & Z. A. ANDRADE, 2006, On the origin of the *Biomphalaria glabrata* hemocytes. *Memórias do Instituto Oswaldo Cruz*, 101 (Suppl. 1): 213–218.

SOWERBY, G. B., I, 1825, *A catalogue of the shells contained in the collection of the late Earl of Tankerville, arranged according to the Lamarckian conchological system; together with an appendix, containing descriptions of many new species*. G. B. Sowerby, London, vii + 92 + xxxiv pp., 9 pls.

SPARKS, J. S., 2004, Molecular phylogeny and biogeography of the Malagasy and South Asian cichlids (Teleostei: Perciformes: Cichlidae). *Molecular Phylogenetics and Evolution*, 30: 599–614.

STAPLES, C. A., K. WOODBURN, N. CASPERS, A. T. HALL & G. M. KLEČKA, 2002, A weight of evidence approach to the aquatic hazard assessment of bisphenol A. *Human and Ecological Risk Assessment*, 8: 1083–1105.

STARMÜHLNER, F., 1979, Distribution of freshwater molluscs in mountain streams of tropical Indo-Pacific islands (Madagascar, Ceylon, New Caledonia). *Malacologia*, 18: 245–255.

STEVENS, A. J., Z. C. WELCH, P. C. DARBY & H. F. PERCIVAL, 2002, Temperature effects on Florida applesnail activity: implications for snail kite foraging success and distribution. *Wildlife Society Bulletin*, 30: 75–81.

STOREY, K. B., 2002, Life in the slow lane: molecular mechanisms of estivation. *Comparative Biochemistry and Physiology A*, 133: 733–754.

STOREY, K. [B.] & J. STOREY, 1997, To freeze or not to freeze. *The Biochemist*, 19: 8–13.

STRONG, E. E., 2003, Refining molluscan characters: morphology, character coding and a phylogeny of the Caenogastropoda. *Zoological Journal of the Linnean Society*, 137: 447–554.

STRONG, E. E., O. GARGOMINY, W. F. PONDER & P. BOUCHET, 2008, Global diversity of gastropods (Gastropoda: Mollusca) in freshwater. *Hydrobiologia*, 595: 149–166.

SUN, J., 2013, *Characterization of the egg and embryonic proteome of* Pomacea canaliculata*, and responses of the proteome to environmental stressors*. PhD Thesis, Hong Kong Baptist University, Hong Kong.

SUN, J., Y. ZHANG, V. THIYAGARAJAN, P.-Y. QIAN & J.-W. QIU, 2010, Protein expression during the embryonic development of a gastropod. *Proteomics*, 10: 2701–2711.

SUN, J., H. MU, H. ZHANG, K. H. CHANDRAMOULI, P.-Y. QIAN, C. K. C. WONG & J. W. QIU, 2013, Understanding the regulation of estivation in a freshwater snail through iTRAQ-based comparative proteomics. *Journal of Proteome Research*, 12: 5271–5280.

SUN, J., M. WANG, H. WANG, H. ZHANG, V. THIYAGARAJAN, P.-Y. QIAN & J.-W. QIU, 2012a, De novo assembly of the transcriptome of an invasive snail and its multiple ecological applications. *Molecular Ecology Resources*, 12: 1133–1144.

SUN, J., H. ZHANG, H. WANG, H. HERAS, M. S. DREON, S. ITUARTE, T. RAVASI, P.Y. QIAN & J.-W. QIU, 2012b, First proteome of the egg perivitelline fluid of a freshwater gastropod with aerial oviposition. *Journal of Proteome Research*, 11: 4240−4248.

SWAINSON, W., 1822 [1821–1823], *Zoological illustrations, or original figures and descriptions of new, rare, or interesting animals, selected chiefly from the classes of ornithology, entomology, and conchology, and arranged on the principles of Cuvier and other modern zoologists*. Series 1, Vols. II–III: pls. 67–192, pp. [i–xxvii]. Baldwin, Cradock & Joy, & W. Wood, London.

TABUGO, S. R. M., M. A. J. TORRES, & C. G. DEMAYO, 2010, Relative warp and correlation analysis based on distances of the morphological shape of the shell of the golden apple snail *Pomacea canaliculata* from Iligan City, Philippines. Pp. 81–85, in: S. Baby & Y. Dan, eds., *2010 International Conference on Environmental Engineering and Applications. 10–12 September, 2010. Singapore.* Proceedings. Institute of Electrical and Electronics Engineers, New York, xiv + 349 pp.

TAKEBAYASHI, T. E., 2013, What are the C and K corpuscles of apple snails? *The Malacologist*, 61: 3–5.

TAMBURI, N. E. & P. R. MARTÍN, 2009a, Reaction norms of size and age at maturity of *Pomacea canaliculata* (Gastropoda: Ampullariidae) under a gradient of food deprivation. *Journal of Molluscan Studies*, 75: 19–26.

TAMBURI, N. E. & P. R. MARTÍN, 2009b, Feeding rates and food conversion efficiencies in the apple snail *Pomacea canaliculata* (Caenogastropoda: Ampullariidae). *Malacologia*, 51: 221–232.

TAMBURI, N. E. & P. R. MARTÍN, 2011, Effects of food availability on reproductive output, offspring quality and reproductive efficiency in the apple snail *Pomacea canaliculata*. *Biological Invasions*, 13: 2351–2360.

TAMBURI, N. E. & P. R. MARTÍN, 2012, Effect of food availability on morphometric and somatic indices of the apple snail *Pomacea canaliculata* (Caenogastopoda, Ampullariidae). *Malacologia*, 55: 33–41.

TAMBURI, N. E. & P. R. MARTÍN, 2013, Allometric and trophic effects on shell morphology of *Pomacea canaliculata* (Caenogastropoda, Ampullariidae) from a geometric morphometrics viewpoint. *Molluscan Research*, 33: 223–229.

TANAKA, K., T. WATANABE, H. HIGUCHI, K. MIYAMOTO, Y. YUSA, T. KIYONAGA, H. KIYOTA, Y. SUZUKI & T. WADA, 1999, Density-dependent growth and reproduction of the apple snail, *Pomacea canaliculata*: a density manipulation experiment in a paddy field. *Researches on Population Ecology*, 41: 253–262.

TANAKA, M. O., A. L. SOUZA & E. S. MÓDENA, 2006, Habitat structure effects on size selection of snail kites (*Rostrhamus sociabilis*) and limpkins (*Aramus guarauna*) when feeding on apple snails (*Pomacea* spp.). *Acta Oecologica*, 30: 88–96.

TEEM, J. L., Y. QVARNSTROM, H. S. BISHOP, A. J. DA SILVA, J. CARTER, J. WHITE-MCLEAN & T. SMITH, 2013, The occurrence of the rat lungworm, *Angiostrongylus cantonensis*, in nonindigenous snails in the Gulf of Mexico region of the United States. *Hawai'i Journal of Medicine and Public Health*, 72 (Suppl. 2): 11–14.

TESANA, S., T. SRISAWANGWONG, P. SITHITHAWORN, T. LAHA & R. ANDREWS, 2009, Prevalence and intensity of infection with third stage larvae of *Angiostrongylus cantonensis* in mollusks from northeast Thailand. *American Journal of Tropical Medecine and Hygiene*, 80: 983–987.

THIENGO, S. C., 1987, Observations on the morphology of *Pomacea lineata* (Spix, 1827) (Mollusca, Ampullariidae). *Memórias do Instituto Oswaldo Cruz*, 82: 563–570.

THIENGO, S. C., 1989, On *Pomacea sordida* (Swainson, 1823) (Prosobranchia, Ampullariidae). *Memórias do Instituto Oswaldo Cruz*, 84: 351–355.

THIENGO, S. C., C. E. BORDA & J. L. B. ARAÚJO, 1993, On *Pomacea canaliculata* (Lamarck, 1822) (Mollusca; Pilidae: Ampullariidae). *Memórias do Instituto Oswaldo Cruz*, 88: 67–71.

THIENGO, S. C., K. A. HAYES, A. C. MATTOS, M. A. FERNANDEZ & R. H. COWIE, 2011, A Família Ampullariidae no Brasil: aspectos morfológicos, biológicos e taxonômicos. Pp. 95–111, in: M. A. Fernandez, S. B. dos Santos, A. D. Pimenta & S. C. Thiengo, org., *Tópicos em Malacologia. Ecos do XIX Encontro Brasileiro de Malacologia*. Sociedade Brasileira de Malacologia, Rio de Janeiro, x + 468 pp.

THIENGO, S. C., A. MALDONADO, E. M. MOTA, E. J. L. TORRES, R. CALDEIRA, O. S. CARVALHO, A. P. M. OLIVEIRA, R. O. SOMÕES, M. A. FERNANDEZ & R. M. LANFREDI, 2010, The giant African snail *Achatina fulica* as natural intermediate host of *Angiostrongylus cantonensis* in Pernambuco, northeast Brazil. *Acta Tropica*, 115: 194–199.

THOMAS, M. & J. AGARD, 1992, Metabolic rate depression in the ampullariid snail *Pomacea urceus* (Müller) during aestivation and anaerobiosis. *Comparative Biochemistry and Physiology A*, 102: 675–678.

TIECHER, M. J., S. BURELA & P. R. MARTÍN, 2014, Mating behavior, egg laying, and embryonic development in the South American apple snail *Asolene pulchella* (Ampullariidae, Caenogastropoda). *Invertebrate Reproduction & Development*, 58: 13–22.

TILL-BOTTRAUD, I., D. JOLY, D. LACHAISE, & R. R. SNOOK, 2005, Pollen and sperm heteromorphism: convergence across kingdoms? *Journal of Evolutionary Biology*, 18: 1–18.

TILLMANN, M., U. SCHULTE-OEHLMANN, M. DUFT, B. MARKERT & J. OEHLMANN, 2001, Effects of endocrine disruptors on prosobranch snails (Mollusca: Gastropoda) in the laboratory. Part III: Cyproterone acetate and vinclozolin as antiandrogens. *Ecotoxicology*, 10: 373–388.

TORRES, M. A., L. R. T. AMARILLO, R. JOSHI, L. SEBASTIAN, Z. BAOANAN & C. G. DEMAYO, 2011, Intra- and Inter-population variability in the golden apple snail *Pomacea canaliculata*. *Australian Journal of Basic and Applied Sciences*, 5: 789–800.

TRAN, C. T., K. A. HAYES & R. H. COWIE, 2008, Lack of genetic diversity in invasive apple snails (Ampullariidae) in Hawaii. *Malacologia*, 50: 351–357.

TRAVERS, M.-A., P. M. DA SILVA, N. LE GOÏC, D. MARIE, A. DONVAL, S. HUCHETTE, M. KOKEN & C. PAILLARD, 2008, Morphologic, cytometric and functional characterisation of abalone (*Haliotis tuberculata*) haemocytes. *Fish and Shellfish Immunology*, 24: 400–411.

TROSCHEL, F. H., 1845, Anatomie von *Ampullaria urceus* und über die Gattung *Lanistes* Montf. *Archiv für Naturgeschichte*, 11: 97–216, pl. 8.

TSAI, H.-C., Y.-S. CHEN & C. M. YEN, 2013, Human Parasitic meningitis caused by *Angiostrongylus cantonensis* infection in Taiwan. *Hawai'i Journal of Medicine and Public Health*, 72 (Suppl. 2): 26–27.

TURNER, R. L., 1994, The effects of hydrology on the population dynamics of the Florida applesnail (*Pomacea paludosa*). *St. Johns River Water Management District, Palatka, Florida, Special Publication*, SJ94–SP3: vi + 31 pp.

TURNER, R. L., 1996, Use of stems of emergent plants for oviposition by the Florida applesnail, *Pomacea paludosa*, and implications for marsh management. *Florida Scientist*, 59: 34–49.

TURNER, R. L., 1998, Effects of submergence on embryonic survival and developmental rate of the Florida applesnail, *Pomacea paludosa*: implications for egg predation and marsh management. *Florida Scientist*, 61: 118–129.

TURNER, R. L. & C. M. McCABE, 1990, Calcium source for protoconch formation in the Florida apple snail, *Pomacea paludosa* (Prosobranchia: Pilidae): more evidence for physiological plasticity in the evolution of terrestrial eggs. *The Veliger*, 33: 185–189.

UESHIMA, E. & Y. YUSA, 2014, Antipredator behaviour in response to single or combined predator cues in the apple snail *Pomacea canaliculata*. *Journal of Molluscan Studies*, Advance Access, doi:10.1093/mollus/eyu057.

UTZ, L. R. P., 2007, First record of *Epistylis plicatilis* (Ciliophora: Peritrichia) attached to *Pomacea canaliculata* (Mollusca: Gastropoda) in southern Brazil. *Zootaxa*, 1454: 49–57.

VAN DER KNAAP, W., C. ADEMA & T. SMINIA, 1993, Invertebrate blood cells: morphological and functional aspects of the haemocytes in the pond snail *Lymnaea stagnalis*. *Comparative Haematology International*, 3: 20–26.

VEGA, I. A., M. A. ARRIBÉRE, A. V. ALMONACID, S. RIBEIRO GUEVARA & A. CASTRO-VAZQUEZ, 2012a, Apple snails and their endosymbionts bioconcentrate heavy metals and uranium from contaminated drinking water. *Environmental Science and Pollution Research*, 19: 3307–3316.

VEGA, I. A., M. C. DAMBORENEA, C. GAMARRA-LUQUES, E. KOCH, J. A. CUETO & A. CASTRO-VAZQUEZ, 2006, Facultative and obligate symbiotic associations of *Pomacea canaliculata* (Caenogastropoda, Ampullariidae). *Biocell*, 30: 367–375.

VEGA, I. A., F. A. DELLAGNOLA, J. A. HURST, M. S. GODOY & A. CASTRO-VAZQUEZ, 2012b, A study of chlorophyll-like and phycobilin pigments in the C endosymbiont of the apple-snail *Pomacea canaliculata*. *Biocell*, 36: 47–55.

VEGA, I. A., C. GAMARRA-LUQUES, E. KOCH, L. BUSSMANN & A. CASTRO-VAZQUEZ, 2005, A study of corpuscular DNA and midgut gland occupancy by putative symbiotic elements in *Pomacea canaliculata* (Caenogastropoda, Ampullariidae). *Symbiosis*, 39: 37–45.

VEGA, I. A., M. GIRAUD-BILLOUD, E. KOCH, C. GAMARRA-LUQUES & A. CASTRO-VAZQUEZ, 2007, Uric acid accumulation within intracellular crystalloid corpuscles of the midgut gland in *Pomacea canaliculata* (Caenogastropoda, Ampullariidae). *The Veliger*, 48: 276–283.

VON BRAND, E., T. YOKOSAWA & Y. FUJIO, 1990, Chromosome analysis of apple snail Pomacea canaliculata. *Tohoku Journal of Agricultural Research*, 40: 81–89.

WADA, T. & K. MATSUKURA, 2007, Seasonal changes in cold hardiness of the invasive freshwater apple snail, *Pomacea canaliculata* (Lamarck) (Gastropoda: Ampullariidae). *Malacologia*, 49: 383–392.

WADA, T. & K. MATSUKURA, 2011, Linkage of cold hardiness with desiccation tolerance in the invasive freshwater apple snail, *Pomacea canaliculata* (Caenogastropoda: Ampullariidae). *Journal of Molluscan Studies*, 77: 149–153.

WADA, T. & K. YOSHIDA, 2000, Burrowing by the apple snail, *Pomacea canaliculata* (Lamarck); daily periodicity and factors affecting burrowing. *Kyushu Plant Protection Research*, 46: 88–93.

WAGNER, J. A., 1827, *Testacea fluviatilia quae in itinere per Brasiliam annis MDCCCXVII – MDCCCXX jussu et auspiciis Maximiliani Josephi I. Bavariae regis augustissimi suscepto collegit et pingenda curavit Dr. J. B. de Spix, quondam ordinis regii coronæ Bavaricæ civilis eques, academiæ scientarum Bavaricæ socius ordinarius, musei regii zoologici, zootomici et ethnographici conservator rel.* C. Wolf, Monachii, iv + [ii] + 36 pp., 29 pls.

WALLACE, G. D. & L. ROSEN, 1969, Studies on eosinophilic meningitis V. Molluscan hosts of *Angiostrongylus cantonensis* on Pacific Islands.

American Journal of Tropical Medicine and Hygiene, 18: 206–216.

WANG, H.-J., 1984, Two upper Jurassic gastropod opercula in China. *Acta Palaeontologica Sinica*, 23: 369–372, pl. 1.

WANG, Q.-P., D.-H. LAI, X.-Q. ZHU, X.-G. CHEN & Z.-R. LUN, 2008, Human angiostrongyliasis. *The Lancet Infectious Diseases*, 8: 621–630.

WATANABE, T., K. TANAKA, H. HIGUCHI, K. MIYAMOTO, T. KIYONAGA, H. KIYOTA, Y. SUZUKI & T. WADA, 2000, Emergence of the apple snail, *Pomacea canaliculata* (Gastropoda: Ampullariidae), after irrigation in a paddy. *Applied Entomology and Zoology*, 35: 75–79.

WEERACHAI, S., P. SITHITHAWORN, K. DUENNGAI, N. KIATSOPIT, R. H. ANDREWS & T. N. PETNEY, 2011, Genetic variation and relationshipsof four species of medically important echinostomes (Trematoda: Echinostomatidae) in South-East Asia. *Infection, Genetics and Evolution*, 11: 375–381.

WHITMAN, D. W. & A. A. AGRAWAL, 2009, What is phenotypic plasticity and why is it important? Pp. 1–63, in: D. W. WHITMAN & T. N. ANANTHAKRISHNA, eds., *Phenotypic plasticity of insects: mechanisms and consequences*. Science Publishers, Inc., Enfield, x + 894 pp.

WINIK, B. C. & A. CASTRO-VAZQUEZ, 2015, Adaptations to frequent oocyte release in the ovary of the invasive snail *Pomacea canaliculata* (Caenogastropoda, Ampullariidae). *Journal of Molluscan Studies*, doi: 10.1093/mollus/eyu078

WINIK, B., N. CATALÁN, C. GAMARRA-LUQUES & A. CASTRO-VAZQUEZ, 2009, Ectaquasperm-like parasperm in an internally fertilizing gastropod. *Invertebrate Biology*, 128: 223–231.

WINIK, B. C., N. M. Y. CATALÁN & O. C. SCHLICK, 2001, Genesis of the apyrene parasperm in the apple snail *Pomacea canaliculata* (Gastropoda, Ampullariidae): an ultrastructural study. *Journal of Molluscan Studies*, 67: 81–93.

WINIK, B., C. SCHLICK & M. CATALÁN, 1994, Fine structure of Sertoli cells in the pond snail *Ampullaria canaliculata* (Gastropoda, Prosobranchia) *Biocell*, 18: 59–73.

WITHERS, P., M. GUPPY & S. PEDLER, 1996, Physiological adjustments during aestivation by the Australian land snail *Rhagada tescorum* (Mollusca: Pulmonata: Camaenidae). *Australian Journal of Zoology*, 45: 599–611.

WONG, P. K., K. L. KWONG & J.-W. QIU, 2009, Complex interactions among fish, snails and macrophytes: implications for biological control of an invasive snail. *Biological Invasions*, 11: 2223–2232.

WONG, P. K., Y. LIANG, N. Y. LIU & J.-W. QIU, 2010, Palatability of macrophytes to the invasive freshwater snail *Pomacea canaliculata*: differential effects of multiple plant traits. *Freshwater Biology*, 55: 2023–2031.

WOOD, T. S., P. ANURAKPONGSATORN, R. CHAICHANA, J. MAHUJCHARIYAWONG & T. SATAPANAJARU, 2005, Predation on freshwater bryozoans by the apple snail, *Pomacea canaliculata*, Ampullariidae, an invasive species in Southeast Asia: a summary report. *Denisia, Neue Serie*, 28: 283–286.

WOOD, T. S., P. ANURAKPONGSATORN, R. CHAICHANA, J. MAHUJCHARIYAWONG & T. SATAPANAJARU, 2006, Heavy predation on freshwater bryozoans by the golden apple snail, *Pomacea canaliculata* Lamarck, 1822 (Ampullariidae). *Natural History Journal of Chulalongkorn University*, 6: 31–36.

WOOD, W., 1828, *Supplement to the Index Testaceologicus; or a catalogue of shells, British and foreign*. W. Wood, London, vi + 59 pp., 8 pls.

YAMANISHI, Y., K. YOSHIDA, N. FUJIMORI & Y. YUSA, 2012, Predator-driven biotic resistance and propagule pressure regulate the invasive apple snail *Pomacea canaliculata* in Japan. *Biological Invasions*, 14: 1343–1352.

YAMAURA, I., T. KOGA, T. MATSUMOTO & T. KATO, 1997, Purification and some properties of endo-1, 4-*β*-D-xylanase from a fresh-water mollusc, *Pomacea insularus* (de Ordigny) [sic]. *Bioscience, Biotechnology, and Biochemistry*, 61: 615–620.

YAMAURA, I. & T. MATSUMOTO, 1993, Purification and some properties of endo-1,4-*β*-D-mannanase from a mud snail, *Pomacea insularus* (de Ordigny) [sic]. *Bioscience, Biotechnology, and Biochemistry*, 57: 1316–1319.

YANG, T.-B., Z.-D. WU & Z.-R. LUN, 2013, The apple snail *Pomacea canaliculata*, a novel vector of the rat lungworm, *Angiostrongylus cantonensis*: its introduction, spread, and control in China. *Hawai'i Journal of Medicine and Public Health*, 72(6) (Suppl. 2): 23–25.

YASEEN, A., A. EBAID & I. KAWASHTI, 1991, Studies on the chromosomal analysis and shell measurements of two species, *Bellamya unicolor* and *Lanistes bolteni* (Prosobranchiata: Gastropoda). *Cytologia*, 56: 503–509.

YOSHIE, H. & Y. YUSA, 2008, Effects of predation on the exotic freshwater snail *Pomacea canaliculata* (Caenogastropoda: Ampullariidae) by the indigenous turtle *Chinemys reevesii* (Testudines: Geoemydidae). *Applied Entomology and Zoology*, 43: 475–482.

YOSHIDA, K., K. HOSHIKAWA, T. WADA & Y. YUSA, 2009, Life cycle of the apple snail *Pomacea canaliculata* (Caenogastropoda: Ampullariidae) inhabiting Japanese paddy fields. *Applied Entomology and Zoology*, 44: 465–474.

YOSHIDA, K., K. HOSHIKAWA, T. WADA & Y. YUSA, 2013, Patterns of density dependence in growth, reproduction and survival in the invasive freshwater snail *Pomacea canaliculata* in Japanese rice fields. *Freshwater Biology*, 58: 2065–2073.

YOSHIDA, K., K. MATSUKURA, N. J. CAZZANIGA & T. WADA, 2014. Tolerance to low temperature and desiccation in two invasive apple snails, *Pomacea canaliculata* and *P. maculata* (Caenogastropida: Ampullariidae) collected in their original distribution area (northern and central Argentina). *Journal of Molluscan Studies*, 80: 62–66.

YOUENS, A. K. & R. L. BURKS, 2008, Comparing applesnails with oranges: the need to standardize measuring techniques when studying *Pomacea*. *Aquatic Ecology*, 42: 679–684.

YOUSIF, F., S. BLÄHSER & G. LÄMMLER, 1980, The cellular responses in *Marisa cornaurietis* experimentally infected with *Angiostrongylus cantonensis*. *Zeitschrift für Parasitenkunde*, 62: 179–190.

YUSA, Y., 2001, Predation on eggs of the apple snail *Pomacea canaliculata* (Gastropoda: Ampullariidae) by the fire ant *Solenopsis geminata*. *Journal of Molluscan Studies*, 67: 275–279.

YUSA, Y., 2004a, Inheritance of colour polymorphism and the pattern of sperm competition in the apple snail *Pomacea canaliculata* (Gastropoda: Ampullariidae). *Journal of Molluscan Studies*, 70: 43–48.

YUSA, Y., 2004b, Brood sex ratio in the apple snail *Pomacea canaliculata* (Gastropoda: Ampullariidae) is determined genetically and not by environmental factors. *Journal of Molluscan Studies*, 70: 269–275.

YUSA, Y., 2006a, Genetics of sex-ratio variation inferred from parent-offspring regressions and sib correlations in the apple snail *Pomacea canaliculata*. *Heredity*, 96: 100–105.

YUSA, Y., 2006b, Predators of the introduced apple snail, *Pomacea canaliculata* (Gastropoda: Ampullariidae): their effectivenss and utilization in biological control. Pp. 345–361, in: R. C. Joshi & L. C. Sebastian, eds., *Global advances in ecology and management of golden apple snails*. Philippine Rice Research Institute, Muñoz, Nueva Ecija, Philippines, x + 588 pp.

YUSA, Y., 2007a, Causes of variation in sex ratio and modes of sex determination in the Mollusca – an overview. *American Malacological Bulletin*, 23: 89–98.

YUSA, Y., 2007b, Nuclear sex-determining genes cause large sex-ratio variation in the apple snail *Pomacea canaliculata*. *Genetics*, 175: 179–184.

YUSA, Y., N. SUGIURA & K. ICHINOSE, 2000, Predation on the apple snail, *Pomacea canaliculata* (Ampullariidae), by the Norway rat, *Rattus norvegicus*, in the field. *The Veliger*, 43: 349–353.

YUSA, Y., N. SUGIURA & T. WADA., 2006b, Predatory potential of freshwater animals on an invasive agricultural pest, the apple snail *Pomacea canaliculata* (Gastropoda: Ampullariidae), in southern Japan. *Biological Invasions*, 8: 137–147.

YUSA, Y. & Y. SUZUKI, 2003, A snail with unbiased population sex ratios but highly biased brood sex ratios. *Proceedings of the Royal Society of London B*, 270: 283–288.

YUSA, Y., T. WADA & S. TAKAHASHI, 2006a, Effects of dormant duration, body size, self-burial and water condition on the long-term survival of the apple snail, *Pomacea canaliculata* (Gastropoda: Ampullariidae). *Applied Entomology and Zoology*, 41: 627–632.

ZHANG, S., Q. Y. YIN, Y. H. LI, M. DING, G. J. XU & F. K. ZHAO, 2007, Molecular and biochemical characterization of *Ba*-EGA, a cellulase secreted by *Bacillus* sp. AC-1 from *Ampullaria crosseans* [sic]. *Applied Microbiology and Biotechnology*, 75: 1327–1334.

ZHOU, W. C., Y. F. WU & J. Q. YANG, 2003, Viability of *Ampullaria* snail in China. *Fujian Journal of Agricultural Sciences*, 18: 25–28.

Revised ms. accepted November 8, 2014

MALACOLOGIA, 2015, 58(1–2): 303–321

INTROGRESSION AND DIFFERENTIATION OF THE INVASIVE SLUG *ARION VULGARIS* FROM NATIVE *A. ATER*

Bjørn A. Hatteland[1,2*], Torstein Solhøy[1†], Christoffer Schander[1,3†], Morten Skage[1,4],
Ted von Proschwitz[5] & Leslie R. Noble[6]

ABSTRACT

The large arionid slug *Arion vulgaris* is an invasive pest dispersing through large parts of Europe and causing considerable damage in gardens, horticulture and agriculture. It is also possible that this so-called “Iberian slug” has an impact on Norwegian ecosystems, displacing or hybridizing with the native black slug *Arion ater*. The taxonomy of the large arionids is complex and confusing, encompassing different anatomical forms and colour varieties. The present study integrates, for the first time, coloration, ligula morphology, genital morphometry, nuclear and mitochondrial DNA in order to differentiate the large arionids found in Norway, *A. vulgaris*, *A. ater* and *A. rufus*. These data revealed a clear separation between *A. vulgaris* and *A. ater* based on the morphology of the genitalia and mtDNA. However, introgression with the red slug *A. rufus* was apparent in approximately half of the *A. ater* specimens analysed, evidenced by ligula morphology, mitochondrial and nuclear DNA. In addition, the mitochondrial COI gene and the nuclear ITS1 gene suggested introgression between *A. ater* and *A. vulgaris*. Phylogenetic analyses that included *A. vulgaris*, *A. ater* and *A. rufus* from other parts of Europe, together with *A. flagellus*, *A. fuscus*, *A. lusitanicus* and *A. nobrei* suggest that *A. vulgaris* is more closely related to *A. ater* and *A. rufus* than to *A. lusitanicus*. This study confirms the uncertainty of identification based solely on coloration and stresses the importance of integrating several approaches to differentiate these large arionids, allowing a better appreciation of their invasive potential, ecological impact and current distribution.

Key words: hybridization, mitochondrial and nuclear DNA, morphometrics, pest slug, Arionidae.

INTRODUCTION

Slugs are common pests in gardens, horticulture as well as in agriculture, especially in cool and moist temperate areas (Barker, 2002; Port & Port, 1986; South, 1992). Many of these slugs are alien species, such as the grey field slug *Deroceras reticulatum* (Müller, 1774), which has been reported to cause extensive damage (e.g., lettuce, cabbage, grasses) (Port & Ester, 2002; South, 1992). Its inadvertent introduction and spread across Europe has led to extensive population admixture, producing a genetically diverse pest species (Foltz et al., 1984). The invasive *Arion vulgaris* (Moquin-Tandon, 1855; also regarded as *A. lusitanicus* Mabille, 1868) has also dispersed across most of Europe, often occurring in high densities due to its high reproductive rate, catholic feeding habits and high survival rate (Kozlowski, 2007; von Proschwitz, 1992). It was first reported in Norway in 1988 and is currently common and locally very abundant as far north as the southern part of northern Norway (Hatteland et al., 2013a). Considerable damage caused by *A. vulgaris* has been reported in gardens, vegetable and strawberry fields (Dolmen & Winge, 1997; Grimm et al., 2000; von Proschwitz & Winge,

---

[1] Department of Biology, University of Bergen, P.O. Box 7803, 5020 Bergen, Norway.

[2] Bioforsk – Norwegian Institute for Agricultural and Environmental Research, Bioforsk Ullensvang, 5781 Lofthus, Norway.

[3] University Museum of Bergen, University of Bergen, P.O. Box 7800, 5020 Bergen, Norway.

[4] Current address: Centre for Ecological and Evolutionary Synthesis (CEES), Department of Biosciences, University of Oslo, P.O. Box 1066, Blindern, 0316 Oslo, Norway.

[5] Göteborg Natural History Museum, P.O. Box 7283, 402 35 Göteborg, Sweden.

[6] School of Biological Sciences, University of Aberdeen, Tillydrone Avenue, Aberdeen, AB24 2TZ, U.K.

[†] This paper is dedicated to Christoffer Schander (1960–2012) and Torstein Solhøy (1942–2013), both of whom were excellent malacologists and inspiring researchers.

*Corresponding author: bjorn.hatteland@bio.uib.no

1994). In addition, it is possible that *A. vulgaris* may have a negative effect on such native slug species as *Arion ater* (Linnaeus, 1758), in Scandinavia (von Proschwitz, 1997), Austria (Reischütz, 1984a,b) and in Britain (Davies, 1987); the number of *A. ater* in a population falls appreciably once *A. vulgaris* becomes noticeable. The reason for this is unknown, but hybridization and predation have been suggested as possible explanations.

The invasive nature of *A. vulgaris* means there is a pressing need to distinguish this species from such native slugs as *A. ater* to avoid misidentifications. Unfortunately, the genus *Arion* poses considerable taxonomic problems, and *Arion* species are thus often misidentified (Noble, 1992; Quinteiro et al., 2005). This is due to intraspecific variation in morphology, colour as well as anatomical characters (Cain & Williamson, 1958; Evans, 1986; Øklans, 1922). Introgression, especially between *A. ater* and *A. rufus* (Linnaeus, 1758) (Evans, 1986), makes this situation even more confusing. However, the large *Arion* slugs can be differentiated using genital characters (Fig. 1); the position of the ligula (a holdfast/stimulatory organ for pulling the spermatophore) and the presence or absence of a lower atrium in the distal part of the genitalia (Noble, 1992). At species-level, however, the arionid group remains problematic, with a combination of morphology and genetics being mandatory to distinguish taxa and potential hybrids.

Arion ater was originally distinguished from its close relative *A. rufus* by colour, the former being black and the latter orange to red (van Regteren Altena, 1955). However, differences in the genitalia that corresponded to these colour variants were described by Pollonera (1889) and Quick (1947), mainly separating the two species by the bulk and relative size of the upper atrium where the ligula is situated. These taxa were even regarded as subspecies, hence *A. ater ater* and *A. ater rufus* (Cain & Williamson, 1958; Quick, 1960), and were distinguished by protein electrophoresis (Burnet, 1972) and multivariate statistical analyses (Noble, 1987). However, Evans (1986) found continuous variation between the two subspecies based on morphometric ratios of the distal genitalia, and Noble (1992) described intermediate variants of the ligula morphology, both authors regarding these as hybrid features. Currently, *A. ater* and *A. rufus* are considered separate species (Anderson, 2005; Falkner et al., 2001).

Arion vulgaris has traditionally been confused with *A. lusitanicus*, and many authors still apply this name to this invasive slug taxon. *Arion lusitanicus* was originally thought to consist of two taxa; *A. lusitanicus* (*sensu* Mabille, 1868) and *A. lusitanicus* (*sensu* Quick = *A. flagellus* (Collinge, 1893; Davies, 1987)). In addition, Noble (1992) recognised two taxa (A and B) from Mont Louis in the Pyrenees of southern France that resembled *A. lusitanicus* based on the ligula morphology. Based on the shape of the ligula and morphometric data, Campbell (2000) added two more taxa, one sampled from the vicinity of Bergen, western Norway, and one from the Pyrenees of Spain, respectively. These were all regarded as hybrids potentially of taxa within the *A. lusitanicus* aggregate. Furthermore, in a molecular phylogeny, the topotype specimens (the Portuguese type localites) of *A. lusitanicus* and *A. flagellus* were grouped in an "Atlantic" clade, while other specimens of *A. lusitanicus* sampled outside the geographic range of the topotype were shown to be polyphyletic, and grouped together with *A. ater* and *A. rufus* (Quinteiro et al., 2005). This latter *A. lusitanicus* is very different from the topotype *A. lusitanicus* based on the form of the spermatophore and internal morphology (Castillejo, 1997), and has recently been regarded as a distinct species, *A. vulgaris* Moquin-Tandon (1855) (Anderson, 2005; Falkner et al., 2002). This is the first name that can be unambiguously used.

It has been proposed that *A. vulgaris* may hybridise with *A. ater*, a supposition supported by declines in the incidence of *A. ater*, and presence amongst the remaining individuals of intermediate colour varieties (T. Solhøy & T. von Proschwitz, pers. obs.) and genital anatomy (von Proschwitz, 2009). Observations from Germany support a similar scenario of hybridization, where the numbers of *A. rufus* declined after the introduction of *A. vulgaris* (Falkner, 1990). Mating experiments have shown that *A. vulgaris* and *A. rufus* are able to mate and subsequently lay eggs (Roth et al., 2012). Other mating studies have investigated sperm exchange between these two species and showed reciprocal spermatophore exchange in mixed pairs (Dreijers et al., 2013) Anecdotal evidence exists also for negative effects of *A. flagellus* on *A. ater* in Britain, although it has been proposed this could derive from differences in their evolutionary tolerance of parasites and pathogens afforded by differences in breeding systems (Noble & Jones,

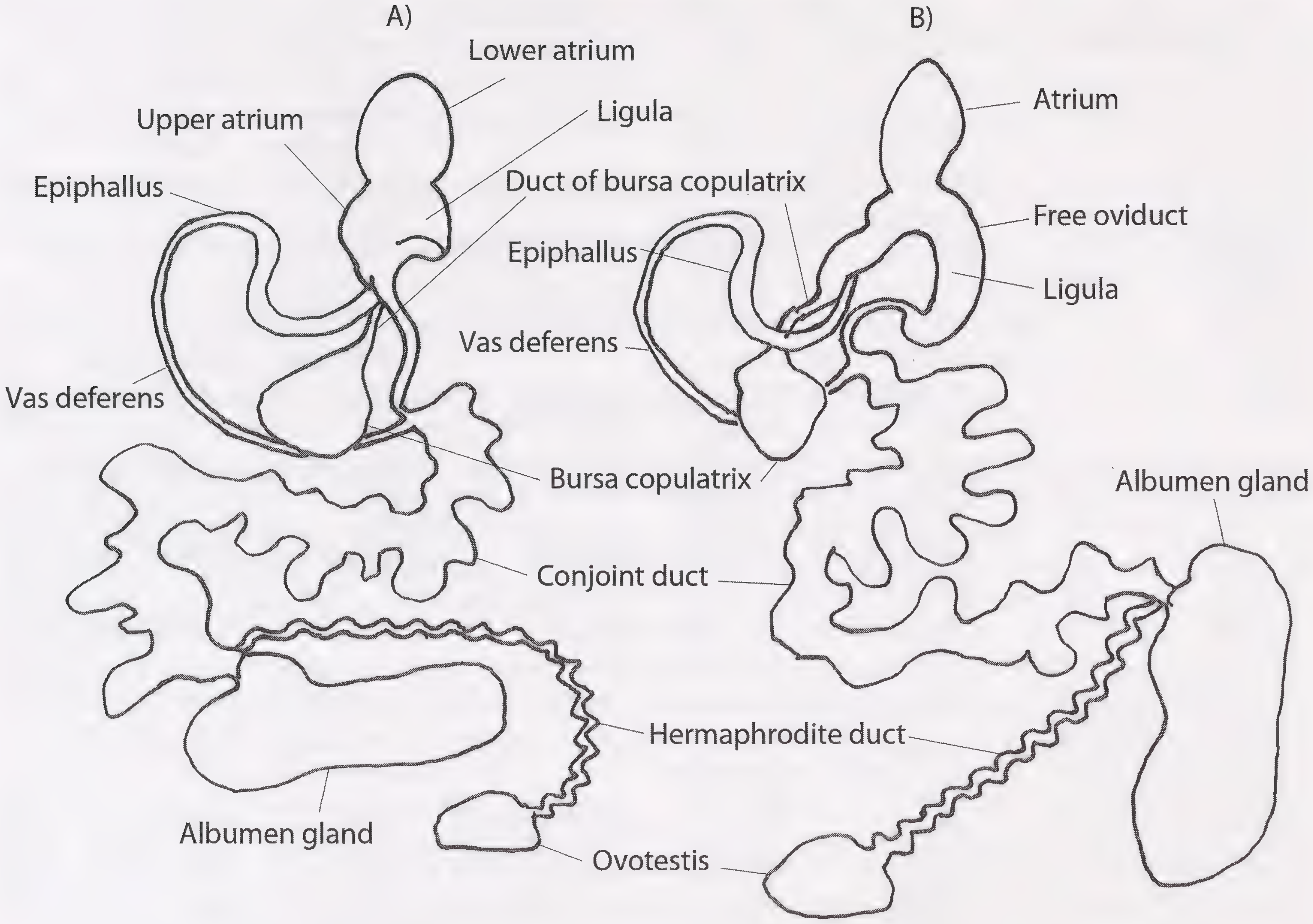

FIG. 1. Overview of measured genital characters used for morphometrics of *Arion ater* (A) and *A. vulgaris* (B).

1996). As an obligatory outcrossing species *A. flagellus* may maintain greater genetic diversity and short-term evolutionary flexibility than the facultative self-compatible *A. ater* (Noble & Jones, 1996). Foltz et al. (1982) found a lack of genetic polymorphism in most *A. ater* populations, thus the decline of *A. ater* might be a consequence of depauperate genetic variability hampering its ability to cope with the dynamics of host-parasite interactions (Hillebrand & Matthiessen, 2009).

The present work is an attempt to clarify the status of these large arionids with special emphasis on *A. vulgaris* and *A. ater* in Norway, by morphometric analyses, ligula anatomy, colour and molecular characterization of mtDNA and nDNA based on multiplex PCR and phylogenetic analyses. For the first time, these approaches are integrated in an attempt to determine potential introgression of exotic terrestrial slugs into the native malacofauna of Norway, affording a better understanding of their invasive potential, ecological impact and current distribution.

MATERIAL AND METHODS

Study Area

Slugs were sampled in seven sites, five of which are close to Bergen, one in Molde, northwestern Norway, and one in Klepp, southwestern Norway. The areas have an oceanic climate with high precipitation throughout the year, mild winters and relatively cool summers. In addition, samples were obtained from eastern Norway, Sweden, Denmark, U.K., France, Portugal, Germany, Iceland and Austria for molecular and phylogenetic analyses (Table 1). All slugs were dissected, and only mature specimens were used for further analyses. Mature specimens were assessed based on the presence of fully developed genitalia.

Sampling Design

All slugs were randomly handpicked and preliminary identification to species was based on colour and external morphology. All specimens

TABLE 1. *Arion* spp. specimens included for phylogenetic analyses. Species identifications are based on genital characters including ligula.

Species	Specimen ID	Location	Accession number	Voucher number	Collected
Arion (*Arion*) *ater* (Linnaeus, 1758)	BAH28	Klepp, Rogaland, Norway	JF950513	ZMBN91243	2006
A. ater	Albus200	Vestby, Akershus, Norway	JF950523	ZMBN91288	2006
A. ater	Wales	Wales, UK	JF950533	ZMBN91286	?
A. ater	SweBAH71	Torsö, Västergötland, Sweden	JQ041671	ZMBN91305	2008
Arion (*Arion*) *rufus* (Linnaeus, 1758)	Germany BAH70	Baden-Württemberg, Germany	JQ041672	ZMBN91304	2005
A. rufus	Denmark BAH21	Silkeborg, Denmark	JQ041668	ZMBN91272	2008
A. rufus	France P2	Col de la Pierre St. Martin, Pyrenees, France	JF950530	ZMBN91285	1993
A. ater x *A. rufus*	BAH51	Sletten, Hordaland, Norway	JF950532	ZMBN91257	2010
A. ater x *A. rufus*	England	Cavedale Gorge, Derbyshire, UK	JF950522	ZMBN91287	?
A. ater x *A. rufus*	BA2	Klepp, Rogaland, Norway	JQ041673	ZMBN91239	2006
A. ater x *A. rufus*	BA10	Klepp, Rogaland, Norway	JF950524	ZMBN91247	2006
A. ater x *A. rufus*	BA23	Klepp, Rogaland, Norway	JF950534	ZMBN91260	2006
A. ater x *A. rufus*	BAH49	Hå, Rogaland, Norway	JF950516	ZMBN91277	2010
Arion (*Arion*) *vulgaris* (Moquin-Tandon, 1855)	BAH52	Bodø, Nordland, Norway	JQ041669	ZMBN91280	2008
A. vulgaris	BA16	Bergen, Hordaland, Norway	JF950527	ZMBN91253	2006
A. vulgaris	BA25	Bergen, Hordaland, Norway	JF950529	ZMBN91266	2006
A. vulgaris	BA11	Molde, Møre og Romsdal, Norway	JF950526	ZMBN91248	2006
A. vulgaris	IcelandBAH72	Reykjavik, Iceland	JQ041670	ZMBN91301	2004
A. vulgaris	Austria	Igls, Innsbruck, Austria	JF950519	ZMBN91289	?
A. vulgaris	A P18	Ax-les-Thermes, Pyrenees, France	JF950521	ZMBN91283	1992
A. vulgaris	B P5	Mont-Louis, Pyrenees, France	JF950520	ZMBN91282	1992
A. vulgaris	Poland	Rzeszów-Slocina, Subcarpathian Region, Poland	EF520640.1		2006
A. vulgaris x *A. ater*	BAH66	Ödsmål, Bohuslän, Sweden	JQ041665	ZMBN91303	2005
Arion (*Mesarion*) *lusitanicus* Mabille, 1868	BAH75	Arrabida, Portugal	JQ041666	ZMBN91306	2010
Arion (*Mesarion*) *nobrei* Pollonera, 1889	BAH77	Luso, Portugal	JQ041667	ZMBN91307	2010
Arion (*Mesarion*) *flagellus* Collinge, 1893	BAH61	Wirral, UK	JF950535	ZMBN91302	?
Arion (*Mesarion*) *fuscus* (Draparnaud, 1805)	BAH48	Sokndal, Rogaland, Norway	JF950531	ZMBN	2010
Arion (*Carinarion*) *silvaticus* Lohmander, 1937	3	Bergen, Hordaland, Norway	JF950517	ZMBN	2007
Arion (*Carinarion*) *circumscriptus* Johnston, 1828	4	Bergen, Hordaland, Norway	JF950518	ZMBN	2007

were photographed in uniform light conditions in the laboratory and killed and stored at -20°C prior to dissections following the procedure of (Evans, 1986; Noble, 1987; Campbell, 2000).

Dissections, Pictures and Morphometrics

Slugs were defrosted for approximately 20 min in warm water, placed under water and dissected in a uniform manner according to the protocol of Noble (1992).

Morphometric analysis was carried out on 54 slugs sampled in western Norway including *A. vulgaris* and *A. ater*, using 14 and 15 characters respectively. Length of organs, and for some (atria, albumen gland, ovotestis) width, was measured for all distal genitalia (Fig. 1) using an adjustable calliper in a standardised way. Some organs were pinned lightly (epiphallus and vas deferens) whilst others were measured under gentle tension. Width of organs was always measured at the widest point and all measurements were repeated (up to three times) by the same person and then averaged to achieve a consistent figure. During this process, specimens were thawed and refrozen for repeated measurements at a different time point. However, freezing and thawing does not alter the shape and size of genitalia in any significant way (Evans, 1986; Noble, 1987; Campbell, 2000), so several cycles of this treatment were not regarded as a confounding factor. In addition, all slugs were weighed initially using Pesola® scales, on a scale graded to 15 g in intervals of 0.1 g, to obtain fresh weight.

Morphometric data were analysed first by Principal Component Analysis (PCA), using the PRINC procedure in SAS/STAT (Version 6) following square root transformations. PCA was used to separate taxa without *a priori* assumptions about classification. Further analyses to produce the best discriminant model of the three taxa were performed using the SAS Stepdisc procedure to test the significance of each character in classification. Finally, Canonical Discriminant Analysis (CDA) (Freund et al., 2003) was performed using this subset of discriminatory characters to achieve the best discriminatory model which separated *A. vulgaris*, *A. ater* and *A. ater-A. rufus* hybrids.

DNA Extraction, Primer Design, Multiplexes and Phylogenetics

DNA was extracted from the foot fringe, using the commercially available E.Z.N.A. Tissue kit (Omega Bio-tek) and the DNeasy Blood & Tissue kit (Qiagen) following manufacturer's instructions, and stored in elution buffer at 4°C.

The universal invertebrate primers LCO1490 and HCO2198 designed by Folmer et al. (1994) were used to amplify the cytochrome c oxidase subunit 1 (COI) gene of *A. vulgaris*, *A. ater* and *A. rufus*, and primers ITS BAB18 S1F and ITS BAB28SR to amplify the internal transcribed spacer (ITS rDNA) region. Each PCR was conducted in 25 µL, containing 12.5 µL GoTaq PCR Mastermix from Promega® (400 µM dNTPs, 3 mM $MgCl_2$ PCR buffer), 1.0 µL of each primer (10 µM), 2.0 µL DNA (10:1 diluted) and 5.5 µL distilled H_2O. Amplifications were carried out in a MJ Research PTC220 Peltier thermal cycler, with cycling conditions of 94°C for 2 min, followed by 5 cycles of 92°C for 60 s, 45°C for 1.5 min, 72°C for 1.5 min, then 30 cycles of 92°C for 30 s, 50°C for 60 s and 72°C for 50 s, and a final cycle of 72°C for 7 min when amplifying the COI sequence. The ITS region, however, was amplified using cycling conditions of 94°C for 2 min, followed by 36 cycles of 92°C for 1 min, 55°C for 1 min and 72°C for 1 min, and a final cycle of 72°C for 20 min. ITS products were then cloned using the TOPO TA cloning kit from Invitrogen®, of which 24 positive colonies were amplified using the universal vector primers M13F and M13R in 50 µL. The cycling conditions for the latter primers were 94°C for 9 min, followed by 26 cycles of 92°C for 1 min, 55°C for 1 min and 72°C for 1.20 min, and a final cycle of 72°C for 7 min.

PCR products were checked and visualized on 1% agarose gels following standard procedures, before purification with ExoSap-IT (GE Healthcare) and sequenced with version 3.1 Big Dye terminator chemistry on an ABI3700 capillary sequencer (Applied Biosystems). The sequences were aligned using the software BioEdit including the multiple alignment function of CLUSTAL W (Hall, 1999). Species-specific primers were designed for *A. vulgaris*, *A. ater* and *A. rufus* (Table 2) using the software PRIMER 3. The three primers for COI have been used previously to study predation by carabid beetles (Hatteland et al., 2011, 2013b).

Two diagnostic PCR multiplexes including the species-specific primers for COI and ITS were used to screen all slug specimens. Amplifications for COI were conducted in 12.5 µL volumes, containing 6.25 µL GoTaq or Qiagen Multiplex PCR Mastermix (dNTPs, HotStarTaq DNA polymerase, 6 mM $MgCl_2$ PCR buffer), 0.25 µL of each primer (10 µM), 0.125 µL BSA (10 mg/ml), 1.0 µL DNA and 3.875 µL dH_2O.

Amplifications for ITS were also carried out in 12.5 µL volumes, containing 6.25 µL GoTaq or Qiagen Multiplex PCR Mastermix, but using 0.5 µL of each primer (10 µM), 2.0 µL DNA (1:9 diluted) and 3.25 µL dH_2O. Cycling conditions for the COI multiplex were 94°C for 2 min, followed by 30 cycles of 92°C for 30 sec, 51°C for 1 min and 70°C for 50 sec, and a final cycle of 68°C for 5 min. The ITS multiplex was used with cycling conditions of 94°C for 2 min, followed by 35 cycles of 92°C for 30 sec, 50°C for 1 min and 72°C for 1 min, and a final cycle of 72°C for 5 min. PCR products were diluted 75:1 and analysed for absolute amplicon sizes using 7.925 µL Hi-Di formamide and 0.075 µL GeneScan™500 Liz size standard (both Applied Biosystems) and then separated using a 48-capillary 3730 DNA Analyzer (Applied Biosystems). The software Genemapper version 4.0 (Applied Biosystems) was used to score electropherograms.

Phylogenetic analyses were performed with maximum parsimony and Bayesian methods using PAUP* version 4.0b10 (Swofford, 1998) and MrBayes version 3.1.2 (Huelsenbeck & Ronquist, 2001; Ronquist & Huelsenbeck, 2003), respectively. Analyses were carried out on a sub-set of selected nucleotide sequences covering all dissimilar haplotypes from the nine species in combination with sequences deposited in the NCBI GenBank database. The best fit model for the data was evaluated using the Akaike information criterion (AIC) implemented in MrModeltest version 2.2 (Nylander, 2004). A GTR + I + G model was selected with flat prior probabilites of nucleotides, invgamma distribution and nucleotide substitutions allowed to vary. Bayesian analysis was run using this model for 1 million generations. A consensus tree was obtained based on the Bayesian analysis with a burn in of 2000. Stationarity was determined based on a constant mean and variance. A consensus tree was also obtained with the parsimony criterion by using a heuristic search adding the sequences randomly and using the tree-bisection-reconnection (TBR) branch-swapping algorithm. Bootstrapping (Felsenstein, 1985) with 500 replicates was used to obtain confidence of nodes.

RESULTS

A total of 26 *A. ater* and 28 *A. vulgaris* specimens were dissected and scored for morphometric data (including ligula), weight, coloration, nDNA and mtDNA (Appendix 1 & 2). In addition, 20 *A. vulgaris*, 13 *A. ater*, 15 *A. rufus*, 1 *A. flagellus*, 2 *A. lusitanicus*, 2 *A. nobrei*, 2 *A. fuscus*, 1 *A. silvaticus*, 1 *A. circum-*

TABLE 2. Primers (5'-3') designed from the COI sequence of the mtDNA (top five primers) and ITS sequence of nrDNA (bottom two primers) to detect *Arion vulgaris*, *A. ater* and *A. rufus*, including size of amplified fragment.

Species	Primer name	Primer sequence	Fragment size (bp)
A. vulgaris	A.I.-Co1-F1	GCCCCCATCTTTACTTTTACTTATTTGCTCC GTATGGTAATAGCCCCGCCAATACG	310
A. vulgaris	A.I.-Co1-R2	FAM-CACCACTGAGAGGAGCC GCTCCAGCCAATACAGGTAAAG	
A. ater	A.a.-Co1-F-new	MTTACTTATCGGTGCGC GCTCCAGCCAATACAGGTAAAG	225
A. rufus	A.r.-Co1-F1	GCCCCCATCTTTACTTTTACTTATTTGCTCC GTATGGTAATAGCCCCGCCAATACG	362
A. ater and *A. rufus*	A.a.-Co1-R1	FAM-CACCACTGAGAGGAGCC GCTCCAGCCAATACAGGTAAAG	
A. rufus,	A. rufus-F	AGGATCATTATCGGTCTCG	547
A. ater and			537
A. vulgaris			544
A. ater, *ater* and *A. vulgaris*	A. ater-R	PET-GGGCAGGAAGAGAAGAACAA	

scriptus as well as 10 possible hybrids between *A. ater* and *A. vulgaris* were included in the genetic analyses. These latter specimens were determined as hybrids based on a large and highly variable ligula in the upper atrium which deviated from *A. ater* in both size and shape.

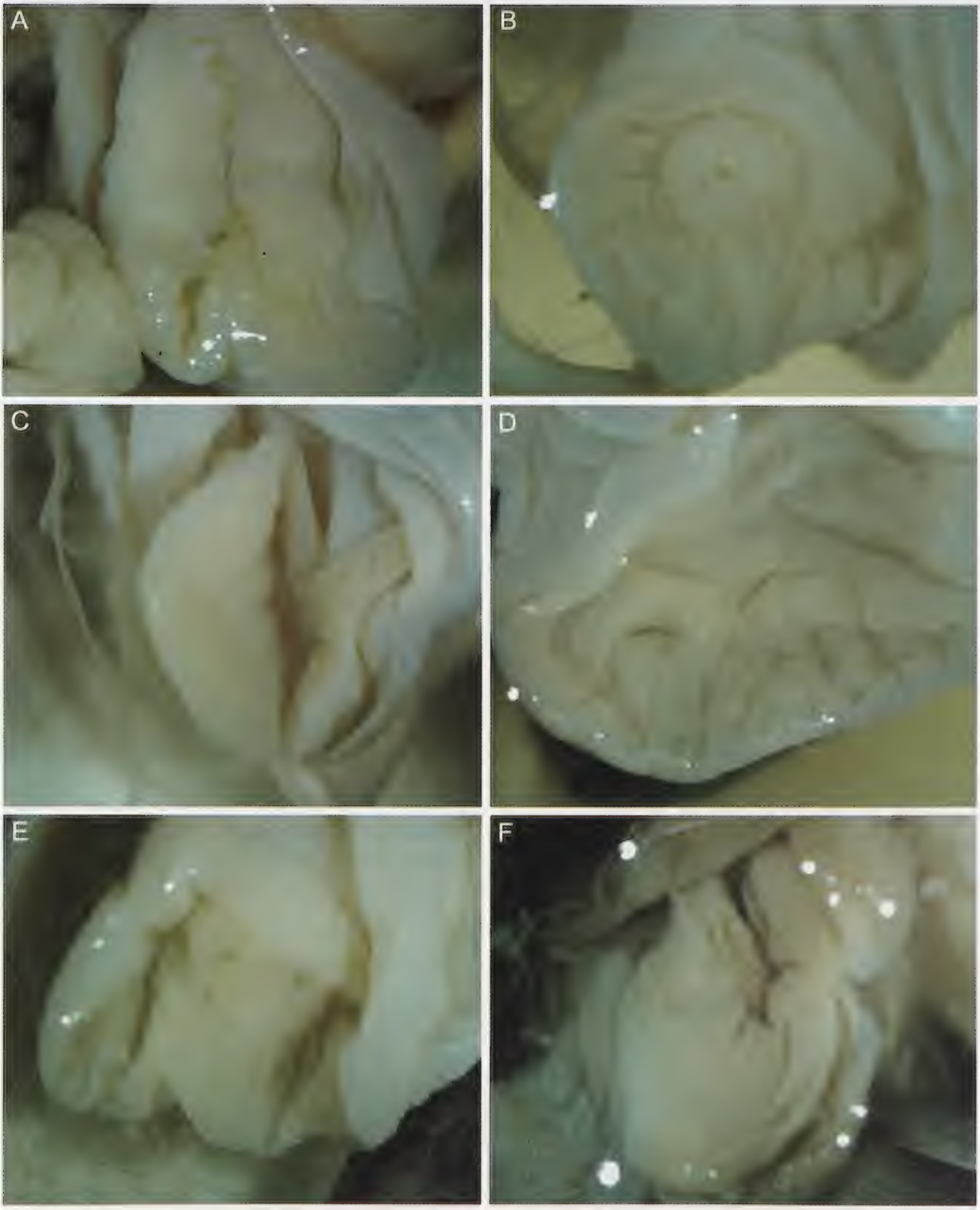

FIG. 2. Ligula types found in *Arion ater* in Norway. A: Typical ligula of *Arion ater*; B–F: Variation in ligula of *A. ater* possibly introgressed with *A. rufus*. Specimens A, B, C, D, E and F corresponds with the specimen codes 10Ø, 22S, 23S, 80S, 77S and 96S in Appendix 1, respectively. Pictures taken using an Olympus DP10 camera connected to a stereomicroscope with 4.8 times magnification.

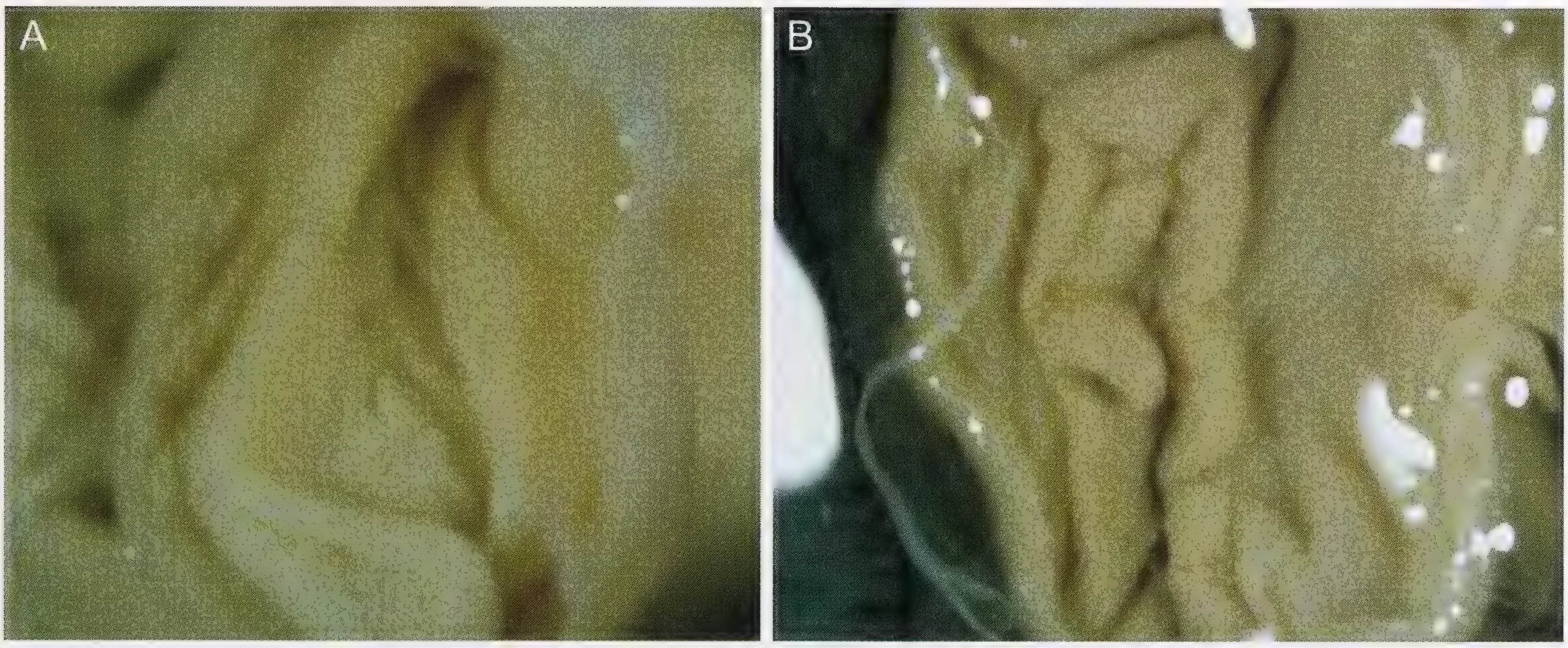

FIG. 3. Ligula types of *Arion vulgaris* in western Norway. A: Typical type (correspond to 67S in Appendix 2); B: Non-typical ligula of *A. vulgaris* (correspond to 12F in Appendix 2). Pictures taken using an Olympus DP10 camera connected to a stereomicroscope with 4.8 times magnification.

It also differed from *A. rufus* having a ligula with several folds and not forming the fleshy collar typical of *A. rufus*. All of these assumed hybrids were sampled in mixed populations of *A. vulgaris* and *A. ater*. Specimens representing different haplotypes based on COI sequences (Table 1) were submitted to GenBank (accession numbers JF950511-JF950535).

Coloration of *A. ater* and *A. vulgaris* was similar in some specimens, confirming earlier studies (Quick, 1960), and making it impossible to assign dark brown specimens to a taxon solely on coloration. Even almost black specimens of *A. vulgaris* were found (2 out of 28 of the specimens scored for morphometrics), leaving only red to brown varieties as reliable markers of identity.

TABLE 3. Principal Component (PCA) and Canonical Discriminant Analysis (CDA) components of morphometrics of the distal genitalia of *Arion vulgaris* and *A. ater*.

Analysis	Axis	Eigen-value	Per-cent	Cum Percent	Canonical Corr
PCA	PC1	5.5153	68.239	68.239	-
	PC2	1.8396	22.761	91.000	-
	PC3	0.3832	4.742	95.742	-
CDA–A	CD1	3.5768	95.376	95.376	0.8840
	CD2	0.1734	4.624	100.000	0.3844
CDA–B	CD1	11.6820	96.437	96.437	0.9598
	CD2	0.2746	2.267	98.704	0.4641

The morphology of the genitalia (including ligula) proved to be distinctive in both *A. vulgaris* and *A. ater* (Figs. 1–3), confirmed through morphometric analyses (Figs. 4, 5). The ligula gave the free oviduct of the former a bulky appearance, but is situated in the upper atrium of *A. ater*, where the epiphallus and bursa copulatrix insert (Fig. 1). Moreover, the ligula of *A. vulgaris* was considerably larger than that of *A. ater*. All *A. vulgaris* specimens in this study were identified as *A. vulgaris* according to the shape of the ligula (Fig. 3A), except for a peculiar ligula in one specimen (Fig. 3B). The ligula of *A. vulgaris* is similar to *A. rufus,* being C-shaped and asymmetrical (Noble, 1992), although the C-shape is less pronounced and both ridges are much longer and thinner than in *A. rufus*. The ligulae of *A. lusitanicus* taxa (including Mabille, 1868) are quite distinct, being much more symmetrical (Noble, 1992).

The ligula of *A. ater* is symmetrical and poorly ornamented, forming a “bowl”, rather than an asymmetrical “C” as found in *A. rufus* (see Noble, 1992). However, approximately 50% of the *A. ater* specimens deviated from this characteristic shape, possibly indicating introgression with *A. rufus*. Possible introgressed specimens were evident in all except the Molde population. A total of six different variants were found, each strikingly different with a consistent ligula shape as also found by Noble (1992) (Fig. 2).

The first two principal components (PCs) (describing 91% of the total variance) clearly

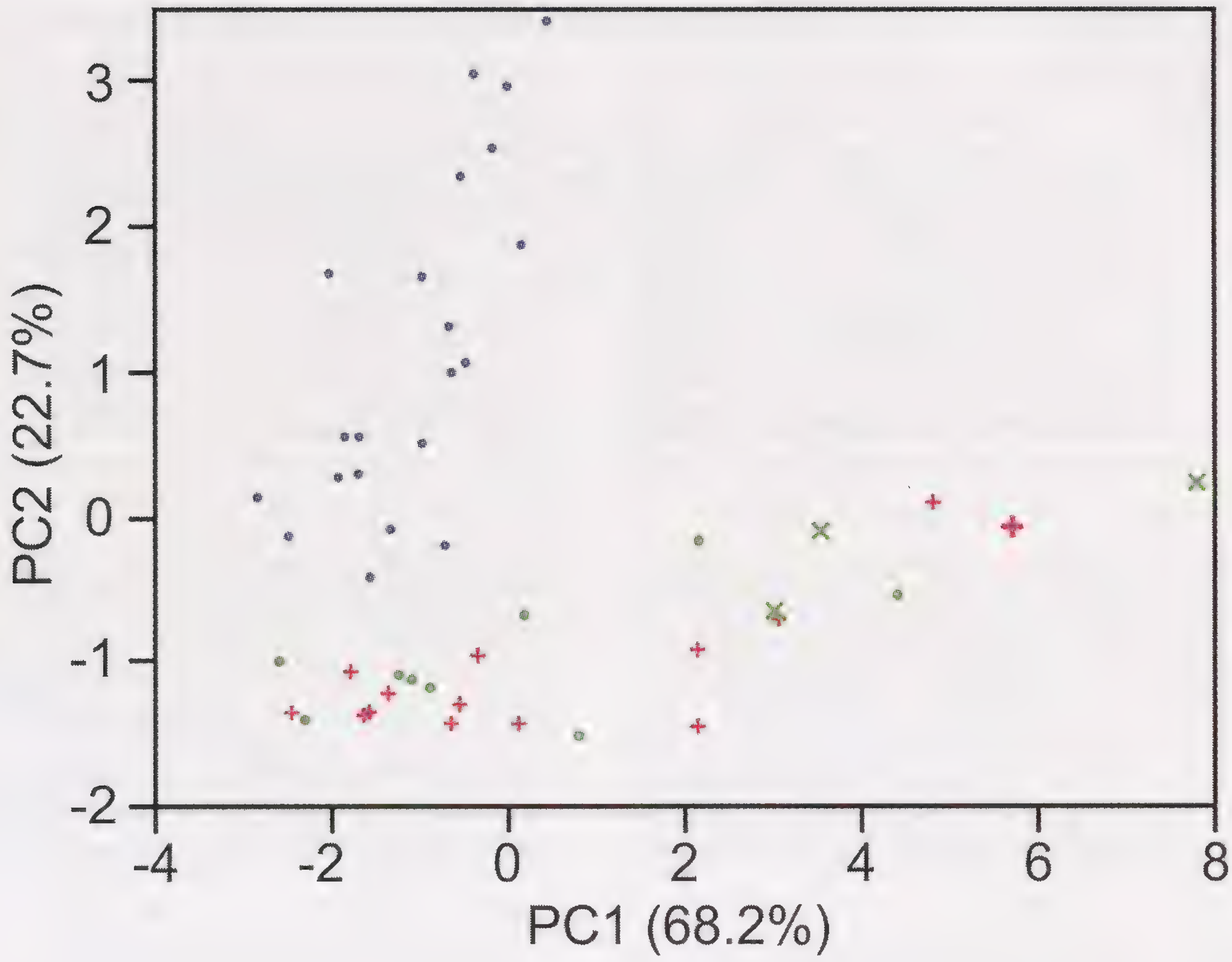

FIG. 4. Principal Component Analysis (PCA) ordination plot of morphometrics of the distal genitalia of *Arion vulgaris* and *A. ater*; blue dots – *A. vulgaris*; green dots – *A. ater* (with *A. ater* ligula & *A. ater* DNA); green crosses – *A. ater* with *A. rufus* DNA but *A. ater* ligula; red crosses – *A. ater* - *A. rufus* hybrids as defined by ligula. First two axes represent 91% of total variance (PC1 = 68%; PC2 = 23%).

separated *A. vulgaris* from *A. ater* based on the morphometrics (Table 3, Fig. 4). Eigenvalues of the first principal component (68% of the total variance) suggest it may be interpreted primarily as a vector describing lengths of the vas deferens, epiphallus and free oviduct (Table 4), with the lengths of the upper atrium and ligula showing lower but still positive loadings. The second principal component (nearly 23% of the total variance) showed a strong positive loading for lengths of the bursa copulatrix and epiphallus (Table 3), with lower but negative loadings for lengths of the vas deferens, free oviduct and upper atrium. *Arion vulgaris* was clearly differentiated from *A. ater* by the second PC, suggesting this species has a relatively longer epiphallus and bursa copulatrix, but shorter vas deference, free oviduct and upper atrium; confirming morphological observations (Noble, 1992). Two clusters are apparent on the first PC, each a mix of *A. ater* and possible *A. ater-A. rufus* hybrids. However, those individuals with a relatively higher PC1 score are predominately from Klepp, a locality where introgression seem still apparent. Two specimens from Sletten have a possible *A. ater-A. rufus* hybrid ligula, but *A. vulgaris* mtDNA as well as PC2 score consistent with *A. vulgaris*.

Stepwise analysis suggested four significant discriminant characters separate *A. ater* and *A. vulgaris* (Table 5). These four characters (lengths of the epiphallus, bursa copulatrix, vas deferens, and upper atrium) were used in a canonical discriminant analysis to produce a strong discriminatory model which was 87.5%

TABLE 4. Eigenvectors of genitalia characters in the Principal Component Analysis (PCA) of morphometrics of the distal genitalia of *Arion vulgaris* and *A. ater*.

Genitalia characters	PC1	PC2	PC3
Epiphallus length	0.50408	0.25999	-0.75021
Vas deferens length	0.52993	-0.26874	0.44116
Free oviduct length	0.49839	-0.17338	0.15417
Ligula length	0.23898	0.04436	0.08206
Upper atrium length	0.28275	-0.17965	0.11220
Upper atrium width	0.16283	0.07457	-0.12417
Bursa copulatrix duct length	0.19671	0.10047	-0.07286
Bursa copulatrix length	0.12007	0.88330	0.42277

TABLE 5. The four significant genitalia characters from the Stepwise analysis.

Genitalia characters	Estimate	nDF	Wald/Score ChiSq	"Sig Prob"
Epiphallus length	-1.18006	1	3.03014	0.0817
Vas deferens length	1.74887	1	7.35874	0.0067
Upper atrium length	2.86354	1	3.85600	0.0496
Bursa copulatrix length	-2.33026	1	4.64053	0.0312

accurate (Wilk's test $p < 0.001$). Morphological observation suggests that the longer upper atrium of the *A. ater-A. rufus* complex is not an unexpected discriminatory character, but the greater length of the bursa copulatrix in *A. vulgaris* has not been noted before. Whilst *A. vulgaris* is clearly differentiated there was no unambiguous clustering of *A. ater* or the various assumed *A. ater* x *A. rufus* hybrid morphologies; *A. ater* specimens are situated at one end of the spectrum, while the assumed hybrids are much more dispersed (Fig. 5).

A 413-bp sequence of the COI gene (mtDNA) was obtained for 29 specimens representing 9

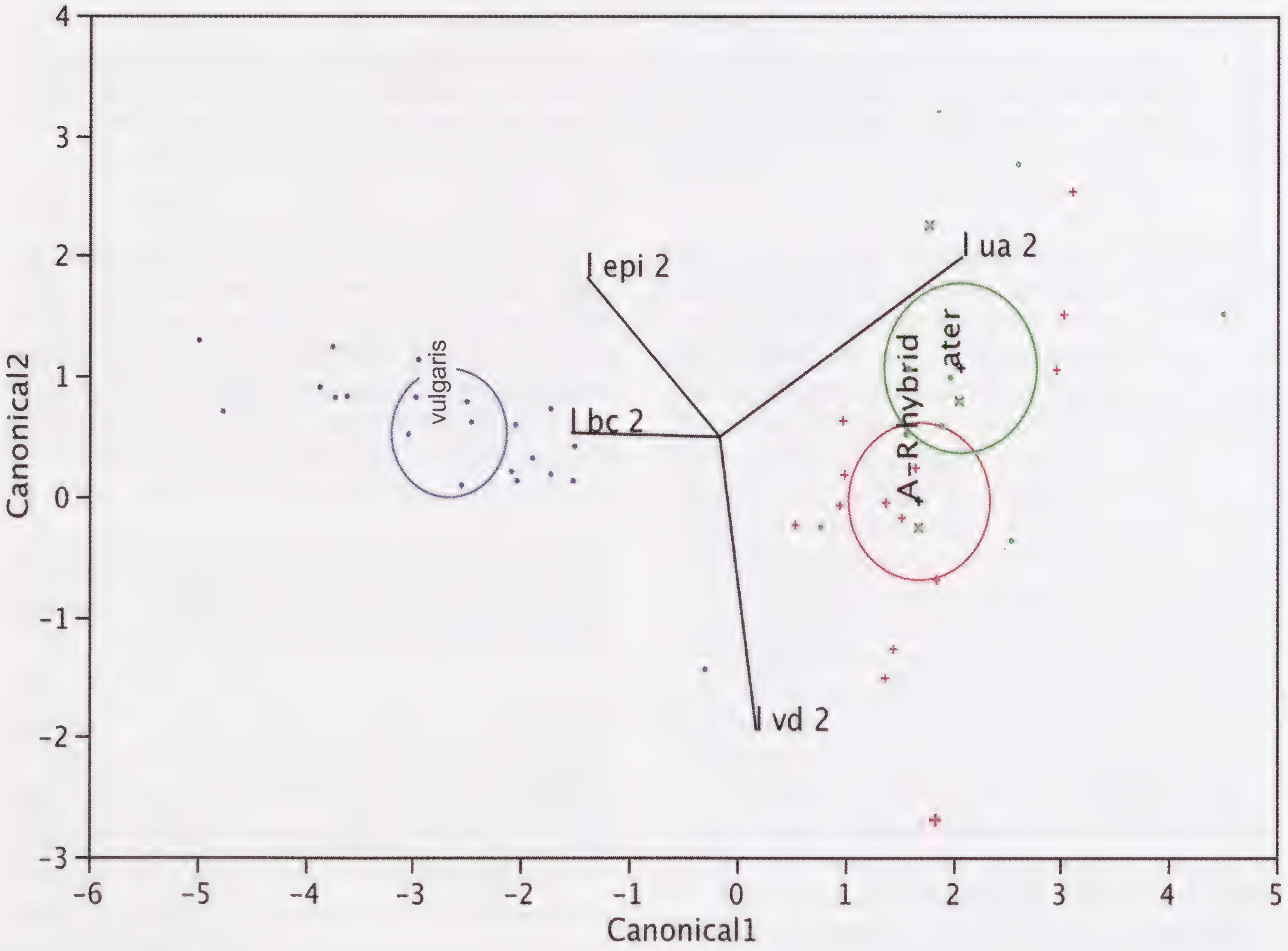

FIG. 5. Canonical Discriminant Analysis (CDA) ordination plot of morphometrics of the distal genitalia of *Arion ater*, *A. ater* x *A. rufus* and *A. vulgaris*. Circles represent 50% contours, i.e. the area in which 50% of the data lies. First two axes represent 100% of variance, producing a discriminatory model which is 87.5%; l epi 2 = length of epiphallus, l bc 2 = length of bursa copulatrix, l ua 2 = length of upper atrium, l vd 2 = length of vas deferens. Hybrids are defined according to morphological and genetic characters.

Arion species; *A. vulgaris*, *A, ater*, *A. rufus*, *A. flagellus*, *A. lusitanicus*, *A. nobrei*, *A. fuscus* and the outgroup species *A. silvaticus* and *A. circumscriptus*. The transition/transversion ratio was 2.31 while an overall bias in the nucleotide frequencies existed towards T, and mean frequencies (A = 0.28, C = 0.16, G = 0.16, T = 0.40) showed homogeneity among taxa (χ^2 = 19.51, df = 84, P = 1.00). The observed sequence divergence ranged from 10.5–13.8% between *A. ater*, *A. vulgaris* and *A. rufus*, whereas variation within species was low (0–1.3%) when restricting comparisons within Scandinavia and central Europe (Germany, Poland and Austria). Previous studies in Poland have shown slightly larger intraspecific variation in what was reported as invasive *A. lusitanicus* (Soroka & Kaluski, 2011). Interestingly, the single *A. vulgaris* specimen sampled in Austria was identical to two of the *A. vulgaris* specimens sampled in Norway, while the Pyrenean *A. vulgaris* (also regarded as *A. lusitanicus* A and B (Noble, 1992)) diverged from Norwegian *A. vulgaris* in the range of 1.2–3.4%. Furthermore, the Iberian taxa (*A. lusitanicus* and *A. nobrei*) diverged from the widespread taxa (*A. vulgaris*, *A. ater* and *A. rufus*) in the range of 16.9–18.6%, while *A. flagellus* diverged similarly from the widespread species (16.2–18.9%) and slightly less from the Iberian taxa (15.5–15.7%). *Arion ater* showed identical COI-sequences comparing Norwegian and Swedish specimens, while *A. ater* sampled in Wales diverged greatly (11.3%) from the Scandinavian specimens. *Arion rufus* showed also high variability when compared with specimens from the UK as well as Pyrenean specimens (0–8.7%).

The suggested introgression between *A. ater* and *A. rufus* was confirmed by the COI and ITS multiplexes, showing species-specific COI and ITS profiles of *A. rufus* respectively in 27% and 23% of the specimens, determined as *A. ater* and *A. ater* x *A. rufus* hybrids based on morphology (Appendix 1). Most of these specimens were sampled from the southwest of Norway (Klepp and Hå populations), but also some from a site in Bergen. No diagnostic pattern was found for potential hybrids, neither for coloration nor ligula shape, although there was a tendency for unusual ligula variants to be coupled with molecular markers suggesting introgression (Appendix 1). Furthermore, *A. vulgaris* COI-sequences were amplified in two specimens with *A. ater* morphology sampled from the same site; Sletten (Bergen), of which one specimen also showed ITS-sequences of *A. vulgaris*. We also amplified ITS-sequences of *A. vulgaris* in one additional specimen identified as *A. ater* as well as ITS-sequences of *A. ater*. Both of these specimens had a ligula anatomy suggesting introgression from *A. rufus* as well as ITS-sequences of *A. rufus*, their coloration was black. All the *A. vulgaris* individuals showed concordance of mtDNA and morphology (Appendix 2). The same concordance was also found between nDNA and morphology in *A. vulgaris*, except for one specimen with an *A. ater* ITS sequence, one with both *A. vulgaris* and *A. ater* ITS profiles and one specimen with *A. vulgaris* and *A. rufus* ITS profiles.

Phylogenetic analyses of the COI-sequences, using the parsimony criterion supported the morphological results, indicating *A. ater* and *A. rufus* grouped together more closely than with *A. vulgaris* (Fig. 6). This finding as well as most of the other topologies was supported by high bootstrapping values. However, the Bayesian analysis suggested that *A. ater* is more closely related to *A. vulgaris*, although this showed a low node support (Fig. 7). In general, the consensus tree based on the Bayesian analysis had low support in all the basal topologies. However, the Iberian taxa, *A. lusitanicus* and *A. nobrei*, was separated from the widespread species *A. vulgaris* (or non-topotype *A. lusitanicus*), *A. ater* and *A. rufus* in both phylogenies. The mtDNA data of the widespread species did not support the morphological identifications for all specimens, which is probably due to introgression. The suggested hybrids between *A. vulgaris* and *A. ater* varied in mtDNA haplotype, most possessing *A. vulgaris* sequences, although some had *A. rufus* haplotypes (Figs. 6, 7).

DISCUSSION

Our results confirm and emphasise differences between *Arion vulgaris* and the *A. ater* aggregate morphologically, although the mitochondrial and nuclear data suggest some introgression between *A. vulgaris* and *A. ater*. Differences between taxa and the existence of hybrids are strongly supported by morphometric data (Figs. 4, 5) and illustrated by the position and form of the ligula (Figs. 1–3). Mitochondrial DNA-sequences show a closer relationship among *A. vulgaris*, *A. ater* and *A. rufus* compared to Iberian taxa such as the topotype *A. lusitanicus* (Figs. 6, 7).

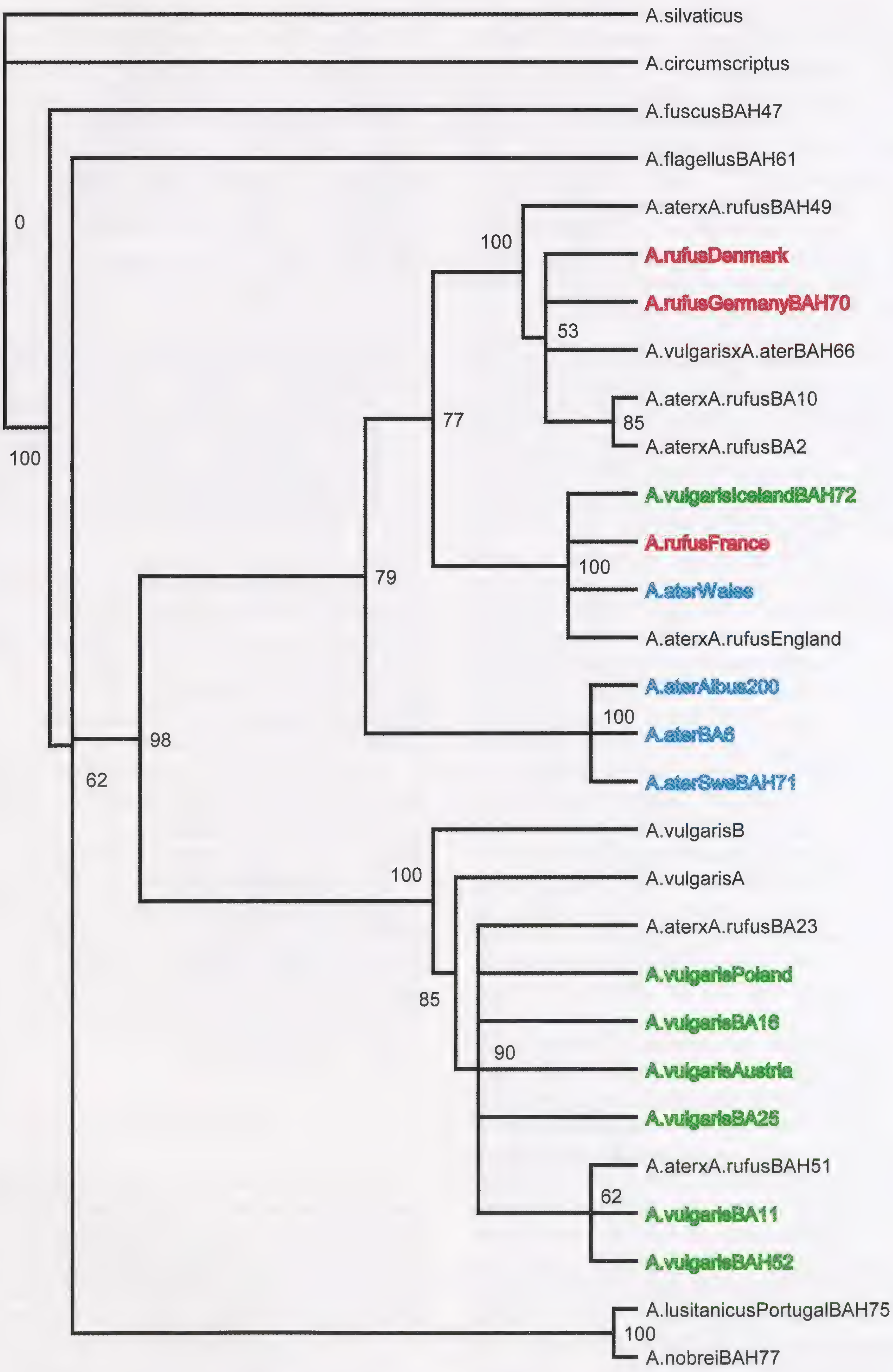

FIG. 6. Phylogenetic consensus tree of COI-sequences of large *Arion* species in Europe using the parsimony criterion, with 500 bootstrapping replicates for node support. Tree length = 357, Consistency index (CI) = 0.6583, Homoplasy index (HI) = 0.3417, Retention index (RI) = 0.8544. Rescaled consistency index (RC) = 0.5624. Species and hybrid names are given based on genital morphology including ligula; green = *A. vulgaris*, blue = *A. ater*, red = *A. rufus*.

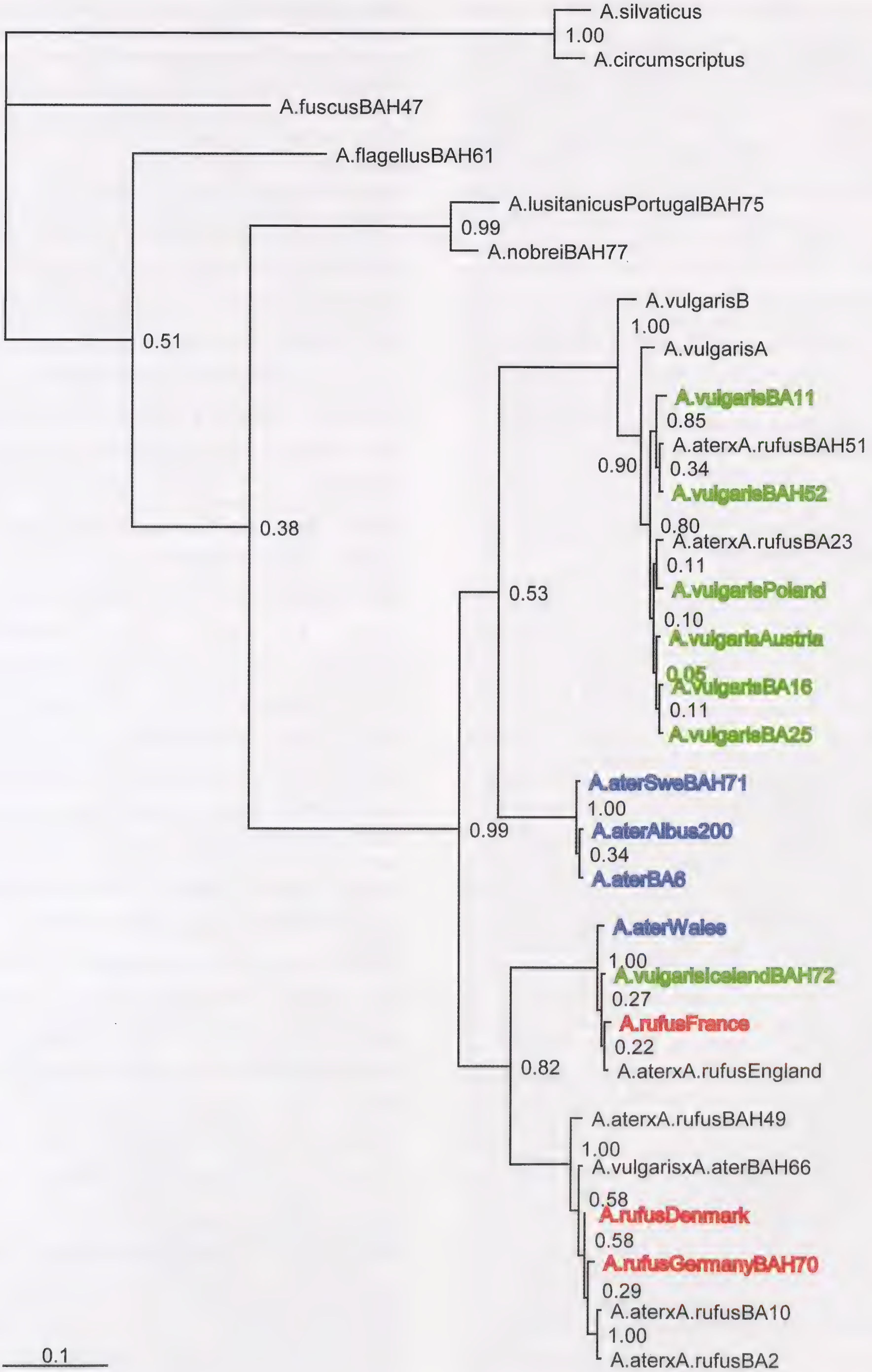

FIG. 7. Phylogenetic consensus tree of COI-sequences of large *Arion* species in Europe using a Bayesian analysis with a GTR + I + G model. Species and hybrid names are given based on genital morphology including ligula; green = *A. vulgaris*, blue = *A. ater*, red = *A. rufus*.

The colour variation in *A. vulgaris* is remarkable; red, brown, dark brown to almost black, clearly overlapping with *A. ater*. However, the brown morph of *A. vulgaris* was the most abundant. Coloration seems to be only partially associated with genital morphology in these large arionids, confirming the previously described uncertainty of identifying these species based on coloration alone (Cain & Williamson, 1958; Evans, 1986). However, coloration of juveniles makes them easier to differentiate (Quinteiro et al., 2005). Juvenile *A. ater* and *A. rufus* lack or have only faint lateral stripes which disappear when black and orange pigments develop (Brohmer et al., 1956; Kerney et al., 1979; Økland, 1922), while the distinct lateral bands of *A. vulgaris* are retained longer, sometimes until maturity (Dolmen & Winge, 1997; von Proschwitz, 1989; von Proschwitz & Winge, 1994). Interestingly, the topotype *A. lusitanicus* always retains these lateral bands to maturity (pers. obs.).

The variability of ligula morphology in *Arion ater* indicates introgression with *A. rufus*. The distinctive and invariable form of the *A. ater* ligula, as Noble described (1992), provides a reliable character to readily distinguish between *A. ater* and potential hybrids. We found the same variation in ligula as outlined by Noble (1992), with the addition of two quite distinct ligula forms (Fig. 2B and 2E), indicative of introgression with *A. rufus*. The same clear distinction was not found in the morphometric analyses (Figs. 4, 5) confirming previous studies using morphometrics (Evans, 1986). *Arion ater* were mainly black (the colour variety var. *atra*), although very dark brown specimens (var. *castanea* – characteristic of *A. ater* x *A. rufus* hybrids) were also found. The var. *atra* colour variety is the commonest in northern Europe including Norway (Økland, 1922), and indicates a lack of introgression, except where var. *castanea* is also recorded, such as in the vicinity of Bergen in the 19th Century (Friele, 1853), where *A. rufus* was introduced. Here are no further records of *A. rufus* in Norway after 1890 (Økland, 1922), until the recent introduction recorded in 2008 in Selbu, central Norway (von Proschwitz & Andersen, 2010). It is therefore likely that *A. rufus* has introgressed with *A. ater* in Norway since the early nineteenth century, leaving a residual mitochondrial signal which has spread to many populations. However, an equally likely explanation is that hybrids between *A. ater* and *A. rufus* have been introduced to Norway, since a wide hybrid zone between these two species has been found in Denmark and northern Germany (Noble & Jones, 1996). A recent introgression of *A. ater*, or *A. ater*-like hybrids, is supported by the finding that most of the individuals from southwest Norway (Klepp and Hå populations) displayed various combinations of ligula morphology, nDNA and mtDNA. If, as suspected (Noble & Jones, 1996), the success of such hybrids is a consequence of heterotic effects then the Klepp population may represent a recent introduction, or an area of extensive introgression. Such hybrid swarms are also common in the British Isles, where pure *A. ater* populations have an increasingly restricted distribution (Noble & Jones, 1996). In such cases of continuing introgression, the genetic signature of less fecund taxa is assimilated (Selander & Hudson, 1976), leaving a residual mtDNA signal, or less common alleles from nuclear markers; these latter are eventually lost from the population by selection or drift. Alternatively, where introgression has been episodic, the result of multiple introductions of limited numbers of individuals, their greater fecundity may cause their genetic signature, in particular their mtDNA, to persist on the genetic background of the endemic taxon. As predicted we found many *A. ater*-like slugs with *A. rufus* mtDNA. A recent study by Rowson et al. (2014) found similar disagreements in taxonomic characters suggesting introgression between large arionids in the British Isles. Studies involving more nuclear markers (e.g. microsatellites) may further elucidate these issues.

Arion vulgaris shows much less variation in ligula morphology, conforming to the "Scandinavian taxon" proposed by Campbell (2000). Furthermore, in terms of mtDNA this taxon was genetically quite different from the Iberian taxa; *A. lusitanicus*, *A. nobrei*, and *A. flagellus*. This distinction was also evident from RAPD markers (Noble & Jones, 1996). In fact, Quinteiro et al. (2005) established that the non-topotype *A. lusitanicus* (*A. vulgaris*) outside the "Atlantic *clade*" (of *A. lusitanicus* (Mabille) and *A. flagellus*) is more related to *A. ater* and *A. rufus* than to the rest of the *A. lusitanicus* aggregate. These findings were confirmed by our COI-sequences, which clustered *A. vulgaris* with *A. ater* and *A. rufus*. However, RAPD markers (Noble & Jones, 1996) suggested close affinities between Austrian *A. vulgaris* and taxa from the Pyrenees, which Noble (1992) described as *A. lusitanicus* forms A and B. Intriguingly COI-sequences also suggest hybrids between *A. vulgaris* and *A. ater*, findings in accordance with studies in Sweden, suggesting hybrids based on genital morphology (von Proschwitz, 2009) and respiration rates (Hagnell et al., 2003). Hybridization between *A. vulgaris* and *A. ater* may be consistent since hybrids between *A. ater* and *A. rufus* obscure the distinctiveness of these taxa, and potential mates may have problems identifying conspecifics. Thus hybrids may be a conduit for gene flow between species which would not otherwise mate. However, ecological differences between the species may limit introgression to hybrid zones. In particular, *A. vulgaris* and *A. ater* differ in habitat preference, where the former is found mainly in highly disturbed areas while the latter is also common in various natural or semi-natural habitats (e.g., moorlands, forests). Hence, hybrids may be predicted to occupy anthropogenic habitats (e.g. gardens, parks), as seems to be the case in our study.

The present work shows the importance of integrating several methods to distinguish between species in this complex group of facultatively self-fertile slugs. Based on these methods we conclude that *A. vulgaris* is quite distinct from *A. lusitanicus*, being more closely related to the *A. ater* aggregate. Furthermore, introgression between *A. vulgaris* and the *A. ater* aggregate seems to occur, possibly maximizing the evolutionary potential and vigour of these similar genomes. However, the ability of many large arions to self-fertilize (Hagnell et al., 2006), producing founding colonies from a single progagule complicates the situation by adding more possibilities for relatedness between generations of arionids. The taxonomic status of these slugs will probably remain controversial.

ACKNOWLEDGEMENTS

We would like to thank Laverne Eagles, Solveig Haukeland and Stine Beate Balevik for assistance in collecting the material. We are also grateful to Geir Dahle for analysing absolute amplicon sizes. Thanks also to the University of Bergen and the Norwegian Research Council for funding the project (project numbers 800233 and 803194).

LITERATURE CITED

ANDERSON, R., 2005, An annotated list of the non-marine Mollusca of Britain and Ireland. *Journal of Conchology*, 38: 607–637.

BARKER, G. M., 2002, *Molluscs as crop pests*. CABI Publishing, Wallingford, U.K., 400 pp.

BROHMER, P., P. EHRMANN & G. ULMER, 1956, *Die Tierwelt Mitteleuropas, Band II: Mollusca*. Von Quelle, Leipzig, 264 pp.

BURNET, B., 1972, Enzyme protein polymorphism in the slug *Arion ater*. *Genetic Research*, 20: 161–173.

CAIN, A. J. & M. WILLIAMSON, 1958, Variation and specific limits in the *Arion ater* aggregate. *Proceedings of Malacological Society London*, 33: 72–86.

CAMPBELL, E. M., 2000, *Investigating the invasive nature of the large arionid slugs of Europe: a study of recent invasions of Arion lusitanicus Mabille in Scandinavia*. PhD thesis. Aberdeen University, Aberdeen, 46 pp.

CASTILLEJO, J., 1997, *Babosas del Noroeste Ibérico*. Universidade de Santiago de Compostela, Santiago de Compostela, Spain, 192 pp.

COLLINGE, W. E., 1893, On the occurrence of *Arion lusitanicus* Mab. in the British Isles, and descriptions of four new varieties. *Annals and Magazine of Natural History*, 12: 414–415.

DAVIES, S. M., 1987, *Arion flagellus* Collinge and *A. lusitanicus* Mabille in the British Isles: a morphological, biological and taxonomical investigation. *Journal of Conchology*, 32: 339–354.

DOLMEN, D. & K. WINGE, 1997, Boasneglen (*Limax maximus*) og iberiasneglen (*Arion lusitanicus*) i Norge; utbredelse, spredning og skadevirkninger. "*Limax maximus* and *Arion lusitanicus* in Norway: distribution, expansion and injurious effects." Report 4: 4–24. In: *Zoological Series*, Vitenskapsmuseet, Trondheim, Norway.

DREIJERS, E., H. REISE & J. M. C. HUTCHINSON, 2013, Mating of the slugs *Arion lusitanicus* auct. non Mabille and *A. rufus* (L.): Different genitalia and mating behaviours are incomplete barriers to interspecific sperm exchange. *Journal of Molluscan Studies*, 79: 51–63.

EVANS, N. J., 1986, An investigation of the status of the terrestrial slugs *Arion ater ater* (L.) and *Arion ater rufus* (L.) (Mollusca, Gastropoda, Pulmonata) in Britain. *Zoologica Scripta*, 15: 313–322.

FALKNER, G., R. A. BANK & T. von PROSCHWITZ, 2001, Check-list of the non-marine molluscan species-group taxa of the states of Northern, Atlantic and Central Europe (CLECOM Area I) and their distribution. *Heldia*, 4: 1–76.

FALKNER, G., T. E. J. RIPKEN & M. FALKNER, 2002, *Mollusques continentaux de France liste de reference annotée et bibliographie*. Museum d`Histoire Naturelle, *Patrimoines Naturels*, 52: 350 pp.

FELSENSTEIN, J., 1985, Confidence limits on phylogenies: an approach using the bootstrap. *Evolution*, 39: 783–791.

FOLMER, O., M. BLACK, W. HOEH, R. LUTZ & R. VRIJENHOEK, 1994, DNA primers for amplification of mitochondrial cytochrome *c* oxidase subunit I from diverse metazoan invertebrates. *Molecular Marine Biology and Biotechnology*, 3: 294–299.

FOLTZ, D. W., H. OCHMAN, J. S. JONES, S. M. EVANGELISTI & R. K. SELANDER, 1982, Genetic population structure and breeding systems in arionid slugs (Mollusca: Pulmonata). *Biological Journal of the Linnean Society*, 17: 225–241.

FOLTZ, D. W., H. OCHMAN & R. K. SELANDER, 1984, Genetic diversity and breeding systems in terrestrial slugs of the families Limacidae and Arionidae. *Malacologia*, 25: 593–605.

FRIELE, J., 1853, *Norske land- og ferskvandsmollusker, som findes i omegnen af Christiania og Bergen* [in Norwegian]. *"Norwegian terrestrial and limnic molluscs in the areas around Christiania and Bergen"*. Feilberg & Landmark. Christiania, Norway, vi + 65 pp.

FREUND, R. J., R. C. LITTELL & L. CREIGHTON, 2003, *Regression using JMP software. 1st ed.* SAS press, Cray, North Carolina, USA, 288 pp.

GRIMM, B., W. PAILL & H. KAISER, 2000, Daily activities of the pest slug *Arion lusitanicus*. *Journal of Molluscan Studies*, 66: 125–130.

HAGNELL, J., C. SCHANDER & T. von PROSCHWITZ, 2003, Hybridisation in arionids: the rise of a super slug? Pp. 221–226, in: G. Dussart, ed., *Slugs & snails: agricultural, veterinary & environmental perspectives*. British Council For Crop Protection Symposium Proceedings, 324 pp.

HAGNELL, J., T. von PROSCHWITZ & C. SCHANDER, 2006, Self-fertilising observed in the invasive Iberian slug *Arion lusitanicus* Mabille 1868. *Journal of Conchology*, 39: 107.

HALL, T. A., 1999, BIOEDIT: a user-friendly biological sequence alignment editor and analysis program for Windows 95/98/NT. *Nucleic Acids Symposium Series*, 41: 95–98.

HATTELAND, B. A., W. O. C. SYMONDSON, R. A. KING, M. SKAGE, C. SCHANDER & T. SOLHØY, 2011, Molecular analysis of predation by carabid beetles (Carabidae) on the invasive Iberian slug *Arion lusitanicus*. *Bulletin of Entomological Research*, 101: 675–686.

HATTELAND, B. A., S. ROTH, A. ANDERSEN, K. KAASA, B. STØA & T. SOLHØY, 2013a, Distribution and spread of the invasive slug *Arion vulgaris* Moquin-Tandon in Norway. *Fauna Norvegica*, 32: 13–26.

HATTELAND, B. A., S. HAUKELAND, S. ROTH, M. B. BRURBERG, I. VAUGHAN & W. O. C. SYMONDSON, 2013b, Spatiotemporal analysis of predation by carabid beetles (Carabidae) on nematode infected and uninfected slugs in the field. *PLoS ONE*, 8(12): eB2142. doi:10.1371/journal.pone.0082142.

HILLEBRAND, H. & B. MATTHIESSEN, 2009, Biodiversity in a complex world: consolidation and progress in functional biodiversity research. *Ecology Letters*, 12: 1405–1419.

HUELSENBECK, J. P. & F. RONQUIST, 2001, MRBAYES: Bayesian inference of phylogeny. *Bioinformatics*, 19: 1572–1574.

KERNEY, M. P., R. A. D. CAMERON & J. H. JUNGBLUTH, 1979, *Die Landschnecken Nord- und Mitteleuropas*. Paul Parey, Hamburg and Berlin, 384 pp.

KOZLOWSKI, J., 2007, The distribution, biology, population dynamics and harmfulness of *Arion lusitanicus* Mabille, 1868 (Gastropoda: Pulmonata: Arionidae) in Poland. *Journal of Plant Protection Research*, 47: 219–230.

LINNAEUS, C., 1758, *Systema naturae*, vol. 1. Stockholm, Salvii, 824 + iii pp.

MABILLE, M. J., 1868, Des limaciens européens. *Revue et Magasin du Zoologie Pure et Appliquee*, 20: 129–146.

MOQUIN-TANDON, A., 1855, *Histoire naturelle des mollusques terrestres et fluviatiles de France* (Atlas), Paris, 92 pp., 54 pls.

NOBLE, L. R., 1987, *The ecological genetics of reproduction in North-West European arionids*. PhD thesis. University of London, London.

NOBLE, L. R., 1992, Differentiation of large arionid slugs (Mollusca, Pulmonata) using ligula morphology. *Zoologica Scripta*, 21: 255–263.

NOBLE, L. R. & J. S. JONES, 1996, A molecular and ecological investigation of the large arionid slugs of North-West Europe: the potential for new pest species. Pp. 93–131, in: W. O. C. Symondson & J. E. Liddell, eds., *The ecology of agricultural pests: biochemical approaches*. Chapman & Hall, London.

NYLANDER, J. A. A., 2004, MrModeltest 2.2. Program distributed by the author. Evolutionary Centre, Uppsala University, Sweden.

ØKLAND, F., 1922, The Arionidae of Norway. *Videnskapsselskapets Skrifter Christiania*, 1922: 1–62.

POLLONERA, A., 1889, Nuove contribuzioni allo studio degli *Arion* europei. *Atti Reale Accademia della Scienze di Torino*, 24: 623–640.

PORT, G. R. & A. ESTER, 2002, Gastropods as pests in vegetable and ornamental crops in Western Europe. Pp. 301–314, in: G. M. Barker, ed., *Molluscs as crop pests*: CABI Publishing, Wallingford, U.K., 400 pp.

PORT, C. M. & G. R. PORT, 1986, The biology and behaviour of slugs in relation to crop damage and control. *Agricultural Zoology Reviews, Intercept, Newcastle-upon-Tyne*, 1: 255–299.

QUICK, H. E., 1947, *Arion ater* (L.) and *A. rufus* (L.) in Britain and their specific differences. *Journal of Conchology*, 22: 249–261.

QUICK, H. E., 1960, British slugs (Pulmonata: Testacellidae, Arionidae, Limacidae). *Bulletin of the British Museum (Natural History) Zoology*, 6: 103–226.

QUINTEIRO, J., J. RODRIGUEZ-CASTRO, J. CASTILLEJO, J. IGLESIAS-PIÑEIRO & M. REY-MÉNDEZ, 2005, Phylogeny of slug species of the genus *Arion*: evidence of monophyly of Iberian endemics and of the existence of relict species in Pyrenean refuges. *Journal of Zoological Systematics & Evolutionary Research*, 43: 139–148.

REISCHÜTZ, P. L., 1984a, Zum massenhaften Auftreten von *Arion lusitanicus* Mabille in den Jahren 1982 und 1983. *Mitteilungen aus dem Zoologischen Gesellschaft, Braunau*, 4: 253–254.

REISCHÜTZ, P. L., 1984b, Zur Schadwirking der „Kapuzinerschnecke“ *Arion lusitanicus* Mabille im Alpengebiet. *Heldia*, 1: 39.

RONQUIST, F. & J. P. HUELSENBECK, 2003, MRBAYES 3: Bayesian phylogenetic inference under mixed models. *Bioinformatics*, 20: 407–415.

SELANDER R. K. & R. O. HUDSON, 1976, Animal population structure under close inbreeding: the land snail *Rumina* in Southern France. *The American Naturalist*, 110: 695–718.

SOROKA, M. & T. KALUSKI, 2011, Genetic studies on the invasive slug *Arion lusitanicus* Mabille, 1868 (Gastropoda: Pulmonata) in Poland. *Folia Malacologica*, 19: 259–265.

ROTH, S., B. A. HATTELAND & T. SOLHØY, 2012, Some notes on reproductive biology and mating behaviour of *Arion vulgaris* Moquin-Tandon 1855 in Norway including a mating experiment with a hybrid of *Arion rufus* (Linnaeus 1758) x *A. ater* (Linnaeus 1758). *Journal of Conchology*, 41: 249–257.

ROWSON, B., R. ANDERSON, J. A. TURNER & W. O. C. SYMONDSON, 2014, The slugs of Britian and Ireland: undetected and undescribed species increase a well-studied, economically important fauna by more than 20%. *PLoSONE* 9 (3): e91907. doi: 10.1371/journal.pone.0091907.

SOUTH, A., 1992, *Terrestrial slugs – biology, ecology and control*. Chapman & Hall, London, 428 pp.

SWOFFORD, D. L., 1998, Paup*. Phylogenetic analysis using parsimony (*and other methods), version 4. Sunderland, M. A. Sinauer Associates.

VAN REGTEREN ALTENA, C. O., 1955, Notes sur les limaces. 3. Sur la présence en France d’ *Arion lusitanicus* Mabille. *Journal de Conchyliologie*, 95: 89–99.

VON PROSCHWITZ, T., 1989, *Arion lusitanicus* Mabille – en för Sverige ny snigelart. „*Arion lusitanicus* Mabille – a new slug species for Sweden“. *Göteborgs Naturhistoriska Museum Årstryck*, 1989: 43–53.

VON PROSCHWITZ, T., 1992, Den spanska skogsnigeln *Arion lusitanicus* Mabille - en art i snabb spridning med människan i Sverige. (with English summary: The Spanish slug *Arion lusitanicus* Mabille – an anthropochorous slug species spreading rapidly in Sweden). *Göteborgs Naturhistoriska Museum*, 1992: 35–42.

VON PROSCHWITZ, T., 1997, *Arion lusitanicus* Mabille and *A. rufus* (L.) in Sweden: a comparison of occurrence, spread and naturalization of two alien slug species. *Heldia*, 4: 137–138.

VON PROSCHWITZ, T., 2009, Faunistical news from the Natural History Muesum, Göteborg 2008 – snails, slugs and mussels – with some notes on the slug *Limacus flavus* (Linnaeus) – refound in Sweden, and *Balea heydeni* von Maltzan – a land snail species new to Sweden. *Göteborgs Naturhistoriska Museum Årstryck*, 2009: 47–68.

VON PROSCHWITZ, T. & A. ANDERSEN, 2010, Rødskogsnegl *Arion rufus* i Sverige og Norge (In Norwegian with English Summary). “Red slug *Arion rufus* in Sweden and Norway”. *Fauna*, 63: 2–7.

VON PROSCHWITZ, T. & K. WINGE, 1994, Iberiaskogsnegl – en art på spredning i Norge. “The Iberian slug – a species expanding in Norway.” *Fauna*, 47: 195–203.

Revised ms. accepted January 22, 2015

APPENDIX 1. Morphological and genetic data of *Arion ater*. All genitalia measurements are given in mm. Specimens denoted 1 and 2 for ligula means *ater* ligula and *ater-rufus* hybrid ligula, respectively. Specimens denoted 1–4 for colour means black, very dark brown, black with a white band above the foot fringe, and very dark brown with a white band above the foot fringe, respectively. Specimens denoted R, V and A in the lowest row means *A. rufus*, *A. vulgaris* and *A. ater*, respectively. Weight/biomass is fresh weight of each individual slug.

	Klepp								Ulset	Sletten								Øygarden				Bolsøya		Frekhaug		
	2K	3K	4K	5K	6K	7K	8K	9K	2U	22S	23S	24S	77S	79S	80S	96S	98S	9Ø	10Ø	59Ø	61Ø	6B	9B	14F	16F	17F
Length of ovotestis	6	6	9	6	6	7	7	5	7	10	7	8	10	6	8	6	10	7	7	7	6	5	5	6	5	7
Width of ovotestis	3	3	4	3	3	3	5	3	4	4	5	5	5	4	5	4	4	4	4	3	4	3	3	4	2	3
Length of epiphallus	12	12	15	15	15	14	13	13	20	16	18	16	18	15	17	13	16	23	17	12	19	19	21	19	19	18
Length of vas deferens	12	13	16	12	16	11	13	13	18	19	20	17	29	21	23	25	28	25	21	-	20	17	13	23	21	15
Length of free oviduct	12	10	11	13	11	10	13	11	14	14	16	11	15	11	17	15	20	24	15	14	12	10	11	12	16	12
Length of ligula	4	5	6	7	6	6	7	6	7	7	7	6	7	8	7	7	7	8	6	6	6	5	7	6	7	6
Length of upper atrium	7	8	8	6	6	7	7	7	10	9	9	9	8	10	10	9	9	9	8	10	10	11	12	9	9	9
Width of upper atrium	4	4	5	4	4	4	5	4	4	4	3	4	5	5	4	4	5	5	4	4	4	4	3	4	5	4
Length of lower atrium	7	8	7	8	7	7	9	7	9	9	9	9	15	9	9	8	7	8	10	6	9	8	8	8	9	9
Length of duct of bursa copulatrix	7	5	7	4	5	6	6	6	8	7	7	6	6	6	8	8	7	8	11	6	6	6	6	8	6	6
Length of bursa copulatrix	6	6	10	6	7	6	7	8	10	10	8	8	8	9	7	10	10	11	8	7	8	8	8	8	7	6
Length of albumen gland	23	24	44	21	26	31	27	24	28	29	27	31	32	27	33	32	28	37	42	30	33	40	35	37	28	28
Width of albumen gland	4	5	9	5	6	6	6	6	8	7	9	7	8	9	8	9	8	6	10	6	8	12	8	9	8	7
Weight/biomass	3	3	4	2	4	3	3	3	11	7	6	7	8	9	8	11	8	14	5	8	10	8	6	14	9	8
Ligula	2	1	1	1	1	2	2	1	2	2	2	1	2	2	1	2	2	2	1	1	2	1	1	1	2	1
Colour	3	3	4	4	4	3	3	3	1	1	1	1	1	1	1	2	1	1	1	1	1	1	1	1	1	1
Mitochondrial DNA *cox1*	R	A	A	R	R	R	R	R	-	V	A	-	A	V	-	R	-	-	A	A	A	A	A	A	R	A
Nuclear ribosomal DNA ITS	A	A	A+R	R	-	A+R	A	A	-	V+R	A+V	-	R	A+R	-	R	-	-	A	A	-	A	A	-	A	A

APPENDIX 2. Morphological and genetic data of *Arion vulgaris*. All genitalia measurements are given in mm. Specimens denoted 1 and 2 for ligula means normal form ligula and hybrid form ligula, respectively. Specimens denoted 1-4 for colour means red-brown, dark brown, very dark brown, and almost black, respectively. Specimens denoted R, V and A in the lowest row means *A. rufus*, *A. vulgaris* and *A. ater*, respectively. Weight/biomass is fresh weight of each individual slug.

	Haukedalen								Morvik					Frekhaug						Bolsøya					Sletten			
	6H	7H	8H	26H	28H	31H	33H	34H	9M	10M	11M	12M	13M	12F	15F	18F	111F	112F	121F	2B	3B	26B	36B	38B	67S	70S	90S	95S
Length of ovotestis	8	12	6	11	9	6	9	7	9	11	8	11	9	7	8	16	10	13	10	6	6	11	9	5	9	7	12	8
Width of ovotestis	6	6	4	5	5	4	4	4	7	6	5	7	8	4	5	6	5	6	6	4	3	4	2	3	6	4	6	5
Length of epiphallus	19	17	15	18	19	22	18	19	20	20	21	22	21	23	22	20	19	21	22	18	17	22	19	14	23	15	21	19
Length of vas deferens	32	30	22	25	23	23	22	23	31	31	25	27	31	28	23	22	20	25	24	18	15	17	15	14	30	-	27	24
Length of free oviduct	14	18	11	13	17	14	14	13	15	19	13	16	17	11	15	13	14	13		9	10	9	7	8	17	13	14	14
Length of ligula	9	13	8	11	12	10	11	11	10	11	10	11	11	10	11	11	11	12	10	10	9	9	8	7	11	10	12	10
Length of upper atrium	7	8	6	8	9	9	9	8	7	7	6	7	6	7	10	8	9	9	9	8	6	9	7	6	9	8	8	8
Width of upper atrium	4	4	3	5	5	5	5	5	4	4	4	4	3	3	6	6	4	6	5	5	4	4	5	4	6	4	5	5
Length of lower atrium	-	-	-	-	-	-	-	-	-	-	-	-	-	-	-	-	-	-	-	-	-	-	-	-	-	-	-	-
Length duct burs cop.	6	8	9	5	7	5	6	6	7	6	6	6	8	6	9	5	5	6	5	6	5	7	5	5	6	-	6	6
Length of bursa cop.	8	10	7	11	11	7	9	10	11	9	10	11	9	11	11	10	9	13	10	12	8	13	7	8	11	-	12	10
Length albumen gland	21	14	20	24	29	36	31	32	19	17	21	23	11	33	38	32	26	48	37	38	24	33	26	26	40	18	24	23
Width albumen gland	7	8	8	7	8	8	8	8	4	6	10	11	4	10	15	11	8	13	10	12	8	7	6	6	11	8	10	5
Weight	12	10	8	6	8	8	5	6	9	13	7	12	8	10	13	16	12	14	16	8	5	6	4	3	16	5	11	7
Ligula	1	1	1	1	1	1	1	1	1	1	1	1	1	2	1	1	1	1	1	1	1	1	1	1	1	1	1	1
Colour	1	1	1	1	3	1	2	4	1	2	1	1	1	2	2	2	1	1	1	3	4	1	2	1	1	1	1	1
MtDNA *cox1*	V	V	V	V	-	V	V	V	V	V	V	V	V	V	V	V	V	V	V	V	V	V	V	V	V	V	V	V
NrDNA ITS	V	-	V	V	V	V	V	V	V	V	V	V	V	-	V	-	A+V	V	V	A	V	V	V	V	V	V	V+R	V

MALACOLOGIA, 2015, 58(1–2): 323–336

MORPHOLOGICAL DEVELOPMENT OF THE RADULA OF FOUR SPECIES OF THE NEOGASTROPOD FAMILY MURICIDAE

Gregory S. Herbert[1]*, María José Pio[2], Guido Pastorino[2], M. G. Harasewych[3],
Yuri I. Kantor[4], Dominique Lamy[5] & Jean-Pierre Pointier[6]

ABSTRACT

Radular ontogenies of four species of the neogastropod family Muricidae are described through comparisons of early post-metamorphic and adult developmental stages, with specific focus on the rachidian (central) tooth. The degree of rachidian transformation during ontogeny varies from minor shape change to addition or loss of structural features important for assigning taxa to subfamilies. Changes include: flattening of the rachidian base and a switch from a short, beak-like to a long, flattened central cusp in the rapanine *Stramonita biserialis*; a switch from variable, asymmetric to regular, symmetric expression of inner lateral denticles in the basal muricid *Timbellus phyllopterus*; curvature of the rachidian base at the margins and separation of the pointed base endpoint from the radular membrane to form a marginal cusp in the muricine *Chicoreus dilectus*; and moderate straightening of the rachidian base in the ocenebrine *Vokesinotus perrugatus*. From these observations and previous work, we propose a plesiomorphic developmental sequence for the Muricidae and provide supporting evidence for the developmental origins of novel features of the muricid radula.

Key words: Muricidae, radula, teeth, development, ontogeny.

INTRODUCTION

The gastropod radula is often modified during development, particularly in the number, shape, and size of teeth, cusps, and denticles (e.g., polyplacophora: Minichev & Sirenko, 1975; pulmonates: Sterki, 1893; pulmonates: Kerth, 1979; trochoideans: Warén, 1990; conids: Nybakken, 1990; Nybakken & Perron, 1998; epitoniids: Page & Willan, 1988; atlantid heteropods: Richter, 1961; patellogastropods: Guralnick & Lindberg, 1999). In many of these examples, developmental modifications were found to mirror key evolutionary transitions between higher taxa, suggesting that evolutionary changes in developmental timing (i.e., heterochrony) may be an important mechanism for generating the kinds of morphological novelty studied by systematists.

Heterochronic mechanisms are thought to have been particularly important in the origins of several subfamily-level, radula morphotypes within the neogastropod family Muricidae (Fujioka 1984, 1985; DiSalvo, 1988; Di Salvo & Carriker, 1994; Herbert et al., 2007; Pastorino et al., 2007; Pastorino & Penchaszadeh, 2009; Pio et al., 2014). However, the early ontogenetic stages of the radula are still unknown for most of the nearly 2,000 species currently assigned to the Muricidae, and coverage is uneven at the level of muricid subfamilies. Prior work on muricid radulae has focused mainly on species of the Rapaninae, Ergalataxinae, and Trophoninae. In particular, there are no observations on radular development for any of the putative basal lineages of the family (e.g., *Timbellus* Gregorio, 1885; *Poirieria* Fischer, 1884; *Paziella* Jousseaume, 1880) recognized by

---

[1]School of Geosciences, University of South Florida, 4202 E. Fowler Ave., Tampa, Florida 33620, U.S.A.
[2]Museo Argentino de Ciencias Naturales, Av. Ángel Gallardo 470, 3er Piso, Lab. 57, C1405DJR Buenos Aires, Argentina.
[3]Department of Invertebrate Zoology, National Museum of Natural History, Smithsonian Institution, P.O. Box 37012, Washington, DC 20013-7012, U.S.A.
[4]A. N. Severtsov Institute of Ecology and Evolution of Russian Academy of Sciences, Leninski Prosp. 33, Moscow 119071, Russia.
[5]As Antilles Mollusques, 6 Lotissement Bel-Air, 97122 Baie-Mahault, GUADELOUPE, French West-Indies; USR 3278 CNRS, EPHE, Université, 52 Ave. Paul Alduy 66860 Perpignan, France.
[6]USR 3278 CNRS, EPHE, Université, 52 Avenue Paul Alduy 66860 Perpignan, France.
*Corresponding author: gherbert@usf.edu

Merle et al. (2011), although these ontogenies might potentially be useful for understanding whether and how heterochrony (evolutionary changes in developmental timing) contributed to the origin and early morphological diversification of the Muricidae. Here, we present new observations on radular development in four species representing three of the eleven subfamilies of the Muricidae, including one basal member of the family: Rapaninae: *Stramonita biserialis* (Blainville, 1832); Muricinae: *Timbellus phyllopterus* (Lamarck, 1822), *Chicoreus dilectus* (A. Adams, 1855); and Ocenebrinae: *Vokesinotus perrugatus* (Conrad, 1846).

MATERIALS AND METHODS

Species were selected based on availability of early post-metamorphic and adult specimens. Radulae were extracted from adult, alcohol-preserved specimens by dissolving dissected proboscis and buccal mass tissues in a concentrated solution of sodium hypochlorite. Both female and male adult specimens were examined; sex determinations for adults were made by visual inspection. Early post-metamorphic snails were harvested directly from egg capsules deposited by adults for three of the four species studied (*T. phyllopterus, C. dilectus, V. perrugatus*) and opportunistic collection of an early post-metamorphic specimen of *S. biserialis* just after settlement on a natural substrate. None of the juveniles examined had more than a whorl of adult sculpture (Figs. 1–4), indicating recent metamorphosis, and two of the four had little or no adult sculpture (Figs. 3, 4).

Radulae of early juvenile snails were recovered by crushing the shells in a shallow Petri dish filled with a concentrated solution of sodium hypochlorite. In some cases, juvenile radulae were extracted together with the odontophore. Radular ribbons were collected with forceps, washed in distilled-water, mounted on stubs with double-sided conductive tape, air-dried, and coated for scanning electron microscopy with Au-Pd. All radulae were examined using a Scanning Electron Microscope (SEM).

Voucher specimens for juvenile and adult radulae are reposited as collective lots in the Museo Argentino de Ciencias Naturales, Buenos Aires, Argentina (MACN). These are as follows: *Chicoreus dilectus* (MACN-In 39550); *Stramonita biserialis* (adult only) (MACN-In 39551); *Stramonita biserialis* (juvenile only) (Yale Peabody Museum No. 28490) *Timbellus phyllopterus* (MACN-In 39552); *Vokesinotus perrugatus* (MACN-In 39553).

Abbreviations and Terminology

The terminology used to describe structural elements of the radula follows Radwin & D'Attilio (1976), Kool (1993) and Herbert et al. (2007) and is illustrated in Figures 2–5. b: rachidian base; cc: central cusp; ild: inner lateral denticle; imc: inner marginal cusp; lc: lateral cusp; mc: marginal cusp; md: marginal denticle; old: outer lateral denticle; omc: outer marginal cusp; rm: radular membrane; s: shoulder; sild: serrated inner lateral denticle.

Following Vokes (1971), a "3-D" base is one in which the rachidian base is not flat or straight along its length but has depth due to the appearance of being angled or bent. A bend in the base can occur at the position of each lateral cusp, which gives the base a V-shape, or at the position of each marginal cusp, which produces a broader, U-shaped or "rectangular" rachidian. The distinction between different types of bending points along the rachidian base was not recognized by Vokes (1971) or Herbert et al. (2007).

RESULTS

Subfamily Rapaninae

Stramonita biserialis (Blainville, 1832)
(Figs. 1, 5–10)

Material Examined

One early post-metamorphic specimen of *Stramonita biserialis* (Yale Peabody Museum No. 28490) with shell length of roughly 2 mm was collected post-settlement from the carapace of a sea turtle at Costa Careyes, Mexico. Nine adult specimens were collected from boulders in the exposed rocky intertidal around Isla Venado, Gulf of Panama, in August 2005 and January 2006.

Ontogeny

Juvenile teeth (Figs. 5, 6): With V-shaped, 3-D base and narrow, curved, central cusp projecting almost 90° from base. Lateral cusps projecting 45° away from rachidian base, positioned close to central cusp, and sharing

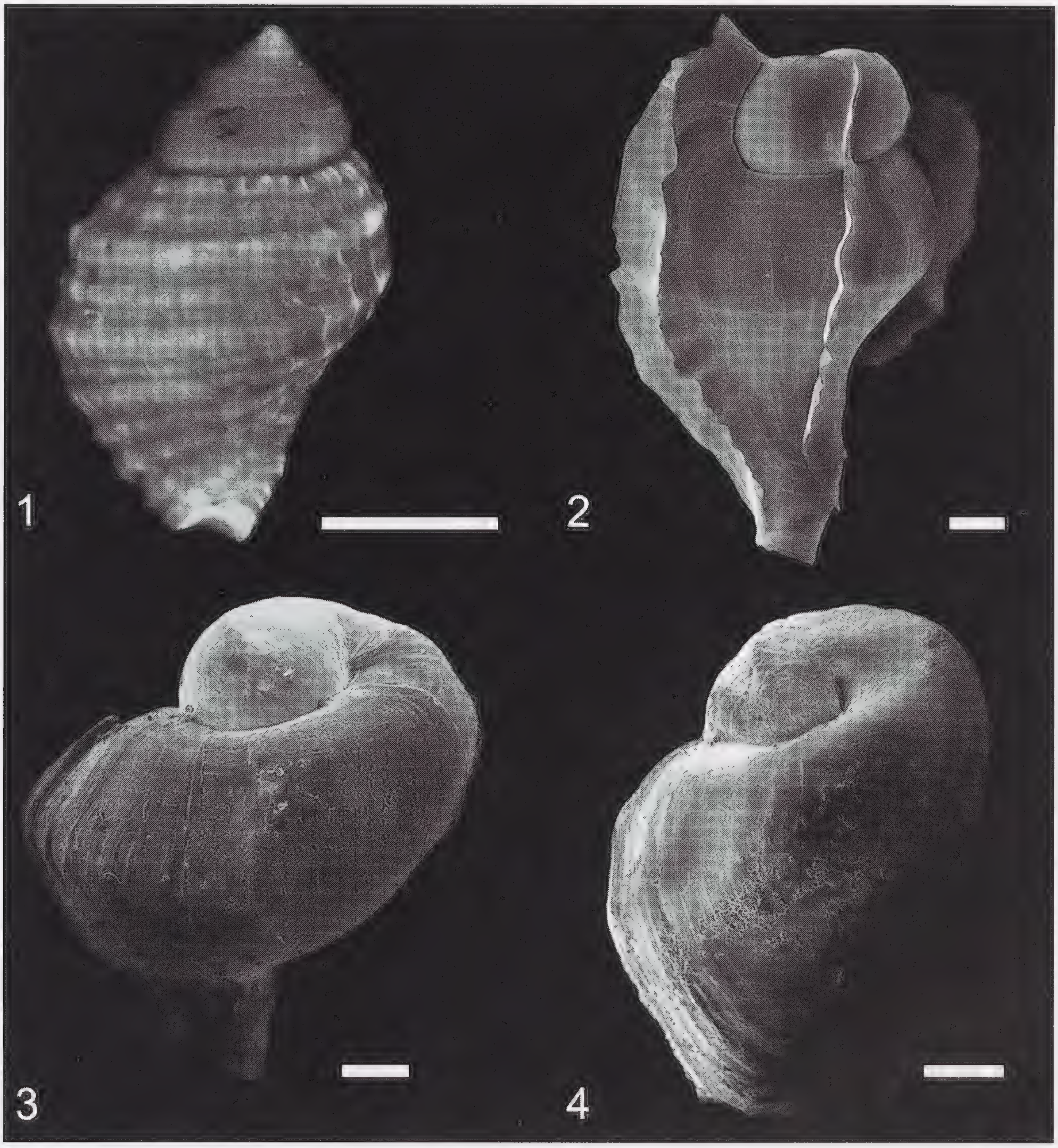

FIGS. 1–4. Dorsal views of juvenile shells. FIG. 1: *Stramonita biserialis*, shell height (SH) = 2.8 mm; FIG. 2: *Timbellus phyllopterus*, SH = 1.5 mm; FIG. 3: *Chicoreus dilectus*, SH = 1.75 mm; FIG. 4: *Vokesinotus perrugatus*, SH = 1.42 mm. Scale bars: Fig. 1 = 1 mm, Figs. 2–4 = 200 μm.

common base with shorter inner lateral denticles. Central and lateral cusps approximately same length. Marginal area with two marginal denticles, including one flanking outer edge of lateral cusp. One marginal cusp, separated from broad, lobe-like extension of rachidian base. Tip of base with prominent, cusp-like end-point. Rachidian base with high, narrow, rounded shoulder.

Adult teeth (Figs. 7–10): With rachidian base slightly bent at lateral cusp position (V-shaped base) and long, straight, triangular central cusp at 45° with rachidian base (Fig. 8). Lateral edges of central cusp near base with subtle serrations. Lateral cusps shorter than central cusp, splayed laterally, and projecting 45° away from rachidian base (co-planar with central cusp). Inner lateral denticle short, strongly serrated along inner edge, splayed laterally, and sharing common base with lateral cusp (Figs. 7, 9). Outer edges of lateral cusps with two or three, small denticles. Marginal area with two marginal denticles (Figs. 8, 10). One marginal cusp separated from

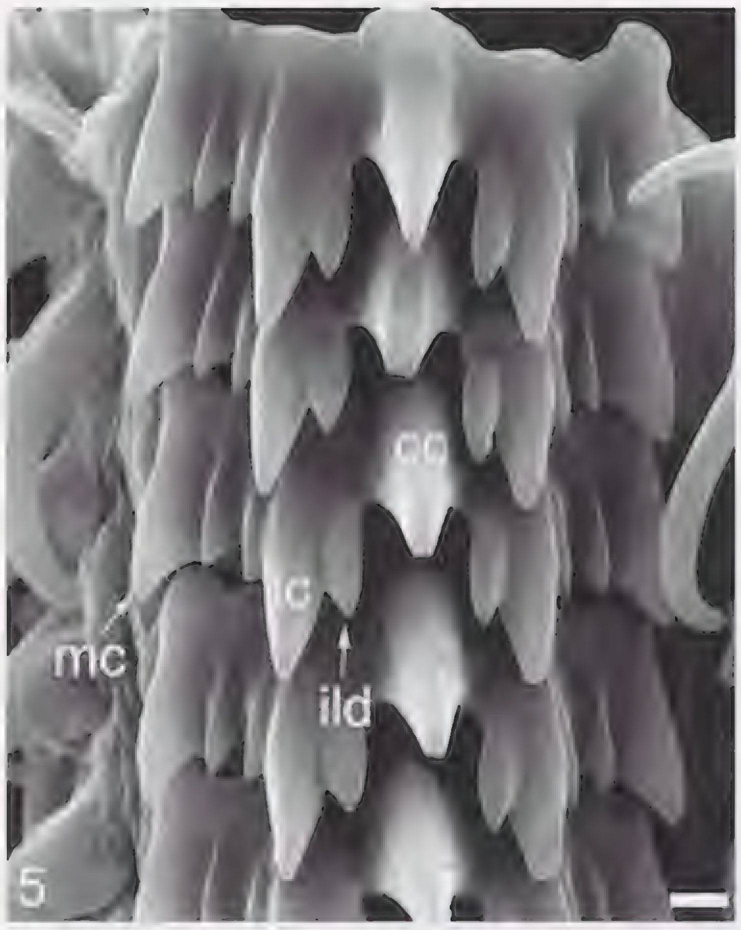
cc
lc
mc
ild
5

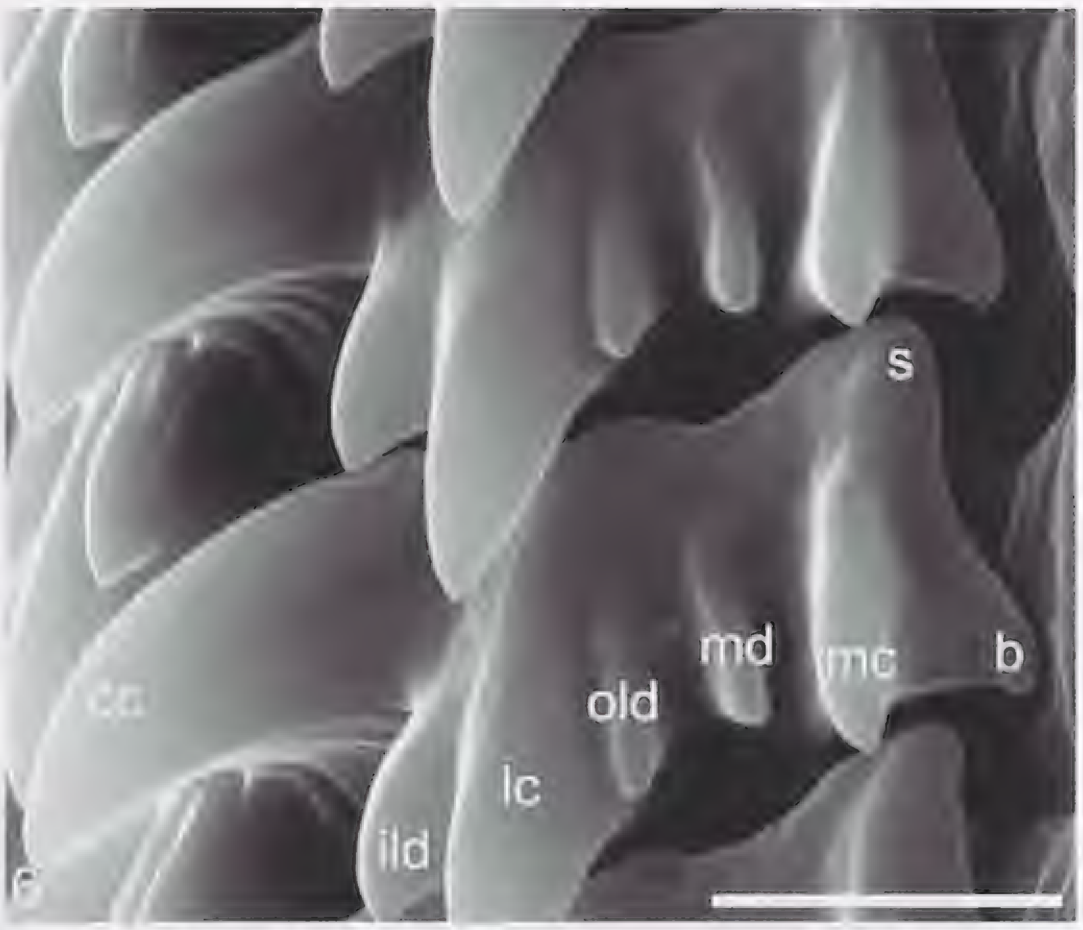
s
md
mc
b
old
cc
lc
ild
6

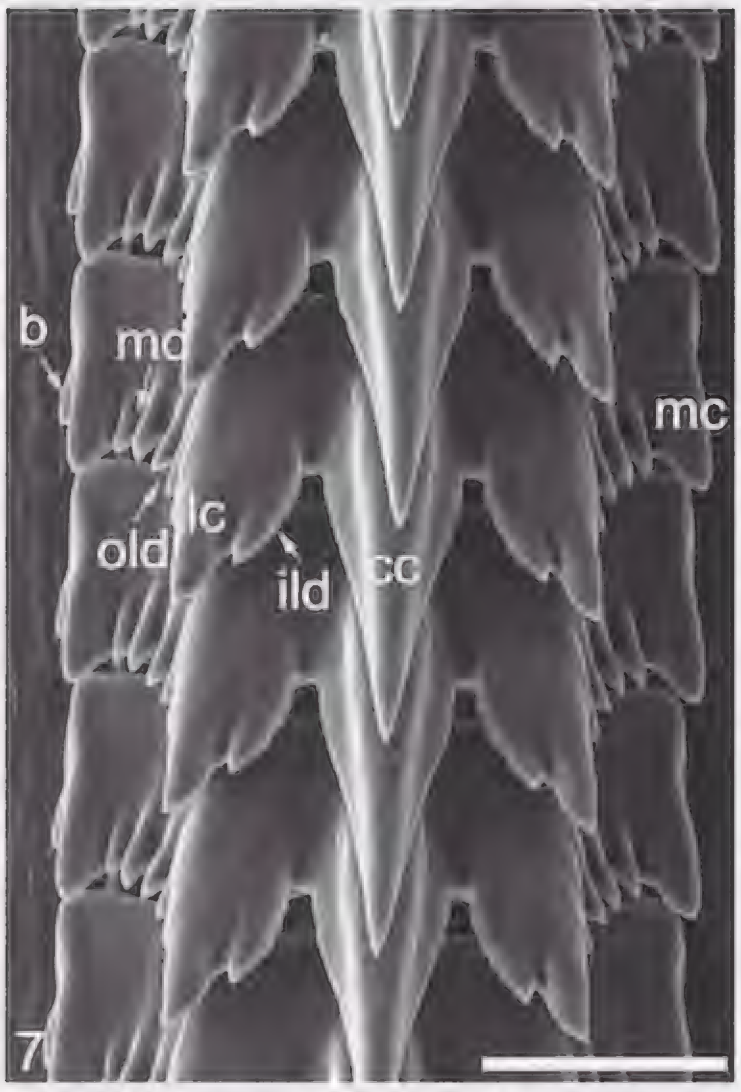
b
md
mc
lc
old
ild
cc
7

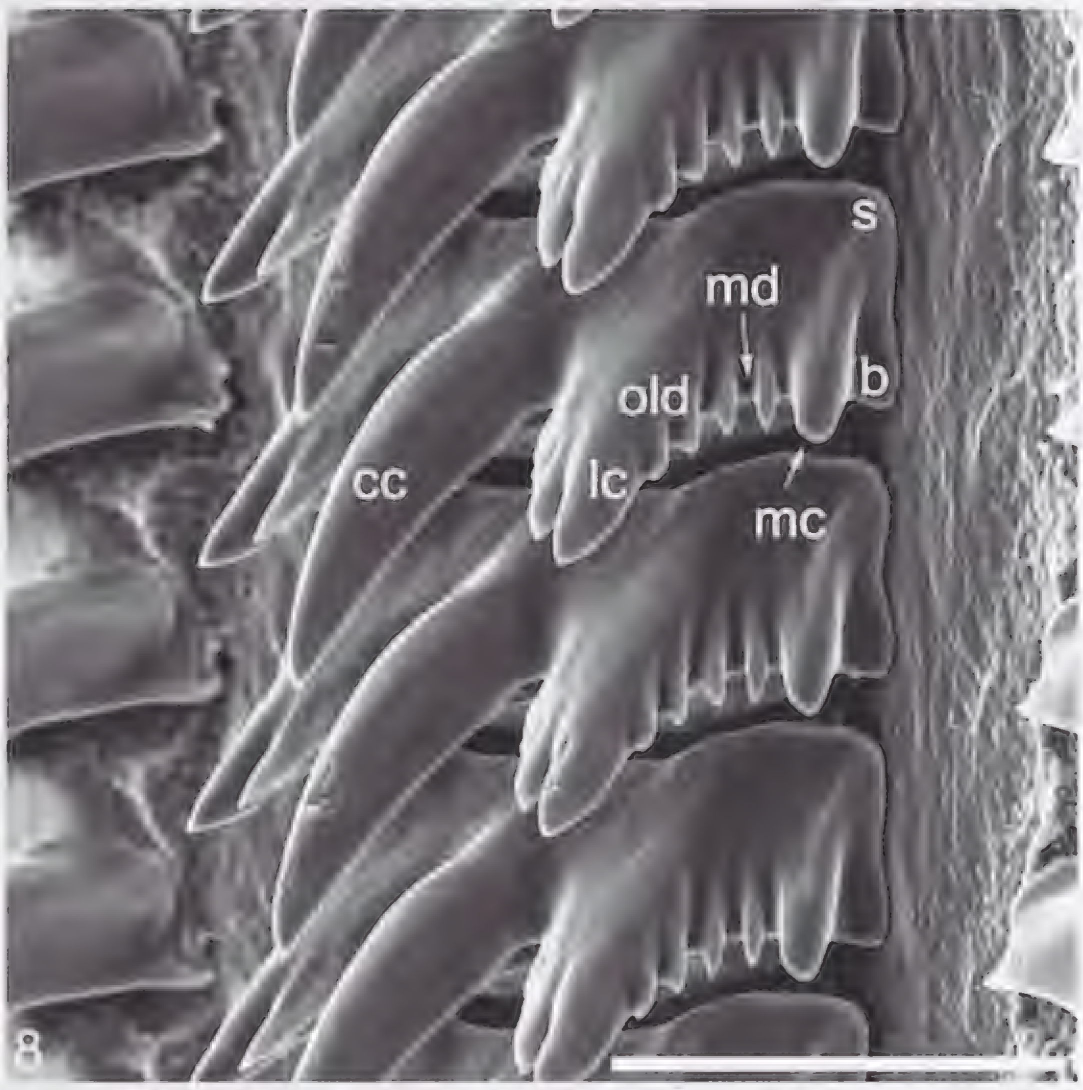
s
md
old
b
cc
lc
mc
8

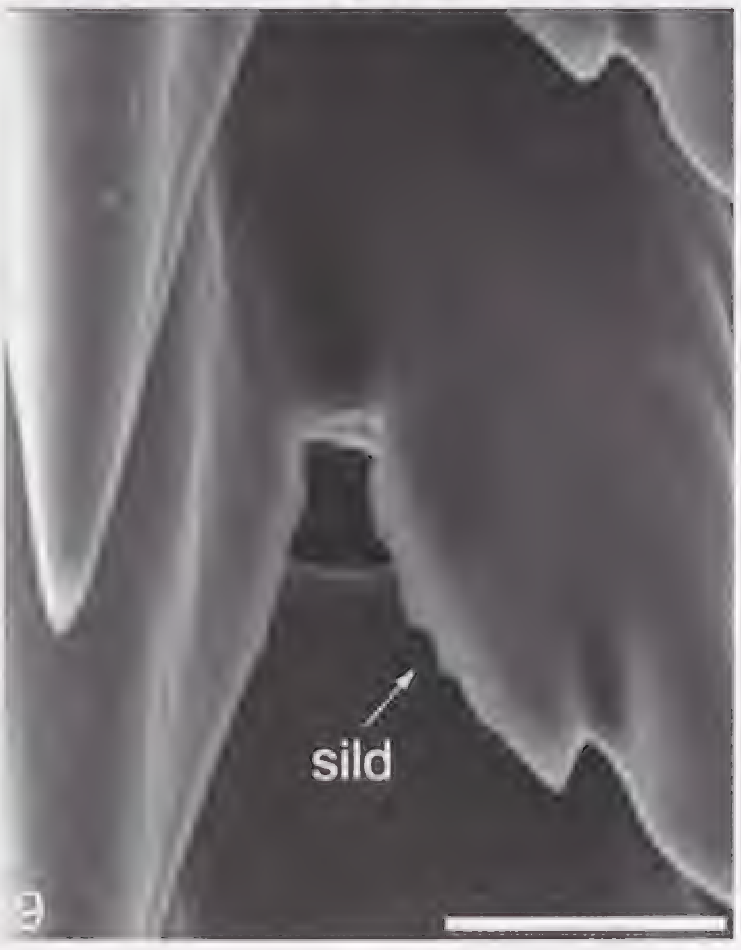
sild
9

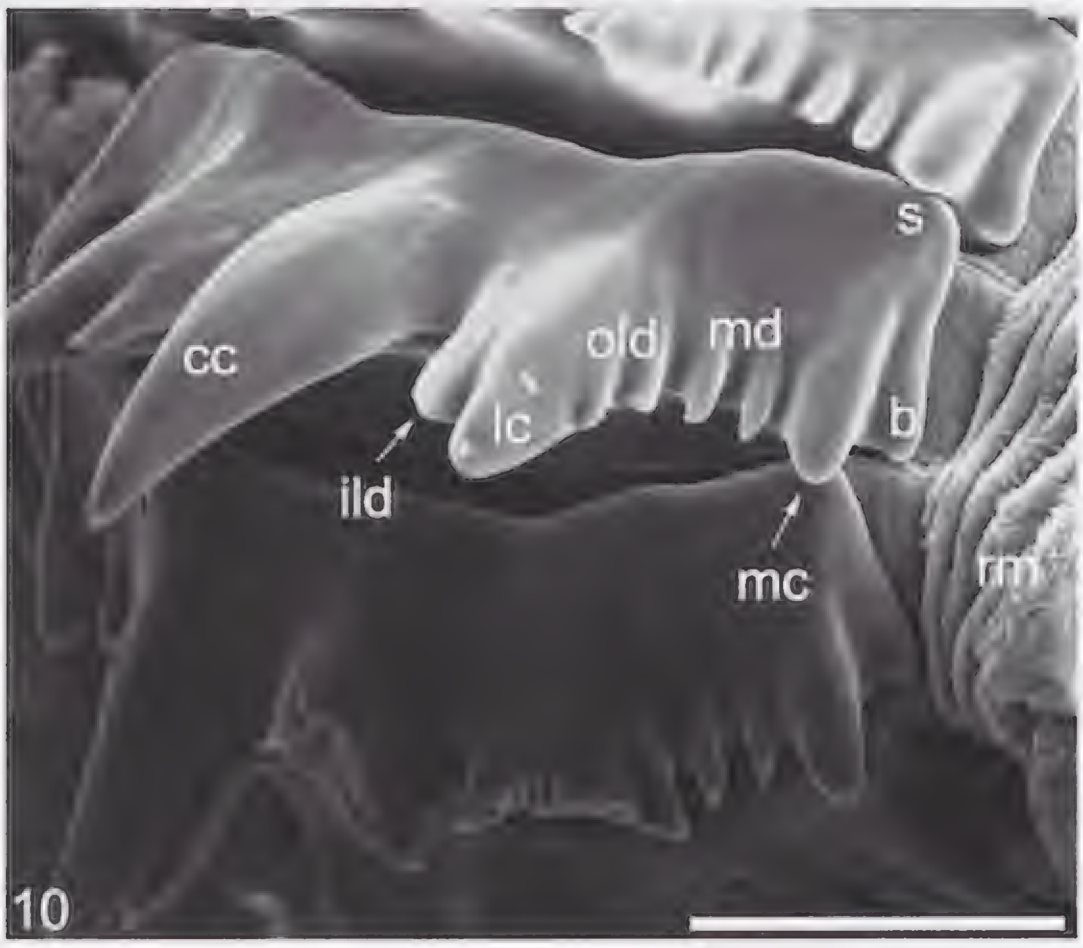
s
cc
old
md
lc
b
ild
mc
rm
10

broad, lobe-like extension of rachidian base (Figs. 8, 10). Lobe-like extension shorter, more rounded than in juvenile. Rachidian base with low, broad shoulder.

Remarks

The ontogeny of *S. biserialis* mirrors that of the Chilean rapanine *Concholepas concholepas* (Bruguière, 1789), as described by Herbert et al. (2007). In both species, adult rachidia have typical rapanine features (e.g., flat rachidian base, a central cusp aligned in the same plane as the lateral cusps, and lateral cusps with a broad, flat base: see Kool, 1987, 1993), while early post-metamorphic individuals have a rachidian that fits the generalized morphology of the subfamily Ocenebrinae (e.g., 3-D rachidian base; short, projecting central cusp; and narrow, conical lateral cusps with appended inner lateral denticles).

The 3-D nature of the juvenile rapanine rachidian base is superficially similar to that of juvenile and adult ocenebrines but differs in having a bend or angle at each lateral cusp, which produces a base with a V-shape. In ocenebrines, the rachidian is angled 90° at the position of each inner marginal cusp, producing a broad U-shape, and sometimes has an additional angle in the middle of the rachidan or at the lateral cusp positions (see *V. perrugata* description below). Another feature of juvenile rapanine rachidia that is superficially similar to that of ocenebrines is a rachidian with pseudo-bifid basal margins (appearance of two cusps). In juvenile rapanines we have studied thus far (*C. concholepas*: Herbert et al., 2007, *S. biserialis*: this study), the bifid morphology is formed by one marginal cusp and a cusp-like ridge at the rachidian base end-point that remains attached to the radular membrane along its entire length. In ocenebrines, however, the bifid morphology is formed by two true marginal cusps, both completely separated from the radular membrane by a narrow, lobe-like feature (Herbert et al., 2007; Pio et al., 2014). Rapanines generally do not retain this pseudo-bifid morphology into adulthood (Kool, 1987, 1993; but see Tan, 2003: fig. 16H), as the ridge at the rachidian base edge becomes less cusp-like in larger juveniles and adults (Fujioka, 1984, 1985; Herbert et al., 2007).

Subfamily Muricinae

Timbellus phyllopterus (Lamarck, 1822)
(Figs. 2, 11–16)

Material Examined

Material used includes seven adults (one male and six females) collected from Basse Terre Island, Guadeloupe and ten newly hatched, direct developing juveniles with shell lengths between 1–2 mm. Juveniles were reared from capsules in aquaria as described by Pointier & Lamy (1985).

Ontogeny

Juvenile teeth: With narrow, flat rachidian base and conical central and lateral cusps projecting 45° from base (Figs. 11, 12). Lateral cusps outwardly splayed. Short, conical inner lateral denticle between central and lateral cusps, closer to lateral cusp but not attached to lateral cusp base. Inner lateral denticles sometimes absent or underdeveloped on one side (Fig. 11). Marginal denticles present as indistinct tubercles (Fig. 12: md). Rachidian base with high rounded shoulder and large, outwardly splayed, cusp-like base endpoint (Figs. 12: b).

Adult teeth: With broad, flat rachidian base, and triangular central and lateral cusps projecting almost 90° from base at point of basal attachment but curved distally (Figs. 13–14). Lateral cusps with slight outward curvature, shorter than central cusp, and bending halfway along their length. Narrow inner lateral denticle (Figs. 13, 14: ild) with slight outward curvature, nearly as long as adjacent lateral cusp, equidistant between lateral and central cusps, and free from both. Marginal area

---

←

FIGS. 5–10. Dorsal and lateral views of rachidian tooth ontogeny of *Stramonita biserialis*. FIGS. 5, 6: Tooth of a juvenile, shell height (SH) = 2.8 mm; FIGS. 7, 8: Tooth of an adult, SH = 31 mm; FIG. 9: Serrated inner lateral denticles of an adult tooth, SH = 31 mm; FIG. 10: Adult radula over the bending plane of the odontophore, SH= 25 mm. Scale bars: Fig. 5 = 2 μm, Fig. 6 = 5 μm, Fig. 7 = 50 μm, Fig. 8 = 100 μm, Fig. 9 = 10 μm, Fig. 10 = 50 μm; b = base; cc = central cusp; ild = inner lateral denticle; lc = lateral cusp; mc = marginal cusp; md = marginal denticle; old = outer lateral denticle; sild = serrated inner lateral denticle.

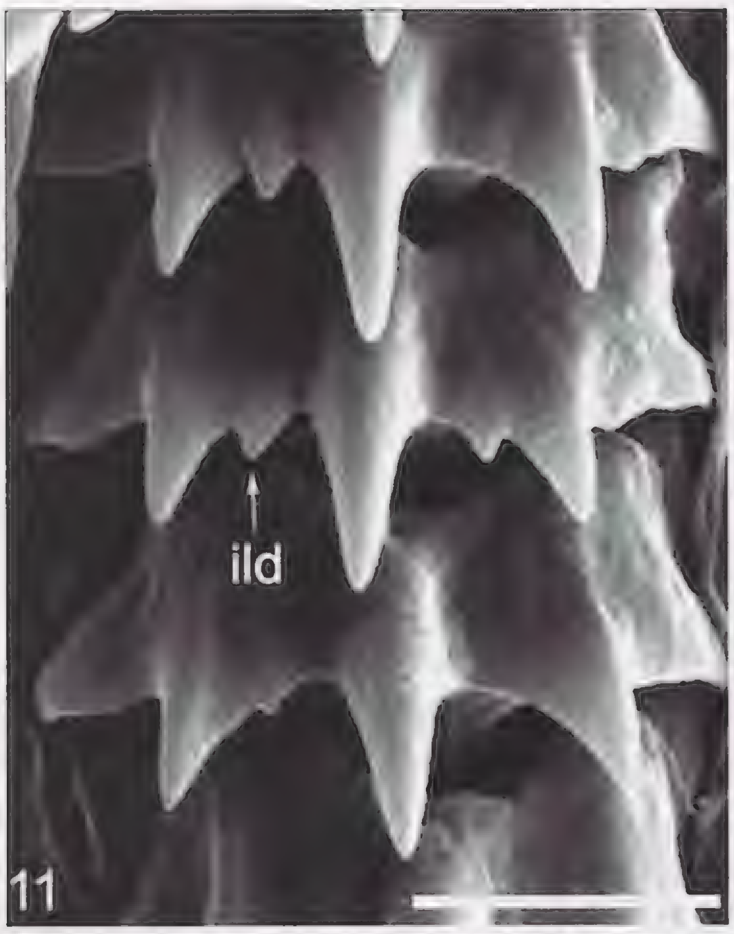
ild
11

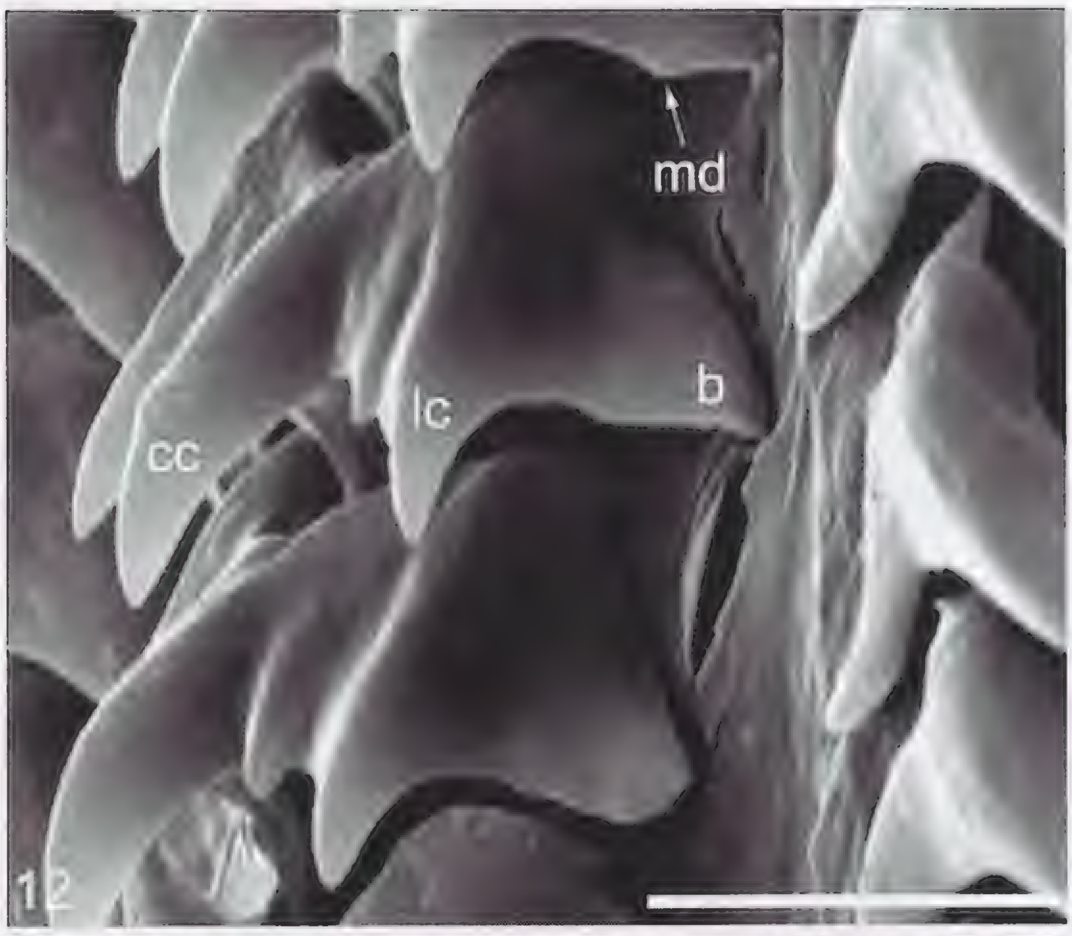
md
b
lc
cc
12

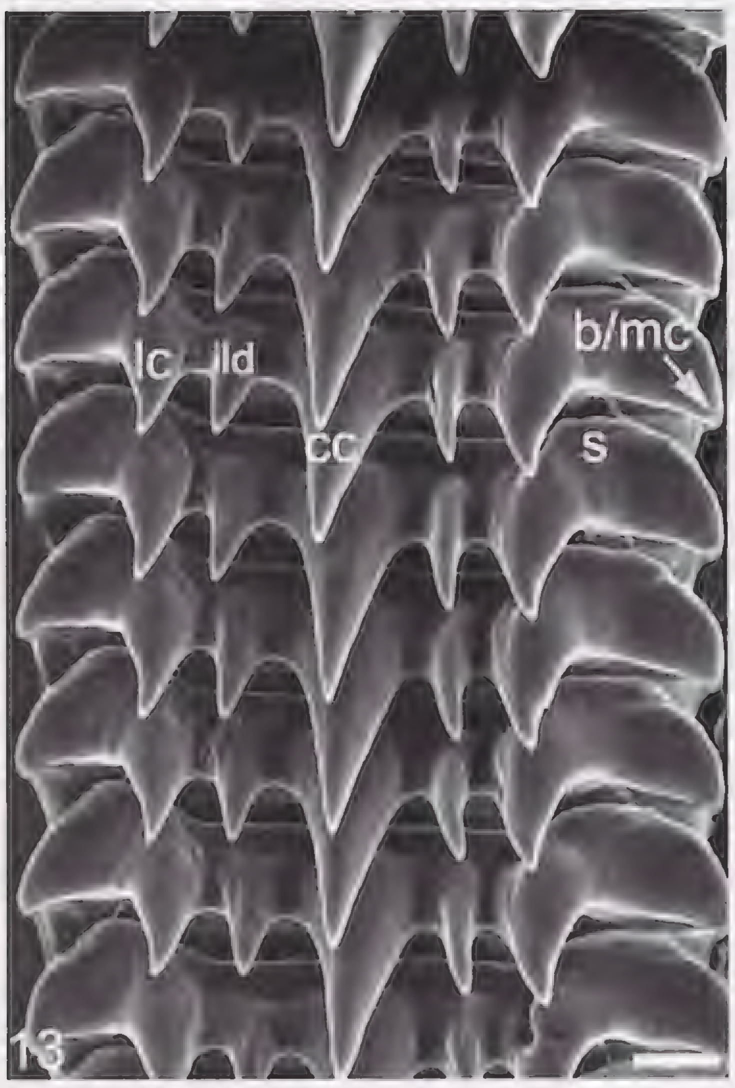
lc
ild
b/mc
cc
s
13

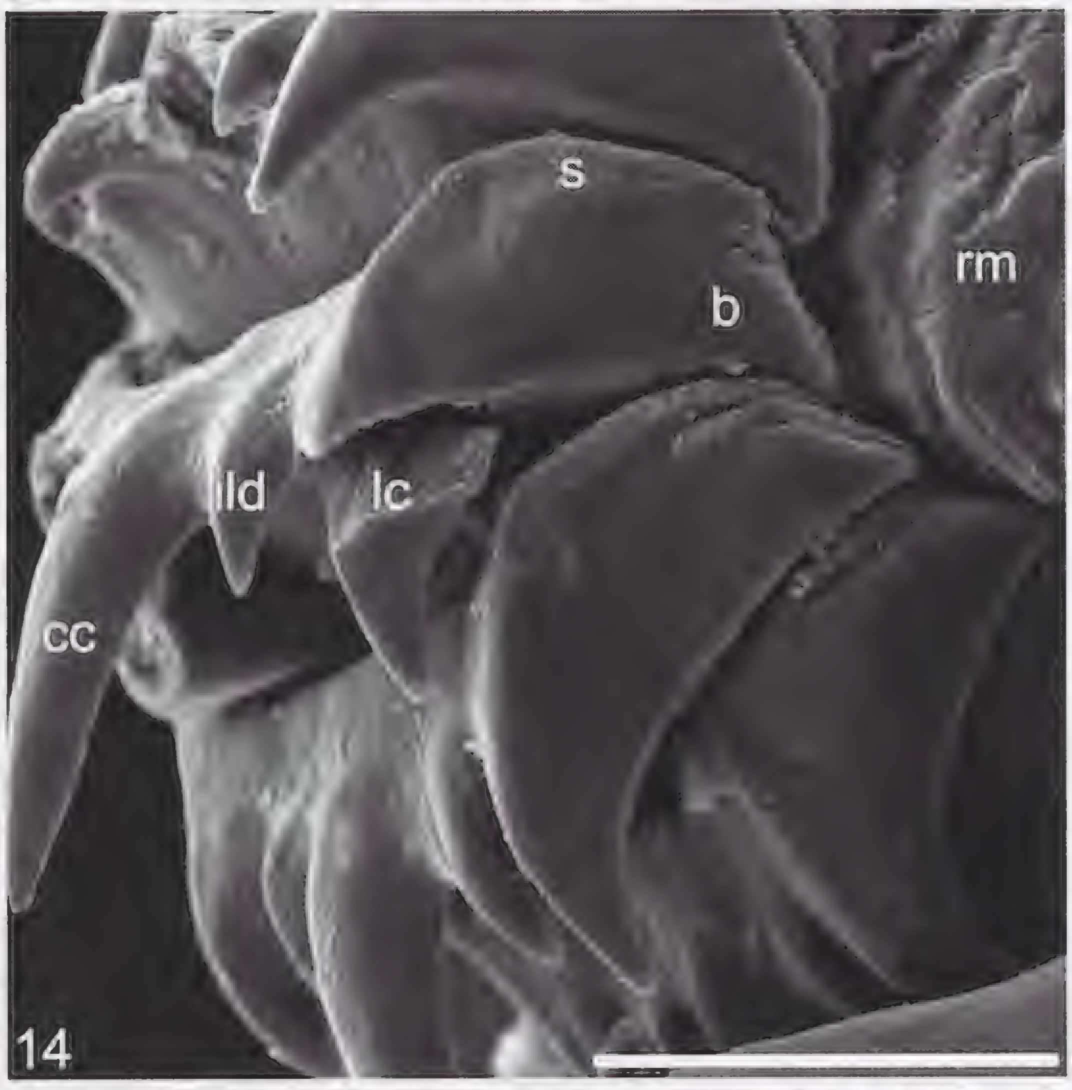
s
rm
b
ild
lc
cc
14

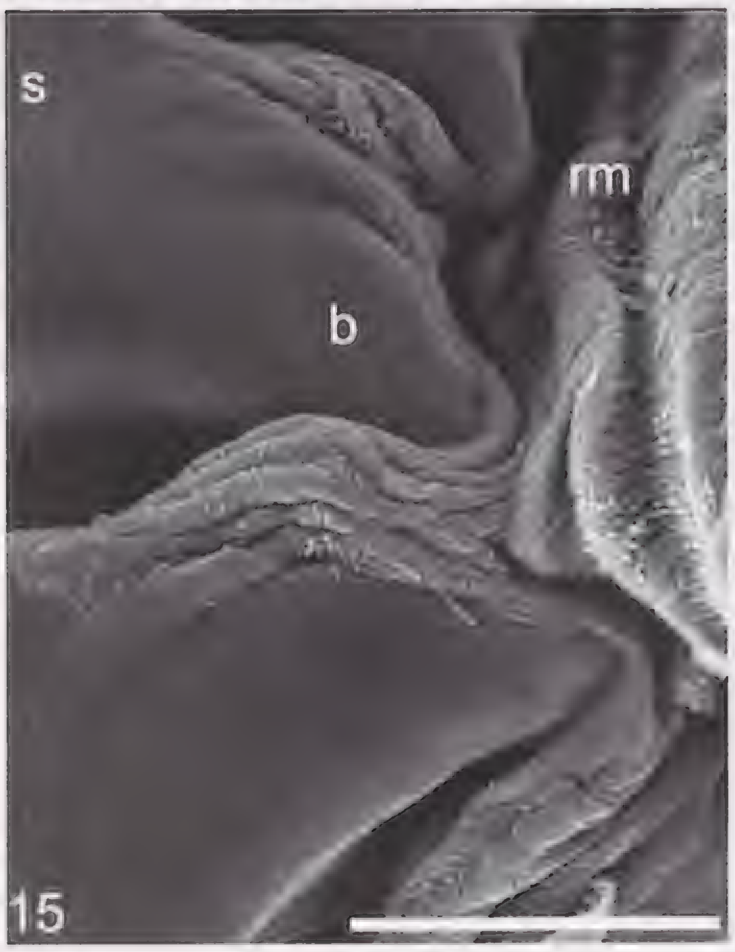
s
rm
b
15

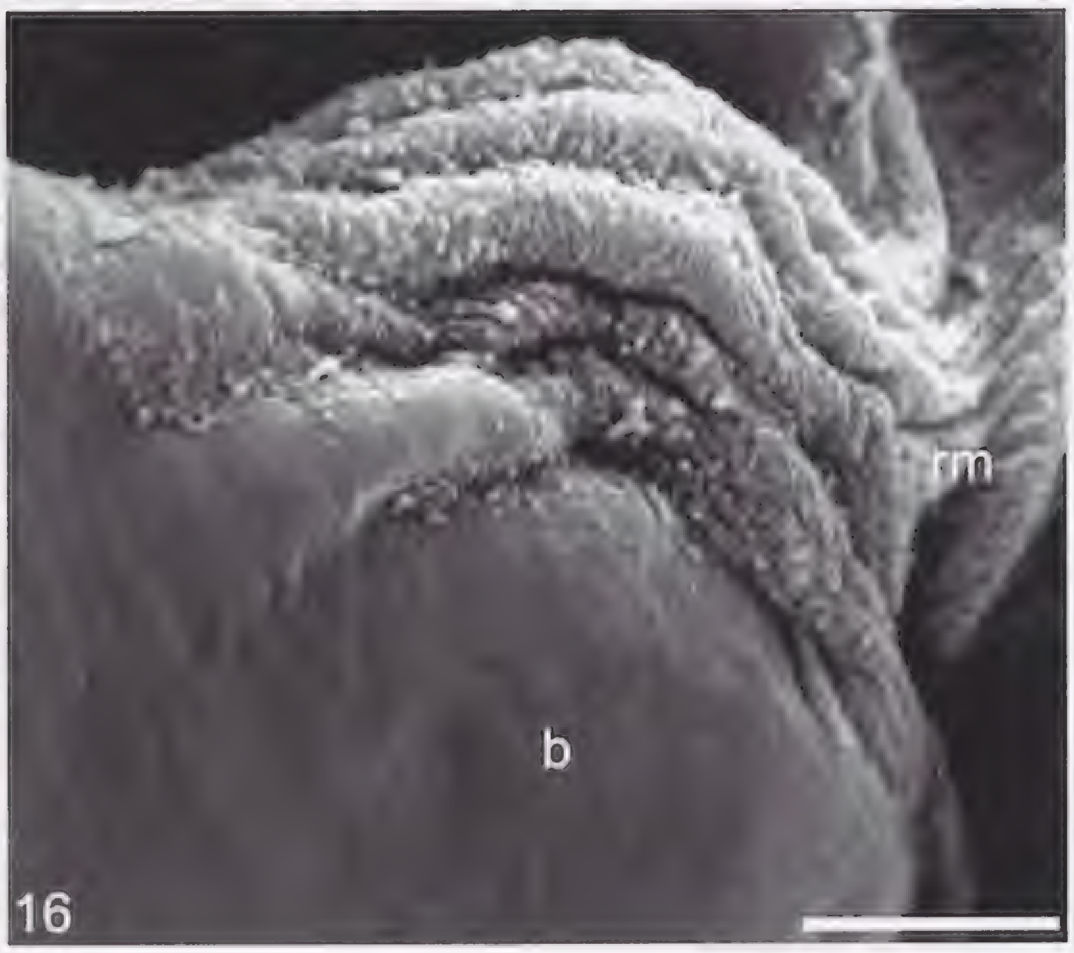
rm
b
16

broad, flat, with no marginal denticles (Fig. 14). Rachidian base with broad, rounded shoulder and broad, rounded, cusp-like endpoint. Outer edge of shoulder with smooth or folded surface (Figs. 15, 16).

Remarks

One of the most notable features of the rachidian teeth of *T. phyllopterus* is ontogenetic change in variability of expression of the inner lateral denticles, which changes from irregular expression in juveniles to regular expression in adults. Rachidia of adults consistently have one inner lateral denticle on each side of the central cusp. In juveniles, however, these structures may be present on both sides of the central cusp as in adults, underdeveloped or absent on just one side (asymmetrical expression), or, less commonly, absent on both sides, all within a single radular ribbon. A second notable feature of the *T. phyllopterus* radula is that there is no clear differentiation between the rachidian base and marginal cusp in either juvenile or adult individuals. Instead, the end of the base is rounded and adherent to the radular membrane along nearly its entire length.

The entire rachidian development of *T. phyllopterus* is remarkably similar to that of *Phyllonotus pomum* (Gmelin, 1791) as described previously by Herbert et al. (2007). Both genera have traditionally been classified as belonging to the Muricinae (Radwin & D'Attilio, 1971, 1976; Ponder & Vokes, 1988; Vokes, 1990, 1992), but morphological and molecular data (Vokes, 1971; Merle, 1999; Barco et al., 2010) suggest that this subfamily is polyphyletic, with *Phyllonotus* Swainson, 1833, belonging to a separate, younger branch (*Hexaplex* group) of true muricines and *Timbellus* Gregorio, 1885, belonging to an as-yet unnamed and much deeper branch.

The fossil record of *Timbellus* Gregorio, 1885, extends back to the Early Paleocene, making it one of the oldest lineages of the Muricidae and one of just three muricid genera to have evolved by that time (Vokes, 1971, 1990, 1992; Garvie, 1991; Merle et al., 2011).

Chicoreus dilectus (A. Adams, 1855)
(Figs. 3, 17–22)

Material Examined

Five juveniles with shell lengths around 1.75 mm were harvested from capsules deposited by adults in laboratory aquaria. Four adults (two males and two females) were collected from sea grass in water 1 m deep in St. Joseph Bay, Florida in June 2007.

Ontogeny

Juvenile teeth (Figs. 17, 18, 21): With narrow, lightly curved rachidian base and long, conical, central and lateral cusps projecting 45° from rachidian base. Lateral cusps slightly splayed, same length as central cusp. Inner lateral denticle conical, thin and shorter than lateral cusps (Fig. 17). No space between inner lateral denticle and adjacent central and lateral cusp. Broad marginal area with one or two low marginal denticles (Figs. 17, 18). Rachidian base with high rounded shoulder and large, outwardly splayed, base point or marginal cusp (Fig. 18) attached over the entirety of its length to radular membrane (Fig. 21). Lobe or extension of rachidian base past marginal cusp absent.

Adult teeth (Figs. 19, 20): With narrow, rectangular rachidian base, long conical lateral cusps, and long, triangular central cusp projecting 45° from rachidian base (Figs. 19, 20). Lateral cusps curving laterally at distal ends, nearly same length as central cusp, with low ripples along the outer edges in the position normally occupied by outer lateral denticles (Figs. 19, 20). Short inner lateral denticle, equidistant between lateral and central cusps, and free from both (Fig. 19). Marginal area short with no marginal denticles and one short, rounded, outwardly splayed marginal cusp (Fig. 20). Marginal cusp free from radular membrane over entire length, separated from membrane by small, lobe-like extension of rachidian base (Figs. 4, 20).

←

FIGS. 11–16. Dorsal and lateral views of rachidian tooth ontogeny of *Timbellus phyllopterus*. FIGS. 11, 12: Tooth of an intracapsular embryo from a closed egg capsule, SH = 1.5 mm; FIG. 13: Tooth of an adult, SH = 63 mm; FIG. 14: Adult radula over the bending plane of the odontophore, SH = 63; FIG. 15: Marginal area of an adult radula; FIG. 16: Detail of the folded marginal area of an adult radula, SH = 63. Scale bars: Fig. 11 = 5 μm, Fig. 12 = 10 μm, Fig. 13 = 20 μm, Fig. 14 = 50 μm, Fig. 15 = 20 μm, Fig. 16 = 5 μm; b = base; b/mc = base/marginal cusp; cc = central cusp; d = denticle; ild = inner lateral denticle; lc = lateral cusp; md = marginal denticle; rm = radular membrane.

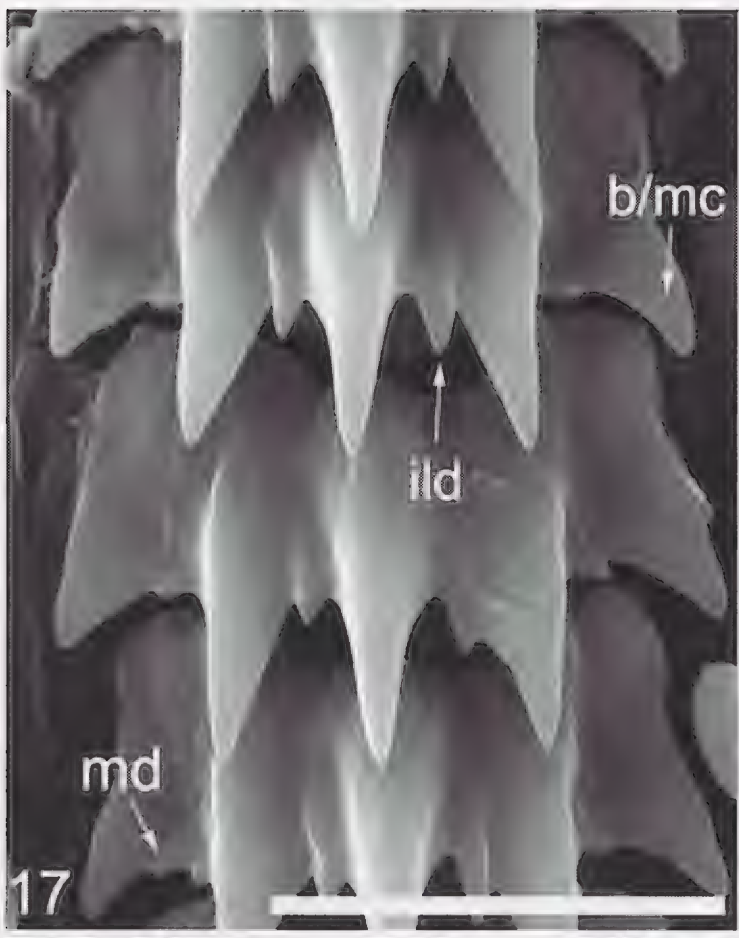
b/mc
ild
md
17

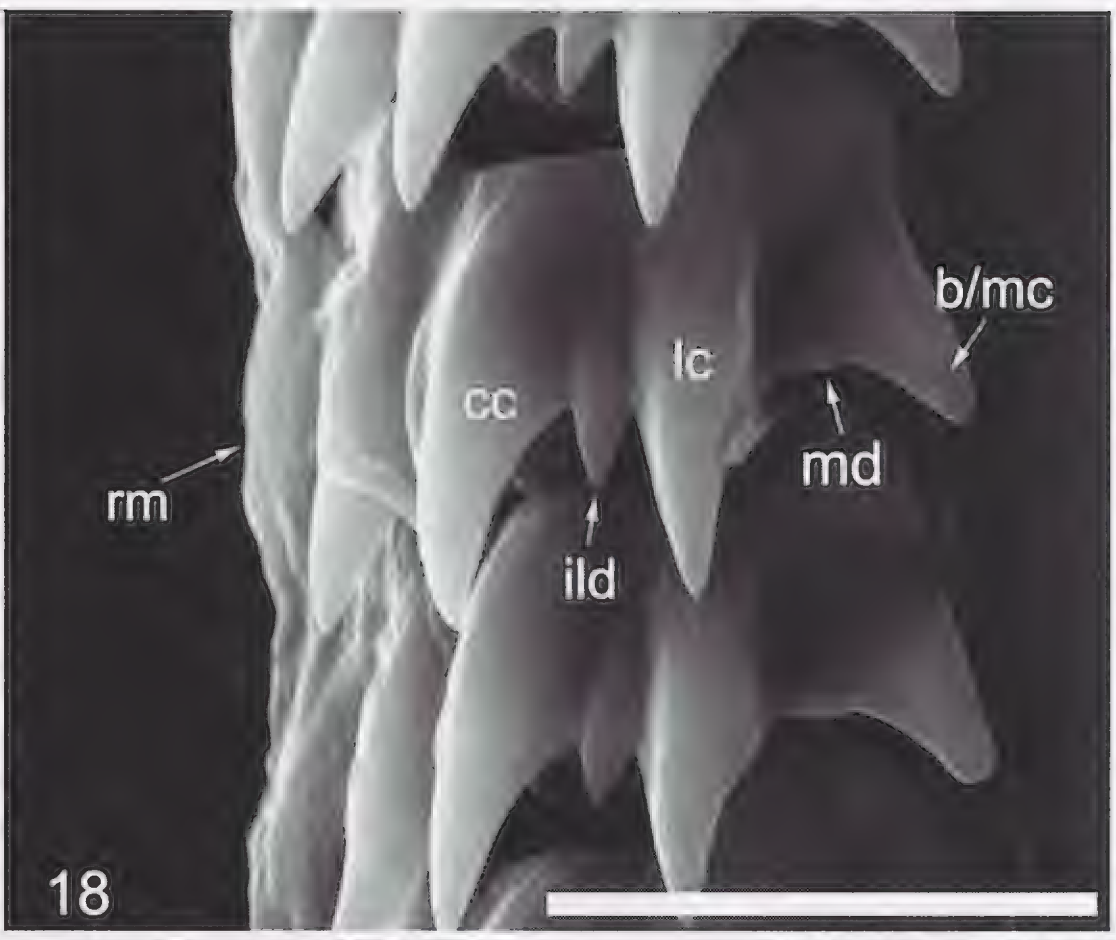
b/mc
lc
cc
md
rm
ild
18

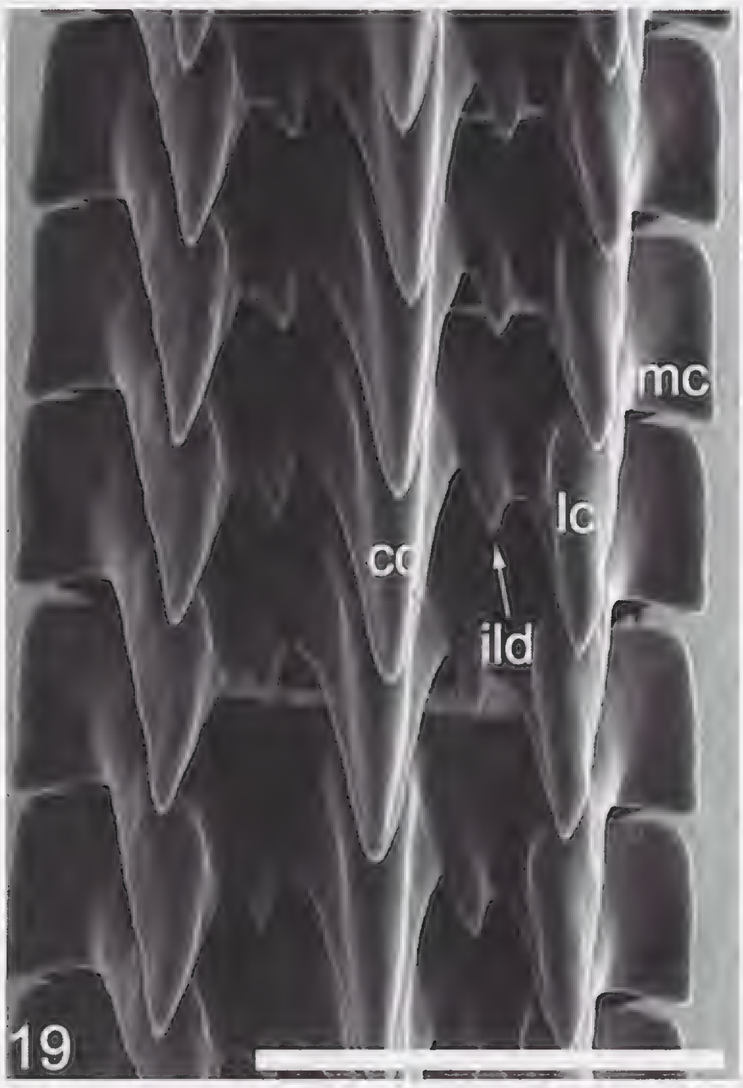
mc
cc
lc
ild
19

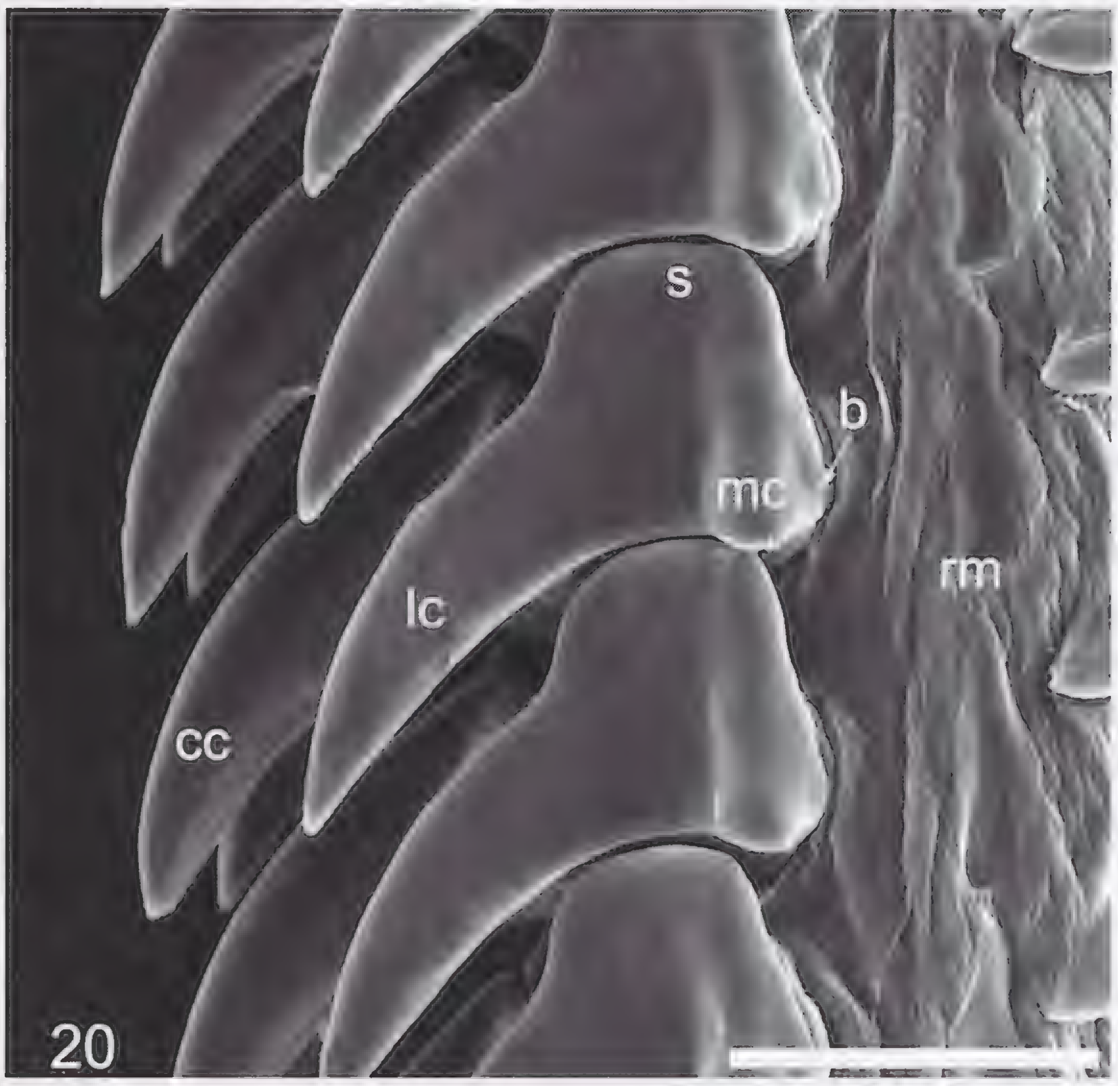
s
b
mc
rm
lc
cc
20

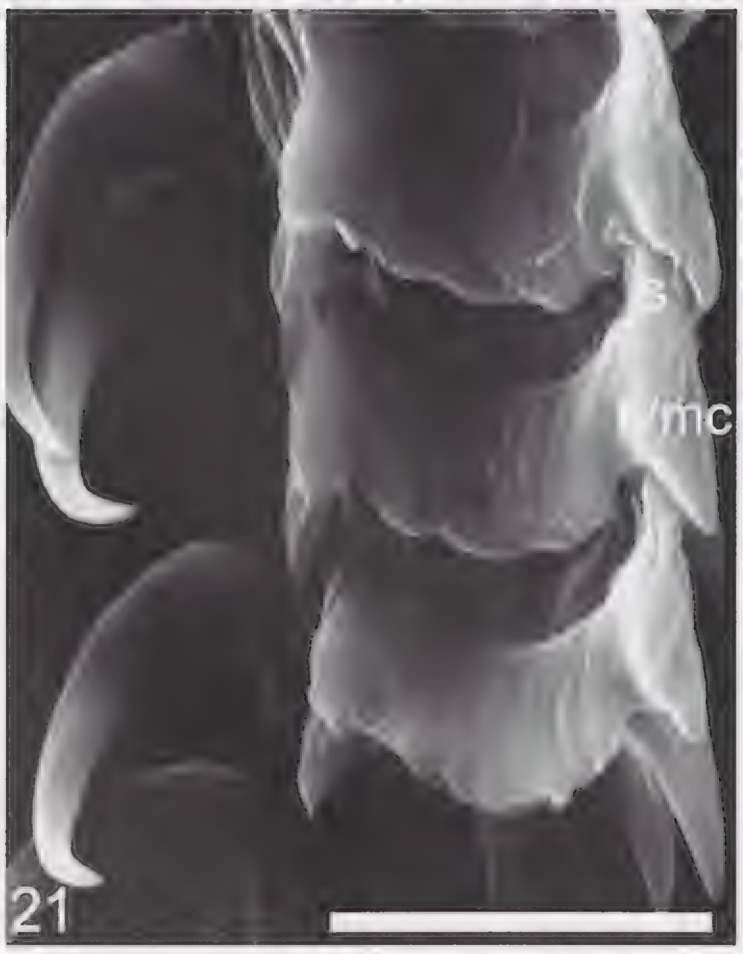
s
/mc
21

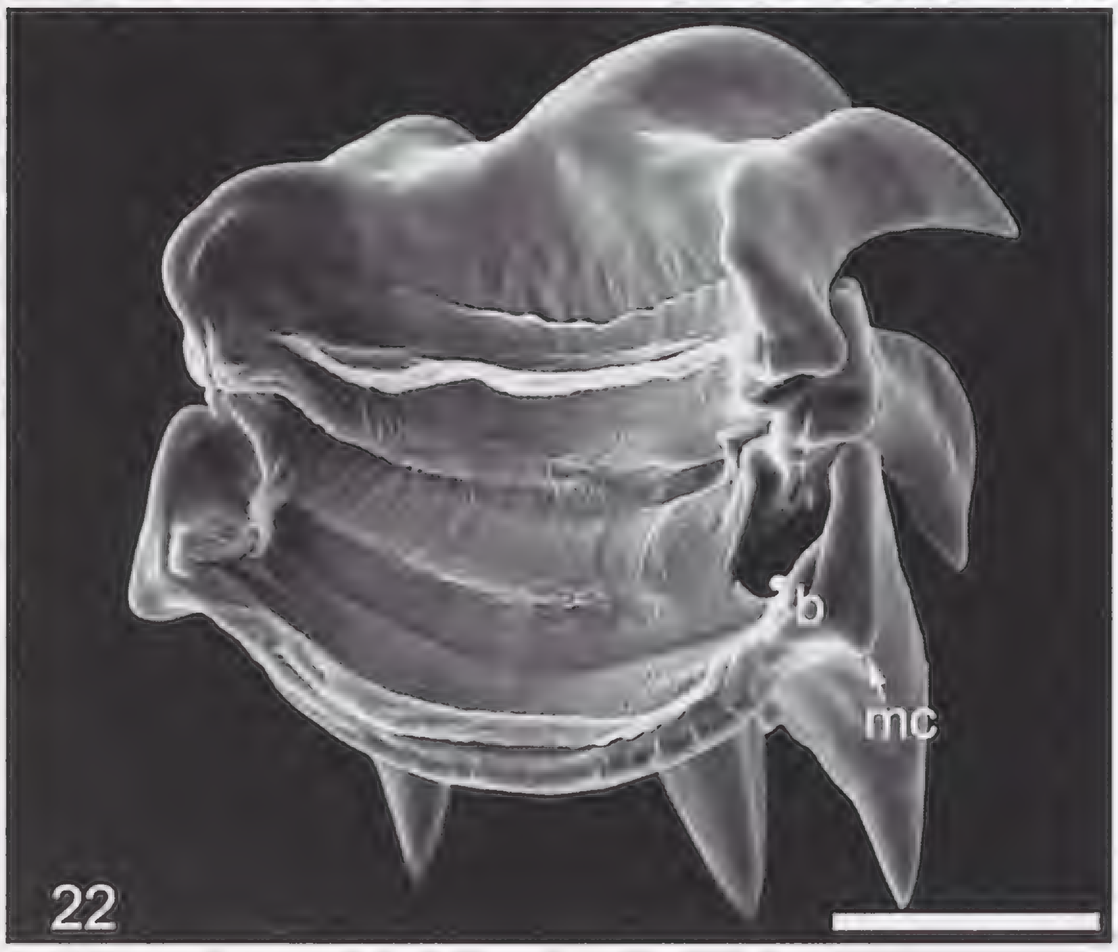
b
mc
22

Remarks

The development of *C. dilectus* is distinct from that of other muricines studied thus far. There is no variable or asymmetric expression of inner lateral denticles in *C. dilectus* as in *P. pomum* or *T. phyllopterus*. Additionally, the marginal cusp, which is long and partially adhered to the radular membrane in juvenile *C. dilectus* (Figs. 17, 18, 21: b/mc), is shorter, more rounded distally, and completely separated from the radular membrane in adults (Figs. 17, 18, 22: mc). Separation of the marginal cusp from the membrane in *C. dilectus* is accompanied by bending of each end of the rachidian base at the position of the lateral cusp so that it forms a 3-D, U-shaped structure (Fig. 22). A by-product of these changes is the formation of a new basal lobe (Fig. 20: b), which is merely the portion of the rachidian base that extends past the now more medially located marginal cusp (Fig. 20). In *P. pomum* and *T. phyllopterus*, no separation of the base endpoint from the radular membrane occurs, leaving the rachidian base and marginal cusp as a single, undifferentiated feature as it appears to be in larval *C. dilectus* (Fig. 21).

Chicoreus dilectus is the only muricid reported thus far to have a rectangular rachidian base. This characteristic is not obvious from frontal or side views of the rachidian and is best viewed from the back side of teeth after they have been separated from the odontophore (Fig. 22).

Subfamily Ocenebrinae

Vokesinotus perrugatus (Conrad, 1846)
(Figs. 4, 23–28)

Material Examined

Six juveniles with shell lengths around 1 mm were harvested from capsules deposited by adults in laboratory aquaria. Ten adults (six females and four males) were collected from sea grass in water 1 m deep in St. Joseph Bay, Florida in June 2007 and preserved in ethanol.

Ontogeny

Juvenile teeth (Figs. 23, 24): With narrow, 3-D base and narrow, short central cusp projecting almost 90° from base. Rachidian base bent at center (V-shape) and at base margins (U-shape). Lateral cusps longer than central cusp and projecting 45° away from rachidian base, positioned close to central cusp, and sharing common base with shorter inner lateral denticle (if present) (Fig. 24). Inner lateral denticles weakly and asymmetrically developed, or absent on most teeth (Fig. 23: ild). Marginal area wide with one larger outer lateral denticle (Figs. 23, 24: old) appended to outer edge of lateral cusp, one to two marginal denticles, and two marginal cusps (Fig. 24: imc, omc). Inner marginal cusp longer than outer marginal cusp but similar in thickness (Fig. 24). Rachidian base with narrow, rounded shoulder (Fig. 24: s). Rachidian base extending laterally past outer marginal cusp forming narrow lobe (Fig. 24: b).

Adult teeth (Figs. 25–28): With broad, 3-D base and short, narrow central cusp projecting between 45–75° from base. Rachidian base slightly bent at center, strongly bent at margins. Lateral cusps same length as central cusp and projecting between 20–50° away from rachidian base, positioned close to central cusp, and sharing common base with shorter inner lateral denticle (Fig. 25). Inner lateral denticles present on all teeth (Fig. 25: ild). Marginal area wide with one outer lateral denticle (Figs. 25, 26: old), one or two marginal denticles (Figs. 25, 26: md), and two marginal cusps (Figs. 26, 27: imc, omc). Inner marginal cusp longer, thicker than outer marginal cusp. Rachidian base with low, narrow, rounded shoulder (Figs. 25, 28: s). Rachidian base extending laterally past outer marginal cusp with narrow lobe. Outer edge of lobe forming short, narrow, cusp-like ridge (Fig. 28: b).

←

FIGS. 17–22. Dorsal and lateral views of rachidian tooth ontogeny of *Chicoreus dilectus*. FIGS. 17, 18: Tooth of an intracapsular embryo from a closed egg capsule, SH = 1.75 mm; FIGS. 19, 20: Tooth of an adult, SH = 52 mm; FIG. 21: Back view of the radula of an intracapsular embryo from closed egg capsule, SH = 1.75 mm. FIG. 22. Back view of an adult radula, SH = 52 mm. Scale bars: Fig. 17 = 10 µm, Fig. 18 = 100 µm, Fig. 19 = 10 µm, Fig. 20 = 50 µm, Fig. 21 = 10 µm, Fig. 22 = 50 µm; b = base; b/mc = base/marginal cusp; cc = central cusp; ild = inner lateral denticle; mc = marginal cusp; lc = lateral cusp; md = marginal denticle; rm = radular membrane.

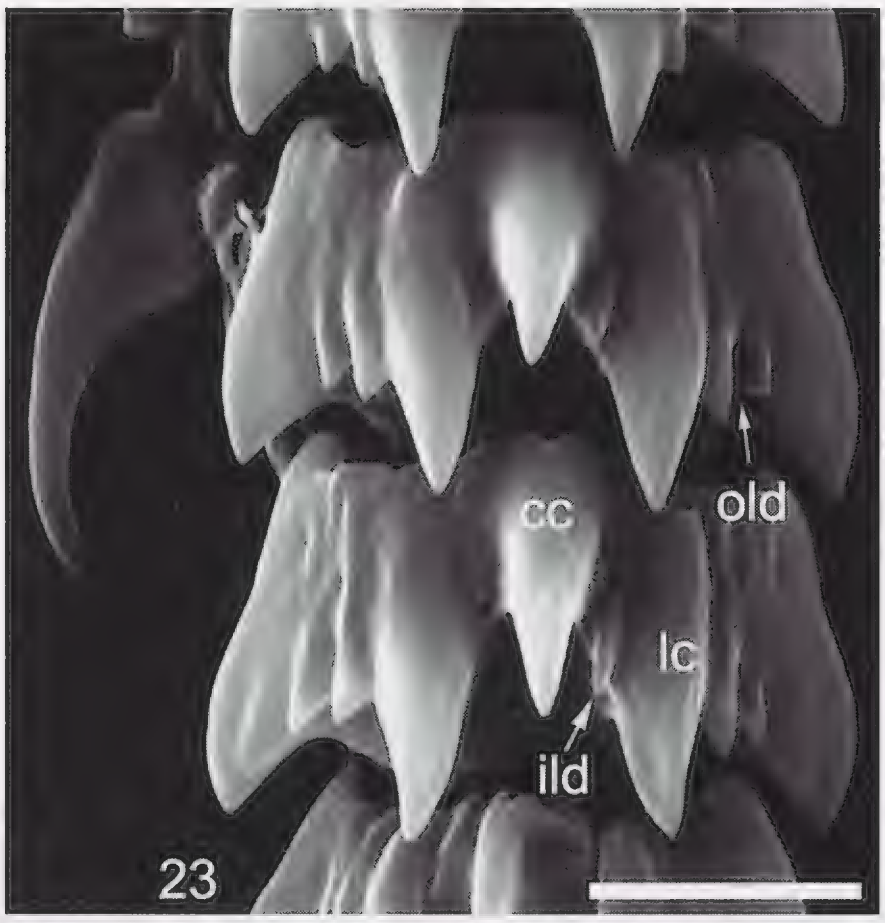
old
cc
lc
ild
23

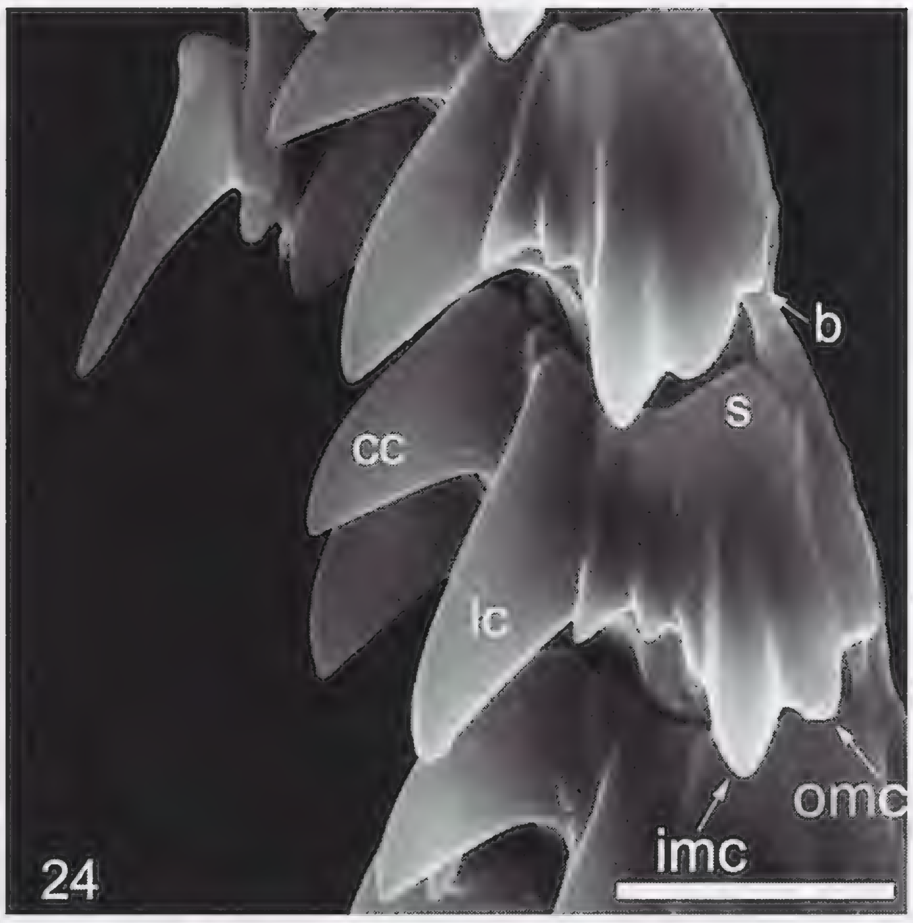
b
s
cc
lc
omc
imc
24

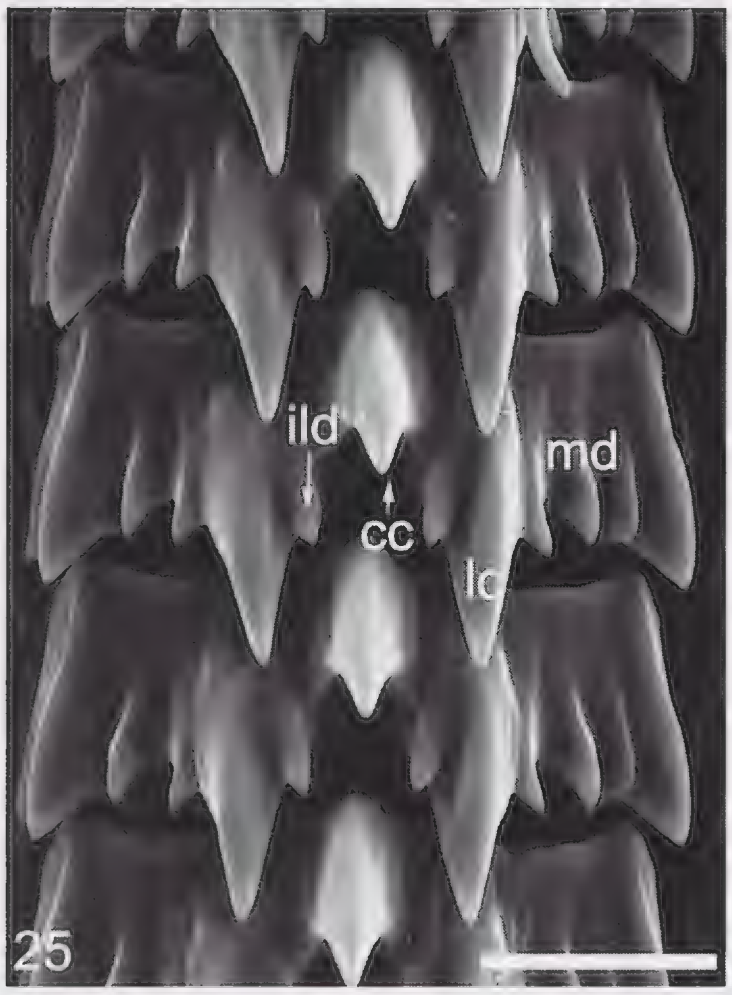
ild
md
cc
lc
25

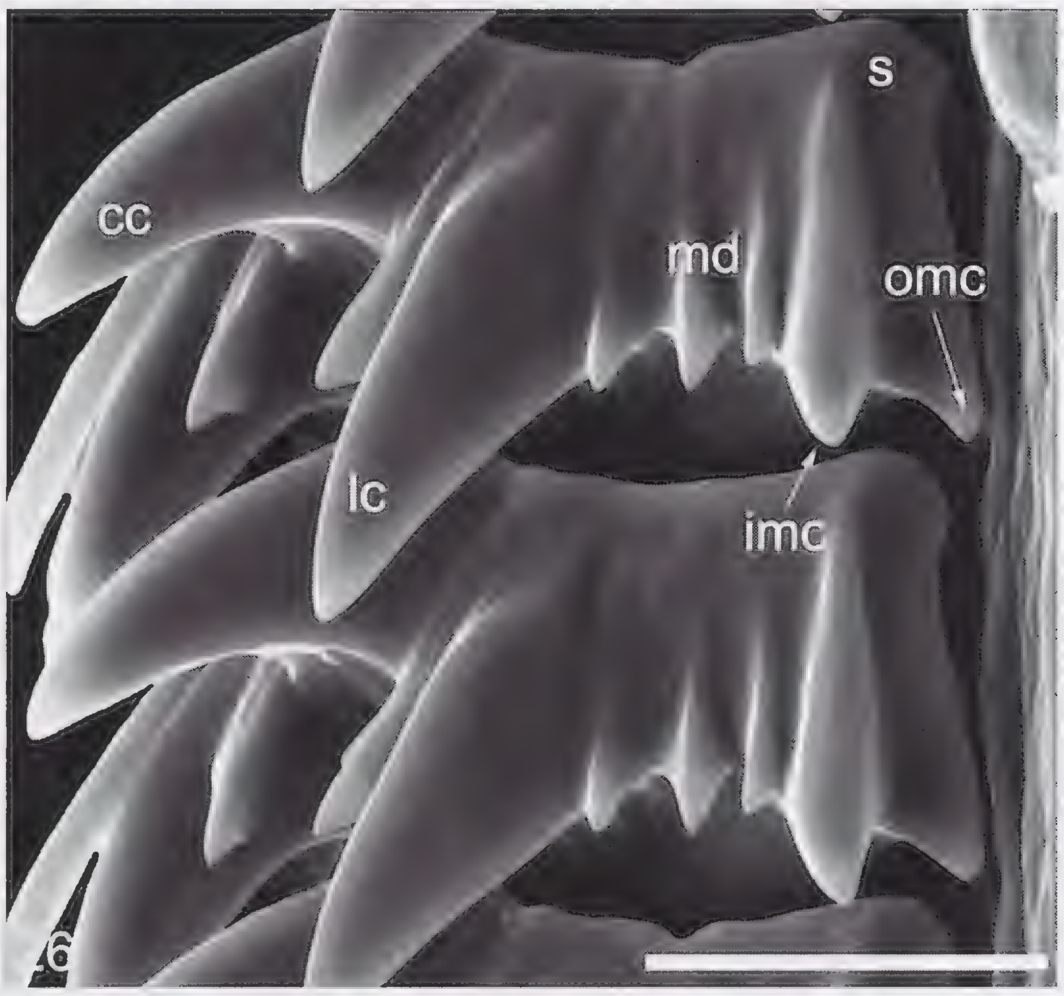
s
cc
md
omc
lc
imc
26

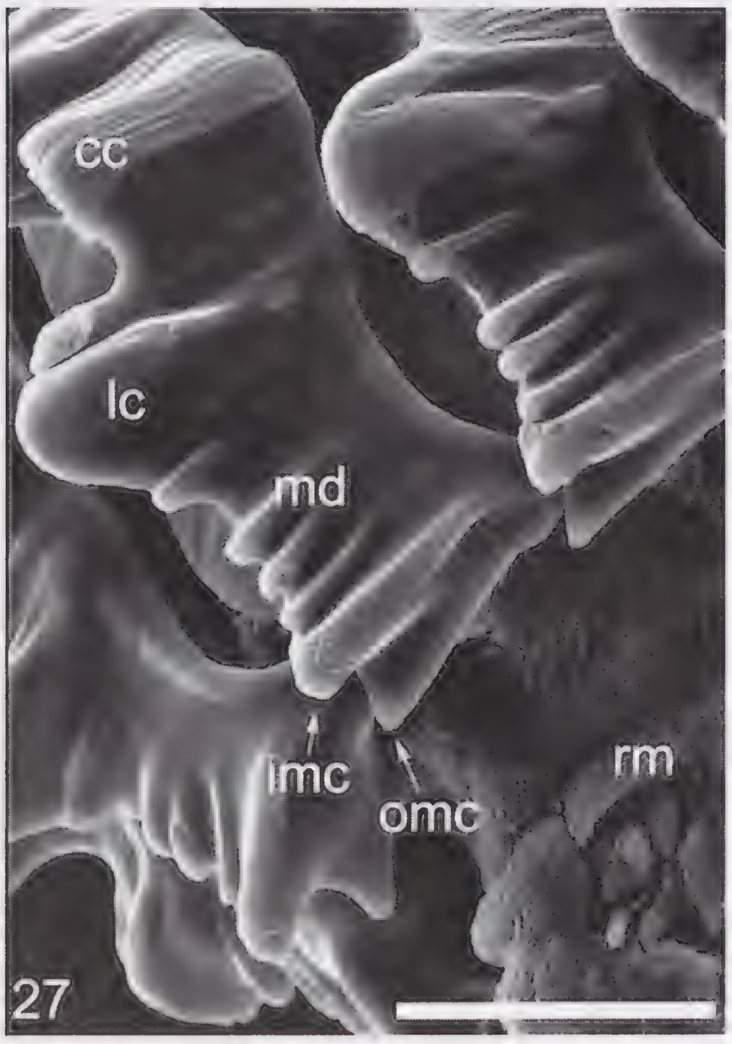
cc
lc
md
imc
omc
rm
27

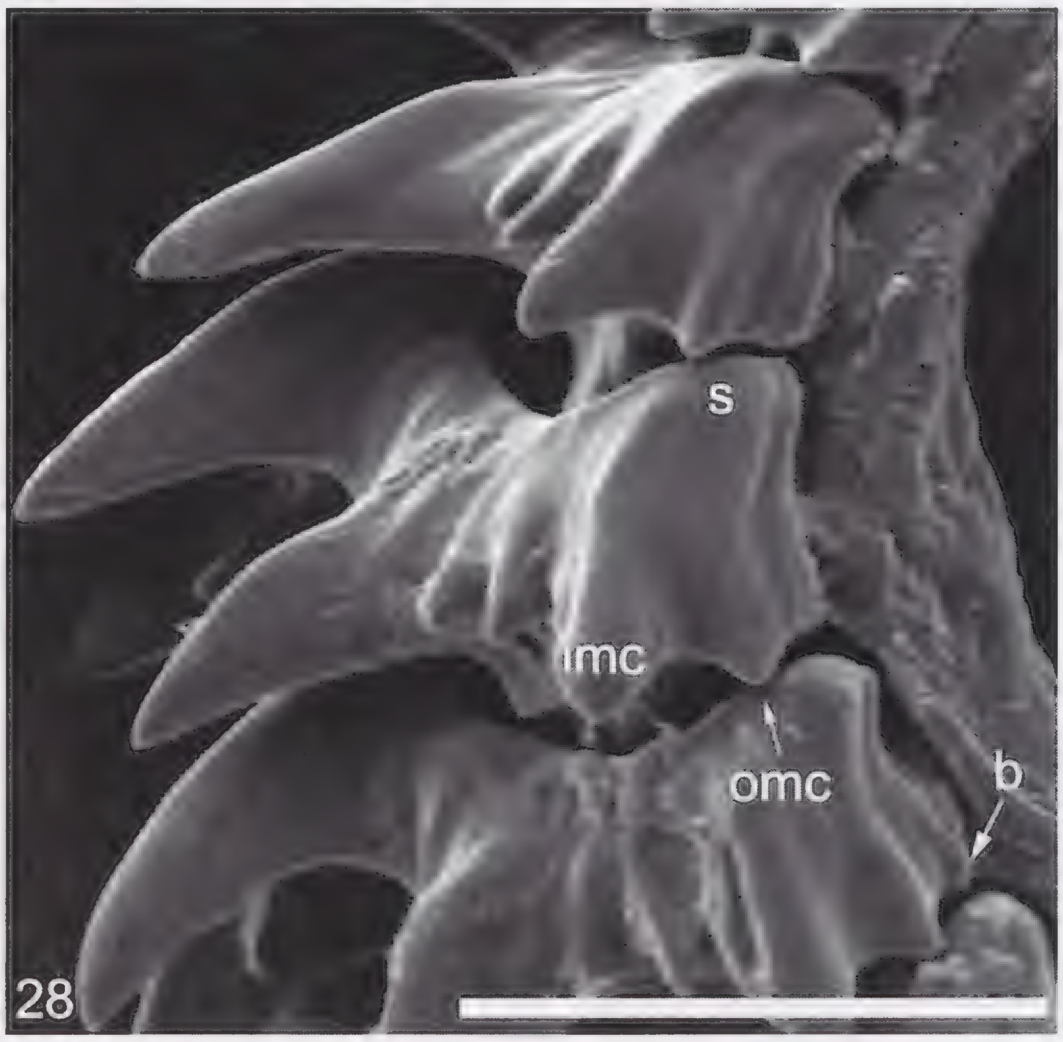
s
imc
omc
b
28

Remarks

The rachidian teeth of *V. perrugata* undergo relatively little shape or structural change between the early post-metamorphic and adult ontogenetic stages, which is similar to the development of another ocenebrine *Urosalpinx cinerea* (Say, 1822) (Herbert et al., 2007). Changes in *V. perrugata* are limited to moderate straightening of the center of the rachidian base, widening of the marginal area, and a shift from irregular to consistent, symmetrical expression of inner lateral denticles.

This species has traditionally been assigned to the genus *Urosalpinx*, but the fossil record of *V. perrugata* can be traced back to the Pleistocene species *Vokesinotus griffini* Petuch, 1991, from which it differs only in size (Petuch, 2003, 2013). The fossil record of *Vokesinotus* extends at least into the late Early Miocene and encompasses a genus-level clade represented by several independent lineages during the Pliocene and Early Pleistocene (Petuch, 1997).

DISCUSSION

Inferring the Plesiomorphic Developmental Sequence for the Muricidae

The rachidia of larval and early post-metamorphic muricids differ in predictable ways from those of adults, regardless of subfamily affiliation. Two differences, in particular, stand out. The smallest juveniles just after metamorphosis (< 1 mm shell length) tend to have a narrow rachidian base relative to conspecific adults, and expression of inner lateral denticles is typically irregular and asymmetric in juveniles but regular and symmetric in adults. The pervasiveness of these developmental trends across the Muricidae (Herbert et al., 2007; Pio et al., 2014; Herbert et al., this study), including within a basal lineage of the family – the genus *Timbellus* – suggests that these characteristics were likely part of the plesiomorphic radular ontogeny of the family. Inner lateral denticles are somewhat uncommon in neogastropods outside the Muricidae, but have been observed in species of Marginellidae, Harpidae, Vexillidae and two undescribed species of the Turbinellidae (Y. Kantor & Bruce Marshall, unpublished data) and Costellariidae (Sasha Fedosov, personal communication). In light of the presence of inner lateral denticles in adults of closely related neogastropods, inner lateral denticles were likely present in adults of the earliest progenitors of the Muricidae. We hypothesize that inner lateral denticles are homologous across the Neogastropoda and typical features of late ontogeny.

Another relatively common developmental pattern observed in some muricids is for early juvenile character states to be extended into adulthood. Examples include the relatively narrow, 3-D rachidia of some adult muricopsines and ocenebrines (Herbert et al., 2007), the asymmetric expression of inner lateral denticles in adult typhines and *Vitularia* (Radwin & D'Attilio, 1976; Houart, 1991; Herbert et al., 2007), and the absence of inner lateral denticles in adults of the muricine *Bouchetia vaubanensis* (Houart, 1986) (Houart & Héros, 2008: fig. 9C) and the rapanine *Vexilla vexillum* (Gmelin, 1791) (Kool, 1987: figs. 30–31). We hypothesize that these examples highlight the important role that developmental modification, specifically paedomorphosis, has played in the evolutionary diversification of the Muricidae. More detailed discussions of the role of developmental change in the evolution of the muricid radula can be found in Herbert et al. (2007) and Pio et al. (2014).

Evolution and Function of a 3-D Rachidian

Vokes (1971) was one of the first systematists to recognize that the rachidian base of muricids is either flat or has depth ("3-D"), and that this character might have phylogenetic significance. A 3-D rachidian tooth is present in larval and early post-metamorphic juveniles of the Ocenebrinae, Rapaninae, and Trophoninae and retained into adulthood in the Ocenebrinae (Herbert et al., 2007). It is also present in some adults of species of the Muricopsinae and

←

FIGS. 23–28. Dorsal and lateral views of rachidian tooth ontogeny of *Vokesinotus perrugatus*. FIG. 23: Tooth of a hatching specimen, SH = 2.8 mm; FIG. 24: Tooth of a hatching specimen, SH = 1.4 mm; FIGS. 25, 26: Tooth of an adult, SH = 25 mm; FIG. 27: Adult radula over the bending plane of the odontophore, SH = 25 mm; FIG. 28: Cusp-like ridge of rachidian base in adult radula, SH = 32 mm. Scale bars: Fig. 23 = 5 µm, Fig. 24 = 5 µm, Fig. 25 = 20 µm, Fig. 26 = 20 µm, Fig. 27 = 25 µm, Fig. 28 = 25 µm; b = base; bmc = bifid marginal cusp; b/mc = base/marginal cusp; cc = central cusp; ild = inner lateral denticle; lc = lateral cusp; old = outer lateral denticle; rm = radular membrane; tmc = third marginal cusp.

Muricinae (Houart, 1992; Herbert et al., 2007; this study). In most other muricids, including the basal lineage *Timbellus*, the rachidian is flat. This is consistent with Vokes' (1971) proposal that a flat rachidian ("muricine" condition) is the plesiomorphic state for the Muricidae.

What Vokes and others (e.g., Herbert et al., 2007) overlooked, however, is that a 3-D rachidian base can result from a bend or angle at a single point (near the rachidian center), at two points (at each lateral cusp, at each marginal cusp, or at each base margin), or at multiple points. In juvenile rapanines and juvenile and adult ocenebrines studied, the base has a single angle near its center to form a V-shape. A flat rachidian base characterizes many species assigned presently to the subfamily Muricinae, but the rachidian base of *C. dilectus* is bent at two points, once at each base margin, near the position of each lateral cusp. Houart (1992) showed similar 3-D morphology for a juvenile of the muricine *Chicoreus torrefactus* (G. B. Sowerby II, 1841). Ocenebrine rachidia are also bent at each of the margins but at the position of each marginal cusp instead of the base margin. Ocenebrine rachidia may also be bent slightly at the lateral cusp positions.

Herbert et al. (2007) proposed that a 3-D rachidian base could be a functional adaptation that helps the tooth withstand mechanical stresses of predatory drilling, a common mode of attack of muricids in which the radula is used along with chemical secretions of the accessory boring organ to bore a hole through the shells of molluscan or barnacle prey. Herbert et al. (2007) based this hypothesis on the fact that a 3-D rachidian is present early in the ontogeny of the rapanine *Concholepas concholepas* when it employs its radula for mechanical drilling of shelled prey but is lost in ontogeny when juveniles begin to kill prey by other means (e.g., toxins) and use the radula primarily for tearing soft flesh (Herbert et al., 2007, and references therein). Drilling is also the predominant form of attack among small ocenebrines and muricopsines, in which the 3-D adult rachidian morphology is expressed in its most extreme form, while a flat rachidian base is more common in muricids that employ toxins and other modes of attack that do not require similar mechanical stresses on radular teeth (reviewed by Herbert et al., 2007).

Evolutionary Innovation at the Rachidian Base

The number of marginal cusps at the rachidian base endpoints has traditionally been used to delineate muricid subfamilies, but here and in previous work (Pio et al., 2014), we have shown that the number of marginal cusps can increase or decrease during normal development within a single individual. In basal muricids, such as *T. phyllopterus*, the adult rachidian base margin is tapered to a dull point (a pseudo-marginal cusp) that is adherent to the radular membrane along its entire length. In other muricids, including adult *C. dilectus* and *S. biserialis,* however, this base margin is detached from the supporting membrane and occupies a more medial position to form a true marginal cusp. In *C. dilectus*, this detachment occurs during ontogeny, and the developmental continuity between the base end-point and marginal cusp in this species reveals that they are homologous structures. The part of the base still adherent to the radular membrane expands in some muricids to form what is often described as a distinct character – the basal lobe (see Kool, 1993). Pio et al. (2014) showed that within the development of *Trophon geversianus* (Pallas, 1774), this lobe can also develop into a pointed structure (a pseudo-marginal cusp) and become detached from the membrane during ontogeny to produce a second (outer) marginal cusp behind the first (inner) marginal cusp. In some species of the Ocenebrinae and Muricopsinae, a new lobe forms again behind the second marginal cusp. The outer edge of this new lobe often takes on a ridged or cusp-like appearance, giving the rachidian margins of these ocenebrines and muricopsines a tri-cusped appearance (Herbert et al., 2007; Pio et al., 2014; Herbert, unpublished data).This process of detachment of the rachidian base end-point from the radular membrane provides a mechanistic explanation for the origin of marginal cusps in general, and the repetition of this single mechanism in some lineages up to three times suggests that acquisition of one or more marginal cusps has likely occurred multiple times in the Muricidae via convergent evolution.

ACKNOWLEDGMENTS

We gratefully acknowledge donation of the juvenile *S. biserialis* by E. A. Lazo-Wasem (Peabody Museum of Natural History, Yale University) and assistance with scanning electron microscopy from Fabian Tricárico (MACN). This work was supported by a grant from the University of South Florida to GSH and a fellowship from Consejo Nacional de Investigaciones Científicas y Técnicas (CONICET) of Argentina to MJP.

LITERATURE CITED

ADAMS, A., 1855, Descriptions of two new genera and several new species of Mollusca, from the collection of Hugh Cuming, Esq. *Proceedings of the Zoological Society of London*, 23: 119–124.

BARCO, A., M. CLAREMONT, D. G. REID, R. HOUART, P. BOUCHET, S. T. WILLIAMS, C. CRUAUD, A. COULOUX & M. OLIVERIO, 2010, A molecular phylogenetic framework for the Muricidae, a diverse family of carnivorous gastropods. *Molecular Phylogenetics and Evolution*, 56: 1025–1039.

BLAINVILLE, H. DE, 1832, Disposition méthodique des espèces Récentes et fossiles des genres pourpre, ricinule, licorne et concholepas de M. de Lamarck et déscription des espèces nouvelles ou peu connues faisant partie de la collection du Muséurn d'Histoire Naturelle de Paris. *Nouvelles Annales du Muséum d'Histoire Naturelle de Paris*, 1: 189–263.

CONRAD, T. A., 1846, Catalogue of shells inhabiting Tampa Bay and other parts of the Florida Coast. *American Journal of Science*, 2: 393–398.

DISALVO, L., 1988, Observations on the larval and post-metamorphic life of *Concholepas concholepas* in laboratory culture. *The Veliger*, 30: 358–368.

DISALVO, L. H. & M. R. CARRIKER, 1994, Planktonic, metamorphic, and early benthic behavior of the chilean loco *Concholepas concholepas* (Muricidae, Gastropoda, Mollusca). *Journal of Shellfish Research*, 13: 57–66.

FUJIOKA, Y., 1984, Remarks on two species of the genus *Drupella* (Muricidae). *Venus*, 43: 44–54.

FUJIOKA, Y., 1985, Systematic evaluation of radular characters inThaidinae (Gastropoda: Muricidae). *Journal of Science of the Hiroshima University (B, 1, Zoology)*, 31: 235–287.

GARVIE, C. L., 1991, Two new species of Muricinae from the Cretaceous and Paleocene of the Gulf Coastal Plain, with comments on the genus *Odontopolys* Gabb, 1860. *Tulane Studies in Geology and Paleontology*, 24: 87–92.

GURALNICK, R. P. & D. R. LINDBERG, 1999, Integrating developmental evolutionary patterns and mechanisms: a case study using the gastropod radula. *Evolution*, 53(2): 447–459.

HERBERT, G. S., D. MERLE & C. S. GALLARDO, 2007, A developmental perspective on evolutionary innovation in the radula of the predatory neogastropod family Muricidae. *American Malacological Bulletin*, 23: 17–32.

HOUART, R., 1991, Mollusca Gastropoda: the Typhinae (Muricidae) from the New Caledonian region with description of five new species. *Mémoires du Muséum National d'Histoire* naturelle, *Zoologie,* (A) 150. *Résultats des Campagnes MUSORSTOM*, 7: 223–241.

HOUART, R., 1992, The genus *Chicoreus* and related genera (Gastropoda: Muricidae) in the Indo-West Pacific. *Mémoires du Muséum National d'Histoire* Naturelle. *Zoologie*, Tome (A) 154: 1–188.

HOUART, R. & V. HÉROS, 2008, Muricidae (Mollusca: Gastropoda) from Fiji and Tonga. In: V. HÉROS, R. H. COWIE & P. BOUCHET, eds., *Tropical Deep-Sea Benthos 25. Mémoires du Muséum National d'Histoire Naturelle*, 196: 437–480.

KERTH, K., 1979, Electron microscopic studies on radular tooth formation in the snail *Helix pomatia* L. and *Limax flavus* L. (Pulmonata, Stylomatophora). *Cell and Tissue Research*, 203: 283–289.

KOOL, S. P., 1987, Significance of radular characters in reconstruction of thaidid phylogeny (Neogastropoda: Muricacea). *The Nautilus*, 101: 117–132.

KOOL, S. P., 1993, Phylogenetic analysis of the Rapaninae (Neogastropoda: Muricidae), *Malacologia*, 35: 155–259.

LAMARCK, J. B. M., 1822, Histoire naturelle des animaux sans vertèbres. Paris, 711 pp.

MERLE, D., 1999, La Radiation des Muricidae (Gastropoda: Neogastropoda) au Paléogène: Approche Phylogénétique et Évolutive. *Ph.D. Dissertation.* Muséum National d'Histoire Naturelle, Paris, i-vi + 499 pp.

MERLE, D., B. GARRIGUES & J. P. POINTIER, 2011, *Fossil and Recent Muricidae of the World. Part I Muricinae*. ConchBooks, Hackenheim, 648 pp.

MINICHEV, A. S. & B. J. SIRENKO, 1974, Development and evolution of radula in Polyplacophora. *Zoologicheskii Zhurnal*, 53: 1133–1139.

NYBAKKEN, J., 1990, Ontogenic change in the *Conus* radula, its form, distribution among the radula types, and significance in systematics and ecology. *Malacologia*, 32(1): 35–54.

NYBAKKEN, J. & F. PERRON, 1988, Ontogenetic change in the radula of *Conus magus* (Gastropoda). *Marine Biology*, 98(2): 239–242.

PAGE, A. J. & R. C. WILLAN, 1988, Ontogenetic change in the radula of the gastropod *Epitonium billeeana* (Prosobranchia: Epitoniidae). *The Veliger*, 30(3): 222–229.

PASTORINO, G. & P. E. PENCHASZADEH, 2009, Egg-capsules, eggs and embryos of *Trophon acanthodes* (Gastropoda: Muricidae) and its new generic position. *Journal of Molluscan Studies*, 75: 337–341.

PASTORINO, G., P. E. PENCHASZADEH & F. SCARABINO, 2007, Egg-capsules, eggs and embryos of the southwestern Atlantic gastropod *Coronium coronatum* (Mollusca: Muricidae). *Journal of Molluscan Studies*, 73: 61–65.

PETUCH, E. J., 1997, *Coastal paleoceanography of eastern North America:* (*Miocene-Pleistocene*). Kendall/Hunt Publishing Company, Dubuque, Iowa, 373 pp.

PETUCH, E. J., 2003, *Cenozoic seas: the view from eastern North America*. CRC Press, Boca Raton, Florida, 328 pp.

PETUCH, E. J., 2013, *Biogeography and biodiversity of western Atlantic mollusks.* CRC Press.

PIO, M. J., G. S. HERBERT & G. PASTORINO, G., 2014, Developmental origins of complex radular characters in the Muricidae: the bifid rachidian edge. *Invertebrate Biology*, 133: 64–73.

POINTIER, J. P. & D. LAMY, 1985, Rearing of *Pterynotus phyllopterus*, Mollusca, Muricidae from Guadalupe (French West Indies). *Proceedings of the Fifth International Coral Reef Congress, Tahiti*, 5: 171–176.

PONDER, W. F. & E. H. VOKES, 1988, A revision of the Indo-west Pacific fossil and Recent species of *Murex* s.s. and *Haustellum* (Mollusca: Gastropoda: Muricidae). *Records of the Australian Museum*, Supplement 8: 1–160.

RADWIN, G. E. & A. D'ATTILIO, 1971, Muricacean supraspecific taxonomy based on the shell and radula. *Western Society of Malacologists, The Echo*, 4: 55–67.

RADWIN, G. E. & A. D'ATTILIO, 1976, *Murex shells of the world: an illustrated guide to the Muricidae*. Stanford University Press, Stanford, California, 284 pp.

RICHTER, G., 1961, Die Radula der Atlantiden (Heteropoda, Prosobranchia) und ihre Bedeutung für die Systematik und Evolution der Familie. *Zeitschrift für Morphologie und Ökologie der Tiere*, 50: 163–238.

STERKI, V., 1893, Growth changes of the radula in land mollusks. *Proceedings of the Academy of Natural Sciences of Philadelphia*, 45: 388–400.

TAN, K. S., 2003, Phylogenetic analysis and taxonomy of some southern Australian and New Zealand Muricidae (Mollusca: Neogastropoda). *Journal of Natural History*, 37: 911–1028.

VOKES, E. H., 1971, The geologic history of the Muricinae and the Ocenebrinae. *Western Society of Malacologists, The Echo*, 4: 37–54.

VOKES, E. H., 1990, Cenozoic Muricidae of the western Atlantic region, Part VIII. *Murex* (s.s.), *Haustellum*, *Chicoreus*, *Hexaplex*; additions and corrections. *Tulane Studies in Geology and Paleontology*, 23: 1–96.

VOKES, E. H., 1992, Cenozoic Muricidae of the western Atlantic region Part IX. *Pterinotus, Poirieria, Aspella, Demomurex, Calotrophon, Acantholabia* and *Attiliosa*, additions and corrections. *Tulane Studies in Geology and Paleontology*, 25: 1–108.

WARÉN, A., 1990, Ontogenetic changes in the trochoidean (Archaeogastropoda) radula, with some phylogenetic interpretations. *Zoologica Scripta*, 19(2), 179–187.

Revised ms. accepted July 16, 2014

MALACOLOGIA, 2015, 58(1–2): 337–347

OVIPOSITION AND EMBRYONIC DEVELOPMENT IN THE VOLUTID SNAIL *ADELOMELON ANCILLA*

Soledad Zabala[1*], Andrés Averbuj[1], Carlos Sanchez Antelo[2],
Pablo E. Penchaszadeh[2] & Gregorio Bigatti[1,3]

ABSTRACT

Intracapsular embryonic development is common in marine gastropods. In many species, embryos obtain nutrition during ontogeny by ingesting substances contained in the intracapsular fluid. South American volutids spawn egg capsules containing relatively few eggs, and development is entirely intracapsular, with young hatching as crawl-away juveniles. The spawning habits, egg capsules morphology and embryonic development of the South American volutid *Adelomelon ancilla* is described in this work. Egg capsules of *A. ancilla* (n = 42) contained 3.0 ± 1.4 (mean ± SD) embryos with a range of 1–6 eggs or embryos. The embryonic morphological changes and body spiralization occur simultaneously with embryo feeding. All embryos within a single egg capsule shared the same developmental stage. No evidence of cannibalism or intracapsular competition was found, suggesting that food is not a limiting resource as in other volutid species. Estimated intracapsular developmental time varied between five and six months (between 12–14°C). The long developmental time and low number of embryos inside the egg capsules, together with late reproductive maturity and longevity of adult individuals, reinforce the statement that the neogastropod *Adelomelon ancilla* is a fragile resource that must be conserved in Argentinean benthic communities.

Keywords: Neogastropoda, Volutidae, Patagonia, egg capsules, intracapsular development.

INTRODUCTION

Intracapsular embryonic development is common in marine gastropods. All neogastropods lay egg capsules that protect their embryos, however, little is known about the structure, composition and intracapsular fluids of these capsules (D'Asaro, 1988; Miloslavich, 1996a, b; Rawlings, 1999; Bigatti et al., 2014). In many species, embryos ingest substances contained in the intracapsular fluid during development, which provide nutrition during ontogeny.

Little is known about the development of the family Volutidae, with the exception of some recently studied South American species (Penchaszadeh & De Mahieu, 1976; Penchaszadeh et al., 1999; Penchaszadeh & Miloslavich, 2001; Penchaszadeh & Segade, 2009; Bigatti et al., 2014). There are significant differences regarding developmental modes among volutids, associated mainly with the geographic region they inhabit (Penchaszadeh et al., 1999), always showing a similar pattern within each group. The first pattern, observed in West African volutids consists of the incubation of one spherical egg capsule in a pedal gland. Developing eggs and ~100,000 nurse eggs are present; hatching mode being a shelled veliger (Marche-Marchad, 1968, 1980). The second mode, found in Indo-Pacific and Australian volutids, consists of an egg mass with numerous capsules attached to hard substrata. Only a single embryo develops per egg capsule; embryonic nutrition remains unknown (Amio, 1963; Knudsen, 1993). Finally, the third mode observed in South American volutids, involves the attachment of large egg capsules to hard substrata, containing few embryos inside, with the exception of the free demersal egg capsules of the volutid *Adelomelon brasiliana* (Penchaszadeh et al., 1999). Embryos feed on

---

[1]LARBIM – CENPAT – CONICET, Bvd. Brown 2915, U9120ACD, Puerto Madryn, Chubut, Argentina.
[2]Museo Argentino de Ciencias Naturales "Bernardino Rivadavia" – CONICET, Av. Ángel Gallardo 470, C1405DJR, Buenos Aires, Argentina.
[3]UNPSJB, Universidad Nacional de la Patagonia San Juan Bosco, Bvd. Brown 3100, Puerto Madryn, Argentina.
*Corresponding author: zabala@cenpat.edu.ar

intracapsular proteic liquid and hatch as crawling juveniles. These species occur in a wide variety of forms, both in the intertidal and the subtidal zones. The embryonic development of these volutids is completed within the egg capsules, without free larval stages (Ponder, 1974; Pechenik, 1986; Miloslavich, 1996a, b; Penchaszadeh & Segade, 2009; Bigatti et al., 2010, 2014). In particular, *Adelomelon ancilla* (Lightfoot, 1786) was not studied before in respect to its oviposition modality and developmental biology.

The marine snail *Adelomelon ancilla* is an edible neogastropod belonging to the family Volutidae, which is distributed along the southern tip of South America, from 35°S (Brazil) in the southwestern Atlantic to Ushuaia in the Beagle Channel (Zabala, 2013), the Malvinas/Falkland islands and northward into the Pacific, reaching central Chile (25°S, Chiloé Island; Castellanos & Landoni, 1992). This species attaches its egg capsules individually to hard substrates, such as empty bivalve shells or stones. Hatching occurs at the crawling stage, after complete intracapsular development while feeding on the intracapsular fluid (Penchaszadeh & De Mahieu, 1976); however, there is no detailed information about its embryonic development. While their gametogenic cycle, diet and population parameters have been well documented (Penchaszadeh et al., 2009; Zabala et al., 2013a, b), further work is necessary to provide a complete description of intracapsular development. Along the Patagonian shore, *A. ancilla* inhabits shallow waters (from 5 m depth) on gravels or mixed bottoms and lives most of the time buried in the substrate. This species is a top-predator of benthic communities, preying principally on other gastropods and on bivalves (Zabala et al., 2013a). The oviposition season occurs from July to November (Winter–Spring) and it is correlated with the gametogenic cycle, both related with the photoperiod (Penchaszadeh et al., 2009). In Golfo Nuevo, the water temperature varies from 9.7°C to 18.3°C (Spring – Fall, respectively), and the photoperiod varies from 9 to 15 h of light.

The aim of this work was to study the oviposition, embryonic development, developmental time, egg capsule morphology and structure of *Adelomelon ancilla* from Patagonian shallow waters. A comparison with other members of the Volutidae family is included.

MATERIALS AND METHODS

Sampling in Patagonian Shallow Waters

Field samples and observations were made monthly from March 2008 to December 2011, in Nuevo Gulf (NG), Patagonia (42°48'S, 64°54'W; Fig. 1). Collection of specimens and egg capsules of *A. ancilla* were performed by SCUBA diving on mixed bottoms at depths between 6 and 10 m. Bottom water temperature was measured *in situ* for the same period of time by Dellatorre et al. (2012).

General Features of Egg Capsules

An extensive investigation on the oviposition process and developmental biology of *Adelomelon ancilla* from the shallow waters of NG was performed. The substrate of oviposition was recorded for each of 84 collected egg capsules. Diameter (maximum width) and height were measured with a 0.1-mm precision digital caliper for all egg capsules.

In order to determinate the number of layers of the egg capsule walls and to assess changes throughout the developmental stages, portions cut from recently laid egg capsules and at hatching were observed under scanning electronic microscopy (SEM). Samples were first fixed in glutaraldehyde in phosphate buffer (pH: 7.4) for 6 h, dehydrated in a graded ethanol series, critical-point dried, mounted and coated with gold in a Denton Vacuum Desk IV. Observation and photography were conducted with a JEOL JSM-6460LV SEM.

In order to test if egg capsules were composed of a calcareous cover as in other volutids (Bigatti et al., 2010), newly laid capsules were treated with 50% hydrochloric acid to determine if CO_2 bubbles were produced. In addition, elemental analysis was performed in recently laid egg capsule, fixed as described above for SEM, with the same microscopy equipped with an EDAX PW 7757/78 X-ray energy scattering microanalyser, for standardless element quantification.

Embryonic Development

Forty two egg capsules were randomly chosen from the total sample and dissected. The number of eggs/embryos per egg capsule was counted under a light microscope, and the intracapsular egg diameter was measured be-

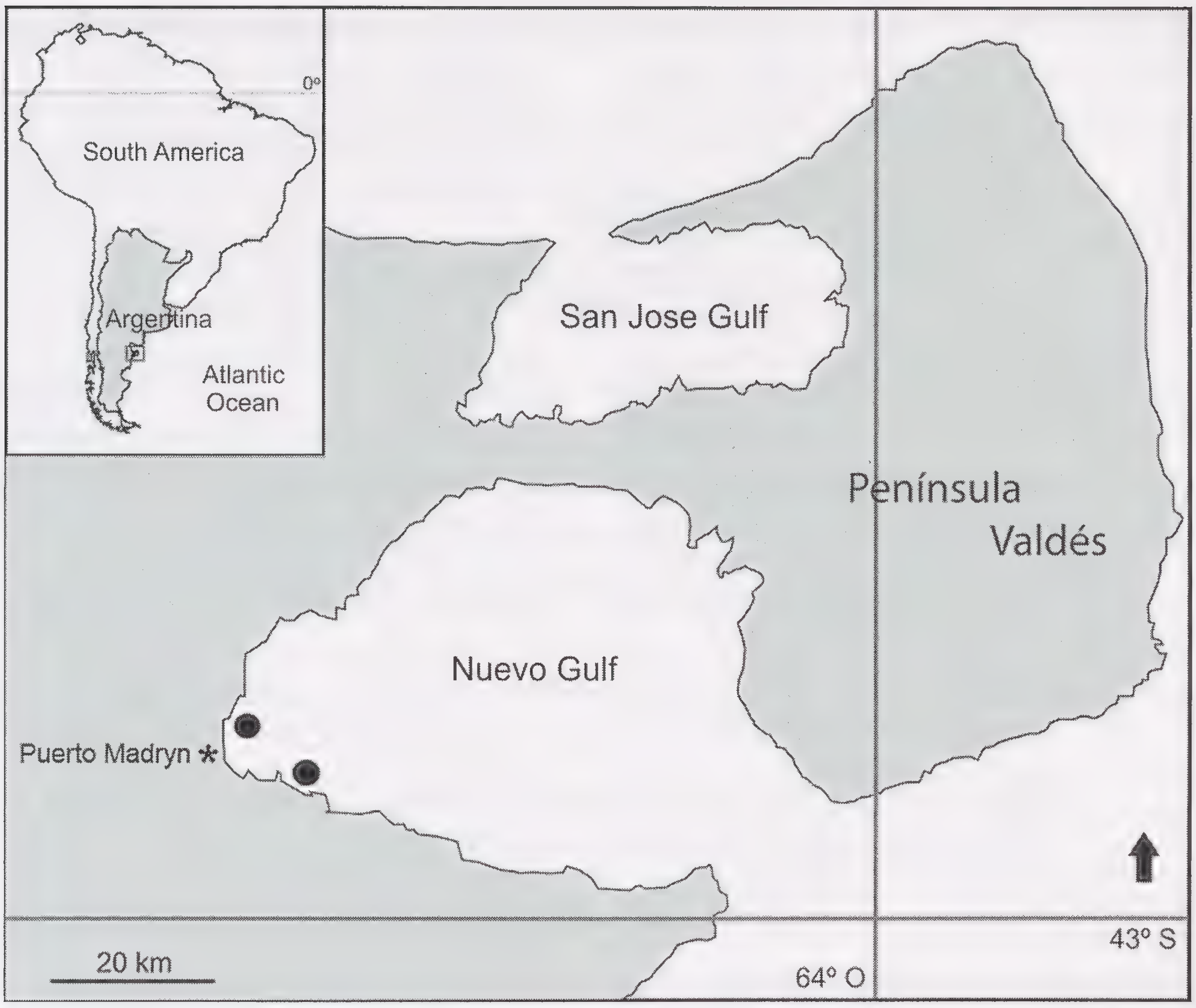

FIG. 1. Sampling site (black dots) of *Adelomelon ancilla* egg capsules in Nuevo gulf.

fore cell division whenever possible. Embryos within the egg capsules were classified into one of six developmental stages: 0 (Egg), 1 (Morula/Gastrula), 2 ("Veliger"), 3 ("Pediveliger"), 4 (Coiling Embryo) and 5 (Hatchling); for a detailed description see Table 1. Total length of the embryos was measured at each developmental stage. In addition, the number of juveniles per egg capsule was counted and measured in all intact egg capsules. All measurements were made with a stereoscopic microscope with a 0.01-mm precision ocular micrometer. Velum size was recorded as the maximum width when expanded.

Throughout the study period, 42 egg capsules in different stages of development, including stage 0 (the female was laying the egg capsule at moment of sampling), were collected in NG and maintained in separate conditioned aquaria. Physical parameters included maintenance of salinity at 35 ppm in accordance with field measurements and a photoperiod of 12:12 h light: dark. Temperature ranged between 12 and 14°C (late spring temperature). Total developmental time was recorded.

RESULTS

General Features of Egg Capsules

Egg capsules measured an average of 32.54 ± 4.61 mm (mean ± SD) in width and 28.80 ± 5.94 mm in height (n = 84). Most egg capsules were attached on the concave side (95.2%) of empty shells of the clam *Eurhomalea exalbida* (92%) or *Ameghinomya antiqua* (8%), both belonging to the family Veneridae (Figs. 2, 3). Egg capsules were deposited on the convex side of empty bivalve shells only in 4.8% of the cases.

Oviposition was observed *in situ* during diving samplings at NG. The process involved several steps. Initially, the female fastened her muscular foot to the substrate where the egg capsules were eventually laid. Then, the soft egg capsule was expulsed through the vagina of the female, covered with her foot, and eventually attached to the substrate probably by pedal gland secretions. Finally, the female fixed and molded the egg capsule with her pedal gland located on the sole of the foot, giving it shape and rigidity. The egg capsules

TABLE 1. Embryonic development of *Adelomelon ancilla.* Values represent mean size ± SD and range (parenthesis).

Embryo stage	Desciption	Mean embryos size (in mm)
Egg	Round and whitish, before cellular cleavage. Polar body present.	0.209 ± 0.053 (N = 15) (0.175–0.220)
Morula/Gastrula	Roundish embryo with >16 cells.	0.219 ± 0.046 (N = 21) (0.200–0.240)
"Veliger"	Embryo with ciliated velum in constant development, mouth and scarce intracapsular fluid into the stomach.	1.523 ± 0.655 (N = 19) (0.880–2.730)
"Pediveliger"	Velum developed, increase of intracapsular fluid into the stomach. Incipient foot.	3.798 ± 0.754 (N = 11) (1.950–4.850)
Coiled embryo	Foot completely developed, resorption of velum; presence of shell gland; beginning of anterior shell calcification.	9.005 ± 1.284 (N = 28) (7.100–10.640)
Hatchling	Juvenile hatches as miniature adult; calcified shell with violet band colors; egg capsules opening visible	10.386 ± 1.074 (N = 47) (7.500–11.380)

are externally white, large rounded and flat (Figs. 2, 3). The test with HCl was negative for the presence of a calcareous cover of the egg capsule. Furthermore, EDAX analysis of layered egg capsule wall showed only peaks for C and O and was negative for the presence of Mg and Ca element peaks. The minimum shell length of females from NG laying egg capsules was 114 mm.

Each capsule contained 3.0 ± 1.4 embryos (mean ± SD) with a range of 1–6 or embryos (n = 42). No plug or opercular opening was observed in any of the studied egg capsules. The hatching area of the egg capsule was predetermined and was always observed as a suture line on one side of the egg capsules, close to its bottom. The egg capsules were composed of different layers according to their developmental stage. Newly

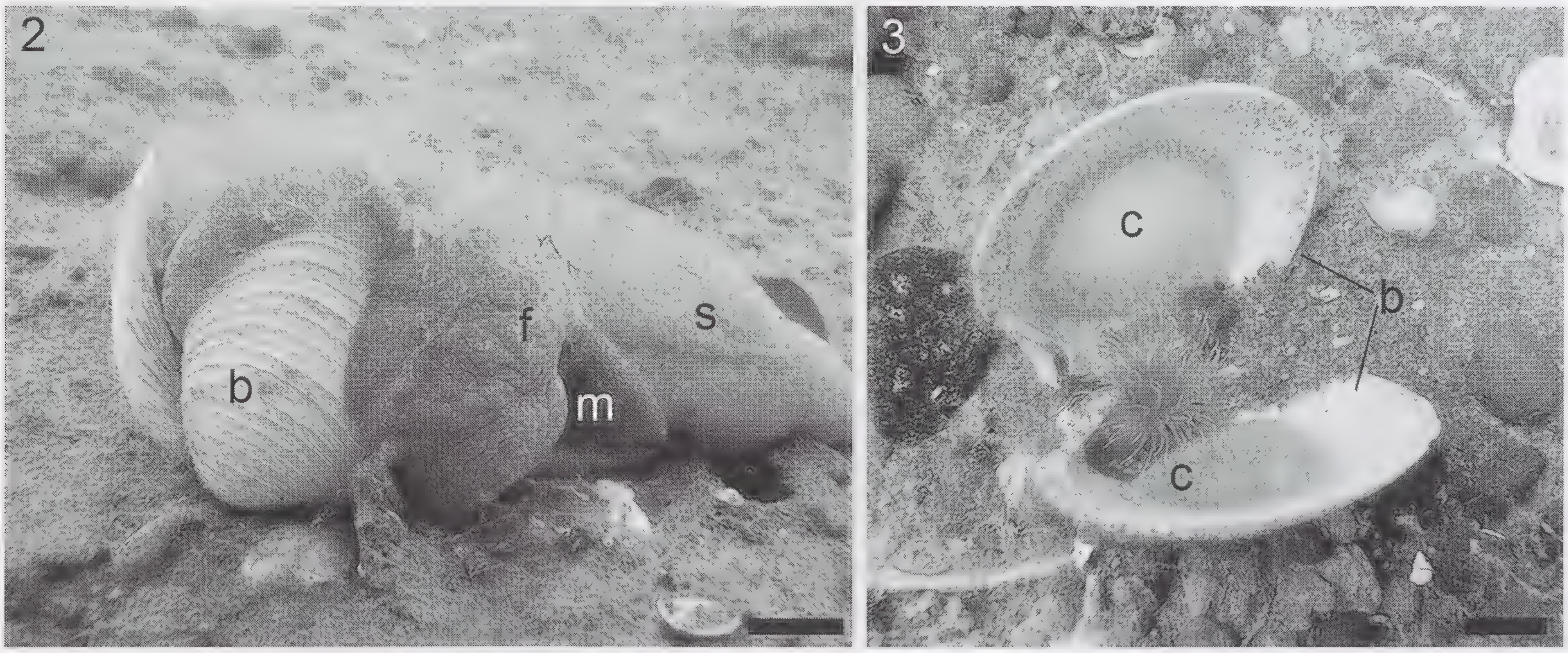

FIGS. 2, 3. Oviposition of *Adelomelon ancilla* in the field. FIG. 2: *A. ancilla* laying an egg capsule onto a bivalve (*Eurhomalea exalbida*) empty shell; FIG. 3: Egg capsules of *A. ancilla* deposited in the concave portion of empty bivalve (*E. exalbida*) shell, note the difference in color that corresponds to early (white) and late (translucent) developmental stages. Abbreviations: b: bivalve shell; c: capsule; f: foot; m: mouth; s: shell. Scale bars: Figs. 2, 3 = 1 cm.

laid egg capsules contained three distinguishable layers (Fig. 4), whereas those found at late stages of development presented only two layers (Fig. 5). The outer and inner layers appeared amorphous in aspect; meanwhile, the medium layer was observed as a laminar structure (Figs. 4, 5). At the same time, the wall's thickness of the inner layer varied depending on development stage. This inner layer was reduced in advanced developmental stages, and completely absent at the hatching stage. At the same time, as embryos grew in size, intracapsular nutrient fluids adhered onto the inner surface of the egg capsule were consumed by juveniles using their radulae. Macroscopically, the intracapsular fluid was characterized by two components: (1) viscous whitish aggregates in which eggs and embryos were immersed and which made the localization and removal of eggs very difficult. This viscous phase decreased in quantity as the embryo development progressed, giving the egg capsule an increasingly transparent aspect; and (2) an almost transparent liquid, which enabled the observation of the embryos inside the egg capsule.

Embryonic Development

Newly laid egg capsules contained uncleaved eggs that measured 0.209 ± 0.053 mm (mean ± SD) in mean maximum diameter. Cell cleavage was spiral and holoblastic with the presence of polar bodies (Fig. 6). The next observed stage was of four cells (Fig. 7), followed by the morula stage (Fig. 8) and then a gastrula (Fig. 9). In all these developmental stages, the size remained approximately the same. The "trochophore" stage was not observed during this study, probably due to its short time of occurrence.

As a general rule, once the "veliger" stage was reached the embryos fed on the intracapsular fluid continuously, and morphological changes (organ formation and body spiralization) ensued. The mouth and stomach were recorded at the "veliger" stage in which embryos were active, showing both rotational and translational movements produced by velum cilliary currents. This stage was divided into an early and a late "veliger", each characterized by the presence of a velum of different size, shape and functionality. The early "veliger" velum was an incipient ciliated band at the anterior region (Fig. 10) that corresponded to the cephalic area of the embryo. Meanwhile, the late "veliger" velum was a lobed-shape structure with a band of cilia involved in feeding and mobility (Figs. 11, 12). At advanced late "veliger" stages, the large ciliated velum increased its size and activity, which produced a current drawing food into the mouth. On the velum area, transparent vacuolar cells (athrocytes) were distinguished (Figs. 11, 12). At this stage, the mouth and visceral mass were clearly observed (Figs. 11, 12), while the body began to appear bottle-shaped. At this stage, the velum size (2.03 mm ± 0.011 (mean ± SD, n = 19)) was equal or larger than the body mass. On occasion, nutrient particles were noted in the embryo's stomach.

At the "pediveliger" stage, a foot began to develop. The velum reached its maximum size (2.60 mm ± 0.14 (mean ± SD, n = 11)) (Fig. 13), and remained active collecting food

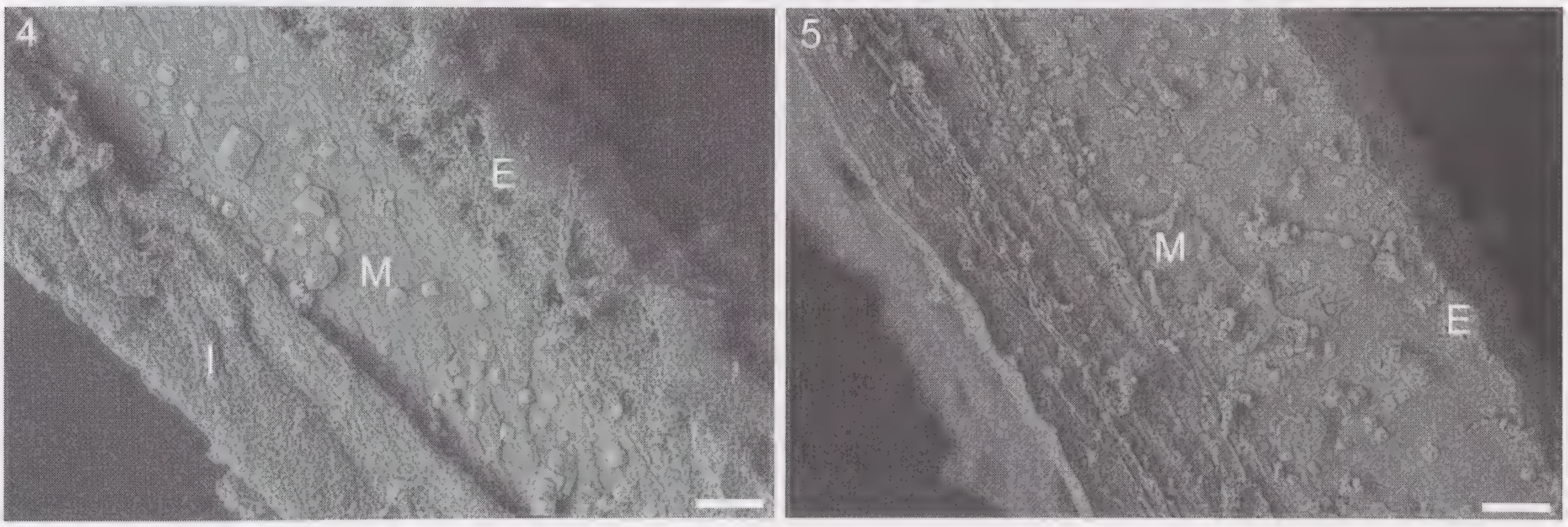

FIGS. 4, 5. Egg capsule wall of *A. ancilla* by Scanning Electron Microscopy (SEM). FIG. 4: Egg capsule recently laid showing 3 layers; FIG. 5: Egg capsule already hatched presenting only 2 layers. Abbreviations: E: external, I: inner, M: medium. Scale bars: Figs. 4, 5 = 20 μm.

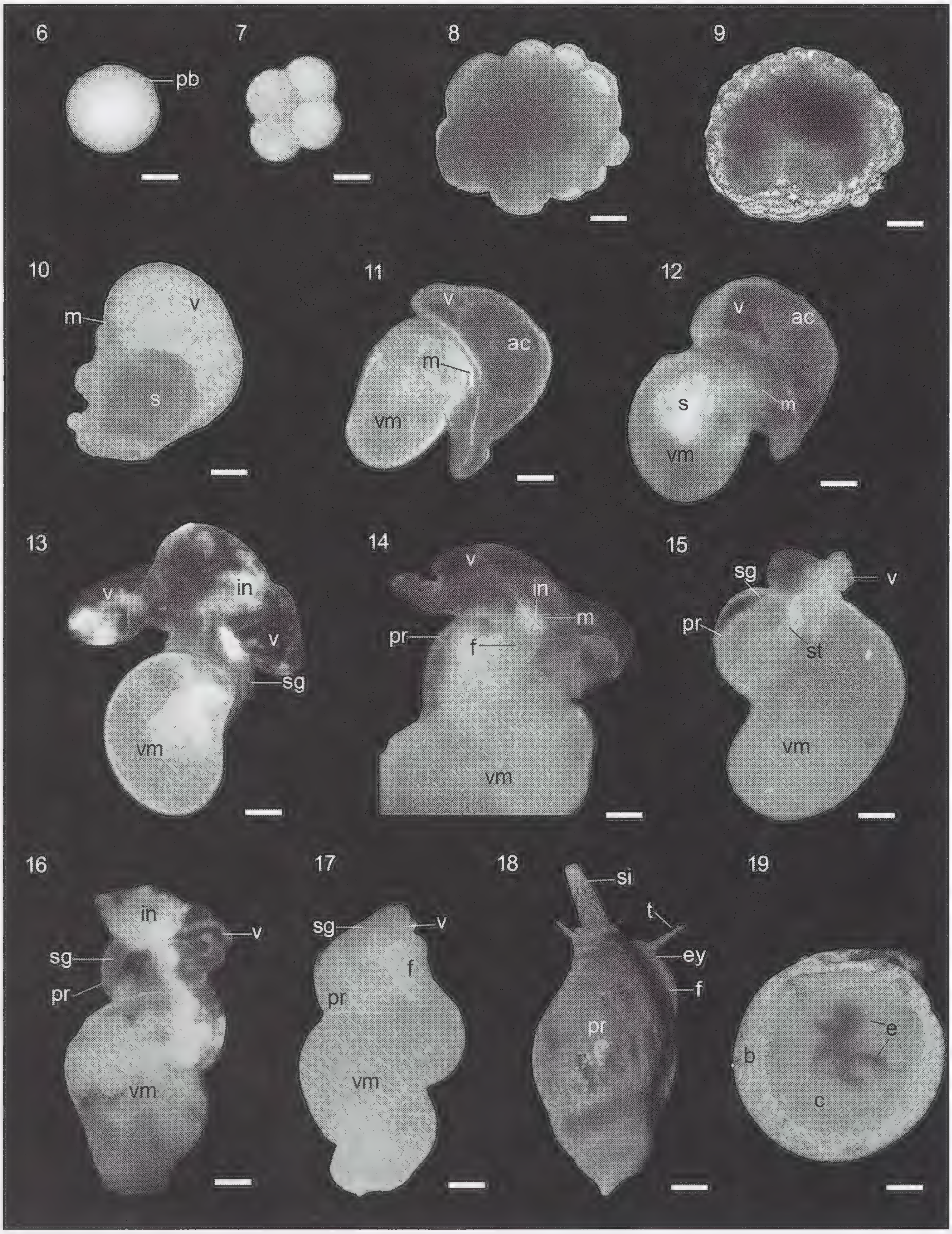

FIGS. 6–19. Embryological development of *Adelomelon ancilla*. FIG. 6: Egg without cleavage. Note the polar lobe; FIG. 7: 4-Cell stage; FIG. 8: Morula; FIG. 9: Gastrula; FIG. 10: Early "veliger" stage with incipient velum; FIG. 11: Embryo "veliger" stage with velum developed; FIG. 12: Embryo "veliger" stage with intracapsular nutrient into the stomach. The velum is expanded and the stomach is visible by transparency. Note the athrocyte cells in the velum; FIG. 13: Early "pediveliger" stage with intracapsular nutrient in the velum and stomach; FIG. 14: "Pediveliger" stage; note the foot and the shell gland; FIG. 15: Embryo in early coiled-shell stage; the shell gland that secretes the protoconch is visible and the velum began to reabsorb; FIG. 16: Coiled-shell embryo; note that ingestion of intracapsular nutrient (white) is still occurring at this stage; FIG. 17: Coiled-shell embryo presenting spiralization, foot and protoconch developed; FIG. 18: Hatchling; FIG. 19: Egg capsule with crawling juveniles (pre-hatchlings) inside. Abbreviations: ac: athrocytes cells; b: bivalve; c: egg capsule; e: embryos; ey: eye; f: foot; in: intracapsular nutrient; m: mouth; pb: polar body; pr: protoconch; s: stomach, sg: shell gland; si: siphon, t: tentacle, v: velum; vm: visceral mass. Scale bars: Figs. 6, 7 = 100 µm, Figs. 8, 9 = 50 µm, Fig. 10 = 300 µm, Figs. 11–13 = 400 µm, Fig. 14 = 500 µm, Fig. 15 = 700 µm, Fig. 16 = 900 µm, Figs. 17, 18 = 1mm, Fig. 19 = 1 cm.

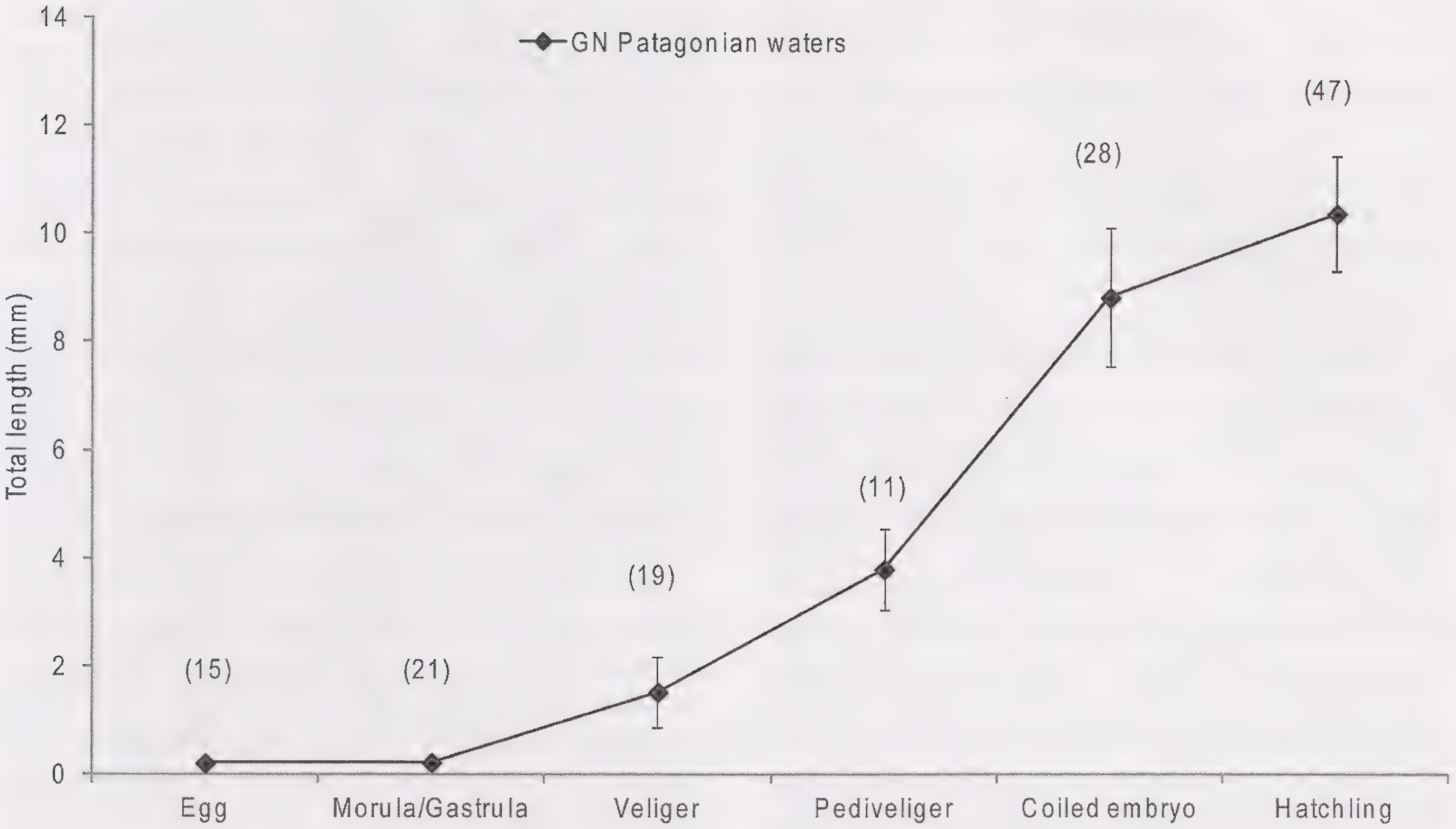

FIG. 20. Size variation throughout development of *Adelomelon ancilla* (bars show SD and parenthesis indicate the number of individuals measured (N) for each stage).

that was ingested and then digested in the stomach (Figs. 13, 14). Associated with this, the embryonic movements decreased. The visceral mass size, filled with intracapsular nutrients, developed faster in relation to the cephalic region. The shell gland appeared as a scalloped edge on the basis of the cephalic structures (Fig. 13).

The coiling embryo stage was characterized by the presence of a greatly reduced velum (1.28 mm ± 0.20 (mean ± SD, n = 28)), which was completely reabsorbed by the end of this stage (Fig. 15). Throughout development of the coiling stage, the embryo was observed increasing degrees of external body coiling; late coiling embryo recorded at least one full-turn of the visceral mass. Calcification of the protoconch, although still thin and fragile, began at this stage by the shell gland situated on the mantle edge (Figs. 15, 16). The deposition of calcium appeared as an antero-posterior directed process, starting at the shell-gland cells which accompanied body growth direction, and finishing at the apex region before embryonic hatching (Figs. 15–17).

The hatchling stage was characterized by the early presence of a fully developed calcified protoconch in the embryo, with the occasional and temporary exception of specific small rounded areas on the apical side of the shell (Fig. 17). Hatchling juveniles had the typical white and pink epidermal pigmentation of the adult clearly visible in the siphon and dorsal side of the foot (Fig. 18). The presence of eyes at the base of the tentacles was also noted. At this stage, the transparent egg capsule wall enabled observation of the embryos crawling behavior (Fig. 19). The presence of the radula could be observed in dissected hatchlings using a stereomicroscope; however, this organ may only be present as an incipient structure in previous stages. For comparison of the embryonic developmental stages sizes see Table 1 and Figure 20.

In general, all embryos that were present within a single egg capsule shared the same developmental stage. Notwithstanding, in a few cases (n = 3 of 42 observed egg capsules), remarkable differences in the total length of embryos were observed. Different developmental stages were rarely present in the same egg capsule (7%; n = 4 egg capsules); when this occurred it was most commonly associated with morphological abnormalities in one or more of those embryos.

The development time of embryos in aquarium was estimated in 5–6 months at 12–14°C water temperature. This time was calculated integrating the developmental time information from three newly laid egg capsules and other egg capsules (n = 42) collected at different developmental stages and maintained in conditioned aquaria until hatching.

DISCUSSION

General Features of Egg Capsules

Adelomelon ancilla females attach their egg capsules to a variety of submerged objects (frequently empty clam shells or stones), which are abundant in the study area and, in the case of some bivalve species, are also part of the species diet (Zabala et al., 2013a). It is remarkable that *A. ancilla* choose mainly concave surfaces (95.2% of cases) to attach their capsules. Curiously, the sympatric volutid *Odontocymbiola magellanica* also deposit egg capsules on submerged objects, but always lay them on the convex side (Bigatti et al., 2010). Nonetheless, egg capsules of the two species never co-ocurred on the same empty shell valve. Furthermore, in contrast with *O. magellanica* (Bigatti et al., 2010), egg capsules of *A. ancilla* lack an external calcium carbonate cover. The absence of a calcareous layer may be associated with increased susceptibility of encapsulated embryos to predation (Rawlings, 1999); however, this may be offset by female's selectivity of (more protective) concave surfaces for oviposition. Such differences between the two sympatric volutids, both top predators of Patagonian benthic communities (Bigatti et al., 2010; Zabala et al., 2013a), could reflect differential use of the resources, thereby preventing niche overlap (prey and/or habitat use).

Gastropod egg capsules are very complex structures; the microstructure is commonly composed of three or four layers (D'Asaro, 1988; Rawlings, 1990, 1994). In *A. ancilla*, it was arranged in three layers, in concordance with others caenogastropods as the volutids *O. magellanica* (Bigatti et al., 2010) and *Voluta ebraea* (Matthews-Cascon et al., 2010), the nassarid *B. cochlidium* (Averbuj, 2009) and others muricids and buccinids (D'Asaro, 1988; Ojeda & Chaparro, 2004). The inner layer of *A. ancilla* egg capsules is reduced and disappears as development advances as reported in other volutids (Matthews-Cascon et al., 2010; Bigatti et al., 2014), mainly as a result of radula action of embryos on the inner egg capsule wall.

Embryonic Development

The embryonic development of *Adelomelon ancilla* (Volutidae, Zidoninae) is direct, without a free larval stage; thus, embryos hatch as crawling juveniles (Penchaszadeh et al., 1999). After a series of cell divisions with few size changes, embryonic growth occurs simultaneously with morphological changes, associated with feeding of the embryos upon development of the velum. In contrast, in the sympatric volutid *Odontomcymbiola magellanica* (Odontocymbiolinae), embryonic development involves three phases: first, slow growth associated to the nutrition resources present in the egg, second, fast growth related to the ingestion of the total solid portion of the intracapsular fluid (major embryo growth), followed by a third phase of slow growth and mostly morphological changes (Bigatti et al., 2014). In *A. ancilla*, the velum disappears before hatching, during the coiling embryo stage. The reabsorption was also observed at an equivalent stage of development in the congeneric *Adelomelon ferrusacci* (Penchaszadeh & Segade, 2009) and *Adelomelon brasiliana* (Penchaszadeh, 1999), although in these species, the velum was not measured. The velum size of *O. magellanica*, is smaller (measured from photographs in Bigatti et al., 2014) than *A. ancilla* velum. *O. magellanica* reduces it velum before "pediveliger", while *A. ancilla* reaches the maximum velum size at that stage. These differences could be related to species differences in feeding behavior strategies and organ formation during intracapsular development, as was previously described.

In this study, we confirm that the embryonic growth and organogenesis of *A. ancilla* is continuous, and is associated with continuous intracapsular feeding. However, there is some disagreement regarding embryonic shell growth features (Romero et al., 2004; Bigatti et al., 2014). In *A. ancilla*, the shell gland was observed at early "pediveliger" stage on the cephalic zone, more specifically in the aperture region of the protoconch, as found by Bigatti et al. (2014). Considering the anterior location of the shell gland it may be interpreted that calcification of the shell in embryos occurs from the aperture zone towards the apex, as was described in *O. magellanica* (Bigatti et al., 2014). If true, this pattern of calcification differs from that proposed by other authors, who have postulated that calcification within other neogastropod species occurs in the opposite direction (from apex to aperture zone), based on the presence of a posterior cap-like shell gland (D'Asaro, 1966; Romero et al., 2004). In *A. ancilla*, the hatchlings showed the apex and other spots lacking calcification (spread around the shell); these areas are subsequently calcified to achieve the final protoconch. This fact might support the existence of other calcification areas on the embryo mantle, complementary to the shell gland situated at the aperture zone. Nevertheless, to answer this query, marking experiments of embryos shells (e.g., with calcein) are needed to correctly determine the shell calcification process.

Studies of early intracapsular nutrition by Rivest (1992) have suggested that larval kidneys (= athrocytes; Bigatti et al., 2014) may be related to incorporation of nutrients without ingestion of food through the mouth. The transparent vacuolar cells distinguished on the velum area of *A. ancilla* could be related to athrocyte cells *sensu* Bigatti et al. (2014). These cells were recognized at early "veliger" stages of development, mainly situated on the central side of the velum. These vacuolar cells have been identified in the sympatric *O. magellanica* (Bigatti et al., 2014), but have not been reported in other published studies of volutid species. This group of cells is commonly reported as larval kidneys in the literature (Rivest, 1992): an example of this is the nassarid *B. globulosus*, which inhabits the same area of *A. ancilla* (Averbuj et al., 2014). Morphological and experimental evidence supports that the large cell size is related to endocytotically absorbed intracapsular proteins and not to stored waste products (Rivest, 1992). Athrocytes cells are present at early stages and resorption occurs during intracapsular metamorphosis in all the neogastropods examined that hatch as juveniles (Rivest, 1992; Averbuj et al., 2014; Bigatti et al., 2014); probably the same could be occurring in *A. ancilla* serving in early nutrient absorption.

The importance of the amount of extraembryonic food sources during development has been discussed by several authors (Fioroni, 1982; Miloslavich, 1996b; Penchaszadeh & Miloslavich, 2001). Abundant intracapsular food in each egg capsule of *Adelomelon ancilla* might explain the similar size of embryos within an egg capsule (embryos rarely differed in size and/or development stage in the same egg capsule). Food would not be a limiting resource allowing the embryos to feed without competition. Moreover, since there was no indication of a decrease in the number of embryos during development, one might conclude that there is no sibling cannibalism. The egg capsules found in the Volutidae are among the largest recorded for caenogastropods (Penchaszadeh et al., 1999), and possibly contain more nutrients than species from other families (Penchaszadeh & Miloslavich, 2001). As an example, biochemical intracapsular liquid analysis of *Voluta musica* demonstrated that there was enough protein and sugar to support its total development (Penchaszadeh & Miloslavich, 2001). In *A. ancilla,* embryos remained within the egg capsule for a few days after hatching, feeding of the remnant intracapsular food by grasping the internal walls by the radula. In contrast, however, in *O. magellanica*, intracapsular food is ingested quickly by embryos, which suggests the existence of intracapsular competition (Bigatti et al., 2014). Smith & Thatje (2013) proposed that the modality and speed of intracapsular ingestion are determinants of sibling feeding competition. Nonetheless, as this two species (e.g. the sympatric *A. ancilla* and *O. magellanica*) belong to different subfamilies, these developmental differences may be phylogenetic.

The embryonic developmental time in *A. ancilla* was estimated between 5–6 months. This is much longer than those recorded for the volutids *O. magellanica*: 2–3 months (Bigatti et al., 2014) and *Z. dufresnei*: 35 days (Roche et al., 2013.) in the northern gulfs of Patagonia. Developmental times are often correlated with embryos size (Spight, 1975). In support of this, the few hatchling embryos of *A. ancilla* achieved a much larger average size (10.4 mm in shell length) compared with *O. magellanica* (8.9 mm in shell length). It is widely assumed that offspring quality increases with size (e.g., Thorson, 1950; Gosselin & Rehak, 2007; Lloyd & Gosselin, 2007; Przeslawski, 2011). Therefore, the larger *A. ancilla* hatchlings are less likely to be affected by such factors as physical stress, predation and starvation (Smith & Thatje, 2013).

The neogastropod *A. ancilla* has an ecological significance in Patagonian shallow waters communities, defined by its high trophic position as a top predator in benthic food webs (Zabala et al., 2013a). The results of the present study: direct development, long developmental time (5–6 months) and presence of few embryos inside each egg capsule, denote the fragility of this species as stated previously on basis of such population parameters as longevity, very low density and late reproductive maturity (Penchaszadeh et al., 2009; Zabala et al., 2013b). All this features indicate that *A. ancilla* is not a recommendable resource for commercial exploitation in Nuevo gulf populations.

ACKNOWLEDGEMENTS

We would like to thank Oscar Wheeler and Eugenia Zavattieri for field assistance; Jaime Groizard for technical support in SEM pictures (ALUAR S.A.). Dr. Livore kindly revised the English writing of the final version of this manuscript. Two anonymous reviewers kindly helped to improve the manuscript. S. Zabala is especially grateful to a postdoctoral fellowship by CONICET. This work was partially supported by the projects PICT 2929, PICT 1232 and PICT 1476.

LITERATURE CITED

AMIO, M., 1963, A comparative embryology of marine gastropods with ecological consideration. *Journal of Shimonoseki University of Fisheries*, 12: 229–358.

AVERBUJ, A., 2009, *Biología reproductiva, crecimiento y dieta del caracol ciego* Buccinanops cochlidium *(Gastropoda: Nassariidae) en Golfo San José, Argentina*. PhD Thesis, Universidad de Buenos Aires, Argentina, 180 pp.

AVERBUJ, A., M. ROCHA & M. S. ZABALA, 2014, Embryonic development and reproductive seasonality of *Buccinanops globulosus* (Nassariidae) (Kiener, 1834) in Patagonia, Argentina. *Invertebrate Reproduction & Development*, doi: 10.1080/07924259.2013.875949.

BIGATTI, G., M. GIRAUD-BILLOUD, I. A. VEGA, P. E. PENCHASZADEH & A. CASTRO-VAZQUEZ, 2010, The calcareous egg capsule of the patagonian neogastropod *Odontocymbiola magellanica*: Morphology, secretion and mineralogy. *Journal of Molluscan Studies*, 76: 279–288.

BIGATTI, G., M. GIRAUD-BILLOUD, I. A. VEGA, P. E. PENCHASZADEH & A. CASTRO-VAZQUEZ, 2014, Embryonic development in the Patagonian red snail *Odontocymbiola magellanica* (Neogastropoda: Volutidae): Morphology and biochemistry. *Zoologischer Anzeiger – Journal of Comparative Zoology*, 253(5): 372–381.

CASTELLANOS DE, Z. J. A. & N. LANDONI, 1992, Catálogo descriptivo de la malacofauna marina magallánica. Neogastropoda, Volutidae, Volutomitridae, Cancellariidae, Olividae y Marginellidae. *Consejo Investigaciones Científicas de la Provincia de Buenos Aires*, 10: 1–43.

D'ASARO, C. N., 1966, The egg capsules, embryogenesis, and early organogenesis of a common oyster predator, *Thais haemastoma floridana* (Gastropoda: Prosobranchia). *Bulletin of Marine Science*, 16: 884–914.

D'ASARO, C. N., 1988, Micromorphology of neogastropod egg capsules. *The Nautilus*, 102(4): 134–148.

DELLATORRE, F. G., J. P. PISONI, P. J. BARÓN & A. L RIVAS, 2012, Tide and wind forced nearshore dynamics in Nuevo Gulf (Northern Patagonia, Argentina): potential implications for cross-shore transport. *Journal of Marine Systems*, 96–97: 82–89.

FIORONI, P., 1982, Entwicklungstypen und Schlupfstadien bei Mollusken - Einige allgemeine Befunde. *Malacolgia*, 22(1–2): 601–609.

GOSSELIN, L. A. & R. REHAK, 2007, Initial juvenile size and environmental severity: the influence of predation and wave exposure on hatching size in *Nucella ostrina. Marine Ecology Progress Series*, 339: 143–155.

KNUDSEN, J., 1993, Redescription of the egg mass of *Melo miltonis* (Griffith and Pidgeon, 1834) (Mollusca, Prosobranchia, Volutidae) *Journal of the Malacological Society of Australia*, 14: 107–112.

[LIGHTFOOT, J.], 1786, [Descriptions of species]. In: *A catalogue of the Portland Museum, lately the property of the Dowager Duchess of Portland, deceased, which will be sold at auction*. Mr. Skinner & Co., London, viii + 194 pp.

LLOYD, M. J. & L. A. GOSSELIN, 2007, Role of maternal provisioning in controlling interpopulation variation in hatching size in the marine snail *Nucella ostrina*. *Biological Bulletin*, 213: 316–324

MARCHE-MARCHAD, I., 1968, Un nouveau mode de dévelopment intracapsulaire chez les mollusques prosobranches néogastropodes: l‘incubation intrapédiose des *Cymba* (Volutidae). *Compte Rendu Hebdomadaire des Séances de l`Academie des Sciences*, 266: 706–709.

MARCHE-MARCHAD, I., 1980, Sur la stratégie de la reproduction chez le genre *Cymbium* Röding, 1798 (Gastropoda, Volutidae). *Haliotis*, 10(2): 94.

MATTHEWS-CASCON, H., C. ROCHA-BARREIRA, P. E. PENCHASZADEH & G. BIGATTI, 2010, Description of egg capsules of *Voluta ebraea* Linnaeus, 1758 (Gastropoda: Neogastropoda). *Comunicaciones de la Sociedad de Malacología del Uruguay*, 9: 237–244.

MILOSLAVICH, P., 1996a, Biochemical composition of prosobranch egg capsules. *Journal of Molluscan Studies*, 62: 133–135.

MILOSLAVICH, P., 1996b, Nurse-egg feeding prosobranchs: a comparative biochemical and electrophoretic analysis of eggs and hatchlings. *American Malacological Bulletin*, 13(1/2): 37–46.

OJEDA, J. A. & O. R. CHAPARRO, 2004, Morphological, gravimetric, and biochemical changes in *Crepidula fecunda* (Gastropoda: Calyptraeidae) egg capsule walls during embryonic development. *Marine Biology*, 144(2): 263–269.

PECHENIK, J. A., 1986, The encapsulation of eggs and embryos by molluscs: an overview. *American Malacological Bulletin*, 4: 165–172.

PENCHASZADEH, P. E. & G. G. DE MAHIEU, 1976, Reproducción de gasterópodos prosobranquios del Atlántico Suroccidental. Volutidae. *Physis*, 35: 145–153.

PENCHASZADEH, P. E., P. MILOSLAVICH, M. LASTA & P. M. S. COSTA, 1999, Egg capsules in the genus *Adelomelon* (Caenogastropoda: Volutidae) from the atlantic coast of South America. *The Nautilus*, 113: 56–63.

PENCHASZADEH, P. E. & P. MILOSLAVICH, 2001, Embryonic stages and feeding substances of the South American volutid *Voluta musica* (Caenogastropoda) during intracapsular development. *American Malacological Bulletin*, 16: 21–31.

PENCHASZADEH, P. E. & M. E. SEGADE, 2009, Spawn characteristics in *Adelomelon ferussacii* (Donovan, 1824) (Gastropoda: Volutidae) from southern Patagonia, Argentina. *The Nautilus*, 123: 172–176.

PENCHASZADEH, P. E., C. S. ANTELO, S. ZABALA & G. BIGATTI, 2009, Reproduction and imposex in the edible snail *Adelomelon ancilla* from northern Patagonia. Argentina. *Marine Biology*, 156(9): 1929–1939.

PONDER, W. F., 1974, The origin and evolution of the Neogastropoda. *Malacologia*, 12(2): 295–338.

PRZESLAWSKI, R., 2011, Notes on the egg capsule and variable embryonic development of *Nerita melanotragus* (Gastropoda: Neritidae). *Molluscan Research*, 31: 152–158.

RAWLINGS, T. A., 1990, Associations between egg capsule morphology and predation among populations of the marine gastropod, *Nucella emarginata*. *Biological Bulletin*, 179: 312–325.

RAWLINGS, T. A., 1994, Encapsulation of eggs by marine gastropods: effects of variation in capsules from on the vulnerability of embryos to predation. *Evolution*, 48(4): 1301–1313.

RAWLINGS, T. A., 1999, Adaptations to physical stresses in the intertidal zone: the egg capsules of neogastropod molluscs. *American Zoologist*, 39: 230–243.

RIVEST, B., 1992, Studies on the structure and function of the larval kidney complex of prosobranch gastropods. *Biological Bulletin*, 182: 305–323.

ROCHE, A., M. MAGGIONI, A. RUMI & M. NARVARTE, 2013, Duration of intracapsular development of *Zidona dufresnei* (Gastropoda: Volutidae) at its Southern distributional limit. *American Malacological Bulletin*, 31(1): 85–89.

ROMERO, M., C. GALLARDO & G. BELLOLIO, 2004, Egg laying and embryonic-larval development in the snail *Thais (Stramonita) chocolata* (Duclos, 1832) with observations on its evolutionary relationships within the Muricidae. *Marine Biology*, 145: 681–692.

SMITH, E. & S. THATJE, 2013, Nurse egg consumption and intracapsular development in the common whelk *Buccinum undatum* (Linnaeus 1758) *Helgoland Marine Research*, 67: 109–120

SPIGHT, T. M., 1975, Factors extending gastropod embryonic development and their selective cost. *Oecologia*, 21: 1–19.

THORSON, G., 1950, Reproductive and larval ecology of marine bottom invertebrates. *Biological Review*, 25: 1–45

ZABALA, S., 2013, *Ecología trófica, crecimiento y reproducción en el gasterópodo* Adelomelon ancilla *en el Golfo Nuevo*. PhD Thesis, Universidad de Buenos Aires, Argentina, 180 pp.

ZABALA, S., G. BIGATTI, F. BOTTO, O. IRIBARNE & D. GALVÁN, 2013a, Trophic relationship and diet composition of a Patagonian gastropod and its epibiotic anemone: combined stable isotopes and conventional dietary approach. *Marine Biology*, 160: 909–919.

ZABALA, S., P. E. PENCHASZADEH, H. O. PANARELLO, M. I. BROGGER & G. BIGATTI, 2013b, Life history parameters in the edible snail *Adelomelon ancilla* from patagonian waters. *Malacologia*, 56: 215–229.

Revised ms. accepted November 19, 2014

MALACOLOGIA, 2015, 58(1–2): 349–360

A NEW SPECIES OF *LAUBIERICONCHA* (BIVALVIA: VESICOMYIDAE) FROM DEEP WATERS OFF ARGENTINA

Javier Signorelli[1]* & Guido Pastorino[2]

ABSTRACT

A new species of bivalve belonging to the family Vesicomyidae, ***Laubiericoncha puertodeseadoi***, n. sp., is described. The material was collected during several cruises to the continental margin of Argentina on board of the R/V "*Puerto Deseado*". The distribution of the genus *Laubiericoncha* is expanded to include the southwestern Atlantic Ocean. The description was done by using morphological characters of the shell and mantle cavity organs. All type material of congeneric species was examined and illustrated. ***Laubiericoncha puertodeseadoi***, n. sp., is characterized by a compressed, subrectangular, elongated, inequilateral shell, with slightly prosogyrous umbo and a well-defined triangular pallial sinus, strong external ligament and ctenidia with two robust demibranchs, foot anteriorly projecting and fused siphons. This new species constitutes the first record of the genus *Laubiericoncha* living on the continental margin off Argentina.

Key words: Vesicomyidae, Argentina, new species, *Laubiericoncha*.

INTRODUCTION

The bivalve family Vesicomyidae, introduced by Dall & Simpson (1901), constitutes one of the six chemosymbiotic groups of bivalves that live around hydrothermal vents, hydrocarbon seeps and whale falls (Cosel & Olu, 2009; Krylova & Sahling, 2010; Taylor & Glover, 2010). Besides Vesicomyidae, species belonging to the families Lucinidae, Mytilidae, Nucinellidae, Solemyidae and Thyasiridae have been reported as being chemosymbiotic.

Vesicomyid species were historically collected in waters from 100 m to 6,400 m depth hosting sulphide-oxiding bacteria in their gills (Sibuet & Olu, 1998; Cosel & Olu, 2008).

The Vesicomyidae was mentioned by Hikida et al. (2003) as living in the Upper Cretaceous of Japan, but these authors did not illustrate its hinge structure, thus its vesicomyid position cannot be confirmed (Amano & Kiel, 2007). However, it has been widely recorded from middle to late Eocene of Washington to Recent by several authors (Otatume, 1942; Kanno et al., 1989; Squires & Goedert, 1991; Amano & Kanno, 2005; Krylova & Sahling, 2006; Kiel & Amano, 2010, among others).

The systematic position of Vesicomyidae is still far from resolved. It has been related to Veneroidea (Scarlato & Starobogatov, 1979), Glossoidea (Keen, 1969; Vokes, 1980; Boss, 1968, 1970, 1982; Bernard, 1983; Allen, 2001; Krylova & Janssen, 2006) and Arcticoidea (Okutani, 1966; Taylor et al., 1973; Slack-Smith, 1998). However, Taylor et al. (2007) left the family Vesicomyidae with an unresolved superfamilial status. They concluded that although Arcticoidea and Glossoidea are usually mentioned as superfamilies, the component, Arcticidae, Trapezidae, Glossidae, Vesicomyidae and Kelliellidae may not be monophyletic. Those works that placed Vesicomyidae in Arcticoidea and suggested a position close to the Veneroidea (Giribet & Wheeler, 2002; Mikkelsen et al., 2006; Taylor et al., 2007). However, the close relationship between *Arctica* and the venerids *Callista* and *Mercenaria*, made Arcticoidea (vesicomyds and articids) non-monophyletic (Giribet & Wheeler, 2002).

Not only is the systematic status of Vesicomyidae under discussion but also the internal structure of clade is as well. The validity of the family was studied by Allen (2001), who revised the genera *Kelliella* Sars, 1870, and

[1]Biología Marina – LARBIM – CENPAT – CONICET, Bvd. Brown 2915, U9120ACD, Puerto Madryn, Chubut, Argentina.
[2]Museo Argentino de Ciencias Naturales "Bernardino Rivadavia", Av. Ángel Gallardo 470 C1405 DJR, Ciudad Autónoma de Buenos Aires, Argentina.
*Corresponding author: jsignorelli@cenpat.edu.ar

Vesicomya Dall, 1886. He suggested that both type species are congeneric, making Vesicomyidae a synonym of Kelliellidae (Glossoidea). However, Krylova & Sahling (2010) rejected this synonymy, keeping both families as valid until new studies are performed. In recent years, several taxonomic studies, in which new taxa were introduced, placed the Vesicomyidae into Glossoidea (Krylova & Janssen, 2006; Cosel & Olu, 2008, 2009; Krylova & Cosel, 2011; Oliver et al., 2011, among others).

The suprageneric classification of Vesicomyidae was recently revised by Krylova & Sahling (2010). They recognized two subfamilies, Vesicomyinae, with only one genus, *Vesicomya*, and Pliocardiinae which groups fifteen genera, including *Laubiericoncha* Cosel & Olu, 2008. In this study, Krylova & Sahling (2010) did not consider genera with such exclusively fossil species as *Adulomya* Kuroda, 1931, *Hubertschenckia* Takada, 1953, and *Pleurophopsis* Van Winkle, 1919. The genus *Laubiericoncha* was introduced for species with two demibranchs by Cosel & Olu (2008) when they described the new species *L. myriamae* from Barbados. In addition, they also included three other species, *L. chuni* (Thiele & Jaeckel, 1931), *L. angulata* (Dall, 1896) and *L. suavis* (Dall, 1913), in the genus. Currently, *L. nanshaensis* (Xu & Shen, 1991) also belongs to this genus (sensu Krylova & Sahling, 2010). Previously, new material collected by Krylova & Janssen (2006: 246, pl. 4 fig. 25) from Edison Seamount, southwest Pacific Ocean, was identified to family level and considered congeneric in *Laubiericoncha* by Cosel & Olu (2008). In addition, Krylova & Janssen (2006) considered as congeneric an undescribed species from Gakkel Ridge in the Arctic Ocean mentioned by Sirenko et al. (1995). Finally, Cosel & Olu (2008) and later Krylova & Sahling (2010) included both unnamed species into *Laubiericoncha*, but highlighting that additional specimens are required to confirm or reject this new taxonomic position.

The shell characters of *Laubiericoncha*, together with some diagnostic anatomical features (i.e., two demibranchs), allow us to recognize it from the other genera of the family. In this paper, we introduced a new species of *Laubiericoncha* from deep waters of the South Atlantic basin.

MATERIAL AND METHODS

The material herein described was collected during several cruises to the continental slope of Argentina on board of the R/V "*Puerto Deseado*". Most of the specimens were collected, with a modified Agassiz dredge, but in one station (24) with bottom trawl net also collected empty shells. One specimen with soft parts was fixed in 96% ethanol. All the other specimens were collected dead, but most of them with both valves still articulated. Critical point dry was used to study several soft parts, including the demibranchs, under the SEM (Philips XL30) at the MACN. Fresh cuts of the valves were coated and photographed at SEM. Type series measures are reported in the Table 1. Type material was deposited in the collection of Museo Argentino de Ciencias Naturales "Bernardino Rivadavia" (MACN-In) and Centro Nacional Patagónico (CNP-Inv).

SYSTEMATIC DESCRIPTION

Order Cardiida Férussac, 1822
Superfamily Glossoidea Gray, 1847
Family Vesicomyidae Dall & Simpson, 1901
Subfamily Pliocardiinae Woodring, 1925

Genus *Laubiericoncha* von Cosel & Olu, 2008.

Type Species: *Laubiericoncha myriamae* von Cosel & Olu, 2008, by original designation.

TABLE 1. Type series measures with ***Laubiericoncha puertodeseadoi***, n. sp.; F: length of fibrous ligament y, N: length of posterior lamellar ligament. Units in mm.

Specimen	Length	Height	Width	F	N
1	110.0	59.3	21.3	26.5	46.0
2	94.7	55.0	18.2	30.0	35.0
3	110.1	62.6	22.8	35.3	40.0
4	131.5	73.1	24.1	36.0	47.3
5	110.6	66.1	21.0	34.5	43.7
6	116.6	61.3	20.7	–	rv only
7	95.0	53.1	20.7	–	34.1 rv only
8	42.1	22.7	6.2	7.3	15.2
9	50.0	28.2	8.5	14.8	20.1
10	47.0	25.5	7.0	¿	15.7
11	80.0	47.7	18.0	25.0	29.8
12	114.0	72.8	21.0	32.8	42.0

Distribution

Western Atlantic basin (this paper), Barbados. Eastern Atlantic: Gulf of Guinea. Eastern Pacific: Panama Bay, Baja California, Gakkel Ridge, Arctic.

Remarks

The morphological differences of *Laubiericoncha* with other large Vesicomyidae were pointed out by Cosel & Olu (2008) in their description of the genus. Species belonging to *Laubiericoncha* can be distinguished from other vesicomyid genera by the combination of shell and anatomical characters. It differs from *Callogonia* Dall, 1889, by the presence of a larger shell with a different outline and hinge configuration characterized by a diverging, thin but prominent cardinals (Cosel & Olu, 2008). *Vesicomya* Dall, 1886, and *Isorropodon* Sturany, 1896, have hinge morphology that is clearly different (Cosel & Salas, 2001; Cosel & Olu, 2008). *Calyptogena, s.s.*, lacks a pallial sinus and has only one demibranch in each gill, whereas *Laubiericoncha* has two demibranchs and a triangular pallial sinus (Cosel & Olu, 2008). *Archivesica* Dall, 1908, is the most similar to *Laubiericoncha*. It also has two demibranchs, but the pallial sinus is

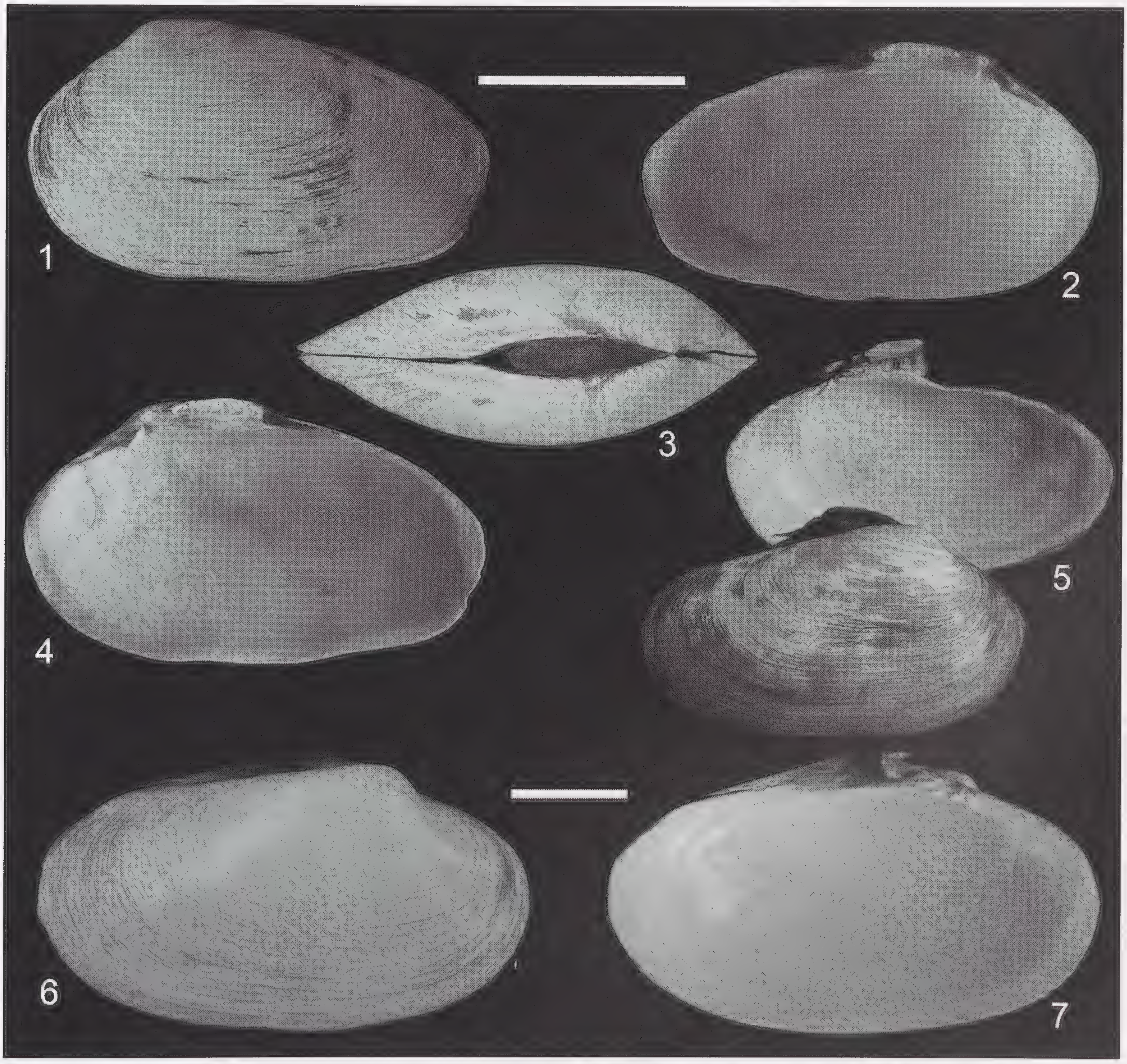

FIGS. 1–7. ***Laubiericoncha puertodeseadoi***, n. sp. FIGS. 1–4: ***Laubiericoncha puertodeseadoi*** holotype, MACN-In 39803; FIG. 5: Paratype MACN-In 39804; FIGS. 6, 7: Paratype CNP-INV 1922. Scale bar: Figs. 1–5 = 5 cm, Figs. 6, 7 = 1 cm.

shorter, broader and blunt (not acute), the shell outline is subquadrate, the umbo is more prominent and the ventral margin is straight. Finally, species belonging to *Laubiericoncha* can be easily distinguished from those vesicomyids with a very elongate shell of the genera *Abyssogena* Krylova et al., 2010, *Ectenagena* Woodring, 1938, *Pleurophopsis* Van Winkle, 1919, and *Adulomya* Kuroda, 1931 (Cosel & Olu, 2008).

Laubiericoncha puertodeseadoi, n. sp. (Figs. 1–28)

Types: Holotype, MACN-In 39803, articulated shell only. Twelve Paratypes from type locality: MACN-In 39804, eight articulated valves and a single right valve; CNP-INV 1921, one complete specimen with soft parts; CNP-INV 1922, a single right valve.

Type Locality: Station 24 of "*Talud Continental I*" expedition on board of R/V "*Puerto Deseado*", 37°54.206'S, 54°2.616'W in 2,419.59 m depth collected on 14/August/2012 with bottom trawl.

Etymology: Dedicated to the crew of the Consejo Nacional de Investigación Científica y Técnica (CONICET)'s ship R/V "*Puerto Deseado*" because of the effort and dedication to get these samples.

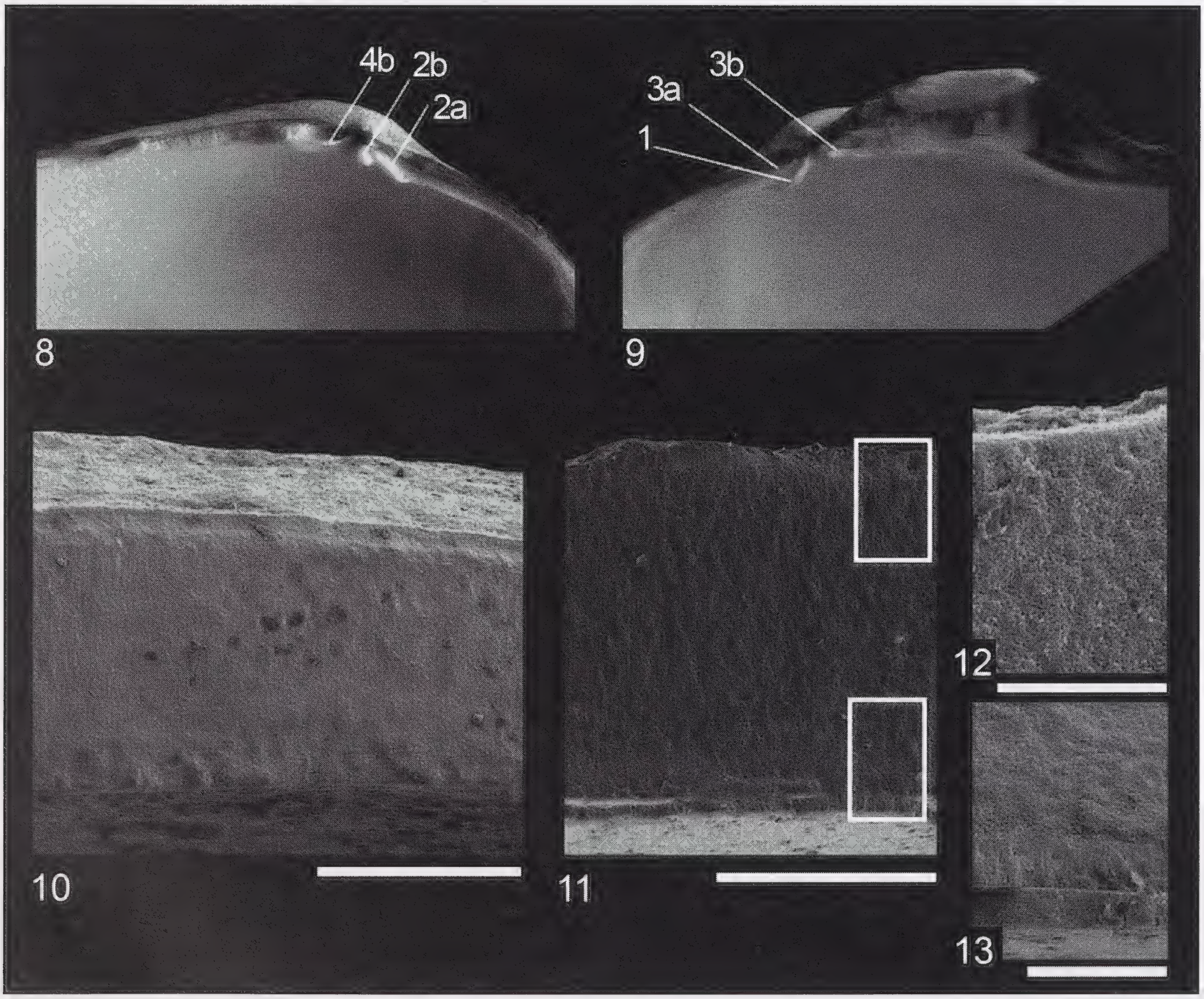

FIGS. 8–13. ***Laubiericoncha puertodeseadoi***, n. sp. FIG. 8: Detail of left hinge; FIG. 9: Detail of right hinge, both from the specimen in fig. 5; FIGS. 10–13: Ultrastructure of the shell; FIGS. 10, 11: General aspect of three layers; FIG. 12: Detail of outer layer with irregular prisms; FIG. 13: Inner layer diffuse with irregular complex crossed lamellar structure. Scale bar: Fig. 10 = 1 mm, Fig. 11 = 500 µm, Fig. 12 = 100 µm, Fig. 13 = 200 µm.

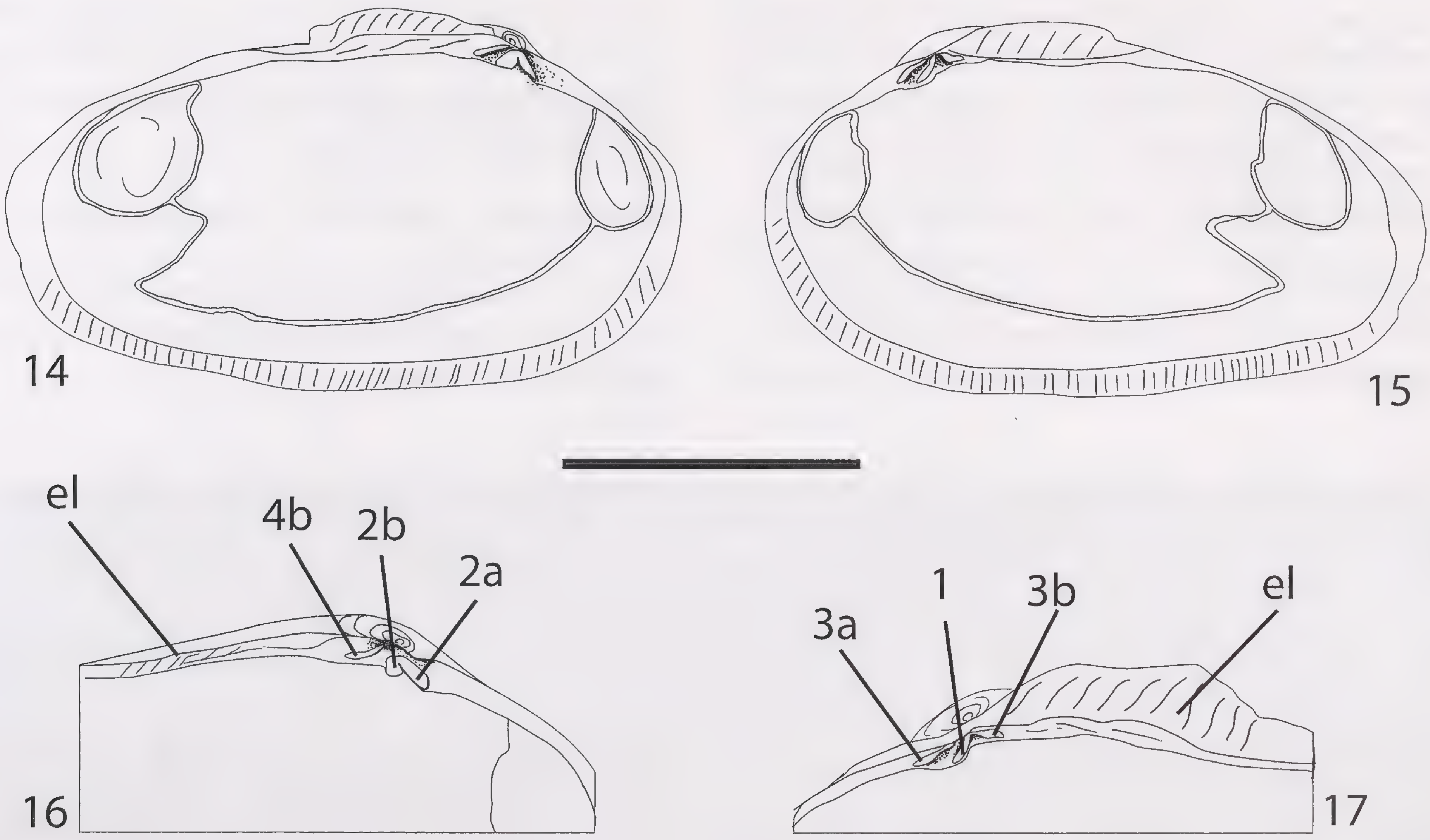

FIGS. 14–17. Schematic drawings of the insides of valves of ***Laubiericoncha puertodeseadoi***, n. sp. FIGS. 16, 17: Hinges of ***L. puertodeseadoi***. Scale bar: 5 cm.

Additional Material Examined: MLP 13918: 2 right valves from St. 42 of *Talud Continental exp.*, 37°59.110'S, 54°41.136'W in 877 m depth collected on 26/May/2013 with modified Agassiz dredge; MLP 13919: 1 articulated specimen, four right and three left valves from St. 56 of *Talud Continental exp.*, 37°54.840'S, 54°2.470'W 2,204 m to 37°55.405'S, 54°2.390'W, in 2,137 m, collected on 09/Sept/2013.

Description

Shell: compressed, moderately thick, large, up to 131 mm of shell length, approximately subrectangular, elongated, inequilateral with slightly prosogyrous umbo located appreciably closer to the anterior end, about 20–30 percent of total length of valves (Figs. 1–7); umbos very close but not touching (Fig. 3); dorsal margin curved, straight in younger specimens, ventral gently convex; anterior margin rounded; posterior margin enlarged, subrectangular to pointed profile; ornamentation comprising irregular, close arranged irregular growth lines; periostracum grey plumbic, yellowish glossy in young specimens, pellucid (Figs. 1, 5); Pallial line impressed, thick, visible all along; pallial sinus shallow and triangular (Figs. 2, 4, 7, 14–15); anterior adductor scar teardrop shaped; posterior adductor scar subcircular, larger; anterior pedal retractor scar deeply impressed, somewhat hidden under the hinge plate, above very close but not touching anterior adductor scar; posterior pedal retractor scar united with posterior adductor scar; external ligament opisthodetic, parivincular, strong, with fibrous layer occupying about 35% of shell length, placed on a thick nymphal plate (Fig. 3); subumbonal pit present and well distinct; hinge plate with a thin and prominent cardinal 1, anteriorly inclined and curved, dorsally surrounded by a curved cardinal tooth comprising the fused 3a and 3b in the right valve (Figs. 9, 17); left valve with, short, thick and fused 2a and 2b cardinal tooth, placed directly under the umbo, 2b descending vertically to the ventral margin of the hinge plate and 2a anteriorly inclined, a laminar cardinal tooth (4b) much longer but thinner and posteriorly inclined complete the left hinge (Figs. 8, 16); shell ultrastructure with an outer layer of reclined, very irregular fibrous prisms; middle layer of very diffuse crossed lamellar structure with barely distinguishable first order lamellae; inner layer very diffuse with irregular complex crossed lamellar structure. The inner and middle layer appear homogeneous at high magnifications (Figs. 10–13).

General Anatomy: Ctenidia with two strong demibranchs, the outer considerably shorter than the inner in the dorsoventral axis, similar in length occupying about half of shell length (Figs. 18–20), food groove clearly visible in both demibranchs (Figs. 21, 22); foot anteriorly projecting, laterally flattened but well developed (Fig. 27); siphons fused, the incurrent slightly larger than excurrent; with very short tentacles along the apertural ring (Figs. 24–26), morphology and size of tentacles looks equal in both siphons; heart elongated antero-posteriorly, with two auricles and one ventricle surrounding the hindgut (Fig. 28).

Distribution

Only known from off Buenos Aires province coast, southwestern Atlantic Ocean in 877–2,204 m depth.

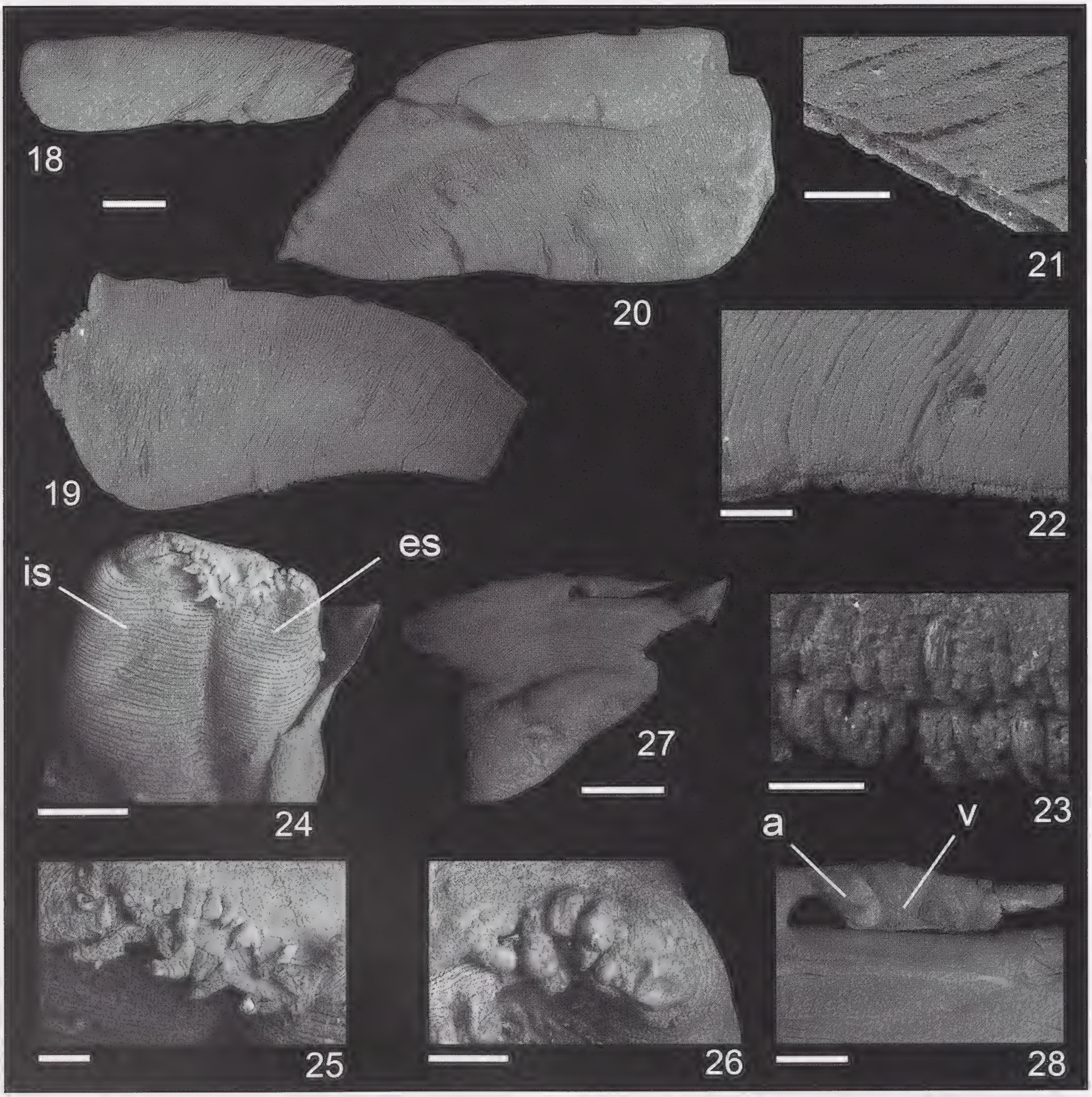

FIGS. 18–28. Soft parts of ***Laubiericoncha puertodeseadoi***, n. sp. FIG. 18: Left outer demibranch; FIG. 19: Left inner demibranch; FIG. 20: Right demibranch; FIG. 21: Food groove of outer demibranch; FIG. 22, 23: Food groove of inner demibranch; FIGS. 24–26: Fused siphons with short tentacles along the apertural ring; is: incurrent siphon, es: excurrent siphon); FIG. 27: Foot anteriorly directed; FIG. 28: Heart; a: auricle, v: ventricle. Scale bar: Figs. 18–20 = 2 mm, Figs. 21, 26, 27 = 200 µm, Fig. 22 = 400 µm, Fig. 23 = 100 µm, Fig. 24 = 4 mm, Figs. 25, 28 = 1 mm.

Remarks

Combination of shell characters and general anatomy undoubtedly placed this new species into the genus *Laubiericoncha*. Shell outline of ***L. puertodeseadoi*** resembles *L. chuni* more than the type species, *L. myriamae* (Figs. 32–34, 29–31, respectively). It has a dorso-posterior area straight and enlarged that goes to the posterior end with a very pronounced angle very similar to *L. chuni*. The posterior end in ***L. puertodeseadoi*** and *L. chuni* is more acute and lower, whereas in *L. myriamae* it is more rounded and placed in the horizontal midline. The rounded ventral margin of *L. angulata* (Figs. 40, 41) makes its shell outline more oval to ellipsoidal, whereas in ***L. puertodeseadoi*** is clearly straight, making it subrectangular. The oval to subcircular shell outline plus a less elongate shell of *L. suavis* (Figs. 35–37), with a less marked posterior end thus distinct from the new species. The external ligament, stronger and larger than that in *L. myriamae*, *L. chuni* and *L. suavis*, easily distinguishing **L.**

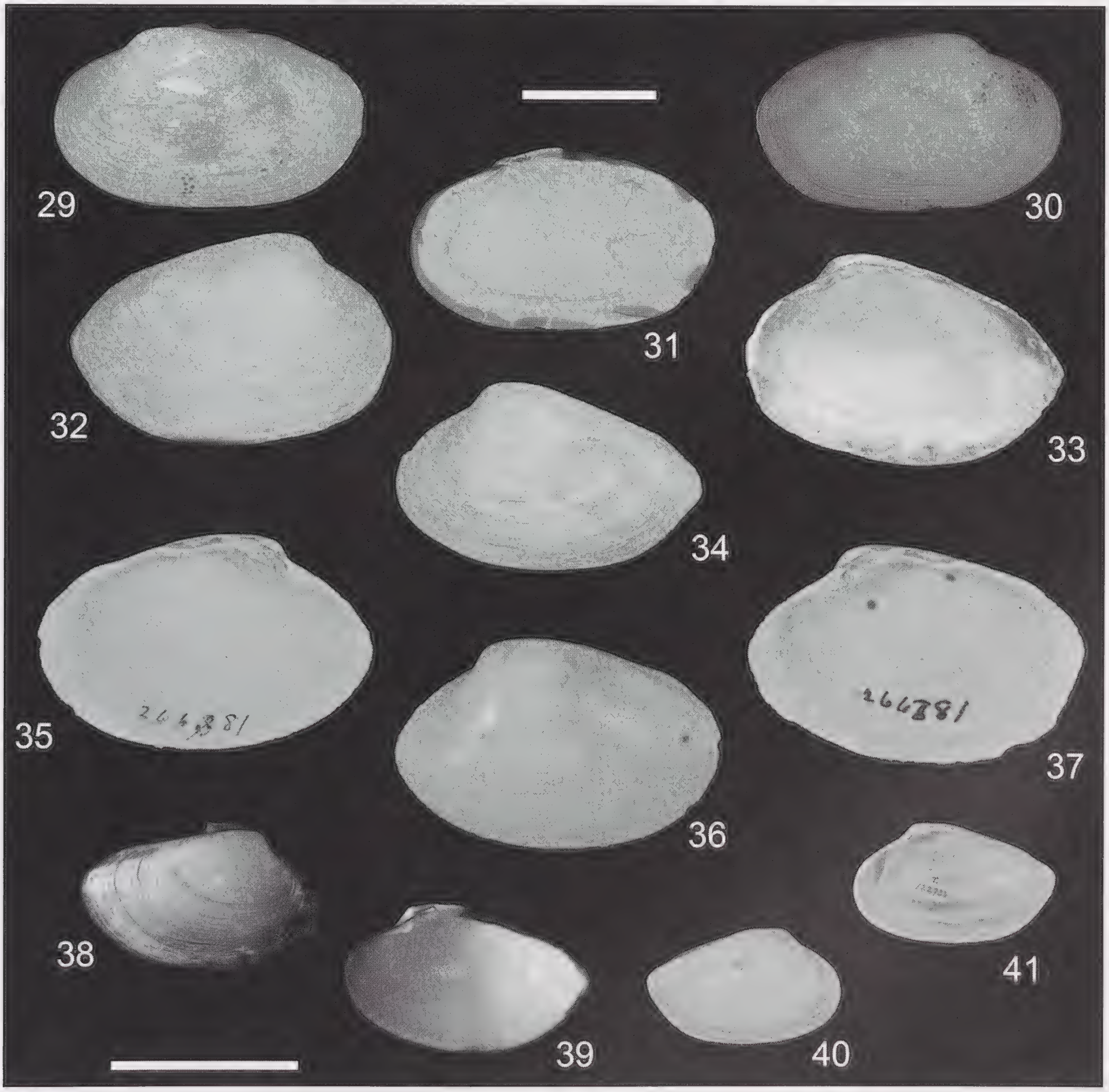

FIGS. 29–41. Species included in the genus *Laubiericoncha*. FIGS. 29–31: *L. myriamae*, holotype MNHN 20550; FIGS. 32–34: *L. chuni*, Lectotype ZMB 77848a; FIGS. 35–37: *L. suavis*, holotype USNM 266881; FIGS. 38, 39: *L. nanshaensis*, holotype SSBII11–10 (no. 30934 in label); FIGS. 40, 41: *L. angulata*, holotype USNM 122933. Scale bar: Figs. 29–34 =4 cm; Figs. 35–41 = 2 cm.

TABLE 2. Morphological features of described vesicomyid species included in the genus *Laubiericoncha.*

	L. puertodeseadoi n. sp.	*L. myriamae* Cosel & Olu, 2008	*L. chuni* (Thiele & Jaeckel, 1931)	*L. angulata* (Dall, 1896)	*L. suavis* (Dall, 1913)	*L. nanshaensis* (Xu & Shen, 1991)
Type locality	Argentine Sea 37°54.206'S, 54°2.616'W, 2419.59 m	Southern part of Barbados accretionary prism, ESE of Trinidad	W of Campo, Cameroon, Gulf of Guinea, 2°00'N, 8°4.3'E, 2492 m	U.S. Fish Commision, st. 3392, 2322 m, hard bottom, Gulf of Panama	W coast of Baja California, W of Tiburon Island (Animas) (25°N, 1345 m)	Nansha Islands, 6°04'N, 113°37'E, 2626 m, 5/June/1985
Type material	MACN-In 39803, holotype	MNHN 20551, holotype	ZMB 88412, 88413, syntypes	USNM 122933, holotype	USNM 266881, holotype	MBM CAS N°SSBII11-10 (N°30934 in label), holotype
Shell	compressed, subrectangular, elongated, posterior end tapering	oblong-oval anterior and posterior end rounded	oblong-oval Posterior end tapering	posterior end tapering	oblong-oval to elliptical anterior and posterior rounded	posterior end tapering
Ultra-structure	Outer layer fibrous prisms; middle layer of very diffuse CL structure, inner layer irregular CCL	?	?	?	?	?
Hinge	Same configuration of type species, RV with 3a shorter; LV with 4b narrower and 2a–2b stronger	RV with cardinal 1 and a fused cardinal 3a and 3b; LV with fused 2a–2b, and posterior laminar cardinal 4b	very similar to type species in tooth shape and size	Like type species, with 3a slightly shorter	Like type species, with 3a shorter and 1 more vertically oriented, LV with 2b shorter and 4b longer	?
Pallial sinus	triangular, less deep than type species, similar to *L. suavis* and *L. chuni*	acute and triangular	triangular, less deep than type species	acute and triangular, high	triangular, less deep than type species	triangular shallower than type species
Ctenidia	two demibranchs	two demibranchs	two demibranchs	?	?	?
Siphons	fused, short with tentacles, no categories of tentacles observed	fused, short with tentacles	fused and short	?	?	?

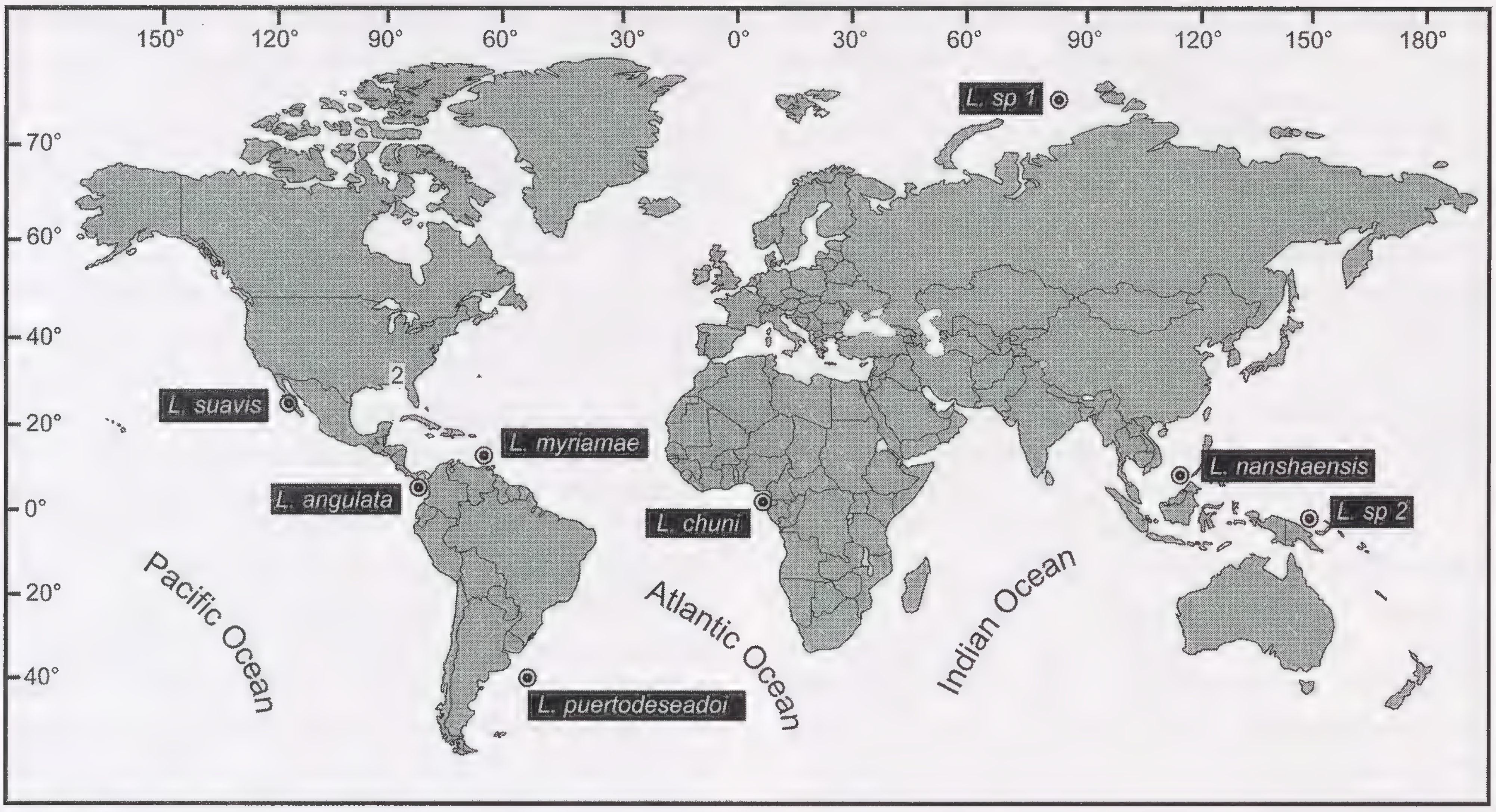

FIG. 42. Global occurrences of the genus *Laubiericoncha*, *L. sp 1* correspond introduced by Sirenko et al., 1995 and *L. sp 2* by Krylova & Janssen, 2006.

puertodeseadoi. The type material of *L. angulata* lacks the ligament; however, the nymphal plate is less developed posteriorly suggesting a smaller ligament. *Laubiericoncha nanshaensis* described from Nansha Islands, South China Sea, is smaller, with a posterior end more acute placed in the horizontal midline, and the pallial sinus is shallower (Figs. 38, 39). All species currently included in *Laubiericoncha* have the same hinge configuration and pallial sinus shape; however, there are some variation in tooth shape, orientation and size that allows distinguishing the valid species (Table 2). The intraspecific variation of ***L. puertodeseadoi*** was not evident. All collected specimens looks equal in hinge morphology, pallial sinus depth and shell outline. Nevertheless only ten articulate shells and eleven single valves were collected during the fieldwork, and additional specimens would be needed to confirm this observation.

Despite the unique specimen collected with soft parts, the morphology of mantle cavity organs of ***L. puertodeseadoi*** is very close to *L. myriamae* and *L. chuni*. Siphons, ctenidia and foot morphology were similar to those observed in *L. myriamae* and *L. chuni*. However, we recognized slight differences, such as a less elongated ctenidia and a stronger foot in the new species. The morphology of soft parts of other members of the genus *Laubiericoncha* is, at the moment, unknown.

DISCUSSION

The family Vesicomyidae was previously registered in the southwestern Atlantic Ocean. Rios (1994, 2009) reported the presence of two species of vesicomyids, that is, *Calyptogena troncosoi* Rios, 2009, and *Vesicomya albida* (Dall, 1889), in the southern coast of Brazil. However the later species was considered into *Kelliella* (Rosenberg, 2014). Previously, Domaneschi & Lopes (1990) described *Calyptogena birmani* off Paraná state, also from the southern coast of Brazil. Within regional context, ***Laubiericoncha puertodeseadoi***, n. sp., constitutes the first record of the family Vesicomyidae, described off Buenos Aires province and the first record of the genus in the southwestern Atlantic Ocean. In recent years, the genus *Laubiericoncha* had been registered in several localities worldwide (Cosel & Olu, 2008; Krylova & Sahling, 2010). After three cruises to the deep canyons off Buenos Aires coast province (Mar del Plata submarine canyon), several specimens of ***Laubiericoncha puertodeseadoi*** were collected between 870–2,200 m depth. The material was found together with gastropods of the families Naticidae and Volutidae characteristic of soft bottoms with no signs of interaction among them.

The taxonomic position of species grouped into the genus *Laubiericoncha* has been widely discussed (Cosel & Salas, 2001, Krylova & Janssen, 2006). These authors noted differences in hinge configuration, pallial sinus and shell outline in a few described species then included in the genera *Callogonia* and *Vesicomya*. Later, Cosel & Olu (2008) introduced the genus *Laubiericoncha* to encompassed four species, the type species, *L. myriamae,* and *L. angulata* (Dall, 1896), *L. chuni* (Thiele & Jaeckel, 1931) and *L. suavis* (Dall, 1913). Finally, Krylova & Sahling (2010) considered *L. nanshaensis* (Xu & Shen, 1991) as a fifth species of the genus. This work confirmed ***Laubiericoncha puertodeseadoi***, n. sp., as the sixth described species of the genus, expanding its distribution to the southwestern Atlantic Ocean. However, there are two additional unnamed species that were tentatively placed in *Laubiericoncha*. They were registered by Sirenko et al. (1995) from Gakkel Ridge in the Arctic (*L. sp 1*; Fig. 42) and by Krylova & Janssen (2006) from Edison Seamount in the southwestern Pacific Ocean (*L. sp 2*; Fig. 42). The new species here described places the genus *Laubiericoncha* in six geographical regions. It was registered in the Caribbean, Argentina, West African, Panamic, Indo Pacific and Arctic basins (Fig. 42). These records make *Laubiericoncha* a widely distributed genus of the family Vesicomyidae which share shell characters, like hinge configuration, pallial sinus form and shell outline, and soft parts, like two demibranchs and fused siphons.

Phylogenetic analysis of the family Vesicomyidae suggested a multiple trans-Pacific migrations between the western and eastern parts of the Pacific Ocean (Kojima et al., 2004). The cladistic relationships of *Laubiericoncha* and other vesicomyid genera were discussed by Decker et al. (2012). In their work, the species *L. chuni* and *L. myriamae* do not form a monophyletic group. They pointed out that taxonomy based on morphology of several genera, including *Laubiericoncha,* did not match with their molecular conclusions. This phylogenetic result agrees with those mentioned by Goffredi et al. (2003) who reported that vesicomyid genera are polyphyletic and need to be morphologically revised. The presence of two demibranchs in *Laubiericoncha* is considered as an ancestral character (Decker et al., 2012). In the Pliocardiinae, this character is also shared by *Archivesica* species and *Phreagena kilmeri* and *Ectenagena extenta* forming a cluster supported by a 99% bootstrap value (Decker et al., 2012). Although *Phreagena kilmeri* and *Phreagena soyoae* were considered synonyms (Kojima et al., 2004; Okutani et al., 2009), some authors considered both species as valid (Krylova & Sahling, 2010; Coan & Valentich-Scott, 2012). Not only the presence of two demibranchs suggest a generic assignment, but also the sharing of hinge configuration, pallial sinus form and shell outline place the new species into *Laubiericoncha*. In our analysis, we considered the genus *Laubiericoncha* as a natural taxon because morphological differences were not observed among valid species that would divide the genus into separate taxa. This discrepancy, between molecular taxa and morphological characters, should be retested. The genera mentioned by Decker et al. (2012) were represented in their analysis by only two species each one. Additional material would be needed to confirm the polyphyletic status of the genus *Laubiericoncha*. Morphological characters of Atlantic species are closely related to Pacific species within the genus *Laubiericoncha*. These evolutionary relationships were mentioned by Peek et al. (2000), who suggested a circumpolar dispersal, with subsequent isolation leading to speciation. In addition, in recent years, different vesicomyid genera were revised and redefined (Cosel & Salas, 2001; Cosel & Olu, 2009; Krylova & Cosel, 2011; Krylova et al., 2010) and none of them questioned the affinities of these genera.

ACKNOWLEDGMENTS

Ellen Strong (USNM), Virginie Heros and Alain Robin (MNHN), Konstantin Lutaenko (Russia) and Matthias Glaubrecht (ZMH) assisted in the revision of type material. We are also grateful to Joseph Carter for his help in the analysis of microstructure of the shell. We acknowledge to CONICET to which both authors belong as members of the “Carrera del Investigador Científico y Técnico”. This contribution was partially supported by the project PICT 2012-1726 from the Agencia Nacional de Promoción Científica y Tecnológica (Argentina).

LITERATURE CITED

ALLEN, J. A., 2001, The family Kelliellidae (Bivalvia: Heterodonta) from the deep Atlantic and its relationship with the family Vesicomyidae. *Zoological Journal of the Linnean Society*, 131: 199–226.

AMANO, K. & S. KIEL, 2007, Fossil vesicomyid bivalves from the North Pacific Region. *The Veliger*, 49(4): 270–293.

AMANO, K. & S. KANNO, 2005, *Calyptogena* (Bivalvia: Vesicomyidae) from Neogene strata in the Joetsu District, Niigata Prefecture, central Japan. *The Veliger*, 47(3): 202–212.

BERNARD, F. R., 1983, Catalogue of the living Bivalvia of the eastern Pacific Ocean: Bering Strait to Cape Horn. *Canadian Special Publication of Fisheries and Aquatic Sciences*, 61: 1–102.

BOSS, K. J., 1968, New species of Vesicomyidae from the Gulf of Darien, Caribbean Sea (Bivalvia; Mollusca). *Bulletin of Marine Science*, 18(3): 731–748.

BOSS, K. J., 1970, Systematics of the Vesicomyidae (Mollusca: Bivalvia). *Malacologia*, 9(1): 254–255.

BOSS, K. J., 1982, *Mollusca.* Pp. 946–1166, in: S. P. PARKER, ed., *Synopsis and classification of living organisms*. New York, McGraw-Hill Book Company, xviii + 1,166 pp.

COAN, E. V. & P. VALENTICH–SCOTT, 2012, *Bivalve seashells of tropical West America. Marine bivalve mollusks from Baja California to northern Peru*. Santa Barbara, California, Santa Barbara Museum of Natural History, 2 vols, 1,258 pp.

COSEL, R. VON & C. K. OLU, 2008, A new genus and new species of Vesicomyidae (Mollusca, Bivalvia) from cold seeps on the Barbados accretionary prism, with comments on other species. *Zoosystema*, 30: 929–944.

COSEL, R. VON & C. K. OLU, 2009, Large Vesicomyidae (Mollusca: Bivalvia) from cold seeps in the Gulf of Guinea off the coasts of Gabon, Congo and northern Angola. *Deep Sea Research II*, 56(23): 2350–2379.

COSEL, R. VON & C. SALAS, 2001, Vesicomyidae (Mollusca: Bivalvia) of the genera *Vesicomya*, *Wisiuconcha*, *Isorropodon*, and *Callogonia* in the eastern Atlantic and the Mediterranean. *Sarsia*, 86(4/5): 333–366.

DALL, W. H., 1886, XXIX. Report on the Mollusca. Part 1. Brachiopoda and Pelecypoda. In Reports on the results of dredging, under the supervision of Alexander Agassiz, in the Gulf of Mexico (1877–1878) and in the Caribbean Sea (1879–1880), by the U.S. Coast Survey Steamer "Blake", Lieut.-Commander C. D. Sigsbee, U.S.N., and Commander J. R. Bartlett, U.S.N., commanding, 1886 + 1889. *Bulletin of the Museum of Comparative Zoology*, 12(6):171–318.

DALL, W. H., 1889, XXIX. Report on the Mollusca. Part 2. Gastropoda and Scaphopoda [with "Addenda and Corrigenda to Part I, 1886", p. 433–452]. In Reports on the Results of Dredging, under the Supervision of Alexander Agassiz, in the Gulf of Mexico (1877–1878) and in the Caribbean Sea (1879–1880), by the U.S. Coast Survey Steamer "Blake", Lieut.-Commander C. D. Sigsbee, U.S.N., and Commander J. R. Bartlett, U.S.N., commanding, 1886 + 1889. *Bulletin of the Museum of Comparative Zoology*, 18: 1–492.

DALL, W. H., 1896, Diagnoses of new species of mollusks from the west coast of America. *Proceedings of the United States National Museum*, 18(1034): 7–20.

DALL, W. H., 1908, Reports on the dredging operations off the west coast of Central America to the Galapagos, to the West coast of Mexico, and in the Gulf of California, in charge of Alexander Agassiz, carried on by the U.S. Fish Commission steamer "Albatross", during 1891, lieut. commander Z. L. Tanner, U.S.N., commanding. XXXVII. Reports on the scientific results of the expedition to the eastern tropical Pacific, in charge of Alexander Agassiz, by the U.S. Fish Commission steamer "Albatross", from October, 1904, to March, 1905, Lieut. commander L. M. Garrett, U.S.N., commanding. XIV. The Mollusca and the Brachiopoda. *Bulletin of the Museum of Comparative Zoology*, 43(6): 205–487.

DALL, W. H., 1913, Diagnoses of new shells from the Pacific Ocean. *Proceedings of the United States National Museum*, 45: 587–597.

DALL, W. H. & C. T. SIMPSON, 1901, The Mollusca of Porto Rico. *United States Fish Commission Bulletin*, 20(1): 351–524.

DECKER, C., K. OLU, R. L. CUNHA & S. ARNAUD-HAOND, 2012, Phylogeny and diversification patterns among vesicomyid bivalves. *PLoS ONE* 7(4): e33359; doi:10.1371/journal.pone.0033359.

DOMANESCHI, O. & S. G. B. C. LOPES, 1990, *Calyptogena* (*Calyptogena*) *birmani*, a new species of Vesicomyidae (Mollusca–Bivalvia) from Brazil. *Malacologia*, 31(2): 363–370.

GIRIBET, G. & W. WHEELER, 2002, On bivalve phylogeny: a high-level analysis of the Bivalvia (Mollusca) based on combined morphology and DNA sequence data. *Invertebrate Biology*, 121(4): 271–324.

GOFFREDI, S. K., L. A. HURTADO, S. HALLAM & R. C. VRIJENHOEK, 2003, Evolutionary relationships of deep-sea vent and cold seep clams (Mollusca: Vesicomyidae) of the "*pacifica/lepta*" species complex. *Marine Biology*, 142(2): 311–320.

HIKIDA, Y., S. SUZUKI, Y. TOGO & A. IJIRI, 2003, An exceptionally well-preserved fossil seep community from the Cretaceous Yezo Group in the Nakagawa area, Hokkaido, northern Japan. *Paleontological Research*, 7(4): 329–342.

KANNO, S., K. AMANO & H. BAN, 1989, *Caylptogena (Calyptogena) pacifica* Dall (Bivalvia) from the Neogene System in the Joetsu District, Niigata Prefecture. *Palaeontological Society of Japan, Transactions and Proceedings*, (n. s.), 153: 25–35.

KEEN, A. M., 1969, Family Vesicomyidae Dall, 1908, P. N664, in: L. R. COX et al., eds., Part N [Bivalvia], Mollusca 6, vols. 1 and 2, xxxvii + 952 pp. In: R. C. MOORE, ed., *Treatise on Invertebrate Paleontology*. Geological Society of America and University of Kansas Press, Lawrence, Kansas.

KIEL, S. & K. AMANO, 2010, Oligocene and Miocene vesicomyid bivalves from the Katalla District, southern Alaska. *The Veliger*, 51(1): 76–84.

KOJIMA, S., K. FUJIKURA & T. OKUTANI, 2004, Multiple trans-Pacific migrations of deep-sea vent/seep-endemic bivalves in the family Vesicomyidae. *Molecular Phylogenetics and Evolution*, 32: 396–406.

KRYLOVA, E. M. & R. von COSEL, 2011, A new genus of large Vesicomyidae (Mollusca, Bivalvia, Vesicomyidae, Pliocardiinae) from the Congo margin, with the first record of the subfamily Pliocardiinae in the Bay of Biscay (northeastern Atlantic). *Zoosystema*, 33(1): 83–99.

KRYLOVA, E. M. & R. JANSSEN, 2006, Vesicomyidae from Edison Seamount (south west Pacific: Papua New Guinea: New Ireland fore-arc basin) (Bivalvia: Glossoidea). *Archiv für Molluskenkunde*, 135: 231–261.

KRYLOVA, E. M. & H. SAHLING, 2006, Recent bivalve molluscs of the genus *Calyptogena* (Vesicomyidae). *Journal of Molluscan Studies*, 72(4): 359–395.

KRYLOVA, E. M. & H. SAHLING, 2010, Vesicomyidae (Bivalvia): current taxonomy and distribution. *PLoS ONE* 5(4): e9957; doi:10.1371/journal.pone.0009957.

KRYLOVA, E. M., H. SAHLING & R. JANSSEN, 2010, *Abyssogena*: a new genus of the family Vesicomyidae (Bivalvia) from deep-water vents and seeps. *Journal of Molluscan Studies*, 76(2): 107–132.

MIKKELSEN, P. M., R. BIELER, I. KAPPNER & T. RAWLINGS, 2006, Phylogeny of Veneroidea (Mollusca: Bivalvia) based on morphology and molecules. *Zoological Journal of the Linnean* Society, 148: 439–521.

OKUTANI, T., 1966, Identity of *Calyptogena* and *Akebiconcha* (Bivalvia, Cyprinidae). *Venus*, 24(4): 297–303.

OKUTANI, T., T. KOSHI–ISHI, T. SATO, T. IMAI & C. KATO, 2009, Vesicomyid fauna in the Chishima (Kurile) Trench: occurrences of a new taxon and *Calyptogena* extent. *Venus*, 68: 15–25.

OLIVER G., C. F. RODRIGUES & M. R. CUNHA, 2011, Chemosymbiotic bivalves from the mud volcanoes of the Gulf of Cadiz, NE Atlantic, with descriptions of new species of Solemyidae, Lucinidae and Vesicomyidae. *ZooKeys*, 113: 1–38.

OTATUME, K., 1942, On the occurrence of fossil *Calyptogena* from the Ishikari Oil-field, Hokkaido. *Journal of the Geological Society of Japan*, 49: 435–437.

PEEK, A. S., B. S. GAUT, R. A. FELDMAN, J. P. BARRY, R. E. KOCHEVAR, R. A. LUTZ & R. C. VRIJENHOEK, 2000, Neutral and nonneutral mitochondrial genetic variation in deep-sea clams from the family Vesicomyidae. *Journal of Molecular Evolution*, 50: 141–153.

RIOS, E. C., 1994, *Seashells of Brazil*, 2nd ed. Editora da Fundaçao Universidade do Rio Grande, Rio Grande, 368 pp.

RIOS, E. C., 2009, *Compendium of Brazilian seashells*. Rio Grande, R.S., viii + 668 pp.

ROSENBERG, G., 2014, *Vesicomya albida* (Dall, 1890). Accessed through: *World Register of Marine Species* at http://www.marinespecies.org/aphia.php?p=taxdetails&id=464335 on 2015-01-16.

SCARLATO, O. A. & Y. I. STAROBOGATOV, 1979, Osnovnye cherty evolyutsii i sistema klassa Bivalvia morfologiya, sistematika i filogeniya mollyuskov. *Trudy Zoologicheskogo Instituta Akademiya Nauk SSSR*, 80: 5–38 [English translation by K. J. Boss & M. K. Jacobson, eds., 1985, *General evolutionary patterns and the system of the class Bivalvia*. Special Occasional Publication no. 5. Cambridge, Harvard University, Massachusetts, 67 + [5] pp.].

SIBUET, M. & K. OLU, 1998, Biogeography, biodiversity and fluid dependence of deep-sea cold-seep communities at active and passive margins. *Deep-Sea Research II*, 45(1–3): 517–567.

SIRENKO, B., V. PETRYASHOV, E. RACHOR & K. HINZ, 1995, Bottom biocoenoses of the Laptev Sea and adjacent areas. *Berichte zur Polarforschung*, 176: 211–221.

SLACK-SMITH, S. M., 1998, Superfamily Glossoidea. Pp. 351–352, in: P. L. Beesley, G. J. B. Ross & A. Wells, eds., *Mollusca: the southern synthesis, part A, Fauna of Australia*, vol. 5. CSIRO, Melbourne, Australia, xvi + 563 pp.

STURANY, R., 1896, Mollusken I (Prosobranchier und Opisthobranchier; Scaphopoden; Lamellibranchier) gesammelt von S.M. Schiff “Pola“ 1890–94. *Denkschriften der mathematisch-naturwissenschaftlichen Klasse der Kaiserlichen Akademie der Wissenschaften, Wien*, 63(2):1–36.

SQUIRES, R. L. & J. L. GOEDERT, 1991, New Late Eocene mollusks from localized limestone deposits formed by subduction-related methane seeps, southwestern Washington. *Journal of Paleontology*, 65: 412–416.

TAYLOR, J. & E. GLOVER, 2010, *Chemosymbiotic bivalves*. Pp. 107–135, in: S. Kiel, ed., *The vent and seep biota*. Springer, Netherlands, x + 340 pp.

TAYLOR, J. D., S. T. WILLIAMS, E. A. GLOVER & O. DYAK, 2007, A molecular phylogeny of heterodont bivalves (Mollusca: Bivalvia: Heterodonta): new analyses of 18S and 28S rRNA genes. *Zoologica Scripta*, 36: 587–606.

TAYLOR, J. D., W. J. KENNEDY & A. HALL, 1973, The shell structure and mineralogy of the Bivalvia. II. Lucinacea–Clavagellacea. Conclusions. *Bulletin of the British Museum* (*Natural History*), *Zoology*, 22(9): 253–294.

THIELE, J. & S. H. F. JAECKEL, 1931, Muscheln der Deutschen Tiefsee Expedition. *Wissenschaftliche Ergebnisse der deutschen Tiefsee-Expedition auf dem Dampfer ‚Valdivia‘ 1898–1899*, 21: 1–110 (159–268).

VOKES, H. E., 1980, Genera of the Bivalvia: a systematic and bibliographic catalogue (revised and updated). *Bulletins of American Paleontology*, 51(232): xxvii + 307 pp.

XU, F. & S. SHEN, 1991, A new species of Vesicomyidae from Nansha Islands waters. *Papers on marine biology of Nansha Islands and adjacent seas. Beijing: China Ocean Press*, 1: 164–166.

Revised ms. accepted January 12, 2015

RESEARCH NOTES

MALACOLOGIA, 2015, 58(1–2): 363–364

THE SUPPOSED TRANSCAUCASIAN ENDEMITE *ADZHARIA RENSCHI* HESSE, 1933 IS A SOUTH AMERICAN *BULIMULUS* SPECIES (GASTROPODA: BULIMULIDAE)

Bernhard Hausdorf

Zoologisches Museum, Universität Hamburg, Martin-Luther-King-Platz 3,
20146 Hamburg, Germany; hausdorf@zoologie.uni-hamburg.de

In his seminal monograph about the anatomy and systematics of the Enidae (Gastropoda: Pulmonata), Hesse (1933) described a new genus and species, *Adzharia renschi*, based on material he received from the Zoological Museum Berlin (ZMB) with the locality data "summit of the pass near Chula in Adzharia". No collector or date is specified on the labels of the type material (ZMB 75980a and b). This genus is characterized by some characters not known from any other enids, such as an odontognath-like jaw. Despite efforts to recollect the supposed Transcaucasian endemite at its type locality in Georgia (Schileyko, 1998; M. Neiber & F. Walther, pers. comm.), no material of this enigmatic species has been found since the original description. Thus, doubts concerning the origin of the type material of *Adzharia renschi* rose.

A re-examination of the lectotype (ZMB 75980a; designated by Kilias, 1971; Figs. 1, 2, height 20.8 mm, 7 whorls) and the paralectotype of *Adzharia renschi* (ZMB 75980b, height 19.4 mm, 6.5 whorls) revealed a distinct microsculpture on the protoconch (Fig. 2) unknown from other enids, but characteristic for Neotropical bulimulids. More precisely, the microsculpture of the protoconch of *Adzharia renschi* consists of small dents in a thimble-like pattern as in some *Bulimulus* species.

The shell of *Adzharia renschi* (Fig. 1) resembles small forms of the variable *Bulimulus bonariensis* (Rafinesque, 1833) (Fig. 3). Some authors distinguish between two subspecies of *B. bonariensis*, namely the broad *Bulimulus b. bonariensis* (Rafinesque, 1833) from northeastern Argentina and Uruguay and the more slender *Bulimulus bonariensis sporadicus* (d'Orbigny, 1835) from Bolivia, Brazil, Paraguay, and northwestern Argentina (Miquel, 1991). According to its dimensions, *Adzharia renschi* Hesse, 1933, is more similar to *Bulimulus bonariensis sporadicus* (d'Orbigny, 1835).

The genitalia of *Adzharia renschi* figured by Hesse (1933: fig. 4B) are similar to those of *B. bonariensis* figured by Schlesch (1935) and Breure (1978: fig. 236, as *B. juyuyensis*; see Miquel, 1991), but the flagellum is longer. The second genital system figured by Hesse (1933: fig. 4A) is characterized by a long diverticulum at the bursa copulatrix. Such a diverticulum does not occur in any bulimulid. In other respects, this genital system resembles the one depicted in the other figure. One possible explanation is that the figured diverticulum was not a part of the genitalia, but a part of another duct that stuck to the bursa copulatrix. It is also possible that the second genital system figured by Hesse (1933: fig. 4A) (or even both) were erroneously combined with the shells, because the soft parts were already separated from the shells when Hesse received them. Unfortunately, these possibilities could not be checked by an examination of the material, because the preparations of the genitalia could not be found in the ZMB (C. Zorn, pers. comm.). The radula figured by Hesse (1933: fig. 4D) with tricuspid central, bicuspid lateral and multicuspid marginal teeth fits the radula of *B. bonariensis sporadicus* figured by Miquel (1991: figs. 52–54). The jaw figured by Hesse (1933: fig. 4C) consists of vertical plaits as the jaw of *Bulimulus* (Schileyko, 1999) and lacks the triangular central piece present in several other bulimulids.

Characters of the shell, the genitalia, the radula and the jaw indicate that the specimens on which Hesse (1933) based the description of *Adzharia renschi* belong to a South American *Bulimulus* species. Consequently, *Adzharia* Hesse, 1933, is a junior synonym of *Bulimulus* Leach, 1814. *Adzharia renschi* Hesse, 1933, might be a junior synonym of *Bulimulus bonariensis sporadicus* (d'Orbigny, 1835). However, the differences in the proportions of the genitalia as figured and described by Hesse (1933) and the small shell leave room for doubt. Without a comprehensive revision of *Bulimulus*, it cannot be excluded that *Adzharia renschi* represents a so far insufficiently known species. The identity of the second genital system is not decisive for the clarification of the synonymy of the name *Adzharia renschi*, because Kilias (1971) designated the figured shell (Figs. 1, 2) as lectotype. In any case, a permutation of locality labels misled Hesse (1933) so that he classified a representative of the Neotropical Bulimulidae, a family with which he was not familiar, as a Palaearctic Enidae.

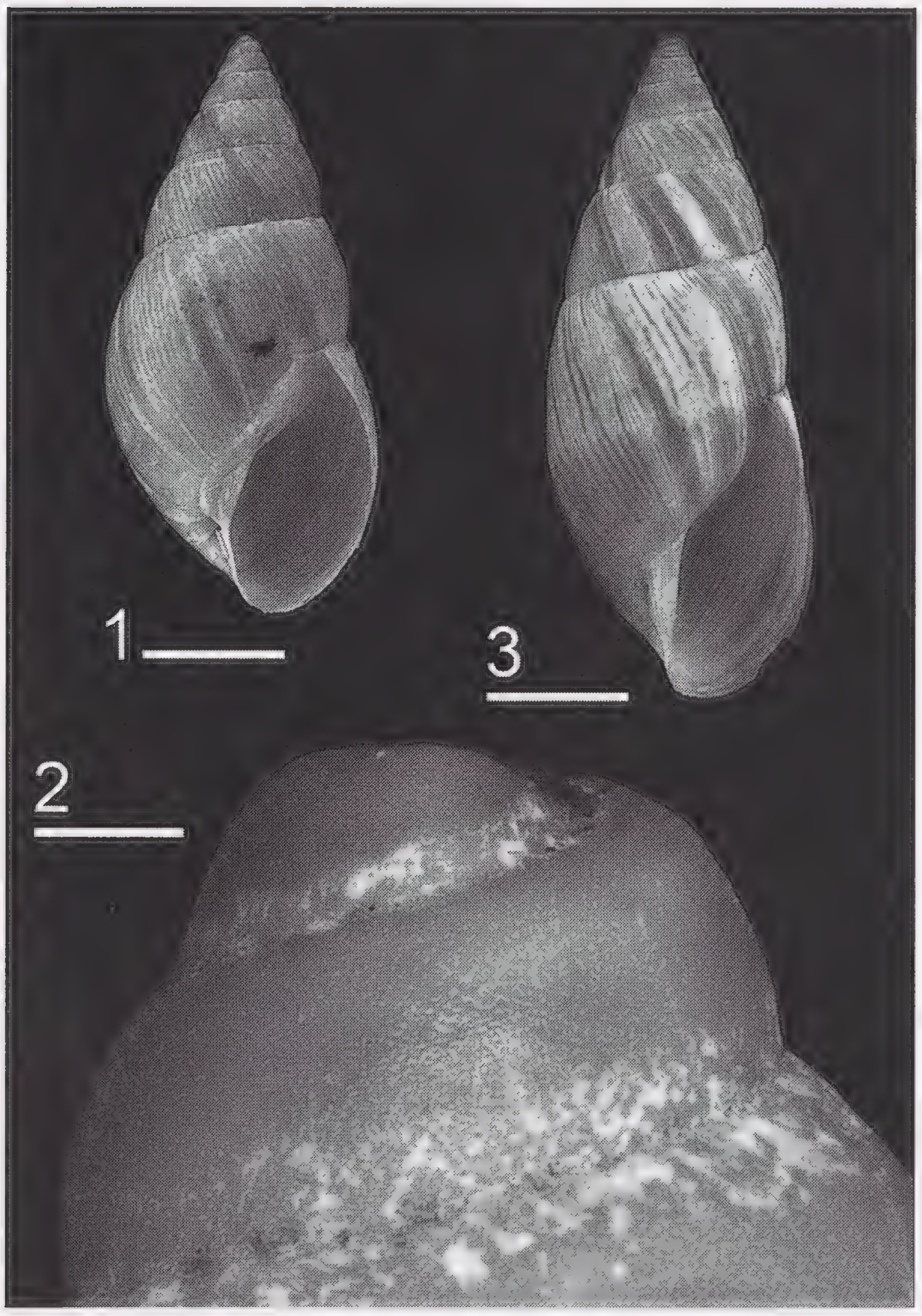

FIGS. 1, 2. *Adzharia renschi* Hesse, 1933, allegedly from Khulo pass, Georgia (lectotype ZMB 75980a). FIG. 1: Shell; FIG. 2: Microsculpture of the protoconch. FIG. 3. *Bulimulus bonariensis sporadicus* (d'Orbigny, 1835) from San Salvador, Paraguay (ZMH 7214). Scale bars: Figs. 1, 3 = 5 mm; Fig. 2 = 0.25 mm.

ACKNOWLEDGMENTS

I am grateful to C. Zorn and M. Glaubrecht (ZMB) for the loan of the type material of *Adzharia renschi*, to S. Miquel for figures and comments concerning *Bulimulus bonariensis*, and to F. Walther for taking the photos. This research was funded by the Volkswagen Foundation.

LITERATURE CITED

BREURE, A. S. H., 1978, Notes on and descriptions of Bulimulidae (Mollusca, Gastropoda). *Zoologische Verhandelingen*, 164: 1–255, pls. 1–22.

HESSE, P., 1933, Zur Anatomie und Systematik der Familie Enidae. *Archiv für Naturgeschichte*, N.F., 2: 145–224.

LEACH, W. E., 1814, *The zoological miscellany; being descriptions of new, or interesting animals.* Nodder & Son, London, 1: 144 pp., 60 pls.

KILIAS, R., 1971, Die Typen und Typoide der Mollusken-Sammlung des Zoologischen Museums Berlin (6). II. Euthyneura, Stylommatophora, Orthurethra, Pupillacea (Enidae). *Mitteilungen aus dem Zoologischen Museum in Berlin*, 47: 215–238.

MIQUEL, S. E., 1991, El género *Bulimulus* Leach, 1814 (Mollusca, Gastropoda, Stylommatophora) en la República Argentina. *Studies on Neotropical Fauna and Environment*, 26: 93–112.

ORBIGNY, A. D', 1835, Synopsis terrestrium et fluviatalium molluscorum, in suo per Americam meridionalem itinere. *Magasin de Zoologie*, 5 (Classe V): 1–44, pls. 61, 62.

RAFINESQUE, C. S., 1833, On 3 n. g. of land shells from Buenos Ayres in South America. *Atlantic Journal and Friend of Knowledge*, 1(5): 165.

SCHILEYKO, A. A., 1998, Treatise on Recent terrestrial pulmonate molluscs. Part 2. Gastrocoptidae, Hypselostomatidae, Vertiginidae, Truncatellinidae, Pachnodidae, Enidae, Sagdidae. *Ruthenica*, Suppl. 2: 129–262.

SCHILEYKO, A. A., 1999, Treatise on Recent terrestrial pulmonate molluscs. Part 3. Partulidae, Aillyidae, Bulimulidae, Orthalicidae, Megaspiridae, Urocoptidae. *Ruthenica*, Suppl. 2: 263–436.

SCHLESCH, H., 1935, Eine neue Subspezies von *Bulimulus* (*Bulimulus*) *sporadicus* Orb. aus Paraguay (*Bul. sporadicus schadei*). *Archiv für Molluskenkunde*, 67: 86–87.

Revised ms. accepted August 14, 2014

MALACOLOGIA, 2015, 58(1–2): 365–369

SENSIBILITY OF THE INVASIVE SNAIL *MELANOIDES TUBERCULATUS* (MÜLLER, 1774) TO SALINITY VARIATIONS

Eder Carvalho da Silva* & Francisco Barros

Federal University of Bahia, Post-Graduate Program in Ecology and Biomonitoring, Benthic Ecology Lab, Rua Barão de Geremoabo, s/n, Ondina, Salvador, Bahia, Brazil

INTRODUCTION

Estuaries are among the most productive systems in coastal zones, but they are also among the most impacted (Kennish, 2002). Human activities, including chemical pollution, nutrient enrichment, overexploitation of natural resources and changes in hydrological regimes, can have a number of effects on estuarine regions. In the last decades, the introduction of alien species has also been reported as an important source of degradation of estuaries (Kennish, 2000, 2002).

Almost all estuaries are affected to some extent by the introduction of invasive species (Carlton, 1989; Carlton & Geller, 1993). Bioinvasions may lead to changes in habitat and trophic organization, a reduction in species diversity, the spread of pathogens, and in extreme cases, the total displacement of native species (Carlton, 1996; Ehrenfeld, 2010; Simberloff et al., 2013).

Despite all of the potential difficulties imposed by a new habitat, invasive species are successful in colonizing new environments due to environmental characteristics (invasibility) and those of the invasive species (invasiveness) (Lodge, 1993; Alpert et al., 2000; Colautti et al., 2006).

Among invasive macroinvertebrates, a group of great importance is the Gastropoda (Carlton, 1999). *Melanoides tuberculatus* (Müller, 1774) is a gastropod that has invaded lakes, rivers and estuaries around the world (Bolaji et al., 2011; Roessler et al., 1977). It is typically a freshwater species, but it can also inhabit brackish waters (Wingard et al., 2008) and is the invasive species with the widest distribution in Brazil (Silva & Barros, 2011). However, there is only one report of this species in Brazilian brackish water (Barroso & Matthews-Cascon, 2009). There is substantial evidence that invader success is related to fast growth and a high rate of reproduction, but enhanced stress tolerance is also important (Weir & Salice, 2011). Previous studies have observed that *M. tuberculatus* is tolerant to several natural and anthropogenic abiotic stressors (Weir & Salice, 2012), but the salinity tolerance of this invasive species is still unknown.

The colonization of new habitats poses challenges to invaders (Richardson et al., 2000), especially in estuarine areas, mainly due to changes in salinity. However, invasive species have characteristics that favor and help overcome these challenges. Thus, this study aims to evaluate the resistance of the invasive snail, *M. tuberculatus*, to salinity.

MATERIALS AND METHODS

Specimens of *M. tuberculatus* (Fig. 1) were collected at four different freshwater sites around Salvador City, Bahia in northeast Brazil (PMP's lake – 12°58'02"S, 38°24'43"W; Passa Vaca River – 12°57'42"S, 38°24'00"W; Stella Maris Lake – 12°55'58"S, 38°19'34"W; and Flamengo's Lake – 12°55'31"S, 38°19'10"W) and acclimatized in an aquarium with sand and macrophytes (*Salvinia auriculata* and *Egeria densa*) for 72 h.

Two salinity tolerance experiments were conducted in the laboratory. The experiments consisted of exposing the *M. tuberculatus* test organisms to different salinities (5, 10, 15, 20, 25, 30, 35, 40 and 45, experiment 1; n = 5) for 48 h.

In the second experiment, all organisms were initially placed into aquaria supplied with freshwater (n = 15). Five aquariums were maintained with freshwater for six weeks (treatment A), five were subjected to weekly increases in salinity (five per week) (treatment B), and the last five were subjected to higher weekly increases in salinity (eight per week) (treatment C).

---

*Corresponding author: edercarvalho514@oi.com.br

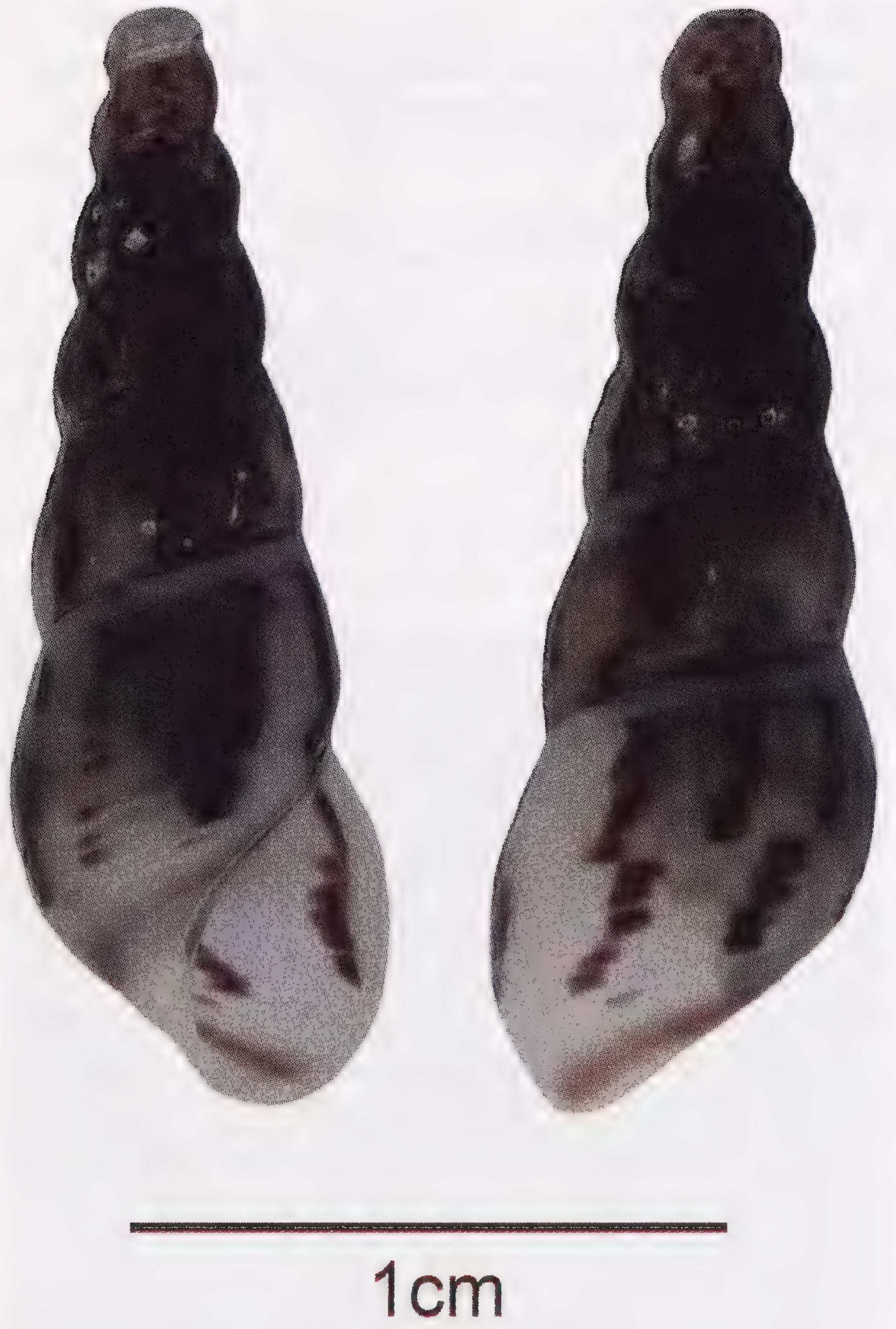

FIG. 1. *Melanoides tuberculatus* from Salvador, Bahia, Brazil.

To assess salinity tolerance (experiment 1), one-way ANOVA between survival (%) and nine treatments was performed (followed by Tukey's test). To assess the resistance of the organisms to gradual increases in salinity (experiment 2), one-way ANOVA was performed followed by Tukey's test between treatments after six weeks.

RESULTS

In experiment 1, we observed that most organisms survived until reaching a salinity of 25 (only 4% mortality) and that the survival rate remained relatively high (74%) until 30 (Fig. 2). The analysis of variance showed significant differences between treatment means ($p < 0.001$). The comparison between paired treatments (Tukey's test) revealed the following: S05 ≅ S10 ≅ S15 ≅ S20 ≅ S25 ≠ S30 ≠ S35 ≅ S40 ≅ S45.

Experiment 2 showed that all treatments led to decreases in survival, especially those above 25 to 30 (five weeks), which resulted in sharp decreases in survival. However, even in extreme salinities (i.e., 45 in treatment C after six weeks), the mean survival rate was greater than 50%, indicating that this species is able to survive in hyperhaline conditions (Fig. 3). The ANOVA results showed significant dif-

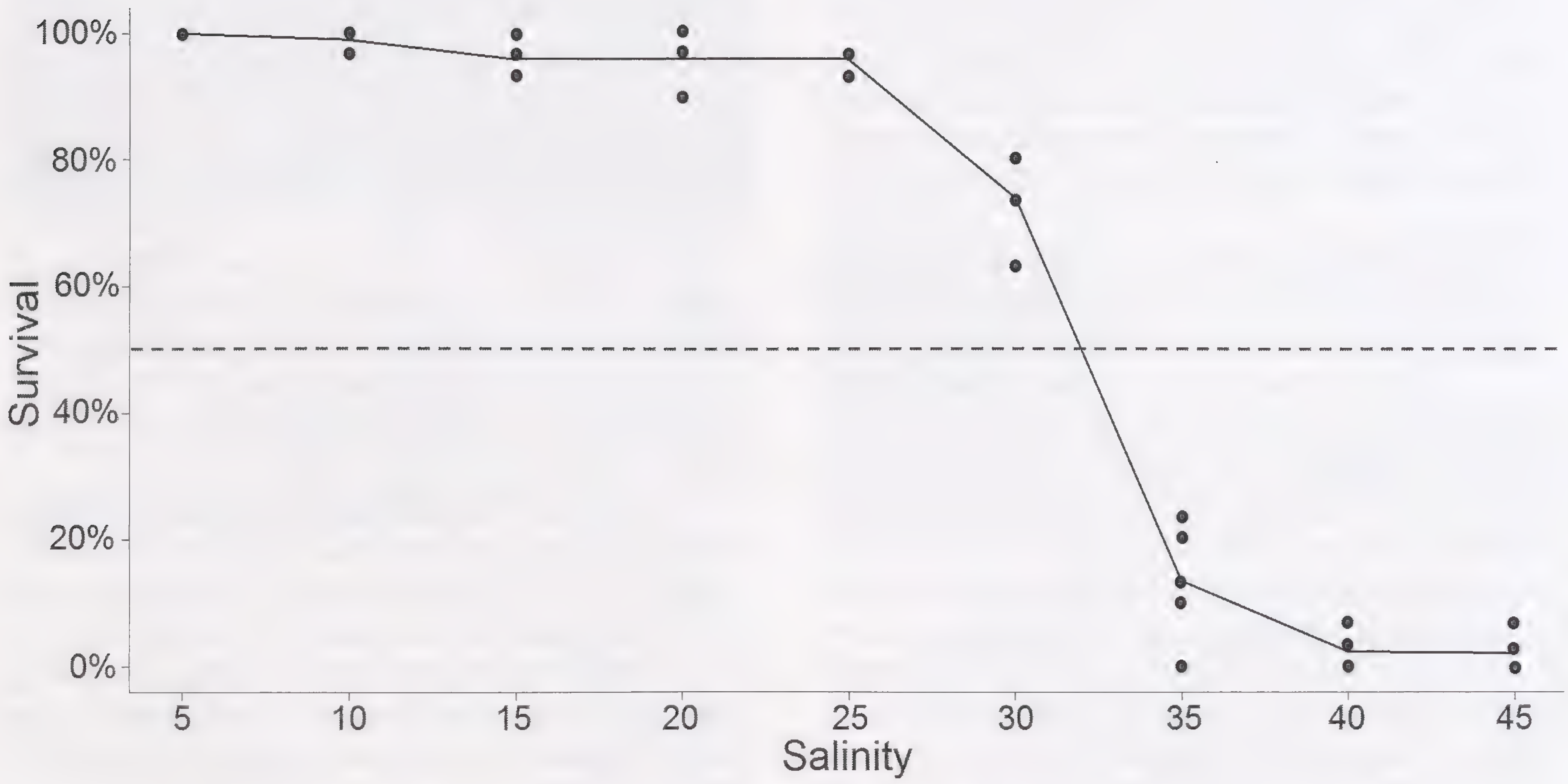

FIG. 2. Survival rate of *Melanoides tuberculatus* exposed to various salinity concentrations. The horizontal dashed line indicates 50% survival. Some points overlap on the graph (n = 5).

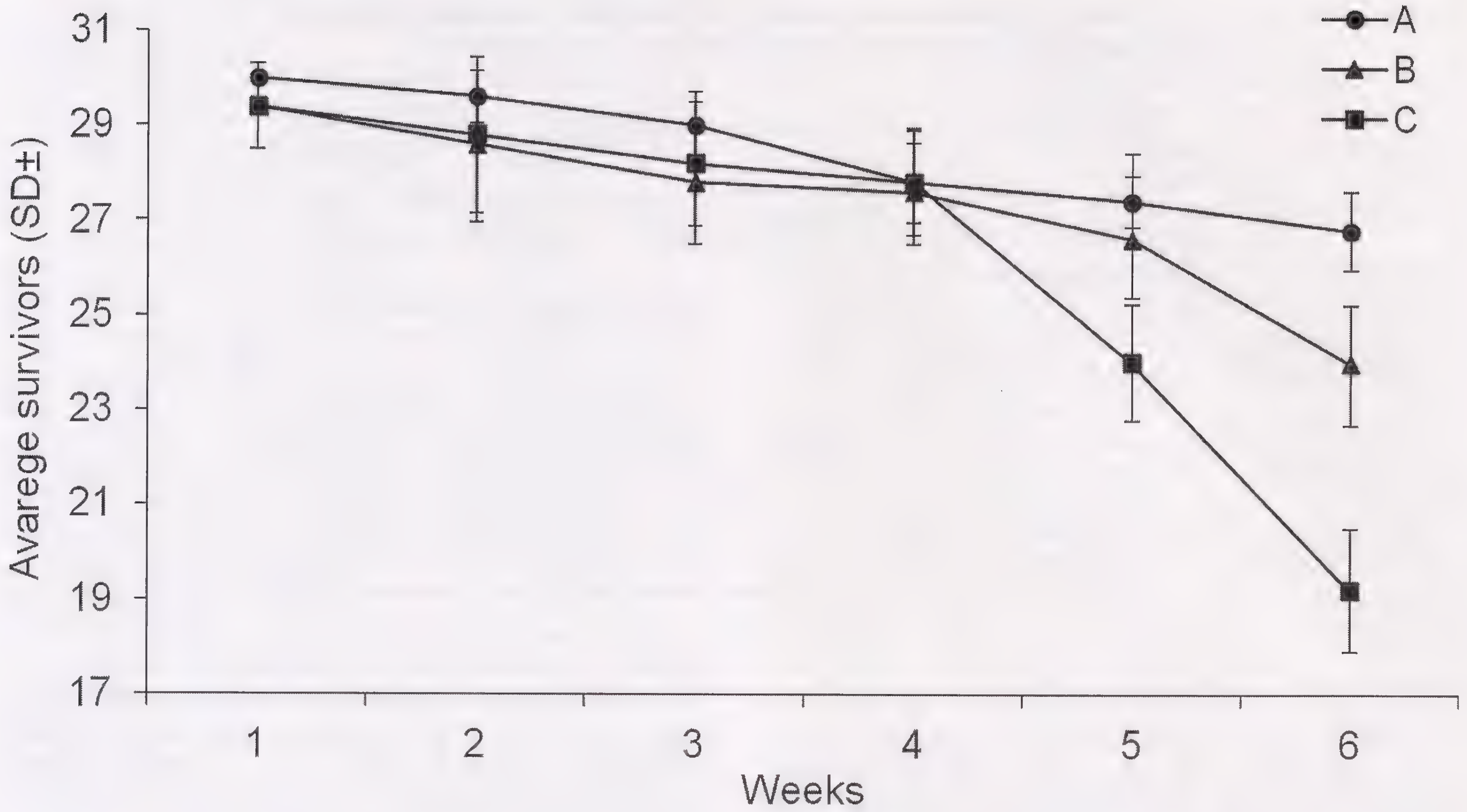

FIG. 3. Average *M. tuberculatus* survivors per week for the three treatments (A, B and C; n = 5). A = water was maintained at < 5 salinity (control); B = weekly increase in salinity of 5; C = weekly increase in salinity of 8.

ferences between the treatment means ($p < 0.001$) and differences between all paired treatments (AB, $p < 0.01$; BC, $p < 0.001$; and AC; $p < 0.001$) (Fig. 4). Thus, we suggest that salinity can influence the survival of this organism because their survival decreased following most of the saline treatments tested; however, resistance to polyhaline conditions of up to 30 was observed without great difficulty.

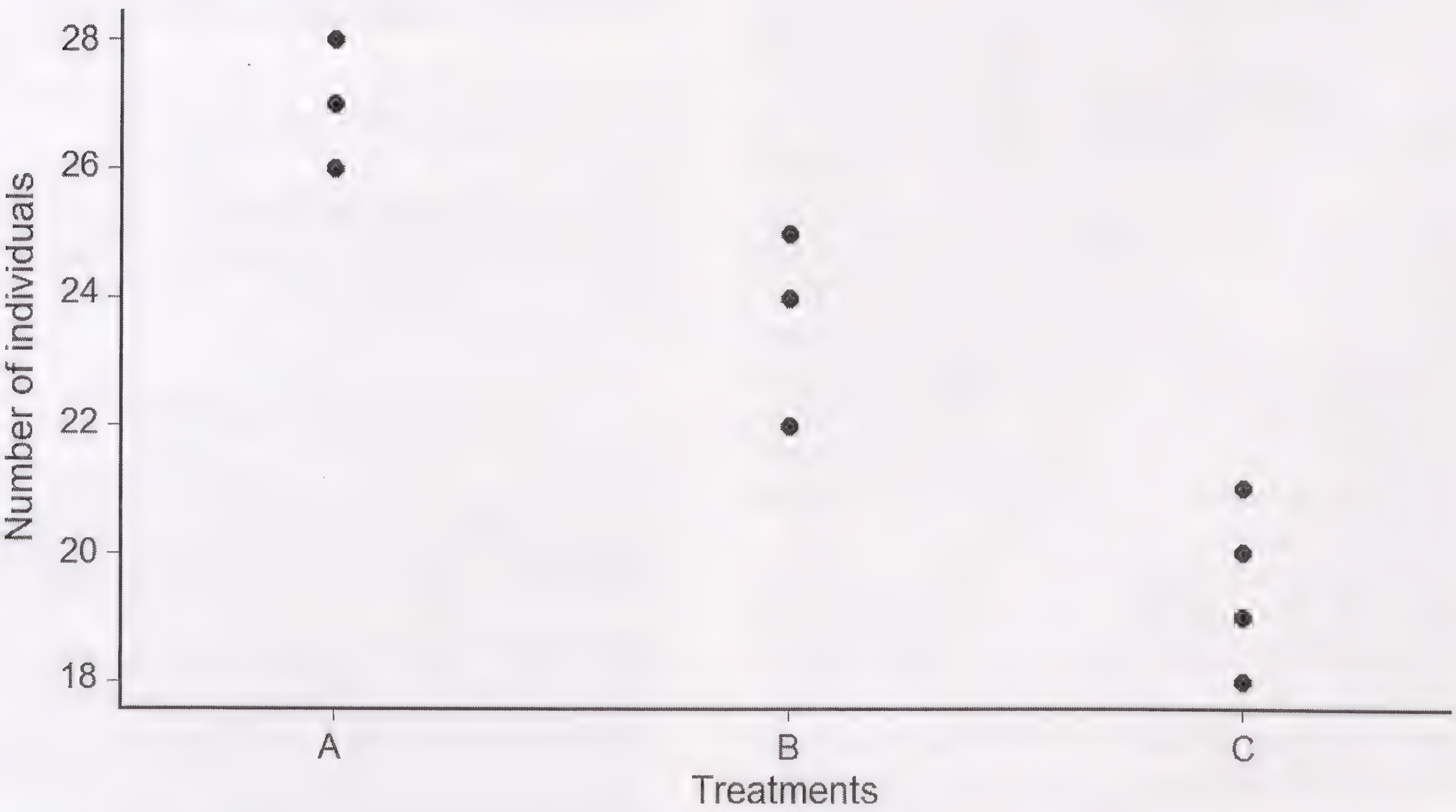

FIG. 4. Graph of the analysis of variance of the number of individuals versus the treatments. Some points overlap on the graph (n = 5).

TABLE 1. Studies that reported salinities tolerated by *Melanoides tuberculatus* (*in situ* and in the laboratory).

References	Sites	Salinity
Barroso & Matthews-Cascon, 2009	*In situ*	30
Englund et al., 2000	*In situ*	34
Roessler et al., 1977	*In situ*	30
Vogler et al., 2012	*In situ*	33
Wingard et al., 2008	*In situ*	33
Barroso & Matthews-Cascon, 2009	Laboratory	35
Bolaji et al., 2011	Laboratory	25
Wingard et al., 2008	Laboratory	45

DISCUSSION

According to Plaziat & Youris (2005), *M. tuberculatus* is an euryhaline species that inhabits low-salinity environments (0.2–3) but is capable of tolerating high salinities (over 23). Several studies are in agreement with the findings of this group and have suggested that *M. tuberculatus* is able to withstand salinities higher than 30 (Table 1), not only under laboratory conditions but also *in situ*. This high tolerance together with the uniparental reproduction of this organism may facilitate its invasion in new environments (e.g., estuaries) (Facon et al., 2008).

Barroso & Matthews-Cascon (2009) have demonstrated the presence of *M. tuberculatus in situ* in high densities in salinities ranging from 0–30; in the laboratory, this organism remained active between salinities of 25 and 35. Other studies have shown similar results, and the highest salinity inhabited by this organism was reported to be between 30 and 34 *in situ* (Roessler et al., 1977; Englund et al., 2000; Wingard et al., 2008; Vogler et al., 2012) and between 25 and 45 in the laboratory (Wingard et al., 2008; Bolaji et al., 2011). Therefore, *M. tuberculatus* can occur in high densities in hyperhaline conditions, demonstrating its ability to adapt to euryhaline conditions.

Melanoides tuberculatus is frequently observed in high densities, which likely increases competition for space and food between exotic and native species (Fernandez et al., 2001; Vogler et al., 2012; Wingard el al., 2008). Although this species is naturally occurring in freshwater environments, our experiment showed that it can adapt to the gradual and abrupt increases in salinity common in typical marine and hyperhaline environments. Thus, this invasive species may cause ecological harm not only in freshwater but also in brackish water (estuaries and mangroves), especially in systems with high organic contents and limited water and flow (Giovanelli et al., 2005).

Melanoides tuberculatus has been previously reported in freshwater systems in northeast Brazil (e.g. Paz et al., 1995; Barroso & Matthews-Cascon, 2009; Santos & Eskinazi-Sant'Anna, 2010; Souto et al., 2011; Silva & Gomes, 2014). However, there have been no reports of its potential invasion of estuaries or of its effects on native benthic communities. Therefore, there is an urgent need for experimental studies to properly understand the potential negative effects of this invasive species on natural benthic assemblages.

ACKNOWLEDGMENTS

This work was supported by FAPESB (PET 0035/2012). F. Barros was supported by CNPq fellowships (303897/2011-2, 239978/2012-9).

LITERATURE CITED

ALPERT, P., E. BONE & C. HOLZAPFEL, 2000, Invasiveness, invasibility and the role of environmental stress in the spread of non-native plants. *Perspectives in Plant Ecology, Evolution and Systematics*, 3: 52–66.

BARROSO, C. X. & H. MATTHEWS-CASCON, 2009, Occurrence of the exotic freshwater snail *Melanoides tuberculatus* (Mollusca: Gastropoda: Thiaridae) in an estuary of north-eastern Brazil. *Marine Biodiversity Records*, 2: 1–4

BOLAJI, D. A., C. A. EDOKPAYI,O. B. SAMUEL, R. O. AKINNIGBAGBE & A. A. AJULO, 2011, Morphological characteristics and Salinity tolerance of *Melanoides tuberculatus* (Muller, 1774). *World Journal of Biological Research*, 4(2): 1–11.

CARLTON, J. T., 1989, Man's role in changing the face of the oceans: biological conservation of near-shore environments. *Conservation Biology*, 3: 265–273.

CARLTON, J. T., 1996, Biological invasion and cryptogenic species. *Ecology*, 77(6): 1653–1655.

CARLTON, J. T., 1999, Molluscan invasions in marine and estuarine communities. *Malacologia*, 41: 439–454.

CARLTON, J. T. & J. B. GELLER, 1993, Ecological roulette: the global transport of nonindigenous marine organisms. *Science*, 261: 78–82.

COLAUTTI, R. I., I. A. GRIGOROVICH & H. J. MACISAAC, 2006, Propagule pressure: a null model for biological invasions. *Biological Invasions*, 8: 1023–1037.

EHRENFELD, J. G., 2010, Ecosystem consequences of biological invasion. Annual *Review of Ecology, Evolution, and Systematics*, 41: 59–80.

ENGLUND, R. A., K. ARAKAKI, D. J. PRESTON, S. L. COLES & L. G. ELDREDGE, 2000, Nonindigenous freshwater and estuarine species introductions and their potential to affcet sportfishing in the lower stream and estuarine regions of the south and west shores of Oahu, Hawaii. *Honolulu. Bishop Museum Technical Report*, 17: 121 pp.

FACON, B., J. P. POINTIER, P. JARNE, V. SARDA & P. DAVID, 2008, High genetic variance in life-history strategies within invasive populations by way of multiple introductions. *Current Biology*, 18: 363–367; doi: 10.1016/j.cub.2008.01.063.

FERNANDEZ, M. A., S. C. THIENGO & L. R. L. SIMONE, 2003, Distribution of the introduced freshwater snail *Melanoides tuberculatus* (Gastropoda: Thiaridae) in Brazil. *The Nautilus*, 117: 78–82.

GIOVANELLI, A., C. L. P. A. SILVA, G. B. E. LEAL & D. F. BAPTISTA, 2005, Habitat preference of freshwater snails in relation to environmental factors and the presence of the competitor snail Melanoides tuberculatus (Muller, 1774). *Memorias do Instituto Oswaldo Cruz*, 100(2): 169–176.

KENNISH, M. J., 2000, *Estuary restoration and maintenance: the National Estuary Program*. CRC Press, Boca Raton, U.S.A., 359 pp.

KENNISH, M. J., 2002, Environmental threats and environmental future of estuaries. *Environmental Conservation*, 29: 78–107.

LODGE, D. M., 1993, Biological invasions: lessons for ecology. *Trends in Ecology & Evolution*, 8: 133–137.

MÜLLER, O. F., 1774, *Vermium terrestrium et fluviatilium, seu animalium infusorium, helminthicorum et testaceorum, non marinorum, succincta historia, ...* Vol. 2. Heineck & Faber, Havniae & Lipsiae, xxxvi + 214 + [x] pp.

PAZ, R. L., T. WATANABE, M. P. M. DIJCK & F. J. P. ABÍLIO, First record of *Melanoides tuberculata* (Müller, 1774) (Gastropoda: Prosobranchia: Thiaridae) in the state of Paraíba (Brazil) and its possible ecological implications. *Revista Nordestina de Biologia*, 10(2): 79–84.

PLAZIAT, J. C. & W. R. YOUNIS, 2005, The modern environments of mollusks in southern Mesopotamia, Iraq: a guide to paleographical reconstructions of Quaternary fluvial palustrine and marine deposits. *Carnets de Geologie/Notebooks on Geology*, Brest, Article 2005/01, 18 pp.

RICHARDSON, D. M., P. PYSEK, M. REJMÁNEK, M. G. BARBOUR, F. D. PANETTA & C. J. WEST, 2000, Naturalization and invasion of alien plants: concepts and definitions. *Diversity and Distributions*, 6: 93–107.

ROESSLER, M. A., G. L. BEARDLEY & D. S. TABB, 1977, New records of the introduced snail *Melanoides tuberculata* (Mollusca: Thiaridae) in south Florida. *Florida Scientist*, 40(1): 87–94.

SANTOS, C. M. & E. M. ESKINAZI-SANT'ANNA, 2010, The introduced snail *Melanoides tuberculatus* (Müller, 1774) (Mollusca: Thiaridae) in aquatic ecosystems of the Brazilian semiarid northeast (Piranhas-Assu River basin, state of Rio Grande do Norte). *Brazilian Journal of Biology*, 70(1): 1–7.

SILVA, E. C. DA & F. BARROS, 2011, Macrofauna bentônica introduzida no Brasil: lista de espécies marinhas e dulcícolas e distribuição atual. *Oecologia Australis*, 15(2): 326–344

SILVA, E. C. DA & L. E. O. GOMES, 2014, *Melanoides tuberculatus* (Müller, 1774): occurrence extension of the invasive gastropod in Bahia, Brazil. *Pan-American Journal of Aquatic Sciences*, 9(2): 145–149.

SIMBERLOFF, D., J. MARTIN, P. GENOVESI, V. MARIS, D. A. WARDLE, J. ARONSON, F. COURCHAMP, B. GALIL, E. GARCÍA-BERTHOU, M. PASCAL, P. PYSEK, R. SOUSA, E. TABACCHI & M. VILÀ, 2013, Impacts of biological invasions: what's what and the way forward. *Trends in Ecology & Evolution*, 28(1): 58–66.

SOUTO, L. S., M. F. G. BRITO & L. C. ROSA, 2011, *Melanoides tuberculatus* (Müller, 1774): a new threat to the conservation of native aquatic species in Sergipe, Brazil. *Scientia Plena*, 7(4): 1–6.

VOGLER, R. E., V. NÚÑEZ, D. E. G. GREGORIO, A. A. BELTRAMINO & J. G. PESO, 2012, *Melanoides tuberculata*: the history of an invader. Pp. 65–84, in: E. M. HÁMALÁINEN & S. JÁRVINEN, eds., *Snails: biology, ecology and conservation*. Nova Science Publishers, New York, xiii + 185 pp.

WEIR, M. S. & C. C. SALICE, 2011, Mananging the risk of invasive species: how well do functional traits determine invasion strategy and success? *Integrated Environmental Assessment Management*, 7: 299–300.

WINGARD, G. L., J. B. MURRAY, W. B. SCHILL & E. C. PHILLIPS, 2008, Red-rimmed melania (*Melanoides tuberculatus*): a snail in Biscayne National Park, Florida – harmful invader or just a nuisance? *U.S. Geological Survey Fact Sheet*, 2008-3006; http://pubs.usgs.gov/fs/2008/3006/ (Accessed 1 May 2014).

Revised ms. accepted December 7, 2014

MALACOLOGIA, 2015, 58(1–2): 371–381

INDEX

Taxa in **bold** are new; pages in *italic* indicate figures of taxa.

Abra 198
  lunella 198
  murrayana 198
Abyssogena 352
Acmaea 204
  kolarovai 204
  peitaihoensis 204, *205*
  testudinaria 204, *206*
  testudinalis var. *minor* 204
Acmaeidae 204
acontes, Anomia 60, 66
Acorylus gouldii 110
Acrilla acuminata 214
acuminata, Acrilla 214
acuta, Physa 169, 171, 172, *173*
adamsi, Arca 15
  Arcopsis 1, 15, *16–18*, 20
adamsiana, Nipponarca 186
Adamussium colbecki 226
Adelomelon ancilla 337, 338, *339–343*, 340, 344, 345
  brasiliana 337, 344
  ferrusacci 344
adiastola, Helobdella 274
Adulomya 350, 352
Adzharia 363
  renschi 363, 364, *364*
Afropomus *247*, 249, 251, 254, 261, 264
  balanoidea *252*
agesilaus, Leptochiton 147, 153
alata, Ostrea 30
alatus, Isognomon 1, 30, *30*, *32*, *33*, 34, 35
alba, Turbonilla garrettiana var. 220, *220*
albida, Vesicomya 357
Alopiinae 225, 226, *228*, 229, 230
alta, Venus 195
  Venus jidoensis var. 195, *196*
alterniplicata, Siphonalia 221
  Siphonaria 221, *221*
altispiralis, Purpura 218, *218*
Alvania concinna 209
alveclata, Purpura 216
ambiguus, Spondylus 56, 57
Ameghinomya antiqua 339
americanus, Spondylus 1, 50, *51–54*, 56, 57, 111, 112
ampullacea, Pila *252*, 275, 280
Ampullaria 248
  (*Pila*) *gigas* 257
  polita 256
ampullariae, Helobdella 273
  Unionicola (*Ampullariatax*) 274
Ampullariidae 233, 245, 246, 248, 249, *250*, *252*, 272, 281, 282
Ampullarioidea 248
Ampullarius 248
Anadara cornea 184
  gubernaculum 184
  inaequivalvis 184
  kagoshimensis 184
  peitaihoensis 184
  (*Scapharca*) *cornea* 184
  subcrenata 184
Anatina pechiliensis 203, *203*
ancilla, Adelomelon 337, 338, *339–343*, 340, 344, 345
angelica, Pila 280
Angiostrongylus cantonensis 274, 279, 280
angulata, Laubiericoncha 350, *355*, 355–358
Angulus sybariticus 110
  tenuis 109, 110
angustata, Barleeia 209, 211
Anomia 5, 65, *117*
  acontes 60, 66
  chinensis 189, 191
  cuticula 189
  cuticulum *191*
  cytaeum 189
  ephippium 60, 65, 66
  nipponensis var. *obsoletocostata* 189, *190*
  nipponensis var. *obsoleto-costata* 189
  outicula 189
  plana 189, 191
  simplex 1, 60, *61*, *62*, *64*, 65, 66, 110, 111, 114, 115
Anomiidae 1, 60, 65, 189
Anomioidea 65
antiqua, Ameghinomya 339
antiquatus, Cardites 70
Aplysia depilans 163
  punctata 162, 163
aquarius, Modiola 195
Arca adamsi 15
  (*Anomalocardia*) *subcrenata* 184
  (*Barbatia*) *interplicata* 183, 187, *187*
  interplicata 187
  kagoshimensis 184
  nodoso crenata 184
  obtusa var. *duplicostata* 185, *186*
  (*Scapharca*) *peitaihoensis* 184, *185*
  subcrenata 184
Arca-nodoso crenata 184
Archivesica 351, 358

Arcidae 4, 184
Arcopsis 5, 110, 115, *117*
  adamsi 1, 15, *16–18*, 20
  interplicata 187
  solida 20
Arctica 349
Arcticidae 349
Arcticoidea 349
Arcuatula 195
  senhousia 195
Arion 304, 306, 313, *314*, *315*
  (*Arion*) *ater* 306
  (*Arion*) *rufus* 306
  (*Arion*) *vulgaris* 306
  ater 303–313, *305*, *309*, *311*, *312*, *314*, *315*, 316, 317, 320, 321
  ater ater 304
  ater rufus 304
  ater var. *atra* 316
  ater var. *castanea* 316
  (*Carinarion*) *circumscriptus* 306
  (*Carinarion*) *silvaticus* 306
  circumscriptus 308, 309, 313, *314*, *315*
  flagellus 303–305, 308, 313, *314*, *315*, 316
  fuscus 303, 308, 313, *314*, *315*
  lusitanicus 303, 304, 308, 310, 313, *314*, *315*, 316, 317
  (*Mesarion*) *flagellus* 306
  (*Mesarion*) *fuscus* 306
  (*Mesarion*) *lusitanicus* 306
  (*Mesarion*) *nobrei* 306
  nobrei 303, 308, 313, *314*, *315*, 316
  rufus 303, 304, 306–308, *309*, 310–313, *311*, *312*, *314*, *315*, 316, 317, 320, 321
  silvaticus 308, 313, *314*, *315*
  vulgaris 303–313, *305*, *310–312*, *314*, *315*, 316, 317, 320, 321
Arionidae 303
aristata, Lithophaga 4
aristatus, Myoforceps 4
asellus, Chiton 148
Asolene 233, 234, *247*, 249, 251, 253, 261, 262, 264
  platae 233, 234, 236, *236–238*, 238–241, *252*, 258, 274
  pulchella 233, 253, 256, 257, 261, 275
  spixii 275
ater, Arion 303–313, *305*, *309*, *311*, *312*, *314*, *315*, 316, 317, 320, 321
  Arion (*Arion*) 306
  Arion ater 304
atra, Arion ater var. 316
Atrina fragilis 49
australis, Plicatula 60

badius, Leptochiton 153
balanoidea, Afropomus 252
ballanodosa, Terebra 219
barbara, Rissoina 179, 209, *209*
Barbatia 5, 110, *117*, 186
  bistrigata 186
  cancellaria 4
  (*Savignyarca*) *virescens* 186
  signata 186
Barleeia angustata 209, 211
basilanica, Limaria 195
  Limaria (*Limaria*) 194, 195
Bdelloidea 274
beana, Entodesma 1, 70, *71–74*, 75, 113
  Lyonsia 70
  Lyonsia (*Philippina*) 70
Beguina semiorbiculata 70
bellanodosa, Terebra 179, 219, *219*
bicolor, Isognomon 34
bidens, Papillifera 225, 226, *227*, *228*, 229, 230
bifascialis, Eulima 212
bilineata, Eulema 212
  Eulima 212, *213*
birmani, Calyptogena 357
biserialis, Stramonita 323, 324, *325–327*, 327, 334
bistrigata, Barbatia 186
  Mesocibota 185, 186
bolteniana, Lanistes 261, 262
bonariensis, Bulimulus 363, 364
  Bulimulus bonariensis 363
bosniensis, Herilla 226, 230
Bouchetia vaubanensis 333
Brachidontes 5, 29, 114, 115, *117*, 118
  exustus 1, 24, *25–28*, 29, 30
  (*Hormomya*) *exustus* 24
  muelleri 30
  mulleri 30
  solisianus 29
brasiliana, Adelomelon 337, 344
brasilianum, Cardium 103
  Laevicardium 103
brasiliensis, Entodesma 75
  Osteodesma 70, 75
braziliensis, Osteodesma 75
brevicula, Littorina 206
bronii, Purpura 216
bronni, Purpura 216
bruneauensis, Pyrgulopsis 174
Buccinanops cochlidium 344
  globulosus 345
Bulimulidae 363, 364
Bulimulus 363
  bonariensis 363, 364
  bonariensis bonariensis 363
  bonariensis sporadicus 363, *364*
  juyuyensis 363
bureri, Rissoina 179, 211, *211*

californica, Lyonsia 75
Callista 349
Callogonia 351, 358
Calyptogena 351
  birmani 357
  troncosoi 357
Calyptraeidae 211
Campaniloidea 248
canaliculata, Pomacea 235, *238*, 239–241, 245, 248, 250–282, *273*
cancellaria, Barbatia 4
candeana, Scissula 110
candidescens, Leucostigma 225, 226, *227*, *228*, 229, 230
cantonensis, Angiostrongylus 274, 279, 280
Cardiidae 1, 98
Cardita sulcata 70
  variegata 70
Carditamera 5, 116, *117*, 118
  floridana 1, 66, *67–69*, 70
Cardites antiquatus 70
  ovalis 70
Carditidae 1, 66
Cardium brasilianum 103
  laevigatum 98, 103
  lamarckii 103
  oviputamen 98, 103
  serratum 98, 103
carinata, Pyrgulopsis 170
carinatus, Lanistes *252*, 275, 280
carnea, Pinna 1, 43, *44–46*, *48*, 49, 112
caroliniana, Polymesoda 98
carpenteri, Glans 70
  Leda 10
  Nuculana 10
  Propeleda 1, 10, *11–13*, 15, 111
carpentieri, Propeleda 10, 15
castanea, Arion ater var. 316
Catadiscus pomaceae 274
catemacensis, Pomacea patula 261, 262
Cercaria pomaceae 274
Chama 5, 112–114, *117*, 118
  exogyra 86
  macerophylla 1, 81, *82–84*, 86, 111, 112
  pellucida 86
Chamidae 1, 81
chemnitzii, Parahyotissa 189
Chicoreus dilectus 323, 324, *325*, 329, *330*, *331*, 331, 334
  torrefactus 334
chinensis, Anomia 189, 191
Chiton asellus 148
  cinereus 148
Chlamys solaris var. *peitaihoensis* 192, *193*
Chlorostoma rustica 204
chuni, Laubiericoncha 350, *355*, 355–358
cimicoides, Leptochiton 153
cinerea, Urosalpinx 333
cinereus, Chiton 148
circumscriptus, Arion 308, 309, 313, *314*, *315*
  Arion (*Carinarion*) 306
Clausiliidae 225, 226, *228*
clavigera, Thais 216, 218, 278
cochlidium, Buccinanops 344
Cochlodina laminata 226, 230
Codakia 5, 113, 116, *117*
  (*Codakia*) *orbicularis* 76
  orbicularis 1, 76, *76–79*, 103
colbecki, Adamussium 226
Collisella peitaihoensis 179, 204
compostellanum, Leptochiton 153
Concholepas concholepas 327, 334
concholepas, Concholepas 327, 334
concinna, Alvania 209
conica, Pila 275
Corbiculidae 92
cornea, Anadara 184
  Anadara (*Scapharca*) 184
corneus, Solen 200
cornuarietis, Marisa *238*, 239, 240, 250, 252, *252*, 255–258, 261, 268, 275, 276, 278–280
Costellariidae 333
costulata, Mangelia 220
Crassostrea 1, 34, 114
  gigas 189
Crassostreinae 114
crenata, Arca nodoso 184
  Arca-nodoso 184
Crepidula ostraeiformis 211, *212*
cristata, Limopsis 21, 24
  Limopsis aff. 1, 21, *21*, *22*
cruciglans, Pyrgulopsis 170
curumim, Pomacea 251, 252
cuticula, Anomia 189
cuticulum, Anomia *191*
Cyclas maritima 92, 98
Cyclocardia velutina 70
  ventricosa 70
Cyclophoroidea 248
Cyrena floridana 92, 98
Cyrenidae 1, 92
cytaeum, Anomia 189

darioi, Leptochiton 147, 148, 153, 154
Delima itala 226
depilans, Aplysia 163
Deroceras reticulatum 303
Dietziella egregia 274
diffusa, Pomacea 248
dilectus, Chicoreus 323, 324, *325*, 329, *330*, *331*, 331, 334
disparile, Paradentalium 4
dobsoni, Mangelia 179, 220

Donacidae 4, 198
Donax 5, 112, 113, *117*, 118
  kiusiuensis 198
  variabilis 4, 115, 116
dufresnei, Zidona 157, 158, *159–162*, 162–164, 345
dunedini, Rissoina 209, *210*
dunedoni, Rissoina 209
duplicostata, Arca obtusa var. 185, *186*

ebraea, Voluta 344
Echinostoma 274, 279–281
  parcespinosum 274
Ectenagena 352
  extenta 358
edulis, Mytilus 174
egregia, Dietziella 274
elongata, Ostrea 187
  Ostrea chemnitzi var. 187, *188*
elongatus, Modiolus (*Modiolusia*) 195
Enidae 364
Entodesma 5, 112–115, *117*, 118
  beana 1, 70, *71–74*, 75, 113
  brasiliensis 75
  inflata 75
  navicula 75
  saxicola 75
ephebicostalis, Trochus 204
ephebocostalis, Trochus (*Livona*) 204, *207*
ephippium, Anomia 60, 65, 66
Epitoniidae 212
Epitonium scalare minor 179, 213
  (*Scalaria*) 213
  (*Scalaria*) *gradata* var. *pygmaea* 213
  (*Scalaria*) *pretiosa* var. *minor* 212, *214*
  (*Scalaria*) *subtilis laevis* 213, 214
  (*Scalaria*) *subtilis* var. *laevis* 213
Ergalataxinae 323
erosa, Geloina 98
Eulema bilineata 212
Eulima bifascialis 212
  bilineata 212, *213*
Eulimidae 212
Euphaedusa fusaniana 226
Eurhomalea exalbida 339, *340*
exalbida, Eurhomalea 339, *340*
exogyra, Chama 86
extenta, Ectenagena 358
exustus, Brachidontes 1, 24, *25–28*, 29, 30
  Brachidontes (*Hormomya*) 24
  Mytilus 24

fabagella, Rupellaria 195
Fabulina (*Moerella*) *peitaihoensis* 198
Felipponea 247, 249, 251, 261, 262, 264
  neritiniformis 252
ferrusacci, Adelomelon 344
figulina, Pomacea 248, 255, 274, 280
flagellata, Pomacea 261, 262, 269
flagellus, Arion 303–305, 308, 313, *314*, *315*, 316
  Arion (*Mesarion*) 306
floridana, Carditamera 1, 66, *67–69*, 70
  Cyrena 92, 98
  Polymesoda 1, 92, *93–97*
Forbesopomus 247, 249, 250
fortunei, Limnoperna 129–132, *133*, *135–137*, 137, 138, 141–143
fragilis, Atrina 49
  Raeta 202, *202*
Fulvia papyracea 103
fusaniana, Euphaedusa 226
fuscus, Arion 303, 308, 313, *314*, *315*
  Arion (*Mesarion*) 306

gaederopus, Spondylus 56
galatheae, Neopilina 4
garrettiana, Turbonilla 220
  Turbonilla (*Chemnitzia*) 221
gascognensis, Leptochiton 153
Gastrochaena 91
  (*Gastrochaena*) *hians* 87
  hians 87, 91
  (*Rocellaria*) *hians* 87
Gastrochaenidae 1, 87
Geloina erosa 98
geversianus, Trophon 334
gibba, Pyrgulopsis 170
gibbosa, Plicatula 1, 57, *58*, *59*, 60
gigas, Ampullaria (*Pila*) 257
  Crassostrea 189
  Strombus 163
glabratum, Monodonta 206
Glans carpenteri 70
glauca, Pomacea 248
globosa, Pila 251, 255–258, 261, 265, 268, 276
globulosus, Buccinanops 344
Gloiobdella michaelseni 274
Glossidae 349
Glossoidea 349, 350
gouldii, Acorylus 110
  Solen 200
gracilis, Pila 252, 275, 280
  Pyrgulopsis 170
gradata, Scalaria 213
Gradatiscala gradata pygmaea 179, 213
gregaria, Nassa 218
gregarius, Nassarius 179, 218
griffini, Vokesinotus 333
Gryphaeidae 1, 2, 35, 65
gubernaculum, Anadara 184

habei, Leptochiton 153
haemophila, Ozmana 274
hakodatensis, Lima 194
  Limaria 194, 195
Harpidae 333
haswelli, Turbellaria 274
haustrum, Pomacea 274
Hawaiarca 186
Helicidae 230
Helobdella adiastola 274
  ampullariae 273, 274
  simplex 274
  triserialis 274
Herilla bosniensis 226, 230
heterospiralis, Littorina 206, *208*
Hexaplex 329
hians, Gastrochaena 87, 91
  Gastrochaena (*Gastrochaena*) 87
  Gastrochaena (*Rocellaria*) 87
  Lamychaena 1, 75, 87, *87*, *88*, *90*, 91, 92
  Pholas 87
hiotis, Pycnodonte 35
hirasei, Volachlamys 192
Hirudinea 274
huarpium, Ozmana 273, 274
Hubertschenckia 350
Hydrobiidae 167, 169
hyotis, Hyotissa 1, 39, 40, *40–42*, 43, 114
  Mytilus 35, 40
  Pycnodonte (*Hyotissa*) 35
Hyotissa 1, 5, 39, 40, 43, 110–114, 116, *117*
  hyotis 1, 39, 40, *40–42*, 43, 114
  mcgintyi 1, 35, *35*, *36*, *38*, *39*, 40, 43, 114

ictericus, Spondylus 56, 57
iheringi, Temnocephala 274
imitatrix, Lophyropsis 147
inaequivalvis, Anadara 184
incongrua, Macoma 198
inflata, Entodesma 75
insularum, Pomacea 248, 249
insularus, Pomacea 275
intermedia, Limopsis 24
interplicata, Arca (*Barbatia*) 183, 187, *187*
  Arcopsis 187
  Barbatia 187
  Verilarca 179, 187
  Verilarca (*Verilarca*) 187
Irus mitis 195
Isognomon 5, 113–115, *117*
  alatus 1, 30, *30*, *32*, *33*, 34, 35
  bicolor 34
  isognomon 34
  isognomum 34
  perna 34
  radiatus 34
isognomon, Isognomon 34
Isognomonidae 1, 30, *30*, *32*, *33*, 34
isognomum, Isognomon 34
isolata, Pyrgulopsis 170
Isorropodon 351
itala, Delima 226
italiana, Medora 226

japonica, Siphonaria 221
jedoensis, Leukoma 195
  Protothaca 195
Jolya rhomboidea 195
juyuyensis, Bulimulus 363

kagoshimensis, Anadara 184
  Arca 184
  Scapharca 184
Kelliella 349, 357
Kelliellidae 349, 350
kerguelensis, Leptochiton 147, 148, 153, 154
kilmeri, Phreagena 358
kiusiuensis, Donax 198
kolarovai, Acmaea 204

labio, Monodonta 204, 206
Laevicardium 5, 113, *117*
  brasilianum 103
  laevigatum 98, 103, 104
  pristis 98, 104
  serratum 1, 86, 98, *99*, *100*, *102*, 103, 104, 115
laevigatum, Cardium 98, 103
  Laevicardium 98, 103, 104
laevis, Epitonium (*Scalaria*) *subtilis* 213, 214
  Epitonium (*Scalaria*) *subtilis* var. 213
lamarckii, Cardium 103
laminata, Cochlodina 226, 230
lamothei, Turbellaria 274
Lamychaena 5, 112, 113, *117*, 118
  hians 1, 75, 87, *87*, *88*, *90*, 91, 92
lanceolata, Limopsis 24
Lanistes *247*, 248–251, 254, 261, 262, 264
  bolteniana 261, 262
  carinatus *252*, 275, 280
  libycus 263, 277
  nyassianus 258
  ovum *238*, 240, 277
lapillus, Nucella 157, 163
Laternula liautaudi 203
  marilina 203
Laternulidae 203
latidens, Leptochiton 153
Laubiericoncha 349–352, *355*, 355–358, *357*
  angulata 350, *355*, 355–358

  chuni 350, *355*, 355–358
  myriamae 350, *355*, 355–358
  nanshaensis 350, *355*, 355–358
  puertodeseadoi 349, 350, *351–354*, 352, 355–358
  suavis 350, 355, *355*, 356, 358
Leda carpenteri 10
Leioselenus 4
Lepidopleurus 154
Leptochiton 147, 148, 153
  agesilaus 147, 153
  badius 153
  cimicoides 153
  compostellanum 153
  darioi 147, 148, 153
  gascognensis 153
  habei 153
  kerguelensis 147, 148, 153
  latidens 153
  medinae 147, 148, 153
  muelleri 153
  pagenstecheri 147, 153
  sanmatiensis 147, 148, *149*, *151*, *152*, 153, 154
Leptochitonidae 147, 148
Lernaeidae 273
Leucostigma candidescens 225, 226, *227*, *228*, 229, 230
Leukoma jedoensis 195
liautaudi, Laternula 203
libertina, Semisulcospira 270
libycus, Lanistes 263, 277
Lima angulata var. *minor* 194
  hakodatensis 194
Limaria 194
  basilanica 195
  hakodatensis 194, 195
  (*Limaria*) *basilanica* 194, 195
  (*Limaria*) *orientalis* 195
  orientalis 195
Limidae 194
Limnoperna fortunei 129–132, *133*, *135–137*, 137, 138, 141–143
Limopsidae 1, 21
Limopsis 5, 110, *117*
  cristata 21, 24
  cristata aff. 1, 21, *21*, 22
  intermedia 24
  lanceolata 24
lineata, Pomacea 248, 255, 265, 274, 275, 280
Lithophaga 4, 5, 114, 115, *117*, 118
  aristata 4
Littorina brevicula 206
  heterospiralis 206, *208*
  obtusata 174
Littorinidae 206
lockensis, Pyrgulopsis 167, 169, 170, 172, *173*
Lophyropsis imitatrix 147
Lucinidae 1, 76, 349
Lucinoidea 81
lunella, Abra 198
lusitanicus, Arion 303, 304, 308, 310, 313, *314*, *315*, 316, 317
  Arion (*Mesarion*) 306
luteostoma, Thais 216
luzonica, Pila 280
Lymnaea stagnalis 277
Lyonsia beana 70
  californica 75
  (*Philippina*) *beana* 70
Lyonsiidae 1, 70

macerophylla, Chama 1, 81, *82–84*, 86, 111, 112
macgintyi, Parahyotissa 35
Macoma 110, 198
  incongrua 198
  murrayi 198
Mactra (*Mactra*) *veneriformis* 201
  quadrangularis 201
Mactridae 200
maculata, Pomacea 239, 240, 248, 249, 251–253, *252*, 255, 257, 262, 263, 267–269, 271, 274, 275, 280, 282
magellanica, Odontocymbiola 344, 345
Mangelia costulata 220
  dobsoni 179, 220
Mangeliidae 220
Maoricrypta monoxyla 164
marcida, Pyrgulopsis 167, 169–171, 173–175, *173*
Marginellidae 333
marilina, Laternula 203
Marisa *247*, 249, 251, 254, 255, 261, 262, 264
  cornuarietis *238*, 239, 240, 250, 252, *252*, 255–258, 261, 268, 275, 276, 278–280
maritima, Cyclas 92, 98
  Polymesoda 92, 98
  Polymesoda (*Pseudocyrena*) 92
mcgintyi, Hyotissa 1, 35, *35*, *36*, *38*, *39*, 40, 43, 114
  Parahyotissa (*Parahyotissa*) 35
medinae, Leptochiton 147, 148, 153, 154
Medora 225, 226, *227*, *228*, 229, 230
  italiana 226
megastoma, Pomacea 274
Melanoides *172*, 174, 175
  tuberculata 167, 169, 170, 172, *173*, 174
  tuberculatus 365, *366*, *367*, 368
Mercenaria 349

merriami, Pyrgulopsis 171
Mesocibota 186
  bistrigata 185, 186
michaelseni, Gloiobdella 274
minor, Acmaea testudinalis var. 204
  Epitonium scalare 179, 213
  Epitonium (*Scalaria*) *pretiosa* var. 212, *214*
  Lima angulata var. 194
  Notolimea 194
  Promantellum 194
  Scalaria pretiosa 212
mitis, Irus 195
Modiola aquarius 195
  subrugosa *194*, 195
Modiolus (*Modiolusia*) *elongatus* 195
  nitidus 195
Moerella rutila 198
Monodonta glabratum 206
  labio 204, 206
  trochiformis 204, *208*
Monoplacophora 4
monoxyla, Maoricrypta 164
muelleri, Brachidontes 30
  Leptochiton 153
mulleri, Brachidontes 30
Muricidae 214, 323, 324, 329, 333, 334
Muricinae 324, 327, 329, 334
Muricopsinae 333, 334
murrayana, Abra 198
  Tellina 198
murrayi, Macoma 198
  Tellina 198
Musculista 195
musica, Voluta 345
Myoforceps 4
  aristatus 4
myriamae, Laubiericoncha 350, *355*, 355–358
Mytilidae 1, 4, 24, 118, 129, 195, 349
Mytilimeria nuttallii 75
Mytilus edulis 174
  exustus 24
  hyotis 35, 40
  roseus 35, 40

nanshaensis, Laubiericoncha 350, *355*, 355–358
Nassa gregaria 218
Nassariidae 218
Nassarius gregarius 179, 218
  (*Hima*) *pauper* 218
Naticidae 357
navicula, Entodesma 75
nelsoni, Rissoina 209, *210*
Neopilina 5, 111, 115, *117*
  galatheae 4
neritiniformis, Felipponea 252
Nipponarca 186
  adamsiana 186
nitidus, Modiolus 195
nobrei, Arion 303, 308, 313, *314*, *315*, 316
  Arion (*Mesarion*) 306
Noetiidae 1, 15
notialis, Solemya 10
Notolimea minor 194
Nucella lapillus 157, 163
Nucinellidae 349
Nuculana carpenteri 10
Nuculanidae 1, 10
nuttallii, Mytilimeria 75
nyassianus, Lanistes 258

obsoletocostata, Anomia nipponensis var. 189
obsoleto-costata, Anomia nipponensis var. 189, *190*
obtusata, Littorina 174
occidentalis, Solemya 1, 6, *6–8*, 10, 111, 115
  Solemya (*Petrasma*) 6
Ocenebrinae 324, 327, 331, 333, 334
Odontocymbiola magellanica 344, 345
Odontocymbiolinae 344
oevis, Scalaria subtilis 213
orbicularis, Codakia 1, 76, *76–79*, 103
  Codakia (*Codakia*) 76
  Venus 76
orientalis, Limaria 195
  Limaria (*Limaria*) 195
Osteodesma brasiliensis 70, 75
  braziliensis 75
ostraeiformis, Crepidula 211, *212*
Ostrea alata 30
  chemnitzi var. *elongata* 187, *188*
  (*Crassostrea*) *pestigris* 189
  (*Crassostrea*) *pes-tigris* 189
  elongata 187
  gigas var. *tientsiensis* 189
  (*Ostrea*) *thomasi* 35
  rosea 40
  thomasi 35
  sellaeformis var. *thomasi* 35
Ostreidae 34, 86, 187
outicula, Anomia 189
ovalis, Cardites 70
  Tellinides 198
ovata, Pila 261, 277
oviputamen, Cardium 98, 103
ovum, Lanistes *238*, 240, 277
  Pila 277
Ozmana haemophila 274
  huarpium 273, 274
Ozmanidae 273

paestana, Siciliaria 225–227, *227*, *228*, 229, 230
pagenstecheri, Leptochiton 147, 153
paludosa, Pomacea 252, 258, 260, 263, 267–269, 272, 274, 275, 277, 278, 280
Papillifera bidens 225, 226, *227*, *228*, 229, 230
papyracea, Fulvia 103
  Pomacea 251, 252
Paradentalium 5, 113, *117*
  disparile 4
Parahyotissa 39, 40, 43
  chemnitzii 189
  macgintyi 35
  (*Parahyotissa*) *mcgintyi* 35
  rosea 35, 40
parcespinosum, Echinostoma 274
Patella peitahoensis 204, *205*
  testudinaria 204
Patellidae 204
Patelloida 204
  pygmaea 204
pauper, Nassarius (*Hima*) 218
Paziella 323
pechiliensis, Anatina 203, *203*
  Purpura alveolata var. 216, *216*
  Rapana 214, *215*
  Rupellaria 195, *196*, *197*
  Solen corneus var. 198, *200*
Pecten solaris var. *peitaihoensis* 192
  teilhardi 192, *192*
Pectinidae 56
peitaihoensis, Acmaea 204, *205*
  Anadara 184
  Arca (*Scapharca*) 184, *185*
  Chlamys solaris var. 192, *193*
  Collisella 179, 204
  Fabulina (*Moerella*) 198
  Patella 204, *205*
  Pecten solaris var. 192
  Scapharca 184
  Tellina (*Tellinides*) *planissima* var. 198, *199*
pellicula, Raeta 202
pellucida, Chama 86
perna, Isognomon 34
perrugatus, Vokesinotus 323, 324, *325*, 327, 331, *332*, *333*, 333
persica, Phyllodina 110
pesmei, Pila 252, 275, 280
pestigris, Ostrea (*Crassostrea*) 189
pes-tigris, Ostrea (*Crassostrea*) 189
petitiana, Tellina 110
Phaedusinae 226
Pholas hians 87
Phreagena kilmeri 358
  soyoae 358
Phyllodina persica 110
Phyllonotus 329
  pomum 329, 331
phyllopterus, Timbellus 323, 324, *325*, 327, *328*, *329*, 329, 331, 334
Physa *172*, 172, 174, 175
  acuta 169, 171, 172, *173*
Physidae 169
Pila *247*, 248–251, 253–255, 258, 260, 261, 264, 268–270, 274, 279, 280
  ampullacea *252*, 275, 280
  angelica 280
  conica 275
  globosa 251, 255–258, 261, 265, 268, 276
  gracilis 252, 275, 280
  luzonica 280
  ovata 261, 277
  ovum 277
  pesmei 252, 275, 280
  polita 252, 275, 280
  scutata 274, 275, 280
  turbinis 280
  virens 265, 275
  virescens 252, 256, 261, 264, 275, 280
Pilidae 248
Pinna 5, 113–115, *117*
  carnea 1, 43, *44–46*, *48*, 49, 112
Pinnidae 1, 43, 49
plana, Anomia 189, 191
planulata, Pyrgulopsis 171
platae, Asolene 233, 234, 236, *236–238*, 238–241, *252*, 258
Pleurophopsis 350, 352
Plicatula 5, 111, 115, 116, *117*
  australis 60
  gibbosa 1, 57, *58*, *59*, 60
Plicatulidae 1, 57
plicatulus, Radix 269
Pliocardiinae 350, 358
Poirieria 323
polita, Ampullaria 256
  Pila 252, 275, 280
Polymesoda 5, 113, *117*
  caroliniana 98
  floridana 1, 92, *93–97*
  (*Geloina*) 98
  maritima 92, 98
  (*Pseudocyrena*) *maritima* 92
Pomacea 233, 234, 241, *247*, 248–251, *250*, 254, 255, 257, 258, 260–262, 264, 265, 267, 270–272, 278, 280, 281
  canaliculata 235, *238*, 239–241, 245, 248, 250–282, *273*
  curumim 251, 252
  diffusa 248
  figulina 248, 255, 274, 280
  flagellata 261, 262, 269

  glauca 248
  haustrum 274
  insularum 248, 249
  insularus 275
  lineata 248, 255, 265, 274, 275, 280
  maculata 239, 240, 248, 249, 251–253, *252*, 255, 257, 262, 263, 267–269, 271, 274, 275, 280, 282
  megastoma 274
  paludosa 252, 258, 260, 263, 267–269, 272, 274, 275, 277, 278, 280
  papyracea 251, 252
  patula catemacensis 261, 262
  scalaris 248, 252, 258, 271, 272, 275
  sordida 248, 255
  urceus 251, 255, 258, 261, 263–265, 268
pomaceae, Catadiscus 274
  Cercaria 274
Pomella 248
pomum, Phyllonotus 329, 331
porrecta, Tryonia 171
pretiosa, Scalaria 21
Pretostrea rosacea 189
pristis, Laevicardium 98, 104
Promantellum minor 194
Propeleda 5, 113, 115, 116, *117*
  carpenteri 1, 10, *11–13*, 15, 111
  carpentieri 10, 15
Protothaca jedoensis 195
Pseudoceratodes 248
puertodeseadoi, Laubiericoncha 349, 350, *351–354*, 352, 355–358
pulchella, Asolene 233, 253, 256, 257, 261, 275
pumila, Tellina 198
punctata, Aplysia 162, 163
Purpura altispiralis 218, *218*
  alveclata 216
  alveolata var. *pechiliensis* 216, *216*
  bronii 216
  bronni 216
  bronni var. *suppressa* 216, *217*
Pycnodonte (*Hyotissa*) *hyotis* 35
  hiotis 35
pygmaea, Epitonium (*Scalaria*) *gradata* var. 213
  Gradatiscala gradata 179, 213
  Patelloida 204
  Scalaria gradata 213
Pyramidellidae 220
Pyrgulopsis *172*, 172, 174
  bruneauensis 174
  carinata 170
  cruciglans 170
  gibba 170
  gracilis 170
  isolata 170
  lockensis 167, 169, 170, 172, *173*
  marcida 167, 169–171, 173–175, *173*
  merriami 171
  sathos 171
  serrata 171
  sulcata 171
  planulata 171
  turbatrix 167, 169, 171–173, *173*

quadrangularis, Mactra 201
quadrasi, Radix 270
quadrata, Sinotaia 270

radiatus, Isognomon 34
Radix plicatulus 269
  quadrasi 270
Raeta fragilis 202, *202*
  pellicula 202
Rapana pechiliensis 214, *215*
  venosa 214
Rapaninae 323, 324, 333
reidi, Solemya 10
renschi, Adzharia 363, 364, *364*
reticulatum, Deroceras 303
rhomboidea, Jolya 195
Rissoidae 209
Rissoina barbara 179, 209, *209*
  bureri 179, 211, *211*
  dunedini 209, *210*
  dunedoni 209
  nelsoni 209, *210*
rochensis, Turbellaria 274
rosacea, Pretostrea 189
rosea, Ostrea 40
  Parahyotissa 35, 40
roseus, Mytilus 35, 40
rufus, Arion 303, 304, 306–308, *309*, 310–313, *311*, *312*, *314*, *315*, 316, 317, 320, 321
  Arion (*Arion*) 306
  Arion ater 304
Rupellaria fabagella 195
  pechiliensis 195, *196*, *197*
rustica, Chlorostoma 204
rutila, Moerella 198

sanmatiensis, Leptochiton 147, 148, *149*, *151*, *152*, 153, 154
sathos, Pyrgulopsis 171
sativa, Scapharca
Saulea 249–251, 254, 261, 264
  vitrea *252*, 253
saxicola, Entodesma 75
Scalaria gradata 213
  gradata pygmaea 213

  pretiosa 212
  pretiosa minor 212
  subtilis 213
  subtilis oevis 213
scalaris, Pomacea 248, 252, 258, 271, 272, 275
Scapharca kagoshimensis 184
  peitaihoensis 184
  sativa 184
Schistosoma 280
Schistosomatidae 274, 280
Scissula 5, 109, 112–114, *117*, 118
  candeana 110
  similis 1, 104, *105*, *106*, *109*, 109, 110
scutata, Pila 274, 275, 280
sellaeformis, Ostrea var. *thomasi* 35
Semelidae 198
semiorbiculata, Beguina 70
Semisulcospira libertina 270
senhousia, Arcuatula 195
serrata, Pyrgulopsis 171
serratum, Cardium 98, 103
  Laevicardium 1, 86, 98, *99*, *100*, *102*, 103, 104, 115
Siciliaria 225
  paestana 225–227, *227*, *228*, 229, 230
signata, Barbatia 186
silvaticus, Arion 308, 313, *314*, *315*
  Arion (*Carinarion*) 306
similis, Scissula 1, 104, *105*, *106*, *109*, 109, 110
  Tellina 104
  Tellina (*Scissula*) 104
simplex, Anomia 1, 60, *61*, *62*, *64*, 65, 66, 110, 111, 114, 115
  Helobdella 274
Sinotaia quadrata 270
Siphonalia alterniplicata 221
Siphonaria alterniplicata 221, *221*
  japonica 221
Siphonariidae 221
Siphopatella walshi 212
Solemya 5, 10, 110, 112, 113, 115, 116, *117*
  notialis 10
  occidentalis 1, 6, *6–8*, 10, 111, 115
  (*Petrasma*) *occidentalis* 6
  reidi 10
  togata 10
  velum 10
Solemyidae 1, 6, 349
Solemyoidea 115
Solen corneus 200
  corneus var. *pechiliensis* 198, *200*
  gouldii 200
  strictus 198, 200
Solenidae 198
Solenomyoidea 115
solida, Arcopsis 20
solisianus, Brachidontes 29
sordida, Pomacea 248, 255
soyoae, Phreagena 358
spixii, Asolene 275
Spondylidae 1, 50, 56
Spondylus 5, 111, 112, 115, *117*
  ambiguus 56, 57
  americanus 1, 50, *51–54*, 56, 57, 111, 112
  gaederopus 56
  ictericus 56, 57
  tenuis 57
sporadicus, Bulimulus bonariensis 363, *364*
stagnalis, Lymnaea 277
Stramonita biserialis 323, 324, *325–327*, 327, 334
Striarca symmetrica 187
strictus, Solen 198, 200
Strombus gigas 163
suavis, Laubiericoncha 350, 355, *355*, 356, 358
subcrenata, Anadara 184
  Arca 184
  Arca (*Anomalocardia*) 184
subrugosa, Modiola *194*, 195
subtilis, Scalaria 213
sulcata, Cardita 70
  Pyrgulopsis 171
suppressa, Purpura bronni var. 216, *217*
  Thais bronni 216
sybariticus, Angulus 110
symmetrica, Striarca 187

talonata, Talonostrea 189
Talonostrea talonata 189
teilhardi, Pecten 192, *192*
Tellina 109, 110
  murrayana 198
  murrayi 198
  petitiana 110
  pumila 198
  similis 104
  (*Scissula*) *similis* 104
  (*Tellinides*) *planissima* var. *peitaihoensis* 198, *199*
  trigonoides 198
Tellinidae 1, 81, 104, 109, 198
Tellinides ovalis 198
Temnocephala iheringi 274
tenuis, Angulus 109, 110
  Spondylus 57
Terebra ballanodosa 219
  bellanodosa 179, 219, *219*
Terebridae 219
testudinaria, Acmaea 204, *206*
  Patella 204

Thais bronni suppressa 216
  clavigera 216, 218, 278
  luteostoma 216
Thiaridae 169, 172
thomasi, Ostrea 35
  Ostrea (*Ostrea*) 35
Thyasiridae 349
tientsiensis, Ostrea gigas var. 189
Timbellus 323, 329, 333, 334
  phyllopterus 323, 324, *325*, 327, *328*, *329*, 329, 331, 334
togata, Solemya 10
torrefactus, Chicoreus 334
Trapezidae 349
Trigonella quadrangularis var. *ventricosa* 200, *201*
trigonoides, Tellina 198
triserialis, Helobdella 274
Trochidae 204
  ephebicostalis 204
  (*Livona*) *ephebocostalis* 204, *207*
trochiformis, Monodonta 204, *208*
troncosoi, Calyptogena 357
Trophon geversianus 334
Trophoninae 323, 333
Tryonia 167, 171, *172*, 172, 174
  porrecta 171
tuberculata, Melanoides 167, 169, 170, 172, *173*, 174
tuberculatus, Melanoides 365, *366*, *367*, 368
turbatrix, Pyrgulopsis 167, 169, 171–173, *173*
Turbellaria haswelli 274
  lamothei 274
  rochensis 274
Turbinellidae 333
turbinis, Pila 280
Turbonilla (*Chemnitzia*) *garrettiana* 221
  garrettiana 220
  garrettiana var. *alba* 220, *220*

Unionicola (*Ampullariatax*) *ampullariae* 274
urceus, Pomacea 251, 255, 258, 261, 263–265, 268
Urosalpinx 333
  cinerea 333

variabilis, Donax 4, 115, 116
variegata, Cardita 70
vaubanensis, Bouchetia 333
velum, Solemya 10
velutina, Cyclocardia 70
Veneridae 81, 195, 339
Veneroidea 349
veneriformis, Mactra (*Mactra*) 201
venosa, Rapana 214
ventricosa, Cyclocardia 70
  Trigonella quadrangularis var. 200, *201*
Venus alta 195
  jidoensis var. *alta* 195, *196*
  orbicularis 76
Verilarca interplicata 179, 187
  (*Verilarca*) *interplicata* 187
Vesicomya 350, 351, 358
  albida 357
Vesicomyidae 349–351, 357, 358
Vexilla vexillum 333
Vexillidae 333
vexillum, Vexilla 333
virens, Pila 265, 275
virescens, Barbatia (*Savignyarca*) 186
  Pila 252, 256, 261, 264, 275, 280
vitrea, Saulea *252*, 253
Vitularia 333
Viviparoidea 248
Vokesinotus 333
  griffini 333
  perrugatus 323, 324, *325*, 327, 331, *332*, *333*, 333
Volachlamys hirasei 192
Voluta ebraea 344
  musica 345
Volutidae 157, 337, 338, 344, 345, 357
vulgaris, Arion 303–313, *305*, *310–312*, *314*, *315*, 316, 317, 320, 321
  Arion (*Arion*) 306

walshi, Siphopatella 212

Zidona dufresnei 157, 158, *159–162*, 162–164, 345
Zidoninae 344

Vol. 49, No. 1	10 Nov. 2006
Vol. 49, No. 2	27 July 2007
Vol. 50, No. 1–2	9 June 2008
Vol. 51, No. 1	19 Mar. 2009
Vol. 51, No. 2	26 Aug. 2009
Vol. 52, No. 1	27 Jan. 2010
Vol. 52, No. 2	7 May 2010
Vol. 53, No. 1	19 Oct. 2010
Vol. 53, No. 2	8 Mar. 2011
Vol. 54, No. 1–2	25 Oct. 2011
Vol. 55, No. 1	17 Sep. 2012
Vol. 55, No. 2	28 Dec. 2012
Vol. 56, No. 1–2	31 Dec. 2013
Vol. 57, No. 1	26 June 2014
Vol. 57, No. 2	17 Oct. 2014

For a full list of the publication dates of Malacologia up to 2008, see:

Coan, E. V., 2008, Publication dates of Malacologia volumes and issues. *Malacologia*, 50(1/2): 361.

INSTRUCTIONS FOR AUTHORS

1. MALACOLOGIA publishes original research on the Mollusca that is of high quality and of broad international interest. Papers combining synthesis with innovation are particularly desired. While publishing symposia from time to time, MALACOLOGIA encourages submission of single manuscripts on diverse topics. Smaller papers of local geographical or systematic content, and of high quality and interest, may be accepted as 'Research Notes'. Nearly all branches of malacology are represented in the pages of MALACOLOGIA.
2. Manuscripts submitted for publication are received with the tacit understanding that they have not been submitted or published elsewhere in whole or in part.
3. Manuscripts must be in English, but may include an expanded abstract in a foreign language as well as the usual brief abstract in English. Both American and British spellings are allowed.
4. Unless indicated otherwise below, contributors should follow the recommendations in the Council of Science Editors (CSE) Scientific Style and Format manual, 7th ed., 2006.
5. Be brief.
6. Manuscripts must be prepared using Microsoft Word® (Windows-version), 12-pitch, Arial font, lines at 1.5 spaces throughout (including the references, tables and figure captions), no added spaces before or after paragraphs, text aligned left, ragged right. Tables, figure captions and figures are to be placed on separate pages at the end of the file. Make the hierarchy of headings within the text simple and consistent. Avoid internal page references.
7. Choose a running title (a shortened version of the main title) of fewer than 50 letters and spaces.
8. For full papers, provide a concise and informative abstract summarizing not only contents but also results. A separate summary is not wanted. Research Notes do not require an added abstract.
9. Supply between five and eight key (topic) words to go at the end of the Abstract for full-length papers.
10. Use the metric system throughout. Micron should be abbreviated µm.
11. Three types of illustrations are accepted: (A) line art figures (black-and-white drawings, diagrams), (B) gray-step figures ("black-and-white" photographs or gray-step drawings) and (C) color figures. Gray-step and color figs. should be saved with a resolution of 300 dpi; line art with 1200 dpi. Illustrations are printed either in one column or the full width of a page of the journal, so plan accordingly. The maximum size of a printed figure is 13.5 x 20.0 cm (preferably not as tall as this so that the caption does not have to be on the opposite page). The figure captions are not to be part of the figure.
12. Lines, letters, and numbers should be thick enough to allow reduction by 30% to 50%. Letters and numbers (Arial font) should be at least 2 mm (line art) or 3 mm (gray-step, color) high after reduction, but avoid letter sizes > 6 mm. In line drawings, the minimum line width of 0.2 mm is required (as measured by final size). Several drawings or photographs may be grouped together as plate.
13. All illustrations should be numbered sequentially and not as lettered sub-series. All figures must be cited in the text in the order in which they appear.
14. Scale lines are required for all none diagrammatic figures, and should be convenient lengths (e.g., "200 µm", not "163 µm"). Magnifications in captions are not acceptable. But object or specimen sizes in a caption are acceptable.
15. Be professional. Sloppy illustrations, labels, borders will not be accepted. If assistance is required of MALACOLOGIA's editorial staff, the author will be charged for the services rendered.
16. A caption should summarize what is shown in an illustration, and should not duplicate information given in the text. Each lettered abbreviation labeling an individual feature in a figure must either be explained in each caption (listed alphabetically), or be grouped in one alphabetic sequence after the Methods section. Use the latter method if many abbreviations are repeated on different figures.
17. Tables are to be used sparingly. All tables must be cited in the text in the order in which they appear. Tables should be composed using the table function of Word (and **not** tab-delimited text).

18. References cited in the text must appear in the Literature Cited section and vice versa. Refer to a recent issue of MALACOLOGIA for bibliographic style, noting especially that serials are cited unabbreviated. Supply information on plates, etc., only if they are not included in the pagination.
19. In systematic papers, synonymies should not give complete citations but should relate by author, date and page to the Literature Cited section. All new type specimens must be deposited in museums where other scientists may study them. Likewise, MALACOLOGIA requires that voucher specimens upon which a paper is based be deposited in a museum where their identity can be verified.
20. For all papers dealing with molluscan species, each such species should include its author and date upon first appearance, with the correct use of parenthesis around an author in the case of a generic assignment other than the original combination. In all taxonomic papers dealing with one to a few species, the original description of each species should be represented in the Literature Cited. In other studies – physiological, ecological, etc. – involving one or a few species, the author should either cite the original description of the taxon/taxa involved or some other work showing its identity.
21. Submitting your manuscript: Send electronically a single manuscript file (including manuscript text, tables, figure captions and figures) together with a cover letter to the editor at georgedavis99@hotmail.com. Contact the editor to determine the method of submission if the manuscript has file sizes exceeding 6 MB. If you do not receive a confirmation letter from the editor with a identifying manuscript number in 6 working days, send a follow up letter of inquiry (without files). Given today's vagaries of viruses, spam, Trojan incursions, transmission errors, etc. communications can be lost. If you do not hear from the editor following the follow up letter of inquiry within three days, contact the graphics editor (tom.wilke@allzool.bio.uni-giessen.de) or the copy editor (genecoan@gmail.com) to pursue the problem. We never ignore any submission.
22. Once the manuscript is accepted, high quality and full resolution graphic files have to be provided. Submit such graphics to the graphics editor (tom.wilke@allzool.bio.uni-giessen.de) as TIFF files. For other formats or any question regarding electronic submission of graphics, contact the graphics editor. Keep the individual file sizes below 5 MB (using the option "LZW compression" will greatly reduce the size of TIFF files).

REPRINTS AND PAGE COSTS

23. Reprints must be ordered from the Business Office at the time proof is returned to the copy editor. Later orders cannot be considered. When 100 or more reprints are ordered, an author will receive 25 additional copies free of charge.
24. PDF files of the paper for personal use are available with a purchase of reprints; free of charge for subscribers to Malacologia. Subscription must include current and two paid-for immediate past and/or future volumes.
25. Page costs must be paid prior to publication. Page cost recovery is required as follows.
    Regular subscribers:*
    - Non-student: 10 pages free (paper < 30 pages), 15 pages free (paper > 30 pages); U.S. $35.00 for each additional page (EAP)
    - Student**: 10 pages free (paper < 30 pages), 15 pages free (paper > 30 pages); U.S. $20.00 EAP

    Non-subscribers:
    - Non-student: 8 pages free (paper < 30 pages), 10 pages free (paper > 30 pages); U.S. $60.00 EAP
    - Student**: 10 pages free (paper < 30 pages), 15 pages free (paper > 30 pages); U.S. $30.00 EAP

    A reduction or elimination of page charges may be possible under certain circumstances by arrangement with the editor. A reduction of page charges may be negotiated for papers exceeding 30 pages.
26. Color figures must be paid-for by the author. Costs are U.S. $300 for the first color page in a paper and U.S. $150 for each subsequent color page.

SUBSCRIPTION PURCHASE

27. Effective with Vol. 57, subscription rates per volume are as follows:
    Personal: U.S. $75.00
    (Student discounted rate: U.S. $40.00)
    Institutional: U.S. $105.00
    Agency and Dealership: U.S. $105.00
    Current volume postage is included for shipment to an American or a Canadian address. Overseas postage is $16.00 per volume. Single and past volumes are available at subscription rates. Postage and handling is $13.00 per volume for shipment to an American or a Canadian address. Overseas postage is $34.00 per volume. Postage for orders weighing over 4 lbs. will be determined by weight.

* Regular subscribers are those who have paid-up subscriptions for the current volume and two immediate past and/or future volumes.

** Students must identify themselves at the time of manuscript submission and also provide the e-mail address of their advisor.

VOL. 58, NO. 1–2 MALACOLOGIA 2015

CONTENTS

FULL PAPERS

Luiz Ricardo L. Simone, Paula M. Mikkelsen & Rüdiger Bieler
Comparative anatomy of selected marine bivalves from the Florida Keys, with notes on Brazilian congeners (Mollusca: Bivalvia) 1

Nicolás Bonel & Julio Lorda
Growth and body weight variability of the invasive mussel *Limnoperna fortunei* (Mytilidae) across habitat and season 129

Marina Güller, María G. Liuzzi & Diego G. Zelaya
A new species of *Leptochiton* (Polyplacophora: Leptochitonidae) from the southwestern Atlantic 147

Mariel Ojeda, Florencia Arrighetti & Juliana Giménez
Morphology and cyclic activity of the digestive gland of *Zidona dufresnei* (Caenogastropoda: Volutidae) 157

Knut Mehler, Kumud Acharya & Donald W. Sada
Spatial and temporal pattern in length-mass regressions of freshwater gastropods in Nevada spring ecosystems 167

Eugene V. Coan, Konstantin A. Lutaenko, Junlong Zhang & Qimeng Sun
The molluscan taxa of A. W. Grabau & S. G. King (1928) and their types . . . 179

Agnese Petraccioli, Teresa Capriglione, Mariastella Colomba, Paolo Crovato, Gaetano Odierna, Ignazio Sparacio & Nicola Maio
Comparative cytogenetic study in four Alopiinae door snails (Gastropoda, Clausiliidae) 225

María J. Tiecher, María E. Seuffert & Pablo R. Martín
Thermal biology of the South American apple snail *Asolene platae* (Caenogastropoda: Ampullariidae) 233

Kenneth A. Hayes, Romi L. Burks, Alfredo Castro-Vazquez, Philip C. Darby, Horacio Heras, Pablo R. Martín, Jian-Wen Qiu, Silvana C. Thiengo, Israel A. Vega, Takashi Wada, Yoichi Yusa, Silvana Burela, M. Pilar Cadierno, Juan A. Cueto, Federico A. Dellagnola, Marcos S. Dreon, M. Victoria Frassa, Maximiliano Giraud-Billoud, Martín S. Godoy, Santiago Ituarte, Eduardo Koch, Keiichiro Matsukura, M. Yanina Pasquevich, Cristian Rodriguez, Lucía Saveanu, María E. Seuffert, Ellen E. Strong, Jin Sun, Nicolás E. Tamburi, María J. Tiecher, Richard L. Turner, Patricia L. Valentine-Darby & Robert H. Cowie
Insights from an integrated view of the biology of apple snails (Caenogastropoda: Ampullariidae) 245

Bjørn A. Hatteland, Torstein Solhøy, Christoffer Schander, Morten Skage, Ted von Proschwitz & Leslie R. Noble
Introgression and differentiation of the invasive slug *Arion vulgaris* from native *A. ater* 303

Gregory S. Herbert, María José Pio, Guido Pastorino, M. G. Harasewych, Yuri I. Kantor, Dominique Lamy & Jean-Pierre Pointier
Morphological development of the radula of four species of the neogastropod family Muricidae 323

Soledad Zabala, Andrés Averbuj, Carlos Sanchez Antelo, Pablo E. Penchaszadeh & Gregorio Bigatti
Oviposition and embryonic development in the volutid snail *Adelomelon ancilla* 337

Javier Signorelli & Guido Pastorino
A new species of *Laubiericoncha* (Bivalvia: Vesicomyidae) from deep waters off Argentina 349

SMITHSONIAN LIBRARIES
3 9088 01815 9327

VOL. 58, NO. 1–2 MALACOLOGIA 2015

CONTENTS

RESEARCH NOTES

Bernhard Hausdorf
The supposed Transcaucasian endemite *Adzharia renschi* Hesse, 1933 is a South American *Bulimulus* species (Gastropoda: Bulimulidae) 363

Eder Carvalho da Silva & Francisco Barros
Sensibility of the invasive snail *Melanoides tuberculatus* (Müller, 1774) to salinity variations 365

INDEX 371

913 Y5 8931
10/03/16 815750 Group

SMITHSONIAN INSTITUTION LIBRARIES
3 9088 01740 4393